PETROLOGY OF THE EARTH'S DEEP CRUST AND UPPER MANTLE AND THE ORIGINS OF MAGMAS IN THE EARTH AND MOON

Headley

David H. Green

A collection of published papers submitted to the University of Tasmania for the degree of Doctor of Science

August, 1988.

SUMMARY

The publications forming this thesis are grouped in three themes:

1. Petrology of the Earth's upper mantle, and of mantle-derived magmas and petrology of lunar magmas (publications in series A, B, C, D).

2. Petrology of the deep crust with emphasis on geothermometry and geobarometry as a means of investigating high pressure/high temperature metamorphism (publications in series E).

3. Roles of volatiles, particularly C-H-O fluids, in deep crust and upper mantle (publications in series B, D).

a. ***Petrology of the Earth's Mantle and of Mantle-derived Magmas:***

The study of the Lizard Peridotite, UK,[A5-7] led to the recognition of four isochemical mineral assemblages for natural lherzolite compositions, i.e. plagioclase lherzolite, aluminous pyroxene + aluminous spinel lherzolite, garnet lherzolite and pargasite lherzolite. These alternative mineral assemblages were inferred to play significant roles in a mineralogically layered upper mantle.[D1] A major thrust of the high pressure/temperature experimental work has been to define the stability fields for these mineral assemblages[D2-6] and to experimentally calibrate mineral reactions and solid solutions[D7,8,10,11,14,15-17] so that they can be used as sensors to determine pressure and temperature of crystallization of natural mantle samples. Theoretical analysis of amphibole stability[E2,B10,B12] led to the prediction that this important water-bearing mineral would be unstable at quite moderate pressures in the Earth's mantle and that at greater depths, even very small amounts of water in the Earth's mantle would produce melting at very low temperatures. This inference was experimentally demonstrated[D5,6,E14] and, based on these experiments, a petrological explanation and prediction of lithosphere/asthenosphere characteristics was presented.[B12,15,D5,9] In this model, the lithosphere/asthenosphere characteristics are directly attributed to the presence of an intergranular, volatile-rich olivine nephelinitic to olivine melilititic melt at temperatures > 1000°C, and at depths in excess of ~ 90 km (P > 28-30 kb). At shallower depths, amphibole stability to temperatures of 1150°C produces

a higher temperature solidus for the mantle so that normal geothermal gradients to not intersect the mantle solidus at depths < 90 kms. The geophysical and geochemical consequences of this model have been explored with an important consequence being the advocacy of the asthenosphere as a region of mantle chemical fractionation(B12,37,D9,20), the deeper levels becoming depleted in a small, highly undersaturated melt fraction and the upper part of the asthenosphere and base of the lithosphere becoming enriched in this melt fraction or in pargasitic amphibole (lithosphere).

In parallel with the investigations of the characteristics of peridotite at high pressure, the behaviour of basaltic liquids at high pressure was also investigated.(B series, C series) The 1967 paper with A.E. Ringwood(B3) was arguably the most influential and quoted paper in basalt petrogenesis over more than a decade. This work systematically explored the liquidus phases of several basalts as functions of pressure and temperature, and most importantly, pioneered the application of the electron microprobe to analyze the 5-50 micron crystals produced in the high pressure experimental charges. The combination of solid media high pressure apparatus and electron microprobe analysis revolutionized experimental petrology with the demonstration that chemically complex, natural rock compositions could be studied quantitatively. Mineral equilibria exactly duplicating natural samples could be studied without ambiguity or extrapolation in the laboratory.

In addition to the pioneering approach to experimental petrology of natural rocks, the 1967 paper presented the concept of adiabatic upwelling as the primary determinant of magma composition and type and integrated major element, trace element and isotopic data into one petrogenetic framework. Controversial statements that trace element and isotopic abundances in magmas were of little or no significance in characterizing melting conditions or mineralogy of magma source rocks [but reflected pre-histories of source rocks and open-system relationships between magmas and wall rocks] were sufficiently provocative to evoke vigorous response, investigation and competition on the basalt petrogenesis theme from the geochemist fraternity. The interaction of experimental petrology and geochemistry has continued to be a powerful approach to understanding the earth's upper mantle.(A9-11,14,18,20,B25,26)

The investigation of processes and products of melting of the upper mantle has continued using an approach emphasizing a synergistic relationship

between natural petrology and experimental petrology. The collection of chemical and petrological data on natural basalts containing high density mantle-derived xenoliths made it possible to characterize the spectrum of liquids formed within the upper mantle[B6,10,18] - these mantle-derived liquids were then studied experimentally to define P,T conditions of origin. This approach led to the recognition of the importance of amphibole fractionation under upper mantle conditions[B18] and to the recognition that many mantle-derived magmas could *not* form from an anhydrous peridotite source.[B6-13] Systematic investigation of the role of water in phase relationships of both peridotite[D5,6] and basalts established conditions of origin for olivine-rich basanite compositions[B17] and, under hydrous conditions, for very siliceous high magnesia andesites and boninites in very low pressure, water-rich environments.[B20,37,39] Similarly, indications of the important effects of $CO_2(CO_3)^=$ solubility at high pressure[B17] led to the participation in, and supervision of G.P. Brey's project on role of CO_2 in the genesis of extremely silica-undersaturated olivine melilitite liquids.[B19,22,24,26]

The techniques and philosophical approach developed for study of petrogenesis of terrestrial basalts led naturally, during the early 1970s, into participation in studies of lunar petrogenesis. Systematic liquidus studies at low and high pressure defined relationships between basalt types and constrained the nature of the lunar interior in a series of, at times, controversial papers. Of particular importance were papers demonstrating conditions of origin for parental Apollo 12, Apollo 15 and Apollo 17 mare basalts.[C1,2,8,9,13]

Most recent work on terrestrial basalt petrogenesis derives from the 'fine structure' now evident in the petrological and chemical data sets from particular tectonic or geographic situations, e.g. 'fine structure' in basalts along the mid-Atlantic ridge. Thus recent projects, largely initiated and supervised Ph.D. projects (Jaques, Jenner, Kuehner, Falloon, Eggins), have addressed the problem of mid-ocean ridge basalt petrogenesis[B28,29,31,39,42] with new rigour and have also unequivocally demonstrated the reality of second stage or multi-stage melting of 'refractory' residual peridotite compositions in convergent margin (including back-arc basin) environments.[B29,35,37,39-41] In these situations, the fluxing role of a water-rich fluid in initiating melting is essential. Experimental data has also combined with mineralogical and

petrological data to demonstrate the importance of magma mixing, including mixing of 'primitive' magmas, in basalt petrogenesis.

b. ***Petrology of the Deep Crust/Geothermometry and Geobarometry***

Investigation of the Lizard Peridotite, U.K.,[A5,6,7] provided an introduction to amphibolite, hornblende granulite and granulite mineral assemblages, albeit of local rather than regional extent, in a dynamothermal aureole to the peridotite. The detailed experimental petrological investigation of the gabbro to eclogite mineral reactions[E1-4,19] provided a demonstration of the usefulness of the piston-cylinder apparatus for study of mineral reactions in the deep crust or in subduction zone P,T regimes. Following the initial gabbro/eclogite work with A.E. Ringwood, this general field was pursued by supervision of and collaboration with graduate students, who have thus been the major contributors in converting a concept or model into well-documented investigations.

The papers on cordierite and garnet granulite stability relations with B.J. Hensen pioneered detailed subsolidus investigations[E20-22] in which the electron microprobe was used to determine mineral compositions, principally Fe/Mg variations, in sliding reactions involving solid solutions. This work resulted in interpretations of deep crustal pressures (~ 10 kb) for very magnesian cordierite assemblages and for sapphirine + quartz assemblages,[E22] which many workers considered excessive. The work has been strikingly vindicated by detailed studies of metamorphic terranes in Antarctica,[E30] emphasizing the interactive roles of the experimental and natural petrology approaches.

This work led naturally to experimental calibration of partition coefficients for Fe/Mg exchange equilibria between garnet and clinopyroxene under conditions of eclogite crystallization.[E5,8,17] Initial work with A. Raheim led to a calibration appropriate to basaltic rocks[E24,C10] and continuation with D.J. Ellis clarified the roles of P,T and other chemical factors to produce the Ellis-Green geothermometer[E28] which is one of the most used mineral geothermometers in deep crust and upper mantle petrology. A parallel project with T. Mori provided data on the two-pyroxene solvus at high pressures and in particular demonstrated quite a strong pressure effect on the solvus.[D8,10] The theme of geothermometry and geobarometry for upper mantle mineral assemblages[D11] was continued by collaboration with S.L. Harley and K.G. Nickel in calibrations aimed at using aluminium and

chromium partitioning between orthopyroxene and garnet as a geobarometer.[D15,17] This work has proven most useful to scientists investigating diamondiferous xenoliths and host rocks and for comparisons with xenolith suites from non-diamondiferous host rocks.

c. *Roles of volatiles, particularly C-H-O fluids in deep crust and upper mantle*

Investigations of the roles of volatiles at high pressure began with studies of the roles of water in peridotite and basalt melting studies summarized previously. Experiments with CO_2 demonstrated a strongly pressure-dependent solubility of $CO_3^=$ in low SiO_2 magmas. Infra-red spectroscopic studies unequivocally demonstrated $CO_3^=$ linkages and clarified the effects of CO_2, H_2O and fluorine solubility on silicate melts at high pressure, using simple system analogues of natural rock melts. The recognition of the importance of $CO_3^=$ in the mantle also led to the study of solid/solid reactions involving enstatite, dolomite and magnesite[D14].

Although these studies indicated an important role for H_2O and CO_2 in magma genesis in the mantle, comparison of mineral compositions sensitive to oxidation state (oxygen fugacity)[D7,13,B37,38] suggested that real mantle oxygen fugacity conditions were low, possibly below conditions of carbonate stability and indicating graphite (diamond) stability together with reduced rather than oxidized fluids. The motivation to experiment with low oxygen fugacity C-H-O fluids led to projects in collaboration with W.R. Taylor, in which new fluid buffering techniques, fluid analysis techniques and complex fluids (C-H-O-S, C-H-O-F) are used routinely in high pressure experiments.[B33,34,37,38,D19] These studies established solubilities of volatile species under highly reduced (CH_4-dominated fluids) conditions and introduced a new concept, 'redox melting'[B37] as particularly applicable to high pressure conditions in lithosphere and asthenosphere where intrinsic oxygen contents may be locally variable and C-H-O fluids may vary rapidly from CO_2 + H_2O fluids to H_2O-dominated to CH_4 + H_2O fluids. The investigations in the more oxidized part of the peridotite -C-H-O system have established conditions of genesis of primary carbonatite magma. Current projects are exploring redox variations in the earth's interior, emphasizing interactions between a reduced 'primitive' interior with (H_2O + CH_4) fluid species and an oxidized crust with (H_2O + CO_2) fluid species. Subduction processes introduce complex interactions between contrasted redox states in the outer 700 km of the earth and, because of the key role played

by C-H-O fluids in determining solidus temperatures and melt compositions, the experimental studies of roles of C-H-O fluids have general significance to all models of the earth's interior and tectonic processes.[B37,40]

CONTENTS

(Volume 1)

SERIES A

Petrology and geochemistry of ultramafic rocks including first documentation of high temperature, high pressure diapiric intrusives, recognition of mineralogical and geochemical fingerprints of residue and later enrichment processes in spinel lherzolite xenoliths and quantification of extreme temperatures required for Archaean peridotitic komatiite liquids.

A11 Cooper, J.A. and Green, D.H., 1969: Lead isotope measurements on lherzolite inclusions and host basanites from western Victorian, Australia. *Earth & Planet. Sci. Lett.* 6: 69-76.

A14 Frey, F. and Green, D.H., 1974: The mineralogy, geochemistry and origin of lherzolite inclusions in Victorian basanites. *Geochim. Cosmochim. Acta.*. 38: 1023-1059.

A15 Green, D.H., 1972: Archaean greenstone belts may include terrestrial equivalents of Lunar Maria? *Earth Plant. Sci. Lett.* 15: 263-270.

A16 Green, D.H., Nicholls, I.A., Viljoen, R. and Viljoen, M., 1975: Experimental demonstration of the existence of peridotitic liquids in earliest Archaean magmatism. *Geology* 3: 11-14.

A17 Green, D.H., 1975: Genesis of Archaean peridotitic magmas and constraints on Archaean geothermal gradients and tectonics. *Geology* 3: 15-18.

A18 Dasch, E.J. and Green, D.H., 1975: Strontium isotope geochemistry of lherzolite inclusions and host basaltic rocks, Victoria, Australia. *Am. J. Sci.* 275: 461-469.

A19 Green, D.H., 1981: Petrogenesis of Archaean ultramafic magmas and implications for Archaean tectonics. In: Kroner, A. (ed.) PRECAMBRIAN PLATE TECTONICS. Elsevier, Amsterdam, 469-489.

A20 (J) Nickel, K.G. and Green, D.H., 1984: The nature of the upper-most mantle beneath Victoria, Australia, as deduced from ultramafic xenoliths. *In* Kornprobst (Ed.) KIMBERLITES. II: THE MANTLE AND CRUST - MANTLE RELATIONSHIPS, 161-178. Elsevier Science Publishers B.V., Amsterdam.

SERIES B

Experimental petrology, petrology and geochemistry applied to understanding of mantle-derived terrestrial magmas with emphasis on use of high pressure liquidus phase relationships and integrated studies of peridotite melting relationships and basalt liquidus relationships.

B1 Green, D.H. and Ringwood, A.E., 1964: Fractionation of basalt magmas at high pressures. *Nature* 201: 1276-1279.

B3 Green, D.H. and Ringwood, A.E., 1967: The genesis of basaltic magmas. *Contrib. Min. & Pet.* 15: 103-190.

B4 Green, T.H., Green, D.H. and Ringwood, A.E., 1967: The origin of high-alumina basalts and their relationships to quartz tholeiites and alkali basalts. *Earth & Planet. Sci. Lett.* 2: 41-51.

B6 (J) Bultitude, R.J. and Green, D.H., 1968: Experimental study at high pressures on the origin of olivine nephelinite and olivine melilite nephelinite magmas. *Earth & Planet. Sci. Lett.* 3: 325-337.

B7 Green, D.H., 1969: The origin of basaltic and nephelinitic magmas in the Earth's Mantle. *Tectonophysics* (Proceedings of Upper Mantle Symposium, Prague 1968) 7: 409-422.

B10 Green, D.H., 1970: The origin of basaltic and nephelinitic magmas. Bennett Lecture, University of Leicester. *Trans. Leicester Lit. Philos. Soc.* 44: 28-54.

B11 Green, D.H. and Hibberson, W., 1970: Experimental duplication of conditions of precipitation of high pressure phenocrysts in a basaltic magma. *Phys. Earth Planet. Int.* 3: 247-254.

B12 Green, D.H., 1971: Compositions of basaltic magmas as indicators of conditions of origin: application to oceanic volcanism. *Phil. Trans. Roy. Soc. Lond.* Ser. A. 268: 707-725.

B13 (J) Bultitude, R.J. and Green, D.H., 1971: Experimental study of crystal-liquid relationships at high pressures in olivine nephelinite and basanite compositions. *J. Petrol.* 12: 121-147.

B15 Green, D.H., 1972: Magmatic activity as the major process in the chemical evolution of the earth's crust and mantle. *Tectonophysics* 13: 47-71.

B17 Green, D.H., 1973: Conditions of melting of basanite magma from garnet peridotite. *Earth Planet. Sci. Lett.* 17: 456-465.

B18 Green, D.H., Edgar, A.D., Beasley, P.H., Kiss, E. and Ware, N.G., 1974: Upper mantle source for some hawaiites, mugearites and benmoreites. *Contrib. Mineral. Petrol.* 48: 33-43.

B19 (J) Brey, G. and Green, D.H., 1975: The role of CO_2 in the genesis of olivine melilitite. *Contr. Mineral. Petrol.* 49: 93-103.

B20 Green, D.H., 1976: Experimental testing of 'equilibrium' partial melting of peridotite under water-saturated, high pressure conditions. *Canadian Mineralogist* 14: 255-268.

B22 (J) Brey, G. and Green, D.H., 1976: Solubility of CO_2 in olivine melilitite at high pressure and role of CO_2 in the Earth's upper mantle. *Contr. Mineral. Petrol.* 55: 217-230.

B23 Green, D.H., Edgar, A.D. and Hibberson, W.O., 1976: Experimental petrology of a highly potassic magma. *J. Petrol.* 17: 339-356.

B24 (J) Brey, G. and Green, D.H., 1977: Systematic study of liquidus phase relations in olivine melilitite + H_2O + CO_2 at high pressures and petrogenesis of an olivine melilitite magma. *Contr. Mineral. Petrol.* 61: 141-162.

B25 (J) Irving, A.J. and Green, D.H., 1976: Geochemistry and petrogenesis of the Newer Basalts of Victoria and South Australia. *J. Geol. Soc., Aust.* 23: 45-66.

B26 Frey, F.A., Green, D.H. and Roy, S.D., 1978: Integrated models of basalt petrogenesis - a study of quartz tholeiites to olivine melilitites from southeastern Australia utilizing geochemical and experimental petrological data. *J. Petrol.* 19: 463-513.

B27 Ryabchikov, I.D. and Green, D.H., 1978: The role of carbon dioxide in the petrogenesis of highly potassic magmas. *Akad. Nauk USSR, Siberian Region, Trudi, Inst. Geol. & Geophys.* Problems of the petrology of the Earth's crust and upper mantle. 403: 49-64.

B28 Green, D.H., Hibberson, W.O. and Jaques, A.L., 1979: Petrogenesis of mid-ocean ridge basalts. In: THE EARTH: ITS ORIGIN, STRUCTURE AND EVOLUTION (ed. M.W. McElhinny). Academic Press, London, pp. 265-290.

B29 Duncan, R.A. and Green, D.H., 1980a: Role of multistage melting in the formation of oceanic crust. *Geology* 8: 22-26.

B31 (J) Jaques, A.L. and Green, D.H., 1980: Anhydrous melting of peridotite at 0-15 kb pressure and the genesis of tholeiitic basalts. *Contrib. Mineral. Petrol.* 73: 287-310.

B33 (J) Foley, S.F., Taylor, W.R. and Green, D.H., 1986: The effect of fluorine on phase relationships in the system $KAlSiO_4$ - Mg_2SiO_4-SiO_2 at 28 kbar and the solution mechanism of fluorine in silicate melts. *Contrib. Mineral Petrol.* 93: 46-55.

B34 (J) Foley, S.F., Taylor, W.R. and Green, D.H., 1986: The role of fluorine and oxygen fugacity in the genesis of the ultrapotassic rocks. *Contrib. Mineral Petrol.* 94: 183-192.

B35 (J) Falloon, T.J. and Green, D.H., 1986: Glass inclusions in magnesian olivine phenocrysts from Tonga: evidence for highly refractory parental magmas in the Tongan Arc. *Earth & Plan. Sci. Lett.* 81: 95-103.

B37 Green, D.H., Falloon, T.J. and Taylor, W.R., 1987: Mantle-derived magmas - roles of variable source peridotite and variable C-H-O fluid compositions. In B.O. Mysen (Ed.): MAGMATIC PROCESSES AND PHYSICOCHEMICAL PRINCIPLES. *Geochem. Soc. Spec. Publ.* 1: 139-154.

B38 (J) Taylor, W.R. and Green, D.H.,, 1987: The petrogenetic role of methane: Effect on liquidus phase relations and the solubility mechanism of reduced C-H volatiles. In B.O. Mysen (Ed.): MAGMATIC PROCESSES AND PHYSICOCHEMICAL PRINCIPLES. *Geochem. Soc. Spec. Publ.* 1: 121-138.

B39 Duncan, R.A. and Green, D.H., 1987: The genesis of refractory melts in the formation of oceanic crust. *Contrib. Mineral Petrol.* 96: 326-342.

B40 Green, D.H., Barsdell, M., Crawford, A.J., Eggins, S.M., Falloon, T.J. and Wallace, M.E., 1988: Petrology of upper mantle processes in the S.W. Pacific. PROCEEDINGS OF THE PACIFIC RIM CONGRESS. A.I.M.M. Victoria: 621-632.

B41 (J) Falloon, T.J., Green, D.H. and Crawford, A.J., 1987: Dredged igneous rocks from the northern termination of the Tofua magmatic arc, Tonga and adjacent Lau Basin. *Aust. J. Earth Sci.* 34(4): 487-506.

B42 (J) Falloon, T.J. and Green, D.H., 1987: Anhydrous partial melting of MORB pyrolite and other peridotite compositions at 10 kbar: implications for the origin of primitive MORB glasses. *Miner. and Petrol.* 37: 181-219.

(Volume 2)

SERIES C

Experimental petrology and petrology of lunar basalts, identification of primitive or parental magmas and use of high pressure experimental studies to deduce the nature of lunar sources.

C1 Green, D.H., Ringwood, A.E., Ware, N.G., Hibberson, W., Major, A. and Kiss, E., 1971: Experimental petrology and petrogenesis of Apollo 12 basalts. *Proc. Second Lunar Science Conference (M.I.T. Press)* Vol. 1: 601-605.

C2 Green, D.H., Ware, N.G., Hibberson, W. and Major, A., 1971: Experimental petrology of Apollo 12 basalts, Part I: Sample 12009. *Earth Planet. Sci. Lett.* 13: 85-96.

C4 Green, D.H. and Ringwood, A.E., 1972: Crystallization of plagioclase in lunar basalts and its significance. *Earth Planet. Sci. Lett.* 14: 14-18.

C7 Green, D.H., Ringwood, A.E., Ware, N.G. and Hibberson, W., 1972: Experimental petrology and petrogenesis of Apollo 14 basalts. *Proc., Third Lunar Science Conference (M.I.T. Press)* Vol. 1, pp. 197-206.

C8 Green, D.H. and Ringwood, A.E., 1973: Significance of a primitive lunar basaltic composition present in Apollo 15 soils and breccias. *Earth Planet. Sci. Lett.* 19: 1-8.

C9 Chappell, B.W. and Green, D.H., 1973: Chemical compositions and petrogenetic relationships in Apollo 15 mare basalts. *Earth Planet. Sci. Lett.* 18: 237-246.

C10 (J) Raheim, A. and Green, D.H., 1974: Experimental petrology of lunar highland basalt composition and applications to models for the lunar interior. *J. Geol.* 82: 607-622.

C13 Green, D.H., Ringwood, A.E., Hibberson, W.O. and Ware, N.G., 1975: Experimental petrology of Apollo 17 mare basalts. *Proc. 6th Lunar Science Conference* Vol. 1: 871-893.

SERIES D

Application of experimental petrology to understanding of the composition, mineralogy, melting relations, physical properties and evolution of the Earth's upper mantle. Includes spinel and garnet peridotite stability relationships and geothermometry and geobarometry, role of pargasitic amphibole in controlling melting relations, role of water and C-H-O fluids with particular emphasis on important roles for fO_2 variation in effects of $CH_4 + H_2O \pm CO_2$ fluids and $H_2O \pm CO_2$ fluids.

D1 Green, D.H. and Ringwood, A.E., 1963: Mineral assemblages in a model mantle composition. *J. Geophys. Res.* 68: 937-945.

D2 Green, D.H. and Ringwood, A.E., 1967: The stability fields of aluminous pyroxene peridotite and garnet peridotite and their relevance in upper mantle structure. *Earth & Planet. Sci. Lett.* 3: 151-160.

D3 Green, D.H. and Hibberson, W., 1970: The instability of plagioclase in peridotite at high pressure. *Lithos* 3: 209-221.

D4 Green, D.H. and Ringwood, A.E., 1970: Mineralogy of peridotitic compositions under upper mantle conditions. *Phys. Earth Planet. Int.* 3: 359-371.

D5 Green, D.H., 1973: Contrasted melting relations in a pyrolite upper mantle under mid-oceanic ridge, stable crust and island arc environments. *Tectonophysics* 17: 285-297.

D6 Green, D.H., 1973: Experimental melting studies on a model upper mantle composition at high pressure under water-saturated and water-undersaturated conditions. *Earth Planet. Sci. Lett.* 19: 37-53.

D7 Green, D.H. and Sobolev, N.V., 1975: Coexisting garnets and ilmenites synthesized at high pressures from pyrolite and olivine basanite and their significance in kimberlitic assemblages. *Contr. Mineral Petrol.* 50: 217-229.

D8 (J) Mori, T. and Green, D.H., 1975: Pyroxenes in the system $Mg_2Si_2O_6$-$CaMgSi_2O_6$ at high pressure. *Earth Planet. Sci. Lett.* 26: 277-286.

D9 Green, D.H. and Liebermann, R.C., 1976: Phase equilibria and elastic properties of a pyrolite model for the oceanic upper mantle. *Tectonophysics* 32: 61-92.

D10 (J) Mori, T. and Green, D.H., 1976: Subsolidus equilibria between pyroxenes in the CaO-MgO-SiO_2 system at high pressures and temperatures. *Am. Mineral.* 61: 616-625.

D11 Mori, T. and Green, D.H., 1978: Laboratory duplication of phase equilibria observed in natural garnet lherzolites. *J. Geol.* 86: 83-97.

D12 (J) Jaques, A.L. and Green, D.H., 1979: Determination of liquid compositions in high-pressure melting of peridotite. *Am. Miner.* 64: 1312-1321.

D13 Ryabchikov, I.D., Green, D.H., Wall, V.J. and Brey, G.P., 1981: The oxidation state of carbon in the Reduced-Velocity Zone. *Geokhimiya* 2: 221-232 (Geochemistry International 1981, 148-158).

D14 Brey, G.P., Brice, W.R., Ellis, D.J., Green, D.H., Harris, K.L. and Ryabchikov, I.D., 1983: Pyroxene-carbonate reactions in the upper mantle. *Earth Planet. Sci. Lett.* 62: 63-74.

D15 Harley, S.L. and Green, D.H., 1982: Garnet-orthopyroxene barometry for
(J) granulites and peridotites. *Nature* 300: 697-701.

D16 Jenner, G.A. and Green, D.H., 1983: Equilibria in the Mg-rich part of
(J) the pyroxene quadrilateral. *Mineralogical Magazine* 47: 153-160.

D17 Nickel, K.G. and Green, D.H., 1985: Empirical geothermobarometry for
(J) garnet peridotites and implications for the nature of the lithosphere, kimberlites and diamonds. *Earth Planet. Sci. Lett.* 73: 158-170.

D18 Gupta, A.K., Green, D.H. and Taylor, W.R., 1987: The liquidus surface of the system forsterite-nepheline-silica at 28 kb. *Amer. J. Sci.* 287: 560-565.

D19 Taylor, W.R. and Green, D.H., 1988: Measurement of reduced peridotite-
(J) C-O-H solidus and implications for redox melting of the mantle. *Nature* 332: 349-352.

SERIES E

Experimental petrology related to crustal rocks, including subduction of oceanic crust, nature of crust/mantle boundary, mineral assemblages of granulite facies and geothermometry and geobarometry applied to crustal rocks.

E1 Ringwood, A.E. and Green, D.H., 1964: Experimental investigations bearing on the nature of the Mohorovicic Discontinuity. *Nature* 201: 566-567.

E2 Green, D.H. and Ringwood, A.E., 1967: An experimental investigation of the gabbro to eclogite transformation and its petrological applications. *Geochim. Cosmochim. Acta.* 31: 767-833.

E3 Ringwood, A.E. and Green, D.H., 1966: An experimental investigation of the gabbro-eclogite transformation and some geophysical implications. *Tectonophysics* 3: 383-427.

E4 Green, D.H. and Lambert, I.B., 1965: Experimental crystallization of anhydrous granite at high pressures and temperatures. *J. Geophys. Res.* 70: 5259-5268.

E5 Green, D.H., 1966: The origin of the 'eclogites' from Salt Lake Crater, Hawaii. *Earth & Planet. Sci. Lett.* 1: 414-420.

E8 Green, D.H., Lockwood, J.P. and Kiss, E., 1968: Eclogite and almandine-jadeite quartz rock from the Guajira Peninsula, Columbia, South America. *Am. Min.* 53: 1320-1335.

E13 Bryhni, I., Fyfe, W.S., Green, D.H. and Heier, K.S., 1970: On the occurrence of eclogite in western Norway. *Contr. Min. Petrol.* 26: 12-19.

E14 Essene, E.J., Hensen, B.J. and Green, D.H., 1970: Experimental study of amphibolite and eclogite stability. *Phys. Earth Planet. Inst.* 3: 378-384.

E17 (J) Irving, A.J. and Green, D.H., 1970: Experimental duplication of mineral assemblages in basic inclusions of the Delegate breccia pipes. *Phys. Earth Planet. Inst.* 3: 385-389.

E18 Green, D.H. and Mysen, B., 1972: Genetic relationships between eclogite and hornblende + plagioclase pegmatite in western Norway. *Lithos* 5: 147-161.

E19 Green, D.H. and Ringwood, A.E., 1972: A comparison of recent experimental data on the gabbro garnet granulite-eclogite transition. *J. Geol.* 80: 277-288.

E20 Hensen, B.J. and Green, D.H., 1971: Experimental study of the

(J) stability of cordierite and garnet in pelitic compositions at high pressures and temperatures, Part I: Compositions with excess alumino-silicate. *Contr. Mineral Petrol.* 33: 309-330.

E21 Hensen, B.J. and Green, D.H., 1972: Experimental study of the
(J) stability of cordierite and garnet in pelitic compositions at high pressures and temperatures, Part II: Compositions without excess alumino-silicate. *Contr. Mineral Petrol.* 35: 331-354.

E22 Hensen, B.J. and Green, D.H., 1973: Experimental study of the
(J) stability of cordierite and garnet in pelitic compositions at high pressures and temperatures, Part III: Synthesis of experimental data and geological applications. *Contr. Mineral. Petrol.* 38: 151-166.

E23 Raheim, A. and Green, D.H., 1974: Talc-garnet-kyanite-quartz schist
(J) from an eclogite-bearing terrane, western Tasmania. *Contr. Mineral. Petrol.* 43: 223-231.

E24 Raheim, A. and Green, D.H., 1974: Experimental determination of the
(J) temperature and pressure dependence of the Fe-Mg partition coefficient for co-existing garnet and clinopyroxene. *Contr. Mineral. Petrol.* 48: 179-203.

E28 Ellis, D.J. and Green, D.H., 1979: An experimental study of the effect
(J) of Ca upon garnet-clinopyroxene Fe-Mg exchange equilibria. *Contr. Mineral. Petrol.* 71: 13-22.

E29 Harley, S.L. and Green, D.H., 1981: Petrogenesis of eclogite inclusions in the Moses Rock Dyke, Utah, USA. *Tschermaks Min. Petr. Mitt.* 28: 131-155.

E30 Ellis, D.J. and Green, D.H., 1985: Garnet-forming reactions in mafic
(J) granulites from Enderby Land, Antarctica - implications for geothermometry and geobarometry. *J. Petrol.* 26(3): 633-662.

INTRODUCTION

The following publications are submitted for consideration for the award of the degree of Doctor of Science at the University of Tasmania. The papers encompass a number of themes and projects generally in the field of igneous and metamorphic petrology, but with contributions in geochemistry and tectonics. The role of experimental petrology and the interaction of natural petrology and experimental petrology are central to the thesis.

It is possible to order the publications into a number of subsets reflecting progression in individual projects or fields over a period of 25 years and I have, for reference purposes, catalogued publications in five series, A to E, and I have retained this grouping and numbering system in the present thesis. However, any sub-division obscures the overlap and continuity in the subjects and the preceding summary deliberately emphasises this by linking publications across the five-fold grouping into three sections on upper mantle petrogenesis, deep crustal metamorphism and roles of volatiles (C-H-O fluids particularly) respectively.

The papers are original and many are co-authored, often with graduate students (15 completed Ph.D., 2 completed M.Sc. students). In co-authored papers, contributions are approximately equivalent or I have been the senior author except in those papers marked (J) where I assess myself as a junior author. Many of these latter papers stem from Ph.D. theses carried out under my supervision. Each paper contains specific acknowledgement of contributions made by others to the work. Papers A5-7 arise from work successfully submitted for a Ph.D. thesis in 1962, but are included here because they illustrate the beginnings to themes followed up in the A series and particularly in D1-D5.

Mrs Karyl Whelan is thanked for her assistance in compiling this thesis in a particularly busy year. I thank Bill Hibberson, Keith Harris, Nick Ware, Elmer Kiss and Wierslaw Jablonski for their essential roles in the technical support so necessary for the experimental and microprobe laboratories. The pleasure of supervision and the companionship of graduate students and of postdoctoral fellows in the adventure and stimulus of scientific research lie at the centre of the work collected in this thesis.

Most importantly, I thank my wife Helen and children for their love, support and understanding through the 25 years of research collected in this thesis.

D.H. Green
21 August, 1988.

Department of Geophysics
Australian National University
Publication No. 292

A4

D. H. GREEN

ALUMINA CONTENT OF ENSTATITE IN A VENEZUELAN HIGH-TEMPERATURE PERIDOTITE

Geological Society of America Bulletin, v. 74, p. 1397–1402, 2 figs., 1 pl., November 1963

Short Notes

D. H. GREEN

ALUMINA CONTENT OF ENSTATITE IN A VENEZUELAN HIGH-TEMPERATURE PERIDOTITE

Abstract: The ARL electron-probe microanalyzer demonstrates high Al_2O_3 content in enstatite augen in high-temperature peridotite and low Al_2O_3 content in recrystallized enstatite. The enstatite augen are zoned in Al_2O_3 content; values are low at the margins, and this decrease is synchronous with or postdates the deformation of the enstatite. The decrease in Al_2O_3 content in the recrystallized enstatite is correlated with a large change in load pressure during emplacement of the peridotite.

Introduction

A recent study of the Lizard (Cornwall) peridotite and its high-temperature aureole (Green, in press) led the author to study the Tinaquillo (Venezuela) peridotite (MacKenzie, 1960) which has many features in common with the Lizard peridotite. One of the most important aspects of the Lizard peridotite study was the recognition of two types of enstatite that differed considerably in Al_2O_3 content. The present note reports the identification and significance of similar aluminous enstatite in the Tinaquillo peridotite.

Comparative Petrography and Chemistry

The Lizard peridotite, during emplacement as a high-temperature but crystalline body, became finely foliated and recrystallized to a fine-grained, granoblastic olivine-enstatite (low Al_2O_3)-diopside (low Al_2O_3)-plagioclase-chromite rock. Its undeformed core of coarse-grained peridotite preserves a primary mineral assemblage of olivine, aluminous enstatite, aluminous diopside, and aluminous spinel. Within the recrystallized peridotite, deformed augen of primary enstatite and diopside are relict from primary assemblage, whereas porphyroblasts of olive-green aluminous spinel mantled with plagioclase are traces of an intermediate stage of recrystallization (Green, in press).

The Tinaquillo peridotite, as described by MacKenzie, does not have a core of undeformed coarse peridotite. However, from MacKenzie's description and the author's study it is clear that this peridodite resembles the recrystallized sheath of the Lizard peridotite in texture (Pl. 1). Enstatite augen[1] are common in the peridotite and diopside is rare; both show bending, fracturing and stages of cataclastic recrystallization toward schlieren of fine recrystallized enstatite. The fine-grained recrystallized material enclosing the augen is dominantly olivine, with subordinate enstatite, diopside, porphyroblastic olive-green spinel, and rare colorless to pale-brown amphibole. The amphibole may replace the pyroxenes, and plagioclase is absent.

As a check on the similarities of the two peridotites a very fresh sample of the Tinaquillo peridotite was analyzed (Table 1). The percentages of both major and minor oxides are very similar.

Alumina Content of Tinaquillo Enstatites

The distribution of Al_2O_3 within the enstatite augen and the recrystallized enstatite was studied by microanalysis. A finely focused electron beam (microprobe) was used, and the intensity of emitted characteristic X radiation was measured. The instrument used was the ARL electron-probe microanalyzer (EMX). Polished thin sections and polished grain mounts were simultaneously coated with a thin carbon film. An electron beam was focused to a spot about 1 μ in diameter; the accelerating

[1] "Phenocrysts" of MacKenzie (1961, p. 313), although he clearly recognized and described the deformed character of the rock and the participation of the enstatites in this deformation (*cf.* p. 305, 313–314).

Geological Society of America Bulletin, v. 74, p. 1397–1402, 2 figs., 1 pl., November 1963

voltage on the beam was 10 kv. The measured-specimen current was 0.045 μ *A* on enstatite, integration time during spot analyses was 1 min 45 sec, and spot analyses were made at 3-, 5-, or 10-μ intervals along the traverses. Observation of contamination spots and of thin exsolution lamellae gave an estimate of the analyzed volume of enstatite as a hemisphere 3 μ in diameter.

TABLE 1. COMPARISON OF CHEMICAL COMPOSITION OF TINAQUILLO (VENEZUELA) AND LIZARD (CORNWALL) PERIDOTITES

Analysts: Tinaquillo: A. J. Easton, Dept. Geophysics, Aust. Nat. Univ., Canberra. Lizard: D. H. Green

	Tinaquillo Princeton Univ. No. V1460 Aust. Nat. Univ. No. 2763	*Lizard* Mean of 4 analyses
SiO_2	44.69	44.77
TiO_2	0.08	0.19
Al_2O_3	3.19	4.16
Fe_2O_3	0.09	..*
FeO	7.54	8.21
MnO	0.14	0.11
MgO	39.80	39.22
CaO	2.97	2.42
Na_2O	0.18	0.22
K_2O	0.02	0.05
H_2O^+	0.38	..*
H_2O^-	0.05	..*
Cr_2O_3	0.45	0.40
NiO	0.26	0.24
P_2O_5	0.04	0.01
CO_2	0.17	n.d.
	100.05	100.00

*Calculated to zero in obtaining preserpentinization composition (*cf.* Green, in press)

The electron-beam scanning technique was first used to seek major inhomogeneities in the Al, Ca, and Fe content in the Tinaquillo augen and the "standard" Lizard enstatites. This enabled positioning of the electron beam for quantitative spot analyses with avoidance of exsolution lamellae of spinel (uncommon) and clinopyroxene (common) when these were found in the Tinaquillo augen.

To obtain an empirical calibration curve, simultaneous analyses for Al (λ_{K_α} = 8.339 Å), Ca (λ_{K_α} = 3.360 Å), and Fe (λ_{K_α} = 1.937 Å) were made at 3-μ intervals on traverses on the analyzed Lizard enstatites and then on a grain mount of the Tinaquillo augen. Intensity of emitted radiation was corrected for slight variation in specimen current. No corrections were applied for absorption or fluorescence of Al radiation by other elements present since all the enstatites were known to be closely similar in major element (Mg, Fe, Si) concentration. Quantitative analyses for Cr and Fe confirmed the close similarity. The presence of clinopyroxene exsolution lamellae in all the pyroxenes prevented any quantitative estimate of CaO content. Correction was not made for background since measurements on olivine and on an enstatite from a meteorite showed background radiation equivalent to less than 0.1 per cent Al_2O_3. Similarly no corrections were made for dead time in the detectors since intensities were low on all samples and the range of standards included the concentration of Al in the unknown specimen.

On the empirical calibration curve each point gives the arithmetic mean of the measured intensities (Fig. 1). At each point a histogram is plotted indicating on the ordinate the spread of intensity values and on the abscissa the frequency of the intensity values. Some intensity values show near-normal distribution; others are irregular and may reflect inhomogeneity in the sample or experimental error. Because of the difficulty of Al_2O_3 determinations (*cf.* Stevens, 1960, p. 9–10) in chemical analysis[2] the author believes errors in the standards could also account for departures of Al_2O_3 determinations from the "line of best fit."

The results show that the Al_2O_3 content of the enstatite augen in the Tinaquillo peridotite is high (range 5–5.5 per cent; mean 5.2) and comparable with that of the primary Lizard enstatites (Fig. 1). Uncommon spinel exsolution lamellae suggest that the true Al_2O_3 content at crystallization could have been slightly higher.

Figure 2 shows the results of a series of analyses across the edges of enstatite augen. A highly polished thin section of the analyzed rock (V1460) was carbon-coated and analyzed under conditions identical to the analysis of the standard enstatites; the results should thus be quantitatively comparable. In Figure 2 the arbitrary intensity values for Al_K radiation have been converted to Al_2O_3 weight percentages utilizing the calibration curve of Figure 1. The microanalyzer showed that the Al_2O_3 content of exsolved clinopyroxene lamellae is not appreciably different from that of the host enstatite. However, occasional spinel rods at varying depths below the

[2] The Lizard enstatites were analyzed for SiO_2, Al_2O_3, MgO and CaO by classical gravimetric methods.

polished surface and small amphibole crystals near the margins of the augen produce anomalously high Al_2O_3. The traverses also confirm the high Al_2O_3 content of the enstatite augen (Al_2O_3 content 4.7–5.7 per cent in the central areas of the augen).

Traverses a, b and c, across the margins of enstatite augen (grain size 0.5–3 mm), show

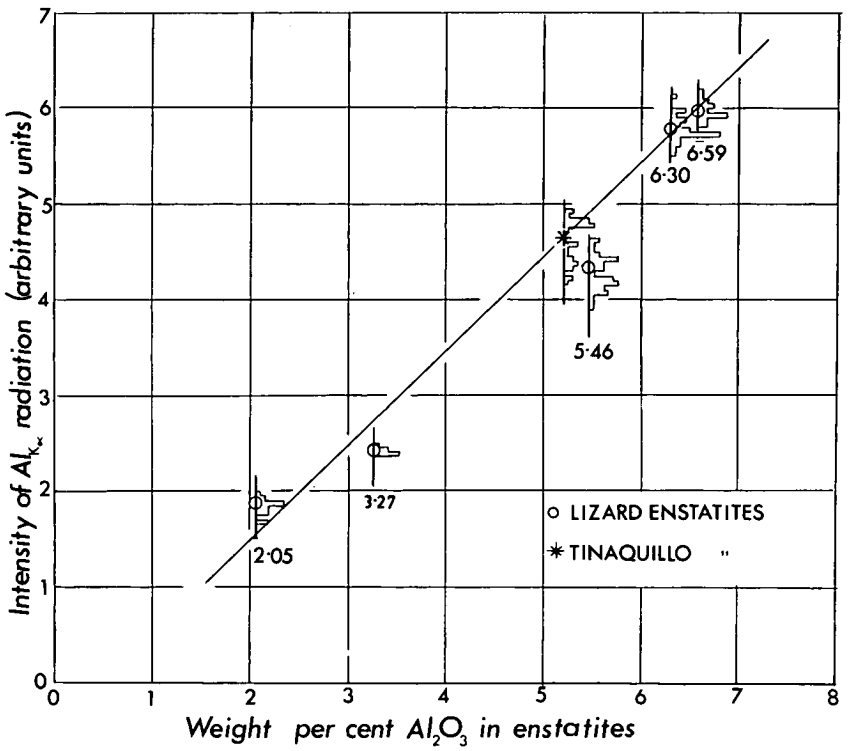

Figure 1. Calibration curve for Al_2O_3 in enstatite

that over distances of 150–200 μ the Al_2O_3 content drops from more than 5 per cent within the augen to 3–3.5 per cent at the margin. The decrease is not linear but steepens toward the margin.

Traverse d begins within a large augen with about 5 per cent Al_2O_3; this value decreases rapidly to 2.5 per cent at the margin, increases to 3.5 per cent in the center of a comparatively large recrystallized enstatite in juxtaposition, then decreases to about 2.8 per cent at the opposite margin of this grain. An anomalous peak near the junction of the two grains is probably due to a change in mineralogy, possibly one of the very small grains of spinel or brown amphibole that characteristically border the enstatite augen.

Traverse e is within an enstatite augen and crosses the edge of a "kink band" due to deformation of the enstatite (Turner and others, 1960). The traverse demonstrates that the normal high Al_2O_3 content of the augen (5 per cent) decreases sharply toward the kink-band boundary and there passes through a minimum of approximately 2.8 per cent Al_2O_3.

In traverses f and g an attempt was made to compare the Al_2O_3 content of adjacent diopside and enstatite grains. No corrections were made for the higher Ca and lower Mg content of the diopside. Traverse f begins within an enstatite augen having about 5.2 per cent Al_2O_3 and extends toward the margin where this value decreases to 4.7 per cent (Fig. 2). It then crosses an included grain (not an exsolution lamella) of "primary" diopside where there is a sharp increase in Al_2O_3. Within the diopside there is a slight decrease in Al_2O_3 toward the augen margin, then an abrupt

decrease in passing back to enstatite with 4.4 per cent Al_2O_3, decreasing to 3.2 per cent at the edge of the augen. Traverse g shows the Al_K intensity of two small adjacent grains of recrystallized diopside (4.8 per cent Al_2O_3 approx.) and enstatite (3.7 per cent Al_2O_3) (Fig. 2). The results of these traverses closely parallel the Lizard results in which primary diopsides containing 6.8–7 per cent Al_2O_3 co-

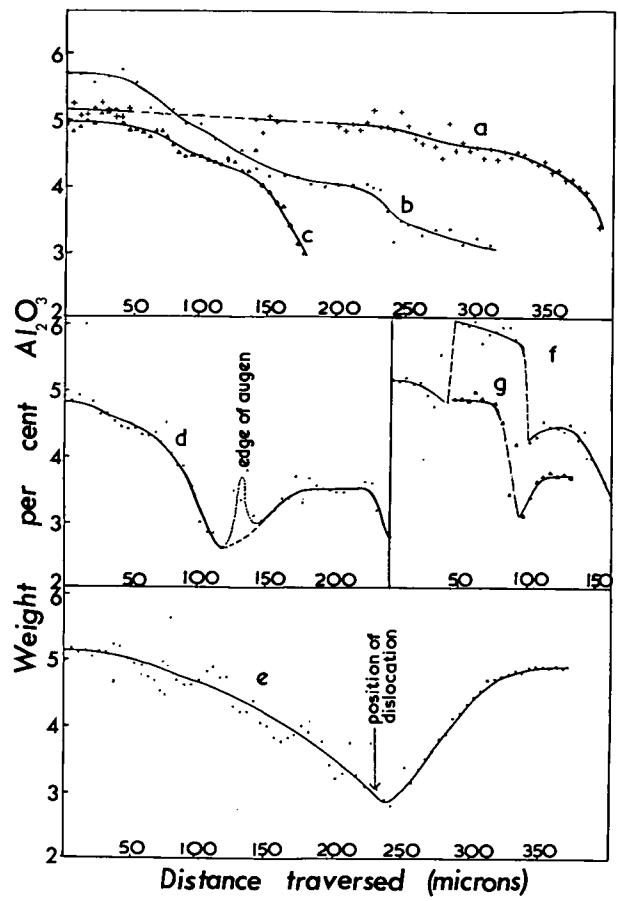

Figure 2. Variation in Al_2O_3 within enstatite augen (*cf.* Pl. 1)

exist with enstatites with 6–6.5 per cent Al_2O_3. A similar relationship holds for the recrystallized enstatite (2–3 per cent Al_2O_3) and diopside (3–5 per cent Al_2O_3).

Conclusions

Quantitative spot analyses using the ARL electron microprobe demonstrate a gradient in Al_2O_3 content from high Al_2O_3 in the core to lower Al_2O_3 at the margin in enstatite augen in the finely foliated Tinaquillo peridotite. Fine-grained, recrystallized enstatite grains of the peridotite contain the lower Al_2O_3 values. Direct comparison of the augen of the Tinaquillo with analyzed enstatites of the Lizard peridotite shows approximately 5.2 per cent Al_2O_3 in the augen.

The data demonstrate that the large pyroxene augen were out of equilibrium, in Al_2O_3 content, with their enclosing fine-grained olivine, enstatite, diopside, spinel, and rare pale-brown hornblende. The porphyroblastic growth of olive-green spinel and its occurrence as tiny grains marginal to the augen and as filling in deformation fractures of the enstatite

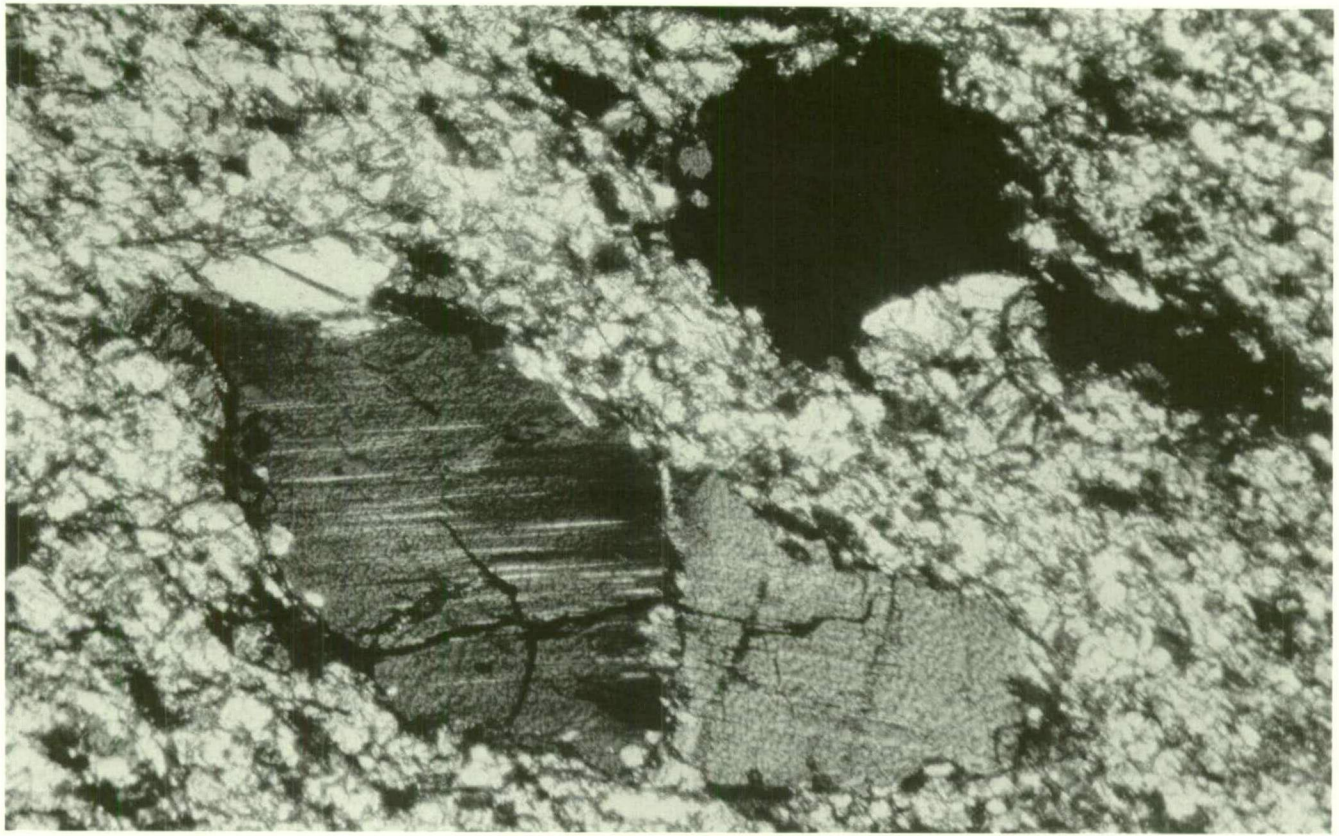

TEXTURE OF TINAQUILLO (VENEZUELA) PERIDOTITE

Large enstatite augen (1.2 mm long) showing kink band, with medium-sized recrystallized enstatite (white) at upper left corner of augen. Isotropic porphyroblast of spinel in upper right, fine material of recrystallized olivine, enstatite, diopside, and spinel. Note exsolution lamellae in the enstatite augen; about × 70

suggest that Al_2O_3 released from earlier coarse aluminous enstatite goes to form aluminous spinel:

$$\underset{\text{aluminous enstatite}}{m\,MgSiO_3 \cdot Al_2O_3} + \underset{\text{olivine}}{Mg_2SiO_4} \rightarrow \underset{\text{spinel}}{MgAl_2O_4} + \underset{\text{enstatite}}{(m+1)\,MgSiO_3}.$$

The Al_2O_3 gradients in the enstatites, particularly the low Al_2O_3 values across a kink-band boundary, show that the loss of Al_2O_3 accompanied or followed deformation (during or after emplacement of the peridotite).

The Tinaquillo peridotite has developed its present texture and foliation because of deformation at a high temperature (*cf.* MacKenzie, 1960) of a coarse-grained rock composed of olivine, aluminous enstatite, aluminous diopside, and accessory spinel. The primary core of the Lizard peridotite is practically identical in chemical composition and texture. As presented elsewhere (Green, in press) the high Al_2O_3 content of co-existing enstatite and diopside can probably be correlated with high pressure at the time of primary crystallization. A considerable decrease in pressure is implied in the instability of the Al pyroxenes during deformation and high-temperature emplacement of the body. It is significent that plagioclase does not occur in the Tinaquillo peridotite, whereas it develops in the Lizard peridotite when pyroxenes and aluminous spinel react to give olivine and plagioclase. This is probably due to pressure difference (*cf.* Green, in press): the depth of final emplacement of the Tinaquillo peridotite was probably greater than that of the Lizard peridotite.

If the deduced change in pressure during recrystallization is a change in load pressure, then vertical movement of the Tinaquillo peridotite through several miles as a high-temperature crystalline diapir must be considered.

The present investigation attests to the petrogenetic importance of the Al_2O_3 substitution in enstatite and to the use of the electron-probe microanalyzer for the study of zoning problems and for spot analyses *in situ* of polished thin sections.

Acknowledgments

Prof. H. H. Hess and Dr. D. B. MacKenzie provided specimens of the Tinaquillo peridotite. Mr. A. J. Easton carried out a carefully checked analysis of the peridotite. Dr. J. F. Lovering instructed and helped the author in the use of the electron-probe microanalyzer.

References Cited

Green, D. H., in press, The petrogenesis of the high-temperature peridotite at the Lizard, Cornwall: Jour. Petrology

MacKenzie, D. B., 1960, High temperature alpine-type peridotite from Venezuela: Geol. Soc. America Bull., v. 71, p. 303–318

Stevens, R. E., 1960, Second report on a co-operative investigation of the composition of two silicate rocks: U. S. Geol. Survey Bull. 1113, p. 1–123

Turner, F. J., Heard, H., and Griggs, D. T., 1960, Experimental deformation of enstatite and accompanying inversion to clinoenstatite: 21st Internat. Geol. Cong., Rept. pt. XVIII, 399–408

Dept. Geophysics, Australian National University, Canberra, Australia
Manuscript Received by the Society, May 16, 1963

A5

The Petrogenesis of the High-temperature Peridotite Intrusion in the Lizard Area, Cornwall

by D. H. GREEN

Department of Geophysics, Australian National University, Canberra

ABSTRACT

The Lizard peridotite produced a high-temperature metamorphic aureole during diapiric emplacement in a period of amphibolite facies regional metamorphism. The peridotite preserves a coarse-grained primary core within a cataclastic, finely foliated and recrystallized marginal shell. Chemical analyses demonstrate the constancy of rock composition in the primary and recrystallized mineral assemblages. The primary mineral assemblage of the peridotite consists of olivine (Fo_{89}), aluminous enstatite, aluminous diopside, and green aluminous spinel. In contrast the mineral assemblage on recrystallization is olivine, enstatite (normal Al_2O_3 content), diopside (normal Al_2O_3 content), plagioclase, and brown chromite. A third assemblage of olivine, pargasite, and brown chromian spinel is developed locally from the plagioclase-bearing assemblage, particularly in contact areas.

Major and trace element analyses of twenty minerals and eight rocks are given. These are compared in detail with peridotites and minerals occurring as accumulates from basaltic magma, as peridotite nodules in basalts and as 'intrusive' peridotites in orogenic areas. It is concluded that the primary minerals of the Lizard peridotite have not crystallized and accumulated from a basaltic magma but have crystallized in a similar environment to that of peridotite nodules in basalts. It is further concluded that the cause of the differences between the *primary* and *recrystallized* assemblages of the peridotite is primarily a difference in load pressure at crystallization. In particular the high alumina content of both enstatite and diopside and the coexistence of pyroxenes+aluminous spinel instead of olivine+anorthite are considered to be a direct consequence of the high load pressure at the initial crystallization of the peridotite.

I. INTRODUCTION

THIS restudy of the Lizard area of south Cornwall has concentrated on a detailed examination of the Lizard peridotite and of the high-grade metamorphic aureole around it. The present paper is devoted to significant aspects of the petrology and mineralogy of the peridotite; a second paper in preparation will cover the petrography, chemistry, and mineralogy of the metamorphic aureole and a third paper will present a general reinterpretation and evaluation of the Lizard geology, particularly structural aspects, from the field work necessarily undertaken in the first stage of the work.

The presence and character of the metamorphic aureole have important implications as to the conditions of emplacement of the peridotite. The peridotite was emplaced in the regionally metamorphosed Landewednack Hornblende Schists (Flett, 1912, 1946), characterized by assemblages with blue-green hornblende, andesine-oligoclase, epidote, and salite. In proximity to the peridotite, assemblages characterized successively by brown-green hornblende, brown hornblende with hypersthene and augite, and typical hypersthene+

[Journal of Petrology, Vol. 5, Part 1, pp. 134–188, 1964]

augite pyroxene granulites are developed in rocks compositionally equivalent (i.e. of basaltic composition) to the Landewednack Hornblende Schists. These assemblages occur in the rocks previously called Traboe Hornblende Schist (Flett, 1912, 1946).

Flett regarded the peridotite as a plug or stock-like intrusive with steep contacts, commonly faulted. At the other extreme Sanders (1955) considered that the peridotite was a flat and fairly thin sheet overlying the metamorphic rocks. Detailed mapping near Porthallow and Porthkerris and also near Predannack and Mullion Cove shows that the peridotite forms a series of domes intruding vertically into the hornblende schists. Similarly the western and north-eastern contacts are also steeply dipping or vertical although rendered complex by the mobile behaviour of the pyroxene granulites in the metamorphic aureole. In contrast, in the south-eastern Lizard, near Cadgwith and Lizard villages, the peridotite forms a sheet overlying the Landewednack Hornblende Schists on an undulating surface dipping at low angles (5°–25°) to the west and north-west (cf. Sanders, 1955).

The general form of the Lizard peridotite is that of a vertical or near-vertical plug-like intrusive, probably elongate in the NNW.–SSE. direction and with several subsidiary domes or apophyses. There is a lip-like extension on the south-eastern margin of the body where the peridotite has intruded at a shallow angle within the flat-lying regional metamorphic rocks.

II. THE LIZARD PERIDOTITE

The Lizard peridotite, about 30 square miles of surface occurrence (Fig. 1), consists of one major and several minor bodies, possibly forming one continuous body at depth. Primary mineral assemblages in the peridotite consist of olivine, orthopyroxene, clinopyroxene, and spinel; plagioclase and aluminous amphibole are of secondary development in areas of high-temperature recrystallization. Serpentinization is general throughout the whole peridotite but quite commonly does not affect more than 50 per cent of the primary phases. The serpentine minerals are of the mesh-texture+bastite+cross-fibre chrysotile group and antigorite in its typical flare texture is rare. Chlorite and fibrous tremolite are common constituents replacing pyroxenes; the spinel shows a sequence of break-down reactions to give relict magnetite surrounded by chlorite and other minerals, and plagioclase is almost invariably replaced by secondary aggregates. The present study has been aimed at the primary, higher temperature assemblages preceding these alterations and the secondary minerals were investigated in so far as they give an indication of the nature of the mineral they replace.

Flett (1912, 1946) regarded the peridotite as a zoned intrusion of three serpentine 'magmas'; an outer 'dunite serpentine', a median 'tremolite serpentine', and a central core and latest intrusion of 'bastite serpentine'. The present investigation has shown that in reality Flett's classification roughly reflects a zoning in

grain-size and degree of mylonitization and recrystallization. It was found practical to classify and map the peridotite on the basis of a division into one *primary assemblage peridotite* and two recrystallized mineral assemblages, the *recrystallized anhydrous* and *recrystallized hydrous* assemblages. The first type

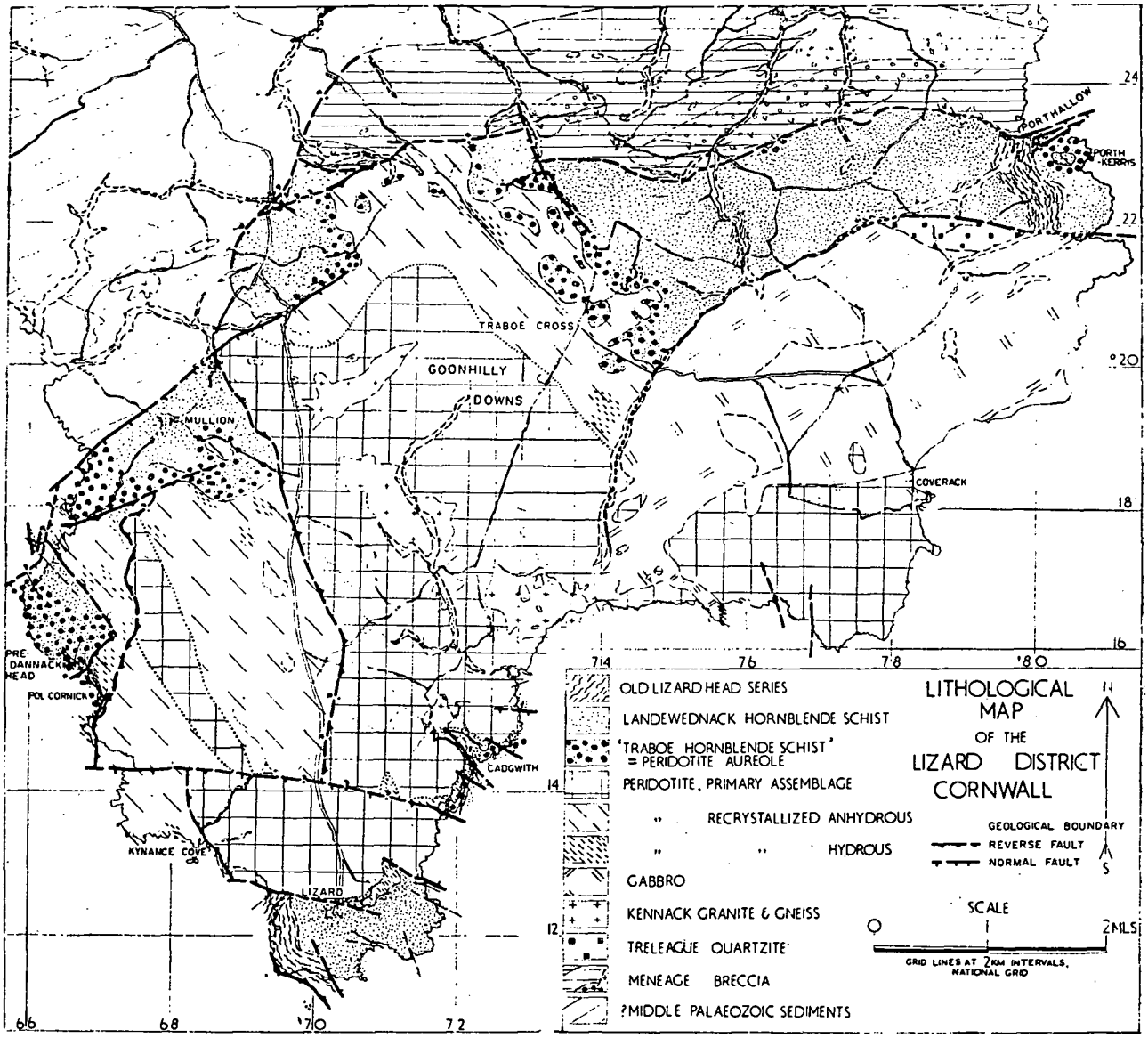

FIG. 1. Lithological map of the Lizard district, Cornwall.

corresponds roughly to the 'bastite serpentine' of Flett and the latter two are included in his 'tremolite serpentine'. The 'dunite serpentine' proved to be a very finely recrystallized and usually completely serpentinized variant of the latter two assemblages.

1. *The primary assemblage*

The peridotite of the primary assemblage has large (5–10 mm) green pyroxene

crystals in rocks varying in colour in hand-specimen from deep red to greenish-black. Most commonly there is some 'grain' or foliation on weathered surfaces due either to mineralogical banding or to parallel 'tails' of fine, recrystallized material with the larger pyroxene crystals.

The rock is a true peridotite rarely having less than 20 per cent or more than 40 per cent pyroxene. The following modal analyses (volume per cent), approximate because of the secondary alteration present, illustrate the variation in the primary rock:

	Specimen 90681		*Specimen* 90683 *Rock analysis V*	
Olivine	21·0	75·5	19·0	64·5
Serpentine replacing olivine	54·5		45·5	
Enstatite	8·5	15·0	15·5	22·5
Serpentine replacing enstatite	6·5		7·0	
Diopside	7·5		12·0	
Olive spinel	2·0		1·0	

The olivine, enstatite, and diopside occur in coarse anhedral texture with curving grain boundaries and uncommon inclusion of one mineral in another. It is a typical igneous, non-directed texture with a clear tendency for the enstatite to form the larger crystals and diopside to occur as a cluster of smaller anhedral grains or more rarely as interstitial plates concave towards equant olivine grains. The enstatite has extremely fine exsolution lamellae and in some cases small exsolved blebs of highly birefringent clinopyroxene. Single crystal X-ray oscillation photographs confirm this identification [the method of Bown & Gay (1959, 1960)] and these augite lamellae exsolve parallel to (100) of the enstatite.

Diopside has a well-developed (100) parting and rarely shows exsolution lamellae of orthopyroxene or serpentine probably having replaced orthopyroxene. Single crystal X-ray oscillation photographs confirm the presence of exsolved enstatite lamellae and the absence in both enstatite and diopside of lamellae of other phases, spinel being particularly sought for in view of the high Al_2O_3–content of the pyroxenes.

Olivine lacks exsolution lamellae or inclusions. The primary spinel is olive green with very abundant, extremely small hexagonal plates of exsolved ilmenite lying on the octahedral planes of the spinel. The primary spinel is of irregular anhedral form suggestive of late interstitial crystallization either by exsolution to grain boundaries or as a late crystallizing phase from the parent magma. Commonly the primary spinel shows a sequence of alteration to give skeletal brown spinel crystals surrounded by aluminous secondary minerals after plagioclase.

Primary banding. The primary assemblage of the peridotite has, in very many outcrops, distinct bands from 1 cm up to about 15 cm thick of peridotite enriched in pyroxene and in some cases with secondary minerals replacing plagioclase. Modal analysis of the analysed (analysis VI) pyroxene-rich band from

Pedn Boar gave a composition with 31 per cent primary diopside, 39 per cent primary enstatite, 15 per cent primary olivine, accessory spinel, and 15 per cent of recrystallized, secondary pyroxene+olivine+plagioclase assemblage. Near Carleon Cove there are several lenses (rather than bands) of pyroxenite, dominantly diopside with some enstatite and probable altered plagioclase. The pyroxene crystals in these lenses are up to 3–4 cm long. North of Polbream Point strong banding in the primary assemblage peridotite is due to diopside and altered plagioclase varying antipathetically to olivine. Some of these bands are now rodingites with relict diopside set in grossularite+chlorite.

More prominent than the pyroxene-rich bands and parallel to them are the 'chromite-serpentine' bands, characteristic of the peridotite core and not observed in either of the recrystallized assemblages. The bands may be more than 2 metres thick but more commonly are about 30 cm thick. The rocks consist of fine, mesh-texture serpentine with common euhedral spinel crystals usually arranged in stringers or lenses parallel to the edge of the band. The spinels do not show a tendency to form at any consistent position in the serpentine band and do not show any typical accumulation textures. The specimens examined covered the primary assemblage peridotite from the west coast, south of Kynance, to Coverack on the north-east coast, and in all specimens the spinel is a deep-brown chromian variety, lacking ilmenite lamellae and showing no evidence of being relict from earlier olive spinel such as occurs in the enclosing peridotite. The only variation now evident is due to secondary alteration to give opaque magnetite relics rimmed by chromian chlorite.

The interpretation of these spinel-serpentine bands based on their petrography is that primarily they were bi-mineralic rocks of coarse olivine and brown chrome spinel in anhedral texture. The megascopic features of the bands show no evidence of accumulative textures nor gravitative segregation, rather the lenticular distribution of the spinel within the bands suggests internal movement parallel to the band. The junctions against the normal pyroxene-bearing peridotite are usually sharp but the bands may bifurcate or lens out or appear to include lenses of the normal peridotite.

2. *The recrystallized anhydrous assemblage*

The recrystallized anhydrous mineral assemblage in the peridotite occurs as a mantling shell to the peridotite body. The rocks are characteristically fine-grained with a variable proportion of pyroxene augen and, on weathered surfaces, a strongly developed ribbing due to selective weathering, picking out the foliation and the schlieren and stringers of different mineralogical composition. Dull-white grains of plagioclase are characteristically present and euhedral, parallel amphibole prisms, typical of the hydrous assemblage, are absent.

In thin section the rocks are of variable grain size, commonly in the range 0·05 mm to 0·5 mm, but usually showing a considerable range even in one thin section. The pyroxene augen are usually from 1 mm to 5 mm, more rarely up to

3 cm. The mineral assemblage is dominantly olivine+enstatite+diopside+plagioclase (calcic labradorite) with pale-brown or orange-brown hornblende as a minor accessory mineral in some examples and with spinel (brown and shades of green) either as lenticular, feldspar-rimmed, porphyroblasts (olive spinel) or as small anhedral crystals (brown chromian spinel).

The olivine does not occur as augen in any example but, on the contrary, is apparently the most readily recrystallizing mineral, forming fine anhedral mosaics or anhedral crystals interstitial to pyroxenes. The recrystallized enstatite is very commonly elongate in the direction parallel to the foliation in thin section and with the '*c*' crystallographic axis defined by the cleavages, perpendicular to this foliation. The plagioclase occurs as anhedral grains, commonly with albite or pericline twinning developed but without compositional zoning. It is very seldom preserved as fresh, clear grains and typically is replaced by turbid aggregates of secondary minerals, including clay minerals and in some cases grossular. The plagioclase or its alteration products usually form stringers parallel to the foliation plane and often broadening out to form rims around skeletal brown spinel or larger olive spinel porphyroblasts. Brown hornblende is absent in many of the recrystallized rocks, in others it may form up to 3–5 per cent of the rock. In some cases the hornblende replaces diopside, in others it is closely associated with plagioclase-rich areas. It is variable in colour with $Z=$ pale orange-brown or pale brown, $Y=$pale yellowish-brown, $X=$colourless, and is optically (+)ve or (—)ve with $2V$ about 90°, $Z \wedge c=12°–17°$. The character and composition vary in relation to the amount of hornblende in the rock, the colour decreasing in intensity with the increasing abundance of the hornblende. In this way the brown hornblende-bearing peridotites pass transitionally into the olivine+colourless pargasite assemblages to be described in the next section.

Olive spinel (rich in $MgAl_2O_4$) occurs in this assemblage only as large anhedral crystals, commonly with exsolved ilmenite lamellae, surrounded by rims of calcic plagioclase or its alteration products. Rarely, the spinel porphyroblast may be of leaf-green or pale-green colour and, in one specimen, is extremely pale blue-green, almost colourless; the edges of such spinels are commonly of deeper green or green-brown colour. The olive spinels with relatively thin plagioclase rims show a continued reaction sequence to yield skeletal brown or opaque spinel relics in the centres of lenticular patches of plagioclase. It is inferred that the large olive spinels originally grew as porphyroblasts during cataclastic recrystallization of the primary assemblage as there are no strain or cataclastic effects evident in the spinels (unlike the pyroxene augen) and there is no deflexion of the fine foliation in the peridotite around the large spinels (Fig. 2).

The petrography of the peridotites of the recrystallized anhydrous assemblage provides evidence for the earlier stability and porphyroblastic growth of aluminous spinel and then later reaction of the spinel with surrounding pyroxene to release alumina forming mantling plagioclase with cores of skeletal

chromium-iron spinel. The earlier stable spinel was an olive-green, pale-green or, rarely, a near-colourless true spinel (approaching $MgAl_2O_4$) but with appreciable chromite and picotite contents and some solid solution of ilmenite.

The proportions of the minerals present vary rapidly across the fine foliation, particularly in the relative proportions of olivine and enstatite. As a result of the breaking apart and recrystallization of the pyroxene augen during movement parallel to the foliation planes, the recrystallized enstatite and diopside commonly occur in distinct lenses or schlieren.

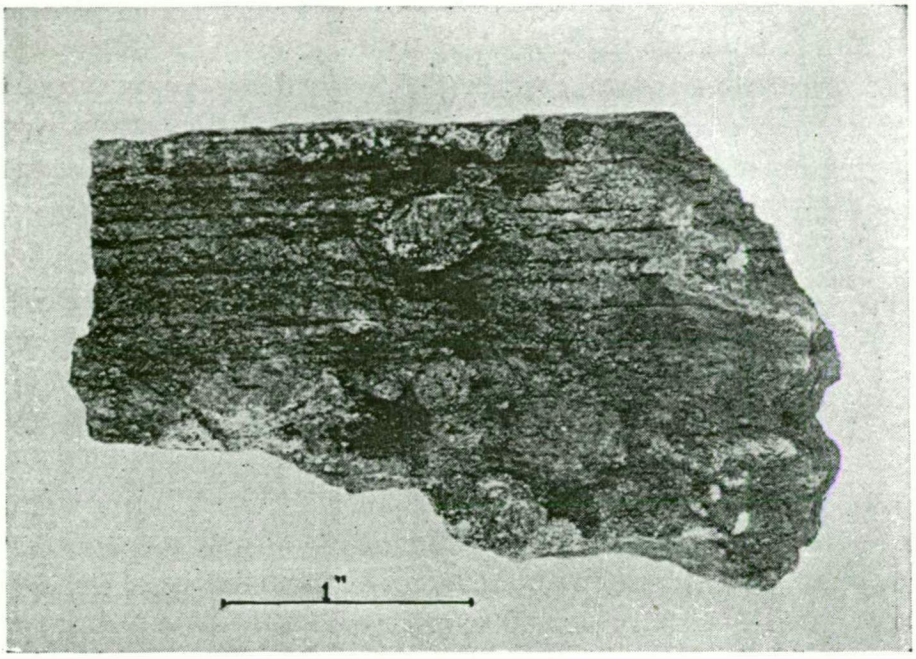

FIG. 2. Spinel porphyroblast in finely foliated, recrystallized peridotite.

At Trevassack and Countybridge Quarries, near the northern margins of the peridotite, at Lawarnick Pit and Pol Cornick on the western margin, and near Porthallow, there are localized occurrences of thin (0·5 cm to 2 cm thick) leucocratic bands parallel to the foliation of the peridotite (Fig. 3). Commonly the bands are extremely planar and a 1-cm band may be traceable for 3–4 metres. Less commonly internal isoclinal folding and distinct lensing make the bands much less continuous. The primary mineral assemblage of the bands is diopside+plagioclase+brown or orange-brown hornblende+enstatite±olivine ±spinel.

The bands are distinctly coarser grained than the enclosing peridotite and the minerals are anhedral, with curving, intergrown boundaries and without cataclastic effects. Hornblende and enstatite (particularly near the contact of the basic band and enclosing ultramafic rock) show crystallographic and dimensional orientation parallel to the band. The petrography of the bands is not diagnostic in determining their genesis but the major and trace element chemistry

strongly indicates an origin by inclusion, and metasomatic reaction with basic xenoliths derived from the marginal pyroxene granulite.

3. *The recrystallized hydrous assemblage*

The recrystallized hydrous assemblage of the peridotite occurs as bands, parallel to the foliation, within the recrystallized anhydrous assemblage throughout much of its area of outcrop. It is particularly characteristic of the zone immediately above the shallow-dipping contact in the south-eastern part of the

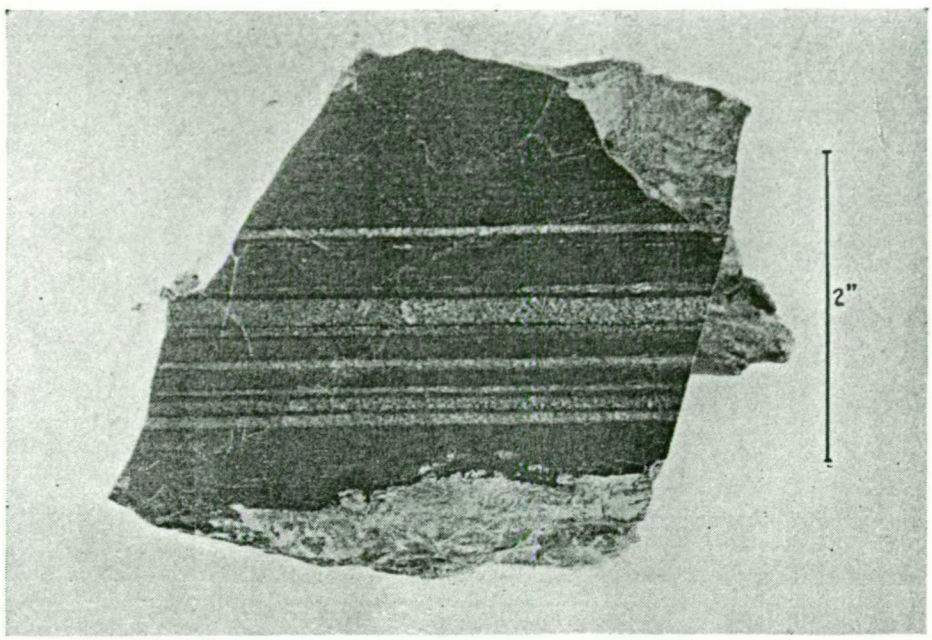

FIG. 3. Finely foliated, recrystallized anhydrous peridotite containing thin basic bands; quarry near Trevassack.

area and also in the area west of the thrust running from Pengersick through George's Cove. The rock type is distinguished by the presence of pale-green amphibole prisms showing parallel alignment in the foliation planes. Plagioclase, pyroxene augen, and porphyroblasts of spinel are normally absent.

The modal composition of a typical specimen (analysis IX), approximate because of the uncertainty that the presence of serpentine and secondary alteration introduces, is as follows:

Olivine, 20·5 per cent; Serpentine replacing olivine, 41 per cent; Pargasite, 36 per cent; Enstatite, 2 per cent; Brown chromian spinel, 0·3 per cent.

The olivine occurs as anhedral crystals from 0·05 to 0·5 mm and is distinctly smaller than, and intergranular to, the larger (0·3 to 2·0 mm) euhedral or subhedral pargasite crystals (Fig. 4). Enstatite is uncommon as small anhedral grains associated with the olivine and small, non-porphyroblastic brown chromian spinels occur commonly as anhedral inclusions within the pargasite or as anhedral grains associated with the olivine aggregate. The pargasite is dimensionally

and crystallographically oriented, the '*c*' axes defining a strong lineation in the foliation plane. In cross-section the crystals are euhedral with development of the (110) prism faces. The pargasite is colourless or extremely faintly green-brown in thin section and with very faint pleochroism. It is biaxial, with $(+)2V$ about 80° and the extinction angle $Z \wedge c = 23°$.

The very fine-grained and finely foliated peridotite (called by Flett the 'dunite peridotite') occurring at the vertical contacts on the west coast is commonly of fine-grained olivine, slightly coarser pargasite and scattered yellow-

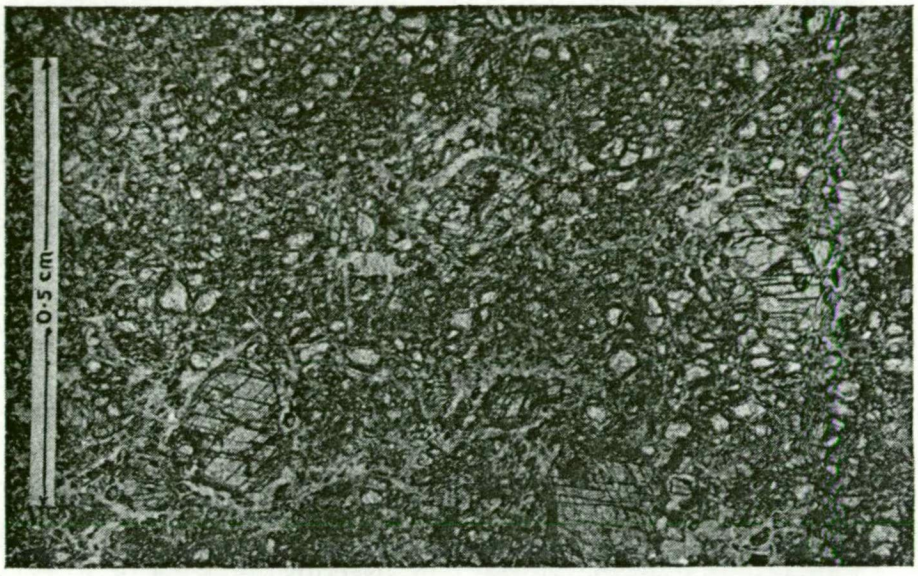

FIG. 4. Euhedral pargasite porphyroblasts in partly serpentinized olivine, recrystallized hydrous peridotite.

brown spinel. These rocks pass transitionally into a fine, interbanded variant of the anhydrous peridotite assemblage with olivine+enstatite+diopside+brown spinel+accessory colourless to pale brown amphibole. At the south-eastern contacts the peridotite, immediately at the contact with the underlying amphibolites, is retrogressively altered to yield relict, euhedral pargasite enclosed in a matte of talc with antigorite, brucite, or magnesite in replacement of the olivine.

III. THE CHEMISTRY OF THE PERIDOTITE

In the Lizard peridotite serpentinization is a secondary, post-crystallization effect and the variable water content in rock analyses introduces an irrelevant complexity into the comparison of the primary rock chemistry. Calculations of this primary rock composition differ considerably depending on whether the serpentinization of olivine and enstatite is assumed to be a replacement reaction at constant volume (cf. Turner & Verhoogen, 1960, pp. 318–19) or a replacement with simple addition of water and no removal of any constituents of the primary composition ('constant composition serpentinization' for brevity).

It is possible to test roughly which process of serpentinization has operated

in two examples (rock analyses V, IX) from the Lizard, as both the rock and its constituent minerals have been analysed. The point-counter analysis of each of the rocks was recalculated to a weight percentage on the alternative hypotheses of serpentinization to obtain two alternative mineralogical compositions and, using the mineral analyses, two calculated rock compositions. These were compared with the whole rock analysis recalculated anhydrous to 100 per cent, assuming alternatively that either the serpentinization reactions at constant volume or at 'constant composition' expressed the process which had operated. Comparison of the four rock analyses thus obtained for each example showed that the hypothesis of 'constant composition serpentinization' yielded similar primary compositions derived from both rock and mineral analyses, whereas the hypothesis of constant volume serpentinization gave two mutually dissimilar primary compositions.

The data favour the hypothesis that in these peridotites serpentinization has proceeded by simple addition of water without massive leaching of MgO (cf. Turner & Verhoogen, 1960, p. 319). The Lizard peridotite has acted as a 'sponge' during serpentinization, not as a channel for large quantities of through-flowing water.

If as a first approximation the serpentinization in the Lizard peridotite is a 'constant composition' process then the primary rock compositions can be readily calculated and compared as in Table 1. The new analyses compare well with the older analyses except that TiO_2 is consistently higher and MnO consistently lower in the new analyses. This is considered to be a more accurate result from improved quantitative methods.

Analyses III, V, and VI are of the primary peridotite assemblage, III and V being normal peridotites and VI being a pyroxene-rich band illustrating (in its high CaO, SiO_2, and Cr_2O_3 and lower MgO) the range in rock composition resulting from the primary banding previously described. All these rocks have similar Mg/Fe ratios. Analysis IV (Flett, 1912, 1946) of a chromite serpentinite band in the primary assemblage is anomalous in several respects. The $\frac{MgO+FeO}{SiO_2}$ ratio is not high enough for a nearly pure olivine rock, indicating either addition of SiO_2 or removal of (Mg,Fe)O. Similarly, the MgO/FeO ratio is appreciably lower than in the other peridotites, CaO is practically absent but Al_2O_3 is only slightly less than in most of the other peridotites.

The analyses of the anhydrous recrystallized peridotite (VII and VIII) and of the hydrous recrystallized assemblage (analysis IX) lie within the composition range defined by the analyses of the primary peridotite assemblage.

The peridotite (analysis X) at the contact with the basic granulite (analysis XII) shows slight metasomatic change from the composition defined by the other analyses, in its lower MgO/FeO ratio and higher SiO_2, FeO, Na_2O, and K_2O contents. The analysis of the granulite in contact with this peridotite is included in Table 1 and illustrates the strong chemical discontinuity across the boundary.

TABLE 1

Rock analyses and analyses calculated anhydrous (i.e. pre-serpentinization composition assuming simple addition of water with volume change during serpentization)

	Dunite Serpentine	*Tremolite Serpentine*	*Bastite Serpentine*	*Chromite Serpentine*	*Primary Peridotite*	*Primary Pyroxene-Rich Band*	*Recrystallized Anhydrous*	*Recrystallized Anhydrous*	*Recrystallized Hydrous*	*Recrystallized Hydrous Contact*	*Recrystallized Basic Band*	*Granulite Contact*
	I	II	III	IV	V	VI	VII	VIII	IX	X	XI	XII
SiO_2	40·12	40·87	39·58	38·58	39·90	44·48	40·02	39·73	40·12	41·22	40·82	48·64
TiO_2	tr.	0 16	0 10	0 08	0 14	0 15	0 20	0 16	0·25	0·23	0·48	0·78
Al_2O_3	0·98	3·93	3·19	2·72	3·74	4·56	4·39	3·13	3·57	4·04	12·83	13·22
Cr_2O_3	0·28	0·25	0·20	0·28	0·33	0·50	0·32	0·40	0·36	0·31	0·14	0·07
Fe_2O_3	6·52	6·17	4·70	8·75	5·92	3·34	3·50	5·03	5·45	5·29	0·95	1·39
FeO	1·21	2·37	2·76	1·02	2·09	3·19	3·81	2·78	2·70	3·82	3·27	7·79
MnO	0·52	0·29	0·34	0·14	0·08	0·07	0·08	0·12	0·10	0·10	0·07	0·16
MgO	35·78	32·86	36·21	35·72	36·21	29·67	33·82	35·91	34·58	31·21	21·23	13·70
CaO	0·12	2·36	1·09	0·07	1·54	5·19	2·75	1·80	2·53	2·17	11·93	9·45
Na_2O	0·24	0·39	0·28	0·44	0·10	0·38	0·21	0·16	0·31	0·58	0·42	2·12
K_2O	0·08	0·04	0·06	0·19	0·02	0·03	0·05	0·06	0·05	0·17	0·10	0·26
H_2O^+	12·17	8·95	10·79	11·03	10·11	7·54	10·10	10·03	9·29	8·86	6·98	1·98
H_2O^-	1·69	1·09	0·51	1·42	0·33	0·56	0·51	0·57	0·45	1·12	0·60	0·15
NiO	0·15	0·17	0·16	0·07	n.d.	n.d.	n.d.	n.d.	n.d.	n.d.	n.d.	n.d.
CO_2	0·15	0·11	0·24	0·04	n.d.	n.d.	n.d.	n.d.	n.d.	n.d.	n.d.	n.d.
P_2O_5	0·10	0·07	0·16	0·03	0·04	0·02	0·00	0·00	0·02	0·00	0·01	0·05
										S=0·38		
FeS_2	0·01	0·01										
	100·12	100·09	100·37	100·58	100·55	99·68	99·76	99·88	99·78	99·50	99·83	99·76
SiO_2	47·07	45·78	44·85	44·24	44·60	48·69	45·12	44·72	44·89	46·32	44·26	49·92
TiO_2	tr.	0·18	0·11	0·09	0·16	0·16	0·23	0·18	0·28	0·26	0·52	0·80
Al_2O_3	1·15	4·40	3·63	3·12	4·18	5·00	4·96	3·52	3·99	4·54	13·95	13·61
Cr_2O_3	0·33	0·28	0·23	0·32	0·37	0·55	0·36	0·45	0·40	0·35	0·15	0·07
Fe_2O_3	—	—	—	—	—	—	—	—	—	—	—	—
FeO	8·37	8·88	7·91	10·19	8·30	6·84	7·87	8·23	8·49	9·65	4·49	9·26
MnO	0·61	0·33	0·39	0·16	0·09	0·08	0·09	0·14	0·11	0·11	0·08	0·16
MgO	41·78	36·84	41·07	41·00	40·45	32·54	37·97	40·48	38·62	35·05	23·04	14·05
CaO	0·14	2·64	1·24	0·08	1·72	5·69	3·10	2·03	2·82	2·44	12·94	9·68
Na_2O	0·28	0·44	0·32	0·50	0·11	0·42	0·24	0·18	0·35	0·66	0·46	2·18
K_2O	0·09	0·04	0·07	0·22	0·02	0·03	0·06	0·07	0·05	0·19	0·11	0·27
NiO	0·18	0·19	0·18	0·08	—	—	—	—	—	S=0·43	—	—
	100·00	100·00	100·00	100·00	100·00	100·00	100·00	100·00	100·00	100·00	100·00	100·00
Mg/Fe	8·89	7·41	9·26	7·19	8·69	8·49	8·62	8·77	8·12	6·46	9·15	2·70
$\frac{Mg \times 100}{Mg+Fe+Mn}$	89·2	87·5	89·0	87·5	89·5	89·4	89·5	89·6	89·0	86·5	89·8	72·8

I. West of Parc Bean Cove. II. Lawarnick Pit. III. Poltesco Mill. IV. East of Kynance Cove [Flett (1912)]. V. Specimen 90683, Goonhilly Downs, near Gwenter. VI. Spec. 90684, The Bees, Pedn Boar. VII. Specimen 90686, Goonhilly Downs, near Kernewas. VIII. Specimen 90692, Goonhilly Downs, Trevassack Quarry. IX. Specimen 90691, Goonhilly Downs, near Kernewas. X. Specimen 90703, Pol Cornick. XI. Specimen 90692, Goonhilly Downs, Trevassack Quarry. XII. Specimen 90703, Pol Cornick.

Analyst (V–XII) D. H. Green with total iron checked by J. H. Scoon for analyses IX and XI.

The analysis (XI) of the recrystallized basic band (cf. p. 140 and Fig. 3) within the anhydrous recrystallized peridotite is high in CaO, Al_2O_3 and particularly, in comparison with the peridotites, high in TiO_2. The low Na_2O content may be real or may be an effect of leaching during the alteration of the primary plagioclase. The trace element concentration (Table 2, measurements by R. S. Allen, Cambridge) shows lower Cr and Ni contents than the peridotites and distinctly higher Si, Li, and V contents. In Ti, Cr, Ni, Sc, and V this band shows an

approach to the compositional characteristics of the surrounding basic rocks and is not typical of the peridotite. The chemical composition favours the interpretation of these bands as drawn-out and metasomatized xenoliths of country rock enclosed in the peridotite in near-contact areas.

In trace element concentrations analyses V, VII, VIII, and IX are practically identical and together define the typical trace-element concentrations of the peridotite. Analysis VI, the primary pyroxene-rich band, differs from the previous analysis but trace element data on the minerals (later tables) clearly

TABLE 2

Trace element data for the Lizard peridotites (p.p.m.)

	V	VI	VII	VIII	IX	X	XI	XII
Ga	—	—	—	—	—	—	—	18
Cr	1800	2800	1950	2200	1800	1950	1000	540
Li	3	3	3	14	14	40	100	40
Ni	2200	1000	1250	2200	2200	1250	550	150
Co	70	46	70	85	70	56	26	220
V	63	125	63	63	63	63	224	220
Zr	—	—	—	—	—	—	—	16
Sc	8	15	7	8	8	8	40	40
Y	—	—	—	—	—	—	—	5
Sr	—	—	—	—	—	—	—	125
Pb	—	—	—	—	—	—	—	—
Ba	—	—	—	—	—	—	—	45

Specimen localities as in Table 1.

show that these differences are due to the relative decrease in olivine and increase in pyroxenes in this type. Analysis X in contact with the basic granulite, differs from the peridotite only in its high Li content; in this feature it resembles the contact granulite (XII) but differs considerably in all other trace elements.

From the rock analyses made during the present study and from the analyses given in the 1912 and 1946 Memoirs on the Lizard area, it is concluded that the variation in composition of the peridotite provides no support for Flett's concept of three separate peridotite magmas. The range of composition expressed in the peridotites of differing mineral assemblages and texture is no greater than the range of composition due to the variation in proportions of olivine, enstatite, and diopside in banding in the primary peridotite assemblage. Immediately at the contact of peridotite and hypersthene granulite country rock there is slight introduction of Na_2O, K_2O, SiO_2, FeO, and possibly TiO_2 into the peridotite.

The inter-relationships of the peridotite types

The previous sections have described the petrographic and mineralogical differences between the three peridotite types and their chemical identity. The present section summarizes the petrographic evidence for the sequence of derivation of one peridotite type from the other.

There is a clear genetic linkage between rocks of the recrystallized anhydrous assemblage and those of the primary assemblage in the presence of bent and fractured augen of diopside and enstatite with common exsolution lamellae in the former rock type. These pyroxenes are exactly analogous to the large pyroxenes with similar or lesser strain effects and with the same type of exsolution lamellae present in the primary assemblage. The first stages of the process of deformation of the primary olivine, diopside, and enstatite and their recrystallization as a finer-grained mineral assemblage are clearly seen in almost all rocks of the primary assemblage.

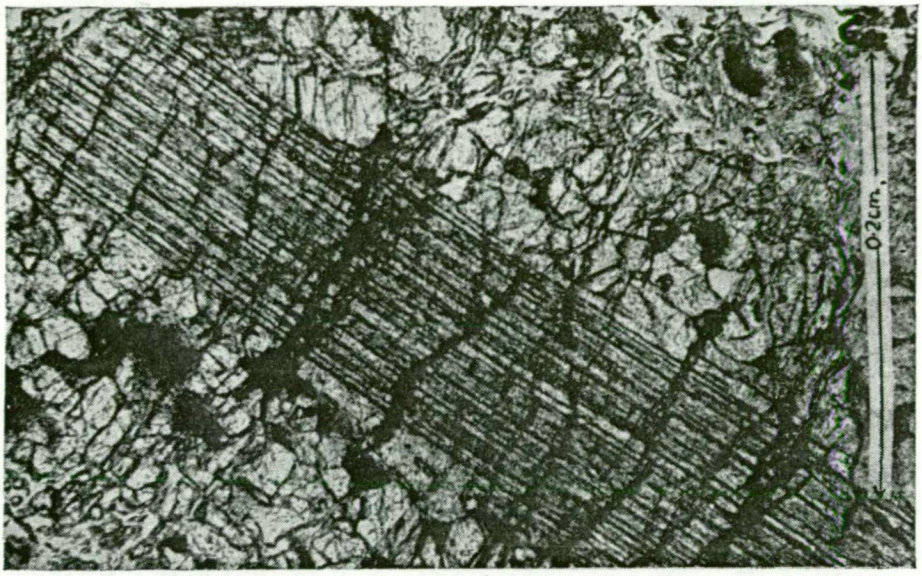

FIG. 5. Primary enstatite augen surrounded by recrystallized enstatite, olivine, saussuritized plagioclase and some diopside.

Thus olivine appears bent and strained and very readily recrystallized to an aggregate of smaller crystals. Diopside has commonly recrystallized to an anhedral mosaic of diopside with some interstitial saussuritized plagioclase, a phase not present in the normal primary assemblage. Enstatite is the most stable of the primary phases under the conditions of deformation and deforms readily by bending or development of 'kink-bands' (Turner, Heard, & Griggs, 1960). With more intense deformation enstatite also develops marginal recrystallization to a mosaic of enstatite (lacking exsolution lamellae), olivine, and plagioclase (Fig. 5).

The recrystallized anhydrous assemblage with its different texture and mineralogy is thus regarded as a cataclastic envelope derived from rock types identical with those of the primary assemblage in the core of the peridotite, by recrystallization during internal deformation.

The petrography also shows that the olivine+pargasite assemblage (the recrystallized hydrous assemblage) developed from and replaced the recrystallized anhydrous assemblage. No example of the reverse sequence has been

observed. The pargasite does not usually show a direct replacement relation to any of the anhydrous phases but probably has developed from the accessory brown hornblende in the anhydrous assemblage, not as a rim growth but as a phase continuously changing in total composition with growth and changing metamorphic environment.

IV. MINERAL CHEMISTRY

A major controversy in the genesis of ultramafic rocks centres on their origin either as accumulates from a basaltic magma of the currently accepted types or as direct crystallization from an ultramafic melt of very different major and minor element concentration from basaltic magmas. For this reason, the analysed minerals from the Lizard are compared in detail with analysed minerals from peridotites of differing modes of occurrence in an attempt to isolate critical differences or similarities which are of genetic significance. Also in the Lizard peridotite, a constancy of bulk rock composition with different mineral assemblages prompts inquiry into compositional changes in the minerals themselves and the evidence of these for changing *P–T* conditions.

1. *Olivine*

In the separation of minerals from the peridotite it was not possible to obtain olivine free from contamination by enstatite or by spinel or magnetite composite grains. However, samples pure enough for composition determinations by the X-ray diffractometer method of Yoder and Sahama (1957) were obtained and the results of these determinations are given in Table 3. Yoder and Sahama estimate the accuracy of their method as ± 4 mol per cent near the forsterite end of the composition range. Thus, within the accuracy of this method, the olivines of the primary and both recrystallized assemblages have the same composition, whereas the olivine from the troctolite at Perprean Cove, Coverack (the first and most mafic intrusion into the peridotite), has a distinctly lower forsterite content.

Partial chemical analyses of two of these olivines are given in Table 4. Since a pure concentrate could not be obtained the olivine was dissolved out from the impurities in 10 per cent HCl. The method gave satisfactory results except for high Al_2O_3 and low SiO_2 values (particularly in Ol. 2) due to the tendency for the precipitated SiO_2 to remain in colloidal form and pass into the R_2O_3 precipitate. The spectrographic determination of Al, using analysed pyroxenes as standards, suggests a more accurate figure for Al_2O_3 would be 0·3 per cent. In trace elements determined on Ol. 1 the higher Cr content and slightly higher Ni, Co, and Zr contents of the Lizard olivine compared with the values given by Ross, Foster, and Myers are probably due to spinel contamination (cf. Table 8).

In Table 5 the molecular ratios $\frac{Mg}{Mg+Fe+Mn} \times 100$, i.e. the proportions of

TABLE 3

Olivine compositions from X-ray diffractometer measurements

Specimen	$2\theta_{130}$		d_{130}	*Fo%*	*Locality*
90683 Primary peridotite assemblage	1. 32·289 2. 32·289	32·289	2·7724	90·3	West of Gwenter
90681 Primary peridotite assemblage	1. 32·289 2. 32·299	32·294	2·7719	91·0	North of Worvas (Olivine analysis Ol. 1)
90689 Recrystallized anhydrous assemblage	1. 32·289 2. 32·293	32·291	2·7723	90·5	Near Rill Cove (Olivine analysis Ol. 2)
90686 Recrystallized anhydrous assemblage	1. 32·299 2. 32·287	32·293	2·7721	90·7	South of Kernewas
90691 Recrystallized hydrous assemblage	1. 32·283 2· 32·287	32·285	2·7728	89·7	South of Kernewas
Troctolite at Coverack	1. 32·229 2. 32·223	32·231	2·7773	83·0	Perprean Cove, Coverack

TABLE 4

Chemical analyses of olivines from 90681 (Ol. 1) and from 90689 (Ol. 2)

		Ol. 1			Ol. 2	
Oxides	*Cations*	*Weight%*	*Cations to 40's*		*Weight%*	*Cations to 40's*
SiO_2	Si	40·75	0·998		39·78	0·982
Al_2O_3	^{z}Al	0·68	0·002	1·000	1·20	0·018
	^{y}Al		0·018			0·017 1·000
TiO_2	Ti	0·18	0·003		0·28	0·005
Fe_2O_3	Fe'''	(assumed)			(assumed)	
		0·00	—		0·00	—
FeO	Fe''	10·05	0·206		10·28	0·212
MnO	Mn	0·13	0·003		0·14	0·003
MgO	Mg	48·01	1·753		47·79	1·758
CaO	Ca	0·00	—	1·987	0·00	— 1·998
Na_2O	Na	n.d.	—		n.d.	—
K_2O	K	n.d.	—		n.d.	—
Cr_2O_3	Cr	tr.	—		tr.	—
NiO	Ni	0·20	0·004		0·16	0·003
		100·00			99·63	

Trace elements (p.p.m.) in Ol. 1:
Cr–850; Ni–4650; Co–220; Zr–16; (Ca–550) (Al–1430)
Sought but not found: Ga, V, Sc, Y, Sr, Pb, Ba.

the magnesian molecule, are compared for the coexisting olivine and orthopyroxene. The analytical and X-ray determinations for the olivines are also compared, suggesting that the X-ray method may yield results 1–2 per cent too high. Within the accuracy of the methods used, the Mg-content as defined above is the same for both coexisting olivine and enstatite.

In Fig. 6 the olivines from the Lizard are compared in their forsterite contents $\left(\text{measured by the molecular ratio } \frac{\text{Mg}}{\text{Mg+Fe+Mn}} \times 100\right)$ with magnesian olivines which have accumulated from basaltic magmas, with olivines from peridotite nodules in basalts and from 'intrusive' peridotites of orogenic belts. The earliest

TABLE 5

Percentage of magnesian molecule $\left(\frac{100 \times \text{Mg}}{\text{Mg+Fe+Mn}}\right)$ *in coexisting enstatite and olivine*

Specimen	*%Enstatite molecule (chemical analyses)*	*%Forsterite molecule*	
		chemical analyses	*X-ray method*
90683 (Primary)	89·5	—	90·3
90681 (Primary)	89·5	89·3	91·0
90684 (Primary band)	89·4	—	—
90686 (Recrystallized)	91·1	—	90·7
90689 (Recrystallized)	89·0	89·1	90·5

olivines from differentiated basaltic magmas (Stillwater, Rhum, and Bushveld Complexes) are of distinctly lower forsterite content than the Lizard olivines which are themselves lower than the analysed olivines from the Webster, Twin Sisters, Dun Mt., and New Caledonian peridotites. On the other hand the analysed Lizard olivines fall within the lower part of the range given by Ross, Foster, and Myers's (1954) analyses from peridotite nodules and match closely with the olivine (optically determined) of the high temperature Tinaquillo peridotite (Mackenzie, 1960) and with analysed olivines from a Tyrol dunite and a picritic sill on Ubekendt Island (Yoder & Sahama, 1957). The differentiated alkaline basaltic intrusions of the Shiant Isles and Black Jack, Gunnedah (Johnston, 1953, and Wilkinson, 1956), contain much more fayalitic olivines.

Olivines from the layered ultramafics of 'alpine type' in New Guinea (Green, 1961) and the Philippines, from the Union Bay Ultramafic Complex, Alaska (Ruckmick & Noble, 1959) and from the Great Dyke, Northern Rhodesia (Worst, 1958), embrace the range of the Lizard olivines and extend to less forsteritic compositions. In summary, the Lizard olivines show a small but

probably significant difference from olivines derived as accumulates from basaltic magmas (cf. Brown, 1956, p. 42) and are similar to olivines in peridotite nodules and in some 'alpine peridotites'.

2. *Enstatite*

Five enstatites from the peridotite have been chemically analysed; O_1, O_2, O_3 are from the primary assemblage and O_4 and O_5 are from the recrystallized anhydrous assemblage. These analyses, with specimen number and locality, and

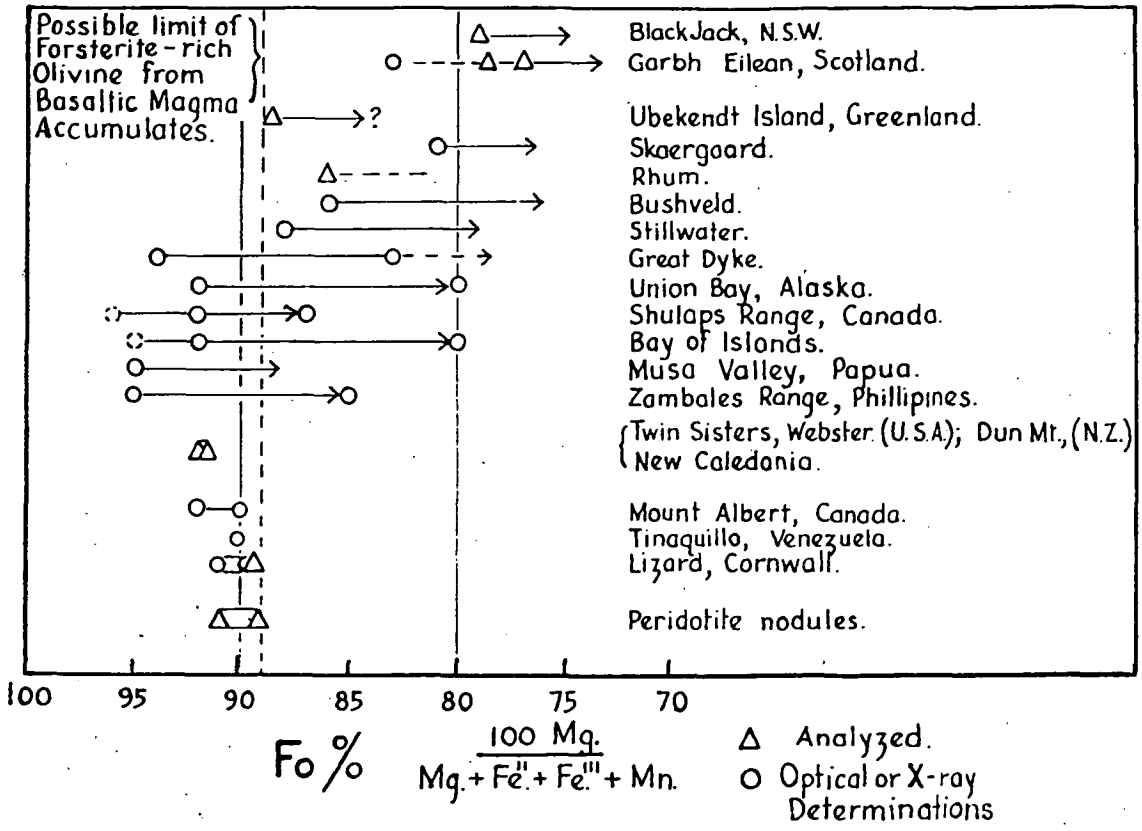

FIG. 6. Comparison of forsterite contents of magnesian olivines from various magmatic origins.

with the calculated structural formulae (on the basis of cations per 6 oxygens and a Z-group total arbitrarily made equal to 2) are given in Table 6. In major elements the two enstatites (O_1 and O_2) from the normal primary peridotite assemblage, although from rocks collected $2\frac{1}{2}$ miles apart, are remarkably similar. The enstatite (O_1) from the pyroxene rich band in the primary assemblage is slightly higher in SiO_2 and lower in Al_2O_3 than the pyroxenes O_1 and O_2 but in all other constituents is very similar. In contrast the enstatites from the recrystallized anhydrous peridotites have higher SiO_2 and lower Al_2O_3 than the primary enstatite and also have higher MgO and lower CaO.

The trace element data provide good confirmation of the analytical results for Cr_2O_3. There appear to be no systematic differences between the orthopyroxenes

TABLE 6

Analyses, structural formulae, and trace-element data for enstatites of the peridotite

Oxides	O_1	O_2	O_3	O_4	O_5
SiO_2	53·26	53·17	54·30	55·67	55·27
Al_2O_3	6·59	6·30	5·46	3·27	2·05
TiO_2	0·17	0·19	0·16	0·23	0·44
Fe_2O_3	0·97	0·74	0·48	*0·00 (Total Fe as Fe_2O_3 = 6·28)	1·21
FeO	5·54	5·80	6·07	5·65	6·00
MnO	0·12	0·11	0·14	0·17	0·14
MgO	31·29	31·21	31·54	33·25	32·69
CaO	2·14	2·11	2·14	1·47	1·88
Na_2O	0·07	0·06	0·01	n.d.	n.d.
K_2O	0·02	0·02	tr.	n.d.	n.d.
Cr_2O_3	0·39	0·67	0·39	0·35	0·53
	100·56	100·38	100·69	100·06	100·21
Cations to 6O's					
Si	1·839 } 2·000	1·842 } 2·000	1·872 } 2·000	1·923 } 2·000	1·920 } 2·000
^{z}Al	0·161 }	0·158 }	0·128 }	0·077 }	0·080 }
^{y}Al	0·107	0·100	0·094	0·057	0·004
Ti	0·004	0·005	0·004	0·006	0·011
Fe‴	0·025	0·019	0·012	0·000	0·032
Fe″	0·160	0·168	0·175	0·163	0·174
Mn	0·004	0·003	0·004	0·005	0·004
Mg	1·610 } 2·005	1·612 } 2·008	1·621 } 2·000	1·712 } 2·007	1·693 } 2·003
Ca	0·079	0·078	0·079	0·054	0·070
Na	0·004	0·004	—	—	—
K	0·001	0·001	—	—	—
Cr	0·011	0·018	0·011	0·010	0·015
Ca	4·2	4·2	4·2	2·8	3·7
Mg	85·7	85·7	85·7	88·5	85·7
ΣFe+Mn	10·1	10·1	10·1	8·7	10·6
$\frac{Mg\times100}{Mg+Fe+Mn}$	89·5	89·5	89·4	91·1	89·0
$\frac{Fe'''}{Fe''+Fe'''}$	0·135	0·102	0·064	—	0·156
Fe″/Mg	0·100	0·104	0·108	—	0·103
^{z}Al/Si	0·0875	0·0857	0·0684	0·0400	0·0417
TRACE ELEMENTS	O_1	O_2	O_3	O_4	O_5
Ga	5	5	5	5	5
Cr	2800	5000	2800	2160	2160
Ni	550	1000	830	550	700
Co	46	56	46	56	46
V	125	170	220	125	170
Zr	—	16	16	—	16
Sc	26	40	40	22	26

Li, Y, Sr, Pb, Ba—sought but not found.

O_1 Specimen 90683, Goonhilly Downs, near Gwenter } primary assemblage.
O_2 Specimen 90681, near Worvas }
O_3 Specimen 90684, The Bees, near Pedn Boar; pyroxene-rich band, primary assemblage.
O_4 Specimen 90686, Goonhilly Downs, near Kernewas } recrystallized anhydrous assemblage.
O_5 Specimen 90689, Rill Cove, Kynance Cliff }

*FeO not determined due to insufficient sample, Fe_2O_3 assumed to be 0·00%.

from the various sources in trace element contents. Comparison of trace elements in coexisting olivine (Ol. 1) and enstatite (O_2) shows the greater concentration of Ni in the olivine ($Ni/Mg \times 10^3 = 6{\cdot}7$) relative to the enstatite $Ni/Mg \times 10^3 = 2{\cdot}2$). The Co shows a similar pattern but Cr and V show the reverse pattern with relative concentration in the enstatite.

CaO *content.* Hess (1960, p. 32) has compared the CaO contents of orthopyroxenes from the layered intrusions of Stillwater, Great Dyke, and Bushweld with the orthopyroxenes of the 'calcium-poor, ultra-mafic' magma series and with pigeonites and inverted pigeonites. The *primary* enstatites of the Lizard have distinctly higher CaO contents (2·14 and 2·11 per cent) than those of the layered complexes (1·35 to 1·93 per cent) but are within the range (1·45 to 2·67 per cent) given by Kuno (1954, p. 33) for high-temperature volcanic orthopyroxenes. Of the enstatites listed by Hess from 'ultramafic magma' most have very much lower CaO contents (0·23 to 1·06 per cent) except for one enstatite (1·96 per cent) from diopside-bearing harzburgite (Leech, 1955, p. 30). The range of CaO contents given by Ross *et al.* (1954, p. 708) for enstatites in 'intrusive' dunites is 0·60 to 1·03 per cent and for enstatites in peridotite nodules is 0·60 to 1·72 per cent, i.e. in both cases lower than the Lizard primary enstatites. The *recrystallized* Lizard enstatites have lower (1·47 and 1·88 per cent) CaO contents, comparable with enstatites from the layered complexes.

The lime content of orthopyroxene has been interpreted as a qualitative and comparative temperature indicator by Kuno (1954, p. 35) and Hess (1960, pp. 31–33) although the parent magma composition is also important (Hess, 1960, p. 31). The occurrence of exsolution lamellae of augite in the orthopyroxenes (including those of the Lizard) is clear evidence of the decreasing solubility of Ca^{++} in the orthopyroxene with falling temperature although the possible effect of pressure changes is uncertain. In the Lizard example, with no change in bulk rock composition, the hypothesis that the enstatites of the recrystallized assemblage formed at a lower temperature than the primary enstatites must be considered. Comparison with other examples sufficiently rich in CaO to crystallize either diopside or plagioclase in addition to orthopyroxene suggests that the recrystallized anhydrous assemblage formed at temperatures similar to those in layered mafic complexes and that the primary assemblage may have crystallized at higher temperatures.

TiO_2 *content.* The Lizard enstatites are low in TiO_2 (except for O_5 with 0·44 per cent) and are very similar in this respect to magnesian orthopyroxenes from mafic magma accumulates, intrusive peridotites, and peridotite nodules.

Cr_2O_3 *content.* The only significant difference between the two primary enstatites O_1 and O_2 is the higher Cr_2O_3 content in O_2. This feature is parallelled in the Cr_2O_3 contents of the coexisting diopsides and in the modal spinel content of the respective rocks (0·8 per cent and 1·7 per cent) and is thus presumably due to different Cr_2O_3 contents of the whole-rock composition.

Hess (1960, p. 24) and Brown (1957) illustrate the enrichment in Cr_2O_3 of the

earliest orthopyroxenes crystallizing from a mafic magma. The range of Cr_2O_3 in the Lizard orthopyroxenes overlaps and extends to higher values the range shown by these basaltic magma pyroxenes and in this feature resembles the enstatite of both 'intrusive' peridotites and peridotite nodules (Fig. 7).

Fe_2O_3 *content.* The enstatites from both primary and recrystallized assemblages contain significant amounts of ferric iron ($Fe^{+++}/Fe^{++} = 0{\cdot}07$ to $0{\cdot}184$). In this respect they differ from the enstatites from peridotite nodules analysed

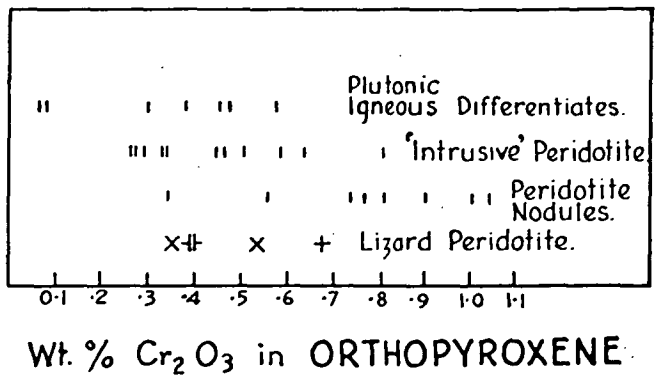

FIG. 7. Variation in Cr_2O_3 (weight per cent) content of orthopyroxenes.

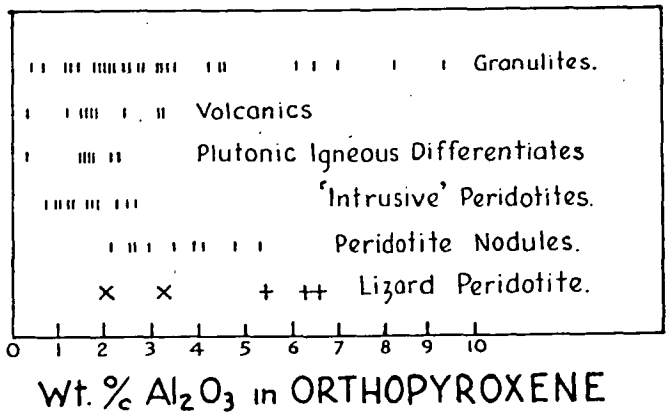

FIG. 8. Variation in Al_2O_3 (weight per cent) content of orthopyroxenes.

by Ross, Foster, and Myers (1954, p. 708) which with one exception (no. 3 with 0·16 per cent Fe_2O_3) are listed with 0·00 per cent Fe_2O_3. Diopsides coexisting with these enstatites contain similar Fe_2O_3 contents to the Lizard diopsides.

Al_2O_3 *content.* The variation in Al_2O_3 (Fig. 8) (and an inverse variation in SiO_2 and MgO) is the most significant feature in the Lizard enstatites and is due to the substitution of ($^{Y}Al\ ^{Z}Al$) for (Mg Si). Hess (1952, p. 177) suggested that this substitution may result in a small decrease in volume of the enstatite and that increased pressure may therefore favour the substitution.[1] As evidence that such a process may occur in natural rocks, Hess draws attention to the extensive substitution of Al for Si in charnockitic and granulite facies hypersthenes, and

[1] In natural assemblages the control on such a pressure-dependent substitution will be whether entry of Al_2O_3 into the enstatite instead of into plagioclase or into spinel increases the density of the whole assemblage, and not simply the possible change in cell-volume of the enstatite.

in enstatites from peridotite nodules in basalts. Eskola (1952, p. 154) draws attention to the very high Al_2O_3 in hypersthene in garnetiferous (i.e. Al_2O_3-rich) granulites. An effect of bulk chemistry and mineralogy on the Al_2O_3-content of the granulite hypersthenes appears in Eskola's results with the low (0·45, 0·68, and 1·25 per cent) Al_2O_3 in hypersthenes coexisting with hornblende and

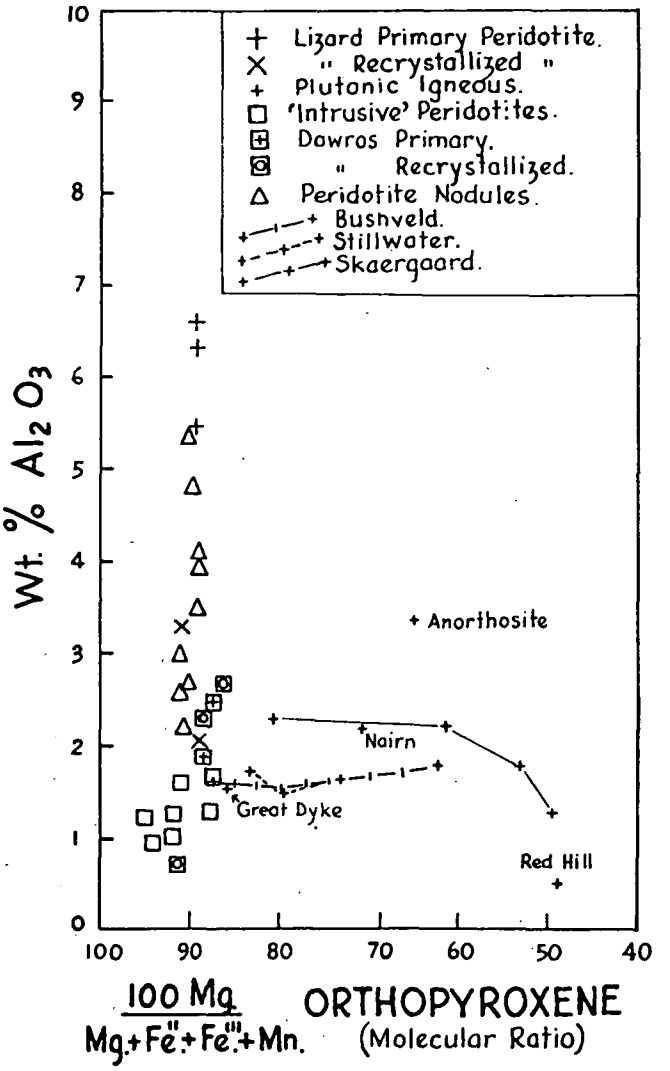

FIG. 9. Al_2O_3 contents of igneous orthopyroxenes in relation to their position in a possible differentiation sequence.

the high (4·51 and 8·26 per cent) Al_2O_3 in hypersthenes coexisting with garnets. Ross, Foster, and Myers (1954, p. 719) note the lower Al_2O_3 contents in enstatites from 'intrusive' peridotites than in enstatites from peridotite nodules but do not comment on any significance to be attached to this.

Fig. 9 is a plot of the Al_2O_3 content of orthopyroxenes against their relative enrichment in MgO $\left(\text{given by the atomic ratio } \frac{Mg}{Mg+Fe+Mn} \times 100\right)$. The pyroxenes are symbolized according to their mode of occurrence and environment, and illustrate a number of trends and fields. The calcium-poor pyroxenes

of the Skaergaard intrusion, including one orthopyroxene and three pigeonites, have Al_2O_3 contents less than 2·5 per cent and decrease with increasing Fe content. Orthopyroxene from the Nairn Gabbro (Labrador) falls close to this rather poorly defined trend. The early formed, more magnesian, orthopyroxenes from the Bushveld and Stillwater Complexes are lower by 0·5 per cent than the Skaergaard pyroxenes but may define a nearly parallel trend. Although the data are very meagre they suffice to show that the early formed pyroxenes in the well-documented differentiated basaltic intrusions have Al_2O_3 contents between 1·5 and 2·5 per cent and in a given intrusion there is very little variation (probably less than the analytical errors) in the range Mg_{88} to Mg_{70}.

The enstatites from peridotite nodules (Ross *et al.*, 1954) are in striking contrast, falling entirely within the range $Mg_{91·5}$ to Mg_{89} and with Al_2O_3 contents ranging from 2·17 to 5·32 per cent, i.e. from near the basaltic magma field to pyroxenes with $2\frac{1}{2}$ times this Al_2O_3 content.

The 'intrusive' peridotites form a cluster within the range Mg_{95} to $Mg_{87·5}$ and with low to very low Al_2O_3 contents. The analysed orthopyroxenes from the Dawros peridotite (Rothstein, 1958) range from $Mg_{91·5}$ to $Mg_{87·5}$ and Al_2O_3 contents from 0·7 per cent to 2·7 per cent. Some of these Rothstein regards as primary igneous pyroxenes, and these fall near the mafic magma field, others are high temperature recrystallizations. One 'igneous' orthopyroxene from a highly aluminous anorthosite (Buddington, 1939) is abnormally high in Al_2O_3.

Orthopyroxenes from volcanic rocks (Kuno, 1954) are not plotted in Fig. 9 but show a considerable scatter in the range Mg_{85} to Mg_{50} and the highest Al_2O_3 content is only 3·12 per cent. In metamorphic granulites the Al_2O_3 contents of the orthopyroxenes show extreme variations with no apparent relationship to Mg content. In general they have a higher Al_2O_3 content than the magmatic pyroxenes.

The primary and recrystallized enstatites of the Lizard fall on the trend defined by the peridotite nodules in the range Mg_{91} to Mg_{89}. O_1 and O_2 are higher (by 1·0 to 1·3 per cent) than, and O_3 lies very close to, the most aluminous of the nodule enstatites; O_4 and O_5 fall within the nodule field and approach the field of the enstatites of Bushveld and Skaergaard type and also that of the Dawros peridotite.

The increased number of analyses available of enstatites, particularly those from peridotite nodules, has shown Ramberg & De Vore's (1951, pp. 206–9) conclusion that hypersthenes between Mg_{80} and Mg_{40} more readily accept Al_2O_3 substitution to be premature.

Boyd and England (1960, p. 49) have carried out the initial stages of an experimental investigation of the solubility of Al_2O_3 in pure enstatite. At a fixed temperature of 1400° C and pressure (18·2 kilobars, i.e. equivalent to about 60 km depth) they have varied the Al_2O_3 content of an $MgSiO_3$–Al_2O_3 mixture and identified the phases formed. They found that at least 14 per cent and possibly 19 per cent Al_2O_3 (weight per cent) can be dissolved in enstatite under these

conditions. Boyd and England consider that their data favour the interpretation that increased pressure at a given temperature increases the solubility limit of Al_2O_3 in enstatite.

In comparison with the experimental work the primary aluminous enstatites of the Lizard are remarkable in containing such a high (6–7 per cent) Al_2O_3 content in a bulk rock composition low (3–5 per cent) in Al_2O_3 and containing two other aluminous phases, diopside and spinel.

Consideration of the distribution of Al_2O_3 in orthopyroxenes of various origins suggests that normal magmatic crystallization could yield orthopyroxenes of maximum Al_2O_3 contents of 2–3 per cent but that the range of Al_2O_3 in peridotite nodules and in peridotites, particularly such as the Lizard, is incompatible with derivation of these rocks as accumulates of known basaltic magma types, at least in upper crustal environments. Since the bulk composition of the primary and recrystallized Lizard assemblages is the same, the different Al_2O_3 contents of the enstatites must be attributed to different temperatures and/or pressures of crystallization.

3. *Diopside*

The five diopsides coexisting with the analysed enstatites (O_1–O_5) have also been analysed and these analyses (numbered C_1–C_5) with structural formulae on the basis of 6 oxygen atoms are given in Table 7. Two other diopsides from the peridotite have also been analysed. Analysis C_6 is of a grey-green diopside (not bright emerald-green as in the primary peridotites) separated from the lenticular, very coarse-grained pyroxenite segregations in the primary assemblage peridotite on the point immediately north of Carleon Cove. Analysis C_7 is of the greyish-white clinopyroxene separated from the basic band (rock analysis XI) within the anhydrous recrystallized assemblage.

Analysis C_8 is the diopside (deep green in colour) separated from the troctolite outcropping in Perprean Cove, near Coverack. The troctolite is intrusive into the peridotite and is itself cut by gabbro dykes. It is the earliest of the post-peridotite intrusions. Analysis C_9 is the pinkish-brown augite separated from a typical specimen of the massive gabbro forming the north shore of Coverack Bay. These pyroxenes were analysed for comparison with those of the peridotite in view of Flett's hypothesis of one magma series embracing the peridotite, troctolite, gabbro, basaltic dykes, and Kennack Gneiss.

Calculations of the structural formulae on the basis of cations for 6 oxygens, and assuming the Z-group cations to be 2·000, give satisfactory results although in every example except C_3 the X, Y-group total is over 2·000.[1] This tendency is most pronounced in the primary peridotite diopsides (C_1 and C_2) with values of 2·028 and 2·024 respectively for X, Y-group cations, and least pronounced in

[1] The same feature is evident in calculating the structural formulae of the pyroxenes from peridotite nodules given by Ross, Foster, and Myers (1954) and seems to be a real feature rather than experimental error.

TABLE 7

Analyses, structural formulae, and trace element data for clinopyroxenes from the Lizard area

	C_1	C_2	C_3	C_4	C_5	C_6	C_7	C_8	C_9
SiO_2	49·83	49·66	51·03	51·93	51·25	51·50	51·38	50·85	51·39
Al_2O_3	7·09	6·80	5·55	4·05	3·80	4·51	4·05	4·49	3·11
TiO_2	0·42	0·31	0·25	0·46	1·12	0·64	1·09	1·06	1·14
Fe_2O_3	1·23	1·37	*0·00	*0·00	1·04	0·53	1·01	1·26	1·31
FeO	2·25	2·38	3·25	2·62	2·30	2·87	2·85	4·08	6·12
MnO	0·10	0·03	0·05	0·08	0·08	0·07	0·10	0 14	0 22
MgO	16·99	17·78	16·98	17·08	16·19	16·29	16·17	16·22	15·66
CaO	20·67	20·36	22·79	23·46	22·63	22·54	22·70	21·22	20·64
Na_2O	0·79	0·36	0·18	0·48	0·70	0·50	0·45	0·49	0·50
K_2O	0·02	0·05	tr.	0·01	0·06	0·05	tr.	tr.	tr.
Cr_2O_3	0·66	0·89	0·43	0·51	0·81	0·73	0·25	0·56	0·07
	100·05	99·99	100·51	100·68	99·98	100·23	100·05	100·37	100·16
Si	1·810	1·805	1·836	1·877	1·873	1·875	1·876	1·858	1·895
^{Z}Al	0·190	0·195	0·164	0·123	0·127	0·125	0·124	0·142	0·105
^{Y}Al	0·113	0·096	0·071	0·049	0·037	0·069	0·050	0·051	0·030
Ti	0·011	0·009	0·007	0·012	0·031	0·018	0·030	0·029	0·032
$Fe^{\cdot\cdot\cdot}$	0·035	0·038	0·000	0·000	0·028	0·014	0·028	0·035	0·036
$Fe^{\cdot\cdot}$	0·068	0·072	0·098	0·079	0·070	0·087	0·087	0·125	0·189
Mn	0·002	0·001	0·002	0·002	0·002	0·002	0·003	0·004	0·007
Mg	0·919	0·963	0·910	0·920	0·882	0·884	0·880	0·883	0·861
Ca	0·806	0·793	0·879	0·909	0·886	0·879	0·888	0·831	0·815
Na	0·057	0·025	0·013	0·033	0·050	0·035	0·032	0·035	0·036
K	—	0·001	—	—	0·003	0·003	—	—	—
Cr	0·017	0·026	0·012	0·015	0·023	0·021	0·007	0·016	0·002
Ca	44·1	42·5	46·5	47·6	47·5	47·1	47·1	44·2	42·7
Mg	50·2	51·6	48·2	48·2	47·1	47·4	46·7	47·0	45·1
$\Sigma Fe+Mn$	5·7	5·9	5·3	4·2	5·3	5·5	6·2	8·8	12·2
$\frac{Mg\times 100}{Mg+Fe+Mn}$	89·7	89·6	90·1	91·8	89·8	89·5	88·1	84·5	78·6
$\frac{Fe^{\cdot\cdot\cdot}}{Fe^{\cdot\cdot}+Fe^{\cdot\cdot\cdot}}$	0·340	0·360	—	—	0·286	0·138	0·244	0·218	0·160
$Fe^{\cdot\cdot}/Mg$	0·074	0·075	—	—	0·079	0·098	0·099	0·142	0·220
$^{Z}Al/Si$	0·1050	0·1080	0·0893	0·0655	0·0677	0·0667	0·0660	0·0764	0·0554
TRACE ELEMENTS	C_1	C_2	†C_3	†C_4	†C_5	C_6	C_7	C_8	C_9
Ga	5	5	—	—	—	7	7	5	7
Cr	4400	6400	5600	7900	4400	5000	5000	6000	1000
Ni	465	465	440	330	250	560	465	260	125
Co	38	32	14	—	20	32	26	22	46
V	380	380	400	420	440	630	630	425	630
Zr	—	16	—	—	30	16	28	28	45
Sc	85	85	80	120	112	100	220	180	180
Y	22	12	46	—	44	22	46	22	26
Sr	—	—	—	—	—	—	—	22	22
Pb	45	45	—	—	—	—	—	—	—
Ba	10	18	—	—	—	—	—	—	—
Li	—	—	—	—	—	—	—	—	—

* Insufficient sample for FeO determination, Fe_2O_3 assumed to be 0·00%

† Extremely small samples, spectrographic determinations on very dilute mixtures so that their accuracy is low.

C_1 Specimen 90683, Goonhilly Downs, near Gwenter
C_2 Specimen 90681, near Worvas
} primary assemblage.

C_3 Specimen 90684, The Bees, Pedn Boar; pyroxene-rich band, primary assemblage.

C_4 Specimen 90686, Goonhilly Downs, near Kernewas
C_5 Specimen 90689, Rill Cove, Kynance Cliff
} recrystallized anhydrous assemblage.

C_6 Specimen 91093, between Carleon Cove and Little Cove; pyroxenite lens, primary assemblage.

C_7 Specimen 90692, (mafic band) Trevassack Quarry; recrystallized anhydrous assemblage.

C_8 Specimen 90974, Perprean Cove, near Coverack; typical troctolite.

C_9 Specimen 91036, North Shore, Coverack Bay; altered olivine gabbro.

the diopsides from the basic band (C_7) and the troctolite and gabbro (C_8 and C_9). Distribution of the cations between Y and Z groups by Hess's method on the basis of balancing charges does not give good results, particularly with the primary pyroxenes C_1 and C_2. This method results in a high value for the X, Y group (usually over 2·02 and for C_1 and C_2 equal to 2·058 and 2·045 respectively) and low value (less than 1·99) for the Z group.

The two diopsides C_1 and C_2 from the primary peridotite are extremely similar. As with the coexisting enstatites, the diopside C_2 is distinctly richer in Cr_2O_3 than C_1. The diopside from the basic band in the recrystallized anhydrous assemblage (C_7) has low Cr_2O_3, a lower Mg/Fe atomic ratio than the peridotite diopsides, and a much higher TiO_2 content. All these factors favour the interpretation of the band as a metasomatized and stretched-out xenolith (cf. p. 144). The diopside from the troctolite (C_8), although of much lower Mg/Fe atomic ratio, has a moderately high Cr_2O_3 content suggesting a link with the peridotite pyroxenes, but also is high in TiO_2 relating it to the augite from the gabbro (C_9). The latter pyroxene has a very low Cr_2O_3 content, a relatively high TiO_2 content, and a distinctly higher MnO content than the peridotite pyroxenes.

As with the coexisting enstatites the most striking variation in the diopsides is in the Al_2O_3 and SiO_2 content. Al_2O_3 is very high (7·09 per cent and 6·80 per cent) in the primary diopsides and distinctly lower (4·05 per cent and 3·80 per cent) in the recrystallized diopsides. This is clearly brought out in the structural formula and since the Na_2O content of the diopsides is not high and does not vary sympathetically with the Al_2O_3 the high alumina content is due to the (^{Y}Al–^{Z}Al) for (Mg–Si) substitution and not to the jadeite substitution (Na–^{Y}Al for Ca-Mg).

The trace element data for the peridotite pyroxenes C_1–C_4 are very similar, probably the only significant difference being the presence of Pb in C_1 and C_2. The pyroxenes C_8 and C_9 illustrate the change from peridotite diopsides to clinopyroxenes from basaltic magmas in the decrease in Cr and Ni and the increase in Sc, V, Zr, and Sr. Analyses C_5, C_6, C_7 show trace element concentrations typical of neither group. In comparison with coexisting olivine and enstatites the peridotite diopsides show lower Ni, Co and higher Cr, V, Sc, and Y contents. The ratio $Ni/Mg \times 10^3 = 1{\cdot}8$ for C_2 and is thus slightly less than that for the coexisting orthopyroxene.

CaO *content*. In Fig. 10 the analysed clinopyroxenes from the Lizard are plotted on a Ca–Mg–Fe diagram and compared with the trends of the early formed pyroxenes from the Skaergaard, Bushveld, Stillwater, Garbh Eilean, and Black Jack intrusions and with the field enclosing the diopsides from peridotite nodules in basalts given by Ross *et al.* (1954).

The diagram illustrates the higher degree of (Mg, Fe) SiO_3 solid solution in the primary diopside C_1 and C_2 and the more Ca-rich character of the recrystallized diopsides C_4, C_5, and C_7. The diopside (C_3) from the pyroxene-rich band and that from the pyroxenite lens (C_6) in the primary assemblage fall closer to

the recrystallized diopsides than the primary diopsides. The primary diopsides fall close to the magnesian extremities of the igneous trends of the Bushveld and Skaergaard pyroxenes and the clinopyroxenes from the troctolite (C_8) and gabbro (C_9) also lie near to these trends. The primary diopsides fall within the field of the nodule pyroxenes but the recrystallized diopsides fall outside it, as do the diopsides of the Webster-Addie 'intrusive' peridotite (Ross *et al.*, 1954; Hess, 1949). The relative increase in Ca-content of the recrystallized diopsides is analogous to the increased Ca-content of granulite augites relative to those of

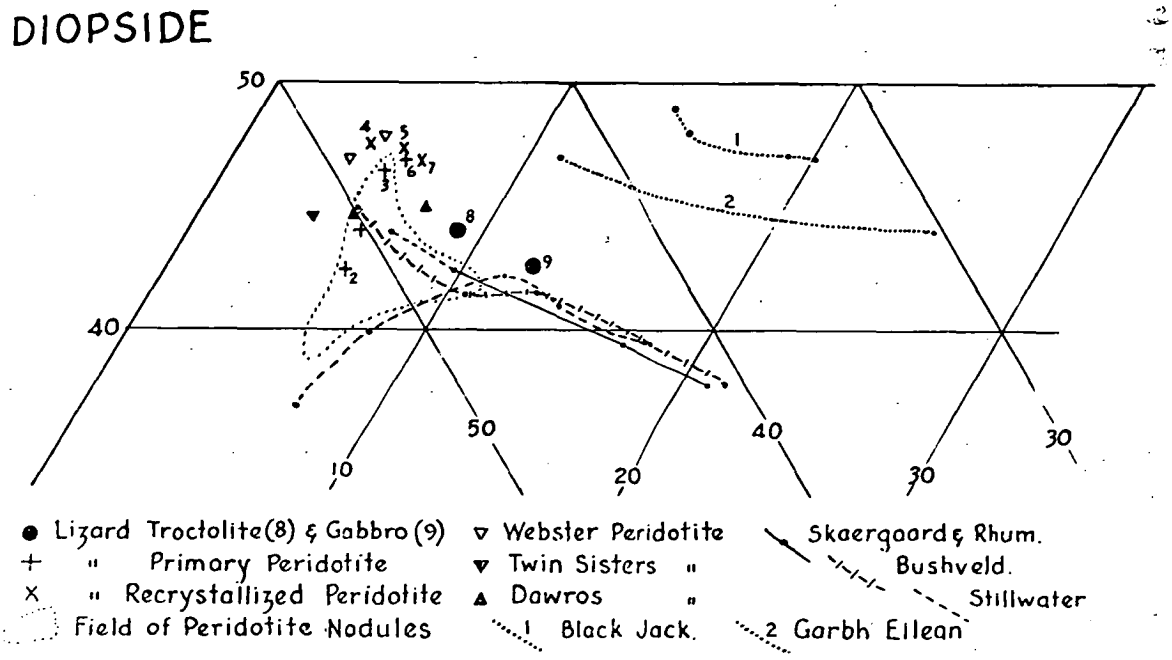

FIG. 10. Ca—Mg—ΣFe plot of Lizard clinopyroxenes.

basic igneous rocks and may indicate a lower temperature of the recrystallized assemblage than the primary assemblage, since in the Lizard peridotite the bulk rock compositions remain the same.

Cr_2O_3 *content*. The Cr_2O_3 content of the diopside is always higher than that of the coexisting enstatite, and in the peridotites is within the range shown by diopsides from peridotite nodules, 'intrusive' peridotites, and by the earliest pyroxenes from the Skaergaard, Bushveld, Stillwater, and Rhum complexes. High Cr_2O_3 in clinopyroxene is typical of the very magnesian members and apparently not characteristic of any specific mode of occurrence or genesis. Ross, Foster, and Myers's conclusion (1954, p. 731) that the high chromian content of the pyroxenes in peridotite nodules seems to be an improbable concentration from a basaltic magma with a few hundredths of one per cent of Cr_2O_3 is not substantiated by comparison of Cr_2O_3 contents of the early pyroxenes from the typical differentiated basaltic magmas (cf. Brown, 1956; Hess, 1960).

The high Cr_2O_3 with high TiO_2 present in the green diopside from the troctolite compares closely with the earliest analysed clinopyroxene of the Skaergaard intrusion (Brown, 1957, analysis 1).

TiO_2 *content.* The diopsides from the peridotite are low in TiO_2 and in this respect differ from the pyroxenes from the troctolite (C_8) and gabbro (C_9) and from the slightly less magnesian Skaergaard, Bushveld, and Stillwater pyroxenes. The pyroxene (C_5) occurring in feldspathic, recrystallized peridotite, north of Kynance Cove, has high Cr_2O_3 (0·81 per cent) but also relatively high TiO_2 (1·12 per cent). The coexisting enstatite similarly has higher TiO_2 than normal in the peridotite and both pyroxenes are slightly but distinctly less magnesian than the other peridotite pyroxenes. Large xenolithic and mobilized sheets of granulite within the peridotite occur in this locality and it is possible that these effects in the pyroxenes are due to contamination of the peridotite.

Al_2O_3 *content.* The Al_2O_3 contents of the diopsides in the peridotite show similar variations to the coexisting enstatites. In all cases the diopside contains more Al_2O_3 than the coexisting enstatite and the main difference between the primary and recrystallized diopsides is the high Al_2O_3 content of the former.

Kushiro (1960) has discussed the substitution of ^zAl for Si in clinopyroxenes from the tholeiitic and alkaline magma series and his analysis brings out the chemical control of this substitution in that deficiency of SiO_2 in the magma increases the ^zAl content of the clinopyroxene. The same feature is brought out in the occurrence of the extremely aluminous clinopyroxenes (fassaites) in metamorphosed limestone xenoliths (Tilley, 1938; Knopf & Lee, 1957).

On the other hand Hess (1960, p. 35) draws attention to the higher Al_2O_3 content of the Stillwater clinopyroxenes than the Bushveld clinopyroxenes, and since he considers the Bushveld and Stillwater magmas to have been practically identical, suggests that the difference may be due to a greater load pressure operative on the Stillwater magma chamber. Hess's reason for this is the analogy with the orthopyroxene crystal structure suggesting that substitution of the smaller ion in the Y-position could cause marked contraction of the unit cell and high pressure could favour increased Al_2O_3 in the clinopyroxene.

In Fig. 11 the Al_2O_3 content of clinopyroxenes is plotted against their Mg enrichment as measured by the ratio $\frac{100\times Mg}{Mg+Fe+Mn}$. The decrease in Al_2O_3 content with differentiation of the Skaergaard intrusion is clearly shown and the Skaergaard clinopyroxenes are distinctly richer in Al_2O_3 than the corresponding clinopyroxenes of the Stillwater and Bushveld Complexes. The early formed clinopyroxene from Rhum (Brown, 1956) falls near the magnesian extremity of the Skaergaard trend. The alkaline differentiated sills of Garbh Eilean (Murray, 1954) and Black Jack (Wilkinson, 1957) have more aluminous pyroxenes than the saturated magmas, the Black Jack sill, in particular, having very high Al_2O_3 in the more magnesian pyroxenes.

The diopsides from 'intrusive' peridotites have either extremely low Al_2O_3 contents (e.g. Twin Sisters, Webster–Addie) or values near those of the mafic magma series (Dawros, Cuba). The diopsides analysed by Ross *et al.* from peridotite nodules are very constant in Mg content at Mg_{88} to Mg_{91} but show a

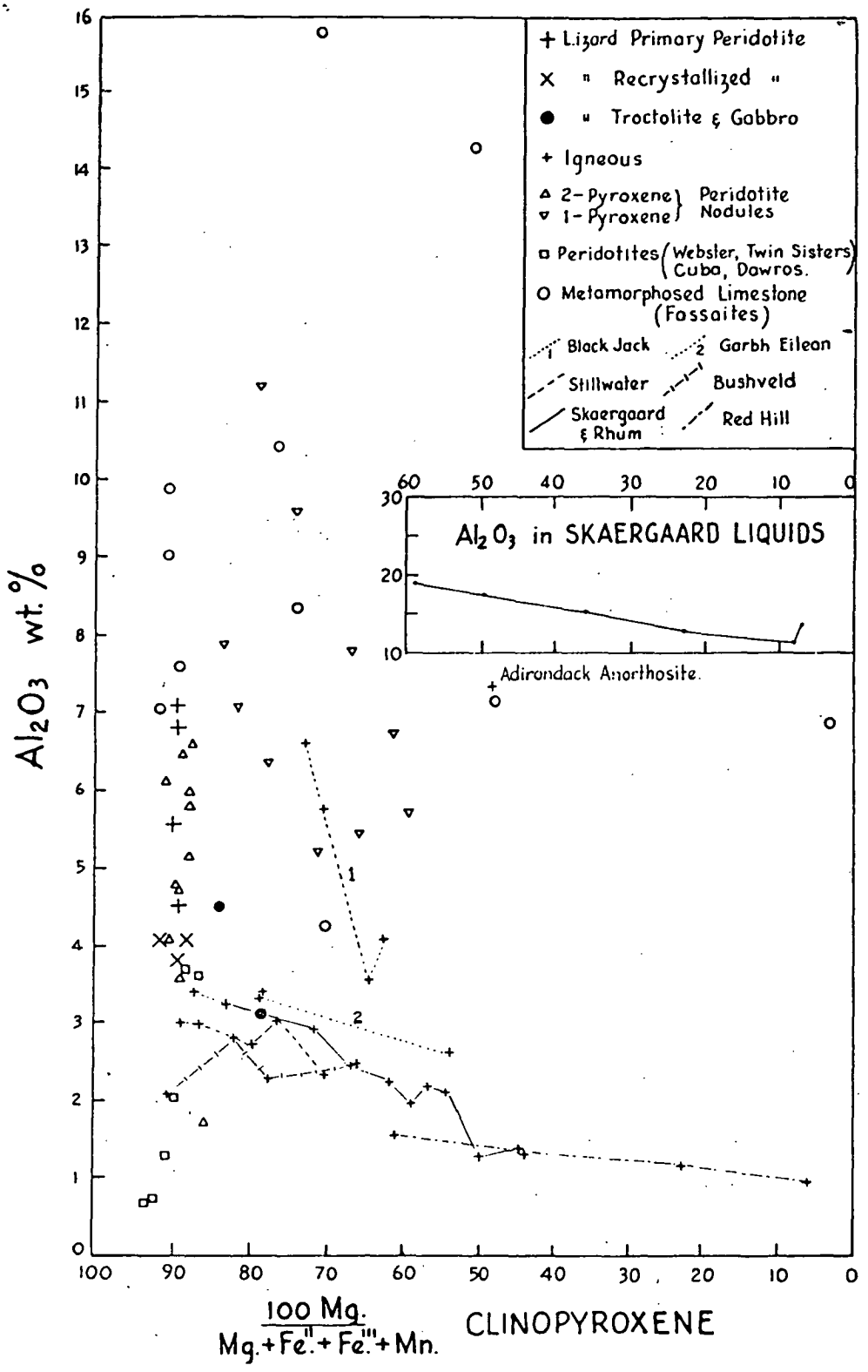

FIG. 11. Al_2O_3 contents of igneous clinopyroxenes in relation to their position in differentiation sequences of basaltic magma.

large range in Al_2O_3 content, one pyroxene (No. 9 of Ross *et al.*) being considerably lower than any others from nodules.[1] Two diopsides from olivine-rich peridotite nodules analysed by Wilshire and Binns (1960) and one from Deriu (1959) fall in the range defined by Ross *et al.* but the diopsides from *pyroxenite* xenoliths given by Wilshire and Binns and by Deriu have a considerable range in both Mg content and Al_2O_3 content. With their low Cr_2O_3 contents and, particularly in Wilshire and Binns's analyses, their high Fe_2O_3/FeO ratios, these pyroxenes are very similar to the fassaites (Tilley, 1938).

In comparing the Lizard primary and recrystallized diopsides, variation in bulk rock composition is eliminated and Hess's suggestion that increased pressure may favour the Al substitution must be considered. In direct comparison with other peridotite pyroxenes the Lizard diopsides, like the enstatites, show great similarity to the diopsides from 2-pyroxene peridotite nodules in basalts.

4. *Cation distributions in coexisting pyroxenes of the peridotite*

Iron-magnesium distribution. It may be shown theoretically that the distribution at equilibrium of mutually substituting cations, A and B, between two phases (A, B)M and (A, B)N is dependent both on temperature and pressure (Ramberg & De Vore, 1951; Kretz, 1961; Mueller, 1961). In particular the theoretical and observed distribution of Fe^{++} and Mg^{++} between coexisting calcium-rich and calcium-poor pyroxenes has been investigated and the relationship

$$(Fe^{++}/Mg^{++})_{Opx} = (Fe^{++}/Mg^{++})_{Cpx} \times K_{Fe}$$

suggested where $(Fe^{++}/Mg^{++})_{Opx}$ and $(Fe^{++}/Mg^{++})_{Cpx}$ are distribution ratios for the calcium-poor and calcium-rich pyroxenes respectively, and K_{Fe} is a numerical function (the distribution coefficient) dependent on temperature and pressure. Kretz (1961)and Bartholomé (1961) have shown that in pyroxene granulites and assemblages crystallizing at 'metamorphic' temperatures $K_{Fe} \simeq 1{\cdot}8$, whereas for rocks crystallizing from a magma (particularly the differentiated basic magmas such as Skaergaard, Stillwater, and Bushveld) $K_{Fe} \simeq 1{\cdot}4$. A further group, the peridotite nodules, have $K_{Fe} = 1{\cdot}2—1{\cdot}3$.

Three of the pairs of coexisting pyroxenes from the Lizard peridotite can be used to define K_{Fe} values, the pairs (O_1, C_1) and (O_2, C_2) from the primary assemblage have $K_{Fe} = 1{\cdot}35$ and $K_{Fe} = 1{\cdot}36$ respectively. The pair from the recrystallized assemblage (O_5, C_5) has $K_{Fe} = 1{\cdot}32$. The small differences between the K_{Fe} values of the different assemblages are probably not significant in relation to the accuracy of analysis. However, the values are distinctly different from those in the metamorphic pyroxene pairs from the aureole of the perido-

[1] The anomalous behaviour of No. 9 is also very apparent when this is plotted with enstatite No. 9 on Fe/Mg and $^{Z}Al/Si$ distribution diagrams (p. 163). Careful reading of Ross, Foster, and Myers's text (p. 697) reveals an error in numbering in their tables. Diopside No. 9 should be No. 10 and does not coexist with enstatite No. 9.

tite. These have K_{Fe} values from 1·57 to 1·75 and will be discussed in a later paper. The values are also very different from pyroxene pairs from the Dawros and Webster-Addie peridotites which have $K_{Fe} = 1·7$. The distribution coefficients of the Lizard peridotite pyroxenes are thus slightly higher than those of peridotite nodules and approach the value for 'igneous' rocks.

Kretz (1961) considers that the effects on the distribution coefficient of variation in minor constituents (CaO and Al_2O_3 particularly) *and of different pressures at crystallization* are negligible in comparison with temperature effects. If this is accepted then the values of K_{Fe} for the Lizard peridotite are evidence for a temperature of crystallization of the Lizard assemblages near, or higher than, that of basic igneous rocks.

Aluminium-silicon distribution. The analyses and calculations of the structural formulae of the pyroxenes have shown a sympathetic variation in the Al_2O_3 content between coexisting diopside and enstatite. Al^{+++} in the pyroxene structure may occur in either the X,Y-positions or in the Z-position and since it is uncommon for Fe^{+++}, Cr^{+++}, or Ti^{++++} to substitute for Si, the simplest substitution involving Al^{+++} to attempt to compare is the Al for Si substitution.

In a purely empirical approach and by analogy with the Fe^{++}/Mg^{++} ratio the distribution ratios $({}^{Z}Al/Si)_{Opx}$ and $({}^{Z}Al/Si)_{Cpx}$ for coexisting orthopyroxenes and clinopyroxenes respectively were calculated and are tabulated in Table 8. Also in Table 8 a distribution coefficient

$$K_{Al} = \frac{({}^{Z}Al/Si)_{Cpx}}{({}^{Z}Al/Si)_{Opx}}$$

is calculated for each pyroxene pair. The primary pyroxenes of the Lizard have aluminium-silicon distribution coefficients of 1·2 to 1·3, whereas the recrystallized assemblages have distribution coefficients of 1·64 and 1·62. The peridotite nodules (Ross, Foster, & Myers, 1954), with a range in Al_2O_3 content in the orthopyroxenes from 2·56 to 5·32 per cent, have significantly constant distribution coefficients in the range 1·14 to 1·35. It is significant that the wrongly numbered 'pair' of Ross, Foster, and Myers's results (No. 9) gives an aberrant result of $K_{Al} = 0·88$, and also $K_{Fe} = 0·9$ (cf. Kretz, 1961).

The two pyroxene pairs from 'intrusive' peridotites (Dawros & Webster-Addie) have higher Al_2O_3 in orthopyroxene than clinopyroxene and have distribution ratios of less than one. On the other hand four metamorphic ultramafic assemblages of lower Mg content (Mg_{73}–Mg_{84}) have distribution ratios in the range 1·50–1·53, closer to the recrystallized Lizard assemblage. A similar assemblage (O'Hara, 1961) differs distinctly and has $K_{Al} = 1·00$. Three igneous pyroxene pairs in the range $Mg_{77·5}$ to $Mg_{87·5}$ from accumulates of basaltic magmas have K_{Al} values of 1·35, 1·14, and 0·82.

The distribution coefficient of one mixture (Si, Al) in coexisting phases may theoretically depend on the ratios of another mixture (Fe, Mg) in the same phases (Kretz, 1961, pp. 365, 370–1). A plot of $(Fe^{++}/Mg^{++})_{Opx}$ against K_{Al} for a

TABLE 8

Aluminium–silicon contents of coexisting pyroxenes (refer to Fig. 12 for plots of compositions)

	ORTHOPYROXENE			CLINOPYROXENE				
No.	100 Mg / Mg+Fe+Mn	Al%	^{z}Al/Si	Al%	^{z}Al/Si	K_{Al}	*Mineralogy*	*Reference*
+1	89·5	6·59	0·0875	7·09	0·1050	1·20	ol–ens–di–sp	Lizard
+2	89·5	6·30	0·0857	6·80	0·1080	1·26	,, ,, ,, ,,	,,
+3	89·4	5·46	0·0684	5·55	0·0780	1·30	,, ,, ,, ,,	,,
×4	91·1	3·26	0·0400	4·05	0·0655	1·64	ol–ens–di–plag	,,
×5	89·0	2·05	0·0417	3·80	0·0677	1·62	,, ,, ,, ,,	,,
1	89·2	3·91	0·0526	5·14	0·0620	1·18	ol–ens–di–sp	Ross *et al.* (1954)
2	89·2	4·10	0·0591	5·97	0·0730	1·23	,, ,, ,, ,,	,, ,, ,, ,,
3	89·8	4·80	0·0679	6·58	0·0916	1·35	,, ,, ,, ,,	,, ,, ,, ,,
4	90·2	5·32	0·0729	6·46	0·0829	1·14	,, ,, ,, ,,	,, ,, ,, ,,
5	91·1	2·56	0·0363	3·56	0·0450	1·24	,, ,, ,, ,,	,, ,, ,, ,,
7	89·4	3·50	0·0525	4·69	0·0645	1·23	,, ,, ,, ,,	,, ,, ,, ,,
8	91·2	2·97	0·0455	4·08	0·0532	1·17	,, ,, ,, ,,	,, ,, ,, ,,
O 13	87·8	1·28	0·0189	0·72	0·0158	0·84	ol–ens–di	,, ,, ,, ,,
O D	86·4	2·69	0·0416	2·05	0·0395	0·95	,, ,, ,,	Rothstein (1957)
H_1	75·9	4·35	0·0670	5·94	0·1006	1·50	hyp–aug–ho–sp–opaques	Howie (1955)
H_2	72·8	4·55	0·0621	5·02	0·0946	1·52	,, ,, ,, ,, ,,	,, ,,
T	83·6	4·24	0·0538	5·17	0·0823	1·53	ol–,, ,, ,, ,, ,, –bi	Muir & Tilley (1958)
R	77·0	1·86	0·0417	2·84	0·0631	1·51	,, ,, ,, ,, plag–opaques	,, ,, ,,
O_1	80·8	4·45	0·0655	4·52	0·0655	1·00	,, ,, ,, ,, ho–sp– ,,	O'Hara (1961)
	87·5	1·61	0·0293	2·08	0·0241	0·82	bronzitite Bushveld	Hess (1960)
	80·7	2·3	0·0465	3·22	0·0625	1·35	gabbro picrite Skaergaard	Brown (1957)
	77·5	2·14	0·0488	3·14	0·0559	1·14	olivine gabbro Hawaii	Muir & Tilley (1957)

series of ultramafic to intermediate igneous and metamorphic rocks gives a large scatter of points with no apparent relationship.

Restricting discussion to magnesian pyroxenes (> 70 per cent enstatite) then a plot of $(^{Z}Al/Si)_{Opx}$ against $(^{Z}Al/Si)_{Cpx}$ (Fig. 12) illustrates an empirical linear relationship for the peridotite nodules. Such nodules are of closely similar

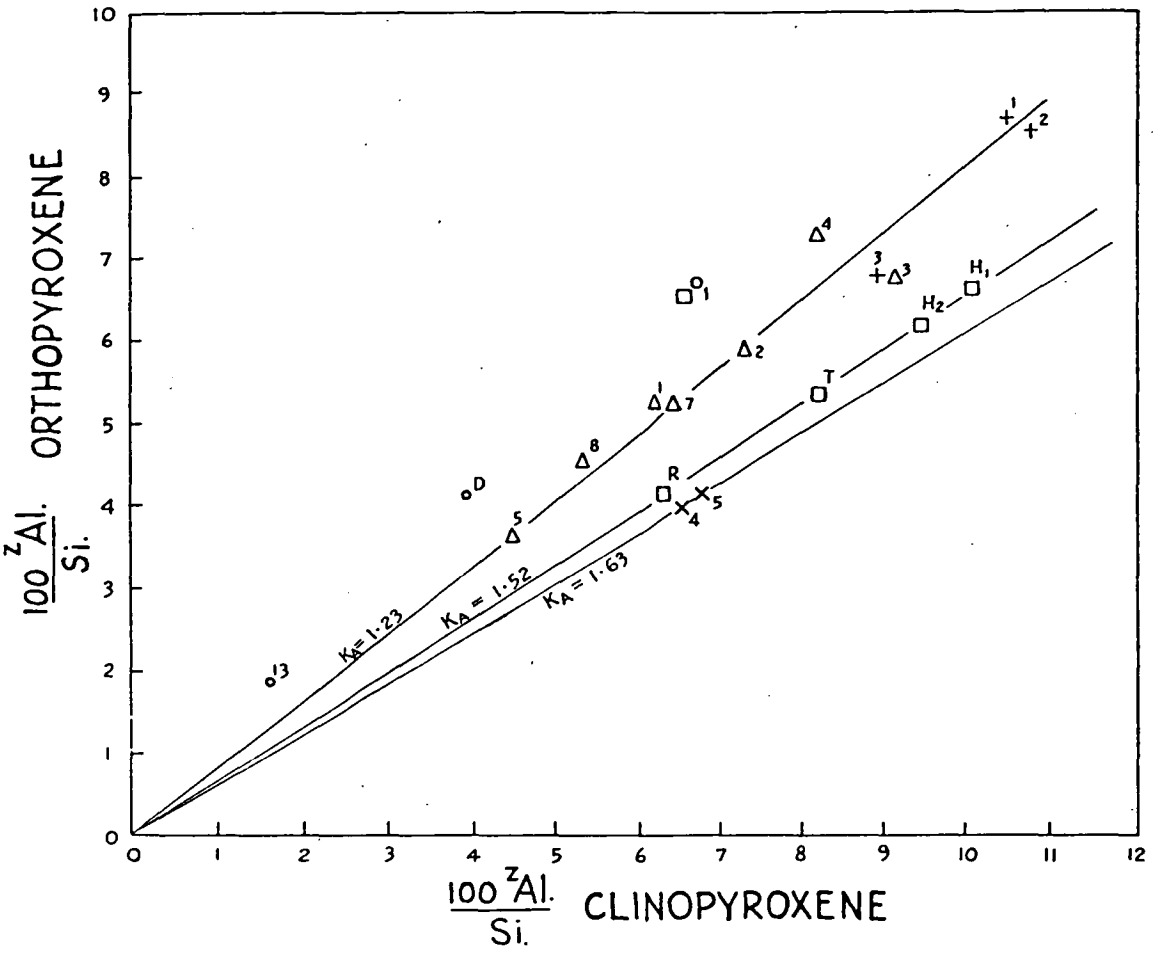

FIG. 12. Aluminium–silicon distribution in coexisting magnesian orthopyroxenes and clinopyroxenes (refer to Table 10). Δ Peridotite nodules; □ metamorphic peridotites; ○ intrusive peridotites; +, × Lizard peridotites.

composition, particularly in Mg-content, but of widely scattered occurrences. The existence of such a relationship is further evidence for a common genesis and physically similar environment of crystallization for these peridotite nodules (Ross *et al.*, 1954). Further, Fig. 12 shows that the primary Lizard pyroxenes fall on the trend defined by the nodules, whereas the recrystallized pyroxenes do not, but have distribution ratios of 1·62 and 1·64. It is considered that as the bulk rock compositions in the primary assemblage and recrystallized assemblages are the same, the Fe^{++}/Mg^{++} ratios and distribution coefficients (K_{Fe}) nearly the same, and minor constituents such as Cr, Fe''', Na closely comparable then this difference in K_{Al} is most reasonably interpretable as directly due to different *pressure* and/or *temperature* conditions of crystallization of the

primary and recrystallized assemblages. The difference in K_{Al} is such that in the peridotite nodules and primary Lizard assemblage relatively more ^{Z}Al goes into the orthopyroxene. With the current experimental work on Al_2O_3–$MgSiO_3$ solid solution at high pressure (Boyd & England, 1960) and the suggested origin of peridotite nodules as xenoliths of mantle material in mind, it is suggested that the difference in the K_{Al}-values for the Lizard peridotite may be due to a difference in *pressure* primarily, and only secondarily in temperature, between the two environments of crystallization (cf. the lack of variation in the Fe^{++}/Mg^{++} distribution coefficient K_{Fe}).

Because of variation in the Mg-content no other K_{Al} values are strictly comparable with the nodules and Lizard results. It may or may not be fortuitous that the four ultramafic granulites with pyroxene analyses given by Muir and Tilley (1958) and Howie (1955) have K_{Al}-values of 1·50–1·53, i.e. near to that of the Lizard recrystallized assemblage. It is considered that the hypothesis warrants further study from the theoretical and experimental angle as well as by examination of K_{Al}-values for pyroxene pairs from highly magnesian peridotites (Mg_{85}–Mg_{95}) in metamorphosed granulite terrains, in hornfels zones and in magmatic accumulates such as the Great Dyke.

5. *Spinel*

Two primary spinels coexisting with O_1 and O_2 and diopsides C_1 and C_2 were separated in quantities sufficient for partial analysis. The spinels were fused directly in potassium hydrogen sulphate and the solution filtered to obtain the small amount of SiO_2 present (probably due to pyroxene composite grains). The procedure given by Ross, Foster, and Myers (1954, p. 718) was then followed although Cr_2O_3 was determined colorimetrically and TiO_2 was not determined chemically. Spectrographic determination, using the analysed enstatites and diopsides as standards, indicated a TiO_2 content of 0·32 per cent in both spinels. As FeO was not determined directly, the structural formulae were calculated assuming a partition of iron as Fe^{++} and Fe^{+++} of the magnitude required to give values of 2·0 for the R^{+++} group and 1·0 for the R^{++} group. The third columns in Table 9 give the recalculated analysis adjusted to these Fe_2O_3 and FeO contents.

The trace element data for the two spinels are given in Table 9 and the results are identical. The very high concentration of Ni ($Ni/Mg \times 10^3 = 35{\cdot}7$; cf. 6·7 for the coexisting olivine) in the spinel is a surprising result and the TiO_2 content is comparable with that of the coexisting diopside and higher than that in the enstatite. Co and V are both concentrated in the spinel phase and Zr is slightly higher than in the coexisting phases. The Ni, Co, and V contents of the Lizard spinels are higher by a factor of about ten than those given by Ross, Foster, and Myers (1954) on the spinels from peridotite nodules. In addition, the Ni/Mg and Ni/Fe ratios for the Lizard spinels are distinctly higher than the coexisting olivine and pyroxenes, whereas in Ross, Foster, and Myers's results from the

nodules these ratios are either similar or slightly higher in the spinel. This discrepancy will require more data before any significance can be evaluated. The spectrographic TiO_2 determinations of the nodule spinels are similar to the Lizard results but the TiO_2 values obtained by chemical methods (Ross *et al.*, p. 710) are much higher.

From the analyses the high proportion of the spinel end member in the

TABLE 9

Partial analyses, trace-element data, and structural formulae of primary spinels

S1 (*Specimen* 90683)			S2 (*Specimen* 90681)		
SiO_2	0·17	0·17	SiO_2	0·35	0·35
Al_2O_3	47·58 Al''' 1·513	47·58	Al_2O_3	46·88 Al''' 1·501	46·88
Fe_2O_3	16·35 Cr''' 0·384	5·07	Fe_2O_3	16·51 Cr''' 0·388	5·40
FeO	n.d. Fe''' 0·103	10·13	FeO	n.d. Fe''' 0·111	10·02
MnO	n.d.	n.d.	MnO	n.d.	n.d.
MgO	19·18 Fe'' 0·229	19·18	MgO	19·06 Fe'' 0·228	19·06
CaO	0·00 Mg'' 0·771	0·00	CaO	0·00 Mg'' 0·771	0·00
Na_2O	n.d.	n.d.	Na_2O	n.d.	n.d.
K_2O	n.d.	n.d.	K_2O	n.d.	n.d.
Cr_2O_3	17·99	17·99	Cr_2O_3	18·08	18·08
TiO_2	n.d.	n.d.	TiO_2	n.d.	n.d.
	101·27	100·12		100·88	99·79

Composition in spinel end members:		Composition in spinel end members:	
75·7% Spinel	$Mg.Al_2O_4$	75·0% Spinel	$MgAl_2O_4$
1·4% Picrochromite	$Mg.Cr_2O_4$	2·1% Picrochromite	$MgCr_2O_4$
17·8% Chromite	$Fe.Cr_2O_4$	17·3% Chromite	$FeCr_2O_4$
5·1% Magnetite	$Fe.Fe_2O_4$	5·5% Magnetite	Fe_3O_4

Composition as by Thayer (1946) $Cr_{19}Al_{76}(Mg_{77})$		Composition as by Thayer (1946) $Cr_{19}Al_{75}(Mg_{77})$	
Cr	$\gg 10^4$	$\gg 10^4$	i.e. $\gg 1\%$ Cr
Co	1000	1000	
Ni	$\simeq 10^4$	$\simeq 10^4$	i.e. $\simeq 1\%$ Ni
V	1000	1000	
Zr	45	45	
Ti	1900	1900	i.e. $TiO_2 = 0{\cdot}32\%$

Sought but not found: Sc, Yr, Ga, Pb, Li, Ba, Sr.

Lizard minerals is very apparent. In the nomenclature of Winchell and Winchell (1959, p. 82) these are true spinels, moderately enriched in the chromite molecule. The observed alteration of the primary spinels to relict deep brown chromite or opaque magnetite surrounded by plagioclase is interpretable as the removal of this high Al_2O_3 and MgO content from the spinel.

A preliminary correlation of the composition of chromian spinel with the character of the enclosing rock by Thayer (1946) brings out the higher $\frac{Mg}{Mg+Fe}$ content of the spinels of 'intrusive' peridotites contrasted with those of the Bushveld and Stillwater Complexes.

Ross, Foster, and Myers's (1954) analyses of spinels from 'intrusive' dunites

and from peridotite nodules show variation in compositions from both sources. Analysis 1 (p. 710) is very similar to the Lizard spinels in its high Al_2O_3 (47·63 per cent) and lower $FeO+Fe_2O_3$ (9·86+2·76 per cent) content and analyses 2 and 7 are similar except in the TiO_2 values determined chemically—all these are from the peridotite nodules. The analysed spinels from the Twin Sisters and Webster-Addie peridotites contain very much lower Al_2O_3 (8·81 and 13·37 per cent) and very much higher Cr_2O_3 (55·17 and 48·48) than the Lizard spinels or those from the peridotite nodules.

6. *Amphibole*

The colourless amphibole characteristic of the hydrous recrystallized assemblage has been separated from two of the analysed rocks; these are the type example, rock analysis IX, and the peridotite immediately in contact with the granulite at Pol Cornick, rock analysis X.

TABLE 10

Analysed amphiboles from the peridotite

	A1 (*Specimen* 90691)			A2 (*Specimen* 90703)	
Oxides	*Cations*	*Weight%*	*Cations per 23 O*	*Weight%*	*Cations per 23 O*
SiO_2	Si	46·19	6·460	44·35	6·251
Al_2O_3	^{Z}Al	12·83	1·540	15·23	1·749
	^{Y}Al		0·577		0·782
TiO_2	Ti	0·90	0·092	0·86	0·091
Fe_2O_3	Fe'''	1·18	0·126	0·38	0·041
FeO	Fe''	2·97	0·344	4·94	0·583
MnO	Mn	0·04	0·008	0·10	0·012
MgO	Mg	18·71	3·898	17·26	3·626
CaO	Ca	12·45	1·865	12·14	1·834
Na_2O	Na	1·87	0·504	2·45	0·669
K_2O	K	0·27	0·050	0·32	0·058
H_2O^+		1·82	—	not determined	—
H_2O^-		0·00	—	0·00	—
Cr_2O_3	Cr	0·80	0·092	0·25	0·027
NiO	Ni	0·08	0·008	n.d.	—
		100·11		98·28	
Cations in Z group (Si, ^{Z}Al)			8·000		8·000
Cations in X+Y group (Mg, Ni, Mn, Fe'', Fe''', Cr, ^{Y}Al)			5·145		5·162
Cations in W group (Na, Ca, K)			2·419		2·561
$100\times\frac{Mg}{Mg+Fe+Mn}$			89·0		85·0
$\frac{Fe'''}{Fe''+Fe'''}$			0·268		0·066

Trace elements in A1 (p.p.m.):

Cr, 10^4	Sc, 40	Co, 22	Ni, 465	V, 224
Zr, 16	Y, 10	Ga, 5	Li, 14	Ba, 18
Sr, 12.	Sought but not found:		Pb.	

The analyses of these two amphiboles and their structural formulae are given in Table 10. The structural formulae were calculated anhydrous on the basis of cations for 23 O-atoms since in one case (analysis A2) there was insufficient sample for a water determination and because of uncertainty that the water in the amphibole is completely driven off in the ignition in Penfield tubing.

The analyses are both of high Al_2O_3 content clearly demonstrating the error of calling the colourless amphibole 'tremolite' (Flett, 1912 and 1946). Analysis A1 contains a considerable amount of Cr_2O_3 and is very high in MgO and low in FeO. The analysis A2 reflects the effects of metasomatism across the peridotite-granulite contact and differs from the typical peridotite amphibole in containing more Na_2O, K_2O, FeO, MnO, and Al_2O_3 and less Cr_2O_3 and MgO.

Both analyses, when the Z-group is arbitrarily made equal to 8·00, have an excess of cations in the X–Y-group. These may be regarded as Mg replacing Ca in the W-group (i.e. cummingtonite substitution) and gives a W-group total of Mg+Ca of 1·996 in A2 and 2·010 in A1. Thus practically the whole of the Na+K cations may be regarded as filling the vacant space position giving a high degree of edenite substitution. Analysing the amphibole composition in terms of these end-members as above (cf. Sundius, 1946; Shido, 1958) shows that the high edenite with moderate tschermackite molecule content places these amphiboles in the pargasite field, the most significant departure from ideal pargasite being the content of the cummingtonite molecule.

V. PETROGENESIS

The Lizard peridotite is an example of different mineral assemblages developed in rocks of the same bulk composition. In discussing the petrogenesis of the peridotite we are thus primarily concerned with the composition changes and the appearance and disappearance of phases as evidence for a changing physical environment.

1. *The role of* Mg–Al *spinel*

The meagre textural evidence from the *primary assemblage* peridotite suggests that aluminous diopside and spinel, in that order, were the last phases to crystallize. The primary spinel (including 75 per cent $MgAl_2O_4$ and 17 per cent $FeCr_2O_4$) in many cases later reacted to give relict chromite surrounded by plagioclase. It is inferred that the following reaction has occurred:

$$\underset{\text{Spinel}}{(MgAl_2O_4 + FeCr_2O_4)} + \underset{\text{Diopside}}{CaMgSi_2O_6} + \underset{\text{Enstatite}}{2MgSiO_3} \rightarrow \underset{\text{(anorthite)}}{CaAl_2Si_2O_8} + \underset{\text{forsterite}}{2Mg_2SiO_4} + \underset{\text{chromite}}{FeCr_2O_4}$$

The evidence from the *recrystallized anhydrous assemblage* is that the rocks passed through a stage in which the olivine and primary pyroxenes were

recrystallizing as the rock was deformed, and in which the olive spinel grew as large porphyroblasts. At a later stage the spinel reacted as above to give the olivine+diopside+enstatite+plagioclase+chromite assemblage, this reaction occurring whilst movement and emplacement of the peridotite was still continuing. Although some of the plagioclase is derived from the spinel reaction, a large part occurs as small anhedral grains with no associated relict chromite. This raises the question whether the five-phase assemblage of olive spinel+plagioclase+diopside+enstatite+olivine was ever a stable one or whether the spinel grew as porphyroblasts in an assemblage without plagioclase.

A possible genetic sequence compatible with the evidence available is given in Figs. 13*a*, *b*. In this analysis the peridotite is regarded as a four-component system of average molecular proportions MgO(+FeO)=56; SiO_2=39; Al_2O_3=2; CaO=3. The minor constituent Cr_2O_3 is regarded as distributing itself between the pyroxenes and Mg–Al spinel or, in stage 3 where Mg–Al spinel is absent, acting as an independent component and increasing the number of phases at equilibrium by one in the addition of brown chromite to the assemblage. Similarly in stage 3 brown hornblende may form an extra accessory phase due presumably to the presence of water as an essential component. The components Na_2O, K_2O, Fe_2O_3, and MnO are regarded as distributing particularly between the pyroxenes and plagioclase.

The alternative possibility that the five-phase assemblage ol–sp–an–ens–di is a stable one would require that the olive spinel be regarded essentially as a Cr_2O_3 phase in a five-component (MgO–CaO–SiO_2–Al_2O_3–Cr_2O_3) system and the Al_2O_3 as distributing between two Al-rich phases (plagioclase and spinel) and two Al-poor phases (pyroxenes).

The main weakness in regarding the sequence from the primary assemblage to the recrystallized, plagioclase-bearing assemblage as a three-stage process in a four-component system is that no rocks with an entire relict assemblage of the character of stage 2 have as yet been found.[1] Such rocks would resemble some of the primary assemblage rocks in that the *only* plagioclase present should be as rims around relict chromite or alternatively that plagioclase should be entirely absent and Mg–Al spinel remain. These rocks should differ from the primary assemblage in being foliated and recrystallized with the spinel not as an interstitial phase but as large porphyroblasts, and the recrystallized pyroxenes containing less Al_2O_3 than the primary pyroxenes.

The absence of this assemblage may be explained by the hypothesis that the marginal zone of recrystallization and movement continually widened during the sequence of recrystallization from the initial environment P_o, T_o (referring

[1] A specimen of the high-temperature peridotite from Tinaquillo, Venezuela, sent to the author by courtesy of Professor H. H. Hess and Dr. D. B. MacKenzie, contains augen of enstatite and rare clinopyroxene set in extremely finely recrystallized olivine, pyroxenes, and rare pale-brown amphibole. Olive spinel is a minor constituent as small or medium-sized (up to 1 mm) porphyroblasts and plagioclase is absent. The rock has the character predicted in stage 2 of Fig. 13. A chemical analysis of this rock yields a bulk composition almost identical with that of the average Lizard peridotite (Table 11, p. 184).

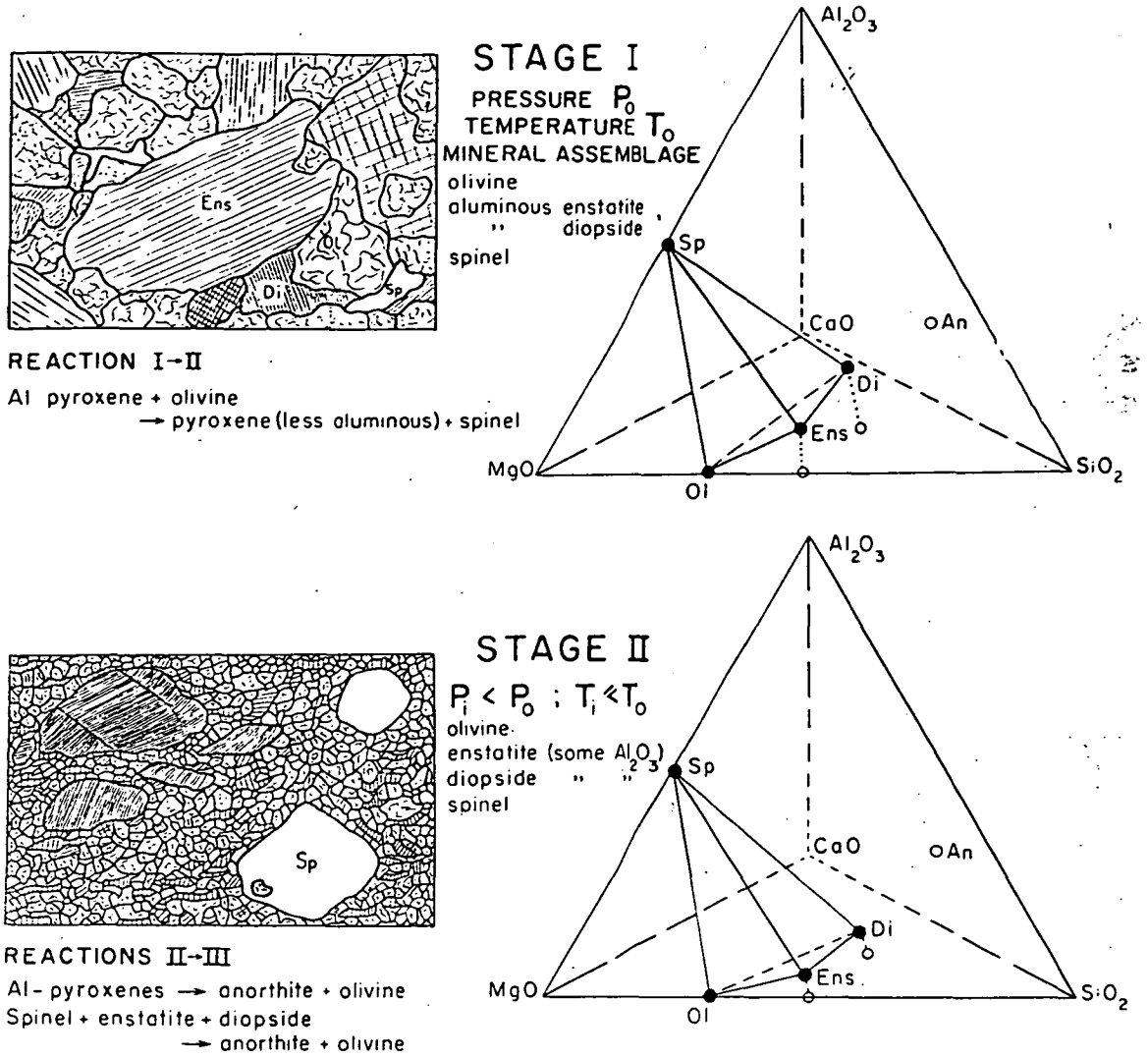

FIG. 13*a*, Sequence of recrystallization in the Lizard peridotite.

to Fig. 13*a*) and that the environment when intrusion and recrystallization of the peridotite finally ceased was P_m, T'_m. Thus any rock of the primary assemblage which recrystallized at an intermediate environment P_i, T_i with porphyroblastic growth of spinel was continually involved in internal movement and recrystallization in passing into the environment P_m, T'_m, i.e. from the stability field of spinel+2-pyroxenes to the stability field of olivine+plagioclase. If the zone of such movement and recrystallization was continually widening in passing from stages 1 to 2 to 3 then the transitional rocks between the primary and recrystallized assemblages would show the assemblage characteristic of the later environment, i.e. strained aluminous primary pyroxenes surrounded by recrystallized mosaics of an–ol–di–ens. This is the observed relationship (e.g. Fig. 5).

In the *recrystallized hydrous* assemblage the variable composition of the pargasite commonly allows the complete elimination of plagioclase, diopside, and enstatite from the assemblage. Cr_2O_3 again appears to act as an

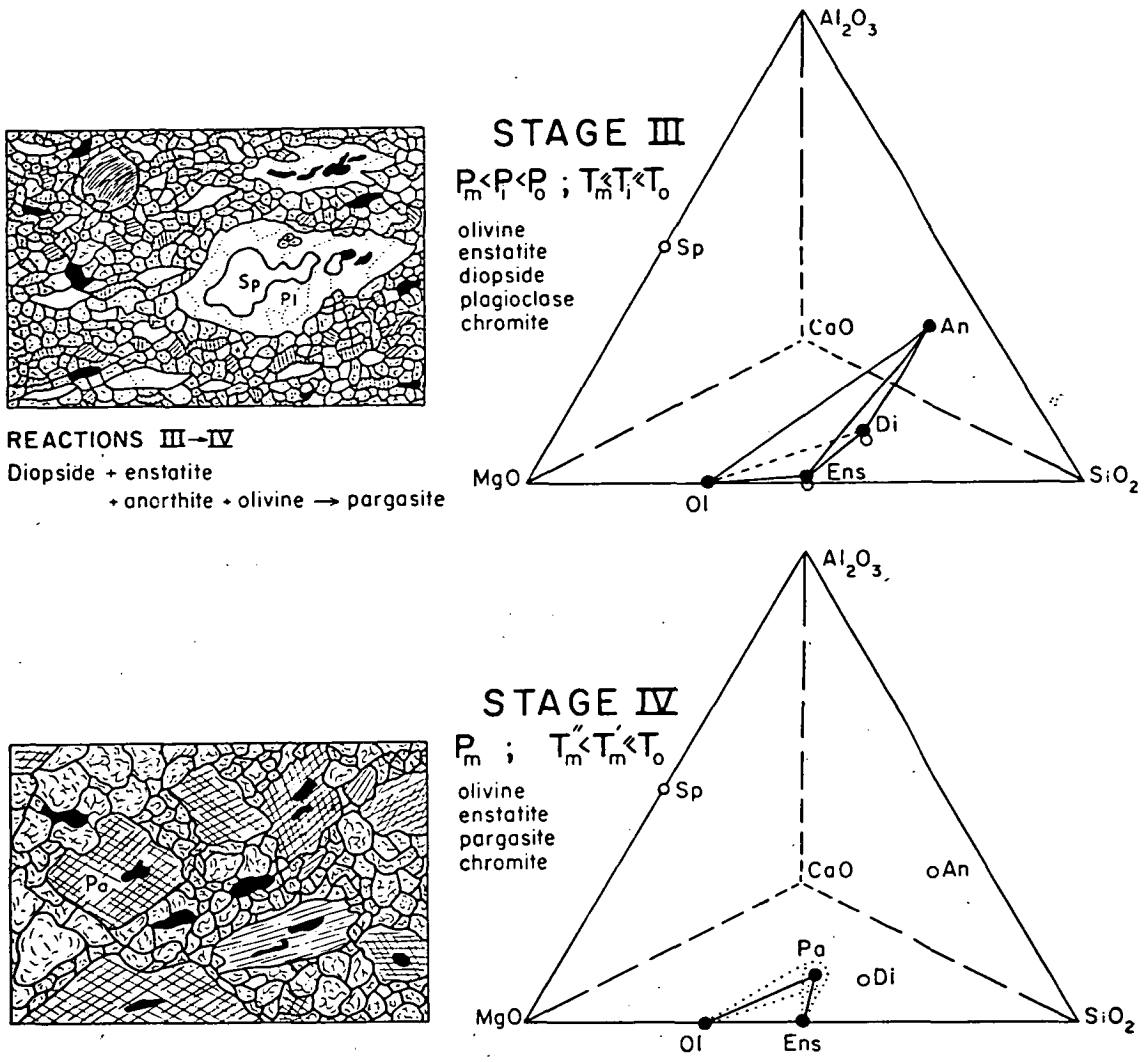

FIG. 13*b*.

independent component and enters into a pale brown, orange-brown, or yellow spinel, presumably Cr_2O_3-rich. Further data are needed on the composition and properties of the spinel in the pargasite assemblage before its significance can be evaluated.

If the peridotite assemblages involving Mg–Al spinel can be interpreted with reference to the four-component system CaO–MgO–Al_2O_3–SiO_2 then the results obtained in the experimental investigations in that system are relevant to the petrogenesis of the peridotite. The investigations of the systems anorthite–forsterite–silica [Anderson (1915) in Bowen (1928)] have shown that at liquidus temperatures in the anhydrous systems at *atmospheric pressure*, pyroxene solid solutions and spinel are in reaction relation while forsterite-anorthite is the stable assemblage. Yoder and Chinner (1960, p. 80) have shown, in an investigation of the system grossular–pyrope–water at high water pressures (P_{H_2O} = 10,000 bars), that anorthite and forsterite are incompatible and pyroxene solid solutions and spinel may coexist at the liquidus. Yoder and Tilley (1961, p. 108)

conclude that the assemblage anorthite+forsterite is unstable at very high load pressure.

The coexistence of plagioclase and olivine in stage 3 of the recrystallization of the Lizard peridotite invites comparison with the low-pressure, high-temperature experimental results. The absence of hydrous phases in the primary assemblage and lack of evidence for a water-rich liquid or vapour phase suggests that the stability together of 2-pyroxenes and spinel is not due to higher P_{H_2O} but rather to higher load pressure+directed pressure in the primary assemblage.

2. *The role of plagioclase*

In the preceding section the absence of plagioclase in typical compositions of the primary assemblage and its presence in the recrystallized anhydrous assemblage is attributed to two factors, the reaction of spinel with pyroxenes and the decreased solubility of Al_2O_3 in the coexisting pyroxenes. It is stressed that in the primary assemblage there is no evidence for the instability of plagioclase as a phase in rocks of appropriate composition (compare its probable occurrence in several bands in the primary assemblage). However, the conclusions reached in the previous section require that olivine and plagioclase should not have coexisted in the primary assemblage. The occurrence of olive spinel stringers in a former plagioclase-rich band is compatible with the existence of an an–di–ens–sp assemblage in the primary peridotite.

If the 10 per cent iron end-member in the pyroxenes and olivines is neglected and the extent of ^{Z}Al for Si substitution in the primary and recrystallized assemblages is taken as 1 ^{Z}Al to 9 Si and O ^{Z}Al to 10 Si respectively, then the reaction in which the aluminous pyroxenes recrystallize to normal pyroxenes and plagioclase may be written as follows:

$$\underset{\text{aluminous enstatite}}{Mg_9Al(AlSi_9)O_{30}} + \underset{\text{aluminous diopside}}{Ca_5Mg_4Al(AlSi_9)O_{30}}$$

$$\rightarrow \underset{\text{plagioclase}}{2CaAl_2Si_2O_8} + \underset{\text{diopside}}{3CaMgSi_2O_6} + \underset{\text{enstatite}}{6MgSiO_3} + \underset{\text{olivine}}{2Mg_2SiO_4}$$

3. *The genetic relationships of the recrystallized peridotite assemblages*

As described previously the hydrous recrystallized assemblage occurs as bands parallel to the foliation in the anhydrous recrystallized assemblage and many thin sections illustrate the derivation of the pargasite-bearing assemblage from the anhydrous assemblage. No examples have been observed in which the opposite genetic sequence occurs, i.e. pargasite→plagioclase+diopside+enstatite. Two hypotheses should be considered as possible explanations of the inter-relationships.

First, the hydrous assemblage may have crystallized under the same temperature and load+directed pressure (P_L+P_S) as the anhydrous assemblage but at a higher P_{H_2O}. This would require that the partial pressure of water varied across

the foliation of the peridotite at any one time during recrystallization and emplacement of the peridotite.

Secondly, the hydrous assemblage may have crystallized retrogressively from the anhydrous assemblage at a different temperature (lower) and/or pressure (lower). Under this hypothesis the peridotite would be regarded as open to water and P_{H_2O} considered essentially constant, or of a low, unidirectional gradient over the interbanded peridotite assemblages at any one time. The explanation for the selective retrogressive hydration of some bands and not of others could be that movement (parallel to the foliation planes) within the peridotite in the later stages of its emplacement became localized in bands. The catalytic effect of internal movement in these bands could be the determining factor causing adjustment of the peridotite minerals to the lower temperature and pressure assemblage. The first hypothesis is considered unlikely as an explanation of the interbanded anhydrous and hydrous assemblages. The presence of accessory brown hornblende in the anhydrous assemblage in many specimens indicates the availability of at least some water during crystallization. The thin basic bands within the peridotite are commonly very rich in brown hornblende, implying that in rocks of different composition but in the same physical environment hornblende grows readily so that the environment cannot be anhydrous. The recrystallized assemblage has a strong augen foliation and the petrographic evidence clearly shows that recrystallization was a dynamic process involving strong internal movement and bending, crushing, and recrystallization of grains. It is difficult to imagine a rock deforming and simultaneously recrystallizing in this way as able to sustain rapidly varying P_{H_2O} gradients.

On the other hand there may well have been a unidirectional P_{H_2O} gradient around the *margin* of the peridotite since the country rock outside the peridotite aureole is a hornblende-rich amphibolite. This effect may explain the characteristic basal zone of pargasite+olivine peridotite, of relatively coarse grain size, in the sheet-like portion of the peridotite near Cadgwith and overlying the hornblende-rich Landewednack Hornblende Schists. The pargasite+olivine assemblage is also present on many of the western contacts of the peridotite. However, this marginal hydration is also consistent with marginal cooling during continuing intrusion and recrystallization of the peridotite, i.e. an effect of lower T rather than higher P_{H_2O}.

In summary of the above discussion it is concluded that the pargasite+olivine assemblage is a lower grade (*lower temperature*, possibly lower pressure) metamorphic assemblage retrogressively and locally derived from the olivine+enstatite+diopside+plagioclase+chromite recrystallized assemblage.

The features of the high grade metamorphic aureole of the peridotite will be described in detail in a separate paper, but some observations are particularly relevant to the present section.

On the contacts of the peridotite, particularly on the west coast, the peridotite directly in contact with the country rock is normally the pargasite-olivine

assemblage. The country rock immediately at the contact is a hornblende+hypersthene+diopside+plagioclase granulite. The contact has the nature of two granoblastic, parallel foliated, metamorphic assemblages recrystallizing in the same physical but different chemical environments. The granulite mineral assemblage is one of the characteristic assemblages developed in the progressive metamorphism of mafic rocks and is typical of the hornblende granulite metamorphic sub-facies using the classification of Turner and Verhoogen (1960). Turner and Verhoogen (1960, p. 557) estimate that 'the granulite facies represents maximum temperatures of regional metamorphism, perhaps of the order of 700° C to 800° C. Pressures normally are high but may in some instances extend down to only a few thousand bars.' The presence of the granulites in the aureole of the peridotite and the occurrence of olivine in some granulites invites comparison with the pyroxene hornfels facies of similar though greater temperature range (Turner & Verhoogen, 1960, p. 525) but the association of hornblende+hypersthene+diopside is against this. In either case a high temperature and a low or moderate pressure environment of crystallization of the granulites is indicated. The same physical environment gives rise to the olivine-pargasite assemblage in the peridotite at the contacts giving a very rough estimate of *P–T* conditions for this assemblage as moderate pressures, and temperatures in the vicinity of 700–800° C. A rather higher temperature and possibly pressure of crystallization is implied for the anhydrous recrystallized assemblage of the peridotite. It is emphasized that in this *P–T* environment there is no suggestion of a liquid phase in the peridotite: both assemblages have metamorphic textures indicative of internal deformation and recrystallization under stress, the hydrous assemblage in parallelism of porphyroblasts, and the anhydrous assemblage in the presence of augen and fine foliation.

4. *The conditions of crystallization of the primary peridotite assemblage*

The primary peridotite assemblage has a coarse grain-size and anhedral texture compatible with deep-seated igneous crystallization or at least of crystallization in a hydrostatic or near-hydrostatic stress environment. Although the banding and incipient augen foliation are ascribed to crystalline flow of the body at a very early stage, this flow has occurred at a rate accommodated in the rock without cataclasis or creation of granulitic or schistose fabrics. The presence of an intergranular fluid phase during this primary flow cannot be ruled out.

One of the most difficult and important of the problems in the petrogenesis of the primary peridotite is the origin of the compositional banding. Three alternative hypotheses for the origin of this banding may be summarized as follows:

(i) Primary accumulative banding, owing its origin to gravitative concentration of different proportions of the normal peridotite phases. Such bands could be modified in texture but not mineral composition by crystalline flow at depth.

(ii) Banding due to streaking out during crystalline flow of inhomogeneities in the peridotite 'magma'.

(iii) Banding due to selective metasomatic change along planes of greater deformation and presumed greater ease of penetration by metasomatising fluids.

The petrographical, chemical and mineralogical evidence is relevant in the discussion of these hypotheses and the following factors are considered to make the first hypothesis improbable:

(*a*) The spinel present in the 'chromite serpentine' bands (primarily olivine+ deep-brown spinel) is very different from the olive spinel of the normal peridotite.

(*b*) The enstatite (O_3) and diopside (C_3) of the pyroxene-rich band are slightly different and the diopside (C_6) of the pyroxenite lens is very different from the typical pyroxenes of the primary peridotite (O_1, O_2, C_3, C_4).

(*c*) The analysis (rock analysis IV) of the 'chromite serpentine' band has a lower MgO/FeO molecular ratio than the other peridotite analyses. This may be a primary feature or it may be an effect during serpentinization.

(*d*) The former presence, in a few bands, of plagioclase, not a normal constituent of the peridotite assemblage.

(*e*) The complete absence of accumulative textures or structures in the bands.

Thus although Rothstein (1957, p. 3) compares the compositional banding in the Lizard peridotite with that of layered accumulates such a comparison is not substantiated by a close examination of the bands as they are now constituted.

The third hypothesis is considered unlikely since the chromite serpentine and pyroxene-rich bands may occur practically side by side and would require very different composition changes to form from the normal massive primary peridotite. The chromite serpentine would require removal of SiO_2, $CaO(Al_2O_3)$ and the pyroxene-rich bands addition of SiO_2, CaO, Al_2O_3, or removal of (Mg, Fe)O.

The second hypothesis is considered to be the most probable of the three on the evidence available. The structural relationships of the banding, the lensing out of the chromite serpentine bands, and the markedly lenticular habit of a few pyroxenite bodies could result from deformation during plastic flow of initially irregularly shaped bodies.

The 'chromite serpentine' bands may have originally been chromite-bearing dunite blocks, possibly a refractory residuum from partial fusion, in the peridotite magma. The pyroxene-rich and pyroxene-plagioclase bands may have been slightly later-crystallizing patches in the peridotite. This origin is particularly suggested for the lenticular pyroxenites near Carleon Cove. The diopside (C_6) from this pyroxenite is higher in TiO_2, and has a lower Mg/Fe″ ratio than the other peridotite pyroxenes. It is also higher in SiO_2 and lower in Al_2O_2 than the primary peridotite diopsides. In all these features it shows a trend towards the more iron-rich diopside from the Coverack troctolite.

In previous discussion the recrystallized assemblages of the peridotite have been interpreted as crystallizing in the same load-pressure and, as movement in

the peridotite ceased, approaching more nearly to the same directed pressure (i.e. the regional stress field) environment as the metamorphic assemblages outside the peridotite.

Since the recrystallized anhydrous assemblage is derived from the primary assemblage by a process of internal deformation and finally complete recrystallization the primary assemblage was clearly not in equilibrium, either mechanically or mineralogically, with the pressure and temperature conditions of crystallization of the marginal recrystallized assemblages. Two alternative explanations must be considered:

1. The primary assemblage is 'exotic' to its present environment and preserves a mineral assemblage formed at different pressures and temperature in another place, in this case most simply interpreted as at a greater depth since the peridotite is an intrusive body. Emplacement of such a body would be by distributed internal movement in the marginal recrystallized assemblage and in fact be a powerful factor in catalysing such recrystallization.

2. The primary assemblage crystallized from a magma essentially in place and the marginal recrystallization is the effect, as crystallization proceeded inwards from the margin, of superimposition of the regional stress field and metamorphic textures on the cooling margin of the peridotite.

In one sense the two hypotheses differ in degree rather than kind since both interpret the marginal foliation and augen texture as due to relative movement between the centre of the intrusion and the wall rock. In the second hypothesis such relative movement could not occur until the entire body was crystallized since the effect of any compression from outside a body containing a liquid core is first to squeeze out such a liquid. It does not seem reasonable to postulate that the augen texture and foliation of the margin is due to 'drag' by the still-liquid core flowing past the crystallized margin. The second hypothesis would mean that a directed pressure due to the regional stress-field would act on the margin of the peridotite but be dissipated by internal deformation there and not transmitted to the core of the body. Since the load pressure on both margin and core would be approximately the same the total pressure on the marginal assemblage could be greater than or equal to the total pressure on the core assemblage—any pressure differences are likely to be small and of short duration for the high temperature of the mineral assemblages means that the rocks would be expected to deform plastically quite readily. In the preceding discussion differences in P_{H_2O} and P_{O_2} between margin and core have not been considered and these effects could conceivably be large. However, since the differences between the two assemblages are not differences in degrees of hydration of phases nor of oxidation (particularly in the pyroxenes and spinel) these explanations appear inadequate. It is concluded that by the second hypothesis the only physical variable to which the large differences in the mineralogy between the primary and recrystallized peridotite assemblages could reasonably be attributed is temperature. The primary assemblage would be the initial high temperature

igneous crystallization at temperature T_1 and pressure P_1, the recrystallized anhydrous assemblage would be a recrystallization in the margin of the peridotite at temperature $T_2 < T_1$ and pressure $P_2 \simeq P_1$. Since during further cooling the primary assemblage in the core must also pass through temperature T_2 at pressure near P_2 an additional reason must be called upon to explain why this zone did not similarly recrystallize. Such a reason could possibly be found in a waning of the regional stress field to give a static rather than dynamic environment.

It is considered that this second hypothesis can be discarded if it can be shown that the differences between the mineralogy of the primary assemblage and the recrystallized assemblage are inconsistent with temperature differences alone but imply large differences in pressure.

On the other hand it is considered that the weight of the evidence from the field study, the petrography and the mineralogy is favourable to the first hypothesis, i.e. that the whole of the peridotite crystallized at a greater depth at temperature T_0 and pressure (essentially load pressure) P_0 and that it moved into a medium-grade regional metamorphic terrain of temperature T_m and pressure (load and directed pressure) P_m entirely as a crystalline body. The peridotite is thus regarded as a crystalline diapir and such a body will only intrude if there is an appreciable rheidity[1] difference between it and the surrounding crystalline materials. The evidence is that when it reached its present crustal environment the peridotite was at a temperature (T'_m) considerably above that (T_m) of the surrounding metamorphic terrain [at temperatures in the vicinity of 500–700° C (Fyfe, Turner, & Verhoogen, 1958)] and produced mineral assemblages regarded as forming at 700–800° C or more. Turner, Heard, and Griggs (1960) have demonstrated experimentally the ability of enstatolites to deform readily without cataclasis at high temperatures and rocks such as the Lizard peridotite and the dunite mylonites of St. Paul's Rocks (Tilley, 1947) show the apparent 'lubricant' effect of olivine readily granulating and recrystallizing in deformed peridotites. It is considered that these characteristics of the peridotite and particularly the fact that the body was at a considerably higher temperature than the country rock determined that the peridotite in its environment (T_0, P_0) of primary crystallization had a lower rheidity than the enclosing country-rock.

If such a peridotite body was in a non-hydrostatic stress-field, then it would flow to minimize the stress-difference and, in the case that the axis of minimum stress was vertical, would intrude as a vertical crystalline diapir. The body would continue to so intrude, at a rate defined by the magnitude of the stress-difference of the regional field and the pseudo-viscosity of the peridotite itself, probably until cooling of the roof and margins of the peridotite and heating of the country-rock destroyed or reversed the rheidity difference. The results of the latter process are seen in the western margin of the peridotite where pyroxene granulites of the peridotite aureole locally intrude and include blocks of the peridotite margin.

[1] Definition of Carey (1954).

In the case of a peridotite diapir where the driving mechanism is the rheidity difference between peridotite and country-rock, and the external stress-field, internal movement would not be uniformly distributed through the body but would be localized in the zone of greatest rheidity difference, i.e. near the margin of the body.

This concept can be looked at another way. At any particular time the margin of the peridotite is subject to a non-hydrostatic stress-field composed of the load pressure component and the directed regional pressure transmitted through the wall rocks. The lower rheidity of the peridotite relative to the country-rocks causes the peridotite at the margin to flow to re-establish a local static stress-field and this is the stress pattern transmitted to the core of the peridotite. The core thus has a tendency to be carried upwards as a passive body while relative movement is localized in the margin.

If this hypothesis of diapiric intrusion of the peridotite in the manner described above and entirely as a crystalline body is valid, then both the margin and core of the peridotite would have been subjected to a range of pressures (load + mean of stress-field) ranging from P_0 to P_m and a range of temperatures from T_0 down to the temperature (T'_m) of the body when it reached its present level (i.e. something above 800° C). Since there was comparatively little internal movement in the peridotite core this has largely preserved the primary assemblage characteristic of P_0, T_0 as a metastable assemblage but the deformation and internal movement in the margin has caused the peridotite there to continuously adjust its mineralogy to approach equilibrium in the changing P, T environment. This has already been postulated to explain the porphyroblastic growth of spinel at some intermediate environment (P_i, T_i) and its later reaction and complete or partial elimination in environment (P_m, T'_m).

A limiting condition on the movement of such a crystalline diapir will be the rate of heat loss to the wall rocks coupled with its relatively slow movement rate. An analysis of this problem, accepting as boundary conditions the possible range of geothermal gradients in the crust, the final temperature of the peridotite as about 800° C and an absence of latent heat of crystallization in the intrusion may give an insight into the distances such a body could reasonably be expected to move.

In the absence of such an analysis and because of the number of assumptions of physical variables involved the only possible proof of the validity of the concept is considered to be in any evidence from the mineral assemblages that $P_0 \gg P_m$. The following factors, treated in detail in preceding sections, are thought to provide such evidence:

1. There is a close analogy in the composition of all its mineral phases, between the primary peridotite assemblage and the minerals of the peridotite nodules in basalts described by Ross, Foster, and Myers (1954). These authors postulated a xenolithic origin for the nodules and (p. 732) that 'the most probable origin of nodule-like inclusions seems to be that they are derived from

the peridotite zone of the earth's crust and that most of them at least came directly from that zone'. The conclusion is entirely interpretive but is consistent with current hypotheses on the origin of basalt magma within the mantle. Even if further data on peridotite nodules show the data of Ross *et al.* to have been selective with regard to the constancy of the $\frac{Mg}{Mg+Fe+Mn}$ content [cf. the data of Wilshire & Binns (1961) and Deriu (1960)] the comparison above remains valid in that rocks of this selected composition have a characteristic phase assemblage implying a similar environment of crystallization.

2. The stability of the assemblage ol–ens_{Al}–di_{Al}–sp in preference to the assemblage ol–ens–di–an in the primary peridotite is incompatible with experimental evidence at atmospheric pressure and with the evidence from basaltic magmas (Bowen, 1928, p. 280; Osborn & Tait, 1952, pp. 428–32). Experimental evidence suggests the reversal of this situation with stability of spinel and pyroxenes together at water pressures of 10,000 bars (Yoder & Chinner, 1960). Since water does not enter as a component into any of these phases it is probable that this relation is pressure-dependent and the ol–ens_{Al}–di_{Al}–sp is a high-pressure assemblage.

3. The high Al_2O_3 contents of the pyroxenes in the primary assemblage and its removal in the recrystallized pyroxenes, in the absence of chemical variation in the rocks, are due to considerable pressure difference rather than any temperature difference between the primary and recrystallized assemblages. This conclusion rests at present on the preliminary experimental work (Boyd & England, 1960) and the suggested volume decrease in pyroxenes on Al_2O_3 substitution (Hess, 1952).

4. Although the use of the distribution coefficient (K_{Fe}) expressing the Fe^{++}/Mg^{++} distribution between coexisting pyroxenes, to deduce temperature of crystallization is not adequately verified in all respects, e.g. its variation with Al_2O_3 or CaO contents and with large pressure changes; the similarity of this coefficient in both primary and recrystallized assemblages is suggestive of similar temperatures of crystallization.

5. The constancy of the distribution coefficient (K_{Al}) expressing the $^{Z}Al/Si$ distribution between coexisting magnesian pyroxenes in nodules and the Lizard primary assemblages, and its very different value in the recrystallized assemblage, may be taken as evidence of a large change in *P–T* conditions. If point 4 above is valid then this change must be in pressure rather than temperature.

None of the factors listed above are adequate in themselves to prove a pressure difference and points 4 and 5 in particular are hypotheses rather than observations. However, it is considered that together they have sufficient weight to justify the conclusion that $P_0 \gg P_m$ and, referring back to p. 177, to justify as a working hypothesis the concept that the core of the Lizard peridotite has an 'exotic' relationship to its present environment. It is considered that the peridotite is a true crystalline diapir, crystallizing initially at a greater depth and

moving vertically within a foliated and cataclastic shell to a much higher crustal level under the influence of a non-hydrostatic regional stress-field. The peridotite was a high-temperature body throughout the whole of such movement but the mineralogical effects (e.g. possibly the lower degree of solubility of enstatite in diopside and diopside in enstatite in the recrystallized assemblage) of any temperature decrease (T_0 to T''_m) are overshadowed by the mineralogical changes following from the change in load pressure (essentially P_0 to P_m).

VI. HIGH-TEMPERATURE PERIDOTITE INTRUSIONS

In contrast to the classical observation that peridotites of alpine type have little or no associated contact metamorphism, very recent work has demonstrated the existence of peridotites in orogenic environments which do possess high grade metamorphic aureloles. The Lizard peridotite is an example of this type. The intrusion was emplaced during regional metamorphism and the operation of a non-hydrostatic stress-field, conditions considered to indicate the deeper zones of an active orogenic belt. In its MgO/FeO ratio, lack of a chilled basaltic margin, lack of interlayered basic rocks, and internal deformed fabric, the intrusion conforms with the criteria of Hess (1938) for 'alpine peridotites'.

The Tinaquillo peridotite in Venezuela (MacKenzie, 1960) shows many similar features to the Lizard peridotite. The peridotite is olivine-rich (Fo_{90} approx.) with lesser enstatite (Ens_{90-92}) either as equant grains or elongate flattened grains parallel to the strong mylonitic foliation. Clinopyroxene occurs but is apparently not as common as in the Lizard peridotite. Thin bands, analogous to the mafic bands in the recrystallized anhydrous assemblage of the Lizard, are brown amphibole (pargasite), plagioclase, orthopyroxene (Ens_{85-90}), and clinopyroxene bearing. The whole of the peridotite is intensely mylonitized and strongly resembles the marginally developed recrystallized anhydrous assemblage of the Lizard. No coarse-grained 'primary assemblage' analogous to that of the Lizard has been recorded and optical determinations suggest that the equant and elongate enstatites are of the same composition (MacKenzie, 1960).

The two intrusions are of similar size and the Tinaquillo has a metamorphic aureole (estimated at 1500 to 2000 metres thick) in which green hornblende of the country-rock gneisses changes to brown hornblende, plagioclase becomes more calcic, and garnet (magnesian pyralspite) becomes increasingly common towards the contact. Augite increases towards the contact and minor hypersthene occurs at the contact. Basic bodies of fine granoblastic 'pseudogabbro', interpreted as included country-rock, characteristically contain hypersthene, augite, red-brown hornblende and calcic plagioclase. Garnet is rare in these included rocks.

The Mount Albert ultramafic complex (Smith & MacGregor, 1960) is about 16 sq. mil in area, i.e. slightly smaller than the Lizard and Tinaquillo peridotites, and consists of dunite, peridotite and enstatite pyroxenite. The authors liken the internal structure to that of salt-domes and propose a similar mechanism of

intrusion. Composition variations in olivine (Fo_{90-92}) enstatite (Ens_{91-97}) and chrome-spinel (35–37 per cent Cr_2O_3 and 10–32 per cent Al_2O_3) are related by the authors to local and variable incorporation of water during intrusion, the areas of high water content giving more highly oxidized magma leading first to crystallization of more magnesian enstatite and more iron-rich spinel and later to more extensive serpentinization in these areas. Such areas are of irregular distribution and unrelated to the primary banding. No details of deformed crystalline textures have been given as yet but presumably the comparison with salt-dome intrusion implies an intrusion largely in the crystalline state.

A metamorphic aureole up to 1000 ft wide partially surrounds the peridotite and the aureole rocks range from greenschists through epidote-amphibolites to garnetiferous hornblende-pyroxene granulite with plagioclase becoming more calcic near the contact. The bulk chemical composition of the rocks shows no significant variation and high-grade metamorphism similar in character to that at the Lizard seems established.

The Dawros Peridotite, Connemara (Rothstein, 1957, 1958, 1961), is a layered peridotite preserving accumulative textures locally but largely overprinted by recrystallization and deformation textures interpreted by Rothstein as originating during movement of the crystalline accumulate (possibly to a higher crustal level) while at a high temperature in an orogenic environment. The mineralogy has previously been compared with the Lizard and embraces similar Mg-rich pyroxenes, comparable with those in the recrystallized assemblage of the Lizard. The rocks in contact with the peridotite appear 'to represent transitions from a hornfels texture to a mylonite' (Rothstein, 1957, p. 18) and garnet, sillimanite, and spinel are developed.

The Cashel Lough–Wheelaun Intrusion (Leake, 1958, 1960), in Galway, Eire, is regarded by Leake as being formed from two magmas, one 'ultramafic' and giving olivine+two-pyroxene+hornblende rocks grading to hornblende pyroxenites and norites with very calcic (An_{86-88}) bytownite, and a basic magma giving labradorite or acid bytownite, hornblende, and apatite. Contact metamorphism with mobilization of pelites, locally containing fragmented blocks of the bytownite-orthopyroxene rock, is extensive with development of cordierite, sillimanite, spinel, corundum, and hypersthene in various rocks.

The relationship of these Connemara intrusions to the type defined by the Lizard, Tinaquillo, and Mt. Albert intrusions is uncertain, the Cashel Lough–Wheelaun Intrusion in particular being more iron- and calcium-rich. Rothstein (1961) has appealed to the postulated effects of high water content of a 'saturated basaltic magma' to explain the absence of plagioclase and the presence of olivine, 2-pyroxenes, and spinel as precipitates from the basaltic magma.

The preceding discussion compares the nature of several high-temperature peridotite intrusions with their contact aureoles, with the features of the Lizard. There is no evidence recorded from these other studies for the close analogy between intrusive peridotites and peridotite nodules which has been stressed for

the Lizard primary assemblage and attributed to a very high load-pressure environment of crystallization for the peridotite nodules and Lizard primary assemblage. It is suspected that such evidence may be found if the Al_2O_3 contents of pyroxene augen in deformed peridotites were compared with the Al_2O_3 contents of fine recrystallized enstatite.

With the demonstration of high-temperature but crystalline peridotite intrusions there still remains the question of whether these bodies were once liquid magmas or magmas with some suspended olivine crystals, at their present composition or whether they were deep-seated accumulates from a more basaltic magma. Rothstein, as previously mentioned, has advocated the second hypothesis while Hess (1960*a*, p. 239) has advocated the first hypothesis. In the second hypothesis the peridotite basal accumulate, when first formed, would be at a higher temperature and thus lower rheidity than the enclosing country-rock but it could not move as a crystalline diapir in response to a stress-field in the manner advocated for the Lizard until any overlying, still-liquid, basic magma had first been squeezed out. Then the peridotite could move and would probably, though not necessarily, follow the preheated channel created by the basic magma. We might expect a sequence of basic to ultramafic intrusion in a given area. It is considered that the hypothesis is a possible one but there is no direct evidence to support it.

The first hypothesis is favoured and it is suggested that a melt or melt+olivine crystals of the composition of the Lizard peridotite did primarily exist at depth. Such a melt would rise by density difference while within the mantle, but probably could not rise through the sialic part of the crust by density difference and would normally cease to move and crystallize at a definite level, possibly at the Mohorovicic Discontinuity, defined by the density of the magma and the density distribution in the sialic column. This is the mechanism proposed by which a high-temperature peridotite magma could enter an environment of cooler rocks. The only mechanism by which the peridotite could then move to higher levels through less dense sialic rocks is the action of the stress-field and the presence of the rheidity difference. It is considered that unless there is the initial magmatic stage there is no mechanism for moving the peridotite out of its initial P–T environment, presumably in the mantle, into the crustal environment with the peridotite having a large temperature and rheidity difference from the crustal environment.

In Table 11 the probable composition (assuming no water and all Fe as FeO) of the Lizard peridotite magma, obtained by averaging analyses V, VII, VIII, and IX (Table 1), is compared with the composition of a typical peridotite nodule (Hess, 1960, p. 179) and with the composition of the enstatite-bearing dunite mylonite from the mid-Atlantic ridge (St. Paul's Rocks, Tilley, 1947). Hess (1960, p. 178) suggests that the peridotite nodule may be representative of some part of the Earth's mantle and the same suggestion is current for the mid-Atlantic ridge peridotite, cf. Hess (1960*a*, p. 237). The analyses of Table 11 are

very similar and invite further investigation of the significance of this composition in mantle petrogenesis (cf. Green & Ringwood, 1963).

Also in Table 11 is given an analysis (4) calculated as an anhydrous rock, of a pillow lava from Cyprus in which the olivine (Fo_{92}) is considered by Gass to be of phenocrystic and not xenocrystic origin. This may represent an ultrabasic liquid which has reached the surface, and it is perhaps significant that it has

TABLE 11

Comparison of average Lizard peridotite with peridotites derived from the mantle and with a pillow lava consisting of over 50 per cent olivine (Fo_{92}) *phenocrysts in a basaltic glass or groundmass*

	1	2	3	4
SiO_2	44·77	43·97	44·35	45·16
TiO_2	0·19	0·17	0·14	0·19
Al_2O_3	4·16	2·89	2·97	4·86
Fe_2O_3	—	1·04	0·67	2·54
FeO	8·21	6·89	7·59	6·90
MnO	0·11	0·13	0·13	0·15
MgO	39·22	41·11	40·80	35·16
CaO	2·42	2·35	2·55	4·19
Na_2O	0·22	0·07	0·20	0·26
K_2O	0·05	nil	0·01	0·05
H_2O^+	—	0·35	0·06	—
H_2O^-	—	0·20	0·03	—
Cr_2O_3	0·40	0·50	0·41	0·54
P_2O_5	0·01	—	0·02	—
CO_2	—	—	0·00	—
NaCl	—	0·09	—	—
NiO	0·24	0·21	0·31	—
	100·00	99·97	100·24	100·00

1. Lizard Average (Anal. V, VII, VIII, IX).
2. St. Paul's Rocks (Tilley, 1947).
3. Peridotite Nodule (Hess, 1960).
4. Ultrabasic Pillow Lava (Gass, 1958).

risen through ultramafic and mafic rocks in an area of high positive gravity anomaly. This analysis is higher in CaO and lower in MgO than the other analyses.

VII. MULTIPLE HYPOTHESES OF ULTRAMAFIC EMPLACEMENT

The recognition of high-temperature peridotite intrusions accentuates the complexity becoming evident in the study of ultramafic rocks occurring in orogenic belts. Such ultramafic rocks include the large layered ultramafic complexes such as the Philippines, Cuba, and Papua characterized by movement and tectonic contacts against enclosing sediments or volcanics. These may preserve excellent accumulative textures, indicating tranquil accumulation from an uncertain magma composition (Green, 1961) or such textures may be destroyed by solid flow as an inhomogeneous crystalline mush (Thayer, 1960). The suggestion by Hess (1960*a*) that such large complexes (he instanced Cuba and

Puerto Rico) are altered sub-oceanic mantle material exposed in young orogenic belts may well be correct since their present environment and attitude seem unrelated to their environment of primary accumulation.

The work of Noble (1960) and others on the Alaskan, zoned stock-like peridotite complexes has demonstrated another type of peridotite characterized mineralogically by the absence of orthopyroxene and plagioclase and the presence of hornblende and of magnetite as major primary phases in some units.

The genesis of the type of serpentinized peridotite sill or sheet in low-grade or unmetamorphosed sediments (Chesterman, 1960, describes a typical example), remains an outstanding problem but the answer is considered to lie in the deformation properties of serpentinized peridotite rather than in an appeal to a low-temperature peridotite magma. The reintrusion of serpentinites as cold intrusions (Taliaferro, 1943, pp. 202–7; Green, 1959, pp. 20–22) demonstrates the readiness of the rock to deform but the actual mechanism of deformation is not well understood.

The data at present seem to force the acceptance of several hypotheses applicable to different peridotite bodies. The one common factor to all these hypotheses is an orogenic environment of relatively large non-hydrostatic stress-fields and characterized by major folding and thrusting. Thus major folding and faulting is the agent bringing possible mantle material present at shallow (3–5 km) depth in the oceanic areas to surface exposure. A non-hydrostatic stress-field is required to bring any peridotite magma or hot crystalline diapir, lacking a density inversion relative to crustal material, from its normal possible level of intrusion (i.e. perhaps at the Mohorovicic Discontinuity) into crustal and sialic rocks. A non-hydrostatic stress-field, at shallow depths, is responsible for the 'cold intrusion' of serpentinized peridotites as slickenside and shear-bounded bodies (Taliaferro, 1943, pp. 202–7).

Thus the term 'alpine-type peridotite' is considered to have significance in designating a peridotite occurring in an orogenic environment but which genetically may have one of several quite distinct origins.

ACKNOWLEDGEMENTS

The research which forms the subject of this paper was carried out in the Department of Mineralogy and Petrology, Cambridge. The restudy of the Lizard peridotite was suggested by Professor C. E. Tilley and the author is grateful to Professor Tilley and also to Dr. S. R. Nockolds for discussions, guidance, and criticism during the period of research. The author acknowledges the instruction and help of Mr. J. H. Scoon in the methods of chemical analysis. The trace-element measurements were made by Mr. R. S. Allen at Cambridge. Other members of the staff of the Department of Mineralogy and Petrology are thanked for discussions and practical help on various occasions.

Professor C. E. Tilley, Cambridge, Professor H. H. Hess, Princeton, Dr. A. E. Ringwood and Dr. I. McDougall, Department of Geophysics, Australian

National University, Canberra, are thanked for the critical reading of this paper and for discussion and suggestions.

The research at Cambridge was made possible by an award of the Royal Commission for the Exhibition of 1851 and this scholarship and the interest of the Commission are gratefully acknowledged.

REFERENCES

BARTHOLOMÉ, P., 1961. Co-existing pyroxenes in igneous and metamorphic rocks. *Geol. Mag.* **98,** 346–8.

BOWEN, N. L., 1928. *The Evolution of the Igneous Rocks* (reprinted 1956, Dover publications).

—— & SCHAIRER, J. F., 1935. The system MgO–FeO–SiO_2. *Amer. Journ. Sci.* **29,** 151–217.

—— & TUTTLE, O. F., 1949. The system MgO–SiO_2–H_2O. *Bull. Geol. Soc. Amer.* **60,** 439–60.

BOWN, M. C., & GAY, P., 1959. Identification of oriented inclusions in pyroxene crystals. *Amer. Min.* **44,** 592–602.

—— —— 1960. An X-ray study of exsolution phenomena in the Skaergaard pyroxenes. *Miner. Mag.* **32,** 379–88.

BOYD, F. R., & ENGLAND, J. L., 1960. Minerals of the mantle. *Ann. Rept. Director Geophysical Lab.*; *Carnegie Inst. Washington Year Book*, **59,** 47–52.

BROWN, G. M., 1956. The layered ultrabasic rocks of Rhum, Inner Hebrides. *Phil. Trans. Roy. Soc. London*, Ser. B 240, 1–53.

—— 1957. Pyroxenes from the early and middle stages of fractionation of the Skaergaard Intrusion, East Greenland. *Miner. Mag.* **31,** 511–43.

BUDDINGTON, A. F., 1939. Adirondack igneous rocks and their metamorphism. *Geol. Soc. Amer. Memoir* 7.

CAREY, S. W., 1954. The rheid concept in geotectonics. *Journ. Geol. Soc. Aust.* **1,** 67–117.

CHESTERMAN, C. W., 1960. Intrusive ultrabasic rocks and their metamorphic relationships at Leech Lake Mountain, Mendocino County, California. *Rept. XXIst Session Internat. Geol. Congr.* Copenhagen, pt. xiii, 208–15.

DERIU, M., 1960. Olivine e pirosseni di noduli inclusi in basalti della Sardegna centro-occidentale. *Periodico di Mineralogia*, **28,** 259–83.

ESKOLA, P., 1952. On the granulites of Lapland. *Amer. Journ. Sci., Bowen Volume*, 133–71.

FLETT, J. S., 1912. The geology of the Lizard and Meneage. *Geol. Surv. Memoir* to sheet 359. 2nd edition 1946 (revised).

FLINT, D. E., DE ALBEAR, J. F., & GUILD, P. W. 1948. Geology and chromite deposits of the Camaguey District, Cuba. *U.S.G.S. Bull.* 954–B.

FYFE, W. S., TURNER, F. J., & VERHOOGEN, J., 1958. Metamorphic reactions and metamorphic facies. *Geol. Soc. Amer. Memoir* 73.

GASS, I. G., 1958. Ultrabasic pillow lavas from Cyprus. *Geol. Mag.* **95,** 241–51.

GONZALES, M. L., PEOPLES, J. W., FERNANDEZ, N. S., & VICTORIO, V., 1957. The ultramafic and mafic rocks of the Zambales Range Luzon, Philippines. *Bull. Geol. Soc. Amer.* **58,** 1736.

GREEN, D. H., 1959. The geology of the Beaconsfield district, including the Anderson's Creek Ultrabasic Complex. *Records of the Queen Victoria Museum, Launceston, Tasmania.* New Series No. 10, 1–26.

—— 1961. Ultramafic breccias from the Musa Valley, eastern Papua. *Geol. Mag.* **98,** 1–26.

—— & RINGWOOD, A. E., 1963. Mineral assemblages in a model mantle composition. *J. Geophys. Res.* **68,** 937–45.

HESS, H. H., 1938. A primary peridotite magma. *Amer. Journ. Sci.* **35,** 321–44.

—— 1949. Chemical composition and optical properties of common clinopyroxenes, Part I. *Amer. Min.* **34,** 621–66.

—— 1952. Orthopyroxenes of the Bushveld type, ion substitutions and changes in unit cell dimensions. *Amer. Journ. Sci., Bowen Volume*, 173–87.

—— 1960. The Stillwater Igneous Complex, Montana. *Geol. Soc. Amer. Memoir* 80.

—— 1960*a*. Caribbean research project progress report. *Bull. Geol. Soc. Amer.* **71,** 235–40.

HOWIE, R. A., 1955. The geochemistry of the charnockite series of Madras, India. *Trans. Roy. Soc. Edinburgh*, **62,** pt. 3, 725–68.

JOHNSTON, R., 1953. The olivines of the Garbh Eilean sill, Shiant Isles. *Geol. Mag.* **90,** 161–71.

KNOPF, A., & LEE, D. E., 1957. Fassaite from near Helena, Montana. *Amer. Min.* **42,** 73–77.

KRETZ, R., 1961. Some applications of thermodynamics to coexisting minerals of variable compositions. Examples: orthopyroxene-clinopyroxene and orthopyroxene-garnet. *Journ. Geol.* **69**, 361–87.

KUNO, H., 1954. Study of orthopyroxenes from volcanic rocks. *Amer. Min.* **39**, 30–45.

KUSHIRO, I., 1960. Si–Al relation in clinopyroxenes from igneous rocks. *Amer. Journ. Sci.* **258**, 548–54.

LEAKE, B. E., 1958. The Cashel Lough–Wheelaun Intrusion, Galway. *Proc. Roy. Irish Acad.* **59B**, 155–203.

—— & SKIRROW, G., 1960. Pelitic hornfelses of the Cashel Lough–Wheelaun Intrusion. *Journ. Geol.* **68**, 23–40.

LEECH, G. B., 1953. Geology and mineral deposits of the Shulaps Range, S.W. British Columbia. *British Columbia Dept. Mines Bull.* 32.

MCDOUGALL, I., 1961. Optical and chemical studies of pyroxenes in a differentiated Tasmanian dolerite. *Amer. Min.* **46**, 661–87.

MACKENZIE, D. B., 1960. High-temperature alpine-type peridotite from Venezuela. *Bull. Geol. Soc. Amer.* **71**, 303–18.

MUELLER, R. F., 1961. Analysis of relations among Mg, Fe and Mn in certain metamorphic minerals. *Geochim. et Cosmochim. Acta.* **25**, 267–96.

MUIR, I. D., & TILLEY, C. E., 1957. Contributions to the petrology of Hawaiian basalts I, the picrite basalts of Kilauea. *Amer. Journ. Sci.* **255**, 241–53.

—— —— 1958. The compositions of co-existing pyroxenes in metamorphic assemblages. *Geol. Mag.* **95**, 403–8.

MURRAY, R. J., 1954. The clinopyroxenes of the Garbh Eilean sill, Shiant Isles. *Geol. Mag.* **91**, 17–31.

NOBLE, J. A., & TAYLOR, H. P., 1960: Correlation of the ultramafic complexes of south-eastern Alaska with those of other parts of North America and the world. *Rept XXIst Session Internat. Geol. Congr. Copenhagen*, pt. xiii, 188–97.

O'HARA, M. J., 1961. Zoned ultrabasic and basic gneiss masses in the early Lewisiom metamorphic complex at Scourie, Sutherland. *Journ. Petrology*, **2**, 248–76.

OSBORN, E. F., & TAIT, D. B., 1952. The system diopside–forsterite–anorthite. *Amer. Journ. Sci., Bowen Volume*, 413–33.

RAMBERG, H., & DE VORE, G. W., 1951. The distribution of Fe^{++} and Mg^{++} in co-existing olivines and pyroxenes. *Journ. Geol.* **59**, 193–210.

ROSS, C. S., FOSTER, M. D., & MYERS, A. T. 1954. Origin of dunites and of olivine-rich inclusions in basaltic rocks. *Amer. Min.* **39**, 693–737.

ROTHSTEIN, A. T. V., 1957. The Dawros peridotite, Connemara, Eire. *Quart. Journ. Geol. Soc. London*, **113**, 1–25.

—— 1958. Pyroxenes from the Dawros peridotite and some comments on their nature. *Geol. Mag.* **95**, 456–62.

—— 1961. A synorogenic peridotite at Dawros, Connemara. *Acta. Geologica (Budapest)*, Tomus VI, 221–32.

RUCKMICK, J. C., & NOBLE, J. A., 1959. Origin of the ultramafic complex at Union Bay, South-eastern Alaska. *Bull. Geol. Soc. Amer.* **70**, 981–1018.

SANDERS, L. D., 1955. Structural observations on the south-east Lizard. *Geol. Mag.* **92**, 231–40.

SHIDO, F., 1958. Plutonic and metamorphic rocks of the Nakoso and Iritono districts in the central Abukuma Plateau. *Journ. Fac. Sci. Univ. Tokyo*, **11**, 131–217.

SMITH, C. H., & MACGREGOR, I. D. 1960. Ultrabasic intrusive conditions illustrated by the Mt. Albert Ultrabasic Pluton, Gaspe, Quebec. *Abst. in Bull. Geol. Soc. Amer.* **71**, 1978.

SUNDIUS, N., 1946. The classification of the hornblendes and the solid solution relations in the amphibole group. *Sveriges Geol. Undersokning Arsbok*, **40**, nr. 4–80, 1–36.

TALIAFERRO, N. L., 1943. The Franciscan–Knoxville problem. *Bull. Amer. Assoc. Petroleum Geologists*, **27**, 109–219.

THAYER, T. P., 1946. Preliminary chemical correlation of chromite with the containing rocks. *Econ. Geol.* **41**, 202–18.

—— 1960. Some critical differences between alpine-type and stratiform peridotite-gabbro complexes. *Rept. XXIst Session Internat. Geol. Congr. Copenhagen*, pt. xiii, 246–59.

TILLEY, C. E., 1938: Aluminous pyroxenes in metamorphosed limestones. *Geol. Mag.* **75**, 81–85.

—— 1947. The dunite-mylonites of St Paul's Rocks (Atlantic). *Amer. Journ. Sci.* **245**, 483–91.

TURNER, F. J., & VERHOOGEN, J., 1960. *Igneous and Metamorphic Petrology*, 2nd ed. (McGraw-Hill).

—— HEARD H., & GRIGGS, D. T., Experimental deformation of enstatite and accompanying inversion to clinoenstatite. *Rept. XXIst Session Internat. Geol. Congr. Copenhagen*, pt. xviii, 399–408.

WILKINSON, J. F. G., 1956. The olivines of a differentiated teschenite sill near Gunnedah, New South Wales. *Geol. Mag.* **93**, 441–55.

WILKINSON, J. F. G., 1957. The clinopyroxenes of a differentiated teschenite sill near Gunnedah, New South Wales. *Geol. Mag.* **94**, 123–34.

WILSHIRE, H. G., & BINNS, R. A., 1961. Basic and ultrabasic xenoliths from volcanic rocks of New South Wales. *Journ. Petrology*, **2**, 185–208.

WINCHELL, A. N., & WINCHELL, D. H., 1959. *Elements of Optical Mineralogy*, Part II, 4th ed. (Wiley).

WORST, B. G., 1958. The differentiation and structure of the Great Dyke of Southern Rhodesia. *Trans. Geol. Soc. South Africa*, **61**, 283–358.

YODER, H. S., & SAHAMA, TH. G., 1957. Olivine X-ray determinative curve. *Amer. Min.* **42**, 475–91.

—— & CHINNER, G. A., 1960. Grossularite–pyrope–water system at 10,000 bars. *Ann. Rept. Director Geophys. Lab.; Carnegie Inst. Washington Year Book*, **59**, 78–81.

—— & TILLEY, C. E., 1961. Simple basalt systems. Ibid. **60**, 106–13.

A 6

Reprinted from THE JOURNAL OF GEOLOGY
Vol. 72, No. 5, September 1964
Copyright 1964 by the University of Chicago
Printed in U.S.A.

THE METAMORPHIC AUREOLE OF THE PERIDOTITE AT THE LIZARD, CORNWALL[1]

D. H. GREEN
Department of Geophysics, Australian National University, Canberra

ABSTRACT

The peridotite in the Lizard area of Cornwall was intruded during a period of regional metamorphism of intensity producing blue-green hornblende amphibolites in rocks of basaltic composition. It is demonstrated that the peridotite has a high-temperature aureole in which assemblages characterized successively by brown-green hornblende, brown hornblende with hypersthene and augite, and typical hypersthene + augite pyroxene granulites are developed in rocks compositionally equivalent to the regional metamorphic assemblage.

Chemical analyses of whole rocks, four hypersthenes, six clinopyroxenes, and five amphiboles are used to compare the metamorphic assemblages with those developed in other metamorphic gradients. In some areas of complex contact of peridotite and granulite or in granulite included within the peridotite, the granulite has become the more mobile rock and locally intrudes and includes blocks of the peridotite margin.

INTRODUCTION

The Lizard Peninsula, southwest Cornwall, consists of metamorphic rocks with peridotite and gabbro intrusions, separated by normal faults and a postulated major thrust zone (Flett and Hill, 1912, 1946) from folded but unmetamorphosed Middle Paleozoic sediments and Carboniferous (Hercynian) granites of Cornwall and Devon. In the restudy of the Lizard area the rock units as described and used in the British Geological Survey Memoir (Flett and Hill, 1912, 1946) were found to be identifiable and mappable in the field, and the nomenclature used by Flett is generally adhered to.

The sequence of rock units in the Lizard area in order of increasing age is given below; their distribution is shown in part in figure 1 and in more detail in the Geological Survey 1 inch to the mile Lizard and Meneage sheet, and in Green (1964).

f) Paleozoic, postmetamorphic rocks outcropping north of the Lizard Boundary Zone.

e) Kennack Gneiss and Microgranite—several small intrusions of microgranite and common irregular dikes and sills of injection gneiss. Lit-par-lit injection during shearing of shallow-dipping basaltic sills in the peridotite has produced mixed hornblende-biotite gneiss and amphibolite sills within the peridotite. Potassium-argon age determinations on the Kennack Gneiss give an Upper Silurian to Lower Devonian age (Caledonian; 350–390 million years) for this event.

d) Basaltic dikes and sills locally forming a dike swarm striking N.NW.–S.SE. Subhorizontal sills are commonly sheared and amphibolitized, whereas feeder dikes are less affected.

c) Gabbro and local troctolite intrusion. The gabbro forms a large crescentic body in the eastern part of the area, intersecting the coast north of Coverack (fig. 1).

b) Peridotite emplacement during regional metamorphism. The peridotite forms a steep-sided diapiric intrusion with a sill-like extension in the southeastern part of the area. The detailed petrology and genesis of the peridotite is discussed elsewhere (Green, 1964).

a) Regionally metamorphosed rocks including
- (1) Hornblende Schist of Landewednack type.
- (2) Old Lizard Head Series, mica schists and metasediments rarely interbedded with, and possibly largely underlying, the Landewednack Hornblende Schists.

The Lizard peridotite was at a high temperature when emplaced in the Landewednack Hornblende Schists (Flett and Hill,

[1] Manuscript received December 5, 1962; revised September 29, 1963.

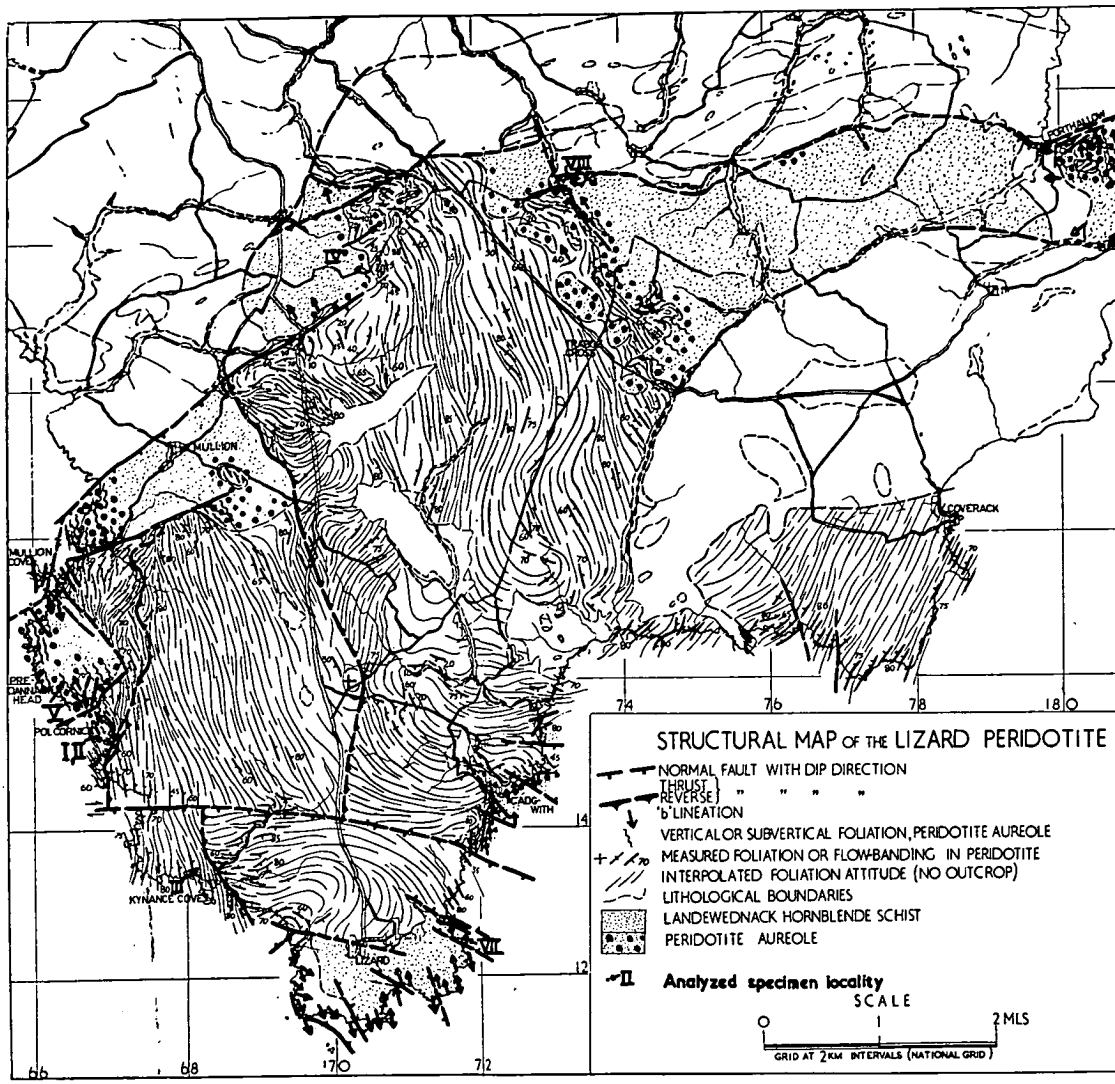

FIG. 1.—Structural map of the Lizard peridotite showing distribution of the metamorphic aureole in relation t peridotite. Also shown are directions of subvertical foliation in the aureole and subhorizontal lineation in the re metamorphic assemblage. See also Green (1964, fig. 1).

1912, 1946). This conclusion is based on the identification of rocks of the pyroxene granulite metamorphic facies and of a metamorphic gradient from these rocks to the normal regional metamorphic assemblage and, second, on the demonstration that this metamorphic gradient is related to the peridotite and not to any other intrusive body. The method of study has been a general petrographic study delimiting the primary mineral assemblages present and their relationship to the peridotite. This has been followed by selection of specimens showing relatively little secondary chloritization and uralitization and typical of the four distinct mineral assemblages in basic rocks revealed by the first stage. These rocks and their ferromagnesian minerals were then chemically analyzed, and trace-element analyses (by R. S. Allen, Cambridge) were carried out. These data are considered adequate to establish the presence of a high-grade metamorphic aureole around the peridotite, contrary to classical observations, and to enable comparison with data from other metamorphic gradients and aureoles. The parallel variation through the metamorphic assemblages of plagioclase and opaque minerals has only been qualitatively studied—plagioclase in particular is commonly partly or completely secondarily altered to "saussurite" or sericitic products, whereas the ferromagnesian minerals remain unaltered.

PETROGRAPHY OF THE METAMORPHIC ASSEMBLAGES

A. BLUE-GREEN HORNBLENDE ASSEMBLAGE

The normal regional metamorphic assemblage of the Landewednack Hornblende Schists (fig. 1) is characterized by blue-green hornblende as the dominant ferromagnesian mineral. Sodic plagioclase, sphene, and magnetite are also typical; and pale-green clinopyroxene (salite) may be present, particularly in more calcic bands. Epidote, grossular, calcite, and quartz are present in bands departing from the normal basaltic composition. The texture of the rocks is very strongly lepidoblastic, locally in hornblende-rich bands becoming nematoblastic or in pyroxene-rich bands becoming granoblastic.

The modal analysis, chemical analysis, and trace-element data for a typical amphibolite (from Pencra Head) are given in table 1, analysis VI.[2] The hornblende, plagioclase (sodic andesine $Ab_{63}An_{37}$), and opaque minerals (magnetite with minor ilmenite) occur in lenses of near-monomineralic composition; and both hornblende and plagioclase show considerable variation in grain size. The hornblende shows the strong and characteristic pleochroism of this assemblage, namely, Z = deep blue-green; Y = very deep green; X = pale yellow to yellow-green.

A pyroxene-rich band (table 1, analysis VII) illustrates the range in composition from the previous typical example—mineralogically this band consists of saussuritized plagioclase and pale-green clinopyroxene (salite) as large anhedral crystals with magnetite (having hematite rims and intergrowth), epidote, blue-green hornblende, and sphene as smaller, less abundant grains.

A third example of the assemblage (table 1, analysis VIII), analyzed by the Geological Survey (Flett, 1912, p. 48), has a very fine-grained and strong lepidoblastic texture. The hornblende needles and prisms are pleochroic in blue-green and green colors but are slightly paler than in the typical specimens.

B. BROWN-GREEN HORNBLENDE ASSEMBLAGE

The characteristic feature of this assemblage is the pleochroic scheme of the hornblende: Z = deep olive-green; Y = very deep brown-green or green-brown; X = pale yellow-green—the blue or blue-green tint of the preceding assemblage is characteristically absent. A pale-green clinopyroxene (salite), ilmenite + magnetite, and intermediate plagioclase (andesine-labradorite) usually occur with the hornblende. Sphene is typically absent; apatite and rare, rounded zircon are present as accessory minerals. In many specimens there is evidence of incipient retrogressive metamorphism with rim-

[2] Trace-element data and key to localities are given in table 1A.

TABLE 1

MODAL COMPOSITIONS (VOLUME PER CENT) AND CHEMICAL ANALYSES OF ROCKS FROM THE LIZARD PERIDOTITE AUREOLE*

	Hornblende Granulite (Contact)	Pyroxene Granulite		Hornblende Granulite	Green-brown Hornblende Amphibolite	Blue-green Hornblende Assemblage		
	(90703)†	(90702)	(90697)	(90696)	(90695)	(90693)	(90694)	(90679)
Plagioclase	33.2	52.1	49.5	44.1	31.8	25.6	.....	.....
Amphibole	35.5	2.0	.....	37.7	57.0	62.0	.....	.....
Clinopyroxene	10.4	5.3	32.9	9.6	2.5	.....	.....	.....
Orthopyroxene	19.9	30.1	5.8	3.8	.....	.....	.....	.....
Opaques	1.0	9.5	9.2	4.8	7.9	9.0	.....	.....
Sphene	.....	.....	.....	.....	.....	3.5	.....	.....
Apatite	.....	.....	0.1	0.2	0.8	.....	.....	.....
Biotite	.....	1.0	1.9	.....	.....	.....	.....	.....
Olivine	.....	.....	0.7	.....	.....	.....	.....	.....
	Analysis No.‡							
	I	II	III	IV	V	VI	VII	VIII
SiO_2	48.64	48.11	46.12	47.26	45.28	45.05	46.72	48.64
TiO_2	0.78	1.73	2.40	1.30	3.22	3.68	2.54	1.90
Al_2O_3	13.22	16.95	14.60	16.85	14.50	13.72	15.41	14.99
Fe_2O_3	1.39	1.15	4.06	1.72	3.27	4.55	6.01	3.42
FeO	7.79	9.92	8.43	9.16	11.17	11.68	5.85	7.76
MnO	0.16	0.23	0.21	0.17	0.27	0.27	0.19	0.30
MgO	13.70	8.48	7.87	7.64	6.93	6.02	4.63	7.76
CaO	9.45	8.45	10.31	11.33	9.98	10.26	14.11	9.60
Na_2O	2.12	2.31	2.67	2.36	3.36	2.58	3.21	3.52
K_2O	0.26	0.39	0.59	0.29	0.35	0.31	0.34	0.52
H_2O+	1.98	1.76	1.97	1.77	1.36	1.44	1.30	1.25
H_2O-	0.15	0.32	0.69	0.00	0.11	0.09	0.13	0.10
P_2O_5	0.05	0.20	0.20	0.10	0.28	0.17	0.21	0.16
Cr_2O_3	0.07	n.d.	n.d.	0.03	0.03	0.03	0.00	n.d.
							S 0.08	CO_2 0.23
							Less O for S −0.03	FeS_2 0.06
	99.76	100.00	100.12	99.98	100.11	99.85	100.70	100.21
Mg/Fe^{++}	3.14	1.52	1.66	1.49	1.11	0.92	1.41	1.78
$Fe^{+++}/Fe^{++}+Fe^{+++}$	0.14	0.09	0.30	0.15	0.21	0.26	0.48	0.32
$100\times Mg/Mg+Fe+Mn$.	72.5	57.5	53.0	55.6	46.2	40.1	41.6	55.1
Norms:								
qz	.....	.....	.....	.....	.....	.....	.....	.....
or	1.7	2.3	3.4	1.5	2.3	1.7	2.2	3.4
ab	18.3	19.9	23.2	18.0	25.1	22.4	23.3	30.8
an	26.6	35.6	26.9	31.2	23.8	25.5	26.7	24.1
ne	.....	.....	.....	.....	2.2	.....	2.3	.....
$CaSiO_3$	8.9	2.6	10.4	8.2	10.3	10.6	18.0	8.6
$MgSiO_3$	17.6	16.3	10.6	8.2	5.6	11.3	11.6	7.6
$FeSiO_3$	6.4	11.5	4.6	5.8	4.3	9.0	2.0	3.5
Mg_2SiO_4	12.0	3.6	6.8	12.7	8.4	2.9	.....	8.6
Fe_2SiO_4	4.8	2.9	3.1	9.9	6.9	2.5	.....	4.2
mt	2.1	1.7	6.2	2.3	5.0	6.9	8.9	5.3
il	1.6	3.4	4.7	2.2	6.2	7.1	4.9	3.7
ap	.....	.1	.1	.....	.2	.1	.1	.1

* Trace-element data and key to localities are given in table 1A.

† Specimen number.

‡ Analyst: D. H. Green (except VIII).

TABLE 1A

TRACE ELEMENTS* AND LOCALITIES OF ANALYZED ROCKS OF THE LIZARD AUREOLE

	I†	II‡	III§	IV‖	V#	VI**	VII††	VIII‡‡
Ga	18	18	18	18	18	22	18	40
Cr	540	465	220	465	320	220	100	20
Li	40	20	14	6	14	20	8	20
Ni	150	150	100	70	46	22	46	90
Co	220	46	180	180	46	220	46	90
V	220	220	380	220	380	425	380	500
Zr	16	45	100	45	100	45	45	300
Sc	40	40	40	40	40	40	40	n.d.
Y	5	12	32	22	32	22	32	50
Sr	125	150	100	100	125	150	170	200
Pb	.....	.....	.....	.....	.....	.....	.....	n.d.
Ba	45	85	60	20	20	45	45	n.d.

* Determined by R. S. Allen, Cambridge.

† Spec. 90703, contact hornblende granulite, Pol Cornick.

‡ Spec. 90702, pyroxene granulite, Pol Cornick.

§ Spec. 90697, pyroxene granulite, Lawarnick Pit.

‖ Spec. 90696, hornblende granulite, near Burnoon.

Spec. 90695, green-brown hornblende amphibolite, Predannack.

** Spec. 90693, blue-green hornblende amphibolite, Pencra Head.

†† Spec. 90694, blue-green hornblende amphibolite, Kilcobben Point.

‡‡ Spec. 90679, blue-green hornblende amphibolite, Lower Relowas Quarry. Rock analysis from Flett (1912, p. 48), trace elements on a similar specimen from the same locality by Butler (1953).

ming of salite and the brown-green hornblende with blue-green hornblende resembling that in the previous assemblage.

Texturally the rocks differ from the blue-green hornblende assemblage in lacking prominent compositional banding; and they have a much less well-defined lepidoblastic texture, in some examples becoming almost xenoblastic. Plagioclase and hornblende are coarser-grained and commonly have curving and embayed mutual boundaries. Although the hornblende crystals are aligned to define a rough foliation, this alignment is not as pronounced as in the blue-green hornblende assemblage, and a lineation defined by hornblende prisms is not developed.

A specimen from Predannack Head was selected as a type specimen for this assemblage; its modal analysis, chemical analysis, and trace-element data are given in table 1, analysis V. The plagioclase is calcic andesine (about $Ab_{53}An_{47}$) and is quite commonly multiply twinned but unzoned and may show strain bending locally. The salite (C_5 analyzed, table 3) is pale green in color and non-pleochroic, and the textural relations show clearly its stability in the assemblage with hornblende and plagioclase.

C. HORNBLENDE-GRANULITE ASSEMBLAGE

The hornblende granulite assemblage is characterized by the presence of brown hornblende as a major component co-existing with both orthopyroxene and clinopyroxene and not in replacement relation to either. The hornblende is brown, without the strong green tint (parallel to *Y*) of the previous assemblage; plagioclase (andesine-labradorite) is more abundant than in the preceding assemblages; and ilmenite, magnetite, pyrite and pyrrhotite, apatite, and zircon are minor or accessory constituents. Texturally the pyroxenes tend to form stubby or equant grains; the plagioclase forms a granoblastic or xenoblastic mosaic; and the hornblende occurs as anhedral grains molded around or between the pyroxenes and plagioclase. Some rocks are massive and fine-grained and suggestive of hornfels (for example, the analyzed rock IV from a basic body within the peridotite), others have a strong foliation and fine banding due to lenticular concentration of hornblende or to absence of hornblende in particular bands.

Brown hornblende of the characteristic type occurs in rocks in which there is now

no orthopyroxene or clinopyroxene preserved. In some of these rocks partial stages of preferential alteration of pyroxenes to secondary minerals leaving the hornblende as relict, comparatively fresh grains, can be seen; but in other examples brown hornblende is accompanied by secondary minerals replacing plagioclase, and the former presence of pyroxene cannot be demonstrated. The brown hornblende may itself be retrogressively altered—in the first stage to a marginal rim of blue-green amphibole and in a later stage to a fine aggregate of colorless or pale-green tremolite-actinolite.

The modal analysis, chemical analysis, and trace-element data for a typical specimen are given in table 1, analysis IV. The rock has a xenoblastic texture with plagioclase (about $Ab_{52}An_{48}$) and hornblende (Z = deep brown, slightly greenish; Y = medium brown; X = colorless to pale yellow-brown) the dominant phases. Colorless augite and pale-pink to pale-green pleochroic hypersthene are minor constituents, the augite occasionally growing as porphyroblasts.

A second specimen analyzed resembles the above in containing hornblende with both hypersthene and augite but has a special significance in being in actual contact with peridotite of the olivine + pargasite assemblage (Green, 1964). The modal analysis, chemical analysis, and trace-element data of the whole rock up to 3 cms. from the contact are given in table 1, analysis I. Even restricted to this zone, the rock shows banding parallel to the contact with variation in augite and hypersthene principally, some bands being essentially hypersthene + hornblende + plagioclase, others being augite + hornblende + plagioclase. In addition the hornblende shows a distinct color change from orange-brown (Z = brown, slightly orange; Y = pale brown; X = colorless) away from the contact to very pale brown (Z = pale brown to buff; Y = buff; X = colorless) at the contact. This color change is not uniform but is particularly marked over the 5 mm. nearest the contact. With the evidence for limited metasomatism across the contact (see p. 549), the change in properties of the amphibole is considered to be due probably to increasing Mg/Fe ratio. Pyrrhotite and rare magnetite are present as accessory minerals.

D. PYROXENE-GRANULITE ASSEMBLAGE

The pyroxene granulite assemblage is characterized by the presence of two pyroxenes (hypersthene and augite) coexisting with plagioclase and ilmenite + magnetite as major constituents. Hornblende is absent or present only in accessory amounts. Olivine, pyrite, pyrrhotite, biotite, apatite, and zircon may be present as accessory minerals. Where present, hornblende is a deep red-brown variety occurring in small intergranular crystals. Biotite is strongly pleochroic from almost colorless to a deep blood-red and occurs in clusters of crystals rather than disseminated evenly through the rock. Zircon occurs in small well-rounded crystals, and olivine is present in very few specimens (cf. Flett and Hill, 1912, p. 51, 54).

In hand specimen the rocks are quite leucocratic with a distinct foliation in part due to mineral alignment but more typically due to a rather lenticular distribution of light and dark minerals, or to slight compositional variation giving a megascopic banding. In thin section the textures are granoglastic to xenoblastic, with the distribution of pyroxene and plagioclase defining a foliation and a granulitic rather than hornfelsic character. Locally either augite or hypersthene may grow as a small porphyroblast. The rocks as a whole are medium- to fine-grained and more leucocratic than any of the preceding assemblages.

The two analyzed specimens (table 1, analyses II and III) were collected respectively from contorted basic granulite, 1 foot from a peridotite contact on the south side of Pol Cornick and from a 6-foot-thick basic sheet with peridotite on either side at Lawarnick Pit near Kynance Cove.

E. CHEMISTRY OF THE ROCKS

In table 1, analyses VI, VII, and VIII illustrate the range of compositional variation in the regional metamorphic assemblage, that is, the blue-green hornblende amphibolite. In both chemical analysis and

normative composition, analyses VI and VIII are comparable with olivine-bearing tholeiitic basalt compositions (Nockolds, 1954) although VIII is abnormally rich in Na_2O. The range in SiO_2 and FeO content defined by these two analyses encompasses the range expressed in analyses I–V. In all other constituents the variation is also restricted (except in analysis I). Analyses II–VI and analysis VIII are all consistent with a parentage as basalt flows, sills, or possibly tuffs. In only one of these rocks is there any normative nepheline present, suggesting that the parental rocks were tholeiitic olivine basalts rather than olivine alkali basalts.

Analysis VII (the diopside + epidote-bearing band in the blue-green hornblende assemblage) is very high in CaO and Fe_2O_3 and low in MgO. Calculation of the norm gives an excess of $CaSiO_3$ over $MgSiO_3$ + $FeSiO_3$ in diopside, and it is considered likely that this horizon originally probably contained calcite either as a cement or as detritus in a basalt tuff. The high TiO_2 and the trace-element data establish a link with the more normal "basalts."

The calculation of the Mg/(Mg + Mn + Fe) × 100 molecular ratios for the analyses accentuates the relative enrichment in MgO of analysis I. This is accompanied by a relative decrease in TiO_2, Al_2O_3, FeO + Fe_2O_3, Na_2O, and K_2O in comparison with the other analyses. The trace-element data shows lower Zr, Y, and V contents than the other analyses and higher Cr, Ni, and Li contents. The specimen analyzed is within 3 cm. from the peridotite contact, and the data are considered to show the presence of magnesia metasomatism over this distance. MgO, Cr_2O_3, and NiO are considered to have moved from the periodotite to "dilute" the previous normal composition. As well as this effect, the analysis (No. X, Green, 1964) of the peridotite immediately in contact with the hornblende granulite is enriched relative to the other peridotite analyses in SiO_2, FeO + Fe_2O_3, Na_2O, and K_2O, and in Li. There seems to have been two-way migration of selected components toward an elimination of the abrupt chemical discontinuity at the contact. Since these effects of composition changes are apparent in the analyzed hornblendes (from peridotite and granulite [see Green, 1964, and table 5]) and pyroxenes (from the granulite, tables 3 and 4) in comparison with analyzed minerals from non-contact rocks, the metasomatism must have taken place at a high temperature and is not an effect during serpentinization of the peridotite and saussuritization and uralitization in the granulite.

Although metasomatism has occurred at this contact, it is very limited. Analyses II and III are from rocks 1 foot and 3 feet, respectively, from similar peridotite contacts on the west coast. Analysis III is not considered to show any evidence of metasomatism in either major or trace elements, except possibly a somewhat higher Ni content than the other basic rocks. Analysis II may show slight MgO enrichment and has higher Ni and lower Y contents. The degree of possible metasomatism in II does not take this rock out of the compositional field of the basalts.

The analyses show clearly that the selected typical rocks of the four assemblages are chemically very closely similar. This similarity is apparent in comparisons of oxide contents, oxidation ratios, major element ratios, ACF plots, and normative compositions. Since the mineral assemblages are very different, the rocks must have crystallized under different physical conditions.

MINERAL CHEMISTRY

A. HYPERSTHENE

The analyses and structural formula of four orthopyroxenes are given in table 2.

All the orthopyroxenes are hypersthenes in the range En_{S72} to En_{S56}, the most magnesian (O_1 and O_2) being from the rocks nearest to the peridotite contact. Analyses O_3 (pyroxene granulite) and O_4 (hornblende granulite) are very similar, O_3 being higher in CaO content and also in TiO_2 content—the TiO_2 content parallels that of the rock which is much higher than in the other hypersthene bearing rocks. The $Fe^{+++}/(Fe^{++} + Fe^{+++})$ ratio is higher for the two orthopyroxenes from the hornblende granulites

TABLE 2

ANALYSES, STRUCTURAL FORMULAS ON THE BASIS OF 6 OXYGENS, AND TRACE-ELEMENT DATA FOR ORTHOPYROXENES FROM GRANULITES

	Weight of Sample for Analysis (Gm.)			
	1.0	1.0	0.7	0.3
	Analysis No.			
	O_1*	O_2†	O_3‡	O_4§
SiO_2	53.69	52.70	51.16	51.49
Al_2O_3	2.09	1.14‖	1.39	1.03
TiO_2	0.33	0.51	1.14	0.25
Fe_2O_3	1.14	1.02	0.85	1.36
FeO	16.20	22.74	24.21	24.75
MnO	0.44	0.63	0.76	0.68
MgO	25.44	20.74	19.15	19.75
CaO	1.31	1.36	1.86	1.46
Na_2O	0.06	0.01	0.08	n.d.
K_2O	0.00	0.00	0.00	n.d.
H_2O-	0.01	0.00	0.04	.....
	100.71	100.85	100.64	100.77
Si	1.932 } 2.000	1.956 } 2.000	1.928 } 2.000	1.944 } 2.000
^{Z}Al	0.068 }	0.044 }	0.063 }	0.046 }
^{Y}Al	0.020	0.005	.....	.....
Ti	0.010	0.013	0.030	0.007
Fe^{+++}	0.031	0.029	Z 0.009	Z 0.010
			Y 0.016	Y 0.029
Fe^{++}	0.486 } 1.984	0.706 } 1.977	0.763 } 1.994	0.781 } 2.009
Mn	0.013	0.020	0.025	0.022
Mg	1.370	1.149	1.078	1.111
Ca	0.051	0.054	0.075	0.059
Na	0.003	0.001	0.007	.....
K	.....	.....	.....	.....
$Fe^{+++}/Fe^{++}+Fe^{+++}$	0.060	0.039	0.032	0.048
Ca	2.6	2.8	3.8	2.9
Mg	70.2	58.6	55.1	55.5
$Fe^{++}+Fe^{+++}+Mn$	27.2	38.6	41.1	41.6
Ga	7	9	18	.....
Cr	630	1,000	465	.....
Ni	400	100	70	.....
Co	100	100	100	.....
V	125	500	630	.....
Zr	45	56	100	.....
Sc	.....	46	85	.....
Y	.....	22	26	.....
Sr	.....	.....	.....	.....
Pb	.....	.....	.....	.....
Ba	.....	.....	.....	.....

* Specimen 90703, rock analysis I, Pol Cornick.
† Specimen 90702, rock analysis II, Pol Cornick.
‡ Specimen 90697, rock analysis III, Lawarnick Pit.
§ Specimen 90696, rock analysis IV, near Burnoon.
‖ Spectrographic comparison of Al contents of O_1, O_2 and O_3 suggests that Al_2O_3 of O_2 should be lower, about 0.60 per cent. Analyst: D. H. Green.

than for the two from the pyroxene granulites. All the hypersthenes are quite low in Al_2O_3, only O_1, with 2.09 per cent, approaching the recrystallized enstatites of the peridotite (Green, 1964). Calculation of the structural formulas on the basis of making the *Z*-group total to 2.000 requires that either Fe^{+++} or Ti^{++++} substitutes to a small degree for Si in O_3 and O_4.

Trace element data have been obtained for O_1, O_2, and O_3 from rocks < 1 inch, 1 foot, and 3 feet from peridotite contacts. Co remains constant in the three hypersthenes but Sc, Zr, Y, V, and Ga all increase distinctly, and Ni decreases with distance away from the peridotite contact. The same trends continue into the recrystallized enstatites of the periodotite. These trends illustrate the differences between the trace-element concentrations in orthopyroxenes derived from a "basaltic" rock and those recrystallizing from a peridotite and the tendency toward convergence at the contacts of the rock types.

B. AUGITE AND SALITE

The analyses, structural formulas, and trace-element data for four augites (C_1–C_4) coexisting with the four analyzed hypersthenes (O_1–O_4) and for two salites (C_5, C_6) from the brown-green and blue-green hornblende amphibolites, respectively, are given in table 3.

The augites show a variation in Mg content comparable with that of the hypersthenes. The Al_2O_3 content is higher than that of the coexisting hypersthene, although the ^{Z}Al substitution and Si deficiency may be very nearly equal in the two pyroxenes. There is no obvious difference between the total Al_2O_3 content of the salites and augites, and both the salites have quite a high ^{Z}Al content.

The Fe_2O_3 content [and $Fe^{+++}/(Fe^{++} + Fe^{+++})$ ratio] is low in the augites from the pyroxene granulites and in the magnesia-rich hornblende granulite from the peridotite contact. In contrast, these values are high in the other hornblende granulite augite (C_4) and particularly high in the two salites. There is a parallel variation in the coexisting hornblendes (p. 554) but it is not so marked in the whole-rock analyses (p. 549). TiO_2 is lowest in the salite (C_6) from the sphene-bearing assemblage and also low in the salite (C_5) from the brown-green hornblende amphibolite, although both these rocks have high TiO_2 contents. In the granulites TiO_2 is highest in C_3 (0.97 per cent), from the most TiO_2-rich of the granulite rock analyses, but is surprisingly lower than the TiO_2 in the coexisting hypersthene (1.14 per cent).

The main difference between the salites and augites is in the CaO content. This is clearly demonstrated in the structural formulas and in figure 2.

Trace-element data for some of the clinopyroxenes are given in table 3. There is no satisfactory evidence for significant differences between the trace-element contents of the salites and the augites, but the data are too meager for any real conclusion.

In figure 2 the augites and salites from the Lizard are compared with the clinopyroxenes from the Madras granulites (Howie, 1955) and with clinopyroxenes coexisting with brown-green hornblende (Shido, 1958, p. 187) and blue-green hornblende (Miyashiro, 1958, p. 256). Shido (1958, p. 187) has suggested that "the maximum value of (Mg + Fe^{++})/Ca ratio increases with increasing grade of metamorphism," and this is in harmony with the concept of greater solid solution of enstatite in diopside and vice versa at higher temperatures. Both the Lizard and Madras augites coexisting with orthopyroxene define smooth curves, the Lizard curve approaching Howie's curve at the iron-rich end but diverging away from it and approaching the igneous tholeiitic pyroxenes at the magnesian end. The two salites coexisting with brown-green hornblende have much lower Mg + ΣFe contents, and in the Lizard examples the salite with the brown-green hornblende has a higher Mg + ΣFe content than that with the blue-green hornblende—in harmony with Shido's and Miyashiro's results.

The changes in composition of the clinopyroxenes in the different assemblages of the

TABLE 3

ANALYSES, STRUCTURAL FORMULAS ON THE BASIS OF 6 OXYGEN AND TRACE-ELEMENT DATA FOR CLINOPYROXENES OF GRANULITES

	Weight of Sample for Analysis (Gm.)					
	0.8	0.6	1.0	0.3	0.4	1.0
	Analysis No.					
	C_1*	C_2†	C_3‡	C_4§	C_5‖	C_6#
SiO_2	52.73	52.00	51.33	51.51	50.37	51.46
Al_2O_3	2.56	1.99	1.98	2.48	2.51	1.89
TiO_2	0.29	0.62	0.97	0.46	0.44	0.23
Fe_2O_3	0.48	0.52	0.70	2.15	2.45	2.96
FeO	6.40	9.11	10.30	10.40	10.08	7.91
MnO	0.13	0.18	0.40	0.19	0.57	0.42
MgO	15.91	14.21	13.25	14.58	11.34	11.76
CaO	21.55	21.13	20.71	18.64	22.53	23.44
Na_2O	0.42	0.34	0.37	0.48	0.49	0.48
K_2O	0.01	0.00 tr.	0.01	0.00 tr.	0.00 tr.	0.04
H_2O-	0.04	0.00	0.01	0.00	0.00	.....
	100.52	100.10	100.03	100.89	100.78	100.59
Si	1.933 } 2.000	1.938 } 2.000	1.931 } 2.000	1.913 } 2.000	1.900 } 2.000	1.928 } 2.000
^{Z}Al	0.067 }	0.062 }	0.069 }	0.087 }	0.100 }	0.072 }
^{Y}Al	0.044	0.025	0.020	0.021	0.012	0.011
Ti	0.008	0.017	0.027	0.013	0.012	0.007
Fe^{+++}	0.013	0.015	0.020	0.060	0.068	0.083
Fe^{++}	0.197	0.284	0.323	0.323	0.318	0.248
Mn	0.002 } 2.010	0.006 } 2.005	0.014 } 1.986	0.006 } 2.006	0.018 } 2.014	0.013 } 1.997
Mg	0.869	0.789	0.721	0.807	0.639	0.657
Ca	0.847	0.844	0.834	0.742	0.912	0.941
Na	0.030	0.025	0.027	0.034	0.035	0.035
K	.....	.....	.....	.....	.....	0.002

* Specimen 90703, rock analysis I, Pol Cornick.
† Specimen 90702, rock analysis II, Pol Cornick.
‡ Specimen 90697, rock analysis III, Lawarnick Pit.
§ Specimen 90696, rock analysis IV, near Burnoon.
‖ Specimen 90695, rock analysis V, Predannack Head.
Specimen 90694, rock analysis VII, Kilcobben Point.
Analyst: D. H. Green.

TABLE 3—*Continued*

	Weight of Sample for Analysis (Gm.)					
	0.8	0.6	1.0	0.3	0.4	1.0
	Analysis No.					
	C_1*	C_2†	C_3†	C_4§	C_5‖	C_6#
$Fe^{+++}/Fe^{++}+Fe^{+++}$...	0.062	0.056	0.077	0.157	0.176	0.250
Ca	44.1	43.6	43.9	38.4	47.1	48.8
Mg	45.2	40.9	38.0	41.8	33.0	34.0
ΣFe+Mn	10.7	15.5	18.1	19.8	19.9	17.2
Ga	5		9		13	9
Cr	850		850		100	46
Li						
Ni	216		46		46	46
Co	46		46		46	100
V	380		1,000		330	224
Zr	28		220		70	45
Sc	85		260		85	180
Y	22		220		22	
Sr	22		5		10	22
Pb						
Ba	10				10	

Lizard basic rocks are thus shown to be closely similar to the changes in compositions of pyroxenes formed under different grades of regional metamorphism.

In table 4 the Fe^{++}/Mg ratios and the distribution coefficient K_{Fe} (Kretz, 1961; Bartholomé, 1961, defined by the relationship $(Fe^{++}/Mg)_{opx} = K_{Fe}(Fe^{++}/Mg)_{cpx}$, are calculated for the coexisting orthopyroxene and clinopyroxene pairs.

be no consistent reason for the different values of table 4. The highest value (1.76) is from the hornblende granulite, possibly a lower-temperature assemblage but occurring very close to the roof of the peridotite and surrounded by peridotite outcrop. The other high value (1.71) is from a more magnesian pyroxene granulite at 1 foot from a peridotite contact, while the lowest value (1.57) is from a much more magnesian *hornblende*

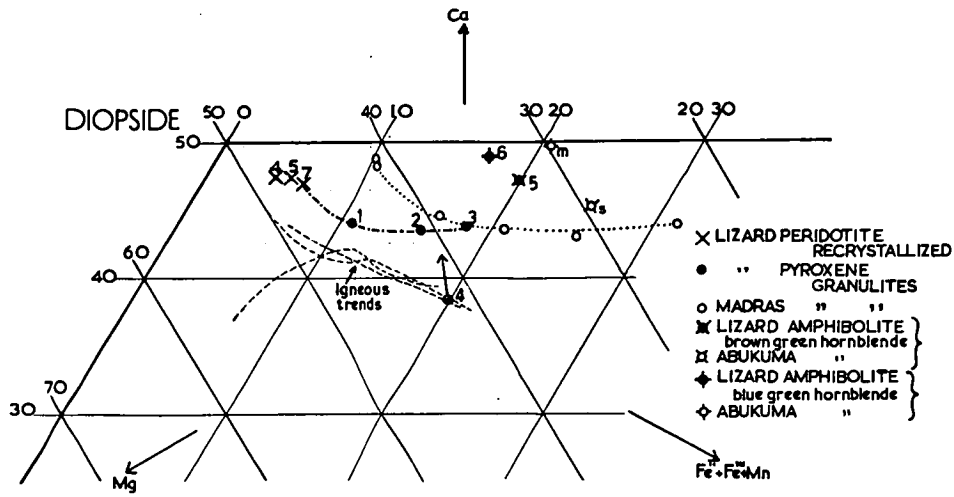

FIG. 2.—Ca-Mg-ΣFe plot for metamorphic clinopyroxenes from the Lizard and comparable localities

TABLE 4

DISTRIBUTION COEFFICIENTS OF METAMORPHIC PYROXENE PAIRS

	C1-01	C2-02	C3-03	C4-04
$(Fe^{++}/Mg)_{cpx}$....	0.226	0.360	0.448	0.400
$(Fe^{++}/Mg)_{opx}$....	0.355	0.615	0.710	0.703
K_{Fe}.....	1.57	1.71	1.59	1.76

Two of the values (1.71 and 1.76) for the distribution coefficients are close to those regarded by Kretz (1961) and Bartholomé (1961) as typical of metamorphic assemblages. Two other results (1.57 and 1.59) are between the typical igneous values (around 1.4) and typical metamorphic values (1.8). All the values are appreciably higher than the K_{Fe} values from within the peridotite (1.3–1.4) (Green, 1964). There appears to

granulite in contact with peridotite. The other low value (1.59) is from a granulite sheet within the peridotite.

If the hypothesis that K_{Fe} is predominantly a temperature-dependent coefficient is accepted as approximately valid, then the Lizard results would be interpreted as indicating temperatures of crystallization of the granulites between the temperatures of regional metamorphic basic granulites (possibly 700°–800° C.) yielding $K_{Fe} \simeq 1.8$ and the temperatures of basic igneous rocks (possibly near 1,000° C.) yielding $K_{Fe} \simeq 1.4$. Since the granulite assemblages are of such local occurrence and are developed in a dynamothermal aureole, temperature gradients are likely to have been steep with resultant variation in K_{Fe} over short distances. The results are at least consistent in that the lowest value (1.31) of K_{Fe} from the Liz-

ard rocks is within the peridotite, the body regarded as the cause of the metamorphism.

C. AMPHIBOLES

The chemical analyses, trace-element data, and structural formulas for two brown hornblendes (A_3 and A_4), a brown-green hornblende (A_5) and a blue-green hornblende (A_6) are given in table 5. The hornblendes were all separated from analyzed rocks except the hornblende A_7, analyzed by Butler (1953) and collected from the same quarry as the analyzed hornblende schist (Flett and Hill, 1912). This hornblende is blue-green (parallel to *Z*) and coexists with diopside, plagioclase (Ab_{40} An_{60}), epidote, and sphene so that it belongs to the "blue-green hornblende assemblage."

Because of uncertainty that the whole of the water content of the amphiboles is removed by the Penfield method of water determination, and since F or Cl was not determined on these amphiboles, the structural formulas are calculated anhydrous on the basis of 23 oxygens. There is a decrease in Mg/Fe^{++} and $Mg/(Mg + \Sigma Fe + Mn)$ ratios from A_3 to A_6, paralleling the changes in the rocks; and only in the most magnesian (analyses I and A_3) is the amphibole more iron-rich than the whole rock. The amphibole A_7 is more magnesian than both A_6 and A_5, illustrating that the color change in the amphiboles is not due to the magnesia content. TiO_2, Al_2O_3, Na_2O, and K_2O show no obvious pattern of variation but the Fe^{+++} content and $Fe^{+++}/(Fe^{++} + Fe^{+++})$ ratio increases from the brown hornblendes, through the green-brown hornblende to the blue-green hornblendes. This is also true of the MnO content. The structural formulas show that the *XY* group total decreases in the same direction, A_3 to A_6; but A_7 shows a reversal of this trend, suggesting possibly that this feature may be related to the Mg content of the amphiboles. In the trace elements Cr and Ni decrease and Ga increases in going from A_3 to A_6; this parallels the trends for the whole-rock analyses for Cr and Ni but not for Ga, which remains very constant.

As the hornblendes form a complex solid-solution series based on alternative substitutions in the basic tremolite structure (Sundius, 1946; Shido, 1958), the structural formulas were calculated in the manner suggested by Shido (1958, p. 178–179) to give the relative proportions of theoretical amphibole end members. The results of these calculations are given in table 6, where they are compared with the two analyzed pargasites from the peridotite (Green, 1964). This type of comparison brings out much greater differences between the amphiboles than would be suspected from the analyses alone. The analyses which have an *XY* group total of less than five imply the possibility of Ca substituting for Mg, that is, a "calcium-cummingtonite" substitution (cf. Shido and Miyashiro 1959, p. 98).

From table 6 the following differences between A_3, A_4, A_5, and A_6 are apparent.

1. The edenite substitution increases, the soda-tremolite substitution decreases, and the glaucophane substitution disappears in the series from blue-green through brown-green to brown hornblendes.

2. The tschermackite substitution, particularly the tschermackite + titano-amphibole substitution, decreases in the series A_6 to A_3, that is, blue-green to brown hornblende.

3. Cummingtonite solid solution is present in the brown hornblende, but theoretical Ca-cummingtonite is present in the brown-green, and particularly the blue-green, hornblende.

A comparison with the pargasites from the peridotite (A_1 and A_2) shows that these continue the trends defined and are similar to the brown hornblendes in the substitutions present, in spite of the different rock compositions. The blue-green hornblende A_7 (analyzed by Butler [1953]) does not conform with the pattern defined but is nearer to the brown hornblende (A_4) than to the blue-green hornblende (A_6) in the character of its substitution. This raises the question of whether the control on the type of substitution is chemical rather than physical environment, since A_7 is nearer to A_4 than

TABLE 5

ANALYSES, STRUCTURAL FORMULAS, AND TRACE-ELEMENT DATA ON AMPHIBOLES

	A₃*	A₄†	A₅‡	A₆§	A₇‖
SiO_2	44.90	46.06	43.46	44.77	45.97
Al_2O_3	11.30	9.14	9.55	11.07	9.01
TiO_2	2.53	1.91	3.24	1.41	0.87
Fe_2O_3	1.57	2.65	3.50	4.81	3.42
FeO	9.00	12.38	14.53	14.17	12.67
MnO	0.13	0.05	0.20	0.37	0.65
MgO	15.22	12.81	10.23	8.43	12.10
CaO	11.49	11.75	11.52	11.26	12.22
Na_2O	1.89	1.73	1.99	1.57	1.12
K_2O	0.43	0.23	0.22	0.37	0.05
H_2O+	1.50	1.76	1.63	1.54	1.78
H_2O-	0.03	0.00	0.02	0.00	0.09
P_2O_5	0.06	0.06	0.07	0.08	.....
					F 0.03
	100.05	100.53	100.16	99.85	99.95
Si	6.451	6.699	6.462	6.634	6.758
ᶻAl	1.549 } 8.000	1.301 } 8.000	1.538 } 8.000	1.366 } 8.000	1.242 } 8.000
ʸAl	0.366	0.271	0.137	0.568	0.322
Ti	0.276	0.210	0.363	0.157	0.097
Fe^{+++}	0.172 } 5.160	0.288 } 5.062	0.391 } 4.990	0.536 } 4.925	0.380 } 5.084
Fe^{++}	1.078	1.507	1.807	1.756	1.555
Mn	0.017	0.009	0.025	0.046	.080
Mg	3.251	2.777	2.267	1.862	2.650
Ca	1.768	1.834	1.835	1.788	1.926
Na	0.517 } 2.371	0.489 } 2.367	0.574 } 2.450	0.451 } 2.310	0.318 } 2.253
K	0.086	0.044	0.041	0.071	0.009
(OH)#	(1.449)	(1.722)	(1.627)	(1.530)	(1.758)
Mg/Fe^{++}	3.02	1.84	1.26	1.06	1.71
Mg×100/ Mg+Fe+Mn	71.9	60.5	50.5	44.3	56.8
$Fe^{+++}/Fe^{++}+Fe^{+++}$	0.14	0.16	0.18	0.23	0.20
Ga	9	13	18	18	50
Cr	1,250	250	220	46	500
Li	.....	.....	.....	3	.....
Ni	220	56	46	32	100
Co	46	46	46	46	70
V	425	250	380	380	200
Zr	45	45	56	45	20
Sc	56	46	46	46	.....
Y	46	46	46	22	.....
Sr	27	22	22	22	.....
Pb	10	10	.....	.....	.....
Ba	56	18	10	45	.....

* Specimen 90703, rock analysis I, Pol Cornick.

† Specimen 90696, rock analysis IV, Burnoon.

‡ Specimen 90695, rock analysis V, Predannack Head.

§ Specimen 90693, rock analysis VI, Pencra Head.

‖ Specimen from Butler (1953), analysis of similar rock VIII, Lower Relowas Quarry. Analysis and trace elements from Butler 1953.

(OH) content in structural formulas calculated on the basis of 24(O, OH) illustrating the deficiency in water in the results, compared with the ideal composition.

A_6 in its Mg/Fe^{++} and $Mg/(Mg + Mn + \Sigma Fe)$ ratios; and the sequence of changes outlined above is also the sequence of Mg/Fe^{++} values.

Shido (1958), Miyashiro (1958), and Shido and Miyashiro (1959) have used the color of the hornblende present in metamorphosed basic rocks as a zone indicator in a regional metamorphic terrain of the Abukuma Plateau and have compared their results with similarly varying amphiboles from the Grampian Highlands of Scotland. lands and Abukuma Plateau (Shido, 1958; Shido and Miyashiro, 1959. There is no clear separation into different fields but only a very generalized tendency for the hornblendes of granulites to have high edenite contents with low tschermackite contents, and for blue-green hornblendes to have low edenite contents or to contain the glaucophane molecule with moderate or high content of tschermackite molecule. The same very general separation is shown by plotting $^{Y}Al + Fe^{+++}$ against $Na + K$ (cf. Shido

TABLE 6

PROPORTIONS OF THEORETICAL AMPHIBOLE END MEMBERS IN ANALYZED AMPHIBOLES FROM THE LIZARD

Symbol†	Peridotite Amphiboles		Ideal Pargasite	Ideal Edenite	Amphiboles from Peridotite Aureole				
	A_1	A_2			A_3	A_4	A_5	A_6	A_7
Tiam	0.184	0.182	.....	.....	0.552	0.420	0.726	0.314	0.194
Cum	0.580	0.648	.....	.....	0.640	0.248	.....	.....	0.336
Ca-Cum	.....	.....	.....	.....	.....	.....	0.016	0.120	.....
Ce*	0.020	.....	.....	.....	.....	.....	.....	.....	0.020
St*	.....	0.016	.....	.....	0.288	0.416	0.700	0.940	.....
Ed*	0.554	0.719	1.000	1.000	0.459	0.325	0.265	.....	0.327
Gl	.....	.....	.....	.....	.....	.....	.....	0.208	.....
Ts*	1.250	1.360	1.600	.....	0.861	0.890	0.862	1.682	1.122
Tr	5.402	5.072	5.400	7.000	5.200	5.700	5.428	4.740	6.000
Total	7.990	7.997	8.000	8.000	8.000	7.999	7.997	7.995	7.999

† Symbols for theoretical end members of the substitutions are those used by Shido (1958) and are as follows: Tiam, $Ca_2Mg\ Ti_4Al_8O_{22}(OH)_2$; Cum, $Mg_2Mg_5Si_8O_{22}(OH)_2$; Ca-Cum, $Ca_2Ca_5Si_8O_{22}(OH)_2$; Ce*, $Ca_4Ca_2Mg_5Al_8O_{22}(OH)_2$; St*, $Na_2Na_2Mg_5Si_8O_{22}(OH)_2$; Ed*, $NaCa_2Mg_5Al_8O_{22}(OH)_2$; Gl, $Na_2Mg_3Al_2Si_8O_{22}(OH)_2$; Ts*, $Ca_2Al_8Al_8Si_8O_{22}(OH)_2$; Tr, $Ca_2Mg_5Si_8O_{22}(OH)_2$.

The characteristic colors of hornblende used correspond with the three assemblages with hornblende defined at the Lizard, with the addition of a lower-grade zone characterized by actinolite in the Abukuma rocks. The incoming of hypersthene characterizes the highest grade Abukuma assemblage (zone D) while brown hornblende, without hypersthene, characterizes the upper part of zone C, typically of brown-green hornblende. One difference from the Lizard sequence is the persistence of sphene in the brown-green hornblende assemblage.

The Lizard hornblendes were compared in the character of their substitutions with hornblendes from hypersthene granulites (Howie, 1955) and from the Grampian High-

1958, p. 182) for the same group of amphiboles, also indicating the greater substitution of $Na + K$ (in edenite and soda-tremolite molecules) relative to tschermackite substitution in the brown and green-brown amphiboles.

To summarize, the analyzed hornblendes from the Lizard rocks show differences in composition and in the degree of solid solution of amphibole end members which justify the use of the color of the amphibole as a significant factor in the classification of these Lizard rocks. Further, these differences are similar to those between the hornblendes of hypersthene granulites of Madras and different zones of regional metamorphic gradients in the Grampian Highlands, Scot-

land, and in the Abukuma Plateau, Japan. It is considered that the variations in the composition of the hornblendes indicate the presence of a metamorphic gradient in the Lizard rocks.

CONCLUSION

A. FACIES CLASSIFICATION OF THE LIZARD ROCKS

In figure 3 the four different Lizard assemblages are compared with characteristic phase assemblages in basic rocks of the almandine-amphibolite facies and the granulite facies[3] (Turner and Verhoogen, 1960). This comparison again leads to the conclusion that the variation in mineralogy of the Lizard rocks must be interpreted in terms of a metamorphic gradient.

The comparison above is with typical regional metamorphic assemblages and not with assemblages of contact metamorphism. The blue-green hornblende assemblage is the characteristic assemblage over a wide area of the Landewednack Hornblende Schist and is a typical assemblage of the almandine-amphibolite facies of regional metamorphism. In particular the association of epidote, a calcic plagioclase, salite, and hornblende is inconsistent with either the albite + epidote hornfels or the hornblende hornfels facies. Similarly the high-grade assemblage with hornblende + hypersthene + augite is characteristically absent from either the hornblende hornfels or pyroxene hornfels facies but typically occurs in the hornblende granulite subfacies of regional metamorphism. The brown-green hornblende assemblage and the pyroxene-granulite assemblage (with the rare occurrence of olivine in the latter) are consistent with either the facies of contact metamorphism or of regional metamorphism.

[3] In using the standard ACF diagrams to correlate the varying mineralogy with metamorphic facies, it is recognized that the diagrams have illustrative value but take no account of variations in bulk composition such as oxidation ratio, Mg/(Mg+Fe) ratio, TiO_2 content, etc. In the author's view these variations are small and can in no way be matched with variation in mineralogy (cf. p. 549).

Another factor which has weighed against the use of the term "hornfels" for any of the Lizard rocks is the lack of hornfels textures in any of the assemblages. The textures are typically foliated and lepidoblastic or granoblastic with distribution of minerals in lenses. These textures imply that movement in the rock has occurred during recrystallization and that recrystallization has not merely been a temperature-induced effect in a static aureole.

Fyfe, Turner, and Verhoogen (1958) give estimates of the P_{H_2O}, T environments of different metamorphic facies and in their figure 108 show how such environments could be intersected in several examples of metamorphic gradients. The Lizard aureole is regarded as a thermal aureole at high but relatively constant pressure in which a regional stress field and relative movement between intrusion and enclosing country rocks have caused development of textures typically of dynamothermal character.

B. DISTRIBUTION OF THE METAMORPHIC ASSEMBLAGES

In figure 1 the distribution of the brown-green hornblende amphibolite, hornblende granulite, and pyroxene granulite is shown by stippling with large dots overprinting the fine-stippling pattern indicating the blue-green hornblende amphibolites.

Hypersthene granulites have been found in bodies of basic rocks surrounded by outcrops of peridotite (e.g., near Traboe Cross and north of Kynance Cove) and in areas immediately in complex contact with the peridotite—as around Pol Cornick, north of Mullion Cove, and at Porthkerris Quarry. The brown-hornblende–bearing rocks have been found in the above localities and also from immediately below the gently dipping peridotite contact near Cadgwith. In the latter area only one specimen of hypersthene + augite granulite, with pyroxenes partly replaced by brown hornblende, has been found. This occurred within 3 feet of the peridotite contact.

The green-brown hornblende assemblage is much more widespread than the higher-

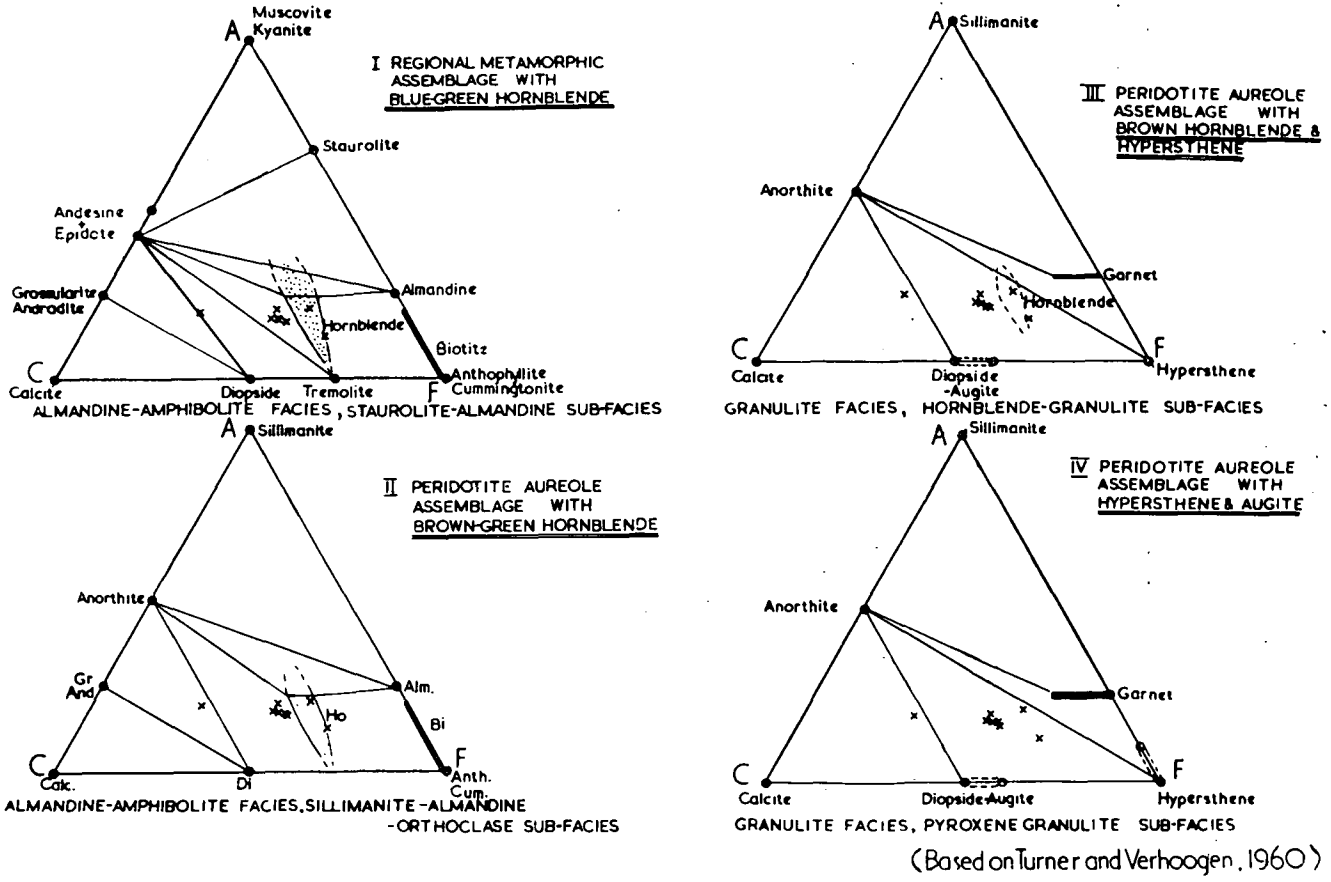

FIG. 3.—Correlation of the Lizard mineral assemblages and whole-rock compositions with those of standard metamorphic facies

grade assemblages and is particularly characteristic of a wide area between Predannack Head and Predannack Wollas. It is possible that there is peridotite at shallow depth in this area, and the same relationship is probably true of the area of vertically foliated hornblende schist north of Mullion Cove. In these western outcrops it is not possible to say how far from the peridotite contact the zone of brown-green hornblende extends, but it is probably around 500 feet. In the northeast part of the area, south of Porthkerris Quarry, the brown-green hornblende assemblage gives way to the blue-green hornblende assemblage at about 350 feet from the peridotite outcrops.

In the southeast, at Devil's Frying Pan near Cadgwith, the flat-lying Landewednack Hornblende Schist from 15 feet below the peridotite contains brown-green hornblende cores with blue-green hornblende rims. At 12 feet below the peridotite, blue-green hornblende is present only as thin rims to the brown-green hornblende. Sphene is still present as an accessory mineral. The transition from brown-green to blue-green hornblende assemblages takes place in a zone from 10 to 20 feet below the base of the peridotite along the southeastern flat-lying contact.

The distribution of the different metamorphic assemblages shown in the previous sections to be characteristic of different grades of metamorphism demonstrates that this metamorphic gradient must be related to the peridotite body. The evidence from detailed mineral chemistry, petrography, and field work is that the Lizard peridotite produced a metamorphic aureole of high-grade character superimposed during moderate-grade regional metamorphism.

C. MOBILIZATION OF GRANULITE IN THE METAMORPHIC AUREOLE

The regional metamorphic blue-green hornblende amphibolite typically has a strong subhorizontal foliation, paralleling the original bedding or flow surfaces, and a strong lineation defined by hornblende prisms. The lineation in most areas plunges N.NW. or S.SE. within the foliation plane and is considered to parallel the intermediate axis of the regional stress field. Within the recrystallized peridotite (Green, 1964) a strong foliation commonly is near vertical and strikes N.NW.–S.SE. This foliation in an intrusive mobile body is considered to define the "b"-"c" plane of the regional stress field, that is, the plane containing intermediate and minimum axes of stress. In the immediate aureole of the peridotite, the brown-green hornblende amphibolites and higher-grade assemblages may show the primary subhorizontal foliation thrown into fluid or rheid folds with subvertical axial planes striking N.NW.–S.SE. (e.g., near Porthkerris and near Mullion Cove) or simply a subvertical N.NW.–S.SE. foliation with gneissic banding but no clear folding. North of Predannack Head, between brown-green hornblende amphibolites to the south and blue-green hornblende amphibolites to the north, the foliation locally bends round from the subhorizontal to the subvertical attitude; and in the intermediate zone are amphibolites of mylonitic texture.

The variation in foliation attitude in the aureole of the peridotite is directly attributed to the effect of elevated temperatures decreasing the rheidity of the amphibolites, leading to their flow in the b-c plane of the stress field. The same effect may be produced by drag of the aureole rocks by the intruding peridotite.

The complexity of the contact between peridotite and granulite at Pol Cornick and Parc Bean is shown in figure 4 (cf. Fox and Teall, 1889). The granulite and peridotite form a series of vertical or near-vertical sheets with either sharp or interbanded contracts, in which it is not possible to determine which rock type is the later, intrusive one. More rarely, the granulite shows injection or infolding of lobes into the peridotite. Careful examination also shows that the foliation of the peridotite may be cut across by foliated granulites, and planar sheets of periodotite between granulite may be cut by granulite "bridges." However, the presence of blocks of granulite (some rounded and

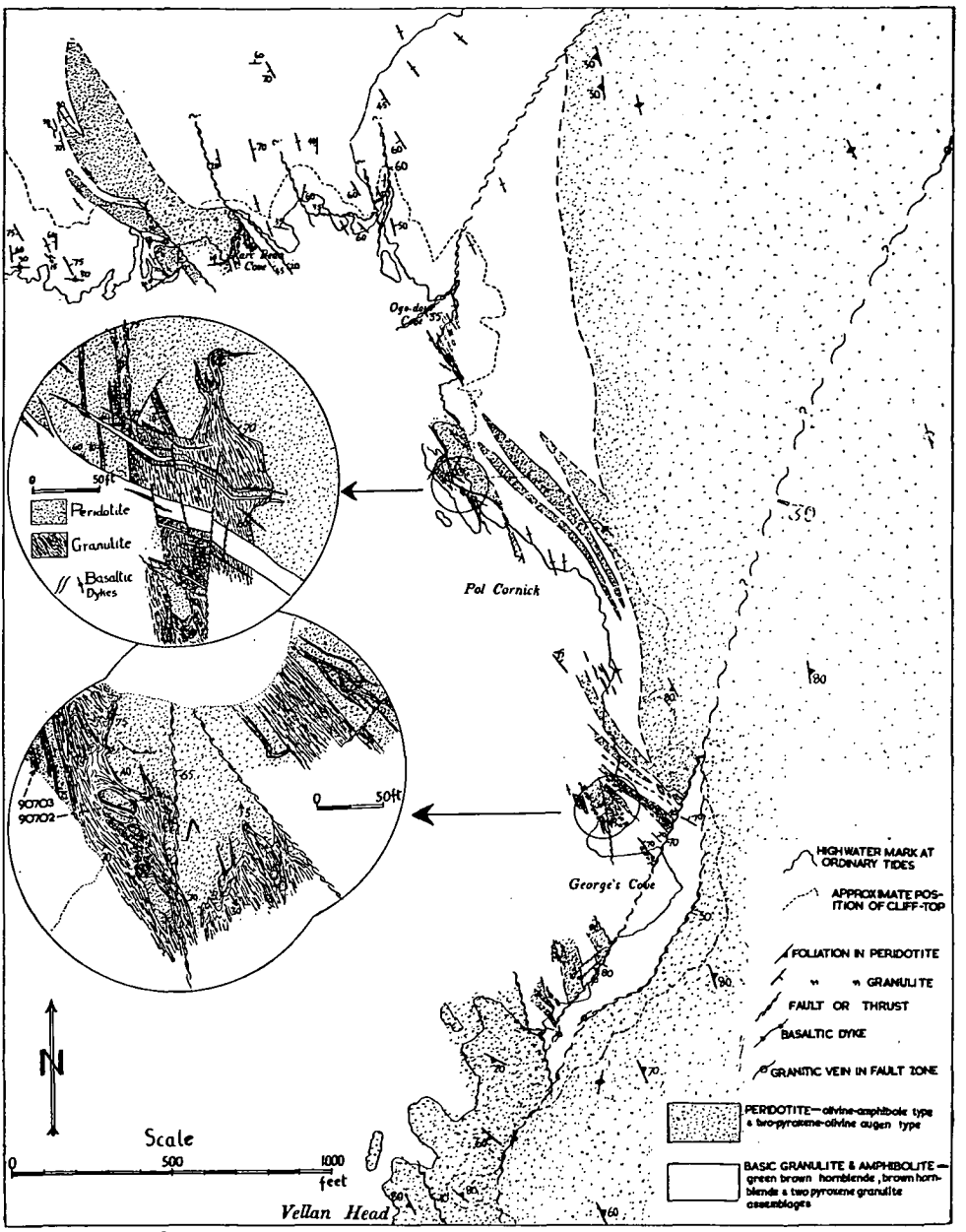

FIG. 4.—Contact area of peridotite and pyroxene and hornblende granulite showing mobilization of granulite, west coast of Lizard Peninsula, south of Predannack Head.

boudin-like, others appearing quite angular) entirely enclosed within granulite provides the clearest evidence for the mobility of the latter. Localities where these relationships are observed are shown in the insets of figure 4 and further occurrences are at Parc Bean Cove (fig. 4) and Lawarnick Pit, near Kynance Cove. The inclusions may be of fine-grained olivine + enstatite + diopside + yellow-brown spinel in the core, passing outward to olivine + pargasite + spinel assemblage, and then into typical hypersthene + augite + plagioclase granulite. In other cases, for example, at Parc Bean, the cores are of olivine + colorless pargasite + orange spinel with increasing amphibole content (and increasing brown color) toward the margin. These bodies are enclosed in pale-brown hornblendite and brown hornblende amphibolite.

The field and petrographic evidence is that the peridotite is the high-temperature body but that locally, in complex contact zones, the highly metamorphosed basic rocks become mobilized and capable of intruding and including blocks of the peridotite. In such cases there is also metasomatic reaction of the type previously discussed (p. 549) between the two rock types. In the immediate-contact zones of the peridotite and especially in any areas of country rock surrounded by peridotite, both peridotite and granulite would approach the same pressure-temperature conditions. If these temperatures are high, then the granulite, being of basaltic composition, is close to its melting range but the peridotite is not. The granulite could, under these conditions, be of lower rheidity than the peridotite and would behave as the more fluid material; inclusions within the peridotite would tend to flow out in sheets parallel to the foliation planes (Green, 1964, fig. 3); and in contact zones the granulite would be capable of intruding and fragmenting the peridotite.

The possibility that the peridotite has caused partial melting of the granulite must be considered. There are no typical igneous textures developed in the granulites, but small patches of coarser grain size or of hornblende-feldspar "pegmatite" occur locally, for example, south of Ogo Dour, and could indicate the former presence of a very local liquid phase. Partial melting cannot be ruled out, and this may be the factor determining the decreased rheidity of the granulite postulated above.

Returning to the discussion of the intrusion mechanism of the peridotite in a previous paper (Green 1964), it has been postulated there that the peridotite at a high temperature (say, 800°–1,000° C.), though crystalline, would have a lower rheidity than the surrounding regional metamorphic amphibolites at say 500°–600° C. However, locally adjacent to the peridotite, this rheidity difference is reversed when the country rocks approach the same temperature as the peridotite. This reversal of rheidity difference would have an important effect on preventing further intrusion of the peridotite.

In the intensity of metamorphism developed in the aureole and in the internal structures of the peridotite itself, the Lizard peridotite is very similar to the Tinaquillo peridotite in Venezuela (MacKenzie, 1960) and the Mount Albert peridotite in Quebec (Smith and MacGregor, 1960).

ACKNOWLEDGMENTS.—The research which forms the subject of this paper was carried out in the Department of Mineralogy and Petrology, Cambridge University. The restudy of the Lizard peridotite was suggested by Professor C. E. Tilley, and the author is grateful to Professor Tilley and to Dr. S. R. Nockolds for discussions, guidance, and criticism during the period of research. The author acknowledges the help and instruction of Mr. J. H. Scoon in the methods of chemical analysis and the courtesy of Dr. S. R. Nockolds and Mr. R. S. Allen in making trace-element measurements available.

Professor C. E. Tilley and Dr. K. S. Heier are thanked for the critical reading of the manuscript.

An award of the Royal Commission for the Exhibition of 1851 made possible the research at Cambridge, and this scholarship and the interest of the Commission are gratefully acknowledged.

REFERENCES CITED

BARTHOLOMÉ, P., 1961, Co-existing pyroxenes in igneous and metamorphic rocks: Geol. Mag., v. 98, p. 346–348.

BUTLER, J. R., 1953, Geochemistry and mineralogy of rock weathering; I. the Lizard area, Cornwall: Geochim. Cosmochim. Acta, v. 4, p. 157–179.

FLETT, J. S., and HILL, J. B., 1912, The geology of the Lizard and Meneage: Geol. Surv. Memoir to sheet 359. (Rev. ed., 1946, J. A. Flett.)

FOX, H., and TEALL, J. J. H., 1889, On the junction of hornblende schist and serpentine in the Ogo Dour district: Roy. Geol. Soc. Cornwall Trans., v. 11, p. 213.

FYFE, W. S., TURNER, F. J., and VERHOOGEN, J., 1958, Metamorphic reactions and metamorphic facies: Geol. Soc. America Memoir 73.

GREEN, D. H., 1964, The petrogenesis of the high-temperature peridotite intrusion in the Lizard area, Cornwall. Jour. Petrology, v. 5, p. 134–188.

HOWIE, R. A., 1955, The geochemistry of the charnockite series of Madras, India: Roy. Soc. Edinburgh Trans., v. 62, pt. 3, p. 725–768.

KRETZ, R., 1961, Some applications of thermodynamics to co-existing minerals of variable compositions. Examples: orthopyroxene-clinopyroxene and orthopyroxene-garnet: Jour. Geology, v. 69, p. 361–387.

MACKENZIE, D. B., 1960, High-temperature alpine-type peridotite from Venezuela: Geol. Soc. America Bull., v. 71, p. 303–318.

MIYASHIRO, A., 1958, Regional metamorphism of the Gosaisyo-Takanuki District in the central Abukuma Plateau: Jour. Fac. Science Univ. Tokyo, v. 11, p. 219–272.

NOCKOLDS, S. R., 1954, Average chemical compositions of some igneous rocks: Geol. Soc. America Bull., v. 65, p. 1007–1032.

SHIDO, F., 1958, Plutonic and metamorphic rocks of the Nakoso and Iritono districts in the central Abukuma Plateau: Jour. Fac. Science Univ. Tokyo, v. 11, p. 131–217.

——— and MIYASHIRO, A., 1959, Hornblendes of basic metamorphic rocks. Jour. Fac. Science Univ. Tokyo, v. 12, p. 85–102.

SMITH, C. H., and MACGREGOR, I. D., 1960, Ultrabasic intrusive conditions illustrated by the Mt. Albert Ultrabasic Pluton, Gaspé, Quebec (abs.): Geol. Soc. America Bull., v. 71, p. 1978.

SUNDIUS, N., 1946, The classification of the hornblendes and the solid solution relations in the amphibole group: Sveriges Geol. Undersokning Arsbök, v. 40, p. 1–36.

TURNER, F. J., and VERHOOGEN, J., 1960, Igneous and metamorphic petrology: 2d ed.: New York, McGraw-Hill Book Co.

A 7

A RE-STUDY AND RE-INTERPRETATION OF THE GEOLOGY OF THE LIZARD PENINSULA, CORNWALL.

D. H. GREEN

Reprinted from
Present Views on Some Aspects of the Geology of Cornwall and Devon.

Published for the 150th Anniversary of the Royal Geological Society of Cornwall
by Oscar Blackford Ltd., Truro, 1964.

A RE-STUDY AND RE-INTERPRETATION OF THE GEOLOGY OF THE LIZARD PENINSULA, CORNWALL

D. H. GREEN

CONTENTS

I. PREVIOUS RESEARCH

The early published investigations of the geology of the Lizard district have been reviewed in sequence by Flett and Hill in the 1912 Geological Survey Memoir and again in the second edition of the Memoir in 1946. The foundations of the understanding of the complex sequence at the Lizard were laid by de la Bêche of the Geological Survey in 1839. A period of controversy and great activity followed in 1880-1900 in which the names of Bonney, Fox and Teall stand out as tackling the broader and more fundamental problems of the area. In 1906-1910 Flett carried out his classic survey, building on the discoveries of his predecessors and correlating evidence to give the detailed and coherent account published in the 1912 Memoir. The quality of the Survey mapping can hardly be surpassed in detail, care and completeness of coverage. Re-mapping in 1959 was not a case of moving established boundaries but rather of re-interpreting in the context of present-day geology, the observable relationships in the coastal exposures, and careful examination of the relatively few outcrops and quarries in the inland areas.

In 1937 Tilley made a detailed study of mineral assemblages in the Old Lizard Head Series at Pistil Ogo and Polkernogo. Also in 1937 and 1939 Hendriks published papers on the structure and stratigraphy of Cornwall in which the broader relationships of the Lizard area and the Lizard-Dodman-Start boundary were discussed. In 1938-39 Scrivenor published a series of short notes on different aspects of the Lizard geology and followed this up in 1949 by a general paper on the Lizard-Start problem. In this paper he concluded that the Landewednack Hornblende Schists are in fact a 'primary' hornblende-plagioclase gneiss formed by consolidation, in a stress field, of an appropriate dioritic magma. Further he disputes Flett's distinction between the

Traboe and Landewednack Hornblende Schists and maintains that the Lizard Boundary is not a major thrust-zone but simply the northern limit of the 'serpentine' and 'hornblende-gneiss intrusions' and their metamorphic effects.

The second edition of the Memoir (1946) revised by Flett, shows very little difference in interpretation south of the Lizard Boundary. Controversy on the Lizard structure and sequence has continued since the publication of the second edition of the Memoir. As mentioned above, Scrivenor's (1949) paper is in sharp conflict with Flett on the major issues. On the other hand, Hendriks (1959), in a paper on the large-scale structures of Cornwall, supports the idea of a major thrust between the Lizard rocks and the Palaeozoic rocks to the north. From exposures in Gerrans Bay, Roseland, where sheared serpentinite occurs in a flat thrust below the Nare Head pillow lava, Hendriks regards the serpentinite as intrusive along the thrust plane and also into the base of the pillow lava itself. This concept is extended to the Lizard as a whole and the 'serpentine' regarded as intrusive during major nappe thrusting in latest Devonian or possibly early Carboniferous time.

The most clearly stated alternatives to Flett's views on the structure and genesis of the main rock types are those of Sanders (1955). Sanders carried out some detailed mapping on the south-eastern corner of the Lizard Peninsula and disputed three of Flett's main conclusions, namely :

(i) The 'serpentine' is a plug or dome-shaped mass intrusive into the mica and hornblende schists which surround it.

(ii) The gneisses at Kennack, and Erisey in the interior of the peninsula, are later intrusives that have risen through the 'serpentine'.

(iii) 'Serpentine' masses up to several acres in extent are included in these gneisses.

Sanders' own conclusions are that the 'serpentine' is a shallow thin sheet in this area, overlying the Landewednack Hornblende Schists and with its base at around the 180-200 ft. level. He regards the intimate mixing of serpentinite, acid gneiss and amphibolite in the Kennack area and south therefrom as a tectonic mixing and the mixed acid-basic gneisses of Kennack, Erisey, Poltesco and Pen Voose as merely the locally migmatized equivalent of the underlying Landewednack Hornblende Schist. Sanders concludes that the Lizard serpentinized peridotite is an intrusive on the thrust plane between the Landewednack Hornblende Schists and an unidentified over-riding block.

The relevant evidence on these conflicting points of view will be discussed in later sections.

II. ROCK SEQUENCE AND RELATIONSHIPS

The rock units and rock types of the Lizard area as defined and used in the 1946 Geological Survey Memoir were found to be identifiable and mappable in the field and the nomenclature used by Flett is generally adhered to. The sequence of rock units in order of increasing age is

f. Palaeozoic, post-metamorphic rocks.
e. Kennack gneiss and microgranite.
d. Basaltic dykes and sills.
c. Gabbro and troctolite.
b. Peridotite.
a $\{a_1$. Old Lizard Head Series.
a_2. Hornblende Schists of Landewednack and Traboe type.

The lithological map (Pl. 1) and locality map (Pl. 2) should be referred to in the following sections.

a_1. The Old Lizard Head Series.

The Old Lizard Head Series is a sequence of dominantly pelitic, thin-bedded rocks which are interbedded with the Landewednack Hornblende Schists. They are typically exposed from Polpeor to Caerthillian Cove and in this south-western corner of the area are considered to underlie the Landewednack Hornblende Schists.

The most common rock type is a quartz + feldspar + muscovite + biotite (or chlorite replacing biotite) schist and garnet-bearing assemblages are not uncommon. Hornblende or actinolite is present in some horizons and there are assemblages transitional to the hornblende + plagioclase assemblage of the Landewednack Hornblende Schist. Tilley (1937) has described in detail the cordierite-bearing assemblages from both south and north of the peridotite body and has drawn attention to the variety of assemblages present, the occurrences of kyanite and sillimanite together near Polkernogo and the occurrence of andalusite south of the peridotite at Pistil Ogo.

Tilley concluded that the rocks were a series of lavas, tuffs, quartzose and pelitic sediments which were folded at a high temperature, undergoing both thermal and dynamic metamorphism.

Tectonically the Old Lizard Head Series is characterized by a sub-horizontal metamorphic foliation parallel to the primary bedding. There is a 'b'-lineation due to mineral and fold-axis orientation on this plane ; the folds are commonly recumbent and plunge in directions from 110° to 160° E. of N. The folding is generally incompetent with fold plunges in a very small area varying from 0°-90° in dip and similarly variable in bearing. In these features the rocks contrast with the regularity of foliation and lineation in the Landewednack Hornblende Schists.

The mineral assemblages of the Old Lizard Head Series are some indication of the complex interplay of thermal and dynamothermal metamorphism that typifies the Lizard. The occurrences of andalusite, cordierite and anthophyllite are suggestive of contact metamorphism in the hornblende-hornfels facies (Fyfe *et al.* 1958, pp.205-211). On the other hand the presence of staurolite, kyanite + sillimanite, almandine and epidote in various assemblages is more indicative of regional metamorphism in the almandine-amphibolite facies (Fyfe *et al.* 1958, p.228). The textures of the rocks are strongly lepidoblastic or granoblastic, with 'eyes' of andalusite or cordierite and elongate amphiboles or biotite, and are of typical dynamothermal character.

a_2. The Hornblende Schists

The Landewednack Hornblende Schists — The hornblende schists of Landewednack type are a monotonous series, at least 250 feet thick, of hornblende + plagioclase amphibolites. They have an extremely regular flat foliation with a pronounced mineral lineation produced by parallelism of hornblende prisms.

The rocks are characterized by medium-grained lepidoblastic texture with subhedral blue-green hornblende prisms ; anhedral, commonly untwinned plagioclase and accessory sphene and magnetite. More calcic bands are common, particularly bands rich in salite and with epidote and less commonly with grossular. Epidote is common and varies from a minor constituent to areas with abundant bands, lenses and even veinlets of epidosite (e.g. Pen Olver). Its distribution probably reflects original calcic bands but also locally either introduction or redistribution of calcic solutions.

In the field the diagnostic features of these rocks are first the dominance of hornblende over other phases and secondly the horizontal foliation and pronounced 'b' lineation, distinguishing the Landewednack type from the Traboe type of hornblende schist. The lineation is due to parallelism of hornblende prisms and to elongation of the feldspar-rich and hornblende-rich lenses in a parallel direction. To a lesser degree it is the axis direction of minor, usually recumbent, folds within the hornblende schists. Such folding is not as common as, but is of a similar style to, that occurring in the Old Lizard Head Series.

The Landewednack Hornblende Schists are intruded by the peridotite, basaltic dykes and Kennack Gneiss. In the south-eastern part of the Peninsula the Landewednack Hornblende Schists are overlain and metamorphosed by the peridotite. *Similarly other contacts with the peridotite are either later fault contacts or contacts showing high grade dynamothermal metamorphism to yield the amphibolite and granulite assemblages called Traboe Hornblende Schist.* (Green 1964a, b).

Field and petrographic data indicate that the Landewednack Hornblende Schists are a metamorphic suite of almandine amphibolite facies, staurolite-almandine sub-facies, derived by regional metamorphism in a stress field with maximum compression directed E.N.E.—W.S.W., normal to the 'b' lineation. From chemical data, (Green 1964b) the pre-metamorphic rocks were a series of basalt lavas and/or sills with some dykes, tuffs and calcareous sediments. There is no evidence of a regional metamorphic gradient in the area in addition to the dynamothermal gradient due to the peridotite ; the exposures in the east, north, west, south and south-east all have assemblages of the same metamorphic grade.

The Traboe Hornblende Schists — Flett (1912, 1946) gave the name Traboe Hornblende Schist to " a grey, feldspathic, non-epidotic and more coarsely crystalline hornblende schist . . . especially common in the district around Traboe and Polkerth. The foliation of these rocks is rough and irregular as contrasted with the flat parallel foliation of the epidotic hornblende schists, and coarse feldspathic veins and lenticles are often to be remarked in it ". Flett also draws attention to the fact that the foliation in the Traboe Hornblende Schist is consistently near-vertical and strikes approximately north-south.

Flett regarded the Traboe Hornblende Schists as intrusive rocks, forming a group of basic injections that immediately preceded the intrusion of the peridotite. He draws attention to the differing mineralogy of the two groups of hornblende schist, particularly to the lack of epidote and garnet, the presence of an augitic rather than a diopsidic pyroxene and the presence in some areas of brown hornblende in the Traboe Hornblende Schists.

The criteria that Flett used to define the Traboe Hornblende Schist are observable and valid ones and can be used to map the distribution of the types of hornblende schist. In the present examination of the Lizard area, careful examination of exposures near Mullion, Ryniau, Kilcobben Point, Devil's Frying Pan, Kildown Point, and particularly around Porthallow and Porthkerris, shows that the Landewednack Hornblende Schist passes transitionally into the Traboe Hornblende Schist. Chemical analyses show that the two rock groups have extremely similar compositions while detailed petrography and mineralogy (Green 1964b) lead to the conclusion that the Traboe Hornblende Schists are almandine amphibolite and granulites facies derivatives of the Landewednack Hornblende Schists. The agent of the dynamothermal metamorphism is the Lizard peridotite.

Near Porthkerris there is a structural and metamorphic transition between hornblende schists of the two types. As the peridotite bodies in the area are approached from south of Porthkerris there is a development of the 'Traboe character' of fluid folding on sub-vertical axial planes striking N.N.W.—S.S.E. or north-south. The pre-metamorphic and sub-horizontal foliation of Landewednack type becomes folded and, in more homogeneous horizons, completely overprinted by the sub-vertical, more irregular Traboe type of foliation. The two metamorphic foliations are consistently explained as forming in the same stress field in rocks of different rheidities[1]. The Landewednack Hornblende Schists are considered to possess a 'b' lineation in a pre-metamorphic S-plane (primary bedding) and the Traboe Hornblende Schists are considered to have a b-c axial plane foliation developed in rocks where the controlling effect of pre-metamorphic foliation was inoperative due to decreased rheidity resulting from higher temperature or varying composition. This effect is well illustrated in several localities where there are foliation 'unconformities'

[1]The rheidity (Carey 1954) of a substance is defined as the time required for the viscous term in the empirical strain equation

$$S = \frac{P}{\eta} + f(P) + \beta t^{\frac{1}{3}} + \frac{Pt}{\mu}$$

(Total Strain = Elastic + plastic + transient + viscous strain)

to become one thousand times as great as the elastic term. It is equal to $\eta/\mu \times 10^3$ seconds where η is a pseudo-viscosity for crystalline materials and μ is the rigidity of the material. The concept of rheidity is particularly necessary in deformation studies in geology since it stresses the importance of the time factor in determining the character, extent and type of deformation. Although numerical values for rheidity can rarely be ascribed to rocks the results of differing rheidities in rocks of different composition are evident in metamorphic and sedimentary terrains (e.g. Carey 1954), the classical examples being the low rheidity and thus fluid behaviour of marble relative to quartzites or gneissic rocks.

in which more massive bands in the Landewednack Hornblende Schists have subvertical foliation of the Traboe type.

The best exposures of the Traboe Hornblende Schist are those around Predannack Wollas and Predannack Head. These are characteristically of the assemblage brown-green hornblende + plagioclase + salite + opaque minerals and with proximity to the peridotite these pass into assemblages characterized by brown hornblende + augite, brown hornblende + augite + hypersthene and augite + hypersthene. Other exposures of the Traboe Hornblende Schists occur north of Kynance Cove, between Mullion Cove and Polurrian Cove, near Meaver and Tresprisson, near Tregadra, Trezise, Traboe, Rosuic, Kernewas, Porthkerris and Porthallow and in a very thin zone below the peridotite contact at Carn Barrow, Devil's Frying Pan and Kildown Point.

It is considered that all the exposures of Traboe Hornblende Schist are to be interpreted as developed in the dynamothermal aureole of the peridotite, acting on the moderate grade regional metamorphic assemblage of the Landewednack Hornblende Schist. There is no evidence that supports Flett's interpretation of these rocks as basic injections related to and immediately preceding the peridotite intrusion.

b. The Lizard Peridotite

The Lizard peridotite has an area of about 20 square miles and consists of one major and several minor bodies, obviously genetically related but of no provable physical connection. Primary mineral assemblages in the peridotite consist of olivine, orthopyroxene, clinopyroxene and spinel; aluminous amphibole and plagioclase are of secondary development in areas of high temperature recrystallization. Serpentinization is general throughout the whole peridotite but quite commonly does not affect more than 50% of the primary phases. The serpentine minerals are of the mesh-texture + bastite + cross-fibre chrysotile group and antigorite in its typical flare texture is not a common constituent. Chlorite and fibrous tremolite are common constituents; the spinel shows a sequence of breakdown reactions to give relict magnetite surrounded by chlorite and other minerals, and plagioclase is almost invariably saussuritized and secondarily altered.

Flett (1912, 1946) regarded the peridotite as a zoned intrusion of three serpentine 'magmas': an outer 'dunite serpentine', a median 'tremolite serpentine' and a central core of 'bastite serpentine'. The present investigation has shown that in reality Flett's classification roughly reflects a zoning in grain size and degree of mylonitization but in part the over-printing effects of serpentinization enter into it. It has been found practicable to classify and map the peridotite on the basis of a division into one primary and two recrystallized mineral assemblages, (Green 1964a). The *primary assemblage*, forming the core of the peridotite, consists of olivine, aluminous enstatite, aluminous and chromium-bearing clinopyroxene and olive green spinel in coarse anhedral texture. By increasing granulation of the olivine and bending and recrystallization of the pyroxene this assemblage passes into the typical *recrystallized anhydrous assemblage* of olivine, enstatite, chromium-bearing clinopyroxene, plagioclase and spinel in granoblastic texture with prominent augen of primary pyroxene

and lenticular porphyroblasts of spinel. The recrystallized anhydrous assemblage may contain orange-brown or pale brown hornblende as a minor accessory, usually replacing clinopyroxene. With increasing water content this passes into the *recrystallized hydrous assemblages* of olivine, pargasite and spinel.

c. Gabbro

Medium and coarse grained gabbro occupies a large part of the Lizard area in the neighbourhood of St. Keverne and its well exposed on the coast and in quarries at Porthoustock. Apart from this area the gabbro occurs in a large number of small dykes in the shore between Coverack and Kennack Sands and in the cliffs from Carn Barrow to Landewednack Church Cove. Inland, outcrops of gabbro occur east of Trenoon, west of Kingey, east of Treveddon, north of Worvas and at Ruan Minor and St. Ruan.

Near Coverack there are small dykes and intrusions of troctolite which are slightly earlier than the gabbro. The gabbro itself ranges from olivine-rich types to clinopyroxene + plagioclase rocks and is commonly strongly secondarily altered. The development of augen, flaser and schlieren gabbros in the small dykes has evoked a classical interpretation[1] of movement of the dyke walls while crystallization of the magma was in progress. The gabbro dykes at Lankidden Point near Carrick Luz show on their western margin a remarkable degree of foliation and high temperature granulation of the primary phases.

The general form of the main gabbro body suggests part of a ring intrusion with the peridotite of the Black Head area (primary assemblage) occupying the core of the ring. The outermost contact of the gabbro striking westwards from Porthoustock is a major curving fault, probably with the north side down-thrown. In a similar way the gabbro abruptly cuts off the marginal, recrystallized phase of the peridotite striking south-east from Traboe, for on strike from this within the gabbro ring, the peridotite has a very different mineral assemblage and direction of foliation. It is likely that across the rather narrow thickness of gabbro at Lankidden there is considerable differential movement and this has resulted in the spectacular development of augen gabbros in this locality.

The gabbro is a late-kinematic or post-kinematic intrusion unaffected by the regional metamorphism and not greatly affected by the regional stress field operative during the emplacement of the peridotite. Augen foliation and schistose structure in the gabbro is due to autometamorphism induced by movement of dyke walls as crystallization and cooling proceeded. The gabbro is very variable in both primary features (grain size, texture and composition) and in secondary features and warrants further detailed study.

d. Basaltic Dykes

Dykes and sills of porphyritic basalt occur commonly on the east coast of the Lizard from Porthoustock to Landewednack Church Cove and less commonly in the

[1] Flett, 1912, pp. 92-99.

peridotite and Traboe Hornblende Schist on the west coast. The least altered of the dykes are porphyritic, commonly with feldspar phenocrysts, less commonly with olivine and pyroxene pseudomorphs set in fine-grained secondary aggregates retaining relict basaltic texture. The dykes are in some cases foliated, the foliation being parallel to the dyke walls, and show mineralogical variation from actinolite-chlorite schists to green-hornblende, plagioclase, sphene amphibolites. The intrusions commonly have fine-grained, chilled contacts against peridotite, gabbro or the Traboe Hornblende Schist.

The dykes intruding the gabbro near Porthoustock form a prominent N.N.W.—S.S.E. trending swarm and this direction probably marks the tension direction of the regional stress field during their intrusion. In the area from Coverack to Landewednack Church Cove the dykes are more irregular but it is noticeable that the N.N.W.—S.S.E. trending sub-vertical dykes tend to retain their massive form whereas sills or shallow-dipping sheets of roughly E.—W. strike are commonly sheared (compare Figs. 1, 2, 3, 4) and invaded by the Kennack injection gneiss. The basaltic dykes cutting the Traboe Hornblende Schist-peridotite contact at Pol Cornick strike N.W.—S.E. and are considered to be part of the same suite.

e. Kennack Gneiss

Kennack Gneiss is the general name given to the late acid intrusives in the Lizard area. These intrusives are shown in the Geological Survey map as occupying quite large areas near Kennack, St. Ruan, Erisey and Goonhilly Downs, but owing to the very poor outcrop it is not possible to delimit accurately the extent of gabbro, serpentine, basaltic dykes and acid gneiss within these areas. Small bosses and irregular bodies of medium grained, non-sheared, quartz + oligoclase + orthoclase + biotite or muscovite microgranite do occur e.g. at the north end of Kennack Sands, but most commonly the coastal exposures show complex intermixtures of gabbro, amphibolite and contaminated acid injection gneiss. At the southern cove at Cadgwith there is a major acid dyke cutting the Landewednack Hornblende Schist and this sends out sills along the Landewednack Hornblende Schist and peridotite contact to the south. Smaller acid veins occur cutting the Landewednack Hornblende Schist in the quarry on the north side of Cadgwith, at Carn Barrow, Kildown Point and Pen Olver. By far the greatest amount of the acid gneiss occurs within the peridotite, particularly in close association with the basaltic dykes and sills.

On Manacle Point, south of Porthoustock, there are a series of basaltic dykes, some of which are intruded and brecciated by leucocratic hornblende dioritic material. These are probably late stage intrusions directly related to the basalt rather than to the acid Kennack Gneiss.

The problem of the age and origin of the Kennack Gneiss — The discussion as to whether the Kennack Gneiss intrusions are older or younger than the serpentinized peridotite with which they occur has continued for over 50 years. Bonney maintained that these rocks are older than the peridotite and that the peridotite is intrusive into them. Lowe in 1900 and 1901 clearly and generally enunciated the evidence for

regarding the gneisses as a series of intrusions penetrating the serpentinite and foliated during their intrusion. Flett (1912 and 1946) gave a review of the controversy and considerable detail of individual exposures of the acid and mixed acid-basic rocks. Flett's conclusions are that the Kennack Gneiss is an injection gneiss of mixed acid and basic magma, intruded into dykes and sills during a period of irregular movement and crystallized to a varied series from a microgranite to foliated and contaminated biotite + hornblende + plagioclase gneiss.

Sanders (1955) returned towards Bonney's view of the age relations of the serpentinite and Kennack Gneiss but introduced the concept of tectonic inclusion as opposed to magmatic intrusion for the serpentinite bodies within the Kennack Gneiss. In the valleys of Cadgwith, Poltesco and Kennack, Sanders considered that the area mapped by the Geological Survey as largely Kennack Gneiss, was in fact (p.236) 'mainly hornblendic gneisses, possibly similar to those south of Landewednack. Locally, the hornblende gneisses merge into hornblende migmatites with granitoid sheets . . .'. Sanders regarded the serpentinized peridotite as a sheet intrusion on a thrust plane and that (p.238) 'the presence beneath the serpentine of hornblende gneisses preserving a generally low regional dip and (at Kennack) containing concordant granitoid sheets and interfoliations, suggests that these are the migmatitized equivalents of the Landewednack and Cadgwith hornblende schists'. He regarded the xenoliths of peridotite within the Kennack Gneiss as 'serpentine removed from the lower levels of the sheet during differential movement'. Areas of serpentinite at sea level i.e. 200 feet below the base of the postulated sheet in the Carn Barrow to Balk area, were interpreted as commonly being landslips or slipped talus blocks.

Sanders' interpretation can be shown to be a false one from careful mapping of excellent coastal exposures from Church Cove to Kennack Sands. The amphibolite component of the mixed injection gneiss + amphibolite bodies is megascopically distinct from the amphibolite of the Landewednack Hornblende Schist in containing relict plagioclase phenocrysts and/or aggregates or schlieren of hornblende replacing former ferromagnesian phenocrysts. There is a continuous and readily observable gradation between massive porphyritic basalt dykes and sills and amphibolites with very strong foliation and orientation of amphibole prisms. The acid injection gneiss commonly follows these sheared amphibolite horizons. In intruding within them the injection gneiss becomes contaminated with crystallization of biotite and hornblende, and introduces alkalis particularly into the amphibolites giving rise to green hornblende + plagioclase + biotite amphibolites. Two localities where the amphibolites derived from the basaltic sills, and amphibolites of the Landewednack Hornblende Schist occur together, are immediately at the base of the peridotite sheet at Kildown Point and Devil's Frying Pan. In both these localities sills of basaltic parentage can be distinguished megascopically by fine grain size, strong and silky foliation and relict plagioclase phenocrysts as augen. Microscopically they are strongly lepidoblastic rocks with a one-generation assemblage of green hornblende and plagioclase. The amphibolites of the Landewednack Hornblende Schist parentage can be distinguished megascopically by coarser grain size, more granoblastic texture and by

plastic folding. Microscopically they have minerals of several generations but characteristically the larger amphiboles have brown cores and retrogressive pale green or colourless rims or there is evidence of the former presence of pyroxene(s) replaced by amphibole aggregates.

There are quite commonly angular unsheared xenoliths of peridotite and more rarely of gabbro within the amphibolite, acid or composite phase of the Kennack Gneiss. The peridotite xenoliths, particularly in the acid rocks, are strongly rimmed with talc, chlorite, tremolite, quartz and carbonate replacing the serpentine and primary minerals.

Four field sketches of exposures which clearly show the relationships of peridotite, gabbro, basaltic intrusions and acid gneiss are shown in Figs. 1, 2, 3 and 4. Fig. 1 shows a clear example of basalt dykes cutting gabbro (intrusive into peridotite) and passing upwards into a sill. The sill contains blocks of peridotite stoped from the peridotite roof of the sill and there is variation in the degree of foliation between the normal sill material and the 'protected' parts between peridotite blocks. The acid gneiss forms a lit-par-lit injection gneiss in the amphibolite and also occurs as a flat vein cutting both gabbro and basaltic dykes. Fig. 2 is a good example of two basaltic sills, both largely altered to amphibolite and with lit-par-lit injection of a a small amount of acid gneiss, connected by a basalt dyke with angular xenoliths. The dyke and patches in the sills retain their primary porphyritic texture very distinctly. Fig. 3 shows a stoped and slightly moved block of peridotite in a dyke of Kennack Gneiss (with small amphibolite stringers) intruding peridotite and gabbro and joining a composite sill of basic and acid material. Fig. 4 is a very complex part of the short platform and cliff-face at the north end of Pen Voose. Gabbro, transitional to flaser gabbro, intrudes peridotite and is itself intruded by irregular basic dykes. Later acid veins follow generally the same channels as the basic dykes and all the rock types are strongly secondarily altered with sericitization, uralitization and other retrogressive processes.

The field evidence from these exposures and from the whole of the Lizard coastline is adequate to reject Sanders' hypothesis that the Kennack Gneiss is the migmatitized equivalent of the Landewednack Hornblende Schists. The general conclusion from the field mapping is that the basaltic magma intruded the peridotite and peridotite-gabbro complex in two main forms—as N.N.W.—S.S.E. trending dykes and as gently north or N.E. dipping sills or sheets. The sills were almost invariably sheared (indicating possibly a regional thrusting or flattening movement) and the following acid intrusions (the Kennack Gneiss) found their greatest ease of penetration along the channels of the basaltic magma, particularly the sheared gently-dipping sills. This explanation differs essentially from that of Flett (1912, 1946) only in that actual mixing of acid and basic magmas is not considered necessary to produce the lit-par-lit composite sills.

f. Palaeozoic Post-Metamorphic Rocks

The 'Lizard Boundary' (Flett 1912, 1946) is the series of faults and unexposed contacts which divides the metamorphic and igneous terrain of the Lizard Peninsula

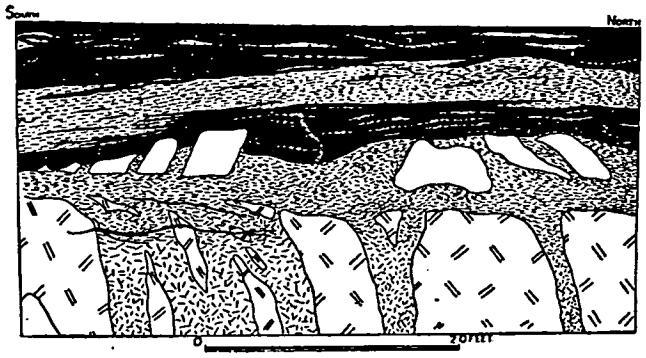

Fig. 1. Cliff section near Whale Rock (for key to stippling see Fig. 4).

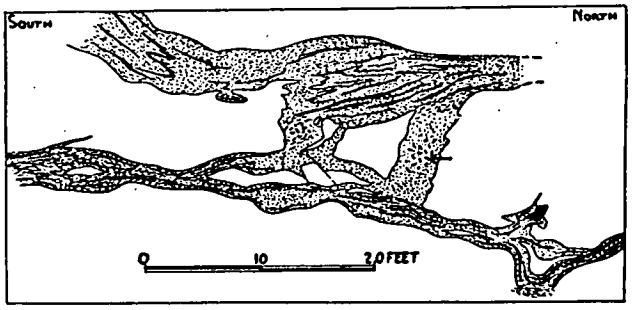

Fig. 2. Cliff section between The Balk and Pen Voose (arrow indicates relatively undeformed pseudomorphs after pyroxene phenocrysts).

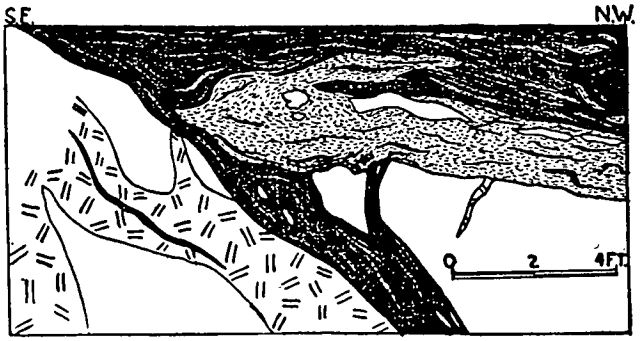

Fig. 3. Cliff section north of Whale Rock.

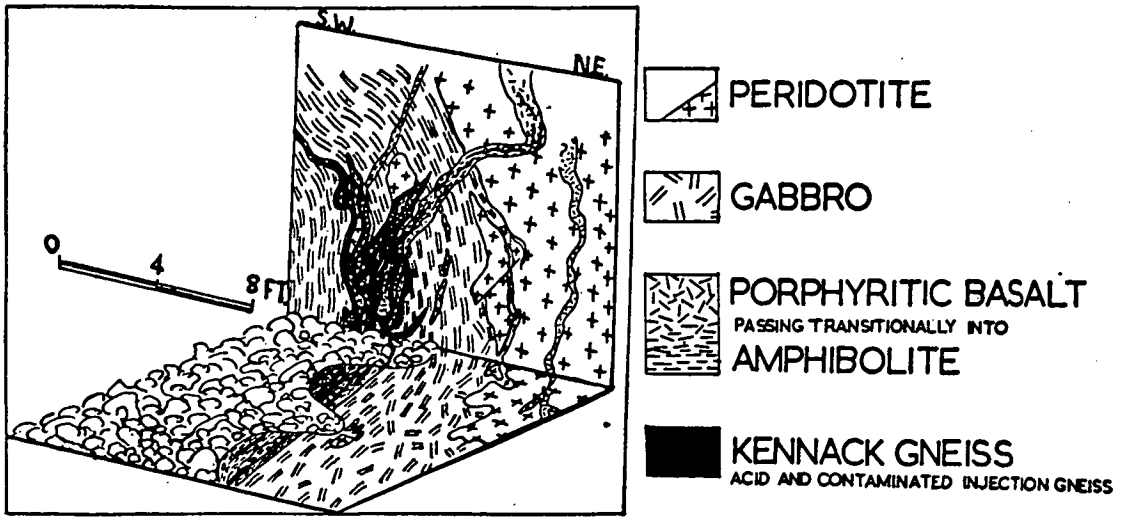

Fig. 4. Cliff section at the northern end of Pen Voose.

from the folded, cleaved but non-crystalline Palaeozoic sediments to the north. On the east coast the boundary immediately south of Porthallow is a normal fault dipping to the south. The rocks to the north have been regarded, particularly by Flett, as a strongly sheared mega-breccia of lenses and pods of more competent rocks, including quartzite, amphibolite, conglomerate and spilite, in incompetent silts and clays. This zone has been called the Meneage Breccia by Flett (1946) and interpreted as a tectonic breccia developed between the overthrust block of the Lizard Complex and the over-ridden Palaeozoic sequence to the north.

In 1949 Scrivenor disputed Flett's conclusion that a major break existed between the Lizard rocks and the Palaeozoic sediments to the north and postulated that the Old Lizard Head Series are the metamorphosed equivalents of the Palaeozoic sediments. A parallel hypothesis is that the Landewednack Hornblende Schists are the metamorphosed equivalents of the Palaeozoic spilites, particularly those of Mullion Island. This latter hypothesis was tested in the present study.

The normal fault emerging at the coast near Polurrian would, if continued along strike, pass north of Mullion Island including the island in the Lizard Complex to the south. Immediately opposite Mullion Island on the mainland at Ryniau the higher grade Traboe Hornblende Schist passes locally into lower grade Landewednack Hornblende Schist with the typical sub-horizontal foliation, N.N.W.—S.S.E. lineation and banded character reflecting primary bedding. Care was therefore taken to examine Mullion Island closely, first for evidence of a metamorphic gradient across the island increasing towards the mainland and secondly to seek evidence of minor faulting as a lead towards the position of any major fault.

The rocks of Mullion Island are predominantly spilitic pillow lava forming several flows and with interbedded chert and black siltstone. The spilites have no metamorphic foliation although some pillows show slight polishing of the pillow surface or local cleavage in the inter-pillow glassy selvages. The thin bedded radiolarian cherts do not show megascopic metamorphic effects but one exposure of a four feet thick horizon of cherts and silts has six recumbent folds in a distance of eight feet, plunging at angles from 5° to 30° in directions from E.N.E. to N.W. — this is very probably a slumping effect or drag due to the overlying basalt flow.

Thin sections of the spilites from the most easterly point on the island (nearest the mainland), the centre, and the most westerly accessible point show variation in the primary features of the basalt (grain-size, texture and degree of crystallinity) but no variation in metamorphic grade. All are characterized by relict fresh, primary pink titan-augite, by albitized plagioclase laths in random texture and interstitial fine chlorite, epidote, opaque oxides, calcite and albite. There is no evidence of any prograde metamorphism of the interstitial material to approach the regional metamorphic assemblage of blue green hornblende, andesine-oligoclase, sphene, epidote, salite. An examination of the former glassy selvage of a pillow shows devitrification and colloform and spherulitic crystallization of chlorite minerals but no directed texture or growth of medium grade metamorphic minerals. The chert bands show colloform and spherulitic crystallization but no evidence of granoblastic recrystallization to give quartzites. A thin section of black siltstone from between two lava flows

contains angular quartz separated by tiny muscovite and pale brown, pleochroic ?stilpnomelane in parallel growth — this is a slate or phyllite in which the growth of muscovite and ?stilpnomelane may be due to metamorphism by the overlying spilite flow.

There are on the island, several small faults striking almost north-south, dipping to the east and with drag effects indicating movement downthrowing to the east. The lack of any metamorphic gradient on the island and the presence of these minor faults is strong evidence for the presence of a major fault, striking north-south and downthrowing to the east, passing between Mullion Island and the mainland. This fault would intersect or be the continuation of the Lizard Boundary Fault at Polurrian (striking N.E.—S.W.) and would to the south probably swing again to a N.E.—S.W. strike as there is no evidence for its presence on Predannack Head. (See Pls. 1 and 2.)

The Treleague Quartzite — Several specimens of more massive sediments in the crush breccia north of Porthallow have angular grains of quartz and feldspar with some secondary growth of chlorite, quartz, sericite and calcite. It may be significant that specimens of Treleague Quartzite (Flett 1946) show a very similar clastic texture and degree of recrystallization to these sediments. The Treleague Quartzite occupies an anomalous position being bounded by faults on all sides, intruded by dolerite sills but clearly not subjected to regional metamorphism of the Old Lizard Head Series and Landewednack Hornblende Schist type. The metamorphics south of the Lizard Boundary are wholly recrystallized, medium-grained lepidoblastic or granoblastic rocks with mineral assemblages characteristic of a moderate grade of regional metamorphism. On the other hand the Palaeozoic rocks are typically of primary igneous textures (spilites) locally modified by shearing, or of primary clastic texture also variably modified by shearing. Many of the rocks are fine grained chlorite phyllites but in any sequence there are beds or lenses preserving more completely the primary sedimentary textures and mineralogy. In summary, the Palaeozoic rocks are characterized by low grade dynamic metamorphism localized in thrust zones and local incompetent horizons.

The conclusions of Flett and Hill (1946) and of P. T. Carr (1960) place the Treleague Quartzite as younger than the metamorphism of the Old Lizard Head Series and Landewednack Hornblende Schist but older than the peridotite, gabbro and basalt igneous intrusions. The present study shows that the regional metamorphism and peridotite intrusion were probably roughly synchronous events but that the basaltic intrusions were of later, Caledonian age. It is considered that there are two possible explanations of the relationships of the Treleague Quartzite, consistent with the fragmentary evidence available :

a. The Treleague Quartzite is a downfaulted block of Lower Palaeozoic sediments, unconformably overlying the Lizard crystalline rocks, post-dating the regional metamorphism and peridotite intrusion but preceding the Caledonian basaltic and acid igneous intrusions. The dolerite sills within the quartzite (Carr 1960) may be the expression in the previously overlying flat quartzites, of the basaltic dyke swarm in the gabbro to the south-east.

b. The Treleague Quartzite is an upthrust block (a horst or thrust lens) of Palaeozoic from beneath a southward-dipping, postulated Hercynian thrust zone forming the Lizard Boundary.

The first of these hypotheses is preferred as more probable.

III. STRUCTURAL GEOLOGY

1. The Form of the Peridotite Intrusion

Flett regarded the peridotite as a plug or stock-like intrusive with steep contacts, commonly faulted. At the other extreme Sanders (1955) considered that the peridotite was a flat and fairly thin sheet overlying the metamorphic rocks.

The detailed mapping of the exposures near Porthallow and Porthkerris (Fig. 5) shows that the peridotite forms a series of domes and anticlinal highs intruding vertically into the hornblende schists. Similarly the small peridotite bodies north of Mullion Cove, near Meaver and at Parc Bean Cove are all small plugs or 'highs' on the roof of a larger peridotite body and are indicative of vertical, diapiric intrusion of the peridotite.

The contact of the major peridotite body on the west coast near Pol Cornick (Green 1964b, Fig. 5) is also steeply dipping or vertical although rendered complex by the mobile behaviour of the pyroxene granulites in the metamorphic aureole. The northern contact around Burnoon and Tregadra is not well exposed but probably is a series of domes plunging to the north — this is interpreted as a roof area of the major peridotite body. The contact area striking south-east from Lower Relowas to Kernewas is steeply dipping to the south-west or locally, near Polkerth, to the east.

The only other area where there are contacts between the regional metamorphic rocks and the peridotite is in the south-eastern part near Cadgwith. It is in this area that Sanders (1955) regarded the peridotite as a sheet overlying the Landewednack Hornblende Schists and this can be shown to be locally true by careful examination of coastal and inland exposures from Kildown Point south to Lizard. The details of the structure in this area can be seen by reference to Pls. 1 and 2, and the perspective diagram, Fig. 6. The base of the peridotite sheet is an undulating surface dipping at low angle (5-20°) to the west and north-west. This contact appears at different levels in the cliffs due to the effects of a series of roughly east-west normal faults.

The peridotite immediately overlying the Landewednack Hornblende Schist is invariably the olivine-pargasite assemblage but 20-30 feet from the contact the peridotite has the coarse, primary assemblage with local rather than general crushing and recrystallization. The banding and incipient augen foliation in the primary peridotite in this area strikes east-west or S.E.—N.W. but is not strongly developed. The pargasite-olivine assemblage also does not show as strongly lepidoblastic texture as in the northern and western outcrops.

At Kildown Point (Fig. 6) foliation in the pargasite-olivine assemblage ten feet above the contact dips at 45° to the south-west, nearer the contact it swings in strike and dip to 70° S.S.W. and then to vertical dip, roughly east-west strike. At three feet

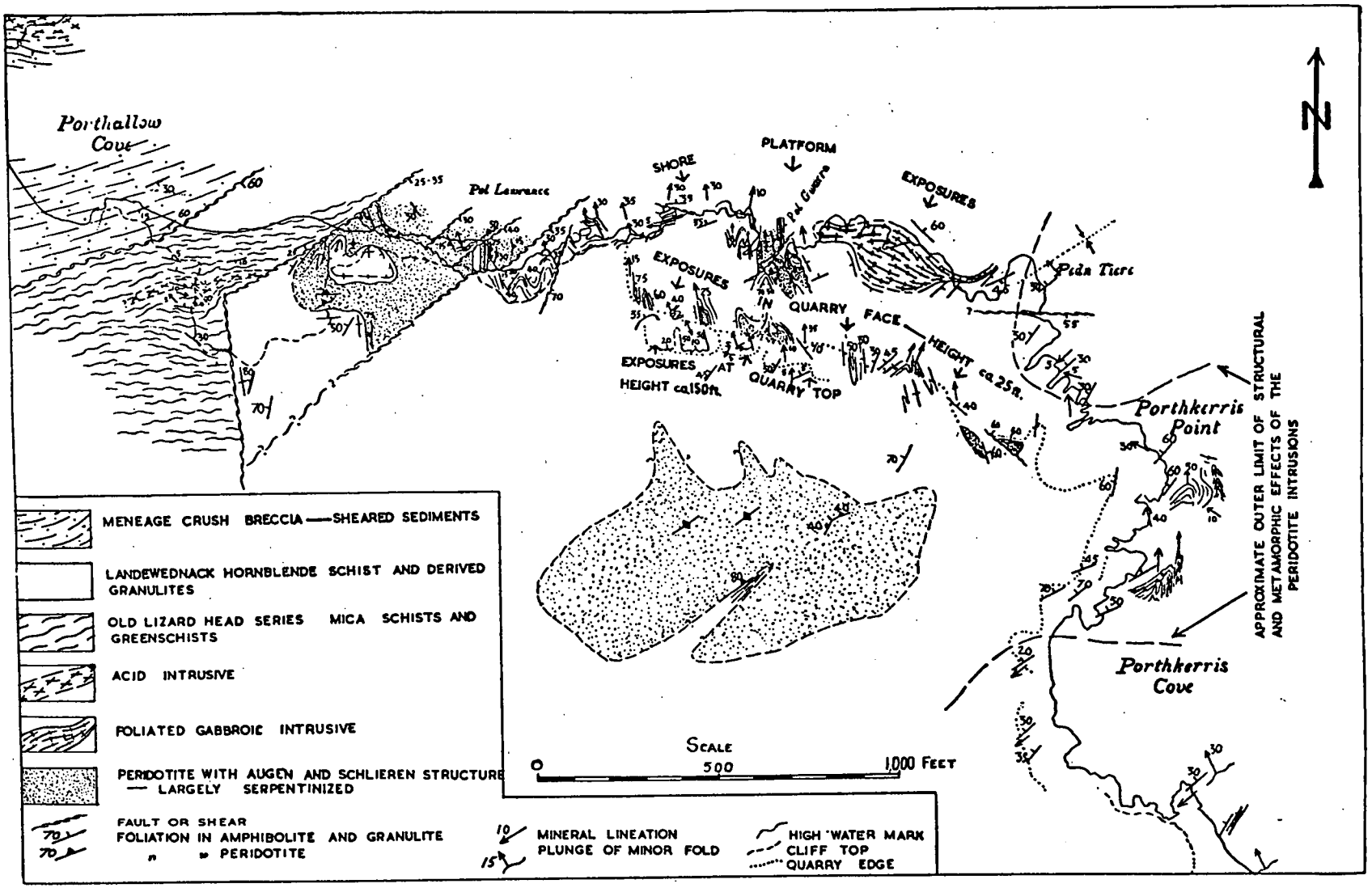

Fig. 5. Detailed geology of the peridotite contacts between Porthallow and Porth kerris Cove.

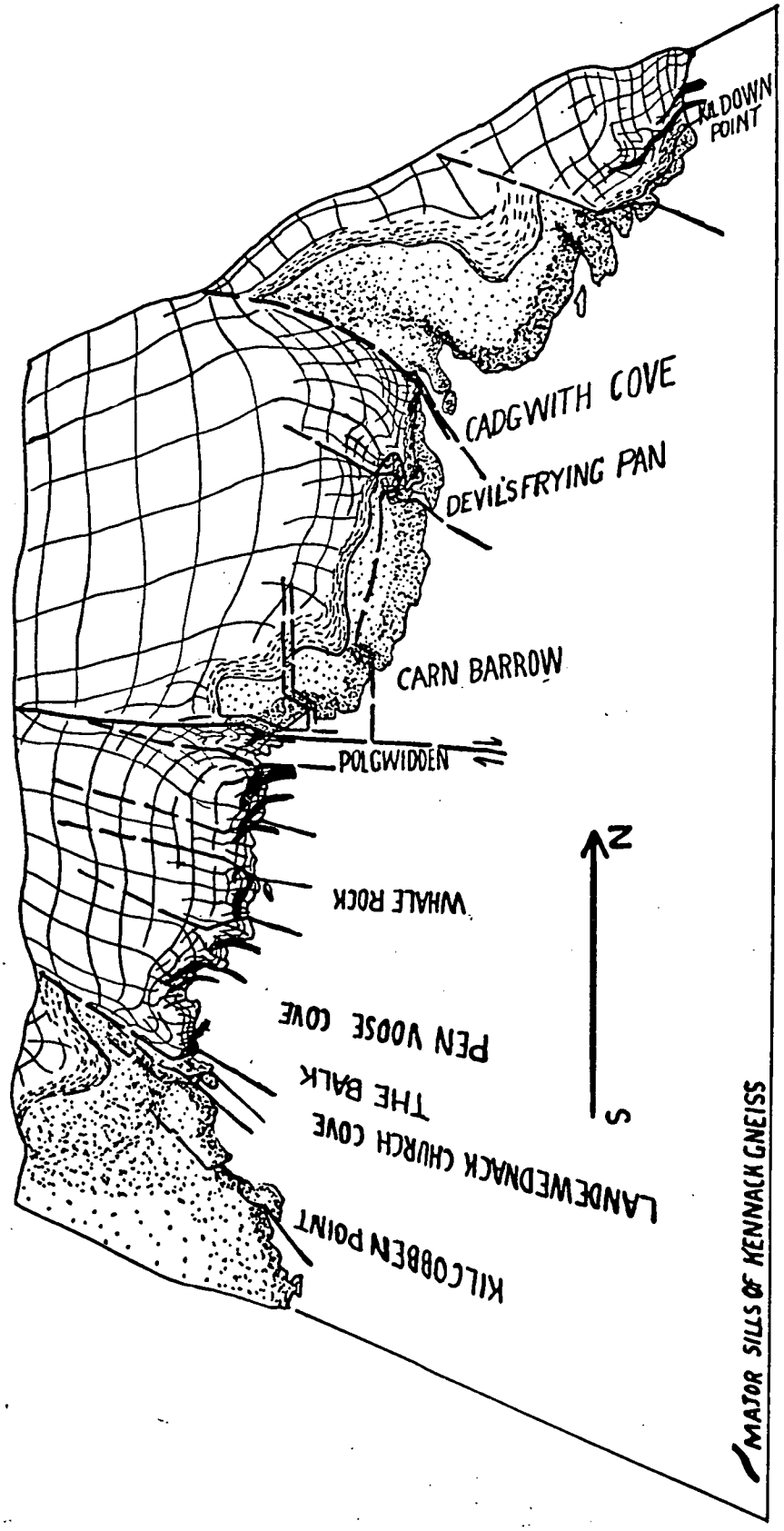

Fig. 6. Perspective sketch of the south-east part of the Lizard Peninsula showing the sheet-like form of the peridotite overlying the Landewednack Hornblende Schist (stippled) and the basal zone of olivine + pargasite peridotite (dashed).

from the contact the foliation strikes east-west and dips at 40° N. and as close to the contact as can be observed it is dipping at 20° to the north. The contact zone itself is slightly obscured by a six inch zone of talc and amphibole and by the intrusion of thin amphibolite and acid gneiss sills along the contact. The general effect is that of drag of the mineral foliation towards an east-west strike and shallow dip paralleling the contact, with increasing proximity to the contact. A similar effect can be seen on the south-west wall of the Devil's Frying Pan where foliation in the pargasite-olivine assemblage swings from 120°/60° N.E. at five feet from the contact to 100°/30° N. nearer the contact. Another structure indicating the same sense of movement occurs at the base of the peridotite within the Devil's Frying Pan on its north-east face. In this case a small drag at the base of the serpentine affects the underlying amphibolite and indicates north over south movement.

The actual plane on which the peridotite overlies the amphibolite is an undulating surface as shown by exposures on Carn Barrow, Kildown Point and Devil's Frying Pan. On the northern side of the sea-entrance to the Devil's Frying Pan the surface has a small-scale drumlinoid appearance with the normal 340° E. of N. lineation but elongation of the drumlin-like domes in the underlying amphibolite in a direction 60° E. of N. The Kildown Point exposure shows a cluster of elongate (1-3 feet) lenses of peridotite plunging at 340° and included within the amphibolite at a level probably about three feet below the base of the peridotite sheet. The amphibolite at this exposure of the flat contact (as at the others, see Green 1964b) shows evidence of high grade metamorphism and the peridotite inclusions have the appearance of more rigid boudins in amphibolite and granulite with fluid folding. Fig. 7 shows a hypothetical sequence by which the peridotite, intruding and metamorphosing the Landewednack Hornblende Schist as a sill-like body, could come to

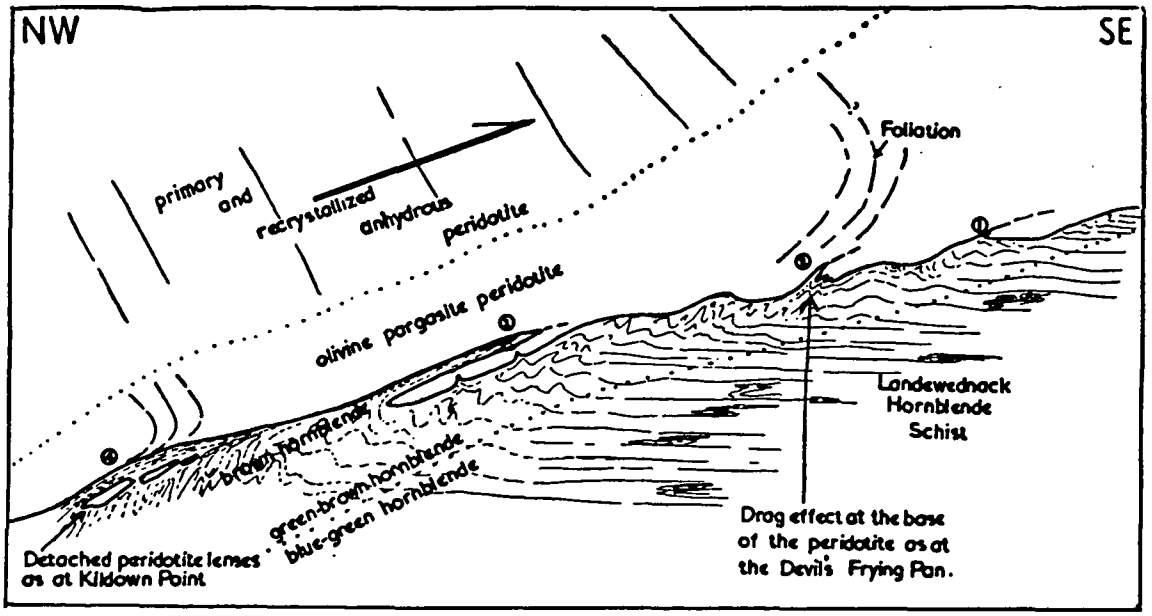

Fig. 7. Diagram illustrating a possible origin for peridotite lenses below the base of the peridotite.

have fragments from its base included within the amphibolites as observed at Kildown Point.

The contacts at Kildown Point and Devil's Frying Pan locally show the presence of the 340° E. of N. 'b' lineation and also fluid folding of Traboe Hornblende Schist type on N.N.W.—S.S.E. axial planes. Later injections of sheared porphyritic basalt sills and acid microgranite or gneiss sills tend to obscure the primary structures.

On a general view the south-eastern contact of the peridotite shows discordance of the contact attitude to the moderately dipping, E.-W. striking foliation of the peridotite but a tendency for this to pass into concordance at the actual contact. This tendency involves drag effects consistent with an overall intrusion of the peridotite from north to south over the Landewednack Hornblende Schists. Effects within the amphibolites themselves are consistent with recrystallization in the regional stress field coupled with local high grade metamorphism by the overlying peridotite sheet.

The general form of the Lizard peridotite is that of a vertical or near-vertical diapiric or plug-like intrusive, probably elongate in the N.N.W.—S.S.E. direction. There is a lip-like extension at the south-eastern end of the peridotite where the peridotite has apparently intruded horizontally as a sill within the flat-lying regional metamorphic rocks.

2. Faulting

Many of the faults of the Lizard are described in earlier studies. However no coherent pattern or even sequence of faulting has emerged and the same faults, particularly those forming the boundaries of the peridotite, have been described by different authors as normal faults and as thrusts.

In the following sections the faults are grouped into a suggested pattern and the field evidence for their character and postulated continuations is given in some detail. It is essential in arriving at the primary structure of the peridotite that these faults be analysed and the movement on them reversed. In this way also a picture of the changing stress field in the area can be built up and this should be consistent with evidence from textures and attitudes of the metamorphic and igneous rocks.

(a) EARLY FAULTING. The earliest series of faults following the emplacement of the peridotite are N.-S. faults in which the core and more central parts of the peridotite are thrust upwards and westwards over the marginal areas. A major fault of this type is exposed in a cove between Lion Rock and Kynance Cove and can be traced north across Kynance Rivulet. In this exposure the fault has a N.N.W. strike and 30°-40° dip to the east. A fault of the same character must lie between Mt. Carlees and Long Alley farms and can then be roughly traced north between peridotite of recrystallized type to the west and peridotite of the primary assemblage and variable foliation attitude to the east. The contact between the hornblende schists and the peridotite from near Penhale to Clahar is not well exposed but the evidence is that the marginal recrystallized phase of the peridotite is absent and peridotite of the primary assemblage and with banding of east-west strike abuts directly against the hornblende schist. It is concluded that this contact is a reverse fault contact in

which the peridotite in the core of the intrusion is thrust westwards over Landewednack Hornblende Schist forming the roof of the body.

A similar fault can be seen half-way up the cliff on the south side of Georges Cove. The fault dips at about 30° to the E.S.E. and brings rocks of the anhydrous recrystallized peridotite assemblage with a consistent N.N.W.—S.S.E. foliation to overlie an extremely complex marginal zone of granulite, amphibolite and olivine-pargasite peridotite with variable foliation trend. On the south side of George Cove the fault zone is intruded by several veins of pink microgranite (Kennack Gneiss) and the fault can be traced north by intermittent outcrops of the microgranite to an exposure in a quarry east of Predannack Wollas. In this quarry an augen-rich peridotite is separated by a shallow east-dipping fault plane from olivine-pargasite peridotite to the west. The fault was located again in a trench between Teneriffe and Isle of Wight farms and can be traced around the hill slope north of Wheal Unity. The former copper mine at Wheal Unity appears to be approximately astride the fault. The northerly limit of the fault is uncertain but is probably cut off by the W.S.W.—E.N.E. reverse fault at Porth Mellin. In this northern area the north-south fault brings a belt of primary assemblage peridotite with slight augen recrystallization over recrystallized hydrous and anhydrous assemblages with strikes of foliation swinging from N.N.W. to N.E.—S.W.

Two other faults in Georges Cove appear to be cut by the reverse fault. One of these strikes N.N.E. and dips steeply E.S.E. and possibly is downthrowing to the E.S.E. The other is a sheared north-south contact between peridotite and granulite.

At Ogo Dour Cove a N.E.—S.W. striking fault dips at 35° S.E. and shows pyroxene and hornblende granulites with lenses of peridotite thrust north-westwards over the green-brown hornblende amphibolites.

The major fault forming the south-west margin of the peridotite at Ryniau has a N.N.W.—S.S.E. strike and dips steeply (75°) to the N.E. On general structural grounds the Predannack area of amphibolites is interpreted as a roof area and the movement on the fault is probably north-east side upthrown i.e. a reverse fault. The age of this fault is unknown.

The general pattern of these faults is that of moderately dipping reverse faults (or steep thrusts) with east over west movement. They post-date the emplacement of the peridotite and act as channels or favourable localities for Kennack Gneiss minor intrusions. The fault near Kynance, as well as a microgranite vein, has several dykes of amphibolite along and near the fault plane — these are sheared and show drag effects consistent with east over west movement. This may be interpreted as later movement on an established fault plane which also acted as a favourable channel for the intrusion of the basaltic dykes. On the other hand the evidence may be interpreted as showing that these north-south faults post-date or are synchronous with the basaltic intrusions. The first alternative seems the more probable since the sense of movement on the faults is generally consistent with the regional stress field and the upward movement of the peridotite at the time of the peridotite intrusion. The absence of deflection of foliation in the peridotite near the fault zones and the

presence of much sheared serpentine within them indicates that the faulting occurred after the main cooling and intrusion of the peridotite, possibly during the waning phase of the regional metamorphism and stress field that accompanied the peridotite intrusion.

(b) TRANSCURRENT FAULTING. At Gew Graze on the west coast of the Lizard there is a major fault zone associated with minor acid intrusion and with hydrothermal alteration to talcose and kaolinitic rocks. The fault has an east-west strike and steep (75°) southerly dip. Well-developed slickensides on a number of major movement faces are horizontal or plunge at 10° E. or W. Other slickenside surfaces within the fault breccia plunge more steeply to the south. On the east coast, south of Carn Barrow and almost directly on strike from this fault, there is a major fault zone striking at 100° E. of N. and dipping at 70-80° S. This fault zone also has subhorizontal slickensides indicating transcurrent movement and also has a strongly developed drag dip of 60° S.S.W. in the Landewednack Hornblende Schist (normal strike and dip 80° E. of N./15° N.).

An attempt to prove the continuity of these faults fails through lack of outcrop between Gwavas and Grochall farms. However on the sides of the small gully running from Grochall to Kynance Cove there is an area of variable foliation strikes at about the place where the postulated fault might cross the gully. North and north-east of this the peridotite is of the strongly foliated, recrystallized type with N.N.W. foliation. South and south-west the peridotite is of the primary assemblage with poorly defined foliation striking east-west. A further important feature is that the north-south trending thrust at Kynance Cove cannot be traced north across Predannack Downs but the same type of fault is present to the north-east near Mt. Carlees. The similarity of the character of the faults at the exposures at Carn Barrow and Gew Graze and the independent evidence of the displacement of the north-south thrust are considered to justify the hypothesis that there is one major fault extending right across the peninsula. The movement on this fault is mainly transcurrent with dextral displacement (north side east movement) but also in part a normal fault movement of south side down in the eastern part of the peninsula accounting for the 200+′ displacement of the base of the peridotite at Carn Barrow. It is possible that the normal fault movement is later than the transcurrent movement.

(c) THE W.S.W.—E.N.E. THRUSTS. There are in the area a group of reverse faults or thrusts striking approximately W.S.W.—E.N.E., dipping at 30° or thereabouts to the south and with the southern block over-riding the northern block. These have the same attitude and sense of movement as that postulated for the Meneage Breccia. These faults could have developed in a Hercynian movement of northward thrusting (Hendriks 1959). The two most clearly demonstrable of these faults occur east of Porthallow (Fig. 5). One, at the centre of Pol Lawrance, carries undulating amphibolite and granulite, developed around the margin of a larger peridotite body, over a smaller peridotite-granulite complex. The other, at the west of Pol Lawrance, carries the peridotite-granulite complex over mica and actinolite schists of the Old Lizard Head Series. Both faults die out to the west against a north-south vertical fault...

A much larger fault with parallel strike, the same sense of movement and a 45° southerly dip occurs on the south side of Mullion Cove. In this case the peridotite is thrust north over granulite and peridotite of the peridotite roof zone and this fault also probably ends against the N.N.W. sub-vertical fault at Ryniau.

The contact north of Burnoon, between the roof area of the peridotite to the south and Landewednack Hornblende Schists and Old Lizard Head Series rocks (unaffected by the dynamothermal aureole of the peridotite) to the north, is probably also a gently dipping reverse fault of south over north movement and W.S.W.—E.N.E. strike. The western limit of the Meneage Breccia and of the Landewednack Hornblende Schist near Bonython, shown as a fault on Pls. 1 and 2, is of uncertain character and may be a sub-horizontal thrust or an intersection of fault and thrust (Flett 1946, p.151).

The main Lizard Boundary running from north of Trelowarren Lodge, by Lower Relowas and Rosemorder to Porthallow is poorly exposed and was not examined in detail in the present study. If the evidence from the coastal exposures and from the Burnoon area is generally valid then the Lizard Boundary in these areas is likely to be a mixture of gently-dipping roughly east-west reverse faults with south over north movement and a series of east-west normal faults downfaulting the over-riding thrust slices of metamorphics against the over-ridden Palaeozoic sediments.

(d) THE EAST-WEST NORMAL FAULTS. The most obvious faults in the Lizard area are the most recent, a series of east-west normal faults downthrowing to both north and south,post-dating the thrusting of the Lizard block over the Palaeozoic sediments to the north. These normal faults are most clearly seen in the cliffs near Lizard and from Lizard to Kennack Sands.

The southern boundary of the peridotite at The Balk is a fault striking E.S.E.—W.N.W. and dipping at 45° to the north. Drag effects in the Landewednack Hornblende Schists immediately to the south indicate a north side down movement and smaller parallel faults, clearly with north side down movement, occur in the cliffs to the south at Kilcobben Point, Church Cove and between Church Cove and The Balk. This boundary fault has been regarded as a thrust by Flett (1946, p.45) on which the peridotite thrust up and southwards over the Landewednack Hornblende Schist. Sanders (1955, p.237) considered the fault to be a normal one and this conclusion is supported by the evidence described above.

The base of the peridotite sheet with its characteristic zone of olivine-pargasite peridotite can be roughly traced from west of The Balk near the 200 ft. contour to near the Methodist Chapel in Lizard. In this area it is cut off by another east-west normal fault, also dipping at 40-50° N. and emerging on the west coast at Pentreath Beach. The vertical displacement on the fault at The Balk is of the order of 200 ft. since the displacement of the base of the peridotite sheet is from a sea-level exposure of olivine-pargasite peridotite, on the north side of the fault, to near the 200 ft. contour. The vertical displacement at Pentreath Beach is probably slightly greater than this.

In the cliff sections from The Balk to Carn Barrow, east-west striking faults of unknown displacement are common and the vertical component of movement on the Carn Barrow transcurrent fault has already been described. The complexity of the Devil's Frying Pan exposures is due to the presence along the southern wall of the 'blow-hole' of a W.N.W.—E.S.E. fault downthrowing to the north and displacing the base of the peridotite sheet with its sills of Kennack Gneiss. There is a major fault at Cadgwith striking N.W.—S.E. along the strike of a microgranite dyke, which has a vertical displacement of about 250 ft. downthrowing to the south. South of Kildown Point a well exposed fault with angular fault breccia dipping at 75° N.N.E. and downthrowing to the north, brings the base of the peridotite sheet from near the 150 ft. contour down to sea-level. North of Enys Head a south-dipping E.-W. fault with a prominent breccia zone, downthrows to the south and on the shore platform on its northern side is olivine-pargasite peridotite overlying amphibolite giving a contact probably of the same character as that at Kildown Point.

The nature of the southern contact of the gabbro at Coverack is not clear but there is no evidence of a major fault. The northern contact at Porthoustock is certainly a major fault striking east-west and curving through a smooth arc to the west to strike north-south. The fault is nowhere exposed but from the distribution of the rock types it is clear that the north and west side is the downthrown side. The problematical relationships of the Treleague Quartzite have already been discussed and Carr (1960) gives evidence for the southern margin of the Quartzite being a normal fault downthrowing to the north.

The fault at East Beach, Porthallow, which brings the Old Lizard Head Series to the south into contact with very sheared sediments of the Palaeozoic sequence, strikes E.N.E.—W.S.W. at the coast and probably swings nearer to E.S.E.—W.N.W. to the west. The fault dips south at 60° and the sediments immediately to the north are dragged from a 15° S.E. to a 60° S.E. dip. The drag effects indicate that this fault also is a normal fault.

The fault at Polurrian Cove on the west coast which forms the northern limit of the peridotite and Traboe type of hornblende schist, strikes N.E.—S.W. and dips at 50° to the south-east. Drag effects on the Palaeozoic sediments are not strongly developed but do indicate a south side down movement. There is a distinct zone of angular fault breccia in this fault zone which suggests a normal fault rather than a steep reverse fault although both alternative explanations are given in the Memoir (1946, p.134). The minor faulting on Mullion Island described previously is consistent with a major fault striking nearly north-south between Mullion Island and the mainland and this is either the continuation of or intersects the Polurrian Fault. Whittard (1961) has reported the coring of 'Devonian slates' 7½ miles south-west of Mullion Cove. This is further evidence that the Lizard Boundary does not continue on the strike of the boundary fault at Polurrian but a continuation of a fault on the trend defined between Mullion Island and the mainland would place this coring on the western side of the Lizard Boundary fault. It is probable that further coring in

the area would reveal as complex a boundary to the Lizard Complex as is present in the land areas.

(e) SUMMARY OF FAULTING. Apart from the faults described and grouped together in the previous sections there are innumerable minor movement planes and faults exposed in the Lizard cliffs. Many of the contacts of contrasted rock types are sheared and the shearing and associated hydrothermal effects result in retrogressive alteration that does much to obscure the primary features of the contacts. In the serpentinized peridotite particularly, practically every joint plane is a movement plane and this 'brecciation' in apparently random manner is largely responsible for the foliation induced in the post-peridotite minor intrusions.

In summary it is possible to recognize in the Lizard three distinct faulting patterns. The earliest pattern is of approximately north-south striking, easterly dipping reverse faults in which the central and more easterly parts of the peridotite complex moved westward over the marginal part of the peridotite and the western metamorphic aureole. These are consistent with late-stage movements in the stress-field of the orientation present during regional metamorphism and peridotite intrusion. A later distinctive series of thrusts or moderately dipping reverse faults strikes roughly E.N.E.—W.S.W. and has a south over-riding north movement—these could be part of a Hercynian system of east-west thrusts and northward thrusting movement. These reverse faults were followed, probably in the Hercynian late orogenic or post-orogenic period by a series of east-west normal faults, downthrowing to both north and south.

IV. THE AGES OF THE LIZARD ROCKS

The palaeontological evidence for the age of the rocks in the Meneage Breccia north of the Lizard Boundary has been summarized by Flett (1946, pp.120-136). An Ordovician age for the Meneage Quartzite remains in dispute and a Lower Devonian age is given as an alternative (Flett 1946, p. 126). The suggested Silurian age for limestone lenses in the Meneage Breccia also needs confirmation and an age of Middle Devonian for plant remains is the only other palaeontogical evidence from this sequence.

Flett (1946, p.24) regarded the movements giving rise to the Meneage Breccia as Hercynian (Carboniferous) in age and causing the thrusting of the *Archaean* Lizard Complex over the lower Palaeozoic rocks. Flett separated the history of the Lizard Complex into two distinct phases — the first a period of high grade regional metamorphism accompanied by the intrusion of the Man of War Gneiss. He regarded the deposition of the Treleague Quartzite as preceding the second phase which was the sequence of genetically related intrusives ranging from the Traboe Hornblende Schist and peridotite to the acid Kennack Gneiss.

Scrivenor in 1949 regarded the Old Lizard Head Series as metamorphosed Lower Palaeozoic and by implication would regard the whole sequence of intrusion and metamorphism in the Lizard as post-Devonian events. Similarly Hendriks (1959, p.255) supported the conclusion that the Old Lizard Head Series were metamor-

phosed Lower Devonian sediments and placed the intrusion of the 'serpentine', as the metamorphosing body, as Upper Devonian or Lower Carboniferous in age.

It is considered that the present study of the Lizard has either confirmed or established the following sequence and relative timing of events.

1. Deposition of a sequence of pelitic sediments, tuffaceous sediments and basalt flows.
2. Local intrusion of acid sills (the Man of War Gneiss).
3. Regional metamorphism of 1 and 2 in a stress field with maximum compression directed E.N.E.—W.S.W. and with intrusion of diapiric peridotite bodies during the regional metamorphism.
4. Intrusion of gabbro — of uncertain time relationship or genetic relationship to either the preceding peridotite or the following basaltic dykes.
5. Intrusion of basaltic dykes and sills with chilled margins and in a stress environment of E.N.E.—W.S.W. relative tension. This implies a large change in stress and temperature environment from stage 3 and thus probably a major time break.
6. Intrusion of acid microgranite probably very closely following stage 5, in a similar stress field and with relationships of basic and acid rocks suggesting incomplete cooling of the former before intrusion by and reaction with the latter.
7. Northward thrusting or reverse faulting of the igneous metamorphic block over Palaeozoic (including Devonian) sediments to the north. This is the Carboniferous (Hercynian) event of previous authors.
8. Post-orogenic normal faulting giving faults of east-west strike and probably occurring in the waning or relaxing phase of stage 7.

With this geologically established sequence in mind, a series of absolute age determinations by the potassium-argon method was undertaken in collaboration with J. A. Miller at the Department of Geodesy and Geophysics, Cambridge. The results of these determinations are summarized in Table 1 in which are also included the measurements by Dodson (1961) on the Lizard rocks.

From the Table the striking feature is the grouping of most of the ages in the 350-390 million years range. In detail it is apparent that both the Oxford and Cambridge results show a slightly younger age for the muscovite from the Old Lizard Head Series than the biotite from the Kennack Gneiss. The total volume technique of argon measurement used at Cambridge gives a slightly greater age than the isotope dilution method used at Oxford — this consistent difference is also apparent in comparative measurements undertaken at Oxford and Cambridge on the Shap granite (Dodson *et al.* 1961). It is particularly encouraging that the hornblendes, containing about one twentieth of the potassium present in the micas, give in three cases ages that are quite closely agreeing with the ages from micas. In particular hornblende and biotite from the same hand-specimen 96392 gave ages of 366 $\pm$ 20 and 397 million years respectively for the Kennack Gneiss.

From these results it can be definitely stated that a 370-390 million year stage marks an 'event' in the crystallization history of the Lizard rocks. The Hercynian granites of south-western England have been dated as about 265 million

TABLE 1: *Age Determinations in the Lizard Area*

Rock Unit	Mineral	% K_2O	No. of determinations	Age (millions of years)	*δt.		Method	Determined at	Specimen No. and Rock Type
Old Lizard Head Series	Muscovite (coarse)	9.03	5	357	3.25	KA,	Total Volume	Cambridge	96388 Muscovite chlorite schist
„ „ „ „	Muscovite (fine)	9.01	5	352	3.21	KA,	Total Volume	Cambridge	96388 „ „ „
„ „ „ „	Muscovite (coarse)	9.17	5	355	3.20	KA,	Total Volume	Cambridge	96391 „ „ „
„ „ „ „	Muscovite (fine)	9.11	5	359	3.27	KA,	Total Volume	Cambridge	96391 „ „ „
„ „ „ „	Muscovite	7.68	3-4	349	—	KA,	Isotope Dilution	Oxford	9372 Muscovite Schist
„ „ „ „	Muscovite I	9.49	3-4	348	—	KA,	Isotope Dilution	Oxford	20557 Muscovite Schist
„ „ „ „	Muscovite II	8.58	3-4	352	—	KA,	Isotope Dilution	Oxford	20557 Muscovite Schist
Landewednack Hornblende Schist	Hornblende	0.375	8	371	3.37	KA,	Isotope Dilution	Cambridge	96396 Blue-green hornblende, plagioclase, sphene amphibolite
„ „ „	Hornblende	0.425	6	442	3.94	KA,	Isotope Dilution	Cambridge	96389 Blue-green hornblende, plagioclase, sphene amphibolite
„ „ „	Biotite	6.4	3-4	369	—	KA,	Isotope Dilution	Oxford	9380 Hornblende, Biotite schist
Traboe Hornblende Schist	Hornblende	0.211	7	357	3.25	KA,	Isotope Dilution	Cambridge	96395 Brown-green hornblende, plagioclase, diopside amphibolite
„ „ „	Hornblende	0.242	7	492	4.43	KA,	Isotope Dilution	Cambridge	96394 Brown hornblende, augite, hypersthene granulite
Kennack Gneiss	Hornblende	0.577	7	366	3.33	KA,	Isotope Dilution	Cambridge	96392 Biotite, hornblende amphibolite
„ „	Biotite	6.97	5	397	3.58	KA,	Total Volume	Cambridge	96392 Biotite, hornblende amphibolite
„ „	Biotite	5.98	5	384	3.47	KA,	Total Volume	Cambridge	96393 Biotite, hornblende amphibolite
„ „	Biotite	7.39	3-4	368 (av.)	—	KA,	Isotope Dilution	Oxford	9406 Granite gneiss
„ „	Biotite	(—	—	352 ± 10	—	Rb-Sr,	Isotope Dilution	Oxford	—) Granite gneiss
		(—	—	353 ± 13	—	Rb-Sr,	Isotope Dilution	Oxford	—)

*δt = Error in age (millions of years) due to a 1% error in proportion of K_2O or volume of radiogenic argon.

years old (Dodson, Miller and York 1961) so that this 'event' cannot be correlated with the Hercynian orogeny. The late thrusting of the Lizard, since it involves Devonian rocks, is probably of this Hercynian phase and thus cannot have greatly modified the general Lizard mineral assemblages *except* that it is very probable that the slightly younger age given by muscovite from the Old Lizard Head Series is due to argon loss on retrogressive alteration (co-existing biotite is partially or completely altered to chlorite, cordierite is altered to secondary products) during the Hercynian thrusting. With their flat-lying foliation, micaceous character and varied lithology it is very plausible that the Old Lizard Head Series should show greater retrogressive effects during a thrusting movement than either the more massive Landewednack Hornblende Schists or the Kennack Gneiss bodies within the peridotite.

With the exception of the rubidium-strontium age of 353 million years all the determinations on the Kennack Gneiss fall in the range 366-397 million years. With the possibility of any argon loss giving a low age, it is probable that the older ages give the true age of intrusion of the Kennack Gneiss — this age of about 390 million years is compatible with the ages of Caledonian granites such as the Shap granite (397 million years) (Dodson *et al.* 1961) the Skiddaw Granite (399 million years) and the Eskdale Granite (383 million years) (Miller, 1961). From these results it is possible to attach an absolute age to events 6 and 5 and to say that the final igneous phase i.e. the acid injection gneiss, and the preceding basic dykes, are of uppermost Silurian or Lower Devonian age and are part of the Caledonian orogenic cycle. This interpretation is compatible with the geological evidence.

The problem of the age of peridotite intrusion still remains. The ages given by muscovite from the Old Lizard Head Series, biotite from the Landewednack Hornblende Schist, one hornblende from the Landewednack Hornblende Schist and one hornblende from the Traboe Hornblende Schist (in the aureole of the peridotite but 800 yards from the nearest peridotite outcrop), are close to the age of the Kennack Gneiss. This does not support the geological evidence of a probable large time break between events 3 and 5 + 6. On the other hand two ages, one of 442 million years from Landewednack Hornblende Schist at Pen Olver, and the other, giving a 492 million year age from brown hornblende in a hypersthene + augite + brown hornblende granulite immediately in contact with the peridotite, are significantly older than the Kennack Gneiss. These older ages are considered to give a 'pointer' back to the earlier, major orogenic event in the Lizard in which, on geological evidence, the regional metamorphism and peridotite intrusion occurred. The actual age of this event is unknown and it would need a concentration of ages around the 490 million year mark before this could be accepted as significant in this problem.

In summary, the interpretation placed on the evidence from age determinations and the geological study is that the Caledonian age of 370-390 million years is a true age for the injection of the Kennack Gneiss. This was also a period of partial or complete argon loss from pre-existing minerals. There was no major recrystallization of the earlier assemblages but probably a general rise in temperature during the period of basic dyke and acid gneiss injection.

The hypothesis that the Old Lizard Head Series are metamorphosed Lower Devonian sediments can no longer be considered; these rocks, the Landewednack Hornblende Schists and the peridotite are at least pre-Caledonian in age, i.e. pre-Devonian or pre-Upper Silurian. The regional metamorphism and peridotite intrusion occurred in a pre-Devonian orogenic event which has not yet been dated more accurately than probably at least 490 million years old. This event cannot as yet be adequately correlated with other early fold systems in Britain but the N.N.W.—S.S.E. direction of fold-axes during the regional metamorphism and peridotite intrusion invites comparison with other 'pre-Cambrian' areas of Britain.

ACKNOWLEDGEMENTS

The research which forms the subject of this paper was suggested to the author by Professor C. E. Tilley and carried out at the Dept. of Mineralogy and Petrology, Cambridge. The guidance of Professor Tilley, Dr. S. R. Nockolds and members of the staff of the above department, is gratefully acknowledged.

The author particularly thanks Mr. and Mrs. S. James, Coverack, Cornwall for their warm hospitality and invaluable help during field-work in 1959-61

REFERENCES

BONNEY, T. G. 1877. On the serpentine and associated rocks of the Lizard district. *Quart. J. Geol. Soc. Lond.*, **33,** 884.

CAREY, S. W. 1954. The rheid concept in geotectonics. *J. Geol. Soc. Aust.*, **1,** 67-117.

CARR, P. T. 1960. The Treleague Quartzite and its associations. *Abstr. Proc. Conf. Geol. Geomorph. S.W. England,* R. geol. Soc. Cornwall, 1960, 9-11.

DODSON, M. H. 1961. Isotopic ages from the Lizard Peninsula, South Cornwall. *Proc. Geol. Soc. Lond.*, **1591,** 13-136.

—— MILLER, J. A. and YORK, D. 1961. Potassium-argon ages of the Dartmoor and Shap Granites. *Nature*, **190,** 800-802.

FLETT, J. S. and HILL, J. B. 1912. The geology of the Lizard and Meneage. *Mem. geol. Surv. U.K.*, 2nd ed., 1946 (revised J. S. Flett).

FYFE, W. S., TURNER, F. J. and VERHOOGEN J. 1958. Metamorphic reactions and metamorphic facies. *Mem. geol. Soc. Amer.*, **73.**

GREEN, D. H. 1964 (a). The petrogenesis of the high-temperature peridotite in the Lizard area, Cornwall. *J. Pet.*, **5,** 134-188.

—— 1964 (b) The metamorphic aureole of the peridotite at the Lizard, Cornwall. *J. Geol.*, Sept., 1964.

HENDRIKS, E. M. L. 1937. Rock succession and structure in south Cornwall, a revision. *Quart. J. geol. Soc Lond.*, **93,** 322-367.

—— 1939. The Start—Dodman—Lizard Boundary-zone in relation to the alpine structure of Cornwall. *Geol. Mag.*, **76,** 385-402.

—— 1959. A summary of present views on the structure of Cornwall and Devon. *Geol. Mag.*, **96,** 253-257.

LOWE, H. J. 1901. The sequence of the Lizard Rocks, I. *Trans. R. geol. Soc. Cornwall,* **12,** 438-466.

—— 1902. The sequence of the Lizard Rocks, II. *Trans. R. geol. Soc. Cornwall,* **12,** 507-534.

MILLER, J. A. 1961. The potassium-argon ages of the Skiddaw and Eskdale Granites. *Geophys. J.*, **6**, 391-393.

—— and GREEN, D. H. 1961 (a). Preliminary age-determinations in the Lizard area. *Nature*, **191**, 159-160.

———————— 1961 (b). Age determinations of rocks in the Lizard (Cornwall) area. *Nature*, **192**, 1175-6.

SANDERS, L. D. 1955. Structural observations on the south-east Lizard. *Geol. Mag.*, **92**, 231-240.

SCRIVENOR, J. B. 1949. The Lizard-Start problem. *Geol. Mag.*, **86**, 377-386.

TILLEY, C. E. 1937. Anthophyllite-cordierite granulites of the Lizard. *Geol. Mag.*, **74**, 300-309.

WHITTARD, W. F. 1961. In discussion to T. D. Allan on 'A magnetic survey in the western English Channel. *Quart. J. geol. Soc. Lond.*, **117**, 169.

PLATE 1. Lithological map of the Lizard district, Cornwall.

PLATE 2. Locality map of the Lizard district, Cornwall.

PLATE 1

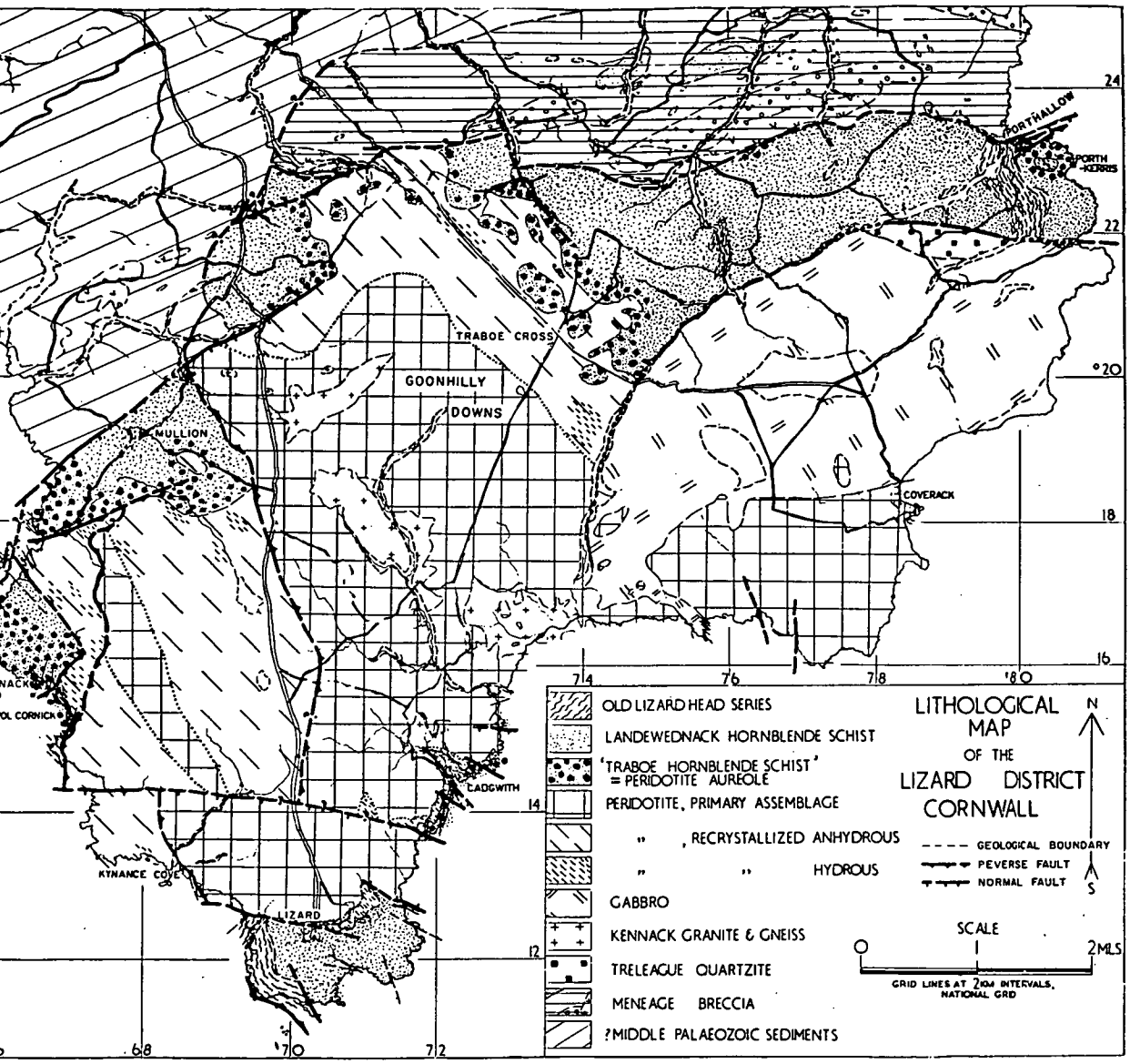
TRABOE CROSS
GOONHILLY DOWNS
MULLION
CADGWITH
KYNANCE COVE
LIZARD
COVERACK
PORTHALLOW
PORTH KERRIS
24
22
20
18
16
14
12
7·4
7·6
7·8
8·0
6·8
7·0
7·2
OLD LIZARD HEAD SERIES
LANDEWEDNACK HORNBLENDE SCHIST
'TRABOE HORNBLENDE SCHIST' = PERIDOTITE AUREOLE
PERIDOTITE, PRIMARY ASSEMBLAGE
" , RECRYSTALLIZED ANHYDROUS
" " HYDROUS
GABBRO
KENNACK GRANITE & GNEISS
TRELEAGUE QUARTZITE
MENEAGE BRECCIA
?MIDDLE PALAEOZOIC SEDIMENTS
LITHOLOGICAL MAP
OF THE
LIZARD DISTRICT
CORNWALL
GEOLOGICAL BOUNDARY
REVERSE FAULT
NORMAL FAULT
N
S
SCALE
0
2MLS
GRID LINES AT 2KM INTERVALS, NATIONAL GRID

PLATE 2

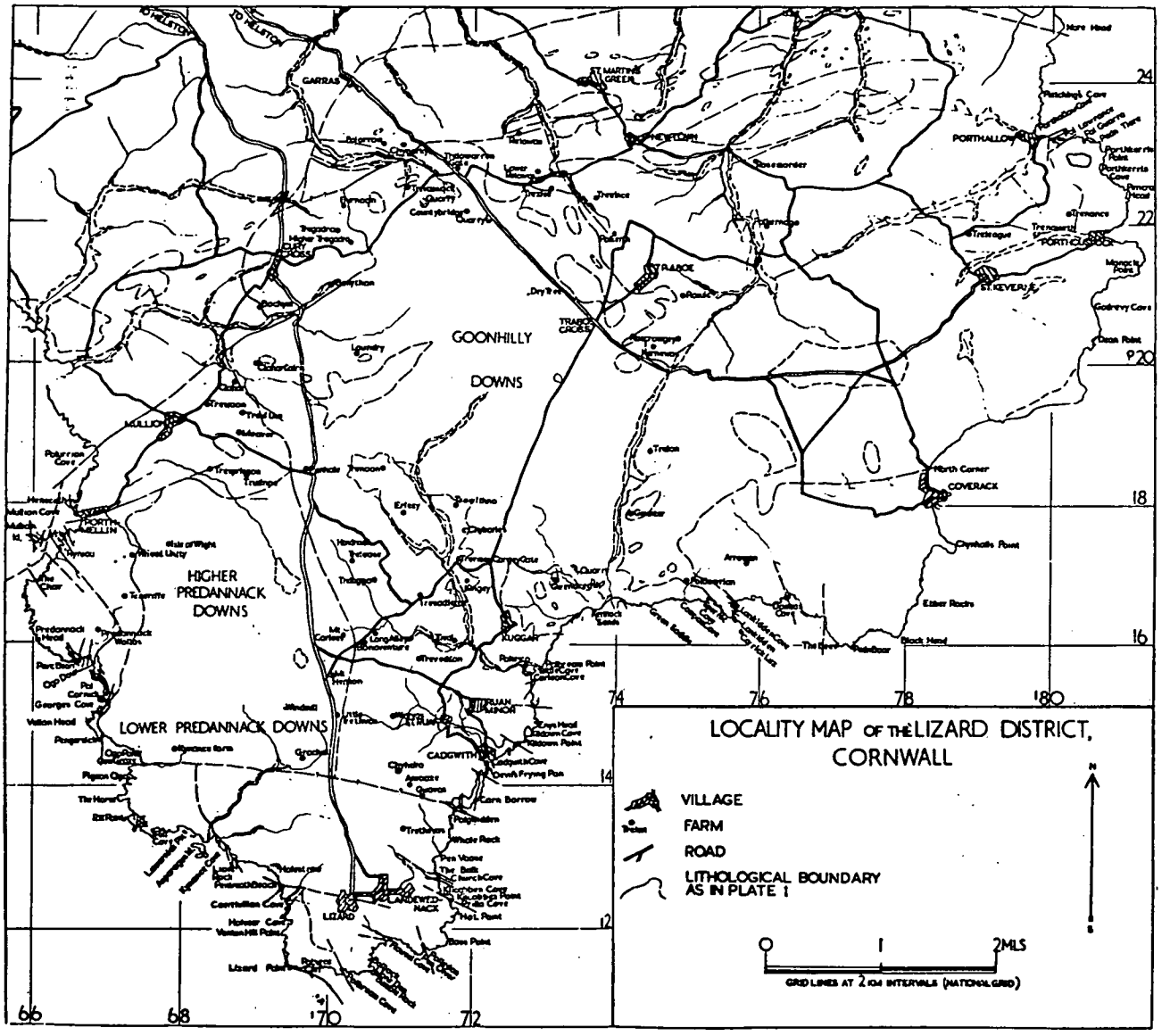
GOONHILLY
DOWNS
HIGHER
PREDANNACK
DOWNS
LOWER PREDANNACK DOWNS
LOCALITY MAP OF THE LIZARD DISTRICT,
CORNWALL
VILLAGE
FARM
ROAD
LITHOLOGICAL BOUNDARY
AS IN PLATE 1
0 1 2MLS
GRID LINES AT 2 KM INTERVALS (NATIONAL GRID)
66
68
70
72
74
76
78
80
12
14
16
18
20
22
24

den Tex, 1965), may then determine the mineral assemblages stable at the given conditions, so that the peridotite high pressure facies is formed at higher temperatures than the eclogite high pressure facies (cf. Sørensen, 1953, p. 83).

5. Ultramafic veins. Veins of bronzitite, dunite, etc. are confined to the ultramafic bodies and do not intrude into the enclosing rocks. This is explained by Bowen and Tuttle (1949) as a result of hydrothermal reactions along fractures in the ultramafic bodies, since experimental work has shown that water vapor unsaturated in SiO_2 may dissolve SiO_2 from orthopyroxene and thus transform it into olivine, or if saturated with SiO_2 may transform olivine into orthopyroxene. Examples of this have for instance been given by Barth (1950) and Sørensen (1954). As emphasized by Barth, this mode of formation of monomineralic rocks is not logically limited to bodies having a dyke-like relation.

III. HIGH-TEMPERATURE PERIDOTITE INTRUSIONS

D. H. Green

A. Introduction

One of the most commonly used arguments for low temperature of emplacement of ultramafic rocks has been the lack of evidence for contact metamorphism, particularly at temperatures compatible with emplacement of ultramafic liquid. However, recent papers on dunites and peridotites occurring in alpine orogenic zones have, in some cases, produced evidence and arguments for moderate or even high-temperature of emplacement of ultramafic rocks. As a recent example, Ragan (1963, p. 561) has deduced that the Twin Sisters dunite was capable of solid flow and intrusive emplacement at temperatures probably of 600 to 700°C but possibly as low as 500°C (Chapter 5-III). Lipman (1964) deduces similar temperatures for the Trinity ultramafic pluton in the Klamath mountains, California, and in this example there is some evidence of increase in metamorphic grade adjacent to some contacts (Lipman 1964, pp. 216–217). Both the Twin Sisters and Trinity ultramafic bodies exhibit evidence for flow as a solid or near-solid, inhomogeneous crystalline body.

The origin of this inhomogeneity in alpine peridotites is often considered to lie in an earlier period of accumulation and gravity stratification (Thayer 1960, p. 257; Green 1961, pp. 6, 22–23; Challis 1965, p. 360) and the nature of the parent magma cannot be specified with any certainty. Challis (1965a, p. 360) has described some of the New Zealand ultramafic bodies, including the classical Dun Mountain locality, and suggests that these bodies represent accumulates in "deep-level magma chambers of a line of upper Palaeozoic volcanoes." Challis considers that the parent magma was probably tholeiitic and may have approached a picrite in composition. One body, Red Hills, has an unfaulted contact locally at which spilitic volcanics are converted to amphibolites and, right at the contact, to pyroxene hornfels (Challis, 1965b). Challis suggests that temperatures at the contact probably did not exceed 800°C and that the magma temperature was about 1200°C (p. 416). It should be emphasized that this is a temperature suggested for a basaltic or picritic magma and not for an ultramafic magma, the ultramafic composition being regarded as the result of accumulation of early crystallizing chromite, olivine, orthopyroxene, and minor clinopyroxene and very complete removal of interstitial basaltic liquid.

These examples of ultramafic rocks, even though they show evidence of moderate temperatures at the time of their emplacement, do not provide any conclusive evidence for the existence of a high-temperature peridotite magma. Rather their features are consistent with accumulation at crustal levels from more basaltic liquids or (liquid + crystal) magmas. It is not proposed to consider these bodies further in this paper; but there are important problems in the nature of the parent magma, the original presence or absence of a basaltic interprecipitate liquid and the mechanism for removal of such an interprecipitate liquid, and in the expected and observed intensities of contact metamorphism.

Further discussion in this paper is limited to a small group of peridotites that have clearly defined dynamothermal aureoles, external form and internal structures resembling those of salt domes, and are of intermediate size (5 to 15 miles diameter). These peridotites have chemical compositions in which Al_2O_3, CaO, Na_2O in particular are minor but essential components (in contrast to the peridotites and dunites of the examples described above where these components are extremely low or of local, sporadic concentration). Mineralogically, these peridotites are characterized by evidence for initial crystallization at high load pressure and for post-crystallization deformation, movement, and recrystallization. Examples of this type of peridotite intrusion include:

1. Tinaquillo, Venezuela (MacKenzie, 1960; Green 1963).
2. Lizard, Cornwall (Green, 1964a,b,c).
3. Mt. Albert, Quebec (Smith and MacGregor, 1960).

These three peridotite bodies have sufficient features in common and the evidence on their nature and emplacement mechanism is sufficiently unambiguous to merit their recognition as a distinctive type of alpine ultramafic intrusion. There are a number of other peridotite intrusions which are similar in some features to the above type but, possibly because of more complex, post-intrusion histories and in part because of insufficiently detailed descriptions, the diagnostic characteristics cannot be so closely matched. Such peridotites include the intrusions of Beni Bousera, Morocco (Milliard, 1959); Lherz, Pyrenees (Lacroix, 1917, Ravier, 1964); Horoman, Japan (Onuki, 1965); and possibly Dawros, Connemara (Rothstein, 1957, 1961).

B. Metamorphic Aureoles

The metamorphic aureoles of the Tinaquillo, Lizard and Mount Albert peridotites are of dynamothermal character and the rocks that have been recrystallized in the aureoles are foliated amphibolites and granulites. Hornfels textures are not developed and the mineral assemblages are not typical of either hornblende hornfels or pyroxene hornfels facies. The peridotites occur in regionally metamorphosed terrains and their emplacement probably occurred during the regional metamorphism. The grade of regional metamorphism is of lower almandine amphibolite facies [i.e., staurolite-almandine subfacies (Turner and Verhoogen, 1960)] in the Lizard and Tinaquillo examples or greenschist facies as in the Mt. Albert example. In all three examples the metamorphic gradient around the ultramafic body affects rocks of predominantly basaltic chemistry.

1. Mineralogy. In the Lizard area the basic rocks outside the metamorphic aureole are characteristically blue-green hornblende amphibolites with sodic plagioclase, sphene and magnetite. Pale green salite, epidote, grossular, calcite and quartz are present in varying proportions in some bands. The outer margin of the peridotite aureole is marked by the change of the hornblende from the distinctive blue-green type to brown-green hornblende. Chemical analyses of two hornblendes from rocks of

closely similar chemistry show that the hornblende color change is matched by a composition change. The contents of the tschermakite, glaucophane, and richterite (soda-tremolite) solid-solution end-members decrease and the contents of the edenite, and cummingtonite solid solutions increase in going from the blue-green to green-brown to brown hornblendes of the aureole (Green 1964b, p. 557).

Accompanying the change in color of the hornblende, the plagioclase becomes more calcic and more abundant, sphene and magnetite are replaced by ilmenite + magnetite and salite appears as a minor constituent in the amphibolites and is not restricted to calcium-rich bands. In the Lizard example, the zone occupied by the green-brown hornblende amphibolites is relatively wide (Green 1964b, p. 560) and, at vertical contacts of the peridotite extends 350 to 500 feet from the peridotite margin and may extend over 1000 feet in some areas.

Higher grade metamorphic assemblages are marked by assemblages of hypersthene + augite + plagioclase ± hornblende + ilmenite + magnetite. The presence or absence of hornblende as a major phase subdivides these near-contact rocks into hornblende granulites and pyroxene granulites. The hornblende is a brown variety, lacking any green coloration in pleochroism, and varying from deep-brown, to very pale brown, almost colorless, probably with increasing Mg/Fe ratio. The plagioclase present in the granulites is andesine-labradorite and the co-existing pyroxenes have compositions matching those of high-grade granulites or intermediate between granulite pyroxenes and magmatic pyroxene pairs. Olivine + orthopyroxene + clinopyroxene + plagioclase assemblages occur and probably represent the highest grade of the aureole indicating that the temperature has locally been adequate to cause the breakdown of hornblende in an undersaturated rock. It may be noted that the bulk compositions of the analyzed rocks from the Lizard aureole are all olivine normative, and in two cases are nepheline normative. In these undersaturated rocks the highest grade assemblages are

olivine + augite + hypersthene + plagioclase + magnetite-ilmenite
augite + hypersthene + plagioclase + magnetite-ilmenite
augite + hypersthene + plagioclase + hornblende + magnetite-ilmenite

It is important in estimating the P-T conditions of this aureole that almandine-pyrope garnet does not occur in any mineral assemblage.

In the Lizard metamorphic aureole there is limited metasomatism over distances of a few inches at the contacts. In the Tinaquillo peridotite, the absence of chemical data on the rocks of the metamorphic aureole makes comparison of metamorphic assemblages more difficult. MacKenzie describes the country rock outside the metamorphic aureole as interlayered hornblende gneiss and plagioclase gneiss. The former rock type consists of roughly 50 per cent oligoclase, 25 per cent quartz and 25 per cent green hornblende while the latter ranges from 90 per cent quartz to 90 per cent albite or oligoclase. The quartz-rich and leucocratic layers are not apparent within the contact aureole and MacKenzie does not describe quartz as a constituent of either the garnet-bearing or hypersthene-bearing granulites. Thus there appear to be chemical differences between the rocks outside the metamorphic aureole and those within it and this makes the evaluation of the metamorphic effects of the peridotite more difficult. There is a possibility of metasomatic interchange with the peridotite but no unequivocal evidence to support this. In the case of the Mt. Albert peridotite, Smith and MacGregor (1960) report essentially constant bulk compositions through the aureole.

MacKenzie distinguishes the outer margin of the metamorphic aureole to the Tinaquillo peridotite by color change of hornblende from green to brown, by the

appearance of pyrope-almandine garnet and by composition change of the plagioclase from albite-oligoclase to andesine. Augite may also appear at the outer edge of the aureole, but only becomes abundant in the inner part of the aureole and is there joined by common garnet and by minor hypersthene. MacKenzie attributes a maximum width to the metamorphic aureole of about 5000 feet. Although the change in mineralogy is certainly partly controlled by changes in bulk chemistry, the inner, near-peridotite rocks with typical hornblende granulite mineralogy (18 per cent augite, 2 per cent hypersthene, 20 per cent pyrope-almandine, 20 per cent brown hornblende, 37 per cent andesine, 2 per cent ilmenite-magnetite) are at a higher metamorphic grade than the surrounding hornblende-oligoclase-quartz gneisses. Within the peridotite, tabular bodies of granoblastic, foliated basic gneiss are in some cases concordant and in some cases discordant to the peridotite foliation. MacKenzie (1964) called these bodies "pseudo-gabbro" and interpreted them as metamorphosed inclusions of country rock (p. 312). This conclusion has been disputed by Thayer and Brown (1961) who preferred a magmatic origin for the "pseudo-gabbro." However, whatever their parentage, the "pseudo-gabbros" are clearly recrystallized metamorphic rocks of basaltic chemistry, and as such invite comparison with the rocks of the inner aureole. Like the rocks of the inner aureole, the mineralogy is that of hornblende granulite with 20 to 30 per cent brown hornblende, about 40 per cent plagioclase (labradorite), 15 per cent augite, 5 to 15 per cent hypersthene and minor ilmenite + magnetite. Small grains of almandine-pyrope garnet occur locally and the rarity of this phase and the increased abundance of hypersthene provide a contrast with the hornblende granulites of the inner part of the metamorphic aureole. While the lack of chemical data again hampers a close comparison, the differences in mineralogy may simply reflect the higher temperatures at similar pressures attained by the bodies included within the peridotite, in contrast to those at external contacts. Thus the left-hand side of equation (1) is favored by higher temperature or lower pressure and this reaction is consistent with the hypersthene + labradorite assemblage within the included basic bodies and the garnet + augite + andesine assemblage outside the peridotite. Free quartz from reaction (1) is unlikely to appear as it would be expected to react with the hornblende present.

$$(1)\quad \underset{\text{hypersthene}}{2(Mg,Fe)SiO_3} + \underset{\substack{\text{anorthite in}\\ \text{plagioclase}}}{CaAl_2Si_2O_8} \rightleftharpoons \underset{\text{garnet}}{Ca(Mg,Fe)_2Al_2Si_3O_{12}} + \underset{\text{quartz}}{SiO_2}$$

A detailed description of the aureole of the Mt. Albert peridotite has not yet been published but Smith and MacGregor (1960) describe the aureole as up to 1000-feet wide and ranging "from greenschist through epidote amphibolite to garnetiferous hornblende-pyroxene granulite" (p. 1978). Plagioclase becomes more calcic towards the contact. The appearance of garnet in the inner aureole invites comparison with the Tinaquillo rather than the Lizard peridotite.

The Horoman and Beni Bousera peridotites, which may be of comparable types to the three just described, have country rocks of pelitic character. The Horoman peridotite (Onuki, 1965, quoting Hunahashi, 1948) has produced cordierite + anthophyllite and cordierite + hypersthene assemblages and conditions of metamorphism appropriate to the pyroxene hornfels facies appear to have been attained. In contrast, the Beni Bousera peridotite (5 km × 15 km) forms the core and culmination of a sequence of metamorphic zones ranging from sericite schists, micaschists (with garnet, staurolite, andalusite), feldspathic gneiss (with biotite, garnet, sillimanite, kyanite) to an inner zone (600-feet wide) mainly of garnet and sillimanite-bearing graphitic gneiss with local occurrence of orthopyroxene-bearing gneiss and also

granulites of pyroxene + garnet + plagioclase + hornblende mineralogy.

2. Textures and structures of the metamorphic aureole. In the Lizard area, the amphibolites outside the metamorphic aureole have nematoblastic to lepidoblastic texture, a well-developed subhorizontal foliation with parallel compositional banding, and a strong lineation striking north-northwest due to alignment of hornblende prisms within the foliation plane. Adjacent to the peridotite, a new subvertical foliation, striking north-northwest, developed in the green-brown hornblende amphibolites and in the granulites. This parallels the foliation developed in the marginal zones of the peridotite and locally can be observed under development as an axial plane foliation where the subhorizontal foliation of the country rock is folded into complex rheid or fluid type folds adjacent to the peridotite. The texture of the metamorphic rocks changes from lepidoblastic to granoblastic in the granulites but a foliation in these rocks is clearly defined by compositional banding and lenticular variations in the proportions of minerals present. In contact areas of complex intermingling of peridotite and contact rocks, the basic granulites locally behaved as the more mobile rocks and were capable of intruding and including fragments of the margin of the peridotite (Green, 1964b, pp. 560–562). There is no clear evidence that partial melting of the granulites occurred.

In the Tinaquillo aureole, the garnet + pyroxene + hornblende granulites of the aureole and the pyroxene-granulites of the included "pseudo-gabbro" bodies are both foliated, gneissic rocks. Foliations in the basic rocks and adjacent peridotite are generally closely conformable.

C. The Peridotites

1. Chemistry. Each of the peridotites displays compositional variation in the form of banding and the average composition cannot be well defined. MacKenzie (p. 305) considers that more than 90 per cent of the Tinaquillo peridotite is dunite but the intensely mylonitized yet unserpentinized character of this body makes petrographic distinction between pyroxenes and olivine extremely difficult. Two analyses of typical, very fresh specimens show compositions matching peridotite rather than dunite (Table 7.1). MacKenzie describes small elliptical plugs of enstatite pyroxenite within the peridotite and also thin, sparsely distributed amphibole- and pyroxene-rich layers.

In the Lizard peridotite, textural differences have been used to define a coarse-grained "primary peridotite" within the core of the body and a finely foliated, recrystallized peridotite, closely resembling the Tinaquillo peridotite, nearer the margins of the body. Both types show compositional variation, but this is more clearly observable in the "primary peridotite" as lenticular compositional banding defined by variation in pyroxene content. However, in the Lizard peridotite, the dominant rock type is peridotite with approximately 60 per cent of olivine; pyroxenites, and chromite-bearing, serpentinized dunites comprise less than 10 per cent of the peridotite. An average composition for the Lizard peridotite is given in Table 7.1 (Green, 1964a, pp. 183–184).

No chemical data on the Mt. Albert peridotite has as yet been published, but Smith and MacGregor (1960) describe it as consisting of interbanded dunite and peridotite with minor enstatite pyroxenite. Onuki (1965) has published analyses from the Horoman peridotite which include rocks from dunite to plagioclase-bearing peridotite. The relative proportions of the various rock types are not specified but two analyses (Nos. 4 and 6 of Onuki, 1965) of peridotite and plagioclase peridotite are listed in Table 7.1. Two analyses of "saxonites" from the Beni Bousera peridotite are also given in Table 7.1. These are calculated anhydrous to enable better comparison with the other analyses. Milliard

TABLE 7.1 Chemical Compositions of High-Temperature Peridotites

	Tinaquillo						
	V1460 (Green, 1963)	V336 (Hess, 1964)	Lizard Average (Green, 1964a)	Beni Bousera 6 (Milliard, 1959)	Beni Bousera 7 (Milliard, 1959)	Horoman 4 (Onuki, 1965)	Horoman 6 (Onuki, 1965)
SiO_2	44.69	43.91	44.77	42.38	43.82	42.55	43.40
TiO_2	0.08	0.06	0.19	...	...	0.04	0.03
Al_2O_3	3.19	2.65	4.16	1.98	5.04	2.10	1.76
Fe_2O_3	0.09	1.44	...	5.21	1.31	1.33	2.01
FeO	7.54	7.23	8.21	6.90	6.20	6.76	6.35
MnO	0.14	0.15	0.11	0.27	0.18	0.11	0.13
MgO	39.80	42.01	39.22	40.13	38.92	44.06	43.15
CaO	2.97	2.02	2.42	2.60	3.88	2.36	2.45
Na_2O	0.18	0.13	0.22	0.39	0.52	0.14	0.19
K_2O	0.02	0.00	0.05	...	...	0.04	0.03
Cr_2O_3	0.45	0.41	0.40	trace	trace	0.24	0.25
NiO	0.26	...	0.24	trace	trace	0.27	0.25
H_2O+	0.38	...	...	...	...	...	...
P_2O_5	0.04	0.00	0.01	0.14	0.13	trace	...
	99.83	100.01	100.00	100.00	100.00	100.00	100.00

(1959) describes the body as garnetiferous saxonite or harzburgite with 50 to 70 per cent olivine, 30 to 50 per cent enstatite and 1 to 2 per cent garnet. The high CaO contents of the analyses indicate that clinopyroxene must also be present.

The comparison of chemical analyses in Table 7.1 illustrates the higher SiO_2/MgO ratio of these peridotites compared with dunites, such as Dun Mountain and Twin Sisters, and implies a pyroxene content of 20 to 40 per cent. Also Table 7.1 illustrates the presence of significant Al_2O_3, CaO, and Na_2O contents, which play an important role in giving rise to mineral phases sensitive to pressure changes. Rocks composed of olivine + chromite or olivine + enstatite + chromite are, in contrast, stable without distinctive mineralogical changes throughout a broad pressure range.

2. Mineralogy. The chemistry of the high-temperature peridotites is such that, under conditions of increasing pressure at high temperatures, three distinct mineral assemblages may form. In order of increasing pressure these are:

1. Olivine + enstatite + diopside + plagioclase + chromite.
2. Olivine + aluminous enstatite + aluminous diopside ± spinel-chromite solid solution.
3. Olivine + enstatite + diopside + garnet (chromian pyrope).

In the presence of water at moderately high temperatures a fourth assemblage of Olivine + pargasite ± enstatite + spinel may also form. (See Chapters 1-II and 12-II for more details.)

The Tinaquillo and Mount Albert peridotites illustrate the second mineral assemblage. In the Tinaquillo peridotite, plagioclase does not occur in any olivine-bearing rocks although MacKenzie (p. 307) does report plagioclase associated with orthopyroxene in thin bands. There is evidence in the Tinaquillo peridotite for two stages of crystallization—an early, coarse-grained stage characterized by highly aluminous clinopyroxene and orthopyroxene and a later stage of recrystallization during deformation characterized by fine grained olivine, pyroxenes of lower

alumina content, porphyroblastic aluminous spinel and minor pargasite (MacKenzie, 1960, pp. 313–314; Green, 1963).

The Lizard peridotite illustrates the derivation of the plagioclase-bearing assemblage by recrystallization of the olivine + aluminous pyroxenes + spinel assemblage under changing P-T conditions. The core of the peridotite preserves the higher pressure assemblage in which enstatite contains up to 6.5 per cent Al_2O_3 and coexisting diopside up to 7.1 per cent Al_2O_3; in both cases the Al_2O_3 is mainly present as Tschermak's silicate $(Ca,Mg)Al_2SiO_6$. The spinel (from 0.5 to 2 per cent of the rock) contains about 50 per cent Al_2O_3 and its textural relations indicate that it was probably the last phase to crystallize. The coarse-grained anhedral, interlocking texture of the core of the Lizard peridotite may be a result of igneous crystallization with a crystallization sequence olivine + enstatite → diopside → spinel. However, the apparent late crystallization of spinel could be a result of decreasing solubility of Al_2O_3 in pyroxenes with decreasing temperature and/or pressure, according to the reaction:

$$(2)\quad \underset{\text{aluminous pyroxene}}{(Ca,Mg)Al_2SiO_6} + \underset{\text{olivine}}{Mg_2SiO_4} \rightleftharpoons \underset{\text{spinel}}{MgAl_2O_4} + \underset{\text{pyroxene}}{(Ca,Mg)MgSi_2O_6}$$

This reaction has been suggested to account for growth of porphyroblastic spinel at the expense of aluminous pyroxenes in both the Lizard and Tinaquillo peridotites (Green, 1963, p. 1401; 1964a, p. 170). The conditions of crystallization of the primary mineral assemblage of the Lizard peridotite and of both the relict primary and recrystallized minerals of the Tinaquillo peridotite were such that olivine and plagioclase were in reaction relationship but plagioclase remained a stable phase in pyroxene-rich bands in the absence of olivine (Green, 1964a, p. 173).

Nearer the margins of the Lizard peridotite, the primary, coarse-grained mineral assemblage is replaced by fine-grained, foliated peridotite with relict augen of large, deformed pyroxene crystals. The recrystallized mineralogy is olivine + pyroxenes + plagioclase + chromite and the reactions giving rise to plagioclase may be written as follows (Green, 1964a, p. 169, 173):

$$(3)\quad \underset{\text{spinell}_{ss}}{(MgAl_2O_4 + FeCr_2O_4)} + \underset{\text{diopside}}{CaMgSi_2O_6} + 2\,\underset{\text{enstatite}}{MgSiO_3} \rightleftharpoons \underset{\text{anorthite}}{CaAl_2Si_2O_8} + 2\,\underset{\text{olivine}}{Mg_2SiO_4} + \underset{\text{chromite}}{FeCr_2O_4}$$

$$(4)\quad \underset{\substack{\text{aluminous}\\\text{enstatite}}}{Mg_9Al_2Si_9O_{30}} + \underset{\substack{\text{aluminous}\\\text{diopside}}}{Ca_5Mg_4Al_2Si_9O_{30}} \rightleftharpoons 2\,\underset{\text{anorthite}}{CaAl_2Si_2O_8} + 3\,\underset{\text{diopside}}{CaMgSi_2O_6} + 6\,\underset{\text{enstatite}}{MgSiO_3} + 2\,\underset{\text{olivine}}{Mg_2SiO_4}$$

The recrystallized pyroxenes have lower Al_2O_3 content and also lower contents of CaO in orthopyroxene and MgO + FeO in clinopyroxene; the plagioclase is labradorite in composition and the spinel is deep-brown or reddish-brown chromite. In their chemistry, the recrystallized orthopyroxene and clinopyroxene are similar to pyroxenes from layered igneous intrusives and are considered to indicate a temperature at recrystallization of around 1000°C. The primary mineral assemblage and the coexisting pyroxenes in particular, indicate conditions of initial crystallization of higher temperature and load pressures of at least 8 and probably less than 15 kb. The best evidence for initial crystallization under high load pressure is the incompatibility of olivine + plagioclase. Experimental studies by Green and Ringwood (1967) on olivine normative basalts including extremely magnesian compositions, and by Green (unpublished) on magnesian olivine + labradorite compositions and peridotite compositions closely matching the Lizard peridotite, indicate that magnesian olivine and calcic plagioclase are unstable together at 1100 to 1200°C at pressures above 10 kb. Kushiro and Yoder

(1964a) and T. H. Green (unpublished), in studies of the forsterite + anorthite system, observe reaction to yield aluminous pyroxenes + spinel above 8 kb at 1200°C.

Additional arguments by Green (1964a) used the high Al_2O_3 content of coexisting orthopyroxenes and clinopyroxene as evidence for high pressure of crystallization. This is supported by the experimental work of Boyd and England (1960b, 1963b) demonstrating an increase in the maximum solubility of Al_2O_3 in enstatite with increase in pressure (at pressures below those necessary to stabilize pyrope garnet). However partition of Al_2O_3 between aluminous pyroxenes and spinel is more complex, and it is uncertain at present whether decrease in Al_2O_3 content in pyroxenes and corresponding increase in the $MgAl_2O_4$ content of coexisting spinel, is a consequence of falling temperature at high but constant pressure, or a consequence of decreasing load pressure at essentially constant temperature (cf. Green, 1963, p. 1401).

In contrast to the Lizard peridotite, the Horoman peridotite appears to contain only the low-pressure olivine + pyroxenes + plagioclase + chromite assemblage. Onuki (1965) and Onuki and Tiba (1965), from a detailed comparison of the Al_2O_3 contents of the pyroxenes, conclude that the Horoman peridotite crystallized under similar conditions to the Lizard recrystallized peridotite assemblage, and at a higher pressure than such peridotites as Twin Sisters, Webster-Adie, Dawros, Cuba, but lower pressure than the Lizard primary peridotite.

The Beni Bousera peridotite is distinctive in preserving the highest pressure, garnet peridotite assemblage (see Chapter 5-IV). Milliard (1959, p. 141) notes an increase in foliation within the peridotite adjacent to the margins with the country rock but does not record any changes in primary mineralogy. In comparison with the mineral assemblage in the country rocks, in particular the presence of sillimanite rather than kyanite, the garnet peridotite assemblage is unstable, and if recrystallization during emplacement occurs at the margins as in the Lizard example, the garnet peridotite should be replaced by the olivine + aluminous pyroxenes ± spinel assemblage. The peridotite of Lherz may provide an example of transition between the garnet peridotite and spinel + aluminous pyroxene peridotite assemblages. Thus the type "lherzolite" (olivine + pyroxenes + spinel) is common but eclogite and garnet + spinel + pyroxenes + olivine assemblages also occur. The pressure required for appearance of garnet is sensitively dependent on the Fe/Mg ratio of the rock types and also on the Al_2O_3 content of the rocks in relation to the amount of pyroxene present; thus, apparently contrasting mineral assemblages may in fact be compatible at a given P-T in varying bulk chemistries.

3. *Texture and structure.* The Lizard peridotite has a coarse-grained core in which primary banding and incipient foliation due to recrystallization show fold patterns and attitudes not closely related to either the margins of the peridotite or the regional stress field. This is mantled by and passes transitionally into peridotite with a well-developed, fine foliation shown by lenticular variation in relative proportions of olivine, pyroxene, and plagioclase. Relict, coarser grains of enstatite and diopside are commonly preserved and have "tails" of recrystallized, pyroxene-rich peridotite paralleling the foliation. Porphyroblastic spinel is surrounded by lenticular mantles of plagioclase. The texture of the peridotite is a consequence of recrystallization during deformation at high temperature rather than a low-temperature cataclastic mylonization. The attitude of the fine foliation in the Lizard peridotite closely follows the attitude of the peridotite/country-rock contact in areas near to the contact but within the body is subvertical and parallels the *b-c* plane of the regional stress field.

In the Tinaquillo peridotite, the body is entirely composed of finely foliated peridotite with very distinctive porphyroclasts of enstatite and diopside and smaller porphyroblastic spinel. The body as a whole is a moderately dipping tabular mass and the foliation in general is conformable, particularly near the southern contact zone. MacKenzie (p. 306, 313) describes remarkable, lath shaped orthopyroxenes in the Tinaquillo peridotite and regards them as formed by translation gliding of favorably oriented crystals.

Smith and MacGregor (1960) liken the internal structure and steep folds defined by peridotite-dunite banding to the internal structure of salt domes and invoke a similar intrusion mechanism, that is, mobility of a crystalline body involving recrystallization and crystal deformation. Smith and MacGregor record areal differences in chrome-spinel and enstatite compositions, unrelated to the primary banding and irregularly distributed through the body. These are attributed to variations in water content during emplacement.

D. Conditions of Emplacement of High-Temperature Peridotites

A temperature of emplacement of approximately 1000°C has been deduced for all three peridotites, based mainly on the chemical characteristics of the pyroxenes and the metamorphic grade of the contact metamorphic rocks. At this temperature, the peridotites are considered to be completely crystalline and owe their mobility to the ease of recrystallization and plastic deformation of olivine at high temperatures. The large temperature difference between the peridotite and the regional country-rock environment determines that the peridotite is the more mobile rock and capable of intrusion in the solid state.

If the temperature of intrusion and the maximum temperature attainable in contact zones or included country-rock is 1000°C, then it is possible to make fairly closely controlled estimates of the load pressures at emplacement of the bodies. The final level of emplacement of the Lizard peridotite was such that olivine + plagioclase were stable in both the peridotite and basic country-rock. At 1000°C this indicates load pressures less than 8 to 9 kb from experimental work of Green and Ringwood (1967), and Kushiro and Yoder (1964a). The absence of garnet in the contact granulites provides confirmatory evidence of a lower load pressure and its presence in the contact zones of both the Tinaquillo and Mount Albert intrusions is consistent with these bodies preserving the higher pressure peridotite assemblage. Thus, in these rocks the reaction of orthopyroxene + plagioclase to yield garnet + clinopyroxene indicates conditions in the high pressure sub-facies of the granulite facies (De Waard, 1964; Ringwood and Green, 1964; Green and Ringwood, 1967). In the Tinaquillo peridotite, the olivine + aluminous pyroxenes + spinel assemblage in the peridotite coexists with the orthopyroxene + clinopyroxene + plagioclase + hornblende assemblage in included gabbroic bodies. The compatibility of these assemblages at 1000°C means that load pressures lie between 9 and 12 kb approximately. The lower temperature of the country rocks immediately outside the peridotite determines that the basic rocks are there within the ga + cpx + plag granulite field. Similar load pressures may be deduced for the Mount Albert peridotite if a temperature of intrusion of the order of 1000°C can be assumed. If the temperature of crystallization of the primary assemblage of the Lizard peridotite is correctly deduced as above 1000°C and nearer to 1200 to 1300°C, then the stability of the olivine + aluminous pyroxenes + spinel assemblage and of plagioclase + orthopyroxene + clinopyroxene indicate pressures probably between 10 and 18 kb.

In the Horoman peridotite, the stability of cordierite and hypersthene in the contact metamorphic rocks implies low-

pressure (pyroxene hornfels) conditions of emplacement, probably at shallower depths than the Lizard peridotite. On the other hand, the presence of ga + cpx and ga + cpx + plag assemblages and the stability of sillimanite rather than kyanite in the contact rocks of the Beni Bousera peridotite imply pressures similar to those of the Tinaquillo and Mount Albert peridotites.

E. Origin of High-Temperature Peridotites

The chemical composition of the high-temperature peridotites is close to a possible mean composition for a peridotite upper mantle and these peridotites have the potential for partially melting to yield 10 to 20 per cent of basaltic magma. Arguments relevant to this hypothesis have been advanced by Green and Ringwood (1963) and Hess (1964). If this hypothesis is valid then the high-temperature peridotites have an important significance in that they represent complete mobilization and intrusion to crustal levels of portions of mantle peridotite. This hypothesis was advocated by Green (1964a) and probably implies the existence of a high-temperature ultramafic liquid or liquid + transported olivine crystals within the mantle. Complete crystallization of such an intrusion occurs in the lower crust or top of the mantle but continued emplacement as a crystalline diapir continues because of temperature and mobility (rheidity) differences between the hot peridotite and cooler country-rocks. This hypothesis would place the high-temperature peridotites as genetically distinct from other alpine ultramafics such as Dun Mountain, Red Hills (New Zealand); Twin Sisters, Klamath Mountains (northwest United States), Musa Valley (Papua), Zambales Range (Philippines), and Camaguey (Cuba).

An alternative hypothesis suggested by recent experimental work on basaltic compositions at high pressure (Green and Ringwood, 1964, and unpublished data; Tilley and Yoder, 1964) is that the initial high-temperature, coarse-grained minerals of the peridotites are accumulates at high load pressure from a picritic or olivine tholeiitic magma. It has been shown (Green and Ringwood, 1964) that the pyroxenes crystallizing at 10 to 20 kb from olivine tholeiite and picritic liquids are rich in Al_2O_3. It is thus conceivable that a picritic or olivine tholeiite magma, held near the base of the crust could precipitate olivine + aluminous pyroxene(s). The residual liquid of alkali basaltic or olivine-poor composition (depending on the depth of differentiation) could then be tapped off and a high temperature, crystalline body of the observed high-temperature peridotite composition be left behind. Slight cooling of such a body would probably cause exsolution of spinel from the pyroxenes and the onset of nonhydrostatic pressure while the crystal accumulate was still hot could cause diapiric, crystalline intrusion to higher crustal levels. This second hypothesis invokes an origin for these peridotites similar to that advocated for the more common alpine ultramafics such as Musa Valley, Dun Mountain, Twin Sisters (see Section A) *except* that the accumulation of crystals from the parental picritic or olivine tholeiitic magma must occur at depths greater than 25 to 30 km whereas the accumulation of such alpine layered complexes as Red Hills and Musa Valley must occur more probably at depths of 5 to 10 km.

It is considered that criteria to distinguish between the hypotheses are at present lacking. Much depends on a knowledge of the type of basaltic liquid produced by partial melting of the mantle at depths of 60 to 150 km. If the liquid formed at minimum temperatures of melting at these depths is picritic with some 30 to 40 per cent normative olivine then the high-temperature peridotites are correspondingly easier to explain as deep-seated crystal accumulates from such a magma. If, on the other hand, the minimum melting liquids are nearer olivine tholeiite with 15 to 20 per cent normative olivine, then it is more difficult or impossible to envisage

peridotites with approximately 60 per cent olivine as accumulates at 10 to 20 kb from such relatively olivine-poor liquids.

Although their primary origin is thus an open and debatable question, the high-temperature peridotites provide clear evidence of the following:

1. Mobility of high-temperature but entirely crystalline peridotite within the crust.
2. Movement of such high-temperature peridotites through distances of 5 to 10 km, implying changes of load pressure of at least 2 to 3 kb.

IV. CHEMICAL AND STRUCTURAL RELATIONS OF ULTRAMAFIC AND FELDSPATHIC ROCKS IN ALPINE INTRUSIVE COMPLEXES

T. P. Thayer

A. Introduction

Igneous rocks of the alpine type, as originally defined by Benson (1927) consist of gabbros as well as ultramafic rocks, and include those rocks commonly called "ophiolites." Benson (p. 6) said alpine igneous rocks "are comprised of the majority of "green-rocks" as considered by Suess (in 1909). These are also the "ophiolitic rocks" as defined by Steinmann (in 1905), in which serpentines and gabbros are intimately associated with amphibolites and diabases. . . . They occur in regions that have been intensely disturbed by overthrusting and alpine orogeny." Peridotite and gabbro were accepted matter-of-factly as members of this family of rocks, and still are by adherents to the ophiolite hypothesis. A conceptual divorce of alpine ultramafites from gabbro and more silicic rocks resulted from Hess' (1938) hypothesis of a primary peridotite magma, and has been carried to its logical conclusions in Lizard by Green (1964a, 1964b), in Venezuela by MacKenzie (1960), and in generation of basalts by Ringwood, MacGregor, and Boyd (1964, p. 148). By outlining some genetic relationships of gabbroic, dioritic, and granophyric rocks to alpine ultramafites, I hope to reemphasize a close kinship that was recognized at least 40 years ago. Like Benson, I regard the ultramafic and gabbroic parts of ophiolite complexes as being identical with, and part of, the alpine igneous rock suite.

At least three distinct types of layered plutonic intrusions composed predominantly of gabbroic and peridotitic rocks can now be recognized in orogenic belts: (1) the alpine, (2) the Duke Island (Chapter 4-II), and (3) the Duluth (Taylor, 1964) or Moxie (Visher, 1961). Despite fundamental differences, similarities in the three kinds of intrusions have led to confusion because distinguishing criteria have not been defined. Six of the principal kinds of features that characterize alpine complexes (Thayer, 1960; 1963a; 1963b; 1964) are as follows:

1. Close areal and structural association of ultramafites, gabbroic, dioritic, and granophyric rocks.
2. Predominance of highly magnesian olivine over pyroxene in ultramafic parts of complexes.
3. Podiform chromite deposits.
4. Flow-layering and related structures and textures that are characteristic of high-grade metamorphic rocks.
5. Complicated structural relations between gabbroic and ultramafic rocks, such as intertonguing of major units along flow-layering; intrusive relations between various facies; and dikes of gabbro in peridotite or vice versa, without chilled margins.
6. Distribution of soda-rich dioritic and

A9

Reprinted from:

EARTH AND PLANETARY SCIENCE LETTERS

A LETTER JOURNAL DEVOTED TO THE DEVELOPMENT IN TIME OF THE EARTH AND PLANETARY SYSTEM

Volume 4, number 2, April 1968

THORIUM, URANIUM AND POTASSIUM ABUNDANCES IN PERIDOTITE INCLUSIONS AND THEIR HOST BASALTS

D. H. GREEN, J. W. MORGAN and K. S. HEIER

pp. 155–166

NORTH-HOLLAND PUBLISHING COMPANY - AMSTERDAM.

This is an offprint of an article which has been published originally in:

Earth and Planetary Science Letters

Editors: P. W. GAST, J. GEISS, W. GENTNER, E. D. GOLDBERG, E. I. HAMILTON, E. PICCIOTTO and R. J. UFFEN.

A letter journal devoted to the development in time of the earth and planetary system.

Monthly. Subscribtion price: vol. 3 and 4, 1968 $ 16.—, Hfl. 58.—.

Orders may be placed with your agent or directly with:

AMSTERDAM
P.O. BOX 103
NORTH HOLLAND PUBLISHING CO.
THE NETHERLANDS

P 8 M 268

To:

☐ Please enter my subscription to **Earth and Planetary Science Letters, vol,** 3 and 4. 1968 at the subscription price of $ 16.—, Hfl. 58.— (per volume)

☐ Please send vol, 1 and 2 of **Earth and Planetary Science Letters** at the price of $ 16.—, Hfl. 58.— (per volume)

☐ cheque enclosed ☐ please bill me

Name: _____

Full address: _____

_____

ZIP-Code: _____

Date :_____ Signature:_____

Printed matter postage please

EARTH AND PLANETARY SCIENCE LETTERS 4 (1968) 155-166. NORTH-HOLLAND PUBLISHING COMP., AMSTERDAM

THORIUM, URANIUM AND POTASSIUM ABUNDANCES IN PERIDOTITE INCLUSIONS AND THEIR HOST BASALTS

D. H. GREEN, J. W. MORGAN * and K. S. HEIER
Department of Geophysics and Geochemistry,
Australian National University, Canberra

Accepted 11 March 1968

The abundances of the radioactive elements uranium, thorium and potassium in six lherzolite inclusions and their host basanites have been determined by neutron activation analysis and γ-ray spectrometry. The lherzolite inclusions have marked differences in K/U, K/Th and smaller differences in Th/U from the basanites. The contents of those elements in lherzolite inclusions are not determined simply by varying degrees of contamination by the host magma. The lherzolites are inferred to be accidental xenoliths in the host magma and their geochemical characteristics are representative of at least some parts of the upper mantle. They are considered to represent residual material left after extraction from mantle pyrolite of an undersaturated basaltic magma or after selective extraction of minor elements by wall-rock reaction processes. Processes of magma extraction from the mantle may lead to strong depletion of K in residual mantle peridotite with very little accompanying depletion in U and Th. The abundances of U, Th and K in the lherzolite inclusions are also compared with various estimates of upper mantle composition based on heat flow data.

1. INTRODUCTION

The abundances and distribution of the radioactive elements potassium, uranium and thorium in the earth's upper mantle are fundamental parameters in the construction of earth models. The earth's upper mantle is considered to be of peridotitic composition and it has been argued that certain types of naturally occurring peridotites are directly derived from the upper mantle [1-5]. However, the natural processes of sampling of the upper mantle, e.g. by basaltic volcanism, kimberlite breccia pipes or extreme tectonic deformation, are such that there is a likelihood of mineralogical and chemical change in the mantle peridotite in transit to shallower levels. In this paper we present data on the abundances of U, Th and K in lherzolite (peridotite) inclusions and in their host magmas and examine the relevance of these data to the relationship between the inclusions and host magma and the wider subject of upper mantle composition and homogeneity.

1.1. *Occurrence and petrology of investigated rocks*

Coarse-grained lherzolite inclusions in undersaturated basaltic rocks are of world-wide distribution and have long attracted interest as possible fragments detached from the earth's upper mantle. The distinctive mineralogy (olivine, aluminous enstatite, aluminous clinopyroxene, aluminous spinel) of the inclusions has been shown to be of high-pressure, high temperature character, and recent experimental studies on relevant simple and complex systems indicate that pressures of at least 8-10 kb but less than 27 kb are required to produce the observed mineralogy at temperatures of around 1000°C or more [3,6,7]. These conditions of crystallization indicate an upper mantle environment but the significance of inclusions in deducing upper mantle chemical composition and characteristics requires a knowledge of their relationships to their host basalts.

Lherzolite inclusions are common in some Tertiary and Quaternary volcanics in Eastern Australia and

* Present address: Australian Atomic Energy Commission, Private Mail Bag, Sutherland, N.S.W.

Tasmania. We have analyzed six inclusions from Quaternary basanite scoria cones in the Newer Volcanics of Western Victoria and south-eastern South Australia (fig. 1). Four of the basanites analyzed are from the same scoria quarries as the inclusions and the basanites themselves contain very small inclusions or xenocrysts. One basanite (2780), also containing lherzolite inclusions, is from Upper Tertiary basalts in north western Tasmania and one alkali olivine basalt (2909) is from Mt. Schank, an eruptive centre 10 miles south of the inclusion-bearing eruptive centre at Mt. Gambier (fig. 1). The samples range over the Newer Volcanics province from its western edge near Mt. Gambier almost to its eastern limit in Central Victoria. The Tasmanian sample is from a petrographically similar but older basanite and provides a link with previous U, Th and K determinations by Compston et al. [8] on tholeiitic and alkaline basalts from the Tasmanian Tertiary province.

The lherzolite inclusions examined were all large (4" - 6" diameter) and were selected after thin section examination of over one hundred inclusions. All six contain (in order of abundance) olivine, enstatite, chrome-diopside and minor spinel and all have coarse-grained, allotriomorphic texture with notable variations in grain size and minor strain effects in olivine and pyroxenes. The samples were selected in an attempt to encompass some of the mineralogical variations ob-

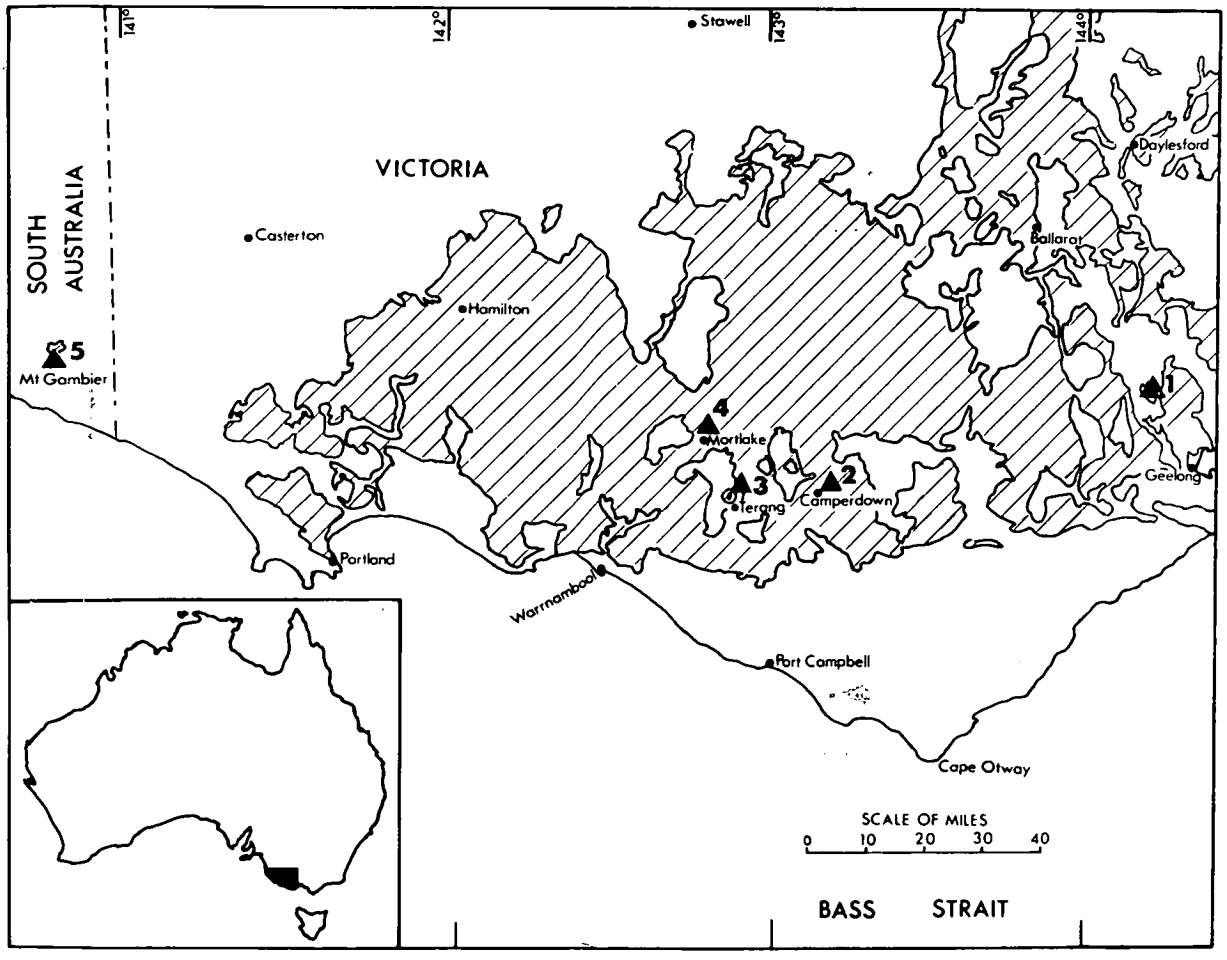

Fig. 1. Locality map showing distribution of Newer Volcanics in Western Virginia and the localities of eruptive centres from which lherzolite inclusions were collected. 1. Anakies. 2. Mt. Leura. 3. Mt. Noorat. 4. Mt. Shadwell. 5. Mt. Gambier.

served in the petrographic examination, particular attention being paid to the presence of accessory minerals which might contain high concentrations of K, U, Th and also the presence or absence of small patches of glass. These patches of glass range from clear, almost colourless, to brown in colour and are typically developed at grain boundaries between clinopyroxene and spinel. The spinel is corroded with development of an opaque rim against the glass and the clinopyroxene is also corroded and apparently replaced by areas of glass containing small crystals of olivine and recrystallized clinopyroxene. In most cases the glass has the appearance of developing in situ at grain boundaries within the inclusion and with no observable connection with the host basanite (partly glassy) surrounding the nodule. Occasionally, veinlets of glass connect internal glass patches with the enclosing basanite. The collection of data on K, U, Th contents of glass-bearing inclusions could help to evaluate whether these inclusions acted as closed or open systems in relation to the surrounding basanite. The following notes indicate the distinctive mineralogical characteristics which led to the choice of the six inclusions:

No. 2604 Olivine-rich lherzolite (dunite) with minor enstatite, rare clinopyroxene and rare deep brown spinel. No glass or internal grain boundary reactions.

No. 2728 Lherzolite with common enstatite, moderately common clinopyroxene and minor yellow-brown spinel. No glass or internal grain boundary reactions.

No. 2642 Lherzolite with common enstatite, clinopyroxene, minor yellow-brown spinel and minor pale yellow-brown hornblende as small grains associated with spinel and clinopyroxene. No melting or internal grain boundary reactions.

No. 2640 Similar to 2642 but spinel is deeper coloured (brown), hornblende is absent but there are extremely rare grains of pale brown phlogopite, in some cases included within olivine or within spinel. No melting or internal grain boundary reactions.

No. 2700 Similar to 2642, 2640, but clinopyroxene more abundant (> orthopyroxene), minor red-brown spinel and rare apatite. Hornblende and phlogopite are absent. The apatite occurs as small anhedral grains filling spaces between olivine and pyroxene crystals; it has no tendency to euhedral form and is very turbid with many small fluid inclusions. Patchy development of colourless glass with small olivine and clinopyroxene euhedra occurs at the expense of clinopyroxene and spinel. The apatite shows no relation in its distribution to the patches of glass but where veinlets of glass extend along grain boundaries to contact apatite, the latter is recrystallized against the glass to clear, inclusion-free apatite with euhedral margin against the glass.

No. 2669 Similar to 2640, 2642 but amphibole, phlogopite and apatite are absent. Clinopyroxene is moderately common and there is minor red-brown spinel. There is prominent grain boundary reaction involving clinopyroxene and spinel with patches of recrystallized, euhedral olivine and clinopyroxene in colourless glass surrounding corroded spinel crystals. There appear to be no 'feeders' of glass from the basalt contact to the areas of glass within this inclusion or in 2700.

2. ANALYTICAL METHODS

Flat slabs (about 200 g) were cut from the selected nodules, carefully cleaned from enclosing basalt and powdered, sieved and quartered with stringent precautions against contamination. From the sample prepared in this way, aliquots were taken for the U and Th measurements and for the K determinations. The analytical method for the K-determinations by neutron activation has been described by Morgan and Goode [9] and the U, Th determination methods are described fully by Morgan and Lovering [10]. Duplicate determinations (separate dissolutions) were made on all samples. U and Th were determined simultaneously on the same aliquot of powdered rock after irradiation for one week. The K determinations were made on separate dissolutions of samples irradiated for only 24 hours [9]. Generally six samples and two comparator standards were included in each batch for irradiation. The precision of all determinations was 3% or better. This was estimated from the sample counting statistics and the standard deviation of the four appropriate comparator sources (i.e. duplicate aliquots of each of the two standards from a batch). The estimated error includes all the uncertainties involved in the determinations except for any systematic errors in the solutions from which the standards were prepared. The accuracy of the methods has been established previously [9, 11, 12].

For the host basalts the K, U and Th determinations by γ-ray spectrometry were carried out using the techniques described by Heier et al. [13]. At the concentration levels in the basalts, the precision of the U and Th determinations is from 3 to 5% and the precision of the K determinations is better than 1% [13]. K determinations by flame photometry [2, 3] carried out by E.

Table 1
Potassium, uranium and thorium abundances in lherzolite nodules and basanites.

Sample No. and locality	Potassium (ppm)	Av.	Uranium (ppm)	Av.	Thorium (ppm)	Av.	Th/U	K/Th	K/U
Lherzolite nodules									
2604 Anakies	70 70	70	0.0227 0.0198	0.0212	0.105 0.104	0.104	4.9	0.67×10^3	3.3×10^3
2728 Mt. Gambier	29 30	30	0.0095 0.0099	0.0097	0.0353 0.0363	0.0358	3.7	0.85×10^3	3.1×10^3
2642 Mt. Leura	15 14	15	0.0186 0.0174	0.0180	* 0.107 0.0771	0.0771	4.3	0.19×10^3	0.8×10^3
2640 Mt. Leura	12, 11 13, 12	12	* 0.0050 0.0030	0.0030	0.0142 0.0137	0.0139	4.6	0.86×10^3	4.0×10^3
2700 Mt. Noorat	109 110	110	0.112 0.115	0.114	0.437 0.477	0.457	4.0	0.24×10^3	1.0×10^3
2669 Mt. Shadwell	90 91	91	0.0400 0.0400	0.0400	0.189 0.214	0.202	5.0	0.45×10^3	2.3×10^3
Basanites	%								
2636 Mt. Leura	2.04 † 2.02 ‡ 2.04		2.3_1		7.2_5		3.1	2.8×10^3	8.8×10^3
2650 Mt. Leura	1.89 † 1.84		2.1_6		6.6_6		3.1	2.8×10^3	8.8×10^3
2705 Mt. Noorat	1.38		1.7_2		5.7_0		3.3	2.4×10^3	8.0×10^3
2679 Mt. Shadwell	1.49 † 1.48		1.6_3		5.7_0		3.5	2.6×10^3	9.1×10^3
2780 Guildford Junction Tasmania	1.39		1.3_2		4.2_5		3.2	3.3×10^3	10.5×10^3
2909 Mt. Schank S. Australia	2.38		2.4_1		8.0_0		3.3	3.0×10^3	9.9×10^3

* Values discarded because of low recovery (< 1%) in chemical separation.
† Determined by flame photometer (E. Kiss, analyst).
‡ Determined by X-ray fluorescence by Dr. B. W. Chappell.

Kiss, are in excellent agreement with the γ-ray spectrometry determinations (table 1).

3. DISCUSSION OF DATA

In the lherzolite inclusions, K, U, Th all show variations in abundance through more than one order of magnitude and this variation cannot be equated to variations in abundances of the major minerals. Correlation between K, U, Th abundances and the minor accessory minerals is equivocal. Thus 2640, which in thin sections contained rare phlogopite grains, and was expected to be richer in K, has the lowest K-content of all, suggesting that the crushed part of the sample contained no phlogopite. On the other hand, the presence of apatite in 2700 may be correlated with the high U, Th abundances in this inclusion. Fission track studies of these inclusions by J. D. Kleeman are in progress and have already demonstrated the high U content of apatite in 2700 (J. D. Kleeman, personal communication). The two specimens containing glass have higher K, U and Th contents than the other samples.

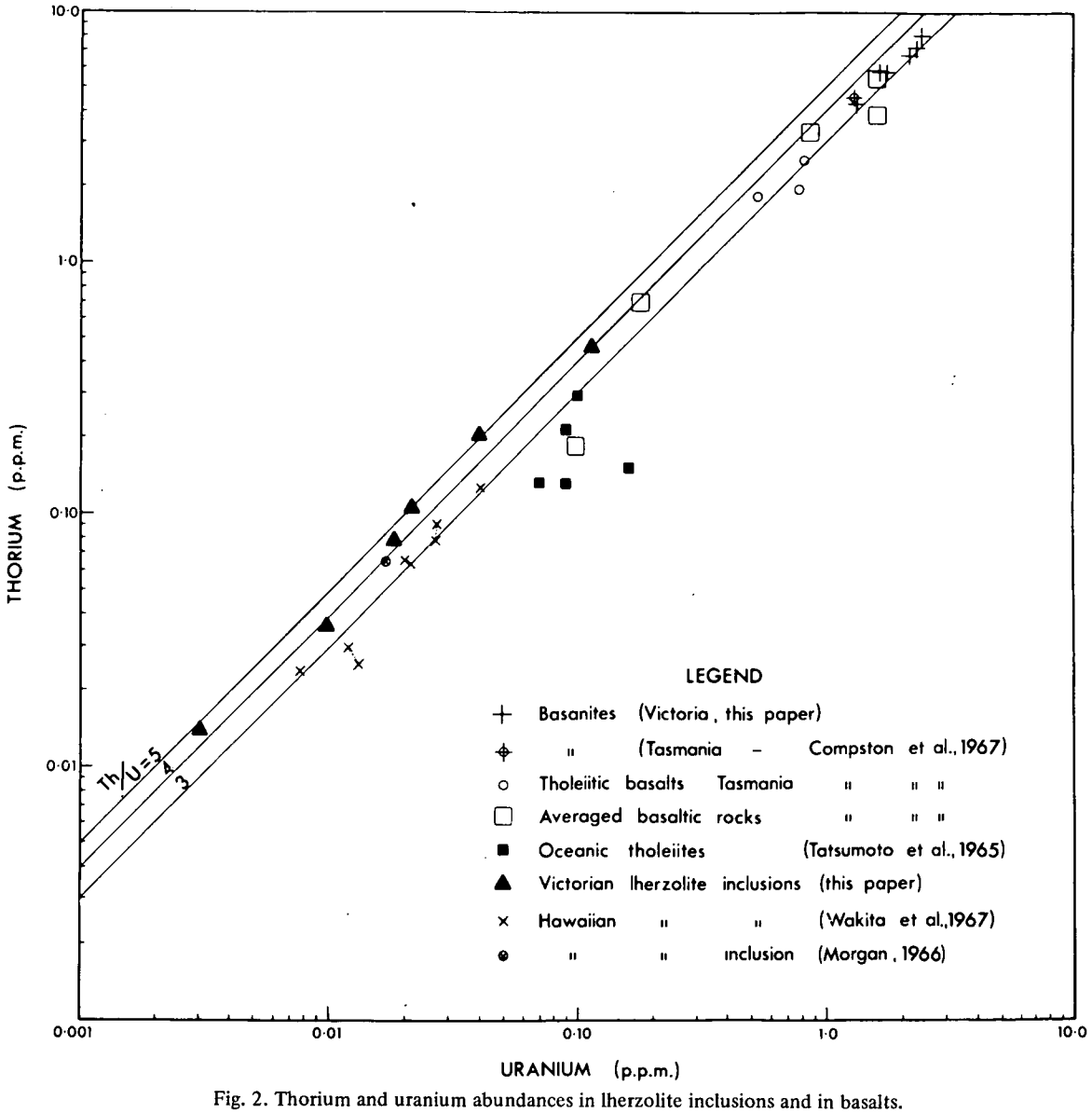

Fig. 2. Thorium and uranium abundances in lherzolite inclusions and in basalts.

Separate regression analyses of the Th, U data (fig. 2) on the six lherzolite inclusions and on the six basanites yield two lines which are statistically indistinguishable at the 95% confidence level in slope and intercept from one another. The meaning of this correlation is not clear to us, it implies that with decreasing U and Th abundances the Th/U ratios regularly increase for this particular selection of data. The conclusion would not apply if data on other basalts and other lherzolites were included (fig. 2). The K, Th and K, U contents of the lherzolites and basanites do *not* show a similar correlation to that of Th and U.

3.1. *Comparison with previous data*

Wakita et al. [14] have recently published data on U, Th contents in lherzolite inclusions in basalts and their data for inclusions from the Hawaiian islands are plotted in fig. 2. There is a range in U, Th abundances similar to that observed in the Victorian province but the Th/U ratios appear to be significantly lower (av. 2.9, range 1.9 - 3.4). These determinations were also made by neutron activation methods, but without interlaboratory comparisons and more extensive data it would be unwise to attach too much significance to the consistency of Th/U ratios within each province

and the consistent difference between the provinces. A determination in this laboratory by Morgan and Lovering of Th, U contents of a single lherzolite nodule from the Salt Lake Crater, Oahu, locality is plotted in fig. 2 and the measured Th/U ratio is 3.8 i.e. higher than those measured by Wakita et al. Wakita et al. also obtained data from lherzolite inclusions from the two other oceanic localities and from six continental localities. The latter inclusions have similar uranium contents to the Victorian and Hawaiian examples but a wider variation in Th contents and thus in Th/U ratios (0.28 to 16). Comparison of our data with those of Wakita et al. supports their statement that there is no indication that oceanic samples have higher uranium and thorium concentrations than inclusions from continental localities. The Victorian data suggest that Th/U ratios for inclusions may be nearly constant for a basalt province of limited extent, but taken in conjunction with the Hawaiian and continental localities [14], suggest that there may be considerable inhomogeneity in Th/U ratios of the lherzolite source material when viewed on a world-wide scale. Such inhomogeneity would, if persistent over a long time interval, considerably influence regional variations in Pb isotopic ratios.

We are not aware of any published data on K contents of inclusions in which the U, Th concentrations have also been measured. Steuber and Murthy [15] measured K contents by isotope dilution methods on five lherzolite inclusions and obtained values of 31 - 190 ppm.

The lherzolite inclusions from Victoria have Th/U ratios ranging from 3.7 to 5.0 (mean 4.4), i.e. consistently higher than their host basanites (ranging from 3.1 to 3.5, mean 3.3). K/Th and K/U ratios show a wider scatter than Th/U ratios but both ratios are consistently lower in the inclusions than in the host basalts. This is particularly evident in K/Th ratios which differ by more than an order of magnitude in some cases. This conclusion remains true if additional data on Tasmanian Tertiary basalts are included. These basalts range from olivine nephelinite to olivine tholeiite [8] and thus cover a range of K contents from 0.5% to 2.0%.

Basalts in general display a wide range of K, U and Th contents and the Tasmanian and Victorian rocks are quite highly enriched in these elements. In figs. 2 and 3, they are compared with averaged K, U, Th contents of other basaltic magma provinces [8] including the Tasmanian and Antarctic Jurassic dolerites, the average Hawaiian tholeiites and the averaged analyses and individual analyses for the low-potassium 'oceanic-tholeiites'. In fig. 4, the K and U contents of the Victorian and Tasmanian Tertiary basalts are compared with individual analyses of both alkaline and tholeiitic basalts from oceanic provinces (mainly the Hawaiian and mid-ocean ridge localities). There are no apparent differences in element ratios between the Victorian and Tasmanian basalts from a continental environment and similar rocks from oceanic environments. There is a tendency for oceanic tholeiites with very low K, U, Th contents to have slightly higher K/Th and lower Th/U ratios than other basalts.

The data plotted in figs. 2, 3, 4 are considered to represent the K, U, Th abundances in basaltic magmas and may be compared with the abundances in the lherzolite inclusions. The Th and U concentrations in the inclusions overlap the lower limits of the basalt spectrum, but it should be noted that the Th/U (4.4) ratio of the Victorian inclusions is higher than that of the oceanic tholeiites (1.8). Differences between the inclusions and the spectrum of basalts are much more apparent in figs. 2 and 3 where it can be seen that although the inclusions and basalts appear to form a continuum in U and Th concentrations they are notably distinct in K concentrations and particularly in their K/Th and K/U ratios. Within the basalt spectrum there is a trend of increasing K/Th with decreasing K and Th concentrations but this trend does not continue into the suite of inclusions.

4. APPLICATIONS OF DATA

4.1. *Lherzolite inclusions in basalts - closed or open systems?*

The analytical data presented clearly demonstrate that the lherzolite inclusions cannot be regarded simply as 'barren' (in K, U, Th), refractory crystal aggregates with a small but variable mixture (e.g. along grain boundaries) of the host basanite. The marked differences in K/Th, K/U and to a lesser degree Th/U ratios show that *either* the inclusions and basanites are chemically distinct systems accidentally brought into juxtaposition and which have not attained chemical or mineralogical equilibrium *or* that there is a

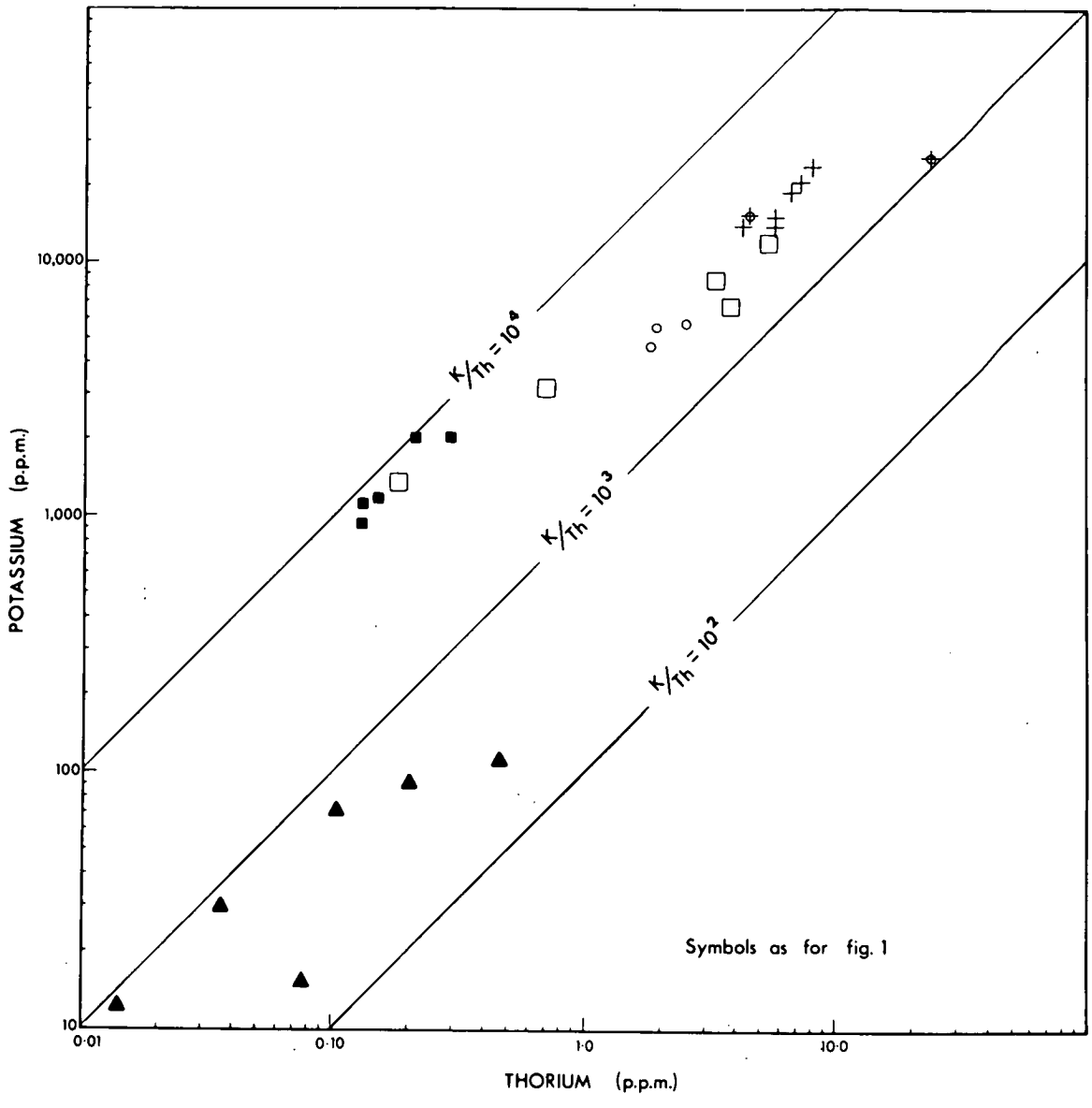

Fig. 3. Potassium and thorium abundances in lherzolite inclusions and in basalts.

very distinctive partition relationship between inclusions and host basanites such that the inclusions preferentially accept Th and U relative to K while the liquid attains higher K/Th, K/U and lower Th/U ratios. Factors unfavourable to the latter interpretation include the variable nature of the accessory minerals (particularly hornblende, phlogopite, apatite which should contain high K, U or Th contents) without large differences in element ratios and the conformity of the glass-bearing and glass-free inclusions. Further evidence against the second hypothesis is provided by a study in progress by J. A. Cooper of this laboratory which has demonstrated very significant differences in Pb isotopic ratios between lead extracted from the lherzolite inclusions and that extracted from the host basanites. No significant differences in $^{87}Sr/^{86}Sr$ ratios between nodule and host basalt were observed by Stueber and Murthy [15].

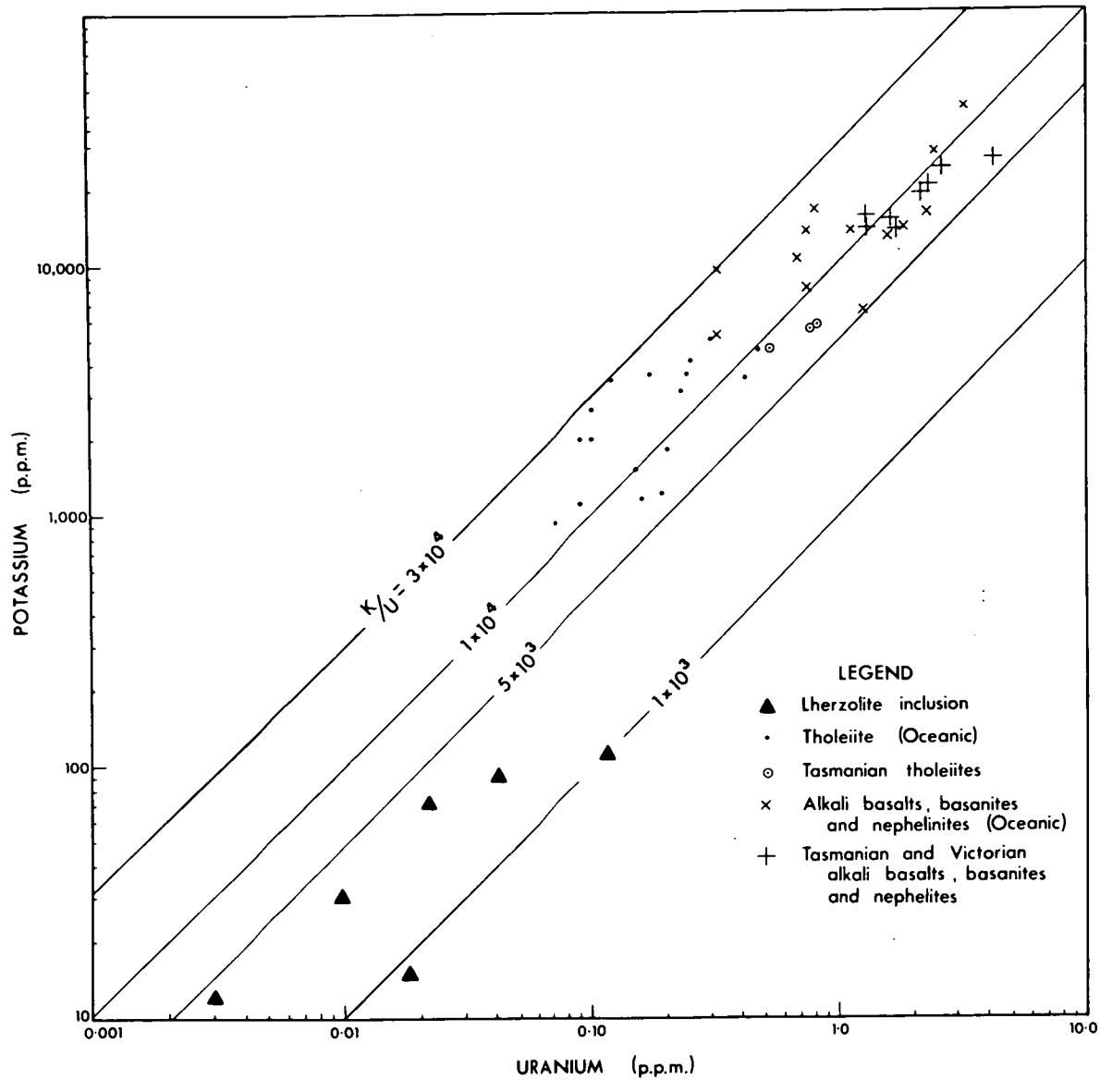

Fig. 4. Potassium and uranium abundances in lherzolite inclusions and in basalts.

A particularly important point in evaluating the origin of the glass in inclusions 2669 and 2700 is that these inclusions, while they have higher K, U and Th contents than the other examples, have lower than average K/Th and K/U ratios and 2669 has the highest Th/U ratio observed. Thus these two inclusions do *not* demonstrate a transition in their K, U, Th characteristics between the lherzolite population and basanite populations as would be expected if the glass were a contaminant penetrating the nodule from the enclosing magma. It may be noted that addition of 1% of basanitic glass would more than double the K content of the inclusions and produce element ratios intermediate between the lherzolite and basanite populations.

4.2. *Lherzolite inclusions as mantle xenoliths*

The preceding discussion accentuates the geochem-

ical differences between the lherzolite inclusions and their host basanites and provides evidence that the lherzolites are accidental rather than cognate inclusions in the basanites. Furthermore, the K, U, Th contents of the inclusions examined appear to be characteristic of the inclusions themselves and not secondary contamination from the enclosing magma. Before the data can be applied to any discussion of upper mantle radioactive element abundances it is necessary to consider hypotheses relating the inclusions to processes of earth differentiation and magma formation.

Stueber and Murthy [15,16] determined potassium, rubidium and strontium abundances and $^{87}Sr/^{86}Sr$ isotopic ratios for some lherzolite inclusions and suggested a specific crust-mantle model in which the source of the lherzolite inclusions was envisaged as a narrow zone beneath both continental and oceanic areas, lying between barren, refractory dunite and underlying primary mantle peridotite ('pyrolite') in continental areas and between basaltic oceanic crust and primary mantle pyrolite in oceanic areas. Stueber and Murthy considered that the lherzolite inclusions represent residual material after basalt extraction from pyrolite at various geological times.

Green and Ringwood [2] in discussing processes of basalt generation in the upper mantle regarded lherzolite inclusions as accidental xenoliths and representative of mantle regions depleted in certain elements either by partial melting or by a process of 'wall-rock reaction'. They showed that primary or parental mantle ('pyrolyte') would, at appropriate pressures, yield an alkali olivine basalt magma by 15-20% melting passing transitionally to an olivine tholeiite magma with higher degrees of melting (30%) under the same load pressures. Once separated from their source region, basaltic magmas ascending through the upper mantle could become further enriched in 'incompatible elements' by processes of wall-rock reaction. The 'incompatible elements' (including K, Ti, P, U, Th, Ba, Rb, Sr, Cs, Zs, Hf and the rare earth elements) are those which are unable to substitute to any appreciable extent in the major minerals of the upper mantle (olivine, aluminous pyroxenes) and are thus considered to be highly concentrated in the lowest temperature melting fraction of pyrolite. The lherzolite inclusions were considered to represent a spectrum of mantle materials ranging from residual material after extraction of an alkali olivine basalt magma, to pyrolite which has been selectively depleted in incompatible elements by wall-rock reaction processes.

If we consider the contents of K, U, Th in the lherzolite inclusions in the light of the above discussion then it is implied that K partitions into a basaltic liquid much more strongly than either U or Th under mantle conditions of pressure, temperature and mineralogy. The production of magmas by varying degrees of partial melting in the mantle and the important role of wall rock reaction in determining the characteristics of the alkali-enriched undersaturated basaltic magmas, taken in conjunction with the data presented, means that movement of basaltic magma from the mantle to the crust is a process which may fractionate K relative to U and Th and also slightly enrich U relative to Th in the crust relative to residual regions of the mantle.

4.3. *Mantle composition and homogeneity*

Stueber and Murthy [15,16] implied a world-wide layer of composition matching that of lherzolite inclusions. From their data on Na, K, Rb and Sr abundances and our own data on K, U, Th abundances, this layer would be variable and inhomogeneous in its composition. Green and Ringwood [2] envisaged intermittent processes of magmatic activity with mantle inhomogeneity resulting from varying degrees of partial melting and wall-rock reaction and consequent varying depletion in the lower melting components of the primary mantle. The model of convective-type movement to generate basaltic magmas which was suggested [2] would place barren and depleted material above a pyrolite zone. Both models suggest that lherzolite inclusion material may be volumetrically important in the uppermost mantle and would influence rates of heat production. The variability of K, U and Th in the specimens examined accentuates the difficulties of any meaningful averaging process, but it is instructive to compare the data with previous estimates of K, U, Th required in the upper mantle by heat flow data or geochemical argument.

Clark and Ringwood [17, p.47] based model compositions for the upper mantle on the premise that basalts contained the total K, U, Th contents previously in the restricted volume of primary mantle which acted as their source. They used a melting relation of three parts basalt to one part refractory resi-

Table 2
Estimates of K, U, Th contents in a peridotitic upper mantle and comparison with lherzolite inclusions.

Region	Depth (km)	K(ppm)	U(ppm)	Th(ppm)	Source
Oceanic upper mantle (Pyrolite)	from 12 km to	2200	0.13	0.52	Clark and Ringwood (1964)
	400 km	500	0.03	0.12	"
	Av. upper 400 km	1300	0.08	0.32	"
Upper mantle beneath Continental Shield (residual)	37-200 km	200	0.01	0.04	"
	200-400 km	1000	0.05	0.20	"
Upper Mantle	M-400 km	500	0.05	0.19	Birch (1965) following Wasserberg et al. (1964)
Oceanic Upper Mantle	M-465 km	1100-1400	0.11-0.14	0.41-0.52	MacDonald (1964) for average mantle with 0.05 ppm U
Continental Upper Mantle	M-465 km	200-250	0.02-0.025	0.07-0.09	"
Oceanic Upper Mantle as source for oceanic tholeiites	Magma segregation at 30-35 km	350	0.025	0.04	from data of Green and Ringwood (1967) and Tatsumoto et al. (1965) on genesis and chemistry of oceanic tholeiites
Lherzolite Inclusions Minimum (2640)	20-50 km approx.	12	0.003	0.014	This paper
Lherzolite Inclusions Maximum (2700)		110	0.114	0.457	"

due and considering the range of K, U, Th contents of natural basalts, with some weighting in favour of tholeiites as volumetrically the more important basalt type, derived the model K, U, Th contents shown in table 2. If compared with Clark and Ringwood's [17] average composition for the oceanic upper mantle as a model for parental pyrolite, then individual nodules would appear to have lost from 92 to 99% of original K, 0-88% original U and 0-65% original Th. Compared to the estimate for the upper 200 km of sub-continental mantle (a refractory residue), individual inclusions are still depleted in K (45-94%) but, in all except one case (2640) are *enriched* in U and Th.

The estimates by Birch [18] and MacDonald [19] were based on the requirements of heat-flow data and utilized crustal element ratios (K/U = 10^4, Th/U = 3.7). The abundances of U and Th within the inclusions encompass the range of abundances in MacDonald's oceanic and continental upper mantle model compositions or show small depletion (2640, 2728) and spread around the mean values of Birch [18]. However, all inclusions may have much less K (80-98% loss of K) than these estimates for the upper mantle. It is particularly to be noted that the K/U and K/Th ratios (0.2×10^4, 0.5×10^3) of the inclusions are very different from the ratios (based on crustal abundance ratios) adopted for their calculations by MacDonald and Birch ($K/U = 1 \times 10^4$, $K/Th = 2.7 \times 10^3$), and differ even more from chondritic ratios ($K/U \approx 7 \times 10^4$, $K/Th \approx 21 \times 10^3$ [24]).

Green and Ringwood [2] considered that the low potassium tholeiites of the mid-oceanic ridges [20] are derived from the mantle by magma segregation (25% melting) from parential peridotite at about 30 km depth and rapid transport of the magma to the sea floor with minimum opportunity for fractionation at shallow depths or for wall-rock reaction. The residual mineralogy would be olivine, lesser orthopyroxene and possibly minor clinopyroxene [21] and if we assume these to contain negligible K, U and Th then the data of Tatsumoto et al. [22] may be used to calculate the K, U, Th abundances in the parental mantle peridotite in an analogous manner to that employed by Clark and Ringwood [17]. The figures are given in

table 2 and comparison of this estimate with the inclusions shows that all the inclusions are relatively depleted in K(68-97%) but only two (2640, 2728) would be regarded as depleted in U and Th.

The analytical data presented in this paper, coupled with that of Wakita et al. demonstrate that lherzolite inclusions have U and Th contents consistent with various models for primary, undifferentiated upper mantle compositions or with moderate degrees of depletion from primary upper mantle material. All, however, show very strong depletion in K, relative to these model compositions. If further studies demonstrate these characteristics to be generally valid, then it is clear that processes of upper mantle differentiation by magmatic activity must be regarded as quite highly variable in the efficiency of extraction of the radioactive trace elements and in particular, the residual peridotite may suffer strong depletion in K without significant depletion in U and Th.

5. CONCLUSIONS

The differences in abundance of K, U, and Th between lherzolite inclusions and their host basanites range from two to three orders of magnitude. There are marked differences in K/U and K/Th ratios and smaller differences in Th/U ratio between inclusions and host rocks which indicate that the contents of these elements in lherzolite inclusions are not determined simply by varying degrees of contamination by the host magma. It is inferred that the lherzolite inclusions are accidental xenoliths preserving, at least in the examples studied, their own geochemical characteristics and thus provide direct information on characteristics of some local parts of the upper mantle (at 20-50 km depth).

The abundances of U and Th in the lherzolite inclusions are relatively high and in these elements, some of the lherzolites may be regarded as suitable source material for low-potassium tholeiitic magmas by direct partial melting. However, this is not the case for K; all the inclusions have too little potassium to produce the observed K-contents of basalts (except for some individual very low potassium tholeiites) by simple partial melting and magma extraction. We conclude that the lherzolite inclusions represent residual material left after extraction of a magmatic component (nephelinite, basanite, alkali olivine basalt) or after selective extraction of minor 'incompatible elements' by wall-rock reaction processes. The data collected show that, if this conclusion is valid, the processes of magma extraction and/or wall-rock reaction lead to a far greater fractionation between K, U and Th than is commonly envisaged. Thus K is preferentially enriched in basaltic magmas relative to U and Th which may be retained in quite large proportion in the residual peridotite. Comparisons of the abundances of K, U, Th in the inclusions with various estimates of upper mantle abundances derived from heat-flow and geochemical argument likewise suggest strong depletion in K, but either no depletion in U and Th or lesser depletion in U and Th when compared with model compositions for both suboceanic and subcontinental mantle.

ACKNOWLEDGEMENTS

We wish to thank Dr. J. F. Lovering and Mr. J. D. Kleeman for critically reading the manuscript.

REFERENCES

[1] W. P. De Roever, Sind die Alpinotypen peridotitmassen vielleicht tektonisch verfrachtete Bruchstücke der Peridoditschale, Geol. Rundschau 46 (1957) 137.
[2] D. H. Green and A. E. Ringwood, Genesis of basaltic magmas, Contr. Mineral. Petrol. 15 (1967) 103.
[3] D. H. Green and A. E. Ringwood, The stability fields of aluminous pyroxene peridotite and garnet peridotite and their relevance in upper mantle structure, Earth Planet. Sci. Letters 3 (1967) 151.
[4] H. H. Hess, The oceanic crust, the upper mantle and the Mayaguez serpentinized peridotite, in: A Study of Serpentinite, ed. C. A. Burk, U.S. National Acad. Science-National Research Council Publication No. 1188 (1964) 169.
[5] A. E. Ringwood, The chemical composition and origin of the earth, in: Advances in Earth Science, ed. P. M. Hurley, M.I.T. Press, Mass. (1966) p. 287.
[6] I. Kushiro and H. S. Yoder, Anorthite-forsterite and anorthite-enstatite reactions and their bearing on the basalt-eclogite transformation, J. Petrol. 7 (1966) 337.
[7] D. H. Green, The stability of plagioclase in peridotitic compositions, unpublished data.
[8] W. Compston, I. McDougall and K. S. Heier, Geochemical comparison of the Mesozoic basaltic rocks of Antarctica, South Africa, South America and Tasmania, Geochim. Cosmochim. Acta 32 (1968).

[9] J. W. Morgan and A. D. T. Goode, Potassium abundances in some ultrabasic and basic rocks, Earth Planet. Sci. Letters 1 (1966) 110.
[10] J. W. Morgan and J. F. Lovering, The determination of uranium and thorium in rocks by neutron activation analysis, Analyt. Chim. Acta 28 (1963) 405.
[11] J. F. Lovering and J. W. Morgan, Comparative uranium and thorium analyses of basic and ultrabasic rocks, Nature 199 (1963) 479.
[12] J. W. Morgan and K. S. Heier, Uranium, thorium and potassium in six U.S.G.S. standard rocks, Earth Planet. Sci.Letters 1 (1966) 158.
[13] K. S. Heier, W. Compston and I. McDougall, Thorium and uranium concentrations, and the isotopic composition of strontium in the differentiated Tasmanian dolerites, Geochim. Cosmochim. Acta 29 (1965) 643.
[14] H. Wakita, H. Nagasawa, S. Uyeda and H. Kuno, Uranium and thorium contents in ultrabasic rocks, Earth Planet. Sci. Letters 2 (1967) 377.
[15] A. M. Stueber and V. Rama Murthy, Strontium isotope and alkali element abundances in ultramafic rocks, Geochim. Cosmochim. Acta 30 (1966) 1243.
[16] A. M. Stueber and V. Rama Murthy, Potassium: rubidium ratio in ultramafic rocks: Differentiation history of the Upper Mantle, Science 153 153 (1966) 740.
[17] S. P. Clark and A. E. Ringwood, Density distribution and constitution of the mantle, Rév. Geophys. 2 (1964) 35.
[18] F. R. Birch, Speculations on the Earth's thermal history, Geol. Soc. Am. Bull. 76 (1965) 133.
[19] G. J. F. MacDonald, Dependence of the surface heat flow on the radioactivity of the Earth, J. Geophys. Res. 69 (1964) 2933.
[20] A. E. J. Engel, C. G. Engel and R. G. Havens, Chemical characteristics of oceanic basalts and the upper mantle, Bull. Geol. Soc. Am. 76 (1965) 719.
[21] T. H. Green, D. H. Green and A. E. Ringwood, The origin of high-alumina basalts and their relationships to quartz tholeiites and alkali basalts, Earth Planet. Sci. Letters 2 (1967) 41.
[22] M. Tatsumoto, C. E. Hedge and A. E. J. Engel, Potassium, rubidium, strontium, thorium, uranium and the ratio of strontium-87 to strontium-86 on oceanic tholeiitic basalt, Science 150 (1965) 886.
[23] J. A. Cooper, The flame photometric determination of potassium in geological material used for potassium-argon dating, Geochim. Cosmochim. Acta 27 (1963) 485.
[24] G. Wasserburg, G. J. F. MacDonald, F. Hoyle and W. A. Fowler, Relative contributions of uranium, thorium and potassium to heat production in the earth, Science 143 (1964) 465.

Printed in the Netherlands

A10

EARTH AND PLANETARY SCIENCE LETTERS 5 (1969) 449-458. NORTH-HOLLAND PUBLISHING COMP., AMSTERDAM

URANIUM DISTRIBUTION IN ULTRAMAFIC INCLUSIONS FROM VICTORIAN BASALTS

J.D.KLEEMAN, D.H.GREEN and J.F.LOVERING

Department of Geophysics and Geochemistry, Australian National University, Canberra, Australia

Received 29 January 1969

The uranium distribution in all phases of nine lherzolite inclusions from the Newer Volcanics of western Victoria has been determined using fission tracks. Primary clinopyroxene has a mean content of 0.30 ppm U in five of the inclusions, and two contain primary apatite with 35 ppm U. Secondary clinopyroxene and apatite crystallizing in equilibrium with glass formed from partial melting of the lherzolites have a much lower abundance. Partition coefficients calculated from the uranium contents in these secondary phases and the glass indicate that a liquid in equilibrium with the primary assemblage would have had to contain 25 to 75 ppm U. Since these abundances are at least ten times those of normal basalts, these inclusions could not have formed as accumulates from a basaltic magma, neither are they the residue from a previous episode of complete magma extraction. However other inclusions containing clinopyroxene with a low uranium abundance could be accumulates or residua.

A model for the uranium distribution in the upper mantle is based on the uranium abundances in the high U primary assemblage. It is consistent with estimates of the upper mantle uranium content, and the uranium contents of basalt magma series calculated from it are consistent with the reported abundances. The petrology and geochemistry of inclusions illustrate a mechanism for limited wall rock reaction, and suggest that potassium may be moved without uranium.

1. INTRODUCTION

Green, Morgan and Heier [1] have recently studied the thorium, uranium and potassium abundances in six peridotite inclusions and their host basalts from the Newer Volcanics of western Victoria. These inclusions provide an important opportunity to study the mineralogy and geochemistry of upper mantle materials, since their primary assemblages could only have formed at moderately high pressures (> 8 kb at 1100°C) [2–4] indicative of upper mantle or very deep crustal conditions.

In this work the uranium distribution has been studied by a technique of registering fission fragment tracks on Lexan plastic prints [5, 6]. Initially the same six inclusions studied in [1] were examined, then a further three were selected to illustrate interesting features.

2. PETROLOGICAL FEATURES

Most aspects of the petrology of these inclusions have been previously described [1, 2], but some new features are included in the description below. For simplicity and clarity primary phases are denoted by I, modified primary phases (retaining the same optic orientation as the parent mineral) by Ia, and secondary, recrystallized phases by II.

The inclusions are peridotites containing the typical four phase lherzolite assemblage of olivine I, orthopyroxene I, clinopyroxene I and spinel I, in order of decreasing modal content. They all have coarse grained textures, but a considerable variation in grain size. Patches of colourless to pale brown glass are observed typically at grain boundaries between clinopyroxene I and spinel I, where both phases appear corroded and replaced by areas of

glass in which there are euhedra of spinel II, clinopyroxene and olivine II. In most cases the glass appears to have developed in situ without any observable connection with the glassy groundmass of the host basalt. In one of the nodules, however, there is continuity between internal glass patches and the glassy groundmass of the basanite; veinlets of brown glass can be observed fingering in from the margins to link up with the internal patches of colourless glass. In many instances the clinopyroxene I is partially melted even where it is not in contact with spinel I. This occurs mainly as rims, but also in bands in the grains, probably following healed cracks. It is seen as a turbid region of clinopyroxene Ia, containing numerous inclusions of glass. Preliminary analyses of these phases indicate that the modified clinopyroxene Ia is poorer in Al_2O_3 and Na_2O compared to the primary phase (clinopyroxene I). Apatite I is present in two inclusions as anhedral, turbid grains, which are rimmed with a new growth of a clear, inclusion-free rim (ApII) where they are in contact with veinlets of glass. The previous report (see ref. [2], p. 181) of primary melilite, based on optical properties only, was a misidentification of this apatite.

The following petrologic notes indicate the distinctive features illustrated by each inclusion.

No. 2604 Olivine-rich lherzolite (dunite) with minor enstatite, rare clinopyroxene I and rare deep brown spinel I. Very rare and narrow reaction zones on some spinel-clinopyroxene areas with small amounts of glass developed.

No. 2728 Lherzolite with common enstatite I, moderately common clinopyroxene I and minor yellow brown spinel I. Local incipient reaction with rare glass. Clinopyroxene is clear, lacks glass inclusions and resembles the clinopyroxene I of other inclusions.

No. 2642 Lherzolite with common orthopyroxene I, clinopyroxene I, minor yellow brown spinel I and minor pale yellow brown hornblende I as small grains associated with spinel and clinopyroxene. Rare incipient reaction between spinel, hornblende and clinopyroxene with rare local glass veinlets.

No. 2640 Similar to 2642, but spinel I is deeper brown. It contains no hornblende but has very rare phlogopite grains.

No. 2700 Similar to 2642, 2640 but clinopyroxene I is more abundant (> orthopyroxene I), minor red brown spinel I and rare apatite I. The turbid apatite I has clear, recrystallized, inclusion-free rim where it is in contact with areas of glass. Glass appears to form at the expense of corroded clin pyroxene I, spinel I and orthopyroxene I and contains euhedra of spinel II, olivine II and clin pyroxene II. Clinopyroxene I has patches modi fied to glass-bearing clinopyroxene Ia. Orthopy ene I has reaction rims of olivine and clinopyro ene where it is in contact with glass areas.

No. 2669 Similar to 2640, 2642 but without amphibole c phlogopite. Clinopyroxene I is common and ha modified clinopyroxene Ia formed as rims or bands. At boundaries between clinopyroxene a red brown spinel I, reactions have yielded glass containing euhedra of olivine II, spinel II and cl nopyroxene II.

No. 2659 Similar to 2669 with abundant clinopyroxene I having extensive alteration (cpx Ia). The brown red spinel has clinopyroxene I and Ia clustered around it and there is abundant colourless to pa brown glass containing euhedral crystals of olivi II, spinel II, clinopyroxene II and plagioclase II.

No. 2683 Similar to 2669 with areas of glass developed ad cent to spinel-clinopyroxene I areas. Orthopyro ene I in reaction relationship with the glass. Sim lar to specimens 2669, 2659, 2700 and 2604 in that a careful search yielded no evidence for physical continuity between the localized interr patches of glass and the glassy groundmass of th host basanite.

No. 2638 This inclusion has undergone internal reaction, a has also been invaded by liquid from the host ba nite. Within the nodule clinopyroxene Ia is seen a transitional relationship with clinopyroxene II Expanding areas of glass finally separate the original clinopyroxene Ia grain into like-orientated parts, which have euhedral outline, indicating ne growth of II. The glass in the interior is practica colourless, but grades to brown near the margin, where it is continuous with the dark brown glass groundmass of the basanite. Continuous interco necting veinlets of glass may be traced througho but are more obvious closer to the contact with host. Near the margin, clinopyroxene Ia is absen all the crystals of clinopyroxene are separated b glass and are euhedral, implying at least an outer zone of new growth (clinopyroxene II). Olivine spinel II and plagioclase II are also present in the glass throughout and only limited, but obvious remnents of spinel I remain. Apatite I is inhomo geneously distributed, being absent in large areas where it is contacted by glass, apatite II is forme at the margin, and apatite II is present closer to the margins as very small isolated crystallites. Or pyroxene is absent from the inclusion, and possi has been eliminated by the large degree of partia melting.

The petrologic evidence for the formation of the

ss by partial melting of some of the primary assem-
ge, particularly clinopyroxene I and spinel I, is sup-
rted by preliminary electron microprobe analyses of
glasses in these interior patches compared with
glass compositions at the borders of inclusions
h as 2638. In 2638 there is a graduation from the
mposition of the glassy groundmass of the basanite
that of the interior glass.

It is not possible to deduce the *P, T* conditions
der which partial melting began, but it is clear that
glass-crystal equilibria now observed indicate low
ssure conditions. The evidence for this includes the
sence of plagioclase crystallites along with olivine
nd clinopyroxene II in some areas, and the strong
ction relationship of orthopyroxene I with the
uids ($Opx + liq_1 = Ol + Cpx + liq_2$). The zoned
ure of the olivine II and clinopyroxene II crystal-
s indicate further that they have grown from the
uid now represented by the glass. As a result of this
wth the present glass composition cannot be taken
that of the partial melt liquid.

FISSION TRACK TECHNIQUE

Techniques for using Lexan plastic to produce fis-
n track and rock texture "prints" have been de-
ibed [5,6], and no modifications have been used in
s work. Discs sixteen millimetres in diameter are
from polished thin sections of the rocks and placed
contact with a sheet of Lexan plastic. This couple
hen irradiated with thermal neutrons at the Hifar
ctor at Lucas Heights, Australia. While these discs
not representative of the rock as a whole, the areas
ected for study include all the petrologic features
the rocks.

Two irradiations were made, one of approximately
$\times 10^{16}$ n cm^{-2}, and the other 2×10^{17} n cm^{-2}.
this way convenient track densities were obtained
m abundances ranging from 43 ppm U to 0.0002
m U. After irradiation the plastic in contact with
rock section is removed, etched and observed as
scribed [5,6], and detailed fission track counts made
h a petrologic microscope at 450 magnifications.

RESULTS

Excellent resolution was obtained on the Lexan plastic prints, and track densities ranging from 1.2×10^4 to 1.3×10^7 tracks cm^{-2} were counted. Figs. 1b and 2b show examples of the print resolution and illustrate some of the type situations encountered. Fig. 1 shows photomicrographs of the rock section and print respectively of 2659, and illustrates the clear primary clinopyroxene I and its modified rim of clinopyroxene Ia, containing blebs of glass. It is seen that the fission track density in the clinopyroxene I is

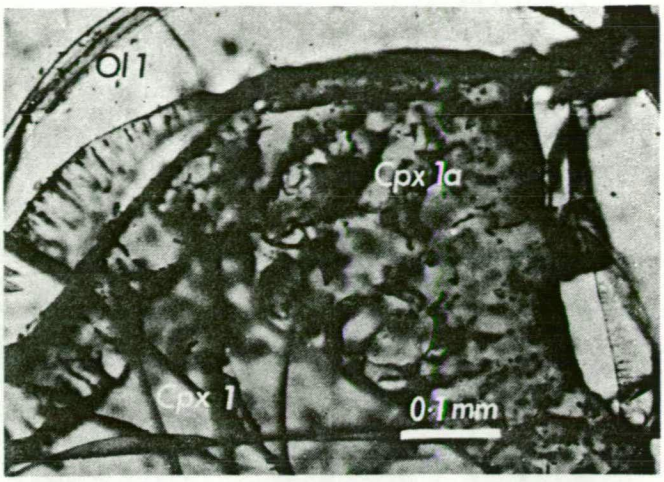

(a)

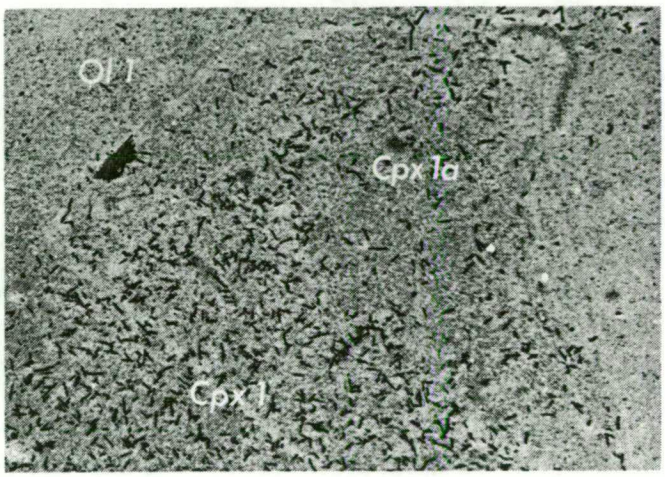

(b)

Fig. 1a. Clear primary clinopyroxene (Cpx I) with its recrystallized rim bearing glass inclusions (Cpx Ia). This example is from inclusion 2659. b. The same area on the fission track print. The recrystallized clinopyroxene (Cpx Ia) has a lower track density, corresponding to 0.035 ppm U, compared to 0.33 ppm for the primary phase (Cpx I).

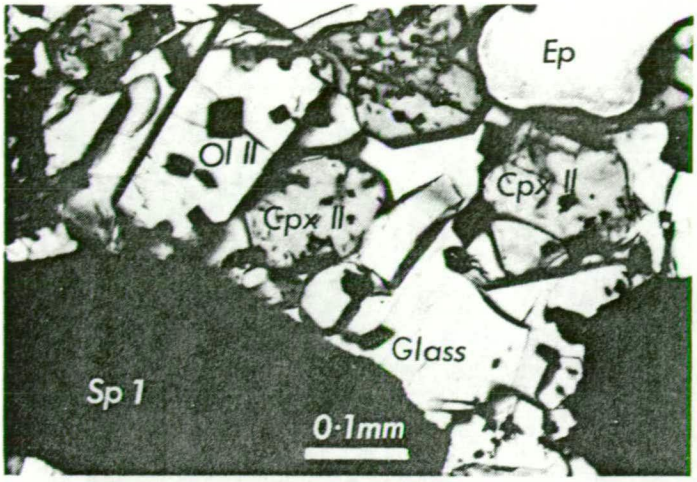

(a)

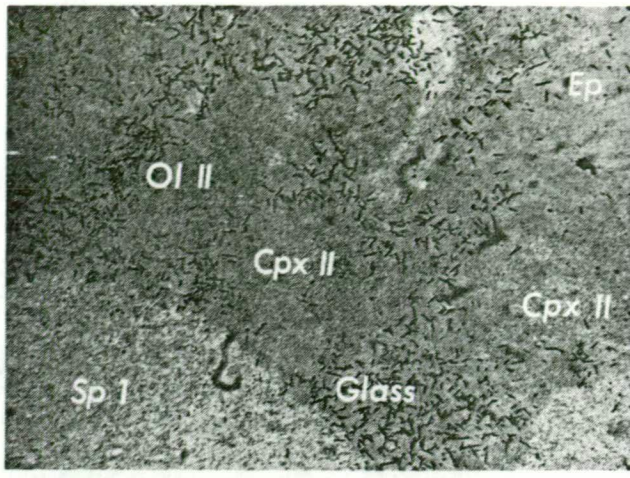

(b)

Fig. 2a. A typical patch of glass in inclusion 2683, with residual spinel I (Sp I) and euhedra of olivine (O1 II), clinopyroxene (
II) and spinel II. Epoxy resin (Ep) is fill – a hole in the slide. b. The same area on the Lexan plastic print. Spinel I, olivine II a
clinopyroxene II all have low abundances (see text), while the glass at this point has 0.7 ppm U.

greater than in its modified rim, while some small concentrations, corresponding to the glass blebs, may be seen in the modified zone. In fact the primary zone there has 0.33 ppm U, while the modified clinopyroxene Ia has 0.035 ppm. Fig. 2 describes the rock section and print illustrating some typical features of 2683. Phases shown are primary, eroded spinel I, glass and crystals of olivine II, clinopyroxene II and spinel II (there is also a hole, filled with epoxy resin, marked Ep).

As described in [6], standard glass discs are used as comparative standards, and from counting the fission track densities in the plastic from the standard as well as the rock sections, the results shown in table 1 are obtained. A blank count is made from the "plastic to plastic" surfaces which arise from the packing arrangement [6] used during irradiation. This blank count could be due to the uranium content of the plastic itself, and possibly also from any surface contamination introduced onto, or improperly removed from, the plastic surface. Care is taken to reduce the surface contamination [6], and the even distribution of the background tracks, together with their geometric arrangement, indicate that this blank count is due to the uranium content within the plastic itself, and not on the surface. The track density of the plastic is equivalent to a uranium content of 0.0001 ppm.

The relative deviations reported depend on the number of tracks counted on the relevant phase as well as the number counted on the standards. Where it significant (i.e. in the very low abundance values) error of the blank count is also involved. Systemat accuracy has been checked with calibration experiments, and by cross checks with other techniques, notably activation and isotope dilution, on the san tektite samples [7]. Systematic errors were found be less than ± 3%.

5. URANIUM PARTITION COEFFICIENTS BETWEEN COEXISTING PHASES

The data in table 2 illustrates the partition of uranium between coexisting crystalline phases and between crystals and silicate liquid. The secondary phases (II) can be considered to be at least in local equilibrium with the glass in contact with them, bu clinopyroxene Ia is thought to have a dynamic rela tionship with the stringers of glass leading from it. The glass has 100–250 times the uranium content of clinopyroxene II adjacent to it, while the uraniu content of the glass in equilibrium with apatite II i around 0.8–1 times that of the apatite II. These partition factors apply to lower pressure condition when compared to the primary assemblage, which formed at pressures greater than 8kb (see above), b provided there only minor compositional differenc the effect of moderate pressures (10–15 kb) shoul

Table 1
Uranium abundance in phases of lherzolite inclusions.

Sample number	Total rock	Clinopyroxene I	Clinopyroxene Ia	Clinopyroxene II	Apatite I	Apatite II	Olivine I	Ortho-pyroxene I	Spinel I	Other	Glass at reaction sites	Interior glass veinlets	Glass veinlets near contact+
2640	0.0030	–	–	–	–	–	0.0002	0.0007	0.0002	Phlogopite 0.0005	–		0.22–0.52
2728	0.0097	0.0057	–	–	–	–	0.0002	0.0006	0.0005	Hornblende 0.0005	–	1.08–1.25	–
2642	0.0180	0.042	–	–	–	–	0.0005	0.0031	0.0002		–	0.36	–
2604	0.0212	0.35	–	–	–	–	0.0007	0.0049	0.0006		0.68	0.12–0.70	–
2700	0.1136	0.28	0.047	–*	38.4	–	0.0006	0.0035	0.0007	–	1.44	0.76–1.32	–
2669	0.0400	0.37	0.037	–	–	–	0.0005	0.0039	0.0003	–	2.45–3.90	1.73–3.84	–
2659	n.a.	0.33	0.035	0.014	–	–	0.0007	0.0022	0.0005	–	2.19–4.26	0.29–2.22	–
2683	n.a.	0.16	0.016	0.012	–	–	0.0005	0.0005	0.0005	–	0.72–2.14	0.41–0.79	–
2638	n.a.	–	0.013	0.016	32.1	5.8	0.0002	–	–	–	2.26–6.06	2.26–6.06	1.85–3.70
Error	–	3%	10%	20%	3%	6%	20–40%	15–40%	25–40%	100%	8–13%	11–20%	11–20%

* Insufficient resolution due to small size.
+ Only 2640 and 2638 included contact zone in fission track specimen.
All figures ppm uranium.

Table 2
Uranium partition between coexisting phases and liquids.

Sample number	Glass veinlets/cpx Ia	Glass patches/cpx II	Glass patches/Ap II	Cpx I/Opx I	Cpx I/Ol I
2604		–	–	71	500
2700	16– 28	–	–	80	470
2669	46–106	–	–	95	740
2659	8– 63	240–253–270	–	150	470
2683	37– 72	97–101–105	–	320	320
2638i	–	194–224–250	0.50–0.84–1.45	–	–
2638ii	–	–	0.86–0.99–1.24	–	–

All figures are ratios between the uranium contents of the minerals indicated.

slight. It is considered that there have not been major changes in the oxidation state of the uranium between high and low pressure conditions. The Fe^{++}/Fe^{+++} ratio in both inclusions and host basalts is high, which indicates that this is a reasonable assumption. In the following sections the liquid/clinopyroxene and liquid/apatite partition coefficients are used to calculate the uranium content of a hypothetical liquid which could have been in equilibrium with the clinopyroxene I (0.30 ppm U) and apatite I (35 ppm U).

On the basis of the apatite, these calculations give a hypothetical liquid with 28–35 ppm U, while from the clinopyroxene data this liquid has 30–75 ppm. These estimates are a factor of 10–100 higher than the abundances observed in basaltic magmas, even the very undersaturated nephelinitic magmas [8].

We conclude that the mineral assemblages in inclusions having clinopyroxene with about 0.3 ppm and/or apatite with about 35 ppm U crystallized in the absence of a basaltic liquid. This applies particularly to the magma in which the inclusions occur, but also applies to any postulated prehistory of the observed mineral assemblage. The data do not rule out the former presence of a vapour or fluid phase, not of basaltic composition, with which the uranium-rich apatite I and clinopyroxene I could have equilibrated. Similarly, any inclusion with clinopyroxene I containing 0.05 ppm U, or less, could have crystallized in equilibrium with a basaltic liquid.

5. IMPLICATIONS OF THE URANIUM DISTRIBUTION ON THE ORIGIN OF THE INCLUSIONS

The various origins suggested for lherzolite inclusions can be summarized into two geochemically d tinguishable hypotheses:

1. They are cognate xenoliths formed in equilibri with the basaltic magma, or its parent, at mode depth. That is, they formed as an accumulative cipitate [9] from the basaltic host magma, or t are residua of the source rock of that magma. I either case there would be geochemical equilibr between basalt liquid and peridotite rock.
2. The lherzolite inclusions represent random, acc tal xenoliths of an upper mantle peridotite whi is inhomogeneous, and varies in composition fr residual refractory peridotite to a primary "pyrolite" * composition [2–4].

If the cognate hypothesis were valid the preced discussion of partition coefficients becomes partic larly important. Calculations based on the uranium content of the clinopyroxene I and apatite I indica that a liquid in equilibrium with inclusions 2604, 2 2669, 2659, 2683 and 2638 would have to contain 30–75 ppm U, a figure 10–100 times the abundan of natural basaltic magmas, including the host mag (1–2 ppm [1]). Even if such a liquid (that is with 30–75 ppm U) was in equilibrium with the lherzol at depth it would have had to be lost and replaced the present host basanite. This conclusion, that the first hypothesis does not explain the uranium distri bution data, is in harmony with previous argument based on mineralogical and petrological grounds [2,10], and on the U, Th and K contents of the inclusions [1].

* Pyrolite is the term given by Ringwood [3,4] to a mode mantle composition of one part basalt to three parts per dotite (see refs. [2,3,4,12]).

The second hypothesis, that the inclusions are enoliths of inhomogeneous upper mantle material, is lequate to explain the mineralogical, petrological nd chemical observations. Inclusions containing inopyroxene I with 0.30 ppm U or with apatite I ontaining 35 ppm cannot be regarded as being re- actory residual material left from a previous episode f complete basaltic magma extraction. On the other nd the low K content reported for these inclusions] argues for a depletion of K, but not of U and Th. is noted that phlogopite is developed patchily in the odules (one example, not studied, contained a small tch with 5% phlogopite). Thus the site of K is not at of U, which is contained in clinopyroxene I and patite (see table 1). Subtle changes, such as small riations in the partial pressure or fugacity of volatile mponents, may cause the breakdown of phlogopite, ith the possibility of volatile transport of K without tendant U. In this instance U would not follow K 1]. However in the event of more severe conditions, y 5% or more partial melting, practically all of both and U would be derived from a rock containing inopyroxene I, apatite and phlogopite, producing an pparent coherence in the behaviour of K and U.

A MODEL FOR URANIUM DISTRIBUTION IN A PERIDOTITIC UPPER MANTLE

The abundance and behaviour of uranium under pper mantle conditions is important for heat flow lculations, in the geochemical evaluation of hypo- eses of basalt genesis and in interpreting lead iso- pe ratios.

A major point established in this study is that anium is present in very significant amounts in nopyroxene crystallized under upper mantle condi- ons. The uranium is homogeneously distributed with- the clinopyroxene I and does not occur as inclusions high U minerals within the clinopyroxene. In ad- tion, an accessory phase, apatite, contains a high anium content. While apatite is clearly stable under pper mantle conditions, it is difficult to attach any neral significance to it. Clinopyroxene, on the other nd, is an essential phase in all recent mantle models, cluding the pyrolite model [3,4,12]. It has been esti- ated to comprise 15–20% of the stable mineral as- mblage of pyroxene pyrolite at depths of 25–75 km. If this clinopyroxene contains 0.30 ppm U (the mean of the group 2604, 2700, 2669, 2659, 2683), then this pyroxene pyrolite would contain approximately 0.05 ppm U.

Heat flow data has been applied to the geochemistry of radiogenic elements and estimates of uranium abundances have been made. The average oceanic upper mantle (upper 400–500 km) is thought to require 0.05–0.08 ppm [13–15]. If there is upward enrichment of U in the upper 400 km the uppermost oceanic mantle is estimated to have 0.13 ppm U [15]. Similar estimates for the upper 200 km of the mantle beneath continental shields give 0.01 ppm U. It is clear from these comparisons that the clinopyroxene content of the pyrolite model is adequate to act as host to 40–100% of the uranium estimated for the uppermost oceanic and continental mantles required to satisfy heat-flow data. With the presence of 0.2% apatite I, the uranium content of this model pyrolite is increased from 0.05 to 0.13 ppm. The evidence from these lherzolite nodules is that the uranium in the upper mantle occurs in the essential phase clinopyroxene and in the accessory phase appatite. It is not held loosely in grain boundaries.

7. URANIUM ABUNDANCES OF BASALT MAGMAS DERIVED FROM A MODEL UPPER MANTLE

A model has been proposed [2,16] to describe the genesis of basaltic magmas and their inter-relationships. It is based on the experimental high pressure investigation of basaltic rocks and the pyrolite upper mantle model composition. A useful test of the present uranium distribution model is to examine the estimated uranium content of magmas generated from such an upper mantle.

At depths of 40–60 km, it is inferred that olivine tholeiite magmas (low-Al, 20% normative olivine) would form by about 30% melting of pyrolite, leaving residual olivine, enstatite and possibly chromite. With the source rock defined above (almost all the U present in a clinopyroxene of content 0.30 ppm and 15–20% modal abundance), such an olivine tholeiite would contain 0.15–0.20 ppm U. The mean content of Hawaiian tholeiite is 0.18 ppm [17]. With lesser degrees of partial melting, liquids are in equilibrium

with a residual clinopyroxene (Ia) as well as olivine and orthopyroxene. However the data shown in tables 1 and 2 show that the uranium is partitioned strongly into the liquid from the relict clinopyroxene. Magmas formed by 20–5% melting would range from alkali olivine basalts to olivine basanites and on this basis would contain 0.2–1.2 ppm U. Olivine nephelinite, formed by less than about 5% melting in the presence of water, would contain more than 0.9–1.2 ppm U. If the pyrolite were to contain 0.2% apatite I (35 ppm U), then the olivine nephelinite would derive an additional 1.2 ppm from this source, to make a total of 2.1–2.4 ppm U. These figures compare very closely with the uranium contents of Hawaiian alkali olivine basalt, akaramite and nephelinites [8,18]. A pyrolite composition with 15–20% clinopyroxene and 0–0.2% apatite containing the uranium abundances noted above, is a suitable source rock for the series of magmas from Hawaiian tholeiites to olivine nephelinites.

However there are difficulties if the same source rock is expected to yield the high alumina (> 15%) oceanic olivine tholeiites, which contain 0.03–0.1 ppm U. The experimental studies [2,19] lead to the conclusion that these magmas segregated from a pyrolite composition at depths 25–35 km, requiring 20–25% melting, and leaving residual olivine, enstatite and minor clinopyroxene. A minor amount of olivine precipitation, between 0–10% would be required to produce the observed variation in natural oceanic tholeiites. Using the same arguments as above the pyrolite model composition would yield magmas with uranium contents greater than those observed. A more suitable parent would be a composition similar to nodule 2642; that is, depleted in U relative to the source rocks of the Hawaiian volcanics.

The attempt to reconcile the experimental and major element analysis data led Green and Ringwood [2] to invoke the process of wall rock reaction to account for high enrichment factors in the "incompatible" elements. The present work indicates that uranium may behave in a compatible fashion during processes of magma generation. An attempt to fit the oceanic tholeiites into this genetic scheme emphasizes the particularly low U-abundances in these magmas, leading to the suggestion that their source rocks have been depleted in U at some previous time and cannot be equated in trace element content with the source rocks for Hawaiian tholeiitic and alkali basalt m
Gast [20] has recently examined trace element
tionation related to the origin of tholeiitic and a
magma types, and concluded that while the abu
dances cannot entirely be explained by fractiona
tallization, partial melting of "accepted upper m
mineral assemblages" is a satisfactory hypothesi
explain many large ion elements.

It has been argued above that the primary cli
roxene I and apatite I bearing assemblages were
equilibrium with a liquid of typical basalt uraniu
content, and yet evidence has been presented to
gest that the inclusions are capable of producing
liquid of plausible uranium content for a basalt.
is stressed that the nodules containing clinopyro
I and apatite I are not in equilibrium during the
forming phase; these two primary phases are onl
present because the extent of partial melting is s
at this stage. One example, 2638, is approaching
librium; there is no clinopyroxene I left, and onl
nants of spinel I, and although there is apatite I
it is rimmed with apatite II where the glass is in
tact.

The relationship of the nodule compositions
pyrolite model composition is not entirely clear.
pyrolite model expresses the average compositio
the relatively large volume of acting as a source f
batches of basaltic magma. This source region ma
inhomogeneous on a hand specimen scale, and th
range of mineralogy in those nodules (containing
pyroxene I with 0.30 ppm U) may reflect this in
mogeneity. These nodules range from dunite (26
to lherzolite (2700, 2659). On the other hand th
range in mineralogy may be the result of a compl
history, involving incomplete magma extraction
some previous time, and resulting in a variation f
"pyrolite" to almost residual, refractory peridoti
Melting of 15% of a particular pyrolite source wo
leave residual olivine, orthopyroxene and minor
clinopyroxene; complete extraction of the magm
would leave only minor residual clinopyroxene h
a uranium content of 0.01–0.05 ppm. However i
the liquid was not extracted, but 1–2% remained
trapped, then this liquid would crystallize during
later cooling, precipitating olivine, enstatite and
cularly clinopyroxene. This crystallization essent
reverses the initial partial melting process, and th
clinopyroxene left when all the liquid is used up

be very similar to the clinopyroxene involved in the initial melting, but will be present in much smaller amounts. This may be a correct interpretation for 2604, which has low modal clinopyroxene I, and a total rock composition of "residual" character, relative to pyrolite or to lherzolite nodules such as 2659, 2700.

8. WALL ROCK REACTION AND ZONE REFINING

It has been argued above that different degrees of a specific upper mantle composition can produce the common basalt magma types with typical uranium abundances, provided that a more depleted source rock (with respect to uranium) is called on to act as source for the oceanic tholeiites. The role of wall rock reaction [2] may be only a minor one in determining uranium abundances; however the data presented illustrate the principle on a small scale. In the inclusions containing apatite, the apatite I becomes recrystallized. Some apatite I is dissolved in the liquid, and it becomes locally saturated with apatite, since a clear rim of apatite II with euhedral outline, is precipitated on the turbid apatite I. Apatite I contains 35 ppm uranium, while apatite II has only about 6 ppm. If the penetrating liquid is saturated with apatite the weight of material dissolved will equal that precipitated, so that uranium will be added without other abundances of the major elements in the liquid. If the apatite is reacted to completion 0.06×10^{-6} g U will be added to the liquid for every gram of lherzolite with 0.2% apatite I present. Similarly, the clinopyroxene I would recrystallize to clinopyroxene Ia under the influence of a basaltic liquid in contact with it, and some would be dissolved and re-precipitated as clinopyroxene II. These secondary phases contain 0.012 to 0.047 ppm uranium, compared with 0.30 ppm in the primary clinopyroxene I. In the absence of an appreciable dissolution of clinopyroxene, that is if the liquid was saturated with clinopyroxene, the uranium would go into the liquid without changing the liquid in other ways. If the model lherzolite with 20% clinopyroxene I is involved in the reaction, then 0.05×10^{-6} g U would be added for every gram of lherzolite whose clinopyroxene is fully transformed. In practice the clinopyroxene I and II and apatite I and II do differ slightly, so that other elements also enter the liquid phase, however the changes in uranium abundance will be proportionately greater. It is important also that if the starting liquid is saturated in these minerals, then these changes will take place without any net latent heat requirement or production. These lherzolite inclusions (especially 2638) show how the trace element content of a penetrating liquid can be changed significantly without simultaneous changes of the same order in major element composition. There are similarities between this mechanism and the zone refining concept of Harris [21] and the wall rock reaction suggested by Green and Ringwood [2].

9. SUMMARY

1. All but one (2638) of the nine inclusions studied show no evidence of the penetration of material from the host basanite, and are considered to be behaving as closed systems with respect to uranium.
2. Most of the uranium is contained primary clinopyroxene I, which has 0.30 ppm U, and in apatite I (35 ppm U) where it is present. The clinopyroxene I is undergoing a readjustment to new conditions, and is becoming involved in partial melting. Its modified equivalent (Ia) is in a dynamic relationship with the partial melting, and has a much lower uranium abundance (0.03 ppm).
3. Secondary phases, apatite II and clinopyroxene II, have euhedral outline against the glass, and are in local equilibrium. Partition factors have been calculated from the U analyses of these phases, and applied to the primary phases to calculate the uranium abundance of a hypothetical liquid which could have been in equilibrium with them. The uranium content of such a liquid is a factor of 10 to 100 times the abundances observed in natural basaltic magmas.
4. Since the partition factors indicate that the lherzolites could not have formed in the presence of any known basaltic liquid, and particularly their present host, the cognate hypothesis is rejected for these inclusions.
5. These lherzolites are accidental xenoliths of an inhomogeneous, peridotitic upper mantle. At least six of them have the potential for producing various amounts of basalt liquid of normal uranium content, and cannot be regarded as refractory residues from a previous episode of complete magma extraction.

6. A model for the uranium distribution in a pyrolitic upper mantle is suggested. The presence of 0.3 ppm U in a clinopyroxene constituting 15–20% of a pyroxene pyrolite would be adequate to account for 40–100% of the uranium content of the upper mantle required by heat-flow data. The possibility of 0–0.2% apatite with 35 ppm U is suggested, supplementing the uranium in the clinopyroxene. This bonus could account for even the highest estimates.
7. If this model is further applied to models of basalt magma genesis, self-consistent quantitative estimates of the uranium contents of basalts are derived.
8. The inclusions are in internal disequilibrium, with a liquid forming as the result of partial reaction principally involving clinopyroxene I and spinel I. The uranium content of this liquid is in the same range as those observed in natural basalts. It is stressed that this liquid is not in equilibrium with the primary assemblage.
9. It is noted that the site of uranium is different from the site of K, which is held in phlogopite. Depletion of K is therefore possible without attendant movement of U if only the phlogopite is affected by any changes which do not alter the clinopyroxene and apatite.

ACKNOWLEDGEMENTS

We thank Professor A.E.Ringwood for critically reading the manuscript. The irradiations were financed by a grant from the Australian Institute of Nuclear Science and Engineering.

REFERENCES

[1] D.H.Green, J.W.Morgan and K.S.Heier, Thorium, uranium and potassium abundances in peridotite inclusions and their hosts, Earth Planet. Sci. Letters 4 (1968) 155.
[2] D.H.Green and A.E.Ringwood, Genesis of basaltic magmas, Contr. Mineral. Petrol. 15 (1967) 103.
[3] A.E.Ringwood, A model of the upper mantle, J. Geophys. Res. 67 (1962) 857.
[4] A.E.Ringwood, The chemical composition and o the earth, in: Advance in Earth Science, ed. P.M. (M.I.T. Press, Cambridge, Mass, 1966) p. 287.
[5] J.D.Kleeman and J.F.Lovering, Uranium distribu rocks by fission-track registration in Lexan plasti Science 156 (1967) 512.
[6] J.D.Kleeman and J.F.Lovering, Uranium distribu studies by fission track registration in Lexan plas prints, Atomic Energy in Australia 10 (1967) 3.
[7] J.W.Morgan and W.Compston, Determination of lite by neutron activation and Philipinite by isoto dilution respectively, personal communication.
[8] E.I.Hamilton, Distribution of some trace element the isotopic composition of strontium in Hawaiia Nature 206 (1965) 251.
[9] M.J.O'Hara, The bearing of phase equilibria studi synthetic and natural systems on the origin and e tion of basic and ultrabasic rocks, Earth-Sci. Rev. (1968) 69.
[10] R.W.White, Ultramafic inclusions in basic rocks f Hawaii, Contr. Mineral. Petrol. 12 (1966) 245.
[11] K.S.Heier and J.W.Rogers, Radiometric determin of thorium, uranium and potassium in basalts and magmatic differentiation series, Geochim. Cosmo Acta 27 (1963) 137.
[12] D.H.Green and A.E.Ringwood, Mineral assemblag model mantle composition, J. Geophys. Res. 68 (937.
[13] F.R.Birch, Speculations on the earth's thermal his Geol. Soc. Am. Bull. 76 (1965) 133.
[14] G.Wasserburg, G.J.F.MacDonald, F.Hoyle and W. Fowler, Relative contributions of uranium, thoriu potassium to heat production in the earth, Scienc (1964) 465.
[15] S.P.Clark and A.E.Ringwood, Density distributio constitution of the mantle, Rev. Geophys. 2 (196
[16] R.J.Bultitude and D.H.Green, Experimental study high pressures on the origin of olivine nephelinite olivine melilite nephelinite magmas, Earth Planet. Letters 3 (1968) 325.
[17] W.Compston, I.McDougall and K.S.Heier, Geoche comparison of the Mesozoic basaltic rock of Anta South Africa, South America and Tasmania, Geoc Cosmochim. Acta 32 (1968) 129.
[18] K.S.Heier, I.McDougall and J.A.S.Adams, Thoriu nium and potassium concentrations in Hawaiian la Nature 201 (1964) 254.
[19] D.H.Green, Origin of basaltic magmas, in: Basalts Poldervaart Treatise on Rocks of Basaltic Compos ed. H.H.Hess and A.Poldervaart (Wiley, N.Y.).
[20] P.W.Gast, Trace element fractionation and the ori tholeiitic and alkaline magma types, Geochim. Co mochim. Acta 32 (1968) 1057.
[21] P.G.Harris, Zone refining and the origin of potassi basalts, Geochim. Cosmochim. Acta 12 (1957) 19

A11

EARTH AND PLANETARY SCIENCE LETTERS 6 (1969) 69-76. NORTH-HOLLAND PUBLISHING COMP., AMSTERDAM

LEAD ISOTOPE MEASUREMENTS ON LHERZOLITE INCLUSIONS AND HOST BASANITES FROM WESTERN VICTORIA, AUSTRALIA

J.A.COOPER and D.H.GREEN

Department of Geophysics and Geochemistry,
Australian National University, Canberra, Australia

Received 1 April 1969

Lead samples extracted from a group of lherzolite inclusions and from their host basanites have been isotopically analyzed. The lead from the basanites varies only slightly in $^{206}Pb/^{204}Pb$ and $^{208}Pb/^{204}Pb$ and is similar to average modern terrestrial lead. The lherzolite lead is isotopically different, showing varying degrees of ^{206}Pb and ^{208}Pb deficiency. On a $^{206}Pb/^{204}Pb$ versus $^{207}Pb/^{204}Pb$ diagram, the data appear to follow the average regression line drawn through a world-wide selection of modern basaltic volcanics. The data require separate immediate source regions, differing in U, Th, Pb relationships, for the lherzolites and basanites and demonstrate that the lherzolites cannot have a cognate relationship to their host basanite. A more detailed analysis of the isotopic data suggests that an evolutionary model of at least two stages is required and calculations based on a two stage model suggest formation of the lherzolites from prior source material with higher μ and lower k values at 2–2.5 billion years ago.

INTRODUCTION

Lherzolite (peridotite) inclusions in undersaturated basalts have aroused interest because of their bearing upon hypotheses about the nature of the Earth's upper mantle. The isotopic composition of lead and strontium in such inclusions provides important constraints on possible relationships between inclusions and their host magmas and may suggest evolutionary changes in the upper mantle which cannot be investigated by other means. Stueber and Murthy [1] reported $^{87}Sr/^{86}Sr$ ratios for whole-rock samples of lherzolite inclusions that were similar to the ratios found in basalts. More recently Leggo and Hutchison [2] found large differences in $^{87}Sr/^{86}Sr$ between basaltic host magmas and lherzolite inclusions from central France. Stueber (in press) [3] reported $^{87}Sr/^{86}Sr$ data in a basanite, lherzolite (whole rock) and on olivine, enstatite and chromediopside separated from the lherzolite. The samples were from Mt. Leura, Camperdown, Victoria. The mineral data, though subject to large uncertainty because of the low abundances involved, show isotopic differences between coexisting minerals consistent with an isochron relationship and an age of 500 m.y. (± a very large uncertainty). The present paper reports lead isotopic analyses for a group of basanites and lherzolite inclusions from the Newer Volcanics of western Victoria and is a continuation of the geochemical studies published previously [5, 6], in part using the same samples.

2. SAMPLE DETAILS

The sampling sites were scoria cones of Pliocene-Recent, Newer Volcanics of western Victoria and southeastern South Australia (see fig. 1, p. 156 of ref. [5]). The lherzolite inclusions consist of the major minerals olivine, enstatite, and chrome diopside in various proportions, with minor spinel and, in some examples, accessory hornblende, phlogopite or apatite. Brief notes on specific samples from which isotopically measurable quantities of lead were obtained, are as follows.

Specimen 2639. Coarse lherzolite with olivine and enstatite, as major phases and clinopyroxene and brown spinel as minor phases. Patches of glass + olivine II * + clinopyroxene II + spinel II strongly developed around skeletal spinel but also not obviously associated with spinel. Clinopyroxene with clinopyroxene Ia on margins.

* The designation of I, Ia, II follow the usage of Kleeman et al. [6] and imply 'primary', 'modified but not recrystallized' and 'recrystallized' phases respectively.

Specimen 2642. Lherzolite with minor pale brown hornblende, and incipient melting only (previously described [5]).

Specimen 2669. Lherzolite with common clinopyroxene with rims of clinopyroxene Ia. Patches of glass with olivine II, clinopyroxene II and spinel II are well developed (previously described [5]).

Specimen 2903. Medium-grained lherzolite rich in clinopyroxene. Incipient melting only at some clinopyroxene and spinel boundaries but there is general development of rims of clinopyroxene Ia about all primary clinopyroxene.

Specimen 2904. Coarse-grained lherzolite with neither melting nor recrystallization of clinopyroxene. Clinopyroxene and spinel moderately common.

Specimen 2697. Coarse lherzolite with clinopyroxene and spinel in lenses or schlieren. Patches of glass with clinopyroxene II, olivine II and spinel II are very well developed in close association with relict spinel. Accessory apatite I occurs as small, extremely turbid crystals.

Specimen 2700. Similar to 2697 with olivine, clinopyroxene, spinel and accessory apatite (previously described [5]).

Notes on other samples from which insufficient lead was obtained are given in table 1. Although the lead determinations are semiquantitative only, it is apparent that lead contents are low and widely variable.

The host basanites contain phenocrystal and groundmass olivine, fine-grained clinopyroxene, plagioclase, opaque mineral and glass. Normative compositions are rich in olivine (15–20%), nepheline (~10%) and albite (10–15%). Four samples were from the same scoria quarries as the analyzed inclusions and one (2642) is of the basaltic shell enclosing an analyzed inclusion. The Mt. Schank (2909) locality is 8 miles south of Mt. Gambier (fig. 1, p. 156 of ref. [5]) and is a scoria cone of olivine basalt which does not contain lherzolite inclusions.

3. Analytical methods

Solid basanite samples were broken to approx. 1 cm pieces and internal pieces, free from cracks and oxidation, were selected. One scoriaceous sample (2642) was also boiled with 3 N HCl, repeatedly rinsed with pure water and then dried. The more coherent lherzolite inclusions were cut into slices from which all contact edges against basanite were removed with a diamond saw. These slices were washed with warm 3 N HCl and pure water and broken into small pieces. Some friable inclusions were broken by hand and only internal pieces selected. These inclusions (2700, 2904) were not acid washed. All samples were ground to < 200 mesh in a tungsten carbide 'Sieb Mill' and 5% of 'Specpure' graphite, previously purified by heating in a vacuum at 1000°C for four hours, was ground with each sample.

Lead was extracted from the samples by approximately 8 hr of vacuum volatilization at 1000°C, following the method of Masuda [7]. The available lherzolite sample size varied from 50 to 300 g and 80 g of basanite were used. The sublimate was dissolved in 50% HNO_3 and the lead extracted by the dithizone technique as previously reported [8]. The final chemical form was either lead oxalate or lead sulphide the latter being used if less than 40 micrograms of lead were available.

An approximate measure of the lead volatilized from the sample (± 30%) was obtained from the quantity of dithizone used in the extraction. From this, approximate Pb contents of the samples have been calculated. These results could be low, depending on the efficiency of the extraction process.

The mass spectrometer is a modified Nuclide machine with 12″ radius of curvature and 60° sector field. The data were collected by the method of Compston et al. [9]. Direct ion collection was used in all cases but one (2700), of particularly low ion beam intensity, when an electron multiplier was required. For all unspiked runs the slower magnetic mode of peak switching was employed. In contrast to the lherzolite samples, for which this procedure consumed the whole yield, the basanites furnished sufficient lead for two runs. To a second aliquot of each of these a ^{207}Pb-^{204}Pb double spike was added. These spike-sample mixtures were measured by the faster method of switching the accelerating voltage [10]. Combination of the two results made possible the removal of mass-dependent fractionation and voltage effects (Compston and Oversby [11]). The spike was calibrated against the standard lead N.B.S. 981 using the Catanzaro values [12] as absolute reference.

The results are reported in 3 tables. Table 1 shows the quantity of lead extracted from lherzolites of low lead content. Tables 2 and 3 list lead isotope measurements and lead content of lherzolite and basanite samples repectively.

4. Discussion of results

The semi-quantitative measure of the lead yield has been used to calculate an approximation to the lead concentration in the sample. The lead concentration in the basanites is approximately 2–5 ppm lead

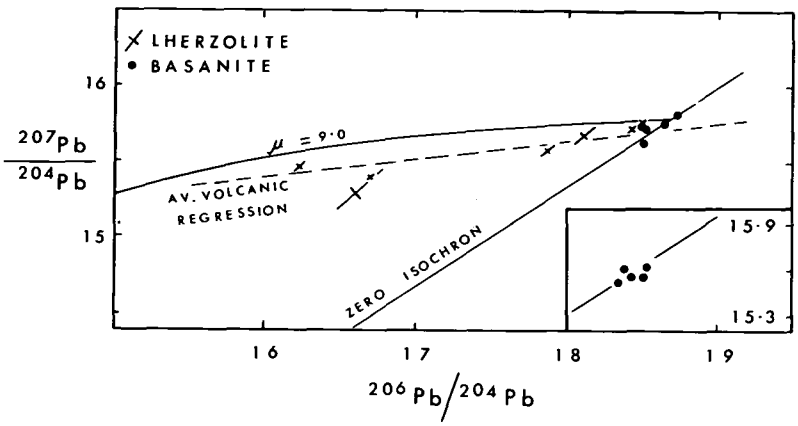

Fig. 1. $^{206}Pb/^{204}Pb$-$^{207}Pb/^{204}Pb$ plot of unspiked lead isotope ratios of whole rock lherzolite and host basanite samples. Also in plot is μ = 8.99 growth curve and meteoritic zero isochron passing through the Primordial Point 9.56, 10.42 [13]. The inset shows the basanite values corrected for fractionation by double spiking calibrated to N.B.S. 981 value.

and the measured and normalized isotopic abundances are listed in table 3 and plotted on figs. 1 and 2. The basanite data fall within the field of modern volcanic leads and the small scatter in the experimental data is reduced by the normalization procedure (inserts to figs. 1 and 2).

The lherzolite inclusions have lead contents ranging over more than an order of magnitude in a manner similar to the uranium and thorium contents [5]. Inclusion 2728 has very low U, Th contents [5], contains clinopyroxene also with very low U content [6] and yielded insufficient lead for isotopic analysis. In contrast, inclusions 2669 and 2700 are relatively rich in U, Th and Pb and have clinopyroxene also with high U contents. Sampling bias therefore exists in the lherzolite data as samples with low lead contents, yielding insufficient lead for mass spectrometry, are automatically excluded. The measured blanks for the

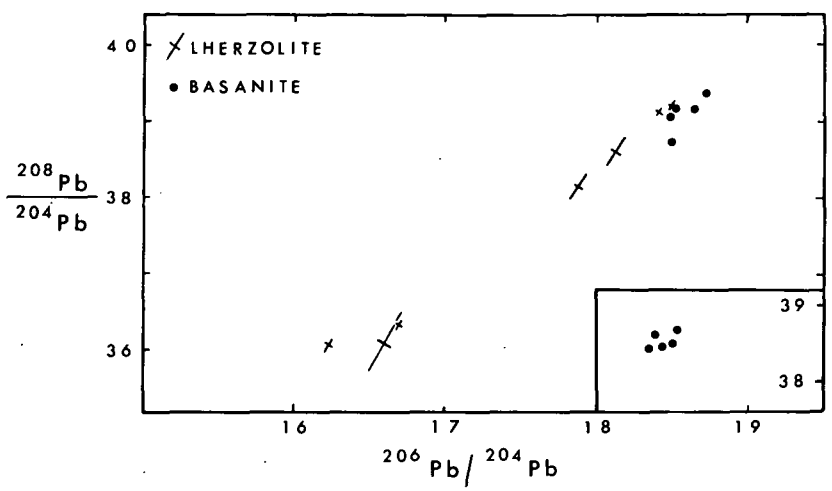

Fig. 2. $^{208}Pb/^{204}Pb$-$^{206}Pb/^{204}Pb$ plot of unspiked lead isotope ratios of whole rock lherzolite and host basanite samples. The inset shows the basanite values corrected for fractionation by double spiking calibrated to N.B.S. 981 value.

Table 1

Approximate lead content and notes on lherzolites from which insufficient lead was extracted for lead isotope measurements.

Sample number and source	ppm Pb	Descriptive notes
2695 Mt. Noorat	0.02	Coarse lherzolite. Incipient reaction between spinel and pyroxene and minor development of margins of clinopyroxene Ia. No glass patches.
2730 Mt. Gambier	0.04	Medium-grained, finely foliated lherzolite with brown spinel and pyroxenes in schlieren and lenticular grains. No melting or alteration of clinopyroxene I or spinel I but rare, very small patches of olivine + pyroxene + semi-opaque phase + glass may be derived from pre-existing amphibole, mica or other phase.
2905 Mt. Noorat	<0.01	Coarse lherzolite with minor development of clinopyroxene Ia and spinel Ia but no general development of glass. Very rare glass patches with euhedral olivine II, clinopyroxene II and spinel II and with distribution suggesting that the glass patches may have replaced some earlier phase.
2906 Mt. Shadwell	<0.01	Very coarse, enstatite-rich lherzolite. Enstatite with exsolved lamellae and irregular patches of spinel, also exsolution lamellae of clinopyroxene.
2907 Mt. Shadwell	0.01	Very coarse lherzolite with little clinopyroxene. No clinopyroxene Ia nor melting at spinel-clinopyroxene boundaries. Rare small glass patches with olivine II, clinopyroxene II and spinel II.
2909 Mt. Schank	0.01	Banded lherzolite, some bands rich in clinopyroxene, orthopyroxene and spinel, others of dunite composition. Pyroxenes with exsolved spinel and pyroxene lamellae. Incipient local melting and development of clinopyroxene Ia. Rare glass patches with clinopyroxene II, olivine II.
2701 Mt. Noorat	0.03	Lherzolite, clinopyroxene moderately common, brown spinel with patchy distribution. No glass patches or clinopyroxene Ia.
2645 Mt. Leura	0.03	Lherzolite with heavy red and irridescent staining of olivine and enstatite due to oxidation along grain boundaries and in cracks. Collected from scoria zone affected by fumarolic activity. Clinopyroxene I with uncommon grain-boundary alteration to Ia.
2728 Mt. Gambier	0.01	See Kleeman et al. [6]. This inclusion has a low uranium content in the total rock and the primary clinopyroxene also has very low U abundance.
2736 Mt. Gambier	0.04	Specimen appears identical to 2730.

analytical procedure amount to 0.18 micrograms and remain a small fraction of the total lead extracted from the sample, even for the lherzolites. Since only one run was possible on each of the lherzolite samples, the normalization procedure is impossible and comparisons of the lherzolite and basanite data are made on the basis of the unspiked results (figs. 1 and 2). The lherzolite inclusions are isotopically different from the host basanites, showing marked depletion in ^{206}Pb and ^{208}Pb, particularly in samples 2700 *, 2903 and 2904.

Since the lead concentration in the lherzolites is

* The small amount of lead extracted from 2700 resulted in a lower level of confidence in its accuracy but the extreme value of $^{206}Pb/^{204}Pb$ remains experimentally significant.

Table 2
Lead isotope data and lead content of lherzolites which yielded sufficient lead for isotopic analysis. (Samples not double spiked.)

Sample number	ppm Pb (extracted)	Micrograms Pb extracted	$^{206}Pb/^{204}Pb$	$^{206}Pb/^{207}Pb$	$^{206}Pb/^{208}Pb$	$^{207}Pb/^{204}Pb$	$^{208}Pb/^{204}Pb$	Lead composition
2639 Mt.Leura	0.3	60	18.42	1.170	0.4708	15.73	39.11	oxalate
2642 Mt.Leura	0.2	40	18.12	1.155	0.4694	15.68	38.60	oxalate
2669 Mt.Shadwell	0.2	50	17.87	1.147	0.4685	15.58	38.14	oxalate
2903 Mt. Noorat	0.09	25	16.70	1.084	0.4594	15.40	36.35	sulphide
2904 Mt.Noorat	0.13	35	16.23	1.049	0.4499	15.47	36.08	sulphide
2697 Mt.Noorat	0.25	100	18.50	1.173	0.4720	15.77	39.20	oxalate
2700 Mt.Noorat	0.2	15	16.6	1.08_6	0.461	15.3	36.1	sulphide, (multiplier)

Table 3
Lead isotope data and approximate lead content of host basanite. Lower figures displaced to the right are figures corrected through double spiking using NBS 981 standard lead as reference calibrator.

Sample	ppm Pb	$^{206}Pb/^{204}Pb$		$^{206}Pb/^{207}Pb$		$^{208}Pb/^{208}Pb$		$^{207}Pb/^{204}Pb$		$^{208}Pb/^{204}Pb$	
2642 Mt. Leura	5	18.65_1	18.53_8	1.183_7	1.187_4	0.4764	0.4793	15.75_7	15.61_2	39.15	38.68
2679 Mt. Shadwell	2	18.49_9	18.43_3	1.183_7	1.185_8	0.4776	0.4793	15.62_8	15.54_5	38.73	38.46
2693 Mt.Noorat	2	18.72_9	18.51_7	1.183_5	1.190_3	0.4754	0.4808	15.82_4	15.55_8	39.40	38.51
2740 Mt.Gambier	2	18.52_1	18.34_7	1.177_4	1.183_0	0.4736	0.4773	15.73_1	15.51_0	39.17	38.44
2909 (JC 45) Mt.Schank	3.5	18.49_2	18.38_4	1.174_3	1.177_7	0.4733	0.4761	15.74_7	15.60_9	39.07	38.61

one to two orders of magnitude below that of the basanite, contamination of the inclusions by lead from their host magma, either during transport or after extrusion must be considered. It is apparent from figs. 1 and 2 that the spread in values of the lherzolite inclusions could in fact be due to mixing of two lead types, one typical of the inclusions and resembling that extracted from 2700, 2903, 2904 and the other type matching the lead in the basanite. Even if this process has occurred, the major observation that the lherzolite inclusions have intrinsic lead isotope ratios differing from their host mama is reinforced. The specimen (2645) selected to test the possible effects of oxidation due to fumarolic activity on the lead content of the lherzolite inclusions contained insufficient lead for isotopic analysis.

5. Evaluation of the volatilization separation of lead

Before the experimental isotope ratios can be applied to petrogenetic aspects, it is necessary to consider the possibility that error may be introduced by isotopic fractionation of lead during volatilization since this technique is used in the initial extraction of the lead. The remixing of the total yield in aqueous solution should cancel out instantaneous, approximately mass dependent, isotopic fractionation effects of the Rayleigh type that occur during volatilization processes from an otherwise homogeneous source. However in a rock system that is 'old' the lead isotope ratios may vary from mineral to mineral due to different U/Pb and Th/Pb ratios in those minerals, provided no recent isotopic equilibrium has occurred. During volatilization, it is possible that lead could be selectively extracted from one or more minerals. This problem does not arise with the recently crystallized basanite samples (Pliocene-Recent) and would not arise with the lherzolite samples if these inclusions were of cognate origin and accumulates or residues from their host magmas.

The work of Kleeman et al. [6] on these lherzolites has clearly shown wide variations in uranium content of different minerals and it may be anticipated that the U/Pb and Th/Pb ratios would also vary. Thus if the efficiency of lead volatilization is less than 100% it remains possible that the lherzolite data obtained are not representative of the whole-rock lead because the extraction process has preferentially favoured the lead in some minerals relative to others. Even in the latter case some conclusions may be drawn. Partial lead extractions from a geologically old lherzolite mineral assemblage could yield a range of lead isotopic contents because of different stability, diffusion or grain size characteristics of the minerals. Such partial extracts should yield a linear distribution of points on the $^{206}Pb/^{204}Pb$ versus $^{207}Pb/^{204}Pb$ diagram, with slope dependent on the age of crystallization of the lherzolite. The line developed would extrapolate back to the initial Pb isotopic ratios of the parent material. Furthermore, if all the lherzolites from a given region had the same initial isotopic ratios and the same age of crystallization, their individual lines would coincide. All partial extractions would lie on this line and have isotopic ratios, relative to ^{204}Pb, greater than the common initial ratio.

Two of the lherzolite samples (2695, 2736) which yielded only a few micrograms of lead, were mixed with more carbon, reground and re-run at the extraction temperature of 1000°C. No further detectable quantities of lead were obtained ($< \frac{1}{2}$ microgram by dithizone extraction, i.e. < 0.002 ppm equivalent) implying a yield of $>90\%$ in the first extraction run. This suggests that the low and variable lead contents of the lherzolites are real features and cannot be attributed to incomplete extraction.

6. Relationship of lherzolite to host magma

The basanite samples form a group with lead isotope ratios plotting near and just to the right of the zero isochron (fig. 1). The normalized values suggest a small but real variation in $^{206}Pb/^{204}Pb$ and in this respect resemble most modern basaltic suites [8]. Two of the lherzolites plot quite close to this group whereas five others have substantially lower $^{206}Pb/^{204}Pb$ and $^{208}Pb/^{204}Pb$ ratios. If the inclusions were cognate, in the sense of having crystallized at depth from the host magmas (O'Hara, p. 401, ref. [13]), then the lead isotope ratios should be the same in both rock types. A similar conclusions would apply if the lherzolites were the refractory residue left after the extraction of their present host magmas from pyrolite, provided that isotopic equilibration was effective during partial melting. The data are clearly incompatible with such relationships and require evolution of the source regions of the basanites and lherzolite inclusions as independent chemical systems for sufficient time to generate the observed isotopic differences. The lherzolites must be interpreted as accidental xenoliths in the basanites. The mineralogy of the lherzolites indicates pressures in excess of 8 kb and temperatures of around 1000°C so that the xenoliths can be attributed to an upper mantle source.

7. Detailed interpretation of the lead isotope ratios

The small variation in the lead isotope ratios of the basanite samples and their similarity to expected modern lead values suggest that a single stage evolution may apply for the parent of this magma. Using

such a premise the $^{238}U/^{204}Pb$ (= μ value) and $^{232}Th/^{235}U$ (= k value) ratios of that parent were about 8.8 and 3.9 respectively (obtained using the unnormalized data which are more relevant to currently accepted constants). The observed Th/U of the Victorian basanites is 3.1–3.5 (Av = 3.25) [5] implying that if a recent separation of this magma from a primeval source region is valid then the basanites were enriched in U relative to Th leaving a residue with Th/U > 3.9. However the normalized data show the percentage $^{208}Pb/^{204}Pb$ variation to be less than half the percentage $^{206}Pb/^{204}Pb$ variation. This implies that after allowing for measurement error and unresolved fractionation effects there remains a small but real variation in the $^{206}Pb/^{204}Pb$ ratio within this group. This suggests that, in common with other basaltic suites, the basanite's parent has also had a complex history. For a two-stage process μ_1 and μ_2 must have been very similar for all but very young values of t_1. Similarly k_1 and k_2 must have been almost identical.

The lead from the lherzolite inclusions is anomalous ("B-type") in terms of a single stage model and roughly defines a straight line on both the $^{207}Pb/^{204}Pb$ versus $^{206}Pb/^{204}Pb$ and $^{208}Pb/^{204}Pb$ versus $^{206}Pb/^{204}Pb$ diagrams. Such a relationship is most simply interpreted as a mixing process involving two different leads, one type similar to that analyzed from 2904 or 2700 and the other type as in the basanites. Such an interpretation would imply significant contamination of the lherzolite by the host basanite and arguments against this have been advanced in earlier papers on these and related inclusions [5, 6]. It may be noted that 2642 and 2639, those samples most resembling the basanites isotopically, do not show evidence of appreciable partial melting or movement of glass within the inclusion whereas partial melting is quite well developed in 2700.

The approximate straight line of the lherzolite points on the two diagrams could also result from the evolution of lead isotopes from a small range of initial ratios. However further details may be calculated only if the time of differentiation is known. Four reasonable values of t_1 were therefore selected. These were 1.5, 2.0, 2.5 and 3.0 b.y. Appropriate μ_1 and μ_2 values were then determined for each sample and t_1 value, assuming two stage evolution from primordial lead isotope ratios [15]. Approximate k_2 values for the second stage were also derived by assuming a primordial k_1 = 3.9 applied to all the samples. (This closely follows a procedure described by Gast [14]). The results are presented in table 4. It is seen that all the samples require a lower μ in the second stage than in the first for all values of t_1. This suggests loss of a component of higher μ value at that time. Unlike the basanites, the lherzolites have not passed through a modern chemical fractionation and the calculated k_2 values may be compared with the direct measurements (Th/U = 3.7–5.0) reported by Green et al. [5]. A t_1 of 2.0–2.5 b.y. produces a more satisfactory range of k_2 values than do the selections of t_1 = 1.5 and 3.0 b.y. Small variations

Table 4
Calculated μ_1, μ_2 and k_2 values for lherzolite lead isotope composition assuming a two stage history, 4 different values for t_1, k_1 = 3.9 and the primordial lead isotope ratios of Murthy and Patterson [15] (Following Gast [14]).

Sample	t_1 (b.y.)	μ_1	μ_2	k_2
2639		8.9	8.3	5.4
2642		8.9	7.2	5.3
2669		8.7	7.1	4.7
2903	1.5	8.6	2.6	4.3
2904		8.8	0.2	26.0
2697		9.0	8.3	5.4
2700		$8._4$	$2._8$	$3._4$
2639		8.9	8.5	5.0
2642		8.9	7.7	4.9
2669		8.7	7.2	4.7
2903	2.0	8.6	4.1	4.0
2904		8.9	2.4	5.2
2697		9.0	8.5	5.0
2700		$8._5$	$4._2$	$3._6$
2639		8.9	8.5	4.7
2642		8.9	7.9	4.6
2669		8.8	7.5	4.5
2903	2.5	8.8	5.0	3.9
2904		9.1	3.6	4.5
2697		9.0	8.5	4.8
2700		$8._6$	$5._0$	$3._7$
2639		9.0	8.6	4.6
2642		9.0	8.0	4.5
2669		8.9	7.7	4.3
2903	3.0	9.0	5.6	3.9
2904		9.5	4.4	4.2
2697		9.0	8.6	4.6
2700		$8._9$	$5._6$	$3._7$

between measured and calculated Th/U ratios on individual samples could be partly due to separate sampling of extremely heterogeneous material, as well as the assumptions made. The comparative small range (8.6–9.1) and the level of the calculated μ_1 values appears to justify the use of an invariant k_1 in the calculations of approximate k_2 values.

In the simplest case the lherzolite data appears to be consistent with a two-stage model in which lherzolites with a range of U/Pb ratios but relatively constant Th/U ratios (~ 4–5), were formed from a parent material with higher U/Pb and lower Th/U ratios, about 2–2.5×10^9 years ago. A similar parent material could have yielded the basanite magma $< 1.0 \times 10^6$ years ago. It is equally consistent with more complex models in which the different lherzolites separated from parent materials at various later times.

It has been argued previously [5, 6] that inclusions such as 2700, 2669 have sufficient U, Th in essential clinopyroxene and accessory apatite and have appropriate major element chemistry to act as source materials for basaltic magmas *. The lead isotope data shows that such materials have widely variable lead isotope ratios and basaltic magmas produced from them would reflect these isotopic variations. It is to be noted that the trend of unnormalized lead isotope measurements on a large number of basic volcanics of world-wide distribution, shown as the dotted line in fig. 1, is not distinguishable from the regression line through the lherzolite data. Thus the spread in lead isotope ratios within the mantle, as deduced from the sampling of modern mantle-derived basalts, could be chronologically related to the spread of lead isotope ratios of xenolithic, crystalline mantle fragments. However no "J-type" anomalous leads occur in the particular lherzolite samples analyzed.

Acknowledgements

The data was reduced with a programme written by P.A.Arriens and adapted for double spike lead work by J.R.Richards. We thank Drs. W.Compston and J.R.Richards for critically reading the draft.

* The K contents are too low but K is regarded as unhomogeneously distributed (in phlogopite, mainly) in basalt source regions [16].

References

[1] A.M.Stueber and V.Rama Murthy, Strontium isotope and alkali element abundances in ultramafic rocks, Geochim. Cosmochim. Acta 30 (1966) 1243.
[2] P.J.Leggo and R.Hutchison, A Rb-Sr study of ultrabasic xenoliths and their basaltic host rocks from The Massif Central, France, Earth Planet. Sci. Letters 5 (1968) 71.
[3] A.M.Stueber, Abundances of K, Rb, Sr and Strontium Isotopes in ultramafic rocks and minerals from Western North Carolina (in press).
[4] D.H.Green and A.E.Ringwood, The genesis of basaltic magmas, Contrib. Mineral. Petrol. 15 (1967) 103.
[5] D.H.Green, J.W.Morgan and K.S.Heier, Thorium, Uranium and Potassium abundances in peridotite inclusions and their host basalts, Earth Planet. Sci. Letters 4 (1968) 155.
[6] J.D.Kleeman, D.H.Green and J.F.Lovering, Uranium distribution in inclusions from Victorian basalts, Earth Planet.Sci. Letters (in press).
[7] A.Masuda, Experimental method for determination of isotopic composition of lead in volcanic rock, J. Earth Sci., Nayoya Univ. 10 (1962) 117.
[8] J.A.Cooper and J.R.Richards, Lead isotopes and volcanic magmas, Earth Planet. Sci. Letters 1 (1966) 259.
[9] W.Compston, J.F.Lovering and M.J.Vernon, The Rubidium-Strontium age of the Bishopville aubrite and its component enstatite and feldspar, Geochim. Cosmochim Acta 29 (1965) 1085.
[10] P.A.Arriens and W.Compston, A method for isotopic ratio measurement by voltage switching, and its application with digital output, Intern. J. Mass Spectr. Ion Phys 1 (1968) 471.
[11] W.Compston and V.Oversby (in press).
[12] E.J.Catanzaro, Absolute isotope abundance ratios of three common lead reference samples, Earth Planet. Sci. Letters 3 (1967) 343.
[13] M.J.O'Hara, Mineral paragenesis in ultrabasic rocks; in: "Ultramafic Rocks", ed. P.J.Wyllie (Wiley and Sons, New York, 1967) p. 393.
[14] P.W.Gast, The isotopic composition of lead from St. Helena and Ascension Islands, Earth Planet. Sci. Letters 5 (1969) 353.
[15] V.Rama Murthy and C.C.Patterson, Primary isochron of zero age for meteorites and the earth, J. Geophys. Res. 3 (1962) 1161.
[16] H.H.Hess, The oceanic crust, the upper mantle and Mayagnes serpentinized peridotite; in: 'A study of serpentinite', Nat. Res. Coun. Publ. 1188 (1964) 169.

A14

Reprinted from

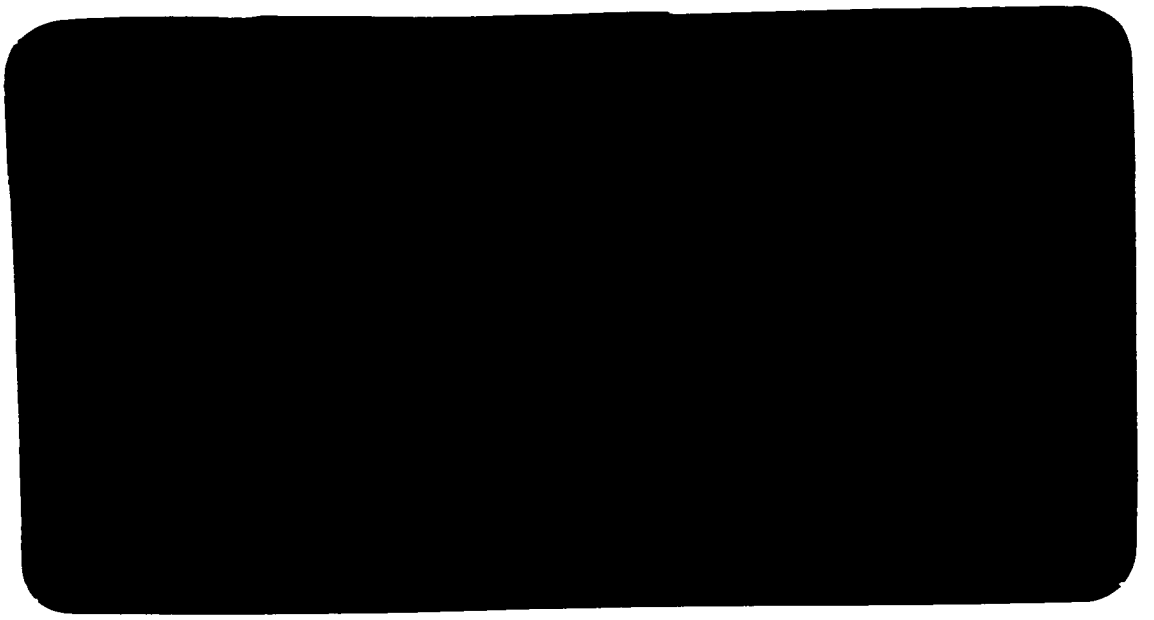

PERGAMON PRESS
OXFORD · NEW YORK

Geochimica et Cosmochimica Acta, 1974, Vol. 38, pp. 1023 to 1059. Pergamon Press. Printed in Northern Ireland

The mineralogy, geochemistry and origin of lherzolite inclusions in Victorian basanites

FREDERICK A. FREY
Dept. of Earth and Planetary Sciences, Massachusetts Institute of Technology, Cambridge, Mass. U.S.A.

and

DAVID H. GREEN
Research School of Earth Sciences, Australian National University, Canberra, Australia

(*Received* 10 *May* 1973; *accepted in revised form* 1 *January* 1974)

Abstract—The mineralogy of lherzolite inclusions in Victorian basanites indicates an upper mantle origin, but a range of temperatures from igneous to metamorphic (subsolidus) is indicated by the mineral compositions. Pyroxene textural features exhibit a slow cooling history consistent with isotopic evidence that these inclusions are accidental xenoliths. Clinopyroxene-rich inclusions (10–20 vol. % cpx) have higher abundances of Ca, Na, Al, Sc, V, Cr and heavy REE, lower $Mg/Mg + Fe^{2+}$, lower Ni abundances, and more fayalitic olivines than clinopyroxene-poor inclusions (<5 vol. % cpx). A surprising result is that the refractory Mg-rich, clinopyroxene-poor inclusions contain the highest abundances of incompatible elements such as P, K, Ti, light REE, Th and U. We believe these inclusions are composed of two components (A and B). Component A determines the major element abundances and primary mineralogy of the inclusions. Based on Ni abundances component A is interpreted as a melting residue rather than a crystallization accumulate. Component B forms a small and varying portion of the inclusions, and it contributes P, K, Ti, light REE, Th and U. This component has the geochemical characteristics of a liquid formed in equilibrium with garnet.

The following model is presented for the origin of lherzolite inclusions. Residual lherzolite (Component A) is left in the lithosphere after partial fusion, and it is later modified by a melt which has migrated to the top of the low velocity zone. Because this liquid (Component B) results from a small degree (<5 per cent) of melting (probably limited by water abundance), and has equilibrated with garnet, it will be very enriched in P, K, Ti, light REE, Th and U. Subsequent cooling and recrystallization forms the present mineralogy. Finally, explosive volcanism, characteristic of silica-undersaturated magmas, incorporates mantle fragments (lherzolite inclusions), and the increasing temperature and decreasing pressure during ascent causes incongruent melting of minor hydrous phases such as phlogopite and amphibole.

INTRODUCTION

LHERZOLITE inclusions are common in basanite scoria cones of the Newer Volcanics in Western Victoria (Southeast Australia). A map of the area showing inclusion locations is shown in GREEN *et al.* (1968) and the basalt hosts are described by IRVING and GREEN (1974). Geochemical characteristics of these inclusions have been previously reported (GREEN *et al.*, 1968; KLEEMAN *et al.*, 1969; COOPER and GREEN, 1969; DASCH and GREEN, in press). The investigations covered K, U and Th abundances, U distribution, Pb-isotopes, and Rb–Sr isotopes. The studies have established that these lherzolite inclusions are xenoliths, having no genetic relationship with their host magmas. The xenoliths preserve evidence of evolution of the source region for the lherzolite inclusions and the source region for the host magmas as separate chemical systems over a long time interval ($>10^9$ yr). The studies also demonstrated that the inclusions preserved their own intrinsic and varied (from

one inclusion to another) geochemical characteristics; that is, contamination by the host magma was absent or at least not detectable. Similar conclusions have been reached for lherzolite inclusions from other localities on the basis of Sr isotopes (LEGGO and HUTCHISON, 1968; PETERMAN *et al.*, 1970; HUTCHISON and DAWSON, 1970; LAUGHLIN *et al.*, 1971; PAUL, 1972) and from rare-earth element abundance data (HERRMANN and WEDEPOHL, 1966; NAGASAWA *et al.*, 1969).

Speculations on the origin of lherzolite inclusions in basalt have suggested two geochemically distinct possibilities: (1) cognate origin as accumulates from their host magmas at moderate to high pressures, and (2) accidental origin in relation to their host magmas, thus providing examples of a major rock type existing in the upper mantle.

The first hypothesis has been advocated in recent years, particularly by O'HARA and MERCY (1963, pp. 278–286) and O'HARA (1967, 1968), as an integral part of models for basalt genesis in which parental hypersthene-normative magmas become nepheline-normative by separation of accumulates of spinel–lherzolite mineralogy. Isotopic studies have shown that the cognate hypothesis is often inapplicable. The principal arguments (variations in mineral composition and equilibration temperatures deduced to be near basaltic liquidus temperatures) previously put forth to support the cognate hypothesis (O'HARA and MERCY, 1963; O'HARA, 1967) are not compelling. The complex temperature history and low temperature of equilibration typically exhibited by lherzolite inclusions (to be discussed) are not consistent with a simple cognate hypothesis.

The Al–Cr correlation in pyroxenes and spinels discussed by O'HARA and MERCY (1963) is not observed in the Victorian inclusions studied (Cr varies correspondingly in spinels and pyroxenes but Al does not), but it is clearly seen in other lherzolite inclusion localities (Kilbourne Hole: CARTER, 1970; San Carlos: Prinz, personal communication; REID, 1972). The recent experimental evidence (DICKEY and YODER, 1972) demonstrating the incongruent melting of Cr-rich diopside ($CaMgSi_2O_6$–$CaCrAlSiO_6$) to liquid plus chromite provides a mechanism for Al–Cr correlations consistent with O'Hara and Mercy's interpretation concerning the presence of a liquid. However, such correlations do not distinguish between an accumulate and a residual origin. An additional complication for the Victorian inclusions is that significant amounts of clinopyroxene and spinel appear to be sub-solidus reaction products.

While the second hypothesis, an accidental or xenolithic origin in relation to their host magmas, has been demonstrated for the Victorian lherzolite inclusions, the more important question of petrogenesis of the lherzolites remains open. It is particularly important to establish whether the inclusions are (1) parental upper mantle composition from which basaltic magma can be derived by partial melting, (2) residue after extraction of a magmatic component, or (3) not related to the *source* of basaltic magmas but are merely geologically older accumulates precipitated at deep crustal or upper mantle levels.

In the following sections, we present data on the petrography, mineralogy, major element abundances, and trace element abundances for six lherzolite inclusions previously analyzed for K, Th and U abundances and U-distribution. These data are used to place constraints on the petrogenesis of the lherzolites.

Petrography and Mineralogy of the Lherzolite Inclusions

Petrography

The lherzolite inclusions contain the typical four-phase assemblage olivine I*, orthopyroxene I, clinopyroxene I and spinel I, but vary considerably in modal proportions of these minerals. They also vary in the abundance of patches of colorless to pale brown glass, occurring typically at grain boundaries between clinopyroxene and spinel, but also within or marginal to olivine and orthopyroxene grains unrelated to clinopyroxene and spinel. These patches of glass contain small euhedra of olivine II + spinel II ± clinopyroxene II ± plagioclase II.

The following petrographic notes indicate the distinctive features illustrated by each inclusion:

No. 2604 Harzburgite with enstatite I, rare clinopyroxene I and rare deep brown spinel I. Very rare and narrow reaction zones on some spinel I–clinopyroxene I boundaries with small amounts of glass developed.

No. 2728 Lherzolite with common enstatite I, moderately common clinopyroxene I and minor yellow brown spinel I. Local incipient reaction at clinopyroxene I–spinel I boundaries with rare formation of glass. Clinopyroxene I is clear and lacks glass inclusions.

No. 2642 Lherzolite with common orthopyroxene I, clinopyroxene I, minor yellow brown spinel I and minor pale yellow-brown hornblende I as small grains associated with spinel I and clinopyroxene I. Rare incipient reaction rims on hornblende I or between spinel I, hornblende I and clinopyroxene I with rare local glass veinlets related to these reaction zones.

No. 2640 Similar to 2642, but with less abundant clinopyroxene I and orthopyroxene I. Spinel I is deeper brown. No hornblende I is present but very rare phlogopite I grains occur, some of which have marginal glass patches.

No. 2700 Similar to 2642 and 2640 but clinopyroxene I is more abundant than orthopyroxene I; minor red brown spinel I and rare turbid apatite I are present. The turbid apatite I has a clear, recrystallized, inclusion-free rim where it is in contact with areas of glass. Glass appears to form at the expense of corroded clinopyroxene I, spinel I and orthopyroxene I and contains euhedra of spinel II, olivine II and clinopyroxene II. Clinopyroxene I has patches modified to glass-bearing clinopyroxene Ia. Orthopyroxene I has reaction rims of olivine II and clinopyroxene II where it is in contact with glass areas.

No. 2669 Similar to 2640 and 2642 but without amphibole I or phlogopite I. Clinopyroxene I is present and has modified clinopyroxene Ia formed as rims or bands. Particularly at boundaries between clinopyroxene I and red-brown spinel I but also apparently unrelated to these phases, there are patches of glass containing euhedra of olivine II, spinel II and clinopyroxene II.

Modal mineralogy

Major element compositions of six Victorian lherzolite inclusions are given in Table 1, and as a comparison, Table 2 cites major element data for peridotites from other areas. The large and variable grain size of constituent minerals prohibit accurate estimation of modes by point-counting of thin sections. Since the compositions of the bulk inclusions (Table 1) and the constituent minerals (Tables 3 and 4) have been determined, it is a simple matter to calculate a mode to 'fit' the major element composition (Table 5). There is a good agreement between the calculated rock composition (from the mode) and the rock analysis for 5 of the 6 inclusions. In inclusion 2669 the Na/Ca of the total rock requires the presence of another phase or phases

* The primary phases are denoted by I, modified primary phases (retaining the same optical orientation as the parent mineral but with inclusions denoting partial melting or exsolution or other evidence of compositional change) are denoted by Ia, and secondary, recrystallized phases by II.

Table 1. Major element composition* of lherzolite inclusions and host basanites, Western Victoria

	Lherzolites						Basanites	
	1 Anakies 2604	2 Mt. Shadwell 2669	3 Mt. Leura 2640	4 Mt. Gambier 2728	5 Mt. Noorat 2700	6 Mt. Leura 2642	7 Mt. Leura 2650	8 Mt. Shadwell 2679
SiO_2	42·69	44·26	43·58	44·42	44·16	45·19	45·03	44·74
TiO_2	0·02	0·00	0·03	0·01	0·00	0·06	3·24	2·75
Al_2O_3	1·07	0·86	1·02	2·13	1·45	2·98	12·97	12·61
Cr_2O_3	0·26	0·36	0·32	0·36	0·41	0·43	0·05	0·04
Fe_2O_3	0·60	0·38	0·81	0·39	0·60	1·50	3·28	2·95
FeO	6·50	7·11	9·27	7·04	7·76	6·30	9·32	8·95
MnO	0·13	0·13	0·15	0·13	0·11	0·13	0·17	0·16
NiO	0·34	0·29	0·30	0·25	0·22	0·27	0·04	0·05
MgO	47·04	46·08	43·68	43·43	42·72	40·56	9·88	12·47
CaO	0·57	0·76	0·97	2·31	2·87	2·50	8·51	8·70
Na_2O	0·05	0·12	0·12	0·18	0·29	0·19	4·06	3·46
K_2O	0·01(70)†	0·02(91)	0·02(12)	0·008(30)	0·014(110)	0·002(15)	2·22	1·78
P_2O_5	0·05	0·02	0·006	0·004	0·039	0·004	1·14	0·52
	99·33	100·41	100·28	100·75	100·75	100·12	99·91	99·18
$\frac{100\,Mg}{Mg + Fe^{2+}}$	92·8	92·0	89·4	91·7	90·7	92·0	65·5	71·4

* Analyses by E. Kiss, R.S.E.S., A.N.U., Canberra by wet chemical (gravimetric, potentiometric and spectrophotometric) techniques.

† Elemental K abundance data in ppm (from GREEN *et al.*, 1968), determined by γ-ray spectrometry.

with higher Na/Ca than any of the analyzed major phases; this is true to a lesser degree for 2604, 2640 and 2700, but is not required for 2642 or 2728. Na-rich glass is most abundant in 2669, present in lesser amounts in 2604, 2640, 2700 and 2642, and absent in 2728.

Nature and origin of glass within lherzolite inclusions

It has been previously inferred on textural grounds and confirmed by the cited K, Th and U abundance, Pb-isotope and U-distribution studies, that the glass within these lherzolite inclusions is internally derived and is not introduced from the host

Table 2. Major element composition of lherzolite inclusions (4, 5) and other peridotities for which REE data exists

	1 Tinquillo Venezuela (GREEN, 1963)	2 Av. Lizard England (GREEN, 1964)	3 Pyrolite (RINGWOOD, 1966)	4 Ataq S. Yemen (VARNE, 1970)	5 Hualalai Hawaii HK61030402 (KUNO and AOKI, 1970)	6 St. Paul's Rocks (MELSON *et al.*, 1967) 7-479	7 7-327	8 8-900
SiO_2	44·69	44·77	45·16	42·84	44·08	44·47	44·82	44·80
TiO_2	0·08	0·19	0·71	—	—	0·07	0·08	0·32
Al_2O_3	3·19	4·16	3·54	1·34	0·47	2·44	3·44	4·68
Cr_2O_3	0·45	0·40	0·43	0·11	0·32	0·55	0·54	0·53
Fe_2O_3	0·09	—	0·46	0·78	1·29	1·43	1·20	3·02
FeO	7·54	8·21	8·04	7·70	7·25	6·33	7·14	4·74
MnO	0·14	0·11	0·14	0·21	0·13	0·14	0·15	0·14
NiO	0·26	0·24	—	—	—	0·33	0·25	0·29
MgO	39·80	39·22	37·47	44·17	45·32	42·88	39·31	36·70
CaO	2·97	2·42	3·08	1·38	0·76	1·15	2·80	4·15
Na_2O	0·18	0·22	0·57	0·40	0·14	0·14	0·17	0·46
K_2O	0·02	0·05	0·13	0·02	<0·05	0·07	0·05	0·12
P_2O_5	0·04	0·01	0·06	—	<0·05	<0·05	<0·05	0·05
	99·45	100·00	99·79	99·44	99·92	100·05	100·00	100·00
$\frac{100\,Mg}{Mg + Fe^{2+}}$	90·4	89·6	89·2	91·1	91·5	91·2	90·8	93·2

Table 3. Major element compositions of minerals from lherzolite inclusions, Western Victoria. Minerals from 2604 by wet chemical analysis, other analyses by electron microprobe. Comparative data for Lizard minerals from GREEN (1964), Ataq lherzolite inclusion from VARNE (1970) and Hualalai inclusions from KUNO and AOKI (1970)

	2604	2669	2640	2728	2700	2642	Lizard 90683	Lizard 90681	Ataq	Hualalai HK61030402
Olivines										
SiO_2	40·84	40·81	39·74	40·87	40·56	40·45		40·75	40·47	40·30
TiO_2	<0·01	0·04	0·03	0·03	0·04	0·04		0·18	—	—
FeO	8·05	8·59	11·72	8·83	9·92	9·30		10·05	9·0	9·20
MnO	0·12	0·11	0·14	0·11	0·11	0·11		0·13	0·16	0·10
NiO	0·40	0·38	0·36	0·37	0·35	0·41		0·20	—	—
MgO	50·04	49·58	47·08	49·45	48·66	49·19		48·01	49·83	50·40
$\frac{100\,Mg}{Mg + \Sigma Fe}$	91·7	91·1	87·7	90·9	89·7	90·4		89·5	90·8	90·8
Orthopyroxenes										
SiO_2	56·39	56·82	56·74	55·61	56·35	56·44	53·26	53·17	55·95	54·22
TiO_2	0·03	0·06	0·17	0·15	0·13	0·14	0·17	0·19	—	0·14
Al_2O_3	2·37	2·18	3·36	3·89	3·31	3·77	6·59	6·30	1·36	4·03
Cr_2O_3	0·41	0·27	0·60	0·44	0·59	0·36	0·39	0·67	0·35	0·64
Fe_2O_3*	0·57	0·18	0·33	0·47	0·45	0·27	0·97	0·74	n.d.	1·15
FeO	4·67	5·19	6·35	5·12	5·61	5·50	5·54	5·80	5·63	4·88
MnO	0·12	0·12	0·08	0·11	0·13	0·12	0·12	0·11	0·19	0·11
MgO	34·38	34·21	31·51	33·15	32·26	32·25	31·29	31·21	36·17	33·60
CaO	0·35	0·35	0·62	0·40	0·64	0·54	2·14	2·11	0·57	1·27
Na_2O	0·08	0·08	0·13	0·06	0·14	0·04	0·07	0·06	0·08	0·17
$\frac{100\,Mg}{Mg + Fe^{2+}}$	92·9	92·2	89·8	92·0	91·1	91·3	91·0	90·6	91·9	92·6
Ca	0·7	0·7	1·3	0·8	1·3	1·1	4·2	4·2	1·0	2·4
Mg	91·5	91·3	88·3	90·7	89·4	89·9	85·7	85·7	91·1	89·0
Fe	7·8	8·0	10·4	8·5	9·3	9·0	10·1	10·1	7·9	8·6
$K_D \frac{(Fe^{2+}/Mg)opx}{(Fe^{2+}/Mg)cpx}$	1·33	1·56	1·22	1·61	1·48	2·00	1·35	1·36	<1·66	1·04
Clinopyroxenes										
SiO_2	53·95	54·35	53·92	53·85	53·41	54·08	49·83	49·66	52·81	52·28
TiO_2	0·10	0·41	0·60	0·68	0·48	0·46	0·42	0·31	0·07	0·29
Al_2O_3	2·51	4·50	5·35	5·39	4·68	4·42	7·09	6·80	3·99	4·25
Cr_2O_3	1·41	0·66	1·27	1·18	1·41	0·73	0·66	0·89	0·09	0·98
Fe_2O_3*	0·45	0·69	1·16	0·39	1·14	0·74	1·23	1·37	0·93	1·01
FeO	1·81	1·56	2·55	1·42	1·86	1·33	2·25	2·38	1·55	2·60
MnO	0·09	0·06	0·09	0·06	0·09	0·05	0·10	0·03	0·12	0·08
NiO	—	—	—	—	—	—	0·06	0·06	—	
MgO	17·66	16·10	15·41	14·82	15·82	15·60	16·99	17·78	16·44	18·59
CaO	21·06	19·86	17·73	19·98	19·39	21·30	20·67	20·36	22·15	19·26
Na_2O	1·23	1·10	1·56	1·63	1·73	1·07	0·79	0·36	1·59	0·81
K_2O	—	—	—	—	—	—	0·02	0·05	0·02	
$\frac{100\,Mg}{Mg + Fe^{2+}}$	94·4	94·9	91·5	94·9	93·8	95·4	93·0	93·0	94·8	92·7
$\frac{100\,Mg}{Mg + \Sigma Fe}$	93·4	92·7	88·5	93·6	90·5	93·4	89·7	89·6	92·5	90·4
Ca	44·3	45·2	42·2	47·6	44·4	47·8	44·1	42·5	47·3	41
Mg	52·0	50·9	51·1	49·1	50·4	48·7	50·2	51·6	48·8	55
Fe	3·7	3·9	6·7	3·3	5·2	3·5	5·7	5·9	3·9	4
mol%(Jd + Ac)	8·7	7·7	10·9	11·4	12·1	7·5	5·7	2·5	11·3	5·7
Spinels										
TiO_2	0·22	0·13	0·45	0·22	0·44	0·13	0·32	0·32		
Al_2O_3	42·63	57·79	40·67	52·26	36·74	58·42	47·58	46·88		
Cr_2O_3	27·76	10·98	25·89	17·59	30·80	11·44	17·99	18·08		

Table 3. (*contd.*)

	2604	2669	2640	2728	2700	2642	Lizard 90683	Lizard 90681	Ataq	Hualalai HK61030402
Spinels (contd.)										
Fe_2O_3†	—	—	2·60	—	2·60	—	5·07	5·40		
FeO	12·75	9·66	12·76	10·08	12·36	9·80	10·13	10·02		
MnO	—	0·11	0·20	0·15	0·22	0·11	—			
NiO	—	0·24	0·23	0·23	0·22	0·25	—			
MgO	16·60	20·32	17·17	19·52	17·17	20·28	19·18	19·06		
$\frac{100\,Mg}{Mg + \Sigma Fe}$	70·1	79·0	68·0	77·5	67·6	78·7	70·0	69·5		
$\frac{100\,Mg}{Mg + Fe^{2+}}$	70	79	72	77·5	72·5	79	77·1	77·1		
Atomic (Cr + Al) to 40	2·00	2·00	1·93	2·00	1·93	2·00	1·90	1·89		
(Mg, Fe) Spinel	70	88·5	67·5	81·5	61·5	88·5	76	75		
(Mg, Fe) Chromite	30	11·5	29	18·5	35·0	11·5	19	19·5		
Magnetite	—	—	3·5	—	3·5	—	5·0	5·5		

* FeO, Fe_2O_3 contents of clinopyroxene and orthopyroxene determined by spectrophotometric methods on separated minerals (5–10 mg): E. Kiss, analyst.

† Fe_2O_3 content of spinel based on structural formulae calculation.

Table 4. Minor phases in lherzolite inclusions of Western Victoria and comparable peridotites. Amphibole 2642, phlogopites and apatites analyzed by electron microprobe

	Amphiboles			Phlogopite		Apatite	
	2642†	Ataq (VARNE, 1970)	Lizard (GREEN, 1964)	2640	2925*	2700	2638*
SiO_2	45·19	44·73	46·19	38·1	40·3	(1·7)	0·2
TiO_2	1·28	0·29	0·96	3·5	0·4	—	0·1
Al_2O_3	15·43	12·58	12·83	17·5	15·0	0·3	0·2
Cr_2O_3	0·97	2·43	0·80	1·4	1·2	—	—
Fe_2O_3	1·27	1·10	1·18	—	—	—	—
FeO	2·04	2·37	2·97	4·0	4·4	0·4	0·1
MnO	<0·03	0·11	0·04	—	—	—	—
NiO	—	—	—	—	—	—	—
MgO	17·98	19·17	18·71	21·3	24·6	0·9	0·7
CaO	10·11	10·95	12·45	—	—	52·3	53·2
Na_2O	3·47	3·84	1·87	0·5	1·3	—	0·9
K_2O	0·04	0·43	0·27	9·8	9·2	0·15	—
P_2O_5	—	—	—	—	—	42·0	42·4
						Cl 1·0	0·9
	97·77	98·00	98·21	96·1	96·4	98·8	98·7
$\frac{Mg}{Mg + Fe^{2+}}$	94·1	93·5	91·8	90·5	91·0		

* Mineral data from inclusions 2638 (KLEEMAN *et al.*, 1969) and 2925 (olivine and phlogopite and large areas of glass + clinopyroxene, etc.) are included for comparative purposes.

† FeO, Fe_2O_3 contents of amphibole 2642 analyzed by E. Kiss, by spectrophotometric methods.

Table 5. Calculated modes (see text) for compositions of Tables 1 and 2. The first column of each pair gives the mode calculated by the least-squares program, (WRIGHT and DOHERTY, 1970) the second column gives the mode calculated by sequential fitting with heavier weighting given to Na, Ca, Al, Cr in determining the clinopyroxene and spinel proportions

	Table 1												Table 2				
	2604		2669		2640		2728		2700		2642		Lizard	Ataq	St. Pauls Rocks		
Olivine	83·4	86	78·3	76	80·5	79	72·4	72·3	75·1	75·3	60·2	61	63	77	70	60	54
Orthopyroxene	13·1	10·5	18·7	19	14·6	15	16·6	15	11·1	10	26·7	24·5	25	17	22	23	22
Clinopyroxene	2·4	2·5	2·8	4	4·8	5	10·0	11	13·7	14	11·3	10·5	10	4	5	14	20
Spinel	1·0	1	0·3	1	0·1	0·8	1·1	1·7	0·2	0·6	2·4	2	2		3	3	4
Amphibole												2		4			
Phlogopite						0·2											
Apatite										0·1							
Grain boundary phase			*							*				*			

* Denotes the presence of glass and olivine II, clinopyroxene II, spinel II. In 2669 and 2700 this forms about 1% of the sample.

basanite. The major element rock and mineral data and the modal calculations (Tables 1–5) show that the glass cannot be entirely derived by partial melting (including incongruent melting) of the major minerals olivine I, orthopyroxene I, clinopyroxene I, and spinel I. Prior to partial melting one or more accessory phases, including a sodium-rich phase, must have been present. This conclusion is supported by petrographic observations on the role of amphibole I and phlogopite I in the lherzolite inclusions (e.g. 2642 and 2640).

Phlogopite I occurs in rare euhedral crystals which may be distributed: (1) randomly throughout the rock (e.g. in 2640 where it occurs at grain boundaries, included within olivine I or pyroxene I, and clustered adjacent to spinel I); (2) intermittently along mylonized fractures (2655-1), or (3) in patches within an inclusion (2925 and 2655-2). In these inclusions, there are examples of a gradation from phlogopite I crystals with sharp boundaries against surrounding crystals, to phlogopite I with corroded form surrounded by glass with included euhedral spinel II and olivine II, to an end stage of patches of glass including euhedral spinel II and olivine II. Patches of glass without associated phlogopite I occur in many inclusions on grain boundaries or entirely enclosed within olivine I, and their derivation from phlogopite I usually cannot be demonstrated. In inclusions 2640, 2655-1, and 2925 the textural relationship to phlogopite I can be observed, and in inclusions 2906 and 2642, patches of glass + olivine II + spinel II + clinopyroxene II show textural evidence for development from pre-existing amphibole I. This process is extensively developed in 2906, but very minor in 2642.

Incongruent melting of hydrous phases in mantle rocks must occur if mantle rock at moderate temperature and high pressure is incorporated in a rapidly ascending magma, which causes a rapid heating accompanied by a large decrease in P_{Load} and P_{H_2O}. An hypothesis of glass formation by partial melting involving clinopyroxene and spinel was presented by KLEEMAN *et al.* (1969). Original patchy distribution of hydrous phases, such as amphibole and phlogopite, explain the observation that in some inclusions there are areas with strong development of glass with relict highly corroded spinel I and clinopyroxene I, whereas elsewhere in

Table 6. Selected analyses of glass developed within lherzolite inclusions. Analyzed by TPD simultaneously at one analytical point.

	2642 Glass developed from amphibole (Table 4)		2700 Glass in large patches and in veinlets			2669 Glass in large patches and in internal veins				
			In vein	In patch	In vein	In patch	In vein	In vein	In vein	In patch
SiO_2	55·2	59·0	67·5	61·2	57·0	65·3	54·5	56·0	53·2	64·8
TiO_2	1·1	0·7	0·5	1·5	1·2	0·5	0·9	0·8	0·8	0·6
Al_2O_3	19·2	19·5	18·6	20·7	20·8	17·9	20·8	20·6	19·9	19·1
FeO	2·1	2·5	2·5	2·5	3·0	1·9	3·8	2·7	3·0	1·9
MgO	8·8	10·5	2·3	2·9	3·3	4·3	4·1	2·7	4·1	2·4
CaO	8·9	4·2	4·0	4·7	6·9	3·2	8·7	8·4	8·0	4·7
Na_2O	4·1	3·6	3·2	5·4	5·9	4·8	5·7	7·1	9·6	4·0
K_2O	0·1	0·05	1·0	1·0	1·1	2·1	1·3	1·3	1·2	1·9
P_2O_5	—	—	0·4	—	0·7	—	—	—	—	—
Cr_2O_3	0·3	—	—	—	—	—	0·2	—	0·3	0·3
$\frac{100\ Mg}{Mg + \Sigma Fe}$	88	88	62	77	66	80	66	64	71	70
Minerals in contact with analyzed glass	amph sp opx ol	amph sp cpx ol	ol sp cpx ap	ol sp cpx	ol sp ap	ol	ol sp cpx	ol sp (cpx)	ol sp	ol cpx
Primary olivine I	(Fo)	90·4		89·7				91·1		
Secondary olivine II	(Fo)	92·1		90·3–91·6				91·3–92·0		

the inclusion, adjacent clinopyroxene I and spinel I show only minor glass development.

Compositions of glass in several lherzolite inclusions and of euhedral crystals in glass areas are given in Tables 6 and 7, respectively. The glasses are chemically heterogeneous and the alkali metal abundances can be correlated with associated amphibole and/or phlogopite. The glass in 2642, derived from amphibole, has very

Table 7. Secondary minerals crystallizing from glass or by recrystallization of primary phases (clinopyroxenes 2642, 2700). Analyses by TPD electron probe

	Clinopyroxenes							Spinels				Plagioclase
	Ia 2642	Ia 2700	II 2669	II 2669	II 2640	II 2925	II 2925	II 2700	II 2669	II 2925	II 2925	II 2925
SiO_2	51·8	52·6	53·5	52·0	52·3	43·5	53·1					54·1
TiO_2	0·7	0·3	0·2	0·3	0·7	4·7	—	1·4	0·5	0·4	0·8	0·2
Al_2O_3	4·7	3·4	5·8	3·9	2·3	9·3	1·7	52·9	32·1	42·4	21·1	28·0
FeO	2·6	2·7	2·6	2·2	5·0	8·7	2·9	10·9	12·6	12·2	23·4	0·7
MgO	18·0	17·3	16·2	16·5	17·4	11·1	16·8	20·6	17·9	20·2	13·2	0·6
CaO	20·7	21·2	18·3	22·6	19·6	22·3	23·6	—	—	—	—	10·3
Na_2O	0·3	0·8	1·1	0·2	0·8	0·5	0·2	—	—	—	—	5·3
K_2O	—	—	—	—	—	—	0·1	—	—	—	—	0·8
Cr_2O_3	—	1·5	2·2	2·0	1·5	—	1·5	14·2	36·7	23·9	41·0	—
NiO	—	—	—	—	—	—	—		0·3	0·4	0·3	—

electron probe (REED and WARE, 1973; GREEN, 1973a) permitting determination of all elements
Total iron only (microprobe), reported as FeO

2640 Glass in basanite and continuous with glass in lherzolite (1–3) glass within lherzolite (4–5)					2925 Large glass areas near relict phlogopite			
1 In basanite	2 Edge lherzolite	3 In small patch	4 In vein	5 In small patch	Near phlog.		Near cpx	
51·3	50·5	59·5	66·2	64·5	52·9	51·8	55·0	SiO_2
2·5	3·4	2·3	1·5	2·0	1·0	1·6	0·6	TiO_2
19·7	19·3	21·6	18·3	18·4	24·2	21·2	21·4	Al_2O_3
7·4	7·5	1·8	1·2	1·4	2·5	5·0	3·9	FeO
2·0	2·8	1·5	1·5	1·6	2·3	2·5	2·0	MgO
4·5	6·9	3·4	1·5	3·0	3·1	4·7	2·8	CaO
6·5	4·8	4·3	3·8	3·3	8·1	7·2	7·7	Na_2O
5·3	4·0	5·6	6·0	5·6	7·0	6·0	6·7	K_2O
1·0	1·1	—	—	—	—	0·2	—	P_2O_5
—	—	—	—	—	—	—	—	Cr_2O_3
33	40	60	68	67	62	47	48	$\frac{100\,Mg}{Mg + \Sigma Fe}$
ol	ol	ol	ol	ol	ol	ol	ol	Minerals in
cpx	cpx	cpx	cpx	opx			cpx	contact with
ilm	sp	phlog		phlog		sp		analyzed
plag		sp				plag		glass
ap								
		87·7				—		Primary olivine I
		90·6				92·1–92·6		Secondary olivine II
		in basanite 81 → 70 (zoned)						

low K_2O and K_2O/Na_2O, which is consistent with an amphibole (Table 4) source for the glass and an absence of pre-existing phlogopite. In contrast, the glass in 2640, observed in contact with corroded phlogopite (Table 4), has very high K_2O and high K_2O/Na_2O. In this case, the Na_2O of the glass cannot be derived entirely from the phlogopite, which implies either the former presence of amphibole or addition of Na_2O by recrystallization of primary clinopyroxene I (1·6 wt.% Na_2O) to secondary clinopyroxene II (0·8 wt.% Na_2O). The very alkali-rich glasses in 2925 have K_2O/Na_2O about unity, indicating a derivation from both phlogopite and amphibole; whereas, only amphibole (with higher K_2O than the 2642 amphibole, cf. Table 4, columns 1 and 2) may have been involved in forming the glasses in 2669 and 2700, which have K_2O/Na_2O greater than 2642 glass but less than 2640 and 2925 glasses.

Inclusion 2640 was examined for information on the degree to which glass from the basanite penetrated the inclusion. The glass in the basanite differs in $100Mg/Mg + \Sigma Fe$ value, FeO, CaO, P_2O_5, MgO and Na_2O from that in the lherzolite, but it shows similar high Al_2O_3 content (Table 6). The chemical intermixing of basanite-derived glass and lherzolite-derived glass occurs only within $\sim 200\ \mu m$ of the inclusion edge (compare analyses 1–5 for 2640 in Table 6).

In addition to alkali metal heterogeneity caused by pre-existing amphibole and phlogopite, the glass within any one inclusion varies considerably in SiO_2 and CaO. The glasses lowest in SiO_2 and highest in CaO (Table 6) are correlated with the absence of small, euhedral, clinopyroxene crystals or neighboring large clinopyroxene

crystals, and such glasses may reflect a metastable fractionation trend. Most of the glasses do contain euhedral crystals of olivine II, spinel II, clinopyroxene II, and occasionally plagioclase. Crystallization of these phases, probably under conditions of rapid growth during quenching of the basanite, may have modified the glass composition; e.g. the high Al_2O_3 content of the glasses in both basanite and lherzolite is possibly due to inhibited plagioclase nucleation (cf. WILKINSON, 1966).

The glass compositions within the lherzolite inclusions show similarities (particularly the high SiO_2 and Al_2O_3 contents, and low MgO and FeO contents) to the glass formed during the quenching of high pressure melting experiments (water-saturated) on peridotite compositions (KUSHIRO *et al.*, 1972; GREEN, 1973b). Detailed study of these experiments (GREEN, 1973b) shows that such siliceous and aluminous glasses result from growth of quench olivine, clinopyroxene, and amphibole (grown during rapid cooling of the experimental charge) which modify the composition of the equilibrium melt along a quench fractionation trend.

The small euhedral olivine II within glass areas is usually more magnesian than the primary olivine I of the lherzolites. The small euhedral clinopyroxene II crystals in glass or the recrystallized areas (Ia) of the primary clinopyroxenes I (cf. KLEEMAN *et al.*, 1969) are variable in composition, but always have lower Na_2O content than clinopyroxene I. The small euhedral spinel II crystals range from very aluminous spinel (2700) to chromian spinel (2925), and their composition does not appear to be related to that of primary spinel I (Tables 3 and 7).

Our results for the glasses within the inclusions, coupled with the results of GREEN *et al.* (1968); KLEEMAN *et al.* (1969); COOPER and GREEN (1969); and DASCH and GREEN (in press) lead to the following conclusions: (1) the host basanite has supplied thermal and mechanical energy resulting in mineralogical changes (recrystallization and melting) within the inclusions, but it has not chemically contaminated the inclusion interiors. (2) Minor accessory phases (particularly phlogopite and pargasitic amphibole) within the inclusions are important loci of *local* incongruent melting. (3) Neither the melting conditions nor the composition of the liquid originally formed can be specified, because the present glass compositions are not those of liquids in equilibrium with primary minerals of the lherzolites under any P,T conditions. (4) During cooling of the basanite and the lherzolite inclusions, growth of quench crystals (olivine, clinopyroxene, and opaque minerals including spinel and, in some cases, plagioclase) from both the basanite liquid and the liquid within the lherzolite inclusions has produced glasses of variable composition which do not match well with observed natural magma types (Table 6).

Crystallization and equilibration conditions of the primary lherzolite mineralogy

Table 3 lists analyses of co-existing major minerals in the lherzolite inclusions, and Table 4 lists analyses of the accessory minerals, apatite (2700 and 2638), phlogopite (2640 and 2925), and amphibole (2642). Microprobe analyses show the primary phases to be homogeneous and without grain to grain compositional variation. Compositional variation does occur where reaction rims (e.g. clinopyroxene I–Ia) are developed.

We have no information on the stability limits of chlor-apatite at high pressure and temperature. Phlogopite (assuming this to be hydrous rather than

fluor-phogopite) is stable in pyrolite composition (with 0·1–0·2 wt.% water) to temperatures between 1150 and 1200°C at 30 kbar, $p_{H_2O} < p_{Total}$ (GREEN, 1973b). In experiments without excess water, pure magnesium phlogopite is stable with forsterite to temperatures of 1150–1200°C at 15–40 kbar (YODER and KUSHIRO, 1969), and with enstatite to temperatures of 1080–1295°C at 10–35 kbar (MODRESKI and BOETTCHER, 1972). In an excess water system with enstatite it is stable to 1050–1190°C at 10–35 kbar (MODRESKI and BOETTCHER, 1972). The maximum thermal stability of pargastic amphibole in pyrolite containing 0·1–0·2 wt.% water is between 1105 and 1200°C at 20–25 kbar, $P_{H_2O} < P_{Load}$ (GREEN, 1972, 1973b).

The degree of mutual solid solution in co-existing pyroxenes, and element partitioning between the major phases, may be used to estimate pressure and temperature conditions of equilibrium for the lherzolites. If the inclusions have existed under varying P,T conditions, e.g. a cooling history following some magmatic event, then various geothermometers may be 'frozen in' at different temperatures. The presence of exsolution lamellae in the lherzolite pyroxenes (microscopic lamellae of clinopyroxene in orthopyroxene in 2642, 2728, and to a lesser extent in 2604; similar sub-microscopic lamellae in 2669, 2700 and 2640; spinel lamellae in orthopyroxene in 2642 and 2728), shows that the inclusions had a cooling history prior to their incorporation into the basanites. The textural characteristics of the inclusions suggest that much of the spinel and clinopyroxene is of late crystallization, probably in part by exsolution from the more abundant orthopyroxene. This interpretation is advocated particularly for spinel occurring in long stringers on grain boundaries in 2728 and, to a lesser extent, in 2640.

Solid solution between co-existing orthopyroxene and clinopyroxene increases with increasing temperature and with decreasing $Mg/Mg + Fe^{2+}$, but decreases with increasing Tschermak's silicate [$(MgCa)Al_2SiO_6$] solid solution (BOYD, 1970). The effects of jadeite, chrome-pyroxene, and acmite components on the clinopyroxene–orthopyroxene solid solution remain unknown. O'HARA (1967, p. 401) estimated clinopyroxene equilibration temperatures in lherzolite inclusions (data obtained from the literature) to be in the range 1130–1330°C at 8–21 kbar, and he inferred that this range coincided with crystallization temperatures for basaltic magmas. Later work (BOYD, 1970; GREEN, 1973a, b; GREEN and RINGWOOD, 1967, 1970) has shown that O'Hara's provisional grid is insufficiently precise to specify equilibration temperatures, although the concept of calibrating such a grid is valid.

Experimental studies on dry basaltic magmas that have olivine, orthopyroxene, and clinopyroxene on or near the liquids (and for which these phases have 100 $Mg/Mg + Fe^{2+}$ = 85–95) show that these magmas have dry liquidi in the temperature range 1250–1450°C (8–21 kbar). At these temperatures, orthopyroxene contains >2·0 wt.% CaO, and co-existing clinopyroxene contains <18 wt.% CaO (GREEN and RINGWOOD, 1967; GREEN and HIBBERSON, 1970). The published data do not yet permit temperature contouring of the two-pyroxene field in the molecular Ca–Mg–Fe plot, but they do demonstrate that the clinopyroxene solid solution is very dependent on $Mg/Mg + Fe^{2+}$ values.

New data on sub-solidus and above-solidus assemblages in pyrolite compositions (GREEN and RINGWOOD, 1970; GREEN, 1973a, b and unpublished data) and on

above-solidus assemblages in a lherzolite (KUSHIRO *et al.*, 1972) provide analyses of co-existing pyroxenes at 20–30 kbar, at temperatures from 900–1300°C. These data confirm that temperatures $\ll$1300°C are required for lherzolite orthopyroxenes (<0·7 wt. % CaO) and clinopyroxenes (>17 wt.% CaO). Because the Al_2O_3, Cr_2O_3, Mg/Mg + Fe^{2+}, and Na_2O contents of pyroxenes crystallized experimentally from pyrolite at 10 kbar, 900–1000°C, 20 kbar, 950–1000°C (GREEN, 1973b) and 30 kbar, 1250°C (GREEN, 1973a), and from lherzolite at 20 kbar, 1050°C (KUSHIRO *et al.*, 1972) are close to the values of the inclusion pyroxenes (Table 3), the experimental data can be used to place limits on the equilibration temperatures of inclusion pyroxenes. The orthopyroxenes of the Victorian lherzolites indicate temperatures $\lesssim$900°C, and the clinopyroxenes indicate temperatures $\lesssim$1050°C. The apparent difference between the two phases implies a cooling history for the inclusions (cf. presence of exsolution lamellae) in which the orthopyroxene compositions were adjusted to lower temperatures. We conclude, therefore, that pyroxene compositions in the lherzolites are incompatible with high pressure equilibrium with basaltic magmas at $T \geq$ 1050°C.

Neglecting the small variation in Mg/Mg + Fe^{2+} among the clinopyroxenes and noting the similarity of all but 2604 in Al_2O_3 content, the variation in Ca–Mg–Fe proportions of the lherzolite clinopyroxenes indicates equilibration temperatures increasing in the order 2642–2728–2669–2700–2604–2640. The Ataq lherzolite (VARNE, 1970) indicates an equilibration temperature of clinopyroxene near that of 2642, whereas Hualalai clinopyroxene (KUNO and AOKI, 1970) indicates temperatures above that of 2640. The Lizard primary clinopyroxenes (GREEN, 1964) indicate temperatures similar to those of 2604 and 2640 (the higher Al_2O_3 contents of Lizard pyroxenes may make the comparison unreliable). The orthopyroxene compositions within the lherzolite inclusions indicate equilibration temperatures increasing in the order 2604–2669–2728–2642–2700–2640 with the Ataq orthopyroxene equilibrating at temperatures near 2642, the Hualalai orthopyroxene equilibrating at temperatures above that of 2640, and the Lizard orthopyroxenes (including exsolution lamellae) equilibrating at temperatures much higher than 2640 ($T >$ 1300°C; CaO = 2·1 wt.%).

The partition of Fe^{2+} and Mg between orthopyroxene and clinopyroxene is temperature-sensitive, and the partition coefficient [$K_D = (Fe^{2+}/Mg)_{opx}/(Fe^{2+}/Mg)_{cpx}$] is consistently lower for igneous pyroxenes (1·3–1·4) than for metamorphic pyroxenes ($\sim$ 1·8). The K_D values for the lherzolite inclusions range from 2·0 to 1·2 and decrease in the order 2642–2728–2669–2700–2604–2640 (Table 3). This order of increasing equilibration temperature is consistent with that indicated by the Ca-content of the clinopyroxene. The temperatures indicated by the K_D values range from igneous (2640 and 2604) to typical metamorphic (2728 and 2642). The K_D value calculated from experimental pyroxene pairs (KUSHIRO *et al.*, 1972; GREEN, 1973b) range from 1·0 to 1·3 at 1050–950°C (assuming no Fe^{3+} in clinopyroxene).

Although the Ca–Mg–Fe proportions in the clinopyroxenes and the pyroxene K_D (Mg, Fe^{2+}) values give the same sequence of relative equilibration temperatures, the orthopyroxene Ca–Mg–Fe proportions do not give the same sequence. Also, the igneous temperature for 2640 indicated by K_D is not consistent with the low

CaO content of the 2640 orthopyroxene (cf. Hualalai and Lizard pyroxenes in Table 3). These inconsistencies may be explained by the probability that the resetting of different geothermometers is determined by kinetics of exchange reactions, unmixing, etc., and thus different geothermometers may record different temperatures. In addition, microprobe analysis as opposed to mineral separation and analysis may yield different compositions for co-existing phases. This factor complicates comparison of Lizard (GREEN, 1964), Hualalai (KUNO and AOKI, 1970), and Ataq (VARNE, 1970) mineral data with that presented in this paper.

It is also relevant to refer to natural rock data for the pyroxene compositions which crystallize on or near the liquidi of basalts at high pressure. Such data are provided by the large 'megacrysts' or high pressure phenocrysts found in many undersaturated magmas. Orthopyroxene 'megacrysts' range from 100 Mg/Mg + Fe^{2+} = 88–82 with CaO contents in the range 2·1–1·45 wt.%. Clinopyroxenes, often associated with orthopyroxenes, range from 100 Mg/Mg + Fe^{2+} = 88–82 with CaO contents from 13·6–20·5 wt.%, most in the range 15–17 wt.% CaO (KUNO, 1964; BINNS, 1969; BINNS *et al.*, 1970; GREEN and HIBBERSON, 1970; IRVING, 1974). These data are consistent with experimental crystallization of liquidus basaltic pyroxenes at high pressures, under dry conditions, or with small water contents, i.e. at temperatures >1100°C. The lherzolite pyroxenes, with much lower mutual solubility at similar or only slightly higher 100 Mg/Mg + Fe^{2+} values, imply equilibration temperatures much less than those at or near the liquidi of basaltic magmas.

The mineralogy of the lherzolite inclusions thus indicates that these rocks were cooled to temperatures below the solidi of the lherzolites, and below the liquidi temperatures of natural basaltic magmas. The high K_D values for Fe^{2+}/Mg partitioning and the low CaO contents of orthopyroxenes suggest temperatures similar to high-grade metamorphic terrains (probably 700–800°C). It should be noted, however, that there is a range of equilibration temperatures among the inclusions; 2642 and 2728 indicate temperatures considerably below those of 2700 and particularly 2640. The evidence of a cooling history implies that the present inclusion mineralogy and modal proportions differ from that originally formed in a higher temperature assemblage. Differences would lie particularly in the presence or absence of accessory minerals and the relative proportions of clinopyroxene and spinel. There is also petrographic evidence for late-stage introduction of mobile components in the presence, in some inclusions, of intergranular sulphide veinlets and in the growth of phlogopite in rare mylonite zones through some inclusions.

Conclusions from petrographical and mineralogical studies

The previous discussion shows that the present characteristics of the lherzolite inclusions have been determined by several distinct processes. During transport from depths >20–30 km to the surface, the inclusions were partially melted, largely as a consequence of incongruent melting of the hydrous phases phlogopite and amphibole, but also involving the major phases of the lherzolites. If the inclusions were at temperatures >1100°C when they were incorporated by the host magma, then the observed melting could be due to decrease in pressure. However, the evidence of low equilibration temperatures (<1000°C) indicated by the lherzolite

pyroxenes, implies that the host magmas have caused both heating and transport of the inclusions, and that the melting in the inclusions is due to both pressure decrease and temperature increase. The melting, followed by quenching and partial crystallization (at eruption) of the partial melt, occurred so rapidly that equilibrium between liquid and the major lherzolite phases has not been attained. Certainly the present glass compositions in the inclusions cannot be taken as the compositions of any equilibrium partial melt fraction of the lherzolites.

Because of the limited and disequilibrium character of the melting, relict (pre-melting) phases are predominant in the lherzolites, and they provide information on the crystallization history of the lherzolites prior to inclusion in the basanites. Our study, like others, (e.g. WHITE, 1966) indicates that the lherzolites have multi-event histories, commonly with an early cooling event from a higher temperature, possibly above or at the solidus, to lower temperature, sub-solidus conditions, probably $<800°C$. In some inclusions there has been late introduction or migration of mobile components including sulphide veinlets, chlorapatite, and probably a K-bearing fluid phase leading to growth of phlogopite in mylonite zones, in probable 'healed' fractures through olivine and enstatite, and along grain boundaries. Although it can be argued from the trace-element and isotopic data that the lherzolites have remained closed systems relative to the enclosing basanite during their rapid transport and eruption, it can equally well be argued that the inclusions may not have remained closed systems since the early high temperature event. They may have been changed chemically by the introduction of small increments of a sulphide-rich phase, water-rich vapor phase, or water-rich silicate melt.

The following sections discuss the major element and trace element compositions of the lherzolites, particularly in relation to the possible original processes of lherzolite formation.

GEOCHEMISTRY OF THE LHERZOLITE INCLUSIONS

In comparing the compositions of the lherzolite inclusions, we evaluate four possibilities that are consistent with an accidental (xenolith) origin for the inclusions. That is, in each case, the basaltic magma mentioned is not the host basanite.

1. The lherzolites are simple residues from basalt magma extraction from a pre-existing ultramafic source rock (pyrolite).

2. The lherzolites are simple accumulates from basaltic magma under high pressure conditions.

3. The lherzolites are residues from basalt magma extraction and contain a trapped liquid component due either to (a) incomplete magma extraction, or (b) later introduction of a small amount of a migratory melt phase.

4. The lherzolites are accumulates from basalt magma under high pressure conditions, and contain an additional component in the manner outlined in 3a or 3b.

Major elements

The lherzolites (excepting 2640, for reasons which become apparent below) may be arranged in order of increasing pyx/ol resulting in the sequence 2604–2669–2700–2728–2642 (Table 5). This is also the sequence of increasing cpx/ol (apart

from 2700 which has anomalously high cpx/opx proportions), of decreasing Mg/Mg + Fe^{2+} in olivine (apart from slight deviation in 2700), and the trend of increasing Ti and Na/Na + Ca in clinopyroxene (provided the 2 vol.% amphibole in 2642 is recast as the anhydrous phases olivine, clinopyroxene, and spinel). The parameters chosen in discussing the sequential grouping are significant in crystal–liquid equilibria.

The mineralogical and chemical sequence defined above may be continued to the Lizard (GREEN, 1964) and Tinaquillo (GREEN, 1963) high temperature peridotites, both with high Ca and Al contents, and thus high modal clinopyroxene. The Ataq lherzolite inclusion (VARNE, 1970) is similar to 2728, but the Hualalai inclusion (KUNO and AOKI, 1970) resembles 2604. A similar sequence of chemical compositions with increasing CaO, Al_2O_3, and Na_2O is seen in the peridotites of St. Paul's Rocks (MELSON *et al.*, 1973; and Table 2). Using the compositions of analyzed minerals from inclusion 2700 as a basis for calculated modes (Table 5), the sequence of St. Paul's Rocks compositions may also be 'fitted' to the lherzolite grouping with the most olivine-rich composition being intermediate between 2669 and 2728 and the most clinopyroxene-rich composition being more clinopyroxene-rich than 2642.

Comparison of total-rock and mineral analyses (Tables 1–4) demonstrates that the variations in total rock composition are not due simply to variations in proportions of mineral phases with constant composition. This is particulary apparent in comparison of Mg/Mg + Fe^{2+} ratios, for this ratio in olivine is lower than in coexisting pyroxenes, yet the most olivine-rich samples (2604 and 2669) have the highest total-rock Mg/Mg + Fe^{2+} values. Lherzolite inclusions at Kilbourne Hole, New Mexico also have major element abundances which can be correlated with changes in mineral chemistry (CARTER, 1970).

Rare earth element abundances in Victorian rocks and minerals

Basanites. REE* concentrations in the host basanites are similar (maximum variation between 2650 and 2679 is 20 per cent) and the relative abundance pattern is typical of highly nepheline-normative basanites or nephelinites (Fig. 1 and Table 8). Compared to the Mt. Shadwell basanite (2679), the Mt. Leura basanites (2650 and GSFC-20) have a more strongly fractionated REE pattern with a lower abundance of HREE and a higher abundance of LREE. This kind of REE fractionation (increasing LREE accompanied by decreasing HREE) is characteristic of liquids which have equilibrated with garnet (KAY and GAST, in press).

The Mt. Leura basanites (2650, GSFC-20) differ in major element composition from the Mt. Shadwell (2679) basanite in higher K_2O/Na_2O, TiO_2 content, and P_2O_5 content, but they are lower in Mg/Mg + Fe^{2+} (Table 1, this paper, and Table 2, PHILPOTTS *et al.*, 1972). Uranium and thorium are more abundant in 2650 (U = 2·2 ppm and Th = 6·7 ppm) than in 2679 (U = 1·6 ppm and Th = 5·7 ppm; GREEN *et al.*, 1968). Since shallow-level fractional crystallization of olivine, pyroxenes and feldspars could not cause the observed REE differences, these

* The symbol REE will be used to designate rare-earth elements. LREE will denote the low atomic number elements La, Ce, Pr and Nd. HREE will denote the high atomic number elements Er, Tm, Yb and Lu.

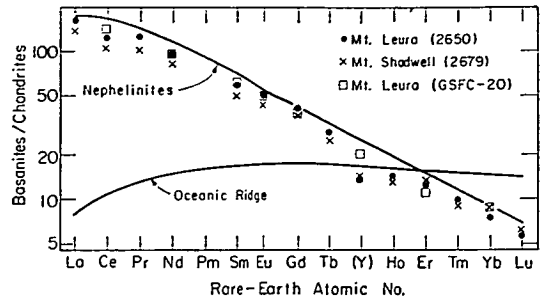

Fig. 1. Victorian basanites (2650, GSFC-20 and 2679) compared to a chondritic REE average (FREY *et al.*, 1968). GSFC-20 from PHILPOTTS *et al.*, 1972. Also shown are an oceanic ridge tholeiitic basalt average (FREY *et al.*, 1968; KAY *et al.*, 1969) and an average for Hawaiian nephelinites (SCHILLING and WINCHESTER, 1969). (In all rare-earth element plots, Y data are plotted in place of Dy.)

chemical differences imply that the Mt. Leura basanite was derived by a smaller degree of partial melting than the Mt. Shadwell basanite.

Lherzolite inclusions. The REE data for eight Victorian inclusions (six studied in this paper, a dunite (RCE) studied by FREY *et al.*, 1971, and a lherzolite (GFSC-20) studied by PHILPOTTS *et al.*, 1972) demonstrate a remarkable spread in REE abundance and distribution patterns. (Table 8, Fig. 2a, b). Compared to the chondritic average La/Yb (1·65) the inclusions range from large relative enrichment in LREE (2604 La/Yb = 37, 2669 La/Yb = 31, 2700 La/Yb = 29, RCE La/Yb = 14, and GSFC-20 La/Yb > 11) to slight enrichment in light REE (2640 La/Yb = 2·8) to slight depletion in LREE (2728 La/Yb = 1·31, 2642 La/Yb = 1·2).

In terms of absolute abundance, those inclusions with LREE-depleted patterns have unfractionated HREE distributions and abundances of HREE from 1 to 2

Table 8. REE abundances* in lherzolite inclusions and host basanites (ppm)

	Lherzolites						Basanites	
	Anakies 2604	Mt. Shadwell 2669	Mt. Leura 2640	Mt. Gambier 2728	Mt. Noorat† 2700	Mt. Leura† 2642	Mt. Leura 2650	Mt. Shadwell 2679
La	0·878	1·74	0·259	0·271	3·37 ± 0·05	0·361 ± 0·006	52·2	45·5
Ce	1·97	2·63	0·59	0·58	2·88 ± 0·10	0·55	108	93
Pr	0·222	0·556	0·101	0·0937	0·477 ± 0·009	0·088 ± 0·002	14·2	11·4
Nd	0·82	2·19	0·50	0·48	1·7 ± 0·2	0·458 ± 0·008	56·3	49·2
Sm	0·133	0·346	0·115	0·165	0·300 ± 0·001	0·187 ± 0·004	10·5	9·10
Eu	0·0331	0·0993	0·0389	0·0683	0·099 ± 0·002	0·0825 ± 0·0002	3·42	2·99
Gd	0·094	0·25	0·14	0·28	0·29 ± 0·02	0·30 ± 0·03	10·1	9·19
Tb	0·013	0·032	0·023	0·048	0·038 ± 0·001	0·061 ± 0·002	1·34	1·18
Ho	0·0113	0·0269	0·0288	0·0737	0·050 ± 0·002	0·110 ± 0·003	0·99	0·95
Er	0·039	0·066	0·084	0·22	0·146 ± 0·001	0·33 ± 0·03	2·5	2·7
Tm	0·0046	0·0090	0·0135	0·0291	0·0211 ± 0·0003	0·0497	0·292	0·281
Yb	0·024	0·056	0·092	0·207	0·117 ± 0·015	0·31 ± 0·02	1·59	1·74
Lu	0·0062	0·0094	0·0158	0·0321	0·0209	0·055 ± 0·005	0·189	0·192
Y‡	0·30	0·73	0·68	1·78	1·20 ± 0·05	2·67 ± 0·01	26·1	26·2

* The REE data reported in Tables 8 and 9 were obtained by a radiochemical neutron activation technique (HASKIN *et al.*, 1968). For ultramafic rocks this technique has a precision of ±5% (FREY *et al.*, 1971) although occasionally poorer precision is obtained for an individual element. The precision of these lherzolite inclusion analyses is indicated for 2700 and 2642, Accuracy is believed comparable to the precision (FREY *et al.*, 1971).

† ± values indicate deviations from the mean of duplicate analyses.

‡ Y data are obtained instead of Dy in this technique (HASKIN *et al.*, 1968).

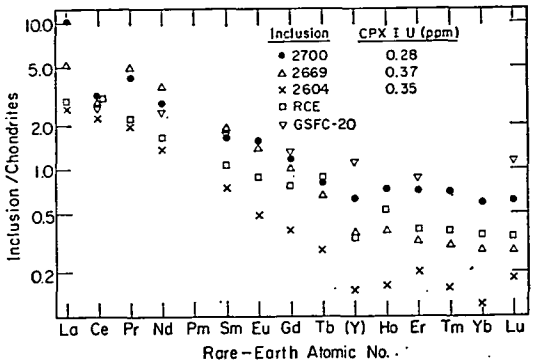

Fig. 2a. Victorian inclusions markedly enriched in light rare-earth elements compared to a chondritic REE average (FREY *et al.*, 1968). Data labeled RCE are for a Mt. Leura dunite (~ 95 vol.% olivine) inclusion (FREY *et al.*, 1971) and data labeled GSFC-20 are for a Mt. Leura lherzolite (~ 7 vol.% cpx) inclusion (PHILPOTTS *et al.*, 1972).

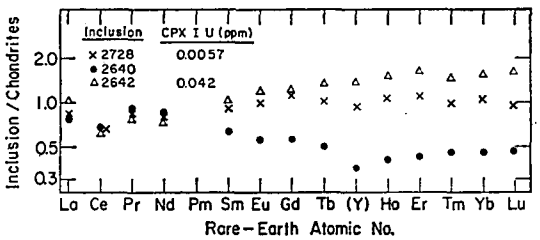

Fig. 2b. Victorian inclusions not markedly enriched in light rare-earth elements compared to the chondritic REE average.

times chondritic abundances and from 0·05 to 0·1 times the abundances in ocean ridge tholeiitic basalts. Those inclusions with LREE-enriched patterns also have unfractionated HREE patterns, but have abundances of HREE from 0·15 to 1·0 times chondritic abundances and 0·0075–0·05 times the abundances in ocean ridge tholeiitic basalts (FREY *et al.*, 1968; SCHILLING, 1971).

Lherzolite minerals. Mineral separates from the lherzolite inclusions are relatively easy to obtain because of the coarse grain-size of the primary minerals (I) and lack of alteration phenomena. Conventional heavy liquid and magnetic separation techniques followed by hand picking of grains (~ 0·5 mm) with a binocular microscope (30 ×) were used. Optically the purity of each separate exceeded 99·9 per cent. There was no difficulty in eliminating composite grains with phases Ia or II attached to primary phases because of the marked difference in magnetic properties (spinel II grains) or color differences in final hand picking. Exsolution lamellae are included with the host mineral.

The REE concentrations of clinopyroxenes from the lherzolite inclusions are given in Table 9 and illustrated in Fig. 3. The REE range in the total rocks is even more apparent in the clinopyroxenes. At one extreme, 2728 has a REE pattern resembling that of ocean ridge tholeiitic basalts, while at the other extreme, 2604 has La/Yb = 57 which exceeds that in the host basanites. LREE enrichment in

Table 9. REE and U abundances* in inclusion minerals (ppm)

	Anakies 2604		Mt. Shadwell 2669	Mt. Leura 2640		Mt. Gambier 2728	Mt. Noorat 2700	Mt. Leura 2642		Mt. Leura 2638
	cpx	opx	cpx	cpx	opx	cpx	cpx	cpx	amph	Apatite
La	26·6	0·686	23·4	5·49	0·0337	1·07	13·0	3·73	8·33	4200
Ce	64·5	1·13	61	15·3	0·10	3·0	17·6	6·6	20·3	8000
Pr	8·43	0·176	9·84	2·38	0·0188	0·68	2·55	1·12	2·04	—
Nd	33·3	0·79	39·4	11·1	0·12	4·1	10·5	5·21	9·22	3400
Sm	5·78	0·146	6·31	2·73	0·0465	1·43	1·98	1·57	2·72	480
Eu	1·58	0·0437	1·865	0·88	0·020	0·62	0·70	0·62	1·13	130
Gd	4·0	0·13	5·0	2·7	0·077	2·4	2·0	2·3	4·34	380
Tb	0·46	0·020	0·58	0·45	0·017	0·42	0·29	0·44	0·76	48
Ho	0·34	0·0187	0·64	0·51	0·030	0·62	0·27	0·68	1·38	—
Er	0·88	0·052	1·45	1·44	0·014	1·75	0·78	1·64	3·64	—
Tm	0·097	0·0091	0·200	0·18	0·0225	0·25	0·11	0·25	0·51	—
Yb	0·47	0·068	1·2	1·02	0·157	1·43	0·53	1·73	3·43	25
Lu	0·095	0·012	0·169	0·183	0·028	0·26	0·10	0·28	0·52	2·5
Y†	9·0	0·557	16·1	13·1	0·84	17·5	5·5	18·6	32	—
U‡	0·35	0·0049	0·37	—	0·0007	0·0057	0·28	0·042	—	32

* For estimates of accuracy and precision see Table 8.
† See Table 8.
‡ U data from (KLEEMAN *et al.*, 1969).

lherzolite inclusions was previously explained (FREY *et al.*, 1971) as a result of interstitial contamination (2 wt.%) by the host basanite. This explanation is no longer valid since the LREE enrichment in these inclusions results from REE contained within clinopyroxene and not from REE-rich interstitial areas between primary lherzolite minerals, or LREE-rich accessory minerals. Although we cannot establish that the REE are uniformly distributed in these clinopyroxenes, the homogeneous U distribution found by KLEEMAN *et al.* (1969) implies that other large ionic-radii trace elements such as REE may be uniformly distributed within

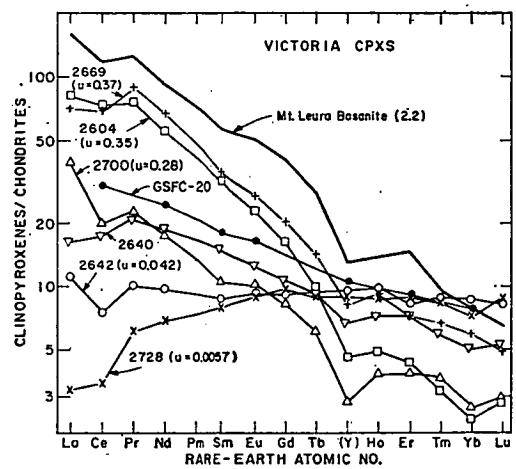

Fig. 3. Clinopyroxenes from Victorian inclusions compared to a chondritic REE average (FREY *et al.*, 1968). Data labeled GSFC-20 from PHILPOTTS *et al.* (1972). In parentheses are the U (cpx I) data of KLEEMAN *et al.* (1970). Also shown for comparison is the Mt. Leura basanite (2650) with a U content of 2·2 ppm.

these clinopyroxenes. In our subsequent interpretations, the clinopyroxene REE data are a key factor. Our interpretations would not be affected if the REE are contained in small phases within the clinopyroxenes. The correlation in clinopyroxene of LREE enrichment and U abundance is remarkable (Fig. 4). Comparison of Fig. 3 and the major element data of Table 3 shows no apparent correlation between REE variations and clinopyroxene major element chemistry (Mg/Mg + Fe^{2+}, Na/Na + Ca, Al_2O_3 content, etc.).

The data from 2642 (Table 9) show that the amphibole contains roughly twice the REE content of the clinopyroxene, but apart from slight enrichment of La and Ce, there is little REE fractionation relative to clinopyroxene. VARNE and GRAHAM (1971) obtained a similar result for REE amphibole/cpx partitioning in a Ataq inclusion, but the REE patterns in both Ataq clinopyroxene and amphibole are highly enriched in LREE, resembling 2604 and 2669 clinopyroxenes. The similar clinopyroxene–amphibole REE partitioning in 2640 and the Ataq inclusion is evidence for REE equilibration. The Lizard peridotite locally contains pargasitic amphibole (Table 4) which has an LREE depleted pattern relative to chondrites (FREY, 1969). Comparison of Table 4 with Table 9 demonstrates that for amphibole also, there is no apparent correlation, except possibly in Na_2O content, between mineral major element data and REE patterns.

We do not have REE data on apatite from 2700, but data from compositionally-similar apatite from another inclusion (2638, Tables 4 and 9) yields apatite/cpx partition coefficients ranging from 120 for La to 9·4 for Lu (FREY and GREEN, unpublished data). Except for La, these values are within a factor of two of the apatite/cpx partition coefficients in the San Marcos Gabbro (TOWELL *et al.*, 1965). In light of recent explanations for the lunar Eu anomaly (GRAHAM and RINGWOOD, 1971; WEILL and DRAKE, 1973), it is noteworthy that at the prevailing oxygen fugacity of these inclusions no evidence is seen for the presence of Eu^{2+}.

Analytical data on enstatites from 2604 and 2640 confirm the previously observed (eg. FREY, 1969) relative enrichment of HREE in clinopyroxene (cpx/opx = 4–10 for HREE) and also demonstrate that orthopyroxene is an even less favorable site than clinopyroxene for LREE (cpx/opx ~ 40–150 for LREE). There is considerable difference in LREE partitioning between the cpx–opx pairs. The 2604 LREE cpx/opx partition coefficients are within the range reported in other rocks (e.g. Winona chondrite, MASON and GRAHAM, 1970; Lizard peridotite, FREY,

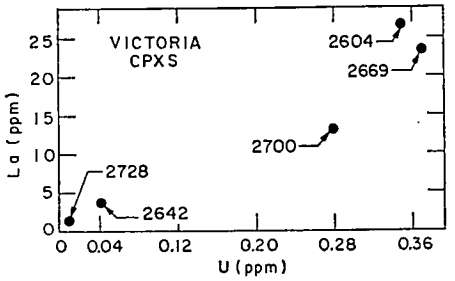

Fig. 4. Correlation of clinopyroxene U abundance with the clinopyroxene abundance of a light rare earth (La). Data not available for 2640 or GSFC-20 clinopyroxenes.

1969; basaltic phenocrysts, ONUMA *et al.*, 1968, and SCHNETZLER and PHILPOTTS, 1970; ultramafic rocks, PHILPOTTS *et al.*, 1972), but the 2640 cpx/opx LREE partition coefficients are considerably larger. The reason for this is unknown, but in studying REE partition coefficients involving a low REE-bearing phase such as orthopyroxene a severe problem is the purity of the phases analyzed. We do not believe that the LREE cpx/opx partitioning difference between 2604 and 2640 is only a result of impurities. A mass balance calculation indicates that 2 wt.% clinopyroxene is required in the 2604 orthopyroxene for the La cpx/opx partition coefficient to be reduced from the 2640 value (160) to that observed in 2604 (40). Our microsopic determinations indicate that the mineral separates contain less than 0·1 vol.% impurity.

Alternative explanations of the differences in LREE cpx/opx partitioning are the higher equilibration temperature deduced for 2640 or the lower $Mg/Mg + Fe^{2+}$ of 2640. The Hualalai inclusion, which has equilibrated at higher temperatures than 2604 and 2640 (Table 3) and has a $Mg/Mg + Fe^{2+}$ similar to 2604 (Tables 1 and 2), is also characterized by very high LREE cpx/opx partition coefficients (about 100 as compared to 20–50 for most cpx/opx pairs). The six coexisting pyroxene pairs from lherzolite inclusions studied by PHILPOTTS *et al.* (1972) do not exhibit as wide a range of LREE cpx/opx values as 2640 and 2604, but the three with higher pyroxene equilibration temperatures (clinopyroxene $Ca/Ca + Mg < 0{\cdot}46$) have higher Ce cpx/opx values (28–35 vs 21–25) than the three with lower pyroxene equilibration temperatures (clinopyroxene $Ca/Ca + Mg > 0{\cdot}46$). We suggest that LREE cpx/opx partitioning may be a sensitive function of temperature. Additional data will be required to confirm this suggestion, but a recent experimental study (CULLERS *et al.*, 1973) indicated that REE cpx/opx partition coefficients increase with increasing temperature.

Mass balances. The modal abundance of minerals (Table 5) may be utilized for REE mass balance calculations. The results yield excellent agreement between calculated whole rock abundances from mode and mineral data and the abundances actually observed. 2604 data show that $\sim$75 per cent of the LREE, $\sim$100 per cent of Sm–Tb and $\sim$ 50 per cent of the HREE are contained in 2·5 vol.% clinopyroxene. By estimating the REE content of olivine (86 vol.%) from cpx/ol partition coefficients and using the observed orthopyroxene (10·5 vol.%) REE abundance (Table 9), a satisfactory ($\pm$20 per cent) whole rock mass balance can be obtained without requiring the presence of an accessory or intersitial grain boundary phase enriched in REE. PHILPOTTS *et al.* (1972) obtained similar results from their analyses of clinopyroxene, orthopyroxene, and olivine from a Victorian inclusion (GSFC-20).

In 2669, the clinopyroxene, orthopyroxene, and olivine (using calculated REE abundances for the latter two phases, obtained from cpx/opx and cpx/ol partition data) account for the REE ($\pm$20 per cent) implying that the glass in this rock does not contribute significantly to the REE concentration in the total rock. The pyroxenes in 2640 contain more than 80 per cent of the total REE, although a better overall mass balance would be obtained with 4–4·5 per cent modal clinopyroxene rather than 5 per cent. The mass balance is very good in 2728 except for a 40 per cent depletion in La and Ce in the calculated abundances (possibly indicating trace amounts of an accessory LREE enriched phase). In 2642 the amphibole and

clinopyroxene contain the bulk of the REE, but the mass balance calculations suggest that amphibole (2 vol.%) and/or clinopyroxene (10·5 vol.%) may be slightly overestimated. In 2700, if the REE partition coefficients (apatite/cpx) of inclusion 2638 are applicable, the 0·1 vol.% apatite contains ~50 per cent of the LREE and ~5 per cent of the HREE in the inclusion.

In summary, considering the various analytical uncertainties, the mass balance calculations give excellent agreement. The REE geochemistry of lherzolite inclusions is dominated by clinopyroxene. The effects of basanite contamination, concentrations in interstitial phases such as glass, and accessory minerals are minimal. Nevertheless, the extremely high REE concentration in an accessory phase such as apatite, demonstrates that such phases in parental lherzolitic compositions strongly influence the characteristics of melt fractions for very low (<1 per cent) degrees of partial melting.

Correlation of REE abundances with modal mineralogy, mineral chemistry, and whole rock major element abundances

Specimens 2604 and 2669 are the most refractory of the six lherzolite inclusions with the highest Mg/Mg + Fe^{2+}, the highest ol/cpx and opx/cpx, and the lowest Na/Na + Ca in clinopyroxene (if amphibole in 2642 is recast as anhydrous minerals). These two inclusions also have the lowest HREE concentrations. In contrast to these refractory characteristics, the two samples are highly enriched in LREE, both in an absolute and relative sense with La/Yb > 30. This degree of LREE enrichment is greater than that of alkali olivine basalts, similar to that in nephelinites, and less than that in highly potassic mafic magmas (eg. minettes and monchiquites) (SCHILLING and WINCHESTER, 1969; KAY and GAST, in press). Except for 2700, these two inclusions also have the highest K, U and Th abundances (GREEN *et al.*, 1968).

Inclusions 2728 and 2642 compared to 2604 and 2669, are less refractory with lower Mg/Mg + Fe^{2+}, ol/cpx, and opx/cpx and contain clinopyroxene (if amphibole in 2642 is recast as anhydrous minerals) with higher Na/Na + Ca. These inclusions contain 3–13 times the HREE abundance of 2604 and 2669, but their REE distribution patterns are nearly chondritic (2728) or LREE-depleted (2642). Thus, these inclusions contain only about 0·2 times the LREE concentration present in 2604 and 2669. The Victorian inclusion, GSFC-20, (PHILPOTTS *et al.*, 1972) and the Ataq inclusion (VARNE, 1970) are similar to 2728 in Mg/Mg + Fe^{2+}, ol/cpx, opx/cpx, and HREE abundances, but unlike 2728 and 2642, they are enriched in LREE (like 2604 and 2669) relative to the chondritic REE distribution. As in 2604 and 2669 the LREE enrichment in GSFC-20 and Ataq inclusions is a result of LREE enrichment (La/Yb > 17) in clinopyroxene (also amphibole in Ataq inclusion, VARNE and GRAHAM, 1971). The Ataq clinopyroxene also has a high U abundance (1·1 ppm, VARNE, 1970). In the Lizard peridotite the characteristics of 2728 and 2642 are more developed. Compared to 2728 and 2642 the average Lizard composition (Tables 1–5) is similar in ol/cpx but lower in Mg/Mg + Fe^{2+}. The Lizard HREE abundances in both total rock and clinopyroxene are similar to those of 2728 and 2642, but the LREE are more strongly depleted in the Lizard peridotite (Figs. 2b, 3 and 6, FREY, 1969).

Lherzolites 2640 and 2700 do not fall into either of the above groupings. Inclusion 2640 resembles 2669 in ol/cpx and opx/cpx, but it has lower Mg/Mg + Fe^{2+} than both 2604 and 2669. In REE abundances and distribution it is intermediate between 2604–2669 and 2728–2642.

Inclusion 2700 differs from all others because of the presence of trace amount of apatite (0·1 vol.%) and its high cpx/opx (>1). In HREE it is intermediate between 2604–2669 and 2728–2642 but it is highly enriched in LREE (La/Yb = 29) like 2604 and 2669. The U-content of 2700 clinopyroxene is slightly lower than that of 2604 and 2669 but very much higher than 2728 or 2642.

Hawaiian lherzolite inclusions have a correlation between mineralogy and REE abundances similar to that observed for the Victorian inclusions, 2604 and 2669, compared to inclusions, 2728 and 2642. A refractory end member (like 2604 and 2669) is the clinopyroxene-poor Hualalai inclusion (KUNO, 1969; KUNO and AOKI, 1970) which has low CaO (0·76 wt.%), low Al_2O_3 (0·47 wt.%), and high Mg/Mg + Fe^{2+} (91·5). Like 2604 and 2669 it has low HREE abundances (0·35 times chondritic average), and is relatively enriched in LREE (La/Yb = 7·2; NAGASAWA *et al.*, 1969). Other Hawaiian lherzolite samples (Salt Lake Crater, KUNO, 1969; JACKSON and WRIGHT, 1970) richer in CaO (>1·9 per cent) and Al_2O_3 (>2 per cent) are presumably clinopyroxene-rich. These inclusions like 2728 and 2642 have HREE abundances 1–3 times the chondritic average and are not relatively enriched in LREE compared to chondrites (NAGASAWA *et al.*, 1969; Frey and Jackson, unpublished).

Three lherzolite inclusions from the Comores Archipelago, Western Indian Ocean, have high HREE abundances (3–5 times chondritic average) and have no relative enrichment in LREE compared to chondrites (La/Yb = 0·5–1·70 (FLOWER, 1971). In these samples, unlike our results, La/Yb systematically decreases as Mg/Mg + Fe^{2+} increases.

A generality in the Victorian and Hawaiian lherzolite data is an approximate correlation of increasing HREE abundances with increasing clinopyroxene (as reflected by CaO). This trend (Fig. 5) is not perfect, since 2700 is obviously an aberrant point, perhaps because of the inclusions analyzed for REE, it is the only one with obvious apatite. A direct correlation of CaO (modal clinopyroxene) and HREE abundances has also been observed for lherzolite inclusions from San Carlos, Arizona (FREY and PRINZ, 1971) but the three Comores inclusions do not show this correlation (FLOWER, 1971).

A similar trend does not exist for LREE in inclusions from Victoria, Hawaii and San Carlos. Inclusions with low CaO abundances sometimes have high LREE abundances (eg. 2604–Victoria and Hualalai–Hawaii), and in a given locality the most refractory inclusions (highest in ol/cpx and Mg/Mg + Fe^{2+}) are characterized by LREE enrichment (La/Yb > 6). Again, the Comores area is an exception.

The CaO–HREE correlation observed in the Victorian, Hawaiian and San Carlos lherzolite inclusions (Fig. 5) is also found in the peridotites of St. Paul's Rocks. Like the lherzolite inclusions these peridotites vary widely in their REE distributions. Five peridotites from St. Paul's Rocks have been analyzed for REE and major elements (FREY, 1970; MELSON *et al.*, 1967; MELSON *et al.*, 1973). Sample 18–900 is enriched in CaO (3·9 wt.%) and Al_2O_3 (4·4 wt.%) with high pyx/ol, and it

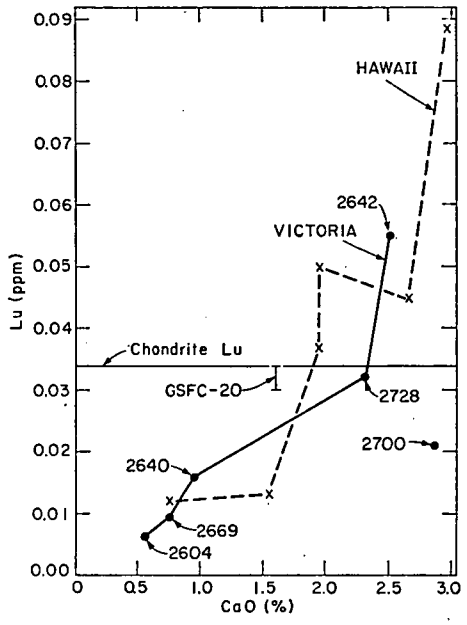

Fig. 5. Correlation of bulk rock CaO abundance (wt.%) with a bulk rock heavy rare earth element (Lu). Victoria data from this work (inclusion 2700 is an aberrant point) except for GSFC-20 (Lu abundance range estimated by extrapolation from Er and Yb abundances) from PHILPOTTS *et al.* (1972). Hawaiian data from NAGASAWA *et al.* (1969), KUNO and AOKI (1970) and FREY and JACKSON (unpublished).

has an HREE abundance five times that of the CaO- and Al_2O_3-poor (1 wt.% and 2·4 wt.%, respectively) samples NE-4 and 7–479. Amphibole rather than clinopyroxene is often present in the St. Paul's peridotites so that the approximate correlation is between HREE and clinopyroxene or amphibole abundance. All the St. Paul's peridotites have La/Yb ratios (3·6–39) greater than the chondritic value (1·65). FREY (1970) and MELSON *et al.*, (1973) considered the possibility that the K, Rb, Sr and REE features of the St. Paul's peridotites resulted from contamination by the associated trace element-rich brown hornblende mylonites. The brown hornblende mylonite has a major element composition resembling alkaline ultrabasic plutonic rocks (MELSON *et al.*, 1973) and an REE pattern similar to the Victoria basanites (FREY, 1970). FREY (1970) and MELSON *et al.* (1973) concluded that the St. Paul peridotite trace element features could not be explained by a simple two end-member mixing model. No clinopyroxene or amphibole separates have been analyzed to determine if the LREE enrichment in St. Paul's Rocks is caused by these primary minerals as it is in lherzolite inclusions.

Abundance of transition metals (Sc, V, Cr, Co *and* Ni) *in inclusions*

The whole-rock data for Sc, V, Cr, Co and Ni in six Victorian inclusions (Table 10) show that Sc, V and Cr abundances are directly proportional to the amount of modal clinopyroxene. A direct correlation between Sc and clinopyroxene has been

Table 10. Whole rock abundances of Sc, V, Cr, Co and Ni (ppm)

Nodule	Modal cpx	Sc*	V†	Cr*‡	Co†	Ni†‡
2604	2·4–2·5	6·5	17·9	1900	119	2750
2669	2·8–4	6·8	22·7	3200	112	2530
2640	4·8–5	7·6	32·2	2790	113	2370
2728	10–11	11·5	52·6	3270	110	2300
2700	11·3–12.5	15·5	55·7	3650	113	2115
2642	13·7–14	14.2	96·7	3950	102	2100

* Analyses done by instrumental neutron activation analysis with accuracy believed to be better than ±5% (GORDON *et al.*, 1968).

† Analyses by spectro-photometry (KISS, in press: cobalt values (ppm) on U.S.G.S. standards by this method are granite G-1 (3·6), granite G-2 (4·9), andesite AGV-1 (15·7), granodiorite GSP-1 (9·0), dolerite W-1 (48), basalt BCR-1 (36), peridotite PCC-1 (112) and dunite DTS-1 (143). Values for vanadium (ppm) are G-1 (15·4), G-2 (32·6), AGV-1 (109), GSP-1 (53) and BCR-1 (401).

‡ Cr and Ni data here are more accurate than those of Table 1.

previously noted (STUEBER and GOLES, 1967). Cr varies directly with clinopyroxene abundance even though spinel is an important Cr host. This is because spinel is equally abundant in these rocks (1–2 vol.%) and spinel Cr abundances are proportional to clinopyroxene Cr abundances (Table 3). An exception is 2669, which has whole-rock Cr abundances significantly higher than those expected from the mineral microprobe analyses.

Co abundances are similar (102–119 ppm) in all six inclusions and they are quite close to the Co average of 110 ppm in ultramafic rocks (STUEBER and GOLES, 1967). The Ni abundances vary over a range of 25 per cent with the highest abundances in the olivine-rich, high $Mg/Mg + Fe^{2+}$ inclusions 2604 and 2669.

PETROGENESIS OF THE LHERZOLITE INCLUSIONS

Examination of the relationships between mineralogy, major element and trace element abundances leads us to the following conclusions:

(1) The REE content of the lherzolites is determined by two independent components which we designate Component A and Component B.

Component A: This component is characterized by an LREE-depleted distribution relative to the chondritic REE distribution. The abundance of clinopyroxene primarily determines the HREE abundance which ranges from <0·5 to at least two times chondritic abundances.

Component B: This component is characterized by an extremely fractionated REE pattern with LREE abundance, nearly 100 times chondritic abundances but HREE only 5–10 times chondritic abundances.

(2) The relationship between major element chemistry, particularly $Mg/Mg + Fe^{2+}$, clinopyroxene/olivine, and HREE abundances can be explained by the hypothesis that the lherzolites are primarily residues from partial melting and basalt extraction at depths <70 km [i.e. approximately above the depth at which garnet is a major residual phase (GREEN and RINGWOOD, 1967; GREEN, 1970; 1971, 1973a, b)]. This hypothesis applies to Component A only. Small amounts (<20 per cent) of melting would leave as a residuum clinopyroxene, orthopyroxene

and olivine, i.e. lherzolite assemblages such as Lizard peridotite, 2642 (anhydrous) and 2728. Such rocks would show moderate depletion in HREE and large depletion in LREE relative to the primary source (pyrolite*). Larger degrees (>20 per cent) of partial melting would leave only olivine, orthopyroxene (with >1·5 per cent CaO, >3 per cent Al_2O_3), and possibly chromite as residual phases. These rocks would be strongly depleted in HREE and extremely depleted in LREE relative to the primary source (pyrolite).

The effects of partial melting on REE abundances were determined by utilizing two trace element partitioning models (total equilibration partial melting and surface equilibration fractional melting, SHAW, 1970). Calculated REE distributions are shown in Fig. 6 for (a) lherzolite residues after 3 per cent (C) and 17 per cent (E, F) melting, (b) garnet–lherzolite residue after 3 per cent (D) melting, and (c) harzburgite residue after 37 per cent melting (G). Initial REE concentrations were taken as two times chondrites, and the partition coefficients used except for orthopyroxene and garnet were similar to the averages of SCHILLING (1971). Recent results for REE partitioning between clinopyroxene–orthopyroxene and clinopyroxene–garnet pairs (MASON and GRAHAM, 1970; SCHNETZLER and PHILPOTTS, 1970; EARLY, in preparation; this work) have been used to determine revised orthopyroxene–liquid and garnet–liquid partition coefficients. There is significant uncertainty in the absolute values of REE partition coefficients (ALBAREDE and BOTTINGA, 1972), but the relative REE partition coefficients are very systematic. Thus, the slopes of REE patterns in Fig. 6 are meaningful. Furthermore, the models can be refined as more is learned about effects of composition, temperature, pressure and kinetics on partition coefficients.

Comparison of lines C and D (Fig. 6) indicates that the presence of garnet (5 wt.%) has only minor effects on the REE distribution in the residual assemblage. At small degrees of melting the residues from both melting models have similar REE abundances, but significant differences, particularly in LREE abundances, appear at higher degrees of melting (E vs F in Fig. 6). Both melting models assume homogeneous solids; that is, solid diffusion is rapid with respect to rates of removal of melt from the solid. In all cases, the greatest LREE depletion of the residue is caused by fractional melting. LREE depletion would be less if the residual solid does not remain homogeneous. No LREE depletion (all REE solid–liquid partition coefficients = 1) would be expected when removal of melt from the system is very rapid with respect to solid state diffusion of the REE.

A comparison of the REE abundances in the calculated residues with those of Victorian inclusion 2642 indicates that except for La, 2642 is consistent with a residue from small amounts (5–10 per cent) of melting (See Fig. 6). We believe the relatively high La abundance (in 2642) reflects Component B. The Lizard peridotite is highly depleted in LREE, as predicted for residues from extensive fractional

* This statement applies whether the source pyrolite had (1) a chondritic REE distribution and 2–4 times chondritic abundances (GAST, 1968; FREY, 1969), (2) slightly LREE depleted distribution and 2–4 times chondritic HREE abundances (as may be required for the source region for mid-oceanic ridge tholeiites), or (3) a slightly LREE-enriched distribution and 2–4 times chondritic HREE abundances (as may be required for the source region for Hawaiian olivine tholeiites).

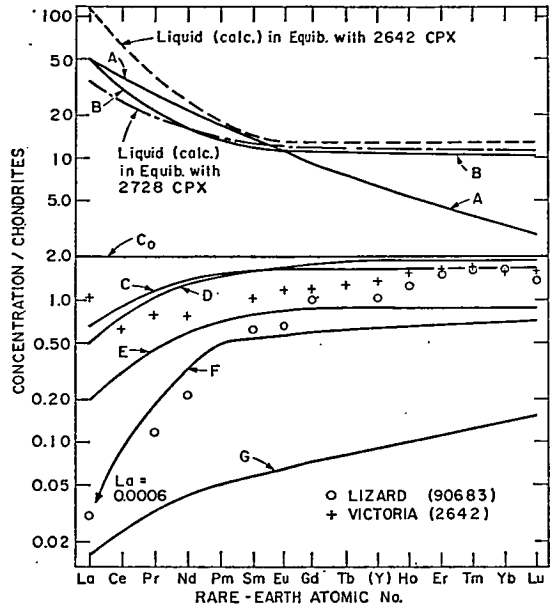

Fig. 6. Legend for Fig. 6 (olivine = oliv, clinopyroxene = cpx, garnet = ga and orthopyroxene = opx):

Initial phases in models

	Assemblage I	Assemblage II
oliv	50%	50%
cpx	25%	20%
ga	—	5%
opx	25%	25%
	melt formed from cpx and opx in 2:1 ratio	melt formed from cpx, ga and opx in a 2:2:1 ratio

A Average derived liquid after 3% fractional melting of assemblage II.

B Average derived liquid after 3% fractional melting of assemblage I.

C Residue solid (ol 51%, cpx 24%, opx 25%) after 3% fractional melting of assemblage I.

D Residue solid (ol 52%, cpx 19%, ga 4%, cpx 25%) after 3% fractional melting of assemblage II.

E Residue solid (ol 60%, cpx 17%, opx 23%) after 17% (total equilibrium) partial melting of assemblage I.

F Residue solid (ol 60%, cpx 17%, opx 23%) after 17% fractional melting of assemblage I.

G Residue solid (ol 79·4%, cpx 0·5%, opx 20·1%) after 37% (total equilibrium) partial melting of Assemblage I.

Also plotted and labeled are: (1) liquids calculated to be in equilibrium with 2642 and 2728 cpx. (2) 2642 lherzolite (+) and Lizard peridotite 90683 (0).

melting (Fig. 6). The similarity of REE distribution in inclusions 2642 and 2728, the Lizard peridotite, and the calculated melting residues is evidence that some peridotitic source rocks have relative REE distributions that are closely approximated by a chondritic REE distribution.

The REE distributions in 2642 and the Lizard peridotite show more relative fractionation from Sm to Lu than the calculated lherzolite residues (C, E and F in Fig. 6). This feature characterizes the theoretical harzburgite and garnet lherzolite residues G and D in Fig. 6). The calculated REE distribution of the lherzolite residues can be more closely matched to the observed REE data by any of the following model changes: (a) including garnet (<5 wt.%) as a residual mineral, (b) increasing the orthopyroxene–liquid REE partition coefficients, or (c) changing the clinopyroxene–liquid REE partition coefficients. The available REE clinopyroxene–liquid partition coefficient data are for Ca-rich clinopyroxenes (SCHNETZLER and PHILPOTTS, 1970), whereas Ca-poor clinopyroxenes were probably present during solid–liquid partitioning. Data for Ca-poor clinopyroxenes are scarce, but such data suggests that unlike Ca-rich clinopyroxenes, Ca-poor clinopyroxenes have significant relative fractionation from Sm to Lu similar to orthopyroxene (ONUMA *et al.*, 1968; SCHNETLZER and PHILPOTTS, 1970; Frey and Green, unpublished).

Figure 6 also shows the calculated liquids A and B which coexist with residues D and C, respectively. Unlike the residual solids the derived liquid HREE abundances are very sensitive to small amounts (<5 wt.%) of garnet (HASKIN and FREY, 1966; GAST, 1968; KAY and GAST, in press). Liquid A has an REE distribution much like that of the Victorian basanites, and liquid B has an REE distribution similar to plateau tholeiites (FREY *et al.*, 1968; SCHILLING, 1971). A precise matching of the basanite pattern with liquid A (i.e. increasing the liquid A LREE to 100–200 times chondritic abundances) would be achieved by less than 1 per cent melting (KAY and GAST, in press).

Component A of inclusions 2642, 2728, 2669 and 2604 has the characteristics expected of a melting residue, and the sequence given would be that of increasing degrees of melting (i.e. decreasing abundance of clinopyroxene, and HREE). Inclusion 2640 is inconsistent because it has low Mg/Mg + Fe^{2+} implying very low degrees of partial melting, but its low clinopyroxene content implies high degrees of partial melting. This sample could be of accumulative origin (see 3 below). Inclusion 2700 is inconsistent in that cpx/opx > 1. The presence of apatite in 2700 and the high LREE content indicate that Component A mineral proportions may be masked by an excessive amount of Component B.

(3) With the evidence presented, we cannot eliminate the possibility that Component A of the lherzolites is an accumulate from a basaltic magma unrelated to the present host basanite. In this hypothesis early accumulates would be Mg-rich olivine (Fo ≥ 90) and orthopyroxene. Later accumulates would contain increasing amounts of clinopyroxene with more Fe-rich olivine (Fo < 90). This hypothesis has been advocated by O'HARA (1968, p. 93) in suggesting that separation of lherzolite accumulates is an integral part of the process by which some hypersthene-normative magmas become nepheline-normative. From the large differences in incompatible element contents between tholeiitic and alkaline magmas and

consideration of the chemical compositions of the natural magmas and lherzolites, the hypothesis requires that the degree of crystallization of the hypersthene-normative magmas must be large (>30 per cent). Since both the accumulate and residue models involve an equilibrium between basaltic liquid and solid phases, arguments based solely on elements strongly partitioned into the liquid (incompatible elements) will not distinguish between residue or accumulate origins for the lherzolites. However, if we consider elements strongly partitioned into the residual or accumulative phases (eg. Mg, Fe, Sc, Cr, Co and Ni), then it may be possible to distinguish the alternatives.

Partial melting (1–30 per cent) of a lherzolite (olivine Fo-89) causes little change in (a) 100 Mg/Mg + Fe^{2+} of the residue (from 89 to 92, approx., GREEN, 1970, 1973b), (b) Ni and Co content of residual olivine, and (c) Cr and Sc content of residual clinopyroxene. However, if we consider an olivine tholeiite (22 per cent normative olivine, GREEN and RINGWOOD, 1967) with olivine on its liquidus (Fo_{90}, containing 2000 ppm Ni), then fractional crystallization of 1–30 wt.% olivine must result in marked changes in (a) 100 Mg/Mg + Fe^{2+} of the liquidus olivine (from 90 to 87·5, 83 and 70 for 10 per cent, 20 per cent and 30 per cent crystallization, respectively, IRVINE and FINDLAY, 1971), and (b) Ni and Co content of the liquidus olivine. As an example, consider an element with a bulk solid–liquid partition coefficient of 10 (typical of Ni in olivine or Cr in clinopyroxene); 30 per cent fractional crystallization of olivine will change the abundance ratio in the derived olivine from $Cs_{\sim 0}/Co = 10$ to $Cs_{30}/Co = 3{\cdot}33$ (Cs_x = solid concentration at x per cent crystallization, Co = initial concentration), whereas 30 per cent fractional melting of lherzolite will change Cs/Co in the residue solid from 1 to 1·38. Similar results can be derived from a total equilibrium model.

In the Victorian inclusions Sc, V and Cr behave similarly to the HREE since their abundances can be correlated with modal clinopyroxene (Table 10). The bulk solid–liquid partition coefficients for Sc, V and Cr in a lherzolite mineralogy are <1 and with increasing degrees of melting, the solid residue becomes increasingly depleted in Sc V and Cr (i.e. the trend from 2642 to 2604 in Table 10). Like the HREE, the solid–liquid partitioning could alternatively be interpreted as a mantle fractional crystallization process.

Olivine–silicate liquid partition coefficients are 2–4 for Co (HENDERSON and DALE, 1970) and 5–20 for Ni (HAKLI and WRIGHT, 1967; HENDERSON and DALE, 1970). For these olivine-rich (>50 vol.%) inclusions, the bulk-solid–liquid partition coefficients for Co and Ni should be greater than unity. In the Victorian inclusions Co abundances vary over a narrow range (<20 per cent), but as expected, the most refractory inclusion (2604) is most enriched in Co (Table 10). Since Ni has a higher bulk solid–liquid partition coefficient than Co, the Ni enrichment is more marked than Co (Table 10) in the refractory (cpx-poor, Mg-rich) inclusions (2604 and 2669) compared to the pyroxene-rich inclusions (2728, 2700 and 2642) or the more Fe-rich inclusion (2640). The approximate 25 per cent variation in Ni abundances (inclusions 2604–2642) is more consistent with the predicted Ni variation in melting residues than the predicted Ni variation in fractional crystallization accumulates. This conclusion is based on the observation that the modal abundance differences (Table 5) and compositional differences (Tables 1 and 3)

require large degrees ($\sim$30 per cent) of melting or crystallization. The latter would cause a much wider Ni abundance variation than that observed, while comparable degrees of melting predict an Ni variation similar to that observed.

The relatively small range in Cr, Co and Ni contents and Mg/Mg + Fe^{2+} in the typical 4-phase spinel–lherzolite assemblages contrasts with the much larger variation of these parameters in dunites, wehrlites, olivine pyroxenites, spinel pyroxenites and garnet pyroxenites which occur more rarely than lherzolite as inclusions in silica-undersaturated basalts. CARTER (1970) found that Ni in olivines from Kilbourne Hole lherzolites varies from 3000 to 2000 ppm compared to a variation from 1500 to <200 ppm in olivine from 3 phase inclusions (lacking orthopyroxene). WHITE (1966) found that Cr_2O_3 varies from 0·5–1·5 wt.% in Hawaiian lherzolite clinopyroxenes, compared to <0·1–1·3 wt.% in clinopyroxenes from wehrlites, dunites and pyroxenites. CARTER (1970) obtained similar Cr_2O_3 clinopyroxene data at Kilbourne Hole.

Based on chemical and textural distinctions between lherzolites and the heterogeneous group of dunites, wehrlites and pyroxenites, WHITE (1966), CARTER (1970), and KUNO and AOKI (1970) concluded that this latter group originated as accumulates from basaltic magmas at low to high pressures. Studies of pyroxenite inclusions in the Victorian province (IRVING, 1974) affirm the accumulative origin of these latter rock types.

Experimental studies at 15–25 kbar on various basaltic magmas (GREEN and RINGWOOD, 1967; BULTITUDE and GREEN, 1968, 1971; GREEN, 1970, 1971; ITO and KENNEDY, 1968) establish that orthopyroxene and clinopyroxene are the dominant phases in near-liquidus crystallization. Initially olivine, orthopyroxene and clinopyroxene must be together on the liquidus of a magma derived from lherzolite, but if the magma segregates and begins to crystallize then the accumulates would be olivine pyroxenites, followed by pyroxenites in many cases, as olivine reacts with liquid to precipitate pyroxene (BULTITUDE and GREEN, 1971). If an olivine tholeiite ($\sim$20 per cent normative olivine) magma moves to shallower depths before crystallizing, then olivine alone may occur on the liquidus but it requires only 5 wt.% olivine fractional crystallization before the equilibrium olivine has perceptibly moved away from the liquidus composition ($\sim$Fo = 90 to Fo = 89 i.e. FeO content of olivine from 9·7 to 10·7 wt.%; IRVINE and FINDLAY, 1972). Orthopyroxene and/or clinopyroxene will join olivine at lower temperatures and, hence, under special conditions, harzburgite, lherzolite or wehrlite accumulates could form containing more Fe-rich olivine than that originally on the liquidus.

To summarize, the very restricted range in (a) modal mineralogy, (b) Mg/Mg + Fe^{2+} and (c) Co and Ni contents of Victorian lherzolite inclusions indicates a residual origin for Component A. Some lherzolites with low Mg/Mg + Fe^{2+} (eg. 2640) may be accumulates, but the majority of lherzolite inclusions with their world-wide occurrence, uniform mineralogy and restricted geochemical ranges are difficult to explain by an accumulate hypothesis.

(4) The data obtained for the incompatible elements (K, P, REE, U and Th) and major elements outline a surprising result: the inclusions most refractory in terms of mineralogy and major element chemistry (2604 and 2669) have the most

LREE-enriched REE patterns and contain greater abundances of the incompatible elements than the least refractory inclusions. We suggest that this result is caused by a variable proportion of a trapped liquid component, designated Component B.

Component B must be extremely fractionated in REE (i.e. high La/Yb) in order to generate the observed 2604 relative REE abundances. Since Component A of 2604 is harzburgite, it has very low REE abundances. If Component A is similar to residue G in Fig. 6, Component B must have La/Yb $\sim$100.* High La/Yb is characteristic of liquids generated by small degrees (<5 per cent) of melting of a garnet-bearing assemblage e.g. highly silica-undersaturated, alkali-rich basalts (KAY and GAST, in press) and kimberlites (FREY *et al.*, 1971). Small quantities (1–2 wt.%) of such liquids added to a harzburgite residue would account for the observed 2604 REE abundances. Adding varying quantities (<0·5 to $\sim$2 wt.%) of Component B to residues (Component A) containing different amounts of clinopyroxene (i.e. residues from various degrees of partial melting) would generate the observed range in lherzolite REE distributions. For example, the four Victorian clinopyroxene-rich (7–14 vol.%) inclusions arranged in order of decreasing Component B are: 2700 (LREE 10 times chondrites), GSFC-20 (LREE 2–4 times chondrites; PHILPOTTS *et al.*, 1972), 2642 (LREE 1 times chondrites), and 2728 (LREE 0·8 times chondrites). The Lizard peridotite (LREE 0·03 times chondrites, FREY, 1969) and an Otago, New Zealand lherzolite inclusion (LREE 0·1 times chondrites, PHILPOTTS *et al.*, 1972) may be examples of pure Component A. In Victoria all the clinopyroxene-poor (<5 vol.%) inclusions studied [2604, 2669 and RCE (FREY *et al.*, 1971)] are LREE-enriched and thus contain significant amounts of Component B. Clinopyroxene-poor inclusions deficient in LREE have been found at San Carlos, Arizona (FREY and PRINZ, 1971).

Although Component B has the REE characteristics of a very undersaturated alkali-rich liquid, we emphasize that it is not present as interstitial material on grain boundaries, but is an integral part of the lherzolite mineralogy. The REE are principally contained in clinopyroxene, but accessory phases (or their reaction and alteration products, e.g. glass) such as phlogopite, apatite and amphibole are the principal hosts for other elements (K, P and U) characteristically enriched in undersaturated basalts. These conclusions result from mineral and bulk rock data which enable mass balance calculations for K, P, REE and U.

(5) The trapped liquid Component B is *not* a portion of the liquid originally in equilibrium with residual lherzolite minerals (Component A) formed in an early partial melting event. The argument for this is as follows. We have deduced that the lherzolites were subsolidus mineral assemblages, equilibrated (prior to inclusion in the host basanite) at various temperatures from about 800°C to 1100°C, and that the mineralogy is the result of Components A and B. Therefore, we cannot use the present mineralogy and values of REE partition coefficients to investigate the precise character of the liquid originally in equilibrium with Component A. However, a qualitative description of the original liquid may be based on the clinopyroxene REE patterns of 2642, 2728 and the Lizard peridotite because these

* The smallest reasonable La/Yb of Component B is 37 (the whole-rock value for inclusion 2604) which is higher than that observed in tholeiitic basalts and most alkali olivine basalts (MASUDA, 1966; FREY *et al.*, 1968; HERMANN, 1968; SCHILLING and WINCHESTER, 1969).

examples have the least Component B. Since the present mineralogy represents subsolidus equilibrium between phases, we may infer that at the higher temperature conditions of partial melting (T = 1200–1400°C), the lherzolites contained no amphibole or phlogopite, contained less orthopyroxene (with >1·5 wt.% CaO). and contained more clinopyroxene (aluminous and sub-calcic) than now present in the inclusions. These sub-calcic clinopyroxenes would probably contain less REE (particularly LREE) than calcic clinopyroxenes (Onuma *et al.*, 1968; Schnetzler and Philpotts, 1970; Frey and Green, unpublished).

Application of calcic clinopyroxene/liquid REE partition coefficients (Schnetzler and Philpotts, 1970) to our clinopyroxene data allows estimation of the minimum absolute REE abundance and minimum relative REE fractionation (e.g. La/Yb) in the liquids coexisting with Component A at 1200–1400°C. This has already been done for the Lizard clinopyroxenes (Frey, 1969). Similar calculations for clinopyroxenes 2642 and 2728 (See Fig. 6) indicate that Component A could represent residual minerals in equilibrium with basalts varying from tholeiitic to alkalic (Frey, 1969, and Fig. 6). These calculated liquids are similar to those expected from partial melting of a lherzolite assemblage (Fig. 6). Our interpretation of lherzolites 2642 and 2604 follows. For 2642: (a) Component A was residual from moderate amounts of partial melting (10–20 per cent). (b) The melt extracted was alkalic (olivine, orthopyroxene and clinopyroxene in the residue but no residual garnet). (c) The magma separated at <70 km, (Green, 1970, 1971). In contrast, for 2604: (a) Component A was residual from high degrees of partial melting (>20 per cent). (b) The melt was tholeiitic (olivine and orthopyroxene residue only; clinopyroxene now in the rock formed in part by exsolution from orthopyroxene (1·5 wt.% CaO originally, now 0·35 wt.% CaO) and in part from the trapped liquid component, see below). For these two examples (2642 and 2604), we now consider the effects on Component A, if the original melt was not *entirely* extracted, but some fraction remained trapped interstitially and later crystallized under subsolidus conditions.

The alkalic melt in equilibrium with Component A of 2642 would have La/Yb > 10 (Masuda, 1966; Frey *et al.*, 1968; Herrmann 1968; Schilling and Winchester, 1969). It is also known that a lherzolite residue (Component A) is always LREE depleted relative to the equilibrium liquid (e.g. Fig. 6). Since the whole rock REE distribution of 2642 is LREE depleted (La/Yb = 1·2) relative to alkalic basalts the addition of small amounts (<1 wt.%) of such basalt (Component B) to Component A (e.g. E and F of Fig. 6) could result in the 2642 bulk rock REE abundances. In this case Component A and Component B may have been in equilibrium. This is *not* the case for the clinopyroxene-poor inclusions (2604 and 2669). These inclusions have the mineralogy expected for residues after tholeiitic basalt formation. However, tholeiitic basalts have La/Yb < 10 (Masuda, 1966; Frey *et al.*, 1968; Herrmann, 1968; Schilling and Winchester, 1969); therefore a tholeiitic liquid could *not* have caused the LREE enrichment of inclusions 2604 and 2669 (La/Yb > 31).

We conclude that, when residual Component A is modified by the addition of a trapped liquid, Component B, then the latter is genetically unrelated to the process of partial melting reflected by residual Component A. Component B is inferred to

be a later migratory fluid phase that locally penetrated regions of the upper mantle (lithosphere) which had previously passed through a partial melting episode.

(6) Our interpretation of the lherzolite inclusions with high-U (0·5–2 ppm) bearing clinopyroxene differs from that of KLEEMAN *et al.* (1969). They suggested that inclusions with high-U clinopyroxenes approached primary mantle compositions with the potential for producing various amounts of basaltic magmas. They also concluded that such inclusions could not be regarded as refractory residues from a previous episode of complete magma extraction. The model we propose is more complex: a parental 'pyrolite' composition undergoes partial melting with loss of a relatively large (probably >5 per cent) melt fraction which leaves residual olivine, orthopyroxene, ±clinopyroxene and ±spinel. This step is followed by cooling and addition of a migratory, highly undersaturated liquid phase. The clinopyroxene enrichment in incompatible trace elements (U and LREE) results from the subsequent crystallization (primarily to clinopyroxene and accessory minerals) of this foreign liquid in the rock initially formed as a refractory residue. The time interval between these two processes cannot be specified, and they may have proceeded as stages in one evolutionary process. The significant point is that after addition of the migratory phase, the mineral assemblage equilibrated at subsolidus, high pressure conditions.

Our model agrees with previous ideas of (a) FREY *et al.* (1971), who suggested that at Dreiser Weiher a lherzolite inclusion had been contaminated by a liquid more enriched in LREE than the host basalt, (b) PHILPOTTS *et al.* (1972), who postulated that a Victorian lherzolite inclusion (GSFC-20) was metamorphosed after contamination by a liquid *unlike* the host basalt and (c) WILSHIRE and TRASK (1971), who found that lherzolite inclusions at Dish Hill, California, contain secondary minerals (amphibole, phlogopite and apatite) as veins and interstitial zones. They tentatively concluded "that solutions from which the amphibole and associated minerals were deposited were derived from lower in the mantle than the peridotite to which they were added, and that they predate the basanite that brought them to the surface." Wilshire (personal communication) has recently observed that some phlogopites in peridotite inclusions (San Carlos, Arizona and Kilbourne Hole, New Mexico) not only predate the basanite but were also incorporated in the inclusions prior to metamorphic deformation.

In the model presented the lherzolite inclusions are considered to represent samples of the lithosphere above the Low Velocity Zone. In terms of modern plate tectonic theory, the oceanic lithosphere is generated at spreading centres such as mid-oceanic ridges or intra-arc basins, and is either carried back into the mantle at subduction zones or, to a more limited extent, further modified to a continental crust and lithosphere structure in the island arc environment. In a continental situation such as Victoria which probably passed through an island arc-like evolutionary stage ~600–500 m yr ago there is obviously scope for conjecture on the origins and timing of formation of components A and B, but the diversity in mineralogy and REE chemistry of the Victorian inclusions is also apparent in Hawaiian inclusions (NAGASAWA *et al.*, 1969) in an oceanic crust and lithosphere situation. We consider that the sequence of events which we propose for the petrogenesis of lherzolite inclusions can be correlated with the simplest model of lithosphere

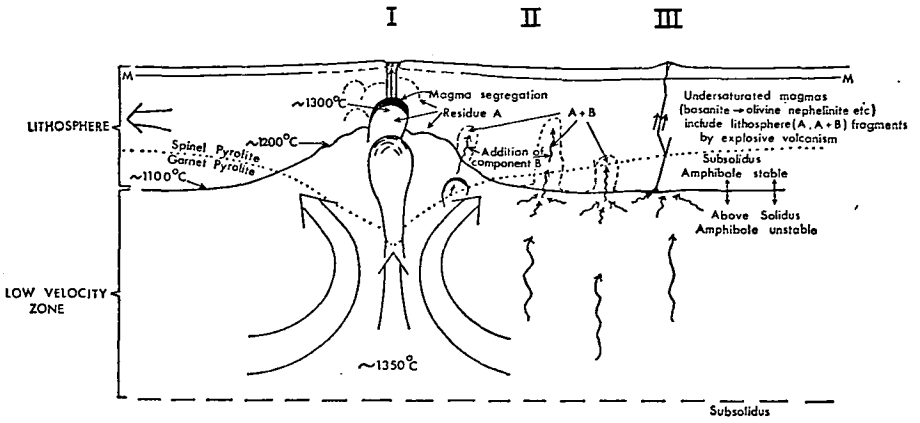

Fig. 7. Model of the magmatic processes occurring at ocean-ridge system leading to formation of peridotitic lithosphere with residual characteristics (component A) and modification of this by addition of component B (small hydrous melt or fluid fraction) as the lithosphere cools and moves away from the ridge axis.

formation, that occurring at mid-oceanic ridges. Referring to Fig. 7, an initial melt from material derived from deep within the Low Velocity Zone leaves residual lherzolite which cools to form the lithosphere. As the lithosphere migrates from the ridge-crest, it cools, crystallizes, and becomes modified by chemical differentiation processes occurring in the Low Velocity Zone (GREEN, 1971). Small amounts of water (0·1–0·2 wt.%) in the Low Velocity Zone lead to development of a <5 wt.% melt fraction in equilibrium with olivine, two pyroxenes, garnet, ilmenite, and possibly phlogopite. GREEN (1971) postulated that this melt migrates to the top of the Low Velocity Zone. With thickening of the lithosphere and stabilization of amphibole at shallow depths (i.e. above the Low Velocity Zone), the migratory melt phase (~olivine nephelinite or more undersaturated composition, GREEN, 1971, 1973a and 1973b) may equilibrate with, and crystallize within, residual peridotite. Later intrusion, and entrainment of lithosphere fragments, by highly undersaturated magmas derived from the Low Velocity Zone, may allow samples of the lithosphere to be brought to the surface. Figure 7 illustrates the major aspects of this hypotheses.

SUMMARY OF CONCLUSIONS

1. The lherzolite inclusions have no cognate or genetic relationship to their host magmas, and thus the inclusions are accidental xenoliths.

2. The lherzolites represent a mix of two geochemically-distinctive components.

Component A is important in terms of major elements, mineralogy and abundances of compatible trace elements, (including Sc, V, Cr, Co, Ni and HREE). Component A has the characteristics of a residuum after basalt (tholeiitic to moderately undersaturated basalt) extraction from a peridotitic (pyrolite) parent.

Component B is important in terms of minor and trace incompatible elements (including K, Ti, P, LREE, Th and U). It has the characteristics of a highly fractionated melt phase such as basanite, olivine nephelinite, olivine leucitite, or other highly silica-undersaturated magmas.

3. Components A and B are not genetically related, i.e. the liquid originally in equilibrium with, and lost from Component A differs from that forming Component B.

4. The sequence of events (a) formation of Component A as a partial melting residue, (b) variable and/or local admixture of Component B with Component A, (c) cooling and recrystallization of both components, and (d) accidental incorporation into a basanite host, are logical steps in the development of the mantle lithosphere + Low Velocity Zone structure within the framework of mid-ocean ridge volcanism and upper mantle dynamics.

5. The HREE abundances in the most clinopyroxene-rich (least refractory) lherzolites approach two times chondritic abundances. Since the proportion of residual clinopyroxene is inversely proportional to the amount of magma extracted, we conclude that the HREE abundances of the upper mantle in the source region, for at least some basaltic magmas, is approximately two times chondritic abundances. It is not possible to deduce unequivocally the LREE abundances of this source region from the lherzolite data as this requires knowledge of the relevant partition coefficients, the proportion of magma extracted, and the proportion of Component B now present in the lherzolites.

Acknowledgements—The technical assistance of E. KISS (Chemical methods of silicate analysis) and N. G. WARE (microprobe analysis of some mineral phases) is gratefully acknowledged. Nuclear irradiations were made at the Massachusetts Institute of Technology nuclear reactor. Research done at M.I.T. was financially supported by the National Science Foundation under grants GA 4463 and GA 25699.

REFERENCES

ALBAREDE F. and BOTTINGA Y. (1972) Kinetic disequilibrium in trace element partitioning between phenocrysts and host lava. *Geochim. Cosmochim Acta* **36,** 141–156.

BINNS R. A. (1969) High pressure megacrysts in basanitic lavas near Armidale, New South Wales. *Amer. J. Sci.* (Schairer Volume) **267A,** 33–49.

BINNS R. A., DUGGAN M. B. and WILKINSON J. F. G. (1970) High pressure megacrysts in alkaline lavas from northwestern New South Wales. *Amer. J. Sci.* **269,** 132–168.

BOYD F. R. (1970) The system $CaSiO_3$-$MgSiO_3$-Al_2O_3. *Carnegie Inst. Wash. Yearb.* **68,** 214–221.

BULTITUDE R. I. and GREEN D. H. (1968) Experimental studies at high pressures on the origin of olivine nephelinite and olivine melilite nephelinite magmas. *Earth Planet. Sci. Lett.* **3,** 325–337.

BULTITUDE R. J. and GREEN D. H. (1971) Experimental study of crystal–liquid relationships at high pressures in olivine nephelinite and basanite compositions. *J. Petrol.* **12,** 121–147.

CARTER J. L. (1970) Mineralogy and chemistry of the Earth's upper mantle based on the partial fusion–partial crystallization model. *Bull. Geol. Soc. Amer.* **81,** 2021–2034.

COOPER J. A. and GREEN D. H. (1969) Lead isotope measurements on lherzolite inclusions and host basanites from Western Victoria, Australia. *Earth Planet. Sci. Lett.* **6,** 69–76.

CULLERS R. L., MEDARIS L. G. and HASKIN L. (1973) Experimental studies of the distribution of rare earths as trace elements among silicate minerals and liquids and water. *Geochim. Cosmochim. Acta* **37,** 1499–1512.

DASCH E. J. and GREEN D. H. (in press) Strontium isotope geochemistry of lherzolite inclusions and host basanites, Victoria, Australia *Amer. J. Sci.*

DICKEY J. S. and YODER H. S. (1972) Partitioning of chromium and aluminum between clinopyroxene and spinel. *Carnegie Inst. Wash. Yearb.* **71,** 384–392.

EARLY T. O. (in preparation) Rare earths in eclogites from the Roberts Victor Kimberlite, South Africa.

FLOWER M. J. (1971) Rare earth element distribution in lavas and ultramafic xenoliths from the Comores Archipelago, Western Indian Ocean. *Contrib. Mineral. Petrol.* **31,** 335–346.

FREY F. A. (1969) Rare earth abundances in a high temperature peridotite intrusion. *Geochim. Cosmochim. Acta* **33,** 1429–1447.

FREY F. A. (1970) Rare earth and potassium abundances in St. Paul's Rocks. *Earth Planet. Sci. Lett.* **7,** 351–360.

FREY F. A., HASKIN L. A. and HASKIN M. A. (1971) Rare earth abundances in some ultramafic rocks. *J. Geophys. Res.* **76,** 1184–1196.

FREY F. A., HASKIN M. A., POETZ J. and HASKIN L. A. (1968) Rare earth abundances in some basic rocks. *J. Geophys. Res.* **70,** 6085–6098.

FREY F. A. and PRINZ M. (1971) Ultramafic nodules from San Carlos, Arizona: mineralogy and chemical composition. *Geol. Soc. Amer. Abstr.* **3**(7), 573–574.

GAST P. W. (1968) Trace element fractionation and the origin of tholeiitic and alkaline magma types. *Geochim. Cosmochim. Acta* **32,** 1057–1086.

GORDON G. E., RANDLE K., GOLES G. G., CORLISS J. B., BEESON M. H. and OXLEY S. S. (1968) Instrumental activation analysis of standard rocks with high-resolution γ-ray detectors. *Geochim. Cosmochim. Acta* **32,** 369–396.

GRAHAM A. L. and RINGWOOD A. E. (1971) Lunar basalt genesis: the origin of the europium anomaly. *Earth Planet. Sci. Lett.* **13,** 105–115.

GREEN D. H. (1963) Alumina content of enstatite in a Venezuelan high temperature peridotite. *Bull. Geol. Soc. Amer.* **74,** 1397–1402.

GREEN D. H. (1964) The petrogenesis of the high temperature peridotite intrusion in the Lizard area, Cornwall. *J. Petrol.* **5,** 134–188.

GREEN D. H. (1970) The origin of basaltic and nephelinitic magmas. *Trans. Leicester Lit. Phil. Soc.* **64,** 28–54.

GREEN D. H. (1971) Compositions of basaltic magmas as indicators of conditions of origin: application to oceanic volcanism. *Phil. Trans. Roy. Soc. Lond. Ser.* **A268,** 707–725.

GREEN D. H. (1972) Magmatic activity as the major process in the chemical evolution of the earth's crust and mantle. *Tectonophysics* **13,** 47–71.

GREEN D. H. (1973a) Conditions of melting of basanite magma from garnet peridotite. *Earth Planet. Sci. Lett.* **17,** 456–465.

GREEN D. H. (1973b) Experimental melting studies on model upper mantle compositions at high pressure under both water-saturated and water-undersaturated conditions. *Earth Planet. Sci. Lett.* **19,** 37–53.

GREEN D. H. and HIBBERSON W. O. (1970) Experimental duplication of conditions of precipitation of high pressure phenocrysts in a basaltic magma. *Phys. Earth Planet. Interiors* **3,** 247–254.

GREEN D. H., MORGAN J. W. and HEIER K. S. (1968) Thorium, uranium and potassium abundances in peridotite inclusions and their host basalts. *Earth Planet. Sci. Lett.* **4,** 155–166.

GREEN D. H. and RINGWOOD A. E. (1967) The genesis of basaltic magmas. *Contrib. Mineral. Petrol.* **15,** 103–190.

GREEN D. H. and RINGWOOD A. E. (1970) Mineralogy of peridotitic compositions under upper mantle conditions. *Phys. Earth Planet. Interiors* **3,** 359–371.

HASKIN L. A. and FREY F. A. (1966) Dispersed and not-so rare earths. *Science* **152,** 299–314.

HASKIN L. A., WILDEMAN T. R. and HASKIN M. A. (1968) An accurate procedure for determination of rare-earth elements by neutron activation. *J. Radioanal. Chem.* **1,** 337–348.

HAKLI T. A. and WRIGHT T. L. (1967) The fractionation of nickel between olivine and augite as a geothermometer. *Geochim. Cosmochim. Acta* **31,** 877–884.

HENDERSON P. and DALE I. M. (1970) The partitioning of selected transition element ions between olivine and groundmass of oceanic basalts. *Chem. Geol.* **5,** 267–274.

HERRMANN A. G. (1968) Die Verteilung der lanthaniden in basaltischen gesteinen. *Contrib. Mineral. Petrol.* **17,** 275–314.

HERRMANN A. G. and WEDEPOHL K. E. (1966) Die Verteilung des Yttriums und der Lanthaniden in einem Olivin-Alkali-Basalt mit Peridotit-Einschlussen. *Contrib. Mineral. Petrol.* **13,** 366–373.

HUTCHISON R. and DAWSON J. B. (1970) Rb, Sr and Sr^{87}/Sr^{86} in ultrabasic xenoliths and host rocks, Lashaine volcano, Tanzania. *Earth Planet. Sci. Lett.* **9**, 87–92.

IRVINE T. N. and FINDLAY T. C. (1972) Alpine-type peridotite with particular reference to the Bay of Islands igneous complex. Publication of the Earth Physics Branch, Department of Energy, Mines and Resources (Ottawa, Canada) **42**(3), 97–128.

IRVING A. J. (in press) Megacrysts from the Newer Basalts and other basaltic rocks of south-eastern Australia. *Bull. Geol. Soc. Amer.*

IRVING A. J. (1974) Pyroxene-rich ultramafic xenoliths in the Newer Basalts of Victoria, Australia. *Neues Jb. Miner. Abh.* **120**, 147–167.

IRVING A. J. and GREEN D. H. (in preparation) The major and trace element geochemistry of the Newer Basalts of southeastern Australia.

ITO K. and KENNEDY G. C. (1968) Melting and phase relationship in the plane tholeiite–lherzolite–nepheline basanite to 40 kilobars with geological implications. *Contrib. Mineral. Petrol.* **19**, 177–211.

JACKSON E. D. and WRIGHT T. L. (1970) Xenoliths in the Honolulu Volcanic Series, Hawaii. *J. Petrol.* **11**, 405–430.

KAY R. and GAST P. W. (in press) The rare-earth content and origin of alkali-rich basalts. *J. Geol.*

KAY R., HUBBARD N. and GAST P. (1970) Chemical characteristics and origin of oceanic ridge volcanic rocks. *J. Geophys. Res.* **75**, 1585–1597.

KISS E. (in press) Pyridylazo-diaminobenzenes as reagents for spectrophotometric determination of cobalt in silicates and meteorites. *Anal. Chim.*

KLEEMAN J. D., GREEN D. H. and LOVERING J. F. (1969) Uranium distribution in ultramafic inclusions from Victorian basalts. *Earth Planet. Sci. Lett.* **5**, 449–458.

KUNO H. (1964) Aluminian augite and bronzite in alkali olivine basalt from Taka-sima, north Kyusyu, Japan. In *Advancing Frontiers in Geology and Geophysics*, pp. 205–220. Osmania University Press.

KUNO H. (1969) Mafic and ultramafic nodules in basaltic rocks of Hawaii. *Geol. Soc. Amer. Mem.* **115**, 189–234.

KUNO H. and AOKI K. (1970) Chemistry of ultramafic nodules and their bearing on the origin of basaltic magmas. *Phys. Earth Planet. Interiors* **3**, 273–301.

KUSHIRO I., SHIMIZU N. and NAKAMURA Y. (1972) Compositions of coexisting liquid and solid phases formed upon melting of natural garnet and spinel lherzolites at high pressures: a preliminary report. *Earth Planet. Sci. Lett.* **14**, 19–25.

LAUGHLIN A. W., BROOKINS D. G., KUDO A. M. and CAUSEY J. D. (1971) Chemical and strontium isotopic investigations of ultramafic inclusions and basalt, Bandera Crater, New Mexico. *Geochim. Cosmochim. Acta* **35**, 107–113.

LEGGO P. S. and HUTCHINSON R. (1968) A Rb–Sr isotope study of ultrabasic xenoliths and their basaltic host rocks from Massif Central, France. *Earth Planet. Sci. Lett.* **5**, 71–75.

MASON B. and GRAHAM A. L. (1970) Minor and trace elements in meteoritic minerals. *Smithson. Contrib. Earth Sci.* **3**, 1–17.

MASUDA A. (1966) Lanthanides in basalts of Japan with three distinct types. *Geochem. J.* **1**, 11–26.

MELSON W. G., HART S. R. and THOMPSON G. (1973) St. Paul's Rocks, equatorial Atlantic: petrogenesis, radiometric ages and implications. *Geol. Soc. Amer. Mem.* **132**, 241–272.

MELSON W. G., JAROSEWICH E., BOWEN V. T. and THOMPSON G. (1967) St. Peter and St. Paul Rocks: a high temperature, mantle derived intrusion. *Science* **155**, 1532–1535.

MODRESKI P. J. and BOETTCHER A. L. (1972) The stability of phlogopite + enstatite at high pressures: a model for micas in the interior of the Earth. *Amer. J. Sci.* **272**, 852–869.

NAGASAWA H., WAKITA H., HIGUCHI H. and ONUMA N. (1969) Rare earths in peridotite nodules: an explanation of the genetic relationships between basalt and peridotite nodules. *Earth Planet. Sci. Lett.* **5**, 377–381.

O'HARA M. J. (1967) Mineral parageneses in ultrabasic rocks. In *Ultramafic and Related Rocks*, (editor P. J. Wyllie), pp. 393–403. John Wiley.

O'HARA M. J. (1968) The bearing of phase equilibria studies in synthetic and natural systems

on the origin and evolution of basic and ultrabasic rocks. *Earth Sci. Rev.* **4**, 69–331.

O'Hara M. J. and Mercy E. L. P. (1963) Petrology and petrogenesis of some garnetiferous peridotites. *Trans. Roy. Soc. Edinburgh* **65**, 251–314.

Onuma N., Higuchi H., Wakita H. and Nagasawa H. (1968) Trace element partition between two pyroxenes and the host lava. *Earth Planet. Sci. Lett.* **5**, 47–51.

Paul D. K. (1972) Strontium isotope studies in ultramafic inclusions from Dreiser Weher, Eifel, Germany. *Contrib. Mineral Petrol.* **34**, 22–28.

Peterman Z., Carmichael I. S. E. and Smith A. L. (1970) Strontium isotopes in Quaternary basalts of southeastern California. *Earth Planet. Sci. Lett.* **7**, 381–384.

Philpotts J., Schnetzler C. and Thomas H. H. (1972) Petrogenetic implications of some new geochemical data on eclogitic and ultrabasic inclusions. *Geochim. Cosmochim. Acta* **36**, 1131–1166.

Reed S. J. B. and Ware N. G. (1973) Quantitative electron microprobe analysis using a Li-drifted silicon detector. *X-Ray Spectrom.* **2**, 69–74.

Reid J. B. (1972) A dual role for lherzolite in the generation of basalt. *EOS* **53**(4), 536.

Ringwood A. E. (1966) Composition and origin of the earth. In *Advances in Earth Science*, (editor P. M. Hurley), pp. 287–365. M.I.T. Press.

Schilling J. G. (1971) Sea-floor evolution: rare-earth evidence. *Phil. Trans. Roy. Soc. London Ser.* **A268**, 663–706.

Schilling J. G. and Winchester J. W. (1969) Rare earth contribution to the origin of Hawaiian lavas. *Contrib. Mineral. Petrol.* **23**, 22–37.

Schnetzler C. and Philpotts J. (1970) Partition coefficients of rare earth elements between igneous matrix material and rock-forming mineral phenocrysts—II. *Geochim. Cosmochim. Acta* **34**, 331–340.

Shaw D. M. (1970) Trace element fractionation during anatexis. *Geochim. Cosmochim. Acta* **34**, 237–242.

Stueber A. M. and Goles G. G. (1967) Abundances of Na, Mn, Cr, Sc and Co in ultramafic rocks. *Geochim. Gosmochim. Acta* **31**, 75–93.

Towell D. G., Winchester J. S. and Spirn R. V. (1965) Rare-earth distribution in some rocks and associated minerals of the batholith of Southern California. *J. Geophys. Res.* **70**, 3485–3496.

Varne R. (1970) Hornblende lherzolite and the upper mantle. *Contrib. Mineral. Petrol.* **27**, 45–51.

Varne R. and Graham A. L. (1971) Rare earth abundances in hornblende and clinopyroxene of a hornblende lherzolite xenolith. Implications for upper mantle fractionation processes. *Earth Planet. Sci. Lett.* **13**, 11–18.

Weill D. F. and Drake M. J. (1973) Europium anomaly in plagioclase feldspar: experimental results and semi-quantitative model. *Science* **180**, 1059–1060.

White R. W. (1966) Ultramafic inclusions in basaltic rocks from Hawaii. *Contrib. Mineral. Petrol.* **12**, 245–314.

Wilshire H. G. and Trask N. J. (1971) Structural and textural relationships of amphibole and phlogopite in peridotite inclusions. Dish Hill, California. *Amer. Mineral.* **56**, 240–255.

Wilkinson J. F. G. (1966) Residual glasses from some alkali basaltic magmas from New South Wales. *Mineral. Mag.* **35**, 847–860.

Wright T. L. and Doherty P. C. (1970) A linear programming and least squares computer method for solving petrologic mixing problems. *Bull. Geol. Soc. Amer.* **81**, 1995–2008.

Yoder H. S. and Kushiro I. (1969) Melting of a hydrous phase: phlogopite. *Carnegie Inst. Wash. Yearb.* **67**, 161–167.

A 15

EARTH AND PLANETARY SCIENCE LETTERS 15 (1972) 263–270. NORTH-HOLLAND PUBLISHING COMPANY

4

ARCHAEAN GREENSTONE BELTS MAY INCLUDE TERRESTRIAL EQUIVALENTS OF LUNAR MARIA?

D.H. GREEN
Department of Geophysics and Geochemistry, Australian National University, Canberra, Australia

Received 5 April 1972

The lower portions of the volcanic sequence of some Archaean greenstone belts include members with crystallized from ultramafic liquids extruded at the earth's surface at 1600–1650°C. These liquids are interpreted as products of 60–80% melting of their mantle source composition which implies more catastrophic conditions of mantle melting than obtained in Palaeozoic, Mesozoic or Recent crust-mantle dynamics. Such conditions may be a consequence of major impacts on the surface of the primitive earth. It is suggested that the production of the lunar maria basins was accompanied by similar impacts on the earth and that such terrestrial maria played an important role in early stages of chemical differentiation of the crust and upper mantle. An hypothesis is presented in which some Archaean greenstone belts are interpreted as very large impact scars, initially filled with impact-triggered melts of ultramafic to mafic composition and thereafter evolving with further magmatism, deformation and metamorphism to the present Archaean greenstone belts.

1. Archaean greenstone belts

An important characteristic of the earth's continental crust is the presence of regions commonly referred to as Archaean granite–greenstone terrains [1–3]. These include irregularly arcuate, synclinal regions dominated by ultramafic, basic and andesitic volcanics ('greenstone belts') which occur within inhomogeneous granodioritic gneiss. Age relationships between the volcanics and the gneisses are not clear. The regional relationships suggest that the gneisses form a basement to the greenstones but there is evidence that intrusions and doming by gneissic acid intrusions is the major cause of the synclinal and arcuate form of the greenstone belts [1, 4–7].

These regions of the earth's crust appear to have been remarkably stable for $> 2.5 \times 10^9$ yr with only thin and slightly deformed sediment cover and without great elevation or extensive erosion. The greenstone belts in many areas have suffered only very low grade metamorphism and preservation of primary minerals and igneous textures is common. In addition, the mineral assemblages of the gneisses and granites are not indicative of high pressure conditions of crystallization, and seismic refraction studies show that normal crustal seismic velocities extend to depths of 30–40 km in shield areas. Thus, these appear to be regions which attained relatively thick, stable, crustal character very early in the earth's history and which preserve evidence of these primitive processes of crustal evolution.

Recent studies of geochemistry of the volcanics of Archaean greenstone belts have emphasized their similarity to basaltic rocks of the ocean floor (particularly the low-K tholeiite magma types) or to mixtures of such rock types with the volcanic characteristic of island environments [8–11]. Such comparisons have emphasized the mantle origin for the volcanics, and the similarity to modern oceanic crustal environments. The authors have, in general, advocated the absence of continental crust or the presence of only very thin sialic plates and presented models of early Archaean geodynamics in terms of the modern theory of plate tectonics involving thin lithospheric plates, shallow subduction zones, and high geothermal gradients [8, 9].

However, a characteristic feature of plate tectonics theory is that the oceanic crust and litosphere is unstable and within relatively short geological time is returned into the mantle along subduction zones.

The oceanic crust and lithosphere undergo further differentiation resulting in island arc magmatism and the gradual accretion and modification of such island arc sequences on continental margins.

In attempting to interpret the Mesozoic and Palaeozoic geological record in terms of plate tectonics theory, the identification of rock types of the oceanic crust and of 'fossil' subduction zones usually rests on the presence of melanges of mixed sedimentary, basaltic and ultramafic sequences, commonly in blueschist and partly in eclogite metamorphic facies, of paired or highly asymmetric metamorphic and lithologic belts and of very linear belts of intense deformation and overthrusting. Thus plate tectonics does not appear to produce cuspate, synclinal troughs dominated by almost unmetamorphosed basaltic volcanics, enclosed and marginally intruded by granodioritic gneiss, and with an absence of high pressure metamorphism (of either low temperature or high temperature character). An instructive analysis of the differences between the early Proterozoic Circum-Ungava Geosyncline, with close analogies to Alpine geosynclines, and the more ancient Archaean greenstone belts is given by Dimroth et al. [12].

It may be argued that the volcanic sequences of at least some of the most ancient greenstone belts are developed on or within primitive sialic crust. Geological evidence is contradictory or not definitive [4–7], and geochronological evidence is as yet inadequate. Geochronological evidence for the existence of metamorphosed sialic (gneissic) terrains of 3.9×10^9 yr in western Greenland [12], of $\geqslant 3.5 \times 10^9$ yr in Minnesota [13] and of $\geqslant 3.4 \times 10^9$ yr in Africa (6) argues for the existence of some areas of moderately thick sailic crust at times $> 3 \times 10^9$ yr. Geochronological studies of upper members of greenstone volcanic sequences and of later clearly transgressive granodiorites and granites shows that some of these volcanic sequences are $\geqslant 3.4 \times 10^9$ yr (Swaziland, S. Africa [14, 15, 17]) $\geqslant 3.3 \times 10^9$ yr (Sebakwian and/or Bulawayan, Rhodesia [6] and $\geqslant 3.0 \times 10^9$ yr (Pilbara, W. Australia [16]). These age determinations are the present older limit on the chronological sequence of exposed surface rocks but, rather intriguingly, these overlap onto the younger limit of lunar chronology as defined by ages of returned crystalline lunar rocks. This aspect of terrestrial and lunar chronology is further discussed in a later section.

2. Implications of unique Archaean volcanism

While a number of workers [8–11] have emphasized the geochemical similarity of basaltic rocks of the Archaean greenstone belts to modern ocean floor basalts and/or to island arc volcanic sequences, it has recently become clear that in *some* Archaean greenstone belts there are ultramafic and mafic volcanics of very distinctive character which are apparently restricted to these ancient magmatic sequences and do not occur in Proterozoic, Palaeozoic or younger sequences. The distinctive character of the lowermost parts of some greenstone sequences suggests that there are important differences between the magmatic activity characteristic of the modern earth and that present, at least locally, $> 3 \times 10^9$ yr ago.

Viljoen and Viljoen [18] have presented convincing evidence for the existence of *peridotitic liquids*, extruded as pillowed lava flows, and forming a major rock type of the lowest units of the greenstone sequence in the Barberton area of Swaziland, southern Africa. The name peridotitic komatiite was given to this distinctive volcanic rock. The same rock type, distinguished by characteristic olivine quench textures and ultramafic composition, has been observed as a major component of the greenstone sequences of the Yilgarn shield of Western Australia [19] and as intrusive sills or extrusive flows in Archaean rocks in Canada [20, 21]. It has been shown experimentally [22] that the temperature of extrusion of ultramafic liquid was at least 1600–1650°C, and that the magma contained $< 1\%$ water. Compositions of peridotitic komatiite magmas are similar to estimates of the bulk composition of the upper mantle in regions acting as sources for modern basalts [23, 24]. The principal differences in $Mg/(Mg + Fe^{2+})$ and in pyroxene/olivine ratios, are consistent with derivation of the peridotitic komatiite by very high degrees of melting (60–80%) of upper mantle pyrolite leaving only olivine (Fo_{93}) as the residual phase. Less olivine-rich magmas (basaltic komatiites [18] or high-magnesian basalts [19]) which overlie or are interbedded with the peridotite flows, may be interpreted as resulting from lower degrees of melting ($< 40\%$ melting) of similar upper mantle pyrolite or possibly as derivative liquids after olivine or olivine + clinopyroxene fractionation from parental peridotitic

komatiite magmas. Thus the characteristics of the distinctive ultramafic and basic magmas of some Archaean greenstone belts are consistent with melting of a mantle of composition close to that of pyrolite [23, 24] but require conditions of melting differing greatly from those operating to yield modern basalts, developed by $< 40\%$ melting under various P, T, P_{H_2O} conditions [24]. If these conclusions are correct, then we are faced with the problem of understanding how at times $> 2.5–3. \times 10^9$ yr ago, the earth's mantle was able to generate liquids reaching the surface at 1600–1650°C and derived by 60–80% melting of their source rock. In the partial melting of a pyrolite source rock, if the degree of melting exceeds ~30%, then residual olivine and orthopyroxene crystals would be separated and 'floating' in the basaltic or picritic magma. The densities of crystals ($\rho = 3.3–3.4$) and liquid ($\rho \simeq 2.7$) are such that, in the earth's gravitational field, liquid and crystals will readily segregate. This is considered to act as a major constraint in modern magma genesis so that parental magmas contain $< 30\%$ olivine and are generated at temperatures of 1200–1400°C by $< 40\%$ melting of the source rock [9, 10]. It appears that to overcome this constraint, extremely rapid upward movement of a crystal + liquid diapir is necessary, so that the liquid is able to entrain residual crystals. The degree of melting may then increase to a very high percentage melting due to pressure decrease along an approximately adiabatic cooling path. If the characteristics of Archaean volcanism as exemplified by peridotitic komatiite and komatiite magmas, are due entirely to processes of internal origin in the Archaean upper mantle, then it may be inferred that convective movements within the upper mantle were very much more rapid and derived from much higher temperature regions (? greater depths) than those characteristic of modern crust–mantle dynamics. This hypothesis encounters severe difficulties in the constraints imposed by the solidus of the upper mantle and the mechanical constraints of lateral movement of primitive lithosphere complementary to magmatic upwelling in the upper mantle.

However, recent lunar studies, arising directly from the Apollo 11–15 landings, have placed new constraints on the origin and early history of the earth–moon system. Geochronological studies on lunar samples and knowledge of the relative cratering history of the lunar surface, have led to the deduction [26] that very high rates of impact cratering prior to $3.8–4.0 \times 10^9$ yr ago would allow only the survival of extensive lava surfaces (such as the lunar maria) formed after 3.85×10^9 yr ago. The early high cratering rate and its exponential decay are attributed to a family of planetesimals in eccentric and inclined solar orbit which was swept up primarily by collision with the earth [26]. If this interpretation of the early history of the earth–moon system is correct then the evolution of the earth's surface at times $> 3 \times 10^9$ yr may be strongly influenced by major impact events. The geochronology of lunar samples [27–30] has shown that major impacts (of size producing maria basins > 300 km in diameter) occurred as late as $3.8–3.9 \times 10^9$ yr ago and that filling of maria basins by volcanism occurred up to at least 3.2×10^9 yr ago. The production of very large impact-produced depressions on the lunar surface on this time scale would be expected to be accompanied by similar impacting of the earth.

In the following discussion a hypothesis is presented suggesting that major impacts on the primitive earth, at times $> 3.0 \times 10^9$ yr ago, played a fundamental role in triggering a distinctive type of volcanism and producing large impact-scars filled with ultramafic and mafic volcanics ('terrestrial maria'). Whereas the lunar maria have been preserved for $> 3 \times 10^9$ yr on the moon, the mobility of the earth's crust caused deformation, metamorphism and further evolution to yield sequences now included amongst Archaean greenstones.

3. Terrestrial maria?

It is envisaged that the primitive earth, following segregation of an iron core and some degree of chemical differentiation of the mantle, possessed a primitive crust with mineralogy and composition determined by low pressure partial melting and crystal fractionation processes (sequence peridotite → quartz tholeiite → tholeiitic andesite → rhyodacite or rhyolite), and by deformation and metamorphism of such rocks [12–14]. While the Na-depleted character of the lunar composition is consistent with anorthitic plagioclase as a major phase of the primitive lunar crust, the primitive terrestrial crust was probably dominated

by intermediate and sodic plagioclase, quartz, K-feldspar and ferromagnesian minerals. Acceptance of Shoemaker's [26] model of lunar impact history would imply that it is most improbable that surface rocks of crystallization age $> 3.8–4 \times 10^9$ yr would occur on the earth (though metamorphic or whole rock Rb/Sr 'ages' greater than this could occur, cf. the 4.5×10^9 yr 'age' for lunar regolith samples [27]). Also it is *not* implied that a primitive sialic crust would be uniformly distributed over the earth nor that convective motions of internal origin and consequent geochemical differentiation of the crust and upper mantle were absent during the pre- 3.8×10^9 yr history of the earth–moon system. It is suggested that if any areas of sialic crust were hit by a very large impact, then a distinctive sequence of events would occur. The location of such an impact scar with a 'stable' sialic region might allow preservation of its distinctive character in spite of the erosive processes and mobility of the earth's crust. In a region of sialic crust, a very large impact structure of 300–500 km diameter (cf. Mare Humorum, Nectaris, Moscoviense) or larger (cf. Mare Orientale, Serenitatis, Imbrium) would result in instantaneous unloading of the impacted region and throwout loading of the surrounding regions. The effect on pressure–temperature covariance in the excavated region relative to the surrounding region is illustrated schematically in fig. 1. The geotherm illustrated in this figure is hypothetical but is much steeper than the estimated modern oceanic geotherm, consistent with a higher radioactive heat production early in the earth's history. A large negative gravity anomaly must result over the impacted area and intensive fracturing would occur below the impacted area, possibly to depths of 60–80 km.

It is suggested that two main processes act to eliminate the instability established by a very large impact. Firstly, the load pressure drop beneath the impact site means that melting of the mantle may occur (figs. 1, 2) at quite deep levels and the degree of melting may be quite high. Uplift of the central floor of the impact requires vertical movement at deeper levels and the presence of a partially molten region underlying a highly fractured zone probably creates favourable conditions for very rapid ascent of large peridotitic diapirs. Such diapirs may reach shallow levels and there separate into liquid and crystal fractions with very high degrees of melting. This process

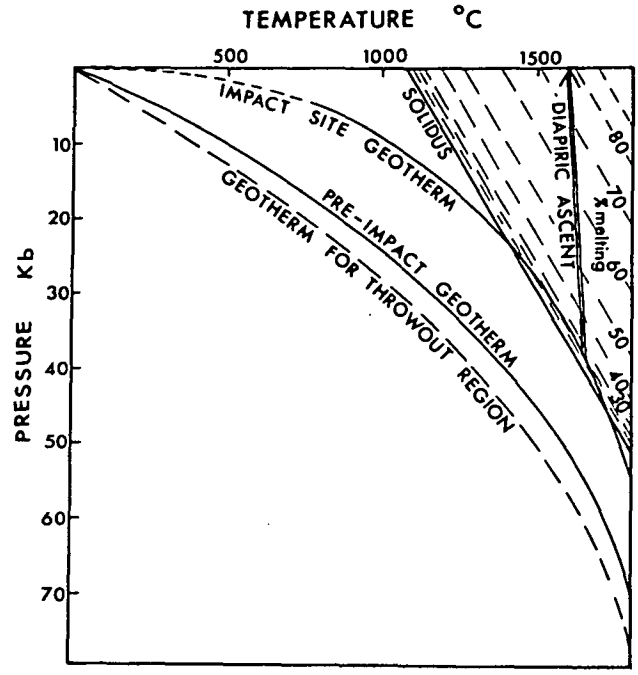

Fig. 1. Hypothetical diagram illustrating the instantaneous effect on a terrestrial geothermal gradient following major impact and unloading (by throwout and brecciation) of a large impact basin. The geotherm is illustrative but is drawn as a steeper geothermal gradient than estimates of the modern oceanic geotherm [34, 35]. Thermal effects of impact are neglected but would produce a transient high temperature at and very near the surface ($P < 5$kb), including impact melting in the ejecta blanket. A region at ~ 100–200 km depth is taken above its solidus by the pressure drop and the diagram shows adiabatic ascent of diapirs from this region to yield magmas reaching the earth's surface at temperatures above 1500°C.

would produce highly fluid peridotitic komatiite magmas leaving minor residual dunite (fig. 2). It is emphasized that the magmas discussed are not direct impact melts. In this model the impact-produced *unloading* produces partial malting at depth, the uplift of the fractured floor initiates diapiric ascent of partially molten peridotite and the process accelerates. The cycles of peridotitic komatiite to basaltic komatiite reported by Viljoen and Viljoen [18] possibly imply the ascent of individual diapirs (fig. 2) rather than a single regional upwelling. Slowing down of the process as the impact basin became filled would lead to power degrees of melting in ascending diapirs or to increased opportunity for crystal fractionation at low pressure with magma types changing to olivine-poor and low-Mg basalts, and possibly to tholeiitic andesite and dacitic derivatives.

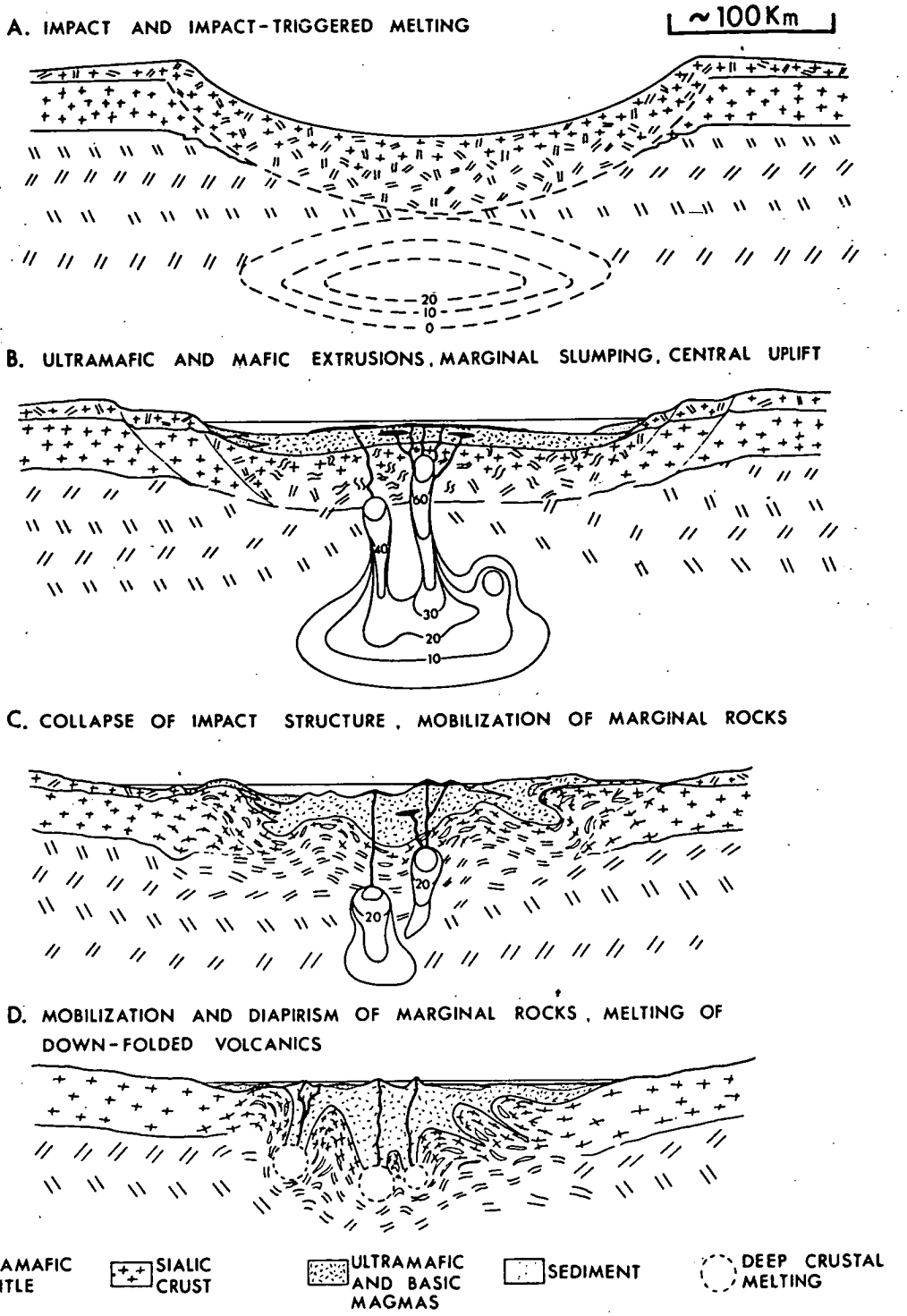

Fig. 2. Diagram illustrating the hypothesis in which some Archaean greenstone belts are suggested as terrestrial equivalents of lunar maria. (A) Primitive sialic crust impacted by very large body excavating large structure of ~ 30–50 km depth, floored with an ejecta blanket overlying brecciated upper mantle rocks. Instantaneous unloading (pressure drop) beneath the impact produces melting and dashed curves illustrate the degree of melting (at ~ 150 km depth). An extremely large negative gravity anomaly would be formed over the impact. (B) Partially melted peridotite rises rapidly into the brecciated impact floor with very great increase in degree of melting and extrusion of very high temperature ultramafic ($\geq$ 1600°C) and basaltic magmas (komatiites). Some marginal slumping and sedimentation. (C) Accelerated inward collapse of impact structure, possibly influenced by regional crustal stresses, but mainly a consequence of increasing temperature and mobility of underlying and marginal mixed ejecta blanket. It is considered that the original crustal component (? granititic) of this would recrystallize, begin to partially melt and intrude or dome the overlying dense ultramafic and mafic lavas. Volcanism changes to more normal basaltic volcanism. (D) Dominant process is the infolding of the ultramafic and mafic volcanics accentuated by upward movement and intrusion of gneiss domes – the basement to the original ultramafic and mafic lava sequence becomes intrusive into that sequence. In the deeper regions, temperatures are sufficiently high to produce remelting (under $P_{H_2O} < P_{Total}$ conditions) of mixed basaltic and 'basement' materials, yielding a second stage of volcanism characterized by andesite and dacitic magmas.

While magmatic activity is considered to be the most rapid and major mechanism responsible for filling the postulated terrestrial 'maria', there are processes which would operate on the earth to eliminate the maria but which have not operated on the moon (at least for the last 3.0 by approx.). With the excavation of a large impact scar through sialic crust and creation of a large gravity anomaly, there is a strong tendency to eliminate the impact structure by lateral flow, or slumping, of the marginal 'highlands' into the maria basin. It is considered that the high gravitational field of the earth, the higher terrestrial geothermal gradient and the lower melting temperature of the postulated primitive terrestrial crust (andesitic) relative to the lunar crust (gabbroic anorthosite) all create conditions favourable to elimination of the terrestrial maria by largely lateral displacement or overthrusting by the primitive sialic crust. The process is illustrated schematically in fig. 2 and is invoked as an explanation for the observation of conformable gneissic granites, intrusive into the base of the greenstone sequences yet regionally underlying the synclinal greenstone sequences and appearing to structurally form the basement to these sequences [4–7]. The effects of erosion and sedimentation (consequent on the existence of a primitive hydrosphere and atmosphere) may also aid in the encroachment of the margins of the impact structure on the central area. In their description of the Onverwacht Group, the lowest group of the Swaziland Sequence, Viljoen and Viljoen [18, 31] note that the upper formation of the Onverwacht Group (Komati Formation) is 3.5 km thick in the type area and consists entirely of altered ultramafic and basic lavas. Interlayered sediments or acid rocks are absent although later felsic intrusives do occur. It is suggested that this formation represents the central or deeper portion of the impact structure whereas the Theespruit Formation, which is in fault contact with the Komati Formation but is interpreted to underlie the Komati Formation, may be in part a facies equivalent of the Komati Formation, formed closer to the margins of the impact structure. The Theespruit Formation consists of 1.9 km of metamorphosed mafic lavas with significant though minor quantities of felsic tuffs and associated poorly bedded chert. There appear to be no rocks described from the Swaziland System which might correspond to the veneer of impact melt, impact tuffs and impact breccia which would initially form the floor to the impact structures (fig. 2). In this context, the thermal effects of frequent and voluminous flows of very high temperature ultramafic and basic magmas may cause metamorphism, partial melting and mobilization of marginal sedimentary intercalations or adjacent older 'sial'.

The result of the process outlined above would be to transform an initially circular impact scar through a 'terrestrial maria' filled with ultramafic and basic lavas and a minimum amount of sediment, to a synclinal but irregularly cuspate or lobate greenstone belt. As the lava sequence of the maria first thickened rapidly and then became infolded with encroaching sial, the possibility of partial melting of the deeper parts of the greenstone sequences would increase. Thus the evolution of the 'terrestrial maria' might continue with the ultramafic and basaltic sequences being overlain by diacitic or rhyodacitic, andesitic and tholeiitic basaltic volcanics and related intrusives, developed by partial melting of peridotitic and basaltic rocks under variable P_{H_2O} conditions at depths of about 30–60 km. If horizontal movements or stresses were as important $> 2.5 \times 10^9$ yr ago as in the Palaeozoic or Mesozoic, then the end result of deformation of large terrestrial maria might be elongate folded greenstone belts such as those of the western Australian Yilgarn shield, rather than the irregular form of the Swaziland Barberton area.

4. Summary

The suggestion that the major impact scars are preserved on Archaean shield regions is not new. An impact origin, with the impact triggering magmatic intrusion and extrusion, has been suggested for Sudbury Lopolith ($\sim 1.7 \times 10^9$ yr old), Vredefort Dome and the Bushveld Complex ($\sim 2 \times 10^9$ yr old) [32, 33]. In this paper, I have used the distinctive characters of the ultramafic and mafic intrusives of some Archaean greenstone belts to argue for a particularly catastrophic type of magmatism adding the hypothesis that this can best be interpreted in terms of major impact. I have attempted to support this hypothesis with the argument that events recorded in some Archaean greenstone belts are nearly synchronous with very large impacts forming the

maria basins on the lunar surface. If this hypothesis (relating a distinctive Archaean magma type (peridotitic komatiite) to an origin by impact-triggered melting) is valid, then it implies that the real age of Archaean greenstone belts in which these distinctive magmas are present would be greater than approximately 3.5×10^9 yr (from present understanding of lunar impact chronology [26]). This aspect of the model is open to testing. Failure of the hypothesis carries the implication of very different upper mantle dynamics and temperature distribution within the Archaean crust and upper mantle. This paper advocates a rather fundamental role for large exogenous impacting bodies in activating chemical differentiation of the crust–mantle system through the volcanism and evolutionary sequences of Archaean greenstone belts. It is emphasized that endogenous processes of crust–mantle differentiation, possibly the precursors of the petrogenetic processes occurring as an integral part of plate tectonics, were probably also in evidence $\sim 3.0 \times 10^9$ yr ago. It is postulated that prior to 3 or 3.5×10^9 yr ago, the *major* geochemical differentiation of the earth was due to initial accretionary processes ($\sim 4.5 \times 10^9$ yr ago) followed by impact-working of the surface and impact-triggered processes in the upper mantle (to $3–3.5 \times 10^9$ yr ago). Since $\sim 3 \times 10^9$ yr, the magnitude and frequency of large impacts on the earth decreased very greatly [26] so that crustal evolution has been dominated by geochemical processes of internal origin (e.g. plate tectonics).

Acknowledgements

The author thanks Drs. M.J. and R.P. Viljoen for their initial stimulation of his interest in the Swaziland rocks, for supply of samples for experimental work and for continuing discussions. The author also acknowledges helpful discussions and manuscript criticism by Professor A.E. Ringwood, Drs. K. Frederiksson, A. Glikson, I.A. Nicholls, V.M. Oversby and W. Compston.

References

[1] C.R. Anhaesser, R. Mason, M.J. Viljoen and R.P. Viljoen, A reappraisal of some aspects of Precambrian Shield geology, Geol. Soc. Am. Bull. 80 (1969) 2175.

[2] A.Y. Glikson, Geosynclinal evolution and the geochemical evolution of early Precambrian systems, Tectonophys. 9 (1970) 397.

[3] A.M. Goodwin, Archaean protocontinental growth and early crustal history of the Canadian Shield, Rept. 23rd Internat. Geol. Congress, Prague 1 (1968) 69.

[4] M.J. Viljoen and R.P. Viljoen, An introduction to the geology of the Barberton granite–greenstone terrain, Geol. Soc. S. Africa Spec. Publ. 2: Upper Mantle Project (1969) 9.

[5] M.J. Viljoen and R.P. Viljoen, A reappraisal of the granite–greenstone terrains of shield areas based on the Barberton model, Geol. Soc. S. Africa Spec. Publ. 2: Upper Mantle Project (1969) 245.

[6] N.W. Bliss and P.A. Stidolph, A review of the Rhodesian Basement Complex, Geol. Soc. S. Africa Spec. Publ. 2: Upper Mantle Project (1969) 305.

[7] A.M. Goodwin and R.H. Ridler, The Abitibi orogenic belt, in: Symposium on Basins and Geosynclines of the Canadian Shield, Geol. Surv. Canada paper 70–40 (1970) 1.

[8] A.Y. Glikson, Primitive Archaean element distribution patterns: Chemical evidence and geotectonic significance, Earth Planet. Sci. Letters 12 (1971) 309.

[9] S.R. Hart, C. Brooks, T.E. Krogh, G.L. Davis and D. Nova, Ancient and modern volcanic rocks: A trace element model, Earth Planet. Sci. Letters 10 (1970) 17.

[10] W.R.A. Baragar, Major element geochemistry of the Noranda volcanic belt, Quebec–Ontario, Can. J. Earth Sci. 5 (1968) 773.

[11] D.C. Green and H. Baadsgaard, Temporal evolution and petrogenesis of an Archaean crustal segment at Yellowknife N.W.T., Canada, J. Petrol. 12 (1971) 177.

[12] L.P. Black, N.H. Gale, S. Moorbath, R.J. Pankhurst and V.R. McGregor, Isotopic dating of very early Precambrian amphibolite facies gneisses from the Godthaab District, West Greenland, Earth Planet. Sci. Letters 12 (1971) 245.

[13] S.S. Goldich, C.E. Hedge and T.W. Stern, Age of the Morton and Montevideo gneisses and related rocks, southwestern Minnesota, Geol. Soc. Am. Bull. 81 (1970) 3671.

[14] H.L. Allsopp, R.D. Davies, A.A.A. de Gasparis and L.O. Nicolaysen, Review of Rb/Sr age measurements from the early Precambrian terrain in the south-eastern Transvaal and Swaziland, Geol. Soc. S. Africa Spec. Publ. 2: Upper Mantle Proeject (1969) 433.

[15] P.M. Hurley, B. Nagy and W.H. Pinson, Age of the Middle Marker Horizon, Onverwacht Group, Swaziland Sequence, South Africa (abstract), Geol. Soc. Am. Abst. with Programs 3 (1971) 609.

[16] W. Compston and P.A. Arriens, The Precambrian geochronology of Australia, Can. J. Earth Sci. 5 (1968) 561.

[17] M.J. Viljoen and R.P. Viljoen, A proposed new classification of the granite rocks of the Barberton region, Geol. Soc. S. Africa Spec. Publ. 2: Upper Mantle Project (1969) 153.

[18] M.J. Viljoen and R.P. Viljoen, Evidence for the existence of a mobile extrusive peridotite magma from the Komati Formation of the Onverwacht Group, Geol. Soc. S. Africa Spec. Publ. 2: Upper Mantle Project (1969) 87.

[19] R.W. Nesbitt, Skeletal crystals forms in the ultramafic rocks of the Yilgarn block, Western Australia; evidence for an Archaean ultramafic liquid, Geol. Soc. Aust. Spec. Publ. 3 (1972) in press.

[20] A.J. Naldrett and G.D. Mason, Contrasting Archaean ultramafic igneous bodies in Dundonald and Clergue Townships, Ontario, Can. J. Earth Sci. 5 (1968) 111.

[21] A.J. Naldrett, Ultramafic and related mafic rocks of the Abitibi origin, in: Symposium on Basins and Geosynclines of the Canadian Shield, ed. A.J. Baer, Geol. Surv. Canada Paper 70–40 (1970) 24.

[22] D.H. Green, I.A. Nicholls, M.J. Viljoen and R.P. Viljoen, Experimental determination of magmatic temperature and crystallization sequence of Archaean peridotitic magma (in preparation).

[23] A.E. Ringwood, Chemical composition and origin of the earth, in: Advances in Earth Science, ed. P.M. Hurley (MIT Press, Cambridge, Mass., 1966) 287.

[24] D.H. Green, The origin of basaltic and nephelinitic magmas (Bennett Lecture), Trans. Leicester Lit. Philos. Soc. 64 (1970) 28.

[25] D.H. Green and A.E. Ringwood, The genesis of basaltic magmas, Contrib. Mineral. Petrol. 15 (1967) 103.

[26] E.M. Shoemaker, Cratering history and early evolution of the moon (abstract), Revised Abstracts of the Third Lunar Science Conference, Lunar Sci. Inst., Houston Publication 88 (1972) 696.

[27] W. Compston, H. Berry, M.J. Vernon, B.W. Chappell and M.J. Kaye, Rubidium-strontium chronology and chemistry of lunar material from the Ocean of Storms, Proc. 2nd Lunar Sci. Conf. 2 (1971) 1471.

[28] D.A. Papanastassiou and G.J. Wasserburg, Rb-Sr ages of igneous rocks from the Apollo 14 mission and the age of the Fra Mauro formation, Earth Planet. Sci. Letters 12 (1971) 36.

[29] G. Turner, J.C. Huneke, F.A. Podosek and G.J. Wasserburg, $^{40}Ar/^{39}Ar$ ages and cosmic-ray exposure ages of Apollo 14 samples, Earth Planet. Sci. Letters 12 (1971) 19.

[30] W. Compston, M.J. Vernon, H. Berry and R. Rudowski, The age of the Fra Mauro formation: A radiometric older limit, Earth Planet. Sci. Letters 12 (1971) 55.

[31] M.J. Viljoen and R.P. Viljoen, The geology and geochemistry of the Lower Ultramafic Unit of the Onverwacht Group and a proposed new class of igneous rock, Geol. Soc. S. Africa Spec. Publ. 2 (1969) 55.

[32] R.S. Dietz, Sudbury structure as an astrobleme, J. Geol. 72 (1964) 412.

[33] W. Hamilton, Bushveld Complex – product of impacts? Geol. Soc. S. Africa Spec. Publ. 1 (1970) 367.

[34] S.P. Clark and A.E. Ringwood, Density distribution and constitution of the mantle, Rev. Geophys. 2 (1964) 35.

[35] A.E. Ringwood, I.D. MacGregor and F.R. Boyd, Petrological constitution of the Upper Mantle, Ann. Rept. Geophys. Lab. Carnegie Inst. Year Book 63 (1964) 147.

A16

Experimental Demonstration of the Existence of Peridotitic Liquids in Earliest Archean Magmatism

D. H. Green, I. A. Nicholls
Research School of Earth Sciences
Australian National University
Canberra, A.C.T., Australia
M. Viljoen, R. Viljoen
Johannesburg Consolidated Investment Company Limited
P.O. Box 2, Randfontein, Transvaal, South Africa

ABSTRACT

An Archean peridotitic komatiite from the Barberton Mountain Land, South Africa, contains relict zoned skeletal olivine crystals with compositions as magnesian as 100 Mg/(Mg + Fe^{2+}) = 93.6. This magnesian olivine is also relatively rich in nickel (0.51 percent NiO) and in chromium (0.18 percent Cr_2O_3). Experimental investigation of the near-liquidus phase relations of peridotitic komatiite as a function of pressure has shown that liquidus olivine for this bulk composition has a composition identical to the observed, most magnesian olivine in the rock. Experimental study of the effect of water on melting relations demonstrates a pronounced, pressure-dependent decrease of liquidus temperature for water-saturated conditions, but further demonstrates that the natural magma contained <0.2 percent H_2O approximately at extrusion. The temperature of the completely liquid peridotitic magma at the Earth's surface was 1650° ± 20°C.

INTRODUCTION

One of the most interesting aspects of recent studies of Archean greenstone terranes has been the recognition and description of a distinctive class of rocks of ultramafic composition, which, on the basis of field relations, pillow structures, and brecciated flow tops, has been interpreted as lava flows, probably extruded in a submarine environment, (Viljoen and Viljoen, 1969a, 1969b; Nesbitt, 1971; Pyke and others, 1973). These ultramafic lava flows exhibit a variety of cooling textures that include evidence for crystallization, settling, and accumulation of olivine phenocrysts. More significantly, they commonly exhibit a texture (now often designated spinifex texture) in which acicular, skeletal crystal forms of olivine, or its alteration products, and pyroxene (in some cases) are grouped in intersecting sheaflike forms. The textures are analogous to quench textures produced experimentally in rapid cooling of olivine-rich silicate melts and have been interpreted as providing clear evidence of extrusion and rapid quenching of ultramafic liquids in a distinctive Archean type of magmatism (Viljoen and Viljoen, 1969a, 1969b; Nesbitt, 1971; Naldrett and Mason, 1968; Pyke and others, 1973).

Salient aspects of the major element chemistry of Archean ultramafic and related Mg-rich mafic rocks have been presented by Viljoen and Viljoen (1969a, 1969b, 1969c), Nesbitt (1971), McCall and Leishman (1971), and Brooks and Hart (1974). We note that a distinctive chemical characteristic of the South African Barberton rocks (that is $CaO/Al_2O_3 > 1$ in weight percent), particularly in the peridotitic rocks, is not equally characteristic of Canadian or Western Australian peridotites, whether they exhibit spinifex texture or evidence of cumulate olivine (Nesbitt, 1971). It may thus be premature to overemphasize the similarities between different Archean terranes for, assuming that the Archean includes rocks >2.5 b.y. old, there is opportunity for secular change in characteristics of magmatism. For example, the conditions of magma genesis that can be deduced from a >3.3-b.y. sequence in South Africa may not be applicable to a >2.7-b.y. sequence in Western Australia. It is clear, however, that the degree of secondary alteration is sufficiently low, and the preservation of primary igneous textures and mineralogy is sufficiently complete in many Archean greenstone belt sequences so that various techniques can be used to unambiguously define the chemical compositions of magmatic liquids and their temperatures of extrusion. In this paper we report results of an analytical and experimental study of peridotitic komatiite from the Barberton Mountain Land, South Africa. From the very

large number of sampled localities this sample was selected as the most olivine-rich peridotite, which is entirely of quench-texture type and has field characteristics of a lava flow, thus preserving relict olivine reasonably interpreted as being of igneous origin.

SAMPLE DESCRIPTION

Sample 49J, taken from the type area of the Komati Formation (Viljoen and Viljoen, 1969a, 1969b), is from a broad zone (~200 m) of peridotitic komatiite that contains narrow, slightly more resistant ridges of an olivine-rich peridotite (~75 percent olivine originally, including both skeletal and equant crystals) and less resistant, intervening areas of peridotite containing less olivine (~55 percent olivine originally). In the latter areas both pillow structures and distinctive quench textures (Viljoen and Viljoen, 1969a, 1969b) occur; the quench textures usually occur in bands or zones several centimeters thick, which are parallel to the over-all trend and the layering of the peridotite horizon. The arrangement of skeletal, elongate olivine crystals within these quench-textured zones is random, without flow orientation (Viljoen and Viljoen, 1969b, Pls. VI, VIII, IX). A considerable textural variation exists, ranging from randomly oriented olivine blades within a matrix of fibrous tremolite and chlorite to interfering packs or bundles of regularly alternating tremolite-chlorite-magnetite-serpentine associations. Sample 49J is of the former type, with original skeletal olivine blades, now altered to serpentine minerals plus magnetite, enclosing numerous well-preserved clear olivine remnants. These remnants preserve a common orientation over the length of individual blades and show mutual interference of blades and strongly skeletal forms.

Electron microprobe analyses of relict primary olivine show that it is zoned from forsterite-rich cores to more fayalite-rich margins (Table 1). Nickel decreases and manganese, chromium, and aluminum increase toward the more fayalitic borders. This olivine is distinctive among terrestrial olivine because of its very high Ni and Cr content. Optical and electron microprobe analyses show that small spinel inclusions are absent, and Cr is present within the olivine lattice. Sobolev (1972) reported as much as 0.08 to 0.11 percent Cr_2O_3 in olivine phenocrysts in meimechite or in olivine occurring with diamond. The Cr_2O_3 content of the olivine described herein is distinctly higher than these values and more than a factor of ten times the Cr_2O_3 content of olivine from alpine peridotite or lherzolite xenoliths in basalt (Sobolev, 1972). Olivine crystallized from *lunar* basaltic magma flows under low f_{O_2} conditions (in equilibrium with metallic iron) have higher Cr content (~0.5 percent CrO) as divalent chromium but, at the f_{O_2} conditions of the lunar magma flows, all Ni is present in the metal phase and does not enter the olivine structure. The association of extreme values of the 100 Mg/(Mg + Fe) ratio, forsterite content, and nickel and chromium contents, is a distinctive characteristic of the primary olivine of these ultramafic lava flows.

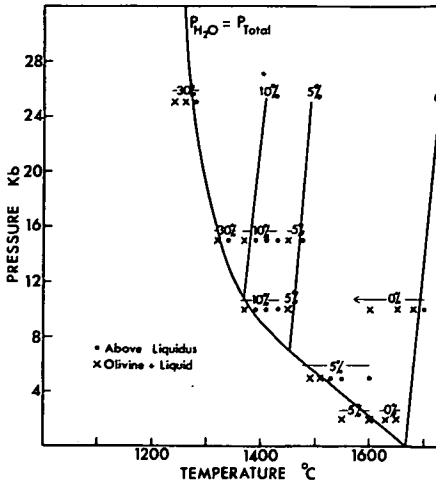

Figure 1. Experimental determination of melting relations of peridotitic komatiite sample 49J. Water content for data points is indicated above each group of data points.

EXPERIMENTAL PETROLOGY

Although the petrographic evidence from the peridotitic komatiite (sample 49J) is consistent with quenching of a liquid whose composition matches that of the rock, it is also possible that the liquid was less olivine-rich, and the

TABLE 1. COMPOSITION OF "FRESHEST" SAMPLE OF PERIDOTITIC KOMATIITE FROM KOMATI FORMATION, ONVERWACHT GROUP, BARBERTON MOUNTAIN LAND, SOUTH AFRICA*

	49J*	Calculated anhydrous with Fe_2O_3 = 1.0%	Most Mg-rich relict olivine (core)	Most Fe-rich relict olivine (nearer edge)
SiO_2	42.38	46.46	41.41	40.45
TiO_2	0.18	0.19	0.0	0.0
Al_2O_3	3.26	3.58	0.0	0.05
Fe_2O_3	5.40	1.00	0.0	0.0
FeO	5.30	9.38	6.27	10.58
MnO	0.19	0.21	0.12	0.18
MgO	30.05	32.97	51.61	47.71
CaO	4.65	5.10	0.19	0.25
Na_2O	0.44	0.49	0.0	0.0
K_2O	0.17	0.18	0.0	0.0
P_2O_5	0.01	0.01	0.0	0.0
Cr_2O_3	0.39	0.43	0.18	0.29
NiO	0.25	0.27	0.51	0.47
H_2O^+	6.63	..	..	
H_2O^-	0.55	..	..	
CO_2	0.20	..	..	
Total	100.05	100.27	100.29	99.98
$\frac{100\ Mg}{Mg + Fe}$		85.0	93.6	89.0

Trace elements 49J: V 88 ppm; Co 119 ppm; Cu 79 ppm; Zn 79 ppm

CIPW norm column 2

Or	Ab	An	Di	Hy	Ol	Ilm	Mt	Chr
1.1	4.2	7.0	14.6	21.7	50.1	0.3	1.4	0.6

Normative plagioclase $Ab_{39}An_{61}$

Note: Analysis of sample 49J by x-ray fluorescence techniques (B. W. Chappell and M. Kaye, analysts), augmented by flame photometry (Na_2O, K_2O), spectrophotometry (FeO, Fe_2O_3), and gravimetric methods (H_2O, CO_2) (E. Kiss, analyst). Olivine analyses by N. G. Ware using A.R.L. wavelength dispersive electron probe x-ray microanalyzer.

* A.N.U. no. 2926.

eridotite composition results from livine accumulation or results from elective metasomatism during alteration f the quench glass or cryptocrystalline aterial initially enclosing the olivine. he experimental study was undertaken o establish whether liquidus olivine or sample 49J bulk composition atched the most Mg-rich olivine in the atural rock as the 100 Mg/(Mg + Fe^{2+}) alues of olivine and *equilibrium* liquid re uniquely related by a partition oefficient at any *P* and *T* (Green and ingwood, 1967; Roeder and Emslie, 970).

It was technically easier to carry out uenching experiments at >2 kb pressure n a piston-cylinder apparatus (Boyd and ngland, 1961) as our 1-atm quenching urnaces do not exceed ~1500°C. Results f dry experimental runs using graphite apsules (in all but one run) and "dry" urnace assemblies (Green and Ringwood, 967) are shown in Figure 1 and Table 2. he liquidus temperature of peridotitic omatiite lies between 1680° and 1700°C t 10 kb and slightly above 1650°C at kb. Liquidus olivine at 1680°C, 10 kb, identical to the natural olivine in Ig-value, Cr_2O_3, CaO, and Al_2O_3 conents but has a lower NiO content. The iO depletion in the experimental livine may be due to f_{O_2} conditions ightly below the Ni-NiO buffer in the raphite capsule and furnace which ould lower the NiO activity in the elt. Oxygen fugacity conditions in ne natural magma must have been ightly higher than in our experimental onditions, although the matching of r content between experimental olivine nd natural olivine shows that the difference was small.

At 10 kb, olivine crystallizes alone down to a temperature of 1450°C where it is joined by orthopyroxene; at 2 kb, however, olivine crystallizes alone down to 1300° ± 40°C where it is joined by clinopyroxene. Fe, Ca, and Cr contents of olivine increase steadily with decreasing temperature. Equilibrium olivine 30°C below the liquidus differs by 1 percent Fo (1.1 wt percent FeO) from liquidus olivine, and the data leave no doubt that the natural, most magnesian olivine in 49J has the composition required for the liquidus phase for 49J bulk composition. In those runs where both quench and equilibrium olivine (Figs. 2, 3) were analyzed, quench olivine is richer in Fe, Cr, Ca, and Al content, again matching the differences between olivine core compositions and quenched, zoned edges to olivine crystals in the natural rock.

Finally, the quench textures produced experimentally are microscale replicas of the spinifex texture of the natural rocks. In the 1650°C run (Fig. 3), marked settling of 5 to 10 μm primary euhedral olivine within the 1-mm capsule produced an exemplary cumulate layer, modeling, again on microscale, the sharply distinct spinifex texture and (granular + interstitial quench) texture layers observed in peridotitic komatiite occurrences (Viljoen and Viljoen, 1969a, 1969b). The contrast between cumulate olivine and blades of quench olivine growing upward into the overlying liquid yields a microscale harrisitic texture.

The experimental data shows that a *dry* magma of peridotitic komatiite composition (specifically as in Table 1) would have an extrusion temperature between 1650° and 1700°C at the Earth's surface. This temperature is 400°C higher than extrusion temperatures of modern olivine tholeiite lava flows. The difficulty of envisaging extrusion at the high temperatures required for anhydrous peridotitic lava flows has led several authors to postulate lowering of the liquidus temperature by high water contents within the ultramafic magma (Brooks and Hart, 1974). To quantify and evaluate this hypothesis, we have determined the water-saturated liquidus and liquidi for 5 percent H_2O and 10 percent H_2O at 10 and 15 kb load pressure (Fig. 1). A water content of 5 percent (by weight) depresses the liquidus temperature by ~230°C at 10 kb, *but* the peridotitic magma is incapable of dissolving 5 percent H_2O at pressures <7 kb (depths <25 km, approximately). Although hydrous peridotitic komatiite magma containing 5 percent H_2O could exist at 1450°C deep in the Archean mantle (>25 km), it must begin to crystallize olivine and release water at ~25 km depth. Our experiments show that during quenching in <30 sec, skeletal olivine crystals nucleate and grow to lengths >100 μm, and euhedral equilibrium olivine crystals nucleate, grow to >20 μm, and settle through distances of >1 mm in <10 min. It is thus impossible that sample 49J magma could have contained 5 percent H_2O at temperatures of ~1450°C, $P > 7$ kb (>25 km depth) and moved to the Earth's surface without nucleation of olivine or loss of water, thus arriving in a supercooled and explosively water-oversaturated state. Even if such a supercooled, water-oversaturated magma were to reach the surface, to be

TABLE 2. COMPOSITIONS OF OLIVINE AND PYROXENES CRYSTALLIZED AT VARIOUS TEMPERATURES

Temperature (°C)	$\frac{100\ Mg}{Mg + Fe}$	Cr_2O_3	CaO	NiO	Capsule
Olivine					
1700 (quench)	(91.0)	0.31	0.29	0.07	C
1680 (quench)	(90.4)	0.29	0.24	0.11	C
1680 equilibrium	93.5	0.17	0.14	0.08	C
1650 (quench)	(89.5)	0.35	0.30	0.09	C
1650 equilibrium	92.4	0.20	0.20	0.07	C
1600 equilibrium	92.8	0.19	0.24	0.24	Pt
1550 equilibrium	91.2	0.27	0.17	0.10	C
1500 equilibrium	90.4	0.30	0.20	0.03	C
1475 equilibrium	90.2	0.30	0.20	0.03	C
1450 equilibrium	89.7	0.32	0.22	0.02	C
1425 equilibrium	88.4	0.31	0.23	0.25	C
1400 equilibrium	88.4	0.32	0.31	0.17	C
1350 equilibrium	88.0	0.30	0.29	0.08	C

Pyroxenes	$\frac{Mg}{Mg + Fe}$	Al_2O_3	Cr_2O_3	CaO	Na_2O	Capsule
1450 orthopyroxene	89.5	1.26	0.42	2.11	0.07	C
1425 clinopyroxene*	88.4	1.66	0.47	3.43	0.10	C
1400 clinopyroxene*	87.9	1.35	0.54	4.31	0.05	C

Note: Analyses of minerals using A.R.L. electron microprobe with wavelength dispersive x-ray analytical system.

* These extremely subcalcic clinopyroxenes may be metastable, and further work is required to explore whether, at this *P* and *T*, orthoenstatite, pigeonite, and diopside all have stability fields or whether only orthopyroxene and diopside may stably co-exist.

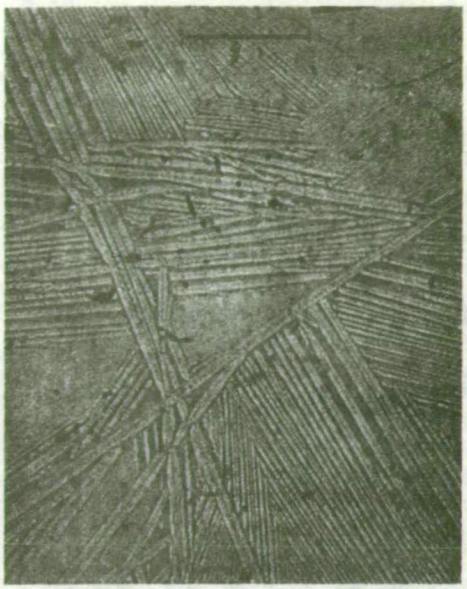

Figure 2. Photomicrograph of polished surface (reflected light) of sample 49J quenched from above liquidus, at 10 kb, 1700°C. Texture is a microscale replica of natural spinifex texture with acicular crystals of olivine, often in parallel bundles, in glass or extremely finely ribbed quench clinopyroxene (center). Scale mark, 100 μm.

Figure 3. Photomicrograph of polished surface (reflected light) of sample 49J quenched from below liquidus, at 10 kb, 1650°C, 10 min run. Texture illustrates gravitational setting of euhedral equilibrium olivine ($Mg_{92.4}$) to base of capsule and growth during quenching of acicular olivine ($Mg_{89.5}$) and quench clinopyroxene in glass. Quench olivine occurs interstitially to primary olivine but also in harrisitic texture with blades roughly perpendicular to accumulation surface. Scale mark, 100 μm.

consistent with field observations, the magma would then have to lose water without violent explosive vesiculation of the lava, and precipitate olivine in the distinctive quench texture. The postulated hydrous magma (5 percent H_2O) would be required to precipitate olivine with compositions beginning from that appropriate to crystallization at 1 atm and ~1650°C rather than the olivine stable at 1 atm and 1450°C (~100 Mg/(Mg + Fe^{2+}) = 89.7). These considerations show that the ultramafic magma did not contain ~5 percent H_2O.

The peridotitic magma flows were probably submarine, and if extruded in deep water, then water pressure of ~1 kb could have been operative at the extrusion surface—this would be sufficient to entrap ~0.5 percent H_2O within the magma flows and depress the liquidus by ~50°C below the anhydrous, 1-atm liquidus temperatures. We conclude that the minimum temperature of extrusion of the peridotite magma (sample 49J composition) was 1620° ± 20°C and that this "low" temperature would require extrusion in very deep water (~1 kb water pressure) and a H_2O content of ~0.5 percent in the peridotite. More probably the extrusion temperature was 1650° ± 20°C, and the water content was <0.2 percent.

CONCLUSIONS

The analytical and experimental data presented here confirm the conclusions of previous authors that Archean greenstone belts contain ultramafic horizons that were extruded as completely liquid peridotite magma flows and were rapidly quenched from above their liquidus temperatures. The temperature of extrusion is established as 1650° ± 20°C for a water content of <0.2 percent. The relatively high water content (>6 percent H_2O) of peridotitic komatiite on which the experimental study was carried out, is a secondary feature and was not present in the magma prior to or during extrusion. The extraordinarily high temperature of peridotite magma indicates magmatic conditions and tectonic processes that are distinctively different from the modern Earth.

REFERENCES CITED

Boyd, F. R., and England, J. L., 1961, Apparatus for phase equilibrium measurements at pressures to 50 kb and temperatures to 1750°C: Jour. Geophys. Research, v. 65, p. 741–748.

Brooks, C., and Hart, S. R., 1974, On the significance of komatiite: Geology, v. 2, p. 107–110.

Green, D. H., and Ringwood, A. E., 1967, The genesis of basaltic magmas: Contr. Mineralogy and Petrology, v. 15, p. 103–190.

McCall, G.J.H., and Leishman, J., 1971, Clues to the origin of Archaean eugeosynclinal peridotites and the nature of serpintinization: Geol. Soc. Australia Spec. Pub., v. 3, p. 281–299.

Naldrett, A. J., and Mason, G. D., 1968, Contrasting Archaean ultramafic igneous bodies in Dundonald and Clergue Townships, Ontario: Canadian Jour. Earth Sci., v. 5, p. 111–145.

Nesbitt, R. W., 1971, Skeletal crystal forms in the ultramafic rocks of the Yilgarn Block, Western Australia: Evidence for an Archaean ultramafic liquid: Geol. Soc. Australia Spec. Pub., v. 3, p. 331–350.

Pyke, D. R., Naldrett, A. J., and Eckstrand, O. R., 1973, Archaean ultramafic flows in Munro Township, Ontario: Geol. Soc. America Bull., v. 84, p. 955–978.

Roeder, P. L., and Emslie, R. F., 1970, Olivine-liquid equilibrium: Contr. Mineralogy and Petrology, v. 29, p. 275–282.

Sobolev, N. V., 1972, Deep-seated inclusions in kimberlites and the problem of the composition of the earth's mantle: Canberra, Australian Natl. Univ., Geol. Dept. Pub., v. 210, p. 1–38 (translated from Russian by D. A. Brown).

Viljoen, M. J., and Viljoen, R. P., 1969a, The geology and geochemistry of the lower ultramafic unit of the Onverwacht Group and a proposed new class of igneous rock, *in* The Upper Mantle Project: Geol. Soc. South Africa Spec. Pub., v. 2, p. 55–85.

—— 1969b, Evidence for the existence of a mobile extrusive peridotitic magma from the Komati Formation of the Onverwacht Group, *in* The Upper Mantle Project: Geol. Soc. South Africa Spec. Pub., v. 2, p. 87–112.

—— 1969c, Evidence for the composition of the primitive mantle and its products of partial melting from a study of the rocks of the Barberton Mountain Land, *in* The Upper Mantle Project: Geol. Soc. South Africa Spec. Pub., v. 2, p. 275–295.

ACKNOWLEDGMENTS

Reviewed by A. E. Ringwood, E. Bence, and J.F.G. Wilkinson.

MANUSCRIPT RECEIVED OCT. 15, 1974

MANUSCRIPT ACCEPTED NOV. 4, 1974

A17

Genesis of Archean Peridotitic Magmas and Constraints on Archean Geothermal Gradients and Tectonics

D. H. Green
Research School of Earth Sciences
Australian National University
Canberra, A.C.T., Australia

ABSTRACT

The experimentally determined extrusion temperature (1650° ± 20°C) for Archean peridotitic komatiite magma implies diapirism of upper mantle peridotite from a depth of at least 200 km. Models of magma genesis are developed in which selective removal of garnet during ascent produces $CaO/Al_2O_3 > 1$ and heavy rare-earth element depletion in the resultant peridotitic or mafic extrusions. Magma genesis can be interpreted with a model of the Archean geotherm, lithosphere, and plate tectonics processes resembling the modern Earth, but this does not account for the distinctive preservation and character of Archean greenstone belts. A preferred model of a steeper Archean geotherm, thin lithosphere (≃50 km), and asthenosphere with approximately 5 percent melting does not allow eclogitization and subduction of basaltic oceanic crust, but it postulates scraping off of such crust against and between primitive sialic nucleii. This model may account for the distinctive characteristics of the Archean greenstone and "granite" terranes.

GENESIS OF PERIDOTITIC KOMATIITE MAGMA

The distinctive characteristics of the peridotic komatiite magma may be used to infer conditions of magma genesis and chemical composition of the Archean mantle. This paper is concerned primarily with the peridotitic komatiite sample 49J (Green, 1972a; Green and others, 1974) and the conditions of extrusion deduced from experimental study of this sample (Green and others, 1974). The magma represented by 49J is unlikely to represent complete melting of the Archean upper mantle because the only process capable of producing the required temperatures at or near the Earth's surface would be impact melting (to be distinguished from *impact-triggered diapirism* and consequent *partial* melting [Green, 1972a, 1972b]). The composition of 49J, if taken as the bulk composition of the upper mantle, is too iron-rich to be suitable as a source composition for modern basalt, although it is suitable in CaO, TiO_2, K_2O, and Na_2 contents (Ringwood, 1966; Green, 1973a, 1973b). The experimental studies on 49J, on pyrolite composition under dry conditions and with 0.2 percent H_2O (Green and Ringwood, 1970; Green, 1973a), on picrite (Green and Ringwood, 1967), and on peridotite (Ito and Kennedy, 1967) show that olivine will remain the liquidus phase of 49J to pressure >40 kb, that orthopyroxene will be the second phase to crystallize at high pressure, and that garnet will be the third phase to crystallize at pressure >40 kb (particularly if 49J contains ~0.2 percent H_2O).

The experimental data show either that the final stage of segregation of 49J peridotitic liquid from a more refractory parent left residual olivine crystals (Mg_{94}) or that the final crystals to dissolve in 49J liquid on route to the surface were olivine (Mg_{94}). Under these conditions, the high CaO/Al_2O_3 ratio of peridotitic komatiite and the slightly light rare earth enriched (relative to chondritic abundances) abundance pattern of the peridotitic komatiite (Whitford, in prep.) would most simply be interpreted as characteristic of the upper mantle source peridotite, that is, source peridotite = x percent 49J liquid + (100 − x) percent olivine (Mg_{94}). This is the simplest interpretation of the data and would indicate an Archean upper mantle composition with important differences from the modern upper mantle. However, the high CaO/Al_2O_3 ratio characteristic of peridotitic komatiite of the Barberton Mountain Land area, and particularly of the Badplaas and Geluk low-alumina basaltic komatiite magma (Viljoen and Viljoen, 1969a, 1969b, 1969c), could possibly be attributed to selective removal of pyrope-rich garnet during the ascent of the source peridotite diapir. This explanation would remove the necessity to postulate regional or temporal variations in the upper mantle source regions: these yield peridotitic liquids with high CaO/Al_2O_3 ratios in the South African Archean but $CaO/Al_2O_3 \sim 1$ for similar peridotitic liquids in Western Australia and Canada (Nesbitt, 1971; McCall and Leishman, 1971; Pyke and others, 1973). A stage of selective garnet removal in the magma genesis processes would be compatible with source regions for Archean magmas with $CaO/Al_2O_3 \leqslant 1$, as for the source regions for modern basalts (for example, pyrolite of Ringwood, 1966; Green, 1973b). The derivation of such a model pyrolite composition for the Archean, closely matching Ringwood's (1966) pyrolite, is illustrated in Table 1.

TABLE 1. DERIVATION OF MODEL PYROLITE COMPOSITION FOR THE ARCHEAN UPPER MANTLE

	Pyrolite*	Archean pyrolite
SiO_2	45.2	44.6
TiO_2	0.7	0.2
Al_2O_3	3.5	3.9
Cr_2O_3	0.4	0.5
Fe_2O_3	0.5	0.7
FeO	8.0	8.4
MnO	0.14	0.2
MgO	37.5	37.4
CaO	3.1	3.7
Na_2O	0.57	0.35
K_2O	0.13	0.12
NiO	0.2	0.3
$\frac{100\ Mg}{Mg + \Sigma Fe}$	88.9	88.0

Note: The model is derived from 65 percent peridotitic komatiite sample 49J (Green, 1972a) + 28 percent olivine ($Mg_{93.5}$) (Green and others, 1974) + 7 percent pyrope-almandine garnet (as experimentally crystallized from pyrolite).

* Ringwood, 1966.

PERIDOTITIC MAGMA GENESIS FROM MODEL PYROLITE UPPER MANTLE COMPOSITION

Dry Pyrolite Source

With an extrusion temperature of ~1650°C (Green and others, 1974), the peridotitic magma (sample 49J composition) must have ascended along a *P-T* cooling and decompression path with dT/dP greater than or equal to the adiabatic gradient, that is, >1°C/kb, approximately (Birch, 1952). If we consider a dry pyrolite source, then the intersection of an adiabatic ascent path for 49J magma and the pyrolite solidus would occur at ~45 kb (150 km) and 1700°C (Fig. 1). This model can be seen as a limiting model for the

Archean geothermal gradient and upper mantle, that is, a geothermal gradient much steeper (at >100 km) than modern estimates but assuming, for this model, a dry upper mantle. (This model must then imply continued post-Archean degassing of the deep mantle to produce the present situation in which the upper mantle contains ~ 0.1 to 0.2 percent H_2O.) The mantle lithosphere would have been thick with subsolidus conditions to depths of 150 km. For this model, 49J would begin as a peridotite diapir at the solidus and as that diapir ascended, the degree of partial melting would increase, successively eliminating clinopyroxene, garnet, and orthopyroxene as residual phases in equilibrium with the liquid. The diapir could pass through a stage (in the 40- to 45-kb pressure interval) where the degree of partial melting was quite high (⩾10 percent) and where olivine, orthopyroxene, and garnet crystals were entrained as a crystal + liquid mush. The density differential between garnet ($\rho = 3.7$) and olivine ($\rho = 3.3$), enstatite ($\rho = 3.3$), and liquid ($\rho < 3.0$), and suitable values for viscosity and shape factors could create flow conditions for the ascending diapir where olivine and enstatite were entrained but garnet settled through the rising diapir and, by its segregation, changed the bulk composition of the diapir (liquid + olivine + enstatite) in a direction of increasing CaO/Al_2O_3 ratio and toward depletion in heavy rare-earth elements ($Yb_{gas}/Yb_{liq} \simeq 5$; Kay and Gast, 1973). By removal of 5 to 10 percent garnet from the original pyrolite diapir and then by continued adiabatic and increasingly rapid ascent of the (liquid + olivine + enstatite) diapir, peridotitic magma units could reach the surface at 1650°C, with compositions characterized by saturation only with olivine (Mg_{94}) at the depth of final magma segregation from residual crystals. With the mechanism of genesis outlined, the Archean upper mantle at depths of ~150 km could have had a bulk composition closely matching the model pyrolite composition for modern upper mantle and with rare-earth content of chondritic relative proportions and at a level of twice-chondritic enrichment (Whitford, in prep.). Enrichment of twice-chondritic abundance levels has also been deduced as characteristic (for heavy rare-earth elements) of the modern upper mantle (Frey and Green, 1974). The suggestion of selective garnet removal accounts for the distinctive CaO/Al_2O_3 ratio of the Barberton rocks without postulating special characteristics of the mantle source. It also accounts qualitatively for the fractionated rare-earth element pattern (Whitford, in prep.), but the very low abundances and uncertainty of partition coefficients at ~1650°C, 45 kb, do not allow rigorous testing of the model by the rare-earth element data.

Pyrolite Source with 0.1 to 0.2 Percent Water

If the Archean upper mantle source region for sample 49J contained a small amount of water (Rubey, 1955; Ringwood, 1966), then the appropriate solidus would be that determined for pyrolite for ~0.2 percent H_2O (Green, 1973a), and melting would be characterized by a large temperature interval over which incipient melting (<10 percent) occurred (Figs. 1, 2). If the Archean geothermal gradient were similar to that (Fig. 2, geotherm I) suggested by Clark and Ringwood (1964), then the Archean lithosphere would be ~ 85 to 95 km thick (Green, 1972a, 1973a), but diapirs producing magma units extruded at 1650°C would have had origins at depths of at least 400 km in the upper mantle and must have moved from such depths to the surface so rapidly as to cause olivine and orthopyroxene entrainment to depths appropriate to 70 to 80 percent melting (Fig. 2). The contrast between this model of extremely deep tapping for peridotite diapirs in the Archean and the ascent of peridotite diapirs from depths of 120 to 130 km in the low-velocity zone, which yields the olivine tholeiite characteristic of *modern* mid-oceanic ridges, is illustrated in Figures 1 and 2.

If the Archean geothermal gradient was similar to that deduced by Clark and Ringwood (1964) to depths of ~90 km but was steeper at deeper levels (Fig. 2, geotherm II) then the Archean lithosphere would have resembled the modern oceanic lithosphere and would be 85 to 95 km thick overlying a low-velocity zone characterized by larger degrees of incipient melting

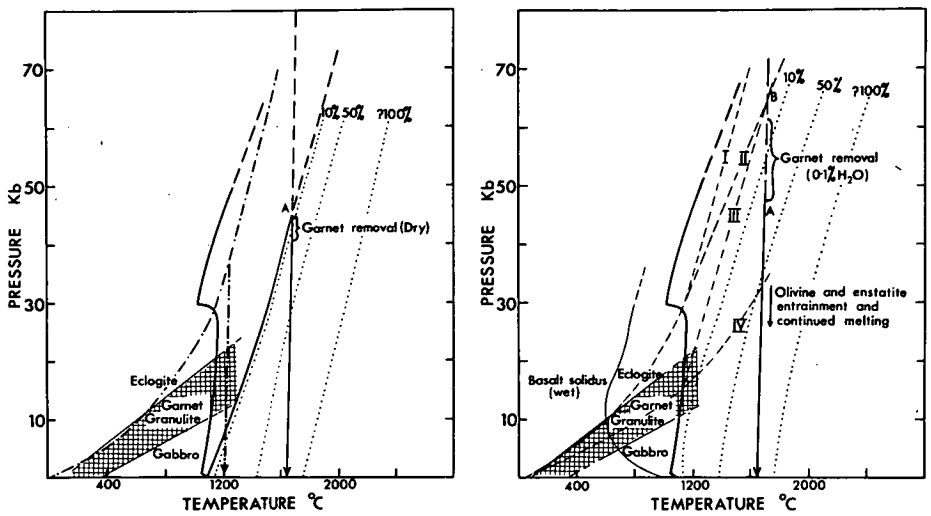

Figure 1 (left). Comparison of genesis of modern oceanic tholeiite volcanism with extrusion of magma units at ~1200°C and Archean peridotitic volcanism with extrusion at ~1200°C and Archean peridotitic volcanism with extrusion at 1650°C. _____ = Solidi for pyrolite under dry conditions and for pyrolite with 0.1 percent H_2O (Green and Ringwood, 1970; Green, 1973a). ..... = Approximate contours showing the degree of partial melting for *dry* pyrolite. _ . _ . _ = Modern geothermal gradient for ocean basins as deduced by Clark and Ringwood (1964 and suggested ascent path for modern diapirism from within low-velocity zone (>90 km depth) to yield magma units extruded at ~1200°C, separating from residual crystals at 10 to 20 kb. A = Minimum depth from which initiation of diapirism in a *dry* Archean mantle could lead to extrusion of peridotitic magma units at 1650°C. Hatched area = Transition of gabbro to eclogite (Green and Ringwood, 1972).

Figure 2 (right). Comparison of alternative geothermal gradients for the Archean with their implications for magma genesis and tectonics. _____ = Solidus for pyrolite containing 0.1 to 0.2 percent H_2O. ..... = Approximate contours showing degree of partial melting for pyrolite + 0.1 percent H_2O. _____ = Solidus for basalt for $P_{H_2O} = T_{total}$ (Lambert and Wyllie, 1970). – – – = Model geothermal gradients for Archean crust and mantle. I = Modern ocean basin regions (from Clark and Ringwood, 1964). II = Model geotherm similar to modern geotherm to depths of ~90 km (that is, subsolidus to 90 km, giving lithosphere of ~90 km thickness) but steeper at deeper levels to intersect sample 49J adiabatic ascent path at ~220 km (B). III = Model geotherm, much steeper than modern geotherm in crust and upper mantle, leading to intersection with pyrolite solidus at ~15 kb (~50 km). Model geotherm is then constrained to be near ~5 percent melting curve for pyrolite to intersect sample 49J adiabatic ascent path at B. IV = Steep geotherm continued to deep levels illustrating instability of situation with high degrees of melting at very shallow depths.

than are envisaged for the modern low-velocity zone (Green, 1970, 1971, 1973a). A geothermal gradient of that or lower value means that basaltic rocks within the crust and lithosphere cool to enter the eclogite stability field. Thus a primitive Archean basaltic crust, like modern oceanic crust, would be potentially gravitationally unstable with an eclogite layer ($\rho \simeq 3.5$) overlying peridotite ($\rho = 3.3$). If the basaltic crust reacted to eclogite, it could sink into the upper mantle, probably initiating subduction processes as suggested for modern plate tectonics (Ringwood and Green, 1966; Ringwood, 1969; Green, 1972a). The model geotherm II intersects the adiabatic ascent path for peridotitic komatiite magma (sample 49J) at ~230 km, 1720°C (Fig. 2, B). These conditions are within the partial melting interval for pyrolite with ~0.1 percent H_2O, and an ascending pyrolite diapir would initially consist of <5 percent melt + olivine, orthopyroxene, garnet, and clinopyroxene. Settling out of garnet from the rising diapir could occur in the manner previously described for dry pyrolite, leading to the distinctively high CaO/Al_2O_3 ratio and heavy rare-earth element depletion (1.2 X chondrites) (Whitford, in prep.) of the peridotitic komatiite.

Several authors (Brooks and Hart, 1972, 1974) have suggested that geothermal gradients, even in the crust, were much steeper in the Archean earth. Model geotherms III and IV (Fig. 2) illustrate this suggestion. For geotherms III and IV, the lithosphere would be ~50 km thick, but the geotherm lies entirely within the garnet granulite stability field and eclogite would not form from basaltic rocks along this geotherm (Green and Ringwood, 1972). Thus basaltic crust overlying peridotitic upper mantle would remain gravitationally stable as it cooled with granulite assemblages ($\rho = 3.0$ to 3.2) overlying peridotite, and there would be no tendency for basaltic oceanic crust to sink in the mantle, thus triggering the subduction process. The modern concepts of plate tectonics could not be directly applied in the Archean if geothermal gradients were as high as III or IV, and in particular, the characteristic removal and further geochemical processing (in the upper mantle) of oceanic crust in subduction zones would not operate if the basalt crust did not cool and transform to eclogite at deeper levels (Ringwood, 1969). In these circumstances, the familiar patterns of island-arc and Andean volcanism above subduction zones would be profoundly modified in the Archean. Tectonics at that time might have been characterized by sialic continental nucleii and thin (50 km) lithosphere beneath both continental and oceanic (basaltic crust) regions. The instability inherent in the existence of the partially molten zone beneath the peridotite lithosphere and the very steep geothermal gradient could lead to thermally activated convective overturns of the lithosphere, but these would not involve the substantial return of areas of basaltic oceanic crust to the upper mantle as eclogite. Basaltic crust would be folded against and between continental nucleii as it was scraped off descending peridotite in a manner analogous to that of the sedimentary horizons during subduction of modern oceanic crust. If folded sequences of thickness ~25 km develop, then they may partially melt (deep crustal melting of amphibolites), leading probably to granodioritic and granitic intrusive and associated volcanism.

In Figure 2, model geotherm IV rises steeply above the peridotite solidus and intersects the adiabatic ascent path for peridotitic komatiite magma at ~100 km, 1680°C, implying that if such a geothermal gradient were possible, the source of peridotitic komatiite magma could have been as shallow as 100 km (that is, similar to modern magmas). This geotherm, however, passes through the 10 percent melting curve for pyrolite + 0.1 percent H_2O) at ~70 km, and the 30 percent melting curve at ~80 km. This is an impossible situation because, for greater than 30 percent melting (and probably for lower degrees of melting), dynamic processes of segregation of magma from crystals must occur rapidly in the Earth's gravitational field. Geotherm IV cannot represent a normal Archean geotherm but could be a short-lived transitory geotherm during diapirism.

Geotherm III is drawn so that immediately below the lithosphere there is an increase in degree of melting from the solidus to ~5 percent melting. The geotherm follows the ~5 percent melting curve to intersect the adiabatic ascent path for sample 49J at ~230 km, 1720°C (Fig. 2, B). This situation, with <5 percent melting, is considered to yield a lithosphere and asthenosphere with sufficient long-term stability for the processes of episodic and cyclic volcanism, sedimentation, and orogeny observed in Archean terranes. It would have much less stability, both in time and in regional extent, than the modern Earth. Diapiric ascent from ~230 km, 1720°C, leading to extrusion of 49J magma at the surface, would follow the path previously outlined with the possible selective depletion of garnet and entrainment of olivine and enstatite as described.

MODELS FOR ARCHEAN TECTONICS

Geotherms II and III serve to illustrate two alternative interpretations of Archean tectonics. Geotherm II would permit a pattern of lithosphere, asthenosphere, magmatism, and plate tectonics similar to that in the modern Earth. Geotherm III requires a much thinner lithosphere and very different behavior of lithospheric plates with no opportunity for subduction of basaltic crust into the upper mantle. In addition, geotherm III precludes the generation of highly undersaturated basaltic magma units such as olivine nephelinite, olivine melilitite, or kimberlite (Green, 1970, 1973b) in the Archean. These magma units require degrees of partial melting and temperatures at appropriate pressures which fall below geotherm III. Both geotherms II and III require initiation of diapiric uprise of peridotite from depths in excess of 200 km. In addition, diapiric uprise must have been very rapid to prevent magma segregation from residual olivine and enstatite when the degree of partial melting was ~30 percent and to entrain these phases to shallow depths and ~70 percent melting. The rate of uprise must have been similar to that of modern basalt containing lherzolite inclusions and high-pressure xenocrysts, but unlike this modern basalt, the Archean peridotitic magma did not contain high H_2O and CO_2 contents and did not erupt explosively from shallow depths. It is, in fact, a characteristic of modern tholeiitic basalt (low water content and derived by relatively high degrees of partial melting [~30 percent] of the mantle) that it rarely moves sufficiently rapidly to the surface to transport lherzolite xenoliths or xenocrysts and, on the contrary, usually reaches the surface having already precipitated some olivine above the depth of magma segregation. The rate of ascent of the peridotitic komatiite diapirs and magma units, the absence of high volatile content, and the large volume of erupted magma sets this magma apart from modern tholeiitic picrite or undersaturated basanite. Elsewhere (Green, 1972a, 1972b) I have suggested that major impacts on the Earth's surface 3 to 4 X 10^9 yr ago would cause large pressure drops due to unloading and could create conditions for rapid upwelling of impact-triggered partial melts from the deep mantle. If further work substantiates the presence of equally high-tempera-

ture peridotite magma flows as young as or younger than 2.7×10^9 yr (possibly Western Australia) and establishes that episodes of ultramafic volcanism are repeated several times and interbedded with major sedimentary units, then it must be inferred that they originate entirely by causes within the Earth and are not a response to unique impact events.

The very rapid ascent and the deep source for the peridotitic lava flows imply, if we seek analogies with modern mid-oceanic-ridge or island-chain tholeiitic volcanism, very rapid separation of the lithospheric plates and much deeper convective motion than at modern tholeiitic volcanic centers. Such differences in the Archean may, possibly, be entirely attributable to high Archean geothermal gradients, but the limiting constraints on rate of ascent of peridotite diapirs are more probably to be found in the rate at which overlying, more viscous asthenosphere and lithosphere can be fractured and laterally displaced at Archean spreading centers.

CONCLUSIONS

Archean ultramafic magma units were extruded at temperatures of at least 1650° ± 20°C. A minimum depth of 200 km in the Archean upper mantle is required for mantle diapirism leading to such ultramafic extrusions. The diapiric upwelling and magma ascent leading to ultramafic extrusions were much more rapid and from deeper levels than those for modern basaltic or picritic volcanism. Models are developed in which peridotite diapirs ascending on adiabatic *P-T* paths from ~200 km pass through a stage of 10 to 20 percent melting in which garnet ($\rho = 3.7$) is selectively left behind and olivine and enstatite ($\rho = 3.3$) are entrained to higher levels and higher degrees (~70 percent) of partial melting. Depletion in garnet yields the $CaO/Al_2O_3 > 1$ and depletion in heavy rare-earth elements (1.2 × chondrite) observed in at least some peridotitic extrusions. Constraints on the Archean geothermal gradient suggested by the distinctive volcanism yield alternative models. One model yields a lithosphere and permits models of plate tectonics similar to the modern Earth but with a steeper geothermal gradient below ~100 km. The second and preferred model suggests a steep geothermal gradient in the lithosphere—a thin (~50 km) lithosphere over an asthenosphere with ~5 percent melting from depths of ~60 km to beyond 200 km. This model has important implications in that any areas of primitive basaltic crust cannot be altered to eclogite (unstable along the high geotherm) and thus cannot develop major gravitational instability of eclogite ($\rho = 3.5$). Thus, basaltic crust is unlikely to be subducted into the upper mantle for further geochemical processing (island-arc volcanism) but instead would be scraped off descending peridotitic lithosphere and folded against or between sialic continental nucleii. Deep crustal melting of such basaltic (+ ultramafic) piles leads to further differentiation of the crust with intrusion of the folded greenstone sequence by granodioritic and granitic magma units. This model may account for the distinctive characteristics of Archean granite/greenstone terranes with local preservation of thick mafic and ultramafic "primitive crust" sequences in largely unmetamorphosed condition. In contrast, modern plate tectonics models involve subduction and removal of such oceanic crustal sequences with only local fragmentary preservation (ophiolite sequences).

REFERENCES CITED

Birch, F., 1952, Elasticity and constitution of the Earth's interior: Jour. Geophys. Research, v. 57, p. 227-286.

Brooks, C., and Hart, S. R., 1972, An extrusive basaltic komatiite from a Canadian metavolcanic belt: Canadian Jour. Earth Sci., v. 9, p. 1250-1253.

—— 1974, On the significance of komatiite: Geology, v. 2, p. 107-110.

Clark, S. P., and Ringwood, A. E., 1964, Density distribution and constitution of the mantle: Rev. Geophysics, v. 2, p. 35-88.

Frey, F. A., and Green, D. H., 1974, The mineralogy and origin of lherzolite inclusions in Victorian basanites: Geochim. et Cosmochim. Acta, v. 38, p. 1023-1060.

Green, D. H., 1970, The origin of basaltic and nephelinitic magmas: Leicester Lit. and Philos. Soc. Trans., v. 64, p. 28-54.

—— 1971, Composition of basaltic magmas as indicators of conditions of origin: Application to oceanic volcanism: Royal Soc. London Philos. Trans., ser. A, v. 268, p. 707-725.

—— 1972a, Magmatic activity as the major process in the chemical evolution of the Earth's crust and upper mantle: Tectonophysics, v. 13, p. 47-71.

—— 1972b, Archaean greenstone belts may include terrestrial equivalents of lunar maria?: Earth and Planetary Sci. Letters, v. 15, p. 263-270.

—— 1973a, Experimental melting studies on a model upper mantle composition at high pressure under water-saturated and water-undersaturated conditions: Earth and Planetary Sci. Letters, v. 19, p. 37-53.

—— 1973b, Conditions of melting of basanite magma from garnet peridotite: Earth and Planetary Sci. Letters, v. 17, p. 456-465.

Green, D. H., and Ringwood, A. E., 1967, The genesis of basaltic magmas: Contr. Mineralogy and Petrology, v. 15, p. 103-190.

—— 1970, Mineralogy of peridotitic compositions under upper mantle conditions: Physics Earth and Planetary Interiors, v. 3, p. 359-371.

—— 1972, A comparison of recent experimental data on the gabbro-garnet granulite-eclogite transition: Jour. Geology, v. 80, p. 277-288.

Green, D. H., Nicholls, I. A., Viljoen, M. J., and Viljoen, R. P., 1974, Experimental demonstration of the existence of peridotite liquids in earliest Archaean magmatism: Geology, v. 3, p. 11-14.

Ito, K., and Kennedy, G. C., 1967, Melting and phase relationships in a natural peridotite to 40 kilobars: Am. Jour. Sci., v. 265, p. 211-217.

Kay, R. W., and Gast, P. W., 1973, The rare earth content and origin of alkali-rich basalts: Jour. Geology, v. 81, p. 653-682.

Lambert, I. B., and Wyllie, P. J., 1970, Low-velocity zone of the Earth's mantle: Incipient melting caused by water: Science, v. 169, p. 764-766.

McCall, G.J.H., and Leishman, J., 1971, Clues to the origin of Archaean eugeosynclinal peridotites and the nature of serpentinization: Geol. Soc. Australia Spec. Pub., v. 3, p. 281-299.

Nesbitt, R. W., 1971, Skeletal crystal forms in the ultramafic rocks of the Yilgarn Block, Western Australia: Evidence for an Archaean ultramafic liquid: Geol. Soc. Australia Spec. Pub., v. 3, p. 331-350.

Pyke, D. R., Naldrett, A. J., and Eckstrand, O. R., 1973, Archean ultramafic flows in Munro Township, Ontario: Geol. Soc. America Bull., v. 84, p. 955-978.

Ringwood, A. E., 1966, The chemical composition and origin of the Earth, *in* Hurley, P. M., ed., Advances in Earth science: Cambridge, Massachusetts Inst. Technology Press, p. 287-356.

—— 1969, Composition and evolution of the upper mantle, *in* Hart, P. J., ed., The Earth's crust and upper mantle: Am. Geophys. Union, Geophys. Mon. 13, p. 1-17.

Ringwood, A. E., and Green, D. H., 1966, An experimental study of the gabbro to eclogite transformation and some geophysical consequences: Tectonophysics, v. 3, p. 383-427.

Rubey, W. W., 1955, Development of the hydrosphere and atmosphere with special reference to the probable composition of the early atmosphere, *in* Poldervaart, A., ed., Crust of the Earth: Geol. Soc. America Spec. Paper 62, p. 631-650.

Viljoen, M. J., and Viljoen, R. P., 1969a, The geology and geochemistry of the lower ultramafic unit of the Onverwacht Group and a proposed new class of igneous rock, *in* The Upper Mantle Project: Geol Soc. South Africa Spec. Pub., v. 2, p. 55-85.

—— 1969b, Evidence for the existence of a mobile extrusive peridotitic magma from the Komati Formation of the Onverwacht Group, *in* The Upper Mantle Project: Geol. Soc. South Africa Spec. Pub., v. 2, p. 87-112.

—— 1969c, Evidence for the composition of the primitive mantle and its products of partial melting from a study of the rocks of the Barberton Mountain Land, *in* The Upper Mantle Project: Geol. Soc. South Africa Spec. Pub., v. 2, p. 275-295.

ACKNOWLEDGMENTS

Reviewed by A. E. Ringwood, E. Bence, and J.F.G. Wilkinson.

MANUSCRIPT RECEIVED OCT. 15, 1974.

MANUSCRIPT ACCEPTED NOV. 4, 1974.

A18

[AMERICAN JOURNAL OF SCIENCE, VOL. 275, APRIL, 1975, P. 461-469]

STRONTIUM ISOTOPE GEOCHEMISTRY OF LHERZOLITE INCLUSIONS AND HOST BASALTIC ROCKS, VICTORIA, AUSTRALIA

E. JULIUS DASCH* and DAVID H. GREEN**

ABSTRACT. Strontium isotope composition (Sr^{87}/Sr^{86}) at time of crystallization of selected, Late Pliocene-Pleistocene nepheline hawaiites and basanites of the Newer Volcanics of Victoria ranges from 0.7038 to 0.7045. Coarse-grained lherzolite inclusions collected from scoria cones in the province have measured whole-rock Sr^{87}/Sr^{86} ratios with a much wider range from 0.7027 to 0.7107. Data for separated minerals of lherzolite inclusions show that the inclusions preserve relict isotopic distributions, differing from that of the host magma, and that the minerals (or at least olivine) do not form closed systems. Collectively these analyses: attest to the accidental nature of the inclusions in the basaltic rocks; indicate relict age and non-equilibrium conditions for component lherzolite minerals; and show that the inclusions, many of which are at least casually similar, probably are not derived from a temporally or geochemically uniform substrate.

INTRODUCTION

The isotopic study of lherzolite inclusions (with mineralogy indicative of an origin deep within the crust or upper mantle) in alkalic basalts is interesting from several viewpoints: (1) the inclusions may be cognate or accidental with respect to host volcanic rocks, (2) minerals from the inclusions may yield internal ages related to mantle events, (3) analyses of a suite of inclusions from a widespread volcanic province may indicate the degree of geographic or vertical homogeneity of the provenance for the inclusions.

Typical lherzolite inclusions contain olivine ($>Fo_{88}$), enstatite, chrome diopside, and chromian spinel. Previous work on strontium isotopes (Leggo and Hutchinson, 1968; Peterman, Carmichael, and Smith, 1970; Stueber, 1969; Stueber and Ikramuddin, 1974; Dasch and Green, 1972), on lead producing elements (Green, Morgan, and Heier, 1968; Kleeman, Green, and Lovering, 1969), on lead isotopes (Cooper and Green, 1969), on rare earth elements (Frey and Green, 1974), and on Victorian and other lherzolites are consistent with or can only be explained by an accidental origin, in relation to their host basalt, for these inclusions.

GEOLOGICAL SETTING AND SAMPLE DETAILS

The lherzolite nodules were collected from scoria cones of the Pleistocene to Recent, Newer Volcanics of western Victoria and southeastern South Australia (fig. 1). The host basalt samples were chosen to include examples of the two distinctive lherzolite-bearing magmas occurring in the province (Irving, ms; Irving and Green, in preparation). Three samples are basanite (from Mt. Porndon and Mt. Leura); one is nepheline hawaiite (2154) from Mt. Noorat, associated with basanites; and two are nepheline mugearite (Anakies) characterizing the second main lherzolite-bearing basalt type in the province.

* Department of Geology, Oregon State University, Corvallis, Oregon 97331 USA
** Research School of Earth Sciences, Australian National University, Canberra, A.C.T., Australia

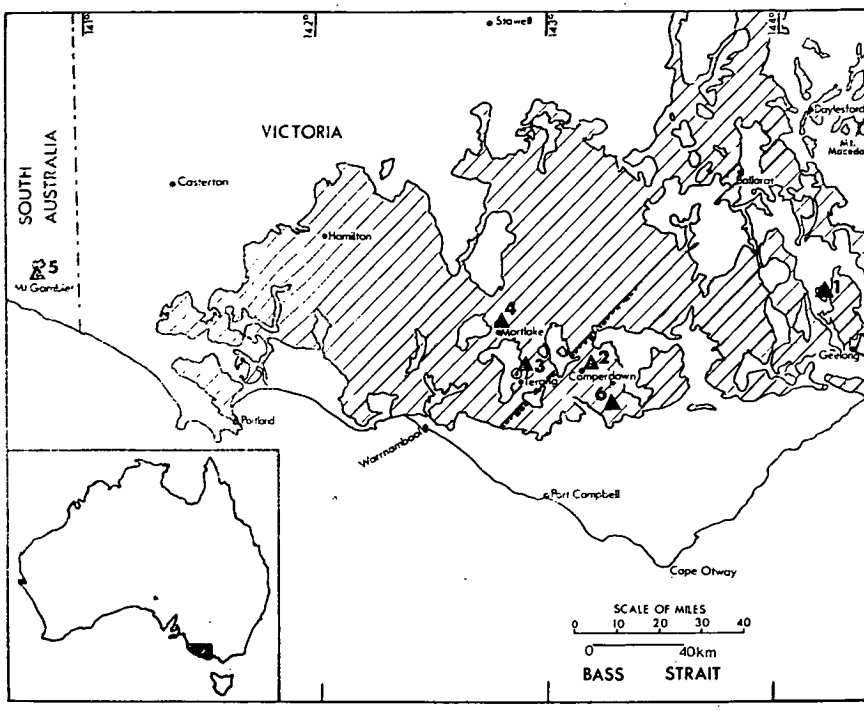

Fig. 1. Locality map with shaded area showing the extent of lava flows of the Newer Volcanics of western Victoria. Sample localities numbered as follows: 1. The Anakies; 2. Mt. Leura; 3. Mt. Noorat; 4. Mt. Shadwell; 5. Mt. Gambier; 6. Mt. Porndon.

The lherzolite samples selected were all large (>20 cm diameter) and free of staining or alteration by fumarolic activity through the scoria. The samples included four (2905, 2639, 2730, and 2736 that had previously been studied for Pb isotopes (Cooper and Green, 1969) but do not include any of those samples previously studied for K, U, Th, or rare earth elements (Frey and Green, 1974; Green, Morgan, and Heier, 1968; Kleeman, Green, and Lovering, 1969). Brief descriptions of the samples are given below, based on analyses of thin sections.

2635 (Mt. Leura).—Coarse lherzolite with olivine > orthopyroxene > clinopyroxene >> orange brown spinel. No development of patches of glass nor alteration of clinopyroxene. No accessory mica, amphibole, or apatite observed.

2639 (Mt. Leura).—Coarse lherzolite with olivine and enstatite as major phases, and clinopyroxene I[1] and brown spinel I as minor phases. Patches of glass + olivine II + clinopyroxene II + spinel II developed

[1] The designation of I, Ia, II follows the usage of Kleeman, Green, and Lovering (1969) and Frey and Green (1974) and imply "primary", "modified" but not "recrystallized", and "recrystallized" phases respectively.

strongly, in some cases, around skeletal spinel but also not obviously associated with spinel. Strong development of clinopyroxene Ia at edges of primary clinopyroxene. Very rare accessory apatite I and rare orange brown hornblende I inclusions within some large orthopyroxene. It is probable that the glass-rich patches derive from incongruent melting of hornblende.

2655 (Mt. Leura).—Coarse lherzolite with olivine > orthopyroxene > clinopyroxene > deep orange spinel. Very rare accessory phlogopite in that part of the sample crushed for whole-rock analysis — but this phase was abundant in and was separated from, a small patch within the xenolith. In this region alteration of phlogopite to patches of glass + olivine II + spinel II was present in varying degree.

2769 (Mt. Leura).—Coarse lherzolite with olivine > enstatite > clinopyroxene > green-brown spinel. Minor development of glass + clinopyroxene II + spinel II + olivine II at some contacts between spinel I and clinopyroxene I but also in isolated patches suggestive of alteration of an earlier accessory mineral.

2905 (Mt. Noorat).—Coarse lherzolite with olivine > enstatite > clinopyroxene > pale green-brown spinel. Spinel is more abundant (~3 percent) in this inclusion than in most of the other nodules. Minor marginal recrystallization of clinopyroxene I to Ia; very rare glass patches with euhedral olivine II; clinopyroxene II and spinel II with distribution of such patches suggesting replacement of an earlier phase such as amphibole or phlogopite (Frey and Green, 1974).

2729, 2730, 2736 (Mt. Gambier).—All three samples are from Mt. Gambier and, although from separate inclusions dispersed within a volcanic breccia, are of a distinctive lherzolite type, differing in hand specimen from the coarser-grained "normal" lherzolites described above and also occurring in the same breccia (for example, 2728 (Frey and Green, 1974; Kleeman, Green, and Lovering, 1969)). These samples are of medium-grained lherzolite with a strong foliation defined by schlieren and lenticular grains of deep brown spinel and pyroxenes. There is no distinct mineralogical banding, and olivine > enstatite > clinopyroxene > spinel. There is no melting or alteration of clinopyroxene I or spinel I, but there are rare, inhomogeneously distributed, very small patches of olivine II + spinel II + feldspar II + glass which probably replace preexisting mica (or amphibole?).

METHODS

Preparation and analyses of all the rocks and minerals reported here were accomplished in laboratories of the Australian National University. Based on unpublished chemical analyses (Irving and Green, in preparation), six samples of host volcanic rocks were selected to cover most of the observed chemical range. For these rocks, which may be classed as basanite, nepheline hawaiite, or nepheline mugearite, SiO_2 varies from

45.3 to 50.3 percent, and K_2O from 1.10 to 2.64 percent (Irving, ms; Irving and Green, in preparation). From several lines of evidence, the rocks fall into at least two chemical groups (Irving, ms; Irving and Green, in preparation) typified by the basanites and nepheline mugearites respectively. Lherzolite inclusions were collected from several of the prominent scoriaceous cones present in the district. The selection was made on the basis of varying mineralogy and lack of distinct metamorphism or of more superficial alteration. One of the typical, very coarse-grained inclusions (2905) was chosen for mineral analyses.

For the basalts and lherzolites, altered and contaminated selvages were sawed off and discarded, and the sawed surfaces were ground and washed prior to crushing and splitting for whole-sample analysis. Sample 2905 was handled with particular care; after crushing and splitting a total-rock sample, minerals were separated magnetically. The final purification of the mineral separates was carried out by hand-picking under a microscope; mineral separates were better than 99 percent pure.

Concentrations of elements listed in table 1 for basalts were determined by X-ray fluorescence, following the procedure of Norrish and Hutton (1969) in which absorption coefficients are measured directly. Sample dissolution for concentrations of Rb, Sr, and Sr isotope composition (tables 2 and 3) took place in the Lunar Sample Laboratory at Australian National University; typical blanks during the study were about 3 Ng Rb and about 2 Ng Sr. The elements were separated by standard techniques of dissolution and ion exchange. The blanks are low, relative to Rb and Sr abundance in the rocks and minerals studied, except for Rb in olivine. Corrections for blanks have been made for the mineral data of table 3 and figure 2.

Isotope ratios for Rb and Sr concentrations were measured on a 6 inch radius-of-curvature, Nier-type mass spectrometer. Strontium isotope data from unspiked aliquots of sample were collected with a 12 inch radius-of-curvature, solid-source instrument in which a Hall effect field controller and anlogue-to-digital converter were employed. The data for tables 1 to 3 record averages from duplicate mass spectrometer runs. The

TABLE 1

Analytical data for whole-rock samples of basalt, New Volcanics, Victoria. Concentrations by X-ray fluorescence. Sr^{87}/Sr^{86} ratios (average of duplicate analyses) normalized to $Sr^{88}/Sr^{86} = 8.3752$

Sample	Location	K%	Rb,ppm	K/Rb	Sr,ppm	Rb^{87}/Sr^{86}	Sr^{87}/Sr^{86}
2101	Anakies	2.36	69.0	342	942	0.211	0.7041
2102	Anakies	2.38	71.5	332	804	0.257	0.7038
2128	Mt. Porndon	1.64	38.3	428	813	0.136	0.7045
2130	Mt. Porndon	1.69	40.3	419	805	0.144	0.7043
2140	Mt. Leura	1.80	42.8	421	925	0.134	0.7043
2154	Mt. Noorat	1.49	41.4	360	937	0.128	0.7045

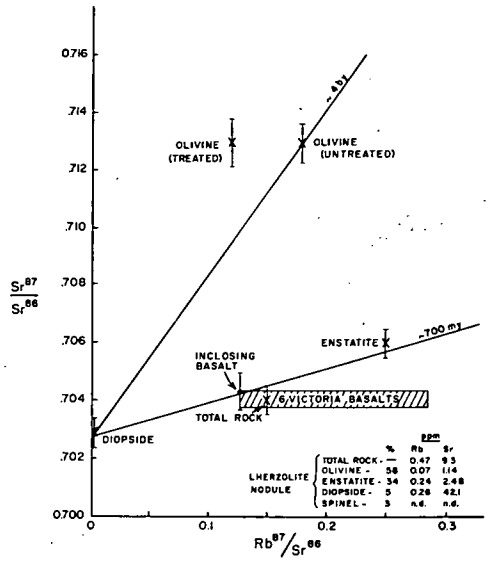

Fig. 2. Sr^{87}/Sr^{86} versus Rb^{87}/Sr^{86} for 6 samples of lherzolite-bearing basaltic rocks, Victoria, Australia.

averaged data of table 3 additionally involves complete duplicate chemistry of phases for 2905, with replicate (in most cases triplicate) runs on individual samples. The analytical uncertainties for the reported Sr^{87}/Sr^{86} ratios (normalized to $Sr^{88}/Sr^{86} = 8.3752$) are about ± 0.0002 (2σ). Several analysis of the Eimer and Amend strontium isotope standard, measured during the period of time when the reported data were obtained, average about 0.7080.

RESULTS AND DISCUSSION

The elemental data for whole-rock samples of basalts (table 1; fig. 1) confirm the petrographic and major element groups, the nepheline mugearites having high K_2O, high Rb, and low K/Rb ratios (samples 2101,

TABLE 2

Analytical data for whole-rock samples of lherzolite nodules, Newer Volcanics, Victoria, Australia. Concentrations by isotope dilution. Averaged Sr^{87}/Sr^{86} ratios normalized to $Sr^{88}/Sr^{86} = 8.3752$

Sample	Rb,ppm	Sr,ppm	Rb^{87}/Sr^{86}	Sr^{87}/Sr^{86}
2905	0.473	9.216	0.148	0.7040
2655	0.428	8.022	0.149	0.7027
2635	12.26	13.95	3.571	0.7062
2639	4.55	45.8	0.287	0.7071
2729	2.34	7.83	0.865	0.7077
2730	2.67	7.37	1.046	0.7093
2736	5.77	7.06	2.360	0.7107
2769	4.83	25.0	0.559	0.7057

TABLE 3

Averaged analytical data for separated minerals and whole-rock sample of lherzolite nodule 2905. Concentrations by isotope dilution. Sr^{87}/Sr^{86} ratios normalized to $Sr^{88}/Sr^{86} = 8.3752$. Data are averages for replicate sets of analyses, including duplicate chemistry (see text). n.d. = not determined

Phase	Approximate percent of nodule	Rb,ppm	Sr,ppm	Rb^{87}/Sr^{86}	Sr^{87}/Sr^{86}
Total rock	100	0.473	9.216	0.148	0.7040
Olivine (untreated)	58	0.072	1.135	0.184	0.7130
(acid-treated)	—	0.050	1.130	0.120	0.7130
Enstatite	34	0.240	2.482	0.250	0.7060
Diopside	5	0.255	42.110	0.015	0.7029
Spinel	3	n.d.	n.d.	n.d.	n.d.
Host basanite	—	41.4	937	0.127	0.7045

2102) relative to the basanites (2128, 2130, 2140). The nepheline hawaiite (2154) has a Rb content very similar to the basanites, but its low K content results in a K/Rb ratio intermediate between the two groups.

The Sr^{87}/Sr^{86} ratios of basaltic host rocks (measured ratios essentially are ratios at time of rock crystallization owing to the low Rb/Sr ratios and young ages of the rocks) range rather narrowly from 0.7038 to 0.7045, although the least and most radiogenic basalts have distinguishable isotopic compositions. The two least radiogenic rocks (2101, 2102) are also the most alkalic and have the highest Rb^{87}/Sr^{86} ratios (table 1).

On an isochron diagram, the Rb-Sr data define a negative trend (fig. 1). Although the trend is based on few data (essentially three point groups), it is of interest to speculate on the significance of negative trends in general. There are limited data available on correlation of Rb/Sr ratios with initial (time of crystalization) Sr^{87}/Sr^{86} ratios from young, supposedly cogenetic basaltic rocks. Where initial, non-zero slopes have been reported, the slopes most commonly are positive. Positive slopes (with built in, positive Rb-Sr ages) may reasonably result from partial melting processes, from contamination by wallrock, or, perhaps more simply, from incomplete isotopic homogenization of a complexly generated magma. Negative slopes for supposedly comagmatic rocks are more difficult to understand, though they also may result from mixing of magmas with different characteristics. Accounting for such a trend by varying degrees of wallrock reaction requires either that a rather siliceous basaltic magma acquires radiogenic strontium, but in the process becomes desilicified, or that a less siliceous basaltic magma acquires less radiogenic strontium along with more siliceous and alkalic components. Alternatively of course, such a trend may indicate that the basalts are not cogenetic.

Data for whole-rock samples of lherzolite inclusions (table 2) show wide ranges for Rb and Sr concentrations and for Sr^{87}/Sr^{86} ratios. We suspect that this variation is largely a consequence of variation in original

minor phases such as amphibole and phlogopite. The three petrographically distinctive lherzolites from Mt. Gambier display a discernible correlation of Rb/Sr and $^{87}Sr/^{86}Sr$ ratios suggesting that careful work on such selected nodules from a single locality may define an isochron relation for parts of the upper mantle. Lack of agreement between Sr^{87}/Sr^{86} ratios of the basalts and most of the lherzolites indicates that the lherzolite nodules were accidentally included in the melt prior to eruption, a conclusion also reached from other work on these and other lherzolite inclusions. The more radiogeneic inclusions point to at least local regions of the asthenosphere more enriched in Sr^{87} than generally is assumed for the lower crust or upper mantle.

Analytical data for separated minerals of lherzolite inclusion 2905 are listed in table 3 and plotted on an isochron diagram in figure 2. Spinel, constituting only ~ 3 percent of the rock (table 3) and containing very small amounts of Rb and Sr, was not analyzed. Of the remaining variables (considering total-rock data as an independent variable in fig. 3), the data define a positive slope except for olivine. The trend is proportional to an age of about 700 m.y., but this number may not have rational significance. Olivine clearly is out of equilibrium with the remaining phases that were measured (similar results have been obtained from lherzolite nodules by Peterman, Carmichael, and Smith (1970), and by Stueber and Ikramuddin (1974).

The distribution of points in figure 2 can result from a variety of processes. Late-stage contamination by exchange with the host basaltic magma is not supported by the data, and the analyses provide evidence for retention of a relict age for the mineral system. Assuming the "isochron" has temporal significance, the age of 700 m.y. could represent a metamorphic age of the lherzolite source or a time of most recent partial

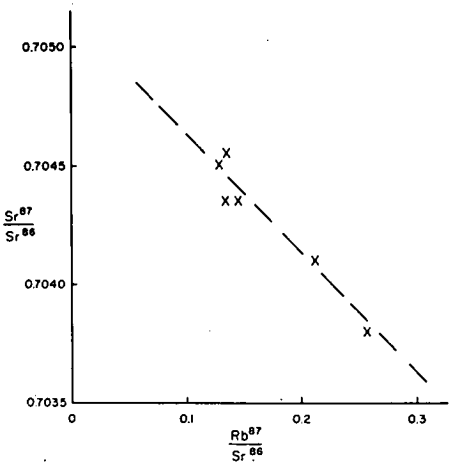

Fig. 3. Sr^{87}/Sr^{86} versus Rb^{87}/Sr^{86} for a whole-rock sample and separated minerals from lherzolite nodule 2905.

melting and magma extraction. It may be noted that the geological evolution of southeastern Australia and Tasmania includes a late Precambrian and Cambrian eugeosynclinal (? island arc) and ophiolite stage, probably applicable to the sub-basalt basement. Assuming an initial Sr^{87}/Sr^{86} ratio equal to that measured for diopside yields an approximate 4 b.y. age for the olivine, it is more likely that the olivine has accepted radiogenic Sr at some time, possibly equilibrating with phlogopite or a grain boundary phase. Unless mineral-selective isotopic homogenization is involved perhaps the most reasonable explanation for the high Sr^{87}/Sr^{86} value (but rather low strontium abundance) for olivine is that it has been contaminated by radiogenic strontium. Points representing the acid treated and untreated olivine (fig. 2) show that although rubidium may reside in intergranular or otherwise easily leached sites, the Sr abundance and isotope composition is a function of the olivine crystals as a whole. It is apparent from the data of table 3 that there is a mass balance discrepancy for rubidium (and probably also for strontium if the estimate of diopside abundance is near to being correct); more rubidium is found in the total rock than in any of the mineral phases. This imbalance indicates that much of the rubidium is in fact located in accessory minerals such as phlogopite, amphibole, or their partial melting products or is dispersed along grain boundaries. These materials, which likely have high Rb-Sr ratios and will in time yield very radiogenic strontium, may be a source for radiogenic contamination of continguous minerals, particularly olivine, perhaps during a late recrystallization or reheating.

ACKNOWLEDGMENTS

We appreciate the preparation and laboratory assistance of Richard Rudowski and M. J. Vernon, and we have benefitted from discussions with W. Compston, A. J. Irving, E. Essene, and A. M. Stueber. Dasch acknowledges the support of a Fulbright Fellowship tenured at Australian National University and an Australian National University Visiting Research Fellowship.

REFERENCES

Cooper, J. A., and Green, D. H., 1969, Lead isotope measurements on lherzolite inclusions and host basanites from western Victoria, Australia: Earth Planetary Sci. Letters, v. 6, p. 69-76.

Dasch, E. J., and Green, D. H., 1972, Strontium isotope geochemistry of lherzolite inclusions and host basaltic rocks, Victoria, Australia: Geol. Soc. America, Abs. with Programs, v. 4, p. 144.

Frey, F. A., and Green, D. H., 1974, The mineralogy, geochemistry and origin of lherzolite inclusions in Victorian basanites: Geochim. et Cosmochim. Acta, v. 38, p. 1-37.

Green, D. H., Morgan, J. W., and Heier, K. S., 1968, Thorium, uranium and potassium abundances in peridotite inclusions and their host basalts: Earth Planetary Sci. Letters, v. 4, p. 155-166.

Irving, A. J., ms, 1971, Geochemical and high pressure experimental studies of xenoliths, megacrysts and basalts from southeastern Australia: Ph.D. thesis, Australian National Univ.

Kleeman, J. D., Green, D. H., and Lovering, J. F., 1969. Uranium distribution in ultramafic inclusions from Victorian basalts: Earth Planetary Sci. Letters, v. 5, p. 449-458.

Leggo, P. J., and Hutchison, R., 1968, A Rb-Sr isotope study of ultrabasic xenoliths and their basaltic host rocks from the Massif Central, France: Earth Planetary Sci. Letters, v. 5, p. 71-75.

Norrish, K., and Hutton, J. H., 1969, An accurate X-ray spectrographic method for the analysis of a wide range of geological samples: Geochim. et Cosmochim. Acta, v. 33, p. 431-453.

Peterman, Z. E., Carmichael, I. S. E., and Smith, A. L., 1970, Strontium isotopes in Quaternary basalts of southeastern California: Earth Planetary Sci. Letters, v. 7, p. 381-384.

Stueber, A. M., 1969, Abundances of K, Rb, Sr, and Sr isotopes in ultramafic rocks and minerals from western North Carolina: Geochim. et Cosmochim. Acta, v. 33, p. 543-553.

Stueber, A. M., and Ikramuddin, M., 1974, Rubidium, strontinum and the isotopic composition of strontium in ultramafic nodule minerals and host basalts: Geochim. et Cosmochim. Acta, v. 38, p. 207-216.

Precambrian Plate Tectonics, by A. Kröner (Editor)
© 1981 Elsevier Scientific Publishing Company, Amsterdam — Printed in The Netherlands

A19

Chapter 19

PETROGENESIS OF ARCHAEAN ULTRAMAFIC MAGMAS AND IMPLICATIONS FOR ARCHAEAN TECTONICS

D. H. GREEN

ABSTRACT

The distinctive peridotitic lavas and intrusives of Archaean greenstone belts imply magma temperatures of $> 1600^{\circ}C$ at near-surface conditions. These magmas are probably produced by two or more stages of melting of rapidly rising peridotite diapirs originating at depths in excess of 200 km in the Archaean mantle. Immediate source compositions for individual lavas imply geochemical heterogeneity in the Archaean upper mantle, similar to that in the modern mantle. The high magmatic temperatures of Archaean magmatism imply differences in the Archaean geotherm. While it is possible that a lithosphere similar to that of the modern earth and a similar pattern of plate tectonics existed in the Archaean, an alternative, preferred model predicts a thinner lithosphere, more active plate movements, instability of eclogite at deep crustal depths and an absence of subduction of oceanic crust.

INTRODUCTION

This chapter focusses attention on the evidence for remarkably high temperatures of extrusion of the Archaean magmas commonly referred to as peridotitic komatiites or "spinifex-textured peridotitic komatiites" and discusses models for petrogenesis of such magmas and the implications of these models for Archaean tectonics. These Archaean magmas are compared with the most magnesian and highest temperature liquids among basalts erupted in the last 500 million years of earth history in an attempt to evaluate possible changes in mantle composition or mantle geothermal gradients with time.

The field occurrences of peridotitic komatiites, particularly the presence of pillow structures, brecciated flow tops and identifiable cooling units, demonstrate that these ultramafic compositions were emplaced as lava flows and shallow intrusives. The variety of quench textures, particularly the acicular, interlocking bladed olivine crystals forming the distinctive "spinifex" texture, and the evidence for crystallization, settling and accumulation of olivine phenocrysts, demonstrates that the original magmas have chilled rapidly but also that there has been, in some cases, opportunity for magma differentiation. The task of identifying liquid compositions, free of accumulate olivine yet sufficiently magnesian to precipitate the most magnesian

olivine observed in the natural rocks, is an important first step. Once the compositions of Archaean liquids are established, the temperature of extrusion of the magmas can be determined. Previously, a peridotitic komatiite from Barberton, South Africa (Viljoen and Viljoen, 1969a, b) was investigated and it was shown that the magma was essentially anhydrous ($< 0.2\%$ H_2O) on eruption and erupted as a completely liquid peridotite magma at a temperature of $1650 \pm 20^\circ C$ (Green et al. 1975). In this paper, quench-textured peridotites and a quench-textured magnesian basalt from Australia and Canada are compared with the Barberton example (49J).

QUENCH-TEXTURED PERIDOTITES

The samples studied experimentally were selected from among those for which major element and trace element data have been obtained (Sun and Nesbitt, 1978; Nesbitt et al., 1979). Samples include typical bladed or acicular olivine quench (49J, 422/95, 331/144) but also include samples containing remarkable dendritic or feathery quench olivine from Yackabindie (331/277, 331/346, 331/347)(Nesbitt, 1971). Rock compositions (calculated anhydrous) and compositional ranges of relict olivines are given in Table 19-I. The dendritic olivine crystals are surprisingly iron-rich, coexist with very magnesian tremolite and do not show compositional zoning from magnesian cores to more iron-rich rims as is observed in Barberton and Mt. Burges bladed olivine quench crystals. Chromium and calcium contents of these olivines are low and variable. In contrast, the bladed olivine crystals of 49J, 422/95 and 331/144 have magnesian core compositions, show slight normal zoning to more Fe-rich rims and consistently contain $> 0.1\%$ Cr_2O_3 and $\geqslant 0.15\%$ CaO.

Table 19-I illustrates the ultramafic compositions of the Barberton and W. Australian rocks, the approach of the Munro Township composition to a picritic composition and the much more siliceous composition of a spinifex-textured basalt (331/338) from the Negri volcanics in the Pilbara area of northwestern Australia.

EXPERIMENTAL PETROLOGY AND PETROGENESIS OF ARCHAEAN QUENCH-TEXTURED PERIDOTITES

The results of the experimental study of the Barberton sample (49J) (Green et al., 1975) are summarized in Fig. 19-1 and Table 19-I. Olivine is the liquidus phase and at 10 kb crystallizes alone (or with accessory chrome spinel) over a temperature interval of $\sim 220^\circ C$ and a compositional range from $Mg_{93.5}$ at the liquidus to $Mg_{89.7}$ at orthopyroxene appearance ($1450^\circ C$). At lower pressures this temperature interval and compositional range would be greater. Experimental studies on pyrolite and Tinaquillo

TABLE 19-I

Composition of Archaean quench-textured peridotitic komatiites (cols. 1—4), and quench-textured basalt (col. 5)

	Barberton 49J	Mt. Burges 331/144/5	Yackabindi 331/346	Munro 422/95	Pilbara 331/338
SiO_2	46.3	46.1	44.9	46.1	55.6
TiO_2	0.19	0.21	0.27	0.4	0.43
Al_2O_3	3.6	5.3	5.4	8.4	11.8
Cr_2O_3	0.43	0.41	0.43	0.46	0.27
NiO	0.27	0.21	0.21	0.13	—
FeO	10.3	10.4	10.0	10.9	9.3
MnO	0.21	0.21	0.20	0.22	0.22
MgO	32.9	30.9	33.1	23.6	12.2
CaO	5.1	5.9	5.2	8.8	7.8
Na_2O	0.49	0.40	0.28	0.84	1.92
K_2O	0.18	0.01	0.00	0.15	0.48
P_2O_5	0.01	0.00	0.00	0.01	0.04
100 Mg/(Mg + Fe)	85	83	85.5	79.4	70.3
Olivine in rock (Mg value)	93.6 → 89.0	92.3 → 74	87.4 → 71	92.7 → 92.3	nil
Liquidus olivine	⩾ 93.5	⩾ 93.6	—	⩾ 91.3	⩾ 86.3
Predicted liquidus olivine $K_D = 0.33$	94.4	93.6	94.6	92.0	87.6
CaO content of liquidus olivine	0.14	0.13	—	0.22	0.16
Cr_2O_3 content of liquidus olivine	0.17	0.15	—	0.15	⩽ 0.10
CaO content of most magnesian olivine in rock	0.19	0.15	n.d.	0.22	—
Cr_2O_3 content of most magnesian olivine in rock	0.18	0.15	n.d.	0.12	—.

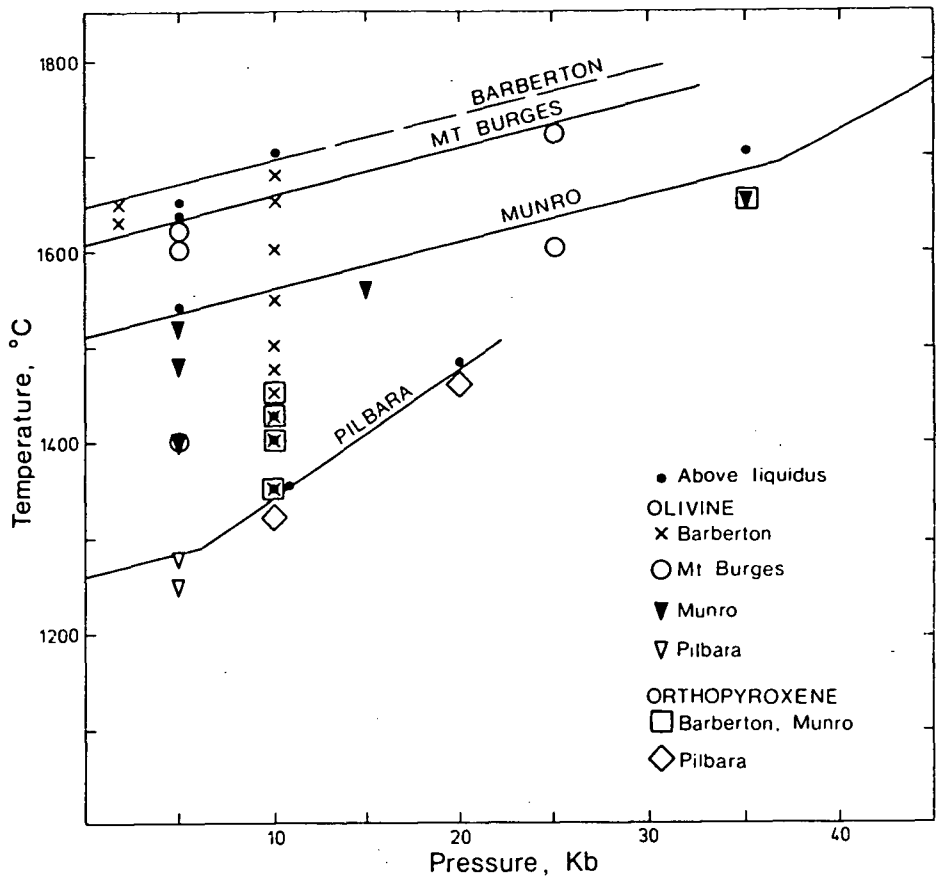

Fig. 19-1. Liquidi and liquidus phases for Archaean quench textured peridotites and basalts (Table 19-I). Symbols indicate the presence of olivine and orthopyroxene in near-liquidus runs.

peridotite composition (Jaques and Green, 1980) determine that orthopyroxene appears at 1270—1320°C at 2 kb.

The experimental studies of Fig. 19-1 and Jaques and Green (1980) are equilibrium partial-melting studies and it should be noted that crystal fractionation of early-formed olivine from peridotitic liquids will produce iron-enrichment and more rapid change in Mg-value of olivine with decreasing temperature.

The crystallization behaviour of Mt. Burges, Munro and Pilbara samples of Table 19-I has also been studied experimentally, using the methods previously described. The use of graphite capsules for sample containers results in lower oxygen fugacity in the charges than is apparently appropriate for the natural rocks. Thus the experimental conditions do not permit assessment of Ni-partitioning between olivine and liquid nor of the precipitation of chrome-spinel since both these aspects of crystallization are sensitive to f_{O_2}. The results of the experimental studies are summarized in Fig. 19-1 and Table 19-I. Olivine is the low-pressure liquidus phase of all samples, and the composition of the olivine obeys, within the experimental uncertainties, the partition relationship $(K_D^{Ol/liq})_{Fe/Mg} = 0.33$ (Table 19-I). Three samples,

Barberton, Munro and Pilbara, give K_D values of 0.39, 0.37 and 0.38 using the compositions of the highest temperature olivine observed and the bulk composition of the charge, assuming all Fe as Fe^{2+}. The inability to quench liquids to glass in Barberton and Mt. Burges compositions prevents direct analysis of olivine-liquid pairs in these peridotitic liquids. For the Pilbara sample, analyses of olivine/glass pairs at 5 kb, 1280°C and 1250°C give $K_D = 0.33$ and 0.32, respectively, and for the Munro sample at 5 kb, 1520°C, an olivine/glass pair gives $K_D = 0.33$. Lower temperature experiments contain much quench olivine and glass compositions are iron-enriched during quenching (cf. Jaques and Green, 1979). The data obtained do not provide unequivocal evidence for variation of $(K_D^{Ol/liq})_{Fe/Mg}$ with temperature, or liquid composition, over a temperature range from 1250°C to 1700°C and for liquids with MgO contents ranging from 12% to 33%. Thus it is appropriate to use $(K_D^{Ol/liq})_{Fe/Mg} = 0.33$ in testing for equilibrium relationships between observed olivine and postulated liquid compositions or for evaluation of the composition of residual olivine in mantle source regions which have yielded particular magma compositions as partial melts.

The experimental study, taken in conjunction with the field evidence for absence of phenocrysts and for extrusion and rapid chilling of the magmas, defines the extrusion temperatures of the magmas. All magmas were essentially anhydrous. Water dissolves in these magmas under high pressure (Green et al., 1975) and saturation with water depresses the liquidus to lower temperature (e.g. to 1510°C for Barberton 49J at 5 kb or to 1300°C at 25 kb). However, such water-bearing magmas cannot move to the surface without rapidly crystallizing olivine as they pass through the olivine + liquid + vapour field. Hydrous peridotitic komatiite magmas must arrive at the surface in partly crystallized state with porphyritic texture — the samples selected for study do not show such textures and were essentially anhydrous magmas. The extrusion temperatures were:

Barberton	(49J)	-1650 ± 20°C;
Mt. Burges	(331/144/5)	-1610 ± 20°C;
Munro	(422/95)	$->1510$°C ($\ll 1610$°C);
Pilbara	(331/338)	-1270 ± 20°C.

Note that the liquidus olivine for the Munro composition studied is Mg_{92} [$K_D = 0.33$] whereas slightly more magnesian olivine cores occur in the natural rock ($Mg_{92.5 \pm 0.2}$). Thus the Munro composition is slightly less magnesian and lower in normative olivine than the parental magma which precipitated the observed ($Mg_{92.5}$) olivines. The extrusion temperature of this parental magma would be >1510°C but $\ll 1610$°C. The spinifex-textured basalt from the Negri volcanics has a liquidus temperature within the range of modern primitive olivine-rich magmas (Green et al., 1979; Duncan and Green, in prep.).

The effect of pressure on all compositions is to increase the liquidus temperature at 4—5°C/kb for the range of pressure over which olivine is the

liquidus phase. In the Pilbara sample orthopyroxene is the liquidus phase at 10 kb and 20 kb and the slope of the orthopyroxene-liquidus is ~ 15°C/kb. In the Munro sample, olivine and orthopyroxene occur together at the liquidus (35 kb, 1680°C) and it is expected that orthopyroxene would be the liquidus phase at higher pressure.

Primary magmas of mantle derivation, which have not suffered olivine or other fractionation between magma segregation at source and extrusion at the earth's surface, should be saturated with olivine and orthopyroxene at some pressure. The two samples, Pilbara and Munro, are potential primary magmas, segregating from residual harzburgite at ~ 6 kb, 1280°C and ~ 35 kb, 1680°C, respectively. In the Pilbara example the residual olivine is $Mg_{87.6}$ and since this is necessarily more magnesian than the original pre-melting source olivine composition, the inference that the Pilbara sample is a primary magma has the connotation that the source peridotite was more Fe-rich (~ Mg_{86}) than modern mantle peridotite (Mg_{89-90}). This inference is *not* supported by the very magnesian liquidus olivine and orthopyroxene of the other samples and an alternative interpretation of the Pilbara sample is preferred. The Pilbara spinifex-textured basalt is inferred to be a derivative magma, having fractionated olivine (15—20%) from a parental magma in which the Mg-value would be ~ 75. Such a parent magma would have separated from residual harzburgite (Mg_{90-91}) at ~ 15 kb, 1500°C.

The Barberton and Mt. Burges compositions have olivine as the liquidus phase up to very high pressures. The compositions are themselves peridotitic and in considering these liquids as partial melts segregating from source peridotite at low pressure, the only residual silicate phase could be highly magnesian olivine (~ Mg_{94}). These liquids may be either formed by very high degrees of melting (60—70%) of source peridotites containing 3—4% CaO, Al_2O_2 (i.e. model peridotites matching those which suffice to account for the spectrum of Phanerozoic natural mantle-derived basaltic compositions and natural mantle-derived peridotites) or, alternatively, by a "normal" (~ 30%) degree of melting of a refractory source peridotite (1.5% CaO, Al_2O_3).

The melting behaviour of two peridotite compositions, pyrolite (Ringwood, 1966) and Tinaquillo lherzolite (Green, 1963) has been studied experimentally (Jaques and Green, 1980) and the trends of liquid compositions for increasing degree of melting have been defined at 2 kb, 5 kb, 10 kb and 15 kb. Figure 19-2 is the (jadeite + Ca Tschermaks silicate) — olivine-quartz diagram (Green, 1970) which provides a convenient summary of the data and a comparison with the Archaean magma compositions from Table 19-I. Barberton, Yackabindie and Mt. Burges compositions must represent sufficiently high degrees of melting of mantle peridotite such that olivine only is the residual phase. The Pilbara composition has an unusually low CaO/Al_2O_3 ratio and its bulk composition may reflect low-temperature secondary alteration. Assuming no such problem, however, the magma composition plots to the

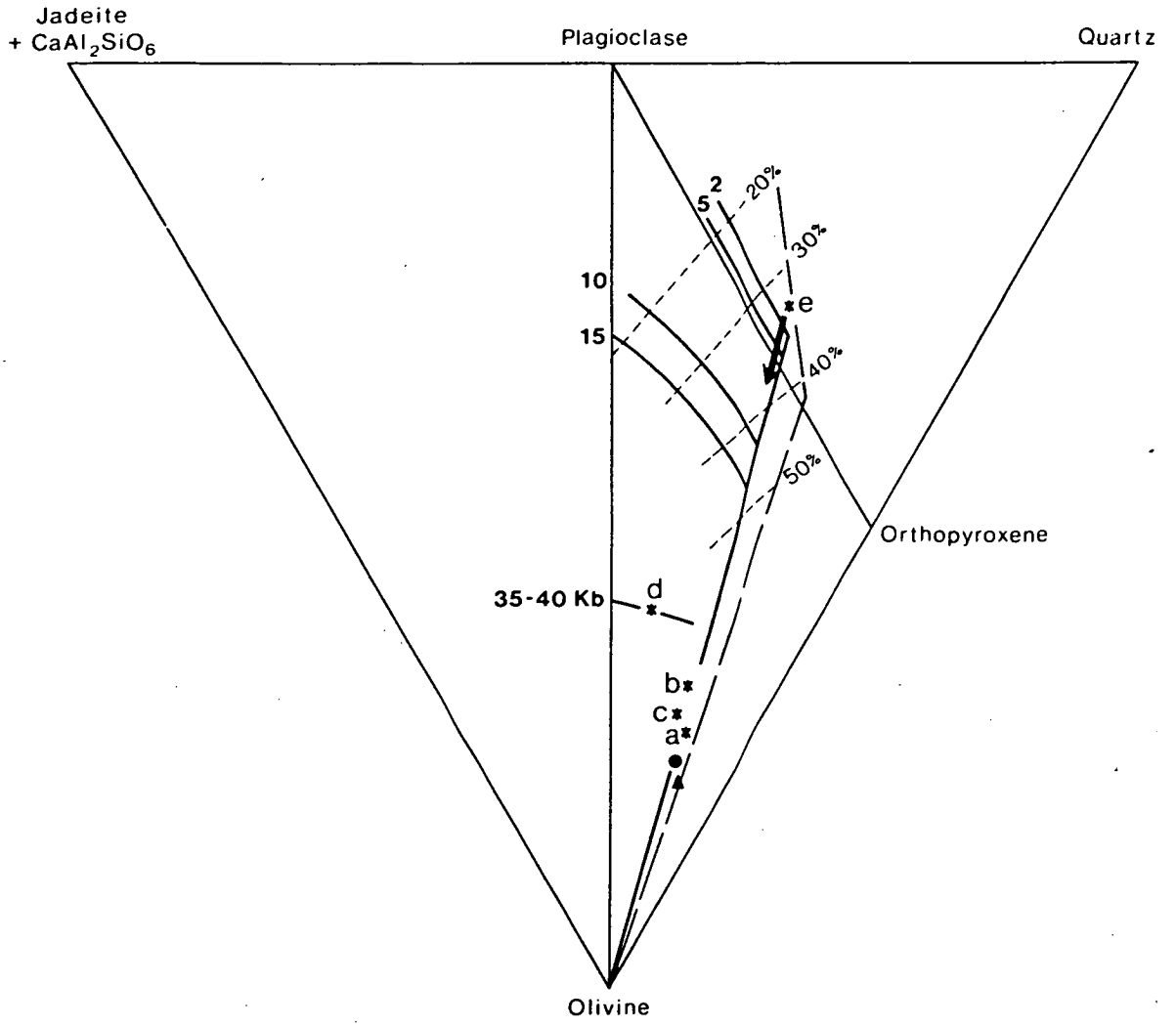

Fig. 19-2. Compositions of liquids derived by equilibrium melting of pyrolite (dark solid lines) at 2, 5, 10 and 15 kb pressure, plotted in the system (jadeite + Ca-Tschermaks silicate) — olivine — quartz (Green, 1970; Jaques and Green, 1980). Short dashed lines indicate percent melting of pyrolite composition, long dashed line shows the compositions of liquids from Tinaquillo lherzolite at 2 kb. Note that the loci of melt compositions follow the ol-opx cotectic until opx is eliminated and then lie on an olivine control line. Co-ordinates calculated from a high-pressure norm in which compositions are cast in terms of the components of the figure together with diopside, ilmenite, magnetite, chromite, orthoclase and apatite. ● = pyrolite; ▲ = Tinaquillo lherzolite; *a* = Barberton; *b* = Mt. Burges; *c* = Yackabindi; *d* = Munro; *e* = Pilbara; (see Table 19-I).

quartz-rich side of the 2 kb and 5 kb olivine + orthopyroxene saturation boundaries but the experimental study indicates olivine and orthopyroxene saturation at ~ 6 kb. This inconsistency, together with the iron-rich nature of the liquidus olivine, suggests that the magma composition results from olivine removal at < 2 kb from a peridotitic komatiite or picritic komatiite melt segregating on the olivine + orthopyroxene saturation line at ~ 15 kb, 45% melting (Fig. 19-2). The Munro composition does not plot on the olivine control line (or on the olivine + orthopyroxene saturation boundary)

for the 2, 5, 10 or 15 kb studies but instead is consistent with separation on an olivine + enstatite co-saturation boundary at $\gg$ 15 kb. The experimental study suggests that magma segregation at a pressure of 35—40 kb with ~ 50% melting of a pyrolite of Tinaquillo peridotite-like source would be appropriate.

THE PROBLEM OF SOURCE COMPOSITION AND HIGH DEGREES OF MELTING OF UPPER-MANTLE PERIDOTITE

Although the highly magnesian and most olivine-rich magmas of Table19-I are peridotite in composition and, in three examples, not very different from estimates of the modern upper-mantle composition, it is not easy to suggest processes of complete melting of the Archaean upper mantle. Apart from impact melting there is no known process which can take a body of upper-mantle peridotite from near-solidus (~ 1000°C at 1 atmosphere pressure, 1500°C at 30 kb) to its liquidus (~ 1700°C at 1 atmosphere, 2000°C at 30 kb) so rapidly that separation of crystals and liquid will not occur during either the heating or decompression (diapirism) process. The strong density contrast between olivine and pyroxene crystals ($\rho \approx 3.3$) and olivine tholeiitic or picritic liquid ($\rho \approx 2.7$) ensures that olivine and pyroxene crystals will rapidly settle within a crystal + liquid magma as soon as the percentage of liquid is sufficient to destroy grain to grain contact, i.e. > 25—30% liquid. In a previous paper (Green, 1975) it was suggested that very rapid diapiric ascent could entrain olivine and pyroxene crystals in initially picritic melts, and as the entrained crystals moved to shallower depths they would dissolve, moving the liquid composition towards peridotite. Rapid ascent of magma (sufficient to entrain peridotite xenoliths ($\rho = 3.3$) from depths in excess of 30 km) does occur in modern basaltic volcanism but it is characteristic of small volume, very under-saturated magmas containing high proportions of dissolved (at high pressure) $(OH)^-$ and $(CO_3)^{2-}$ and apparently does *not* occur in olivine tholeiitic or tholeiitic picrite magmas, i.e. it is characteristic of small-volume partial melts of the modern mantle and magmas which characteristically show explosive eruptions.

Arndt (1977) has carefully considered the problem of liquid segregation from an ascending crystal + liquid diapir and has argued that peridotitic liquids represent remelting or continued melting of residual peridotite following extraction of picritic or basaltic melts at deeper levels. There is sufficient flexibility within this general model to account for the variation in both major element and trace element characteristics. Effective separation of a small melt fraction (< 5%) at pressures within the garnet peridotite stability field will produce residual peridotite which may then melt to ~ 30% to yield olivine-rich magmas which are strongly depleted in incompatible elements but not depleted in heavy rare earths. By contrast, a high degree of melting (~ 30%) initially produces liquids with the same relative incom-

patible elements as the source peridotite and leaves only residual olivine and orthopyroxene. If a small amount of this liquid does not leave the source peridotite but remains as an intergranular film, then continued ascent of the now very refractory peridotite *bulk* composition may yield a second-stage magma of high Mg-value but still with incompatible element contents which are similar to the source. i.e. two or more processes of high-degree melting with incomplete magma extraction do not produce strong fractionation of incompatible element contents, whereas complete extraction of small melt fractions produces maximum fractionation within the incompatible element group. Two or more processes of high-degree (20—30%) melting and incomplete magma extraction produce large differences in the major element compositions of liquids, successive melts being increasingly dominated by olivine and orthopyroxene as the only residual phases contributing to the later stage melts.

Sun and Nesbitt (1978) have considered the implications of incompatible element contents in Archaean magmas, particularly the REE, and have argued that the Archaean mantle was chemically heterogeneous and that the degree of heterogeneity was similar to that deduced for the source regions of modern ocean-basin basalts. The experimental study reinforces this conclusion since only olivine and orthopyroxene are potential residual phases for all magmas and the REE contents of these phases are negligible. The source region for the Pilbara spinifex-textured basalt was enriched in light rare-earth elements (LREE) relative to heavy rare earth (HREE) but the converse is true for Mt. Burges, Yackabindi and Munro — the latter being the most strongly depleted in REE (Fig. 19-3). The Barberton sample is almost chondritic in its REE relative abundances, with only slight LREE/HREE enrichment. There is no simple correlation between REE and major element abundances of the immediate source regions. The implications of hypothetical simple batch melting of source compositions [all of which had 2 x chondritic HREE abundances (Dy → Yb)] are illustrated in Fig. 19-3. The La abundance of the source regions would then range from 10 x chondritic to ~ 0.45 x chondritic, the Ca contents from ~ 2% to ~ 4.5% and the % melting of the source regions from 25% to 90%.

To summarize, the compositional variation of the Archaean magmas is such that inhomogeneity of the immediate source regions is required with no apparent simple relation between major element abundances and incompatible element abundances. If we accept the reasonable hypothesis that melting in excess of ~ 30% of any source peridotite must result in segregation of magma but that the efficiency of separation of liquid from residue is variable and further that magma may segregate from residual crystals at lower degrees of melting, then we have a model for the Archaean mantle which has the flexibility to produce the observed variations in Archaean ultramafic and basic liquids. The major conclusion

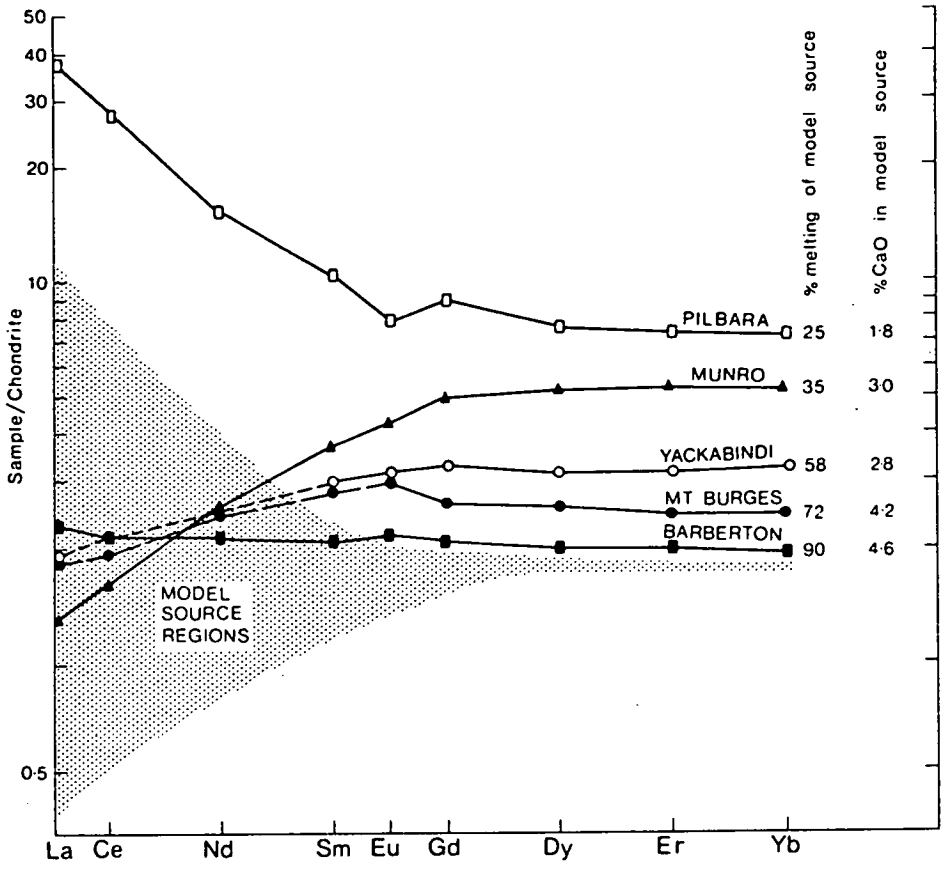

Fig. 19-3. Rare earth abundance data for composition of Table 19-I (from Sun and Nesbitt, 1978). Note that there is little fractionation among the heavy rare earths (Dy → Yb). The shaded area illustrates the range of rare earth abundances in model source regions *assuming* that all source regions have twice chondritic abundances of Dy, Er and Yb. This model would require the source regions to vary in CaO content (see figure) and imply degrees of partial melting from 25% to 90%. The figure illustrates the necessity for the immediate source peridotites of these magmas to be chemically inhomogeneous as the possible residual phases, olivine and orthopyroxene have negligible REE contents.

is that the Archaean upper mantle is not obviously less geochemically complex than the modern earth's mantle in its variability of major element and incompatible element abundances and that processes of incompatible element (particularly LREE) enrichment and depletion by migration of low % melting liquids in the mantle were operative in the Archaean mantle.

COMPARISON OF ARCHAEAN MAGMA GENESIS WITH PHANEROZOIC PERIDOTITIC AND BASALTIC MAGMA GENESIS

The discussion of the previous section incorporated the concept of diapirism of partially molten mantle peridotite as the immediate cause of magma segregation and ascent in the Archaean upper mantle. In addition the details of magma chemical composition require chemical inhomogeneity of the source peridotite compositions. These are concepts which have been applied to the modern earth and it is important to compare the nature of

modern and Phanerozoic magmatic activity with that of the Archaean to understand differences and similarities and their significance.

Diapirism and emplacement of peridotite "magma" at upper mantle and crustal levels has been demonstrated for "high-temperature peridotite" intrusions such as Mt. Albert, Lizard, Tinaquillo, Serrania del Ronda and Beni Bousera (see Wyllie, 1967 for summary). The chemical compositions of these peridotite diapirs are similar to, or slightly more refractory than, the compositions of Barberton, Mt. Burges or Yackabindi of Table 19-I. Typically these intrusions, although at high temperature ($> 1000°C$) causing dynamothermal metamorphism of adjacent country rocks to pyroxene granulite or pyroxene hornfels facies assemblages, are largely or completely crystalline. The emplacement process has resulted in cataclasis, recrystallization and production of distinctive augen and foliated textures within the peridotites which preserve evidence of initial crystallization of the peridotite mineralogy at pressures in excess of 10 kb and temperatures in excess of 1200°C.

Recent publications (e.g. Kirby, 1979) equating these complexes with "ophiolites" may well be correct if the term "ophiolite" is applicable to any mechanically emplaced (?overthrust, ?obducted) sliver of oceanic crust juxtaposed against continental crust. This nomenclature, however, obscures the important distinction between the high-temperature and relict high-pressure lherzolite mineralogy of these ultramafic complexes and the highly refractory harzburgite tectonite and layered, accumulative dunite, peridotite, pyroxenite and gabbro sequences of the deep-seated portions of "classical" ophiolites. The latter are characteristically low-pressure magmatic sequences and relate to segregation and fractionation of picritic and magnesian quartz tholeiite magmas derived from mantle peridotitic source rocks.

The concept of mantle peridotite diapirism is also an integral part of most discussions of modern basalt petrogenesis. The primary magmas which are parental to the common mid-ocean ridge basalts are considered to be picritic (Table 19-II), i.e. 20—30% melt fractions segregating from residual peridotite at pressures of ~ 20 kb and temperatures of around 1450°C (Green et al., 1979). Extrusion temperatures of common magmas are normally nearer 1250°C (Table 19-II, column 1) and reflect olivine crystallization and removal from primary picritic magmas (liquidus ~ 1350°C, 1 atmosphere). There are, however, examples of picritic melts rich in olivine which have quench textures ("spinifex-textures", leading to application of the term komatiitic by some authors) and must have been emplaced at and quenched from temperatures of ~ 1350°C (Gansser et al., 1979). Continued ascent of diapirs of residual peridotite after segregation of tholeiitic picrite magma may produce second stage melts, segregating from residual harzburgite at pressures of 5—8 kb and a temperature of ~ 1350°C (Table 19-II, column 3) (Duncan and Green, 1980, in prep.). Extrusion temperatures for such second-stage melts range from $< 1300°C$ to 1350°C,

TABLE 19-II

Compositions of very magnesian Phanerozoic extrusives

	Olivine tholeiite glass from Atlantic ocean floor (1)	Inferred picritic parent magma for common MORB (2) (cf. column 1)	2nd stage melt of mantle peridotite (parental magma for Troodos upper pillow lavas, Cyprus (3)	High-Mg andesite or "Boninite" (Cape Vogel, Papua-New Guinea) (4)	Howqua Peridotite (Cambrian) Victoria, Australia (5)
SiO_2	49.7	48.3	52.4	57.6	50.9
TiO_2	0.72	0.60	0.30	0.2	0.01
Al_2O_3	16.4	13.7	11.7	7.5	0.73
FeO	7.9	7.9	8.4	10.7	10.4
MnO	0.12	0.12	0.15	0.2	0.19
MgO	10.1	16.7	15.8	17.1	37.2
CaO	13.1	10.9	10.7	5.1	0.58
Na_2O	2.0	1.65	0.70	0.6	0.03
K_2O	0.01	0.01	0.10	0.4	0.03
Cr_2O_3	0.07	0.06	—	—	—
NiO	0.03	0.08	—	—	—
$\frac{100\,Mg}{Mg + \Sigma Fe}$	71	79	77	74	86
Observed liquidus olivine	Fo_{89}	$Fo_{91.5}$	Fo_{91}	[Clinoenstatite Mg_{92}]	Fo_{94}
Liquidus temperature at 1 atmosphere	1230°C	1350°C	1350°C	1360°C	?

(1) DSDP3-18 from Frey et al. (1974); (2) Green et al. (1979); (3) Duncan and Green (1980, in prep.); (4) Dallwitz et al. (1966); (5) Peridotite with cumulate olivine, clinoenstatite and bronzite phenocrysts in a rapidly quenched devitrified matrix (Crawford, 1980).

the lower-temperature magmas being porphyritic with olivine and/or orthopyroxene phenocrysts or fractionated by removal of olivine.

There are other Phanerozoic extrusive rocks which are characterized by very magnesian phenocrysts of clinoenstatite (replacing protenstatite), bronzite or, less commonly, olivine in a quenched matrix. This group includes the "high-magnesium andesites" of Cape Vogel, Papua-New Guinea (Dallwitz et al., 1966), and the Marianas trench (Dietrich et al., 1978) and the "boninites" of the Bonin Islands. These magmas are silica-rich relative to other primary, mantle-derived basalts (cf. Table 16-II). It appears probable that these magmas have their liquidus temperatures lowered by dissolved water at their conditions of origin (work in progress) and their porphyritic character reflects crystallization during ascent, accompanied by boiling-off of water and crystallization en route to the surface. An extreme example of this magma type is possibly the Howqua peridotite (Crawford, 1980). This remarkable rock contains very magnesian olivines (Mg_{94}), having similar Cr_2O_3 and NiO contents but lower CaO than those in olivine of the Archaean peridotitic komatiites. In this largely accumulate rock only the interstitial matrix and zoned phenocryst rims show evidence of rapid quenching. Extrusion temperatures for this rock are as yet not determined but also may be lowered by high water content. These examples of magnesium and silica-rich magmas appear to be characteristic of island-arc settings but the role of water in their petrogenesis and their tectonic significance remains uncertain. There is as yet no compelling evidence that this high-Mg, very high-SiO_2 and porphyritic (clinoenstatite and bronzite phenocrysts) magma type is represented among Archaean magmas. There are some compositional similarities but marked mineralogical and petrographic differences from the Archaean high-Mg, high-SiO_2 spinifex-textured basalt (cf. Table 19-I, column 5, and Table 19-II, column 4).

To summarize, the concepts of mantle diapirism, magma segregation at different pressures and temperatures leading to local mantle chemical heterogeneity, and continued ascent of peridotite diapirs after segregation of a melt fraction, are all encompassed within recent models of magma production in the modern and Phanerozoic earth. In particular these concepts are advanced in models of magma genesis at mid-ocean ridge or back-arc basin spreading centres. The principal difference between Archaean ultramafic and basaltic petrogenesis and Phanerozoic ultramafic and basaltic petrogenesis is in the *maximum* temperature of magma extrusion, i.e. $\sim 1350°C$ on the Phanerozoic earth and $\sim 1650°C$ on the Archaean earth.

THE IMPLICATIONS OF VERY HIGH EXTRUSION TEMPERATURES OF ARCHAEAN MAGMAS

The determination of the *P-T* conditions of segregation of a primary magma from mantle peridotite source rock also locates a point on a temperature/depth profile in the earth at the time of magma production. The concept

of mantle diapirism, however, implies that this is a point on a perturbed geotherm. To establish a point on the geothermal gradient prior to diapiric upwelling of the upper mantle, it is necessary to extrapolate the *P-T* conditions reached by the peridotite diapir at the depth of magma segregation back to deeper levels — to the depth of origin of the ascending diapir itself. A large, ascending peridotite diapir can be considered, as a first approximation, to follow an adiabatic cooling path as it moves towards the earth's surface, and for a largely crystalline, olivine-dominated peridotite the adiabatic gradient is approximately 1°C/kb (Birch, 1952). If melting occurs, then the latent heat of melting and the higher compressibility of melt relative to crystals will increase the adiabatic gradient. Extrapolation of magma extrusion temperatures to deeper levels at an adiabatic gradient of 1°C/kb thus yields *minimum* values for the temperature distribution in the upper mantle.

The adiabatic ascent paths for peridotite diapirs and segregated magmas may be superimposed in *P-T* diagrams showing the melting behaviour of a suitable model mantle peridotite composition. Experimental studies of two peridotite compositions [pyrolite (Ringwood, 1966) and Tinaquillo lherzolite (Green, 1963)] have established the solidi, % melting contours and liquid and residual phase compositions over the pressure range 0—15 kb (Jaques and Green, 1979, 1980). The data for pyrolite, which is closer to Barberton 49J composition in Na and K contents than is Tinaquillo lherzolite, are summarized in Fig. 19-4. The solidus for pyrolite is strongly dependent on the presence or absence of water and on the water content. Accepting that the interior of the earth is still degassing and that the modern upper mantle contains small water contents (< 0.3—0.4% H_2O), it may be argued that the Archaean upper mantle could not have been anhydrous. The solidus for pyrolite with $H_2O \sim 0.1\%$ H_2O is therefore considered most appropriate and this results in an important region of "incipient" or small degree of partial melting between this solidus and the position of the anhydrous solidus. With increasing temperature above the position of the anhydrous solidus, the effect of the water in controlling the melt fraction is progressively less important and the % melt contours approach those for anhydrous melting above the anhydrous solidus. The intersection of minimum adiabatic ascent paths for Barberton, or Mt. Burges, or Yackabindie peridotite magmas with solidi and % melting contours for pyrolite (Fig. 19-4) shows that only at

Fig. 19-4. Implication of very high extrusion temperature for models of Archaean geotherm. Heavy solid lines give solidi for pyrolite compositions under anhydrous conditions and with a water content $\leqslant 0.4\%$ H_2O. The fine dashed lines indicate percent melting of anhydrous pyrolite and are approximately correct for $> 20\%$ melting if the mantle contains $\sim 0.1\%$ H_2O. The heavy dashed lines represent two model geotherms (see text) and the hatched area illustrates conditions of the gabbro—garnet granulite—eclogite reactions. Superimposed on this diagram are the extrusion temperatures and minimum adiabatic ascent paths for peridotite diapirs yielding the magmas of Table 19-I and Fig. 19-1. Points *A* and *B* mark the deduced conditions of magma segregation of Pilbara and Munro compositions, respectively (see text). The shaded, above-solidus region denotes the *P-T* conditions of modern mantle diapirism and magma genesis.

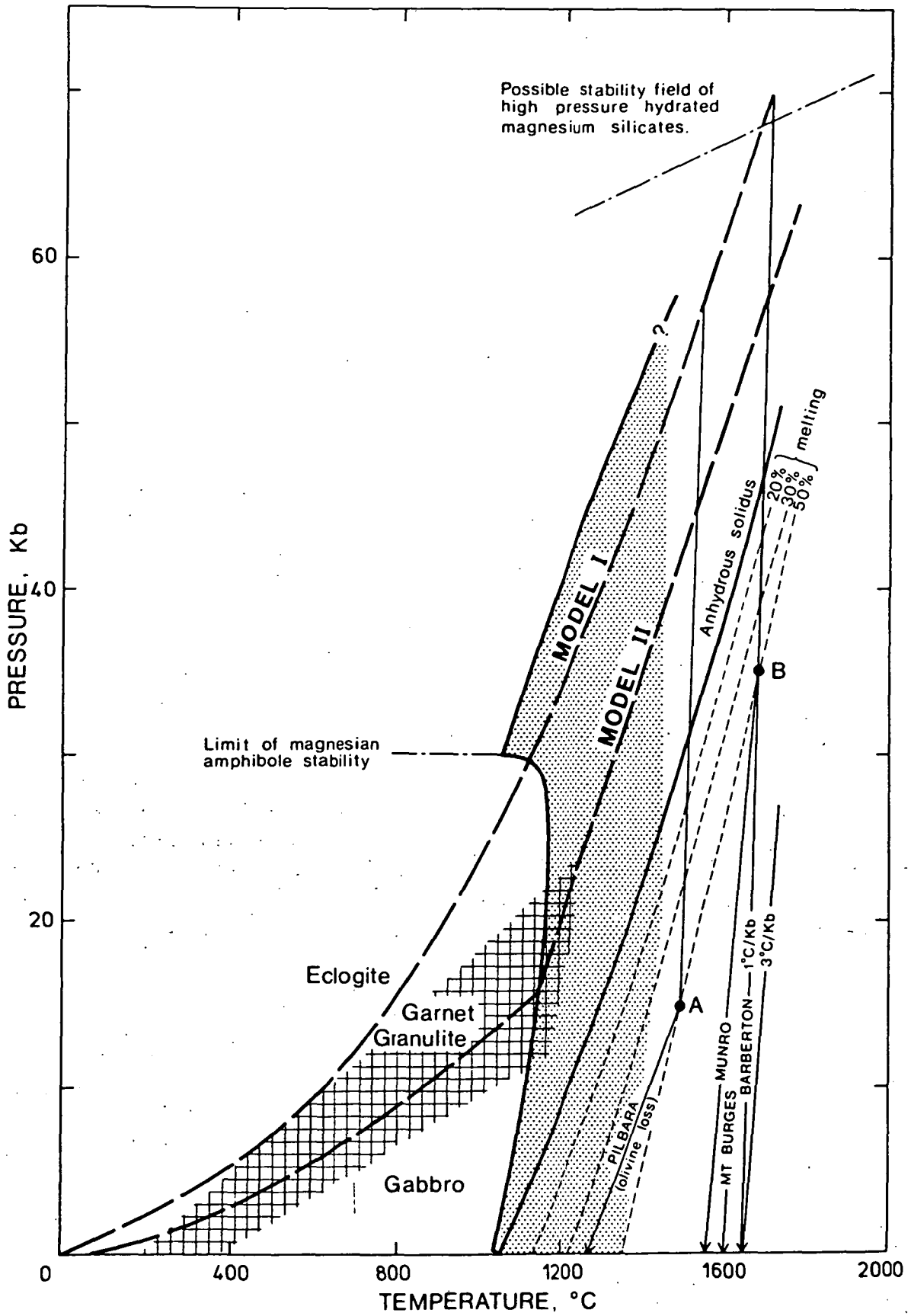
Possible stability field of high pressure hydrated magnesium silicates.
60
40
20
0
PRESSURE, Kb
400
800
1200
1600
2000
TEMPERATURE, °C
MODEL I
MODEL II
?
Anhydrous solidus
20%
30%
50%
melting
Limit of magnesian amphibole stability
Eclogite
Garnet Granulite
Gabbro
A
B
PILBARA (olivine loss)
MUNRO
MT BURGES
BARBERTON
1°C/Kb
3°C/Kb

depths of > 200 km would the degree of melting be similar (< 5%, probably 1—2%) to that inferred for the modern low velocity zone (Green and Lieberman, 1976) with its attendant lithosphere/asthenosphere tectonic and dynamic implications. Estimates of the modern geothermal gradient in oceanic regions (e.g. Clark and Ringwood, 1964) yield depths of ~ 400 km for intersection with peridotitic adiabatic ascent paths. The implications of steeper Archaean geotherms, to yield depths of origin of peridotite diapirs of ~ 200 km, were explored by Green (1975). Two possibilities with very different tectonic implications are illustrated in Fig. 19-4.

Model I suggests a geotherm similar to that estimated for ocean basin regions of the modern earth down to depths of ~ 100 km (30 kb) and implies a crystalline lithosphere of ~ 90 km thickness overlying a low velocity zone with 1—2% melt present. As illustrated in Fig. 19-4, this geotherm lies within the eclogite stability field for basaltic compositions. Basaltic rocks, cooling from igneous temperature to conditions on the regional geotherm, should recrystallize to eclogite mineralogy if they remain essentially anhydrous and reaction rates permit. At depths greater than 100 km, the model I geotherm departs from the Clark and Ringwood (1964) geotherm to higher temperatures to give an intersection with adiabatic peridotitic diapir ascent paths at depths of 200—250 km (> 60 kb). The plate tectonics of an Archaean earth with mean geothermal gradient similar to the model I geotherm would probably be much like that of the modern earth — the 90 km lithosphere and 1—2% melting in the low velocity zone being major controlling parameters to lithospheric plate dimensions and relative velocities between lithospheric plates and deeper mantle. In addition, the stability, along the mean geothermal gradient, of dense eclogite ($\rho = 3.4$—3.5) rather than basalt or gabbro ($\rho = 3.0$—3.1) mineralogy would ensure that formation of basaltic crust was only a transitional stage in mantle geochemical differentiation. With a model I geotherm, it would be expected that the Archaean earth should show evidence of subduction of basaltic oceanic crust, of linear zones containing glaucophase schist and eclogite mélanges and linear volcanic/intrusive belts in which an important role for water in magma genesis and evolution from peridotitic source rocks (as opposed to "wet" melting of deep crustal, basaltic or other rocks) could be demonstrated. An important implication of model I geotherm is that highly undersaturated basanitic and nephelinitic magmas, formed by < 5% melting in the presence of H_2O and $(CO_3)^{2-}$ in the garnet peridotite field, should occur among Archaean intrusives or volcanics, as they do in Phanerozoic and modern volcanics.

Model II suggests a steeper geotherm which intersects the pyrolite + 0.1% H_2O solidus at ~ 50 km, implying a lithosphere of only ~ 50 km thickness. The geotherm passes rapidly into conditions of 5—10% melting of pyrolite and is arbitrarily drawn to higher pressures following approximately the

5% melting content. The combination of thin lithosphere and greater melt fraction in the asthenosphere suggests that an Archaean earth with model II mean geotherm would be characterized by an absence of large, thick, slow moving, lithospheric plates, and by a relatively unstable set of thinner plates, particularly with respect to basaltic volcanism. Basaltic volcanism would be restricted to types derived by $> 5\%$ melting of pyrolite and thus olivine leucitites, olivine melilitites, olivine nephelinites and nepheline-rich basanites should not occur among Archaean extrusives or intrusives.

The second major consequence of a model II geotherm is that this geotherm remains within the stability field of garnet + clinopyroxene + plagioclase ± quartz mineral assemblages in basaltic rocks. Therefore, Archaean basaltic crust overlying peridotitic upper mantle would have no tendency to react to eclogite on cooling and would remain gravitationally stable ($\rho = 3.0$—3.2 overlying $\rho = 3.3$—3.4). The concepts that the gabbro $\rightleftharpoons$ eclogite reaction in thick oceanic crust may trigger subduction (Ringwood and Green, 1966) and that further geochemical processing of basaltic crust is responsible for Andean volcanism, would not be relevant to an Archaean earth if the basaltic crust could not cool sufficiently to transform to eclogite at deeper levels. It has been suggested (Green, 1975) that with a model II geotherm, thermally activated convective overturn of a thin Archaean lithosphere (~ 50 km) would not involve substantial return of basaltic crust to the upper mantle as eclogite but rather the basaltic crustal sequences would be scraped off the underlying convecting peridotite and folded against sialic continental nuclei in a manner analogous to the fate of ocean-floor sedimentary sequences during subduction of modern oceanic crust. If deeper levels of such infolded basaltic sequences (Archaean greenstone belts) attains depths of ~ 25 km then they may partially melt leading to granodioritic and granitic intrusives and associated volcanism. Green (1975) proposed that a model II geotherm, while permitting sialic crust and associated continental processes from sedimentation to deep crustal metamorphism and anatexis, would imply greater movement rates of smaller lithospheric plates to both the thinner lithosphere and the higher melt fraction in the mantle beneath the lithosphere.

In summary, the observations of Phanerozoic and modern volcanism are consistent with processes operating within the shaded area of Fig. 19-4, i.e. a *P-T* region bounded by the solidus for pyrolite + 0.1% H_2O, the extrusion temperatures of $\sim 1350°C$ for primitive, anhydrous magmas, and the adiabat for peridotite diapirs extrapolated from 20 kb, 1450°C (depth of magma segregation of tholeiitic picrite parental to MORB). The mean geothermal gradient for oceanic regions for the modern earth passes through ~ 30 kb, 1100°C, implying a lithospheric thickness of ~ 90 km and a low velocity zone or asthenosphere with 1—2% melt (composition of highly undersaturated olivine melilitite or olivine nephelinite). The voluminous tholeiitic volcanism of Phanerozoic and modern basaltic provinces results

from perturbation of the mean geothermal gradient by diapiric upwelling of peridotite diapirs from depths of 100—180 km, such upwelling occurring beneath rifted plate margins in mid-oceanic ridges or back-arc basins. Although convective motion of deeper mantle levels is implied in the general plate-tectonic model, the character and rate of such movements is not such as to provide sufficient instability to produce *rapidly ascending* and thus adiabatically cooling peridotite diapirs from deeper (> 180 km), higher temperature, levels of the upper mantle. This statement derives directly from the apparent absence among Phanerozoic or modern extrusives of anhydrous magmas extruded at temperatures above 1350°C and of anhydrous liquids of more olivine-rich composition than picrite.

In contrast, Archaean basaltic and ultramafic volcanism requires upwelling and peridotitic diapirism which tap deeper levels at higher temperatures, extending *at least* to the minimum (1°C/kb) Barberton adiabat of Fig. 19-4 and probably to higher temperatures and greater depths. It is possible that the Archaean thermal regime reflects an increase in the efficiency and magnitude of *convective* heat loss from the deep mantle, i.e. heat lost through mantle mass transport and consequent volcanism. If this is so then the mean Archaean geotherm, in non-volcanic areas, and consequent lithosphere thickness may not be very different from those of the modern earth, [model I geotherm of Fig. 19-4). It is more probable, however, that increased heat loss is both conductive, reflected in a higher mean geothermal gradient, and convective [model II geotherm of Fig. 19-4). In this case the Archaean lithosphere would be much thinner (~ 50 km), crustal and lithospheric temperatures higher and the nature of Archaean basaltic magmatism restricted to hypersthene normative or mildly undersaturated basaltic magmas (i.e. excluding olivine melilitites, olivine nephelinites and basanites). This model also implies that Archaean basaltic crust overlying residual mantle peridotite would not react to eclogite (with consequent gravitational instability), and thus would not return via a subduction-like process for further geochemical processing in the upper mantle.

SUMMARY AND CONCLUSIONS

Extrusion temperatures of South African and Western Australian Archaean peridotitic komatiite magmas were greater than 1600°C and the mineralogy of the residue from magma segregation is highly magnesian olivine (Mg_{93-94}) alone. Peridotitic komatiite from Canada has slightly lower extrusion temperature (~ 1540°C) and is inferred to have segregated from residual harzburgite at ~ 35—40 kb, ~ 1700°C. The immediate source compositions for these high-temperature liquids differed in minor and trace element compositions, and the combination of experimental petrological and geochemical data suggests that the Archaean upper mantle was as geochemically heterogeneous as the modern upper mantle, some regions having

been enriched and others depleted in incompatible trace elements. Archaean magma genesis can be interpreted in terms of mantle diapirism, i.e. similar processes to those operating in modern mid-ocean ridge or back-arc basin spreading centres. The principal differences lie in the maximum temperatures of extrusion of Archaean magmas which are 300—350°C above those of modern or Phanerozoic magmas. The different temperature regime for magma extrusion implies differences between the Archaean geothermal gradient and that of the modern earth. By superimposing model Archaean geotherms on the known high-pressure melting behaviour of model upper mantle compositions, two different models for Archaean lithosphere/asthenosphere can be presented.

Model I implies a lithosphere of similar thickness (~ 90 km) to that of the modern earth and predicts similar processes of eclogitization of basaltic crust and of subduction of oceanic crust. This model predicts that intrusives, extrusives or differentiates of highly undersaturated magmas (olivine nephelinites, olivine melilitites etc.) should occur within the Archaean. The principal differences from the modern earth are in higher temperatures within the upper mantle and a more efficient heat loss by convective processes (i.e. more active mantle diapirism and consequent magmatic activity).

Model II implies a thin Archaean lithosphere (~ 50 km) and higher subcrustal and lithosphere temperatures such that basaltic rocks do not react to eclogite on cooling to the geotherm. This model predicts that Archaean basaltic crust will not be subducted as eclogite for further geochemical differentiation in the upper mantle but rather will be folded against and between sialic continental nuclei (Archaean granite/greenstone terranes). Model II further predicts that Archaean basaltic volcanism or intrusives and their differentiates will be restricted to hypersthene-normative or mildly undersaturated liquids, i.e. exclusive of olivine-rich basanites, olivine nephelinites etc. Model II predicts a different type of tectonics in the Archaean with much more convective heat loss by higher temperature diapirism from deeper levels of the upper mantle (200—250 km minimum for source depth of Archaean diapirs). The transition from a model II Archaean earth to the modern earth would be gradual and transitional except that the onset of eclogite stability along mean geothermal gradient might be expected to have an important signature within the geological record as a change from granite/greenstone terranes to appearance of eclogite-bearing mélanges, absence of thick, synclinal volcanic sequences dominated by basalt or basalt + peridotite and pronounced linearity of metamorphic/magmatic orogenic belts.

The interpretation of the distinctive Archaean magmatism in terms of mantle convection and heat loss has been the focus of this paper. However, it is possible that, in seeking understanding of processes within the earth prior to 3.5 Ga ago, the effects of major impacts on the earth's surface must be considered (Green, 1972). The energy impacted to enter regions of the earth's crust by impact phenomena in the 4.5 to 4.0 Ga period and the

reaction of the earth to major impacts such as produced Mare Orientale on the moon must be considered in earth models which encompass the geology of the earliest Archaean.

With continuing programmes of field geology, geochronology and geochemistry of Archaean terranes it should be possible to test the relevance of model I or model II geotherms by the predictions on eclogite stability, geochemistry of basaltic magmas etc. which are intrinsic to each model. Similarly the applications of lunar impact chronology to the early history of the earth may lead to predictions which are testable in areas of the oldest Archaean shields.

REFERENCES

Arndt, N. T., 1977. Ultrabasic magmas and high degree melting of the mantle. Contrib. Mineral. Petrol., 64: 205—221.

Birch, F., 1952. Elasticity and constitution of the earth's interior. J. Geophys. Res., 57: 227—286.

Clark, S. P. and Ringwood, A. E., 1964. Density distribution and constitution of the mantle. Rev. Geophys., 2: 35—88.

Crawford, A. J., 1980. The petrology of the Howqua peridotite: a clinoenstatite-bearing cumulate from a refractory ultramafic magma. Contrib. Mineral. Petrol., (in press).

Dallwitz, W. B., Green, D. H. and Thompson, J. E., 1966. Clinoenstatite in a volcanic rock from the Cape Vogel area, Papua. J. Petrol., 7: 375—403.

Dietrich, V., Emmermann, R., Oberhansli, R. and Puchelt, H., 1978. Geochemistry of basaltic and gabbroic rocks from the West Mariana basin and the Mariana Trench. Earth Planet. Sci. Lett., 39: 127—144.

Duncan, R. A. and Green, D. H., 1980. The role of multistage melting in the formation of oceanic crust. Geology, 8: 22—26.

Duncan, R. A. and Green, D. H., in prep. The petrogenesis of second-stage melts and their role in the formation of oceanic crust.

Frey, F. A., Bryan, W. B. and Thompson, G., 1974. Atlantic ocean floor: geochemistry and petrology of basalts from legs 2 and 3 and the Deep Sea Drilling Project. J. Geophys. Res., 79: 5507—5527.

Gansser, A., Dietrich, V. J. and Cameron, W. E., 1979. Palaeogene komatiites from Gorgona Island. Nature, 278: 545—546.

Green, D. H., 1963. Alumina content of enstatite in a Venezuelan high temperature peridotite. Geol. Soc. Am. Bull., 74: 1397—1402.

Green, D. H., 1970. The origin of basaltic and nephelinitic magmas. Trans. Leicester Lit. Philos. Soc., 64: 28—54.

Green, D. H., 1972. Archaean greenstone belts may include terrestrial equivalents of Lunar maria? Earth Planet. Sci. Lett., 15: 263—270.

Green, D. H., 1975. Genesis of Archaean peridotitic magmas and constraints on Archaean geothermal gradients and tectonics. Geology, 3: 15—18.

Green, D. H., Nicholls, I. A., Viljoen, M. J. and Viljoen, R. P., 1975. Experimental demonstration of the existence of peridotite liquids in earliest Archaean magmatism. Geology, 3: 11—14.

Green, D. H. and Liebermann, R. C., 1976. Phase equilibria and elastic properties of a pyrolite model for the oceanic upper mantle. Tectonophysics, 32: 61—92.

Green, D. H., Hibberson, W. O. and Jaques, A. L., 1979. Petrogenesis of mid-ocean ridge basalts. In: M. W. McElhinny (Editor), The Earth: Its Origin, Structure and Evolution. Academic Press, London, pp. 265—290.

Jaques, A. L. and Green, D. H., 1979. Determination of liquid compositions in high pressure melting of peridotite. Am. Mineral., 64: 1312—1321.

Jaques, A. L. and Green, D. H., 1980. Anhydrous melting of peridotite at 0-15 kb pressure and the genesis of tholeiitic basalts. Contrib. Mineral. Petrol., 73: 287—310.

Kirby, G. A., 1979. The Lizard complex as an ophiolite. Nature, 282: 58—61.

Nesbitt, R. W., 1971. Skeletal crystal forms in the ultramafic rocks of the Yilgarn block, western Australia: evidence for an Archaean ultramafic liquid. Geol. Soc. Austr. Spec. Publ., 3: 331—350.

Nesbitt, R. W., Sun, S. S. and Purvis, A. C., 1979. Komatiites: geochemistry and genesis. Can. Mineral., 17: 165—186.

Ringwood, A. E., 1966. The chemical composition and origin of the earth. In: P. M. Hurley (Editor), Advances in Earth Science. M.I.T. Press, Cambridge, Mass., pp. 287—356.

Ringwood, A. E. and Green, D. H., 1966. An experimental study of the gabbro to eclogite transformation and some geophysical consequences. Tectonophysics, 3: 383—427.

Sun, S. S. and Nesbitt, R. W., 1978. Petrogenesis of Archaean ultrabasic and basic volcanics: evidence from rare earth elements. Contrib. Mineral. Petrol., 65: 301—325.

Viljoen, M. J. and Viljoen, R. P., 1969a. The geology and geochemistry of the lower ultramafic unit of the Onverwacht Group and a proposed new class of igneous rock. In: The Upper Mantle Project. Geol. Soc. S. Afr. Spec. Publ., 2: 55—85.

Viljoen, M. J. and Viljoen, R. P., 1969b. Evidence for the existence of a mobile extrusive peridotite magma from the Komati Formation of the Onverwacht Group. In: The Upper Mantle Project. Geol. Soc. S. Afr. Spec. Publ., 2: 87—112.

Wyllie, P. J. (Editor), 1967. Ultramafic and Related Rocks. John Wiley & Sons, New York, N.Y., 464 pp.

A20

Kimberlites. II: The Mantle and Crust—Mantle Relationships, by J. Kornprobst (Editor), pp. 161—178
© 1984 Elsevier Science Publishers B.V., Amsterdam — Printed in The Netherlands

THE NATURE OF THE UPPER-MOST MANTLE BENEATH VICTORIA, AUSTRALIA AS DEDUCED FROM ULTRAMAFIC XENOLITHS

by K.G. NICKEL and D.H. GREEN

Abstract - Utramafic inclusions from two neighbouring localities in Victoria, Australia include lherzolites with and without hydrous phases, wehrlites, pyroxenites, and hornblendites.

Mineral chemistry provides evidence for equilibrium crystallization for individual nodules at a depth near 45 km but over a range of temperatures. Temperature estimates yield systematic differences with anhydrous assemblages > phlogopite-bearing assemblages > amphibole-bearing assemblages.

Bulk rock variation of MgO, CaO, Al_2O_3 and compatible element contents in lherzolite and harzburgite has been modelled as an early partial melting event, giving rise to various degrees of depletion. The extracted liquid was of picritic composition.

Amphiboles in lherzolites are developed independently and postdate the partial melting event, as a response to near-isochemical metamorphic reaction, consequent on addition of water. The hydration events predate but are not precursor conditions for production of basanite. Hydration-metasomatism occurs in the uppermost mantle above the LVZ, the source region for basanites lies at deeper levels (?LVZ). The emplacement and passage of alkaline magmas through the lithosphere/upper mantle may be the cause of local metasomatism and of hydration.

Wehrlites, pyroxenites, hornblendites and some lherzolites are precipitates from magmas fractionating and/or crystallizing at mantle depths. Observable wall-rock reaction is extremely restricted (about 1 cm) as evidenced by composite xenoliths.

INTRODUCTION

The xenoliths and megacrysts found in the Victorian Newer Volcanics have drawn much attention in recent years because of their abundance and great variety. Work has been carried out concentrating on various aspects including isotope studies (Cooper & Green, 1969; Dasch & Green, 1975), uranium distribution (Kleeman et al., 1969) and on various types, e.g. megacrysts (Irving, 1974c), pyroxene-rich xenoliths (Irving, 1974a; Ellis, 1976), lherzolites (Frey &

Green, 1974), composite xenoliths (Irving, 1980), as well as their host basalts (Frey et al., 1978; Green, 1973a; Irving & Green, 1976).

These papers have shown that most lherzolites represent accidental xenoliths brought up from the upper mantle and that pyroxene-rich xenoliths are high-pressure precipitates from either the host magma or preceeding magmas.

Papers on hydrous phases and on metasomatism in the upper mantle (e.g. Best, 1975; Boettcher & O'Neil, 1980; Carswell 1975: Embey-Isztin, 1976; Francis, 1976a,b; Green, 1970[b], 1973a,b; Green & Ringwood, 1967; Kesson & Price, 1972; Lambert & Wyllie, 1968; Lloyd & Bailey, 1973; Menzies & Murthy, 1980[b]; Varne, 1970; Wass, 1980; Wass et al., 1980; Wass & Rogers, 1980; Wilshire et al., 1980; Wilshire & Trask, 1971) have studied and interpreted the role of amphibole and phlogopite in upper mantle xenoliths and there are differing views on the relationship of such hydrous phases to magma genesis and on the pervasive or local character of amphibole-producing metasomatism.

Amphibole and phlogopite have been reported as rare or minor phases in xenoliths from the Newer Volcanics (Ellis, 1976; Frey & Green, 1974; Wass & Irving, 1976), but recently Hollis (1981) and Sutherland & Hollis (1983) reported localities at the maar-type volcanoes Lake Bullenmerri and Lake Gnotuk (38°15'S, 143°8'E), at which amphibole-bearing xenoliths are common. The present work describes xenoliths from Lake Bullenmerri and near-by Mt. Leura (Singleton & Joyce, 1969), concentrating on petrography, mineral and bulk chemistry and the application of these data to deduce a model of mantle evolution beneath the eruption centres.

PETROGRAPHY AND MINERALOGY

Host rocks

At both Lake Bullenmerri and Mt. Leura the host rocks to the xenoliths are vesicular basanites (table B of appendix) containing small zoned olivine phenocrysts and uncommon clinopyroxene phenocrysts in a groundmass of clinopyroxene, olivine, plagioclase, ilmenite, nepheline, apatite and glass. Megacrysts of amphibole, clinopyroxene and anorthoclase have reacted borders against groundmass; amphibole and anorthoclase megacrysts are relatively common at Lake Bullenmerri.

Xenoliths

The xenoliths have been grouped on grounds of mineralogical, textural and chemical differences into several types:

A - Lherzolites (ol>opx>cpx>sp±amph±mica)

-1 without hydrous phases or remnants thereof

-2 amphibole bearing

-3 phlogopite bearing

-4 with sites of former hydrous phases, now only present as secondary assemblages of glass, olivine and clinopyroxene (Frey & Green, 1974)
-5 amphibole and phlogopite bearing
-6 Fe-rich (amphibole bearing)
-7 layered or banded

B - Wehrlites (ol > cpx ± amph ± sp ± opx ± mica ± ap)
C - Harzburgites (ol > opx > sp ± amph)
D - Hornblendites (amph > mica > ilm ± cpx ± opx ± titanomag ± ol)
E - Composite xenoliths (two or more different rock-types in one specimen)
F - Pyroxenites (gt, cpx, opx ± sp ± amph)
G - Cumulate textured wehrlite (ol > cpx, amph, phlo)

The textures of lherzolites, wehrlites and harzburgites are classified following Mercier & Nicolas (1975) into protogranular, porphyroclastic and recrystallized (equigranular or tabular), but it must be noted that most samples represent transitional types. Rock descriptions are given in the appendix.

Mineral chemistry

Analyses of the constituent phases are listed in table 1. The spinel lherzolites show the typical range of compositions observed in many localities (e.g. Basaltic Volcanism Study Project, 1981; Frey & Green, 1974; Frey & Prinz, 1978; Kuno, 1969; Kuno & Aoki, 1970; Maaloe & Aoki, 1977; Ross et al., 1954; White, 1966) with olivine in the range Fo_{88-92} and principal variations being the Al_2O_3 content of pyroxenes and the Cr/Cr+Al ratio of spinel.

The wehrlites and lherzolites of groups A-5 to A-7 and group B have olivine in the range of Fo_{82-90}, compatible with the interpretation that they are of cumulate origin from a basaltic liquid.

The group C harzburgite shows affinities with the group A lherzolites and is very refractory in terms of Mg-values of olivine and orthopyroxene and in the high Cr/Al-ratio of spinel. The amphibole is similarly Mg-rich and high in Cr_2O_3, but is the most Na-rich of all amphiboles analysed and contains moderately high K_2O.

The group D hornblendites are markedly more Fe-rich than all other assemblages and this pattern continues in the composite xenoliths in which amphibole-phlogopite veinlets occur. By contrast the pyroxenites examined are Mg-rich and highly aluminous, with compositions resembling those of the lherzolite suite. Consistent with the highly magnesian clinopyroxenes (Mg 89-91), the garnets are also highly magnesian (Mg 79-82) but with low Cr_2O_3 contents (lower then coexisting clinopyroxene).

The distinctive cumulate textured wehrlite (group G) has mineral compositions closest to those of group B wehrlites and group D hornblendites.

Table 1: Averages of microprobe analyses of mineral phases of xenoliths: Mg/Mg+Fe(ol)= Mg-nb of coexisting olivine; BME= Lake Bullenmerri, LE= Mt. Leura

Group	A-1										
Sample	BME-54			BME-69			BME-99			BME-160	
Phases	opx	cpx	sp	opx	cpx	sp	opx	cpx	sp	opx	cpx
Na2O		0.70			0.81			1.51			1.18
MgO	33.08	16.70	20.07	33.21	17.08	20.36	33.33	15.91	18.86	32.99	16.28
Al2O3	4.75	5.49	52.69	4.74	5.25	50 39	3.77	5.39	44.18	5.03	6.26
SiO2	55.02	52.66		54.97	52.83		55.71	53.42		54.49	52.18
CaO	0.84	20.82		0.71	20.58		0.77	19.70		0.78	19.81
Cr2O3	0.47	0.93	15.70	0.41	0.97	17.45	0.48	1.38	25.27	0.45	1.11
FeO	5.86	2.70	10.41	5.76	2.48	11.03	5.94	2.69	11.68	6.02	2.78
Mg/Mg+Fe(ol)	90.58			90.48			90.34			90.03	

Group	A-1										
Sample	160	LE-00			LE-50			LE-532			LE-532
Phase	sp	opx	cpx	sp	opx	cpx	sp	opx	cpx	sp	opx
Na2O			2.28			2.12			1.24		
MgO	20.09	32.75	15.48	20.06	33.85	15.69	20.97	33.81	16.24	16.90	33.07
Al2O3	51.15	5.55	7.25	55.45	2.76	5.17	29.46	3.03	4.67	34.87	4.40
SiO2		53.79	51.60		56.41	53.86		56.15	53.35		54.89
CaO		0.82	19.22		0.75	18.03		0.71	19.98		0.63
TiO2	0.31		0.38	0.29		0.27	0.52				
Cr2O3	16.16	0.41	0.97	11.97	0.61	2.06	37.72	0.66	2.01	34.48	0.37
FeO#	11.46	6.23	2.99	11.05	5.59	2.71	15.03	5.64	2.54	13.37	6.08
Mg/Mg+Fe(ol)		90.03			90.84			90.66			

Group	A-1						A-2					
Sample	LE-532		LE-2664				BME-9				BME-15	
Phase	cpx	sp	opx	cpx	sp		opx	cpx	sp	amph	opx	cpx
Na2O	1.69			0.92				2.31		3.45		1.68
MgO	15.70	20.66	34.39	16.26	19.39		35.57	15.24	13.14	17.04	32.76	15.08
Al2O3	6.28	52.67	3.03	4.19	45.68		0.86	3.34	16.75	10.22	4.58	6.68
SiO2	52.70		56.12	53.49			57.59	54.84		42.12	55.09	52.59
K2O										0.96		
CaO	19.39		0.32	21.97			0.26	19.26		9.42	0.64	20.08
TiO2	0.38									0.34		0.41
Cr2O3	1.08	13.97	0.34	1.23	22.96		0.25	2.95	52.57	3.19		0.51
FeO#	2.79	11.42	5.49	1.91	11.05		5.55	2.07	16.88	2.95	6.93	2.97
Mg/Mg+Fe(ol)	90.27		90.94				91.02				88.64	

Group	A-2										
Sample	BME-15		BME-27				BME-58				BME-62
Phase	sp	amph	opx	cpx	sp	amph	opx	cpx	sp	amph	opx
Na2O		3.33		1.71		3.26		2.18		3.28	
MgO	20.24	17.07	33.69	15.68	20.14	17.33	32.76	14.93	19.77	17.22	34.02
Al2O3	58.04	15.20	4.25	5.94	58.57	15.08	4.64	7.19	51.93	15.15	2.60
SiO2		42.51	54.97	52.65		43.42	54.72	52.66		43.35	56.45
K2O		1.01				0.92				1.57	
CaO		10.70	0.54	20.71		9.78	0.69	18.27		9.82	0.38
TiO2		1.86		0.24		1.63				1.20	
Cr2O3	10.44	0.78	0.25	0.77	10.16	0.66	0.48	1.21	15.96	1.50	0.28
FeO#	11.28	4.09	6.13	2.37	10.11	3.26	5.96	2.92	11.47	3.85	6.27
Mg/Mg+Fe(ol)			90.17				90.60				

table 1 (ctd.)

Group	A-2										
Sample	BME-62			BME-74				BME-134			
Phase	cpx	sp	amph	opx	cpx	sp	amph	opx	cpx	sp	amph
Na2O	1.39		3.57		1.55		2.97		2.33		3.89
MgO	15.81	18.12	17.94	33.08	15.96	18.82	16.91	34.47	15.34	15.55	16.90
Al2O3	4.73	47.95	14.05	3.63	5.14	47.68	14.28	1.80	4.28	33.04	12.45
SiO2	53.56		42.73	55.62	53.46		42.45	56.61	54.69		41.58
K2O			n.d.				0.92				0.32
CaO	21.07		10.43	0.39	20.44		10.79	0.24	19.62		9.44
TiO2			0.54				1.14				0.36
Cr2O3	1.07	20.74	1.49	0.29	1.06	19.71	1.68	0.28	1.54	35 24	2.25
FeO#	2.37	12.26	3.23	6.39	2.39	12.61	3.81	6.30	2.21	15.42	3.48
Mg/Mg+Fe(ol)	89.75			89.18				89.73			

Group	A-2										
Sample	BME-139				BME-147				BME-161		
Phase	opx	cpx	sp	amph	opx	cpx	sp	amph	opx	cpx	sp
Na2O		1.87		3.50		2.67		4.02		1.67	
MgO	33.01	15.11	19.40	17.31	34.43	15.34	13.63	18.44	33.16	15.62	19.71
Al2O3	3.60	6.25	53.64	14.70	2.12	4.70	27.13	13.63	3.89	5.77	51.83
SiO2	55.66	53.32		42.80	55.93	53.71		43.64	55.62	53.22	
K2O				1.22				0.57			
CaO	0.62	19.75		10.45	0.38	19.61		10.03	0.39	20.32	
TiO2				0.90				0.31			
Cr2O3	0.22	0.79	15.02	0.99	0.31	1.47	41.74	1.95	0.24	0.99	15.80
FeO#	6.97	3.00	11.84	3.94	6.61	2.50	17.38	3.57	6.18	2.42	11.37
Mg/Mg+Fe(ol)	88.60				89.36				89.69		

Group	A-2											
Sample	161	BME-166				BME-167				LE-2641		
Phase	amph	opx	cpx	sp	amph	opx	cpx	sp	amph	opx	cpx	
Na2O	2.86		1.01		3.49		1.38		3.35		1.18	
MgO	16.00	34.31	16.02	20.23	17.47	33.04	15.47	20.32	16.68	34.17	15.95	
Al2O3	13.83	3.30	4.86	52.81	14.65	4.52	6.60	55.49	14.59	3.17	4.99	
SiO2	40.51	55.70	53.11		42.45	54.87	52.54		40.39	56.36	53.26	
K2O	0.86				0.20				n.d.			
CaO	10.34	0.28	21.72		10.99	0.41	20.40		9.77	0.28	21.57	
TiO2	1.27		0.24		1.33		0.36		1.62		0.22	
Cr2O3	1.36	0.27	1.00	15.42	1.19	0.25	0.90	11.54	0.95	0.22	0.92	
FeO#	3.53	5.94	2.09	10.54	3.03	6.53	2.42	11.22	3.66	5.79	1.95	
Mg/Mg+Fe(ol)			90.53				89.50				90.56	

Group	A-2		A-3							
Sample	LE-2641		LE-67				LE-68			
Phase	sp	amph	opx	cpx	sp	phlo	opx	cpx	sp	phlo
Na2O		3.32		1.61				1.72		0.74
MgO	20.52	18.16	33.75	16.15	19.28	21.10	33.17	15.68	20.46	19.69
Al2O3	52.21	14.38	4.13	5.73	46.96	17.26	4.66	6.53	54.22	16 64
SiO2		43.02	55.54	53.18		37.48	55.40	52.86		34.27
K2O		n.d.				9.61				8.67
CaO		10.99	0.71	19.56			0.71	19.51		
TiO2		1.32				2.65				2.86
Cr2O3	16.52	1.13	0.53	1.22	21.77	1.58	0.41	0.90	14.29	0.98
FeO#	9.66	2.99	5.33	2.54	11.55	3.73	5.66	2.68	10.69	3.79
Mg/Mg+Fe(ol)				91.46				90.92		

table 1 (ctd.)

Group	A-4										
Sample	BME-48			BME-144			BME-162			LE-4	
Phase	opx	cpx	sp	opx	cpx	sp	opx	cpx	sp	opx	cpx
Na2O		2.04			1.34			1.23			2.10
MgO	34.56	15.83	16.14	33.37	15.86	19.92	33.41	16.04	19.92	32.20	15 01
Al2O3	1.61	2.97	27.70	3.82	5.70	53.28	3.89	5.6753.19		5.74	7.94
SiO2	57.54	55.33		55.17	53.04		55.41	53.02		54.19	52.25
CaO	0.34	20.24		0.46	20.60		0.42	20.52		0.68	18.53
TiO2											0.44
Cr2O3	0.34	1.44	40.60	0.27	0.90	14.53	0.20	1.00	13.73	0.32	0.67
FeO#	5.46	2.16	14.01	6.66	2.56	11.35	6.48	2.53	11.69	6.39	3.07
Mg/Mg+Fe(ol)	91.20			89.09			89.37			89.53	

Group	A-4									
Sample	LE-4	LE-19			LE-544			LE-2662		
Phase	sp	opx	cpx	sp	opx	cpx	sp	opx	cpx	sp
Na2O			1.92			1.03			1.42	
MgO	20.49	35.34	16.69	14.63	33.90	16.07	20.47	34.72	16.84	18.26
Al2O3	59.10	1.21	2.23	18.71	3.42	4.76	52.80	2.26	3.53	34.61
SiO2		57.26	54.64		55.45	52.71		56.83	54.52	
CaO		0.35	19.14		0.33	21.84		0.33	20.39	
TiO2						0.32				
Cr2O3	7.93	0.26	3.49	50.46	0.32	1.04	14.48	0.30	1.43	34.76
FeO#	10.49	5.58	1.92	15.81	6.21	2.24	11.21	5.18	1.87	11.51
Mg/Mg+Fe(ol)		90.91			89.94			91.50		

Group	A-5					A-6					
Sample	BME-143					BME-47			BME-154		
Phase	opx	cpx	sp	amph	mica	opx	cpx	amph	opx	cpx	sp
Na2O		2.09		3.01	0.79		1.41	3.29		1.76	
MgO	33.10	15.39	19.71	16.78	20.35	33.13	15.85	18.03	32.67	15.45	14.55
Al2O3	4.91	6.99	51.22	14.76	17.13	1.96	3.47	13.47	2.38	4.34	28.22
SiO2	54.17	51.66		42.53	37.98	56.17	54.20	44.34	56.06	53.67	
K2O				1.78	9.17						
CaO	0.84	18.94		10.47		0.51	20.85	10.53	0.39	20.03	
TiO2	0.20	0.78	0.43	3.59	6.04						0.29
Cr2O3	0.54	1.26	16.48	1.35	1.27	0.26	1.11	1.72	0.30	1.70	37.55
FeO#	5.99	2.89	11.60	3.75	4.27	7.97	3.08	4.29	7.58	3.06	18.12
Mg/Mg+Fe(ol)	90.39					86.85			87.12		

Group	A-6	A-7				B					
Sample	BME15	BME-137				BME-18				BME-51	
Phase	amph	opx	cpx	sp	amph	opx	cpx	sp	amph	cpx	sp
Na2O	2.85		0.60		2.66		1.81		4.09	2.36	
MgO	16.06	33.99	16.12	20.67	16.43	35.14	16.08	11.26	19.12	15.26	11.24
Al2O3	12:22	3.11	4.64	59.55	13.99		1.80	11.83	9.42	2.88	13.89
SiO2	41.47	56.00	53.14		39.94	58.28	55.22		45.98	55.11	
K2O	1.23				0.80				0.56		
CaO	10.32	0.31	22.57		11.21	0.36	21.35		10.03	20.36	
TiO2	1.25				1.54			0.20	0.60		
Cr2O3	2.24		0.61	8.47	0.96		1.44	58.14	2.26	1.42	56.07
FeO#	4.31	6.59	2.20	10.64	3.52	6.22	2.29	18.66	3.02	2.62	18.80
Mg/Mg+Fe(ol)		89.67				89.79				89.81	

table 1 (ctd.)

Group	B										
Sample	BME51	BME-135		BME142	(cumul.)BME-152(matrix)				LE-27		
Phase	amph	cpx	amph	cpx	opx	cpx	cpx	amph	opx	cpx	sp
Na2O	4.48	1 63	4.10	2.06		1.35	1.44	3.06		1.37	
MgO	19.36	15.92	18.62	15.59	30.72	14.67	15.13	15.31	33.09	15.52	19.66
Al2O3	9.86	2.22	10 13	1.70	5.03	7.56	6.69	14.24	4.27	6.05	52.99
SiO2	46.96	54.97	45.94	54.60	52.74	50.33	50.63	40.84	55.12	52.41	
K2O	0.66		0.83					1.23			
CaO	9.97	21.23	9.78	20.38	0.92	19.79	19.51	10.36	0.72	20.46	
TiO2	0.25		0.89		0.37	1.02	0.83	3.28		0.43	0.21
Cr2O3	1.74	1.20	1.87	2.11	0 22	0.35	0.53	0.37	0.40	0.80	15.15
FeO#	3.20	2.84	3.83	3.57	10.01	4.94	5.25	6.63	6.40	3.00	12 07
Mg/Mg+Fe(ol)		87.92		85.40		83.39	82.63			89.75	

Group	B	C			D						
Sample	LE-27	BME-163			BM-117			BME-156			
Phase	phlo	opx	sp	amph	amph	phlo	ilm	amph(a)	amph(b)	phlo	opx
Na2O	0.70			4.61	2.85	0.99		2.71	2.76	0.94	
MgO	20.56	35.17	12.46	19.14	12.08	14.40	9.38	12.48	13.83	14.71	26.23
Al2O3	16.68	2.27	14.66	10.53	14.96	16.38	1.09	14.87	14.45	16.45	4.75
SiO2	36.99	56.57		46.00	40.21	36.87		39.97	40.76	36.26	52.30
K2O	9.01			0.62	1.76	9.14		1.78	1.20	8.93	
CaO	0.37	0.32		9.28	9.87			10.06	10.39		0.91
TiO2	4.72			0.20	5.06	8.90	52.16	4.42	3.76	7.21	0.26
Cr2O3	0.97		56.07	3.04							
FeO#	4.25	5.30	16.64	2.59	10.07	11.89	37.00	10.54	9.55	12.01	15.60
Mg/Mg+Fe(ol)		91.44			72.69			73.41			

Group	D		E(including F)								
Sample	BME-156		(lherzolite)			BME-109		(vein)			Le-00
Phase	cpx	ilm	opx	cpx	sp	amph	Tr-amp	amph	phlo	cpx	phlo
Na2O	1.13			1.69		3.38	3.31	3.39	1.17	1.90	0 92
MgO	13.56	8.67	33.59	15.65	15.56	17.51	17.02	16.79	21 02	15.23	20 97
Al2O3	7.17	0.82	2.64	4.50	36.44	13.80	13.19	13.28	16.62	5.18	16.32
SiO2	50.16		55.95	53 94		43.39	43.10	45.01	39.68	53.73	38.11
K2O						0.79	1.11	1.31	9.06		9.30
CaO	19.28		0.57	19.50		10.06	10.12	10.01		18.93	
TiO2	1.13	52.51				0.48	2.08	2.66	4.39	0.27	4.34
Cr2O3			0.46	1.40	31.01	2.10	1.80				1.74
FeO#	7.52	37.84	6.79	3.34	16.23	4.10	4.58	7.02	6.69	4.77	3 84
Mg/Mg+Fe(ol)				88.94							90.80

Group	E(including F)											
Sample	(lherzolite)				(cpx'te)		BME-116	(transition)			(gt-px'te)	
Phase	opx	cpx	sp	amph	cpx	sp	opx	cpx	sp	amph	gt	cpx
Na2O		1.66		3.30	1.60			1.50		2.85		1.66
MgO	34.11	16.00	18.93	17.95	15.46	20.06	33.31	15.39	22.25	15.66	20.55	15.22
Al2O3	3.06	5.14	43.71	15.26	6.33	50.03	4.92	7.17	64.07	14.66	23.86	7.52
SiO2	55.96	53.59		44.00	52.78		54.79	52.71		39.03	41.89	52.74
K2O				0.98						0.74		
CaO	0.47	20.12		10.48	20.43		0.54	20.26		10.15	4.64	19.98
TiO2				0.52						1.07		
Cr2O3	0.35	1.24	24.29	1.80	1.01	17.82		0.51	3.37	0.57	0.22	0.31
FeO#	5.70	2.26	12.16	3.42	2.31	11.14	6.12	2.45	9.51	3.69	8.25	2.60
Mg/Mg+Fe(ol)	90.70											

Group	E(incl. F)					G			
Sample	116	(gt-px)BME-114 (cpx'te)				BME-168			
Phase	opx	opx	cpx	gt	amph	opx	cpx	amph	phlo
Na20			1.50		3.19		2.22	3.25	0.76
MgO	32.41	32.00	15.09	19.98	17.15	29.77	14.57	15.28	18.58
Al203	5.84	5.45	7.23	23.80	17.16	4.49	7.34	14.87	17.29
Si02	54.19	54.24	52.57	41.31	42.14	53.35	51.66	41.98	37.37
K20					0.80			1.65	8.87
CaO	0.49	0.51	20.16	4.76	10.11	0.98	18.00	9.89	
Ti02					0.54		0.56	3.40	4.79
Cr203		0.34							
FeO#	6.42	7.53	3.17	9.42	4.24	11.20	5.49	7.32	7.97
Mg/Mg+Fe(ol)							80.76		

CONDITIONS OF CRYSTALLIZATION OF LHERZOLITE XENOLITHS

Element partitioning

Plots of Fe/Mg ratios of the phases olivine, orthopyroxene, clinopyroxene and dispersed pargasitic amphibole all reveal linear relationships with varying degrees of scatter. $(Fe/Mg)_{ol}$ vs. $(Fe/Mg)_{cpx}$ shows some scatter of data points but a systematically lower $K_D = (Fe/Mg)_{cpx} / (Fe/Mg)_{ol}$ for amphibole bearing assemblages than for anhydrous or phlogopite bearing lherzolites. Uncertainty in Fe2+/Fe3+ of clinopyroxenes prevents meaningful temperature estimates, but lower temperatures of crystallization of the amphibole bearing assemblages are inferred using an empirical experimental calibration (Mori & Green, 1978).

Positive correlation is present between (Cr/Al) of spinel, orthopyroxene, clinopyroxene, and amphibole, and plots of $(Cr/Al)_{opx}$ vs. $(Cr/Al)_{sp}$ or $(Cr/Al)_{cpx}$ both show weak systematic grouping of the amphibole bearing and amphibole-free data.

The exchange of Al for Si provides further evidence for equilibrium between phases.Plots of $(Al(IV)/Si)_{cpx}$ vs. both $(Al(IV)/Si)_{opx}$ or $(Al(IV)/Si)_{amph}$ yield strong linear relationships for all data except low-alumina wehrlites.

To summarize the element partitioning data for coexisting minerals, the regularity of compositional relationships shows that olivine - two pyroxenes - spinel and amphibole (where present) are coexisting phases, equilibrated under varying P,T conditions in a limited range of bulk compositions. In particular, amphibole is an equilibrium phase within the assemblage in which it occurs and does not reflect disequilibrium or arrested replacement process by super-imposed metasomatic events.

The limited number of samples containing phlogopite does not permit a similar analyses of element partitioning relations between phlogopite and other phases.

Geothermometry/barometry from mineral equilibria

The currently available geothermometers and geobarometers all show considerable uncertainties and deviations from each other (Carswell & Gibb, 1980)[b], so that the determination of absolute numbers is likely to include large uncertainties. However, internal consistency has been demonstrated for some models and the indications for relative temperature distributions are regarded as meaningful.

The thermometer of Wells (1977) is preferred to that of Wood & Banno (1973), because of the highly magnesian character of the lherzolites and their pyroxenes. The range of calculated temperatures for lherzolites is 810° to 1070° C. The distribution is not random, but shows correlation with mineralogy (fig. 1), the lowest recorded temperatures occuring in amphibole-bearing types, intermediate temperatures in phlogopite bearing types and higher temperatures in anhydrous types.

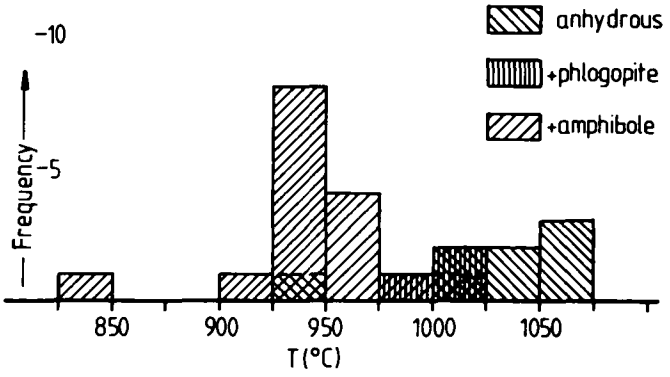

Fig. 1: Histogram of temperature estimates for lherzolite xenoliths by the method of Wells (1977) in relation to their mineralogy

Most anhydrous lherzolites do not show pyroxene exsolutions. Thus they do not retain textural evidence of their cooling history but rather record only one relatively high temperature of equilibration. Dasch & Green (1975) obtained evidence from Sr-isotopes and Rb/Sr systematics for an "age" of approx. 700 Ma, which they suggested was related to late Precambrian/Cambrian magmatic activity, the lherzolites representing residual mantle from such magma segregation and thus recording a high temperature event or events within the mantle. The isotopic age may record events when the region was part of an oceanic regime (Crawford, 1983; Crawford & Keays, 1978) with a high geothermal gradient.

The hydrous lherzolites on the other hand commonly show exsolutions in

pyroxenes and thus record a re-equilibration (cooling) history. The water may have helped in the process of annealing recrystallization.

The P-conditions for the lherzolites cannot be determined with reliability, because no general accepted experimental data exist for a geobarometer for spinel lherzolites. Only the stability region for spinel in peridotitic systems can be used, giving the range of app. 8 - 20 kb. Assuming a depth-selective sampling process, the two pyroxenites which contain garnet are inferred to come

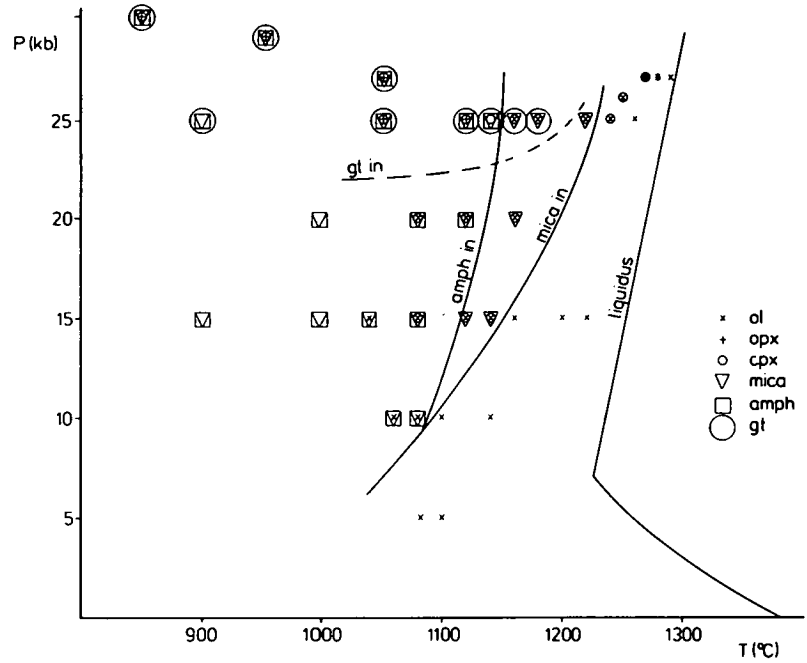

fig. 2: Above-solidus phase diagram for basanite No. 2650 + 10% ol for a water content of 4.5 wt.%.

from similar depths and have been used for the estimation of P. The barometer based on the reaction enstatite + Mg-tschermak's molecule = garnet in the form of Harley & Green's (1982) equation was applied, yielding values of 12 to 16 kb, depending on the method of temperature estimation employed (Wells, 1977; Ellis & Green, 1979).

table 2

P (kb)	15	15	BME-168
T (°C)	1120	1080	
Mg#(ol)	79-80	73-75	80.8
Mg#(cpx)	81-83	76-78	82.6
Mg#(mica)	81-82	79	80.6
Mg#(amph)	absent	74-78	78.8

P,T are experimental conditions, Mg# = Mg/Mg+Fe

A second approach towards a P-estimation utilizes the experimental data obtained in a liquidus phase study on the basanite of Mt. Leura (No. 2650 + 10% ol, Green, 1973a). A diagram of the phases coexisting

with liquid for this compostion containing 4.5% H_2O is given in fig. 2.

The mineralogy of cumulate wehrlite BME-168 (group G) has been compared with the experimentally produced phases and the bracketing conditions for the phases of BME-168 are listed in table 2, again pointing towards pressures around 15 kb and thus supporting the restricted depth sampling model.

COMPLEXITIES OF THE UPPER MANTLE SOURCE REGION FOR LHERZOLITE XENOLITHS

Bulk rock chemistry

Discussion of bulk rock chemistry must bear in mind three constraining difficulties: (a) coarse grain size and restricted sample size (most are < 20 cm) make representative sampling difficult; (b) mineral banding enhances the problem of representative sampling; (c) concentrations of Na, K, Ti, P are very low and detection limits of XRF analyses are similar to abundance levels, so that large relative errors can result.

To overcome problems with Na_2O-analyses at levels which are near the detection limit of XRF analyses for lherzolites, harzburgites and wehrlites, the Na--content of the bulk rock has been calculated from modal abundances (derived by a least-square fit) of analysed minerals. Analyses of bulk rock compositions are listed in table 3.

On the basis of bulk rock chemistry, subsets can be distinguished. The AFM--diagram (fig. 3) shows a single linear trend for hydrous and anhydrous lherzolites and the harzburgite, clearly separated from the data points of wehrlites, Fe-rich lherzolites and the cumulate BME-168. The wehrlites and Fe-rich lherzolites may be interpreted as following a different cumulate trend. Lherzolites of group A-5 and A-7 however fall off both trends, indicating different histories.

In chemical variation diagrams of the type MgO (wt-%) vs. oxides or trace elements the wehrlites, Fe-rich lherzolites and other cumulates do not form clear trends, but tend to scatter. This may be seen as evidence that those do not belong to one single group. They may originate in different events and represent cumulates from different sources (e.g. picrite, basanite).

The lherzolites (except groups A-5 and A-7) on the other hand exhibit regular linear variations with MgO for a number of oxides and trace elements (fig. 4). The best correlations are given with Al_2O_3 and CaO, showing a very welldefined rectilinear trend. A straight line chemical variation in oxides or oxide ratios is suggestive of a mixing line for those elements.

Na_2O, BaO, Sr and Zr show only a very weak or no correlation with MgO. However, the variations of these elements in most of the amphibole-bearing lherzolites are within the compositional spectrum of the anhydrous lherzolites. Efforts have been made to analyse for K_2O, P_2O_5, Rb, Y and Nb. The detected

table 3: chemical analyses of bulk rocks from Lake Bullenmerri, normalised to 100% on volatile free basis

Group	A-1			A-2						A-3
Sample	69	99	160	9	134	162	167	139	15	143
Na2O	0.14	0.12	0.14	0.19	0.32	0.19	0.19	0.72	0.40	0.16
MgO	44.12	44.25	40.26	45.95	44.41	42.26	40.65	38.35	37.99	40.36
Al2O3	1.65	1.69	2.91	0.72	1.25	2.12	2.75	3.69	3.86	2.62
SiO2	43.72	44.36	45.19	43.87	43.15	44.64	44.30	44.51	44.95	44.80
K2O				0.03	0.03			0.17	0.03	0.08
CaO	1.47	1.72	2.60	0.67	1.22	2.20	2.64	3.49	3.54	2.54
TiO2	0.04	0.05	0.10	0.02	0.04	0.06	0.11	0.17	0.17	0.08
FeO#	8.10	7.98	8.01	7.70	8.80	7.67	8.58	8.26	8.27	8.62
Cr2O3	0.33	0 42	0.39	0.39	0.35	0.46	0.37	0.41	0.41	0.41
MnO	0.14	0.13	0.14	0.12	0 15	0.13	0.14	0.14	0.14	0.13
NiO	0.30	0.29	0.28	0.32	0.32	0.28	0.27	0.23	0.24	0.27
Zr	2	9	4	2	5	3	5	32	16	10
Sc	10	8	9.4	6	7	11	12	16	15	11
V	49	42	55	30	36	56	63	89	86	58

Group	A-5	A-6		A-7	B					C
Sample	143	154	47	137	18	135	142	51	152	163
Na2O	0.64	0.30	0.55	0.81	0.51	0.46	0.25	0.82	0.40	0.24
MgO	36.09	41.68	38.37	30.96	44.01	42.58	42.39	41.77	38.12	46.90
Al2O3	4.30	1.54	2.45	7.64	1.04	1.04	0.70	1.71	1.73	0.68
SiO2	45.67	43.34	44.40	44.15	42.30	42.13	41.60	42.36	42.02	43.39
K2O	0.08	0.04	0.14	0.09	0.07	0.06	0.10	0.11	0.04	0.02
CaO	4.74	1.60	2.88	6.24	2.50	2.98	1.83	3.96	3.65	0.63
TiO2	0.45	0.14	0.07	0.44	0.10	0.11	0.10	0.07	0.31	0.02
FeO#	7.02	10.44	10.33	6.24	8.32	9.85	12.17	8.00	13.19	7.27
Cr2O3	0.67	0.40	0.44	0.84	0.39	0.34	0 33	0.51	0.20	0.38
MnO	0.12	0.15	0.18	0.11	0.15	0.15	0.23	0.14	0.13	0.13
NiO	0.22	0.29	0.24	0.21	0.28	0.27	0.29	0.26	0.22	0.31
P2O5		0.01	0.04	0.05	0.35			0.35		0.04
Zr	19	21	29	42	2	36	72	24	13	5
Sc	19	7	13	30	8	7	5	12	9	7
V	121	43	72	180	39	37	23	54	71	24

Group	D		E/F			G
Sample	117	156	114	116G	116C	168
Na2O	2.11	1.53	1.11	1.11	1.36	0.51
MgO	12.35	13.27	16.96	17.27	19.52	31.09
Al2O3	14.14	12.43	13.94	14.72	11.75	4.14
SiO2	38.12	43.40	48.06	47.37	47.84	43.60
K2O	1.77	0.93	0.07	0.04	0.13	0.23
CaO	9.90	12.38	12.83	12.94	13.95	6.12
TiO2	7.48	4.10	0.14	0.19	0.33	0.71
FeO#	8.83	11.73	6.49	5.95	3.90	13.71
Cr2O3	0.01	0.05	0.15	0.15	1.01	0.07
MnO	0.11	0.13	0.19	0.19	0.08	0.17
NiO	0.02	0.02	0.04	0.04	0.07	0.15
P2O5		0.01	0.02	0.01		0.03
Zr	55	46	26	11	10	42
Sc	22	27	53	47	39	13
V	549	449	219	221	218	133

FeO# = Fe_{tot} as FeO
oxides in wt.%, trace
elements in ppm.
116G = garnet-pxte
116C = cpxte.

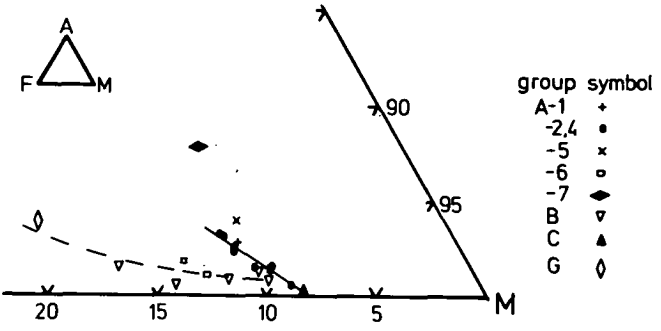

fig. 3: AFM-diagram for bulk rock compositions of nodules, A = Al_2O_3 + Cr_2O_3, F = FeO_{tot}, M = MgO, legend of groups see text

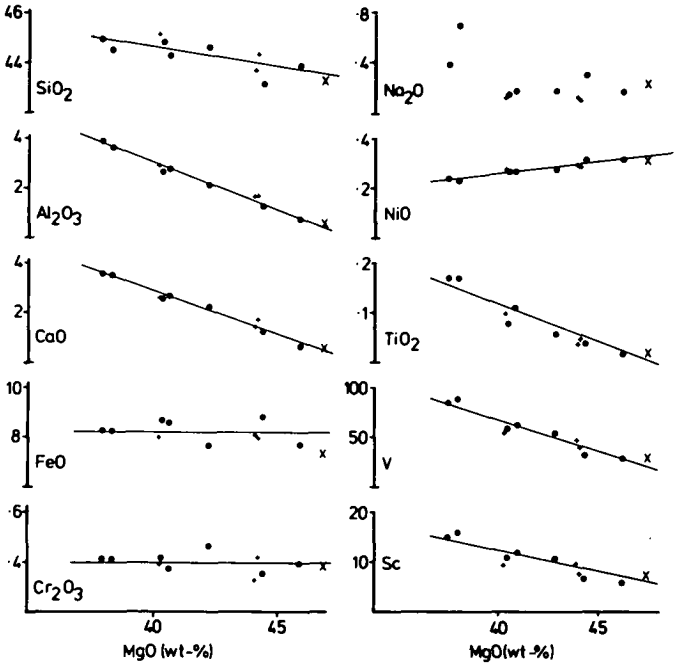

fig. 4: MgO (wt.%) vs. oxides (wt.%) and trace elements (ppm) of lherzolites and harzburgite. Crosses anhydrous lherzolites (group A-1), Dots: hydrous lherzolites (groups A-2 and A-4), X = harzburgite (group C)

range (K_2O < 0.03%, P_2O_5 < 0.04%, Rb < 3 ppm, Y < 3 ppm, Nb < 2 ppm) was in each case close to the detection limit of XRF analyses, hence their variation cannot provide significant trends. Nonetheless the low concentraions of K_2O, P_2O_5, Rb, Y and Nb in both hydrous and anhydrous lherzolites argues that these elements have not been added in large, significant amounts to the hydrous lherzolites. However, sample BME-139 shows unusual high values for Na_2O, K_2O, Nb as well as Sr, Ba and Zr. This sample has an exceptionally high modal abundance of amphibole (app. 15%) and thus may provide evidence for metasomatic chemical change. It should be noted that the sample is small, and thus the exceptional values may also be due to non-representative sampling.

The group A-5 sample is not only unusual in containing both amphibole and phlogopite, but also in being Mg-poor. It is consistent with the trends for the lherzolites for most elements, but shows strong deviation in Ti and Cr and minor deviations in Fe and Ca.

Group A-7 sample is essentially in disagreement with the trends for the other lherzolites for every element, but particularly for TiO_2, Cr_2O_3, FeO and SiO_2. Although it is relatively Mg-poor, its Mg-value is still high (89.8), and although it is very rich in Cr_2O_3, it has a low 100 x Cr/Cr+Al ratio (6.8). This sample is also unusual in MgO vs. NiO, where all other groups show identical behaviour.

Origin of amphibole

Composite xenoliths from Lake Bullenmerri and Mt.Leura (sample no's BME-109, -114, -116 and LE-00, described in appendix) do not show evidence for changes in major element composition in lherzolite wall-rocks at distances beyond app. 1 cm from contacts with pyroxenite, hornblendite or veins of phlogopite. The absence of pervasive metasomatism and presence of steep chemical gradients are supportive of models of a very limited wallrock-magma interaction (Irving, 1980; Wilshire et al., 1980).

Because of the observed limited nature of wall-rock metasomatism we conclude that the occurence of pargasitic amphibole as a disseminated phase, particularly in large nodules (up to 20 cm diameter), in which no vein is present, is evidence for an origin by a process other then chemical addition (metasomatism) to the wall-rock by veining magma. This conclusion is consistent with the bulk-rock composition arguments presented previously.

Hornblendite BME-156 contains a patch consisting mainly of Cr-free, Ti-rich, low-Mg pyroxenes within a matrix of poikilitic amphibole. The matrix amphibole of the pyroxenite has a higher Mg-value (72.1) than that of the enclosing hornblendite (67.7) (amphiboles b and a of BME-156, table 1). From the chemical character of the patch in relation to its host and the textural evidence we

interpret the pyroxenite as a precipitate from a magma, which later precipitated the intergrown amphibole and mica. We thus interpret the hornblendite as precipitate from a magma rather then vapor-phase fluid on the basis of this sample and on the similarity of hornblende compositions to near liquidus phases of basanite and nepheline mugearite (cf. Irving, 1971).

The conclusion that kaersutitic hornblendites are precipitates from a magma and that the magma has very limited capabilities of wallrock-metasomatism does not exclude a less direct relationship between disseminated amphiboles in lherzolites and pyroxenite/hornblendite veining systems. The amphibole precipitating magmas are hydrous (cf. Green, 1973a) and so may release excess H_2O while crystallizing. This water then may enter the lherzolites (Rovetta, 1981) and cause widespread hydration reactions such as cpx+sp+H_2O=amph. Thus the amphibole produced in this way is uniformly distributed through the lherzolite, nucleation sites being determined by local chemical composition (e.g. cpx-sp-contact). This contrasts with the expectation of a zonal arrangement or gradient in amphibole abundance, if the H_2O-rich fluid is also a source of major components of the amphibole (i.e. a strongly metasomatising fluid).

PETROGENESIS OF THE UPPERMOST MANTLE BENEATH VICTORIA

The linear character of the chemical variations in the lherzolite nodules makes it possible to model the composition of the nodules as residual mantle compositions for varying degrees of extraction of partial melts. As a source composition one of the most fertile lherzolite nodules (BME-15) has been chosen. This nodule is closely comparable with model mantle compositions in both major elements and trace element concentrations (cf. Green et al., 1979; Ringwood, 1966; Frey et al., 1978) (table 4a) and with compositions of fertile sp--lherzolite nodules from other localities (Jagoutz et al., 1979).

If we apply a batch melting model to this source composition then the oxide compositions of the extracted partial melt must lie on the extended trendlines for the oxide variations within the nodules themselves. Matching of MgO, Al_2O_3-, CaO can be acchieved using olivine melilitites or basanites as extracted melts, but this matching produces source compositions with extremely high TiO_2 and Na_2O (i.e.>1wt.%) and requires 5 - 30 % melt extraction to produce the observed lherzolite range. Models of this type are thus inconsistent with observed minor element variations of the nodules. These models are also inconsistent with experimental studies suggesting depths of 80-100 km rather then 40-60 km for magma segregation for these magmas and degrees of partial melting around 5% (Green, 1973a; Frey et al., 1978).

It has previously been suggested that the lherzolite mineralogy may reflect

early magmatic events associated with oceanic lithosphere in the late Precambrian (Crawford, 1983; Crawford & Keays, 1978; Dasch & Green, 1975). Experimental results on parental ocean floor basalts (Green et al., 1979) argue that picritic liquids are extracted from mantle beneath mid-ocean ridges. We have therefore chosen a liquid composition resembling closely a possible parental picrite for MORB (DSDP 3-18+17%ol, Green et al., 1979, table 4a), but also constrained to fit the lherzolite trend lines passing through the model source (BME-15). The result of the mixing calculations is shown in table 4b. The fit is generally very good for all oxides including TiO_2. The least satisfactory fit is for FeO. It should be noted that even though Na_2O shows only weak correlation with the MgO in the nodules and hence some scatter in the

Table 4a: Comparison of model mantle and parental picrite with fertile nodule compositions (wt.%, trace elements in ppm)

	a	b	BME-15	DSDP(a)	model picrite
Na2O	0.40	0.57	0.40	1.65	1.65
MgO	38.80	37.50	37.99	16.70	17.70
Al2O3	4.40	3.50	3.86	13.70	12.80
SiO2	45.00	45.20	44.95	48.30	48.10
K2O	0.003	0.13	0.03	0.01	0.01
CaO	3.40	3.10	3.54	10.90	10.80
TiO2	0.17	0.71	0.17	0.60	0.62
FeO#	7.60	8.60	8.27	7.90	7.90
Cr2O3	0.45	0.43	0.41	0.06	0.06
MnO	0.11	0.14	0.14	0.12	0.12
NiO	0.26	0.20	0.24	0.08	0.08
Zr*	15.5		16		
Sc*	20		15		
V*	75		86		

Pyrolite a from Green et.al., 1979
b from Ringwood, 1966
* from Frey et.al., 1978

Table 3b: Mantle source compositioins calculated as composition of residual nodule + X % picrite = source

nodule	139	144	167	162	160	99	69	134	9	163	15
X %	2.6	10.6	11.8	16.5	16.9	21.8	22.9	25.0	27.7	29.9	0
Na2O	0.72	0.32	0.36	0.43	0.40	0.45	0.49	0.65	0.59	0.66	0.40
MgO	38.05	37.86	38.03	38.02	38.07	38.13	38.15	38.11	38.06	38.20	37.99
Al2O3	3.85	3.69	3.95	3.87	4.04	4.10	4.21	4.14	4.06	4.31	3.86
SiO2	44.88	45.03	44.86	45.02	44.88	44.86	44.81	44.74	44.97	44.84	44.95
K2O	0.17	0.00	0.00	0.00	0.00	0.00	0.00	0.03	0.02	0.02	0.03
CaO	3.70	3.41	3.61	3.61	3.58	3.69	3.61	3.62	3.47	3.68	3.54
TiO2	0.18	0.14	0.17	0.15	0.20	0.17	0.17	0.19	0.19	0.20	0.17
FeO#	8.30	8.52	8.52	7.67	8.15	7.90	8.07	8.65	7.74	7.47	8.27
Cr2O3	0.40	0.37	0.33	0.39	0.38	0.34	0.27	0.28	0.30	0.28	0.41
MnO	0.14	0.13	0.14	0.13	0.14	0.13	0.14	0.14	0.12	0.13	0.14
NiO	0.23	0.25	0.25	0.25	0.23	0.24	0.25	0.26	0.25	0.24	0.24

source estimates is expected. the calculated values for Na_2O are consistent with or only slightly higher than those for model mantles and fertile nodules. The misfit of sample BME-139 has previously been related to the exceptionally high pargasite content of this nodule.

The chemical variations within the lherzolites, including both hydrous and anhydrous examples, can thus be satisfactorily explained by early partial melting events, linking residue, melt and source by relations such as 70.1% residue (harzburgite BME-163) + 29.9% melt (picrite) = source (lherzolite BME-15). Compositions of lherzolites are simple mixtures between residue and melt and thus reflect incomplete segregation.

The presence of hydrous phases and their textural relationships with clinopyroxene and spinel suggest that a fluid phase, composed mainly of water, entered the rocks and changed their mineralogy in a more or less isochemical way. The water entering the lherzolites may however contain trace amounts (ppm) of elements. Changes in chemistry for major oxides are then undetectable, but may be significant for some trace elements. The quantitative effect on trace element concetrations such as REE cannnot be assessed at this stage as sufficient data are not available.

The cumulates transported with the lherzolites are difficult to model and to recognize, because they may either stem from the period of early partial melting event(s) or may be derived from later magmatic transits including early eruptions of the host magma suite. Re-crystallization of these cumulates occurs as evidenced by the metamorphic growth of garnet in the pyroxenites. Original textures are thus largely eliminated. Only in those cases where cumulus textures are well preserved it is possible to infer the character of a parental magma. This is the case for BME-168, which for this reason has been placed into a separate group (G). The preservation of excellent cumulate texture is consistent with an origin from basanites related to but slightly preceeding the eruption of the host basanite.However earlier, unrelated basanite sources are not excluded (Basu & Murthy, 1977).

SUMMARY OF THE EVOLUTION OF THE UPPERMOST MANTLE BENEATH VICTORIA

1. Lherzolites are the major rock type of the uppermost mantle (lithosphere) of the region at a depth of less then 60km, probably around 45km.
2. This part of the subcontinental lithosphere records an early history of extraction of picrite basalt of oceanic type from a relatively homogeneous mantle comparable to the model mantle "pyrolite".
3. The chemical variation of the lherzolites can be modeled by varying degrees of extraction of such a liquid, thereby creating lateral and horizontal chemical mantle heterogeneity with varying degrees of depletion.

4. Pargasitic amphibole in the lherzolites is developed by a near-isochemical hydration reaction of the phases of the lherzolites, particularly involving spinel and clinopyroxene. Other then addition of water and in a few rare cases of small amounts of Na_2O and K_2O possibly, there is no evidence for addition of other components in other then trace (ppm) amounts.
5. Hydration-metasomatism occurs within the lithosphere and predates or is contemporaneous with transits through the lithosphere of the alkaline host magma. The lithosphere is not the source region of the alkaline magmas so that the presence of amphibole or phlogopite cannot be taken as evidence that mantle metasomatism is a precursor event to alkaline magmatism.
6. Hydration-metasomatism changes the mineralogy of parts of the lithosphere introducing mineralogical heterogeneity, whithout inducing major chemical heterogeneity additional to that produced by earlier partial melting events.
7. Within the lithosphere, segregated bodies of magma from the earliest magmatic event(s) and later batches of magma passing through the lithosphere may crystallize, either partially or completely, giving rise to cumulates such as pyroxenites, hornblendites, wehrlites and Fe-rich lherzolites. Cumulates are often recrystallized. The existence of pockets, lenses, dykes and veins of this nature adds further to the present heterogeneous character of the lithosphere.
8. Wallrock-reaction (metasomatism) by magmas fractionating under mantle pressure is very restricted and contributes only very locally to the chemistry and mineralogy of the lithosphere. However magmas may release water upon crystallization at mantle depths and produce widespread hydration reactions in the lherzolites (and early cumulates). Thus it seems more likely that alkaline magmatism is a precursor to hydration-metasomatism of the uppermost mantle rather than vice versa.

Acknowledgements

The research leading to this paper was carried out at the Geology Department, University of Tasmania with financial support from the Australian Research Grants Scheme and the University of Tasmania. We like to thank Dr. Rick Varne, Dr. Ian Nicholls and Mr. Arthur Day for helpful assistance and discussions during the collection of the nodules. We also thank Drs. David Ellis and Simon Harley, Mr. Neil Ortez, Mr. Scott Kuehner and Mr. Wayne Taylor for stimulating discussions, Dr. Ron Berry for help with the computing of models and Mr. Wieslaw Jablonski for assistance on the microprobe.

B1

FRACTIONATION OF BASALT MAGMAS AT HIGH PRESSURES

By

Dr. D. H. GREEN

and

Prof. A. E. RINGWOOD

(*Reprinted from Nature, Vol.* 201, *No.* 4926, *pp.* 1276–1279, *March* 28, 1964)

(*Reprinted from Nature, Vol.* 201, *No.* 4926, *pp.* 1276–1279, *March* 28, 1964)

FRACTIONATION OF BASALT MAGMAS AT HIGH PRESSURES

By Dr. D. H. GREEN and Prof. A. E. RINGWOOD
Department of Geophysics, Australian National University, Canberra

ALTHOUGH basalts seem to exhibit a continuous spectrum of chemical compositions, combined petrographic and chemical studies have led to the general recognition of two magma types, alkali basalt and tholeiitic basalt, with their respective differentiation series[1]. The tholeiitic suite is characterized by the presence of normative hypersthene and modal hypersthene or pigeonite, while the alkali basalt suite is characterized by normative olivine with nepheline and modal high-CaO augite or titan-augite[1]. In the tholeiitic suite, fractionation at low pressure is dominated by early crystallization of olivine and by the reaction relationship of magnesian olivine to orthopyroxene. Fractional crystallization at low pressures leads to an increase in the silica saturation of the residual liquid. In the alkali basalt suite, crystallization of olivine with CaO-rich clinopyroxene continues the state of critical undersaturation in silica in the early stages of fractionation.

From examination of natural cases of differentiation in the crust and from experimental investigations, there appears to be no plausible way in which an alkali basalt liquid could be derived from a parental tholeiitic liquid, or vice versa, by processes of fractional crystallization at low pressure. However, Yoder and Tilley[1] have shown that, at pressures of 20 kb. and greater, crystallization in a variety of basaltic compositions is dominated by the phases pyrope-almandine garnet and omphacitic clinopyroxene. They have suggested that the position of a co-tectic between these two phases may be pressure sensitive and thus that fractional melting of garnet peridotite at different pressures could produce the two magma suites. Yoder and Tilley also suggested that separation of garnet from a primitive basalt liquid would leave a liquid typical of the alkali basalt suite, whereas separation of omphacite would leave a liquid crystallizing at low pressures as a member of the tholeiitic suite.

As an alternative hypothesis Powers[2], Tilley[3] and Macdonald[4] have discussed the possibility that the field of primary crystallization of orthopyroxene from tholeiitic magma might be substantially increased by high pressure. Excess crystallization of orthopyroxene could move the residual liquid into the critically undersaturated field of the alkali basalt. Our experimental results support this latter hypothesis.

The preliminary experiments reported here are in the intermediate pressure range, 10–20 kb. The experiments have been carried on a basalt composition very close to the estimate by Macdonald and Katsura[5] of the 'parent magma' for olivine tholeiite from Kilauea Iki.

Experimental runs were made in a single-stage high-pressure apparatus of the type designed by Boyd and England[6]. The basalt mixture was fused to a glass, finely ground, dried over iron powder and re-analysed for FeO and Fe_2O_3 to check the oxidation state. The sample was loaded into a platinum capsule and compressed in a pellet press. The sample was brought to the desired pressure, and the temperature quickly raised and held at the desired value for one hour. The run was quenched to about 200° C in less than 30 sec by switching off power to the furnace. Quenching yielded glass with variable amounts of quench clinopyroxene. The capsules were not sealed by welding in these initial runs and in all cases there has been access of small amounts of water from dehydration of the talc pressure medium. Because of this effect our temperatures are appreciably lower than the liquidus temperatures for similar dry basalt compositions[1,7].

Following Boyd and England[8], no corrections have been made for friction, and pressure determinations are believed to be accurate to ± 5 per cent in an absolute sense and in a relative sense, comparing run to run, to better than 2 per cent. Temperature measurement by platinum–platinum 10 per cent rhodium thermocouple is estimated to be accurate to $\pm 10°$ C with a variation of $\pm 5°$ C about the control point.

Parts of the sample were powdered and examined optically and by X-ray diffraction. In partial melting runs olivine, enstatite, garnet and clinopyroxene are readily recognized from their optical properties and also their characteristic euhedral forms in the melt. X-ray diffraction was useful in confirming the presence of olivine and garnet and the absence of amphibole in the partial melting runs. An electron probe micro-analyser (Applied Research Laboratories, *EMX* model) was used to make a direct quantitative analysis of the primary crystals. The crystals were 10–100μ in their longest dimensions and were distinguishable on a polished surface of the sample. Traverses were made across the mineral in 2μ steps, the diameter of the electron beam being about 1μ and the volume of analysis (that is, the volume from which characteristic X-rays were emitted) was a hemisphere of 3–4μ diameter. Analyses were made simultaneously for $Fe_{K\alpha}$, $Ca_{K\alpha}$ and $Al_{K\alpha}$. Quantitative determinations of total iron as FeO, CaO, and Al_2O_3 were obtained by direct calibration with analysed enstatites and diopsides (from 2–7 per cent Al_2O_3), analysed basaltic glasses, and analysed garnets. Corrections were made for background, variation in beam current and for detector dead-time but not for inter-element absorption or fluorescence effects.

Five or more different grains in each run were analysed

Table 1. SUMMARY OF EXPERIMENTAL PARTIAL MELTING RUNS

Pressure (kb.)	Temperature (° C)	Primary phases present	Remarks
		Olivine tholeiite	
10	1,250	Ol+opx+liq.*	Ol≫opx.
12½	1,250	Ol+opx+?cpx+liq.	Opx>ol.
15	1,300	Ol+opx+cpx+liq.	Opx≫cpx>ol.
20	1,300>T>1,200†	Opx+liq.	No garnet or olivine.
20	1,300	Opx+liq.	Opx less abundant than in previous run.
		Picrite	
15	1,300	Ol+opx+?cpx+liq.	Ol>opx; estimate Ol 25%; Opx 10%.
20	1,325	Opx+liq.	No olivine, liquid entirely quench products.
25	1,300	Garnet megacrysts+opx laths in fine cpx (? quench) aggregate	Uncertain liquidus run.

* The 'liquid' appears in the sample as glass or as a quench, metastable clinopyroxene possessing a characteristic texture, or as mixtures of these components.

† Thermocouple contamination.

since only by repeated analysis could it be determined whether the volume of analysis was entirely within the mineral grain or passed through the grain to include glass or mantling quench clinopyroxene below the grain. The determination of CaO, iron as FeO, and Al_2O_3 enabled the calculation of SiO_2 and MgO assuming that the minerals consisted of simple end-members of their solid solution series.

In Table 1 are given the results of partial melting runs on olivine tholeiite composition (Table 3, col. 1) and on a picrite composition (Table 3, col. 5). The first composition lies centrally within the olivine tholeiite volume of the Ne.-Cpx.-Ol.-Quartz tetrahedron[1] and the second composition is within this volume but very close to the Ol.-Cpx.-Plag. plane of critical undersaturation[1].

The most significant result from the olivine tholeiite runs is the replacement of olivine by orthopyroxene as the primary liquidus phase as pressure increases from 10 to 20 kb. In the higher pressure part of the range, orthopyroxene possesses an extensive primary crystallization field, while olivine is not observed. It is clear from this behaviour that the course of fractionation of an olivine tholeiite between 10 and 20 kb. will be very different from the familiar low-pressure behaviour.

Table 2 contains the results of the electron probe analyses of the primary phases present in the partial melting runs. Probable errors are difficult to estimate; the precision of measurement with the electron probe on a homogeneous standard is better than 2 per cent of the amount present for Al_2O_3 and CaO and better than 1 per cent for FeO in the concentrations dealt with. However, the small size of the crystals, and particularly the uncertainty of their thickness in relation to the depth of penetration of the electron beam, results in a greater uncertainty. This is particularly important in measure-

Table 2. Compositions of Primary Phases present in Partial Melting Runs

	Olivine tholeiite									Picrite	
	10 kb. 1,250° C		12·5 kb. 1,250° C		15 kb. 1,300° C			20 kb. 1,200–1,300° C	20 kb. 1,300° C	15 kb. 1,300° C	
	Olivine	Ortho-pyroxene	Olivine	Ortho-pyroxene	Olivine	Ortho-pyroxene	Clino-pyroxene‡	Orthopyroxene	Ortho-pyroxene	Olivine	Ortho-pyroxene
SiO_2	40·1	54·3	39·7	53·2	39·7	53·9	50·9	50·0	51·4	41·1	54·9
Al_2O_3	not detected*	5·0	n.d.*	6·7	n.d.*	6·4	8·3	9·8	9·3	n.d.*	5·2
FeO	13·8	8·4	15·9	8·3	15·4	6·4	5·4	13·6	9·0	8·4	5·3
MgO	46·1	30·5	44·4	29·1	44·9	30·4	22·1	24·2	27·3	50·5	32·0
CaO	not detected†	1·8	n.d.†	2·7	n.d.†	2·9	13·3	2·4	3·0	n.d.†	2·6
Mol. ratio $\frac{Mg}{Mg+Fe}$	85·5	86·6	83·4	86·2	83·9	89·5	88	76·0	84·5	91·5	91·5

* Less than 0·5% † Less than 0·2% ‡ Sub-calcic augite $Ca_{13}Mg_{83}Fe_5$

ment of CaO in the orthopyroxene since interference by mantling quench clinopyroxene or glass will give a high and incorrect CaO value. It is estimated that the error is less than ± 5 per cent of the amount present for Al_2O_3 and FeO but probably greater for CaO in orthopyroxene.

The orthopyroxenes separating from the olivine tholeiite are aluminous (Table 2) and the alumina content increases with pressure between 10 kb and 20 kb. There is an apparent exception in that in our results the Al_2O_3 content of the 15-kb. orthopyroxene is very close to that of the 12·5-kb. run. The runs are at different temperatures and it must be emphasized that these reconnaissance runs at the different pressures are random points between the solidus and liquidus, and in comparing compositions between runs we are not necessarily comparing the same degree of crystallization. There is a lower Al_2O_3 content in the orthopyroxene crystallizing from the picrite at 15 kb. than that from the olivine tholeiite at the same pressure.

The two runs at different temperatures at 20 kb. show that the orthopyroxene formed at the higher temperature is more magnesium-rich than the more abundant enstatite formed at the lower temperature. A trend to iron-enrichment (relative to magnesium) of the liquid during fractionation thus continues to operate at 20 kb.

The results provide information on the course of fractionation followed by a basaltic liquid crystallizing at depths of about 35–70 km (10–20 kb.). At lower pressures fractionation in the olivine tholeiite and in the picrite is determined in its initial stages by the crystallization of olivine. At higher pressures than 20 kb. the course of liquid variation will be determined by the crystallization of garnet and omphacitic clinopyroxene[1].

As enstatite is the only primary phase present in the olivine tholeiite at 20 kb., the composition of the remaining liquid can be calculated assuming different degrees of crystallization. In Table 3 we have done this assuming 20 and 25 per cent crystallization of the olivine tholeiite at 20 kb. In these calculations we have used the composition of the orthopyroxene observed at 1,300° C. In col. 4 we have calculated the liquid composition assuming 30 per cent crystallization and using the composition of the orthopyroxene observed in the run between 1,200° C and 1,300° C. We have not been able accurately to determine the percentage of crystals and glass in the various runs. An estimate of the two 20-kb. runs is 15 ± 5 per cent crystalline at 1,300° C and 25 ± 5 per cent crystalline in the lower temperature run.

The decrease in $\frac{Mg}{Mg + \Sigma Fe + Mn}$ molecular ratio at 20 and 25 per cent crystallization results from using the magnesium-rich orthopyroxene formed at 1,300° C for both calculations. A much smaller change is produced if the enstatite from the 1,200°–1,300° C run is used in the calculations (col. 4).

Table 3. Calculated Residual Liquid Compositions assuming Varying Degrees of Crystallization of Analysed Phases of Table 2

	1 Olivine tholeiite	2 20% Enstatite crystallized (enstatite as found in 20 kb., 1,300° C run)	3 25% Enstatite crystallized	4 30% Enstatite crystallized (enstatite as found in 20 kb., 1,200–1,300° C run)	5 Picrite	6 Picrite with 25% olivine, 10% enstatite crystallized
SiO_2	47·35	46·3	46·0	46·2	45·78	46·1
TiO_2	2·04	2·5	2·7	2·9	1·94	2·9
Al_2O_3	13·20	14·2	14·5	14·7	12·52	18·5
Fe_2O_3	0·92	1·1	1·2	1·3	0·82	1·3
FeO	9·31	9·4	9·4	7·5	8·20	8·6
MnO	0·15	0·2	0·2	0·2	0·15	0·2
MgO	14·68	11·4	10·5	10·6	18·90	4·8
CaO	10·27	12·3	12·7	13·6	9·74	14·5
Na_2O	1·75	2·20	2·32	2·50	1·65	2·54
K_2O	0·08	0·10	0·11	0·12	0·08	0·12
P_2O_5	0·21	0·26	0·28	0·30	0·20	0·31
Cr_2O_3	0·04	0·04	0·04	0·04	0·03	0·04
K feld.	0·5	0·6	0·6	0·6	0·5	0·6
Na plag.	14·8	17·0	16·3	14·7	14·1	17·4
Ca plag.	27·8	28·4	28·7	28·7	26·4	38·7
Di	17·2	25·1	26·3	29·8	16·2	25·9
Hy	14·3	—	—	—	3·5	—
Ol	19·6	21·0	18·7	14·7	33·9	7·1
Ne	—	1·0	2·0	3·4	—	2·3
Ap	0·5	0·6	0·6	0·6	0·5	0·7
Mt	1·4	1·6	1·7	1·9	1·2	1·9
Ilm	3·9	4·7	5·1	5·5	3·7	5·4
$\frac{100\ Mg}{Mg+Fe+Mn}$	71·6	65·7	63·7	68·1	78·8	46·1

It is apparent from Table 3 that the effect of fractionation by crystallization of aluminous orthopyroxene is to produce a residual liquid containing normative nepheline. Even with 20 per cent crystallization the liquid has changed from having 14 per cent normative hypersthene to contain 1 per cent normative nepheline. The compositions in cols. 2, 3 and 4 are close to naturally occurring alkali basalts[1,9]. Although containing normative nepheline, the compositions are quite low in Na_2O and K_2O, particularly the latter. This is a consequence of our original olivine tholeiite composition being low in Na_2O and very low in K_2O.

At 15 kb. the picrite composition (Table 3, col. 5) crystallized out both orthopyroxene and olivine. The composition of the residual liquid is recalculated (col. 6) assuming 25 per cent olivine and 10 per cent enstatite (cf. Table 1) have crystallized out and have the compositions given in Table 2. The liquid composition obtained contains normative nepheline but is higher in Al_2O_3 (18 per cent) than normal alkali basalts. This results from the lower Al_2O_3 content of the enstatite from the picrite at 15 kb. and demonstrates the essential role of the Al_2O_3 content of the orthopyroxenes in leaving liquids of normal basaltic character. While separation of non-aluminous enstatite could produce nepheline normative rocks these would have Al_2O_3 contents inconsistent with normal basalt types.

Our data demonstrate that between 15 and 20 kb., aluminous orthopyroxene crystallizes as the liquidus phase from a range of basalt compositions between quartz tholeiite and tholeiitic picrite. An olivine tholeiite magma, beginning to crystallize at a depth of about 60 km, will yield aluminous orthopyroxene and not olivine as the first crystals. Separation of these crystals may give a residual liquid typical of alkali basalt magma. This process is invoked to explain the relationships of magma types in the Hawaiian Islands where the main volcanism is of olivine tholeiite character, but followed in the waning phases of activity of each centre by thin veneers of alkali basalt and its derivatives[3]. At a currently active vent, Kilauea Iki, the magma is of olivine tholeiite composition[5] and there is seismic evidence[10] for a depth of accumulation of the magma at 50–60 km. Cooling at this depth of accumulation would provide the conditions we have defined under which the olivine tholeiite magma of Kilauea Iki could yield an alkali basalt magma by fractionation.

While we consider that this mechanism of derivation of an alkali basalt magma from a parental olivine tholeiite is a very plausible explanation for the sequence of Hawaiian rocks, it seems inadequate for the large provinces of alkali basalt magma without tholeiites, for example, Japan[9] and S.E. Australia. Direct partial melting of both alkali basalt and tholeiitic basalt magma from a parental peridotite seems a more probable origin for such occurrences.

The experimental observations on the picrite com-

position are relevant to the problem of partial melting of peridotite since the compositions of the olivine ($Fo_{91\cdot5}$) and the aluminous enstatite ($Ens_{91\cdot5}$, 5·2 per cent Al_2O_3) crystallizing at 15 kb. are typical of the olivine and enstatite occurring in peridotite nodules in basalt (ref. 11 and Green and Easton, unpublished data). Arguments have been presented elsewhere[12,13] that the composition of peridotite nodules is very close to that of the upper mantle, this composition being capable of providing a basaltic fraction by partial melting leaving residual, refractory dunite. We have shown that at 15–20 kb. a basaltic liquid may cross the composition boundary between alkali basalt and olivine tholeiite by crystallization or solution of aluminous orthopyroxene ± olivine. In the picrite, this process can occur with the crystalline phases in equilibrium with the liquid being of the same composition as those occurring in peridotite nodules. From this we suggest that if melting occurs in the peridotite assemblage (olivine + aluminous enstatite + aluminous chrome-dropside ± spinel) at 15–20 kb. then with a low degree of partial melting the liquid will be of alkali basalt type in equilibrium with olivine + aluminous enstatite in the parent peridotite. If there is no separation of this liquid and melting continues to a higher temperature then aluminous enstatite + some olivine will go into the liquid, changing it into the olivine tholeiite field.

Preliminary runs in peridotite compositions show that the olivine + aluminous pyroxenes ± spinel assemblage will be stable at near-solidus conditions to at least 100 km. Following the foregoing discussion we suggest that the extent of fractional melting of this assemblage will largely determine whether an alkali basalt or an olivine tholeiite liquid is generated. At a greater depth, at present unknown, the olivine + pyroxenes + garnet (garnet peridotite) assemblage becomes stable. The course of progressive partial melting in this assemblage may differ considerably from that in the olivine + aluminous pyroxenes ± spinel assemblage[1].

We thank Dr. F. R. Boyd and Mr. O. R. McClunin of the Geophysical Laboratory, Washington, for assistance in setting up the high-pressure apparatus, and Prof. C. E. Tilley, Prof. H. Kuno, Dr. K. S. Heier and Dr. I. McDougall for their advice.

[1] Yoder, H. S., and Tilley, C. E., *J. Petrology*, **3**, 342 (1962).
[2] Powers, H. A., *Amer. J. Sci.*, 5th Ser., **30**, 57 (1935).
[3] Tilley, C. E., *Quart. J. Geol. Soc. Lond.*, **106**, 37 (1950).
[4] Macdonald, G. A., *Bull. Geol. Soc. Amer.*, **60**, 1541 (1949).
[5] Macdonald, G. A., and Katsura, T., *Pacific Sci.*, **15**, 358 (1961).
[6] Boyd, F. R., and England, J. L., *J. Geophys. Res.*, **65**, 741 (1960).
[7] Tilley, C. E., Yoder, H. S., and Schairer, J. F., *Carnegie Inst. Washington Year Book*, **62**, 77 (1963).
[8] Boyd, F. R., and England, J. L., *J. Geophys. Res.*, **68**, 311 (1963).
[9] Kuno, H., *J. Petrology*, **1**, 121 (1960).
[10] Eaton, J. P., and Murata, K. J., *Science*, **132**, 925 (1960).
[11] Ross, C. S., Foster, M. D., and Myers, A. T., *Amer. Mineralogist*, **39**, 693 (1954).
[12] Kushiro, I., and Kuno, H., *J. Petrology*, **4**, 75 (1963).
[13] Green, D. H., and Ringwood, A. E., *J. Geophys. Res.*, **68**, 937 (1963).

Printed in Great Britain by Fisher, Knight & Co., Ltd., St. Albans.

Contr. Mineral. and Petrol. 15, 103—190 (1967)

B3

I

The Genesis of Basaltic Magmas

D. H. Green and A. E. Ringwood

Department of Geophysics and Geochemistry, Australian National University, Canberra, Australia

Received December 12, 1966

Contents

Abstract. This paper reports the results of a detailed experimental investigation of fractionation of natural basaltic compositions under conditions of high pressure and high temperature. A single stage, piston-cylinder apparatus has been used in the pressure range up to 27 kb and at temperatures up to 1500° C to study the melting behaviour of several basaltic compositions. The compositions chosen are olivine-rich (20% or more normative olivine) and include olivine tholeiite (12% normative hypersthene), olivine basalt (1% normative hypersthene) alkali olivine basalt (2% normative nepheline) and picrite (3% normative hypersthene). The liquidus phases of the olivine tholeiite and olivine basalt are olivine at 1 Atmosphere, 4.5 kb and 9 kb, orthopyroxene at 13.5 and 18 kb, clinopyroxene at 22.5 kb and garnet at 27 kb. In the alkali olivine basalt composition, the liquidus phases are olivine at 1 Atmosphere and 9 kb, orthopyroxene with clinopyroxene at 13.5 kb, clinopyroxene at 18 kb and garnet at 27 kb. The sequence of appearance of phases below the liquidus has also been studied in detail. The electron probe micro-analyser has been used to make partial quantitative analyses of olivines, orthopyroxenes, clinopyroxenes and garnets which have crystallized at high pressure.

These experimental and analytical results are used to determine the directions of fractionation of basaltic magmas during crystallization over a wide range of pressures. At pressures corresponding to depths of 35—70 km separation of aluminous enstatite from olivine tholeiite magma produces a direct fractionation trend from olivine tholeiites through olivine basalts to alkali olivine basalts. Co-precipitation of sub-calcic, aluminous clinopyroxene with the orthopyroxene in the more undersaturated compositions of this sequence produces derivative liquids of basanite type. Magmas of alkali olivine basalt and basanite type represent the lower temperature liquids derived by approximately 30% crystallization of olivine-rich tholeiite at 35—70 km depth. At depths of about 30 km, fractionation of olivine-rich tholeiite with separation of both olivine and low-alumina enstatite, joined at lower temperatures by sub-calcic clinopyroxene, leads to derivative liquids with relatively constant SiO_2 (48 to 50%) increasingly high Al_2O_3 (15—17%) contents and retaining olivine + hypersthene normative chemistry (5—15% normative olivine). These have the composition of typical high-alumina olivine tholeiites. The effects of low pressure fractionation may be superimposed on magma compositions derived from various depths within the mantle. These lead to divergence of the alkali olivine basalt and tholeiitic series but convergence of both the low-alumina and high-alumina tholeiites towards quartz tholeiite derivative liquids.

The general problem of derivation of basaltic magmas from a mantle of peridotitic composition is discussed in some detail. Magmas are considered to be a consequence of partial melting but the composition of a magma is determined not by the depth of partial melting but by the depth at which magma segregation from residual crystals occurs. Magma generation from parental peridotite (pyrolite) at depths up to 100 km involves liquid-crystal equilibria between basaltic liquids and olivine + aluminous pyroxenes and does not involve garnet. At 35—70 km depth, basaltic liquids segregating from a pyrolite mantle will be of alkali olivine basalt type with about 20% partial melting but with increasing degrees of partial melting, liquids will change to olivine-rich tholeiite type with about 30% melting. If the depth of magma segregation is about 30 km, then magmas produced by 20—25% partial melting will be of

high-alumina olivine tholeiite type, similar to the "oceanic tholeiites" occurring on the sea floor along the mid-oceanic ridges.
Hypotheses of magma fractionation and generation by partial melting are considered in relation to the abundances and ratios of trace elements and in relation to isotopic abundance data on natural basalts. It is shown that there is a group of elements (including K, Ti, P, U, Th, Ba, Rb, Sr, Cs, Zr, Hf and the rare-earth elements) which show enrichment factors in alkali olivine basalts and in some tholeiites, which are inconsistent with simple crystal fractionation relationships between the magma types. This group of elements has been called "incompatible elements" referring to their inability to substitute to any appreciable extent in the major minerals of the upper mantle (olivine, aluminous pyroxenes). Because of the lack of temperature contrast between magma and wall-rock for a body of magma near to its depth of segregation in the mantle, cooling of the magma involves complementary processes of reaction with the wall-rock, including selective melting and extraction of the lowest melting fraction. The "incompatible elements" are probably highly concentrated in the lowest melting fraction of the pyrolite. The production of large overall enrichments in "incompatible elements" in a magma by reaction with and highly selective sampling of large volumes of mantle wall-rock during slow ascent of a magma is considered to be a normal, complementary process to crystal fractionation in the mantle. This process has been called "wall-rock reaction". Magma generation in the mantle is rarely a simple, closed-system partial melting process and the isotopic abundances and "incompatible element" abundances of a basalt as observed at the earth's surface may be largely determined by the degree of reaction with the mantle or lower crustal wall-rocks and bear little relation to the abundances and ratios of the original parental mantle material (pyrolite).
Occurrences of cognate xenoliths and xenocrysts in basalts are considered in relation to the experimental data on liquid-crystal equilibria at high pressure. It is inferred that the lherzolite nodules largely represent residual material after extraction of alkali olivine basalt from mantle pyrolite or pyrolite which has been selectively depleted in "incompatible elements" by wall-rock reaction processes. Lherzolite nodules included in tholeiitic magmas would melt to a relatively large extent and disintegrate, but would have a largely refractory character if included in alkali olivine basalt magma. Other examples of xenocrystal material in basalts are shown to be probable liquidus crystals or accumulates at high pressure from basaltic magma and provide a useful link between the experimental study and natural processes.

Introduction

Basaltic rocks, by virtue of their widespread occurence in both oceanic and continental regions, occupy a unique position in igneous petrogeny. It is widely believed that basaltic magmas are derived from the earth's mantle. Basalts accordingly contain a vast reservoir of information, the correct interpretation of which should throw a great deal of light on the chemical and mineralogical nature of the mantle. Petrologists have long recognized the existence of a number of different types of basalt characterized by distinctive chemical and mineralogical properties, e.g. alkali basalts, olivine tholeiites, high-alumina basalts and quartz tholeiites. The main theme of this paper is a detailed experimental study of the relationships between the principal magma types, their fractionation trends at various pressures and their derivation by partial melting processes in the peridotitic mantle.
Recent workers have attempted to systematise the classification and nomenclature of basaltic rocks and the reader is referred particularly to the excellent summaries of previous and present views on basalt classification by YODER and TILLEY (1962, p. 346—348, 349—356), MACDONALD and KATSURA (1964), COOMBS (1963), KUNO (1960). We shall adhere to a classification of basaltic rocks similar to that accepted by YODER and TILLEY (1962) and MACDONALD and KATSURA

(1964). Since our main concern is with chemistry rather than the modal mineralogy of basaltic rocks, it is convenient to accept a classification directly based on CIPW normative mineralogy (i.e. an indirect chemical classification). The "basalt tetrahedron" of YODER and TILLEY (1962; Fig. 1) is a convenient and simple illustration of this method of classification of basaltic rocks. The principal classes of

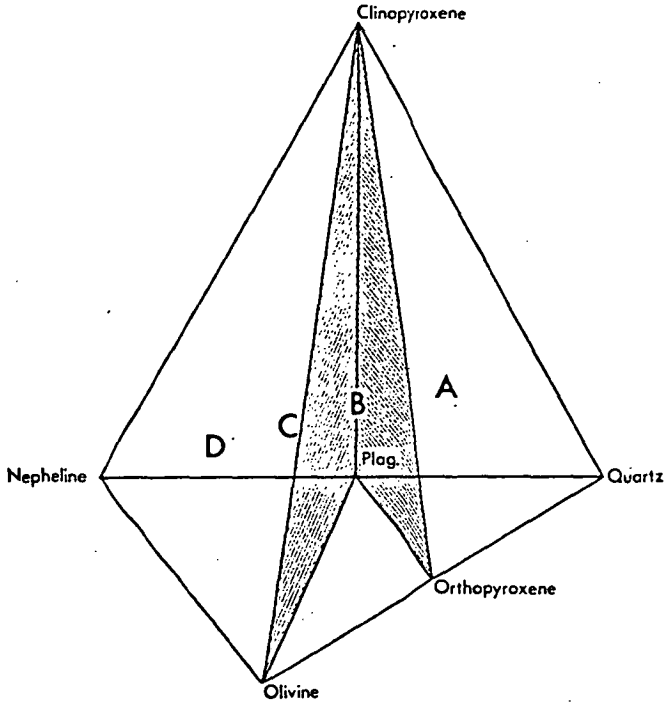

Fig. 1. Diagrammatic representation of the major mineralogy of basalts using the "basalt tetrahedron" (YODER and TILLEY, 1962). The plane olivine—clinopyroxene—plagioclase is referred to as the "critical plane of undersaturation". *A* field of quartz tholeiites; *B* field of olivine tholeiites; *C* field of alkali olivine basalts; *D* field of olivine basanites

basalts are clearly represented as primary phase volumes in this figure. The following terms are used to define these principal magma types:

Tholeiite or tholeiitic suite: basalts characterised by the presence of normative hypersthene.

Quartz Tholeiite: — basalts with normative quartz and hypersthene.

Olivine Tholeiite: — basalts with normative olivine and hypersthene. *Olivine basalt* is used for brevity and convenience in nomenclature for basalts falling within this group but having low (0—3%) normative hypersthene content. This convention is similar to the use of the term by YODER and TILLEY (1962).

Alkali[1] *Olivine Basalt:* — basalts characterised by the presence of normative olivine and nepheline but with normative nepheline less than 5%.

Basanite: — basalts characterized by normative olivine and nepheline and with more than 5% nepheline.

Olivine Nephelinite: — basalt-like rocks without normative albite and typically with olivine, diopside and nepheline as the major normative minerals.

[1] The term alkali olivine basalt is preferred to the more grammatically correct "alkaline olivine basalt" or "alkalic olivine basalt" (MACDONALD and KATSURA, 1964, p. 89) for reasons of common usage and euphony.

The use of a classification based on the calculation of the CIPW norm enables objective grouping of analyzed basalts but it creates an artificial clarity of classification which is absent from the natural rocks. Apart from uncertainties introduced by the quality of chemical analyses and by post-magmatic or late magmatic changes in oxidation state, it is clear that the "critical plane of undersaturation" (Fig. 1) dividing olivine + nepheline normative basalts from olivine + hypersthene normative basalts is a finite zone of indeterminacy in basalt classification. Thus, POLDERVAART (1962, 1964) argued that a group of hypersthene-normative basalts were nevertheless petrographically and genetically related to the alkali olivine basaltic suite. These hypersthene-normative alkali olivine basalts characteristically have $Ab - 2\,En_{Hy} - 1.5\,Fs_{Hy} > 0$, while olivine tholeiites have values $Ab - 2\,En_{Hy} - 1.5\,Fs_{Hy} < 0$ (Ab, En_{Hy}, Fs_{Hy} are the normative albite, enstatite in hypersthene, and ferrosilite in hypersthene, respectively). YODER and TILLEY (1962, p. 404) expressed similar uncertainty about the affinities of olivine basalts with low normative hypersthene contents. The data complied by COOMBS (1963) and his definition of an "indicator ratio" to classify the basalt magma types are in good agreement with POLDERVAART's criteria for separation of the two suites. On the other hand, MACDONALD and KATSURA (1964) use a simple total alkalies ($Na_2O + K_2O$ in weight per cent) vs silica plot to distinguish magmas of alkali olivine basalt type from the tholeiitic suite.

The test of any chemical method of classification is in comparison with the modal mineralogy, i.e. (a) the presence of phenocrystal and groundmass olivine in the alkali olivine basalt and absence of calcium-poor pyroxene; (b) the presence of calcium-poor pyroxene and partially resorbed or mantled phenocrystal olivine in the olivine tholeiites. However, such petrographic classification is frequently nondefinitive because of uncertainty in identification of groundmass and because of the presence of common glass within the rock. In general, these methods of basalt classification work equally well for rocks removed from the transition zone between alkali olivine basalts and olivine tholeiites but all are subjective and may be mutually inconsistent when applied to rocks within the transition zone. Nevertheless a fundamental point is that all the above attempts at classification recognise the existence of a continuous spectrum of basalt compositions between alkali olivine basalt magmas and olivine tholeiites.

Previous Investigations

The general question of possible fractionation trends of alkali olivine basalt and tholeiites at low pressure has been fully discussed by YODER and TILLEY (1962). These authors point out that the "critical plane of silica undersaturation" Cpx — Ol — Plag (Fig. 1) separating the alkali basalts from the olivine tholeiites represents a "thermal barrier" for fractionation at low pressures and that under normal low pressure conditions, fractionation trends in basaltic magmas move *away* from this plane on either side. The recognition of different basalt magma types and of a continuous spectrum of compositions between alkali basalts and tholeiites has accordingly posed a major problem in petrogenesis. One of the earliest hypotheses aimed at solving this problem involves the separation of hypersthene in place of olivine from olivine tholeiite magmas, leading to derivative

liquids of alkali basalt type (Holmes and Harwood, 1932; Powers, 1935, p. 65; Larsen, 1940, p. 926; Macdonald, 1949, p. 1576; and Tilley, 1950, p. 45.).
An important step in the study of basalt fractionation was the initiation of detailed experimental work at high pressures on natural basalts (Yoder and Tilley, 1962; Green and Ringwood, 1964; Tilley and Yoder, 1964). Yoder and Tilley (1962, p. 507) appealed to the removal of garnet from a parental liquid at high pressures to produce an alkali basaltic liquid while, in contrast, removal of omphacite and effective enrichment of garnet in the liquid would produce tholeiite-type liquids. Calculations of the effects of extracting either garnet or omphacite from actual basaltic compositions as extruded at the surface show that the residual liquids do not possess typical basaltic compositions and do not follow the trend suggested (pages 153—156). Accordingly this hypothesis must be rejected in its simplest form. Nevertheless, Yoder and Tilley's results are important since they demonstrated a new control of fractionation in basalt magmas at high pressure and that the low pressure "thermal divide" between alkali basalts and their derivatives and olivine tholeiites and their derivatives was absent at high pressure.
Green and Ringwood (1964) demonstrated experimentally that orthopyroxene replaced olivine as the liquidus phase in an olivine-rich tholeiite at pressures from 13 to 18 kb. The orthopyroxene was shown to be rich in Al_2O_3 and the extraction of aluminous orthopyroxene gave a very direct fractionation trend from olivine tholeiites to derivative alkali olivine basalt magmas. These experiments, although of a preliminary and reconnaissance nature, strongly supported earlier hypotheses on the role of hypersthene crystallization and demonstrated a fundamental change in the fractionation of olivine-rich basaltic magmas at modest pressures. The data provided a simple and very direct fractionation trend from olivine and hypersthene normative olivine tholeiites to olivine and nepheline normative alkali olivine basalt by separation of a single phase.

Present Investigation

This paper presents the results of some 120 experimental runs over the period 1963—1966 investigating the melting relations of selected olivine-rich basaltic rocks. The study was aimed at extending and confirming the preliminary data on the role of aluminous orthopyroxene in basalt fractionation and obtaining further information on the possible direction of fractionation of basalts and effects of partial melting in the mantle at moderate to high pressures. Our approach to the problem has been to select an olivine tholeiite composition considered for petrographic reasons to be a possible "primitive" composition. The nature, compositions and proportions of phases which crystallize between the liquidus and solidus of the olivine tholeiite have been determined over a wide range of pressures. This information, together with knowledge of the original composition, allows the fractionation trends and compositions of residual liquids to be established for different load pressure conditions. Within a limited range of pressures (between 12 and 18 kb) it was found by these means that the residual liquid was fractionating directly *towards* the alkali olivine basalt field. Accordingly, a new basalt composition lying on the general path of fractionation of the olivine tholeiite, and intermediate in composition between the olivine tholeiite and a typical alkali olivine basalt was prepared. The composition of this basalt would be obtained by a

comparatively small degree of crystallization of the parental olivine tholeiite within the specified pressure interval. This second basalt had a composition lying close to the critically undersaturated plane (Fig. 1), possessing 1 % of normative hypersthene. A detailed study of the crystallization behaviour of this second basalt, called "olivine basalt" for convenience (YODER and TILLEY, 1962) was then carried out. It was found that within the above pressure range, the residual liquids resulting from crystallization of the olivine basalt followed a fractionation trend directly across the critically undersaturated plane and into the alkali olivine basalt field. The fractionation trend was followed further into the critically undersaturated field in an exactly analogous way by the detailed study of a typical alkali olivine basalt with a composition just within the critically undersaturated field.

The objective, in studying the crystallization behaviour of a series of related basaltic compositions linked by a common fractionation trend between 12 and 18 kb, was to established the nature and limitations of this fractionation trend in the most unambiguous way possible. Assumptions and extrapolations concerning the proportion of phases which crystallize, their compositions, and changes in oxidation states are minimised by this procedure. Some doubts had previously been expressed regarding the implications of GREEN and RINGWOOD'S (1964) preliminary results and interpretation on the fractionation of the parental olivine tholeiite (O'HARA, 1965; TILLEY and YODER, 1964) because of the degree of crystallization which was assumed, and because of possible changes in oxidation state. The present methods of investigation should remove these doubts.

These methods also yield results directly applicable to problems of partial melting and magma segregation in the mantle. If the liquidus phases of the basaltic compositions are also stable in the sub-solidus mineral assemblage of a "parental peridotite" then the partial melting process can be regarded essentially as the reverse of the fractionation process. In this way we are able to apply our results to problems of partial melting deep within the mantle and attempt deductions on the nature and proportions of the basaltic liquids derived by partial melting.

a) "Primary" Basaltic Liquids

In a project designed to study the fractionation trends of basaltic magmas at high pressure it is obviously desirable to select those compositions which exist as liquids at depth and are not the end result of processes of crytallization and fractionation, or of contamination, at upper crustal levels. The liquids formed by processes of partial melting or complete melting of mantle rock are commonly referred to as" primary magmas" or "primary liquids" and these liquids may be considerably different in chemistry from the major basaltic magma types which we see extruded in bulk at the earth's surface. O'HARA (1965, p. 19—27) has given a thoughtful review and analysis of the arguments on the nature of primary basaltic liquids and concludes that the composition of extrusive basalt magmas is the product of the interplay of two processes (p. 27):

"(i) Partial melting of the mantle, yielding primary magmas which vary in composition according to the pressure, partial pressure of volatiles and degree of overheating which accompany the process.

(ii) Continuous crystallization differentiation during the movement of the liquids to the surface."

These general conclusions indicate that the compositions of liquids or glasses observed in natural rocks may not provide a reliable guide to liquid compositions at depth.

Studies of the currently active Kilauea and Mauna Loa volcanoes of Hawaii demonstrate most convincingly the role of fractionation at shallow levels in producing a series of bulk compositions ranging from picrite with over 30% normative olivine to tholeiites with variable normative quartz (Muir and Tilley, 1963; Macdonald and Katsura, 1961; Murata and Richter, 1966a, b). The low-pressure fractionation in these Hawaiian tholeiites is dominated by settling of olivine. The most undersaturated basaltic glass from Kilauea Iki (1959 eruption) contains only 6.5% normative olivine (Macdonald and Katsura, 1961) but Macdonald and Katsura clearly recognize the role of olivine settling in making their estimate of the *average magma* composition for the 1959 Kilauea Iki lava lake. These authors note the tendency for the bulk composition of the erupted magma to become more mafic as the eruption proceeds and their estimated composition for the lava lake contains 18% normative olivine. The olivine tholeiite composition chosen for this study matches very closely with Macdonald and Katsura's estimated 1959 average Kilauea Iki lava lake composition[2]. The chosen olivine tholeiite composition also compares closely with a weighted average composition for the first eruptive phase of Kilauea Iki in 1959 (Murata and Richter, 1966b) although the Al_2O_3 content is higher (13.1% compared to 11.4%) in our olivine tholeiite composition. There is, of course, no compelling evidence that these estimates represent the bulk composition of a Kilauean liquid at 30—60 km. However, the relatively rapid ascent of the Kilauea Iki magma (Eaton and Murata, 1960) deduced from seismic evidence suggests that, particularly in the most vigorous extrusive phase or slightly thereafter, the bulk composition of erupted magma may be virtually unmodified from the liquid composition existing at considerable depth (20—60 kms).

The estimation of liquid compositions at depth from the evidence of natural extrusive magmas is thus somewhat subjective and requires detailed investigations of the type which have been undertaken at Hawaii. Limitations may be deduced by restricting attention to extrusive bulk compositions with high $Mg/Mg+Fe^{++}$ values, as the generalization that the liquidus ferro-magnesian silicates are enriched in Mg relative to Fe, appears well founded. This limitation directs attention towards olivine-rich, picritic rocks but the distinction between possible primary liquids and shallow level accumulative picrites is currently impractical.

An alternative, more direct approach to this problems is to seek the composition of liquids forming at the minimum melting temperatures under high pressure in peridotitic compositions such as are believed to be present in the upper mantle. O'Hara (1963a, p. 71—77; 1963b, p. 116—118), Davis (1964, p. 165—171) and Davis and Schairer (1965) have presented data relevant to this problem. O'Hara (1963a, 1963b) made a preliminary study of melting relations in various

[2] Macdonald and Katsura (1961) list $Al_2O_3 = 12.9\%$ for the "parent magma" for the 1959 lava lake samples but this is derived from the average of columns 2 and 3, Table 1, and should be 12.1%. This error was followed in our own work with the Al_2O_3 content of the prepared olivine tholeiite being 13.1%.

mixes of natural minerals separated from a garnet peridotite and an eclogite. He reported lower solidus temperatures in olivine + garnet + pyroxene mixes than in simple garnet + pyroxene mixtures and, comparing his data with that of YODER and TILLEY (1962) on quartz-bearing eclogites, concluded that the whole range of garnet + pyroxene assemblages must be considered a thermal barrier at 30 kb between lower temperature liquids in either olivine-bearing or quartz-bearing eclogitic rocks. If this conclusion is valid then a quartz-bearing eclogite, or a liquid of that composition, cannot be derived by partial melting of a garnet peridotite at 30 kb.

DAVIS (1964) and DAVIS and SCHAIRER (1965) have reported results on the system diopside—forsterite—pyrope at 40 kb. The minimum liquidus temperature in this system is at $1670 \pm 10°C$ and at a composition $Di_{47}\,Py_{47}\,Fo_6$. DAVIS and SCHAIRER deduce that the primary liquid for melting of the Ol + Ga + Cpx + Opx assemblage in the CaO-MgO-Al_2O_3-SiO_2 system will have a composition of approximately $Di_{47}\,Py_{47}\,Ens_3\,Fo_3$. Expressed in the CIPW norm to illustrate the approximate low pressure mineralogy, this composition gives $An_{32}\,Di_{22}\,Ens_{26}\,Fo_{20}$.

Thus, the studies at both 30 kb and 40 kb suggests that the compositions of liquids derived by partial melting of peridotite would contain around 20% or more olivine if expressed in the low pressure CIPW norm. Such liquids would be similar to rocks transitional between olivine tholeiites with around 10% olivine and tholeiitic picrites with 25—30% of olivine.

b) Basaltic Compositions Chosen for Study

In the previous section, evidence from natural volcanic sequences and from experimental studies at high pressure has been summarized, leading to the conclusion that liquids derived from partial melting of peridotite will have 20% or more normative olivine. In the initial selection of an olivine tholeiite composition for experimental study we used the estimate by MACDONALD and KATSURA (1961) of a "parental magma" composition of the Kilauea Iki 1959 lava lake. The composition used contains 20% olivine in the CIPW norm and, when expressed in an ideal eclogite norm, contains 46% garnet, 50% pyroxene, 4% ilmenite or alternatively 46% garnet, 49% pyroxene (Di + Jd + Ens) 3% olivine, 2% rutile depending on the assumed role of TiO_2. This compares closely in terms of mineral proportions, though not in mineral compositions, with DAVIS and SCHAIRER'S (1965) estimate of the reaction point Ol + Ga + Cpx + Opx + *Liq* at 40 kb in garnet, two-pyroxene, olivine assemblage, i.e. $Pyrope_{47}\,Diopside_{47}\,Ens_3\,Fo_3$. It is considered therefore that the olivine tholeiite composition is significant and relevant in studies of fractionation of basalts at high pressure. Conversely tholeiitic basalts with less than about 12% normative olivine cannot be considered "primary" basaltic liquids in the sense of being derived without fractionation from depths of more than 40 kms within the earth and are not relevant compositions for study of basalt fractionation at pressure in excess of 10 kb. Picritic compositions with more than 20% normative olivine (CIPW norm) may also be important as possible liquids or liquid + crystal derivatives from parental mantle peridotite.

The choice of an alkali basalt composition for experimental study was influenced both by the observed and inferred fractionation trends of the olivine tholeiite

towards an alkali olivine basalt between 12 and 18 kb, and by petrological considerations of a more general nature. Thus most alkali olivine basalt liquids, as observed in extrusive or chilled rocks, have probably progressed some way along a low pressure fractionation trend controlled by olivine separation. The average "alkali basalt" (mostly olivine-bearing) of the Hawaiian Islands listed by MacDonald and Katsura (1964) contains 14% normative olivine and neither hypersthene nor nepheline in the norm. The average Hawaiian alkali olivine basalt listed by Kuno et al. (1957) contains 18% normative olivine and the average from Japan (Kuno, 1960) contains 17% normative olivine. The composition chosen for study contains high normative olivine (26%), low normative nepheline (2%) but

Table 1. *Chemical compositions, CIPW norms and "eclogite" norms of compositions used experimentally*

	Olivine tholeiite	Olivine basalt	Alkali olivine basalt	Picrite
SiO_2	46.95	47.05	45.39	45.51
TiO_2	2.02	2.31	2.52	1.93
Al_2O_3	13.10	14.17	14.69	12.44
Fe_2O_3	1.02	0.42	1.87	0.92
FeO	10.07	10.64	12.42	8.67
MnO	0.15	0.16	0.18	0.15
MgO	14.55	12.73	10.37	18.79
CaO	10.16	9.87	9.14	9.67
Na_2O	1.73	2.21	2.62	1.64
K_2O	0.08	0.44	0.78	0.08
P_2O_5	0.21	—	0.02	0.20
	100.04	100.00	100.00	100.00
$\frac{100\,Mg}{Mg+Fe^{++}}$ (atomic ratio)	72.0	68.1	59.8	79.4
CIPW Norms				
Or	0.6	2.7	4.5	0.5
Ab	14.7	18.9	18.0	13.9
Ne	—	—	2.2	—
An	27.6	27.3	26.2	26.3
Di	17.0	17.6	15.7	16.5
Hy	12.3	1.3	—	2.8
Ol	21.9	27.2	25.8	34.6
Ilm	3.8	4.4	4.8	3.7
Mt	1.4	0.6	2.9	1.3
Ap	0.5	—	—	0.4
"Eclogite" Norm — assuming TiO_2 in ilmenite, small "K_2O" solubility in acmite-omphacite. Garnet is $Ca_{0.5}$ (Mg, Fe)$_{2.5}$ $Al_2Si_3O_{12}$ in all compositions.				
Pyroxene	50	52	47	40
Garnet	46	44	46	43
Olivine	—	—	2	13
Quartz	tr	tr	—	—
Ilmenite	4	4	5	4

is appreciably more iron-rich ($100\,Mg/Mg + Fe^{++} = 60$) than the olivine tholeiite composition ($100\,Mg/Mg + Fe = 72$). Analyses of alkali olivine basalts and basanites containing peridotite inclusions with the moderately high pressure mineralogy of olivine + aluminous pyroxenes + spinel show that these have $100\,Mg/Mg + Fe^{++}$ ratios between 60 and 70. These basalts, because of their transported xenolithic material, may be assumed to be derived, without fractionation of olivine, from depths greater than 20 km (BULTITUDE and GREEN, unpublished). Such basalts also have high normative olivine contents (>15%). It is considered that the chosen alkali olivine basalt composition is consistent with the available geological evidence on the estimation of compositions of critically undersaturated basaltic liquids derived without fractionation from depths of 20 km or more.

The olivine basalt composition was calculated as the arithmetic mean of the olivine and alkali olivine basalt compositions. As was previously discussed, it was also chosen to lie along the fractionation trend of the olivine tholeiite between 12 and 18 kb.

The compositions and CIPW norms of the glasses as used in the experiments are given in Table 1. Also given are "eclogite norms" based on calculation of garnets of composition $Ca_{0.5}\,(Mg, Fe)_{2.5}\,Al_2Si_3O_{12}$ and assuming solid solution of the minor orthopyroxene in some compositions in the calcium-rich pyroxene. The "eclogite norms" contain olivine in all four compositions if TiO_2 is calculated as rutile but only the picrite contains significant olivine if TiO_2 is calculated as ilmenite. Both the olivine tholeiite and olivine basalt lie essentially on the garnet + pyroxene join with neither quartz nor olivine, but the alkali olivine basalt contains 2% olivine and the picrite contains 13% olivine in eclogite nineralogy. All three basaltic compositions lie close to, but on the olivine-poor side of, the suggested minimum melting composition at 40 kb, using the simple Di-Fo-Pyrope system as a guide.

Experimental Procedure

a) Preparation of Basaltic Glasses

The glasses of olivine tholeiite, tholeiitic picrite and alkali olivine basalt were prepared from natural analyzed Hawaiian basalts with added MgO and $Fe + Fe_2O_3$ to obtain the desired compositions. The olivine tholeiite and tholeiitic picrite were prepared from a quartz tholeiite of the Pololu Series, Hawaii, and, as a result, have the low K_2O and Na_2O contents typical of these particular flows. After adding the MgO, Fe and Fe_2O_3 in calculated proportions, the components were intimately mixed and then fused to a glass. The alkali olivine basalt was similarly prepared from an analyzed Hawaiian alkali olivine basalt. The olivine basalt composition was prepared entirely by reacting mixtures of A. R. chemicals, in the required proportions, then adding Fe in the required amount and fusing the mixture to a glass.

Fusion of the basaltic compositions was carried out in either platinum tubes or crucibles at temperatures of 1,400—1,500° C. Oxidation was prevented by fusing in an argon atmosphere in contact with graphite at about 1,500° C. Loss of iron due to solution in the platinum containers during fusion was monitored in several control experiments and calculated amounts of Fe were added to compensate for this effect. After checking for homogeneity by examination in refractive index liquids, the glasses were finely ground and then analyzed in duplicate for FeO and Fe_2O_3 content. The compositions were calculated to 100% using the figures for FeO and Fe_2O_3 determined by analysis. The compositions obtained are listed in Table 1. In all cases the initial material was entirely glass — even the picrite was quenched without the formation of quench olivine.

b) Apparatus and Methods

The experimental runs were carried out using a single-stage, piston-cylinder apparatus similar to that described by Boyd and England (1960a, b, 1963). The techniques used have been described previously (Green and Ringwood, 1967). In the melting runs reported in this paper, exclusion of water from the sample is essential. This was attained by enclosing the sample in a platinum tube of 0.006″ wall thickness with both ends sealed by welding. In addition the furnace assembly used contained an inner boron nitride sleeve between the talc and graphite cylinders and the boron nitride, graphite and all ceramic components were dried for 1 hour at 1,000° C in an argon atmosphere. To minimise the loss of iron to the platinum capsule, the periods of runs were limited to 1 hour at temperatures less than 1,400° C and to shorter times at temperatures greater than 1,400° C. Temperatures were measured by a Pt-Pt10%Rh thermocouple in contact with the charge. Variation of recorded temperature during a run was smaller than $\pm 5°$ C whilst the temperature gradient across the sample was smaller than 10° C. No correction was made for the effect of pressure on the thermocouple EMF. Ignoring this latter factor, the maximum error in determination of charge temperature was 15° C. In practice however, the relative errors in series of runs were much smaller than this. Thus, experimental runs spaced 5° apart and carried out with identical procedures were internally consistent and yielded reproducible results. Sample pressures were calculated from the load pressure on the 3″ ram, assuming a −10% pressure correction for friction and imperfect pressure transmission in the furnace assembly (Green, Ringwood and Major, 1966). The absolute accuracy of pressure measurement is estimated at $\pm 3\%$.

c) Examination of Sample

Small portions of the sample were crushed and examined optically in refractive index liquids. This usually served to identify the phases present and the degree of melting. X-ray powder diffraction methods were used particularly to confirm the identification of olivine in the presence of clinopyroxene. Provided there was no access of water to the charge, little difficulty was found in quenching liquids to glass at pressures of 18 kb or lower. In some runs, particularly at 27 kb, there was patchy development of quench clinopyroxene (in part nucleating on primary crystals) but this was usually readily distinguishable from primary crystals by its feathery or fine-aggregate texture, by uneven extinction and by higher refractive indices than any primary clinopyroxene present.

Several fragments of most of the partial melting runs were mounted in epoxy resin and polished for use with the electron microprobe. These polished surfaces were excellent in showing the form and distribution of the primary phases, the quench clinopyroxene and the glass. Slight differences in hardness and in reflectivity were adequate to enable the phases to be clearly distinguished in reflected light.

d) Microprobe Methods and Calibration

An electron probe X-ray micro-analyser (Applied Research Laboratories model E.M.X.) was used for quantitative analysis for selected elements in olivine, enstatite, clinopyroxene and garnet in many of the experimental runs, particularly those near the liquidus. The electron beam of the microprobe was focussed to about 1 micron diameter, giving a volume of analysis (i.e. the volume from which characteristic X-rays were detectable) of 2—3 microns diameter and similar depth. An accelerating voltage of 12 kV, emission current of 60—100 mA and a specimen current of 0.04 micro-amps were used. Spot analyses were made at intervals of 1 to 10 microns with an integration time of 70 seconds. Analyses for Fe, Ca and Al were made simultaneously using K_α radiation. Corrections were made for specimen current fluctuations and for background but inter-element and matrix absorption and fluorescence effects were avoided by using calibration curves from glasses of known pyroxene composition. These glasses, prepared specifically for this project from carefully weighed A. R. chemicals, are enstatite ($100\,Mg/Mg + Fe = 90$) with 2.0% CaO to which were added Al_2O_3 contents from 0—20% and a second series of aluminous hypersthene ($100\,Mg/Mg + Fe = 75$; $Al_2O_3 = 8.0\%$) with variable CaO content from 0—8%. After fusion at 1,500—1,600° C and quenching to glass, these compositions were checked for iron content by analysis. The calibration curve for Fe was also based on analyzed olivines. Calibration curves for higher CaO contents in

clinopyroxenes were based on a series of glasses of variable SiO_2, Al_2O_3, TiO_2, CaO, MgO, Na_2O and K_2O contents prepared by T. H. GREEN. During analysis of crystals in the high pressure runs, frequent re-analysis of several standards provided a means of monitoring machine drift. The determinations of Fe, Ca and Al (reported as oxides in accordance with normal petrographic practice) are considered accurate to ± 0.2 weight percent on large homogeneous samples. The limit of detection for Ca and Al with the methods used was 0.1% Ca and 0.2% Al_2O_3 respectively. These estimates of accuracy and limits of detection are derived from the reproducibility of results on standards and from the linearity of the calibration curves. Slightly greater uncertainties derive from the nature of the crystals in the high pressure runs — these will be discussed in later sections.

Since the analyses of crystals are only partial analyses, the compositions of pyroxenes, olivines and garnets must be calculated assuming stoichiometry of the crystals and considering the major solid solution end members only i.e. Ca, Mg, Fe silicates or aluminosilicates. Components such as Mn or Ni silicates were neglected. In the clinopyroxenes, TiO_2 and Na_2O may be present in minor amounts but are not considered in the present study. Olivine was calculated as forsterite, fayalite and larnite solid solution, orthopyroxene and clinopyroxene as enstatite, ferrosilite, wollastonite and Al_2O_3 solid solution, and garnet as grossular, almandine and pyrope solid solution. The latter calculation gives a calculated Al_2O_3 content which compares quite closely with the measured Al_2O_3, particularly since Fe^{+++} is assumed to be zero.

e) Changes in Fe Content and Oxidation State

The use of platinum capsules for the experimental runs means that loss of Fe to solid solution in the platinum and resulting oxidation of remaining FeO, may be of sufficient importance to materially change the chemistry and thus the mineralogy of the basalts. To evaluate this effect, semi-micro chemical analyses for FeO and Fe_2O_3 were carried out on 2—8 mg samples from some of the experimental runs. The results of these analyses are given in Table 2. The loss of iron is greater than from the subsolidus runs previously reported (GREEN and RINGWOOD, 1967) and averages about 20—25% of the total iron present. In most cases there is slight reduction of the iron rather than oxidation and this may be attributed to the presence of hydrogen and a reducing environment within the graphite furnace sleeve.

The changes in iron content and oxidation state are not so large as to destroy the basaltic chemistry or even the general character of the normative mineralogy. The normative olivine and hypersthene or nepheline contents of the most altered compositions are calculated in Table 2. The olivine contents in the tholeiitic basalts are considerably decreased and hypersthene is conversely increased. In the alkali olivine basalt compositions both olivine and nepheline decrease but the compositions remain nepheline normative.

The chemical composition of the sample cannot be considered constant for the length of the experimental run and it is uncertain whether observed crystals in glass maintained equilibrium with the changing bulk chemistry throughout the length of the run. Microprobe examination of samples has demonstrated that there may be a range in $Mg/Mg+Fe$ contents of crystals, controlled by their position in the sample capsule. Crystals which have formed near the edge of the sample are more magnesian than those at the centre — this has been particularly well shown for olivine. In addition some orthopyroxene, olivine and garnet crystals have shown zoning in Fe content — this zoning is the reverse of normal igneous zoning and crystal cores are more iron-rich than crystal edges. This effect is attributed to gradual loss of Fe from the sample with the result that outer zones of crystals either maintain equilibrium with the changing liquid composition while crystal cores do not, or alternatively the outer zones of crystals have grown during the latter part of the experimental runs. Either process would produce the observed zoning of crystals.

A method of evaluating the effect of Fe-loss in relation to the compositions of crystals formed during the experimental runs is to compare the partition coefficients for liquidus crystal-magma equilibria observed in natural basalts with the partition coefficients observed in the experiments. In considering the partition of Mg and Fe between liquidus olivine and liquid, it is convenient to define a partition co-efficient

$$K_{O,L} = \left(\frac{Mg}{Mg+Fe^{++}}\right)_{Olivine} \Big/ \left(\frac{Mg}{Mg+Fe^{++}}\right)_{Liquid}.$$

Table 2. *Loss of iron and change in oxidation state during experimental runs*

Run No.	Composition	Conditions			FeO		Fe_2O_3		Total Fe as FeO	
		Temp. (°C)	Press. (kb)	Time (hrs)	initial	final	initial	final	initial	Final
55	Olivine tholeiite A	1200	9	2	10.07	8.31	1.02	0.21	10.99	8.50
56	Olivine tholeiite A	1250	9	1	10.07	7.10	1.02	0.94	10.99	7.76
413	Olivine tholeiite A	1370	9	1	10.07	6.92*	1.02	2.61*	10.99	9.27
141	Olivine tholeiite A	1375	9	1	10.07	6.42	1.02	1.60	10.99	7.86
451	Olivine tholeiite A	1440	22.5	1/2	10.07	8.33	1.02	0.88	10.99	9.12
447	Olivine tholeiite A	1450	22.5	20 min	10.07	8.27	1.02	1.40	10.99	9.53
445	Olivine tholeiite A	1510	27	20 min	10.07	8.07	1.02	1.11	10.99	9.07
Mean of olivine tholeiite runs		—	—	—	10.07	7.63+	1.02	1.25+	10.99	8.7
130	Alkali basalt	1250	18	1	12.42	10.00	1.87	1.14	14.10	11.03
124	Alkali basalt	1400	18	1	12.42	8.23**	1.87	3.90**	14.10	11.73
412	Alkali basalt	1440	27	1/2	12.42	7.60	1.87	0.29	14.10	7.86
496	Alkali basalt (Mix 2)	1310	13.5	1/2	13.06	10.25	0.17	0.70	13.21	11.88
396	Olivine basalt	1360	18	1	10.64	7.09++	0.42	1.15++	11.02	8.13
764	Olivine basalt	1300	13.5	50 min	10.64	8.72	0.42	0.82	11.02	9.46
474	Picrite	1520	18	1/2	8.67	6.48	0.92	0.47	9.50	6.90

Analyst: E. Kiss

	Compositions after experiments	*Initial compositions*
* Norm contains	17.1% Hypersthene 13.6% Olivine	(12.3% Hy, 21.9% Ol)
+ Norm contains	14.6% Hypersthene 16.9% Olivine	(12.3% Hy, 21.9% Ol)
** Norm contains	0.2% Nephelene 19.5% Olivine	(2.2% Ne, 25.8% Ol)
++ Norm contains	8.1% Hypersthene 17.5% Olivine	(1.3% Hy, 27.2% Ol)

From the experimental results (see pages 132—134) on the three basaltic compositions at 4.5 and 9 kb, the partition coefficients can be calculated assuming either that the "liquid" composition is that of the original mix before Fe-loss during the experiment or that the liquid composition is close to the average of the compositions analysed for FeO, Fe_2O_3 after the melting experiments (Tables 2 and 3). The examples of partition coefficients in natural basalts are the maximum values obtained and only include those with olivine determined by chemical, X-ray or refractive index measurements. The effect of olivine accumulation or of the olivine phenocrysts present representing crystal-liquid equilibrium at temperatures lower than the liquidus, will be to yield *low* values for the natural partition coefficients.

Table 3. *Partition coefficients between olivine and liquid composition in experimental and natural examples*

	Olivine in equilibrium with initial mix composition			Olivine in equilibrium with average composition after Fe loss	
	$\left(\frac{100\,Mg}{Mg+Fe}\right)_{Ol}$	$\left(\frac{100\,Mg}{Mg+Fe^{++}}\right)_{Liq}$	$K_{O,L}$	$\left(\frac{100\,Mg}{Mg+Fe^{++}}\right)_{Liq}$	$K_{O,L}$
Olivine Tholeiite	92	72	1.28	78	1.18
Olivine Basalt	90	68	1.32	73	1.23
Alkali Olivine Basalt	83	60	1.38	69	1.20
		Mean Value	1.33		

	Natural examples of maximum partition coefficients between phenocryst olivine and whole rock composition		
	$\left(\frac{100\,Mg}{Mg+Fe}\right)_{Ol}$	$\left(\frac{100\,Mg}{Mg+Fe^{++}}\right)_{Liq}$	$K_{O,L}$
1959 Kilauea 1st phase (Muir and Tilley, 1963)	89	66	1.35
1959 Kilauea Pele's hair (MacDonald and Katsura, 1961)	87.5	62.5	1.40
1887 Mauna Loa (Yoder and Tilley, 1962)	87	62.5	1.39
1868 Kilauea flow (Muir and Tilley, 1963)	81	62	1.31
1868 Kilauea flow (Muir and Tilley, 1963)	88	59.5	1.48
1868 Kilauea tachylyte (Muir and Tilley, 1963)	81.5	53.5	1.52

In both the experimental and natural examples the partition coefficient apparently increases with decreasing values of $100\,Mg/Mg+Fe^{++}$ for the liquid (Table 3). However within the range $60 < 100\,Mg/Mg+Fe^{++} < 75$ there is close similarity between the values of the natural partition coefficients and the partition coefficients for the experimental runs provided that the initial, pre-run, composition is used as the liquid composition. The comparison of partition coefficients thus suggests that the iron loss from the sample occurs after most of the crystal growth, at least in the central parts of the sample capsule.

In summary, the evidence we have obtained on the magnitude and time dependence of the loss of Fe to the platinum capsule, leads to the conclusion that this effect is not a major factor in the experiments reported herein in modifying either the major element chemical composition or the nature of the crystalline phases of the experimental runs.

Experimental Results

Detailed descriptions of the results of individual runs on the several compositions are given in Tables 4—7. Photographs of typical phases in polished sections are

Table 4. *Details of experimental partial melting runs on olivine tholeiite composition*

Run No.	Pressure (kb)	Temp. (°C)	Time (mins)	Phases present*	Comments
A1	1 atmos.	1,200	30	Ol + Px + Pl + Glass	Low degree (~30%) of melting. Orthopyroxene not identifiable.
A4	1 atmos.	1,240	30	Ol + Pl + ?Mt + Glass	Glass > crystals. Plagioclase approx. 10—15%. No pyroxene identifiable. Minor brown spinel (?magnetite$_{ss}$) possibly due to oxidation.
A2	1 atmos.	1,260	30	Ol + Pl + Glass	Plagioclase definite but very weak reflections.
A6	1 atmos.	1,280	30	Ol + ?Mt + Glass	Common olivine (~10%), minor brown spinel (?magnetite, probably due to oxidation (capsule burst during run).
A7	1 atmos.	1,320	20	Ol + ?Mt + Glass	Uncommon olivine, rare ?magnetite$_{ss}$. Near liquidus run.
A8	1 atmos.	1,340	20	Ol + Glass	Very, very rare olivine, essentially liquidus run.
142	4.5	1,350	60	Ol + Glass	Olivine as very uncommon small euhedra. Very near liquidus.
485	9.0	1,100	180	Ol + Px + Pl + Spinel	Plagioclase common. Olivine more common than in 1210°C, 1230°C runs. Spinel as moderately common small green to green-brown equant grains. Orthopyroxene not identifiable optically.
459	9.0	1,210	180	Ol + Opx + Cpx + Pl + Glass	Minor segregated glass, also intergranular, with plagioclase. Ol and Cpx as small anhedra. Opx as large laths.
453	9.0	1,230	180	Ol + Opx + Cpx + Glass	Coarser grained and with more glass than following run. Plagioclase identification (X-ray) uncertain.
439	9.0	1,230	60	Ol + Opx + Cpx + Glass	Near solidus run with fine Cpx and Ol, larger Opx with Cpx or Ol inclusions. No definite plagioclase (X-ray).
436	9.0	1,250	60	Ol + Opx + Cpx + Glass	Glass moderately common but crystals > glass. Cpx > Opx + Ol. Opx as large euhedra, olivine as smaller euhedra, clinopyroxene as abundant subhedral or euhedral small crystals.
434	9.0	1,270	60	Ol + Opx + Glass	Much greater partial melting than in previous run. Glass > Crystals, Ol > Opx. No definite Cpx.
431	9.0	1,290	60	Ol + Opx + Glass	Olivine common. Orthopyroxene uncommon. No clinopyroxene.
426	9.0	1,310	60	Ol + Glass	Olivine common.
423	9.0	1,330	60	Ol + Glass	Olivine moderately common, euhedral.
417	9.0	1,350	60	Ol + Glass	Olivine as uncommon, euhedral crystals. Very near liquidus.
413	9.0	1,370	60	Glass + quench cpx	Rare quench clinopyroxene.
141	9.0	1,375	60	Glass + quench cpx	Rare quench clinopyroxene.

84	10.1	1,100	120	Ol + Px + Pl + Spinel	Similar to 9 kb, 1,100°C run, olivine reflections weak.
488	11.3	1,100	150	Px + Pl + Spinel	Olivine absent, plagioclase much decreased from 10.1 kb run and spinel more abundant.
762	11.3	1,370	40	Ol + Opx + Glass	Moderately common large orthopyroxene laths, less common small olivine euhedra. Comparable crystallization to 13.5 kb, 1380°C run.
487	12.4	1,100	180	Px + Pl + Spinel	Plagioclase decreased from run 488. No definite garnet. Spinel moderately common.
469	13.5	1,100	180	Px + Pl + Ga + Amphibole	Minor plagioclase reflections, weak garnet reflections but optically distinctive as porphyroblasts. Spinel minor or absent. Minor amphibole.
461	13.5	1,180	180	Opx + Cpx + Pl + Spinel	Predominantly clinopyroxene + orthopyroxene. Plagioclase definitely present but less abundant than at 13.5 kb, 1,100°C. Spinel moderately common. Orthopyroxene is very distinctive as large porphyroblasts with both spinel and plagioclase inclusions. Clinopyroxene, in contrast, occurs as small equant granules. No glass.
456	13.5	1,220	180	Opx + Cpx + ?Pl + Spinel + Glass	Orthopyroxene and clinopyroxene similar to 13.5 kb, 1,180°C run. Opx porphyroblasts contain included spinel and rare included plagioclase. Glass as intergranular low R.I. continuum, more abundant than discrete low R.I. plagioclase grains at 13.5 kb, 1180°C. Plagioclase identification probable from X-ray data.
441	13.5	1,220	60	Opx + Cpx + ?Pl + Spinel + Glass	Similar to previous 3hr run but with less low R.I. material. Opx porphyroblasts smaller than in 3 hr run. Plagioclase probably present. Very near solidus.
782	13.5	1,250	60	Opx + Cpx + Pl + Spinel	Mainly very fine-grained clinopyroxene with uncommon small euhedral orthopyroxene porphyroblasts. Minor spinel. Moderately common disconnected amoeboid patches of low R.I. plagioclase. No definite glass. Solidus run. Plag. approx. 15%.
438	13.5	1,270	60	Opx + Cpx + Spinel + Glass	Crystals > glass. Mainly fine, subhedral clinopyroxene with uncommon orthopyroxene as larger crystals. Intergranular continuum and some segregations of glass. Minor pale green spinel.
432	13.5	1,290	60	Opx + Cpx + Spinel + Glass	Very similar to 1,270°C run. Glass more common. Minor spinel identifiable on polished surface.
425	13.5	1,310	60	Opx + Cpx + Glass	Common small equant clinopyroxene, less common large orthopyroxene laths. Crystals > glass.

Table 4 (continued)

Run No.	Pressure (kb)	Temp. (°C)	Time (mins)	Phases present*	Comments
428	13.5	1,350	60	Opx + Cpx + Glass + quench cpx	Glass > crystals. Opx > Cpx. Large euhedral orthopyroxenes and very uncommon large clinopyroxene crystals. Clinopyroxene clearly primary and in part intergrown with othopyroxene.
424	13.5	1,380	60	Opx + Glass + quench cpx	Common (10—15%) (Plate IB) euhedral orthopyroxene. Rare quench clinopyroxene, in part nucleating on othopyroxene margins.
143	13.5	1,400	60	Opx + Glass	Uncommon large orthopyroxene crystals in glass. Some crystal settling possible. Near-liquidus run.
773	13.5	1,360	5	Cpx + ? Spinel + Glass + quench cpx	Poorly crystallized fine granular clinopyroxene, minor probable spinel and intergranular glass.
772	13.5	1,380	5	Opx + Cpx + Glass + quench cpx	Mainly poorly crystallized granular and feathery clinopyroxene. Rare orthopyroxene cores.
781	13.5	1,400	5	Opx + ? Cpx + Glass + quench cpx	Mainly feathery, granular and some rather clear clinopyroxene crystals + glass. Uncommon but distinctive orthopyroxene commonly with clinopyroxene rims or patchy "intergrowth" of clinopyroxene.
774	13.5	1,420	5	Glass + quench cpx	Glass with rare, feathery clinopyroxene.
761	13.5	1,380	40	Opx + Glass + quench cpx + residual Ga	The initial material for this run was crystallized to garnet + clinopyroxene at 30 kb, 1,100° C, 4 hrs. The run consisted of abundant glass, moderately common clear, medium to large orthopyroxene laths with borders and outgrowths of feathery quench clinopyroxene. No primary clinopyroxene. Some glass areas contain small, perfectly spherical, garnet residual crystals, some with rutile inclusions.
113	18.0	1,300	60	Cpx + Ga + ? Glass	Very near to solidus, small percentage of low R.I., amoeboid grains may be glass or plagioclase.
131	18.0	1,325	60	Cpx + Ga + Glass	Garnetless than in previous run. Glass intergranular and in small segregations.
125	18.0	1,350	60	Cpx + Ga + Glass	Minor garnet (euhedral), mainly fine clinopyroxene with intergranular glass. Crystals > glass.

121	18.0	1,370	60	Cpx + Glass	Garnet absent, orthopyroxene not identifiable. Fine-grained clinopyroxene + common glass (~40%).
122	18.0	1,375	60	Opx + Cpx + Glass	Well crystallized orthopyroxene and clinopyroxene crystals, some in parallel intergrowth. Abundant glass, and some possible quench clinopyroxene. Cpx > Opx.
118	18.0	1,380	60	Opx + Cpx + Glass + quench cpx	Large primary orthopyroxene and clinopyroxene as both separate and intergrown crystals. Cpx > Opx. Common quench clinopyroxene.
114	18.0	1,400	60	Opx + Cpx + Glass + quench cpx	Large, clear, primary orthopyroxene and clinopyroxene set in glass or glass + feathery quench clinopyroxene. Opx > Cpx.
454	18.0	1,420	30	Opx + Glass + quench cpx	Rare, large euhedral crystals of orthopyroxene in glass + minor quench clinopyroxene. Very near liquidus.
123	18.0	1,425	60	Opx + Glass + quench cpx	Rare, large euhedral crystals of orthopyroxene in glass + minor quench clinopyroxene. Very near liquidus.
448	22.5	1,410	20	Cpx + Ga + Glass	Common large euhedral garnet. Major phase is rather fine-grained, subhedral clinopyroxene. Minor glass generally intergranular, rarely as small segregations.
449	22.5	1,430	20	Cpx + Glass	Abundant fine-grained subhedral clinopyroxene in glass. Crystals > glass.
451	22.5	1,440	30	Cpx + Glass + quench cpx	Glass + common quench clinopyroxene. Some clinopyroxene is probably primary but difficult to distinguish from quench.
447	22.5	1,450	20	Glass + quench cpx	Mainly glass with patches of quench clinopyroxene.
783	27.0	1,430	30	Cpx + Ga	Medium-sized subhedral garnet and fine grained clinopyroxene. Glass absent or as very rare and very small patches. Solidus run.
442	27.0	1,450	20	Cpx + Ga + Glass	Common euhedral garnet and fine-grained clinopyroxene. Minor intergranular glass. Near-solidus run.
444	27.0	1,490	20	?Cpx + Ga + Glass + quench cpx	Moderately common euhedral garnet. Very common quench clinopyroxene, some clinopyroxene *may* be primary.
445	27.0	1,510	20	Glass + quench cpx	Mainly glass but some clinopyroxene considered to be of quench origin. Above liquidus.

* Abbreviations used are as follows: Ol — olivine, Opx — orthopyroxene, Cpx — clinopyroxene, Ga — garnet, Pl — plagioclase.

Table 5. *Details of partial melting experiments on olivine basalt composition*

Run No.	Pressure (kb)	Temp. (°C	Time (mins)	Phases present	Comments
784	9.0	1,240	60	Ol + Cpx + Glass	Abundant very fine anhedral clinopyroxene. Minor olivine (slightly larger, subhedral). About 40% glass.
787	9.0	1,260	60	Ol + Opx + Cpx + Glass	Abundant small anhedral clinopyroxene. Moderately common olivine, rare orthopyroxene laths. About 60% glass.
418	9.0	1,280	60	Ol + Glass	Uncommon, small euhedral olivine in glass.
764	13.5	1,290	50	Opx + Cpx + Spinel + Glass	Rare orthopyroxene, abundant fine clinopyroxene, probable minor spinel with intergranular glass locally expanding into small segregations. Estimated glass (30%).
767	13.5	1,310	50	Opx + Cpx + Glass + quench cpx	Large orthopyroxene laths and some large clinopyroxene crystals. Opx > Cpx. Quench clinopyroxene common.
419	13.5	1,320	60	Opx + ?Cpx + Glass	Large orthopyroxene laths with rims and some parallel growth of clinopyroxene, in glass. No definite primary clinopyroxene and none identified with microprobe (Plate Ic).
770	13.5	1,330	50	Opx + Glass + quench cpx	Uncommon, well formed orthopyroxene, some quench clinopyroxene but no definite primary clinopyroxene.
397	18.0	1,320	60	Cpx + Ga + Glass	Moderately common large, subhedral garnet with abundant fine grained clinopyroxene. Glass intergranular with some small segregations.
400	18.0	1,330	60	Cpx + Ga + Glass	Uncommon garnet, small subhedral clinopyroxene with some outgrowth of quench cpx. No orthopyroxene identifiable. Less garnet and more glass than previous run. Crystals > Glass.
405	18.0	1,335	60	Opx + Cpx + Glass + quench cpx	Large orthopyroxene laths and large clinopyroxene crystals, in some cases in parallel growth, also as distinct crystals. Common fine, anhedral and feathery quench clinopyroxene. Glass > Primary crystals.
398	18.0	1,340	60	Opx + Glass + quench cpx	Rare large orthopyroxene crystals, rimmed by feathery clinopyroxene but this is not in parallel growth as in previous run. Very near liquidus.
402	18.0	1,340	60	Opx + Glass + quench cpx	Large orthopyroxene crystals, slightly more common than in previous run, in fine-grained equant and feathery clinopyroxene and glass. No clinopyroxene in parallel growth with orthopyroxene.
396	18.0	1,360	60	Glass + quench cpx	Glass with patchy quench clinopyroxene including both feathery and anhedral forms.

404	27.0	1,420	60	Cpx + Ga + Glass
407	27.0	1,450	60	Ga + Glass + quench cpx
415	27.0	1,460	20	Ga + Glass + quench cpx
410	27.0	1,470	60	Ga + Glass

Abundant garnet and clinopyroxene, in similar proportions. Intergranular glass — approx. 20—30% melting.
Garnet as medium-sized and large euhedral crystals either in feathery, turbid quench clinopyroxene or in clear glass (Fig. 2D). No definite primary clinopyroxene.
Similar to previous run but garnet smaller and less abundant. Patchy development of quench clinopyroxene and other areas of glass + garnet. No evidence for primary clinopyroxene.
Rare garnet is spherical or amoeboid showing clear resolution effects. Glass is colourless and has grossly lost Fe to the platinum capsule. Garnet interpreted as early crystallizing liquidus phase, later being redissolved in the liquid as the composition changed due to Fe loss.

given in Fig. 2. A number of generalizations on the habits and appearance of the various crystalline phases apply to all the compositions. Olivine, when appearing on or near the liquidus, occurs as euhedra of short prismatic or pseudohexagonal habit (crystal size 5—25 microns) — the latter form, with strong development of the hkl or h0l, 0kl faces, is particularly diagnostic. Prismatic crystals show straight extinction and moderate to high birefringence, pseudohexagonal or rhombic sections show symmetrical extinction. When present in assemblages near the solidus with abundant clinopyroxene, olivine is distinguished from the latter by more euhedral and slightly larger crystals and by higher birefringence.

Orthopyroxene is very distinctive in the experimental runs with a greater tendency towards euhedral form and large, inclusion-free crystals than any other mineral present. In near-liquidus runs the orthopyroxene crystallizes as elongate prisms terminated by the basal pinacoid, in some cases with minor development of the hkl, 0kl or h0l faces. Crystals are commonly 40—400 microns long and 10—50 microns thick (Fig. 2B, C). The orthopyroxene is optically distinctive in having straight extinction with low birefringence in prismatic sections. In runs well below the solidus (1,100° C) the orthopyroxene remains fine-grained and cannot be distinguished optically from clinopyroxene. In runs close to the solidus, and particularly in the runs at 9 kb and 13.5 kb on the olivine tholeiite composition where there has been access of small amounts of water in 3-hour runs, the orthopyroxene grows as very distinctive, large porphyroblasts which contain uncommon small inclusions of spinel, clinopyroxene and plagioclase. In some near-liquidus runs in which clinopyroxene is a co-existing primary phase as uncommon large crystals, the orthopyroxene shows included and marginal parallel intergrowth of clinopyroxene. In runs in which orthopyroxene and liquid are the only phases, the orthopyroxene does not show this intergrowth with clinopyroxene but may show some nucleation of quench clinopyroxene as feathery outgrowths, particularly at crystal corners (Fig. 2C).

Primary clinopyroxene occurs typically as small (2—10 microns) equant or short, prismatic crystals

Table 6. *Details of partial melting experiments on alkali olivine basalt composition*

Run No.	Pressure (kb)	Temp. (°C)	Time (mins)	Phases present	Comments
A3	1 atmos.	1,220	30	Ol + Cpx + Pl + ?Mt + Glass	About 50% melting. Common olivine, plagioclase and clinopyroxene, minor deep brown $spinel_{ss}$.
A5	1 atmos.	1,240	30	Ol + Pl + Glass	About 30% crystals, olivine and plagioclase in similar abundance. No semi-opaque $spinel_{ss}$.
A10	1 atmos.	1,250	30	Ol + Glass	Uncommon olivine, very near liquidus.
A9	1 atmos.	1,260	30	?Mt + Glass	Minor brown spinel ($magnetite_{ss}$) possibly due to some oxidation.
788	9.0	1,180	60	Ol + Cpx + Pl + Spinel + Glass	Near solidus run. Olivine (minor) with abundant fine equant clinopyroxene, uncommon spinel and common low R.I. plagioclase + some glass (probably) intergranular and amoeboid patches.
401	9.0	1,220	60	Ol + Cpx + Glass	Olivine and clinopyroxene as small euhedral or subhedral crystals. Clinopyroxene identified by microprobe. Glass > Crystals.
786	9.0	1,240	60	Ol + Glass	Olivine crystals in glass. Clinopyroxene not identifiable optically nor by X-ray means.
399	9.0	1,260	60	Ol + Glass	Small euhedral olivine in glass. Rare quench clinopyroxene.
785	11.3	1,270	60	?Ol + Cpx + Opx + Glass	Moderately common small euhedral to subhedral crystals of clinopyroxene, probable minor olivine and rare orthopyroxene laths. Glass ≫ crystals.
523	13.5	1,250	60	Cpx + Glass	Abundant small anhedral clinopyroxenes in intergranular glass. No definite spinel. Crystals > glass.
521	13.5	1,270	45	Cpx + Glass	Medium grained anhedral or subhedral clinopyroxene in glass. No orthopyroxene. Glass > crystals.
420	13.5	1,290	60	Opx + Cpx + Glass + quench cpx	Rare large orthopyroxene and clinopyroxene primary crystals in glass and quench clinopyroxene in feathery and aggregate textures.
494	13.5	1,290	30	?Opx + Cpx + Glass + ?quench cpx	Small subhedral clinopyroxene and possibly some orthopyroxene with glass and minor ?quench clinopyroxene outgrowths and anhedral aggregates. Apparently much greater crystallization than previous run.
501	13.5	1,295	30	Glass + quench cpx	Patchy development of fine aggregates of anhedral clinopyroxene in glass, probably entirely quench but may be primary.
497	13.5	1,300	30	?Opx + ?Cpx + Glass + quench cpx	Small, rectangular crystals of probable orthopyroxene with clinopyroxene outgrowths and similar crystals of clinopyroxene with quench outgrowths. Abundant glass and anhedral quench clinopyroxene aggregates.

496	13.5	1,310	30	Glass + quench cpx	No primary crystals. Very little quench clinopyroxene.
130	18.0	1,250	60	Cpx + Ga + Glass	Mainly fine clinopyroxene with moderately common garnet as larger subhedral crystals. Minor (~10%) intergranular glass, mauve-coloured.
128	18.0	1,300	60	Cpx + Glass	Abundant granular clinopyroxene with intergranular and segregated mauve-coloured glass. About 50% glass.
132	18.0	1,320	60	Cpx + Glass	Uncommon large clinopyroxene crystals in glass + rare quench cpx.
133	18.0	1,335	60	Glass + quench cpx	Some patches of feathery and fine aggregate quench clinopyroxene.
126	18.0	1,350	60	Glass + quench cpx	Some patches of feathery and fine aggregate quench clinopyroxene.
403	27.0	1,360	60	Cpx + Ga + Glass	Abundant garnet and clinopyroxene with minor intergranular glass and small segregations showing brownish or mauve colour. Near solidus run.
406	27.0	1,400	60	Cpx + Ga + Glass	Euhedral garnet and sub-hedral, equant clinopyroxene in common brownish glass. Cpx > Ga.
416	27.0	1,430	30	Ga + Glass + quench cpx	Euhedral garnet, locally in clear glass, more commonly in feathery, turbid quench clinopyroxene.
412	27.0	1,440	30	Glass + quench cpx	No garnet. Patchy quench clinopyroxene.

without characteristic crystal form. In runs where there is a high glass content and relatively few clinopyroxene crystals, the latter form larger (up to 50 microns), stubby prismatic crystals, distinguished from orthopyroxene by inclined extinction and much higher birefringence. The distinction by optical means between olivine and primary clinopyroxene is often difficult and X-ray data are commonly necessary. The identification as primary or quench clinopyroxene is very difficult in some runs where the quench clinopyroxene forms fine-grained anhedral aggregates. More commonly the quench clinopyroxene is feathery, turbid, without crystal form and with wavy extinction. In some runs at 22.5 or 27 kb, larger crystals of clinopyroxene are distinguished as quench products by small inclusions of turbid, low R.I. material either in stringers or randomly distributed. Primary clinopyroxene crystals in these runs are clear and have lower refractive indices than enclosing quench clinopyroxene.

In the compositions studied in this paper, plagioclase appears only in runs at temperatures close to the solidus. Under these conditions plagioclase could not be distinguished from glass by optical means and was identified by X-ray diffraction methods.

In subsolidus or near-solidus runs, garnet forms euhedral or subhedral crystals usually from 10—20 microns grain-size and commonly containing included pyroxene or other phases. In near-liquidus runs garnet is euhedral, without inclusions and up to 50 microns grain-size (Fig. 2D).

a) Crystallization at 1 Atmosphere

Olivine is the liquidus phase in the olivine tholeiite and alkali olivine basalt compositions at 1 Atmosphere. The appearance of minor, deep brown spinel (? $magnetite_{ss}$) in some runs near the liquidus (Tables 4 and 6) and not in others, may be attributed to the effects of oxidation

Table 7. *Details of partial melting experiments on picrite composition*

Run No.	Pressure (kb)	Temp. (°C)	Time (mins)	Phases present	Comments
614	13.5	1,320	40	Ol + Opx + Cpx + Glass + quench cpx	Opx uncommon but as large phenocrysts.
623	13.5	1,340	40	Ol + Opx + Cpx + Glass	Glass approx. 40—50% of run. Opx as uncommon large porphyroblasts. Cpx > Ol.
572	13.5	1,360	30	Ol + Glass	Abundant euhedral olivines.
612	13.5	1,360	40	Ol + Opx + Glass	Common olivine, very rare orthopyroxene.
479	13.5	1,380	30	Ol + Glass	Euhedral olivine + glass.
618	18.0	1,350	40	Ol + Ga + Cpx + ? Glass	Near solidus run. Minor garnet. Minor olivine. Small amount of intergranular low R.I. phase may be glass.
462	18.0	1,370	30	Ol + Cpx + Glass	Crystals > glass. Small equant clinopyroxene with minor olivine.
465	18.0	1,390	30	Ol + Cpx + Glass + quench cpx	Euhedral olivine. Crystals < glass + quench cpx. No orthopyroxene.
476	18.0	1,400	20	Ol + Opx + ? Cpx + Glass + quench cpx	Common olivine. Uncommon orthopyroxene, some with parallel Cpx intergrowth. No definite separate primary Cpx.
467	18.0	1,410	30	Ol + Opx + ? Cpx + Glass + quench cpx	Common olivine. Uncommon orthopyroxene, some with parallel Cpx intergrowth. No definite separate primary Cpx.
468	18.0	1,430	30	Ol + Glass	Moderately common olivine euhedra.
620	22.5	1,430	20	Ol + Cpx + Ga + ? Spinel + Glass	Near solidus run. Mainly. Mainly Cpx + minor garnet + minor olivine + minor brownish high R.I. phase (? Spinel or Mg-rich ilmenite).
621	22.5	1,450	20	Cpx + Glass + quench cpx	Near liquidus run. Uncommon large clinopyroxene with quench outgrowths of Cpx.
615	22.5	1,460	20	Glass + quench cpx	Above liquidus.
625	27.0	1,200	120	Cpx + Ga + Ol + ? Magnetite-ulvospinel	Common garnet and clinopyroxene. Minor olivine. Minor semi-opaque (possibly magnetite-ulvospinel$_{ss}$).
619	27.0	1,450	20	Cpx + Ga + ? Spinel	Subsolidus run. Common garnet and clinopyroxene. Minor translucent, high R.I. grains may be spinel$_{ss}$.
473	27.0	1,480	20	Cpx + Ga + ? Spinel + Glass	Near solidus run. Cpx and Ga well crystallized. Possible minor olivine. Minor high R.I. phase (spinel$_{ss}$ or ilmenite$_{ss}$).
475	27.0	1,500	20	Opx + Cpx + Ga + Glass + quench cpx	Uncommon garnet euhedra, uncommon orthopyroxene laths. Common Cpx but most is probably quench clinopyroxene. Possible olivine, minor high R.I., birefringent rutile or Mg-ilmenite ?
616	27.0	1,510	20	Glass + quench cpx	Above liquidus.
474	27.0	1,520	20	Glass + quench cpx	

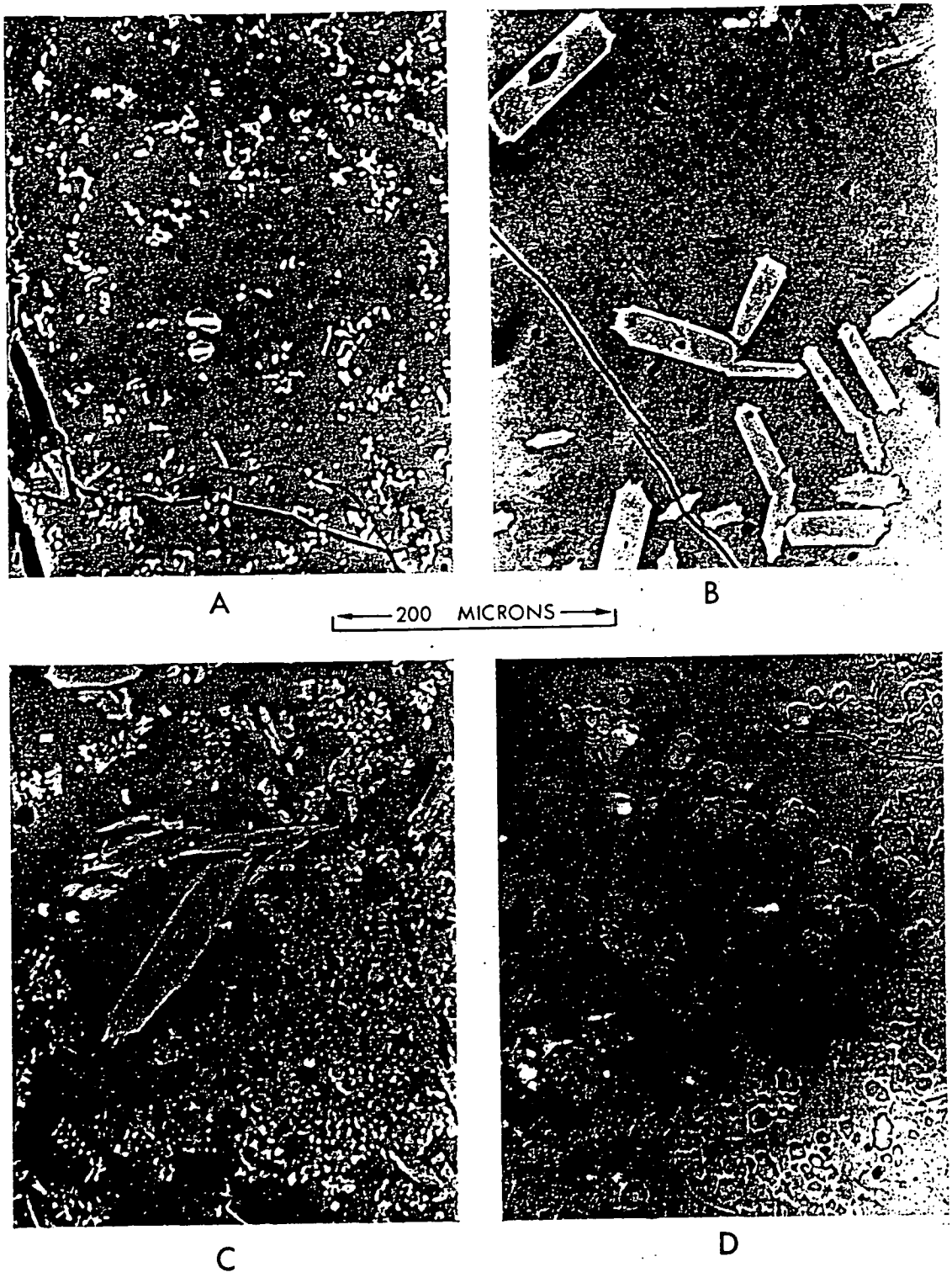

Fig. 2A—D. Polished mounts for electron microprobe analyses showing crystalline phases in glass at various pressures. A. Olivine (small, highly reflecting grains) and orthopyroxene (larger, lath-shaped) crystals in glass. Olivine tholeiite at 9 kb, 1,290° C. White trace across larger orthopyroxenes shows path of electron beam during microprobe analyses. B. Orthopyroxene crystals in glass. Olivine tholeiite at 13.5 kb, 1380° C. Incipient nucleation of quench clinopyroxene particularly at corners of orthopyroxene. C. Large orthopyroxene and fine aggregates of quench clinopyroxene. Olivine basalt at 13.5 kb, 1,320° C. D. Garnet crystals and patchy aggregates of finegrained quench clinopyroxene (right hand side of picture) in 27 kb, 1,450° C run

either due to loss of iron to the platinum capsule or, in some cases, to splitting of the sample capsule during the run. The liquidus of the olivine tholeiite is at approximately 1,340° C and that of the alkali olivine basalt at about 1,260° C. In both compositions plagioclase is the second phase to appear (at 1,260° C in the olivine tholeiite and at 1,240° C in the alkali olivine basalt). Clinopyroxene appears at a similar temperature (1,220 ± 10° C) in both compositions and thus, in the olivine tholeiite composition there is a temperature interval of about 30° C over which precipitation of olivine and plagioclase together will determine the fractionation trend.

b) Crystallization at 9 kb

The liquidus phase in all three basalt compositions studied at 9 kb is olivine. In the olivine tholeiite composition olivine is the only phase crystallizing from the liquidus at 1,360 ± 10° C[3] down to 1,300° C. In the olivine basalt the liquidus was not accurately established but seems unlikely to be higher than 1,310° C and both orthopyroxene and clinopyroxene begin crystallizing with olivine between 1,260° C and 1,280° C. In the alkali olivine basalt composition, olivine occurs on the liquidus at 1,270 ± 10° C and co-exists with liquid alone down to 1,230 ± 10° C. At 9 kb, there is in all three compositions, a temperature interval of about 40° C or more in which separation of olivine alone will govern the early stages of fractionation of these basaltic liquids. It is of interest that the composition with the *lowest* normative olivine content (the olivine tholeiite) has the highest liquidus temperature at 9 kb and the largest temperature interval for the two phase olivine + liquid assemblage. This composition has the highest $Mg/Mg + Fe^{++}$ value and lowest $Na_2O + K_2O$ content and the liquidus temperatures show a dependence on alkali content and iron-enrichment closely analogous to that observed at atmospheric pressure by Tilley, Yoder and Schairer (1965).

In the 1.290° C run on the olivine tholeiite composition, olivine is joined by orthopyroxene (Plate IA) and the assemblage ol + opx + liquid is stable down to 1,260 ± 10° C. At this temperature the composition is less than 50% crystallized. However, the appearance of clinopyroxene as a primary phase in the 1,250° C run also results in greatly increased degree of crystallization. There is an apparent decrease in the abundance of olivine in the 1,210 to 1,250° C runs in comparison with runs at both higher and lower temperatures. The increase in olivine in going from 1,210° C down to 1,100° C may be attributed to decreasing solubility of Al_2O_3 in pyroxenes with decreasing temperatures — it is accompanied by an increase in spinel and in plagioclase (c.f. Green and Ringwood, 1967) and implies reactions

$$\text{olivine} + \text{plagioclase} \rightleftharpoons \text{aluminous pyroxenes}_{ss}$$
$$\text{spinel} + \text{plagioclase} \rightleftharpoons \text{aluminous pyroxenes}_{ss}.$$

The lower abundance of olivine in the interval 1,210° C—1,250° C in comparison with runs at higher temperatures implies a reaction relationship between olivine and liquid — this will be further discussed in a later section, but it may be noted that the precipitating phase, replacing olivine, is not enstatite or hypersthene but aluminous clinopyroxene.

Plagioclase may be present as a minor phase at 1,230° C, 9 kb, and is definitely present in the near-solidus run at 1,210° C. The very late appearance and small content of plagicclase in this composition at 9 kb contrast with the major role that this phase plays in the atmospheric pressure runs.

Olivine is again the liquidus phase in the olivine basalt at 9 kb. Both orthopyroxene and clinopyroxene begin crystallizing at similar temperatures (about 1,260° C) but the orthopyroxene is a very minor phase. The degree of crystallization shows a marked increase with the appearance of clinopyroxene. At a lower temperature (1,240° C) clinopyroxene increases in abundance at the expense of both orthopyroxene (no longer observed) and olivine.

In the alkali olivine basalt composition, orthopyroxene does not appear at 9 kb and olivine is joined by clinopyroxene in the 1,220° C run. Clinopyroxene in this run forms medium sized euhedra (up to 10—15 microns), not distinguishable optically from olivine but clearly identifiable with the microprobe. In this composition the first appearance of clinopyroxene is apparently not accompanied by an abrupt increase in the degree of crystallization. At 1,180° C, a near-solidus run contains mainly clinopyroxene with a moderate amount of plagio-

[3] The uncertainty in temperature reflects the spacing of runs at 10° C—20° C intervals and does not include the estimated precision or absolute accuracy of temperature measurement (see page 114).

clase, minor olivine and minor spinel. This assemblage differs from the subsolidus run at 1,100° C (GREEN and RINGWOOD, 1967) only in having lower plagioclase and olivine contents.

c) Crystallization at 11.3 kb

Only two runs, both aimed at establishing the phases present close to the liquidus, were carried out at 11.3 kb. In the olivine tholeiite composition, a run at 1,370° C showed large orthopyroxene euhedra and less common but well crystallized olivine euhedra. Either phase may be the liquidus phase (at 1380 ± 10° C) but it is clear that both phases are important in the early stages of fractioning of the olivine tholeiite at this pressure. Since olivine is absent in the subsolidus assemblage in this composition at 1,100° C, 11.3 kb (GREEN and RINGWOOD, 1967), there is either a subsolidus reaction (e.g. spinel + orthopyroxene + clinopyroxene = olivine + anorthite) to yield olivine above 1,100° C or an incongruent melting relationship in the opx + cpx + plag + spinel assemblage.

A second run, at 11.3 kb 1,270° C, was carried out on the alkali olivine basalt composition. This run yielded glass as the major phase but with quite common clinopyroxene and rare orthopyroxene. The firm identification of olivine was not possible.

d) Crystallization at 13.5 kb

In contrast to the important role of olivine at 9 kb, this phase does not occur at 13.5 kb in any composition studied except the picrite. Orthopyroxene is the liquidus phase in both the olivine tholeiite and olivine basalt compositions and both orthopyroxene and clinopyroxene occur near or on the liquidus in the alkali olivine basalt. In the olivine tholeiite composition, there is an extensive field of crystallization of orthopyroxene alone (Fig. 2B) from a temperature of 1,400° C or slightly greater, down to about 1,360° C. Orthopyroxene is then joined by clinopyroxene and these two phases crystallize together down to 1,300° C. At 1,350° C orthopyroxene is more abundant than clinopyroxene and both occur as large, well-formed crystals. In this run, glass is more common than crystals but in the 1,310° C run crystals are more abundant than glass and the small, equant or short, prismatic crystals of clinopyroxene are much more abundant than the distinctive large orthopyroxene laths. Spinel first appears in the 1,290° C run and remains a minor phase down to a temperature between 1,100° C and 1,180° C where garnet first appears.

Plagioclase does not appear in the olivine tholeiite until practically at the solidus at 1,250° C approximately (for the dry composition). In 1 hr and 3 hr runs at 1,220° C, the presence of minor amounts of glass and uncertainty in plagioclase identification are attributed to access of small amounts of water to the charge, resulting in depression of the solidus. The 3 hr run at 1,180° C showed appreciable plagioclase, but less than observed at 1,100° C — this could result from the presence of minor glass in the run or from increasing solubility of Al_2O_3 in the pyroxenes at higher temperatures. The replacement of the px + plag + spinel assemblage by px + plag + ga with decreasing temperature at 13.5 kb is matched by the same reactions with increasing pressure at 1,100° C (GREEN and RINGWOOD, 1967).

The liquidus phase in the olivine basalt at 1,330° C is also orthopyroxene but in this composition there is a much smaller temperature interval before appearance of the second phase, clinopyroxene. Definite primary clinopyroxene first appears at 1,310° C but in this run is less abundant than orthopyroxene. There is a marked increase in the degree of crystallization between 1,310° C and 1,290° C and in the latter run clinopyroxene is much more abundant than the orthopyroxene.

In the alkali olivine basalt composition, a run for 60 min at 1,290° C, 13.5 kb is very near the liquidus with a very few large euhedral crystals of both orthopyroxene and clinopyroxene. The composition of the glass used is given in Table 1. In a later series of runs, a new batch of glass of slightly different composition (normative olivine 28%; normative nepheline 3.1%; normative diopside 16.0%) was used for 30 min runs at 1,290° C to 1,310° C. In these runs it is difficult to distinguish fine-grained anhedral quench clinopyroxene from aggregates of fine-grained primary clinopyroxene. None of these runs contain large crystals of either orthopyroxene or clino- pyroxene but the 1,290° C and 1,300° C runs both contain uncommon medium-sized rectangular laths with straight extinction and very low birefringence which are probably orthopyroxene. These crystals have rims and outgrowths of quench clinopyroxene.

At 1,270° C and 1,250° C the alkali olivine basalt crystallizes to clinopyroxene and glass and orthopyroxene is not identifiable.

The picrite differs from the three compositions described above in that olivine and not pyroxene is the liquidus phase at 13.5 kb. The liquidus temperature was not established but is greater than 1,380° C. Orthopyroxene is the second phase to appear — it is present in a 40 minute run at 1,360° C but only olivine was observed in a 30 minute run at the same temperature. There is a rather abrupt increase in degree of crystallization between 1,360° C and 1,340° C and clinopyroxene is the major phase at 1,340° C. Olivine continues to remain stable with both the orthopyroxene and clinopyroxene down to at least 1,320° C. The roles of orthopyroxene and clinopyroxene in the picrite composition are similar to those in the olivine basalt composition in that orthopyroxene appears at the higher temperature but there is only a small temperature drop before the crystallization of abundant clinopyroxene.

e) Crystallization at 18 kb

In all compositions, except the alkali olivine basalt, the liquidus phase at 18 kb is the same as that observed at 13.5 kb. Orthopyroxene is the liquidus phase in the olivine tholeiite and olivine basalt composition but in the alkali olivine basalt composition, orthopyroxene does not appear at all at 18 kb and clinopyroxene is the liquidus phase. The temperature interval over which orthopyroxene alone co-exists with the liquid is much smaller at 18 kb than 13.5 kb in the olivine tholeiite and olivine basalt compositions.

The liquidus of the olivine tholeiite at 18 kb is about 1,430° C and orthopyroxene co-exists with liquid down to 1400° C or 1,410° C. At 1,400° C, 1,380° C and 1,375° C both pyroxenes form large crystals, in some cases showing parallel intergrowth of the two pyroxene types. In the lower temperature runs clinopyroxene is more abundant than the orthopyroxene and at 1,370° C orthopyroxene is not identifiable, the run consisting entirely of clinopyroxene + liquid. The disappearance of orthopyroxene at lower temperatures in the partial melting interval is analogous to the behaviour of the alkali olivine basalt at 13.5 kb. The runs at 18 kb differ from those at lower pressures in showing the appearance of garnet at temperatures above the solidus. Garnet first appears at 1,350° C and increases in abundance in lower temperature runs. The solidus at 18 kb is close to 1,300° C giving a partial melting or crystallization interval of about 130° C.

The behaviour of the olivine basalt at 18 kb is notable for the very small temperature interval over which crystallization and rapid changes in phase assemblages occur. The liquidus is at $1{,}350 \pm 10$° C and duplicate runs at 1,340° C both yielded orthopyroxene + liquid. At 1,335° C, the mineral assemblage consists of large primary orthopyroxene and primary clinopyroxene with liquid but at 1,330° C orthopyroxene is not present, the degree of crystallization is much greater and garnet appears as a minor phase with the abundant clinopyroxene. The solidus for this composition is near 1,300° C. The sequence of appearance of phases in the olivine basalt matches that observed in the olivine tholeiite but the different fields for the various phase assemblages are compressed into a melting interval of about 50° C.

The liquidus of the alkali olivine basalt at 18 kb is at 1,325° C approximately. The rare clinopyroxenes present in the 1,320° C run are large and well crystallized but there is an abrupt increase in the degree of crystallization between 1,320° C and 1,300° C. Clinopyroxene is the only primary crystalline phase present in the 1300° C run but garnet is moderately common at 1,250° C.

In the picrite composition, olivine is still the liquidus phase at 18 kb and is joined by orthopyroxene in the 1,410° C and 1,400° C runs. In these runs there is no definite identification of primary clinopyroxene but this becomes a major phase and orthopyroxene disappears in the 1,390° C and 1,370° C runs. Minor garnet first appears in a near-solidus run at 1,350° C Unlike orthopyroxene, olivine persists as a stable phase right through to the subsolidus assemblage.

f) Crystallization at 22.5 kb

At 22.5 kb, clinopyroxene is the liquidus phase in both the olivine tholeiite and the picrite compositions. No runs have been carried out at this pressure on either the alkali olivine basalt or olivine basalt compositions. In the olivine tholeiite composition, the amount of clino-

pyroxene crystallizing increases rapidly over a small temperature interval. A run at 1,410° C, only 30—40° C below the liquidus, contains common garnet and is very near the solidus. The crystallization interval in the picrite at 22.5 kb is also small. Clinopyroxene appears to be the liquidus phase at 1,450° C and there is only minor glass present at 1,430° C. In the picrite composition, garnet and olivine appear at similar temperatures and there is also a small amount of a brownish high R.I. phase. The determination of the solidus is particularly difficult in this composition due to outgrowths of quench clinopyroxene on the abundant primary clinopyroxene crystals.

g) Crystallization at 27 kb

In all three basaltic compositions, garnet is the liquidus phase at 27 kb and is joined by clinopyroxene at about 10° C below the liquidus. In the picrite composition garnet, clinopyroxene and orthopyroxene all appear together in the near-liquidus run at 1,500° C. Orthopyroxene disappears at lower temperature (between 1,480° C and 1,500° C) and minor amounts of either $spinel_{ss}$ or $ilmenite_{ss}$ occur. The run at 1,480° C is very near the solidus and a run at 1,430° C is below the solidus. The latter run does not contain detectable olivine but olivine is a minor but definite phase at 27 kb, 1,200° C. The melting interval of the picrite at 30 kb is an extremely small one of about 40° C — the melting interval of similar compositions at atmospheric pressure is about 375° C (1,425° C to 1,050° C, cf. TILLEY, YODER and SCHAIRER, 1965).

In the olivine tholeiite composition the liquidus is at about 1,500° C and the solidus at 1,430° C. Garnet is probably the liquidus phase although the presence of quench clinopyroxene in the 1.490° C run makes the absence of primary clinopyroxene difficult to establish. The presence of euhedral garnet in clear glass in parts of the olivine basalt runs (at 1,450° C and 1,460° C) and in the alkali olivine basalt run at 1,430° C demonstrates that garnet is the liquidus phase in these compositions (Fig. 2D). The quench clinopyroxene forms feathery and turbid aggregates and, in some cases, quite large anhedral crystals which are distinguishable as quench rather than primary crystals only by their patchy occurrence, the presence of characteristic lines of small inclusions and the absence of a change in refractive index at edges against feathery, definite quench material. Garnet and clinopyroxene are the only phases observed in the crystallization sequence. The solidus of the alkali olivine basalt at 30 kb is about 1,350° C giving a melting interval for this composition of about 90° C. The solidus of the olivine basalt was not determined.

h) Stability of Orthopyroxene as a Liquidus Phase in the 9—18 kb Pressure Interval

YODER (1964) found enstatite as a liquidus phase in the forsterite-albite system at 9 kb but interpreted the enstatite as metastable, proxying for olivine. Extending this interpretation, TILLEY and YODER (1964) suggested, as a possible interpretation of GREEN and RINGWOOD's (1964) results, that orthopyroxene appearing as a liquidus phase from basaltic liquids at moderate pressure might also be metastable, crystallizing in place of clinopyroxene. Arguments against this interpretation may be developed from the observed readiness of clinopyroxene to nucleate, even during quenching; from the experimental runs in which both orthopyroxene and clinopyroxene occur as co-existing phases and from the restriction of orthopyroxene as a liquidus phase to a definite pressure interval. To demonstrate the stability of orthopyroxene, rather than either garnet or clinopyroxene, as the liquidus phase at 13.5 kb in the olivine tholeiite composition, the glass was run for 4 hrs at 27 kb, 1,100° C. This yielded an assemblage of fine-grained clinopyroxene and common, larger subhedra or euhedra of garnet. The garnet + clinopyroxene assemblage was then re-run for 1 hr at 1,380° C, 13.5 kb yielding an assemblage of euhedral orthopyroxene, uncommon relict garnet and glass + minor quench clinopyroxene. The relict garnet shows clear evidence of partial solution and is not a stable phase under these conditions. The opx + liquid

assemblage obtained from an eclogite (ga + cpx) starting material is the same as that obtained under the same run conditions using glass starting material. The runs carried out in the olivine tholeiite for only 5 mins. at 13.5 kb demonstrate that clinopyroxene, rather than orthopyroxene, may crystallize metastably in very short runs but these runs also show that at temperatures of 1,400° C, run lengths of about 5 minutes may be sufficient to allow nucleation and moderate growth of stable liquidus phases. These observations effectively refute Tilley and Yoder's (1964) suggestion that the orthopyroxene reported in our earlier runs was a product of metastable crystallization.

i) Microprobe Analyses of Crystals in Partial Melting Runs

Microprobe analyses of olivine, pyroxenes and garnets are listed in Tables 8—12. The analysis of clinopyroxene was only practical in runs in which this phase grew as large well-formed crystals, i.e. near-liquidus runs. The determination by direct analysis of only three elements (Fe, Ca and Al) means that the contents of Ti and Na are unknown — these constituents are unlikely to be of significance in either olivine or orthopyroxene but the clinopyroxene may have appreciable Ti (0.5—2% TiO_2) and low Na (0.5% Na_2O) contents if comparison is made with early-formed clinopyroxenes of natural basalts. This is further substantiated by later microprobe analyses in this laboratory of clinopyroxenes in other basaltic compositions by T. H. Green and R. F. Bultitude (unpublished data). These analyses include direct determination of Na, Ti contents of the clinopyroxenes.

j) Olivine Analyses (Table 8)

The olivines in all compositions show an extremely low Al_2O_3 content and a low but measurable CaO content of 0.3%. This compares closely with the 0.4% CaO in olivine from Kilauean tholeiites reported in a preliminary study by Murata, Bastron and Brannock (1965). Liquidus olivines have consistently higher Mg/Mg + Fe molecular ratios than olivines formed below the liquidus and the correlation of nominal temperature with Mg/Mg + Fe ratios for a given composition gives an independent check on the reliability of relative temperature intervals between runs. On this basis the olivine (100 Mg/Mg + Fe = 92.2) at 4.5 kb, 1,350° C in the olivine tholeiite is closer to the liquidus than the olivine (100 Mg/Mg + Fe = 90.8) at 10 kb, 1,350° C. The partition of magnesium and iron between liquidus olivine and liquid composition has previously been discussed and an empirical mean partition coefficient of 1.33 has been derived for the relationship between basaltic liquid and liquidus olivine or orthopyroxene of composition range $92 > 100\,Mg/Mg + Fe > 82$. This empirical partition coefficient is defined by the ratio

$$\left(\frac{100\,Mg}{Mg+Fe}\right)_{Crystal} \Big/ \left(\frac{100\,Mg}{Mg+Fe^{++}}\right)_{Liquid} = K_{O,L}.$$

In each run, ten separate olivine crystals were analyzed and the analysis of each crystal is the mean of 3 to 10 separate spot analyses 2 to 3 microns apart. The analysis given in Table 8 is the mean of the ten separate crystal analyses. It was observed that some olivine crystals showed slight zoning with more iron rich cores than rims. Also it was observed that crystals located close to the platinum

Table 8. *Compositions of olivines analysed by electron microprobe. Fe, Ca, Al determined by direct analysis; other components calculated*

	Olivine tholeiite								Olivine basalt	Alkali olivine basalt	
Pressure (kb)	4.5	9.0	9.0	9.0	9.0	9.0	9.0	9.0	9.0	9.0	9.0
Temp. (°C)	1,350	1,350	1,330	1,310	1,290	1,270	1,250	1,230	1,280	1,260	1,220
SiO_2	41.1	40.9	40.8	40.7	40.3	40.2	39.9	39.8	40.7	39.6	39.2
Al_2O_3	n.d.**	n.d.	n.d.	n.d.	n.d.	n.d.	n.d.	n.d.	n.d.	n.d.	n.d.
FeO	7.7	8.9	9.9	10.3	12.3	12.9	14.0	14.7	10.1	16.1	18.0
MgO	50.9	49.9	49.0	48.7	47.1	46.6	45.8	45.2	48.9	44.0	42.5
CaO	0.3	0.3	0.3	0.3	0.3	0.3	0.3	0.3	0.3	0.3	0.3
$\frac{100\,Mg}{Mg+Fe}$ (mol)	92.2	90.9	89.8	89.4	87.2	86.4	85.3	84.7	89.6	83.0	80.8
Mol. Proportions											
Fo	91.8	90.6	89.5	89.0	86.8	86.1	84.9	84.3	89.3	82.7	80.5
Fa	7.8	9.0	10.1	10.6	12.8	13.5	14.7	15.3	10.3	16.9	19.1
La	0.4	0.4	0.4	0.4	0.4	0.4	0.4	0.4	0.4	0.4	0.4
Coexisting Crystalline phases	Nil	Nil	Nil	Nil	Opx*	Opx*	Opx* + Cpx	Opx + Cpx + ?Plag	Nil	Nil	Cpx*

* Denotes crystalline phase analyzed by electron microprobe.
** "not detected", i.e. $Al_2O_3 < 0.2\%$.

wall of the capsule were slightly poorer in iron than those near the centre of the capsule. As an example the FeO content of a large olivine grain (25 μ traverse) in the 10 kb, 1,350° C, olivine tholeiite run ranged from 9.3% FeO in the centre to 9.0% FeO at the edge and averaged 9.2% FeO. In the mount as a whole the mean FeO content of the crystals ranged from 9.2% FeO to 8.7% FeO in two crystals located near the capsule wall. The mean FeO content of all the crystals was 8.9%. The variation from 8.7% FeO to 9.3% FeO represents a change in the 100 Mg/Mg + Fe ratio from 91.1 to 90.5. Similarly the maximum variation in crystal composition in the olivine of the 10 kb, 1,260° C run on the alkali olivine basalt composition is from 15.5% FeO to 16.6% FeO with an average of 16.1% FeO. This variation represents a change in 100 Mg/Mg + Fe ratio from 83.6 to 82.4 with a mean of 83.0. Thus we consider that there is an uncertainty in composition of about ± 0.3% forsterite in olivines around Fo_{90} and about ± 0.6% forsterite in olivines around Fo_{80}. This uncertainty derives from real variations in 100 Mg/Mg + Fe ratio of crystals with position in the mount and may be a consequence of Fe loss to the Pt crucible at the margins of the sample or of small temperature gradients within the sample capsule.

k) Orthopyroxene Analyses

The analyses of orthopyroxenes listed in Table 9 also demonstrate an increase in FeO content and decrease in the 100 Mg/Mg + Fe ratio with decrease in temperature at a given pressure. The partition of Fe and Mg between liquid and liquidus crystals where orthopyroxene is the liquidus phase is similar to runs in which olivine is the liquidus phase (cf. Table 10). The orthopyroxenes are distinctive in all cases in having a moderate or high Al_2O_3 content, similar to or higher than that observed in enstatites of the Ol + Opx + Cpx + Sp assemblage of peridotite nodules, and higher than the Al_2O_3 contents of orthopyroxenes crystallizing at low pressure from basaltic or andesitic magmas. At any given pressure, the Al_2O_3 content of orthopyroxene increases with decrease in temperature, as long as no other co-existing Al_2O_3-rich phase appears. At constant temperature, the Al_2O_3 content of orthopyroxene increases with increase in pressure (cf. runs on olivine tholeiite at 1,400° C, 13.5 kb and 18 kb), provided closely similar phase assemblages are compared. Alternatively, comparing orthopyroxenes of similar 100 Mg/Mg + Fe ratios, those crystallized at higher pressure, have higher Al_2O_3 contents.

The series of analyses of orthopyroxenes from the olivine tholeiite composition at 13.5 kb best illustrate the change in orthopyroxene composition with increasing degree of crystallization. The liquidus orthopyroxene at 1,400° C contains only 3.8% Al_2O_3 but this increases to 7.8% Al_2O_3 in the 1,310° C run. The run at 1,290° C reverses this trend with a drop in Al_2O_3 to 6.4%. We attribute the lower Al_2O_3 content of the 1,290° C orthopyroxene to the first appearance of spinel as a co-existing phase — this will alter the partition relationship of Al_2O_3 between liquid and crystallizing orthopyroxene. The Al_2O_3 content of the liquidus orthopyroxene at 18 kb is greater than that of the liquidus orthopyroxene at 13.5 kb in both the olivine basalt and olivine tholeiite compositions. The contrast between the Al_2O_3 content of the orthopyroxene in the olivine basalt, 18 kb 1,340° C

Table 9. *Compositions of orthopyroxenes analyzed by electron microprobe. Fe, Ca, Al determined by direct analysis, other components calculated assuming ideal orthopyroxene composition*

	Olivine tholeiite								Olivine basalt			Alkali olivine basalt
Pressure (kb)	9.0	9.0	9.0	13.5	13.5	13.5	13.5	13.5	18.0	18.0	13.5	18.0	18.0	13.5
Temp. (°C)	1,290	1,270	1,250	1,400	1,380	1,350	1,310	1,290	1,420	1,400	1,320	1,340	1,335	1,290
SiO_2	54.5	53.9	52.9	55.9	54.4	53.8	52.5	53.1	54.9	53.4	53.8	51.8	54.3	50.6
Al_2O_3	4.9	5.4	6.9	3.8	5.7	6.0	7.8	6.4	5.1	7.3	6.4	10.0	5.9	10.6
FeO	7.8	8.3	9.1	5.5	6.5	7.2	8.7	9.7	5.8	6.4	6.6	6.5	6.4	9.7
MgO	30.0	29.6	28.5	32.8	31.2	30.2	28.3	28.3	32.0	30.4	30.3	29.5	30.8	26.6
CaO	2.9	2.8	2.6	2.0	2.2	2.8	2.7	2.5	2.2	2.5	2.9	2.2	2.6	2.5
$\frac{100\,Mg}{Mg+Fe}$ (mol)	87.3	86.4	84.9	91.4	89.6	88.2	85.3	83.9	90.8	89.5	89.1	89.0	89.6	83.0
Mol. Proportions														
Ens	78.1	77.0	74.4	84.5	80.6	78.1	74.1	74.2	82.5	78.6	78.4	76.2	79.8	69.9
Fs	11.3	12.1	13.3	8.0	9.4	10.5	12.7	14.3	8.3	9.2	9.6	9.4	9.3	14.3
Wo	5.5	5.3	5.0	3.7	4.2	5.2	5.1	4.8	4.0	4.7	5.4	4.2	4.8	4.8
Al_2O_3	5.1	5.6	7.3	3.8	5.8	6.2	8.1	6.7	5.2	7.5	6.6	10.2	6.1	11.0
Coexisting Crystalline phases	Ol*	Ol*	Ol* + Cpx	Nil	Nil	Cpx	Cpx*	Cpx + Sp**	Nil	Cpx*	Nil	Nil	Cpx*	Cpx*

* Denotes crystalline phase analyzed by electron microprobe.

** Spinel has approximately 14% FeO, 70 ± 5% $Al_2O_3 < 1.3$% CaO.
(Calculated composition assuming $FeAl_2O_4$, $MgAl_2O_4$ solid solution 14% FeO, 67.3% Al_2O_3, 18.7% MgO.)

Table 10. *Comparison of 100 Mg/Mg + Fe^{++} values of liquidus olivine and liquidus orthopyroxene crystals*

	Liquidus olivine			Liquidus orthopyroxene		
	Pressure (kb)	Temp. (°C)	$\frac{100\,Mg}{Mg+Fe^{++}}$	Pressure (kb)	Temp. (°C)	$\frac{100\,Mg}{Mg+Fe^{++}}$
Olivine Tholeiite	4.5	1350	92.2	13.5	1400	91.4
„ „	9	1350	90.9	18	1420	90.8
Olivine Basalt	9	1280	89.6	13.5	1320	89.1
„ „				18	1335	89.6
„ „				18	1340	89.0
Alkali Olivine Basalt	9	1260	83.0	13.5	1290	83.0

(10% Al_2O_3) run and the 1,335° C (5.9% Al_2O_3) run is not readily understood but may be an effect of the presence of aluminous clinopyroxene (9.9% Al_2O_3) in the 1,335° C run and its absence in the 1,340° C run.

The CaO content of the orthopyroxene is lower (2.0—2.2% CaO) in runs in which there is no co-existing clinopyroxene and increases to 2.5 or 2.8% CaO in these runs in which stable clinopyroxene occurs. This is shown by the olivine tholeiite runs at 13.5 kb and 18 kb and the olivine basalt runs at 18 kb but the olivine basalt 13.5 kb 1,320° C run and the 9 kb olivine tholeiite runs are exceptions to this generalization.

Table 11. *Compositions of clinopyroxenes analyzed by electron microprobe. Fe, Ca, Al determined by direct analysis, other components calculated assuming ideal clinopyroxene composition and little or no Na or Ti substitution*

	Olivine tholeiite		Olivine basalt	Alkali olivine basalt		
Pressure (kb)	13.5	18.0	18.0	9.0	13.5	18.0
Temp. (°C)	1,310	1,400	1,335	1,220	1,290	1,320
Analysis No.	1	2	3	4	5	6
SiO_2	49.3	52.3	50.7	49.4	49.2	49.1
Al_2O_3	11.3**	7.3	9.9	9.0	11.2	11.0
FeO	8.3	6.0	5.5	9.5	9.0	7.6
MgO	21.2	25.1	23.1	16.9	20.9	19.5
CaO	9.9	9.3	10.8	15.2	9.7	12.8
$\frac{100\,Mg}{Mg+Fe}$	82.1	88.2	88.2	76.1	80.6	82.1
Mol. Proportions						
Ens	56.5	66.0	61.0	46.1	56.0	52.5
Fs	12.4	8.8	8.1	14.5	13.5	11.3
Wo	19.1	17.6	20.6	29.5	18.6	24.6
Al_2O_3	12.0	7.6	10.3	9.9	11.9	11.6
Coexisting						
Crystalline phases	Opx*	Opx*	Opx*	Ol*	Opx*	Nil

* Denotes crystalline phase analyzed by electron microprobe.

** Doubtful value, possibly too high due to interference from glass. Crystals are very small.

l) Clinopyroxene Analyses

Four of the analyzed clinopyroxenes of Table 11 co-exist with orthopyroxene + liquid, one co-exists with olivine + liquid and one co-exists only with liquid. The four clinopyroxenes which co-exist with orthopyroxene are lower in CaO content and may be classified as sub-calcic augites. Within this group there is an increase in CaO content with decrease in temperature (analyses 2 and 3) and the more magnesian clinopyroxenes have higher CaO contents at similar temperatures than more iron-rich clinopyroxenes (analyses 1 and 3, Fig. 3). These relationships are a consequence of the widening of the Opx-Cpx immiscibility gap (Boyd and Schairer, 1964; Davis and Boyd, 1966) with decreasing temperature and the narrowing of this gap with increasing Fe-content or decreasing Mg/Mg + Fe content of the pyroxenes.

In contrast to the four clinopyroxenes described above, the pyroxene compositions in equilibrium with the alkali olivine basalt liquid at 1,320° C, 18 kb and in equilibrium with olivine + liquid at 1,220° C, 9 kb (analysis 4), lie outside the pyroxene immiscibility gap for their compositions and P-T conditions. These pyroxenes are richer in CaO than those co-existing with orthopyroxene.

Table 12. *Garnet compositions determined by electron microprobe. Fe, Ca, Al determined by direct analysis, other components calculated*

	Olivine basalt		
Pressure (kb)	18	18	27
Temp. (° C)	1,330	1,320	1,460
SiO	41.6	41.4	42.1
Al_2O_3	23.3	22.6	23.9
FeO	11.5	11.8	8.7
MgO	16.9	16.6	19.5
CaO	6.4	6.6	5.7
Al_2O_3 *	23.6	23.6	24.0
$\frac{100\,Mg}{Mg+Fe}$ (mol.)	72.3	71.5	80.0
Mol. Proportions			
Almandine	23.0	23.6	17.2
Pyrope	60.5	59.4	68.3
Grossular	16.5	17.0	14.5
Coexisting			
Crystalline Phases	Cpx	Cpx	Nil

* Al_2O_3 value calculated from FeO, CaO values assuming garnets are ideal almandine-pyrope-grossular solid solutions.

The clinopyroxenes generally contain more Al_2O_3 than the co-existing orthopyroxene although more data is needed to substantiate this. Thus clinopyroxene analyses 2 and 5 have similar or slightly greater Al_2O_3 contents than their co-existing orthopyroxenes but clinopyroxenes 1 and 3 have much greater Al_2O_3 contents than co-existing orthopyroxene. The 100 Mg/Mg + Fe values for the clinopyroxenes are consistently lower than co-existing olivine or orthopyroxene.

The analyzed clinopyroxenes and co-existing orthopyroxenes have been projected on to the experimentally determined phase diagram for the $CaMgSi_2O_6$-$MgSiO_3$ system at atmospheric pressure (Boyd and Schairer, 1964). Davis (1963) and Davis and Boyd (1966) have demonstrated that the position of the pyroxene solvus at a given temperature is virtually unaffected by pressure. The data from the microprobe analyses demonstrate that the width of the pyroxene solvus is greatly decreased by increasing Fe content. Surprisingly, the solubility of diopside-hedenbergite in enstatite-hypersthene is less than that determined for the simple magnesian system, but the solubility of orthopyroxene in calcic clinopyroxene is much greater. The data of Fig. 3 demonstrate preliminary

results in a method of obtaining a pyroxene-diagram for natural basaltic magmas at high pressures.

m) Garnet Analyses

In the olivine basalt composition, two garnets co-existing with clinopyroxene at 18 kb and the liquidus garnet at 27 kb have been analyzed. As the oxidation state of iron cannot be determined with the microprobe the garnets are assumed to contain no andradite molecule but to consist entirely of grossular + almandine + pyrope solid solutions. With this assumption it is possible to calculate

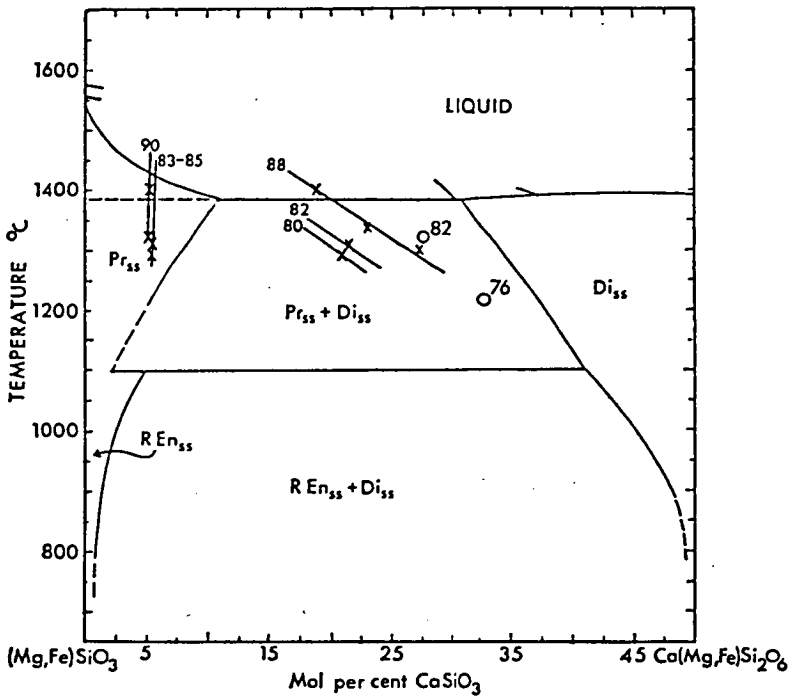

Fig. 3. Diagram illustrating the degree of solid solubility in co-existing orthopyroxene and clinopyroxene. The pyroxene solvus for pure $MgSiO_3$—$CaMgSi_2O_6$ is taken from Boyd and Schairer (1964) and the compositions of the pyroxenes observed in the partial melting runs on basalt are projected on to this solvus. × = two pyroxene + liquid assemblages; ○ = clinopyroxene + liquid only; 90, 88 etc. values of 100 Mg/Mg + Fe for the pyroxene — note that the clinopyroxene always has a lower 100 Mg/Mg + Fe ratio than the co-existing orthopyroxene

the whole garnet composition from the Fe and Ca determinations. The Al_2O_3 contents calculated in this way compare well with the directly determined Al_2O_3.

No phases co-existing with garnet have been analyzed but the liquidus garnet at 27 kb with 100 Mg/Mg + Fe = 80 is much more iron-rich than the liquidus olivine at 9 kb (100 Mg/Mg + Fe = 89.6) or the liquidus orthopyroxene at 13.5 kb (100 Mg/Mg + Fe = 89.1) or 18 kb (100 Mg/Mg + Fe = 89.0).

Fractional Crystallization of Basaltic Magmas

The nature of the fractionation trend and the derivative liquid compositions from any primitive basaltic magma may be determined if we know the composition of the crystalline phase or phases and the proportions of liquid and crystals.

Our data show that the nature of the liquidus phase, the sequence of appearance and nature of other phases, and the temperature interval for crystallization are strongly dependent on load pressure. The data on which the following discussion is based are shown in Figs. 4, 5, 6 and 7. Principal fractionation trends at several different pressures are compared in Figs. 8 and 9.

a) Fractionation at Upper Crustal Levels (<15 km)

The behaviour of the three basalts during fractionation in the upper continental crust or within the oceanic crust or uppermost mantle (i.e. at pressures <5 kb)

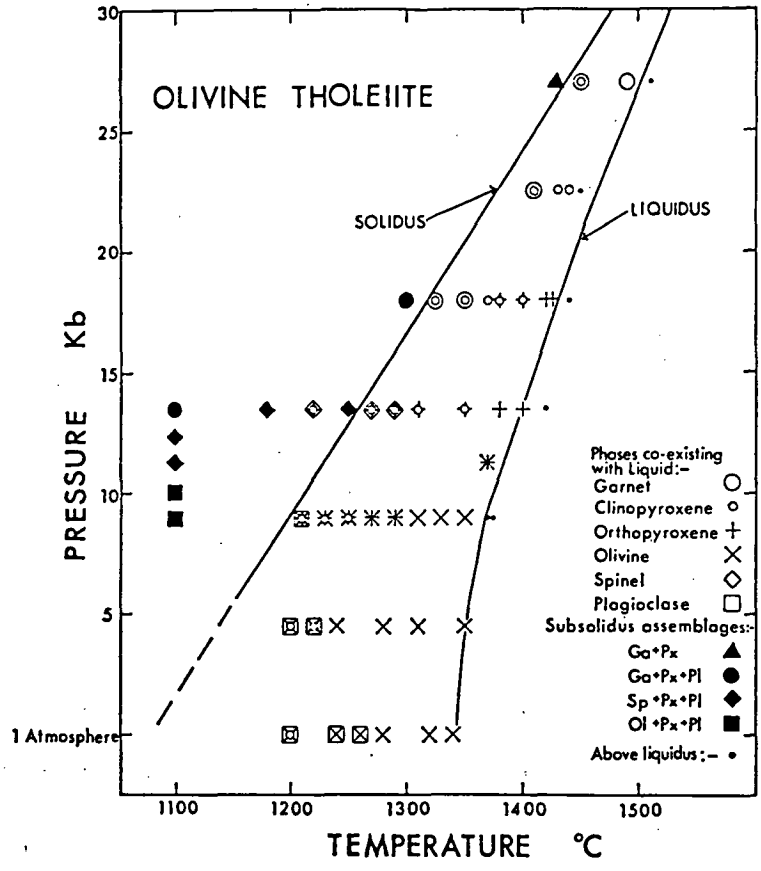

Fig. 4. Detail of melting experiments carried out on the olivine tholeiite composition at high pressures. Run descriptions are given in Table 4

can be discussed on the basis of the experimental results at atmospheric pressure on the olivine tholeiite and alkali olivine basalt compositions. A further, most important, source of information on the fractionation of basaltic magmas at low pressures is the detailed and comprehensive study of basalt melting relations at 1 Atmosphere carried out by TILLEY, YODER and SCHAIRER (1963, 1964, 1965). The observed sequence of appearance of phases at atmospheric pressure (Table 4) and in particular the appearance of plagioclase before clinopyroxene, could also have been deduced by comparison of the olivine tholeiite and alkali olivine basalt with the chemical compositions and crystallization sequences of the basalts studied by YODER and TILLEY (1962); TILLEY, YODER and SCHAIRER (1963, 1964, 1965) and YAGI (1964). Although the early crystallization of olivine in the olivine tholeiite composition results in a fractionation trend of SiO_2, Al_2O_3, and CaO

enrichment at low pressure, the appearance of very calcic plagioclase as the second phase curtails the Al_2O_3 and CaO enrichment trend (Table 13), instead maintaining the well documented, tholeiitic fractionation to iron-rich, Na + K enriched quartz tholeiites with 50% or more SiO_2 and 12—14% Al_2O_3.

As the olivine tholeiite composition was initially derived from an estimate by Macdonald and Katsura (1961) for the average magma composition of the 1959—1960 Kilauea Iki lava lake, it is of interest to compare the low pressure

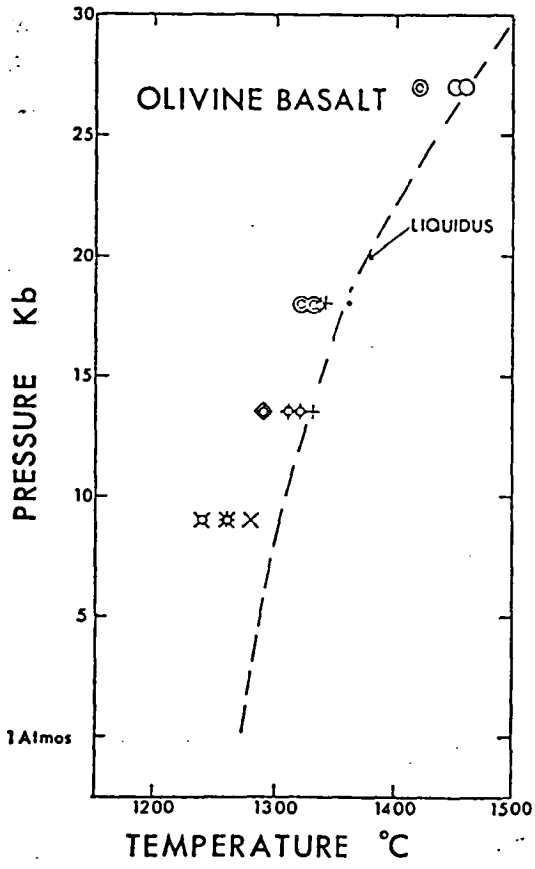

Fig. 5

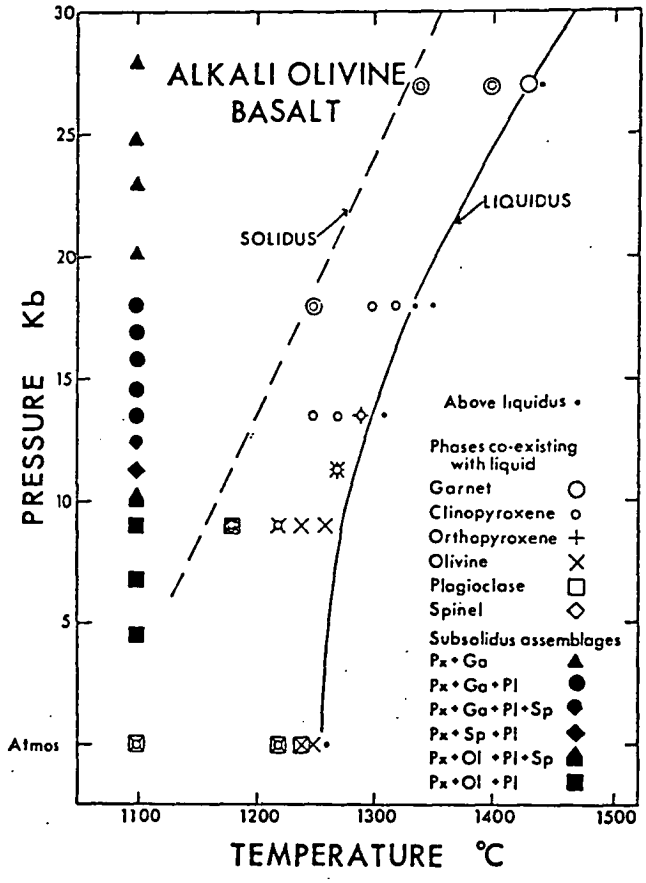

Fig. 6

Fig. 5. Detail of melting experiments on the olivine basalt composition at high pressures. Symbols are the same as those in Figs. 4 and 6. Run descriptions are given in Table 5

Fig. 6. Detail of melting and subsolidus experiments on the alkali olivine basalt composition. Run descriptions are given in Table 6

fractionation trend of the olivine tholeiite with the thoroughly documented fractionation trends of the 1959—1960 Kilauea Iki eruption. Tilley, Yoder and Schairer (1963, 1964, 1965) have shown experimentally that rocks and glasses derived from the 1959—1960 Kilauea Iki and other Kilauean eruptions contain olivine as the liquidus phase and that olivine alone remains the liquidus phase even into the field of quartz-normative liquids. The same conclusion also follows from the quartz-normative composition for the low magnesia terminus of the olivine control lines in the 1950—1960 Kilauea Iki differentiation series of Murata and Richter (1966a, b). Tilley et al. (op. cit.) have shown that clinopyroxene is usually the second phase to crystallize from Kilauean lavas but may appear simultaneously with plagioclase or be very closely followed by plagioclase. The

Table 13. *Hypothetical fraction of the olivine tholeiite at Atmospheric pressure*

Nature and estimated percentage of minerals		15% Olivine (Fo_{88})		18% Olivine (Fo_{88}) 12% Plagioclase (An_{80})	
Composition of crystal extract					
SiO_2		40.0		43.1	
Al_2O_3		—		13.4	
FeO		14.3		8.7	
MgO		45.7		27.4	
CaO		—		6.4	
Na_2O		—		1.0	
Composition of residual liquid					
	(Initial liquid)				
SiO_2	46.95	48.1		48.6	
TiO_2	2.02	2.4		2.9	
Al_2O_3	13.10	15.5		13.0	
Fe_2O_3	1.02	1.2		1.4	
FeO	10.07	9.3		10.7	
MnO	0.15	0.2		0.2	
MgO	14.55	9.0		9.1	
CaO	10.16	12.0		11.8	
Na_2O	1.73	2.0		2.0	
K_2O	0.08	0.1		0.1	
P_2O_5	0.21	0.2		0.3	
CIPW Norm					
Or	0.67	0.7		0.8	
Ab	14.7 } 42.9	16.8 } 50.5		16.7 } 43.9	
An	27.6	33.0		26.4	
Di	17.0	20.2		24.6	
Hy	12.3	15.3		20.2	
Ol	21.9	7.1		3.2	
Ilm	3.8	4.6		5.5	
Mt	1.4	1.8		2.0	
Ap	0.5	0.5		0.6	
$\frac{100\,Mg}{Mg+Fe^{++}}$	72.1	63.3		60.3	

appearance of plagioclase before clinopyroxene in our olivine-tholeiite composition and the relatively early appearance of plagioclase in relation to the Kilauea Iki fractionation (MURATA and RICHTER, 1965) are attributed to compositional differences. Thus the analyses that MACDONALD and KATSURA (1961, Table 1, analyses 2 and 3) used to estimate their parent magma do not fall on MURATA and RICHTER's (1966a, b) differentiation trend but are distinctly higher in Al_2O_3 (cf. page 110 and footnote). The experimental and natural studies of low pressure fractionation are sufficient to form the conclusion that separation of olivine, plagioclase and clinopyroxene, in that order, from the chosen olivine tholeiite composition will result in derivative liquid compositions equivalent to Fe-enriched quartz tholeiites, with normal Al_2O_3 contents. At these low pressure conditions,

derivative liquids from the olivine tholeiite composition will move out of the undersaturated olivine tholeiite field into the oversaturated quartz-tholeiite field (Fig. 1).

The results from the alkali olivine basalt composition are consistent with results from similar rocks studied experimentally by Tilley, Yoder and Schairer (1963, 1964, 1965) and Yoder and Tilley (1962). The effect of olivine and calcic plagioclase separation would be to increase the normative nepheline content and also the SiO_2 content. The relatively early appearance of plagioclase prevents any large increase in Al_2O_3 content. The appearance of clinopyroxene amongst the phases crystallizing would result in either an increase or possibly slight decrease of normative nepheline content depending upon the composition of the particular pyroxene. In general terms, crystal fractionation at low pressures of compositions close to our alkali olivine basalt would yield liquids retaining normative nepheline but becoming richer in SiO_2, alkalis, Al_2O_3 (in early fractionation stages) and Fe/Fe + Mg ratio. Some hawaiites and mugearites are probably natural examples of this low pressure fractionation trend (Muir and Tilley, 1961) although Tilley, Yoder and Schairer (1965) have recently suggested that crystal flotation involving plagioclase enrichment with extraction of olivine and clinopyroxene may be involved in the genesis of hawaiite and mugearite.

Although the olivine basalt composition contains 1% of normative hypersthene, fractionation at low pressure may produce residual liquids closer to those derived from the alkali olivine basalt than from the olivine tholeiite. As in the other compositions, the crystallization sequence at atmospheric pressure is probably olivine-plagioclase-clinopyroxene. Separation of olivine and calcic plagioclase will result in a small increase in normative hypersthene content but the appearance of clinopyroxene may reverse this trend and even produce nepheline-normative liquids. This may occur if the clinopyroxene has sufficiently high (Mg, Fe) SiO_3 solid solution and low Al_2O_3 + Na (Al, Fe^{+++}) Si_2O_6 solid solution to yield a hypersthene normative composition. The olivine basalt and compositions derived from it in early stages of low pressure fractionation belong to the transitional group of rocks discussed by Poldervaart (1964), which are hypersthene normative but show crystallization and fractionation sequences more typical of the alkali basalt suite. Although a nepheline normative liquid *may* be produced by low pressure fractionation from the olivine basalt composition it must be emphasized that this can only result after crystallization of large amounts of olivine, plagioclase, clinopyroxene and titanomagnetite — the residual liquid would in fact be trachytic and not basaltic.

b) Fractionation at about 15—35 km Depth

The experimental partial melting runs carried out at 9 kb provide the data on which the following discussion is based. The liquidus phase in all compositions studied is olivine but the second phase to crystallize is orthopyroxene in the olivine tholeiite, orthopyroxene + sub-calcic clinopyroxene in the olivine basalt and clinopyroxene in the alkali olivine basalt. This contrasts with the atmospheric pressure sequence of crystallization in which plagioclase is the second phase to crystallize. In addition to the late appearance of plagioclase at 9 kb, the experimental results suggest that the early crystallizing olivine may bear a reaction

relationship towards clinopyroxene. In discussion of the experimental results it was noted that there was a decrease in intensity of olivine as clinopyroxene became more abundant in the assemblages. However, olivine does not entirely disappear in any of the compositions, and microprobe analyses show that, in the olivine tholeiite at least, the olivine continues to become more Fe-rich even after crystallization of clinopyroxene commences. Our data therefore suggest that olivine partially reacts with liquid to precipitate aluminous, calcic clinopyroxene. This implies that it is possible to derive residual liquid compositions from these olivine-rich compositions which do not have olivine on the liquidus at 9 kb, but instead have clinopyroxene or clinopyroxene + orthopyroxene as liquidus phases. Furthermore, these derivative liquids, if crystallized at atmospheric pressure would have either olivine or plagioclase, or both, as liquidus phases. These aspects of basalt fractionation are being intensively studied by T. H. Green (Department of Geophysics and Geochemistry, Australian National University) and his results provide a much more complete documentation of the relationships than our present data.

The compositions of residual liquids can be calculated using the analyzed minerals of Tables 8, 9 provided that an estimate can be made of the proportions of crystals present. This can be done approximately by visual methods and the use of polished surfaces offers the possibility of modal analyses either on the specimen itself or on photographic reproductions of the surface. In the present paper we have used the known compositions of olivines and orthopyroxenes crystallized at various temperatures to estimate the proportions of crystals present. In a previous section we have discussed the empirical relationship between the molecular ratio 100 Mg/Mg + Fe^{++} of a basaltic liquid and the same ratio of its liquidus olivine.

An empirical partition coefficient $K_{O,L}$ has been defined as

$$\left(\frac{100\,Mg}{Mg+Fe}\right)_{Olivine} \Big/ \left(\frac{100\,Mg}{Mg+Fe^{++}}\right)_{Liquid} = K_{O,L}$$

and for $(100\,Mg/Mg+Fe)_{Olivine}$ between 83 and 92, $K_{O,L}$ has a mean value of 1.33 at 9 kb. $K_{O,L}$ increases slightly with decreasing values of $(100\,Mg/Mg+Fe)_{Olivine}$ but as a first approximation the mean value of 1.33 is used in the following calculations (Table 3).

At 9 kb, the liquidus olivine of the olivine tholeiite at a temperature of about 1,360° C has $100\,Mg/Mg+Fe = 92$. At a lower temperature, e.g. 1,310° C, the olivine is more abundant and has $(100\,Mg/Mg+Fe)_{Olivine} = 89.4$. Olivine of this composition is the liquidus phase of the glass present in the run, and assuming the empirical relationship that $K_{O,L} = 1.33$ the liquid at this temperature has $(100\,Mg/Mg+Fe^{++})_{Liquid} = 89.4/1.33 = 67.2$. The first appearance of orthopyroxene in the olivine tholeiite is at 1,290° C, 9 kb and in a similar way the residual liquid at this temperature may be calculated to have the value $(100Mg/+Fe^{++}) = 65.6$. The ratio [MgO]/[FeO] where [MgO] and [FeO] are expressed in weight percent can then be calculated for the residual liquid

$$\frac{[MgO]}{[FeO]_{Liquid}} = 1.07.$$

Since orthopyroxene is extremely rare in the 1,290° C run the residual liquid must be derived from the original composition by extraction of olivine alone. The olivine at 1,290° C 9 kb contains 12.3% FeO and 47.1% MgO and if the percentage of olivine crystals present is m% then

$$\frac{[MgO]}{[FeO]}_{\text{Liquid}} = \frac{14.55 - \frac{m}{100} \times 47.1}{10.07 - \frac{m}{100} \times 12.3} = 1.07.$$

$$\text{i.e. } m = 11.1\%.$$

The composition of the liquid phase, assuming 11% crystallization of olivine as analyzed at 1,290° C, 9 kb, is given in Table 14.

Between 1,290° C and about 1,260° C the olivine tholeiite composition consists of olivine, orthopyroxene and liquid. The first appearance of clinopyroxene was at 1,250° C. Both olivine and orthopyroxene have been analyzed from this run and have $(100\,Mg/Mg+Fe)_{Opx} = 84.9$ and $(100\,Mg/Mg+Fe)_{Ol} = 85.3$ respectively. The residual liquid has a calculated $100\,Mg/Mg+Fe^{++})_{Liquid} = 64$ but to calculate the degree of crystallization, the relative proportions of olivine and orthopyroxene crystallizing between 1,290° C and 1,250° C must be estimated. If this crystal extract consists of 25% olivine and 75% orthopyroxene then its composition is

SiO_2	49.66%
Al_2O_3	5.23%
FeO	10.38%
MgO	32.83%
CaO	2.10%

and, using the liquid composition determined at 1,290° C, the percentage of olivine + orthopyroxene crystals precipitating between 1,290° C and 1,250° C may be calculated as 3.4%, i.e.

0.9% Olivine
2.5% Orthopyroxene.

This method of estimation of degree of crystallization is potentially very useful, particularly as more data on liquid and liquidus phase partition coefficients become available. Using the estimates of degrees of crystallization obtained in this way as a guide, Table 14 contains the calculated compositions of the liquid phase in the olivine tholeiite at about 1,290° C assuming 11% crystallization of olivine, and about 1,250° C assuming 12% crystallization of olivine and 3% crystallization of orthopyroxene.

The appearance of clinopyroxene at 1,250° C appears to coincide with a relatively rapid increase in the proportion of crystals present. Although no analysis of the clinopyroxene was possible, its composition may well be similar to the clinopyroxenes which co-exist with orthopyroxene at 1,290° C, 13.5 kb and 1,310° C, 13.5 kb in the alkali basalt and olivine tholeiite composition. The clinopyroxene at 9 kb, 1,230° C would probably contain a lower Al_2O_3 content but similar CaO content and similar $100\,Mg/Mg+Fe$ ratio to that from the alkali olivine basalt at 1,290° C, 13.5 kb. In Table 14 an approximate residual liquid composition assuming 30% crystallization (12% olivine, 4% orthopyroxene, 14% clinopyroxene) has been calculated for the olivine tholeiite at 9 kb and about 1,230° C.

Table 14. *Fractionation of the olivine tholeiite at 9 kb*

P, T conditions (kb) (°C)		9 1,290		9 1,250		9 1,230	
Nature and estimated percentage of crystals		11% Olivine		12% Olivine 3% Ortho-pyroxene		12% Olivine 4% Orthopyroxene 14% Clinopyroxene	
Composition of Crystal Extract							
SiO_2		40.3		42.5		45.9	
Al_2O_3		—		1.4		6.2	
FeO		12.3		13.0		11.3	
MgO		47.1		42.3		31.6	
CaO		0.3		0.8		5.0	
Composition of Liquid Phase							
	(Initial liquid)						
SiO_2	46.95	47.6		47.6		47.3	
TiO_2	2.02	2.3		2.4		2.9	
Al_2O_3	13.10	14.8		15.2		16.1	
Fe_2O_3	1.02	1.1		1.2		1.5	
FeO	10.07	9.8		9.6		9.5	
MnO	0.15	0.2		0.2		0.2	
MgO	14.55	10.5		9.5		7.2	
CaO	10.16	11.4		11.8		12.4	
Na_2O	1.73	2.0		2.0		2.5	
K_2O	0.08	0.1		0.1		0.1	
P_2O_5	0.21	0.2		0.2		0.3	
CIPW norm of Liquid Phase							
Or	0.67	0.7		0.7		0.8	
Ab	14.7 } 42.9	16.5 } 48.3		16.8 } 49.6		21.0 } 54.2	
An	27.6	31.1		32.1		32.4	
Di	17.0	19.2		20.2		22.5	
Hy	12.3	13.8		12.9		5.2	
Ol	21.9	12.2		10.5		10.1	
Ilm	3.8	4.3		4.6		5.5	
Mt	1.4	1.6		1.8		2.1	
Ap	0.5	0.5		0.5		0.6	
$\frac{100\,Mg}{Mg+Fe^{++}}$	72.1	65.5		64.3		57.2	

If the Al_2O_3 content of the clinopyroxene is lower than the value used (cf. the clinopyroxene from the alkali basalt at 9 kb, 1,220° C) the resulting liquid will have higher Al_2O_3 and higher normative anorthite content.

The calculated compositions of Table 14 illustrate the fractionation trend of the olivine tholeiite assuming quite low degrees of crystallization at pressures around 9 kb, i.e. depths of 30—35 kms. The derivative liquids are very distinctive in showing very little change in SiO_2 content and in normative olivine content once fractionation has proceeded to the stage of separation of both pyroxene and olivine (Fig. 8). In contrast, Al_2O_3, CaO and Na_2O are steadily enriched in the residual liquid as fractionation proceeds (Figs. 8, 9) and the resulting compositions have high normative plagioclase contents. The derivative liquids are classifiable as high-alumina olivine tholeiites and closely resemble analyses of high

alumina olivine tholeiites, "oceanic tholeiites" or "high-alumina basalts" given by Yoder and Tilley (1962), Engel, Engel and Havens (1965) and Kuno (1960). It must be emphasized that the enrichment in CaO, Al_2O_3 and Na_2O is caused by the absence of plagioclase as an early-crystallizing phase and by the co-precipitation of olivine and orthopyroxene, maintaining an olivine normative character and essentially constant SiO_2 content. The appearance of clinopyroxene does not greatly modify this trend *provided* that the clinopyroxene is sub-calcic (i.e. co-existing with orthopyroxene) and of low or moderate Al_2O_3 content. The increasing proportion of low-calcium pyroxenes extracted as fractionation proceeds results in decreasing normative hypersthene — in terms of the basalt tetrahedron (Yoder and Tilley, 1962), residual liquids from the olivine tholeiite fractionate rapidly towards the plagioclase apex of the olivine tholeiite volume and also fractionate slightly towards the Cpx-Ol-Plag plane of critical undersaturation (Fig. 1).

In the alkali olivine basalt composition, the analyses of both olivine and clinopyroxene at 9 kb 1,220° C can be used to calculate a possible residual liquid composition (Table 15) assuming 15% crystallization (5% olivine, 10% clinopyroxene). As with the olivine tholeiite, fractionation produces little change in SiO_2 content but an increase in Al_2O_3, Na_2O and normative plagioclase contents, and a decrease in $100\,Mg/Mg+Fe^{++}$ ratio (Figs. 8, 9). The absence of orthopyroxene and more calcic nature of the clinopyroxene prevent marked enrichment in CaO content though it must be pointed out that a higher proportion of olivine to clinopyroxene than that assumed in Table 15 would result in more marked increase in Al_2O_3 content and increasing SiO_2 and CaO contents. In terms of normative minerals, the separation of olivine and clinopyroxene results in increased nepheline and derivative liquids remain critically undersaturated with low or moderate degrees of fractionation.

The analytical data on phases crystallized from the olivine basalt composition at 9 kb are insufficient for a quantitative discussion of fractionation. However, the appearance of both orthopyroxene and clinopyroxene with olivine in the 9 kb, 1,260° C run will cause derivative liquids to move towards high Al_2O_3, CaO, and Na_2O contents while maintaining approximately constant SiO_2. Derivative liquids would almost certainly become nepheline-normative with sufficient fractionation. The absence of orthopyroxene in the 1,240° C, 9 kb run indicates a more calcic clinopyroxene and fractionation beyond this temperature would probably show decreasing CaO content.

In general, analyses of natural high-Al_2O_3 basalts in the literature have higher SiO_2 contents than the calculated compositions. Closer similarity in this component would be produced if a slightly greater proportion of olivine crystallized before the appearance of orthopyroxene and we anticipate that this would happen in the olivine tholeiite at slightly lower pressures than 9 kb. We anticipate a transition with increasing pressure between the low pressure fractionation trend to quartz tholeiite without Al_2O_3 enrichment and the higher pressure trend to high-alumina olivine tholeiites or high-alumina alkali olivine basalts. Increasing pressure will enlarge the temperature interval between the appearance of olivine and plagioclase and will also gradually extend the field of orthopyroxene crystallization into olivine-normative (particularly with $Ol > 15\%$) compositions. Thus

Table 15. *Fractionation of alkali olivine basalt at 9 kb*

P, T conditions (kb) (°C)		9 1,270		9 1,220	
Nature and estimated percentage of crystals		Nil		5% Olivine 10% Clinopyroxene	
Composition of crystal extract					
SiO_2				46.0	
Al_2O_3				6.0	
FeO				12.3	
MgO				25.5	
CaO				10.2	
Composition of liquid phase					
	(Initial liquid)				
SiO_2	45.39			45.3	
TiO_2	2.52			3.0	
Al_2O_3	14.69			16.2	
Fe_2O_3	1.87			2.2	
FeO	12.42			12.4	
MnO	0.18			0.2	
MgO	10.37			7.7	
CaO	9.14			9.0	
Na_2O	2.62			3.1	
K_2O	0.78			0.9	
P_2O_5	0.02			—	
CIPW norm					
Or	4.5			5.5	
Ab	18.0	48.7		19.0	52.0
An	26.2			27.5	
Ne	2.2			3.9	
Di	15.7			14.2	
Ol	25.8			21.0	
Ilm	4.8			5.7	
Mt	2.9			3.2	
$\frac{100\,Mg}{Mg+Fe^{++}}$	59.8			52.5	

the same parent magma may fractionate to yield high-alumina basalts of slightly different SiO_2 contents and normative olivine and hypersthene contents depending on the particular pressure in the 5—10 kb range at which fractionation occurs.

Kuno (1960, p. 125) considers that high-alumina basalts are chemically transitional between tholeiites and alkali basalts, except in Al_2O_3 content. Yoder and Tilley (1962, p. 416—417) also note that high-alumina basalts are not restricted to either the tholeiites or alkali basalt and include analyses of hawaiites within the group. Our data suggests that at 8—10 kb pressure there is no well defined thermal divide close to the Ol-Cpx-Plag plane of critical undersaturation but rather this fractionation trend runs obliquely to this "plane" and directly towards plagioclase enrichment. Thus, while a "parental" olivine tholeiite with low

normative hypersthene content may fractionate with moderate degree of crystallization to yield nepheline-normative, high-Al_2O_3 residual liquids, parental olivine tholeiites with higher normative hypersthene are unlikely to yield nepheline-normative residual liquids but would produce high-Al_2O_3, olivine tholeiites (5—15% normative olivine).

c) Fractionation at 35—70 km Depth

The experimental partial melting runs carried out at 13.5 and 18 kb provide the data on which the following discussion is based. The liquidus phases in all compositions studied, except the picrite[4], are pyroxenes, and orthopyroxene plays a dominant role in the early stages of fractionation within this depth interval. Clinopyroxene appears early in the fractionation sequence and, if accompanied by orthopyroxene, is a very sub-calcic variety. Both clinopyroxene and orthopyroxene are aluminous. Garnet does not appear above the solidus at 13.5 kb but appears late in the crystallization sequence at 18 kb. Spinel and plagioclase appear near the solidus at 13.5 kb but are absent at 18 kb.

The compositions of derivative liquids from the basaltic compositions can be calculated using the analyzed minerals of Tables 9, 11 provided that an estimate can be made of the proportions of crystals present. The mineral analysis data show that co-existing olivine and orthopyroxene have almost identical ratios of 100 Mg/Mg + Fe, at least for values of this ratio between 85 and 90 (Table 10). Also, where the compositions have orthopyroxene as the liquidus phase, this has a similar 100 Mg/Mg + Fe ratio to the liquidus olivine observed at lower pressure. For these reasons it is possible to use the empirical partition coefficient

$$\left(\frac{100\,\mathrm{Mg}}{\mathrm{Mg}+\mathrm{Fe}}\right)_{\mathrm{Opx}} \Big/ \left(\frac{100\,\mathrm{Mg}}{\mathrm{Mg}+\mathrm{Fe}^{++}}\right)_{\mathrm{Liquid}} = 1.33$$

to obtain an estimate of the degree of crystallization in the olivine tholeiite (cf. pages 143—144). At 13.5 kb, orthopyroxene is the only phase present on the liquidus and very uncommon clinopyroxene first appears in the 1,350° C run. The calculated proportion of orthopyroxene crystallized between the liquidus and the first appearance of clinopyroxene is 14.5%, using the composition of the orthopyroxene in the 1,350° C, 13.5 kb run in the calculations. This is in good agreement with the amount of orthopyroxene observed optically. At 18 kb, clinopyroxene is absent in the 1,425° C and 1,420° C runs but moderately common in the 1,400° C run. Assuming separation of orthopyroxene (as analyzed at 1,400° C, 18 kb) alone between the liquidus and 1,400° C the percentage of orthopyroxene crystallized may be calculated as 12.5%. This is likely to be an over-estimate as clinopyroxene probably appears at about 1,410° C.

In Table 16 we have calculated derivative liquid compositions assuming 15% crystallization of orthopyroxene alone at 13.5 kb and crystallization of 10% orthopyroxene + 5% clinopyroxene at 18 kb. The derivative liquids are very similar in chemistry and in normative mineralogy although the extraction of

[4] Orthopyroxene occurred as the liquidus phase in the picrite at 1,325° C, 18 kb in the preliminary runs reported by Green and Ringwood, 1964. The absence of olivine presumably resulted from the access of water, possibly with some resulting oxidation, and suppression of the liquidus temperature by about 100° C.

sub-calcic clinopyroxene at 18 kb results in a residual liquid with slightly higher hypersthene and lower anorthite content. Both compositions lie very close to the "critical plane of undersaturation" in the basalt tetrahedron (Fig. 1) and are olivine-rich basalts of the type transitional between olivine tholeiite and alkali olivine basalt. In chemistry and normative mineralogy the calculated compositions are very close to the "olivine basalt" composition chosen for detailed study and further fractionation beyond 15% crystallization can be best interpreted from the experimental results on this and the alkali olivine basalt. However it is worth noting that crystallization below 1,350° C at 13.5 kb in the olivine tholeiite involves extraction of both orthopyroxene and co-existing sub-calcic clinopyroxene. Thus the nature of the crystal extract remains rich in SiO_2 and in hypersthene molecule, and derivative liquids will move into the nepheline normative field. A similar relationship holds for the 1,380° C and 1,375° C runs at 18 kb. The disappearance of orthopyroxene in the 1,370° C 18 kb run would result in extraction of much higher CaO content in the crystalline phase and the appearance of garnet in the 1,350° C run would further divert the fractionation trend away from the direct path from hypersthene-normative to nepheline-normative olivine basalts.

In the olivine basalt composition at 13.5 kb there is a temperature interval of 10—20°C over which orthopyroxene alone separates from the liquid. Our data are insufficient to use the pyroxene compositions to estimate the degree of crystallization at 13.5 kb and instead we have calculated the derivative liquid composition assuming 10% crystallization of orthopyroxene as indicated by optical examination of polished surfaces. At 18 kb the orthopyroxene co-existing with liquid at 1,340°C has a lower 100 Mg/Mg + Fe ratio (89.0) than the orthopyroxene co-existing with clinopyroxene + liquid in the lower temperature and more extensively crystallized run at 1,335°C. This is apparently in conflict with the empirical partition relationship between liquid and orthopyroxene discussed previously. However the co-existing clinopyroxene at 1,335°C has 100 Mg/Mg + Fe = 88.2 so that the mean value of this ratio for the crystalline phase is <89.0. It is clear however that very little orthopyroxene may be extracted at 18 kb from the olivine basalt before the appearance of subcalcic clinopyroxene. In Table 17 we have calculated a residual liquid at 18 kb assuming crystallization of 5% orthopyroxene + 10% clinopyroxene as analyzed at 1,335°C, 18 kb. The residual liquids calculated for 10% crystallization at 13.5 kb and 15% crystallization at 18 kb are very closely similar. Both show decreased SiO_2 content from the original liquid and both are nepheline normative with over 2% nepheline and 24% normative olivine. In both chemistry and normative mineralogy these compositions are very close to the alkali olivine basalt composition and the experimental results on the latter composition may be used to further investigate the fractionation trend beyond 10 and 15% crystallization. The appearance of minor orthopyroxene at the liquidus of the alkali olivine basalt composition at 13.5 kb, supports the estimate of 10% orthopyroxene crystallized from the olivine basalt at 13.5 kb. These two compositions effectively demonstrate that orthopyroxene may crystallize from nepheline-normative magmas at moderate pressure and that in the chosen compositions it is the dominant role of orthopyroxene which determines the liquid fractionation trend from olivine-rich tholeiite to alkali olivine basalt.

Table 16. *Fractionation of olivine tholeiite at 13.5 kb and 18 kb*

P, T conditions (kb) (°C)		13.5 1,350		18 1,400	
Nature and estimated percentage of crystals		15% Ortho-pyroxene		10% Orthopyroxene + 5% Clinopyroxene	
Composition of crystal extract					
SiO_2		53.8		53.0	
Al_2O_3		6.0		7.3	
FeO		7.2		6.3	
MgO		30.2		28.6	
CaO		2.8		4.8	
Composition of liquid Phase					
	(Initial liquid)				
SiO_2	46.95	45.7		45.9	
TiO_2	2.02	2.4		2.4	
Al_2O_3	13.10	14.3		14.1	
Fe_2O_3	1.02	1.2		1.2	
FeO	10.07	10.6		10.7	
MnO	0.15	0.2		0.2	
MgO	14.55	11.9		12.1	
CaO	10.16	11.3		11.1	
Na_2O	1.73	2.0		2.0	
K_2O	0.08	0.1		0.1	
P_2O_5	0.21	0.2		0.2	
CIPW norm of liquid Phase					
Or	0.6	0.6		0.6	
Ab	14.7 } 42.9	17.3 } 47.6		17.3 } 46.7	
An	27.6	29.7		28.8	
Di	17.0	20.5		20.3	
Hy	12.3	0.2		2.0	
Ol	21.9	24.9		24.2	
Ilm	3.8	4.5		4.6	
Mt	1.4	1.8		1.8	
Ap	0.5	0.5		0.5	
$\frac{100\,Mg}{Mg+Fe^{++}}$	72.1	66.7		66.9	

The residual liquids from the alkali olivine basalt, assuming 10% crystallization of orthopyroxene + clinopyroxene at 13.5 kb and 20% crystallization of clinopyroxene at 18 kb (Table 18) suggest that derivatives with higher normative nepheline contents, approaching olivine-rich basanites, may be produced. If both orthopyroxene and clinopyroxene crystallize together, the CaO content of derivative liquids remain roughly constant and the derivative liquids show increasing nepheline and diopside contents and decreasing albite and anorthite contents. Continuation of this trend appears appropriate for derivation of basanites. However, if orthopyroxene is absent, extraction of calcic clinopyroxene results in decreasing CaO content and atypical basaltic chemistry. The change in normative mineralogy is towards lower diopside content but the ratio of nepheline to albite

Table 17. *Fractionation of olivine basalt at 13.5 kb and 18 kb*

P, T conditions (kb) (°C)		13.5 1,310	18 1,335
Nature and estimated percentage of minerals		10% orthopyroxene (as at 1,320°C, 13.5 kb)	5% orthopyroxene 10% clinopyroxene
Composition of crystal extract			
SiO_2		53.8	51.9
Al_2O_3		6.4	8.6
FeO		6.6	5.8
MgO		30.3	25.6
CaO		2.9	8.1
Composition of residual liquid			
	(Initial liquid)		
SiO_2	47.10	46.4	46.3
TiO_2	2.31	2.6	2.7
Al_2O_3	14.15	15.0	15.1
Fe_2O_3	0.42	0.5	0.5
FeO	10.64	11.1	11.5
MnO	0.16	0.2	0.2
MgO	12.71	10.8	10.4
CaO	9.86	10.6	10.2
Na_2O	2.21	2.5	2.6
K_2O	0.44	0.5	0.5
CIPW norm of residual liquid			
Or	2.7	3.0	3.3
Ab	18.9	16.8	17.8
Ne	—	2.4	2.3
An	27.3	28.1	27.8
Di	17.6	19.9	18.6
Hy	1.3	—	—
Ol	27.2	24.2	24.3
Ilm	4.4	5.0	5.1
Mt	0.6	0.7	0.8
$\frac{100\,Mg}{Mg+Fe^{++}}$	68.1	63.4	61.8

with 20% clinopyroxene extracted is almost the same as for 10% (orthopyroxene + clinopyroxene) extraction. Extraction of clinopyroxene alone (if this is similar in composition to that analyzed at 1,335°C, 18 kb) appears likely to yield compositions unlike natural basanites or olivine nephelinites. The possible derivation by fractionation of these more extremely undersaturated liquids is currently being studied and factors such as the appearance of spinel or garnet and the Na_2O content of the liquidus clinopyroxenes are potentially important in this problem.

Without microprobe analyses of the phases crystallizing from the picrite, it is not possible to quantitatively discuss the fractionation of this composition. However the normative composition is such that the picrite is essentially the same as the olivine basalt composition with the addition of about 9% more olivine. The

Table 18. *Fractionation of alkali olivine basalt at 13.5 kb and 18 kb*

P, T conditions (kb) (°C)		13.5 1,280	18 1,310
Nature and estimated percentage of minerals		2.5% orthopyroxene + 7.5% clinopyroxene (as at 13.5 kb, 1,290°C)	20% clinopyroxene (as at 18 kb, 1,320°C)
Composition of crystal extract			
SiO_2		49.6	49.1
Al_2O_3		11.0	11.0
FeO		9.2	7.6
MgO		22.3	19.5
CaO		7.9	12.8
Composition of residual liquid			
	(Initial liquid)		
SiO_2	45.39	44.9	44.5
TiO_2	2.52	2.8	3.2
Al_2O_3	14.69	15.1	15.6
Fe_2O_3	1.87	2.1	2.3
FeO	12.42	12.8	13.6
MnO	0.18	0.2	0.2
MgO	10.37	9.1	8.1
CaO	9.14	9.3	8.2
Na_2O	2.62	2.9	3.3
K_2O	0.78	0.9	1.0
P_2O_5	0.02	—	—
CIPW norms of residual liquids			
Or	4.5	5.5	6.1
Ab	18.0	15.7	17.4
Ne	2.2	4.9	5.6
An	26.2	25.3	24.8
Di	15.7	17.1	13.2
Hy	—	—	—
Ol	25.8	23.2	23.6
Ilm	4.8	5.3	6.1
Mt	2.9	3.0	3.3
$\frac{100\,Mg}{Mg+Fe^{++}}$	59.8	56.1	51.5

melting runs at 13.5 kb and 18 kb are in excellent agreement with this conclusion as olivine is the liquidus phase at both pressures and following precipitation of a moderate amount of olivine, orthopyroxene followed closely by clinopyroxene separates from the residual liquid. We conclude that initially the picrite would fractionate by separation of olivine to yield a composition with 25 ± 3% normative olivine, 4% normative hypersthene. Further fractionation by separation of orthopyroxene or of orthopyroxene + clinopyroxene accompanying the olivine would yield nepheline normative liquids closely analogous to those derived from the olivine basalt composition.

The appearance of orthopyroxene rather than olivine as the liquidus phase at 18 kb, 1,325°C under "wet" melting conditions (GREEN and RINGWOOD, 1964) suggests the possibility that low partial pressures of water may suppress the temperature of appearance of olivine to a greater degree than orthopyroxene. This aspect of high pressure fractionation needs to be further explored experimentally.

d) Fractionation at about 70—100 km Depth

The experimental results at 22.5 kb and 27 kb are relevant to discussion of fractionation below 70 km depth. At 22.5 kb, clinopyroxene is the liquidus phase in all three basaltic compositions and also in the picrite. By analogy with the clinopyroxene in the alkali basalt at 20 kb, such clinopyroxenes are likely to contain CaO contents greater than the liquid, high Al_2O_3 content, and may also contain moderate Na_2O as jadeite solid solution. Fractionation by separation of clinopyroxene at this pressure would produce lower SiO_2 contents, lower CaO contents and lower 100 Mg/Mg + Fe ratios. Depending on the Na_2O content of the clinopyroxene, hypersthene normative liquids could possibly yield derivative nepheline-normative liquids but high degrees of crystallization would be required and resultant liquids would be atypical of basalt in having low CaO contents.

At 27 kb, garnet is the liquidus phase in the olivine basalt and alkali olivine basalt compositions and possibly garnet alone occurs on the liquidus of the olivine tholeiite at 27 kb. In all three cases, there is a relatively small drop in temperature before the appearance of clinopyroxene. The melting interval in all compositions and particularly in the picrite is quite small at 27 kb so that quite large amounts of a phase may precipitate over a small temperature interval.

We have calculated a residual liquid composition (Table 19) assuming 10% crystallization of garnet from the olivine basalt and using the composition of the garnet analyzed from the 27 kb, 1,460°C run. The effect of garnet extraction from this particular composition is to produce a nepheline-normative (0.6% Ne) liquid. This result supports the conclusions of YODER and TILLEY (1962) that the plane of critical undersaturation is not a thermal divide at 27—30 kb and, in particular, that extraction of garnet may produce liquids of alkali basalt type. However, separation of 10% garnet without the appearance of clinopyroxene is rather doubtful in the compositions studied, particularly in the olivine tholeiite where clinopyroxene possibly occurs with garnet at the liquidus. Extraction of garnet results in increased SiO_2 content and particularly in decreased Al_2O_3 content and is not as "efficient" as aluminous orthopyroxene in developing nepheline-normative residual liquids, e.g. while extraction of 10% garnet from the olivine basalt at 27 kb produces a residual liquid with 0.6% nepheline, extraction of 10% aluminous orthopyroxene at 13.5 kb produces a liquid with 2.4% normative nepheline. Extraction of garnet with its high Al_2O_3/SiO_2 ratio causes a decrease in normative anorthite and this imposes a rather severe restriction on the amount of garnet which can be extracted while retaining a basalt-like chemistry and normative mineralogy.

Calculations of the effects of extracting 10% garnet from the alkali-olivine basalt demonstrate an increase in normative nepheline content (from 2.2% to 4.0%) and decrease in normative anorthite content (from 26.2% to 21.5%). Similar

Table 19. *Fractionation of olivine basalt at 27 kb*

P, T conditions (kb) (°C)	Composition of initial liquid	27 1,460 Residual liquid after extraction of 10% garnet (1,460°C, 27 kb)
SiO_2	47.10	47.6
TiO_2	2.31	2.5
Al_2O_3	14.15	13.0
Fe_2O_3	0.42	0.5
FeO	10.64	10.9
MnO	0.16	0.2
MgO	12.71	12.0
CaO	9.86	10.3
Na_2O	2.21	2.5
K_2O	0.44	0.5
Norms		
Or	2.7	3.1
Ab	18.9	20.0
Ne	—	0.6
An	27.3	22.7
Di	17.6	23.0
Hy	1.3	—
Ol	27.2	25.2
Ilm	4.4	4.7
Mt	0.6	0.7
$\frac{100\,Mg}{Mg+Fe^{++}}$	68.1	66.3

extraction of 10% garnet from the olivine tholeiite decreases the normative hypersthene from 12.3% to 10.1% and normative anorthite from 27.6% to 23.3%. To obtain a nepheline normative liquid from the olivine tholeiite would require separation of more than 30% garnet without the appearance of clinopyroxene. This requirement is in direct conflict with our experimental data. Furthermore, it would produce non-basaltic residual liquids.

In the picrite composition at 27 kb, garnet, orthopyroxene and clinopyroxene all occur very close to the liquidus and the direction of fractionation cannot be estimated. Olivine is not a liquidus phase in the picrite at 27 kb suggesting that this composition is not appropriate as a "minimum melting liquid" derived by partial melting of mantle peridotite. We would anticipate that such a liquid would have olivine, with orthopyroxene or possibly clinopyroxene, as liquidus phases — these being the major phases of the residual peridotite with which the liquid would be in equilibrium.

We conclude that separation of garnet or a garnet-rich mixture of garnet + clinopyroxene may produce nepheline normative liquids from compositions rich in olivine but poor in hypersthene. Such fractionation, if significant, must be restricted in basaltic rocks as extraction of garnet with its high-Al_2O_3 content leads to residual liquids inconsistent with basaltic chemistry. If this process is significant in producing liquids (at 27 kb or similar pressures) which are parental to the low pressure divergent alkali olivine basalt and olivine tholeiite sequences, then

in general alkali olivine basalts should have lower Al_2O_3/SiO_2 ratios than olivine tholeiites of similar Al_2O_3 or SiO_2 content. This is the reverse of the observed situation cf. MACDONALD and KATSURA (1964, Table 9, p. 124) and the association of higher Al_2O_3 and lower SiO_2 contents with alkali olivine basalts relative to olivine tholeiites of similar 100 Mg/Mg + Fe^{++} ratios, is consistent with fractionation control by aluminous orthopyroxene rather than garnet.

Discussion of the role of garnet in the basaltic compositions at 27—30 kb may be irrelevant if these particular compositions are appreciably divergent from the

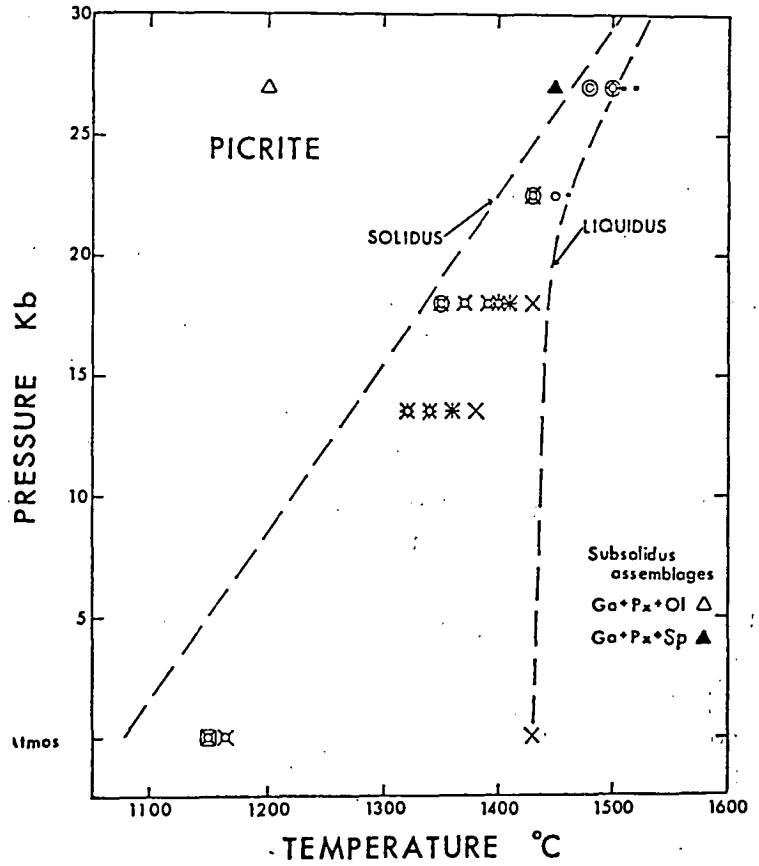

Fig. 7. Detail of melting and subsolidus experiments carried out on the picrite composition at high pressure. Solidus and liquidus positions are approximate only. Data at 1 Atmosphere is entirely interpreted from the literature (TILLEY, YODER and SCHAIRER, 1963, 1964, 1965). Symbols are the same as those of Figs. 4 and 6

composition of liquids which are partial melting derivatives of a mantle peridotite composition and thus in equilibrium with residual crystals of that peridotite. The presence of clinopyroxene and garnet on or very near the liquidus in these compositions suggests that at 27 kb these liquids could be in equilibrium with residual eclogite — rather than residual peridotite or dunite. Experimental work in progress in this laboratory has shown that garnet is unstable at 27 kb, 1,500°C in several peridotite compositions which are appropriate chemically for derivation of basaltic magmas leaving residual dunite or enstatite peridotite. Such compositions contain olivine + orthopyroxene + clinopyroxene ± spinel at the solidus at 27 kb and liquids derived from them by partial melting at this pressure may be expected to have one or more of these phases on the liquidus (cf. pages 160, 166, 167). It appears that the picrite composition may be closer to the composition of liquids

which may be derived from parental peridotite at 27 kb, particularly if in fact orthopyroxene is the liquidus phase at 27 kb, $1{,}500°C < T < 1{,}510°C$.

e) Summary of Fractionation Trends

The data and discussions of previous sections demonstrate that an olivine-rich tholeiite magma may fractionate to yield distinctive basaltic magma types at different pressures. These fractionation trends are depicted in Figs. 8—10.

(i) *Low Pressure or Shallow Crustal Fractionation* (< 15 km depth). Fractionation under these conditions is dominated by olivine as the liquidus phase with clinopyroxene and/or plagioclase appearing at lower temperatures. The field of olivine + liquid in compositions with 20—25% normative olivine may cover a wide temperature interval and, because of the Bowen reaction relationship, olivine remains the liquidus phase, in many compositions, into the quartz-normative tholeiite field. Thus, in the olivine tholeiites, olivine may show a reaction relationship with liquid, and fractionation of olivine-rich tholeiitic liquids (such as the olivine tholeiite) may yield quartz-normative residual liquids.

(ii) Fractionation at about 15—35 km Depth. Early stages of fractionation are dominated by olivine as at low pressure but the olivine is joined by orthopyroxene as the second phase in the olivine tholeiite composition and possibly the olivine basalt composition and by clinopyroxene in the alkali olivine basalt composition. Plagioclase only appears at temperatures very near the solidus. The crystallization of relatively large proportions of olivine and pyroxene(s) *before* the appearance of plagioclase contrasts with the crystallization sequence at low pressure and results in a marked increase in Al_2O_3 while retaining a relatively constant SiO_2 content at about 47—49% SiO_2. In this load pressure or depth interval an olivine tholeiite will not fractionate to yield an oversaturated quartz-tholeiite but instead will fractionate to yield high-Al_2O_3 olivine tholeiites (5—10% normative olivine).

(iii) Fractionation at about 35—70 km Depth. In this depth interval, olivine does not appear as the liquidus phase except in the picrite composition. Fractionation is dominated by separation of aluminous orthopyroxene or orthopyroxene + subcalcic augite. In either case magnesium-iron metasilicate is the major component removed with lesser but important amounts of alumina and calcium metasilicate. Extraction of these pyroxenes results in decrease in SiO_2 content, increase in $Na_2O + K_2O$ content and smaller percentage increases in Al_2O_3 and CaO contents. The fractionation trend yields olivine-rich, alkali basaltic magmas (i.e. nepheline normative) from parental olivine-rich tholeiitic magmas, and is in direct contrast to the shallow crustal fractionation trend of olivine tholeiites towards olivine-poor or quartz tholeiitic magmas.

(iv) Fractionation at about 70—100 km Depth. The appearance of garnet as the liquidus phase, without clinopyroxene, means that separation of garnet alone may occur over a very limited temperature interval and result in a fractionation trend producing higher SiO_2 + alkalis, lower Al_2O_3, MgO + FeO and approximately constant CaO in derivative liquids. The early appearance of clinopyroxene accompanying the garnet and the separation of garnet + clinopyroxene would change the fractionation trend, probably retaining an overall basaltic chemistry for the residual liquids but leading to increased FeO/MgO, increased K_2O, TiO_2 and possibly Na_2O, depending on the Na_2O content of the clinopyroxene.

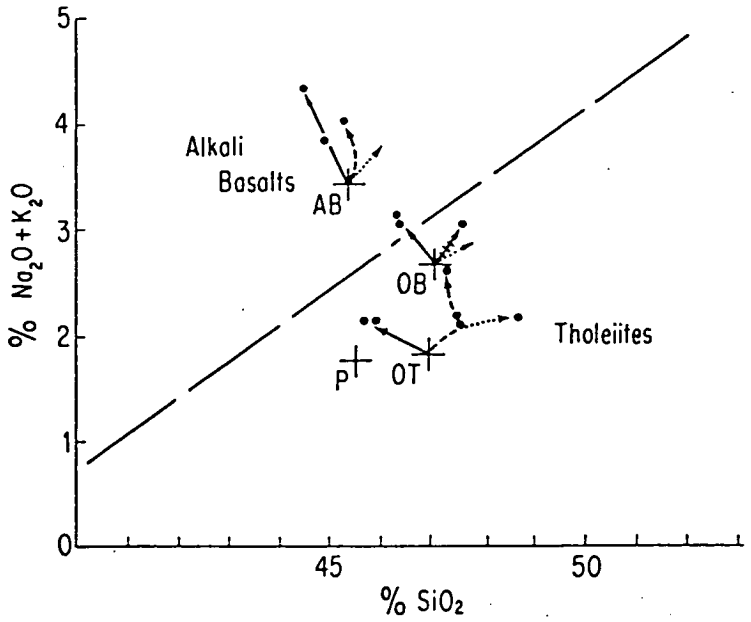

Fig. 8. Total alkalies vs silica plot for the compositions used in the experimental melting study. The line dividing the alkali basalt from the tholeiite fields is from MACDONALD and KATSURA (1964). *AB* alkali olivine basalt composition (Table 1); *OB* olivine basalt composition (Table 1); *OT* olivine tholeiite composition (Table 1); *P* Picrite (Table 1). • Calculated composition (Tables 12—19). ·····→ Fractionation trend at atmospheric pressure; -----→ fractionation trend at about 9 kb (30 km); ——→ fractionation trend at about 13—18 kb (40—60 km); -|-|-|→ fractionation trend at about 27 kb (100 km)

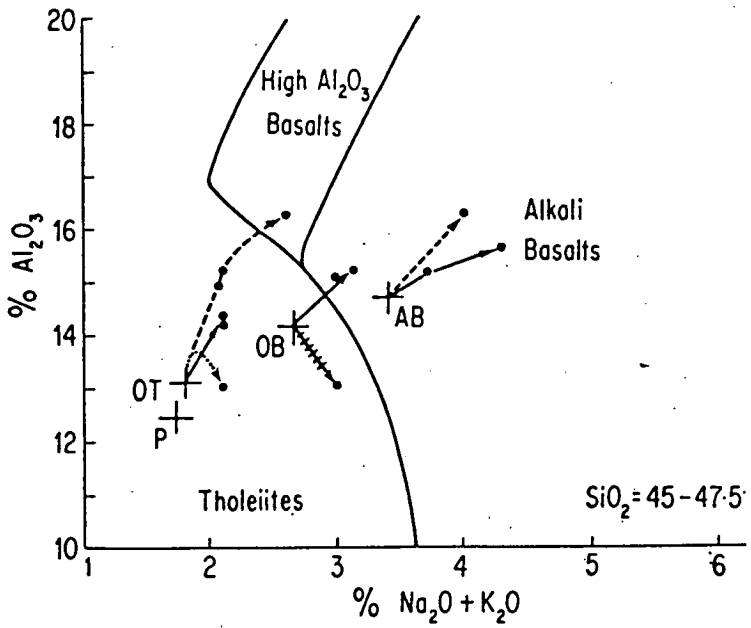

Fig. 9. Diagram for total alkalies v alumina for the compositions used in the experimental study and for the calculated fractionation trends of Tables 12—19. Basalt field boundaries from KUNO (1960). Symbols as in Fig. 8

If basaltic magmas in general are derived by partial melting of a peridotitic mantle at a depth of 100 to 150 km and segregate from residual unmelted peridotite at a depth of 100 km or less then the above diverse fractionation would argue for the recognition of one "primary" basaltic magma (an olivine-rich and

hypersthene-normative composition) and three derivative magma types of similar status:

(a) the alkali olivine basalt magma,
(b) the high alumina olivine tholeiite magma,
(c) the olivine tholeiite and quartz tholeiite magmas of low alumina content.

It must be emphasized that no sharp division between these magma types would be anticipated but rather a continuity in compositions since all may have the same parental liquid. The experimental data provide support for the concept that

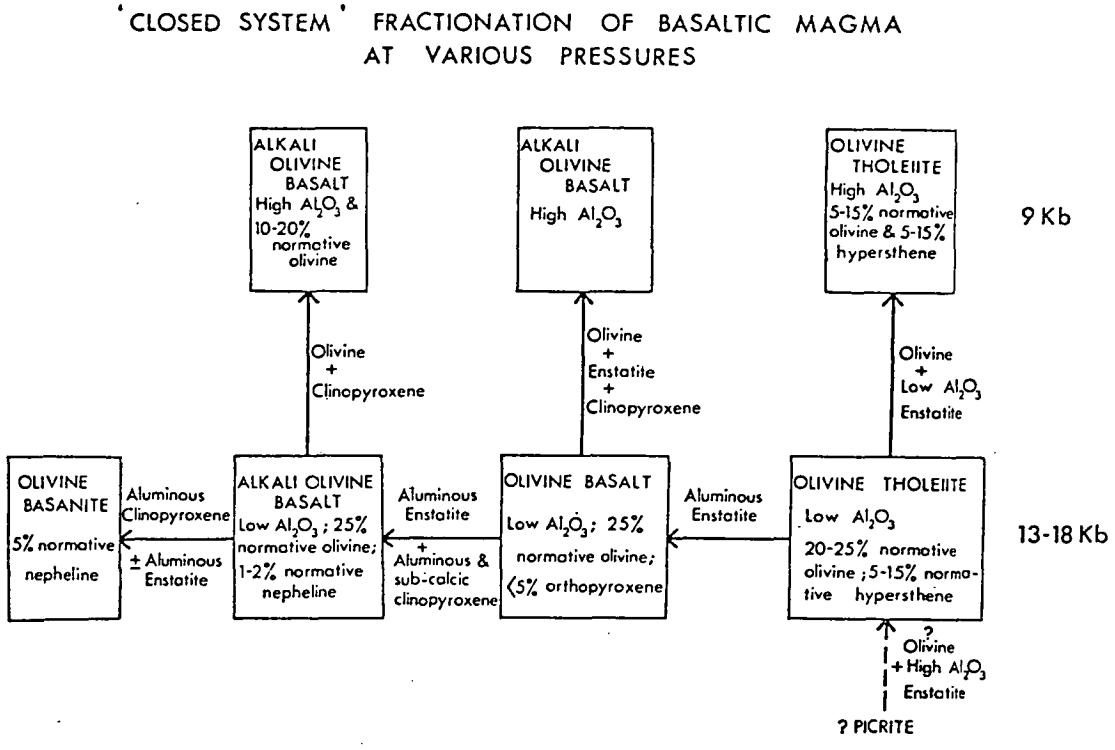

Fig. 10. Diagrammatic summary of the effects and directions of fractionation of basaltic liquids at moderate to high pressures. Refer also to Figs. 8 and 9 for plots of fractionation trends on the conventional "alkalies vs silica" and "alkalies vs alumina" diagrams

high-alumina basalts, like alkali olivine basalts, require recognition as a specific magma type indicative of origin or fractionation with a defined depth interval of the mantle cf. TILLEY (1950), KUNO (1960), GREEN, GREEN and RINGWOOD (1967). Rocks derived from these two magma types, and also those derived from a "parental" olivine tholeiite magma, most commonly reflect the effects of low pressure fractionation super-imposed on the chemistry of the liquid actually derived from the mantle. Low pressure fractionation of alkali olivine basalts will only increase the divergence of these liquids from liquids of the olivine or quartz tholeiite type (cf. pages 107—111), thus facilitating recognition of the type of magma derived from the mantle. In contrast, high alumina olivine tholeiites, if allowed to fractionate at shallow depth, will do so by precipitation of plagioclase, olivine and clinopyroxene. Derivate liquids, if separated, will move towards tholeiites with lower Al_2O_3 and finally into the quartz tholeiite field. The effect of low pressure fractionation on high-alumina olivine tholeiites and on "parental" olivine-rich tholeiite is to produce a convergence of derivative liquids, making identification of the nature of the mantle-derived magma more difficult.

Consideration of low pressure fractionation of basaltic magmas leads to a concept of two-fold division of magmas into nepheline-normative and hypersthene-normative types separated by a thermal divide (YODER and TILLEY, 1962). The study of fractionation at high pressure accentuates the transitional and continuous character of chemical variation in magma types but delimits three distinctive trends of fractionation characteristic of certain pressure intervals. These three trends require consideration in any petrogenetic classification of basaltic rocks.

The Generation of Basaltic Magmas

In the previous sections we have discussed the fractionation of basaltic magmas at various depths in the mantle and demonstrated mechanisms by which a "primitive" olivine-rich tholeiite magma may produce derivative liquids of alkali olivine basalt, high-alumina basalt or quartz tholeiite type. An important alternative hypothesis (e.g. KUNO, 1960; KUSHIRO and KUNO, 1963) maintains that the compositions of the principal basaltic magmas are determined by the depth in the mantle at which partial melting occurs rather than by subsequent fractionation processes. The data obtained from our experiments are used in the following sections to evaluate this hypothesis in detail.

An essential prerequisite to a discussion of the generation of basaltic magmas in the mantle is a consideration of the mineralogical and chemical constitution of the upper mantle. We will take up this subject in the next section, proceed then to the physical conditions of magma formation and finally investigate the chemical and mineralogical equilibria involved and their effect upon the composition of the resultant magma.

a) Chemistry and Mineralogy of Parental Mantle

It can be argued plausibly on general petrological and geochemical grounds that the chemical composition of the primary undifferentiated upper mantle should be somewhere between those of typical basalt and typical alpine peridotite. A chemical and petrological model for the upper mantle based upon this postulate has been developed by RINGWOOD (1962a, b; 1966a, b), GREEN and RINGWOOD (1963) and GREEN (1966a). In this model, the primary undifferentiated composition of the upper mantle is assumed equal to approximately 1 part of basalt to 3 parts of peridotite. This primary composition is called pyrolite (pyroxene-olivine rock). It is emphasized that the 3:1 proportion is not regarded as critical or unique, and substantial variations in this ratio are possible. Nevertheless an approximate 3:1 ratio is suggested by certain geochemical considerations and is convenient for the formulation of a specific model. The composition of pyrolite as derived by RINGWOOD (1966a) is given in Table 20.

An important property of compositions close to pyrolite is the ability to crystallize in four distinct mineralogical assemblages over the range of P, T conditions existing in the upper mantle. These are

1. Olivine + amphibole ± enstatite ± spinel (Ampholite);
2. Olivine + pyroxenes + plagioclase + chromite (Plagioclase pyrolite);
3. Olivine + aluminous pyroxenes ± spinel (Pyroxene pyrolite);
4. Olivine + pyroxenes + garnet (Garnet pyrolite).

The stability fields of these mineral assemblages for the model pyrolite composition given in Table 20 are currently under experimental investigation. A preliminary outline of the pyrolite stability fields was given by RINGWOOD, MACGREGOR and BOYD (1964), and RINGWOOD (1966b). Our latest experimental results require some modifications of the earlier boundaries of pyrolite stability fields but these are not of a fundamental nature. Much of the revision is caused by the necessity to introduce a pressure correction to earlier results because of non-uniform distribution of pressure in the furnace assemblies (GREEN et al., 1966). A provisional outline of stability fields for the pyrolite composition (Table 20) according to our latest experimental results is given in Fig. 11.

Table 20
Model composition of pyrolite (RINGWOOD, 1966a)

SiO_2	45.16
TiO_2	0.71
Al_2O_3	3.54
Fe_2O_3	0.46
FeO	8.04
MnO	0.14
MgO	37.47
CaO	3.08
Na_2O	0.57
K_2O	0.13
Cr_2O_3	0.43
NiO	0.20
P_2O_5	0.06

For the present purposes, it is important to observe that the boundary between the stability fields of pyroxene pyrolite and garnet pyrolite intersect the pyrolite solidus at a depth of 100 km. *Thus, the formation of magmas by fractional melting of pyrolite at depths smaller than 100 km would occur in the stability field of olivine + aluminous pyroxenes. Garnet would not play a significant role in the genesis of magmas by fractional melting at depths smaller than 100 km.* These considerations constitute a serious objection to the views of YODER and TILLEY (1962), O'HARA (1965) and others, that the principal basalt magma types are formed by direct partial melting of "garnet peridotite" in the upper mantle. In order to stabilise garnet at shallower depths in the mantle, a pyrolite composition possessing a much higher ratio of R_2O_3 ($Al_2O_3 + Cr_2O_3 + Fe_2O_3$) to total pyroxene than appears reasonable would need to be assumed. Furthermore, a model invoking such a composition would encounter further difficulties because of the tendency for garnet to melt incongruently to aluminous enstatite at an early stage of fractional melting in ultramafic compositions, so that magmas produced at relatively low pressures (15—30 kb) are in equilibrium with residual olivine and aluminous pyroxene for a very wide range of possible mantle compositions.

b) Physical Processes of Magma Generation

The formation of a magma in the mantle requires the supply of a large amount of thermal energy, in excess of 100 cals per gram of magma, to a localised region. Physical processes, e.g. thermal conduction, radioactive heat generation, mass transfer, which might be responsible for the supply of this energy operate on a comparatively long time scale. In contrast, the time scale required for separation of crystals from liquid within the mantle directly by gravity or indirectly by deformational processes ultimately of gravitational origin, is probably smaller by orders of magnitude. Because of these conditions, the formation of magmas in the mantle will almost always be the result of *partial* melting rather than of complete melting. Where a substantial degree of partial melting occurred throughout a large volume, the magma will tend to segregate from residual crystals into a self-contained magma body which thereafter evolves

independently of the refractory residuum with which it was formerly associated. The degree of fractional melting which is required before the magma separates from residual crystals doubtless varies according to physical conditions, but perhaps ranges mostly between 20 and 40 percent (by volume).

Many processes of magma generation have been advocated in the past, e.g. melting by relief of pressure. localised melting caused by liberation of energy during earthquakes, melting caused by accumulation of heat in regions characterised by a high concentration of radioactivity, and melting connected with rising "convection" cells or "advective movement" in the mantle. After an examination of possibilities, the authors are of the opinion that the only generally

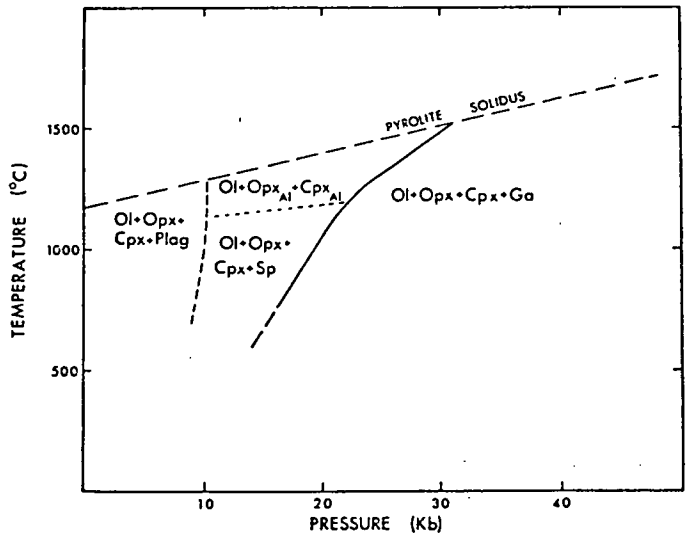

Fig. 11. Preliminary experimental determination of the stability fields of different mineral assemblages in the pyrolite composition of Table 20. The data are for an anhydrous composition and do not include the "ampholite" (olivine + amphibole ± enstatite) assemblage

satisfactory mechanism for producing basalt magmas and their observed distribution over the face of the earth and through geologic time, is some process connected with "convection" or "advection" in the mantle. Such processes have been advocated by many authors (e.g. HOLMES, 1926, 1927; VERHOOGEN, 1954). Accordingly we will base our discussion of magma generation on this type of process. Nevertheless it should be pointed out that much of the following discussion is of a general nature and could be applied to some other models of magma generation.

The condition for gravitational instability in the mantle is that the actual temperature gradient should exceed the adiabatic gradient. This condition is therefore most favourable in the upper few hundred kilometers of the mantle, where the geothermal gradient is greatly in excess of the adiabatic gradient. Indeed, as shown by CLARK and RINGWOOD (1964) it is probable that the density of the mantle actually decreases with depth down to 100 km or so in many regions. Although the outermost mantle many be potentially gravitationally unstable, the triggering-off of an actual instability leading to some form of mass-transfer requires other favourable conditions controlled particularly by rheological properties and by the presence of horizontal inhomogeneities in density, caused either

by temperature or chemical differences. Because of the close approach of the actual temperature gradient to the melting point gradient in the uppermost mantle, this region will constitute a zone of low strength and high mobility as previously pointed out by numerous authors. Also, horizontal inhomogeneities are most pronounced in the upper mantle. All these factors contribute towards the occurrence of mass transfer processes in the upper mantle, and their essential restriction to this region.

Processes of mass transfer in the upper mantle are commonly referred to as "convection" a term which characteristically applies to quasiregular, thermally generated motions in a viscous fluid. The analogy has frequently been applied to the earth and it has been argued e.g. Vening Meinesz (1952, 1962), Runcorn (1962) that the mantle is characterised by regular arrays of convection cells, extending as deep as the core. Such schemes appear unrealistic and implausible for many reasons. Elsasser (1963) has provided a stimulating discussion of the subject, and argued convincingly for restriction of mass transport processes to the upper mantle. Furthermore he emphasizes the probable extreme irregularity both in time and configuration, of the processes to be expected in the upper mantle. An additional complication in the models which we shall discuss is that mass motions are accompanied by partial melting and chemical differentiation, and are hence irreversible. Clearly, "convection" in the conventional sense is not an ideal term[5] to apply to such complex processes.

The model for magma generation which we have in mind is given in Fig. 12. It is characterised by a highly specific relationship between the actual temperature distribution and the pyrolite solidus, as shown in the diagram. Gravitational instability in the upper mantle combined with a suitable combination of horizontal inhomogeneity and rheological properties causes a source-mass (S) of solid pyrolite to rise diapirically (in the manner of a salt dome) from the low-velocity zone. It is possible that the initial triggering-off was connected with stresses associated with seismic activity, i.e. the diapir may be derived from an earthquake source-region; however this is not essential. The rising diapir is sufficiently large and hence possesses sufficient thermal inertia in relation to its velocity, so that it cools adiabatically and does not interact by thermal conduction with the surrounding mantle. The adiabatic gradient, of the order of 0.3° C/km (Birch, 1952) is much smaller than the gradient of the pyrolite solidus. Accordingly partial melting in the rising diapir will occur as the temperature of the diapir, following the adiabat from S, intersects the solidus at F (Fig. 12). This causes an increase of the density contrast between rising diapir and surrounding mantle and accordingly, an increase in its rate of upward movement. We assume that the partially melted diapir remains adiabatic. As it rises, and the pressure decreases further, the degree of partial melting increases. The absorption of latent heat accordingly steepens the effective adiabatic gradient, and the temperature of

[5] In a previous paper (Ringwood and Green, 1966) we adopted the term "advection" for the process, following Elsasser (1963). Although this term adequately specifies the complexity of the mass transport envisaged, it also carries the implication that the horizontal dimensions of the motions greatly exceed the vertical dimensions. This may not necessarily apply in the upper mantle.

the rising diapir (now a crystal-liquid mush) behaves as shown. It is probable that at this stage, the velocity of upward movement is sufficiently slow to permit the liquid component of the mush to remain in chemical equilibrium with the residual unmelted crystals. Eventually, the degree of partial melting becomes sufficiently extensive (20—40%) so that the liquid segregates from residual refractory crystals, and forms an independent, homogeneous magma body. This may be termed the stage of *magma segregation* (M, Fig. 12). From this stage

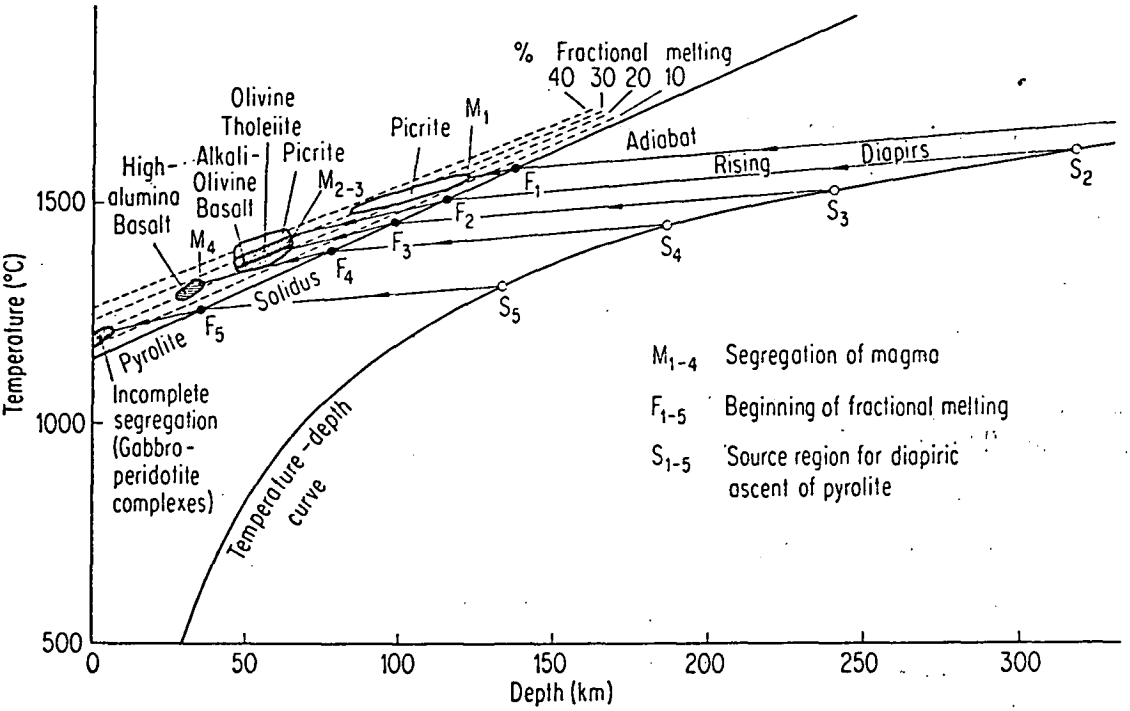

Fig. 12. A model for magma formation by fractional melting of mantle pyrolite. S_1—S_5 represent arbitrary source regions from which there is diapiric ascent of bodies of subsolidus pyrolite to intersect the pyrolite solidus at points F_1—F_5. Partial melting begins at these points and the rising crystal-liquid mushes follow the courses indicated until segregation of magma from residual crystals at M_1—M_4. The nature of the magma is determined by equilibria occurring at M_1—M_4 and not at F_1—F_4

onwards, the magma is no longer in equilibrium with the residual crystals with which it was originally associated. Instead, it may fractionate independently by cooling and crystal settling as it rises towards the surface.

The above outline suggests that the processes of magma generation in the mantle are more complex than sometimes assumed. Thus the initial source region (S) of the rising solid diapir, which may be associated with seismic activity, is probably much deeper than the point (F) at which the earliest liquid forms by fractional melting. As we shall see, the chemical composition of the liquid first formed at (F) is sensitively dependent upon depth. However, the magma which finally segregates at the much shallower level (M) may have an entirely different composition. As long as crystals and liquid in the rising crystal mush remain in chemical equilibrium, as appears likely, the nature of the liquid will change continuously with pressure, and will retain no "memory" of its earlier, deeper

origin. The overall chemistry of the magma is in fact, not determined until it segregates from residual refractory crystals at M. Thus the depth of *magma segregation* M is decisive in determining the nature of the magma. This depth may not be related in any simple manner to the initial depth of partial melting (F). Accordingly, in subsequent sections, we will discuss the partial melting of pyrolite according to the depths at which magma may segregate from residual crystals.

c) Partial Melting of Pyrolite — General Discussion

The rationale of the pyrolite model was to select a composition which on fractional melting would yield a generally "basaltic" magma, leaving an unmelted residuum similar in composition to peridotite or dunite. In one sense, fractional melting may be regarded as the reverse of fractional crystallization, providing that the nature of the crystalline phases are similar in both cases. This relationship is independent of the actual proportions of phases which may be present. We have seen that at depths between about 30 kms and 100 kms, the mineral assemblage of pyrolite at the solidus consists essentially of olivine, aluminous enstatite and aluminous subcalcic clinopyroxene. The experiments upon the crystallization of basalt magmas at different pressures showed that the principal magma types could be derived by the separation of olivine and aluminous pyroxenes in various proportions according to P, T conditions and magma compositions. Moreover the Fe/Mg ratios of olivines and pyroxenes occurring near the liquidi of the experimental basaltic compositions are similar to the Fe/Mg ratios of olivines and pyroxenes of mantle-derived ultramafic material such as kimberlite inclusions, peridotite nodules and alpine peridotites. Because of these relationships, we are able to apply our results on fractional crystallization of basalt magmas to fractional melting of pyrolite within the above depth range. The inferred relationships are summarized in Fig. 13 and elaborated in the following sections.

d) Depth of Magma Segregation 0—15 km

It has long been known that at atmospheric pressure, the field of crystallization of olivine extends into quartz normative basaltic compositions. Accordingly, it is possible to derive quartz tholeiite from an olivine tholeiite magma by early crystallization of olivine, followed by segregation of crystals from magma, so that Bowen's reaction relationship is prevented. Conversely, segregation of small amounts of magma from fractional melting of pyrolite under restricted conditions may yield an oversaturated tholeiite magma together with residual dunite (Reay and Harris, 1964).

Boyd et al. (1964) showed that a pressure of a few kilobars was sufficient to prevent the incongruent melting of enstatite. T. H. Green is currently studying this relationship in natural basaltic magmas (personal communication). He finds that saturated tholeiites may form by fractional melting of pyrolite in the depth interval 0—15 km. Below this depth, the olivine reaction relationship does not occur, and the liquid fractions are always olivine-normative.

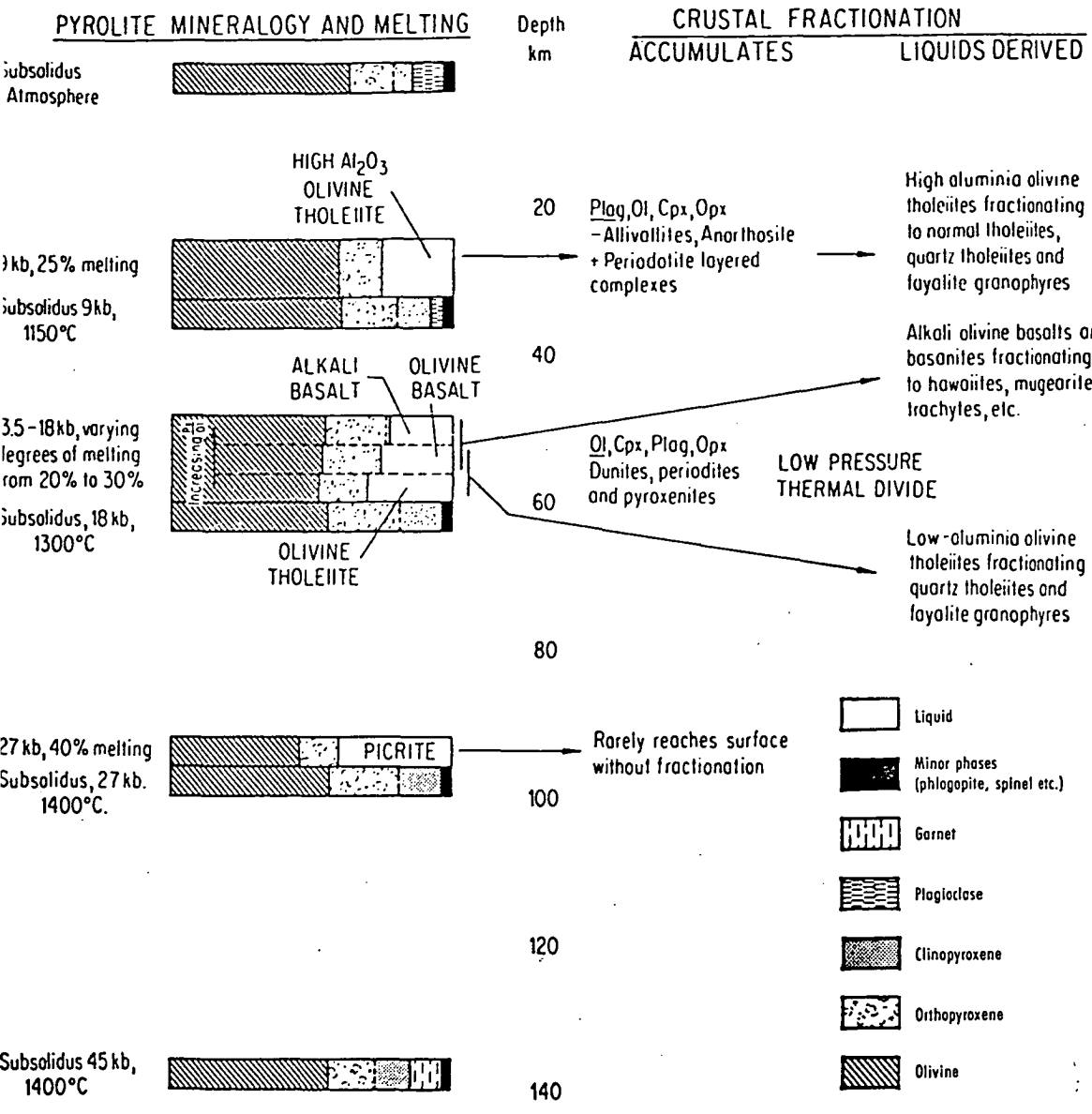

Fig. 13. Diagram illustrating the variation in the near-solidus mineralogy of pyrolite, the degree of partial melting and nature of both the liquid and the refractory residuum at various depths within the mantle

e) Depth of Magma Segregation 15—35 km

Results of experimental crystallization of the olivine tholeiite are given in Table 14. At 1,250° C, the separation of about 12 percent of olivine (Fo_{91-86}) and 3 percent of orthopyroxene (En_{87}, $Al_2O_3 = 5\%$) produced a residual liquid similar to high-alumina olivine tholeiite. Since the liquid is saturated with these phases under the stated conditions, it would be possible to increase these proportions to any desired amount without affecting liquid composition, e.g. 60 percent of olivine and 15 percent of enstatite (5% Al_2O_3) could be added, giving a bulk composition essentially identical to pyrolite. It follows that fractional melting of 20—25% of pyrolite followed by magma segregation under these P, T conditions would yield a high alumina olivine tholeiitic liquid.

This liquid might thus be erupted directly to the surface after segregation or it might undergo crystal fractionation at a slightly higher level under closed system conditions leading to even greater enrichment in Al_2O_3 due to separation of olivine and pyroxenes as previously discussed.

f) Depth of Magma Segregation 35—70 km

The compositions of liquidus orthopyroxenes from the olivine tholeiite and olivine basalt are close to the compositions of natural orthopyroxenes of the olivine + aluminous orthopyroxenes + spinel mineral assemblage in peridotites. Previously GREEN and RINGWOOD (1964) have noted that near-liquidus olivine and orthopyroxene from the picrite composition at 13.5 kb closely match the compositions of olivine and orthopyroxene from the olivine + aluminous pyroxenes + spinel assemblage of lherzolite nodules. Olivine was not observed during the crystallization of olivine tholeiite or of the olivine basalt at 12—20 kb. However it was present on the liquidus of the picrite composition. It follows from a consideration of these three compositions that the olivine tholeiite and olivine basalt are almost saturated with olivine between 12—20 kb. We have already noted that they are saturated with highly aluminous orthopyroxene. Accordingly, a fairly large degree of fractional melting of pyrolite under these conditions would yield an olivine tholeiite magma closely resembling our chosen composition, but containing slightly more normative olivine. Such an olivine tholeiite would be in equilibrium with a refractory assemblage of olivine + aluminous orthopyroxene possessing Fe/Mg ratios identical to natural peridotite nodules.

The crystallization experiments upon picrite, olivine tholeiite and olivine basalt at 12—20 kb showed that these magmas would fractionate by means of the crystallization of substantial amounts of aluminous orthopyroxene ± aluminous clinopyroxene to the composition of alkali-olivine basalts. Thus we see that an alkali olivine basalt (with a slightly higher content of normative olivine than the one which we investigated), can be in equilibrium with olivine + aluminous enstatite ± aluminous clinopyroxene. This assemblage would be identical on cooling at pressure to the assemblage found in many lherzolite nodules which are commonly found in alkali olivine basalts and basanites (pages 181—185). These relationships show that olivine-rich alkali basalt may be formed by direct fractional melting of pyrolite.

Whether an olivine tholeiite or an alkali olivine basalt is formed by melting and magma segregation under these conditions depends simply upon the extent of partial melting. With a relatively small degree (~20%) of partial melting of pyrolite, the residual crystals consist of olivine, abundant aluminous enstatite ± aluminous clinopyroxene, and the liquid has the composition of an olivine-rich alkali basalt. However, as the temperature is increased, the extent of partial melting increases, the clinopyroxene and then a large amount of aluminous orthopyroxene enter the liquid, changing its composition to an olivine tholeiite at about 30 percent partial melting. The situation is exactly the reverse of fractional crystallization of the olivine tholeiite.

The series of liquids developed by different degrees of partial melting at 35 to 70 km would be lower in SiO_2 content and in Al_2O_3 content than the series of liquids developed at 9 kb (30 km approx.) with similar degrees of melting of

pyrolite. This is because the ratio of pyroxene/olivine, and particularly of orthopyroxene/olivine in the residual crystals is always higher at 13.5—18 kb than at 9 kb for a given degree of partial melting. In addition the residual pyroxene at 13.5—18 kb contains more Al_2O_3 in solid solution, resulting in lower Al_2O_3 content of the liquid fractions.

g) Depth of Magma Segregation Around 90 km

We have argued that the mineralogy of pyrolite at depths of around 90 km (P ~27 kb) and temperatures near the basalt solidus or liquidus (1,420—1,520°C) will consist essentially of olivine + aluminous enstatite + aluminous clinopyroxene. Garnet is absent from this assemblage but we have shown that garnet is a major phase in the subsolidus assemblages of the basaltic compositions at 27 kb and is the liquidus phase of at least two of the three basaltic compositions at 27 kb. These relationships demonstrate that the three basaltic compositions chosen are not compositions which may be derived by direct partial melting and magma segregation from pyrolite at 27 kb. Compositions which could be derived by partial melting of pyrolite at 27 kb should have olivine + orthopyroxene or olivine + clinopyroxene as liquidus phases or near-liquidus phases. The appearance of orthopyroxene near the liquidus of the picrite composition at 27 kb suggests that this composition is closer to being an appropriate partial melt at this pressure and re-inforces the previous arguments that liquids derived by partial melting and magma segregation at pressures near 30 kb (i.e. 100 km) would have the chemistry of picrites with over 30% normative olivine.

The deduced and observed nature and behaviour of the partial melt at 27 kb illustrates the important role which buffering by residual crystals may play in liquid fractionation. If a picritic liquid is segregated free from residual olivine + pyroxenes and fractionates essentially as a closed system then garnet and clinopyroxene will be the major phases controlling fractionation. If, however, a picritic liquid does not segregate from residual crystals but begins to crystallize again then garnet and olivine are incompatible and will react principally to form aluminous enstatite + olivine. Garnet as a phase will have no role in either the fractionation sequence or in the solidus assemblage at 27 kb unless some segregation of partial melt and residual crystals occurs.

Application of the Hypotheses of Partial Melting and Fractionation to Natural Basaltic Provinces

The conclusions on partial melting in the upper mantle and basalt fractionation at high pressure which have been detailed in previous sections should be relevant to discussions of any basaltic magma province. However, we will briefly apply our conclusions to an interpretation of the causes of the main features of Hawaiian volcanism, and the rather distinctive basaltic magmas of the mid-oceanic ridges.

a) Hawaiian Volcanism

The extensive chemical data on Hawaiian basalts published by MACDONALD and KATSURA (1964) and their review of the main features of the individual volcanoes, together with the review by YODER and TILLEY (1962), serve as the basis for the

following discussion. The major eruptive phase of each of the Hawaiian volcanoes comprises voluminous, rapid and rather homogeneous eruptions of olivine tholeiite to quartz tholeiite liquids. The average lava compositions for each of seven major volcanoes is quartz normative but all workers recognize the important role that fractionation at very shallow depths (2—5 km) exercises in producing the variations in lava composition and particularly the trend to quartz-normative tholeiites. The liquids derived from the mantle and "parental" for the low pressure sequence of fractionation, are probably of olivine tholeiite composition, but neighbouring volcanoes may show lava compositions of a consistently distinctive character, e.g. the Pololu Series of Kohala is distinctive in low K_2O, low TiO_2 and high-Al_2O_3 contents and in high Al_2O_3/SiO_2 ratio. Individual lavas are closely similar if not identical to the high-Al_2O_3 "oceanic" tholeiites of Engel, Engel and Havens (1965). The early, voluminous tholeiites of the Hawaiian Islands pass *transitionally* to an upper zone of interlayered tholeiite and alkali olivine basalt types — the transitional nature of this change of magma type is most significant, as is the restriction of the alkali olivine basalts to the late, waning stage of activity of any particular volcano. In some volcanoes [of Kohala type (Macdonald and Katsura, 1964)] the upper zone containing alkali olivine basalts is disconformably overlain by a thin veneer of mugearite and related rocks, i.e. lavas derived by shallow level fractionation of the alkali olivine basalts. A similar relationship appears to hold for Piton des Neiges volcano, Reunion Id. (Upton and Wadsworth, 1965).

Geophysical studies on the currently active Kilauea volcano indicate that seismic activity correlatable with the ascent of magma for the 1959-60 eruption of Kilauea Iki was first observed at depths of 50—60 km. A reasonable interpretation of this is that 50—60 km marks the depth at which magma segregated and accumulated as a discrete body. We have shown that magma segregation following a high degree of partial melting at 35—70 km will produce olivine tholeiite magmas. If these magmas move rapidly from this depth to shallow levels and then fractionate to a variable extent at 2—5 km, the observed sequence of early tholeiitic series will result. Rapid and voluminous tholeiite eruptions will continue as long as the melting process is active and the zone of pyrolite is not exhausted of its basaltic component. Variations towards high-alumina tholeiites, e.g. Pololu Series, will result if fractionation occurs at intermediate depths (20—30 km) or alternatively if magma segregation for other volcanoes occurs at shallower depths ($\sim$30 km) than deduced for Kilauea. The latter explanation is preferred.

In the waning phase of activity of each volcano the ascent of magma batches becomes less frequent and cooling at the depth of segregation may occur. Cooling of an olivine tholeiite liquid at 35—70 km depth will cause crystallization of aluminous enstatite and the magma composition will change towards alkali olivine basalt. The Hawaiian sequence of rock types, the transitional nature of the change from tholeiitic series to alkali olivine basalt and the relative volumes of tholeiite and alkali types are all consistently explained by the hypothesis of high pressure fractionation of olivine tholeiite during waning phases of activity. Like the tholeiitic series, the alkali olivine basalt magmas may accumulate and differentiate in shallow level magma chambers. It is significant that the most undersaturated rocks of the late alkali olivine basalt series appear to be basanites, i.e. compositions

near the suggested limit of fractionation towards nepheline-enrichment at 35—70 km. Some Hawaiian volcanoes have a much later period of eruption of olivine nephelinites and nephelinites but these seem unlikely to be derived by extreme fractionation at 35—70 km of the alkali olivine basalt series.

The Hawaiian volcanic province is one in which the observed proportions and sequence of magma types support an hypothesis of origin of alkali olivine basalt magma by crystal fractionation of olivine tholeiite at 35—70 km depth. Complete transition between the magma types occurs at the depth of fractionation but later, shallow level fractionation of most liquids has imposed the effects of the low pressure thermal divide between the nepheline-normative and hypersthene-normative rock series leading to a greater chemical separation of the magma series. Perhaps the most notable effect of low pressure fractionation is that the average composition of the tholeiitic series for the Hawaiian volcanoes is almost exactly saturated in silica with either minor olivine or quartz in the norm (MACDONALD and KATSURA, 1964). These liquids represent the effects of precipitation of some 20% (if olivine only precipitated) to 30% (olivine $\pm$ clinopyroxene $\pm$ plagioclase) of crystals at very shallow depths from the olivine-rich tholeiitic liqudis present at 35—70 km depth. Geophysical data showing the existence of high density and seismically fast material at shallow depths beneath the central regions of Hawaiian volcanoes (STRANGE, WOOLLARD and ROSE, 1965; FURUMOTO, THOMPSON and WOOLLARD, 1965) may be consistent with such olivine-rich, low pressure accumulative material.

b) Oceanic Ridge Volcanism

In recent years, papers by ENGEL and ENGEL and their co-workers have focussed attention on the distinctive chemical characteristics of basalts dredged from the ocean floor at depths around 3,000 metres and located along the mid-oceanic ridges (Mid-Atlantic Ridge, Indian Ocean ridges, and the East Pacific Rise). Earlier analytical work by WISEMAN (1940) and independent work by NICHOLLS, NAWALK and HAYS (1964) support the conclusions of ENGEL and ENGEL (1964a, b), ENGEL, FISHER and ENGEL (1965) and ENGEL, ENGEL and HAVENS (1965) that a characteristic magma is of olivine tholeiitic character with $SiO_2 = 49$—50%, $Al_2O_3 = 15$—17%, $Na_2O = 2.5$—3.0%, $K_2O < 0.3\%$ and $100\ Mg/Mg + Fe^{++} \sim 65$. This composition is closely similar to the high-alumina, olivine tholeiite composition derived by fractionation of low-Al_2O_3, olivine-rich tholeiite at 9 kb (pages 142—148) and also interpreted as a direct product of magma segregation from mantle pyrolite at depths around 30 kms.

ENGEL and ENGEL (1964b) and ENGEL, ENGEL and HAVENS (1965) have argued that these high-alumina olivine tholeiites are the only "primary" basaltic magma generated by partial melting within the mantle and that other tholeiitic and alkali magmas are derived by processes of crystal differentiation and volatile transfer, mainly in volcanic conduits at depths less than 3 km. The possible directions of fractionation of high-alumina olivine tholeiites at various pressures are at present under study by Mr. T. H. GREEN and his data is unfavourable to any hypothesis of crystal fractionation at shallow depths leading to alkali olivine basalt compositions (T. H. GREEN, personal communication).

There is an alternative process consistent both with our results on high pressure fractionation and partial melting and with the observed features of chemistry and distribution of volcanics along the mid-oceanic ridges. The high-Al_2O_3 olivine tholeiites have chemical compositions appropriate for liquids segregated from a pyrolite composition at the comparatively shallow depth of about 30 kms. With about 25% melting and segregation of the magma from pyrolite at about 30 kms depth, high-Al_2O_3 olivine tholeiitic liquids could be produced leaving residual olivine + low-Al_2O_3 enstatite. Apart from the probable dropping of minor (0—10% approx.) olivine during ascent, the high-Al_2O_3 olivine tholeiites show little chemical change consequent on low pressure fractionation. These magmas thus approach the simplest model of partial melting with extraction of a rather constant proportion of magma from a given volume of pyrolite and transport of the magma through the oceanic crust with a minimum of chemical change by either fractionation or processes of wall-rock reaction. In comparison with other tholeiitic provinces it may be relevant that the environment of intrusion or extrusion of the oceanic tholeiites requires 3—5 km less vertical travel than the exposed Hawaiian tholeiites and there is no thin zone of near-surface material of low density to be penetrated.

The distinctive chemical compositions of the oceanic tholeiites seem to require particularly intense or active upward movement of mantle such that separation of magma and crystals does not occur until depths of about 30 km. If the proposed rapid mantle upwelling process in any part of the mid-oceanic ridge begins to wane in intensity it is probable that the zone of magma segregation will move to greater depths and also the frequent, fissure type of eruption will change towards a localized and central type of eruption. If this process occurs then there will be a gradual transition from high-alumina olivine tholeiite to low-alumina olivine tholeiite or to alkali olivine basalt.

c) Other Provinces

The Hawaiian alkali olivine basalts are interpreted as the product of crystal fractionation of olivine tholeiite magma. Other basaltic provinces of regional extent are characterized by alkali-type magmas ranging from alkali olivine basalt to nephelinites and excluding the tholeiitic suite entirely. Kuno (1960) has drawn attention to this feature in Japan and correlated the distribution of the alkali series with a region characterized by particularly deep melting of the mantle. The Tertiary volcanic provinces of Eastern Australia are almost entirely of the alkali olivine basalt + basanite + nephelinite type. In contrast Tertiary basalts of Western Australia and the Jurassic dolerites of Tasmania are tholeiitic. The Tasmanian tholeiitic province, as well as the much more widespread Jurassic Ferrar dolerites of Antarctica and Karroo dolerites of South Africa form distinctive magma provinces. Other examples could be cited supporting the observation that basaltic provinces of regional extent may be typified by alkali olivine basalt magmas alone or by tholeiitic magmas alone. Examples such as these are interpreted as direct partial melting products from the mantle, with relatively constant conditions of melting and magma segregation over the region. Extensive fractionation at low pressure within the crust appears to be a normal characteristic of the continental tholeiitic series.

Trace Element Contents and Isotopic Ratios of Basaltic Rocks in Relation to Partial Melting and Fractionation Processes

The relationships between basalt magma types which have been deduced in previous sections, are based on a consideration of the relative concentrations of the major elements (Si, Al, Fe, Mg, Ca, Na and Ti). These elements largely determine the normative and modal mineralogy and thus the classification of basaltic magma types. However, the minor elements K, Ti, P, and trace elements U, Th, Ba, Cs, Rb, Sr, Zr, Hf and the rare earth group, are frequently much more abundant in alkali olivine basalts than predicted by simple crystal fractionation from olivine-rich tholeiite or by differences in degree of partial melting of the same parental peridotite. Isotopic ratios also show variations amongst basalts which must be considered in formulating hypotheses in their origin. In this section trace element behaviour and isotopic ratios amongst basalts are briefly reviewed and the data derived in this way are applied to formulate a more detailed discussion of the partial melting and fractionation processes within the mantle.

a) Enrichment in K_2O and Associated Elements

The high-alumina olivine tholeiites (oceanic tholeiites) have been interpreted as the result of simple melting of 20—25% pyrolite mantle and extraction of basalt with a minimum of fractionation. In this case their K_2O content of 0.1—0.2% may be used to estimate an average K_2O content of 0.03—0.05% for their source region, assuming no retention of K_2O in residual olivine or enstatite. Many alkali olivine basalts and continental tholeiites contain 0.5 to 1% K_2O and their derivation by simple partial melting from such a source would require that these magmas represent extraction of 5% or less of liquid. Alternatively some additional process of K_2O enrichment must be postulated for these magmas.

In the Hawaiian volcanic province, comparison of average Hawaiian alkali olivine basalt with average Hawaiian tholeiite (MACDONALD and KATSURA, 1964) shows an increase of 100% or more in K_2O content in the alkali series. This cannot be accounted for by 10—30% fractionation or the difference between 20% and 30% partial melting of the same pyrolite parental material. In the Hawaiian example there is a smaller but similar inconsistency in the P_2O_5 contents whereas TiO_2 variation between the suites is broadly consistent with the suggested major element fractionation. The abundances of U and Th in alkali olivine basalts compared to tholeiites in Hawaii are greater by factors of 3 to 5 instead of 1.5 to 2 as expected in the simple crystal fractionation model (HEIER and ROGERS, 1963; HEIER, McDOUGALL and ADAMS, 1964; HAMILTON, 1965; TATSUMOTO, HEDGE and ENGEL, 1965). Nephelinites and melilite nephelinites are in even more marked contrast having over five times the U and Th contents of the tholeiites (HEIER et al., 1964; HAMILTON, 1965). Although data are meagre and commonly not easily correlated with total rock chemistry, there appears to be a similar contrast in abundance in tholeiites and alkali olivine basalts for Ba (ENGEL et al., 1965; LE MAITRE, 1962), for Zr (ENGEL et al., 1965; NAUGHTON and BARNES, 1965) and probably for Cs and Hf. Recent data for Rb and Sr contents of basalts are much more extensive and demonstrate a much greater enrichment of Rb in the alkali olivine basalt series (TATSUMOTO et al., 1965; HAMILTON, 1965; ENGEL et al., 1965; LESSING and CATANZARO, 1963). Strontium shows a similar pattern although

enrichment is not as marked as for rubidium. The limited data on Sr contents of nephelinites and melilite nephelinites show extremely high Sr contents (Hamilton, 1965).

As well as large enrichment factors in the alkali olivine basalts, the above-mentioned elements show relative fractionation within the group (as might be expected from the rather diverse elements included). There is an independent and rather random variation of K_2O, TiO_2 and P_2O_5 among basalts (Green, 1966) e.g. there exist tholeiites with $TiO_2 < 1\%$ and others with $TiO_2 > 2.5\%$; low TiO_2 may be coupled with high K_2O or low K_2O etc. Heier and Rogers (1963) noted a correlation of high Th/U ratios with high K_2O contents while Gast (1965) noted that high K/Rb ratios (> 1000) occurred in the oceanic tholeiites with very low K_2O contents and that this ratio decreased (down to 350) with increasing K_2O contents through the tholeiitic and alkali olivine basalt series. Continental tholeiites with K_2O contents similar to the oceanic alkali olivine basalts have even lower K/Rb ratios of about 200 (Heier et al., 1965; Compston et al., 1966; Gunn, 1965).

The data summarized above suggest that the process or processes which determine the abundances of the group of elements discussed above, are sufficiently selective to produce marked fractionation within the group. This conclusion is further illustrated and supported by recent studies of rare-earth element distributions in basalts (Haskin, Frey, Schmitt and Smith, 1966; Schilling and Winchester, 1966). The total rare earth content of basalts ranges from around 100 ppm for high-alumina oceanic tholeiites and a Kilauean tholeiite, 174 ppm for a composite sample of 282 continental basalts, 280—430 ppm for oceanic island alkali basalts and 530 ppm for a continental alkali olivine basalt. As a group, the rare earth elements are enriched in terms of their total abundance in basalts in similar manner to K, Rb, Sr etc. The overall enrichment in rare-earth abundances is accompanied by marked fractionation within the rare-earth group (Haskin et al., 1966; Schilling and Winchester, 1966). The high-alumina oceanic tholeiites are distinctive amongst basalts so far analyzed in having low rare-earth abundances and a distribution pattern similar to the chondritic abundance pattern, although there is relative depletion (compared to chondrites) in the lightest rare-earth elements (La, Ce, Pr). Hawaiian tholeiites show low or moderate degrees of overall enrichment and maximum enrichment factors, relative to the chondrite pattern, for Pr and Nd. Alkali olivine basalts, and basanites, show greater enrichment than tholeiites throughout the rare earth series but particularly in the lightest rare earth elements (enrichment factors, relative to a low-potassium tholeiite, of 2.5 to 3.5 for La compared to factors around 1.2 for Lu; Schilling and Winchester, 1966). Nephelinite and melilite nephelinite from Hawaii show enrichment factors relative to tholeiite which range from over 10 for La to about 1.1 for Lu (Schilling et al., 1966). The processes which lead to enrichment in the rare earth elements in alkali olivine basalts and basanites relative to olivine tholeiites, also lead to marked fractionation within the rare earth group. Elements which are heavier than Gd have abundances in alkali olivine basalts and basanites which appear consistent with the fractionation or partial melting relationships outlined in previous sections. Elements which are lighter than Gd (and have progressively larger ionic radii) have abundances which are inconsistent

with the simple fractionation model and resemble K, Rb, Sr etc. in their abundance relationships.

b) Isotopic Abundances and Fractionation

Data obtained from basaltic rocks indicate a rather constant initial Sr^{87}/Sr^{86} ratio of 0.703—0.704 (FAURE and HURLEY, 1963; HEDGE and WALTHALL, 1963; LESSING and CATANZARO, 1964; HEIER, COMPSTON and MCDOUGALL, 1965; GAST, 1966). LESSING and CATANZARO (1964) found no differences in Sr^{87}/Sr^{86} ratio between Hawaiian basalts of tholeiitic and alkali basalt types. This is supported by data given by HAMILTON (1965), POWELL, FAURE and HURLEY (1965) and POWELL and DE LONG (1966) and is consistent with a simple crystal fractionation relationship for these two magma series. However both POWELL et al. (1965) and HAMILTON (1965) noted that the highly undersaturated, low-SiO_2 nephelinites and melilite nephelinites from Oahu (Honolulu Series) have distinctly lower Sr^{87}/Sr^{86} ratios than either the tholeiites or the alkali olivine basalts. This problem was further amplified by POWELL and DE LONG (1966) with extensive data from the Honolulu Series, Oahu (basanites to melilite nephelinites) showing that this series has consistently lower Sr^{87}/Sr^{86} ratios than the tholeiitic Koolau Series, Oahu. However, four specimens of the Waianae Series, Oahu, including tholeiite, alkali basalt, hawaiite and rhyodacite gave low Sr^{87}/Sr^{86} ratios similar to the highly undersaturated Honolulu Series. Current data from Hawaii appear to suggest that a given Sr^{87}/Sr^{86} ratio is characteristic for a particular volcanic centre or series and not for a specific magma type.

GAST, TILTON and HEDGE (1964) found consistent differences in the Sr^{87}/Sr^{86} ratio for alkali olivine basalts and their differentiates from two oceanic islands, Gough Island ($Sr^{87}/Sr^{86} = .7045$) and Ascension Island ($Sr^{87}/Sr^{86} = .7025$). They observed that these differences in Sr^{87}/Sr^{86} were accompanied by differences in Pb^{206}/Pb^{204} ratios while Pb^{208}/Pb^{204} ratios were closely similar. GAST et al. concluded that the isotopic differences between equivalent magma types on the two islands reflect differences in the source regions of the mantle, i.e. higher Rb/Sr in the mantle acting as source for the Gough Id. basalts and higher U/Pb but not Th/Pb for the Ascension Id. source. It is relevant that LE MAITRE (1962) pointed out compositional differences between the alkali olivine basalt series of the two islands, the Gough Id. rocks having higher K_2O contents and K_2O/Na_2O ratios than those from Ascension Id.

The compilation of Sr^{87}/Sr^{86} data by GAST (1966) further suggests that regional variations in Rb/Sr in mantle source regions may cause the observed variation in Sr^{87}/Sr^{86} ratios and that this is not coupled to rock type. There is some evidence that basalt series characterized by high K_2O contents such as the alkali olivine basalts of Gough Id. and Samoa or the quartz tholeiites of Tasmania and Antarctica also have the highest Sr^{87}/Sr^{86} ratios and the lowest ratios are found in series with relatively low K_2O contents or K_2O/Na_2O ratios such as the high-alumina oceanic tholeiites (TATSUMOTO, HEDGE and ENGEL, 1965) or the Ascension and St. Helena Id. alkali olivine basalts (GAST, 1966). GAST's (1966) compilation also illustrates the greater abundance of basalts with $Sr^{87}/Sr^{86} > .705$ from continental areas rather than oceanic areas, a result accentuated by the work of HEIER et al. (1965) and COMPSTON et al. (1966) on Jurassic continental tholeiites.

Tatsumoto et al. (1965) found that the Rb/Sr ratios of high-alumina oceanic tholeiites was too low to account for the observed Sr^{87}/Sr^{86} ratios, assuming an initial Sr^{87}/Sr^{86} ratio of .6984 for the earth system. These authors concluded that the magmas either were not representative of their source in Rb/Sr ratio or alternatively that the source region had changed its Rb/Sr ratio during earlier evolution from a high value of Rb/Sr to the present low value (0.011) observed in the oceanic tholeiites.

Inconsistencies in isotopic abundances and parent element abundances are even more apparent in the U-Th-Pb system (Gast et al., 1964; Tatsumoto, 1966a, b; Gast, 1966). These authors have postulated multistage differentiations of the source material to account for differences between the U/Pb and Th/Pb ratios of the basalts and the ratios required by the observed Pb^{208}/Pb^{204}, Pb^{207}/Pb^{204}, Pb^{206}/Pb^{204} and assumed primordial abundance ratios. In addition, heterogeneity in U-Th-Pb in the mantle source region seems to be required by the data.

c) Inferences from Minor Element and Isotopic Studies

The data briefly summarized in previous sections lead to the following general conclusions:

(i) Processes other than simple crystal fractionation in a "closed-system" magma are necessary to account for observed abundances of the elements (K, Ti, P, Ba, Cs, Rb, Sr, U, Th and the lighter rare earth elements) in tholeiitic and alkali olivine basalt magmatic series.

(ii) Not only are these elements fractionated as a group but there is also fractionation within the group leading to changes in abundance ratios such as K/Rb, K/Ti, K/Zr, Rb/Sr etc. and in relative abundances of elements of the rare earth group.

(iii) The simple concept of partial melting in which elements strongly partitioned into the liquid fraction preserve the abundance ratios of the parental mantle does not account for the observed relationships of the highly enriched elements nor for observed isotopic ratios. In particular the abundance ratios Rb/Sr, U/Pb, Th/Pb of a magma probably differ from the ratios of the original parental mantle and may not be simply related to the strontium or lead isotopic ratios present in the magma.

(iv) Variations in isotopic ratios amongst basalts require that the basaltic magmas interact with regions of mantle or crust which have differed for considerable lengths of time in their Rb/Sr, U/Pb and U/Th ratios. This implies inhomogeneity in distribution of these elements within at least the uppermost mantle.

(v) In highly fractionated derivatives of basaltic magmas the late differentiates may show higher Sr^{87}/Sr^{86} ratios. Examples of the process, e.g. Skaergaard granophyres (Hamilton, 1963) and Gough and Ascension Id. trachytes (Gast et al., 1965) suggest that fractionation of basaltic magmas, even at low pressure, is not a simple, closed-system process.

The elements K, Rb, U, Zr etc. which show relatively high enrichment factors in the alkali olivine basalts have the common property that all of them are incapable, because of their ionic radii and valency states, of appreciable substitution in the major minerals of pyrolite, i.e. in olivine, orthopyroxene, chromian clinopyroxene and possibly spinel or garnet. This group of elements is the same as that con-

sidered by HARRIS (1957) to be concentrated by processes of "zone refining" in the mantle and referred to as "incompatible elements" by RINGWOOD (1966a). Both authors stressed the crystal-chemical factors controlling the behaviour of these elements in the mantle and concluded that these "incompatible elements" would be strongly partitioned into any liquid fraction present in the mantle. In the absence of a liquid phase, these elements are considered to be present in the mantle in minor phases such as phlogopite, Mg-ilmenite. apatite or other phases stable under upper mantle pressure, temperature conditions (HARRIS, 1957; HESS, 1964).

In contrast to the behaviour of the highly enriched elements, for which we shall adhere to the term "incompatible elements" (RINGWOOD, 1966a) other minor elements such as Mn, Cr, Ni or trace elements (Cu, Co, Ga, V, Y) show comparatively small variations between tholeiitic and alkali olivine basaltic series and appear consistent with the simple crystal fractionation or partial melting hypotheses. These elements all substitute comparatively readily in the major minerals (olivine + pyroxenes $\pm$ spinel $\pm$ garnet) of the mantle and in the liquidus phases of basaltic magmas. In the present context, these elements have been grouped as "compatible elements" referring to their crystal-chemical properties in relation to the major mineral phases of the mantle.

d) Wall-Rock Reaction

The hypothesis that fractional crystallization of olivine tholeiite magma at 35—70 km depth yields derivative alkali olivine basalt liquids requires cooling of the magma body against its wall-rock environment. Cooling of a magma leading to partial crystallization may occur by two main processes —

(i) heat transfer by conduction to cooler wall-rock without intermixing of material, or

(ii) by reaction with and solution of crystalline material incorporated into the magma.

The relative importance of these two processes probably differs at different depths and for different magmatic provinces. At shallow crustal depths the large temperature contrast between wall-rock and magma *usually* results in chilling of the magma in a zone near the contact so that the remaining liquid is isolated in a protective sheath of rock with similar chemistry. Under these conditions there is a minimum of chemical exchange between magma and wall-rock and the magma may behave essentially as a closed system during any fractionation process.

At greater depths in the mantle, particularly near the depth of segregation of basaltic magmas, there may be little temperature contrast between magma and mantle wall-rock. Under such conditions, cooling of a magma may proceed mainly by a process of "wall-rock reaction". We envisage the nature of this reaction as solution of low-melting components from the wall-rock and their incorporation into the magma, accompanied by precipitation of the liquidus phase of the basalt. The concept of "wall-rock reaction" is closely related to the "zone-refining" concept discussed by HARRIS (1957) and our arguments have been considerably influenced by this earlier paper. However "wall-rock reaction" is applied in a much broader sense and to a wider spectrum of basalts than was attempted by HARRIS. In addition "zone refining" is a defined physico-chemical process and,

in its geological application, was coupled to models of solution of roof material, magma convection and bottom precipitation and also to specific models of mantle temperature distribution (HARRIS, 1957, p. 199).

In considering the mantle environment of a magma near its depth of segregation, the chemical nature of the wall-rock will, in general, be that of pyrolite or a refractory peridotite composition or some composition intermediate between these extremes. Ascent of the magma near its source within the mantle may be by processes of stoping or by displacive intrusion. In both cases the contacts between magma and wall rock will not be chilled but will be diffuse with a gradual decrease in the ratio of liquid to crystals away from the magma body. Mantle material which is processed by the magma body by stoping or by marginal reaction may lose its low melting fraction into the basaltic liquid and the nature and proportion of the liquid fraction thus extracted will depend on the temperature of the magma and the temperature reached by the wall-rock. Lower temperature basaltic magmas will clearly be able to melt and extract only a small proportion of the potential basaltic magma in any incorporated mantle material but this small fraction may be highly enriched in elements which are not readily accepted by the major mantle minerals, i.e. the incompatible elements. In contrast, higher temperature basaltic magmas may extract almost all the potential basaltic liquid from enclosed pyrolite blocks and there would be little or no selective enrichment or fractionation in the lowest melting components of pyrolite.

In the particular case of an olivine tholeiite magma segregated at 35—70 km depth in the mantle, cooling of the magma by the "wall-rock reaction" process would include solution of the lowest melting fraction from any stoped or accessible wall-rock material and the complementary process of precipitation of the liquidus phase, i.e. aluminous enstatite. As this cooling continues, the major element chemistry of the liquid would trend towards alkali olivine basalt composition with slightly decreasing Mg/Fe ratio. The magma would also, because of cooling and changing Mg/Fe ratio, be able to melt successively smaller fractions from any stoped mantle peridotite with which it is in contact. The lowest melting fraction and most easily extracted elements from pyrolite are the "incompatible" elements previously discussed. These elements could become highly enriched in the magma depending on the amount of mantle material processed through the magma and on the proportion of mantle material soluble in the magma. The process of crystal fractionation at depths near that of magma segregation in the mantle is considered to be *normally* accompanied by "wall-rock reaction" leading to enrichment in incompatible elements to a degree greater than is possible by closed system fractionation alone. It is also apparent that with extraction of extremely small amounts of liquid from the mantle wall-rock, the opportunity for fractionation between elements is greatly enhanced. Much more data is needed on partition relationships for the incompatible elements in both major and minor minerals of the pyrolite composition. For instance, it has been suggested (GREEN, 1967) that the inverse relationship between K/Rb ratios and K_2O contents (GAST, 1965) could be a consequence of melting and wall-rock reaction involving a major phase with low K_2O content but high K/Rb ratio (possibly pyroxenes) and a minor phase with high K_2O content and low K/Rb ratio (possibly phlogopite). It has been shown (HASKIN et al., 1965) that garnet in eclogite is enriched relative to

clinopyroxene in the heavier rare earths. Aluminous enstatite is chemically similar to pyrope-almandine garnet and, if similarly enriched in the heavier rare earths, in a liquid-orthopyroxene or clinopyroxene-orthopyroxene partition, could be a major factor in producing the light-element enriched rare earth pattern of alkali olivine basalts. A knowledge of orthopyroxene-liquid, clinopyroxene-liquid and phlogopite-liquid partition relationships at high pressures would probably show methods by which fractionation could yield liquid fractions with Rb/Sr, U/Th, U/Pb and Th/Pb ratios different from those in either the initial pyrolite source for the magma or the mantle material processed by the wall-rock reaction mechanism.

A corollary of the "wall-rock reaction" mechanism is that zones of pyrolite which are still potential sources for basaltic magma in major element chemistry, may acquire lower abundances and different element-ratios for the incompatible elements by being "processed" through an early magmatic cycle. The application of this to the origin of lherzolite nodules in basalts is discussed in the following section. Batches of magma or accumulates from magmas formed in early magmatic cycles may remain as segregated bodies within the mantle and develop isotopic ratios for Sr and Pb which are of local extent and very different from the ratios in subjacent pyrolite. Such bodies may be intersected by later ascending magmas, and, if their content of incompatible elements is extracted by wall-rock reaction, may modify the composition and isotopic ratios of the later magma batch.

To summarize, the fractional crystallization and slow ascent of an olivine tholeiitic magma at 35—70 km depth or the slow ascent of an alkali olivine basalt magma derived by direct partial melting at 35—70 km, would be accompanied by extensive and highly selective reaction with mantle wall-rock. This would cause overall enrichment in incompatible elements and selective fractionation amongst them. The process would also lead to heterogeneity in incompatible element distribution and ratios in the mantle, creating the necessary conditions for development of varied Pb-isotope ratios and, to a less marked degree, Sr^{87}/Sr^{86} ratios in different mantle regions.

It is important to note that enrichment in incompatible elements accompanies fractionation of an olivine tholeiite magma near its depth of segregation so that magmas enriched in incompatible elements at 35—70 km depth are of alkali olivine basalt type. Enrichment in incompatible elements while retaining tholeiitic affinities requires that an olivine tholeiite magma cools and fractionates at lower pressures i.e. along the trend towards high-Al_2O_3 tholeiites or towards quartz tholeiites. This aspect of wall-rock reaction is treated in more detail in the following section.

e) Wall-Rock Reaction at Lower Pressures

Under some conditions it is possible that an environment suitable for extensive wall-rock reaction may occur under lower pressure conditions, e.g. if magma segregation occurs at higher levels in the mantle or if continued magmatic activity causes wall-rock temperatures in the lower crust or top of the mantle to approach the magma temperature. There are important differences between the nature of the highly enriched "incompatible elements" in a process of wall-rock reaction at low pressure in comparison with wall-rock reaction at high pressure. At high

pressure, plagioclase is not a stable phase in the wall-rock mineralogy, and strontium behaves as an incompatible element since it does not readily enter either clinopyroxene or orthopyroxene. At low pressure, plagioclase is a major stable phase in the wall-rock mineralogy and as strontium substitutes for calcium in plagioclase, strontium will behave as a "compatible element" in fractionation or reaction processes. In addition, at sufficiently low pressure, plagioclase may be a liquidus or near-liquidus phase and as strontium is preferentially enriched in plagioclase (Wilkinson, 1959; Heier, 1962, p. 436), precipitation of this phase will prevent marked enrichment of strontium in a fractionating basaltic liquid at very low pressure.

Titanium may exhibit similar differences in behaviour at high and low pressure particularly if ilmenite or titanomagnetite have the character of relatively refractory phases at low pressure in intermediate or acidic compositions. Changes in redox potential between mantle and lower crust environments may also potentially alter the role of titanium.

The Jurassic tholeiites of Antarctica, South Africa and Tasmania are considered to be possible examples of magmas which have trace element contents determined in large part as a result of wall-rock reaction and fractionation processes occurring at low pressure, and in these particular continental examples, in a crustal rather than upper mantle environment. The Ferrar Dolerites (Antarctica) and Tasmanian dolerites are highly enriched in K, Rb, U, Th but are conversely low in Sr and Ti in comparison with olivine and quartz tholeiites from oceanic islands or oceanic ridges (Compston et al., 1966). In the Ferrar Dolerites there is strong K_2O enrichment accompanying increasing SiO_2 oversaturation in the sequence of magmas ranging from olivine tholeiite (0.38% K_2O, 50.40% SiO_2) to pigeonite quartz tholeiites (1.27—1.76% K_2O, 55.25—55.87% SiO_2) (Gunn, 1962, 1966). The initial Sr^{87}/Sr^{86} ratios for both Tasmanian and Antarctic tholeiites are consistently above 0.710, in contrast to the much lower values (0.702—0.704) found in alkali olivine basalts or tholeiites of oceanic areas.

It is suggested that the parental olivine tholeiite magmas for these intrusions began to crystallize at crustal levels giving rise to a spectrum of magma compositions for individual intrusions ranging from oversaturated, iron-rich pigeonite tholeiite to more magnesian olivine tholeiite (Gunn, 1962, 1966). The period of slow ascent of very large volumes of basic magma through the lower crust established conditions suitable for selective extraction of a low-melting fraction from the wallrock environment. The nature of this extraction process presents some difficulty if the average lower crust is of intermediate or acid composition, unless it is a partial melting process with migration of the liquid phase into the basaltic magma. The elements enriched in the basaltic magma are considered to be those least able to substitute in the major phases of the surrounding wallrock, i.e. in pyroxenes, plagioclase, quartz and possibly hornblende and ilmenite or titanomagnetite. The contaminating material would be anticipated to have high Sr^{87}/Sr^{86} ratios and lead isotopic ratios consistent with geologically old crustal material. Heier et al. (1965), Compston et al. (1966) and Gast (1966) have discussed more fully the role of contamination processes by crustal material enriched in Sr^{87}/Sr^{86} in deriving the particular chemistry of the Tasmanian and Antarctic tholeiites. Compston et al. (1966) present arguments favouring a highly selective contamina-

tion rather than wholesale assimilation by average crustal material. The process of wall-rock reaction detailed previously goes some way towards indicating a mechanism for such selective contamination but requires that the average lower crustal material will only be melted to a very limited extent by the tholeiitic magmas and that the bulk of the wall-rock material would remain as refractory residue. A lower crust of anhydrous granulitic or anorthositic composition (RINGWOOD and GREEN, 1966a, b; T. H. GREEN, 1966) would possibly be suitable wall-rock material for the process and effects outlined above. The alternative explanation for the particular chemical compositions of the Tasmanian and Antarctic quartz tholeiites requires a mantle source region of high K, U, Th etc. content and high Sr^{87}/Sr^{86} ratio (HEIER et al., 1965; COMPSTON et al., 1966).

If the conclusions on the behaviour of Sr at low and high pressure are correct then rocks enriched in incompatible elements at low pressure should be characterized by rapid increases in such ratios as K/Sr and Rb/Sr whereas basalts enriched in incompatible elements at high pressures should show relatively small changes in K/Sr and Rb/Sr through quite large variations in overall incompatible element abundances. Without making an exhaustive literature search we have assembled data in Table 21 which supports this hypothesis. In the oceanic tholeiite to basanite series with K contents increasing by a factor of 20 and Rb contents increasing by a factor of 40, the K/Sr ratio only varies between 10 and 21 and the Rb/Sr between 0.01 and 0.07. In contrast the K-enriched quartz tholeiites, with K contents only 10 times the K content of oceanic tholeiites, have K/Sr ratios increasing with increasing K content to a maximum near 90. The Rb/Sr ratio increases to 25—40 times the Rb/Sr ratio of the oceanic tholeiites. In contrast, tholeiites and quartz tholeiites of Hawaii do not show large enrichments in K_2O contents nor large changes in K/Sr or Rb/Sr ratios.

f) Summary

The slow ascent of magmas at considerable depth within the mantle, if accompanied by cooling and partial crystallization, would also cause selective enrichment in the incompatible element content (wall-rock reaction). Repetition of such processes would produce a mantle which is quite inhomogeneous in incompatible element content and, over geological time, would become inhomogeneous in Sr and Pb isotopic ratios. Less commonly, and possibly only in continental areas, slow ascent of magmas in the lower crust or uppermost mantle would be accompanied by partial crystallization and by selective enrichment in incompatible elements extracted from the wall-rock under conditions of lower pressures. The abundances of K, Rb, Ba and probably U, Th relative to major or trace compatible elements may be used to determine whether a given magma has been altered in chemistry by wall-rock reaction. The difference in partition behaviour of Sr at low and high pressures (consequent on the stability or instability of plagioclase) leads to the promising possibility of using such ratios as K/Sr or Rb/Sr to distinguish between the effects of deep-level wallrock reaction or a shallow-level process. In attempting the interpretation of isotope and trace-element abundance data there seems little relevance in the simple model of melting in which a liquid composition is determined at source (particularly in trace element and isotopic ratio contents) and thereafter remains essentially a

Table 21. *Comparison of K/Sr and Rb/Sr for various average and individual basalts. Enrichment in incompatible elements in the first 5 rock types is considered to have occurred at low pressure, enrichment in the remainder is considered to have occurred at high pressure*

K (%)	K/Sr	Rb (ppm)	Rb/Sr	Sr (ppm)	Rock and locality	Reference
1.20	88	55	0.4	137	Average Pigeonite tholeiite, Antarctica	Compston et al. (1966)
0.67	54	31	0.25	125	Average Hypersthene tholeiite, Antarctica	Compston et al. (1966)
0.86	66	33	0.25	130	Average Hypersthene tholeiite, Tasmania	Compston et al. (1966)
0.31	31	12	0.12	100	Olivine tholeiite, Antarctica	Compston et al. (1966)
		55	0.18	310	Columbia R. Plateau, Oregon	Faure and Hurley (1963)
2.57	13	40	0.02	1,980	Basanite, Tasmania (Tertiary)	Compston et al. (1966)
1.53	20	14	0.02	770	Alkali olivine basalt (Tertiary)	Compston et al. (1966)
1.20	20	30	0.05	600	Average Alkali basalt	Tatsumoto et al. (1965)
1.64	11	21	0.015	1,436	Hawaiite, Hawaii	Hamilton (1965)
0.80	19	16	0.04	413	Alkali olivine basalt, Hawaii	Hamilton (1965)
0.51	10	10	0.02	515	Ankaramite, Hawaii	Hamilton (1965)
		47	0.04	1,249	Alkali olivine basalt Hawaii	Faure and Hurley (1963)
		42	0.07	568	Alkali olivine basalt Samoa	Faure and Hurley (1963)
		32	0.04	643	Alkali olivine basalt Ascension	Faure and Hurley (1963)
0.57	21	20	0.07	270	Tholeiitic basalt Tasmania (Tertiary)	Compston et al. (1966)
0.31	12	10	0.04	250	Average Hawaiian tholeiite	Compston et al. (1966)
0.50	22	10	0.04	230	Average non-submarine tholeiite	Tatsumoto et al. (1965)
0.41	10	8	0.02	391	Quartz dolerite, Oahu	Hamilton (1965)
0.50	15	11	0.03	335	Quartz dolerite (vein), Oahu	Hamilton (1965)
0.34	11	5	0.02	297	Tholeiite, Mauna Loa, Hawaii	Hamilton (1965)
0.13	11	1.2	0.01	115	Average oceanic tholeiite	Tatsumoto et al. (1965); Compston et al. (1966)

closed system except for depletion by fractional crystallization. There are great uncertainties in use of trace element and isotopic data obtained from basaltic rocks rich in incompatible elements to deduce element abundances and geochemical pre-histories for the mantle source region and such attempts should be viewed with caution.

The Significance of Cognate Xenoliths in Basalt Petrogenesis

a) Peridotite Nodules

Coarse-grained inclusions of peridotite have a sporadic but world-wide occurrence as inclusions in alkali olivine basalts, basanites, nephelinites and melilite nephelinites. The most abundant type of nodule may be classed as lherzolite and has the mineral assemblage olivine (Fo_{85-92}), aluminous enstatite, aluminous chrome-diopside (also with appreciable Na_2O content) and minor spinel ($MgAl_2O_4$-rich). Other types, less common and of more restricted occurrence, ranging from dunite through wehrlite to clinopyroxene (FRECHEN, 1948, 1963), are probably genetically distinct (de ROEVER, 1963; WHITE, 1966).

The lherzolite inclusions commonly have the character of xenoliths of previously consolidated rocks showing internal effects of deformation, cataclasis, grain-boundary recrystallization and dimensional or crystallographic orientation of minerals (DEN TEX, 1963). There may be internal evidence of disequilibrium and reaction between phases and the minerals of the inclusion are clearly not in equilibrium with the enclosing basaltic liquid — orthopyroxene, spinel and clinopyroxene all showing clear evidence of partial reaction. The lherzolite nodules apparently do not occur in olivine tholeiitic magmas or their derivatives (WHITE, 1966). The proportions of olivine, pyroxenes and spinel are variable amongst individual nodules but the order of abundance is almost invariably olivine $\gg$ enstatite $>$ chrome-diopside $>$ spinel. Compilations of modal analyses by VILMINOT (1965) from Rocher du Lion, Velay, France and WHITE (1966) from Hawaii indicate a greater frequency of nodules with modes containing olivine from 90—65% and pyroxenes from 10—35%. The ratio of orthopyroxene to clinopyroxene is usually between 2:1 and 3:1. Both authors plot modal data obtained from the literature giving a wider scatter and including types with clinopyroxene in excess of olivine (cf. BROTHERS, 1960). Spinel is almost ubiquitous as a minor phase (1—4%) and accessory minerals noted in the literature on nodules and in a study (GREEN — in preparation) of Eastern Australian examples, include phlogopite, hornblende, sulphides, melilite, plagioclase (An_{90} and An_{65}; WHITE, 1966) and garnet.

Nodules show evidence of internal disequilibrium — thus some Australian examples show reaction between clinopyroxene and spinel at mutual grain boundaries to yield fine grained plagioclase, olivine and chromite aggregates. WHITE (1966, p. 289—293) notes that enstatites in some inclusions are of variable Al_2O_3 content and may be zoned in Al_2O_3 content. Comparison of the mineralogy and bulk chemical composition of lherzolite nodules with the chemical compositions of high temperature peridotite intrusions (GREEN, 1963, 1964) and with other peridotites (GREEN and RINGWOOD, 1963), coupled with the internal evidence of disequilibrium in the peridotites themselves, demonstrates that the mineral assemblage of the lherzolite inclusions is unstable at high temperatures at upper

crustal levels. Preliminary experimental work indicates that the olivine + aluminous pyroxenes + spinel assemblage is stable at pressures > 8 kb approx. at 1100°C in compositions close to those of the lherzolite nodules. The temperature at which the mineral assemblages of individual nodules reached equilibrium is probably variable but the degree of solid solution of the two pyroxenes is very much less than the experimentally crystallized pyroxene pairs at 1300—1400°C (p. 138, Fig. 3). The CaO content of most orthopyroxenes is <1.0% CaO and commonly around 0.5% CaO (ROSS, FOSTER and MYERS, 1954; WHITE, 1966; GREEN and EASTON, unpublished data) and the orthopyroxene very commonly has exsolution lamellae of clinopyroxene indicating a history involving cooling from an earlier, higher temperature environment. The low CaO content of olivine (<0.1% CaO; WHITE, 1966) also suggests temperatures rather less than volcanic temperatures or the temperatures of the experimental high pressure runs previously reported. These features suggest that the lherzolite nodules were at temperatures of less than 1000°C before inclusion in their host basalts. The partition of Mg and Fe^{++} between co-existing pyroxenes in lherzolite nodules has been discussed by several authors (KRETZ, 1961; BARTHOLOME, 1961; DEN TEX, 1963; GREEN, 1964; WHITE, 1966) and, in some cases, used to suggest temperatures of equilibrium crystallization of the nodules similar to or greater than those of igneous, basaltic rocks. The distribution coefficients (K_D) for the analyzed orthopyroxene and clinopyroxene pairs (Tables 9, 11) obtained experimentally range from 1.14 to 1.27 and are thus distinctly higher than the values for igneous rocks (0.7 approx.) and somewhat higher than those of lherzolite nodules (around 1.0), cf. DEN TEX, 1963; WHITE, 1966. A considerable uncertainty in the use of mineralogical criteria for estimation of crystallization temperature is that different indicators may be "frozen in" at different stages of cooling.

Hypotheses of origin of the lherzolite nodules must be consistent with the above observations and may be broadly grouped into four possibilities:

1. Lherzolite nodules are accumulates of crystals precipitated from olivine-rich picritic or basaltic magmas at moderate to high pressures.

2. Lherzolite nodules are xenoliths of "parental mantle" from which a basaltic magma can still be derived under appropriate melting conditions.

3. Lherzolite nodules are xenoliths of residual, refractory mantle peridotite after basaltic magma has been removed.

4. Lherzolite nodules are xenoliths of mantle peridotite which have been selectively depleted in those "incompatible elements" which do not readily substitute in the major minerals of the peridotite.

In the simplest statement of the first hypothesis, a crystal accumulate relationship to the magmas *in which they occur* fails to account for the evidence of cataclasis, deformation and recrystallization in the lherzolite nodules. The estimated equilibration temperature of <1000°C and the compositions of pyroxenes and spinel are inconsistent with liquidus temperature equilibrium with a basaltic magma. It would be necessary to postulate an earlier precipitation from another magmatic event, cooling of the accumulates with variable cataclastic effects and accidental incorporation in a later magmatic event. The chemistry and mineralogy of the lherzolite inclusions would require that the initial precipitating

phases were dominantly very magnesian olivine, with much smaller quantities of aluminous enstatite and/or sub-calcic, aluminous clinopyroxene. This type of mineral accumulate is possible from magmas such as the olivine basalt, olivine tholeiite or picrite compositions at pressures around 5—10 kb. We might expect such accumulative rocks to be initially inhomogeneous, possibly ranging from dunite to pyroxenite and also controlled in their bulk chemistry by the presence or absence of trapped, interprecipitate magma. Later cooling would be accompanied by exsolution of Al_2O_3 from aluminous pyroxenes to form spinel, exsolution of orthopyroxene from subcalcic clinopyroxene and could give rise to the observed mineralogy of the nodules. This hypothesis may be applicable to a limited degree but must rest on a postulated earlier history of the nodules which cannot be directly and unequivocally deduced from the present observed chemistry and mineralogy of the nodules.

The second hypothesis has been adopted by KUSHIRO and KUNO (1963) with calculations of the degree of partial melting needed to extract basalts of average Hawaiian and Japanese types from average lherzolite nodule composition. KUSHIRO and KUNO (1963) show that only 2—9% of basalt magma could be extracted from the lherzolite before one or more of the oxides TiO_2, P_2O_5 or K_2O goes to zero. Approximately 8% of an average high-Al_2O_3, oceanic tholeiite (ENGEL, ENGEL and HAVENS, 1965) could be extracted before TiO_2 and Na_2O of the average nodule composition used by KUSHIRO and KUNO go to zero. These small degrees of partial melting seem incompatible with the relatively high $Mg/Mg+Fe^{++}$ ratios of some basaltic liquids and pose mechanical difficulties in segregating such a small liquid fraction from residual crystals. The difficulties in obtaining basaltic chemistry, particularly the contents of incompatible elements such as K, U, Th etc. are even more formidable if average nodule compositions (e.g. VILMINOT, 1965) rather than selected individual nodules are used as model parental material.

The third hypothesis has been advocated by de ROEVER (1961, 1963), O'HARA and MERCY (1963) and OXBURGH (1964a, b) and is supported by the very low K_2O (MORGAN and GOODE, 1966), TiO_2, P_2O_5 and, to a lesser extent, Na_2O, contents of the lherzolite nodules. Referring to the previous discussion of partial melting in the mantle, the nature of residual peridotite will differ considerably depending on whether an olivine tholeiite or alkali olivine basalt magma is extracted. The appreciable Na_2O, CaO and Al_2O_3 contents and the opx:cpx ratios of 3:1 or 2:1 in very many lherzolites imply that, if the nodules are residua after basalt extraction, the magma extracted was of alkali olivine basalt type and not of olivine tholeiite type. The presence of glass (with crystallites of olivine, clinopyroxene and plagioclase) apparently developed at the expense of clinopyroxene+spinel in some Australian lherzolite inclusions, implies that at least some inclusions are capable of yielding a liquid fraction at magmatic temperatures and cannot be regarded as completely refractory residues. The third hypothesis, i.e. that lherzolite nodules are residual mantle from which a basaltic magma has been extracted, is probably valid for many lherzolite nodules. The previous arguments indicate that the magma extracted from pyrolite to yield compositions of the lherzolite nodules is of alkali olivine basalt rather than olivine tholeiite type. With this type of limitation the third hypothesis passes transitionally into the fourth, i.e. that

lherzolite nodules are "residual" in character only in their content of incompatible elements but have not suffered a general partial melting process.

The fourth hypothesis has been suggested by Hess (1964) and further discussed by Ringwood (1966a) and Green (1967). The hypothesis postulates that lherzolite nodules are "residual", in comparison with pyrolite in their contents of elements such as K, Ba, U, Th, Rb, Sr, Zr, Ti, P and to a lesser extent, Na and the rare earths. The selective depletion in these elements, with little change in Ca, Al, Fe etc. could be a consequence of the process of wall-rock reaction previously discussed. Thus, fragments of pyrolite included in alkali olivine basalt magma would be expected to lose any very low melting fraction into the magma — it is assumed that this low melting fraction will be highly enriched in the incompatible elements K, Ba, U, Th, Rb, Sr, Zr, P and Ti. Of the major minerals of the lherzolite, clinopyroxene may partially react with loss of jadeite component to the liquid phase. By this hypothesis, the enrichment in incompatible elements in alkali olivine basalts is a complementary process to the depletion of these elements in any fragments of mantle accidentally incorporated into a body of magma. The third and fourth hypotheses, which differ in degree rather than in kind, probably together provide an adequate explanation of the mineralogy and chemical compositions of lherzolite inclusions.

b) The Restriction of Lherzolite Nodules to Critically Undersaturated Basaltic Magmas

Both of the preferred hypotheses postulate an initially accidental inclusion of peridotitic mantle material into ascending basaltic magma. The mechanical difficulty of upward transport of xenoliths of density 3.3 in magma of density approximately 2.7 may impose some limitation on the nature of host basalts. On the other hand, the present experimental work and discussion offers a direct reason for the restriction of the lherzolite nodules to undersaturated, alkali olivine basalts, basanites etc. and their absence in olivine tholeiites or quartz tholeiites. The data and discussion on basalt fractionation and on partial melting of pyrolite demonstrated that an alkali olivine basalt liquid may be in equilibrium with olivine, aluminous orthopyroxene and aluminous clinopyroxene near its depth of segregation at 35—70 kms (cf. Green and Ringwood, 1964). If lherzolite nodules have the character suggested in either the third or fourth hypotheses then they will behave essentially as refractory xenoliths in alkali olivine basalt with little internal melting and without disaggregation of the nodule.

In contrast to their behaviour in alkali olivine basalt magma, lherzolite nodules would be unstable if enclosed in an olivine tholeiite magma at 35—70 kms depth. An olivine tholeiite or tholeiitic picrite magma at these depths will be saturated in magnesian olivine and magnesian, aluminous enstatite but will completely dissolve any aluminous clinopyroxene introduced into it.

A lherzolite nodule which is included in an olivine tholeiite magma at 35—70 kms depth will partially melt with spinel, aluminous clinopyroxene and some aluminous enstatite entering the tholeiitic liquid, i.e. probably some 20—30% of the original inclusion would melt. Under these conditions a lherzolite inclusion would disintegrate although residual xenocrysts of magnesian olivine or chromite might remain, cf. Muir and Tilley (1964).

An additional reason for the absence of lherzolite nodules in tholeiitic magmas is that tholeiitic liquids extruded at the surface have in many cases undergone low pressure fractionation towards quartz tholeiites. The Hawaiian tholeiites illustrate this trend very well. Any magma which has fractionated by crystal settling at low pressure will no longer retain mantle xenoliths of high pressure mineralogy.

c) Pyroxene Xenocrysts and Pyroxenite Xenoliths

The experimental evidence on the important role of aluminous pyroxenes in basalt fractionation at high pressure suggests a critical examination of the xenolithic and xenocrystal material in basalts for natural examples of high pressure accumulates. The xenoliths of pyroxenite and "eclogite" occurring in olivine nephelinite tuff at Salt Lake Crater, Oahu, have assumed significance in some discussions of the hypothesis that the earth's upper mantle is of eclogitic composition. The experimental data previously presented offer a direct explanation of the occurrence, chemistry and petrography of these xenoliths as accumulates at high pressure and temperature from an undersaturated magma (KUNO, 1964; GREEN, 1966). The inclusions show features supporting an origin as sub-calcic clinopyroxene $\pm$ olivine accumulates from undersaturated, olivine-rich basaltic magma at pressures of 13—18 kb. Cooling, following initial precipitation, would cause a decrease in solubility of Al_2O_3 in the clinopyroxene and also result in exsolution of orthopyroxene from the low-calcium clinopyroxene. High temperature aluminous pyroxenes would exsolve Al_2O_3 as spinel initially but on further cooling into the stability field of pyrope-almandine garnet, spinel and pyroxene would react to yield garnet + olivine (cf. garnet coronas around spinel) or garnet may have exsolved directly from aluminous pyroxene. We infer that the Hawaiian "eclogites" were originally high pressure, high temperature accumulates from undersaturated magma and are non-equlibrium assemblages showing partial adjustment to lower temperature but still high pressure conditions. Both olivine (minor) and clinopyroxene (major) were probably included in the initial precipitate minerals.

KUNO (1964) described aluminian bronzite (4.4% Al_2O_3) and aluminian augites (4.9—10.3% Al_2O_3, 0.5—0.9% Na_2O) as phenocrysts or xenocrysts in an alkali olivine basalt or hawaiite from Japan and concluded that these phases crystallized from the magma at high pressures. The magma composition contains 50% SiO_2, 16% Al_2O_3 and is olivine + hypersthene normative. Our experimental data suggest that liquid and crystals of these compositions could be in equilibrium at about 9 kb. KUNO (1964) also refers to a quotation by HESS (1952) of an unpublished analysis of aluminous orthopyroxene (with almost 8% Al_2O_3) in alkali olivine basalt from western Texas. JAMIESON (1966) has reported olivine phenocrysts and orthopyroxene phenocrysts and aggregates in picritic basalts from the Nuanetsi province, Rhodesia. These orthopyroxenes are interpreted by JAMIESON as products of crystallization at high pressure from a picritic magma.

We have observed very rare coarse-grained pyroxenite (opx + cpx) xenoliths in lherzolite-bearing alkali olivine basalts from western Victoria. These show complex exsolution textures consistent with a high temperature origin and may be high pressure, high temperature accumulates from their host magma. Large single crystals of black, glassy-looking clinopyroxenes are not uncommon in basalts

containing lherzolite nodules in eastern Australia and these may represent crystallization products at high pressure from their host magma.

These examples of "xenoliths" and "xenocrysts" are interpreted as natural examples of material crystallized from basaltic liquids at high pressure. Many other examples undoubtedly occur and the accumulation of data on such occurrences should provide an excellent linkage with experimental studies such as that presented in this paper.

Acknowledgements. We thank Dr. I. McDougall, Professor F. J. Turner and Mr. T. H. Green for helpful comments and criticisms of a preliminary draft of this paper, and Dr. K. S. Heier for a critical reading of this manuscript. We also thank Mrs. I. Ginn, W. Hibberson and G. Milburn for their parts in preparation of the manuscript and diagrams. W. Hibberson and A. Major assisted in many of the experimental runs.

References

Bartholomé, P.: Co-existing pyroxenes in igneous and metamorphic rocks. Geol. Mag. 98, 346—348 (1961).

Birch, F.: Elasticity and constitution of the earth's interior. J. Geophys. Research 57, 227—286 (1952).

Boyd, F. R., and J. L. England: Apparatus for phase equilibrium measurements at pressures up to 50 kb and temperatures up to 1750° C. J. Geophys. Research 65, 741—748 (1960a).

— — The quartz-coesite transition. J. Geophys. Research 65, 749—756 (1960b).

— — Effect of pressure on the melting of diopside, $CaMgSi_2O_6$ and albite $NaAlSi_3O_8$ in the range up to 30 kb. J. Geophys. Research 68, 311—323 (1963).

— — and B. T. C. Davis: Effects of pressure on the melting and polymorphism of enstatite, $MgSiO_3$. J. Geophys. Research 69, 2101—2109 (1964).

—, and J. F. Schairer: The system $MgSiO_3$—$CaMgSi_2O_6$. J. Petrology 5, 275—309 (1964).

Brothers, R. N.: Olivine nodules from New Zealand. Rept. Intern. Geol. Congr. 21st Session Norden 13, 68—81 (1960).

Clark, S. P., and A. E. Ringwood: Density distribution and constitution of the mantle. Rev. Geophys. 2, 35—88 (1964).

Compston, W., I. McDougall, and K. S. Heier: Geochemical comparison of the Mesozoic basaltic rocks of Antarctica, South Africa, South America and Tasmania. Geochim. et Cosmochim. Acta (1966) (in press).

Coombs, D. S.: Trends and affinities of basaltic magmas and pyroxenes as illustrated on the diopside-olivine-silica diagram. Min. Soc. Am. Special Paper 1, 227—250 (1963).

Davis, B. T. C.: The system enstatite-diopside at 30 kilobars pressure. Carnegie Inst. Wash. Year Bk. 62, 103—107 (1963).

— The system diopside-forsterite-pyrope at 40 kilobars. Carnegie Inst. Wash. Year Bk. 63, 165—171 (1964).

—, and F. R. Boyd: The join $Mg_2Si_2O_6$—$CaMgSi_2O_6$ at 30 kilobars pressure and its application to pyroxenes from kimberlites. J. Geophys. Research 71, 3567—3576 (1966).

—, and J. F. Schairer: Melting relations in the join diopside-forsterite-pyrope at 40 kilobars and at one atmosphere. Carnegie Inst. Wash. Year Bk. 64, 123—134 (1965).

Den Tex, E.: Gefügekundliche und geothermometrische Hinweise auf die tiefe, exogene Herkunft lherzolithischer Knollen aus Basaltlaven. Neues Jahrb. Mineral. Monatsh. 9/10, 225—236 (1963).

De Roever, W. P.: Mantelgesteine und Magmen tiefer Herkunft. Fortschr. Mineral. 39, 96—107 (1961).

— Ein Versuch zur Synthese der verschiedenen Ansichten zur Herkunft der Mafitknollen vom Maarvulkan Dreiser Weiher in der Eifel. Neues Jahrb. Mineral. Monatsh. 9/10, 243—250 (1963).

Eaton, J. P., and K. J. Murata: How volcanoes grow. Science 132, 925—938 (1960).

ELSASSER, W. M.: Early history of the earth, chap. 1, p. 1—30. In: Earth science and meteoritics in honour of F. G. HOUTERMANS, edited by J. GEISS and E. GOLDBERG. Amsterdam: North Holland Publ. Co. 1963.
ENGEL, A. E. J., and C. G. ENGEL: Composition of basalts from the Mid-Atlantic Ridge. Science 144, 1330—1333 (1964a).
— — Igneous rocks of the East Pacific Rise. Science 146, 477—485 (1964b).
— — and R. G. HAVENS: Chemical characteristics of oceanic basalts and the upper mantle. Bull. Geol. Soc. Am. 76, 719—734 (1965).
ENGEL, C. G., R. L. FISHER, and A. E. J. ENGEL: Igneous rocks of the Indian Ocean Floor. Science 150, 605—610 (1965).
FAURE, G., and P. M. HURLEY: The isotopic composition of strontium in oceanic and continental basalts: application to the origin of igneous rocks. J. Petrology 4, 31—50 (1963).
FRECHEN, J.: Die Genese der Olivinausscheidungen vom Dreiser Weiher (Eifel) und Finkengebirg (Siebengebirge). Neues Jahrb. Mineral. Abh. 79A, 317—406 (1948).
— Kristallisation, Mineralbestand, Mineralchemismus und Förderfolge der Mafitite vom Dreiser Weiher in der Eifel. Neues Jahrb. Mineral. Monatsh. 9/10, 205—225 (1963).
FURUMOTO, A. S., N. J. THOMPSON, and G. P. WOOLLARD: The structure of Koolau Volcano from seismic refraction studies. Pacific Sci. 19, 306—315 (1965).
GAST, P. W.: Terrestrial ratio of potassium to rubidium and the composition of the earth's mantle. Science 147, 858—860 (1965).
— Isotope geochemistry of volcanic rocks, to be published in: Basaltic rocks (H. H. HESS, ed.). New York: J. Wiley & Sons — Interscience 1966.
— G. R. TILTON, and C. E. HEDGE: Isotopic composition of lead and strontium from Ascension and Gough Islands. Science 145, 1181—1185 (1964).
GREEN, D. H.: Alumina content of enstatite in a Venezuelan high temperature peridotite. Bull. Geol. Soc. Am. 74, 1397—1402 (1963).
— The petrogenesis of the high temperature peridotite in the Lizard area, Cornwall. J. Petrology 5, 134—188 (1964).
— The origin of basaltic magmas; to be published in: Basaltic rocks (H. H. HESS, ed.). New York: J. Wiley & Sons — Interscience 1967.
— The origin of the "eclogites" from Salt Lake Crater, Hawaii. Earth and Planetary Sci. Letters 1, 414—420 (1966b).
—, and J. EASTON: A contribution to mineralogy of lherzolite inclusions in alkali olivine basalts from western Victoria (in preparation) 1966.
— — and A. E. RINGWOOD: Mineral assemblages in a model mantle composition. J. Geophys. Research 68, 937—945 (1963).
— — — Fractionation of basalt magmas at high pressures. Nature 201, 1276—1279 (1964).
— — — An experimental investigation of the gabbro to eclogite transformation and its petrological applications. Geochim. et Cosmochim. Acta (1967) (in press).
GREEN, T. H.: High pressure experiments on the genesis of anorthosites. (In preparation, 1966).
GREEN, T. H., D. H. GREEN, and A. E. RINGWOOD: The origin of high-alumina basalts and their relationships to quartz tholeiites and alkali basalts. Earth and Planetary Sci. Letters 2, 41—52 (1967).
— A. E. RINGWOOD, and A. MAJOR: Friction effects and pressure calibration in a pistoncylinder apparatus at high pressure and temperature. J. Geophys. Research 71, 3589—3594 (1966).
GUNN, B. M.: Differentiation in Ferrar Dolerites, Antarctica. New Zealand J. Geol. Geophys. 5, 820—863 (1962).
— Layered intrusions in Ferrar Dolerites, Antarctica. Min. Soc. Am. Special Paper 1,124—133 (1963).
— K/Rb and K/Ba ratios in Antarctic and New Zealand tholeiites and alkali basalts. J. Geophys. Research 70, 6241—6247 (1965).
— Modal and element variation in Antarctic tholeiites. Geochim. et Cosmochim. Acta 30, 881—920 (1966).
HAMILTON, E. I.: The isotopic composition of strontium in the Skaergaard intrusion, East Greenland. J. Petrology 4, 383—391 (1963).
— Distribution of some trace elements and the isotopic composition of strontium in Hawaiian lavas. Nature 206, 251—253 (1965).

Harris, P. G.: Zone refining and the origin of potassic basalts. Geochim. et Cosmochim. Acta 12, 195—208 (1957).

Haskin, L. A., F. A. Frey, R. A. Schmitt, and R. H. Smith: Meteoritic, solar and terrestrial rare-earth distributions. In: Physics and Chemistry of the Earth, vol. 7. pp. 167—321 New York: Pergamon 1966.

Hedge, C. E., and F. G. Walthall: Radiogenic strontium-87 as an index of geologic processes. Science 140, 1214—1217 (1963).

Heier, K. S.: Trace elements in feldspars — a review. Norsk. Geol. Tidsskr. 42, 415—454 (1962).

— W. Compston, and I. McDougall: Thorium and uranium concentrations, and the isotopic composition of strontium in the differentiated Tasmanian dolerites. Geochim. et Cosmochim. Acta 29, 643—659 (1965).

— I. McDougall, and J. A. S. Adams: Thorium, uranium and potassium concentrations in Hawaiian lavas. Nature 201, 254—256 (1964).

—, and J. W. Rogers: Radiometric determination of thorium, uranium and potassium in basalts and in two magmatic differentiation series. Geochim. et Cosmochim. Acta 27, 137—154 (1963).

Hess, H. H.: Orthopyroxenes of the Bushveld type, ion substitutions and changes in unit cell dimensions. Am. J. Sci. Bowen Volume 173—178 (1952).

— The oceanic crust, the upper mantle and the Mayaguez serpentinized peridotite. In: A study of serpentinite (C. A. Burk, ed.). U. S. National Acad. Science — National Research Council Publ. No. 1188, 169—174 (1964).

Holmes, A., and H. F. Harwood: Petrology of the volcanic fields east and southeast of Ruwenzori, Uganda. Quart. J. Geol. Soc. London 88, 370—442 (1932).

Jamieson, B. G.: Evidence on the evolution of basaltic magma at high pressures. Nature 212, 243—246 (1966).

Kretz, R.: Some applications of thermodynamics to co-existing minerals of variable composition. Examples: orthopyroxene-clinopyroxene and orthopyroxene-garnet. J. Geol. 69, 361—387 (1961).

Kuno, H.: High-alumina basalt. J. Petrology 1, 121—145 (1960).

— Aluminian augite and bronzite in alkali olivine basalt from Taka-sima, north Kyusyu, Japan. In: Advancing frontiers in geology and geophysics. Hyderabad: Osmania Univ. Press 1964.

— K. Yamasaki, C. Iida, and K. Nagashima: Differentiation of Hawaiian magmas. Japan. J. Geol. and Geography, Trans. 28, 179—218 (1957).

Kushiro, I.: The liquidus relations in the systems forsterite-$CaAl_2SiO_6$-silica and forsterite-nepheline-silica at high pressures. Carnegie Inst. Wash. Year Bk. 64, 103—108 (1965).

—, and H. Kuno: Origin of primary basalt magmas and classification of basaltic rocks. J. Petrology 4, 75—89 (1963).

Larsen, E. S.: Petrographic province of central Montana. Bull. Geol. Soc. Am. 51, 887—948 (1940).

Le Maitre, R. W.: Petrology of volcanic rocks, Gough Island, South Atlantic. Bull. Geol. Soc. Am. 73, 1309—1340 (1962).

Lessing, P., and E. J. Catanzaro: Sr^{87}/Sr^{86} in Hawaiian lavas. J. Geophys. Research 69, 1599—1601 (1964).

Macdonald, G. A.: Hawaiian petrographic province. Bull. Geol. Soc. Am. 60, 1541—1595 (1949).

—, and T. Katsura: Variations in the lava of the 1959 eruption in Kilauea Iki. Pacific Sci. 15, 358—369 (1961).

— — Chemical composition of Hawaiian lavas. J. Petrology 5, 82—133 (1964).

MacGregor, I. D., and A. E. Ringwood: The natural system enstatite-pyrope. Carnegie Inst. Wash. Year Bk. 63, 161—163 (1964).

Morgan, J. W., and A. D. T. Goode: Potassium abundances in some ultrabasic and basic rocks. Earth and Planetary Sci. Letters 1, 110—112 (1966).

Muir, I. D., and C. E. Tilley: Contributions to the petrology of Hawaiian basalts. I. The picrite basalts of Kilauea. Am. J. Sci. 255, 241—253 (1957).
— — The tholeiitic basalts of Mauna Loa and Kilauea. Pt. 2 of: Contributions to the petrology of Hawaiian basalts. Am. J. Sci. 261, 111—128 (1963).
— — Basalts from the northern part of the rift zone of the Mid-Atlantic Ridge. J. Petrology 5, 409—434 (1964).
Murata, K. J.: A new method pf plotting chemical analyses of basaltic rocks. Am. J. Sci. 258-A (Bradley volume), 247—252 (1960).
— H. Bastron, and W. W. Brannock: X-ray determinative curve for Hawaiian olivines of composition Fo_{76-88}. U.S. Geol. Survey Profess. Papers 525-C, 35—37 (1965).
—, and D. H. Richter: The settling of olivine in Kilauean magma as shown by lavas of the 1959 eruption. Am. J. Sci. 264, 194—203 (1966a).
— — Chemistry of the lavas of the 1959—60 eruption of Kilauea volcano, Hawaii. U.S. Geol. Survey Profess. Papers 537-A, 1—26 (1966b).
Naughton, J. L., and I. L. Barnes: Geochemical studies of Hawaiian rocks related to the study of the upper mantle. Pacific Sci. 19, 287—290 (1965).
Nixon, P. H., O. von Knorring, and J. M. Rooke: Kimberlites and associated inclusions of Basutoland: a mineralogical and geochemical study. Am. Mineralogist 48, 1090—1132 (1963).
O'Hara, M. J.: Melting of garnet peridotite and eclogite at 30 kilobars. Carnegie Inst. Wash. Year Bk. 62, 71—77 (1963a).
— The join diopside-pyrope at 30 kilobars. Carnegie Inst. Wash. Year Bk. 62, 116—118 (1963b).
— Primary magmas and the origin of basalts. Scot. J. Geology 1, 19—40 (1965).
— and E. L. P. Mercy: Petrology and petrogenesis of some garnetiferous peridotites. Trans. Roy. Soc. Edinburgh 45, 251—313 (1963).
Oxburgh, E. R.: Petrological evidence for the presence of amphibole in the upper mantle and its petrogenetic and geophysical implications. Geol. Mag. 101, 1—19 (1964).
Poldervaart, A.: Aspects of basalt petrology. J. Geol. Soc. India 3, 1—14 (1962).
— Chemical definition of alkali basalts and tholeiites. Bull. Geol. Soc. Am. 75, 229—232 (1964).
Powell, J. L., G. Faure, and P. M. Hurley: Strontium 87 abundance in a suite of Hawaiian volcanic rocks of varying silica content. J. Geophys. Research 70, 1509—1513 (1965).
—, and S. E. De Long: Isotopic composition of strontium in volcanic rocks from Oahu. Science 153, 1239—1242 (1966).
Powers, H. A.: Composition and origin of basaltic magma of the Hawaiian Islands. Geochim. et Cosmochim. Acta 7, 77—107 (1955).
Ringwood, A. E.: A model for the upper mantle. J. Geophys. Research 67, 857—867 (1962a).
— A model for the upper mantle, 2. J. Geophys. Research 67, 4473—4477 (1962b).
— The chemical composition and origin of the earth. In: Advances in earth science (P. M. Hurley, ed.), p. 287—356. Boston, U.S.A.: M.I.T. Press 1966a.
— The mineralogy of the mantle. In: Advances in earth science (P. M. Hurley, ed.), p. 357—417. Boston, U.S.A.: M.I.T. Press 1966b.
—, and D. H. Green: An experimental investigation of the gabbro-eclogite transformation and some geophysical implications. Tectonophysics 3, 383—427 (1966).
— I. D. MacGregor, and F. R. Boyd: Petrological constitution of the upper mantle. Carnegie Inst. Wash. Year Bk. 63, 147—152 (1964).
Ross, C. S., M. D. Foster, and A. T. Myers: Origin of dunites and of olivine-rich inclusions in basaltic rocks. Am. Mineralogist 39, 693—737 (1954).
Schilling, J. G., and J. W. Winchester: Rare-earths in Hawaiian basalts. Science 153, 867—870 (1966).
Strange, W. E., G. P. Woollard, and J. C. Rose: An analysis of the gravity field over the Hawaiian Islands in terms of crustal structure. Pacific Sci. 19, 381—389 (1965).

Tatsumoto, M.: Isotopic composition of lead in volcanic rocks from Hawaii, Iwo Jima and Japan. Geophys. Research 71, 1721—1733 (1966a).
— Genetic relations of oceanic basalts as indicated by lead isotopes. Science 153, 1094—1101 (1966b).
— C. E. Hedge, and A. E. J. Engel: Potassium, rubidium, strontium, thorium, uranium, and the ratio of strontium-87 to strontium-86 in oceanic tholeiitic basalt. Science 150, 886—888 (1965).
Tilley, C. E.: Some aspects of magmatic evolution. Quart. J. Geol. Soc. London 106, 37—61 (1950).
—, and H. S. Yoder: Pyroxene fractionation in mafic magma at high pressures and its bearing on basalt genesis. Carnegie Inst. Wash. Year Bk. 63, 114—121 (1964).
— —, and J. F. Schairer: Melting relations of basalts. Carnegie Inst. Wash. Year Bk. 62, 77—84 (1963).
— — — New relations on melting of basalts. Carnegie Inst. Wash. Year Bk. 63, 92—97 (1964).
— — — Melting relations of volcanic tholeiite and alkali rock series. Carnegie Inst. Wash. Year Bk. 64, 69—82 (1965).
Upton, B. G., and W. J. Wadsworth: Geology of Reunion Island, Indian Ocean. Nature 207, 151—154 (1965).
Verhoogen, J.: Petrological evidence on temperature distribution in the mantle of the earth. Trans. Am. Geophys. Union 35, 85—92 (1954).
Vilminot, J. C.: Les enclaves de peridotite et de pyroxenolite à spinelle dans le basalt du Rôcher du Lion (Chaine du Deves, Haute-Loire). Bull. soc. franç. minéral. et crist. 88, 109—118 (1965).
White, R. W.: Ultramafic inclusions in basaltic rocks from Hawaii. Beitr. Mineral. u. Petrog. 12, 245—314 (1966).
Wilkinson, J. F. G.: The geochemistry of a differentiated teschenite sill near Gunnedah, New South Wales. Geochim. et Cosmochim. Acta 16, 123—150 (1959).
Wilshire, H. G., and R. A. Binns: Basic and ultrabasic xenoliths from volcanic rocks of New South Wales. J. Petrology 2, 185—208 (1961).
Yagi, K.: Pillow lavas of Keflavik, Iceland, and their genetic significance. J. Fac. Sci., Hokkaido Univ., Ser. IV 12, 171—183 (1964).
Yoder, H. S.: Genesis of principal basalt magmas. Carnegie Inst. Wash. Year Bk. 63, 97—100 (1964).
—, and C. E. Tilley: Origin of basalt magmas: an experimental study of natural and synthetic rock systems. J. Petrology 3, 342—532 (1962).

D. H. Green and A. E. Ringwood
Department of Geophysics and Geochemistry,
Research School of Physical Sciences,
The Australian National University,
Box 4, P.O. Canberra/Australia

B4

EARTH AND PLANETARY SCIENCE LETTERS 2 (1967) 41-51. NORTH-HOLLAND PUBL. COMP., AMSTERDAM

THE ORIGIN OF HIGH-ALUMINA BASALTS AND THEIR RELATIONSHIPS TO QUARTZ THOLEIITES AND ALKALI BASALTS

Trevor H. GREEN, D. H. GREEN and A. E. RINGWOOD
Department of Geophysics and Geochemistry.
Australian National University. Canberra, Australia

Received 9 November 1966

Experimental crystallization of olivine tholeiite (20% olivine) at 9 kb shows that olivine and, to a lesser extent, orthopyroxene are the early crystallizing phases, joined at lower temperatures by clinopyroxene and plagioclase. This contrasts with atmospheric crystallization of olivine first, joined at lower temperatures by plagioclase and clinopyroxene. In high-alumina olivine tholeiite (6% olivine) however, clinopyroxene is the liquidus phase at 9 kb, joined at lower temperatures by plagioclase, while from 0-6.8 kb plagioclase is the liquidus phase joined by olivine and clinopyroxene. Alkali basalt and olivine basalt have olivine and clinopyroxene as important near-liquidus phases at 9 kb, compared with olivine and plagioclase at atmospheric pressure. Quartz tholeiite contains olivine, together with plagioclase and clinopyroxene near the liquidus at atmospheric pressure, but at 4.5 kb and 6.8 kb plagioclase and clinopyroxene alone were evident.

These results show that derivation of quartz-normative tholeiites from olivine-normative parent magmas is only possible at depths of less than 15 km, while at depths of 15-35 km high-alumina basalts of tholeiitic or alkalic affinities and only slightly enriched in silica are obtained from olivine tholeiite or olivine basalt parents. At depths of 35-60 km fractionation of olivine-rich magmas is largely governed by aluminous pyroxenes and the derivative liquids trend towards undersaturated alkali basalts.

The inter-relationships of the three major magma types, quartz tholeiite, high-alumina basalt and alkali basalt, in such volcanic provinces as Japan are explained by magma segregation or fractional crystallization over specific depth ranges. Thus alkali basalts are derived at 35-60 km depth, high-alumina basalts at 15-35 km and quartz tholeiites at less than 15 km.

1. INTRODUCTION

In classification and in petrogenetic studies of basaltic rocks, the tholeiitic basalt series and alkali basalt series have long been recognized as distinctive magma types [1]. More recently a third group of basalts, designated the high-alumina basalts, has assumed greater significance with the recognition that basalts of this type are widespread and of significant volume [2-12]. Some authors have argued that a distinctive high-alumina basalt magma is a 'primary' or 'primitive' liquid derived from the mantle. The experimental projects forming the basis of this paper are aimed at establishing mechanisms of fractionation which could relate the high-alumina basalt magmas to the tholeiitic and alkali basalt magmas, and produce a coherent pattern of basalt fractionation and inter-relationships stemming from common source materials within the upper mantle.

In a review paper in 1950, Tilley [5] recognized high-alumina basalt as a distinctive type. Tilley's recognition was based on aphyric basalts characterized by Al_2O_3 contents of 16-18%, occurring in the Medicine Lake area of California [2-4]. Kuno [6], in a more detailed petrographical and chemical study of the high-alumina basalt type, pointed to many examples of high-alumina basalts in Japan, and proposed that the high-alumina basalt type represented a primary magma series of similar status to the alkali basalt magma series and the tholeiitic magma series. Kuno [6] considered that the high-alumina basalt primary magma was derived by partial melting of the mantle at depths intermediate between the depths of origin of tholeiite and alkali basalt magmas. He pointed out that high-alumina basalts may have either tholeiitic or alkalic affinities and that the three magma types are completely gradational. However by plotting Al_2O_3 against $Na_2O + K_2O$ for various ranges of silica content, Kuno illustrated the differences in chemistry between tholeiites, high-alumina basalts and alkali basalts and defined compositional fields for the magma types (cf. fig. 3).

Table 1
Compositions and CIPW norms of the synthetic basaltic glasses used in the experimental work.

Rock type	Olivine Tholeiite I	Olivine Tholeiite II	Olivine Tholeiite III	Olivine Tholeiite IV	Saturated Tholeiite	Olivine Basalt	Alkali Basalt
SiO_2	46.9	49.7	50.3	51.5	52.9	47.1	45.4
TiO_2	2.0	1.6	1.7	1.7	1.5	2.3	2.5
Al_2O_3	13.1	15.9	17.0	16.7	16.9	14.2	14.7
Fe_2O_3	1.0	0.5	1.5	0.4	0.3	0.4	1.9
FeO	10.1	8.1	7.6	8.1	7.9	10.6	12.4
MnO	0.2	0.2	0.1	0.1	0.2	0.2	0.2
MgO	14.5	10.5	7.8	7.7	7.0	12.7	10.4
CaO	10.2	10.7	11.4	11.5	10.0	9.9	9.1
Na_2O	1.7	2.6	2.8	2.8	2.7	2.2	2.6
K_2O	0.1	0.2	0.2	0.2	0.6	0.4	0.8
P_2O_5	0.2	-	-	-	-	-	-
CIPW norms							
Qz	-	-	-	-	1.3	-	-
Or	0.6	1.2	1.1	1.1	3.5	2.7	4.5
Ab	14.7	22.0	23.7	23.2	22.8	18.9	18.0
Ne	-	-	-	-	-	-	2.2
An	27.6	31.1	33.3	32.7	32.2	27.3	26.2
Di	17.0	17.7	18.9	19.8	14.2	17.6	15.7
Hy	12.3	9.7	11.9	15.9	22.6	1.3	-
Ol	21.9	14.5	6.2	4.1	-	27.2	25.8
Ilm	3.8	3.0	2.2	3.2	2.8	4.4	4.8
Mt	1.4	0.7	3.2	0.6	0.4	0.6	2.9
Ap	0.5	-	-	-	-	-	-

Yoder and Tilley [13] criticized Kuno's proposal that high-alumina basalt represented a primary magma type and proposed that high-alumina basalts were derived from alkali or tholeiite basalt parent magmas. They also suggested that the high-alumina character could be attributed to a high normative plagioclase content and concluded that some process delaying the crystallization of plagioclase from basaltic magma could explain the derivation of high-alumina basalts. This could be achieved by high water pressure tending to increase the plagioclase content of residual liquids during fractional crystallization [13-16]. However, Kuno [6] had previously argued that the lack of any evidence for higher water pressure in the natural high-alumina basalts was very unfavourable to this hypothesis.

Recent work on dredge samples from ocean ridge areas [7-12] has shown that high-alumina basalts have a far more widespread significance than was previously recognized. Engel et al. [9] maintain that these basalts, which they termed oceanic tholeiites, are the principal or possibly the only primary magma generated in the upper mantle under the oceans. These authors have suggested that the widespread flows of oceanic tholeiites at abyssal depths in the oceans tend to change to flows with alkalic affinities at shallower depths, and finally to distinctly alkali basalts on oceanic islands [7-10].

High pressure experimental work on several basalt compositions ranging from olivine tholeiite to high-alumina olivine tholeiite and high-alumina quartz tholeiite, and olivine basalt to alkali olivine basalt is described in this paper. The compositions of the basaltic glasses prepared are given in table 1. The olivine-rich tholeiite (column I) is close to estimates of a parental magma for the 1959 Kilauea Iki lava lake [17], and lies centrally within the olivine tholeiite volume of fig. 1. The oceanic tholeiite

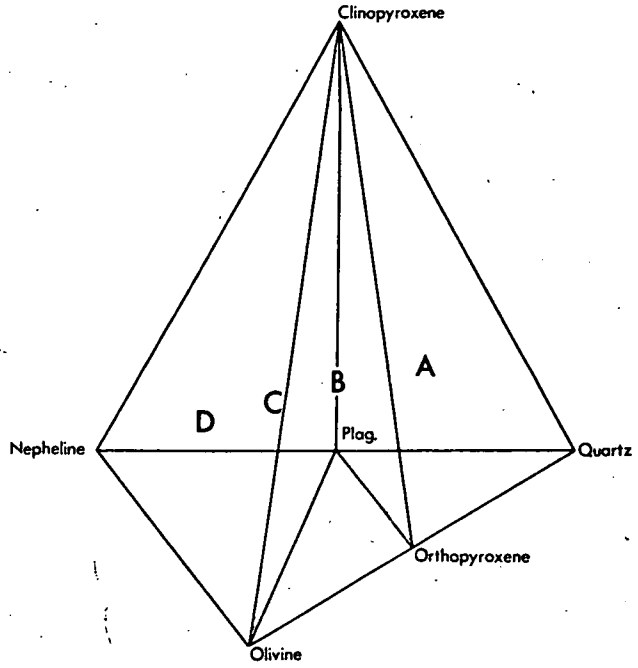

Fig. 1. Basalt tetrahedron showing the oversaturated quartz tholeiite field (a), the olivine tholeiite field (b), the olivine basalt field (c) and the alkali basalt trending to basanite field (d). The shaded olivine-plagioclase-clinopyroxene plane marks the critical plane of silica undersaturation while the shaded orthopyroxene-plagioclase-clinopyroxene plane marks the plane of silica saturation.

or high-alumina tholeiite (column III) composition is almost identical with the average oceanic tholeiite of Engel et al. [9] and is a particularly important composition in discussions of the genesis and inter-relationships of the high-alumina basalts. This composition contains only 6% normative olivine. To provide a composition intermediate between olivine tholeiites I and III, an olivine tholeiite composition with 14% normative olivine and moderately high alumina content was also prepared (column II). Two additional compositions, both with high alumina contents, but with 4% normative olivine (column IV) and 2% normative quartz (column V) respectively, were prepared to investigate the relationships between the high-alumina basalt and the quartz tholeiite magma types.

The olivine basalt (table 1, column IV) and alkali olivine basalt (column VI) are close to magma compositions falling along the direct fractionation trend between olivine-rich tholeiites (e.g. column I) and basanites [19]. This fractionation trend has been shown by Green and Ringwood [18,19] to be operative in the 12 to 18 kb pressure range and the compositions are important in the present context in illustrating fractionation trends in liquids ascending from 35-60 km depth and undergoing further fractionation in shallower regions.

The results of this experimental work demonstrate that high-alumina basalts of either tholeiitic or alkalic affinities may be derived by simple partial melting or fractional crystallization processes in a strictly limited range of depths in the mantle. When combined with other experimental work on the origin of basalts [18-20], a simple unified picture on the origin of the various major basalt magma types emerges.

2. EXPERIMENTAL

The basalt glasses were prepared either from natural analyzed basalts or from mixes of A.R. chemicals by melting under controlled redox conditions. After fine grinding, analyses for FeO and Fe_2O_3 contents (A.J. Easton and E.Kiss, analysts) gave a further check on the chemical compositions. The basaltic compositions have been crystallized at closely spaced temperature intervals between the liquidus and solidus at pressures up to 18 kb, using a piston-cylinder, high pressure and high temperature apparatus similar to that described by Boyd and England [21,22]. The experimental techniques involved have been described fully elsewhere [23]. A pressure correction of -10% has been applied [24], but since the pressure range 0-9 kb is below the range of pressures for which this apparatus is best suited, the resulting pressures on the sample may not be known to the ±3% accuracy claimed for the 15-40 kb pressure range. However this uncertainty will not affect the overall features of fractional crystallization observed with increasing pressure.

At the conclusion of a run the nature and proportion of mineral phases present have been determined by optical and X-ray methods. In suitable runs, where the crystals are large enough, quantitative analysis of the crystals has been carried out using an electron probe microanalyzer (Applied Research Laboratories, model EMX). The analyses of actual crystal phases present in the partial melting runs enables detailed calculation of fractionation trends in the 0-9 kb pressure range.

3. RESULTS

The most important results are summarized in the accompanying diagram (fig. 2).

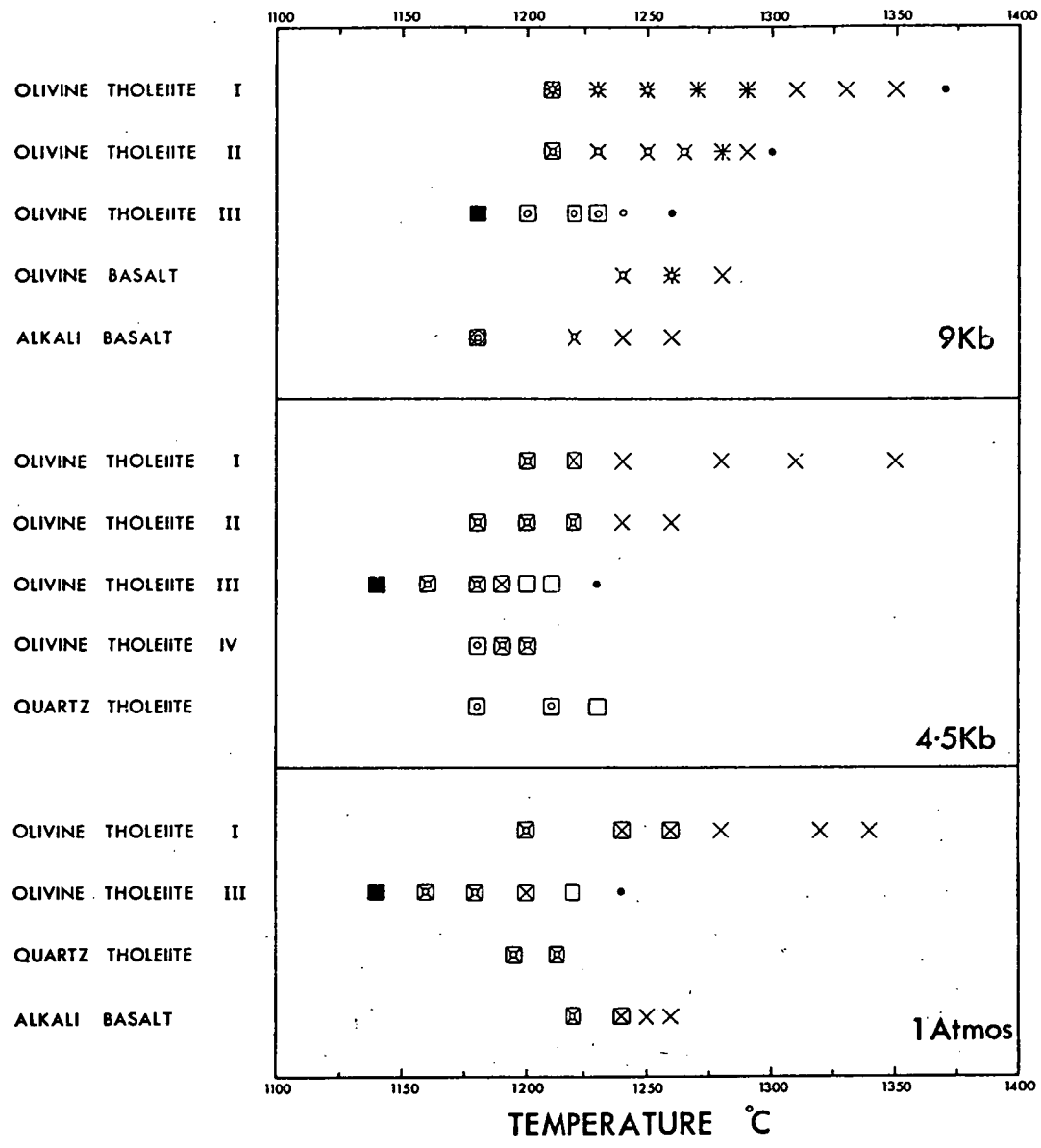

Fig. 2. Results of the atmospheric, 4.5 kb and 9 kb high temperature experimental runs.
• Above liquidus. ■ Below solidus. Phases co-existing with liquid: × Olivine. + Orthopyroxene. □ Plagioclase. o Clinopyroxene. ◇ Spinel.

3.1. *Crystallization at atmospheric pressure*

The sequence of crystallization in olivine tholeiites I, III, quartz tholeiite and alkali basalt has been investigated at atmospheric pressure.

In olivine tholeiite I, olivine is the liquidus phase at 1340°C and is joined by plagioclase (1260°C) and then clinopyroxene (1200°C). In olivine tholeiite II, a similar sequence of crystallization at atmospheric pressure is indicated by comparison with results at 2.3 kb (olivine at 1230°C joined by plagioclase and clinopyroxene below 1190°C). Plagioclase is the liquidus phase (1220°C) in olivine tholeiite III, and is followed by olivine (1200°C) and clinopyroxene (1180°C). In the quartz tholeiite composition, plagioclase, clinopyroxene and olivine are present at 1212°C and 1195°C. Finally in the alkali basalt, olivine is present on the liquidus ($\geq$ 1250°C) joined by plagioclase (1240°C) and clinopyroxene (1220°C). In all compositions at atmospheric pressure where olivine is the only phase crystallizing, the degree of crystallization is slight (< 10%) but when it is joined by a second phase (plagioclase or clinopyroxene) the degree of crystallization increases rapidly.

3.2. *Crystallization at* 4.5 *kb*

The crystallization sequence at 4.5 kb has been studied in the five tholeiite compositions and in each of the olivine tholeiites (except IV) a similar sequence to that found at atmospheric pressure has been obtained. The only significant difference is that the liquidus temperatures and temperatures of appearance of phases are slightly higher at 4.5 kb than at atmospheric pressure. In the olivine tholeiite IV however, at 1200° plagioclase and minor olivine and clinopyroxene were present but at 1190°C and 1180°C only plagioclase and clinopyroxene were evident. For comparison, a run at 2.3 kb and 1180°C on this composition showed common plagioclase and olivine and only minor clinopyroxene. In the high-alumina quartz tholeiite plagioclase appears at 1230°C and is joined by clinopyroxene at 1210°C. The same two phases are present at 1180°C. Olivine was not identified in this composition at 4.5 kb.

3.3. *Crystallization at* 6.8 *kb*

In olivine tholeiite III, plagioclase is the liquidus phase (1230°C) but it is joined by both olivine and clinopyroxene at only 10°C lower temperature. This compares with a 20°C temperature interval between the appearance of the three phases in this composition at 4.5 kb and reflects the enlargement of the field of crystallization of clinopyroxene with increasing pressure. In the olivine tholeiite IV, plagioclase is also the liquidus phase at 1230°C and is joined by clinopyroxene at lower temperatures (1220°C and 1210°C). No olivine was identified in this composition at this pressure. A similar sequence of crystallization occurs in the high-alumina quartz tholeiite composition with plagioclase appearing at 1230°C followed by pyroxene at 1220°C. No olivine is evident.

3.4. *Crystallization at* 9 *kb*

In olivine tholeiite I olivine is the liquidus phase at 1350°C and the next phase to appear is orthopyroxene at 1290°C followed by clinopyroxene at 1250°C; plagioclase does not definitely appear until just above the solidus at 1210°C. In olivine tholeiite II, olivine and minor orthopyroxene are the near-liquidus phases at 1280°C and are joined by clinopyroxene at 1265°C, while plagioclase again only appears at 1210°C, just above the solidus. In both compositions the degree of crystallization increases markedly with the appearance of clinopyroxene. Clinopyroxene is the liquidus phase at 1240°C in olivine tholeiite III, and it is followed by plagioclase at 1230° C. Olivine does not appear in this composition at 9 kb. In the olivine basalt, olivine alone is present at 1280°C and is joined by clinopyroxene and orthopyroxene at 1260°C but at 1240°C no orthopyroxene is evident. The alkali olivine basalt has olivine as the liquidus phase (1260°C) joined by clinopyroxene (1220°C) and by plagioclase and spinel (1180°C) just above the solidus.

The experimental runs at 9 kb on olivine tholeiites I, II, alkali olivine basalt and olivine basalt all show a decrease with falling temperature in the amount of olivine present after clinopyroxene appears as a crystalline phase. This suggests that olivine partially reacts with liquid to precipitate aluminous calcic clinopyroxene (ref. [19], pp. 142-143, 157).

3.5. *Crystallization at pressures greater than* 9 *kb*

The fractional crystallization of olivine-rich basaltic magmas has been described in detail elsewhere [19]. The main result is that above 9 kb olivine is replaced as the liquidus phase by orthopyroxene and/or clinopyroxene in these compositions (olivine tholeiite I, olivine basalt and alkali olivine basalt).

3.6. *Summary of results*

(a) Olivine occurs in the partial melting field of the quartz tholeiite at atmospheric pressure but is absent at 4.5 and 6.8 kb. In olivine tholeiite IV, olivine is present near the liquidus, but is not evident near the solidus at 4.5 kb. It is absent in this composition at 6.8 kb.

(b) The field of crystallization of olivine becomes smaller as the pressure is increased from 0-9 kb. The degree of crystallization is low where olivine is the only crystallizing phase.

(c) The liquidus olivine at 9 kb may partially or completely react with liquid at lower temperatures to precipitate clinopyroxene.

(d) There is an expansion of the field of crystallization of ortho- and clinopyroxene as the pressure is increased from 0 to 9 kb. This is accompanied over the same pressure range by the suppression of crystallization of plagioclase to near-solidus temperatures in all compositions except olivine tholeiites III, IV and quartz tholeiite. Plagioclase is the liquidus phase in olivine tholeiite III, up to 6.8 kb, then at 9 kb, where clinopyroxene is the liquidus phase, plagioclase is present at only 10°C below the liquidus.

4. PRINCIPAL FRACTIONATION TRENDS

4.1. *Low pressure regime*

The presence of olivine in the quartz tholeiite composition at atmospheric pressure and its

absence at 4.5 kb, indicates that it is only possible for liquids fractionating from olivine tholeiites to cross the plane of silica saturation (fig. 1) into the quartz tholeiite field at depths corresponding to pressures of less than 4.5 kb. The occurrence of olivine near the liquidus at 4.5 kb in the olivine tholeiite IV composition illustrates that the fractionation trend towards the plane of silica saturation persists to greater depths than those corresponding to this pressure in compositions with some normative olivine. Thus olivine-normative tholeiitic compositions may fractionate towards the plane of silica saturation (fig. 1) at depths of up to about 20 km, but the plane can only be crossed, producing quartz normative tholeiitic liquid derivatives, by fractionation at depths of less than about 15 km.

4.2. *Moderate pressure regime*

As the pressure increases from 4.5 to 9 kb the field of crystallization of pyroxenes is enlarged at the expense of the crystallization of plagioclase and, to some extent, olivine (e.g. olivine tholeiite III). The effect of co-precipitation of olivine and low-calcium pyroxenes is to produce derivative liquids with relatively constant SiO_2 content (47-50% SiO_2), high Al_2O_3 (15-17% Al_2O_3) and with slightly increasing alkali content. Thus the derivative lower temperature liquids from the olivine tholeiite compositions are high-alumina olivine tholeiite types (with lower normative olivine content than the parent magma). In terms of the basalt tetrahedron (fig. 1) the residual liquids move directly towards the plagioclase apex of the olivine tholeiite volume. For parent magma compositions initially near the critical plane of silica undersaturation (e.g. olivine basalt) similar fractionation processes take place with the resulting main fractionation trend towards the plagioclase apex, but in addition slight movement towards the critical plane of silica undersaturation occurs. The resulting liquids are of high-alumina type with alkali affinities. In the case of the fractionation of alkali olivine basalt at 9 kb separation of olivine and pyroxene yield liquids high in alumina but the alkali content is too high for these liquids to be classed as high-alumina basalts according to Kuno's diagrams [6] (see fig. 3).

For the olivine tholeiite compositions the limit of the Al_2O_3 enrichment trend is close to olivine tholeiite III. In this composition the relatively early appearance of plagioclase would produce lower alumina contents in derivative liquids at 9 kb. Extraction of minor clinopyroxene (the liquidus phase in olivine tholeiite III at 9 kb) before plagioclase appears could carry the alumina enrichment trend a little further than this composition, but liquids obtained in this way would be lower in lime than those derived by fractionation of olivine and orthopyroxene alone.

The apparent reaction relationship between olivine and clinopyroxene at 9 kb in the olivine-rich basalts indicates that it is possible for these liquids to fractionate by separation of olivine and some pyroxene to yield derivative liquids which have clinopyroxene instead of olivine as their liquidus phase. These derivative liquids will be high-alumina olivine-poor tholeiites similar to olivine tholeiite III. Although olivine plays no part in the crystallization of such compositions at 9 kb, at lower pressures olivine may appear in the melting interval at higher temperatures than clinopyroxene.

Thus the liquid compositions produced by fractionation of basaltic compositions in the pressure range 4.5-9 kb are characterized by high-alumina contents. If these liquids undergo further fractionation by separation of both olivine and plagioclase at less than 4.5 kb, quartz-normative compositions with normal alumina contents may result. There is no fractionation trend from high-alumina tholeiite to alkali basalt under the experimental conditions applied in this work.

4.3. *Higher pressure regime*

Both orthopyroxenes and clinopyroxenes separating from the olivine-rich basalts in the 12-20 kb range are rich in Al_2O_3. Fractional crystallization by separation of these magnesian and aluminous pyroxenes gives derivative liquids of decreasing SiO_2 content, only slightly increasing Al_2O_3 content and rather rapidly increasing alkali content. The fractionation trends are from parental olivine tholeiite compositions (similar to olivine tholeiite I, table 1) to derivative olivine basalt and alkali olivine basalt compositions. This spectrum of basaltic liquids may further fractionate at lower pressures, e.g. to high-alumina compositions in the 4.5-9 kb range, but the fractionation trends [18, 19] in the 12-20 kb range do not lead to residual liquids of high-alumina type.

4.4. *Calculation of fractionation trends*

Although the high pressure experiments have been mainly carried out at 9 kb, it is likely that over a pressure range of 5-10 kb the same olivine tholeiite or olivine basalt parent magma may fractionate to yield high-alumina basalts of tholeiitic or alkalic affinities respectively. Over

Table 2
Calculated derived liquid compositions for olivine tholeiite I, II, III and alkali basalt at 9 kb.
Results for olivine tholeiite I and alkali basalt from Green and Ringwood [19].
(Ol = olivine, Cpx = clinopyroxene, Opx = orthopyroxene, plag = plagioclase.)

Rock type	Olivine tholeiite I				Olivine tholeiite II			Olivine tholeiite III			Alkali basalt	
Temperature (°C)		1290	1250	1230		1280	1265		1230	1220		1220
Nature and estimated % of crystal	Nil (initial liquid)	11% Ol	12% Ol 3% Opx	12% Ol 4% Opx 14% Cpx	Nil	3% Ol 1% Cpx	4% Ol 12% Cpx	Nil	10% Cpx	20% Cpx 10% plag	Nil	5% Ol 10% Cpx
Composition												
SiO_2	46.9	47.6	47.6	47.3	49.7	50.0	50.1	50.3	50.3	49.9	45.4	45.3
TiO_2	2.0	2.3	2.4	2.9	1.6	1.6	1.8	1.7	1.8	2.1	2.5	3.0
Al_2O_3	13.1	14.8	15.2	16.1	15.9	16.5	17.8	17.0	17.9	17.4	14.7	16.2
Fe_2O_3	1.0	1.1	1.2	1.5	0.5	0.5	0.6	1.5	1.7	2.1	1.9	2.2
FeO	10.1	9.8	9.6	9.5	8.1	8.2	8.5	7.6	7.9	9.6	12.4	12.4
MnO	0.2	0.2	0.2	0.2	0.2	0.2	0.2	0.2	0.2	0.2	0.2	0.2
MgO	14.5	10.5	9.5	7.2	10.5	9.2	7.7	7.8	6.8	6.3	10.4	7.7
CaO	10.2	11.4	11.8	12.4	10.7	10.9	10.1	11.4	10.8	10.0	9.1	9.0
Na_2O	1.7	2.0	2.0	2.5	2.6	2.7	3.0	2.8	3.0	3.0	2.6	3.1
K_2O	0.1	0.1	0.1	0.1	0.2	0.2	0.2	0.2	0.2	0.3	0.8	0.9
P_2O_5	0.2	0.2	0.2	0.3	-	-	-	-	-	-	-	-
CIPW norm of liquid phase												
Or	0.6	0.7	0.7	0.8	1.2	1.2	1.2	1.1	1.2	1.5	4.5	5.5
Ab	14.7	16.5	16.8	21.0	22.0	22.8	25.4	23.7	25.4	25.4	18.0	19.0
An	27.6	31.1	32.1	32.4	31.1	32.4	34.5	33.3	34.8	33.3	26.2	27.5
Ne	-	-	-	-	-	-	-	-	-	-	2.2	3.9
Di	17.0	19.2	20.2	22.5	17.7	17.6	12.6	18.9	15.3	13.4	15.7	14.2
Hy	12.3	13.8	12.9	5.2	9.7	10.4	12.2	11.9	12.9	15.7	-	-
Ol	21.9	12.2	10.5	10.1	14.5	11.9	9.7	6.2	5.1	4.5	25.8	21.0
Ilm	3.8	4.3	4.6	5.5	3.0	3.0	3.4	2.2	2.5	3.0	4.8	5.7
Mt	1.4	1.6	1.8	2.1	0.7	0.7	0.9	3.2	3.4	4.0	2.9	3.2
Ap	0.5	0.5	0.5	0.6	-	-	-	-	-	-	-	-

this pressure range the relative proportions of olivine and pyroxenes crystallizing from the different compositions will vary, so that high-alumina compositions of slightly different SiO_2 and CaO contents and differing normative nepheline, olivine and hypersthene contents may accordingly be formed, depending on the pressure at which fractionation occurs.

The actual compositions of derivative liquids can be determined by measuring the compositions of crystallizing phases using the electron probe microanalyzer, estimating the relative proportions of these phases present and then calculating the composition of the residual liquid. The results of these calculations are given in table 2.

Examination of table 2 shows that the liquid derived from olivine tholeiite I with only 15% crystallization closely approaches the composition of olivine tholeiite II. In turn the liquid derived from olivine tholeiite II with 16% crystallization is very similar to the olivine tholeiite III composition. The termination of the alumina-enrichment trend from olivine tholeiite I to III is indicated by the calculated liquid composition after 10% crystallization of clinopyroxene from olivine tholeiite III. For greater degrees of crystallization plagioclase will appear halting

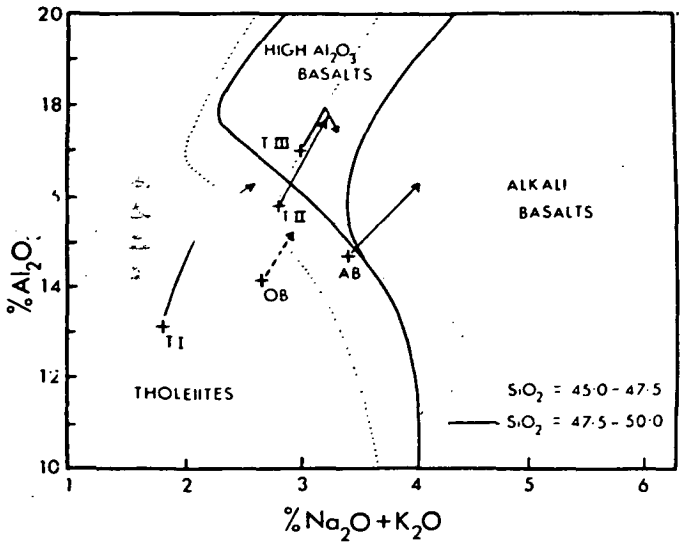

Fig. 3. Diagram for total alkalies against alumina for the compositions used in the experimental study (table 1). Calculated fractionation trends from table 2 are also plotted, as well as predicted trends. (Basalt field boundaries from Kuno [6].)

T I = olivine tholeiite I
T II = olivine tholeiite II
T III = olivine tholeiite III
OB = olivine basalt
AB = alkali basalt
⟶ calculated fractionation trend
⇢ predicted fractionation trend
····· SiO_2 = 45.0-47.5
— SiO_2 = 47.5-50.0

the alumina-enrichment trend. The liquid derived from the alkali olivine basalt also shows a high-alumina content, and similarly the liquid derived from the olivine basalt would also have a high-alumina content, although this could not be verified by analysis of the crystalline phases because of their small size (olivine only could be analyzed at 9 kb).

The fractionation trends to high-alumina compositions are best illustrated by plotting the initial and derived liquid compositions on Kuno's [6] Al_2O_3 against Na_2O + K_2O diagrams (fig. 3). These diagrams clearly distinguish tholeiitic, high-alumina and alkali magma types for different ranges of SiO_2 content and show the fractionation trends at 9 kb extending into the high-alumina field.

5. FRACTIONAL MELTING

In the previous sections the fractional crystallization of various basaltic compositions has been described and these results applied to determination of liquid trends resulting from fractional crystallization in closed systems at different pressures. In this section we consider the problem of formation of the different types of basalt magma in the mantle by direct fractional melting followed by magma segregation at different depths. Provided the nature of the crystallizing phases are the same, fractional melting may be considered as the reverse process of fractional crystallization. The parent mantle from which basalt magmas may be derived is believed to be equivalent in composition to a mixture of approximately 3 parts of peridotite to 1 part of basalt (termed pyrolite) [19, 25]. This pyrolite composition crystallizes essentially as olivine + aluminous enstatite + aluminous sub-calcic clinopyroxene for depths between about 35 and 100 km with plagioclase probably appearing at near-solidus temperatures between 15 and 35 km [19, 25]. The experimental work in the 0-18 kb range on the basalt compositions described in this paper showed that olivine and aluminous pyroxenes, in varying proportions, were the key phases in governing the fractionation trends connecting the various main magma types. Thus the phases crystallizing from the basalts studied are similar to the phases in the pyrolite at corresponding pressures, so that the fractional crystallization results should be applicable to the reverse case of fractional melting of pyrolite.

There have been many suggestions for mechanisms causing partial melting and magma formation in the upper mantle, but the most generally satisfactory process is the model involving fractional melting connected with rising "convection" cells in the mantle [19, 27, 28]. A crystal-liquid mush will result from the onset of partial melting, but as long as the crystals and liquid remain together, equilibrium between the crystals and liquid will be maintained over the changing pressure-temperature conditions caused by the upward movement of the mush. As partial melting during the upward "convective" motion proceeds, a critical point will be reached at which liquid becomes segregated from the complementary residual crystals. The degree of melting required before separation takes place will depend on the physical conditions but may well range between 20-40% by volume. The resulting magma body will then evolve independently of the refractory residuum with which it was originally associated. The depth at which partial melting begins is not significant in governing the nature of the liquid finally extruded at the earth's surface. Instead, the depth at which the magma segregation takes place and the subsequent rate of progress (governing the amount of fractional crystallization of the magma) to the

earth's surface are the key factors in governing the composition of the magma finally extruded.

5.1. *Depth of magma segregation* 0-15 *km*

Application of results on the quartz tholeiite and olivine tholeiite IV indicate that magma segregation under pressure-temperature conditions corresponding to these depths would yield a low melting quartz tholeiite liquid fraction and a refractory dunite residuum. If segregation is incomplete then pseudostratiform gabbro-peridotite complexes, or stratiform anorthosite-gabbro-peridotite complexes may result.

5.2. *Depth of magma segregation* 15-35 *km*

In sections 3.4, 4.2 it was shown that in olivine tholeiites I, II, olivine basalt and alkali olivine basalt, olivine and moderately low-alumina orthopyroxene are the near-liquidus phases at depths of 15-35 km and these crystal phases are in equilibrium with high-alumina basaltic liquids. Thus fractional crystallization at these depths led to alumina enriched liquids. Similarly in the reverse case of partial melting of pyrolite at these depths and at the same temperatures, high-alumina liquids will be in equilibrium with an olivine + orthopyroxene crystalline fraction, though in this case the bulk composition will probably consist of 60% olivine, 15% orthopyroxene and about 25% high-alumina basaltic liquid. Thus segregation of liquid from partially melted pyrolite at these depths will yield high-alumina basalt liquids, leaving a refractory olivine + pyroxene residuum (note the Ol/Px ratio in this residuum is higher at this depth range than the Ol/Px ratio in the 35-60 km depth range discussed below; also the alumina content of the pyroxene in this residuum is lower than in pyroxenes found in residua formed at greater depths [19]). The liquid so formed may rise to the surface as high-alumina basalts or may undergo fractional crystallization at shallow levels (0-15 km) yielding quartz tholeiite derivative liquids complementary to residual stratified anorthosite-peridotite complexes.

5.3. *Depth of magma segregation* 35-60 *km*

The presence of olivine and aluminous orthopyroxene near the liquidus in picrite [19] and aluminous orthopyroxene on and near the liquidus in olivine tholeiite I at 12-18 kb indicates that for a fairly large degree of partial melting of pyrolite, magma segregation at these depths will yield olivine tholeiite magma with a residuum of olivine and some orthopyroxene. This magma may be extruded as olivine tholeiite or it may undergo fractional crystallization at shallower levels as outlined previously (sections 4.1, 4.2). However with a smaller degree of partial melting a much larger proportion of aluminous enstatite ± aluminous clinopyroxene is left in the unmelted residuum and the composition of the liquid is that of an olivine-rich alkali basalt. These relationships are discussed in greater detail elsewhere [19]. The alkali basalt may also undergo further fractionation at shallower levels (sections 4.1, 4.2).

6. ORIGIN OF HIGH-ALUMINA BASALTS

As described in sections 4 and 5 the results of this experimental work show that the critical factor in explaining the derivation of high-alumina basalts is the depth (about 15-35 km) at which magma segregation from partially melted pyrolite or the depth (again about 15-35 km) at which fractional crystallization of parent olivine tholeiite or alkali basalt takes place. No outside influence of water pressure need be called upon to explain the alumina enrichment trend [13-16].

The voluminous high-alumina tholeiites (oceanic tholeiites) described from dredge samples from the ocean floor at around 3000 metres depth on the mid-oceanic ridges (Mid-Atlantic Ridge, Indian Ocean ridges and the East Pacific Rise) deserve special consideration because of their widespread occurrence and distinctive chemical characteristics [7-12]. They have an overall uniform composition in terms of major element chemistry and have minor and trace element contents typical of 'primitive' material [9]. The experimental work described in this paper and its application to fractional melting and crystallization processes in the upper mantle show that large scale magma segregation from partially melted pyrolite at a depth of about 20-30 km will produce high-alumina basaltic liquids. If these liquids move rapidly to the surface then apart from some minor crystallization of olivine, there will be little chance for major fractionation of the magma at shallower levels, or for the selective reaction and contamination between magma and wall rocks which would cause modification of the 'primitive' trace element distribution [19].

Alkali basalts typically cap the oceanic tholeiites either on volcanic oceanic islands or on seamounts. The experimental data (sections 3, 4) indicate that these basalts were probably derived by magma segregation or fractional crystallization processes at greater depths than

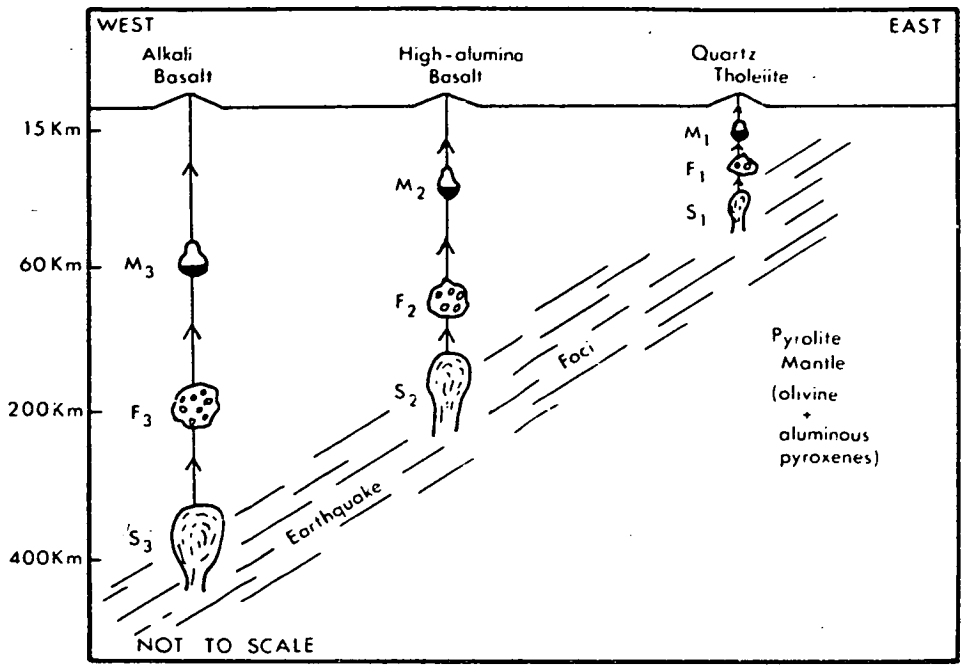

Fig. 4. Diagrammatic profile across Japan (from Kuno [29]) showing the interpreted relationship between the depth of earthquake foci. the depth of initial upward movement of pyrolite, the depth of magma segregation and the nature of the basalt magma erupted at the earth's surface.

S_1, S_2, S_3 = loci of initial upward movement of pyrolite mass
F_1, F_2, F_3 = beginning of partial melting
M_1, M_2, M_3 = depths at which magma segregation occurs
[N.B. Nature of the basalt erupted at the surface depends on the depth of magma segregation (M_1, M_2, M_3), not on the depth of onset of partial melting (F_1, F_2, F_3).]

the oceanic tholeiite. Our results show that there is no apparent way in which alkali basalt can form by fractional crystallization processes from oceanic tholeiite (equivalent to olivine tholeiite III of this work, section 4.2).

Similar arguments to those outlined for the origin of the oceanic tholeiites may also be applied to explain the origin of the high-alumina basalts of the Pololu Series, Hawaii [26] and the high-alumina basalts of Japan and California.

7. GENETIC RELATIONSHIPS BETWEEN QUARTZ THOLEIITES, HIGH-ALUMINA BASALTS AND ALKALI BASALTS

Kuno [6, 29] has described field relationships between alkali basalts, high-alumina basalts (of both alkalic and tholeiitic affinities) and tholeiites in Japan. He points out that the alkali basalt province falls to the west of a boundary line separating areas of earthquake foci at depths of greater than 200 km (west of boundary line) from those at shallower depths, while the tholeiitic basalt province corresponds to the zone of shallower earthquake foci at 50-200 km depth (east of the boundary line). The high-alumina basalts fall in an area approximately intermediate between these two zones. Kuno maintained that there was a definite link between the depth of earthquake foci and the basalt magma type and proposed that alkali basalt magmas were derived at depths greater than 200 km, tholeiitic magmas at depths less than 200 km and high-alumina magmas at intermediate depths between the alkali basalts and tholeiites.

Our work supports Kuno's view that the depth of origin governs the basalt type produced (fig. 4) but the actual depths of origin interpreted from our results are grossly different from Kuno's figures (e.g. magma segregation or fractional crystallization at depths of

(1) 35-60 km alkali basalts
(2) 15-35 km high-alumina basalts
(3) 0-15 km quartz tholeiites).

Deep earthquake foci may be related to the upward movement of a pyrolite mass which eventually partially melts at higher levels and finally undergoes magma segregation (fig. 4). The depth at which magma segregation takes place is critical in governing the composition of the basalt finally extruded. Magma segregation

is only likely after substantial (e.g. 20-40%) partial melting, and the degree of partial melting will largely be governed by the depth from which the rising mass originated, as masses originating from greater depths will possess more superheat and undergo greater melting at shallower levels. Hence alkali basalts may be derived from pyrolite masses rising from great depths which have then undergone sufficient partial melting at 35-60 km depth to allow magma segregation at these levels, while the other basalt types are derived from pyrolite masses which initially rise from shallower levels and do not undergo sufficient partial melting to allow magma segregation until depths of less than 35 km are reached. Thus on this model the correlation between earthquake foci and magma type may still be explained, though not by direct magma segregation at the depths of earthquake foci as proposed by Kuno [6, 29].

REFERENCES

[1] W. Q. Kennedy, Trends of differentiation in basaltic magmas, Am. J. Sci. 25 (1933) 239.

[2] H. A. Powers, The lavas of the Modoc Lava-Bed quadrangle, California, Am. Min. 17 (1932) 253.

[3] H. Williams, Geology of the Lassen Peak National Park, California, Univ. Calif. Dept. Geol. Sci. 21 (1932) 195.

[4] C. A. Anderson, Volcanoes of the Medicine Lake Highland, California, Univ. Calif. Dept. Geol. Sci. (1941) 347.

[5] C. E. Tilley, Some aspects of magmatic evolution, Quart. J. Geol. Soc. London 106 (1950) 37.

[6] H. Kuno, High-alumina basalt, J. Petrol. 1 (1960) 121.

[7] A. E. J. Engel and C. G. Engel, Composition of basalts from the Mid-Atlantic Ridge, Science 144 (1964) 1330.

[8] A. E. J. Engel and C. G. Engel, Igneous rocks of the East Pacific Rise, Science 146 (1964) 477.

[9] A. E. J. Engel, C. G. Engel and R. G. Havens, Chemical characteristics of oceanic basalts and the upper mantle, Bull. Geol. Soc. Am. 76 (1965) 719.

[10] C. G. Engel, R. L. Fisher and A. E. J. Engel, Igneous rocks of the Indian Ocean floor. Science 150 (1965) 605.

[11] G. D. Nicholls, A. J. Nalwalk and E. E. Hays, The nature and composition of rock samples dredged from the Mid-Atlantic Ridge between 22°N and 52°N, Marine Geol. 1 (1964) 333.

[12] J. D. H. Wiseman, The John Murray Expedition 1933-'34, Publ. Brit. Mus. (Nat. Hist.) Geol. Mineral Invest. 3 (1940) 1.

[13] H. S. Yoder and C. E. Tilley, Origin of basaltic magmas: an experimental study of natural and synthetic rock systems, J. Petrol. 3 (1962) 342.

[14] H. S. Yoder, Synthetic basalt, Carnegie Inst. Wash. Yearbook 53 (1954) 106.

[15] I. D. Muir and C. E. Tilley, Basalts from the northern part of the rift zone of the Mid-Atlantic Ridge. J. Petrol. 5 (1964) 409.

[16] W. Hamilton, Origin of high-alumina basalt, andesite and dacite magmas. Science 146 (1964) 635.

[17] G. A. Macdonald and T. Katsura, Variations in the lava of the 1959 eruption in Kilauea Iki. Pacific Science 15 (1961) 358.

[18] D. H. Green and A. E. Ringwood, Fractionation of basalt magmas at high pressures, Nature 201 (1964) 1276.

[19] D. H. Green and A. E. Ringwood, The genesis of basalt magmas. Dept. Geophys. Geochem. Aust. Nat. Univ. Publ. 444 (1966) 118.

[20] T. H. Green, unpublished work.

[21] F. R. Boyd and J. L. England, Apparatus for phase-equilibrium measurements at pressures up to 50 kilobars and temperatures up to 1750°C, J. Geophys. Res. 65 (1960) 741.

[22] F. R. Boyd and J. L. England, Effect of pressure on the melting point of diopside. $CaMgSi_2O_6$ and albite $NaAlSi_3O_8$ in the range up to 50 kilobars, J. Geophys. Res. 68 (1963) 311.

[23] D. H. Green and A. E. Ringwood, An experimental investigation of the gabbro-eclogite transformation and its petrological applications, Geochim. Cosmochim. Acta, in press (1966).

[24] T. H. Green, A. E. Ringwood and A. Major, Friction effects and pressure calibration in a piston-cylinder apparatus at high pressure and temperature, J. Geophys. Res. 71 (1966) 3589.

[25] D. H. Green and A. E. Ringwood, Mineral assemblages in a model mantle composition, J. Geophys. Res. 68 (1963) 937.

[26] G. A. Macdonald and T. Katsura, Chemical composition of Hawaiian lavas, J. Petrol. 5 (1964) 82.

[27] A. Holmes, Contributions to the theory of magmatic cycles, Geol. Mag. 63 (1926) 306.

[28] J. Verhoogen, Petrological evidence on temperature distribution in the mantle of the earth. Am. Geophys. Union Trans. 35 (1954) 85.

[29] H. Kuno, Origin of Cenozoic petrographic provinces of Japan and surrounding areas, Bull. Volc. Ser. 2, 20 (1959) 37.

B6

Reprinted from:

EARTH AND PLANETARY SCIENCE LETTERS

A LETTER JOURNAL DEVOTED TO THE DEVELOPMENT IN TIME OF THE EARTH AND PLANETARY SYSTEM

Volume 3, number 4, January 1968

EXPERIMENTAL STUDY AT HIGH PRESSURES ON THE ORIGIN OF OLIVINE NEPHELINITE AND OLIVINE MELILITE NEPHELINITE MAGMAS

R. J. BULTITUDE and D. H. GREEN

pp. 325–337

NORTH-HOLLAND PUBLISHING COMPANY - AMSTERDAM.

EARTH AND PLANETARY SCIENCE LETTERS 3 (1967) 325-337. NORTH-HOLLAND PUBLISHING COMP., AMSTERDAM

EXPERIMENTAL STUDY AT HIGH PRESSURES ON THE ORIGIN OF OLIVINE NEPHELINITE AND OLIVINE MELILITE NEPHELINITE MAGMAS

R. J. BULTITUDE and D. H. GREEN

Department of Geophysics and Geochemistry, Australian National University, Canberra, Australia

Received 5 December 1967

The compositions of basaltic rocks containing high pressure xenoliths are used to select olivine nephelinite and picritic nephelinite compositions for study of high pressure melting and crystal fractionation relationships. In the olivine nephelinite composition (26% normative olivine) under anhydrous conditions, olivine is the liquidus phase up to 18 kb and is joined by clinopyroxene at lower temperatures. At 27 kb, clinopyroxene is the liquidus phase and both garnet and clinopyroxene occur in runs near the liquidus at 36 kb. A similar sequence is found in the picritic nephelinite (36% normative olivine) but olivine persists as the liquidus phase up to 27 kb and garnet is the liquidus phase at 31.5 kb and 36 kb. Orthopyroxene was not observed in the melting interval of either composition under dry conditions. Experiments were carried out in which water added to the sample resulted in lowering of the liquidus temperature by 150–250°C at pressures of 13.5–30 kb. Under these conditions olivine is the liquidus phase up to 18 kb. At pressures of 18–22.5 kb in the olivine nephelinite and 22.5–27 kb in the picritic nephelinite aluminous *orthopyroxene* is the major near-liquidus phase (at temperatures of 1150°C–1250°C). Minor olivine and garnet accompany the orthopyroxene.

Electron microprobe analyses of pyroxenes, olivine and garnet enable calculation of high pressure fractionation trends for both the dry melting and wet melting conditions. While fractionation under dry conditions at high pressure may account for some of the variation among natural undersaturated magmas, the fractionation trend does not conform to the natural chemical variation in the series olivine basanite → olivine nephelinite → olivine melilite nephelinite. However, the fractionation trend at 18–27 kb under 'wet' conditions ($P_{H_2O} < P_{load}$) is dominated by orthopyroxene and separation of orthopyroxene accompanied initially by minor olivine, and at lower temperatures by garnet, produces derivative liquids closely matching the olivine nephelinite → olivine melilite nephelinite series.

The results provide evidence for development of the highly undersaturated olivine and melilite nephelinite lavas by either extreme fractionation of picritic magmas or by low degrees of partial melting of the mantle at depths of 60–100 km. An essential factor in their genesis is the presence of small amounts of water so that the magmas are produced at temperatures of 150–250°C below that required for dry magma production.

1. INTRODUCTION

Olivine nephelinites and olivine melilite nephelinites represent the most undersaturated lavas of basaltic kindred. Olivine nephelinites are characterized mineralogically by the presence of olivine, calcium-rich clinopyroxene and nepheline as major phases and by the absence of modal plagioclase. Olivine melilite nephelinites have, in addition to the above characteristics, melilite present as a minor or major phase. The high degree of undersaturation of these volcanics is also evident in the high normative nepheline content with minor normative albite or leucite in the olivine nephelinites and in the presence of normative nepheline, leucite and larnite in the melilite olivine nephelinites.

Olivine nephelinites and related rock types occur in two different associations:

(a) They occur with alkali olivine basalts and basanites in volcanic provinces in both oceanic and continental areas. In the Hawaiian province, eruption of these highly undersaturated lavas is character-

istic of a stage of 'post-erosional rejuvenation' of some volcanic centres (Oahu, West Maui and Kauai [1]). In this province nephelinites do not appear to be associated with the main eruptive cycle encompassing the early tholeiitic series to the late alkali olivine basalt series. In other provinces, there are as yet no grounds for separation of the highly undersaturated nephelinites from associated basanites and alkali olivine basalts.

(b) Nephelinites and melilite nephelinites also occur in association with alkaline plutonic rocks and carbonatites. These occurrences are restricted to stable continental areas and are not accompanied by major quantities of less undersaturated basaltic magmas.

A wide variety of hypotheses have been propounded for the genesis of the nephelinites and their associates. The hypothesis most relevant to the present work is that put forward by Winchell [2] to explain the origin of the Honolulu Series of Oahu, Hawaii. Winchell could see no way in which the nepheline and melilite bearing lavas could have been derived by fractional crystallization processes involving the separation of olivine. He observed, however, that if hypersthene, rather than olivine, crystallized from the primitive olivine basalt, typical of Hawaii, nepheline basanite and ultimately olivine nephelinite and melilite nephelinite would be obtained. He suggested that crystallization at depth, under high pressures, or with an abundance of mineralizers might cause hypersthene to crystallize instead of olivine.

Our approach to the problem of origin of the nephelinites has been to seek lavas providing evidence for direct derivation from upper mantle levels without super-imposed effects of low pressure fractionation at near-surface levels. Xenoliths of lherzolite, garnet

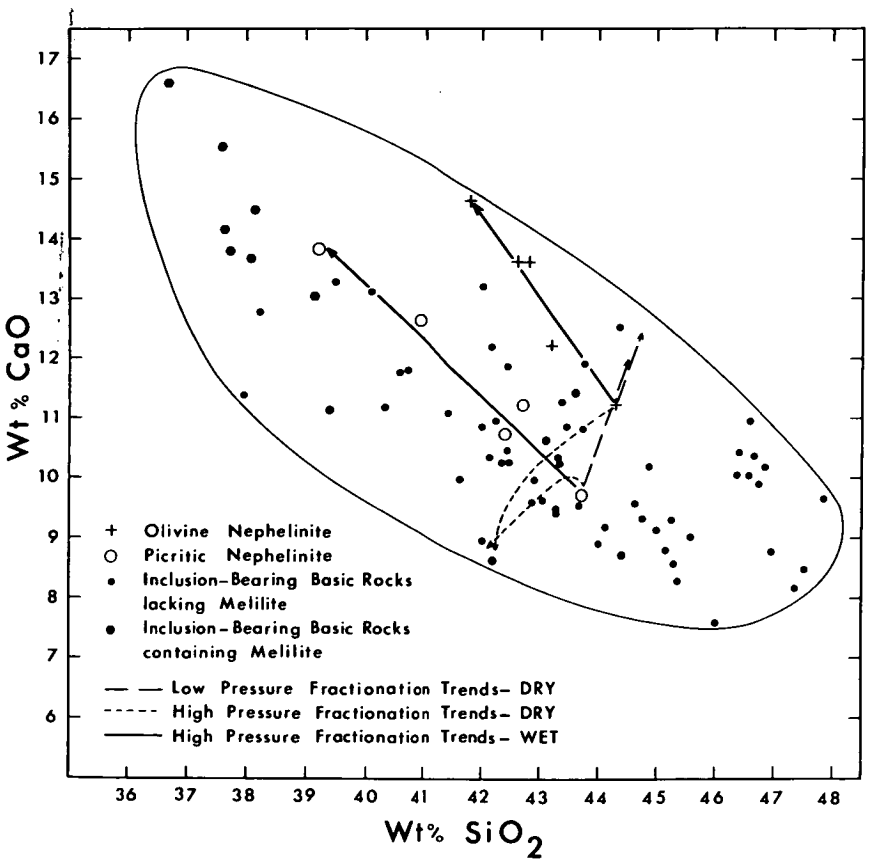

Fig. 1. Variation of lime versus silica in basaltic rocks which contain xenoliths of high pressure mineralogy. Analyses were calculated to 100%, omitting H_2O and CO_2 contents. The calculated fractionation trends (table 5) for the olivine nephelinite and picritic nephelinite are also shown.

pyroxenite, or spinel pyroxenite or xenocrysts of highly aluminous orthopyroxene and clinopyroxene, which occur in some alkaline magmas, have mineral compositions indicative of crystallization at pressures greater than 8–10 kb [3, 4]. The enclosing magmas are thus inferred to have ascended from depths in excess of 30 km without appreciable fractionation. These magmas range from alkali olivine basalts to olivine melilite nephelinites and their range of composition is illustrated in the CaO versus SiO_2 and alkalies versus SiO_2 plots of figs. 1 and 2. It is considered that the range of compositions illustrated in figs. 1 and 2 could represent a genetically related series at their depth of origin and the aim of the experimental study is to determine possible fractionation trends, at various pressures, of compositions lying rather centrally within the field of fig. 1. Green and Ringwood [4] have shown that alkali olivine basalts and basanites with up to 5% normative nepheline can be derived by crystallization of aluminous orthopyroxene and clinopyroxene from olivine-rich tholeiitic magmas at depths of 35–70 km. They indicated that the limit of fractionation along this trend at 35–70 km under dry conditions appeared to be olivine-rich basanites (p. 151) and did not establish a mechanism of formation of the extremely undersaturated nephelinites.

The nephelinite compositions used in the present experiments are listed in table 1. The olivine nephelinite was based on analyses of a limburgite from Japan [5] and an olivine fourchite from Antarctica [6]. Both contain lherzolite inclusions, have low Fe_2O_3 contents and very low normative albite contents placing them close to the olivine basanite-olivine nephelinite boundary using a normative classification. The picritic nephelinite was calculated by adding approximately 15% olivine (Fo_{80}) to the olivine nephelinite composition to obtain the desired composition with about 35% normative olivine. The rationale of

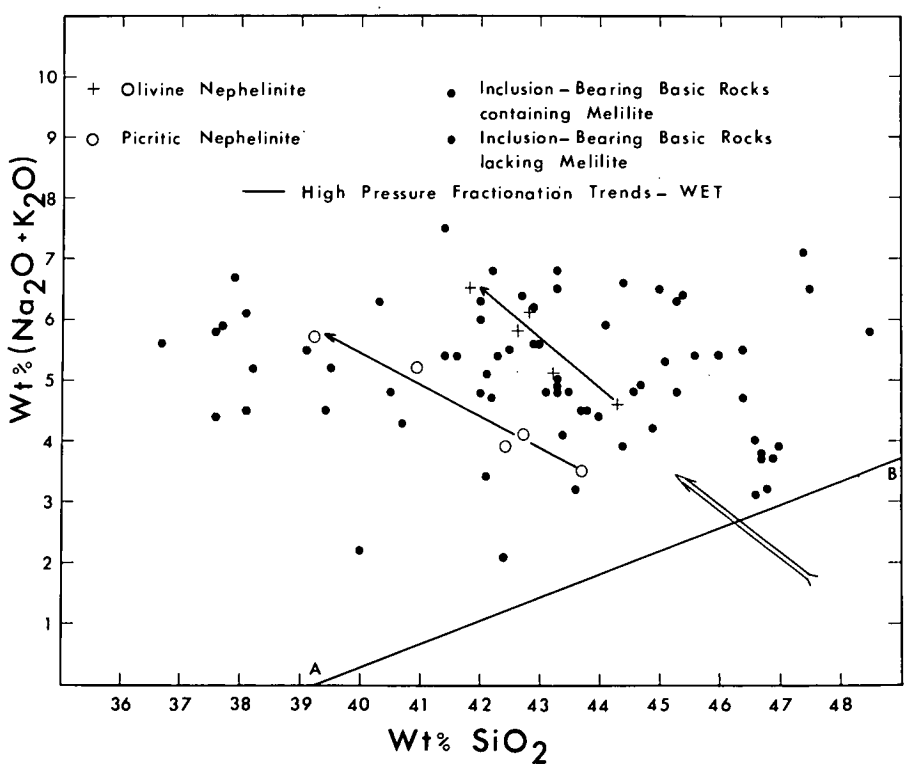

Fig. 2. Variation of alkalies versus silica in the basaltic rocks plotted in fig. 1. The calculated fractionation trends of table 5 are plotted and the large arrow defines a similar fractionation trend at 13–18 kb for the series of basaltic compositions studied experimentally by Green and Ringwood [4]. The line AB is the boundary between the tholeiitic and alkalic fields for the Hawaiian province as defined by MacDonald and Katsura [1].

Table 1
Compositions of the synthetic nephelinitic glasses used in the experimental work.

Rock type	Olivine nephelinite	Picritic nephelinite
SiO_2	44.3	43.7
TiO_2	1.5	1.3
Al_2O_3	14.2	12.3
Fe_2O_3	0.5 *	1.1 *
FeO	9.7 *	10.8 *
MnO	0.2	0.2
MgO	13.3	17.0
CaO	11.2	9.7
Na_2O	3.6	2.7
K_2O	1.0	0.8
P_2O_5	0.5	0.4
CIPW norms		
Or	6.1	4.5
Ab	2.0	3.4
Ne	15.3	10.6
An	19.4	19.2
Di	26.4	21.7
Ol	25.9	35.7
Ap	1.3	1.0
Il	2.9	2.4
Mt	0.7	1.6

* Determined by E. Kiss, analyst A.N.U.

this selection was that a primitive picritic nephelinite generated at 60 km or more, could precipitate olivine within the mantle before picking up lherzolite nodules at depths of 30–40 km. Previous studies strongly suggested that liquids derived by partial melting at depths of 60 km or more would approach the compositions of picrites.

2. EXPERIMENTAL METHODS

The nephelinite compositions were prepared from analytical reagent chemicals, fused in an argon atmosphere, finely ground under acetone and re-analysed for FeO and Fe_2O_3. The experimental runs were carried out in a single stage, piston-cylinder apparatus similar to that described by Boyd and England [7, 8]. Details of the furnace assemblages and experimental techniques involved have been fully described elsewhere [3]. A pressure correction of −10% has been applied to all nominal pressure readings [9].

Both graphite and platinum capsules have been used in 'dry' and 'wet' runs. In 'dry' runs the platinum capsules were sealed by welding to prevent access of water. There is some loss of iron from the sample to the Pt container during a run but this has been monitored both by microprobe analyses and wet chemical analyses of samples after the runs. We have shown that the loss of iron for the experimental procedures used is usually less than 20–25% of the total iron present and there is only a small change in the oxidation state. The effect of Fe-loss on the chemical and normative composition can of course be calculated and even in one or two runs of long duration in which 75% of the iron was lost the change in normative mineralogy is only from a picritic nephelinite to an olivine-rich basanite. As a further test of the validity of use of Pt capsules, graphite capsules were used extensively in 1 hour runs on the picritic nephelinite and to a lesser extent on the olivine nephelinite composition. Graphite capsules cannot be sealed and the entry of small amounts of water into the experimental charges resulted in variable lowering of the liquidus from run to run and in the presence of minor amphibole in a number of near-solidus runs. The comparison of runs using graphite and platinum capsules under dry conditions showed consistent sequences of crystallization with both containers but demonstrated uncertainty in the determination of solidus and liquidus temperatures using the graphite capsules.

'Wet' runs were conducted using a simple talc sleeve surrounding the graphite furnace sleeve. The nature and sequence of appearance of phases in both graphite and platinum capsules were mutually consistent. Small droplets of water were added to the capsules, the sample powder was then added and gently compressed. Neither type of capsule could be sealed by welding. In a few cases, there was movement of alumina and silica-rich melt (derived probably from the pyrophyllite spacer) into the sample capsule. Runs were carried out using boron nitride spacers to eliminate this factor and as a further check bulk analyses of the most important runs were carried out by microprobe traverses (5–10μ beam size) across the sample. The use of alternate capsule materials and the analytical results obtained eliminate compositional

change of the sample as the factor determining the nature of the crystalline phases formed in the experiments.

The nature and proportion of mineral phases present were determined by X-ray and optical methods. In runs in which crystals were large enough, quantitative analyses of the crystals were carried out using an electron probe microanalyser (Applied Research Laboratories, model EMX). The analyses of actual crystal phases present in the partial melting runs enabled detailed calculation of fractionation trends.

3. RESULTS

3.1. **Olivine nephelinite**

3.1.1. *Dry conditions*

The liquidus temperature is close to 1370°C at 1 atmosphere, 1410°C at 18, 1420°C at 22.5 and 1545°C at 36 kb. Olivine is the liquidus phase up to 18 kb. At 1 atmosphere there is a large temperature interval in which olivine crystallizes alone, being joined by both clinopyroxene and plagioclase some 200°C below the liquidus. With increasing pressure, the temperature interval between the appearance of olivine and clinopyroxene progressively decreases. Plagioclase was not observed at pressures above 1 atmosphere. At 22.5 kb olivine and clinopyroxene occur together in a near-liquidus run. At 27 kb clinopyroxene is the liquidus phase and garnet appears only in runs close to the solidus; olivine is absent. Garnet and clinopyroxene occur together in runs near the liquidus at 36 kb.

3.1.2. *Wet conditions*

At pressures less than 18 kb, olivine is the liquidus phase at temperatures of 1150–1250°C and is joined by amphibole at lower temperatures. However, at 18 kb and 22.5 kb, large orthopyroxene euhedra occur in runs near the liquidus at temperatures of 1150°C–1250°C. Olivine is generally a minor constituent and is completely absent from some runs. Minor garnet often co-exists with the orthopyroxene. The mineral assemblages encountered at 18 kb and 22.5 kb are orthopyroxene + olivine + liquid, orthopyroxene + garnet + olivine + liquid, orthopyroxene + garnet + liquid.

3.2. **Picritic nephelinite**

3.2.1. *Dry conditions*

Under dry conditions olivine is the liquidus phase to pressures slightly in excess of 27 kb and is followed by clinopyroxene. The liquidus temperature changes from 1415°C at 9 kb, to 1530°C at 27 kb and 1610°C at 36 kb. At pressures greater than 18 kb clinopyroxene is followed closely by garnet. Garnet is the liquidus phase at 31.5 kb, 1570°C, and 36 kb, 1600°C, and is joined by clinopyroxene at slightly lower temperatures.

3.2.2. *Wet conditions*

Wet runs at 18 kb yield near-liquidus assemblages at 1200–1300°C in which olivine is the principal crystalline phase. Clinopyroxene is also common. Orthopyroxene occurs in minor quantities. At higher pressures (22.5 kb–27 kb) orthopyroxene is the dominant crystalline phase, occurring generally as large tabular crystals often containing small inclusions of garnet and olivine. In runs near the liquidus, the olivine is much less abundant than orthopyroxene and garnet may be absent. In runs with a greater degree of crystallization, garnet and orthopyroxene may be the major phases with minor olivine.

With the particular experimental techniques used, the amount of water retained in the sample cannot be controlled and this may differ from run to run and particularly differs with variations in furnace assemblies or type of sample capsule. The effective depression of the liquidus of the compositions by the addition of water ranged from 150°C to 250°C. Near-liquidus runs with orthopyroxene as the major phase were obtained at 1150°C and as high as 1280°C at pressures of 22.5 and 27 kb. The sequence of crystallization in these experiments was thus inferred by comparisons of relative proportions of primary and quench phases or glass rather than by comparison of run temperatures. It is important to note that the nature and sequence of phases crystallizing, and particularly the role of orthopyroxene, were the same for runs in both platinum and graphite capsules. Mutually consistent results were also obtained using boron nitride or pyrophyllite spacers in the furnace assemblages.

4. FRACTIONAL CRYSTALLIZATION OF OLIVINE NEPHELINITE MAGMAS

The nature of the fractionation trend and the derivative liquid compositions from any magma may be determined if the composition of the crystalline phase or phases, the proportions of liquid and crystals and the composition of the parent magma are known. Liquidus and near-liquidus phases in the two nephelinite compositions have been analysed using the electron microprobe and the proportions of crystals and glass estimated, thus allowing fractionation trends at various pressures to be calculated.

4.1. Fractionation trends under dry conditions

At low pressures the dominant role of olivine separation from both the olivine nephelinite and picritic nephelinite leads to increasing SiO_2 content in derivative liquids and will not produce olivine melilite nephelinites from the chosen compositions. However, at pressures of 22.5 to 36 kb, by crystallization of various proportions of clinopyroxene, garnet and minor olivine, it is possible to move from the picritic nephelinite towards more undersaturated compositions. A calculated fractionation trend at 36 kb is shown in fig. 1. To produce decreasing SiO_2 content in derivative liquids, it is necessary for the accumulating phases to include a high proportion of clinopyroxene. Microprobe analyses of the near-liquidus clinopyroxenes demonstrate a high CaO content (14–17%) and the dry high pressure fractionation trend produces liquids of decreasing CaO content as well as decreasing SiO_2. Liquids produced are unlike the natural olivine melilite nephelinites. Also, extraction of relatively large amounts of material is necessary to effect a small change in SiO_2 content, e.g. the decrease in SiO_2 content of the picritic nephelinite from 43.7% to 42.1% is effected by extraction of 20% clinopyroxene + 10% garnet (as analyzed at 36 kb, 1560°C).

Similarly, in the olivine nephelinite composition the extraction of clinopyroxene (30%) alone at 27 kb would give rise to the high pressure fractionation trend shown in fig. 1. At 36 kb, separation of garnet with clinopyroxene would limit the silica depletion yielding compositions at intermediate points along the illustrated high pressure dry fractionation trend.

The results of the dry melting experiments will be reported in more detail in a separate paper but they are unfavourable to the hypothesis that a parent olivine nephelinite magma approaching the chosen compositions could fractionate to yield olivine melilite nephelinite derivative liquids under dry conditions at depths up to 130–140 km.

4.2. Fractionation trends under wet conditions

The experimental data briefly described in previous sections demonstrate the important role of orthopyroxene in near-liquidus runs in the olivine nephelinite at 18 kb and 22.5 kb and in the picritic nephelinite at 22.5 kb and 27 kb. In tables 2, 3 and 4, the results of microprobe analyses of phases in the wet melting runs are presented. Olivine and orthopyroxene show decreasing values of (100 Mg)/(Mg + Fe) with increasing degrees of crystallization * but there is a reversal of this trend at the appearance of garnet. Garnet has a much lower (100 Mg)/(Mg + Fe) ratio than co-existing olivine or orthopyroxene and thus the mean (100 Mg)/(Mg + Fe) value for the crystallizing phases would be at some intermediate value. The Al_2O_3 contents of the orthopyroxenes are moderately high and show some scatter which may be attributed to analytical error or to difficulties due to the presence of poikilitically included olivine or garnet. For orthopyroxene in equilibrium with garnet (± olivine, ± liquid) there is a decrease in Al_2O_3 with increasing pressure. The Al_2O_3 content of orthopyroxene co-existing with garnet at 22.5 kb, ~ 1250°C, is 5–6% and at 27 kb, ~ 1250°C is 3.5–4%. These values are in good agreement with Al_2O_3 contents of orthopyroxene in the assemblage Ol + Opx + Cpx + Ga in pyrolite (peridotite) compositions under the same physical conditions [10].

CaO contents of the orthopyroxenes are rather variable, possibly in part due to analytical difficulties, but most orthopyroxenes do not co-exist with clinopyroxene and therefore are not saturated in $CaSiO_3$ solid solution. The one clinopyroxene (18 kb,

* There are differences in the results obtained with similar degrees of crystallization between platinum and graphite capsules. These can be attributed to iron loss in the platinum capsules. The magnitude of this effect is to change the (100 Mg)/(Mg + Fe) ratio of the near liquidus orthopyroxene in the picritic nephelinite from around 89 in graphite capsules to 92 in platinum capsules and from 87 to 92 in the olivine nephelinite.

Table 2

Compositions of olivines analysed by electrin microprobe. Fe, Ca, Al determined by direct analysis; SiO_2, MgO calculated. WET conditions. (Opx = orthopyroxene, Cpx = clinopyroxene, Ga = garnet, Amp = amphibole, Gr = graphite, Pt = platinum.)

Rock type	Picritic nephelinite										Olivine nephelinite		
Pressure (kb)	13.5	13.5	18.0	18.0	22.5	22.5	22.5	24.8	27.0	27.0	18.0	18.0	18.0
Temperature (°C)	1220	1200	1250	1190	1450	1245	1230	1200	1280	1260	1210	1200	1200
Sample container	Pt	Pt	Pt	Pt	Gr	Pt	Pt	Pt	Gr	Pt	Pt	Pt	Gr
Time (min)	15	15	15	15	60	15	15	60	60	15	15	15	60
Composition													
SiO_2	40.9	40.5	40.4	40.4	40.4	40.7	40.3	40.6	39.9	40.4	40.5	39.8	40.1
Al_2O_3	n.d.	n.d.	n.d.	n.d.	n.d.	n.d.	n.d.	n.d.	n.d.	n.d.	n.d.	n.d.	n.d.
FeO	9.4	11.5	11.8	12.5	11.9	10.5	12.5	11.0	14.7	12.4	11.5	15.1	13.5
MgO	49.6	47.8	47.6	47.0	47.3	48.6	46.8	48.2	45.3	47.1	47.8	44.9	46.2
CaO	0.1	0.2	0.2	0.1	0.4	0.2	0.4	0.2	0.1	0.1	0.2	0.2	0.2
$\frac{100\ Mg}{Mg + Fe^{++}}$ (mol)	90.4	88.1	87.8	87.0	87.6	89.2	87.0	88.6	84.6	87.1	88.1	84.1	85.9
Mol. proportions													
Fo	90.2	87.8	87.6	86.9	87.1	88.9	86.4	88.4	84.5	88.0	87.8	83.9	85.7
Fa	9.7	11.8	12.2	13.0	12.3	10.8	13.0	11.4	15.3	11.9	11.8	15.8	14.1
La	0.1	0.3	0.3	0.1	0.6	0.3	0.6	0.3	0.2	0.1	0.3	0.3	0.3
Coexisting crystalline phase	–	–	Opx + Cpx	Opx(?) + Ga * + Amp	Opx * + Cpx + Ga + Amp	Amp	Opx * + Ga + Amp	–	Opx * + Ga	Opx + Ga	–	Opx + Cpx *	Opx *

* Denotes crystal phase analyzed by probe.

n.d. = not detected.

Table 3
Compositions of orthopyroxenes analysed by electron microprobe. Fe, Ca, Al determined by direct analysis; MgO, SiO_2 calculated. WET conditions.
(Ol = olivine, Cpx = clinopyroxene, Ga = garnet, Amp = amphibole, Gr = graphite, Pt = platinum.)

Rock type	Picritic nephelinite										Olivine nephelinite					
Pressure (kb)	22.5	22.5	22.5	22.5	22.5	22.5	27.0	27.0	27.0	27.0	18.0	18.0	18.0	18.0	22.5	22.5
Temperature (°C)	1450	1290	1270	1270	1260	1230	1280	1240	1240	1100	1290	1270	1260	1200	1230	1200
Sample container	Gr	Gr	Gr	Pt	Pt	Pt	Gr	Pt	Pt	Pt	Gr	Pt	Pt	Gr	Gr	Gr
Time (min)	60	60	60	15	15	15	60	15	60	60	60	15	15	60	60	60
Composition																
SiO_2	51.8	54.8	54.4	54.2	53.9	53.7	54.7	55.0	56.0	55.4	54.3	54.8	55.3	54.6	53.9	54.3
Al_2O_3	8.8	4.9	4.7	5.8	6.1	6.3	4.2	5.7	3.6	3.6	5.6	5.2	4.6	4.7	4.8	5.2
FeO	9.5	7.1	8.6	7.0	7.1	7.5	8.8	4.5	5.3	8.0	7.3	5.9	5.2	8.2	10.4	8.1
MgO	28.2	32.1	30.5	31.1	30.9	30.2	30.1	33.8	33.7	31.9	31.1	32.0	32.6	30.6	29.0	30.7
CaO	1.7	1.1	1.8	1.9	2.0	2.3	2.2	1.0	1.4	1.2	1.7	2.1	2.3	1.9	1.9	1.7
$\frac{100\,Mg}{Mg + Fe^{++}}$ (mol)	84.1	88.9	86.3	88.8	88.6	87.8	86.0	93.0	91.9	87.7	88.3	90.6	91.8	86.9	83.2	87.1
Mol. proportions																
En	73.7	82.6	79.2	80.3	79.7	78.3	78.6	85.9	86.1	82.6	80.4	82.3	83.6	79.5	76.0	79.6
Fs	13.9	10.3	12.6	10.1	10.3	10.9	12.8	6.5	7.6	11.6	10.6	8.5	7.4	11.9	15.3	11.8
Wo	3.2	2.1	3.4	3.5	3.7	4.3	4.1	1.8	2.6	2.2	3.1	3.8	4.2	3.6	3.6	3.1
Al_2O_3	9.3	5.1	4.9	6.0	6.3	6.6	4.4	5.8	3.7	3.7	5.8	5.4	4.8	4.9	5.1	5.4
Coexisting crystalline phases	Ga	Ol	Ga	Ol + Ga	Ol + Cpx + Ga	Ol * + Ga + Amp	Ol * + Ga	Ol + Ga *	Ol	Ga *	Ga	Ol + Ga + Sp	Ol	Ol *	Ol + Ga *	Ol + Ga *

* Denotes crystal phase analysed by probe.

Table 4
Composition of garnets and clinopyroxene analysed by electron microprobe. The elements involved below have been determined by direct analysis. WET conditions. (Ol = olivine, Opx = orthopyroxene, Gr = graphite, Pt = platinum.)

	Garnet				Clinopyroxene	
Rock type	Picritic nephelinite		Olivine nephelinite			
Pressure (kb)	27.0	27.0	22.5	22.5		18.0
Temperature (°C)	1240	1100	1230	1200		1200
Sample container	Pt	Pt	Gr	Gr		Pt
Time (min)	15	60	60	60		15
Composition						
SiO_2	42.3	42.5	41.4	41.4	SiO_2	49.5
TiO_2	0.8	0.9	1.0	0.7	TiO_2	0.7
Al_2O_3	22.9	22.9	22.8	23.2	Al_2O_3	15.5
FeO	6.1	9.3	10.7	9.1	FeO	8.2
MgO	19.6	18.6	17.3	19.3	MgO	12.5
CaO	7.5	6.5	6.7	6.6	CaO	12.1
					Na_2O	1.3
					K_2O	–
	99.2	100.7	99.9	100.0		99.8
$\frac{100\ Mg}{Mg + Fe^{++}}$ (mol)	85.1	78.1	74.2	79.0		73.1
Mol. proportions						
Almandine	11.9	18.2	21.5	17.4	En	39.4
Pyrope	68.9	65.2	61.4	66.4	Fs	14.5
Grossular	19.1	16.5	17.2	16.2	Wo	27.5
					Jd	2.7
					Al_2O_3	15.9
Co-existing crystalline phases	Ol + Opx	Opx *	Ol + Opx *	Ol + Opx *		Ol * + Opx

* Denotes crystal phase analysed by probe.

1200°C) analyzed is very aluminous and shows much less (Mg,Fe)SiO_3 solid solution than clinopyroxenes co-existing with orthopyroxene at 1350–1400°C [4].

Calculated fractionation products at 18–27 kb for both nephelinite compositions are presented in table 5 using estimates of the percentages of crystals consistent with observations of the sequence of appearance of crystals and their relative abundances. It may also be noted that microprobe analyses of the quench or glassy portions of samples with major orthopyroxene show compositions consistent with the calculated derivative liquids, in particular showing compositions with only 38–39% SiO_2.

Precipitation of relatively small amounts of aluminous orthopyroxene produces residual liquids significantly poorer in SiO_2 and MgO and richer in TiO_2, Al_2O_3, FeO, CaO and alkalies than the original nephelinite compositions. Normative K-feldspar and albite disappear, normative olivine decreases, while normative anorthite, leucite, nepheline and larnite increase. The trend is, therefore, towards more undersaturated nephelinite and melilite nephelinite compositions (table 5). The conformity of the experimentally determined fractionation to the trend of compositional variation in natural inclusion-bearing rocks is well shown in figs. 1 and 2. Comparison with the natural rocks indicates that the Al_2O_3 and CaO contents of the residual liquids, derived from the olivine nepheli-

Table 5

Fractionation of olivine nephelinite and picritic nephelinite under WET conditions. (Ol = olivine, Opx = orthopyroxene, Ga = garnet.)

Rock type	Olivine nephelinite					Picritic nephelinite				
Pressure (kb)		18.0	22.5	22.5	22.5		22.5	22.5	22.5	27.0
Nature and estimated % of crystals	Nil (initial liquid)	15% Opx + 5% Ol	10% Opx	15% Opx + 10% Ga	20% Opx + 10% Ga	Nil (initial liquid)	10% Opx	10% Opx + 5% Ol **	20% Opx + 10% Ga * + 5% Ol **	20% Opx + 15% Ga
Composition		Residual liquids					Residual liquids			
SiO_2	44.3	42.6	43.2	42.8	41.8	43.7	42.4	42.7	40.9	39.2
TiO_2	1.5	1.9	1.7	1.9	2.0	1.3	1.4	1.5	1.8	2.0
Al_2O_3	14.2	16.9	15.2	14.8	15.6	12.3	13.1	13.7	13.5	13.7
Fe_2O_3	0.5	0.6	0.6	0.7	0.7	1.1	1.2	1.3	1.7	1.8
FeO	9.7	9.8	9.7	10.1	10.3	10.8	11.2	11.2	12.4	12.5
MnO	0.2	0.3	0.2	0.3	0.3	0.2	0.2	0.2	0.3	0.3
MgO	13.3	8.0	11.6	9.1	7.6	17.0	15.3	13.8	11.0	10.5
CaO	11.2	13.6	12.2	13.6	14.6	9.7	10.7	11.2	12.6	13.8
Na_2O	3.6	4.5	4.0	4.8	5.1	2.7	3.0	3.2	4.0	4.4
K_2O	1.0	1.3	1.1	1.3	1.4	0.8	0.9	0.9	1.2	1.3
P_2O_5	0.5	0.6	0.6	0.7	0.7	0.4	0.4	0.4	0.6	0.6
	100.0	100.1	100.1	100.1	100.1	100.0	99.8	100.1	100.0	100.1
$\frac{100\ Mg}{Mg + Fe^{++}}$ (mol)	71.0	59.2	68.1	61.6	56.8	73.8	70.8	68.7	61.2	59.9
CIPW norm of liquid phase										
Or	6.1	–	–	–	–	4.5	2.0	2.5	–	–
Lc	–	6.1	5.2	6.1	6.5	–	2.9	2.4	5.6	6.1
Ab	2.0	–	–	–	–	3.4	–	–	–	–
Ne	15.3	20.7	18.4	22.0	23.4	10.6	13.7	14.7	18.4	20.1
An	19.4	22.0	20.0	15.0	15.5	19.2	19.4	20.0	15.0	13.6
Di	26.4	26.9	29.3	31.3	25.9	21.7	24.9	26.6	23.6	14.4
Ol	25.9	15.8	21.6	16.3	15.9	35.7	31.6	28.2	25.4	27.6
Cs	–	2.9	0.3	2.9	6.3	–	–	–	4.6	10.5
Ap	1.3	1.3	1.3	1.6	1.6	1.0	1.0	1.0	1.3	1.3
Il	2.9	3.6	3.2	3.6	3.8	2.4	2.7	2.9	3.5	3.8
Mt	0.7	0.9	0.9	0.9	0.9	1.6	1.9	1.9	2.6	2.6
	100.0	100.2	100.2	99.7	99.8	100.1	100.1	100.2	100.0	100.0

* Analysis of garnet from run 1196 (27 kb, 1240°C).

** Analysis of olivine from run 1210 (22.5 kb, 1230°C).

nite in particular, are rather high for the degree of SiO_2 undersaturation. This, however, is due at least in part to the relatively high amounts of CaO and Al_2O_3 present in the initial composition. A CaO content of 9–10% would have been much closer to that found in the majority of natural, nodule-bearing rocks (fig. 1). The picritic nephelinite with 9.7% is ideal in this respect.

The appearance of garnet as a crystalline phase coexisting with orthopyroxene modifies the fractionation trend, preventing further Al_2O_3 enrichment. Normative anorthite now decreases quite rapidly together with diopside and olivine (less rapidly) while leucite, nepheline and larnite increase. If sufficient orthopyroxene is extracted to lower the SiO_2 content of the residual liquid to less than that of garnet, precipitation of garnet causes the SiO_2 content to decrease further. Olivine occurs in most cases in very minor quantities. Olivine extraction therefore will not greatly effect the compositions of the residual liquids. Slight decreases in MgO and FeO and increases in the other oxides occur. If sufficient other material has been extracted so that the SiO_2 contents of the liquid residua have been lowered to less than approximately 39–40%, olivine precipitation will also cause a slight decrease in SiO_2. This is particularly relevant to the calculated derivative liquids of table 5 in that olivine may be their liquidus phase at pressures < 18 kb and further fractionation at higher levels in the mantle or crust may further decrease SiO_2. The trend of the melilite bearing lavas of fig. 1 with $SiO_2 < 38\%$ suggests that olivine separation at lower pressures * may play an important role. The role of lower pressure fractionation by olivine separation will produce an overprinting effect on the high pressure fractionation trend leading to scatter of compositions into a band (figs. 1 and 2).

5. CONCLUSIONS

5.1. Role of water in genesis of extremely undersaturated magmas

We regard the experiments reported as of a reconnaissance nature but demonstrating the extremely important role that small amounts of water may play in the generation of magmas in the deep mantle. Experiments in which the water content of the sample can be carefully controlled are clearly necessary – we assume in our experiments that $P_{H_2O} < P_{load}$ but varies from run to run. A similar effect to that reported here is apparent in the observation [11] of orthopyroxene as the liquidus phase in a picrite at 18 kb under 'wet' melting conditions but the appearance of olivine as the liquidus phase in later experiments under dry conditions [4].

We conclude that in olivine-rich or picritic compositions, crystallization of orthopyroxene continues further into the undersaturated field with increasing depression of the liquidus by high P_{H_2O}. Under *dry* conditions at 18 kb, the limit of crystallization of orthopyroxene is reached in basanite compositions with about 5% normative nepheline [4], but if, during fractional crystallization, the water content of the magma also rises then this limit is no longer operative and crystallization of orthopyroxene continues to lower temperatures. Separation of orthopyroxene-rich accumulates will take derivative liquids to olivine nephelinite and olivine melilite nephelinite compositions. If parent compositions are sufficiently picritic then olivine in minor amount may accompany the orthopyroxene. The orthopyroxene may in turn be joined by clinopyroxene at lower pressure or garnet at higher pressure. It is probable that the extremely undersaturated olivine melilite nephelinite magmas may only be derived at pressures of 22–27 kb from picritic parental magmas and that generation of these magmas requires the separation of garnet with the orthopyroxene. Our evidence strongly indicates that olivine nephelinites and olivine melilite nephelinites cannot form from *anhydrous* parent magmas by any fractionation process at depths < 140 km and that the magmas, at their depth of origin, are hydrous magmas. They would form at temperatures considerably below those at which *dry* mantle peridotite could produce appreciable quantities of magma [4].

The frequent occurrence of nephelinites as tuffs and in breccia pipes is consistent with explosive eruption of water-rich magmas. The large, corroded brown kaersutites or 'basaltic hornblende' crystals which occur in some olivine nephelinites may form by partial crystallization at intermediate depths of the water-

* The pressures referred to must be > 8 kb as the rocks of fig. 1 contain xenoliths of peridotite with mineral assemblages inconsistent with very low pressure crystallization.

rich magma. If olivine nephelinites crystallize at moderate depths without escape of their water content then hornblendite and biotite hornblendite bodies could result [12].

5.2. Wall rock reaction in undersaturated magmas

The minor elements, K, P, Ti and trace elements U, Th, Ba, Sr, Rb, Zr, Hf and the rare earth group are frequently greatly enriched in the highly undersaturated nephelinites and melilite nephelinites. It may also be noted that the degree of fractionation within the rare earth group is greater than for other basalt magmas [15]. Because of their inability to readily substitute in the major phases of the mantle (olivine, pyroxenes, spinel, garnet), these elements are considered to be distributed in the mantle in minor phases such as phlogopite, apatite, Mg-ilmenite etc. [4, 13, 14].

The terms 'zone refining' [13] and 'wall rock reaction' [4] have been applied to processes by which these elements are selectively extracted from wall rock material and highly enriched in a magma during ascent and slow cooling in the mantle. Because of their comparatively low temperature, hydrous olivine nephelinite or olivine melilite nephelinite magmas would be able to melt or dissolve only a very small fraction of any mantle wall-rock. This fraction, it is considered, would be highly enriched in the 'incompatible elements' (K, P, Sr, Rb, U, Th, rare earths etc.). Our conclusions on the hydrous nature and lower temperature of olivine nephelinite and olivine melilite nephelinite magmas lead to the expectation that these magmas would show enrichment processes which are even more selective than those operating in the olivine tholeiite → basanite series, and which consequently lead to more notable fractionation between geochemically similar elements.

5.3. Olivine nephelinites as partial melting products from the mantle

In applying our results to partial melting of the mantle it is necessary to consider the mineralogy of the parent mantle ('pyrolite') under appropriate *P, T* conditions. The stability fields in pyrolite of olivine + aluminous pyroxenes ± spinel and olivine + aluminous pyroxenes + garnet assemblages have recently been described [10] and are very relevant in discussions of partial melting of the mantle. At temperatures of 1200°–1300°C, olivine + aluminous pyroxenes ± spinel are stable to pressures of 21.5 kb (1200°C) or 24 kb (1300°C) and olivine + aluminous pyroxenes + garnet are stable at higher pressures. The compositions of olivine, orthopyroxene and garnet obtained near the liquidi of the olivine and picritic nephelinites are very similar in Mg/(Mg + Fe) ratio, in Al_2O_3 content and in CaO content to those phases in the pyrolite at similar conditions [10]. The data suggest that hydrous olivine melilite nephelinite magma could form at temperatures of 1150–1250°C at pressures of 22.5–27 kb by a small degree of partial melting of pyrolite leaving residual olivine, aluminous enstatite (4–6% Al_2O_3) and garnet. The components entering the liquid phase would be derived from accessory phases in the pyrolite, from aluminous clinopyroxene and to a small degree from garnet, olivine and aluminous orthopyroxene. With a greater degree of partial melting, increasing amounts of garnet and orthopyroxene and possibly minor olivine enter the liquid, changing it to a picritic nephelinite composition in equilibrium with residual aluminous enstatite and olivine. Further melting at this depth (75–100 km) would yield alkaline and tholeiitic picrite lavas.

Olivine nephelinite magmas may be derived by direct partial melting of pyrolite under wet conditions at depths of 60–70 km (18 kb–22.5 kb) yielding a small proportion of liquid in equilibrium with residual olivine, enstatite, garnet and/or clinopyroxene. Liquids at this depth would not be as olivine-rich as picritic nephelinites originating at greater depths and would probably contain 40% SiO_2 or more.

In applying our data to natural occurrences we suggest that olivine nephelinites such as those of Hawaii have formed at depths of around 60 km as a result of waning of the tholeiitic and alkali olivine basalt eruptive activity giving increased opportunity for migration and concentration of water and other volatile components in residual magma. As a result, the liquidus is lowered, allowing fractionation to proceed to the extremely undersaturated magma types. In continental regions, the occurrences of olivine nephelinites with little or no associated olivine basanite, alkali olivine basalt or tholeiite are interpreted as direct partial melting products from mantle peridotite at depths of around 80–100 km. The role of water is essential in lowering melting temperatures sufficiently to produce melting along the subcontinental geother-

mal gradient. An extension of the trend of volatile enrichment and silica impoverishment probably leads to low temperature kimberlitic magmas at depths of around 100 km.

The present work adds a qualifying condition to a major conclusion of Green and Ringwood [4], i.e. that 'garnet would not play a significant role in the genesis of magmas by fractional melting at depths smaller than 100 km'. The dry melting experiments reinforce this statement but the wet melting experiments indicate that the statement is valid for *anhydrous* melting only. If the mantle solidus is lowered sufficiently by water entering the liquid phase then garnet-liquid equilibria do play a role in determining the composition of highly undersaturated olivine melilite nephelinite liquids at depths of 60–100 km.

REFERENCES

[1] G. A. Macdonald and T. Katsura, Chemical composition of Hawaiian lavas, J. Petrol. 5 (1964) 82.

[2] H. Winchell, Honolulu series, Oahu, Hawaii, Bull. Geol. Soc. Am. 58 (1947) 1.

[3] D. H. Green and A. E. Ringwood, An experimental investigation of the gabbro to eclogite transformation and its petrological implications, Geochim. Cosmochim. Acta 31 (1967) 767.

[4] D. H. Green and A. E. Ringwood, The genesis of basaltic magmas, Contr. Mineral. Petrol. 15 (1967) 103.

[5] M. Yamaguchi, Petrogenic significance of ultrabasic inclusions in basaltic rocks from southwest Japan, Mem. Fac. Sci., Kyushu Univ. 15 (1964) 163.

[6] C. N. Fenner, Olivine fourchites from Raymond Fosdick Mountains, Antarctica, Bull. Geol. Soc. Am. 49 (1938) 367.

[7] F. R. Boyd and J. L. England, Apparatus for phase equilibrium measurements at pressures up to 50 kilobars and temperatures up to 1750°C, J. Geophys. Res. 65 (1960) 741.

[8] F. R. Boyd and J. L. England, Effect of pressure on the melting of diopside, $CaMgSi_2O_6$, and albite, $NaAlSi_3O_8$, in the range up to 30 kilobars, J. Geophys. Res. 68 (1963) 311.

[9] T. H. Green, A. E. Ringwood and A. Major, Friction effects and pressure calibration in a piston-cylinder apparatus at high pressure and temperature, J. Geophys. Res. 71 (1966) 3589.

[10] D. H. Green and A. E. Ringwood, The stability fields of aluminous pyroxene peridotite and garnet peridotite and their relevance in upper mantle structure, Earth Planet. Sci. Letters 3 (1967) 151.

[11] D. H. Green and A. E. Ringwood, Fractionation of basalt magmas at high pressures, Nature 201 (1964) 1276.

[12] R. Varne, The petrology of Moroto Mountain, eastern Uganda, Proc. Geol. Soc. London 1629 (1966) 23.

[13] P. G. Harris, Zone refining and the origin of potassic basalts, Geochim. Cosmochim. Acta 12 (1957) 195.

[14] H. H. Hess, The oceanic crust, the upper mantle and the Mayageuz serpentinized peridotite. In: A study of serpentinite (C. A. Burke, ed.), U.S. Nat. Acad. Sci. – National Research Council Publ. No. 1188 (1964) 169.

[15] J. G. Schilling and J. W. Winchester, Rare earths in Hawaiian basalts, Science 153 (1966) 867.

Tectonophysics - Elsevier Publishing Company, Amsterdam
Printed in The Netherlands

THE ORIGIN OF BASALTIC AND NEPHELINITIC MAGMAS IN THE EARTH'S MANTLE

D.H. GREEN

Department of Geophysics and Geochemistry, Australian National University, Canberra, (Australia)

(Received March 6, 1969)

SUMMARY

Over the past ten years, the availability of solid-media high pressure apparatus capable of generating pressures up to 50 kbar at closely controlled temperatures (to 1,700°C) has led to a rapid acceleration of direct experimental studies of both simple systems and natural rocks under high pressure conditions. These studies have been most fruitful in elucidating possible genetic relationships among basalts and it is now possible to erect a rather complete and self-consistent model in which a peridotitic mantle, by processes of partial melting, magma segregation and further magma fractionation, may produce liquids ranging in composition from olivine melilite nephelinite to olivine tholeiite.

INTRODUCTION

The compositions of basic magmas within the mantle are determined by three main processes:

(a) The partial melting and magma segregation process - for a given volume of parental peridotite, the composition of the basaltic liquid formed and the nature and proportions of the residual crystalline phases, will be determined by the degree of partial melting and the P, T, P_{H_2O} conditions at which the magma segregates from residual crystals and becomes an independent chemical system.

(b) Crystal fractionation processes - after segregation, a magma may move slowly towards the surface or be held at various depths with opportunity for cooling and crystal fractionation en route. Low pressure (depths <10–15 km) crystal fractionation is very common, particularly amongst tholeiitic magmas and leads to the divergent trends of tholeiitic magmas towards quartz tholeiitic and alkali magmas towards hawaiites, mugearites, trachytes, etc. Crystal fractionation at deeper levels produces the trend to high-alumina olivine basalts characteristic of depths of 20–35 km, the trend to alkali olivine basalts and, in the presence of water, towards olivine basanites and olivine nephelinites at depths of 40–70 km, and the trend to olivine nephelinites and olivine melilite nephelinites (in the presence of water) at depths of 60–100 km. Magmas produced by fractionation at deeper

levels may further fractionate at lower pressures, particularly by the separation of olivine, leading to further diversification and, in some cases, obliteration of chemical characteristics which would identify their primary source conditions.

(c) Wall-rock reaction process - this is considered to be a normal corollary to crystal fractionation of a magma near its depth of segregation and is the process mainly determining abundances of the "incompatible elements" in basaltic magmas.

The complexity of magma genesis will be reflected in complexity of the residual mantle peridotite and in segregations of accumulate phases which may impart a high degree of chemical inhomogeneity, particularly in abundances of "incompatible elements", to regions of the mantle which have been subject to partial melting or to the through-flow of basaltic magmas from deeper levels.

VARIATIONS AMONGST NATURAL BASALTS AND NEPHELINITES

A principal variation amongst natural basalts is the degree of saturation expressed modally by the presence or absence of quartz, hypersthene, nepheline, plagioclase, or melilite. While recognizing the diversity of natural basalts most workers have also recognized the essential continuity and transition in chemical composition between the various basalts. Basaltic magma provinces commonly contain a large part of the compositional spectrum, in some cases in apparently random time and spatial relationship, but in other cases in an ordered sequence, e.g., Hawaii. These features have led to the concept that there are simple genetic relationships between the basic magma types and hypotheses of crystal fractionation, contamination or differentiation by other processes have been advanced to relate one magma type to another. Of all the possible processes of magmatic differentiation, crystal fractionation is the most demonstrable in terms of natural examples. However, crystal fractionation may occur at any depth between the original segregation of a magma and its final crystallization. This summary outlines the results of experimental studies aimed at investigating the role that crystal fractionation at high pressure, under dry or wet conditions, may play in generating the spectrum of basaltic compositions.

It is convenient for the purposes of these studies to adopt a chemical (normative) rather than mineralogical (modal) classification of basic rocks and the nomenclature used is given below.

Tholeiite: basalt with normative hypersthene.

Olivine tholeiite: basalt with normative hypersthene and olivine, hypersthene $> 3\%$.

Olivine basalt: with normative olivine and with 0–3% normative hypersthene, no normative nepheline.

Alkali olivine basalt: with normative olivine and nepheline, nepheline $< 5\%$.

Olivine basanite: basalt with normative olivine, nepheline and albite, nepheline $> 5\%$, albite $> 5\%$.

Olivine nephelinite: basalt-like composition with major normative olivine, and nepheline, albite $< 2\%$; normative orthoclase and/or leucite, no normative larnite.

Olivine melilite nephelinite: basalt-like composition with normative olivine, nepheline, leucite and larnite.

In the sequence olivine tholeiite to olivine melilite nephelinite, SiO_2 content decreases from 47–49% to <38% while alkalis ($Na_2O + K_2O$) increase (from 1.5% to 5–7%) and CaO also increases, particularly in the olivine basanite to olivine melilite nephelinite compositions. Al_2O_3 contents are similar in the more silica-rich basalts but decrease significantly in olivine melilite nephelinite compositions. However, a further variation in basalt compositions is apparent in the recognition of distinctive high-alumina basalts (Tilley, 1950; Kuno, 1960), aphyric basalts with normative olivine and either normative hypersthene or low normative nepheline contents but with Al_2O_3 contents distinctly higher than "normal" olivine tholeiites or alkali olivine basalts of similar SiO_2 and $Na_2O + K_2O$ contents (Kuno, 1960).

PARENTAL MAGMAS

A first step in elucidating the origin and interrelationships of basaltic magmas is to establish the effects of low-pressure fractionation and to identify those magmas which existed as liquids at depth within the mantle and have not been modified in composition by later, low-pressure fractionation. For convenience, such magmas are herein called "parental magmas". O'Hara (1965) has argued that most basalts observed at the surface have chemical compositions and exhibit crystallization sequences which have been determined by low-pressure crystal fractionation processes. Excellent documentation on the effects of low-pressure fractionation in diversifying the compositions of basalts from an individual eruptive centre, and thus presumably from a single mantle source, is provided by the studies of the olivine and quartz tholeiite eruptions of Kilauea, Hawaii, e.g., Murata and Richter (1966) and many earlier authors. In the Kilauea example, however, seismic activity at depths of about 60 km closely preceded the 1959 Kilauea Iki eruption and there are plausible arguments for considering that the mean composition of the 1959–60 eruption represented quite closely the magma originally existing at 60 km depth and relatively rapidly transported to the surface (cf., Green and Ringwood, 1967b, pp.109–111). Other arguments from studies of simple systems (e.g., Davis and Schairer, 1965) also provide some guide to parental magma compositions in demonstrating that liquids derived by partial melting of peridotitic source rocks will be rich in normative olivine. An extremely useful indication of "parental magmas", unmodified by near-surface fractionation processes, is provided by those basalts which contain xenoliths and xenocrysts of high-pressure origin and with density (3.3-3.4) considerably higher than that of the enclosing magma. Lherzolite (olivine + aluminous pyroxenes + aluminous spinel) inclusions are probably the most common inclusions but are restricted to undersaturated rocks from alkali olivine basalts through olivine melilite nephelinite to alnoitic and kimberlitic magmas. There is sufficient data on the stability of plagioclase, aluminous pyroxenes, and spinel to show that the lherzolite mineral assemblages indicate temperatures near 1,000°C and pressures between 8–10 kbar and 20–25 kbar. The presence of the lherzolite inclusions shows that the particular host magma travelled rapidly (sufficiently rapid to transport the xenoliths) from depths of greater than 30–35 km. Although these magmas

may have suffered some contamination during rapid passage through the crust, their compositions cannot have been modified by crystal fractionation above the level at which the lherzolite inclusions were collected. The lherzolite inclusions are considered to be accidental xenoliths (White, 1966; Green and Ringwood, 1967b; Green et al., 1968) and estimates of their conditions of equilibration indicate a minimum depth of origin of the host liquid. More definitive knowledge of the history of an individual magma batch can be obtained for those magmas which contain "xenocrysts"[1] of high-pressure origin, usually partly resorbed and with low-pressure reaction rims. A magma batch, after segregation from residual peridotite at some depth may begin to cool and crystallize at any depth during its movement to the earth's surface and the nature and composition of the liquidus crystals will be characteristic of the magma composition and the P,T conditions of crystallization. It is thus possible to take such a magma and crystallize it experimentally under a variety of P,T conditions until liquidus crystals are obtained matching those "xenocrysts" observed in the natural basalt. These experiments have been successfully carried out for a number of olivine basalts and basanites, and demonstrate equilibrium between basalts and "xenocrysts" at pressures of 13–18 kbar. In most cases the high-pressure phenocrysts are pyroxenes, olivine, spinel or amphibole (ρ = 3.2–3.8 approx.) and their transport to the surface implies rather rapid movement of the magmas ($\rho \approx$ 2.7–2.8) from depth and precludes the possibility of further crystal fractionation.

Thus by selecting those basalts with xenoliths or xenocrysts demonstrably of high-pressure origin, it is possible to eliminate chemical variation due to low-pressure fractionation and to establish a range or trend of chemical variations among basalts imposed by processes acting within the mantle (or deepest continental or orogenic crust) i.e., at $P > 8$–10 kbar. The CaO vs. SiO_2 plot of Fig.1 (Bultitude and Green, 1968a) exemplifies such variation and includes rocks ranging from olivine basalts, transitional between olivine tholeiites and alkali olivine basalts, through alkali olivine basalts, olivine basanites, olivine nephelinites to olivine melilite nephelinites. It should be emphasized that the variation of Fig.1 is probably not imposed by a single process of magmatic differentiation but is a composite of a number of processes acting at various depths in excess of about 30–35 km.

FRACTIONATION AT HIGH PRESSURES–DRY CONDITIONS

The previous discussion goes some way towards defining the problem and indicating the basaltic compositions which are relevant for experimental studies but does not provide information on the actual processes operating to produce the observed variations amongst the "parental basaltic liquids". However, direct experimental studies of natural basaltic compositions at high pressure have demonstrated processes of crystal fractionation which relate some of the major basalt types.

---

[1]The term "high-pressure phenocryst" is more appropriate for the particular crystals under discussion but implies a knowledge of a genetic relationship between crystal and host magma which must be demonstrated in each case.

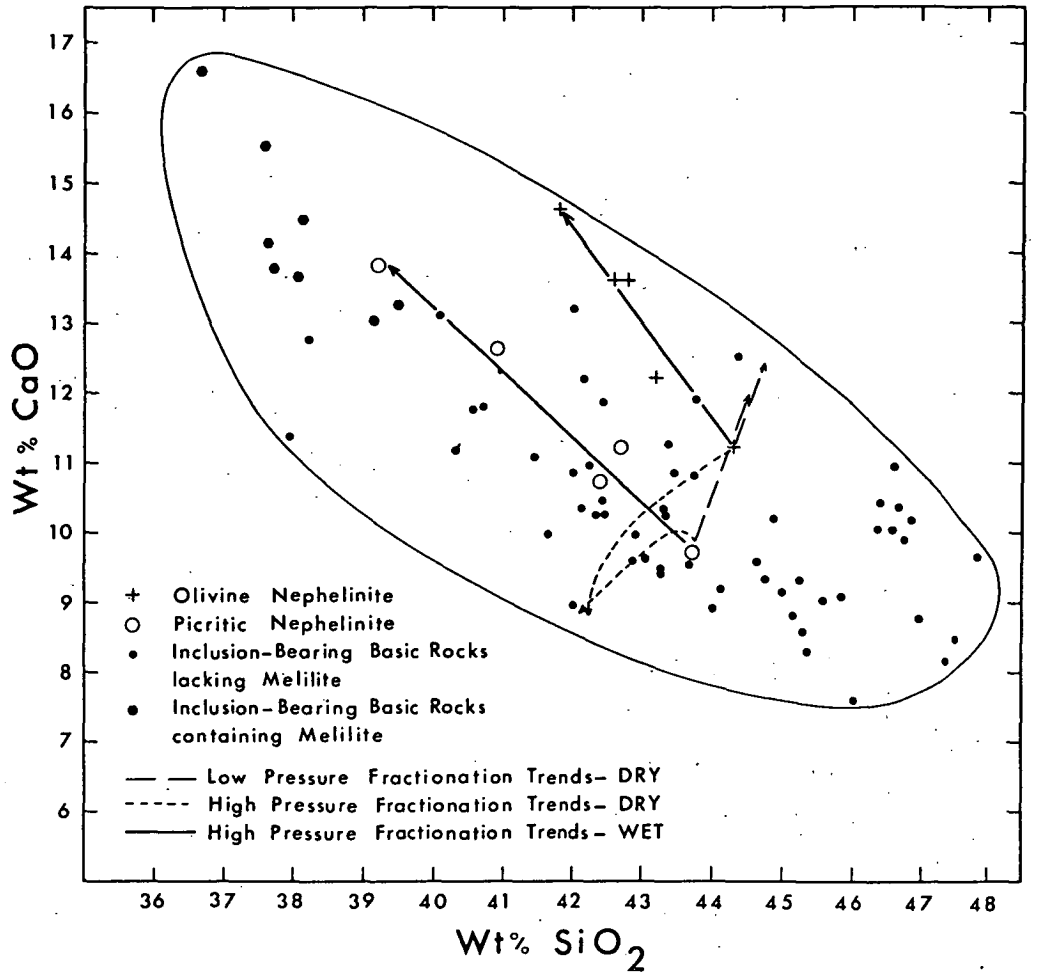

Fig.1. Variation of lime vs. silica in basaltic rocks which contain xenoliths of high-pressure mineralogy. Calculated fractionation trends for two olivine nephelinite compositions under dry and "wet" conditions are shown (from Bultitude and Green, 1968a).

High-alumina basalts

It has been shown (Green et al., 1967; Green and Ringwood, 1967b) that olivine-rich, low-alumina tholeiite magma, under dry conditions, crystallizes olivine, orthopyroxene and clinopyroxene as near-liquidus phases at pressures near 9 kbar and plagioclase does not appear until near the solidus. In contrast, at atmospheric pressure, orthopyroxene does not appear in the crystallization sequence until quartz-normative compositions are attained. Also there is a much greater temperature and composition range over which olivine is the only phase crystallizing, and plagioclase appears relatively early in the crystallization sequence, at temperatures higher than or similar to clinopyroxene. The fractionation trend of olivine tholeiitic magma at depths of 15–35 km will markedly enrich liquids in Al_2O_3 while retaining almost constant SiO_2 contents. Derivative liquids are rich in normative plagioclase, and contain both normative olivine (10–15%) and normative hypersthene or minor normative nepheline. Such magmas are the" basalts

of high-alumina type" including the high-alumina olivine tholeiites (oceanic tholeiites) of the mid-oceanic ridges, and high-alumina olivine basalts, transitional towards alkali basalts, such as those of Medicine Lake, California.

Olivine tholeiites, olivine basalts and alkali olivine basalts

At pressures of 13–18 kbar, orthopyroxene is the liquidus phase of olivine-rich (≈ 20% normative olivine) tholeiite, and olivine, followed closely by orthopyroxene, is the liquidus phase of tholeiitic picrite (≈ 30%normative olivine)(Green and Ringwood, 1964, 1967b; Tilley and Yoder, 1964). It has been shown (Green and Ringwood, 1967b) that separation of orthopyroxene from the olivine tholeiite will produce a very direct fractionation trend through olivine basalt to alkali olivine basalt (≈ 25% normative olivine, 2% nepheline). The orthopyroxene is joined by clinopyroxene as compositions with low normative nepheline contents are attained and the limit of fractionation under dry conditions at 13 kbar appears to be an olivine basanite with about 5% nepheline, 20–25% olivine. In more olivine-rich compositions, olivine and orthopyroxene have been observed as liquidus phases at 18 kbar, 1,400°C in an olivine basanite composition (9% Ne, 6% Ab, 34% Ol) and fractionation to yield more undersaturated basanites with 5% Ab, 11% Ne, 30% Ol appears possible. Under dry conditions it does not seem possible to produce olivine nephelinite or olivine melilite nephelinite magmas by fractionation of olivine-rich basanites at pressures <30 kbar (Bultitude and Green, 1968a, b).

In the depth range of 35–70 km, orthopyroxene plays a dominant role in producing a fractionation trend in dry basaltic magmas which leads from higher temperature olivine tholeiite magmas to lower temperature olivine basanite magmas.[1] To produce the undersaturated members of the fractionation series from the olivine tholeiitic members, about 30–40% crystallization is required. Clinopyroxene may join orthopyroxene in the more undersaturated part of the trend and both orthopyroxene and clinopyroxene contain moderate to large amounts of Al_2O_3 as (Ca, Mg)Al_2SiO_6 solid solution. The aluminous nature of the pyroxenes plays an important role in preventing marked Al_2O_3 enrichment accompanying the trend to lower SiO_2 contents and more undersaturated compositions.

At pressures above 20 kbar (≈ 70 km) the fractionation of basaltic compositions under dry conditions is dominated by clinopyroxene and garnet. Separation of various proportions of garnet and pyroxene may change magma composition to more or less undersaturated types (Yoder and Tilley, 1962) but the mechanisms require high degrees of crystallization and do not appear effective in producing the observed chemical variations.

---

[1] Dr. Kushiro, in his discussion of this paper, refers to the necessity for liquids derived from a peridotite source rock to have olivine as a liquidus phase. This was fully recognized by Green and Ringwood (1967b, pp.166–167). However, careful consideration of the experimental data published on a range of basalt compositions shows that while olivine must be present on the liquidus of an olivine tholeiite magma formed by partial melting at 18 kbar, further cooling results in precipitation of major orthopyroxene with only very minor olivine. The bulk composition of the accumulate phases is dominated by orthopyroxene.

FRACTIONATION AT HIGH PRESSURES-WET CONDITIONS

At the present time, experimental techniques to adequately control and measure water pressures or compositions of a vapour phase in solid media apparatus have not been developed. However, by simple, empirical methods, using pressure media which dehydrate during a high temperature run, or by adding small drops of water to the sample capsule, it is possible to depress the liquidi of basalts in reproducible manner and study the effects of crystallization of basaltic liquids under conditions in the range P_T = 10–40 kbar, $P_{H_2O} < P_T$. Using a dried sample enclosed in a crimped but not welded Pt capsule and a simple talc furnace assembly (Green and Ringwood, 1967a, pp.773–774) the liquidi of basalts can be depressed 100° ± 20°C in the pressure range 13–30 kbar. Using the same techniques but also adding a small drop of water to the sample, the liquidi can be lowered 180° ± 30°C in the same pressure range.

The most notable effect of lowering of the liquidi by the presence of water is the enlargement of the field of crystallization of orthopyroxene at the expense of olivine and clinopyroxene, both in terms of temperature and pressure range over which it crystallizes in a given composition, and in terms of the basaltic compositional range in which orthopyroxene becomes a liquidus or near-liquidus phase. Bultitude and Green (1968) have shown that orthopyroxene plays a dominant role in the fractional crystallization of olivine nephelinite and picritic nephelinite compositions at 18–27 kbar at temperatures of 1,150°–1,250°C. The dry liquidi were in the range 1,400°-1,530°C with olivine, clinopyroxene and garnet as liquidus and near-liquidus phases. Further work has shown that an alkali olivine basalt (Green and Ringwood, 1967b) with clinopyroxene as the liquidus phase at 18 kbar, 1,320°C, has orthopyroxene as the liquidus phase at 18 kbar, 1,300°C in the presence of a small amount of water. A preliminary outline of the liquidus relationships under anhydrous and under "wet conditions" for an olivine-rich basanite composition is illustrated in Fig.2 and demonstrates the dominant role of orthopyroxene in the 1,200°–1,300°C temperature range[1].

The data demonstrate that, provided water is available in the source regions of the basalts, fractionation by separation of orthopyroxene as the only or major crystallizing phase, extends over the composition range from olivine tholeiite to olivine nephelinite. In sufficiently olivine-rich compositions, olivine may be a co-precipitating phase and the orthopyroxene is joined by clinopyroxene or by garnet at lower temperatures. The effect of fractional crystallization by separation of aluminous orthopyroxene is to deplete the residual liquid in SiO_2, while strongly enriching it in CaO and

[1] Experiments carried out since the preparation of this article have utilized sealed Pt capsules containing known, controlled quantities of water. These experiments have confirmed the role of orthopyroxene as a major near-liquidus phase in olivine-rich basanite (11% Ab, 11% Ne) containing 2–5% water at pressures of 22–27 kbar and temperatures of 1,250–1,350°C. The use of sealed capsules eliminates the possibility of sample compositional change due to loss of alkalies or to addition of silica as the factor responsible for appearance of near-liquidus orthopyroxene (cf., discussion of this paper by Dr. I. Kushiro). The role of orthopyroxene in the olivine nephelinite and picritic nephelinite compositions (Bultitude and Green, 1968a) has not yet been confirmed with sealed capsules.

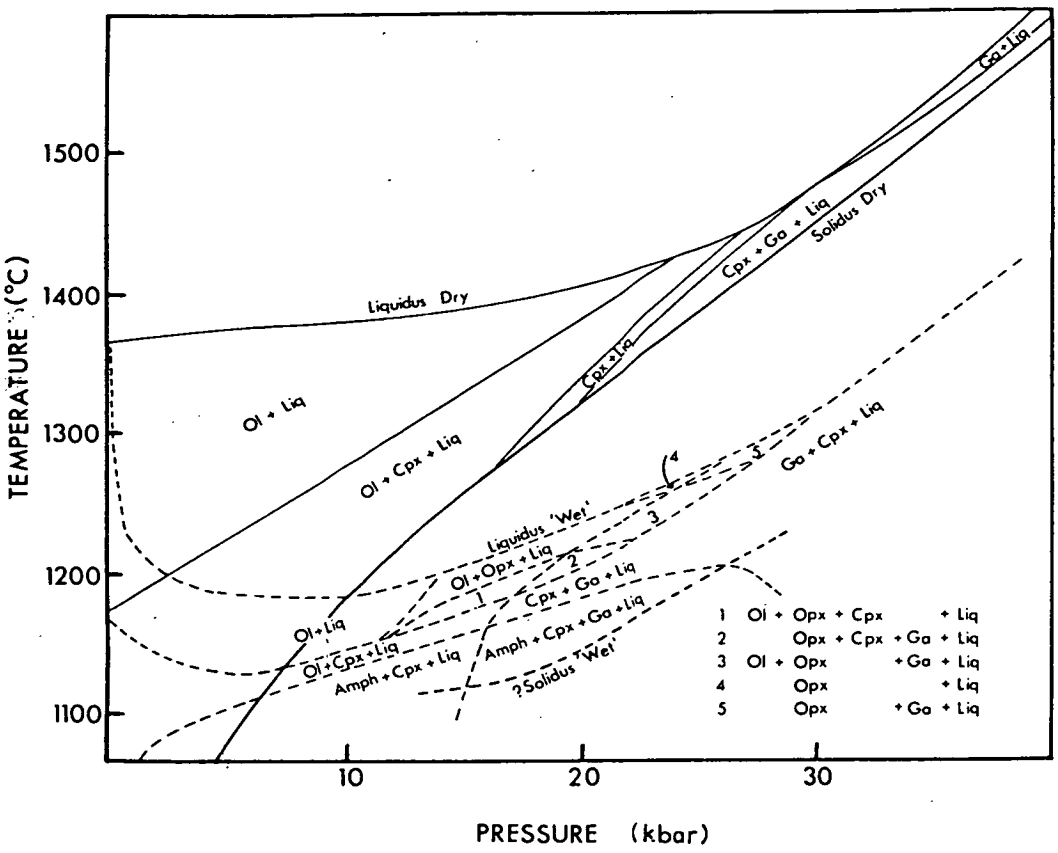

Fig.2. Preliminary outline of the crystallization sequences between liquidus and solidus at various pressures for an olivine-rich basanite composition. Solid lines indicate relationships under dry conditions, dotted lines indicate "wet" conditions ($O < P_{H_2O} \leq P_{Total}$).

alkalies. The residual liquids define the fractionation trend illustrated in Fig.1, with olivine melilite nephelinite being the most undersaturated product reached by separation of aluminous orthopyroxene joined by pyrope-almandine garnet (Bultitude and Green, 1968a).

The experimental studies, although still in the exploratory stage, strongly indicate that olivine basanites (with > 10% nepheline), olivine nephelinites and olivine melilite nephelinites are hydrous magmas at their depth of origin in the mantle. The highly undersaturated magmas may be derived from depths of 60–100 km and at temperatures of 100°C–200°C below the anhydrous solidus of olivine basanite. It is inferred that during fractional crystallization of a tholeiitic picrite or olivine tholeiite, the water content of the magma may increase, leading to lower temperature and more highly undersaturated derivative liquids. A number of features of olivine nephelinite volcanism, particularly its explosive character and the common presence of hornblende "xenocrysts", are indicative of moderate to high water contents of the natural rocks.

The inferred processes and products of basalt fractionation under both wet and dry conditions are summarized in Fig.3.

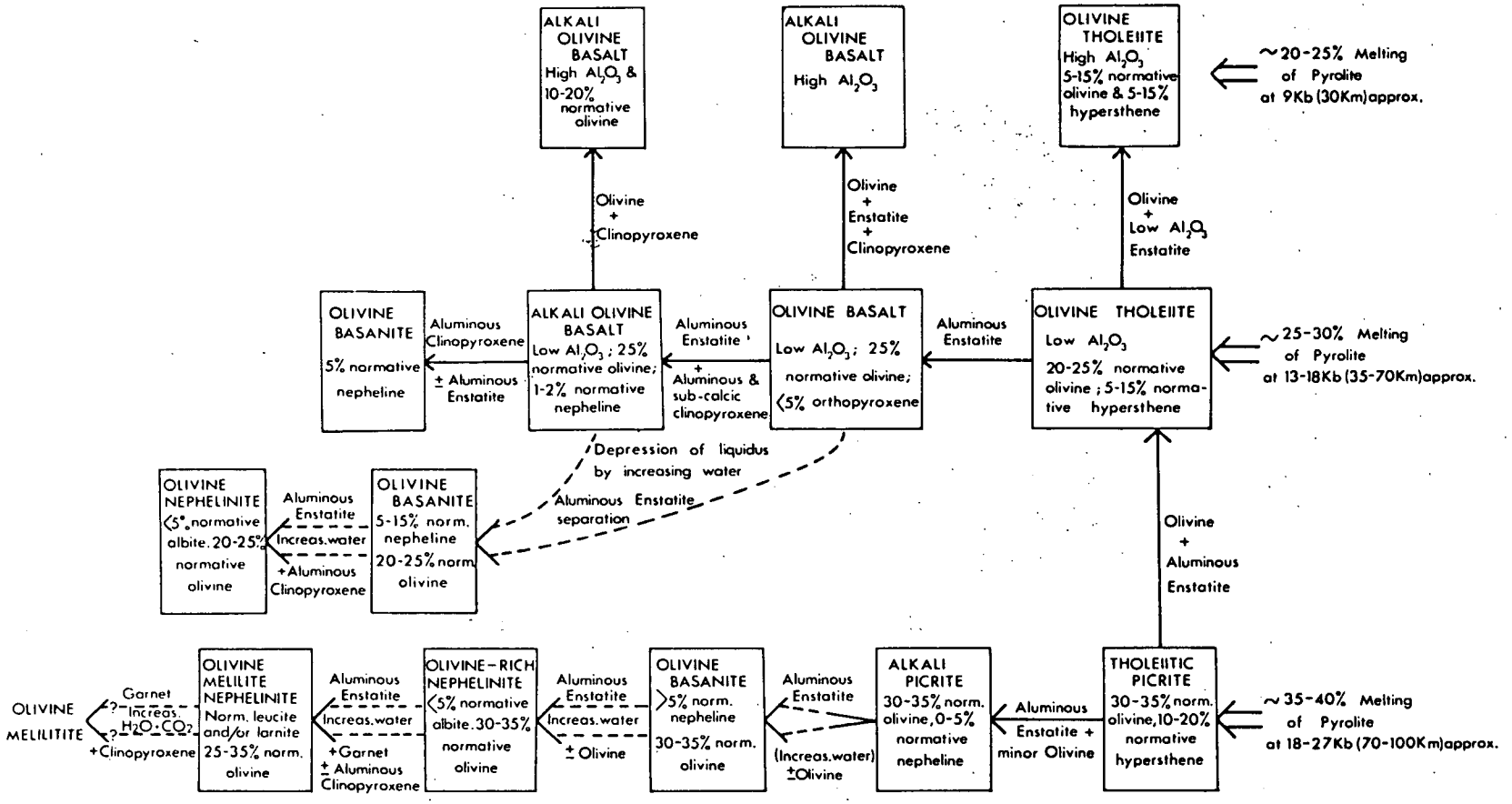

Fig.3. Summary of deduced crystal fractionation relationship between various basaltic magmas at moderate to high pressures. Upper part of the diagram is from Green and Ringwood (1967b, fig.10).

PARTIAL MELTING IN THE MANTLE

It is assumed that the average mantle composition, in regions unaffected by earlier extraction of basaltic magmas, is that of a peridotite capable of providing 20–30% of basaltic liquids or 40% of picritic liquids, by partial melting leaving residual olivine and enstatite. A specific model composition, the "pyrolite" composition of Ringwood (1966), is used in the following discussion although it is recognized that some inhomogeneity must be expected, particularly in regions which have been subjected to any earlier melting or wall-rock reaction processes. The stability fields of plagioclase pyrolite, pyroxene pyrolite, spinel + pyroxene pyrolite and garnet pyrolite have been experimentally determined by Green and Ringwood (1967c). Similar data for another peridotitic composition have been published by Ito and Kennedy (1967) and for relevant simple systems or component mineral assemblages by MacGregor (1966, 1967). In the pyrolite composition (Fig. 4), assemblages of olivine + orthopyroxene + clinopyroxene + plagioclase + chromite are stable on the solidus to pressures of 12 kbar. Partial melting in the 7-12 kbar range would eliminate plagioclase and take some pyroxene + olivine into the liquid phase, the latter being of high-alumina olivine tholeiite composition (Green and Ringwood, 1967b). In the 12–27 kbar pressure range, *dry* melting of pyrolite involves equilibria between liquid, olivine, aluminous orthopyroxene and aluminous clinopyroxene. Early-formed liquids in the 12–18 kbar range are alkali olivine basalt with a low degree of melting (5–20%) passing with increasing melting to olivine basalt and olivine tholeiite. In the 18-27 kbar range, early-formed liquids ($\approx$ 35–40% melting) are of picritic olivine tholeiite type under dry conditions. Alkali picrites *may* be developed with a lower degree (30–35%) of melting in the 18–27 kbar pressure range.

In the presence of water the pyrolite solidus is moved to lower temperatures so that the solidus intersects the garnet pyrolite field at depths of 60–80 km at a temperature of 1,250°C. Early-formed liquids at depths of 70–100 km under wet conditions may be in equilibrium with olivine, orthopyroxene, garnet and clinopyroxene. It is inferred that olivine melilite nephelinite liquids may form by direct partial melting at these conditions and with an increasing degree of melting, all clinopyroxene, much garnet and minor orthopyroxene and olivine enter the liquid phase changing it to olivine nephelinite composition. Olivine nephelinite liquids would be in equilibrium with residual olivine, aluminous enstatite and possibly chromite, Increasing degree of melting, with incorporation of aluminous enstatite and some olivine into the liquid, would yield olivine basanite and alkali picrite liquids. It may be noted that reaction relationships observed in the 13–27 kbar interval in the crystallization of the complex basalt compositions imply incongruent melting relationships in the pyrolite. Thus at low degrees of partial melting (22–27 kbar) clinopyroxene yields orthopyroxene + components added to an olivine melilite nephelinite liquid and, at higher degrees of melting, garnet yields aluminous orthopyroxene + components added to olivine nephelinite liquid. The role of Cr_2O_3 in melting remains uncertain. In the subsolidus assemblages Cr_2O_3 is concentrated in garnet, spinel or pyroxenes but on melting, any of these phases could possibly yield a liquid component with residual, refractory chromite.

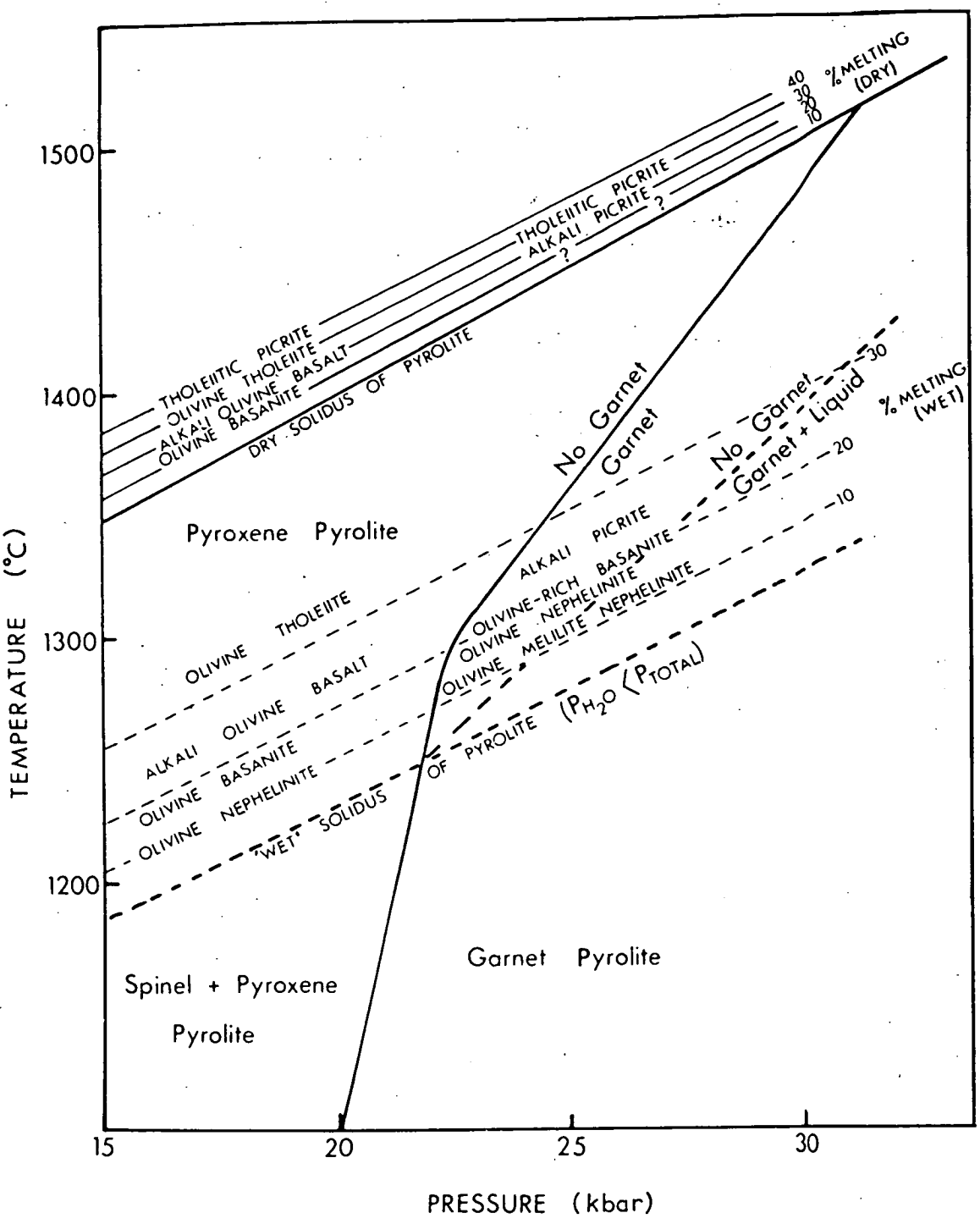

Fig.4. Diagram showing possible relationships between partial melting of pyrolite under dry conditions (solid lines) with resultant production of certain magma types, and partial melting under "wet" conditions. (Compare with Green and Ringwood, 1967b, fig.12, and 1967c, fig.1.)

WALL-ROCK REACTION AND SELECTIVE ELEMENT ENRICHMENT

The previous discussion of basaltic magma relationships has been based on a consideration of the relative concentrations of the major elements (Si, Al, Fe, Mg, Ca, Na and Ti) which largely determine the normative and modal mineralogy, and thus the classification, of basaltic rocks. However, the minor elements (K, Ti and P) and trace elements (U, Th, Ba, Cs, Rb, Sr, Zr, Hf and the rare earth group) are frequently much more abundant in the undersaturated magmas than predicted by the simple crystal fractionation relationships of differences in degrees of partial melting outlined in the previous section. It has been argued (Green and Ringwood, 1967b) that this group of elements ("incompatible elements") may be highly enriched in a fractionating magma by a process of "wall-rock reaction" In an environment with little temperature contrast between magma and wall-rock, as is likely for a magma near its depth of segregation, cooling and crystallization of the magma involves complementary processes of reaction with wall-rock including selective melting and extraction of the lowest melting fraction. The incompatible elements are considered to be present mainly in accessory minerals, such as phlogopite, apatite, ilmenite and are likely to be highly concentrated in the lowest melting fraction of pyrolite. As the liquidus of a fractionating magma moves to lower temperatures, particularly with increasing content of water, the incorporation of material would become increasingly selective leading to relative fractionation between geochemically similar elements and extreme enrichment in the liquid of those elements least able to substitute in the major and minor minerals of the wall-rock. The hydrous character of the extremely undersaturated magmas adds a further factor to wall-rock reaction processes. It is likely that these liquids are not saturated with water at their depth of origin[1] and the vapour pressure of water in the magma may be less than that in wall-rock containing accessory phases such as hornblende or phlogopite. Water existing as a vapour phase in the wall rock may migrate into the magma. Hydrous phases in the wall rock may break down to residual anhydrous products and a vapour phase migrating into the magma. Under the high-pressure, high-temperature conditions, element transport in a vapour phase may be both highly efficient and selective. Thus both their relatively low temperature and hydrous character are inferred to be major factors favouring enrichment in incompatible elements and fractionation between elements in the olivine nephelinite and olivine melilite nephelinite magmas. For example, nephelinite and melilite nephelinite from Hawaii show enrichment factors for the rare earth elements relative to tholeiite which range from over 10 for La to about 1.1 for Lu (Schilling and Winchester, 1966). Alkali olivine basalts have enrichment factors relative to tholeiite of 2.5-3.5 for La and around 1.2 for Lu. Only by careful consideration of both major and minor element abundances will it be possible to evaluate the rel. ative roles of partial melting, crystal fractionation and wall-rock reaction in determining the chemical composition of a basaltic magma.

---

[1]Preliminary data from this laboratory (N. Gray, personal communication, 1968) indicate that depression of basaltic liquidus by 100°C at 22.5 kbar is effected by 2–3% water, while a depression of 200°C is effected by 5–7% water. Boettcher and Wyllie (1967) report solubilities of about 30% water in silicate melts at pressures above 15 kbar.

CONCLUSIONS

The compositions of basic magmas within the mantle are determined by three main processes:

(a) The partial melting and magma segregation process - for a given volume of parental peridotite, the composition of the basaltic liquid formed and the nature and proportions of the residual crystalline phases, will be determined by the degree of partial melting and the P, T, P_{H_2O} conditions at which the magma segregates from residual crystals and becomes an independent chemical system.

(b) Crystal fractionation processes - after segregation, a magma may move slowly towards the surface or be held at various depths with opportunity for cooling and crystal fractionation en route. Low-pressure (depths $< 10-15$ km) crystal fractionation is very common, particularly amongst tholeiitic magmas and leads to the divergent trends of tholeiitic magmas towards quartz tholeiites and alkali magmas towards hawaiites, mugearites, trachytes, etc. Crystal fractionation at deeper levels produces the trend to high-alumina olivine basalts characteristic of depths of 20–25 km, the trend to alkali olivine basalts and, in the presence of water, towards olivine basanites and olivine nephelinites at depths of 40–70 km, and the trend to olivine nephelinites and olivine melilite nephelinites (in the presence of water) at depths of 60–100 km. Magmas produced by fractionation at deeper levels may further fractionate at lower pressures, particularly by the separation of olivine, leading to further diversification and, in some cases, obliteration of chemical characteristics which would identify their primary source conditions.

(c) Wall-rock reaction process - this is considered to be a normal corollary to crystal fractionation of a magma near its depth of segregation and is the process mainly determining abundances of the "incompatible elements" in basaltic magmas.

The complexity of magma genesis will be reflected in complexity of the residual mantle peridotite and in segregations of accumulate phases which may impart a high degree of chemical inhomogeneity, particularly in abundances of "incompatible elements", to regions of the mantle which have been subject to partial melting or to the through-flow of basaltic magmas from deeper levels.

ACKNOWLEDGEMENTS

Although the author is responsible for this summary paper, the data and conclusions stem largely from joint projects with A.E. Ringwood and with T.H. Green, R.J. Bultitude and N.H. Gray at the Australian National University. The work of others (particularly F.R. Boyd, K. Ito, G.C. Kennedy, I. Kushiro, I.D. MacGregor, M.J. O'Hara, C.E. Tilley and H.S. Yoder) in the field of experimental petrology of basalts at high pressures has also been most useful in preparing this summary. The author is grateful to W. Hibberson for technical assistance.

REFERENCES

Boettcher, A.L. and Wyllie, P.J., 1967. Hydrothermal melting curves in silicate-water systems at pressures greater than 10 kbar. Nature, 216: 572–573.

Bultitude, R.J., and Green, D.H., 1968a. Experimental study at high pressures on the origin of olivine nephelinite and olivine melilite nephelinite magmas. Earth Planetary Sci. Letters, 3: 325–337.

Bultitude, R.J. and Green, D.H., 1968b. Experimental crystallization of olivine nephelinite at high pressures and temperatures. In press.

Davis, B.T.C. and Schairer, J.F., 1965. Melting relations in the join diopside–forsterite–pyrope at 40 kbar and at one atmosphere. Carnegie Inst. Wash., Year Book, 64: 123–134.

Green, D.H. and Ringwood, A.E., 1964. Fractionation of basalt magmas at high pressures. Nature, 201: 1276–1279.

Green, D.H. and Ringwood, A.E., 1967a. An experimental investigation of the gabbro to eclogite transformation and its petrological applications. Geochim. Cosmochim. Acta, 31: 767–833.

Green, D.H. and Ringwood, A.E., 1967b. The genesis of basaltic magmas. Contr. Mineral Petrol., 15: 103–190.

Green, D.H. and Ringwood, A.E., 1967c. The stability fields of aluminous pyroxene peridotite and garnet peridotite and their relevance in upper mantle structure. Earth Planetary Sci. Letters, 3: 151–160.

Green, D.H., Morgan, J.W. and Heier, K.S., 1968. Th, U, K abundances in peridotite inclusions and their host basalts. Earth Planetary Sci. Letters, 4: 155–166.

Green, T.H., Green, D.H. and Ringwood, A.E., 1967. The origin of high-alumina basalts and their relationships to quartz tholeiites and alkali basalts. Earth Planetary Sci. Letters, 2: 41–51.

Ito, K. and Kennedy, G.C., 1967. Melting and phase relations in a natural peridotite to 40 kbar. Am. J. Sci., 265: 519–538.

Kuno, H., 1960. High-alumina basalt. J. Petrology, 1: 121–145.

MacGregor, I.D., 1966. The stability fields of spinel- and garnet-bearing peridotites. Ann. Rept. Geosciences Div. 1965–66, S.W. Centre for Advanced Studies, 6–8.

MacGregor, I.D., 1967. Stability fields of garnet- and spinel-peridotites. Ann. Rept. Geosciences Div. 1966–1967, S.W. Centre for Advanced Studies, 14–19.

Murata, K.J. and Richter, D.H., 1966. The settling of olivine in Kilauean magma as shown by lavas of the 1959 eruption. Am. J. Sci., 264: 194–203.

O'Hara, M.J., 1965. Primary magmas and the origin of basalts. Scot. J. Geol., 1: 19–40.

Ringwood, A.E., 1966. The chemical composition and origin of the earth. In: P.M. Hurley (Editor), Advances in Earth Sciences. M.I.T. Press, Cambridge, Mass., pp.287–356.

Schilling, J.G. and Winchester, J.W., 1966. Rare-earths in Hawaiian basalts. Science, 153: 867–869.

Tilley, C.E., 1950. Some aspects of magmatic evolution. Quart. J. Geol. Soc. London, 106: 37–61.

Tilley, C.E. and Yoder, H.S., 1963, 1964. Pyroxene fractionation in mafic magma at high pressure and its bearing on basalt genesis. Carnegie Inst. Wash., Year Book, 62: 77–84, 63: 114–121.

White, R.W., 1966. Ultramafic inclusions in basaltic rocks from Hawaii. Contr. Mineral. Petrol., 12: 245–314.

Yoder, H.S. and Tilley, C.E., 1962. Origin of basalt magma: an experimental study of natural and synthetic rock systems. J. Petrol., 3: 342–532.

B10

THE ORIGIN OF BASALTIC AND NEPHELINITIC MAGMAS

* *The Bennett Lectures*

THE ORIGIN OF BASALTIC AND NEPHELINITIC MAGMAS

Preface by M. J. LeBas

In the past it has been the task of the 'hard-rock' geologist to observe and describe rocks as they occurred. In recent decades, the art of description (petrography) has been supplemented by the science of experimentation. The experiments have been directed at trying to imitate, on a laboratory scale, the processes which are believed to have occurred in nature.

The particular field of petrogenesis studied by Dr. Green is that of the basaltic magmas. The work has been done in the Department of Geophysics and Geochemistry within the Research School of Physical Sciences of the Australian National University at Canberra, Australia, where he is a Senior Fellow.

The origin of basaltic magmas which are so abundantly extruded from volcanoes over the whole world, undoubtedly gives us the key to the origin of all igneous rocks. It also tells us a great deal about the chemical and physical processes that have taken place over geological time in the Earth's crust and mantle. In the near future, we should be in a position to theorize on how the material beneath the crust of the earth, say that below Europe, has changed with geological time; perhaps quite a different state of affairs exists beneath the Atlantic.

In the 1960s the experimental investigations on basaltic rocks have become fairly sophisticated and so rather restricted to a specialist band of geologists, physicists and chemists. This being the case, it is necessary every now and again to explain to one's fellow geologists what is happening. Dr. Green's *Bennett Lecture* does just this.

Together with Professor Ringwood at Canberra, Dr. Green subjected rocks to high temperatures (1,000 - 1,500° C) and pressures (approx. 10,000 - 30,000 atmospheres, or 10 - 30 kilobars), and then 'watched' to see how the mineral components reacted during progressive crystallization under various physical conditions. From this study has emerged a hypothesis which is able to account for the known variations in time of the basaltic lavas of the world. This hypothesis, though it may be the leading one at present, is not without its rivals, and an interesting and instructive controversy is arising.

The lecture demonstrates that it is permissible to re-enact geological history in a crucible. Firstly, it reviews mineralogical evidence for the nature of the upper mantle which is considered to be the source of basaltic magmas, and defines the various magma types. Secondly, it describes what happens when model ultrabasic rock begins to melt, and traces various alternative consequences. Thirdly, it reconciles these observations on synthetic rocks with observations made on actual rocks such as the extrusive and intrusive basaltic magmas of Hawaii, Antarctica, and Iceland.

Dr. Green concludes by showing that, according to their experiments, it is possible for basaltic magmas to develop by partial (1% or more)

* Delivered in the Department of Geology in the University of Leicester on 10th November 1969.

melting of the ultrabasic upper mantle of the earth. He postulates on this evidence that the upper mantle has a particular composition, and "pyrolite" is the name he gives to the hypothetical rock. He further shows that primary melts derived from pyrolite can have different chemical compositions depending on the depth at which they were produced and the water content of the parent pyrolite — also, that each of these melts can change its composition through fractional crystallization. This will depend on the length of time that the melts remain at the various depths. Volcanic eruptions occur whenever some geological incident brings such melts to the surface.

THE ORIGIN OF BASALTIC AND NEPHELINITIC MAGMAS

by

D. H. GREEN

1. INTRODUCTION

Basaltic magmas are derived from the earth's mantle. Investigation of the origins of diverse magmas and deduction of the nature of the earth's upper mantle composition and mineralogy are two complementary problems. In this lecture, I will briefly review ideas on the nature of the Earth's upper mantle, as deduced from geological processes which sample the upper mantle and from constraints imposed on their source region by basalt magmas themselves. This will lead to derivation of a specific model composition for the upper mantle. The mineralogical variation with depth for this composition has been studied experimentally. The influence of a small (0.1 - 0.2%) quantity of water in the upper mantle source region is treated in some detail showing that this will lead to the formation of a low velocity zone within the upper mantle, characterized by very small degrees of partial melting.

The variations among natural basalts are briefly reviewed to select those magmas of direct mantle derivation. The experimental crystallization of such basaltic magmas under pressures and temperatures equivalent to upper mantle conditions and with various water contents, allows the recognition of conditions at which these magmas may be in equilibrium with olivine, enstatite, and possibly clinopyroxene, and spinel or garnet i.e. the residual phases of a source peridotite composition. In this way, an attempt is made to outline an internally consistent model of source composition, derivative liquids, peridotitic residues, and magmatic accumulates from the primary liquids under high and low pressure.

2. NATURAL PROCESSES SAMPLING THE UPPER MANTLE

(a) *Kimberlite Pipes* Kimberlite pipes transport xenoliths and xenocrysts of high-pressure type from depths of 80 kilometres or more. The dominance of peridotite xenoliths over rare eclogite (quartz-free), kyanite eclogite and grosspydite xenoliths has previously been noted (Ringwood 1966a). The peridotites themselves commonly consist of olivine + enstatite + rare chromite, olivine + enstatite + garnet, olivine + enstatite + clinopyroxene and olivine, enstatite, clinopyroxene and garnet. Magnesium-rich ilmenite, or phlogopite may occur as minor phases in some samples. The mineral assemblages of the peridotites indicate temperatures well below their solidus — this is apparent in the low Al_2O_3 content (1 - 2% Al_2O_3) of orthopyroxene coexisting with garnet and in the generally low degree of solid solution between orthopyroxene — clinopyroxene pairs (Boyd 1967, Green and Ringwood 1969). This is particularly important in evaluating attempts to use the olivine + orthopyroxene + garnet assemblage of some kimberlite inclusions to argue that residues from basalt magma extraction from the mantle source rock should be olivine + orthopyroxene + garnet ± clinopyroxene (O'Hara 1968, Carswell and Dawson 1970)

rather than olivine + aluminous orthopyroxene + aluminous clinopyroxene (Green and Ringwood 1967a, b). However the garnet: pyroxene ratio of many kimberlite xenoliths is such that at temperatures near their solidi (200 - 600° C above their probable equilibration temperature, depending on the water content of the source rock at the time of melting), the garnet would be taken up in the aluminous pyroxene solid solutions giving olivine + orthopyroxene ± clinopyroxene mineralogy. This would be valid for depths of 80 - 150 kilometres in the upper mantle. There is no unique composition for peridotite inclusions in kimberlite, they exhibit a small range in $\frac{100\,Mg}{Mg+Fe^{++}}$ ratio from ~89 to ~93, and relatively larger variations in CaO, Al_2O_3, Na_2O and TiO_2 contents. They are probably residue from basalt magma extraction but represent re-equilibration of the residual phases at temperatures well below the peridotite solidus. Their contents of minor elements such as Ba, Rb, K, etc. are likely to be grossly contaminated by their host 'magma' (kimberlite); this process can be seen in the growth of secondary carbonates, serpentine or phlogopite in some inclusions.

The inclusions of kimberlite thus suggest an upper mantle which is inhomogeneous and at least partially residual in nature and in which magnesian olivine and orthopyroxene are the most abundant phases. Their investigation appears unlikely to lead to the selection of a specific individual xenolith composition as representative of any part of the upper mantle.

(b) *Xenoliths in Alkali Olivine Basalts, Basanites and Nephelinites*

Olivine-rich and nepheline normative magmas quite commonly contain xenoliths of coarse-grained lherzolite with the typical mineral assemblage of olivine > enstatite > clinopyroxene > spinel. Hornblende, phlogopite, and apatite occur as accessory minerals in some examples. There is variation from sample to sample in the relative proportions of the major and minor minerals and in the presence or absence of particular accessory minerals. The pyroxenes are characteristically aluminous (2 - 5% Al_2O_3 in orthopyroxene) and the degree of solid solution between the two pyroxenes indicates temperatures below the solidus temperatures for the lherzolites. The spinel is aluminous spinel with variable chromite solid solution and the stability of the olivine + aluminous pyroxenes + spinel assemblage relative to lower or higher pressure alternatives indicates pressures at equilibration of > 8 kb and < 30 kb, probably < 23 kb. The lherzolite inclusions have a limited range of $\frac{100\,Mg}{Mg+Fe^{++}}$ values from > 88 to < 92. Detailed geochemical and isotopic studies (see Cooper and Green 1969, for references) demonstrate that the lherzolites (at least the intensively studied examples) are accidental xenoliths with no cogenetic or cognate relationship to their host magmas. It has been inferred that the lherzolite inclusions include residual peridotite after magma extraction, but range from such refractory residue to materials which have not suffered partial melting and *complete* magma extraction but may have lost a small low temperature melt or fluid phase. Again it is possible to ascertain which lherzolites are not refractory and residual in character, only after detailed geochemical study, and it is not yet possible to select a specific lherzolite composition as appropriate for a mean upper mantle composition. Rather it appears that the mantle

source region for the lherzolite inclusions is appreciably inhomogeneous on the hand-specimen scale.

Other coarse-grained inclusions occur with the dominant lherzolite and include olivine orthopyroxenites, websterites, spinel websterites, and garnet clinopyroxenite. These compositions have lower $\frac{100\,Mg}{Mg+Fe^{++}}$ ratios, decreasing approximately in the order listed above, and show clear evidence of exsolution and partial reaction and recrystallization of the assemblages in a high pressure cooling history following initial crystallization. These inclusions are interpreted as random xenoliths of small bodies of *high pressure* (> 10 kb) accumulates and accumulates + entrapped liquid. Another group of xenoliths, which may occur with or without the lherzolite xenoliths described above, includes dunites ($Fo_{87.5}$ - Fo_{84}) with minor chromian spinel, clinopyroxene and minor plagioclase, and possibly related wehrlites and olivine clinopyroxenites (Jackson and Wright 1970). This group contains more iron-rich olivine than the lherzolite inclusions and the mineral assemblages lack the clear evidence of a high pressure cooling history which is evident in the garnet pyroxenites. They are interpreted as accumulates or recrystallized accumulates from basaltic magmas at shallower depths (< 20 kilometres approximately). Inclusions of olivine gabbro, gabbro, and anorthosite (approximately An_{80}) are interpreted as accumulates from shallow magma chambers (< 10 kilometres). Ultimately the detailed study of xenolithic inclusions and their host magmas, together with knowledge of the crystallization sequence in various basalt magma types, should provide important evidence on the natural processes of crystallization and fractionation of basaltic magmas at various depths.

(c) *High-temperature peridotite intrusions* There are some peridotite intrusions, usually of dome or plug-like form and emplaced in metamorphic terrains, which have high temperature, dynamothermal, metamorphic aureoles. The peridotites themselves provide evidence of initial crystallization at high pressure and high temperature (to olivine + aluminous pyroxene + spinel) and subsequent movement as high temperature crystalline diapirs to emplacement in the crust at lower pressures. The mineralogy of these peridotites is olivine > enstatite > clinopyroxene > spinel (high pressure assemblage). The major element composition and mineralogy is such that these rocks could potentially yield some proportion of basaltic magma by partial melting but detailed geochemical studies such as that of Frey (1969) show evidence for more complex history and selective depletion in some elements by an earlier melting or volatile-extraction process. Inhomogeneity within the peridotites due to lenses or bands of dunite or pyroxenite and modal variation within the peridotite again pose difficulty in selecting a valid mean composition for these mantle-derived peridotites.

To summarize, at least three geological processes sample materials which, because of their high pressure mineralogy, demonstrably crystallized under upper mantle conditions. All three processes indicate the importance of peridotitic composition with major olivine, enstatite as the second most abundant phase, essential clinopyroxene and a minor but essential alumina-rich phase which may be plagioclase, spinel or garnet depending on the final P, T conditions of equilibration. In all three processes, there is a

problem of representative sampling and inhomogeneity. The partially residual or depleted character of many samples, relative to a potential basalt source composition, has already been demonstrated. These factors illustrate the difficulty of natural mantle-sampling processes in determining the mean upper mantle composition.

3. THE PYROLITE MODEL FOR THE UPPER MANTLE

If basaltic magmas are liquids derived from the upper mantle as products of partial melting then it would be possible to estimate the source-rock composition if the compositions of liquid and residue and their relative proportions were known. This is the rationale of the 'pyrolite' -model for the mean upper mantle composition and it is emphasized that this approach is a general one (Ringwood 1962). Green and Ringwood (1963) calculated a specific pyrolite composition by combining an average basalt composition (Nockolds 1954) and very refractory dunite in the proportions 1:3. The proportion 1:3 was chosen to yield Al_2O_3 and CaO contents similar to those of the natural mantle-derived peridotites of the previous section and also similar to an estimated upper mantle composition based on the chondritic earth model. Later experimental work on basaltic compositions permitted more restrictive limitations on the nature of liquids and residues in basalt genesis. Ringwood (1966a) calculated a second pyrolite composition using Hawaiian olivine tholeiite as the liquid and harzburgite (olivine 80%, enstatite 19%, chromite 1%) as the residue. These were combined in the 1:3 ratio to give the composition, shown in column 9 of table 1, which has orthopyroxene : olivine and pyroxene : Al_2O_3 ratios much closer to those of the mantle-derived peridotites. With the models of liquid compositions, nature of residues, and proportions of liquid : residue (which are developed later in this lecture) one could calculate many such 'pyrolite' compositions, and if the concept of a mean upper mantle composition (acting as the source for a variety of magma types) has any validity then these calculated compositions should be very similar. Also as more extensive studies of mantle-derived peridotites become available, these may provide closer constraints by indicating trends of increasingly residual character from 'pyrolite'. At the present time the pyrolite composition of Ringwood (1966a) appears adequate in deriving internally-consistent models of mantle composition and basalt genesis, at least to the level of precision currently possible.

The stability relations of various mineral assemblages for the pyrolite composition have been experimentally determined (fig. 1) (Green and Ringwood 1967a, 1969; Green and Hibberson 1970). The boundary for the disappearance of spinel at high temperature to yield the olivine + aluminous pyroxenes assemblage and the boundary for appearance of garnet from the latter assemblage are sensitive to bulk composition, particularly the pyroxene : R_2O_3 proportions. In the pyrolite composition of Green and Ringwood (1963), spinel persists to the solidus and there is no distinct inflexion in the boundary for the appearance of garnet from the olivine + aluminous pyroxenes + spinel assemblage. In considering partial melting of the pyrolite composition (Ringwood 1966a) under dry conditions, the first liquids will be in equilibrium with olivine + pyroxenes + plagioclase at low pressures, olivine + aluminous pyroxenes at intermediate pressures and olivine + aluminous pyroxenes + garnet at high pressures. With increasing degree of melting, the minerals in equilibrium with the

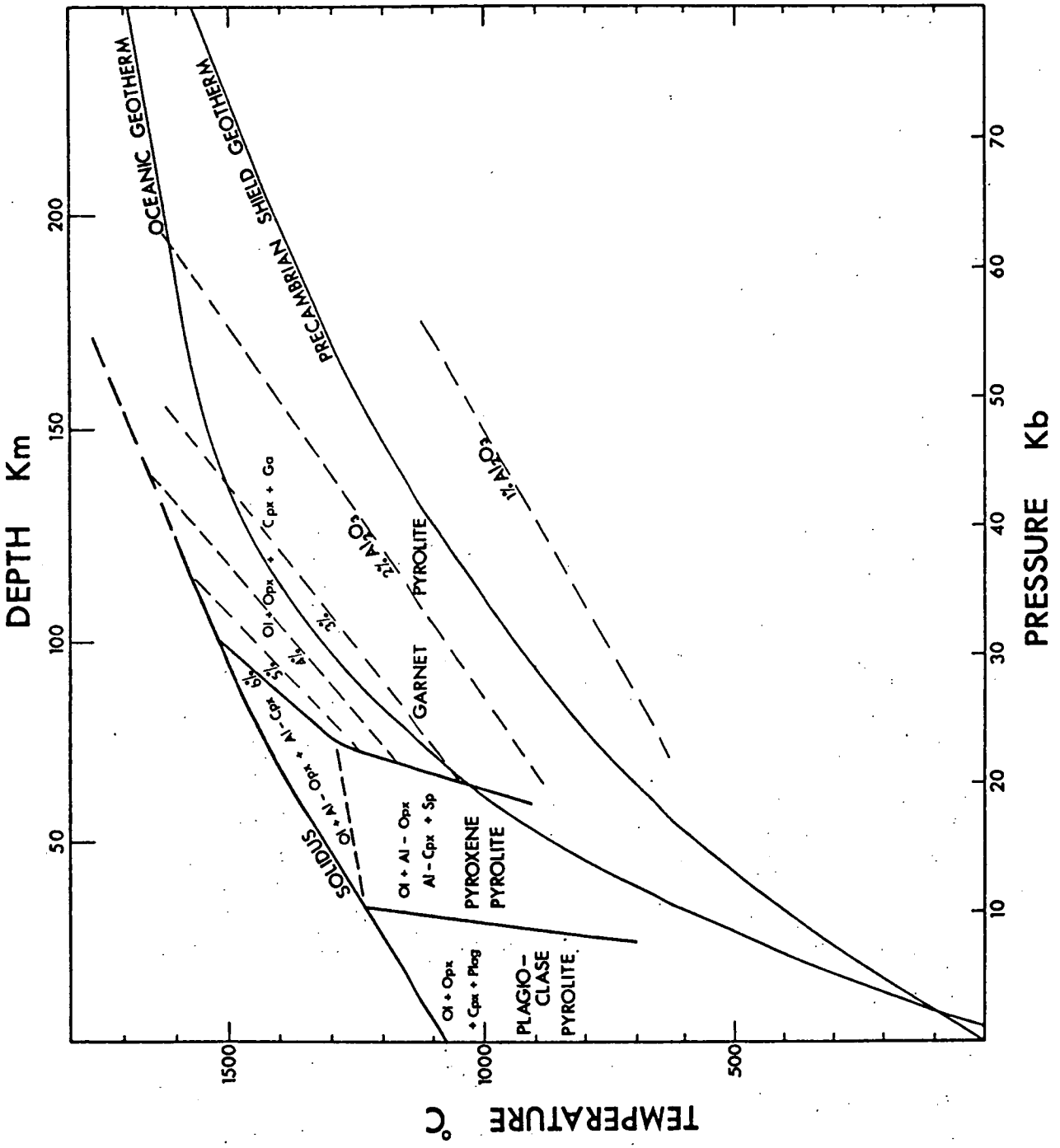

FIG. 1 (Green and Ringwood 1967a). Diagram illustrating the P, T, fields of different mineral assemblages in pyrolite composition under anhydrous conditions. The figures 1% Al_2O_3, 2% Al_2O_3, 3%, 4% etc. refer to the Al_2O_3 content of orthopyroxene in equilibrium with garnet, clinopyroxene and olivine in the garnet pyrolite field. Positions of two estimated geothermal gradients are also shown.

melt disappear in the order: plagioclase followed by clinopyroxene, clinopyroxene; and garnet followed by clinopyroxene (up to 36 kb) in the difference phase fields. Enstatite and major olivine remain as the residual minerals for quite high degrees of melting at pressures above 5 kb.

If the solidus of the pyrolite is lowered by the presence of water, then the characteristic mineralogy at the solidus and the nature of liquids developed in equilibrium with the near-solidus mineralogy will both differ. The presence of water causes crystallization of amphibole in the subsolidus mineralogy, but amphibole stability is limited at high pressure and this mineral breaks down to olivine + pyroxenes + garnet + water. Experimental studies indicate that for the pyrolite composition containing 0.1 - 0.2% H_2O, amphibole breaks down at pressures above 28 - 29 kb at 1,000° C yielding a subsolidus assemblage of olivine + pyroxenes + garnet + rare phlogopite (Green and Ringwood 1969). The solidus for pyrolite containing 0.1 - 0.2% water will have the form shown in figure 2 (Green 1970). Within the amphibole stability field, the subsolidus assemblage will contain 10 - 15% amphibole, and the P_{H_2O} for this mineral assemblage will determine the solidus at some value below the solidus for $P_{H_2O}=O$. At higher pressure, the solidus for the particular P_{H_2O} value will intersect the amphibole breakdown curve for the same P_{H_2O} value. The solidus will then migrate through a series of such intersections to the intersection of the amphibole breakdown and solidus curves for $P_{H_2O} = P_{total}$ If another fluid phase such as CO_2 is present in the upper mantle such that P_{H_2O} is some value $P_2 < P_{fluid} = P_{solid}$ then the solidus will only be depressed to the intersection of amphibole breakdown and solidus curves for $P_{H_2O} = P_2$.

If we consider a load pressure of 25 kb it is apparent from figs 1, 2 that partial melting of anhydrous pyrolite would require temperatures of around 1,450°C and initial liquids would be in equilibrium with olivine + aluminous enstatite + aluminous clinopyroxene. At these temperatures the extent of mutual pyroxene solid solution is large so that the clinopyroxene in equilibrium with the liquid would be subcalcic (~11% CaO). In contrast, in the presence of 0.1 - 0.2% water in the source pyrolite, melting would begin at around 1,100° C and initial liquids would be in equilibrium with olivine, enstatite (~3% Al_2O_3, fig. 1), clinopyroxene, and garnet. The amount of garnet present in the pyrolite composition would be ~7%. The pyroxenes at the solidus would show a very much lower degree of mutual solid solution so that the clinopyroxene in equilibrium with early liquids would be calcium rich (> 20% CaO).

An estimated geothermal gradient (Clark and Ringwood 1964, Ringwood 1966b) is illustrated in fig. 2. This does not intersect the anhydrous solidus for pyrolite but does intersect the solidus for pyrolite containing a small amount of water. Because the degree of melting at temperatures above the solidus is strongly controlled by the limited initial water content of the source rock (fig. 3), the amount of liquid present will remain small for a rather large temperature interval above the solidus. The effect of small quantities of water in the upper mantle is thus to cause a region beginning at depths of 80 - 100 kilometres in which there is

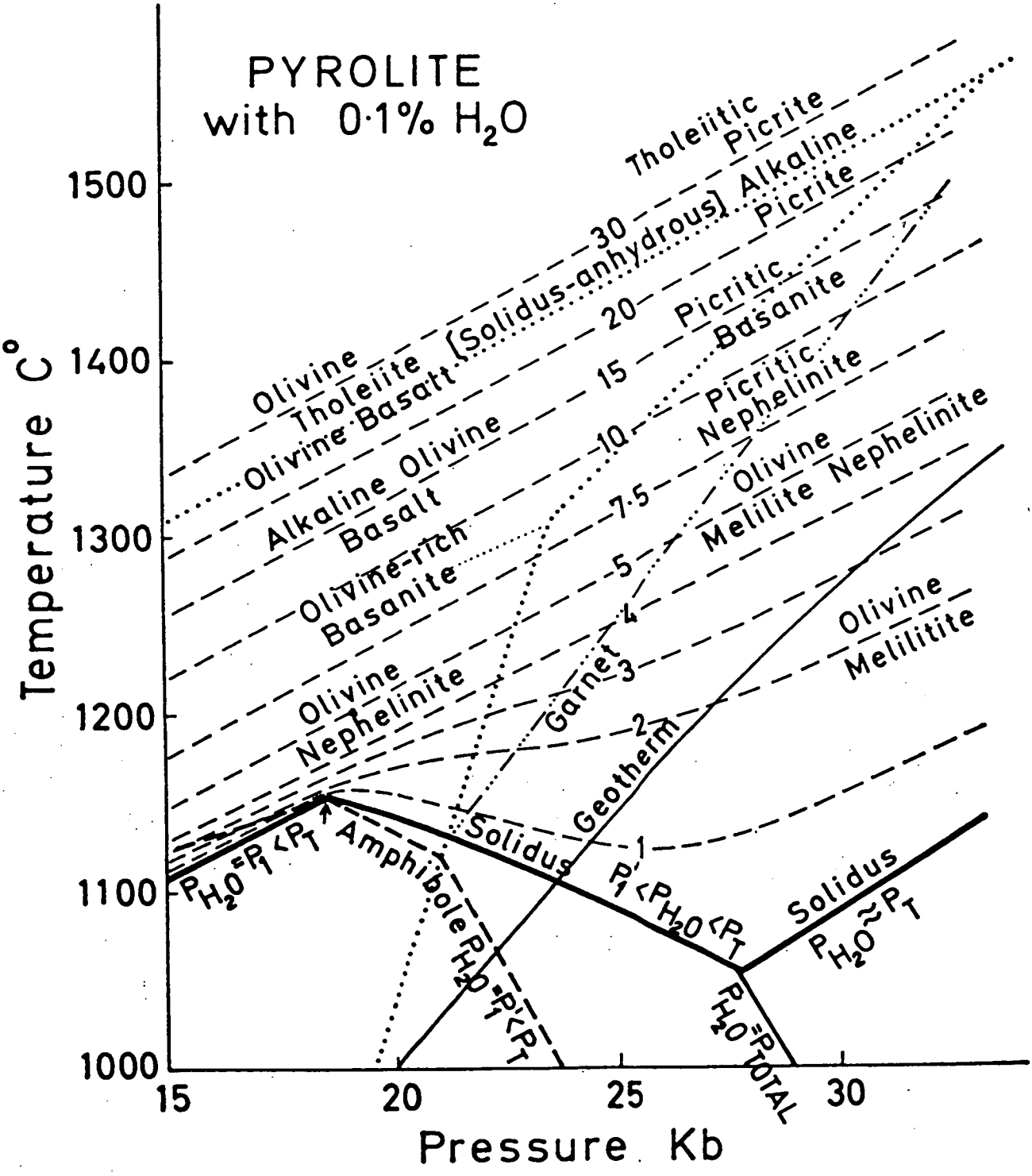
PYROLITE
with 0·1% H_2O
Temperature C°
1500
1400
1300
1200
1100
1000
15
20
25
30
Pressure Kb
Tholeiitic Picrite
30
Olivine Tholeiite (Solidus-anhydrous) Alkaline Picrite
20
Olivine-Basalt
15
Picritic Basanite
Alkaline Olivine Basalt
10
Picritic Nephelinite
Olivine-rich Basanite
7·5
Olivine Melilite Nephelinite
5
Olivine Nephelinite
4
Garnet
3
Olivine Melilite
2
Geotherm
1
Solidus
$P_{H_2O} = P_1 < P_T$
Amphibole
$P_{H_2O} = P_1 < P_T$
$P_1 < P_{H_2O} < P_T$
Solidus
$P_{H_2O} \simeq P_T$
$P_{H_2O} = P_{TOTAL}$

normally present a small (< 5%) melt fraction. It is considered that this region corresponds to the seismic low velocity zone, the small melt fraction producing low seismic velocity and high seismic attenuation. The lower boundary of the low-velocity zone may be caused either by decreasing water content or by entry of water into higher pressure silicate phases.

The discussion in this section has illustrated the very sensitive controls exerted by P, T and P_{H_2O} in determining the mineralogy and solidus temperature of the model pyrolite composition. Attention in the following section is directed at the liquidus phases of basaltic magmas at high pressures since if these magmas are derived from the pyrolite composition by partial melting then the liquidus phases of the basalt and the residual phases in pyrolite at a given P, T and % melting must match one another. The study of the liquidus and near-liquidus phases of basalts at high pressure also shows the possible fractionation trends which a basalt magma, separated from its source peridotite, may follow at various depths in the upper mantle and crust.

4. CRYSTALLIZATION OF BASALTIC MAGMAS AT HIGH PRESSURE

(a) *Basalt nomenclature used* In studies of basalts where the chemical composition of a magma is the principal concern, it is convenient to adopt a normative (i.e. indirect chemical) classification rather than a modal (mineralogical) classification. The nomenclature used is as follows:

Tholeiite: basalt with normative hypersthene
Quartz tholeiite: basalt with normative hypersthene and quartz
Olivine tholeiite: basalt with normative hypersthene and olivine, hypersthene > 3%
Olivine basalt: with normative olivine and with 0-3% normative hypersthene; no normative nepheline
Alkali olivine basalt: with normative olivine and nepheline; nepheline < 5%

FIG. 2 (Green 1970). Diagram illustrating the amphibole stability limit at high pressure and the solidus for pyrolite composition containing approximately 0.1% H_2O. Also shown (dotted lines) are the solidus for anhydrous pyrolite and the boundary for appearance of garnet (from Green and Ringwood 1967a). The numbered dashed curves show the % liquid present above the solidus and the petrochemical character of these liquids is indicated. The geothermal gradient shown is the oceanic geotherm illustrated by Ringwood (1966b).

The positions of the curves on this diagram, other than the anhydrous boundaries, are estimated from reconnaissance experiments on the solidus and amphibole stability in pyrolite with 0.1-0.2% water and by experiments establishing the degree of depression of the liquidus temperatures of various basalts by addition of known amounts of water.

Ordinate — Temperature within the earth.

Abscissa — P_{total} = Load Pressure or Solid Pressure.

P_{H_2O} = equilibrium water pressure.

P_I = water pressure along solidus for pyrolite with 0.1% H_2O.

P_I varies along the solidus to P'_I and an arrow indicates the intersection of the solidus with a subsolidus breakdown curve for amphibole at $P_{H_2O} = P'_I$ also (amphibole $\longrightarrow$ pyroxenes + garnet + olivine + water).

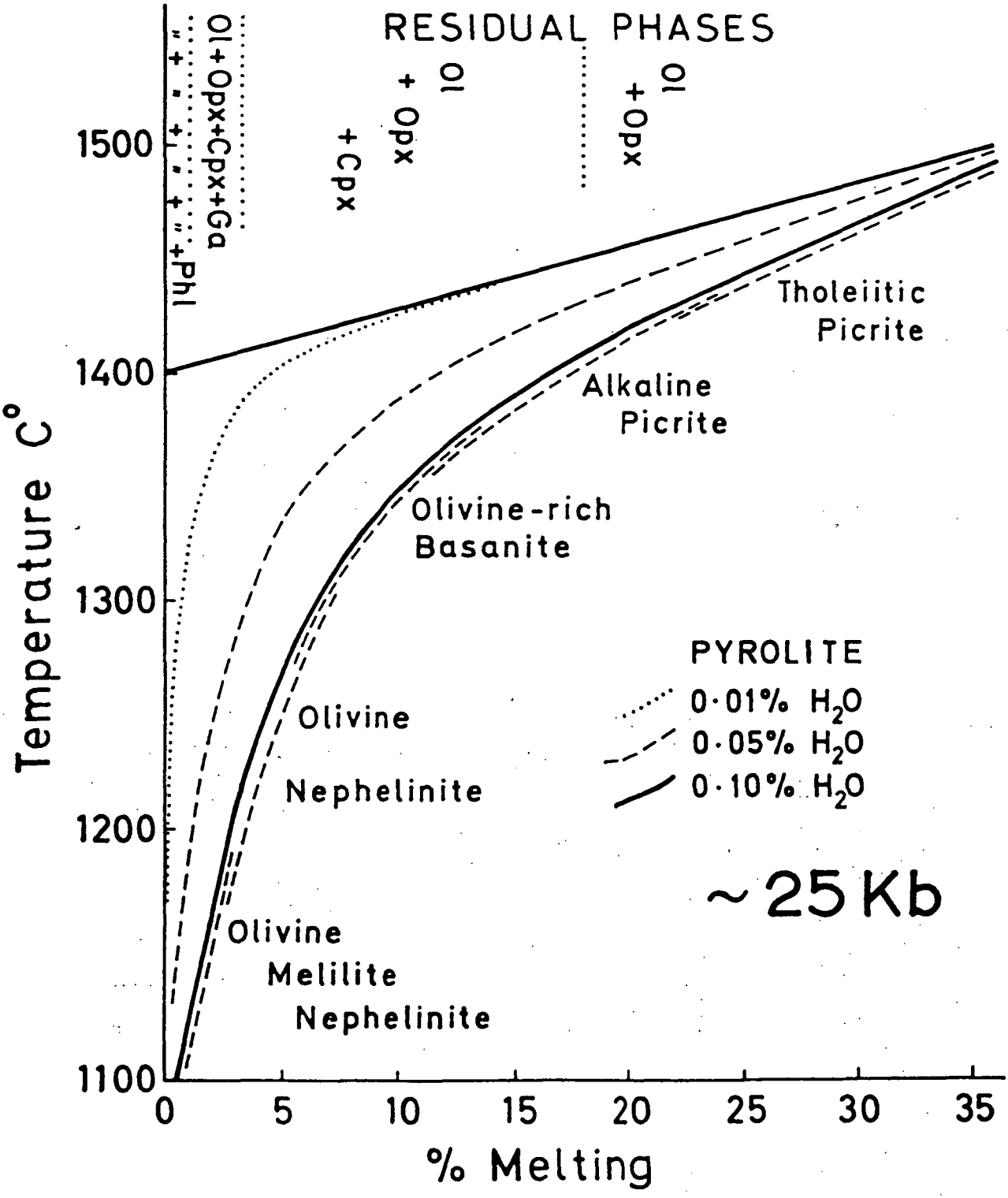

FIG. 3 (Green 1970). Diagram contrasting the melting behaviour of anhydrous pyrolite with melting in pyrolite compositions containing 0.01, 0.05 and 0.10% H_2O. The nature of the residual phases and the petrochemical character of the liquids derived are shown for example with 0.10% H_2O.

Basanite: basalt with normative olivine, nepheline and albite and with nepheline > 5%, albite > 2%
Olivine nephelinite: basalt-like composition with major normative olivine and nepheline; albite < 2%; normative orthoclase and/or leucite, but no normative larnite
Olivine melilite nephelinite: basalt-like composition with normative olivine, nepheline, leucite and larnite.

The principal variation between the above magma types is the degree of silica saturation. Most workers recognize continuity and transition in chemical composition between the various basalts. Silica content decreases from 47 - 49% in the olivine tholeiites to < 38% in olivine melilite nephelinite; alkalis ($Na_2O + K_2O$) increase and CaO also increases, paricularly in the nephelinitic compositions. A further variation in basalt compositions is apparent in the recognition of distinctive high-alumina basalts (Tilley 1950; Kuno 1960). These are aphyric basalts with normative olivine and either normative hypersthene or low normative nepheline contents but with Al_2O_3 contents distinctly higher (at 16 - 20% Al_2O_3) than 'normal' olivine tholeiites or alkali olivine basalts of similar SiO_2 and $Na_2O + K_2O$ contents (Kuno 1960).

(b) *Selection of relevant basaltic magmas* The detailed studies of the active Hawaiian volcanoes convincingly demonstrate the importance of low pressure, near-surface crystal fractionation in determining the composition of the magma finally extruded at the surface. In selecting basalts for study under simulated upper mantle compositions, it is clearly necessary to seek those liquids which have been derived from the upper mantle without opportunity for crystal fractionation at shallow levels. One group of basalts obeying this restriction is the suite from alkali olivine basalts, through basanites, olivine nephelinites, olivine melilite nephelinites to olivine melilitites, which contain high density ($\rho \sim 3.3$) xenoliths and xenocrysts of high pressure mineralogy. These magmas clearly cannot have undergone any crystal fractionation at pressures less than those at which the xenoliths were picked up. As a group, these magmas are Mg-rich, rather high in normative olivine, and with SiO_2 contents ranging from $\sim$ 49% SiO_2 (some olivine trachybasalts) to $\sim$ 36% (olivine melilitites). There is of course no reason to suppose that this whole spectrum is related by crystal fractionation or by different degrees of partial melting at any one pressure (depth) but there clearly must be processes operative in the upper mantle capable of yielding each magma type by partial melting of pyrolite or by crystal fractionation of a higher temperature magma at some depth within the upper mantle. The experimental petrologist can directly evaluate the possible inter-relationships for these magmas.

In selecting an olivine tholeiite magma for experimental study at high pressures one cannot use the high-pressure inclusion criterion since this class of basalts does not contain such inclusions. However, the detailed studies of the 1959 - 60 Kilauea Iki eruption of Hawaii have provided evidence for the relatively rapid movement of a magma batch from depths of approximately 60 kilometres to the earth's surface, and eruption of that magma batch in episodic extrusions which ranged from very olivine-rich picrite to olivine-poor tholeiite. These episodic eruptions could be monitored for volume and magma composition, allowing an estimate of the mean composition of the lava lake in which the extrusions accumulated. The mean composition was estimated as an olivine-rich

	Olivine Tholeiite	Olivine Basalt	Picrite	Alkali Basalt	Olivine-rich basanite (Mt. Leura, Victoria) (Green, unpublished)	Picritic Basanite	Olivine nephelinite	Picritic Nephelinite	Pyrolite (Ringwood 1966)
	(Green and Ringwood, 1967b)					(Bultitude & Green, 1968, 1970)			
	1	2	3	4	5	6	7	8	9
SiO_2	46.95	47.05	45.51	45.39	44.63	44.50	44.30	43.70	45.16
TiO_2	2.02	2.31	1.93	2.52	2.92	1.30	1.50	1.30	0.71
Al_2O_3	13.10	14.17	12.44	14.69	11.67	12.00	14.20	12.30	3.54
Fe_2O_3	1.02	0.42	0.92	1.87	2.95	0.80	0.50	1.10	0.46
FeO	10.07	10.64	8.67	12.42	9.39	10.60	9.70	10.80	8.04
MnO	0.15	0.16	0.15	0.18	0.15	0.20	0.20	0.20	0.14
MgO	14.55	12.73	18.79	10.37	13.85	16.70	13.30	17.00	37.47
CaO	10.16	9.87	9.67	9.14	7.68	9.90	11.20	9.70	3.08
Na_2O	1.73	2.21	1.64	2.62	3.65	2.80	3.60	2.70	0.57
K_2O	0.08	0.44	0.08	0.78	2.00	0.80	1.00	0.80	0.13
P_2O_5	0.21		0.20	0.02	1.03	0.40	0.50	0.40	0.06
Cr_2O_3									0.43
$\frac{100\ Mg}{Mg+Fe++}$	72.00	68.10	79.40	59.80	72.50	73.70	71.00	73.80	89.20
CIPW Norms									
Or	0.60	2.70	0.50	4.50	11.70	4.50	6.10	4.50	1.10
Ab	14.70	18.90	13.90	18.00	12.00	6.20	2.00	3.40	4.70
Ne				2.20	10.20	9.40	15.30	10.60	
An	27.60	27.30	26.30	26.20	9.80	18.00	19.40	19.20	6.60
Di	17.00	17.60	16.50	15.70	18.70	22.80	26.40	21.70	6.70
Hy	12.30	1.30	2.80						15.40
Ol	21.90	27.20	34.60	25.80	25.80	34.40	25.90	35.70	62.70
Ilm	3.80	4.40	3.70	4.80	5.60	2.40	2.90	2.40	1.40
Mt	1.40	0.60	1.30	2.90	4.30	1.20	0.70	1.60	0.60
Ap	0.50		0.40		2.00	1.00	1.30	1.00	0.10
Chr									0.70

TABLE I COMPOSITION OF BASALTIC GLASSES USED FOR EXPERIMENTAL STUDIES OF CRYSTALLIZATION AT HIGH PRESSURES

tholeiite containing ~18% normative olivine (Macdonald and Katsura 1961) or 17% normative olivine (Murata and Richter 1966). Green and Ringwood (1967b) used an olivine tholeiite composition modelled closely on Macdonald and Katsura's estimate as a reasonable inferred composition for an olivine tholeiite magma derived from the upper mantle with little or no low pressure fractionation.

(c) *Crystal fractionation — olivine tholeiite to alkali olivine basalt* The compositions and CIPW norms of some of the basalt types which have been studied experimentally are listed in Table 1. The experimental results for olivine tholeiite (fig. 4) show olivine as the liquidus phase at low pressure, orthopyroxene at intermediate pressure, clinopyroxene at about 20 kb, and garnet at 27 kb. Electron probe analyses of the near-liquidus crystals and estimation of the percentage crystallization allow calculation of the derivative liquid compositions. In this way it has been shown that, at atmospheric pressure, parental olivine tholeiite will yield derivative quartz tholeiite liquids, at about 9 kb derivative liquids will be characteristically high-alumina olivine tholeiites, and at 13 - 18 kb derivative liquids will move rapidly into the nepheline-normative field. The validity of the major role of orthopyroxene in defining the trend from parental olivine tholeiite to derivative alkali olivine basalt was confirmed by experiments on an olivine basalt, an alkali olivine basalt, and on a picrite composition, the latter being saturated in olivine to higher pressures than the other three compositions but having orthopyroxene as the second phase to crystallize at 13 - 18 kb. It is emphasised that the calculation of crystal fractionation trends must be carried out on all oxide components of the basalt — plots of oxide trends, or projections into 'simple component planes' can be extremely misleading and should be used only for illustrative and not deductive purposes. In fig. 5, the molecular norms of the experimental compositions and of their calculated derivatives (Green and Ringwood 1967b) have been plotted as they would appear on a plane approximately parallel to the base of the 'basalt tetrahedron' (Qz - Ol - Cpx - Ne) of Yoder and Tilley (1962). The calculated fractionation trends are shown as solid lines — these show the possible fractionation behaviour of a magma batch of the chosen composition if cooled at the pressures indicated. Thus at 13.5 kb the olivine tholeiite (OT_1) crystallizes orthopyroxene alone near the liquidus and fractionation produces the trend illustrated. At the same pressure, a second olivine tholeiite (OT_2), prepared by adding 5% more olivine (Fo_{90}) to the initial olivine tholeiite, crystallizes olivine alone (see fig. 4). However, at 13.5 kb it obviously cannot fractionate by olivine separation *through* the point OT_1. Thus before the liquid crystallizes 5% olivine, orthopyroxene appears and dominates the further crystal extract giving the trend shown as a dashed curve for 13.5 kb. A similar relationship is apparent between the picrite (PB) and olivine basalt (OB) at 13 - 18 kb. These compositions and their crystallization paths illustrate clearly that although olivine must appear (at appropriate P, T) with orthopyroxene as a liquidus phase for any liquid derived by partial melting of a pyrolite source rock, the olivine is a minor phase in the crystal accumulate formed if the magma separates and begins to crystallize at depths equivalent to 12 - 18 kb. The type of crystal accumulate formed would be an olivine orthopyroxenite. When clinopyroxene joins the precipitating phases, any olivine not removed from contact with the liquid may react with liquid. A reaction (olivine + $\text{liquid}_1 \longrightarrow$ clinopyroxene + liquid_2) has been observed

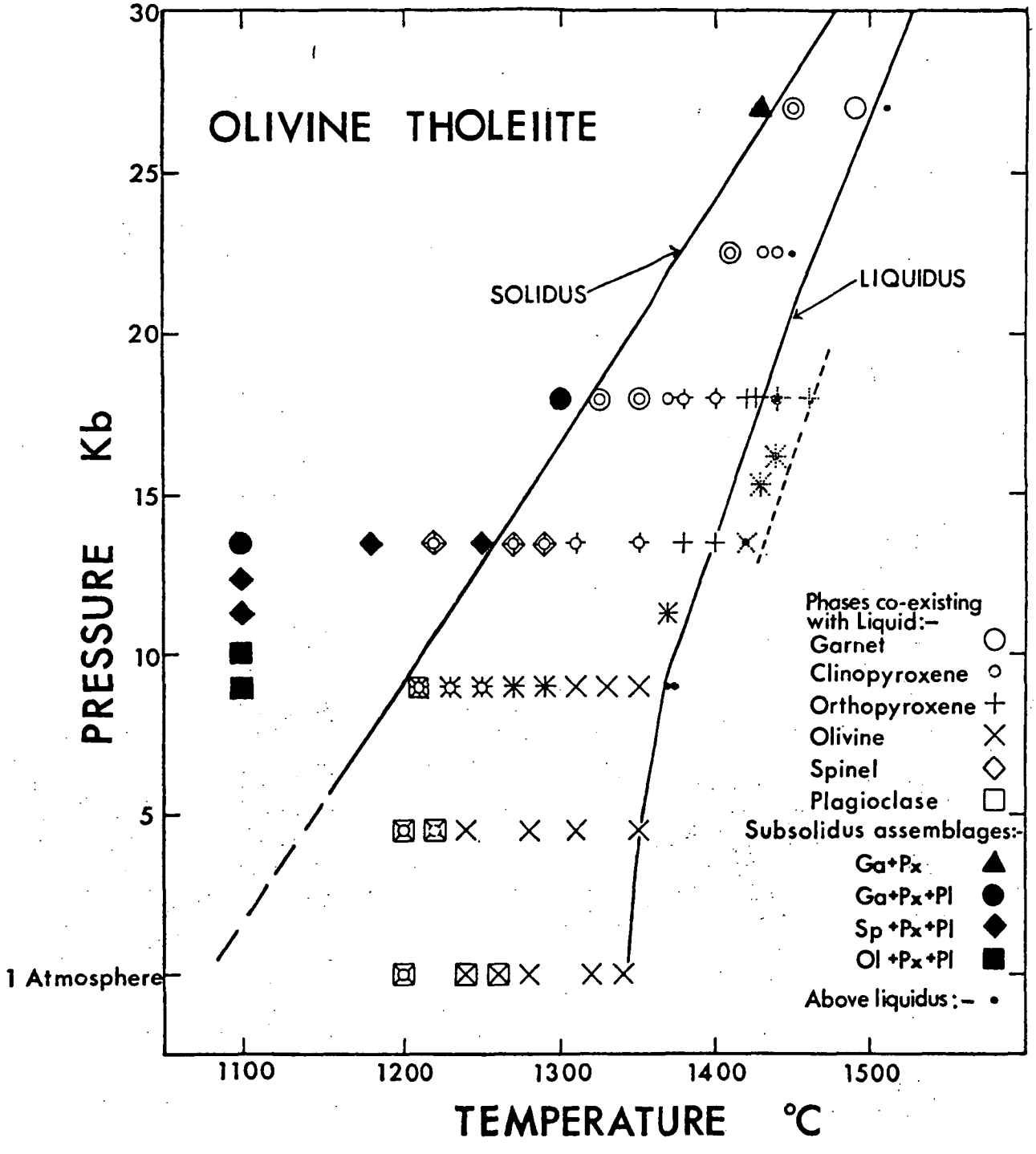

FIG. 4 (Green 1969b). Experimental crystallization of olivine tholeiite (Table 1) at various pressures. Data (dotted symbols) for an olivine-enriched tholeiite was prepared by addition of 5% olivine (Fo_{90}) to the olivine tholeiite of Table 1.

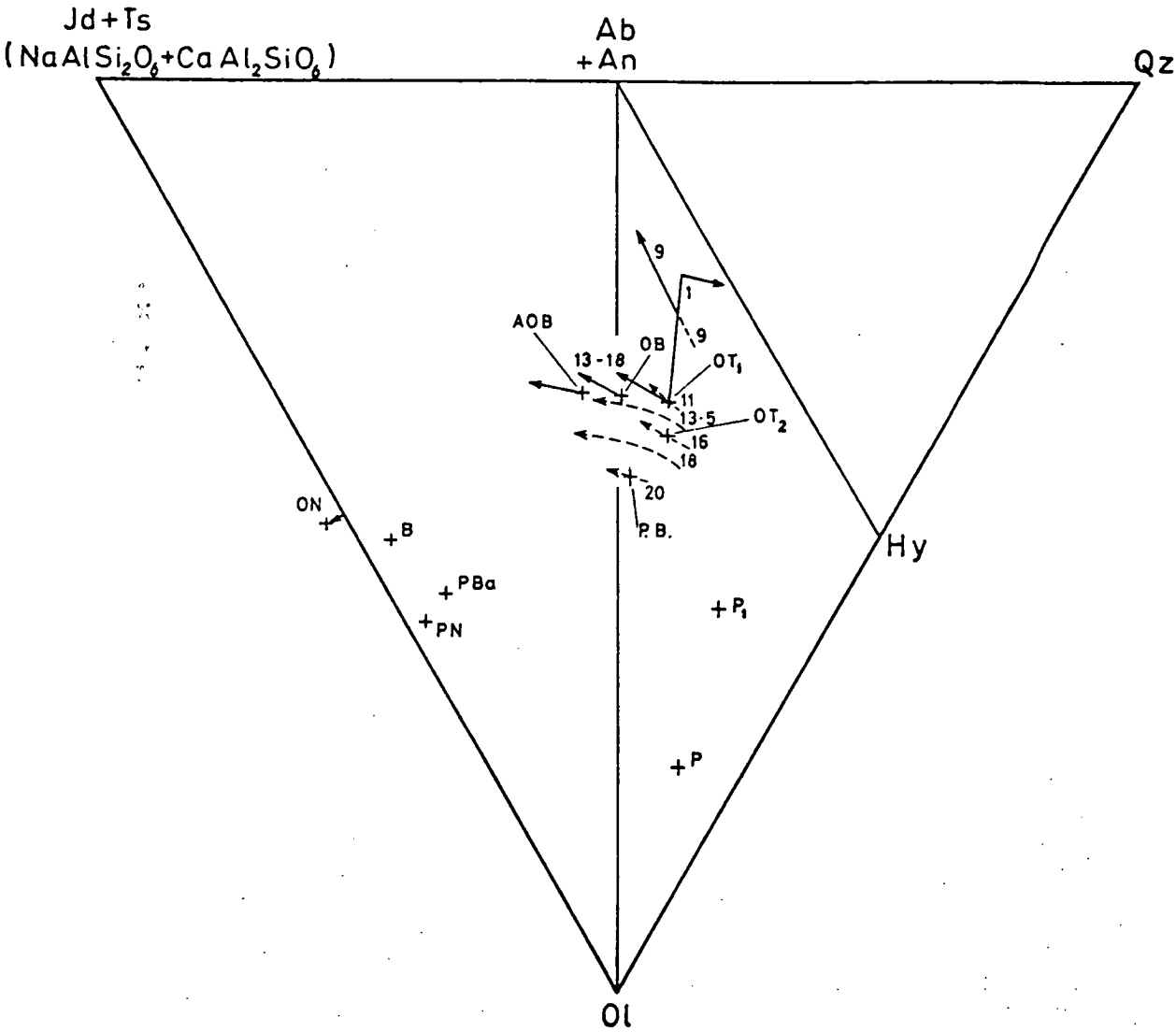

FIG. 5 Plot of experimental compositions of Table 1 and calculated fractionation trends, on the surface (Jadeite + Ca-Tschermak's silicate) — Olivine — Quartz. Co-ordinates calculated from the Ab, An, Ne, Hy, Ol components of the molecular norm as follows:

$Jd + Ts = Ab + An + Ne$

$Qz = Ab + An - Ne + \frac{Hy}{2}$

$Ol = Ol + \frac{Hy}{2}$

OT_1 = Olivine tholeiite
OT_2 = Olivine tholeiite (OT_1) + 5% olivine Fo_{90}
OB = Olivine basalt
AOB = Alkali olivine basalt
PB = Picrite
PBa = Picritic basanite
B = Olivine-rich basanite
ON = Olivine nephelinite
PN = Picritic nephelinite
P = Pyrolite
P_1 = Pyrolite – 40% Olivine

Solid lines: calculated fractionation trends (Green and Ringwood 1967b) at various pressures (9kb, 13 - 18 kb).

Dotted lines: estimated trends for liquids in equilibrium with olivine and orthopyroxene at various pressures (numbers indicate the pressures).

in some undersaturated compositions at pressures up to 31.5 kb (Bultitude and Green 1970). Accumulates lacking primary olivine and consisting only of aluminous orthopyroxene + aluminous clinopyroxene may thus be formed, and at lower temperatures the disappearence of orthopyroxene and later appearance of spinel or garnet may yield clinopyroxenite, spinel clinopyroxenite or garnet clinopyroxenite accumulates.

(d) *Crystal fractionation — basanite to olivine nephelinite* The compositions of some highly undersaturated basaltic magmas which have been studied experimentally are given in Table 1 and plotted on Fig. 5. The compositions were selected from amongst basalts containing high pressure lherzolite xenoliths, and thus should closely approach the compositions of magmas existing in the upper mantle. All are olivine-rich and, under dry conditions, olivine is the liquidus phase up to 20 kb or to 32 kb depending on the specific composition. Clinopyroxene is the second phase to crystallize over a large pressure range and becomes the liquidus phase over a small pressure interval in the olivine nephelinite and olivine-rich basanite compositions. At higher pressure, clinopyroxene is either joined by garnet on the liquidus or garnet becomes the liquidus phase, joined by clinopyroxene slightly below the liquidus. Details of the experimental studies, with analytical data on the near-liquidus phases are given by Bultitude and Green (1970). In the picritic basanite composition, orthopyroxene appears in the crystallization sequence at 18 kb over a very small temperature interval after the crystallization of 5 - 8% olivine and prior to appearance of clinopyroxene. In the picritic nephelinite composition at 22.5 kb, orthopyroxene again makes a very brief appearance in the crystallization interval, after the precipitation of some olivine and clinopyroxene. Orthopyroxene does not appear in the crystallization sequences for the olivine nephelinite or olivine-rich basanite at any pressure under dry conditions.

The fractionation trends at various pressures have been calculated from the analytical data on the liquidus phases. Low-pressure fractionation is dominated by olivine and yields derivative liquids of higher silica content and rapid iron enrichment. At pressures of 18 - 27 kb, fractionation of these particular liquids is dominated by clinopyroxene with minor olivine or garnet. Derivative liquids become more undersaturated but there is marked calcium depletion accompanying the silica depletion. At pressures greater than 27 kb crystal fractionation is controlled by garnet + clinopyroxene separation. Evaluation of fractionation controlled by these phases is particularly important since O'Hara (1968) considers that eclogite (i.e. garnet + clinopyroxene) fractionation is the process by which magmas such as alkali olivine basalts, basanites, nephelinites, etc. become highly enriched in 'incompatible elements' (such as K, P, Ti, Rb, Sr, U, Th, etc.) relative to olivine tholeiites. O'Hara (1968 pp. 117 - 118) suggests 50% ecologite fractionation will be important in trace element enrichment but will have little effect on the major element composition of the basalts. O'Hara and Yoder (1967, p. 110) similarly invoke eclogite fractionation to account for enrichment in trace elements, but also invoke eclogite fractionation from parental tholeiitic picrite to produce residual liquids with abundant olivine, nepheline, larnite, leucite and kalsilite in the CIPW norm. The quantitative evaluation of fractionation by garnet + clinopyroxene separation at pressures of 27 - 36 kb from the picritic basanite and nephelinite compositions by Bultitude and Green (1970) shows that large

degrees of crystallization are required to produce small changes in silica content and in degree of undersaturation. Such fractionation is accompanied by depletion in calcium and enrichment in iron relative to magnesium. These effects are inconsistent with characteristics on natural magmas of mantle derivation which show increasing Ca-contents with increasing degree of undersaturation and demonstrate similar or higher $\frac{Mg}{Mg+Fe^{++}}$ values for the very undersaturated magma types, relative to olivine tholeiites. Separation of garnet and clinopyroxene under upper mantle conditions undoubtedly occurs in specific cases (xenoliths of garnet clinopyroxenite in the Delegate or Salt Lake Crater tuffs are in part probably examples of such accumulates) but it is concluded that it is not the process responsible for the natural magma series from olivine-rich tholeiite to olivine nephelinite and olivine melilitite.

Experiments on the effect of water on the liquidus phases of the basanite and nephelinite compositions of table 1 (Bultitude and Green 1968, Green 1969a, b) show that whereas olivine and clinopyroxene or clinopyroxene alone may be the liquidus phases under dry conditions (liquidus 1,400 - 1,450° C, 20 - 30 kb), if the liquidus is depressed to 1,200 - 1,300° C by the addition of 2 - 5% water, then olivine and orthopyroxene, or olivine, orthopyroxene and clinopyroxene may occur at or near the liquidus. This effect has been substantiated for the olivine-rich basanite composition and an alkali olivine basalt composition with experiments using sealed capsules and known quantities of water (Green 1969a, b, Green and Hibberson 1969). It should be noted that the near-liquidus clinopyroxene under dry conditions at 1,400 - 1,450° C is rather sub-calcic, and with the rapid widening of the pyroxene miscibility gap at lower temperature, such a composition would be represented by orthopyroxene and clinopyroxene. Thus depression of the liquidus by the addition of water may bring in orthopyroxene as a liquidus phase, not as a consequence of any major compositional shift of the cotectic between olivine and orthopyroxene (cf. Kushiro 1969), but as a direct consequence of the sensitive temperature dependence of the pyroxene solid solutions.

The important near-liquidus role of orthopyroxene in water-bearing basanitic and nephelinitic magmas at high pressure may permit fractionation of magmas through olivine-rich basanites to olivine nephelinites at 20 - 25 kb and through picritic basanites and picritic nephelinites to olivine melilite nephelinites at $\sim$ 27 kb.

5. APPLICATION OF BASALT CRYSTALLIZATION STUDIES TO PARTIAL MELTING

If we consider an olivine tholeiite magma then the experimental studies (Green and Ringwood 1967b) have shown that by separation of approximately 15% crystals at 13 - 18 kb we may produce an olivine basalt magma type. The crystal extract would be dominantly orthopyroxene with very minor olivine. Further crystallization ($\sim$15%) of orthopyroxene, now joined by sub-calcic clinopyroxene and possibly still accompanied by very minor olivine, will produce a liquid of alkali olivine basalt type. If crystals have remained in contact with the liquid, then we have a chemical system in which an alkali olivine basalt liquid is in equilibrium with minor olivine, minor sub-calcic clinopyroxene and major orthopyroxene. The proportion of crystals to liquid is approximately 30:70 but it will not

affect the composition of either liquid or crystals nor the equilibrium between them if we grossly change the proportions of the crystals adding a very large amount of olivine, a little more orthopyroxene but no more clinopyroxene so that the proportion of crystals to liquid becomes approximately 80:20. We are now considering a total composition which is peridotitic, and have a model of partial melting or batch melting of that total composition. By increasing the temperature on the peridotitic bulk composition we can envisage all the clinopyroxene, major orthopyroxene and minor olivine entering the melt and changing the melt composition back through olivine basalt to reach olivine tholeiite at a stage of about 30% melting.

This discussion illustrates the way in which the experimental studies on basalt crystallization can be applied to a model of partial melting. This reasoning can *only* be applied if the observed liquidus phases of the series of basaltic liquids are the same as the observed phases in the postulated source composition at the same P and T. This particularly applies to $\frac{Mg}{Mg+Fe}$ ratio — a basalt with olivine of Fo_{80} as the liquidus phase could not be in equilibrium with a peridotite having olivine Fo_{90} under any conditions. In this example a prediction that a basalt with similar normative mineralogy but suitably higher $\frac{Mg}{Mg+Fe}$ ratio would have olivine of Fo_{90} as liquidus phase at the same pressure, is probably valid. The situation is more complex with the pyroxenes, however, for the extent of mutual solid solution of calcium-rich and calcium-poor pyroxenes is very dependent on both temperature and $\frac{Mg}{Mg+Fe}$ ratio. Thus if a particular basalt had a clinopyroxene of $\frac{100\,Mg}{Mg+Fe} = 80$ as the liquidus phase at a particular pressure it is difficult to predict whether a more magnesian basalt of the same normative mineralogy will have orthopyroxene or clinopyroxene or even olivine as the liquidus phase at the same pressure, since the pyroxene solid solution limits will be considerably different (less extensive) for the more magnesian pyroxenes. This discussion illustrates the caution that is necessary when attempting to extrapolate from simple iron-free systems to natural basalts, and emphasizes the limitations of projections in which Mg and Fe are equated and on which basalts, peridotites, and mineral compositions of very different $\frac{Mg}{Mg+Fe}$ ratio are plotted with attempts to derive generalized liquidus phase fields and cotectics (e.g. O'Hara 1968). Such techniques may have illustrative value if applied to closely coherent groups of compositions, but remain qualitative and invalid for deductive purposes unless augmented by treatment of the total chemical composition.

(a) *Pyrolite as a source rock for the experimentally studied basalts* In the discussion of basalt crystallization and fractionation it was suggested that by about 30% crystallization of olivine tholeiite at 13 - 18 kb, derivative alkali olivine basalt magmas could be obtained. The accumulate would be dominated by aluminous orthopyroxene, with minor sub-calcic clinopyroxene and minor olivine. Referring to the detail of the analyzed basalts (Green and Ringwood 1967b), the olivine tholeiite and olivine basalt compositions (table 1) had liquidus olivine and orthopyroxene with

$\frac{100\,Mg}{Mg+Fe} \sim 90$, whereas the more iron-rich alkali olivine basalt had liquidus olivine (9 kb) and orthopyroxene (13.5 kb) with $\frac{100\,Mg}{Mg+Fe}$ = 83. In general terms, liquids which could be in equilibrium with the pyrolite $\left(\frac{100\,Mg}{Mg+Fe} = 89\right)$ or residual assemblages from the pyrolite must be relatively magnesian basalts i.e. $\frac{100\,Mg}{Mg+Fe} \sim 68 - 73$. In this respect the alkali olivine basalt composition of Table 1 is unsuitable for direct derivation from a pyrolite source, but a more magnesian composition of similar normative mineralogy is predicted to show similar crystallization behaviour with a slightly higher liquidus temperature and possibly slightly enhanced role of orthopyroxene crystallization at > 13 kb.

Referring to fig. 1, it is apparent that the phases which were invoked in the postulated crystal fractionation of olivine tholeiite to alkali olivine basalt are the same as the phases at the anhydrous pyrolite solidus within the pressure range 10 - 13 kb. This applies to a more detailed comparison of $\frac{Mg}{Mg+Fe}$ ratios and of alumina contents of the pyroxenes (Green and Ringwood 1969). Furthermore, the limited partial melting data on the pyrolite (Green and Ringwood, 1967a) shows that clinopyroxene rapidly enters the liquid and disappears from the residue leaving olivine and enstatite only. The studies on basalt crystallization and mineralogy of pyrolite at high pressure may be integrated to suggest a model of partial melting at depths of 13 - 18 kb. At these depths, if the pyrolite source rock is anhydrous, then the first liquid at the solidus will be in equilibrium with olivine, aluminous orthopyroxene, and aluminous clinopyroxene — a liquid saturated with these phases will be nepheline-normative, i.e. an alkali olivine basalt or, at low degrees of melting at about 18 kb, an olivine-rich basanite (Bultitude and Green 1970). Up to 15 - 20% melting, clinopyroxene will remain among the residual phases and the liquids will remain nepheline-normative, though decreasingly so with increasing temperature. Since all the phases existing in the source rock are Fe-Mg solid solutions, it is considered that melting with increasing temperature will be nearer to a linear process (as illustrated in fig. 3) than a eutectic and 'stepped' process (O'Hara 1968) although different 'gradients' of the various solid-solution cotectics may produce some non-linearity in the % melting *vs.* temperature curve. For degrees of melting greater than 15 - 20%, clinopyroxene will be absent from the residual phases and the liquid, saturated only with olivine and aluminous enstatite, will become increasingly hypersthene normative changing through olivine basalt to olivine-rich tholeiite ($\sim$ 22% olivine, 15% hypersthene, at 13 kb; $\sim$ 27% olivine, 13% hypersthene at 18 kb).

At lower pressures ($\sim$ 9 kb) the experimental studies permit a similar deduction that liquids developed at 15-20% melting will be in equilibrium with olivine, enstatite (lower Al_2O_3 content), and minor clinopyroxene and such liquids will be high-alumina olivine tholeiites (10-15% normative olivine). With higher degrees of melting, clinopyroxene, orthopyroxene and minor olivine enter the melt changing it to olivine tholeiite of low Al_2O_3 type with high normative olivine and hypersthene contents. At higher pressures,

$\sim$ 22 kb, initial melts may be olivine-rich or picritic basanite, and change through alkali picrites to tholeiitic picrites with increasing melting.

The preceding discussion has considered partial melting in a source pyrolite composition which is anhydrous. However, it has been inferred in previous sections that some mantle derived magmas, such as olivine nephelinite or olivine melilitite, are hydrous magmas at their depth of origin implying that the mantle source region is itself water bearing. The effects on the near-solidus mineralogy and solidus temperature of water contents of 0.1 - 0.2% have been discussed in earlier sections, and now must be integrated with the basalt melting data under both wet and dry conditions.

(b) *Partial melting of a hydrous pyrolite mantle: andesitic or nephelinitic magmas?* Turning to the nature of liquids derived by partial melting of a hydrous peridotite source, there are two hypotheses in the current literature which could hardly be more diametrically opposed or mutually exclusive. Each is based on experimental data which are probably correct. Kushiro *et. al.* (1968) and Kushiro (1969) have studied melting relations in the systems enstatite + water, and forsterite + diopside + silica + water, and inferred that enstatite melts incongruently to forsterite + quartz normative liquid under high water pressures (up to 30 kb water pressure). A similar incongruent melting relationship for enstatite is inferred for water undersaturated conditions i.e. $P_{H_2O} < P_{total}$ These results are extrapolated to the melting of more complex olivine + enstatite + clinopyroxene-bearing assemblages in the presence of a minor water-rich fluid phase in the upper mantle, and lead to the hypothesis that liquids developed from such a source will be silica-oversaturated, specifically, quartz tholeiites or andesites. Such silica-rich magmas ($SiO_2 > 50\%$) might also form from parental olivine tholeiite by crystal fractionation at high water pressures (Kushiro *et. al.* 1968).

In contrast, Bultitude and Green (1968) had experimented on the role of water in depressing the liquidus of very undersaturated natural magmas (olivine nephelinites, Table 1), and reported a major role for orthopyroxene as a near-liquidus phase at 20 - 30 kb, $P_{H_2O} < P_{total}$, temperature 150 - 250° C below the anhydrous solidus. From these studies it was inferred that highly undersaturated olivine melilite nephelinite, olivine nephelinite, and olivine-rich basanite magmas could form by partial melting of a pyrolite source (i.e. be in equilibrium with residual olivine, orthopyroxene, $\pm$ clinopyroxene, $\pm$ garnet) at pressures of 20 - 30 kb. It was inferred that parental olivine tholeiite could fractionate to these silica-poor magmas ($SiO_2 \sim 42\%$) by crystal fractionation in the presence of small but essential water contents.

Kushiro (1969) considered that Bultitude and Green's data were in error due to the experiments being carried out in crimped (rather than welded) Pt capsules with the result that the sample composition had altered during the run. Precautions against this had been taken by Bultitude and Green, and the use of the microprobe to analyze charges after runs effectively restricted any such sample leaching or contamination to very selective migration of alkali elements. Confirmation of the effect, using sealed platinum capsules and known quantities of water, was obtained for olivine-rich basanite composition (Table 1, column 5, reported in Green 1969a (footnote) and 1969b). In anhydrous runs on this composition, clinopyr-

oxene is the liquidus phase at 1,470° C and 27 kb, joined by garnet at lower temperature. With 2% H_2O, the liquidus is depressed to ~1,340° C, and olivine (minor) joined by orthopyroxene and then by clinopyroxene is the crystallization sequence. An analogy with Kushiro's data is suggested by the appearance of olivine at higher pressure in the hydrous runs but the important role of orthopyroxene is confirmed and is considered to be largely an effect of lowering the liquidus temperature and widening the pyroxene miscibility gap. Thus a magma, which at the high temperature of the anhydrous liquidus will crystallize a clinopyroxene with moderate CaO content, cannot precipitate this same phase as a single pyroxene at lower temperatures because of the wider pyroxene miscibility gap. Instead the magma may precipitate two pyroxenes, either of which may be the liquidus phase depending on bulk composition. The implication of these experiments to mantle melting is considered in a later section.

Kushiro *et. al's.* (1968) experiments on the systems enstatite + water were in part repeated, and similar results were obtained on the roles of olivine + enstatite in the subsolidus and persistence of olivine in the melting interval. Unambiguous interpretation of the data is difficult owing to solubility of silica in the vapour phase and indeterminacy of liquid and vapour compositions. It is clear however that the total fluid phase (liquid + vapour) is silica-oversaturated and Kushiro *et. al's.* experiments with low water contents provide evidence that in the vapour-absent region the liquid phase may also be silica-oversaturated. To test the applicability of the extrapolation from the simple system to natural basalt, experiments have been carried out in a quartz tholeiite composition (Green and Ringwood, 1967, Table 1, column 2) in the presence of 15% and 30% water at a load pressure of 22.5 kb. The quartz tholeiite contains 21% normative hypersthene and 2.5% normative quartz but olivine is the liquidus phase at atmospheric pressure — it is a typical basalt showing reaction between early-formed olivine and silica-oversaturated liquid. At 22.5 kb, with 15% water, the liquid is undersaturated with water (i.e. no vapour phase) and the liquidus is at 1,070 ± 15° C. The liquidus phase is clinopyroxene and garnet joins the clinopyroxene at about 1,050° C. With 30% water, the liquid is saturated with water (i.e. vapour phase coexists with liquid) and the liquidus lies between 1,000° C and 1,050° C. Clinopyroxene is the liquidus phase and garnet joins the clinopyroxene between 1,000° C and 970° C. Olivine does not appear in either the water-saturated or water-undersaturated runs, and the identification and presence of phases has been carefully checked with the electron microprobe. To further eliminate the possibility that absence of olivine was not due to nucleation difficulties, the quartz tholeiite was seeded with 6.4% olivine. This is sufficient to make the bulk composition exactly saturated i.e. with 26% normative hypersthene and no normative quartz or olivine. For this composition, the seed olivines entirely disappeared and clinopyroxene was the liquidus phase at 1,080° C (15% H_2O) and clinopyroxene and garnet appeared together in a near-liquidus run at 1,000° C (30% H_2O). The experiments show that olivine does not occur as a liquidus or near-liquidus phase in either a silica-oversaturated or exactly silica-saturated tholeiite at 22.5 kb either under water-saturated (30% H_2O) or water-deficient (15% H_2O) conditions. This pressure is within the range (up to 30 kb water pressure) in which Kushiro *et. al.* (1968) report incongruent melting of enstatite to forsterite + silica-oversaturated liquid. Thus, at least at this pressure, the inference from the simple system study cannot be

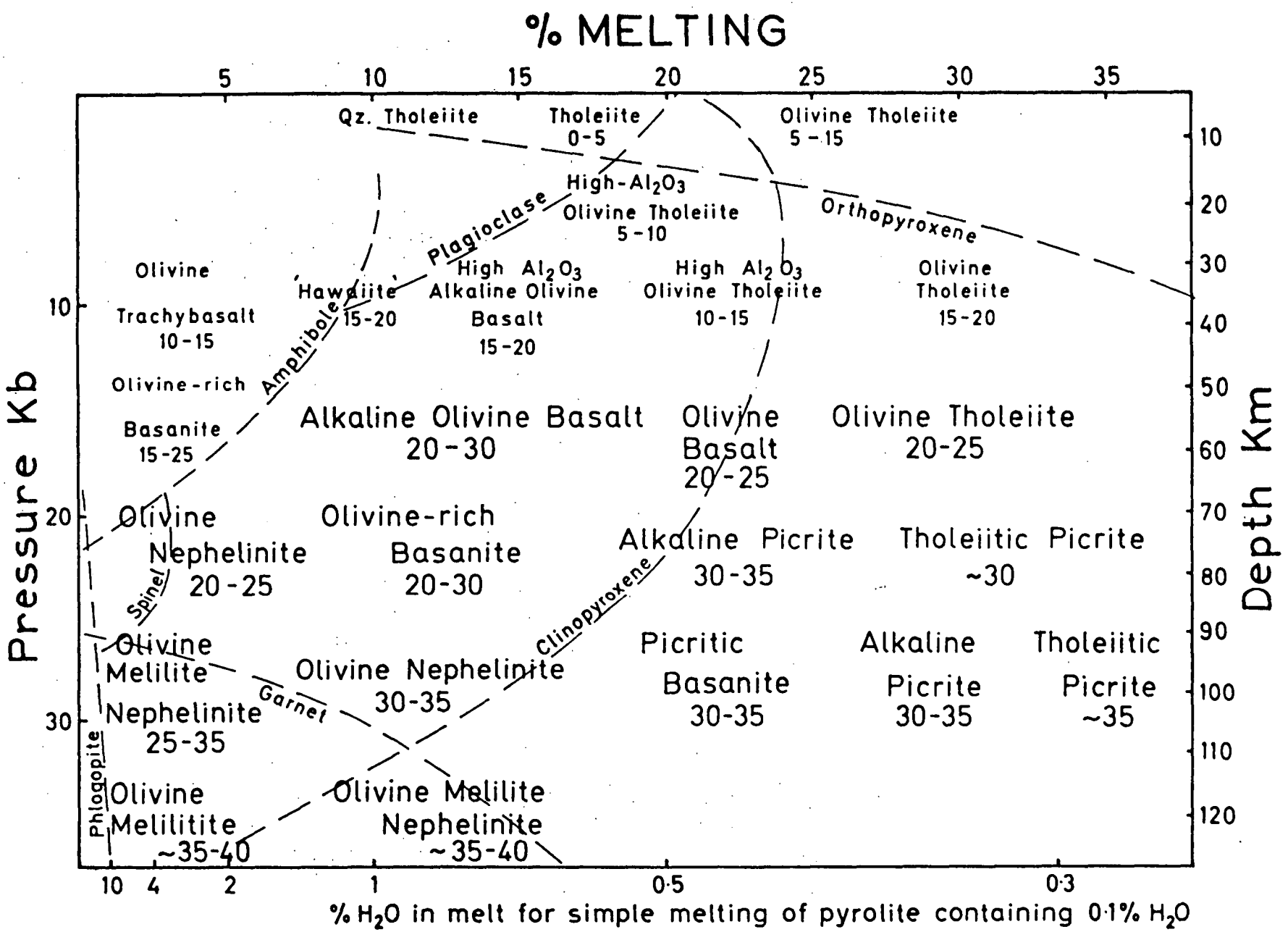
% MELTING
5
10
15
20
25
30
35
Qz. Tholeiite
Tholeiite
0-5
Olivine Tholeiite
5-15
High-Al2O3
Olivine Tholeiite
5-10
Plagioclase
Orthopyroxene
Amphibole
Olivine
Trachybasalt
10-15
Hawaiite
15-20
High Al2O3
Alkaline Olivine
Basalt
15-20
High Al2O3
Olivine Tholeiite
10-15
Olivine
Tholeiite
15-20
Olivine-rich
Basanite
15-25
Alkaline Olivine Basalt
20-30
Olivine
Basalt
20-25
Olivine Tholeiite
20-25
Olivine
Nephelinite
20-25
Olivine-rich
Basanite
20-30
Alkaline Picrite
30-35
Tholeiitic Picrite
~30
Spinel
Clinopyroxene
Olivine
Melilite
Nephelinite
25-35
Olivine Nephelinite
30-35
Picritic
Basanite
30-35
Alkaline
Picrite
30-35
Tholeiitic
Picrite
~35
Garnet
Phlogopite
Olivine
Melilitite
~35-40
Olivine Melilite
Nephelinite
~35-40
Pressure Kb
10
20
30
Depth Km
10
20
30
40
50
60
70
80
90
100
110
120
10
4
2
1
0·5
0·3
% H2O in melt for simple melting of pyrolite containing 0·1% H2O

extrapolated and applied to a typical basalt. It is considered most improbable that a quartz-normative tholeiitic or andesitic liquid can coexist with olivine (i.e. have olivine as its liquidus phase) under upper mantle conditions (P > 10 kb) even at high water pressures.

Thus the hypothesis that quartz tholeiitic or andesitic liquids may be derived by direct partial melting of a source peridotite composition in the presence of water in the upper mantle is rejected, and the contrasted hypothesis that such wet melting produces extremely undersaturated magmas from the pyrolite source is pursued in the following section.

(c) *Nephelinitic magmas from partial melting of hydrous pyrolite*

Experiments referred to in previous sections have shown that very undersaturated basanite and olivine nephelinites may form in equilibrium with residual magnesian olivine, orthopyroxene and calcic clinopyroxene at pressures of 18 - 35 kb, provided temperatures of melting are depressed 100 - 250° C below the anhydrous solidus by the presence of water. Olivine nephelinite magmas may form at 18 - 22 kb in equilibrium with residual olivine, enstatite, and clinopyroxene. The presence of garnet in the residual phases with olivine, enstatite, and clinopyroxene at pressures of ~ 27 kb will produce early liquids of low alumina and high calcium content (i.e. olivine melilite nephelinite and olivine melilitite). It may be noted that the temperature — pressure regime under discussion (i.e. T ~ 1,200° C, P > 18 kb) is largely outside the stability field of amphibole, so that this phase does not occur at the solidus, particularly at pressure > 25kb. For conditions ~ 18 kb amphibole will appear at the solidus at sufficiently high water pressure —— liquids in equilibrium with amphibole at low degrees of partial melting (P = 10 - 18 kb) are probably potassium-rich and range from basanites near 18 kb to olivine trachybasalts near 9 kb.

6. SUMMARY OF PARTIAL MELTING RELATIONSHIPS

Figures 2, 3 and 6 present, in diagrammatic form, an integrated model for derivation of basalt types ranging from olivine trachybasalt and hawaiite to olivine melilitite and to tholeiitic picrite. It is emphasized that the magma types shown are restricted to magmas of direct mantle derivation. Processes of crystal fractionation at crustal levels or at deeper levels may modify these magma types producing other magmas not represented in these figures. Also it is *not suggested* that *all* rocks classifiable as 'hawaiite', quartz tholeiite or alkali olivine basalt etc. are derived as partial melts from pyrolite in the manner indicated. Rather the figures illustrate the petrochemical characteristic of the particular liquid formed *if partial melting of pyrolite occurs* at the designated conditions. In general terms, liquids formed in equilibrium with pyrolite source rock must be very magnesian ($\frac{100\,Mg}{Mg+Fe^{++}} = 68 - 73$), whereas if any liquid segregates from

FIG. 6 (Green 1970). A petrogenetic grid for mantle-derived basaltic magmas. Various basalt magma types are assigned to a % Melt, Pressure grid (implying also specific % H_2O and temperature of melting, see figs. 2 and 3) in which they are regarded as partial melting products of a pyrolite composition containing 0.1% H_2O. The numbers placed with each basalt type refer to the normative olivine content of this liquid at its depth of origin — because of the expansion of the olivine crystallization field at low pressure most basalts will precipitate olivine before other phases if fractionation occurs at *lower* pressures. The dashed boundaries marked with a mineral name show that this mineral will occur among the residual phases remaining after extraction of magma types to the left of the boundary. Olivine is present in equilibrium, i.e. is a residual phase in the pyrolite composition for all the magma types, *cf.* fig. 3.

the source rock and begins to cool and crystallize, then separation of olivine, pyroxenes, garnet, or amphibole will all produce iron-enrichment in the derived liquids. The ratio $\frac{100\,Mg}{Mg+Fe^{++}}$ for a basalt is thus a sensitive indicator of the prehistory of a particular magma, but there is a practical difficulty in that any oxidation of iron in the magma or rock will produce falsely high $\frac{100\,Mg}{Mg+Fe^{++}}$ ratios.

In figs. 2, 3 and 6, tholeiitic magmas are produced with high degrees of partial melting, with olivine and enstatite remaining as residual phases. The water contents of these magmas, if they have developed from a source rock with 0.1% H_2O, would be only 0.3 to 0.4% H_2O. This water content would depress the tholeiite liquidus to only 30 - 50° C below the anhydrous liquidus. Tholeiitic magmas would form from a pyrolite source with about 0.1% H_2O at temperatures only 30 - 50° C below the temperature at which similar melts would form from *anhydrous* pyrolite and little difference in chemical composition would be expected between the two tholeiites. This is very different from the situation when very low degrees of partial melting are considered (fig. 3) for then the relatively water-rich magmas form at very much lower temperatures than anhydrous melts and the liquid-residue equilibria may be significantly different.

The conclusions on basalt petrogenesis outlined in figs. 2, 3 and 6 will undoubtedly require refinement and modification as further detailed studies proceed. However, these figures are intended to give a framework in which the increasingly detailed studies of natural basalt provinces can be viewed with greater insight as to possible magma source conditions and magma inter-relationships. Finally the acceptance or rejection of petrogenetic models such as figs. 2, 3 and 6 will be based on the natural basalts themselves, and there is a great deal of information still to be obtained. A specific example of how the P, T history of a particular magma (an olivine basalt from Auckland Is.) can be deduced is presented by Green and Hibberson (1969), and the same techniques can be applied to a very large range of natural, 'xenocryst'-bearing magma compositions. In the example quoted, it was shown that olivine, orthopyroxene, and clinopyroxene closely matching the compositions of 'xenocrysts' in the olivine basalt, were liquidus and near-liquidus phases for the host magma composition at 14 - 16 kb and 1,200 ± 20° C. For the basalt liquidus to occur at that P, T, then the basalt must have contained 2% water. Furthermore, since the liquidus phases had $\frac{100\,Mg}{Mg+Fe} = 86 - 87$, the liquid could not have been a direct partial melt from pyrolite with $\frac{100\,Mg}{Mg+Fe} = 89$, but had probably already fractionated some way along the path towards alkali olivine basalt by separation of the observed orthopyroxene, clinopyroxene, and minor olivine at depths of about 50 - 55 kilometres.

7. TRACE ELEMENTS IN BASALTS — WALL-ROCK REACTION AND SOURCE INHOMOGENEITY

In the preceding discussion, the emphasis has been on the major element composition of basaltic magmas, since this determines the mineralogy and forms the basis of classification of basaltic rocks. In attempting to relate olivine tholeiitic and alkali olivine basalt magmas by crystal fractionation or different degrees of melting of a pyrolite source, Green and Ringwood (1967b) noted that there was a group of elements including K, Ti, P, Ba, Sr, Rb, Zr, Hf, U, Th, Pb, and the lighter rare earth elements, which show enrichment factors in Hawaiian alkali olivine basalts which are greater than would be produced by 30% crystallization of a parental olivine tholeiite or the difference between 20% melting (alkali olivine basalt) and 30% melting of the pyrolite source rock. These highly enriched elements ("incompatible elements") are those which do not substitute readily in the major minerals of the upper mantle, but probably form rare accessory phases. These elements are expected to be strongly partitioned into any melt fraction, so that for partial melting in excess of about 5% their concentration should closely reflect the %-melting and source composition only, and be essentially independent of the relative proportions of olivine, enstatite and clinopyroxene remaining in the residue.

Green and Ringwood (1967b) suggested an additional mechanism of concentrating incompatible elements in a fractionating magma by a process called 'wall-rock reaction'. In this process, it was envisaged that a body of magma could, under some conditions, cool by reaction with, and solution of, the lowest melting fraction of any wall-rock material with which it was in contact. This process was considered to be an important one for bodies of magma in a region of little temperature contrast between magma and wall-rock (i.e. a magma body near its depth of segregation from source pyrolite or for a large magma body with a relatively long residence time in the crust and undergoing crystal fractionation at low pressures). The latter aspect of wall-rock reaction was applied particularly to the fractionated and 'incompatible element enriched' quartz tholeiites of Tasmania and Antarctica.

With the recognition that the genesis of the undersaturated basanites, nephelinites, etc. (the magma with the highest enrichment factors for the incompatible elements) requires the presence of water, a further factor in selective element enrichment was suggested (Green 1969a, b). If hydrous accessory minerals such as phlogopite, amphibole, apatite, etc. are stable in the upper mantle then there exist conditions with $P^{\text{wall-rock}}_{H_2O} < P^{\text{wall-rock}}_{\text{fluid}} \leq P_{\text{solid}}$ A body of magma moving through such an environment may be very undersaturated in water and $P^{\text{magma}}_{H_2O}$ may be less than $P^{\text{wall-rock}}_{H_2O}$. Hydrous phases in the wall rock may break down under the influence of the neighbouring magma and water may migrate into the magma.. The concept of wall rock reaction was modified to include the movement of a fluid phase containing incompatible element concentrations or diffusion of incompatible elements through a fluid phase from wall-rock to magma.

In an important paper, Gast (1968) discussed the trace-element enrichment in basalt magmas derived by partial melting, and showed that the strongly enriched 'incompatible element' contents of alkali olivine basalts, basanites, etc. would result if these magmas were produced by

very low degrees of melting (3 - 7%) of their source peridotite. Olivine tholeiites from the mid-oceanic ridge environments, with very low potassium and other incompatible element contents, were regarded as derived by 20 - 30% melting of a source rock which had previously suffered partial melting. Hawaiian olivine tholeiites, enriched in incompatible elements when compared with many oceanic ridge olivine tholeiites, were grouped with the alkali olivine basalts as products of smaller degrees of partial melting. This suggested relationship is inconsistent with figs. 4 and 6. Fig. 6 could reasonably account for the differences between Hawaiian magma types on the basis of different degrees of partial melting (provided alkali olivine basalts are in general formed by up to 20% melting, and commonly much less than this) of a pyrolite source rock, but the same source rock could not also yield the oceanic tholeiites (high-alumina olivine tholeiites) with their characteristically depleted incompatible element contents, by 15 - 20% melting in a single-stage process.

Consideration of incompatible element variations between rocks which are essentially similar in major element content, leads to the concept of inhomogeneity in incompatible element contents in the source region. Gast's (1968) suggestion of 2-stage melting, the first extracted melt being of small volume but highly enriched in incompatible elements, may be important. An additional suggestion has been made that the upper mantle source region may be vertically zoned in incompatible element concentrations (Green 1970) due to upward migration within the low velocity zone of a fluid phase. This fluid phase is envisaged as water-rich and possibly CO_2-rich, or possibly, a very small, water-rich, silicate melt fraction. The presence of a free fluid phase within the low velocity zone may permit the upward migration of incompatible elements, which do not readily substitute in olivine, pyroxenes, or garnet, until they are 'fixed' by entering a small silicate melt fraction in the upper part of the low velocity zone. In this way, source regions with 'depleted' and 'enriched' patterns of incompatible element abundance could be developed in the lower or upper part respectively of the low velocity zone. The particular tectonic or dynamic mechanism of partial melting (i.e. mantle diapirism, 'fault' tapping of the low velocity zone etc.) would determine which source region was involved in magma production.

8. CONCLUSIONS

The understanding of basalt magma genesis and of upper mantle composition are mutually dependent problems and both require a close integration of studies of geochemical and geophysical aspects of natural basalts, and experimental studies under simulated (P, T, P_{H_2O}) upper mantle conditions. I have, in this lecture, developed a model of basalt genesis in which the source composition (pyrolite) is regarded as essentially homogeneous in major elements but inhomogeneous or chemically zoned in content of incompatible elements and accessory minerals. The low velocity zone of the upper mantle is interpreted as a region in which, due to the instability of amphibole in pyrolite containing 0.1 - 0.2% H_2O at depths in excess of 80 - 100 kilometres, there is a very small (<5%) degree of partial melting. The nature of this liquid fraction is highly undersaturated olivine nephelinite or olivine melilitite. Ascent and extrusion of basaltic magmas may occur when the low velocity zone is tapped rather directly

by major rift or fault systems. More voluminous magmas, which are also usually products of much greater degrees of partial melting, form when there is diapiric upwelling of material from the low velocity zone to higher levels in the mantle or lower crust (Green and Ringwood 1967; Green 1970).

Magma types ranging from tholeiitic picrite to olivine melilitite and olivine trachybasalt are assigned to a petrogenetic grid in which the depth (pressure) of magma segregation, the degree of partial melting of the source rock, the water content, and approximate temperature of the magma, are specified. While this model can account for variations in major element abundances and normative mineralogy among basalts, there are variations in abundances of K, Rb, Ba, the rare-earths, etc. (incompatible elements), which are inconsistent with a model involving a constant source composition for all mantle derived basalts. Abundances of incompatible elements in the magmas are partly determined by the source composition at magma segregation but may be further enriched by wall-rock reaction processes in the upper mantle or in the continental crust. Source inhomogeneity appears to be required to account for variations in incompatible element abundances and such inhomogeneity may be a characteristic feature within the low velocity zone, the upper part of which is considered to have 'enriched' and the lower part a 'depleted' pattern of incompatible element contents.

REFERENCES

BOYD, F. R., 1967. Electron probe study of diopsidic pyroxenes from kimberlite. *Carnegie Inst.Washington Year Bk.*, **65**, 252 - 260.

BULTITUDE, R. J. and GREEN, D. H., 1968. Experimental studies at high pressures on the origin of olivine nephelinite and olivine melilite nephelinite magmas. *Earth Planetary Sci.Let.*, 3, 325 - 337.

BULTITUDE, R. J. and GREEN, D. H., 1970. Experimental study of crystal-liquid relationship at high pressures in olivine nephelinite and basanite compositions. *J.Petrol.* (In press).

CARSWELL, D. A. and DAWSON, J. B., 1970. Garnet peridotite xenoliths in South African kimberlite pipes and their petrogenesis. *Contr.Mineral.Petrol.*, **25**, 163 - 184.

CLARK, S. P. and RINGWOOD, A. E., 1964. Density distribution and constitution of the mantle. *Rev.Geophys.*, **2**, 35 - 88.

COOPER, J. A. and GREEN, D. H., 1969. Lead isotope measurements on lherzolite inclusions and host basanites from Western Victoria, Australia. *Earth Planetary Sci.Let.*, **6**, 69 - 76.

FREY, F. A., 1969. Rare earth abundances in a high temperature peridotite intrusion. *Geochim.Cosmochim.Acta.*, 33, 1429 - 1447.

GAST, P. W., 1968. Trace element fractionation and the origin of tholeiitic and alkaline magmas types. *Geochim.Cosmochim.Acta.*, 32, 1,057 - 1,086.

GREEN, D. H. 1969a. The origin of basaltic and nephelinitic magmas in the earth's mantle. *Tectonophysics*, 7, 409 - 422.

GREEN, D. H., 1969b. A review of experimental evidence on the origin of basaltic and nephelinitic magmas. *Pyhs.EarthPlanetaryInteriors*, 3, 221 - 235.

GREEN, D. H., 1970. Compositions of basaltic magmas as indicators of conditions of origin: application to oceanic volcanism. *Phil.Trans.Roy.Soc.London*, (In press).

GREEN, D. H. and HIBBERSON, W., 1969. Experimental duplication of conditions of precipitation of high pressure phenocrysts in a basaltic magma. *Phys. EarthPlanetaryInteriors*, 3, 247 - 254.

GREEN, D. H. and HIBBERSON, W., 1970. Instability of plagioclase in peridotite at high pressures. *Lithos*, 3, 209 - 221.

GREEN, D. H. and RINGWOOD, A. E., 1967a. The stability fields of aluminous pyroxene peridotite and garnet peridotite and their relevance in upper mantle structure. *Earth Planetary Sci.Let.*, 3, 151 - 160.

GREEN, D. H. and RINGWOOD, A. E., 1967b. The genesis of basaltic magmas. *Contr.Mineral.Petrol.*, **15**, 103 - 190.

GREEN, D. H. and RINGWOOD, A. E., 1967c. An experimental study of the gabbro to eclogite transformation and its petrological applications. *Geochim. Cosmochim.Acta.*, **31**, 767 - 833.

GREEN, D. H. and RINGWOOD, A. E., 1969. Mineralogy of peridotitic compositions under upper mantel conditions. *Phys.EarthPlanetaryInteriors*, **3**, 359 - 371.

JACKSON, E. D. and WRIGHT, T. L., 1970. Xenoliths in the Honolulu Volcanic Series, Hawaii. *J.Petrol.*, **11**, 405 - 430.

KUNO, H., 1960 . High-alumina basalt. *J.Petrol.*, **1**, 121 - 145.

KUSHIRO, I., 1969. Discussion of paper "The origin of basaltic and nephelinitic magmas in the earth's mantle". *Tectonophysics*, **7**, 427 - 436.

KUSHIRO, I., YODER, H. S. and NISHIKAWA, M., 1968. Effect of water on the melting of enstatite. *Geol.Soc.Amer.Bull.*, **79**, 1,685 - 1,692.

MACDONALD, G. A. and KATSURA, T., 1961. Variations in the lava of the 1959 eruption in Kilauea Iki. *Pacific Sci.*, **15**, 358 - 369.

MURATA, K. J. and RICHTER, D. H., 1966. Chemistry of the lavas of the 1959 - 60 eruption of Kilauea volcano, Hawaii. *U.S.Geol.Surv.Profess.Papers*, **537-A**, 1 - 26.

NOCKOLDS, S. R., 1954. Average chemical compositions of some igneous rocks. *Geol.Soc.Amer.Bull.*, **65**, 1,007 - 1,032.

O'HARA, M. J., 1968. The bearing of phase equilibria studies in synthetic and natural systems on the origin and evolution of basic and ultrabasic rocks. *Earth Sci.Rev.* **4**, 69 - 133.

O'HARA, M. J. and YODER, H. S., 1964. Formation and fractionation of basic magmas at high pressures. *Scottish J.Geol.*, **3**, 67 - 117.

RINGWOOD, A. E., 1962. A model for the upper mantle. *J.Geophys.Res.*, **67**, 857 - 867.

RINGWOOD, A. E., 1966a. The chemical composition and origin of the earth. p. 287 - 356 in *Advances in Earth Science*, ed. P. M. Hurley. M.I.T. Press, Cambridge, Mass.

RINGWOOD, A. E., 1966b. The mineralogy of the mantle. p. 357 - 417 in *Advances in Earth Science*, ed. P. M. Hurley. M.I.T. Press, Cambridge, Mass.

TILLEY, C. E., 1950. Some aspects of magmatic evolution. *Quart.J.Geol.Soc., London*, **106**, 37 - 61.

ACKNOWLEDGMENTS

The writer is grateful to Professor Sylvester-Bradley and Dr. M. J. Le Bas for their invitation to deliver this lecture and it is hoped that its publication will be of some value in summarizing a current view of a rapidly advancing and somewhat controversial aspect of igneous petrology. I also take this opportunity to gratefully acknowledge the stimulating collaboration with Professor A. E. Ringwood, the instruction and stimulus of Professor C. E. Tilley, and the essential role of Professor J. C. Jaeger and academic and technical colleagues at the Australian National University.

B11

EXPERIMENTAL DUPLICATION OF CONDITIONS OF PRECIPITATION OF HIGH-PRESSURE PHENOCRYSTS IN A BASALTIC MAGMA

D. H. GREEN and W. HIBBERSON

Department of Geophysics and Geochemistry, Australian National University, Canberra

Reprint from: **PHYS. EARTH PLANET. INTERIORS**

NORTH-HOLLAND PUBLISHING COMPANY - AMSTERDAM

printed from:
70, *Phys. Earth Planet. Interiors* 3, 247–254. North-Holland Publishing Company, Amsterdam
inted in the Netherlands

EXPERIMENTAL DUPLICATION OF CONDITIONS OF PRECIPITATION OF HIGH-PRESSURE PHENOCRYSTS IN A BASALTIC MAGMA

D. H. GREEN and W. HIBBERSON

Department of Geophysics and Geochemistry, Australian National University, Canberra

ı olivine basalt from the Auckland Islands contains partially sorbed "xenocrysts" of orthopyroxene, clinopyroxene and mi- r olivine. Electron probe microanalyses of these crystals con- m their similarity to near-liquidus crystals obtained experi- ıntally in tholeiitic and alkali olivine basalts at high pressures. high pressure experimental study of the host olivine basalt monstrates that orthopyroxene and clinopyroxene are near- uidus phases at 11–18 kb but the degree of solid solution be- een the pyroxenes crystallized from the dry magma is much eater than that observed in the natural pyroxenes. Addition of ıter to the experimental runs results in lowering of the liquidus the basalt and in the appearance of orthopyroxene, clinopyroxene and olivine as near-liquidus phases at 13–18 kb, 1130–1230 °C. A close correspondence between chemical compositions of the natural "xenocrysts" and the experimental near-liquidus pyroxenes and olivine is obtained and the conditions of the precipitation of the "xenocrysts" from their host magma are inferred to be near 14–16 kb and 1200 °C. The host magma contained ~2% H_2O at these conditions to produce the requisite depression of the liquidus. The "xenocrysts" are regarded as high pressure phenocrysts giving natural evidence of high pressure magmatic fractionation controlled largely by separation of orthopyroxene.

Introduction

Recent experimental studies on the melting behaviour ' natural basalts at high pressures have led to the rmulation of hypotheses of magma generation and actionation at depths in the mantle. To test such ypotheses we require evidence from the natural basalts emselves on their pre-eruption history. Many basalts ıve suffered low pressure fractionation to various egrees, so that their chemical compositions bear little lation to the compositions of liquids originally exist- g at depth. This is particularly true of tholeiitic ba- lts. However, among the undersaturated basalts, some kali olivine basalts, olivine basanites, olivine nephe- ıites etc. contain high density lherzolite and pyroxenite enoliths of high pressure mineralogy. These liquids ıve clearly not fractionated by crystal settling at allow depths (less than those from which the xeno- hs were acquired) and their rapid movement to the rface provides minimal opportunity for contamina- on by digestion of crustal material. Many of these erzolite-bearing magmas also contain large single ystals ("xenocrysts") including clinopyroxene, olivine, thopyroxene, spinel and amphibole. These "xenocrysts" (with the exception of olivine) were out of equilibrium with the magma during the final stages of crystallization and show evidence of resorption and reaction. It is a reasonable hypothesis that these crystals are the liquidus or near-liquidus phases of their host magma at depths greater than or similar to those at which the magmas picked up the lherzolite xenoliths. This hypothesis can be experimentally tested for any given magma and "xenocryst" assemblage and if it can be demonstrated that there are unique P, T conditions at which the host magma has liquidus or near-liquidus phases which match the observed xenocrysts in mineralogy and chemical composition, then these P, T conditions may be those at which the magma batch was held, however briefly, allowing some crystallization before final rapid movement to the surface. Although this characterization of P, T environment for the "magma-xenocryst" assemblage does not identify the initial source-region of the magma batch, it does demonstrate a compositional point and a fractionation trend and process which was operating at depth in the particular magma batch. In this way evidence from the natural rocks can be used to evaluate and test rival hypotheses of magma generation and fractionation within the mantle.

An olivine basalt from Mt. Eden plug, Auckland Id., Southern Ocean, was collected and examined by Dr. J. B. Wright* and the presence of both orthopyroxene and clinopyroxene as large, vitreous, corroded crystals was noted. The basalt also contains lherzolite inclusions with the typical olivine, enstatite, clinopyroxene and pale brown spinel assemblage but the "xenocrysts" contrast in size and colour with crystal fragments detached from these xenoliths.

2. Chemical compositions of xenocrysts and host magmas

Several features of the chemical and normative composition (table 1) of the host magma are worthy of comment. The norm contains a small amount of hypersthene but falls within the alkali basalt field using the

TABLE 1

Chemical composition of olivine basalt, Mt. Eden plug, Auckland Id. Otago University No. 19594, A.N.U. No. 2900. Analyst E. Kiss, A.N.U.

SiO_2	46.55	
TiO_2	3.18	CIPW Norm
Al_2O_3	12.70	Or 5.6
Fe_2O_3	2.98	Ab 24.8
FeO	9.72	An 18.9
MnO	0.17	Di 17.7
MgO	10.63	Hy 2.7
CaO	8.66	Ol 18.8
Na_2O	2.95	Ap 1.3
K_2O	0.95	Ilm 6.1
P_2O_5	0.60	Mt 4.4
H_2O^+	0.67	
CO_2	0.24	Normative feldspar
Cr_2O_3	0.06	$Or_{11}Ab_{51.5}An_{37.5}$
NiO	0.04	D.I. = 30.4
CoO	0.01	
	100.11	

$\frac{100\ Mg}{Mg+Fe^{++}}$ (atomic ratio) = 66.2

criteria of POLDERVAART (1964). Petrographically it is an alkali olivine basalt in that olivine occurs as both phenocrysts and crystallites, co-precipitating with the clinopyroxene and with no evidence of a reaction relationship with the liquid. The composition also lies within the Hawaiian alkali olivine basalt field on an Na_2O+K_2O vs SiO_2 diagram. The basalt is an example illustrating the continuity of composition between the nepheline-normative alkali olivine basalts and hypersthene normative olivine tholeiites (YODER a TILLEY, 1962 p. 353). It lies close to the "plane critical undersaturation" of the latter authors.

The normative plagioclase composition is andesi ($Ab_{58}An_{42}$) and is more typical of hawaiite compo tion than alkali olivine basalt if a comparison is ma with Hawaiian lavas (MACDONALD and KATSUR 1964). However the low SiO_2 content and hi $Mg/(Mg+Fe^{++})$ ratio of the basalt is typical of alk olivine basalts and alkali picrites. Except for normati feldspar composition, the host basalt falls close to t alkali olivine basalt point in all the criteria used TILLEY and MUIR (1964) in their characterization members of the alkali olivine basalt to trachyte magr series. The term "olivine basalt" is used in this pap for the magma but affinities to alkali olivine basalts a recognized. The points of similarity to some hawaiit are noted and may be linked to data (unpublishe showing that some hawaiites are magmas formed with the deep crust or mantle ($P \geq 8$ kb) and that not hawaiites can be regarded as products of alkali olivi basalt fractionation in shallow magma chambers.

The compositions of the large phenocrysts present the magma have been determined using the electr probe microanalyzer and empirical calibration curv based on analyzed minerals and synthetic glasses (GREEN and RINGWOOD, 1967a). Analyses of sever crystals and of different areas within one crystal der onstrated small but real variations in composition the most magnesian and most iron rich compositio obtained for both pyroxenes are listed in table 2. T orthopyroxene and clinopyroxene (table 2) have a hi degree of mutual solid solution (i.e. high CaO in orth pyroxene, low CaO in clinopyroxene). They differ this respect from the co-existing pyroxenes of lherzol inclusions in basalts (ROSS, FOSTER and MYERS, 195 and are also more iron-rich than the lherzolite asser blages (olivines, enstatites and clinopyroxenes wi $100\ Mg/(Mg+Fe^{++}) = 92$–$89$).

The contrast between the clinopyroxene "xenocrys compositions and the composition of the recrystallis outermost rim, presumed to be in equilibrium with t basalt magma during crystallization at or near the su face, is clearly shown in table 2. The recrystallized ri is markedly different in TiO_2 content, CaO content ar hypersthene solid solution, and shows smaller diffe ences in Na_2O and Al_2O_3 contents.

* Ahmadu Bello University, Zaria, Nigeria.

TABLE 2

Chemical compositions of orthopyroxene, clinopyroxene and olivine xenocrysts in olivine basalt. Analyses by electron probe microanalyzer

		Orthopyroxene		Clinopyroxene		Recrystallized rim
SiO_2		56.0	56.0	54.6*	52.9*	50.5
TiO_2		0.2	0.3	0.45	0.65	2.2
Al_2O_3		3.0	3.6	3.4	4.3	2.8
Cr_2O_3		—	—	—	—	1.3*
FeO		8.1	8.6	5.9	6.5	6.7
MgO		31.6	31.0	20.7	19.1	14.2
CaO		2.1	2.1	16.0	15.6	21.9
Na_2O		<0.1	<0.1	0.7	0.7	0.5
		101.1	101.7	101.7	99.7	100.1
Molecular ratios	Ca	4	4	32	33	46
	Mg	84	83	59	56	41
	Fe	12	13	9	11	13
$\frac{100\ Mg}{Mg+Fe^{++}}$		87.4	86.5	86.2	84.0	79.1

Partial analyses of olivines

Olivine partially enclosed by orthopyroxene xenocryst ($Ca_4Mg_{84}Fe_{12}$)

	FeO	CaO	Al_2O_3	$\frac{100\ Mg}{Mg+Fe^{++}}$
Part against orthopyroxene	12.8	0.1	0.1	86.9
Zoned edge against basalt	28.9	0.3	0.6	67.2
Olivine phenocryst – continuously zoned, strongly zoned on edge				
Centre	18.8	—	—	80.0
Outer edge	29.6	—	—	66.5

*Values calculated from other elements assuming normal pyroxene molecules in solid solution.

A single olivine grain was observed to be partially enclosed by an orthopyroxene "xenocryst" and has closely similar $Mg/Mg+Fe^{++}$ value to the orthopyroxene (table 2). The crystal is not significantly zoned except at the margin contacting the basalt where a sharp compositional gradient leads to more iron-rich olivine with a minimum $Mg/(Mg+Fe^{++})$ value of 67.2. An euhedral olivine phenocryst has a core composition Fo_{80} with very sharp marginal zoning to at least $Fo_{66.5}$ at the outer edge.

Experimental study of the crystallization behaviour of the olivine basalt

Anhydrous conditions: The experimental methods used have been described previously (GREEN and RINGWOOD, 1967a, 113–117). The starting material for the runs was a glass prepared from the analysed basalt and rechecked after fusion for FeO and Fe_2O_3 content. The effect of Fe-loss to the platinum capsule, previously shown to be of minor importance (op. cit. p. 115–117) and not significantly affecting the sample mineralogy, has been further minimised by shorter run times. As a further confirmatory measure, some runs were carried out in graphite capsules demonstrating the same sequence of appearance of phases at 13.5 kb. Runs in both platinum and graphite at 13.5 kb and at 1330 °C and 1320 °C all yielded orthopyroxene + clinopyroxene + liquid. The similarity of degree of crystallization and of the 100 $Mg/(Mg+Fe^{++})$ values (83.0) of the clinopyroxenes in both 1330 °C and 1320 °C runs in graphite suggests that there is no actual difference in degree of crystallization between these runs. The more magnesian compositions of the pyroxenes from the run in platinum at 1330 °C may be due to this run being nearer the liquidus or to some iron loss. The latter effect may also have caused the appearance of orthopyroxene (100 $Mg/(Mg+Fe^{++}) = 86.4$) alone in the one hour run at 1325 °C. Microdetermination of FeO (10.3%) and Fe_2O_3 (0.97%) in the 30 min. run at 13.5 kb 1320 °C in platinum confirms the relatively small change in chemical and normative composition produced by iron loss within the run times used. Microprobe methods and the accuracy of analyses are as previously described (GREEN and RINGWOOD, 1967a).

The crystallization behaviour of the Auckland Island olivine basalt is almost identical to that of the olivine basalt studied by GREEN and RINGWOOD (1967a). Comparison of the compositions shows higher normative olivine and Al_2O_3 in the previous composition but otherwise very similar chemical and normative compositions. Details of experimental runs are given in table 3. Olivine is the liquidus phase at 9 kb and is joined by clinopyroxene as the second phase. At 13.5 kb orthopyroxene and clinopyroxene occur together near the liquidus. Orthopyroxene is the major phase, or possibly the only phase on the liquidus, but at lower temperatures, clinopyroxene is more abundant. At 18 kb clinopyroxene appears to be the liquidus phase and orthopyroxene probably appears over a very restricted lower temperature interval. In comparison with the previous data on olivine basalt (GREEN and RINGWOOD, 1967) the present composition has a slightly more re-

TABLE 3

Experimental crystallization of Auckland Island olivine basalt at various pressures and temperatures

Pressure (kb)	Temperature (°C)	Time (mins)	Sample capsule	Results
A. *Dry conditions*				
9.0	1280	30	Pt	Olivine+glass. Very near liquidus
9.0	1260	30	Pt	Olivine+clinopyroxene+glass
11.3	1320	30	Pt	Above liquidus
11.3	1310	30	Pt	Clinopyroxene+rare orthopyroxene+minor olivine. Clinopyrox with rare parallel growth of orthopyroxene
13.5	1350	30	Pt	Above liquidus
13.5	1330	30	Pt	Uncommon orthopyroxene and clinopyroxene+glass. Very near uidus
13.5	1330	60	Graphite	Clinopyroxene+orthopyroxene+glass Clinopyroxene > orthopyroxene
13.5	1325	60	Pt	Orthopyroxene+glass
13.5	1320	30	Pt	Clinopyroxene+rare orthopyroxene+glass Cpx ⩾ Opx
13.5	1320	60	Graphite	Clinopyroxene+orthopyroxene+glass Cpx > Opx
13.5	1300	30	Pt	Clinopyroxene+minor orthopyroxene+glass (~30% crystallizati
18.0	1380	60	Graphite	Above liquidus
18.0	1370	60	Graphite	Clinopyroxene+glass. Cpx may be quench
18.0	1360	60	Graphite	Clinopyroxene+possible rare orthopyroxene+glass
B. *"Wet" conditions*				
13.5	1200	30	Pt	Olivine+glass. Very near liquidus
13.5	1190	30	Pt	Olivine+orthopyroxene+glass. Opx > ol
13.5	1180	30	Pt	Olivine+orthopyroxene+glass. Opx ⩾ ol
13.5	1160	30	Pt	Olivine+orthopyroxene+clinopyroxene+glass. Opx > Cpx. Mi olivine. Possible amphibole
13.5	1150	30	Pt	Olivine+orthopyroxene+clinopyroxene+glass
13.5	1130	30	Pt	Olivine+orthopyroxene+amphibole+glass. Clinopyroxene not c tain
18.0	1260	30	Pt	Orthopyroxene+glass. Very near liquidus
18.0	1240	30	Pt	Orthopyroxene+clinopyroxene+glass. Opx > Cpx
18.0	1200	30	Pt	Orthopyroxene+clinopyroxene+glass. Orthopyroxene and clino roxene intergrowths well developed Opx ≃ Cpx
C. *Controlled Water Contents*				
15.3	1200	20	Pt	*With 3% H_2O.* Above liquidus
14.4	1200	30	Pt	*With 2% H_2O.* Above liquidus
14.4	1170	30	Pt	*With 2% H_2O.* Orthopyroxene+clinopyroxene+rare olivine. C common
15.3	1200	20	Pt	*With 2% H_2O.* Rare large orthopyroxene, no definite olivine.
15.3	1170	30	Pt	*With 2% H_2O.* Common orthopyroxene and possible rare olivine

stricted field of orthopyroxene crystallization. The analytical data on the pyroxene compositions (table 4) demonstrate a very high degree of hypersthene solid solution in the clinopyroxene and somewhat lower Al_2O_3 contents in both pyroxenes than those observed in the previous olivine basalt. The clinopyroxenes have compositions suggestive of very magnesian pigeonites but comparison with the sub-calcic (9–10% CaO) clinopyroxenes previously obtained experimentally does not provide any evidence as yet for a compositional break between augites, sub-calcic augites and compositic near to pigeonite. The coexistence of orthopyroxer with slightly varying CaO content with this range clinopyroxene compositions suggests that we are de ing with the "roof" of the two-pyroxene miscibil gap, the orthopyroxene side being "steep" (i.e. Ca content varies only slightly with temperature and w Mg/(Mg+Fe^{++}) ratio) while the clinopyroxene si in contrast is "shallow" and the hypersthene solid so tion rapidly increases for small increases in temperatu

TABLE 4

mpositions of phases crystallized from the olivine basalt under dry conditions in sealed platinum capsules or in graphite capsules with "dry" (talc+boron nitride) furnace assemblies

Pressure (kb)	11.3		13.5		13.5	
Temperature (°C)	1310		1330		1320	
Sample capsule	Platinum		Platinum		Graphite	
Time	30 mins		30 mins		60 mins	
Phases present	Ol+Cpx+Glass		Opx+Cpx+Glass		Opx+Cpx+Glass	
Analyzed phase	Olivine	Clino-pyroxene	Ortho-pyroxene	Clino-pyroxene	Ortho-pyroxene	Clino-pyroxene
SiO_2	40.0*	53.5*	55.0*	54.4*	54.0*	53.0*
TiO_2	—	(0.6)+	0.4	0.5	0.4	0.7
Al_2O_3	<0.2	3.9	4.1	3.8	4.0	4.0
Fe_2O_3	—	—	—	—		
FeO	14.2	9.4	8.4	8.1	10.3	9.9
MgO	45.5*	27.2*	29.9*	27.9*	28.9*	27.0*
CaO	0.3	5.3	2.2	5.1	2.4	5.2
Na_2O	—	(0.2)+	<0.05	0.2	<0.05	0.25
Molecular proportions Ca	0.4	10.5	4.5	10.0	4.5	10.5
Molecular proportions Mg	84.8	75.0	82.5	77.5	79.7	74.5
Molecular proportions Fe	14.8	14.5	13.0	12.5	15.8	15.0
$\frac{100\ Mg}{Mg+Fe^{++}}$	85.1	83.6	86.3	86.0	83.3	83.0

Calculated value.
Value assumed from analyses of similar clinopyroxenes.

r decreases in $Mg/(Mg+Fe^{++})$ ratio. A similar effect evident in the simple system diopside-enstatite (DAs and BOYD, 1966) and is reported for the system edenbergite-ferrosilite at 20 kb by LINDSLEY (this volme).

Wet" Conditions: Apparatus for sealing of water in e small high pressure capsules was not available when e majority of the experiments were carried out so that e techniques of running with an unknown but fairly producible water contents were followed (BULTITUDE nd GREEN, 1968). Approximately 1 mgm (~5%) of ater was added to the sample and the platinum capule crimped but not welded. The high pressure furnace ssembly used a simple talc cylinder (see GREEN and INGWOOD, 1967b fig. 1) in which dehydration of the lc and use of open (non-welded) platinum capsules ad previously (GREEN and RINGWOOD, 1964) produced depression of the liquidus of an olivine tholeiite composition by approximately 100 °C. Use of these techques produced a depression of the liquidus of the ivine basalt of about 130 °C at 13.5 kb and 100 °C at 18 kb. It might be anticipated that runs with this technique would yield rather random points between liquidus and solidus but in fact the careful repetition of the same run procedure produced a series of runs at 13.5 kb and 18 kb in which the order of decreasing temperature is also the order of increasing degree of crystallization as illustrated by the regular sequence of appearance of phases, and the regular decrease of the ratio $100\ Mg/(Mg+Fe^{++})$ in the phases. These data suggest that the technique produces similar but unknown activity of water in the experimental runs. Several later experiments carried out with sealed Pt capsules and known water contents yielded crystallization products consistent with the previous work and showing that the observed depression of the liquidus required water contents of 2–3% (table 3). The earlier technique of running with appreciable but unknown water activity has been criticized by O'HARA (1968) and KUSHIRO (1968) but the data obtained on this particular composition give no grounds for suspecting change of sample composition by transport of components in an aqueous phase either moving into or out of the sample capsule.

TABLE 5

Compositions of analyzed crystals obtained in crystallization of olivine basalt at 13.5 kb and 18 kb under "wet" conditions lowering of liquidus by ~120 °C by the addition of water.

Phase	Temperature (°C)	100 Mg / (Mg+Fe++ (atomic) ratio)	Molecular proportions Ca	Mg	Fe	Weight per cent Al_2O_3	CaO
A. *At 13.5 kb*							
Olivine	1200	86.9	0.2	86.7	13.1	<0.2	0.2
Olivine	1190	86.9	0.2	86.7	13.1	<0.2	0.2
Orthopyroxene		90.0	3.4	87.1	9.6	1.7	1.8
Olivine	1180	84.8	0.2	84.6	15.2	<0.2	0.2
Orthopyroxene		88.1	3.6	85.2	11.3	1.7	1.9
Olivine	1160	81.4	0.2	81.2	18.6	<0.2	0.2
Orthopyroxene		84.3	4.0	81.2	14.8	4.4	2.0
Clinopyroxene			no consistent analyses				
Olivine	1150	80.0	0.3	79.8	19.9	<0.2	0.3
Orthopyroxene		83.3	4.0	80.0	16.0	4.3	2.0
Clinopyroxene		83.3	32.0	56.6	11.3	6.1	≥15.2
Olivine	1130	81.0	0.2	80.8	19.0	<0.2	0.2
Orthopyroxene		82.8	4.0	79.5	16.5	4.5	2.0
Amphibole		—	not analyzable				
B. *At 18 kb*							
Orthopyroxene	1260	89.3	3.8	85.9	10.3	2.4	2.0
Orthopyroxene	1240	86.1	3.9	82.8	13.3	2.5	2.0
Clinopyroxene		83.5	30.4	58.0	11.6	5.5	≥14.0
Orthopyroxene	1200	85.6	3.9	82.3	13.8	3.1	2.0
Clinopyroxene		83.2	35.5	53.4	11.1	5.9	16.2

Coexisting orthopyroxene and clinopyroxene

	13.5 kb 1150 °C		18 kb 1240 °C		18 kb 1200 °C	
	Opx	Cpx	Opx	Cpx	Opx	Cpx
SiO_2	51.1*	51.7*	55.3*	52.8*	54.9*	52.3*
TiO_2	—	0.6	0.4	0.7	0.4	0.7
Al_2O_3	4.5	6.1	2.5	5.5	3.1	5.9
FeO	10.4	6.9	8.8	6.8	9.1	6.4
MgO	29.4*	19.3*	30.9*	19.2*	30.5*	17.5*
CaO	2.0	≥15.2	2.0	≥14.0	2.0	16.2
Na_2O	—	0.3	—	1.0	—	1.0

* Calculated values.

The depression of the liquidus of the olivine basalt to 1200 °C at 13.5 kb resulted in appearance of olivine as the liquidus phase, closely followed by orthopyroxene and joined by clinopyroxene as the third phase. At 1130 °C, amphibole may replace clinopyroxene as the latter was not definitely identified. It may also be noted that the olivine coexisting with amphibole at 1130 °C is more magnesian than that at higher temperature. Olivine is present throughout the crystallization interval studied but remains a minor phase and does not perceptibly increase in abundance, in contrast with t large increase in abundance of the orthopyroxene a clinopyroxene. The orthopyroxene analyses (table show CaO contents consistently lower than those o tained from orthopyroxenes at 1320–1330 °C. Al_2 contents in the higher temperature orthopyroxenes a low but increase in the 1160–1130 °C runs. The clin pyroxene analyzed at 1150 °C has higher Al_2O_3 co tent than coexisting orthopyroxene and, most signi cantly, has a very much higher CaO content than t

inopyroxenes analyzed from 1320 °C and 1330 °C
ns.

The experimental runs at 18 kb yielded orthopy-
xene as the liquidus phase, joined by clinopyroxene at
wer temperatures. Orthopyroxene is slightly more
agnesian than coexisting clinopyroxene and has lower
l_2O_3 content (cf. GREEN and RINGWOOD, 1967a). The
inopyroxene compositions have CaO contents of
–16%. The most reliable clinopyroxene analyses ob-
ined from the runs were those at 18 kb, 1200 °C; in
ost runs the crystals were smaller than orthopyroxene
d with quench outgrowths and were analyzed with
fficulty. The Na_2O contents of the clinopyroxenes in
uilibrium with the olivine basalt liquid increase with
creasing pressure – thus in both the dry and "wet"
ns at 13.5 kb, the clinopyroxenes contained 0.2–0.3%
a_2O with apparently slightly lower contents in the
gher temperature clinopyroxenes. At 18 kb however
e clinopyroxenes contain 1.0% Na_2O, probably in
deite solid solution.

A puzzling feature of the compositions listed in
ble 5 is that olivine has a consistently lower 100
g/(Mg+Fe^{++}) ratio than co-existing orthopyroxene
the "wet" runs. This differs from the pattern previ-
sly obtained at 9 kb, 1290–1250 °C (GREEN and
NGWOOD 1967a) where olivine has essentially the
me 100 Mg/(Mg+Fe^{++}) ratio as co-existing ortho-
roxene. Except for the 13.5 kb, 1150 °C run, co-
isting pyroxene pairs have clinopyroxene with lower
0 Mg/(Mg+Fe^{++}) ratio than coexisting orthopy-
xene. The differences are very small at 13.5 kb, 1320–
30 °C i.e. where the compositional differences be-
een the two pyroxenes are relatively small, but are
ger in the 18 kb, 1240–1200 °C runs. The partition
efficients for Fe and Mg between pyroxene pairs in
tural rocks are such that the clinopyroxene is rela-
ely enriched in magnesium although for magnesian
neous pyroxene pairs the coefficients approach unity.
e apparent reversal of this trend in the experimental
ns may in part be due to appreciable Fe^{+++} contents
ot determinable by microprobe analyses) in the clino-
roxenes or may be a real feature of the high temper-
ure of equilibration of these assemblages.

*mparison of natural xenocryst compositions with ex-
imentally crystallized phases:* The experiments under
conditions show that olivine, orthopyroxene and clinopyroxene (the three natural xenocryst phases) occur together on the liquidus at 11.3 kb, 1310 °C; the two pyroxenes occur without olivine on the liquidus at 13.5 kb and olivine occurs on the liquidus at 9 kb. The analyzed synthetic phases are similar or slightly lower in 100 Mg/(Mg+Fe^{++}) value than the natural xenocryst phases and it is probable that accurate matching of this parameter could be obtained at 11–12 kb and appropriate temperature (1310–1320 °C). However, the analyzed clinopyroxene at 11.3 kb and the pyroxene pairs at 13.5 kb are very different in composition from the natural pyroxenes, particularly in the extremely sub-calcic nature of the clinopyroxene and the slightly higher CaO content of the synthetic orthopyroxene.

Comparison of tables 2 and 5 shows that the natural pyroxene compositions are very closely matched by analyzed pyroxenes from "wet" runs at 13.5 kb and 18 kb. CaO contents in both pyroxenes, TiO_2 contents, 100 Mg/(Mg+Fe^{++}) ratios and Na_2O contents are closely matched. In detail the Na_2O content of the natural clinopyroxenes (0.7%) is between the values for the 13.5 kb (0.3) and 18 kb (1.0) clinopyroxene; the CaO content of the natural orthopyroxene is slightly greater and the CaO content of the more Fe-rich natural clinopyroxene slightly lower than the 18 kb, 1200 °C pyroxene pair. These differences suggest that a pressure of 14–16 kb and a temperature slightly above 1200 °C would yield near-liquidus pyroxenes identical to the natural xenocrysts. It may be noted also that while olivine precedes orthopyroxene in the crystallization sequence at 13.5 kb, and is absent at 18 kb, it should occur together with orthopyroxene on the liquidus at about 15 kb. The natural pyroxenes encompass a small range in 100 Mg/(Mg+Fe^{++}) ratio and thus represent crystal/liquid equilibria over a small range of P, T conditions such as might be anticipated in a cooling magma chamber or in a static or slow moving feeder dyke. The range of experimental conditions in the wet melting experiments appears to exceed the range required to produce the observed compositional variations.

4. Conclusions

The experimental study of the crystallization of the Auckland Id. olivine basalt has shown that the olivine basalt can precipitate, as near-liquidus phases, crystals which closely match the observed partly resorbed "xe-

nocrysts" within the basalt. This matching of liquidus and xenocryst phases in chemical composition and in paragenesis can only be achieved experimentally over a very small P, T range. In particular, the possible temperature of precipitation is rather closely fixed by the observed degree of solid solution between co-existing pyroxenes and the load pressure at precipitation may be deduced from the relative roles of pyroxene or olivine as liquidus phases and by the Na_2O content of the clinopyroxene. It is considered that the "xenocrysts" are not of accidental origin but are cognate, high-pressure phenocrysts precipitated from the host olivine basalt at depths of around 50–55 kms, (load pressure 14–16 kb) and a temperature close to 1200 °C. These conditions of precipitation require that the basalt liquidus was depressed about 130 °C below the dry liquidus – this is consistent with the presence of approximately 2% water within the magma at the depth of precipitation of the crystals.

The inferred high pressure phenocrysts have lower 100 $Mg/(Mg+Fe^{++})$ values than that inferred for parental mantle material or those values present in lherzolite or garnet peridotite xenoliths (100 $Mg/(Mg+Fe^{++})$ ~88–92). Thus the composition of the Auckland Id. olivine basalt is not considered to be that of a direct partial melt from mantle peridotite but rather to be a liquid produced from some more primitive parent magma by fractional crystallization at depths ≥ 50 km. While it is not possible to unequivocally deduce the nature of this parent magma, the Auckland Id. olivine basalt magma provides natural evidence of a process of fractional crystallization operating at about 50 km depth and "quenched" by the rapid eruption of both liquid and precipitating phases. This fractionation trend is dominated by pyroxene separation and in particular, by orthopyroxene. Although olivine accompanies the near-liquidus pyroxenes in the experiments, it is volumetrically a minor percentage of the precipitated material i.e. the precipitated material would be olivine-poor pyroxenite and not peridotite mineralogy. In chemical composition, the estimated crystal extract at 14–16 kb is very similar to that deduced for the olivi basalt and alkali olivine basalt by GREEN and RIN WOOD (1967a). The calculated fractionation trend 14–16 kb, ~1200 °C, deduced for the Auckland olivine basalt predicts more hypersthene-normati tholeiitic compositions as parental to the observed h basalt and predicts nepheline-normative alkali olivi basalts as lower temperature derivative liquids fr the host basalt. The data support and extend the cc clusions of GREEN and RINGWOOD (1964, 1967a) on t dominant role of orthopyroxene and orthopyroxene clinopyroxene crystallization at 13–18 kb in produci a spectrum of basaltic liquids from olivine tholeiite basanite. It has been demonstrated that it is possil to characterize in a rather unequivocal manner, t P, T conditions and water content of some magm within the upper mantle, prior to rapid extrusion.

Acknowledgements

We thank Dr J. B. Wright for originally bringing t Auckland Id. basalt and its xenocrysts to our att tion. The technical assistance of Mr E. H. Pedersen the preparation of microprobe mounts is gratefu acknowledged.

References

BULTITUDE, R. J. and D. H. GREEN (1968) Earth Planet. Letters **3**, 325.

DAVIS, B. T. C. and F. R. BOYD (1966) J. Geophys. Res. **71**, 35

GREEN, D. H. and A. E. RINGWOOD (1964) Nature **201**, 127

GREEN, D. H. and A. E. RINGWOOD (1967a) Contr. Mine Petrol. **15**, 103.

GREEN, D. H. and A. E. RINGWOOD (1967b) Geochim. Cosr chim. Acta **31**, 767.

KUSHIRO, I. (1968) Upper Mantle Committee Symposium, Ab Proc. XXIII Internat. Geol. Congr. Prague. 11.

LINDSLEY, D. H. (in press).

MACDONALD, G. A. and T. KATSURA (1964) J. Petrol. **5**, 82.

O'HARA, M. J. (1968) Earth Sci. Rev. **4**, 69–133.

POLDERVAART, A. (1964) Geol. Soc. Am. Bull. **75**, 229.

ROSS, C. S., M. D. FOSTER and A. T. MYERS (1954) Am. Mine ogist **39**, 693.

TILLEY, C. E. and I. D. MUIR (1964) Geol. Foren. Stockh Forh. **85**, 434.

YODER, H. S. and C. E. TILLEY (1962) J. Petrol. **3**, 342.

B12

Phil. Trans. Roy. Soc. Lond. A. **268**, 707–725 (1971) [707]
Printed in Great Britain

V. PETROGENESIS AND DISCUSSION

Composition of basaltic magmas as indicators of conditions of origin: application to oceanic volcanism

By D. H. Green
Department of Geophysics and Geochemistry,
Australian National University, Canberra

Basaltic magmas are formed by partial melting of a source rock of peridotitic composition (pyrolite) under upper mantle conditions. Experimental studies of the mineralogy of pyrolite and the melting relations of various basaltic magmas under high-pressure conditions are integrated in an attempt to present an internally consistent model of source composition, derived liquid compositions and residual mantle compositions. The role of a small (0.1 %) content of water in the upper mantle is treated in some detail. The presence of the low velocity zone in the upper mantle is attributed to a small (< 5 %) degree of melting of pyrolite containing approximately 0.1 % water. The small liquid fraction present in the low-velocity zone is highly undersaturated olivine nephelinite or olivine melilite nephelinite. Other magma types of direct upper mantle derivation ranging from olivine trachybasalt to olivine melilitite and to tholeiitic picrite are assigned to a genetic grid expressing the depth (pressure) of magma segregation, the degree of partial melting of the source pyrolite, the water content and approximate temperature of the magma. While this genetic model can account for variations in major element abundances and normative mineralogy among basalts, there are variations in abundances of the incompatible elements, particularly K, Rb, Ba, and the rare earths, which are inconsistent with a model invoking a constant source composition for all mantle-derived basalts. Additional factors producing source inhomogeneity, particularly in incompatible element abundances, include the possibility of two-stage melting and of chemical zoning within the low-velocity zone. It is suggested that vertical migration of a fluid or incipient melt phase, enriched in H_2O, CO_2 and incompatible elements, occurs within the low-velocity zone.

The evolution of continental and oceanic rift systems and of the Hawaiian volcanic province is discussed in relation to the depths and conditions of magma genesis derived from the models of magma genesis.

Introduction

Basaltic magmas are derived by partial melting of source rock of peridotitic composition and knowledge of possible magma and residue relations allows estimation of source compositions from observed natural basalts and peridotites. This is the rationale of the 'pyrolite' model composition for the Earth's upper mantle and it is emphasized that the method is a general one capable of revision and refinement as knowledge of magma/residue pairs is extended. At the present stage the model pyrolite composition of Ringwood (1966*a*) provides a suitable framework and reference composition to employ in the search for internally consistent models of primary mantle composition, derived liquids, refractory residues and magmatic accumulates.

The pyrolite composition crystallizes in four anhydrous mineral assemblages under near-solidus upper mantle conditions (Green & Ringwood 1967*a*, 1969). At temperatures near the anhydrous solidus, these four assemblages are:

(i) olivine + orthopyroxene + clinopyroxene + plagioclase + minor chromite [$P \leq 9$ kbar (0.9 GN m^{-2})];

(ii) olivine + orthopyroxene + clinopyroxene + minor spinel + minor plagioclase (pyroxenes moderately aluminous with 3–4 % Al_2O_3) [P = 9–12 kbar (0.9–1.2 GN m^{-2})].

(iii) olivine + aluminous orthopyroxene + aluminous clinopyroxene (pyroxenes with 6–8 % Al_2O_3) [P = 12–30 kbar (1.2–3.0 GN m^{-2})].

(iv) olivine + orthopyroxene + clinopyroxene + garnet [P > 30 kbar (3 GN m^{-2})].

In melting anhydrous pyrolite, the first drop of liquid formed at a given pressure will be in equilibrium with one of the mineral assemblages listed above and with increasing degree of melting, the residual phases will change in composition and be eliminated one by one, some possibly melting incongruently, e.g.

$$\text{clinopyroxene} + \text{liquid}_1 \rightarrow \text{olivine} \pm \text{orthopyroxene} + \text{liquid}_2.$$

The composition of the partial melt will thus change with the degree of melting as the solid phases buffering it also change. Because of the olivine-rich nature of the source composition, all partial melts will be saturated with respect to olivine. Experimental studies on melting of pyrolite (Green & Ringwood 1967*a*), on picritic and basaltic compositions, and consideration of the abundance of enstatite in the modal pyrolite mineralogy at pressures of 10 to 30 kbar (1–3 GN m^{-2}), show that enstatite will be the second last phase to disappear during progressive melting at pressures of 5 to 50 kbar (0.5–4.0 GN m^{-2}). Thus self-consistency arguments imply that basalts derived directly by partial melting of pyrolite composition will have olivine and enstatite and may have plagioclase, clinopyroxene, spinel or garnet as liquidus phases at appropriate pressure and temperature conditions.

Recent geophysical studies have confirmed the existence of a low velocity zone in the upper mantle, beginning at depths of 80 to 120 km and extending to around 200 km (Archambeau, Flinn & Lambert 1969). It has also been argued that the characteristics of the low-velocity zone indicate that this is a region in which a small percentage of interstitial liquid is present in the mantle pyrolite. Estimates of the continental or oceanic geothermal gradients (Clark & Ringwood 1964) and knowledge of the anhydrous pyrolite solidus show that the geotherm would lie well below the anhydrous solidus at this depth interval (see figure 1). Either there is considerable error in the estimates of average geothermal gradients or some other factor depresses the solidus of the mantle to lower temperatures in this depth interval. Recent studies of the role of water under upper mantle conditions show that small (0.1 to 0.2 %) quantities of water in upper mantle pyrolite provide a solution to this dilemma. Experimental studies of olivine nephelinite magmas showed that derivation of these extremely undersaturated magmas from pyrolite is possible provided these magmas were hydrous (2 to 10 % H_2O) and formed by partial melting of a pyrolite source rock at temperatures 150 to 250 °C below the anhydrous pyrolite solidus (Bultitude & Green 1968, Green 1969*a*, *b*). Studies of the stability of the hydrous mineral amphibole in basaltic and peridotitic compositions (Green & Ringwood 1967*c*; Lambert & Wyllie 1968; Green & Ringwood 1969) showed that this mineral was unstable relative to the assemblage garnet + pyroxene (± olivine) + water at pressures above 25 to 30 kbar (2.5–3.0 GN m^{-2}), $P_T = P_{H_2O}$, T = 1000 °C. In particular, it has been shown that, in pyrolite composition containing 0.1 to 0.2 % H_2O, the olivine + amphibole + pyroxene(s) assemblage is stable at 1000 °C at pressures less than 28 to 29 kbar (2.8–2.9 GN m^{-2}) but is replaced by olivine + pyroxenes + garnet + minor phlogopite + water at higher pressures (Green & Ringwood 1969). The depth limitation on amphibole stability in the upper mantle has a large effect on the character of the pyrolite solidus. This is illustrated in figure 1 which contrasts the solidus for anhydrous pyrolite with the solidus for pyrolite containing approximately 0.1 % H_2O. At low pressures amphibole is present at the solidus and the latter is determined by some value of $P_{H_2O} = P_1 < P_{total}$. At higher pressures this solidus for $P_{H_2O} = P_1$ intersects the breakdown

curve for amphibole at $P_{H_2O} = P_1$ and the solidus migrates through a series of such intersections to the intersection of solidus and amphibole breakdown for $P_{H_2O} = P_{total}$. If some other fluid phase such as CO_2 is present then P_{H_2O} may only attain some value

$$P_{H_2O} = P_2 < P_{fluid} = P_{total}$$

and the solidus would be appropriate for this value of P_{H_2O}.

It is apparent from figure 1 that a geotherm such as that shown, which would not intersect the anhydrous pyrolite solidus, will intersect the solidus for pyrolite containing 0.1 % H_2O at a depth of approximately 80 km. In figure 1, the dashed curves illustrate the degree of melting at

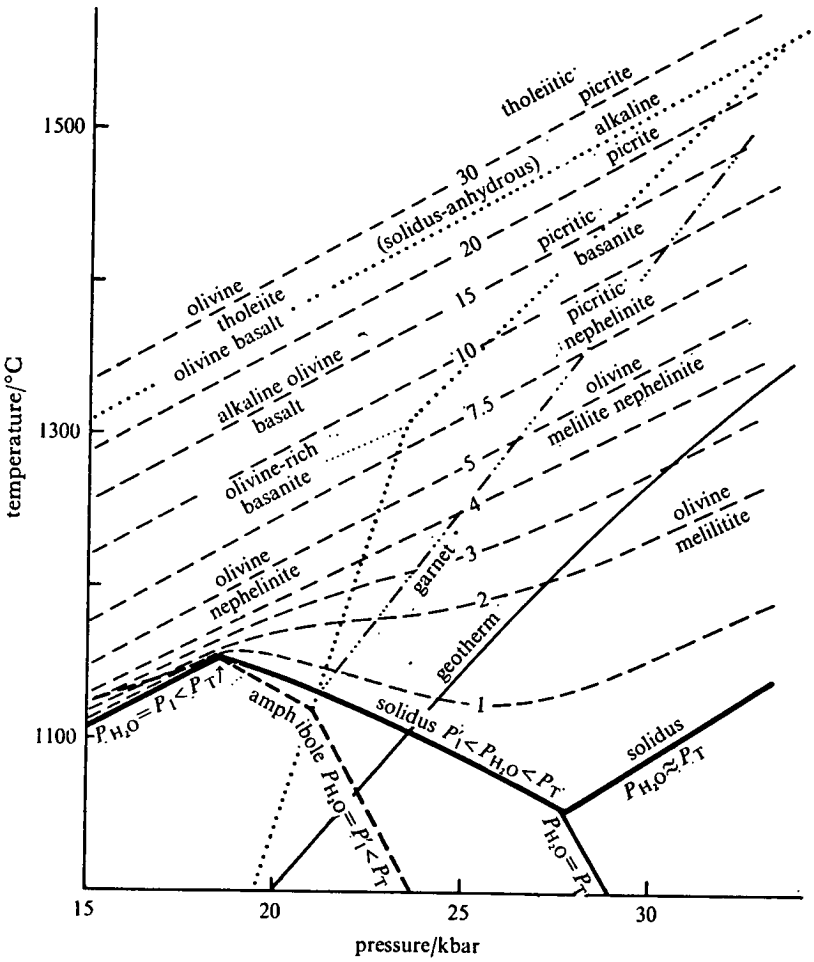

FIGURE 1. Diagram illustrating the amphibole stability limit at high pressure and the solidus for pyrolite composition containing approximately 0.1 % H_2O. Also shown (dotted lines) are the solidus for anhydrous pyrolite and the boundary for appearance of garnet (from Green & Ringwood 1967*a*). The numbered dashed curves show the % liquid present above the solidus and the petrochemical character of these liquids is indicated. The geothermal gradient shown is the oceanic geotherm illustrated by Ringwood (1966*b*).

The positions of the curves on this diagram, other than the anhydrous boundaries, are estimated from reconnaissance experiments on the solidus and amphibole stability in pyrolite with 0.1 to 0.2 % water and by experiments establishing the degree of depression of the liquidus temperatures of various basalts by addition of known amounts of water. P_{H_2O}, equilibrium water pressure; P_1, water pressure along solidus for pyrolite with 0.1 % H_2O.

P_1 varies along the solidus and an arrow indicates the intersection of the solidus with a subsolidus breakdown curve for amphibole at $P_{H_2O} = P_1'$ also (amphibole $\rightleftarrows$ pyroxenes + garnet + olivine + water).

temperatures above the solidus and this is further illustrated and contrasted with the anhydrous case in figure 2. It is apparent that melting in a pyrolite source with a low and limited amount of water produces a condition where the amount of liquid formed remains small over quite large temperature and depth variations, i.e. small temperature perturbations in the low-velocity zone or small changes in depth within the zone do not produce extremely large variations in the percentage of melt and thus in the seismic properties. If the low-velocity zone is itself compositionally zoned (see later sections) so that the amount of water decreases with depth below 120 to 150 km then this will limit or prevent melting at deeper levels.

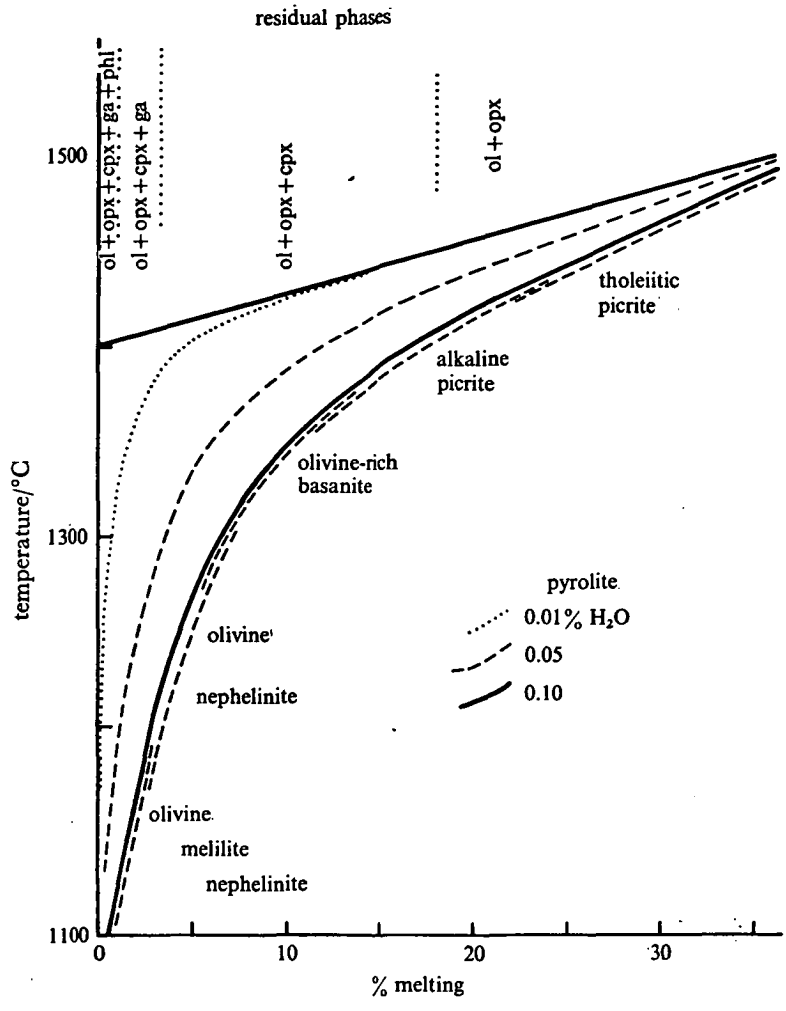

FIGURE 2. Diagram contrasting the melting behaviour of anhydrous pyrolite with melting in pyrolite compositions containing 0.01, 0.05 and 0.10% H_2O. The nature of the residual phases and the petrochemical character of the liquids derived are shown for the example with 0.10% H_2O.

The hypothesis that melting occurs in a hydrous pyrolite source has important implications in that pyrolite contains both orthopyroxene and clinopyroxene and the mutual solid solution between these phases is very temperature dependent. Similarly, the Al_2O_3 solubility in pyroxenes is both temperature and pressure dependent. Thus a liquid produced with a very small degree of melting of anhydrous pyrolite at 1400 °C, 25 kbar (2.5 GN m^{-2}) would be in equilibrium with olivine, aluminous enstatite ($\sim$ 6% Al_2O_3, 2.2% CaO) and aluminous

subcalcic clinopyroxene (~ 8 % Al_2O_3, 11 % CaO), whereas the liquid produced with a similarly small degree of melting at 25 kbar, 1150 °C (hydrous pyrolite source) would be in equilibrium with olivine, enstatite (~ 3 % Al_2O_3, < 1.5 % CaO) clinopyroxene (~ 5 % Al_2O_3, > 20 % CaO) and garnet (or spinel) (Green & Ringwood 1967*a*, 1969).

The discussion in this section has centred on the choice of a model composition for the upper mantle acting as source for basaltic magmas and on illustrating the very sensitive controls exerted by P, T and P_{H_2O} in determining the mineralogy and solidus temperature of this composition. In the following section, the liquidus phases of basalts at high pressures are briefly reviewed in the context of self-consistency with derivation from the pyrolite model.

Liquidus minerals of basaltic compositions at high pressures

In seeking to establish models in which basaltic magmas are derived by partial melting of a peridotite source rock, a principal constraint, imposed by self-consistency, is that the liquidus phases of the postulated melt must be the same as the residual phases of the postulated source rock at the appropriate P, T, P_{H_2O} conditions. Experimental study of basaltic compositions at high pressures, both dry, and with various water contents, serves to identify the nature of the liquidus phases which can then be compared with the data on solidus and near-solidus mineralogy of pyrolite to determine whether the basalt studied is a possible derivative liquid from the pyrolite source at some P, T, P_{H_2O}. It must be emphasized that the feasibility of using this method depends entirely on obtaining accurate chemical compositions of the mineral phases—comparison must include degree of pyroxene solid solution, Al_2O_3 content of pyroxenes and, most importantly, the Mg/Mg + Fe ratios of the mineral phases. The combined use of experimental high-pressure crystallization techniques utilizing complex natural basalts and electron microprobe analyses of the mineral phases synthesized is essential in this type of study.

Two examples of basalt suites studied experimentally are briefly summarized below. Studies of olivine tholeiite and high alumina olivine tholeiite (Green & Ringwood 1964, 1967*b*; Green, Green & Ringwood 1967; Green 1969*b*; Tilley & Yoder 1964) under *dry* conditions show that these liquids may have magnesian olivine and aluminous orthopyroxene occurring together on the liquidus at a specific pressure. At 9 kbar (0.9 GN m^{-2}), the liquid with olivine, enstatite and clinopyroxene together on the liquidus has about 10 to 15 % normative olivine, 10 to 15 % normative hypersthene and has high Al_2O_3 content (15 to 16 %). Liquids with olivine and enstatite only on the liquidus at 9 kbar have higher olivine and hypersthene contents and lower Al_2O_3 contents (Green & Ringwood 1967*b*, Green *et al.* 1967). At 12 kbar (1.2 GN m^{-2}), a liquid with olivine and enstatite together on the liquidus contains 20 % normative olivine, 12 to 14 % hypersthene and lower Al_2O_3 content (13 to 14 %) (Green & Ringwood 1967*b*). At 15 to 16 kbar (1.5 to 1.6 GN m^{-2}), a liquid with olivine and enstatite together on the liquidus has 26 % normative olivine, 12 % hypersthene, and 12 to 13 % Al_2O_3. At 18 kbar (1.8 GN m^{-2}), the tholeiitic liquid would contain 28 % olivine, 12 % hypersthene and 11 to 12 % Al_2O_3 (Green 1969*b*). These experiments illustrate the variation in the nature of tholeiitic liquids which can be produced at various depths from the pyrolite source rock, provided the degree of melting is sufficient to eliminate all the plagioclase, and most of the clinopyroxene from the source pyrolite at 9 kbar, all the spinel and clinopyroxene at 12 kbar and all the clinopyroxene together with appreciable olivine and aluminous enstatite at 15 to 18 kbar.

Experiments on the effect of water on the liquidus phases of undersaturated basalts (Bultitude & Green 1968, Green 1969*a*, *b*) show that whereas olivine and clinopyroxene or clinopyroxene alone may be the liquidus phases under dry conditions (liquidus 1400 to 1450 °C, 20 to 30 kbar (2 to 3 GN m^{-2}), if the liquidus is depressed to 1200 to 1300 °C by the addition of 2 to 5 % water, then olivine and orthopyroxene, or olivine, orthopyroxene and clinopyroxene may occur at or near the liquidus. This effect has been substantiated with experiments using sealed capsules and known quantities of water (Green 1969*a*, *b*; Green & Hibberson 1969). It should be noted that the near-liquidus clinopyroxene under dry conditions at ~ 1400 to 1450 °C is rather subcalcic and with the rapid widening of the pyroxene immiscibility gap at lower temperature, such a composition would be represented by orthopyroxene and clinopyroxene. Thus the depression of the liquidus by the addition of water may bring in orthopyroxene as a liquidus phase, not as a consequence of any major compositional shift of the cotectic between olivine and orthopyroxene (cf. Kushiro 1969) but as a direct consequence of the sensitive temperature dependence of the pyroxene solid solutions. The experiments show that very undersaturated basanites and olivine nephelinites may form in equilibrium with residual magnesian olivine, orthopyroxene and calcic clinopyroxene at pressures of 18 to 35 kbar (1.8 to 3.5 GN m^{-2}) provided the solidus of the source rock is depressed 100 to 250 °C below the anhydrous solidus, with consequent changes in source-rock mineralogy and in the nature of liquids formed at or near the solidus. It may be noted that the temperature, pressure régime under discussion, i.e. $T \sim 1200$ °C, $P \geqslant 18$ kbar (1.8 GN m^{-2}) is largely outside the stability field of amphibole so that this phase does not occur at the solidus, particularly at pressures > 25 kbar (2.5 GN m^{-2}). Phlogopite remains stable, and may be a minor but very significant phase in the subsolidus mineralogy.

Summary of basalt magma and pyrolite relations

Figures 1 to 3 present, in diagrammatic form, an integrated model for derivation of basalt types ranging from olivine trachybasalt and 'hawaiite' to olivine melilitite and to tholeiitic picrite. It is emphasized that the magma types shown are restricted to those magmas of direct mantle derivation as evidenced by the presence within them of xenoliths or xenocrysts of high-pressure mineralogy or in the case of tholeiitic magmas, as deduced from geophysical data. Processes of crystal fractionation at crustal levels may modify these magma types producing other magmas classifiable as basanite, trachybasalt or hawaiite but differing chemically and mineralogically from the types represented in figures 1 to 3.

In figures 2 and 3, tholeiitic magmas are produced with high degrees of partial melting (~ 30 %) and only olivine and enstatite remain in the residue. The water contents of such magmas, if developed from a source rock with 0.1 % H_2O, would be only 0.3 to 0.4 % H_2O. It is to be noted that such magmas would form only 30 to 50 °C below the temperature at which tholeiitic magmas would form from anhydrous pyrolite and little compositional difference would be anticipated between tholeiites developed from an anhydrous pyrolite and those from a hydrous pyrolite source.

The curve for the appearance of garnet in the anhydrous pyrolite composition is shown in figure 2 and this intersects the anhydrous solidus at > 30 kbar (3 GN m^{-2}). If the source rock contains 0.1 % H_2O then the lower part of this curve lies within the amphibole stability field and garnet may not appear until amphibole disappears at the solidus with a reaction possibly represented by amphibole $\rightleftharpoons$ olivine + garnet + pyroxene + liquid.

The curve for the appearance of garnet *above* the solidus for 'wet' pyrolite is shown schematically. Contours in figure 2 illustrate the variation in degree of melting at temperatures above the solidus and the petrologic character of the liquids for various degrees of melting is also shown. Since the source is regarded as having a fixed water content and all of this is partitioned into the liquid at the solidus (except below ~ 18 kbar (1.8 GN m^{-2}) where amphibole has a minor role immediately above the solidus) the water content of the various magma types can also be read from figure 2.

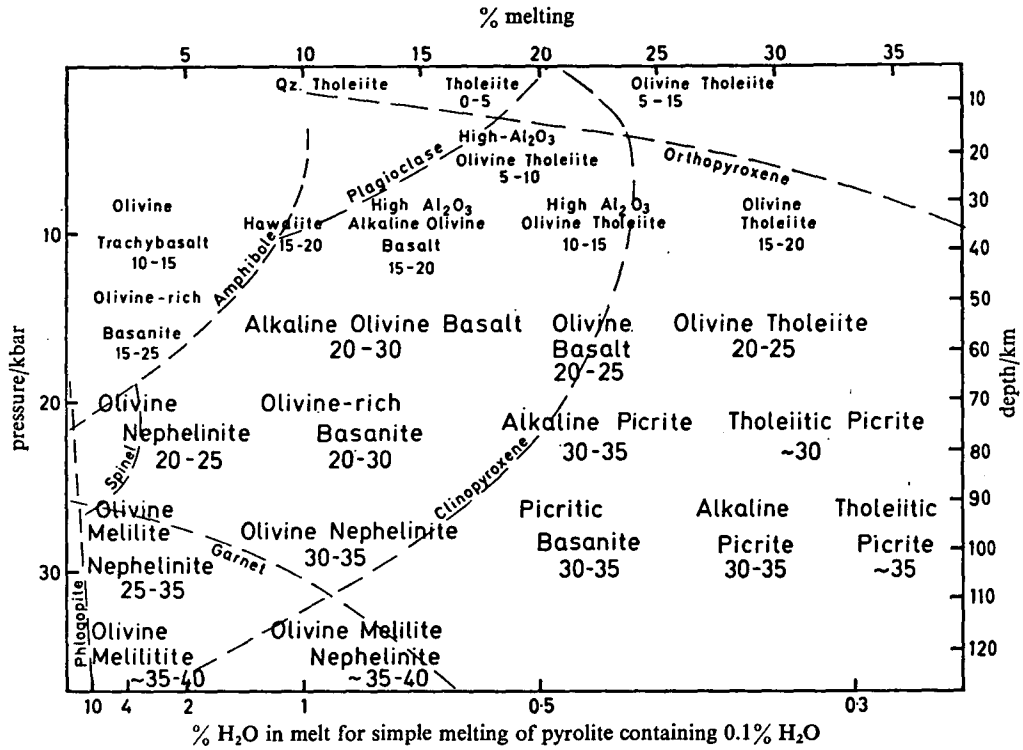

FIGURE 3. A petrogenetic grid for mantle-derived basaltic magmas. Various basalt magma types are assigned to a % melt, pressure grid (implying also specific % H_2O and temperature of melting, see figures 1 and 2) in which they are regarded as partial melting products of a pyrolite composition containing 0.1 % H_2O. The numbers placed with each basalt type refer to the normative olivine content of this liquid at its depth of origin—because of the expansion of the olivine crystallization field at low pressure most basalts will precipitate olivine before other phases if fractionation occurs at lower pressures. The dashed boundaries marked with a mineral name show that this mineral will occur among the residual phases remaining after extraction of magma types to the left of the boundary. Olivine is present in equilibrium, i.e. is a residual phase in the pyrolite composition, for all the magma types of this figure.

In figure 3, the arguments of figures 1 and 2 are synthesized to present a pressure (or depth) against % melting grid for a source pyrolite with 0.1 % H_2O, in which characteristic natural magma types are assigned to a pigeon-hole specifying their depth of magma segregation, the degree of partial melting (with implication of temperature as in figures 1 and 2) their water content and the nature of mineral phases with which they were in equilibrium at the point of magma segregation and which will remain in the more refractory peridotitic residue. The magma types appearing on figure 3 include only these liquids developed in equilibrium with residual peridotite—these magmas may in turn be modified by crystal fractionation as they move from the depth of magma segregation to eruption at the Earth's surface.

The conclusions on basalt petrogenesis summarized in figures 1 to 3 will undoubtedly require modification and refinement as further detailed studies proceed—the olivine trachybasalt to high alumina olivine basalt series and the olivine nephelinite to alkaline picrite series are currently under more intensive study. However, the relation outlined in figures 1 to 3 are considered sufficiently well founded to justify an attempt to use this petrogenetic grid to make deductions about the nature of melting processes responsible for rift valley, oceanic ridge and oceanic island volcanism.

Minor and trace elements in basalts—source inhomogeneity

The relations expressed in figures 1 to 3 are considered to account for differences between basalt types in major element chemical composition, normative and modal mineralogy and in ratios such as $Mg/(Mg+Fe^{2+})$, $Na/(Na+Ca)$. However, there is a group of elements, referred to as incompatible elements by Green & Ringwood (1967*b*) and including K, Ti, P, Ba, Sr, Rb, Zr, Hf, U, Th, Pb and the lighter rare earth elements, which show variations in basalts that cannot be accounted for by the hypothesis of a constant source (pyrolite) composition and single stage melting of the character illustrated in figure 3. These elements are those which would be so strongly partitioned into the basaltic liquid that for partial melting in excess of about 5 % their concentration should closely reflect the % melting and source composition only. Their concentration would be largely independent of relative proportions of olivine, orthopyroxene and clinopyroxene in the residual phases. On this basis and from figure 3, high-alumina olivine tholeiites such as occur commonly in the mid-oceanic ridge environment, should have K contents intermediate between those of alkali olivine basalts and parental low-alumina tholeiites. Comparison of K contents of Hawaiian alkali olivine basalts and Hawaiian low-alumina olivine tholeiites shows that these magma types are roughly consistent with magma genesis at 50 to 60 km according to the relations of figure 3. However, the same source rock could not produce the very low-potassium tholeiites (of both low-alumina and high-alumina type) with the similar degrees of melting implied by figure 3. Differences in rare-earth element fractionation patterns between Hawaiian tholeiitic basalts and low-potassium tholeiitic rocks from the oceanic ridges, and between low-potassium and high-potassium basalts from oceanic ridges, further illustrate the dilemma (Green & Ringwood 1967*b*; Gast 1968; Green 1969*b*; Kay, Hubbard & Gast 1970). Green & Ringwood (1967*b*) called on processes of wall rock reaction to account for selective enrichment of the incompatible elements in the more undersaturated rocks but this will not account for differences between various olivine tholeiitic magmas. Gast (1968) clearly delineated the problem and, considering the trace element data of paramount importance, interpreted alkaline magmas such as the Hawaiian alkali magma series as products of very small degrees (3 to 7 %) of partial melting of the peridotite source. The low-potassium olivine tholeiites of the mid-oceanic ridges were interpreted as products of 20 to 30 % melting. Olivine tholeiites of Hawaiian type, which have higher K_2O contents and r.e. abundances showing enrichment in the light r.e., were grouped with the alkaline basalts on the basis of their trace element contents. The inference that parental Hawaiian olivine tholeiite is produced by very small degrees of partial melting is inconsistent with the phase equilibrium studies on the roles of olivine, enstatite and clinopyroxene as liquidus phases and mantle residual phases for these different magma types. Gast (1968) also advocated a two-stage melting process. The source rock for the low potassium olivine tholeiites was regarded (p. 1077) as having

previously been depleted, particularly in incompatible elements, by an earlier partial melting event in which a very small magmatic fraction was extracted.

Further geochemical data on oceanic basalts, particularly the studies of r.e. element distributions by Kay *et al.* (1970), Frey, Haskin, Poetz & Haskin (1968) and Schilling (1969), lends support to the concept that differences in incompatible element contents reflect source characteristics. Muir & Tilley (1964) and Nicholls (1964) both describe high-alumina olivine basalts transitional between olivine tholeiite and high-alumina alkali olivine basalt. Both papers describe dredged samples from the crestal region of the oceanic ridge but those described by Muir & Tilley have high K_2O contents (0.4 to 0.6 % K_2O), whereas that described by Nicholls has K_2O = 0.09 %. The abundance of r.e. elements in at least one of Muir & Tilley's samples is enriched in lighter rare earths (Frey *et al.* 1968; Kay *et al.* 1969), whereas Nicholls's sample would be expected to show the depletion of light r.e. elements characteristic of other low-potassium oceanic basalts (Kay *et al.* 1970).

If basalts with marked differences in incompatible element contents, but with similar major element composition were randomly distributed in space and time then one might conceive of a mantle source region which is irregularly and randomly inhomogeneous due to effects of variable degrees of magma extraction at various times in the past. However, several authors, notably Gast (1968), Schilling (1969) and Kay *et al.* (1970) have argued that the regular appearance of the low-potassium tholeiite at mid-oceanic ridge crests suggests that this magmatic process taps a widespread and relatively homogeneous source region of the mantle. Basalts with high K_2O contents and high contents of other incompatible elements relative to the low-potassium tholeiites do occur at abyssal depths in the ocean basins. Commonly they occur on the flanks of the ridges rather than within the median valley (Aumento 1967, 1968; Kay *et al.* 1970) and rock types range fom high-alumina alkali olivine basalts to olivine basanite (Melson, Jarosewich, Cifelli & Thompson 1967). The occurrence of high-potassium basalts is particularly characteristic of seamounts which locally are symmetrically developed on either side of the median valley (Aumento 1967, 1968) or from chains moving away from the ridge crest in the direction of oceanic plate movement (Menard 1969). These occurrences show that an oceanic crustal locality, which taps a source of low-potassium tholeiite when at the ridge crest, may later tap a second source region as it moves away from the ridge crest. The second source region characteristically provides magmas relatively enriched in incompatible elements.

It appears that there are two independent controls on the chemical characteristics of major oceanic basalt magma types. These are the conditions (P, T, P_{H_2O}) of melting and the nature of the source composition. The source composition is envisaged as relatively constant in major element content and thus in mineralogy but variable in content of incompatible elements and accessory phases such as phlogopite or apatite. It is suggested that the upper mantle is vertically zoned in its content of incompatible elements and that this chemical zoning results from the upward migration within the low-velocity zone of a separate fluid phase. This is envisaged as water-rich, possibly CO_2-rich and may be a very small water-rich silicate melt fraction. This concept is illustrated in figures 4 and 6. The movement of incompatible elements within or through a fluid phase has been discussed by Green (1969*b*) and Frey (1969) gives an excellent illustration of the operation of this process as regards r.e. elements. Frey shows that selective depletion of light rare earths occurs in a dehydration reaction (amphibole → pyroxene) in a metamorphic aureole and that enrichment in light rare earths occurs in neighbouring rocks (highly magnesian peridotite) in which amphibole is stable and crystallizes under the ambient

conditions at the expense of magnesian pyroxenes and olivine. A similar effect on a large scale and over long periods of time is envisaged within the low-velocity zone. The presence of a free fluid phase ($H_2O \pm CO_2$) in this region permits the upward migration of incompatible elements which are strongly rejected by the major minerals in the low-velocity zone (olivine, aluminous pyroxenes, garnet) until they are 'fixed' by entering a small silicate melt fraction in the upper part of the low-velocity zone or possibly by entering minor hydrous phases (particularly amphibole) at the base of the lithosphere. Referring to the r.e. elements, the presence of garnet in the low-velocity zone and its increasing abundance at deeper levels (Green & Ringwood 1967*a*) would strongly influence the r.e. distribution pattern as the heavy rare earths would be strongly partitioned into the garnet (Gast 1968), whereas the light rare earths would strongly partition into the fluid phase relative to garnet, clinopyroxene or enstatite (Frey 1969). In this way contrasted r.e. distribution patterns would be developed within the low-velocity zone. To summarize, it is suggested that the upper part of the low-velocity zone has relative abundances of incompatible elements matching those of olivine-rich tholeiite of Hawaiian type (e.g. average Kilauea Iki lava lake), whereas the lower part of the low-velocity zone has the relative abundances of incompatible elements of an oceanic ridge low-potassium olivine tholeiite. In both regions, the actual concentrations of the incompatible elements in the source rocks, are one-fifth to one-third those of the characteristic tholeiitic magmas.

The mantle lithosphere overlying the low-velocity zone is considered to be inhomogeneous on a smaller, local scale reflecting diapiric emplacement of mantle from the low-velocity zone, local magma segregation and magma channels, and local accumulates from basaltic

---

LEGEND TO FIGURE 4

FIGURE 4. Illustration of possible processes relating rift valley volcanism to continental rifting and the creation of new oceanic crust with a typical mid-oceanic rift system. The mantle lithosphere is in part refractory, residual peridotite in which minor amphibole may occur if water is available. The low-velocity zone is of pyrolite composition containing, in the upper part at least, about 0.10% H_2O. Amphibole is unstable in the low-velocity zone and this results in a region of partial melting with $< 5\%$ of highly undersaturated and volatile-enriched magma in the upper part of the low-velocity zone. Vertical migration of a H_2O-rich fluid phase is considered to cause chemical zoning within the low-velocity zone, the lower part becoming depleted, and the upper part enriched, in incompatible elements.

Stage I. Local tapping of magmas present and potentially available within the low-velocity zone—parental magma types are olivine nephelinites and olivine melilitites, characteristic of small degrees of partial melting at depths of 80 to 120 km. A zone of partially depleted pyrolite is produced within the low-velocity zone.

Stage II. With appreciable crustal thinning under tension, the upwelling of material from the low-velocity zone becomes important leading to both lateral and vertical movements within the low velocity zone. Volcanism of the characteristic stage I type may continue with the depth of magma segregation now near 60 to 70 km (olivine-rich basanite) but also with the diapiric upward movement of material from the low-velocity zone (Green & Ringwood 1967*b*, figure 12) magmas produced by $> 5\%$ partial melting and with segregation at $\leqslant 60$ km may appear (alkali olivine basalts, olivine basalts, olivine tholeiites). The source of the pyrolite diapirs is considered to be the upper part of the low-velocity zone.

Stage III. With rifting apart of the continental crust and mantle lithosphere, pyrolite upwelling to shallow depths ($\sim$ 30 km or less) will occur. This may bring partially depleted pyrolite (the source region for stage I magmas) to depths of $\sim$ 30 km causing a second melting stage—20 to 25% melt will yield high-alumina olivine tholeiites and the two-stage melting will produce very low contents of incompatible elements in these magmas. Continuation of the rifting process will lead to upwelling of pyrolite from deeper within the low velocity zone and having the incompatible element contents typical of this zone. It is conjectured that the upper part of the low velocity zone moves with the overlying plate, the rate of such movement decreasing with depth and reversing at some depth to flow towards the ocean-floor spreading centre. Tectonic activity within the lithosphere plates on either side of the spreading centre may tap magmas from the low-velocity zone yielding volumetrically small extrusions of extremely undersaturated magma types—such centres would move with the lithosphere plate.

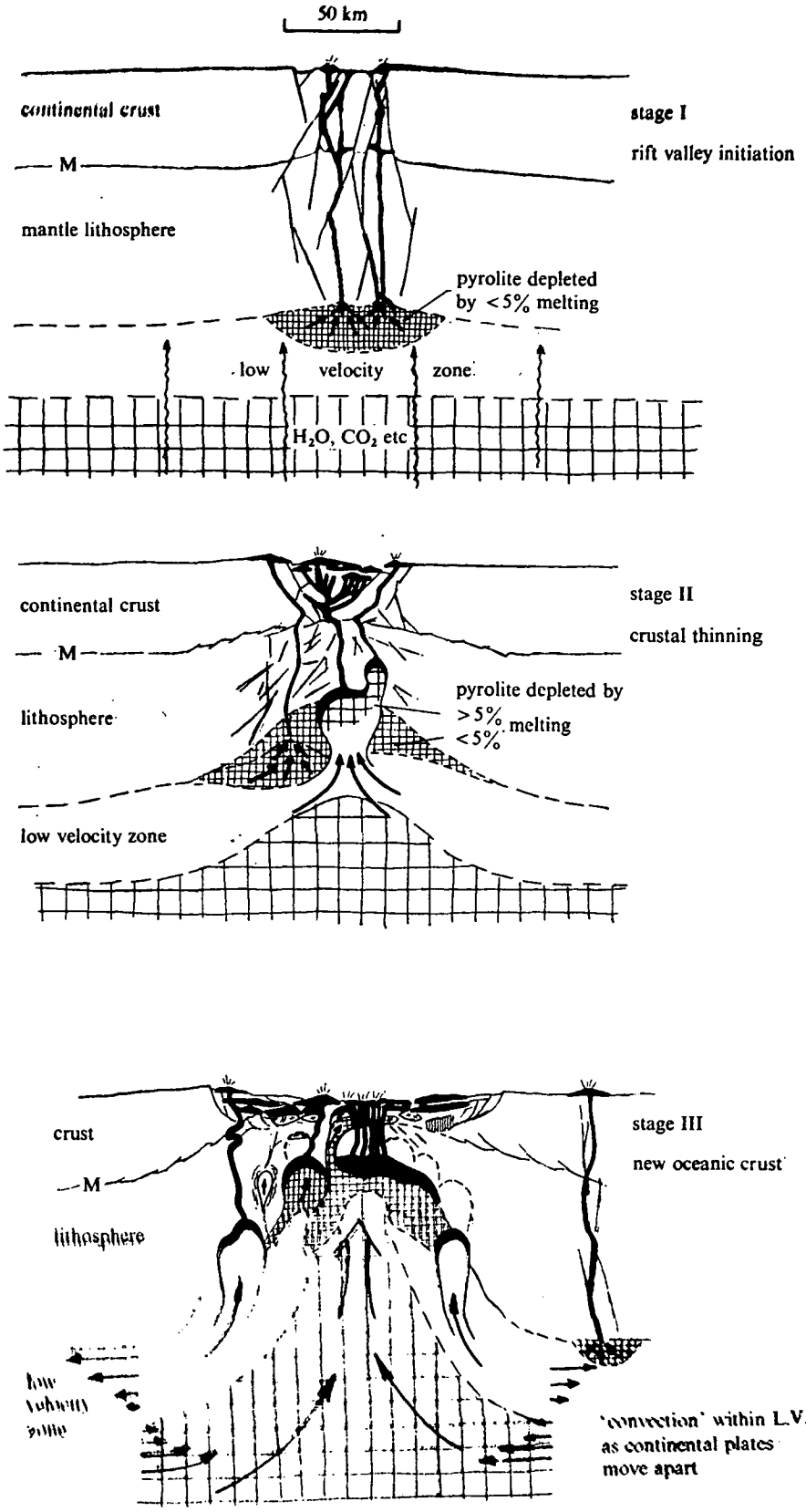

FIGURE 4. For legend see facing page.

magmatism. It is considered to range from refractory harzburgite to near-primitive pyrolite. This is the region sampled by explosive eruption of hydrous magmas from the low velocity zone and the detailed geochemistry of lherzolite inclusions is currently revealing the variation and complex history of this mantle region (Leggo & Hutchison 1968; Kleeman, Green & Lovering 1969; Cooper & Green 1969).

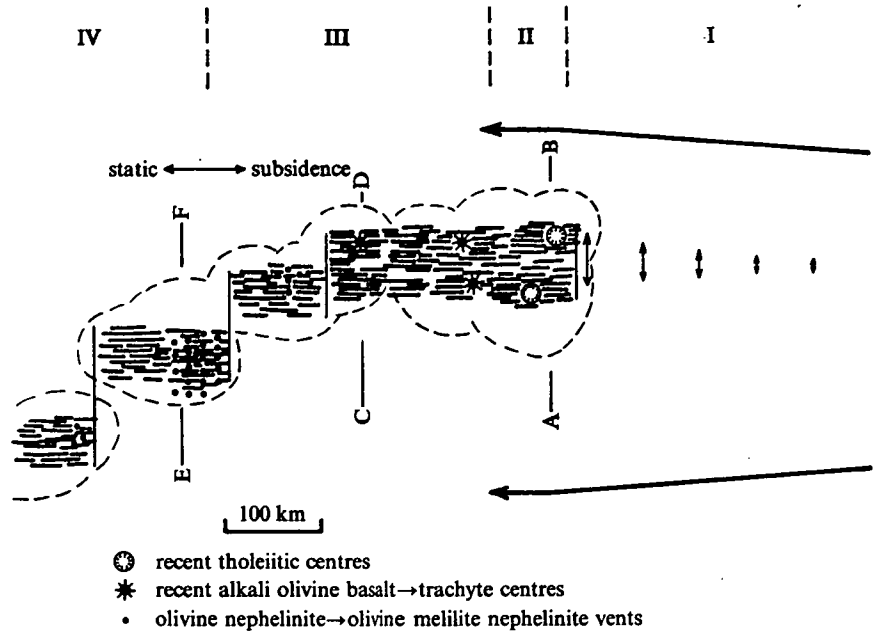

FIGURE 5. Hypothesis outlining the origin of a chain of volcanic islands on a moving oceanic plate. The diagram represents an idealized plan of the Hawaiian Islands. It is suggested that divergence of flow vectors, such as could be produced by a plate moving over an imperfect sphere, leads to a zone of tension. Intermittent failure of the lithosphere leads to rapid upwelling from the low velocity zone, a short-lived stage of active volcanism with creation of new oceanic crust, subjacent dyke swarms (illustrated diagrammatically) and a broad carapace of extruded lavas.

Stage I. Zone of stress build-up in lithosphere due to divergent plate movement vectors.

Stage II. Failure of lithosphere, stress release. Active volcanism with formation of new crust and growth of individual tholeiitic dome in 1 to 2 Ma.

Stage III. Decay of volcanism with source now emplaced within and moving with the oceanic plate; consolidation of new crust and lithosphere.

Stage IV. Local rejuvenation of volcanism with transverse tensional faulting tapping magmas directly from the low-velocity zone. This has been correlated with a hinge zone between a region of crustal loading and subsidence and a static zone (Jackson & Wright 1970).

Diagrammatic sections illustrating the volcanism are given in figure 6. AB represents a section approximately through Kilauea and Mauna Loa, Hawaii. CD represents a section through East Maui. EF represents a section through Oahu.

APPLICATION TO RIFT VALLEY AND OCEANIC VOLCANISM

In previous sections detailed models of basalt petrogenesis and of upper mantle chemical variation have been presented. These models are now applied to specific natural volcanic provinces in figures 4 to 6. These figures and their detailed legends are largely self-explanatory. Although figure 4 differs in some respects, it owes much to models of oceanic ridge volcanism developed by Aumento (1967), Oxburgh & Turcotte (1968), Gast (1968), Cann (1968), Vogt, Schneider & Johnson (1969), Ringwood (1969) and Gass (1970). It is drawn with the African rift system, the Afar depression and the Red Sea and Gulf of Aden areas as natural parallels to

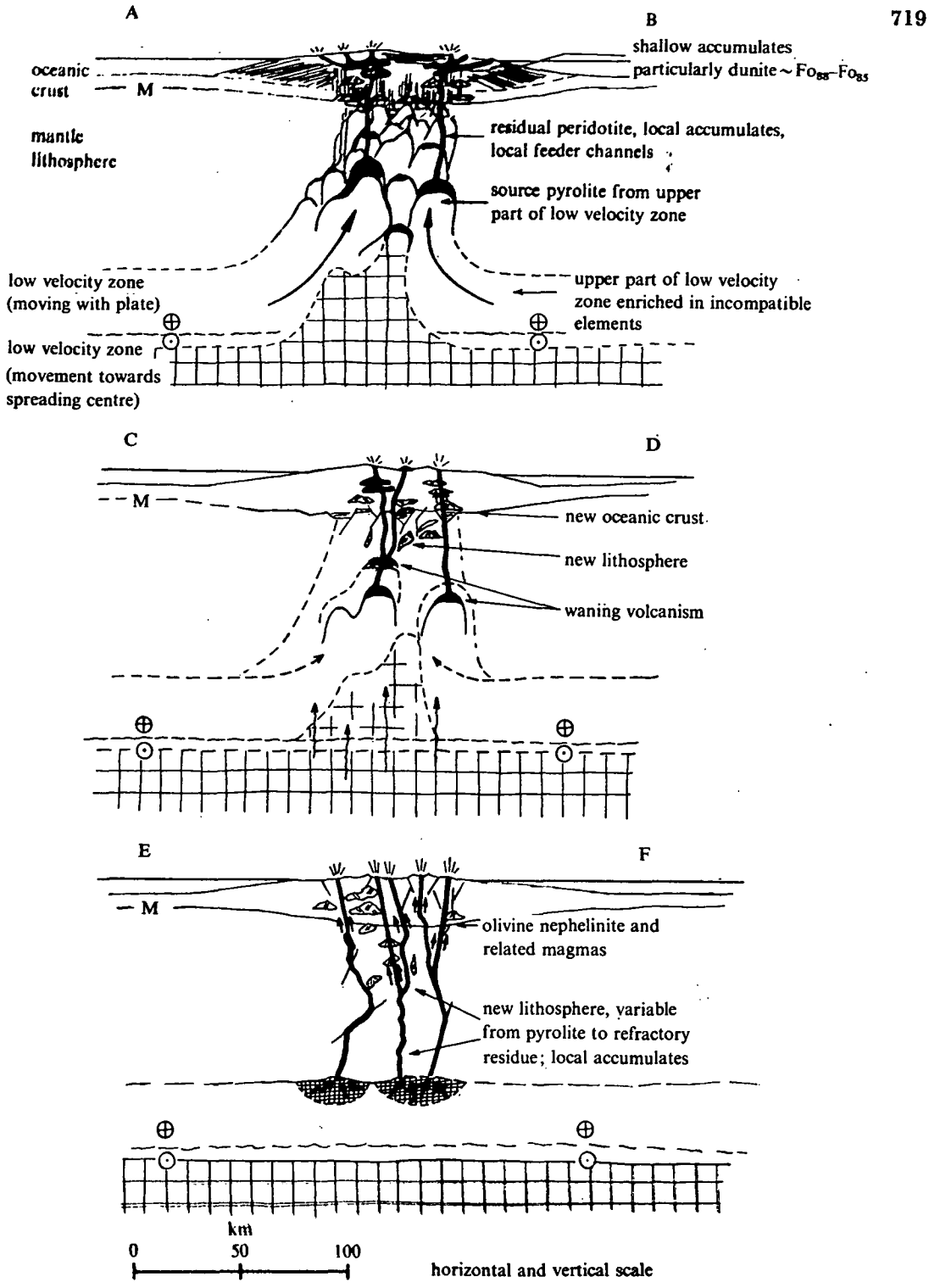

FIGURE 6. Evolutionary stages of oceanic volcanic islands with particular reference to the Hawaiian Islands. See figure 5 for location of sections AB, CD and EF.

AB. Stage of rapid cone building, development of new oceanic crust and new lithosphere from very rapid upwelling of pyrolite from the upper part of the low-velocity zone. Magmas of olivine tholeiite type formed by around 30 % melting at a depth of magma segregation of 40 to 60 km. In the later stages of cone formation, residence of magma batches within the volcanic pile becomes common with consequent precipitation of low pressure accumulates, particularly dunite with olivine of composition Fo_{88}–Fo_{85}.

CD. Stage of waning volcanism. The re-establishment of the lithosphere/low-velocity zone boundary and movement of the newly created lithosphere with the overlying plate. Magmas produced from smaller degrees of partial melting (< 20 %) at depths of magma segregation of 40 to 70 km or from high-pressure crystal fractionation of magma batches relict from tholeiitic volcanism. Magmas of alkali olivine basalt series.

EF. Faulting rejuvenates local minor volcanism. Magma tapped directly from upper part of the low-velocity zone (cf. figure 4, stage I) and is volatile-enriched, olivine-rich basanite, olivine nephelinite or olivine melilite nephelinite. Explosive eruption from various depths entrains xenoliths of lower crust and upper mantle rock types.

the three stages of the model. In stage III, the model illustrates an example of two-stage melting in which a mantle volume which earlier yielded a small olivine nephelinite melt fraction, later undergoes a second melting at much shallower levels to produce low-potassium olivine tholeiites. While this can account for the magma types appearing early in the rifting process, it is difficult to envisage a 'steady state' process as the oceanic rift widens in which the source material reaching the rift area always undergoes a preliminary low degree of partial melting as it approaches the crest. This difficulty has influenced the choice of a model in which the lower part of the low-velocity zone has the low-potassium characteristics as a general feature. Although the movement towards the spreading centre is shown as localized within the lower part of the low-velocity zone, this movement could be distributed through a much greater depth interval and thus be substantially vertical at the ridge areas. The model does however require the establishment of a source region enriched in incompatible elements, probably at the top of the low-velocity zone, very early in the evolution of the oceanic crust–lithosphere system. This is attributed to the 'degassing' mechanism within the low-velocity zone previously discussed. The figure 4, stage III diagram, illustrates an example of a peridotite diapir reaching crustal levels (< 10 km) and differentiating in place to a layered complex of gabbroic accumulates and harzburgite residue. Also, diapiric ascent of a small, detached, high-temperature peridotite along a line of structural weakness is illustrated. These aspects of emplacement of ultramafic complexes at oceanic ridges are discussed in more detail elsewhere (Green 1970).

Figures 5 and 6 illustrate a model for the development of an oceanic chain of volcanic islands due to migration of a tensional fracture, approximately parallel to the plate movement vector but probably offset by transform faults, through a moving oceanic lithosphere. The fracture of the lithosphere is considered to produce a very rapid upwelling from the low-velocity zone, resulting in high degree ($\sim 30\ \%$) of melting at 40 to 60 km depth and very rapid building of the main cone phase. As the creation of new crust and lithosphere is not a continuous process, the lower part of the low-velocity zone does not normally attain depths suitable for partial melting, although it may be noted that the low-potassium tholeiites of the Pololu Series, Kohala, may be derived from this deeper source material. As the volcanoes enter the waning phase with magmas of the alkali olivine basalt suite, the pyrolite source lies within the lithosphere and moves with it. From geochronological data the time between stages I and III for Kauai Island (McDougall 1964) is $\geqslant 4$ Ma. If the Pacific plate is moving at 5 cm a^{-1} this implies a displacement of the $\geqslant 200$ km during the complete life cycle of a Hawaiian volcano.

Conclusions

Experimental studies of the high-pressure behaviour of basalts and potential mantle source material have been used to derive a detailed model of magma evolution and upper mantle composition. It is considered that in this way petrological data on characteristics of different types of oceanic volcanism can be used to place important constraints on the nature of processes occurring in the upper mantle. An important concept developed in this paper is that of mantle source inhomogeneity with a specific suggestion that the upper part of the low-velocity zone is enriched in incompatible elements relative to deeper levels. The petrochemical character of basalt magmas reflects these source characteristics as well as the conditions of partial melting and later magma fractionation.

References (Green)

Archambeau, C. B., Flinn, E. A. & Lambert, D. G. 1969 Fine structure of the upper mantle. *J. geophys. Res.* **74**, 5825–5866.

Aumento, F. 1967 Magmatic evolution on the mid-Atlantic ridge. *Earth Planet. Sci. Lett.* **2**, 225–230.

Aumento, F. 1968 The mid-Atlantic ridge near 45° N. II. Basalts from the area of Confederation Peak. *Can. J. Earth Sci.* **5**, 1–21.

Bultitude, R. J. & Green, D. H. 1968 Experimental study at high pressures on the origin of olivine nephelinite and olivine melilite nephelinite magmas. *Earth Planet. Sci. Lett.* **3**, 325–337.

Cann, J. R. 1968 Geological processes at mid-ocean ridge crests. *Geophys. J. R. Astr. Soc.* **15**, 331–341.

Clark, S. P. & Ringwood, A. E. 1964 Density distribution and constitution of the mantle. *Rev. Geophys.* **2**, 35–88.

Cooper, J. A. & Green. D. H. 1969 Lead isotope measurements of lherzolite inclusions and host basanites from Western Victoria, Australia. *Earth Planet. Sci. Lett.* **6**, 69–76.

Frey, F. A., Haskin, M. A., Poetz, J. & Haskin, L. A. 1968 Rare earth abundances in some basic rocks. *J. geophys. Res.* **73**, 6085–6098.

Frey, F. A. 1969 Rare earth abundances in a high temperature peridotite intrusion. *Geochim. cosmochim. Acta* **33**, 1429–1447.

Gast, P. W. 1968 Trace element fractionation and the origin of tholeiitic and alkaline magma types. *Geochim. cosmochim. Acta* **32**, 1057–1086.

Gass, I. G. 1970 The evolution of volcanism in the junction area of the Red Sea, Gulf of Aden, and Ethiopian rifts. *Phil. Trans. Roy. Soc. Lond.* A **267**, 369.

Green, D. H. 1969*a* The origin of basaltic and nephelinitic magmas in the earth's mantle. *Tectonophysics* **7**, 409–422.

Green, D. H. 1969*b* A review of experimental evidence on the origin of basaltic and nephelinitic magmas. *Phys. Earth Planetary Interiors* **3**, 221–235.

Green, D. H. 1970 Peridotite–gabbro complexes as keys to petrology of mid-oceanic ridges: discussion. *Bull. Geol. Soc. Am.* **81**, 2161–2166.

Green, D. H. & Hibberson, W. 1969 Experimental duplication of conditions of precipitation of high pressure phenocrysts in a basaltic magma. *Phys. Earth Planet. Interiors* **3**, 247–254.

Green, D. H. & Ringwood, A. E. 1964 Fractionation of basalt magmas at high pressures. *Nature, Lond.* **201**, 1276–1279.

Green, D. H. & Ringwood, A. E. 1967*a* The stability fields of aluminous pyroxene peridotite and garnet peridotite and their relevance in upper mantle structure. *Earth Planet. Sci. Lett.* **3**, 151–160.

Green, D. H. & Ringwood, A. E. 1967*b* The genesis of basaltic magmas. *Contr. miner. Petrol.* **15**, 103–190.

Green, D. H. & Ringwood, A. E. 1967*c* An experimental study of the gabbro to eclogite transformation and its petrological applications. *Geochim. cosmochim. Acta* **31**, 767–833.

Green, D. H. & Ringwood, A. E. 1969 Mineralogy of peridotitic compositions under upper mantle conditions. *Phys. Earth Planet. Interiors* **3**, 359–371.

Green, T. H., Green, D. H. & Ringwood, A. E. 1967 The origin of high-alumina basalts and their relationships to quartz tholeiites and alkali basalts. *Earth Planet. Sci. Lett.* **2**, 41–52.

Jackson, E. D. & Wright, T. L. 1970 Xenoliths in the Honolulu Volcanic Series. *J. Petrology* (in the Press).

Kay, R., Hubbard, N. J. & Gast, P. W. 1970 Chemical characteristics and origin of oceanic ridge volcanic rocks. *J. geophys. Res.* **75**, 1585–1613.

Kleeman, J. D., Green, D. H. & Lovering, J. F. 1969 Uranium distribution in ultramafic inclusions from Victorian basalts. *Earth Planet. Sci. Lett.* **5**, 449–458.

Kushiro, I. 1969 Discussion of paper; the origin of basaltic and nephelinitic magmas in the Earth's mantle. *Tectonophysics* **7**, 427–436.

Lambert, I. B. & Wyllie, P. J. 1968 Stability of hornblende and nature of the low velocity zone. *Nature, Lond.* **219**, 1240.

Leggo, P. J. & Hutchison, R. 1968 Rb–Sr study of ultrabasic xenoliths and their basaltic host rocks from the Massif Central, France. *Earth Planet. Sci. Lett.* **5**, 71–77.

McDougall, I. 1964 Potassium-argon ages from lavas of the Hawaiian Islands. *Bull. Geol. Soc. Am.* **75**, 107–128.

Melson, W., Jarosewich, E., Cifelli, R. & Thompson, G. 1967 Alkali olivine basalt dredged near St Paul's Rocks, Mid-Atlantic Ridge. *Nature, Lond.* **215**, 380–381.

Menard, H. W. 1969 Growth of drifting volcanoes. *J. geophys. Res.* **74**, 4827–4838.

Muir, I. D. & Tilley, C. E. 1964 Basalts from the northern part of the rift zone of the mid-Atlantic ridge. *J. Petrology* **5**, 409–434.

Nicholls, G. D. 1965 Basalts from the deep ocean floor. *Miner. Mag.* **34**, 373–388.

Oxburgh, E. R. & Turcotte, D. L. 1968 Mid-ocean ridges and geotherm distribution during mantle convection. *J. geophys. Res.* **73**, 2643–2661.

Ringwood, A. E. 1966*a* The chemical composition and origin of the earth. In *Advances in Earth Science* (ed. P. M. Hurley), pp. 287–356. Cambridge, Mass.: M.I.T. Press.

Ringwood, A. E. 1966*b* Mineralogy of the mantle. In *Advances in Earth science* (ed. P. M. Hurley), pp. 357–417. Cambridge, Mass.: M.I.T. Press.

Ringwood, A. E. 1969 Composition and evolution of the upper mantle. In *The Earth's crust and upper mantle* (ed. P. J. Hart), pp. 1–17. Am. Geophys. Union, Geophys. Monograph 13.

Schilling, J. G. 1969 Red Sea floor origin: rare-earth evidence. *Science, N.Y.* **165**, 1357–1360.

Tilley, C. E. & Yoder, H. S. 1964 Pyroxene fractionation in mafic magma at high pressures and its bearing on basalt genesis. *Yb. Carnegie Inst. Wash.* **63**, 114–121.

Vogt, P. R., Schneider, E. D. & Johnson, G. L. 1969 The crust and upper mantle beneath the sea. In *The Earth's crust and Upper mantle* (ed. P. J. Hart), pp. 556–617. Am. Geophys. Union, Geophys. Monograph 13.

Discussion

Dr M. J. O'HARA (*University of Edinburgh*). The term pyrolite is ill defined and frequently changing, both in terms of chemistry and mineralogy (O'Hara 1968*a*, pp. 105–113). Believers should specify which version they credit at any moment, and remember that the 'pyrolite models' *assume* the composition of the residual mantle, the composition of the primary partial melt magma, and the proportion of that liquid produced, ensuring a circular debate on the three most pressing questions of upper mantle petrology. The assumptions are, moreover, unsatisfactory in detail and lead to a postulated mantle composition which is *critically* different from that based on observed ultrabasic inclusions in kimberlite.

The pyrolite model cannot explain the chemistry of some important magmas, nor the origin of garnet–harzburgite nodules in kimberlite, whereas they are explained by a model based on real garnet–lherzolite nodules in kimberlite which can also explain all other observations accounted for by the pyrolite model (O'Hara 1970). The pyrolite model may not be satisfactory for the suboceanic mantle except in so far as *any* ultrabasic material would be.

Dr D. H. Green's latest hypothesis of magma origins by variable partial melting of 'damp' peridotites is based upon the observation that the orthopyroxene primary phase volume extends far into critically undersaturated compositions at high-water vapour pressures, although restricted to hypersthene saturated compositions in the absence of water. I have doubted the adequacy of composition control in the original experiments on which this observation is based (O'Hara 1968*a*, p. 103) and look forward to seeing the new data on which the hypothesis is now based. Meantime I am impressed by the results of wet melting experiments carried out in the systems forsterite–silica, forsterite–diopside–silica, forsterite–Ca Tschermak's molecule–silica, forsterite–nepheline–silica, forsterite–diopside–anorthite–silica, natural tholeiite and natural high alumina basalt, by such workers as Chinner, Kushiro, Tilley and Yoder at the Geophysical Laboratory; and in the synthetic basalt–andesite system by T. H. Green and Ringwood at Canberra, which show the effect that the presence of water greatly reduces the extension of the orthopyroxene primary phase volume into critically undersaturated compositions; in fact it causes an expansion of the olivine primary phase volume into silica oversaturated compositions (O'Hara 1968*a*). This is the precise opposite of the situation required by Dr Green's hypothesis and it may, therefore, be premature to accept this hypothesis as a model to explain magma generation under the oceanic crust.

I turn now to the difficulties identified by several speakers concerning magma genesis under the mid-ocean ridges. The assumption that the ocean-floor tholeiites are primary magmas is the cause of these difficulties, which melt away when a more sophisticated model is adopted. The compositions of most ocean-floor tholeiites lie on the boundary of the primary phase volume of olivine at 2 to 5 kbar (0.2 to 0.5 GN m^{-2}), but outside it at higher pressures. They cannot

therefore be formed as primary partial melts of olivine-rich rocks at higher pressures. Worse, many of their compositions do not lie on the boundary of, or within, the primary phase volume of orthopyroxene at any pressure, hence they cannot under any circumstances be primary magmas derived from enstatite-bearing peridotites remotely similar to alleged upper mantle compositions. These difficulties are removed if it is accepted that olivine crystals have formed and fractionated in substantial amounts during the ascent of the magma. This argument has been developed in detail elsewhere (O'Hara 1968*b*).

The calculation which purports to show that eclogite fractionation, followed by olivine fractionation, results in erupted liquids of too high an Fe/Fe + Mg ratio is invalid because it *assumes* the pyrolite model for the upper mantle, which has previously *assumed* that the basalt used in its calculation has *not* suffered eclogite fractionation. I suggest that it has, and that there are, therefore, two eclogite fractionation events concealed within Dr Green's calculation. This underlines my earlier point that the pyrolite model is unsatisfactory because it assumes the answers to the very questions it is used to answer, with predictable results.

References (M. J. O'Hara)

O'Hara, M. J. 1968*a* *Earth Sci. Rev.* **4**, 69–133.
O'Hara, M. J. 1968*b* *Nature, Lond.* **220**, 683–686.
O'Hara, M. J. 1970 *Phys. Earth Planet. Interiors* **3**, 236–245.

Written Reply to Discussion by M. J. O'Hara (D. H. Green)

The criticisms by Dr M. J. O'Hara are all-embracing, generalized and unsubstantiated by argument or comparable experiments. His alternative hypothesis (O'Hara & Yoder, 1967; O'Hara 1968) is given in general terms and has not been tested by simple arithmetical calculation, experimental investigation or even by examination for self-consistency. The misrepresentation in O'Hara's discussion of the term 'pyrolite' should be apparent from the 'Introduction' in my paper in this Symposium (see also Ringwood 1970, p. 135; Green 1970). Pyrolite is a clearly defined but general term for a hypothetical *chemical* composition; precisely two pyrolite compositions have been calculated (Green & Ringwood 1963; Ringwood 1966) and the later calculation reflects advance in factual knowledge of the high-pressure crystallization of olivine tholeiite and picrite magmas (Green & Ringwood, 1964, 1967*b*). Experimental data on the subsolidus mineralogy of these calculated pyrolite compositions have been obtained over some years and the present knowledge is presented in Green & Ringwood (1969).

The pyrolite model *assumes only* that observed primary basalts are derived from a *peridotitic source rock* by partial melting. The only competing assumption to this is that basalts are derived from an eclogitic source rock—this is apparently not supported by O'Hara. Basalt magmas themselves place strong constraints on their source composition. Examples of alkali basalts, basanites, olivine nephelinites, etc., sometimes contain dense (ρ = 3.2–3.4) high pressure, xenoliths or xenocrysts which can be shown to be derived from $P > 10$ kbar (1 GN m^{-2}) and in some cases (Green & Hibberson 1969) from $P = 14$ to 16 kbar (1.4 to 1.6 GN m^{-2}). Such magmas are unmodified by crystal fractionation processes at low pressure. Examination of 94 analyses of such basalts of world-wide occurrence shows an extremely strong concentration of the atomic ratio 100 Mg/(Mg + Fe^{2+}) in the range 63 to 73. For a basalt of a given 100 Mg/(Mg + Fe^{2+}) ratio, the liquidus olivine, or residual olivine of a potential source peridotite, is

uniquely fixed—the Mg/Fe partition relation can be established from natural phenocryst/basalt data and from experimental studies of basalt crystallization. Basalts with 100 Mg/(Mg + Fe^{2+}) = 63 to 73 could be in equilibrium with olivine of 100 Mg/(Mg + Fe^{2+}) = 87 to 92. The pyrolite of Ringwood (1966*a*) has 100 Mg/(Mg + Fe^{2+}) = 89. Similarly, spinel lherzolite xenoliths in undersaturated basalts, high temperature peridotite intrusions, garnet lherzolite xenoliths in kimberlite have 100 Mg/(Mg + Fe^{2+}) $\approx$ 88 to 92. The pyrolite model interprets the latter rock types as ranging from possible 'pyrolite' composition to peridotites residual after extraction of a basaltic magma or volatile-rich component from 'pyrolite'. This aspect of the relationship of pyrolite composition to natural peridotites is treated in more detail in Green (1970) and Kleeman, Green & Lovering (1969).

The preceding discussion illustrates the search for an *internally consistent model* which can relate specific, observed natural basalt magmas to one another, to a potential source peridotite composition and to observed, natural, mantle-derived peridotites. It is indeed an assumption that such rock types are genetically and not accidentally related, yet this is an assumption that O'Hara (1968) also makes, though in an arbitrary manner, by selecting a particular garnet lherzolite xenolith (in kimberlite) composition as a source peridotite. O'Hara has not examined his models (O'Hara & Yoder 1967; O'Hara 1968) for internal consistency and, even more frustrating for the reader, does not express the models in terms of actual magma compositions, degrees of melting, composition of accumulates, etc. It is difficult not to emphasize the inadequacy and futility of attempting to evaluate complex magma compositions (> 10 components), with their highly significant variations in such diagnostic ratios as Mg/(Mg + Fe^{2+}), Na/(Ca + Na), Na/(Na + K), etc. by considering projections into pseudo-quaternary systems ('Al_2O_3' = $Al_2O_3 + Fe_2O_3 + Cr_2O_3 + Na_2O + K_2O + TiO_2$; 'CaO' = $CaO - 3\frac{1}{3}P_2O_5 + 2Na_2O + 2K_2O$; 'MgO' = $MgO + FeO + NiO + MnO - TiO_2$; '$SiO_2$' = $SiO_2 - 2Na_2O - 2K_2O$, O'Hara 1968, p. 87). One can attempt to evaluate the O'Hara & Yoder (1967) and O'Hara (1968, p. 118.) models for internal consistency in the following way.† Accepting O'Hara's 1968, garnet lherzolite source, then the source has 100 Mg/(Mg + Fe^{2+}) $\leqslant$ 92 as deduced from the natural rocks. The partial melt (20 %) at 30 kbar (3 GN m^{-2}) is postulated (O'Hara 1968, p. 118; O'Hara & Yoder, 1967, p. 115) to be a tholeiitic picrite—this magma must have 100 Mg/(Mg + Fe^{2+}) $\leqslant$ 72 if it is less than 20 to 30 % melt of the source rock. The picrite is postulated to precipitate some olivine and orthopyroxene (decreasing the liquid 100 Mg/(Mg + Fe^{2+}) value), before passing through a reaction of these phases with liquid to precipitate garnet and clinopyroxene ('eclogite'). O'Hara (1968) postulates 50 % eclogite fractionation of such a magma followed by a further 40 % of olivine crystallization to yield derivative nepheline-rich magmas observed at the earth's surface. Applying the Mg/Fe partition factors for the various phases and their compositions as observed in experiments one can show that the derivative magmas would have 100 Mg/(Mg + Fe^{2+}) < 55‡ and probably < 50—the actual observed magmas of demonstrable direct mantle derivation have 100 Mg/(Mg + Fe^{2+}) = 63 to 73.

O'Hara's discussion of this type of calculation illustrates his failure to evaluate critically the implications of *his own model* in terms of specific compositions. For a quantitative evaluation of the role of eclogite fractionation based on experimental high-pressure data, analysed minerals etc., the reader is referred to Bultitude & Green (1971, in press).

† I would strongly urge that the authors themselves attempt such evaluation. In this way one could hopefully see whether the model is a viable alternative to the pyrolite basalt genesis models.

‡ Such magmas would have liquidus olivine of 100 Mg/(Mg + Fe^{2+}) = 80 to 83.

Turning to the role of water in basalt fractionation and partial melting, a central point is again the danger of attempting to extrapolate from simple 2 or 3 component systems to > 10 component systems. The relevant experimental data on (alkali basalt + water) and (basanite + water) compositions are referred to in Green & Hibberson (1969) and Green (1969*b*, p. 229), and on (quartz tholeiite + water) and (tholeiite + water) compositions in Green (1970*c*).

It should also be noted that Kushiro (1970) found that the low melting composition in the system Fo–Ne–SiO_2–H_2O lay in the nepheline normative volume and commented that this brought the simple system studies closer to the observations on natural rock compositions. Actually, the enhanced role of orthopyroxene crystallization in nepheline-normative, olivine-rich compositions in the presence of water, is due not so much to contraction of the olivine crystallization field in favour of orthopyroxene but rather is due to the broadening of the pyroxene miscibility gap at lower temperature, introducing orthopyroxene additional to or in place of clinopyroxene. While I do not accept the validity of O'Hara's comments, I would emphasize that the calculation of model pyrolite composition(s) is bound to require future refinement and that some of the details of the petrogenetic model will probably be proved wrong or inadequate—the paper is presented as the current status in a rapidly progressing branch of petrology.

References (additional to the preceding paper)

Bultitude, R. J. & Green, D. H. 1971 Experimental study of crystal–liquid relationships at high pressures in olivine nephelinite and basanite compositions. *J. Petrology* (in the press).

Green, D. H. 1970 The origin of basaltic and nephelinitic magmas. Bennett Lectures, Leicester University, *Trans. Leicester Philos. Soc.* (in the Press).

Green, D. H. & Ringwood, A. E. 1963 Mineral assemblages in a model mantle composition. *J. Geophys. Res.* **68**, 937–945.

Kushiro, I. 1970 The system forsterite–nepheline–silica–water. *Yb. Carnegie Instn Wash.* **68**, 240–241.

O'Hara, M. J. 1968 The bearing of phase equilibria studies on synthetic and natural systems on the origin and evolution of basic and ultrabasic rocks. *Earth Sci. Rev.* **4**, 69–133.

O'Hara, M. J. & Yoder, H. S. 1967 Formation and fractionation of basic magmas at high pressures. *Scottish J. Geol.* **3**, 67–117.

B 13

Experimental Study of Crystal–Liquid Relationships at High Pressures in Olivine Nephelinite and Basanite Compositions

by R. J. BULTITUDE[1] *and* D. H. GREEN

Department of Geophysics and Geochemistry, Australian National University, Canberra, Australia

(*Manuscript received 26 February 1970*)

ABSTRACT

The crystallization sequences in olivine-rich nephelinitic and basanitic compositions have been experimentally studied under dry conditions at pressures up to 36 kb. Electron microprobe analyses of olivines, clinopyroxenes, garnets, and orthopyroxenes enable calculation of possible crystal fractionation trends for these magmas at various pressures. Low-pressure fractionation is dominated by olivine and yields derivative liquids of higher silica content and showing rapid iron enrichment. At pressures of 18–27 kb, fractionation is controlled by aluminous clinopyroxene with minor olivine or garnet. Derivative liquids show marked depletion in calcium accompanying silica depletion and increasing degree of undersaturation. At pressures greater than 27 kb, crystal fractionation is controlled by garnet+clinopyroxene separation. Chemical analyses of these phases allow quantitative calculations of possible fractionation which show that large degrees of crystallization are required to produce quite small changes in silica content and in degree of undersaturation. In addition, fractionation by garnet and clinopyroxene separation is accompanied by depletion in calcium content in the more undersaturated rocks and high degrees of crystallization are necessarily accompanied by enrichment in iron relative to magnesium. These effects are inconsistent with the characteristics of natural magmas of mantle derivation in the range from alkali olivine basalts to olivine melilitites. It is concluded that separation of garnet and clinopyroxene under upper mantle conditions does not produce the natural magma series from olivine-rich tholeiite to olivine nephelinite and olivine melilitite. The transient role of orthopyroxene over a very small P, T range in the melting interval of two of the experimental compositions suggests that an olivine-rich basanite may be developed by small degrees of partial melting of a source pyrolite under dry conditions at 60–80 km depth. This liquid, which would form in equilibrium with residual olivine, aluminous orthopyroxene, and aluminous clinopyroxene, would contain approximately 5 per cent normative orthoclase, 5 per cent albite, 12 per cent nepheline, 20 per cent anorthite, 22 per cent diopside, and 31 per cent olivine.

INTRODUCTION

OLIVINE nephelinites occur as lavas and minor intrusives, usually of small volume, in many Tertiary and Quaternary volcanic provinces in both oceanic and continental environments. They are characterized mineralogically by the presence of olivine, calcium-rich pyroxene, and nepheline as major phases and by the absence of modal plagioclase. These rocks appear to pass transitionally to basanites (with both modal plagioclase and nepheline) and, with increasing degree of undersaturation, to the olivine–melilite nephelinites. In the Hawaiian volcanic province, eruption of olivine nephelinite and olivine–melilite nepheli-

[1] Present address: Bureau of Mineral Resources, P.O. Box 378, Canberra, Australia.

nite is characteristic of a stage of post-erosional rejuvenation of some volcanic centres (Macdonald & Katsura, 1964) but in other provinces there appears to be no clear separation of the highly undersaturated nephelinites from associated basanites and alkali olivine basalts.

The use of simple silicate systems as models for the melting and crystallization behaviour of natural basalts becomes increasingly difficult in undersaturated rocks as these rocks characteristically contain high contents of TiO_2, K_2O, P_2O_5, i.e. modal ilmenite, potassic feldspar, and apatite. Similarly, attempts to project normative compositions on to selected mineral planes within 4 or 5 component systems may become extremely misleading in terms of the real crystal–liquid equilibria involved and attention is particularly directed to the importance of the $CaTiAl_2O_6$, $(Ca,Mg)Al_2SiO_6$, and $NaFe^{+++}Si_2O_6$ solid solutions in pyroxenes from these rocks. The alternative approach, followed in the present paper, is the direct experimental study of natural volcanic rocks. The experimental petrologist who adopts this approach must demonstrate the relevance of the selected, specific compositions to the particular problem under investigation. The aim of the present investigation was to explore the nature of the liquidus and near-liquidus phases of olivine nephelinites at high pressures, thus obtaining factual data on possible courses of fractional crystallization and partial melting processes at depth. For this purpose the olivine nephelinite composition used should be that of a liquid derived directly from the upper mantle, without opportunity for fractionation at shallower levels and with minimal opportunity for contamination by crustal materials. Magmas which contain xenoliths of lherzolite, pyroxenite, or garnet pyroxenite (with mineralogies indicating pressures in excess of 8–10 kb at approximately 1000 °C) or high-pressure phenocrysts of aluminous pyroxenes, cannot have been modified by low-pressure fractional crystallization. The rapidity of eruption required to transport the xenoliths ($\rho \simeq 3{\cdot}3$) would allow little opportunity for contamination by crustal material. Magmas of this character range in composition from alkali olivine basalt and olivine trachybasalt to olivine–melilite nephelinite, ãlnoite and kimberlite and Table 1 illustrates the chemical variation between basanite and olivine–melilite nephelinites. Attention is directed to the high 100 $Mg/(Mg+Fe^{++})$[1] ratios and to the differences as well as the transitional variation between the rocks listed (contrast MgO contents of 1 and 2, and Al_2O_3, MgO and alkali contents of 11, 12). It is not suggested that these individual lavas are genetically related by a single, simple crystal fractionation or partial melting process within the upper mantle but we do infer that all closely represent liquid compositions originally existing at various depths in the upper mantle.

For the experimental study, a glass was prepared of the composition called olivine nephelinite in Table 2. This was modelled on analyses 2 and 3 of Table 1 with the particular aim of establishing whether any process of crystallization at high pressures could lead to a trend of decreasing SiO_2 and Al_2O_3 content

[1] Possibly slightly exaggerated by some oxidation of Fe^{++} to Fe^{+++} in some examples.

TABLE 1

Selected analyses of host magmas containing lherzolite inclusions, ranging from basanite to olivine–melilite nephelinite

	1	*2*	*3*	*4*	*5*	*6*	*7*	*8*	*9*	*10*	*11*	*12*	*13*
SiO_2	45·4	44·1	43·8	43·7	42·9	42·1	42·0	40·7	39·4	37·9	37·6	37·6	36·7
TiO_2	2·5	1·3	1·8	3·9	2·7	2·9	2·1	2·7	3·4	3·2	2·5	2·6	1·8
Al_2O_3	13·7	14·1	13·6	15·4	10·5	11·3	11·6	8·8	9·5	11·9	12·3	8·2	13·1
Fe_2O_3	3·6	3·7	3·1	3·1	4·7	5·5	4·3	6·0	5·1	6·3	6·2	6·5	5·7
FeO	9·3	9·2	8·5	8·7	8·2	8·4	7·9	8·3	10·7	9·6	7·6	5·7	9·9
MnO	0·2	0·2	0·2	0·2	0·2	0·3	0·2	0·2	0·2	0·2	0·1	0·2	0·3
MgO	9·6	13·6	12·1	8·2	14·4	13·1	11·6	16·4	13·9	11·5	12·4	18·6	8·8
CaO	8·3	9·2	11·9	9·5	10·0	10·1	13·2	11·8	11·2	11·4	14·1	15·5	16·6
Na_2O	4·2	4·1	3·5	4·2	3·8	3·9	4·5	3·1	3·0	5·3	4·9	2·9	3·7
K_2O	2·3	1·8	1·0	2·2	1·8	1·6	1·5	1·2	1·5	1·5	0·9	1·5	1·9
P_2O_5	1·0	0·8	0·6	0·9	1·0	0·8	0·9	0·8	2·3	1·3	1·4	0·9	1·6
$\frac{100\,Mg}{Mg+Fe^{++}}$	64·8	69·2	71·9	62·5	75·9	73·7	72·6	77·9	70·0	68·0	74·3	85·2	61·4
CIPW Norms													
Or	13·4	10·6	6·1	12·8	10·6	8·9	—	—	8·9	—	—	—	—
Lc	—	—	—	—	—	—	7·0	5·6	—	6·9	4·4	6·9	8·7
Ab	7·1	6·2	3·6	9·4	3·6	3·2	—	—	2·0	—	—	—	—
Ne	15·0	15·1	13·9	14·2	15·3	15·6	20·2	14·5	12·3	23·9	21·6	13·3	16·7
An	11·7	14·2	17·8	16·7	6·0	8·1	7·0	6·0	7·9	4·0	8·9	5·0	13·1
Di	17·9	20·7	29·7	19·2	29·4	27·8	39·5	36·7	25·7	25·5	21·1	16·7	12·4
Ol	21·2	21·7	18·6	13·3	20·6	17·3	13·1	21·0	22·9	16·8	18·4	27·8	19·2
Cs	—	—	—	—	—	—	1·3	0·4	—	3·6	7·4	14·1	13·1
Ap	2·4	1·8	1·3	2·1	2·4	1·8	2·1	1·8	5·3	3·0	3·4	2·0	3·6
Ilm	4·6	2·4	3·4	7·2	5·0	5·1	4·0	5·1	6·4	5·9	4·6	4·9	3·3
Mt	5·1	5·4	4·4	4·4	6·7	7·7	6·0	8·6	7·2	9·0	8·8	9·4	8·1

1. Basanite, Armidale (Wilshire & Binns, 1961).
2. Olivine fourchite, Raymond Fosdick Mts., Antarctica (Fenner, 1938).
3. Limburgite, Sukumozuka, Japan (Harumoto, 1952).
4. Basanitoid, Hut Point Peninsula, Antarctica (Forbes & Kuno, 1965).
5. Basanite, Prindle Volcano, Alaska (Forbes & Kuno, 1965).
6. Monchiquite, Murrumburrah, N.S.W. (Harvey & Joplin, 1941).
7. Olivine nephelinite, Todd's Quarry, Arapohue, New Zealand (Black & Brothers, 1965).
8. Olivine nephelinite, Grove Farm Quarry, Kauai, Hawaii (White, 1966; Washington & Keyes, 1926).
9. Olivine nephelinite, Scottsdale, Tasmania (D. H. Green, unpublished analysis).
10. Olivine nephelinite, Salt Lake Crater, Oahu, Hawaii (Forbes & Kuno, 1965).
11. Olivine–melilite nephelinite, Kalihi flow, Oahu, Hawaii (Winchell, 1947).
12. Olivine–melilitite, Hochbol, Swabia, Germany (Ernst, 1936).
13. Olivine–melilite nephelinite, Nagahama, Japan (Harumoto, 1952).

with increasing CaO in derivative liquids. The picritic nephelinite glass results from the addition of approximately 15 per cent olivine (Fo_{80}) to the olivine nephelinite and the picritic basanite is a composition with higher normative albite and lower nepheline. The compositions are more strongly undersaturated than any previously investigated for high pressure melting relations, the alkali olivine basalt of Green & Ringwood (1967*b*) having 2 per cent normative nepheline and the basanite of Ito & Kennedy (1968) having 11 per cent nepheline, 16 per cent albite, and 12 per cent olivine.

TABLE 2

Compositions and CIPW norms of highly undersaturated glasses used in experimental study

	Picritic basanite	*Olivine nephelinite*	*Picritic nephelinite*		*Picritic basanite*	*Olivine nephelinite*	*Picritic nephelinite*
SiO_2	44·5	44·3	43·7	*Or*	4·5	6·1	4·5
TiO_2	1·3	1·5	1·3	*Ab*	6·2	2·0	3·4
Al_2O_3	12·0	14·2	12·3	*Ne*	9·4	15·3	10·6
Fe_2O_3	0·8[1]	0·5[1]	1·1[1]	*An*	18·0	19·4	19·2
FeO	10·6[1]	9·7[1]	10·8[1]	*Di*	22·8	26·4	21·7
MnO	0·2	0·2	0·2	*Ol*	34·4	25·9	35·7
MgO	16·7	13·3	17·0	*Ap*	1·0	1·3	1·0
CaO	9·9	11·2	9·7	*Ilm*	2·4	2·9	2·4
Na_2O	2·8	3·6	2·7	*Mt*	1·2	0·7	1·6
K_2O	0·8	1·0	0·8				
P_2O_5	0·4	0·5	0·4				
$\frac{100\ Mg}{Mg+Fe^{++}}$	73·7	71·0	73·8				

[1] Determined by E. Kiss, Department of Geophysics and Geochemistry, A.N.U.

EXPERIMENTAL METHODS

Experiments were carried out in a piston-cylinder apparatus using techniques previously described (Green & Ringwood, 1967*a*, 1967*b*; Bultitude & Green, 1968). To decrease the effect of water released by dehydration of talc, all runs utilized a boron-nitride sleeve between the talc pressure medium and the graphite furnace sleeve. Sealed platinum capsules were used in most experiments on the olivine nephelinite and in some runs on the picritic nephelinite. Graphite capsules were used for runs on the picritic nephelinite and picritic basanite and for a few runs on the olivine nephelinite. The problem of Fe-loss from the sample to the Pt capsule has been evaluated by Green & Ringwood (1967*b*) and later experiments in both graphite and platinum capsules on olivine tholeiite (Green, 1969*b*) and an olivine basalt (Green & Hibberson, 1969) confirmed that the nature of the liquidus phase was independent of the capsule used. In the present investigation, the comparison of runs using platinum and graphite capsules under 'dry' conditions showed consistent sequences of crystallization with both capsules but demonstrated an uncertainty in the determination of solidus and liquidus temperatures using the graphite capsules. This is attributed to the access of small and random amounts of water to the unsealed graphite capsules during the run and may result in runs at nominally lower temperatures being nearer to the liquidus than higher temperature 'drier' runs (cf. Fig. 3, olivines at 13·5 kb and 27 kb, 1500 °C). In the platinum capsules, the compositions of liquidus olivine is 2–3 mol. per cent richer in forsterite than olivine in similar near-liquidus runs in graphite capsules. This is attributed to iron loss over the run-times used (5 mins at 1550 °C, 10 mins at 1500 °C, 15 mins at 1450–1500 °C). Ito & Kennedy (1968) report a similar effect in comparing runs (10 mins at 1550 °C) in platinum (Fo_{90}), graphite (Fo_{87}), and iron (Fo_{86}) capsules.

The nature of the mineral phases present was determined on crushed portions of the sample by optical and X-ray methods and commonly by examination of polished surfaces in reflected light and by electron-probe micro-analyser (Applied Research Laboratories, model EMX). The latter technique enabled chemical analysis of the phases present in many of the partial melting runs. Mineral and synthetic glass standards, with compositions close to those of unknown minerals, were used to establish empirical calibration curves for the electron-probe analyses. Knowledge of the original liquid composition and the composition of the near liquidus crystals were combined with estimates of the degree of crystallization to establish liquid fractionation paths at various pressures.

EXPERIMENTAL RESULTS

a. Olivine nephelinite. The experimental data are plotted in Fig. 1. The slope of the liquidus (dT/dP) is small at low pressure but increases distinctly above 20 kb as clinopyroxene and then garnet appear on the liquidus. No attempt was made to locate the solidus but the runs at 1 atm, 1100 °C and 36 kb, 1480 °C are near-solidus with no definite observation of melting. Runs at 27 kb, 1400 °C (10 per cent melting), 9 kb 1240 °C (20–30 per cent melting) and 1 atm 1150 °C (20–30 per cent melting) also provide evidence for the pronounced narrowing of the crystallization interval at higher pressures as observed in other olivine basalts (Yoder & Tilley, 1962; Green & Ringwood, 1967*b*; Ito & Kennedy, 1968). At 1 atm, approximately 25–30 per cent olivine separates from the liquid before clinopyroxene and plagioclase appear at approximately 200 °C below the liquidus. At higher pressures plagioclase is not observed in the melting interval and the temperature interval over which olivine alone crystallizes progressively decreases up to 22·5 kb where olivine and clinopyroxene occur together near the liquidus. At higher pressures garnet appears in the crystallization interval and joins clinopyroxene on the liquidus at 36 kb. Spinel is present as rare medium-size euhedral crystals in a run at 27 kb 1460 °C, but its tentative identification in many other runs as submicroscopic crystallites is interpreted as a quench feature. It is probable that any increase in oxidation state would cause the early appearance of spinel and this may account for its apparently random occurrence in only one run throughout the studied P, T interval. Spinel is present in the subsolidus assemblages at 10–25 kb (Bultitude & Green, 1970) and probably appears very close to the solidus in this pressure interval (Green & Ringwood, 1967*b*; Ito & Kennedy, 1968).

The experiments at 22·5 kb demonstrate a most important reaction relationship. Olivine appears on the liquidus but is absent at lower temperatures, implying the reaction

$$\text{olivine} + \text{liquid}_1 \longrightarrow \text{clinopyroxene} + \text{liquid}_2.$$

At 18 kb there is a more subjective interpretation of a similar reaction relationship as the amount of olivine in the 1360 °C and 1340 °C runs is estimated as lower than the amount in the 1380 °C run.

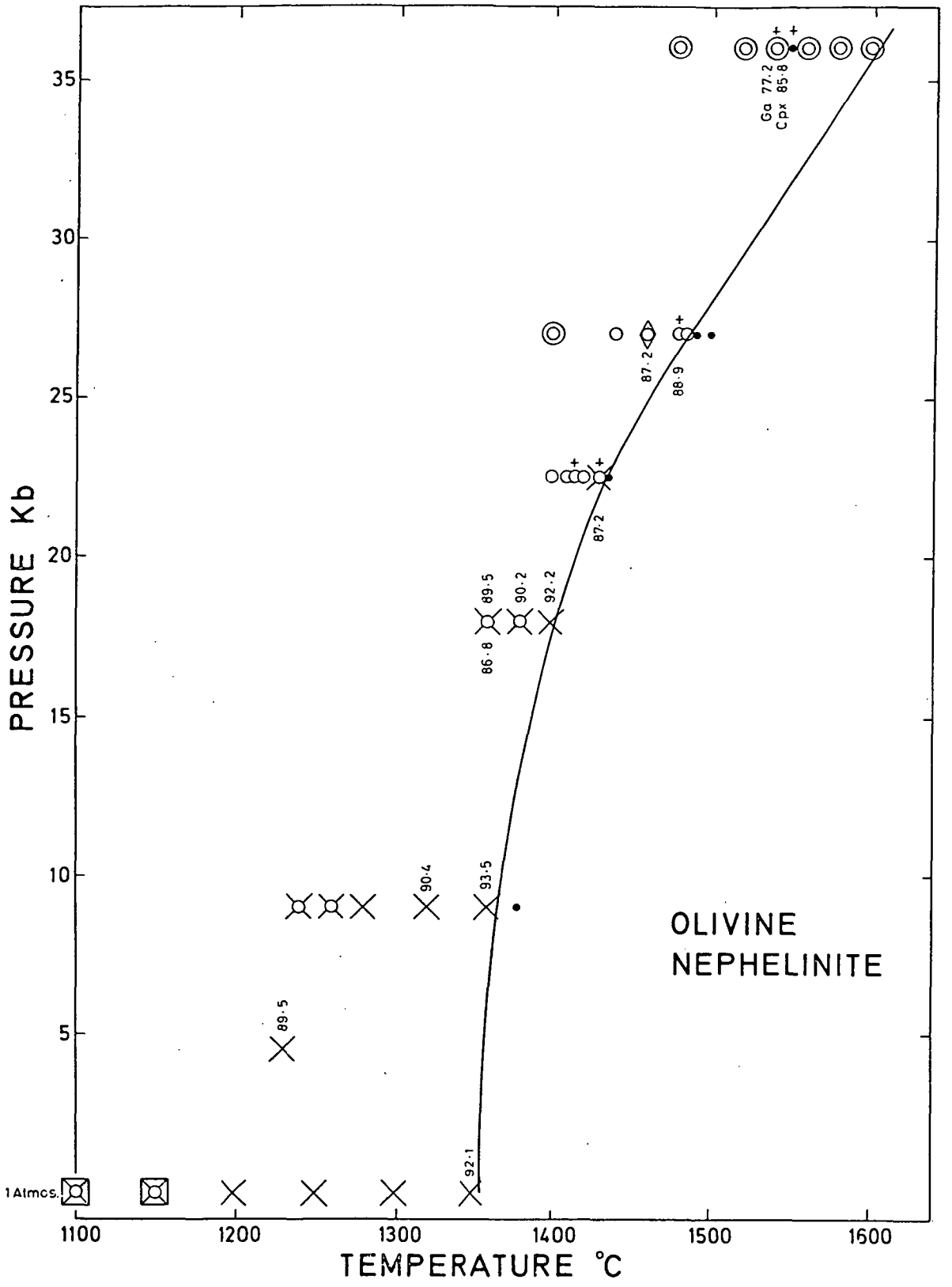

FIG. 1. Crystallization sequence for olivine nephelinite at various pressures. All experiments in platinum capsules except for those marked with a small cross (graphite capsules). Liquidus shown by solid line, solidus not determined. The numbers *above* the data points show the 100 Mg/(Mg+Fe) (atomic ratio) value for olivine as analysed by electron microprobe. Numbers *below* the data points show the 100 Mg/(Mg+Fe) value for clinopyroxene.

Phases coexisting with liquid are shown as follows:

× Olivine
○ Clinopyroxene
◯ Garnet
□ Plagioclase
◊ Spinel
● Above liquidus

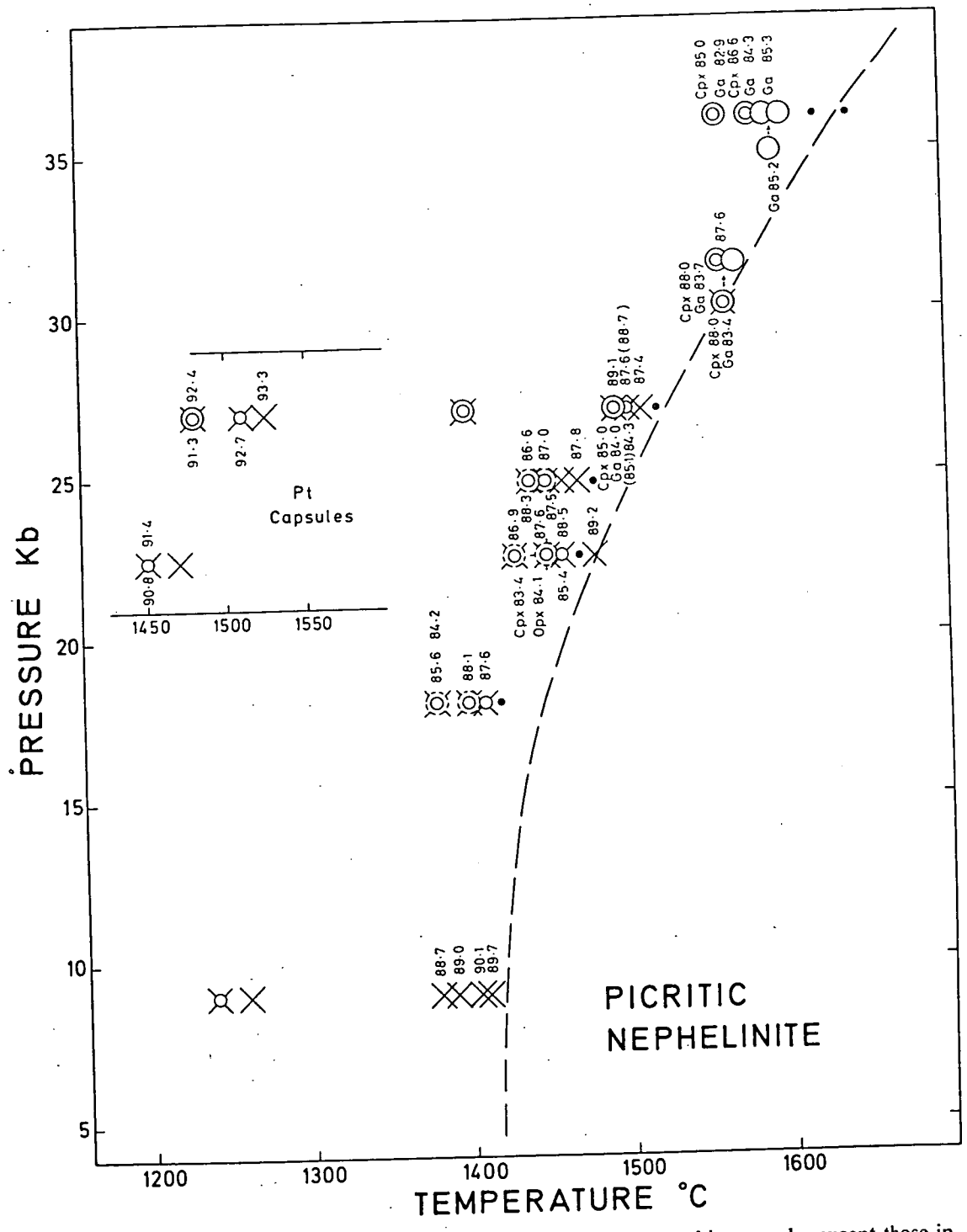

FIG. 2. Crystallization sequence for picritic nephelinite. All runs in graphite capsules except those in insert (platinum capsules). Liquidus is approximate only. The numbers *above* the data points show the 100 Mg/(Mg+Fe) values for analysed olivine, those *below* the data points show the 100 Mg/(Mg+Fe) value for clinopyroxene. Where both garnet and clinopyroxene occur and have been analysed the 100 Mg/(Mg+Fe) values for the individual phases are shown explicitly. Symbols used as in Fig. 1 with also + indicating the presence of orthopyroxene (at 1450 °C, 22·5 kb).

b. Picritic nephelinite (Fig. 2). As graphite capsules were used for most runs on the picritic nephelinite, the liquidus curve was not accurately established but the degree of crystallization and the high 100 $Mg/(Mg+Fe^{++})$ ratio of the phases showed that runs extremely close to the liquidus were obtained at 9 kb, 22·5 kb, 27 kb, 31·5 kb, and 36 kb. Depression of the liquidus by access of water appears to have occurred particularly in the 18 kb and 24·8 kb runs. These runs contain more Fe-rich olivine than that observed near the liquidus at other pressures.

The data show that olivine is the liquidus phase in this composition up to 29–30 kb and that garnet rather than clinopyroxene is the liquidus phase at 31·5 kb and 36 kb. Clinopyroxene is the second phase to appear up to approximately 28–29 kb where garnet and clinopyroxene should appear practically together. Rare garnet, occurring as small equant and occasionally euhedral crystals, was identified optically at 18 kb, 22·5 kb, and 24·8 kb. Interference from quench amphibole reflections and the low abundance of the isotropic phase prevented firm identification of garnet by X-ray diffraction and no microprobe analyses were obtained of garnet at pressures below 27 kb. For this reason, the recording of garnet in the lower temperature runs at pressures below 27 kb, while consistent with data on less undersaturated compositions (Green & Ringwood, 1967*b*) should be regarded with caution and the presence of rare spinel is an alternative. On the other hand, garnet was analysed from the 27 kb, 1500 °C run and is a major phase in the 27 kb, 1400 °C run and in runs at higher pressure.

Two runs carried out at 1450 °C, 22·5 kb, in graphite capsules, both contained orthopyroxene but a run at the same nominal conditions in a platinum capsule contained only olivine, clinopyroxene and glass. Experiments at 1455 °C and 1460 °C in graphite capsules contained olivine, clinopyroxene and quench products, and at 1430 °C contained olivine, clinopyroxene and minor ?garnet. Orthopyroxene was not observed at higher or lower pressures. The data suggest that the picritic nephelinite composition crystallizes orthopyroxene over a very restricted P, T interval and that this mineral reacts with liquid at lower temperatures as follows

$$\text{orthopyroxene}+\text{clinopyroxene}_1+\text{liquid}_1 \rightarrow \text{clinopyroxene}_2 \pm \text{garnet}+\text{liquid}_2.$$

A similar reaction relationship of orthopyroxenes with liquid was observed at 9–20 kb in various compositions by Green & Ringwood (1964, 1967*b*), Green *et al.* (1967), Tilley & Yoder (1964) and Ito & Kennedy (1968). In the picritic nephelinite, olivine shows a reaction relationship with liquid at 31·5 kb, analogous to that observed in the olivine nephelinite at 22·5 kb.

c. Picritic basanite (Fig. 3). A limited amount of data was obtained on the crystallization of the picritic basanite between 13 kb and 32 kb. All runs were carried out in graphite capsules. Olivine remains the liquidus phase at 31·5 kb but at this pressure it reacts with liquid at lower temperature to yield garnet,

clinopyroxene, and liquid. At 13·5 kb olivine is joined by clinopyroxene as the second phase to crystallize. At 18 kb, orthopyroxene is the second phase to appear and reacts with liquid at lower temperatures to yield clinopyroxene. At

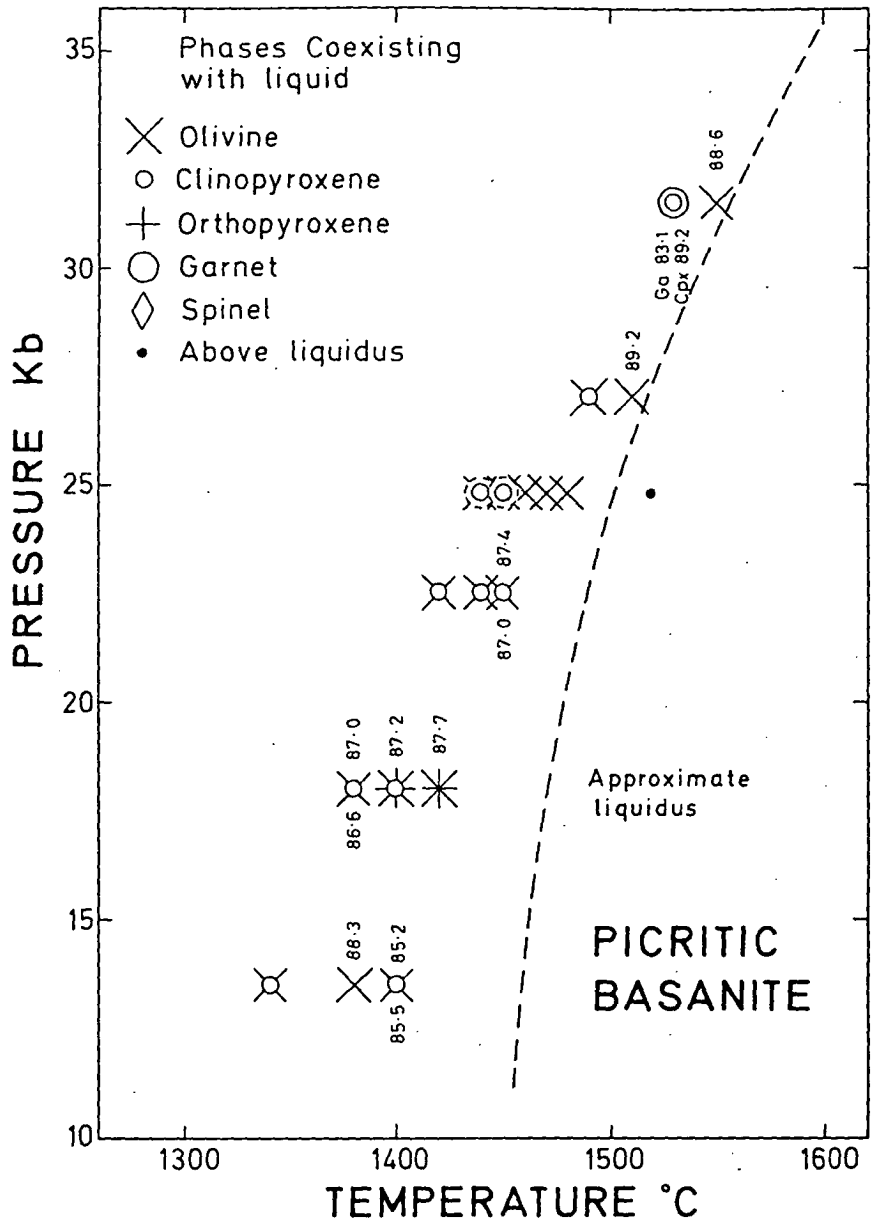

FIG. 3. Crystallization sequence for picritic basanite composition. All experiments in graphite capsules. Numbers *above* the data points give the 100 Mg/Mg+Fe ratio of analysed olivine, those *below* the data points give the 100 Mg/(Mg+Fe) value for the clinopyroxene. Symbols as shown, also as in Figs. 1 and 2.

higher pressures orthopyroxene does not appear and clinopyroxene is again the second phase to crystallize. Probable rare garnet was optically identified at 24·8 kb, 1440 °C and 1450 °C, and appears as a minor phase in the 31·5 kb, 1530 °C run.

MICROPROBE ANALYSES OF NEAR-LIQUIDUS PHASES

a. Olivine. Microprobe analyses for Fe, Ca, Al, and in some cases Mg, allow calculation of olivine composition (neglecting Mn_2SiO_4). The olivines have extremely low Al_2O_3 contents (< 0·2 per cent, which is indistinguishable from background) and low but measurable CaO contents (0·4 per cent, analytical range 0·3–0·5 per cent). This value compares with 0·4 per cent CaO in olivine from Kilauean tholeiites (Murata *et al.*, 1965) and 0·3 per cent CaO in olivines from basalts crystallized at pressures up to 9 kb (Green & Ringwood, 1967*b*). There is no evidence that either higher pressure or the increasing degree of undersaturation from olivine tholeiite to picritic nephelinite is effective in increasing the monticellite solid solution in near-liquidus olivine from basic magmas.

The molecular ratios (100 Mg/(Mg+Fe) for analysed olivines are plotted on figs. 1, 2, and 3. At a given pressure, olivine becomes more fayalitic with increasing degree of crystallization[1] but the 100 Mg/Mg+Fe value of olivine appearing at the liquidus appears to be independent of pressure as long as no other phase accompanies the olivine. From the runs in graphite capsules, the molecular ratio $[Mg/(Mg+Fe)]_{olivine}/[Mg/(Mg+Fe)]_{liquid}$ at the liquidus is approximately 1·25, and the liquidus olivine in the olivine nephelinite (platinum capsules) should have 100 Mg/(Mg+Fe) = 89 rather than 92–93. There is an apparently anomalous increase in 100 Mg/(Mg+Fe) ratio of olivine with increasing crystallization at 27 kb in the picritic nephelinite composition. This is associated with the appearance of appreciable garnet which has a much lower 100 Mg/(Mg+Fe) ratio. Thus the 100 Mg/(Mg+Fe) ratios of residual liquids and of the total crystal extract appear to steadily decrease as fractionation proceeds rather than showing sharp inflexions at the onset of garnet separation.

b. Orthopyroxene (Table 4). Only one analysis of orthopyroxene, from the picritic nephelinite at 22·5 kb, 1450 °C, was obtained. This is an aluminous bronzite with 100 Mg/(Mg+Fe) = 84. The analysed orthopyroxene coexists with ?garnet but primary olivine and clinopyroxene were not identified. In a second run at 22·5 kb, 1450 °C, the assemblage olivine (100 Mg/(Mg+Fe) = 87·6), orthopyroxene, clinopyroxene and ?garnet were identified, but no microprobe analysis of the orthopyroxene or clinopyroxene was possible.

c. Clinopyroxene (Table 3). The determination of Si, Ti, Al, Fe, Mg, Ca, Na, and K yields oxide totals for the pyroxenes which range from 98·4 to 100·8 (assuming all Fe as FeO). Calculations of structural formulae (Table 3) illustrate the high Al for Si substitution and yield '$X+Y$' group totals which are generally between 2·0 and 2·1. The cation excess in the $(X+Y)$ group may reflect minor olivine solid solution in the pyroxene or may be a consequence of bias in the MgO or SiO_2 calibration curves. Attention is directed towards the low TiO_2 content of the pyroxenes in comparison with TiO_2 contents of natural low-pressure clinopyroxenes from undersaturated basalts and nephelinites. The

[1] The effect of depression of the liquidus by access of water to runs in graphite capsules has previously been mentioned.

analysed clinopyroxenes are aluminous augites with low to very low calcium contents. In detail the compositions of the pyroxenes show effects of control by pressure, temperature and host magma composition. All clinopyroxenes plot within the one-pyroxene field as roughly defined at various temperatures by the analysed orthopyroxene–clinopyroxene pairs from natural basalts and from pyrolite (Green & Ringwood, 1967*b*, 1969; Green & Hibberson, 1969).

In the olivine nephelinite composition, near-liquidus clinopyroxenes show increasing Al_2O_3 contents [as (Mg, Ca)Al_2SiO_6 (Tschermak's silicate) substitution] and increasing (En+Fs)/(En+Fs+Wo) ratios with increasing pressure up to 27 kb. The appearance of garnet at 36 kb correlates with a clinopyroxene of much lower Tschermak's silicate content, higher jadeite and lower (En+Fs)/(En+Fs+Wo) ratio. Pyroxenes crystallizing from the picritic basanite at 18, 22·5, and 27 kb provide a useful comparison with those from the olivine nephelinite under similar *P*, *T* conditions. The pyroxenes from the picritic basanite have lower Tschermak's silicate, slightly lower jadeite content (increasing with pressure) and higher (En+Fs)/(En+Fs+Wo) ratios (also increasing with pressure) than those from the olivine nephelinite. The pyroxene in the 13·5 kb, 1400 °C run on the picritic basanite appears to be anomalously high in Tschermak's silicate and jadeite in relation to the other pyroxenes from this composition.

In the picritic nephelinite, clinopyroxenes are generally intermediate between clinopyroxenes from the olivine nephelinite and picritic basanite (comparing runs at similar *P*, *T*) in their Tschermak's silicate and jadeite contents, but have lower 100 Mg/(Mg+Fe) ratios and higher (En+Fs)/(En+Fs+Wo) ratios. These pyroxenes, particularly those analysed from the 27 kb runs, are very subcalcic and it is only the very high temperature of the runs which allows this pyroxene composition to crystallize as a single clinopyroxene phase rather than an orthopyroxene+clinopyroxene pair (cf. Green & Hibberson, 1969). Jadeite content of the pyroxenes increases with increasing pressure, and with decreasing temperature at constant pressure, although there is some scatter possibly attributable to analytical error. Tschermak's silicate shows a marked decrease at 36 kb where garnet is a major phase. In the runs at 22·5 kb, the ratio (En+Fs)/(En+Fs+Wo) initially increases with falling temperature to a maximum near 1450 °C and then decreases; it may be noted that the appearance of orthopyroxene in two runs at 1450 °C, 22·5 kb, appears to coincide with this maximum. Higher values of (En+Fs)/(En+Fs+Wo) are attained in clinopyroxenes at 27–36 kb but these are from runs at considerably higher temperature and thus with increased solubility of (En+Fs) in the clinopyroxene.

d. Garnet (Table 4). As Fe^{+++} and Mn were not determined in the microprobe analyses, garnet compositions were assumed to consist of grossular+almandine +pyrope solid solutions. The small content of Ti as Ti-andradite solid solution was ignored. SiO_2 contents were calculated assuming stoichiometry, and Al_2O_3 contents calculated in a similar way agreed very well with the direct determinations.

TABLE 3. *Compositions of clinopyroxenes analysed by electron microprobe.* Si, Ti, Al, Fe, Mg, Ca, Na, K, *determined by direct analysis*

	Olivine nephelinite					*Picritic basanite*				
Pressure (kb)	18	22·5	27	27	36	13·5	18	22·5	27	31·5
Temperature (°C)	1360	1430	1480	1460	1540	1400	1380	1450	1490	1530
Capsule	Pt	Gr	Gr	Pt	Gr	Gr	Gr	Gr	Gr	Gr
SiO_2	50·6	49·1	48·6	48·2	52·0	49·1	49·1	49·4	48·6	48·9
TiO_2	0·9	0·7	0·6	0·7	0·8	0·9	0·6	0·6	0·4	0·4
Al_2O_3	10·3	11·5	12·8	13·1	10·5	10·8	9·6	9·5	10·3	9·4
FeO	4·1	4·0	3·6	4·0	4·1	5·0	4·9	4·9	4·7	4·7
MgO	15·1	15·4	16·2	15·4	13·9	16·6	17·8	18·4	20·7	21·6
CaO	17·3	17·2	16·7	15·5	16·4	16·0	17·1	16·0	14·7	13·4
Na_2O	1·3	1·4	1·4	1·4	2·6	1·2	1·0	1·3	1·4	1·6
K_2O	—	0·1	—	0·1	—	—	—	—	—	—
Total	99·6	99·4	99·9	98·4	100·3	99·6	100·1	100·1	100·8	100·0
$\frac{100\ Mg\ (mol.)}{Mg+Fe}$	86·8	87·2	88·9	87·2	85·8	85·5	86·6	87·0	88·6	89·2
$\frac{100\ Mg\ (mol.)}{Mg+Fe}$ for coexisting olivine	89·5					85·2	87·0	87·4		
Number of ions on the basis of 6 oxygens										
Si } Z	1·824	1·776	1·743	1·754	1·869	1·784	1·777	1·781	1·706	1·757
Al } Z	0·176	0·224	0·257	0·246	0·131	0·216	0·223	0·219	0·294	0·243
Al	0·262	0·267	0·286	0·314	0·314	0·247	0·185	0·184	0·141	0·154
Ti	0·024	0·020	0·017	0·020	0·022	0·024	0·017	0·017	0·011	0·011
Fe	0·123	0·122	0·108	0·122	0·123	0·153	0·148	0·147	0·140	0·140
Mg } $X+Y$	0·812	0·830	0·866	0·835	0·746	0·899	0·958	0·988	1·159	1·157
Ca	0·667	0·667	0·642	0·604	0·631	0·622	0·662	0·618	0·564	0·516
Na	0·091	0·100	0·099	0·101	0·182	0·083	0·069	0·091	0·099	0·112
K	—	0·004	—	0·004	—	—	—	—	—	—
Z	2·00	2·00	2·00	2·00	2·00	2·00	2·00	2·00	2·00	2·00
$X+Y$	1·98	2·01	2·02	2·00	2·02	2·03	2·04	2·05	2·11	2·09
Mol. proportions										
En	44·5	44·4	45·8	45·2	43·2	47·1	49·0	51·3	54·4	57·4
Fs	6·8	6·5	5·7	6·6	7·1	8·0	7·6	7·6	6·9	7·0
Wo	36·5	35·7	33·9	32·7	36·6	32·6	33·9	32·0	27·8	25·6
Jd	2·5	2·7	2·6	2·7	5·3	2·2	1·8	2·4	2·4	2·8
Al_2O_3	9·7	10·7	12·0	12·8	7·8	10·2	7·8	6·7	8·5	7·3
Coexisting crystalline phase	Ol[1]	Ol	Nil	Nil	Ga[1]	Ol[1]	Ol[1]	Ol[1]	Ol	Ga[1]

TABLE 3 (*cont.*)

	Picritic nephelinite																
Pressure (kb)	22·5	22·5	22·5	22·5	22·5	24·8	24·8	27	27	27	27	27	27	31·5	31·5	36	36
Temperature (°C)	1460	1455	1450	1440	1430	1450	1440	1510	1510	1500	1500	1490	1480	1565	1560	1580	1560
Capsule	Gr	Gr	Pt	Gr	Gr	Gr	Gr	Gr	Pt	Gr	Gr	Gr	Pt	Gr	Gr	Gr	Gr
SiO_2	50·1	48·2	51·0	47·9	48·5	48·1	49·0	49·2	50·1	48·3	49·1	48·7	48·5	49·5	49·8	51·5	50·1
TiO_2	0·4	0·4	0·5	0·6	0·6	0·5	0·5	0·4	0·3	0·5	0·4	0·4	0·5	0·3	0·4	0·3	0·4
Al_2O_3	7·4	10·4	9·8	10·1	9·5	10·5	10·7	9·8	9·2	11·2	10·0	10·5	10·2	9·2	10·2	6·8	7·6
FeO	6·3	6·5	3·8	6·5	6·5	5·1	4·7	6·8	3·4	6·5	6·6	6·1	3·9	5·0	4·9	5·9	6·2
MgO	20·7	21·0	21·0	18·3	18·2	20·1	19·8	22·3	24·1	19·5	21·1	19·5	22·8	20·6	20·1	21·3	19·6
CaO	14·3	12·8	12·4	15·4	15·7	14·4	13·7	9·3	11·1	13·0	11·6	13·5	12·3	14·0	13·3	13·4	14·0
Na_2O	0·9	0·8	1·2	1·2	1·2	1·2	1·5	0·9	1·4	1·1	1·0	1·0	1·3	1·4	1·3	1·3	1·6
Total	100·1	100·1	99·7	100·0	100·2	99·9	99·9	98·7	99·6	100·1	99·8	99·7	99·5	100·0	100·0	100·5	99·5
$\frac{100\,Mg\,(mol.)}{Mg+Fe}$	85·4	85·3	90·8	83·5	83·4	87·5	88·3	85·3	92·7	84·3	85·0	85·1	91·3	88·0	88·0	86·6	85·0
$\frac{100\,Mg\,(mol.)}{Mg+Fe}$ for coexisting olivine	88·5	88·5	91·4	87·0	86·9	87·0	86·6			87·6	89·1	88·7	92·4	87·6			
Number of ions on the basis of 6 oxygens																	
Si } Z	1·808	1·736	1·812	1·742	1·761	1·734	1·758	1·777	1·780	1·738	1·766	1·758	1·738	1·778	1·781	1·841	1·819
Al } Z	0·192	0·264	0·188	0·258	0·239	0·266	0·242	0·223	0·220	0·262	0·234	0·242	0·262	0·222	0·219	0·159	0·181
Al	0·124	0·178	0·222	0·175	0·167	0·181	0·211	0·194	0·164	0·214	0·190	0·205	0·169	0·166	0·211	0·130	0·146
Ti	0·011	0·011	0·013	0·017	0·017	0·013	0·013	0·011	0·009	0·013	0·011	0·011	0·013	0·009	0·011	0·009	0·011
Fe	0·191	0·195	0·113	0·197	0·196	0·154	0·140	0·206	0·100	0·197	0·199	0·184	0·116	0·151	0·146	0·176	0·188
Mg	1·112	1·128	1·112	0·992	0·984	1·082	1·059	1·200	1·276	1·047	1·130	1·050	1·217	1·103	1·072	1·134	1·060
Ca	0·553	0·494	0·472	0·601	0·611	0·557	0·526	0·360	0·423	0·502	0·447	0·523	0·472	0·540	0·509	0·513	0·545
Na	0·065	0·056	0·081	0·083	0·083	0·082	0·104	0·065	0·098	0·078	0·069	0·069	0·090	0·099	0·090	0·090	0·113
Z	2·00	2·00	2·00	2·00	2·00	2·00	2·00	2·00	2·00	2·00	2·00	2·00	2·00	2·00	2·00	2·00	2·00
X+*Y*	2·06	2·06	2·01	2·07	2·06	2·07	2·05	2·04	2·07	2·05	2·05	2·04	2·07	2·07	2·04	2·05	2·06
Mol. proportions																	
En	55·2	55·2	58·4	49·3	49·2	53·7	54·2	60·7	64·0	52·7	54·7	52·9	61·5	55·3	55·1	57·6	[54·0
Fs	9·5	9·5	5·9	9·7	9·8	7·6	7·2	10·4	5·0	9·8	9·6	9·3	5·9	7·6	7·5	8·9	9·6
Wo	27·4	24·2	24·8	29·9	30·6	27·6	26·9	18·2	21·2	25·3	25·2	26·4	21·5	27·1	26·2	26·1	27·9
Jd	1·6	1·4	2·1	2·1	2·1	2·0	2·6	1·6	2·5	2·0	1·7	1·7	2·3	2·5	2·3	2·3	2·9
Al_2O_3	6·3	9·6	8·7	8·9	8·3	9·1	9·1	9·1	7·4	10·2	8·8	9·7	8·8	7·5	8·9	5·1	5·6
Coexisting crystalline phases	Ol[1]	Ol[1]	Ol[1]	Ol[1]	Ol[1]	Ol[1]	Ol[1]		Ol	Ol[1]	Ol[1]+ Ga[1]	Ol[1]+ ?Ga	Ol[1]+ Ga	Ol[1]+ Ga[1]	Ga[1]	Ga[1]	Ga[1]

[1] Denotes crystalline phase analysed by probe.
Abbreviations used: Ol = olivine, Ga = garnet, Sp = spinel, Pt = platinum, Gr = graphite.

TABLE 4

Compositions of garnets and orthopyroxene analysed by electron microprobe. Ti, Al, Fe, Mg, Ca *determined by direct analysis*; SiO_2 (*unless otherwise indicated*) *calculated*

Composition	*Olivine nephelinite*	*Picritic nephelinite*							*Picritic basanite*	*Orthopyroxene from picritic nephelinite*
Pressure (kb)	36	27	31·5	31·5	36	36	36	36	31·5	22·5
Temperature (°C)	1540	1500	1565	1560	1595	1590	1580	1560	1530	1450
Capsule	Gr	Gr	Gr	Gr	Gr	Gr	Gr	Gr	Gr	Gr
SiO_2	41·7[1]	43·2	42·8	43·1	42·9	42·9	42·9	42·9	40·9	51·8
TiO_2	1·1	0·6	0·7	0·9	0·5	0·7	0·6	0·8	0·5	—
Al_2O_3	22·5	22·5	22·8	22·3	22·7	22·7	22·8	22·8	23·6	8·8
FeO	8·8	7·2	7·1	7·0	6·5	6·4	6·8	7·3	7·2	9·5
MgO	16·6	21·2	20·1	20·1	20·9	20·8	20·6	20·0	19·8	28·2
CaO	9·3	5·2	6·4	6·7	6·0	6·1	6·1	6·5	6·4	1·7
Total	100·0	99·9	99·9	100·1	99·5	99·6	99·8	100·3	98·4	100·0
$\frac{100\,Mg\ (mol.)}{Mg+Fe}$	77·2	84·0	83·4	83·7	85·2	85·3	84·3	82·9	83·1	84·1
		Mol. proportions								
Pyrope	58·0	75·1	70·0	69·7	72·4	72·3	71·4	69·3	69·8	*En* 73·7
Almandine	17·4	14·2	13·9	13·4	12·6	12·6	13·4	14·3	14·0	*Fs* 13·9
Grossular	24·6	10·7	16·0	16·8	15·1	15·1	15·1	16·4	16·2	*Wo* 3·2
										Al_2O_3 9·3
Coexisting crystalline phases	Cpx[2]	Ol[2]+ Cpx[2]	Ol[2]+ Cpx[2]	Cpx[2]	Nil	Nil	Cpx[2]	Cpx[2]	Cpx[2]	Ga + ?Ol + ?Cpx

[1] Si determined by probe analysis. [2] Denotes crystal analysed by probe.
Abbreviations used: Ol = olivine. Cpx = clinopyroxene, Ga = garnet, Gr = graphite.

The 100 Mg/(Mg+Fe) ratio for garnet is in all cases lower than that of the coexisting clinopyroxene or olivine but is greater than that of the parent composition. This is particularly valid where garnet occurs alone at the liquidus. Thus crystallization of garnet enriches residual liquids in Fe relative to Mg although this effect is not as marked as with olivine extraction. The CaO contents of garnet are around 6·0 per cent (15 per cent grossular) in all cases except for the higher grossular content in the garnet from the olivine nephelinite at 36 kb. Bultitude & Green (1970) have pointed out the importance of grossular-rich garnet in this composition in subsolidus assemblages at high pressure. The grossular content of garnet at 36 kb in the picritic nephelinite increases at lower temperatures.

Partition coefficients [$K = (Fe/Mg)_{Ga}/(Fe/Mg)_{Cpx}$] range from 1·1–1·8 for the garnet–pyroxene pairs. This assumes as a first approximation that all Fe is as Fe^{++} in both phases. The values for K provide some data towards calibration of the temperature dependence of this partition coefficient (cf. Banno & Matsui, 1965; Lovering & White, 1969).

INTERPRETATION OF EXPERIMENTAL DATA

Partial melting models

The experimental data on crystallization of the nepheline-rich compositions can be examined to evaluate the possibility that these compositions, or others closely related to them, could be derived as direct partial melts from a peridotitic source rock. It is assumed that the relevant peridotitic source rock is similar to the pyrolite III composition of Green & Ringwood (1967*b*, 1969), and thus to the spinel lherzolite and garnet lherzolite occurring as high temperature peridotite intrusions and accidental, mantle-derived, xenoliths in undersaturated basalts and in kimberlites. This assumption requires olivine $\gg$ enstatite $>$ clinopyroxene $\geqslant$ garnet or $>$ spinel in the potential source rock. Furthermore, the residual phases with which any partial melt would initially be in equilibrium, must include olivine and orthopyroxene and may include clinopyroxene and/or garnet or clinopyroxene and/or spinel. The postulated source rock has 100 Mg/(Mg+Fe^{++}) $\simeq$ 88–90 so that residual phases would have similar or greater Mg-enrichment if an internally consistent model is to be set up. From this reasoning we can infer that if the basaltic compositions studied have *olivine+orthopyroxene*$\pm$clinopyroxene+garnet or spinel, as near-liquidus phases, and further that if the olivine and orthopyroxene have 100 Mg/(Mg+Fe) = 88–90 for these P, T conditions, then the liquid present is a possible partial melt from a pyrolite source rock at that P and T.

When examined in this way, the high-pressure crystallization data show that only the picritic basanite (at 18 kb) and the picritic nephelinite (at 22·5 kb) have olivine and orthopyroxene together in their melting intervals under dry conditions. The picritic basanite has olivine as the liquidus phase up to 31·5 kb.

TABLE 5

Calculated compositions of liquids which could be parental to, or derived from, the olivine nephelinite composition by solution or precipitation of the liquidus and near-liquidus phases at various pressures. Compositions of minerals used in the calculations are given in Tables 3 and 4 and the proportions of minerals in the chosen extract were estimated from observation of the experimental runs

Pressure (kb)	—	18	22·5	22·5	27	36	36	36	36	36	36	36
Temperature (°C)	—	1360	1430	<1430	1460	>1540	>1540	>1540	1540	1540	1540	1540
% *Crystallization*	Nil	−30	−20	−40	−30	+20	+20	+20	−20	−20	−20	−30
Crystal extract	(Initial Liquid)	10% Ol +20% Cpx	20% Cpx	40% Cpx	30% Cpx	15% Cpx +5% Ga	10% Cpx +10% Ga	5% Cpx +15% Ga	15% Cpx +5% Ga	10% Cpx +10% Ga	5% Cpx +15% Ga	20% Cpx +10% Ga
SiO_2	44·3	43·0	43·1	41·2	42·4	45·1	44·8	44·4	43·0	43·6	44·2	42·6
TiO_2	1·5	1·9	1·7	2·0	1·9	1·4	1·4	1·4	1·6	1·6	1·6	1·7
Al_2O_3	14·2	17·3	14·9	16·0	14·6	14·1	14·7	15·1	14·4	13·6	12·9	14·0
Fe_2O_3	0·5	0·7	0·6	0·8	0·7	0·4	0·4	0·4	0·6	0·6	0·6	0·7
FeO	9·7	11·3	11·1	13·5	12·1	8·9	9·2	9·3	10·9	10·5	10·2	11·5
MnO	0·2	0·3	0·2	0·3	0·3	0·2	0·2	0·2	0·2	0·3	0·2	0·3
MgO	13·3	7·7	12·8	11·9	12·3	13·4	13·7	13·8	13·0	12·7	12·6	12·6
CaO	11·2	11·0	9·7	7·2	9·3	11·6	11·5	11·1	10·4	10·7	11·2	10·0
Na_2O	3·6	4·7	4·2	5·1	4·4	3·3	3·3	3·1	4·0	4·2	4·3	4·4
K_2O	1·0	1·4	1·2	1·6	1·4	0·8	0·8	0·8	1·2	1·25	1·3	1·4
P_2O_5	0·5	0·7	0·6	0·8	0·7	0·4	0·4	0·4	0·6	0·6	0·6	0·7
$\frac{100\,Mg}{Mg+Fe^{++}}$	71·0	54·9	67·3	61·1	64·5	72·6	72·6	72·5	68·0	68·3	68·7	66·2
Or	6·1	8·3	7·2	9·4	7·7	4·8	4·8	4·8	4·9	6·4	6·0	3·9
Lc	—	—	—	—	0·4	—	—	—	2·0	0·7	1·4	3·5
Ab	2·0	0·6	0·6	—	—	4·7	3·6	4·7	—	—	—	—
Ne	15·3	21·2	19·0	23·4	20·1	12·5	13·0	11·6	18·3	19·3	19·8	20·1
An	19·4	22·0	18·1	16·2	15·9	21·3	23·0	24·0	17·6	14·8	12·0	14·2
Di	26·4	22·9	21·4	11·4	21·0	26·2	25·2	22·1	24·6	28·1	32·5	24·9
Ol	25·9	18·6	28·3	33·1	28·8	26·1	26·4	27·5	27·3	25·1	22·9	27·4
Ap	1·3	1·7	1·5	1·9	1·7	1·0	1·0	1·0	1·3	1·3	1·3	1·7
Ilm	2·9	3·6	3·2	3·8	3·6	2·6	2·6	2·6	3·0	3·0	3·0	3·2
Mt	0·7	1·0	0·9	1·2	1·0	0·6	0·6	0·6	0·9	0·9	0·9	1·0

Clinopyroxene is the second phase to appear at pressure < 18 kb and a more subcalcic clinopyroxene is the second phase to appear at pressure > 18 kb. However, at 18 kb orthopyroxene is the second phase to appear at $\sim$ 1420 °C and accompanies the olivine over a very small crystallization interval before clinopyroxene first joins ($\sim$ 1400 °C) and then eliminates the orthopyroxene (by 1380 °C). The liquidus olivine for the picritic basanite has composition 100 Mg/(Mg+Fe^{++}) = 89·5 and the olivine coexisting with orthopyroxene has 100 Mg/(Mg+Fe^{++}) = 87·7 (1420 °C) to 87·2 (1400 °C). It may be inferred (cf. Green & Ringwood, 1967*b*, pp. 143–4) that approximately 5–8 per cent olivine crystallized from the picritic basanite prior to the appearance of orthopyroxene. The values of the ratio 100 Mg/ (Mg+Fe^{++}) for the liquidus olivine and orthopyroxene are a little low ($\sim$ 87·5) compared with that estimated for the potential source rock ($\sim$ 88–90). It is inferred by the above arguments that a basanitic liquid of normative composition:

Or	Ne	Ab	An	Di	Ol	Ap	Mt	Ilm
5·0	10·0	7·0	19·0	24·0	30·0	1·0	1·0	2·5

and with 100 Mg/(Mg+Fe^{++}) = 72–73, is a possible direct derivative (cf. Table 7) from a pyrolite source rock at 18 kb, $T \simeq 1420$ °C, leaving residual olivine and orthopyroxene only. If clinopyroxene remains in the residual phases then the calculations of Table 7 suggest that a slightly more undersaturated basanitic liquid with normative composition:

Or	Ne	Ab	An	Di	Ol	Ap	Mt	Ilm
5·5	11·5	4·5	19·0	26·0	28·0	1·0	1·5	3·0

and 100 Mg/(Mg+Fe^{++}) = 71–72, could be derived from a peridotitic source rock. Spinel would not occur in the residue and the pyroxenes in the residue should contain rather high Al_2O_3 contents. These possible liquids derived from the mantle source peridotite would have around 44·5 per cent SiO_2, 12–13 per cent Al_2O_3, 10 per cent CaO, 3·0 per cent Na_2O, 0·8 per cent K_2O.

The picritic nephelinite has olivine as the liquidus phase at 22·5 kb ($\sim$ 1480 °C) and clinopyroxene appears at $\sim$ 1460 °C. Orthopyroxene is apparently the third phase to appear, accompanied by a very small amount of isotropic spinel or garnet. At slightly lower temperatures orthopyroxene is absent, apparently being eliminated by the more abundant low-calcium clinopyroxene. The orthopyroxene and clinopyroxene at 1440–1460 °C have low values of 100 Mg/ (Mg+Fe^{++}) in relation to the postulated source peridotite but we infer that at 22·5 kb an undersaturated, olivine-rich basanitic liquid is a possible partial melt of the pyrolite at $\sim$ 1450 °C leaving residual olivine, orthopyroxene, and clinopyroxene, and possibly also spinel. Such a liquid would have a normative composition of approximately:

Or	Ne	Ab	An	Di	Ol	Ap	Mt	Ilm
5·5	12·0	4·5	20·0	22·0	31·0	1·0	2·0	3·0

with 100 $Mg/(Mg+Fe^{++})$ = 71–72, and would contain approximately 44 per cent SiO_2, 13 per cent Al_2O_3, 10 per cent CaO, 3·0 per cent Na_2O, 0·9 per cent K_2O.

The absence of orthopyroxene in the crystallization interval of the olivine nephelinite composition, and its transitory appearance within very small P, T fields in the picritic basanite and picritic nephelinite compositions, implies that it is not possible to derive olivine nephelinite liquids with < 2 per cent normative albite or even more undersaturated olivine melilite nephelinites by direct partial melting of *dry* peridotite (pyrolite) at pressures up to 36 kb. The most undersaturated liquids developed in equilibrium with residual olivine, aluminous enstatite and aluminous, calcium-poor pyroxene appear to be picritic basanites with about 44 per cent SiO_2, 4 per cent Na_2O+K_2O and with approximately 5 per cent normative albite, 12 per cent nepheline, and 30 per cent olivine. These may be derived by small degrees of partial melting at 60–75 km depth.

Crystal fractionation models

As an alternative to direct partial melting from a pyrolite source, the low-SiO_2, highly undersaturated magmas may be products of fractional crystallization of more saturated magmas at high pressures. The experimental data can be used to evaluate possible mechanisms and directions of crystal fractionation at various pressures. The calculations and discussion below assume a discontinuous model of crystal fractionation rather than continuous extraction and removal of liquidus phases with continuously falling temperature. Thus a magma at $P_1 T_1$ is envisaged as moving to P_2, T_1, then cooling slowly to $P_2 T_2$ with equilibrium being approximately maintained between magma and crystals over the temperature interval $T_1 \rightarrow T_2$. Extraction of crystals at $P_2 T_2$ occurs as the magma is tapped and moves to the surface leaving a residual accumulate.

a. Olivine control. Separation of olivine dominates the early crystallization of all compositions up to 22·5 kb and of the two picritic compositions up to 27 kb. Olivine separation decreases the high normative olivine contents but does not change the degree of undersaturation as measured by the Ne/Ab ratio. Derived liquids have higher SiO_2 contents and show a rapid decrease in 100 $Mg/(Mg+Fe^{++})$ ratio due to the strong Mg-enrichment in olivine relative to liquid and the high concentrations of Mg and Fe in the olivine phase (Green & Ringwood, 1967*b*, p. 143). It may be noted that the large proportions of olivine which O'Hara (1968, p. 118) suggests separate from magmas derived by partial melting of the upper mantle, will inevitably produce large changes in 100 $Mg/(Mg+Fe^{++})$ ratio of the liquids.

b. Clinopyroxene control. In all three compositions crystallization in the 18–25 kb interval is initially controlled by olivine separation, but olivine is joined at slightly lower temperature by clinopyroxene (or rarely orthopyroxene and clinopyroxene) and some of the early crystallized olivine reacts with liquid to

TABLE 6

Calculated compositions of liquids which could be parental to, or derived from, the picritic nephelinite composition by solution or precipitation of the liquidus and near-liquidus phases at various pressures. Compositions of minerals used are given in Tables 3 and 4

Pressure (kb) *Temperature* (°C) % *Crystallization* *Crystal extract*	Nil (Initial liquid)	22·5 1460 −10 7% Ol +3% Cpx	22·5 ~1450 −15 5% Ol[1] +8% Cpx[1] +2% Opx[1]	22·5 1430 −25 5% Ol +20% Cpx	27 1500 −20 2% Ol +12% Cpx +6% Ga	27 1480 −30 5% Ol +15% Cpx +10% Ga[2]	36 >1595 +10 10% Ga	36 1590 −10 10% Ga	36 1580 −20 10% Ga +10% Cpx	36 1560 −30 20% Ga +10% Cpx	36 1560 −30 15% Ga +15% Cpx	36 1560 −30 10% Ga +20% Cpx
SiO_2	43·7	43·8	43·2	42·7	43·0	42·8	43·6	43·8	43·0	43·0	42·6	42·1
TiO_2	1·3	1·4	1·5	1·6	1·5	1·6	1·2	1·3	1·4	1·6	1·6	1·6
Al_2O_3	12·3	13·4	13·3	13·9	12·2	12·1	13·2	11·1	11·6	10·0	11·1	12·0
Fe_2O_3	1·1	1·2	1·3	1·5	1·4	1·6	1·0	1·2	1·3	1·6	1·6	1·6
FeO	10·8	10·9	11·2	11·8	11·7	12·7	10·4	11·3	11·9	12·2	12·5	12·8
MnO	0·2	0·2	0·2	0·2	0·2	0·3	0·2	0·2	0·2	0·2	0·3	0·3
MgO	17·0	14·5	14·5	14·7	15·5	13·1	17·4	16·6	16·1	15·7	15·8	15·8
CaO	9·7	10·3	10·1	8·7	10·0	10·6	9·4	10·1	9·8	10·0	9·4	8·8
Na_2O	2·7	2·9	3·1	3·3	3·2	3·6	2·5	3·0	3·2	3·6	3·6	3·4
K_2O	0·8	0·9	0·9	1·1	1·0	1·1	0·7	0·9	1·0	1·1	1·1	1·1
P_2O_5	0·4	0·4	0·5	0·5	0·5	0·6	0·4	0·4	0·4	0·6	0·6	0·6
$\frac{100\ Mg}{Mg+Fe^{++}}$	73·8	71·6	71·0	69·0	70·1	64·7	75·0	72·4	70·6	69·6	69·3	68·8
Or	4·5	5·2	5·5	6·6	6·1	6·1	3·9	5·5	6·1	6·6	6·1	6·6
Lc	—	—	—	—	—	0·4	—	—	—		0·4	—
Ab	3·4	4·7	4·0	3·6	0·6	—	5·8	2·4	0·2	0·6	—	0·6
Ne	10·6	10·8	12·0	13·1	14·4	16·5	8·3	12·3	14·7	16·2	16·5	15·4
An	19·2	20·8	19·8	19·9	15·8	13·6	23·2	14·2	14·2	7·9	10·9	14·2
Di	21·7	22·3	21·6	19·4	24·8	28·8	17·1	26·8	25·7	30·2	26·9	21·0
Ol	35·7	30·6	31·2	34·1	32·5	28·0	37·5	33·5	33·7	31·5	33·6	35·7
Ap	1·0	1·0	1·2	1·1	1·1	1·3	0·8	1·0	1·0	1·5	1·3	1·3
Ilm	2·4	2·6	2·9	3·0	2·9	3·0	2·3	2·4	2·7	3·0	3·0	3·0
Mt	1·6	1·8	1·9	2·1	2·0	2·3	1·4	1·9	1·9	2·3	2·3	2·3

[1] Ol, Cpx from 22·5 kb, 1455 °C run; Opx from 22·5 kb, 1450 °C run.

[2] Ga from 27 kb, 1500 °C run.

precipitate clinopyroxene. Fractionation may be controlled by clinopyroxene alone (at higher pressures) or by clinopyroxene and minor olivine. In the picritic basanite composition, 30 per cent crystallization of olivine (8 per cent) and clinopyroxene (22 per cent) at 18 kb would produce a more undersaturated liquid with lower SiO_2 and CaO, and higher Al_2O_3, alkali content and K_2O/Na_2O ratio than the original. The process is inefficient in that 30 per cent crystallization only decreases the SiO_2 content from 44·5 to 43·6 per cent and the liquid retains minor normative albite. However, the 100 $Mg/(Mg+Fe^{++})$ ratio shows a marked decrease and it is apparent that if large degrees of crystallization of this type are invoked the derivative liquids must be notably more iron-enriched than the parental liquids. The role of Na_2O in the clinopyroxene (1 per cent at 18 kb to 1·5 per cent at 27 kb) curtails the Na_2O enrichment and leads to an increase in K_2O/Na_2O ratio of the derived liquids.

In the olivine nephelinite composition, calculated derivative liquids at 18, 22·5, and 27 kb show similar trends of decreasing SiO_2 and CaO contents and increasing degree of undersaturation. Again the process is 'inefficient' in that high degrees of crystallization are required to effect relatively small changes in SiO_2 content and in degree of undersaturation and such high degrees of crystallization necessarily decrease the 100 $Mg/(Mg+Fe^{++})$ ratio. The effect of clinopyroxene separation alone at 22·5–27 kb produces a more rapid decrease in SiO_2 but also rapidly depletes derivative liquids in CaO. Similar effects are apparent in the picritic nephelinite at 22·5 kb where olivine and pyroxene separation occurs. In this composition the transitory appearance of orthopyroxene with olivine and clinopyroxene may initially produce liquids with lower SiO_2 and *higher* CaO and alkali contents but the effect operates over a very small temperature and composition range and is then swamped by the clinopyroxene separation leading to lower CaO contents.

c. Garnet control. In the picritic nephelinite composition separation of garnet alone may occur at pressures greater than 30 kb. The calculation of a garnet-controlled fractionation trend at 36 kb shows that derived lower temperature liquids show slight silica increase, marked alumina decrease and slight increases in CaO and Na_2O content. Lower temperature liquids show slightly higher Ne/Ab ratios and lower 100 $Mg/(Mg+Fe^{++})$ ratios.

d. Garnet+clinopyroxene control. At pressure greater than 27 kb all compositions have garnet+clinopyroxene as the major phases near or on the liquidus. The relative proportions of garnet and pyroxene are difficult to estimate, and calculations of fractionation trends have been made assuming different relative proportions, particularly for the olivine nephelinite and picritic nephelinite compositions at 36 kb. The composition of the garnet separating is pyrope-almandine but clinopyroxene is aluminous, sub-calcic augite with low jadeite content. Jadeite solid solution becomes a little more important and the $(Ca, Mg)Al_2SiO_6$ solid solution less important at 36 kb. However, none of the experimental pyroxenes could be called omphacite and an accumulate of garnet

TABLE 7

Calculated derivative liquids from picritic basanite composition assuming degrees of crystallization estimated from optical examination of crushed and polished mounts. Compositions of minerals used in calculations are given in Tables 3 and 4. Alternative proportions of phases in the crystal extract are given in some cases due to the difficulty of estimating degree of crystallization and proportions of phases

Pressure (kb)		18	18	18	27	27	31·5	31·5	31·5
Temperature (°C)		1420	1420	1380	1490	1490	1530	1530	1530
% Crystallization		−8	−15	−30	−20	−20	−15	−30	−30
Crystal extract	Nil	5% Ol[1] +3% Opx	10% Ol[1] +5% Opx	8% Ol +22% Cpx	10% Ol[2] +10% Cpx	5% Ol[3] +15% Cpx	10% Cpx +5% Ga	20% Cpx +10% Ga	25% Cpx +5% Ga
SiO_2	44·5	44·5	44·6	43·6	44·4	43·9	44·2	43·7	43·2
TiO_2	1·3	1·4	1·5	1·7	1·6	1·5	1·5	1·7	1·7
Al_2O_3	12·0	12·7	13·6	14·1	13·8	13·1	11·6	11·1	12·1
Fe_2O_3	0·8	0·9	0·9	1·2	1·0	1·0	0·9	1·1	1·1
FeO	10·6	10·6	10·5	12·2	11·4	11·6	11·4	12·8	13·0
MnO	0·2	0·2	0·2	0·3	0·2	0·2	0·2	0·3	0·3
MgO	16·7	14·7	12·4	12·9	12·1	14·1	15·8	14·8	14·7
CaO	9·9	10·7	11·5	8·8	10·5	9·6	9·7	9·4	9·3
Na_2O	2·8	3·0	3·3	3·7	3·4	3·2	3·2	3·5	3·4
K_2O	0·8	0·9	0·9	1·2	1·0	1·0	0·9	1·1	1·1
P_2O_5	0·4	0·4	0·5	0·6	0·5	0·5	0·5	0·6	0·6
$\frac{100\ Mg}{Mg+Fe^{++}}$	73·7	71·2	67·9	65·4	65·4	68·4	71·0	67·4	66·8
Or	4·5	5·5	5·5	7·2	6·1	6·1	5·5	6·6	6·6
Lc	—	—	—	—	—	—	—	—	—
Ab	6·2	4·5	4·7	6·0	6·2	5·2	5·2	3·6	2·0
Ne	9·4	11·1	12·7	13·8	12·3	12·0	11·9	14·2	14·5
An	18·0	18·7	19·4	18·0	19·2	18·4	14·4	11·1	14·4
Di	22·8	25·6	27·7	18·0	23·8	21·7	24·3	25·9	22·9
Ol	34·4	29·7	24·6	30·9	26·7	31·2	33·1	32·4	33·7
Ap	1·0	1·0	1·2	1·3	1·3	1·1	1·3	1·3	1·3
Ilm	2·4	2·7	2·9	3·2	3·0	2·9	2·9	3·2	3·2
Mt	1·2	1·4	1·4	1·8	1·4	1·4	1·4	1·6	1·6

Superscripts indicate that crystal compositions from other experimental runs have been used in the calculations.
[1] 1450 °C, 22·5 kb Picritic Nephelinite composition. [2] 1510 °C, 27 kb. [3] 1450 °C, 22·5 kb.

and aluminous, subcalcic augite would not be called an 'eclogite' if the term has its usual petrological meaning.

The term 'eclogite fractionation' was used by Yoder & Tilley (1962) in their pioneering work on basalt fractionation at high pressures and applied to a process of separation of pyrope-almandine and omphacitic clinopyroxene, i.e. the minerals of eclogite. However, O'Hara & Yoder (1967) and O'Hara (1968) used the term loosely to include fractionation controlled by garnet and pyroxene, the compositions of the near liquidus pyroxenes being unknown but assumed to be aluminous and subcalcic (O'Hara, 1968, p. 94). The differences between the two models are very great; the concept of separation of omphacitic pyroxene involves separation of a phase with >52 per cent SiO_2, high Na_2O content and containing normative albite, nepheline and little or no normative anorthite. Separation of aluminous, subcalcic clinopyroxene removes a phase with < 49 per cent SiO_2, $\geqslant 8$ per cent Al_2O_3, low Na_2O content and high normative anorthite and olivine contents. The ambiguity of the terminology and the lack of precise definition of either magma compositions or of high-pressure crystal extracts, prevents unequivocal evaluation of the 'eclogite fractionation' hypothesis as expressed in O'Hara (1968). It is emphasized that the use of projections in which Ca, Na, and K, and Fe and Mg are equated is necessarily inadequate and misleading unless accompanied by detailed, element by element, treatment of the multicomponent basalt systems. The type of error that this can lead to is exemplified by the inference made by O'Hara (1968, p. 94) that all basalts having clinopyroxene and garnet as liquidus phases at approximately 30 kb must lie in the locus of liquids derived by 'eclogite fractionation' and that therefore 'eclogite fractionation' does not lead to abnormal or non-basaltic chemical compositions in residual liquids. This type of argument can be applied in a 3-component system for liquids lying along a univariant cotectic but is inadequate for an n-dimensional surface between garnet and pyroxene in an $(n+1)$-component system. A simple example illustrates this point. Two basalts, differing in degree of undersaturation as expressed by Hy/Ol or Ne/Ab ratio, may have exactly the same ratio of 100 $Mg/(Mg+Fe^{++})$ and both have garnet and clinopyroxene on their liquidi at approximately 30 kb. Fractionation by garnet or pyroxene or combinations thereof from either basalt will decrease the 100 $Mg/(Mg+Fe^{++})$ ratio and cannot lead to the other composition. In general terms, compositions lying on the garnet+pyroxene 'surface' are not all mutually attainable by 'eclogite fractionation' and are not all of basaltic composition.

It is possible to use the experimental and analytical data on the undersaturated basanitic and nephelinitic compositions to calculate possible liquids obtained from the chosen compositions by separation of garnet and clinopyroxene. In attempting to judge whether the processes may be active in natural basalt evolution, it is necessary to compare calculated derivative liquids and calculated fractionation trends with natural mantle-derived basalt compositions and compositional trends. The use of basalts containing high-pressure xenoliths

to define these primary or primitive compositional trends will undoubtedly improve as more attention is paid to these particular basalts but the selected analyses listed in Table I and the alkalis *vs.* SiO_2 and CaO *vs.* SiO_2 (Fig. 4) plots (Bultitude & Green, 1968) provide a useful frame of reference. Attention is drawn to the high values of the 100 Mg/(Mg+Fe^{++}) ratio for these basalts and the absence of any consistent trend of variation of this ratio for 36 per cent $< SiO_2 <$ 46 per cent.

In the picritic basanite at 31·5 kb, 1530 °C, clinopyroxene is more abundant than garnet and calculations of 30 per cent crystallization with 2:1 and 5:1 clinopyroxene:garnet ratios yield liquids with lower SiO_2, lower 100 Mg/(Mg+Fe^{++}) and lower Ab/Ne ratios. CaO decreases as SiO_2 decreases and Al_2O_3 remains almost constant. In the olivine nephelinite composition both clinopyroxene and garnet occur on the liquidus at 36 kb, 1540 °C, and possible parental liquids can be calculated for this composition, assuming 20 per cent crystallization of garnet and pyroxene to reach the olivine nephelinite composition from a higher temperature parent. Similarly, derivative liquids assuming 20 or 30 per cent crystallization of the olivine nephelinite have been calculated and the calculations thus demonstrate the fractionation trend produced by approximately 37 per cent crystallization of garnet and clinopyroxene (3:1, 1:1, and 1:3 proportion) *through* the initial chosen olivine nephelinite composition. If clinopyroxene and garnet are present in similar proportions then SiO_2, CaO, Al_2O_3, and 100 Mg/(Mg+Fe^{++}) decrease with increasing alkalis. If garnet:clinopyroxene = 3:1 then SiO_2 and CaO remain almost constant and alumina decreases as alkalis increase. If garnet:clinopyroxene = 1:3, then SiO_2 and CaO decrease and Al_2O_3 increases with crystal fractionation. In all cases, large degrees of crystallization are required to produce relatively small increases in degree of undersaturation (to leucite-normative olivine nephelinites) and small decreases in SiO_2 content. In addition the trend to more undersaturated compositions is coupled with *decrease* in CaO content and in 100 Mg/(Mg+Fe^{++}) ratio, in disagreement with the relationships shown by the natural rocks. For the picritic nephelinite composition, garnet is joined by clinopyroxene near 1580 °C at 36 kb and separation of garnet with pyroxene produces trends similar to those already outlined; to produce larger depletion in SiO_2 content, clinopyroxene must be dominant in the precipitate but this leads to marked depletion in CaO and also decrease in 100 Mg/(Mg+Fe^{++}) ratio.

To summarize, separation of garnet and clinopyroxene from these undersaturated basaltic compositions at 27–36 kb will produce liquids which are slightly lower in SiO_2 and more undersaturated than the parent liquids. The process is 'inefficient' in the sense that large degrees of crystallization are required to effect small changes in degree of undersaturation and it appears most improbable that a 'hypersthene-normative picritic basalt' (O'Hara & Yoder, 1967, p. 103; O'Hara, 1968, p. 117) (with 46–47 per cent SiO_2 probably) could fractionate to yield picritic basanite or picritic nephelinite compositions, much

less the olivine–melilite nephelinites with 38 per cent SiO_2, by separation of garnet and aluminous clinopyroxene. It should be noted that the higher SiO_2 content of a hypersthene-normative picritic basalt may be greater than that of the garnet+aluminous pyroxene extract. Fractionation would in this case yield derivative liquids with *higher* SiO_2 contents. The high degrees of crystal fractionation required to produce small changes in degree of undersaturation will produce changes in 100 $Mg/(Mg+Fe^{++})$ ratio such that the more undersaturated olivine–melilite nephelinite and olivine nephelinites are more iron-rich than basanites, alkali olivine basalts, and tholeiitic picrites. This relationship is not observed amongst natural basalts of direct mantle derivation. Similarly the requirement that to give appreciable SiO_2 depletion, clinopyroxene must exceed garnet in the accumulate phases, has the corollary that CaO content will decrease with SiO_2; this is the opposite of the observed relationship in the natural rocks (Fig. 4).

We do not wish to infer that separation of garnet+clinopyroxene from basaltic magmas does not occur in natural basalts but rather that it is not the process which gives rise to the observed spectrum of basalts from tholeiites to olivine–melilite nephelinites. This series of magmas is considered to be derived by direct melting of a pyrolite source rock containing small amounts of water (Bultitude & Green, 1968; Green, 1969*a*, *b*) or by fractionation of hydrous, olivine-rich picritic magmas from parental tholeiitic picrite through to olivine-melilite nephelinite at $\sim$ 27 kb or from parental olivine tholeiite through to olivine nephelinite at $\sim$ 18 kb. Fractionation under these conditions is dominated by orthopyroxene, initially accompanied by minor olivine and joined by clinopyroxene or garnet at lower temperatures. The partial melting hypothesis is preferred mainly because even the relatively small degrees of orthopyroxene (+ other phases) separation which have been suggested will produce iron-enrichment in the derived liquids. Separation of garnet and clinopyroxene may occur in natural magmas and may modify the chemical variations imposed in the partial melting relationship. Thus some of the scatter in the CaO *vs* SiO_2 plot of lherzolite-bearing basalts (Fig. 4) may be due to both olivine separation (lower pressure) or garnet+clinopyroxene separation from the liquids derived by partial melting.

In experimental studies of the xenoliths of the Delegate breccia pipe, Irving & Green (1969) have shown that some xenoliths represent an initial layered assemblage of garnet and aluminous clinopyroxene, and are probably accumulates from earlier undersaturated batches of magma. It may be noted that these xenoliths are Fe-rich (Irving & Green, 1969; Lovering & White, 1969) and probably represent accumulates or accumulates+trapped liquid from magmas which are more Fe-enriched than those of Table 1 and which may not have reached the surface at all. A similar hypothesis may account for the features of the Salt Lake Crater xenoliths, ranging from magnesium-rich pyroxenites to more iron-rich garnet pyroxenite.

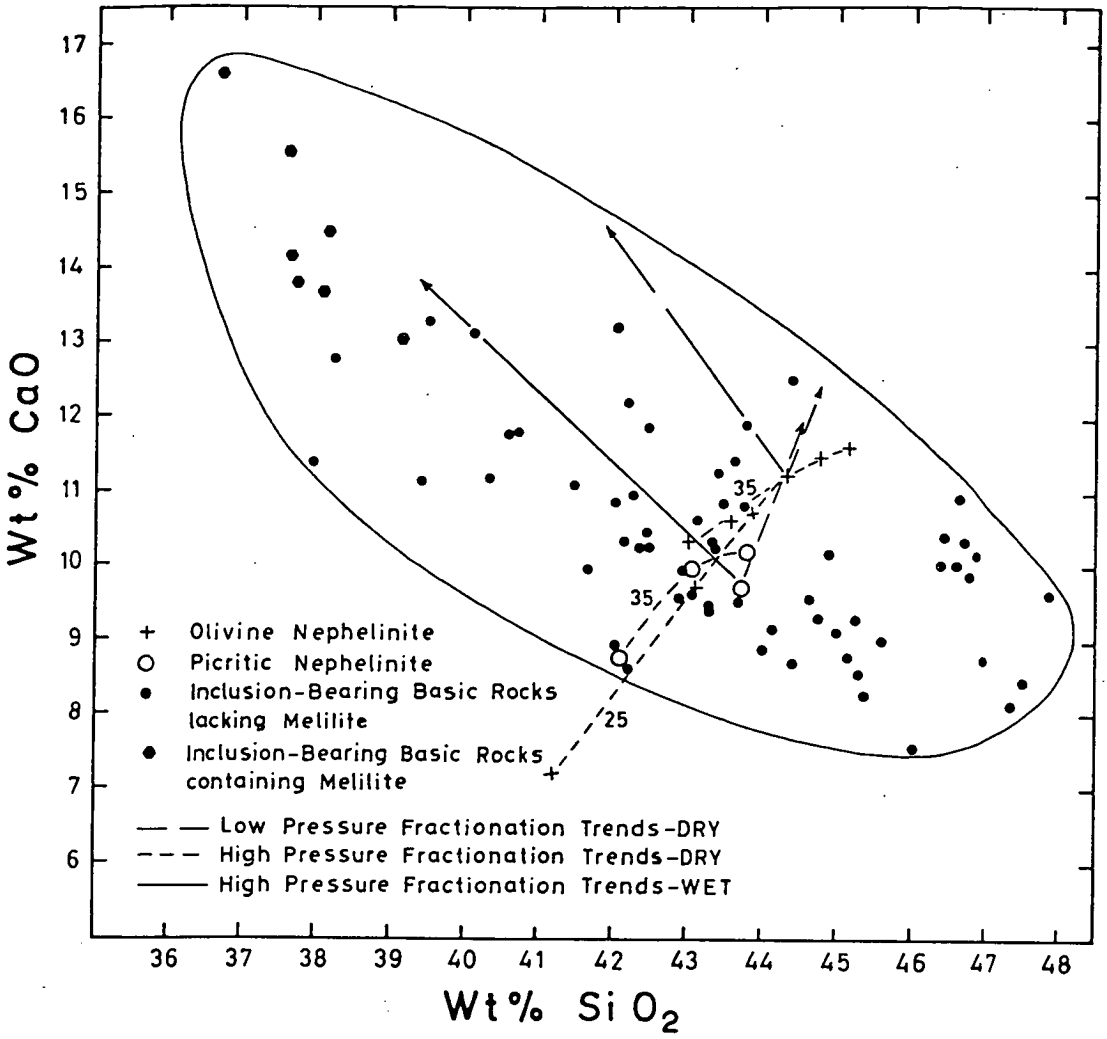

FIG. 4. CaO *vs.* SiO_2 variation amongst natural alkali basalts, basanites, olivine nephelinites, and olivine melilitites which contain inclusions of lherzolite, pyroxenite or garnet pyroxenite with high pressure mineralogy (> 8 kb). The fractionation trends shown for the olivine nephelinite and picritic nephelinite at various pressures are derived from Tables 5 and 6 (dry fractionation) and from Bultitude & Green (1968) (wet fractionation controlled largely by orthopyroxene separation). The trend marked '35' passing through the olivine nephelinite composition is determined by clinopyroxene and garnet separation at 35 kb (Table 5). The trend marked '25' for this composition is determined by extraction of clinopyroxene only at 25 kb (Table 5). For the picritic nephelinite composition separation of garnet alone initially yields liquids with higher CaO and SiO_2 content but the co-precipitation of clinopyroxene reverses this trend (Table 6). The low pressure, dry fractionation trends in both compositions are controlled by olivine separation.

CONCLUSIONS

Experimental study of the crystallization behaviour at high pressures of picritic basanite, olivine nephelinite, and picritic nephelinite shows that the near-liquidus fractionation trends are dominated by olivine up to 18 kb, by aluminous clinopyroxene between 18 and 27 kb and by aluminous clinopyroxene with garnet at pressures of 27 kb and higher. Microprobe analyses of the near-liquidus phases illustrate the high $(Ca,Mg)Al_2SiO_6$ solid solution and low

jadeite solid solution in the pyroxene up to 36 kb and also demonstrate the iron-enrichment trend in the liquid [i.e. depletion in the ratio 100 Mg/(Mg+Fe^{++})] which must accompany any fractionation by separation of olivine, clinopyroxene, or garnet.

Orthopyroxene appears over an extremely limited temperature interval in the picritic basanite at 18 kb and the picritic nephelinite at 22·5 kb. This feature is used to suggest that an olivine-rich basanite may be developed by partial melting of a source pyrolite composition under dry conditions at 60–80 km depth. This liquid, which would be in equilibrium with residual olivine, aluminous orthopyroxene, and aluminous clinopyroxene (and possibly spinel), would contain approximately 44 per cent SiO_2, 4 per cent Na_2O+K_2O, 13 per cent Al_2O_3, and 10 per cent CaO. Its normative composition would include approximately 5 per cent orthoclase, 5 per cent albite, 12 per cent nepheline, 20 per cent anorthite, 22 per cent diopside, and 31 per cent olivine. The liquid would be magnesium-rich with 100 Mg/(Mg+Fe^{++}) = 71–72. The experiments suggest that it is not possible to derive liquids of more undersaturated character (olivine nephelinite, olivine–melilite nephelinite) and with lower SiO_2 contents down to $\sim$ 38 per cent SiO_2, by partial melting of *dry*, peridotitic compositions in which olivine and enstatite are major phases and thus present in equilibrium with any partial melts. This conclusion applies for pressures up to approximately 36 kb.

Alternative schemes of derivation of the olivine nephelinite and olivine–melilite nephelinite magmas by fractional crystallization of a more saturated basanitic or nephelinitic parent are examined quantitatively. It is shown that while separation of olivine, aluminous clinopyroxene, or clinopyroxene+garnet may account for some variation in the chemical composition of mantle-derived basalts, these processes cannot produce a trend linking tholeiitic picrite or even alkaline picrite with olivine nephelinite and olivine–melilite nephelinite. In particular, separation of garnet and aluminous clinopyroxene does not produce the observed variation among the undersaturated magmas. The principal objections to this hypothesis, as applied to the rock types under investigation, are the 'inefficiency' of the process requiring large degrees of crystal fractionation to produce relatively small changes in SiO_2 content and degree of undersaturation. This would inevitably produce significant decrease in Mg/(Mg+Fe^{++}) ratio in the derivative liquids, a feature not observed in the natural rocks. Similarly the necessity for clinopyroxene to outweigh garnet in the accumulates to produce significant SiO_2 depletion, in parent magmas with 43–46 per cent SiO_2, will cause CaO to decrease also; this contradicts the natural magmas relationships. Garnet+clinopyroxene fractionation may be significant in generating kimberlitic, alnoitic or olivine melilitite liquids from *parental* olivine–melilite nephelinites ($\sim$ 38 per cent SiO_2) (Green, 1969*a*, fig. 3). The production of the olivine nephelinite and olivine–melilite nephelinite magmas is believed to require the presence of small amounts of water in the source region of the upper mantle. These magmas may be produced by low degrees of partial

melting of a pyrolite upper mantle containing 0·1–0·2 per cent H_2O at depths of 80–120 km (Bultitude & Green, 1968; Green, 1969*a*, *b*).

REFERENCES

BANNO, S., & MATSUI, Y., 1965. Eclogite types and the partition of Mg, Fe and Mn between clinopyroxene and garnet. *Proc. Jap. Acad.* **41**, 716–21.

BLACK, P. M., & BROTHERS, R. N., 1965. Olivine nodules in olivine nephelinite from Tokatoka, Northland. *N.Z. J. Geol. Geophys.* **8**, 62–80.

BULTITUDE, R. J., & GREEN, D. H., 1968. Experimental study at high pressures on the origin of olivine nephelinite and olivine melilite nephelinite magmas. *Earth planet. Sci. Lett.* **3**, 325–37.

—— 1970. Highly undersaturated rocks under upper mantle conditions. *Nature, Lond.* (in press).

ERNST, T., 1936. Der Melilith-Basalt des Westberges bei Hofgeismar, nordlich von Kassel, ein Assimilationsprodukt ultrabasischer Gesteine. *Chemie. Erde*, **10**, 631–66.

FENNER, C. N., 1938. Olivine fourchites from Raymond Fosdick Mountains, Antarctica. *Bull. geol. Soc. Am.* **49**, 367–400.

FORBES, R. B., & KUNO, H., 1965. The regional petrology of peridotite inclusions and basaltic host rocks. Upper Mantle Symposium, New Delhi. *Internat. Union Geol. Sci.* 161–79.

GREEN, D. H., 1969*a*. The origin of basaltic and nephelinitic magmas in the Earth's mantle. *Tectonophysics*, **7**, 409–22.

—— 1969*b*. A review of experimental evidence on the origin of basaltic and nephelinitic magmas. *Phys. Earth planet. Inter.* **5** (in press).

—— & HIBBERSON, W., 1969. Experimental duplications of conditions of precipitation of high pressure phenocrysts in a basaltic magma. Ibid. **5** (in press).

—— & RINGWOOD, A. E., 1964. Fractionation of basaltic magmas at high pressures. *Nature, Lond.* **201**, 1276–9.

—— —— 1967*a*. An experimental study of the gabbro to eclogite transformation and its petrological applications. *Geochim. cosmochim. Acta*, **31**, 767–833.

—— —— 1967*b*. The genesis of basalts. *Contr. Miner. Petrol.* **15**, 103–90.

—— —— 1969. Mineralogy of peridotitic compositions under upper mantle conditions. *Phys. Earth planet. Inter.* **5** (in press).

HARUMOTO, A., 1952. Melilite-nepheline-basalt, its olivine nodules and other inclusions from Nagahama, Japan. *Mem. Coll. Sci. Univ. Kyoto*, Ser. B, **20**, 311–22.

HARVEY, M., & JOPLIN, G. A., 1941. A note on some leucite bearing rocks from New South Wales with special reference to an ultrabasic occurrence at Murrumburrah. *J. R. Soc. N.S.W.* **74**, 419–42.

IRVING, A. J., & GREEN, D. H., 1969. Experimental duplication of mineral assemblages in basic inclusions of the Delegate breccia pipes. *Phys. Earth planet. Inter.* **5** (in press).

ITO, K., & KENNEDY, G. C., 1968. Melting and phase relations in the plane tholeiite-lherzolite-nepheline basanite to 40 kilobars with geological implications. *Contr. Miner. Petrol.* **19**, 177–211.

LOVERING, J. F., & WHITE, A. J. R., 1969. Granulitic and eclogitic inclusions from basic pipes at Delegate, Australia. Ibid. **21**, 9–52.

MACDONALD, G. A., & KATSURA, T., 1964. Chemical composition of Hawaiian lavas. *J. Petrology*, **5**, 82–133.

MURATA, K. J., BASTRON, H., & BRANNOCK, W. W., 1965. X-ray determinative curve for Hawaiian olivines of composition Fo_{76-88}. *Prof. Pap. U.S. geol. Surv.* **525–C**, 35–7.

O'HARA, M. J., 1968. The bearing of phase equilibria studies in synthetic and natural systems on the origin and evolution of basic and ultrabasic rocks. *Earth Sci. Rev.* **4**, 69–113.

—— & YODER, H. S., 1967. Formation and fractionation of basic magmas at high pressures. *Scot. J. Geol.* **3**, 67–117.

TILLEY, C. E., & YODER, H. S., 1964. Pyroxene fractionation in mafic magma at high pressures and its bearing on basalt genesis. *Yb. Carnegie Instn. Wash.* **63**, 114–21.

WASHINGTON, H. S., & KEYES, M., 1926. Petrology of Hawaiian Islands V; the Leeward Islands. *Am. J. Sci.* **12**, 336–52.

WHITE, R. W., 1966. Ultramafic inclusions in basaltic rocks from Hawaii. *Contr. Miner. Petrol.* **12**, 245–314.

WILSHIRE, H. S., & BINNS, R. A., 1961. Basic and ultrabasic xenoliths from volcanic rocks of New South Wales, *J. Petrology*, **2**, 185–208.

WINCHELL, H., 1947. The Honolulu Series, Oahu, Hawaii. *Bull. geol. Soc. Am.* **58**, 1–48.

YODER, H. S., & TILLEY, C. E., 1962. Origin of basalt magmas: an experimental study of natural and synthetic rock systems. *J. Petrology*, **3**, 342–532.

B15

Tectonophysics
Elsevier Publishing Company, Amsterdam – Printed in The Netherlands

MAGMATIC ACTIVITY AS THE MAJOR PROCESS IN THE CHEMICAL EVOLUTION OF THE EARTH'S CRUST AND MANTLE

D.H. GREEN

Department of Geophysics and Geochemistry, Australian National University, Canberra, A.C.T. (Australia)

(Received November 15, 1971)

ABSTRACT

Green, D.H., 1972. Magmatic activity as the major process in the chemical evolution of the earth's crust and mantle. In: A.R. Ritsema (Editor), *The Upper Mantle. Tectonophysics*, 13(1–4): 47–71.

Hypotheses of continental drift or plate tectonics require the formation of new oceanic crust at mid-oceanic ridges and imply the further modification or continued evolution towards continental type of crust in island arcs and orogenic belts. Volcanism is the main process by which chemical differentiation by partial melting of parental upper-mantle peridotite occurs to yield, firstly, basaltic oceanic crust and, in a second and more complex melting stage, "andesitic" continental crust. Further differentiation of the continental crust may occur with deep crustal melting leading to enrichment of the upper crust in silica-rich and alkali-rich intrusives. The evolutionary trend of the processes of magmatism is towards a gravitationally and thermally stable, layered earth. The geological record suggests that the modern patterns of volcanism and plate tectonics have persisted for more than a billion years, as the mechanism of earth differentiation. However, the oldest exposed parts of the crust (>2.5 b.y.) provide evidence for a characteristically different type of magmatic activity implying very high degrees of melting of the upper mantle at very shallow depths. It is suggested that the "greenstone belts" of the Archaean shields may be the folded and metamorphosed terrestrial equivalents of lunar maria and formed contemporaneously with the lunar maria. Major impacts are considered to have triggered partial melting at depths of 150–300 km and diapiric ascent from these depths produced characteristic ultramafic magmas. Further evolution of the "terrestrial maria" was controlled by endogenous processes producing andesitic volcanism and in-folding of the maria to yield the "greenstone belts".

INTRODUCTION

In approaching the problem of the chemical evolution of the earth's crust and upper mantle, a first step is to consider the examples of crust–mantle differentation operating in active volcanic regions. Such an approach leads inevitably to consideration of the large-scale dynamics of the earth and it is a debatable point whether the geochemical differentiation of the earth's upper mantle is the prime cause or a major consequence of large

horizontal movements of the earth's crust (plate tectonics). The period of the International Upper Mantle Project has seen great advances in understanding the processes and conditions of magma genesis, the characterization of associated tectonic and volcanic environments and in the present and past patterns of crustal movement. It is the purpose of this paper to attempt to summarize a current view of the interaction and interdependence of magmatic activity and the dynamics of the earth's crust and upper mantle. It is also important to consider whether recent and current processes of geochemical evolution of the earth are adequate to interpret the geological record or whether very different processes or conditions operated in earlier stages of earth evolution.

CRUST–MANTLE DIFFERENTIATION AS EXEMPLIFIED BY RECENT BASALTIC VOLCANISM

The source region

The similarity of basaltic volcanism occurring in both continental and oceanic crust environments, the observations of the depths of seismicity associated with volcanism and geophysical arguments based on heat-flow, all demonstrate that the source of basaltic magmas is within the upper mantle. It is now clear that the major rock type of the upper mantle is peridotite, with olivine and lesser orthopyroxene as its major mineral phases. The constraints on upper-mantle mineralogy imposed by seismic velocity characteristics, including the demonstration of pronounced seismic anisotropy in the uppermost mantle, are consistent with olivine-rich peridotite in which the forsterite content of the olivine is close to Fo_{90}. Closer characterization of the nature of the upper mantle is possible from examination of the products of natural processes of upper-mantle sampling. The dominance of peridotite among high-pressure xenoliths in kimberlite pipes and in explosively erupted undersaturated basalts, and the presence of peridotite in high-temperature intrusives or exposed on fracture zones on the ocean floor, confirm the major role of peridotite and subordinate, local role of other high-pressure rocks such as eclogite, garnet pyroxenite and spinel pyroxenite. The natural peridotites of these occurrences have olivine with Mg-values★ in the range 88–94. Detailed geochemical studies (including isotopic, rare-earth and uranium-distribution studies) of peridotite inclusions in undersaturated basalts and in kimberlites have demonstrated that these inclusions are not high-pressure cognate accumulates from their host magmas or preceding magma batches but are unrelated, accidental xenoliths of sub-crustal origin (Leggo and Hutchison 1968, Kleeman and Cooper, 1970). Each of these peridotite occurrences show variability in proportions of major and minor phases (olivine, orthopyroxene, clinopyroxene, garnet, spinel, phlogopite, amphibole, apatite, ilmenite) and several attempts have been made to estimate average compositions from a large number of samples (Table I).

★ Mg-value is used as an abbreviation for the atomic ratio $100\ Mg/(Mg+Fe^{2+})$.

TABLE I

Estimated compositions for the upper mantle by various authors compared with compositions of Archaean ultramafic extrusives from "Greenstone belts"

	1	2	3	4	5	6	7	8	9
SiO_2	45.16	45.0	43.8	45.1	42.86	46.63	46.46	47.10	44.80
TiO_2	0.71	0.07	0.02	0.5	0.33	0.34	0.19	0.30	0.23
Al_2O_3	3.54	3.01	1.45	4.1	6.99	3.02	3.58	6.55	5.26
Cr_2O_3	0.43	0.41	0.45	0.3	0.18	–	0.43	–	–
Fe_2O_3	0.46	1.28	1.61	2.0	0.36	1.00	1.00	1.00	1.00
FeO	8.04	6.70	6.75	7.9	8.97	9.63	9.38	7.66	9.46
MnO	0.14	0.11	0.12	0.2	0.14	0.18	0.21	0.21	0.18
NiO	0.20	0.25	0.29	0.2	0.20	–	–	–	–
MgO	37.47	39.7	44.0	36.7	35.07	34.23	32.97	30.17	34.34
CaO	3.08	3.15	1.38	2.3	4.37	4.79	5.10	6.77	4.35
Na_2O	0.57	0.24	0.15	0.6	0.45	0.15	0.49	0.22	0.35
K_2O	0.13	0.04	0.03	0.02	0.003	0.03	0.18	0.02	0.03
P_2O_5	0.06	–	–	0.1	–	–	0.01	–	–

Columns 6–9 have been recalculated from original data to 100% anhydrous and with Fe_2O_3 arbitrarily made 1.00%.

Column 1. Pyrolite model composition (Ringwood, 1966).

Column 2. Mean of analyses of 20 spinel lherzolite xenoliths from Rocher du Lion, Haute-Loire (Vilminot, 1965; quoted by Hutchison et al., 1970).

Column 3. Mean of analyses of 40 spinel lherzolite xenoliths from Dreiser Weiher, Eifel, W. Germany (Hutchison et al., 1970, col.4).

Column 4. Estimated upper-mantle composition from which volatiles (H_2O, CO_2, Cl) have been lost but without any basalt removal by partial fusion (Nicholls, 1967).

Column 5. Estimated upper-mantle composition, based on genetic relationship by partial fusion, partial crystallization model to account for ultramafic inclusions in basalts, (Carter, 1970).

Column 6. Average peridotitic komatiite Barberton area, South Africa (Viljoen and Viljoen, 1969b).

Column 7. Freshest sample of quenched peridotitic komatiite (Sample 49J). Demonstrated ultramafic liquid (Green et al., in preparation) from Barberton area, South Africa.

Column 8. Peridotite with quench texture, Scotia, western Australia (Nesbitt, 1971).

Column 9. Peridotite with quench texture, Mt. Ida, western Australia (Nesbitt, 1971).

A complementary approach is to compare the chemistry of natural mantle-derived peridotites with that of natural basalts to evaluate whether the peridotites are capable of yielding basalt magmas by reasonable partial melting processes. Where this has been done, the peridotites have been found to be partially residual and depleted in particular elements, e.g., light rare-earth elements, potassium, uranium, thorium, titanium, sodium and phosphorus. The depleted or residual character is seen first in those elements ("incompatible elements") which do not substitute readily in the major phases of the mantle peridotite and are highly concentrated in any initial melt fraction. Thus an alternative approach to deduction of upper-mantle composition, prior to basalt extraction, is to use the composition of natural basalt, combining this with the possible residual minerals (identified by experimental study of the liquidus phases of mantle-derived basalts under upper-mantle pressure–temperature conditions) to yield a parental upper-mantle composition (Green and Ringwood, 1963, Green, 1970b). A further constraint applied, in order to fix the proportions in which liquid (basalt) and residue (olivine, enstatite, chromite) are combined, is that the major element abundances (Si, Mg, Fe, Ca, Al) of the parental composition should be close to those of the more Fe-, Ca- and Al-rich natural mantle samples mentioned above. This approach led to the calculation of model "pyrolite" composition for the upper mantle (Ringwood, 1966) and at the present time this composition (Table I) serves as a reasonable estimate of parental upper-mantle composition in those regions yielding basaltic magmas in Tertiary to Recent times. The principal uncertainties in this composition are in TiO_2 content (high because of the use of Hawaiian olivine tholeiite in the calculation of pyrolite) and possibly K_2O and P_2O_5. These are components most likely to be inhomogeneously distributed in the upper mantle since they form accessory minerals such as titanian phlogopite, ilmenite or apatite – for these components the concept of a single parental mantle composition may be misleading, whereas the concept may remain valid for major elements and those trace elements readily substituting in the minerals olivine, orthopyroxene, clinopyroxene, spinel or garnet.

The model pyrolite composition is capable (in terms of major elements) of yielding basaltic magmas of observed composition and leaving residual peridotite, again consistent with natural peridotite samples. The pyrolite composition may crystallize in a variety of mineral assemblages, stable at the solidus under various load-pressure and water-pressure conditions:

(a) Olivine + enstatite + diopside + plagioclase + chromite (on solidus for dry conditions up to approximately 9 kbar).

(b) Olivine + enstatite + pargasitic amphibole ± diopside ± spinel (on solidus in the presence of water up to approximately 29 kbar).

(c) Olivine + aluminous enstatite + aluminous diopside ± aluminous spinel (on solidus for dry conditions from 9 kbar to approximately 30 kbar).

(d) Olivine + enstatite + diopside + garnet (on dry solidus at pressures $>$ 30 kbar, on wet solidus at pressures $>$ 29 kbar approximately).

Physical conditions of melting

The solidi of several peridotite compositions have been determined as functions of pressure and temperature under dry conditions (Ito and Kennedy, 1968; Kushiro et al., 1968; Green and Ringwood, 1967b). The sequence of disappearance of phases with increasing degrees of melting in the pyrolite composition is spinel (or garnet at 30–35 kbar) followed by clinopyroxene, orthopyroxene and olivine. Green (1970b) illustrated an essentially linear plot of percentage melting against temperature above the solidus, but Wyllie (1971) argued for a stepped character. It is in fact probable that the different cotectics involved, as phases successively disappear into the melt, will have different slopes on a temperature vs. percentage melt plot – this is illustrated in Fig. 3 and 4.

Kushiro et al. (1968) have determined the solidus for a peridotite composition for water-excess conditions ($p_{H_2O} = p_{total}$) and data on the solidus for pyrolite composition (with 10% H_2O) are illustrated in Fig. 1.

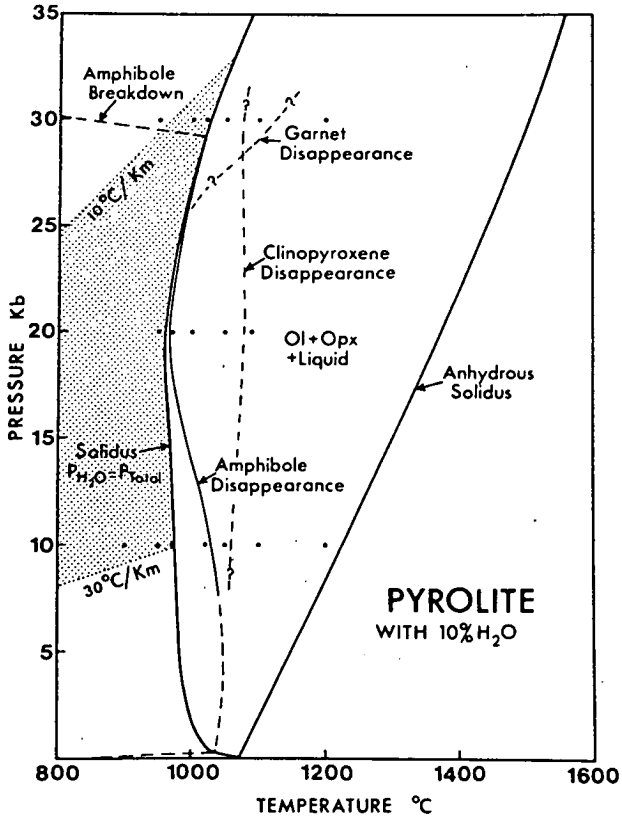

Fig. 1. Solidus and melting relations for pyrolite with excess water. Experimental data points shown by individual black dots. The stippled area illustrates the conclusion that reasonable geothermal gradients (as given by *p-t* estimates in exhumed metamorphic terrains of orogenic belts) may intersect the upper-mantle melting curve for $p_{H_2O} = p_{total}$ at very shallow depths.

Attention is drawn to the high-pressure limit of amphibole stability and to the disappearance of amphibole very close to the solidus at 10 kbar and 20 kbar. The amount of melt present increases rapidly immediately above the solidus at 10 kbar and probably also at

20 kbar, largely as a consequence of the high-water content (10% of the total system). This is in contrast to the situation where the source region contains very small amounts of water (Fig. 3, 4). In the latter case, the liquid is undersaturated in water either at the solidus (in the amphibole stability region) or at temperatures only slightly above the solidus and becomes increasingly undersaturated in water (with increasing liquidus temperature) as the amount of melting increases. Thus the amount of melting is effectively buffered by the amount of water present (Fig. 3,4; Ringwood, 1969; Green, 1970b; Wyllie, 1971).

Whether or not melting occurs in a given region of the upper mantle will be determined by the local geothermal gradient and its relationship to the mantle solidus. Fig. 1 and 2 indicate that estimated geothermal gradients may intersect a region of melting in the upper mantle if water is present whereas in dry conditions no melting would occur except under extremely high geothermal gradients.

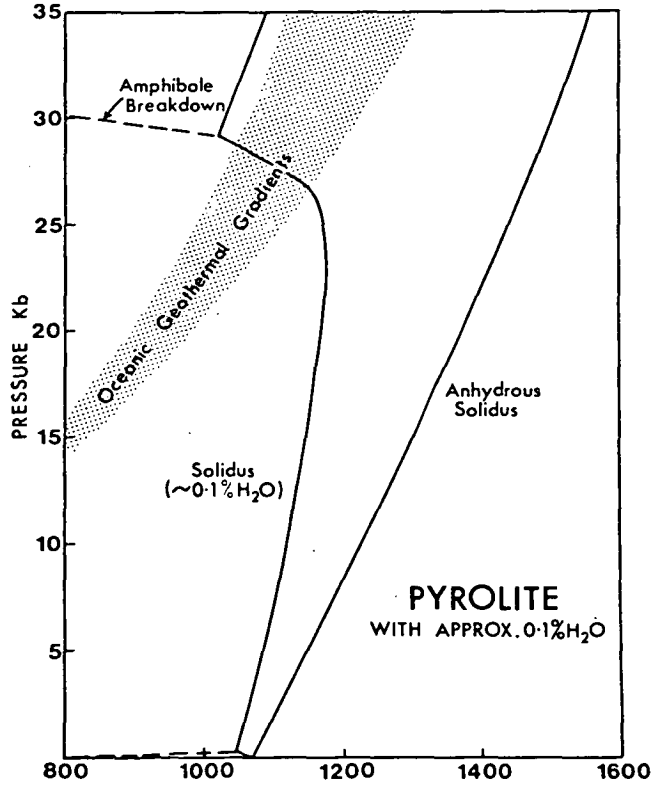

Fig. 2. Deduced solidus for pyrolite with ~0.1% H_2O in which amphibole is present in sub-solidus assemblages up to ∿ 30 kbar where the breakdown curve amphibole ⇌ olivine + pyroxenes + garnet + water for $p_{H_2O} = p_{total}$ intersects the pyrolite solidus for $p_{H_2O} = p_{total}$. At lower pressures $p_{H_2O} < p_{total}$ at the solidus. The stippled area illustrates a range of oceanic geothermal gradients which intersect the solidus at depths of 70–100 km. Comparison with Fig. 5 shows that the degree of partial melting along such geothermal gradients will remain very small.

A region of partial melting in the upper mantle affects seismic and deformational properties, producing marked decrease in the shear velocity, increase in seismic attenuation, decrease in compressional velocity, and a decrease in strength of the material producing a

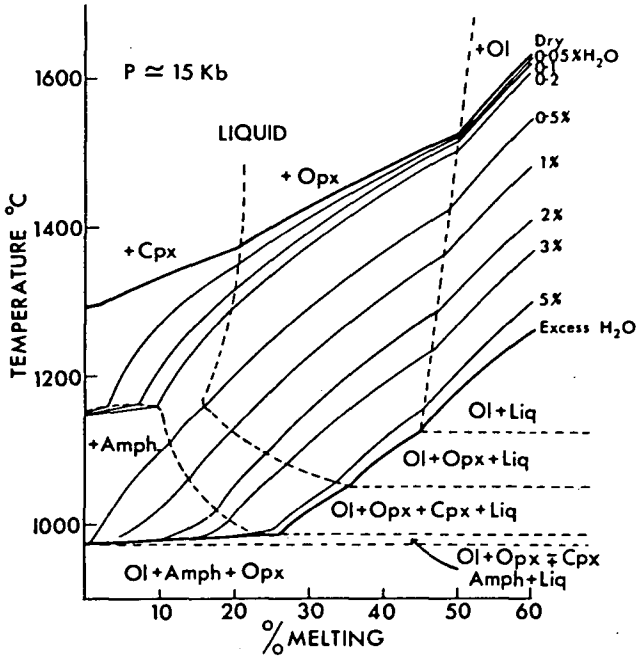

Fig. 3. Plot of percentage melting against temperature at approx. 15 kbar for pyrolite under anhydrous conditions and with various water contents. The solidus is at ∿ 1280°C, ∿ 1150°C or 970°C depending on whether the pyrolite is dry, with minor amphibole ($p_{H_2O} < p_{total}$ and buffered by amphibole and its breakdown products) or with excess water ($p_{H_2O} = p_{total}$). The nature of residual phases in equilibrium with the liquid is also shown. This diagram is based on deductions and internal consistency using the information of Fig. 1, knowledge of the pyrolite composition and of compositions of high-temperature pargasitic amphibole, and magnitude of the depression of liquidi of basalts and the stability field of amphibole and pyroxenes in various basaltic magmas with controlled water contents.

region of potential flow. It is inferred that the presence of the low-velocity zone in the upper mantle is a direct consequence of partial melting in the manner illustrated in Fig. 2 and it is this characteristic of the mantle which determines the distinction between lithosphere and asthenosphere. (Lambert and Wyllie, 1968; Green, 1970b, 1971). In many regions of the earth, particularly beneath ocean basins and "younger" continental crust, the low-velocity zone begins at depths of 70–100 km and extends to depths of 150–200 km. This situation is probably best explained by a zone of melting in a "water-deficient" mantle with $p_{H_2O} < p_{total}$ (Fig. 2), i.e., with minor amphibole present in the lithosphere and breaking down, due to increased pressure, at the top of the low-velocity zone. Beneath "shield areas" of the continents, the low-velocity zone may be absent or apparent only in a broad v_s minimum – in these regions the geotherm may fail to intersect the solidus, even for $p_{H_2O} = p_{total}$ or alternatively the mantle in this region may be refractory and *dry*. In active orogenic regions, particularly in mantle regions overlying the dipping Benioff zones of arc-trench systems, there are regions of anomalous mantle in which low seismic velocities and high seismic attenuation persist to very shallow depths (30–40 km). It is suggested that in these regions, melting may occur in a mantle in which amphibole is a major sub-solidus phase and in which $p_{H_2O} = p_{total}$ (see Fig. 1).

The mechanism by which a partial melt, particularly for conditions of only 1–2%

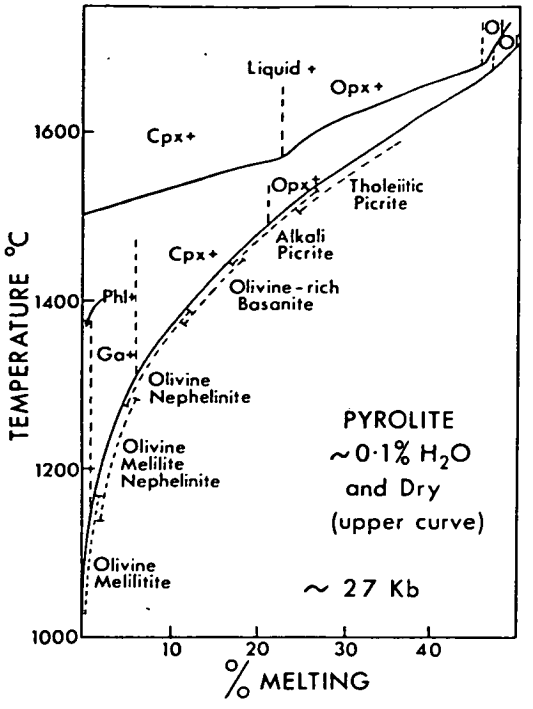

Fig. 4. Plot of percentage melting against temperature at approximately 27 kbar (modified slightly from Green, 1970b, 1971).Curves are shown for anhydrous pyrolite and for pyrolite with 0.1% H_2O. The nature of the residual phases in both cases and of the deduced composition of the melt for melting with 0.1% H_2O are also shown.

melting, may be tapped from its source rocks, remains uncertain. However, there are strong geochemical arguments that magmas formed by very small degrees of melting do reach the earth's surface (Gast, 1968; Bultitude and Green, 1968) and equally strong arguments that other magma types (particularly the voluminous olivine tholeiites) are products of high degrees of partial melting. It has been suggested (Green and Ringwood, 1967a) that high degrees of melting of the upper mantle occur as a consequence of diapiric upwelling of large masses from within the low-velocity zone. If such diapirs are large and cool essentially adiabatically then the amount of melt will increase as the mass moves towards the surface. Melting of greater than about 30% is difficult to envisage, except in an extremely rapidly moving diapir, because the settling of residual olivine and orthopyroxene in the earth's gravitational field will lead to segregation of magma from residual crystals.

Nature of partial melting products of the upper mantle

While Fig. 1 and 2 outline the conditions under which partial melting may occur in the upper mantle, it is equally important to know the chemical composition of the liquids and how this varies with pressure, temperature, water content and degree of melting. The chemical composition of the liquids is buffered by the residual crystalline phases and both

experimental studies on model pyrolite composition and consideration of the major element chemistry of natural peridotites leads to the inference that olivine (Fo_{88-93}) and enstatite must remain as residual phases, buffering the liquid, even up to > 40% partial melting. The mineralogy of the peridotite source rock is very sensitive to temperature, pressure and water content. Thus there is a very temperature-sensitive solid solution of orthopyroxene within clinopyroxene such that small degrees of partial melting at 1400°C ("dry peridotite") at 60–100 km would yield liquids in equilibrium with olivine, aluminous orthopyroxene and sub-calcic aluminous clinopyroxene (~ 10% CaO). However, for partial melting of peridotite with 0.1% H_2O, small degrees of melting at ~ 1200°C would yield liquids in equilibrium with olivine, orthopyroxene and clinopyroxene (~ 16–20% CaO) and possibly minor spinel, garnet or amphibole. For partial melting of peridotite with ~ 1.0% H_2O, small degrees of melting at ~ 1050°C would yield liquids buffered by olivine, orthopyroxene (low Al_2O_3), clinopyroxene (low Al_2O_3, CaO > 20%) and amphibole or, at higher pressures, garnet. The chemical compositions of the liquid developed by partial melting will thus differ depending on the water content of the source rock. For conditions of dry melting, initial melts will range from high-alumina olivine basalts at ~ 30 km to olivine-rich basanites or alkali picrites at 60–100 km (Green and Ringwood, 1967b). However, it is considered improbable that the mantle is dry, except possibly in regions in which a low-velocity zone does not exist and sub-crustal seismic velocities are high. In regions where a well-defined low-velocity zone exists below depths of 70–100 km it is more probable that the mantle has a small water content and that melting occurs at the solidus for $p_{H_2O} < p_{total}$ in Fig. 2, 4 and 5. For this case, the experimental studies of basalt crystallization with known water contents, allow the deduction of a detailed petrogenetic grid (Green, 1970a, b, 1971) expressing the chemical characteristics of magmas as a function of degree of partial melting, load pressure, temperature, water content (assuming a fixed water content of the source rock) and character of the residual phases. This petrogenetic grid is illustrated in percentage melting vs. temperature (at 15 and 27 kbar) and percentage melting vs. pressure (variable temperature) plots of Fig. 3, 4, 5 and 6.

Combination of Fig. 1–6 yields a model for present-day volcanism which relates the geophysical observations on the lithosphere and the low-velocity zone to petrological models of above-solidus and sub-solidus conditions in the source peridotite and to the nature of potential magmas existing in the earth's mantle.

EVOLUTION OF MODERN OCEANIC CRUST

The past 10–15 years has seen a major re-orientation of geological concepts of evolution of continental, orogenic and oceanic regions of the earth's crust. This stems largely from wide acceptance of geological and geophysical evidence that large-scale horizontal movements of continents (continental drift) have occurred in Palaeozoic, Mesozoic and Cenozoic time. Carey (1955, 1958) in several perceptive and stimulating papers, presented

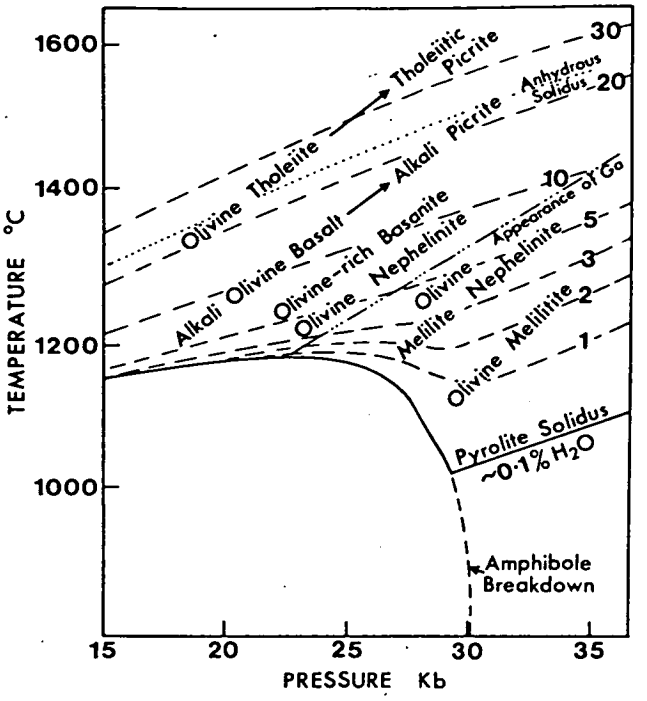

Fig. 5. Diagram illustrating the variation in compositions of liquids formed by various degrees of melting of pyrolite with 0.1% H_2O. Pyrolite solidus as in Fig. 2; diagram slightly modified from Green (1970b, 1971).

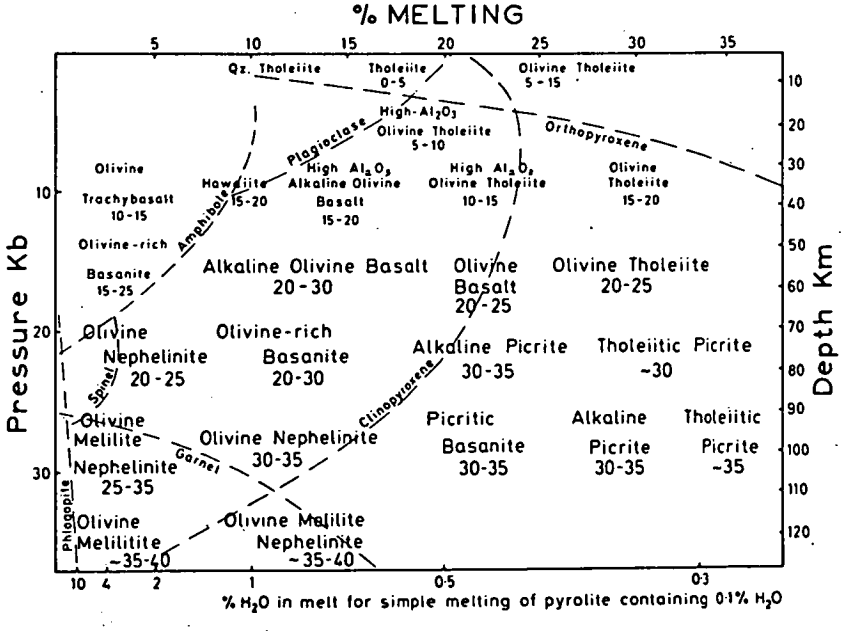

Fig. 6. Petrogenetic grid for magmas derived from the upper mantle by direct partial melting of pyrolite with 0.1% H_2O (from Green 1970b, 1971). The numbers placed with each basalt type refer to the normative olivine content of this liquid at its depth of origin. The dashed boundaries marked with a mineral name show that this mineral will occur amongst the residual phases remaining after extraction of magma types to the left of the boundary. Olivine is present as a residual phase for all magma types of this figure.

geological, topographical and geophysical arguments for continental drift and gave detailed reassemblies of earlier continental configurations which more recent work has vindicated to a very great extent. Carey (1958) recognized that his hypothesis implied the generation of new, geological young, oceanic crust and suggested evolutionary stages in this process from the rift valley stage, through a "Red Sea stage" to an "Atlantic stage" of evolution. Carey (1958, p.179) related the rifting process to "dilatational tectonic ascent of crystalline sima" and noted (p.190) that the rise of isotherms in these areas would increase the probability of volcanism. Impressed by the apparent lack of evidence for destruction of oceanic crust, Carey (1958, 1970) linked the continental drift reconstructions with an hypothesis of an expanding earth.

The rapid expansion in marine geophysical and geological work has been largely responsible for the change of emphasis from "continental drift" through "sea-floor spreading" (Dietz, 1961; Hess, 1962; Vine and Mathews, 1963) to the current emphasis on "plate tectonics" (Le Pichon, 1968; Isacks et al., 1968; McKenzie, 1969). In these more recent concepts, the oceanic ridges are locations of active basaltic volcanism and the oceanic lithosphere (crust of 6–6.5 km/sec layer, upper mantle with ~ 8 km/sec layer) is considered to be formed at the ridge crest and to become older and increasingly sediment-covered as it moves away from the ridge crest.

The characteristic basalts of the central rift areas of the oceanic ridges are olivine tholeiites with variable olivine contents (Miyashiro et al., 1969, Cann, 1971). They range from high-alumina olivine tholeiites to low-alumina tholeiite and exhibit variable degrees of low-pressure crystal fractionation. Parental magmas have low water contents and require high degrees of melting of a pyrolite source at relatively shallow depths (20–60 km approx.). This is consistent with upwelling of material from the lower part of the low-velocity zone to produce high degrees of melting, magma segregation at 10–20 kbar, 1350–1450°C and development of basaltic crust and underlying partly residual peridotitic lithosphere. As the crust-lithosphere moves away from the central rift area, cooling and crystallization lead to thickening of the lithosphere and establishment of the low-velocity zone (Fig. 7).

The formation of oceanic volcanic islands and sea-mounts and of island chains (e.g., Hawaiian Islands) away from the oceanic ridge crests, points to continued evolution of the oceanic lithosphere with addition of volcanic material differing from that characteristic of the oceanic ridges. Oceanic island volcanoes may be of two types:

(a) Isolated volcanoes or seamounts which have long histories of eruption, apparently only of undersaturated magmas or their derivatives, and which appear to move with the oceanic crust. In the model illustrated in Fig. 7 the source of these magmas lies in the upper part of the low-velocity zone and the cause of the magmatic activity may be a structural control within the lithosphere or anomalous characteristics within the upper part of the low-velocity zone.

(b) Island chains such as the Hawaiian Islands in which the individual volcanoes are built within 1–2 m.y. and in which the centre of active volcanism migrates in a direction opposed to that of the plate movement. In the model of Fig. 7 (see also Green, 1971, for

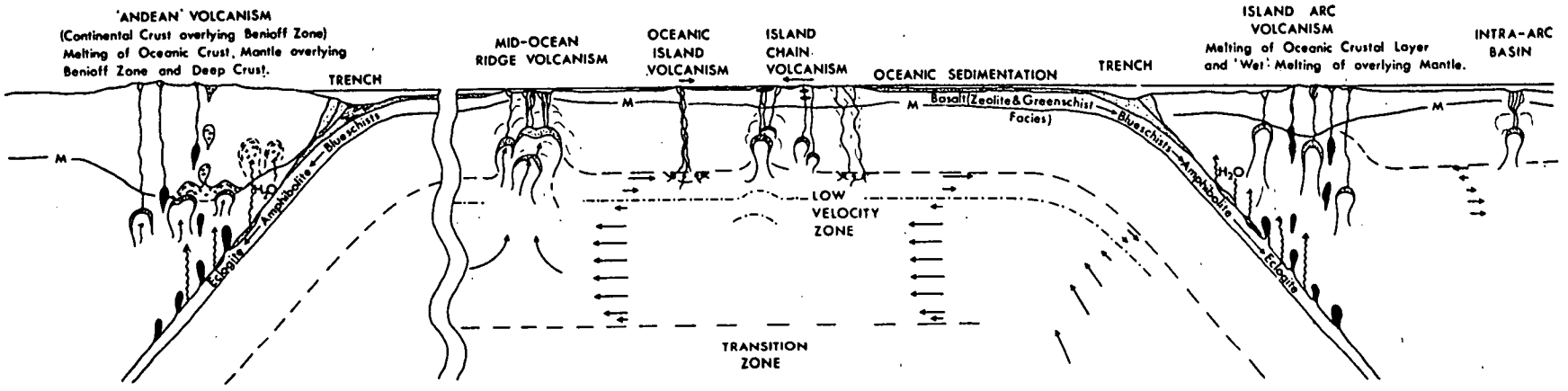

Fig. 7. Schematic diagram illustrating the petrogenetic processes of significance in the plate tectonics hypothesis. The initial formation and later local modification by volcanism and sedimentation of the basaltic oceanic crust is shown. Two examples of downgoing lithospheric slabs, one in the island-arc situation, one at a continent-ocean boundary are also illustrated and the complexity of magma genesis beneath such regions is emphasized. Patterned areas capping peridotite diapirs indicate segregation of basaltic magmas, black areas rising from the Benioff zone indicate andesitic or dacitic magmas of the calc-alkaline suite and areas with patterns of crosses indicate deep crustal melting and rhyolitic or granitic (s.l.) intrusions. Stippling indicates sediment or metamorphosed sedimentary cover. See also Ringwood (1969); Green (1971).

more details), the prime cause of local tensional failure of the lithosphere, with consequent volcanism, is considered to lie in the lower part of the low-velocity zone (the region of return flow of Fig. 7).

Thickening of the basaltic layer of the oceanic crust will occur beneath oceanic volcanic islands, and basaltic sequences with higher incompatible element contents (Green, 1971, fig. 6) may come to comprise a significant portion of the oceanic crust. Also, the increasing sediment thickness on the oceanic crust as it moves away from the ridge produces a significant chemical addition.

To summarize, the evolution of the crust in oceanic regions results from separation of upper-mantle pyrolite into an overlying basaltic layer and an underlying partly residual peridotitic lithosphere. The effects of low-pressure crystal fractionation (yielding peridotitic and gabbroic accumulates, and quartz normative basalts), oceanic island volcanism, sedimentation, metamorphism and metasomatism add to the geochemical complexity of the oceanic crust but do not invalidate the major feature that it is primarily a result of partial melting of part of the upper mantle. If the pyrolite composition is taken as the model composition for the upper mantle and olivine tholeiite is the dominant parental magma of the intrusions and extrusions of the oceanic crust, then one may estimate that 20–30% melting of the source region has occurred. A basaltic layer of the oceanic crust of 7 km implies that 20–35 km of underlying peridotite must be regarded as refractory and residual. If the oceanic lithosphere is around 80 km thick, then between one-half and three-quarters of the lithosphere above the low-velocity zone is essentially undepleted in terms of its magmatic component or has been depleted by loss of a very small melt fraction. This emphasizes that the convective-type movements in the upper mantle in the region of the oceanic ridges are complex, probably with ascent of individual diapirs which may or may not follow appropriate *p-t* paths to produce high degrees of melting. In terms of the discussion of the composition of the descending lithosphere developed in the following section, the estimates of compositions and thicknesses used above imply that there is little compositional difference between the average composition of the peridotite of the lithosphere and peridotite of the low-velocity zone. The sub-Moho lithosphere is envisaged as compositionally variable from pyrolite to harzburgite (residual olivine + enstatite + trace chromite) with local, minor bodies of gabbro, spinel pyroxenite or garnet pyroxenite from pockets of entrapped magma or magmatic accumulates.

CRUSTAL EVOLUTION IN ISLAND ARCS

Recent researches have produced compelling evidence that the oceanic crust and lithosphere, created by mantle upwelling at the mid-oceanic ridges, are "consumed", "destroyed" or "modified" by return movement deep into the mantle beneath the trench-island arc systems. Seismological evidences on the existence of the Benioff zone of deep focus earthquakes, the analysis of stress patterns associated with these earthquakes and

the existence of a dipping slab of low seismic attenuation and high seismic velocities beneath the Benioff zone, have combined to produce a model in which the relatively cool lithosphere descends into the mantle, maintaining its identity and contrast in physical properties down to depths of at least 600–700 km (Isacks et al., 1968; McKenzie, 1969). The cause of initial localization of a trench-arc system is uncertain but may be related to continental margins or to development of abnormally thick basaltic crust, for example, beneath island chains such as Hawaii. It has been suggested (Ringwood and Green, 1966) that gravitational instability due to conversion of the lower part of a basaltic crust to eclogite ($\rho \simeq 3.5$) overlying mantle peridotite ($\rho \simeq 3.3$) may initiate the sinking of the lithospheric slab. Analysis of the thermal regime of the downgoing slab shows that the temperatures within the slab remain lower than those in the surrounding mantle down to very great depths (Oxburgh and Turcotte, 1970; Minear and Toksöz, 1970). Polymorphic phase changes of mantle minerals to denser phases (such as olivine to spinel structure, pyroxene to garnet structure etc.; Ringwood, 1971) will occur at shallower depths in the cool slab than in the surrounding mantle. This effect will act as a major factor in driving a convective-type motion to depths of at least 700 km and in producing a long-term mixing or overturning process operative within the earth's outer 1000 km approximately (Ringwood, 1971).

Although the major part of the descending lithosphere is peridotite with the main contrast between the downgoing slab and the surrounding mantle being in temperature rather than composition, the presence of the layer of oceanic crust forming the upper ~ 10 km of the lithosphere is of major geochemical and petrological importance. It is clear that much of the basaltic part of the oceanic crust is carried into the mantle and the conversion of dry basalt and gabbro ($\rho \simeq 3.1$) to eclogite ($\rho \simeq 3.5$), mentioned previously, may be an important part of the driving mechanism in plate tectonics. The mineralogical evidence from blue-schist metamorphic terranes argues that mixed sedimentary + igneous sequences can be highly deformed and carried to depths of 20–30 km while relatively cool ($< 400°C$) and a number of authors have argued that such sequences have been carried down by descending lithospheric plates before being rapidly tectonically uplifted to their present exposure (Ernst, 1970; Coleman, 1971). The presence in the oceanic crust of major quantities of metasedimentary or other rocks, less mafic than basalts, would counteract the effects of the basalt to eclogite reactions in producing a density inversion in the lithosphere. Gravitational forces will act to detach such sequences from the downgoing slab or to inhibit the slab's downward motion.

Oceanic crustal rocks carried down with the descending lithosphere become subject to increasing temperature and pressure. The upper surface of the lithosphere will be heated by conductive heat transfer from the overlying mantle above the Benioff zone and possibly by frictional heat along the Benioff zone. The effects of the increase in pressure and temperature on the oceanic crustal rocks will be to produce metamorphic assemblages passing through glaucophane schists, amphibolites and garnet amphibolites to eclogites and biotite eclogites.

The reaction of amphibolite to eclogite is a direct consequence of the instability of

amphibole relative to garnet + pyroxene + water at high pressures and will take place at depths of 70–100 km depending on the degree of silica saturation of the rock. (Fig. 1, 2). Basaltic rocks which have remained dry, or with very low water contents, may react to eclogite or hornblende eclogite at shallower depths (20–30 km). An important feature associated with the metamorphic reactions (largely dehydration reactions) within the basalt layer is the loss of water – water may move along the Benioff zone or alternatively may move into the overlying wedge of mantle and crust above the Benioff zone. This is illustrated schematically in Fig. 7. In those regions where the temperature in the upper mantle above the Benioff zone is below ~ 1000°C, access of water at depths < 100 km will lead to increased abundance of amphibole (up to a maximum of ~ 30% for pyrolite composition containing pargasitic amphibole). This causes a decrease in density and seismic velocity but probably has little effect on seismic attenuation. On the other hand, if the temperature of any region of the overlying mantle to which water has access is at a temperature > 1000°C, then melting will occur wherever the effective local water content is > 0.3% of the mantle composition (Fig. 3). The amount of melting is controlled by the temperature and amount of water present. Melting, whether local or widely distributed, will decrease density and seismic velocity, and will markedly increase seismic attenuation of the region affected.

If the Benioff zone is overlain by a continental (e.g., Andean), rather than island arc, region (Fig. 7) then crustal rock types (containing quartz + K-feldspar + sodic-plagioclase etc. as essential minerals) rather than peridotite may exist at depths of 60–70 km (James, 1971). Movement of water from below the Benioff zone into crustal regions of this type may produce melting at temperatures of around 700°C – such magmas would be of granitic or granodioritic composition and either water-saturated or near-saturated. Vertical movement of such water-rich magmas would be extremely limited (Burnham, 1967) but gneissic intrusions and migmatitic zones of batholithic dimensions may result from crustal rocks which had previously been through complex histories of metamorphism and dehydration. Attention is directed to this aspect of the model (Fig. 7) which suggests that regions of relatively high temperature metamorphism and migmatization may immediately overlie regions of high-pressure, low-temperature metamorphism. Later uplift of the high-pressure metamorphics may be responsible for the paired metamorphic belts of orogenic regions (Miyashiro, 1961).

The possible effects of dehydration reactions within the downgoing slab considered above are particularly important in the example of the breakdown of amphibolite to eclogite (Lambert and Wyllie, 1968, Essene et al., 1970). If the temperature within the basaltic crust is less than ~ 700°C (Hill and Boettcher, 1970, Lambert and Wyllie, 1968) when any amphibolite is carried through the hornblende breakdown reactions at 70–100 km, then biotite eclogites will form with loss of water and no melting in the basaltic layer. Melting may occur in the overlying mantle (with water access) but in this case the magmas produced will be those formed by wet melting of peridotite composition and will be liquids in equilibrium with olivine (~ Fo_{90}) + enstatite ± amphibole ± clinopyroxene. However,

if the basaltic crust is already at temperatures in excess of ~ 700°C when it is carried through hornblende breakdown reactions at 70–100 km then melting of the basaltic layer will occur with formation of liquids in equilibrium with garnet + clinopyroxene ± quartz ± kyanite ± biotite. Chemical inhomogeneity within the basaltic layer, particularly intermixed metasedimentary materials, may locally produce low-melting fractions saturated with almandine + kyanite + plagioclase. Magmas formed by partial melting of the basaltic layer, in equilibrium with the residual phases noted above, will be silica-rich, of lower $Mg/(Mg + Fe^{2+})$ ratio than liquids derived from peridotite, and will range from rhyodacitic or dacitic to andesitic in composition (Green and Ringwood, 1968, 1969). It is important that such liquids result from a two-stage melting of the primary mantle peridotite and that these andesitic to dacitic liquids are not formed in equilibrium with magnesium-rich peridotite. Thus andesitic and dacitic liquids have clinopyroxene, plagioclase, garnet or quartz and not olivine or orthopyroxene as liquidus phases at high pressures and for various water contents, and furthermore have 100 $Mg/(Mg + Fe^{2+})$ ratios of 50–55 rather than 65–70 as for primary melts from the upper mantle. Magmas formed from the basaltic layer at the amphibolite $\rightleftharpoons$ eclogite + hydrous melt reaction boundary will tend to have high water contents, their eruption at the surface would be explosive, and crystallization (of amphibole, biotite, clinopyroxene) must begin at considerable depth below the earth's surface due to the shape of the liquidus and decreasing solubility of water with decreasing pressure.

Bodies of eclogite (biotite eclogite) which were initially relatively dry or which formed from amphibolite at temperatures below the beginning of melting, may be carried deeper into the mantle with the descending lithosphere. Melting of such material may occur at depths > 100 km. The percentage melting vs. temperature characteristics of melting under these conditions are not clear but the chemical characterization of the melt would probably be andesitic (in equilibrium with garnet and clinopyroxene at $p > 30$ kbar) as quartz and biotite would more readily enter the melt. The amount of water in the source rock would effectively buffer the amount of melting and melts would be undersaturated in water and able to move to relatively shallow depths before the onset of crystallization (pyroxene, olivine, plagioclase).

The preceding discussion, summarized in Fig. 7, emphasizes the varied and complex conditions of melting which can be operative in the island arc-trench system. Magmatism may be characterized as follows:

(1) *Melting of peridotite overlying the Benioff zone* may occur under conditions of high water pressures or water contents if water or water-saturated melt migrates from the basaltic crust of the descending lithosphere into the overlying mantle. Magmas produced by this process will be olivine-normative basalts (if they are formed in equilibrium with olivine + enstatite at $p > 5$ kbar approx.) but their specific geochemistry will be dependent on the degree of partial melting and the chemical and mineralogical composition of the source rock. Magmas produced by 10–30% melting under conditions of high water pressures would have residual olivine, enstatite and amphibole and the magmas may be of olivine

tholeiite or high Al olivine tholeiite composition. With lower degrees of melting (lower water contents or lower temperatures) magmas of shoshonite type with high K/Na ratios may form as a result of the increasing amount of amphibole (containing Na, Ti, Ca, Al) left as a residual phase. Because of high water contents, the decreasing solubility of water at lower pressures and the *p-t* shapes of liquidi for various water contents, tholeiitic, high-alumina basaltic or shoshonitic magmas formed in the manner outlined above, must begin to crystallize at 1–3 kbar (4–12 km). Thus there is a greater likelihood of such magmas reaching the earth's surface in a partly crystallized state, and furthermore there is increased opportunity for crystal fractionation and the eruption at the earth's surface of fractionated rather than parental magmas.

(2) *Melting of the basaltic crust of the upper part of the descending lithosphere* may occur abruptly at depths of 70–100 km due to breakdown of amphibolite to eclogite and the release of water, provided the temperature in the basaltic rocks is $\gtrsim 700°C$. Melting may only begin at deeper levels in the downgoing slab if temperatures at 70–100 km are $< 700°C$ but reach 1000–1200°C at deeper levels (100–150 km) and exceed the solidus temperatures for biotite + quartz eclogites. Melts derived from the basaltic layer will be in equilibrium with garnet + clinopyroxene (and possibly amphibole at 70–80 km depth) and are inferred to be of the calc-alkali suite ranging from andesite (or basaltic andesite) to dacite or rhyodacite in composition (Green and Ringwood, 1968, 1969). Such liquids would be quartz-normative, with varying water contents dependent on the water content and mineralogy of their source regions, and would have lower 100 $Mg/(Mg + Fe^{2+})$ values than basaltic magmas derived from the overlying lithosphere. Those magmas initially with high water contents would tend to crystallize before reaching the surface whereas those with low water contents (e.g., high degrees of melting of biotite + quartz eclogite source) could reach the surface with little or no crystallization.

(3) *Melting of thickened continental crust overlying the descending lithosphere* may occur under the influence of water released by dehydration reactions in the descending plate. The composition of liquids would be rhyolitic to rhyodacitic but the high water contents of such liquids would render them more likely to crystallize within the crust. However, the overall effect would be an upward migration of the low melting fraction in the form of migmatitic gneisses, mantled gneiss domes or gneissic granites.

(4) *Melting of peridotite (pyrolite) under "normal" (oceanic ridge pattern) conditions* may occur with upwelling of material from the low-velocity zone in those regions behind the island arcs (intra-arc basins; Karig, 1971) where the crust and lithosphere are of oceanic rather than continental character and local sea-floor spreading centres seem to operate. Such magmas, if formed by high degrees of melting, would be olivine tholeiite to high-alumina basalt and would be almost anhydrous.

The preceding discussion illustrates the considerable variety of magma generation processes which may occur in island arcs. Further complexity is introduced by possibilities of magma mixing, by differing fractionation trends controlled by p_{H_2O}, p_{O_2} variation and by opportunity for magma contamination during passage through a thick crust of conti-

nental or island-arc type. Quantitative evaluation of the overall chemical fractionation of oceanic crust to island-arc crust is difficult at the present stage of knowledge, but the overall trend of chemical differentiation is apparent. Thus the importance of andesites, dacites and rhyodacites of the calc-alkali suite, and of basaltic andesites, andesites, and more silica-rich derivatives of the island-arc tholeiite suite (Jakes and White, 1971) lies in the observation that even though these silica-rich rocks may be deeply buried and metamorphosed under eclogite facies conditions, the resultant mineral assemblages with quartz, sodic plagioclase and potassium feldspar or mica as major phases, will not attain densities greater than mantle peridotite. Thus a crust of andesitic or more silica-rich composition does not have the potential for gravitational instability that is present in a crust or lower crust of basaltic composition. Processes of high-grade metamorphism and partial melting occurring in the roots of island arcs or in thickened continental crust of orogenic regions may further enhance the chemical differentiation of the crust–mantle system by concentrating granitic rock types in the upper crust leaving residual pyroxene granulitic to anorthositic compositions in the lower crust (Green, 1969).

CRUSTAL EVOLUTION THROUGHOUT GEOLOGICAL TIME

The three-stage evolution of continental crust discussed in the previous sections may be summarized as:

(1) Basaltic oceanic crust developed by partial melting of peridotitic mantle.

(2) Mixed basaltic-andesitic-rhyodacitic crust developed by second-stage melting of oceanic crust and by further magma extraction from peridotitic mantle.

(3) Stable and mature continental crust developed by regional metamorphism, migmatization and ascent of granitic and granodioritic intrusives, enriching upper crust and depleting lower crust in low melting components.

These stages of evolution are an integral part of mantle–crust convective motions in which effective overturn and mixing of upper-mantle material to depths of at least 600–700 km occurs over times of the order of 100 m.y. The processes are coupled to a specific earth structure and evolution involving the existence of lithospheric plates, a well-defined low-velocity zone (asthenosphere) and descent of cooler lithospheric slabs to depths of at least 600–700 km. Nevertheless the processes are fundamentally a geochemical differentiation of the earth whereby low melting components become concentrated in the crust, and the mantle becomes increasingly refractory. The processes move towards a gravitationally and thermally stable layered earth.

It is necessary to examine and interpret the geological record to ascertain how far back in geological time the present pattern of geodynamics and geochemical evolution persists. The presence of linear orogenic belts, including metamorphic belts and ophiolite complexes, the occurrences of andesitic extrusives and intrusives and the characteristics of eugeosynclinal sedimentation provide evidence for existence of the island-arc type of environ-

ment throughout the Palaeozoic, extending back for at least one billion years. Similarly the presence of old tholeiitic basalt provinces and of old graben structures with intrusives of the alkali-basalt and olivine nephelinite suites or their low-pressure derivatives argues that the processes of basalt generation in the upper mantle were not substantially different in the Palaeozoic. Finally, palaeomagnetic data identify past continental configurations and demonstrate large relative horizontal movement of continental plates for the last one billion years.

THE ARCHAEAN CRUST

In the stable continental shield regions, the "mobile belts" (Anhaeusser et al., 1969) appear to have some similarities to orogenic belts of the Palaeozoic, but these transect older "cratons" or stable blocks which form the oldest ($2.5 \cdot 10^9$ year) identifiable units of the earth's crust now exposed at the surface. These regions, often referred to as granite–greenstone terrains, are well exposed and described from southern Africa, western Australia and northern Canada (Goodwin, 1968; Anhaeusser et al., 1969; Viljoen and Viljoen, 1969a; Glikson, 1970). These areas include irregularly arcuate or cuspate synclinal areas dominated by ultramafic, basic, and andesitic volcanics which occur within inhomogeneous granodioritic gneiss. Age relationships between the volcanics and the gneisses are not clear. The regional relationships suggest that the gneisses form a basement to the greenstone but there is evidence that intrusion and doming by gneissic acid intrusions is the major cause of the synclinal and arcuate form of the greenstones (Viljoen and Viljoen, 1969a). Later, clearly transgressive, intrusives range from granodiorite to potassic granites and the shield regions are also characteristically cut by basic to ultramafic dykes (including such major structures as the Great Dyke of Rhodesia). The greenstone belts in many areas have suffered only very low-grade metamorphism and preservation of primary minerals and structures (such as pillow structures, vesicles, etc.) is common. The mineral assemblages of the gneisses and granites are also not indicative of high-pressure conditions. Typical crustal seismic velocities extend to depths of 30–40 km. These regions appear to have been remarkably stable for $\geqslant 3$ b.y. with only thin and slightly deformed sediment veneers and without great elevation or extensive erosion. It appears probable that the granite–greenstone terrains of the continental shields represent processes of crust–mantle differentiation which are characteristic of an early stage of earth-evolution. This conclusion is further supported by the nature of the ultramafic and mafic magmas which form a major part of the greenstone sequences.

Viljoen and Viljoen (1969b) have presented convincing evidence for existence of ultramafic liquids, extruded as fluid magmas in an aqueous environment and forming the major rock type of the lowest units of the greenstone sequence in the Barberton area of South Africa. Viljoen and Viljoen (1969b) used the name peridotitic komatiite to refer to this distinctive volcanic rock. Rocks of apparently identical character occur in the green-

stone sequences of the Yilgarn shield in western Australia (Glikson, 1970; Nesbitt, 1971), and as intrusive sills in Archaean rocks in Canada (Naldrett and Mason, 1968). It has been shown experimentally (Green et al., in preparation) that the temperature of extrusion of the ultramafic liquid listed in Table I (49J) was at least 1600–1650°C. The magma was essentially anhydrous (containing $< 1\%$ H_2O) and is similar in major element composition to the "pyrolite" estimate for the present upper-mantle composition in the source regions for basalt magmas. The sample studied experimentally, unequivocally existed as a liquid at the earth's surface and was rapidly quenched giving the characteristic textures (which also have been reproduced in laboratory quenching studies). Other peridotitic magmas, which texture, mineralogy and field occurrence prove to have been entirely liquid, are also listed in Table I and are even closer to the "pyrolite" model composition. Experimental studies show that olivine (Fo_{93}) alone is on the liquidus of the peridotitic komatiite composition up to very high pressures ($\sim$ 40 kbar) and the principal differences (in 100 Mg/(Mg + Fe) and in pyroxene/olivine ratios) between the komatiite and pyrolite compositions are consistent with derivation of the komatiite by very high degree of melting (60–80%) of pyrolite leaving only olivine (Fo_{93}) as a residual phase. The peridotitic komatiite flows are overlain and interbedded with olivine and pyroxene-rich rocks which have been referred to as basaltic komatiites by Viljoen and Viljoen (1969c) or as high-magnesian basalts (Nesbitt, 1971). The chemical compositions of these basalt types are indicative for a genesis from more olivine-rich parents at low pressure. Their genesis may reflect olivine settling and extraction from parental peridotitic komatiite magma at or near the earth's surface or alternatively they may be direct partial melts (and thus with high Mg-values) of a pyrolite source rock with magma segregation occurring at very low pressures. For the latter mechanism, the degree of melting would be lower (up to 40% melting) than that required to develop peridotitic komatiite magmas.

The characteristics of the distinctive ultramafic and basic magmas of the Archaean greenstone belts are consistent with melting of a mantle of composition close to that of pyrolite (at least in major elements) but require conditions of melting differing greatly from those operating to yield modern basalts. The magma compositions, considered in relation to modern basalts and a pyrolite-like source composition, imply very rapid diapiric ascent of mantle-source rock and may also be indicative of a much steeper geothermal gradient in the upper 100–200 km. If such conditions were entirely caused by endogenous processes, then they imply that the earth up to 2.5 b.y. ago was evolving from a more primitive (higher temperature? more rapid and deeper convection?) state towards the present layered state. Archaean volcanism and crust formation, as exemplified in rocks of 2.5 – 3.5 b.y. old, would help establish constraints on early temperature and cooling history of the earth, time of core and crust formation, and ultimately on models of chemically homogeneous accretion vs. sequential accretion. One can state that study of Archaean volcanism requires that, if these rocks owe their characteristics entirely to processes and conditions existing within the earth, the dynamics and temperature distribution within the solid earth differed greatly from the present; yet the existence of a hydrosphere, some form of atmosphere and some

processes of erosion and sedimentation were already established.

However, the results of lunar studies, arising directly from the Apollo 11–15 moon landings, show that an alternative hypothesis (Green, in preparation) for the granite-greenstone terrains might be considered. Briefly stated, this hypothesis suggests that the ultramafic–mafic sequences of the "greenstone" areas are the equivalents of the lunar maria and the "granite" areas are the equivalents of the lunar highlands. Whereas these structures have been preserved for > 2.5 b.y. on the essentially rigid crust of a more rapidly cooling moon, they have been highly deformed, mobilized, re-intruded and metamorphosed by endogenous processes acting in the outer part of a more slowly cooling and highly mobile earth (Fig. 8). On the moon, the maria basins are considered to be of impact origin, the impacting bodies being extremely large at an early stage of the moon's history, but the maximum size of impacting bodies decreasing with time. The filling of the impact-produced depressions with lava flows produced by varying degrees of partial melting in the lunar interior (Ringwood and Essene, 1970) is a secondary process, probably consequent on uplift of the impact basin floor and diapirism in the lunar interior. Geochronological studies of lunar samples confirm an age of ~ 4. 6 b.y. for the moon as a whole but show that the ages of crystallization of individual igneous rocks range from 4.1 to 2.9 b.y. (Compston et al., 1971a,b).

The principal reasons which have led the author to suggest that the Archaean greenstone belts are deformed terrestrial equivalents of lunar maria may be summarized as follows:

(1) The extremely high temperature of the ultramafic and mafic magmas forming the lower part of the greenstone sequences and their origin by such very high degrees of melting of a peridotitic mantle, suggest more catastrophic and rapid magma genesis than is observed in endogenous processes of magma genesis in Tertiary and Recent volcanism. Major impact could provide such instantaneous triggering of deep mantle-melting (Fig. 8).

(2) The cuspate and irregular form of greenstone belts suggest inward and roughly radial collapse and encroachment of sialic rock-types on a deep, magma-filled basin rather than any similarity to linear orogens of eugeosynclinal or island arc sequences.

(3) The geochronology of lunar events show that major impacts occurred on the moon up to 3. 8 – 3. 9 b.y. ago and possibly younger, and filling of maria by volcanism occurred up to 2. 9 b.y. ago. The earth should have received similar or greater intensity of large impacts, at times synchronous with the formation of the Archaean granite – greenstone terranes. Such structures are unlikely to be preserved on the highly mobile earth's crust in the same manner as the lunar maria.

Finally, just as on the moon there are many impact craters which post-date the major maria, so one might look for similar-sized events on the earth's surface. Some larger lunar craters such as Tycho (70 km diameter) appear to have associated volcanism and Dietz (1964) has presented cogent arguments for an impact origin and impact-triggered magmatism for the Sudbury structure (40 km diameter, age 1. 7 b.y.). Dietz (1964, p.432) stated "My search for the terrestrial analogy of a lunar mare led me to Sudbury, as an example of a sufficiently large impact event on earth to trigger magmatism. In this context, the Sud-

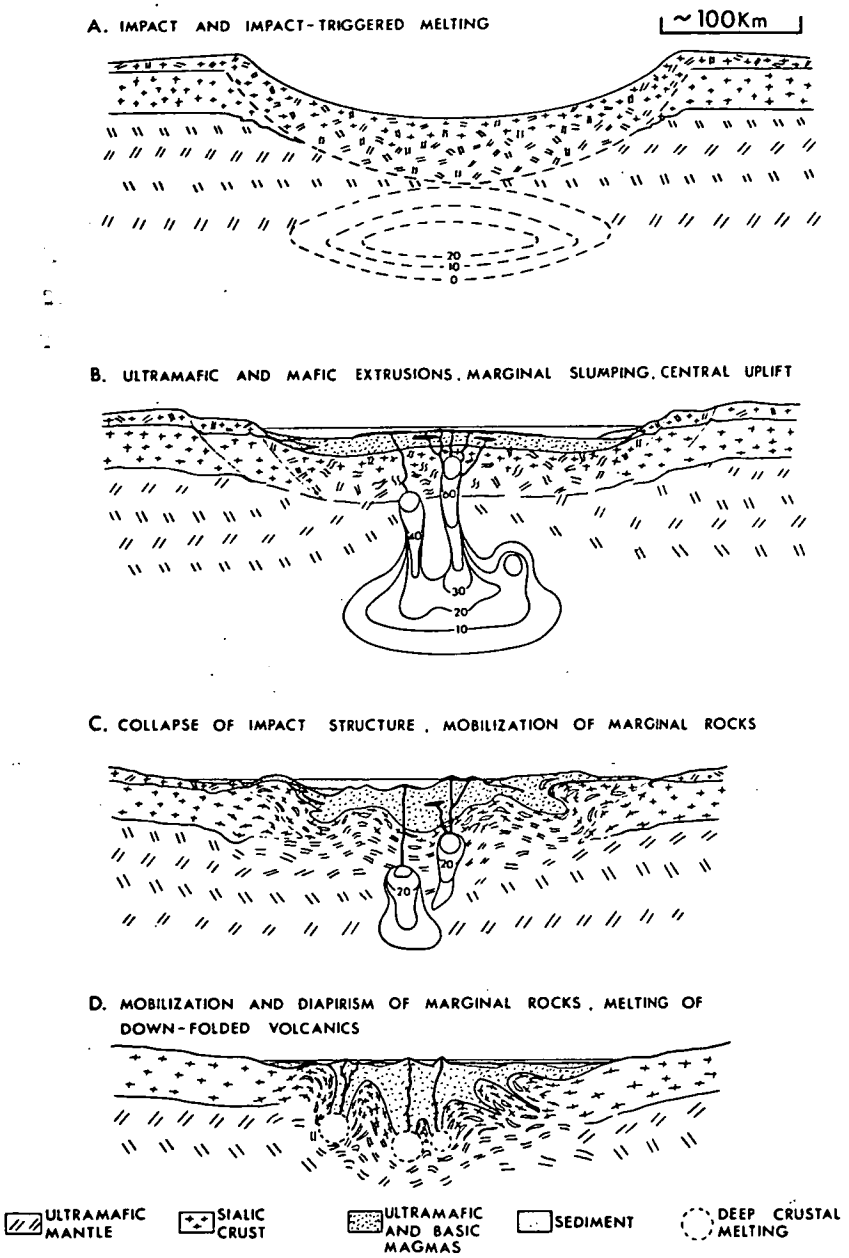

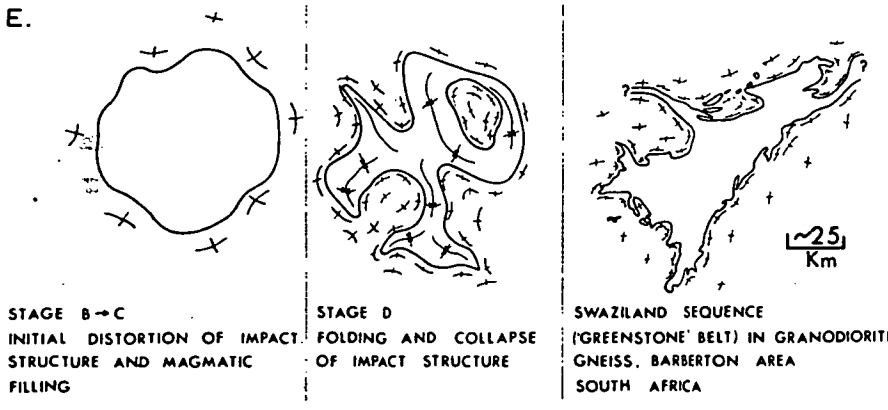

STAGE B→C
INITIAL DISTORTION OF IMPACT STRUCTURE AND MAGMATIC FILLING

STAGE D
FOLDING AND COLLAPSE OF IMPACT STRUCTURE

SWAZILAND SEQUENCE ('GREENSTONE' BELT) IN GRANODIORITIC GNEISS, BARBERTON AREA SOUTH AFRICA

bury structure may be the terrestrial analogue of a small lunar mare". The identification of other impact and possible impact structures on the shield regions is continuing. The "terrestrial maria" hypothesis suggests an even greater and more fundamental role for large exogenous impacting bodies in activating chemical differentiation of the mantle–crust system through the volcanism and evolutionary sequences of the Archaean greenstone belts (Fig. 8).

ACKNOWLEDGEMENTS

I wish to acknowledge the benefit of many discussions on the themes in this paper with W. Compston, A.E. Ringwood and A.J.R. White. I thank W. Hibberson for preparation of the diagrams.

REFERENCES

Anhaeusser, C.R., Mason, R., Viljoen, M.J. and Viljoen, R.P., 1969. A reappraisal of some aspects of Precambrian shield geology. *Geol. Soc. Am. Bull.*, 80: 2175–2200.

Armstrong, R.L., 1971. Isotopic and chemical constraints on models of magma genesis in volcanic arcs. *Earth Planet. Sci. Lett.*, 12: 137–142.

Bultitude, R.J. and Green, D.H., 1968. Experimental study at high pressures on the origin of olivine nephelinite and olivine melilite nephelinite magmas. *Earth Planet. Sci. Lett.*, 3: 325–337.

Burnham, C.W., 1967. Hydrothermal fluids at the magmatic stage. In: H.A. Barnes (Editor), *Geochemistry of Hydrothermal Ore Deposits.* Holt, Rinehart and Winston, New York, N.Y., pp. 34–76.

Cann, J.R., 1971. Major element variations in ocean-floor basalts. *Philos. Trans. R. Soc. Lond., Ser. A.*, 268: 495–505.

Carey, S.W., 1955. The orocline concept in geotectonics, I. *Pap. Proc. R. Soc. Tasmania*, 89: 255–288.

Carey, S.W., 1958. The tectonic approach to continental drift. In: *Continental Drift: a symposium.* Geol. Dep. Univ. Tasmania Publication, pp. 177–355.

Fig. 8. Diagram illustrating an hypothesis (Green, in preparation) in which the Archaean greenstone belts are suggested as terrestrial equivalents of lunar maria. (A) Primitive sialic crust impacted by very large body excavating large structure of ~ 30 km depth, floored with ejecta blanket overlying brecciated upper-mantle rocks. Instantaneous unloading (pressure drop) beneath the impact produces melting and dashed curves illustrate the degree of melting (at ~ 150 km depth). An extremely large negative gravity anomaly would be formed over the impact. (B) Partially melted peridotite rises rapidly into the brecciated impact floor with very great increase in degree of melting and extrusion of very high temperature ultramafic (1600°C) and basaltic magmas (komatiites). Some marginal slumping and sedimentation. (C) Accelerated inward collapse of impact structure, possibly influenced by regional crustal stresses, but mainly a consequence of increasing temperature and mobility of underlying and marginal mixed ejecta blanket. It is considered that the original crustal component (granitic?) of this would recrystallize, begin to partially melt and intrude or dome the overlying dense ultramafic and mafic lavas. Volcanism changes to more normal basaltic volcanism. (D) Dominant process is the infolding of the ultramafic and mafic volcanics accentuated by upward movement and intrusion of gneiss domes – the basement to the original ultramafic and mafic lava sequence becomes intrusive into that sequence. In the deeper regions, temperatures are sufficiently high to produce remelting (under $p_{H_2O} < p_{total}$ conditions) of mixed basaltic and "basement" materials, yielding a second stage of volcanism characterized by andesitic and dacitic magmas. (E) The "plan view" diagrams illustrate stages B – D and compares the model with the irregularly synclinal structure of a South African greenstone belt (Viljoen and Viljoen, 1969c).

Carey, S.W., 1970. Australia, New Guinea and Melanesia in the current revolution in concepts of the evolution of the earth. *Search*, 1: 178–189.

Carter, J.L., 1970. Mineralogy and chemistry of the earth's upper mantle based on the partial fusion-partial crystallization model. *Geol. Soc. Am. Bull.*, 81: 2021–2034.

Coleman, R.G., 1971. Plate tectonic emplacement of upper mantle peridotites along continental edges. *J. Geophys. Res.*, 76: 1212–1222.

Compston, W., Berry, H., Vernon, M.J., Chappell, B.W. and Kaye, M.J., 1971a. Rubidium-strontium chronology and chemistry of lunar material from the Ocean of Storms. *Proc. Lunar Sci. Conf.*, 2 nd, M.I.T. Press, Cambridge, Mass., 2: 1471–1486.

Compston, W., Vernon, M.J., Berry, H. and Rudowski, R., 1971b. The age of the Fra Mauro formation: a radiometric older limit. *Earth Planet. Sci. Lett.*, 12: 55–58.

Dietz, R.S., 1961. Continent and ocean basin evolution by spreading of the sea-floor. *Nature*, 190: 854–857.

Dietz, R.S., 1964. Sudbury structure as an astrobleme. *J. Geol.*, 72: 412–434.

Ernst, W.G., 1970. Tectonic contact between the Francisican melange and the Great Valley sequence: crustal expression of a late Mesozoic Benioff zone. *J. Geophys. Res.*, 75: 886–901.

Essene, E.J., Hensen, B.J. and Green, D.H., 1970. Experimental study of amphibolite and eclogite stability. *Phys. Earth Planet. Inter.*, 3: 378–384.

Gast, P.W., 1968. Trace element fractionation and the origin of tholeiitic and alkaline magma types. *Geochim. Cosmochim. Acta*, 32: 1057–1086.

Glikson, A.Y., 1970. Geosynclinal evolution and geochemical affinities of early Precambrian systems. *Tectonophysics*, 9: 397–433.

Goodwin, A.M., 1968. Archaean proto-continental growth and early crustal history of the Canadian shield. *Int. Geol. Congr., 23rd, Prague, 1968, Rep.*, 1: 68–89.

Green, D.H., 1970a. A review of experimental evidence on the origin of basaltic and nephelinitic magmas. *Phys. Earth Planet. Inter.*, 3: 221–235.

Green, D.H., 1970b. The origin of basaltic and nephelinitic magmas. *Trans. Leicester Lit. Philos. Soc.*, 64: 26–54.

Green, D.H., 1971. Compositions of basaltic magmas as indicators of conditions of origin: application to oceanic volcanism. *Philos. Trans. R. Soc. Lond., Ser. A*, 268: 707–725.

Green, D.H., in preparation. Archaean greenstone terrains: possible terrestrial equivalents of lunar maria.

Green, D.H. and Ringwood, A.E., 1963. Mineral assemblages in a model mantle composition. *J. Geophys. Res.*, 68: 937–945.

Green, D.H. and Ringwood, A.E., 1967a. The genesis of basaltic magmas. *Contrib. Mineral. Petrol.*, 15: 103–190.

Green, D.H. and Ringwood, A.E., 1967b. The stability fields of aluminous pyroxene peridotite and garnet peridotite and their relevance in upper mantle structure. *Earth Planet. Sci. Lett.*, 3: 151–160.

Green, D.H., Nicholls, I.A., Viljoen, M.H. and Viljoen, R.P., in preparation. Experimental study of extremely high temperature ultramafic volcanic extrusions.

Green, T.H., 1969. Experimental fractional crystallization of quartz diorite and its application to the problem of anorthosite origin. In: Y.W. Isachsen (Editor), *Origin of Anorthosite and Related Rocks.* Memoir 18 of New York State Museum and Science Service, pp. 23–30.

Green, T.H. and Ringwood, A.E., 1968. Genesis of the calc-alkaline igneous rock suite. *Contrib. Mineral. Petrol.*, 18: 105–162.

Green, T.H. and Ringwood, A.E., 1969. High pressure experimental studies on the origin of andesites. In: A.R. McBirney (Editor), *Proceedings of the Andesite Conference.* State of Oregon, Dept. of Geology and Mineral Industries Bull., 65: 21–32.

Hess, H.H., 1962. History of ocean basins. In: *Petrologic Studies: a Volume to Honour A.F. Buddington.* Geol. Soc. Am., New York, N.Y., pp. 599–620.

Hill, R.E.T. and Boettcher, A.L., 1970. Water in the earth's mantle: melting curves of basalt–water and basalt–water–carbon dioxide. *Science*, 167: 980–982.

Hutchison, R., Paul, D.K. and Harris, P.G., 1970. Chemical composition of the upper mantle. *Mineral. Mag.*, 37: 726–729.

Isacks, B., Oliver, J. and Sykes, L.R., 1968. Seismology and the new global tectonics. *J. Geophys. Res.*, 73: 5855–5900.

Ito, K. and Kennedy, G.C., 1968. Melting and phase relations in a natural peridotite to 40 kilobars. *Am. J. Sci.*, 265: 519–538.

Jakes, P. and White, A.J.R., 1971. Compositions of island arcs and continental growth. *Earth Planet. Sci. Lett.*, 12: 224–230.

James, D.E., 1971. Andean crustal and upper mantle structure. *J. Geophys. Res.*, 76: 3246–3271.

Karig, D.E., 1971. Origin and development of marginal basins in the Western Pacific. *J. Geophys. Res.*, 76: 2542–2561.

Kleeman, J.D. and Cooper, J.A., 1970. Geochemical evidence for the origin of some ultramafic inclusions from Victorian basanites. *Phys. Earth Planet. Inter.*, 3: 302–308.

Kushiro, I., Syono, Y. and Akimoto, S., 1968. Melting of a peridotite nodule at high pressures and high water pressures. *J. Geophys. Res.*, 73: 6023–6029.

Lambert, I.B. and Wyllie, P.J., 1968. Stability of hornblende and a model for the low velocity zone. *Nature*, 219: 1240–1241.

Leggo, P.J. and Hutchison, R., 1968. Rb–Sr study of ultrabasic xenoliths and their basaltic host rocks from the Massif Centrale, France. *Earth Planet. Sci. Lett.*, 5: 71–77.

Le Pichon, X., 1968. Sea-floor spreading and continental drift. *J. Geophys. Res.*, 73: 3661–3697.

McKenzie, D.P., 1969. Speculations on the consequences and causes of plate motions. *Geophys. J.*, 18: 1–32.

Minear, J.W. and Toksöz, M.N., 1970. Thermal regions of a downgoing slab and the new global tectonics. *J. Geophys. Res.*, 75: 1397–1420.

Miyashiro, A., 1961. Evolution of metamorphic belts. *J. Petrol.*, 2: 277.

Miyashiro, A., Shido, F. and Ewing, M., 1969. Diversity and origin of abyssal tholeiite from the Mid-Atlantic Ridge near 24° and 38° north latitude. *Contrib. Mineral. Petrol.*, 23: 38-52.

Naldrett, A.J. and Mason, G.D., 1968. Contrasting Archaean ultramafic igneous bodies in Dundonald and Clergue Townships, Ontario. *Can. J. Earth Sci.*, 5: 111–142

Nesbitt, R.W., 1971. Skeletal crystal forms in the ultramafic rocks of the Yilgarn block, Western Australia; evidence for an Archaean ultramafic liquid. *Geol. Soc. Aust., Spec. Publ.*, 3, in press.

Nicholls, G.D., 1967. Geochemical studies in the ocean as evidence for the composition of the mantle. In S.K. Runcorn (Editor), *Mantles of the Earth and Terrestrial Planets.* Interscience, New York, N.Y., pp. 285–304.

Oxburgh, E.R. and Turcotte, D.L., 1970. The thermal structure of island arcs. *Geol. Soc. Am. Bull.*, 81: 1665–1688.

Ringwood, A.E., 1966. The chemical composition and origin of the Earth. In: P.M. Hurley (Editor), *Mineralogy of the Mantle.* M.I.T. Press Cambridge, Mass., pp. 287–356.

Ringwood, A.E., 1969. Composition and evolution of the upper mantle. In: P.J. Hart (Editor), *The Earth's Crust and Upper Mantle – Geophys. Monogr. 13.* Am. Geophys. Union, Washington, D.C., pp. 1–17.

Ringwood, A.E., 1971. Phase transformations and mantle dynamics. *Aust. Natl. Univ., Dep. Geophys. Geochem., Publ.*, 999, preprint.

Ringwood, A.E. and Essene, E.J., 1970. Petrogenesis of Apollo 11 basalts, internal constitution and origin of the moon. In: A.A. Levinson (Editor), *Proc. Apollo 11 Lunar Science Conference.* Pergamon Press, London, 1: 769–799.

Ringwood, A.E. and Green, D.H., 1966. An experimental investigation of the gabbro-eclogite transformation and some geophysical consequences. *Tectonophysics*, 3: 383–427.

Viljoen, M.J. and Viljoen, R.P., 1969a. An introduction to the geology of the Barberton granite-greenstone terrain. In: *Upper Mantle Project. Geol. Soc. S. Afr., Spec. Publ.*, 2: 9–28.

Viljoen, M.J. and Viljoen, R.P., 1969b. Evidence for the existence of a mobile extrusive peridotitic magma from the Komati Formation of the Onverwacht Group. In: *Upper Mantle Project. Geol. Soc. S. Afr., Spec. Publ.*, 2: 87–112.

Viljoen, M.J. and Viljoen, R.P., 1969c. The geology and geochemistry of the lower ultramafic unit of the Onverwacht Group and a proposed new class of igneous rock. In: *Upper Mantle Project. Geol. Soc. S. Afr. Spec. Publ.*, 2: 55–85.

Vine, F.J. and Matthews, D.H., 1963. Magnetic Anomalies over oceanic ridges. *Nature*, 199: 947–949.

Wyllie, P.J., 1971. Role of water in magma generation and initiation of diapiric uprise in the mantle. *J. Geophys. Res.*, 76: 1328–1338.

B17

EARTH AND PLANETARY SCIENCE LETTERS 17 (1973) 456–465. NORTH-HOLLAND PUBLISHING COMPANY

4

CONDITIONS OF MELTING OF BASANITE MAGMA FROM GARNET PERIDOTITE

D.H. GREEN
Department of Geophysics and Geochemistry, Australian National University, Canberra, A.C.T., Australia

Received 15 August 1972
Revised version received 27 October 1972

Experimental studies have been carried out at high pressures and temperatures, to determine the crystallization behaviour of olivine-rich basanite composition with various known water contents. Between 25 kbar and 30 kbar, in the temperature range from 1200°C to 1300°C and with water contents in the magma from 2% to 7% H_2O, the olivine basanite has orthopyroxene, garnet, clinopyroxene and olivine on or near the liquidus. There is, at these conditions, a fractionation trend from higher-temperature olivine-rich basanite to lower-temperature olivine nephelinite produced by progressive crystallization (or, with increasing temperature, progressive melting) of the phases orthopyroxene, garnet, clinopyroxene and olivine. The analyzed compositions of near-liquidus phases in the olivine-rich basanite are closely similar to the residual phases present in pyrolite (+ 0.2% H_2O) in a partially melted run at ~ 30 kbar, 1250°C. The data are consistent with a specific model in which partial melting of pyrolite + (0.2–0.4)% H_2O at 30 kbar, 1250°C yields 6% olivine-rich basanite magma. The residual peridotite contains 60% olivine, 18% orthopyroxene, 14% clinopyroxene and 18% garnet. It is concluded that magmas present in the low velocity zone are highly undersaturated and nephelinerich (olivine nephelinites to olivine melilitites).

1. Introduction

A recent controversy has arisen over the nature of the liquid formed by partial melting of hydrous peridotitic compositions at upper mantle pressures. The controversy arises directly from the results and interpretation of experimental studies. One approach, based mainly on study of high pressure melting relations in simple systems such as enstatite–water [1], diopside–forsterite–silica–water [2], and nepheline–forsterite–silica–$CaAl_2SiO_6$–water [3], has demonstrated an expansion of the liquidus field of olivine with increasing water pressures. This led to the prediction that liquids derived by partial melting of peridotite (i.e., in equilibrium with residual olivine) with $P_{H_2O} = P_{Total}$ (excess water) would be oversaturated in silica [1–5]. It was suggested that such liquids would be andesitic or quartz tholeiitic in character. Thus, the liquid present in the low velocity zone of the mantle, and in the regions of anomalously low seismic velocity and high seismic attenuation beneath island arcs, was inferred to be of andesitic or quartz tholeiitic character. Apparent confirmation of this hypothesis is provided by direct partial melting of a peridotite composition under water-saturated conditions at 20–26 kbar [5]. With conditions such that ~ 20% melting occurred, it was found that the composition of glass in the experimental run was very rich in silica, alumina and lime – very broadly andesitic or dacitic in character. I have obtained similar results by partial melting of a model mantle peridotite (pyrolite) composition at 20 kbar, but have demonstrated that the siliceous and aluminous glasses formed are metastable products modified by the quench crystallization of olivine, clinopyroxene, amphibole and mica during rapid cooling of the original equilibrium melt phase in the experimental runs [18].

Further critical testing of the hypothesis of derivation of andesite by wet melting of peridotite has confirmed the reality and very great importance of the expansion of the liquidus field for olivine in tholeiitic basalts under high water pressures. Nicholls and Ringwood [6] have shown that quartz tholeiitic basalt (but not andesite) may be in equilibrium with residual peridotite mineralogy (olivine, orthopyroxene, clinopyroxene) from 10 kbar to almost 20 kbar, provided the water content of the magma is greater than 5% (10 kbar) to 15% (~ 17 kbar).

These experiments, together with preliminary experiments at 22.5 kbar [7] show that quartz normative basalts, andesites or dacites do not have olivine as a liquidus phase (i.e., cannot be derived by equilibrium partial melting of a peridotitic mantle) at pressures >20 kbar (depths >70 km) even under water-saturated conditions.

The other side of the controversy has grown from experiments on the high pressure melting behaviour of olivine tholeiite, alkali basalt [8–10], basanite and olivine nephelinite compositions [11, 12] in which an expansion of the liquidus field of orthopyroxene into nepheline-rich compositions was reported at pressures in excess of 10 kbar under conditions of low water contents ($P_{H_2O} < P_{Total}$). Since orthopyroxene and olivine (± clinopyroxene ± garnet) were liquidus phases of olivine-rich basanite and olivine nephelinite magmas when the liquidus was depressed by the addition of water, it was inferred that these highly silica-undersaturated magmas could be direct partial melts of upper mantle peridotite provided the mantle contained small ($<0.5\%$) water contents and the degree of partial melting of the source region was small. Early criticism of the experimental methods suggesting compositional change of the sample was answered by preliminary reporting of experiments in sealed capsules and by electron micropole analysis of the bulk charge after experiments [12].

The present paper details the confirmation of the role of orthopyroxene as a liquidus phase of a nepheline-rich basanite in the presence of known water contents of the magma, compares the composition of the liquidus phases of the basanite with the compositions of residual phases in the model pyrolite composition at similar P, T conditions and leads to firm specification of the conditions of origin of olivine-rich basanite in the Earth's mantle. The paper is a critical testing of one 'pigeon-hole' in the petrogenetic grid for mantle-derived magmas presented previously [7, 13] as a working hypothesis for the petrogenesis of basaltic magmas (of the non-orogenic magmatic associations).

2. Experimental methods

2.1. *Selection of basanite*

The basanite used in the experimental study was collected from Mt. Leura, Western Victoria, and is from the Quaternary Newer Volcanics. The scoria cone from which the basanite was collected contains abundant lherzolite xenoliths, minor high-pressure pyroxenite and garnet pyroxenite xenoliths and moderately common xenocrysts of aluminous pyroxenes. The characteristics of these xenoliths establish that this magma contains included fragments of upper mantle rock types and thus has not suffered compositional change by crystal fractionation at depths $<30-40$ km (10 kbar) [7, 9, 10]. The sampled basanite was from a more massive block within the scoria. It is fine-grained, vesicular, with small zoned olivine and rare zoned clinopyroxene phenocrysts in a fine-grained groundmass including plagioclase laths, ilmenite, clinopyroxene, olivine, nepheline and glass. In selecting chips for analysis, care was taken to exclude xenoliths or xenocrysts – this may have also led to exclusion of some phenocrystal olivine. The basanite as analyzed (table 1) contained 18% normative olivine whereas previous experiments [11, 12] had led to the inference that magmas of direct mantle derivation at 25–30 kbar should contain ~25% normative olivine. It was reasoned that a primary basanite, if derived at 25–30 kbar, could have dropped olivine prior to picking up mantle xenoliths at 10–20 kbar and then rapidly moving to the surface. Thus 10% olivine (Fo_{90}) was added to the basanite before melting to the glass used in experimental runs. The composition of the glass (analysed for Fe_2O_3, FeO used in the experiments is given in table 1. Microprobe analysis of several different batches of glass confirmed this composition. The normative composition shows high normative nepheline and olivine – it may be described as an olivine-rich basanite.

2.2. *Pyrolite composition*

The model pyrolite composition [14] (see table 5) contains $>50\%$ olivine in all subsolidus high pressure mineral assemblages. To facilitate the study of both subsolidus and melting relations, experiments were carried out on a composition [15] which is that of pyrolite less 40% olivine ($Mg_{91.6}Fe_{8.1}Ni_{0.2}Mn_{0.1}$). Provided olivine always remains as an equilibrium phase, the results on the (pyrolite–40% olivine) composition are directly applicable to pyrolite except that the composition and proportion of olivine present must be modified by calculating the effect of adding olivine

Table 1
Compositions and CIPW norms of natural basanite from Mt. Leura, Camperdown, Victoria (column 1), theoretical composition after addition of analyzed olivine (column 2) and analyzed composition of glass used in experiments (column 3). Also listed (column 4), is the composition of the liquid calculated after extraction of 10% orthopyroxene + 1% olivine from the basanite. These are estimated proportions of phases in the run at 1250°C, 27 kbar illustrated in fig. 2 and the compositions used in the calculations are those analyzed from this experiment. The analyzed compositions of the glass (using both the ARL electron probe and the new TNO instrument) are given in columns 5 and 6. The high Fe content in the ARL analysis is probably in error and the low Na_2O content may be an effect of volatilization by the electron beam although a defocussed 50 μ beam was used. All analyses are calculated to anhydrous compositions; the glass in the experimental run actually contains a high water and CO_2 content.

	Basanite 2650	Olivine-rich basanite 2650+10% olivine (Fo_{90})	Prepared glass for experiments	Column 3 less (10% orthopyroxene + 1% olivine)	Averaged glass composition	
					TNO probe	ARL probe
	1	2	3	4	5	6
SiO_2	45.0	44.6	44.7	43.5	43.7	43.1
TiO_2	3.2	2.9	2.9	3.2	3.1	3.2
Al_2O_3	13.0	11.7	11.7	12.6	13.6	11.6
Fe_2O_3	3.3	3.0	1.8	2.0 } 12.4	–	
FeO	9.3	9.4	10.5	10.6	12.3	14.6
MnO	0.2	0.15	0.15	0.15	–	0.2
MgO	9.9	13.9	13.9	11.8	11.5	12.6
CaO	8.5	7.7	7.7	8.4	8.2	8.2
Na_2O	4.1	3.65	3.65	4.1	4.3	3.3
K_2O	2.2	2.0	2.0	2.2	2.3	2.2
P_2O_5	1.1	1.0	1.0	1.1	0.9	(1.0)
Cr_2O_3	0.05	0.05	–	–	–	–
NiO	0.05	0.08	–	–	–	–
$\frac{100Mg}{Mg+Fe^{2+}}$	65.5	72.5	70	66.5	–	–
$\frac{100Mg}{Mg+Fe_{Tot}}$	59	67	67	63	62.5	60.5
CIPW Norm						
Or	13.0	11.8	11.8	13.0	13.6	12.9
Ab	14.5	12.8	11.5	7.1	3.4	3.8
An	10.6	9.6	9.6	9.5	11.0	10.5
Ne	11.0	9.8	10.5	15.0	17.9	12.9
Di	19.6	17.6	17.7	20.2	19.4	19.5
Ol	17.8	26.2	28.4	23.5	26.7	32.0
Ilm	6.1	5.5	5.5	6.1	5.9	6.0
Mt	4.8	4.3	2.6	2.9	–	–
Ap	2.6	2.4	2.4	2.6	2.1	2.4
Chr	0.1	0.1				

as above. This also may cause small compositional shifts in $100Mg/Mg+Fe^{2+}$ value in co-existing phases in equilibrium with the olivine.

2.3. *Experimental techniques*

Experiments were carried out in a piston-cylinder apparatus. Samples were sealed in silver-palladium ($Ag_{75}Pd_{25}$ to ~1200°C at 27 kbar, $Ag_{50}Pd_{50}$ to ~1300°C at 27 kbar) capsules or Pt capsules at higher temperatures. The desired water content (using 10–15 mg samples) was added to the capsule by microsyringe and its retention checked by weighing before and after welding of the capsule. For every small quantities of water (<2%) the weighing error for 10–15 mg charges for this method is prohibitively large. For such

conditions, particularly for the melting studies [(pyrolite –40% olivine) + 0.3% H_2O] a starting mix was prepared in which the desired water content was reacted into a 100-mg sample (large capacity run) at 15 kbar, 1000°C. This yielded a subsolidus mineral assemblage dominantly of olivine + enstatite + amphibole with the bulk composition containing the desired water content. The solidus and melting relations were determined using this starting material.

Results are also presented for a run in which basanite glass was placed in a graphite capsule together with approximately 20% H_2O. The sample could not be sealed so that the water (and CO_2, CO, C) content of the charge was not fixed. Nevertheless, several runs using this technique produced beautifully quenched charges (see fig. 2) in which primary crystals occurred in glass without any nucleation or outgrowth of quench phases. Because of the nature of these rather fortuitous runs, it has been possible to analyze both primary crystals and co-existing nepheline-rich glass. In contrast, quenching of sealed samples with known water contents in Ag–Pd or Pt capsules always produced mixtures of large primary crystals together with quench clinopyroxene, amphibole, biotite and metastable residual glass.

2.4. *Microprobe analyses*

Most microprobe analyses reported in this paper were carried out using an electron probe produced by Technisch Physische Dienst, Delft Technical University, Delft, The Netherlands. This more recent version of the instrument described by Fontijn et al. [17], uses a Li-drifted Silicon detector (Ortec type 77016-041655) for quantitative X-ray analysis. This detector has an active area of 12.6 mm^2 and an 8-micron thick Be window. The detector is placed 7.5 cm from the specimen. Spectra were recorded with 100-sec counting time on a Northern Scientific (NS 710) multichannel pulse height analyser at a count rate of around 4000 counts per sec. Peak intensities were measured by summing counts over 100–140 eV bands for each peak. Resolution of the energy spectrum is such that the full width at half maximum of the MnK_α peak is about 170 eV and the Na, Mg, Al and SiK_α peaks were well-resolved.

The analytical conditions employed an electron beam-accelerating voltage of 15 kV, a probe diameter of < 1 micron and a probe current of 3 nanoamps (compared with 30–50 nanoamps for analyses with the ARL microprobe). The instrument allowed the quantitative analysis for 11 elements (Na, Mg, Al, Si, P, K, Ca, Ti, Cr, Mn, Fe) simultaneously at each point. The analyzed volume was about 5 cubic microns. The instrument is ideal for the fine grain size and possible quench zoning of phases in experimental runs, and the problems of returning to the same analysis point, or of surface damage with repetitive analysis for different elements, or of high specimen currents, in earlier use of the ARL microprobe, are avoided.

The correction procedures for quantitative analysis using the instrument will be fully described by S.J.B. Reed and N.G. Ware. Analyses of minerals of known composition permit the estimation of accuracy of analysis as ± 2% relative at concentration levels above 10 weight percent for all elements except Na. Most Na analyses were in the concentration range 1–5 weight percent and the estimated error is from ± 0.2 weight percent at the lower end of this range to ± 0.5 weight percent at higher levels. The lower accuracy for Na results from uncertainty in background correction and interference from the tail of the Mg-peak. The limit of detection is 0.1 weight percent for K to Fe and 0.2% for Na, Mg, Al, Si and P.

3. Experimental results

The phases olivine, clinopyroxene, orthopyroxene, garnet, biotite, amphibole and ilmenite all appear in the melting interval of the basanite for various water contents, at pressures between 1 atmosphere and 36 kbar. The detailed study of the stability fields and compositional variations in these phases will be reported elsewhere as these data bear on the possible fractionation trends for hydrous basanite magmas under upper mantle conditions. In this paper, only the nature of the liquidus phases for various water contents will be discussed and these data are summarized in fig. 1. Increasing water content slightly expands the field of olivine to higher pressures but this effect is minor in this composition compared to the effect in tholeiitic compositions [6]. At pressures around 25 kbar, the field of clinopyroxene (aluminous and with low calcium content [11]) as a liquidus phase, either alone or together with olivine, is replaced at lower temperatures by a small field in which orthopyroxene, ± clinopyroxene, + olivine

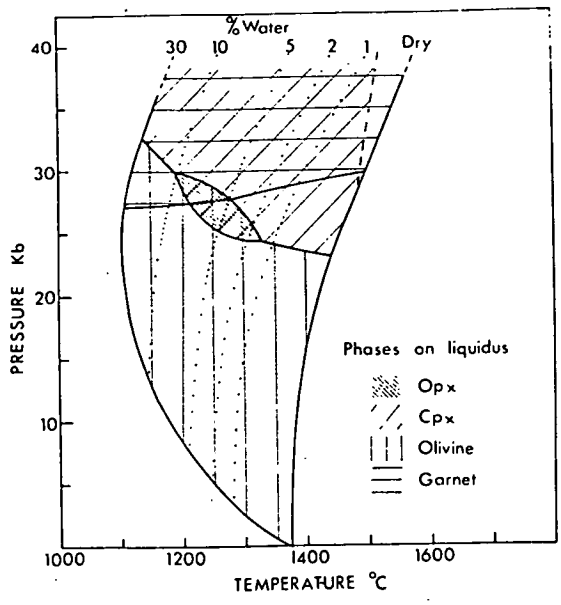

Fig. 1. With increasing water content in the basanite glass its liquidus moves from the anhydrous liquidus to the water-saturated liquidus. The positions of the liquidi for 1, 2, 5 and 10% water are shown – although well located in the 20–30 kbar pressure interval, they are approximate only at lower pressure. The diagram illustrates the nature of the liquidus phases at a given pressure temperature and water content. The restricted field in which orthopyroxene occurs on or near the liquidus is the most noteworthy feature of this diagram.

or (at higher pressure) orthopyroxene, garnet, ± clinopyroxene, ± olivine occur on or very close to the liquidus. Experimental results for a few key runs in this field are given in table 2. Within the small field in which orthopyroxene is a near-liquidus phase, olivine is the coexisting phase at lower pressures (and lower water contents, high temperatures) and is joined by clinopyroxene either at the liquidus or at slightly lower temperatures. For a given water content, clinopyroxene increases in abundance below the liquidus and orthopyroxene reacts out. A similar effect is present at higher pressures (e.g., 29 kbar, 6% H_2O) where orthopyroxene and garnet are liquidus phases but at lower temperatures the orthopyroxene reacts with liquid and is replaced by increasing clinopyroxene, + garnet ± olivine (see table 2). In one run (table 2) at 29 kbar, 1240°C, 6% H_2O part of the charge consisted of a near-liquidus assemblage of orthopyroxene (100 Mg/Mg+Fe = 84.9) and garnet (100 Mg/Mg+Fe = 73.5) with quench but the majority of the run was garnet ($Mg_{69.5}$) + clinopyroxene (Mg_{82}) (table 2 with the greater abundance and more Fe-rich character of these phases implying a higher degree of crystallization. This observation may be explained by a temperature gradient within the charge or inhomogeneity in distribution of water through the sample.

Use of Ag–Pd capsules prevented iron loss to the sample capsule so that the Mg-values (100 Mg/Mg+Fe^{2+}) of the phases crystallizing are a reliable indication of the degree of crystallization. The most magnesian orthopyroxene (apart from orthopyroxene in runs in Pt capsules – see table 2) is Mg_{88} occurring with olivine, on the liquidus, at 27 kbar, 1250°C, 5% H_2O. A run at nominally the same conditions yielded olivine, orthopyroxene ($Mg_{86.1}$) and clinopyroxene while garnet appeared at 1240°C, coexisting with more Fe-rich enstatite ($Mg_{85.6}$). The most Fe-rich orthopyroxene ($Mg_{84.8}$) observed in the experiments occurs in the 29 kbar, 1220°C, 6% H_2O run and coexists with olivine, clinopyroxene and garnet.

The compositions of pyroxenes in table 1 provide further data on the pyroxene miscibility gap. Orthopyroxene with ~2% CaO and clinopyroxene with 13–15% CaO (Mg_{83} – Mg_{85}) are in equilibrium at 1220–1270°C – these compositions lie towards the high-Mg and low-Ca end of the range of compositions of natural high pressure pyroxene phenocrysts occurring in undersaturated magmas.

Table 3 lists the compositions of olivine, orthopyroxene, dinopyroxene and garnet coexisting in a run on (pyrolite–40% olivine) composition at 30 kbar, 1250°C in the presence of 0.3% H_2O. At these conditions there is sufficient melting to eliminate phologopite and ilmenite (both present below 1200°C at 30 kbar) but the composition or proportion of melt phase cannot be determined directly from the experimental run. While the composition of the melt cannot be directly analyzed we do know that the melt is in equilibrium with the phases olivine, orthopyroxene, clinopyroxene and garnet and we know the compositions of each of these solid solutions, particularly in terms of 100 Mg/Mg + Fe, Al_2O_3 in pyroxene, Na and Ca contents of pyroxene, Cr_2O_3 and TiO_2 contents of pyroxenes and garnets. Given the compositions in table 3 we may predict that the compositions of crystals in pyrolite + 0.2% H_2O (i.e., 40% olivine $Mg_{91.6}$ added to the residual minerals) at 1250°C, 30 kbar would be slightly more magnesian (Mg_{89-90} rather than Mg_{87-88}) than those of table 3 but in other respects would be almost identical.

Table 2
Compositions of coexisting mineral phases near the liquidus of basanite at various pressures and for various water contents.

Run conditions	29 kbar, 1260°C, 6% H_2O			29 kbar, 1220°C, 6% H_2O				29 kbar, 1240°C, 6% H_2O*		27 kbar, 1250°C, 5% H_2O			27 kbar, 1240°C 5% H_2O				27 kbar, 1250°C, 4.5% H_2O	25 kbar, 1300°C, 2% H_2O	
Sample capsule	$Ag_{50}Pd_{50}$			$Ag_{50}Pd_{50}$				$Ag_{50}Pd_{50}$		$Ag_{50}Pd_{50}$			$Ag_{50}Pd_{50}$				$Ag_{50}Pd_{50}$	Pt	
Phase	Opx	Ga	Cpx**	Opx	Ga	Cpx	01	Ga	Cpx	Opx	Cpx	01	Opx	Cpx	Ga	01	Opx	Opx	Cpx
SiO_2	55.1	41.8	53.4	54.4	42.1	53.7	39.9	42.7	54.2	53.5	52.3	40.1	55.3	54.1	42.8	40.7	55.7	56.3	51.5
TiO_2	0.2	0.7	0.7	0.2	1.2	0.4	–	1.1	0.6	0.3	1.0	–	0.2	0.5	0.9	–	0.3	0.4	1.0
Al_2O_3	4.1	23.0	6.4	5.6	22.5	5.4	–	24.0	5.8	6.1	7.3	–	4.2	5.8	23.1	0.2	4.7	6.6	9.4
Cr_2O_3	–	0.3	–	–	0.2	0.2	–	0.2	0.2	0.2	0.3	–	–	0.1	0.5	–	0.2	–	0.2
FeO	8.5	9.5	6.3	8.8	10.7	6.1	15.7	11.6	6.5	8.0	5.5	13.1	8.8	6.3	9.7	14.0	7.4	5.1	3.4
MnO	–	0.2	–	–	0.3	–	–	0.3	–	–	–	–	–	–	0.1	–			
MgO	29.2	18.7	17.7	27.6	18.1	18.3	43.2	14.7	16.6	27.7	17.2	45.6	29.3	18.5	19.0	45.1	30.3	31.3	19.0
CaO	2.0	5.8	13.8	2.2	6.9	14.1	0.2	5.6	15.2	2.6†	14.5	0.1	2.3	13.7	6.1	0.2	2.1	2.3	13.4
Na_2O	0.2	–	1.9	0.2	–	1.6	–	–	2.2	0.3	1.7	–	0.2	1.6	–	–	0.1	0.3	1.9
Mol. proportions																			
100Mg/Mg+Fe	86.0	77.7	83.3	84.8	75.3	84.1	83.0	69.5	82.0	86.1	84.8	86.1	85.6	83.9	77.8	85.4	88.0	91.7	91.0
Ca	4.1	14.7	31.8	4.6	17.0	31.8		15.9	35.0	5.4	33.9		4.5	30.8	15.4		4.1	4.7	31.4
Mg	82.5	66.4	56.8	80.9	62.4	57.4		58.3	53.3	81.4	56.0		81.7	58.1	65.9		84.3	87.4	62.4
Fe	13.4	18.9	11.4	14.5	20.6	10.8		25.8	11.7	13.2	10.1		13.8	11.1	18.7		11.6	7.9	6.2

* Part of this run contains orthopyroxene and garnet in quench; the orthopyroxene and garnet are very similar to those in the 1260°C, 29 kbar run. Most of the run consists of the more Fe-rich garnet and clinopyroxene listed in this table, implying a greater degree of crystallization.

** The low 100 Mg/Mg + Fe ratio and higher Al_2O_3 content suggest that this analyzed area may have included some quench clinopyroxene.

† CaO content too high, analysis is of thin orthopyroxene rimmed by clinopyroxene.

Table 3
Compositions of coexisting mineral phases crystallized from the (pyrolite – 40% olivine) composition at 30 kbar, 1250°C with the presence of 0.3 ± 0.1% H_2O in the sample. Raw analyses totalled 102.5 – 103% due to incorrect specimen current; they have been recalculated to 100%.

	Orthopyroxene	Clinopyroxene	Garnet*	Olivine**
SiO_2	55.5	53.6	40.8	44.5
TiO_2	0.5	0.9	1.4	0.1
Al_2O_3	3.4	4.9	20.8	1.6
Cr_2O_3	0.6	1.2	1.8	–
FeO	7.1	4.6	9.0	10.7
MnO	–	–	0.2	–
MgO	31.0	17.8	20.2	42.9
CaO	1.7	15.1	5.8	0.5
Na_2O	0.2	1.9	–	–
100Mg/Mg+Fe	88.5	87.4	< 80.0	87.8
Ca	3.3	34.8	14.1	
Mg	85.7	56.0	68.8	
Fe	11.0	8.2	17.1	

* Calculation of structural formula suggests that the garnet analysis contains a small admixture of olivine.
** Olivine grains were < 5μ and thus analysis reflects admixture of orthopyroxene.

Table 4
Composition of residual liquid (column 1) after crystallization of 10% orthopyroxene + 8% garnet + 5% clinopyroxene + 2% olivine (Extract of column 2) from the basanite in table 1, column 3. The compositions of phases used are those analyzed at 29 kbar, 1220°C (table 2).

	Residual liquid 1	Crystal extract 2
SiO_2	43.1	48.6
TiO_2	3.7	0.6
Al_2O_3	12.1	10.5
Fe_2O_3	2.4 } 12.9	0.1
FeO	10.8 }	9.5
MnO	0.1	0.1
MgO	10.6	24.0
CaO	8.3	5.9
Na_2O	4.7	0.4
K_2O	2.7	–
P_2O_5	1.3	–
	99.8	–
100Mg/Mg+Fe^{2+}	63.9	82.0
Or	16.0	–
Ab	4.4	3.4
An	4.0	26.9
Ne	19.2	–
Di	23.2	1.9
01	19,6	23.2
Ilm	7.0	1.1
Mt	3.5	0.2
Ap	3.1	–
		Hy 43.3

Table 1 contains calculated compositions of liquids in equilibrium with olivine and orthopyroxene. Because of the nature of the well-quenched run (fig. 2), the estimate of 10% orthopyroxene + 1% olivine crystallization can be checked against the actual analysis of the glass (table 1). The data demonstrate that liquids with higher Ne/Ab, approaching olivine nephelinites, can be in equilibrium with olivine and orthopyroxene. In the second example (table 4), the composition of residual liquid, coexisting with olivine, orthopyroxene, clinopyroxene and garnet, is also close to olivine nephelinite. The compositions of these phase crystallizing from the basanite are more Fe-rich than the equivalent phases in the pyrolite at similar P, T conditions but it is a small extrapolation to state that liquids with normative compositions closely similar to those in columns 5, 6 (table 1) or column 2 (table 4) but with 100Mg/Mg + Fe^{2+} = 68 – 70 could be in equilibrium with residual pyrolite mineralogy.

4. Conditions of genesis of basanite and olivine nephelinite magmas

The experiments described demonstrate that at pressures of 25 – 30 kbar, temperatures of 1200–1300°C and with water contents in magmas of about 2 – 7%,

Mem: 33

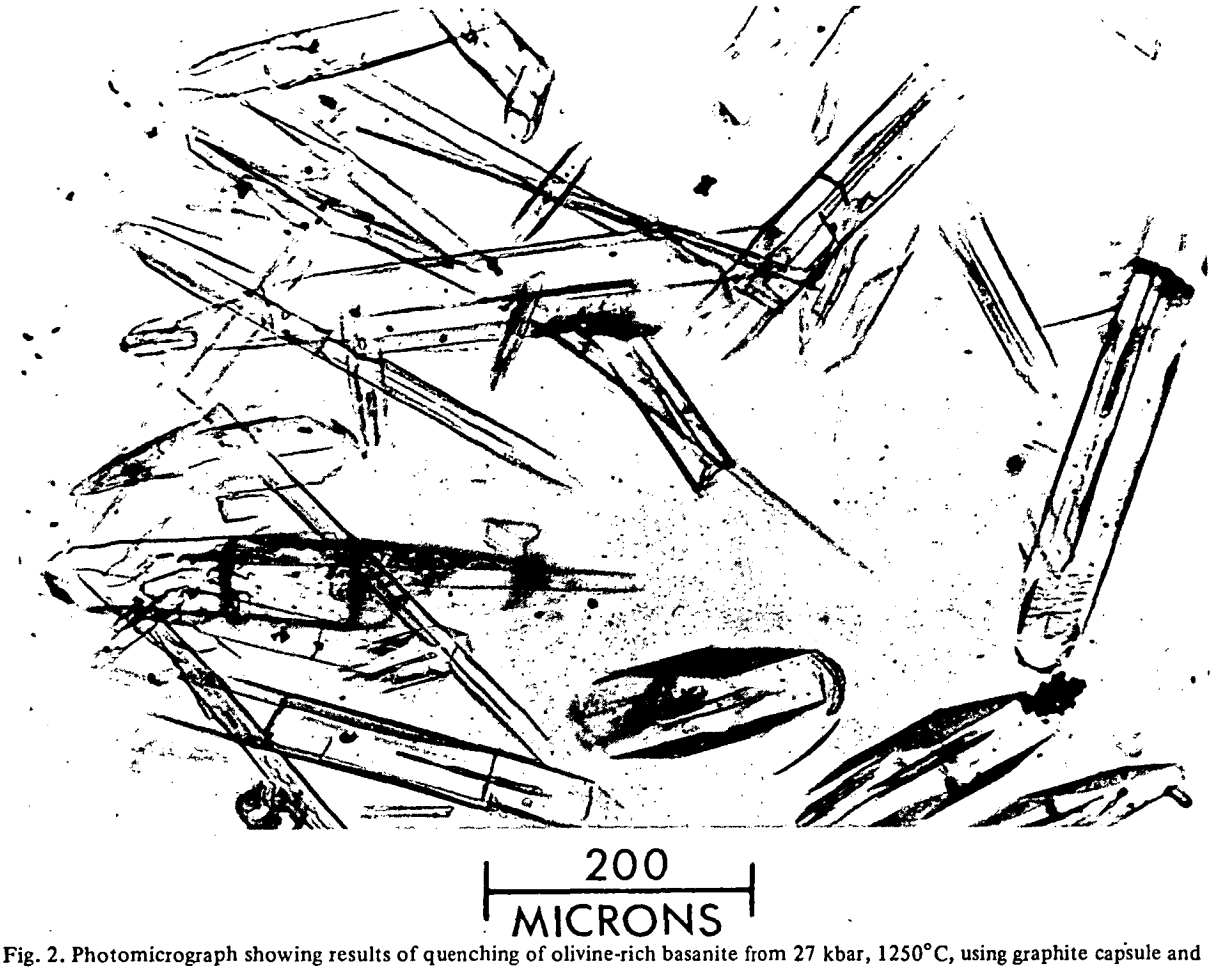

Fig. 2. Photomicrograph showing results of quenching of olivine-rich basanite from 27 kbar, 1250°C, using graphite capsule and uncontrolled water content. Crystals are orthopyroxene with rare olivine (both analyzed). Glass composition (table 1, columns 5, 6) approaches olivine nephelinite. Comparable runs in sealed AgPd capsules with known water contents suggest > 5% H_2O and electron probe analysis of the glass, including analysis for carbon, indicates a high CO_2 content in the glass.

there is a liquid fractionation trend or continuum of liquid compositions ranging from olivine-rich basanite to olivine nephelinite. The crystalline phases which are in equilibrium with these liquids and which determine the fractionation trend are orthopyroxene, garnet, clinopyroxene and olivine. It has been further shown that the nature and the compositions of the liquidus phases along this fractionation trend are the same* as those existing in pyrolite at similar P, T conditions provided the pyrolite contains ~0.2% H_2O and is thus itself partially melted. All these observations are consistent with a model [7, 13] of magma genesis in which olivine-rich basanite is a product of partial melting of pyrolite composition at 25–30 kbar, 1200–1300°C, in the presence of small water contents and with the prediction that with lower degrees of melting liquids are of olivine nephelinite character. In table 5, this model is evaluated in terms of the specific pyrolite and basanite compositions used. Since K_2O and P_2O_5 are not present in measurable amounts in olivine, orthopyroxene, clinopyroxene or garnet at these conditions the concentration of these

* The small differences in 100 Mg/Mg + Fe^{2+}, Cr content, and Ti content reflect the problem that ideally the comparison should be of phases exactly on the liquidus of the basanite. In practice, the runs contain > 5% crystals and any components strongly partitioned into the crystals (such as Mg, Cr, Ni) will quickly show differences in concentration between the partial melting situation (pyrolite experiments) and crystal fractionation situation (basanite experiments).

Table 5
Evaluation of the partial melting model relating olivine-rich basanite to model pyrolite composition. Columns 2 and 4 give compositions of the residue after extraction of 6% and 8%, respectively, of the olivine basanite of table 1, column 3. Columns 3 and 4 show that this residual composition can be matched by the proportions of minerals shown at the top of the column. The compositions of orthopyroxene, garnet, and clinopyroxene are taken from table 3 but the olivine composition used in the calculations was that of natural olivine (Mg_{90}) from a lherzolite xenolith.

	Pyrolite	Pyrolite – 6% Basanite	60% Olivine 18% Orthopyroxene 14% Clinopyroxene 8% Garnet	Pyrolite – 8% Basanite	61% Olivine 20% Orthopyroxene 12% Clinopyroxene 7% Garnet
	1	2	3	4	5
SiO_2	45.16	45.3	45.1	45.2	45.0
TiO_2	0.71	0.6	0.4	0.5	0.3
Al_2O_3	3.54	3.0	3.0	2.8	2.8
Cr_2O_3	0.43	0.4	0.4	0.4	0.4
Fe_2O_3	0.46	0.4	8.4	0.3	8.5
FeO	8.04	7.9		7.8	
MnO	0.14	0.1	0.1	0.1	0.1
MgO	37.47	39.1	39.1	39.5	39.6
CaO	3.08	2.8	2.9	2.7	2.7
Na_2O	0.57	0.4	0.3	0.3	0.3
K_2O	0.13	0.01	0.0	(–0.03)	0.0
P_2O_5	0.06	0.0	0.0	(–0.02)	0.0
	99.79	100.1	99.7	99.6	99.7
$\frac{100Mg}{Mg+Fe^{2+}}$	89.2	89.8		90.0	

components in the basanite and pyrolite effectively determine the degree of partial melting. It is seen from table 5 that there is internal consistency in the model for partial melting of pyrolite yielding 6% olivine-rich basanite magma. The residual peridotite contains 60% olivine, 18% orthopyroxene, 14% clinopyroxene and 8% garnet, all phases being of the compositions observed in pyrolite at ~ 30 kbar, 1250°C. The model would require that the pyrolite contained 0.2% H_2O (for ~ 3% water in the magma) to 0.4% H_2O (for ~ 6% water in the magma). The only component in table 5 which does not 'fit' at the level of accuracy permitted by the microprobe data is TiO_2 – this is too high in the model pyrolite composition. The pyrolite is a 'model' [7, 9, 14, 16] composition and can claim no virtue other than that it also yields olivine-rich tholeiite magma of Hawaiian-type leaving residual olivine and orthopyroxene only, by ~ 30% melting at 15 – 20 kbar. If the mean mantle composition in the source region for the Victorian basanite contained different K_2O and P_2O_5 contents, then clearly a different specific melting relation could be calculated. It is possible that an equally good fit for another 'model pyrolite' composition could be obtained by other combinations of the five phases (basanite, olivine, orthopyroxene, clinopyroxene and garnet). The approach used in this paper does not specify a unique mantle source composition but does test whether a postulated mantle composition could yield observed magma types.

To summarize, the data presented in this paper demonstrate the internal consistency of the pyrolite model mantle composition and a petrogenetic scheme for magma genesis in which the nature of the melt phases for small degrees of melting at pressure > 20 kbar is strongly undersaturated nephelinitic or basanite magma [7, 13]. The data show that liquids containing < 7% H_2O which are in equilibrium with olivine, orthopyroxene, clinopyroxene and garnet as residual phases are highly undersaturated, alkali-rich, silica-poor magmas at pressures > 20 kbar and by implication argues that the silica-rich, oversaturated quartz tholeiitic, andesitic or dacitic magmas cannot also be in equilibrium with the same four residual phases [see also 6, 7]. The consistency of the trend

from studies of dry melting relationships through the present studies leads to the prediction that magmas derived by even smaller degrees of melting and containing > 7% water will be more alkali-rich and more strongly undersaturated. Thus, the present study strongly reinforces the model of the low-velocity zone previously presented [13] in which the nature of a < 2% melt fraction in the low velocity zone is predicted to be of olivine nephelinite to olivine melilitite character.

Acknowledgements

The high pressure melting experiments have been carried out by W.O. Hibberson and chemical analysis of basanite by E. Kiss. The microprobe analyses were made both possible and remarkably satisfying to carry out through the efforts of Dr. S.J.B. Reed and N.G. Ware in installing and testing the new 'TNO' microprobe.

References

[1] I. Kushiro, H.S. Yoder and M. Nishikawa, Effect of water on the melting of enstatite, Geol. Soc. Am. Bull. 79 (1968) 1685.
[2] I. Kushiro, The system forsterite–diopside–silica with and without water at high pressures, Am. J. Sci. 267A (1969) 269.
[3] I. Kushiro, Systems bearing on melting of the upper mantle under hydrous conditions, Carnegie Inst. Washington Year Book 68 (1970) 240.
[4] H.S. Yoder, Calcalkalic andesites: experimental data bearing on the origin of their assumed characteristics, Oregon Dept. Geol. Mineral. Ind. Bull. 65 (1969) 77.
[5] I. Kushiro, N. Shimizu and Y. Nakamura, Compositions of coexisting liquid and solid phases formed upon melting of natural garnet and spinel lherzolites at high pressures: A preliminary report, Earth Planet. Sci. Letters 14 (1972) 19.
[6] I.A. Nicholls and A.E. Ringwood, Effect of water on olivine stability in tholeiites and the production of silica-saturated magmas in the island arc environment, Contrib. Mineral. Petrol. (in press) 1972.
[7] D.H. Green, The origin of basaltic and nephelinitic magmas (Bennett Lecture), Trans. Leicester Lit. Philos. Soc. 64 (1970) 28.
[8] D.H. Green and A.E. Ringwood, Fractionation of basaltic magmas at high pressures, Nature 201 (1964) 1276.
[9] D.H. Green and A.E. Ringwood, The genesis of basaltic magmas, Contrib. Mineral. Petrol. 15 (1967) 103.
[10] D.H. Green and W. Hibberson, Experimental duplication of conditions of precipitation of high pressure phenocrysts in a basaltic magma, Phys. Earth Planet. Inter. 3 (1970) 209.
[11] R.J. Bultitude and D.H. Green, Experimental studies at high pressures on the origin of olivine nephelinite and olivine melilite nephelinite magmas, Earth Planet. Sci. Letters 3 (1968) 325.
[12] D.H. Green, The origin of basaltic and nephelinitic magmas in the earth's mantle, Tectonophysics 7 (1969) 409.
[13] D.H. Green, Compositions of basaltic magmas as indications of conditions of origin: application to oceanic volcanism, Philos. Trans. R. Soc. London Ser. A.268 (1971) 707.
[14] A.E. Ringwood, The chemical composition and origin of the earth, in: P.M. Hurley, ed., Advances in Earth Science (M.I.T. Press, Cambridge, Mass., 1966) 287.
[15] D.H. Green and A.E. Ringwood, Mineralogy of peridotitic compositions under upper mantle conditions, Phys. Earth Planet. Inter. 3 (1967) 359.
[16] D.H. Green and A.E. Ringwood, Mineral assemblages in a model mantle composition, J. Geophys. Res. 68 (1963) 937.
[17] L.A. Fontijn, A.B. Bok and J.G. Kornet, The TPD Electron Probe X-ray Micro-Analyzer; in: G. Mollenstedt and K.H. Gaukler, eds., Fifth Intern. Cong. X-ray Optics and Microanalysis (1969) 261.
[18] D.H. Green, Composition of glasses quenched from partial melting of pyrolite under high pressure, water-saturated conditions, submitted for publication.

Contrib. Mineral. Petrol. 48, 33—43 (1974)
© by Springer-Verlag 1974

B 18

Upper Mantle Source for Some Hawaiites, Mugearites and Benmoreites

D. H. Green, A. D. Edgar*, P. Beasley, E. Kiss, and N. G. Ware

Research School of Earth Sciences, Australian National University, Canberra, Australia

Received July 22, 1974

Abstract. Chemical analyses of over seventy lavas or dykes containing spinel lherzolite inclusions of high pressure mineralogy, show that most host magmas are of alkali olivine basalt or basanite composition with relatively rare olivine nephelinites, and olivine melilitites. The 100 Mg/Mg+Fe^{++} ratios of host magmas display a strong maximum at about Mg_{70} consistent with partial melting of source peridotite with olivine of Fo_{88-90}. In contrast to these primary magmas, there occur some host magmas with 100 Mg/Mg+Fe^{++}<60 and with chemical compositions resembling those of classical hawaiite, mugearite, and nepheline benmoreite magmas. It is inferred that these magmas have been produced by crystal fractionation, within the upper mantle, of parental basanites or alkali olivine basalts. The presence of kaersutitic hornblende xenocrysts accompanying the lherzolite inclusions, and the nature of the chemical variation between associated basanites and nepheline benmoreites suggests that crystal fractionation has been dominated by kaersutitic hornblende, together with olivine and, in some cases, probably clinopyroxene. The mantle-derived nepheline benmoreite magmas also show similarities to some plutonic nepheline syenites.

Introduction

The occurrence of "mafic phonolite" lava containing lherzolite inclusions with typical high pressure mineralogy in north-eastern Otago, New Zealand led Wright (1966) and Price and Green (1972) to suggest that (phonolitic) lavas of this type might originate by crystal fractionation at high pressure within the upper mantle. The "mafic phonolite" (Price and Green, 1972) represented the most highly fractionated liquid of direct upper mantle derivation of any described to that time and contrasted in its chemical composition (particularly MgO, CaO, alkalies, SiO_2 and Mg/Mg+Fe contents) with the alkali olivine basalts, basanites, olivine nephelinites etc. more commonly occurring as hosts to lherzolite inclusions and, by this criterion, of direct upper mantle derivation. In an attempt to chemically characterize the nature of upper mantle derived liquids, over seventy samples from the Tertiary to Recent basalt provinces in Eastern Australia and Tasmania have been analyzed (Fig. 1).

Of the lherzolite-bearing rocks, 37 are from Tasmania, 10 from Eastern Victoria, 6 from south-eastern Queensland, 10 from the Bowen Basin, central Queensland and west of Townsville, 10 from north Queensland, and 2 from the Atherton area north Queensland. These samples were largely supplied by Drs. Sutherland, Wellman, Ewart, and Stephenson. Details of the geochemistry and petrology of these and other rocks in these provinces will be published elsewhere by the donors. In addition Irving (1971) and Irving and Green (1974) list 49 analyses of lherzolite-

* Permanent address: Dept. of Geology, University of Western Ontario, London, Canada.

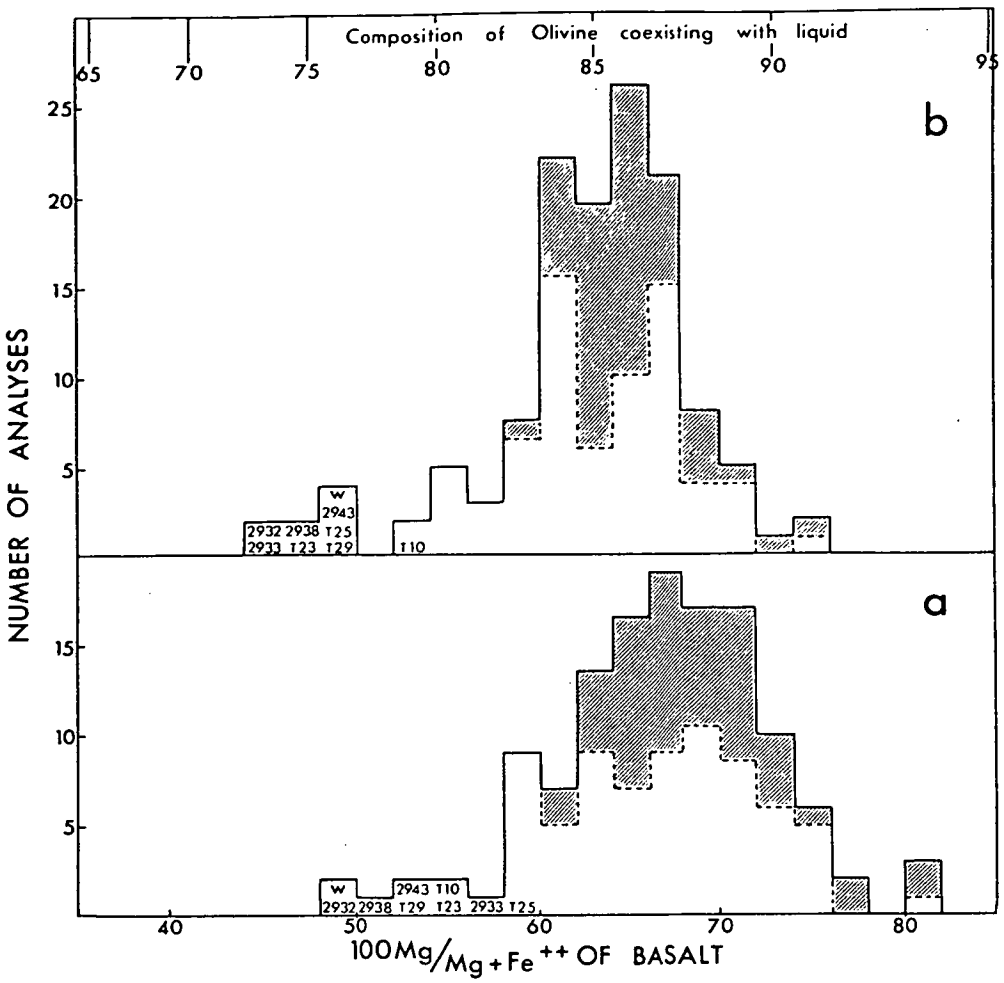

Fig. 1a and b. Histograms showing distribution of $\frac{100Mg}{Mg + Fe^{++}}$ values for 130 lherzolite-bearing volcanic rocks of Tertiary to Recent age occurring in Eastern Australia. Specimen numbers for most fractionated examples (lowest Mg-values) are as follows: W—Waipiata "mafic phonolite" (Price and Green, 1972): 2932 2933, 2938 northern Bowen Basin basalts (F. L. Sutherland): T10, T23, T25, T29 Tasmanian Tertiary Basalt province: 2943 Mt. Mitchell, south-eastern Queensland Main Range Volcanics (A. Ewart). Fig. 1a was compiled using the Fe^{+++}/Fe^{++} of the natural rock as analyzed but in Fig. 1b, for rocks other than those from within Victoria, Fe_2O_3/FeO (wt-%) was adjusted to 0.15, as a reasonable, though arbitrary, value for all unaltered basaltic magmas. The Mg-value was calculated from this adjusted FeO content. The western Victorian rocks were also corrected for oxidation of FeO to Fe_2O_3 using oxidation ratios deduced by Irving (1971) as appropriate for the different magma types

bearing basalts from the Newer Volcanics of Western Victoria and South Australia. These data have also been compiled in Fig. 1.

Variation of Atomic Ratio $\frac{100Mg}{Mg + Fe^{++}}$ (Mg-Value) in Lherzolite-Bearing Basalts

Tertiary to Recent basalts containing lherzolite xenoliths show a slightly skewed (to lower Mg-values) distribution (Fig. 1) with a maximum between Mg_{66} and Mg_{72}, using the Fe_2O_3/FeO ratios as observed in the analyzed rocks; or near Mg_{65} using the Fe_2O_3/FeO ratios corrected to an assumed oxidation ratio Fe_2O_3/FeO =

0.15 (for basalts other than the Newer Basalts of Victoria—see legend to Fig. 1). Green (1971, p. 723) noted that a collection of 94 analyses of lherzolite-bearing basalts from the literature showed a strong concentration of Mg-value in the range 63–73. Empirical data on the partition relationship between Mg-values of olivine and liquid at equilibrium (Cawthorn *et al.*, 1973; Green and Ringwood, 1967; Roeder and Emslie, 1970) lead to the conclusion that olivine in equilibrium with liquid of Mg-value $= 70 \pm 2$ must be of composition Fo_{88} to Fo_{90}. Thus, liquids with Mg-values of 70 ± 2, if derived by $< 20\%$ melting of a peridotitic source rock, place a major constraint on the source peridotite as containing olivine of Fo_{88-90} composition.

If the basalts of mantle origin with the higher Mg-values define the Mg-value of olivine in the source region for basalts as Fo_{88-90}, and if the upper mantle, on the scale sampled in a melting and magma extraction event, is approximately homogeneous in Mg-value, then those basalts of Fig. 1 with Mg-value < 70 have undergone crystal fractionation of ferro-magnesian phases within the upper mantle.

In most cases, the degree of crystal fractionation and resulting change in Mg-value is small (eg. examples studied by Wilkinson and Binns, 1969; Green and Hibberson, 1970a), but in the Waipiata "mafic phonolite" (Price and Green, 1972) and in 6 or 7 examples with Mg-values < 50 (Fig. 1) the degree of crystal fractionation is large, as measured by the change in Mg-value. These fractionated magmas are examined in more detail, particularly in relation to chemical variation within the classical basalt fractionation series. Nomenclature is based on the use of "Differentiation Index" (normative Or+Ab+Ne+Qz) and normative An/An+Ab and follows that used by Coombs and Wilkinson (1969).

Alkalies vs Silica Variation

In Fig. 2, the conventional total alkalies vs silica diagram clearly identifies the lherzolite host magmas as alkalic, many of them strongly so. The average Hawaiian fractionation trend from alkali olivine basalts, through hawaiite, mugearite and benmoreite to trachyte (Macdonald and Katsura, 1964) and a Hebridean fractionation trend from hawaiite to 2 benmoreite(s) (from Muir and Tilley, 1964) are plotted in Fig. 1 and demonstrate that the fractionated lherzolite-bearing "basalts" have affinities with classical hawaiites and mugearites. One example (2943) from Mt. Mitchell, S.E. Queensland, plots to the low SiO_2 side of a Hebridean benmoreite and three samples from northern Bowen Basin plot close to or on the alkali-rich side of the Hebridean mugearite. The comparison of the analyses in Table 1 and in Figs. 2, 3, 4 substantiates the classification of the Mt. Mitchell sample as a benmoreite, transitional to nepheline benmoreite (Coombs and Wilkinson, 1969). The most fractionated (2932) of the Bowen Basin samples is a nepheline mugearite while another fractionated sample (2938) is hawaiite, transitional to mugearite. As shown in Table 1, fractionated Tasmanian magmas are not as rich in alkalies but display a large spread in SiO_2 so that normatively they range from rather typical hawaiites (23,29) to highly undersaturated (18% Ne) nepheline hawaiite (25) (Table 1). The Tasmanian province also contains unfractionated (in the sense of Mg-value > 70) lherzolite-bearing magmas which range from mildly undersaturated alkali olivine basalt to extremely undersaturated basanites (Mg_{71}, Mg_{75}

Table 1. Compositions and CIPW norms of fractionated examples of lherzolite-bearing magmas syenite

	Benmoreite (Hebrides) (Tilley and Muir, 1964)	Nepheline Benmoreite (Mt. Mitchell S.E. Queensland) 2943	Benmoreite (Hawaii) (Tilley and Muir, 1964)	Nepheline Mugearite (near Mt. Leslie, north. Bowen Basin, central Queensland) 2932	Hawaiite (Redcliffe plateau, northern Bowen Basin Central Queensland) 2938	Average Mugearite (Hawaii) (Macdonald and Katsura, 1964)	Hawaiite (near Kingston, southern Tasmania) 23
SiO_2	56.73	54.60	57.97	50.64	50.54	51.90	49.21
TiO_2	1.81	1.00	1.06	2.03	2.50	2.57	2.41
Al_2O_3	16.83	17.68	18.56	17.30	17.03	16.65	16.07
Fe_2O_3	3.16	2.21	1.82	2.96	2.73	4.25	4.72
FeO	6.13	5.82	4.81	7.31	7.62	6.17	7.78
MnO	0.22	0.17	0.24	0.13	0.13	0.21	0.17
MgO	1.10	3.70	1.95	3.93	4.55	3.56	5.40
CaO	3.28	3.91	3.32	5.83	6.10	6.30	7.15
Na_2O	6.39	6.44	6.74	5.86	4.96	5.22	4.48
K_2O	3.94	3.80	2.79	3.12	2.82	2.01	1.74
P_2O_5	0.41	0.67	0.54	0.89	1.02	0.93	0.86
$\frac{100\,Mg}{Mg+Fe^{++}}$	24.2	53.1	42.0	48.9	51.5	50.5	55.3
Or	23.2	22.5	16.7	18.4	16.6	11.7	10.3
Ab	48.2	37.8	56.6	30.3	34.0	44.0	36.2
An	5.4	8.1	12.0	11.7	15.9	16.1	18.6
Ne	3.4	9.4	0.3	10.4	4.3	—	0.9
Di	7.2	5.7	0.7	9.4	6.3	7.0	9.1
Hy	—	—	—	—	—	2.8	—
Ol	3.7	10.2	7.8	9.5	11.7	4.8	11.4
Mt	4.5	3.2	2.6	4.3	4.0	6.3	6.8
Ilm	3.6	1.9	2.1	3.9	4.7	4.9	4.6
Ap	1.0	1.6	1.3	2.1	2.4	2.4	2.1
An/An + Ab	10.1	17.6	17.5	27.9	31.8	26.8	34.0
DI	74.8	69.7	73.6	59.1	55.9	55.7	47.4

on Fig. 2), olivine nephelinite (Mg_{70}) and olivine melilite nephelinite (Mg_{76}). The more mafic Bowen Basin host basalts are more restricted in composition and are basanites transitional to alkali olivine basalts. The S.E. Queensland samples include three rather similar basanites (Mg_{61}–Mg_{63}) but in addition an alkali olivine basalt (Mg_{69}) and a fractionated, hypersthene normative hawaiite (Mg_{58}, DI = 41, 100 An/Ab + An = 38).

The rather random sampling of lherzolite-bearing basalts in Eastern Australia illustrates a large variation in chemistry and normative mineralogy and, perhaps surprisingly, yields data showing that some mantle-derived liquids are quite highly evolved or fractionated and should be classified as hawaiites, mugearites

with comparisons with classical examples of hawaiite, mugearite, benmoreite and nepheline

Average Hawaiite (Hawaii) (Macdonald and Katsura, 1964)	Nepheline Hawaiite (Flinty Marsh, southeastern Tasmania) 10	Nepheline Hawaiite (Runnymede, southern Tasmania) 25	Nepheline Benmoreite (mafic phonolite) N.E. Otago, N. Zealand (Price and Green, 1972)	Average alkali syenite (vareity Larvikite) (Nockolds, 1954)	Average nepheline syenite (Nockolds, 1954)	Average nepheline monzonite (Nockolds, 1954)
48.60	45.75	42.71	48.17	57.2	56.0	51.8
3.16	2.42	2.85	2.28	1.7	0.7	1.5
16.49	14.04	13.20	13.97	17.9	21.5	20.5
4.19	3.54	6.95	4.18	2.3	2.4	2.8
7.40	10.42	8.79	8.02	4.2	2.0	4.1
0.18	0.21	0.28	0.20	0.1	0.2	0.1
4.70	7.41	7.02	5.69	1.5	0.6	2.2
7.79	7.71	9.84	7.03	4.4	2.0	6.2
4.43	4.74	5.28	6.46	5.8	8.9	6.5
1.60	2.45	1.84	2.88	4.0	5.4	4.1
0.69	1.31	1.25	1.12	0.6	0.2	0.5
53.0	55.9	58.7	55.8	38.8	33.7	49.2
9.5	14.5	10.9	17.0	23.9	31.5	23.7
35.1	17.7	10.6	21.4	46.6	32.5	23.9
20.6	9.8	6.9	0.7	10.6	2.8	14.7
1.1	12.1	18.4	17.9	1.4	23.6	16.4
10.8	16.3	27.1	21.2	5.9	4.2	10.0
—	—	—	—	—	—	—
8.6	16.8	7.7	8.5	2.9	0.2	1.3
6.0	15.1	10.1	6.0	3.3	3.5	4.2
6.1	4.6	5.4	4.3	3.2	1.4	4.8
1.7	3.1	2.9	2.7	1.5	0.4	1.0
37.0	35.6	39.5	3.2	18.5	8.0	38.2
45.7	45.3	39.5	56.3	71.9	87.6	64.0

and benmoreites and their nepheline-bearing equivalents. In the following section the most fractionated example, from Mt. Mitchell, is described in more detail, substantiating the high pressure origin of the lherzolite inclusions and describing the modal mineralogy and xenocrystal material present in this "basalt".

The Mt. Mitchell Nepheline Benmoreite

The nepheline benmoreite contains olivine phenocrysts in a trachytic (texturally) groundmass of alkali feldspar laths, olivine, clinopyroxene, opaque minerals and probable minor nepheline. The phenocryst olivine ranges from Fo_{83} to $< Fo_{51}$

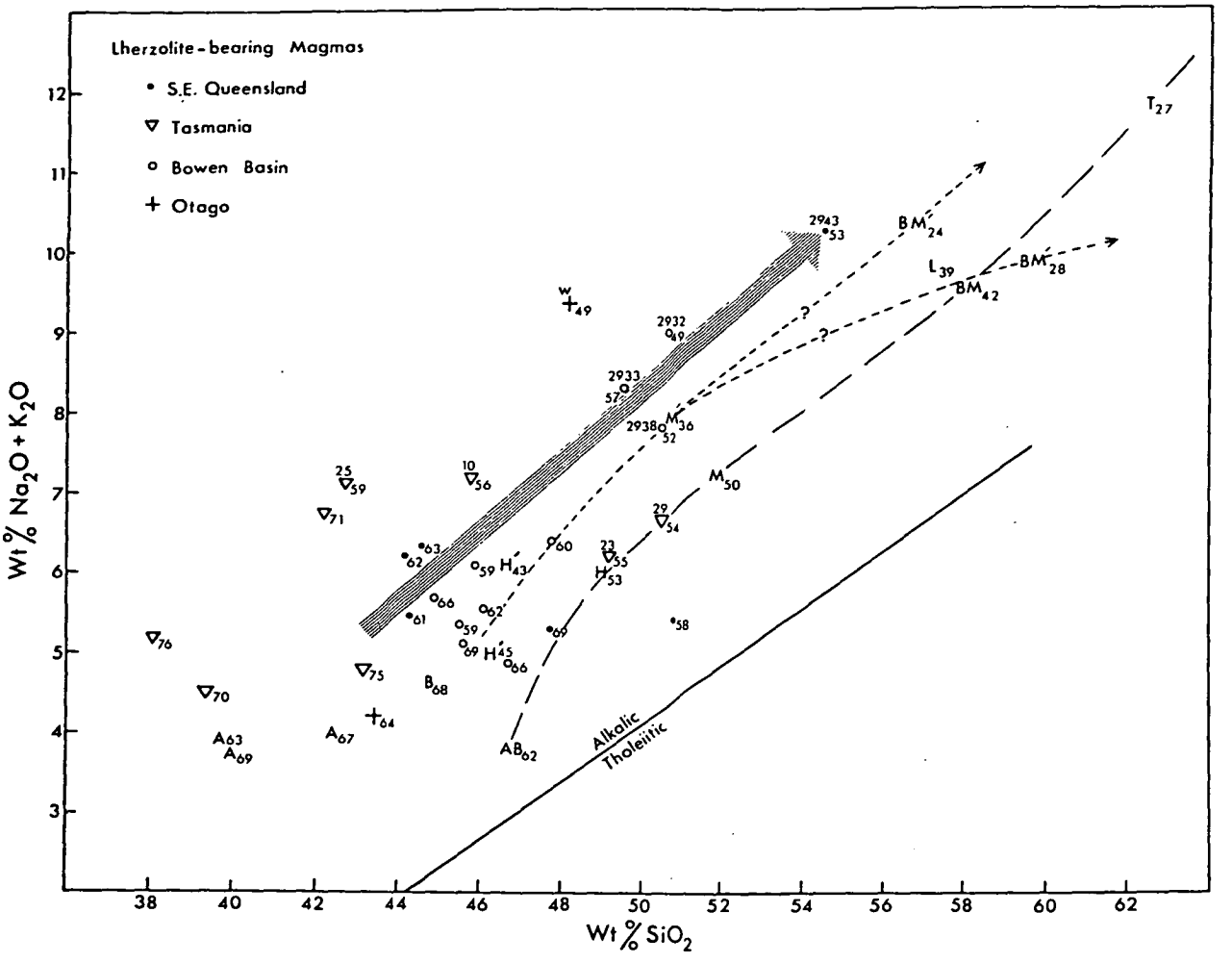

Fig. 2. Total alkalies (Na_2O+K_2O) vs SiO_2 diagram showing relationships of fractionated, lherzolite-bearing liquids to the classical fractionation series of Hawaii and of the Hebridean province, and also to less fractionated, lherzolite-bearing basalts, basanites etc. from the same province. The Mg-value for each analysis is noted next to the analysis and specimen numbers are given for the fractionated basalts discussed in this paper. Solid-line: boundary between alkalic and tholeiitic fields in Hawaii (Macdonald and Katsura, 1964). Dashed line: Fractionation trend for averaged alkali basalt (*AB*), hawaiite (*H*) mugearite (*M*), benmoreite (*BM*) and trachyte (*T*) from Hawaii (Macdonald and Katsura, 1964). Averaged basanite is "*B*". Short-dashed line: Similar fractionation sequences with individual analyzed rocks (*H'*, *M'*, *BM'*) from the Hebridean Province (Tilley and Muir, 1964). *A* Plots of amphibole (Mg-values indicated) xenocrysts in Mt. Mitchell nepheline benmoreite. Possible fractionation trend linking the Mt. Mitchell rock with basanites and kaersutite is shown as a shaded arrow

and is strongly zoned with more Mg-rich cores. The alkali feldspar is largely anorthoclase but varies from potassic oligoclase (Ca:Na:K = 26:86:8) to anorthoclase (Ca:Na:K = 3:56:41) in analyzed crystals (Table 2). In addition to the fine grained groundmass there are occasional megacrysts with anhedral, corroded shape and reaction rims against the groundmass. The megacrysts include anorthoclase ($Ca_{10}Na_{75}K_{15}$ in core to $Ca_{11}Na_{64}K_{25}$ at rim), ilmenite with titanomagnetite rims (Table 2) and Ti-poor kaersutite (Table 2). The megacrysts are not derived from the lherzolite inclusions but could be fragments of phases crystallized from the host benmoreite or similar magma at higher pressures.

Table 2. Electron microprobe analyses of mineral phases in nepheline benmoreite from Mt. Mitchell and in enclosed lherzolite xenolith

	Zoned olivine phenocrysts			Groundmass feldspar		Core of anortho-clase mega-cryst	Rim of titano-magnetite on core of ilmenite	Ilmenite mega-cryst	Separate Kaersutite megacrysts in nepheline benmoreite			Lherzolite xenolith			
				potassic oligo-clase	anortho-clase							Oli-vine	Ortho-pyro-xene	Clino-pyro-xene	Spinel
SiO_2	40.1	38.4	34.8	61.1	66.0	65.3	—	—	39.7	42.3	39.8	40.4	55.0	51.8	—
TiO_2	—	—	—	—	—	—	25.4	51.5	5.2	3.2	4.6	—	<0.07	0.3	—
Al_2O_3	0.6	0.2	0.35	24.4	19.9	21.7	1.6	0.3	14.2	12.3	14.2	—	3.8	6.5	58.9
Fe_2O_3	—	—	—	—	—	—	—	—	—	—	—	—	—	—	2.3
FeO	16.1	20.9	40.2	0.6	0.3	<0.1	67.0	42.7	10.3	11.6	13.0	9.8	6.3	2.4	8.2
MnO	0.2	0.2	1.1	—	—	—	0.9	0.9	—	—	—	—	<0.08	<0.08	
MgO	43.2	40.1	23.6	0.4	0.4	0.15	2.5	3.8	13.2	13.4	11.9	50.0	34.3	15.8	21.8
CaO	0.25	0.2	0.4	5.1	0.5	1.8	—	—	10.6	10.4	9.8	<0.05	0.37	20.8	—
Na_2O	—	—	—	7.3	6.3	7.5	—	—	2.3	2.9	2.8	—	<0.1	1.3	—
K_2O	—	—	—	1.3	7.1	2.3	—	—	1.4	1.0	1.3	—	—	—	—
Cr_2O_3	—	—	—	—	—	—	not determined		—	—	—	—	0.2	0.8	8.9
$\frac{100\,Mg}{Mg + Fe^{++}}$	82.8	77.3	51.1	—	—	—	—	—	69.5	67.5	62.0	90.1	90.5	92.1	82.5
									assuming no Fe_2O_3						

The mineralogy of the lherzolite inclusion (Table 2) is in sharp contradistinction to the host magma consisting of coarse-grained olivine (Fo_{90}), aluminous enstatite, aluminous diopside and aluminous, chromian spinel (Table 2). The high pressure character of the lherzolite assemblage is apparent in the highly aluminous character of the spinel and of the pyroxenes. The mineral assemblage indicates pressures in excess of 7–8 kb, at higher pressure than the stability field of the alternative olivine + plagioclase + pyroxenes mineral assemblage (Green and Hibberson, 1970b; Kushiro and Yoder, 1964). A more specific designation of P, T conditions of crystallization of the lherzolite mineralogy is not yet possible but would establish a minimum depth of fractionation and origin of the nepheline benmoreite magma.

Petrogenesis of Mt. Mitchell Nepheline Benmoreite

Figs. 2, 3 and 4 illustrate the relationship of the nepheline benmoreite composition to the lherzolite bearing basanites from S. E. Queensland, to the generalized alkali basalt fractionation trend from Hawaii and the Hebridean province, and to the compositions of the kaersutite megacrysts occurring within the nepheline benmoreite. The data suggest that crystal fractionation of a parental basanite could lead to nepheline benmoreite of the composition of the Mt. Mitchell rock provided that kaersutitic amphibole was a major phase and possibly the dominant phase involved in crystal fractionation. From experimental studies on basanite (Green, 1973 and unpublished data) and nepheline mugearite (Irving, 1971 and Irving and Green, in preparation) Ti-rich amphibole occurs near the liquidus for appropriate compositions and water contents from 5–25 kb, and phases accompanying the amphibole include olivine, clinopyroxene and biotite. A dominance of olivine in the crystal extract would lead to increase rather than decrease in TiO_2, CaO, and to excessively rapid depletion in normative olivine and in Mg-value. Dominance of clinopyroxene at high pressure has equally obvious disadvantages. Suitably chosen combinations of olivine, clinopyroxene and ilmenite might provide an alternative crystal extract but lack the supporting evidence provided by the kaersutites in the rock and are not supported by experimental data on basanite crystallization (Green, unpublished data). Price and Green (1972) noted the presence of kaersutite megacrysts in the Waipiata "mafic phonolite" and suggested a similar genetic role for amphibole and olivine in controlling crystal fractionation of basanite to yield the Waipiata "mafic phonolite". Irving (1974) has collected data on the abundant kaersutitic amphibole megacrysts from the Victorian Newer Volcanics and has emphasized the importance of this phase in deep-crustal and upper mantle crystal fractionation of hydrous undersaturated basaltic magmas (see also Kesson and Price, 1973).

The compositions of amphiboles crystallizing from a basaltic melt are sensitively variable in TiO_2 content, Ti/Al ratio, Na_2O, K_2O and CaO contents and the compositional dependence on P, T, % H_2O, and magma composition have not yet been determined. With ability of amphibole to take up Fe^{+++}, amphibole crystallization may lead to quite high degrees of crystallization of an original magma batch without a large decrease in the $Mg/Mg+Fe^{++}$ ratio (implying addition of O_2 to the magma and an externally buffered magma batch). If crystal fractionation is controlled by olivine + clinopyroxene + ilmenite as accumulate

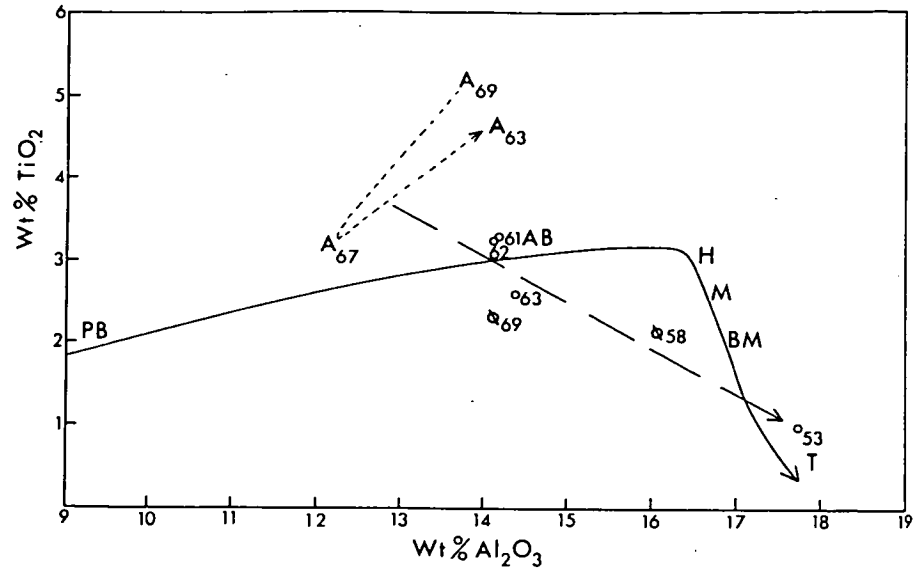

Fig. 3. TiO_2 vs Al_2O_3 diagram showing the Mt. Mitchell nepheline benmoreite (Mg_{53}) in relation to the amphibole xenocrysts within the rock (*A*) and to basanites Mg_{61}, Mg_{62}, Mg_{63}) occurring in the same province. The basalts Mg_{69} and Mg_{58} do *not* lie near the kaersutite-controlled postulated fractionation trend in Fig. 2. For comparison, the alkali basalt fractionation trends from picrite basalt (*PB*) to trachyte are also shown

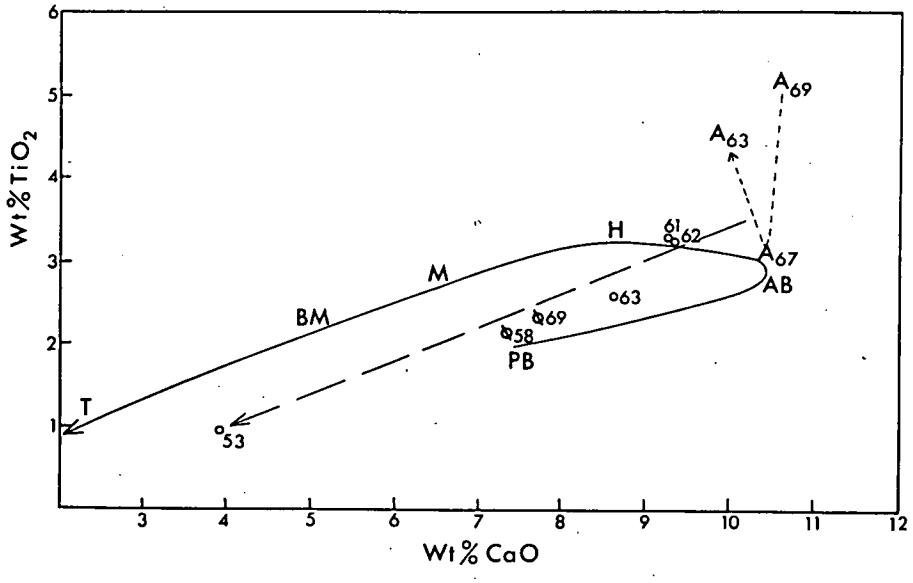

Fig. 4. TiO_2 vs CaO diagram, symbols as in Fig. 2. Note that if amphibole was dominating crystal fractionation and changed in composition from $Mg_{69} \rightarrow Mg_{67} \rightarrow Mg_{63}$ then the fractionation trend on these diagrams should be curved rather than linear

phases then large amounts of olivine and clinopyroxene precipitate before ilmenite appears, leading to rapid decrease in Mg-value. The sequential appearance of phases of such contrasted composition as olivine, clinopyroxene, ilmenite or titano-magnetite and plagioclase (as at low pressure) lead to distinct inflections in

chemical variation diagrams such as Figs. 2–4. The nature of the variation curves relating Hawaiian and Hebridean alkali picrites, alkali olivine basalts, hawaiites etc. (Figs. 2–3) suggest that crystal fractionation is dominated in the suites by olivine (alkali picrite to alkali basalt), olivine + clinopyroxene (alkali olivine basalt to hawaiite), and clinopyroxene + olivine + (titanomagnetite or ilmenite) + plagioclase (hawaiite through benmoreite) (cf. Le Maitre, 1962). This pattern of crystal fractionation is consistent with a low pressure environment and differentiation at crustal levels, commonly within the volcanic structure. The evidence presented herein shows that there occur hawaiites, mugearites, benmoreites and nepheline-rich equivalents (Coombs and Wilkinson, 1969) which have been derived most probably by crystal fractionation from parental basanites within the upper mantle ($P_{Load} > 8$ kb). Furthermore, the data suggest that kaersutitic hornblende is the major phase, accompanied by olivine, and in some cases, probably by clinopyroxene, controlling crystal fractionation. The different fractionation regimes are to some extent convergent but there are differences in Mg-values [at equivalent differentiation indices (Table 1)], in SiO_2, TiO_2, K/Na, relative to parental basanite etc. which will probably serve to distinguish the product of the different fractionation regimes. The possibility of using chemical variation patterns to identify the depth at which fractionation occurred in a given alkaline basaltic province depends on accumulation of further data on suites of lherzolite-bearing basalts from provinces such as those so well represented in Eastern Australia.

In Table 1 we have listed analyses of average larvikite (alkali syenite), nepheline syenite and nepheline monzonite in order to illustrate the similarity in composition between the Mt. Mitchell nepheline benmoreite and these plutonic rocks. Principal differences occur in MgO content and Mg-value. We use this comparison to infer that some plutonic syenite and nepheline syenite magmas may be of mantle origin. The lack of evidence of basaltic or nephelinitic intrusions or bodies of accumulate pyroxenites, peridotites etc. occurring in field association with a syenite complex, does not provide evidence against an origin of the syenite as a fractionation product of undersaturated basaltic magma but may provide evidence that such fractionation occurred within the upper mantle rather than near the depth of emplacement within the crust.

Conclusions

Sampling of magmas containing lherzolite inclusions of upper mantle origin in Eastern Australia has led to the identification of fractionated magmas classifiable on both a modal and normative basis as hawaiites, mugearites and benmoreites and their more undersaturated equivalents, nepheline hawaiites, nepheline mugearites and nepheline benmoreites. The phases controlling crystal fractionation and yielding these derivative magmas from parental alkali olivine basalts and basanites are probably olivine, kaersutitic amphibole and clinopyroxene. In particular the data presented suggest a dominant role for kaersutitic amphibole in leading to decreasing TiO_2 content, increasing SiO_2 content, and relatively small change in Mg-value. The origin of some plutonic syenite complexes may be in intrusion of "mantle-fractionated" magmas rather than fractionation of magmas at crustal levels near the depth of emplacement of the complex.

References

Cawthorn, R. G., Ford, C. E., Biggar, G. M., Bravo, M. S., Clarke, D. B.: Determination of the liquid in experimental samples: discrepancies between microprobe analysis and other methods. Earth Planet. Sci. Litt. **21**, 1–5 (1973)

Coombs, D. S., Wilkinson, J. F. G.: Lineages and fractionation trends in undersaturated volcanic rocks from the east Otago volcanic province (New Zealand) and related rocks. J. Petrol. **10**, 440–501 (1969)

Green, D. H.: The origin of basaltic and nephelinitic magmas. Trans. Leicester Lit. Philos. Soc. **64**, 28–54 (1970)

Green, D. H.: Conditions of melting of basanite magma from garnet peridotite. Earth Planet. Sci. Lett. **17**, 456–465 (1973)

Green, D. H., Hibberson, W. O.: Experimental duplication of conditions of precipitation of high pressure phenocrysts in balsaltic magma. Phys. Earth Planet. Interiors **3**, 247–254 (1970a)

Green, D. H., Hibberson, W.: The instability of plagioclase in peridotite at high pressure. Lithos **3**, 209–221 (1970b)

Green, D. H., Ringwood, A. E.: The genesis of basaltic magmas. Contrib. Mineral. Petrol. **15**, 103–190 (1967)

Irving, A. J.: Geochemical and high pressure experimental studies of xenoliths, megacrysts and basalts from south-eastern Australia. Unpublished Ph. D. thesis, Aust. National. Univ. Canberra (1971)

Irving, A. J.: High pressure megacrysts in the Newer Basalts of southeastern Australia. J. Geol. (in press, 1974)

Irving, A. J., Green, D. H.: Geochemistry and petrogenesis of the Newer Basalts of Victoria and South Australia. (In preparation, 1974)

Kesson, S., Price, R. C.: The major and trace element chemistry of kaersutite and its bearing on the petrogenesis of alkaline rocks, Contrib. Mineral. Petrol. **35**, 119–124 (1972)

Kushiro, I., Yoder, H. S.: Anorthite-forsterite and anorthite-enstatite reactions and their bearing on the basalt-eclogite transformation. J. Petrol. **7**, 337–62 (1966)

Le Maitre, R. W.: Petrology of volcanic rocks, Gough Island, South Atlantic. Geol. Soc. Am. Bull. **73**, 1309–40 (1962)

Macdonald, G. A., Katsura, T.: Chemical composition of Hawaiian lavas. J. Petrol. **5**, 82–133 (1964)

Nockolds, S. R.: Average chemical compositions of some igneous rocks. Geol. Soc. Am. Bull. **65**, 1007–32 (1954)

Price, R. C., Green, D. H.: Lherzolite nodules in a "mafic phonolite" from north east Otago, New Zealand. Nature, Physic. Sci. **235**, 133–134 (1972)

Roeder, P. L., Emslie, R. F.: Olivine-liquid equilibria. Contrib. Mineral. Petrol. **29**, 275–285 (1970)

Tilley, C. E., Muir, I. D.: Intermediate members of the oceanic basalt-trachyte association. Geol. Foren. Stockholm Forh. **85**, 434–43 (1962)

Wilkinson, J. F. G., Binns, R. A.: Hawaiite of high pressure origin from north-eastern New South Wales. Nature **222**, 553–555 (1969)

Wright, J. B.: Olivine nodules in a phonolite of the East Otago alkaline province, New Zealand. Nature **210**, 519 (1966)

Dr. D. H. Green
Research School of Earth Sciences
Australian National University
Box 4, P. O.
Canberra, Australia

Contrib. Mineral. Petrol. 49, 93—103 (1975)
© by Springer-Verlag 1975

B19

The Role of CO_2 in the Genesis of Olivine Melilitite

Gerhard Brey and David H. Green

Research School of Earth Sciences, Australian National University, Canberra, Australia

Received November 12, 1974

Abstract. The nature of the near-liquidus phases for a mantle-derived olivine melilitite composition have been determined at high pressure under dry conditions and with various water contents. Olivine and clinopyroxene occur on or near the liquidus and there are no conditions where orthopyroxene crystallizes in equilibrium with the olivine melilitite. We have determined the effect on the liquidus temperature and liquidus phases of substituting CO_2 for H_2O on a mole for mole basis at 30 kb, using olivine melilitite + 20 wt% H_2O at $X_{CO_2} = 0$ and $X_{CO_2} = (CO_2)/(H_2O + CO_2)$ (mole fraction) = 0.25, 0.5, 0.75 and 1.0 (i.e. olivine melilitite + 38 wt% CO_2). Experiments were buffered by the MH or NNO buffers. At 30 kb, CO_2 is only slightly less soluble than water for $X_{CO_2} < 0.5$ as judged by the slight increase in liquidus temperature on mole-for-mole substitution of CO_2 for H_2O and at 30 kb, 1200° C, $X_{CO_2} = X_{H_2O} = 0.5$ the olivine melilitite contains 8.8 wt% H_2O and 21 wt% CO_2 in solution. For $X_{CO_2} \to 1$ the CO_2 saturated liquidus is depressed ~70° C below the anhydrous liquidus and the magma dissolves approx. 17% CO_2 at 30 kb, 1400° C, $X_{CO_2} \to 1$, $X_{H_2O} \to 0$. Infrared spectra of quenched glasses have absorption bands characteristic of $CO_3^{=}$ and OH^- molecules and no evidence for HCO_3^-. The effect of $CO_3^{=}$ molecules dissolved in the olivine melilitite at high pressure is to suppress the near-liquidus crystallization of olivine and clinopyroxene and bring orthopyroxene and garnet on to the liquidus. We infer that olivine melilitite magmas may be derived by equilibrium partial melting (<5%) of pyrolite at 30 kb, 1150–1200° C, provided that both H_2O and CO_2 are present in the source region in minor amounts. Preferred conditions are $0 < X_{CO_2} < 0.5$, $0.5 < X_{H_2O} < 1$, and at low oxygen fugacities (<Ni-NiO buffer). Residual phases are olivine, orthopyroxene, clinopyroxene and garnet.

Introduction

A principal aim of petrologists and geochemists has been to account for the wide spectrum of basaltic compositions derived from the upper mantle. Green (1970, 1971, 1973a) presented model petrogenetic grids in which mantle-derived magmas are attributed to partial melting of a pyrolite upper mantle with low water content ($\simeq$ 0.1–0.2% H_2O) and are assigned to specific degrees of partial melting, pressure or depth of magma segregation and nature of residual peridotite mineralogy. Testing of this grid for a specific olivine basanite composition (Green, 1973b) led to an internally consistent model in which 6% melting of pyrolite containing 0.2% H_2O at about 29 kb, 1250° C, leaving residual garnet lherzolite, would produce the specific olivine basanite magma. It was suggested that smaller degrees of melting, and higher pressure, lower temperature conditions would yield olivine nephelinite or olivine melilitite magmas. The present investigation was undertaken to explore this suggestion and also to evaluate whether such highly undersaturated magmas could be derived by melting in the presence of H_2O only in the upper mantle pyrolite or also required the presence of CO_2 in the source region. The latter possibility is suggested by extensive natural evidence (in kimberlites, carbonatites, fluid inclusions in olivine, sampled volcanic gases) that CO_2 is

released from the upper mantle, and by experimental evidence that carbon (as CO_2 possibly) was soluble in nephelinitic glass at ~30 kb (Green, 1973b). Also Eggler (1973) has shown that CO_2 is soluble in several simple silicate systems at high pressure and CO_2 solubility in a melt of diopside composition increases with increasing pressure. Kushiro (1973) also suggested that the presence of oxides of polyvalent components such as P_2O_5, TiO_2, and probably CO_2, in magmas might shift liquidus boundaries towards silica-poor compositions encouraging production of more silica undersaturated liquids.

In the present paper we report experiments on a natural olivine melilitite composition at high pressures under dry conditions, with variable water contents and with variable H_2O/CO_2 ratios. The experiments were carried out under conditions of the magnetite/haematite or nickel/nickel oxide buffers or alternatively were "buffered" by the graphite and other components of the high pressure furnace assembly.

Experimental Methods

Analyses of melilitite-bearing and larnite-normative lavas which contain lherzolite inclusions and are thus of mantle derivation are sufficiently uncommon and sufficiently variable that selection of an average composition for experimental study is probably not very meaningful. We selected for our experimental study an olivine melilitite from Laughing Jack Marsh, near Lake St. Clair, Tasmania (Sutherland, 1973). The rock contains olivine (larger crystals zoned from (100 Mg)/(Mg+Fe) = 89.5 in the cores to (100 Mg)/(Mg+Fe) = 79 on rims), and titaniferous clinopyroxene phenocrysts, and xenocrysts and xenoliths of typical spinel lherzolite and its minerals. The ground mass consists of melilitite, nepheline, clinopyroxene, ilmenite and apatite. Chips free of obvious xenoliths or probable xenocrysts were selected and crushed. The analyzed powder (Table 1) was fused to glass, and re-analyzed for Fe_2O_3 and FeO contents (by spectrophotometric methods) and for other major elements by the electron probe (Table 1).

Experiments were carried out in a piston-cylinder apparatus using piston-in technique and a pressure correction of −10% of nominal piston pressure (calibrated on quartz-coesite at 1100° C, 32 kb, and albite → jadeite + quartz at 600° C, 16.2 kb). Samples were sealed in silver palladium capsules (mainly Ag_{50} Pd_{50}) below 1250° C and in platinum capsules above 1250° C. Run duration varied from 5 to 30 min depending on the capsule material used (shorter time for Pt capsules to minimise iron loss). Sample size was 8–10 mg with added water (microsyringe, checked by weighing before and after welding) where desired. Runs with pure water were carried out both unbuffered (i.e. "buffered" approximately by the graphite furnace and presence of water from talc dehydration in the environment external to the sample—our experiments demonstrate that this gives conditions of oxygen fugacity lower than the Ni-NiO buffer) and with the magnetite-haematite external buffer. Runs containing CO_2 (added as silver oxalate; Boettcher *et al.*, 1973) were enclosed in an external capsule containing the magnetite-haematite buffer, or in some runs, the Ni-NiO buffer. The double capsule method used for buffering employed an inner capsule with >10 mg sample and an outer capsule containing approximately 100 mg of the buffer assemblage. In all cases examination of the buffer immediately adjacent to the sample capsule by x-ray and/or optical means demonstrated the presence of both components of the buffering reaction although the directions of the change of the buffers were towards magnetite and metallic nickel respectively. Metallic nickel strongly alloyed with the silver palladium capsules but did not detectably (in the runs reported in this paper) pass into the silicate melt of the inner capsule. Iron loss from experiments in Ag_{50} Pd_{50} capsules did not exceed 2 wt% FeO as shown by defocussed beam microprobe analyses of the charges.

Electron Microprobe Techniques. Mineral analyses were carried out using the TPD electron microprobe (Fontijn *et al.*, 1969) and an energy dispersive analytical system (Reed and Ware, 1973). Conditions of analysis were as described by Green (1973a).

Table 1. Compositions of natural rock and of glass used in experiments

	Olivine melilitite 2927 Laughing Jack Marsh, Tasmania	Prepared glass for experiment
	1	2
SiO_2	37.1	39.4
TiO_2	2.7	2.9
Al_2O_3	9.3	9.8
Fe_2O_3	4.2	— (1.2)
FeO	9.0	12.6 (10.3)
MnO	0.2	0.4
MgO	15.9	16.3
CaO	12.8	13.4
Na_2O	3.7	3.7
K_2O	1.4	1.4
P_2O_5	1.3	(1.3)
H_2O^+	1.6	—
CO_2	0.3	—
C.I.P.W. Norms		
an	5.1	5.8
lc	6.6	6.5
ne	17.2	17.1
di	19.0	13.4
ol	29.1	36.3
cs	8.5	10.9
mt	6.2	1.8
il	5.2	5.2
ap	3.2	3.1

1 = Analysis by XRF methods, spectrophotometry for FeO, Fe_2O_3, flame photometry for Na_2O.

2 = Analysis by electron microprobe, with FeO, Fe_2O_3 determined by spectrophotometry, P_2O_5 not determined, value taken from natural rock.

Infrared Spectrophotometry of Glasses. The glasses were finely ground, mixed with KBr and pressed into discs. The infrared spectra were obtained on a Perkin-Elmer MODEL 457 Grating Infrared Recording Spectrophotometer in the frequency range of 4000 cm^{-1} to 250 cm^{-1}.

Experimental Data

Experiments have been carried out on the olivine melilitite with added water, water + graphite, and water + silver oxalate. The double capsule method with outer oxygen buffer assemblage was used for runs with water and silver oxalate and for some runs at 30 kb with water alone.

a) Runs under Dry Conditions and with Various Water Contents. Reconnaissance studies have been carried out between 25 kb and 40 kb with water contents from 0–40 wt %. The positions for liquidi at dry conditions, 10% and 20% H_2O are shown in Fig. 1. Near-liquidus phases are olivine, olivine and clinopyroxene, clinopyroxene and, in one experiment (Nr. 4477, 40 kb, 1160° C, 20% H_2O), garnet, olivine and clinopyroxene. Quench mica, quench amphibole and ?apatite are

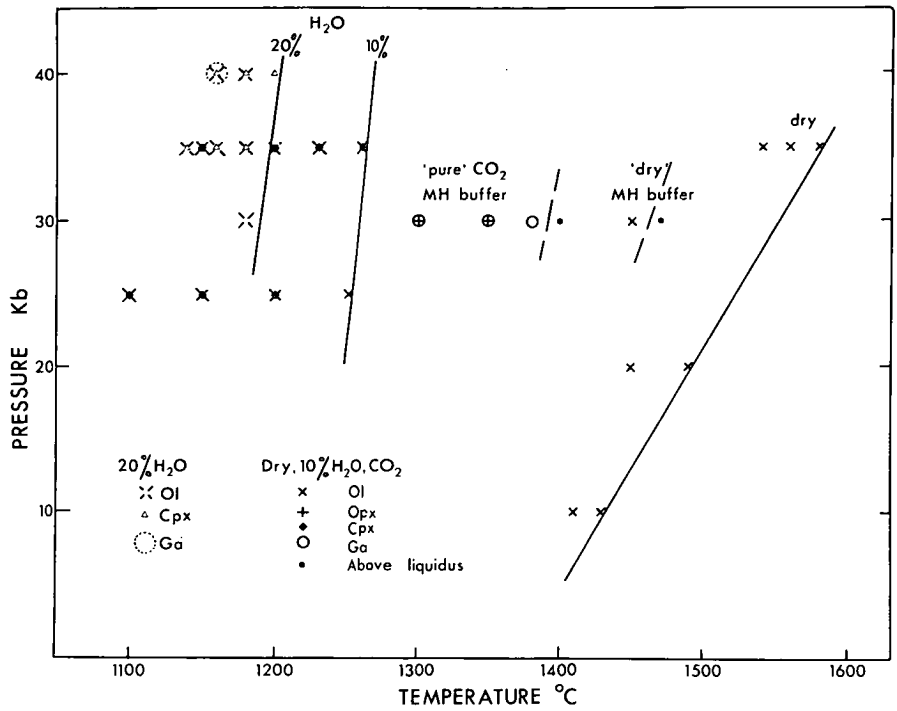

Fig. 1. Liquidi for dry, H_2O- and CO_2-containing experiments. The positions of the liquidi are either estimated from Mg-values of phases and their abundances or bracketted by experiments. The liquidi for dry and CO_2-containing experiments at 30 kb with MH buffer have been lowered by migration of hydrogen into the charge from the external MH-buffer. This depression corresponds to about 1% H_2O as inferred from experiments on basanite (Green, 1973a)

common but orthopyroxene was not found under any conditions and all analysed near-liquidus clinopyroxenes were calcium-rich.

b) Runs with Water and Graphite Added. A quick reconnaissance of possible effects of carbon solubility at low oxygen fugacities was carried out using mixtures of glass + 5 wt % C and varying water contents (10–30 wt%). In some runs at 30 kb, orthopyroxene and orthopyroxene + garnet occurred near the liquidus but other runs at similar temperatures yielded clinopyroxene, or clinopyroxene + garnet + olivine. Gas release after the runs and examination of polished mounts showed variation in the extent to which carbon remained as graphite or was oxidized with loss of hydrogen from the charge and it was apparent that equilibrium within the volatile species and the liquid was not attained. The appearance of orthopyroxene warranted further study of the roles of CO_2 and water.

c) Runs with Known CO_2 and H_2O Contents. Boettcher *et al.* (1973) used silver oxalate ($Ag_2C_2O_4$) as a means of adding CO_2 to silicate charges under controlled water and oxygen fugacities, because silver oxalate decomposes at moderate temperatures to elementary silver (inert towards the silicate melt) and CO_2. Boettcher *et al.* (1973) found it necessary to maintain relatively high oxygen fu-

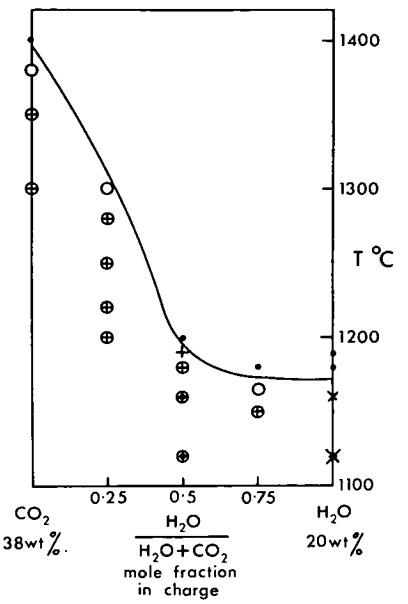

Fig. 2. Position of liquidus and phase relations for olivine-melilitite at 30 kb as a function of X_{H_2O} in the presence of an external MH-buffer. Note that between $X_{H_2O} = 0.5-1.0$ experiments were carried out vapour-undersaturated and vapour-oversaturated between $X_{CO_2} = 0.5-1.0$. For key to symbols see Fig. 1

gacity in the charge by using an external magnetite-haematite buffer and double capsule technique (Eugster and Skippen, 1967) to ensure a pure CO_2-H_2O mixture in the free vapour phase. We wished to carry out our experiments under conditions, at least in part, where there is no free vapour phase and to explore the effect on liquidus temperature and nature of liquidus phases of mole for mole replacement of H_2O by CO_2, both volatile species being dissolved in the silicate melt, at least for low CO_2 contents. One series of runs on the join olivine melilitite—(H_2O + CO_2) ($X_{H_2O} = 1$–0, $X_{CO2} = 0$–1) was carried out at 30 kb with magnetite-haematite external buffer. In runs with no vapour phase, hydrogen fugacity within the silicate melt is buffered by the magnetite-haematite buffer and oxygen fugacity in the melt is lower than that of the buffer assemblage (Whitney, 1972). Similarly, in runs with higher CO_2 content in which there is a free vapour phase, oxygen fugacity is lower than the magnetite-haematite buffer depending on the CO_2/H_2O ratio of the vapour phase (Boettcher *et al.*, 1973).

The CO_2-free runs contained 20 wt% H_2O entirely dissolved in the silicate liquid at 30 kb, $T > 1160°$ C; water-free runs contained 38 wt% CO_2 but this was not entirely dissolved in the liquid and a vapour phase was present. Results of experiments are shown in Fig. 2 as functions of temperature and $X_{H_2O} = (H_2O)/(H_2O + CO_2)$ (mole fraction). The liquidus temperature increases only $\sim 20°$ C from $X_{H_2O} = 1$ to $X_{H_2O} = 0.5$, no free vapour phase was observed and CO_2 is apparently soluble in the melt for CO_2/H_2O (mol) ≤ 1. Liquidus temperature increases sharply and a vapour phase is present above the liquidus for $X_{H_2O} = 0.25$ and $X_{H_2O} = 0$. The CO_2-saturated liquidus is 70° C below the liquidus for "dry" conditions (magnetite-haematite buffered, no added H_2O or CO_2). However, runs ostensibly with "pure CO_2" or "dry" runs which used the external MH buffer

Table 2. Compositions of phases analysed in selected runs

Sample	5172	5010		5004		5001	5041	5041
Run conditions	1160° C $X_{H_2O}=1$	1180° C $X_{H_2O}=0.5$		1160° C $X_{H_2O}=0.5$		1160° C $X_{H_2O}=0.5$	1380° C $X_{CO_2}=1$	1380° C $X_{CO_2}=1$
Phase	ol	ga	opx	ga	cpx	ti-magn.	ga	q-carb.
SiO_2	41.0	41.6	54.0	41.7	53.6	—	42.1	0.3
TiO_2	—	0.8	0.1	0.5	0.4	22.75	0.6	—
Al_2O_3	—	21.4	5.3	21.6	4.5	2.65	22.9	0.3
Cr_2O_3	—	0.7	0.3	0.2	—	0.67	0.3	—
FeO[a]	8.7	10.8	9.2	10.2	8.6	68.95	7.7	8.3
MnO	—	0.3	—	0.3	0.3	—	0.5	0.5
MgO	49.8	19.8	29.6	19.8	18.4	4.22	20.7	19.7
CaO	0.4	4.9	1.4	5.8	12.8	0.77	5.2	24.3
Na_2O	—	—	0.2	—	1.5	—	—	—
K_2O	—	—	—	—	—	—	—	0.1
Mg/Mg+Fe	91.1	76.5	85.1	77.6	79.2	9.8	82.7	—
Mg	—	67.3	82.8	66.7	56.7	—	71.9	44.9
Ca	—	12.0	2.7	14.0	28.4	—	13.1	42.4
Fe	—	20.7	14.5	19.3	14.9	—	15.0	12.7

[a] All Fe reported as FeO; andradite contents of garnet (see text) calculated from structural formulae.

were in fact not water-free. This is demonstrated by the OH^- vibrations in the infra-red spectra for these experiments (Fig. 3). We infer that rapid migration of hydrogen from the buffer assemblage into the charge reduced the liquidus temperature to that appropriate for about 1% H_2O. A higher liquidus temperature was obtained for unbuffered, dry runs (Fig. 1) where there is no source of hydrogen immediately external to the sample capsule. Thus the liquidus for olivine melilitite + CO_2 should also be at higher temperatures than that observed for the MH buffered run.

With increasing CO_2 content, the liquidus phases change from olivine for runs with pure water, to garnet (?+opx) for $X_{H_2O} = 0.75$, orthopyroxene for $X_{H_2O} = 0.5$, and garnet for $X_{H_2O} = 0.25$ and $X_{H_2O} = 0$. Below the liquidus, orthopyroxene $\pm$ clinopyroxene crystallize together with garnet. Quench phases are mica, amphibole, clinopyroxene, apatite and carbonate and in all runs except those containing only CO_2, the quenching process yields crystalline products and not glass. The quench character of mica and amphibole is demonstrable both on textural and compositional grounds in comparison with co-existing primary phases. However the carbonate (analysis Table 2) is iron-rich dolomite and is interpreted as quench on the basis of absence of euhedral crystal shapes and interstitial habit in relation to both euhedral primary phases and euhedral to subhedral quench mica and amphibole.

In run 5001 at 1160° C, $X_{H_2O} = 0.5$, titanomagnetite was present and analyzable. The occurrence of titanomagnetite rather then ilmenite and the high andradite content of analyzed garnets (Table 2) contrasts with natural TiO_2-

bearing garnetiferous mantle-derived assemblages (garnet peridotites, eclogites) in which garnets are characteristically low in andradite and, where accessary ilmenite occurs, the ilmenite contains very low Fe_2O_3 in solid solution (Green and Sobolev, 1974). Thus we infer that the experiments buffered (for hydrogen fugacity) with the magnetite-haematite buffer created oxygen fugacity conditions within the capsules which are unrealistically high for natural mantle conditions. Further experiments will use the Ni-NiO buffer or the innate buffering qualities of the high pressure graphite furnace assembly (f_{O_2} < Ni-NiO buffer). Our experiments to date with the Ni-NiO buffer have yielded no evidence for reduced carbon after the run (cf. Boettcher *et al.*, 1973) and equilibrium calculations by Holloway and Reese (1974) in the system C—O—H to 10 kb, 1200° C leave open the possibility that graphite is unstable or stable but does not precipitate (for reasons of sluggish nucleation) at our experimental conditions.

Solubility of Carbon Dioxide in Olivine Melilitite

Eggler (1973) has shown that the solubility of CO_2 in silicate melts at high pressure is dependent on composition, being higher (e.g. up to 9.5 wt% at 20 kb, 1500° C) in diopside melt than in albite melt (e.g. <1 wt% at 20 kb, 950° C). Eggler's data also show that CO_2 is more soluble in a given melt in the presence of water than under dry conditions. Semi-quantitative electron probe analyses for carbon in basanite-nephelinite glass (Green, 1973) at 29 kb, 1250° C gave approximately 5% C, i.e. 18% CO_2, dissolved in the glass together with unknown water content.

The solubility of CO_2 can be indirectly determined in some of our experiments. The run at 30 kb, 1400° C, $X_{H_2O} = 0$ quenched to a clear, pale brown glass. Microprobe analyses of this glass consistently gave totals (83 ± 0.5 wt%) compared with analyses of starting glass giving totals of (100 ± 0.5%) and the same relative proportions of other oxides. Infra-red absorption spectra (Fig. 3) of this glass shows, as well as strong SiO_4^{4-} and CO_3^{2-} absorbances, some effect of $(OH)^-$. From these data, our best estimate for solubility of CO_2 in olivine melilitite saturated with CO_2 under conditions of $X_{H_2O} \to 0$ is 17 wt% CO_2. For $X_{H_2O} = 0.5$ at 30 kb, 1200° C the charge is above the liquidus and there is apparently no vapour phase present. Thus the liquid contains 8.8 wt% H_2O, 21 wt% CO_2 in solution.

We have attempted to investigate the manner of solution of CO_2 in the silicate melt by the methods of infra-red spectrography. This method was restricted to experiments which yielded glass and were free of primary crystals and either free or with <1% of quench carbonate. We were able to directly compare spectra for glasses listed in Table 3.

The infra-red spectra (Fig. 3) were compared with known spectra of silicates, carbonates and bicarbonates. The 30 kb, 1470° C "H_2O-free", CO_2-free glass (run 5050) shows strong absorbances at frequencies around 1000 cm^{-1} and 500 cm^{-1} due to SiO_4^{4-} groupings but the bands are not as sharply defined as in crystalline silicates. The 30 kb, 1400° C, $X_{H_2O} = 0$, $X_{CO_2} = 1$ glass (run 5040) shows additional absorbance bands between 1600 cm^{-1} and 1400 cm^{-1} (doublet with maxima at 1530 cm^{-1} and 1420 cm^{-1}) and a band at 850 cm^{-1} overlapped by

Table 3. Run details for experiments containing glasses subjected to infra-red spectrography

No.	Composition	CO_2 added as	H_2O	Buffer	P (kb)	T (° C)	Capsule	Products at the end of run
5050	Ol-melilitite Table 1	—	—	MH	30	1470	Pt	pale brown glass
5040	Ol-melilitite Table 1	$Ag_2C_2O_4$	—	MH	30	1400	Pt	pale brown glass very little q-carb.
5041	Ol-melilitite Table 1	$Ag_2C_2O_4$	—	MH	30	1380	Pt	Ga + brown glass very little q-carb.
1893	Basanite, Green (1973b)	enclosed in graphite capsule	present, but unknown amount		29	1260	Graphite	brown glass
2650	Basanite, Green (1973b)	starting material, glass						

SiO_4^{4-} absorbance. Comparison of spectra for the basanite starting glass (CO_2 and H_2O free) and the glass quenched from 29 kb, 1260° C (unknown H_2O and CO_2 contents) (run 1893) shows in addition to the SiO_4^{4-} absorbance bands, an absorbance band at 3450 cm^{-1} attributable to OH^- bonding in the melt, and an absorbance band at 1400 cm^{-1} (in this case, this is not a doublet). Absorbance bands between 1400 cm^{-1} and 1600 cm^{-1} correspond to the vibration-mode of the CO_3^{2-} molecule and comparison with spectra of crystalline carbonates show that doublets in this region appear mainly with alkali-carbonates, single peaks with carbonates of divalent cations. There is no evidence for HCO_3^- bonding in run 1893 as the bicarbonate molecule should produce strong absorbance between 1600 cm^{-1} and 1700 cm^{-1}. Ernst and Schwab (1972) suggested the existence of CO_4^{4-} at high pressure, analogous to SiO_4^{4-} but this possibility cannot be evaluated in the infra-red spectra. In organic compounds where C is surrounded by four oxygens, the main infra-red absorbance is around 1100 cm^{-1} and would be obscured by the SiO_4^{4-} absorbance.

The infra-red spectra clearly demonstrate the presence of both $CO_3^=$ and OH^- molecules in the complex melts quenched to glass at high pressures. The presence of OH^- molecules in a silicate melt may lead to breaking of Si-O chains, enhancing the activities of components containing individual SiO_4-tetrahedra (such as olivine) and depressing the activities of components for chain-silicates. The CO_3^{2-} molecule, with two free bonds available, apparently enhances the formation of linked Si-O chains, increasing the activity of pyroxene relative to olivine components in the melt. Kushiro (1973) also suggested that polyvalent elements (P, C, Ti) lead to polymerization of SiO_4^{4-} tetrahedra in the melt whereas monovalent elements prevent such polymerization. However, these arguments are inadequate to explain the enhanced role of orthopyroxene relative to clinopyroxene nor the enhancement of garnet crystallization in the presence of CO_2. It is possible that $CO_3^=$ bonding with $Ca^=$ within the melt is an additional factor.

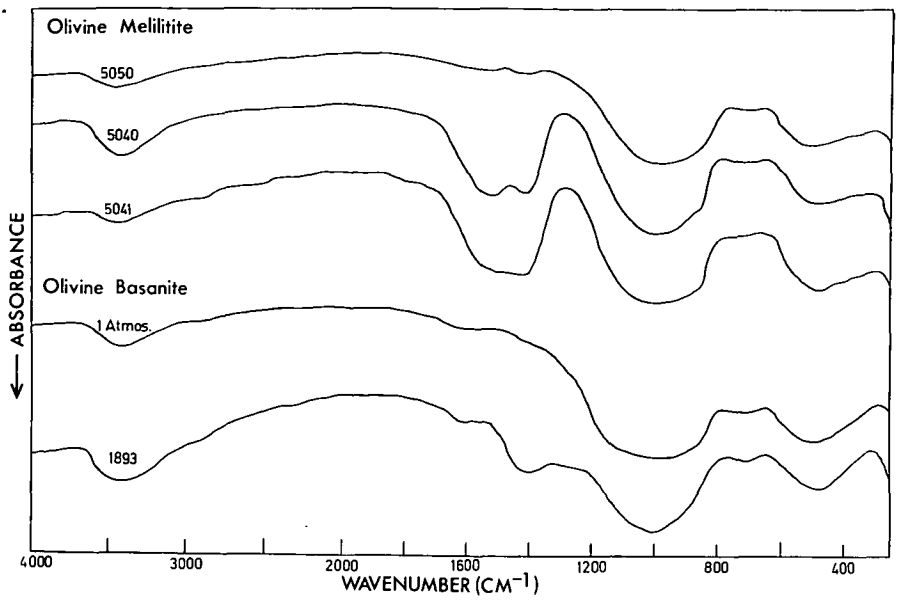

Fig. 3. Infra-red spectra from glasses as described in Table 3. Absorbance bands around 3450 cm^{-1} are due to OH^- vibrations, carbonate molecules show strong absorbance between 1400 cm^{-1} and 1600 cm^{-1} and around 850 cm^{-1}, and SiO_4^{4-} bands lie around 1000 cm^{-1} and 500 cm^{-1}

Genesis of Olivine Melilitite

We have approached this problem in the context of the petrogenetic grid (Green, 1970, 1971) in which various primary basaltic liquids are assigned to specific melting conditions of a common source rock, pyrolite. The reconnaissance studies of dry melting relationships and of the melting of olivine melilitite together with various water contents yielded no evidence for the existence of P, T, % H_2O conditions at which olivine melilitite liquid could be in equilibrium with the appropriate residual phases of pyrolite at the same P, T (i.e. olivine, enstatite, clinopyroxene and garnet). The experiments reported in this paper however show that CO_2 has a high solubility in the olivine melilitite at high pressure, particularly in presence of water. The solution of CO_2 in the melt changes the activities of components within the melt leading to suppression of olivine and clinopyroxene as near-liquidus phases, the appearance of orthopyroxene on and near the liquidus and the enhanced role of near-liquidus garnet.The roles of olivine and clinopyroxene near the liquidus at ~1160° C, 30 kb, $X_{H_2O} = 1$ and of orthopyroxene and garnet near the liquidus at ~1160° C, 30 kb, $X_{H_2O} = 0.75$ allow the prediction that at $P \simeq 30$ kb, $T \sim 1160°$ C and $X_{H_2O} \sim 0.8$–0.9 the olivine melilitite will have olivine, enstatite, clinopyroxene and garnet together on the liquidus. The compositions of olivine, orthopyroxene, clinopyroxene and garnet (Table 2) at 30 kb, ~1160° C are similar to those in pyrolite at the same P, T either with 0.1–0.2% water or with 0.2 water + 0.2% CO_2 (Green, 1973a and unpublished data). These P, T conditions are >100° C above the solidus for pyrolite + 0.2% H_2O (Green,

1973b). We infer that in the presence of CO_2 and H_2O and at least within the range $X_{CO_2} = 0.1$–0.3, the nature of the liquid formed by low degrees of partial melting of pyrolite at 30 kb, 1150–1200° C is olivine melilitite of composition similar to that investigated. The degree of partial melting of pyrolite for these conditions is probably $\leq 5\%$.

Further experiments are in progress at several pressures, varying f_{O_2} and X_{H_2O} and temperature. The experiments on olivine basanite (Green, 1973a; Green, Brey and Hibberson, unpublished data) and olivine melilitite lead us to infer that the presence of CO_2 and H_2O are necessary for derivation of such highly undersaturated magmas as olivine melilitite from pyrolite. In the absence of CO_2 but presence of 0.1–0.2% H_2O the most highly undersaturated liquids which can be derived from pyrolite at 30–35 kb are olivine basanite or possibly olivine nephelinite. It is possible that higher pressure and higher CO_2/H_2O proportions may change the nature of the liquid present in pyrolite at 5% melting towards even more SiO_2 undersaturated magma than that studied. In particular, the close similarities between basaltic kimberlite and olivine melilitite compositions and the common association of both rock types with carbonatites and carbonate minerals are common geological observations consistent with the role of CO_2 in magma genesis advocated in this paper.

Acknowledgements. We thank W. Hibberson for assistance in carrying out experimental high pressure runs, N. Ware for instruction in electron microprobe analysis and J. Ogilvie for instruction in infrared spectrometry. We thank J. F. G. Wilkinson and T. Mori for critical reading of the manuscript.

References

Boettcher, A. L., Mysen, B. O., Allen, J. C.: Techniques for the control of water fugacity and oxygen fugacity for experimentation in solid-media high-pressure apparatus. J. Geophys. Res. **78**, 5898–5901 (1973)

Eggler, D. H.: Role of CO_2 in melting processes in the mantle. Ann. Rept. Dir. Geophys. Lab., Washington **72**, 457–467 (1973)

Ernst, T., Schwab, R.: A new theory on the formation and ascent of basic magmas with special respect to the undersaturated series. 24th Inst. Geol. Congr., Proc. **14**, 28 (1972)

Eugster, H. P., Skippen, G. B.: Igneous and metamorphic reactions involving gas equilibria. Res. in Geochemistry **2**, 492–510 (1967)

Fontijn, L. A., Bok, A. B., Kornet, J. G.: The TPD electron probe X-ray micro-analyser. In: G. Mollenstedt and K. H. Gaukler, eds., Fifth Intern. Cong. X-ray Optics and Micro-analysis, 261 (1969)

Green, D. H.: The origin of basaltic and nephelinitic magmas. Trans. Leicester Lit. Phil. Soc. **64**, 28–54 (1970)

Green, D. H.: Compositions of basaltic magmas as indicators of conditions of origin: application to oceanic volcanism. Phil. Trans. Roy. Soc. London, Ser. A **268**, 707–725 (1971)

Green, D. H.: Conditions of melting of basanite magma from garnet peridotite. Earth Planet. Sci. Lett. **17**, 456–465 (1973a)

Green, D. H.: Experimental melting studies on model upper mantle compositions at high pressure under both water-saturated and water-undersaturated conditions. Earth Planet. Sci. Lett. **19**, 37–53 (1973b)

Green, D. H., Sobolev, N. V.: Co-existing garnets and ilmenites synthesized at high pressures from pyrolite and olivine basanite and their significance for kimberlitic assemblages. (Submitted for publication) 1974

Holloway, J. R., Reese, R. L.: The generation of N_2-CO_2-H_2O fluids for use in hydrothermal experimentation. I. Experimental method and equilibrium calculations in the C-O-H-N system. Am. Mineralogist **59**, 587–597 (1974)

Kushiro, J.: Regularities in the shift of liquidus boundaries in silicate systems and their significance in magma genesis. Ann. Rept. Dir. Geophys. Lab. Washington **72**, 497–502 (1973)

Reed, S. J. B., Ware, N. G.: Quantitative electron microprobe analysis using a lithium drifted silicon detector. X-ray Spectrometry **2**, 69–74 (1973)

Sutherland, L. V.: Igneous rocks, central plateau. In: The Lake Country of Tasmania. Roy. Soc. of Tasmania Symp., Nov. 1972, 43–54 (1973)

Whitney, J. A.: The effect of reduced H_2O fugacity on the buffering of oxygen fugacity in hydrothermal experiments. Am. Mineralogist **57**, 1902–1908 (1972)

Dr. D. H. Green
Research School of Earth Sciences
Australian National University
P. O. Box 4
Canberra 2600, Australia

Canadian Mineralogist
Vol. 14, pp. 255-268 (1976)

B20

EXPERIMENTAL TESTING OF "EQUILIBRIUM" PARTIAL MELTING OF PERIDOTITE UNDER WATER-SATURATED, HIGH-PRESSURE CONDITIONS

D. H. GREEN
Research School of Earth Sciences, Australian National University, Canberra

Abstract

Experimental aspects of studies of water-saturated melting of peridotite compositions are reviewed and it is shown that problems of grain size of starting materials, extent of iron loss, iron oxidation state, and problems of electron probe microanalysis need to be evaluated. The reality of quench outgrowth and nucleation of phases during quenching of high-pressure runs is demonstrated and the method of determination of equilibrium liquid by analysis of glasses in quenched runs is shown to give erroneous results for wet melting of peridotite. The use of bulk and mineral compositional data, together with crystal/liquid partition data, to calculate equilibrium melt compositions in favorable cases is shown to yield reliable results. This is demonstrated by reversal experiments in which the liquidus temperatures and phases of the postulated melt match with the residual phases of the peridotite at the appropriate pressure and temperature.

Water-saturated melting of peridotitic compositions in island arc environments will produce parental basalts of magnesian quartz tholeiite (10 kbar, 1100-1200°C) to olivine tholeiite composition (20 kbar, 1100-1200°C) with 25-35% melting. Lower degrees of melting at 10-20 kbar will only produce more undersaturated magmas with higher normative olivine or nepheline contents. Andesites or dacites are not possible melting products of peridotitic source rocks at depths greater than 30 km.

Sommaire

L'aspect expérimental d'études effectuées sur la fusion de péridotites en présence d'eau est étudiée et la conclusion qu'on en tire est celle-ci: il faut réévaluer les problèmes de la dimension des grains des matériaux de départ, de la perte du fer, de l'état d'oxydation du fer et des problèmes de microanalyse à la sonde électronique. Nous pouvons démontrer la réalité de l'excroissance trempée et de la nucléation de nouvelles phases pendant la trempe d'essais à haute pression; on y démontre aussi que la pratique de déterminer le liquide d'équilibre par l'analyse de verres (liquides trempés) donne des mauvais résultats en cas de fusion par voie humide de la péridotite. Par contre, on obtient de bons résultats en utilisant les données de composition minéralogiques et les données sur les répartitions cristal/liquide pour calculer les compositons de liquides d'équilibre dans des cas favorables. Ceci peut se démontrer dans plusieurs expériences "renversées" pendant lesquelles les températures du liquidus et les phases sur le liquidus en question correspondent aux phases résiduelles de la péridotite à des températures et pressions appropriées. La fusion de péridotites en milieux saturés en eau, comme dans les arcs insulaires, produira des basaltes du genre tholéiite quartzique magnésien (10 kbar, 1100-1200°C) ou tholéiite à olivine (20 kbar, 1100-1200°C) avec une fusion de 25 à 35%. Une fusion moins poussée, soit 10-20%, produira uniquement des magmas sous-saturés contenant plus d'olivine normative ou de néphéline. Les andésites ou dacites ne peuvent provenir de péridotites par fusion partielle à des profondeurs plus grandes que 30 km.

(Traduit par le journal)

Introduction

The melting behavior of peridotitic compositions under water-saturated conditions at high pressure has become a matter of controversy amongst experimental petrologists. Rather diametrically opposed interpretations of apparently simple experiments make it easy for the non-specialist to adopt the viewpoint that anything remains possible as a melting product of the upper mantle and it must appear to many earth scientists that hypotheses of magma genesis can remain unconstrained by knowledge of mantle melting behavior under water-saturated conditions. A principal controversy is whether siliceous (>55% SiO_2), highly quartz-normative liquids can be derived as equilibrium partial melts of peridotite at pressures >10 kbar, under water-saturated conditions. A recent paper by Nehru & Wyllie (1975) illustrates the problems but in reporting their own data and emphasizing the experimental difficulties encountered, these authors do not equally emphasize that these experimental difficulties have been foreseen, and minimized or surmounted by other groups using different approaches.

Problems and Comparisons in Experimental Methods

Four separate laboratories (Kushiro *et al.* 1968, 1972; Mysen & Boettcher 1975a; Nehru &

Wyllie 1975; and Green 1972, 1973a,b) have studied the melting relationships of peridotitic compositions under water-saturated conditions. In three studies (Kushiro *et al.* 1968; Milhollen *et al.* 1974 and Nehru & Wyllie 1975; and Green 1972, 1973) the solidus was placed between 950°C and 1000°C at 5 to 30 kbar. Mysen & Boettcher (1975a,b) placed solidi for four peridotite compositions at much lower temperatures (<800°C at 25-30 kbar for the least-refractory compositions). The detection of the solidus was based in the first instance in *all* the investigations on the optical examination of the charge and included textural changes indicating the appearance of an intergranular melt phase. Additional criteria include the identification of quenched glass and the distinction of quenched glass derived from the silicate dissolved in the vapor phase from that derived from a silicate melt. These observations are subjective and Green (1973a) attempted to obtain an objective result by analyzing amphibole compositions above and below the optically determined solidus. It was shown that the amphibole changed in Na/K and Ti/K across the 'solidus' with the higher temperature amphibole having lower K_2O contents. Furthermore, knowledge of the bulk composition and coexisting mineral compositions at 10 kbar and 1000°C and 970°C, showed that at 1000°C another phase (additional to olivine, pyroxenes and amphibole) was required with a higher K/Na ratio than all the crystalline phases — this phase was correlated with the optically observed intergranular melt phase. No such phase was required, however, in the 970°C run and the compositions of amphibole, pyroxene and olivine were such as to satisfy the bulk composition without requiring the presence of an additional K-enriched phase. Mysen & Boettcher (1975a, p. 533) did not give full cognizance to these bases on which Green (1973a) had determined the solidus at 10 kbar and published data (Mysen & Boettcher 1975b, Table 4, 1975a, Fig. 3) purporting to show *no* change in amphibole composition across their solidus (which they placed at 800-840°C). If the equilibrium solidus for Mysen & Boettcher's composition is at ~1000°C instead of ~820°C, then their only published analysis of above-solidus amphibole is that at 1100°C and is obviously very different (0.04% K_2O, 1.2% Na_2O) from those at lower temperatures (0.11-0.32% K_2O, 2.0-2.6% Na_2O). However, the real significance of these (and other) analyses in Mysen & Boettcher's work could only be gauged after a very careful microprobe study of the primary and secondary mineralogy in the natural rock starting materials. The samples used by Mysen & Boettcher (1975a,b) in their study were natural rocks crushed to <200 mesh, i.e. mineral fragments (and aggregates) up to 70 microns diameter. I have repeated experiments on a natural lherzolite of known mineralogy (Frey & Green 1974) using identical run times, temperatures, and water content to those used by Mysen & Boettcher at 15 kbar on lherzolite B. These new data show persistence of zoned, unequilibrated relicts of primary minerals up to at least 1100°C and the only effect on primary minerals at temperatures <950°C appears to be minor solution-rounding of original mineral grains by the large amount of vapor phase (16-22 wt. % H_2O) present. Quench glass from the vapor phase forms thin films on most mineral grains. New growth of amphibole apparently occurs in some lower temperature runs but the dominance of relict, original mineral grains means that such new crystallization may reflect a local chemical system and certainly cannot be assumed to be equilibrium crystallization of the bulk composition.

The failure to reach equilibrium using natural mineral mixes was carefully documented by Råheim & Green (1974) using minerals ground to <10 microns and run times greatly in excess of those used by Mysen & Boettcher (1975a,b). It should be noted that any increase in reaction rates attributed to the presence of a free vapor phase results from a very effective increase in intergranular diffusion rates (Ahrens & Schubert 1975) and a free vapor phase is ineffective in increasing reaction rates controlled by intracrystalline diffusion of coarsely crystalline starting materials. A more detailed appraisal of the problems inherent in the use of coarsely crystalline starting materials will be published elsewhere based on detailed examination of melting relations of a natural lherzolite (–200 mesh) at 15 kbar, 870°C to 1200°C, water-saturated conditions. There are, however, several areas in which the experimental techniques normally used in the Canberra laboratory offer distinct advantages in reducing experimental uncertainties.

Nehru & Wyllie (1974) document the problem of iron loss in their melting runs at 20 kbar, 900°C-1250°C, and it is clear from their techniques that Mysen & Boettcher (1974a,b) must have similar iron losses which, when combined with the presence of relict starting materials ensure that any use of Mg/Mg+Fe values in their charges must be highly suspect. Rather than the flattened pillow-shaped sample capsule containing 2-3mg of samples used by these groups, our own sample geometry remains cylindrical, and uses 10-20 mg of sample, recoverable as a coherent cylinder or series of discs which can be monitored for Fe-loss in tra-

verses from wall to wall. In subsolidus or near-solidus assemblages, Fe loss to container walls is limited and, under suitable run conditions, restricted to the marginal areas. In runs with a high proportion of melt, iron loss is pervasive throughout the charge (c.f. Nehru & Wyllie 1975) and the depletion of iron during such an experiment is commonly recorded in reverse zoning of olivine (or other) crystals from iron-rich core to magnesian margins (documented by Green & Ringwood 1967b and Green 1973a).

In the Canberra experiments the iron loss and the oxidation state of iron have been carefully monitored as standard practice in any project by direct microanalysis by spectrophotometric methods of the bulk samples after runs (Green & Ringwood 1967a,b; Kiss 1974). This can be done on 1-2 mg samples and it is surprising indeed that other laboratories have failed to apply this technology and persisted in experiments in which either both iron loss and oxidation state remain unmonitored or oxidation state is controlled (at unknown Fe^{3+}, Fe^{2+} values) using an external hydrogen buffer while iron loss remains undetermined. It has also long been known that the piston cylinder apparatus, using a graphite furnace and either talc, talc + boron nitride or talc + pyrex glass sleeves surrounding the graphite heater, produces high hydrogen fugacities and low oxygen fugacities within the Pt or Ag-Pd sample container. This was illustrated in the FeO, Fe_2O_3 data of Green & Ringwood (1967a,b, and later papers), particularly by Banno & Green (1968) in studies of the system diopside + albite + magnetite + quartz and by the Green & Sobolev (1975) demonstration of very low Fe_2O_3 content of ilmenites crystallized under a wide range of water contents. Nehru & Wyllie (1975) note determinations by a number of workers showing that using the single capsule method and the standard 'dry' or 'wet' furnace assemblies, oxygen fugacities in the sample capsule are close to the NNO buffer and usually between the NNO and MW buffers. Experiments in our laboratory on stability of buffer assemblages confirms $f(O_2)$ conditions < NNO for our normal run procedures. Mysen & Boettcher (1975a,b) concur in this assessment and refer to their own experiments under these conditions as 'f_{H_2} (NNO)' (e.g. 1975b, p. 557, p. 577) or f_{H_2} > NNO. Curiously, they refer to experiments by Green, using the same type of furnace assembly, as 'unbuffered (f_{H_2})' (1975b, p. 554). In fact, in the experiments reported by Green (1973a,b) the charges were buffered by the furnace assembly, the oxidation state of iron was determined (cf. Table 1) and microprobe analyses of the bulk sample were carried out routinely for all major elements and reported simply as 100Mg/Mg + ΣFe ratios for the charges (Green 1973a, Tables 1-9). Only at 10 kbar, 1200°C (100Mg/Mg + Σ Fe = 89.7, initially 85.2), 10 kbar, 1100°C (100 Mg/Mg + Fe = 86.4) and 20 kbar, 1100°C (100 Mg/Mg + Fe = 85.7, initially 85.2) was there appreciable iron loss from the charge. These iron losses were much lower than those reported by Nehru & Wyllie (1975) and relfect the lower sample/metal capsule ratio and longer run times used by Nehru & Wyllie. These authors recognized their dilemma in that shorter run times resulted in failure of the crushed rock (− 200 mesh) to reach equilibrium and longer run times resulted in excessive iron loss. These problems were minimized in the Canberra work by the use of a sintered oxide mix (grain size < 5 microns, olivine + pyroxenes + plagioclase mineralogy) as starting material, larger sample/metal capsule ratios and empirically established run times, and the resultant charges were carefully checked for bulk composition by the methods noted above. These data refute the contention of Mysen & Boettcher (1975a,b) that no significance can be attached to changes

TABLE 1: SPECTROPHOTOMETRIC DETERMINATION OF FeO AND Fe_2O_3 IN SAMPLES AFTER HIGH-PRESSURE RUNS

Composition	$\%H_2O$	Pressure (kbar)	Temp (°C)	Time (hrs)	Sample Capsule	Initial		Final	
						FeO	Fe_2O_3	FeO	Fe_2O_3
Pyrolite - 40% olivine	2	15	1000	24	$Ag_{75}Pd_{25}$	8.1	0.5	8.2	0.3
Pyrolite - 40% olivine	10	15	1000	6.5	$Ag_{75}Pd_{25}$	8.1	0.5	8.1	0.6
Pyrolite - 40% olivine	10	15	900	31	$Ag_{75}Pd_{25}$	8.1	0.5	7.7	0.4
Glass 1	15	10	1180	0.5	$Ag_{50}Pd_{50}$	7.9	0.6	5.8	1.0
Glass 1 + 3% Ol	15	10	1180	0.5	$Ag_{50}Pd_{50}$	7.9	0.6	5.5	0.9
Glass 3 + 2% Ol	15	10	1080	0.5	$Ag_{75}Pd_{25}$	6.8	0.5	5.5	1.1
Glass 3 + 1% CaO	15	10	1060	0.5	$Ag_{75}Pd_{25}$	6.7	0.5	6.4	0.5
Glass 5 + 10% Opx	20	20	1100	0.25	$Ag_{75}Pd_{25}$	8.9	0.5	8.0	0.5

E. Kiss, analyst

in 100 Mg/Mg + Σ Fe values of minerals and that there is no validity in the use of this ratio to test for equilibrium between quenched glass and olivine crystals (in experiments carried out at f_{O_2} < NNO buffer).

It is useful to comment on two further technical aspects of the experimental studies. Green (1973a) added 10 wt. % water to the (pyrolite – 40% olivine) composition (Green & Ringwood 1967c) yielding experiments equivalent to (pyrolite + 6% water). The charges after the runs were coherent, and either 'rock-like' to 'coherent but readily crushable' — such samples are readily mounted and polished so that textures and crystal/melt/vapor relationships can be readily observed. Nehru & Wyllie (1975) used a partly serpentinized peridotite containing 5.7% water and apparently obtained similar coherent charges (Nehru & Wyllie 1975, Fig. 2). However, in our recent experiments on lherzolite (–200 mesh) + 16-22% water (duplicating Mysen & Boettcher's 1975a,b sample mixes), the sample is recovered as an incoherent white powder, pouring cleanly from the capsule as a disaggregated mineral powder, most grains being coated with glass films quenched from the vapor phase and/or silicate melt. Textural relationships in this material are much more obscure and the high proportion of vapor phase results in appreciable composition change in the condensed phases (cf. the occurrence of forsterite in subsolidus assemblages of the enstatite+H_2O system—Kushiro *et al.* 1968).

A second aspect of the experimental studies is the identification of quench borders on primary crystals. Green (1972) noted that 0.5 micron

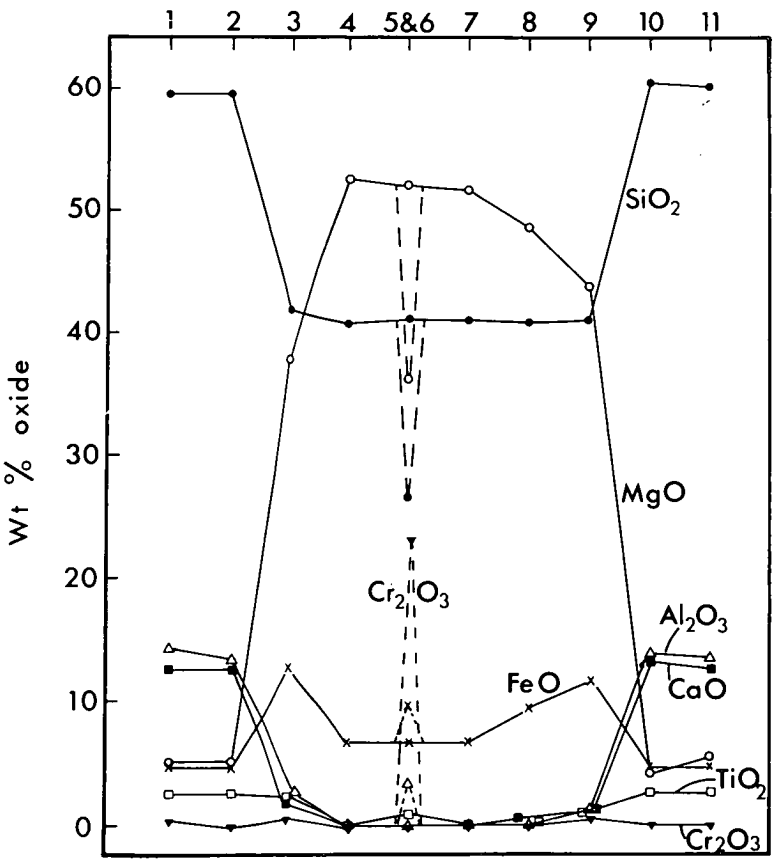

FIG. 1. Analytical data from (pyrolite - 40% olivine) composition at 10 kbar, 1200°C, 10% H_2O added, showing analyses of olivine crystals (4,5,7), typical analyses of glass areas free of olivine crystals (1,2,10,11), and three analyses at the edges of olivine crystals (3,8,9) showing iron enrichment and partial admixture of glass (<3% CaO, Al_2O_3, >10% FeO). The analytical data from a tiny chromite grain (6) of 1-2 micron diameter and included in olivine are also shown.

quench borders on 10-micron olivine crystals result in >33% volume increase of crystallized olivines and Green (1973a) published an analysis of quench olivine ($Fo_{84.5}$) outgrowth on primary olivine (Fo_{93}). Nehru & Wyllie (1975) and Mysen & Boettcher (1975a,b) did not find such borders, suggesting that such borders are <2 micron (approx.) thick in their experiments. Raw analytical data for such a quench border outgrowth obtained by the TPD microprobe (<0.5 micron beam, energy dispersive analytical system; Reed & Ware 1973, 1975) are illustrated in Figure 1. The only grain boundary effect able to produce these variations in X-ray intensities is real iron enrichment at the grain boundary. "Correction" of the border analysis for glass admixture (calculated by assuming no CaO in the olivine border) and high TiO_2 yielded the olivine composition ($Fo_{84.5}$) given by Green (1973a).

Previous Experimental Testing of Equilibrium Melt Compositions

Experimental studies of simple systems are of great value in suggesting explanations of observed crystallization behavior of natural complex melts (e.g., the incongruent melting of enstatite at low pressures and the appearance of olivine phenocrysts and pigeonite reaction rims in quartz normative basalts) but are of qualitative value only for prediction of crystallization behavior in complex natural rock compositions. From studies of the enstatite+water system and then of related systems such as Fo+Di+Qz+H_2O and Fo+Ne+Qz+H_2O, Kushiro (1970, and earlier papers) argued that water-saturated melting of peridotite would produce quartz-normative liquids at pressures to at least 25 kbar. Green (1970) took a natural quartz-normative tholeiite displaying the classical low-pressure olivine+liquid$_1$⇌subcalcic pyroxene + liquid$_2$ reaction relationship and showed that, at 22.5 kbar, $P(H_2O)=P$(total), this composition did not have olivine as the liquidus phase (as would be predicted if the Kushiro hypothesis applied to this natural rock composition). Addition of olivine *crystals* sufficient to make the bulk composition exactly silica-saturated (neither quartz nor olivine in the norm) resulted in solution of the olivine and clinopyroxene was again the liquidus phase. The data showed that a typical natural quartz tholeiite could not be a direct partial melt of a peridotitic source rock at 22.5 kbar, even under water-saturated conditions. This method of testing hypotheses of partial melting by establishing P, T, $\%H_2O$, conditions where a given magma has the same liquidus phases (of the same composition) as the residual phases of the postulated source composition, is of general application and has been followed consistently in the formulation and testing of a petrogeneic grid for basaltic magmas (Green & Ringwood 1967a; Green 1970, 1971, 1972, 1973a,b,c; Brey & Green 1975) and for lunar magmas (Green *et al.* 1975, Longhi *et al.* 1974). Nicholls & Ringwood (1973) evaluated the pressure range over which quartz tholeiites, saturated tholeiite and olivine tholeiite crystallized olivine as their liquidus phase under water-saturated conditions, establishing that the silica-saturated tholeiite could be derived by partial melting of a peridotite source under water-saturated conditions up to pressures between 17 kbar and 20 kbar. Nicholls (1974) carried out similar studies on andesite and basaltic andesite compositions showing that olivine was a liquidus phase to 5 kbar (andesite) and 10-15 kbar (two basaltic andesite compositions) under water-saturated conditions. These studies demonstrated the great importance of water in expanding the liquidus role of olivine to higher pressures in hydrous silica-rich magma compositions as predicted by Kushiro *et al.* (1968). A similar but less marked effect was noted in highly undersaturated magmas (Green 1973c) but in these compositions a more genetically important effect is the appearance of orthopyroxene in addition to or replacing clinopyroxene as a near-liquidus phase accompanying olivine (Green 1970, p. 43; 1971, p. 725). The results of the experimental studies under water-saturated conditions on both the postulated source compositions and on natural magmatic liquids from andesite to olivine tholeiite, were synthesized into an internally consistent picture (Green 1973a,b; Nicholls & Ringwood 1974) in which it was shown that the most siliceous liquids derived by partial melting of pyrolite at 10 kbar were magnesian quartz tholeiites (~55% SiO_2) or basaltic andesites and at 20 kbar were magnesian olivine tholeiites (~49% SiO_2).

These conclusions were opposed by Mysen & Kushiro (1974), Boettcher (1975), and Mysen & Boettcher (1975a,b) who affirmed that their experimental methods were adequate to attain equilibrium, that the compositions of glasses obtained in their experimental runs were unmodified by quenching problems, and that such glass compositions were those of equilibrium liquids appropriate to the P, T conditions of their experiments. Nicholls & Ringwood (1973) synthesized a glass of composition matching that obtained by Kushiro *et al.* (1968) in melting of a lherzolite at 26 kbar, 1190°C, $P(H_2O)=P$(total) and showed that its water-saturated liquidus at 26 kbar was at 940°C, not 1190°C, and that clinopyroxene, not olivine, was the liquidus

phase. Mysen & Kushiro (1974) ignored the temperature discrepancy but argued that liquids derived from an olivine-bearing residue need not have olivine as a liquidus phase at the *P, T* conditions of melting if a reaction relationship existed between olivine and liquid. Mysen & Boettcher (1975b) (see also Mysen & Kushiro 1974) tested a glass from a much lower temperature partial melting run (940°C, at 15 kbar) and prepared a glass of the composition analyzed in the lherzolite melting run (coexisting with olivine, orthopyroxene, clinopyroxene, amphibole and spinel). This glass did not crystallize olivine or amphibole as liquidus phases at 15 kbar although its liquidus temperature (>950°C) was close to that of the partial melting run and amphibole appeared between 950°C and 930°C. Furthermore, addition of 9.4% olivine to the supposedly olivine-saturated composition did *not* result in olivine crystallization. Mysen & Boettcher (1975b) considered that these results supported their conclusions on genesis of highly siliceous liquids and did not recognize that their data at 940°, 15 kbar were inconsistent with the detail of their model and also greatly aggravated the problems for their higher temperature, equally siliceous 'equilibrium liquids' (Mysen & Boettcher 1975b, Table 9).

New Data on Water-Saturated Melting of Pyrolite

The conclusions by Mysen & Boettcher (1975a) that their peridotite solidi were at temperatures <950°C prompted a careful examination of the pyrolite melting relations at 15 kbar to augment the previously published data at 10 kbar and 20 kbar (Green 1973a,b).* Optical examination of crushed sample (mounted in refractive index oils) and of the polished surfaces of uncrushed samples showed a distinctive textural change between 970°C and 1000°C with runs at temperatures ≥ 1000°C showing interstitial glass and quench phases. Analyses of coexisting minerals are given in Table 2 and plotted in terms of 100 Mg/Mg+ΣFe vs. temperature in Fig. 2. The disappearance of primary amphibole (acicular, feathery amphibole at higher temperatures is more siliceous and Fe-rich and is a quench phase, cf. Green 1973a Tables 4,5,8,9) and appearance of ilmenite between 1000°C and 1020°C coincides with a marked increase in Mg/Mg+Fe value of olivine, orthopyroxene and clinopyroxene. These changes require the presence of a large melt fraction (>15%) at 1020°C. The consistency of Mg-value of orthopyroxene and olivine between 900°C and 970°C and the small increase in this value in both orthopyroxene and olivine (the most accurately analyzable phases) at 1000°C suggest that a small melt fraction is present at 1000°C. Unlike the 10 kbar data (Green 1973a) there is no distinctive change in Na/K ratio of amphibole between 970°C and 1000°C. The TiO_2-content of the amphibole increases with increasing temperature at constant pressure (Table 2) and decreases with increasing pressure at constant temperature (Table 2 and Green 1973a Tables 6,7,12). Ilmenite is a coexisting accessory phase at 20 kbar, probably also at 15 kbar and 10 kbar, but was only

TABLE 2. COMPOSITIONS OF MINERALS SYNTHESIZED IN (PYROLITE - 40% OLIVINE) COMPOSITION (GREEN 1973a TABLE 1) UNDER WATER-SATURATED CONDITIONS AT 15 KBAR

Temp. °C	900	930	950	970	1000	1020	1050
Time (hrs)	31	29	25	20	6	4	5
$\frac{100\ Mg}{Mg+\Sigma Fe}_{olivine}$	n.a	83.9	83.8	83.3	84.2	85.7	86.4
	Amph	Amph	Amph	Amph	Amph	Ilm	
SiO_2	46.7	46.3	45.7	46.0	44.5	1.0	
TiO_2	1.1	1.2	1.4	1.5	1.7	54.9	
Al_2O_3	12.1	11.5	12.0	11.8	13.2	0.5	
FeO	5.4	5.2	5.2	5.4	5.6	27.6	
MgO	19.2	19.0	18.3	18.5	18.7	12.9	
CaO	10.5	10.8	11.4	11.2	10.0	0.4	
Na_2O	1.8	1.9	2.1	2.05	2.1	-	
K_2O	0.45	0.5	0.6	0.5	0.5	-	
Cr_2O_3	1.0	1.2	1.2	1.0	1.3	2.3	
$\frac{100\ Mg}{Mg+\Sigma Fe}_{Amph}$	86.3	86.7	86.3	85.9	85.7	45.4	
	Opx	Opx	Opx	Opx	Opx	Opx	Opx
SiO_2	54.1	54.7	54.5	54.3	54.2	55.6	55.0
TiO_2	0.3	0.3	0.3	0.4	0.4	0.3	0.3
Al_2O_3	3.8	3.4	3.7	3.9	3.8	2.3	2.0
FeO	9.5	9.5	9.6	9.5	9.1	8.2	7.9
MgO	30.5	30.5	30.6	30.1	30.3	31.9	32.5
CaO	0.8	0.8	0.9	1.0	1.1	1.0	1.2
Cr_2O_3	0.8	0.6	0.7	0.8	0.8	0.5	1.0
MnO	0.2	0.2	0.1	0.1	0.2	0.2	0.1
$\frac{100\ Mg}{Mg+\Sigma Fe}_{Opx}$	85.1	85.2	85.1	85.0	85.6	87.4	88.0
		Cpx	Cpx	Cpx	Cpx	Cpx	Cpx
SiO_2		53.6	53.0	52.1	52.5	53.5	53.1
TiO_2		0.7	0.5	0.7	0.7	0.8	0.4
Al_2O_3		3.3	3.2	4.0	4.3	3.1	2.6
FeO		4.6	4.3	4.4	4.6	4.1	4.0
MgO		16.5	17.4	17.2	17.1	17.6	18.0
CaO		20.3	20.4	20.5	20.2	20.2	21.0
Na_2O		0.3	0.3	0.3	-	0.1	-
Cr_2O_3		0.7	0.8	0.8	0.7	0.6	0.8
$\frac{100\ Mg}{Mg+\Sigma Fe}_{Cpx}$	n.a	86.4	87.8	87.4	86.8	88.4	88.9

*A new batch of (pyrolite-40% olivine) sintered mix was used with composition as given by Green (1973a Table 1) except that it contained 8.1% FeO and 0.5% Fe_2O_3.

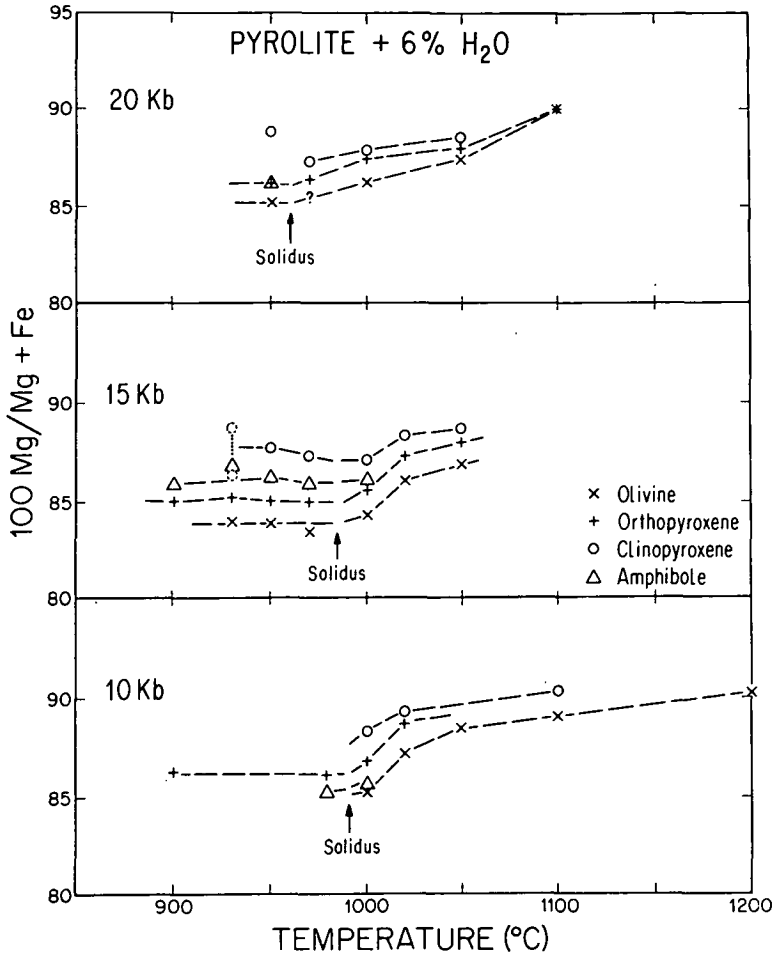

FIG. 2. Plot of temperature versus 100 Mg/Mg+ΣFe for minerals analyzed from (pyrolite - 40% olivine) + 10% H_2O at 10 kbar and 20 kbar (Green 1973a) and at 15 kbar (Table 2, this paper). The position of the solidus is shown at each pressure, as deduced from optical and mineral composition data.

sufficiently large and analyzable above the amphibole breakdown at 15 kbar and 20 kbar.

In view of the discussions by Mysen & Boettcher (1975a,b) on $f(H_2)$ $f(O_2)$ and oxidation state it is important to note that the analyses of the charges after experiments show little or no iron loss and very high FeO/Fe_2O_3 ratios (Table 1). This is confirmed by the ilmenite analyses (Table 2; Green 1973 Table 10) which demonstrate little or no Fe_2O_3 solid solution and are compatible with real mantle conditions (Green & Sobolev 1975). Note also that the differences in 100 Mg/Mg+ΣFe values of coexisting amphiboles, olivine and clinopyroxenes (Fig. 2) when compared with data from natural assemblages in which Fe^{3+} and Fe^{2+} are separately determined (Frey & Green 1974) show that there is little or no Fe^{3+} in amphibole in the 15 kbar runs, and probably small Fe^{3+} contents in the 10 kbar and 20 kbar amphiboles (shorter run times in the 10 kbar, 20 kbar runs, starting mix with 0.8% Fe_2O_3, compared with 0.5% Fe_2O_3 for the 15 kbar runs). The new experimental data confirm that the water-saturated solidus for pyrolite lies between 970°C and 1000°C at 15 kbar, consistent with the interpolation from the previous 10 kbar and 20 kbar data. The upper limit of amphibole stability lies between 1000°C and 1020°C at 15 kbar, slightly higher than interpolated from the 10 kbar and 20 kbar data. The new data give no support to Mysen & Boettcher's (1975a,b) contention that solidi of their perido-

tites, in some cases of more refractory compositions than (pyrolite – 40% olivine) composition, lie at or below 900°C. I consider that these latter solidi were incorrectly determined, errors being caused by lack of equilibrium in the coarsely crystalline starting mixtures and the difficulty of distinguishing vapor-phase quench from silicate-melt quench particularly in bulk compositions where the proportion of vapor phase is high and extremely high in relation to the small proportion of reactive silicate solid phases in a coarse-grained mineral mixture.

Experimental Testing of Calculated Equilibrium Partial Melts of Pyrolite

Previous sections reviewed the evidence against acceptance of silicate glass compositions (analyzed from partial melting runs on peridotite compositions) as equilibrium liquids due to the problems caused by quench outgrowth of primary crystals and the appearance of quench clinopyroxene, amphibole, and possibly chlorite. Green (1973a) used knowledge of the bulk composition of the charge (before and after runs), the composition of mineral phases present, the relative proportions of mineral phases where more than one was present, and the empirical partition coefficient $(Fe/Mg)_{ol}/(Fe/Mg)_{liquid}=0.3$ (Roeder & Emslie 1971) to calculate equilibrium partial melts at 10 kbar, 1200°C; 10 kbar 1100°C; and 20 kbar, 1100°C. These liquids were considerably less siliceous than the analyzed glasses at the appropriate *P, T* conditions and were used to outline a petrogenetic grid for water-saturated melting of pyrolite (Green 1973a; Fig. 3). This work concluded that the most silica-saturated liquids obtainable by partial melting of pyrolite at 20 kbar, water-saturated conditions, were olivine-poor tholeiites (<10% normative olivine).

If this method of derivation of melt compositions is to earn more credence than the discredited method discussed previously then it is obviously necessary to test these calculated melts in the same manner outlined previously. Thus if the calculated equilibrium melt from the 20 kbar, 1100°C run is indeed a partial melt from pyrolite, its water-saturated liquidus should

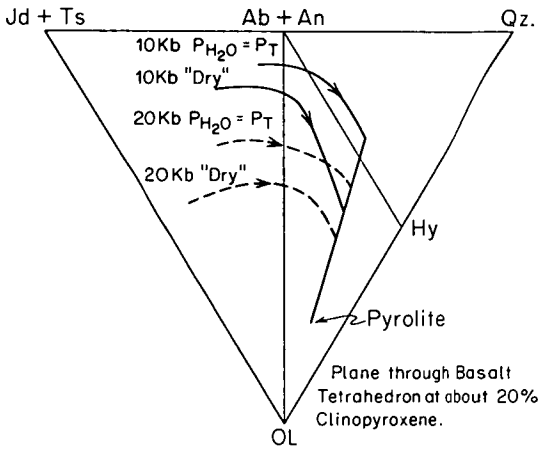

FIG. 3. *Schematic* diagram illustrating the partial melting trend (i.e. trace of liquid compositions with increasing degrees of melting) of pyrolite at 10 kbar and 20 kbar. The "dry" curves refer to melting paths for pyrolite + 0.1% H_2O approximately (Green 1970, 1971, 1973a). The $P_{H_2O} = P_T$ paths refer to water-saturated melting. The low-temperature parts of the curves are cotectic melting paths in which olivine and one or two pyroxenes are residual phases and the beginning of melting involves at least olivine, two pyroxenes, amphibole and spinel. The compositions of residual pyroxenes are of course quite different in the 'dry' and $P_{H_2O} = P_T$ cases. For higher degrees of melting, olivine alone is the residual phase. The different compositions at which the partial melting trends intersect the olivine control line are determined by the data in this paper and in Green (1973a, 1970, 1971) and Green & Ringwood (1967b). Note the relevance of behavior in the simple system Fo-Qz (Kushiro *et al.* 1969) in which water-saturated melting of olivine + enstatite assemblages produces a quartz-normative liquid at 20 kbar, and the simple system Ne-Fo-Qz (Kushiro 1972) in which the water-saturated beginning of melting lies in the nepheline-normative field.

TABLE 3. CALCULATED EQUILIBRIUM LIQUIDS FROM WATER-SATURATED MELTING OF PYROLITE (GREEN 1973a) AND PREFERRED COMPOSITIONS AFTER EXPERIMENTAL TESTING

	10 kbar, 1200°C		10 kbar, 1100°C		20 kbar, 1100°C	
	1	2	3	4	5	6
	Initial	Preferred	Initial	Preferred	Initial	Preferred
SiO_2	54.6	53.8	56.1	55.5	49.4	49.8
TiO_2	2.2	2.0	2.5	2.5	2.7	2.6
Al_2O_3	10.7	9.7	12.4	12.3	12.5	12.0
Fe_2O_3	1.5(0.6)*	0.3	1.7(0.5)*	0.5	0.5(0.5)*	0.5
FeO	6.9(7.9)*	9.1	5.8(6.9)*	6.8	8.9(8.9)*	9.0
MnO	0.2	0.2	0.1	0.1	0.2	0.2
MgO	11.9	14.1	9.3	9.3	11.5	12.6
CaO	9.4	8.6	9.5	10.4	10.9	10.4
Na_2O	1.9	1.7	2.0	2.0	2.1	2.0
K_2O	0.4	0.4	0.5	0.5	0.5	0.5
Cr_2O_3	0.1	0.1	0.1	0.1	0.2	0.2
Qz	6.3	3.0	11.1	8.5	-	-
Or	2.4	2.4	3.0	3.0	3.0	3.0
Ab	16.1	14.4	16.9	16.9	17.9	17.0
An	19.5	18.0	23.4	23.1	23.3	22.3
Di	21.7	19.6	18.9	22.9	25.0	23.6
Hy	27.5	38.2	19.4	20.2	14.5	18.0
Ol	-	-	-	-	10.1	10.2
Chr	0.2	0.2	0.2	0.2	0.3	0.3
Ilm	4.2	3.8	4.7	4.8	5.2	5.0
Mt	2.2	0.4	2.6	0.7	0.7	0.7
$\frac{100\ Mg}{Mg+Fe^{2+}}$	73	73.5	70.5	70.5	70	71.5

* FeO, Fe_2O_3 as analyzed on initial glasses (E. Kiss, analyst).

lie at 20 kbar, 1100°C and olivine and orthopyroxene should either be the liquidus phases or become liquidus phases after addition of <5% (approx.) of either phase. Similar strictures apply to the 10 kbar calculated liquid compositions.

The compositions tested experimentally are listed in Table 3, columns 1, 3 and 5. These compositions were prepared as glasses and the actual analyzed contents of FeO and Fe_2O_3 are listed in Table 3. The iron loss to AgPd capsules is small (Table 1) but, as is anticipated, greater than that in the largely crystalline (pyrolite −40% olivine) compositions at lower temperature and longer run times (Table 1). Experimental data for these compositions are given in Table 4.

10 kbar, 1200°C

The calculated equilibrium liquid for 10 kbar, 1200°C was found to crystallize olivine as the liquidus phase, as predicted, but at $T<1200$°C, probably at 1160-1170°C (there is some uncertainty due to optical identification of olivine in the crushed mounts of some runs but its absence in that part of the sample mounted for electron probe analysis). Addition of 3%, 5% and 10% olivine (Fo_{93}) crystals showed that ~10% olivine must be added before rare, euhedral olivine ($Fo_{90\text{-}91}$) persisted as the liquidus phase at 1180°C. From these data it is inferred that the initial calculated equilibrium liquid was slightly too siliceous and high in normative quartz and the more olivine-rich composition listed in Table 3 column 2 is thus preferred. Column 2 lists the estimate of the liquid derived by ~35% equilibrium partial melting of pyrolite at 10 kbar, 1200°C, water-saturated conditions leaving residual olivine (Fo_{90}) and a trace of chrome spinel. This equilibrium partial melt composition should be contrasted with the analyzed glass compositions (Green 1973a. Table 2 column 6, 7) demonstrating the strong effects of quench crystallization.

10 kbar, 1100°C

The calculated equilibrium liquid (glass 3) for 10 kbar, 1100°C was found to crystallize enstatite and diopside (Table 4) at 10 kbar, 1080°C and to be above its liquidus temperature at 1100°C. For the pyrolite−40% olivine composition at 10 kbar, 1100°C the residual phases were olivine (Mg_{89}) and clinopyroxene (Mg_{90}). Addition of 5% olivine to glass 3 yielded olivine (Mg_{88}) and orthopyroxene (Mg_{90}) as near-liquidus phases at 1100°C and addition of 1% CaO to glass 3 yielded clinopyroxene (Mg_{89}) alone as near-liquidus phase at 10 kbar, 1100°C. It is clear that glass 3 is compositionally extremely close to a liquid which has its 10 kbar, water-saturated liquidus at 1100°C and which is saturated by olivine, orthopyroxene and clinopyroxene at that temperature. It is particularly notable that the clinopyroxene crystallized as the near-liquidus phases from glass 3 (and modified glass 3) compositions at 10 kbar, ~1100°C, is compositionally identical within analytical error with that of the residual clinopyroxene at 10 kbar, 1100°C in

TABLE 4. DETAILS OF EXPERIMENTAL RUNS ON CALCULATED EQUILIBRIUM MELT COMPOSITIONS (GREEN 1973a) AND ON VARIANTS MADE BY ADDING SMALL QUANTITIES OF OLIVINE, ORTHOPYROXENE AND CaO.

Composition†	Run No.	Pressure (kbar)	Temp (°C)	Time (mins)	Products (observed in polished mount).
1	4406	10	1200	30	Quench (above liquidus)
1	4418	10	1180	30	Quench (very rare olivine seen in crush)
1	4488	10	1180	30	Quench
1	4497	10	1170	30	Quench (very rare olivine seen in crush).
1 + 3% Ol*	4501	10	1180	30	Quench
1 + 3% Ol	4503	10	1160	30	Quench
1 + 5% Ol	4507	10	1180	30	Quench
1 + 5% Ol	4515	10	1160	15	Quench
1 + 5% Ol	4518	10	1150	15	Ol_{90}+Quench
1 + 5% Ol	4508	10	1140	30	$Ol_{88\text{-}92}$+Quench
1 + 10% Ol	4540	10	1180	15	$Ol_{90\text{-}91}$+Quench
3	4410	10	1100	30	Quench
3	4412	10	1080	30	Opx_{88}+Cpx_{88}
3 + 2% Ol	4506	10	1120	30	Quench
3 + 2% Ol	4509	10	1110	30	Opx_{89}+Quench
3 + 2% Ol	4504	10	1100	30	Opx_{91}+Quench
3 + 5% Ol	4519	10	1120	15	Quench
3 + 5% Ol	4524	10	1100	15	$Ol_{86\text{-}88}$+$Opx_{89\text{-}90}$+Quench
3 + 1% CaO*	4525	10	1100	15	Cpx_{89}+Quench
3 + 1% CaO	4534	10	1080	15	$Cpx_{87\text{-}88}$+Quench
3 + 1% CaO	4547 4550	10	1060	30	Opx_{85}+Cpx_{86}+Quench
5	4541	20	1120	15	$Cpx_{88.5}$+Quench
5	4535	20	1110	35	$Cpx_{88.5}$+Quench
5	4408	20	1100	60	Cpx_{88}+Quench
5	4417	20	1080	60	Ol_{85}+Cpx_{87}+Quench
5	4419	20	1060	60	Ol_{82}+Cpx_{86}+Quench
5 + 5% Enst.*	4552	20	1110	20	$Ol_{85\text{-}86}$+Cpx_{88}+Quench
5 + 5% Enst.	4546	20	1100	20	Ol_{86}+Cpx_{88}+Quench
5 + 5% Enst.	4551	20	1080	20	$Opx_{84\text{-}85}$+Cpx_{86}+Quench
5 + 5% Enst.	4559	20	1080	20	$Ol_{83\text{-}84}$+Cpx_{87}+Quench
5 + 10% Enst.	4572	20	1140	15	Quench
5 + 10% Enst.	4571	20	1130	15	Opx_{86}+Cpx_{87}+Quench
5 + 10% Enst.	4568	20	1120	15	$Opx_{85\text{-}86}$+$Cpx_{86\text{-}88}$+Quench
5 + 10% Enst.	4564	20	1100	15	Ol_{86}+$Opx_{86\text{-}88}$+Cpx_{88}+ Quench
5 + 10% Enst.	4563	20	1100	15	Opx_{85}+Cpx_{86}+Quench

†See Table 3

*Olivine added was finely ground (<20μm) olivine from lherzolite 2604 (Frey & Green 1974) of composition Mg_{93}. Enstatite added was finely ground (<10x30μm laths) enstatite from enstatite eclogite (Green 1969) and was of composition Mg_{85}, 0.9% Al_2O_3, 0.5% CaO. CaO was added as Analar $CaCO_3$, so that in fact these runs contained 0.9 wt.% CO_2 in addition to 15 wt.% H_2O.

All runs at 10 kbar contained 15 wt.% H_2O, those at 20 kbar contained 20 wt.% H_2O. At 10 kbar, experiments at <1100°C were carried out in $Ag_{75}Pd_{25}$ capsules, those at >1100°C used $Ag_{50}Pd_{50}$ capsules. At 20 kbar all experiments were carried out in $Ag_{75}Pd_{25}$ capsules.

For Run No. 4564, read 1110°C.

TABLE 5: COMPOSITIONS OF LIQUIDUS AND NEAR-LIQUIDUS PHASES OF LIQUIDS OF TABLE 3. COMPARE WITH RESIDUAL PHASES AT SIMILAR *P,T*. FOR PYROLITE - 40% OLIVINE (GREEN 1973a).

	Glass 3		Glass 3 + 5% Ol		Glass 3 + 1% CaO			Glass 5	Glass 5		Glass 5 + 5% Enst.		Glass 5 + 10% Enst.			
	10 kbar, 1080°C		10 kbar, 1100°C		10 kbar, 1100°C			20 kbar, 1120°C	20 kbar, 1080°C		20 kbar, 1100°C		20 kbar, 1110°C			
	Opx	Cpx	Ol	Opx	Cpx	Q-Cpx	Q-Cpx	Cpx	Ol	Cpx	Ol	Cpx	Ol	Opx	Cpx	Q-Amp
SiO_2	56.9	54.5	41.0	54.4	54.3	53.9	48.8	53.5	40.9	53.8	40.5	53.3	40.2	56.7	54.6	44.9
TiO_2	0.2	0.4	-	0.2	0.3	0.6	4.0	0.4	-	0.4	-	0.4	-	0.2	0.2	2.9
Al_2O_3	0.4	1.0	-	0.6	1.0	1.7	6.8	1.3	-	2.0	-	2.1	-	1.2	1.6	11.0
FeO	8.0	4.3	11.1	6.6	4.1	5.6	7.6	4.1	14.4	4.5	12.7	4.1	13.3	8.1	4.2	9.9
MnO	-	-		-	-	-		-	0.1	-	0.1	-	-	0.1	-	-
MgO	32.3	18.7	47.7	33.0	18.5	18.5	15.6	17.9	45.5	17.8	46.3	17.3	46.4	31.9	18.1	15.9
CaO	1.9	20.2	0.2	1.6	20.8	18.9	16.9	21.4	0.4	20.5	0.1	20.9	0.1	1.3	20.1	9.7
Na_2O	-	-	-	-	-	-	0.2	-	-	0.1	-	-	-	-	-	1.7
Cr_2O_3	0.4	0.9	-	-	1.0	0.8	0.1	1.4	-	1.0	0.1	1.8	-	0.5	1.1	.2
	87.8	88.5	88.4	89.9	89.0	85.5	78.4	88.6	84.9	87.5	86.5	88.2	86.1	87.6	88.5	74.2

(pyrolite – 40% olivine + 10% H_2O; Green 1973a). In the (pyrolite – 40% olivine) composition, orthopyroxene was not present in the polished mount but rare grains were identified optically in the crushed portion of the charge and the abundance of orthopyroxene at 10 kbar, 1050°C suggests that 10 kbar, 1100°C is very close to the temperature of disappearance of orthopyroxene as a residual phase in water-saturated melting of pyrolite. As Mysen & Kushiro (1974) have pointed out, if olivine and quartz-normative liquid are in a reaction relationship (to precipitate orthopyroxene at lower temperature) under water-saturated conditions at 10 kbar, then the liquid separated from an olivine-bearing residue may have orthopyroxene, not olivine as its liquidus phase. However addition of olivine to that liquid must result in persistence of olivine, either in place of or additional to orthopyroxene. These are precisely the relationships observed in the glass 3 composition and its modifications by CaO and olivine addition.

20 kbar, 1100°C

The calculated equilibrium liquid (glass 5) at 20 kbar, 1100°C has clinopyroxene as its liquidus phase at 1120°C, with olivine appearing between 1100°C and 1080°C. Addition of 5% enstatite crystals resulted in solution of enstatite and precipitation of olivine and clinopyroxene as liquidus phases, but addition of 10% enstatite resulted in persistence of some cores of relict enstatite (low Al, low Ca) and reaction of rims and smaller crystals to more Mg-rich, aluminous and calcic enstatites (cf. Table 4 footnote, and Table 5) and coprecipitation of clinopyroxene (1130°C, 1120°C) or clinopyroxene and olivine (1110°C). Compositions of liquidus pyroxene in the glass 5 and related compositions are agai very close to the residual pyroxenes in (pyrolit 40% olivine) at 20 kbar, 1100°C (orthopy roxene, possible primary clinopyroxene cores t quench clinopyroxene; see Green 1973a Tab 8) and 20 kbar, 1050°C (orthopyroxene an clinopyroxene). This compositional similarit shows that the Al_2O_3, TiO_2, Na_2O, and Mg-value as well as the normative composition, of the ca culated equilibrium liquid are about right for th liquid in equilibrium with the observed residu pyrolite mineralogy. Column 6, Table 3 lists th preferred composition, slightly richer in enst tite and lower in diopside content than glass which has the correct liquidus phases of th correct composition to be a water-saturated pa tial melt from pyrolite at 20 kbar, 1100±20°C Note that the difference from the original ca culated liquid (glass 5) implies that the roughl estimated ratio of 3:2 for residual olivine:orth pyroxene in the original partial melting ru (Green 1973a Table 8) was too low, and a 5: ratio would have been better. The 'reverse partial melting experiments confirm that equil brium partial melting of pyrolite under wate saturated conditions at 20 kbar, 1100°C wi produce 27±1% melt of magnesian olivine th leiite composition (~10% normative olivin ~18% normative hypersthene and having SiO content of ~50%) leaving residual olivin orthopyroxene and possibly minor clinopyroxen The contrast between this equilibrium melt an the highly siliceous quenched glass composition (with their water-saturated liquidi at 950°C 1000°C) obtained at 20 kbar, 1100°C accentu ates the quenching problem in partial meltin experiments. Even in above-liquidus and nea liquidus runs, the water-saturated basaltic liquic

id not quench to clear glass but grew quench utgrowths on primary phases (Table 4) and ucleated fibrous or acicular amphibole and ?)mica or chlorite laths during quenching. The roblem is aggravated when such basaltic liq-ids are interstitial to common crystals which row during quenching and act as nucleation ites for quench phases.

Conclusions

The data presented in this paper, when com-ined with the previously published data on the artial melting relationships of pyrolite under vater-saturated conditions (Green 1973a,b) de-ine the compositions of liquids formed by aturated melting of pyrolite at 10 kbar, 1100°C nd 1200°C, and 20 kbar, 1100°C. It has been hown that, provided the bulk composition of he peridotite charge is known, (iron loss is ıonitored and oxygen fugacity maintained :NNO buffer), the mineral compositions anal-zed, and the relative proportions of minerals stimated, then it is possible to use this informa-ion together with known equilibrium crystal/ iquid partition relationships to calculate equili-rium liquid compositions (Green 1973a). It is hen possible to test and confirm the reliability nd accuracy of the calculated liquids by run-ing these compositions at the appropriate P, T, $'(H_2O)$ conditions to confirm that their liquidus emperatures and liquidus phases match those of he residual peridotite. This general approach to stablishing a petrogenetic grid for mantle mag-na genesis has now been demonstrated for dry nelting (Green & Ringwood 1967b,c), water-ndersaturated melting (Green 1970, 1971, 973c), and water-saturated melting. In the first wo cases, it was possible to use petrological and eological arguments to identify the natural man-le-derived liquids and to use these compositions s the basis for the petrogenetic studies. In the ıtter case, although it has often been suggested hat the distinctive basaltic and andesitic magmas f island arcs are the products of water-saturated nelting of the upper mantle, it has not been pos-ible (in the absence of transported high-pressure enoliths) to objectively identify mantle-derived, nfractionated liquids in the island arc environ-ıent. The investigation of water-saturated melt-ıg of pyrolite is thus more completely an empi-ical, experimental exercise with the complemen-ary aspects of partial melting experiments on eridotite and liquidus studies on potential melt roducts as presented in this paper.

The data presented by Green (1973a,b) and in ıis paper show that at 10 kbar, 1100°C, under water-saturated conditions, the pyrolite composition will contain 28±1% liquid with a composition classifiable as a magnesian quartz tholeiite or magnesian basaltic andesite composition (Table 3, columns 3, 4). With increasing degrees of melting, clinopyroxene and olivine enter the melt until at 10 kbar, 1200°C the pyrolite is 35±1% molten and the liquid is a magnesian quartz tholeiite (Table 3, column 2). Higher degrees of melting, dissolving further olivine, will produce olivine-poor tholeiitic liquids with very low Al_2O_3, CaO, Na_2O contents. The compositions of liquids nearer the pyrolite solidus cannot as yet be uniquely determined since calculation of such liquids would require knowledge of the relative proportions of olivine, pyroxenes and amphibole (at 1000°C) among the residual crystals. However, the increasing modal abundance of orthopyroxene and clinopyroxene, the reaction relationship between olivine and liquid to precipitate pyroxene, and the strong partitioning of Na, K, Ti into the liquid relative to pyroxenes and olivine, show that liquids at <1100°C, 10 kbar are unlikely to have >55% SiO_2 and will decrease in SiO_2 and increase in $Na_2O + K_2O$ towards the solidus. Unpublished data on partitioning of Na_2O and K_2O between amphibole and liquid between 10 kbar and 20 kbar, 1000°C to 1150°C shows that $(Na_2O)_{liquid}/(Na_2O)_{amphibole} \approx 2$ and $(K_2O)_{liquid}/(K_2O)_{amphibole} > 2$. Thus the amphibole present at 1000°C, 10 kbar (Green 1973a) can be used to predict that the coexisting equilibrium liquid contains 4% Na_2O (approx.) and >0.6% K_2O — such liquids, with 50-55% SiO_2 and >14% Al_2O_3 would be olivine-normative and possibly nepheline-normative. The experimental studies show that the most silica-oversaturated liquids which can be derived from water-saturated partial melting of pyrolite at 10 kbar (30-40 km depth) are magnesian quartz-rich tholeiites with <10% normative quartz (Fig. 3). There is no temperature at which andesites with >55% SiO_2, >10% normative quartz, can be derived as equilibrium partial melting products of pyrolite at >10 kbar. The evidence herein and previously published (Green 1973a) on the problems of quenching of hydrous liquids show that analyses of siliceous glasses present in experimental runs do not represent equilibrium liquids even at 10 kbar, and cannot be used as evidence of the nature of magmas derived by water-saturated melting of peridotitic compositions.

At 20 kbar, 1100°C, the pyrolite composition contains 27 ± 1% melt under conditions of $P_{H_2O} = P_{Total}$ and the melt is of magnesian olivine tholeiite composition. Lower degrees of melting increase the importance of residual

pyroxenes but Na_2O, K_2O and TiO_2 remain strongly partitioned into the melt phase so that liquids are deduced to be more undersaturated and would probably become nepheline-normative between 1050°C and 1000°C. The presence of residual ilmenite at 1000°C and 970°C shows that the TiO_2 concentration in the liquid at these temperatures is sufficient to precipitate ilmenite — further data are required but unpublished experiments on basanite and mugearite composition (Irving & Green, unpublished) and on potassic mafurite composition (Edgar *et al.* in press) show that the TiO_2 content of such a liquid will exceed 3% TiO_2. Partition coefficients for $(Na_2O)_{cpx}/(Na_2O)_{liquid}$ suggest that the liquid at 20 kbar, 1100°C would contain > 3.0% Na_2O. At temperatures > 1200°C at 20 kbar, liquids may become slightly richer in SiO_2 and lower in normative olivine, up to the temperature at which orthopyroxene is no longer a residual phase (1200-1250°C approx.). Such liquids will be of magnesian, olivine-poor tholeiite composition. Quartz tholeiites, basaltic andesites, andesites or more siliceous liquids cannot be equilibrium partial melts from pyrolite under any conditions at pressures > 20 kbar.

Source-Peridotite Geochemistry in Island Arc Environments

It has previously been suggested (Green 1973a, p. 42) that some of the distinctive geochemical characteristics of magmas in the island arc environment may arise because the source peridotite producing the parental olivine-poor tholeiites to quartz tholeiite magmas (island arc tholeiitic series) is not of pyrolite composition but is of partly-depleted pyrolite composition. This 'depleted pyrolite' is envisaged as having lost a basaltic melt fraction (<10% melt) in an earlier mid-ocean ridge or 'Hawaiian' type of magmatism and lithosphere formation. The 'depleted pyrolite', having lost a magmatic component under conditions of water-undersaturated melting, is mobilized as a source for further magmatism by access of water from subducted oceanic crust and lithosphere in the island arc environment, leading to conditions of water-saturated or near-saturated melting. An additional factor which must be considered in the geochemistry of island arc magmatism is the possibility that significant compositional change to peridotite overlying the Benioff zone is effected either by components transported through a vapor phase or by addition of a small water-saturated melt fraction from the subducted oceanic crust (Ringwood & Green 1966; Gre & Ringwood 1968; T. H. Green 1972; Nicho & Ringwood 1973; Ringwood 1974). These fa tors emphasize that it is probably incorrect consider the model pyrolite composition as t likely source composition for island arc ma matism. However the experimental study pyrolite and the information on residual perid tite mineralogy permit inferences on the effe of variation in a source peridotite compositi on the nature of the melting products.

If the source peridotite in island arc regio is depleted from pyrolite by the earlier loss of basaltic fraction, then the K_2O, TiO_2, Na_2O co tents (and geochemically related trace elemer Sr, Ba, Rb, *REE*, Zr, etc.) will be strongly d pleted whereas SiO_2, MgO, FeO, Al_2O_3 and Ca would have suffered less relative change. Wate saturated melting of such source material (st with subsolidus mineralogy of olivine, pyro enes, amphibole, spinel) will produce a low proportion of liquid than is present in pyrolite a particular near-solidus temperature because depletion of the low-melting fraction. At high temperatures the liquids will be similar to tho from pyrolite at the same *T*, *P*, $\%H_2O$ in tern of SiO_2, MgO, FeO, CaO, Al_2O_3 contents b will be distinctly lower in Na/Ca, K/Ca, TiC *REE* etc. It is suggested that three of the mo important characteristics of some island a magma series are indicative of, or at least co sistent with, such a depleted source region. Th the low TiO_2 content characteristic of island a basalts, in comparison with basalts from ocean or stable continental environments, cannot l attributed to the presence of a relatively TiC enriched phase (amphibole, ilmenite, phlogopit *in equilibrium with* a TiO_2-poor liquid but wou be a characteristic of a partly-depleted source r gion. Secondly, a most distinctive characterist of many, but not all, island arc basalt-andesit dacite series is the extremely calcic nature phenocryst plagioclase (Whitford 1975). Basal of such series may contain plagioclase phen crysts up to An_{93} whereas the most calcic plagi clases crystallizing from basalts of oceanic stable crust environments are An_{85}. It is su gested that parental magmas to those crystalli ing plagioclase $>An_{90}$ are derived from sour peridotites with much lower Na/Ca ratio th that of pyrolite. A third characteristic of son island arc magmas series is the low abundan of the *REE* and the relative *LREE*-depletion this is consistent with a source peridotite whi has previously lost a small, incompatible el ment-enriched basaltic fraction.

It may be inferred from the experimental st dies of eclogite-facies melting (Green & Rin

ood 1968; T. H. Green 1972) and from studies f natural pegmatites associated with eclogite in igh-pressure metamorphic terranes (Green & lysen 1972) that small degrees of melting of ibducted eclogitic crust will yield silicic mag-as of high K/Na ratio. The variation of K_2O ontents, occurrence of basalt and andesites with $Sr/^{86}Sr>0.703$ and with *LREE*-enriched char-icteristics, may primarily be due to variable roportions of added low-temperature melt frac-on from subducted oceanic crust (cf. Ringwood 974). *Alternatively*, variations in these incom-atible-element abundances and related isotopic ariations may reflect prior differences in source-eridotite composition. Frey & Green (1974) ave shown that lherzolites from the upper litho-here show at least two stages of development - an initial stage (A) of formation as residual ierzolite from a partial melting event, and a econd stage (or stages; B) of variable and local nrichment in incompatible trace elements hrough either an added small melt fraction livine melilite nephelinite) or migration through H_2O-rich vapor phase. Differences in incom-atible-element contents in parental island arc nagmas may thus reflect differences in the ex-nt to which stage(s) B have modified the litho-here composition, e.g. if *older* crust/lithosphere egions are reactivated then resultant orogenic r island arc magmas are incompatible-element nriched and may have high $^{87}Sr/^{86}Sr$ ratios. In ontrast, if *younger* crust/lithosphere regions, articularly of oceanic crust, are reactivated nen the source peridotite and resultant magmas ould be depleted in incompatible-element con-nts, have low Na/Ca ratios, etc. The purpose f the preceding discussion is to indicate the type f geochemical complexity which might be ex-ected in the island arc situation — the geo-hemical 'fingerprints' of such complexity of the ource region act as overprints of fine detail on arental magma compositions defined in the resent experimental study. The experimental artial melting and crystallization studies, with eir emphasis on the mineral phases and major-ement compositions of liquids and crystals, re adequate to define the prime characteristics .g. andesite or basalt, olivine-normative or uartz-normative, high Al or low Al) of perido-te-derived liquids under water-saturated con-itions but do not strongly constrain trace ele-ents, particularly incompatible trace elements. has been conclusively demonstrated that the elting products of peridotitic mantle, at depths f magma segregation of >30 km, are basaltic n the broad sense) and andesites, dacites or hyodacites are not possible products of direct artial melting of peridotitic mantle. As dis-cussed in earlier papers, the parental water-rich basalt magmas in the island arc situation will necessarily partly crystallize, and most commonly fractionate, by extraction of olivine, pyroxene, amphibole, plagioclase and titanomagnetite as they move toward the surface, yielding derivative, silica-enriched andesites, dacites, etc.

References

AHRENS, T. J. & SCHUBERT, G. (1975): Gabbro-eclogite reaction rate and its geophysical significance. *Rev. Geophys. Space Phys.* **13**, 383-400.

BANNO, S. & GREEN, D. H. (1968): Experimental studies on eclogites: the roles of magnetite and acmite in eclogitic assemblages. *Chemical Geology* **3**, 21-32.

BOETTCHER, A. L. (1975): Experimental igneous petrology. *In* U.S. National Report 1971-1974 to IUGG. 75-79 (*Amer. Geophys. Union*).

BREY, G. & GREEN, D. H. (1975): The role of CO_2 in the genesis of olivine melilitite. *Contr. Mineral. Petrology* **49**, 93-103.

EDGAR, A. D., GREEN, D. H. & HIBBERSON, W. O. (1967): Experimental petrology of a highly potassic magma. *J. Petrology* **17**, (in press).

FREY, F. A. & GREEN, D. H. (1974): The mineralogy, geochemistry and origin of lherzolite inclusion in Victorian basanites. *Geochim. Cosmochim. Acta* **38**, 1023-1059.

GREEN, D. H. (1970): The origin of basaltic and nephelinitic magmas (Bennett Lecture). *Trans. Leicester Lit. Philos. Soc.* **64**, 28-54.

——— (1971): Composition of basaltic magmas as indicators of conditions of origin: application to oceanic volcanism. *Phil. Trans. Roy. Soc. London A*, **268**, 707-725.

——— (1972): Magmatic activity as the major process in the chemical evolution of the crust and mantle. *In* The Upper Mantle (A. R. Ritsema, ed.). *Tectonophys.* **13**, 47-71.

——— (1973a): Experimental studies on a model upper mantle composition at high pressure under water-saturated and water-undersaturated conditions. *Earth Planet. Sci. Lett.* **19**, 37-53.

——— (1973b): Contrasted melting relations in a pyrolite upper mantle under mid-oceanic ridge, stable crust and island arc environments. *Tectonophys.* **17**, 285-297.

——— (1973c): Conditions of melting of basanite magma from garnet peridotite. *Earth Planet. Sci. Lett.* **17**, 456-465.

——— & RINGWOOD, A. E. (1967a): An experimental investigation of the gabbro to eclogite transformation and its petrological implications. *Geochim. Cosmochim. Acta* **31**, 767-833.

——— & ——— (1967b): The genesis of basaltic magmas. *Contr. Mineral. Petrology* **15**, 103-190.

——— & ——— (1967c): The stability fields of aluminous pyroxene peridotite and garnet peridotite and their relevance in upper mantle structure. *Earth Planet. Sci. Lett.* 3, 151-160.

———, ———, HIBBERSON, W. O. & WARE, N. G. (1975): Experimental petrology of Apollo 17 mare basalts. *Proc. 6th Lunar Sci. Conf.* 1, 871-893.

——— & SOBOLEV, N. V. (1975): Coexisting garnets and ilmenites synthesized at high pressures from pyrolite and olivine basanite and their significance for kimberlitic assemblages. *Contr. Mineral. Petrology* 50, 217-229.

GREEN, T. H. (1972): Crystallization of calc-alkaline andesite under controlled high pressure hydrous conditions. *Contr. Mineral Petrology* 34, 150-166.

——— & RINGWOOD, A. E. (1968): Genesis of the calc-alkaline igneous rock suite. *Contr. Mineral. Petrology* 18, 105-162.

KISS, E. (1974): Synthesis of a sulphonated ferroin reagent for chelating iron (II) in strong acid. Spectrophotometric determinations of the oxidation state of iron in silicates. *Anal. Chim. Acta* 72, 127-144.

KUSHIRO, I. (1970): Systems bearing on melting of the upper mantle under hydrous conditions. *Carnegie Inst. Wash. Yearbook* 68, 240-245.

——— (1972): Effect of water on the composition of magmas formed at high pressures. *J. Petrology* 13, 311-334.

———, SYONO, Y. & AKIMOTO, S. (1968): Melting of a peridotite nodule at high pressures and high water pressures. *J. Geophys. Res.* 73, 6023-6029.

———, YODER, H. S. & NISHIKAWA, M. (1968): Effect of water on the melting of enstatite. *Geol. Soc. Amer. Bull.* 79, 1685-1692.

LONGHI, J., WALKER, D., GROVE, T. L., STOLPER, R. M. & HAYS, J. F. (1974): The petrology of the Apollo 17 mare basalts. *Proc. 5th Lunar Sci. Conf.* 1, 447-470 (Pergamon).

MILHOLLEN, G. L., IRVING, A. J. & WYLLIE, P. J. (1974): Melting interval of peridotite with 5.7 percent water to 30 kilobars. *J. Geol.* 82, 575-587.

MYSEN, B. O. & KUSHIRO, I. (1974): A possible mantle origin for andesite liquids: discussion of a paper by Nicholls and Ringwood. *Earth Planet. Sci. Lett.* 21, 221-229.

——— & BOETTCHER, A. L. (1975a): Melting of a hydrous mantle: I. Phase relations of natural peridotite at high pressures and temperatures with controlled activities of water, carbon dioxic and hydrogen. *J. Petrology* 16, 520-548.

——— & ——— (1975b): Melting of a hydrous mantle: II. Geochemistry of crystals an liquids formed by anatexis of mantle peridotit at high pressures and high temperatures as function of controlled activities of water, hydr gen and carbon dioxide. *J. Petrology* 16, 549-59

NEHRU, C. E. & WYLLIE, P. S. (1975): Compos tions of glasses from St. Paul's peridotite partiall melted at 20 kilobars. *J. Geol.* 83, 455-471.

NICHOLLS, I. A. (1974): Liquids in equilibriu with peridotitic mineral assemblages at high w ter pressures. *Contr. Mineral. Petrology* 4 289-316.

——— & RINGWOOD, A. E. (1973): Effect water on olivine stability in tholeiites and the pr duction of silica-saturated magmas in the islan arc environment. *J. Geol.* 81, 285-300.

——— & ——— (1974): A possible mant origin for andesitic liquids: discussion of pap by Nicholls and Ringwood. *Earth Planet. Sc Lett.* 21, 221-229.

RAHEIM, A. & GREEN, D. H. (1974): Experiment determination of the temperature and pressu dependence of the Fe/Mg partition coefficie for coexisting garnet and clinopyroxene. *Cont Mineral. Petrology* 48, 179-203.

REED, S. J. B. & WARE, N. G. (1973): Quantitativ electron microprobe analysis using a lithiun drifted silicon detector. *X-ray Spectrometry* 69-74.

——— & ——— (1975): Quantitative ele tron microprobe analysis of silicates using energ dispersive X-ray spectrometry. *J. Petrology* 1 499-519.

ROEDER, P. L. & EMSLIE, R. F. (1970): Olivin liquid equilibrium: *Contr. Mineral. Petrology* 2 275-289.

RINGWOOD, A. E. (1974): The petrological evol tion of island arc systems. *J. Geol. Soc. Lon* 130, 183-204.

——— & GREEN, D. H. (1966): Experimental i vestigation of the gabbro to eclogite transform tion and some geophysical consequences. *Tect nophys.* 3, 383-427.

WHITFORD, D. J. (1975): *Geochemistry and P trology of Volcanic Rocks from the Sunda Ar Indonesia.* Ph.D. thesis, R.S.E.S. Australian Na Univ.

Manuscript received November 1975, emended Ja uary 1976.

(Reprinted in Canada from The Canadian Mineralogist, Vol. 14, Part 3, August 1976)

B22

Contrib. Mineral. Petrol. 55, 217–230 (1976)

Contributions to Mineralogy and Petrology
© by Springer-Verlag 1976

Solubility of CO_2 in Olivine Melilitite at High Pressures and Role of CO_2 in the Earth's Upper Mantle

Gerhard P. Brey and David H. Green

Research School of Earth Sciences, Australian National University, Canberra

Abstract. The positions of the liquidi and the near-liquidus phases of olivine-melilitite + CO_2 have been determined under MH-buffered and 'furnace-buffered' conditions up to 40 kb. It is found that CO_2 alone lowers the liquidus compared to 'dry' conditions, yet its influence is minor compared to H_2O. The major role of CO_2 is to favour the growth of orthopyroxene and garnet over that of olivine at least at high pressures. CO_2-contents of glasses from experiments just above the liquidus (MH-buffered) were determined as 5.1 % at 10 kb; 7.5 % at 20 kb, 9.3 % at 30 kb and 10–11 % (estimated) at 40 kb. Experiments on (pyrolite − 40 % olivine) + H_2O + CO_2 show that CO_2 occurs under mantle conditions as carbonate under subsolidus conditions and dissolved in a melt above the solidus. At 30 kb, the solidus lies between 1,000° C and 1,050° C for vapour-saturated conditions, at $X_{H_2O} = 0.5 = X_{CO_2}$ and at $X_{H_2O} = 0.9$, $X_{CO_2} = 0.1$.

Introduction

The important effects of CO_2 on phase relationships at high pressures in simple systems [3, 4] and in highly undersaturated magmas [1] have shown that processes of magma generation in the upper mantle will be strongly affected by the presence or absence of CO_2. It is important to determine the solubility of CO_2 in silicate melts under H_2O-absent conditions as a function of pressure, temperature and melt compositions, and particularly to determine CO_2 solubility in the presence of H_2O and varying H_2O:CO_2 proportions. Initial data in simple systems [3, 4] show that the solubility of CO_2 increases with increasing pressure and is dependent on the composition of the silicate melt. The presence of H_2O enhances the solubility of CO_2 [1, 3].

The solubility of CO_2 in dry or hydrous silicate melt at a given pressure can be determined by increasing CO_2 content until no further depression of the liquidus is observed and (if quench crystallization is not a problem) bubbles from a separate vapour phase are observed. If the depression of the liquidus by added CO_2 is

not large then this method is insensitive. Many *dry* silicate melts containing only CO_2 as a dissolved vapour phase, quench to clear glass and the CO_2 content in such glasses may be determined directly or indirectly. Mysen and Seitz [19] used radioactive carbon and fission track (β-track) counting of the CO_2-containing glass to estimate CO_2-contents. In this paper we report gas chromatographic determination of CO_2-contents of glasses of olivine melilitite and diopside compositions up to 40 kb at temperatures slightly above the liquidi. We also have determined the effect of CO_2 on the liquidus temperature and the nature of liquidus phases of the olivine melilitite composition and gathered further information on experimental techniques suited for investigation of silicate systems.

Experimental Methods

The experimental methods and the starting material (olivine melilitite from Laughing Jack Marsh, Tasmania) were described previously [1]. The use of pyrex glass (to prevent water migrating from the outermost talc sleeve into the neighbourhood of the capsule) causes a slight uncertainty in the accuracy of pressure measurement as, unlike boron nitride (with which the calibration experiments were carried out [1], the pressure correction for pyrex glass may be temperature dependent. The oxygen fugacity in the samples has been held within narrow but unknown limits either using a double capsule method (magnetite-haematite + water buffer determines hydrogen fugacity in inner capsule) or a single capsule (furnace assembly determines hydrogen fugacity in inner capsule at values close to and slightly greater than the water + Ni-NiO buffer). We emphasize that both techniques 'buffer' oxygen to a first approximation but at different values of f_{O_2}. Olivine melilitite glass and $Ag_2C_2O_4$ (generally equivalent to 38 wt % CO_2) were mixed in a mortar and then welded into a plantinum capsule. H_2O-saturated experiments were carried out in single $Ag_{50}Pd_{50}$ capsules for 20 min with f_{O_2} 'buffered' by the furnace assembly ($f_{O_2} \leqq$ NNO buffer). Experiments with diopside + CO_2 utilized two different starting materials:

(a) Crystalline diopside (Tem-Pres) + $Ag_2C_2O_4$ (corresponding to 20% CO_2) runs in double Pt capsules with external MH buffer applied.

(b) A mechanical mix of MgO, SiO_2 (silicic acid fired at 1,000° C) and $CaCO_3$, which was dried at 500° C, loaded into Pt capsules, dried again for several hours and then immediately welded. The runs were buffered by the furnace assembly ($f_{O_2} \leqq$ NNO).

Electron Microprobe Techniques

A TPD electron microprobe [6] with an energy dispersive analytical system [21, 22] was used for mineral and glass analyses. Conditions of analysis and evaluation of accuracy are given by Reed and Ware [22].

Infrared Spectrophotometry of Glasses

The glasses were finely ground, mixed with KBr, dried at 110° C and then pressed into discs. The infrared spectra were obtained on a Perkin-Elmer Model 257 Grating Infrared Recording Spectrophotometer in the frequency range of 4,000 cm^{-1} to 625 cm^{-1}.

Quantitative Analysis of CO_2 and H_2O

CO_2 and H_2O have been analysed simultaneously with a Hewlett-Packard 185B CHN (Carbon, Hydrogen, Nitrogen) analyser. Lindgren *et al.* [15] used this method successfully for larger amounts (50–100 mg) of rock samples and have described the analytical procedure in detail. The CHN analyser at ANU is set up for the analysis of very small amounts of sample ($\sim$0.5 mg) of organic substances.

Analysis of silicate glasses in such amounts yields results comparable with other methods (Table 2). The sample (glass splits from experimental runs) is placed at the end of a rod in an aluminum container, kept in the gas stream in a separate chamber at about 70° C for several minutes to eliminate atmospheric gases and is then pushed into the combustion furnace (1,055° C). A combustion time of 55 secs is routinely used for organic samples and an increase to 90 seconds yields a small increase in CO_2 content for the silicate glasses. Larger combustion times gave the same yield (Table 2). The H_2O and CO_2 released are carried into a gas chromatographic system by a continuous helium stream and separated in a column filled with Porapak Q-80–100 mesh column packing. CO_2 and water then sequentially enter a thermal conductivity detector. The detector develops electrical signals proportional to the concentration of H_2O or CO_2 respectively in the carrier gas. The peak area of the signal is measured by an electronic integrator and compared to that of a standard sample. The accuracy of the method is ± 0.1 % at 16 % CO_2 (using Ag_2CO_3 as a standard).

Experimental Results

(a) Olivine Melilitite + $Ag_2C_2O_4$ (MH Buffer, Double Capsule)

The characteristics of near-liquidus runs at pressures to 40 kb are shown in Fig. 1 for olivine melilitite + 38 wt. % CO_2 (= molar equivalent of 20 wt % H_2O).

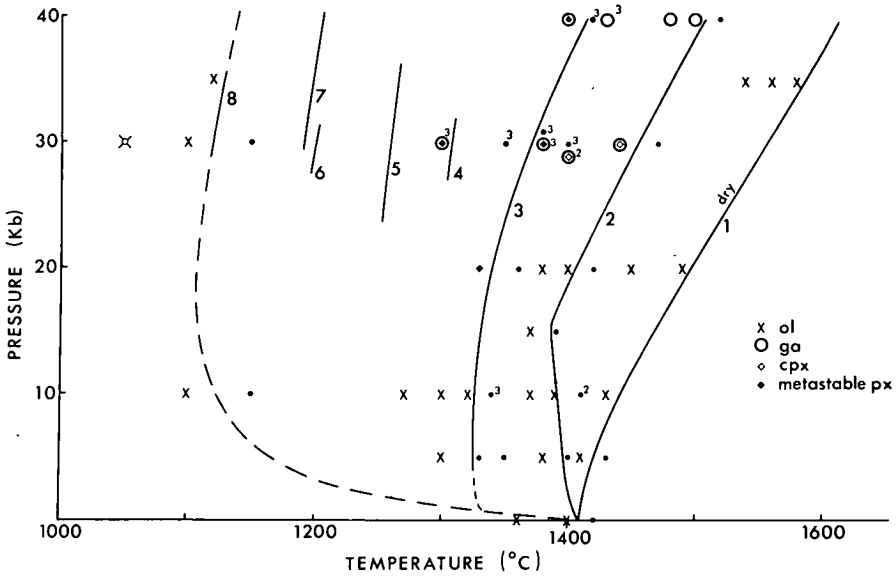

Fig. 1. Liquidi and near-liquidus phases for olivine-melilitite + various amounts of volatiles added. These are indicated by large numbers. *1* Olivine-melilitite without volatiles, buffered by furnace assemblage. *2* Olivine-melilitite + 38 wt % CO_2, buffered by furnace assemblage. *3* Olivine-melilitite + 38 wt % CO_2, MH buffer, *4* Olivine-melilitite + H_2O + CO_2 with $X_{H_2O} = 0.25$, $X_{CO_2} = 0.75$ (wt % added equivalent to 20 wt % H_2O at $X_{H_2O} = 1$, $X_{CO_2} = 0$), MH buffer. *5* Olivine-melilitite + 10 wt % H_2O ($X_{H_2O} = 1$, $X_{CO_2} = 0$) buffered by furnace assemblage. *6* Olivine-mellilitite + H_2O + CO_2 with $X_{H_2O} = 0.5 = X_{CO_2}$ (wt % added equivalent to 20 wt % H_2O at $X_{H_2O} = 1$, $X_{CO_2} = 0$) MH buffer. *7* Olivine-melilitite + 20 wt % H_2O ($X_{H_2O} = 1$, $X_{CO_2} = 0$), buffered by furnace assemblage. *8* Olivine-melilitite + 40 wt % H_2O, buffered by furnace assemblage. $P-T$ conditions and results are shown only for those experiments which have not been published previously (Brey and Green, 1975). Small numbers indicate the relationship of individual data points to the particular liquidi, in those cases where such relationships are not obvious

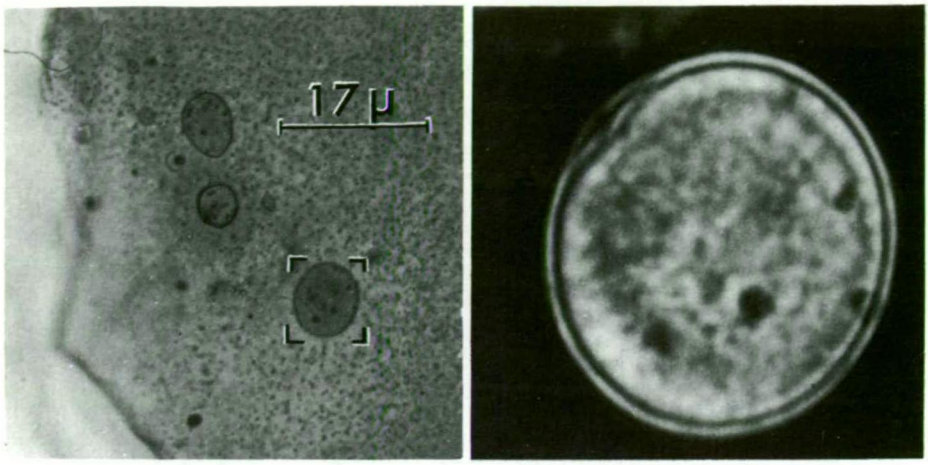

Fig. 2a and b. Carbonate droplets in olivine-melilitite glass (30 kb, 1,350° C, MH-buffer), (a) plane light; (b) nicols crossed

Olivine is the near-liquidus phase at 5 and 10 kb, pyroxene at 20 kb, garnet and pyroxene at 30 kb and garnet and pyroxene at 40 kb.

The silicate phases are euhedral although olivine and pyroxene show minor quench outgrowth. The silicate minerals and large silver globules are accumulated at the bottom of the capsule. Microscopically, the glass is clear and pale brown coloured in most areas with minor patchy occurrences of sub-microscopic 'dust' of fine? gas bubbles or silver globules. Macroscopically the colour varies considerably from run to run from olive green to dark brown (green colours more common at lower pressures). Large, spherical cavities, easily seen macroscopically, indicate the presence of free vapour phase. Small carbonate spheres (up to 10 μ diameter, see Fig. 2) occur at pressures >20 kb, increasing in number with increasing pressure. A small gas bubble, slightly removed from the centre, can be seen in the large spheres. These spheres are more common near the large vapour phase cavities and particularly aligned along the margins of cavities, in some cases being connected with the cavities through channels. Quench phases occur at 10 kb, and in those runs at 30 kb with less CO_2 added (12–18 %). Quench phases consist of unidentified, elongate, clear minerals radiating from a nucleation point and intergrown with interstitial carbonate. *X*-ray photographs yield only very diffuse lines and the phases were not identified. We were not able to consistently bracket the liquidus within a small temperature interval at 30 kb and 40 kb (Fig. 1), probably due to migration of H_2 from the buffer into the inner capsule (this is necessary anyway to make the buffer work). Hydrogen up to the equivalent of 1 % H_2O (Fig. 6b) migrates into the inner capsule. At these low amounts, only a slight variation in H_2O content causes a large variation in liquidus temperature. Since we wished to determine the effect of CO_2 alone on the liquidus temperature, the availability and access of hydrogen from the outer buffer capsule was a source of considerable uncertainty. We therefore carried out experiments using the single capsule "furnace buffered" method and minimized the potential sources of water and

hydrogen in the furnace assembly, by using pyrex glass rather than boron nitride, by firing the furnace components at 1,000° C and storing them dry until immediately before the run. We were not completely successful (note that the outermost sleeve of the furnace assembly is made of talc) as weak OH^- bands appear in infrared spectra of glasses, but the following observations show that we greatly decreased the availability of hydrogen during the "furnace buffered" runs. A sensitive test for the presence of water in a mafic silicate melt is to crystallize it under P, T conditions where amphibole or phlogopite would crystallize, provided water is present, and use X-ray diffraction to detect the presence of these hydrated phases. Thus, two capsules with olivine melilitite $+CO_2$ with and without the outer MH buffer capsule were kept above their liquidi for 10 min at 30 kb and then dropped to 900° C and kept there for 20 min. Biotite and ? amphibole crystallized in the MH buffered run whereas neither phase was detected in the single capsule dry furnace-buffered run.

(*b*) *Olivine Melilitite* $+ CO_2$ (*"Dry, Furnace-Buffered"*)

The liquidus is 50–80° C higher then that for MH buffered runs. Olivine is the near-liquidus phase up to 20 kb, followed by garnet+clinopyroxene at 30 kb and garnet only at 40 kb. The glasses are light brown under the microscope and generally clear. Carbonate droplets as in MH buffered runs are very rare at 30 kb, more common at 40 kb. In runs with lower CO_2 contents (8–14 % CO_2, not in the 16–18 % CO_2 runs) unidentified quench phases similar to those in MH buffered runs occur at 30 kb and at 40 kb (38 % CO_2). The stable silicate phases in below-liquidus runs are euhedral except for olivine which shows minor feathery quench outgrowth. Microprobe analyses of olivines at $\leqq 20$ kb show decreasing Mg-values with decreasing temperature, consistent with equilibration at increasing degree of crystallization. The primary garnet crystals (numerous, but small) in the 30 kb–40 kb runs show an unusually wide range in their composition (Fig. 3) in individual runs. A tentative explanation is that this reflects Fe-loss to the capsule since the variation is principally in Mg/Fe and previous work has shown that early formed crystals may only partially readjust to changing Mg/Fe of liquid during an experimental run [9].

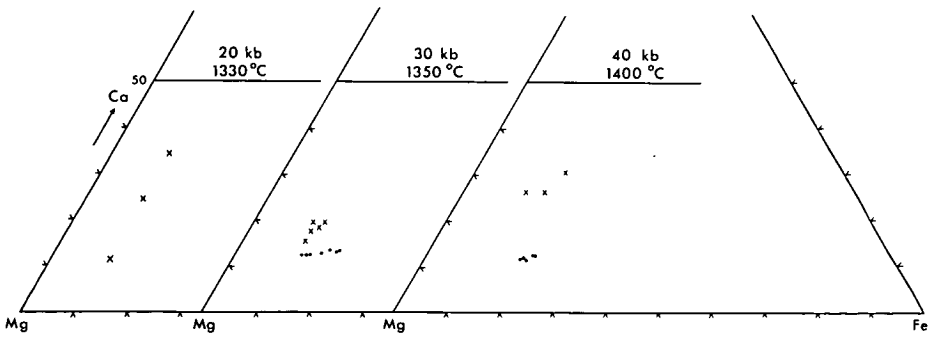

Fig. 3. Ca—Mg—Fe diagram illustrating the compositions of near-liquidus phases (dots = garnets, crosses = pyroxenes), MH-buffer

There is a small decrease in grossular content of garnet between 30 kb and 40 kb which may indicate changing partition relationships between garnet and liquid. The pyroxene compositions vary widely (Fig. 3) and plot within the probable two-pyroxene miscibility gap (Mori, personal communication) but extend towards the orthopyroxene and clinopyroxene limbs. Our short run durations probably do not allow the pyroxenes to reach their stable compositions[1] [16].

(c) *Olivine Melilitite + Excess H_2O (~40 %) (Furnace-Buffered)*

An approximate position for the liquids of olivine melilitite under H_2O-saturated conditions is shown in Fig. 1. Near liquidus phases at 10, 30 and 35 kb are olivine and olivine and clinopyroxene.

(d) *Olivine Melilitite (Dry, CO_2-free, 0 kb)*

Runs under vacuum in spec. pure Fe-capsules have olivine as the liquidus phase (Fig. 1).

(e) *Diopside + CO_2*

These experiments were carried out to compare our CO_2 solubility data obtained with a gas chromatograph with those obtained by the fission track method [19]. A MH buffered run in a Pt capsule at 30 kb, 1,660° C failed because the capsule melted after 3 min. The glass from a MH buffered run at 20 kb, 1,580° C, 5 min, was yellow due to migration of Fe through the Pt capsule into the charge. A run with crystalline diopside + silver oxalate (single Pt capsule, furnace-buffered) at 30 kb, 1,660° C yielded diopside + a layer of graphite (*X*-ray identification) between charge and Pt-capsule after 12 min. Only runs with the MgO, SiO_2, $CaCO_3$ mixture under unbuffered conditions where extreme precautions could be taken to eliminate water and hydrogen from the external environment were successful. Run conditions and products are shown in Table 1. Our position of the

Table 1. Run conditions and products of diopside mixture (MgO, SiO_2, $CaCO_3$, no buffer applied)

Run No.	*P*(kb)	*T*(°C)	Run duration (min)	Run products
5941	30	1,660	8	di + V
5943	30	1,700	10	colorless glass + V; di at lower end (away from hot spot) of capsule
5945	30	1,730	8	colorless glass + V

[1] Longer run times would be required for pyroxenes to exsolve to their equilibrium conditions but would result in so great a loss of Fe to the Pt containers at these high temperatures that results would be of little value. Since our concern is for solubility of CO_2 in the melt phase we prefer to tolerate the absence of equilibrium in the pyroxene solid solutions.

melting point between 1,660° C and 1,700° C at 30 kb corrected pressure (33 kb nominal pressure) does not necessarily disagree with that of Eggler [3] (1,630° C at 30 kb nominal pressure) because of the different experimental techniques (piston-out at Geophysical Laboratory and piston-in at ANU), the uncertainties of pressure correction using pyrex glass and the uncertainty in temperature measurement.

Composition of a CO_2-rich Vapour Phase

It is not possible to analyse the composition of a vapour phase under run conditions in a piston cylinder apparatus. In runs in which only glass and vapour phase are present, it is possible to deduce relative solubilities of different oxide components in the vapour phase if the glass composition differs from that of the starting mix. Analyses of quenched glasses from runs above the liquidus of both olivine melilitite and diopside show persistent deviations from the composition of the starting material (Fig. 4). The analyses of the quenched glasses were normalised

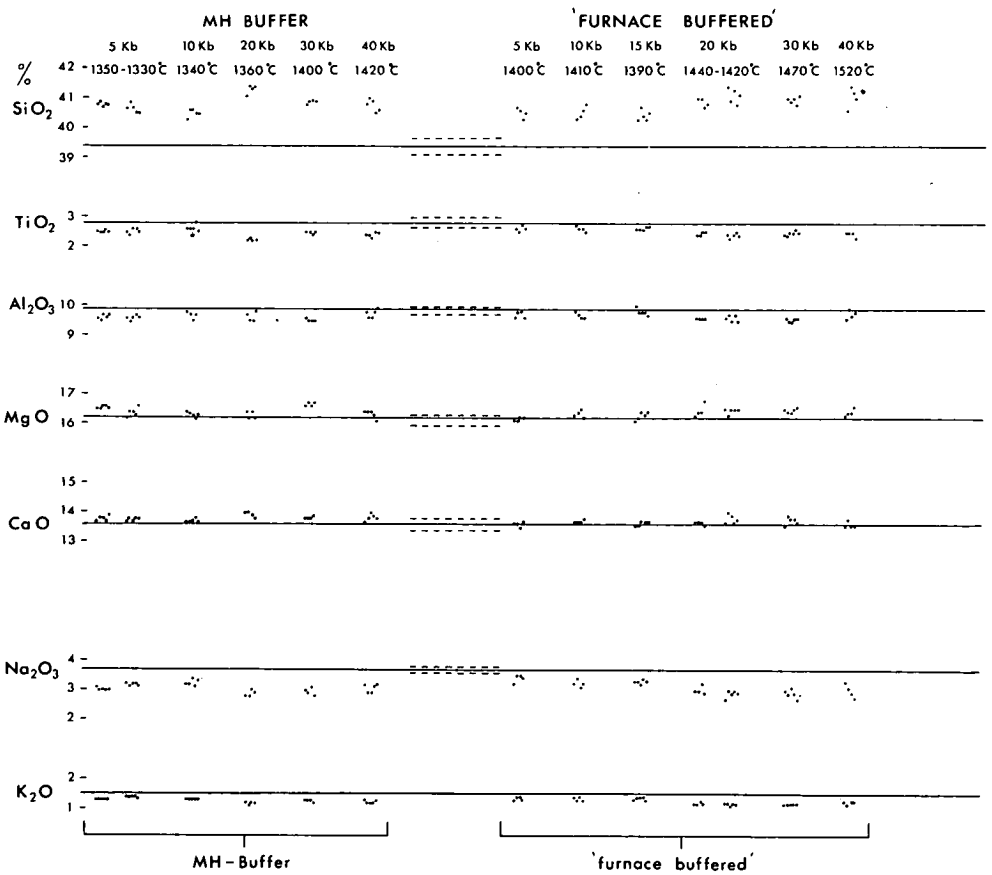

Fig. 4. (a) Compositions of quenched olivine-melilitite glasses + CO_2 compared with average starting composition (shown by solid line with the dashed lines indicating the range of values as analysed on the starting glass (by T. P. D. electron probe))

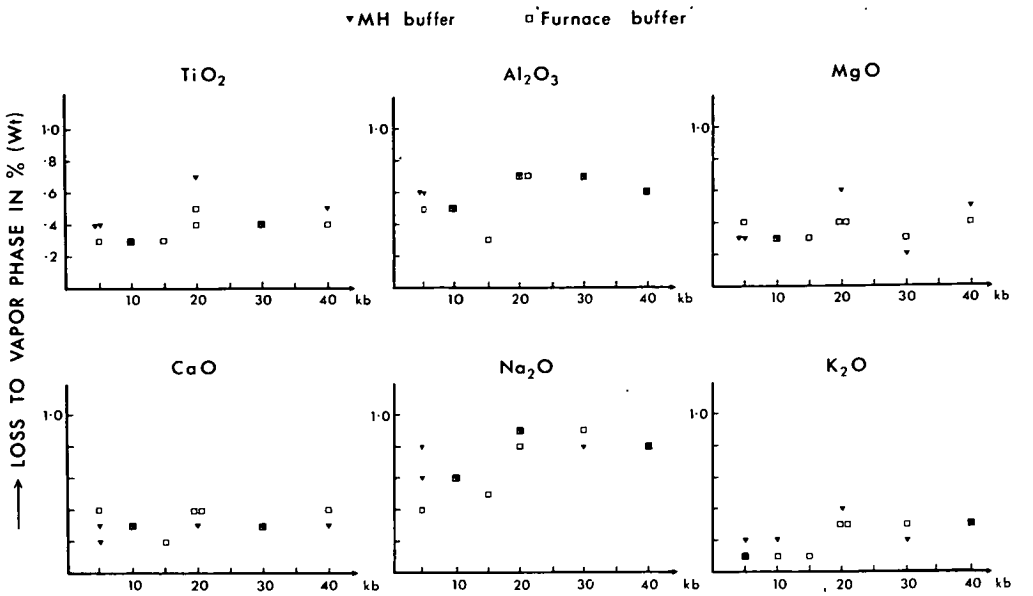

Fig. 4. (b) Loss to vapour phase in wt %, assuming that SiO_2 was not soluble in vapour phase. Analyses of glasses are those in Table 3

Table 2. CO_2 content of diopside glasses (run conditions Table 1) measured with the Hewlett-Packard 185 B CHN analyser

Run No.	*P* (kb)	*T* (°C)	Combustion time (sec)	$\%CO_2$	$\%H_2O$	Eggler *et al.* at 30 kb, 1,625° C
5945	30	1,730	55	5.4	–	
5945	30	1,730	55	5.1	–	4.8 % CO_2
5945	30	1,730	90	6.2	–	
5945	30	1,730	120	5.8	–	
5943	30	1,700	90	5.9	–	

to 100 % and corrected for Fe loss to the capsule (this correction was <25 % of the Fe originally present). This procedure assumes initially that FeO is not soluble in a CO_2 vapour phase. Fig. 4a shows that SiO_2 contents are 1–2 wt % greater than in the starting mix, while MgO, CaO are slightly greater and Na_2O, K_2O, Al_2O_3 and TiO_2 are lower. Our interpretation of these relative changes is that SiO_2 is only slightly soluble in a CO_2 vapour phase, whereas all the other elements including Fe are appreciably dissolved. The apparent solubility of TiO_2 in the vapour phase is surprising to us and it is conceivable that Ti could alloy with the Pt capsule [24]. In the diopside composition MgO seems to be relatively enriched in the vapour phase leading to decrease of MgO/CaO (mol. ratio) of the glass (from 0.92 in the starting glass to 0.89 in the CO_2-saturated glass).

Table 3. Average glass analyses of olivine-melilitite + CO_2 corrected for Fe-loss by increasing the measured FeO content to an arbitrary 12.8% FeO

	MH Buffer						
	5 kb 1,350° C	5 kb 1,330° C	10 kb 1,340° C	20 kb 1,360° C	30 kb 1,400° C	40 kb 1,420° C	Average starting mix I + II
SiO_2	40.8	40.7	40.5	41.3	40.9	40.8	39.4
TiO_2	2.5	2.5	2.6	2.2	2.5	2.4	2.8
Al_2O_3	9.6	9.6	9.7	9.6	9.5	9.8	9.9
FeO	12.8	12.8	12.8	12.8	12.8	12.8	12.8
MgO	16.5	16.4	16.3	16.3	16.6	16.3	16.2
CaO	13.8	13.8	13.7	13.9	13.8	13.8	13.6
Na_2O	3.0	3.2	3.2	2.9	3.0	3.0	3.7
K_2O	1.3	1.4	1.3	1.2	1.3	1.2	1.5
	"Furnace-buffer"						
	5 kb 1,400° C	10 kb 1,410° C	15 kb 1,390° C	20 kb 1,440° C	20 kb 1,420° C	30 kb 1,470° C	40 kb 1,520° C
SiO_2	40.5	40.5	40.4	40.9	41.1	41.0	41.0
TiO_2	2.6	2.6	2.6	2.5	2.4	2.5	2.5
Al_2O_3	9.7	9.7	9.8	9.6	9.6	9.6	9.7
FeO	12.8	12.8	12.8	12.8	12.8	12.8	12.8
MgO	16.2	16.3	16.3	16.4	16.5	16.5	16.4
CaO	13.6	13.7	13.7	13.7	13.8	13.8	13.7
Na_2O	3.4	3.2	3.3	3.0	2.9	2.9	3.0
K_2O	1.4	1.4	1.4	1.2	1.2	1.2	1.3

Solubility of CO_2 in Olivine Melilitite

(a) *Data from Microprobe and Infrared Spectra*

Microprobe analyses of quenched glasses of olivine melilitite + CO_2 give totals considerably lower than 100%. We interpreted the difference as the amount of CO_2 dissolved in the glass [1].

The data yield a curve of apparent CO_2 solubility as a function of pressure for runs just above the liquidus (Fig. 5a). Both curves (MH buffered and furnace-buffered) become steeper around 20 kb and the curve for MH buffered runs lies at slightly higher CO_2 content. These relationships are confirmed qualitatively by a plot of pressure vs CO_3^{2-}/SiO_4^{4-} (from IR absorption bands) of the same runs (Fig. 5b). This ratio represents the weighted peak area of the CO_3^{2-} and SiO_4^{4-} bands in infrared spectra. At high pressure (30 kb) the values for the MH curve are too high because of the presence of separate carbonate (see experimental results) inclusions in the glass.

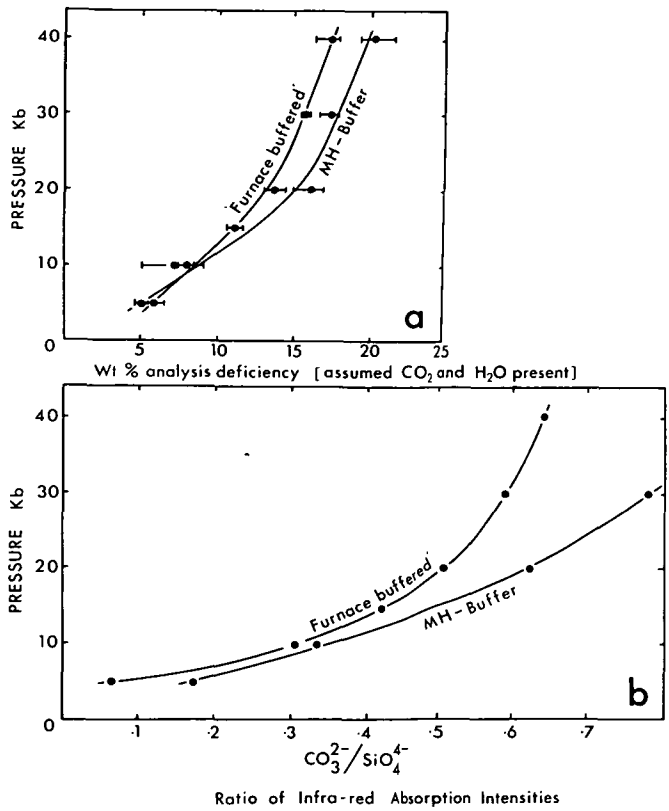

Fig. 5. (a) Olivine melilitite glasses equilibrated with CO_2 at above liquidus temperatures at various pressures, deficiency from 100 wt % in oxide totals obtained by TPD electron probe calibrated against standards and against starting glass correctly analysing at 100 wt % total oxides. Each point is the average of 4–5 analyses. The glasses are from runs just above the liquidus. (b) Ratio of infra-red absorption intensities (measured by area beneath peaks) of the same runs as in Fig. 5(a)

(*b*) *Direct Measurement by Gas Chromatography*

Eggler et al. [5] showed that the indirect microprobe method gives too high CO_2 values when calibrated against the CO_2-contents determined by the fission track method [19]. Since our sample size is larger, we have been able to use gas chromatography to directly determine CO_2 and H_2O in our glasses. The Hewlett-Packard 185B analyser was used for this purpose. Table 2 shows a comparison of our data with that from Eggler et al. [5] at 30 kb.

We find that approximately 6 % CO_2 is soluble in a diopside melt at 30 kb. We believe that this is comparable with Eggler's et al. [5] 4.8 % because of the pressure uncertainty and the analytical uncertainties.

To determine the CO_2 content in olivine melilitite, clear glass pieces were handpicked under the microscope to avoid Ag-globules and carbonates. The results are plotted in Fig. 6a, as a function of pressure (analyses of MH-buffered runs from above the liquidus except at 40 kb, where some garnet occurs). Fig. 6b,

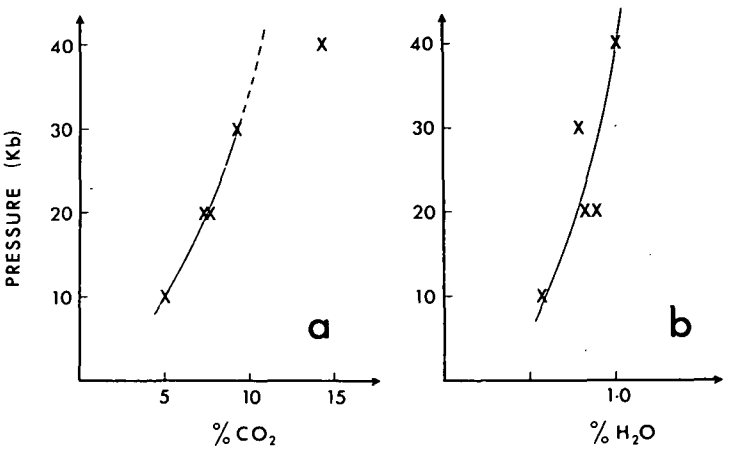

Fig. 6. (a) Wt % CO_2 in olivine-melilitite glasses of runs just above the liquidus determined by the Hewlett-Packard 185B CHN analyser. (b) The simultaneously determined H_2O content in these glasses. Analyst: Laboratory Dr. Fildes

shows the simultaneously determined H_2O content. The carbonate droplets are sufficiently common in the 40 kb run that it was impossible to separate them effectively and their presence causes the high CO_2 content. From the 10–30 kb data and the curvatures in Fig. 5a, b we estimate, that 10–11 % CO_2 is dissolved in olivine melilitite at 40 kb.

Conclusions

Fig. 1 clearly shows that CO_2 suppresses the liquidus temperature of an olivine melilitite liquid. The effect of CO_2 alone is very much smaller than that of H_2O; for example, the liquidus at 30 kb is lowered by about 80° C (compared to dry liquidus) for CO_2 saturated conditions, but is lowered by about 400° C for H_2O saturated conditions. The presence of H_2O at high total pressures increases the influence and solubility of CO_2 considerably, e.g. CO_2 dissolved in the melt at 30 kb lies between 12 and 21 % (Fig. 2 in [1]) and the liquidus is lowered by about 350° C for $X_{H_2O}=0.5$ (for 20% H_2O present at $X_{H_2O}=1.0$, Fig. 1). Olivine as a liquidus phase is restricted to lower pressures than under dry conditions or with only H_2O present, and the roles of garnet and orthopyroxene are enhanced by CO_2.

Carbonate droplets in a silicate glass are commonly interpreted as quench products of an immiscible carbonate liquid [14, 13].

If this inference is correct then we can infer the presence of an immiscible carbonate liquid coexisting with the olivine melilitite liquid at 30 kb and 40 kb and our observations suggest that the dry carbonate liquid contains excess CO_2 over carbonate stoichiometry. Higher pressure and the presence of small amounts of H_2O increase the number of carbonate droplets. Any interpretation concerning the genesis of carbonatites is premature because of too few experimental results,

difficulties in analysing the droplets and the unknown role of H_2O (in runs with H_2O the textural relationships are obscured by quench features).

The solubility of CO_2 in olivine melilitite increases with increasing pressure, at least up to 40 kb. The rate of increase in solubility with pressure becomes less at pressures above 20 kb (Figs. 5 and 6). The influence of temperature is very small compared with that of pressure and could not be established with our methods.

Discussion

Various possibilities for the occurrence of CO_2 in the mantle are discussed [11, 12]. Experimental evidence exists for two of them:

(a) CO_2 is soluble in an interstitial silicate melt, if the $P-T$ conditions are above the solidus of a peridotitic mantle composition $+H_2O+CO_2$ [1, 3].

(b) CO_2 occurs in carbonates. Newton and Sharp [20] show in experiments up to 45 kb that forsterite $+CO_2$ is an incompatible assemblage for most likely mantle conditions and reacts to enstatite + magnesite. Our preliminary experiments at 10–30 kb on (pyrolite 40 % ol)+excess H_2O and CO_2 (MH buffered, $X_{H_2O}=X_{CO_2}=0.5$) show that at 950° C, enstatite + diopside + olivine + CO_2 is stable at low pressures ($\leqq 17$ kb), enstatite + dolomite at intermediate pressures (20, 25 kb) and diopside + magnesite at high pressures ($\geqq 30$ kb) (see Table 4).[2] Thus a CO_2-rich vapour phase will not coexist with olivine at depths in the upper mantle along subsolidus conditions of the stable oceanic or continental geotherm (estimated [2]). We have also (Table 4) determined the solidus for (pyrolite − 40 % olivine) at 30 kb for excess H_2O+CO_2 ($X_{H_2O}=0.5$, $X_{CO_2}=0.5$ and $X_{H_2O}=0.9$, $X_{CO_2}=0.1$). Larger grain sizes (especially orthopyroxene), less inclusions in minerals and the disappearance of two phases (Table 4) at 1,050° C indicate the position of the solidus between 1,000° C and 1,050° C for vapour excess conditions ($X_{H_2O}=1$, $X_{H_2O}=0.9$ and $X_{H_2O}=0.5$). We have found no evidence for melting at 950° C in pyrolite at 10 kb $P\leqq 30$ kb for $X_{H_2O}=1$ or $X_{H_2O}=0.5$, $X_{CO_2}=0.5$. These results are in conflict with those of Mysen and Boettcher [17, 18]. The latter authors did not observe the olivine + pyroxene + $CO_2 \rightleftharpoons$ pyroxene + carbonate reaction and we have comparable experiments to theirs showing the absence of equilibrium using crushed (200 mesh, $\leqq 75$ microns) natural rocks as starting materials. Internal inconsistencies in their data and observations on experiments duplicating their techniques lead us to serious doubts on many of Mysen and Boettcher's experiments. The theoretical treatment of CO_2+H_2O effects on the peridotite solidi [17, 18] is erroneous due to high solubility of CO_2 in the silicate melt, dependence of CO_2 solubility on H_2O content of the melt and the non-ideality of CO_2+H_2O vapours [10]. Also, there will be a large difference in the effects of CO_2 on melting in hydrous silicate systems at conditions where the appropriate solidi cross the ol + cpx + $CO_2 \rightleftharpoons$ opx + dolomite reaction boundary (cf. [23]). Our new data are consistent with the inference [7, 8] that the effect

[2] These results are confirmed by our experiments in the simple system $CaMgSi_2O_6+2\ MgCO_3+3\ MgSiO_3$ (Brey and Green, in prep.). See also Kushiro et al. (1975, Earth Planet. Sci Lett. 28, 116–120) for confirmatory data.

Table 4. Experimental data on (pyrolite -40% olivine) $+12\%$ $CO_2+5\%$ H_2O (MH buffer, $X_{H_2O}=0.5$) and on (pyrolite -40% olivine) $+2.5\%$ $CO_2+9\%$ H_2O (MH buffer, $X_{H_2O}=0.9$)

Run No.	Pressure (kb)	Temperature (°C)	Run duration (hrs)	X_{H_2O}	Run products identified
6005	10	950	6	0.5	ol + amph + ? opx + cpx + vapour phase quench
6003	15	950	6	0.5	ol + ? (run lost CO_2+H_2O)
6009	17	950	6	0.5	ol + amph + ? opx + cpx + vapour phase quench
6001	20	950	6	0.5	amph + opx + cpx + dolomite[1] + vapour phase quench
6004	25	950	6	0.5	amph + opx + cpx + ga + dolomite[2] + vapour phase quench
5923	30	950	3	0.5	opx + cpx + ga + rutile + magnesite[3] + vapour phase quench
5919	30	1,000	3	0.5	opx + cpx + ga + rutile + magnesite[4] + vapour phase quench
5931	30	1,050	1	0.5	opx + ga + rutile + quench (liquid + vapour phase)
5925	30	950	3	0.9	ol + opx + cpx + ga + Ti-magnetite + ? phlogopite + vapour phase[5] quench
5921	30	1,000	3	0.9	ol + opx + cpx + ga + Ti-magnetite + ? phlogopite + vapour phase quench
5932	30	1,050	1	0.9	opx + ga + Ti-magnetite + quench (liquid + vapour phase[6] quench

Analyses of primary carbonate (1, 2, 3, 4) and quench carbonate (5, 6)

	1	2	3	4	5	6
SiO_2	7.0	3.2	2.2	3.1	7.7	5.1
TiO_2			0.8	0.8		
Al_2O_3	1.0	0.5	0.3	0.3	0.3	1.2
FeO	2.1	2.3	7.5	8.2	6.8	4.6
MgO	17.9	20.1	39.9	38.4	18.2	15.2
CaO	30.6	27.3	2.3	2.7	25.1	24.1
	58.6	53.4	53.0	53.5	58.1	50.2
Mg (molecular proportions)	43.7	49.0	87.9	85.5	45.5	43.3
Ca (molecular proportions)	53.5	47.9	3.6	4.3	45.0	49.3
Fe (molecular proportions)	2.8	3.2	9.2	10.2	9.5	7.3

of small quantities of water, with or without CO_2 ($CO_2 < H_2O$), in the upper mantle is to produce a region of small degrees of partial melting at depths $\cong 85$ kms, the CO_2 and H_2O being dissolved in the melt phase and the melt phase having the composition of highly silica-undersaturated basalt magma (Olivine nephelinite or basanite for $X_{CO_2}=0$, $X_{H_2O}=1$, olivine melilitite for $X_{CO_2}\approx 0.2$, $X_{H_2O}\approx 0.8$ ([1] and unpublished data). If the temperature distribution in the mantle is such as to be below the pyrolite solidus, then CO_2 will be present in dolomite (low pressure) or magnesite ($\geqq 30$ kb) as an accessory phase.

Acknowledgements. The assistance of W. O. Hibberson in experimental techniques and of N. G. Ware in microprobe analyses are greatly appreciated. We thank Dr. Fildes and assistants, John Curtin School of Medical Research, A. N. U., for carrying out the CO_2 and H_2O determinations. We acknowledge the benefit of many discussions with T. Mori.

References

1. Brey, G., Green, D.H.: The role of CO_2 in the genesis of olivine melilitite. Contrib. Mineral. Petrol. **49**, 93-103 (1975)
2. Clark, S.P., Ringwood, A.E.: Density distribution and constitution of the mantle. Rev. Geophys. **2**, 35-88 (1964)
3. Eggler, D.H.: Role of CO_2 in melting processes in the mantle. Am. Rept. Div. Geophys. Lab., Washington, **72**, 457-467 (1973)
4. Eggler, D.H.: Effect of CO_2 on the melting of peridotite. Ann. Rept. Div. Geophys. Lab., Washington, **73**, 215-224 (1974)
5. Eggler, D.H., Mysen, B.O., Seitz, M.G.: The solubility of CO_2 in silicate liquids and crystals. Ann. Rept. Div. Geophys. Lab., Washington **73**, 226-228 (1974)
6. Fontijn, L.A., Bok, A.B., Kornet, J.G.: The TPD electron probe X-ray micro-analyser. In: (G. Mollenstedt and K.K.Gaukler, eds.), Fifth Intern. Cong. *X*-ray Optics and Microanalysis, **261**, (1969)
7. Green, D.H.: The origin of basaltic and nephelinitic magmas (Bennett Lecture) Trans. Leicester Lit. Philos. Soc. **64**, 28-54 (1970)
8. Green, D.H., Liebermann, R.C.L.: Phase equilibria and elastic properties of a pyrolite model for the oceanic upper mantle. Tectonophysics (in press) (1975)
9. Green, D.H., Ringwood, A.E.: The genesis of basaltic magmas. Contrib. Mineral. Petrol. **15**, 103-190 (1967)
10. Greenwood, H.J.: The compressibility of gaseous mixtures of carbon dioxide and water between 0 and 500 bars pressure and 450° and 800° centigrade. Am. J. Sci., Schairer Vol. 267-A, 191-208
11. Irving, A.J., Wyllie, P.J.: Melting relationships in $CaO—CO_2$ and $MgO—CO_2$ to 36 kilobars with comments on CO_2 in the mantle. Earth and Planetary Science Letters **20**, 220-225 (1973)
12. Irving, A.J., Wyllie, P.J.: Subsolidus and melting relationships for calcite, magnesite and the join $CaCO_3—MgCO_3$ to 36 kilobars. Geochim. Cosmochim. Acta **39**, 35-53 (1975)
13. Koster van Groos, A.F.: The effect of high CO_2 pressures on alkalic rocks and its bearing on the formation of alkalic ultrabasic rocks and the associated carbonatites. Am. J. Sci. **275**, 163-185 (1975)
14. Koster Van Groos, A.F., Wyllie, P.J.: Liquid immiscibility in the system $Na_2O—Al_2O_3—SiO_2—CO_2$ at pressures to 1 kilobar. Am. J. Sci. **264**, 234-255 (1966)
15. Lindgren, F.T., Stevens, G.R., Jensen, L.C.: Elemental C, H and N microanalysis of crushed rock and soil samples. J. Am. Oil Chem. Soc. **49**, No. 4, 208-214 (1972)
16. Mori, T., Green, D.H.: Pyroxenes in the system $Mg_2Si_2O_6—CaMgSi_2O_6$ at high pressure. Earth Planet. Sci. Lett. **26**, 277-286 (1975)
17. Mysen, B.O., Boettcher, A.L.: Melting of a hydrous mantle: 1. Phase relations of natural peridotite at high pressures and temperatures with controlled activitites of water, carbon dioxide and hydrogen. J. Petrol. **16**, 520-548, (1975a)
18. Mysen, B.O., Boettcher, A.L.: Melting of a hydrous mantle: 2. Geochemistry of crystals and liquids formed by anatexis of mantle peridotite and high temperatures as a function of controlled activities of water, hydrogen and carbon dioxide. J. Petrol. **16**, 549-593 (1975b)
19. Mysen, B.O., Seitz, M.G.: Trace element partitioning determined by beta track mapping: an experimental study using carbon and samarium as examples. J. Geophys. Res. **80**, No. 17, 2627-2635 (1974)
20. Newton, R.C., Sharp, W.E.: Stability of forsterite $+ CO_2$ and its bearing on the role of CO_2 in the mantle. Earth Planet. Sci. Lett. **26**, 239-244 (1975)
21. Reed, S.J.B., Ware, N.G.: Quantitative electron microprobe analysis using a lithium drifted silicon detector. *X*-ray Spectrometry **2**, 69-74 (1973)
22. Reed, S.J.B., Ware, N.G.: Quantitative electron microprobe analysis of silicates using energy-dispersive *X*-ray spectrometry. J. Petrol. **16**, 499-519 (1975)
23. Wyllie, P.J., Huang, W.: Influence of mantle CO_2 in the generation of carbonatites and kimberlites. Nature **257**, 297-299 (1975)
24. Hansen, M., Constitution of binary alloys. Sec. ed. New York, N.Y.: McGraw-Hill Book Co. 1958

Received November 21, 1975/Accepted November 25, 1975

B 23

Experimental Petrology of a Highly Potassic Magma

by A. D. EDGAR,* D. H. GREEN and W. O. HIBBERSON

Research School of Earth Sciences, Australian National University, Canberra

(*Received 25 March 1975; in revised form 22 September 1975*)

ABSTRACT

The melting behaviour of a highly potassic biotite mafurite of the Central African olivine leucitite kindred has been studied experimentally as a function of pressure (to 30kb) temperature, and water content (0%, 5%, 15%, 25%, and 40% H_2O). Olivine is the liquidus phase up to 30 kb for all water contents studied except for anhydrous (clinopyroxene on the liquidus) and 15% H_2O (phlogopite on the liquidus) conditions. Analyses of phases crystallizing from the biotite mafurite show that pressure has very little effect on the composition of clinopyroxene which is extremely calcium-rich, and low in Al_2O_3 and TiO_2 for all conditions investigated. Phlogopite has low TiO_2 content and titanphlogopite cannot be a refractory phase in the upper mantle causing Ti-depletion in partial melts in equilibrium with titanphlogopite. There are apparently no conditions where the extremely potassic biotite mafurite could be a partial melt from pyrolite but derivation from an olivine+clinopyroxene+phlogopite+ilmenite assemblage occurring as 'enriched' patches in the upper mantle, is possible. Liquids in equilibrium with phlogopite as a residual phase at ~30 kb would be olivine nephelinites with approximately 5% K_2O, $Na_2O/K_2O \geqslant 1$ and $TiO_2 > 5+$. Crystal elutriation with transported residual phlogopite reacting (phlogopite+liquid 1 $\rightleftharpoons$ olivine+liquid 2) at lower pressures provides a mechanism for K-enrichment and generating $Na_2O/K_2O < 1$.

INTRODUCTION

HIGHLY potassic mafic and ultramafic lavas with the geochemical and mineralogical features given below occur mainly in continental and island arc environments. This paper is concerned only with the continental varieties of these rocks of which the best-known examples are those of the Bufumbira region of E. Africa (Holmes & Harwood, 1937; Holmes, 1950; Bell & Powell, 1969; Cundari & Le Maitre, 1970) and the Leucite Hills, Wyoming (Cross, 1897; Carmichael, 1967). Although these rocks show a wide range of compositions (cf. Bell & Powell, 1969) and corresponding plethora of names, they may be characterized by high K_2O/Na_2O (some with exceptional K_2O contents), TiO_2, Rb, Zr, Nb, La, and Y. These rocks contain combinations of the K-rich minerals sanidine, leucite, kalsilite, phlogopite together with olivine, titaniferous salite, plagioclase, and nepheline.

A critical discussion of the theories of genesis of these lavas is given by Bell & Powell (1969). Any hypothesis for their origin must account for the extreme enrichment of K_2O, TiO_2, and elements normally associated with more highly differentiated silicic rocks, but which in these rocks are associated with high MgO and CaO contents and low SiO_2. Thus differentiation from an alkali

* Permanent address: Dept. of Geology, University of Western Ontario, London, Canada.

basaltic magma without some extreme form of crustal contamination, or assimilation, is unlikely to produce their peculiar geochemistry. Lack of basaltic rocks in most highly potassic ultramafic provinces also tends to preclude derivation from a basaltic parentage. On the basis of Sr-isotope data Bell & Powell (1969) suggest that the most likely of any assimilation or contamination hypotheses would be mixing of nephelinitic magma with sialic material or carbonatitic magma with sial.

The presence of xenoliths of mica pyroxenite and/or augite peridotite in high potash lavas (Holmes, 1952; Carmichael, 1967) has been used to infer that these rocks are the products of partial melting of mica-bearing ultrabasic assemblages at sub-crustal depths. The high levels of Sr, Nb, Zr etc. are difficult, although not impossible, to explain by this mechanism.

No high pressure experimental studies have as yet been done on the origin of lavas of this type. The present paper describes a reconnaissance investigation of an extremely K-rich and Ti-rich lava at pressures from 10–30 kb under conditions ranging from anhydrous to water saturated. The main objectives are to present analytical data on the compositions of the principal crystalline phases (clinopyroxene, olivine, phlogopite), and to determine the partition relations between these phases and their coexisting liquids.

Although the composition we have used may not be appropriate as the composition of parental magma of classical potash-rich ultramafic provinces such as Birunga (cf. Holmes, 1950; Cundari & Le Maitre, 1970), it was chosen to determine the effects of extreme K-enrichment on phase relations of liquids at high pressure and particularly to define the $P,T,\%\ H_2O$ conditions under which such liquids were saturated with a potassic phase.

STARTING MATERIAL

Starting material consisted of a synthetic glass of composition very similar to that of biotite mafurite from S.W. Uganda (Holmes, 1942, p. 212, Anal. D.). The principal constituents of this biotite mafurite are olivine, clinopyroxene, kalsilite, perovskite, and biotite with xenoliths of glimmerite (near-monomineralic phlogopite rock) and minor biotite peridotite (Holmes, 1942) suggestive of an upper mantle origin. The Fe_2O_3 content of the analysis of Holmes was reduced to give a $\frac{100\ Mg}{Mg+Fe}$ ratio of 75 (Table 1) appropriate to a liquid derived from a pyrolite or peridotite source with residual olivine of about Fo_{90} (Green, 1973*a*). Comparison of this analysis with a postulated parental composition (Holmes, 1950; Cundari & Le Maitre, 1970) deduced as olivine-rich ugandite (Holmes & Harwood, 1937, p. 61, Anal D), shows that the biotite mafurite of the present study is significantly higher in $\frac{K_2O}{Na_2O}$, TiO_2, CaO, BaO and SrO and lower in Al_2O_3 and in $\frac{100\ Mg}{Mg+Fe}$.

The glass was prepared by mixing oxides in the required proportions, sintering at 1000 °C and fusing in a Pt-crucible to a homogeneous glass at approximately 1400 °C for about 2 minutes to minimize loss of Fe to the Pt container and volatilization of the alkalis. The composition of the glass as analysed by microprobe is also shown in Table 1.

TABLE 1

Composition of starting material

	a	*b*
SiO_2	41·5	42·6
TiO_2	4·9	5·3
Al_2O_3	8·0	8·3
Fe_2O_3	0·6	0·2 *
FeO	9·5	7·8 *
MgO	16·1	15·8
CaO	10·2	10·7
Na_2O	0·7	0·8
K_2O	7·3	7·1
P_2O_5	0·4	n.d.
Cr_2O_3	0·15	0·2
NiO	0·05	n.d.
MnO	0·2	n.d.
BaO	0·35	n.d.
SrO	0·2	n.d.
TOTAL	100·15	98·8
$\frac{100\ Mg}{Mg+Fe}$	75·0	77·6
Lc	34·1	33·1 †
Ac	1·8	0·5
Di	7·4	16·3
Ol	33·1	26·7
Il	9·3	10·0
Cr	0·3	0·6
Ap	1·1	1·1
ns	0·9	0·8
Ca_2SiO_4	12·0	9·5
Ne	—	1·4

a, desired glass composition, biotite mafurite (Holmes, 1942).

b, glass composition, normalized to 98·8% to allow for constituents not analysed by electron microprobe, but added to original mix.

n.d., not determined.

* determined by spectrophotometry, E. Kiss, analyst.

† CIPW norm calculated with added P_2O_5, NiO, MnO, BaO and SrO not analysed for by microprobe but added to mixture.

EXPERIMENTAL PROCEDURE

All experiments were done in a piston-cylinder apparatus using techniques described by Green & Ringwood (1967*a*,*b*) and Bultitude & Green (1968, 1971). Iron and graphite capsules were used for the anhydrous runs while hydrous

experiments were done in Pt, $Ag_{50}Pd_{50}$ or $Ag_{75}Pd_{25}$ capsules depending on the temperature required. Problems of Fe loss to Pt capsules have been discussed previously by Green & Ringwood (1967*b*), Green (1969), and Green & Hibberson (1969). Problems caused by random entry of water in 'dry' runs using graphite capsules are discussed by Bultitude & Green (1971) while a comparison of graphite, platinum, and iron capsules is made by Ito and Kennedy (1968). Gibb (1971) has shown that iron loss to Ag–Pd alloys is considerably less than to Pt. Short run times were used to minimize Fe loss, particularly at high temperatures.

Crystalline phases and glass were identified in crushed portions of the charges and their compositions determined on polished surfaces by the TPD energy dispersive electron microprobe system (Reed & Ware, 1973). In addition to determining compositional changes under different conditions and partition ratios between different phases, the probe determinations allowed distinction between primary and 'quench' crystals.* These are considered in a later section.

EXPERIMENTAL RESULTS

Results of anhydrous experiments and hydrous runs with 5, 15, 25, and 40 wt. per cent H_2O are given in Table 2 and shown in Fig. 1. Compositions of solid phases are given in Tables 3–6.

(*a*) *Dry Runs.* Liquidus temperatures for anhydrous experiments ranged from 1490 °C at 10 kb to 1625 °C at 30 kb, olivine being the primary phase at lower pressures and clinopyroxene at high pressures (Fig. 1). No runs were made at 20 kb but by analogy with work on nephelinitic compositions (Bultitude & Green, 1971) the slope of the liquidus may be steeper at lower pressures than at higher pressure.

At 10 kb olivine of slightly decreasing $\frac{100\,Mg}{Mg+Fe}$ value (Table 4) is the only solid phase between 1480 and 1370 °C.

At 30 kb and 1620 °C, rare, and possibly primary, clinopyroxene was observed. No olivine was detected in this run, suggesting that clinopyroxene is the primary phase at high pressure under anhydrous conditions.

(*b*) *5% H_2O.* Results of experiments with 5% H_2O (Fig. 1) show that the liquidus temperatures are lowered by 200–300 °C relative to anhydrous conditions. 'Quench' phlogopite was an ubiquitous phase and 'quench' clinopyroxenes were common in all of the hydrous experiments. Microprobe analyses of typical 'quench' phlogopites and clinopyroxenes (Table 3) show their distinctive chemical differences from primary varieties.

Olivine is the primary phase up to 30 kb although the narrowing of this field

* Primary is used here to denote a crystalline phase grown at the *P*, *T* condition of the experiment. It does not necessarily imply a phase which crystallizes at the liquidus. 'Quench' denotes a phase formed during cooling from the run temperature to ambient temperature.

TABLE 2

Results of experimental runs

	(°C)	(kb)	Time (min)	Capsule	Products
(a)	*Anhydrous*				
	1500	10	5	C	Gl(76) *
	1480	10	5	Fe	Ol(91), Gl(76)
	1450	10	5	Fe	Ol(89), Gl
	1400	10	5	Fe	Ol(89), Gl(70)
	1370	10	5	Fe	Ol(88), Gl(66)
	1650	30	5	C	Gl
	1620	30	5	C	cpx(?), Gl
(b)	*5 weight % H_2O added*				
	1300	10	5	Pt	Q.Ph(87)
	1250	10	5	Pt	Ol(91)
	1230	10	5	Pt	Ol(92)
	1200	10	10	$Ag_{50}Pd_{50}$	Ol(89), Q.Ph(75)
	1150	10	10	$Ag_{50}Pd_{50}$	Ol(87), cpx(90), Ph(89)
	1330	20	5	Pt	Q.Ph(90)
	1330	20	3	Pt	Ol(92), Q.Ph(82)
	1300	20	5	Pt	Ol(93)
	1250	20	10	$Ag_{50}Pd_{50}$	Ol(89), Ph(91)
	1200	20	10	$Ag_{50}Pd_{50}$	Ol(87), Ph(90), cpx(88)
	1500	30	5	Pt	Q.Ph(94)
	1450	30	5	Pt	Q.Ph(91), Q.cpx(82)
	1400	30	5	Pt	Q.Ph(87), Q.cpx(87)
	1370	30	5	Pt	Q.Ph(92), Q.cpx(89)
	1330	30	5	Pt	Q.cpx(88), Q.Ph
	1300	30	10	Pt	Ol(92), Q.Ph(89)
	1250	30	20	$Ag_{50}Pd_{50}$	Ph(83), cpx(87)
	1200	30	20	$Ag_{50}Pd_{50}$	Ph(82), cpx(83)
(c)	*15 weight % H_2O added*				
	1250	10	10	Pt	Q.Ph(89)
	1200	10	10	$Ag_{50}Pd_{50}$	Q.Ph(86)
	1180	10	10	$Ag_{50}Pd_{50}$	Ol(92), Q.Ph(84)
	1150	10	10	$Ag_{50}Pd_{50}$	Ol(90), Q.Ph(82)
	1100	10	10	$Ag_{75}Pd_{25}$	Ol(88), Ph(90), cpx(90)
	1050	10	30	$Ag_{75}Pd_{25}$	Ph(82), cpx(78), ilm(31)
	1300	20	5	Pt	Q.Ph(90), Q.cpx(78)
	1240	20	10	$Ag_{50}Pd_{50}$	Q.Ph(86), Q.cpx(62)
	1200	20	10	$Ag_{50}Pd_{50}$	Ol(91), Q.Ph(86)
	1170	20	10	$Ag_{75}Pd_{25}$	Ol(90), Q.Ph(84)
	1150	20	15	$Ag_{75}Pd_{25}$	Ol(88), Ph(90), Q.cpx(58)
	1100	20	15	$Ag_{75}Pd_{25}$	Ol(87), Ph(90), cpx(91)
	1250	30	10	$Ag_{50}Pd_{50}$	Q.Ph(88)
	1200	30	10	$Ag_{50}Pd_{50}$	Ph(93)
	1175	30	10	$Ag_{75}Pd_{25}$	Ph(92), cpx(90)
	1150	30	30	$Ag_{75}Pd_{25}$	Ph(89), cpx(90), Q.ilm(17)
	1100	30	30	$Ag_{75}Pd_{25}$	Ph(86), cpx(87), ilm(38)
(d)	*25 weight % H_2O added*				
	1150	20	10	$Ag_{75}Pd_{25}$	Ol(89), Q.Ph(79)
	1100	20	10	$Ag_{75}Pd_{25}$	Ol(88), Ph(91), cpx(91)
	1050	20	20	$Ag_{75}Pd_{25}$	cpx(90), Ph, ilm
(e)	*40 weight % H_2O added*				
	1150	30	10	$Ag_{75}Pd_{25}$	Ol(90)
	1100	30	10	$Ag_{75}Pd_{25}$	Ol(86), ilm(46), Q.Ph(67), Q.cpx(64)
	1050	30	30	$Ag_{75}Pd_{25}$	Ol(77), Ph(83), cpx(82), ilm(28)

* Bracketed numbers indicate $\frac{100\ Mg}{Mg\ \ Fe}$ values.

Abbreviations: Gl, glass; Ol, olivine; Ph, phlogopite; cpx, clinopyroxene; Ilm, ilmenite; Q, quench.

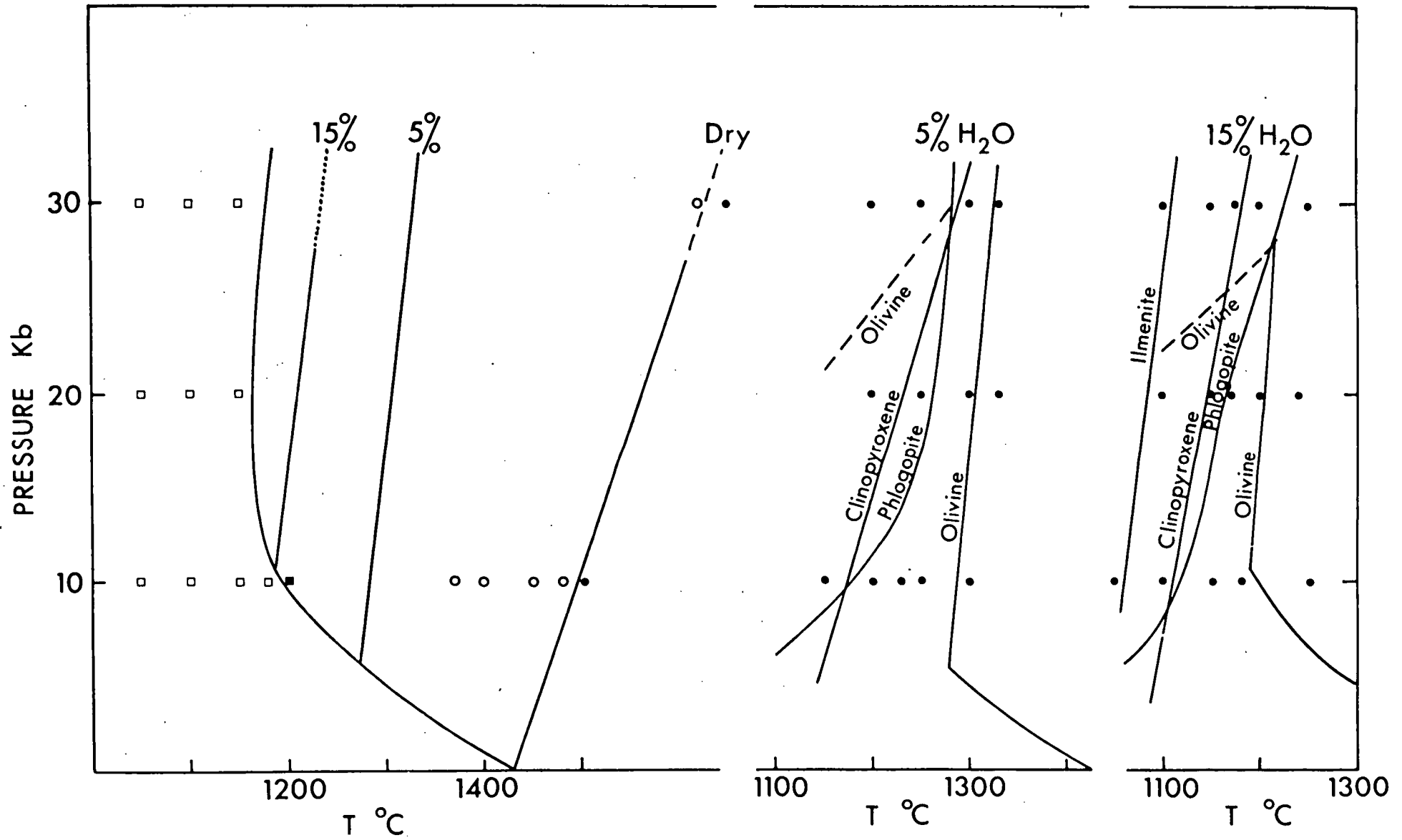

FIG. 1. Summary of experimental data for highly potassic biotite mafurite. The left diagram shows subsolidus (open symbols) and above-solidus runs for water-saturated and anhydrous conditions and the positions of the liquid for 5 % and 15 % H_2O. Olivine is the liquidus phase along liquidi shown as solid lines.

with increasing pressure (Fig. 1) suggests that some other phase, possibly clinopyroxene or phlogopite, may become the primary phase at higher pressures. At pressures slightly less than 30 kb the second phase to appear is phlogopite, closely followed by clinopyroxene as a third phase. At 30 kb olivine is present at 1300 °C but only clinopyroxene and phlogopite were present at 1250 °C showing the presence of a reaction relationship between olivine and liquid.

Following initial crystallization of olivine the compositions of the residual liquids are probably similar to those analysed for dry runs at 10 kb since both are close to the f_{O_2} of Ni–NiO. Unfortunately direct analyses of glass were impossible due to the abundance of 'quench' material in the charges. With crystallization of phlogopite, the K_2O, MgO, Al_2O_3, and SiO_2 contents of the liquid decrease while crystallization of clinopyroxene produces a decrease in CaO and SiO_2.

(*c*) *15% H_2O*. Results of runs with 15% H_2O (Fig. 1) indicate a further lowering of liquidus temperatures, the liquidus at pressures up to 10 kb representing water-saturated conditions. At 15% H_2O the primary phase field of olivine is restricted to pressures slightly under 30 kb, above this pressure phlogopite becomes the liquidus phase. Between 1050 °C at 10 kb and 1200 °C at 30 kb olivine was not detected. Below these temperatures ilmenite coexists with phlogopite and clinopyroxene.

(*d*) *Water-Saturated Runs*. Experiments to determine the primary phases under conditions of water saturation were done with 20% H_2O at 20 kb and 40% H_2O at 30 kb (Table 2). Phase relations under conditions of water saturation (Fig. 1) indicate olivine as the liquidus phase up to 30 kb and 1150 °C with phlogopite and clinopyroxene appearing at lower temperatures. With decreasing temperature olivine is no longer present and phlogopite, clinopyroxene, and ilmenite are the stable phases.

DETERMINATION OF PRIMARY AND 'QUENCH' PHASES

The greatest experimental difficulty in this study has been the distinction between primary and 'quench' phlogopite, clinopyroxene, and, to a lesser degree, ilmenite. Textures in polished sections and chemical analyses were used to distinguish such phases.

'Quench' phlogopite usually occurred as sheaves often with a wispy appearance or as elongated laths, both with complex habits. These are similar to the textures noted by Forbes & Flower (1974) for synthetic Ti-rich phlogopites. In contrast, primary varieties usually occurred as shorter laths with simple habit. In addition the 'quench' types were fairly strongly pleochroic whereas primary crystals generally had weak pleochroism. Texturally, primary and 'quench' clinopyroxenes are more difficult to distinguish but the 'quench' varieties tend to have stronger mauve colour and faint pleochroism.

Table 3 shows selected examples of primary and 'quench' phlogopites, clinopyroxenes, and ilmenites, illustrating differences in their chemistry. Relative to

primary varieties, 'quench' phlogopite is characterized by higher TiO_2, and lower Al_2O_3 and $\frac{100\,Mg}{Mg+Fe}$ ratios. The latter values in 'quench' varieties are much lower than in coexisting primary olivines, whereas in primary phlogopites the $\frac{100\,Mg}{Mg+Fe}$ value is comparable to that of the other primary phases (cf. Table 3). Compari-

TABLE 3
Analyses of 'quench' and primary phases

	Phlogopite				*Clinopyroxene* *		*Ilmenite* *	
Pressure (kb)	10	10	30	30	20	20	30	30
Temp. (°C)	1150	1100	1250	1175	1150	1100	1150	1100
Wt. % H_2O added	15	15	15	15	15	15	15	15
'Quench' (Q) *or Primary* (P)	Q	P	Q	P	Q	P	Q	P
SiO_2	40·3	39·6	43·0	41·2	40·6	53·9	1·96	0·38
TiO_2	4·68	2·47	2·4	1·3	9·15	0·71	49·8	55·3
Al_2O_3	10·1	13·1	10·2	13·3	4·80	0·52	1·22	0·41
Cr_2O_3	—	0·51	—	0·3	0·26	0·40	—	0·79
FeO	8·62	4·80	5·6	3·9	11·00	3·06	40·4	31·2
MnO	—	—	—	—	0·22	—	0·62	0·48
MgO	21·9	23·6	22·9	24·6	8·32	17·3	4·63	10·72
CaO	—	0·23	0·1	0·1	23·5	24·1	1·09	0·47
K_2O	9·71	9·84	10·1	10·2	0·18	0·06	0·34	0·27
TOTAL	95·3	94·2	94·8	94·9	98·03	100·05	100·06	100·02
$\frac{100\,Mg}{Mg+Fe}$	82	90	88	92	58	91	17	38

Clinopyroxene and ilmenite analyses were normalized to 100 per cent and are reported to three significant figures only.

son of 'quench' and primary clinopyroxenes (Table 3) shows the former have much higher TiO_2 and Al_2O_3 values with lower SiO_2 and $\frac{100\,Mg}{Mg+Fe}$ values. The principal differences between primary and 'quench' ilmenite are the higher SiO_2 and lower TiO_2 and $\frac{100\,Mg}{Mg+Fe}$ values in the 'quench' type.

The stability of phlogopite in the present system may be compared with known phase relations of phlogopite in simple systems. The work of Modreski & Boettcher (1973) in the system K_2O–MgO–CaO–Al_2O_3–SiO_2–H_2O shows that phlogopite *may* be stable under the conditions of the present study. The presence of FeO in the present study might be expected to lower the phlogopite stability temperature whereas the high TiO_2 contents are known to raise the temperature of stability of phlogopite (Forbes & Flower, 1974).

MICROPROBE ANALYSES OF PHASES

Olivine

Analyses of primary olivines crystallized under various conditions show the principal differences to be decreasing Mg-values (*i.e.* $\frac{100\,Mg}{Mg+Fe}$) with increasing degree of crystallization at constant pressure (Table 2). However this parameter appears to be independent of pressure at liquidus temperatures provided olivine is the only primary crystalline phase. Bultitude & Green (1971) report similar independence of Mg-value of liquidus olivine with pressure for compositions akin to olivine nephelinites and basanites.

All olivines have detectable CaO contents ranging from a minimum of 0·1% CaO at 30 kb, 1150 °C to a maximum of 1·1% CaO at 10 kb, 1370 °C–1480 °C. Although there is considerable scatter in the data, the CaO content of olivine is directly proportional to temperature and inversely proportional to pressure and appears to correlate with TiO_2 (up to 0·35% at 10 kb, 1400 °C) and K_2O (up to 0·2% at 10 kb, 1400 °C). These values are considerably higher than those reported for olivines crystallized from basaltic compositions (Green & Ringwood, 1967*b*) or from olivine nephelinitic and basanitic compositions (Bultitude & Green, 1971) and may be petrogenetically significant. However, it is also possible that submicroscopic inclusions of glass or quench cause both the high values of CaO, TiO_2, and K_2O and the scatter in the data. Such inclusions will not significantly affect MgO and FeO values.

Clinopyroxene (Table 4)

The clinopyroxenes crystallized at 10, 20, and 30 kb from 1050 °C to 1250 °C with various water contents are all extremely CaO-rich with $\frac{Ca}{Ca+Mg} > 0{\cdot}47$ and in most cases >0·5. In addition, the pyroxenes are low in Al_2O_3, particularly in comparison with pyroxenes crystallized from basanitic and nephelinitic magmas at pressures to 30 kb (Bultitude & Green, 1971; Green, 1973*c*). The clinopyroxenes lie in the one-pyroxene field of the pyroxene quadrilateral for 10–30 kb and do *not* approach compositions appropriate for equilibrium with Ca-poor pyroxene at the relevant temperature (Davis & Boyd, 1966; Mori & Green, 1975; Mori, 1975). The K_2O contents of the pyroxenes are high and the apparently random scatter suggests that high values may be due to inclusions of liquid or phlogopite. As with the olivine analyses, such inclusions will not greatly affect CaO, MgO, or FeO values. For pyroxenes crystallizing near the liquidus, the estimated partition coefficient $\frac{K_2O \text{ in liq}}{K_2O \text{ in cpx}}$ must be greater than 20. The TiO_2 content of clinopyroxene shows a systematic inverse relationship to pressure: the three experiments at 1050 °C, 10, 20, and 30 kb are all saturated with both phlogopite and ilmenite and the TiO_2 content decreases from 1·9% at 10 kb to

0·6% at 30 kb. Plotting of Ti *vs* Al substitution suggests a further pressure dependence in that at 30 kb the substitution is Ti+2 Al (for Mg+2Si possibly) whereas at 10 kb the substitution appears to be Ti+Al (for Mg+Si possibly). At each pressure the maximum TiO_2 content in clinopyroxene occurs in those runs with coexisting ilmenite.

Comparison of clinopyroxene analyses (Table 4) with analyses of natural clinopyroxenes from K-rich volcanics of Leucite Hills, Wyoming; West Kim-

TABLE 4

Compositions of clinopyroxenes analysed by microprobe

Wt. % H_2O added	5	5	5	5	15	15
Pressure (kb)	10	20	30	30	10	10
Temp. (°C)	1150	1200	1250	1200	1100	1050
SiO_2	53·4	53·4	52·9	52·7	53·2	51·3
TiO_2	1·12	1·02	1·29	1·31	1·02	1·91
Al_2O_3	0·81	1·19	1·92	1·89	0·71	1·11
Cr_2O_3	0·29	0·35	0·29	0·26	0·26	0·14
FeO	3·23	4·08	4·42	5·28	3·40	7·29
MnO	—	—	0·21	—	—	—
MgO	17·00	16·9	15·9	14·8	16·8	14·3
CaO	24·0	22·7	22·5	23·0	24·5	23·6
Na_2O	—	—	0·33	0·40	—	0·17
K_2O	0·12	0·32	0·32	0·28	0·18	0·17
$\frac{100\ Mg}{Mg+Fe}$	90	88	87	83	90	78
Coexisting Phase(s)	Ph, Ol	Ph, Ol	Ph	Ph	Ol, Ph	Ph, Ilm
Cations for 6 Oxygens	4·00	3·99	4·01	3·98	4·01	4·01

Wt. % H_2O added	15	15	15	15	25	25	40
Pressure (kb)	20	30	30	30	20	20	30
Temp. (°C)	1100	1175	1150	1100	1100	1050	1050
SiO_2	53·9	53·8	54·4	53·7	53·5	52·9	53·4
TiO_2	0·71	0·54	0·53	0·62	0·93	1·13	0·63
Al_2O_3	0·52	0·71	0·85	0·97	1·02	1·34	2·00
Cr_2O_3	0·40	0·28	0·23	0·20	0·59	0·49	—
FeO	3·06	3·58	3·44	4·23	2·04	3·36	5·78
MnO	—	—	0·22	0·13	—	—	—
MgO	17·3	18·2	16·9	16·5	17·1	17·0	14·9
CaO	24·1	22·9	23·3	23·5	24·0	23·7	22·9
Na_2O	—	—	—	—	—	—	—
K_2O	0·06	—	0·13	0·22	—	0·12	0·37
$\frac{100\ Mg}{Mg+Fe}$	91	90	90	87	91	90	82
Coexisting Phase(s)	Ol, Ph	Ph	Ph	Ph, Ilm	Ph, Ilm	Ph, Ilm	Ph, Ilm
Cations for 6 Oxygens	3·99	4·00	3·99	4·00	4·00	4·00	3·99

All analyses normalized to 100 % and are reported to three significant figures only.

berley, Western Australia (Carmichael, 1967), and central New South Wales (Cundari, 1973) shows that the natural pyroxenes also show the distinctive characteristics of very high CaO, very low Al_2O_3, and low TiO_2. It appears that pressure has remarkably little effect on the compositions of clinopyroxenes crystallized from highly potassic magmas (similar to that used in this study).

Phlogopite (Table 5)

The phlogopites synthesized from the mafurite contain appreciable titan-phlogopite solid solution particularly at higher temperatures at all pressures.

TABLE 5

Compositions of phlogopites analysed by microprobe

Wt. % H_2O added	5	5	5	5	5	15	15	15
Pressure (kb)	10	20	20	30	30	10	10	20
Temp. (°C)	1150	1250	1200	1250	1200	1100	1050	1150
SiO_2	40·5	39·5	40·6	40·3	39·4	40·4	39·5	41·5
TiO_2	4·0	3·7	3·2	4·0	3·9	2·5	3·5	2·3
Al_2O_3	13·9	14·6	13·8	13·6	13·8	13·4	13·0	13·0
Cr_2O_3	0·2	0·9	0·2	0·1		0·5	0·1	0·4
FeO	4·9	4·2	4·6	7·4	8·2	4·9	8·3	4·7
MnO		0·2		0·1				
MgO	22·3	22·5	22·9	19·8	20·3	24·1	21·3	23·6
CaO	0·2	0·3	0·4	0·6	0·2	0·2	0·5	0·1
K_2O	10·0	10·2	10·1	9·9	10·3	10·0	9·6	10·5
TOTAL	96·0	96·1	95·8	95·8	96·1	96·0	95·8	96·1
$\frac{100\ Mg}{Mg+Fe}$	89	91	90	83	82	90	82	90
Coexisting Phase(s)	Ol, cpx	Ol	Ol, cpx	cpx	cpx	cpx, Ol	cpx, ilm	Ol, cpx
Cations for 22 Oxygens	15·58	15·66	15·68	15·56	15·68	15·77	15·83	15·74
SiO_2		40·8	41·5	41·7	40·9	40·9	41·8	39·8
TiO_2		2·1	1·3	1·3	1·9	1·7	2·1	1·6
Al_2O_3		13·6	13·6	13·5	13·5	13·7	13·5	14·5
Cr_2O_3		0·2	0·4	0·3	0·1		0·6	
FeO		4·6	3·6	3·9	5·3	6·6	4·3	8·1
MnO					0·1			
MgO		24·2	25·0	24·9	23·6	22·7	23·8	21·9
CaO		0·2	0·2	0·1	0·2	0·2	0·2	0·1
K_2O		10·3	10·3	10·4	10·4	10·1	9·7	10·1
TOTAL		96·0	95·9	96·1	96·0	96·0	96·0	96·1
$\frac{100\ Mg}{Mg+Fe}$		90	93	92	89	86	91	83
Coexisting Phase(s)		Ol, cpx	—	cpx	cpx	cox, Ilm	Ol, cpx	cpx, Ilm
Cation for 22 Oxygens		15·79	15·80	15·81	15·81	15.77	15·64	15·82

Omitted readings below

% H2O 15 15 15 15 15 25 40

P 20 30 30 30 30 20 30

T 1100 1200 1175 1150 1100 1100 1050

Various chemical and physical controls on TiO_2 content of phlogopite are apparent in the data of Table 5. At 1050 °C, the two phlogopites crystallized at 10 kb and 30 kb are of Mg_{82} and Mg_{83} composition respectively and both coexist with ilmenite, clinopyroxene, and liquid. The large difference in TiO_2 content (3·5% TiO_2 at 10 kb, 1·6% TiO_2 at 30 kb) suggests that increasing pressure decreases the TiO_2 content of phlogopite. At 1100 °C and 1150 °C phlogopites (Mg_{89-91}) also show decreasing TiO_2 with increasing pressure for assemblages (liquid + olivine ± clinopyroxene) but the absence of ilmenite and possible variations in TiO_2 content of the liquid do not allow the effects of pressure to be isolated from chemical effects. At 1200 °C, two runs at 30 kb with 15% H_2O and 5% H_2O yielded charges with very different degrees of crystallization and different phlogopite compositions, *i.e.* Mg_{93}, 1·3% TiO_2 liquidus phlogopite at 30 kb, 1200 °C, 15% H_2O and Mg_{82}, 3·9% TiO_2 coexisting with clinopyroxene, at 30 kb, 1200 °C, 5% H_2O. Two factors may explain the very different TiO_2 contents. If the liquidus phlogopite in the 15% H_2O run defines $\frac{TiO_2 \text{ in liquid}}{TiO_2 \text{ in phlogopite}}$ then either the liquid (after clinopyroxene separation) in the 5% H_2O run contains 14–16% TiO_2 or the partition coefficient for $\frac{TiO_2 \text{ in liquid}}{TiO_2 \text{ in phlogopite}}$ is markedly decreased for more iron-rich phlogopite. It is probable that both factors operate, and further support for compositional control of TiO_2 content is provided by comparison of the 30 kb and 20 kb data. At 20 kb, phlogopites crystallized between 1250 °C and 1100 °C (from charges with different water contents but similar degrees of crystallization) are of Mg_{90-91} composition and decrease steadily in TiO_2 content with decreasing temperature. However, at 30 kb, with 15% H_2O, phlogopites crystallized between 1250 °C and 1050 °C *increase* slightly in TiO_2 content at lower temperature, correlating with decreasing Mg-value for phlogopite and increasing degree of crystallization.

Our reconnaissance experiments provide evidence that if a given liquid has phlogopite as its liquidus phase over an appreciable temperature and pressure range (*e.g.* with various water contents at high pressure) then the partition relationship $\frac{TiO_2 \text{ in liquid}}{TiO_2 \text{ in phlogopite}}$ increases with decreasing temperature, and decreases with decreasing pressure. There is also compositional control in that TiO_2 more readily substitutes in more Fe-rich phlogopites and $\frac{TiO_2 \text{ in liquid}}{TiO_2 \text{ in phlogopite}}$ decreases with decrease in Mg-value of liquid and phlogopite.

The partitioning of iron and magnesium between coexisting phases is such that $\left(\frac{Mg}{Mg+Fe}\right)_{Ilm} \ll \left(\frac{Mg}{Mg+Fe}\right)_{liq} < \left(\frac{Mg}{Mg+Fe}\right)_{Ol} < \left(\frac{Mg}{Mg+Fe}\right)_{Cpx} \approx \left(\frac{Mg}{Mg+Fe}\right)_{Ph}$ for $T > 1000$ °C and $\left(\frac{Mg}{Mg+Fe}\right)_{Ph}$ between 0·8 and 0·95 approximately.

The TiO_2 content of the phlogopites of the present study may be compared with the analyses of phlogopites from the Leucite Hills, Wyoming, many of which occur as phenocrysts. Carmichael (1967, Table 6, p. 42) reports an average TiO_2 value (from 12 phlogopites) of 1·95 with a range of 1·8–2·1. These values are slightly higher than those at high pressures and water contents reported in Table 5 but much lower than the values for lower pressures and lower water contents of this study. Comparison of other elements in the phlogopites of Leucite Hills with the synthetic ones of this study shows that the Leucite Hills samples have higher $\frac{100\,Mg}{Mg+Fe}$ number and lower Al_2O_3. The phlogopite phenocrysts from West Kimberley (Western Australia) potassic lavas are much more Ti-rich and generally lower in $\frac{100\,Mg}{Mg+Fe}$ ratio than the experimental phlogopites. Phlogopites from olivine leucitite lavas in New South Wales (Cundari, 1973) are extremely Ti-rich and are of low-pressure origin.

Analyses of phlogopites of undoubted mantle origin are few. However, Dawson *et al.* (1970, Table 7) report a high-Ti phlogopite from a mica–garnet lherzolite xenolith in lavas from Lashaine volcano, Northern Tanzania with $>9\%$ TiO_2. Frey & Green (1974) report phlogopites with low TiO_2 (0·4%) and moderate TiO_2 (3·5%) in spinel lherzolite xenoliths from Victoria. Forbes & Flower (1974) have shown that synthetic titanphlogopites (containing about 10 wt. % TiO_2) are stable to higher temperatures at high pressure than phlogopite without TiO_2.

Forbes & Flower (1974) have used the simple system study to suggest that titanphlogopite may be a refractory phase during magma generation at relatively low pressures, remaining as a residual phase retaining high contents of incompatible elements, particularly K and Ti. Forbes & Flower (1974) suggest that the low TiO_2 and K_2O contents of abyssal tholeiites of the ocean basins are due to their equilibration with residual titanphlogopite. This hypothesis is inconsistent with the data presented in this paper which show that over the pressure and temperature range associated with basalt genesis, the conditions for equilibrium between phlogopite and liquid are such that $\frac{(TiO_2)_{liq}}{(TiO_2)_{phlog}} \geqslant 4$ and $\frac{(K_2O)_{liq}}{(K_2O)_{phlog}} \geqslant 0{\cdot}5$. Forbes and Flower's hypothesis would predict $\frac{(TiO_2)_{liq}}{(TiO_2)_{phlog}} < 1$ and $\frac{(K_2O)_{liq}}{(K_2O)_{phlog}} \simeq 0{\cdot}02$ for genesis of abyssal tholeiites ($TiO_2 \sim 1{\cdot}5\%$, $K_2O \sim 0{\cdot}15\%$).

Ilmenite

Ilmenites (Table 6) crystallized from the mafurite are close to $MgTiO_3$–$FeTiO_3$ solid solutions with minor Cr_2O_3 and Al_2O_3 solid solution but no Fe_2O_3 solid solution (cf. Green & Sobolev, 1975). Ilmenite appears relatively late in the crystallization sequence (*i.e.* with clinopyroxene of Mg-value < 87) after

crystallization of olivine, clinopyroxene, and phlogopite *except* under water-saturated conditions (40% H_2O) at 30 kb. With 40% water at 30 kb, olivine is the liquidus phase but ilmenite (Mg_{46}) is the second phase to appear (at 1100 °C, with olivine, Mg_{86}). This ilmenite is the most Mg- and Cr-rich of those synthesized and compares closely with ilmenites synthesized from pyrolite at similar

TABLE 6

Compositions of ilmenites† determined by electron microprobe*

Wt % H_2O added	15	15	40	40
Pressure (kb)	10	30	30	30
Temperature (°C)	1050	1100	1100	1050
SiO_2	—	0·38	—	—
TiO_2	55·6	55·3	56·7	53·9
Al_2O_3	0·25	0·41	0·34	0·48
Cr_2O_3	0·20	0·79	1·71	0·47
FeO	34·7	31·2	27·4	36·0
MnO	0·23	0·48	0·26	0·28
MgO	8·68	10·72	13·12	7·98
CaO	0·29	0·47	0·33	0·65
K_2O	0·14	0·27	0·07	0·26
$\frac{100\ Mg}{Mg+Fe}$	31	38	46	28
Coexisting Phase(s)	cpx	cpx, Ph	ol	cpx, Ph
Cations for 6 Oxygens	4·02	4·03	4·01	4·06

* The ilmenite crystals are small (<15μ) and the variable contents of CaO, K_2O, Al_2O_3, and SiO_2 may be attributed in part or wholly to interference from phases enclosing the ilmenite.

† All analyses have been normalized to 100 % and are reported to three significant figures only.

P and *T* (Green & Sobolev, 1975). The presence of excess water and thus of a free vapour phase may mean that some components, *e.g.* K?, are partitioned into the vapour phase in sufficient quantity to materially change the composition of the silicate melt phase. The data indicates that the liquid in equilibrium with ilmenite at ~30 kb, 1100 °C contains ~5> TiO_2 (in magma composition calculated to 100% anhydrous).

PETROGENETIC IMPLICATIONS

The experimental data place constraints on hypotheses of derivation of highly potassic liquids from upper mantle source rocks. The mafurite has olivine as liquidus phase over a wide pressure, temperature, and $\%H_2O$ range and thus either this composition, or compositions derived from the mafurite by subtraction of some olivine, could be a partial melt from an olivine-rich source rock. The mafurite is, however, not saturated with orthopyroxene at any pressure, temperature, or $\%H_2O$ and the extremely CaO-rich compositions of the clinopyroxenes crystallizing from the mafurite suggest that this composition is well

removed from orthopyroxene saturation. It is therefore most improbable that the mafurite or compositions resembling it could be derived by partial melting of an orthopyroxene-bearing source rock. Similar conclusions apply to garnet, in the source rock and potassium-rich liquids in equilibrium with garnet at ~30 kb would need to contain higher Al_2O_3 contents than the mafurite used. We were surprised that a liquid with such a high K_2O-content and K_2O/Na_2O ratio, did not crystallize phlogopite as its liquidus phase over a much wider temperature and pressure range. In retrospect, a composition with lower MgO, higher Al_2O_3 and lower $\frac{K_2O}{Na_2O}$ would have given lower liquidus temperatures and possibly had a wider P,T field for near-liquidus phlogopite. Modreski & Boettcher (1972, 1973) and Forbes & Flower (1974) show that pure phlogopite and particularly titanphlogopite remain stable up to >1250 °C and >1350 °C respectively at $P > 15$ kb for vapour absent conditions, yet phlogopite does not occur on the water-undersaturated liquidi for 5% H_2O at any pressure or for 15% H_2O until 30 kb, ~1230 °C. Thus our data show that some magnesian lavas, if at $T >$ 1200 °C, may become extremely enriched in K_2O without crystallizing a K-rich phase.

The relationships of the liquidus and primary fields for olivine and phlogopite for 15% H_2O suggest a possible mechanism for enrichment of magmas in K_2O during movement to the surface. At 30 kb, 1200 °C, 15% H_2O, the mafurite consists of primary phlogopite (Mg_{93}) and liquid. Since phlogopite crystallizes alone over a small temperature interval, the liquid at the appearance of clinopyroxene is lower in K_2O than the mafurite composition. We have, at $1175° < T < 1200$ °C, a situation in which a liquid containing suspended phlogopite crystals at 30 kb, could move to lower pressures and pass from the phlogopite+liquid field to the olivine+liquid field (Fig. 1). The consequence of this reaction relationship would be to enrich the liquid in K_2O and Al_2O_3 and to decrease its MgO content. The relative densities and shape factors for phlogopite and olivine crystallizing from a melt are such that phlogopite could very readily be transported in a moving magma column whereas under the same conditions of movement, olivine crystals would settle out. Extensive studies of crystallization of a nepheline mugearite composition (Irving & Green, in preparation) and olivine-rich basanite composition (Green, 1973*b*, and unpublished data) at high temperature and pressure and with various water contents show that for these compositions, there also exist P,T conditions where they are saturated with olivine, clinopyroxene, and phlogopite or clinopyroxene and phlogopite. Movement of magma could produce winnowing of crystals with olivine and clinopyroxene settling out, phlogopite being carried to lower pressure but reacting with liquid with precipitation of olivine to produce liquid of higher K/Na ratio and Al_2O_3 content.

The highly magnesian character of K-rich lavas such as the mafurite or olivine leucitites of central New South Wales (Cundari, 1973) argues against extensive

crystal fractionation as a factor in their genesis (since this would produce Mg-values <65 in the fractionated liquids) but a reaction relationship in which phlogopite (Mg_{93}, 25% MgO) dissolves in the melt with co-precipitation of olivine (Mg_{91}, 49% MgO) would inhibit Fe-enrichment. A further factor which affects the Mg-value of K-rich magmas and which is very difficult to evaluate is the possibility of increasing f_{O_2} and Fe^{+++} content of the magma as it moves towards the surface. Both the bulk compositions and the crystallization sequences (titanomagnetite rather than ilmenite or armalcolite) of K-rich magmas (Cundari,1973; Carmichael, 1967) suggest extrusion under conditions of relatively high f_{O_2} (cf. Carmichael, 1967).

CONCLUSIONS

The reconnaissance study of the crystallization of an extremely K-rich lava as a function of pressure, temperature, and water content suggests that it is not possible to derive magmas of this type by partial melting of a mantle source lherzolite or garnet lherzolite (*e.g.* pyrolite) character. It is possible that local, atypical mantle regions of olivine+clinopyroxene+phlogopite+ilmenite mineralogy (established by earlier processes of partial melting, migration of minor melt or fluid phases) could partially melt to yield K-rich magmas of the olivine leucitite kindred.

Our data show that for basaltic liquids to exist in equilibrium with olivine and phlogopite at ~50–100 kms then the liquid must contain $>5\%$ K_2O. The K/Na ratio of such phlogopite-saturated liquids is unknown but we have also shown that for magnesian phlogopites (Mg_{90} approx.), TiO_2 is partitioned into the liquid and does not remain in phlogopite as a refractory component. A further peculiarity of the K-rich magma is that over the whole pressure and temperature range investigated, the clinopyroxenes crystallized are close to pure diopside–hedenbergite solid solutions with very little TiO_2, Al_2O_3, or $(Mg,Fe)SiO_3$ solid solution. Explanations for this behaviour, when viewed against the compositions of clinopyroxenes crystallized from liquids with similar CaO contents such as basalts, basanites, olivine nephelinites and olivine melilitite (Green & Ringwood, 1967; Bultitude & Green, 1968, 1970; Green, 1973*c*; Brey & Green, 1975) may be sought in the nature of bonding and structure within the silicate melts. It appears that high concentrations of K^+ atoms inhibit the formation of Ca–Al and Ca–Ti bonds and of $MgSiO_3$-silicate chains within the melt.

The studies of melting of pyrolite composition under water-undersaturated conditions (Green, 1973*a*,*b*) established conditions at ~30 kb 1000–1150 °C, where incipient melting occurs and liquids, at very low degrees of melting, are in equilibrium with olivine, orthopyroxene, clinopyroxene, garnet, ilmenite, and phlogopite. The earlier studies (Green, 1971, 1973*a*; Brey & Green, 1975) show that liquids from pyrolite at these conditions will have the character of olivine nephelinite. The present study shows that liquids in equilibrium with residual phlogopite will contain $>5\%$ K_2O. Data on the Na/Ca partition between clino-

pyroxene and liquid at 30 kb and the CaO content of clinopyroxene in pyrolite (Green, unpublished data) show that such liquids would also contain a high Na_2O content with $K_2O/Na_2O \approx 1$. The present study has suggested a mechanism whereby such potassic olivine nephelinite liquids could become enriched in K_2O by crystal elutriation, with transport of phlogopite crystals to shallower depths. This process, which leads to the reaction

$$\text{phlogopite} + \text{liquid 1} \rightleftharpoons \text{olivine} + \text{liquid 2}$$

with decreasing pressure, will enrich the liquid in K_2O and Al_2O_3. This process may modify basaltic liquids in their K/Na ratio and may be important in some alkaline basaltic provinces but will not produce the extreme depletion in Na_2O and very high K_2O/Na_2O ratios characteristic of many magmas of olivine leucitite kindred. Our experimental study suggests that extremely high K_2O/Na_2O ratios must be characteristic of their source region, or some process of Na depletion, which does not involve crystal fractionation or partial melting, must be invoked.

ACKNOWLEDGEMENTS

We thank J. F. G. Wilkinson for critical reading of the manuscript and N. G. Ware, E. H. Pedersen and E. Kiss for technical assistance.

REFERENCES

BELL, K., & POWELL, J. L., 1969. Strontium isotopic studies of alkalic rocks. The potassium rich lavas of the Birunga and Toro–Ankole regions, East and Central Equatorial Africa. *J. Petrology*, **10**, 536–72.

BORLEY, G. D., 1967. Potash rich rocks from Southern Spain. *Miner. Mag.* **36**, 364–79.

BREY, G., & GREEN, D. H., 1975. The role of CO_2 in the genesis of olivine melilitite magma. *Contr. Miner. Petrol.* **49**, 93–104.

BULTITUDE, R. J., & GREEN, D. H., 1971. Experimental study of crystal–liquid relationships at high pressures in olivine nephelinite and basanite compositions. *J. Petrology*, **12**, 121–47.

CARMICHAEL, I. S. E., 1967. The mineralogy and petrology of the volcanic rocks from the Leucite Hills, Wyoming. *Contr. Miner. Petrol.* **15**, 24–66.

CROSS, W., 1897. Igneous rocks of the Leucite Hills and Pilot Butte, Wyoming. *Am. J. Sci.* 4, 115–41.

CUNDARI, A., 1973. Petrology of the leucite-bearing lavas in New South Wales, *J. geol. Soc. Aust.* **20**, 465–92.

—— & LE MAITRE, R. W., 1970. On the petrogeny of the leucite-bearing rocks of the Roman and Birunga volcanic regions. *J. Petrology*, **11**, 33–47.

DAWSON, J. B., POWELL, D. G., & REID, A. M., 1970. Ultrabasic xenoliths and lava from the Lashaine volcano, Northern Tanzania. *Ibid.* **11**, 519–48.

FORBES, W. C., & FLOWER, M. F. J., 1974. Phase relations of titanphlogopite, $K_2Mg_4TiAl_2Si_6O_{20}(OH)_4$; a refractory phase in the Upper Mantle? *Earth planet. Sci. Lett.* **22**, 60–6.

GIBB, F. G. F., 1971. Crystal–liquid relationships in some ultrabasic dykes and their petrological significance. *Contr. Miner. Petrol.* **30**, 103–18.

GREEN, D. H., 1969. A review of experimental evidence on the origin of basaltic and nephelinitic magmas. *Phys. Earth planet. Interiors*, **5**, 221–35.

—— 1973*a*. Experimental melting studies on a model upper mantle composition under water saturated and water under-saturated conditions. *Earth planet. Sci. Lett.* **19**, 37–53.

—— 1973*b*. Contrasted melting relations in a pyrolite upper mantle under mid-oceanic ridge, stable crust and island arc environments. *Tectonophysics*, **17**, 285–97.

—— 1973*c*. Conditions of melting of basanite magma from garnet peridotite. *Earth planet. Sci. Lett.* **17**, 456–65.

—— & HIBBERSON, W., 1969. Experimental duplication of conditions of precipitation of high pressure phenocrysts in a basaltic magma. *Phys. Earth planet. Interiors*, **3**, 247–54.

—— & RINGWOOD, A. E., 1967*a*. An experimental study of the gabbro to eclogite transformation and its petrological applications. *Geochim. cosmochim. Acta*, **31**, 767–833.

—— —— 1967*b*. The genesis of basalts. *Contr. Miner. Petrol.* **15**, 103–90.

—— & SOBOLEV, N. V., 1975. Coexisting garnets and ilmenites synthesized at high pressures from pyrolite and olivine basanite and their significance for kimberlite assemblages. *Ibid.*, **50**, 217, 229.

HOLMES, A., 1942. A suite of volcanic rocks from south-west Uganda containing kalsilite (a polymorph of $KAlSiO_4$). *Miner. Mag.* **26**, 197–217.

—— 1950. Petrogenesis of katungite and its associates. *Am. Miner.* **35**, 772–92.

—— 1952. The potash ankaratrite–melaleucitite lavas of Nabugando and Mbuga Craters, South-West Uganda. *Trans. geol. Soc. Edinb.* **15**, 187–213.

—— & HARWOOD, F., 1937. The petrology of the volcanic area of Bufumbira. *Mem. geol. Surv. Uganda*, **3**, pt. 2, 1–300.

IRVING, A. J., & Green, D. H., 1975. Experimental evidence for the role of kaersutite fractionation in the alkaline magma series at high pressures (in preparation).

ITO, K., & KENNEDY, G. C., 1968. Melting and phase relations in the plane tholeiite–lherzolite–nepheline basanite to 40 kilobars with geological implications. *Contr. Miner. Petrol.* **19**, 177–211.

MODRESKI, P. J., & BOETTCHER, A. L., 1973. Phase relationships of phlogopite in the system K_2O–MgO–CaO–Al_2O_3–SiO_2–H_2O to 35 kilobars: a better model for micas in the interior of the earth. *Am. J. Sci.* **273**, 385–414.

MORI, T., 1975. Pyroxenes in the system CaO–MgO–FeO–SiO_2 at 1200 °C, 15 kb and 30 kb (in preparation).

—— & GREEN, D. H., 1975. Pyroxenes in the system $CaMgSi_2O_6$–$Mg_2Si_2O_6$ at high pressure. *Earth planet. Sci. Lett.* **26**, 277–86.

REED, S. J. B., & WARE, N. G., 1973. Quantitative electron microprobe analysis using a Li-drifted silicon detector, *X-ray Spectrometry*, **2**, 69–74.

ROEDER, P. L., & EMSLIE, R. F., 1970. Olivine–liquid equilibrium. *Contr. Miner. Petrol.* **29**, 275–89.

YODER, H. S., & KUSHIRO, I., 1969. Melting of a hydrous phase: phlogopite. *Am. J. Sci.* **267***A*, 558–82.

B24

Contrib. Mineral. Petrol. 61, 141 – 162 (1977)

Contributions to Mineralogy and Petrology
© by Springer-Verlag 1977

Systematic Study of Liquidus Phase Relations in Olivine Melilitite $+H_2O$ $+CO_2$ at High Pressures and Petrogenesis of an Olivine Melilitite Magma

G. Brey* and D.H. Green**

Research School of Earth Sciences, Australian National University, P.O. Box 4, Canberra, A.C.T. 2600, Australia

Abstract. Near-liquidus phase relationships of a spinel lherzolite-bearing olivine melilitite from Tasmania were investigated over a P, T range with varying x_{H_2O}, x_{CO_2}, and f_{O_2}. At 30 kb under MH-buffered conditions, systematic changes of liquidus phases occur with increasing x_{CO_2} ($x_{CO_2}=CO_2/CO_2+H_2O+$olivine melilitite). Olivine is the liquidus phase in the presence of H_2O alone and is joined by clinopyroxene at low x_{CO_2}. Increasing x_{CO_2} eliminates olivine and clinopyroxene becomes the only liquidus phase. Further addition of CO_2 brings garnet + orthopyroxene onto the liquidus together with clinopyroxene, which disappears with even higher CO_2. The same systematic changes appear to hold at higher and lower pressures also, only that the phase boundaries are shifted to different x_{CO_2}. The field with olivine + clinopyroxene becomes stable to higher x_{CO_2} with lower pressure and approaches most closely the field with garnet + orthopyroxene + clinopyroxene at about 27 kb, 1160° C, $x_{CO_2}\sim 0.08$ and $x_{H_2O}\sim 0.2$ (i.e., 6–7% CO_2 + 7–8% H_2O). Olivine does not coexist with garnet + orthopyroxene + clinopyroxene under these MH-buffered conditions. Lower oxygen fugacities do not increase the stability of olivine to higher x_{CO_2} and do not change the phase relationships and liquidus temperatures drastically. Thus, it is inferred that olivine melilitite 2927 originates as a ~5% melt (inferred from K_2O and P_2O_5 content) from a pyrolite source at about 27 kb, 1160° with about 6–7% CO_2 and 7–8% H_2O dissolved in the melt. The highly undersaturated character of the melt and the inability to find olivine together with garnet and orthopyroxene on the liquidus (in spite of the close approach of the respective liquidus fields) can be explained by reaction relationships of olivine and clinopyroxene with orthopyroxene, garnet and melt in the presence of CO_2.

* *Present address and address for offprint requests:* Mineralogisches Institut der Technischen Universität, Welfengarten 1, D-3000 Hannover, Federal Republic of Germany

** *Present address:* Dept. of Geology, University of Tasmania, Box 252C, G.P.O., Hobart, Tasmania 7001, Australia

Introduction

The importance of CO_2 (in addition to H_2O) in influencing the nature of partial melting of peridotite under upper mantle conditions and controlling the formation of highly undersaturated magmas has been demonstrated by experiments in simple systems (Eggler, 1973, 1975; Wyllie and Huang, 1976) and in natural rock compositions (Brey and Green, 1975, 1976). Highly undersaturated basaltic compositions such as the olivine melilitite from Laughing Jack Marsh, Tasmania (see below) are inferred to be derived by small degrees of partial melting from a peridotitic composition. It has been shown (Brey and Green, 1975) that olivine and olivine+clinopyroxene are the liquidus phases of this olivine melilitite up to 40 kb under dry conditions and in the presence of H_2O alone, but that garnet+orthopyroxene are liquidus phases at similar p, T conditions, when sufficient CO_2 is present in addition to H_2O. The purpose of this paper is to map out stability fields of near liquidus phases of this olivine melilitite as a function of P, T, H_{H_2O}, X_{CO_2} and f_{O_2} and thus set up a specific model for the origin of this olivine melilitite. The study shows the influence of *two* active (towards a silicate melt) volatile components on the liquidus and liquidus phases of a basaltic composition and emphasises the systematic variation of variables and their effects on liquidus phase relations. The shape of the liquidus surface makes it possible to deduce the simultaneous solubility of H_2O and CO_2 in the melt at a constant pressure. The following section shows a schematic liquidus surface of a system olivine melilitite$-H_2O-CO_2$ and outlines how the experiments were designed to obtain maximum information.

The presence of a volatile component soluble in a silicate melt and therefore not inert towards it, lowers the liquidus temperature of that melt. At any given pressure addition of increasing proportions of the volatile component to the melt results in further lowering of the liquidus temperature until the saturation value is reached. Further addition of the volatile component does not change the liquidus temperature except insofar as components from the melt are partitioned into the free vapor phase, thereby changing the melt composition and thus increasing its liquidus temperature. The presence of two volatile components similarly lowers the liquidus temperature, but now the effect is a function of both the amount and the proportion of the two components. Figure 1 shows a schematic diagram of the liquidus surface of a system olivine melilitite$-H_2O-CO_2$ at a fixed pressure. Olivine melilitite is presented here as one component. H_2O is more soluble than CO_2 in the olivine melilitite melt (Brey and Green, 1976) and lowers the liquidus temperature more rapidly than CO_2. This results in a liquidus of two curved, intersecting surfaces as shown in Figure 1. The dashed lines represent isotherms at equal temperature intervals, the thick solid line marks the boundary between liquids with a free vapor phase present and fluid absent liquids. The isotherms are kinked where they cross this boundary. This is seen more clearly in an isobaric polythermal projection of the liquidus surface onto the plane olivine melilitite$-H_2O-CO_2$ (shown also schematically in Fig. 1). The geometry of the liquidus surface gives a tool to experimentally establish the shape of the liquidus surface at a particular

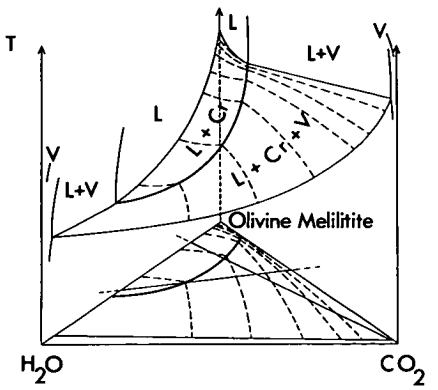

Fig. 1. Schematic liquidus surface at constant pressure of the system olivine melilitite $-H_2O-CO_2$ and the projection of the liquidus surface onto the plane olivine melilitite $-H_2O-CO_2$. Dashed lines are isotherms, the thick solid line is the vapor saturation boundary

pressure and to find how much H_2O and CO_2 are soluble simultaneously in olivine melilitite at a particular liquidus temperature. Basically, two joins in the system olivine melilitite $-H_2O-CO_2$ provide the maximum information:

a) Starting on the olivine melilitite-H_2O side at a chosen vapor undersaturated composition, more and more CO_2 is added and the liquidus temperature is established for each composition. The liquidus temperature should go through a minimum when the vapor saturation boundary is crossed.

b) Starting again from the olivine melilitite-H_2O side at a chosen vapor-undersaturated composition, H_2O is replaced mole for mole by CO_2. The liquidus temperature increases only slightly until the vapor saturation boundary is reached and then it increases rapidly.

Experimental Methods

Starting composition for this study was glass made from a spinel lherzolite bearing olivine melilitite from Laughing Jack Marsh, Tasmania. The chemical composition and a short petrographic description are given by Brey and Green (1975). Experiments were carried out with a piston-cylinder apparatus and a -10% friction correction was applied for the piston-in technique. No pressure correction was applied for the emf of the $Pt/Pt_{90}Rh_{10}$ thermocouple. The double capsule method was used in experiments with an external buffer which was in most cases the MH buffer and for reconnaissence studies the NNO buffer. Experiments with no external buffer are buffered by the furnace assembly with hydrogen fugacities $\geq$NNO. Capsule materials for the experiments were $Ag_{77}Pd_{23}$ up to 1180° C, $Ag_{50}Pd_{50}$ up to 1250° C and Pt for higher temperatures. The outer capsule in experiments with an external buffer was made of Pt in most cases and rarely of Au or $Ag_{50}Pd_{50}$. Run times varied from 10–30 min. The shorter run times were used in earlier experiments, where there were some difficulties in maintaining the MH-buffer over longer periods of time.

The compositions (olivine melilitite 2927: H_2O: CO_2) used in this study are shown in Figure 2 in mol.-% and are given in Table 1 in mol.- and wt.-%. It is purely arbitrary how to calculate the molecular weight of a rock composition and several methods are in use. We have used the expression $\Sigma\{$[gram formula weight of oxide] $\times$ [molecular fraction of oxide]$\}$ = molecular weight of the rock composition. This method yields a molecular weight of 59.74 for olivine melilitite 2927.

Mineral analyses were carried out with a TPD electron microprobe. Analytical procedures and accuracy are described by Reed and Ware (1973, 1975).

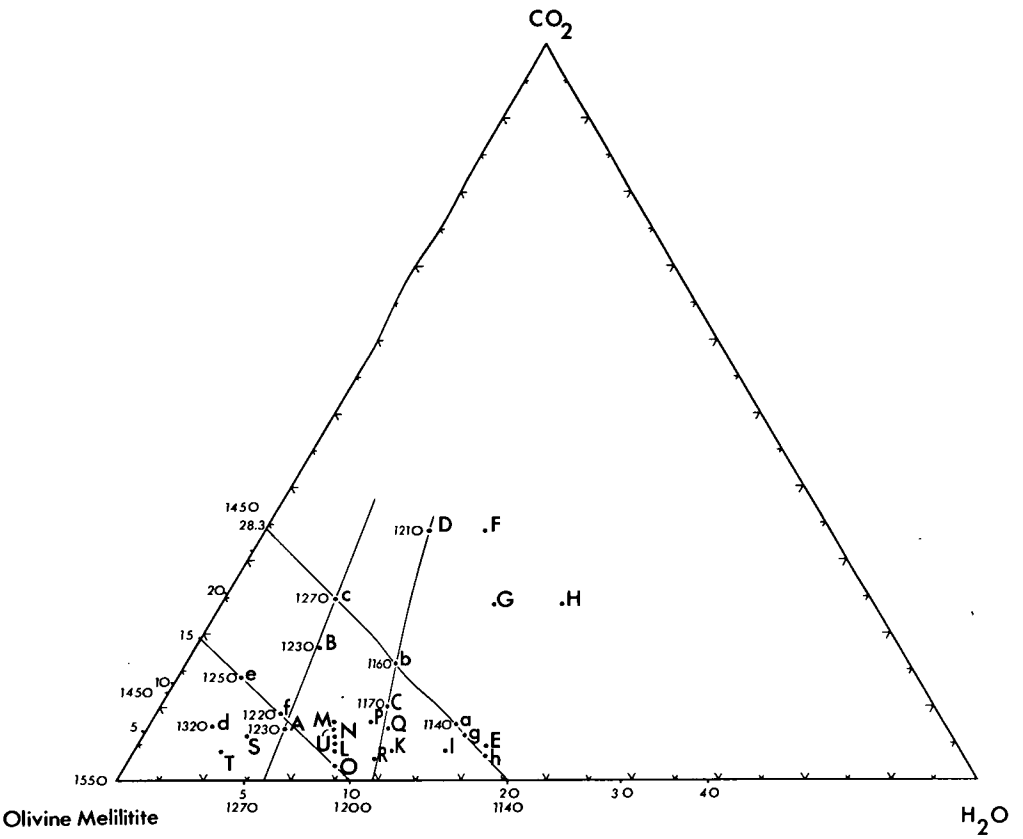

Fig. 2. The system olivine melilitite–H_2O–CO_2 in Mol-%. *A, B, C ... a, b, c* mark compositions used in the experiments. Numbers 5–40 are wt.-% of H_2O and CO_2, other numbers are experimentally determined liquidus temperatures

Experimental Results

Olivine Melilitite + H_2O + CO_2 at 30 kb under MH-Buffered Conditions

The liquidus surface and the nature of the liquidus phases in this system were established at 30 kb under MH-buffered conditions. The two boundary systems olivine melilitite-H_2O and olivine melilitite-CO_2 and four joins I, II, III and IV (Fig. 2) were investigated.

a) Olivine Melilitite-H_2O. The presence of H_2O lowers the liquidus temperature rapidly from 1550° C for dry conditions to about 1110° C for H_2O saturated conditions (Fig. 3a and b). Olivine is the liquidus phase for any H_2O-content under MH- and furnace-buffered (~NNO) conditions (Fig. 3). A solubility of 30–34 wt.% H_2O in olivine melilitite at 30 kb was found by adding more and more H_2O to the charge until no further lowering of the liquidus temperature

Table 1. Starting compositions in the system olivine melilitite $2927 + H_2O + CO_2$

	Molecular %			wt %		
	$2927 : H_2O : CO_2$			$2927 : H_2O : CO_2$		
A	77.0	16.0	7.0	88.5	5.5	6.0
B	68.0	14.0	18.0	79.5	5.0	15.5
C	63.6	26.4	10.0	80.6	10.1	9.3
D	46.7	19.3	34.0	60.2	7.5	32.3
E	54.7	40.8	4.5	77.8	17.5	4.8
F	40	26	34	54.9	10.8	34.4
G	44	32	24	61.7	13.5	24.8
H	36	40	24	54.8	18.4	26.9
J	60	36	4	81.3	14.7	4.0
K	66	30	4	84.6	11.6	3.8
L	73	23	4	88.1	8.4	3.6
M	71	21	8	85.3	7.6	7.1
N	72	22	6	86.7	8.0	5.3
O	74	24	2	89.5	8.8	1.8
P	67	25	8	83.3	9.4	7.3
Q	65	28	7	82.7	10.7	6.6
R	69	28	3	86.6	10.6	2.8
S	82	12	6	91.1	4.0	4.9
T	86	10	4	93.5	3.3	3.2
U	71.5	21.5	7	86.0	7.8	6.2
a	57.0	35.4	7.6	77.8	14.6	7.7
b	59.5	24.6	15.9	75.6	9.5	14.9
c	62.2	12.9	24.9	73.6	4.6	21.8
d	85.1	7.4	7.4	91.7	2.4	5.9
e	78.7	7.3	14.0	86.3	2.4	11.3
f	76.7	14.2	9.1	87.5	4.9	7.7
g	56.5	37.5	6.0	78.2	15.6	6.2
h	55.4	41.3	3.3	78.8	17.7	3.4

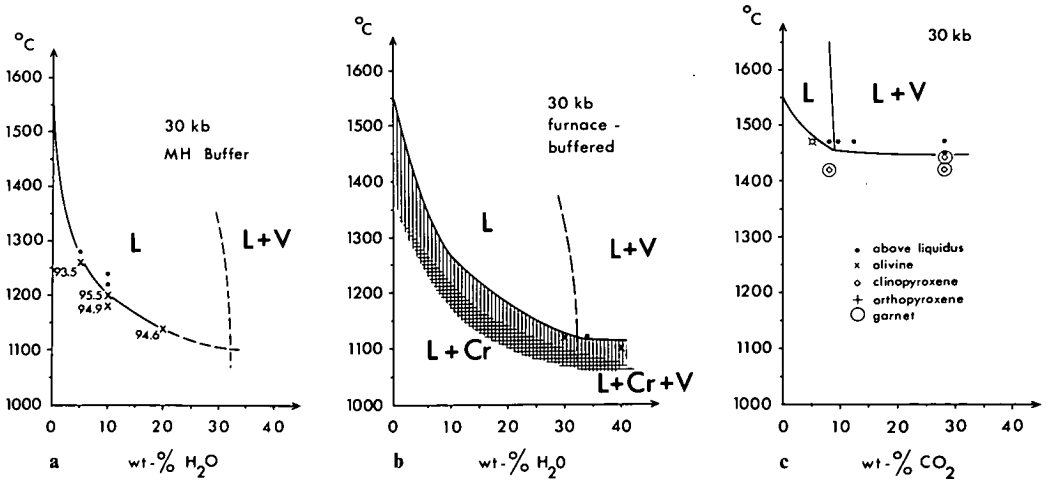

Fig. 3a. Liquidus of olivine melilitite 2927 at 30 kb with various amounts of H_2O added. Numbers are forsterite content in olivine. **b** Determination of maximum solubility of H_2O in olivine melilitite 2927 at 30 kb. Liquidus temperatures interpolated from experiments at 25 and 35 kb (Brey and Green, 1975). Vertical lines represent a field with olivine alone as liquidus phase, the hatched area with olivine and clinopyroxene. **c** Liquidus and liquidus phases of olivine melilitite 2927 at 30 kb with various amounts of CO_2 added.

occurred (Fig. 3b). The single capsule method (under furnace-buffered conditions) was used for this purpose, since the temperature is known more accurately (estimated ± 10° C) than with the double capsule method (estimated ± 15°).

b) Olivine Melilitite-CO_2. CO_2 lowers the liquidus temperature of olivine melilitite only by about 100° C (Fig. 3c) from 1550° C to 1450° C. No external buffer was applied for these experiments (in Pt-capsules) with olivine melilitite $+CO_2$ and great care was taken to keep the influence of the furnace assembly to a minimum by drying the furnace assembly at 110° C until just before the run. Direct measurement showed that 9 wt.% CO_2 is soluble in olivine melilitite at 30 kb (Brey and Green, 1976) and the experiments with various amounts of CO_2 added, show that no further lowering of the liquidus occurs with more than 8–10% CO_2 added. Olivine is the liquidus phase for volatile-free conditions. It is joined by pyroxene with increasing CO_2-content. Garnet and pyroxene are the liquidus phases for more than 8 wt.% CO_2 present. The pyroxenes vary widely in composition, but MgO is always greater than CaO, TiO_2 varies from about 0.5–2.5%, Al_2O_3 from 7–11% and SiO_2 from 47–53%. Some pyroxenes have about 0.6% TiO_2, 8% Al_2O_3, 52% SiO_2, 19% MgO and 10–11% CaO and approach closely clinopyroxene compositions found in experiments with pyrolite –40% ol at 30 kb, 1450° C (Mori, 1976). Most other clinopyroxenes are interpreted as metastable nucleation products (rather than quench products, no quench pyroxenes appear in runs above the liquidus) from the starting glass under run conditions, which could not exsolve to their equilibrium composition(s) due to short tun times and probably slower reaction rates in runs with only CO_2 (compared to those with H_2O present also). Nucleation problems of pyroxenes are discussed by Mori (1976, accepted for publication). Since Fe-loss would have been too great for longer run times, the metastability of the pyroxenes was accepted as unavoidable, since the main interest was to establish the liquidus temperature of the original starting material.

c) Olivine Melilitite–H_2O–CO_2, Profile I. It was intended that in profiles I and II (Fig. 4a and b), H_2O should be replaced mole by mole by CO_2, i.e., the profiles should be parallel to the H_2O–CO_2 side of the triangle olivine melilitite-H_2O–CO_2. Due to a mistake in calculating the molecular proportions, they are somewhat oblique to that side, but the desired information is still fully obtainable.

The liquidus temperature for olivine melilitite +10% H_2O lies between 1200 and 1220° C at 30 kb. The liquidus temperature increases only slightly when H_2O is replaced by CO_2 until H_2O/H_2O+CO_2 ~0.34. At higher CO_2, lower H_2O contents, the temperature increases rapidly due to the intersection with the vapor-saturation boundary (see "Introduction"). The near-liquidus phases change from olivine to olivine+clinopyroxene to pyroxene (probably orthopyroxene and clinopyroxene–see discussion under "Mineral chemistry").

d) Olivine Melilitite–H_2O–CO_2, Profile II. The ratios and amounts of volatiles in solids along this join are identical to those in the preliminary experiments with H_2O and CO_2 under MH-buffered conditions described by Brey and Green

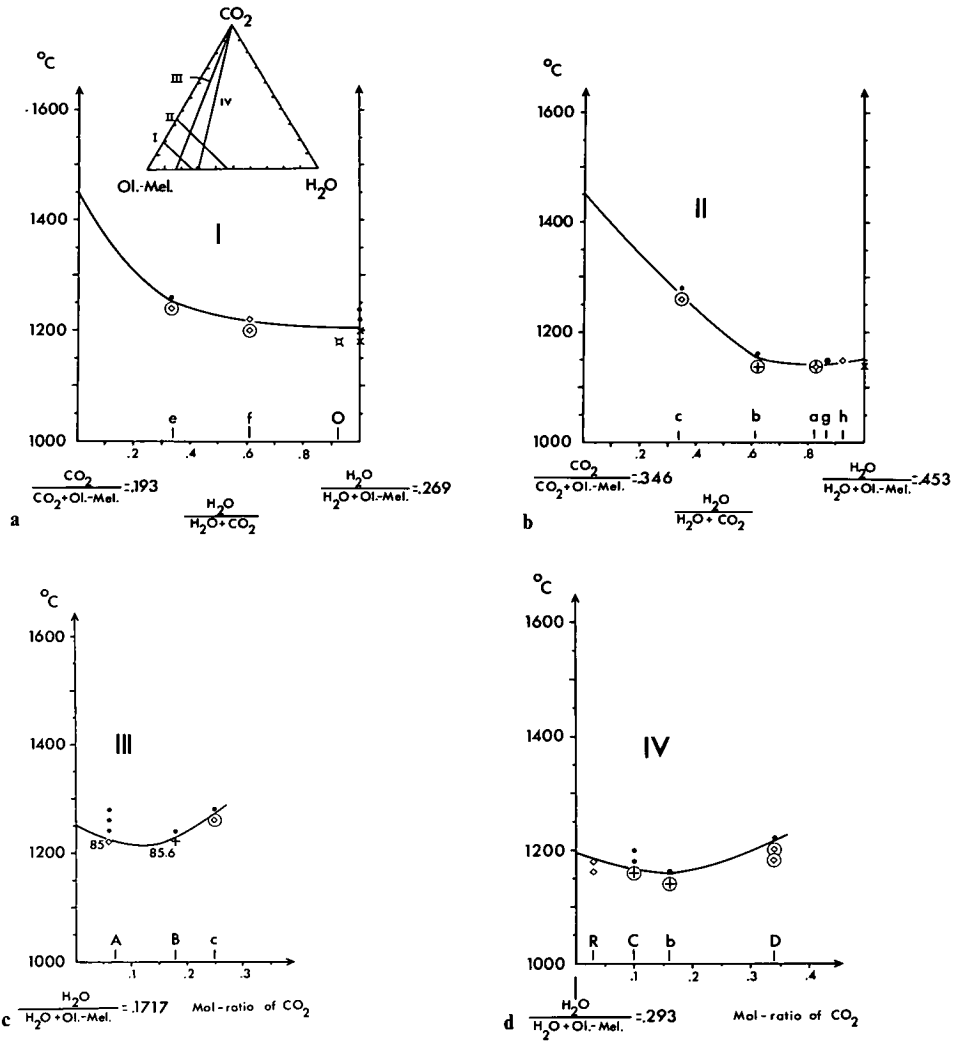

Fig. 4a–d. Liquidi at 30 kb (MH buffer) along joins (*I–IV*) in the system olivine melilitite-H_2O-CO_2

(1975). However, systematic differences were found in liquidus temperatures (30–40° C lower in the experiments) which are attributed to slightly different furnace geometry and less accurate "hot-spot" positioning. There are also minor differences of interpretation of near-liquidus phases [the Mg-rich pyroxenes in runs with CO_2 only were interpreted as very small orthopyroxenes with quench outgrowth (Brey and Green, 1975)].

As in profile I, there is only a slight increase of the liquidus temperature in the vapor undersaturated region, when H_2O is replaced by CO_2, and a sharp increase when the vapor-saturation boundary is crossed. Near-liquidus phases change from olivine ($x_{H_2O}=1$) to olivine+clinopyroxene, followed by

clinopyroxene, then by garnet + pyroxene (probably ortho- and clinopyroxene, see discussion below), then garnet + orthopyroxene and garnet + pyroxene ($x_{H_2O} = 0$).

e) Olivine Melilitite – H_2O – CO_2, Profile III (Fig. 4c). In such profiles, the H_2O/olivine melilitite ratio is kept constant and more and more CO_2 is added. The liquidus temperature is lowered with addition of CO_2 under vapor-undersaturated conditions and goes through a minimum at the vapor-saturation boundary. The liquidus phases change from olivine to clinopyroxene to orthopyroxene and to garnet + pyroxene.

f) Olivine Melilitite – H_2O – CO_2, Profile IV (Fig. 4d). The liquidus temperature again goes through a minimum when the vapor-saturation boundary is crossed. The liquidus phases are olivine, followed by clinopyroxene, garnet + orthopyroxene and garnet + pyroxene.

From the results of the above series of experiments and the results of additional experiments with varying ratios of olivine melilitite: H_2O: CO_2 (Fig. 2 and Table 1), the isotherms (50° C intervals) of the liquidus surface at 30 kb and the vapor-saturation boundary were constructed (Fig. 5). The position of the 1150° C isotherm is not very well defined, since there are only small differences in acutal liquidus temperatures of these H_2O-rich compositions near the 1150° C isotherm. These differences cannot be resolved with our technique. The best fit construction of isotherms in the vapor oversaturated region would appear to be slightly curved isotherm projections rather than the straight line projections of the simple system diopside – H_2O – CO_2 (Eggler, 1973). This may reflect increasing solution of solids in the increasing amount of vapor phase with increasing distance from the vapor-saturation boundary. This effect would produce a continuous change in coexisting melt composition and liquidus temperature. The slope of the liquidus surface is very steep near the join olivine melilitite-CO_2 but decreases with increasing distance (Fig. 5). Multiple changes of liquidus phases occur in the vapor-undersaturated region (Fig. 7) and should be indicated by small kinks in liquidus temperatures (Eggler and Mysen, 1976). However, these changes in slope are so minor that they cannot be resolved with our experimental techniques and the projections of the isotherms have therefore been drawn as smooth curves.

One major kink in these projections is prominent, i.e. when the vapor-saturation boundary is crossed. This intersection lies in the orthopyroxene + garnet field (see Fig. 7). All kinks of the 1400–1150° C isotherms were joined by a smooth curve to give the vapor-saturated boundary in the system olivine melilitite – H_2O – CO_2 (Fig. 5). The position is fixed on the olivine melilitite-CO_2 join by a quantitative determination (9 wt.% CO_2) and on the olivine melilitite-H_2O join by adding more and more H_2O until no further lowering of the liquidus was observed (30–34%, see Fig. 3b). Two runs with H_2O and CO_2 from above the liquidus (compositions c and e) quenched to dusty brown coloured glasses which were analysed quantitatively for CO_2 and H_2O. The results plot closely to the estimated vapor-saturation boundary (Fig. 5). The shaded area in Figure 5 indicates the estimated error in its position. The bound-

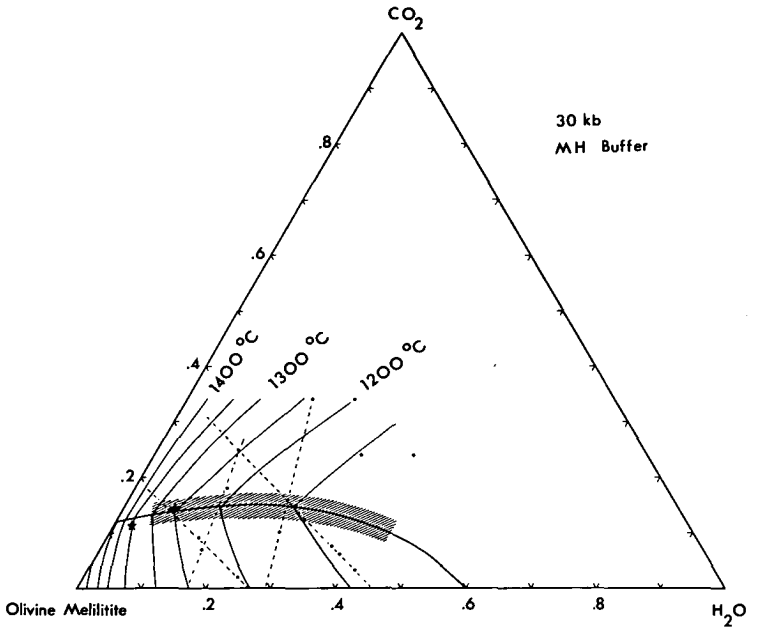

Fig. 5. Experimentally determined projections of the isotherms of the liquidus surface of the system olivine melilitite 2927 – H_2O – CO_2 (Mol-%) at 30 kb. The vapor saturation boundary joins the inflexion "points" in the isotherm projections and the shaded area represents the estimated error in the determination of the vapor saturation boundary. The stars represent analysed H_2O and CO_2 contents in glasses quenched from experiments above the liquidus (run no. 6152, 30 kb, 1260° C, comp. e – 8.8% CO_2, 0.9% H_2O and run no. 6245, 30 kb, 1280° C, comp. c – 11.7% CO_2, 2.7% H_2O)

ary is bent towards the CO_2 corner indicating an increasing CO_2 solubility with increasing H_2O – content, which was found also by Eggler (1973) in the diopside – H_2O – CO_2 system. The amount of CO_2 dissolved in the melt at the vapor saturation boundary is plotted in Figure 6 against the simultaneously dissolved amount of H_2O. Figure 6 shows that up to 14% CO_2 compared with only 9% in the H_2O free system together with 10% H_2O can be dissolved in olivine melilitite melt at 30 kb. The liquidus temperatures decrease with increasing H_2O content, but the negative temperature dependence of CO_2 solubility (Brey and Green, 1976) is only very small, so that the presence of H_2O must be responsible for the increase in CO_2 solubility.

The composition of the vapor phase (H_2O/CO_2 ratio) coexisting with melt can be determined only approximately by constructing isobaric, isothermal sections. Figure 8 shows such sections at 1150° C, 1200° C, and 1300° C as they are constructed from the available experiments. This figure illustrates the approximate composition of the vapor phase (in terms of H_2O, CO_2) coexisting with liquid at the liquidus temperatures at 30 kb in the system olivine melilitite – H_2O – CO_2. These approximate vapor compositions were used to estimate the oxygen fugacities in the system olivine melilitite – H_2O – CO_2 under fluid oversa-

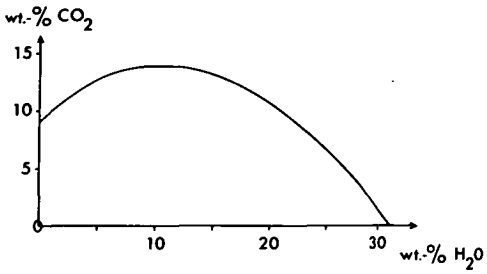

Fig. 6. Solubility of CO_2 in olivine melilitite 2927 at the liquidus at 30 kb as a function of H_2O content. The solubility data are taken from Figure 5 (vapor saturation boundary) and calculated in wt.-%

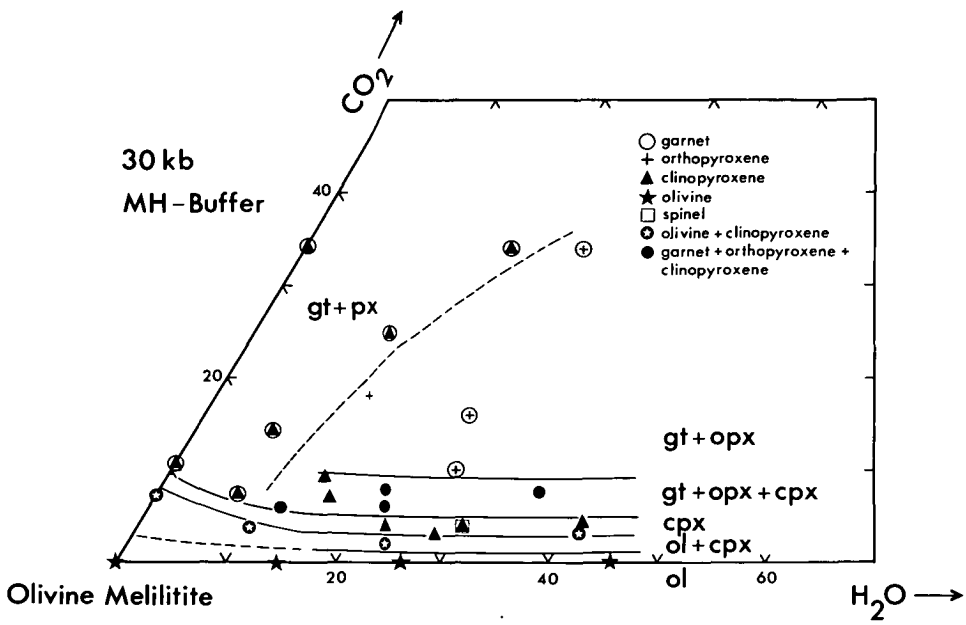

Fig. 7. Near-liquidus phases in the system olivine melilitite 2927 – H_2O – CO_2 at 30 kb

turated conditions. An external MH buffer was applied in most experiments except in those with CO_2 only. This keeps the hydrogen fugacity in all experiments at a low, but constant level and ensures that a free vapor phase is practically composed only of CO_2 and H_2O (except for dissolved solids). The oxygen fugacity varies throughout the system olivine melilitite – H_2O – CO_2 with varying H_2O/CO_2 ratios and also depends on the presence or absence of a free vapor phase. Assuming ideal behaviour of a free $CO_2 + H_2O$ vapor phase and that there are no other components other than CO_2 and H_2O, it is possible to approximately calculate oxygen fugacities as a function of varying CO_2/H_2O ratios with respect to an externally applied buffer (Boettcher et al., 1973). We have used the rough estimates of vapor compositions shown in Figure 8 to calculate the oxygen fugacities in the system olivine melilitite – H_2O – CO_2 (Fig. 9). The oxygen fugacity for a free vapor phase with H_2O alone

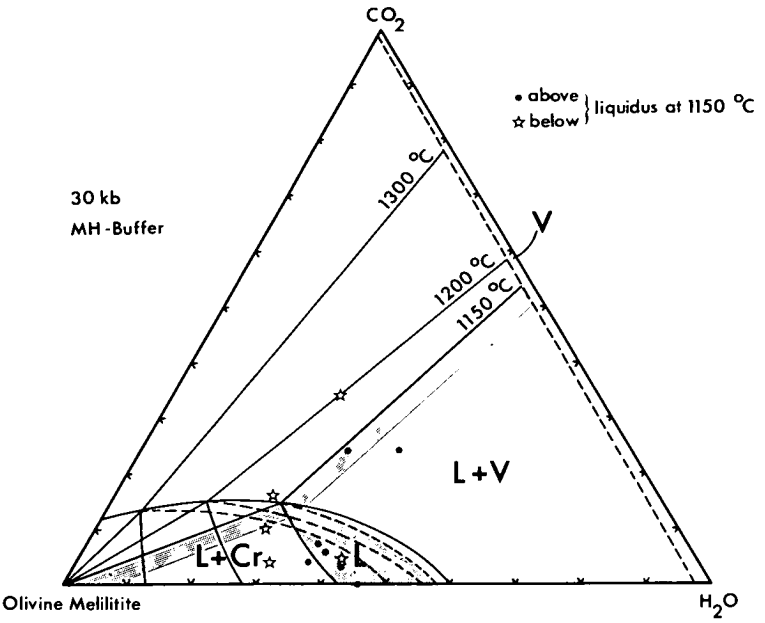

Fig. 8. Approximate composition (H_2O, CO_2) of the vapor phase (V_{1150}, V_{1200}, V_{1300}) in the system olivine melilitite – H_2O – CO_2 coexisting at 30 kb with liquid at liquidus temperatures. Compositions were determined by constructing isobaric, isothermal sections

is that of the external MH buffer. It decreases slowly with increasing CO_2-content (relative to the MH buffer), but falls rapidly and approaches the oxygen fugacity of the NNO buffer only for $x_{H_2O} < 0.1$ in the vapor phase. Such calculations cannot be carried out for fluid absent conditions, since there is not enough information about the activities of H_2O and CO_2 in silicate melts, but oxygen fugacities are certainly lower compared to vapor present conditions (Whitney, 1972). The lines of equal oxygen fugacities in the vapor-undersaturated region given in Figure 9 are estimated by assuming that the oxygen fugacity does not change for a fixed x_{H_2O}, if the temperature remains the same. Since the liquidus temperature increases from the vapor-saturation boundary to the join olivine melilitite-H_2O, a temperature correction has to be applied which moves the lines of equal oxygen fugacity towards the H_2O corner.

The experimental results presented show, that under otherwise very similar conditions, varying H_2O/CO_2 ratios bring different phases onto the liquidus of olivine melilitite 2927. Further experiments with varying olivine melilitite: H_2O:CO_2 (Fig. 2) showed that there are systematic changes of near-liquidus phases with increasing distance from the join olivine melilitite-H_2O (Fig. 7). At 30 kb, olivine is the only liquidus phase in the presence of H_2O. It is joined by clinopyroxene for small amounts of CO_2. More CO_2 eliminates olivine and clinopyroxene alone is the liquidus phase, except in one run (comp. K), where magnetiterich spinel (Table 2) is present also. Increasing CO_2 introduces

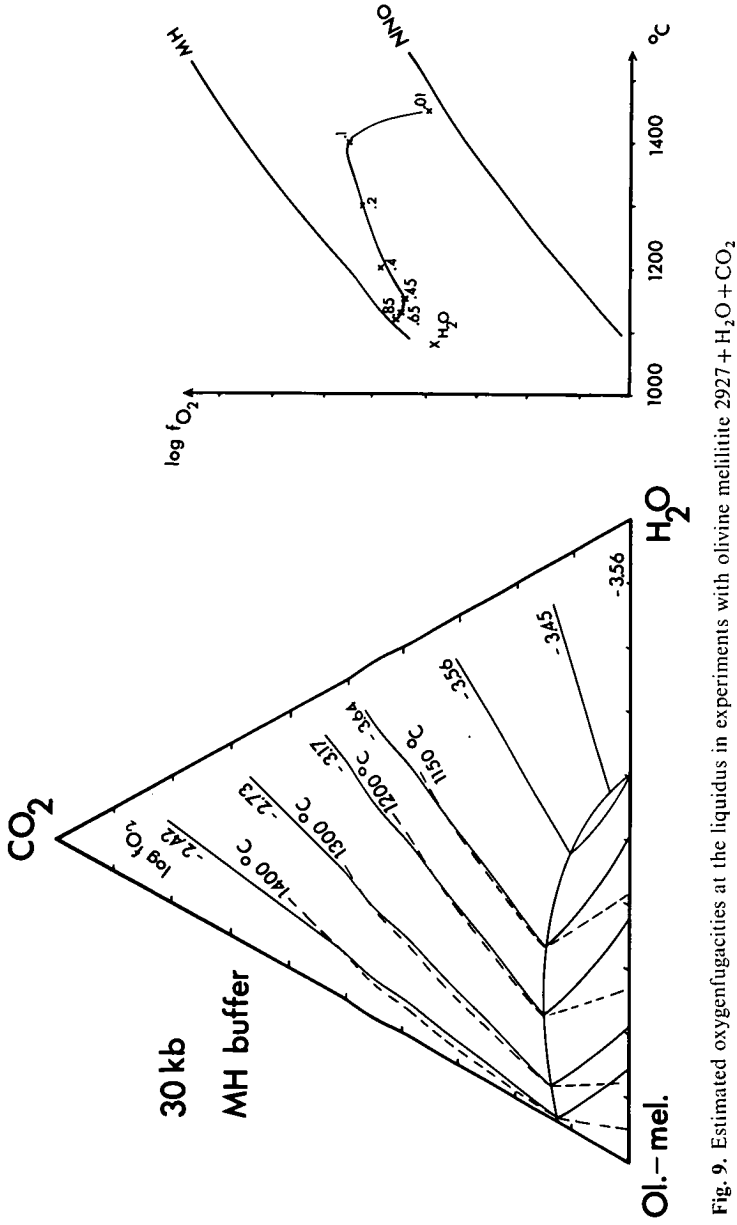

Fig. 9. Estimated oxygenfugacities at the liquidus in experiments with olivine melilitite 2927 + H_2O + CO_2

garnet and orthopyroxene as liquidus phases and clinopyroxene disappears with even higher CO_2. Titanomagnetite occurs in some H_2O- and CO_2-rich runs, but is large enough to be analysed in very few of them. A separate field garnet-+pyroxene (optically a clinopyroxene) for CO_2-rich compositions is shown in Figure 7, where the actual nature of the pyroxene cannot be accurately established for reasons similar to those given above for runs with olivine melili-

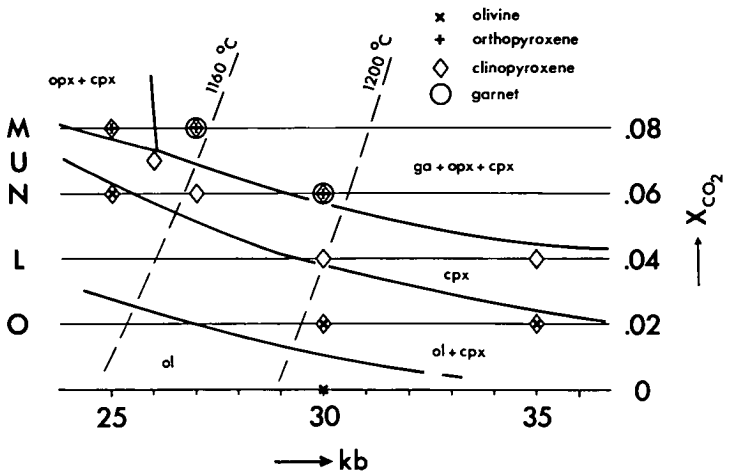

Fig. 10. Change of liquidus phases with pressure along a compositional join O-L-N-U-M (see Fig. 2)

tite + CO_2. The MgO-rich nature of the pyroxenes was demonstrated there and, since, with increasing temperature (the liquidus temperature increases towards the join olivine melilitite-CO_2), the clinopyroxene structure can take in more orthopyroxene component, we infer that the stable pyroxene would be clinopyroxene. Compositions A, f and B with only pyroxenes on their liquidi are not consistent with the systematic changes of liquidus phases with increasing x_{CO_2} outlined above, but the pyroxenes are joined immediately by garnet at somewhat lower temperature (comp. F, Fig. 11 and Table 2). Random failure of garnet to nucleate in the short run time may account for these three inconsistencies.

Olivine Melilitite + H_2O + CO_2 at Various Pressures under MH-Buffered Conditions

The influence of pressure on the nature of liquidus phases in the system olivine melilitite – H_2O – CO_2 was examined for the compositional sequence O-L-N-U-M (Fig. 2) from 25–35 kb. A diagram outlining liquidus phase boundaries as a function of pressure and molecular ratio of CO_2 is given in Figure 10. Olivine is the liquidus phase at 30 kb in the presence of H_2O alone under MH-buffered and "Furnace-buffered" conditions (see above) and will certainly be so at lower pressures also. It is joined by clinopyroxene under "furnace-buffered" conditions at 35 kb (Brey and Green, 1975) and it is expected that the same holds under MH-buffered conditions also, so that a field with olivine alone as liquidus phase wedges out towards higher pressure (Fig. 10). The olivine + clinopyroxene field widens at lower pressures to higher molecular ratios of CO_2 (N) and diminishes at higher pressures (O; note that clinopyroxene alone is the liquidus phase at 40 kb under "furnace-buffered" conditions in the presence

of H_2O alone – see Brey and Green, 1975). At all pressures investigated, a field with clinopyroxene alone borders the olivine + clinopyroxene field towards compositions with higher molecular ratios of CO_2. The clinopyroxene field becomes somewhat wider and moves towards H_2O-richer compositions (L) with increasing pressure (i.e., it expands at the expense of the olivine and olivine + clinopyroxene field) and becomes narrower and moves to CO_2-richer compositions (N, U) at lower pressures. The phase boundary which marks the appearance of garnet and orthopyroxene in addition to clinopyroxene as liquidus phases lies at higher CO_2 contents at lower pressure (27 kb) and lower CO_2 contents at higher pressures (30 kb) (cf. compositions M + N). Garnet disappears as a liquidus phase between 27 kb and 25 kb and orthopyroxene and clinopyroxene alone are liquidus phases at 25 kb and $x_{CO_2} = 0.08$ (M). As at 30 kb, none of the compositions examined within the system olivine melilitite $- H_2O - CO_2$ simultaneously crystallized all four phases olivine, orthopyroxene, clinopyroxene and garnet in a near-liquidus run. The closest approach to four-phase crystallization is ~27 kb, composition M. Addition of < 5% olivine to the olivine melilitite composition (implying precipitation of some olivine from the primary magma before picking up lherzolite inclusions) may cause the olivine + clinopyroxene field to adjoin the garnet + orthopyroxene field. A further point is that reaction relations exist between crystals and liquid so that, within the accuracy and reproducibility of experiments and the necessity to run slightly *below* the liquidus to obtain phases for identification and analysis, it might be regarded as rather fortuitious, if any one run did obtain all four phases on the liquidus.

Olivine Melilitite + H_2O + CO_2 under Hydrogen Fugacities Higher than that of the MH Buffer

One variable which has not been adequately investigated so far in this study is oxygen fugacity. Oxygen fugacities lower than those created by the MH buffer may increase the stability of olivine as a liquidus phase to higher CO_2 contents and thus establish conditions of four-phase saturation. Hydrogen and oxygen fugacities created by the MH buffer are almost certainly lower and higher, respectively than those in the mantle. This is indicated by the occurrence of ilmenite rather than titanomagnetite (observed in our MH buffered experiment) as the Ti-bearing phase in garnet lherzolite nodules, by the low Fe^{3+} content in ilmenites, clinopyroxenes and garnets from lherzolite nodules and by the occurrence of graphite and diamond in mantle derived products. However, experiments to duplicate such conditions by applying an external NNO buffer or using the innate oxygen fugacity of the furnace assemblage (slightly lower than NNO) were not very successful. NNO is an unsuitable buffer material at these high temperatures as nickel rapidly migrates through the capsule walls into the charge and changes the starting composition. No graphite was detected in furnace-buffered runs (hydrogen fugacity > NNO), but it is not known what the composition of the gas species is in a C-O-H system at such high hydrogen fugacities and total pressures. Inhomogeneities in mineral assemblages within individual runs and inconsistencies from run to run mitigate against rigorous

experiments and obscure the application of the results obtained under low oxygen fugacities. Some conclusions may, however, be drawn from these experiments:

a) liquidus temperatures are somewhat higher than under MH-buffered conditions either due to different oxygen fugacities or to some reduction of CO_2 or possibly due to a systematic temperature error between the two types of furnace assemblies.

b) the stability of olivine is not obviously increased to higher (added) CO_2 contents.

c) the presence of one or more carbon species dissolved in the melt brings orthopyroxene and garnet onto the liquidus of olivine melilitite under f_{O_2} conditions near NNO, as well as under MH-buffered conditions.

Mineral Chemistry of Liquidus Phases

a) At 30 kb. Olivines are 20–30 microns diameter in CO_2-free runs, but only a few microns in runs with CO_2. Clinopyroxene is also < 10 microns grain size, except in compositions T, S and A, where it occurs as up to 30 microns laths. Orthopyroxene occurs as up to 40 microns long needles with quench-clinopyroxene outgrowth. Garnet is euhedral and up to 20 microns. It is clear in runs close to the liquidus, but contains tiny, unidentified inclusions at lower temperatures. Quench phases are clinopyroxene, phlogopite, amphibole, (?) apatite and carbonate.

Selected microprobe analyses (normalised to 100%) of minerals from some experiments are given in Table 2 – the complete presentation of analyzed phases is plotted in Figure 11 and a listing of individual analyses is obtainable from the authors on request. Garnets and clinopyroxenes contain appreciable amounts of Fe^{3+} in these MH-buffered experiments. This is apparent in high totals of the structural formulae. If not corrected for Fe^{3+}, Mg-values of garnets and clinopyroxenes are too low with respect to equilibrium with coexisting olivine, orthopyroxene or liquid (Table 2). If Fe^{3+} contents in clinopyroxenes are calculated according to a method proposed by Ryburn et al. (1976), the resulting Mg-values ($Mg/Mg+Fe^{2+}$) are consistent with equilibrium between the coexisting phases (Table 2). No correction for Fe^{3+} was applied in plotting analyses from individual runs in the pyroxene quadrilateral (Fig. 11).

Olivine from runs with olivine melilitite $+ H_2O$ (i.e., CO_2-free) under MH-buffered conditions has a higher forsterite content (93.5–95.5, Figs. 3 and 11) than under furnace-buffered ($<$ NNO) conditions (89–90). Forsterite content in olivines from experiments (also MH-buffered) with compositions O and T, where small amounts of CO_2 are present, is 91 and 90, respectively (Fig. 11 and Table 2). It is 93 in composition h with a rather long run time (60 mins compared with 10 and 15 min, indicating Fe-loss). A possible explanation for lower Mg-values in the presence of CO_2 is that CO_2 changes the distribution coefficient of Fe^{2+} and Mg between liquids and crystals. Mg-values of olivines vary with different oxygen fugacities (see above), but we do not expect that the difference in oxygen fugacities between CO_2-free and CO_2-containing runs so closely spaced is so great that it could cause the change in forsterite content

Table 2. Selected mineral analyses of runs with olivine melilite + H_2O + CO_2

Run No.	6119	6370		6460	6366		6626			6051			6320		6525		6476		
p[kb]	30	30		30	30		30			30			30		25		27		
T[°C]	1200	1180		1180	1180		1180			1160			1150		1140		1140		
time [min]	20	10		30	10		30			20			15		30		30		
Compo-	10%																		
sition	H_2O	O		L	N		M			C			K		M		M		
Phase	ol	ol	cpx	cpx	ga	"opx"	cpx	ga	"opx"	cpx	ga	opx	Ti-magn.	cpx	spinel	opx	cpx	ga	opx	cpx
SiO_2	41.6	41.6	50.7	50.9	41.5	51.3	51.3	41.6	53.0	52.3	41.7	55.1	1.9	51.6	0.3	54.0	50.7	41.4	53.0	50.8
TiO_2	–	–	0.5	0.5	0.9	0.7	0.5	0.4	0.3	0.3	0.6	–	23.3	0.4	2.7	0.1	0.5	0.9	0.2	0.6
Al_2O_3	–	–	6.2	6.5	21.7	6.2	7.7	21.7	5.1	6.0	21.9	3.7	1.4	5.0	20.0	5.1	6.6	20.9	6.2	7.4
Cr_2O_3	–	–	0.5	0.6	0.3	0.1	0.2	0.9	0.2	0.5	0.4	–	–	0.3	2.1	0.3	0.7	0.8	0.2	0.5
FeO	4.6	8.7	5.9	5.7	8.4	8.3	5.5	8.5	7.4	5.8	10.4	7.9	58.5	6.5	60.0	7.5	6.7	9.2	7.8	6.4
MnO	–	–	–	–	0.2	–	–	0.2	–	–	0.2	–	–	–	0.2	–	–	0.3	–	–
MgO	53.7	50.0	15.3	16.0	19.8	19.5	16.5	20.3	20.0	16.2	18.8	31.4	2.3	16.8	14.3	31.2	15.1	19.3	31.2	16.0
CaO	0.2	0.3	19.3	18.4	7.3	12.7	16.2	6.4	12.7	17.1	6.1	1.5	3.3	18.1	0.3	1.8	17.9	7.3	1.4	16.4
Na_2O	–	–	1.5	1.6	–	1.2	2.1	–	1.4	1.8	–	0.4	0.5	1.3	–	–	1.8	–	–	1.9
K_2O	–	–	–	–	–	–	0.2	–	–	–	–	–	–	–	–	–	–	–	–	–
Si	0.996	1.000	1.859	1.858	2.971	1.859	1.857	2.976	1.908	1.898	2.999	1.921		1.887		1.882	1.857	2.985	1.848	1.850
Ti	–	–	0.013	0.013	0.047	0.019	0.013	0.023	0.008	0.009	0.033	–		0.010		0.003	0.015	0.047	0.006	0.015
Al	–	–	0.269	0.280	1.831	0.267	0.329	1.832	0.217	0.256	1.859	0.150		0.217		0.209	0.286	1.778	0.256	0.318
Cr	–	–	0.015	0.016	0.018	0.004	0.006	0.049	0.006	0.015	0.022	–		0.007		0.008	0.020	0.043	0.005	0.015
Fe	0.091	0.177	0.181	0.173	0.503	0.251	0.166	0.508	0.233	0.177	0.627	0.232		0.198		0.219	0.207	0.555	0.226	0.195
Mn	–	–	–	–	0.010	–	–	0.011	–	–	0.012	–		–		–	–	0.017	–	–
Mg	1.913	1.815	0.836	0.869	2.177	1.052	0.889	2.169	1.073	0.877	2.015	1.630		0.918		1.621	0.824	2.072	1.622	0.866
Ca	0.004	0.008	0.759	0.718	0.559	0.494	0.628	0.493	0.489	0.665	0.467	0.57		0.709		0.065	0.703	0.560	0.53	0.640
Na	–	–	0.107	0.112	–	0.085	0.144	–	0.096	0.124	–	0.030		0.095		–	0.128	–	–	0.137
K	–	–	–	–	–	–	0.010	–	–	–	–	–		–		–	–	–	–	–
Total	3.004	3.000	4.039	4.039	8.056	4.031	4.042	8.061	4.020	4.021	8.032	4.020		4.041		4.006	4.039	8.057	4.016	4.037
Mg-value	95.5	91.1	82.2	83.4	80.8	80.8	84.2	81.0	82.8	83.2	76.2	87.6		82.2		88.1	80.0	78.9	87.8	81.6
Fe^{3+} coor.			89.1	89.3			91.1			86.5				88.3			86.6			87.8

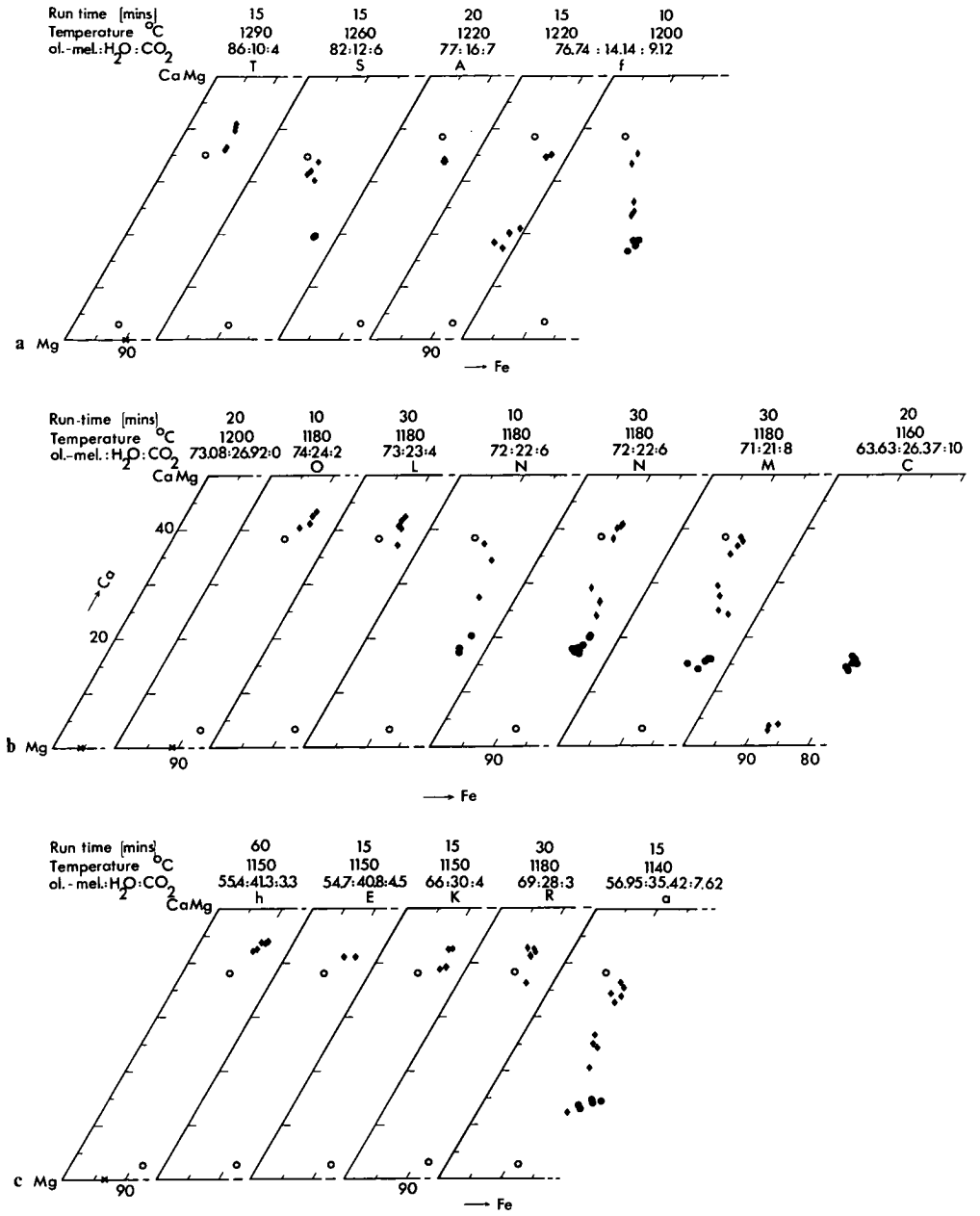

Fig. 11a–c. Ca-Mg-Fe diagrams of near liquidus phases at 30 kb. *Crosses* represent olivine, *diamonds* are pyroxenes and *dots* garnets. Stars represent pyroxene compositions from Mori and Green (1976)

of olivine (see Fig. 9). Our preference is to attribute the effect on K_D to the presence of CO_2.

Compositions of pyroxenes are compared in Fig. 11 with the compositions of coexisting orthopyroxene and clinopyroxene obtained by Mori and Green (1976, submitted for publication) on (pyrolite III − 40% olivine) + H_2O at 30 kb, 1150° C, 1200° C and 1250° C and at 40 kb, 1300° C (these runs were carried out under $f_{H_2} >$ NNO and the minerals contain little or no Fe^{3+}). Clinopyroxene coexisting with olivine is always Ca-rich (Table 2) and plots on the Ca-rich side of clinopyroxene coexisting with orthopyroxene in pyrolite under similar p,T conditions (Fig. 11). It is therefore inferred that these clinopyroxenes are not saturated in orthopyroxene. Compositions with a higher molecular ratio of CO_2 have only clinopyroxene on their liquidus (L, E, K.R). The clinopyroxenes are still Ca-rich (Table 1) and plot on the Ca-side of the clinopyroxene in pyrolite, but on average, appear to be closer in composition to the clinopyroxene limb of the two pyroxene field (Fig. 11). These compositions (L, E, K,R) are also inferred to be saturated only in clinopyroxene and not in orthopyroxene. Even higher molecular ratios of CO_2 (N, M, S. a) bring garnet onto the liquidus as well. The garnet compositions within individual runs vary mainly in Fe/Mg ratio. Rims of larger garnets are always Mg-richer than the cores, which reflects Fe-loss to the sample container. Grossular content in garnet increases with increasing temperature (Fig. 11 and Table 2). Clinopyroxenes are now of lower Ca-content and plot on the Mg-side of clinopyroxenes co-existing with orthopyroxene under similar p, T conditions in pyrolite (N, M, S, a, see also A, f). In most of these runs, a second Mg-rich pyroxene group (marked in Table 2 as "opx") exists which plots somewhere in the middle of the pyroxene solid solution gap. This second group is interpreted as metastable sub-calcic clinopyroxene, so that in these runs, garnet, orthopyroxene and clinopyroxene should coexist. This interpretation reflects the problem of orthopyroxene failing to nucleate and long persistence of subcalcic clinopyroxenes proxying for 2-pyroxenes (opx + Ca-rich cpx) encountered in other studies (Mori, 1976; Green, 1976). The subcalcic clinopyroxenes are usually somewhat poorer in Ti, Na and Al and richer in Si than the Ca-rich clinopyroxenes (Table 2). Clinopyroxene disappears when the molecular ratio of CO_2 is increased (C, b, F) and garnet + orthopyroxene (with compositions plotting on the orthopyroxene limb of the pyroxene solid solution gap (Fig. 11) are the liquidus phases.

b) Mineral Chemistry at 25, 27 and 35 kb. Analyses of primary phases are given in Table 2 and plotted in the pyroxene quadrilateral (Fig. 12) together with compositions of ortho- and clinopyroxene obtained by Mori and Green (1976) on pyrolite (see above). Again those clinopyroxenes coexisting with olivine (N, O) or occurring as the only liquidus phase (M, N, L) plot on the Ca-rich side of, or coincide with, the calcic pyroxene limb of the two-pyroxene field as defined by experiments in pyrolite. In contrast to the 30 kb experiments, clino- and orthopyroxenes exsolve to their equilibrium compositions at 25 kb and 27 kb (M, Fig. 12) and plot closely with the pyroxenes in pyrolite from similar temperatures.

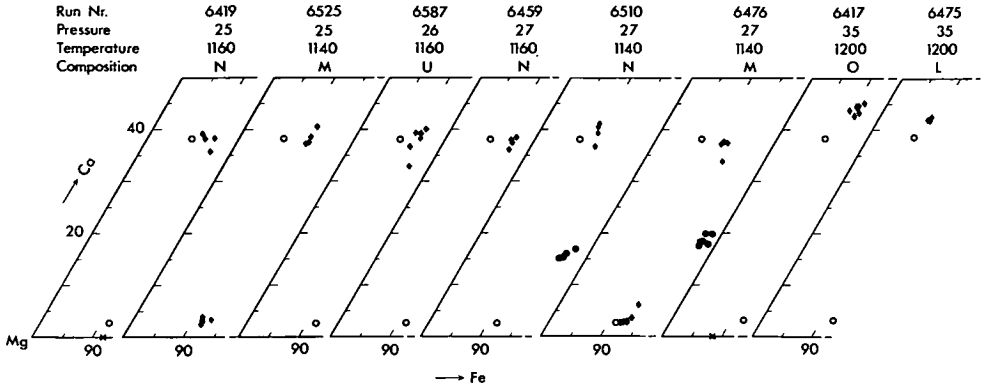

Fig. 12. Ca-Mg-Fe diagrams of liquidus phases from 25–35 kb. Symbols as in Figure 11

Ortho- and clinopyroxene compositions in olivine melilitite $2927 + H_2O + CO_2$ from 25–35 kb are very similar to those in pyrolite under similar p, T conditions with respect to Ti, Mg, Ca and Na contents, but have markedly higher Al and lower Si contents (Table 2; Mori and Green, 1976). Because of higher oxygen fugacities, total Fe content is also higher in clinopyroxenes from this study than in those from pyrolite.

Garnet coexists with clinopyroxene at 27 kb, 1140° C in composition N (> 20° below liquidus) and at the same conditions M (< 20° below liquidus). The latter garnets are more grossularrich than the former and both are slightly higher in grossular content than the garnets from 30 kb at similar temperatures. All garnets are very similar to those from pyrolite under similar conditions except for lower Cr-content and higher Fe^{3+} content.

Conclusions

Experimental studies on olivine melilitite $+ H_2O + CO_2$ using an external MH buffer ensure low f_{H_2}, high f_{O_2} and the persistence of CO_2 rather than more reduced carbon species in experimental runs. However, the compositions of minerals, particularly titanomagnetite, garnet (with $andradite_{ss}$) and clinopyroxene (with Fe^{3+} substitution), crystallized in the experiments, contrast with those of natural garnet lherzolites of mantle derivation (containing ilmenite, garnet and clinopyroxene all with low Fe^{3+} contents). Thus, the f_{O_2} conditions of the MH-buffered experiments render them not strictly applicable to natural mantle processes. However, it has also been shown that similar liquidus temperatures and similar near-liquidus roles for olivine, orthopyroxene, clinopyroxene and garnet are observed at hydrogen fugacities > NNO. It is thus concluded that the experimental results obtained with the MH buffer are applicable to natural conditions with reference to the effects of CO_2 and H_2O on the liquidus temperatures and silicate liquidus phases of olivine melilitite 2927.

Olivine was not observed to coexist with orthopyroxene, clinopyroxene and garnet as a liquidus phase under any *P*, *T*, x_{H_2O} and x_{CO_2} investigated. A narrow

field of clinopyroxene always separates an olivine+clinopyroxene field from an orthopyroxene+clinopyroxene+garnet field. This suggests either that olivine melilitite 2927 is not a partial melting product of a four-phase lherzolite source in the presence of H_2O and CO_2 (e.g., Cl could be an additional important vapor phase component as suggested by high Cl contents in sodalites – see Brey 1976b, unpublished Ph.D. thesis) *or* that its composition was slightly changed (by loss of olivine) on its way to the surface *or* (and) that there is a reaction relationship in the source region involving olivine.

The last possibility is suggested by experiments in the simple system diopside+forsterite+CO_2. Eggler (1975) describes the melting of this assemblage at pressures greater than 27 kb by the reaction diopside+forsterite+$CO_2 \leftrightharpoons$ enstatite+liquid, showing that both diopside and forsterite melt incongruently. Frey et al. (1976, submitted for publication) deduced models for the origin of olivine melilitite 2927 from a garnet lherzolite source (pyrolite) in the presence of H_2O and CO_2 by selective melting of components from the major silicate phases and formulated a hypothetical reaction similar to the one given here: olivine+clinopyroxene (diopside, jadeite, etc. solid solution)+(melt$_1$ containing H_2O) $\xrightarrow{+CO_2}$ (melt$_2$ containing monticellite+H_2O+CO_2)+garnet+orthopyroxene. Such a reaction also implies (at least in a simple system) that there should be a phase boundary in a p, T, x_{H_2O}, x_{CO_2} space, along which olivine, orthopyroxene, clinopyroxene and garnet are coexisting. In the complex system olivine melilitite-H_2O-CO_2 with extensive solid solutions in the minerals involved, such a reaction boundary will be a multivariant field. The probability of experimentally locating and intersecting with the four-phase saturation field in the presence of the reaction relationship and so many controlling variables is considered to be quite low. Thus, we would argue that conditions of origin for olivine melilitite 2927 in terms of the variables studied should be sought where the field for olivine+clinopyroxene as liquidus phases approaches most closely to that of orthopyroxene+clinopyroxene+garnet.

The field with clinopyroxene as the only liquidus phase diminishes with decreasing pressure whereas that of olivine+clinopyroxene expands to higher CO_2 contents (Fig. 10). This pressure dependence of the role of near-liquidus phases suggests that olivine melilitite 2927 can be a partial melting product of a peridotitic source at pressures around 27 kb (=incoming of garnet) and temperatures between 1160°–1180° C with 7–8% H_2O and 6–7% CO_2 dissolved in the melt.

The effects of five variables (pressure, temperature, x_{H_2O}, x_{CO_2} and f_{O_2}) were investigated in this study. Possible combinations of these variables give a rather wide field to experiment with and, contrary to the view expressed above, there may not be a *unique* solution (P, T, $\%H_2O$, $\%CO_2$, f_{O_2}) to the problem of the origin of this olivine melilitite. Definite constraints for such conditions are set by the incoming of a field orthopyroxene+clinopyroxene+garnet. However, as shown in Figure 7 at 30 kb, these three phases can coexist over a wide range of H_2O/CO_2 ratios, where x_{CO_2} (the amount of CO_2 present) is fixed and x_{H_2O} can vary widely. This may mean that the compositions, derived by low degrees of partial melting in the presence of H_2O and CO_2, are buffered

as to the approximate percentage of melt by temperature and amount of H_2O present, but are critically controlled as to degree of silica undersaturation (as measured by normative larnite + leucite contents) by the amount of CO_2 present. The meaning of this is illustrated in the following discussion: Olivine nephelinite may be the smallest melt fraction ($\sim 5\%$, Frey et al., 1976) which reaches the surface of the earth consequent on partial melting of a periodotitic source *in the presence of H_2O (no CO_2) alone.* The presence of small amounts of CO_2 ($x_{CO_2} = CO_2/CO_2 + H_2O + \text{melt} \cong 0.07$ in the melt) will change the composition of a 5% melt fraction to an olivine melilitite like 2927, the degree of melting being primarily determined by temperature and the amount of H_2O present. The product of higher degrees of partial melting, be it by increasing temperature or H_2O content but maintaining x_{CO_2} constant, will be olivine nephelinite whose chemical characteristics are somewhat different (e.g. CaO/Na_2O is higher; see Frey and Green, 1976) to that derived by melting in the presence of H_2O alone. Increasing x_{CO_2} for the same degree of partial melting will make the composition of the melt more olivine and larnite normative.

Acknowledgements. We thank W. Hibberson for assistance in carrying out high pressure experiments, N. Ware for instruction in electron microprobe analysis and Dr. Fildes and assistants for quantitative CO_2 and H_2O determinations. We benefitted greatly from discussions with T. Mori and Dr. R.I. Ryabchikov.

References

Boettcher, A.L., Mysen, B.O., Allen, J.C.: Techniques for the control of water fugacity and oxygen fugacity for experimentation in solid-media high-pressure apparatus. J. Geophys. Res. **78**, 5898–5901 (1973)

Brey, G.: CO_2 solubility and solubility mechanisms in silicate melts at high pressures. Contrib. Mineral. Petrol. **57**, 215–221 (1976a)

Brey, G.: Carbon dioxide in highly undersaturated basaltic magmas. Unpublished Ph.D. thesis, Australian National University (1976b)

Brey, G., Green, D.H.: The role of CO_2 in the genesis of olivine melilitite. Contrib. Mineral. Petrol. **49**, 93–103 (1975)

Brey, G.P., Green, D.H.: Solubility of CO_2 in olivine melilitite at high pressures and role of CO_2 in the earth's upper mantle. Contrib. Mineral. Petrol. **55**, 217–230 (1976)

Eggler, D.H.: Role of CO_2 in the melting processes in the mantle. Ann. Rept. Dir. Geophys. Lab., Washington **72**, 457–467 (1973)

Eggler, D.H.: Peridotite-carbonate relations in the system $CaO\text{-}MgO\text{-}SiO_2\text{-}CO_2$. Ann. Rept. Dir. Geophys. Lab., Washington **74**, 468–474 (1975)

Eggler, D.H., Mysen, B.O.: The role of CO_2 in the genesis of olivine melilitite: discussion. Contrib. Mineral. Petrol. **55**, 231–236 (1976)

Frey, F.A., Green, D.H., Roy, S.D.: Integrated models of basalt petrogenesis: A study of olivine tholeiites to olivine melilitites from South Eastern Australia utilising geochemical and experimental petrological data. (In press)

Green, D.H.: Orthopyroxene in the lunar interior and constraints on early lunar differentiation. Lunar Science Institute, Lunar Science **VII**, 336 (1976)

Mori, T.: Experimental study on pyroxene equilibria in the system $CaO\text{-}MgO\text{-}FeO\text{-}SiO_2$. J. Petrol. (in press, 1976)

Mori, T., Green, D.H.: Laboratory duplication of phase equilibria observed in natural garnet lherzolites. J. Geol. (in press, 1976)

Reed, S.J.B., Ware, N.G.: Quantitative electron microprobe analysis using a lithium drifted silicon detector. X-ray Spectrometry 2, 69–74 (1973)

Reed, S.J.B., Waren, N.G.: Quantitative electron microprobe analysis of silicates using energy-dispersive X-ray spectrometry. J. Petrol. **16**, 499–519 (1975)

Ryburn, R.J., Råheim, A., Green, D.H.: Determination of the p, T paths of natural eclogites during metamorphism – record of subduction. A correction to a paper by Råheim and Green (1975). Lithos **9**, No. 2, 161–164 (1976)

Whitney, J.A.: The effect of reduced H_2O fugacity on the buffering of oxygen fugacity in hydrothermal experiments. Am. Mineralogist **57**, 1902–1908 (1972)

Wyllie, P.J., Huang, W.: Carbonation and melting reactions in the system $CaO - MgO - SiO_2 - CO_2$ at mantle pressures with geophysical and petrological applications. Contrib. Mineral. Petrol. **54**, 79–107 (1976)

Received January 4, 1977/Accepted January 20, 1977

B25

GEOCHEMISTRY AND PETROGENESIS OF THE NEWER BASALTS OF VICTORIA AND SOUTH AUSTRALIA

By A. J. IRVING and D. H. GREEN

(With 1 Table and 6 Figures)

(MS received 19 March 1975; revised MS received 5 October 1975)

ABSTRACT

The Pliocene-Recent Newer Basalts province contains a large variety of magma types: quartz tholeiite, olivine tholeiite, olivine basalt, alkali olivine basalt, hawaiite, K-rich hawaiite, nepheline basanite, transitional olivine analcimite and olivine nephelinite (normatively low-K basanite to low-K nepheline mugearite), nepheline hawaiite, K-rich nepheline hawaiite, and nepheline mugearite. Despite some spatial restriction of the different magmas, there is no well-defined compositional progression with time. Many of the alkaline lavas contain Cr-diopside lherzolite-series xenoliths and must be of direct upper-mantle derivation.

Based on systematics of Mg-values (100 Mg/Mg + Fe^{2+} ratios) coupled with data for the olivine-liquid equilibrium and the results of other experimental studies, it is deduced that most of the basanitic magmas are primary melts of garnet-peridotite mantle, essentially unmodified by crystal fractionation. The nepheline hawaiites and nepheline mugearites are considered to be fractionated liquids derived from basanites by progressive removal of mainly olivine and kaersutite *at mantle pressures.* The hawaiites may be similarly related to alkali olivine-basalt parental liquids. The olivine tholeites and olivine basalts cannot be primitive mantle melts and must have undergone fractionation of olivine and perhaps pyroxene. The quartz-tholeiite and K-rich hawaiitic magmas are probably products of low-pressure fractionation processes.

A synthesis of chemical data for Tertiary-Quaternary basaltic lavas from throughout eastern Australia reveals that nepheline basanite is the most widespread mantle-derived magma type, and that the high-pressure lineage nepheline basanite → nepheline hawaiite → nepheline mugearite → nepheline benmoreite is much more important than previously recognized.

INTRODUCTION

The Tertiary volcanics of Victoria and south-east South Australia were extruded in two distinct episodes. The first, in the Palaeocene to Early Miocene, is represented by the Older Volcanics, which occur as eroded plugs and flow remnants chiefly in Gippsland (eastern Victoria), but also sporadically to the north and west of Melbourne (see Singleton & Joyce, 1969; Edwards, 1938*a*). Post-Miocene volcanic activity is represented by the Newer Volcanics, which were erupted chiefly from Late Pliocene to Recent over large areas of Victoria (the Western District Plains, Werribee Plains, and Central Highlands) and in a small region in the far southeast of South Australia (see Fig. 1).

The Newer Volcanics comprise over 99 per cent basaltic rocks, with minor trachytic rocks, and accordingly the term Newer Basalts has been commonly used, and will be used here, to denote the post-Miocene basaltic rocks of the province. The Newer Basalts represent a continental mixed tholeiitic-alkaline basaltic suite, with a wide variety of basalt types in space and time, and an abundance of xenoliths and megacrysts of high-pressure origin (see Irving, 1974*a*, *b*). In attempting to derive a petrogenetic scheme for the genesis and evolution of basaltic magmas in a single province, we have relied not so much on field and petrographic aspects, as on major-element geochemistry and the application of data from experimental studies. Trace-element data for a selection of the samples studied here have also been obtained, and their implications for petrogenesis will be discussed in a separate paper.

Previous studies of the Newer Volcanics have collectively encompassed most of the province in varying detail. Petrological studies include Howchin (1901), Jutson (1905), Stanley (1909, 1910), Grayson & Mahony (1910), Skeats & Summers (1912), Fenner (1921), Orr (1927), Mahony (1931), Skeats & James (1937), Edwards (1938*b*), Hills (1938), Edwards & Crawford (1940), Coulson (1938, 1941, 1954), Gill (1947), Condon (1951), Solomon (1952), Yates (1954), Hanks (1955), and Spencer-Jones *in* Boutakoff

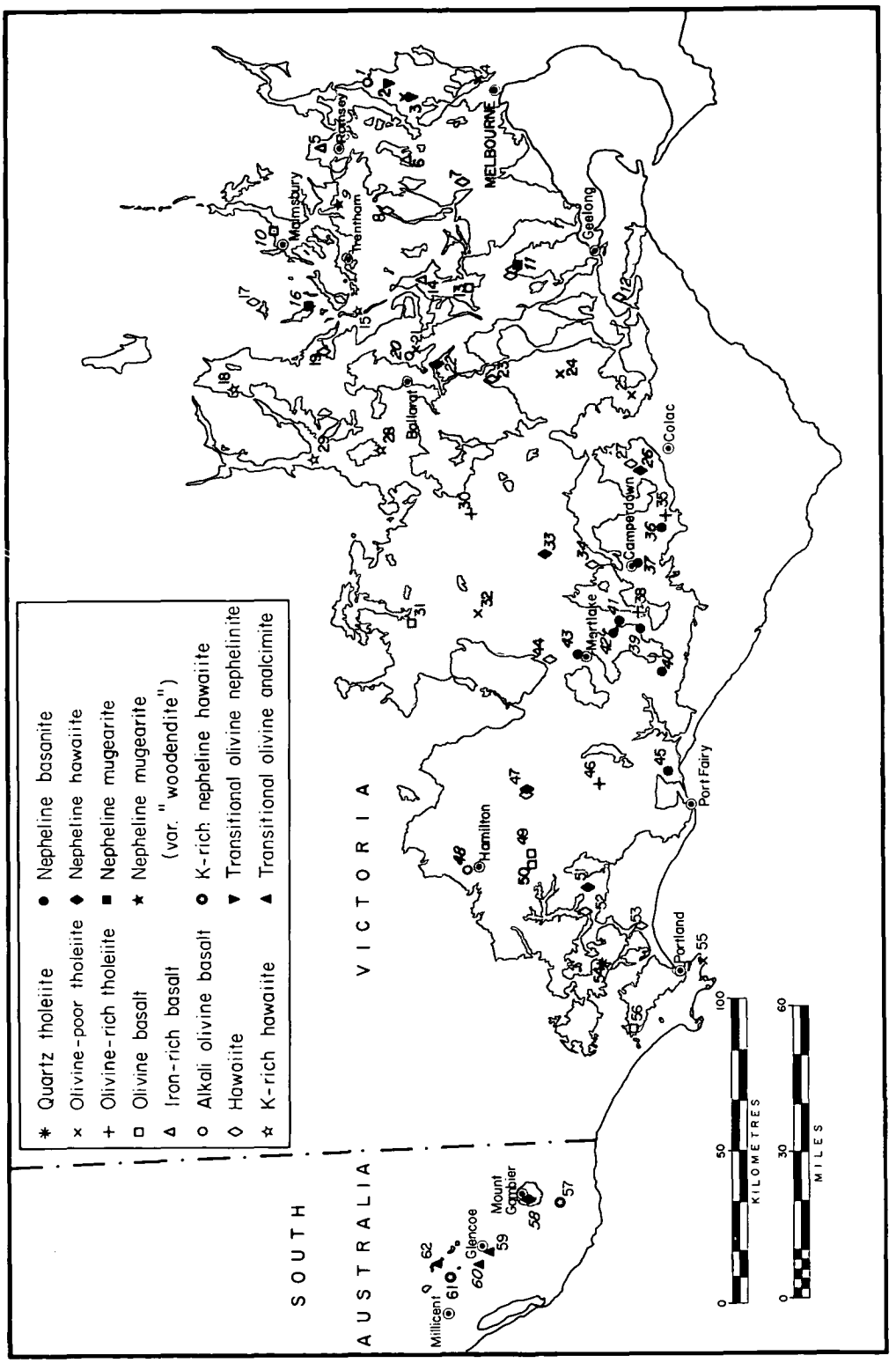
* Quartz tholeiite
× Olivine-poor tholeiite
+ Olivine-rich tholeiite
□ Olivine basalt
△ Iron-rich basalt
○ Alkali olivine basalt
◇ Hawaiite
☆ K-rich hawaiite
● Nepheline basanite
◆ Nepheline hawaiite
■ Nepheline mugearite
★ Nepheline mugearite (var. "woodendite")
⊙ K-rich nepheline hawaiite
▼ Transitional olivine nephelinite
▲ Transitional olivine analcimite
SOUTH AUSTRALIA
VICTORIA
MELBOURNE
Geelong
Colac
Ballarat
Malmsbury
Kyneton
Trentham
Camperdown
Mortlake
Hamilton
Port Fairy
Portland
Millicent
Glencoe
Mount Gambier
KILOMETRES
MILES

(1963). The most extensive contribution of chemical data was that of Edwards (1938*b*).

Geomorphological studies, such as those of Hills (1938), Gill (1950), Ollier & Joyce (1964), Ollier (1967), Singleton & Joyce (1971), have provided much of the knowledge of relative ages of lavas within the province. The stratigraphic relationships between certain lavas and Pleistocene aeolian calcarenite dunes have also been used to evaluate relative ages (e.g. Sprigg, 1952; Coulson, 1938; Boutakoff, 1963). The rather limited K-Ar dating of the Newer Basalts (McDougall *et al.*, 1966; Rahman & McDougall, 1972; Wellman, 1974) has been confined mainly to lava flows rather than eruptive centres, but indicates ages ranging from 4.5 to 0.57 m.y. Evidence of more recent activity in South Australia is contained in aboriginal legends (Hossfeld, 1950), and ^{14}C– dating of material from tuffs suggests ages of 5000 to 6000 years at Tower Hill (Gill, 1967), and 1400 to 4800 years at Mount Gambier (Gill, 1955; Dury & Langford-Smith, 1968).

In his classic study of the Newer Volcanics of central Victoria, Edwards (1938*b*) recognized a group of trachytic rocks and a group of basaltic rocks. The trachytic rocks are confined to the Macedon-Trentham district, where they occur as isolated, steep-sided plugs and domes (e.g. Blue Mountain, Babbingtons Hill, Hanging Rock, The Camel's Hump). They include sölvsbergites, phonolites, and anorthoclase trachytes, and appear on geomorphological grounds (e.g. Ollier, 1967) to be older than nearby basaltic lavas; this is confirmed by recent K-Ar and Rb-Sr dating which indicate an age of 6.3 m.y. (Dasch *et al.*, 1972). Thus aside from the unusual 'woodendite' from Racecourse Hill, Woodend, these acidic to intermediate members of the Newer Volcanics appear to be temporally distinct from the basaltic rocks. They can be also distinguished by their limited geographic extent and the lack of a continuous chemical spectrum between the two groups (as shown by the analyses of Edwards, 1938*b*). It is thus doubtful whether the trachytic volcanics represent classical products of shallow-level crystal fractionation from Newer Basalt parent magmas (as postulated by Edwards), and it appears probable that they are quite distinct[1]. Both these and the unusual hypersthene trachyandesites associated with more typical basaltic rocks in the Mount Gisborne district (Edwards & Crawford, 1940) have been excluded from this study.

Edwards divided the basaltic rocks of central Victoria into several types (e.g. Ballan type, etc.) based largely on criteria of petrography and field relationships, with lesser regard to chemical features. Unfortunately, these petrographic types do not necessarily have particularly well defined chemical compositions. Many of the flows sampled are quite oxidized, and Edwards' use of 'iddingsite' as a key mineral in several types undoubtedly served to obscure primary chemical features.

APPROACH IN THE PRESENT STUDY

Sampling Considerations

Fresh lava samples were collected from the whole province, but attention was focussed on the

Fig. 1. Distribution of magma types within the Newer Basalts province (stippled). Cr-diopside lherzolite series xenoliths are present at localities numbered in italics. *Key to localities:*

1. Mt Frazer
2. Bald Hill
3. Mt Ridley
4. Merri Creek (flow)
5. Melbourne Hill
6. Mt Holden
7. Mt Cottrill
8. Mt Bullengarook
9. Racecourse Hill (Woodend)
10. Green Hill
11. The Anakies
12. Mt Moriac
13. Mt Wallace
14. Mt Gorong
15. Leonard's Hill
16. Mt Franklin
17. Mt Consultation
18. Mt Mooloort
19. Smeaton Hill
20. Mt Warrenheip
21. Dunnstown (flow)
22. Mt Bunninyong
23. Mt Mercer
24. Gow's Hill
25. Mt Gellibrand
26. Red Hill
27. Warrion Hill
28. Mt Callender
29. Mt Mitchell
30. Mt Widderin (flow)
31. The Bald Hill
32. Mt Hamilton
33. Mt Elephant
34. Mt Kurweeton
35. Stoneyford (flow)
36. Mt Porndon
37. Mt Leura
38. Marida Yallock (flow)
39. Terang (flow)/Mt. Terang
40. Mt Warrnambool
41. Noorat (flow)/Mt Noorat
42. Kolora (flow)
43. Mt Shadwell
44. Mt Flat Top (Mondilibi)
45. Tower Hill
46. Hawkesdale (flow)
47. Mt Rouse
48. Mt Bainbridge
49. Mt Napier
50. Flow west of Mt Napier
51. Mt Eccles (Lake Surprise Crater)
52. Flow near Lake Condah
53. Tyrendarra flow
54. Mt Eckersley
55. Cape Grant (flow)
56. Mt Kincaid
57. Mt Schank
58. Mt Gambier (Brown Lake)
59. The Bluff
60. Mt Watch
61. Mt Burr
62. Mt McIntyre

[1] The $^{87}Sr/^{86}Sr$ initial ratio of 0.7103 ± 0.0024 measured for nine sölvsbergites and soda trachytes (Dasch *et al.*, 1972) is inconsistent with their derivation from any of the basaltic lavas of the province with $^{87}Sr/^{86}Sr$ ratios of 0.7035-0.7045: Dasch & Green, 1975; Stueber, 1969; Stuckless & Irving, 1976).

volcanic hills rather than the more extensive lava plains, since the former were found to be the more likely sites for xenoliths and/or megacrysts of demonstrable high-pressure origin. Multiple samples were analysed from some localities, especially if lavas of several different ages appeared to be present; the rims of several lherzolite bombs were also analysed for comparison with associated lavas.

Analytical Methods

Rock samples were prepared for analysis by breaking down sawn slices with the aid of a steel splitter to fragments about 1 cm^3 in size (taking care to exclude foreign matter), and crushing the resulting 60 to 90 g of material to −150 B.S. mesh in a tungsten carbide Sieb mill. For all but six samples, chemical analyses for Si, Ti, Al, Fe, Mn, Mg, Ca, K, and P were carried out by X-ray fluorescence spectrometry. The fused borate button sample technique of Norrish & Hutton (1969) was employed, buttons being prepared in duplicate, and in some cases triplicate, for each sample. Measurements were made on a Phillips 1220 spectrometer for 74 of the samples and on a Siemens SRS instrument for a further 15. Element absorption corrections were made using the parameters of Norrish & Hutton (1969). A synthetic glass containing suitable amounts of the elements of interest was used as a standard after calibration against the USGS standard rocks GSP-1, AGV-1, BCR-1, W-1, and PCC-1. The overall precision of the XRF analyses is better than 1 percent relative for Si, Ti, Al, Fe, Mn, Ca, and K, and 2 percent for Mg and P. For two samples (2976 and 2977), homogeneous glasses were prepared in duplicate and analysed by energy-dispersive electron microprobe (N. G. Ware, analyst), with a precision of about 2 percent relative for all elements.

All Na analyses were performed by flame photometry with a precision of better than 1 percent relative. In some cases, K determinations were made concurrently on the same solutions and showed excellent agreement with values obtained by XRF. Determinations of FeO (in duplicate), total H_2O, H_2O-, CO_2, or loss on ignition were made using classical methods.

Totals of analysed oxide weight percentages for the XRF and microprobe analyses are between 99.5 and 100.5 in 73 percent of cases, and below 99 in only 9 percent of cases (8 analyses). The reasons for the few low totals are not entirely apparent, although the samples in question (all basanites, nepheline hawaiites, and nepheline mugearites) typically have relatively high trace-element concentrations (A. J. Irving, unpubl. data).

The analyses of samples 2636, 2650, 2679, and RAB-5 were made exclusively by wet chemical methods, the first three by E. Kiss, and the fourth by G. I. Z. Kalocsai.

Treatment of Analytical Data

In order to permit more meaningful intercomparisons, we decided to recalculate the primary analytical data in several ways. First, adjustments were made to the observed Fe_2O_3/FeO ratios; secondly, five analyses were corrected for suspected lherzolite contamination; and thirdly, the analyses were normalized free of volatiles to total 100 percent. The selection of the appropriate pre-eruptive Fe_2O_3/FeO ratio in a given case is largely arbitrary owing to uncertainty as to the extent of oxidation during or after the eruption process. Nevertheless, some attempt has been made to resolve this difficulty because of the significant effect of Fe_2O_3 content on the norm (and hence to some extent nomenclature) and on other important petrological parameters such as 100 Mg/Mg $+Fe^{2+}$ ratio[1].

Several criteria were used to judge sample contamination by lherzolite xenolithic material. Five samples containing abundant olivine (and chrome spinel) xenocrysts and having usually high Mg-values relative to samples of otherwise similar chemistry, were suspect, and in these cases appropriate amounts of olivine (of Fo_{90} composition) were subtracted from the primary analyses (as indicated below) to decrease their normative olivine contents to 'normal'. Unusually high Ni and Cr contents were also indicative of likely lherzolite contamination. Nevertheless, a rigorous correction for lherzolite debris is not possible, and the principal precaution was in the initial selection of samples free of obvious debris.

From the primary analytical data, a number of chemical groups of basalts are apparent, and in the following discussion the nomenclature outlined below is anticipated. A survey of the primary data suggested that a Fe_2O_3/FeO ratio of 0.20 may be a realistic minimum for the basanites from all centres except Mount Leura, for the tholeiites (many of which show petrographic evidence of oxidation, *e.g.* 'iddingsite', hematite), for the olivine basalts, for the hawaiites, and for the nepheline hawaiites. In ten examples the measured natural Fe_2O_3/FeO ratios are slightly less than 0.20 and have been retained on recalculation. Three samples (2139, 2140, 2141) of the very fresh basanites from Mount Leura have consistent Fe_2O_3/FeO ratios close to 0.25, as do the two fresh samples (2178, 70-1022) of K-rich nepheline hawaiites from South Australia, and therefore that value has been employed in these cases. In the absence of objective criteria, a Fe_2O_3/FeO ratio of 0.25 has also been adopted for the three K-rich hawaiites, the four olivine analcimites, the two olivine nephelinites, the 'woodendites', and the three iron-rich basalts (all of which show some petrographic evidence of secondary oxidation). The nepheline mugearites of the Anakies (east) and Mount Franklin appear fresh, yet have systematically high Fe_2O_3/FeO ratios; a ratio of 0.50

[1] The 100 Mg/Mg + Fe^{2+} ratio will be designated for convenience as the 'Mg-value'.

TABLE I

Major-element chemical data and CIPW weight percent norms for Newer Basalts lavas.

ROCK TYPE	Quartz Tholeiite	Olivine Tholeiites										Iron-rich Basalts			Olivine Basalts						Alkali Olivine Basalts		
LOCALITY	Mt. Eckersley	Merri Creek	Gow's Hill	Mt. Gellibrand	Mt. Ridley	Mt. Hamilton	Dunnstown	Cape Grant	Merida Yallock	Hawkesdale	Mt. Widderin	Stoneyford	Mt. Holden	Melbourne Hill	Mt. Gorong	The Bald Hill	Mt. Rincaid	Mt. Wallace	Green Hill	W. of Mt. Napier	Mt. Napier	Mt. Warrenheip	Mt. Bainbridge
SAMPLE	2177	GA 1061	69-1016	69-1018	2962	69-1022	2205	70-1221	2152	69-1019	69-1026	2125	2961	69-1034	69-1006	69-1023	69-1020	69-1009	69-1033*	2966	2185	71-003*	2201*	69-1021*
SiO_2	53.53	50.96	51.47	50.70	51.51	51.89	50.15	52.14	50.11	51.23	49.83	50.11	49.64	49.86	49.09	49.69	49.23	50.70	49.58	49.50	49.98	47.65	47.37	48.14
TiO_2	1.80	1.82	1.71	2.07	2.18	2.09	3.47	2.09	1.89	1.71	1.73	2.06	3.13	3.32	3.40	2.06	1.88	2.05	2.65	2.03	2.11	2.41	2.43	2.15
Al_2O_3	15.32	14.25	14.86	14.30	13.49	15.31	15.86	14.64	14.56	15.08	14.88	13.89	15.28	15.88	17.20	14.36	14.37	14.85	13.86	13.64	14.26	15.08	14.80	14.11
Fe_2O_3	1.59	1.68	1.78	1.92	1.73	1.72	1.86	1.63	1.85	1.80	1.90	1.76	2.46	2.46	2.38	1.87	1.87	1.73	1.85	1.09	1.76	1.86	1.83	1.89
FeO	7.94	9.31	8.90	9.60	8.65	8.58	9.30	8.14	9.26	8.99	9.51	9.55	9.85	9.83	9.53	9.37	9.37	8.65	9.25	9.43	8.81	9.31	9.13	9.45
MnO	0.11	0.17	0.20	0.16	0.18	0.14	0.13	0.16	0.17	0.18	0.17	0.16	0.18	0.16	0.14	0.16	0.16	0.14	0.15	0.18	0.16	0.17	0.17	0.16
MgO	6.52	8.82	8.13	7.95	8.24	6.13	5.34	6.60	8.48	7.15	8.49	8.74	4.78	4.46	3.76	8.67	9.19	7.36	8.45	10.24	8.41	9.49	9.46	9.43
CaO	8.38	8.78	8.40	8.90	9.30	8.86	8.51	9.28	8.75	8.62	8.60	8.60	8.39	7.10	7.17	8.45	9.10	8.40	8.20	8.93	8.93	8.02	8.47	9.51
Na_2O	3.65	3.02	3.34	3.24	3.08	3.62	3.49	3.76	3.37	3.97	3.45	3.55	3.73	3.87	4.14	3.47	3.20	3.73	3.45	3.47	3.74	3.10	3.54	3.49
K_2O	0.85	0.88	0.90	0.81	1.19	1.28	1.40	1.16	1.15	0.96	1.09	1.17	1.51	2.09	2.32	1.42	1.26	1.78	1.88	1.06	1.38	2.09	1.96	1.21
P_2O_5	0.31	0.31	0.30	0.35	0.45	0.39	0.48	0.40	0.40	0.31	0.34	0.41	1.05	0.98	0.87	0.47	0.37	0.60	0.68	0.43	0.46	0.81	0.84	0.45
Fe_2O_3/FeO	0.20	0.18	0.20	0.20	0.20	0.20	0.20	0.20	0.20	0.20	0.20	0.18	0.25	0.25	0.25	0.20	0.20	0.20	0.20	0.12	0.20	0.20	0.20	0.20
100 Mg/Mg+Fe^{2+}	59.4	62.8	61.9	59.6	62.9	56.0	50.6	59.1	62.0	58.6	61.4	62.3	38.5	44.7	41.3	62.0	63.6	60.3	62.0	65.9	63.0	64.5	64.9	64.0
Orig. Sum	100.05	99.94	100.41	100.03	99.50	100.14	100.10	99.27	100.21	100.04	100.26	99.10	100.59	100.14	99.77	100.43	100.30	100.12	100.22	99.73	99.98	99.84	100.25	100.49
Nat. Fe_2O_3/FeO	0.82	0.18	0.55	0.24	0.62	0.58	0.59	0.60	1.33	1.29	1.13	0.18	2.07	0.99	1.50	0.25	0.42	0.73	0.71	0.12	0.39	0.93	0.58	0.60
H_2O^+	1.79	1.67	1.12	0.67	1.36	0.72	0.63	2.61	0.95	1.13	1.16	0.06	1.70	1.18	1.08	0.72	0.75	1.08	0.87	0.61	0.08	1.57	1.29	0.68
H_2O^-																							0.70	
CO_2	0.18		0.05	0.08		0.03	0.06		0.06	0.04	0.03	0.06		0.06	0.03	0.05	0.03	0.43	0.05		0.10	0.10	0.08	0.42
qz	1.04	-	-	-	-	-	-	-	-	-	-	-	-	-	-	-	-	-	-	-	-	-	-	-
or	5.01	5.20	5.31	4.76	7.03	7.57	8.28	6.86	6.82	5.64	6.47	6.92	8.92	12.35	13.72	8.36	7.43	10.51	11.10	6.26	8.18	12.32	11.58	7.15
ab	30.88	25.55	28.28	27.45	26.06	30.62	29.51	31.82	28.53	33.61	29.16	30.00	31.56	32.71	32.83	29.38	26.89	31.33	28.89	27.46	28.83	22.76	20.61	22.80
an	22.90	22.73	22.90	22.06	19.47	21.73	23.47	19.64	21.19	20.48	21.90	18.52	20.49	19.77	21.49	19.42	21.13	18.50	16.75	18.51	18.01	21.07	18.69	19.26
ne	-	-	-	-	-	-	-	-	-	-	-	-	-	-	1.17	-	0.10	0.13	0.18	1.01	1.53	1.87	5.07	3.64
di	13.61	15.32	13.60	16.13	19.28	16.10	12.77	19.41	15.98	16.52	15.08	17.43	11.84	7.42	6.99	15.79	17.52	15.68	15.82	18.66	18.89	10.85	14.45	20.24
hy	20.11	16.77	16.04	14.53	15.49	11.39	11.31	8.60	4.95	3.28	2.84	2.16	9.64	8.01	-	0.23	-	-	-	-	-	-	-	-
ol	-	7.83	7.26	7.52	4.98	5.21	6.23	6.42	15.30	13.87	17.69	17.52	5.62	7.45	11.85	19.08	19.76	16.03	17.95	21.65	16.92	21.90	20.37	19.01
mt	2.30	2.44	2.58	2.78	2.51	2.49	2.70	2.36	2.68	2.61	2.76	2.55	3.56	3.56	3.45	2.72	2.72	2.51	2.68	1.58	2.55	2.70	2.65	2.74
il	3.42	3.46	3.24	3.92	4.14	3.96	6.59	3.97	3.60	3.24	3.29	3.91	5.94	6.30	6.46	3.91	3.57	3.90	5.02	3.86	4.00	4.62	4.61	4.08
ap	0.73	0.73	0.72	0.84	1.05	0.93	1.15	0.94	0.94	0.75	0.82	0.98	2.44	2.33	2.05	1.12	0.88	1.42	1.60	1.00	1.09	1.91	1.98	1.87
an/ab+an	42.6	47.1	44.7	44.6	42.8	41.5	44.3	38.2	42.6	37.9	42.9	38.2	39.4	37.7	39.6	39.8	44.0	37.1	36.7	40.3	38.5	48.1	47.6	45.8
D.I.	36.9	30.8	33.6	32.2	33.1	38.2	37.8	38.7	35.4	39.3	35.6	36.9	40.5	45.1	47.7	37.7	34.4	42.0	40.2	34.8	38.5	36.9	37.3	33.6

ROCK TYPE	Alkali Olivine Basalts	Hawaiites													K-rich Hawaiites			Nepheline Basanites			
LOCALITY	Mt. Fraser	Camperdown	Toowoomba (QLD.)	Mt. Bullangarook	Mt. Rouse	Mt. Consultation	Lake Condah	Tyrendarra	Mt. Kurweeton	Mt. Mercer	Warrion Hill	Mt. Cottrill	Smeaton Hill	Mt. Moriac	Mt. Flat Top	The Anakies (N)	The Anakies (W)	Mt. Callender	Mt. Mitchell	Mt. Hooloort	Mt. Porndon		
SAMPLE	69-1036*	2149*	71-1058*	2960	2968	2959	2965	2964	71-024*	69-1014	2121	69-1004	2970	69-1011**	2969	2118*	69-1013**	69-1028	69-1029	69-1030	2127*	2128*	2130*	2131*
SiO_2	48.00	46.79	49.63	48.59	49.69	49.69	49.55	48.02	48.71	49.12	49.40	50.06	49.28	48.20	48.59	50.16	48.74	49.32	47.82	48.37	46.38	46.21	45.34	45.15
TiO_2	2.14	2.62	1.66	3.27	2.14	2.93	2.11	2.26	2.41	2.26	2.23	2.14	2.59	2.35	2.30	2.10	2.36	2.61	2.88	2.53	2.51	2.51	2.87	2.89
Al_2O_3	13.91	13.60	13.87	14.78	13.16	14.65	13.69	13.87	13.33	14.58	13.97	15.08	15.30	13.99	13.95	14.99	14.59	16.36	15.02	15.11	12.53	12.38	12.28	12.22
Fe_2O_3	1.85	2.06	1.78	2.01	1.30	1.88	1.80	1.94	1.94	1.86	1.87	1.68	1.91	1.87	1.83	1.81	1.89	2.35	2.44	2.36	2.01	2.00	2.07	2.08
FeO	9.27	10.28	8.88	10.03	9.17	9.33	8.99	9.69	9.70	9.31	9.34	8.40	9.57	9.33	9.13	9.06	9.44	9.41	9.75	9.45	10.07	9.98	10.34	10.41
MnO	0.16	0.18	0.18	0.17	0.17	0.17	0.17	0.19	0.16	0.16	0.16	0.14	0.18	0.18	0.18	0.16	0.18	0.17	0.17	0.16	0.17	0.17	0.18	0.18
MgO	11.39	9.78	10.86	6.59	10.36	6.85	9.51	9.22	9.66	8.57	8.94	7.75	6.48	9.56	9.16	7.45	8.31	4.89	6.95	7.53	11.25	11.71	11.90	11.94
CaO	8.35	9.00	7.73	8.51	9.09	7.83	9.08	9.01	8.83	8.46	8.45	8.89	7.86	8.59	9.16	7.86	8.07	7.12	8.08	7.36	8.35	8.56	8.34	8.29
Na_2O	3.23	3.34	3.23	3.47	3.43	3.68	3.51	3.67	3.30	3.53	3.65	3.77	4.23	3.49	3.73	4.12	4.50	4.39	3.83	3.94	3.76	3.54	3.73	3.83
K_2O	1.18	1.60	1.71	1.87	1.08	2.22	1.14	1.52	1.40	1.54	1.44	1.54	1.75	1.84	1.46	1.73	1.20	2.38	2.15	2.36	2.07	2.01	2.06	2.11
P_2O_5	0.51	0.76	0.47	0.71	0.41	0.78	0.45	0.61	0.56	0.61	0.55	0.55	0.85	0.60	0.51	0.56	0.72	1.00	0.91	0.81	0.90	0.90	0.89	0.89
Fe_2O_3/FeO	0.20	0.20	0.20	0.20	0.14	0.20	0.20	0.20	0.20	0.20	0.20	0.20	0.20	0.20	0.20	0.20	0.20	0.25	0.25	0.25	0.20	0.20	0.20	0.20
100 Mg/Mg+Fe^{2+}	68.6	62.9	68.5	53.9	66.8	56.7	65.3	62.9	64.0	62.2	63.0	62.2	54.7	64.6	64.1	59.5	61.1	48.1	55.9	58.7	66.6	67.6	67.2	67.2
Orig. Sum	100.36	99.62	99.38	100.44	99.78	100.69	99.38	99.88	100.07	100.14	100.60	100.16	99.53	100.35	100.35	100.00	100.45	99.80	100.20	100.44	98.26	99.16	99.04	99.21
Nat. Fe_2O_3/FeO	0.67	0.21	0.26	1.82	0.14	0.82	0.25	0.22	0.37	0.68	0.22	0.45	0.36	0.16	0.70	0.59	0.50	0.48	0.72	0.64	0.37	0.41	0.23	0.24
H_2O^+	0.46	0.35	2.47	1.79	0.57	1.20	0.64	0.75	1.13	0.53	0.28	0.42	0.67	0.87	0.96	0.49	1.17	1.07	1.11	1.42	0.60	0.33	0.24	0.32
H_2O^-		0.23																			0.11	0.09	0.11	0.12
CO_2	0.03	0.07							0.08	0.07	0.07	0.07		0.32		0.07	0.06	0.20	0.09	0.14	0.03	0.13	0.08	0.10
or	7.00	9.43	10.11	11.05	6.38	13.12	6.74	8.98	8.26	9.11	8.49	9.08	10.34	10.87	8.63	10.24	7.09	14.05	12.68	13.95	12.25	11.88	12.16	12.46
ab	24.93	19.97	27.24	28.08	27.73	29.79	28.31	22.41	26.21	28.01	28.53	29.23	30.67	22.11	23.50	30.42	28.92	31.00	24.96	25.20	15.47	14.93	12.56	11.52
an	19.93	17.38	18.30	19.23	17.32	16.90	18.23	16.88	17.41	19.39	17.47	19.69	17.59	17.07	17.01	17.27	16.07	17.91	17.45	16.56	11.18	11.93	10.67	9.90
ne	1.31	4.51	0.05	0.69	0.70	0.73	0.75	4.68	0.93	0.98	1.28	1.44	2.78	4.02	4.37	2.41	4.96	3.33	4.02	4.42	8.84	8.15	10.30	11.32
di	14.64	18.11	13.74	15.05	20.32	13.79	19.35	19.39	18.44	15.09	16.93	16.89	13.03	17.54	20.37	14.71	15.71	8.97	13.62	11.93	19.64	19.87	20.03	20.49
ol	24.23	20.86	23.75	15.13	20.65	15.59	18.96	19.14	20.04	18.99	19.06	15.86	15.94	19.82	17.93	17.00	18.37	14.03	16.12	17.80	22.81	23.44	23.71	23.70
mt	2.69	2.98	2.58	2.91	1.88	2.73	2.61	2.81	2.81	2.70	2.71	2.43	2.77	2.71	2.65	2.62	2.74	3.41	3.53	3.42	2.92	2.89	3.00	3.02
il	4.06	4.97	3.15	6.21	4.06	5.56	4.01	4.29	4.58	4.28	4.24	4.06	4.92	4.46	4.37	3.98	4.48	4.96	5.46	4.81	4.76	4.76	5.45	5.49
ap	1.21	1.79	1.09	1.65	0.95	1.81	1.05	1.42	1.32	1.46	1.30	1.31	1.98	1.39	1.19	1.34	1.67	2.36	2.16	1.92	2.14	2.14	2.11	2.11
an/ab+an	44.4	46.5	40.2	40.6	38.5	36.2	39.2	43.0	39.9	40.9	38.0	40.3	36.5	43.6	42.0	36.2	35.7	36.6	41.2	39.7	42.0	44.4	45.9	46.2
D.I.	33.2	33.9	37.4	39.8	34.8	43.6	35.8	36.1	35.4	38.1	38.3	39.7	43.8	37.0	36.5	43.1	41.0	48.4	41.7	43.6	36.6	35.0	35.0	35.3

TABLE I—*(continued)*

ROCK TYPE	Nepheline Basanites														Nepheline Hawaiites							
LOCALITY	Mt. Porndon				Mt. Leura					Mt. Noorat				Kolora	Mt. Shadwell			Mortlake	Mt. Terang	Terang	Mt. Warrnambool	Tower Hill	Noorat	Red Hill**
SAMPLE	2132*	2134*	2135*	2136*	2139*	2140*	2141*	2650*	2636*	2156*	71-017*	71-026*	RAB-5*	2161*	2164*	71-028*	2679*	2191*	2167*	2169*	2963*	2170	2154*	2122**
SiO_2	45.37	45.94	46.82	46.04	44.98	44.98	44.96	45.15	44.32	45.59	45.29	45.40	45.82	46.36	45.16	45.04	45.03	45.43	46.11	46.26	47.19	46.81	46.26	48.22
TiO_2	2.89	2.70	2.53	2.72	3.04	3.01	3.03	3.25	3.48	2.52	2.43	2.72	2.98	2.57	2.81	2.83	2.77	2.87	2.50	2.58	2.55	2.41	2.72	2.20
Al_2O_3	12.48	12.87	13.02	12.77	13.20	13.22	13.37	13.00	12.72	12.28	12.00	12.64	13.09	12.85	13.55	13.65	12.69	13.98	13.32	13.85	13.35	14.02	13.15	13.30
Fe_2O_3	2.06	1.78	1.28	2.06	2.52	2.52	2.52	2.51	2.64	1.85	1.94	2.01	2.12	2.00	1.99	2.00	1.98	2.01	1.91	1.94	1.28	1.89	2.06	1.88
FeO	10.31	10.46	10.92	10.30	10.08	10.09	10.06	10.04	10.55	10.00	9.70	10.04	10.58	10.01	9.97	9.98	9.89	10.03	9.55	9.68	10.42	9.79	10.30	9.41
MnO	0.18	0.18	0.18	0.18	0.18	0.18	0.18	0.17	0.17	0.18	0.17	0.17	0.16	0.18	0.18	0.18	0.16	0.18	0.17	0.17	0.19	0.17	0.18	0.18
MgO	11.71	10.44	10.63	10.41	10.11	10.00	9.71	9.91	9.58	12.65	13.76	11.59	10.38	10.60	10.53	10.22	12.55	8.99	10.05	9.61	10.17	8.95	9.67	9.32
CaO	8.31	8.58	8.70	8.70	8.55	8.51	8.45	8.53	8.57	8.14	7.96	8.33	8.45	8.64	8.96	8.81	8.76	8.65	9.65	9.57	9.39	8.99	8.65	9.34
Na_2O	3.69	3.93	3.49	3.78	4.01	4.20	4.29	4.07	4.03	3.86	3.95	4.13	3.97	3.77	3.79	4.16	3.49	4.51	3.79	3.41	3.45	4.04	4.18	3.72
K_2O	2.10	2.16	1.74	2.12	2.21	2.20	2.28	2.23	2.48	2.01	1.95	2.08	1.94	2.05	2.06	2.16	1.79	2.36	2.14	2.10	1.41	2.14	1.83	1.77
P_2O_5	0.89	0.94	0.68	0.92	1.11	1.09	1.15	1.14	1.46	0.91	0.85	0.90	0.51	0.96	0.99	0.97	0.89	0.99	0.81	0.82	0.60	0.80	1.00	0.66
Fe_2O_3/FeO	0.20	0.16	0.12	0.20	0.25	0.25	0.25	0.25	0.25	0.19	0.20	0.20	0.20	0.20	0.20	0.20	0.20	0.20	0.20	0.20	0.12	0.19	0.20	0.20
100 $Mg/Mg+Fe^{2+}$	66.9	64.0	63.5	64.3	64.1	63.9	63.2	63.7	61.8	69.3	71.7	67.3	63.6	65.4	65.3	64.6	69.3	61.5	65.2	63.9	63.5	62.0	62.6	63.8
Orig. Sum	99.88	99.38	98.53	98.70	98.89	98.90	98.46	100.15	99.53	99.09	99.95	100.02	100.19	99.79	99.25	99.90	100.42	99.24	100.30	100.32	99.60	99.55	99.51	99.48
Nat. Fe_2O_3/FeO	0.28	0.16	0.12	0.23	0.27	0.29	0.27	0.35	0.46	0.19	0.35	0.33	0.48	0.26	0.32	0.39	0.33	0.36	0.59	0.66	0.12	0.19	0.50	0.21
H_2O^+	0.32	0.35	0.24	0.27	0.41	0.17	0.21	0.10	0.52	0.11	0.20	0.21	0.31	0.93	0.86	0.90	0.58	0.10	0.76	1.53	0.66	0.33	0.48	0.45
H_2O^-	0.09	0.12	0.08	0.13	0.21	0.06	0.07	0.06	0.22	0.04			0.10	0.43	0.26		0.16						0.18	
CO_2	0.06	0.07	0.13	0.12	0.05	0.07	0.08	0.07	0.11	0.06	0.07	0.08	-	0.06	0.19	0.08	0.13	0.05	0.07	0.05		0.10	0.06	0.19
or	12.43	12.79	10.30	12.52	13.05	13.00	13.49	13.14	14.62	11.89	11.51	12.27	11.46	12.13	12.19	12.74	10:57	13.93	12.62	12.42	8.33	12.63	10.78	10.46
ab	12.67	13.42	17.21	14.34	12.86	12.48	12.47	13.81	12.07	12.53	11.07	11.78	13.47	15.68	11.88	10.64	12.21	11.26	11.14	13.65	16.86	15.22	17.31	20.24
an	11.26	11.05	14.72	11.60	11.47	10.71	10.45	10.63	9.29	10.21	9.27	9.82	12.15	12.04	13.85	12.18	13.67	10.94	13.03	16.27	16.78	13.83	11.71	14.37
ne	10.06	10.76	6.66	9.55	11.42	12.48	12.91	11.16	11.92	10.91	12.09	12.52	10.90	8.79	10.93	13.30	9.37	14.57	11.33	8.24	5.60	10.25	9.77	6.09
di	19.51	20.55	19.47	20.69	19.15	19.73	19.36	19.55	19.13	19.51	19.79	20.64	21.40	19.89	19.49	20.34	19.27	20.68	23.93	20.91	21.06	20.76	19.99	22.47
ol	23.50	21.50	23.37	20.98	20.01	19.65	19.21	19.18	19.09	25.34	26.82	22.75	20.69	21.42	21.08	20.23	24.67	17.94	18.53	18.87	21.29	18.12	19.91	17.95
mt	2.99	2.58	1.86	2.98	3.65	3.65	3.65	3.64	3.82	2.68	2.81	2.91	3.07	2.90	2.89	2.89	2.87	2.91	2.77	2.81	1.86	2.73	2.99	2.73
il	5.48	5.13	4.80	5.16	5.78	5.72	5.75	6.17	6.61	4.78	4.61	5.16	5.65	4.88	5.33	5.38	5.26	5.44	4.74	4.90	4.84	4.58	5.16	4.18
ap	2.10	2.23	1.62	2.17	2.63	2.57	2.73	2.71	3.46	2.15	2.02	2.14	1.21	2.26	2.35	2.30	2.08	2.34	1.91	1.95	1.39	1.89	2.38	1.53
an/ab+an	47.0	45.2	46.1	44.7	47.1	46.2	45.6	43.5	43.5	44.9	45.6	45.5	47.4	43.4	53.8	53.4	52.8	49.3	53.9	54.4	47.1	47.6	40.4	41.5
D.I.	35.2	37.0	34.2	36.4	37.3	38.0	38.9	38.2	38.6	35.3	34.7	36.6	35.8	36.6	35.0	36.7	32.2	39.8	35.1	34.3	32.8	38.1	37.9	36.8

TABLE I—*(continued)*

ROCK TYPE	Nepheline Hawaiites							K-rich Nepheline Hawaiites		Nepheline Mugearites								Olivine Nephelinites		Olivine Analcimites			
LOCALITY	Mt. Elephant		Mt. Sunninyong	Mt. Rouse	Mt. Eccles	Mt. Gambier		Mt. Schank	Mt. Burr	The Anakies (E)				Mt. Franklin		Woodend		Mt. Ridley	Bald Hill	Mt. Watch		Mt. McIntyre	Murrumburrah (N.S.W.)
SAMPLE	71-007**	2194**	69-1027*	2967	2176	2180*	2183*	2178	70-1022	2101*	2102*	71-050*	2111*	69-1031*	2209*	2206A*	2206B*	2976	2977	71-010*	70-1174*	71-008	M3
SiO_2	47.58	47.64	47.22	46.64	47.54	48.43	48.34	47.46	47.30	49.63	48.88	49.87	50.31	48.87	48.78	48.14	48.64	43.6	43.8	43.85	43.75	44.09	42.06
TiO_2	2.44	2.44	2.28	2.75	2.22	2.38	2.35	3.11	3.14	2.18	2.19	2.19	2.19	2.26	2.26	2.34	2.32	3.8	3.7	3.64	3.68	3.87	4.29
Al_2O_3	13.21	12.96	14.96	13.82	13.79	13.57	13.41	14.43	14.52	15.45	15.41	15.49	15.40	15.71	15.77	12.44	12.33	10.3	11.6	9.17	9.37	10.56	10.99
Fe_2O_3	1.91	1.92	1.79	1.91	1.97	1.85	1.89	2.25	2.27	3.47	3.45	3.47	3.46	3.64	3.66	2.09	2.08	2.4	2.6	2.39	2.50	2.42	2.56
FeO	9.59	9.59	8.97	9.58	9.83	9.52	9.44	9.00	9.09	6.94	6.90	6.93	6.92	7.28	7.32	8.34	8.32	9.7	10.2	9.57	10.00	9.69	10.22
MnO	0.18	0.18	0.16	0.19	0.17	0.17	0.17	0.16	0.16	0.16	0.16	0.15	0.17	0.16	0.16	0.16	0.15	0.1	0.1	0.17	0.18	0.18	0.19
MgO	9.70	9.77	8.95	9.42	9.72	8.69	8.88	7.35	7.20	6.41	7.20	7.18	6.56	6.48	6.55	9.38	8.94	10.4	9.2	15.54	15.18	12.03	13.20
CaO	8.42	8.64	7.91	8.21	8.77	9.58	9.58	7.51	7.58	6.78	6.52	6.37	6.67	6.82	6.84	8.32	8.30	11.5	12.7	10.33	10.66	11.88	10.72
Na_2O	4.02	3.95	4.70	4.32	3.83	3.52	3.69	4.63	4.59	5.43	5.74	4.92	5.64	5.01	4.90	4.20	4.37	5.3	4.1	4.14	3.40	3.89	3.78
K_2O	2.10	2.07	2.23	2.26	1.50	1.69	1.68	3.02	3.04	2.91	2.87	2.77	2.84	2.89	2.87	3.23	3.17	1.0	0.7	0.35	0.39	0.36	1.17
P_2O_5	0.85	0.84	0.83	0.91	0.66	0.58	0.57	1.08	1.11	0.64	0.68	0.65	0.64	0.88	0.89	1.35	1.39	1.9	1.3	0.84	0.88	1.02	0.82
Fe_2O_3/FeO	0.20	0.20	0.20	0.20	0.20	0.19	0.20	0.25	0.25	0.50	0.50	0.50	0.50	0.50	0.50	0.25	0.25	0.25	0.25	0.25	0.25	0.25	0.25
100 Mg/Mg+Fe^{2+}	64.3	64.5	64.0	63.7	63.8	61.9	62.6	59.3	58.5	62.2	65.1	64.9	62.8	61.3	61.4	66.7	65.7	65.6	61.6	74.3	73.0	68.9	69.7
Orig. Sum	100.98	98.70	100.32	100.87	100.54	100.30	100.27	99.50	99.57	99.40	100.20	99.92	99.14	99.35	98.81	100.46	99.55	100.4[a]	100.1[a]	99.84	99.73	99.51	99.46
Nat. Fe_2O_3/FeO	0.30	0.23	0.37	0.38	0.29	0.19	0.34	0.25	0.25	0.70	0.80	0.62	0.89	0.56	0.50	1.27	1.21	1.02	1.51	0.99	1.02	0.61	0.48
H_2O^+	0.31	0.22	0.22	1.35	0.32	0.27	0.17	0.18	0.27	0.39	0.08	1.54	1.16	1.30	1.19	1.63	1.11	2.8[b]	2.9[b]	1.33	1.85	1.75	2.27
H_2O^-		0.12								0.28		0.90	0.48		0.40					0.88	1.17	1.46	0.66
CO_2	0.07	0.13	0.05		0.18	0.08	0.18	0.09	0.08	0.54	0.04	0.10	0.54	0.08	0.08	0.08	0.07			0.05	0.11	0.05	0.64
or	12.41	12.23	13.18	13.36	8.86	9.99	9.94	17.86	17.98	17.16	16.96	16.39	12.07	17.05	16.96	19.09	18.74	5.91	4.14	2.07	2.33	2.15	6.90
ab	18.95	18.77	17.25	16.05	21.18	21.63	20.81	18.26	17.92	24.38	21.87	27.72	31.98	24.69	24.74	15.79	17.83	10.74	10.89	11.46	12.37	12.92	3.60
an	11.80	11.52	13.11	11.64	16.00	16.21	15.08	9.68	10.05	9.19	7.78	11.99	10.63	11.87	12.55	5.56	4.65	1.36	11.18	5.41	9.15	10.25	9.54
ne	8.16	7.94	12.20	11.11	6.08	4.42	5.62	11.30	11.30	11.69	14.46	7.53	8.54	9.57	9.05	10.68	10.35	18.48	12.89	12.74	8.87	10.85	15.39
di	19.83	20.99	16.75	18.79	18.82	22.38	23.30	16.64	16.48	16.29	16.16	12.35	14.69	13.09	12.55	21.65	22.13	34.78	35.08	32.11	30.30	33.64	30.56
ol	19.49	19.20	18.61	18.98	20.42	16.79	16.69	14.54	14.40	10.60	12.00	13.31	11.41	12.09	12.45	16.58	15.60	13.64	12.02	23.83	24.28	16.92	20.21
mt	2.77	2.78	2.60	2.77	2.85	2.68	2.74	3.26	3.29	5.03	5.00	5.02	5.02	5.28	5.31	3.02	3.01	3.48	3.77	3.47	3.62	3.51	3.70
il	4.63	4.63	4.33	5.22	4.22	4.52	4.47	5.91	5.97	4.14	4.16	4.15	4.15	4.30	4.30	4.44	4.40	7.22	7.03	6.91	6.98	7.35	8.15
ap	1.98	1.95	1.97	2.11	1.56	1.37	1.35	2.55	2.62	1.52	1.61	1.53	1.51	2.08	2.10	3.20	3.28	4.50	3.02	2.00	2.09	2.42	1.95
an/ab+an	38.4	38.0	43.2	42.0	43.0	42.8	42.0	34.6	35.9	27.4	26.2	30.2	25.0	32.5	33.7	26.0	20.7	11.2	50.7	32.1	42.5	44.2	72.6
D.I.	39.5	38.9	42.6	40.5	36.1	36.0	36.4	47.4	47.2	53.2	53.3	51.6	52.6	51.3	50.8	45.6	46.9	35.1	27.9	26.3	23.6	25.9	25.9

Analyses recalculated to total 100.00 free of volatiles and natural Fe_2O_3/FeO ratios adjusted as shown.

* Localities where Cr-diopside lherzolite xenoliths are present.

** Samples have been corrected for contamination by lherzolite debris (see text).

a: sum of microprobe analysis of glass, with natural Fe_2O_3/FeO ratio; *b*: loss on ignition of natural-rock powder.

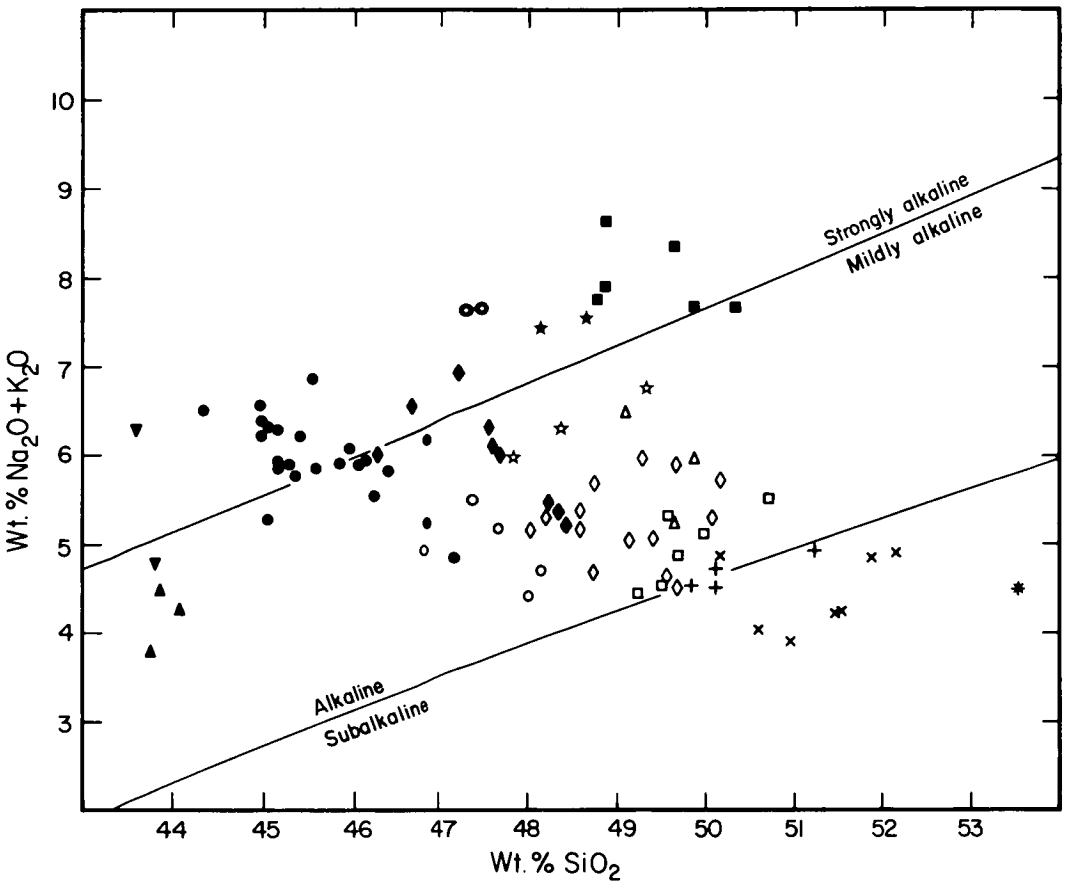

Fig. 2. Alkalis *versus* silica plot for analysed Newer Basalts lavas. Symbols as for Fig. 1. Alkaline/subalkaline dividing line after Irvine & Baragar (1971); strongly alkaline/mildly alkaline dividing line after Saggerson & Williams (1964).

(the minimum natural value) has been used for all six samples.

The recalculated data are presented in Table I, together with CIPW weight percent norms, the original oxide totals obtained by analysis, and the natural Fe_2O_3/FeO ratios; for each sample, the presence or apparent absence of Cr-diopside lherzolite xenoliths is also indicated. A comparison of the norms in Table I with those computed from the primary analytical data reveals that the adjustments of Fe_2O_3/FeO ratio have removed minor normative quartz in four of the tholeiites, and most significantly have in many cases introduced normative nepheline in place of normative hypersthene.

Nomenclature

The basaltic rock nomenclature scheme adopted is based largely on chemistry, normative mineralogy, and a number of derived indices. It is essentially the same as that used by Green & Ringwood (1967), supplemented by the scheme of Coombs & Wilkinson (1969) for alkaline rocks. A plot of $Na_2O + K_2O$ *versus* SiO_2 (Fig. 2) also serves to illustrate the distinction between subalkaline (tholeitic) rocks and alkaline rocks if the dividing line proposed by Irvine & Baragar (1971) is used. The term olivine basalt has been used to denote transitional rocks with 0 to 2% normative hypersthene or 0 to 0.5% normative nepheline.

The alkaline rocks have been subdivided using Coombs & Wilkinson's plot of normative plagioclase composition *versus* Thornton-Tuttle differentiation index (D.I. $\equiv qz + ab + or + ne + lc$). A narrow, natural division of the rock analyses is discernible at a normative plagioclase composition of An_{44} (see Fig. 3), and this has been used to divide alkali olivine basalts and (nepheline) basanites from hawaiites and nepheline hawaiites. This classifies most rocks carrying modal labradorite as alkali olivine basalts or basanites (*cf.* Coombs & Wilkinson, 1969, p. 493). The highly nepheline-normative lavas of The Anakies (east) and Mount Franklin, which have normative plagio-

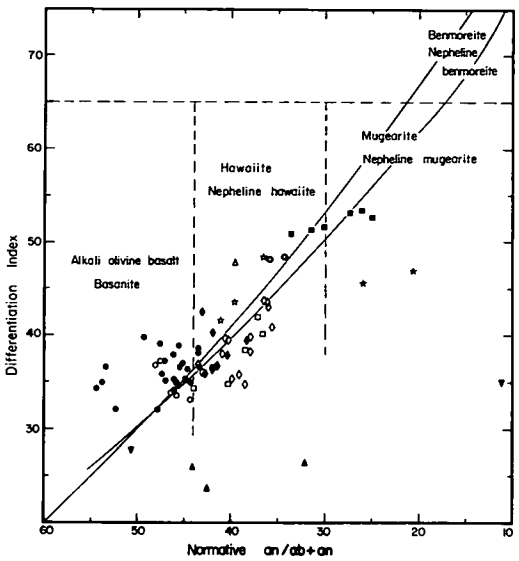

Fig. 3. Plot of Thornton-Tuttle Differentiation Index *versus* normative plagioclase composition for alkaline Newer Basalts lavas. Symbols as for Fig. 1. See text for details of nomenclature. Diagonal lines are Hebridean and Hawaiian trends after Coombs & Wilkinson (1969).

clase compositions of An $_{25.0}$ to An$_{33.6}$ but carry modal feldspar of calcic oligoclase composition, have all been called nepheline mugearites. Coombs & Wilkinson advocated that a K_2O:Na_2O ratio of 1:2 be used to differentiate between hawaiites and alkali olivine basalts on the one hand and trachyandesites and trachybasalts on the other. On this basis, a proportion of all the spatially associated lavas here termed basanites would be nepheline trachybasalts, and many of the nepheline hawaiites would be nepheline trachyandesites and trachyandesites. Rather than use further names prefixed by 'trachy' (chiefly because of the textural connotation of this term and general disagreement on its use), modifying phrases such as 'K-rich' have been used where appropriate with the other names defined above.

Several samples lacking modal feldspar have been termed olivine nephelinite and olivine analcimite on the basis of their petrography. Chemically, however, these particular samples differ markedly from true olivine nephelinites (which have very low normative albite contents). On a normative basis, these lavas would be unusual types of basanite, nepheline hawaiite, and nepheline mugearite, highly enriched in normative diopside.

CHEMICAL AND PETROGRAPHIC FEATURES OF THE NEWER BASALTS

Although there is a continuous variation in chemical composition among the majority of analysed basalts (see Figs 2 and 3), a number of chemical/petrographic types can be distinguished.

Quartz Tholeiite

The only quartz-normative tholeiite so far found among the Newer Basalts is that from Mount Eckersley, a geomorphologically very old volcano near Heywood. Minor (1%) normative quartz persists after correction for secondary oxidation and is apparently a primary feature. The rock is relatively rich in plagioclase, which, with uncommon olivine (partly iddingsitized), forms phenocrysts in a medium-grained intersertal groundmass of plagioclase, pale brownish clinopyroxene, opaque laths, and interstitial turbid material (probably altered glass).

Olivine Tholeiites

The tholeiites from Gows Hill, Mount Gellibrand, Mount Hamilton, Dunnstown, Cape Grant, Merri Creek, and Mount Ridley (lower flow) are distinctly richer in normative hypersthene and poorer in normative olivine than the tholeiitic flows near Mount Widderin, Hawkesdale, Marida Yallock, and Stoneyford (the last being an example from the extensive 'Stony Rises' between Colac and Camperdown). The rocks of the second group are transitional to olivine basalts. The flows at Merri Creek and Cape Grant have been dated respectively at 2.2 m.y. (McDougall *et al.*, 1966) and 2.8—3.1 m.y. (Rahman & McDougall, 1972). All these rocks consist of plagioclase and olivine phenocrysts in a groundmass of plagioclase with pale greenish-brown clinopyroxene, granular or rod-like opaque, and rare turbid altered glass (cf. McInerny, 1929, p. 152). Most are medium grained (doleritic), and petrographically resemble Edwards' 'Malmsbury type'. The majority of the oligoclase-, andesine-, and labradorite-bearing basalts studied by Edwards (1938*b*) from the Malmsbury-Trentham-Romsey district are samples of flows between the volcanic hills and are dominantly tholeiites or transitional olivine basalts (2-20% normative hypersthene). On the other hand, most of Edwards' samples from volcanic *hills* are petrographically distinct and alkaline in chemistry (if the relatively high Fe_2O_3 contents of some of his analyses are taken into account).

The rock from a flow in the operating quarry at Dunnstown (dated at 3.9 m.y. by McDougall *et al.*, 1966) differs from other tholeiitic rocks analysed in having more P_2O_5 and K_2O and much higher TiO_2 and Fe/Mg ratio. It is

noticeably plagioclase-phyric, with microphenocrysts of olivine set in a very fine-grained groundmass composed largely of feldspar and abundant titanomagnetite granules.

Olivine Basalts

The olivine basalts from Mount Kincaid (dated at 2.4 m.y. by I. McDougall, *pers. comm.*, 1972), Mount Wallace, Mount Napier, The Bald Hill (near Tatyoon), and Green Hill (near Malmsbury) are petrographically similar to the olivine tholeiites, but are richer in olivine phenocrysts. The samples from Mount Napier and the nearby Stony Rises are strictly hawaiites in terms of major elements (1–1.5% normative *ne*), but trace-element data (A. J. Irving, unpublished) indicate their affinities to the tholeiites. The Green Hill sample contains orange-brown biotite in the groundmass, and Edwards (1938*b*) classed this lava and those of several other nearby hills as andesine basalt (his 'Ballan type'). Like the tholeiitic rocks, the olivine basalts do not in general contain xenoliths of Cr-diopside lherzolite; however, in the specimen from Green Hill several small (5 cm across), somewhat altered fragments were positively identified by their relict chrome diopside, enstatite, and chrome spinel.

Alkali Olivine Basalts

The alkali olivine basalts from Mount Frazer, Mount Warrenheip, Mount Bainbridge, and a flow at Camperdown (near the swimming pool) all contain Cr-diopside lherzolite xenoliths. The lavas consist of olivine phenocrysts in a groundmass of olivine, plagioclase, titanaugite, and a little apatite. The Mount Frazer samples contain much crystal debris from disaggregated lherzolite xenoliths. The rock from Mount Bainbridge (an old volcano geomorphologically) is slightly coarser grained than the others and contains a little iddingsite and carbonate; associated lherzolite xenoliths are small and rather altered.

Hawaiites

Hawaiite lavas occur at Mts Cottrill, Mercer, Rouse, Flat Top, Bullengarook, Kurweeton, and Moriac, Warrion Hill, Smeaton Hill, Lake Condah, Tyrendarra and The Anakies (middle and western cones[1]). Cr-diopside lherzolite xenoliths are present at Mts Kurweeton and Moriac, and the Anakies, and aluminous pyroxene megacrysts occur at these four localities and at Mt Bullengarook. The Mount Rouse lava occurs as a massive flow interbedded with scoria of nepheline hawaiite composition. These basalts are characterized by SiO_2 48.0–50.2%, TiO_2 2.0–3.2%, K_2O 1.1–2.2%, and P_2O_5 0.41–0.85%, and are petrographically similar to the alkali basalts (except for the doleritic lava from Warrion Hill)[2].

For purposes of comparison, an analysis of a Cr-diopside lherzolite-bearing olivine basalt transitional to hawaiite from the Toowoomba Council Quarry, Queensland, has been included in Table 1.

K-rich Hawaiites

The rocks from Mts Callender, Mitchell, and Mooloort, three of the numerous vesicular basalt domes in the area west and north of Ballarat, are distinctive in possessing higher contents of K_2O (2.2–2.4%), TiO_2 (2.5–2.9%), and P_2O_5 (0.8–1.0%), and much lower Mg-values than the other rocks termed hawaiites. In thin section, they are seen to contain olivine phenocrysts in a fluidal ('trachytic') groundmass of andesine laths, titanaugite, abundant titanomagnetite, apatite, and minor nepheline. The lava from Leonards Hill, south of Daylesford (Orr, 1927) is petrographically and chemically very similar, and contains anorthoclase megacrysts. None of these rocks contain lherzolite xenoliths.

Nepheline Basanites

The rocks forming the conspicuous scoria and lava cones of Mts Porndon, Leura, Noorat, Shadwell, Terang, and Warrnambool, and Tower Hill (and no doubt others) in the Colac-Mortlake-Port Fairy area on the southern part of the Western Plains are nepheline basanites. With the exception of Tower Hill, all these eruptive centres are characterized by the presence of Cr-diopside lherzolite xenoliths; the majority also have Al-augite-rich pyroxenite xenoliths, and pyroxene and anorthoclase megacrysts (see Irving, 1974*a*, 1974*b*). Singleton & Joyce (1969) have convincingly demonstrated a continuous graduation in this region from the many simple tuff maars (*e.g.* Lake Purrumbete, Lake Keilambete) through maars with 'nested' scoria cones (*e.g.* Tower Hill, Mt Leura) to scoria cones with little sign of earlier tuffs deposits (*e.g.* Mt Noorat).

[1] The Anakies are three aligned vesicular basalt and scoria cones situated 27 km north of Geelong.

[2] The rocks from The Anakies (west) and Mt Moriac contain fine crystal debris (largely olivine) derived from lherzolite xenoliths, and accordingly 5% and 6% olivine (Fo_{90}), respectively, have been subtracted from the primary analyses (to bring normative *ol* contents close to those of the other hawaiites).

Chemically, the basanites are characterized by SiO_2 contents of 44.3–47.2% and with the exception of the Mount Warrnambool lava, relatively high P_2O_5 contents (0.8–1.5%). It should be emphasized that rocks from lava flows between the scoria cones are generally *not* basanites but tholeiites transitional to olivine basalts. Although it is possible that conduits beneath some of the present cones were the sources for surrounding tholeiitic flows (*e.g.* the 'Stony Rises' around Mt Porndon), it is more probable that most of the lava plains were produced by multiple fissure eruptions.

In a detailed study, eight samples from Mount Porndon were analysed. This complex volcano is unusual in having scoria cones and massive basalt flows enclosed by an almost complete basaltic ring barrier, the whole on top of a broad, thick lava disc sitting on the tholeiitic plains (see Skeats & James, 1937; Ollier, 1967). Samples of scoria (2127-2130), flows (2134, 2136), basalt from the ring barrier (2135), and the skins of two lherzolite/wehrlite bombs (2131, 2132) were analysed: all were found to be quite similar in composition, although the scoria samples are more magnesian. The other basanites of the province are chemically similar to those from Mount Porndon, except that those from Mount Leura are notably richer in P_2O_5, TiO_2, and to a lesser extent K_2O, and have lower Mg-values (61.8–64.1). Microscopically, the basanites are characterized by plagioclase of andesine-labradorite composition and by groundmasses containing apatite with interstitial brown glass and/or nepheline. The samples from the Mount Porndon ring barrier (2135, 2136) and from Mount Warrnambool are doleritic.

Nepheline Hawaiites

The nepheline hawaiites from Mt Eccles (Lake Surprise Crater), Mt Rouse, Red Hill, Mt Gambier, Mt Bunninyong, Mt Elephant, and a flow south of Mt Noorat (the last five containing Cr-diopside lherzolite xenoliths) are petrographically very similar to the basanites. They are also chemically gradational to the basanites in possessing SiO_2 contents of 46.3–48.4%, normative plagioclase of composition $An_{38.0}$–$An_{43.2}$ and relatively low D.I. (35–43).[1]

The samples from Mount Eccles, from the Stony Rises near Lake Condah to the west, and from the well-defined flow at Tyrendarra are very similar in composition. The last two are strictly hawaiites, but the normative nepheline contents for all three range only from 0.8 to 6.1%. This is in accord with Boutakoff's (1963) suggestion that these Stony Rises formerly represented an immense lake of lava derived from Mount Eccles, and that this was eventually tapped at the southwest margin, from which the extremely fluid Tyrendarra flow travelled south some 45 km to a point beyond the present coastline.

Nepheline Mugearites

The nepheline mugearites from the eastern cone of The Anakies and Mount Franklin are chemically very distinctive in having SiO_2 contents of 48.9–50.3%, Al_2O_3 15.4–15.8%, rather sodic normative plagioclase ($An_{25.0}$–$An_{33.6}$), high D.I. (50-53), and high K_2O (2.1–2.9%). Cr-diopside lherzolite xenoliths and anorthoclase megacrysts are abundant at both these localities. The very thin basalt rims (3–6 mm thick) surrounding lherzolite nodules from The Anakies (bulk sample 71–050) are very similar in chemistry to the other samples (which include cone material (2102) and peripheral flows). The Anakies (east) lavas consist of phenocrysts of olivine in a groundmass rich in plagioclase (calcic oligoclase) with titanomagnetite granules, prismatic clinopyroxene, uncommon apatite grains, and interstitial nepheline with minor alkali feldspar, the last two being particularly conspicuous in the slightly coarser-grained samples from flows. The Mount Franklin samples are similar but contain in addition small patches of brown glass.

The unusual Cr-diopside lherzolite-bearing rock (given the local name 'woodendite' by Skeats & Summers, 1912) occurring in a quarried flow on Racecourse Hill, Woodend, shows affinities with the nepheline mugearites and is conveniently described with them. Material from this site, all of which is slightly oxidized, gives a K-Ar age of 6.7 m.y. (Wellman, 1974). Although Skeats & Summers report the type rock to be glassy, the two specimens analysed in the present study consist of small phenocrysts of iddingsitized olivine and prismatic pale clinopyroxene in a groundmass charged with opaque granules and composed largely of nepheline with some simply-twinned alkali feldspar and acicular apatite. Despite the absence of modal plagioclase, these rocks are chemically K-rich

[1] The primary analyses of the samples from Mt Elephant (2) and Red Hill (1) have been adjusted for probable contamination by disaggregated lherzolite xenoliths by subtraction of 8% and 5% olivine, (Fo_{90}), respectively.

nepheline mugearites, although they differ slightly from the younger lavas of The Anakies and Mount Franklin in having lower Al_2O_3 and Na_2O and higher CaO, K_2O, and P_2O_5 (1.4%).

K-rich Nepheline Hawaiites

According to Sprigg (1952), evidence from physiography and aeolianite stratigraphy suggests that the Newer Basalts of South Australia were erupted in two distinct periods. The basalts of the Millicent-Glencoe region, including those of Mts Burr, McIntyre, and Watch, and The Bluff, were probably erupted in the Late Pliocene or Early Pleistocene, whereas activity at Mount Gambier and Mount Schank to the east began in the late Pleistocene. Despite this apparent age difference, the analysed samples from Mount Burr and Mount Schank are chemically almost identical. Furthermore, they are distinctive in having relatively high K_2O (3.0%), TiO_2 (3.1%), P_2O_5 (1.1%), and K_2O:Na_2O ratio (almost 2:3, making them strictly nepheline trachyandesites according to Coombs & Wilkinson, 1969). Lherzolite xenoliths are apparently absent at both localities. In thin section, these lavas are seen to be composed of olivine phenocrysts in a medium-grained groundmass of andesine laths, titanaugite prisms, olivine grains, titanomagnetite octahedra, abundant thin apatite needles, tiny grains of red-brown amphibole(?), and interstitial nepheline.

Olivine Nephelinites

A re-examination of two localities north of Melbourne, Mount Ridley (upper quarried flow) and Bald Hill, which were briefly described by Hanks (1955), has confirmed the occurrence of olivine nephelinite lavas. The Mount Ridley flow overlies a flow of olivine tholeiite. These basalts lack lherzolite xenoliths and consist of phenocrysts of olivine in a groundmass of titanaugite laths, titanomagnetite granules, apatite needles, and interstitial nepheline and minor analcime. These rocks are chemically different, however, from true olivine nephelinites such as those in Tasmania (Sutherland, 1969*a*, 1974; D. H. Green, unpubl. data) and within the Older Volcanics of Victoria (Edwards, 1938*a*). Normatively, they are varieties of basanite and nepheline mugearite, although they differ significantly from the basanites of the Western District in their lower K_2O, SiO_2, and Al_2O_3, coupled with higher CaO, TiO_2, and P_2O_5. The lavas from Runnymede, Tasmania (Green *et al.*, 1974) and Wee Jasper, N.S.W. (Kesson, 1972) are furthe examples of these unusual rocks.

Olivine Analcimites

The lavas of Mount Watch, Mour McIntyre, and The Bluff lack feldspar an consist of phenocrysts of olivine in a fluida groundmass of titanaugite prisms, olivin grains, titanomagnetite granules, acicula apatite, and interstitial isotropic analcime. Th analcime in the Mount Watch examples, whic in part exhibits icositetrahedral form and con centric or radial arrangements of inclusions was tentatively identified as leucite by Fehlber (1968). The presence of leucite would no accord with the very low K_2O and moderatel high Na_2O contents of the rocks, and X-ra powder photography proves the dominan groundmass mineral at all three localities t be analcime. The rock from Mount McIntyr contains uncommon titanaugite phenocryst and minor orange-brown amphibole (?) in it groundmass, and that from The Bluff (whic was not analysed) has small patches of nephe line and carbonate. Typical Cr-diopside lherzo lite xenoliths are present at Mount Watch, bu apparently absent at other localities. Chemi cally these olivine analcimites are unusual i having very low K_2O (0.4%) and high P_2O_5 (0.8–1.0%), TiO_2 (3.6–3.9%), and Mg values (68.9–74.3). They are very differen (especially in SiO_2, K_2O, and Mg-values) from the analcimites listed by Wilkinson (1962 1968), but do resemble the olivine analcimite from the Cooktown region, northern Queens land (Morgan, 1968), and from Murrum burrah, N.S.W. (see Table 1, sample M3 Cundari, 1973; Harvey & Joplin, 1941). Rare very small Cr-diopside lherzolite xenoliths are present in the Murrumburrah samples.

Normatively, the South Australian olivine analcimites are unusual varieties of nepheline hawaiite rather than olivine nephelinite, and except for higher Mg-values and lower P_2O_5 and alkalis, show similarities to the olivine nephelinites from Mount Ridley and Bald Hill Both are characteristically very rich in normative diopside (>30%).

Iron-rich Basalts

The basalts from Mount Gorong, Mount Holden, and Melbourne Hill have notably lower Mg-values (41.3, 38.5, and 44.7) than other analysed members of the Newer Basalts All three are relatively rich in P_2O_5 (0.9–1.0%) and TiO_2 (3.1–3.4%), but the first is nepheline-normative and the last two hypersthene-normative. They show subtrachytic

textures and are relatively rich in plagioclase, titanomagnetite, and apatite. The Melbourne Hill basalt, in which the olivine is almost completely iddingsitized, contains minor red-brown amphibole, and the Mount Gorong example contains red-brown biotite. These rocks may have affinities with some of the hawaiites, but rather than name them specifically, we refer to them simply as iron-rich basalts. Material from another site on Melbourne Hill analysed by Edwards (1938*b*) is chemically quite different from sample 69-1034 (having K_2O = 4.2%), and should probably be termed trachyandesite. A sample from the latter site has been dated at 4.2 m.y. by Rahman & McDougall (1972).

SPATIAL AND TEMPORAL DISTRIBUTION OF NEWER BASALTS MAGMAS

Members of most of the chemically distinctive lava types are geographically grouped in sub-provinces (Fig. 1). Aside from the apparently extensive tholeiite and olivine basalt plains, good examples are the volcanic hills composed of basanite, of K-rich hawaiite, and of olivine tholeiite. The olivine nephelinites occur at the eastern, and olivine analcimites at the western, extremities of the province. The restriction of the very young basanitic volcanoes and maars to the southern margin of the province coincides approximately with a zone of anomalously high electrical conductivity centred beneath Colac at depths less than 50 km, which may represent a region of partial melting in the upper mantle or a receding thermal high related to the volcanism (Bennett & Lilley, 1973). The nepheline mugearite and K-rich nepheline hawaiite cones are both confined to restricted parts of the province, and there is some tendency for hawaiite volcanoes to be concentrated in the southeastern section.

The geochronology of the Newer Basalts is only imperfectly known. As outlined above, there are relatively few isotopic ages (especially for the volcanic hills) and much of the available evidence derives from geomorphological considerations (e.g. Ollier & Joyce, 1964; Ollier, 1967); however, some generalized relationships can be deduced. In broad terms, there is the suggestion of a time sequence from a tholeiitic flood plain or shield through superposed hawaiitic volcanoes to basanitic volcanoes, although very few of the investigated centres contain more than one basalt type. In detail, however, this sequence is invalid. Among the very old volcanoes of the Portland-Hamilton area, there is the quartz tholeiite of Mount Eckersley, but also the alkali olivine basalt of Mount Bainbridge. Also, the olivine tholeiites of the Stony Rises and in particular Mount Hamilton are almost certainly as young as most of the alkaline lavas (see Ollier, 1967). Again, the hawaiites and nepheline hawaiites of Mounts Gambier, Rouse, and Eccles and the Tyrendarra flow are probably younger than most of the basanites, and, as mentioned above, the almost identical lavas of Mounts Burr and Schank appear to be widely separated in time.

Thus, in summary, it appears that in the interval from about 4.5 m.y. to sub-historic times the province has developed by recurring eruptions of a variety of subalkaline and alkaline magmas, which although to a certain degree spatially restricted, did not form a well-defined compositional progression with time.

CRITERIA FOR RECOGNITION OF PRIMARY AND DERIVATIVE MAGMAS

It is generally agreed by petrologists that basaltic magmas are generated by processes of partial melting in the Earth's mantle. An objective in the study of basaltic rocks is to extrapolate from features of erupted lavas to processes of magma generation and evolution. Such an extrapolation is at first sight intractable, because an erupted lava is likely to have had a very complex history, beginning with the partial melting process itself, and involving subsequent crystal fractionation, contamination, or both at all levels up to the surface. There are, however, a number of characteristics in some lavas which provide constraints on the extent of these processes.

According to the weight of current isotopic and other trace-element geochemical evidence, Cr-diopside-spinel lherzolite-series xenoliths in basalts represent accidental, modified samples of the Earth's upper mantle (see Frey & Green, 1974). It can thus be argued that basalts containing these dense fragments must have moved directly and rapidly from the mantle to the surface without significant modification by crystal fractionation (*i.e.* settling) processes at shallow crustal levels (Green, 1969, 1970*a*; Maaløe, 1973). Xenoliths of other ultramafic rocks, rich in aluminous pyroxenes, as well as aluminous pyroxene megacrysts, may also imply mantle derivation for the lavas containing them (see Irving, 1974*a*, 1974*b*). Thus, an erupted basalt liquid containing any of these high-pressure inclusions must be either (a) a primary partial melt of the mantle, or (b) a derivative of such a primary melt pro-

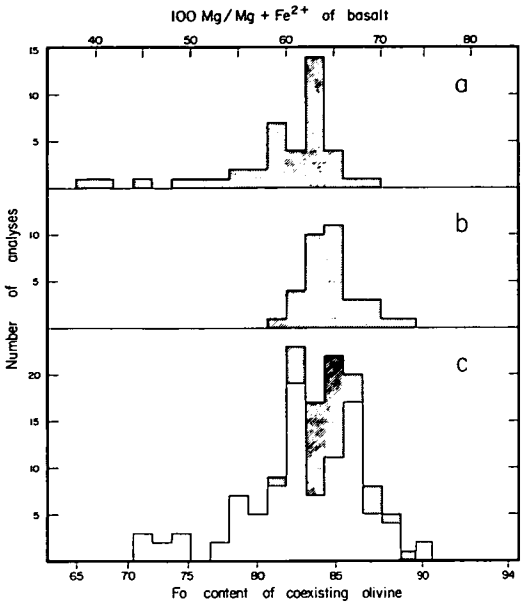

Fig. 4. Histograms of Mg-values and compositions of coexisting olivines (for $K_D^{OL-LIQ} = 0.33$):

(a) Newer Basalts magmas lacking Cr-diopside lherzolite-series xenoliths. Fe_2O_3/FeO ratios adjusted as discussed in text.

(b) Newer Basalts magmas containing Cr-diopside lherzolite-series xenoliths. Multiple analyses were averaged for Racecourse Hill, The Anakies (east) (2 groups) Mts Franklin, Warrenheip, Elephant, Porndon (2 groups), Leura (2 groups), Shadwell (2 groups), Gambier, and Watch. Fe_2O_3/FeO ratios adjusted as discussed in text. Data for all analysed samples before and after adjustment are illustrated by Green *et al.* (1974, fig. 1).

(c) Data of (b) combined with data for 95 lherzolite-bearing basaltic magmas from other eastern Australian Tertiary-Quaternary provinces (Fe_2O_3/FeO adjusted to 0.15). Most of the latter data are unpublished (*see* Green *et al.*, 1974), the remainder being from Binns *et al.* (1970), Wass (1971), Lovering & White (1969), Cundari (1973), and Table I.

duced by crystal fractionation processes *at high pressures.*

Possibly the most important equilibrium pertinent to processes of partial melting in the upper mantle is that between olivine, th most abundant upper mantle phase, an basaltic liquid. Experimental studies a zero pressure (Grove *et al.*, 1973) and atmosphere (Roeder & Emslie, 1970) indicat a value of 0.33 for the distribution coefficient $K_D^{OL-LIQ} = (\frac{Fe}{Mg})OL/(\frac{Fe}{Mg})LIQ$. An alter native way of expressing this relation is $X_{OL} = 100X_{LIQ} \div [X_{LIQ} + K_D (100 - X_{LIQ})]$ where $X = 100\ Mg/Mg+Fe^{2+}$. A summary o data for Mg-value of liquids (X_{LIQ}) and Fe content of coexisting olivines (X_{OL}) was given by Cawthorn *et al.* (1973). Data from experi mental studies on terrestrial and Ti-poor luna compositions at pressures up to 30 kb also yield K_D^{OL-LIQ} near 0.33, thus demonstrating that pressure has a negligible effect on the equilibrium.

Recent estimates of the chemical composition of the undepleted Earth's upper mantle by Carter (1970), Ringwood (1966), and Nicholls (1967) have Mg-values of 87.4 to 89.3[1], and the olivines of these peridotitic assemblages would have similar values. I compositions in the range Fo_{86} to Fo_{90} are considered, this would imply equilibrium with basaltic liquids with Mg-values between 66 and 75 (for $K_D^{OL-LIQ}=0.33$). Melts which are primary on the basis of this criterion commonly contain high-pressure inclusions; but since the presence of inclusions at the surface depend ultimately only on the vigour of the final eruption, it is possible to have primary melt that lack inclusions. Mg-values below 66 would imply some history of crystal fractionation in the basalt. Because of the necessarily rather subjective estimation of pre-eruptive Fe_2O_3 contents, the $100\ Mg/Mg+Fe^{2+}$ ratio is far from an ideal parameter, but in the absence of data on such partition relationships as Mg/Ni and Mg/Co, it is the most definitive index of ferromagnesian crystal fractionation processes.

In Figure 4 the Mg-values of basaltic magmas containing and lacking Cr-diopside lherzolite xenoliths are compared. Also shown are the compositions of olivine coexisting with liquid for $K_D^{OL-LIQ} = 0.33$. The lherzolite bearing magmas can be consistently interpreted as primary liquids or slightly fractionated liquids derived from peridotite containing olivine of composition Fo_{87-90}. The lherzolite

[1] Hutchison *et al.* 1970) have listed average compositions of French spinel lherzolites in basalts (Mg value = 91.0-92.6) and South African peridotite xenoliths in kimberlite (Mg-value = 94.7). These and the estimate of Harris *et al.* (1967) (with an Mg-value of 91.0) are considered to be depleted compositions (see Frey & Green, 1974).

free magmas show a greater spread of Mg-values, consistent with equilibrium with olivine of composition Fo_{65-85}. On this basis, it is deduced that the majority of the lherzolite-free basalts have undergone some crystal fractionation, and, in particular, the quartz tholeiite and olivine tholeiites cannot be interpreted as primary liquids but have probably lost olivine.

The widespread presence in erupted lavas of xenoliths of crustal material suggests that the possibility of contamination by such material should always be entertained, although it can be argued that any lava containing inclusions of high-pressure (>10 kb) origin is unlikely to have had the opportunity for crustal contamination, even if crustal xenoliths were incorporated en route to the surface. Isotopic parameters such as $^{87}Sr/^{86}Sr$ ratio can provide more definitive evidence of the extent of contamination processes: the $^{87}Sr/^{86}Sr$ ratios for 14 examples (of all major chemical types) from the Newer Basalts are within the normal range for uncontaminated modern basalts (Dasch & Green, 1975; Stueber, 1969; Stuckless & Irving, 1976).

GENESIS OF THE NEWER BASALTS MAGMAS

The detail of interpretations regarding the development of the Newer Basalts province as a whole is necessarily limited by its complexity in both space and time, and discussion is here confined to likely processes and physical conditions involved in the evolution of the major basalt types. Observations made on the lavas themselves and their inclusions have been integrated with evidence from relevant experimental studies.

Basanitic Magmas

On the basis of criteria detailed above, the only examples of the Newer Basalts which could have developed as direct upper mantle melts are the majority of the basanites, including some of the transitional olivine analcimites (low-K 'basanites'). The Mount Frazer alkali olivine basalt (Mg-value = 68.6) could also be primary, but in view of the very high normative olivine content of this sample the possibility of contamination with xenocrystal olivine must be considered. Some of the basanites, notably those from Mount Leura, cannot be primary melts on the grounds of low Mg-values. The more magnesian basanites commonly contain megacrysts which attest to crystallization and possible crystal fractionation of these or related magmas at high pressures. The extent of fractionation may not have been very great, and many of the basanites are probably only slightly removed in composition from their parental mantle melts.

Recent experimental studies (Green, 1973*a*) on a Mount Leura basanite (2650) with 10% added olivine (Fo_{90}) indicate that the Victorian basanite magmas may be derived by small degrees (about 5%) of partial melting of hydrous mantle peridotite (containing about 0.1–0.3% water) at pressures of 25–30 kb (*i.e.* depths of 80-100 km). At these pressures residual mantle peridotite contains garnet as well as olivine, orthopyroxene, and clinopyroxene Green, 1973*b*). Data for the rare-earth elements in basanites from Victoria (Frey & Green, 1974; F. A. Frey, unpubl.) and elsewhere (Kay & Gast, 1974) affirm that such magmas must form by very small degrees of partial melting of peridotite containing garnet as a residual phase.

The relatively high contents of Ti, K, and P characteristic of basanites are also consistent with such small degrees of melting and these elements (especially K and P) are particularly enriched in the Victorian basanites. In the source peridotite these 'incompatible' elements are contained in early-melting accessory phases such as amphibole, mica, apatite, ilmenite, and titanoclinohumite, and it is notable that pargasite, phlogopite, and apatite are present in some Victorian Cr-diopside lherzolite xenoliths (Frey & Green, 1974). The basanites from Mount Leura, which have exceptionally high K, Ti, and P, have a higher Fe-Mg ratio than those of, say, Mount Porndon and Mount Noorat, and some part of their enrichment in incompatible elements may have been produced by small amounts of fractionation (major olivine with some clinopyroxene and/or orthopyroxene) from a more typical basanite parent.

The very low K contents of the transitional olivine analcimites virtually exclude source regions containing mica. Coupled with the very high Ti and P contents of these magmas, this suggests that apatite and ilmenite or perhaps titanoclinohumite were the important accessory phases at subsolidus conditions in their source regions. Such apparent regional variation in the accessory mineralogy, minor element chemistry and isotope chemistry of upper mantle peridotite also emerges from studies of Cr-diopside lherzolites (*e.g.* Frey & Green, 1974; Frey & Prinz, 1971 and unpubl. data, Dasch & Green, 1975). Both the olivine analcimites and the more fractionated olivine nephelinites transitional to basanites probably originated by slightly lower degrees of partial

melting, possibly at deeper levels than the more typical basanites (*cf.* Bultitude & Green, 1971).

Hawaiitic and Mugearitic Magmas

All the analysed samples of hawaiite, nepheline hawaiite, and nepheline mugearite have Mg-values less than 66 and are thus considered to be derivative magmas rather than primary mantle melts. Over two-thirds of the investiated examples of these magma types are associated with Cr-diopside lherzolite xenoliths, implying that, at least in these cases, the crystal fractionation processes responsible were operative at mantle pressures. Such a high-pressure origin cannot be excluded for the remainder of these lavas.

Nepheline hawaiites and nepheline mugearites

In terms of Newer Basalt lavas now observed at the surface, the only candidates as primary melts parental to the hawaiitic and mugearitic magmas appear to be basanite, transitional olivine analcimite, and possibly a more primitive alkali olivine basalt type. The spatial restriction of the transitional olivine analcimites and their very low K contents would seem to exclude them as parents of widespread significance; however, several lines of evidence suggest a link at high pressures between the more typical basanites, the nepheline hawaiites, and the nepheline mugearites.

A lherzolite-bearing flow of nepheline hawaiite (2154) occurs at Noorat, immediately southeast of the complex basanite volcano Mount Noorat, from which it is possibly derived. More definitive evidence of a link between the basanite, nepheline hawaiite, and nepheline mugearite magmas is provided by the chemistry of the clinopyroxene megacrysts found within examples of each. General similarities are evident amongst all these megacrysts; however the occurrence at one nepheline mugearite centre (Mt Franklin) of clinopyroxene megacrysts with compositions representing an extension of the chemical trend defined by clinopyroxenes in the basanites at Mount Noorat suggests a continuous compositional variation in liquids precipitating the clinopyroxenes and a genetic relationship between these two magma types in particular (*see* Irving, 1974*b*).

Nepheline mugearite 2102 from The Anakies (east) has been the subject of an extensive experimental investigation (Irving & Green, 1972, and unpubl. data). From this study, it was concluded that the nepheline mugearite and nepheline hawaiite magmas could be derived from hydrous basanitic parental liquids by high pressure (12-20 kb) crystal fractiona processes involving the removal particularly o kaersutitic amphibole, with olivine, apatite aluminous clinopyroxene, and biotite in vary ing proportions. Further evidence for th important role of amphibole in producing thi magmatic lineage is provided by trace elemen data, and in particular by the observed de crease in K/Rb ratio from basanites througl nepheline hawaiites to nepheline mugearite (A. J. Irving, unpubl.). Particular difference in contents of incompatible minor and trac elements (*e.g.* K, Ti, P, Ba, Sr, Rb, etc. between otherwise similar magmas (compar P_2O_5 contents (0.6% and 0.9%) of th nepheline mugearites from The Anakies (east and Mt Franklin) are interpreted as largely inherited chemical traits of parent magmas Even though the contents of these element can be modified by crystal fractionation pro cesses, large differences in concentration ar more probably determined by variations i accessory mineralogy and partial melting pro cesses in the primitive upper mantle sourc regions.

Hawaiites

In calculating fractionation trends fron basanite to nepheline mugearite, we have foun that the effect of kaersutite subtraction wa largely to decrease the Ca:Na ratio in th derivative liquids without significantly alterin the normative nepheline content. It is thus pre dictable that just as the nepheline hawaiite may be related to the basanites by a fractiona tion model involving chiefly amphibole control so the hawaiites of the Newer Basalts (whic differ primarily in lower normative *ne*) ma be related to an alkali olivine basalt parent. A role for aluminous orthopyroxene in suc fractionation may be indicated by the presenc of megacrysts of this mineral in the hawaiit at The Anakies (west) and in the Kyogl hawaiite (Wilkinson & Binns, 1969). Although with the possible exception of the Moun Frazer lava, alkali olivine basalt magmas o demonstrable direct upper mantle derivatio are not present among the Newer Basalts, a the observed alkali olivine basalt magmas ca be related to a more primitive type by scheme involving minor olivine and pyroxen fractionation at upper mantle levels.

K-rich hawaiitic magmas

The K-rich hawaiites of the Ballarat regio and the K-rich nepheline hawaiites of Sout Australia are possibly low-pressure fraction tion products of other (high-pressure) hawaiit

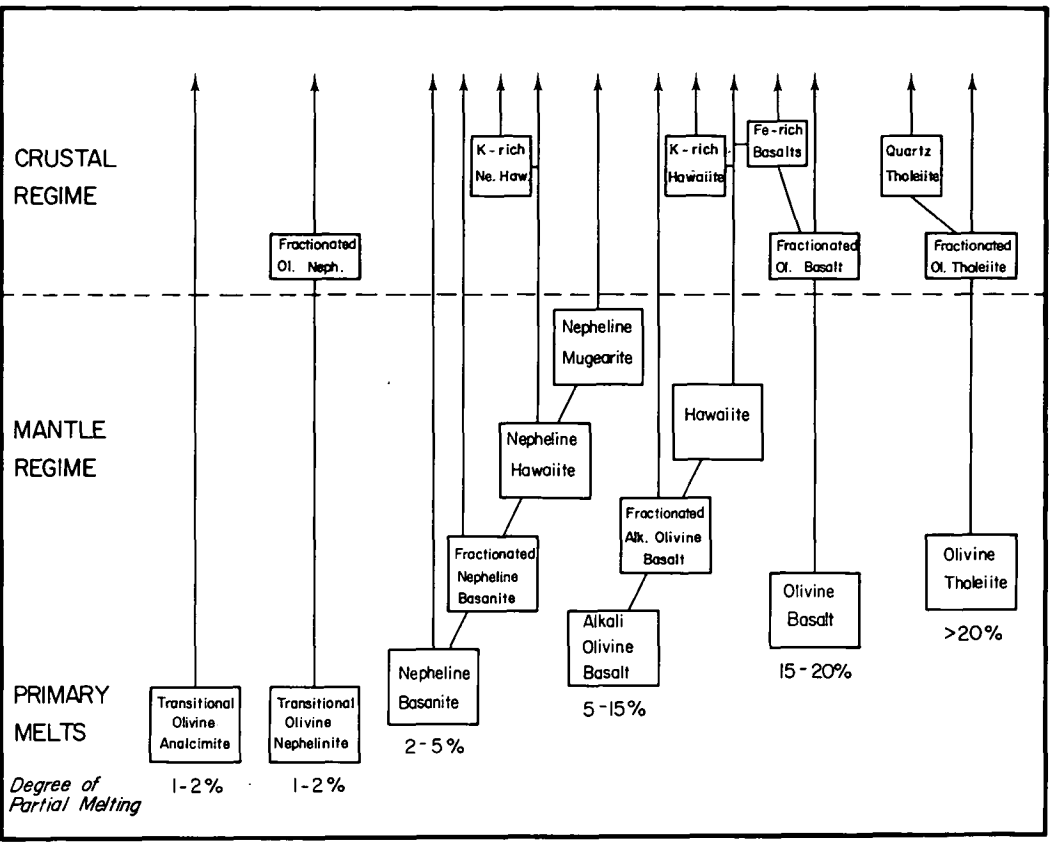

Fig. 5. Schematic summary of primary melts and magmatic lineages for the Newer Basalts magmas. Approximate degrees of partial melting are after Green (1970*b*, 1973*a*) and Kay & Gast (1974). Vertical scale has only partial depth significance.

nagmas respectively (which in each case are present in the near vicinity). All these lavas are relatively iron-rich (with Mg-values less than 60), and are also very noticeably enriched in K, Ti, and P. There is no conclusive evidence as to the pressures at which these magmas might have fractionated, although the systematic absence of high-pressure inclusions is consistent with a relatively low-pressure origin. Experimental data (Irving & Green, unpubl.) suggest that the fractionation at pressures less than 5 kb (even under wet conditions) of mugearitic and hawaiitic magmas will be controlled by olivine and eventually clinopyroxene and plagioclase over a temperature interval of at least 120°C, which would result primarily in a marked iron-enrichment trend accompanied by enhanced incompatible element contents in derivative liquids. The three iron-rich basalts show some similarities to the K-rich hawaiites, yet differ in terms of lower K and Mg-value. It is probable that these lavas represent examples of more extreme (and perhaps multiple) low-pressure fractionation of magmas which may have ranged in bulk composition from olivine basalt to hawaiite.

Tholeiite and Olivine Basalt Magmas

The tholeiitic and olivine basalt magmas of the Newer Basalts are too high in Fe/Mg to be primary magmas produced by relatively large degrees (greater than 20%) of partial melting of mantle peridotite (*cf.* Green & Ringwood, 1967). The tholeiites of Gows Hill, Mount Gellibrand, Mount Hamilton, Dunnstown, Cape Grant, Merri Creek, Mount Ridley and Mount Eckersley, which have Mg-values of 50.6–62.9 and are poor or lacking in normative olivine (0.7–8%), are most likely fractionates of more olivine-rich tholeiite magmas at very low pressures, probably less than 5 kb (*cf.* Green *et al.*, 1967; Green, 1970*b*). The olivine basalts from Bald Hill, Mount Kincaid, and

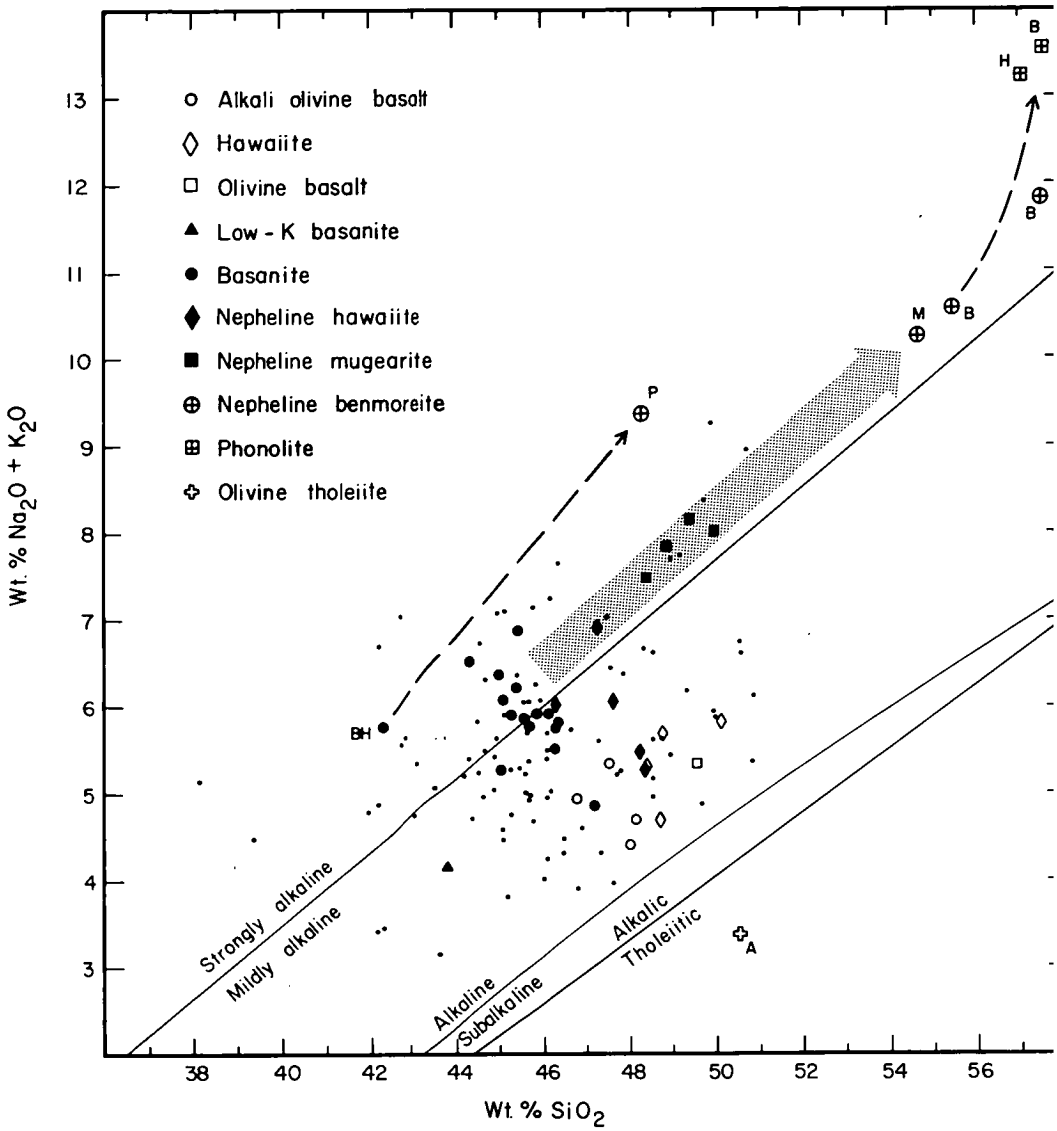

Fig. 6. Alkalies *versus* silica plot for Cr-diopside lherzolite-bearing magmas from eastern Australia a elsewhere. Data for the Newer Basalts magmas (large symbols) averaged as in Fig. 4b (low basanite = transitional olivine analcimite). Small dots refer to 95 other eastern Australi magmas (volatile-free), as in Fig. 4c. Other abbreviations and data sources are A = Andov Tasmania (Sutherland, 1974), BH = Black Head, New Zealand (Price & Taylor, 1973), P Pigroot, New Zealand (Price & Green, 1972), M = Mt Mitchell, Queensland (Green *et a* 1974), B = Bokkos, Nigeria (Price & Irving, unpubl.), H = Heldburg, E. Germany (Price Irving, unpubl.). Dividing lines as for Fig. 2, with alkalic/tholeiitic dividing line after Ma Donald & Katsura (1964).

Mount Wallace and the olivine tholeiites transitional to them from Marida Yallock, Hawkesdale, Mount Widderin, and Stoneyford have, in general, slightly higher Mg-values (58.6–63.6) and much greater normative olivine contents (13.9–19.8). Such differences are explicable in terms of different conditio of melting of source peridotite and thus d ferent normative olivine/hypersthene ratios f parental magmas, with the further complic tion of variable olivine or (olivine + pyr xene) fractionation at low pressures.

Summary

A schematic summary of the suggested arental melts and magmatic lineages for the Newer Basalts is presented in Fig. 5.

COMPARISON WITH OTHER CAINOZOIC VOLCANICS OF EASTERN AUSTRALIA

The Newer Basalts province contains a wide ange of lava compositions from quartz holeiite to basanite. A particular feature of the rovince is the development of hawaiitic and ugearitic lavas, yet very young examples of ven more evolved alkaline magmas such as enmoreite, trachyte, phonolite, and alkali hyolite are apparently lacking, in contrast to heir occurrence among Tertiary-Quaternary olcanics elsewhere in eastern Australia. In ddition, extremely undersaturated lavas, like he olivine nephelinites and olivine melilitites f Tasmania and the Victorian Older Volanics, appear to be absent from the Newer asalts (see Sutherland, 1969*b*).

In Figure 6 we compare the (Na_2O+K_2O) *s.* SiO_2 variation for lherzolite-bearing Newer asalts magmas with that for over 90 lherzote-bearing magmas from elsewhere in eastern ustralia. With one remarkable exception, an livine tholeiite from Tasmania (Sutherland, 974), the lherzolite-bearing magmas plot ithin the alkaline field (as defined by Irvine Baragar, 1971, or Macdonald & Katsura, 964) or within the strongly alkaline field (as efined by Saggerson & Williams, 1964). asanite is the most widespread mantle-derived agma type. The trend from basanite through epheline hawaiite to nepheline mugearite as a igh-pressure magma series, which is particularly discernible among the Newer Basalts, ay be extrapolated to the distinctive nephene benmoreite from Mount Mitchell, Southast Queensland (Green *et al.*, 1974). The unusual mafic nepheline benmoreite (or phonolite) from Pigroot in the East Otago province of New Zealand (Price & Green, 1972) may be similarly related to basanites of the same province. We have suggested on the basis of experimental and other evidence that fractionation of kaersutitic amphibole is largely responsible for this high-pressure lineage, and the observed association of kaersutite megacrysts with many magmas of this series throughout eastern Australia (see Wass & Irving, 1976) is supporting evidence. As demonstrated in Nigeria and Eastern Germany (Irving & Price, 1974), continued fractionation can produce high-pressure phonolites, which may also be represented in eastern Australia. As studies following that of Binns *et al.* (1970) are beginning to reveal, such evolved members of high-pressure alkaline magma series are much more important throughout eastern Australia than previously recognized.

ACKNOWLEDGEMENTS

We wish to thank Professor A. J. R. White, Dr I. McDougall, Mr R. Overton, and Dr T. H. Green for collecting several of the samples, and Dr R. A. Binns for permission to use an unpublished analysis. XRF analyses of most samples were made at the Australian National University with the expert assistance of P. H. Beasley; 15 XRF analyses were obtained at Macquarie University through the generosity of Dr R. H. Flood. Special thanks are due to E. Kiss for his highly skilled efforts in carrying out the majority of the wet chemical determinations, and to A. Powell for preparation of numerous thin sections. The critical comments of Professor D. S. Coombs are greatly appreciated.

REFERENCES

ENNETT, D. J., & LILLEY, F. E. M., 1973: Electrical conductivity structure in the southeast Australian region. *Geophys. J. Roy. astr. Soc., 37*, pp. 191-206.

INNS, R. A., DUGGAN, M. B., & WILKINSON, J. F. G., 1970: High pressure megacrysts in alkaline lavas from northeastern New South Wales. *Am. J. Sci., 269*, pp. 132-168.

OUTAKOFF, N., 1963: The geology and geomorphology of the Portland area. *Mem. geol. Surv. Vict., 22.*

ULTITUDE, R. J., & GREEN, D. H., 1971: Experimental study of crystal-liquid relationships at high pressure in olivine nephelinite and basanite compositions. *J. Petrol., 12*, pp. 121-147.

CARTER, J. L., 1970: Mineralogy and chemistry of the earth's upper mantle based on the partial fusion-partial crystallisation model. *Bull. geol. Soc. Am., 81*, pp. 2021-2034.

CAWTHORN, R. G., FORD, C. E., BIGGAR, G. M., BRAVO, M. S., & CLARKE, D. B., 1973: Determination of the liquid composition in experimental samples: discrepancies between microprobe analysis and other methods. *Earth planet. Sci. Lett., 21*, pp. 1-5.

CONDON, M. A., 1951: The geology of the lower Werribee River, Victoria. *Proc. Roy. Soc. Vict., 63*, pp. 1-24.

COOMBS, D. S., & WILKINSON, J. F. G., 1969: Lineages and fractionation trends in undersaturated volcanic rocks from the East Otago volcanic province (New Zealand) and related rocks. *J. Petrol., 10,* pp. 440-501.

COULSON, A., 1938: The basalts of the Geelong district. *Proc. Roy. Soc. Vict., 50,* pp. 251-257.

COULSON, A., 1941: The volcanoes of the Portland district. *Proc. Roy. Soc. Vict., 53,* pp. 394-402.

COULSON, A., 1954: The volcanic rocks of the Daylesford district. *Proc. Roy. Soc. Vict., 65,* pp. 113-124.

CUNDARI, A., 1973: Petrology of the leucite-bearing lavas in New South Wales. *J. geol. Soc. Aust., 20,* pp. 465-492.

DASCH, E. J., & GREEN, D. H., 1975: Strontium isotope geochemistry of lherzolite inclusions and host basaltic rocks, Victoria, Australia. *Am. J. Sci., 257,* pp. 461-469.

DASCH, E. J., WELLMAN, P., & MILLAR, D. J., 1972: Age and strontium isotope geochemistry of highly differentiated volcanic rocks from the 'Newer Volcanics', southeastern Australia (abstr.). *Abstracts with Programs, Geol. Soc. Am. Mtgs., 4,* pp. 483-484.

DURY, G. J., & LANGFORD-SMITH, T., 1968: Australian geochronology: Checklist 3. *Aust. J. Sci., 30,* pp. 304-306.

EDWARDS, A. B., 1938*a*: Petrology of the Tertiary Older Volcanic rocks of Victoria. *Proc. Roy. Soc. Vict., 51,* pp. 73-98.

EDWARDS, A. B., 1938*b*: The Tertiary volcanic rocks of central Victoria. *Q.J. geol. Soc. Lond., 94,* pp. 243-320.

EDWARDS, A. B., & CRAWFORD, W., 1940: The Cainozoic volcanic rocks of the Gisborne district, Victoria. *Proc. Roy. Soc. Vict., 52,* pp. 281-311.

FENNER, C., 1921: The craters and lakes of Mount Gambier, South Australia. *Trans. Roy. Soc. S. Aust., 45,* pp. 169-205.

FREY, F. A., & GREEN, D. H., 1974: The mineralogy, geochemistry and origin of lherzolite inclusions in Victorian basanites. *Geochim. cosmochim. Acta, 38,* pp. 1023-1059.

FREY, F. A., & PRINZ, M., 1971: Ultramafic nodules from San Carlos, Arizona: mineralogy and chemical composition (abstr.). *Abstracts with Programs, Geol. Soc. Am. Mtgs., 3,* pp. 573-574.

GILL, E. D., 1947: Ecklin Hill—a volcano in the Western District of Victoria. *Vict. Naturalist, 64,* pp. 130-134.

GILL, E. D., 1950: An hypothesis relative to the age of some Western District volcanoes, Victoria. *Proc. Roy. Soc. Vict., 60,* pp. 189-194.

GILL, E. D., 1955: Radiocarbon dates for Australian archaeological and geological samples. *Aust. J. Sci., 18,* pp. 49-52.

GILL, E. D., 1967: Evolution of the Warrnan bool-Port Fairy coast and the Tower Hi eruption, Western Victoria, *in* JENNINGS, J. N & MABBUTT, J. A. (eds.), *Landform Studie from Australia and New Guinea.* ANU Pres pp. 340-364.

GRAYSON, H. J., & MAHONY, D. J., 1910: Th geology of the Camperdown and Mount Ele phant districts. *Mem. geol. Surv. Vict., 9.*

GREEN, D. H., 1969: The origin of basaltic an nephelinitic magmas in the earth's mantl *Tectonophysics, 7,* pp. 409-422.

GREEN, D. H., 1970*a*: A review of experimenta evidence on the origin of basaltic an nephelinitic magmas. *Phys. Earth planet. In teriors, 3,* pp. 221-235.

GREEN, D. H., 1970*b*: The origin of basaltic an nephelinitic magmas. *Trans. Leicester lit. phi Soc., 44,* pp. 26-54.

GREEN, D. H., 1973*a*: Conditions of melting o basanite magma from garnet peridotite. *Eart planet. Sci. Lett., 17,* pp. 456-465.

GREEN, D. H., 1973*b*: Experimental meltin studies on a model upper mantle compositio at high pressure under water-saturated an water-undersaturated conditions. *Earth planet Sci. Lett., 19,* pp. 37-53.

GREEN, D. H., & RINGWOOD, A. E., 1967: Th genesis of basaltic magmas. *Contr. Miner Petrol., 15,* pp. 103-190.

GREEN, D. H., EDGAR, A. D., BEASLEY, P., KISS E., WARE, N. G., 1974: Upper mantle sourc for some hawaiites, mugearites and ben moreites. *Contr. Miner. Petrol., 48,* pp. 33 43.

GREEN, T. H., GREEN, D. H., & RINGWOOD, A. E. 1967: The origin of high-alumina basalts an their relationships to quartz tholeiites an alkali basalts. *Earth planet. Sci. Lett., 2,* pp 41-51.

GROVE, T. L., WALKER, D., LONGHI, J., STOLPER E., & HAYS, J. F., 1973: Petrology of roc 12002 and origin of picritic basalts at Oceanu Procellarum. *Proc. Fourth Lunar Sci. Conf. Geochim. cosmochim. Acta, Suppl. 4, Vol. 1* pp. 995-1011.

HANKS, W., 1955: Newer Volcanic vents and lava fields between Wallan and Yuroke, Victoria *Proc. Roy. Soc. Vict., 57,* pp. 1-16.

HARRIS, P. G., REAY, A., & WHITE, I. G., 1967: Chemical composition of the upper mantle. *J. geophys. Res., 72,* pp. 6359-6369.

HARVEY, M., & JOPLIN, G. A., 1941: A note on some leucite bearing rocks from New South Wales with special reference to an ultrabasic occurrence at Murrumburrah. *J. Proc. Roy. Soc. N.S.W., 74,* pp. 419-422.

HILLS, E. S., 1938: The age and physiographic relationships of the Cainozoic volcanic rocks of Victoria. *Proc. Roy. Soc. Vict., 51,* pp. 112-139.

HOSSFELD, P. S., 1950: The late Cainozoic history of the southeast of South Australia. *Trans. Roy. Soc. S. Aust., 73,* pp. 232-279.

HOWCHIN, W., 1901: Notes on the extinct volcanoes of Mount Gambier and Mount Schank, South Australia. *Trans. Roy. Soc. S. Aust., 25,* pp. 54-62.

HUTCHISON, R., PAUL, D. K., & HARRIS, P. G., 1970: Chemical composition of the upper mantle. *Miner. Mag., 37,* pp. 726-729.

IRVINE, T. N., & BARAGAR, W. R. A., 1971: A guide to the chemical classification of the common volcanic rocks. *Canad. J. Earth Sci., 8,* pp. 523-548.

IRVING, A. J., 1974*a*: Pyroxene-rich ultramafic xenoliths in the Newer Basalts of Victoria, Australia. *N. Jb. Miner. Abh., 120,* pp. 147-167.

IRVING, A. J., 1974*b*: Megacrysts from the Newer Basalts and other basaltic rocks of southeastern Australia. *Bull. geol. Soc. Am., 85,* pp. 1503-1514.

IRVING, A. J., & GREEN, D. H., 1972: Experimental study of phase relationships in a high-pressure mugearitic basalt as a function of water content (abstr.). *Abstracts with Programs, Geol. Soc. Am. Mtgs., 4,* pp. 550-551.

IRVING, A. J., & PRICE, R. C., 1974: Mantle-derived phonolitic rocks from Nigeria, Eastern Germany and New Zealand (abstr.). *EOS, Trans. Am. geophys. Union, 55,* p. 487.

JOYCE, E. B., 1971: A study of maars in the post-Miocene volcanics of southeastern South Australia (abstr.). *Abstr. ANZAAS 43rd Congress,* Brisbane, p. 72.

JUTSON, J. T., 1905: Notes on the volcanic history of Mount Shadwell. *Vict. Naturalist, 22,* p. 8.

KAY, R. W., & GAST, P. W., 1974: The rare earth content and origin of alkali-rich basalts. *J. Geol., 81,* pp. 653-682.

KESSON, S. E., 1972: Basic alkaline rocks. Unpub. Ph.D. thesis, Australian National University, Canberra.

LOVERING, J. F., & WHITE, A. J. R., 1969: Granulitic and eclogitic inclusions from basic pipes at Delegate, Australia. *Contr. Miner. Petrol., 21,* pp. 9-52.

MAALØE, S., 1973: Temperature and pressure relations of ascending primary magmas. *J. geophys. Res., 78,* pp. 6877-6886.

MACDONALD, G. A., & KATSURA, T., 1964: Chemical composition of Hawaiian lavas. *J. Petrol., 5,* pp. 82-133.

MAHONY, D. J., 1931: Alkaline Tertiary rocks near Trentham and at Drouin, Victoria. *Proc. Roy. Soc. Vict., 43,* pp. 123-129.

MCDOUGALL, I., ALLSOPP, H. D., & CHAMALAUN, F. H., 1966: Isotopic dating of the Newer Volcanics of Victoria, Australia, and geomagnetic polarity epochs. *J. geophys. Res., 71,* pp. 6107-6118.

MCINERNY, K., 1929: The building stones of Victoria, Part II. The igneous rocks. *Proc. Roy. Soc. Vict., 41,* pp. 121-159.

MORGAN, W. R., 1968: The geology and petrology of Cainozoic basaltic rocks in the Cooktown area, north Queensland. *J. geol. Soc. Aust., 15,* pp. 65-78.

NICHOLLS, G. D., 1967: Geochemical studies in the ocean as evidence for the composition of the mantle, *in* RUNCORN, S. K. (ed.), *Mantles of the Earth and Terrestrial Planets.* Interscience, pp. 285-304.

OLLIER, C. D., 1967: Landforms of the Newer Volcanic Province of Victoria, *in* JENNINGS, J. N., & MABBUTT, J. A. (eds), *Landform Studies from Australia and New Guinea.* A.N.U. Press, pp. 315-339.

OLLIER, C. D., & JOYCE, E. B., 1964: Volcanic physiography of the Western Plains of Victoria. *Proc. Roy. Soc. Vict., 77,* pp. 357-376.

ORR, D., 1927: An olivine-anorthoclase-basalt from Daylesford. *Proc. Roy. Soc. Vict., 40,* pp. 34-44.

PRICE, R. C., & GREEN, D. H., 1972: Lherzolite nodules in a 'mafic phonolite' from north-east Otago, New Zealand. *Nature phys. Sci., 235,* pp. 133-134.

PRICE, R. C., & TAYLOR, S. R., 1973: The geochemistry of the Dunedin Volcano, East Otago, New Zealand: rare earth elements. *Contr. Miner. Petrol., 40,* pp. 195-205.

RAHMAN, A., & MCDOUGALL, I., 1972: Potassium-argon ages on the Newer Volcanics of Victoria. *Proc. Roy. Soc. Vict., 85,* pp. 61-69.

RINGWOOD, A. E., 1966: The chemical composition and origin of the Earth, *in* HURLEY, P. M. (ed.), *Advances in Earth Science.* M.I.T. Press, pp. 287-356.

ROEDER, P. L., & EMSLIE, R. F., 1970: Olivine-liquid equilibrium. *Contr. Miner. Petrol., 29,* pp. 275-289.

SAGGERSON, E. P., & WILLIAMS, L. A. J., 1964: Ngurumanite from southern Kenya and its bearing on the origin of rocks in the northern Tanganyika alkaline district. *J. Petrol., 5,* pp. 40-81.

SINGLETON, O. P., & JOYCE, E. B., 1969: Cainozoic volcanicity in Victoria. *Geol. Soc. Aust. spec. Publ. 2,* pp. 145-154.

SKEATS, E. W., & JAMES, A. V. G., 1937: Basaltic barriers and other surface features of the Newer Basalts of Western Victoria. *Proc. Roy. Soc. Vict., 49,* pp. 245-278.

SKEATS, E. W., & SUMMERS, H. S., 1912: The geology and petrology of the Macedon district. *Geol. Surv. Vict. Bull. 24.*

SOLOMON, M., 1952: The volcanic deposits of southeast South Australia as sources of quarry stone. *Min. Rev. (Adelaide), 93,* pp. 133-137.

SPRIGG, R. C., 1952: The geology of the South-East Province, South Australia, with special reference to Quaternary coastline migrations and modern beach developments. *Geol. Surv. S. Aust. Bull., 29.*

STANLEY, E. R., 1909: Complete analysis of the Mount Gambier Basalt, with petrographical descriptions. *Trans. Roy. Soc. S. Aust., 33,* pp. 82-100.

STANLEY, E. R., 1910: Lherzolite and olivine from Mount Gambier. *Trans. Roy. Soc. S. Aust., 34,* pp. 63-68.

STUCKLESS, J. S., & IRVING, A. J., 1976: Strontium isotope geochemistry of megacrysts and host basalts from southeastern Australia. *Geochim. cosmochim. Acta, 40,* pp. 209-213.

STUEBER, A. M., 1969: Abundances of K, Rb, Sr and Sr isotopes in ultramafic rocks and minerals from western North Carolina. *Geochim. cosmochim. Acta, 33,* pp. 543-553.

SUTHERLAND, F. L., 1969*a*: A review of the Tasmanian Cainozoic volcanic province. *Geol. Soc. Aust. spec. Publ., 2,* pp. 133-144.

SUTHERLAND, F. L., 1969*b*: A comparison of the Cainozoic volcanic provinces of Victoria and Tasmania. *Proc. Roy. Soc. Vict., 82,* pp. 179-186.

SUTHERLAND, F. L., 1974: High-pressure inclusions in tholeiitic basalt and the range of lherzolite-bearing magmas in the Tasmanian volcanic province. *Earth planet. Sci. Lett., 24,* pp. 317-324.

WASS, S. Y., 1971: Studies on some basaltic rocks in New South Wales. Unpub. Ph.D. thesis, University of Sydney, Sydney.

WASS, S. Y., & IRVING, A. J., compilers, 1976: XENMEG: a catalogue of occurrences of xenoliths and megacrysts in volcanic rocks of eastern Australia. *Spec. Publ. Aust. Mus.,* in press.

WELLMAN, P., 1974: Potassium-argon ages on the Cainozoic volcanic rocks of eastern Victoria, Australia. *J. geol. Soc. Aust., 21,* pp. 359-376.

WILKINSON, J. F. G., 1962: Mineralogical, geochemical and petrogenetic aspects of an analcite-basalt from the New England District of New South Wales. *J. Petrol., 3,* pp. 192-214.

WILKINSON, J. F. G., 1968: Analcimes from some potassic igneous rocks and aspects of analcime-rich assemblages. *Contr. Miner. Petrol., 18,* pp. 252-269.

WILKINSON, J. F. G., & BINNS, R. A., 1969: Hawaiite of high pressure origin from north-eastern New South Wales. *Nature, Lond. 222,* pp. 553-555.

YATES, H., 1954: The basalts and granitic rocks of the Ballarat district. *Proc. Roy. Soc. Vict., 66,* pp. 63-101.

*Dr A. J. Irving,**
Dr R. H. Green,
Research School of Earth Sciences,
Australian National University,
P.O. Box 4, Canberra, A.C.T. 2600.

**Present address:*
The Lunar Science Institute,
3303 NASA Road 1,
Houston, Texas, U.S.A. 77058.

B26

Extract from
Journal of Petrology
Vol. 19, No. 3

Integrated Models of Basalt Petrogenesis: A Study of Quartz Tholeiites to Olivine Melilitites from South Eastern Australia Utilizing Geochemical and Experimental Petrological data

F. A. FREY, D. H. GREEN *and* S. D. ROY

UNIVERSITY OF TASMANIA
GEOLOGY DEPARTMENT
PUBLICATION No. 336

OXFORD
AT THE CLARENDON PRESS

Integrated Models of Basalt Petrogenesis: A Study of Quartz Tholeiites to Olivine Melilitites from South Eastern Australia Utilizing Geochemical and Experimental Petrological Data

by F. A. FREY,[1] D. H. GREEN[2] *and* S. D. ROY[1]

[1] *Department of Earth and Planetary Sciences, Massachusetts Institute of Technology, Cambridge, Massachusetts 02139 U.S.A.;* [2] *Department of Geology, University of Tasmania, Hobart, 7001, Australia*

(*Received 25 February 1977; in revised form 26 August 1977*)

ABSTRACT

The Tertiary to Recent basalts of Victoria and Tasmania have mineralogical and major element characteristics of magmas encompassing the range from quartz tholeiites to olivine melilitites. Abundances of trace elements such as incompatible elements, including the rare earth elements (REE), and the compatible elements Ni, Co and Sc, vary systematically through this compositional spectrum. On the basis of included mantle xenoliths, appropriate 100 Mg/Mg + Fe^{+2} (68–72) and high Ni contents many of these basalts represent primary magmas (*i.e.*, unmodified partial melts of mantle peridotite). For fractionated basalts we have derived model primary magma compositions by estimating the compositional changes caused by fractional crystallization of olivine and pyroxene at low or moderate pressure. A pyrolite model mantle composition has been used to establish and evaluate partial melting models for these primary magmas. By definition and experimental testing the specific pyrolite composition yields parental olivine tholeiite magma similar to that of Kilaeau Iki, Hawaii (1959–60) and residual harzburgite by 33 per cent melting. It is shown that a source pyrolite composition differing only in having 0·3–0·4 per cent TiO_2 rather than 0·7 per cent TiO_2, is able to yield the spectrum of primary basalts for the Victorian–Tasmanian province by ~4 per cent to ~25 per cent partial melting. The mineralogies of residual peridotites are consistent with known liquidus phase relationships of the primary magmas at high pressures and the chemical compositions of residual peridotite are similar to natural depleted or refractory lherzolites and harzburgites. For low degrees of melting the nature of the liquid and of the residual peridotite are sensitively dependent on the content of H_2O, CO_2 and the CO_2/H_2O in the source pyrolite.

The melting models have been tested for their ability to account for the minor and trace element, particularly the distinctively fractionated REE, contents of the primary magmas. A single source pyrolite composition can yield the observed minor and trace element abundances (within at most a factor of 2 and commonly much closer) for olivine melilitite (4–6 per cent melt), olivine nephelinite, basanite (5–7 per cent melt), alkali olivine basalt (11–15 per cent melt), olivine basalt and olivine tholeiite (20–25 per cent melt) *provided that* the source pyrolite was already enriched in strongly incompatible elements (Ba, Sr, Th, U, *LREE*) at 6–9 × chondritic abundances and less enriched (2·5–3 × chondrites) in moderately incompatible (Ti, Zr, Hf, Y, *HREE*) prior to the partial melting event. The source regions for S.E. Australian basalts are similar to those for oceanic island basalts (Hawaii, Comores, Iceland, Azores) or for continental and rift-valley basaltic provinces and very different in trace element abundances from the model source regions for most mid-ocean ridge basalts. We infer that this mantle heterogeneity has resulted from migration within the upper mantle (LVZ or below the LVZ) of a melt or fluid (H_2O, CO_2-enriched) with incompatible element concentrations similar to those of olivine melilitite, kimberlite or carbonatite. As a result of this migration, some mantle regions are enriched in incompatible elements and other areas are depleted.

Although it is possible, within the general framework of a lherzolite source composition, to derive the basanites, olivine nephelinites and olivine melilitites from a source rock with chondritic *relative* REE abundances at 2–5 × chondritic levels, these models require extremely small degrees of

melting (0·4 per cent for olivine melilitite to 1 per cent for basanite). Furthermore, it is not possible to derive the olivine tholeiite magmas from source regions with chondritic relative REE abundances without conflicting with major element and experimental petrology arguments requiring high degrees (≥15 per cent) of melting and the absence of residual garnet. If these arguments are disregarded, and partial melting models are constrained to source regions with chondritic relative REE abundances, then magmas from olivine melilitites to olivine tholeiites can be modelled if degrees of melting are sufficiently small, *e.g.*, 7 per cent melting for olivine tholeiite. However, the source regions must be heterogenous from ~1 to ~5 × chondritic in absolute REE abundances and heterogeneous in other trace elements as well. This model is rejected in favor of the model requiring variation in degree of melting from ~4 per cent to ~25 per cent and mantle source regions ranging from LREE-enriched to LREE-depleted relative to chondritic REE abundances.

INTRODUCTION

In recent years, two approaches have produced major advances in knowledge of the origin of basalts and the mineralogical and chemical nature of the upper mantle. First, experimental study of near-liquidus phase relations of basalts and near-solidus phase relations of potential source rocks has defined internally consistent models in which liquids of the basalt spectrum from olivine melilitite to olivine tholeiite can be assigned to a pressure, temperature and per cent melting grid. Residual phases have been specified for origins of these liquids as partial melts of a particular model source peridotite composition, i.e., pyrolite (Green & Ringwood, 1967; Green, 1970*a*, *b*, 1971, 1973*a*, *b*). The second approach uses differences in trace element contents of basalts and a knowledge of crystal/liquid partition relationships to model processes of partial melting and test possible magma/residue pairs. In this approach, the rare earth elements (REE) have been very important since they show distinctive relative abundance patterns amongst natural basalts. These REE abundance differences reflect the characteristic and very different solid/liquid partition relationships for major mantle minerals such as olivine, pyroxenes, garnet and amphibole (Gast, 1968; Schilling, 1971; Kay & Gast, 1973).

If the upper mantle source region for basalts is of constant composition and if no processes other than partial melting and crystal fractionation act to change the compositions of magmatic liquids, then these two approaches must be mutually consistent and should suffice to define the mantle source composition, the conditions of melting and nature of residue. However, Green (1968) assembled data for the minor elements, Na, K, Ti, P to show that their variable abundances in magmas of similar type (particularly tholeiites and alkali olivine basalts) were such that inhomogeneity in these elements in the source regions was required by simple partial melting models. In addition, the inability of simple crystal fractionation models to explain differences in trace element contents and in isotopic ratios among tholeiites and alkali olivine basalts, etc., led Green & Ringwood (1967) to advance the concept of 'wall-rock reaction'. In this process, a body of magma was considered, at least in those cases where there was little temperature contrast between wall rock and magma, to act as an open system, extracting from the wall rocks a small low melting fraction, highly enriched in the 'incompatible elements'*.

* 'Incompatible elements' are those elements which, because of their ionic radii and valency do not readily substitute in the major minerals of the mantle (or of the deep crust if that is the source or wall-rock region being considered) and are strongly enriched in the liquid relative to coexisting major minerals.

This low melting fraction was added to the magma which at the same time would be precipitating its liquidus phases of olivine or pyroxene. By this process, magmas could acquire trace element and isotopic compositions that are not related to their original source region. The pessimistic inference that trace element studies were not useful in constraining basalt genesis was convincingly countered by Gast's (1968) use of REE data to argue for extremely small degrees of melting for silica-undersaturated basalts and to argue for two-stage melting to account for the light REE-depleted characteristics of the source region for mid-ocean ridge basalts.

In this study, we have obtained major and trace element data for a wide spectrum of mantle-derived liquids from a geographically and temporally limited volcanic province. In addition, experimental studies on several of these mantle-derived liquids and on similar liquids place constraints on conditions of partial melting and residual mineralogy. Our objective is to use these data to test whether it is possible to construct internally consistent models for genesis of the spectrum of basalts from a common source peridotite. If this is not possible or reasonable then an alternative approach is to evaluate the type and degree of heterogeneities between source regions or complexities of 'contamination' of basalts which must be invoked in their petrogenesis. The basalt province sampled, south-eastern Australia, is of continental as opposed to ocean basin type and the limitations on the source region for this province can be compared to two dissimilar ocean basin regions, *viz*, the Hawaiian Islands and to mid-ocean ridge basalts.

SELECTION AND DESCRIPTION OF SAMPLES

We have selected basalt samples from the Tertiary–Recent basalt provinces of Tasmania and western Victoria, at the southern end of the very extensive Tertiary–Recent basalt provinces occurring throughout eastern Australia (Browne, 1939). Sample selection was based on recent geochemical and petrological studies of the Newer Volcanics of western Victoria (Irving & Green, 1976) and the availability of basalts from eastern Australia with the common characteristics that they contain spinel lherzolite xenoliths (Green *et al.*, 1974; Sutherland, 1974; Irving & Green, 1976).

The Tasmanian basalts were derived from a large number of eruptive centers in rather deeply dissected terrain which produced valley-filling flows rather than extensive lava plains or major central volcanoes (Sutherland, 1969). The age of volcanism in Tasmania is Oligocene–Miocene (20–30 m yr) and the compositions of basalts cover the extreme range from olivine melilitite to olivine tholeiite and quartz tholeiite (Sutherland, *ibid.*). The Newer Volcanoes of western Victoria are of late Pliocene, Pleistocene and Recent age ($\geqslant$4·5 m yr to ~5000 yr) and the compositional range, although not extending to compositions as undersaturated as the Tasmanian basalts, is from olivine-rich basanites to olivine tholeiites and quartz tholeiites. As in the Tasmanian province, there are many eruptive centers and no large central volcanoes in the Newer Volcanics of western Victoria, but topographic relief on the pre-basalt surface has been covered to form extensive basalt plains.

Brief field and petrographic descriptions of the samples are given in Table 1 and major element compositions and normative mineralogy are given in Table 2.

TABLE 1

Specimen details for basalts for which major element and trace-element data have been obtained

Specimen and Locality	*Rock Type*	*Phenocrysts*	*Microphenocrysts*	*Groundmass*	*Comments*
	(a) *Normative Classification* (b) *Modal Classification*				
2177—Lava flow Porters Quarry, Mt. Eckersley, W. Victoria	(a) Quartz tholeiite (b) Olivine tholeiite	Ol	Pl	Pl, Cpx, Ilm, Gl	(Irving & Green, 1976) Note low normative diopside content.
T14—Lava flow Andover, Tasmania	(a) Olivine tholeiite (b) Olivine tholeiite	Ol		Pl, Cpx, Opaques, Gl-mesotasis	(Sutherland, 1974) Contains lherzolite xenoliths and pyroxene megacrysts.
69-1018—Ejecta Mt. Gellibrand, W. Victoria	(a) Olivine tholeiite (b) Olivine tholeiite	Ol	Ol	Cpx, Pl, Ilm, Gl- mesostasis	(Irving & Green, 1976)
2152—Lava flow Marida Yallock, W. Victoria	(a) Olivine tholeiite (b) Olivine basalt	Ol	Ol	Ol, Cpx, Pl, Ilm, Gl-mesostasis	(Irving & Green, 1976) Clinopyroxene is colourless. Note higher K_2O relative to 2177 and 69-1018.
69-1026—Lava flow Mt. Widderin, W. Victoria	(a) Olivine basalt (b) Alkali olivine basalt	Ol	Ol	Ol, Cpx, Pl, Opaques, Gl-mesostasis	(Irving & Green, 1976) Clinopyroxene zoned from colourless to pale mauve.

69-1036—Ejecta Mt. Frazer, W. Victoria	(a) (b)	Alkali olivine basalt Alkali olivine basalt	Ol	Ol	Ol, Cpx, Pl, Opaques, Mesostasis	(Irving & Green, 1976) Note higher Mg-value (Table 2) and presence of lherzolite xenoliths.
2128 Ejecta Mt. Porndon 2650 Ejecta Mt. Leura 2679 Ejecta Mt. Shadwell W. Victoria	(a) (b)	Basanite Basanite	Ol	Ol, Cpx, Pl	Ol, Cpx, Pl, Ne, Opaques, Gl-mesostasis	(Green, 1972*a*; Irving & Green, 1976) All contain lherzolite xenoliths; Note differences in Na_2O, K_2O, P_2O_5, TiO_2 contents and particularly lower Mg-value and higher Na_2O, etc. of 2650.
2896—Small plug Lughrata, Flinders Id, Tasmania	(a) (b)	Basanite Olivine nephelinite	Ol	Ol	Ol, Cpx (titanaugite), Ne, Opaques, Ap	(Sutherland & Kershaw, 1971) Contains lherzolite xenoliths.
2854—Small plug Scottsdale, Tasmania	(a) (b)	Olivine nephelinite Olivine nephelinite	Ol	Ol, Cpx	Ol, Cpx, Ne, Opaques, Ap, mesostasis-Gl	Contains lherzolite xenoliths. Note lower SiO_2, Al_2O_3 and alkalis and higher CaO, TiO_2 and MgO contents than basanites.
2860—Small plug Scottsdale, Tasmania	(a) (b)	Olivine nephelinite Nephelinite	—	—	Medium-grained Cpx, Ne, Ap, Opaques, Gl + Zeolites	No lherzolite xenoliths, coarser grained phase intimately mixed with olivine nephelinite 2854. Note low Mg-value and enrichment in CaO, Al_2O_3, Na_2O, K_2O, P_2O_5 relative to 2854.
2927—Small plug Laughing Jack Marsh, Tasmania	(a) (b)	Olivine melilitite Olivine melilite nephelinite	Ol, Cpx	Ol, Cpx, Mel	Cpx, Mel, Ilm, Ne, Ap	(Brey & Green, 1974) Contains lherzolite xenoliths.

TABLE 2

Compositions and CIPW norms of basalts studied

	1	2*	3	4	5	6*
Locality	*Mt. Eckersley W. Victoria*	*Andover Tasmania*	*Mt. Gellibrand W. Victoria*	*Marida Yallock W. Victoria*	*Mt. Widderin W. Victoria*	*Mt. Frazer W. Victoria*
Sample No.	*2177*	*T14*	*69-1018*	*2152*	*69-1026*	*69-1036*
SiO_2	53·53	50·57	50·70	50·11	49·83	48·00
TiO_2	1·80	1·95	2·07	1·89	1·73	2·14
Al_2O_3	15·32	13·57	14·30	14·56	14·88	13·91
Fe_2O_3	1·59	1·77	1·92	1·85	1·90	1·85
FeO	7·94	9·68	9·60	9·26	9·51	9·27
MnO	0·11	0·18	0·16	0·17	0·17	0·16
MgO	6·52	8·51	7·95	8·48	8·49	11·39
CaO	8·38	9·96	8·90	8·75	8·60	8·35
Na_2O	3·65	2·90	3·24	3·37	3·45	3·23
K_2O	0·85	0·54	0·81	1·15	1·09	1·18
P_2O_5	0·31	0·36	0·35	0·40	0·34	0·51
$\frac{100\ Mg}{Mg + Fe^{++}}$ $\left(\text{for } \frac{Fe^{+++}}{Fe} = 0{\cdot}15\right)$	59·4	61·0	59·6	62·0	61·4	68·6
$\frac{100\ Mg}{Mg + Fe^{++}}$ $\left(\text{for } \frac{Fe^{+++}}{Fe} \text{ as analyzed}\right)$	68·3	61·0	60·4	75·2	73·1	74·8
Qz	1·0	—	—	—	—	—
Or	5·0	3·2	4·8	6·8	6·5	7·0
Lc	—	—	—	—	—	—
Ab	30·9	25·1	27·5	28·5	29·2	24·9
Ne	—	—	—	—	—	1·3
An	22·9	22·9	22·1	21·2	21·9	19·9
Di	13·6	20·4	16·1	16·0	15·1	14·6
Hy	20·1	19·7	14·5	5·0	2·8	—
Ol	—	1·7	7·5	15·3	17·7	24·2
Cs	—	—	—	—	—	—
Mt	2·3	2·2	2·8	2·7	2·8	2·7
Ilm	3·4	3·8	3·9	3·6	3·3	4·1
Ap	0·7	0·9	0·8	0·9	0·8	1·2

PRIMARY AND DERIVATIVE MAGMAS

Since our purpose is to use major and trace element constraints to elucidate problems of mantle composition and magma genesis, a first step is to identify those magmas which are primary melts from the upper mantle; that is, mantle-derived magmas that have been unmodified by crystal fractionation or other processes either during movement to the earth's surface or following emplacement. We utilize three criteria. First, the presence of spinel lherzolite xenoliths in a basalt establishes that the magma has ascended from depths $\geqslant$30 km without crystal fractionation and with meagre opportunity for chemical interaction with wall-rock environments.

Secondly, the evidence from natural lherzolite xenoliths in kimberlites and basalts, from diapiric intrusives of high temperature and high pressure peridotites and from refractory dunites and harzburgites exposed in ophiolite complexes, consistently indicates that the least refractory upper mantle peridotite compositions have 100 Mg/(Mg + Fe^{++}) (Mg-values) $\simeq$ 88–89. Basaltic magmas derived from such a source peridotite must have Mg-values ~ 68–75 for up to about 30 per cent melting (using $K_{D_{(Ol/Liq)}}^{(Fe/Mg)} = 0{\cdot}3$, Roeder & Emslie, 1970). Applying these criteria

TABLE 2 (*continued*)

	7*	8*	9*	10*	11*	12	13*
Locality	*Mt. Porndon Victoria*	*Mt. Shadwell W. Victoria*	*Mt. Leura W. Victoria*	*Lughrata Flinders Id.*	*Scottsdale N.E. Tasmania*		*Laughing Jack Marsh Tasmania*
Sample No.	*2128*	*2679*	*2650*	*2896*	*2854*	*2860*	*2927*
SiO_2	46·21	45·07	45·13	42·87	39·88	40·23	38·26
TiO_2	2·51	2·78	3·25	2·73	3·42	3·66	2·72
Al_2O_3	12·38	12·71	13·00	11·29	9·60	13·76	9·58
Fe_2O_3	2·00	1·95	2·04	2·34	2·64	2·26	2·11
FeO	9·98	9·93	10·45	11·39	13·08	10·99	10·95
MnO	0·18	0·16	0·17	0·18	0·20	0·18	0·24
MgO	11·71	12·57	9·90	12·17	14·11	5·40	16·40
CaO	8·56	8·76	8·51	8·78	11·37	14·09	13·19
Na_2O	3·54	3·48	4·07	4·68	3·03	4·08	3·77
K_2O	2·01	1·80	2·22	2·16	1·55	3·19	1·43
P_2O_5	0·90	0·81	1·14	1·37	1·10	2·16	1·35
$\frac{100\ Mg}{Mg + Fe^{++}}$ $\left(\text{for } \frac{Fe^{+++}}{Fe} = 0{\cdot}15\right)$	67·6	69·3	62·8	65·6	65·8	46·6	72·8
$\frac{100\ Mg}{Mg + Fe^{++}}$ $\left(\text{for } \frac{Fe^{+++}}{Fe} \text{ as analyzed}\right)$	70·9	71·4	65·5	70·7	70·0	54·0	76·0
Qz	—	—	—	—	—	—	—
Or	11·9	10·6	13·1	12·8	—	—	—
Lc	—	—	—	—	7·3	15·1	6·7
Ab	14·9	11·8	13·3	3·3	—	—	—
Ne	8·2	9·6	11·5	19·7	14·0	19·1	17·4
An	11·9	13·7	10·7	3·4	8·1	10·0	5·1
Di	19·9	19·6	19·6	25·2	25·9	23·6	11·7
Hy	—	—	—	—	—	—	—
Ol	23·4	24·6	20·0	23·8	28·7	11·0	36·0
Cs	—	—	—	—	3·0	5·7	11·6
Mt	2·9	2·8	3·0	3·4	3·9	3·8	3·1
Ilm	4·8	5·3	6·2	5·2	6·6	7·1	5·2
Ap	2·1	1·9	2·7	3·2	2·6	5·2	3·2

* Basalts containing xenoliths of high pressure spinel herzolite.

to the basalts of Table 2, analyses 6, 7, 8, 10, 11, 13, covering the range from alkali olivine basalt to olivine melilitite, are identified as primary partial melts from upper mantle peridotite. Analyses 2 and 9 are identified as melts modified by some crystal fractionation (probably olivine or olivine + pyroxene separation) within the upper mantle prior to inclusion of upper mantle xenoliths. Analyses 1, 3, 4, 5 and 12 are fractionated liquids in which the depth of crystal fractionation cannot be specified. If we are to make valid comparisons of these fractionated magmas with other primary magmas, it is necessary to make some estimate of the proportion and nature of the crystals extracted and to calculate back to a model parental basalt. Olivine is a liquidus phase at 1 atmosphere for all compositions of Table 2 and using the relationship $K_{D_{Ol/Liq}}^{Fe/Mg} = 0{\cdot}3$, it is possible to model the effects of low pressure fractional crystallization and add olivine of appropriate composition until a liquid composition is reached which would have olivine of Fo_{88-90} as its liquidus phase. Calculated 'primary' liquids for analyses 1–5 are listed in Table 3. For analysis 9, the listed composition in Table 3 is that derived previously by addition

TABLE 3

Simple models of 'primitive' basalts derived by olivine-addition to the fractionated basalts of Table 2

	1'	*2'*	*3'*	*4'*	*5'*	*9'*	*12'*
	2177	*T14*	*69-1018*	*2152*	*69-1026*	*2650*	*2860*
	+14 per cent	*+12·5 per cent*	*+15 per cent*	*+10 per cent*	*+12 per cent*	*+10 per cent*	*+25 per cent*
	Olivine	*Olivine*	*Olivine*	*Olivine*	*Olivine*	*Ol(Fo_{90})*	*Olivine*
SiO_2	51·8	49·4	49·2	49·1	48·7	44·7	40·1
TiO_2	1·57	1·73	1·77	1·70	1·53	2·9	2·73
Al_2O_3	13·3	12·0	12·2	13·1	13·2	11·7	10·3
Fe_2O_3	1·4	1·6	1·6	1·7	1·7	1·8	1·7
FeO	8·6	10·1	10·1	9·6	9·9	10·5	12·2
MnO	0·10	0·16	0·14	0·15	0·15	0·15	0·14
MgO	11·8	12·9	13·5	12·3	12·9	13·9	15·3
CaO	7·3	8·8	7·6	7·9	7·6	7·7	10·6
Na_2O	3·17	2·57	2·77	3·03	3·05	3·65	3·05
K_2O	0·74	0·48	0·69	1·03	0·97	2·0	2·39
P_2O_5	0·27	0·32	0·30	0·36	0·30	1·0	1·62
$\frac{100\,Mg}{Mg + Fe^{++}}$	71·0	69·5	70·5	69·5	69·9	70·2	69·0
Qz	—	—	—	—	—	—	—
Or	4·4	2·8	4·1	6·1	5·7	11·8	—
Lc	—	—	—	—	—	—	11·2
Ab	26·8	21·3	23·5	25·6	25·8	11·5	—
Ne	—	—	—	—	—	10·5	14·2
An	19·9	20·0	18·8	19·1	19·5	9·6	7·5
Di	11·7	17·4	13·7	14·3	13·1	17·7	16·8
Hy	20·3	15·8	12·4	4·5	2·3	—	—
Ol	11·3	16·3	21·2	23·8	27·5	28·4	34·3
Cs	—	—	—	—	—	—	4·4
Mt	2·0	2·3	2·3	2·5	2·5	2·6	2·5
Ilm	3·0	3·3	3·4	3·2	2·9	5·5	5·3
Ap	0·6	0·8	0·7	0·9	0·7	2·4	3·9

of 10 per cent olivine (Fo_{90}) to basanite 2650. This composition has been experimentally tested and conditions established where the olivine-rich basanite melt could be a partial melt from garnet peridotite (Green, 1973*a*).

Our third criterion for identifying primary magmas involves compatible trace elements such as Sc, Cr, Co and Ni. These elements have mineral/liquid partition coefficients exceeding unity for at least one major upper mantle phase such as olivine, garnet and pyroxenes. As a result, their abundances in a magma are very sensitive to fractional crystallization of mafic minerals (e.g., the ratio c^l/c_0 decreases from 1 to 0·39 for 10 per cent fractionation of a phase with a constant solid/liquid partition coefficient of 10; see also, Fig. 1 of Gast, 1968). Thus, the abundance of these elements can be utilized to identify the most primitive magmas in a suite of basalts. Furthermore, if (1) the upper mantle abundance can be accurately estimated and (2) partition coefficients are known as a function of temperature, pressure and composition, then the compatible element concentration of primary magmas can be calculated. In particular, Ni abundances have been used to identify magmas which have experienced very little olivine fractionation (*e.g.*, Gast, 1968; Kay *et al.*, 1970; Sun & Hanson, 1975*a*, *b*; Allegré *et al.*, 1977). Although it is established that mineral/liquid partition coefficients of compatible trace elements are very temperature dependent (*e.g.*, olivine/liquid partition coefficients vary from ~1 at 1600 °C, Nesbitt & Sun, 1976 to >20 at <1200 °C, Leeman, 1973), the compositional dependence of these partition coefficients is poorly understood (Irvine, 1974; Duke, 1976; Hart *et al.*, 1976). Thus, the abundance of these elements cannot be used to quantitatively evaluate partial melting models. Nevertheless, the abundance of compatible trace elements can provide general constraints on petrogenetic models. For example, if compositional dependence of partition coefficients is ignored, 1 per cent to 20 per cent partial melts of lherzolite are estimated to range in Ni from 90 to 670 ppm, in Co from 27 to 80 ppm and in Sc from 15 to 28 ppm (Cr values were not calculated since Cr is not a trace element in upper mantle pyroxenes; the surprisingly low Ni and Co concentrations forming the lower boundary stem from Leeman's (1973) experimental studies; see Appendix for values of partition coefficients and source concentrations used in the model calculations). The Ni, Co and Sc abundances in the Australian basalts studied lie within these broad ranges. Because crystallization and removal of olivine and pyroxenes from a cooling magma causes a rapid decrease in the abundance of these compatible elements, basaltic liquids with compatible trace element abundances at the high end of the calculated range can be inferred to be primary magmas. In particular, six basalts (6, 7, 8, 10, 11 and 13 in Table 2) have Ni abundances $\geqslant$320 ppm (all other samples studied have Ni $\leqslant$280 ppm), and these six basalts are those identified by the first two criteria as primary partial melts of peridotite.

CONDITIONS OF MELTING

The compositions of Table 3, together with the possible primary compositions on Table 2 (6, 7, 8, 10, 11, 13) comprise a suite of compositions with olivine of Fo_{88-90} as a low pressure liquidus phase. It is possible to use the results of experimental

studies of natural basalts at high pressure to evaluate whether these compositions may also have multiply saturated liquidi with orthopyroxene, or orthopyroxene + clinopyroxene, etc. as liquidus phases in addition to olivine at high pressure. If such conditions exist then we can calculate a model source composition and residual mineralogy from knowledge of the liquid composition and composition of the residual phases. However, such model source compositions are arbitrary in the sense that the experimental studies constrain phase compositions but not the proportions of liquid and residual minerals. In this study, we use the model pyrolite composition of Ringwood (1966) as a reference source composition. For each primary mantle liquid, the K_2O and P_2O_5 contents of pyrolite and the liquid define the degree of melting, since we assume that K_2O and P_2O_5 are completely partitioned into the melt. This assumption is based on the extremely low P_2O_5 and K_2O contents of the liquidus phases of basaltic magmas and the absence of phlogopite on the liquidus of basaltic magmas at high pressures unless K_2O-contents are very high (>5 per cent for biotite mafurite composition, Edgar *et al.*, 1976). Although ilmenite or other Ti-rich phases do not occur on the high pressure liquidi of the basaltic compositions considered in this paper, TiO_2 contents are not negligible in the garnet, clinopyroxene and orthopyroxene occurring as residual phases in partial melting experiments on pyrolite or as liquidus phases of basaltic magmas. Na_2O is similarly partitioned into pyroxene, particularly at high pressure, so that Na_2O and TiO_2 cannot be regarded as 'incompatible' elements in partial melting models.

By using K_2O and P_2O_5 contents in the primary basalts to define the degree of pyrolite melting, we calculate the bulk composition of the residue (or two bulk compositions if K_2O and P_2O_5 contents do not yield the same value of per cent melting). This residual composition is calculated into a modal mineralogy by one of two methods. The first method is used for very undersaturated magmas and follows the approach used for modeling the origin of the olivine-rich basanite, 2650 + 10 per cent olivine (Green, 1973*a*). The compositions of olivine, orthopyroxene, clinopyroxene and garnet analyzed from a partial melting experiment on pyrolite—40 per cent olivine + 0·3 per cent H_2O at 30 kb, 1200 °C (Mori & Green, 1978) are used to calculate the mode of the residual bulk composition. In all cases, very close matching of residual bulk composition and bulk composition of an appropriate mix was possible (except for TiO_2 which is ~0·2–0·3 per cent in the mineral mix compared with 0·5–0·6 in the pyrolite residue).

A second modelling method was used for the alkali olivine basalt and tholeiitic magmas since for these magmas the possible *P*, *T*, per cent H_2O conditions of genesis cover a wider spread, and the nature of model residues would be quite different depending on whether residual orthopyroxene contained 4·5 per cent Al_2O_3 or 2·5 per cent Al_2O_3 or whether melting occurred in the garnet lherzolite or spinel lherzolite field. As in the previous method, basaltic K_2O and P_2O_5 contents are used to define the degree of melting of pyrolite and hence, the bulk composition of the residue. However, the residual mineralogy is calculated as a 'high pressure norm' using information from high pressure experimental studies to choose appropriate (specific examples are given later) mineral compositions (Al in

pyroxenes, Na in pyroxene, Ti in garnet and pyroxene, etc.) for inferred P, T conditions of magma segregation.

Olivine Tholeiites (69-1018, 2177, T-14)

The tholeiites are fractionated liquids which are not in equilibrium with olivine of Mg-value $\geqslant 88$. Simple models of crystal fractionation involving extraction of olivine alone are used to derive possible parental compositions of Table 3 (1′, 2′, 3′), these new compositions having liquidus olivine $\geqslant Mg_{88}$. However, when compared with olivine tholeiite and olivine basalt compositions which have been shown by high pressure studies to have olivine and orthopyroxene as liquidus phases or with the most magnesian olivine tholeiite glasses or aphyric basalts amongst Hawaiian or ocean floor basalts, it is apparent that the Mt. Eckersley and Mt. Gellibrand tholeiites have excessively low normative diopside and CaO contents and very high Al_2O_3/CaO. It is commonly argued that the earth's upper mantle should have Al_2O_3/CaO ratio which is close to that of chondrites *i.e.*, $\sim 1{\cdot}2$, and that basalts derived by high degrees of melting leaving mainly olivine and orthopyroxene as residual phases, should have $Al_2O_3/CaO \simeq 1{\cdot}2$. If melting leaves residual clinopyroxene, and Al_2O_3 contents of both pyroxenes are not very high, then $(Al_2O_3/CaO)_{melt} > 1{\cdot}2$. However, it is difficult to generate Al_2O_3/CaO of 1·8 and 1·6 by partial melting leaving residual clinopyroxene and it is more probable that the olivine tholeiites 2177 and 69-1018 have undergone low pressure fractionation by settling out of olivine and calcium-rich clinopyroxene, or by crystallization of olivine, Ca-rich clinopyroxene and plagioclase. Attempts to model such low pressure fractionation are too arbitrary but addition of clinopyroxene as well as olivine to 69-1018 would yield a more reasonable parental tholeiite composition. This conclusion is even more applicable to tholeiite 2177 and the presence of plagioclase phenocrysts in this sample suggest the possible presence of accumulate plagioclase.

If we consider the simplest model for 69-1018 in which (69-1018 + 15 per cent olivine) is taken as a possible primary magma then the K_2O and P_2O_5 contents of pyrolite (Ringwood, 1966) fix the degree of partial melting at 20 per cent. The mineralogy of the residual composition (Table 4) can be calculated as 70 per cent olivine, 21·5 per cent orthopyroxene, 7 per cent clinopyroxene, 1·5 per cent (chromite + ilmenite). If clinopyroxene as well as olivine were added to 69-1018 in correcting for crystal fractionation then this more Ca-rich model parent magma would require a higher degree of partial melting and clinopyroxene would be less abundant or absent from the residue. The compositions of the residual pyroxenes for the simple melting model are such that the mean pyroxene contains 4·2 per cent Al_2O_3 and 0·1 per cent Na_2O. This Al_2O_3 content (*i.e.*, ~3·8–3·9 per cent Al_2O_3 in orthopyroxene) is less than the Al_2O_3 content of orthopyroxene coexisting with aluminous spinel at $T > 1200$ °C, 15–20 kb or with garnet at 30 kb, >1350 °C. These model calculations, considered together with experimental studies at high pressure defining liquidus temperatures and liquidus phase relationships for olivine tholeiitic magmas, show that garnet is not a residual phase for the olivine tholeiite (69-1018) parent magma.

TABLE 4

Comparisons of residual compositions for derivation of different magmas from a common source pyrolite with compositions calculated by combinations (modes) of minerals from pyrolite at 30 kb, 1200 °C. This method of calculation of models for partial melting and model mineralogy of residual peridotite is applied for the highly undersaturated compositions. The first column is the calculated residual composition, the second column is the close match calculated from the mode listed in the lower part of the table. For the alkali olivine basalt 69-1036 and tholeiite 69-1018, the residual mineralogy is calculated (as discussed in the text) by calculation of a high pressure 'norm' on the basis of assumed pyroxene compositions

Magma Composition }	*Olivine melilitite*		*Olivine nephelinite*				*Basanite*		*Alkali olivine basalt*			*Olivine tholeiite*	*Olivine tholeiite kilauea*
	2927		*2927*		*2896*		*2896*		*2650 + 10 per cent olivine*		*69-1036*		*69-1018 + 15 per cent olivine*	*(Table 5, col. 2)*
Per cent melting based on K_2O	*9*		*—*		*6*		*—*		*6*		*11*		*20*	*33*
Per cent melting based on P_2O_5	*—*		*5*		*—*		*4*		*6*		*11*		*20*	*33*
SiO_2	45·85	45·77	45·55	45·58	45·35	45·44	45·27	45·39	45·3	45·1	44·92		44·23	43·9
TiO_2	0·52	0·24	0·60	0·27	0·48	0·25	0·63	0·26	0·6	0·4	0·53		0·45	0·01
Al_2O_3	2·94	3·10	3·22	3·31	3·05	3·04	3·22	3·17	3·0	3·0	2·26		1·36	0·06
Fe_2O_3	0·30	—	0·37	—	0·34	—	0·38	—	0·4	—	0·29		0·16	—
FeO	7·75	8·00	7·89	8·23	7·84	8·09	7·90	8·51	7·9	8·4	7·91		7·53	6·95
MnO	0·13	0·14	0·14	0·14	0·14	0·14	0·13	0·14	0·1	0·1	0·14		0·14	0·1
MgO	39·55	39·43	38·58	38·96	39·10	39·30	38·53	38·67	39·1	39·1	40·80		43·63	47·5
CaO	2·08	2·08	2·55	2·50	2·72	2·73	2·84	2·84	2·8	2·9	2·43		1·95	0·38
Na_2O	0·25	0·27	0·40	0·31	0·31	0·34	0·40	0·35	0·4	0·3	0·24		0·02	—
K_2O	—	—	0·06	—	—	—	0·04	—	0·01	—	—		—	—
P_2O_5	(–0·06)	—	—	—	(–0·02)	—	—	—	—	—	—		—	—
Cr_2O_3	0·47	0·39	0·46	0·43	0·46	0·42	0·45	0·44	0·4	0·4	0·48		0·53	0·6
NiO	0·22	0·23	0·21	0·23	0·21	0·23	0·21	0·23	0·2	—	0·24		0·25	0·3
$\frac{100\,Mg}{Mg + \Sigma Fe}$	89·6		89·3		89·6		89·0		89·8		89·9		91·1	92·3
											A	B C		
Olivine	56		56·5		59		58		60		63·0	63·0 63·0	70	80·8
Orthopyroxene	30		26		22·5		22·5		18		25·5	22·5 26·0	21·5	18·4
Clinopyroxene	7		9·5		11·5		12		14		9·5	9·5 10·5	7	—
Garnet	7		8		7		7·5		8		2·0	5·0 —	—	—
Spinel	—		—		—		—		—			— 0·5	} 1·5	—
Chromite	—		—		—		—		—					0·8

The Mt. Eckersley tholeiite (2177) is, as noted previously, a fractionated tholeiite in which olivine, clinopyroxene and plagioclase crystallization may all have contributed to the derivation of the analyzed rock composition. The very high Al_2O_3/CaO and relatively low CaO/Na_2O ratios are attributed to clinopyroxene and plagioclase separation and it is possible that the degree of crystallization required to generate 2177 from the parental magma was as high as 40–50 per cent. Incompatible trace elements could thus be enriched by factors of up to 2 in 2177 relative to the primary magma. However, the relative proportions of K_2O, P_2O_5 and TiO_2 among the tholeiites suggest that the source region for 2177 had a higher K_2O content than the sources for tholeiites 69-1018 and T14.

The Andover, Tasmania tholeiite (T14), although a fractionated rather than primary mantle-derived liquid, has much lower Al_2O_3/CaO and higher CaO/Na_2O ratios than 69-1018 and 2177. Both values are consistent with high degrees of melting leaving little residual clinopyroxene with a low jadeite content. The presence of lherzolite xenoliths and high pressure pyroxene megacrysts show that addition or subtraction of plagioclase cannot have occurred and high pressure fractionation by olivine, orthopyroxene and minor clinopyroxene may have led to slight increase in Al_2O_3/CaO and decrease in CaO/Na_2O relative to the primary magma. The simplest model of reversing crystal fractionation (Table 3, 2′) by addition of 12·5 per cent olivine yields a parental tholeiite composition similar to 69-1018 + 15 per cent olivine but with higher normative diopside and lower normative olivine contents. We infer from experimental studies on tholeiitic magmas that this liquid could be a partial melt produced by 20–25 per cent melting of a pyrolite source leaving olivine, orthopyroxene and very little clinopyroxene in the residue. The depth of magma segregation was probably not more than 50 km. Comparison of TiO_2, P_2O_5 and K_2O abundances with those of 69-1018 suggest that the source region for T14 had similar P_2O_5 and TiO_2 contents but a lower K_2O content than the source for 69-1018.

It is useful to compare models for genesis of the Victorian tholeiites with the model for genesis of a primitive Kilauean olivine tholeiite since the calculation of the pyrolite composition (Ringwood, 1966) was based on the composition of a Kilauean olivine tholeiite (although, in retrospect, not a very primitive tholeiite since its liquidus olivine would be $\sim Mg_{84}$). Probably the best estimates of primitive Kilauean olivine tholeiite can be derived from the detailed analyses of the 1959–60 Kilauea Iki eruption by Murata & Richter (1969) which define the mean compositions of the first eruptive phase and permit an estimate of the mean erupted lava composition through the 2nd → 17th eruptive phases. These two estimates (Table 5) are possible primary magma compositions. The more magnesian composition (column 2) implies a greater depth of magma segregation from residual olivine and orthopyroxene, and it has a more magnesian liquidus olivine. Experimental studies on two olivine tholeiite compositions (with 22 per cent olivine, 14·6 per cent MgO and 26 per cent olivine, 16·3 per cent MgO, respectively, Green & Ringwood, 1967; Green, 1970*a*) establish conditions at which magmas such as those of Table 5 are in equilibrium with residual olivine and orthopyroxene. These data define an internally consistent model in which the chosen pyrolite composition

TABLE 5

Model for melting of primitive Kilauean tholeiitic magma from pyrolite source. Column 1 is the weighted average composition for lava of the 1st eruption phase (Murata & Richter, 1966, Table 8, col. 1). Column 2 is the estimated mean composition of 2nd–17th eruptive phases based on the oxide variation curves for summit magmas and the mean of 17 per cent MgO suggested by Murata & Richter (ibid, p. A24). Column 3 is the calculated residue (composition and mode) for pyrolite composition given 33 per cent melting and extraction of liquid composition of column 2. Column 4 is the calculated composition of residual orthopyroxene—this is probably too low in Al_2O_3 for equilibrium with the liquid of column 2 at ~15 kb, 1350–1400 °C and suggests that the 'pyrolite composition' should have ~3·9 per cent Al_2O_3 rather than 3·54 per cent Al_2O_3—the residual orthopyroxene would then contain ~3 per cent Al_2O_3

	1	*2*	*3*	*4*
SiO_2	48·2	47·3	43·9	58·3
TiO_2	2·24	2·1	0·01	—
Al_2O_3	11·4	10·5	0·06	0·3
Fe_2O_3	1·5	1·5	—	—
FeO	10·2	10·3	6·95	4·8
MnO	0·18	0·2	0·1	0·1
MgO	13·9	17·0	47·5	34·7
CaO	9·7	8·5	·38	1·4
Na_2O	1·89	1·7	—	—
K_2O	0·44	0·4	—	—
P_2O_5	0·22	0·2	—	—
Cr_2O_3	—	—	0·6	0·4
NiO	—	—	0·3	—
$\frac{100\ Mg}{Mg + Fe^{++}}$			MODE	
for liquid	70·8	74·5	80·8 per cent Olivine	
for liquidus olivine ($K_D = 0·3$)	89·0	91	18·4 per cent Enstatite 0·8 per cent Chromite	

yields liquids appropriate to primary Kilauean tholeiite magma by ~33 per cent melting at ~17 kb, 1400 °C leaving residual harzburgite (80·8 per cent olivine, 18·4 per cent enstatite, 0·8 per cent chromite). For this model, K_2O, P_2O_5, TiO_2 and Na_2O contents all require 33 per cent melting and the residual enstatite contains <2 per cent CaO, consistent with the absence of clinopyroxene in the residue.

Olivine Basalt (2152)

The Marida Yallock olivine basalt is a fractionated liquid and calculation of the simplest fractionation model (olivine extraction) yields a possible mantle-derived parental magma with ~24 per cent normative olivine (Table 2, 4′). The lower degree of silica undersaturation and lower TiO_2, P_2O_5, K_2O and Na_2O contents relative to 69-1036 (see next section) suggest that 13–17 per cent melting would be required to generate this liquid. Also, garnet would be absent or less abundant as a residual phase (c.f. next section) and the residue would be a lherzolite with 5–10 per cent residual clinopyroxene, ~25 per cent residual enstatite.

Alkali Olivine Basalts (69-1036, 69-1026)

The Mt. Frazer basalt (69-1036) is a primary, mantle-derived melt on the basis of the criteria discussed previously. However, the Mt. Widderin basalt (69-1026) requires the addition of ~12 per cent olivine to obtain a composition having equilibrium liquidus olivine > Mg_{88} (Table 3). Olivine is the low pressure liquidus phase and hence olivine fractionation is possible. It is also possible that there was fractionation at high pressure involving pyroxenes and olivine. Comparison of the compositions of 69-1036 and 69-1026 + 12 per cent olivine (*i.e.*, the simplest model of crystal fractionation for genesis of 69-1026 from a primary, mantle-derived melt) shows that the lower TiO_2, Na_2O, K_2O and P_2O_5 contents of the latter are consistent with a slightly larger melt fraction than the Mt. Frazer basalt. We have no detailed high pressure studies of an alkali basalt composition similar to 69-1036, especially in the presence of water. The closest analogues are the relatively Fe-rich alkali olivine basalt of Green & Ringwood (1967) and the olivine basalt from Auckland Id. (Green & Hibberson, 1970). Both of these basalts are multiply saturated with olivine, orthopyroxene and clinopyroxene at moderate pressures (<20 kb) and may be partial melts from lherzolite leaving olivine, orthopyroxene and clinopyroxene as residual phases. The petrogenetic grid for melting of a pyrolite source with ~0·1–0·2 per cent H_2O (Green, 1970*b*, 1973*b*) suggests that at pressures of 25–30 kb increasing degrees of melting will lead from olivine-rich basanite at ~6 per cent melt through alkali picrite and picritic olivine basalt to tholeiitic picrite at ~35 per cent melting. Since garnet is a residual phase in melting of pyrolite + 0·2 per cent H_2O at 30 kb up to a temperature of 1350 °C (Green, 1973*b*) and the estimated degree of melting at 1350 °C is 10–15 per cent (Green & Liebermann, 1976), magmas of alkali picrite character may be derived by partial melting leaving residual garnet. In addition, if water contents of >0·2 per cent occur in the source pyrolite then 10–15 per cent rather than 5–6 per cent partial melting may occur at 30 kb, 1250 °C so that liquids in equilibrium with garnet lherzolite mineralogy at these conditions may be olivine-rich alkali basalt or alkali picrite rather than olivine-rich basanite. From these arguments it may be inferred that primary, alkali picrite magmas may be derived by moderate degrees of partial melting at 30 kb, leaving olivine, orthopyroxene, clinopyroxene and minor garnet as residual phases.

With the model pyrolite composition of Ringwood (1966), the K_2O and P_2O_5

contents of the Mt. Frazer alkali olivine basalt (69-1036) are such that the basalt would be produced by ~11 per cent melting with no K_2O or P_2O_5 remaining in the residue. Three models for the residual mineralogy (Table 4) have been calculated appropriate to different P, T conditions of melting.

Model A

$P \sim 30$ kb, $T \sim 1300$ °C, 11 per cent melting leaving a garnet lherzolite residue (62·2 per cent olivine, 25·4 per cent enstatite, 9·2 per cent diopside, 2·3 per cent garnet and 0·8 per cent ilmenite). This model assumes that orthopyroxene in equilibrium with garnet at these conditions contains ~4·8 per cent Al_2O_3 and clinopyroxene contains ~7 per cent Al_2O_3, 2·3 per cent Na_2O.

Model B

$P \sim 25$ kb, $T \sim 1200$ °C, 11 per cent melting leaving a garnet lherzolite residue (62·5 per cent olivine, 21·8 per cent enstatite, 9·9 per cent clinopyroxene, 5·0 per cent garnet and 0·8 per cent ilmenite). This model assumes that orthopyroxene contains ~5·1 per cent Al_2O_3, 2·2 per cent Na_2O.

Model C

$P \sim 15$–20 kb, $T \sim 1300$ °C, 11 per cent melting leaving a lherzolite residue (62·2 per cent olivine, 26 per cent enstatite, 10·6 per cent diopside, 0·4 per cent chromite and 0·8 per cent ilmenite). The mean Al_2O_3 content of the residual pyroxenes is ~6 per cent. Within our knowledge of the effects of variations in P, T and water-content on magma composition, all three models are possible residual mineralogies for primary, olivine-rich alkali basalts. In later sections we use trace element data to discriminate between these models.

The presence of residual ilmenite is an embarrassment in all these models since ilmenite is not likely to be a liquidus phase of the alkali olivine basalt at any pressure. Residual ilmenite stems from the use of Hawaiian tholeiite in formulating the pyrolite model; in particular, the high average TiO_2 content of Hawaiian alkali olivine basalts (3·0 per cent TiO_2) and Hawaiian tholeiites (2·1–2·9 per cent TiO_2, Macdonald & Katsura, 1964) relative to the basalts from Victoria and Tasmania. If the source pyrolites for the latter alkali olivine basalts contains 0·3–0·4 per cent TiO_2, then residual ilmenite would not appear in models A, B, C and the models would be consistent with the absence of ilmenite as a high pressure liquidus phase.

Basanites (2128, 2679, 2650)

Previously, Green (1973*a*) argued that basanite 2650 is not a primary mantle partial melt, and that it lost some olivine prior to entrainment of the lherzolite inclusions. Experimental studies (Green, *ibid.*) on a model primary melt composition, 2650 + 10 per cent olivine (9′ in Table 3), showed that this composition is a possible partial melt from garnet peridotite leaving residual olivine, orthopyroxene, clinopyroxene and garnet at ~27 kb, 1200–1300 °C provided there is sufficient water content in the source region to yield a water content in the magma of 3–7 per cent H_2O. Analyses of olivine, pyroxenes and garnet from (pyrolite–40

per cent olivine) composition at 30 kb, 1250 °C were used to calculate a specific model for the genesis of the 2650 + 10 per cent olivine magma; *i.e.*, 6 per cent melting of pyrolite leaving residual lherzolite of mineralogy 60 per cent olivine, 18 per cent orthopyroxene, 14 per cent clinopyroxene and 8 per cent garnet*. The similarities in composition between basanites 2128, 2679 and 2650 are such that very similar conditions of partial melting and residual mineralogy are estimated for all three basanites. The differences in K_2O, P_2O_5 and TiO_2, the lower Ne/Ab and higher CaO/Na_2O ratio of the Mt. Porndon (2128) and Mt. Shadwell (2679) basanites relative to the Mt. Leura magma (2650 + 10 per cent olivine) suggests that the former basanites represent slightly higher degrees of melting (~6·5 per cent for 2128, Mt. Porndon, and 7·0–7·3 per cent melting for 2679, Mt. Shadwell).

Olivine Nephelinite (2896)

The Lughrata olivine nephelinite (2896) is transitional between the basanites and Tasmanian olivine (melilite) nephelinites (2854, 2927) in SiO_2 and Al_2O_3 contents, Al_2O_3/CaO, and degree of undersaturation but is richer in Na_2O, K_2O and P_2O_5 (but not in TiO_2) contents. Compositionally, it is most similar to the parental olivine basanite (2650 + 10 per cent olivine) and similar conditions of magma genesis (~30 kb, 1200–1250 °C, 5–10 per cent H_2O in magma) are inferred. In particular, it is considered that CO_2 did not play a significant role in determining the melt composition in contradistinction to its role in the genesis of the olivine melilitite 2927 (Brey & Green, 1975, 1976). The higher Na_2O, K_2O and P_2O_5 contents and lower CaO/Na_2O ratio of 2896 in comparison with (2650 + 10 per cent olivine) indicate that 2896 olivine nephelinite was derived by <6 per cent melting. Specific models of partial melting, calculated from the P_2O_5 and K_2O contents of 2896 and pyrolite and from the analyzed olivine, pyroxenes, and garnet in (pyrolite–40 per cent olivine) at 30 kb, 1200 °C are listed in Table 4.

Olivine Melilitite (2927) and Olivine Nephelinite (2854)

It has been shown that olivine melilitite 2927 has olivine, orthopyroxene, clinopyroxene and garnet on or near its liquidus near 30 kb, 1150–1200 °C (Brey & Green, 1975; Brey, unpublished data) provided that the magma contains ~8 per cent H_2O, 6 per cent CO_2 in solution. Similarly, it has been shown that olivine, orthopyroxene, clinopyroxene and garnet are residual phases in pyrolite + 0·2 per cent H_2O at 30 kb and 1200 °C. The K_2O and P_2O_5 concentrations in the pyrolite model source and melilitite 2927 define the degree of partial melting of 2927 as 5 per cent (based on P_2O_5) or 9 per cent (based on K_2O). The mineralogy of the residue for the two models is calculated in Table 4 using the compositions of minerals in pyrolite–40 per cent olivine at 30 kb, 1200 °C (Mori & Green, 1976). The residual garnet lherzolite (Table 4) contains similar proportions of garnet and clinopyroxene and differs from the residue previously calculated for the basanites in the higher clinopyroxene and olivine and lower orthopyroxene content of the basanite residue. The differences in liquid composition and residual mineralogy for

* The TiO_2 anomaly persists and residual ilmenite would appear in the model if the source pyrolite contained 0·7 per cent TiO_2, but not if it contained 0·4 per cent TiO_2.

similar degrees of partial melting at similar pressure (30 kb) and temperature (1200–1250 °C) are attributed to the roles of the volatile species, H_2O and CO_2. The source for the basanite had very low CO_2 and $CO_2/H_2O + CO_2$, whereas that for the melilitite had ~0·7–1 per cent CO_2, and $CO_2/CO_2 + H_2O \sim 0{\cdot}2$ (mol. ratio) (Brey & Green, 1975).

Comparison of the Scottsdale olivine nephelinite (2854) with the experimentally studied basanite and olivine melilitite samples suggests that conditions of genesis similar to those for the olivine melilitite should be applicable (cf. low SiO_2, low Al_2O_3, high CaO in 2854). However, there are significant differences in degree of silica undersaturation, Na_2O, TiO_2 and P_2O_5 contents between the magmas. It is possible that compositional differences in these primary magmas are subtly explained by differences in $H_2O:CO_2$ proportions in the source region, the olivine nephelinite being a similar melt fraction but from a source region with higher $H_2O:CO_2$ proportions than that for olivine melilitite.

SUMMARY OF PETROGENETIC MODELS BASED ON MAJOR ELEMENTS

We have shown that the suite of mantle-derived magmas from olivine melilitite (2927) to alkali-olivine basalt (69-1036) can be derived by partial melting of a common source composition. The mineralogy of the residual peridotites is consistent with known high pressure liquidus relationships of the respective basalts. There is greater uncertainty in genesis of the olivine basalt and olivine tholeiite parent magmas since the effects of crystal fractionation on primary magmas must be estimated. Tholeiitic parental magmas form by 20–25 per cent melting (cf. 33 per cent melting for Kilauean parental olivine tholeiite magma) leaving olivine, orthopyroxene, minor clinopyroxene and chromite as residual phases. Clinopyroxene and garnet become increasingly important as residual phases through the sequence of decreasing partial melting (Table 4); that is, olivine basalt (~15 per cent) → alkali olivine basalt (11 per cent) → basanite (6 per cent). The CaO/Na_2O ratio of a melt reflects the CaO/Na_2O ratio (diopside/jadeite) of coexisting clinopyroxene provided that diopside and jadeite activities in the melt are approximately proportional to CaO, Na_2O concentrations. The decreasing CaO/Na_2O ratios of the primary mantle melts from alkali olivine basalt (69-1036) to olivine nephelinite (2896) support the models of progressively lower degrees of melting with the melts equilibrated with increasingly jadeite-rich clinopyroxenes. This trend is sharply reversed in the olivine nephelinite (2854) and olivine melilitite (2927) from Tasmania; both have very high CaO/Na_2O ratios. For these magmas it is probable that diopside activity in the melt is dramatically reduced by Ca bonding with $(CO_3)^=$ within the melt (Brey & Green, 1975, 1976; Brey, 1976; Eggler & Mysen, 1976) and thus, the concentration ratio $(CaO/Na_2O)_{melt}$ is no longer simply related to the activity ratio $(diopside/jadeite)_{melt}$.

The sensitivity of the compositions of liquids formed by small degrees of melting (~5 per cent) to the proportions of H_2O and CO_2 in the source is well illustrated by the calculations presented (Table 4); thus, the residue to the olivine melilitite (5 per cent melt) has high orthopyroxene/olivine and garnet/clinopyroxene ratios compared with the residues for the basanite (6 per cent melt) and olivine nephelinite

(2896, 4 per cent melt). The experimental studies of pyrolite melting in the presence of CO_2 (Brey & Green, 1976 and unpublished data) and of the liquidus relations of 2927 and other extremely undersaturated liquids show that the melting of peridotite in the presence of CO_2 involves incongruent melting of clinopyroxene in the manner: olivine + clinopyroxene (diopside, jadeite, etc., solid solution) + ($melt_1$ containing H_2O + CO_2) → ($melt_2$ containing larnite + nepheline + H_2O + CO_2) + garnet + orthopyroxene. This type of melting leads to an increasing garnet to clinopyroxene ratio in the residue as melting proceeds. In the light of this effect, the differences in liquid composition and residue mineralogy among 2927, 2854, 2896 and 2650 are due in part to the small difference in degree of melting but more particularly due to a decreasing CO_2/H_2O in the order 2927 > 2854 > 2896 ⩾ 2650.

PETROGENETIC MODELS BASED ON REE

Mantle peridotites exposed in the crust (*e.g.*, ultramafic inclusions in basalt, alpine peridoties, and peridotite members of ophiolite sequences) range widely in composition, especially in trace elements (*e.g.*, Fisher *et al.*, 1969; Philpotts *et al.*, 1972; Frey & Green, 1974; Kay & Senechal, 1976; Loubet *et al.*, 1976). These compositonal variations may represent mantle heterogeneity, but at least in part they result from processes of magma formation and events occurring during transport to the crust. Since we have no precise model-independent constraints on trace element abundances in the mantle source of basalts, our approach is to consider a range of plausible initial models. In particular, as one model we adopt the pyrolite composition based on Hawaiian basalt compositions. Because an inevitable consequence of this model is an upper mantle source with a significant relative light REE (LREE) enrichment compared to chondritic REE abundances, we have also evaluated a peridotitic model with near-chondritic relative REE abundances in the mantle source. In the following discussion, we consider some of the quantitative implications of these models.

We focus initially upon the REE because of their geochemical similarity. A signifcant result of REE studies on basalts has been the observation that different basalt types are characterized by different REE abundances (especially relative abundances), and that basalts of similar type (*i.e.*, similar major element composition) from diverse geographic areas usually have surprisingly similar REE abundances (*e.g.*, continental tholeiitic diabases, Philpotts & Schnetzler, 1968; alkalic basalts, Herrman, 1968; Philpotts *et al.*, 1972; Kay & Gast, 1973; Sun & Hanson, 1975*a*, *b*). However, among tholeiitic basalts there is also a strong correlation of relative REE abundances with tectonic setting; in particular, tholeiites from ocean floor distant from islands are depleted in LREE relative to tholeiites from continents and oceanic islands.

In the section on conditions of melting in this paper we utilized major element (including P_2O_5 and K_2O) contents and experimental petrology results to construct petrogenetic models (Table 4). We now evaluate these models in terms of REE geochemistry. Our objective is to determine if the basaltic source rocks differ in key geochemical parameters such as La/Yb (also K/Rb, Zr/Hf, etc.). Compared with

TABLE 6

Trace element abundances (ppm)[1]

	Tholeiites			*Olivine and alkali olivine basalts*		
	Mt. Eckersley, W. Victoria	*Andover, Tasmania*	*Mt. Gellibrand, W. Victoria*	*Marida Yallock, W. Victoria*	*Mt. Widderin, W. Victoria*	*Mt. Frazer, W. Victoria*
Locality	*2177*	*T-14*	*69-1018*	*2152*	*69-1026*	*69-1036*
Sc	19·9 ± 0·3	26	23 ± 1	22 ± 1	22 ± 0·5	23 ± 1
V	151	142	184	170	171	170
Cr	249 ± 4	312	240 ± 10	300 ± 8	257 ± 8	388 ± 4
Co	40	59	66 ± 2	89	—	56
Ni	141	103	190	280	278	364
Cu	—	61	—	—	51	—
Zn	—	118	—	—	—	—
Rb	23	9	17·5	24	21	24
Sr	430	373	392	531	471	543
Ba	320	125	180	590	1200	350
Y	99	27	26	62	55	27
Zr	142	146	133	142	151	152
Nb	—	—	—	—	—	—
Hf	3·7 ± 0·2	3·7	3·6 ± 0·1	3·7 ± 0·1	3·8 ± 0·2	3·9 ± 0·2
La	47·8 ± 0·5	17·6	15·9 ± 0·2	50·3 ± 0·4	51 ± 1	23 ± 1
Ce	100 ± 2	44·7	38 ± 3	130 ± 10	180 ± 7	49 ± 4
Nd	49·4 ± 0·7	22	19 ± 2	47 ± 1	51 ± 0·5	23 ± 2
Sm	12·4 ± 0·3	5·08	4·9 ± 0·3	10·3 ± 0·4	12·2 ± 0·1	5·53 ± 0·01
Eu	4·0 ± 0·1	1·85	1·62 ± 0·05	3·1 ± 0·1	3·53 ± 0·03	2·02 ± 0·04
Tb	2·0 ± 0·2	0·80	0·8 ± 0·1	1·7 ± 0·2	1·7 ± 0·1	0·87 ± 0·04
Ho	2·56 ± 0·06	0·90	0·8 ± 01	1·95 ± 0·05	2·0 ± 0·1	0·98 ± 0·06
Yb	5·1 ± 0·2	1·9	1·8 ± 0·2	3·4 ± 0·1	3·9 ± 0·2	1·77
Lu	0·77 ± 0·01	0·28	0·27 ± 0·03	0·46 ± 0·05	0·50 ± 0·05	0·23
Th	2·7 ± 0·3	2·2	2·1 ± 0·2	3 ± 0·2	2·7 ± 0·1	2·9 ± 0·2
U	0·5	0·2	0·7	0·8	1·2	1·1

1. In general: Ba, Sc, Co, Hf, Ta, REE and Th determined by instrumental neutron activation at MIT. Precision for 10 samples analysed in duplicate is indicated by ± deviation from the mean: accuracy indicated by standard rock data reported in Frey *et al.*, 1974. V and Ni determined at ANU by wet chemical methods (analyst, E. Kiss); Rb, Sr, Y, Zr, Nb and U determined at ANU by X-ray fluorescence (analysts, P. Beasley, A. Irving, S. Kesson). Exceptions are T-14 (all elements not determined by INAA were

absolute abundance variations, these ratios change little during geological processes (Gast, 1968). If such ratios vary in the mantle sources for basalts, then an extensive, probably complex, sequence of geochemical processes must have affected upper mantle rocks.

Our most detailed experimental constraints are for nepheline–normative basalts, especially basanitic compositions (Green, 1973*a*); therefore, in the detailed evaluation of models based on experimental petrology, major and trace element compositions, we consider first, the basanites.

Basanites (2650, 2679, 2128)

The three basanites studied and another Mt. Leura sample studied by Philpotts *et al.* (1973) have very similar REE abundances (Table 6 and Fig. 1) (maximum deviation for La, Sm, Eu and Tb is <10 per cent, and for Ce, Nd, Ho, Yb and Lu <22 per cent). Considering that three volcanic centers are represented and two different analytical techniques were used, the similarity is remarkable. As mentioned earlier these rocks are also similar in major element composition (both Mt. Leura samples require ~10 per cent olivine addition to be considered as primary magmas). Evidently, the source composition (major element and REE), degree of melting and residual mineralogy for these basanites have been very similar.

TABLE 6 (*continued*)

	Basanites			*Olivine (melilite) nephelinites*			
Locality	*Mt. Porndon, W. Victoria*	*Mt. Shadwell, W. Victoria*	*Mt. Leura, W. Victoria*	*Lughrata, Flinders Id.*	*Scottsdale, Tasmania*		*Laughing Jack Marsh, Tasmania*
	2128	*2679*	*2650*	*2896*	*2854*	*2860*	*2927*
Sc	19·4 ± 0·2	21	18	14·3 ± 0·3	18·7 ± 0·5	9·8 ± 0·7	23·8 ± 0·6
V	175	177	173	143	194	173	229
Cr	400 ± 15	310	219	520 ± 20	410 ± 20	11 ± 2	510 ± 20
Co	55	57	50	57	66	42 ± 3	66
Ni	375	342	263	405	366	64	458
Cu	—	44	47	—	—	—	—
Zn	—	135	154	—	—	—	—
Rb	40	36	45	27	12	27	29
Sr	862	830	950	1380	1250	2060	1440
Ba	510	460	590	300	250	475	530
Y	28	24	25	29	28	44	31
Zr	298	281	327	354	320	445	243
Nb	—	62	68	—	97	—	99
Hf	7·3 ± 0·3	6·3	—	9 ± 0·3	8·6 ± 0·2	10·5 ± 0·3	5·9 ± 0·1
La	48·7 ± 0·3	45·5	52·2	67 ± 3	62·2 ± 0·2	103 ± 2	75 ± 5
Ce	101 ± 3	93	108	144 ± 7	140 ± 1	180 ± 30	160 ± 5
Nd	44·3 ± 0·2	49·2	56·3	63 ± 3	57·2 ± 0·1	77 ± 10	64 ± 4
Sm	9·7 ± 0·2	9·1	10·5	12·7 ± 0·2	11·9 ± 0·3	18 ± 1	12·3 ± 0·2
Eu	2·98 ± 0·05	2·99	3·42	4·1 ± 0·1	3·9 ± 0·2	6 ± 0·3	3·67 ± 0·01
Tb	1·23 ± 0·03	1·18	1·34	1·55 ± 0·08	1·5 ± 0·1	2·4 ± 0·2	1·6 ± 0·2
Ho	1·10 ± 0·1	0·95	0·99	1·41	1·16	1·7 ± 0·2	1·32
Yb	1·7	1·74	1·59	1·7 ± 0·2	1·42	1·9 ± 0·1	1·80
Lu	0·21	0·19	0·19	0·22 ± 0·4	0·175	0·20 ± 0·02	0·27 ± 0·05
Th	5·6 ± 0·1	5·7	6·7	8 ± 1	6·6 ± 0·3	12 ± 2	11 ± 2
U	1·3	1·6	2·2	2·1	2·3	3·8	2·5

determined by XRF at Macquarie University, data from L. Sutherland, personal communication, 1975), 2650 and 2679 (Rb, Sr, Ba, Cu, Zn, Y, Zr, Nb and U were determined by XRF at ANU, analyst, B. Chappell; Th and U by gamma ray spectrometry, Green *et al.*, 1968 and 69-1026 (Ba, V, Ni and Cu determined by emission spectrography at ANU, A. Irving, analyst); REE by radiochemical neutron activation; Frey & Green, 1974.

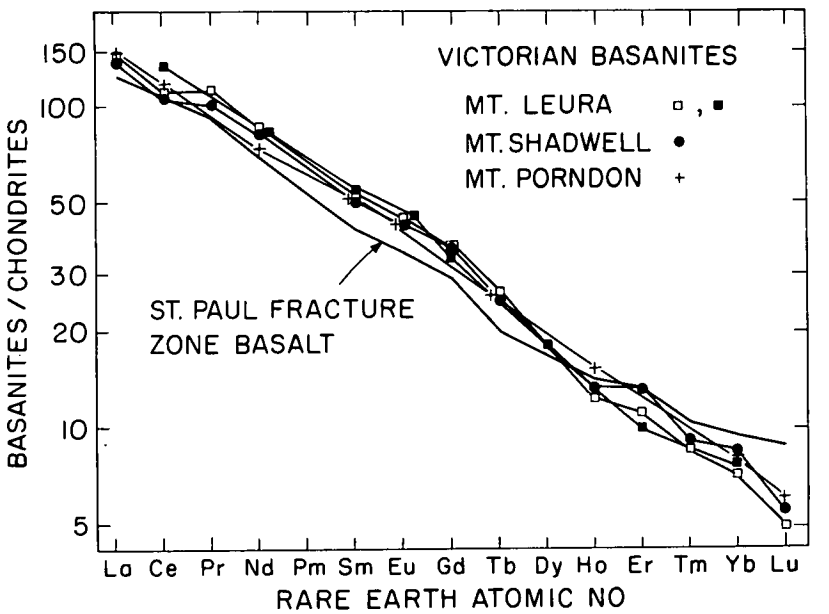

FIG. 1. REE abundances in four basanites from the Younger Basalts of Victoria compared to a chondritic average (Frey *et al.*, 1968). Shown for comparison are the REE data for a basanite (10·9 per cent normative nepheline) dredged from the St. Paul fracture zone (Frey, 1970*a*). Nd isotopic studies have been done on this basalt by DePaolo & Wasserburg (1976*a*).

A pyrolite source model for basanite 2650 requires 6 per cent melting (based on K_2O and P_2O_5 contents, Table 4). In addition to the degree of melting (F) the evaluation of an equilibrium melting model ($C^L/C_0 = 1/(D + F - DF)$, Shaw, 1970) requires a knowledge of mineral/liquid partition coefficients (D) and the proportion of residual mineral phases coexisting with a 6 per cent melt (C^L = liquid concentration, C_0 = source concentration). At 30 kb and 1250 °C, the residual mineral proportions are 14 per cent cpx, 8 per cent ga, 18 per cent opx and 60 per cent ol (Table 4). In an equilibrium model with this residue mode any reasonable

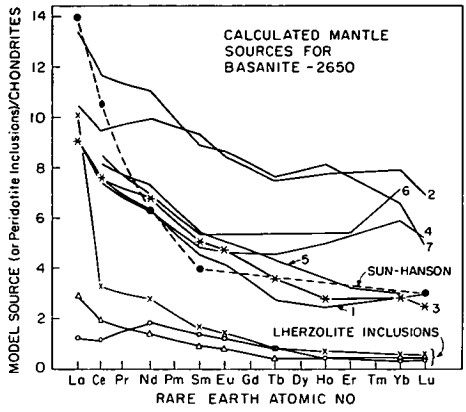

FIG. 2. REE abundances in seven calculated mantle sources for basanite 2650. In the model calculations, equation 11 of Shaw (1970) was utilized with per cent melting equal to 6 per cent, residual mode equal to 60 per cent olivine, 18 per cent orthopyroxene, 14 per cent clinopyroxene and 8 per cent garnet and the seven sets of REE partition coefficients given in the Appendix. Results from the preferred set of REE P.C. (no. 3) are designated by *. Shown for comparison is the mantle source proposed by Sun & Hanson (1975*b*) and REE abundances in 3 lherzolite inclusions (2700 (×)), Victoria, Australia, Frey & Green, (1974); SAL-3(○), Salt Lake Crater, Hawaii, Frey, unpublished; PA-10(△), San Carlos, Arizona, Frey & Prinz (1978).

set of REE partition coefficients (see Appendix) requires that the upper mantle source have a higher LREE/HREE ratio than chondrites. Specifically, we find that this model requires a source with a LREE content of 9–13·5 × chondrites and HREE content of 2·5–7·5 × chondrites (Fig. 2). Although similar in HREE to some of our models, the REE content of the mantle source for alkalic basalts determined by Sun & Hanson (1975*a*) has significantly higher fractionation of LREE relative to HREE (La/Yb = 7·5 and 5·3, for Sun & Hanson model, and model 3 of Fig. 2, respectively).

As an alternative model, we arbitrarily chose 1 per cent melt as a reasonable lower melting limit for basanite 2650, and calculated the REE abundances of the source using the same residual minerals, initial mode (Table 4) and seven sets of partition coefficients (see Appendix) that were used in the pyrolite model evaluation. The results demonstrate that if basanite 2650 is a 1 per cent melt three of the partition coefficient sets yield mantle sources with nearly chondritic REE distributions at concentration levels 2–3 times chondrites (Fig. 3). These models are in agreement with other conclusions that the upper mantle has REE (at least HREE) abundances equal 2–4× chondrites (Gast, 1968; Frey *et al.*, 1968; Frey,

1969; Kay & Gast, 1973; Frey & Green, 1974). We consider that models 1, 3 and 5 in Fig. 3 are consistent with a source having chondritic relative REE abundances. Since relative REE abundances in ordinary chondrites commonly differ by up to 20 per cent (Nakamura, 1974) small deviations from a chondritic average are not unexpected.

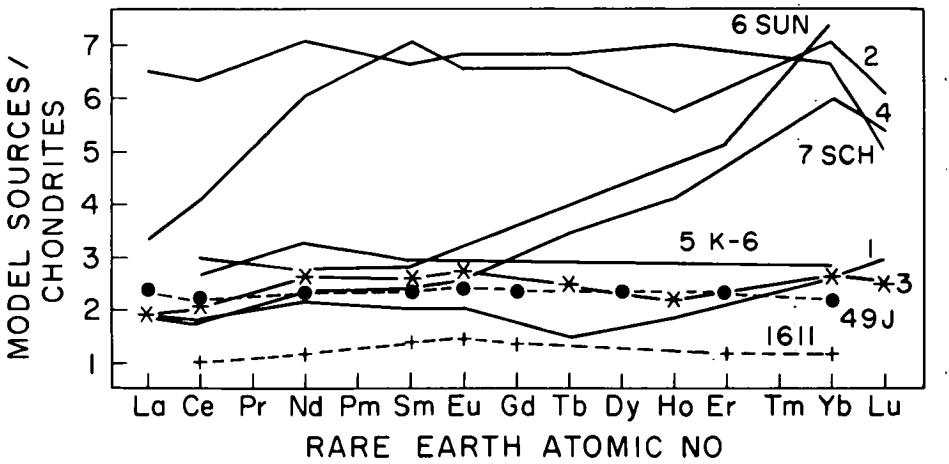

FIG. 3. REE abundances in seven calculated mantle sources for basanite 2650. In the model calculations, equation 15 of Shaw (1970) was utilized with per cent melting equal to 1 per cent, an initial mode equivalent to that used in Fig. 2 models; that is, 57·2 per cent olivine, 17 per cent orthopyroxene, 16 per cent clinopyroxene, 8·5 per cent garnet and 1·3 per cent phlogopite + ilmenite + apatite, and the seven sets of REE partition coefficients given in the Appendix. Results from the preferred set of REE P.C. (no. 3) are designated by *. Shown for comparison are REE abundances in a spinifex textured peridotitic komatiite from South Africa (49J of Sun & Nesbitt, 1978) and a garnet lherzolite inclusion in kimberlite (1611 of Shimizu, 1975).

Olivine Nephelinite (2896)

Like Hawaiian nephelinites (Fig. 4), this basalt is strongly enriched in LREE (La/Yb = 39). On the basis of major element composition we deduced that this basalt resulted from a smaller degree of melting than the basanites; and that it equilibrated with a residue of higher garnet/clinopyroxene ratio (Table 4). Because the K_2O/P_2O_5 ratio of 2896 differs from that of pyrolite (1·53 and 2·17, respectively) two models were developed on the basis of major element composition. The 6 per cent melt model, based on K_2O content, leads to a source with LREE of ~13× chondrites, and this enrichment differs significantly from the model 3 source for the basanite (Fig. 2). However, the 4 per cent melting model, based on P_2O_5 content, leads to REE abundances in the source rock that are within ±10 per cent (except Ho (16 per cent) and Lu (21 per cent)) of the REE abundances in the model source for basanite 2650 (Fig. 5). Therefore, the basanites and this olivine nephelinite could have originated from a mantle source with a similar major element and REE content. In addition to LREE and P_2O_5, the higher Sr, Zr, Hf and Th contents in 2896 are consistent with this magma originating by a smaller degree of melting than basanite 2650.

If the source rock for basalt 2896 had a near chondritic REE distribution, then

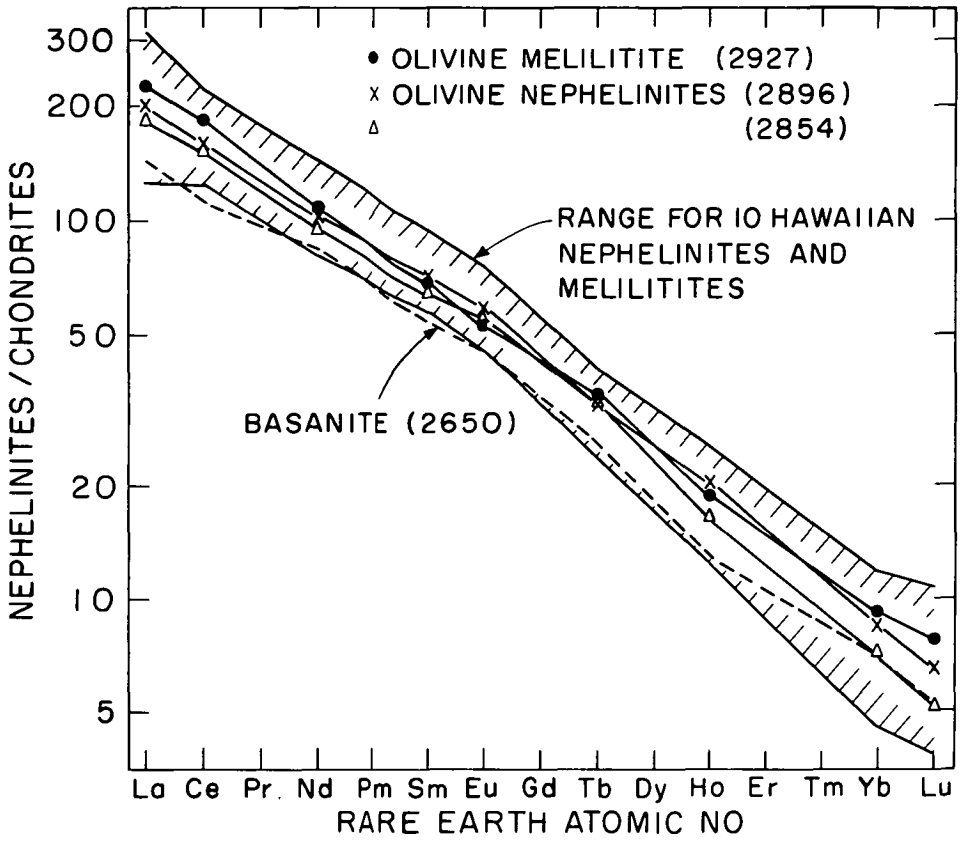

FIG. 4. REE abundances in olivine melilitite, 2927 (●), and olivine nephelinites 2896 (×) and 2854 (△) compared to a chondritic average (Frey *et al.*, 1968). Shown for comparison are REE data for the Victorian basanite, 2650 and the range for 10 Hawaiian alkalic basalts with more than 19 per cent normative nepheline (Schilling & Winchester, 1969; Kay & Gast, 1973; Frey & Jackson, unpublished).

the high light REE content in 2896 (relative to the basanites) requires a degree of melting less than 1 per cent. For example, 0·6 per cent melting is sufficient for identical light REE abundances in the source rocks for 2650 and 2896 (Fig. 6). At 30 kb and 1200 °C, we calculate the theoretical subsolidus modal proportions of pyrolite as 54·1 per cent olivine, 23·8 per cent orthopyroxene, 11·1 per cent clinopyroxene, 8·6 per cent garnet, 1·4 per cent phlogopite, 0·9 per cent ilmenite and 0·15 per cent apatite (note that apatite is assumed to be completely melted at 0·6 per cent melting). If it has these amounts of initial garnet and clinopyroxene, the model source rock (with nearly chondritic relative REE abundances) for 2896 is enriched by 20 to 40 per cent in HREE relative to the source rock for basanite 2650 (Fig. 6). In order to reduce this HREE discrepancy, the amount of residual garnet must be decreased from ~8·5 per cent to ~6·5 per cent.

Olivine Melilitite (2927) and Olivine-Nephelinite (2854)

The olivine melilitite (2927) from Tasmania is highly enriched in LREE and its REE abundances are well within the narrow (factor of 2 to 3) range established by

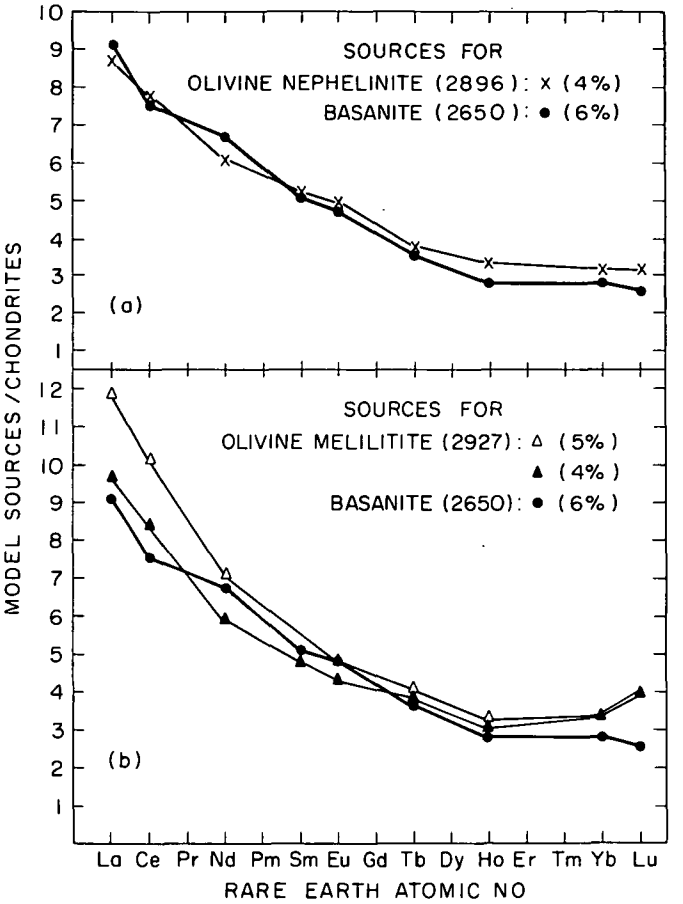

FIG. 5. Upper (a): REE abundances in the calculated mantle source for olivine nephelinite 2896 (×). In the model calculation, equation 11 of Shaw (1970) was utilized with 4 per cent melting, residual mode equal to 58 per cent olivine, 22·5 per cent orthopyroxene, 12 per cent clinopyroxene and 7·5 per cent garnet and REE partition coefficient set number 3 (see Appendix). Shown for comparison is model 3 for basanite 2650 from Fig. 2. Lower (b): REE abundances in the calculated mantle sources for olivine melilitite 2927 (△, ▲). In the model calculations, equation 11 of Shaw (1970) was utilized with degree of melting equal to 4 or 5 per cent, residual mode equal to 56·5 per cent olivine, 26 per cent orthopyroxene, 9·5 per cent clinopyroxene and 8 per cent garnet. Shown for comparison is model 3 for basanite 2650 from Fig. 2.

10 highly silica undersaturated (>19 per cent normative nepheline) Honolulu series basalts from Oahu (Fig. 4). Since the K_2O/P_2O_5 ratio in 2927 differs significantly from the pyrolite ratio (1·06 and 2·17, respectively) we developed two petrogenetic models based on major element composition. The model based on K_2O (implying that 2927 resulted from 9 per cent melting) requires a source with REE abundances (La = 21× chondrites, Lu = 3·8× chondrites) very different from the source for Victorian basanites but the model based on P_2O_5 (2927 as a 5 per cent melt with 8 per cent residual garnet, Table 4) requires a source rock with REE abundances that deviate <35 per cent (except for Lu, 58 per cent) from the 2650 source (Fig. 5). Decreasing the degree of melting for 2927 to 4 per cent decreases the difference in REE abundances of the 2650 and 2927 sources to <15 per cent except for Yb (19 per cent) and Lu (56 per cent). Compared to basanite 2650, a

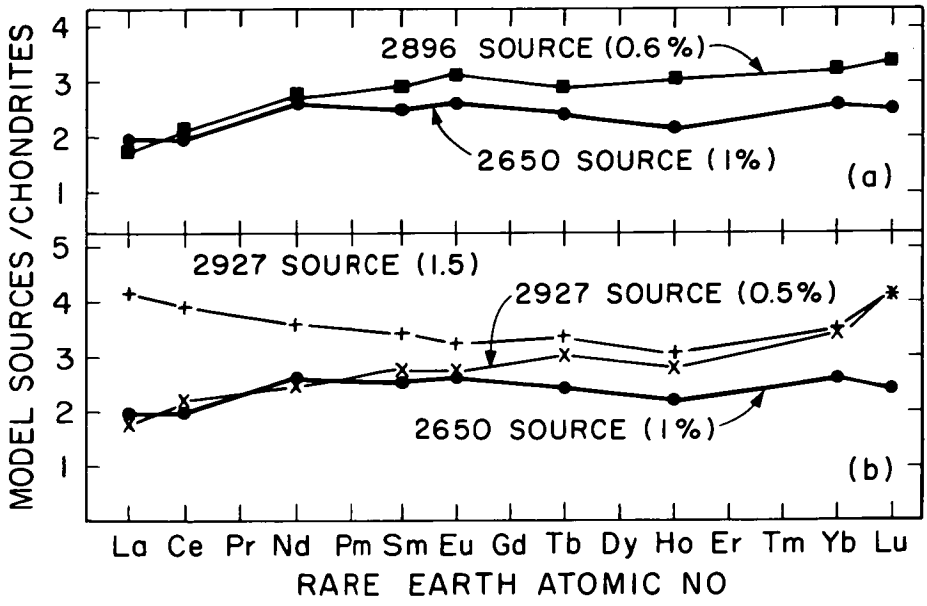

FIG. 6. Upper (a); REE abundances in the calculated mantle source for olivine nephelinite 2896 (■). In the model calculation, equation 15 of Shaw (1970) was utilized with per cent melting equal to 0·6 per cent, an initial mode of 54·1 per cent olivine, 23·8 per cent orthopyroxene, 11·1 per cent clinopyroxene, 8·6 per cent garnet and 2·4 per cent phlogopite + ilmenite + apatite, and REE partition coefficient set number 3 (see Appendix). Shown for comparison is model 3 for basanite 2650 from Fig. 3. Lower (b): REE abundances in the calculated mantle sources for olivine melilitite 2927 (×, +). In the model calculations, equation 15 of Shaw (1970) was utilized with per cent melting equal to 0·5 or 1·5 per cent, an initial mode as for 2896 (Fig. 6*a*) and REE partition coefficient set number 3 (see Appendix). Shown for comparison is model 3 for basanite 2650 from Fig. 3. Note that the 1·5 per cent melting model for 2927 requires a factor of 2 absolute LREE enrichment compared to the calculated source for 0·5 per cent melting and the basanite 2650 source.

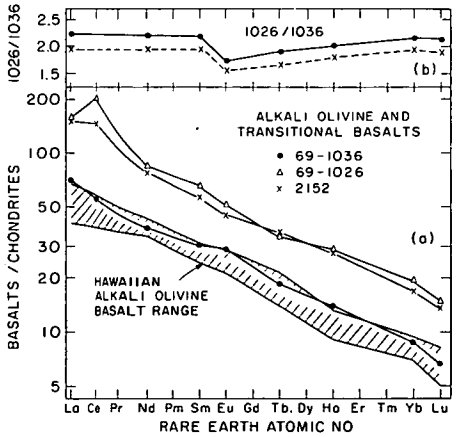

FIG. 7. Lower: REE in 3 alkali olivine and transitional basalts from the Younger Basalts of Victoria compared to a chondritic average (Frey *et al.*, 1968). Shown for comparison is the REE range for 5 Hawaiian alkali olivine basalts (1·9 to 4·5 per cent normative nepheline) (Schilling & Winchester, 1969; Kay & Gast, 1973; Frey & Jackson, unpublished). Upper: REE abundances in alkaline-olivine basalt 69-1026 compared to alkali olivine basalt 69-1036. Dashed line includes effect of 12 per cent olivine addition to original composition of 69-1026 (5′ in Table 3). Note the linear ordinate scale.

lower degree of melting for melilitite 2927 is consistent not only with P_2O_5 and LREE abundances, but also with the relative Sr, Y, Nb, Th and U concentrations; however, the lower Zr and Hf contents of 2927 are inconsistent with this model.

The olivine nephelinite from Scottsdale, Tasmania (2854) has REE abundances 10–20 per cent lower (Table 5 and Fig. 4) than the olivine melilitite (2927) implying a degree of melting range of 4·4 to 6 per cent compared to 4 to 5 per cent for 2927. A slightly higher degree of melting for olivine nephelinite (2854) is consistent with relative Na_2O, P_2O_5, Sr, REE, Y, Th and U contents, but relative K_2O, Zr and Hf abundances are inconsistent with this implication. The degree of REE fractionation is similar in 2927 and 2854 (La/Yb = 42 and 44, respectively). Thus, the REE data are consistent with major element implications that 2854 and 2927 resulted from similar degrees of melting, and that each basalt equilibrated with similar proportions of residual olivine, pyroxenes and garnet. The enrichment of incompatible elements and depletion of compatible elements Ni, Cr, V, Co, Sc in the nephelinite 2860 are generally consistent with derivation of this liquid from 2854 parental basalt by processes of crystal fractionation.

As with the olivine nephelinite (2896), near-chondritic relative REE abundances in the source rock for olivine melilitite (2927) require very low degrees of melting. For example, in order to have identical light REE abundances in the source rocks for basanite (2650) and olivine melilitite (2927) the degree of melting for 2927 must be about 0·5 per cent (Fig. 6). Note that the model source rocks for 2896 (0·6 per cent melting) and 2927 (0·5 per cent melting) are very similar, each having a small but significant depletion in LREE relative to the chondritic distribution (Fig. 6). As discussed for the 2896 model, in order to have identical HREE contents in the source rocks for 2650, 2896 and 2927 the residual amount of garnet for 2896 and 2927 must be decreased from about 8·5 per cent to 6·5 per cent (for 2896 and 2927 models, the initial mode of the source rock was determined from the mineralogy of pyrolite at 30 kb and 1200 °C).

An alternative set of models can be calculated if the source rocks are required to have a near chondritic relative REE distribution but the absolute abundance of the REE group is allowed to vary. An example model (Fig. 6) is derivation of melilitite 2927 by 1·5 per cent melting of a source with pyrolite mineralogy at 30 kb and 1200 °C but REE abundances varying from 3 to 4 times chondrites compared to the 2650 source rock (30 kb, 1250 °C) with REE contents varying from 1·9 to 2·7 times chondrites.

Having established the geochemical features of upper mantle models for highly nepheline–normative basalts, we now evaluate the geochemical features of less-silica undersaturated basalts. We are particularly interested in determining if similar source compositions can yield highly nepheline–normative basalts, alkali olivine basalts and tholeiitic basalts.

Alkali-Olivine Basalts (69-1036, 69-1026)

The alkali olivine basalt from Mt. Frazer (69-1036) has REE abundances falling within (or very close to) the abundance range of five Hawaiian alkali olivine basalts

(Fig. 7*a*). By using the degree of melting as 11 per cent (based on K_2O and P_2O_5 contents relative to pyrolite) and REE mineral/liquid partition coefficients (*e.g.*, set 3 was used for reasons outlined in the Appendix), the REE content of the peridotite source for alkali olivine basalt (69-1036) was evaluated for each of the model residual mineralogies proposed earlier (Table 4). If the residue contains 5 per cent

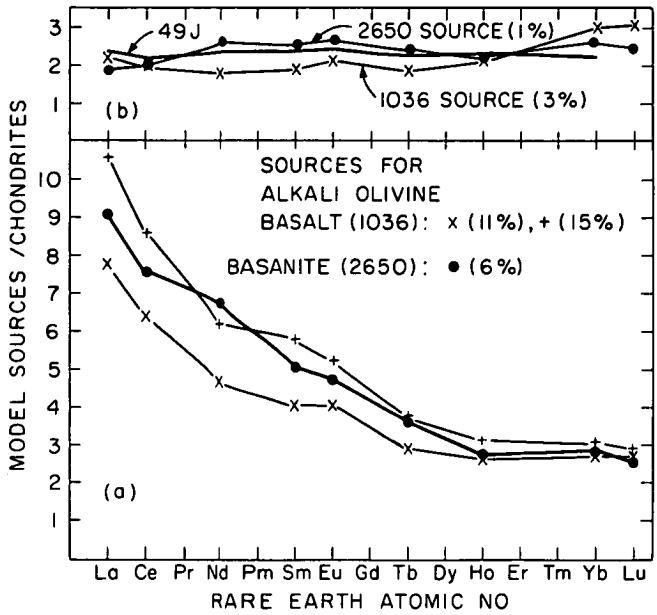

FIG. 8. Lower (a): REE abundances in the calculated mantle source for alkali olivine basalt 69-1036 (×, +). In the model calculations, equation 11 of Shaw (1970) was utilized with degree of melting equal to 11 or 15 per cent, residual model equal to 63 per cent olivine, 22·5 per cent orthopyroxene, 9·5 per cent clinopyroxene and 5 per cent garnet, and REE partition coefficient set number 3 (see Appendix). Shown for comparison model 3 for basanite 2650 from Fig. 2. Upper (b): REE abundances in the calculated mantle source for alkali olivine basalt 69-1036 (×). In the model calculation, equation 15 of Shaw (1970) was utilized with per cent melting equal to 3 per cent, an initial mode of 55·8 per cent olivine, 21·5 per cent orthopyroxene, 13·1 per cent clinopyroxene, 8 per cent garnet and 1·6 per cent phlogopite + ilmenite + apatite, and REE partition coefficient set number 3 (see Appendix). Shown for comparison is model 3 for basanite 2650 from Fig. 3 and the REE data for a spinifex textured peridotitic komatiite from South Africa (49J of Sun & Hanson, 1978).

garnet (model B, Table 4), the predicted parental REE abundances in the source garnet–peridotite are quite similar to the model parental REE abundances for basanite 2650 (Fig. 8*a*). The REE contents of the model source rocks differ by <15 per cent with the largest discrepancies occurring for LREE.

We consider the <15 per cent differences in LREE to be excellent agreement for two reasons: (1) it is probably unrealistic to expect the absolute abundances of trace elements in the upper mantle to vary by <15 per cent. For example, by accurate multiple analyses (11) of a single basalt flow Haskin *et al.* (1971) found that La abundance varied by ±20 per cent while other REE varied by about ±10 per cent; (2) increasing the degree of melting for 69-1036 to 15 per cent requires a mantle source with LREE slightly higher than the 2650 model parent; thus, the

REE range of the 69-1036 source resulting from variation of melting degree from 11 to 15 per cent encompasses the REE abundances of the 2650 model (Fig. 8*a*).

Compared to the garnet-bearing sources, a garnet-free source (model C, Table 4) for the Mt. Frazer basalt must have significantly lower HREE contents and a more strongly fractionated REE distribution (for 11 per cent melting La = 7·7 × chondrites, Lu = 0·95× chondrites). These REE abundances are not consistent with the REE abundances in the model sources for more undersaturated basalts such as the basanites and nephelinites (Figs. 2 and 5).

Although we utilized only K_2O and P_2O_5 abundances to infer that 69-1036 resulted from 11 per cent melting, this degree of melting relative to 6 per cent for basanite 2650 is consistent with several other incompatible element abundances. For example, an element with a solid/liquid P.C. = 0 should be enriched in 2650 relative to 69-1036 by a factor of 1·83. The observed 2650/69-1036 abundance ratios are K = 1·09, Rb = 1·88, Sr = 1·75, Zr = 2·15, La = 2·29, Th = 2·59, U = 1·82 and P = 1·96. Although certainly not exact, the range of ratios are broadly consistent with the predicted factor of 1·83 (note values less than 1·83 imply s/l P.C. significantly > 0 which is realistic for elements such as Sr).

As with basanite 2650 we also desire to evaluate for alkali–olivine basalt 69-1036 the implications of a model requiring nearly chondritic relative REE abundances in the mantle source. If an initial garnet peridotite mantle mode is estimated for pyrolite at 25 kb and 1200 °C and 69-1036 is considered to represent a 3 per cent melt, then REE abundances in the source rock for basalt 69-1036 range from 1·8 to 3·1 times chondrites. Within this range, the abundance of each REE is within ±30 per cent of the REE abundance in the source rock required if basanite 2650 is a 1 per cent melt (Fig. 8*b*). Note that both model source peridotites have REE distributions sub-parallel to a South African spinifex-texture peridotitic komatiite (49J in Fig. 8*b*). This agreement is comparable to that based on the pyrolite model (cf., Figs. 8*a*, *b*). However, a factor of 3 enrichment in 69-1036 relative to 2650 is expected for incompatible elements and as shown earlier, a comparison of incompatible element abundances in basanite 2650 and basalt 69-1036 indicates this enrichment factor is only ~2.

Olivine basalt, 69-1026, from Mt. Widderin has relative REE abundances very similar to the Mt. Frazer (69-1036) alkali–olivine basalt (Fig. 7*a*, *b*); however, even with the addition of 12 per cent olivine to basalt 69-1026 its REE content is nearly twice that of the Mt. Frazer basalt (Table 5, Fig. 7*b*). Other incompatible elements are equally, or less, abundant in 69-1026 relative to 69-1036; for example, abundance ratios are P = 0·7, K = 0·9, Rb = 0·9, Sr = 0·9, Zr = 1·0, Hf = 1·0, and Th = 0·9. The relative abundance of Y (69-1026/69-1036 = 2·3), an element with geochemical features similar to HREE, confirms the high REE content of the 69-1026 basalt. Although on the basis of major elements we concluded that basalt 69-1026 could be derived by a slightly higher degree of melting from the same source rock as basalt 69-1036 (except, possibly for a small, <25 per cent difference in P), it is evident that the source peridotite for basalt 69-1026 must have been enriched by nearly a factor of 2 in REE and Y relative to the peridotite source for

basalt 69-1026. Despite this difference in absolute REE content, the relative REE abundances in these sources must have been quite similar.

Olivine Basalt (2152)

A REE-enriched source is also required for the Marida Yallock olivine basalt (2152). On the basis of major elements, we deduced that this basalt resulted from a higher degree (13–17 per cent) of melting than the Mt. Frazer alkali olivine basalt (69-1036). Consistent with this deduction, the incompatible elements (P, K, Rb, Sr, Zr, Hf, Th and U) have an abundance in 2152 relative to 69-1036 ranging from 0·7 to 1·0. However, REE and Y abundances in 2152 are about a factor of two higher than in the 69-1036 basalt (Fig. 7*a*). Therefore, a REE- and Y-enriched peridotite source similar to that for 69-1026 is required for the Marida Yallock basalt.

Tholeiites (69-1018, T-14)

The least fractionated tholeiites (69-1018, T-14) studied have similar REE abundances (Fig. 9) differing by only about 10 per cent in LREE. Since both tholeiites are presumed to originate by high degrees of melting (≥20 per cent) and low-pressure fractionation (olivine and pyroxene loss) is not an effective way to change abundance ratios of incompatible elements (Fig. 1 of Gast, 1968), the REE abundances in their respective source rocks probably differed by <10 per cent. Except for the common (but unique to Hawaiian tholeiites) relative La decrease in Hawaiian tholeiites, the REE abundances in these Australian thoeliites lie within the abundance range established by Hawaiian tholeiites (Fig. 9).

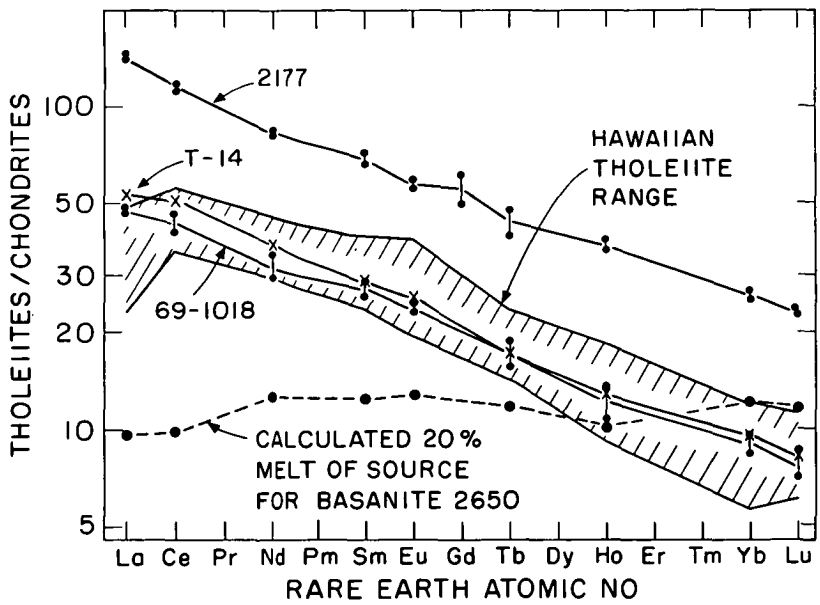

FIG. 9. REE in 3 Victorian tholeiites compared to a chondritic average (Frey *et al.*, 1968). For 69-1018 and 2177, the double points connected by a vertical line indicate data for duplicate analyses. Shown for comparison is the REE range for 7 tholeiites from Kilauea, Hawaii (Haskin *et al.*, 1966; Schilling & Winchester, 1969: Masuda *et al.*, 1974; Frey, unpublished). Also indicated (dashed line) are the REE data for a model liquid derived by 20 per cent equilibrium melting of the source which can generate the REE abundances of basanite 2650 by 1 per cent melting; that is, model 3 in Fig. 3.

Using the same set of REE partition coefficients as for the nepheline–normative basalt calculations, degree of melting equal to 20 per cent (determined from K_2O and P_2O_5 contents) and the calculated residual mineral mode (Table 4), the REE abundances in the tholeiitic source rock have been determined. From La through Ho the REE abundances in the source rock are within 18 per cent of those determined for basanite 2650 based on 6 per cent melting of pyrolite and alkali–olivine basalt 69-1036 based on 11 per cent melting of pyrolite (Fig. 10*a*). The 20

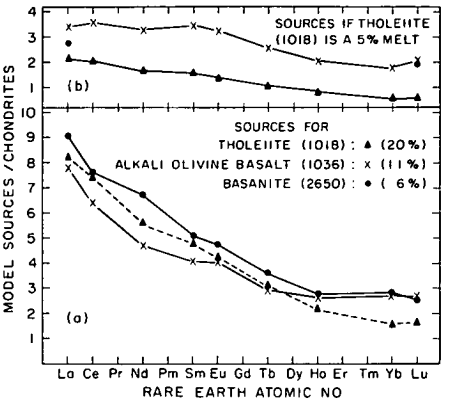

FIG. 10. Lower (a): REE abundances of the calculated mantle source for tholeiite 69-1018 (△). In the model calculation, equation 11 of Shaw (1970) was utilized with 20 per cent melting, a residual mode of 69·9 per cent olivine, 21·6 per cent orthopyroxene, 7·2 per cent clinopyroxene and 1·2 per cent spinel, and REE partition coefficient set number 3 (see Appendix). Shown for comparison are model 3 for basanite 2650 (Fig. 2) and alkali–olivine basalt 69-1036 (Fig. 8). Upper (b): REE abundances in the calculated mantle source for tholeiite 69-1018 (△). In the model calculation, equation 15 of Shaw (1970) was used with per cent melting equal to 5 per cent, an initial mode of 54·1 per cent olivine, 27 per cent orthopyroxene, 16 per cent clinopyroxene and 2·9 per cent phlogopite + spinel + ilmenite + apatite, and REE partition coefficient set number 3 (see Appendix). Note that even if tholeiites are produced by such low degrees of melting, the source is relatively LREE enriched. The upper curve (×) shows this result even with the most favorable set of REE partition coefficients (*i.e.*, those of Schilling, 1971, 1975b; set number 7 of this paper, see Appendix. These are favorable because the relatively high solid/liquid values maximize the extent of REE fractionation during melting). A relatively LREE enriched source is required for 5 per cent equilibrium melting. A somewhat less fractionated source (● symbols) is required by a fractional melting model (equation 14 of Shaw, 1970) utilizing Schilling's REE partition coefficients.

to 45 per cent differences in HREE content are significant. These discrepancies could be resolved by changes in the model for tholeiite petrogenesis, for example, by increasing the role of clinopyroxene in the residue, assuming that significant fractionation of clinopyroxene occurred after the melting event or by small amounts of garnet as a residual mineral. Since the major element compositions of tholeiites (69-1018 and T14) are not consistent with an increased role for clinopyroxene and garnet in the source region, the source rock for these tholeiites may have been depleted in HREE (20–45 per cent) relative to the sources for nepheline–normative basalts. Despite the HREE abundance differences in the sources we believe the less than factor of 2 variation in REE abundances of mantle sources for basalts ranging from olivine tholeiite to olivine melilitite (17·4 per cent normative Ne) demonstrates a remarkable and meaningful internal consistency of the pyrolite model.

Relative to the basanites, tholeiite 69-1018 (also T14) is depleted in other incompatible elements such as Rb, Sr, Zr, Hf, Th and U by factors ranging from 0·3 to 0·5. Since there is a factor of 3·33 difference in degree of melting for the tholeiite (20 per cent) and basanites (6 per cent), a depletion in the tholeiite of 0·3 is expected for elements that are totally excluded from the residual minerals. Therefore, the observed depletions are consistent with bulk solid–liquid partition coefficients ranging from zero to ~0·07 for Rb, Sr, Zr, Hf, Th and U.

The capability and internal consistency of the pyrolite model in deriving nepheline–normative basalts and tholeiitic basalts from a source with uniform major element composition and nearly uniform (within a factor of two) incompatible trace element contents (*e.g.*, REE) does not exist if the mantle source of nepheline–normative basalts is assumed to have near-chondritic relative REE abundances. For example, 20 per cent melting of the peridotite source that yields basanite 2650 as a 1 per cent melt creates a liquid with relative REE abundances very similar to the source, in this case nearly chondritic (Fig. 9). For an olivine–pyroxene residual mineralogy (*i.e.*, no residual garnet) as required by the high pressure liquidus phase relationships, even much lower degrees of melting, such as 5 per cent, cannot account for the LREE enrichment in these tholeiites unless the source is relatively enriched in LREE (La/Yb = 3·3 to 5·7 relative to chondritic value of 1·6, see Fig. 10*b*). Thus, if nepheline–normative basalts originate from a mantle with near-chondritic relative REE abundances, as proposed by Kay & Gast (1973), and if the partial melting models (Green & Ringwood, 1967; Green, 1971; this paper) are correct for tholeiitic basalts, then a different mantle source is required for tholeiitic basalts and nepheline–normative basalts.

Tholeiite (2177)

Because the major element composition of tholeiite 2177 is considerably evolved from a primary composition, we have not developed a detailed petrogenetic model for this basalt. Nevertheless, minor and trace element abundances in this basalt reflect some key geochemical features of the source rock. For example, the abundance ratios 2177/69-1018 are $TiO_2 = 0{\cdot}87$, $P_2O_5 = 0{\cdot}89$, $K_2O = 1{\cdot}05$, Rb = 1·3, Sr = 1·1, Zr = 1·1, Th = 1·3, U = 0·7, Cr = 1·0, Co = 0·8 and Ni = 0·7 but REE and Y are enriched in 2177 by factors of 2·4 to 3·8 (Table 5 and Fig. 9). Because of the similar abundances in other trace elements, this enrichment in REE and Y cannot be accounted for by extensive fractional crystallization. Apparently, tholeiite 2177 has been derived from a relatively REE and Y-rich source material similar to the source rocks for the olivine basalts 69-1026 and 2152 (cf., Fig. 7*a*).

COMPOSITIONAL HETEROGENEITIES IN THOLEIITE SOURCE ROCKS

Tholeiitic basalts with similar major element compositions but widely different incompatible element abundances, *e.g.*, P, LREE and Ba, occur in many localities, especially on or near oceanic islands (*e.g.*, O'Nions & Pankhurst, 1974; Schilling, 1975*a*; O'Nions *et al.*, 1976). Relatively high incompatible element abundances are usually accompanied by more radiogenic isotopic ratios; therefore, these abundance variations can be interpreted in terms of mantle heterogeneity (*e.g.*,

Schilling, 1973; Hart *et al.*, 1973). Attempts to explain a wide abundance range of LREE in tholeiitic and alkali–olivine basalts by varying degrees of melting of a homogeneous source are often unrealistic in terms of major elements. For example, O'Nions & Gronvold, *ibid.*) stated that Icelandic tholeiitic and alkalic basalts can be generated by variable degrees (5–30%) of melting of a homogeneous source. However, the factor of 6·5 difference in Ce abundance for Icelandic tholeiites from Kerlingarfjoll is significantly greater than the maximum variation (<factor of 3) predicted by their model for 5–30 per cent melts (cf., Figs. 2 and 7 of O'Nions & Gronvold, *ibid.*). Since it is unlikely that magmas with a tholeiitic major element composition can form from a homogeneous source over a partial melting range of <6 to >30 per cent, we believe that a homogeneous (on a trace element basis) source for these tholeiites is not a viable model. Similar criticisms are valid for the more than factor of 5 variation in degree of melting invoked by Treuil & Joron (1975, p. 166) to explain LREE abundance variations in basalts along the Reykjanes Ridge—Iceland transect reported by Schilling (1973).

As an alternative to a heterogeneous mantle source composition, non-equilibrium melting models have been proposed (O'Nions & Pankhurst, 1974; Flower *et al.*, 1975) to explain LREE abundance and Sr isotopic variations in basalts, but these models fail to explain other important features of the compositional data (Sun *et al.*, 1975: O'Nions *et al.*, 1976; Hoffman & Hart, 1975). O'Nions *et al.* (1976) have interpreted their most recent trace element data for Icelandic tholeiites in terms of compositionally heterogeneous mantle sources.

EVALUATION OF PETROGENETIC MODELS

Pyrolite-based models

There are two attractive features of an upper mantle source with a fractionated (LREE enriched) REE distribution relative to chondrites.

(1) Perhaps the most important problem resolved by this model is the difficulty associated with deriving tholeiitic and nepheline–normative basalts from a common source with chondritic relative REE abundances. In fact, if as commonly accepted, tholeiitic basalts result from larger degrees of peridotite melting (>20 per cent) than nepheline–normative basalts (<20 per cent), then the different REE abundances in olivine tholeiites (continental and island occurrences) and nepheline–normative basalts cannot be accounted for by melting a source with a chondritic relative REE distribution. However, if the mantle source for nepheline–normative basalts is relatively enriched in LREE as implied by the pyrolite-based model (Fig. 3), then it is possible that the different basaltic types form from a mantle with similar relative REE abundances.

(2) The LREE enrichment of the mantle source required by the pyrolite model is consistent with geochemical features of Cr-diopside lherzolite and related ultramafic inclusions in basalts. These inclusions are accidental upper mantle xenoliths and their mineralogy and composition reflect the nature of the upper mantle overlying the source region of the host basalts. The geochemical history of many inclusions is complex (Frey & Green, 1974; Frey & Prinz, 1978), but a

common geochemical feature is that these inclusions are relatively enriched in LREE (*e.g.*, LREE 3–12× chondrites and HREE 0·1–1·5× chondrites, Varne & Graham, 1971; Philpotts *et al.*, 1972; Frey & Green, 1974; Frey & Prinz, 1978). None of the inclusions have REE abundances which overlap the range calculated for the parental mantle source (Fig. 2), but many inclusions such as PA-10 from San Carlos, Arizona have $(La/Yb)_{chondrites} \ll (La/Yb)_{PA\text{-}10} < (La/Yb)_{model\ mantle\ source}$ and absolute REE abundances decreased by about a factor of five compared to the model source rocks (Fig. 2). These differences and their general depletion in basaltic constituents such as CaO, Al_2O_3, etc. are consistent with inclusions, such

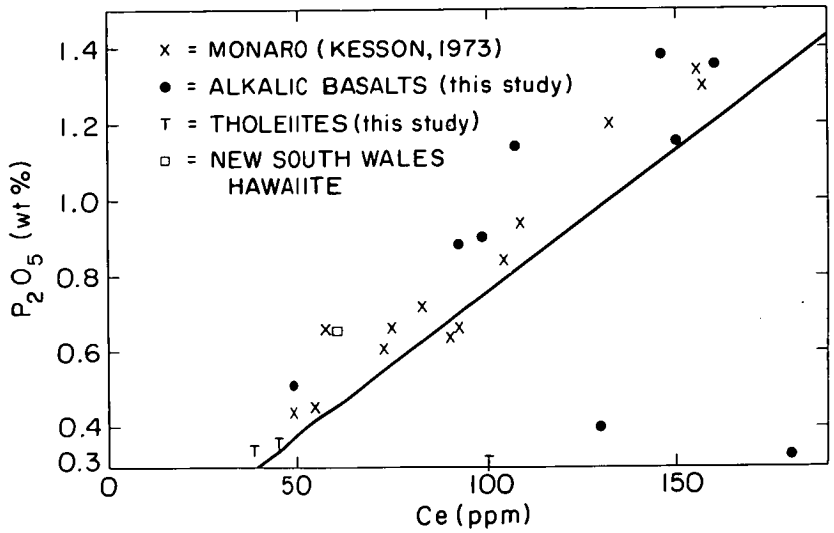

FIG. 11. Correlation of P_2O_5 and Ce abundances in Australian basalts. Solid line indicates a P_2O_5/Ce ratio of 75 which is typical for primary alkalic basalts (Sun & Hanson, 1975*a*, *b*).

as PA-10, having an origin as residues from large degrees of melting of a source with REE abundances similar to models 1, 3 and 5 in Fig. 2.

A drawback of a model requiring basaltic sources to have relative enrichment in LREE compared to chondrites is the increased complexity; that is, if the bulk earth has chondritic relative REE abundances, then a poorly understood upper mantle process must be invoked to create this LREE enrichment (*e.g.*, Fig. 7 of Frey & Green, 1974). However, the criticism is partially negated by the common occurrence of upper mantle xenoliths with LREE enrichment.

In addition, pyrolite-based models demonstrate the incompatible nature of phosphorus and the more complex nature of potassium geochemistry. Previously, we utilized P_2O_5 and K_2O abundances to infer the degrees of melting required to generate various primary basalts. However, among alkalic basalts P_2O_5 content is strongly correlated with LREE (and other incompatible elements) abundances (Fig. 11) but K_2O content correlates poorly with incompatible trace element abundances (Fig. 7 of Sun & Hanson, 1975*a*). As a result, melting models based on P_2O_5 contents lead to more uniform mantle source compositions than models

based on K_2O (*e.g.*, Fig. 5); thus P_2O_5 contents appear to be a more reliable index reflecting differing degrees of melting. Although the more random K_2O variation can be interpreted as resulting from a heterogeneous mantle distribution of phlogopite, it may also reflect the relatively complex geochemistry of alkali metals; in particular, their solubility in fluid phases and sensitivity to alteration phenomena.

Models based on chondritic relative REE abundances in basaltic source rocks

In addition to a variety of geochemical arguments that imply the bulk earth has chondritic abundances for non-volatile elements, such as the REE (Ringwood, 1966; Anders, 1971; Larimer, 1971) there are several attractive features of models with chondritic relative REE abundances in the upper mantle.

(1) Igneous rocks ranging from Archaean greenstones and ultramafic lavas (Sun & Nesbitt, 1976; Herrmann *et al.*, 1976) to modern oceanic floor and island tholeiites (Baffin Island: O'Nions & Clarke, 1972; Iceland: Shimokawa & Masuda, 1972; O'Nions *et al.*, 1976; oceanic ridge basalts: Kay *et al.*, 1970; Bryan *et al.*, 1976) have relative REE abundances similar to that of chondrites (certainly much closer to a chondritic REE distribution than the calculated parents for the pyrolite model in Fig. 2). Because all of these basalts are believed to result from greater than 20 per cent melting (>50 per cent for ultramafic lavas, Green, 1975), their REE distributions strongly imply a mantle source with a nearly chondritic REE distribution.

(2) Some garnet-peridotite inclusions in kimberlites and spinifex textured peridotitic komatites have REE abundances that are almost identical to chondrites (Fig. 3).

(3) Preliminary data from Sm–Nd isotopic systematics in oceanic alkalic basalts (specifically, a St. Paul fracture zone basalt and Atlantic ocean island basalts) require that such basalts are not derived from *ancient* source regions which are significantly enriched in LREE relative to chondrites (DePaolo & Wasserburg, 1976*a*, *b*; Richard *et al.*, 1976). These results do not preclude a LREE enrichment process in the mantle source shortly before the melting event generating the alkalic basalt. However, the results provide strong evidence that the mantle source for these alkalic basalts had a Sm/Nd ratio equal to or higher than chondrites for the bulk of earth history. Furthermore, Nd isotopic data (DePaolo & Wasserburg, 1976*b*) for continental rocks are consistent with a chondritic REE distribution for the bulk earth. Although these are major deductions based on limited isotopic data, we believe the results are very important because of the similarity of these basalts (*e.g.*, St. Paul fracture zone basalt, Fig. 1) to the nepheline–normative basalts we have studied, and the general similarity of alkalic basalts on a world-wide basis (Schwarzer & Rogers, 1974: Sun & Hanson, 1975*b*).

(4) The largest volume crustal exposures of upper mantle rocks, that is alpine peridotites, are typically strongly depleted in LREE relative to chondrites (Frey, 1969; 1970*b*; Frey *et al.*, 1971; Loubet *et al.*, 1975). This observation contrasts with the ubiquitous relative LREE enrichment in continental crustal rocks (sediments, granites, basalts). Mass balance calculations illustrate that the bulk earth has chondritic REE abundances if 25 per cent of the mantle contains REE as in high-

temperature peridotites (Frey, 1969) and 75 per cent of the mantle has retained chondritic REE abundances (Frey *et al.*, 1971).

(5) Sun & Hanson (1975*a*) have utilized geochemical arguments to conclude that the mantle source for nepheline–normative basalts must be relatively enriched in LREE. However, we do not believe that their primary argument is compelling; in fact, we suggest that an important assumption in their reasoning, that the solid/liquid partition coefficient for P is *much* smaller than that for Ce, is incorrect. Because the Sun and Hanson conclusion is important to an understanding of alkalic basalt petrogenesis we will discuss in detail their geochemical arguments and key asumptions.

Because Ce and P are often classed as incompatible elements, there is a tendency to expect similar geochemical behavior (*e.g.*, Fig. 11). Nevertheless, their different positions in the periodic table suggest that the geochemical behavior of P and Ce are likely to be considerably different. Contrary to the assumption of Sun & Hanson, we suggest that its likely that P solid/liquid (solids are olivine, pyroxene and garnet) partition coefficients are larger than those for Ce. Our suggestion results from several observations: (1) P abundance data in rock-forming silicate minerals indicates that small but significant amounts of P may substitute for tetrahedral silicon, especially in olivine, pyroxene and garnet (Tables 2 and 4, Koritnig, 1965), (2) determinations of P in garnets and coexisting basaltic liquids at pressures from 18–45 kb indicate a garnet/glass partition coefficient varying from 0·09 to 0·29 with a value of 0·15 at 30 kb and 1400 °C (Thompson, 1975). A value of 0·15 exceeds the Ce s/l partition coefficients (olivine, pyroxine and garnet) used in 9 of the 10 sets of REE partition coefficients used to calculate Fig. 2 (see Appendix). (3) phenocryst/matrix determinations of P partitioning in Hawaiin tholeiites indicates $D_P^{cpx/l} = 0{\cdot}009$, $D_P^{opx/l} = 0{\cdot}014$ and $D_P^{ol/l} = 0{\cdot}043$ (Anderson & Greenland, 1969). These values are comparable to or greater than the Ce partition coefficients used in our models 1 and 3, $D_{Ce}^{cpx/l} = 0{\cdot}04$, $D_{Ce}^{opx/l} = 0{\cdot}0009$, $D_{Ce}^{ol/l} = 0{\cdot}0008$ and $D_{Ce}^{garnet/l} = 0{\cdot}0033 - 0{\cdot}021$. Thus, we conclude that the interesting linear relationship between P and Ce identified by Sun & Hanson (Fig. 6*a*, 1975*b*; and Fig. 1, this paper) results from similar bulk solid/liquid partition coefficients for Ce and P and Sun (personal communication, 1976) is in agreement with this alternative explanation. As a result, these data cannot be used to establish that the mantle source rock was relatively enriched in LREE compared to the chondritic REE distribution.

(6) Kay & Gast (1973) also demonstrated that less than 3 per cent (typically $<1{\cdot}5$ per cent) melting is required to generate the highly fractionated REE abundances of alkalic basalts from a garnet peridotite with chondritic relative REE abundances. A drawback to such models is that there may be important physical problems in accumulating a 1 per cent melt so that it may rise to the surface. Sleep (1974) has outlined the physical parameters which are important in magma segregation, but his results do not preclude separation of 1 per cent melts in narrow, <1 km conduits.

(7) These models require that tholeiitic basalts are derived from a mantle source that is compositionally distinct from the source of alkalic basalts. This is not an

improbable conclusion because it is well known that the source region for mid-oceanic ridge tholeiites is geochemically distinct from the source region of more alkalic oceanic island basalts. Furthermore, in areas such as Hawaii where nepheline–normative basalt eruptions follow eruptions of voluminous tholeiitic magmas there are uniformly distinct Sr isotopic differences between magma types (Lanphere, personal communication, 1976).

If a lherzolite source model, such as pyrolite, is abandoned, it is possible to devise petrogenetic models for deriving tholeiites from a mantle source with chondritic relative REE abundances. For example, Helmke & Haskin (Fig. 4, 1973) showed that the apparent parental magma of Steens Mountain basalts could originate by 20 per cent fractional melting of a source with REE abundances equal to 10× chondrites if the residual bulk solid/liquid partition coefficients ranged from ~0·7 for Lu to ~0·07 for La (these partition coefficients are similar to those determined from Takashima clinopyroxene megacrysts, P.C. set 2 in Appendix). Alternatively, if the source had REE abundances equal to 5× chondrites, the bulk solid/liquid partition coefficients are halved (these values are similar to the $D_{REE}^{cpx/l}$ in P.C. set 3, see Appendix). The important implication of these models is that the residual solid has REE partition coefficients similar to clinopyroxene; thus, the source must be almost totally composed of clinopyroxene (very much unlike pyrolite with only 10–20 per cent clinopyroxene). Although clinopyroxene-rich rocks occur in the upper mantle (*e.g.*, Reid & Frey, 1971; Beeson & Jackson, 1970; Wilshire & Shervais, 1975; Wilkinson, 1976), there is no evidence that mantle clinopyroxenites are sufficiently abundant to account for the voluminous continental plateau tholeiites.

CONSTRAINTS ON PETROGENETIC MODELS FROM OTHER TRACE ELEMENT ABUNDANCES

Abundances of first series transition elements Sc, V, Co and Ni and the incompatible elements Rb, Sr, Ba, Y, Zr, Hf, Th and U can be utilized to test the petrogenetic models based on REE and major elements. Although initial mantle compositions and mineral/liquid partition coefficients must be estimated (Table 7 and Appendix), these values are known sufficiently well to test the plausibility of petrogenetic models.

For the lherzolite residues (5–10 per cent garnet) in Table 4, the compatible trace elements Sc, V, Co and Ni have bulk solid/liquid partition coefficients ranging from <1 (V) to >1 (Co and Ni); thus, they differ in degree of compatibility. Vanadium bulk solid/liquid partition coefficients range from 0·2 to 0·3; therefore, the low percent melting models (Table 7) yield the highest calculated V contents. In each case, the lower abundances calculated from the pyrolite model (Table 7) are closest to the observed values (±25 per cent, except ~50 per cent for 2896). However, the uncertainty in the source rock V content precludes elimination of the low per cent melting models based on chondritic relative REE abundances in the source rock. Bulk solid/liquid Sc partition coefficients are near unity, and as a result, both models predict Sc contents within ±33 per cent of the observed values (Table 7). Co and Ni bulk solid/liquid partition coefficients exceed unity (especially

TABLE 7

Comparison of model trace element abundances[a] *to observed abundances* (ppm)

	Sc	*V*	*Co*	*Ni*	*Cu*	*Zn*	*Rb*	*Sr*	*Ba*	*Y*	*Zr*	*Hf*	*Th*	*U*
Mantle Source Concentration[b]	*20*	*75*	*110*	*2000*	*100*	*50*	*1*	*27·5*	*8·75*	*5·25*	*15·5*	*0·39*	*0·15*	*0·64*
Olivine Melilitite (2927):														
Observed	24	229	66	458	—	—	29	1440	530	31	243	5·9	11	2·5
5 per cent Melt Model	16	229	48	279			15(20)	350(550)	147	30	260	5·2	2·5(3)	0·67(0·8)
1·5 per cent Melt Model	15	234	32	120–222[c]			31	590	352	33	623	12·5	6(10)	1·6(2·7)
0·5 per cent Melt Model	15	239	26	83–207[c]			45	747	585	35	1037	20·7	10(30)	2·7(8)
Olivine Nephelinite (2896):														
Observed	14	143	57	405	—	—	27	1380	300	29	354	9	8	2·1
4 per cent Melt Model	16	216	44	227	—	—	17·5(25)	380(687)	176	31·5	312	10	3·0(3·8)	0·8(1)
0·6 Melt Model	15	239	27	89–212[c]	—	—	43	728	549	34·8	972	31	9·4(25)	2·5(6·7)
Basanite (2650):														
Observed + 10 per cent olivine	18	157	50–83[e]	263–641[e]	47	154	41	863	535	23	297	—	6·1	2·0
6 per cent Melt Model	16	198	53	323	1667	833	13	291	126(146)	27	223	7·2	2·2(4)	0·58(0·67)
1 per cent Melt Model	15	202	28	94–205[c]	—	—	35	560	440	32	779	25	7·5(15)	2·0(2·1)
Alkali Olivine Basalt (69–1036):														
Observed	23	170	56	364	—	—	24	543	350	27	152	3·9	2·9	1·1
11 per cent Melt Model	19·6	208	63	454	—	—	8(9)	201(250)	74	27	130	4·2	1·26(1·36)	0·34(·36)
3 per cent Melt Model	15	213	41	195–268[c]	—	—	21	429	220	31	390	12·6	3·8(5)	1(1·33)
Olivine Tholeiite (69-1018):														
Observed + 15 per cent olivine	23	160	66–70[e]	190(302)[e]	61[f]	118[f]	15·2	341	156	23	116	3·1	1·8	0·6
20 per cent Melt Model	28	193	80	670	500	250	4·7(5)	124(138)	41(44)	24	75	2·4	0·7(0·8)	0·19(0·2)

[a] Calculated on the basis of equilibrium melting with partition coefficients listed in Table A-2.

[b] Sources for mantle values: Sc, V, Co and Ni from the reasonably uniform content in lherzolites (Goles, 1967; Fisher *et al.*, 1969; Shaw, 1972; Frey & Green, 1974; Wedephol, 1975; Frey & Prinz, 1976; Sun & Nesbitt, 1976). Rb from Goles (1967), Griffin & Murthy (1969), Shaw (1972), Philpotts *et al.*, (1972) and Wedepohl (1975). Sr, Y, Ba, Zr and Hf values are 2·5 times chondritic abundances. Th and U from Wedepohl (1975). Goles (1967), Shaw (1972) and Haines & Zartman (1973). Cu and Zn are ordinary chondrite abundances.

[c] High values for Hakli & Wright (1967) data; low values for Leeman (1973) data.

[d] Values within parentheses are calculated for D = 0.

[e] Higher values are corrections for olivine fractionation.

[f] Values are for tholeiite T-14.

Ni). Therefore, low per cent melting models yield the lowest calculated Co and Ni abundances. The higher estimates from the higher per cent melting models (pyrolite-based) are in better accord with the observed values. In particular, Co contents are more accurately predicted by the pyrolite-based model. Because the Co content of the source rock peridotite may be known within ±15 per cent, this better agreement is a significant result favoring the pyrolite based model. Although the initial source Ni content is probably known within ±25 per cent, neither model accurately predicts the observed Ni abundances (the pyrolite model estimates are closest to the observed abundances). It is the strong temperature dependence of Ni olivine/liquid partitioning (Leeman, 1973) which causes low (<200 ppm) estimates for the low per cent melting models. Because the temperature and compositional dependence of Ni olivine/liquid partitioning are not yet firmly established, the Ni abundance data cannot be quantitatively used to evaluate the proposed petrogenic models.

For the incompatible trace elements (except the relatively volatile element Rb) initial source concentrations were assumed as equal to 2·5 times the chondritic abundance level (Table 7), since this is the typical enrichment of HREE required in the source rocks for all models (*e.g.*, Figs. 2, 3, 5, 6, 8 and 10). With this assumption and estimated partition coefficients (see Appendix), the pyrolite-based models (relatively higher per cent melting models in Table 7) account for Y, Zr and Hf abundances within ±45 per cent (generally within ±15 per cent). Models based on a source rock with relative REE abundances as in chondrites can also account for Y abundances, but Zr and Hf abundances in the basalts can only be explained if bulk solid/liquid partition coefficients of 0·05 are used instead of 0·01. This change in partition coefficients is well within the uncertainty in such values, especially when the compatible nature of Ti (note, Ti, Zr and Hf form group 4b in the periodic table) in alkalic basalts is considered (*e.g.*, Sun & Hanson, 1975*b*, estimate a Ti solid/liquid partition coefficient of 0·2). Also, Helmke & Haskin (1973) found that a genetic relationship among Steens Mountain basalts (Oregon, U.S.A.) requires bulk solid/liquid Hf partition coefficients ranging from 0·18 to 0·66.

If the mantle source rock for basalts contains 1 ppm Rb (Table 7) and 2·5 times chondritic abundances for Sr, Ba, U and Th, then the pyrolite-based model cannot account for the abundances of these elements in the basalts (even if bulk solid/liquid partition coefficients of zero are used). Sources based on a chondritic relative REE distribution (*i.e.*, low per cent melt models, Table 7) are more consistent with the basaltic data. However, these results do not negate pyrolite-based models, because the abundances of these elements in basalts are strongly correlated with LREE (*e.g.*, Fig. 11 of Sun & Hanson, 1975*b*); thus, the relative enrichment of LREE required in the pyrolite-based sources may also be accompanied by similar enrichments in Rb, Sr, Ba, Th and U. Generally, a factor of 3 increase in initial concentration (above the C_0 chosen in Table 7) is required for good agreement between observed and calculated values based on the pyrolite model. A factor of 3 increase (7·5× chondrites) is equivalent to that required for LREE (Figs. 2, 5, 8 and 10*a*) and similar to initial source abundance proposed by Sun & Hanson (Table 4, 1975*b*).

It is generally observed that the Cu content of tholeiites exceeds that in nepheline normative basalts (Prinz, 1967) and that the Cu content of alkali basalts ranges only from 40–50 ppm (Kesson, 1973; Sun & Hanson, 1975*b*; Irving, unpublished data for Victorian basalts described in Irving & Green, 1976). These data indicate that Cu is not an incompatible element during alkaline basalt petrogenesis, and an interesting implication is that a sulfide melt has equilibrated (as a residual or fractionated phase) with alkalic basalts. Furthermore, Cu concentrations in all basalts are much lower than expected if the source rocks had chondritic Cu abundances (*e.g.*, if the bulk solid/liquid Cu partition coefficient is 0·1, 6 per cent melting of a chondritic source for basanite 2650 yields a calculated Cu content of 650 ppm instead of the observed 50 ppm, see also Table 7). In addition to the inference of equilibration with a sulfide phase, it is possible that basaltic sources are depleted in Cu relative to chondrites as a result of core (Fe–Ni–S) formation. Although to a lesser extent, similar conclusions are required for Zn (Table 7).

Although abundances of these trace elements do not distinguish between our end-member models, the abundance ratio of these elements provide confirmatory evidence for some of our earlier conclusions. For example, P_2O_5/Ce ratios average about 90 (in agreement with a Sun & Hanson (1975*b*) value of 75 $\pm$ 15, 1975), significantly lower than the chondrite ratio of >2000, but the three samples (2177, 2152, 69-1026) with unusually high REE contents have anomalously low P_2O_5/Ce values of $\leqslant$31 (Table 8). These basalts also have unusually low Zr/Ce, Sr/Ce and K_2O/Ce (Table 8).

As discussed earlier and reflected by K_2O/Ce and Rb/Ce variations, potassium and rubidium do not behave as systematically as other incompatible elements. Kay & Gast (1973) also found that Rb abundances are not correlated with Sr, Ba and REE contents and detailed studies of a single flow often demonstrate that K and Rb contents are quite variable (*e.g.*, Hart *et al.*, 1971). Some additional process, such as alkali loss in aqueous fluids, may affect K_2O and Rb abundances.

In all samples the Zr/Ce ratio is significantly lower than the chondritic value (by more than a factor of two with a tendency to decrease with increasing degree of SiO_2 undersaturation, Table 8). Two possible interpretations are: (1) Zr is preferentially retained relative to Ce in the source rock, and it is, like Ti, not totally incompatible; this conclusion is consistent with models based on a chondritic relative distribution of REE, or (2) Ce has been enriched relative to Zr in the source region: this conclusion is consistent with the pyrolite-based models. In contrast, except for the 3 REE-rich basalts (2177, 2152, 69-1026), Sr/Ce values are within 30 per cent of the chondritic value. Apparently, Sr is slightly less incompatible than Ce, and this is in agreement with relative partition coefficients in likely upper mantle minerals.

The low TiO_2/Zr values relative to chondrites implies that Ti is more compatible than Zr (in agreement with mineral/liquid P.C. data), and the decreasing ratio with increasing alkalinity suggests that Ti is most compatible at low degrees of melting (in agreement with inferences based on experimental results). TiO_2/Sc ratios exceed the chondritic ratio by more than a factor of 5, almost certainly reflecting the compatible nature of Sc; that is, a strong preference for incorporation into

TABLE 8

Key element ratios in Australian basalts

	Chondrites[a]	*Tholeiites*			*Olivine and Alkali Olivine Basalts*			*Basanites*			*Olivine (melilite)*		*Nephelinites*	
		2177	*T-14*	*69-1018*	*2152*	*69-1026*	*69-1036*	*2128*	*2679*	*2650*	*2896*	*2854*	*2860*	*2927*
P_2O_5/Ce	2200(75 ± 15)[b]	31	81	92	31	19	104	89	87	106	97	82	123	84
Zr/Ce	7·7	1·4	3·3	3·5	1·1	0·8	3·1	3·0	3·0	3·0	2·5	2·3	2·5	1·5
Sr/Ce	13·5	4·3	8·3	10·3	4·1	2·6	11·1	8·5	8·9	8·8	9·6	8·9	11·4	9·0
K_2O/Ce	710	85	121	213	88	61	241	199	194	206	148	109	173	89
Rb/Ce	2·1	0·23	0·20	0·47	0·18	0·12	0·49	0·40	0·39	0·42	0·19	0·09	0·15	0·18
TiO_2/Zr	175	127	134	156	133	115	141	84	99	99	76	106	80	112
TiO_2/Y	517	182	722	796	305	315	793	896	1158	1300	928	1166	811	877
TiO_2/Sc	137	904	750	900	859	786	930	1294	—	—	1881	1807	3643	1143
Zr/Y	3·0	1·43	5·4	5·1	2·3	2·7	5·6	10·6	11·7	13·1	12·2	11·4	10·1	7·8
Zr/Hf	44	38	39	37	38	40	39	41	45	—	39	37	42	41
Zr/Nb	16								4·5	4·8				
Th/U	3·1	5·4	11[c]	3	3·8		2·6	4·3	3·6	3·1	3·8	2·9	3·2	4·4

[a] Chondritic values from Wedepohl (1975) and Sun & Nesbitt (1976).
[b] Terrestrial alkalic basalt average proposed by Sun & Hanson (1975*a*, *b*).
[c] U value is probably incorrect.

pyroxenes and garnet relative to a coexisting liquid. Also, the high (relative to chondrites) and increasing TiO_2/Y and Zr/Y ratios with increasing alkalinity reflect the affinity of Y for garnet (Lambert & Holland, 1974). As expected in a garnet-bearing source, Y is more compatible than TiO_2.

Zr/Hf ratios are quite constant (37–42) throughout the basalt suite confirming that mineral/liquid partitioning processes during basalt petrogenesis are unable to fractionate these elements. Th/U ratios have more scatter, but this may only reflect the large uncertainty in the U data.

CONCLUSIONS

(1) In the Tertiary–Recent basaltic provinces of Victoria and Tasmania, there are systematic variations in composition from quartz and olivine tholeiites, through alkali olivine basalt, basanite and olivine nephelinite to an extremely silica undersaturated olivine melilitite. Primary magmas, consistent with derivation by partial melting of a peridotite with olivine of Fo_{88-89}, can be identified in the alkali olivine basalt to olivine melilitite part of this continuum but olivine tholeiites are fractionated by olivine, olivine + pyroxene or olivine + pyroxene + plagioclase extraction, most commonly at low pressures.

(2) The systematic variation in major element composition is matched by systematic abundance changes in minor elements P, K, Ti and in compatible and incompatible trace elements, particularly in the abundance and relative fractionation of the REE.

(3) Information on (a) the phase relationships during melting of lherzolite (pyrolite) containing 3·5 per cent Al_2O_3, 3·1 per cent CaO; (b) the liquidus phases of natural primary basalts as functions of P, T, per cent H_2O, per cent CO_2; and use of (c) mass balance calculations enabled us to calculate specific partial melting models for the various primary basalts. In these models, the per cent melting of the model sources was most consistently determined by P_2O_5 contents of the source and basaltic magma, assuming this component to be 'perfectly' incompatible and entirely partitioned into the liquid, even at very small degrees of melting.

(4) The significance attached to P_2O_5 contents is supported by the strong correlation (throughout the basalt spectrum) of P_2O_5 abundance with the abundance of other incompatible elements, particularly the light REE, Sr, Ba, Zr, Hf, Th and U. P_2O_5 abundance does not correlate as well with K and Rb abundances and it is possible that alkali–metal abundances have been affected by loss of volatile-rich phases and/or late stage alteration of some samples. The correlation of P_2O_5 abundance with other incompatible elements contents, the low P partition coefficients (<0·05) between mantle minerals (olivine and pyroxenes) and melt and the absence of apatite or other P-rich phases on the liquidi of primary basalts all imply that for homogeneous source models of magma genesis, the P_2O_5 contents of primary magmas can be used to infer degrees of partial melting.

(5) We have shown that a single source lherzolite composition very close to that of the model pyrolite, calculated primarily as a source composition for Hawaiian olivine tholeiite magma (Ringwood, 1966), can yield the spectrum of primary basalts for the Victorian–Tasmanian province by ~4 per cent to ~25 per cent

melting. The model source lherzolite (pyrolite) for Victorian and Tasmanian basalts contains 0·3–0·4 per cent TiO_2, i.e., considerably lower than that for the source lherzolite (pyrolite of Ringwood, *ibid.*, for Hawaiian tholeiite (0·7 per cent TiO_2). The mineralogies of residual peridotites are consistent with known liquidus phase relationships of the primary magmas and the chemical compositions of residual peridotite are similar to natural depleted or refractory lherzolites and harzburgites. The degree of partial melting, nature of residual mineralogy and thus the compositions of the melts, are sensitive to P, T, and, particularly for low degrees of melting, the presence of H_2O, CO_2 and the CO_2/H_2O ratio in the source region.

(6) We have tested the melting models, based on major element abundances and experimental petrology, for their ability to account for the minor and trace element, particularly REE, contents of the primary magmas. A major conclusion is that *a single source lherzolite (pyrolite) model composition can yield the observed REE contents (within at most a factor of 2, commonly much closer) for olivine melilitite (4–6 per cent melts), basanite (5–7 per cent melts), alkali olivine basalts (11–15 per cent melts) and olivine tholeiites (20–25 per cent melts) provided that the source region was already relatively enriched in LREE (LREE ~7–9× chondrites, HREE ~2<5–3× chondrites) prior to the partial melting event.*

(7) These models also satisfactorily account (within the current uncertainties of partition coefficients) for abundances of the compatible elements Ni, Co, Sc and V, the moderately incompatible elements Ti, Zr, Hf, Y and the strongly incompatible elements Ba, Sr, Th, and U provided that the abundances of moderately incompatible elements are enriched in the source to values of 2·5 to 3× chondrites, *i.e.*, similar to HREE, and the strongly incompatible elements are enriched in the source to values of 6 to 9× chondrites, *i.e.*, similar to the LREE enrichment.

(8) It is possible, within the general framework of a lherzolite (pyrolite) source composition (~3–5 per cent Al_2O_3, 3–4 per cent CaO, Fo_{89-90}) to derive the highly silica undersaturated *basanites*, *olivine nephelinite* and *olivine melilitite* from a source rock with chondritic relative REE abundances, but with absolute REE abundance at 2–5× chondritic values. These models require extremely small degrees of melting (0·4 per cent for olivine melilitite to 1 per cent for basanite) but do not contravene the major element or experimental petrology constraints for the major phases olivine, pyroxenes and garnet (although they may be inconsistent with roles of accessory minerals such as phlogopite, apatite or ilmenite). However, it is *not* possible to derive the olivine tholeiite magmas possessing LREE-enriched patterns from a source rock with chondritic REE abundances if the experimental petrology and major element arguments are accepted that such magmas require high degrees of melting (>15 per cent), without residual garnet and only minor clinopyroxene. If experimental petrology constraints are disregarded, the REE abundances in Victorian tholeiites (and most continental plateau tholeiites) can be modeled by partial melting of a source with chondritic relative REE abundances (2 to 5× chondrites in absolute abundance) if the degree of melting is small (<10 per cent) and clinopyroxene and/or garnet are major residual phases. For example, the REE abundances of a Victorian tholeiite could be derived by <5 per cent melting of a spinel lherzolite (7 per cent residual clinopyroxene, no residual garnet) source

rock with near-chondritic relative REE abundances at 1 to 2× chondrites in absolute REE abundance. Although models can be formulated to derive tholeiites and alkaline basalts from a source with chondritic relative REE abundances, these sources must be heterogeneous in other trace element abundances. However, mantle heterogeneity is not a drawback of this model because mantle heterogeneity is required when comparing the mantle source compositions of tholeiites from Hawaii, continents and other islands (*e.g.*, Iceland) and the ocean floor. Furthermore, there is isotopic evidence (Sr, Pb, Nd) that tholeiitic basalts are derived from mantle sources that have had a markedly different history than the sources for nepheline–normative basalts. An important feature of Nd isotopic variations is that the source regions for most oceanic basalts have possessed fractionated non-chondritic REE patterns for long periods of time (DePaolo & Wasserburg, 1976*a*, *b*; Richard *et al.*, 1976). Since we do not believe that experimental petrology constraints on the nature of residual mineralogy should be disregarded, we prefer partial melting models requiring high degrees of melting, particularly for tholeiitic magmas, and source peridotites ranging from LREE-enriched to LREE-depleted relative to chondritic REE abundances.

(9) Considered in relation to source regions for other well-studied basaltic provinces, the source regions for Victorian and Tasmanian basaltic are similar to those for oceanic island basalts (Hawaii, Comores, Iceland, Azores) or for continental and rift valley basaltic provinces and very different from the model source regions for most mid-ocean ridge basalts. These differences are attributed to mantle heterogeneity resulting from selective mobility of elements which are strongly incompatible with respect to the major mantle minerals olivine, orthopyroxene, clinopyroxene and garnet and possibly also incompatible relative to the accessory minerals ilmenite, phlogopite and sulphide (liquid), i.e., P, LREE, Ba, Sr, U, Th and Ta. We infer that this heterogeneity has resulted from migration within the upper mantle (LVZ or below the LVZ) of a melt or fluid (possibly $H_2O + CO_2$-enriched supercritical fluid) with REE concentrations similar to olivine melilitite, kimberlite or carbonatite, thereby depleting some mantle regions and enriching others. The concept of a chemically zoned LVZ produced by melt or fluid (<2 per cent melt?) migration from lower to upper part of the LVZ (Green, 1971; Green & Liebermann, 1976) is consistent with this inference. On the other hand, we cannot readily rationalize a process of this nature or any other process which could produce a LREE-enriched source of local ('hot spot', 'mantle plume') character in the *deep* mantle and an overlying *shallow* LREE-depleted mantle source for mid-ocean ridge tholeiites (*e.g.*, Schilling, 1973).

(10) The mantle heterogeneity inferred for basalt source regions and which we suggest is explained by mobility of a LREE-enriched melt or fluid phase within the LVZ and base of the lithosphere (cf., Frey & Green, 1974) has developed and is continually developing throughout geological time. The LVZ may be a region in which differentiation rather than homogenization of mantle lherzolite occurs, and it is possibly only in the oceanic ridge setting (diapirism of lower part of LVZ through upper LVZ and lithosphere) and subduction setting (involving lithosphere, possibly with downward drag of underlying LVZ) that there is a *tendency* to mix

and homogenize the uppermost mantle. The mantle beneath the LVZ, assuming this to be characterized by absence of melt and also by mineral structures (within the transition zone) whose partition relationships for the minor and trace elements are unknown, *may be* regarded as a reservoir with 2× chondritic incompatible element abundances and with chondritic relative abundances of REE.

ACKNOWLEDGEMENTS

The research leading to preparation of this paper was carried out at Department of Earth and Planetary Sciences, M.I.T., Cambridge (F. A. Frey and S. D. Roy), and at the Research School of Earth Sciences, A.N.U., Canberra (D. H. Green). Research at M.I.T. was supported by Earth Sciences Section, National Science Foundation, NSF Grant DES-75-02900. The technical assistance of E. Kiss, P. Beasley (A.N.U.) and the M.I.T. nuclear reactor are gratefully acknowledged. A. J. Irving provided samples and some analytical data from Western Victorian basalts and we acknowledge the benefit of discussions with A. J. Irving, S. R. Hart, P. J. Leeman, and G. Brey. F. A. Frey thanks the Research School of Earth Sciences, A.N.U., for a Visiting Fellowship during 1976 which enabled completion of the project, and D. H. Green acknowledges the support of Department of Earth and Planetary Sciences, M.I.T., in making several short visits possible during the progress of the project.

REFERENCES

ALLÈGRE, C. J., TREUIL, M., MINSTER, J. F., MINSTER, B., & ALBARÈDE, F., 1977. Systematic use of trace element in igneous process. *Contr. Miner. Petrol.* **60**, 57–76.

ANDERS, E., 1971. How well do we know 'cosmic' abundances? *Geochim. cosmochim. Acta*, **35**, 516–22.

ANDERSON, A. T., & GREENLAND, L. P., 1969. Phosphorous fractionation diagram as a quantitative indicator of crystallization differentiation of basaltic liquids. *Geochim. cosmochim. Acta*, **33**, 493–505.

BEESON, M. H., & JACKSON, E. S., 1970. Origin of the garnet pyroxenite xenoliths at Salt Lake Crater, Oahu. *Spec. Pap. Mine. Soc. Am.* **3**, 95–112.

BREY, G. P., 1976. CO_2 solubility and solubility mechanisms in silicate melts at high pressures. *Contr. Miner. Petrol.* **57**, 215–21.

—— & GREEN, D. H., 1975. The role of CO_2 in the genesis of olivine melilitite. *Contr. Miner. Petrol.* **49**, 93–103.

—— —— 1976. Solubility of CO_2 in olivine melilitite at high pressures and role of CO_2 in the Earth's upper mantle. *Contr. Miner. Petrol.* **55**, 217–30.

BROWNE, W. R., 1939. The Cenozoic igneous rocks of Australia. *Proc. Sixth Pac. Sci. Congr.*, 881–7.

BRYAN, W. B., THOMPSON, G., FREY, F. A., & DICKEY, J. S., 1976. Inferred geologic settings and differentiation in basalts from the Deep-Sea Drilling Project. *J. geophys. Res.* **81**, 4285–304.

DEPAOLO, D. J., & WASSERBURG, G. J., 1976*a*. Nd isotopic variations and petrogenetic models. *Geophys. Res. Lett.* **3**, 249–56.

—— —— 1976*b*. Inferences about magma sources and mantle structure from variations of 143Nd/144Nd. *Geophys. Res. Lett.* **3**, 743–6.

DUKE, J. M., 1976. Distribution of the period four transition elements among olivine, calcic clinopyroxene and mafic silicate liquid: experimental results. *J. Petrol.* **17**, 499–521.

EDGAR, A. D., GREEN, D. H., & HIBBERSON, W. O., 1976. Experimental petrology of a highly potassic magma. *Ibid.* **17**, 339–56.

EGGLER, D. H., & MYSEN, B. O., 1976. The role of CO_2 in the genesis of olivine melilitite: Discussion. *Contr. Miner. Petrol.* **55**, 231–6.

FISHER, D. E., JOENSU, O., & BOSTROM, K., 1969. Elemental abundances in ultramafic rock and their relation to the upper mantle. *J. geophys. Res.* **74**, 3865–73.

FLOWER, M. F. J., SCHMINCKE, H.-U., & THOMPSON, R. N., 1975. Phlogopite stability and the $^{87}Sr/^{86}Sr$ step in basalts along the Reykjanes Ridge. *Nature*, **254**, 404–6.

FREY, F. A., 1969. Rare earth abundances in a high-temperature peridotite intrusion. *Geochim. cosmochim. Acta*, **33**, 1429–47.

—— 1970*a*. Rare earth and potassium abundances in St. Paul's rocks. *Earth planet. Sci. Lett.* **7**, 351–60.

—— 1970*b*. Rare earth abundances in alpine ultramafic rocks. *Phys. Earth planet. Interiors*, **3**, 323–30.

—— BRYAN, W. B., & THOMPSON, G., 1974. Atlantic Ocean floor: Geochemistry and petrology of basalts from Legs 2 and 3 of the Deep-Sea Drilling Project, *J. geophys. Res.* **79**, 5507–27.

—— & GREEN, D. H., 1974. The mineralogy, geochemistry and origin of lherzolite inclusions in Victorian basanites. *Geochim. cosmochim. Acta*, **38**, 1023–59.

—— HASKIN, L. A., & HASKIN, M. A., 1971. Rare earth abundances in some ultramafic rocks. *J. geophys. Res.* **76**, 2057–70.

—— HASKIN, M. A., POETZ, J., & HASKIN, L. A., 1968. Rare earth abundances in some basic rocks. *Ibid.* **73**, 6085–98.

—— & PRINZ, M., 1978. Ultramafic inclusions from San Carlos, Arizona: Petrologic and geochemical data bearing on their petrogenesis. *Earth planet. Sci. Lett.* **38**, 129–76.

GAST, P. W., 1968. Trace element fractionation and the origin of tholeiitic and alkaline magma types. *Geochim. cosmochim. Acta*, **32**, 1057–86.

GOLES, G. G., 1967. Trace elements in ultramafic rocks. *In*: *Ultramafic and Related Rocks* (ed. P. J. WYLLIE) Wiley, New York.

GREEN, D. H., 1968. Origin of basaltic magmas. *In*: *Basalts* (eds. H. H. HESS and A. POLDERVAART) Vol. 2, Interscience, New York.

GREEN, D. H., 1970*a*. A review of experimental evidence on the origin of basaltic and nephelinitic magmas. *Phys. Earth planet. Interiors*, **3**, 221–35.

—— 1970*b*. The origin of basaltic and nephelinitic magmas. *Trans. Leicester Lit. Phil. Soc.* **64**, 28–54.

—— 1971. Compositions of basaltic magmas as indicators of conditions of origin: applications to oceanic volcanism. *Phil. Trans. R. Soc. London, Ser. A.*, **268**, 707–25.

—— 1973*a*. Conditions of melting of basanite magma from garnet peridotite. *Earth planet. Sci. Lett.* **17**, 456–65.

—— 1973*b*. Experimental melting studies on a model upper mantle composition at high pressure under water-saturated and water-undersaturated conditions. *Ibid.* **19**, 37–53.

—— 1975. Genesis of Archaean peridotitic magmas and constraints on Archaean geothermal gradients and tectonics. *Geology*, **3**, 15–18.

—— EDGAR, A. D., BEASLEY, P., KISS, E., & WARE, N. G., 1974. Upper mantle source for some hawaiites, mugearites and benmoreites. *Contr. Miner. Petrol.* **48**, 33–43.

—— & HIBBERSON, W. O., 1970. Experimental duplication of conditions of precipitation of high pressure phenocrysts in a basaltic magma. *Phys. Earth planet. Interiors*, **3**, 247–54.

—— & LIEBERMANN, R. C., 1976. Phase equilibria and elastic properties of a pyrolite model for the oceanic upper mantle. *Tectonophysics*, **32**, 61–92.

—— MORGAN, J. W., & HEIER, K. S., 1968. Thorium, uranium and potassium abundances in peridotite inclusions and their host basalts. *Earth planet. Sci. Lett.* **4**, 155–66.

—— & RINGWOOD, A. E., 1967. The genesis of basaltic magmas. *Contr. Miner. Petrol.* **15**, 103–90.

GRIFFIN, W. L., & MURTHY, V. R., 1969. Distribution of K, Rb, Sr and Ba in some minerals relevant to basalt genesis. *Geochim. cosmochim. Acta*, **33**, 1389–414.

HAINES, E. L., & ZARTMAN, R. E., 1973. Uranium concentration and distribution in six peridotite inclusions of probable mantle origin. *Earth planet. Sci. Lett.*, **20**, 45–53.

HÄKLI, J. A., & WRIGHT, T. L., 1967. The fractionation of nickel between olivine and augite as a geothermometer. *Geochim. cosmochim. Acta*, **31**, 877–84.

HART, S. R., DAVIS, K., KUSHIRO, I., & WATSON, E. B., 1976. Partitioning of nickel between olivine and silicate liquid. *Abstracts with Programs, Geol. Soc. Am.* **8**, 906–7.

—— GUNN, B. M., & WATKINS, N. O., 1971. Interlava variation of alkali elements in Icelandic basalt. *Am. J. Sci.* **270**, 315–18.

—— SCHILLING, J.-G., & POWELL, J. L., 1973. Basalts from Iceland and along the Reykjanes Ridge: Sr isotope geochemistry. *Nat. Phys. Sci.* **246**, 104–7.

HASKIN, L. A., FREY, F. A., SCHMITT, R. A., & SMITH, R. H., 1966. Meteoritic, solar, and terrestrial rare-earth distributions. *Phys. Chem. Earth*, **7**, 167–321.

—— HELMKE, P. A., PASTER, T. P., & ALLEN, R. O., 1971. Rare-earths in meteoritic, terrestrial and lunar matter. *In*: *Activation Analysis in Geochemistry and Cosmochemistry* (eds. A. O. BRUNFELT and E. STEINNES) Universitetsforlaget, Oslo.

HELMKE, P. A., & HASKIN, L. A., 1973. Rare-earth elements, Co, Sc, Hf in the Steens Mountain basalts. *Geochim. cosmochim. Acta*, **37**, 1513–30.

HERRMANN, A. G., 1968. Die verteilung der Lanthaniden in basaltischen Gesteinen. *Contr. Miner. Petrol.* **17**, 275–314.

—— BLANCHARD, D. P., HASKIN, L. A., JACOBS, J. W., KRAKE, D., KOROTEV, R. L., & BRANNON, J. C., 1976. Major, minor and trace element compositions of peridotitic and basaltic komatiites from the Precambrian crust of Southern Africa, *Contr. Mineral. Petrol.* **59**, 1–12.

HOFMANN, A. W., & HART, S. R., 1975. An assessment of local and regional isotopic equilibrium in a partially molten mantle. *Ann. Rept. Dept. Terr. Mag.* **74**, 195–210.

IRVINE, T. N., 1974. Simple and multiple oxides in magmatic rock systems. *Yb. Carnegie Instn. Wash.* **73**, 300–16.

IRVING, A. J., & GREEN, D. H., 1976. Geochemistry and petrogenesis of the Newer basalts of Victoria and South Australia. *J. geol. Soc. Aust.* **23**, 45–66.

KAY, R., HUBBARD, N. J., & GAST, P. W., 1970. Chemical characteristics and origin of oceanic ridge volcanic rocks. *J. geophys. Res.* **75**, 1585–613.

—— & GAST, P. W., 1973. The rare earth content and origin of alkali-rich basalts. *J. Geol.* **81**, 653–82.

—— & SENECHAL, R. G., 1976. The rare earth geochemistry of the Troodos ophiolite complex. *J. geophys. Res.* **81**, 964–70.

KESSON, S. E., 1973. The primary geochemistry of the Monaro alkaline volcanics, Southeastern Australia—evidence for upper mantle heterogeneity. *Contr. Miner. Petrol.* **42**, 93–108.

KORITNIG, S., 1965. Geochemistry of phosphorous—I. The replacement of Si^{4+} by P^{5+} in rock-forming silicate minerals. *Geochim. cosmochim. Acta*, **29**, 361–71.

LAMBERT, R. S.-J., & HOLLAND, J. G., 1974. Yttrium geochemistry applied to petrogenesis utilizing calcium-yttrium relationships in minerals and rocks. *Geochim. cosmochim. Acta*, **38**, 1393–414.

LARIMER, J. W., 1971. Composition of the earth: chondritic or achondritic. *Ibid.* **35**, 769–86.

LEEMAN, W. P., 1973. Partitioning of Ni and Co between olivine and basaltic liquid (abstract). *EOS*, **54**, 1222.

LOUBET, M., SHIMIZU, N., & ALLÈGRE, C. J., 1975. Rare earth elements in alpine peridotites. *Contr. Miner. Petrol.* **53**, 1–12.

MACDONALD, G. A., & KATSURA, T., 1964. Chemical compositions of Hawaiian lavas. *J. Petrology*, **5**, 82–133.

MASUDA, Y., YAGI, S., & ASAYAMA, T., 1974. Instrumental neutron activation analysis of 13 trace elements in volcanic rocks. *Bull. Univ. Osaka Pre. Ser. A*, **23**, 203–13.

MORI, T., & GREEN, D. H., 1978. Laboratory duplication of phase equilibria observed in natural garnet lherzolites. *J. Geol.* **86**, 83–97.

MURATA, K. J., & RICHTER, D. H., 1966. Chemistry of the lavas of the 1959–60 eruption of Kilauea Volcano, Hawaii. *Prof. Pap. U.S. geol. Surv.*, **537-A**, 1–26.

NAKAMURA, N., 1974. Determination of REE, Ba, Fe, Mg, Na and K in carbonaceous and ordinary chondrites. *Geochim. cosmochim. Acta*, **38**, 757–75.

NESBITT, R. W., & SUN, S. S., 1976. Geochemistry of Archaean spinifex-textured peridotites and magnesium and low magnesium tholeiites. *Earth planet. Sci. Lett.* **31**, 433–53.

O'NIONS, R. K., & CLARKE, D. B., 1972. Comparative trace element geochemistry of Tertiary basalts from Baffin Bay. *Ibid.* **15**, 436–46.

—— & GRÖNVOLD, K., 1973. Petrogenetic relationships of acid and basic rocks in Iceland: Sr isotopes and rare-earth elements in Late and Postglacial volcanics. *Ibid.* **19**, 397–409.

—— & PANKHURST, R. J., 1974. Petrogenetic significance of isotope and trace element variations in volcanic rocks from the Mid-Atlantic. *J. Petrol.* **15**, 603/34.

—— —— & GRONVOLD, K., 1976. Nature and development of basalt magma sources beneath Iceland and the Reykjanes Ridge. *Ibid.* **17**, 315–38.

PHILPOTTS, J. A., & SCHNETZLER, C. C., 1968. Genesis of continental diabases and oceanic tholeiites in light of rare-earth and barium abundances and partition coefficients. *In*: *Origin and Distribution of the Elements* (ed. L. H. AHRENS) Pergamon, Oxford.

—— —— & THOMAS, H. H., 1972. Petrogenetic implications of some new geochemical data on eclogitic and ultrabasic inclusions. *Geochim. cosmochim. Acta*, **36**, 1131–66.

PRINZ, M., 1967. Geochemistry of basaltic rocks: Trace elements. *In*: *Basalts* (eds. H. H. HESS and A. POLDERVAART) Vol. 1, Interscience, New York.

REID, J. B., & FREY, F. A., 1971. Rare earth distributions in lherzolite and garnet pyroxenite xenoliths and the constitution of the upper mantle. *J. geophys. Res.* **76**, 1184–96.

RINGWOOD, A. E., 1966. The chemical composition and origin of the Earth. *In*: *Advances in Earth Science* (ed. P. M. HURLEY) MIT Press, Cambridge, Mass.

RICHARD, P., SHIMIZU, N., & ALLÈGRE, C. J., 1976. $^{143}Nd/^{146}Nd$, a natural tracer: an application to oceanic basalts. *Earth planet. Sci. Lett.* **31**, 269–78.

ROEDER, P. L., & EMSLIE, R. F., 1970. Olivine-liquid equilibrium. *Contr. Miner. Petrol.* **29**, 275–89.

SCHILLING, J.-G., 1971. Seafloor evolution: Rare-earth evidence. *Phil. Trans. R. Soc. London, Ser. A.*, **268**, 663–706.

—— 1973. Iceland mantle plume: Geochemical study of the Reykjanes Ridge. *Nature*, **242**, 565–71.

—— 1975*a*. Azores mantle blob: Rare-earth evidence. *Earth planet. Sci. Lett.* **25**, 103–15.

—— 1975*b*. Rare-earth variations across 'normal segments' of the Reykjanes Ridge 60–53 °N, Mid-Atlantic Ridge 29 °S and East Pacific Rise, 2–19 °S and evidence on the composition of the underlying low velocity layer. *J. geophys. Res.* **80**, 1459–73.

—— & WINCHESTER, J. W., 1969. Rare earth contribution to the origin of Hawaiian lavas. *Contr. Miner. Petrol.* **23**, 22–37.

SCHWARZER, R. R., & ROGERS, J. J. W., 1974. A worldwide comparison of alkali olivine basalts and their differentiation trends. *Earth planet. Sci. Lett.* **23**, 289–96.

SHAW, D. M., 1970. Trace element fractionation during anatexis. *Geochim. cosmochim. Acta*, **34**, 331–40.

—— 1972. Development of the early continental crust. Part 1. Use of trace element distribution coefficient models for the Proto-Archaean crust. *Can. J. Earth Sci.* **9**, 1577–95.

SHIMIZU, N., 1975. Rare earth elements in garnets and clinopyroxenes from garnet lherzolite nodules in kimberlites. *Earth planet. Sci. Lett.* **25**, 26–32.

SHIMOKAWA, T., & MASUDA, A., 1972. Rare-earths in Icelandic Neovolcanic rocks. *Contr. Miner. Petrol.* **37**, 39–46.

SLEEP, N. H., 1974. Segregation of magma from a mostly crystalline mush. *Bull. geol. Soc. Am.* **85**, 1225–32.

SUN, S. S., & HANSON, G. N., 1975*a*. Origin of Ross Island basanitoids and limitations upon the heterogeneity of mantle sources for alkali basalts and nephelinites. *Contr. Miner. Petrol.* **52**, 77–106.

—— —— 1975*b*. Evolution of the mantle: geochemical evidence from alkali basalt. *Geology*, **3**, 297–302.

—— & NESBITT, R. W., 1978. Petrogenesis of Archaean ultrabasic and basic volcanics and mantle evolution: Evidence from rare earth elements *Contr. Mineral. Petro.* **65**, 301–325.

—— TATSUMOTO, M., & SCHILLING, J.-G., 1975. Mantle plume mixing along the Reykjanes Ridge axis: Lead isotopic evidence. *Science*, **190**, 143–7.

SUTHERLAND, F. L., 1969. A review of the Tasmanian Cainozoic Volcanic Province. *Spec. Publ. geol. Soc. Aust.*, **2**, 133–44.

—— 1974. High pressure inclusions in tholeiitic basalt and the range of lherzolite-bearing magmas in the Tasmanian Volcanic province. *Earth planet. Sci. Lett.* **24**, 317–24.

—— & KERSHAW, R. C., 1971. The Cainozoic geology of Flinders Id., Bass Strait. *Pap. Proc. R. Soc. Tasmania*, **105**, 151–77.

THOMPSON, R. N., 1975. Is upper mantle phosphorous contained in sodic garnet. *Earth planet. Sci. Lett.* **26**, 417–24.

TREUIL, M., & JORON, J., 1975. Utilisation des elements hygromagma-tophiles pour la simplification de la modelisation quantitative des processes magmatiques. Exemples de L'Afar de de la dorsale MedioAtlantique, *Soc. Ital. Min. Petrol. XXXI*, 125–74.

VARNE, R., & GRAHAM, A. L., 1971. Rare earth abundances in hornblende and clinopyroxene of a hornblende lherzolite xenolith: Implications for upper mantle fractionation processes. *Earth planet. Sci. Lett.* **13**, 11–18.

WEDEPOHL, K. H., 1975. The contribution of chemical data to assumptions about the origins of magmas from the mantle. *Fortschr. Miner.* **52**, 141–72.

WILKINSON, J. F. G., 1976. Some subcalcic clinopyroxenites from Salt Lake Crater, Oahu, and their petrogenetic significance. *Contr. Miner. Petrol.* **58**, 181–201.

WILSHIRE, H. G. & SHERVAIS, J. W., 1975. Al-augite and Cr-diopside ultramafic xenoliths in basaltic rocks from Western United States. *Phys. Chem. Earth*, **9**, 257–72.

APPENDIX

COMMENTS ON PARTITION COEFFICIENT (P.C.) SETS

Partition coefficients for REE are listed in Table A-1 and those for other elements listed in Table A-2.

For the reasons outlined below, we believe that P.C. sets 1, 3 and 5 of Table A-1 are the best sets for evaluating basalt petrogenesis. These P.C. sets are consistent with a wide range of coexisting mineral partitioning data, but their absolute P.C. values are near the minimum of the range determined from phenocryst/matrix pairs. We suggest these values are most reasonable because errors such as impure mineral separates or disequilibrium tend to increase values of P.C. when the s/l P.C. values are <1 (except for HREE in garnet, REE s/l P.C. are <1 for all anhydrous rock-forming minerals coexisting with a basaltic melt).

Following, for each mineral, we present additional rationale for perferring P.C. sets 1, 3 and 5.

Olivine and orthopyroxene: All REE solid/liquid P.C. for ol and opx are $\leqslant 1$ (except $D^{opx/l}_{HREE}$ of P.C. set 6); therefore, the range of $D^{ol/l}_{REE}$ and $D^{opx/l}_{REE}$ values in P.C. sets 1 to 5 has a negligible effect on relative REE abundances in a coexisting liquid, and uncertainties in $D^{ol/l}_{REE}$ and $D^{opx/l}_{REE}$ are unimportant in our treatment of basalt petrogenesis.

Garnet: Experimental studies of a basalt at high P and T (Harris & Nicholls, 1978) demonstrate that HREE garnet/liquid P.C. decrease with increasing temperature; thus, the lower $D^{gar/l}_{REE}$, such as in P.C. sets 1, 3 and 5, are applicable to upper mantle melting processes.

(g) Data used by Schilling in his model calculations (e.g., Schilling 1975*b*). These data are selected from phenocryst/matrix results. Garnet and olivine data are similar to set 2. The $D^{cpx/l}_{HREE}$ values lie between the cpx/liquid values of sets 1 and 2 but $D^{cpx/l}_{LREE}$ values exceed those of all other data sets. Thus, the importance of cpx in causing REE fractionation is minimized in this partition coefficient set. $D^{opx/l}_{REE}$ values are higher than in all other data sets. Therefore, the role of opx is maximized in this data set. The $D^{opx/l}_{Sm}$ value (0·08) is near that determined experimentally (0·056) at 20 kb and 1025 °C in the simple system Fo–Ab–An–SiO_2–H_2O (Mysen, 1976). The relative values of $D^{cpx/l}_{REE}$ and $D^{opx/l}_{REE}$ (*i.e.*, $D^{cpx/opx}_{REE}$) are inconsistent with REE partitioning in 20 pairs of coexisting cpx-opx. For example, $D^{cpx/opx}_{HREE}$ exceed 2 in all natural pyroxene pairs whereas this data set has $D^{cpx/opx}_{HREE} < 1{\cdot}2$.

TABLE A-1

REE partition coefficient sets

	Set 1[a]				*Set 2*[b]				*Set 3*[c]	*Set 4*[d]
	cpx	*opx*	*ol*	*gar*	*cpx*	*opx*	*ol*	*gar*	*gar*	*gar*
La	0·02	0·0005	0·0005	0·001	0·084	0·0021	0·0021	0·003	0·004	0·003
Ce	0·04	0·0009	0·0008	0·0033	0·166	0·004	0·0033	0·007	0·021	0·007
Nd	0·09	0·0019	0·0013	0·0184	0·382	0·0083	0·0055	0·033	0·087	0·033
Sm	0·14	0·0028	0·0019	0·0823	0·736	0·0147	0·0098	0·161	0·217	0·161
Eu	0·16	0·0036	0·0019	0·1333	0·753	0·0171	0·0088	0·284	0·320	0·284
Tb	0·19	0·0059	0·0019	0·2568	0·97	0·0303	0·0097	1·2	0·70	1·2
Ho	0·195	0·0089	0·0020	1·083	1·03	0·0468	0·0103	3·5	1·4	3·5
Yb	0·20	0·0286	0·0040	4·0	1·01	0·1443	0·0202	9·84	4·03	9·84
Lu	0·19	0·038	0·0048	7·0	0·95	0·19	0·0238	13	5·7	13

	Set 5[e]				*Set 6*[f]				*Set 7*[g]			
	cpx	*opx*	*ol*	*gar*	*cpx*	*opx*	*ol*	*gar*	*cpx*	*opx*	*ol*	*gar*
La									0·18	0·026	0·0089	0·0035
Ce	0·096	0·0014	0·0005	0·003	0·11	0·003	0·0006	0·003	0·256	0·0325	0·009	0·0083
Nd	0·18	0·0029	0·0009	0·019	0·14	0·005	0·0007	0·015	0·40	0·0508	0·010	0·039
Sm	0·26	0·005	0·0013	0·107	0·24	0·01	0·0012	0·096	0·57	0·079	0·0105	0·205
Eu									0·61	0·099	0·011	0·418
Tb	0·31	0·0106	0·0016	1·27	0·48	0·032	0·0024	1·92	0·645	0·153	0·0128	1·6
Ho	0·28	0·0136	0·0014	2·57	0·51	0·051	0·0026	4·63	0·62	0·24	0·0152	5
Yb	0·23	0·0192	0·0011	4·20	0·54	0·09	0·0027	11·48	0·56	0·47	0·023	9·26
Lu									0·54	0·59	0·027	10

cpx = clinopyroxene, opx = orthopyroxene, ol = olivine, gar = garnet.

(a) The cpx data are for cpx megacrysts from an Auckland Island olivine basalt (hypersthene normative but petrographic and some compositional features indicate affinities with alkali–olivine basalts). Green & Hibberson (1970) determined that the cpx megacrysts are compositionally equivalent to liquidus cpx precipitated from the host basalt at 14–16 kb and 1200 °C. The $D_{Sm}^{cpx/l}$ determined from the megacryst/basalt ratio (0·14) is near the value of 0·08 for diopside/liquid determined by Mysen and Seitz (1975) at 20 kb and 1340 °C in a Di–Ab–An system. In general, these $D_{REE}^{cpx/l}$ values form the lower range obtained from phenocrysts/matrix studies (e.g., Schnetzler & Philpotts, 1970). Orthopyroxene/liquid REE partition coefficients ($D_{REE}^{opx/l}$) have been determined from $D_{REE}^{cpx/l}$ (based on Auckland Island megacrysts) and the fairly uniform REE abundance ratios in 20 paris of coexisting cpx–opx (Frey, 1972: data from Onuma *et al.*, 1968; Frey, 1969; Nagasawa *et al.*, 1969; Schnetzler & Philpotts, 1970; Philpotts *et al.*, 1972; Frey & Green, 1974; Frey, 1974) according to ($D_{REE}^{cpx/l}$)/(mean $D_{REE}^{cpx/opx}$). Similarly, olivine REE partition coefficients are determined from a mean of ol/cpx REE ratios (10 pairs, Frey, 1972) and the $D_{REE}^{cpx/l}$ values. The resulting $D_{REE}^{ol/l}$ values are broadly similar to the phenocryst matrix data of Higuchi & Nagasawa (1964). Garnet/liquid REE partition coefficients ($D_{REE}^{gar/l}$) are determined from $D_{REE}^{cpx/l}$ values by utilizing the mean of the fairly narrow range of REE partitioning between cpx and garnet in 21 coexisting pairs (Haskin *et al.*, 1966; Reid & Frey, 1970; Philpotts *et al.*, 1972; Ridley & Dawson, 1975; Mitchell & Carswell, 1976). Experimental partitioning values for Ho and Yb in coexisting cpx and garnet crystallized from a basalt at 30 kb and 1220 °C (Harris & Nicholls, 1978) fall within the range of this natural mineral data. The resulting garnet/liquid partition coefficients for HREE are similar to the experimental data of Shimizu & Kushiro (1975).

(b) The cpx data are for cpx megacrysts from the alkali–olivine basalt at Takashima, Japan (Onuma *et al.*, 1968). In general, these values form the upper range obtained from phenocryst matrix studies. $D_{REE}^{opx/l}$ values, determined as in set 1 by using the mean of cpx/opx ratios, are similar to solid/liquid partition coefficients for opx megacrysts from Takashima (Onuma *et al.*, 1968) and Auckland Island (Frey, 1974). Also, as in set 1, olivine REE partition coefficients are determined by using a mean of ol/cpx REE abundance ratios. The resulting $D_{REE}^{ol/l}$ are similar to the phenocryst/matrix data of Schnetzler and Philpotts (1970). The $D_{REE}^{gar/l}$ values are from a Kakanui garnet xenocryst/host basalt pair (Philpotts *et al.*, 1972). This $D_{REE}^{gar/l}$ set is consistent with $D_{Ho}^{gar/l}$ and $D_{Yb}^{gar/l}$ (3·9 and 8·3, respectively) determined from experimental study of a natural basalt at 30 kb and 1220 °C (Harris & Nicholls, 1978). The $D_{REE}^{cpx/gar}$ values for set 2 lie within but near the upper bound of $D_{REE}^{cpx/gar}$ values in 20 natural coexisting cpx-gar pairs.

(c and d) The cpx, opx and olivine partitioning data are the same as for set 1. In set 3, garnet data are from Shimizu & Kushiro (1975) and in set 4 the garnet data are the same as in set 2. In P.C. sets 3 and 4, the cpx/garnet values lie on the low end of the range of cpx/garnet values in 21 coexisting natural pairs.

(e) This partition coefficient data set is from Kay & Gast (1973). Dy values are listed in the Tb row and Er values are in the Ho row. Although slightly higher, these values are generally within a factor of 2 of set 1.

(f) This data set is based on Kakanui cpx xenocryst/host basalt REE abundance ratios (Philpotts *et al.*, 1972) and the $D_{REE}^{cpx/gar}$, $D_{REE}^{cpx/opx}$ and $D_{REE}^{cpx/ol}$ values used by Sun & Hanson (table 3, 1975). Dy values are listed in the Tb row and Er values are in the Ho row. These $D_{REE}^{cpx/l}$ values are intermediate between the $D_{REE}^{cpx/l}$ values of sets 1 and 2. $D_{REE}^{opx/l}$ and $D_{REE}^{gar/l}$ data are similar to values of set 2, and $D_{REE}^{ol/l}$ data are similar to values of set 1.

TABLE A-2

Partition coefficients

	Partition Coefficients				*Data Sources*
Element	*Garnet*	*Cpx*	*Opx*	*Olivine*	
Sc	6·5	3·1	1·1	0·25	(1 thru 8)
V	0·27	1·5	0·3	0·09	(1, 2, 3, 8, 9)
Co	2	1·2	2	6·5–1·3	(1 thru 10, variation for olivine results from temperature dependence, 1120–1420 °C, Leeman, 1973)
Ni	0·8	4–2	5–3	35–3·8	(1–4, 7–13)
Rb	0·02	0·05	0·02	0·01	(11, 14, even lower cpx values implied by 15 and 16)
Sr	0·014	0·165	0·016	0·016	(2, 5, 11, 14–16)
Y	1·4	0·20	0·009	0·002	(same as Ho in P.C. set 3, Table A-1)
Ba, Zr, Hf	bulk solid/liquid P.C. arbitrarily set = 0·01				
Cu, Zn, Th, U	bulk solid/liquid P.C. arbitrarily set = 0·00 to 0·01				

1. Taylor *et al.*, 1969.
2. Coleman *et al.*, 1965.
3. Lindstrom, 1976.
4. Dale & Henderson, 1972.
5. Onuma *et al.*, 1968.
6. Paster *et al.*, 1974.
7. Leeman & Scheidegger, 1977.
8. Ewart *et al.*, 1973.
9. Bougault & Hekiman, 1974.
10. Leeman, 1973.
11. Shaw, 1972.
12. Gunn, 1971.
13. Hakli & Wright, 1967.
14. Philpotts & Schnetzler, 1970.
15. Shimuzu, 1974.
16. Hart & Brooks, 1974.

Clinopyroxene: $D^{cpx/l}_{HREE}$ values may also decrease with increasing temperature, but data are scarce and the effect may be small (Harris & Nicholls, 1978). Cullers *et al.* (1973) found that diopside/aqueous liquid REE P.C. increased with increasing temperature, but important, possibly unrealistic, assumptions must be made to apply their data to basaltic magma petrogenesis. However, with such assumptions, their inferred cpx/silicate liquid REE P.C. are similar to those of P.C. sets 1, 3, 4 and 5. Furthermore, the 1 atm, 1295 °C experimental results for $D^{diopside/l}_{REE}$ (in simple system Ab–An–Di, Grutzeck *et al.*, 1974) are identical, within error limits, to the cpx P.C. of set 5.

An important feature of aluminous cpx megacrysts, presumably formed at high pressure, is that they cause greater REE fractionation than cpx phenocrysts. For example, the Takashima megacryst augite has 8·8 wt. per cent Al_2O_3 and $D^{cpx/l}_{Ce}/D^{cpx/l}_{Yb} = 0·16$, the Kakanui xenocrystic augite has 7·9 wt. per cent Al_2O_3 and $D^{cpx/l}_{Ce}/D^{cpx/l}_{Yb} < 0·2$, and the Auckland Island megacryst cpx has $Al_2O_3 = 5·3$ wt. per cent and $D^{cpx/l}_{Ce}/D^{cpx/l}_{Yb} = 0·2$, whereas cpx phenocryst/matrix pairs (9) have $D^{cpx/l}_{Ce}/D^{cpx/l}_{Yb} > 0·2$ (mean ~0·4, Fig. 2 of Schnetzler & Philpotts, 1970). Typically, cpx megacrysts compared to the host basalt have $D^{cpx/l}_{La}/D^{cpx/l}_{Yb}$ ~0·1, and this value is consistent with an experimental value of 0·11 obtained for liquidus cpx (>6·1 wt. per cent Al_2O_3) crystallized from a basalt at 15 kb and 1080 °C (Harris & Nicholls, 1978). Thus, we believe that P.C. sets 1, 3 and 4 with low $D^{cpx/l}_{REE}$ values and $D^{cpx/l}_{La}/D^{cpx/l}_{Yb} = 0·1$ are best for evaluating basalt petrogenesis.

SUMMARY

On the basis of the above discussion, the most realistic set of $D^{min/l}_{REE}$ values are P.C. sets 1 and 3. In the models of this paper, very similar results were obtained for P.C. sets 1, 3 and 5 and we have

no basis for discriminating among these P.C. sets. For simplicity in the text and Figs. 6, 7, 9 and 11, we have emphasized results based on P.C. set 3 because calculated model sources using P.C. set 3 have chondritic relative HREE abundances for basanite 2650 (Figs. 2 and 3).

REFERENCES*

BOUGAULT, H., & HEKINIAN, R., 1974. Rift valley in the Atlantic ocean near 36° 50′ N: Petrology and geochemistry of basaltic rocks. *Earth planet. Sci. Lett.*, **24**, 249–61.

CULLERS, R. L., MEDARIS, L. G., & HASKIN, L. A., 1973. Experimental studies of the distribution of rare earths as trace elements among silicate minerals and water. *Geochim. cosmochim. Acta*, **37**, 1499–1512.

COLEMAN, R. B., LEE, D. E., BEATTY, L. B., & BRANNOCK, W. W., 1965. Eclogites and eclogites: Their differences and similarities. *Bull. geol. Soc. Am.* **76**, 483–508.

DALE, I. M., & HENDERSON, P., 1972. The partition of transition elements in phenocryst-bearing basalts and the implications about melt structure. *24th Int. Geol. Cong. Proc.* **10**, 105–11.

EWART, A., BRYAN, W. B., & GILL, J. B., 1973. Mineralogy and geochemistry of the younger volcanic islands of Tonga, S.W. Pacific. *J. Petrol.*, **14**, 429–65.

FREY, F. A., 1972. Partitioning of rare earth elements among coexisting phases in ultramafic rocks. Abstracts of Int. Conf. on Distribution and Partition of Trace Elements and Origin of Volcanic Rocks, Newport, R.I.

FREY, F. A., 1974. Rare-earth element abundances in megacrysts from alkali-olivine basalts. *EOS*, **55**, 474.

GRUTZECK, M., KRIDELBAUGH, S., & WEILL, D., 1974. The distribution of Sr and REE between diopside and silicate liquid. *Geophys. Res. Lett.* **1**, 273–5.

GUNN, B. M., 1971. Trace element partition during olivine fractionation of Hawaiian basalts. *Chem. Geol.* **8**, 1–13.

HARRIS, K. L., & NICHOLLS, I. A., 1978. An experimental study of the partitioning of selected rare earth elements between garnet, clinopyroxene, amphibole and liquids of andesitic and basaltic composition. *Geochim. cosmochim. Acta* (in press).

HART, S. R., & BROOKS, C., 1974. Clinopyroxene-matrix partitioning of K, Rb, Cs, Sr and Ba. *Geochim. cosmochim. Acta*, **38**, 1799–806.

HIGUCHI, H., & NAGASAWA, H., 1969. Partition of trace elements between rock-forming minerals and the host volcanic rocks. *Earth planet. Sci. Lett.* **7**, 281–7.

LEEMAN, W. P., & SCHEIDEGGER, K. F., 1977. Olivine/liquid distribution coefficients and a test for crystal–liquid equilibrium. *Ibid.* **35**, 247–257.

LINDSTROM, D. J., 1976. Experimental study of the partitioning of the transition metals between clinopyroxene and coexisting silicate liquid. Ph.D. Thesis, Univ. of Oregon, Eugene.

MITCHELL, R. H., & CARSWELL, D. A., 1976. Lanthanium, samarium and ytterbium abundances in some southern African garnet lherzolites. *Earth planet. Sci. Lett.* **31**, 175–8.

MYSEN, B., 1976. Partitioning of samarium and nickel between olivine, orthopyroxene and liquid; preliminary data at 20 kbar and 1025 °C. *Ibid.* **31**, 1–7.

MYSEN, B. O., & SEITZ, M. G., 1975. Trace element partitioning determined by beta track mapping: an experimental study using carbon and samarium as examples. *J. geophys. Res.* **80**, 262–35.

NAGASAWA, H., WAKITA, H., HIGUCHI, H., & ONUMA, N., 1969. Rare earths in peridotite nodules: an explanation of the genetic relationship between basalt and peridotite nodules. *Earth planet. Sci. Lett.* **5**, 337–81.

ONUMA, N., HIGUCHI, H., WAKITA, H., & NAGASAWA, H., 1968. Trace element partition between two pyroxenes and the host lava. *Ibid.* **5**, 47–51.

PASTER, T. P., SCHAUWECKER, D. S., & HASKIN, L. A., 1974. The behavior of some trace elements during solidification of the skaergarrd layered series. *Geochim. cosmochim. Acta*, **38**, 1549–77.

PHILPOTTS, J. A., & SCHNETZLER, C. C., 1970. Phenocryst-matrix partition coefficients for K, Rb, Sr and Ba with applications to anorthosite and basalt genesis. *Geochim. cosmochim. Acta*, **34**, 307–22.

REID, J. B., & FREY, F. A., 1970. Rare earth distributions in lherzolite and garnet pyroxenite xenoliths and the constitution of the upper mantle. *J. geophys. Res.* **76**, 1184–96.

RIDLEY, W. I., & DAWSON, J. B., 1975. Lithophile trace element data bearing on the origin of peridotite xenoliths, ankaramite and carbonatite from Lashaine Volcano, N. Tanzania. *In Phys. Chem. Earth* (eds. L. H. AHRENS, J. B. DAWSON, A. R. DUNCAN and A. J. ERLANK) Pergamon Press, Oxford.

SCHNETZLER, C. C., & PHILPOTTS, J. A., 1970. Partition coefficients of rare-earth elements between igneous matrix material and rock-forming mineral phenocrysts—II. *Geochim. cosmochim. Acta*. **34**. 331–40.

SHIMIZU, N., 1974. An experimental study of the partitioning of K, Rb, Cs, Sr and Ba between clinopyroxene and liquid at high pressures. *Ibid.* **38**, 1789–98.

SHIMIZU, N., & KUSHIRO, I., 1975. The partitioning of rare earth elements between garnet and liquid at high pressures: preliminary experiments. *Geophys. Res. Lett.* **2**, 413–16.

TAYLOR, S. R., KAYE, M., WHITE, A. J. R., DUNCAN, A. R., and EWART, A., 1969. Genetic significance of Co, Cr, Ni, Sc and V contents of andesites, *Geochim. Cosmochim. Acta*. **33**, 275–86.

* Certain references are to be found in the References list for the main section of this paper.

Garnet Compositions at Broken Hill, New South Wales, as Indicators of Metamorphic Processes

by R. L. STANTON[1] *and* K. L. WILLIAMS[2]

[1] *Department of Geology, University of New England, Armidale, New South Wales, Australia.*
[2] *Department of Geology and Geophysics, University of Sydney, Sydney, New South Wales, Australia*

(*Received 31 May 1977; in revised form 16 January 1978*)

ABSTRACT

Electron microprobe analyses of garnets in the finely bedded 'banded iron formations' (BIF) of the Willyama Complex at Broken Hill reveal marked compositional changes from one garnet to the next on a scale of 1–2 mm. Further, systematic analytical traverses across bedding and along bedding show the compositions of the garnets to change markedly from one fine bed to the next, but to remain extremely uniform within individual beds.

In view of the minuteness of the domains involved it appears evident that compositional variation cannot be attributed to variations in metamorphic pressures, temperatures or oxygen fugacities. Neither can they be attributed to variation in garnet-matrix partition functions, as most of the garnets occur in one simple matrix—quartz.

It is concluded that in spite of the high (sillimanite) grade of the relevant metamorphism, any equilibration of garnet compositions, and hence any associated inter-grain metamorphic diffusion, has been restricted to a scale of less than 1 mm; that garnet compositions here reflect original rock composition on an ultra-fine scale, and have no connotations concerning metamorphic grade; that, hence, the garnets must derive from a single precursor material, earlier suggested to be a manganiferous chamositic septechlorite; and that the between-bed variation : within-bed uniformity of garnet composition reflects an original pattern of chemical sedimentation—a pattern preserved with the utmost delicacy through a period of $\approx 1800 \times 10^6$ years and a metamorphic episode of sillimanite grade.

INTRODUCTION

In several recent contributions concerned with the metamorphosed 'banded iron formations' and their associated rocks of the Willyama Complex at Broken Hill (Stanton, 1975; 1976; Stanton & Roberts, in press) it was concluded that the regional metamorphism concerned had been essentially of 'closed system' kind. From this it was deduced that the resulting metamorphic minerals derived essentially from specific sedimentary-diagenetic precursor minerals, rather than from progressive sequences of mineral reactions. Two important lines of evidence leading to these conclusions were the apparent preservation of primary patterns of chemical sedimentation in the 'banded iron formations', and of substantial, systematic, differences in the compositions of the latters' garnets over distances of centimetres or less.

These two problems—of metamorphic diffusion distances and of short-range intergrain differences in garnet composition—are of course closely related and of ancient vintage. Earlier opinion (e.g. Harker, 1893) favoured the limitation of regional metamorphic diffusion to very small distances, and well into this century Harker (1932) noted 'The study of metamorphosed rocks . . . makes it appear that the mineral formed at any given point depends upon the composition of the rock

Printed in Great Britain at the Spottiswoode Ballantyne Press
by William Clowes & Sons Limited, London, Colchester and Beccles

THE ROLE OF CARBON DIOXIDE IN THE PETROGENESIS OF HIGHLY POTASSIC MAGMAS

I.D. Ryabchikov
Inst. for the Genesis of Ore Deposits
Academy of Sciences of the USSR
Moscow. USSR

and

D.H. Green *
Dept. of Geology
University of Tasmania
Hobart 7001 Australia

Abstract

Experiments at 30 Kb confining pressure show that the liquidus of an anhydrous, highly potassic biotite mafurite liquid is depressed by ~150°C in the presence of CO_2-vapour and that up to 10.6 wt % CO_2 can be dissolved in the biotite mafurite (30 Kb, 1380°C) as the carbonate molecule. Olivine is the liquidus phase at the anhydrous, CO_2-free liquidus (30 Kb 1510°C), at the CO_2-saturated liquidus (30Kb, 1360°C), and at the H_2O-saturated liquidus (30 Kb, 1160°C) but within the system biotite mafurite - H_2O-CO_2 there exist vapour-undersaturated liquidus fields for olivine, clinopyroxene, orthopyroxene and phlogopite at appropriate contents of H_2O and CO_2. Analyses of olivines, clinopyroxene, orthopyroxene and phlogopite are presented and it is shown that the Ti-content of phlogopite is positively related to temperature and is much higher in the phlogopites crystallized under f_{H_2} conditions of the MH-buffer than in phlogopites crystallized at similar P,T under f_{H_2} conditions near the NNO-buffer. The experimental study further illustrated the dramatic effect of $(CO_3)^=$ on the liquidus phase relations of the highly potassic magma. It may be inferred that, in the presence of both H_2O and CO_2 and at very small degrees of melting of mantle peridotite such that phlogopite is not eliminated as a residual phase, liquid compositions will be highly potassic and strongly undersaturated. The source rock for natural highly potassic magmas may be locally enriched in phlogopite but contains the normal mantle residual phases olivine, orthopyroxene, clinopyroxene ± garnet.

* Previous address: Research School of Earth Sciences, Australian National University, Canberra 2601, Australia.

Introduction

The work of Academician V.S. Sobolev has provided outstanding contributions to our understanding of petrology and the physico-chemical processes active in the upper mantle. His contributions include detailed mineralogical studies of kimberlites, mantle xenoliths and crystalline phases including diamonds, investigations of high pressure,metamorphic and igneous rocks and microinclusions in their minerals. V.S. Sobolev considered the subcrustal processes leading to the formation of highly potassic rocks. He proposed a hypothesis ascribing the genesis of highly potassic magmas to anatexis in portions of mantle enriched in phlogopite by earlier metasomatic processes (Sobolev, 1973).

Rocks extremely rich in potassium are among the most enigmatic of magmatic rocks. Processes which may result in selective enrichment in potassium in the upper mantle environment are still not clearly understood. Geochemical characteristics of potassium-rich magmas, and particularly the presence in them of ultramafic inclusions containing phlogopite (Holmes, 1952; Carmichael, 1967) indicate that volatiles may be important in their genesis.

Previous experimental studies in the biotite mafurite-H_2O system provided information on phase relations in magmas in the presence of high K concentrations and on the stability of phlogopite in a highly potassic ultramafic composition as a function of P,T and % H_2O conditions (Edgar, Green and Hibberson, 1976). The present work complements these studies in attempting to gauge the possible role of CO_2 in addition to H_2O in the genesis of highly potassic magmas.

Starting Material

A new batch of synthetic glass very close in composition to that used in experimental work by Edgar, Green, and Hibberson (1976) was prepared by sintering a mixture of oxides at 1000°C and fusing in a Pt

TABLE 1

Composition of Starting Material

	a	b	c	
SiO_2	41.5	42.6	42.02	0.11
TiO_2	4.9	5.3	4.93	0.05
Al_2O_3	8.0	8.3	8.02	0.04
Fe_2O_3	0.6	0.2*	0.12*	0.00
FeO	9.5	7.8*	9.07*	0.02
MgO	16.1	15.8	16.14	0.21
CaO	10.2	10.7	10.54	0.12
Na_2O	0.7	0.8	0.55	0.11
K_2O	7.3	7.1	7.26	0.02
P_2O_5	0.4	n.d.	n.d.	
Cr_2O_3	0.15	0.2	0.15	0.03
NiO	0.05	n.d.	n.d.	
MnO	0.2	n.d.	n.d.	
BaO	0.35	n.d.	n.d.	
SrO	0.2	n.d.	n.d.	
Total	100.15	98.8	98.8	
$\frac{100\ Mg}{Mg + Fe}$	75.0	77.6	76.05	

a: desired glass composition biotite mafurite (Holmes, 1942).

b: glass composition used as starting material by Edgar, Green and Hibberson (1976).

c: starting glass composition used in this work with standard deviations from 5 points analysed by electron microprobe.

Compositions b and c are normalized to 98.8% to allow for constituents not analysed by electron microprobe but added to original mix.

* determined by spectrophotometry, E. Kiss, analyst.

n.d.: not determined.

crucible at 1400°C for about 2 minutes. This composition is very similar to biotite mafurite from S.W. Uganda (Holmes, 1942, p. 212, Anal. D). The principal constituents of this biotite mafurite are olivine, clinopyroxene, kalsilite, perovskite and biotite with xenoliths of glimmerite (almost monomineralic phlogopite rock) and minor biotite peridotite (Holmes, 1942) suggestive of upper mantle origin. The comparison of this composition with that of postulated highly potassic ultramafic parent magma (olivine-rich ugandite) was discussed earlier (Edgar, Green, Hibberson, 1976).

The composition of starting glass used in this study is shown in Table 1 together with the composition of biotite mafurite (Holmes, 1942) and starting glass used in previous work (Edgar, Green and Hibberson, 1976).

Experimental Procedure

Experiments were carried out in a piston-cylinder apparatus using piston-in-technique and a pressure correction of -10% of nominal piston pressure (T.H. Green *et al.* 1966). The desired amounts of starting glass together with known amounts of distilled water and silver oxalate (used as a source for CO_2) were weighed into Pt, $Ag_{50}Pd_{50}$ or $Ag_{75}Pd_{25}$ capsules and the capsules sealed by welding. The capsule type varied with the temperature of experiment: above 1250°C, Pt capsules were used, whereas below 1250°C, silver-palladium alloys were preferred due to the lower iron losses in these capsules. The amount of biotite mafurite used varied from 10 to 20 mg depending upon the percentage of volatiles in the runs.

To prevent the reduction of CO_2 to graphite, haematite + magnetite + H_2O external buffers were used in all runs. Inasmuch as only H_2 fugacity is equalized through the walls of Pt or AgPd capsules, and water equilibrium pressure in the inner capsules was not equal to total pressure, actual oxygen fugacities of runs were lower than those for HM buffer. Values

varied from f_{O_2} close to NNO or QFM buffers for runs when no H_2O was added to the starting mixture, up to values close to f_{O_2} for HM buffer for runs with large amounts of water.

Crystalline phases and quenched glass were identified optically in crushed portions of the charges, and their compositions were determined on polished surfaces by the TPD energy dispersive electron microprobe system (Reed and Ware, 1973). Homogeneous glasses from some anhydrous runs were analysed for CO_2 using a Hewlett-Packard 185B CHN analyser. Details of analytical procedure may be found elsewhere (Lindgren *et al.* 1972; Brey and Green, 1976).

Experimental Results

Results of "anydrous"* experiments and runs with various amounts of H_2O and/or CO_2 added are given in Table 2 and illustrated by Figs. 1, 2 and 3. Compositions of solid phases and glasses are given in Tables 3-7.

The majority of experiments was carried out at 30 kbar. The comparison of the results of runs without H_2O or CO_2 added with the series of experiments for biotite mafurite + 30 wt.% CO_2 composition show that in both cases olivine is the first phase crystallizing from the melt. However, the liquidus temperature for the CO_2-saturated composition is approximately 120^{o} lower than that for volatile-free biotite mafurite, suggesting substantial solubility of carbon dioxide in silicate liquid. In fact, the analyses of quenched glasses from biotite mafurite + 30 wt.% CO_2 runs have shown 10.4 wt.% CO_2 at $1380^{o}C$, 30 kbar and 10.9 wt.% CO_2 at $1370^{o}C$, 30 kb giving an average of 10.6 wt.% CO_2. This value is only slightly higher than the CO_2 solubility in olivine melilitite melts (Brey

---

* Small amounts of water could have been present in "anhydrous" runs due to hydrogen diffusion through the walls of capsules. This effect was, however, minimized by using MH-H_2O external buffer.

and Green, 1976; Brey, 1976). Both magmas contain high Mg,Ca contents but very different K and Na contents.

Although olivine was the liquidus phase for both volatile-free and CO_2-saturated compositions, the second crystallizing phase was clinopyroxene in the first case and orthopyroxene in the second. The same tendency was observed in the runs with both CO_2 and H_2O: at sufficiently high concentrations of carbon dioxide, clinopyroxene is replaced by orthopyroxene. It appears from the results of our experiments that approximately 6 wt.% CO_2 is necessary to bring orthopyroxene to the liquidus in biotite mafurite composition at 30 kb. This result is similar to that obtained by G. Brey and D.H. Green (1975) for olivine melilitite.

A series of runs at various pressures with biotite mafurite + 6.8% H_2O + 16.5% CO_2 (H_2O:CO_2 = 1:1 mole ratio,mixture equivalent to 15 wt.% H_2O) composition has shown that orthopyroxene persists at the liquidus with decreasing pressure down to at least 20 kbar.

Phlogopite was not found as a liquidus phase at 30 kb in our experiments containing CO_2. It should however, appear as the first crystallizing phase in H_2O-rich and CO_2-poor compositions as can be seen from Figs. 1 and 2, which combine our experimental data with those for the biotite mafurite + H_2O join (Edgar, Green and Hibberson, 1976). From Fig. 2, it can be seen that at 10-11% H_2O, phlogopite should start to crystallize at 1240°-1250°C, whereas in our experiments with 10.7% H_2O and 8.7% CO_2, primary phlogopite appears between 1160° and 1140°C (see Table 2). These data imply that large amounts of CO_2 strongly suppress the stability of phlogopite. This effect is, however, not so evident in the series of runs with lower CO_2 concentrations: for the mixtures with 3.7% H_2O; 3.0% CO_2 and 2.4% H_2O; 5.9% CO_2, the crystallization temperatures of phlogopite are higher than for the biotite mafurite + H_2O join with equivalent water content (5 wt.% H_2O) (see Fig. 1a). In fact, biotite mafurite + 2.4% H_2O + 5.9% CO_2 yielded the highest temperature of

TABLE 2

Results of Experimental Runs

Run Numbers	°C	(kb)	Time (min)	Capsule	Products
			a. Runs without H_2O or CO_2 added		
7048	1560	30	5	Pt	Gl(83), Q.Cpx(88)
7051	1520	30	5	Pt	Gl(81-83), Q.Cpx(87)
7052	1480	30	10	Pt	Ol, Gl(84), Q.Cpx(87)
7054	1460	30	10	Pt	Ol(94), Gl(82)
7053	1440	30	10	Pt	Ol(91), Cpx(89) Gl
			b. 30 wt.% CO_2 added ($CO_2/H_2O + CO_2 = 1$)		
7056	1380	30	10	Pt	Gl(88)
7058	1370	30	10	Pt	Gl(88)
7057	1360	30	10	Pt	Ol(93), Q.Cpx(84-91), Gl
7055	1340	30	10	Pt	Ol, Opx(90), Q.Cpx(85), Gl
			c. 2.4 wt.% H_2O and 5.9 wt.% CO_2 added ($CO_2/CO_2 + H_2O = 0.5$)		
7105	1400	30	3	Pt	Gl(77)
7098	1380	30	10	Pt	Opx(91), Cpx(89), Q.Ph(76), Gl(73)
7094	1340	30	10	Pt	Opx(90), Cpx(88), Q.Ph(69), Gl(74)
6654	1300	30	20	Pt	Opx(87), Cpx(82), Ph(82)
			d. 3.7 wt.% H_2O and 3.0 wt.% CO_2 added ($CO_2/CO_2 + H_2O = 0.25$)		
7086	1300	30	20	Pt	Ol(89.5), Cpx(87), Q.Ph(73)
7095	1280	30	20	Pt	Ol(89), Cpx(85), Q.Ph(77)
7085	1250	30	20	Pt	Ol(84), Cpx(81), ?Ph(82)
7089	1200	30	20	$Ag_{75}Pd_{25}$	Ol(84), Cpx(82), Ph(84)
			e. 6.8 wt.% H_2O and 16.5 wt.% CO_2 added ($CO_2/CO_2 + H_2O = 0.5$)		
7074	1160	20	20	$Ag_{75}Pd_{25}$	Opx(88), Ph(83), Q.Cpx(66)
7064	1170	25	20	$Ag_{75}Pd_{25}$	Opx(88), Q.Ph(79), Q.Cpx(78)
7066	1220	30	20	$Ag_{50}Pd_{50}$	Opx(88), Q.Ph(73)
7060	1200	30	20	$Ag_{50}Pd_{50}$	Opx(89), Q.Ph(80), Q.Carb
7075	1160	30	20	$Ag_{75}Pd_{25}$	Opx(87), Q.Ph(73), Q.Cpx(70)
			f. 10.7 wt.% H_2O and 8.7 wt.% CO_2 added ($CO_2/CO_2 + H_2O = 0.25$)		
7106	1200	30	20	Pt	Opx(88), Q.Ph(80), Q.Carb
7076	1180	30	20	$Ag_{50}Pd_{50}$	?Cpx(82), Q.Ph(77)
7082	1160	30	20	$Ag_{75}Pd_{25}$	?Cpx(83), Q.Ph(76)
7080	1140	30	20	$Ag_{75}Pd_{25}$	Opx(86), Cpx(81), Ph(82)
			g. 15 wt.% H_2O added ($CO_2/CO_2 + H_2O = 0$)		
7096	1160	30	20	$Ag_{75}Pd_{25}$	Cpx(79), Ph(80)

Abbreviations: Ol is olivine; Opx is orthopyroxene; Cpx is clinopyroxene; Ph is biotite; Gl is glass; Carb is carbonate; Q. is quench.

Bracketed numbers indicate 100 Mg/Mg + Fe values.

TABLE 3

Compositions of quench (Q) and primary (P) phlogopites analysed by microprobe (normalized to total 96%)

Run Numbers	7098	7097	6654	7086	7095	7085	7089	7074	7064
Wt.% H_2O added	2.4	2.4	2.4	3.7	3.7	3.7	3.7	6.8	6.8
Wt.% CO_2 added	5.9	5.9	5.9	3.0	3.0	3.0	3.0	16.5	16.5
$CO_2/CO_2 + H_2O$	0.5	0.5	0.5	0.25	0.25	0.25	0.25	0.5	0.5
Pressure (kb)	30	30	30	30	30	30	30	20	25
Temperature (°C)	1380	1340	1300	1300	1280	1250	1200	1160	1170
Quench (Q) or primary (P) phlogopite	Q	Q	P	Q	Q	P	P	P(?)	Q
Coexisting primary phases	Opx(91) Cpx(89)	Opx(90) Cpx(88)	Opx(87) Cpx(82)	Ol(89) Cpx(87)	Ol(89) Cpx(85)	Ol(84) Cpx(81)	Ol(84) Cpx(82)	Opx(88)	Opx(88)
SiO_2	41.9	40.6	38.1	39.0	38.8	39.0	38.7	40.4	41.7
TiO_2	7.5	9.2	8.0	8.4	7.6	7.1	5.8	5.5	6.5
Al_2O_3	10.4	11.4	14.7	12.4	12.6	14.2	14.7	14.0	11.2
Cr_2O_3	-	-	0.3	-	-	-	0.1	0.3	-
FeO	7.9	10.6	7.0	9.9	9.0	6.9	6.6	7.3	8.9
MnO	-	-	-	-	-	-	-	-	-
MgO	16.0	13.1	17.5	15.3	17.2	17.9	19.4	20.4	17.1
CaO	1.9	1.1	-	0.9	0.1	0.5	0.1	-	0.2
K_2O	10.4	10.0	10.5	10.1	10.6	10.5	10.5	10.7	10.5
100 Mg/Mg + Fe	78.4	68.8	81.6	73.4	77.2	82.3	83.9	83.2	77.4
Cations for 22 oxygens									
Si	6.06	5.92	5.45	5.68	5.63	5.59	5.55	5.64	6.02
Ti	0.81	1.01	0.87	0.92	0.83	0.77	0.62	0.58	0.70
Al	1.76	1.94	2.49	2.13	2.17	2.41	2.49	2.31	1.89
Cr	-	-	0.03	-	-	-	0.01	0.03	-
Fe	0.95	1.29	0.84	1.21	1.10	0.82	0.80	0.86	1.07
Mg	3.43	2.84	3.72	3.34	3.72	3.81	4.14	4.26	3.65
Ca	0.29	0.17	-	0.14	0.02	0.07	0.01	-	0.04
K	1.91	1.86	1.93	1.87	1.95	1.91	1.92	1.91	1.93
Total	15.21	15.03	15.36	15.28	15.42	15.39	15.54	15.57	15.30

Run Numbers	7066	7060	7075	7106	7076	7082	7080	7096
Wt.% H_2O added	6.8	6.8	6.8	10.7	10.7	10.7	10.7	15
Wt.% CO_2 added	16.5	16.5	16.5	8.7	8.7	8.7	8.7	0
$CO_2/CO_2 + H_2O$	0.5	0.5	0.5	0.25	0.25	0.25	0.25	0
Pressure (kb)	30	30	30	30	30	30	30	30
Temperature (°C)	1220	1200	1160	1200	1180	1160	1140	1160
Quench (Q) or primary (P) phlogopite	Q	Q	Q	Q	Q	Q	P	P
Coexisting primary phases	Opx(88)	Opx(89)	Opx(87)	Opx(88)	?Cpx(82)	?Cpx(83)	Opx(86) Cpx(81)	Cpx(79)
SiO_2	40.4	42.0	44.8	43.0	38.5	38.7	40.5	39.1
TiO_2	7.0	6.3	6.4	5.7	6.5	7.2	5.1	5.0
Al_2O_3	12.8	11.7	12.6	11.6	13.0	13.3	13.6	13.4
Cr_2O_3	-	-	-	-	-	-	0.2	-
FeO	9.6	7.8	8.8	7.1	9.3	9.3	7.3	8.7
MnO	-	-	-	-	-	-	-	-
MgO	16.3	17.3	13.1	17.7	17.5	16.9	18.6	19.1
CaO	0.4	0.3	0.2	-	1.0	0.4	0.2	0.5
K_2O	10.1	10.7	10.1	11.0	10.1	10.2	10.4	10.2
100 Mg/Mg + Fe	75.1	79.8	72.6	81.6	76.8	76.4	81.9	79.6
Si	5.84	6.02	6.36	6.14	5.60	5.61	5.80	5.66
Ti	0.75	0.68	0.69	0.61	0.71	0.78	0.54	0.54
Al	2.09	1.98	2.11	1.94	2.23	2.27	2.30	2.28
Cr	-	-	-	-	-	-	0.02	-
Fe	1.16	0.93	1.04	0.85	1.14	1.13	0.88	1.05
Mg	3.50	3.69	2.76	3.75	3.79	3.66	3.96	4.11
Ca	0.07	0.04	0.03	-	0.16	0.06	0.04	0.08
K	1.87	1.95	1.82	1.99	1.89	1.89	1.91	1.88
Total	15.29	15.29	14.81	15.28	15.52	15.41	15.45	15.60

TABLE 4

Compositions of olivines analysed by microprobe (normalized to 100%)

Run Numbers	7054	7053	7057	7086	7095	7085	7089
Wt.% H_2O added	0	0	0	3.7	3.7	3.7	3.7
Wt.% CO_2 added	0	0	30	3.0	3.0	3.0	3.0
$CO_2/CO_2 + H_2O$	-	-	1	0.25	0.25	0.25	0.25
Pressure (kb)	30	30	30	30	30	30	30
Temperature (°C)	1460	1440	1360	1300	1280	1250	1200
Coexisting primary phase(s)	-	Cpx(89)	-	Cpx(87)	Cpx(85)	Cpx(81) Ph(82)	Cpx(82) Ph(84)
SiO_2	41.5	40.2	41.2	40.7	40.8	39.6	39.8
TiO_2	0.1	0.1	0.2	-	-	0.2	-
Al_2O_3	-	-	0.2	-	-	0.4	-
FeO	5.8	10.5	6.9	10.3	10.4	15.2	15.2
MgO	52.0	48.5	50.4	48.6	48.3	44.2	44.7
CaO	0.6	0.6	0.9	0.4	0.6	0.4	0.3
K_2O	-	0.1	0.2	-	-	-	-
100 Mg/Mg + Fe	94.1	89.2	92.9	89.4	89.2	83.9	84.0
Cations for 4 oxygens							
Si	1.00	0.99	1.00	1.00	1.00	0.99	1.00
Ti	0.002	0.002	0.004	-	-	0.004	-
Al	-	-	0.006	-	-	0.01	-
Fe	0.12	0.22	0.14	0.21	0.21	0.32	0.32
Mg	1.87	1.78	1.82	1.78	1.77	1.66	1.68
Ca	0.02	0.02	0.02	0.01	0.02	0.01	0.01
K	-	0.003	0.005	-	-	-	
Total	3.01	3.01	3.00	3.00	3.00	2.99	3.01

Run Numbers	7055	7098	7097	6654	7074	7064	7066	7060	7075	7106	7080
Wt.% H_2O added	0	2.4	2.4	2.4	6.8	6.8	6.8	6.8	6.8	10.7	10.7
Wt.% CO_2 added	30	5.9	5.9	5.9	16.5	16.5	16.5	16.5	16.5	8.7	8.7
$CO_2/CO_2 + H_2O$	1	0.5	0.5	0.5	0.5	0.5	0.5	0.5	0.5	0.25	0.25
Pressure (kb)	30	30	30	30	20	25	30	30	30	30	30
Temperature (°C)	1340	1380	1340	1300	1160	1170	1220	1200	1160	1200	1140
Coexisting primary phases(s)	Ol	Cpx(89)	Cpx(88)	Cpx(82 Ph(82)	Ph(83)	-	-	-	-	-	Cpx(81) Ph(82)
SiO_2	54.2	55.5	55.4	54.3	54.9	55.4	54.5	55.0	54.8	57.7	56.0
TiO_2	0.6	0.3	0.4	0.6	0.3	0.2	0.3	0.2	0.3	-	0.1
Al_2O_3	5.1	3.4	3.2	4.3	3.5	2.2	2.9	3.4	3.6	1.8	1.8
Cr_2O_3	0.5	0.5	0.4	0.3	0.6	0.2	0.5	0.6	0.3	-	-
FeO	5.5	5.6	6.0	7.7	7.4	7.7	7.6	7.0	8.4	7.5	9.0
MgO	30.7	31.8	31.2	30.1	32.1	32.6	31.7	32.4	30.3	31.6	31.2
CaO	3.4	2.9	3.3	2.6	1.3	1.65	2.4	1.4	2.3	1.3	1.9
Na_2O	-	-	-	-	-	-	-	-	-	-	-
K_2O	0.1	-	0.1	-	-	-	0.1	-	-	0.1	-
100 Mg/Mg + Fe	90.9	90.9	90.2	87.4	88.5	88.3	88.2	89.1	86.6	88.3	86.1
Cations for 6 oxygens											
Si	1.88	1.92	1.92	1.90	1.91	1.93	1.91	1.91	1.92	2.00	1.96
Ti	0.01	0.01	0.01	0.02	0.008	0.01	0.01	0.005	0.01	-	0.004
Al	0.21	0.14	0.13	0.18	0.14	0.09	0.12	0.14	0.15	0.07	0.075
Cr	0.01	0.01	0.01	0.01	0.02	0.01	0.01	0.02	0.01	-	-
Fe	0.16	0.16	0.17	0.23	0.22	0.22	0.22	0.20	0.24	0.22	0.26
Mg	1.59	1.64	1.62	1.57	1.67	1.70	1.66	1.68	1.58	1.63	1.63
Ca	0.13	0.11	0.12	0.10	0.05	0.06	0.09	0.05	0.09	0.05	0.07
Na	-	-	-	-	-	-	-	-	-	-	-
K	0.05	-	0.003	-	-	-	0.003	-	-	0.005	-
Total	3.99	3.99	4.00	3.99	4.00	4.01	4.02	4.01	4.00	3.97	4.00

TABLE 1. Compositions of primary and quench clinopyroxenes analyzed by microprobe (normalized to 100%)

Run Numbers	7052	7053	7057	7055	7098	7098	7097	6654	7086	7095
Wt.% H_2O added	0	0	0	0	2.4	2.4	2.4	2.4	3.7	3.7
Wt.% CO_2 added	0	0	30	30	5.9	5.9	5.9	5.9	3.0	3.0
$CO_2/CO_2 + H_2O$	-	-	1	1	0.5	0.5	0.5	0.5	0.25	0.25
Pressure (kb)	30	30	30	30	30	30	30	30	30	30
Temperature (°C)	1480	1440	1360	1340	1380	1380	1340	1300	1300	1280
Quench (Q) or primary (P)	Q	P	Q	Q	P	Q	P	P	P	P
Coexisting primary phase(s)	Ol	Ol(91)	Ol(93)	Ol,Opx(90)	Opx(91)	Opx(91),Cpx(89)	Opx(90)	Ph(82) Opx(87)	Ol(89)	Ol(89)
SiO_2	46.1	49.5	46.8	47.1	53.0	47.8	52.1	48.2	51.7	52.4
TiO_2	5.4	2.6	4.3	3.8	0.5	3.6	1.1	1.3	1.1	1.0
Al_2O_3	8.9	6.6	8.9	7.5	4.4	9.3	5.1	11.1	5.0	3.5
Cr_2O_3	0.2	0.6	0.3	0.2	0.8	0.2	0.6	0.3	0.7	0.4
FeO	5.2	3.3	4.3	6.7	4.5	6.4	5.3	6.1	4.7	5.1
MgO	19.2	15.6	16.6	21.9	21.7	17.4	22.3	15.8	18.0	16.6
CaO	13.0	21.1	18.3	11.4	14.6	14.6	12.8	15.5	18.1	20.9
Na_2O	0.3	0.2	0.2	-	0.34	0.5	0.3	0.4	0.4	-
K_2O	1.6	0.5	0.3	1.3	-	0.1	0.3	1.3	0.3	0.1
100 Mg/Mg + Fe	86.9	89.3	87.3	85.4	89.5	82.9	88.2	82.2	87.2	85.4
Cations for 6 oxygens										
Si	1.68	1.81	1.71	1.72	1.90	1.73	1.87	1.76	1.87	1.91
Ti	0.15	0.07	0.12	0.10	0.01	0.10	0.03	0.04	0.03	0.03
Al	0.38	0.29	0.38	0.32	0.19	0.40	0.22	0.48	0.21	0.15
Cr	0.01	0.02	0.01	0.01	0.02	0.01	0.02	0.01	0.02	0.01
Fe	0.16	0.10	0.13	0.20	0.14	0.20	0.16	0.18	0.14	0.15
Mg	1.04	0.85	0.90	1.19	1.16	0.94	1.19	0.86	0.98	0.90
Ca	0.51	0.83	0.72	0.45	0.56	0.57	0.49	0.60	0.70	0.82
Na	0.02	0.02	0.01	-	0.02	0.03	0.02	0.03	0.03	-
K	0.07	0.03	0.02	0.06	-	0.01	0.01	0.06	0.01	0.007

Run Numbers	7085	7089	7074	7064	7075	7076	7082	7080	7096
Wt.% H_2O added	3.7	3.7	6.8	6.8	6.8	10.7	10.7	10.7	15
Wt.% CO_2 added	3.0	3.0	16.5	16.5	16.5	8.7	8.7	8.7	0
$CO_2/CO_2 + H_2O$	0.25	0.25	0.5	0.5	0.5	0.25	0.25	0.25	0
Pressure (kb)	30	30	20	25	30	30	30	30	30
Temperature (°C)	1250	1200	1160	1170	1160	1180	1160	1140	1160
Quench (Q) or primary (P)	P	P	Q	Q	Q	?P	P	P	P
Coexisting primary phase(s)	Ol(84),Ph(82)	Ol(84),Ph(84)	Opx(88) Ph(83)	Opx(88)	Opx(87)	-	-	Ph(82) Opx(86)	Ph(80)
SiO_2	50.3	51.3	46.8	50.6	42.9	53.2	52.9	53.5	52.0
TiO_2	1.0	0.8	4.8	1.9	12.3	0.8	0.7	1.3	1.4
Al_2O_3	3.0	5.1	3.5	5.1	5.6	2.9	3.6	3.1	2.3
Cr_2O_3	0.3	0.3	0.1	0.1	0.2	0.2	0.3	0.2	0.4
FeO	6.6	5.5	12.8	9.1	10.2	5.3	5.6	6.6	5.7
MgO	16.1	16.6	14.0	17.8	12.8	15.0	15.2	16.3	14.3
CaO	21.3	19.4	17.4	14.4	12.5	22.1	20.2	17.9	22.7
Na_2O	0.6	0.5	0.4	0.7	0.2	0.4	1.4	0.4	0.7
K_2O	0.6	0.6	0.2	0.1	3.2	0.1	0.1	0.5	0.3
100 Mg/Mg + Fe	81.3	84.4	66.0	77.8	69.1	83.4	83.0	81.5	81.7
Cations for 6 oxygens									
Si	1.87	1.88	1.78	1.86	1.63	1.95	1.94	1.95	1.93
Ti	0.03	0.02	0.14	0.05	0.35	0.02	0.02	0.04	0.04
Al	0.13	0.22	0.16	0.22	0.25	0.12	0.15	0.13	0.10
Cr	0.01	0.01	0.003	0.004	0.01	0.005	0.01	0.006	0.01
Fe	0.21	0.17	0.41	0.28	0.32	0.16	0.17	0.20	0.18
Mg	0.89	0.91	0.79	0.97	0.72	0.82	0.83	0.89	0.79
Ca	0.85	0.76	0.71	0.57	0.51	0.87	0.79	0.70	0.90
Na	0.04	0.03	0.03	0.05	0.02	0.03	0.10	0.03	0.05
K	0.03	0.03	0.01	0.005	0.15	0.006	0.005	0.02	0.01
Total	4.06	4.02	4.03	4.01	3.97	3.98	4.01	3.97	4.01

TABLE 7. Compositions of glasses analysed by microprobe (normalized to 100%).

Run Numbers	B.M.*	7048	7051	7052	7054	7056	7058	7105	7098	7097
Wt.% H_2O added		0	0	0	0	0	0	2.4	2.4	2.4
Wt.% CO_2 added		0	0	0	0	30	30	5.9	5.9	5.9
$CO_2/CO_2 + H_2O$		-	-	-	-	1	1	0.5	0.5	0.5
Pressure (kb)		30	30	30	30	30	30	30	30	30
Temperature (°C)		1560	1520	1480	1460	1380	1370	1400	1380	1340
Coexisting primary phase(s)		-	-	Ol	Ol(94)	-	-	-	Opx(91) Cpx(89)	Opx(90) Cpx(88)
SiO_2	42.4	44.4	43.9	44.5	44.6	46.6	46.6	43.7	42.0	42.4
TiO_2	5.0	5.3	5.3	5.3	5.3	5.2	5.3	4.7	5.5	5.4
Al_2O_3	8.1	8.3	8.2	8.4	8.5	8.3	8.4	7.8	8.7	8.8
Cr_2O_3	0.15	0.1	0.1	0.1	0.2	-	-	-	-	-
FeO	9.5	5.9	6.1	5.5	5.9	4.1	4.4	8.8	9.5	8.8
MgO	16.3	17.0	17.1	17.0	15.8	17.4	17.4	16.5	14.9	14.4
CaO	10.6	11.1	11.2	11.2	11.5	11.3	11.3	10.9	11.0	11.3
Na_2O	0.6	0.4	0.4	0.5	0.4	-	-	-	0.35	0.35
K_2O	7.3	7.6	7.6	7.5	7.8	7.1	6.6	7.4	8.1	8.6
Total	100	100	100	100	100	87.2	86.1	84.4	86.0	85.9
100 Mg/Mg + Fe	75.4	83.7	83.2	84.6	82.7	88.4	87.7	77.0	73.7	74.6

* Biotite mafurite starting glass (see Table 1).

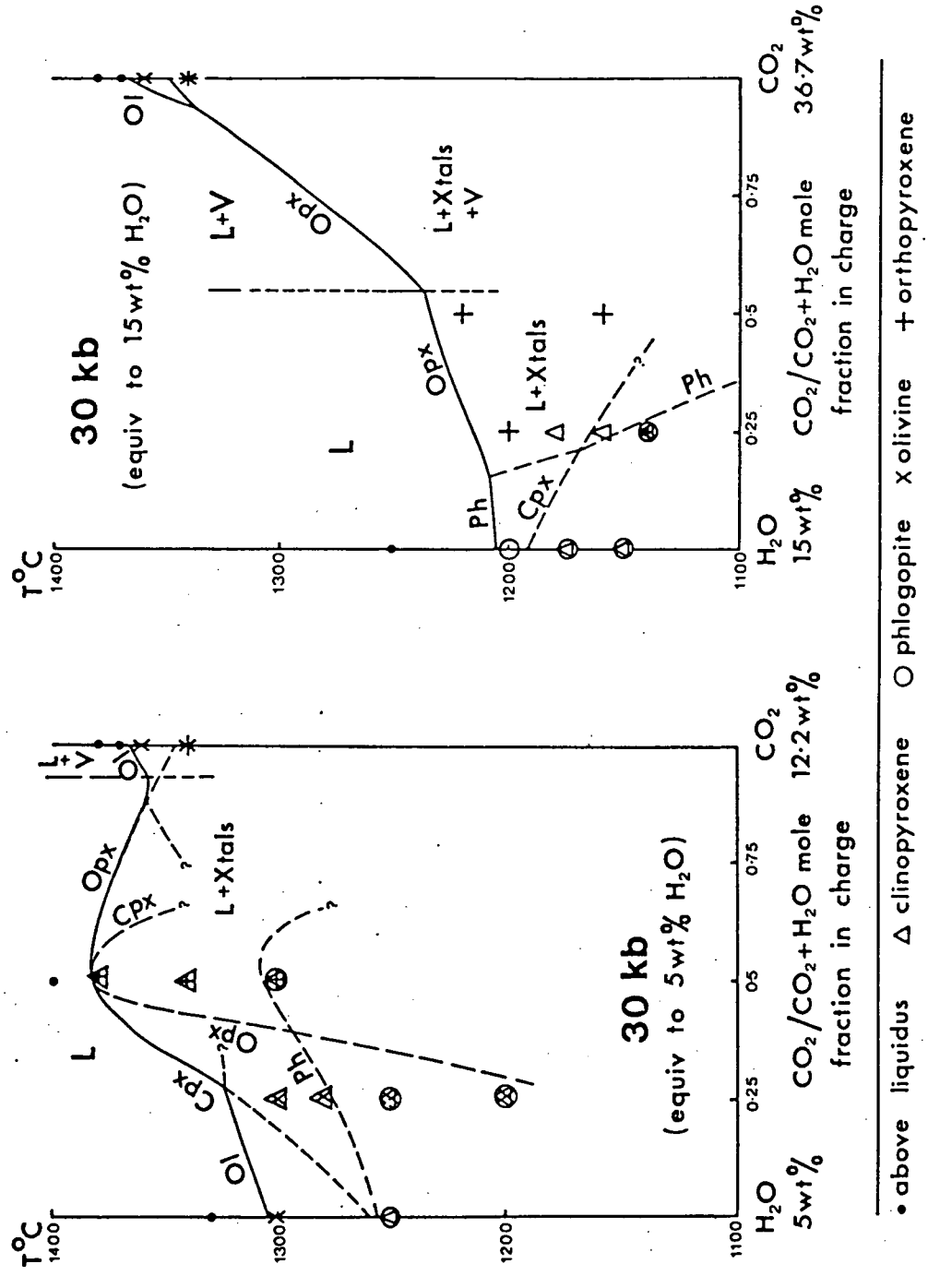

Fig. 1 Phase relations for biotite mafurite at 30 kbar as a function of $CO_2/CO_2 + H_2O$ values in the charge in the presence of an external MH-buffer. Data for compositional joins equivalent to 5 wt.% H_2O (a) and to 15 wt.% H_2O (b). Data for the biotite mafurite - H_2O side were taken from Edgar, Green and Hibberson (1976). Note that at low $CO_2/CO_2 + H_2O$ values, experiments were carried out vapour-undersaturated but were vapour-oversaturated for high $CO_2/CO_2 + H_2O$ values. Phase boundaries are based on the experiments shown and on constraints imposed by fig. 2 and attempts to contour the liquidus surface of fig. 2 for temperature. Ol is olivine; Opx is orthopyroxene; Cpx is clinopyroxene; Ph is phlogopite, L is liquid, V is vapour.

crystallization for primary phlogopite (above 1300°C at 30 kbar) ever observed in experimental runs. It should be, however, kept in mind that phlogopite is not a liquidus phase in these runs and it crystallizes from a liquid enriched in potassium compared with biotite mafurite due to the preceding crystallization of olivine or pyroxenes.

Primary phlogopites from our runs are characterized by slightly lower Mg/Mg + Fe values than co-existing olivines or orthopyroxenes, whereas previously published experimental results for biotite mafurite + H_2O join (Edgar, Green and Hibberson, 1976) show the opposite relation. These differences may be attributed to the fact that our experimental runs were carried out under much more oxidizing conditions than the previous work, and part of the iron in our phlogopites is present in trivalent state. We infer that $Mg^{2+}/Mg^{2+} + Fe^{2+}$ values would be higher than the measured Mg/Mg + total Fe values, derived from microprobe analyses. In the earlier runs (Edgar, Green and Hibberson, 1976) the lower f_{O_2} values would cause little difference between $\frac{Mg^{2+}}{Mg + Fe^{2+}}$ and $\frac{Mg}{Mg+\text{total Fe}}$ values.

TiO_2 contents of our primary phlogopites are somewhat higher than in phlogopites from biotite mafurite + H_2O compositions (Edgar, Green and Hibberson, 1976) synthesized under similar T,P and % H_2O conditions. This may be due to either the differences in oxidation states or to the effect of CO_2 dissolved in the melt on the activity of titanium. We carried out a run without CO_2, but with 15% H_2O at 30 kbar, 1160°C with oxygen fugacity controlled by haematite-magnetite buffer which yielded phlogopite with relatively high TiO_2 content (5 wt. % TiO_2). This result favours the first of the above explanations. Our experiments confirmed the previously observed (Edgar, Green, and Hibberson, 1976) positive correlation between TiO_2 contents of phlogopite and temperatures of equilibration with melt or negative correlation with H_2O content in the system. In fact, primary phlogopites synthesized at 30 kbar, 1300°C, 2.4% H_2O, 5.9% CO_2, are characterized by the highest titanium concentrations

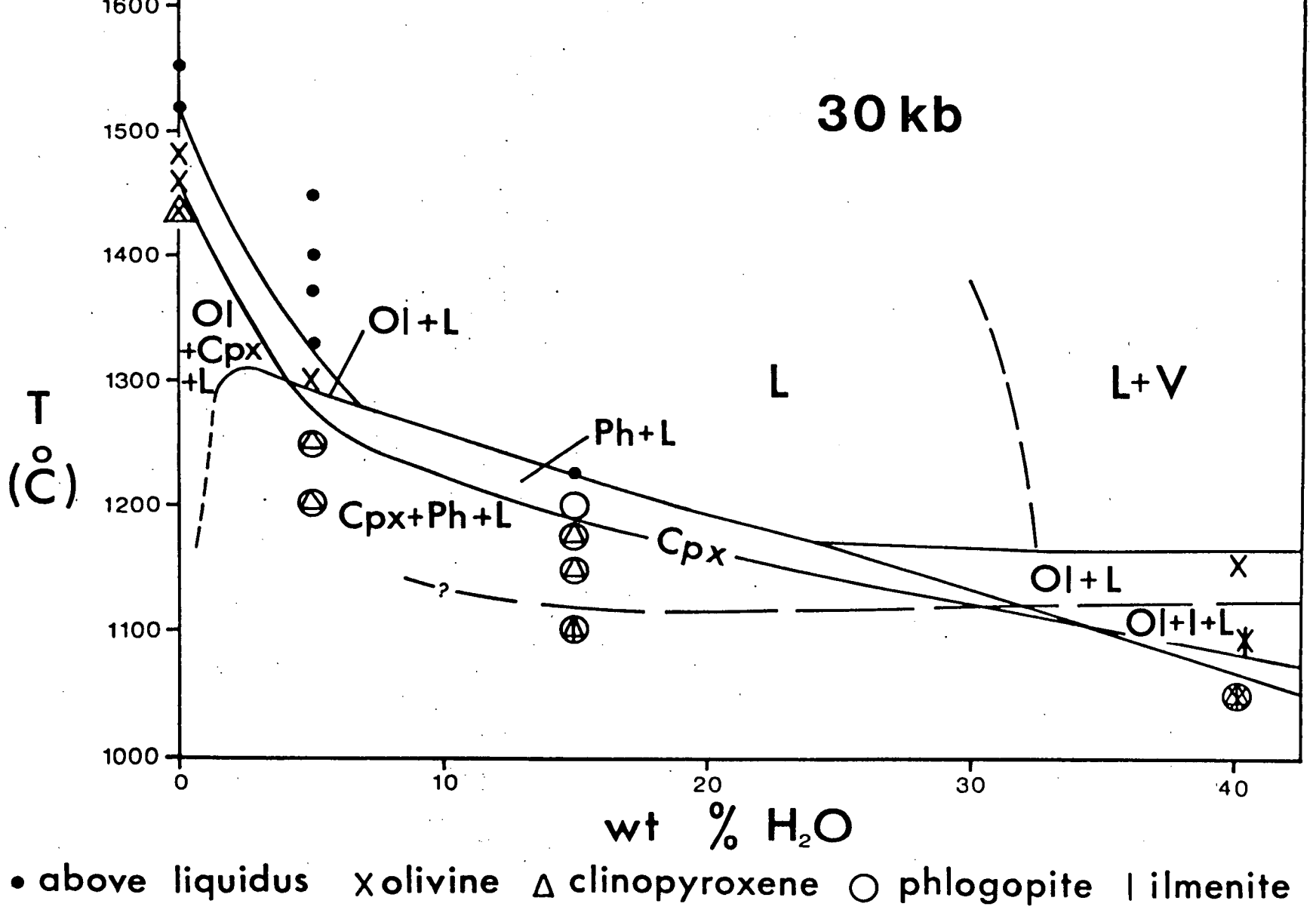

Fig. 2 Phase relations for biotite mafurite at 30 kbar as a function of water content. Data for 5% H_2O, 15% H_2O and 40% H_2O are taken from Edgar, Green and Hibberson (1976) and for anhydrous biotite mafurite from present work.

(8.1% TiO_2). The results of the present study and that of Edgar *et al.* 1976 demonstrate that TiO_2 content of phlogopite positively correlates with increased temperature, increased Fe^{++}/Mg ratio and increased Fe^{+++} content (higher f_{O_2}) and inversely correlates with increased pressure. Of these controls the temperature and Fe^{+++} contents may be the most important.

Distinction between primary and quench phlogopites in the present work was possible on the basis of higher Mg/Mg + Fe values in the former, these values being slightly lower than the Mg-values of coexisting primary orthopyroxene or olivine and similar to clinopyroxene, and on the basis of their textural features. Primary phlogopite in many cases formed equant euhedral grains and in some cases formed very large poikilitic crystals, whereas quench phlogopite usually occurred as elongated laths with complex habits.

Analyses of primary clinopyroxenes show lower Mg/Mg + Fe values than coexisting olivines or orthopyroxenes. As in the case of phlogopite, this atypical relationship may be explained by the presence of a part of the iron as Fe^{3+}. Primary clinopyroxenes are characterized by much lower TiO_2 and Al_2O_3 and higher Cr contents than quench clinopyroxenes. This difference is particularly well illustrated by the comparison of primary and quench clinopyroxenes from the same run carried out at 30 kbar, 1380°C with 2.4% H_2O and 5.9% CO_2 (see Table 6). CaO contents of clinopyroxenes are variable and reach minimum values at higher temperatures in clinopyroxenes coexisting with orthopyroxenes. Clinopyroxenes which are not coexisting with orthopyroxene contain higher CaO contents but those clinopyroxenes crystallized from melts containing CO_2 characteristically contain lower CaO contents than those precipitated from CO_2-free liquids. These relationships suggest that activity of diopside component in the melt is reduced by bonding of Ca^2 and CO_3^{2-} within the melt.

In the products of three runs, it was possible to analyse both quenched glass and primary crystals. $\left(K_D^{Mg/Fe}\right)^{\ell/c} = (Mg/Fe)^{melt}/(Mg/Fe)^{crystals}$ values are 0.30 for olivine and 0.33 for orthopyroxene which is in the range of K_D values measured for these minerals and melts of various compositions (Green and Ringwood, 1967; Roeder and Emslie, 1970). $\left(K_D^{Mg/Fe}\right)^{\ell/c}$ values for phlogopite and clinopyroxene reflect the Fe^{+++} present in these phases.

Petrogenetic Implications

Previous experiments (Edgar *et al.* 1976) demonstrated that over a wide P,T, % H_2O range orthopyroxene did not appear within the melting interval of biotite mafurite, implying that the melt of biotite mafurite composition was not derived through the partial melting of a mantle mineral assemblage including Ol + Cpx + Opx with water as the only volatile component. In contrast, the present study demonstrates that, in the presence of CO_2 in addition to H_2O, biotite mafurite melt may become saturated with respect to orthopyroxene thereby allowing the possibility of generation of silicate liquids similar to biotite mafurite magma in the course of the partial melting of mineral assemblages typical for upper mantle peridotite. The appearance of orthopyroxene in the melting range of this silica-undersaturated, highly calcic and alkaline (potassic) rock results from drastic reduction in the activities of CaO and alkalis due to the interaction of these components with $(CO_3)^=$ complexes. A similar effect was observed in a number of other silicate + H_2O + CO_2 systems (Eggler, 1974; Brey and Green, 1975) and was anticipated on the basis of general consideration of the interaction of basic cations with acid volatile compounds (Ryabchikov and Kogarko, 1963; Kushiro, 1975).

In order to apply the results of our experiments to the elucidation of the composition of silicate liquids which may be derived during the

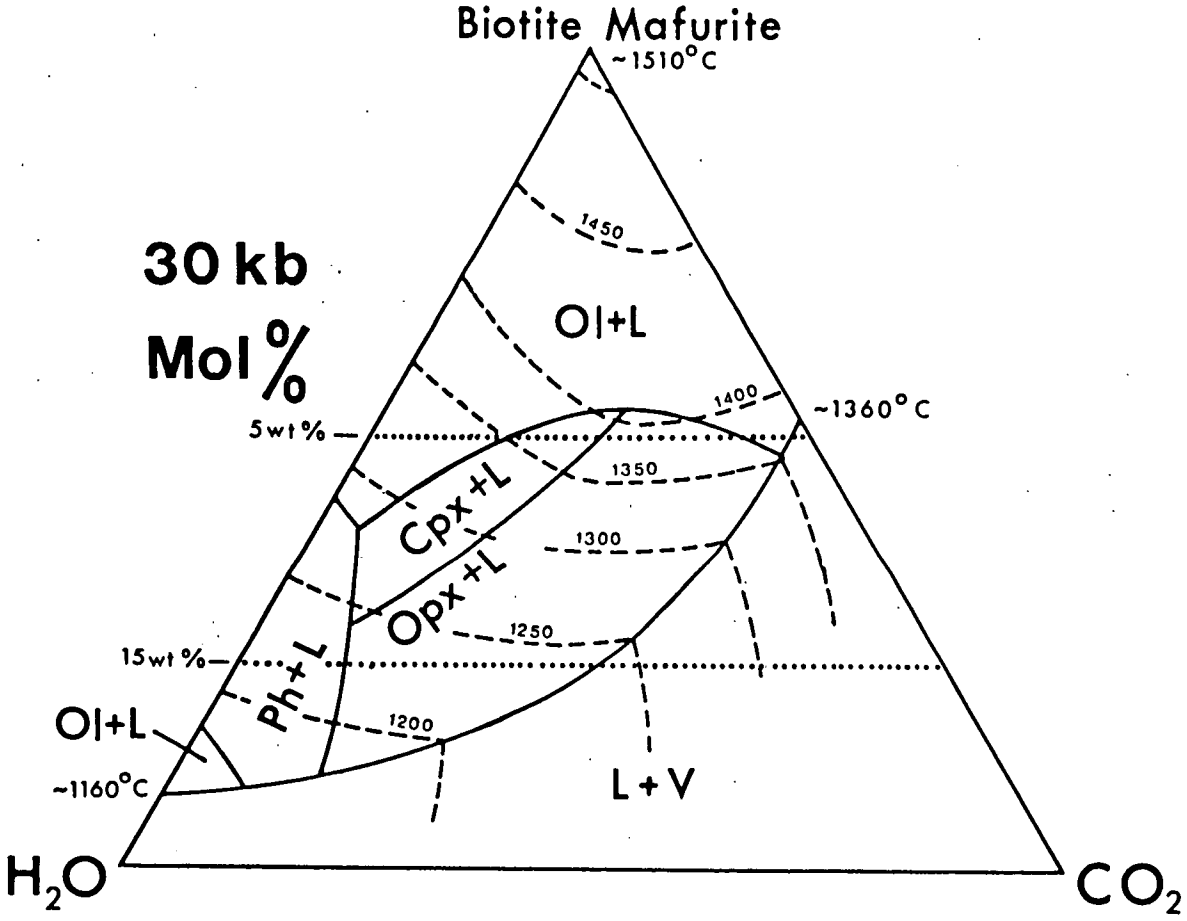

Fig. 3 Schematic diagram showing approximate position of liquidus fields of various minerals in the system biotite mafurite-H_2O-CO_2 at 30 kbar. Molecular weight of biotite mafurite is assumed to be equal to 308.3 g (equivalent to 8 oxygen atoms).

partial melting of phlogopite-bearing mantle we constructed a schematic diagram showing the position of the liquidus fields of various minerals in biotite mafurite as a function of H_2O and CO_2 concentrations in the melt (Fig. 3). The vapour saturation boundary is tentatively drawn in the compositional triangle by analogy with the data for olivine melilitite (Brey and Green, 1977). Although boundaries between the liquidus fields of the various crystalline phases are drawn as lines, they are more probably bands in which two neighbouring phases coexist with liquid (cf. Brey and Green, 1977). It can be seen from this diagram that there are three 'points' where three crystalline phases may simultaneously coexist with the liquid of biotite mafurite composition: A - Ph + Opx + Cpx + Liq; B - Opx + Ol + Cpx + Liq; C - Ph + Ol + Cpx + Liq.

Point A corresponds to $CO_2/CO_2 + H_2O \approx 0.15$. The phase assemblage at this point includes phlogopite but not olivine, and therefore we may infer that if the $CO_2/CO_2 + H_2O$ ratio in the melt is approx. 0.1-0.2, then the silicate liquid coexisting with Ph + Ol + Opx + Cpx assemblage should be characterized by approximately the same K_2O content (~7 wt.%) as the investigated biotite mafurite, but it would be somewhat less silicic. On the other hand, inasmuch as clinopyroxenes in our experiments contain less Na_2O than subsolidus clinopyroxenes in pyrolite under comparable P,T conditions (Green, 1973), we may expect that partially melted phlogopite-bearing pyrolite should yield silicate liquid with higher Na_2O content than biotite mafurite. Near-liquidus clinopyroxenes in the olivine melilitite + H_2O + CO_2 system at 30 kbar are characterized by approximately the same Na_2O concentrations as subsolidus pyrolite (Brey and Green, 1975), and consequently, melts equilibrated with phlogopite-bearing mantle mineral assemblage should contain Na_2O in similar amounts to olivine melilite (3-4 wt.% Na_2O) and K/Na ratio in such melts may be estimated as equal to 1.2-1.5.

Point B with $CO_2/CO_2 + H_2O \tilde{\sim} 0.7$ corresponds to Ol + Opx + Cpx + Liq phase assemblage in which phlogopite is absent, and therefore silicate melts with $CO_2/CO_2 + H_2O > 0.5$ in equilibrium with Ph + Ol + Opx + Cpx would contain more than 7 wt.% K_2O, and thus have K/Na > 1.5.

At point C, $CO_2/CO_2 + H_2O \tilde{\sim} 0.05$, and since the phase assemblage does not include orthopyroxene, we may conclude that liquids with low $CO_2/CO_2 + H_2O$ ratios equilibrated with Ph + Ol + Opx + Cpx would contain about 7 wt.% K_2O, but they should be more silicic and probably less calcic and less alkaline than liquids with higher CO_2 contents in equilibrium with the same assemblage (cf. Green, 1973).

It must be noted that garnet did not appear among the near-liquidus minerals at 30 kbar in the biotite mafurite composition. This mineral, however, was found in the melting interval of another highly potassic magmatic rock (olivine leucitite, Cundari and O'Hara, 1976) at pressures above 30 kbar and therefore it might be expected that the above conclusions should be also qualitatively valid for the melting of Ph + Ol + Opx + Cpx + Gar phase assemblage at pressures higher then 30 kbar.

Summing up the results of the present study, we may state that in the presence of both H_2O and CO_2 at high pressures, very small degrees of melting of a lherzolite such that phlogopite is not eliminated as a residual phase will yield a highly potassic, silica-undersaturated liquid composition. The source rock for such magmas may be locally enriched in phlogopite but contains the normal mantle residual phases olivine + orthopyroxene + clinopyroxene ± garnet. The parental magmas of olivine leucitite, ugandite or biotite mafurite type are inferred to be products of very small degrees of partial melting of phlogopite-bearing lherzolite in the presence of both H_2O *and* CO_2 in the source region.

Acknowledgements

This work has been done when one of the authors (I.D.R.) was visiting the Research School of Earth Sciences, Australian National University under the Australian-USSR Agreement on Scientific Exchange. I.D.R. thanks R.S.E.S. A.N.U. for hospitality and making available research facilities. The instruction of W.O. Hibberson in experimental techniques and of N.G. Ware in microprobe analyses are greatly appreciated. We thank Dr. Fildes and her assistants, John Curtin School of Medical Research, A.N.U. for carrying out CO_2 determinations. We acknowledge the benefit of many discussions with G.P. Brey and T. Mori (R.S.E.S., A.N.U.) and with Dr. A. Cundari (University of Melbourne).

References

Brey, G.P., 1976, CO_2 solubility and solubility mechanisms in silicate melts at high pressures. Contrib. Mineral. Petrol., v. 57, 215-221.

Brey, G.P. and Green, D.H., 1975, The role of CO_2 in the genesis of olivine melilitite. Contrib. Mineral. Petrol., v. 49, 93-104.

Brey, G.P. and Green, D.H., 1976, Solubility of CO_2 in olivine melilitite at high pressures and role of CO_2 in the earth's upper mantle. Contrib. Mineral. Petrol., v. 55, 217-230.

Brey, G.P. and Green, D.H., 1977, Petrogenesis of olivine melilitite. Contrib. Mineral. Petrol.(in press)

Carmichael, I.S.E., 1967, The mineralogy and petrology of the volcanic rocks from the Leucite Hills, Wyoming. Contrib. Mineral. Petrol., v. 15, 24-66.

Cundari, A. and O'Hara, M.J., 1976, Experimental study at atmospheric and high pressures of a mafic leucitite from New South Wales, Australia. In: Progress in Experimental Petrology. Third Progress Report, NERC Publ. Ser. D N6, Manchester and Edinburgh.

Edgar, A.D., Green, D.H. and Hibberson, W.O., 1976, Experimental petrology of a highly potassic magma. Jour. Petrology, v. 17, part 3, 339-356.

Eggler, D., 1974, Effect of CO_2 on the melting of peridotite. Ann. Rept. Dir. Geophys. Lab., Washington, Y.B. 73, 215-224.

Green, D.H., 1973, Conditions of melting of basanite magma from garnet peridotite. Earth Planet. Sci. Lett., v. 17, 456-465.

Green, D.H., and Ringwood, A.E., 1967, The genesis of basaltic magmas. Contrib. Mineral. Petrol., v. 15, 103-190.

Green, T.H., Ringwood, A.E. and Major, A., 1966, Friction effects and pressure calibration in a piston-cylinder apparatus at high pressure and temperatures. Jour. Geophys. Res., v. 71, 3589-3594.

Holmes, A., 1942, A suite of volcanic rocks from south-west Uganda containing kalsilite (a polymorph of $KAlSiO_4$). Mineral. Mag.,v.26,197-217.

Holmes, A., 1952, The potash ankaratrite-melaleucitite lavas of Nabugando and Mbugo craters, south-west Uganda. Trans. geol. Soc. Edinb., v. 15, 187-213.

Kushiro, I., 1975, On the nature of silicate melt and its significance in magma genesis: regularities in the shift of the liquidus boundaries involving olivine, pyroxene, and silica minerals. Am. J. Sci., v. 275, 411-431.

Lindgren, F.T., Stevens, G.R. and Jensen, L.C., 1972, Elemental C, H and N microanalysis of crushed rock and soil samples. J. Am. Oil Chem. Soc., v. 49, 208-214.

Reed, S.J.B. and Ware, N.G., 1973, Quantitative electron microprobe analysis using a lithium drifted silicon detector. X-ray Spectrometry, v. 2, 69-74.

Roeder, P.L. and Emslie, R.F., 1970, Olivine-liquid equilibrium. Contrib. Mineral. Petrol., v. 29, 275-289.

Ryabchikov, I.D. and Kogarko, L.N., 1963, The effect of anionic substitution on the acidity of magmatic melt (in Russian). Geokhimiya, N3.

Sobolev, V.S., 1975

B28

9. Petrogenesis of Mid-ocean Ridge Basalts

D. H. GREEN, W. O. HIBBERSON
and A. L. JAQUES

Abstract

The liquidus and near-liquidus crystallization of primitive, mid-ocean ridge basalt (DSDP3-18-7-1) has been studied experimentally from 0–15 kbar. Olivine is the liquidus phase at low pressure (<12 kbar) and is joined by plagioclase (An_{78}) and clinopyroxene at lower temperature. Calcium-rich clinopyroxene becomes the liquidus phase at ≥12 kbar and there is no liquidus or near-liquidus field for orthopyroxene. Orthopyroxene addition experiments confirm that the liquid composition is not close to saturation with orthopyroxene. The low-pressure experiments show that DSDP3-18-7-1 could be a derivative liquid by olivine fractionation from a more olivine-rich parent. Olivine addition experiments show that a picritic composition (83 per cent DSDP3-18-7-1 + 17 per cent olivine) is saturated with olivine + orthopyroxene at ~20 kbar, 1430 °C.

An earlier model for genesis of mid-ocean ridge, high-Al_2O_3 olivine tholeiites by magma segregation from pyrolite at 9–10 kbar is retracted. The primary magma for high-Al_2O_3 mid-ocean ridge olivine tholeiites is considered to be tholeiitic picrite, segregated from residual harzburgite at ~20 kbar, 1430 °C. The primary tholeiitic picrite contains ~25 per cent normative olivine, with SiO_2 ~48 per cent, MgO ~16 per cent, 100Mg/(Mg+Fe) ≈ 79, ~600 p.p.m. Ni and was strongly depleted in incompatible elements. The experimental studies show that there can be no simple genetic relationship between the primary tholeiitic picrite magmas which are parental to common mid-ocean ridge basalts, and the residual harzburgite or accumulate peridotite, pyroxenite, anorthosite or troctolite of ophiolite complexes. Similarly, the tholeiitic picrite magmas cannot precipitate the highly calcic plagioclase (>An_{80}) or magnesian clinopyroxene (>Mg_{88}) megacrysts which they sometimes contain. It is argued that there must exist, in mid-ocean ridge environments, a second magma type with high SiO_2 (>50 per cent?), very high CaO/Na_2O and very low TiO_2. This magma type, and its fractionation products, are assigned a complementary relation to ophiolite complexes, and it is suggested that both arise as a consequence of shallow emplacement and second-state melting of diapirs of refractory lherzolite or harzburgite.

The experimental data on DSDP3-18-7-1 are used to calculate a model source composition which differs significantly from previous estimates of the source pyrolite

for mid-ocean ridge basalts. The source pyrolites for mid-ocean ridge tholeiites and "Hawaiian" or "incompatible element enriched" tholeiites are both considered to occur within the upper mantle and to characterize a chemically zoned low-velocity zone.

1. Introduction

The production and emplacement of basaltic magmas at mid-ocean ridges is volumetrically the most important step in the geochemical differentiation of the Earth's mantle. A common view is that this process yields a basaltic oceanic crustal layer about 10 km thick, overlying residual upper mantle peridotite of dunite, harzburgite or lherzolite character. The basaltic crustal layer is considered to be lithologically complex but with an idealized depth profile grading downwards from pillow lavas, through a sheeted dolerite dyke complex, to an underlying layer rich in gabbro and dolerite intrusions which individually pass downwards into layered accumulate sequences of gabbro, anorthosite, pyroxenite, troctolite and peridotite. The effects of low-grade metamorphism, particularly hydration reactions, on this idealized crustal section, produce chemical change and patchy alteration to greenschists and amphibolites.

There is a common view that the tectonically-emplaced associations of deep-sea sediments, pillow lavas, dolerites, gabbros, layered mafic-ultramafic complexes and ultramafic tectonites (collectively called the "ophiolite suite") occurring in many orogenic belts are uplifted sections through the oceanic crust. Furthermore, many authors have recognized that both ocean floor basalts and basalts of ophiolite suites commonly include lavas that have been fractionated by separation of olivine, pyroxene and plagioclase from more magnesian parental lavas. It has been inferred that the layered accumulate sequences of the oceanic crust and of ophiolite suites were formed as the complementary accumulates to the fractionation of mid-ocean ridge basalts (Bonatti *et al.*, 1971; Cann, 1974; Davies, 1971; Melson and Thompson, 1970; Moores and Vine, 1971; Hodges and Papike, 1976).

The rapid accumulation of data from the DSDP program and the FAMOUS project and the application of a variety of geochemical analytical tools to the study of ocean floor basalts have brought about a situation in which it should be possible to define more closely the processes of magma formation beneath mid-ocean ridges, the compositions of source rocks, and the nature of crystal fractionation processes and of crystalline accumulates. One essential ingredient to understanding of mid-ocean ridge magmatism is a knowledge of the phase relationships of both magmas and possible source compositions. In this paper we present part of our data gathered for this

purpose and explore the relevance of the data to the general model of oceanic crust and ophiolite genesis.

2. "Primary" Magmas

Mid-ocean ridge basalts are the products of crystallization of magmas consisting of silicate liquid, variable proportions of phenocrysts and xenocrysts (Donaldson and Brown, 1977) and very minor inclusions of immiscible sulphide liquid (Mathez, 1976). Analyses of quenched glasses avoid the problem of contamination by xenocrysts and enrichment by settling of phenocrysts and are a reasonable first step towards establishing the compositions of parental, mantle-derived liquids and derivative, fractionated liquids. Since the first phases to crystallize from mid-ocean ridge basalts are magnesian olivine, magnesian clinopyroxene and calcic plagioclase, the most "primitive" liquids can be selected as those glass analyses having the highest Mg/(Mg+Fe) and/or Ca/(Ca+Na) ratios.

We use the term "primary magma" to refer to a magma which has not changed composition by crystal fractionation, contamination or volatile loss between the time of *magma segregation* from residual crystals of the source rock and the time of extrusion and quenching. Green and Ringwood (1967) discussed the concept of an "event" (time and depth) of magma segregation and showed that "primary magma" compositions are determined by crystal–liquid equilibria between residue and melt at the conditions of magma segregation. The ascent of a peridotite diapir consisting of crystalline residue and a minor liquid fraction, both changing composition with changing pressure and temperature during movement of the diapir, is considered to be the prime cause of magma generation in the upper mantle (Verhoogen, 1954; Green and Ringwood, 1967). Readjustment of equilibrium, i.e. change in composition of crystals and liquid, will occur until the liquid segregates from the solid residue (this will happen rapidly if the melt fraction exceeds 20–30 per cent, Green and Ringwood, 1967; Arndt, 1977). We refer to the liquid at this point as a *primary* liquid and the experimental petrologist, given the composition (including H_2O, CO_2 contents) of such a primary liquid, sets out to establish the P, T conditions at which it is multiply saturated with the inferred residual minerals; i.e. in the case of a peridotite source and basaltic magma, saturated with olivine ± orthopyroxene ± clinopyroxene ± garnet, spinel or plagioclase.

The above model of melting and magma segregation is the simplest one and we can devise more complex models. It is possible that a peridotite diapir at, say, 60 km depth may contain 10 per cent melt, half of which may segregate as basalt A leaving entrapped liquid among the residual crystals. We now have effectively a new source peridotite composition which may

continue to rise and, as the melt fraction increases with decreasing depth, segregate a further melt fraction as basalt B derived by 20 per cent melting at ~20 km depth. If basalts A and B are sampled at the surface, both are primary magmas in the sense used here and the experimental petrologist should be able to define the depth of magma segregation and nature of residual minerals for each of basalt A and B. The source compositions for basalts A and B will, however, differ and the experimental petrologist cannot proceed further to relate these source compositions. Thus conceptual models such as the "dynamic melting model" of Langmuir *et al.* (1977) or the models of sequential batch extraction of Arndt (1977) are equally suited to establishment of "depth of magma segregation" by the experimental approach, but differ from the simple partial melting or batch melting and extraction model in that the "source composition" is not fixed but varies from an original "undepleted" mantle composition towards increasingly refractory residual compositions.

Other models of melting of mantle peridotite which include mixing of already segregated magmas or include fractional melting (i.e. a melt (A) formed at T_1 is segregated from reaction with residual crystals; at $T_1 + \Delta T$ a second melt (A') forms from residual crystals, segregates and is added to A, etc. (Presnall, 1969)) are not amenable to the experimental approach, i.e. the compositions of the liquids so formed differ from those originally in equilibrium with residual crystals and one cannot correlate liquidus phases of the observed liquids with residual phases for the (unknown) individual increments of magma.

In a sequence of earlier related papers (see review by Green, 1976*a*), it has been profitable to explore the range of primary magmas which can be explained by the simple model of batch partial melting and magma segregation based on

(a) a constant anhydrous source peridotite composition (P and T variable);
(b) a constant source peridotite composition but with addition of variable amounts of water (P, T, per cent H_2O variable);
(c) a constant source peridotite composition but with variable H_2O and CO_2 contents (P, T, per cent CO_2 variable).

However, even from the earliest of these papers, it has been accepted that the constant source peridotite composition is an oversimplification (Green and Ringwood, 1967; Green, 1968, 1970, 1971; Frey and Green, 1974; Frey *et al.*, 1978) and that inhomogeneity, particularly in incompatible element contents, was present in the upper mantle source regions for basalts. The study of mantle derived xenoliths and of mantle-derived peridotite diapirs (Lizard, Tinaquillo, Beni Bousera, Serrania del Ronda) is one way of

exploring mantle inhomogeneity and detailed geochemical studies emphasize that peridotites of these types have complex histories (Frey, 1969; Frey and Green 1974; Frey and Prinz, 1977). However, the relationship of such peridotites to basalt genesis is unclear and it is therefore necessary to examine the basalts themselves to investigate mantle inhomogeneity. If specific basalts can be identified as primary basalts and the nature of the melting conditions and residue specified, then source compositions can be estimated and compared. The use of basalts to determine regional and/or depth variations of mantle composition is still some way off, but this approach may well be important in understanding mantle and crust evolution—it is already apparent that models of mantle evolution based on trace element abundances and isotopic measurements (e.g. U/Pb and Pb isotopes; RB/Sr and Sr isotopes, Sm/Nd and Nd isotopes) need to be constrained by petrogenetic models which consider phase equilibria, major element geochemistry and well-determined element partition coefficients. The converse of this statement is equally valid.

2.1. Primary Basalts of the Ocean Floor

The arguments favouring an upper mantle composition of peridotite with 3–4 per cent CaO, 3–4 per cent Al_2O_3 and dominated (>50 per cent) by olivine (Fo_{88-90}) have been given elsewhere. If we consider equilibrium partial melting of such source peridotite to leave a more refractory residue (olivine of Mg_{88-92}) then liquids should have Mg values (Mg/(Mg+Fe))= 0.68–0.78 for up to approx. 30 per cent melting (Green and Ringwood, 1967; Roeder and Emslie, 1970; Green, 1970, 1971).

Most ocean floor basalts have Mg values less than this (and contain less than 9 weight per cent MgO) and have probably undergone pre-eruptional fractional crystallization of olivine, spinel and in many cases, plagioclase and pyroxene (e.g. Kay *et al.*, 1970; Miyashiro *et al.*, 1969; Shido *et al.*, 1971; Frey *et al.*, 1974; Bryan *et al.*, 1976; Bryan and Moore, 1977). The apparent cut-off at about 9 weight per cent MgO and 200 p.p.m. Ni (Mg value $\simeq$65) led Kay *et al.* (1970) to suggest that these features typified relatively undifferentiated basalts. More magnesian lavas with Mg values of 68–72 have been reported by Frey *et al.* (1974) at DSDP 3-14, 18, by Melson *et al.* (1977) in a survey of abyssal glasses, and by Blanchard *et al.* (1976) and Bence and Taylor (1977) for DSDP 37-332B. Sampling by submersibles in the rift zone of the mid-Atlantic Ridge in the FAMOUS area has provided a large suite of highly magnesian glasses (Mg_{70-72}), e.g. Bryan and Moore (1977), Langmuir *et al.* (1977), Melson *et al.* (1977).

Examination of analyses of these relatively unfractionated basalts reveals that most have high Al_2O_3 content (>16 per cent), Al_2O_3/CaO ratios of

≈ 1.3, high MgO (9–10 weight per cent), mostly low TiO_2 (<0.75 weight per cent), low Na_2O (<2.5 weight per cent), and high CaO/Na_2O ratios (>5). Fractionation by olivine, plagioclase and clinopyroxene will lead to decrease in Mg value and in Ca/Na. Silica contents are mostly in the range 48–49 weight per cent and the percentage of normative olivine ranges from about 10 to 20, averaging 12–14 per cent.

A basalt glass from the south Atlantic (Frey *et al.* 1974, Leg 3, Site 18, Sample 3-18-7-1) was chosen for experimental study. Frey *et al.* (1974) showed that this glass ($Mg_{69.5}$) which contains microphenocrysts of olivine ($Fo_{89.7-89.2}$) and of plagioclase (An_{79}) is strongly depleted in light rare-earth elements and has very low contents of large-ion lithopile (LIL) elements together with high NiO and Cr_2O_3 contents. The compositional characteristics of this basalt strongly suggests that it may be parental to other ocean floor basalts by olivine and plagioclase fractionation and, on the basis of its Mg value and olivine microphenocryst composition, it is a possible primary melt from mantle peridotite containing olivine (Mg_{88-92}). This basalt is not reported to contain megacrysts of olivine ($>Mg_{90}$) or calcic plagioclase ($\sim An_{85-95}$) unlike other examples of ocean floor glasses (Donaldson and Brown, 1977; Bryan *et al.*, 1976; Blanchard *et al.*, 1976).

The experimental study was directed towards establishing the liquidus phases for the chosen basalt, with the hope that some condition would be found at which olivine, orthopyroxene and possibly clinopyroxene occurred together on the liquidus, this condition then defining the probable depth of magma segregation from residual harzburgite or lherzolite for this particular magma.

3. Experimental Petrology of a Mid-ocean Ridge Basalt

The composition of the glass prepared for experimental study is listed in Table 1. Experiments at 0 kbar were carried out by placing ~20 mg sample in spec-pure iron capsules which were sealed in evacuated silica tubes and suspended in a 1-atm quenching furnace. Since previous experience, particularly on lunar compositions, had demonstrated that plagioclase nucleation and crystallization could be sluggish using glass starting material, the low-pressure (0 kbar, 5 kbar) runs used a fine-grained crystalline sample prepared by devitrifying a 250 mg sample of the glass to pyroxene + plagioclase + olivine assemblage at 0 kbar, 1050 °C, 5 h. To confirm that plagioclase observed at 0 kbar, 1210 °C (Run A520, Table 2) was stable and not relict from the starting material and to provide coarser crystals for microprobe analysis, a repeat run at 0 kbar, 1210 °C used a starting mix of (90 per cent glass + 10 per cent Run A520).

The problem of sample containers in experimental melting studies has been explored in lunar studies (O'Hara *et al.*, 1975; O'Hara and Humph-

Table. 1. Compositions used in experimental study.

	Glass of DSDP3-18-7-1 Composition	91 per cent DSDP3-18 +9 per cent olivine Mix D	83 per cent DSDP3-18 +17 per cent olivine Mix E
SiO_2	49.7	48.9	48.3
TiO_2	0.72	0.65	0.60
Al_2O_3	16.4	14.9	13.7
FeO	7.9	7.9	7.9
MnO	0.12	0.12	0.12
MgO	10.1	13.6	16.7
CaO	13.1	11.9	10.9
Na_2O	2.0	1.80	1.65
K_2O	0.01	0.01	0.01
Cr_2O_3	(0.07)†	(0.06)†	(0.06)†
NiO	(0.03)†	0.05	0.08
CIPW Norms			
Or	0.06	0.05	0.05
Ab	16.7	15.2	14.0
An	35.9	32.6	29.9
Di	23.4	21.3	19.5
Hy	10.0	9.1	8.3
Ol	12.6	20.5	27.1
Ilm	1.4	1.25	1.1
100 Mg/(Mg+Fe)	70.9	75.4	79.0

† These components were not added to the synthetic mix but the values given are those for the natural rock (Frey *et al.*, 1974)

eys, 1977; Green *et al.* 1975). Noble metal capsules (Pt, AgPd) result in Fe oss to the container and sample compositions must be monitored carefully. At low pressure (<5 kbar approx.) graphite capsules precipitate metallic ron from the charge. High-purity magnetic iron has similar problems at oth low and high pressure. Spec-pure iron is suitable at low and high ressure except that Fe_2O_3 in the charge must be assumed to be reduced to eO and the sample bulk composition after the run should be monitored to heck for composition change either by addition of iron or reduction of FeO o metallic iron. Graphite is suitable as a container at pressures ≥ 10 kbar in he sense that the C–$(CO_3)^{2-}$ oxygen buffer appears to lie below the QFM xygen buffer, but poses an uncertain risk at high pressure as (CO_3^{2-}) is oluble in natural basalts at high pressure and has been shown to affect the ature of phases on the liquidus at high pressure (Brey and Green, 1975, 977). The best technique available for dry experiments is to use graphite apsules but to carry out confirmatory near-liquidus runs in spec-pure Fe

capsules to ascertain that depression of liquidus and change of liquidus phases due to $(CO_3)^{2-}$ solubility have not occurred. The experiments in spec-pure Fe capsules must be monitored for gain of FeO.

The experimental techniques and composition used however are unsuitable for evaluation of the role of chrome spinel—trace quantity of Cr_2O_3 was not added to the DSDP 3-18 composition—and the low f_{O_2} of the experiments would have inhibited spinel crystallization. Thus in the discussion and application of our experiments we cannot comment on the presence or absence of chrome spinel as a near-liquidus phase in DSDP 3-18.

In the present study, spec-pure Fe capsules were used at 5 kbar and both graphite and spec-pure Fe were used at $\geqslant 10$ kbar. The compositions of above-liquidus runs at 0, 10, 12 and 13 kbar were determined by electron microprobe analysis. This confirmed that there was no composition change in graphite capsules at 10, 12 and 13 kbar, and only very minor addition of Fe in the spec-pure Fe capsule at 0 kbar, but that the above liquidus run in spec-pure Fe at 10 kbar had absorbed iron to change its Mg value from 69.5 to 67.7 (i.e. 7.85 per cent FeO → 8.25 per cent FeO).

The composition of near-liquidus crystalline phases and of glass were determined by electron microprobe analysis and the phase relationships and compositional data are summarized in Fig. 1 and Table 2. At low pressure (0 kbar, 5 kbar) olivine (Mg_{88}) is the liquidus phases and crystallizes alone over a 10–30 °C temperature interval. Plagioclase (An_{78}) is the second phase to appear at both 0 kbar and 5 kbar. Analyses of crystal and liquid compositions show that 3 ± 0.5 per cent olivine crystallized from the melt at 0 kbar prior to the liquid reaching the plagioclase saturation surface. At 5 kbar and 10 kbar, less olivine crystallizes before reaching the plagioclase saturation surface and at 10 kbar the liquid becomes saturated with clinopyroxene and plagioclase together (within the resolution of the experimental data) and after separation of ~ 1 per cent olivine. The effect of pressure in the 0–10 kbar interval on the anhydrous, near-liquidus crystallization is to move the olivine–plagioclase cotectic towards more olivine-rich composition, and to expand the field of clinopyroxene crystallization towards both olivine- and plagioclase-rich compositions. The composition of plagioclase at its first appearance also becomes less anorthite-rich at higher pressure (An_{78}–0 kbar, An_{77}–5 kbar, An_{73}–10 kbar, An_{69}–12 kbar)—this may be attributed to the appearance and coprecipitation of calcium-rich clinopyroxene, but the analytical data also show a decrease in

$$\frac{(Ca/Na)_{plag}}{(Ca/Na)_{liq}}$$

with increasing pressure.

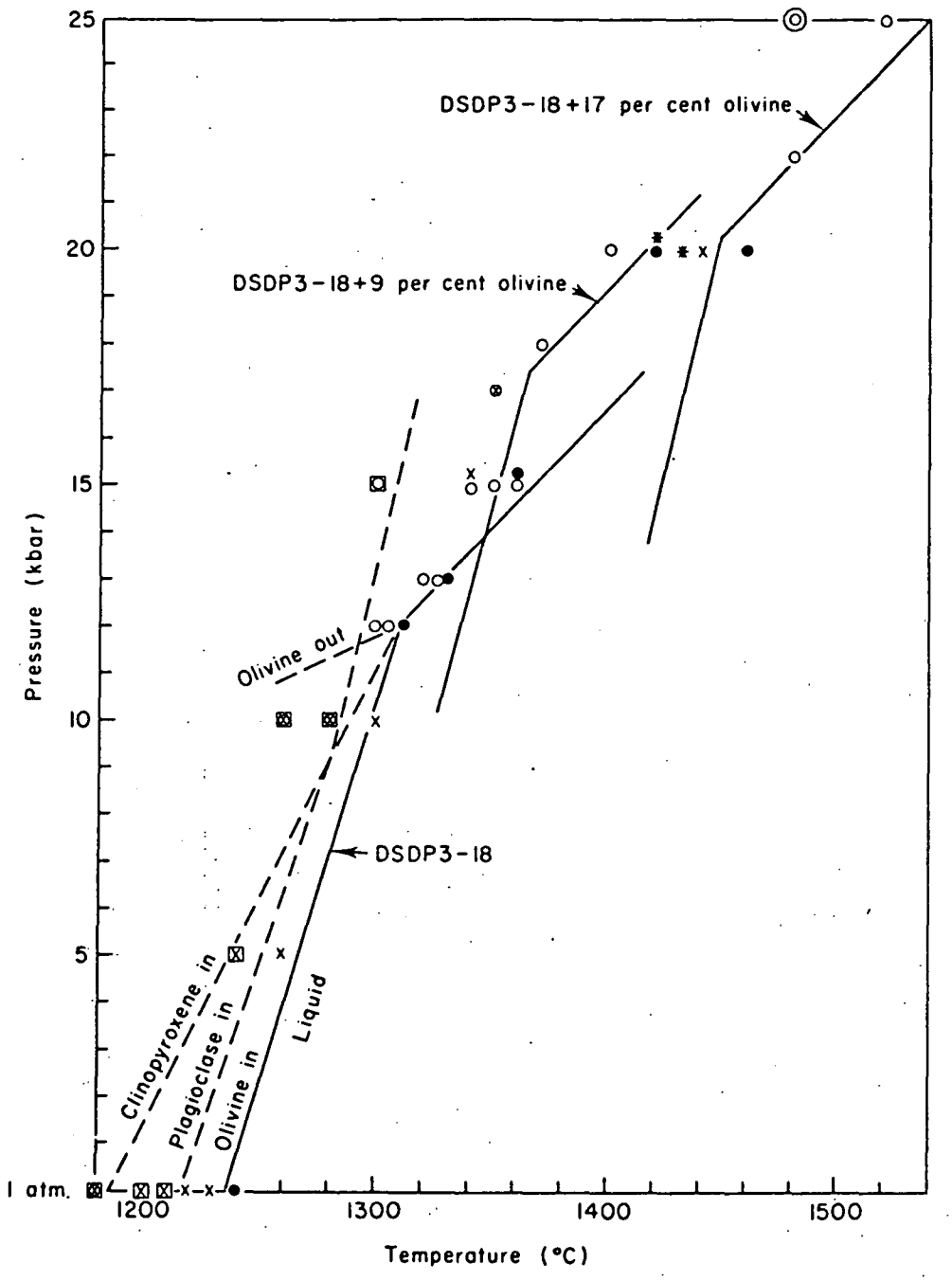

Fig. 1. Experimental determination of liquidus and near-liquidus phases for olivine tholeiite DSDP3-18-7-1 and olivine-enriched compositions (see text). ●, Above liquidus; ×, olivine; +, orthopyroxene; ○, clinopyroxene; ○, garnet; □, plagioclase.

Table 2. Details of melting experiments on DSDP3-18 composition and derivative compositions A, B, C, D, E (see text and Table 1)

Run no.	Starting material	Capsule	Temperature (°C)	Pressure (kbar)	Time (h)	
A517	Crystallized mix	Fe	1240	0	1	Glass ($Mg_{69.2}$)
A498	Crystallized mix	Fe	1230 ± 10	0	1	Olivine (Mg_{88}) + Glass ($Mg_{68.8}$)
A493	Crystallized mix	Fe	1220	0	1.25	Olivine + glass
A520	Crystallized mix	Fe	1210	0	2	Olivine ($Mg_{86.8}$) + plagioclase (An_{78}) + glass (Mg_{67})
A521	90 per cent glass 10 per cent A520	Fe	1210	0	2	Olivine ($Mg_{86.5}$) + plagioclase (An_{78}) + glass
A519	Crystallized mix	Fe	1200	0	1.5	Olivine + plagioclase + glass
A514	Crystallized mix	Fe	1180	0	2	Olivine + plagioclase ± clinopyroxene + glass (fine grained)
5535	Glass	Fe	1260	5	1	Olivine ($Mg_{87.8}$) + glass ($Mg_{68.8}$)
5532	Glass	Fe	1240	5	1	Olivine ($Mg_{87.5}$) + plagioclase (An_{77}) + glass ($Mg_{67.4}$)
5548	Glass	C	1300	10	0.5	Glass ($Mg_{69.5}$) + very rare olivine ($Mg_{88.7}$)
5555	Glass	C	1280	10	0.5	Olivine ($Mg_{87.5}$) + clinopyroxene (Mg_{88}) + plagioclase (An_{73}) + glass ($Mg_{67.5}$)
5551	Glass	C	1260	10	0.65	Olivine ($Mg_{83.4}$) + clinopyroxene ($Mg_{85.6}$) + plagioclase (An_{71}) + glass (Mg_{61})
5537	Glass	Fe	1280	10	1	Glass ($Mg_{67.7}$)
5544	Glass	Fe	1280	10	0.5	Glass + very rare olivine
5543	Glass	Fe	1260	10	0.5	Olivine ($Mg_{86.5}$) + clinopyroxene (Mg_{87}) + plagioclase (An_{72}) + Glass (Mg_{63})
5575	Glass	C	1310	12	0.5	Glass (Mg_{70})
5590	Glass	C	1305	12	0.5	Clinopyroxene ($Mg_{88.3}$) + glass ($Mg_{68.5}$)
5578	Glass	C	1300	12	0.5	Clinopyroxene (very rare) + glass
5587	Glass	C	1290	12	0.5	Clinopyroxene ($Mg_{83.5}$) + plagioclase (An_{69}) + glass (Mg_{62})
5565	Glass	C	1330	13	0.5	Glass ($Mg_{69.5}$)
5586	Glass	C	1325	13	0.5	Glass ($Mg_{69.5}$)
5596	Glass	C	1325	13	0.5	Clinopyroxene ($Mg_{88.5}$) + Glass ($Mg_{69.5}$)
5571	Glass	C	1320	13	0.5	Clinopyroxene (Mg_{88}) + Glass ($Mg_{68.5}$)
5591	Glass	C	1320	13	0.5	Clinopyroxene ($Mg_{87.8}$) + Glass† (Mg_{67})
5569	Glass	C	1310	13	0.5	Clinopyroxene (Mg_{87}) + Glass†
5561	Glass	C	1360	15	0.5	Clinopyroxene (Mg_{88}) + Glass ($Mg_{68.5}$)
5563	Glass	C	1350	15	0.65	Clinopyroxene ($Mg_{87.5}$) + Glass ($Mg_{67.5}$)
5560	Glass	C	1340	15	0.5	Clinopyroxene ($Mg_{85.5}$) + Glass (Mg_{65})
5558	Glass	C	1300	15	0.5	Clinopyroxene (Mg_{76}) + Plagioclase (An_{66}) + Glass†
T16	Mix A	C	1360	12	1	Rare orthopyroxene (Mg_{99}–Mg_{91}) + glass
T20	Mix A	Fe	1350	12	1	Rare orthopyroxene + glass

T14	Mix A	C	1340	12	1	Orthopyroxene + calcic clinopyroxene + glass(+ relict $MgSiO_3$)
T12	Mix A	C	1320	12	1	Orthopyroxene ($Mg_{88.7}$) + clinopyroxene (Mg_{91}) + glass(+ relict $MgSiO_3$)
T15	Mix B	C	1330	12	1	Glass
T18	Mix B	Fe	1320	12	1	Orthopyroxene (Mg_{91}–Mg_{86}) + glass
T13	Mix B	C	1320	12	1	Orthopyroxene (Mg_{89}) + glass
T11	Mix B	C	1310	12	1	Relict orthopyroxene rimmed by low-Ca clinopyroxene + glass†
T19	Mix B	Fe	1300	12	1	Relict orthopyroxene rimmed by low-Ca clinopyroxene + glass†
T24	Mix C	C	1315	12	1	Glass
T22	Mix C	Fe	1310	12	1	Very rare clinopyroxene + glass
T25	Mix C	Fe	1300	12	1	Calcic clinopyroxene ($Mg_{89.3}$, 19 per cent CaO, 3.9 per cent Al_2O_3) + glass
T230	Mix D	C	1310	12	1	Olivine ($Mg_{90.5}$) + glass
T228	Mix D	C	1360	15	1	Glass
T229	Mix D	C	1340	15	1	Olivine ($Mg_{90.3}$) + clinopyroxene ($Mg_{90.3}$, 15.2 per cent CaO, 6.5 per cent Al_2O_3) + glass
T232	Mix D	C	1350	17	0.4	?Olivine + clinopyroxene (Mg_{90}, 7–12 per cent CaO, 3.6–7.1 per cent Al_2O_3) + glass†
T234	Mix D	Fe	1370	18	0.25	Clinopyroxene (Mg_{88}, 13.5–14.5 per cent CaO, 8.5 per cent Al_2O_3) + glass†
T233	Mix D	C	1370	18	0.5	Clinopyroxene + glass†
T235	Mix D	Fe	1420	20	0.5	Clinopyroxene (Mg_{89}, 12.5–13.5 per cent CaO, 8.5 per cent Al_2O_3) + glass†
T226	Mix D	C	1420	20	0.75	Glass
T227	Mix D	C	1400	20	0.75	Clinopyroxene ($Mg_{88.5}$, 14.5 per cent CaO, 9.8 per cent Al_2O_3) + glass†
T240	Mix E	C	1460	20	0.25	Glass
T245	Mix E	Fe	1450	20	0.25	Olivine (Mg_{90}) + glass (Mg_{75})
T241	Mix E	C	1440	20	0.25	?Olivine + glass
T244	Mix E	C	1430	20	0.25	Olivine ($Mg_{91.5}$) + glass ($Mg_{78.5}$)
T247	Mix E	Fe	1430	20	0.2	?Olivine + orthopyroxene ($Mg_{90.5}$, 2.6 per cent CaO, 5.5 per cent Al_2O_3) cores to low-Ca clinopyroxene + glass
T243	Mix E	C	1420	20	0.25	?Olivine + orthopyroxene (Mg_{92}, 2.7 per cent CaO, 5.3 per cent Al_2O_3) + glass†
T239	Mix E	C	1480	22	0.25	?Olivine + low calcium clinopyroxene + glass†
T238	Mix E	C	1520	25	0.25	Clinopyroxene + glass†
T237	Mix E	C	1480	25	0.35	Clinopyroxene + garnet + glass†

† Glass is accompanied by common quench clinopyroxene, analyses of glass are not reliably those of liquid in equilibrium with primary crystals.

Table 3. Compositions of near-liquidus calcic pyroxenes for DSDP3-18-7-1 and DSDP3-18+9 per cent olivine.

	DSDP3-18-7-1				91 per cent DSDP3-18 +9 per cent olivine	
P (kbar)	12	12	15		15	20
T (°C)	1305	1290	1360		1340	1420
			Low Al†	High Al†		
SiO_2	51.6	50.7	53.2	51.5	52.8	52.6
TiO_2	0.3	0.5	0.1	0.3	0.3	0.3
Al_2O_3	7.2	8.9	5.3	8.3	6.5	8.4
FeO	4.4	6.0	4.7	4.1	4.5	4.5
MnO	—	—	—	—	—	—
MgO	18.5	17.5	19.4	17.1	23.0	20.8
CaO	17.6	15.6	17.0	18.4	12.5	12.9
Na_2O	0.4	0.6	0.4	0.2	0.4	0.5
100 Mg/(Mg+Fe)	88.3	83.8	88.1	88.2	90.2	89.3

† The pyroxenes show a range of Al–Si solid solution.

Between 10 kbar and 12 kbar, olivine is replaced as the liquidus phase by clinopyroxene. The clinopyroxene (Table 3) is calcium-rich and has Fe/Mg partition coefficient with respect to the liquid

$$\frac{(Fe/Mg)_{cpx}}{(Fe/Mg)_{liq}} = 0.3 \pm 0.03,$$

which is similar to that for olivine (cf. Cawthorn *et al.* 1973). At 13 kbar and 15 kbar, calcium-rich clinopyroxene remains the liquidus phase and earlier studies on a variety of basaltic compositions suggest that clinopyroxene will be replaced by garnet on the liquidus phase between 20 and 30 kbar.

The experimental study confirms that the microphenocrysts present in the natural rock have compositions appropriate to low pressure liquidus and near liquidus phases of a liquid matching the glass composition, i.e. the olivine or plagioclase are not xenocrysts. (Note that the small difference ($Mg_{89.7}$ to $Mg_{88.7}$) between most Mg-rich microphenocryst and experimental liquidus olivine (10 kbar, graphite) compositions could be explained by reduction of Fe^{3+} present in the natural magma, to Fe^{2+} in the experiments.) The experimental study also confirms that liquids such as the glass from DSDP 3-18 are incapable of precipitating at any pressure either the anorthite-rich plagioclase ($>An_{80}$) or olivine of $>Mg_{90}$ composition or chrome-rich, aluminium-poor diopside ($>Mg_{88}$) which are observed as megacrysts in some ocean floor basalts, including glassy basalts similar to DSDP 3-18

(Donaldson and Brown, 1977). The experimental study also confirms that if DSDP 3-18 is not a primary liquid in the sense used herein, but has evolved by crystal fractionation from a more primitive magma, then, provided that crystal fractionation occurred at < 10 kbar, olivine is the only crystalline phase involved, i.e. a more primitive melt lies along the olivine-addition fractional crystallization path from DSDP 3-18. If crystal fractionation had occurred between 10 kbar and 12 kbar, then both olivine- and calcium-rich clinopyroxene may have separated and if at pressures $\geqslant 12$ kbar, then clinopyroxene only may have separated. It should be noted however that the possibility of clinopyroxene fractionation at $P \geqslant 12$ kbar to yield DSDP 3-18 is ruled out if the constraint of an ultimate peridotite source is accepted. Thus addition of Ca-rich clinopyroxene to DSDP 3-18 liquid would produce liquids moving further away from the olivine field and further into the liquidus field of clinopyroxene. Higher pressure would accentuate this problem and the problem also exists for postulated olivine + clinopyroxene crystal fractionation, which in addition would move liquids further away from the liquidus field of orthopyroxenes (see following discussion).

3.1. Possible Derivation of DSDP 3-18 from Peridotite Source Rock

Olivine ($\sim Mg_{89}$) is the liquidus phase of DSDP 3-18 in the 0–10 kbar pressure interval and this liquid could be derived from a mantle peridotite by partial melting and magma segregation at depths to about 35 km provided the degree of melting of the peridotite was sufficient to melt out all phases other than olivine (and chrome-rich spinel probably). We return to discuss this model in a later section, but we note at this point that extremely pure dunites are rather uncommon in nature, whereas harzburgites and lherzolites in which orthopyroxene is a major phase are relatively much more common. We prefer to investigate further for a model of derivation in which olivine and one or more pyroxenes remain as residual phases.

The melting relations of two peridotite compositions (pyrolite (Ringwood, 1966) and Tinaquillo peridotite (Green 1963)) in the pressure range 0–15 kbar are currently being investigated (Jaques and Green, in preparation) and in Fig. 2 we summarize our data on the solidus and phase stability at above-solidus conditions. We have also plotted the 20, 30 and 40 per cent melting contours for both compositions. For our present purpose it is only necessary to point out that olivine and orthopyroxene are present as residual phases in both compositions over the entire P–T range defined by the liquidus of DSDP 3-18, i.e. if DSDP 3-18 was a primary melt from either peridotite, then olivine and *orthopyroxene* should occur together on its liquidus at some P, T condition. The liquidus of DSDP 3-18 overlaps the

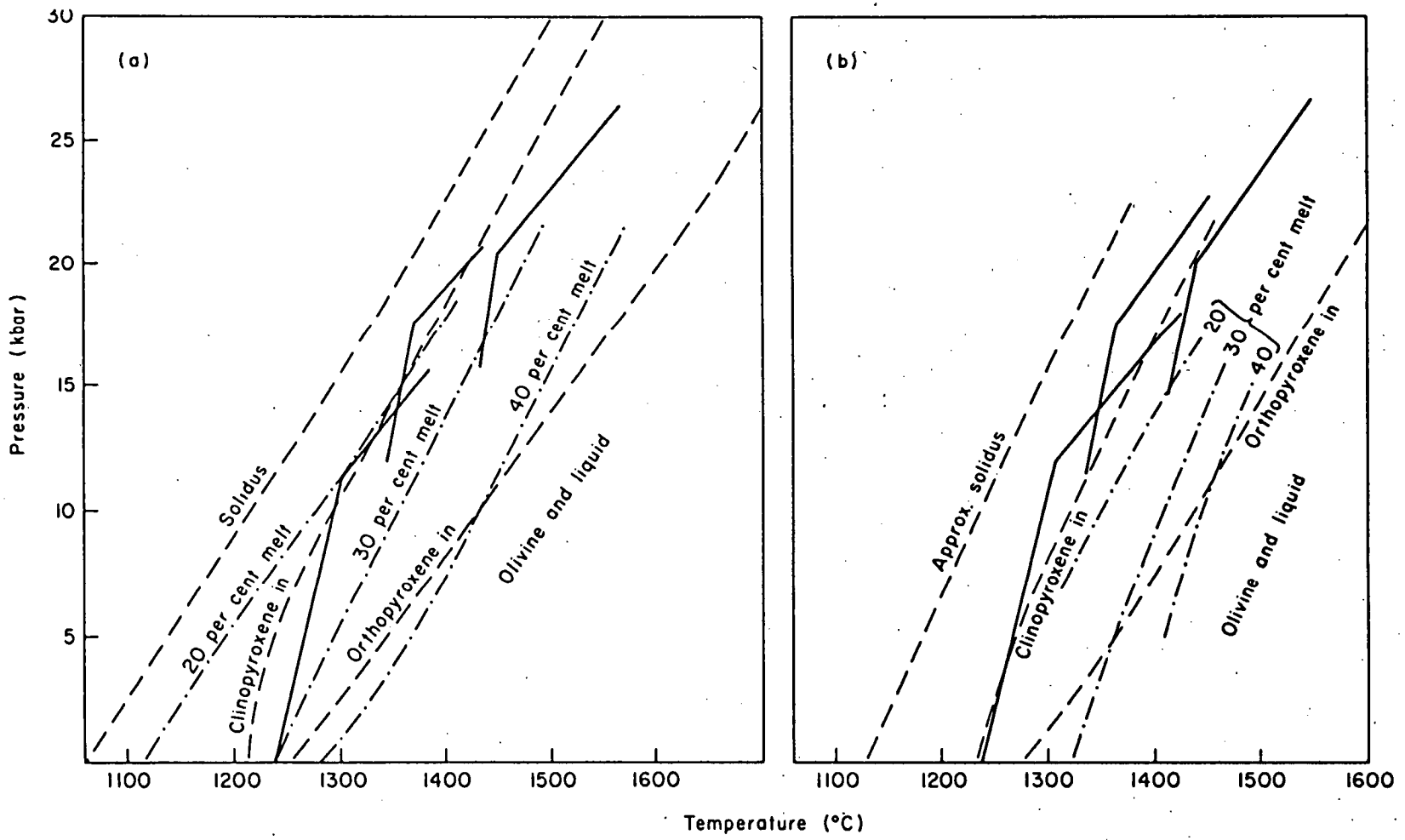

Fig. 2. (a) Summary of partial melting data for pyrolite composition showing solidus and boundaries marking the disappearance of phases above the solidus. Also shown are percentage melting contours and (solid lines) the positions of the liquidi from Fig. 1. (b) Summary of partial melting data for Tinaquillo peridotite composition showing solidus and boundaries marking the disappearance of phases above the solidus. Also shown are percentage melting contours and (solid lines) the positions of the liquidi from Fig. 1.

field for residual clinopyroxene for Tinaquillo peridotite except at low pressure and overlaps the clinopyroxene field for pyrolite only between 10 and 13 kbar. The absence of orthopyroxene and the presence of a calcium-rich pyroxene alone or with olivine is therefore prohibitive for direct derivation of DSDP 3-18 by equilibrium partial melting of peridotites with compositions similar to pyrolite or Tinaquillo peridotite.

Harzburgite and enstatite-bearing dunite are common highly refractory peridotites ($>Mg_{90}$) occurring in nature whereas wehrlite or chrome diopside-bearing dunite (enstatite-free) are very uncommon among refractory peridotites ($>Mg_{90}$). We take these observations on natural rocks as support for the general relevance of compositions close to pyrolite or Tinaquillo peridotite, i.e. peridotites with high normative hy/di ratios, and the general applicability of the olivine + orthopyroxene constraint in evaluating primary magmas and their conditions of genesis.

In earlier studies of both terrestrial and lunar basalts, it was found that orthopyroxene occurred as a liquidus phase between the *P*-dependent liquidus fields of olivine (lower pressure) and clinopyroxene (higher pressure) (Green and Ringwood, 1967; Ito and Kennedy, 1968; Green *et al.*, 1971, 1975). In addition it has been observed that the composition of the first calcic pyroxene to crystallize in coexistence with olivine, becomes less calcic, i.e. approaches the orthopyroxene–clinopyroxene solvus, with increasing pressure (Bultitude and Green, 1971) and clinopyroxenes coexisting with orthopyroxene on anhydrous liquidi are extremely subcalcic indeed (Green and Ringwood, 1967; Bultitude and Green, 1971; Green and Hibberson, 1970; Green *et al.* 1971, 1975). It has also been shown that orthopyroxene, present at high temperature, may react out at lower temperature in the melting interval. Finally, the careful study of liquidus pyroxenes of lunar basalts has shown that there exist experimental difficulties in the metastable nucleation and growth of subcalcic ("pigeonitic") clinopyroxenes in place of the stable coexisting orthopyroxene–clinopyroxene pair (Green, 1976*a*,*b*, and unpublished data on a wide range of subcalcic near-liquidus pyroxenes from lunar compositions studied at high pressure). It has proved very difficult to experimentally define the pyroxene miscibility gap at high pressure in the complex natural systems but our incomplete results suggest that clinopyroxene (Mg_{85}–Mg_{90}) coexisting with orthopyroxene on the liquidi of basalts at 10–15 kbar, 1300–1400 °C should contain not less than 12 weight per cent CaO and not more than 14 weight per cent CaO.

Against this background it is necessary to examine critically our data on clinopyroxene composition and conditions of crystallization to ascertain if DSDP-18 could be saturated with orthopyroxene at conditions slightly different from those tested, or is very close to saturation with orthopyroxene

or is indeed saturated with orthopyroxene but crystallization of metastable clinopyroxene has obscured this. The compositions of subliquidus pyroxenes from DSDP3-18 at pressures below 12 kbar and of liquidus pyroxenes at and above 12 kbar are calcium-rich (Tables 3 and 4) and unlike compositions occurring on the solvus limb, at least with our present state of knowledge.

Table 4. Compositions of residual phases (near-liquidus at 20 kbar, 1420–1430 °C) for composition E (83 per cent DSDP3-18 + 17 per cent olivine). Also compositions of residual spinel in pyrolite at 15 kbar, 1400 °C coexisting with olivine and orthopyroxene only, and spinel inclusion within olivine megacrysts (Donaldson and Brown, 1977).

	Olivine	Orthopyroxene	Spinel (Jaques and Green, in progress)	Spinel xenocryst (Donaldson and Brown, 1977)
SiO_2	40.9	54.8	—	—
TiO_2	—	<0.1	1.2	0.4
Al_2O_3	—	5.5	19.2	24.2
FeO	8.2	4.9	17.8	15.3
MgO	50.4	32.0	17.8	15.3
CaO	0.4	2.8	—	—
Na_2O	—	—	—	—
K_2O	—	—	—	—
Cr_2O_3	—	(1.2)†	43.5	44.4
NiO	(0.4)†	(0.05)†	—	—
100 Mg/(Mg+Fe)	91.6	92.1	64	64

† Values from residual pyroxene and olivine in pyrolite at 15 kbar, 1400 °C. Note that Cr_2O_3 and NiO were not added to DSDP3-18 mix.

Orthopyroxene Addition Experiments

To test further for orthopyroxene saturation or nearness thereto, we have added enstatite to DSDP3-18. Three mixes were used:

A. 91 per cent DSDP3-18 (glass) + 9 per cent $MgSiO_3$ (Tem-Pres synthetic clinoenstatite);
B. 91 per cent DSDP3-18 (glass) + 9 per cent bronzite (Mg_{86}, 0.9 per cent Al_2O_3, 0.5 per cent CaO);
C. 95 per cent DSDP3-18 (glass) + 5 per cent bronzite (Mg_{86}, 0.9 per cent Al_2O_3, 0.5 per cent CaO).

In each case the pyroxene added was sufficiently different from anticipated liquidus orthopyroxene for the chemical distinction between relict seed

cores to pyroxenes and equilibrium orthopyroxene to be readily made by electronprobe analysis. The seeds were respectively more magnesian and less magnesian than the liquidus pyroxene of DSDP3-18. The seed pyroxenes were crushed to $< 10\,\mu m$ but grain size was very variable. Experiments were run at 12 kbar, 1300–1360 °C in graphite and spec-pure iron capsules. In mix C, the liquidus was at ~1310 °C and calcium-rich pyroxene (≥19 per cent CaO, $Mg_{89.3}$) was the liquidus phase, orthopyroxene seeds disappeared and there was no low-calcium (<10 per cent CaO) pyroxene present. For mix B, the liquidus at 12 kbar was 1325 °C and the liquidus phase was orthopyroxene. The charge contained small cores of orthopyroxene with compositions approaching the seed crystals surrounded by rims of orthopyroxene with Mg_{89-91}, 2.4 per cent Al_2O_3, 2.2 per cent CaO. Similarly, for mix A, the liquidus temperature was ~1360 °C and near-liquidus runs contained rare relict seed cores (orthopyroxene up to Mg_{99}), new "equilibrium" orthopyroxene (Mg_{91}, 2.4 per cent Al_2O_3, ~3.0 per cent CaO) and metastable or quench low-calcium clinopyroxene (<Mg_{91}). At 12 kbar, 1320 °C and 1310 °C (i.e. just above the liquidus temperature of DSDP3-18), mix A contained relict seed orthopyroxene (Mg_{100}), orthopyroxene ($Mg_{92.3}$, 2.2 per cent Al_2O_3, 2.8 per cent CaO) and calcium-rich clinopyroxene ($Mg_{89.6}$, 2.8 per cent Al_2O_3, 10.1 per cent CaO). The experiments confirm the difficulty in nucleating coexisting orthopyroxene and calcium-rich pyroxene rather than metastable low-calcium clinopyroxene and expose the limitations of the seeding technique in that the seeds only partially react, and act as nucleii for new crystal growth. However, the experiments confirm that DSDP3-18 lies in the liquidus field of calcium-rich pyroxene at 12 kbar, and that it does not lie on the two pyroxene boundary. The orthopyroxene addition experiments demonstrate that the two-pyroxene boundary intersects the DSDP3-18 to orthopyroxene join at compositions between DSDP3-18 + 5 per cent orthopyroxene and DSDP3-18 + 10 per cent orthopyroxene. It may be noted that this result is consistent with earlier studies in the 9–13.5 kbar interval (Green and Ringwood, 1967; T. H. Green *et al.*, 1967; Green, 1970) in which orthopyroxene accompanied or preceded clinopyroxene precipitation in compositions having higher normative hy/di or (hy + ol)/(di + an) ratios than DSDP3-18. The various data partially define the primary liquidus fields of olivine, orthopyroxene, clinopyroxene, plagioclase within the "basalt tetrahedron" (Yoder and Tilley, 1962) at 9–13 kbar, anhydrous conditions.

Olivine Addition Experiments

Previous studies have demonstrated that pressure has the effect of increasing the activity of pyroxene components at the expense of olivine in olivine-rich liquids and that a liquid which at low pressure has olivine on its liquidus,

followed at lower temperature by clinopyroxene, may, at a higher pressure, have olivine replaced by orthopyroxene or orthopyroxene + clinopyroxene (Green and Ringwood, 1967; Green, 1970). The results of the experiments on DSDP3-18 demonstrated that this magma could originate by olivine extraction from a more olivine-rich parent magma. We have, on these grounds, added olivine to DSDP3-18 to evaluate whether, at higher pressure and temperature, an olivine-enriched magma could be both saturated in olivine and orthopyroxene (± calcic clinopyroxene), and thus a possible primary melt from mantle peridotite, and also parental to DSDP3-18 by extraction of olivine alone at lower pressures.

Two mixes were prepared by addition of natural olivine ($Mg_{91.7}$) to DSDP3-18 glass. The olivine was crushed to < 10 μm and mixed with the powdered glass. Bulk compositions of the two mixes (composition D: 91 per cent DSDP3-18 + 9 per cent olivine; composition E: 83 per cent DSDP3-18 + 17 per cent olivine) are given in Table 1. Composition D has olivine as liquidus phase ≤ 15 kbar, olivine and clinopyroxene (Mg_{90}, 7–12 per cent CaO, 3.5–7 per cent Al_{23}) on the liquidus at 17 kbar, ~1360 °C and clinopyroxene (13–14 per cent CaO, 8.5 per cent Al_2O_3) as liquidus phase at 18 kbar, 1370 °C and 20 kbar, 1400 °C. It is at present uncertain whether the clinopyroxene lies within the pyroxene solvus at 17–18 kbar, 1360–1370 °C or on the calcium-rich side of the diopside limb. The range of CaO and Al_2O_3 contents in the 17 kbar, 1360 °C run suggest metastable low-calcium clinopyroxene in place of orthopyroxene + calcic clinopyroxene.

Composition E has olivine as the liquidus phase at 20 kbar, 1450 °C, but olivine and orthopyroxene (Mg_{92}, 2.8 per cent CaO, 5.5 per cent Al_2O_3) occur together at 20 kbar, 1430 °C. The presence of near-liquidus orthopyroxenes accompanying olivine was confirmed in both graphite and spec-pure iron capsules. (Note the minor FeO addition in the latter and the barely significant difference in liquidus temperature in C and Fe capsules.) At 22 kbar, clinopyroxene (stable or metastable low-calcium clinopyroxene) and olivine occur very close to the liquidus and similar clinopyroxene occurs on the liquidus at 25 kbar, 1520 °C. Garnet joins clinopyroxene at 25 kbar, 1480 °C but does not appear in the near-liquidus runs at lower pressure.

4. A Primary Parental Magma

We infer from the olivine addition studies that a picritic magma containing ~25 per cent normative olivine and parental to DSDP3-18 by the separation of 15–17 per cent olivine (mean composition ~Mg_{91}), has appropriate liquidus phases, olivine and orthopyroxene, to be a primary magma derived at high pressure from mantle orthopyroxene-bearing peridotite. In particular, the depth of magma segregation for this primary, picritic magma is

~70 km (~20 kbar) at a temperature of ~1430 °C leaving residual olivine ($Mg_{91.5}$) and orthopyroxene (Mg_{92}, 5.5 per cent Al_2O_3, 2.8 per cent CaO). From the nickel content of DSDP3-18 and of olivine phenocrysts and xenocrysts and the similar contents of nickel in olivine (Mg_{89-92}) of mantle derived lherzolites, it may be inferred that the primary, picritic parental magma would contain ~600 p.p.m. Ni. The Ni content of source peridotite and potential primary liquids will provide an important constraint (cf. Frey *et al.*, 1978) on models of magma genesis, but uncertainties in the compositional and temperature effects on the partition coefficient for Ni between olivine and liquids are as yet not resolved (Leeman and Scheidegger, 1977; Hakli and Wright, 1967; Mysen, 1976). The predicted Ni content of ~600 p.p.m. for the DSDP3-18 parent magma is similar to that (670 p.p.m. Ni) modelled for a primitive tholeiite melting at ~17 kbar, 1400 °C leaving harzburgite residue (Frey *et al.*, 1978).

4.1. Retraction of an Earlier Model of Mid-ocean Ridge Petrogenesis

In earlier papers (Green and Ringwood, 1967; T. H. Green *et al.*, 1967; Green, 1970, 1971) the experimental data then available was used to infer that high Al_2O_3 (>14 per cent Al_2O_3) olivine tholeiites (~10 per cent normative olivine) were primary melts from mantle peridotite (pyrolite) at ~20 per cent melting, leaving residual olivine, orthopyroxene and very minor calcium-rich pyroxene, at a depth of magma segregation of ~30 km (9 kbar). Direct studies of melting of pyrolite and Tinaquillo lherzolite at 0–15 kbar (Jaques and Green, unpublished data) show that liquids derived at these conditions are indeed enriched in Al_2O_3/CaO relative to liquids at ~15 kbar but differ from liquids such as DSDP3-18 in lower Al_2O_3 contents, higher SiO_2 contents and higher alkali contents. Similarly, other studies (Green *et al.*, 1974) have confirmed a low pressure fractionation trend towards Al_2O_3 and Al_2O_3/CaO enrichment (Green and Ringwood, 1967) at low pressure (5–10 kbar), but derivative liquids are hawaiitic and mugearitic rather than high-Al_2O_3-olivine tholeiites.

The earlier model emphasized that olivine fractionation was important in magma genesis in the mid-ocean ridge situation, but envisaged primary parental magmas with ~10 per cent normative olivine (~49 per cent SiO_2, >14 per cent Al_2O_3, ≥12 per cent CaO). This model is now retracted and we support the view, earlier advocated by O'Hara (1968), that primary, parental magmas in the mid-ocean ridge situation include picrites with ~25 per cent normative olivine, ~48 per cent SiO_2, ~13–14 per cent Al_2O_3, ~11 per cent CaO. We do not infer that magmas of this composition are the only primary, parental magmas, but rather that this is one primary magma

whose probable conditions of genesis can now be delineated and which will yield, by crystallization and settling out of olivine, highly magnesian liquids such as DSDP3-18 and similar compositions (Melson *et al.*, 1977).

As noted above, our conclusion that a primary parental magma for mid-ocean ridge magmatism is tholeiitic picrite rather than olivine tholeiite, is in agreement with O'Hara (1968). However, O'Hara inferred that the primary picrite was derived by melting at ~30 kbar (>~100 km) whereas our data shows that this pressure is too high and the depth of magma segregation is around 70 km. Similarly, O'Hara inferred that the primary magma was formed in equilibrium with olivine + orthopyroxene + garnet ± clinopyroxene (i.e. a garnet harzburgite residue). Our data show that garnet is absent both for the near-liquidus experiments on DSDP3-18 + olivine, and for the melting studies on pyrolite and Tinaquillo peridotite at 20 kbar, 1400–1500 °C. We infer that clinopyroxene is also absent as a residual phase. The absence of garnet is a key factor in controlling rare earth fractionation in the partial melting process and is consistent with the absence of heavy rare earth element depletion in DSDP3-18 and similar mid-ocean ridge basalts (Group I of Bryan *et al.*, 1976).

Our study of the petrogenesis of one of the more primitive mid-ocean ridge basalts has provided evidence for a deep origin and a post-segregation history of crystal fractionation and cooling (from ~1430 °C to ~1230 °C) during movement to the Earth's surface. Other authors (including Donaldson and Brown, 1977; Flower *et al.*, 1977; Clarke and Pedersen, 1976; Esson *et al.*, 1975) have presented evidence for picritic melts in mid-ocean ridge and ?pre-ridge volcanism (western Greenland, Hebridean province). Variations in Na_2O/CaO, K_2O/Na_2O, TiO_2/CaO, or TiO_2/Al_2O_3 in such primary picritic melts may originate by:

1. *Variation in degree of melting.* Lower degrees of melting produce liquids with higher K_2O/Na_2O, TiO_2/CaO, etc., and the liquids trend towards alkali picrite.
2. *Difference in source composition.* This particularly includes earlier processes of magma extraction leaving more refractory peridotite with lower Na_2O/CaO, TiO_2/CaO ratios. There may also have been earlier melt addition (Green, 1971; Frey and Green, 1974; Frey *et al.*, 1978) enriching the source in incompatible elements with increase in CaO/Al_2O_3, TiO_2/CaO, etc.

Further work is required to evaluate whether the entire spectrum of mid-oceanic ridge basalts derive from primary *picritic melts.* Alternatively, the spectrum may include examples which are derivative from primary *olivine tholeiite* to *alkali olivine basalt* (Green and Ringwood, 1967; Green, 1971) segregated from mantle peridotite at *shallower depths.* Primary

basalts formed in the latter way should have Mg-values of 75 ± 3, ~ 500 p.p.m. Ni, but have lower normative olivine and higher SiO_2 contents than the picritic magmas deduced in this study.

5. Ophiolites in Relation to Mid-ocean Ridge Petrogenesis

The experimental data obtained on DSDP3-18 and the olivine-enriched compositions define the possible crystal accumulates and residues which can be formed as complementary rocks to the melting-out of the parent magma or its low pressure fractionation. The residual minerals at ~ 20 kbar, 1430 °C would be olivine (Mg_{92}) and enstatite (+Cr-spinel)† but, although these are appropriate to harzburgite, the composition of the orthopyroxene, with >5 per cent Al_2O_3, >2.5 per cent CaO, is unlike that of orthopyroxene of harzburgite associated with ophiolites (<1.5 per cent Al_2O_3, <1 per cent CaO) (England and Davies, 1973; Moores, 1969). Residual harzburgite from extraction of DSDP3-18 + 17 per cent olivine at 20 kbar, 1430 °C would recrystallize as lherzolite (plagioclase or spinel lherzolite) at lower temperatures and would not equate chemically or mineralogically with non-cumulate harzburgite observed as "basement" to many ophiolite complexes.

If DSDP3-18 or olivine-enriched parents were to segregate from mantle peridotite at <20 kbar, then wehrlite (DSDP3-18 at 12 kbar) or dunite (DSDP3-18 at <12 kbar, or picritic parental magmas at <20 kbar) would be *residual* rock types. The common occurrence of non-accumulate harzburgite, the less common occurrence of enstatite-free dunites, the rarity of wehrlite and the accumulative nature of at least some observed wehrlites and dunites, are inconsistent with this model.

A picritic magma of DSDP3-18 + 17 per cent olivine composition can produce low-pressure accumulates of dunite (olivine ($\leqslant Mg_{92}$) + ?chrome spinel), olivine + plagioclase (more iron-rich and sodic than Fo_{87} and An_{79}, respectively), or olivine, diopside and plagioclase. There is no possibility of magmas such as DSDP3-18 or the picritic parental magma producing accumulates containing magnesian orthopyroxene ($\geqslant Mg_{87}$) or calcic plagioclase ($\geqslant An_{80}$). Similarly, it is characteristic that plagioclase precipitation should precede clinopyroxene precipitation in magmas such as

† It has been noted previously that our experiments do not allow an appraisal of the near-liquidus role of spinel for DSDP3-18 or derivative compositions. However, the experimental melting studies of pyrolite and Tinaquillo peridotite composition show that spinel ($100Cr/(Cr+Al) \approx 65$, $TiO_2 = 1.2$ per cent) would be present as a very minor residual phase at 20 kbar, 1430 °C.

DSDP3-18 or similar high-Al_2O_3 ocean floor basalts. The first clinopyroxene to appear in DSDP3-18 at low pressure has Mg-value of ~88 and is unlike the most magnesian clinopyroxenes occurring in rocks with cumulus texture in at least some ophiolite complexes (Mg_{92}, Mg_{94}; England and Davies, 1973). The uncommon chrome diopside megacrysts (Mg_{91}) in mid-ocean ridge basalts (Donaldson and Brown, 1977) are also inconsistent with precipitation from DSDP3-18 or picritic parental magmas.

We conclude that the primary picritic magma which we have identified as parental to DSDP3-18 and similar basalts, has no genetic relationship to ophiolite complexes having the following characteristics:

(a) basement of non-cumulate harzburgite with olivine $>Mg_{91}$, orthopyroxene (Mg_{91}, <1.5 per cent Al_2O_3, <1 per cent CaO), and lacking clinopyroxene and/or plagioclase;
(b) cumulate sequences containing plagioclase more anorthite-rich than An_{79}, clinopyroxene more Mg-rich than Mg_{88}, or orthopyroxene more Mg-rich than approx. Mg_{87}.

These characteristics are in fact typical of most ophiolite complexes and it follows that ophiolite complexes are related to some other magma type than the more primitive and common mid-ocean ridge basalts (i.e. magmas similar to DSDP3-18). Similarly, the megacrysts of very calcic plagioclase and magnesian clinopyroxene occurring in some mid-ocean ridge basalts have no genetic relation to their host magma and are more probably genetically related to the accumulates of ophiolite complexes. Curiously, highly magnesian orthopyroxene megacrysts do not occur in mid-ocean ridge basalts, although their role as accumulate phases in ophiolite complexes and residual phases in non-cumulate harzburgite is equally problematical. We suggest the need to explore several alternative and probably complementary hypotheses on the petrogenesis of ophiolite complexes. We consider that there is no single tectonic setting for development of ophiolite complexes—probable tectonic settings include:

(i) *Island arcs.* Ophiolite complexes may develop in complementary relation to genesis and fractionation of primitive highly magnesian island-arc tholeiites (boninites, high-Mg andesites of Cape Vogel, Marianas Trench, etc.; Dallwitz *et al.*, 1966; Green, 1973).
(ii) *Mid-oceanic ridge environments,* as complementary residues and accumulates to second-stage melting of refractory peridotite diapirs at shallow depths to yield highly magnesian, silica-rich olivine tholeiites, or quartz tholeiites rarely if every seen as extrusive magmas and yielding eruptive rocks only after crystal fractionation. The shallow "extrusive" diapir model of Moores (1969) may be applicable, the

bulk composition of the diapir resembling the composition of Lizard or Tinaquillo lherzolites or possibly even more refractory, i.e. low Na/Ca, low K, Ti, etc., contents, due to loss of an earlier melt fraction, perhaps identified as the "typical" mid-ocean ridge basalts.

(iii) *Back-arc basin environments*, e.g. Lau basin; possibly transitional between (i) and (ii) in that limited access of water activates melting of refractory lithosphere, residual from a previous melting episode.

The origin of megacrysts in mid-ocean ridge basalts may be found in the passage of primary picrite magmas, segregating at ~60–70 km, (or their olivine-depleted derivatives) through accumulates and incompletely crystallized magma chambers of shallow, second-stage melting, diapirs occurring at depths of 1–15 km. The two different depth regimes for origins of picrites and "ophiolite" layered sequences provides opportunity for entrainment of xenocrysts and xenoliths from the latter within the picritic magmas. This model provides opportunity for magma mixing to occur and is sufficiently complex to make testing difficult. Possibly the most rewarding area for further study is a search for primitive liquids or fractionation products of primitive liquids, which originate in the postulated shallow depth, second-stage of partial melting, i.e. liquids which leave harzburgite residue, precipitate plagioclase of An_{80-95}, clinopyroxene of Mg_{89-95}, and orthopyroxene of Mg_{89-92}, in early accumulates. Liquids with these characteristics should have high SiO_2 contents (>50 per cent), high CaO contents (>12 per cent) with low Na_2O contents (<1.5 per cent) and should be quartz normative or with small normative olivine contents. Our conclusions that high Ca, low Na liquids, unlike common mid-ocean ridge basalts such as DSDP3-18, are required to account for precipitation of megacrysts in mid-ocean ridge basalts and to produce the accumulate sequences of ophiolite complexes, are similar to those of Donaldson and Brown (1977) and Hodges and Papike (1976).

6. Composition of the Upper Mantle Source Region for Mid-ocean Ridge Basalts

Our experimental study defines two rather different possible origins for DSDP3-18 (and by inference, similar mid-ocean ridge basalts). First, DSDP3-18 may be a primary magma segregating from residual dunite at pressures less than 12 kbar, i.e. depths <~40 km. The composition of residual olivine (i.e. liquidus olivine for DSDP3-18) is best determined by the most magnesian microphenocrysts in DSDP3-18 (Frey *et al.*, 1974). These authors did not determine the NiO content of the olivine but this may be approximated as 0.4 weight per cent from partition data (Leeman and

Scheidegger, 1977) or from other analyses of similar olivine (e.g. Hodges and Papike, 1976). Similarly, the occurrence of spinel inclusions in early olivine phenocrysts, the presence of spinel megacrysts and the melting studies of pyrolite and Tinaquillo peridotite suggest that chrome-rich spinel should be a residual phase for DSDP3-18 in low-pressure magma segregation. The composition of spinel given in Table 4, column 4, is assumed to be a reasonable estimate of residual spinel—it is close to residual spinel compositions in pyrolite and Tinaquillo peridotite.

It is thus possible to calculate model source composition for DSDP3-18 by mixing calculations using DSDP3-18, olivine ($Mg_{89.7}$) and chrome–spinel (Mg_{64}). The approach used herein does not determine an estimate of the proportions of these phases. In Table 5, column A, we list source and residue compositions assuming 30 per cent melting—this figure being derived from the intersection of the liquidus for DSDP3-18 with the 30 per cent melting contour for pyrolite. This choice is not unreasonable for self-consistency as shown by comparison of key element contents (Na_2O, CaO, Al_2O_3, SiO_2, MgO) between "source peridotite" (A) and pyrolite (Ringwood, 1966) compositions (Table 5).

The second class of models for derivation of DSDP3-18 are those which derive a parental picritic magma (DSDP3-18 + 17 per cent olivine) by magma segregation at ~20 kbar (70 km) bearing residual harzburgite. Our experiments determine phase compositions (Tables 1, 3 and 4) but not the relative proportions. In Table 5 we have calculated two model sources and residue compositions (columns B, C) on the arbitrary assumption that the degree of partial melting of the source is 24 per cent, there is 1 per cent residual spinel and the residue is either an orthopyroxene-poor (column B) or orthopyroxene-rich (column C). The relative proportions were chosen to yield ~3–4 per cent CaO and 4–5 per cent Al_2O_3 in the source composition, i.e. compositions similar to previous estimates of upper mantle "pyrolite" composition (Table 5), and hence with the same support from natural occurrences of peridotite (Green and Ringwood, 1963, 1967). In calculating the model source compositions and residue compositions, it should be noted that because residual olivine contains 0.4 per cent CaO and no detectable (i.e. < 0.2 per cent) Al_2O_3, and, because spinel contains high Al_2O_3 and no CaO, it is possible to choose proportions of the four phases to yield "chondritic" CaO/Al_2O_3 ratios for the source (cf. Ringwood, 1975; Sun and Nesbitt, 1977). However the TiO_2 content, TiO_2/Al_2O_3 and/or TiO_2/CaO ratios of all phases are so low that it is not possible to calculate model source composition with "chondritic" ratios for these elements—the possible source compositions are all depleted in TiO_2. Similar conclusions apply (more strongly) to the incompatible elements K_2O, P_2O_5, Rb, Sr, light rare earth elements, etc., based on the composition of DSDP3-18 and estimates

Table 5. Compositions of model source compositions (see text), i.e. model pyrolite compositions, based on: A, DSDP3-18 + dunite residue; B, picrite (from DSDP3-18) + enstatite-poor harzburgite residue; C, picrite + enstatite-rich harzburgite residue; D is the favoured model adjusted from B and C to bring the source and residue compositions into the spectrum of lherzolite compositions of Kuno and Aoki (1970).

	A		B		C		D (favoured model)		Pyrolite (Ringwood, 1966) (based on Hawaiian tholeiite)	Pyrolite (Ringwood, 1975) (based on mid-ocean ridge tholeiite)
Melt (per cent)	30		24		24		24			
Olivine (per cent)	69‡		65†		50†		57.5†			
Orthopyroxene (per cent)	—		10†		25†		18†			
Spinel (per cent)	1‡		1†		1†		0.5†			
	Source	Residue	Source	Residue	Source	Residue	Source	Residue		
SiO_2	44.3	39.9	43.5	42.2	45.6	44.7	45.0	43.9	45.2	46.1
TiO_2	0.24	—	0.16	0.02	0.17	0.03	0.17	0.04	0.71	0.2
Al_2O_3	5.7	0.34	4.0	0.97	4.8	2.1	4.4	1.4	3.5	4.3
FeO	9.6	10.0	7.9	7.9	7.4	7.2	7.6	7.5	8.6	8.2
MnO	0.12	0.11	0.12	0.12	0.11	0.11	0.11	0.11	0.14	—
MgO	37.1	48.0	40.0	47.6	37.3	43.7	38.8	45.9	37.5	37.6
CaO	4.6	0.43	3.2	0.71	3.5	1.2	3.4	0.95	3.1	3.1
Na_2O	0.66	—	0.40	—	0.40	—	0.40	—	0.57	0.4
K_2O	0.003	—	0.003	—	0.003	—	0.003	—	0.13	0.03
Cr_2O_3	0.46	0.63	0.50	0.74	0.74	0.96	0.45	0.58	0.43	—
NiO	0.29	0.40	0.28	0.35	0.23	0.28	0.26	0.32	0.20	—
100 Mg/(Mg + Fe)	87.3	89.5	90.1	91.5	90.0	91.5	90.1	88.6	89.1	

† Mineral compositions of Table 3, columns 1–3

‡ Spinel from Table 4, column 4; olivine is $Mg_{89.7}$ from Frey *et al.* (1974) (with 0.4 per cent NiO added)

of the relevant residue/liquid partition coefficients (Frey *et al.*, 1978). It is thus not reasonable to use preconceptions of "chondritic" mantle chemistry to model the proportions of phases in the source/residue/melt equilibrium. It is however reasonable to turn to natural mantle-derived peridotites to enquire whether independent evidence from this source permits choice between models such as A, B and C of Table 5.

Kuno and Aoki (1970) assembled chemical data on spinel lherzolite inclusions in basalt from many localities. It is generally accepted that these rocks are random xenoliths of the upper part of the subcrustal lithosphere and that, although they include examples of accumulates from basaltic magmas, they are predominantly residual after extraction of basaltic magmas from parental lherzolite (Kuno and Aoki, 1970; Frey and Green, 1974). Likewise, high-temperature lherzolite diapirs such as Tinaquillo, Lizard, Serrania del Ronda, Beni Bousera, etc., are interpreted as residual upper-mantle compositions, depleted by loss of a small melt fraction. Kuno and Aoki (1970) show that lherzolite compositions are variable in Mg/Fe ratios and that there is systematic change in Ca, Al, Cr, Ti and Na + K associated with Mg/Fe variation. These systematic compositional changes are consistent with melting and magma extraction. These inferences on the origin of natural lherzolites, if accepted, provide a discriminant to choose between models A, B and C, i.e. the calculated source/residue pairs should lie within the spread of natural residue/?source peridotite compositions. On this basis, model A is not appropriate as it produces a chemical trend lying athwart the natural rock trends and either source or residue compositions lie outside the compositional range of the natural rocks. Models B and C are generally compatible with the natural rock trends except that both are too high in Cr_2O_3. In detail, the plots of individual oxides against Mg/Fe (Kuno and Aoki, 1970) suggest that B is too low and C is too high in orthopyroxene and/or olivine in the residue. These "errors" are corrected in model D, in which a "favoured model" for source and residue is calculated. It is emphasized that this model source is capable of yielding a variety of residual compositions with differing olivine to orthopyroxene ratios dependent on conditions of melting and magma extraction (Fig. 2). It is also emphasized that model D is constrained only by the compositions of the phases involved in the postulated partial melting and magma extraction event and by the applicability and compositional spread of the natural peridotite compositions.

Model D may be evaluated using information on rare earth concentrations. Frey and Green (1974) showed that although light rare earth elements showed large fractionation among lherzolite inclusions and intrusive lherzolites, the heavy rare earth's were correlated with CaO-content and the degree of refractoriness of the lherzolites and, in the least

refractory lherzolites (~3 per cent CaO) approach concentrations of 2× chondrites and flat, unfractionated patterns (Tb → Lu). Frey *et al.* (1978) analysed the significance of trace-element and major-element variations in a suite of tholeiitic to olivine melilite basalts from both Victoria and Hawaii to infer that the mantle source peridotites had 2.5–3.0× chondritic abundances of the heavy rare earths. Model D, using the rare earth element contents of Frey *et al.* (1974) for DSDP3-18, implies that the source region had a heavy rare earth concentration of 2.2× chondrites but showed very strong light rare earth element depletion. Thus the model deduced on phase equilibria and major element considerations is consistent with constraints implied by heavy rare earth abundances of mantle-derived basalts and mantle-derived lherzolites.

The model source composition, i.e. "pyrolite"-yielding mid-ocean ridge basalts matching DSDP3-18, is very similar in major elements to the pyrolite of Ringwood (1966) which has been so extensively studied experimentally. It is significantly lower in its orthopyroxene to olivine ratio and higher in Al_2O_3 content, so that there will be some differences in the roles of subsolidus spinel and Al_2O_3 content of pyroxenes in the spinel pyrolite field and the proportions of garnet in the garnet–pyrolite field (Green and Ringwood, 1970; Green and Liebermann, 1976). Differences in CaO and Na_2O between the two compositions have complementary effects, but the principal difference between the two model compositions is in incompatible element contents exemplified by TiO_2 (0.71 per cent and 0.17 per cent) and K_2O (0.13 per cent and 0.003 per cent). The difference in Mg/(Mg+Fe) value is a significant one and may be attributed to the rather low Mg-value of the basalt used in the original Ringwood (1966) calculation—an "error" only apparent with the benefit of hindsight! Ringwood (1975, Table 5-4) calculated a pyrolite source composition for mid-ocean ridge tholeiite on the basis of the earlier petrogenetic model of segregation at 4–10 kbar from residual harzburgite. Taking the heavy rare earth concentration of "primary" oceanic tholeiite as 12× chondrites and assuming a source concentration of ~2× chondrites, Ringwood inferred 17 per cent melting to yield a primitive mid-ocean ridge tholeiite (KD-11 of Kay, Hubbard and Gast, 1970); leaving residual orthopyroxene-rich (33 per cent enstatite, 67 per cent olivine) harzburgite. The experimental data presented herein necessitate revision of Ringwood's calculation in that KD-11 is too Fe-rich (100Mg/(Mg+Fe) = 64) and the earlier petrogenetic model is now retracted in favour of a picritic parental magma. Thus, although the calculated model D source and Ringwood's (1975) model pyrolite agree (somewhat fortuitously bearing in mind the different basalts and models) in TiO_2, Al_2O_3 and Na_2O contents, the differences in CaO, Mg-value and particularly in MgO, SiO_2 and Opx/Ol ratio are significant for mantle mineralogy and

petrogenesis and the source composition D is preferred as a more closely constrained estimate of upper-mantle composition for the source region of mid-ocean ridge basalts. This conclusion applies strictly only to DSDP3-18 or its derivative melts, but in so far as the petrographic and major element characteristics of DSDP3-18 are common to many mid-ocean ridge basalts (cf. Melson *et al.*, 1977) the deduced composition may have wide application.

Frey *et al.* (1978) have shown that the pyrolite compositon of Ringwood (1966) (or a slightly modified composition with 0.3–0.4 per cent TiO_2) which was based on Hawaiian olivine tholeiite composition, is a suitable source composition for a suite of south-east Australian basalts ranging from olivine tholeiite to olivine melilitite. On the basis of the recognized similarity of these continental "rift" basalt sequences to oceanic-island or light rare earth element-enriched oceanic basalts (as typified by Hawaii, Reunion, Azores, etc.) it has previously been argued that a world-wide source pyrolite of composition close to Ringwood's (1966) estimate exists or develops at the upper part of the low-velocity zone (LVZ) (Green, 1971; Green and Liebermann, 1976). This hypothesis contrasts with an alternative (e.g. Schilling 1973, 1975) view that the appropriate mantle source composition for these basalts occurs as "plumes" or "mantle blobs" rising from a *deep* mantle region underlying a more refractory peridotite (light rare earth-depleted, etc.) acting as a source for mid-ocean ridge basalts. In the context of the model for the LVZ developed by Green and Liebermann (1976), we suggest that our present study defines a composition of the lower, depleted part of the LVZ. We consider that the process of migration of incompatible elements, i.e. depletion in the deeper part of the LVZ and enrichment in the upper levels, occurs through the migration of a small melt fraction (<2 per cent melt) with composition of olivine melilitite to kimberlitic character (Green, 1971; Brey and Green, 1977; Frey *et al.*, 1978; Green and Liebermann, 1976). Although we have, by the nature of the approach used, identified two important pyrolite compositions, i.e. incompatible-element enriched or "Hawaiian type" and incompatible element depleted or "mid-ocean ridge type", the discussion above should illustrate that we envisage a continuum of such compositions and a dynamic situation in which incompatible element contents reflect both "old" events of depletion and enrichment and the presently active migration within the LVZ. Thus the model predicts minor variations and inhomogeneities in incompatible element contents in both "enriched" and "depleted" parts of the LVZ. The need for such source inhomogeneity has been noted in the detailed studies in the ridge-crest areas of the mid-Atlantic Ridge (Blanchard *et al.*, 1976; Bryan *et al.*, 1976). The time-integrated effects and overprinting of depletion and enrichment events in upper-mantle source regions for basalts are becoming apparent in the

ombination of trace element and isotopic studies, particularly Rb/Sr and m/Nd systematics (De Paolo and Wasserburg, 1976; O'Nions *et al.*, 1977). : is our view that the time scale for migration of interstitial melt and evelopment of chemical zoning in the LVZ is short (10–20 million years) ompared to the "life" of oceanic crust/lithosphere (100–200 million years) r to the "cycle" of deep mantle convection (? 1 billion years) implied by the ersistence of Benioff zones to depths of ~700 km.

In the model which we propose for derivation of mid-ocean ridge basalts, ~7 km of basaltic oceanic crust implies ~21 km refractory harzburgite esidue. Since the lithosphere thickens to ~90 km at distance from the nid-ocean ridge crests, it is clear that the lithosphere itself should not be egarded as refractory harzburgite but as a mix of lherzolite → harzburgite → lunite containing both country-rock to intrusive diapirs, diapirs that have ost large melt fractions (harzburgites) or small melt fractions (e.g. Lizard or inaquillo peridotites) and accumulates of dunite and troctolite and wehrlite esulting from fractional crystallization of picritic parent magmas *en route* to he surface. At shallower depths, both within the crust and at the rust/mantle interface, we envisage complexes of residual harzburgite, and ccumulate sequences of peridotite, pyroxenite and gabbro representing mplacement, second-stage melting and crystal fractionation within diapirs f refractory lherzolite or harzburgite, these being characterized by highly alcic plagioclase (>An_{80}), accumulate magnesian orthopyroxene and linopyroxene.

7. Conclusions

1) The experimental study of one of the most magnesian glass composi- ions among mid-ocean ridge basalts (DSDP3-18-7-1) has shown that this omposition is not a possible melt from a lherzolite source peridotite unless nelting and magma segregation occurs at shallow depths (<35 km) leaving esidual chrome–spinel-bearing dunite. This model is not favoured as it mplies source and residue peridotite compositions which are unlike natural nantle lherzolite compositions.

(2) Olivine addition experiments (i.e. testing of the hypothesis that SDP3-18-7-1 is not a primary magma but is derived from a primary nagma by olivine fractionation at low pressure) have demonstrated that a icritic parental composition (83 per cent DSDP3-18-7-1 + 17 per cent livine ($Mg_{91.7}$)) is a possible melt from mantle lherzolite leaving harzburgite olivine ($Mg_{91.5}$) + enstatite (Mg_{92}, 5.5 per cent Al_2O_3) + ?spinel) as residue. he conditions of melting and magma segregation are 20 kbar (~70 km epth) and ~1430 °C.

(3) It is inferred that tholeiitic picrite magmas with ~25 per cent normative olivine are important primary magmas in mid-ocean ridge petrogenesis. An earlier hypothesis that the primary basalts of the mid-ocean ridges are high-Al_2O_3 olivine tholeiites (~10 per cent olivine) segregating from residual harzburgite or lherzolite at ~30 km depth is retracted in the light of the new experimental data in favour of the picritic model (O'Hara, 1968).

(4) Primary magmas of tholeiitic picrite or their derivatives such as DSDP3-18-7-1 cannot precipitate the highly magnesian clinopyroxene ($>Mg_{88}$) or highly calcic plagioclase ($>An_{80}$) megacrysts which occur in some mid-ocean ridge basalts, nor can they precipitate those accumulate sequences of ophiolite complexes which contain highly calcic plagioclase, magnesian orthopyroxene ($>Mg_{87}$ approx.) or highly magnesian diopside ($>Mg_{88}$ approx.). Similarly, primary magmas of this type cannot be genetically related as liquid/residue pairs to highly refractory harzburgites of ophiolite complexes in which the orthopyroxene and olivine have very low contents of Al_2O_3 (<1.5 per cent in orthopyroxene) and CaO (<0.3 per cent in olivine, <2.0 per cent in orthopyroxene) and these constituents are not redistributed in the rock on subsolidus recrystallization. To summarize, the experimental study precludes a direct genetic relationship between ophiolite complexes (with the character designated) and the type of mid-ocean ridge basalt represented by tholeiitic picrite or olivine tholeiite magmas studied in this project.

(5) We postulate that, in the mid-ocean ridge environment, there must occur primary magmas, and particularly fractionated magmas derived from them, which segregated from Na-poor, Ti-poor depleted peridotite at very shallow depths leaving harzburgite residue. These postulated primary magmas would have high SiO_2 contents, high MgO contents, very low Na_2O/CaO ratios, low TiO_2 and K_2O contents and would be quartz-normative or low in normative olivine content. These magmas and their fractionation products are considered to be complementary to the harzburgites and accumulate sequences of ophiolite complexes. The extrusive diapir model of Moores (1969) may be appropriate for the emplacement and characteristics of these complexes.

(6) We have used the information obtained on DSDP3-18-7-1 and olivine-enriched derivatives to constrain the composition of the source peridotite and to obtain a preferred model composition. This pyrolite composition differs slightly but significantly from previous estimates of upper-mantle compositions.

(7) We support a model of the lithosphere and asthenosphere (LVZ) in which the source pyrolite for mid-ocean ridge tholeiites is considered as representative of the lower, depleted part of the LVZ and the incompatible element-enriched pyrolite composition (Ringwood, 1966) previously stu-

died is considered representative of the upper, enriched part of the asthenosphere (LVZ). Both types of pyrolite source (and compositional variants between them) are considered to be of general, world-wide occurrence beneath oceanic crust and the time scale of enrichment and depletion processes is short compared with the "life" of oceanic crust/lithosphere segments. The factors determining which source region is actively involved in diapirism and magma production are the particular tectonics and dynamics of the area, i.e. a "leaky transform" fault, an oceanic island chain (migrating fracture) or a continental rift may trigger diapirs only from the upper part of the LVZ. By contrast, the continued movement apart of major lithospheric plates at a spreading centre or mid-ocean ridge involves upwelling from deeper levels and upper mantle overturn which taps diapirism from the deep, incompatible-element depleted regions of the LVZ.

Acknowledgements

This study was partly completed at the Research School of Earth Science, the Australian National University, and partly at the Department of Geology, University of Tasmania, the latter part being supported by the Australian Research Grants Committee. All authors, but particularly D. H. Green, acknowledge the stimulus and leadership of Professors J. C. Jaeger and A. L. Hales—the influence of J. C. Jaeger determined the establishment of experimental petrology at The Australian National University and the stimulus of A. L. Hales has ensured that pyrolite and the upper mantle have remained very much subjects for continuing reappraisal and review.

References

Arndt, N. (1977). Ultrabasic magmas and high-degree melting of the mantle. *Contr. Mineral Petrol.* **64**, 205–221.

Bence, A. E. and Taylor, S. R. (1977). Petrogenesis of Mid-Atlantic Ridge basalts at DSDP Leg 37 Holes 332A and 332B from major and trace element geochemistry. *Initial Repts Deep Sea Drilling Program* **37**, 705–710.

Blanchard, D. P., Rhodes, J. M., Dungan, M. A., Rodgers, K. V., Donaldson, C. H., Brannon, J. C., Jacobs, J. W. and Gibson, E. K. (1976). The chemistry and petrology of basalts from Leg 37 of the Deep Sea Drilling Project. *J. geophys. Res.* **81**, 4231–4247.

Bonatti, E., Honnorez, J. and Ferrara, G. (1971). Peridotite–gabbro-basalt complex from the equatorial mid-Atlantic ridge. *Phil. Trans. R. Soc. A* **268**, 385–402.

Brey, G. and Green, D. H. (1975). The role of CO_2 in the genesis of olivine melilitite. *Contr. Mineral. Petrol.* **49**, 43–103.

Brey, G. and Green, D. H. (1977). Systematic study of liquidus phase relations in olivine melilitite + H_2O + CO_2 at high pressures and petrogenesis of an olivine melilitite magma. *Contr. Mineral. Petrol.* **61**, 141–162.

Bryan, W. B. and Moore, J. C. (1977). Compositional variations of young basalts in the mid-Atlantic Ridge rift valley near lat. 36°49'N. *Bull. geol. Soc. Am.* **88**, 556–564.

Bryan, W. B., Thompson, G., Frey, F. A. and Dickey, J. S. (1976). Inferred geological settings and differentiation in basalts from the Deep Sea Drilling Project. *J. geophys. Res.* **81**, 4285–4304.

Bultitude, R. J. and Green, D. H. (1971). Experimental study of crystal liquid relationships at high pressures in olivine nephelinite and basanite compositions. *J. Petrol.* **12**, 121–147.

Cann, J. R. (1974). A model for oceanic crustal structure developed. *Geophys. J. R. astronom. Soc.* **39**, 169–187.

Cawthorn, R. G., Ford, C. E., Biggar, G. M., Bravo, M. S. and Clarke, D. B. (1973). Determination of liquid composition in experimental samples: discrepancies between microprobe analysis and other methods. *Earth planet. Sci. Lett.* **21**, 1–5.

Clarke, D. B. and Pedersen, A. K. (1976). Tertiary volcanic province of West Greenland. In *Geology of Greenland* (A. Escher and W. S. Watt, eds), Geological Survey of Greenland, pp. 365–385.

Dallwitz, W. B., Green, D. H. and Thompson, J. B. (1966). Clinoenstatite in a volcanic rock from Cape Vogel, Papua. *J. Petrol.* **7**, 375–403.

Davies, H. L. (1971). Peridotite-gabbro complexes in Eastern Papua: an overthrust of oceanic crust and mantle. *Bur. Miner. Resour. Australia Bull.* **128**, 1–47.

De Paolo, D. J. and Wasserburg, G. J. (1976). Nd isotopic variations and petrogenetic models. *Geophys. Res. Lett.* **3**, 249–254.

Donaldson, C. H. and Brown, R. W. (1977). Refractory megacrysts and magnesium-rich melt inclusions within spinel in oceanic tholeiites: indications of magma mixing and parental liquid composition. *Earth planet. Sci. Lett.* **37**, 81–89.

England, R. N. and Davies, H. L. (1973). Mineralogy of ultramafic cumulates and tectonites from eastern Papua. *Earth planet. Sci. Lett.* **17**, 416–425.

Esson, J., Dunham, A. C. and Thompson, R. N. (1975). Low-alkali, high-calcium olivine tholeiite laves from the Isle of Skye, Scotland. *J. Petrol.* **16**, 488–497.

Flower, M. F. J., Robinson, P. T., Schmincke, H. U. and Ohnmacht, W. (1977). Magma fractionation systems beneath the mid-Atlantic Ridge at 36–37°N. *Contr. Mineral. Petrol.* **64**, 167–195.

Frey, F. A. (1969). Rare earth abundances in a high-temperature peridotite intrusion. *Geochim. cosmochim. acta* **33**, 1429–1447.

Frey, F. A. and Green, D. H. (1974). The mineralogy, geochemistry and origin of lherzolite inclusions in Victorian basantites. *Geochim. cosmochim. acta* **38**, 1023–1059.

Frey, F. A. and Prinz, M. (1977). Ultramafic inclusions from San Carlos, Arizona: Petrologic and geochemical data bearing on their petrogenesis. *Earth planet. Sci. Lett.* **38**, 129–176.

Frey, F. A., Green, D. H. and Roy, S. D. (1978). Integrated models of basalt petrogenesis: a study of quartz tholeiites to olivine melilitites from S.E. Australia utilizing geochemical and experimental petrological data. *J. Petrol.* **19**, 463–513.

Frey, F. A. Bryan, W. B. and Thompson, G. (1974). Atlantic Ocean floor: geochemistry and petrology of basalts from Legs 2 and 3 of the Deep Sea Drilling Project. *J. geophys. Res.* **79**, 5507–5527.

Green, D. H. (1963). Alumina content of enstatite in a Venezuelan high temperature peridotite. *Bull. geol. Soc. Am.* **74**, 1397–1402.

Green, D. H. (1968). Origin of basaltic magmas. In *Basalts* (H. H. Hess and A. Poldervaart, eds), Wiley-Interscience, New York, London, Sydney, Vol. 2, pp. 835–862.

Green, D. H. (1970). The origin of basaltic and nephelinitic magmas. *Trans. Leicester lit. phil. Soc.* **64**, 28–54.

Green, D. H. (1971). Compositions of basaltic magmas as indicators of conditions of origin: application to oceanic volcanism. *Phil. Trans. R. Soc. A* **268**, 707–725.

Green, D. H. (1973). Experimental studies on a model upper mantle composition at high pressure under water-undersaturated and water-saturated conditions. *Earth planet. Sci. Lett.* **19**, 37–53.

Green, D. H. (1976*a*). Experimental petrology in Australia—a review. *Earth Sci. Rev.* **12**, 99–138.

Green, D. H. (1976*b*). Orthopyroxene in the lunar interiors and constraints on early lunar differentiation. *Proc. Seventh Lunar Sci. Conf.* **1**, 336–338.

Green, D. H. and Hibberson, W. O. (1970). Experimental duplication of conditions of precipitation of high pressure phenocrysts in a basaltic magma. *Phys. Earth planet. Interiors* **3**, 247–254.

Green, D. H. and Liebermann, R. C. (1976). Phase equilibria and elastic properties of a pyrolite model for the oceanic upper mantle. *Tectonophysics* **32**, 61–92.

Green, D. H. and Ringwood, A. E. (1963). Mineral assemblages in a model upper mantle composition. *J. geophys. Res.* **68**, 937–945.

Green, D. H. and Ringwood, A. E. (1967). The genesis of basaltic magmas. *Contr. Mineral. Petrol.* **15**, 103–190.

Green, D. H. and Ringwood, A. E. (1970). Mineralogy of peridotitic compositions under upper mantle conditions. *Phys. Earth planet. Interiors* **3**, 359–371.

Green, D. H., Ringwood, A. E., Hibberson, W. O. and Ware, N. G. (1975). Experimental petrology of Apollo 17 mare basalts. *Proc. Sixth Lunar Sci. Conf.* **1**, 871–893.

Green, D. H., Edgar, A. D., Beasley, P., Kiss, E. and Ware, N. G. (1974). Upper mantle source for some hawaiites, mugearites, and benmoreites. *Contr. Mineral. Petrol.* **48**, 33–43.

Green, D. H., Ringwood, A. E., Ware, N. G., Hibberson, W. O., Major, A. and Kiss, E. (1971). Experimental petrology and petrogenesis of Apollo 12 basalts. *Proc. Second Lunar Sci. Conf.* **1**, 601–615.

Green, T. H., Green, D. H. and Ringwood, A. E. (1967). The origin of high alumina basalts and their relationships to quartz tholeiites and alkali basalts. *Earth planet. Sci. Lett.* **2**, 41–52.

Hakli, J. A. and Wright, T. L. (1967). The fractionation of nickel between olivine and augite as a geothermometer. *Geochim. cosmochim. acta* **31**, 877–884.

Hodges, F. N. and Papike, J. J. (1976). DSDP Site 34: magmatic cumulates from oceanic layer 3. *J. geophys. Res.* **81**, 4135–4151.

Ito, K. and Kennedy, G. C. (1968). Melting and phase relations in the plane tholeiite-lherzolite-nepheline basanite to 40 kbar with geological implications. *Contr. Mineral. Petrol.* **19**, 177–211.

Kay, R., Hubbard, N. J. and Gast, P. W. (1970). Chemical characteristics and origin of oceanic ridge volcanic rocks. *J. geophys. Res.* **75**, 1585–1613.

Kuno, H. and Aoki, K. (1970). Chemistry of ultramafic nodules and their bearing on the origin of basaltic magmas. *Phys. Earth planet. Interiors* **3**, 273–301.

Langmuir, C. H., Bender, J. F., Bence, A. E. and Hanson, G. N. (1977). Petrogenesis of basalts from the Famous area: Mid-Atlantic Ridge. *Earth planet. Sci. Lett.* **36**, 133–156.

Leeman, W. P. and Scheidegger, K. F. (1977). Olivine/liquid distribution coefficients and a test for crystal/liquid equilibrium. *Earth planet. Sci. Lett.* **35**, 247–257.

Mathez, E. A. (1976). Sulphur solubility and magmatic sulphides in submarine basalt. *J. geophys. Res.* **81**, 4269–4276.

Melson, W. G. and Thompson, G. (1970). Layered basic complex in oceanic crust, Romanche Fracture equatorial Atlantic Ocean. *Science, N.Y.* **168**, 817–820.

Melson, W. G., Byerly, G. R., Nelen, J. A., O'Hearn, T., Wright, T. L. and Vallier, T. (1977). A catalog of the major element chemistry of abyssal volcanic glasses. *Mineral Sciences Investigations: Smithsonian Contributions to the Earth Sciences* **19**, 31–60.

Miyashiro, A. Shido, F. and Ewing, M. (1969). Diversity and origin of abyssal tholeiite from the Mid-Atlantic Ridge near 24° and 30° north latitude. *Contr. Mineral. Petrol.* **23**, 38–52.

Moores, E. M. (1969). Petrology and structure of the Vourinos ophiolitic complex of northern Greece. *Geol. Soc. Am. spec. Paper* **118**, 1–74.

Moores, E. M. and Vine, F. J. (1971). The Troodos Massif, Cyprus and other ophiolites as oceanic crust: evaluation and implications. *Phil. Trans. R. Soc. A* **268**, 443–466.

Mysen, B. (1976). Partitioning of samarium and nickel between olivine, orthopyroxene and liquid: preliminary data at 20 kb and 1025 °C. *Earth planet. Sci. Lett.* **31**, 1–7.

O'Hara, M. J. (1968). Are ocean-floor basalts primary magmas. *Nature Lond.* **220**, 683–686.

O'Hara, M. J. and Humphries, D. J. (1977). Problems of iron gain and loss during experimentation on natural rocks: the experimental crystallization of five lunar basalts at low pressures. *Phil. Trans. R. Soc. A* **286**, 313–330.

O'Hara, M. J., Humphries, D. J. and Waterston, S. (1975). Petrogenesis of mare basalts: implications for chemical mineralogical and thermal models for the moon. *Proc. Sixth Lunar Sci. Conf.* **1**, 1043–1055.

O'Nions, R. K., Hamilton, P. J. and Evensen, N. M. (1977). Variations in $^{143}Nd/^{144}Nd$ and $^{87}Sr/^{86}Sr$ ratio on oceanic basalts. *Earth planet. Sci. Lett.* **34**, 13–22.

Presnall, D. C. (1969). The geometrical analysis of partial fusion. *Am. J. Sci.* **267**, 1178–1194.

Roeder, P. L. and Emslie, R. F. (1970). Olivine–liquid equilibrium. *Contr. Mineral. Petrol.* **29**, 275–289.

Ringwood, A. E. (1966). The chemical composition and origin of the earth. In *Advances in Earth Science* (P. M. Hurley, ed.), M.I.T. Press, Cambridge, Mass., pp. 287–356.

Ringwood, A. E. (1975). *Composition and Petrology of the Earth's Mantle*, McGraw-Hill, New York.

Schilling, J. G. (1973). Iceland mantle plume: geochemical study of the Reykjanes Ridge. *Nature, Lond.* **242**, 565–571.

Schilling, J. G. (1975). Azores mantle blob: rare-earth evidence. *Earth planet. Sci. Lett.* **25**, 103–115.

Shido, F., Miyashiro, A. and Ewing, M. (1971). Crystallization of abyssal tholeiites. *Contr. Mineral. Petrol.* **31**, 251–266.

Sun, S. S. and Nesbitt, R. W. (1977). Chemical heterogeneity of the Archaean mantle, composition of the earth and mantle evolution. *Earth planet. Sci. Lett.* **35**, 429–488.

Verhoogen, J. (1954). Petrological evidence on temperature distribution in the mantle of the Earth. *Trans. Am. geophys. Union* **35**, 85–92.

Yoder, H. S. and Tilley, C. E. (1962). Origin of basalt magmas: an experimental study of natural and synthetic rock systems. *J. Petrol.* **3**, 342–532.

B29

Role of multistage melting in the formation of oceanic crust

R. A. Duncan, D. H. Green
Department of Geology, University of Tasmania
Hobart, Tasmania 7001, Australia

ABSTRACT

Picritic liquids, formed by 20% to 30% partial melting of upper-mantle "pyrolite" at 60- to 70-km depth and a temperature of 1,400 to 1,450 °C, are parental to the majority of ocean-floor basalts. Other more-refractory liquids must be generated beneath mid-ocean spreading ridges to provide a source for the very refractory megacrysts entrained by ocean-floor tholeiites and for some cumulate sequences in ophiolites (thought to be segments of oceanic crust). Such liquids have the composition of extremely LREE-depleted magnesian quartz tholeiite (LREE = light rare-earth element) or olivine-poor tholeiite and are derived by small degrees (5% to 10%) of anhydrous melting of refractory lherzolite diapirs at shallow depths (≤25 km). These liquids are termed "second-stage" melts because they are extracted from lherzolite diapirs, which are the residue of a previous partial melting of upper-mantle "pyrolite" that yielded first-stage picritic liquids. Rocks representative of these second-stage melts can be recognized among the uppermost lavas in several ophiolites.

INTRODUCTION

It has been proposed that the primary magma for high-Al_2O_3 mid-ocean ridge olivine tholeiites is tholeiitic picrite (O'Hara, 1968). Experimental studies by Green and others (1979) have shown (1) that such picritic liquids (Table 1) are multiply saturated in olivine and orthopyroxene at ~20-kb pressure (equivalent to depths of 60 to 70 km) and a temperature of 1,430 °C and (2) that such liquids may reasonably be derived by ~30% partial melting of upper-mantle lherzolite. Many ocean-floor basalts can be genetically related to these primary liquids by pre-eruptional fractional crystallization of olivine, spinel, plagioclase, and pyroxene (Frey and others, 1974; Bryan and others, 1976; Bryan and Moore, 1977). Other studies (Blanchard and others, 1976; Flower and others, 1977; Bender and others, 1978), however, have emphasized the chemical and mineralogic variability of ocean-floor basalts and have stressed the requirement of a range in composition of primary liquids. This variability in primary-liquid composition may develop from complex processes of fractional melting and crystallization and from magma mixing (for example, the "dynamic melting" model of Langmuir and others, 1977) as well as from upper-mantle chemical heterogeneity.

If such complexity exists, it is important to isolate and understand the petrogenesis of "extreme" or "end member" parental liquids because these are components for magma mixing, starting points for fractional crystallization, and so forth. This paper draws attention to the existence of extremely LREE-depleted magnesian quartz tholeiite or olivine-poor tholeiite liquids (whose representative counterparts have been recognized in several ophiolites) and relates their genesis to residual diapirs from which picritic liquids have earlier been extracted. Such two-stage melting [and more complex multistage melting(?)] of upper-mantle source rocks may be an important mechanism in the formation of ocean crust.

PROBLEMS IN RELATING OPHIOLITES TO OCEANIC CRUST FORMATION

A popular hypothesis argues that ocean-floor basalts, dredged samples of gabbroic and ultramafic cumulates, and dredged samples of ultramafic tectonites are complementary components (fractionated liquids, shallow-level cumulates, and refractory residue, respectively) formed by mantle diapirism of lherzolite with consequent partial melting and magma segregation at shallow depths. It is also held that ophiolites occurring in orogenic zones are tectonically emplaced slices of oceanic crust. The above model of ocean-crust development and correlation of ophiolites with ancient oceanic crust can be tested for internal consistency by examination of the nature of cumulate mineral phases of ophiolite complexes (and similar dredged plutonic rocks) and by comparison with the products of low-pressure fractional crystallization of ocean-floor basalts.

The experimental studies of crystallization of primitive ocean-floor basalts (olivine tholeiite and tholeiitic picrite, Green and others, 1979) show that complementary cumulates would contain olivine ($<Mg_{91.5}$), plagioclase ($<An_{80}$), clinopyroxene ($<Mg_{88}$), and pigeonite or orthopyroxene ($<Mg_{87}$). Those

TABLE 1. HIGH-MgO ROCKS FROM OPHIOLITES, THE OCEAN FLOOR, AND ISLAND ARCS

	1	2	3	4	5	6	7	8	9	10	11	12	13
SiO_2	45.57	48.95	54.2	52.4	48.3	49.7	48.19	43.6	43.7	53.9	53.3	58.5	52.5
TiO_2	0.19	0.29	0.4	0.3	0.6	0.72	0.37	0.04	0.01	0.3	0.6	0.3	0.4
Al_2O_3	4.92	9.63	15.4	11.7	13.7	16.4	16.05	1.4	0.47	12.7	14.4	10.3	10.0
FeO*	9.17	8.84	7.9	8.4	7.9	7.9	9.10	7.4	8.2	8.6	9.9	9.5	9.7
MnO	0.16	0.14	0.16	0.15	0.12	0.12	0.16	0.11	0.15	0.19	n.d.	0.2	0.2
MgO	35.45	22.51	8.7	15.8	16.7	10.1	11.10	45.6	46.0	9.8	7.8	14.1	16.7
CaO	4.23	8.91	11.5	10.7	10.9	13.1	13.85	0.95	0.77	12.7	12.4	5.9	9.2
Na_2O	0.26	0.60	1.6	0.7	1.65	2.0	1.03	..	..	1.4	1.7	0.8	1.0
K_2O	0.05	0.12	0.1	0.1	0.01	0.01	0.03	..	..	0.4	0.1	0.4	0.3
Cr_2O_3	n.d.	n.d.	n.d.	n.d.	(0.06)	(0.07)	0.10	0.58	0.39	n.d.	n.d.	n.d.	n.d.
NiO	n.d.	n.d.	n.d.	n.d.	(0.08)	(0.03)	0.03	0.32	0.25	n.d.	n.d.	n.d.	n.d.
Mg/(Mg + Fe)	0.873	0.819	0.662	0.770	0.790	0.709	0.658	0.916	0.909	0.671	0.583	0.726	0.747

Note: (1) Troodos upper pillow lava, ultramafic (Gass, 1958). (2) Troodos upper pillow lava, ultramafic, Kalvasos (average) (Searle and Vokes, 1969). (3) Troodos upper pillow lava (Smewing and Potts, 1976). (4) Inferred parental liquid for Troodos magnesian quartz tholeiites. (5) Inferred picritic parental liquid for olivine tholeiites (Green and others, 1979). (6) DSDP3-18-7-1 (Frey and others, 1974). (7) Lau Basin olivine basalt (Hawkins, 1976). (8) Harzburgite residue after extraction of picritic liquids (Green and others, 1979). (9) Basal harzburgite (average of eight), Troodos (Menzies and Allen, 1974). (10) Laves supériéurs, Baër-Bassit, Syria (Parrot, 1977). (11) Average of five basaltic glasses from DSDP 236, Indian Ocean (Melson and others, 1977). (12) Clinoenstatite-bearing high-MgO andesite, Cape Vogel (Dallwitz, 1968). (13) Spinifex-textured basalt, Pilbara block, Western Australia (Sun and Nesbitt, 1978a). All analyses recalculated to 100%, volatile-free.
*Total Fe.

layered sequences within ophiolites with these specific mineralogic compositions may be reasonably related to the picrites, and the more common olivine tholeiites and Fe-Ti–rich quartz tholeiites, of the ocean floors. However, ophiolites commonly contain more highly refractory mineral compositions than those listed above, particularly within the basal layered sequences. These are cumulates that contain plagioclase as calcic as An_{95}, clinopyroxene as magnesian as Mg_{94}, and orthopyroxene as magnesian as Mg_{92}. Underlying harzburgite tectonites contain refractory olivine ($>Fo_{91}$), very little Al_2O_3, and magnesian orthopyroxene ($>Mg_{91}$) (for example, England and Davies, 1973; Pallister and Hopson, 1979; Juteau and Whitechurch, 1979). Minerals of these compositions cannot have precipitated from primary picritic liquids or their derivatives. Similarly, the megacrysts of calcic plagioclase ($>An_{85}$), chrome spinel, and (rarely) magnesian chrome diopside ($>Mg_{88}$) observed in ocean-floor olivine tholeiites from widespread localities (Donaldson and Brown, 1977) cannot have precipitated from their host magmas.

The extremely refractory compositions of megacrysts in ocean-floor basalts, of dredged coarse-grained plutonic rocks, and of cumulate sequences in ophiolites (inferred to have formed at mid-ocean ridges) argue for the existence in the mid-ocean ridge environment of a second distinctive primary magma type unlike the tholeiitic picrites parental to the majority of "normal" ocean-floor basalts. This magma type should be magnesian quartz tholeiite having 52% to 53% SiO_2, 15% to 16% MgO, very little Na_2O and TiO_2, and a very high CaO/Na_2O ratio (Green and others, 1979). That picritic parental liquids cannot be solely responsible for oceanic crust formation may also be inferred from the nature of the noncumulate harzburgite present as the basal unit in many ophiolites. Although harzburgite (at high pressure and temperature) is the expected residue after extraction of the picritic fraction from upper-mantle lherzolite at 60- to 70-km depth, the residual orthopyroxene contains >5% Al_2O_3 and >2.5% CaO; the residual harzburgite is thus much too Al_2O_3 and CaO-rich to be correlated with the very depleted harzburgite tectonites of ophiolites (for comparison, see Table 1, analyses 8 and 9). These highly refractory harzburgites are, however, compatible with an origin as a residue from a shallow-depth second-stage partial melting of rather refractory peridotite.

Experimental work (in progress) indicates that these magnesian silicic melts are multiply saturated in olivine and orthopyroxene at 7 to 8 kb and ~1,360 °C and thus could be derived by second-stage melting of residual peridotite with magma segregation at ≤25 km. The degree of melting is small [5% to 10% estimated from experimental melting of depleted lherzolite (A. L. Jaques and D. H. Green, in prep.)], and the magmas are prone to crystal fractionation at shallow depth. Emplacement and deformation of the source diapirs result in mutually intrusive contacts between residual harzburgite tectonites (now appropriately low in Al_2O_3 and CaO) and cumulate sequences.

Magmas produced by second-stage melting are likely to form only 10% to 20% of the ocean crust, are difficult to identify if fractionated, and could commonly be interfingered with magmas of first-stage melting parentage. We believe that rocks representative of such magmas, however, can be recognized among the uppermost lava series of several ophiolites.

EVIDENCE FROM OPHIOLITES FOR TWO-STAGE MELTING

At the Troodos ophiolite, Cyprus, the pillow lavas overlying the sheeted-dike complex have been divided into two units, the upper and lower pillow lavas, on the basis of a metamorphic discontinuity (Moores and Vine, 1971; Gass and Smewing, 1973). The sheeted-dike complex grades into the overlying lower pillow lavas; the two together are termed the axis sequence in view of their postulated comagmatic relationship by formation at an axial spreading ridge (Smewing and others, 1975). The upper pillow lavas were later erupted onto this basement, probably outside the axial zone of hydrothermal convection from the fact that they have been metamorphosed only as far as zeolite facies whereas those of the axis sequence have reached greenschist facies.

The upper pillow lavas at Troodos include lavas enriched in

cumulate olivine (Fo_{90} to $Fo_{91.7}$) as well as slightly fractionated olivine basalt (Table 1, analyses 1, 2, and 3). Removal of olivine from the one and addition of small amounts of olivine to the other would produce magnesian quartz tholeiite; a magma with this composition would be appropriate for the precipitation of the most-magnesian olivine observed in these lavas. Gass (1958) reported olivine-phyric ultramafic lavas within the upper pillow lavas that contain groundmass anorthite ($\sim An_{95}$), diopside, and hypersthene. Such a magma, therefore, is capable of precipitating orthopyroxene at low pressures and may be parental to appropriately calcic plagioclase.

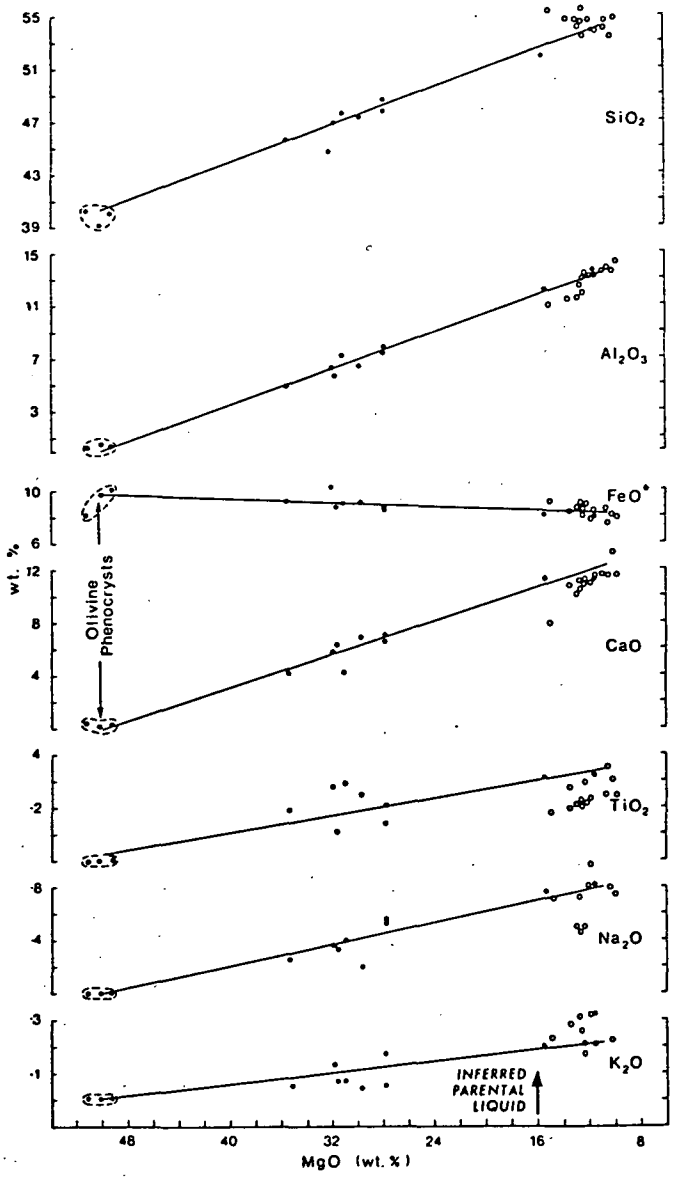

Figure 1. Chemical variation among ultramafic lavas (olivine cumulates) and olivine-phyric basalts from the upper pillow lavas at the Troodos ophiolite, Cyprus. Compositions for olivine phenocrysts in the ultramafic lavas from Searle and Vokes (1969). Major-element analyses are (closed circles) from Gass (1958), Searle and Vokes (1969), Kay and Senechal (1976) and (open circles) from Simonian and Gass (1978). The linearity exhibited indicates that most variation can be explained by olivine addition or removal. The parental magma for these lavas (broad arrow near bottom) has been inferred from these variation diagrams with the constraint that such a liquid [Mg/(Mg + Fe) = 0.77] must be in equilibrium with the most-magnesian olivine observed ($Fo_{91.7}$).

We have used the reported chemical variation among upper pillow lavas (Fig. 1) to determine the composition of a parental liquid for these samples. Such a liquid must be in equilibrium with the most magnesian olivine observed ($Fo_{91.7}$); this implies a Mg/(Mg + Fe^{+2}) ratio of 0.77 (Roeder and Emslie, 1970). The determined Troodos parental liquid (Table 1) is higher in SiO_2 and MgO and lower in TiO_2, Al_2O_3, CaO, and Na_2O than either DSDP3-18-7-1, one of the least-fractionated basaltic glasses recovered from the Mid-Atlantic Ridge (Frey and others, 1974), or 95-1, a highly magnesian basalt from a back-arc basin (Lau Basin, see Hawkins, 1976). These differences cannot be explained by low-pressure crystal fractionation and are significant in identifying a primary magma type that is capable of precipitating the orthopyroxene and the refractory olivine, clinopyroxene, and plagioclase phenocryst compositions reported. We infer that such liquids result from small degrees of melting of upper-mantle peridotite that has already given up its picritic component and thus constitute "second-stage" melts of the upper-mantle diapirs.

Smewing and Potts (1976) and Kay and Senechal (1976) reported REE abundances for Troodos complex rocks. All analyses have LREE-depleted patterns; the lower pillow lavas and some of the upper pillow lavas exhibit patterns typical of ocean-floor basalts elsewhere. Other samples from upper pillow lavas, however, such as 103A, have distinctly more severe depletion of LREE; Smewing and Potts (1976) concluded that the magmas responsible were derived from a more-depleted source than that for the axis-sequence magmas. This is consistent with the major-element composition of our proposed second-stage primary magma which reflects melting from a source earlier depleted in its basaltic component. We concur with Smewing and Potts (1976) who argued from REE data that several primary magmas are required for the generation of the Troodos ophiolite. These different primary magmas may be closely related by virtue of being successive melts from a single upper-mantle lherzolite diapir, or the primary magmas may be only broadly related in that they represent products of first-stage and second-stage melting of different upper-mantle diapirs.

Such second-stage magmas are not unique to Troodos. At the Baër-Bassit ophiolite in northeastern Syria, two pillow-lava series have been recognized (Parrot, 1977). The uppermost is distinctly richer in SiO_2 and MgO and poorer in TiO_2 and Na_2O than the underlying tholeiitic pillows and dikes. Parrot (1977) reported that an average modal analysis of samples from the Baër-Bassit upper pillow lavas contains from 1% to 7% orthopyroxene and from 6% to 8% olivine; the bulk of the rock is clinopyroxene and glass. Although these lavas are perhaps slightly poorer in Al_2O_3 at the same degree of fractionation (Table 1), their chemical composition compares closely with the upper pillow lavas at Troodos. No ultramafic lavas of the Troodos type have been reported from Baër-Bassit. At the Semail ophiolite in Oman, a similar distinction between upper and lower lava series has been made (Smewing and others, 1976).

A search of ocean-floor basaltic glass compositions (Melson and others, 1977) reveals a small number of samples which could be related, by high-level fractional crystallization, to primary liquids similar to those that we suggest are derived by second-stage melting. An average glass composition for samples recovered at DSDP site 236, for example, in the Somali Basin (Table 1) is more fractionated than those from basaltic pillow lavas at the two ophiolites [Mg/(Mg + total Fe) = 0.58 and 0.63 to 0.67, respectively], so that addition of the precipitated phases (principally olivine and clinopyroxene) would yield a

parent primary liquid which should be very similar to the proposed parent magma of the Troodos upper pillow lavas.

That basalts of such refractory compositions are rare in the ocean basins is expected because their parent magmas constitute only 10% to 20% of the total oceanic crust and their off-axis eruptions may be overlapped and buried by the more voluminous, axial, first-stage melts and derivative melts (Fig. 2). Also, liquids derived by small degrees of melting (5% to 10%) of the residual diapir may be difficult to separate from the diapir on emplacement at the base of the crust and hence never reach the surface as pillow lavas (this may explain the often diffuse and irregular "contact" between the basal harzburgite and the lowermost ultramafic sequences in many ophiolites). Such magnesian quartz tholeiite melts may possibly reach the surface only when afforded a zone of weakness such as transform faults (Simonian and Gass, 1978) and otherwise solidify lower in the crust as gabbroic bodies. It appears that some samples of ocean-floor basalts do have refractory compositions like those of the uppermost pillow lavas of several ophiolites. Confirmation that such rocks are related to primary liquids like the second-stage melts inferred at Troodos will be important not only in demonstrating an origin for the refractory megacrysts common in mid-ocean ridge basalts and in dredged gabbroic rocks from the ocean basins, but also in supporting the contention that petrogenetic relationships defined in ophiolites can be extended to the mid-ocean ridge environment.

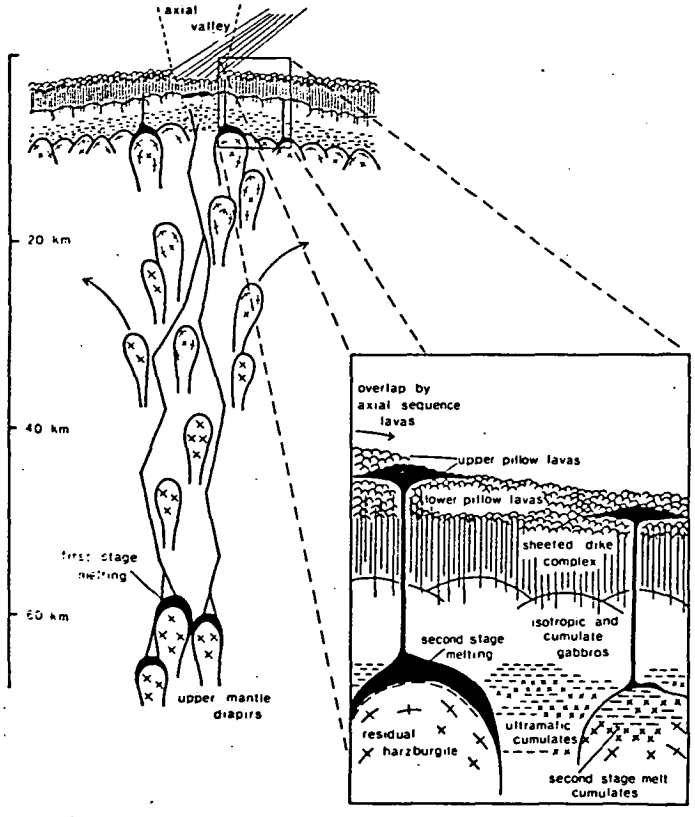

Figure 2. Multistage melting in the formation of oceanic crust. Picritic liquids are derived by 20% to 30% melting of upper-mantle diapirs of "pyrolite" at 60- to 70-km depth and temperatures of 1,400 to 1,450 °C; this process leaves a lherzolite residue. These "first-stage" liquids precipitate olivine as they rise directly to crustal magma chambers beneath mid-ocean spreading ridges, where they differentiate to produce the majority of ocean-floor basalts. Continued upwelling of residual lherzolite diapirs results in small degrees (5% to 10%) of "second-stage" melting at shallow depth (5 to 25 km). Second-stage melts may be segregated during slightly off-axis intrusion of the residual diapirs beneath new oceanic crust, and a very refractory harzburgite diapir remains. Such second-stage magmas may intrude the upper pillow lavas (as in the Troodos example) and may interfinger with first-stage magmas erupting at the axial valley.

COMPARISON WITH OTHER HIGHLY MAGNESIAN MAGMAS

In island arcs, unusual magmas exist that show some similarities in chemical composition (particularly in Mg content) and mineralogy to the proposed parental second-stage melts at Troodos. Examples are the distinctive clinoenstatite-bearing high-MgO andesites of Cape Vogel, Papua New Guinea (Dallwitz, 1968, Table 1) and the "boninites" of the Bonin Islands (Kuroda and Shiraki, 1975). But there are significant differences: (1) chemical variation in Cape Vogel lavas is controlled by pyroxene fractionation, whereas the Troodos lavas exhibit olivine control; (2) the Cape Vogel and Bonin Islands magmas have distinctly lower Ca/Al ratios, do not show such extreme Ca/Na values, and are not as depleted in K and other incompatible elements; and (3) the very strong LREE depletion of the Troodos second-stage lavas is not seen in the high-MgO island-arc rocks (Sun and Nesbitt, 1978b).

Several authors have argued that these island-arc occurrences of high-MgO, high-SiO_2 andesites or boninites are derived by hydrous melting of refractory lherzolite. Experimental petrology results allow a wide range of *P-T* conditions over which it is possible to derive hypersthene-normative and silica-oversaturated to silica-undersaturated melts from a lherzolite source, provided variable quantities of water are available (Green, 1973).

Within Archean greenstone terranes are distinctive high-MgO, high-SiO_2 (>51% SiO_2, >15% MgO) rocks that have the texture of rapidly quenched liquids (called "spinifex-textured basalts" by Sun and Nesbitt, 1978a, or "pyroxenitic komatiites" by Arndt and others, 1977). We suspect that the petrogenesis of these magmas will prove to be very similar to that proposed for the second-stage melts at Troodos, that is, anhydrous melting and magma segregation from a lherzolite (pyrolite to refractory harzburgite) source at shallow depths (≤25 km). There are, however, problems with this analogy. Among Archean spinifex-textured basalts with major-element contents similar to those of the inferred parent for Troodos upper pillow lavas (Table 1) are examples (Sun and Nesbitt, 1978a) with strong LREE depletion, slight LREE enrichment, and strong LREE enrichment. In addition, there are variations in Ca/Na, Ca/Al, Na/K, and so forth that do not permit the Archean komatiite nomenclature to be simply equated to the Troodos lavas.

CONCLUSIONS

We hesitate to assign tectonic regimes to particular magma compositions. Probably no single tectonic setting generates all ophiolites. We agree, however, with previous studies (Gass, 1958; Moores and Vine, 1971; Gass and Smewing, 1973; Smewing and others, 1975; Smewing and Potts, 1976) that the Troodos ophiolite at Cyprus was formed at a mid-ocean spreading ridge and that the high-MgO, high-SiO_2, and low-TiO_2 rocks present within the upper pillow lavas were not derived from young island-arc volcanism but resulted from second-stage melts that segregated from refractory lherzolite diapirs at shallow depths (≤25 km).

As summarized in Figure 2, we envisage the refractory lherzolite diapirs as slightly off-axis intrusions that result from continued upwelling of upper-mantle diapirs after extraction at 60- to 70-km depth and temperatures of 1,400 to 1,450 °C of a major melt fraction (20% to 30%) consisting of picritic liquids.

REFERENCES CITED

Arndt, N. T., Naldrett, A. J., and Pyke, D. R., 1977, Komatiitic and iron-rich tholeiitic lavas of Munro Township, Northeast Ontario: Journal of Petrology, v. 18, p. 319–369.

Bender, J. F., Hodges, F. N., and Bence, A. E., 1978, Petrogenesis of basalts from the Project FAMOUS area: Experimental study from 0 to 10 kbars: Earth and Planetary Science Letters, v. 41, p. 277–302.

Blanchard, D. P., and others, 1976, The chemistry and petrology of basalts from Leg 37 of the Deep Sea Drilling Project: Journal of Geophysical Reserach, v. 81, p. 4231–4246.

Bryan, W. B., and Moore, J. G., 1977, Compositional variations of young basalts in the Mid-Atlantic Ridge rift valley near lat 36°49′N: Geological Society of America Bulletin, v. 88, p. 556–570.

Bryan, W. B., and others, 1976, Inferred geological settings and differentiation in basalts from the Deep Sea Drilling Project: Journal of Geophysical Research, v. 81, p. 4285–4304.

Dallwitz, W. B., 1968, Chemical composition and genesis of clinoenstatite bearing volcanic rocks from Cape Vogel, Papua: A discussion: International Geological Congress, 23rd, Prague, Proceedings, v. 2, p. 229–242.

Donaldson, C. H., and Brown, R. W., 1977, Refractory megacrysts and magnesium-rich melt inclusions within spinel in oceanic tholeiites: Indicators of magma mixing and parental liquid compositions: Earth and Planetary Science Letters, v. 37, p. 81–89.

England, R. N., and Davies, H. L., 1973, Mineralogy of ultramafic cumulates and tectonites from eastern Papua: Earth and Planetary Science Letters, v. 17, p. 416–425.

Flower, M.F.J., and others, 1977, Magma fractionation systems beneath the Mid-Atlantic Ridge at 36–37°N: Contributions to Mineralogy and Petrology, v. 64, p. 167–195.

Frey, F. A., Bryan, W. B., and Thompson, G., 1974, Atlantic ocean floor: Geochemistry and petrology of basalts from Legs 2 and 3 of the Deep Sea Drilling Project: Journal of Geophysical Research, v. 79, p. 5507–5527.

Gass, I. G., 1958, Ultrabasic pillow lavas from Cyprus: Geological Magazine v. 95, p. 241–251.

Gass, I. G., and Smewing, J. D., 1973, Intrusion, extrusion and metamorphism at constructive margins: Evidence from the Troodos Massif, Cyprus: Nature, v. 242, p. 26–29.

Green, D. H., 1973, Contrasted melting relations in a pyrolite upper mantle under mid-oceanic ridge, stable crust and island arc environments: Tectonophysics, v. 17, p. 285–297.

Green, D. H., Hibberson, W. O., and Jaques, A. L., 1979, Petrogenesis of mid-ocean ridge basalts, *in* McElhinny, M. W., ed., The Earth: Its origin, structure and evolution: London, Academic Press, p. 265–290.

Hawkins, J. W., 1976, Petrology and geochemistry of basaltic rocks of the Lau Basin: Earth and Planetary Science Letters, v. 28, p. 283–297.

Juteau, T., and Whitechurch, H., 1979, The magmatic cumulates of Antalya (Turkey): Evidence of multiple intrusions in the magma chamber: International Ophiolite Symposium, Cyprus, Abstracts of Papers Submitted, p. 41–42.

Kay, R. W., and Senechal, R. G., 1976, The rare earth geochemistry of the Troodos ophiolite complex: Journal of Geophysical Research, v, 81, p. 964–970.

Kuroda, N., and Shiraki, K., 1975, Boninite and related rocks of Chichijima, Bonin Islands, Japan: Shizuoka University, Reports of the Faculty of Science, v. 10, p. 145–155.

Langmuir, C. H., and others, 1977, Petrogenesis of basalts from the FAMOUS area: Mid-Atlantic Ridge: Earth and Planetary Science Letters, v. 36, p. 133–156.

Melson, W. G., and others, 1977, A catalog of the major element chemistry of abyssal volcanic glasses: Mineral Scinece Investigations: Smithsonian Contributions to Earth Sciences, v. 19, p. 31–60.

Menzies, M., and Allen, C., 1974, Plagioclase lherzolite–residual mantle relationships within two eastern Mediterranean ophiolites: Contributions to Mineralogy and Petrology, v. 45, p. 197–213.

Moores, E. M., and Vine, F. J., 1971, The Troodos Massif, Cyprus, and other ophiolites as oceanic crust: Evaluation and implications: Royal Society of London Philosophical Transactions, v. 268, p. 443–466.

O'Hara, M. J., 1968, Are ocean-floor basalts primary magmas?: Nature, v. 220, p. 683–686.

Pallister, J. S., and Hopson, C. A., 1979, Samail ophiolite magma chamber: II, Evidence from the cryptic variation and mineral chemistry: International Ophiolite Symposium, Cyprus, Abstracts of Papers Submitted, p. 38.

Parrot, J. F., 1977, Assemblage ophiolitique du Baër-Bassit et terms effusifs du volcano-sédimentaire: Paris, Office de la Recherche Scientifique et Technique Outre-Mer, Travaux et Documents, no. 72, 333 p.

Roeder, P. L., and Emslie, R. F., 1970, Olivine-liquid equilibrium: Contributions to Mineralogy and Petrology, v. 29, p. 275–289.

Searle, D. L., and Vòkes, F. M., 1969, Layered ultrabasic lavas from Cyprus: Geological Magazine, v. 106, p. 515–530.

Simonian, K. O., and Gass, I. G., 1978, Arakapas fault belt, Cyprus: A fossil transform fault: Geological Society of America Bulletin, v. 89, p. 1220–1230.

Smewing, J. D., and Potts, P. J., 1976, Rare-earth abundances in basalts and metabasalts from the Troodos Massif, Cyprus: Contributions to Mineralogy and Petrology, v. 57, p. 245–258.

Smewing, J. D., Simonian, K. O., and Gass, I. G., 1975, Metabasalts from the Troodos Massif, Cyprus: Genetic implications deduced from petrography and trace element geochemistry: Contributions to Mineralogy and Petrology, v. 51, p. 49–64.

Smewing, J. D., and others, 1976, Similar ophiolite sequences from the Troodos Massif, the Oman Mountains and the Baër-Bassit region of Syria: EOS (American Geophysical Union Transactions), v. 57, p. 412.

Sun, S. S., and Nesbitt, R. W., 1978a, Petrogenesis of Archaean ultramafic and basic volcanics: Evidence from rare earth elements: Contributions to Mineralogy and Petrology, v. 65, p. 301–325.

———1978b, Geochemical regularities and genetic significance of ophiolitic basalts: Geology, v. 6, p. 689–693.

ACKNOWLEDGMENTS

Reviewed by R. A. Frey and E.M. Moores. R. A. Coish also made comments on an early version of the manuscript. R. A. Duncan acknowledges support through a Queen's Fellowship in Marine Science from the Australian government.

MANUSCRIPT RECEIVED JUNE 6, 1979

MANUSCRIPT ACCEPTED OCTOBER 26, 1979

B 31

Contrib. Mineral. Petrol. 73, 287–310 (1980)

Contributions to Mineralogy and Petrology
© by Springer-Verlag 1980

Anhydrous Melting of Peridotite at 0–15 Kb Pressure and the Genesis of Tholeiitic Basalts

A.L. Jaques* and D.H. Green

Department of Geology, University of Tasmania, Hobart, Tasmania 7001, Australia

Abstract. The anhydrous melting behaviour of two synthetic peridotite compositions has been studied experimentally at temperatures ranging from near the solidus to about 200° C above the solidus within the pressure range 0–15 kb. The peridotite compositions studied are equivalent to 'Hawaiian' pyrolite and a more depleted spinel lherzolite (Tinaquillo peridotite) and in both cases the experimental studies used peridotite *–40% olivine* compositions. Equilibrium melting results in progressive elimination of phases with increasing temperature. Four main melting fields are recognized; from the solidus these are: olivine (ol)+orthopyroxene (opx)+clinopyroxene (cpx)+Al-rich phase (plagioclase at low pressure, spinel at moderate pressure, garnet at high pressure)+liquid (L); ol+opx+cpx+Cr-spinel+L; ol+opx+Cr-spinel+L: ol±Cr-spinel+L. Microprobe analyses of the residual phases show progressive changes to more refractory compositions with increasing proportion of coexisting melt i.e. increasing Mg/(Mg+Fe) and Cr/(Cr+Al) ratios, decreasing Al_2O_3, CaO in pyroxene.

The degree of melting, established by modal analysis, increases rapidly immediately above the solidus (up to 10% melting occurs within 25°–30° C of the solidus), and then increases in roughly linear form with increasing temperature.

Equilibrium melt compositions have been calculated by mass balance using the compositions and proportions of residual phases to overcome the problems of iron loss and quench modification of the glass. Compositions from the melting of pyrolite within the spinel peridotite field (i.e. ~15 kb) range from alkali olivine basalt (<15% melting) through olivine tholeiite (20–30% melting) and picrite to komatiite (40–60% melting). Melting in the plagioclase peridotite field produces magnesian quartz tholeiite and olivine-poor tholeiite and, at higher degrees of melting (30–40%), basaltic or pyroxenitic komatiite. Melts from Tinaquillo lherzolite are more silica saturated than those from pyrolite for similar degrees of partial melting, and range from olivine tholeiite through tholeiitic picrite to komatiite for melting in the spinel peridotite field.

The equilibrium melts are compared with inferred primary magma compositions and integrated with previous melting studies on basalts. The data obtained here and complementary basalt melting studies do not support models of formation of oceanic crust in which the parental magmas of common mid-ocean ridge basalts (MORB) are attributed to segregation from source peridotite at shallow depths (≦ 25 km) to leave residual harzburgite. Liquids segregating from peridotite at these depths are more silica-rich than common MORB.

1. Introduction

It is now generally accepted that basaltic magmas result from partial melting of a peridotitic upper mantle. Previous melting studies on natural basalt and peridotite, and simple system analogues (e.g., Green and Ringwood 1967a; Ito and Kennedy 1967; Green 1970, 1971, 1973a, b, 1976b; Kushiro 1969; Nicholls 1974; Eggler 1974, 1978) have shown that varying degrees of partial melting of peridotite under different conditions (*P*, *T*, volatile content) may give rise to a wide spectrum of basaltic compositions. The results of these studies have been integrated to produce a petrogenetic grid (Green 1971, 1973b) for the origin of a range of natural basaltic compositions occurring in the ocean basins and on stable continental regions.

* *Present address:* Bureau of Mineral Resources, P.O. Box 378, Canberra City 2601, Australia

0010-7999/80/0073/0287/S04.80

To date, formulation and experimental testing of the petrogenetic grid have relied largely on basalt crystallisation studies i.e. examination of liquidus and near liquidus mineralogy of mantle-derived basaltic liquids. However, because of the uncertainties of identifying primary magmas among basalts of tholeiitic composition (which, unlike alkali basalts, generally do not carry mantle xenoliths as evidence of their primary nature) direct melting studies of peridotite are necessary to more closely constrain conditions of origin of tholeiitic magmas.

Here we present the results of a study of the anhydrous melting of two different peridotites at 0–15 kb pressure. Our data show that the equilibrium liquid compositions formed over a relatively wide melting interval are broadly of tholeiitic composition. The experimentally determined liquid compositions and residual mineralogy are then used to examine models for the genesis of oceanic crust and ophiolites, and various other naturally occurring magnesian tholeiites.

2. Compositions of the Oceanic Upper Mantle

Evidence supporting the hypothesis of an upper mantle comprised of olivine (Mg_{88-92})[1], orthopyroxene, clinopyroxene, and minor spinel (or garnet) and containing approximately 3–4 wt.% CaO and Al_2O_3 each has been discussed elsewhere (e.g., Ringwood 1975 for a review). Previous experimental studies (see Green 1976a, for review) and, more recently, integration with detailed trace element modelling (Frey et al. 1978) have shown that a calculated peridotite composition – similar to pyrolite III (Ringwood 1966) – is capable of yielding a wide range of basalt compositions ranging from olivine melilitite through alkali olivine basalt to olivine tholeiite under varying conditions and degrees of partial melting[2]. We have therefore chosen Ringwood's (1966) pyrolite as representative of mantle composition in areas of oceanic island volcanism. Although originally proposed as a general, conceptual term we use 'pyrolite' in this paper for one specific composition (Ringwood 1966) to enable direct comparison with previous studies on this composition and melting studies on other possible upper mantle compositions. Pyrolite is also a reasonable approximation of upper mantle composition in areas of continental alkali basalt volcanism (Frey et al. 1978). This model composition is LREE-enriched and enriched in incompatible elements relative to the source region for most mid-ocean ridge basalts (Frey et al. 1978; Green et al. 1979). For the latter basalts (MORB), trace element and isotopic studies (e.g., Gast 1968; Kay et al. 1970; Bryan et al. 1976) indicate a more refractory peridotite source, depleted in incompatible elements. Accordingly we have selected a spinel lherzolite, Tinaquillo peridotite (Green 1963) as a specific composition representative of depleted mantle peridotite. In addition to having slightly lower CaO and Al_2O_3 content than the pyrolite composition used, Tinaquillo peridotite is depleted in TiO_2 and incompatible elements, including REE (Philpotts et al. 1972), and is more magnesian than pyrolite. Tinaquillo lherzolite is also of similar composition to the less depleted of the spinel lherzolites examined by Kuno and Aoki (1970), Frey and Green (1974) and Frey and Prinz (1977), and to estimates of the upper mantle composition based on averages of spinel lherzolite compositions (e.g., Harris et al. 1967; Maaloe and Aoki 1977), although CaO and Al_2O_3 contents are higher for Tinaquillo than Maaloe and Aoki's (1977) average oceanic mantle. Tinaquillo lherzolite is also more depleted in incompatible elements than the mantle source composition suggested for DSDP basalt 3–18 by Green et al. (1979). We have chosen two peridotite compositions which, although similar in major elements, represent the two ends of a compositional spectrum in their content of incompatible elements.

In addition to the mantle heterogeneity reflected in basaltic rocks, detailed geochemical studies of peridotite xenoliths in basalts, high temperature peridotites and peridotitic komatiites (e.g., Frey and Green 1974; Frey and Prinz 1977; Frey et al. 1978; Sun and Nesbitt 1977, 1978a) have shown that the mantle chemistry is complex, and many source regions have apparently been enriched by addition of a small incompatible element-enriched melt fraction, whereas others have been depleted. Green (1971) and Green and Lieberman (1976) have presented a model of chemical zoning within the mantle, suggesting that the deeper part of the Low Velocity Zone (LVZ) is depleted in incompatible elements and overlain by an enriched layer, due to continuous upward migration of a small melt fraction (<2% melt) of olivine

[1] In this paper we use Mg-value for the ratio 100 Mg/(Mg+Fe^{++}) and *Mg-value* for the ratio 100 Mg/(Mg+ΣFe). The two numbers differ for rocks or liquids where Fe^{++} and Fe^{+++} can be measured or estimated but are identical for microprobe analyses of olivine, orthopyroxene and clinopyroxene where Fe^{+++} is assumed to be absent, particularly under the experimental run conditions of low f_{O_2}. For spinel analyses, the use of stoichiometry constraints permits calculation of Fe^{+++} and Fe^{++}

[2] The TiO_2 content of Ringwood's (1966) pyrolite composition is now known to be too high for other than the Hawaiian province and 0.3–0.4 wt.% TiO_2 is probably a more reasonable estimate for other provinces and other mantle peridotite compositions (Frey et al. 1978)

melilitite composition. With reference to this model, we suggest that the peridotite compositions selected may be reasonable *approximations* to the upper and lowermost parts of the LVZ of the mantle, i.e. source regions for magmas of oceanic islands and midocean ridges respectively, but we emphasize that we envisage a *continuum* of mantle compositions from enriched to highly depleted and refractory peridotite.

3. Experimental Technique

3.1 Preparation of Starting Mixes

Starting mixes were prepared from analytical reagent grade chemicals, carefully ground under acetone (< 5 μm) and sintered at 1000° C. The initial mix was then recrushed under acetone and heated to 1000° C in a sealed evacuated silica tube with a quartz-fayalite-magnetite buffer. A split from the mixes was then analysed for FeO and Fe_2O_3 by spectrophotometry. The compositions prepared are presented in Table 1. These compositions are of pyrolite and Tinaquillo lherzolite modified by the extraction of 40% olivine to facilitate identification of minor phases. The validity of this approach has been discussed previously (e.g., Green and Ringwood 1970), and is here re-affirmed by the fact that all runs, including the highest temperature experiments, where oversaturated in olivine. While the use of these modified compositions is relevant to peridotite melting studies in that the correct residual phases are always present, it does introduce a small error in regard to the Mg-value of the starting mix. Ideally the composition of the olivine removed should be that of the equilibrium residual olivine for each particular P, T and degree of melting. Since this is impractical, olivine of an average residual composition was removed ($Mg_{91.6}Fe_{8.1}Ni_{0.2}Mn_{0.1}$ for pyrolite and $Mg_{91.9}Fe_{8.0}Ni_{0.0}Mn_{0.1}$ for Tinaquillo lherzolite). For low to moderate degrees of melting the olivine compositions removed are slightly more magnesian than the equilibrium olivine for the original peridotite compositions, and, thus, the mix compositions and phase compositions are slightly too iron-rich for low degrees of melting. The extraction of olivine also produces slightly greater change in Mg-value of residual phases with increasing temperature (percent melting) for the modified peridotite composition than for the unmodified peridotite, due to the decrease of buffering effect of the larger amounts of olivine. However, these errors are small, and more than compensated by the improved quenching characteristics due to high proportions of glass to crystals, and the greater accuracy and ease of modal analyses. In addition the higher Fe-content is partly counteracted by the iron loss from the charge (see below).

3.2 Apparatus and Methods

Experiments were carried out in solid media (piston-cylinder) high pressure apparatus using a piston-in technique and a pressure correction of minus 10% nominal piston pressure. Pressures have been previously calibrated on the quartz ⇄ coesite transition at 1100° C, 32 kb, and albite ⇄ jadeite + quartz at 600° C, 16.2 kb by Brey and Green (1975), and the error in pressure measurement is considered to be ±3% at ~15 kb but may increase to ±20% at < 3 kb. Temperatures (±5° C) were measured by a Pt – Pt 10% Rh thermocouple. No correction was made for the effect of pressure on the thermocouple emf.

Table 1. Compositions of pyrolite (Ringwood 1966) and Tinaquillo lherzolite (Green 1963) and pyrolite minus 40% olivine ($Mg_{91.6}Fe_{8.1}Ni_{0.2}Mn_{0.1}$) and Tinaquillo minus 40% olivine ($Mg_{91.9}Fe_{8.0}Mn_{0.1}$) compositions used in experiments

	Pyrolite	Pyrolite −40% ol	Tinaquillo lherzolite	Tinaquillo −40% ol
SiO_2	45.2	47.9	44.95	47.5
TiO_2	0.71	1.18	0.08	0.13
Al_2O_3	3.54	5.91	3.22	5.35
Fe_2O_3	0.48	0.20*	0.09	0.15
FeO	8.04	8.63	7.58	7.38
MnO	0.14	0.13	0.14	0.18
MgO	37.5	28.8	40.03	32.8
CaO	3.08	5.14	2.99	4.97
Na_2O	0.57	0.95	0.18	0.30
K_2O	0.13	0.22	0.02	0.03
P_2O_5	–	0.06	0.01	0.02
NiO	0.20	0.13	0.26	0.43
Cr_2O_3	0.43	0.72	0.45	0.75
CIPW Norms				
Or	0.8	1.3	0.1	0.2
Ab	5.0	8.0	1.5	2.5
An	6.6	11.2	7.9	13.2
Di	6.8	11.0	5.4	9.0
Hy	15.8	26.5	18.0	30.8
Ol	62.5	38.2	65.9	42.5
Il	1.3	2.2	0.2	0.3
Mt	0.7	0.3	0.1	0.2
Cr	0.6	1.0	0.6	1.1
100 Mg/(Mg + Fe^{++})	89.3	85.6	90.3	88.8
100 Mg/(Mg + Fe)	88.7	85.4	90.4	88.6

* FeO by spectrophotometry – P. Robinson, analyst

Pyrex glass sleeves with graphite inserts were used in the 0.5 inch diameter furnace assemblies to minimize hydrogen diffusion from dehydration of the outer talc sleeve. Experiments on the stability of buffer assemblages using this furnace assembly indicate prevailing f_{O_2} conditions < NNO (Green 1976b; D. Gust, personal communication 1979). However, the comparatively high Fe^{3+} contents of residual spinels (see below) suggests the f_{O_2} in our runs may have been greater than this, as a consequence of alloying of Fe with the Pt capsule according to the reaction $Pt + 3FeO \rightleftarrows (Fe, Pt)_{SS} + Fe_2O_3$. Because iron loss is dependent on run duration the Fe^{3+}/Fe^{2+} ratios of the spinels are not considered a reliable indicator of prevailing f_{O_2}. Samples (15–20 mg) were contained in sealed Pt capsules and preheated at 900°–1000° C for 8–12 h packed in metallic iron powder in an attempt to presaturate the Pt capsule in iron. All runs were anhydrous and the powdered starting mix was dried overnight at 110° C. Several short duration runs were made using unsealed spec-pure iron capsules. These experiments produced a lower f_{O_2}, did not yield chrome spinel, and, in some cases, the charges dissolved iron from the capsule and contained dispersed small spheres of metallic iron.

The 1-atmosphere partial melting experiments were carried out in a 1-atmosphere quenching furnace using 20 mg samples in spec-pure iron capsules sealed in evacuated silica tubes. These samples also resulted in f_{O_2} below the QFM buffer and the charge dissolved additional iron. For these reasons phase relations only, and no compositional data, are presented for the 1-atmosphere experiments.

3.3 Microprobe Analyses

The charge was recovered as a coherent cylinder of residual crystals and glass. A small portion of one split was crushed and examined optically in refractive index oil. The other split was mounted, polished, and examined optically in reflected light and by scanning electron microscope. Optimization of the backscattered and secondary electron images enabled clear resolution and discrimination of all phases (except for fine-grained runs near the solidus), including melt and quench crystals, up to X 2000 magnification. Discrimination of phases was based on form and contrast using the backscattered electron image in which 'brightness' is dependent on the mean atomic number of the phases in the target. In this way quench phases e.g. quench clinopyroxene rims on primary phases, can be distinguished from primary phases because of the higher Ti, Al, and Fe contents in the quench phase compared to the primary equilibrium phase. Scanning electron microscope photographs of some of the experimental charges are given by Jaques and Green (1979).

Simultaneous quantitative analysis for 10 elements (Na-Fe) was made using a JEOL JX50A electron microprobe – scanning electron microscope fitted with an energy dispersive (EDAX) analytical system following the method of Reed and Ware (1975). Operating conditions employed an accelerating voltage of 15 kV, beam current of 3 nA, a beam diameter of less than 0.5 μm, and 100 s counting time. Glass analyses and analyses of the bulk charge were made using rapid reduced area scans to minimize alkali volatilization and ensure representative analysis. At least 5 analyses of each phase, including glass and bulk charge, were made for each run: some 2000 analyses were acquired during the study. All iron analyses are reported as weight percent FeO unless otherwise stated.

3.4 Iron Loss

A number of studies (e.g., Merrill and Wyllie 1973; Green 1973b, 1976; Stern and Wyllie 1975) have documented loss of iron from the sample to platinum group metal capsules during experiments, and shown that the extent of iron loss is particularly dependent on temperature and run duration. Jaques and Green (1979), in a re-examination of iron loss in partial melting experiments, showed that iron is lost preferentially from the charge in the order liquid > olivine > pyroxene, and that this preferential iron loss commonly results in nonequilibrium crystal-liquid and crystal-crystal (e.g., olivine – orthopyroxene) Fe/Mg partitioning, due to the different rates of adjustment of phases to the iron loss. On a local scale this is demonstrated by reverse zoning of larger crystals and by the fact that smaller crystals are generally more magnesian than cores of larger ones. Jaques and Green (1979) stressed that even where iron loss was minimized by presaturation techniques, the extent of compositional interchange between sample and container needed to be carefully evaluated. Capsule materials other than Pt (e.g., graphite, molybdenum, spec-pure iron) are difficult to seal and thus f_{O_2} can be only poorly controlled, and H_2O or CO_2 may gain access to the charge with consequent change to the degree of melting and nature of residual phases.

We have used Pt in our experiments but circumvented excessive iron loss from the charge, and the consequent effect on the compositions of phases, by carrying out repeated runs of varying duration, and monitoring the extent of the iron loss by analysis of the bulk charge after the run. From this, optimum run conditions, in terms of attainment of equilibrium and minimum iron loss, were established. Iron loss in these experiments was also monitored by examining the Fe-Mg partitioning between residual phases using the core composition of large (> 20 μ) orthopyroxene crystals, which re-adjust more slowly to iron loss, as a reference. Since the $K_D^{ol\text{-}opx}$ (where $K_D^{A\text{-}B} = (Fe/Mg)^A/(Fe/Mg)^B$ is known to be insensitive to temperature and pressure and has been determined experimentally as 1.1 ± 0.1 (e.g., Matsui and Nishazawa 1974; Mori and Green 1978), we have used this relationship to test the Fe-Mg partitioning between olivine and orthopyroxene for equilibrium. In all except the shortest duration runs, olivine compositions are 1 to 4 mol% more magnesian than the equilibrium value. Data obtained during this and previous partial melting studies (e.g., Green 1976b, c; Jaques and Green 1979) show that the observed olivine – glass Fe/Mg partitioning is variable, being dependent on temperature and run duration (i.e., the extent of iron loss) and on quench modification of the glass, and therefore is of little use in determining equilibrium in situations where iron loss has occurred. Similarly the observed olivine compositions in an experiment cannot be used to constrain the Mg-value of equilibrium melt unless first corrected for the effect of Fe-loss.

3.5 Determination of Liquid Compositions and Percentage Melting

The problem of growth of metastable, non-equilibrium phases, both as discrete crystals and as rims and outgrowths on primary phases, during quenching of the charge, and the consequent modification of melt compositions in partial melting experiments is well known (Green 1973b, 1976b; Cawthorn et al. 1973; Nicholls 1974). Jaques and Green (1979) re-examined the problem of quench modification of the partial melt compositions with the aid of the scanning electron microscope coupled to the energy-dispersive microprobe, and found that significant quenching problems occur both at comparatively low degrees of melting ($\leqq 10\%$) where the solid/liquid proportion is high, and at high degrees of melting (30–40%) where olivine and low Ca-pyroxene readily quench from the low viscosity, magnesian liquid. They also showed that the combined effects of iron loss and quenching result in glass compositions significantly more silica-rich, and containing less FeO and MgO and generally more Al_2O_3 and CaO, than the equilibrium liquids calculated by either crystal-liquid element partition data or mass balance after allowing for iron loss. For these reasons, equilibrium liquids have been *calculated* by mass balance from a knowledge of the composition and proportions of the residual phases.

The proportions of residual phases were established by point-counting of scanning electron microscope photographs of the polished mount using a transparent 10 × 9 cm grid. A minimum of 1200 points were counted in replicate and averaged. Point counting of phases was not possible for the high degree melting runs where olivine or olivine + chrome spinel were residual phases because of strong crystal settling within the charge, even in runs of short duration. For these experiments, the equilibrium liquid composition was calculated by mass balance assuming a $K_D^{ol/liquid}$ of 0.3 (Roeder and Emslie 1970; Green and Ringwood 1967a) after correcting for iron loss from the charge (cf. Green 1973b). The use of this fixed K_D may introduce a small error since we have found that Fe-Mg partitioning between olivine and liquid is pressure dependent at pressures above 5 kb, and K_D increases with pressure resulting in more magnesian equilibrium liquids at higher pressure for olivine of the same composition (unpublished data).

Liquid compositions were calculated by mass balance after conversion of the volume percent modes to weight percent modes using appropriate mineral densities (Tröger 1956). The liquid density was calculated by the method of Bottinga and Weill (1970) using the least modified, most magnesian glass composition (obtained by reduced area rapid scans) with adjustment for the effect of pressure on the density (Kushiro et al. 1976). Iteration of the

Table 2. Comparison glass and calculated melt composition, and estimated errors

	10 kb 1300° C				10 kb 1450° C			
	Glass	37% melt	39%[a] melt	41% melt	Glass	71% melt	73% melt	75% melt
SiO_2	51.3	49.3	49.8	49.9	52.4	51.5	51.2	51.0
TiO_2	2.8	3.0	2.7	2.6	1.6	1.7	1.6	1.6
Al_2O_3	12.4	12.8	12.5	12.1	7.9	8.2	8.0	7.8
FeO[b]	8.9	9.0	9.0	8.5	8.8	9.9	9.5	9.5
MnO	–	0.1	0.1	0.1	–	0.1	0.1	0.1
MgO	10.4	11.5	12.0	13.4	20.7	19.8	21.0	21.7
CaO	11.8	11.2	10.9	10.6	7.1	7.2	7.0	6.8
Na_2O	1.9	2.5	2.4	2.3	1.2	1.3	1.3	1.3
K_2O	0.5	0.6	0.6	0.5	0.3	0.3	0.3	0.3
CIPW Norm								
Or	3.0	3.6	3.6	3.0	1.8	1.8	1.8	1.8
Ab	16.1	21.2	20.3	19.5	10.2	11.0	11.0	11.0
An	23.8	21.9	21.6	21.2	15.3	15.7	15.1	14.6
Di	28.0	27.1	26.2	25.2	15.9	16.1	15.7	15.3
Hy	23.0	3.2	7.2	9.7	44.7	40.0	37.4	36.1
Ol	0.8	17.2	16.0	16.5	9.2	12.2	16.0	18.2
Il	5.3	5.7	5.1	4.9	3.0	3.2	3.0	3.0
100 Mg/(Mg+Fe)	67.6	69.5	70.4	73.8	80.7	78.1	79.7	80.3

[a] Percent melting is of pyrolite minus 40% olivine composition
[b] Total iron as FeO

mass balance calculations to overcome the density difference between the equilibrium liquid and the analysed glass made negligible difference to the resultant liquid composition. Compared to the analysed glass compositions (available on request) the calculated liquids are more magnesian, have higher FeO content, lower SiO_2 and, generally, lower Al_2O_3 and CaO contents (Table 2), (see also Jaques and Green 1979). An additional uncertainty in the composition of the calculated liquids is the Fe_2O_3 content of the melt, and, consequently, calculated 100 Mg/(Mg+Fe^{2+}) ratios, since change in oxidation state may occur during the run. In Tables 4 and 5 calculated 100 Mg/(Mg+Fe^{2+}) ratios assume no change in Fe_2O_3 content and 100 Mg/(Mg+Fe) ratios assume all Fe as Fe^{2+}.

3.6 *Errors and Limitations*

Errors involved in the calculation of the equilibrium liquids are difficult to define precisely. Errors in point counting may be as high as 2 volume percent for phases present in excess of 5% due to inhomogeneous distribution, and crystal settling. The effect of a 2% error in the determination of the percentage of melting is shown in Table 2 for the melting of pyrolite at 10 kb, 1450° C (residual olivine and chrome spinel) and 10 kb 1300° C (residual olivine, orthopyroxene and chrome spinel). Uncertainty of ±2% in estimation of percentage melting produces small differences in Mg-value and normative compositions, which do not however overlap the composition of analyzed glass in the runs.

We have not been able to adequately discriminate residual phases in the low degree melting range i.e. within 25° C of the solidus, due to the fine grain size of the charge. Long run times to obtain sufficiently large crystals result in excessive iron loss and a non-equilibrium residual assemblage. An additional problem is the nucleation of stable calcic pyroxene: residual clinopyroxenes, particularly at low pressure, showed a range of calcium contents, some being sub-calcic (see later).

4. Melting Relations

Data on the experimental runs are presented in Table 3. The phase relations of the melting of both pyrolite and Tinaquillo lherzolite at 50° C intervals from the solidus to above the orthopyroxene-out curve are plotted as a function of T and P in Fig. 1. Also shown are the pyrolite solidus and subsolidus relations previously defined by Green and Ringwood (1967b, 1970). The position of the Tinaquillo lherzolite solidus is shown as approximate only, but appears to lie some 30°–40° C above the pyrolite solidus, reflecting its more refractory composition. The subsolidus assemblage at low pressure (0–10 kb) consists of olivine, orthopyroxene, clinopyroxene and plagioclase (plus minor accessory ilmenite, chrome spinel, apatite); at pressures above 10 kb this assemblage is replaced by olivine, aluminous pyroxenes and spinel, and above 25–30 kb by olivine, pyroxenes and garnet (Green and Ringwood 1967b).

Three main fields have been defined within the melting range studied for anhydrous melting of both peridotites. From near the solidus these are: olivine+orthopyroxene+clinopyroxene+chrome spinel+liquid, olivine+orthopyroxene+chrome spinel+liquid, and olivine±chrome spinel+liquid. Incomplete data close to the solidus indicate the presence of a narrow field in which an aluminous phase – plagioclase at low pressure, aluminous spinel at moderate pressure and garnet at high pressure (≧30 kb, Green and Ringwood 1976b) – coexists with olivine, 2 pyroxenes and liquid. Our data, though incomplete, indicate that this phase melts within 25°–30° C of the solidus (in the case of aluminous spinel by solid solution change to chrome spinel, Fig. 4). The clinopyroxene-bearing field for these peridotites extends some 75°–100° C above the solidus and expands at low pressure (<5 kb), particularly in the case of pyrolite. The upper stability limit of orthopyroxene lies approximately 150°–200° C above the solidus of both peridotites and the field expands slightly with pressure. The liquidus of either peridotite has not been determined but the pyrolite 1-atmosphere liquidus is approximately 1700°–1750° C by comparison with the data for peridotitic komatiite 49J (Green et al. 1975).

The melting relations defined here (together with the pyrolite melting runs of Green and Ringwood 1967b) are broadly similar to those established by Ito and Kennedy (1967) and Mysen and Kushiro

Table 3. Experimental run data

Run No.	P (kb)	T (°C)	Time (hours)	Capsule	100 Mg/(Mg + Fe) Charge	Phases present[a]
Pyrolite minus 40% olivine						
A555	0	1170	5	Fe	–	Ol + Opx + Cpx + L
A554	0	1200	2.5	Fe	–	Ol + Opx + Cpx + L
A556	0	1225	3	Fe	–	Ol + Opx + L
A553	0	1250	2	Fe	–	Ol + L
958	2.25	1100	2	Pt	85.8	Ol + Opx + Cpx + Pl + Sp + L
T-149	2	1150	3.5	Pt	88.2	Ol + Opx + Cpx + Sp + L
T-111	2	1200	2	Pt	86.0	Ol + Opx + Sp + L
T-107	2	1250	2	Pt	89.5	Ol + Opx + Sp + L
T-185	2	1250	0.5	Pt	86.5	Ol + Opx + Sp + L
T-133	2	1300	1	Pt	87.1	Ol + Sp + L
T-147	5	1200	2.5	Pt	87.2	Ol + Opx + Cpx + Sp + L
T-186	5	1200	0.75	Pt	86.2	Ol + Opx + Cpx + Sp + L
T-104	5	1250	2	Pt	86.9	Ol + Opx + Sp + L
T-167	5	1250	0.75	Pt	86.2	Ol + Opx + Sp + L
T-102	5	1300	2	Pt	87.2	Ol + Opx + Sp + L
T-166	5	1300	0.5	Pt	86.5	Ol + Opx + Sp + L
T-119	5	1350	2	Pt	88.9	Ol + Opx + Sp + L
T-158	5	1350	0.33	Pt	87.0	Ol + Sp + L
956	6.75	1200	2	Pt	85.5	Ol + Opx + Cpx + Sp + L
892	9	1200	2	Pt	86.7	Ol + Opx + Cpx + Sp + L
T-100	10	1250	2	Pt	86.1	Ol + Opx + Cpx + Sp + L
T-140	10	1250	1	Fe	84.6	Ol + Opx + Cpx + L
T-89[b]	10	1300	2	Pt	86.9	Ol + Opx + Sp + L
T-118	10	1350	2	Pt	87.0	Ol + Opx + Sp + L
T-139	10	1350	0.5	Fe	85.1	Ol + Opx + L
T-90	10	1400	2	Pt	88.0	Ol + Opx + Sp + L
T-157	10	1400	0.33	Pt	86.6	Ol + Opx + Sp + L
T-101	10	1450	2	Pt	89.7	Ol + Sp + L
T-138	10	1450	0.25	Fe	83.3	Ol + L
T-148	15	1350	2.5	Pt	87.7	Ol + Opx + Cpx + Sp + L
T-142	15	1400	1	Pt	86.2	Ol + Opx + Sp + L
T-184	15	1450	0.5	Pt	88.4	Ol + Opx + L
T-143	15	1500	0.75	Pt	88.8	Ol + Opx + Sp + L
T-150	15	1550	0.33	Pt	89.2	Ol + L
Tinaquillo lherzolite minus 40% olivine						
T-134	2	1200	2	Pt	90.0	Ol + Opx + Cpx + Sp + L
T-161	2	1200	4	Pt	90.1	Ol + Opx + Cpx + Sp + L
T-123	2	1250	2	Pt	90.0	Ol + Opx + Sp + L
T-121	2	1300	2	Pt	94.8	Ol + Opx + Sp + L
T-199	2	1300	0.5	Pt	89.2	Ol + Opx + Sp + L
T-162	2	1350	0.5	Pt	90.6	Ol + Sp + L
T-163	5	1200	4	Pt	89.4	Ol + Opx + Cpx + Pl + Sp + L
T-132	5	1250	1	Pt	89.0	Ol + Opx + Cpx + Sp + L
T-129	5	1300	2	Pt	90.8	Ol + Opx + Sp + L
T-180	5	1300	0.5	Pt	89.5	Ol + Opx + Sp + L
T-120	5	1350	2	Pt	91.0	Ol + Opx + Sp + L
T-154	5	1400	0.33	Pt	90.0	Ol + Sp + L
T-135	10	1250	2	Pt	89.0	Ol + Opx + Cpx + Sp + L
T-128	10	1300	2	Pt	90.0	Ol + Opx + Cpx + Sp + L
T-136	10	1350	1	Pt	89.2	Ol + Opx + Sp + L
T-137	10	1400	1	Pt	91.3	Ol + Opx + Sp + L
T-141	10	1400	1	Pt	91.4	Ol + Opx + Sp + L
T-155	10	1450	0.5	Pt	90.7	Ol + Sp + L
T-165	10	1500	0.33	Pt	90.8	Ol + Sp + L
T-156	15	1350	3	Pt	91.0	Ol + Opx + Cpx + Sp + L
T-145	15	1400	1	Pt	90.4	Ol + Opx + Sp + L
T-194	15	1400	0.33	Pt	–	Ol + Opx + Sp + L
T-183	15	1450	0.5	Pt	90.6	Ol + Opx + L
T-216	15	1450	0.33	Pt	–	Ol + Opx + L
T-218	15	1500	0.33	Pt	–	Ol + Opx + L
T-164	15	1550	0.5	Pt	91.8	Ol + L

Ol: olivine; Opx: orthopyroxene; Cpx: clinopyroxene; Sp: spinel; Pl: plagioclase; L: liquid (glass)

[a] Primary phases only, excludes quench pyroxene and/or olivine present in most runs

[b] Additional experiments by Jaques and Green (1979)

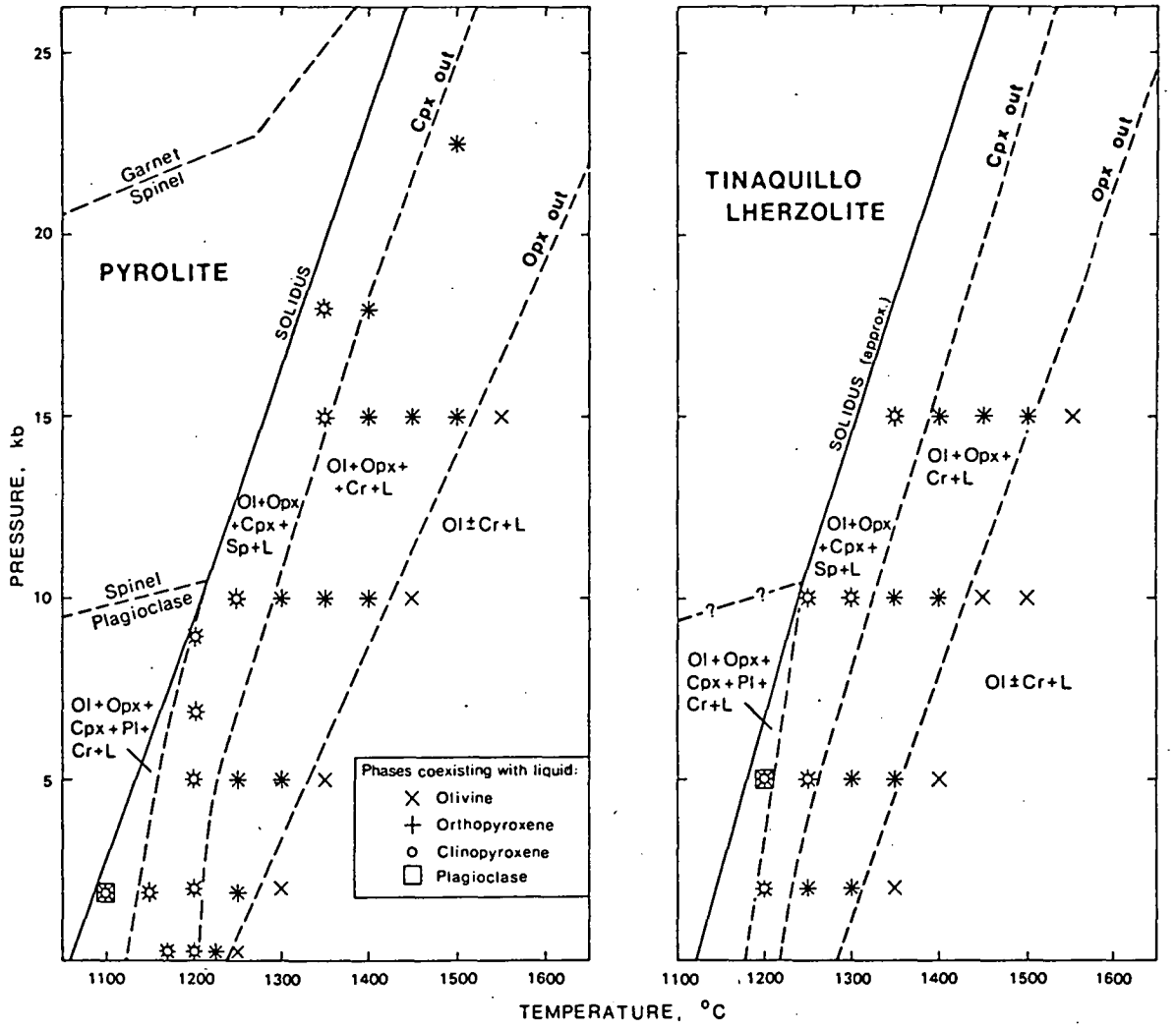

Fig. 1. *P-T* diagram for melting of pyrolite (composition of Ringwood 1966) and Tinaquillo lherzolite. Ol: olivine; Opx: orthopyroxene; Cpx: clinopyroxene; Sp: spinel; Cr: chrome spinel; Pl: plagioclase; L: liquid. Data for 18 and 22.5 kb pyrolite runs from Green and Ringwood (1967b). Plagioclase-spinel peridotite and spinel-garnet peridotite transition boundaries from Green and Ringwood (1970). The solidus and subsolidus boundaries for Tinaquillo lherzolite are estimated

(1977) for the anhydrous melting of garnet peridotite at 0–40 kb, and 25 and 35 kb respectively. Ito and Kennedy (1967) did not define a field in which clinopyroxene was a residual phase but noted that garnet and clinopyroxene melted within a temperature interval of approximately 50° C above the solidus at high pressure. The presence of residual orthopyroxene at low pressure (< 5 kb) in our experiments is in agreement with the 1-atmosphere data of Ito and Kennedy (1967) but conflicts with the incongruent melting behaviour of orthopyroxene in the MgO-SiO_2 system. This illustrates very well the contrast between the abrupt disappearance of a phase and change in melt proportions characteristic of simple, pure Mg systems (Kushiro 1969; Presnall et al. 1979), and the gradual reaction and disappearance of a phase over a moderately large temperature interval in complex Fe-Mg systems.

The percentage of melt obtained from the melting of pyrolite and Tinaquillo lherzolite at 15 kb and 10 kb is plotted as a function of temperature in Fig. 2. Satisfactory determination of the percentage of melting at less than about 10% melting was not achieved due to the experimental difficulties already discussed. From Fig. 2 is seen that the amount of melt increases rapidly in the initial stages of melting, and then increases at a steady rate. Comparison of pyrolite and Tinaquillo lherzolite shows that more liquid can be extracted from pyrolite: approximately 20% melt can be derived from pyrolite before clinopyroxene disappears but only about 12–15% melt can be derived from Tinaquillo before clinopyroxene is

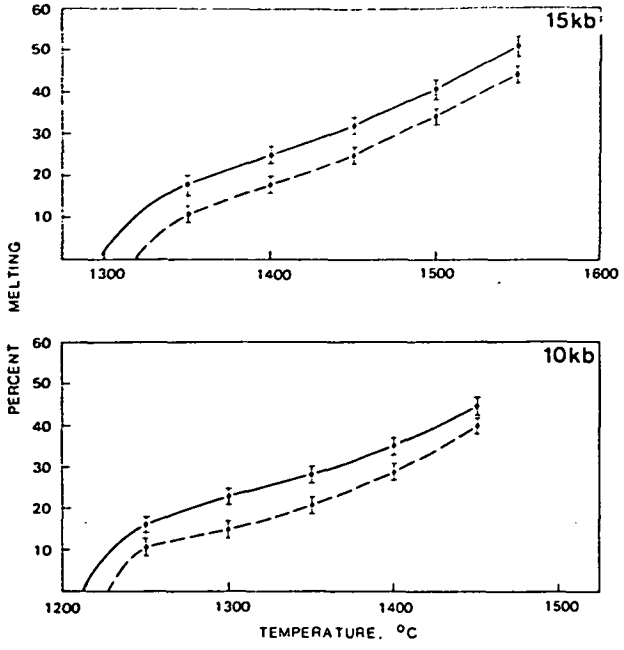

Fig. 2. Percent melting versus temperature for melting of pyrolite *(solid line)* and Tinaquillo lherzolite *(dashed line)*. Note that percent melting is of peridotite compositions, not the experimental (minus 40% olivine) compositions shown in Fig. 3. Bars indicate ±2% error in determination of liquid

exhausted. Mysen and Kushiro (1977) claim that the anhydrous melting relations of peridotite resemble those of simple systems and that melting may approximate an invariant character. This conclusion is not supported by our data (Fig. 2). Our data do not permit evaluation of the melting behaviour between the 50° C intervals to determine if minor inflexions (cf. Kushiro 1969), or steps (Wyllie 1971), occur as phases disappear from the residue. Presnall (1969) has shown graphically that equilibrium melting is a continuous process and we interpret our results as demonstrating the 'smoothing effect' of Fe-Mg, Al-Cr, Al-Si, Na-Ca, solid solutions in the percent melt versus temperature plot. Following the initial stages of melting, where the amount of melt increases rapidly, the percentage of melting increases approximately linearly as a function of temperature. The melting behaviour observed in our experiments bears similarities with that predicted by O'Hara (1968, Fig. 8, stages 3–5), although the observed melting interval is less than that suggested in his model.

Modal variation (volume %) of the residue phases for the modified (−40% olivine) peridotite compositions are shown in Fig. 3. In each case the melt fraction increases while the proportion of residual phases decreases regularly. Ito and Kennedy (1967) also observed a progressive decrease in the proportion of residual phases and eventual elimination of the phase from the residue. Although the melting of orthopyroxene in the complex composition differs from that in the CaO-MgO-SiO_2 system (Kushiro 1969) and the CaO-MgO-Al_2O_3-SiO_2 system (Presnall et al. 1979), comparison of the relative proportions of olivine and orthopyroxene at 2 and 5 kb with the 10 and 15 kb experiments show that the field of orthopyroxene expands with pressure as previously noted (e.g., Green and Ringwood 1967a). Melts produced by moderate degrees of melting at low pressure are oversaturated in SiO_2, and become olivine normative at higher pressure (Tables 4 and 5).

We have not carried out melting experiments in the high degree melting range (>50% melting) since degrees of partial melting of this order may not be geologically feasible. All our experiments at high degrees of melting (≧40%) showed strong crystal settling of olivine in the fluid komatiitic liquid, and we agree with Arndt (1977) that the high settling velocities will probably mean that high degrees (40–80%) of melting of peridotite are unlikely to be attained, since before that degree of melting is reached, a highly fluid picritic-komatiite liquid will segregate from the source peridotite. Green et al. (1975) proposed that peridotitic liquids required unusually rapid rates of diapiric ascent to counter the settling problem, and Arndt (1977) proposed that peridotitic komatiites result from a process of sequential melting.

5. Compositions of Residual Phases

5.1 Olivine

All runs are oversaturated in olivine. Variation in olivine composition, expressed as changes in Mg-value, with temperature are shown in Fig. 4. Olivine adjusts readily to iron loss from the charge and, consequently, where the $K_D^{ol/opx}$ between the analysed olivine and the cores of large orthopyroxene grains show the analysed olivine to be out of equilibrium (i.e., excessively magnesian due to iron loss, as is the case for almost all our runs), the equilibrium olivine composition has been calculated using a $K_D^{ol/opx} = 1.1$. Where olivine is the only residual phase the equilibrium olivine composition has been calculated prior to iron loss, using the analysis of the bulk charge (obtained by rapid reduced area, ~250 μ, scans) and the original bulk composition.

Olivine Mg-values progressively increase with temperature (%melting) from less than 88 near the pyrolite solidus to approximately 95 at 15 kb 1550° C (~50% melting) where olivine is the only residual phase. For the Tinaquillo lherzolite composition, residual olivine is more magnesian and Mg-values range from 90 near the solidus to approximately 95 (~44% melting). Calcium contents for olivine in both peridotites lie in the range 0.2 to 0.4 wt. %, and decrease with increasing temperature (%melting).

The rates of adjustment to iron loss from the charge differ for olivine and liquid, or olivine, pyroxene and spinel, and preclude any meaningful examination of Fe-Mg partitioning between phases where iron loss has occurred.

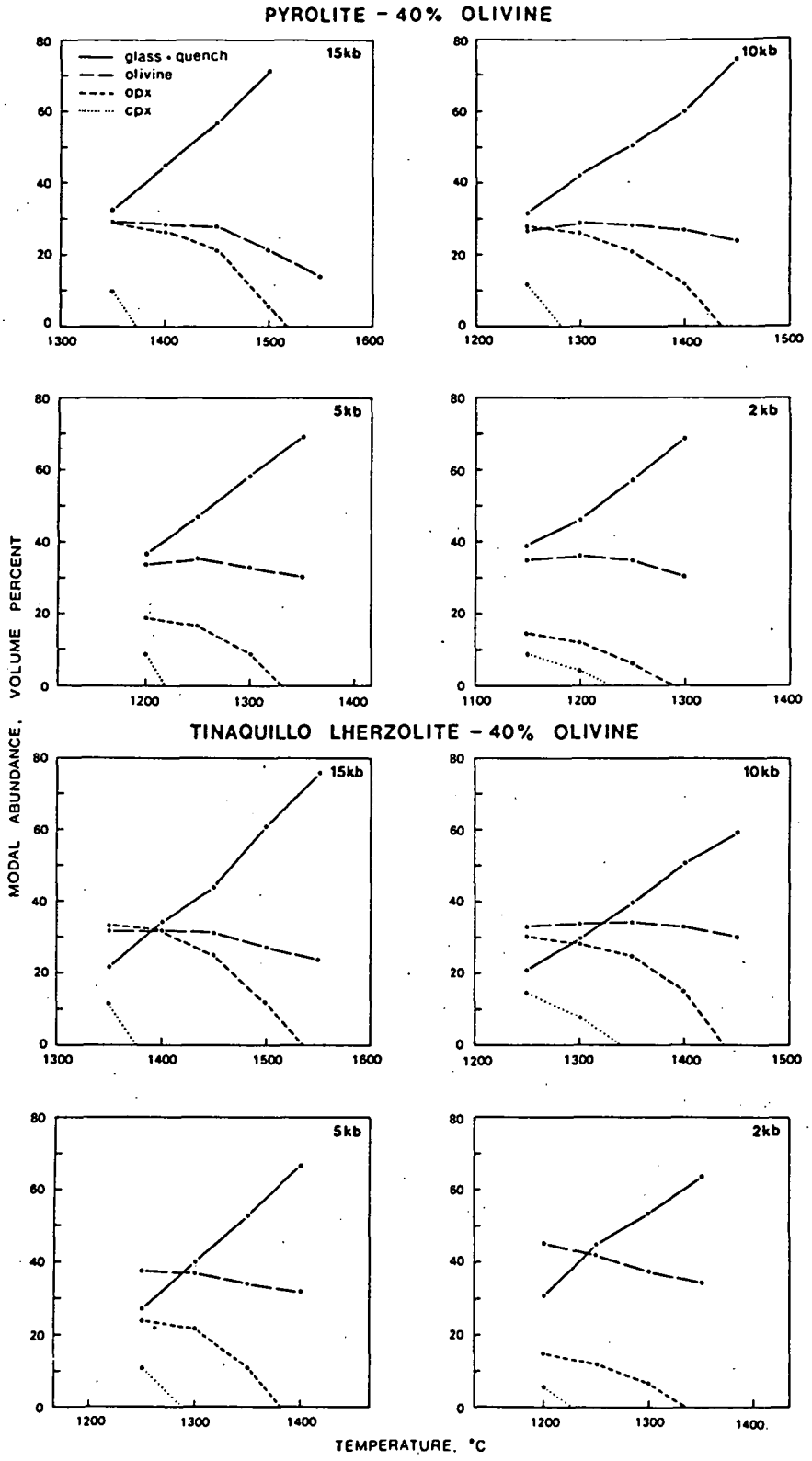

Fig. 3. Modal variation (volume percent) of run products with temperature. Residual spinel present at 0–1.5 volume percent is omitted. All quench material counted as melt

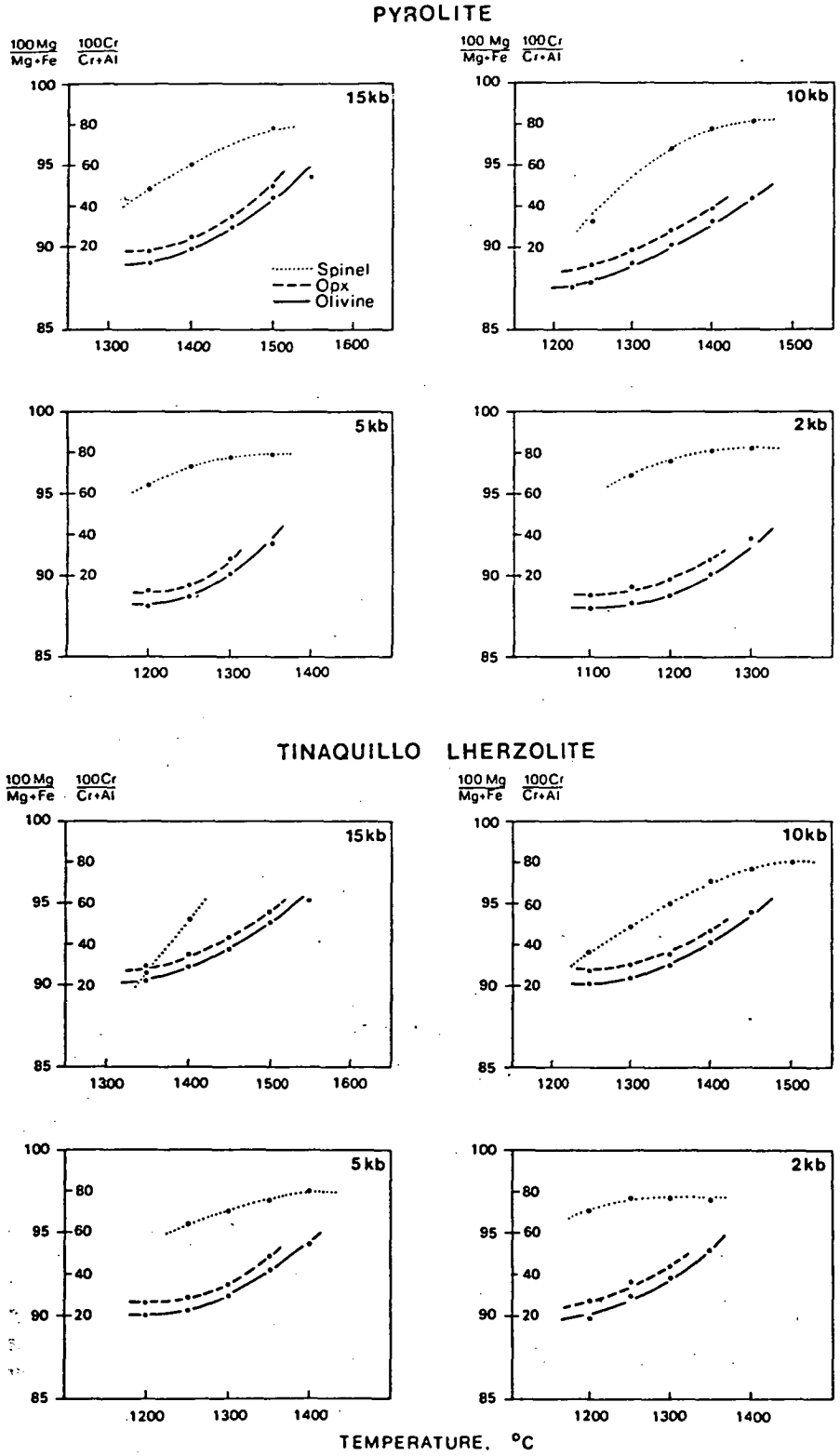

Fig. 4. Variation in 100 Mg/(Mg+Fe) of olivine and orthopyroxene, and 100 Cr/(Cr+Al) of spinel with temperature (see text fo derivation of olivine compositions in runs experiencing iron loss)

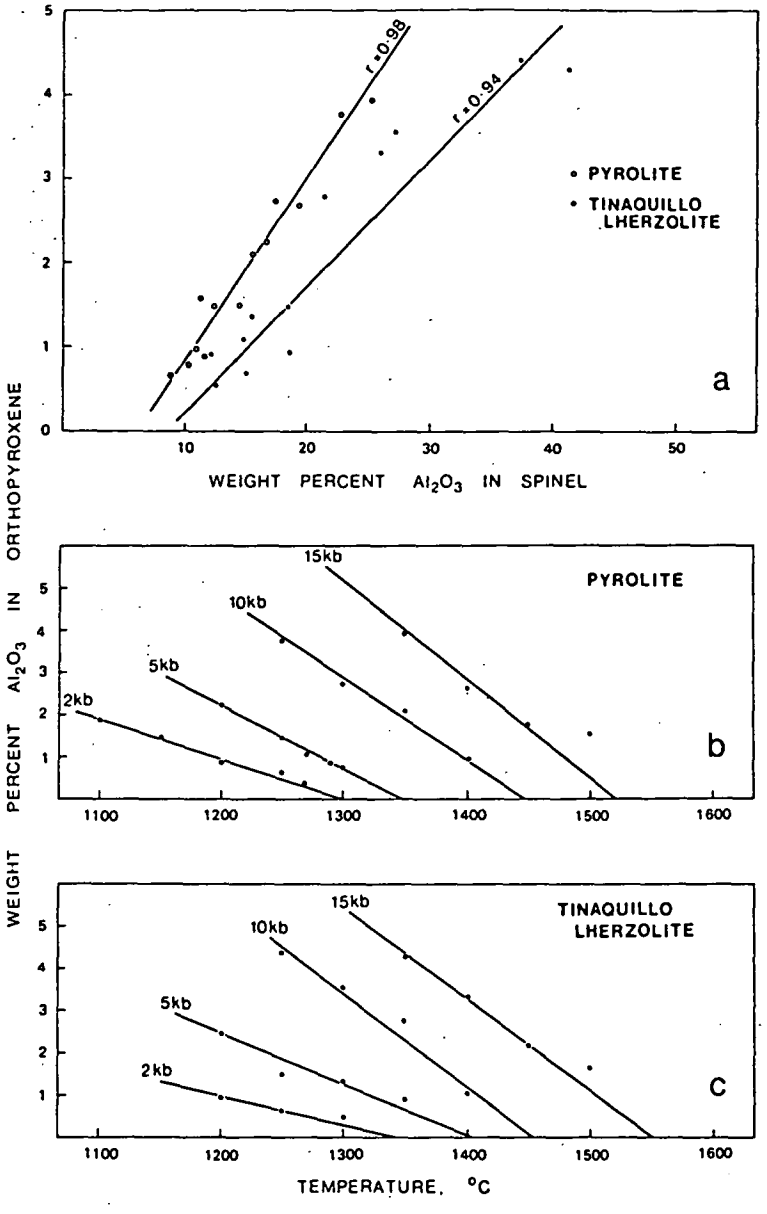

Fig. 5. a Variation in weight percent Al_2O_3 in spinel with weight percent Al_2O_3 in orthopyroxene. b, c Variation in weight percent Al_2O_3 in orthopyroxene with temperature. Stars are for melting of pyrolite + 0.3 wt.% H_2O (DH Green, unpubl.)

5.2 *Spinel*

Tables of spinel analyses are available from the authors on request, and compositional variation, expressed as 100 Cr/(Cr + Al) ratios, with temperature is shown in Fig. 4. Variation in spinel composition is dominantly Cr-Al substitution in trivalent cations, and spinels become increasingly chrome-rich with increasing degree of melting until a maximum 100 Cr/(Cr + Al) ratio of ~ 80 is reached. Spinels of this composition are highly refractory, containing ~ 55–58 wt.% Cr_2O_3, similar to chrome spinels from alpine peridotites and tectonite harzurgite in ophiolites. The *Mg-values* (56–75 in pyrolite, 70–77 in Tinaquillo lherzolite) increase with increasing temperature, a consequence of increasing degree of melting, and of iron-loss. Compared to chrome spinels from alpine peridotites, ophiolites and stratiform intrusions the experimental spinels are deficient in iron, reflecting both substantial subsolidus re-equilibration of the natural rocks, and, possibly, iron loss from the experimental charge. Calculated Fe^{3+} contents are significant ($Fe^{3+}/(Cr^{3+}+Al^{3+}+Fe^{3+}) = 0.06-0.14$ in pyrolite and 0.04 to 0.10 in Tinaquillo lherzolite) and may reflect increased Fe^{+++}/Fe^{++} of the charge, due to Fe alloying with the Pt capsule.

Chrome spinels near the solidus at low pressure (2–5 kb) are distinctly more chrome-rich than those at higher pressure (10–15 kb). This is consistent with the melting of different subsolidus assemblages of plagioclase + chrome spinel (< 10 kb) and aluminous spinel + aluminous pyroxenes (> 10 kb), and the presence of a plagioclase-field immediately above the solidus at low pressure. The distribution coefficient $K_D = (Al/Cr)_{cp}/(Al/Cr)_{Sp}$ is greater than unity, in accord with experimental data from simple Cr-bearing systems (Dickey and Yoder 1972) and natural peridotites. The Al_2O_3 content of orthopyroxene shows a direct correlation with the Al_2O_3 of coexisting spinel (Fig. 5a), and the Cr/(Cr + Al) ratios of spinel correlate with the Cr/(Cr + Al) ratio of coexisting orthopyroxene at constant pressure. Both correlations appear dependent on bulk composition as well as temperature and pressure (Fig. 5) as might be expected if Cr-Al substitution in spinel is non-ideal

(Wood and Nicholls 1978). As for clinopyroxene, the $K_D^{Cr_2O_3\ clinopyroxene/spinel}$ is greater than unity indicating that Cr is preferentially partitioned into spinel; the K_D, at low pressure are higher than at higher pressure.

5.3 Orthopyroxene

Tables of orthopyroxene analyses are available from the authors on request. The Mg-values of large orthopyroxene grains (Fig. 4) increase with temperature (percent melting) from about Mg_{89} near the pyrolite solidus to Mg_{93-94} at the orthopyroxene-out curve. Orthopyroxene from the melting of Tinaquillo lherzolite is slightly more refractory, with Mg-values of 91 to 94. Orthopyroxene grains are commonly zoned with rims which are 1–2 mol% more magnesian, due to iron loss. Al_2O_3 and CaO contents decrease with increasing temperature, and compositions near the orthopyroxene-out curve have very low CaO and Al_2O_3 contents (1–2%). The linear decrease of Al_2O_3 in orthopyroxene with increasing temperature (Fig. 5b, c) is further evidence that melting is a continuous process, and that melting is dominated by solid solution behaviour rather than eutectic behaviour. Alumina contents in orthopyroxene are higher at higher (10 to 15 kb) pressure for similar degrees of melting, and coexisting liquids (Tables 4, 5) are lower in Al_2O_3. The data imply that Al_2O_3 solubility in pyroxene increases with pressure over this pressure range. The solubility of Al_2O_3 in orthopyroxene in spinel peridotite and plagioclase peridotite is at present in dispute (cf. MacGregor 1974; Obata 1976; Presnall 1976). Stroh (1976) has shown that the addition of Fe and Cr to the simple system MgO-SiO_2-Al_2O_3 markedly affects the activities of phases at equilibrium. Because of the complexity of interplay of pressure and temperature, varying % melting, liquid composition and spinel composition, the data is not analyzed further in terms of mineral equilibria or P, T dependence of Al_2O_3 solubility in phases. The data on orthopyroxene compositions indicate a strong site preference of Al for the tetrahedral position and that this preference increases with temperature. Chromium contents and 100 Cr/(Cr + Al) ratios increase with temperature (percentage melting). Orthopyroxene at 2 and 5 kb has noticeably lower chromium contents than those at 10 and 15 kb, but coexists with more chromium-rich spinel.

5.4 Clinopyroxene

Analyses of clinopyroxene compositions are available from the authors on request and are plotted in the relevant pyroxene quadrilateral in Fig. 6. The clinopyroxenes are of diopsidic composition, have low jadeite component, and comparatively low calcium contents. As for orthopyroxene, Al_2O_3 contents are greater at higher pressure for similar degrees of melting and decrease with increasing temperature (decreasing Al_2O_3 content of liquid). Cr_2O_3 contents and 100 Cr/(Cr + Al) ratios increase with increasing temperature and, as for orthopyroxene, Cr_2O_3 contents are higher at higher pressure (10–15 kb) for similar degrees of melting reflecting changes in the Cr/Al partitioning between spinel and pyroxene with increasing pressure.

Clinopyroxenes analysed within a single run exhibited a range of CaO contents, especially at low pressure: the analyses presented are the more calcic examples of the range. The compositions of the residual clinopyroxenes need to be critically examined, particularly in view of the fact that clinopyroxene coexisting with orthopyroxene on anhydrous liquidi are commonly highly subcalcic (e.g., Green and Ringwood 1967a). More importantly, Green (1976c) has demonstrated the experimental difficulties which exist in the nucleation and growth of subcalcic 'pigeonitic' pyroxenes. Previous studies have shown that the pyroxene miscibility gap narrows, and the field of Ca-poor clinopyroxene contracts towards the En – Di join, with increasing pressure (e.g., Mori 1978; Hensen 1973). However data available at low pressure are mostly restricted to the En – Di and Fs – Hd joins (see Mori 1978 for summary), and only in a few cases have experiments been reversed. Compared to the solvus defined by pyroxenes that have crystallized from basaltic magmas (e.g., Atkins 1969; Wager and Brown 1967; Hodges and Papike 1976), the residual clinopyroxenes examined here are decidedly less calcic. Comparison with experimental data shows that residual clinopyroxenes at 15 kb 1350° C lie within the 15 kb 1200° C solvus of Mori (1978) in the Ca-Mg-Fe-SiO_2 system, and both residual pyroxenes are in reasonable agreement (Ca-px slightly less calcic) with the En – Di solvus defined by Lindsley and Dixon (1976). Residual clinopyroxenes at low pressure are less calcic than those defined in En – Di exsolution and dissolution experiments under similar P – T conditions (Warner and Luth 1974; Mori and Green 1975; Lindsley and Dixon 1976).

However, a lack of data in Fe-bearing systems means that the composition of clinopyroxene coexisting with orthopyroxene at high temperature under anhydrous conditions and 0–10 kb pressure range is not adequately constrained. Given this uncertainty, we have tentatively accepted the compositions of the most calcic, low alumina clinopyroxenes in our experiments as equilibrium compositions. The possibility that the equilibrium residual clinopyroxene is more calcic does not greatly affect our calculations of the equilibrium liquid compositions if we can assume that the modal abundance of a more calcic pyroxene would be less than that of a less calcic clinopyroxene, i.e. that chemical equilibrium obtains for Ca-Mg-Fe partitioning between the liquid and the total residual pyroxene components regardless of their appearance as orthopyroxene, subcalcic or calcic clinopyroxene. This assumption appears reasonable for Ca-Mg-Fe but is unlikely to hold for elements such as Al, Ti, Na, and Cr whose partitioning into pyroxene as minor components is likely to be strongly influenced by the nature of the pyroxene.

6. Equilibrium Melt Compositions

The compositions of equilibrium partial melts for each P and T studied have been calculated by mass balance using the data on phase compositions and proportions. These liquid compositions and their CIPW norms are presented in Tables 4 and 5. The basaltic liquids are classified on a normative basis following Green and Ringwood (1967a). Some of the liquids are of komatiitic composition; we have used the terms peridotitic, pyroxenitic and basaltic komatiite in a broad sense only since opinion differs as to the classification criteria of magmas of the komatiite suite.

6.1 Pyrolite

At 15 kb liquid compositions range from olivine basalt (Mg_{67} i.e. 100 Mg/(Mg + ΣFe) = 67) at 18% melting with residual olivine, orthopyroxene, clinopyroxene and spinel, through olivine tholeiite (Mg_{70-75}) with residual olivine, orthopyroxene and chrome

Table 4. Calculated equilibrium melt compositions – Pyrolite

P kb	15	15	15	15	15	10	10	10	10	11	5	5	5	5	2	2	2	2
T°C	1350	1400	1450	1500	1550	1250	1300	1350	1400	1450	1200	1250	1300	1350	1150	1200	1250	1300
% melt of Pyrolite	18	25	32	41	51	16	23	28	35	44	20	25	31	38	21	24	31	39
SiO_2	49.0	49.3	50.0	50.5	49.6	49.7	49.8	50.3	50.6	51.2	52.1	52.4	52.6	52.8	52.8	53.0	53.3	52.5
TiO_2	3.2	2.5	2.1	1.7	1.4	3.2	2.7	2.3	1.9	1.6	3.0	2.6	2.3	1.8	2.8	2.6	2.2	1.8
Al_2O_3	12.9	11.7	10.3	8.3	7.0	14.5	12.5	11.3	9.6	8.0	14.9	13.2	11.3	9.1	15.1	13.5	11.0	8.9
Fe_2O_3	0.7	0.5	0.4	0.3	0.2	0.7	0.5	0.4	0.3	0.3	0.6	0.5	0.4	0.3	0.6	0.5	0.4	0.3
FeO	9.5	9.1	9.6	9.7	9.3	8.2	8.5	8.9	9.5	9.2	7.3	7.1	8.4	8.9	7.2	7.3	8.1	9.0
MnO	0.1	0.2	0.2	0.1	0.1	0.2	0.1	0.1	0.1	0.1	0.1	0.1	0.1	0.2	0.1	0.1	0.1	0.1
MgO	11.6	13.2	16.0	20.3	24.9	10.2	12.0	13.9	17.6	21.0	8.9	9.9	12.9	17.2	8.7	10.5	13.3	17.9
CaO	9.1	10.7	9.2	7.4	6.1	9.1	10.9	10.1	8.3	7.0	9.5	11.4	9.7	7.9	9.4	9.7	9.4	7.7
Na_2O	3.1	2.3	1.8	1.4	1.1	3.3	2.4	2.0	1.6	1.3	2.8	2.3	1.9	1.5	2.7	2.3	1.8	1.5
K_2O	0.7	0.5	0.4	0.3	0.3	0.8	0.6	0.5	0.4	0.3	0.6	0.5	0.4	0.3	0.6	0.5	0.4	0.3
CIPW Norm																		
Qt_z	–	–	–	–	–	–	–	–	–	–	0.8	1.1	0.7	–	2.2	2.3	2.0	–
Or	4.1	3.0	2.4	1.8	1.8	4.7	3.6	3.0	2.4	1.8	3.6	3.0	2.4	1.8	3.6	3.0	2.4	1.8
Ab	26.2	19.5	15.2	11.9	9.3	27.9	20.3	16.9	13.5	11.0	23.7	19.5	16.1	12.7	22.9	19.5	15.2	12.7
An	19.2	20.1	18.8	15.5	13.3	22.4	21.6	20.4	17.8	15.1	26.3	24.2	21.1	17.2	27.3	25.0	20.8	16.7
Di	20.9	26.5	21.5	17.0	13.5	18.3	26.1	23.9	18.7	15.7	16.7	25.9	21.7	17.6	15.5	18.5	20.7	17.2
Hy	1.1	7.3	21.8	32.4	31.3	2.5	8.3	19.2	29.0	37.9	22.1	20.6	33.0	44.5	22.3	26.0	34.1	42.7
Ol	21.1	18.1	15.6	17.8	27.8	16.8	14.3	11.7	14.3	15.0	–	–	–	2.2	–	–	–	5.0
Mt	1.1	0.7	0.6	0.4	0.3	1.0	0.7	0.6	0.4	0.4	0.9	0.7	0.6	0.4	0.9	0.7	0.6	0.4
Il	6.1	4.8	4.0	3.2	2.7	6.1	5.1	4.4	3.6	3.0	5.7	4.9	4.4	3.4	5.3	4.9	4.2	3.4
100 Mg/(Mg+Fe^{++})	68	72	75	79	83	69	72	74	77	80	68	71	73	77	69	72	75	78
100 Mg/(Mg+Fe)	67	71	74	79	82	67	70	73	76	80	67	70	72	77	67	71	74	78

Table 5. Calculated equilibrium melt compositions – Tinaquillo lherzolite

P kb	15	15	15	15	15	10	10	10	10	10	5	5	5	5	2	2	2	2
T°C	1350	1400	1450	1500	1550	1250	1300	1350	1400	1450	1250	1300	1350	1400	1200	1250	1300	1350
% melt of Tinaquillo lherzolite	11	18	25	34	44	11	15	21	29	40	14	21	29	39	17	24	29	36
SiO_2	47.3	48.0	48.4	49.6	50.4	47.9	49.0	50.2	50.5	51.6	50.3	51.4	51.5	51.8	54.0	53.6	53.3	52.9
TiO_2	0.5	0.4	0.3	0.2	0.2	0.2	0.3	0.3	0.2	0.2	0.3	0.3	0.2	0.2	0.4	0.3	0.3	0.2
Al_2O_3	14.8	12.8	11.8	9.2	7.3	15.7	14.8	12.5	10.5	7.8	18.4	13.9	10.4	8.5	17.2	12.7	10.8	8.7
Fe_2O_3	0.8	0.5	0.4	0.3	0.2	0.8	0.6	0.4	0.3	0.2	0.6	0.4	0.3	0.2	0.6	0.4	0.3	0.2
FeO	9.2	8.4	9.0	9.0	8.3	8.5	7.6	7.6	8.6	8.2	6.1	7.3	8.4	8.3	4.6	6.9	7.7	8.2
MnO	0.3	0.2	0.2	0.2	0.1	0.3	0.2	0.2	0.1	0.2	0.1	0.1	0.1	0.1	0.1	0.1	0.1	0.2
MgO	14.6	15.4	18.1	22.4	26.3	13.3	13.7	15.5	19.2	23.9	10.3	13.5	18.6	22.9	9.0	13.6	16.9	20.8
CaO	11.0	13.2	11.0	8.5	6.7	11.8	12.6	12.3	9.9	7.4	12.5	12.1	9.8	7.5	12.9	11.5	9.9	8.2
Na_2O	1.3	1.0	0.7	0.5	0.4	1.3	1.1	0.9	0.6	0.5	1.3	0.9	0.6	0.5	1.1	0.8	0.6	0.5
K_2O	0.2	0.1	0.07	0.05	0.04	0.2	0.1	0.09	0.06	0.04	0.1	0.09	0.06	0.05	0.1	0.07	0.06	0.05
CIPW Norm																		
Qt_z	–	–	–	–	–	–	–	–	–	–	–	–	–	–	7.7	4.0	1.9	–
Or	1.2	0.6	0.4	0.3	0.2	1.2	0.6	0.5	0.4	0.2	0.6	0.5	0.4	0.3	0.6	0.4	0.4	0.3
Ab	11.0	8.5	5.9	4.2	3.4	11.0	9.3	7.6	5.1	4.2	11.0	7.6	5.1	4.2	9.3	6.8	5.1	4.2
An	34.0	30.1	28.9	22.7	18.0	36.4	35.2	29.8	25.8	18.9	44.1	33.6	25.5	20.8	41.7	30.9	26.6	21.4
Di	16.6	28.4	20.6	15.5	12.1	17.9	22.0	25.0	18.7	14.2	14.4	21.0	18.5	13.1	17.9	21.0	18.0	15.4
Hy	11.7	9.3	22.1	35.5	42.8	12.4	17.9	25.3	36.6	47.3	26.9	35.1	42.7	49.1	21.2	35.6	46.9	54.7
Ol	23.2	21.5	20.7	20.6	22.6	19.3	13.4	10.4	12.6	14.4	1.4	0.7	6.9	11.8	–	–	–	3.1
Mt	1.2	0.7	0.6	0.4	0.3	1.2	0.9	0.6	0.4	0.3	0.9	0.6	0.4	0.3	0.9	0.6	0.4	0.3
Il	1.0	0.8	0.6	0.4	0.4	0.4	0.6	0.6	0.4	0.4	0.6	0.6	0.4	0.4	0.8	0.6	0.6	0.4
100 Mg/(Mg+Fe^{++})	74	77	78	83	85	74	76	78	80	84	75	77	80	83	78	78	80	82
100 Mg/(Mg+Fe)	73	76	78	82	85	72	75	78	80	84	73	76	79	83	76	77	79	82

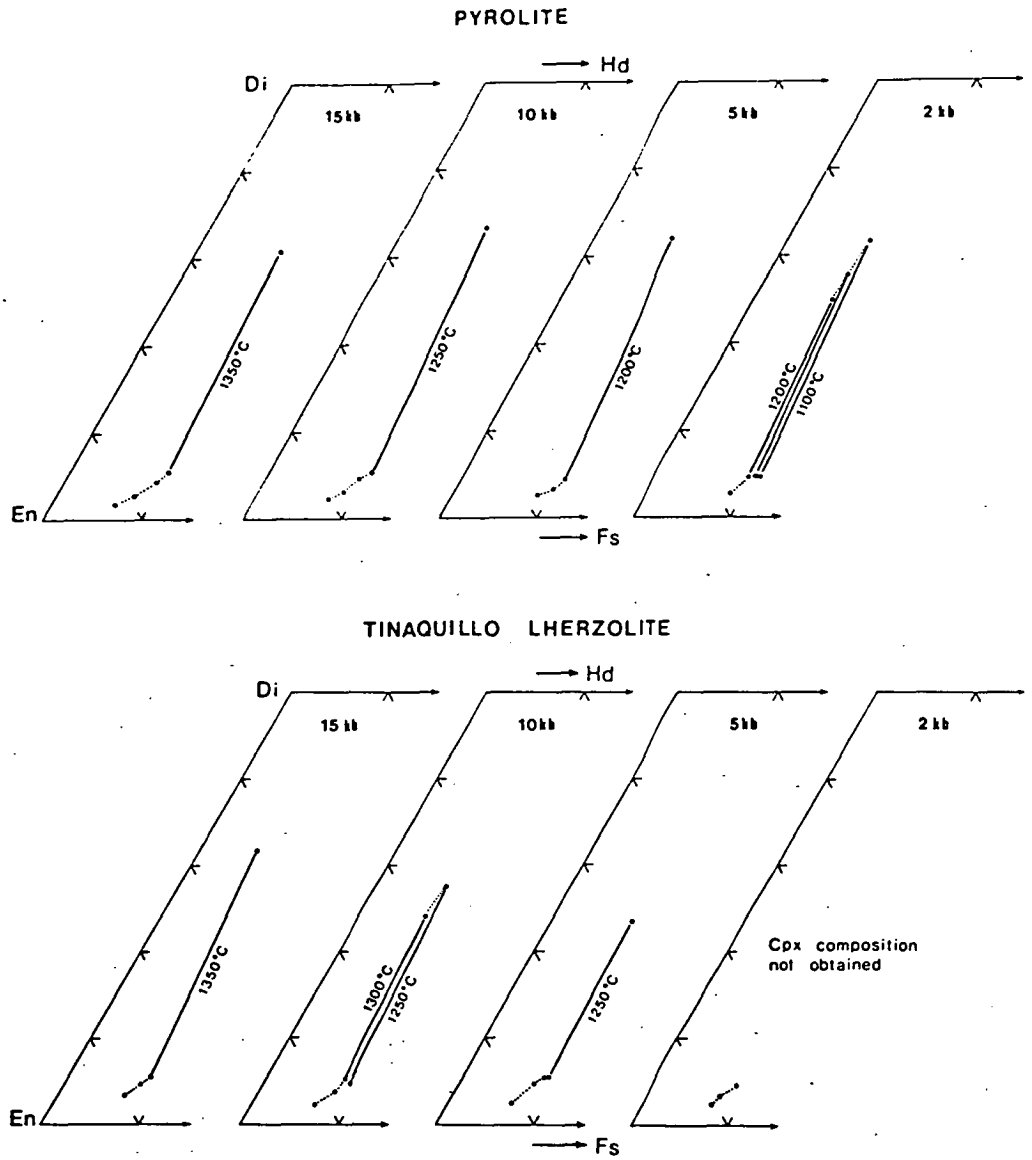

Fig. 6. Pyroxene quadrilateral showing compositions of residual pyroxenes

spinel (20–30% melting) to tholeiitic picrite to komatiite (Mg_{80}) at 40–50% melting in equilibrium with residual olivine.

Liquids at 10 kb range from olivine basalt (16% melting) with residual olivine, ortho- and clinopyroxene and spinel through olivine tholeiite (residual olivine, orthopyroxene and chrome spinel) to pyroxene-rich komatiite at 44% melting leaving residual olivine and chrome spinel. Compared to the partial melts at 15 kb, liquids at 10 kb are more aluminous and have a higher normative hy/ol ratio.

Partial melts at low pressure – 5 and 2 kb – are distinctly more silica saturated than those at high pressure, due to expansion of the primary field of olivine into quartz-normative basaltic compositions at the expense of orthopyroxene (as shown by the decrease in modal abundance of residual orthopyroxene relative to that at higher pressure). Liquids range from quartz tholeiite to pyroxenitic komatiite at higher degrees of partial melting. Quartz tholeiites produced by lower degrees of partial melting have considerably higher abundances of Al_2O_3 and incompatible elements than those produced by large degrees of melting. Melts at low pressure are also distinctly more aluminous for similar degrees of partial melting than those at high pressure where the coexisting residual pyroxenes are aluminous (cf. Green and Ringwood 1967a).

Variation of oxide percentages with percent melting for each pressure are shown in Fig. 7. Silica con-

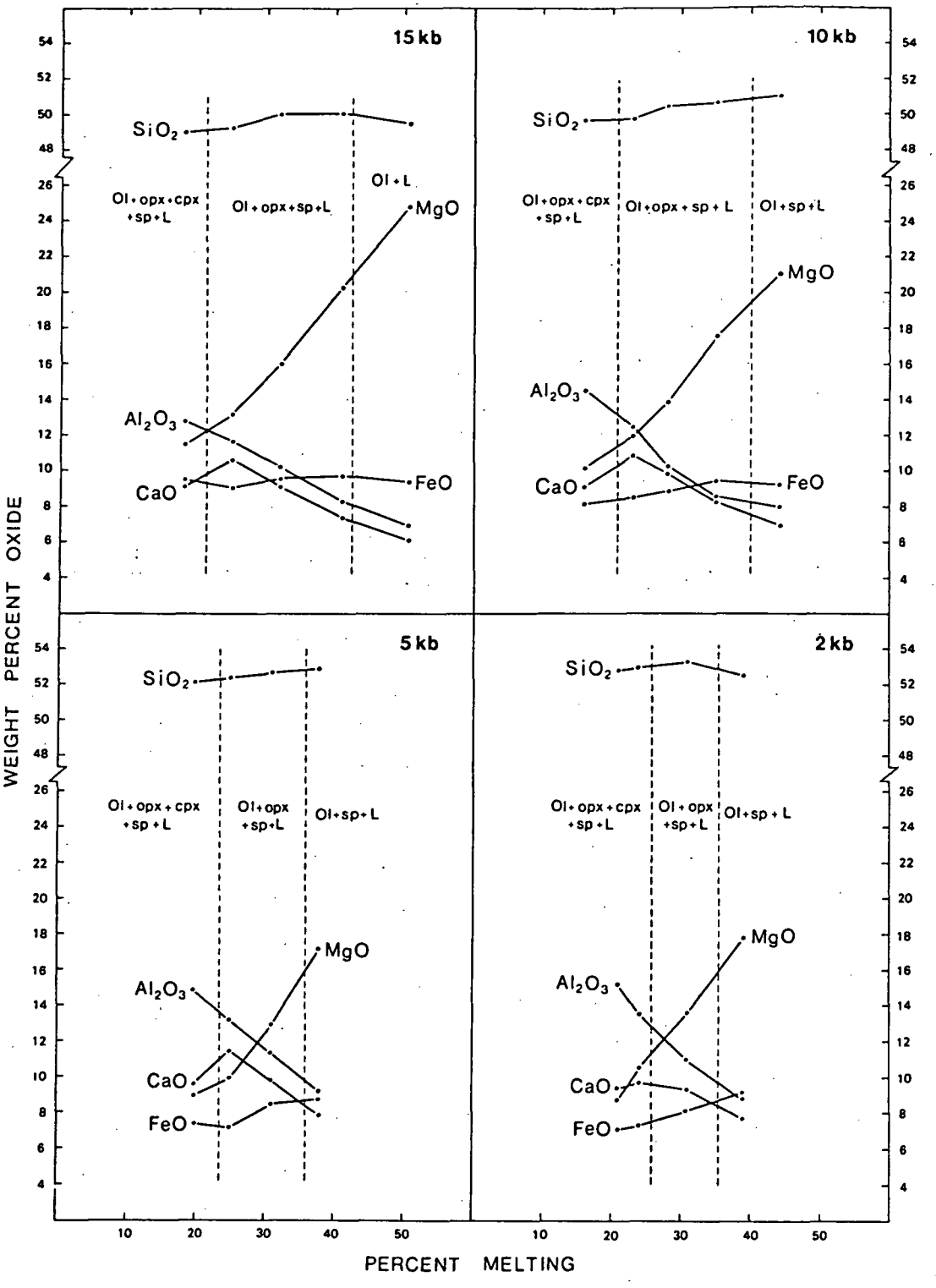

Fig. 7. Chemical trends of pyrolite equilibrium liquids with percentage melting. 'Percent melting' refers to pyrolite, not pyrolite – 40% olivine composition

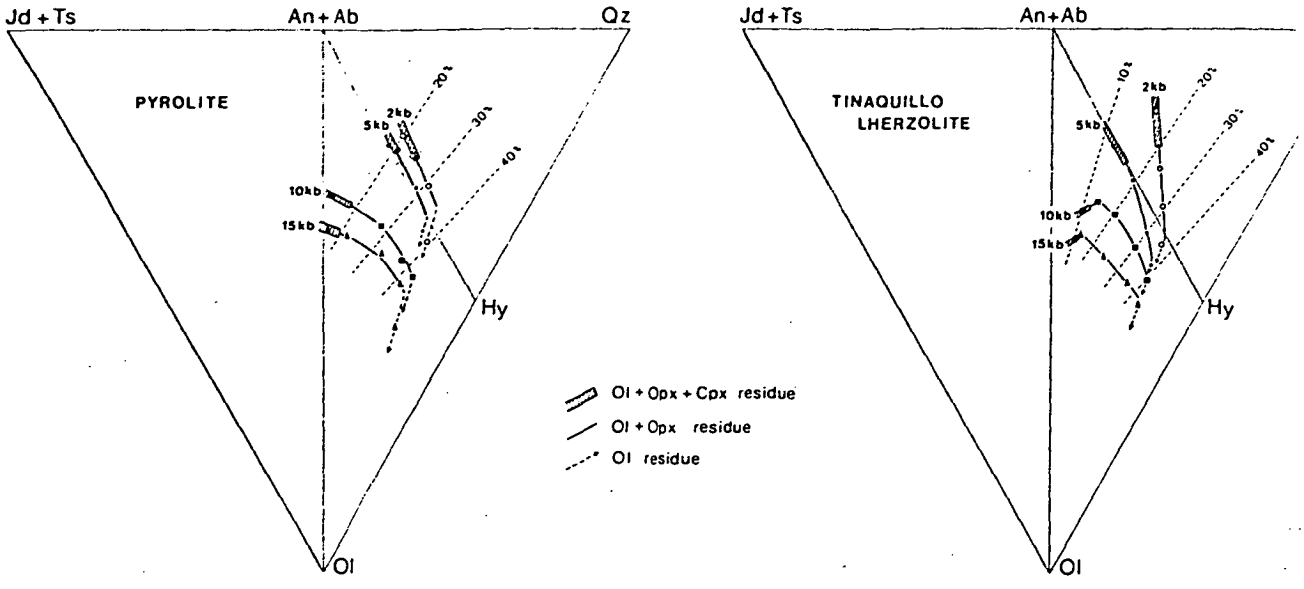

Fig. 8. Equilibrium melt composition plotted on the surface (Jadeite + Ca-Tschermak's silicate) – Olivine – Quartz. Co-ordinates calculate from the Ne, Ab, An, Hy, Ol, Qz components of the molecular norm as follows: Jd + Ts = Ab + An + Ne; Qz = Ab + An − Ne + Hy/2 Ol = Ol + Hy/2. *Dashed lines* indicate percent melting

tents and the degree of silica saturation (at 10 kb and 15 kb) increase with increasing degree of melting to a maximum at, or near, the orthopyroxene-out boundary, then decrease as the liquid becomes more magnesian by melting of residual olivine. MgO contents increase sharply as the residue becomes more refractory at higher degrees of melting. Al_2O_3 contents decrease regularly with increasing degree of melting as do Ti, Na, and K which are readily partitioned into the melt. CaO contents increase as the liquid moves with increasing degree of melting from the olivine – two pyroxene residue field to the olivine-orthopyroxene field but then decrease, following the elimination of calcic clinopyroxene as a residual phase. The Al_2O_3/CaO ratio, therefore, changes with percent partial melting: at low degrees of partial melting (olivine, orthopyroxene and clinopyroxene in the residue) the Al_2O_3/CaO ratio of the liquid is higher than that of the source peridotite, whereas at high degrees of melting (olivine or olivine + minor orthopyroxene residual) the Al_2O_3/CaO ratio of the liquid is constant and closely matches that of the source peridotite. Similarly the Al_2O_3/TiO_2 and CaO/TiO_2 ratios increase with increasing degree of partial melting until the ratio of the source peridotite is reached, as predicted by Sun and Nesbitt (1977). For pyrolite the Al_2O_3/TiO_2 ratios range from 4 to 5, and CaO/TiO_2 ratios from 3 to 4, and are generally lower than commonly observed in 'primitive' magmas from either oceanic island or ocean floor tholeiites, reflecting the high TiO_2 content of the pyrolite composition based on Hawaiian tholeiite.

Partial melting trends are well illustrated on the normative (Jadeite + Tschermak's silicate) – Quartz – Olivine diagram (Green 1970) which approximates a plane at ~20% diopside parallel to the base of the 'Basalt Tetrahedron' (Qz-Fo-Ne-Di). The equilibrium partial melts (data plotted in molecular norms) define curvilinear melting paths (Fig. 8a) which show an initial trend towards increasingly hypersthene-normative compositions due to progressive melting of pyroxene from the residue. Liquids formed by high degrees of melting lie on an olivine control line since olivine is the only residual phase. The melting trends clearly demonstrate the increasingly olivine-normative nature of partial melts at high pressure (i.e., 10 kb liquids are more *hy*-normative than those at 15 kb) and show the extension of partial melts at low pressure into the quartz-normative field.

It is clear from the trends that liquids derived by lower degrees of partial melting at high pressure will cross the critical plane of silica undersaturation to alkaline compositions. This accords with previous studies which suggested that alkali olivine basalt could be derived by approximately 10–15% melting of pyrolite at pressures greater than 10 kb (Green and Ringwood 1967a; Green 1970, 1971) under dry conditions or with small contents of H_2O and CO_2.

Partial melts at low pressure, however, do not trend toward the critical plane of silica undersaturation, and low degree (< 10%) partial melts will be saturated to oversaturated in silica, probably aluminous quartz tholeiite, in equilibrium with residual olivine, orthopyroxene, clinopyroxene, plagioclase

and chrome spinel. At high degrees of partial melting at low pressure, quartz tholeiite liquids cross the plane of silica saturation to olivine normative compositions.

6.2 Tinaquillo Lherzolite

Partial melts from Tinaquillo lherzolite at 15 kb range from olivine tholeiite Mg_{73} at approximately 11% melting with residual olivine, orthopyroxene, clinopyroxene and chrome spinel though tholeiitic picrite Mg_{77} with residual olivine, orthopyroxene and chrome spinel to komatiite Mg_{84} at about 35–45% melting in equilibrium with residual olivine.

Liquids at 10 kb show a similar compositional range over the melting interval 11 to 40% melting, resembling that at 15 kb except that 10 kb liquids contain more normative hypersthene and lower normative olivine.

Partial melts at low pressure (2 and 5 kb) and low degrees of melting are quartz tholeiite or tholeiite lying practically on the Hy-Plag-Di plane. The quartz tholeiite and tholeiite melts at low degrees of partial melting are highly aluminous e.g., 17–18 wt.% Al_2O_3 with high normative An+Ab content. With higher degrees of melting, liquids change to olivine-poor tholeiite composition.

Liquids produced by melting of Tinaquillo lherzolite, although distinctly more magnesian (e.g., Mg_{73-85} compared to Mg_{67-80}), show similar trends to those of pyrolite on the (Jd+Ts)-Qz-Ol diagram (Fig. 8b). Melt compositions tend toward hypersthene-normative compositions until orthopyroxene is eliminated, and then lie on an olivine control line by melting of residual olivine. Melts at higher pressure, 15 kb, are more olivine-normative than those at lower pressure, and melts at low pressure extend into quartz normative compositions. Compared to the partial melts from pyrolite, Tinaquillo liquids are markedly more hypersthene normative at similar degrees of melting and very poor in Ti, Na, and K reflecting the refractory nature of Tinaquillo lherzolite. For example 11% melting of Tinaquillo peridotite (at 15 kb) yields an olivine tholeiite whereas the same amount of melting of pyrolite will produce an alkali basalt. The more *hy*-normative nature of the Tinaquillo liquids is clearly demonstrated on the (Jd+Ts)-Qz-Ol diagram (Fig. 8b). Although, like pyrolite melts, the Tinaquillo liquids trend toward the critical plane of silica undersaturation, the 11% melts are well displaced from it. It appears, therefore, that alkaline liquids can only be obtained from refractory peridotites like Tinaquillo at very low degrees of melting (<5%?) at high pressure (≧20 kb). In addition, the very low abundances of incompatible elements (especially REE) in Tinaquillo lherzolite (Philpotts et al. 1972) argue that alkali basalts cannot be derived from depleted lherzolites similar to Tinaquillo lherzolite.

6.3 Comparison With Basalt Melting Studies

Reversal of the calculated equilibrium melts i.e. crystallization of each of the liquids at the particular P and T conditions, presents a formidable task. However, previous melting studies on a range of basaltic compositions provide a comparison for the calculated partial melts. The results of the complementary studies are broadly consistent but differ in detail of liquid compositions (compare Fig. 8 with Fig. 5, Green 1970 or Fig. 3, Green 1976).

Green (1970, 1971) inferred from available anhydrous melting studies on olivine tholeiite and high-alumina tholeiite compositions (Green and Ringwood 1967a; T.H. Green et al. 1968) that liquids with olivine, orthopyroxene and clinopyroxene as liquidus phases at 9 kb contained ~10–15% normative olivine, 10–15% normative hypersthene and high Al_2O_3 content (15–16 wt.%), whereas liquids with olivine and orthopyroxene only as liquidus phases have higher normative hypersthene and olivine, and lower Al_2O_3 content. These studies also suggested that basalts with olivine and orthopyroxene on their liquidi contained approximately 20% normative olivine, 12–14% normative hypersthene and 13–14 wt.% Al_2O_3 at 12 kb; ~25% normative olivine, ~12% normative hypersthene and 12–13 wt.% Al_2O_3 at 15–16 kb; and ~28% normative olivine, ~12% normative hypersthene at 18 kb (Green 1970, 1971).

In comparison, data from the partial melting of pyrolite indicate that olivine tholeiite melts at 10 kb are in equilibrium with residual olivine and orthopyroxene and, although they contain 12–15% normative olivine, they are somewhat richer in normative hypersthene and have lower Al_2O_3 contents than inferred from the basalt crystallization data. This study also indicates that partial melts of pyrolite at 10 kb in equilibrium with residual olivine, orthopyroxene *and clinopyroxene* are of olivine basalt composition. Similarly, partial melting of pyrolite at 15 kb produces olivine tholeiite liquids with less normative olivine (15–20%) and less Al_2O_3 (10–12.5 wt.%) than implied by the basalt crystallization studies. The derivation of alkali olivine basalt at low degrees of partial melting at pressure ≧15 kb leaving residual olivine, orthopyroxene, clinopyroxene and spinel – also supported by the melting study by Thompson (1974) on a relatively primitive alkali olivine basalt from Skye (Mg=65, ~3% normative Ne) – is supported

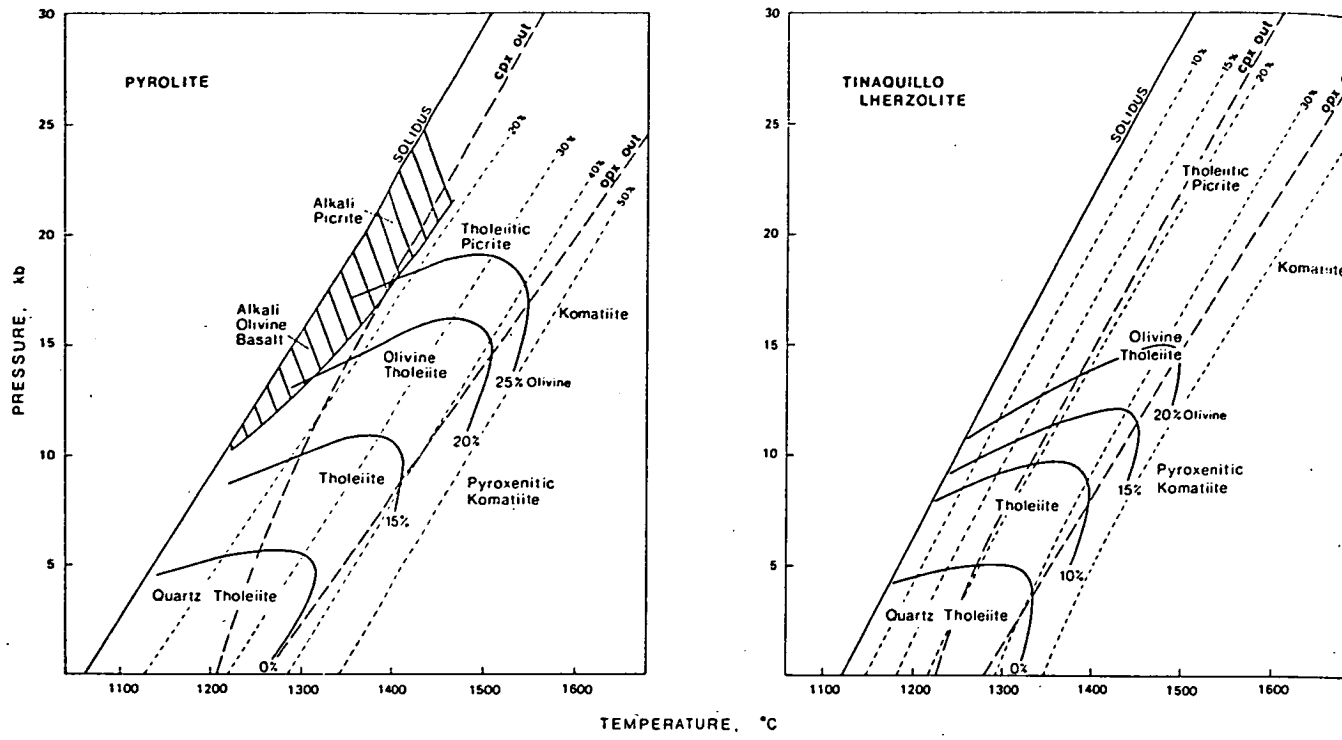

Fig. 9. *P-T* diagram for partial melting of pyrolite and Tinaquillo lherzolite indicating compositions of liquids generated. *Long-dashed lines* indicate disappearance of residual phases, *short-dashed lines* indicate percentage melting, and *solid lines* indicate percent normative olivine in the melt

by the present study. However our data do not directly bear on the genesis of more undersaturated rocks since it is now well established that such magmas are generated in presence of H_2O, and, for more undersaturated rocks, CO_2 (e.g., Green 1970; 1971; Eggler 1974, 1978; Brey and Green 1975).

The derivation of alkali olivine basalt at low degrees of melting is restricted to pressures > 10 kb, and is favoured by source peridotites with high incompatible element content. At lower pressures (< 10 kb), liquids are enriched in Al_2O_3 and, for low degrees of melting, have high Al_2O_3/CaO ratios – this is consistent with the pattern predicted from the basalt melting studies, and reflects the low Al_2O_3 content of residual pyroxenes at low pressure. However, the effect is most evident in quartz tholeiites and olivine-poor tholeiites, and does not produce liquids resembling ocean-floor tholeiites with ~10% olivine and 15–17% Al_2O_3. Thus, the earlier model for derivation of ocean floor tholeiites (Green and Ringwood 1967a; Green 1971), involving segregation of high alumina olivine tholeiite magmas at about 30 km depth, has been abandoned in the light of the new data presented here and in recent studies of ocean-floor basalts (Green et al. 1979; Jaques and Green, unpublished data).

The melting studies on both peridotite and basalt are in agreement that melts become more olivine normative at higher pressure. We suggest that approximately 20–30% melting of pyrolite and lherzolite similar to Tinaquillo lherzolite at 20 kb will produce olivine-rich tholeiite and tholeiitic picrite with approximately 25% normative olivine. Studies by Green et al. (1979) and Stolper (1980) have shown that primary picritic magmas of this composition are likely parents to high alumina olivine tholeiites (mid-ocean ridge basalts) by separation of about 15% olivine, and that these tholeiitic picrite parents segregated at about 60–70 km depth at temperatures of about 1400°–1450° C.

6.4 Summary on Equilibrium Melt Composition

From our results and the foregoing discussion we conclude that:

1. Olivine tholeiites and tholeiitic picrites result from moderate to large degrees of partial melting (10–30% depending on the nature of the source peridotite; 20–30% for pyrolite) at pressures greater than 7–8 kb in equilibrium with olivine + orthopyroxene + chrome spinel ± clinopyroxene;

2. Partial melting at low pressure (5 kb or less) produces quartz tholeiites and tholeiites, and, at high

degrees of partial melting, silica-rich olivine-poor tholeiites resembling basaltic and pyroxenitic komatiiite. Melts at low pressure are distinctly more aluminous than those at high pressure, and, at low degrees of melting, are of high-alumina quartz tholeiite composition;

3. Alkali basalts, and more undersaturated rocks, result from less than 15% melting at pressures greater than 10 kb, and probably greater than 15 kb, to leave a residue of olivine + orthopyroxene + clinopyroxene ± spinel or garnet depending on the pressure;

4. Olivine-rich (peridotitic) komatiites result from high degrees of partial melting (>40%) at pressures greater than 10 kb to leave residual olivine, or at higher pressures, olivine + orthopyroxene.

These results are integrated in *P-T* diagrams for both pyrolite and Tinaquillo lherzolite (Fig. 9). Our results are thus consistent with evidence from trace elements which suggest that tholeiites are derived by comparatively large degrees of partial melting (20–30%), whereas alkali basalts result from less than 15 percent of partial melting (e.g., Gast 1968; Sun and Hanson 1975; Frey et al. 1978). Trace element abundances in komatiites suggest comparatively large degrees of partial melting, and, in many cases, melting of a mantle source strongly depleted in incompatible elements (e.g., Arndt 1977; Arth et al. 1977).

7. Effect of Volatiles in the Genesis of Tholeiitic Basalts

Volatiles, particularly H_2O and CO_2, exert a marked influence on melting of peridotite, affecting the character of the solidus, the stability of residual phases and the melt compositions, particularly at low degrees of melting.

The very low H_2O contents (<0.5 wt.%) and low $Fe^{3+}/(Fe^{2+}+Fe^{3+})$ of fresh basaltic glasses suggest that water is not important in the genesis of ocean floor basalts (Moore 1970; Bryan and Moore 1977; Langmuir et al. 1977). Moreover, analysis of glass-vapour inclusions in olivine and plagioclase phenocrysts quenched in glassy rims of pillow basalts from mid-ocean ridge spreading centres suggests that the source region may be virtually anhydrous (Delaney et al. 1978). Very low water contents were also found in a similar study of Hawaiian pillow lavas (Muenow et al. 1979) implying that olivine tholeiites in ocean basins in general are derived by water-undersaturated melting of a nearly anhydrous upper mantle. Our experimental study under anhydrous conditions is therefore directly appropriate to the genesis of these basalts.

Our results can be compared with those for water-saturated melting of pyrolite. Since the principal effect of water-saturated melting, at moderate to large degrees of melting, is to expand the field of olivine (Kushiro 1972), the silica content of the equilibrium melts under anhydrous conditions may be taken as a *minimum* for similar degrees of melting under hydrous conditions. Comparison of the anhydrous partial melts of pyrolite (Table 4) with those from hydrous melting of pyrolite (Green 1976b; Nicholls 1974) shows that for similar degrees of partial melting the hydrous melts are distinctly more siliceous, and lower in CaO, MgO, and FeO, due to expansion of the field of olivine and of diopside at the expense of orthopyroxene. For example, 28% melting of pyrolite under anhydrous conditions at 10 kb produces an olivine tholeiite (12% normative *Ol*, 50 wt.% SiO_2), whereas 28% of pyrolite under water-saturated conditions produces a magnesian quartz tholeiite containing ~9% normative quartz and ~56 wt.% SiO_2 (Green 1973, 1976b). At lower pressure, 5 kb, 25% dry melting produces a quartz tholeiite with ~1% normative quartz (Table 4) whereas 25% melting under water-saturated conditions produces a magnesian 'andesite' with ~15% normative quartz (Nicholls 1974). In both these examples the hydrous melt is distinctly more siliceous, containing about 6 wt.% more SiO_2 than an equivalent melt under anhydrous conditions. The anhydrous melting data therefore provide a useful comparison with previous studies of hydrous melting of peridotite.

8. Partial Melting and the Oceanic Crust-Ophiolite Model

Popular models for the formation of ocean crust (e.g., Cann 1974; Christensen and Salisbury 1975; Dewey and Kidd 1977) equate ophiolites with oceanic crust generated at present day spreading centres, and regard the various lithologies of both as cogenetic. Thus, the layered cumulate gabbro and peridotite of oceanic layer 3 and ophiolites are generally regarded as accumulation of phases involved in low pressure crystal fractionation of the overlying basaltic lavas in a magma chambers(s) beneath an axial zone of crustal dilation (as evidenced by dyke swarms). The tectonite harzburgite-dunite of ophiolites is generally interpreted as the refractory residue remaining after partial melting which generated the primitive basalts of the pillow lavas.

A consequence of ophiolite analogue models for oceanic crust is the implication that partial melting and magma segregation occurred at shallow depth. However, models invoking shallow segregation of MORB (high alumina olivine tholeiites) are at vari-

ance with the results of experimental petrology. We have shown in this work that partial melting of peridotite at shallow depths within the plagioclase peridotite field (25 km or less) will produce quartz tholeiite or olivine-poor tholeiite and *not* MORB-type olivine tholeiite magmas. Comparisons of the 5–10 kb liquids determined in this study with the most Mg-rich glasses of MORB show that the latter are richer in normative olivine, diopside and anorthite. In a novel experimental study aimed at investigating the origin of MORB, Stolper (1980) has independently reached a similar conclusion. Melting studies on primitive MORB high-alumina olivine tholeiites place the depth of magma segregation for their parent tholeiitic picrites at 60–70 km (Green et al. 1979). Residual orthopyroxene from tholeiitic picrite segregation at 60–70 km contains relatively high Al_2O_3 and CaO contents and thus the residual peridotite from tholeiitic picrite extraction will recrystallize at lower temperature to spinel lherzolite rather than highly refractory harzburgite. In addition, there is a major discrepancy in the nature of near-liquidus phases for olivine tholeiites and cumulate sequences in ophiolites, as basalts such as DSDP 3–18 (or their picritic parents) are incapable of yielding cumulate sequences containing abundant magnesian orthopyroxene (Mg_{87-90}) and highly calcic plagioclase such as occur in a number of ophiolites (e.g., England and Davies 1973; Church and Riccio 1977; Coleman 1977), and in stratiform masses in the ocean basins (e.g., Hodges and Papike 1976). On these grounds, Green et al. (1979) proposed that such ophiolite cumulate sequences crystallized from magnesian lavas characterized by high SiO_2 contents (> 50 wt.% SiO_2, low normative olivine) and high CaO/Na_2O ratio, and suggested that these magmas might arise by second-stage melting of a refractory peridotite diapir at shallow depth.

Duncan and Green (1980) have suggested that examples of such 2nd stage melting may include the Ti-poor lavas of the Troodos Complex (Smewing et al. 1975; Simonian and Gass 1978). Our data for the melting of Tinaquillo peridotite, a relatively refractory lherzolite inferred to have been depleted by a previous melting event, show that Ti-poor magnesian quartz tholeiites with high Al_2O_3/TiO_2 ratios can be generated by anhydrous melting of depleted peridotite at low pressure. We believe that the Ti-poor silica-rich basalts of the Upper Pillow Lavas of the Troodos complex are comparable to the magnesian quartz tholeiite liquids in our anhydrous melting experiments at low pressure, and differ significantly from the more silica-rich high-Mg andesites or 'bonínites', which may represent water-saturated melting of refractory peridotite at shallow depth (Green 1973, 1976b). Magnesian quartz tholeiites or olivine-poor tholeiites such as the Ti-poor, severely LREE depleted lavas of Troodos (UPL) show no evidence of excess water, or of addition of an incompatible element enriched fluid, and it is suggested that they may arise by anhydrous melting and magma segregation from a depleted peridotite diapir at shallow level. (cf. Duncan and Green 1980). A similar model has been proposed by Smewing et al. (1975) and Smewing and Potts (1976) who invoked a continuous melting process to explain the progressive depletion in incompatible elements (especially REE) of the Troodos Upper Pillow Lavas.

9. Partial Melting and Continental Flood Basalts

Continental flood basalts are characterized by an overall chemical uniformity, notably high SiO_2 and Al_2O_3 and low MgO contents; many are more appropriately termed iron-enriched tholeiitic andesites (e.g., Thompson 1975; Wilkinson and Binns 1977). A feature of most flood basalts is their enrichment in incompatible elements and high $^{87}Sr/^{86}Sr$ ratios relative to ocean floor tholeiites. Most flood basalts have Mg-values too low to be considered primary magmas derived from magnesian (pyrolite-like) mantle peridotite, and extensive olivine fractionation is commonly invoked in their petrogenesis (e.g., Cox 1972; McDougall 1976). However, mafic olivine-rich lavas have been documented in several areas of flood volcanism, chiefly the Tertiary volcanic province of Baffin Island – West Greenland (Clarke 1970; Clarke and Pedersen 1976) and the Nuanetsi Province of Rhodesia (Cox 1972; Cox and Jamieson 1974).

Clarke (1970) and Clarke and Pedersen (1976) suggested from the abundance of olivine microphenocrysts and skeletal olivine that the mafic olivine tholeiites of the Baffin Island – West Greenland region represent primary magmas. Clarke (1970) inferred from comparison with the phase relations in model peridotite projections that Baffin Island olivine tholeiites containing approximately 18–20 wt.% MgO and 27–30% normative olivine might represent primary magmas derived from partial melting of garnet peridotite at about 30 kb. Associated mafic picrites and more felsic tholeiites were considered to form by olivine accumulation and fractionation respectively (Clarke 1970). Compared to the partial melts presented here, the Baffin Island – West Greenland olivine tholeiites are lower in SiO_2 and richer in normative olivine, suggesting segregation at greater depth. Similarly, they are slightly more olivine normative than the tholeiitic picrite composition studied experimentally by Green et al. (1979) which segregated at about 60–70 km, suggesting that they may,

as suggested by Clarke (1970), represent primary magmas segregated at about 80–100 km depth.

Cox (1972) and Cox and Jamieson (1974) inferred that the Nuanetsi olivine tholeiites containing ~15 wt.% MgO at the base of the Karroo might represent primary magmas segregated from residual harzburgite at about 35 km depth since many of the lavas had olivine and orthopyroxene as liquidus and near-liquidus phases at 7–10 kb. While, like the Baffin Island – West Greenland basalts, the Nuanetsi lavas show strong evidence of olivine control, Cox and Jamieson (1974) invoke polybaric crystal fractionation of both olivine and orthopyroxene. Many of the Nuanetsi lavas containing 12–16 wt.% MgO compare with the pyrolite partial melts at 10 kb in equilibrium with olivine and orthopyroxene (although Al_2O_3 and CaO contents are higher in the experimental melts), suggesting that they might be derived at comparatively shallow depths, 25–40 km, by about 20–35% partial melting. The high abundances of incompatible elements, especially K_2O, in the Nuanetsi lavas indicate that they were derived from a mantle more enriched in incompatible elements (especially K_2O) than pyrolite.

10. Basaltic Komatiites

Pyroxenitic and basaltic komatiites (Arndt et al. 1977), high-Mg basalts (Williams 1972) or spinifex-textured basalts (Sun and Nesbitt 1978a), a group of lavas characterized by high SiO_2 contents (50–55 wt.% SiO_2; low normative olivine or normative quartz) and high MgO contents (10–20 wt.%) are intermediate between peridotitic komatiites and tholeiitic basalts. Opinion is divided as to whether these lavas represent primary magmas formed by lower degrees of melting than peridotitic komatiites, or whether they represent differentiates of more peridotitic primary magmas (e.g., Arth et al. 1978; Sun and Nesbitt 1978a). Compositionally many of these magnesian basalts resemble the magnesian olivine poor tholeiites and quartz tholeiites in our low pressure melting experiments (except for TiO_2, Na_2O, and K_2O), suggesting that they might represent primary magmas segregating from residual peridotite at about 25–40% melting in the plagioclase peridotite stability field, probably ~5 kb.

11. Conclusions

(1) Equilibrium melting under anhydrous conditions results in progressive elimination of phases with increasing T. Four main fields are recognized; from the solidus these are: ol + opx + cpx + aluminous phase (plag, sp or ga) + L; ol + opx + cpx + Cr spinel + L; ol + opx + Cr spinel + L; ol ± Cr spinel + L. The residual phases progressively change composition to more refractory compositions with increasing proportion of coexisting melt i.e. increasing 100 Mg/(Mg + Fe) and Cr/(Cr + Al) ratios, decreasing Al_2O_3 and CaO in pyroxene etc.;

(2) The degree of melting increases rapidly immediately above the solidus (up to 10% melting occurs within 25–30° C of the solidus) and then increases in roughly linear form with increasing T;

(3) Equilibrium melt compositions from pyrolite within the spinel peridotite field range from alkali olivine basalt (< 15% melting) through olivine tholeiite (20–30%) and picrite to komatiite (40–60% melting). Melting in the plagioclase-peridotite field produces magnesian quartz tholeiite and olivine-poor tholeiite with high alumina contents due to expansion of the primary field of olivine at low pressure. Liquids in equilibrium with olivine, pyroxenes and an aluminous phase (plagioclase, Al-spinel or garnet) result from low degrees of partial melting (< 10%) and are enriched in incompatible elements;

(4) Melts from spinel lherzolite are more silica saturated than those from pyrolite for similar degrees of melting. This is primarily a result of higher alkali contents in pyrolite composition. Melts within the spinel peridotite field range from olivine tholeiite through tholeiitic picrite to komatiite with increasing degree of melting. Although similar (in major elements) olivine tholeiite magmas can be derived from both pyrolite and Tinaquillo lherzolite, the degree of melting for such liquids is lower and the depth of melting is greater for the Tinaquillo lherzolite parent;

(5) The results of the peridotite melting study support melting studies on 'primitive' high-alumina olivine tholeiites from the ocean floor, and indicate that such magmas result from 10–30% melting (depending on the peridotite source composition) at depths of 60–70 km. The liquidus and near-liquidus phase relations of such basalts are not consistent with oceanic crust models based on the Troodos, Papua, and Betts Cove ophiolites, and the primary magmas which generated the tectonite and accumulate sequences of these ophiolites are considered to be magnesian quartz tholeiite or olivine-poor tholeiite formed by partial melting and magma segregation from refractory peridotite in the plagioclase-peridotite field (10–25 km depth);

(6) Like most MORB, tholeiitic basalts in other tectonic regions appear to have undergone low pressure crystal-fractionation. Two examples of primary magmas in continental and continental-margin areas may be the olivine-rich lavas of Baffin Island – West

Greenland, and of the Nuanetsi province. Our partial melting data are consistent with the derivation of the Baffin Island picritic tholeiites (~30% normative olivine) by partial melting of garnet peridotite (Clarke 1970), and the Nuanetsi olivine tholeiites (10–15% normative olivine) by 20–35% melting at 25–40 km depth:

(7) Basaltic komatiites (12–20% MgO, <5% normative olivine) may be primary magmas derived by 25–40% melting of plagioclase peridotite, magma segregation occurring at 15–25 km.

Acknowledgements. We thank W.O. Hibberson, K.L. Harris, W.C. Doran, and P. Robinson for technical assistance and Dr. A. McKee and B.J. Griffin for instruction in the use of the SEM-microprobe at Hobart. N.G. Ware kindly provided access to the TPD probe at ANU Canberra for comparative studies. Jaques gratefully acknowledges receipt of an Australian Government Scholarship. The project was supported by ARGC grant to D.H. Green. R.J. Arculus and J. Knutson are thanked for comments on the manuscript. Jaques publishes with the permission of the Director, Bureau of Mineral Resources, Geology and Geophysics.

References

Arndt NT (1977) Ultrabasic magmas and high degree melting of the mantle. Contrib Mineral Petrol 61:205–221

Arndt NT, Naldrett AJ, Pyke DR (1977) Komatiitic and iron-rich tholeiitic lavas of Munro Township, northeast Ontario. J Petrol 18:319–369

Arth JG, Arndt NT, Naldrett AJ (1977) Genesis of Archaean komatiites – trace element evidence from Munro Township, Ontario. Geology 5:590–594

Atkins FB (1969) Pyroxenes of the Bushveld Intrusion, South Africa. J Petrol 10:222–249

Bottinga Y, Weill FF (1970) Densities of liquid silicate systems calculated from partial molar volumes of oxide components. Am J Sci 269:169–192

Brey G, Green DH (1975) The role of CO_2 in the genesis of olivine melilitite. Contrib Mineral Petrol 49:93–103

Bryan WB, Moore JG (1977) Compositional variations of young basalts in the Mid-Atlantic Ridge rift valley near lat. 36°49'N. Geol Soc Am Bull 88:556–570

Bryan WB, Thompson G, Frey FA, Dickey JS (1976) Inferred geological settings and differentiation in basalts from the Deep Sea Drilling Project. J Geophys Res 81:4285–4304

Cann JR (1974) A model for oceanic crustal structure developed. Geophys J R Astron Soc 39:169–184

Cawthorn RG, Ford CE, Biggar GM, Bravo MS, Clarke DB (1973) Determination of the liquid composition in experimental samples: discrepancies between microprobe analyses and other methods. Earth Planet Sci Lett 21:1–5

Christensen NI, Salisbury MH (1975) Structure and constitution of the lower oceanic crust. Rev Geophys Space Phys 13:57–86

Church WR, Riccio L (1977) Fractionation trends in the Bay of Islands ophiolite of Newfoundland: polycyclic cumulate sequences in ophiolites and their classification. Can J Earth Sci 14:1156–1165

Clarke DB (1970) Tertiary basalts of Baffin Bay: possible primary magma from the mantle. Contrib Mineral Petrol 25:203–224

Clarke DB, Pedersen AK (1976) Tertiary volcanic province of West Greenland. In: A Escher, WS Watts (eds) Geology of Greenland. Geol Surv Greenland, pp 365–385

Coleman RG (1977) Ophiolites. Springer-Verlag, Berlin

Cox KG (1972) The Karroo volcanic cycle. J Geol Soc London 128:311–336

Cox KG, Jamieson BG (1974) The olivine-rich lavas of Nuanetsi: a study of polybaric magmatic evolution. J Petrol 14:269–301

Delaney JR, Muenow D, Ganguly J, Royce D (1977) Anhydrous glass-vapour inclusions from phenocrysts in oceanic tholeiite pillow basalts. Trans Am Geophys Union 58:530

Dewey JF, Kidd WSF (1977) Geometry of plate accretion. Geol Soc Am Bull 88:960–968

Dickey JS, Yoder HS Jr (1972) Partitioning of chromium and aluminium between clinopyroxene and spinel. Carnegie Inst Washington Yearb 71:384–392

Duncan RA, Green DH (1980) The role of multi-stage melting in the formation of oceanic crust. Geology 8:22–28

Eggler DH (1974) Volatiles in ultrabasic and derivative rock systems. Carnegie Inst Washington Yearb 73:215–224

Eggler DH (1978) The effect of CO_2 upon partial melting of peridotite in the system Na_2O-CaO-Al_2O_3-MgO-SiO_2-CO_2 to 35 kb, with an analysis of melting in a peridotite-H_2O-CO_2 system. Am J Sci 278:305–343

England RN, Davies HL (1973) Mineralogy of ultramafic cumulates and tectonites from eastern Papua. Earth Planet Sci Lett 17:416–425

Frey FA, Green DH (1974) The mineralogy, geochemistry and origin of lherzolite inclusions in Victorian basanites. Geochim Cosmochim Acta 38:1023–1059

Frey FA, Green DH, Roy SD (1978) Integrated models of basalt petrogenesis: a study of quartz tholeiites to olivine melilitites from S.E. Australia utilizing geochemical and experimental petrological data. J Petrol 19:463–513

Frey FA, Prinz M (1977) Ultramafic inclusions from San Carlos, Arizona: Petrologic and geochemical data bearing on their petrogenesis. Earth Planet Sci Lett 38:129–176

Gast PW (1968) Trace element fractionation and the origin of tholeiitic and alkaline magma types. Geochim Cosmochim Acta 32:1057–1086

Green DH (1963) Alumina content of enstatite in a Venezuelan high temperature peridotite. Geol Soc Am Bull 74:1397–1402

Green DH (1970) The origin of basaltic and nephelinitic magmas. Trans Leicester Lit Phil Soc 64:26–54

Green DH (1971) Compositions of basaltic magmas as indicators of conditions of origin; application to oceanic volcanism. Phil Trans R Soc London 268A: 707–725

Green DH (1973a) Contrasted melting relations in a pyrolite upper mantle under mid-oceanic ridge, stable crust and island arc environments. Tectonophysics 17:285–297

Green DH (1973b) Experimental melting studies on a model upper mantle composition at high pressure under water-saturated and water-undersaturated conditions. Earth Planet Sci Lett 19:37–53

Green DH (1976a) Experimental petrology in Australia – A review. Earth Sci Rev 12:99–138

Green DH (1976b) Experimental testing of 'equilibrium' partial melting of peridotite under water-saturated, high pressure conditions. Can Mineral 14:255–268

Green DH (1976c) Orthopyroxene in the lunar interior and constraints on early lunar differentiation. Lunar Sci VII:336–338

Green DH, Hibberson WO, Jaques AL (1979) Petrogenesis of mid-ocean ridge basalts. In: MW McElhinny (ed) The Earth: its origin, structure and evolution. Academic Press, pp 265–299

Green DH, Lieberman RC (1976) Phase equilibria and elastic properties of a pyrolite model for the oceanic upper mantle. Tectonophysics 32:61–92

Green DH, Nicholls IA, Viljoen M, Viljoen R (1975) Experimental demonstration of the existence of peridotite liquids in earliest Archaean magmatism. Geology 3:11–14
Green DH, Ringwood AE (1967a) The genesis of basaltic magmas. Contrib Mineral Petrol 15:103–190
Green DH, Ringwood AE (1967b) The stability fields of aluminous pyroxene peridotite and garnet peridotite and their relevance in upper mantle structure Earth Planet Sci Lett 3:151–160
Green DH, Ringwood AE (1970) Mineralogy of peridotitic compositions under upper mantle conditions. Phys Earth Planet Inter 3:359–371
Green TH, Green DH, Ringwood AE (1967) The origin of high alumina basalts and their relationships to quartz tholeiites and alkali basalts. Earth Planet Sci Lett 2:41–51
Harris PG, Reay A, White IG (1967) Chemical composition of the upper mantle. J Geophys Res 72:6359–6369
Hensen BJ (1973) Pyroxenes and garnets as geothermometers and geobarometers. Carnegie Inst Washington Yearb 72:527–534
Hodges FN, Papike JJ (1976) DSDP Site 334: magmatic cumulates from oceanic layer 3. J Geophys Res 81:4135–4151
Ito K, Kennedy GC (1967) Melting and phase relations in a natural peridotite to 40 kilobars. Am J Sci 265:519–538
Jaques AL, Green DH (1979) Determination of liquid compositions in experimental, high pressure melting of peridotite. Am Mineral 64:1312–1321
Kay R, Hubbard NJ, Gast PW (1970) Chemical characteristics of ocean ridge volcanic rocks. J Geophys Res 75:1585–1613
Kuno H, Aoki K (1970) Chemistry of ultramafic nodules and their bearing on the origin of basaltic magmas. Phys Earth Planet Int 3:273–301
Kushiro I (1969) The system forsterite – diopside – silica with and without water at high pressures. Am J Sci 267A:269–294
Kushiro I (1972) Effect of water on the composition of magmas formed at high pressures. J Petrol 13:311–334
Kushiro I, Yoder HS, Mysen BO (1977) Viscosities of basalt and andesite melts at high pressures. J Geophys Res 81:6351–6356
Langmuir CH, Bender JB, Bence AE, Hanson GN, Taylor SR (1977) Petrogenesis of basalts from the FAMOUS area: Mid-Atlantic Ridge. Earth Planet Sci Lett 36:133–156
Lindsley DH, Dixon SA (1976) Diopside-enstatite equilibria at 850°–1400° C, 5–35 kb. Am J Sci 276:1285–1301
Maaloe S, Aoki K (1977) The major element composition of the upper mantle estimated from the composition of lherzolites. Contrib Mineral Petrol 64:161–173
MacGregor ID (1974) The system MgO-Al_2O_3-SiO_2: Solubility of Al_2O_3 in enstatite for spinel and garnet peridotite compositions. Am Mineral 50:110–119
Matsui Y, Nishazawa O (1974) Iron (II)-magnesium exchange equilibrium between olivine and calcium-free pyroxene and a temperature range 800° to 1300° C. Bull Soc Mineral Cristallogr 97:122–130
McDougall I (1976) Geochemistry and origin of basalt of the Columbia River Group, Oregon and Washington. Geol Soc Am Bull 87:777–792
Merrill RB, Wyllie PJ (1973) Absorption of iron by platinum capsules in high pressure rock melting experiments. Am Mineral 58:16–20
Moore JG (1970) Water content of basalt erupted on the ocean floor. Contrib Mineral Petrol 28:272–279
Mori T (1978) Experimental study of pyroxene equilibria in the system CaO-MgO-FeO-SiO_2. J Petrol 19:45–65
Mori T, Green DH (1975) Pyroxenes in the system $Mg_2Si_2O_6$-$CaMgSi_2O_6$ at high pressure. Earth Planet Sci Lett 26:277–286
Mori T, Green DH (1978) Laboratory duplication of phase equilibria observed in natural garnet lherzolites. J Geol 86:83–97
Muenow DW, Graham DG, Liu NWK, Delaney JR (1979) Water poor glass-vapour inclusions in phenocrysts from Hawaiian tholeiitic pillow basalts. Earth Planet Sci Lett 42:71–76
Mysen BO, Boettcher AL (1975) Melting of a hydrous mantle: II. Geochemistry of crystals and liquids formed by anatexis of mantle peridotite at high pressures and high temperatures as a function of controlled activities of water, hydrogen, and carbon dioxide. J Petrol 16:549–593
Mysen BO, Kushiro I (1977) Compositional variations of coexisting phases with degree of melting of peridotite in the upper mantle. Am Mineral 62:843–865
Nicholls IA (1974) Liquids in equilibrium with peridotitic mineral assemblages at high water pressures. Contrib Mineral Petrol 45:289–316
Nicholls IA, Ringwood AE (1973) Effect of water on olivine stability in tholeiites and the production of silica saturated magmas in the island arc environment. J Geol 81:285–300
Obata M (1976) The solubility of Al_2O_3 in orthopyroxenes in spinel and plagioclase peridotites and spinel pyroxenite. Am Mineral 61:804–816
O'Hara MJ (1968) The bearing of phase equilibria studies in synthetic and natural systems on the origin and evolution of basic and ultrabasic rocks. Earth-Sci Rev 4:69–133
Philpotts JA, Schnetzler CC, Thomas HH (1972) Petrogenetic implications of some new geochemical data on eclogitic and ultrabasic inclusions. Geochim Cosmochim Acta 36:1131–1166
Presnall DC (1969) The geometrical analysis of partial fusion. Am J Sci 267:1178–1194
Presnall DC (1976) Alumina content of enstatite as a geobarometer for plagioclase and spinel lherzolites. Am Mineral 61:582–588
Presnall DC, Dixon JR, O'Donnell Th, Dixon SA (1979) Generation of mid-ocean ridge tholeiites. J Petrol 20:3–36
Reed SJB, Ware NG (1975) Quantitative electron microprobe analysis of silicates using energy-dispersive x-ray spectrometry. J Petrol 16:499–519
Ringwood AE (1966) The chemical composition and origin of the earth. In: PM Hurley (ed) Advances in Earth Science, pp 287–356
Ringwood AE (1975) Composition and petrology of the earth's mantle. New York, McGraw-Hill
Roeder PL, Emslie RF (1970) Olivine-liquid equilibrium. Contrib Mineral Petrol 29:275–289
Simonian KO, Gass IG (1978) Arakapas fault belt, Cyprus: A fossil transform fault. Geol Soc Am Bull 89:1220–1230
Smewing JD, Potts PJ (1976) Rare-earth abundances in basalts and metabasalts from the Troodos Massif, Cyprus. Contrib Mineral Petrol 57:245–258
Smewing JD, Simonian KO, Gass IG (1975) Metabasalts from the Troodos Massif, Cyprus: Genetic implication deduced from petrography and trace element geochemistry. Contrib Mineral Petrol 51:49–64
Stern CR, Wyllie PJ (1975) Effect of iron absorption by noble metal capsules on phase boundaries in rock melting experiments at 30 kb. Am Mineral 60:681–689
Stolper E (1980) A phase diagram for mid-ocean ridge basalts: preliminary results and implications for petrogenesis (in press)
Stroh JM (1976) Solubility of alumina in orthopyroxene plus spinel as a geobarometer in complex systems. Applications to spinel-bearing alpine-type peridotite. Contrib Mineral Petrol 54:173–188
Sun SS, Hanson GN (1975) Origin of Ross Island basanitoids and limitations on the heterogeneity of mantle sources for alkali basalts and nephelinites. Contrib Mineral Petrol 52:77–106
Sun SS, Nesbitt RW (1977) Chemical heterogeneity of the Archaean mantle, composition of the earth and mantle evolution. Earth Planet Sci Lett 35:429–448
Sun SS, Nesbitt RW (1978a) Petrogenesis of Archaean ultrabasic

and basic volcanics: Evidence from rare earth elements. Contrib Mineral Petrol 65:301–325

Thompson RN (1975) Primary basalts and magma genesis II. Snake River plain, Idaho, U.S.A. Contrib Mineral Petrol 52:157–164

Tröger WE (1956) Optische Bestimmung der gesteinbildenden Minerale. Teil 1. E. Schweizerbart'sche Verlagsbuchhandlung, Stuttgart

Wager LR, Brown GM (1968) Layered igneous rocks. Oliver and Boyd, London

Warner RD, Luth WC (1974) The diopside-orthoenstatite two-phase region in the system $CaMgSi_2O_6$ – $Mg_2Si_2O_6$. Am Mineral 59:98–109

Wilkinson JFG, Binns RA (1977) Relatively iron-rich lherzolite xenoliths of the Cr-Diopside suite: a guide to the primary nature of anorogenic tholeiite andesite magmas. Contrib Mineral Petrol 65:199–212

Williams DAC (1972) Archaean ultramafic, mafic and associated rocks, Mt. Monger, Western Australia. J Geol Soc Austr 19:163–188

Wood BJ, Nicholls J (1978) The thermodynamic properties of reciprocal solid solutions. Contrib Mineral Petrol 66:389–400

Wyllie PJ (1979) Kimberlite magmas from the system peridotite-H_2O-CO_2. In: FR Boyd, HOA Meyer (eds) Kimberlites, Diatremes and Diamonds: their geology, petrology and geochemistry. Proc. 2nd Int Kimberlite Conference. American Geophysical Union, Washington, pp 319–338

Wyllie PJ (1971) The dynamic earth: Text book in geosciences. John Wiley, New York

Received September 17, 1979; Accepted May 7, 1980

B33

Contrib Mineral Petrol (1986) 93:46–55

Contributions to Mineralogy and Petrology
© Springer-Verlag 1986

The effect of fluorine on phase relationships in the system $KAlSiO_4 - Mg_2SiO_4 - SiO_2$ at 28 kbar and the solution mechanism of fluorine in silicate melts

Stephen F. Foley, Wayne R. Taylor, and David H. Green
Geology Department, University of Tasmania, Box 252C, Hobart, Tasmania, Australia 7001

Abstract. Phase relationships in the system kalsilite-forsterite-quartz with fluorine added by direct substitution for oxygen were examined at 28 kb. A large liquidus field for fluorphlogopite exists with approx. 4 wt% F added to the system and the thermal stability of phlogopite is increased by ~300° C relative to the water saturated system. Fluorine expands the phase volume of enstatite relative to forsterite so that the peritectic point PHL+EN+FO+L, a model for melting of a phlogopite harzburgite, lies in the silica-undersaturated field. Experimental phlogopites have excess Si which correlates with F content and are Al-deficient. The high Si contents indicate solid solution with an end member intermediate between tri- and di-octahedral micas. Glasses with compositions analogous to partial melts from phlogopite harzburgite were examined by infrared spectroscopy in the mid- and far-IR regions. Results show that fluorine polymerises the melt by bonding with all the network modifying cations K, Mg and Al. At higher F contents, but still less than 1 wt%, tetrahedral $KAlO_2$-groups are complexed by fluorine and removed from the aluminosilicate network simultaneously polymerising and increasing the Si/(Si+Al) ratio of the network. However, when HF rather than F is present, the overall effect will be to depolymerise melts due to the effect of OH released by dissolution of HF. The presence of abundant Si-F bonds is considered unlikely even in silica-rich magmas: the viscosity decrease characteristic of fluorine-bearing melts can be attributed to the formation of fluoride complexes.

Introduction

Fluorine has long been recognised as an important constituent of late-stage granitic melt-fluid systems where, along with other anionic elements, it exerts control on the distribution of economically important metals such as Sn. Experimental studies of the effect of HF on silicate melt equilibria have been restricted to silica-rich melts, where a large depression of the liquidus temperature and expansion of the quartz liquidus phase volume relative to feldspar has been found (Wyllie and Tuttle 1961; Manning et al. 1980).

The role of fluorine in basic melts has been neglected because of the generally low content of fluorine in common basaltic rocks; typically less than 500 ppm (Aoki et al. 1981; Schilling et al. 1980). However, fluorine is abundant in potassium-rich mafic rocks such as lamproites, and shows a positive correlation with potassium content (Aoki et al. 1981). The probable importance of fluorine in lamproite petrogenesis has been emphasised recently by Jaques et al. (1984), who predicted increased stability for fluormica over hydroxymica.

The system kalsilite-forsterite-quartz (Ks-Fo-Qz) was chosen for experimental studies of the fluorine effect on silicate melts because it is the potassic analogue of the base of the basalt tetrahedron of Yoder and Tilley (1962), and is thus relevant for ultrapotassic rocks. This paper reports experimental results and an investigation of the solution mechanism of fluorine in silicate melts: the implications for ultrapotassic rock genesis are discussed in a companion paper (Foley et al. in prep.).

Experiments were run at 28 kbar to enable direct comparison with the studies of Gupta and Green (in prep.) on the system Ks-Fo-Qz in volatile-free conditions and with H_2O and CO_2. The rationale behind this choice is compatibility with the earlier studies in the system nepheline-forsterite-quartz (Gupta, Green and Taylor (in prep.); Windom and Boettcher 1981). The pressure of 28 kb is taken to represent the approximate pressure at the top of the low velocity zone defined by the high pressure stability limit of pargasitic amphibole (Green and Liebermann 1976). However, there are indications that in the presence of fluorine, the stability limit of pargasite will be expanded to higher temperatures and pressures (Holloway and Ford 1975).

Experimental methods

Experiments were run in solid media piston-cylinder apparatus with 0.5 inch furnace assemblies with talc/pyrex sleeves. A 10% pressure correction was used and pressures are accurate to within 0.5 kbar. Temperatures were measured with a $Pt/Pt_{90}Rh_{10}$ thermocouple within 0.5 mm above the sample capsule and are accurate to approximately ±10° C. No correction was made for the effect of pressure on emf of the thermocouple.

Starting materials were synthetic kalsilite, Al_2O_3, MgO, SiO_2 and MgF_2. Kalsilite was prepared by sintering a mixture of K_2CO_3, Al_2O_3 and SiO_2 at 750° C for 10 h after slowly increasing the temperature from 500° C over two days to minimise loss of K_2O. MgF_2 was prepared by heating analytical reagent grade MgO in an excess of 50% HF and evaporating to dryness. The MgF_2 was then heated at 450° C for several hours to eliminate all traces of H_2O. Both kalsilite and MgF_2 were checked for purity by X ray diffraction. All starting materials were stored in a desiccator and dried thoroughly before use.

Fluorine was added as MgF_2 by direct substitution for MgO,

Offprint requests to: W.R. Taylor

i.e. by the exchange vector F_2O_{-1}. Most experiments were conducted with 4% F_2O_{-1}, meaning that 4 atom % of the oxygen in the starting composition was replaced by fluorine. This is approximately equal to 4 wt% F for the compositions used.

Minerals from Ks-Fo-Qz-F were analysed with a JEOL JXA 50A electron microprobe with integrated wavelength (F and Cl) and energy dispersive (all other elements) systems with operating conditions of 15 kV and 5×10^{-8} A. F and Cl were calibrated on synthetic MgF_2 and natural scapolite standards respectively. The Ks-Fo-Qz-H_2O analyses were made at routine EDAX operating conditions (15 kV, 7×10^{-10} A). Volatilisation of alkalis from fluormicas at the higher current was checked by reanalysing at 7×10^{-10} A, and found to be minimal. Detection limits were approximately 0.20 wt% for fluorine and 0.04 wt% for chlorine.

Results

Phase relationships

Experimental results are listed in Table 1. Phases encountered were forsterite, enstatite, phlogopite, kalsilite, sanidine and quartz, identified optically and by microprobe. Primary phlogopite was not difficult to identify: it occurred as large hexagonal plates (RI 1.54: Shell and Ivey 1969), usually with easily distinguishable thin feathery quench outgrowths. Quench crystals of phlogopite and enstatite occurred in the more Mg-rich compositions, but only phlogopite formed quench crystals from compositions outside its own primary phase field. Enstatite crystals occurred as stubby laths usually more elongate than olivines, although enstatite vs. olivine was always confirmed with the microprobe. Kalsilite, sanidine and quartz are reported only where confirmed by microprobe, since all these minerals formed lath-shaped crystals with refractive indices slightly greater than the glass. Residual MgF_2, easily recognised by its low RI (1.38), was found only in a preliminary 1,250° C run of short duration (composition 1 with 10% F_2O_{-1}; not listed in Table 1). It was absent from all other runs, which are much closer to liquidus temperatures.

Figure 1 presents the results for 4% F_2O_{-1} projected onto the Ks-Fo-Qz face from the corresponding fluorine end-members $KAlSiF_8 - Mg_2SiF_8 - SiF_4$. It is thus a prismatic projection along the F_2O_{-1} exchange vector from a plane within the prism because of the addition of fluorine by direct substitution. It is not a saturation surface projected from the apex of a tetrahedron as in the H_2O and CO_2 systems, but the differences in projection angles are not large enabling reasonable comparisons to be made. Phase boundaries were located by optical estimates of relative abundances of phases present and, in more Mg-poor compositions, by probe analyses of glasses. Glass analyses could not be used in the Mg-rich compositions (1, 2, 3, 4, 7) due to modification by quench crystal formation.

In the dry system Ks-Fo-Qz at 28 kbar MgO-rich liquids crystallise forsterite and enstatite and their compositions move towards a FO + EN + SAN + L peritectic, and from there to a PHL + SAN + KS + L eutectic in the case of silica-undersaturated compositions (Fig. 2). Both these four-phase points lie in the silica-undersaturated region delimited by the FO-SAN join. Luth (1967) studied the water-saturated Ks-Fo-Qz system at pressures up to 3 kbar. In comparison with the water-saturated system at 28 kbar, crystallisation paths are similar except for the presence of leucite at low pressures. Compositions defined by EN-SAN-PHL crystallise through the QZ + PHL + EN + L peritectic at all

Table 1. Experimental run data at 28 kb pressure

Run No.	% F	Composition	Mix	Duration (mins)	Temp. (°C)	Phases
1372	10	Ks44Fo39Qz17	1a	60	1,350	Phl, L
1373	10	Ks44Fo39Qz17	1a	45	1,450	Phl, L
1378	10	Ks44Fo39Qz17	1a	30	1,480	Ol, Phl, 2xL
1380	10	Ks44Fo39Qz17	1a	30	1,510	Phl, 2xL
1375	10	Ks44Fo39Qz17	1a	30	1,550	L
1385	4	Ks44Fo39Qz17	1	30	1,480	Ol, Phl, L
1387	4	Ks44Fo39Qz17	1	40	1,500	Ol, Phl, L
1390	4	Ks44Fo39Qz17	1	25	1,540	Ol, L
1391	4	Ks15Fo50Qz35	2	25	1,540	En, L
1393	4	Ks15Fo50Qz35	2	40	1,480	En, L
1395	4	Ks15Fo50Qz35	2	50	1,430	En, Phl, L
1399	4	Ks33Fo45Qz22	3	45	1,450	En, Phl, L
1400	4	Ks33Fo45Qz22	3	55	1,480	En, Phl, Ol, L
1401	4	Ks33Fo45Qz22	3	50	1,510	En, L
1404	4	Ks17Fo63Qz20	4	40	1,530	En, Ol, L
1407	4	Ks17Fo63Qz20	4	30	1,560	En, Ol, L
1408	4	Ks17Fo63Qz20	4	20	1,590	En, L
1409	4	Ks50Fo15Qz35	5	45	1,400	Phl, L
1412	4	Ks50Fo15Qz35	5	35	1,450	Phl, L
1413	4	Ks50Fo15Qz35	5	30	1,480	L
1419	4	Ks50Fo15Qz35	5	90	1,340	Phl, San, L
1414	4	Ks78Fo15Qz7	6	40	1,480	L
1417	4	Ks78Fo15Qz7	6	45	1,420	Phl, Ks, L
1418	4	Ks78Fo15Qz7	6	60	1,380	Phl, Ks, L
1421	4	Ks78Fo15Qz7	6	40	1,450	Phl, L
1425	4	Ks42Fo25Qz33	7	40	1,440	Phl, En, L
1427	4	Ks42Fo25Qz33	7	30	1,470	Phl, En, L
1438	4	Ks48Fo8 Qz44	8	180	1,300	Phl, L
1441	4	Ks48Fo8 Qz44	8	144	1,340	Phl, L
1449	4	Ks48Fo8 Qz44	8	800	1,240	Phl, San, L
1450	4	Ks48Fo8 Qz44	8	600	1,270	Phl, L
1455	4	Ks39Fo18Qz43	9	200	1,350	Phl, Qz, L
1457	4	Ks39Fo18Qz43	9	150	1,410	Phl, L
1458	4	Ks39Fo18Qz43	9	60	1,450	L
1459	4	Ks39Fo18Qz43	9	345	1,290	Phl, Qz, L
1469	4	Ks36Fo10Qz54	10	200	1,320	Phl, Qz, L
1473	4	Ks36Fo10Qz54	10	150	1,380	Phl, Qz, L
1475	4	Ks36Fo10Qz54	10	180	1,410	L

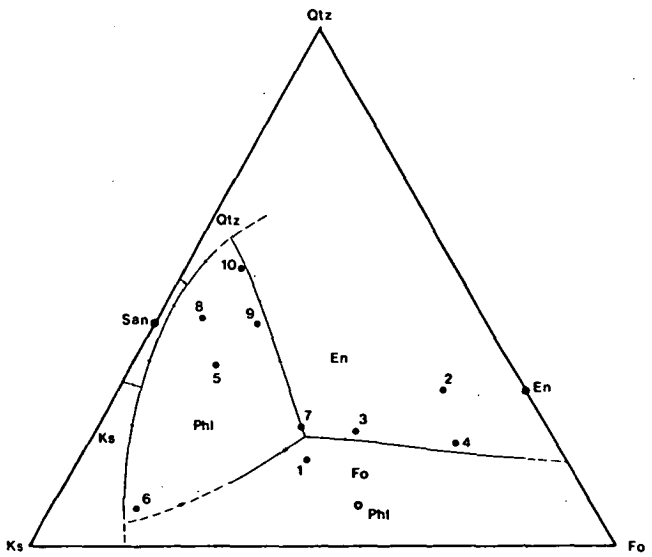

Fig. 1. Liquidus phase fields at 28 kb and 4% F_2O_{-1}. Numbers mark starting compositions as listed in Table 1. o = pure mineral composition

pressures from 1 to 28 kbar. The phlogopite phase volume expands greatly with increasing pressure, so that the EN + FO + PHL + L peritectic lies at much more Mg-rich compositions at mantle pressures than was estimated by Sekine and Wyllie (1982).

The phase diagram for 4% F_2O_{-1} at 28 kbar broadly resembles the water-saturated, fluorine-free system (Fig. 2) in having a large primary phase volume for phlogopite, plus primary phase volumes for the same six minerals (En, Fo, Phl, Ks, San and Qz). However, the fluorine-bearing system differs in that the fluorphlogopite has a much greater thermal stability (max. 1,490–1,500° C) than hydroxyphlogopite (<1,200° C: Gupta and Green in prep.). This may be attributed to the lack of K-H repulsion in fluorphlogopite. This repulsion exists in hydroxyphlogopite due to orientation of the O-H bond directly away from neighbouring octahedral cations and towards the interlayer potassium cations (McCauley et al. 1973). The EN + PHL phase boundary is not a peritectic reaction despite its extension apparently lying outside the join EN – PHL. This is an artifact of the projection due to Phl_{ss} and liquid compositions lying outside the plane of projection. As in the H_2O-saturated system, the intersection of the FO + PHL phase boundary with the extension of the FO – PHL join forms a thermal maximum. Liquids with compositions to the silica-rich side of this divide will fractionate either through the EN + FO + PHL + L peritectic point or across the phlogopite phase field to either the PHL + SAN + QZ or PHL + SAN + KS eutectics. Compositions to the silica-poor side of the PHL – FO join and its extension will fractionate through the KS + FO + PHL + L peritectic point or across the phlogopite phase field towards the KS + SAN + PHL eutectic.

In the fluorine-bearing system the primary phase field of enstatite relative to forsterite is enlarged compared to the volatile-free system, so that the EN + FO phase boundary is in a similar position to that in the CO_2-saturated system (Fig. 2). The position of this phase boundary is frequently taken to indicate the degree of polymerisation of the melt (Eggler 1974; Kushiro 1975). Expansion of the enstatite phase volume at the expense of forsterite with the addition of fluorine thus suggests that fluorine causes polymerisation of the melt.

The peritectic point PHL + EN + FO + L is a simple system analogue for a phlogopite harzburgite. The position of this point indicates that partial melting of a phlogopite harzburgite in H_2O-free conditions but in the presence of fluorine would produce a silica-undersaturated magma lying to the silica-poor side of the forsterite-sanidine join at

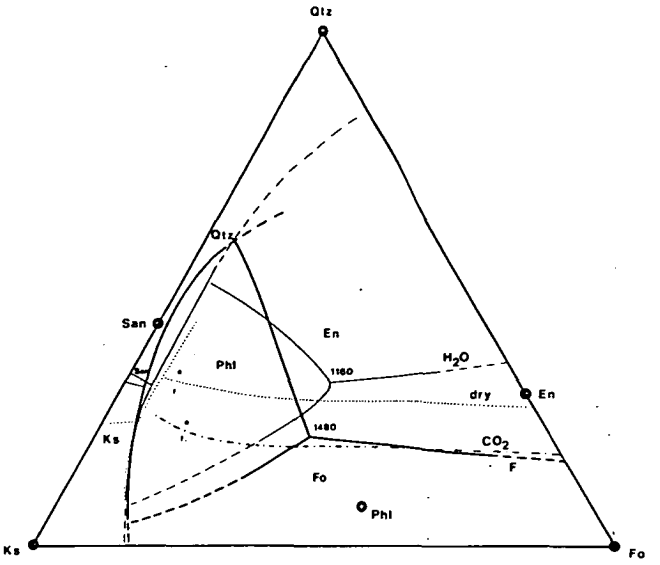

Fig. 2. Comparison of data for Ks-Fo-Qz at 28 kb with various volatiles. e/f marks enstatite-forsterite boundary in dry and CO_2-present systems where there is no phlogopite field. Phase fields for H_2O, CO_2 and volatile-free systems are from Gupta and Green (in prep.)

1,480° C. In contrast, in the water saturated system, the first melt would be in the more silica saturated part of the system delineated by the joins between forsterite, enstatite and sanidine at 1,160° C.

Several experiments were run with composition 1 with 10% F_2O_{-1}. Near-liquidus runs contained a very minor immiscible liquid phase rich in Mg and F. The immiscibility may extend above the liquidus, but this could not be ascertained because of the abundance of quench crystals in the above liquidus run. With 10% F_2O_{-1}, composition 1 lies just inside the primary phase volume of phlogopite, indicating expansion of the phlogopite phase volume with increasing fluorine. However, because of the apparent immiscibility which occurs at high fluorine contents, it is unlikely that phlogopite will melt congruently at any fluorine content.

Mineral compositions

Enstatites have alumina contents varying between 0.5 and 1.9 wt% (Table 2) but with no strong correlation with temperature or accompanying phases. These alumina contents

Table 2. Representative compositions of enstatites from experimental products at 28 kb and 4% F_2O_{-1}. (analyses normalised to 100%)

Mix No.	2	2	2	3	3	3	4
Temperature (°C)	1,430	1,480	1,540	1,450	1,480	1,510	1,530
Coexisting phases	Phl			Phl	Phl, Ol		ol
SiO_2	59.56	59.64	59.52	58.92	59.27	58.74	59.11
Al_2O_3	0.54	0.70	0.77	1.69	0.99	1.86	1.41
MgO	39.90	39.66	39.71	39.40	39.73	39.39	39.48
Si	1.990	1.992	1.989	1.969	1.981	1.964	1.975
Al	0.021	0.028	0.030	0.066	0.039	0.073	0.056
Mg	1.987	1.974	1.977	1.962	1.979	1.963	1.966
Sum	3.999	3.994	3.996	3.998	4.000	4.000	3.997

Table 3. Representative compositions of micas in experimental products: Mixes 1–10 have 4% F_2O_{-1}, mix 1a has 10% F_2O_{-1}

Mix No.	1	1	3	3	5	5	5	6	6	7	7	7
Temp. (°C)	1,480	1,500	1,480	1,450	1,340	1,400	1,450	1,380	1,420	1,440	1,470	1,490
Coexisting phases	ol	ol	ol, en	en	san			ks	ks	en	en	en
SiO_2	43.12	42.87	43.83	44.12	46.37	44.19	45.17	41.73	41.39	44.53	44.04	43.40
Al_2O_3	13.03	13.32	12.72	12.26	11.43	12.05	11.85	14.76	15.75	11.82	12.75	12.41
MgO	27.59	27.39	26.93	27.44	24.03	26.93	26.42	26.41	26.03	26.64	26.77	27.26
K_2O	10.84	10.68	10.75	10.79	11.33	10.75	11.07	11.31	10.90	10.91	10.90	10.89
F	5.41	5.73	5.76	5.39	6.84	6.09	5.20	5.78	5.93	6.10	5.54	6.04
Si	6.030	6.011	6.137	6.156	6.539	6.206	6.318	5.880	5.823	6.256	6.153	6.109
Al	2.148	2.200	2.099	2.015	1.900	1.994	1.941	2.451	2.613	1.956	2.098	2.058
Mg	5.750	5.724	5.618	5.707	5.053	5.636	5.473	5.546	5.458	5.577	5.575	5.718
K	1.934	1.910	1.920	1.919	2.038	1.925	1.961	2.034	1.957	1.956	1.944	1.955
Sum	15.863	15.844	15.773	15.797	15.529	15.760	15.693	15.911	15.849	15.745	15.770	15.840
F	2.348	2.464	2.606	2.364	3.211	2.611	2.226	2.620	2.671	2.721	2.504	2.649

Table 3 (continued)

Mix No.	8	8	8	8	9	9	9	10	1a	1a	1a
Temp. (°C)	1,240	1,270	1,300	1,340	1,290	1,350	1,410	1,380	1,510	1,480	1,450
Coexisting phases	san				qz	qz		qz		ol	ol
SiO_2	46.52	45.89	47.33	45.36	48.89	46.95	45.99	47.83	42.26	43.25	42.46
Al_2O_3	11.55	10.96	11.77	11.54	10.33	10.29	10.45	9.79	11.45	11.33	11.17
MgO	24.05	25.39	23.36	25.57	23.64	25.21	26.42	25.15	26.96	26.32	26.84
K_2O	11.01	10.98	11.08	10.97	11.03	10.94	10.94	10.62	12.05	11.61	12.37
F	6.88	6.78	6.45	6.56	6.10	6.60	6.20	6.62	7.09	7.49	7.16
Si	6.547	6.472	6.617	6.387	6.794	6.594	6.452	6.693	6.104	6.212	6.122
Al	1.915	1.821	1.939	1.916	1.693	1.703	1.728	1.615	1.939	1.918	1.899
Mg	5.045	5.338	4.869	5.367	4.896	5.278	5.526	5.245	5.778	5.636	5.769
K	1.976	1.975	1.976	1.970	1.955	1.960	1.958	1.896	2.210	2.128	2.275
Sum	15.483	15.605	15.401	15.640	15.338	15.535	15.663	15.448	16.031	15.962	16.065
F	3.123	3.037	2.871	3.046	2.713	2.923	2.842	2.845	3.239	3.429	3.275

were mostly greater than those of enstatites in water-saturated runs at 28 kbar (Gupta and Green in prep.).

Phlogopites show a large range in composition between the different mixes used (Table 3). Phlogopites in the more magnesian mixes are closer to the ideal $K_2Mg_6Al_2Si_6O_{20}F_4$ than those in less magnesian mixes. Phlogopites in silica-rich compositions (10, 9, 8, 5) have excess silica (>6 cations), less Mg and Al, and have a lower average octahedral occupancy. Micas from composition 6 are distinct in having high Al and no excess Si. Excess silicon correlates positively with fluorine in approximately 1:1 proportions. This and other correlations are illustrated in Figs. 3 and 4. Individual substitution mechanisms are difficult to isolate because of scatter in the data and also compositional dependence of substitutions, which is indicated by deviation of data from linearity in Fig. 3 (especially for the Al-rich micas of composition 6). The coupling of Si with F requires substitution for O* as well as Mg and Al to charge balance (where O* is oxygen on the OH site). Dependence of the F/O* of mica on the F/O of bulk composition is to be expected, and is indicated by higher F contents of micas in the experiments with 10% F_2O_{-1} on composition 1. These contain F/F+O*) ratios of 0.81–0.86 (bulk composition ratio = 0.182) relative to 0.59–0.61 with 4% F_2O_{-1} (bulk composition = 0.077). The micas in the 10% F_2O_{-1} runs have an excess of K over the ideal 2 cations per formula unit. This excess is significantly greater than analytical uncertainty. Excess alkalis have been described previously in Si-rich micas from a melilitic rock by Hazen et al. (1981), who assigned Na to octahedral sites. However, octahedral K is difficult to envisage in view of its larger ionic radius (1.33 Å vs. 0.97 Å for Na): this problem cannot be resolved with the data available here.

The chemistry of the experimental micas in the fluorine-bearing system indicate substitution with a mica end-member intermediate between trioctahedral and dioctahedral micas. Where this end-member is present, octahedral site occupancies are lower than in pure trioctahedral micas (Fig. 4), which can be attributed to a higher average octahedral cation charge (increase in Al and decrease in Mg). In the tetrahedral sites, Si is present in excess of the six cations per formula unit of the pure phlogopite end-member (Fig. 3). The existence of such an intermediate end-member is suggested by the lack of any known micas with between 4.3 and 5 octahedral cations, which would be expected in the case of solid solution between trioctahedral and dioctahedral micas (Seifert and Schreyer 1971; Green 1981). The experimental micas are compared to other known intermediate micas in Fig. 4. Amongst the natural micas, only those from ultrapotassic rocks show an excess of Si, a depletion

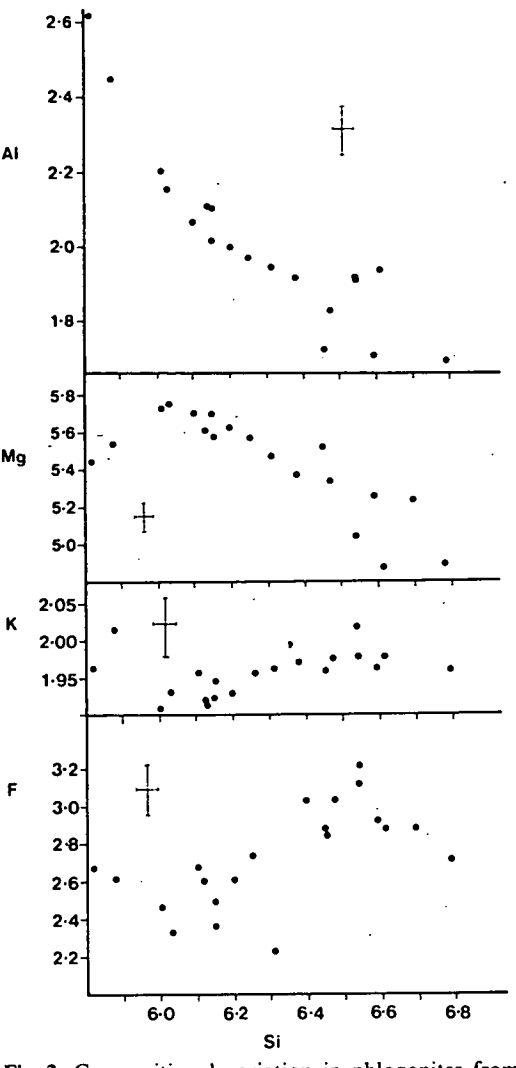

Fig. 3. Compositional variation in phlogopites from 4% F_2O_{-1} runs. Ions are calculated on 44 cation valencies per formula unit. Cross hairs denote analytical uncertainty

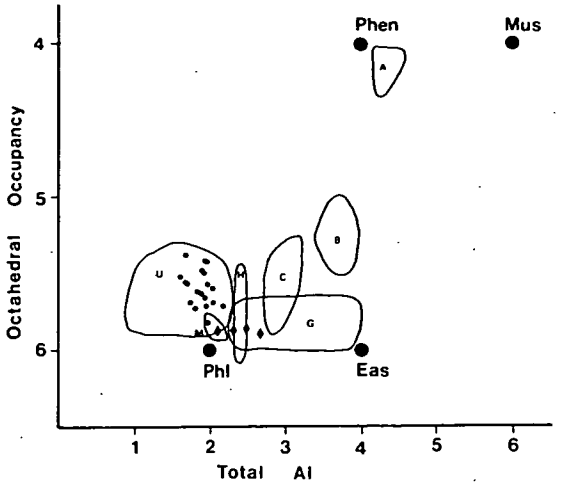

Fig. 4. Plot of total Al vs. octahedral site occupancy for phlogopites for fluorine-present experimental runs: Field *M* = magnesian compositions (1, 3, 7); ● = silicic compositions (10, 9, 8, 5); ○ = comp. 6; Other fields marked are: *U*, natural lamproitic micas; *H*, micas from H_2O-saturated system (Gupta and Green, in prep.); *G*, granitic micas (Green 1981). Fields A, B and C are synthetic intermediate micas of Green (1981). *Phl*, phlogopite; *Eas*, eastonite; *Phen*, phengite, *Mus*, muscovite

in Al and a decrease in octahedral site occupancy similar to the fluormicas in the experiments. These include micas from silica-poor melilitic rocks (Velde 1979) which may be related to the lamproites (Gallo et al. 1984; Best et al. 1968).

Analyses of micas from the water-saturated Ks-Fo-Qz system (Gupta and Green in prep.) show less compositional variation than those in the F system. Some have excess Si but show no variation in Al (2.3–2.5 cations). Cation variation diagrams (Figs. 4 and 5) show that the substitutions here are much simpler, and that excess Si is achieved by

$$2\,Mg^{VI} + Al^{IV} = Si^{IV} + Al^{VI} + [\,]^{VI}.$$

Mica substitution schemes can thus be expected to change with F/OH ratios with more variability occurring in F-rich than OH-rich micas.

The dissolution mechanism of fluorine in silicate melts

As noted earlier, the movement of the FO+EN phase boundary towards more silica-undersaturated compositions with the addition of fluorine indicates polymerisation of the melt. The position of this phase boundary is similar to that in the CO_2 saturated system (Fig. 2) in which the melt is polymerised by complexing of carbonate ions with one or more cations (Brey and Green 1975; Eggler and Rosenhauer 1978; Taylor 1985).

The mechanism of melt polymerisation in the presence of fluorine was investigated by infrared spectroscopy. Composition 1 was chosen for infrared study because of its proximity to the PHL+EN+OL+L peritectic point. Glasses were prepared at 1 atm for infrared studies: high pressure experimental products could not be used due to the abundance of quench crystals in the above liquidus runs. Even a small amount of crystalline material results in sharp, intense peaks in the infrared spectra, which mask the broader absorptions of the glasses. The structure of glasses and liquids of the same composition are known to be similar (Seifert et al. 1981; Taylor et al. 1980; Mysen et al. 1982).

Spectroscopic methods

Spectra were obtained using a DIGILAB FTS-20E Fourier Transform interferometric spectrometer in the regions 4,000–400 cm^{-1} (mid-infrared) and 500–100 cm^{-1} (far-infrared). The use of these regions permits study of absorption bands characteristic of vibrations in the aluminosilicate network (mid-IR) and those of network modifying cations, especially uni- and divalent (far-IR). Crystal-free glasses of composition 1 were prepared with 0.9 wt%, 0.3 wt% and no fluorine at 1 atm. For mid-IR, 1.5 to 2 mg of glass were thoroughly dispersed in approximately 200 mg KBr and then pressed into a disc. Samples for far-IR (2–3 mg) were prepared by mixing with nujol and mounting the mixture between two high density polyethylene plates.

Absorption bands in the glasses caused by vibrations involving fluorine atoms were characterised by comparing them with crystalline fluoride samples. This approach is justified by the existence of short-range order in silicate glasses (reviewed by Bottinga et al. 1981): the structural

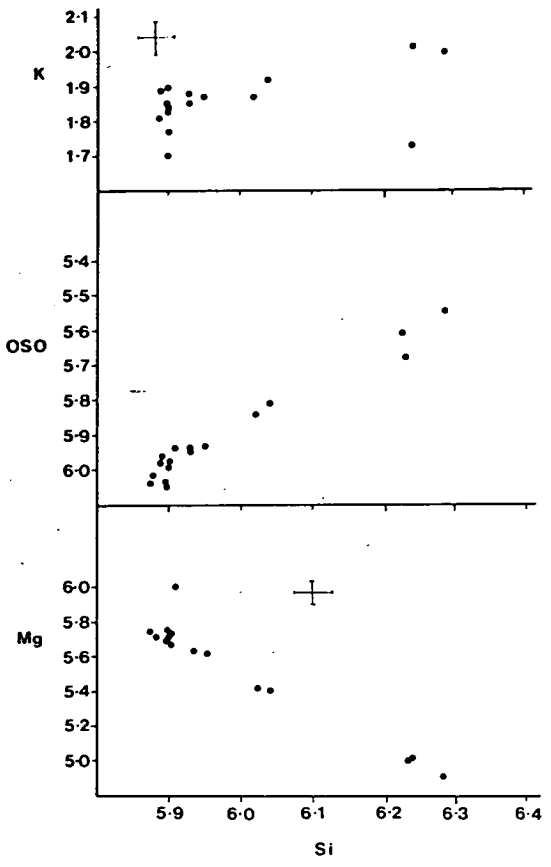

Fig. 5. Compositional variation in phlogopites from the H_2O saturated Ks-Fo-Qz system of Gupta and Green (in prep.). Cross hairs denote analytical uncertainty

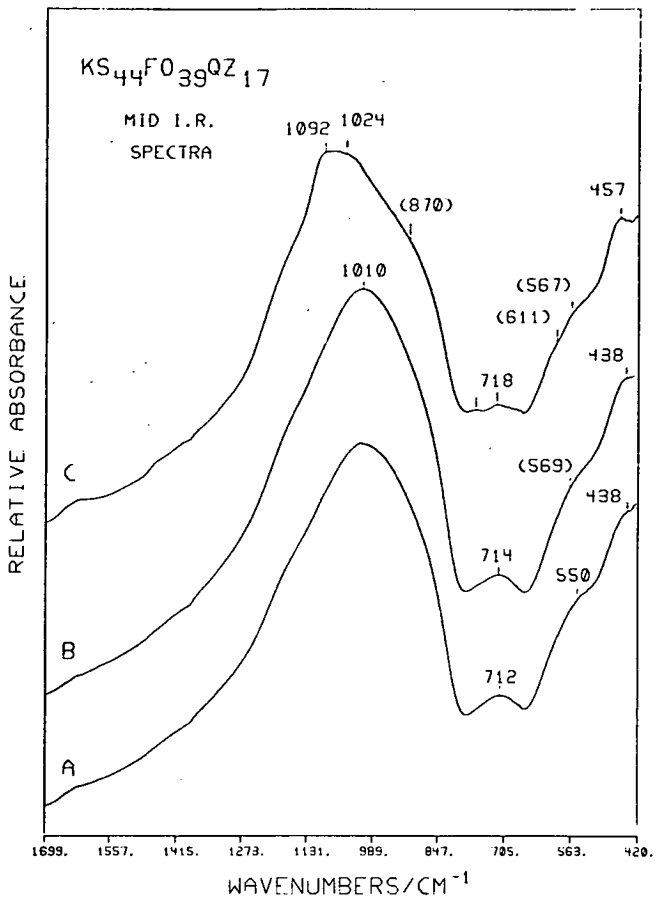

Fig. 6. Mid infrared spectra of composition 1 glasses (1 atm) with no fluorine (A), 0.3 wt% F (B) and 0.9 wt% F (C)

sites remain comparable with crystalline material, but have a greater variability in bond angles as shown by NMR studies (Dupree and Pettifer 1984) resulting in broad absorption envelopes. The fluorides used were AlF_3, MgF_2, KF and K_2SiF_6. AlF_3, MgF_2 and KF were obtained as fluorides and heated to 450° C to eliminate H_2O, but since KF is strongly hygroscopic (prepared from $KF \cdot 2H_2O$) not all the H_2O could be removed. Synthetic cubic hieratite (K_2SiF_6; Palache et al. 1951) was used to characterise Si-F bond absorptions in octahedral co-ordination. There are no known minerals with tetrahedral Si-F bonds (Allmann 1971). Hieratite was prepared by the reaction

$$K_2CO_3 + SiO_2 + 6\,HF = K_2SiF_6 + 3\,H_2O + CO_2.$$

Reactants were mixed thoroughly and placed in a teflon beaker with H_2O added to make the reaction with HF less violent. After reaction the mixture was dried to a gel on a hotplate and then at room temperature to avoid loss of SiF_4 from K_2SiF_6 which occurs at above 427°C. All crystalline fluorides were checked by X-ray diffraction and stored in an oven at 110° C until used.

Spectroscopic results

Basic melts: The high frequency region of the mid infrared spectrum (1,300–800 cm^{-1}) contains a broad envelope of absorption bands which are assigned to symmetric and asymmetric stretching vibrations of bridging (BO) and non-bridging (NBO) Si-O bonds. In simple binary metal oxide – silica glasses with high NBO/Si the bridging and non-bridging Si-O vibrations can be resolved into two distinct envelopes (Ferraro and Manghnani 1972), but this is not possible in more complex glasses. Lower frequency mid-IR absorptions are due to a mixture of Al-O stretching vibrations and rocking (O motion perpendicular to the Si-O-Si plane) and bending (O motion in the Si-O-Si plane) motions of bridging oxygen bonds (Laughlin and Joannopoulos 1977).

The spectra for the three compositions studied here are given in Fig. 6. These show little difference between 0 and 0.3 wt% F, but more difference with greater amounts of fluorine. The broad high frequency envelope shows a shift to higher wavenumbers due to a larger component at approximately 1,100 cm^{-1}. This is clearly seen in Figure 7, which shows difference spectra generated by computer subtraction of the digital spectra: these highlight the structural changes resulting from substitution of fluorine for oxygen. Difference spectra for (0.9–0 wt% F) and (0.3–0 wt% F) are compared on the same vertical scale in Fig. 7. The change in the high frequency region is seen to be due to addition of at least two absorption bands at approximately 1,100 and 1,200 cm^{-1}, and removal of absorption near 950 cm^{-1}. Studies of simpler silicate and aluminosilicate glasses have demonstrated that a shift to higher frequencies may be due to an increase in the degree of polymerisation of the silicate anions or an increase in the Si/(Si + Al) ratio of the silicate

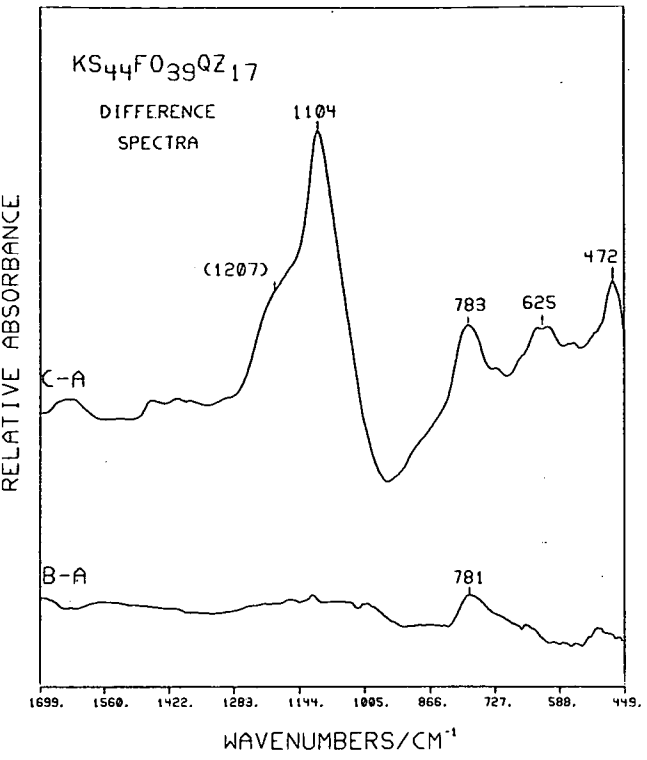

Fig. 7. Mid infrared difference spectra. Fluorine-free glass (A in Fig. 6) subtracted to reveal the effect of fluorine on the silicate network. A, B and C as in Figure 6. The shift of the silicate network stretching frequencies to higher wavenumbers (1,100–1,200 cm^{-1}) indicates polymerisation

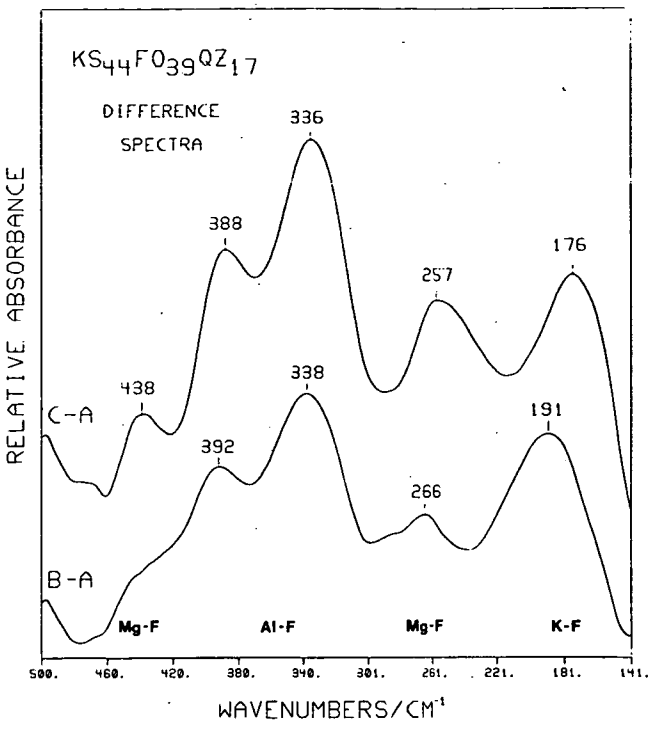

Fig. 8. Far infrared difference spectra showing absorption bands characteristic of fluoride bonds with Al, Mg and K as defined by pure fluoride minerals. A, B and C as in Fig. 7

network (Tarte 1967; Furukawa et al. 1981; White 1975; Seifert et al. 1982). The new bands in the region 1,100–1,200 cm^{-1} cannot be assigned to specific anionic units as vibrations in more polymerised structures will be coupled through bridging bonds (Furukawa et al. 1981). The calculated IR spectra of Furukawa et al. (1981) for sodium silicate melts predict the occurrence of absorption bands in the 750–800 cm^{-1} region for $(Si_2O_6)^{4-}$ chains and more polymerised units, but not for less polymerised units. The appearance of an absorption band at 780 cm^{-1} together with the shift to higher wavenumbers in the high frequency envelope for the fluorine-bearing glasses (Figs. 6 and 7) suggests that fluorine is causing polymerisation of the silicate network.

The far-IR region contains absorptions due to "cage-like" vibrations of cations of larger size and co-ordination number than the mid-IR region (Rao and Elliott 1981). The precise frequencies are dependent on cation mass, co-ordination number, bond length and the nature of the network attachment and the effective charge of the co-ordinating anion. In general, an increase in size or co-ordination number of the cation leads to absorption at lower wavenumbers (Tarte 1965, 1967; Rao and Elliott 1981; Kovach et al. 1975). The far-IR region thus contains information on the bonding characteristics of the network modifying cations (particularly K and Mg) in the Ks-Fo-Qz glasses.

The far-IR difference spectra in Fig. 8 correspond to the samples for which the mid IR difference spectra are given in Fig. 7. The effect of fluorine on the far-IR spectra is pronounced; bonding interactions with all network modifying cations are seen, and these are evident even at low fluorine contents where there is no corresponding effect in the mid-IR region. The far-IR absorption bands are assigned with reference to the simple fluoride mineral samples which have similar co-ordination environments to species in the melts.

The far-IR and mid-IR spectra can be explained by the following mechanism of fluorine dissolution. At low fluorine contents, fluorine initially forms bonds with network modifying cations without appreciably altering the aluminosilicate network. At higher fluorine contents, tetrahedral $KAl^{IV}O_2$ groups are complexed by fluorine and removed from the aluminosilicate network simultaneously polymerising and increasing the Si/(Si+Al) ratio of the network, resulting in the shift of the high frequency mid-IR absorption envelope to higher wavenumbers. This polymerising action of fluorine is in accord with calculations made by Tsunawaki et al. (1981) from Raman spectra of fluorine-bearing calcium silicate glasses. These authors observed polymerisation in glasses where fluorine was added by direct substitution, but not where CaF_2 was added to compositions with constant CaO/SiO_2. The fluorine in these melts lowers a_{CaO} by forming $Ca^{2+} - F^-$ complexes and raises a_{SiO_2} in the network.

In natural silicate melts the solution mechanism will differ in detail due to the presence of water, the dominant fluorine species then being HF (Munoz and Eugster 1969). In this case fluorine will behave in a similar manner, bonding with network modifiers, but the dissolution of HF will result in the release of water which will have a depolymerising effect. Examples of possible reactions showing the complexing of fluorine with network modifiers are:

$$(Mg_2SiO_4) + 2\,HF = (MgSiO_3) + (MgF_2) + H_2O, \quad (1)$$

$$(KAl^{IV}O_2) + 4\,HF = (Al^{VI}F_3) + (KF) + 2\,H_2O. \quad (2)$$

The effect on the silicate network is clearly seen by

$$2\,(KAl^{IV}Si_2O_6) + 4\,HF = (KAl^{IV}Si_3O_8 \cdot SiO_2) + (KF) + (Al^{VI}F_3) + 2\,H_2O. \quad (3)$$

Water is known to dissolve in silicate melts both as hydroxyl groups and, particularly at higher total water contents, as molecular H_2O (Stolper 1982). The formation of hydroxyl ions depolymerises the melt due to breakage of bridging bonds to form two non-bridging bonds. It is not certain whether this process is concentrated on Si-O-Si bonds (Burnham 1975, 1979a) or on Al-O-Si bonds (de Jong and Brown 1980; Taylor 1985), but this uncertainty does not have any bearing on the broad depolymerising effect discussed here. Evidence for depolymerisation is seen in the expansion of the liquidus phase volumes of less polymerised minerals such as olivine relative to enstatite (Kushiro 1972; Mysen 1977). The polymerising action of fluorine will thus be masked by the depolymerising action of the H_2O released by HF dissolution. In the presence of mixed H_2O-HF fluids, the forsterite-enstatite phase boundary in the system Ks-Fo-Qz can be expected to show overall depolymerisation.

Silicic melts. The solution mechanism for HF outlined above for basic melts contradicts the popular assumption that HF dissolves in granitic melts by Si-F bond formation. Consideration of the applicability of the HF solution mechanism for silicic melts is therefore necessary.

Many workers studying silicic melts have assumed that HF dissolves by a process analagous to H_2O in that Si-O-Si bridging bonds are broken resulting in tetrahedral Si-F bonds and a depolymerised melt (e.g. Burnham 1979b; Bailey 1977; Collins et al. 1982). This is based on the similarity of ionic radii of O (1.32 Å) and F (1.33 Å) (Buerger 1948) and the assignment of mid infrared absorption bands in alkali- and alkaline earth-silicate glasses to Si-F bonds (Kumar et al. 1961, 1965).

However, it has been shown above that the dissolution of HF, at least in basic melts, is a two-stage process in which the depolymerisation is due to H_2O released by HF dissolution, so that the assumption of Si-F bond formation as a major process is not justified. Manning (1981) also proposed a two-stage dissolution process for HF but with Si-F bonds as the intermediate stage occurring prior to hydrolysis: the infrared spectra of H_2O-free, fluorine-bearing glasses lead us to prefer the process represented by Equations 1–3. A process similar to that in basic melts causing an increase in Si/(Si+Al) of the network is supported by the observed expansion of the quartz phase volume with respect to feldspars on addition of fluorine (Wyllie and Tuttle 1961; Kovalenko 1977; Manning et al. 1980).

A number of arguments have been put forward, particularly in the Russian literature, that despite an increase in the proportion of Si-F bonds in silicic relative to basic melts, the proportion of Si-F bonds will still be very minor (Kogarko and Krigman 1973; Kogarko et al. 1968; Kogarko and Ryabchikov 1978; Mitchell 1967). Arguments include the absence of minerals with tetrahedral Si-F bonds, immiscibility between silica-rich and alkali-fluoride-rich melts (Kogarko 1967), the predominance of alkali fluoride in vapours in equilibrium with silicic melts, and thermodynamic calculations. In addition, acid-base theory predicts that reactions will proceed in favour of the formation of bonds of maximum and minimum polarity (Ramberg 1952; Kogarko 1974). Thus, reactions of the type

$$4\,MF + SiO_2 = SiF_4 + 2\,M_2O \quad (4)$$

where M = any cation, will favour the left side due to the higher electronegativity of F relative to O and Si relative to all other common cations in silicate melts.

Attempts in this study to form tetrahedral Si-F bonds in glasses for infrared study failed, producing instead crystalline fluorosilicates containing octahedral (SiF_6) units. Crystallisation of fluorosilicates is common in pressurised experiments on fluorine-bearing compositions (Wyllie and Tuttle 1961; Glyuk and Anfilogov 1973; Manning et al. 1980). The assignment of absorption bands to tetrahedral Si-F bonds by Kumar et al. (1961, 1965) is considered to be erroneous, as bands due to more polymerised silicate units will occur in the regions described by Kumar et al. (Ito et al. 1967; Mitchell 1967; Furukawa et al. 1981). Reference to the fluorosilicate mineral spectra shows that any Si-F bonds in this region would be octahedral, probably due to octahedral (SiF_nO_{6-n}) units and not tetrahedral (SiF_nO_{4-n}) units.

Mysen and Virgo (1985) reported Raman spectra for glasses on the joins SiO_2-AlF_3 and SiO_2-NaF, and they suggested that tetrahedral Si-F bonds are important, particularly on the SiO_2-AlF_3 join. However, these results are inappropriate for extrapolation to complex natural silicate melts as they used fully polymerised SiO_2 melts as a starting point for fluorine addition. The compositions studied here in the system Ks-Fo-Qz contain an array of structural species which form a better analogy for natural silicate melts. Also, the addition of fluorine as fluorides is less suitable for studying the structural effect of fluorine than is direct substitution of fluorine for oxygen, because the effect due to fluorine cannot be isolated from the effect due to the accompanying cation. Tsunawaki et al. (1981) have demonstrated that addition of fluorine as fluoride does not cause polymerisation, whereas addition of the same amount of fluorine by direct substitution does.

The larger viscosity decrease in silicic melts on fluorine addition (Kozakevitch 1954, Kumar et al. 1961) has been used as evidence for melt depolymerisation and Si-F bond formation. Dingwell et al. (1985) and Dingwell and Mysen (1985) confirmed the large viscosity decrease due to fluorine in melts in the system $SiO_2-Na_2O-Al_2O_3$ where fluorine was added by direct substitution for oxygen. It is important to note that 'polymerisation' as used in this paper refers to the aluminosilicate network, whereas viscosity reflects the overall structure of the melt. The polymerisation state of the aluminosilicate network, which can be represented by the EN+FO phase boundary, is more useful for considering the composition of partial melts produced in the mantle because the phase volumes of the silicate minerals reflect their relative stabilities as residual phases. The viscosity decrease in fluorine-bearing silicate melts relative to fluorine-free melts can be attributed to the formation of fluoride complexes incorporating cations which form part of the aluminosilicate network in fluorine-free melts (Equations 1-3). We found no evidence in the present study to support the proposal of Dingwell et al. (1985) that the decrease in viscosity is due to tetrahedral Si-F bond formation.

Acknowledgments. Financial support for this study was provided by University of Tasmania (SFF) and Commonwealth (WRT) postgraduate awards and ARGS support to DHG for the experimental laboratory. Technical assistance was provided by KL Harris and NW Davies. This work has benefitted at various stages from discussions with, or comments from, AK Gupta, KL Harris, AL Jaques, DJ Ellis and W Schreyer.

References

Allmann R (1971) Fluorine. In: Wedepohl KH (ed) Handbook of Geochemistry Section 9A, 6pp

Aoki K, Ishikawa K, Kanisawa S (1981) Fluorine geochemistry of basaltic rocks from continental and oceanic regions and petrogenetic application. Contrib Mineral Petrol 76:53–59

Bailey JC (1977) Fluorine in granitic rocks and melts: a review. Chem Geol 19:1–42

Best MG, Henage LF, Adams JAS (1968) Mica peridotite, wyomingite, and associated potassic igneous rocks in northeastern Utah. Am Mineral 53:1041–1048

Bottinga Y, Weill DF, Richet P (1981) Thermodynamic modeling of silicate melts. In: RC Newton, A Navrotsky, BJ Wood (eds) Thermodynamics of minerals and melts: Adv Phys Geochem 1:207–245

Brey GP, Green DH (1975) The role of CO_2 in the genesis of olivine melilitite. Contrib Mineral Petrol 49:93–103

Buerger MJ (1948) The structural nature of the mineraliser action of fluorine and hydroxyl. Am Mineral 33:744–746

Burnham CW (1975) Water and magmas: a mixing model. Geochim Cosmochim Acta 39:1077–1084

Burnham CW (1979a) The importance of volatile constituents. In: HS Yoder (ed) The Evolution of the Igneous Rocks: Fiftieth Anniversary perspectives. pp 439–482. Princeton University Press, Princeton, New Jersey

Burnham CW (1979b) Magmas and hydrothermal fluids. In: HL Barnes (ed) Geochemistry of hydrothermal ore deposits. pp 71–136 Wiley

Collins WJ, Beams SD, White AJR, Chappell BW (1982) Nature and origin of A-type granites with particular reference to southeastern Australia. Contrib Mineral Petrol 80:189–200

de Jong BHWS, Brown GE (1980) Polymerisation of silicate and aluminate tetrahedra in glasses, melts, and aqueous solutions – I. Electronic structure of $H_6Si_2O_7$, $H_6SiAlO_7^-$, and $H_6Al_2O_7^{2-}$. Geochim Cosmochim Acta 44:491–511

Dingwell DB, Mysen BO (1985) The effect of water and fluorine on the viscosity of albite melt at high pressure: a preliminary investigation. Earth Planet Sci Lett 74:266–274

Dingwell DB, Scarfe CM, Cronin DJ (1985) The effect of fluorine on viscosities in the system $Na_2O-Al_2O_3-SiO_2$: implications for phonolites, trachytes and rhyolites. Am Mineral 70:80–87

Dupree E, Pettifer RF (1984) Determination of the Si-O-Si bond angle distribution in vitreous silica by magic angle spinning NMR. Nature 308:523–525

Eggler DH (1974) Effect of CO_2 on the melting of peridotite. Carnegie Inst Washington Yearb 73:215–224

Eggler DH, Rosenhauer M (1978) Carbon dioxide in silicate melts, II, Solubilities of CO_2 and H_2O in $CaMgSi_2O_6$ (diopside) liquids and vapors at pressures to 40 kb. Am J Science 278:64–94

Ferraro JR, Manghnani MH (1972) Infrared absorption spectra of sodium silicate glasses at high pressures. J Appl Phys 43:4595–4599

Furukawa T, Fox KE, White WB (1981) Raman spectroscopic investigation of the structure of silicate glasses. III. Raman intensities and structural units in sodium silicate glasses. J Chem Phys 75:3226–3237

Gallo F, Giametti F, Venturelli G, Vernia L (1984) The kamafugitic rocks of San Venanzo and Cupaello, central Italy. N Jahrb Mineral Mh 5:198–210

Glyuk DS, Anfilogov VN (1973) Phase equilibria in the system granite-H_2O-HF at a pressure of 1000 kg/cm^2. Geochem Int 10:321–325

Green DH, Liebermann RC (1976) Phase equilibria and elastic properties of a pyrolite model for the oceanic upper mantle. Tectonophysics 32:61–92

Green TH (1981) Synthetic high-pressure micas compositionally intermediate between the dioctahedral and trioctahedral mica series. Contrib Mineral Petrol 78:452–458

Hazen RM, Finger LW, Velde D (1981) Crystal structure of a silica- and alkali-rich trioctahedral mica. Am Mineral 66:586–591

Holloway JR, Ford CE (1975) Fluid absent melting of the fluorhydroxy amphibole pargasite to 35 kilobars. Earth Planet Sci Lett 25:44–48

Ito H, Yanagase T, Suginohara Y, Miyazaki N (1967) Studies on the structure of molten fluoride-silicate systems by infrared absorption spectra. Chem Abs 67:68972g from Nippon Kinzoku Gakkaishi 31:290–295

Jaques AL, Lewis JD, Smith CB, Gregory GP, Ferguson J, Chappell BW, McCulloch MT (1984) The diamond bearing ultrapotassic (lamproitic) rocks of the West Kimberley region, Western Australia. In: Kornprobst J (ed) Kimberlites I: Kimberlites and related rocks. p 225–254

Kogarko LN (1967) Lamination area in melts of the system Si, Al, Na//O, F. Dokl Akad Nauk Earth Sci Sec 176:203–205

Kogarko LN (1974) Role of volatiles. In: H Sorensen (ed) The alkaline rocks, pp 474–487 Wiley, New York

Kogarko LN, Krigman LD (1973) Structural position of fluorine in silicate melts (according to melting curves). Geochem Int 10:34–40

Kogarko LN, Ryabchikov ID (1978) Volatile components in magmatic processes. Geochem Int 15:9–32

Kogarko LN, Krigman LD, Sharudilo NS (1968) Experimental investigations of the effect of alkalinity of silicate melts on the separation of fluorine into the gas phase. Geochem Int 5:782–790

Kovach JJ, Hiser AL, Karr C (1975) Far-infrared spectroscopy of minerals. In: C Karr (ed) Infrared and Raman spectroscopy of lunar and terrestrial minerals. p 231–254 Academic Press, London, New York

Kovalenko NI (1977) The reactions between granite and aqueous hydrofluoric acid in relation to the origin of fluorine-bearing granites. Geochem Int 14:108–118

Kozakevitch P (1954) Viscosity of blast furnace slags. Rev Metall Mem Sci 51:569–587

Kumar D, Ward RG, Williams DJ (1961) Effect of fluorides on silicates and phosphates. Disc Faraday Soc 32:147–154

Kumar D, Ward RG, Williams DJ (1965) Infrared absorption of some solid silicates and phosphates with and without fluoride additions. Trans Faraday Soc 61:1850–1857

Kushiro I (1972) Effect of water on the compositions of magmas formed at high pressures. J Petrol 13:311–334

Kushiro I (1975) On the nature of silicate melt and its significance in magma genesis: regularities in the shift of the liquidus boundaries involving olivine, pyroxene and silica minerals. Am J Sci 275:411–431

Laughlin RB, Joannopoulos JD (1977) Phonons in amorphous silica. Phys Rev B 16:2942–2952

Luth WC (1967) Studies in the system $KAlSiO_4-Mg_2SiO_4-SiO_2-H_2O$: I, Inferred phase relations and petrologic applications. J Petrol 8:372–416

Manning DAC (1981) The effect of fluorine on liquidus phase relationships in the system Qz-Ab-Or with excess water at 1 kb. Contrib Mineral Petrol 76:206–215

Manning DAC, Hamilton DL, Henderson CMB, Dempsey MJ (1980) The probable occurrence of interstitial Al in hydrous, F-bearing and F-free aluminosilicate melts. Contrib Mineral Petrol 75:257–262

McCauley JW, Newnham RE, Gibbs GV (1973) Crystal structure analysis of synthetic fluorphlogopite. Am Mineral 58:249–254

Mitchell A (1967) Reactions of calcium silicates in solution in liquid calcium fluoride. Trans Faraday Soc 63:1408–1417

Munoz JL, Eugster HP (1969) Experimental control of fluorine reactions in hydrothermal systems. Am Mineral 54:943–959

Mysen BO (1977) The solubility of H_2O and CO_2 under predicted magma genesis conditions and some petrological and geophysical implications. Rev Geophys Space Phys 15:351–361

Mysen BO, Virgo D (1985) Interaction between fluorine and silica in quenched melts on the joins SiO_2-AlF_3 and SiO_2-NaF determined by Raman spectroscopy. Phys Chem Minerals 12:77–85

Mysen BO, Virgo D, Seifert FA (1982) The structure of silicate melts: implications for chemical and physical properties of natural magmas. Rev Geophys Space Phys 20:353–383

Palache C, Berman H, Frondel C (1951) Dana's system of mineralogy II pp 103–104 Wiley, New York

Ramberg H (1952) Chemical bonds and distribution of cations in silicates. J Geol 60:331–355

Rao KJ, Elliott SR (1981) Characteristic vibrations of cations in glasses. J Non-Cryst Solids 46:371–378

Schilling J-G, Bergeron MB, Evans R (1980) Halogens in the mantle beneath the North Atlantic. Phil Trans R Soc London A 297:147–178

Seifert F, Schreyer W (1971) Synthesis and stability of micas in the system $K_2O-MgO-SiO_2-H_2O$ and their relations to phlogopite. Contrib Mineral Petrol 30:196–215

Seifert F, Mysen BO, Virgo D (1981) Structural similarity of glasses and melts relevant to petrological processes. Geochim Cosmochim Acta 45:1879–1884

Seifert F, Mysen BO, Virgo D (1982) Three-dimensional network melt structure in the systems $SiO_2-NaAlO_2$, $SiO_2-CaAl_2O_4$ and $SiO_2-MgAl_2O_4$. Am Mineral 67:696–717

Sekine T, Wyllie PJ (1982) Phase relationships in the system $KAlSiO_4-Mg_2SiO_4-SiO_2-H_2O$ as a model for hybridisation between hydrous siliceous melts and peridotite. Contrib Mineral Petrol 79:368–374

Shell HR, Ivey KH (1969) Fluorine micas. US Bur Mines Bull 647:291pp

Stolper EM (1982) The speciation of water in silicate melts. Geochim Cosmochim Acta 46:2609–2620

Tarte P (1965) The determination of cation co-ordination in glasses by infra-red spectroscopy. In: JA Prins (ed) Physics of non-crystalline solids. pp 549–565 Wiley, New York

Tarte P (1967) Infra-red spectra of inorganic aluminates and characteristic vibrational frequencies of AlO_4 tetrahedra and AlO_6 octahedra. Spectrochim Acta 23A:2127–2143

Taylor M, Brown GE, Fenn PM (1980) Structure of silicate mineral glasses III, $NaAlSi_3O_8$ supercooled liquid at 805° C and the effects of thermal history. Geochim Cosmochim Acta 44:109–119

Taylor WR (1985) The role of C-O-H fluids in upper mantle processes: a theoretical, experimental and spectroscopic study. Ph.D thesis, University of Tasmania, Hobart

Tsunawaki Y, Iwamoto N, Hattori T, Mitsuishi A (1981) Analysis of $CaO-SiO_2$ and $CaO-SiO_2-CaF_2$ glasses by Raman spectroscopy. J Non-Cryst Solids 44:369–378

Velde D (1979) Trioctahedral micas in melilite-bearing eruptive rocks. Carnegie Inst Washington Yearb 78:468–475

White WB (1975) Structural interpretation of lunar and terrestrial minerals by Raman spectroscopy. In: C Karr (ed) Infrared and Raman spectroscopy of lunar and terrestrial minerals. p 325–358 Academic Press, London New York

Windom KE, Boettcher AL (1981) Phase relations for the joins jadeite-enstatite and jadeite-forsterite at 28 kb and their bearing on basalt genesis. Am J Sci 281:335–351

Wyllie PJ, Tuttle OF (1961) Experimental investigation of silicate systems containing two volatile components. Part II. The effects of NH_3 and HF in addition to H_2O on the melting temperatures of albite and granite. Am J Sci 259:128–143

Yoder HS, Tilley CE (1962) Origin of basalt magmas: an experimental study of natural and synthetic rock systems. J Petrol 3:342–532

Received May 21, 1985 / Accepted January 6, 1986

Contrib Mineral Petrol (1986) 94:183–192

DHG

Contributions to Mineralogy and Petrology
© Springer-Verlag 1986

B34

The role of fluorine and oxygen fugacity in the genesis of the ultrapotassic rocks

Stephen F. Foley*, Wayne R. Taylor, and David H. Green
Geology Department, University of Tasmania, Box 252C, Hobart, Tasmania, Australia 7001

Abstract. The effects of H_2O, CO_2, CH_4 and HF on partial melting of a model phlogopite harzburgite mantle are considered with regard to the production of ultrapotassic magmas. Fluorine has a polymerising effect in H_2O-poor conditions, but in the presence of abundant H_2O where HF rather than F is dominant, the overall effect is depolymerisation. Methane also dissolves by forming $(OH)^-$ groups, and so has a depolymerising effect. Group I ultrapotassic rocks (lamproites) probably originate from primary magmas with SiO_2 contents ranging from around 40 wt% to at least 52 wt%. This range can be explained by differing depths of origin from a similar source with a similar reduced H_2O-CH_4-HF volatile mixture. The formation of silica-rich initial melts from a model phlogopite harzburgite is assisted by the presence of CH_4 and HF. Dissociation of less than 0.1 wt% H_2O, driven by H_2 loss, is sufficient to cause oxidation during emplacement to observed oxidation states. Silica-poor ultrapotassic rocks could be produced at higher pressures in a reduced environment, or in an oxidised environment with high $CO_2/(CO_2+H_2O)$ ratios.

Group II (African Rift) potassic rocks may originate in H_2O-poor conditions in which fluorine will maintain a large phlogopite phase field, so that initial melts will be magnesian and silica-undersaturated.

Introduction

The ultrapotassic rocks are a compositionally heterogeneous group of rocks in which volatile species (H_2O, CO_2, F, Cl SO_2) are more abundant than in less alkaline rocks. Experimental studies on natural ultrapotassic rock compositions (Edgar et al. 1976; Barton and Hamilton 1979, 1982; Ryabchikov and Green 1978; Arima and Edgar 1983a, b) and simple systems (Wendlandt and Eggler 1980a, b; Gupta and Green in preparation) at high pressures have been limited to consideration of the effect of H_2O and CO_2 on phase relationships as a guide to petrogenesis. These studies have emphasised the stability of mica under H_2O-rich conditions, and the different roles of H_2O and CO_2 in stabilising more depolymerised and polymerised anhydrous silicate minerals respectively.

In this paper we extend the discussion of volatiles to include fluorine and methane. The effect of fluorine will be greater in ultrapotassic rocks than in other mafic rocks because fluorine correlates positively with K content (Aoki et al. 1981). Jaques et al. (1984) suggested that H_2O+HF-rich volatile mixtures are important in generating lamproite magmas and that F would increase the stability of mica. Our studies of the fluorine solution mechanism and phase relationships in the system kalsilite-forsterite-quartz (Ks-Fo-Qz; Foley et al. 1986a) provide more evidence for the role of fluorine in ultrapotassic rock genesis.

Methane has not been considered important in the past mainly due to models for the oxidation state of the upper mantle during magma genesis which presuppose stability of carbonates forming oxygen buffer reactions with f_{O_2} close to that of the FMQ and MW buffers (Eggler 1978; Wyllie 1978, 1979). However, measurements of intrinsic oxygen fugacity and oxygen barometry on megacrysts and xenoliths believed to be derived from the mantle (Arculus et al. 1984; Haggerty and Tompkins 1983) indicate that the oxidation state of the mantle is likely to be heterogeneous, including regions with f_{O_2} as low as that of the IW buffer. The relative importance of reduced and oxidised environments in the mantle within the range noted above is currently the subject of much debate (*see* discussions by Ryabchikov et al. 1981, Eggler and Baker 1982, Arculus 1985, Taylor 1985, Woermann and Rosenhauer 1985): we therefore consider variations in oxygen fugacity on ultrapotassic rock genesis, and develop a model for the production of lamproites in a F-rich reduced environment.

Ultrapotassic rock nomenclature

Ultrapotassic rocks can be divided into three groups based on their chemistry and rock associations (Barton 1979). These groups may be viewed as end members between which a number of transitional types occur. They represent a variety of potassic liquids which reflect variations in source composition, degree of partial melting, volatile abundances and compositions (including fluorine) and oxygen fugacity to name but a few. These groups are described in detail by Foley et al. (1986b), and their more important characteristics, which need to be taken into account in petrogenetic models, are summarised here:

1. Group I: Lamproites, typically occurring without other associated magma types, have high K_2O and low Al_2O_3 (frequently perpotassic: $K/Al>1$). Na_2O and CaO contents are low, and SiO_2 is variable. TiO_2 contents are high and are characteristic of individual areas, and are highest in rocks from stable contental areas. The lamproites have high Mg-numbers [100 Mg/(Mg+Fe)] and may carry lherzolite and harzburgite xenoliths of high pressure origin (Jaques et al. 1984; Sheraton and Cundari 1980).

2. Group II rocks, typified by the Toro Ankole volcanics in the western branch of the East African Rift Valley, have low SiO_2

* *Present address and address for offprint requests:* Abteilung Kosmochemie, Max-Planck-Institut für Chemie, Saarstraße 23, Postfach 3060, D-6500 Mainz, FRG

Table 1. Fluorine contents of micas from natural lamproites and related rocks

F wt%	F ions	Locality & description	Sample	Reference
2.46	1.069	Leucite Hills, wyomingite	B	1*
2.38	1.029	Leucite Hills, orendite	SK 36	2
2.51	1.084	Leucite Hills, orendite	SK 36	2
4.11	1.784	Leucite Hills, orendite	SK 36	2
2.95	1.279	Leucite Hills, orendite	SK 36	2
4.52	1.996	Leucite Hills, wyomingite	SK 9	2
4.86	2.214	Leucite Hills, madupite	SK 23	2
0.84	0.362	Holsteinsborg, lamproite	5944	3
0.74	0.319	Holsteinsborg, lamproite	5944	3
0.24	0.104	Holsteinsborg, lamproite	5944	3
0.87	0.391	Holsteinsborg, lamproite (core)	5622	3, 4
0.88	0.384	Holsteinsborg, lamproite (core)	5622	3, 4
nd	–	Holsteinsborg, lamproite (rim)	5622	3, 4
2.69	1.187	SE Spain, jumillite	SP059	5
1.35	0.598	SE Spain, jumillite	SP059	5
2.07	0.917	SE Spain, jumillite	SP059	5
1.25	0.537	SE Spain, fortunite	SP081	5
0.97	0.419	SE Spain, fortunite	SP081	5
1.52	0.666	SE Spain, fortunite	SP081	5
2.40	1.058	SE Spain, lamproite	2	6*
1.4	0.621	Gaussberg, olivine leucitite	4755	7*
1.42	0.638	Gaussberg, olivine leucitite (gd)	2780	–
1.93	0.871	Gaussberg, olivine leucitite (gd)	4882	–
1.95	0.883	Gaussberg, olivine leucitite (gd)	2780	–
4.01	1.843	Priestley Peak, alkali melasyenite	3949C	8
3.91	1.786	Priestley Peak, alkali melasyenite	3949C	8
4.07	1.860	Priestley Peak, alkali melasyenite	3949C	8
5.55	2.589	Prairie Creek, Ark, olivine lamproite	PK 1/19	9*
5.32	2.449	Prairie Creek, Ark, olivine lamproite	PK 1/19	9*
5.74	2.673	Prairie Creek, Ark, olivine lamproite	PK 1/19	9*
5.06	2.343	Utah, melilite peridotite	Y127	10*
3.76	1.681	Sierra Nevada, high-K basanite	MP410	11*
2.91	1.314	Sierra Nevada, high-K basanite	MP410	11*
3.56	1.579	Sierra Nevada, high-K basanite	B5	11*
3.69	1.701	Sierra Nevada, high-K basanite	M74B	11*
2.88	1.284	Sierra Nevada, high-K basanite	M74B	11*

New analyses unless denoted (*); gd, groundmass; new analyses by JEOL JXA 50A microprobe (wavelength dispersive system) with topaz and synthetic MgF_2 standards

References. 1, Carmichael 1967; 2, Kuehner et al. 1981; 3, Scott, 1977; 4, Scott 1981; 5, Venturelli et al. 1984; 6, Fuster et al. 1967; 7, Sheraton and Cundari 1980; 8, Sheraton and England 1980; 9, Scott-Smith and Skinner 1984; 10, Velde 1979; 11, Van Kooten 1980. Chlorine (detection limit <0.05 wt%) was not detected in any of the new analyses

and Al_2O_3 (not perpotassic) but higher CaO than lamproites. TiO_2 contents are comparable to group I and higher than group III. The Toro Ankole rocks are related to more sodic undersaturated rock types to the south by a northward increase in K_2O and decrease in SiO_2 (Pouclet 1980a, b; Pouclet et al. 1984). The potassic rocks of the Toro Ankole volcanic field occur together with carbonatitic lavas (Von Knorring and DuBois 1961; Nixon and Hornung 1973). Xenoliths are rich in phlogopitic mica and clinopyroxene.

3. Group III rocks (Roman Province type) are rich in CaO and Al_2O_3 and poor in TiO_2. They have Mg-numbers up to about 68, but the majority are more differentiated. Group III rocks occur exclusively in orogenic environments. Various processes including crustal interaction (Hawkesworth and Vollmer 1979) and magma mixing (Barton et al. 1982) may be important in their genesis. They are not dealt with further here because of the difficulty of isolating primary magma compositions.

Fluorine in ultrapotassic magmas

Fluorine is most abundant in Group I rocks, ranging up to 0.8 wt%. Examples of fluorine contents in lamproitic rocks are 0.20 to 0.54 wt% for West Kimberley, Australia (Jaques et al. 1984), 0.59–0.76 wt% for the Leucite Hills, USA (Kuehner et al. 1981; Aoki et al. 1981) and 0.33 wt% for Gaussberg, Antarctica (Sheraton and Cundari 1980). Group II rocks range up to 0.28 wt% in the katungites and melilitic rocks of the Toro Ankole field (Holmes 1937; Holmes and Harwood 1932; Edgar and Arima 1981) with generally lower values in the less potassic rock types to the south. Group III rocks contain the lowest amounts of fluorine amongst the ultrapotassic rocks, generally less than 0.2 wt% (Fornaseri et al. 1963; Iddings and Morley 1915), although data are sparse for this group. The understanding of the behaviour of fluorine in magmatic systems is therefore particularly important for elucidating the petrogenesis of the lamproites.

Fluorine contents in phlogopite phenocrysts/xenocrysts in lamproitic rocks are frequently high (see Table 1). Natural mica compositions from ultrapotassic rocks have been reviewed by Arima and Edgar (1981) and Bachinski and Simpson (1984), but their data lacked fluorine contents.

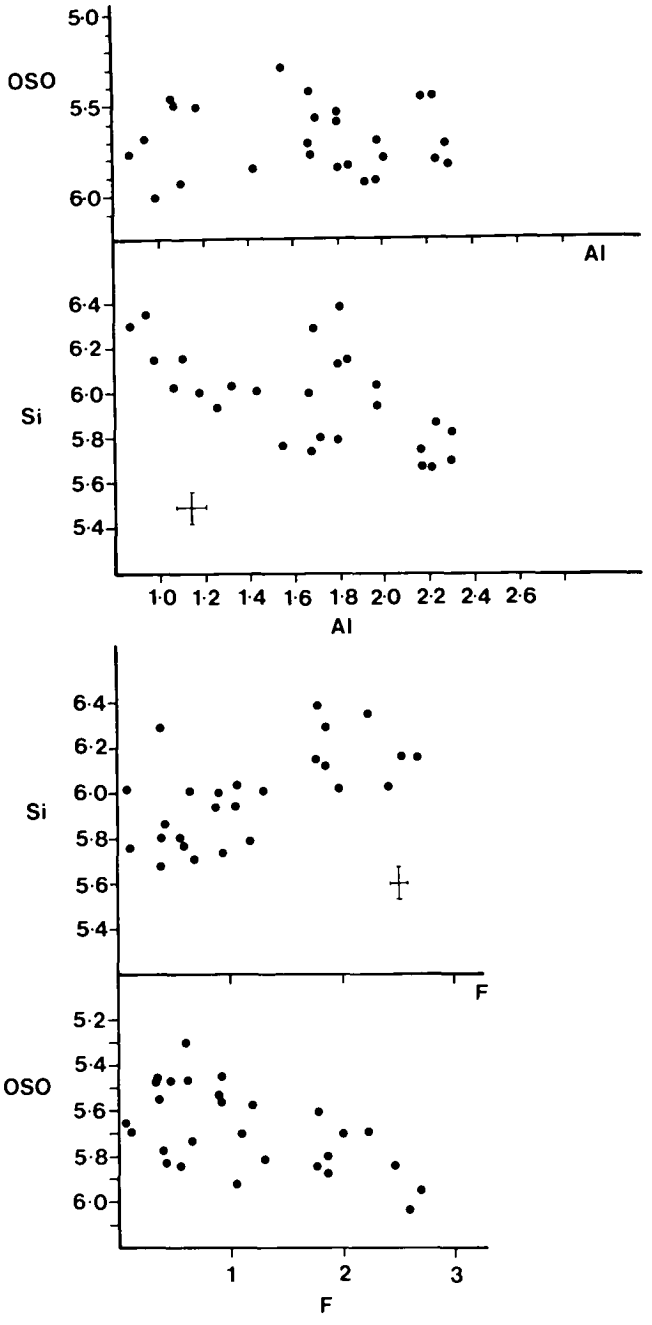

Fig. 1. Compositional variation in natural ultrapotassic micas from Leucite Hills, Gaussberg Holsteinsborg, Southeastern Spain and Priestley Peak (Antarctica). OSO = Octahedral site occupancy

Foley et al. (1986a) showed that synthetic micas in the system Ks-Fo-Qz with fluorine have more complex compositional variations than micas in the same system under water-saturated, fluorine-free conditions, so that natural mica compositions can be expected to vary with F/OH ratios.

Micas crystallising from melts containing relatively small amounts of fluorine, such as ultrapotassic melts, can be expected to have high F/OH ratios since micas are very efficient at removing fluorine from a melt (Munoz and Eugster 1969). Ion variation plots of natural micas (Fig. 1) show several broad trends amongst ultrapotassic rocks as a

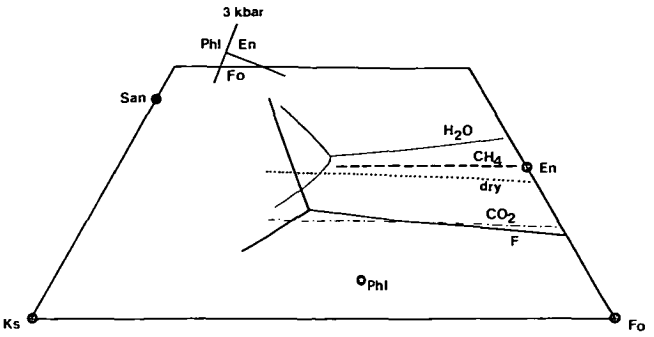

Fig. 2. Part of the system Ks-Fo-Qz showing the relative positions of the enstatite – forsterite phase boundary in the presence of vairous volatile species discussed in the text. The boundary for CH_4 is estimated from its position in the Ne-Fo-Qz system, taken from Gupta et al. (in preparation). The position with HF is uncertain, but can be expected to be close to the CH_4 position. The data for the water-saturated Ks-Fo-Qz system at 3 kbar are taken from Luth (1967)

group, but these are not necessarily reproduced in rocks from a single area, especially where fluorine content is low. Si and F do show a positive correlation, but the ratio is nearer 1:2 than the 1:1 in the experimental micas, indicating more complex substitution relationships. No simple correlation of fluorine with any other cation is seen, although this may be partly due to scatter between ultrapotassic rock localities.

The alumina contents of many ultrapotassic rock micas are much lower than any of the experimental micas. This is probably a consequence of the peralkaline and, in the case of lamproites, often perpotassic, nature of the melts. The experiments are restricted to K = Al, whereas K is frequently in excess of Al in lamproitic rocks. The dominant Al substitution in the natural micas appears to be a Tschermak-type substitution indicated by the Si = 2 Al slope and large variation in Al relative to octahedral occupancy (Fig. 1). The low Al-content of natural ultrapotassic rock micas will reflect both the low Al content of the melt and the F/OH ratio. For a constant K/Al, Si in micas is likely to increase with F towards more silica-rich whole-rock compositions. The substitution mechanisms cannot be formulated in detail as they are complicated by other cations, particularly Ti and Fe (*see* discussion by Arima and Edgar 1981), which are not present in the Ks-Fo-Qz system. The difference between fluormicas and hydroxymicas in the system Ks-Fo-Qz indicates that coupled substitutions of specific cations with F, O and OH on the (OH) site, as discussed by Bohlen et al. (1980), are probably important. As an example, the $Fe^{2+} - F$ avoidance principle (Rosenberg and Foit 1977; Sanz and Stone 1979) should cause coupling of F with cations other than Fe^{2+}.

The effect of fluorine on the compositions of melts generated in the mantle is best represented by the polymerisation state of the aluminosilicate network. The most convenient simple system indicator for this in Ks-Fo-Qz is the movement of the forsterite-enstatite phase boundary (Fig. 2) since these two minerals are likely to be major components of the mantle residuum. The phase equilibrium and spectroscopic data for the Ks-Fo-Qz system (Foley et al. 1986a) indicate that fluorine polymerises the aluminosilicate network. However, in most geological conditions H_2O will be present in excess of fluorine, so that HF will be the

dominant fluorine species. HF will dissolve by a reaction in which the polymerising effect of F is counterbalanced by the depolymerising effect of H_2O released by HF dissolution (Foley et al. 1986a). Under these conditions the overall effect will be an increase in the liquidus phase volume of the most depolymerised phase, resulting in the production of more silica-rich melts (ol, en, san normative). In the event of H_2O-poor but F-rich conditions, melts generated in the mantle will be silica-undersaturated (ol, san, lc normative) as modelled by the PHL + EN + FO + L peritectic point (Fig. 2).

Oxygen fugacity and ultrapotassic magmas

Oxygen fugacity will also be an important controlling factor of melt polymerisation, particularly affecting the behaviour of carbon. CO_2 has been found to polymerise silicate melts by forming carbonate complexes with network-modifying cations. This causes expansion of the phase volume of enstatite relative to that of forsterite (Fig. 2) so that lower silica partial melts result (Brey and Green 1975; Eggler 1974, 1978; Ryabchikov and Green 1978). Experiments investigating the solution of CO_2 in silicate melts of the same composition at widely differing f_{O_2} have shown that the amount of carbonate dissolved in the melt, and thus the polymerisation, increases with increasing f_{O_2} (Brey and Green 1976).

At low f_{O_2} methane will be the dominant carbon species. Recent studies by Taylor (1985) have shown that the solubility of reduced carbon in simple system silicate melts is limited to 1,000–2,000 ppm before saturation and crystallisation of graphite occurs. This small amount of carbon is probably contained as atomic carbon on cation vacancies and defect sites as envisaged by Freund et al. (1980, 1983) for silicate minerals. Methane dissolution is accompanied by reduction in the stoichiometry of the silicate network (i.e. $O/Si < 2$) (Taylor 1985). The enstatite-forsterite phase boundary in the methane-saturated system Ne-Fo-Qz (f_{O_2} < IW buffer) is to the silica-rich side of its position in the volatile-free system. Thus, in a very reduced environment with H_2O, CH_4 and HF, depolymerisation will be at a maximum, and melts produced will be more silica-rich than those in source regions containing H_2O, CO_2 and HF. In a reduced C–O–H fluid at mantle pressures (f_{O_2} between the iron-wustite buffer and ~2 log units above IW) the H_2O/CH_4 ratio will vary greatly with f_{O_2}, temperature and presssure, but there will always be a significant amount of H_2O (Taylor 1985).

Intrinsic f_{O_2} measurements on mantle derived xenoliths and xenocrysts indicate two distinct oxygen fugacities may be prevalent in the upper mantle; one reduced near the IW buffer and the other oxidised near QFM (Arculus and Delano 1981; Arculus et al. 1984). However, this data is sparse at present and these may represent extremes of a continuum of oxygen fugacities in the mantle, with the majority of measurements clustering around the MW buffer (O'Neill and Wall 1982, Arculus 1985).

What evidence then, is there of the oxygen fugacity in ultrapotassic magma source regions? CO_2 contents are variable between ultrapotassic rock groups: Group II rocks are rich in CO_2, frequently with carbonates present in the groundmass, whereas Group I rocks, in most cases, have very low CO_2 contents. However, the source regions of CO_2-poor rocks need not have been poor in carbon if oxygen fugacity was low.

Foley (1985) studied early crystallising chrome-spinels which form inclusions in olivine phenocrysts in lamproites, and experimentally calibrated the ferric number [100 $Fe^{3+}/(Fe^{3+}+Fe^{2+})$] of spinel as an oxygen fugacity sensor. Spinels from various lamproites show a wide range in oxygen fugacities for different lamproitic rocks, and these differences are also seen in the Fe_2O_3 content of leucites. There may be a large disparity (up to 4 log units) between the f_{O_2} indicated by the spinel (more reduced) and the f_{O_2} given by the whole rock analysis by the equation

$$\ln f_{O_2} = \left[\ln(X^{Fe_2O_3}_{melt}/X^{FeO}_{melt}) - \left(\frac{b}{T} + c + \Sigma k_i X_i\right)\right] \cdot \frac{1}{a} \quad (1)$$

which is rearranged from Kilinc et al. (1983). In Eq. (1), a, b, c and d are constants, X = mole fraction, and k_i are empirical constants for each oxide component i. Ultrapotassic rocks may therefore have experienced oxidation during emplacement, and this effect must be allowed for in deducing source conditions.

Diffusion of H_2 out of an ascending magma into the surrounding rock has been proposed by Sato [1978] as a possible oxidation mechanism. H_2 can originate by dissociation of water represented by the equilibrium

$$H_2O = H_2 + \frac{1}{2} O_2. \quad (2)$$

which will be driven to the right by diffuse H_2 loss. Arculus and Delano (1981) reserved judgement on this model, noting that a spread of oxidation states would be expected in resulting melts due to differing degrees of H_2O dissociation: this is precisely what is seen in the lamproite spinels (Foley 1985).

In considering oxidation during magma ascent, we have to assume an oxygen fugacity for the source mantle. In H_2O-rich, CO_2-poor conditions suggested by analyses of lamproites, the f_{O_2} is best represented by the CW buffer (carbon-water) which is the locus of points on the carbon saturation surface where X_{H_2O} is a maximum. This lies roughly midway between the IW and WM buffers at temperatures and pressures likely to represent diamond stability in the mantle (Taylor 1985). There is no direct evidence for the oxygen fugacity of lamproite magmas in the mantle: it is also possible that melt generation is triggered by the introduction of a water-rich volatile phase. This may be more oxidised than CW if not constrained by carbon saturation. In this case the survival of diamonds in lamproites could be attributed to sluggish diamond breakdown reactions.

However, for the following discussion we will assume a starting f_{O_2} equivalent to the CW buffer in order to assess (a) the oxidation model given by reaction (2), and (b) the relevance of reduced fluids to lamproite petrogenesis. As shown in the following sections, many of the features of lamproites can be explained by a model of a reduced source with oxidation during emplacement. Under these conditions diamonds may be stable in the lamproite source region. This model is limited to the lamproites as CO_2 may be important for Group II rocks, and the applicability of the spinel f_{O_2} sensor of Foley (1985) is limited by compositional differences. Whilst this discussion contrasts the extremes of oxidation, a continuum between the two is most realistic for application to natural magmas.

A model for the Fe_2O_3/FeO ratio of an ascending lamproitic magma

The following thermodynamic model estimates the amount of H_2O dissociation which would be required to cause an increase in Fe_2O_3/FeO of the order inferred from compositions of phenocrysts (Foley 1985) which crystallised during emplacement of a lamproitic magma.

Whilst non-volatile components of the liquid and solid phases of a magma are likely to remain relatively constant during ascent, those of the fluid or vapour phase, particularly H_2, are likely to be lost more readily via diffusion and outgassing. The amount of H_2O dissociation which can occur must be affected by the magma ascent rate. The survival of mantle-derived ultramafic nodules and diamonds in some lamproites indicates that eruption times must be relatively short. The approximation used here that exchange with the surroundings is limited to hydrogen only is more realistic under these conditions because of the fast diffusion rate of H_2. The calculation which follows contains much thermodynamic idealisation, but it is only intended to give an approximate value for H_2O dissociation. It is sufficient to demonstrate that the resulting wt% H_2O dissociated is not unreasonably high and that this mechanism may be realistic for the oxidation of magmas during ascent.

Mo et al. (1982) have determined the partial molar volumes of FeO and $FeO_{1.5}$ in silicate liquids as a function of temperature. Since $\bar{V}_{FeO}$ is less than $\bar{V}_{FeO_{1.5}}$ and noting the relation

$$\left(\frac{\partial \mu_i}{\partial P}\right)_T = \bar{V}_i \qquad (3)$$

FeO will have the lowest chemical potential (μ) at high pressures, and should be favoured over $FeO_{1.5}$ in silicate melts at depth. It is assumed that $\bar{V}_i$ is independent of pressure (i.e. no compressibility terms).

A melt containing a variable ratio of $FeO_{1.5}$/FeO is not an oxygen buffer but responds to changes in the intensive parameters P, T, f_{O_2} etc. (Carmichael and Nicholls 1967). When a magma ascends rapidly from depth two extreme forms of behaviour can be considered, i.e. closed system and open system behaviour. The model presented here considers a limited open system case in which escape of H_2 is the only exchange with the surrondings. In the closed system case, μO_2 of the system will change because of the equilibrium

$$FeO + \tfrac{1}{2}O_2 \rightleftarrows FeO_{1.5} \qquad (4)$$

so that

$$\mu O_2 = 2\mu_{FeO_{1.5}} - 2\mu_{FeO} \qquad (5)$$

The closed system case was considered by Mo et al. (1982) from which they proposed that the oxygen fugacity in the source regions of basic magmas is greater than that at the surface. Calculations from their equations give f_{O_2} conditions at high pressures several orders of magnitude higher than the MW buffer, which are geologically unreasonable. The implied reduction during transport to the surface is also the opposite of observed crystallisation sequences in spinel and leucite.

In the "limited open system" case considered further here, the intrinsic f_{O_2} of the system is assumed to be maintained (i.e. μO_2 constant) during ascent due to diffusive H_2 loss via the reaction

$$FeO + \tfrac{1}{2}H_2O = \tfrac{1}{2}H_2\uparrow + FeO_{1.5} \qquad (6)$$

The closed and open system emplacement paths are contrasted in Fig. 3a.

A magma originating at depth may have its f_{O_2} determined by an oxygen buffer reaction in the source region (Ryabchikov et al. 1981, Eggler 1983) such as

$$\underset{\text{olivine}}{6Fe_2SiO_4} + O_2 = \underset{\text{spinel}}{2Fe_3O_4} + \underset{\text{opx}}{6FeSiO_3}$$

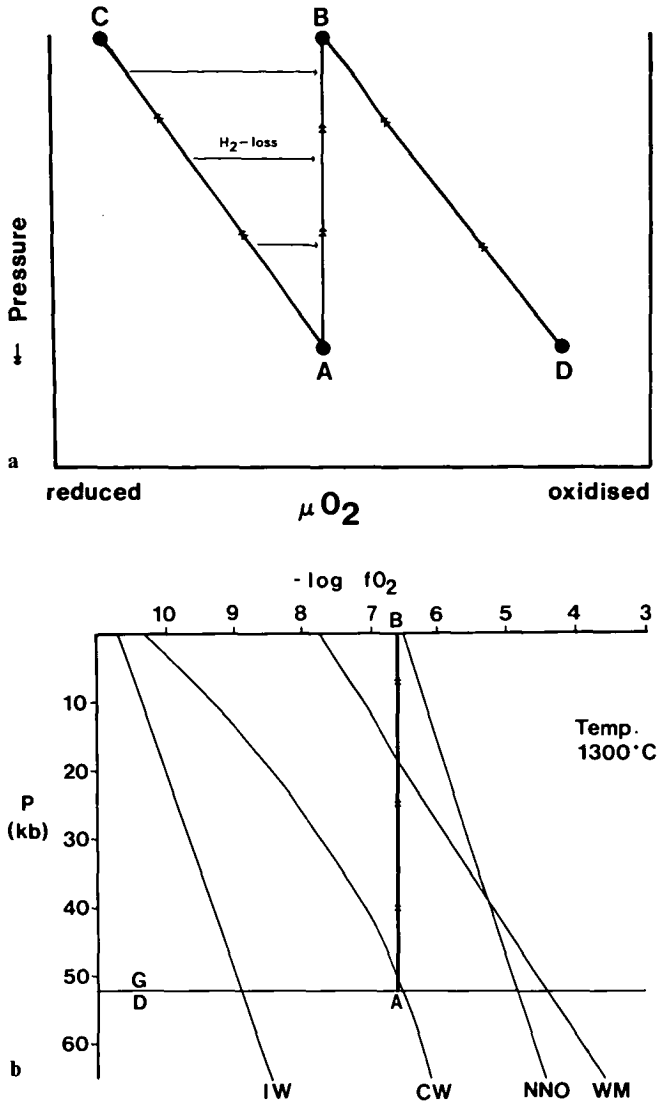

Fig. 3. **a** Schematic $P-\mu O_2$ diagram illustrating the difference between closed and open system cases of the model discussed in the text. A – B is the open system emplacement path considered here; A – C is the closed system emplacement from the same conditions at depth (A); D – B is closed system emplacement resulting in the same oxidation state at the surface (considered by Mo et al. 1982). **b** Emplacement path used (A – B) for calculations of water dissociation compared to buffer curves iron-wustite (IW) graphite-water (CW), nickel-nickel oxide (NNO) and wustite-magnetite (WM) at 1,300° C. Path maintains f_{O_2} from the diamond-graphite transition boundary (G/D; from Kennedy and Kennedy 1976) to the surface near NNO, which correspoonds to the surface f_{O_2} of the Gaussberg olivine leucitite (Foley 1985)

or possibly a vapour phase reaction involving graphite (or diamond) plus C–O–H–S vapour (Eggler and Baker 1982, Woermann and Rosenhauer 1985). During ascent, however, the magma will not be buffered (unless it contains an abundant phenocryst assemblage capable of acting as a buffer; Carmichael and Nicholls 1967) and hence the Fe^{3+}/Fe^{2+} ratio of the melt may change.

In our model system $FeO-FeO_{1.5}-H_2O$ we consider the case of isothermal ascent in which the oxygen potential of the system remains constant. O_2 is gained from the dissociation of H_2O in order to maintain μO_2. Differentiating Eq. (5) with respect to pressure at constant temperature we get

$$0=\left(\frac{\partial \mu_{O_2}}{\partial P}\right)_T=\left[\frac{\partial \mu_{FeO_{1.5}}}{\partial P}-\frac{\partial \mu_{FeO}}{\partial P}\right] \tag{7}$$

Using the standard relation

$$\mu_i=\mu_i^0+RT\ln a_i, \tag{8}$$

noting

$$\left(\frac{\partial \ln a_i}{\partial P}\right)_T=V_i^0, \tag{9}$$

rearranging and integrating over pressure, we get

$$\ln\left(\frac{a_{FeO}}{a_{FeO_{1.5}}}\right)^{P\,bar}-\ln\left(\frac{a_{FeO}}{a_{FeO_{1.5}}}\right)^{1\,bar}=\frac{V^0_{FeO_{1.5}}-V^0_{FeO}}{RT}(P-1) \tag{10}$$

but

$$\ln(\gamma^P_{FeO}/\gamma^1_{FeO})=\frac{\bar V_{FeO}-\bar V^0_{FeO}}{RT}(P-1) \tag{11}$$

and similarly for $FeO_{1.5}$ (where γ_i is the activity coefficient of i). Therefore

$$\left(\frac{X_{FeO}}{X_{FeO_{1.5}}}\right)^P=\left(\frac{X_{FeO}}{X_{FeO_{1.5}}}\right)^1\cdot\exp\left[\frac{(\bar V_{FeO_{1.5}}-\bar V_{FeO})}{RT}(P-1)\right] \tag{12}$$

For the calculation X^1_{FeO} and $X^1_{1.5}$ are known, let $X^1_{H_2O}=0$ and applying the mass balance constraint

$$X^P_{FeO}+X^P_{FeO_{1.5}}+X^P_{H_2O}=1 \tag{13}$$

$X^P_{H_2O}$ can be calculated from Eq. (13) where

$$X^P_{FeO}=\left[\exp\left(\frac{(\bar V_{FeO_{1.5}}-\bar V_{FeO})}{RT}(P-1)\right)\cdot\left(\frac{X^1_{FeO}}{X^1_{FeO_{1.5}}}\right)\right]\cdot X^P_{FeO_{1.5}} \tag{14a}$$

and

$$X^P_{FeO_{1.5}}=\frac{1+\frac{1}{2}X^1_{FeO}}{\left[1.5\left(\exp\left(\frac{(\bar V_{FeO_{1.5}}-\bar V_{FeO})}{RT}(P-1)\right)\cdot\left(\frac{X^1_{FeO}}{X^1_{FeO_{1.5}}}\right)\right)+1\right]} \tag{14b}$$

The calculation based on the simple $FeO-FeO_{1.5}-H_2O$ system may be extended to natural compositions assuming an ideal solution of liquid components so that the activities of FeO, $FeO_{1.5}$ and H_2O may be represented by their mole fractions. In this model H_2O is assumed to act as an "inert dilutant" and does not affect $(\bar V_{FeO_{1.5}}-\bar V_{FeO})$ of the liquid.

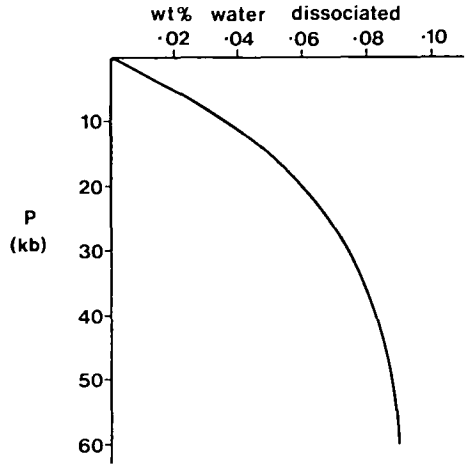

Fig. 4. Curve showing the amount of water dissociation required to maintain constant oxygen fugacity with depth. Calculation is made from variation of partial molar volumes of FeO and Fe_2O_3 with pressure in the system $FeO-FeO_{1.5}-H_2O$

The assumption of ideal solution of H_2O rather than setting activity as a function of $X^2_{H_2O}$ (Burnham 1979; Nicholls 1980) is insignificant considering the approximate nature of this calculation, making a difference of only 0.01 wt% H_2O to the result noted below. The emplacement path chosen for a model lamproitic magma (A → B in Fig. 3b) is from a relatively reduced source. The source condition (A in Fig. 3b) is at the intersection of CW with the diamond-graphite transition boundary (Kennedy and Kennedy 1976). For the end-point (B in Fig. 3b) the oxidation state at near-surface conditions of a melt yielding the glassy olivine leucitite of Gaussberg, Antarctica is chosen, since this is a pristine example of a lamproitic volcanic rock (Foley 1985). The Gaussberg composition has a median value for primary lamproite magmas for both surface oxidation state (Foley 1985) and for wt% FeO, which is the only compositional parameter of the rock which affects this calculation (total Fe as FeO in Gaussberg = 6% compared to a range of 4–8% for primary lamproites; Barton and Hamilton 1978, Jaques et al. 1984, Foley et al. 1986b). This is not intended to imply that the Gaussberg magma originated at 52 kbar, indeed it is argued in the next section that the more silicic lamproite magmas originate at much shallower levels. By the above calculation, 0.09 wt% H_2O must dissociate between A (52 kbar) and the surface to maintain the f_{O_2} of the system at 1,300° C. The form of the curve in Fig. 4 indicates that the rate of increase of $FeO_{1.5}/FeO$ will increase towards the surface, with half of the water dissociation ocurring in the uppermost 15 kbar. Dissociation of water in the order of 0.1 wt% water does not appear unreasonably high, and is consistent with the 0.07 wt% calculated by Mathez (1984) for oxidation between the iron-wustite and quartz-fayalite-magnetite buffers. This small amount of dissociation will be lessened if the near-surface oxidation by degassing of carbon species proposed by Mathez (1984) also operates.

Genesis of ultrapotassic rocks with a range of silica contents

The fluorine rich lamproites range in silica content from 40 to 60 wt% and, whilst accumulation of olivine and crys-

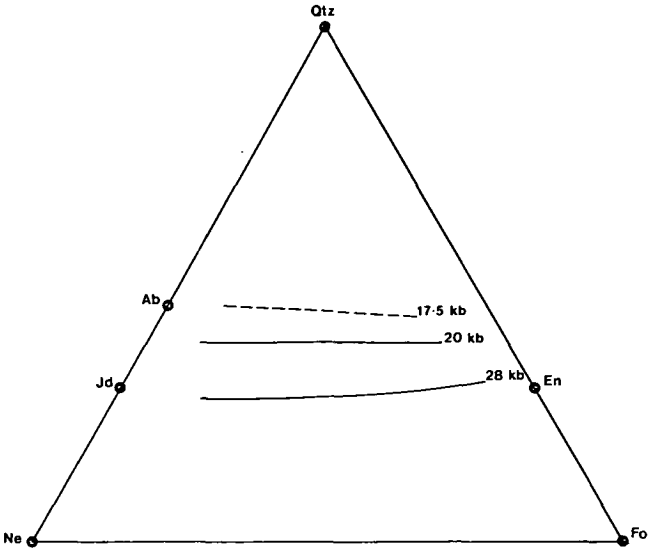

Fig. 5. The effect of pressure on the forsterite-enstatite phase boundary in the water-saturated Ne-Fo-Qz system showing shift to more silica-undersaturated compositions at higher pressures. Positions taken from Kushiro (1972; 17.5 and 20 kbar) and Gupta and Green (in preparation; 28 kbar)

tal fractionation is important (Jaques et al. 1984), a range in primary magma silica contents seems likely. West Australian lamproite compositions considered to be primary range in silica content from approximately 40 to 52 wt% (Atkinson et al. 1984; Jaques et al. 1984). Primary lamproite magmas from other regions may have even higher silica contents: a Leucite Hills orendite with 55 wt% silica has been found to crystallise olivine, orthopyroxene, clinopyroxene and garnet at its liquidus at 27 kbar, indicating that it may represent a primary melt from the mantle (Barton and Hamilton 1982).

Experimental work on dry compositions and with mixed H_2O+CO_2 volatiles indicates that for the more silicic magmas to be primary, the H_2O/CO_2 ratio would have to be extremely high because of the polymerising effect of CO_2 leading to lower silica partial melts. The presence of HF will assist the formation of silica-rich melts by the process outlined previously, so that the effect of any CO_2 present will be lessened. If conditions are sufficiently reduced for CH_4 to be important rather than CO_2, then this will further assist the production of silica-rich melts.

Compositions with lower silica contents are represented among Group I and Group II ultrapotassic rocks. Referring to the Ks-Fo-Qz system, there are two ways by which melting of the model phlogopite harzburgite may give rise to silica-undersaturated melts: 1. by increasing CO_2/H_2O, demonstrated by movement of the FO+EN phase boundary (Fig. 2) or 2. by increasing pressure. It has been shown in both Ne-Fo-Qz and Ks-Fo-Qz systems that the FO+EN phase boundary moves to more silica-poor compositions with increasing pressure (Kushiro 1968, 1980), and that in Mg-poor compositions the phase volume of sanidine also expands (Wendlandt and Eggler 1980a). Figure 5 illustrates, from the data of Kushiri (1972) and Gupta and Green (in preparation) in the Ne-Fo-Qz system, that this holds for water saturated systems. The same source giving rise to silicic leucite lamproites may therefore produce more silica-undersaturated melts at higher pressures without any difference in volatile composition, i.e. in a CO_2-free mantle. It is not necessary to appeal to widely differing volatile compositions to explain the silica variation in likely primary magmas within a given locality, for example, the West Kimberley lamproite suite. A greater depth of origin for primary olivine lamproite compositions from West Kimberley in a reduced environment is in accord with the occurrence of diamonds being commonest in the Mg-rich, Si-poor lamproites (Atkinson et al. 1984; Jaques et al. 1984).

The position of the PHL+EN+FO+L peritectic point will depend critically on the stability of phlogopite. Since there can be no phlogopite field in fluorine-free conditions with CO_2 as the only volatile, the composition of the first melt from a model (phlogopite) harzburgite will vary greatly in both SiO_2 content and Ks/Fo ratio with $H_2O/(H_2O+CO_2)$. The liquidus phase field for phlogopite is reduced at moderate $CO_2/(CO_2+H_2O)$ ratios (Ryabchikov and Green 1978; Wendlandt and Eggler 1980c; Arima and Edgar 1983a). The position for PHL+EN+FO+L under H_2O-saturated conditions given by Sekine and Wyllie (1982) is considered to be erroneous (too low Fo) due to an extensive extrapolation from the low pressure data of Luth (1967). The data of Gupta and Green (in preparation) at 28 kbar indicate that the phlogopite phase field will be much larger (see Fig. 2). The large difference in the position of the PHL+FO+EN+L peritectic point at 3 kbar and 28 kbar (Fig. 2) indicates that the Ks/Fo ratio of melts must be strongly dependent on pressure, but compositions at intermediate pressures can only be estimated due to the lack of data. The argument put forward above that more silica-rich lamproites may originate at shallower depths corresponds to this expected variation in Ks/Fo ratio with pressure: the Gaussberg olivine leucitite (51 wt% SiO_2) has an MgO content of 8 wt% and K_2O in excess of 11 wt%, whereas typical West Kimberley olivine lamproites (40–43 wt% SiO_2) have MgO in excess of 20 wt% and K_2O of 4–5 wt%, and yet both these lamproite types have high Mg-number and carry mantle-derived nodules. The addition of fluorine to a mixed volatile system will greatly enlarge the phase volume of phlogopite, increasing the Fo/Ks ratio and leading to more magnesian melts regardless of silica content.

These arguments for a reduced source may be more applicable in some regions of lamproite magmatism than others, because lamproites from different localities differ both in their range of probable primary magma compositions and in their oxidation state at near-surface conditions as measured by spinel phenocryst compositions. The variation in spinel phenocryst compositions does not correlate with silica content of the rock in different lamproite regions, indicating that the effectiveness of oxidation during emplacement may differ greatly.

Application to other ultrapotassic rock groups

The source region for Group II rocks of the Toro Ankole volcanic field was probably poor in H_2O. This is indicated by low H_2O contents of volcanic gases in African Rift volcanoes (Bailey 1978, 1980), and by the occurrence of carbonatites in the Toro Ankole field. The Ks-Fo-Qz analogue of a source poor in H_2O and with lower F than Group I rocks (though still F-rich relative to most basaltic rocks) would move initial melts to more Si-poor, K-rich compositions, possibly giving rise to rocks akin to katungite. The

oxidation state in the source regions of Western Rift rocks is poorly known, though volcanic gases (Bailey 1978) and dissolved methane of possible volcanic origin in Lake Kivu to the south of the Virunga field (Burke 1963, discussed by Gerlach 1980) may indicate a reduced environment at depth. However, in a reduced environment, carbon saturation should occur at low concentrations so that transportation of carbon in the melt will be limited: a much greater amount of carbon would dissolve in a melt (as carbonate) in a more oxidised environment. A reduced source should therefore result in carbon-poor volcanics regardless of the oxidation state at the surface, unless emplacement takes place as a melt + fluid system, and oxidation of the fluid occurs preferentially. If the source is oxidised, the presence of fluorine will maintain a phlogopite phase field so that melts will still have an appreciable MgO content.

The above discussion covers, in general terms, the effect of mixed C – H – O – F volatiles on ultrapotassic rock genesis, but does not address differences in source composition, and so cannot hope to explain the origin of the entire spectrum of potassic rocks. A number of esperimental studies on ultapotassic rocks (Arima and Edgar 1983a, b; Ryabchikov and Green 1978; Edgar et al. 1976; Barton and Hamilton 1979) indicate that discussion of a phlogopite harzburgite may be inappropriate for some compositions. This is backed up by studies of ultramafic xenoliths (Lloyd and Bailey 1975; Lloyd 1981) which show that the fluid which supplies K-enrichment to the mantle is reacting with the mantle rocks causing progressive elimination of orthopyroxene and even olivine in favour of mica and clinopyroxene. The observed northward increase in K and decrease in Si of the western rift lavas (Pouclet 1980b) may be related to a northward increase in the fluid component of the mantle source. Studies of such xenoliths provide insight into the K-enrichment processes, and may provide evidence of the nature and oxidation state of volatile mixtures at depth.

Conclusion

The arguments developed above from evidence in the system Ks-Fo-Qz with added fluorine support the suggestion of Jaques et al. (1984) that fluorine is an important controlling factor in lamproite petrogenesis. Many lamproites may originate in a reduced mantle, in which case the range in silica contents of primary magmas can be explained by variation in the depth of origin, with more silica-poor magmas originating at greater depths. The dissociation of less than 0.1 wt% water is sufficient to cause oxidation during transport from a reduced mantle to the oxidation states observed in lamproites at the surface. The effects of F, C/H ratio and f_{O_2} on a phlogopite harzburgite analogue as a source for ultrapotassic rocks can be tested by high-pressure experiments on natural ultrapotassic rock compositions with variations in these parameters. Individual areas of ultrapotassic volcanism can then be examined in the light of these experimental studies, combined with information gathered from the rocks themselves on fluid phase composition, oxidation state and pressure-temperature crystallisation path.

Acknowledgements. Financial support for this study was provided by University of Tasmania (SFF) and Commonwealth (WRT) postgraduate awards and ARGS support to DHG for the experimental laboratory. SM Kuehner, BH Scott-Smith, AJ Crawford and JW Sheraton kindly supplied samples from which micas were analysed for fluorine. The helpful comments of KL Harris, EJ Reid, AL Jaques, SM Kuehner, DJ Ellis, AJ Crawford and TJ Falloon have greatly assisted this work.

References

Aoki K, Ishikawa K, Kanisawa S (1981) Fluorine geochemistry of basaltic rocks from continental and oceanic regions and petrogenetic application. Contrib Mineral Petrol 76:53–59

Arculus RJ (1985) Oxidation status of the mantle: past and present. Ann Rev Earth Planet Sci 13:75–95

Arculus RJ, Delano JW (1981) Intrinsic oxygen fugacity measurements: techniques and results for spinels from upper mantle peridotites and megacryst assemblages. Geochim Cosmochim Acta 45:899–913

Arculus RJ, Dawson JB, Mitchell RH, Gust DA, Holmes RD (1984) Oxidation states of the upper mantle recorded by megacryst ilmenite in kimberlite and type A and B spinel lherzolites. Contrib Mineral Petrol 85:85–94

Arima M, Edgar AD (1981) Substitution mechanisms and solubility of titanium in phlogopites from rocks of probable mantle origin. Contrib Mineral Petrol 77:288–295

Arima M, Edgar AD (1983a) High pressure experimental studies on a katungite and their bearing on the genesis of some potassium-rich magmas of the west branch of the African Rift. J Petrol 24:166–187

Arima M, Edgar AD (1983b) A high pressure experimental study on a magnesian-rich leucite lamproite from the West Kimberley area, Australia: petrogenetic implications. Contrib Mineral Petrol 84:228–234

Atkinson WJ, Hughes FE, Smith CB (1984) A review of the kimberlitic rocks of western Australia. In: Kornprobst J (ed) Kimberlites I: Kimberlites and related rocks, pp 195–224

Bachinski SW, Simpson EL (1984) Ti-phlogopites of the Shaw's Cove minette: a comparison with micas of other lamprophyres, potassic rocks, kimberlites and mantle xenoliths. Am Mineral 69:41–56

Bailey DK (1978) Continental rifting and mantle degassing. In: Neumann ER, Ramberg IB (eds) Petrology and Geochemistry of continental rifts, D Riedel, p 1–13

Bailey DK (1980) Volcanism, earth degassing and replenished lithosphere mantle. Phil Trans Soc Lond Ser A 297:309–322

Barton M (1979) A comparative study of some minerals occurring in the potassium-rich alkaline rocks of the Leucite Hills, Wyoming, the Vico volcano, western Italy, and the Toro-Ankole region, Uganda. Neues Jahrb Mineral Abh 137:113–134

Barton M, Hamilton DL (1978) Water-saturated melting relations to 5 kilobars of three Leucite Hills lavas. Contrib Mineral Petrol 66:41–49

Barton M, Hamilton DL (1979) The melting relationships of a madupite from the Leucite Hills, Wyoming, to 30 kb. Contrib Mineral Petrol 69:133–142

Barton M, Hamilton DL (1982) Water-undersaturated melting experiments, bearing upon the origin of potassium-rich magmas. Mineral Mag 45:267–278

Barton M, Varekamp JC, van Bergen MJ (1982) Complex zoning of clinopyroxenes in the lavas of Vulsini, Latium, Italy: evidence for magma mixing. J Volcanol Geotherm Res 14:361–388

Bohlen SR, Peacor DR, Essene EJ (1980) Crystal chemistry of a metamorphic biotite and its significance in water barometry. Am Mineral 65:55–62

Brey GP, Green DH (1975) The role of CO_2 in the genesis of olivine melilitite. Contrib Mineral Petrol 49:93–103

Brey GP, Green DH (1976) Solubility of CO_2 in olivine melilitite at high pressures and role of CO_2 in the earth's upper mantle. Contrib Mineral Petrol 55:217–230

Burke K (1963) Dissolved gases in East African Lakes. Nature 198:568–569

Burnham CW (1979) The importance of volatile constituents. In: The Evolution of the Igneous rocks – Fiftieth Anniversary Per-

spectives. Yoder HS (ed) Princeton University Press, New Jersey, pp 439–482
Carmichael ISE (1967) The mineralogy and petrology of the volcanic rocks from the Leucite Hills, Wyoming. Contrib Mineral Petrol 15:24–66
Carmichael ISE, Nicholls JW (1967) Iron-titanium oxides and oxygen fugacities in volcanic rocks. J Geophys Res 72:4665–4687
Edgar AD, Arima M (1981) Geochemistry of three potassium-rich ultrabasic lavas from the west branch of the African Rift: interferences on their geneses. Neues Jahrb Mineral Monatsh H12:539–552
Edgar AD, Green DH, Hibberson WO (1976) Experimental petrology of a highly potassic magma. J Petrol 17:339–356
Eggler DH (1974) Effect of CO_2 on the melting of peridotite. Carnegie Inst Washington Yearb 73:215–224
Eggler DH (1978) The effect of CO_2 upon melting in the system $Na_2O-CaO-Al_2O_3-SiO_2-CO_2$ to 35 kb, with an analysis of melting in a peridotite $-H_2O-CO_2$ system. Am J Sci 278:305–343
Eggler DH (1983) Upper mantle oxidation state: evidence from olivine-orthopyroxene-ilmenite assemblages. Geophys Res Lett 10:365–368
Eggler DH, Baker DR (1982) Reduced volatiles in the system C–O–H: implications to mantle melting, fluid formation, and diamond genesis. In: Akimoto S, Manghnani M (eds) High pressure research in geophysics. Center for Academic Publications, Tokyo, pp 237–250
Foley SF (1985) The oxidation state of lamproitic magmas. Tschermaks Mineral Petrogr Mitt 34:217–238
Foley SF, Taylor WR, Green DH (1986a) The effect of fluorine on phase relationships in the system $KAlSiO_4-Mg_2SiO_4-SiO_2$ and the solution mechanism of fluorine in silicate melts. Contrib Mineral Petrol 93:46–55
Foley SF, Venturelli G, Green DH, Toscani L (1986b) The ultrapotassic rocks: Characteristics, Classification, and constraints for petrogenetic models. Earth Sci Rev (in press)
Fornaseri M, Ventriglia U, Scherillo A (1963) La regione vulcanica dei Colli Albani, Vulcano Laziale. CNR Rome
Freund F, Kathrein H, Wengeler H, Knobel R, Heinen HJ (1980) Carbon in solid solution in forsterite – a key to the untractable nature of reduced carbon in terrestrial and cosmogenic rocks. Geochim Cosmochim Acta 44:1319–1333
Freund F, Wengeler H, Kathrein H, Knobel R, Oberheuser G, Maiti GC, Reil D, Kotz J (1983) Hydrogen and carbon derived from dissolved H_2O and CO_2 in minerals and melts. Bull Mineral 106:185–200
Frost BR (1979) Mineral equilibria involving mixed volatiles in a C–O–H fluid phase: the stabilities of graphite and siderite. Am J Science 27:1035–1059
Fuster JM, Gastesi P, Sagredo J, Fermoso ML (1967) Las rocas lamproiticas del SE de Espana. Estud Geolog 23:35–69
Gerlach TM (1980) Chemical characteristics of the volcanic gases from Nyiragongo lava lake and the generation of CH_4-rich fluid inclusions in alkaline rocks. J Volcanol Geotherm Res 8:177–189
Haggerty SE, Tompkins LA (1983) Redox state of Earth's upper mantle from kimberlitic ilmenites. Nature 303:295–300
Hawkesworth CJ, Vollmer R (1979) Crustal contamination versus enriched mantle: $^{143}Nd/^{144}Nd$ and $^{87}Sr/^{86}Sr$ evidence from the Italian volcanics. Contrib Mineral Petrol 69:151–165
Holmes A (1937) The petrology of katungite. Geol Mag 74:200–219
Holmes A, Harwood HF (1932) Petrology of the volcanic fields east and south-east of Ruwenzori, Uganda. J Geol Soc London 88:370–439
Iddings JP, Morley EW (1915) Contributions to the petrography of Java and Celebes. J Geol 23:231–245
Jaques AL, Lewis JD, Smith CB, Gregory GP, Ferguson J, Chappell BW, McCulloch MT (1984) The diamond bearing ultrapotassic (lamproitic) rocks of the West Kimberley region, Western Australia. In: Kornprobst J (ed) Kimberlites I: Kimberlites and related rocks, pp 225–254
Kennedy CS, Kennedy GC (1976) The equilibrium boundary between graphite and diamond. J Geophys Res 81:2467–2470
Kilinc AI, Carmichael ISE, Rivers ML, Sack RO (1983) The ferric-ferrous ratio of natural silicate liquids equilibrated in air. Contrib Mineral Petrol 83:136–140
Kuehner SM, Edgar AD, Arima M (1981) Petrogenesis of the ultrapotassic rocks from the Leucite Hills, Wyoming. Am Mineral 66:663–677
Kushiro I (1968) Compositions of magmas formed by partial zone melting of the earth's upper mantle. J Geophys Res 73:619–637
Kushiro I (1972) Effect of water on the compositions of magmas formed at high pressures. J Petrol 13:311–334
Kushiro I (1980) Changes with pressure of degree of partial melting and K_2O content of liquids in the system $Mg_2SiO_4-KAlSiO_4-SiO_2$. Carnegie Inst Washington Yearb 79:267–271
Lloyd FE (1981) Upper mantle metasomatism beneath a continental rift: clinopyroxenes in alkali mafic lavas and nodules from South West Uganda. Mineral Mag 44:315–323
Lloyd FE, Bailey DK (1975) Light element metasomatism of the continental mantle: the evidence and the consequences. Phys Chem Earth 9:389–416
Luth WC (1967) Studies in the system $KAlSiO_4-Mg_2SiO_4-SiO_2-H_2O$. I. Inferred phase relations and petrologic applications. J Petrol 8:372–416
Mathez EA (1984) Influence of degassing on oxidation states of basaltic magmas. Nature 310:371–375
Mo X, Carmichael ISE, Rivers ML, Stebbins JB (1982) The partial molar volume of Fe_2O_3 in multicomponent silicate liquids and the pressure dependence of oxygen fugacity in magmas. Mineral Mag 45:237–245
Munoz JL, Eugster HP (1969) Experimental control of fluorine reactions in hydrothermal systems. Am Mineral 54:943–959
Nicholls JW (1980) A simple thermodynamic model for estimating the solubility of H_2O in magmas. Contrib Mineral Petrol 74:211–220
Nixon PH, Hornung G (1973) The carbonatite lavas and tuffs near Fort Portal, western Uganda. Inst Geol Sci Overseas Geol Mineral Res 41:168–179
O'Neill HS, Wall VJ (1982) Oxygen fugacities from the assemblage olivine-orthopyroxene-spinel. Research School Earth Sciences, Australian National University, Annual Report, pp 177–179
Pouclet A (1980a) Les laves du rift de l'Afrique centrale; revue des données pétrographiques et chimiques. Essai de magmatologie. Rapp Annu Mus Afr Centr 1979:81–128
Pouclet A (1980b) Contribution à la systématique des laves alcalines, les laves du rift de l'Afrique centrale (Zaire-Uganda). Bull Volcanol 43:527–540
Pouclet A, Menot R-P, Piboule M (1984) Differenciation des laves de l'Afrique Centrale (Rift Ouest) Contribution de l'analyse statistique multivariée. Neues Jahrb Mineral Abh 149:283–308
Rosenberg PE, Foit FF (1977) $Fe^{2+}-F$ avoidance in silicates. Geochim Cosmochim Acta 41:345–346
Ryabchikov ID, Green DH (1978) The role of carbon dioxide in the petrogenesis of highly potassic magmas. In: Problems of petrology of the earth's crust and upper mantle. Inst Geol Geofiz Nauka Novosibirsk 403:49–64
Ryabchikov ID, Green DH, Wall VJ, Brey GP (1981) The oxidation state of carbon in the reduced-velocity zone. Geochem Int 18:148–158
Sanz J, Stone WEE (1979) NMR study of micas. II. Distribution of Fe^{2+}, F^-, and OH^- in the octahedral sheet of phlogopites. Am Mineral 64:119–126
Sato M (1978) Oxygen fugacity of basaltic magmas and the role of gas-forming elements. Geophys Res Lett 5:447–449
Scott BH (1977) Petrogenesis of kimberlites and associated potassic lamprophyres from central West Greenland. Ph D thesis, Edinburgh University
Scott BH (1979) Petrogenesis of kimberlites and associated potassic lamprophyres from central west Greenland. In: Boyd FR, Meyer HOA (eds) Kimberlites, diatremes and diamonds: their

geology, petrology, and geochemistry. Am Geophys Union, pp 190–205
Scott BH (1981) Kimberlite and lamproite dykes from Holsteinsborg, West Greenland. Medd om Grøn. Geosci 4:1–24
Scott-Smith BH, Skinner EMW (1984) A new look at Prairie Creek, Arkansas. In: Kornprobst J (ed) Kimberlites. I. Kimberlites and related rocks, pp 255–283
Sekine T, Wyllie PJ (1982) Phase relationships in the system KAlSiO$_4$–Mg$_2$SiO$_4$–SiO$_2$–H$_2$O as a model for hybridisation between hydrous siliceous melts and peridotite. Contrib Mineral Petrol 79:368–374
Sheraton JW, Cundari A (1980) Leucitites from Gaussberg, Antarctica. Contrib Mineral Petrol 71:417–427
Sheraton JW, England RN (1980) Highly potassic mafic dykes from Antarctica. J Geol Soc Aust 27:129–135
Taylor WR (1985) The role of C–O–H fluids in upper mantle processes: a theoretical, experimental and spectroscopic study. Ph D thesis, University of Tasmania, Hobart
Van Kooten GK (1980) Mineralogy, petrology, and geochemistry of an ultrapotassic basaltic suite, central Sierra Nevada, California, USA. J Petrol 21:651–684
Velde D (1979) Trioctahedral micas in melilite-bearing eruptive rocks. Carnegie Inst Washington Yearb 78:468–475
Venturelli G, Capedri S, di Battistini G, Crawford AJ, Kogarko LN, Celestini S (1984) The ultrapotassic rocks from southeastern Spain. Lithos 17:37–54
Von Knorring O, du Bois CGB (1961) Carbonatitic lava from Fort Portal area in western Uganda. Nature 192:1064–1065
Wendlandt RF, Eggler DH (1980a) The origins of potassic magmas: I. Melting relations in the systems KAlSiO$_4$–Mg$_2$SiO$_4$–SiO$_2$ and KAlSiO$_4$–MgO–SiO$_2$–CO$_2$ to 30 kilobars. Am J Sci 280:385–420
Wendlandt RF, Eggler DH (1980b) Stability of sanidine + forsterite and its bearing on the genesis of potassic magmas and the distribution of potassium in the upper mantle. Earth Planet Sci Lett 51:215–220
Wendlandt RF, Eggler DH (1980c) The origins of potassic magmas: II. Stability of phlogopite in natural spinel lherzolite and in the system KAlSiO$_4$–MgO–SiO$_2$–H$_2$O–CO$_2$ at high pressures and high temperatures. Am J Sci 280:421–458
Woermann E, Rosenhauer M (1985) Fluid phases and the redox state of the Earth's mantle: extrapolations based on experimental, phase-theoretical and petrological data. Fortschr Mineral 63:263–349
Wyllie PJ (1978) Mantle fluid compositions buffered in peridotite-CO$_2$–H$_2$O by carbonates, amphibole, and phlogopite. J Geol 86:687–713
Wyllie PJ (1979) Magmas and volatile components. Am Mineral 64:469–500

Received May 21, 1985/Accepted June 9, 1986

835

Earth and Planetary Science Letters, 81 (1986/87) 95–103
Elsevier Science Publishers B.V., Amsterdam – Printed in The Netherlands

[1]

Glass inclusions in magnesian olivine phenocrysts from Tonga: evidence for highly refractory parental magmas in the Tongan arc

Trevor J. Falloon and David H. Green

Geology Department, University of Tasmania, Hobart, Tasmania 7001 (Australia)

Received May 20, 1986; revised version received September 8, 1986

During the 1984 "Natsushima" cruise to the North Tonga arc, fresh volcanic rocks were recovered from the Tongan forearc. Olivine phenocrysts in some of the dredged rocks are highly magnesian (Fo_{94}) and contain large (up to 0.2 mm) glass inclusions. The glass inclusion chemistry, as analysed by electron microprobe, is characterized by high CaO (> 13 wt.%) and low Na_2O (< 0.8 wt.%) contents, resulting in very high CaO/Na_2O ratios (18–29). Such high CaO/Na_2O ratios in glasses provide a ready explanation for the occurrence of extremely calcic plagioclase (up to An_{100}) in the Tongan arc lavas. The prevalence of magma mixing and the existence of a spectrum of liquids, ranging to the extremely refractory glasses analysed, is a characteristic of this intra-oceanic island arc environment. High P_{H_2O} is not important in precipitation of extremely calcic plagioclase from common low CaO/Na_2O liquids, although water plays a significant role in controlling melting in refractory source compositions.

1. Introduction

One of the important aims of petrological studies in island arcs is to determine the nature of "parental" and "primary" magmas for different magma series commonly observed (calc-alkaline, island arc tholeiite, boninite, etc.). However, most volcanic rocks of these series are phenocryst-rich and lie on compositional trend lines in which effects of crystal fractionation, contamination, magma mixing and volatile loss can be reasonably proven or inferred. It is commonly not possible to identify parental or primary compositions in these magma series without somewhat arbitrary assumptions.

It is possible to avoid these complications by studying glass inclusions in early crystallizing phases of island arc magmas, such as Cr-spinels, olivines and orthopyroxenes. These trap small samples of their host magma, preserving them as inclusions [1,2]. The only problem with this approach is to see through the effects of post-entrapment interaction between the host mineral and the glass inclusion.

We present here the compositions of trapped glass inclusions in very magnesian olivine (Fo_{94}) phenocrysts which occur in highly magnesian lavas dredged from the forearc of the North Tonga

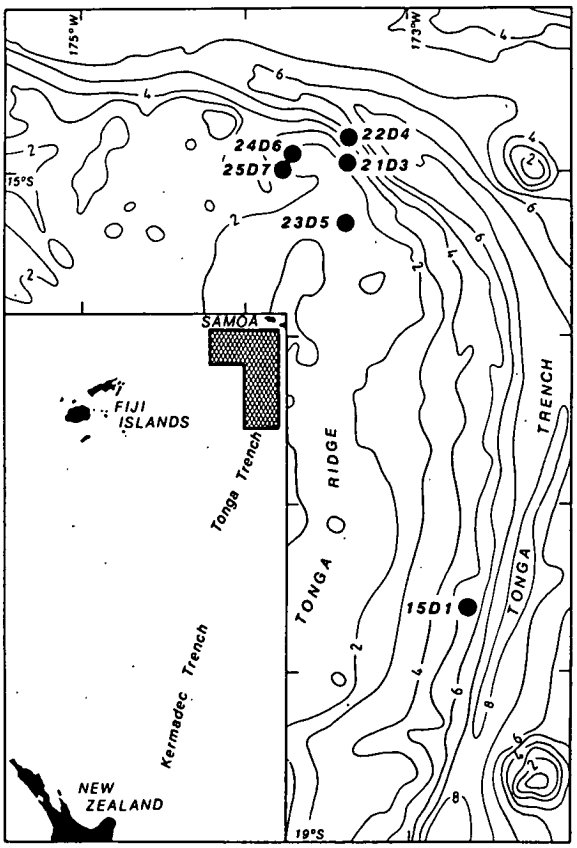

Fig. 1. Locality map of northern Tonga, showing locations of dredged igneous rocks [4]. High magnesian lavas were recovered from stations 21, 23, 24 and 25.

0012-821X/86/$03.50 © 1986 Elsevier Science Publishers B.V.

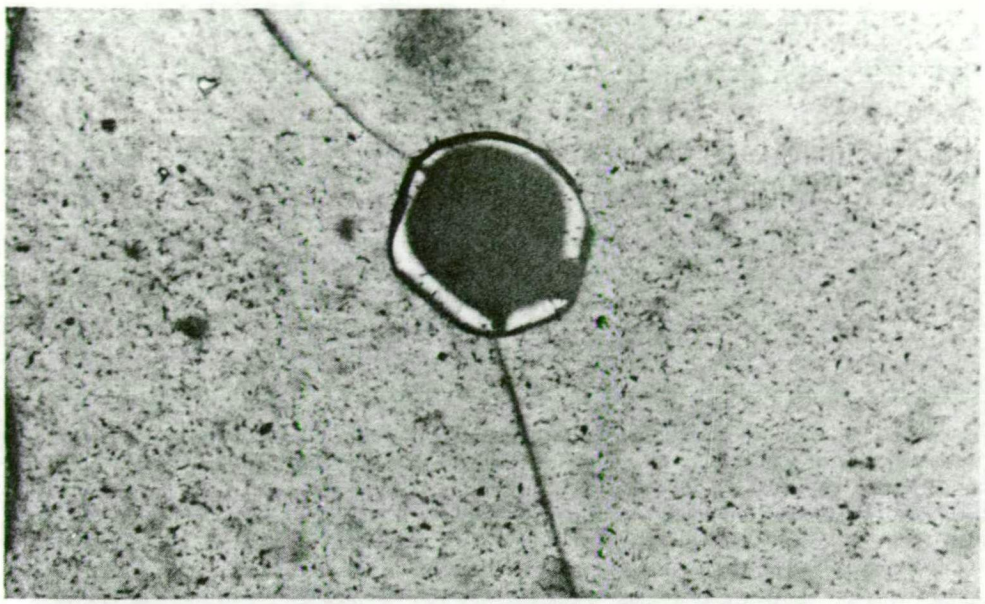

Fig. 2. An example of a well quenched glass inclusion in a magnesian olivine phenocryst (Fo_{94}), sample 5-25, station 23, crossed nicols, magnification 16×.

ridge during the 1984 cruise of the "Natsushima" [3,4]. The location of the dredged magnesian lavas is shown in Fig. 1; details of the location, petrography and geochemistry of the dredged rocks are given in Falloon and Green [4]. The particular samples reported here are 3-24 and 5-25 from stations 21 and 23 respectively (see [4]).

2. Petrography

The glass inclusions occur in large (< 1–5 mm) olivine phenocrysts, which have euhedral to resorbed grain boundaries and contain euhedral Cr-spinel inclusions. The olivines are very magnesian, with Fo_{94} in the cores, and rim compositions

Fig. 3. Well developed quench pyroxenes in a glass inclusion in an olivine phenocryst, sample 3-24, station 21, crossed nicols, magnification 6.3×.

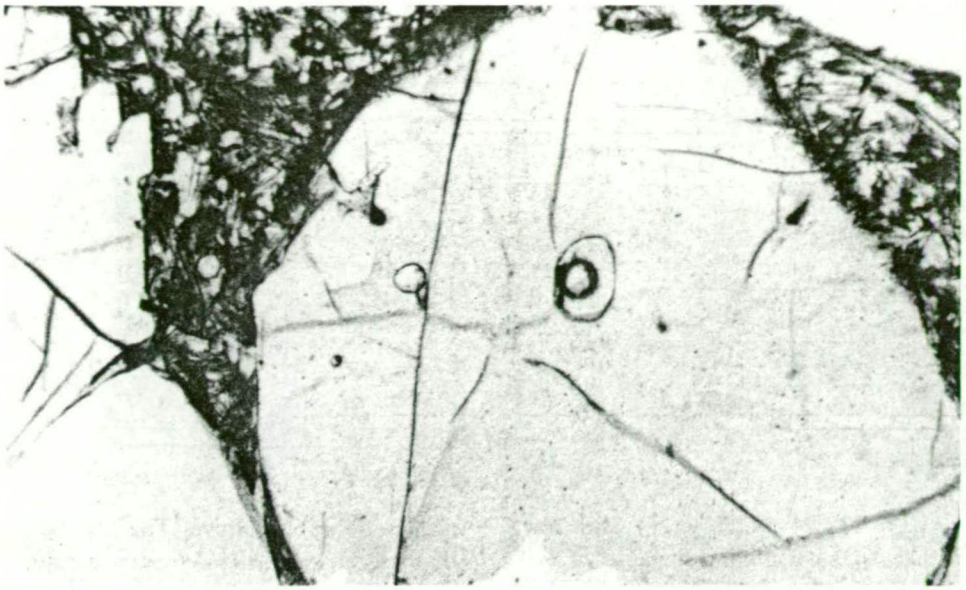

Fig. 4. An example of a breached glass inclusion in a magnesian olivine phenocryst (Fo_{94}). Groundmass of the host lava consists of pyroxene and glass. A smaller glass inclusion occurs to the left of the breached inclusion. Sample 5-25, station 23, plane polarised light, magnification 6.3×.

ranging from Fo_{85} to Fo_{88}; the latter are close to being in equilibrium with the quenched matrix of the host magma (Mg# = 0.706, Mg# = Mg/(Mg + Fe_t), Fe_t = total iron as FeO); however the magnesian cores are significantly out of equilibrium. The glass inclusions range in size from < 0.05 to 0.2 mm (Fig. 2). The glass in most of the inclusions has been effectively chilled, so that no quench crystals are visible under either optical or scanning electron microscopes. In some olivines, however, the glass inclusions display well developed quench pyroxenes (Fig. 3) of ferro-augite composition. No amphiboles or any other hydrous phases have been detected in any of the inclusions. The glass inclusions also have a trapped volatile component, evidenced by an empty vapour bubble (Fig. 4): we have not yet found examples of unbreached fluid inclusions.

3. Composition of the glass inclusions

The compositions of the glass inclusions were determined by a JEOL JXA-50A microprobe with an energy-dispersive analytical system. A composition range was observed with centres of large inclusions giving most magnesian compositions (6–8 wt.% MgO) and rims of larger inclusions and cores and rims of small inclusions giving more Fe-rich compositions (2–5 wt.% MgO, 4–5 wt.% FeO) relative to MgO. This effect is attributed to growth of quench olivine on the walls of inclusions and thus the cores of large inclusions give the closest approach to the original entrapped liquid.

Compositions of some of the glass inclusions in the olivine phenocrysts are listed in Table 1. The glass totals from the electron microprobe are approximately 95 wt.% indicating the possibility of H_2O dissolved in the glasses. This is currently being tested, using an infra-red microprobe technique. The glass compositions have all been modified by the host olivine, as evidenced by their low Mg# numbers (62–73), which are not in equilibrium with the host olivine core composition, assuming a K_d (equilibrium distribution coefficient for Fe and Mg between olivine and liquid) of 0.3 [5] and a $Fe^{2+}/(Fe^{2+} + Fe^{3+})$ ratio of 0.9. The olivine host becomes progressively more Fe-rich towards the glass inclusion; however it is difficult to establish the exact composition of the olivine immediately adjacent to the glass, due to glass-olivine overlap. The glasses have high SiO_2 contents (58–62 wt.%), low TiO_2 contents (0.19–0.22 wt.%), and high CaO contents (13.4–14.9 wt.%)

TABLE 1

Olivine glass inclusion microprobe analyses

	1	2	3	4	5	6	7	8
SiO_2	58.64	61.82	61.78	61.08	60.68	60.26	60.80	60.88
TiO_2	0.22	0.21	0.19	–	–	0.19	–	–
Al_2O_3	12.38	14.18	14.27	13.99	12.24	12.31	12.42	13.41
FeO	6.91	4.31	4.17	4.21	6.59	6.28	5.99	4.80
MgO	7.52	3.71	3.59	6.27	6.06	6.03	5.95	5.03
CaO	13.41	14.78	14.89	13.57	13.55	13.89	14.18	14.77
Na_2O	0.62	0.75	0.85	0.74	0.48	0.71	0.49	0.85
K_2O	0.19	0.16	0.16	0.15	0.30	0.20	0.17	0.18
Cl	0.10	0.08	0.10	–	0.11	0.12	–	0.07
Mg#	0.66	0.60	0.61	0.73	0.62	0.63	0.64	0.65

Analyses 1, 2, 6, 7, 8 are spot analyses, 3, 4, 5 are broad area scan analyses.
Glass totals normalised to 100%.

relative to Al_2O_3 (12.24–14.27 wt.%) and low Na_2O (0.48–0.85 wt.%) contents. Because of the high CaO contents, the inclusions have high CaO/Al_2O_3 ratios (0.97–1.14) and exceptionally high CaO/Na_2O ratios (18–29).

Under the electron beam, especially during spot analysis, Na_2O may volatilize, resulting in anomalously low Na_2O contents. This problem was investigated by (1) comparing spot and broad area scans of the same inclusion, and (2) by monitoring the counts on Na with time, for a spot analysis. Both approaches confirmed that Na-volatilization was not a problem, using the very low beam current (0.7 nA) and spot and area scan techniques described above. The low Na_2O contents of these inclusions is definitely a primary feature.

4. Chemical affinities of the calculated parental magma composition

To establish the original magma chemistry sampled by a glass inclusion prior to post-entrapment processes it is necessary to incrementally add back olivine to the most magnesian glass compositions analysed. Two assumptions required are the $Fe^{2+}/(Fe^{3+} + Fe^{2+})$ ratio of the glass (0.9), and the Fe-Mg K_d between olivine and liquid (0.3). The relatively reduced $Fe^{2+}/(Fe^{3+} + Fe^{2+})$ ratio

TABLE 2

Refractory melts developed in oceanic tensional settings

	1	2	3	4	5	6
SiO_2	48.3	50.42	52.4	54.72	58.09	50.9
TiO_2	0.6	0.34	0.3	0.15	0.14	0.6
Al_2O_3	13.7	15.75	11.7	9.57	7.11	14.4
FeO	7.9	8.59	8.4	7.22	9.22	6.9
MnO	0.1	0.16	0.1	–	–	0.1
MgO	16.7	9.78	15.8	17.15	20.70	12.1
CaO	10.9	14.67	10.7	10.50	3.91	13.6
Na_2O	1.7	0.99	0.7	0.54	0.62	1.4
K_2O	0.1	0.01	0.1	0.15	0.21	0.1
Total	100.0	100.71	100.2	100.00	100.00	100.1
Mg#	0.79	0.67	0.77	0.81	0.80	0.76

1 = primary MORB magma composition, olivine tholeiite DSDP3-18-7-1 [25]+17% Fo_{91} [12].
2 = Lau Basin basalt glass analysis 123 95-12 [26].
3 = inferred Upper Pillow lava parental liquid [6].
4 = calculated parental magma composition in equilibrium Fo_{94} olivine.
5 = Cape Vogel, parental magma composition [27].
6 = xenocryst melt inclusions [8].

of 0.9 was chosen as the Cr-spinels which also occur as inclusions in the olivine phenocrysts, have very low Fe^{3+} contents ($Fe^{3+}/(Fe^{3+} + Al + Cr) \sim 0.06$) suggesting relatively low f_{O_2} in the original magma which crystallized the magnesian olivines. An example of a calculated magnesian magma composition, in equilibrium with Fo_{94} olivine, is given in Table 2 (analysis 4). The calculated Tongan composition in terms of its high CaO, high CaO/Na_2O and CaO/Al_2O_3 ratios has geochemical affinities to proposed second-stage melts developed in oceanic tensional environments [6,7], such as the Upper Pillow Lavas from the Troodos ophiolite, Cyprus, and basalts from the Lau Basin (examples given in Table 2). Compared to stage-one melts, which are parental to typical MORB, second-stage melts have characteristically higher SiO_2 and CaO, and lower TiO_2 and Na_2O contents. A typical stage-one parental composition to MORB is given in Table 2 (analysis 1), it has a CaO/Na_2O ratio of 6.41 and a CaO/Al_2O_3 ratio of 0.79. The Tongan composition and other second-stage melts have CaO/Na_2O ratios $> \sim 14$ and CaO/Al_2O_3 ratios $> \sim 0.9$. Magmas of these characteristics have so far not been identified from major mid-ocean ridge tectonic environments, however several compositions have been identified which have a second-stage melt "fingerprint". These are (1) xenocryst melt inclusions (Table 2, analysis 6, from the Mid-Atlantic Ridge [8], (2) basaltic glass from DSDP Site 236, Indian Ocean [9], (3) basaltic glass from the Costa Rica rift zone [10]. All these samples have higher CaO/Na_2O and CaO/Al_2O_3 ratios than typical MORB. It is possible that more extreme compositions, such as those from Tonga, Troodos and the Lau Basin are involved in the production of ocean crust but are not directly observed due to processes such as magma mixing.

The Tonga composition shows the closest affinities to the inferred parental liquid to the Troodos ophiolite, Cyprus, but contains higher SiO_2 (54.7 compared to 52.4 wt.%) and lower Na_2O contents (0.54 compared to 0.7 wt.%) and TiO_2 contents (0.15 compared to 0.3 wt.%). Such compositions may be a characteristic of forearc tensional environments. Boninites are another primitive magma composition which have been recovered from the forearc regions of West Pacific island arcs. These are distinctly different from the

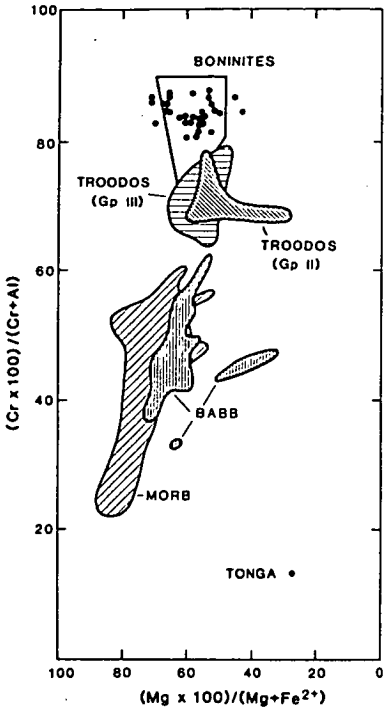

Fig. 5. 100Cr/(Cr+Al) and 100Mg/(Mg+Fe) variations in spinel inclusions in magnesian olivine phenocrysts from North Tonga (Falloon, unpublished data) compared with spinels from back-arc basin basalts (BABB), mid-ocean ridge basalts, boninites [18], and Troodos Upper Pillow lavas [7].

Troodos, Tongan and Lau Basin compositions, in their characteristically high SiO_2 and very low CaO contents, which result in low CaO/Na_2O and characteristically low CaO/Al_2O_3 ratios ($\sim < 0.6$). Although there are distinct major element differences between the primitive Tongan liquid identified and boninites, the Tongan composition does have geochemical affinities to boninites in terms of Cr-spinel compositions. Cr-spinels also occur as euhedral inclusions in the magnesian olivines containing the glass inclusions. They have very high Cr# > 0.80, overlapping with Cr-spinels from boninites, and are distinctly more Cr-rich than spinels from Troodos (Cr# < 0.80), (Fig. 5). The similarity in Cr-spinel compositions between the Tongan and boninite compositions indicates that they were derived from similar depleted mantle sources. There appears to be a spectrum of primitive magma compositions being supplied to the forearc and possibly back-arc regions of intra-oceanic island arcs.

The compositions in Table 2 are plotted in Fig. 6, for comparison with equilibrium partial melt compositions from a MORB pyrolite composition (Falloon and Green, unpublished results) and a more depleted peridotite composition; Tinaquillo lherzolite ([11] and Green et al. unpublished results). The stage-one melt S_1, is the MORB parental composition from Green et al. [12] (DSDP3-18-7-1 + 17 wt.% Fo_{91}), which is a primary melt at 20 kbar, segregating from an upper mantle peridotite (M, Fig. 6) at 1420°C leaving a harzburgite residue (R, Fig. 6). The residual diapir from this first stage melting event may continue to rise adiabatically and generate an additional melt fraction at some shallower depth. The range of second-stage melts (S_2, S_3, S_4, S_5, S_6) indicate a range of depleted residual mantle sources. Experimental studies on the Troodos parental composition (S_3), suggest it is a primary magma, having segregated from depleted upper mantle peridotite at about 25 km, 1360°C leaving a harzburgite residue, with a water content of 0.5–1.0 wt.% [7]. The position of the Tongan primitive magma identified from the olivine glass inclusions (S_4), indicates a pressure of melt segregation of < 5 kbar under anhydrous conditions in equilibrium with a harzburgite residue or at slightly higher pressures (7–8 kbar), similar to the Troodos composition but at higher water pressures. The position of the boninite parental composition (S_5) requires it to have the most depleted of mantle sources. Experimental work by Jenner [13] indicates that boninite compositions may derive from quite shallow levels (< 5 kbar), provided water is present. The position of the Lau Basin glass (S_2) and the xenocryst melt inclusion (S_6) suggests that they are possible primary magmas at pressures of < 8 kbar under anhydrous conditions, leaving a lherzolite residue from a mantle source similar to typical MORB but more depleted in Na_2O and TiO_2. Although this inference is compatible with the Jd + CaTs–Ol–Qz plot, it is not consistent with low pressure cotectic melts plotted in the Di–Ol–Qz plane of the basalt tetrahedron. The compositions

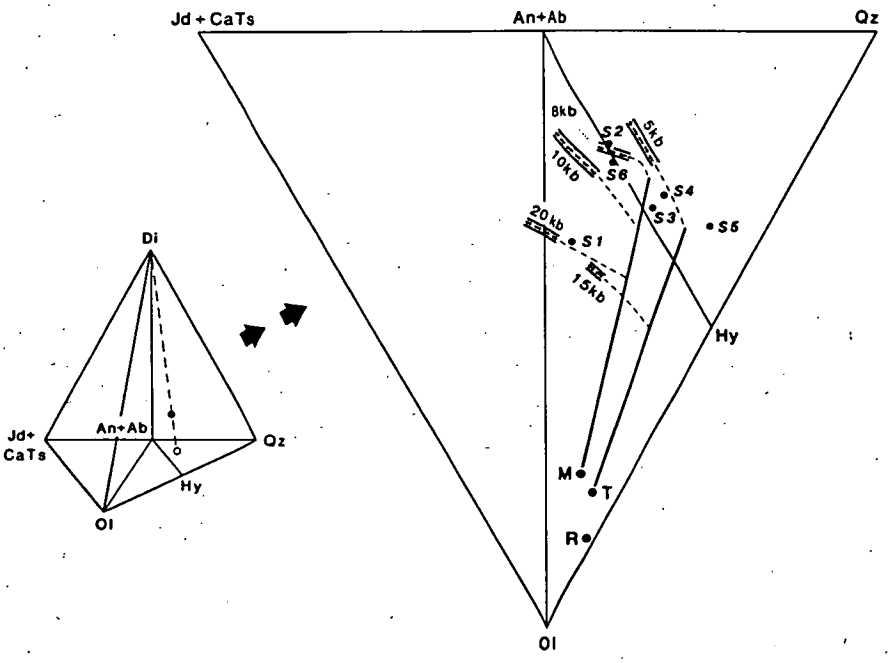

Fig. 6. CIPW molecular norm projection from Di onto the base of the basalt tetrahedron Jd + CaTs–Oliv–Qtz. M is a MORB pyrolite composition (Falloon and Green, unpublished data), T is Tinaquillo lherzolite [11] and R is the residual mantle composition after removal of stage-one melt composition S_1 (DSDP3-18-7-1 + 17 wt.% Fo_{91} [12]) from MORB pyrolite. Compositions S_1 to S_6 are taken from Table 2, analyses 1–6 respectively. Lines represent cotectics derived from the experimental melting of MORB pyrolite (Falloon, unpublished data) and Tinaquillo lherzolite ([11], Green et al., unpublished data). Solid lines represent locus of liquids in equilibrium with olivine only. Dashed lines represent locus of liquids in equilibrium with olivine and orthopyroxene only and dashed area represents locus of liquids in equilibrium with olivine and orthopyroxene and clinopyroxene.

(S_2, S_6) plot above the ol + opx + cpx + l cotectic, lying in the cpx phase volume in the Di–Ol–Qz projection from An + Ab. This suggests that S_2 and S_6 are fractionated compositions, having undergone olivine fractionation from more picritic parents.

5. Implications for calcic plagioclase in island arc and mid-ocean ridge basalts

The origin of extremely calcic plagioclase phenocrysts and megacrysts is a problem common to basalts both from island arcs and mid-ocean ridges [8,14–16]. Plagioclase in dredged lavas from the North Tonga arc occurs as both discrete phenocrysts and in large glomeroporphyritic clusters, either by itself or associated with clinopyroxene and orthopyroxene. Plagioclase can be either euhedral or subhedral, commonly displaying evidence of resorption. The plagioclase is extremely calcic, phenocryst core compositions range from An_{81} to An_{100}, and most plagioclase cores are $> An_{90}$. These calcic plagioclase phenocrysts are not in equilibrium with the host rock in which they are found. This is demonstrated in Fig. 7 where the straight line shows the empirical relationship between the 100Ca/(Ca + Na) ratio of a bulk composition and the most anorthitic plagioclase which can crystallize from that composition under *anhydrous conditions*. The empirical relationship only holds for rocks of basaltic composition of between 15 and 25% normative diopside, thus the relationship is applicable to MORB and the Tongan compositions. The line was constructed from the experimental studies listed in the caption of Fig. 7 and consisted of taking the most anorthitic plagioclase that crystallized, in a particular bulk composition, regardless of pressure or temperature. Thus the relationship shown in Fig. 7 is a more general relationship than the Drake [17] approach which requires some independent means of determining temperature before a plagioclase composition can be determined. The relationship in Fig. 7 emphasises the strong relationship between plagioclase composition and the 100Ca/(Ca + Na) ratio of the bulk rock composition. For anhydrous conditions, the plagioclase phenocryst cores in the Tongan lavas are out of equilibrium with their host rocks, i.e. they are hosted in rocks which have lower Ca/(Ca + Na)

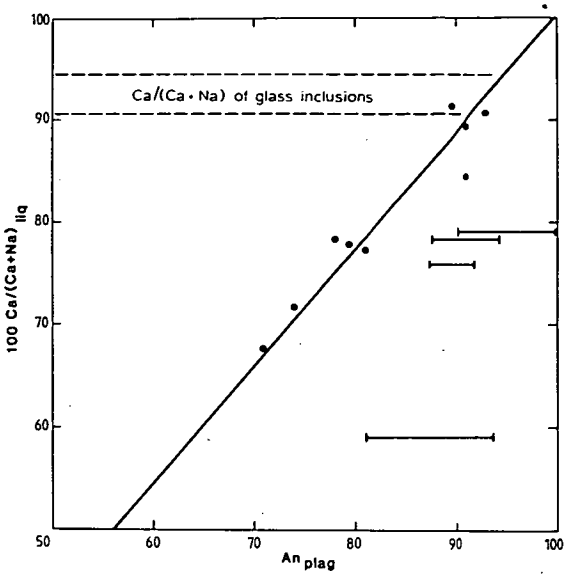

Fig. 7. The empirical relationship between the Ca/(Ca + Na) ratio of a bulk composition and the most anorthite-rich plagioclase capable of crystallizing under anhydrous conditions regardless of pressure and temperature (restricted to basaltic compositions of between 15 and 25 wt.% normative diopside). The line is based on the experimental studies [7,12,19–23]. ● = the data points taken from the above experiments. Bars indicate the range in plagioclase core compositions from dredged lavas from the North Tonga arc (Falloon, unpublished data).

ratios than would be expected, similar results are found for MORB (see [16, Fig. 16]). An increase in P_{H_2O} is commonly cited in the literature, as an explanation of very anorthite-rich plagioclase in basaltic magma, based on experimental work in simple systems [15]. However, this effect in complex systems has so far not been demonstrated experimentally. Increasing P_{H_2O} will lower the plagioclase liquidus relative to clinopyroxene and orthopyroxene [28], causing a less anorthite-rich plagioclase to crystallize, due to enhanced pyroxene fractionation. At the present time, P_{H_2O} can not be considered as having an important effect on the liquidus plagioclase composition, rather the bulk composition of the magma as reflected in its Ca/(Ca + Na) ratio, will have the determining role.

The relationship in Fig. 7 requires the existence of magmas with 100Ca/(Ca + Na) ratios of between 78 and 100 to account for the calcic plagioclase phenocrysts. The glass inclusions in the olivine phenocrysts from Tonga have 100 Ca/

(Ca + Na) ratios of between 91 and 94 (Fig. 7), and thus provide a ready solution to the problem of calcic plagioclase phenocrysts in the Tongan arc magmas. These calcic magmas may not be represented or seen in island arc and MORB lava piles due to the efficiency of processes such as magma mixing, which modify and mask primary compositional characteristics. This effect is illustrated in Fig. 8 where the CaO/Na_2O ratios of Tongan lavas are plotted against MgO contents. The inferred fractionation path of the primitive liquid composition, identified from glass inclusions, is also illustrated. The fractionation of mafic phases such as olivine will have little effect on the CaO/Na_2O ratio whereas the pyroxenes will have a slight (orthopyroxene) to major (clinopyroxene) effect on the CaO/Na_2O ratio. The primitive Tongan composition will fractionate mafic phases until plagioclase saturation is reached and the plagioclase composition which crystallizes will be very calcic. These partially crystallized liquids, containing plagioclase and other phenocrysts can then be mixed with magmas of lower CaO/Na_2O ratios. Thus the bulk rock compositions from dredged and emergent island samples (Fig. 8) may represent the mixing of at least two liquids, one of which is defined by the melt inclusions, and the other by the quenched glasses and aphyric groundmass compositions of the host rocks; this suggests similar ol + opx control but with lower CaO/Na_2O ratios. Some of the groundmass compositions for the Tongan lavas have significantly lower CaO/Na_2O ratios than some of the whole rock compositions. This could be explained by contributions from magmas of high CaO/Na_2O ratios being mixed into the more common low CaO/Na_2O ratio magmas. In Fig. 8 several different mixing lines are shown to illustrate this point. Mixing may occur at any point along the fractionation trend of the primitive Tonga composition, accounting for the scatter in data points seen in this diagram.

Acknowledgements

Financial support for this study was provided by a Commonwealth postgraduate award to T.J.F. and a grant from the Department of Science and Technology. Technical assistance was provided by W. Jablonski. Thanks to A.J. Crawford for helpful discussions of this work. Thanks also to the captain and crew of the "Natsushima" and to chief scientists E. Honza and K. Lewis and fellow shipboard scientists.

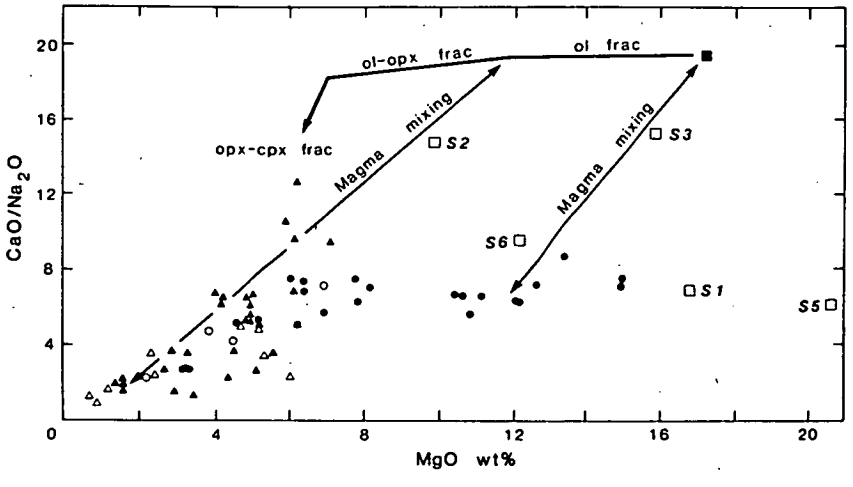

Fig. 8. CaO/Na_2O ratio versus MgO wt.% for Tonga lavas from the Tonga islands (▲) [24], and dredged lavas from the North Tongan arc (●) [4]. ■ = is the primitive magma composition identified from glass inclusions in olivines. Compositions labelled S_1, S_2, S_3, S_4, S_5, and S_6 are from Table 2. O = groundmass compositions from dredged lavas from the North Tonga arc (Falloon, unpublished data). △ = calculated groundmass compositions for lavas from the Tongan islands [24]. Thick solid line is the inferred fractionation path for the primitive magma composition identified from melt inclusions..

References

1 A.T. Anderson, Evidence for a picritic, volatile-rich magma beneath Mt. Shasta, California, J. Petrol. 21, 743–799, 1974.

2 E.B. Watson, Glass inclusions as samples of early magmatic liquid: Determinative method and application to a south Atlantic basalt, J. Volcanol. Geotherm. Res. 1, 73–84, 1976.

3 E. Honza, K.B. Lewis and Shipboard Party, A Marine Geological and Geophysical Survey of the Northern Tonga Ridge and Adjacent Lau Basin, Natural Resources of Tonga, Field Report 1, in press, 1986.

4 T.J. Falloon and D.H. Green, Dredged igneous rocks from the Northern Termination of the Tofua Magmatic Arc, Tonga and adjacent Lau Basin, submitted to N.Z. J. Geol. Geophys.

5 P.L. Roeder and R.F. Emslie, Olivine-liquid equilibrium, Contrib. Mineral. Petrol. 29, 275–289, 1970.

6 R.A. Duncan and D.H. Green, Role of multistage melting in the formation of oceanic crust, Geology 8, 22–26, 1980.

7 R.A. Duncan and D.H. Green, The genesis of refractory melts in the formation of oceanic crust, submitted to Contrib. Mineral. Petrol., 1986.

8 C.H. Donaldson and R.W. Brown, Refractory megacrysts and magnesian-rich melt inclusions within spinel in oceanic tholeiites: indicators of magma mixing and parental magma composition, Earth Planet. Sci. Lett. 37, 81–89, 1977.

9 W.G. Melson, G.R. Byerly, J.A. Nelen, T. O'Hearn, T.L. Wright and T. Vallier, A catalog of major element chemistry of abyssal volcanic glasses, Smithsonian Contrib. Earth Sci. 19, 31–60, 1977.

10 L.K. Autio and J.M. Rhodes, Costa Rica rift zone basalts: geochemical and experimental data from a possible example of multistage melting, in: J.R. Cann, M.G. Langseth, J. Honnorez, R.P. Von Herzen and S.M. White, Initial Reports of the Deep Sea Drilling Project 69, pp. 729–745, U.S. Government Printing Office, Washington, D.C., 1984.

11 A.L. Jaques and D.H. Green, Anhydrous melting of peridotite at 0-15 kb pressure and the genesis of tholeiitic basalts, Contrib. Mineral. Petrol. 73, 287–310, 1980.

12 D.H. Green, W.O. Hibberson and A.L. Jaques, Petrogenesis of mid-ocean ridge basalts, in: The Earth: Its origin, Structure and Evolution, M.W. McElhinney, ed., pp. 265–299, Academic Press, London, 1979.

13 G.A. Jenner, Petrogenesis of high-Mg andesites: an experimental and geochemical study with emphasis on high-Mg andesite from Cape Vogel, P.N.G., Ph.D. Thesis, University of Tasmania, Hobart, Tasmania, 1983.

14 J.B. Gill, Orogenic Andesites and Plate Tectonics, 385 pp., Springer-Verlag, New York, N.Y., 1981.

15 R.J. Arculus and K.J.A. Wills, The petrology of plutonic blocks and inclusions from the Lesser Antilles island arc, J. Petrol. 21, 743–799, 1980.

16 D.S. Stakes, J.W. Shervais and C.A. Hopson, The volcanic-tectonic cycle of the FAMOUS and AMAR Valleys, Mid-Atlantic Ridge (36 47° N): evidence from basalt glass and phenocryst compositional variations for a steady state magma chamber beneath the Valley midsections, AMAR, J. Geophys. Res. 89, 6995–7028, 1984.

17 M.J. Drake, Plagioclase-melt equilibria, Geochim. Cosmochim. Acta 50, 457–465, 1976.

18 H.J.B. Dick and T. Bullen, Chromian spinel as a petrogenetic indicator in abyssal and alpine-type peridotites and spatially associated lavas, Contrib. Mineral. Petrol. 86, 54–76, 1984.

19 D.H. Green, A.E. Ringwood, N.G. Ware and W.O. Hibberson, Experimental petrology and petrogenesis of Apollo 14 basalts, Proc. 3rd Lunar Sci. Conf. 1, pp. 197–206, 1972.

20 J.F. Bender, F.N. Hodges and A.E. Bence, Petrogenesis of basalts from the project FAMOUS area: experimental study from 0 to 15 kbars, Earth Planet. Sci. Lett. 41, 277–302, 1978.

21 T. Fujii and H. Bougault, Melting relations of a magnesian abyssal tholeiite and the origin of MORBs, Earth Planet. Sci. Lett. 62, 283–295, 1983.

22 M.A. Dungan, P.E. Long and J.M. Rhodes, The petrography, mineral chemistry and one-atmosphere phase relations of basalts from Site 395, in: W.G. Melson, P.D. Rabinowitz et al., Initial Reports of the Deep Sea Drilling Project 45, pp. 461–477, U.S. Government Printing Office, Washington, D.C., 1978.

23 H. Fukuyama and K. Hamuro, Melting relations of Leg 46 Basalts at atmospheric pressure, in: L. Dmitriev, J. Heirtzler et al., Initial Reports of the Deep Sea Drilling Project 46, pp. 215–226, U.S. Government Printing Office, Washington, D.C., 1978.

24 A. Ewart, W.B. Bryan and J.B. Gill, Mineralogy and geochemistry of the younger volcanic islands of Tonga, S.W. Pacific, J. Petrol. 14, 429–465, 1973.

25 F.A. Frey, W.B. Bryan and G. Thompson, Atlantic Ocean Floor Geochemistry and Petrology of Basalts from Legs 2 and 3 of the Deep Sea Drilling Project, J. Geophys. Res. 79, 5507–5527, 1974.

26 J.W. Hawkins and J.T. Melchior, Petrology of Mariana Trough and Lau Basin basalts, J. Geophys. Res. 90, 11431–11468, 1985.

27 D.A. Walker and W.E. Cameron, Boninite primary magmas: evidence from the Cape Vogel Peninsula, P.N.G., Contrib. Mineral. Petrol. 83, 150–158, 1983.

28 T. Sekine, T. Katsura and S. Aramaki, Water saturated phase relations of some andesites with application to the estimation of the initial temperature and water pressure at the time of eruption, Geochim. Cosmochim. Acta 43, 1367–1376, 1979.

B37

Magmatic Processes: Physicochemical Principles
© The Geochemical Society, Special Publication No. 1, 1987
Editor B. O. Mysen

Mantle-derived magmas—roles of variable source peridotite and variable C–H–O fluid compositions

D. H. GREEN, T. J. FALLOON and W. R. TAYLOR
Geology Department, University of Tasmania, GPO Box 252C, Hobart, Australia 7001

Abstract—The system forsterite–nepheline–quartz is a useful simple system analogue of melting relations in upper mantle peridotite. The liquidus phase fields at 28 kbar differ from those at low pressure by expansion of the enstatite field at the expense of forsterite. The system illustrates a large field of liquid compositions, from model basanites to model quartz tholeiites, which can be derived from one peridotite source. More refractory source compositions permit a greater compositional range of derivative liquid compositions than more fertile compositions and in particular are required as source or parent compositions for enstatite-rich liquids.

The effects of C–H–O volatiles on melting relationships have been explored with H_2O, CH_4 and CO_2–vapour saturated experiments. The effect of water is to expand the olivine field and depress liquidus temperatures by 350–400°C, but liquids at low degrees of melting of a model peridotite remain nepheline–normative. The effect of CO_2 is most marked with liquids moving to increasingly undersaturated compositions. Methane saturation produces a similar liquidus depression but results in OH^- solution, low carbon solubility and a reduced melt structure, *i.e.*, Si:O < 1:2.

The studies in the simple Fo–Ne–Qz system are matched by melting studies of several peridotite compositions and by liquidus studies on a variety of magnesian primary magmas from different tectonic settings. Mid-ocean ridge basalts are most commonly deriviative from picritic parents at 15–20 kbar although some low-olivine to quartz tholeiite liquids are probably primary from approximately 8 kbar pressure. However, other primary magmas such as high-magnesium quartz tholeiites and olivine-poor tholeiites and the very siliceous, low-calcium boninite liquids, are derived from much more refractory source rocks than MORB and require two-stage or multistage melting processes. The role of C–H–O fluids in fluxing such multi-stage melting on convergent margins is very important. An additional source of water, accompanied by low f_{O_2} *conditions (i.e.,* $H_2O > CH_4$ fluids) is identified in the redox-interaction of oxidized lithosphere with $CH_4 > H_2$ fluids degassing from the deep earth.

INTRODUCTION

N SEEKING to unravel the complexities of magma genesis in the earth's upper mantle, experimental petrologists have successfully demonstrated the diversity of basaltic magmas which can arise from the same source composition by variation of pressure (depth of magma segregation) and temperature (degree of partial melting) (see BASALTIC VOLCANISM STUDY PROJECT, 1981, and references therein). In addressing the same problem, isotope geochemists have demonstrated that mantle-derived magmas have formed from isotopically different sources or reservoirs which have remained isolated and with considerably different ratios of radiogenic elements for long periods of time (BASALTIC VOLCANISM STUDY PROJECT, 1981, and references therein). Some studies of trace element geochemistry have helped to link these two approaches (*e.g.*, FREY *et al.*, 1978), particularly by emphasizing the role played by large differences in partition coefficients between residual crystals and liquids for different elements and have introduced concepts of distinctive behaviour for 'compatible' vs 'incompatible' elements, 'LIL-element', 'HFS' elements, 'light' vs 'heavy' rare earth elements etc.

It is possible that the mantle source regions for primary magmas may be relatively homogeneous in major and compatible elements but quite widely variable in incompatible elements, *i.e.*, those which are perceived as mobile because of high solubility in mantle fluid phase(s) or in small, volatile-rich melt phases. This view finds support from studies of mantle lherzolite samples which provide evidence for multievent histories including late stage enrichment in incompatible elements (BASALTIC VOLCANISM STUDY PROJECT, 1981) and from the recognition of mantle-derived peridotites which are extremely depleted in incompatible elements yet retain major element chemistry with large 'basaltic component' (CaO, $Al_2O_3 > 3$ weight percent; FREY and GREEN, 1974; MENZIES, 1983; KURAT *et al.*, 1980; FREY *et al.*, 1985).

In this paper our major concern is to demonstrate that the mantle source regions for basaltic magmas are inhomogeneous in terms of major elements and that the inhomogeneity arises principally from multistage melting of more primitive mantle lherzolite. Our further purpose is to elaborate the role of C–H–O fluids in controlling the presence or absence of melting and to present arguments for redox-interactions between oxidized ($H_2O + CO_2$)

lithosphere and reduced ($CH_4 + H_2$) deeper mantle, within the tectonic framework of large-scale subduction and transform faulting along convergent margins of lithospheric plates.

We will firstly present data on a simple system forsterite (Fo)–nepheline (Ne)–silica (Qz), as a convenient means of illustrating the principles involved in the study of the multicomponent natural system.

A SIMPLE SYSTEM ANALOGUE FOR BASALT GENESIS (Fo–Ne–Qz)

YODER and TILLEY (1962) introduced the concept that the broad family of basalts, from olivine nephelinites, through basanites, alkali olivine basalts, picrites, olivine tholeiites to quartz tholeiites and basaltic andesites, could be pictured as a continuum of compositions within the 4-component tetrahedron with apices represented by olivine, quartz, cinopyroxene and feldspathoids. Since that time experimental petrologists have devoted much effort to defining, as functions of pressure and volatile content, the liquidus fields and cotectics, thermal divides and liquid evolution paths within the tetrahedron. Parallel approaches to the problem have used natural basaltic compositions and simple system analogues.

The system forsterite–nepheline–quartz (Fo–Ne–Qz) serves as a simplified analogue of basalt/peridotite in that it contains low melting liquids enriched in sodium aluminosilicate and large liquidus fields for olivine and enstatite. The system has been studied at 28 kbar under dry conditions by WINDOM and BOETTCHER (1981) and GUPTA *et al.* (1986). A pressure of 28 kbar approximates that near the top of the Earth's Low Velocity Zone beneath oceanic lithosphere, *i.e.*, depths of 80–90 km. In terms of mantle magma genesis, the most important boundary in Fo–Ne–Qz is the cotectic between olivine and enstatite which defines the range of liquids formed by increasing degrees of melting of mantle peridotite in the presence of residual olivine and enstatite.

Initial melts (Figure 1) of a model mantle, *i.e.*, olivine + enstatite + jadeite, are 'basanitic' with similar normative nepheline and albite contents. The partial melting involves the reaction Forsterite (Fo) + Jadeite (Jd) → Enstatite (En) + Liquid as the enstatite liquidus surface crosses the Fo–Jd join. With increasing temperature, liquids traverse the base of the simplified basalt tetrahedron passing from nepheline-normative compositions into hypersthene-normative compositions.

We wish to consider melting of two model peridotite compositions, a relatively 'fertile' peridotite

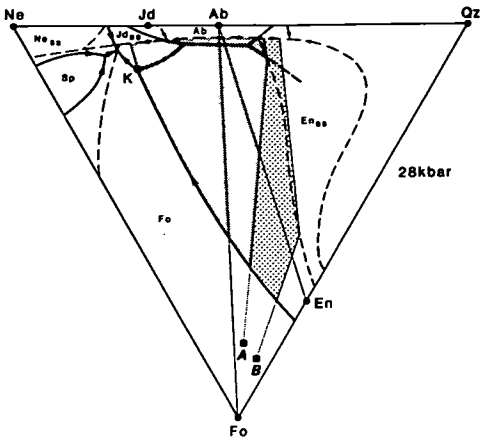

FIG. 1. Liquidus surface of the system Ne–Fo–Qz [weight percent] at 1 bar (dashed lines) and 28 kbar (solid lines) (see text for source references). Liquids formed by melting of a jadeite–enstatite–forsterite assemblage vary from composition K along the olivine–enstatite cotectic until enstatite or olivine is eliminated from the residue. The heavily shaded area includes all liquid compositions which can be derived from model peridotite A by single stage melting at 28 kbar to 1 bar. The more refractory peridotite composition B can yield liquids within the same area but *also* within the lightly shaded area.

(A) (enriched in the low-melting components), and a relatively 'refractory' peridotite (B). It is clear from Figure 1, that although the initial melt composition in each peridotite is the same (at the Fo–En–Jd invariant point) the more refractory peridotite will traverse further along the olivine–enstatite cotectic before enstatite is eliminated as a residual phase. The liquid then moves to 100% melting along the olivine control line passing through the bulk compositions A or B. The positions of the liquidus phase boundaries at 1 bar pressure (SCHAIRER and YODER, 1961) are also illustrated (boundaries to shaded fields of Figures 1 and 2). Liquids formed at 28 kbar along the olivine–enstatite cotectic will crystallize olivine at lower pressure and move towards the 1 bar olivine–enstatite reaction boundary or olivine–albite cotectic as appropriate. The shaded area in Figure 1 illustrates the range of derivative liquids which could be formed by anhydrous melting of both compositions A and B at 28 kbar, followed by crystal fractionation at lower pressure. The area marked by lighter shading includes derivative liquid compositions which could *not* be formed from peridotite A by anhydrous melting followed by crystal fractionation at lower pressure but *could* be formed from the more refractory composition B. In a later section we use this simple system analogue approach to demonstrate that very different

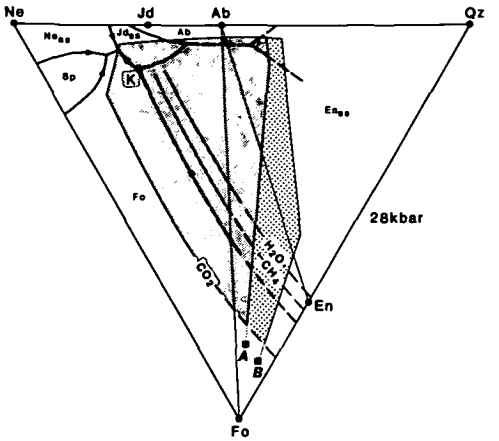

FIG. 2. As for Figure 1 but with the positions of the vapour-saturated cotectic between olivine and enstatite shown for H_2O, CH_4 and CO_2 saturated conditions at 28 kbar. The effect of C–H–O volatiles is to expand the field of possible liquids from peridotites A and B but the restriction of liquids lying in the lightly shaded areas to source compositions such as B, remains valid.

source peridotite compositions are required for MORB and boninite parent magmas.

The effect of C–H–O fluids on melting in the Fo–Ne–Qz system

In Figure 2, the position of the forsterite-enstatite cotectic at 28 kbar in the vapour-absent Fo–Ne–Qz system is compared with the positions of the same cotectic under vapour-saturated conditions, the three specific cases illustrated being H_2O-saturated, CO_2-saturated and CH_4-saturated (EGGLER, 1978; TAYLOR, 1985; GREEN *et al.*, 1986). The effect of water is to expand the olivine field at the expense of enstatite (KUSHIRO, 1972) but liquids at low degrees of partial melting remain strongly silica-undersaturated and nepheline-normative (EGGLER, 1975). Water enters the melt as OH^-, causing depolymerization by hydrolysis of Al–O–Si and Si–O–Si bonds and depression of the liquidus by 350–400°C. In contrast, CO_2 enters the melt at CO_3^{2-} in the form of metallocarbonate complexes resulting in melt polymerization and marked expansion of the liquidus field of enstatite at the expense of forsterite (see earlier discussions by EGGLER, 1978; BREY and GREEN, 1975, 1976; MYSEN and BOETTCHER, 1975; MYSEN *et al.*, 1980, and others on related systems). Liquids at low degrees of melting are nepheline-rich (Ne > Ab) and approach simple system analogues of olivine nephelinite.

Under CH_4-saturated conditions, liquidus temperatures are depressed by 80–90°C at 28 kbar (see also EGGLER and BAKER, 1982). Electron microprobe, gas chromatographic analyses and infrared spectroscopic studies show carbon solubilities up to 0.2% carbon (*i.e.*, ~0.25% CH_4 or ~0.7% CO_2 equivalent) and OH solution equivalent to 2–3 weight percent H_2O. The effect of methane-saturation is to expand the field of olivine at the expense of enstatite (Figure 2) but to a lesser extent than H_2O-saturation (see also EGGLER and BAKER, 1982). The infrared spectroscopic study of quenched glasses shows changes in the absorption bands attributed to the aluminosilicate network which suggest an increase in the Si:O ratio (*i.e.*, >1:2) of the network (TAYLOR, 1985; TAYLOR and GREEN, 1987). Thus, under methane-saturated conditions, melts may become *reduced* and contain small dissolved carbon and larger OH^- contents. On decompression, without redox-interaction with wall-rocks, such melts will exsolve $CH_4 + H_2$. It is noteworthy that initial melts near the low temperature minimum melting for jadeite–enstatite–forsterite, remain nepheline normative in all three cases illustrated in Figure 2. However, the degree of undersaturation is sensitively dependent on the fluid phase present.

In considering melting in the upper mantle, the evidence from mantle-derived liquids and xenoliths, from the presence of graphite and diamond and fluid inclusions within mantle samples, argue that mantle fluids are dominated by the C–H–O system. In considering melting in the upper mantle, it is necessary to consider possible variations on fluid phase compositions within the C–H–O system and whether particular source regions may be characterized by particular fluid phase characteristics. The simple system analogue illustrated in Figure 2 shows that variation in fluid phase composition will not invalidate one of the major conclusions from Figure 1, that is, that some specific liquids and potential source peridotite compositions cannot be related to each other because of limitations imposed by their major element compositions and phase relations.

FLUID-CONTROLLED MELTING IN THE UPPER MANTLE

The importance of water in determining the pressure–temperature conditions and form of the mantle solidus is well determined from studies on peridotite compositions (KUSHIRO, 1968; GREEN, 1973; MYSEN and BOETTCHER, 1975). The model 'pyrolite' composition studied (GREEN, 1973) may

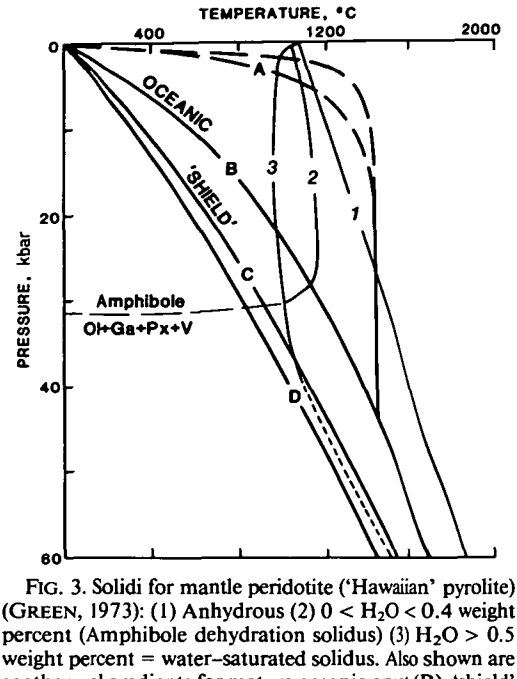

FIG. 3. Solidi for mantle peridotite ('Hawaiian' pyrolite) (GREEN, 1973): (1) Anhydrous (2) $0 < H_2O < 0.4$ weight percent (Amphibole dehydration solidus) (3) $H_2O > 0.5$ weight percent = water-saturated solidus. Also shown are geothermal gradients for mature oceanic crust (B), 'shield' regions (C, D) and near-mid ocean spreading centres (A) (BASALTIC VOLCANISM PROJECT, 1981; Figure 9.5.7). Ol, olivine; Px, pyroxene; Ga, garnet; V, vapour.

be referred to as 'Hawaiian pyrolite' composition as the 'melt' component in the 'melt + residue' model used to calculate the model 'pyrolite' composition (RINGWOOD, 1966), was based on Hawaiian olivine tholeiite liquids, *i.e.*, enriched in TiO_2, K_2O and incompatible elements relative to MORB. In Figure 3, the solidi for three distinctive water contents are illustrated:

(1) Anhydrous solidus

(2) Dehydration solidus; pargasitic hornblende is present on the solidus below 28–29 kbar but the water content is less than approximately 0.4 weight percent.

(3) Water-saturated solidus; pargasitic hornblende is present on the solidus but water content exceeds approximately 0.4 weight percent so that water is present in excess and sub-solidus assemblages coexist with a water-rich fluid.

In Figure 3 we illustrate geothermal gradients appropriate to thermal upwelling beneath spreading centres (A), beneath 'old' oceanic crust and lithosphere (B) and beneath ancient Archean crust and lithosphere (C, D) (BASALTIC VOLCANISM PROJECT, 1981; Figure 9.5.7, p. 1180). The presence or absence of a region of partial melting along geotherms B, C and D and the depth to such a region is clearly sensitively controlled by the role of water, specifically by the activity of water.

Recognising that carbon, as well as water, is a component of mantle fluids adds further complexity to the determination of the mantle solidus. It is necessary to determine the activity of water in the C–H–O system under mantle conditions. TAYLOR (1985, 1986) has presented a thermodynamic model of this system appropriate to mantle pressures and temperatures. Results may be presented, following FROST (1979) as isobaric, isothermal diagrams plotting $\log f_{O_2}$ vs X_C* defined as the mole fraction of carbon relative to hydrogen in the bulk fluid.

In Figure 4 and Table 1 we illustrate results at 30 kbar, 1327°C showing the carbon–saturation surface bounding the metastable carbon–oversaturated fluid field (TAYLOR 1985, 1986). The strong dependence of fluid composition on oxygen fugacity is very clear in Figure 4 and Table 1 and it is noteworthy that graphite coexists with fluid approaching pure water in composition at f_{O_2} = IW + 1 to 2 log units.

The composition of C–H–O fluids present along geothermal gradients in Archean shield and in oceanic crust regions (taken from Figure 9.5.7, p. 1180, BASALTIC VOLCANISM STUDY PROJECT, 1981) can be calculated from this thermodynamic

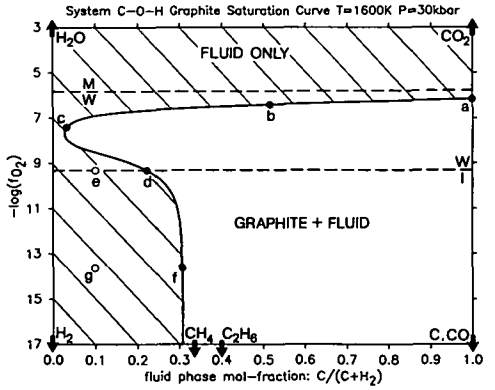

FIG. 4. $\log f_{O_2}$ vs $X_C \left[= \text{mol fraction } \frac{C}{(C+H_2)} \right]$ diagram at 1600 K (1327°C), 30 kbar showing the graphite saturation surface, stable fluid-only pseudo-divariant region (blank) and X_C-independent traces of IW and MW oxygen buffers. Arrows indicate the off-scale positions of the six C–O–H volatile species, filled circles ('a' to 'f') on the graphite saturation surface correspond to fluid compositions given in Table 1. The maximum mol fraction of H_2O on the graphite saturation curve is reached at point C.

* $X_C = x_{CO} + x_{CO_2} + \frac{1}{3}x_{CH_4} + \frac{2}{5}x_{C_2H_6}$.

Table 1. Fluid compositions at selected points in Figure 6; T = 1600 K, P = 30 kbar

	EQUILIBRIUM FLUIDS Mol percent species*									
	$-\log f_{O_2}$	X_C	X_O	H_2O	CO_2	CO	H_2	CH_4	C_2H_6	$V^{mix}cm^3/mol$
**	6.15	1.000	1.000	0	97.1	2.9	0	0	0	30.27
	6.40	0.510	0.671	48.5	49.3	1.6	0.4	0.1	0	24.21
†	7.40	0.032	0.339	94.1	2.3	0.2	1.5	1.9	0	17.90
‡	9.30	0.220	0.091	26.9	0.1	0.1	7.8	63.3	1.8	25.60
‡	9.30	0.100	0.192	57.4	0	0	12.7	29.7	0.2	21.05
	13.60	0.306	0.001	0.2	0	0	8.7	87.7	3.4	28.69
	13.60	0.100	0.004	0.2	0	0	68.8	29.9	0	19.83

** f_{O_2} = GCO, † f_{O_2} = GW(max.x_{H_2O}), ‡ f_{O_2} = IW.
* round-off error = ±0.1 mol percent.

model provided that we assume that graphite or diamond is a stable accessory mantle mineral. The C–H–O fluid composition at any pressure and temperature is only fixed if f_{O_2} is also known—in Figure 5 (GREEN *et al.*, 1986) we calculate fluid compositions for the two geothermal gradients assuming f_{O_2} = FMQ, IW + 2 log units and IW, respectively. The results in Figures 4 and 5 demonstrate that if mantle f_{O_2} conditions are near IW to IW + 2 or 3 log units, then mantle fluids are dominated by water or water + methane. In the presence of a mixed fluid, (H_2O + CH_4), pargasitic hornblende will reach a maximum thermal stability near $a_{H_2O} \sim 0.5$ (see study by HOLLOWAY (1973) on pargasite + CO_2 + H_2O)—an interpretation supported by studies in progress in which subsolidus amphibole + garnet lherzolite crystallized at 25 kbar, 1100°C in the presence of graphite and an f_{O_2}–buffered fluid phase of CH_4:$H_2O \sim$ 1:1.

There is evidence from measurements of intrinsic oxygen fugacity of mantle minerals, of deep-seated igneous intrusions and from identification of reduced gases (CH_4) evolving from MORB glasses and from submarine volcanic centres (ARCULUS *et al.* 1984; SATO and VALENZA, 1980; WELHAN and CRAIG, 1979, 1983) that the earth's mantle in the source regions for basaltic magmas is reduced with $f_{O_2} \sim$ IW to IW + 1 to 2 log units. These interpretations are not unchallenged and others, for example, EGGLER (1983) and MATTIOLI and WOOD 1986) infer higher mantle f_{O_2} conditions. At near-surface and shallow crustal conditions, mineral assemblages of igneous rocks indicate $f_{O_2} \geq$ FMQ (HAGGERTY, 1978; SATO, 1978). Thus, the earth's lithosphere may be seen broadly as a transition zone or boundary layer between deeper mantle with f_{O_2} ~ IW and mantle fluids dominated by CH_4, H_2O + H_2 and near-surface conditions with $f_{O_2} \sim$ FMQ and fluids dominated by H_2O, CO_2. The consequences of this redox interaction, coupled with the sensitivity of the mantle solidus to a_{H_2O}, are explored more fully elsewhere (GREEN *et al.*, 1986) but are presented in summary form in the following section and Figures 6 and 7 which also build upon ideas canvassed by others including WYLLIE (1978, 1979, 1980), WOERMANN and ROSENHAUER (1985), EGGLER (1978), EGGLER and BAKER (1982), RYABCHIKOV *et al.* (1981) and GREEN (1973).

Mantle degassing and magma genesis: Oceanic lithosphere

We adopt the view that the earth's upper mantle *beneath the asthenosphere* is at $f_{O_2} \sim$ IW ± 1 log unit and that this region contains C–H–O fluids, possibly remnant from primordial entrapped volatiles, and minor carbon (diamond) contents. (In adopting this view we recognize that alternative views of higher oxygen fugacity (QFM to MW) are also current and our purpose is to explore the 'reduced mantle' model.) The fluids will be dominated by $CH_4 > H_2O > H_2$, C_2H_6 (*cf.* GOLD and SOTER, 1980, 1983). The transition from these reduced conditions towards more oxidized lithosphere will result in fluid change with increase in H_2O:CH_4 (Figures 4 and 5) but the oceanic geothermal gradient will lie within a field of partial melting at P > 28–29 kbar (Figure 3) due to instability of pargasitic hornblende and the role of water in depressing the mantle solidus. Provided that fluid concentrations are low, this region of partial melting will be a fluid-absent region in which a minor melt phase can accommodate continuously variable f_{O_2} via melt structure redox changes (SiO variation) with solubility of OH^- and minor carbon, and at higher f_{O_2}, by increasing solubility of CO_3^{2-}. At depths < 90 km, the stability of pargasitic hornblende at $f_{O_2} \sim$ IW + 1 to 3 log units creates a lid

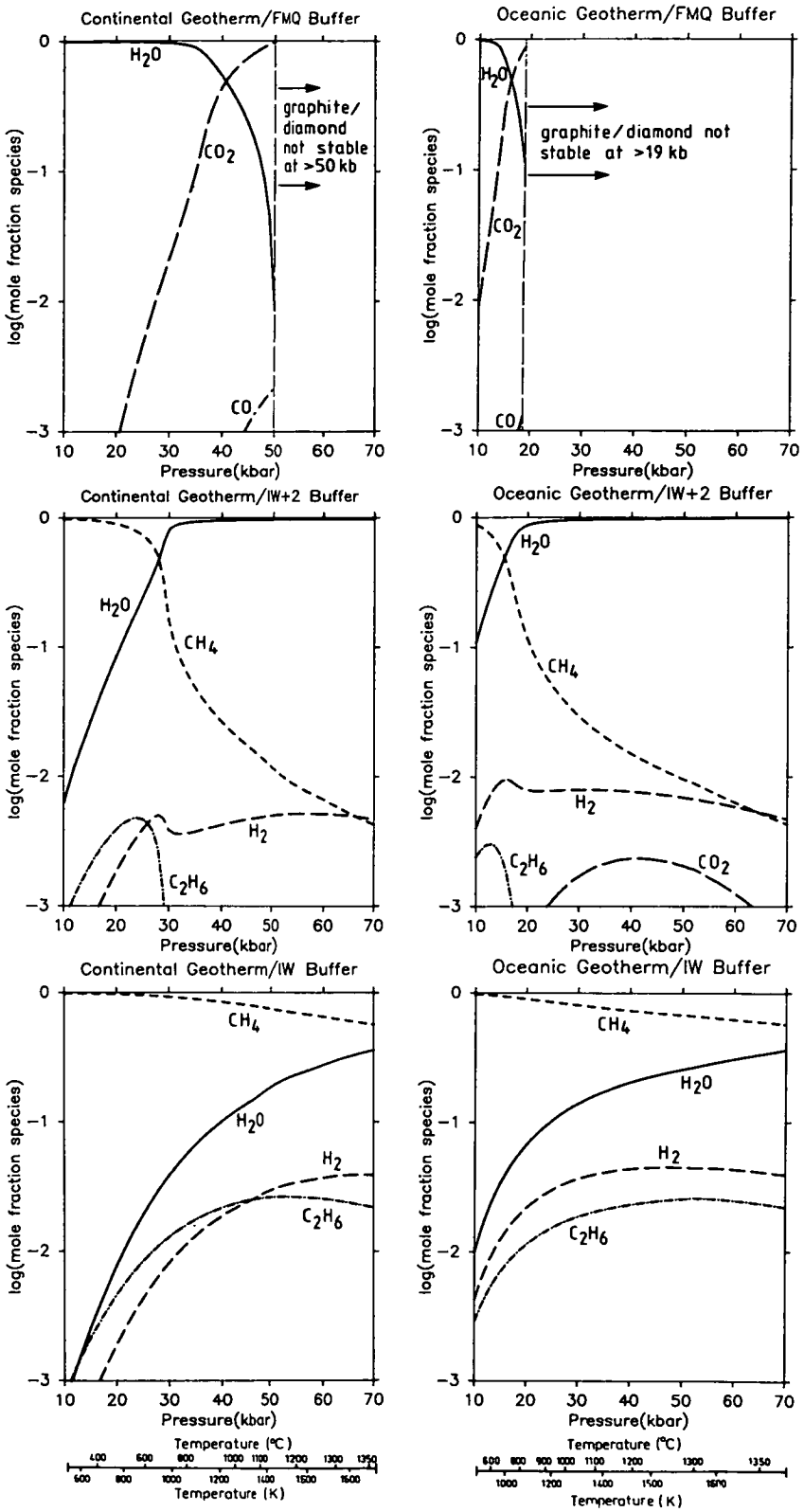

FIG. 5. Fluid compositions along model 'oceanic' and 'shield' geotherms (BASALTIC VOLCANISM STUDY PROJECT, 1981; Figure 9.5.7, p. 1180) assuming fluid coexists with graphite/diamond and with specific f_{O_2}'s corresponding to IW, IW + 2 log units and FMQ buffers.

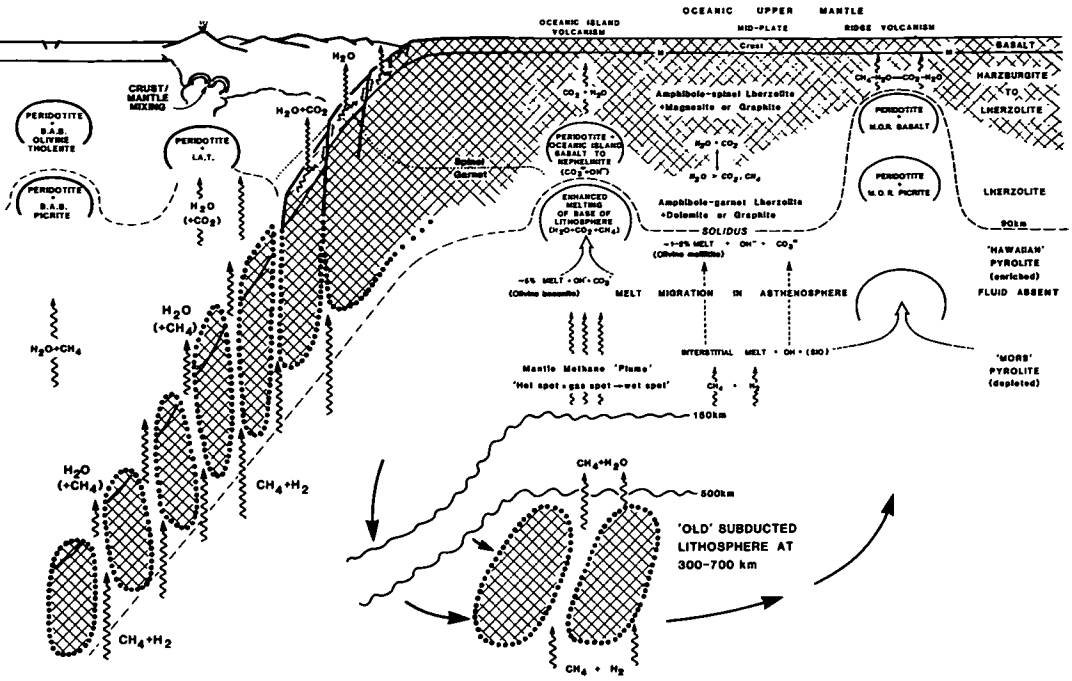

FIG. 6. Schematic model of the oceanic lithosphere and asthenosphere. The lithosphere is variable in composition due to melt extraction and fluid enrichment events and is envisaged as variably oxidized from FMQ (shaded areas) to ~IW + 1 to 2 log units (blank areas of lithosphere). The asthenosphere is a fluid-absent region in which C–H–O volatiles are dissolved in a small melt fraction (1–2% melt) which migrates towards the top of the asthenosphere or base of the lithosphere. Source regions for Hawaiian-type island chains (hot-spots) are in the upper part of the asthenosphere or base of the lithosphere. Source regions for MORB are in the lower part of the asthenosphere. The mantle is degassing reduced fluids ($CH_4 + H_2$) and the asthenosphere is a fluid-absent region with intrinsic oxygen content and fugacity varying from ~IW to IW + 2 to 3 log units—this variation is accommodated in change of melt structure from reduced (Si:O > 1:2) to contain OH^- and CO_3^{2-} (f_{O_2} ~ IW + 2 to 3 log units). The patterned symbol on the oceanic lithosphere signifies f_{O_2} ~ FMQ, *i.e.*, 'oxidized' lithosphere. In the convergent margin or subduction plate boundary scenario, the oxidized lithosphere is portrayed as penetrated along fracture zones by $CH_4 + H_2$ fluids from subjacent mantle. The redox-interactions produce H_2O-rich fluids which strongly influence melting relations above or within the subducted lithosphere. Thus, even at depths below those at which hydrated minerals of the oceanic crust and lithosphere have been lost, the 'slab' may be a source of H_2O-rich fluids. Abbreviations for primary magmas developed within the schematic diapirs are: M.O.R. = mid-ocean ridge; I.A.T. = island arc tholeiite; B.A.B. = back-arc basin. See text for further discussion, including the genesis of boninite parent magmas.

to the partially molten layer because any interstitial melt migrating upwards from the asthenosphere will crystallize to pargasite-bearing lherzolite containing graphite or dolomite ± graphite (GREEN, 1973; EGGLER, 1978; WYLLIE, 1978; GREEN *et al.*, 1986).

In Figure 6, the asthenosphere beneath oceanic crust is a fluid-absent region separating methane-rich fluids in the deep mantle from H_2O-rich and $H_2O + CO_2$ fluids in the lithosphere. It is a zone of decoupling between lithospheric plates and underlying mantle, a zone of increased seismic attenuation and decreased seismic velocity (GREEN and LIEBERMANN, 1976; GREEN, 1973; EGGLER, 1978; WYLLIE, 1978) and most importantly, a zone of chemical differentiation rather than homogenization due to the migration of an interstitial melt phase towards the top of the asthenosphere. The character of the interstitial melt is extremely undersaturated olivine melilitite to olivine nephelinite (GREEN, 1971; GREEN and LIEBERMANN, 1976; BREY and GREEN, 1976; WYLLIE, 1979; EGGLER, 1978; WENDLANDT and MYSEN, 1980) and apart from enriching the upper part and depleting the lower part of the asthenosphere in incompatible elements, the high Ca/Al ratio of olivine melilitite will decrease the Ca/Al ratio of the lower part of the astheno-

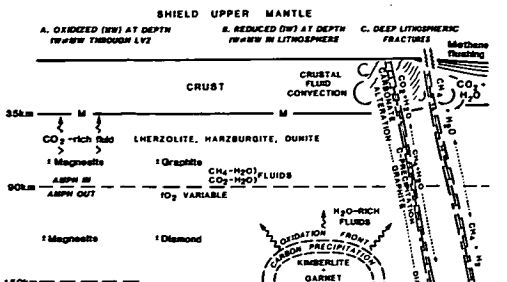

FIG. 7. Schematic model for the continental lithosphere beneath Archean/Proterozoic shield regions. See text for detailed discussion. The deep mantle is degassing ($CH_4 + H_2$) fluids that interact with oxidized lithosphere. (A) suggests a deep, thin asthenospheric layer (partial melting) in which the f_{O_2} change from mantle or lithosphere is accommodated within the fluid-absent melt. (B) suggests a mechanism of 'redox' melting (see text) in which diamond-bearing garnet harzburgite is left as a residue from oxidation of $CH_4 + H_2$ to $H_2O + C$ with extraction of water-rich kimberlitic melt. (C) suggests a role for deep lithosphere fractures in localizing mantle fluid release and interaction of these fluids with oxidized crustal fluids at shallow depths.

sphere and increase the Ca/Al ratio of the uppermost part. The extent of chemical differentiation will be related to: (a) the age of the lithosphere, (b) the extent to which volumes of old lithosphere/asthenosphere are preserved near transform fault/spreading centre intersections or at spreading axes themselves, and (c) depth within the asthenosphere. The base of the lithosphere will also become enriched in incompatible elements, hosted particularly in pargasitic hornblende, phlogopite and apatite as minor and accessory phases. In Figure 6, the lower part of the asthenosphere is depicted as a fluid-absent region at low f_{O_2} (IW to IW + 1 log unit) which has the incompatible element contents appropriate to MORB source (abbreviated as 'MORB' pyrolite) whereas the upper part of the asthenosphere has f_{O_2} near IW + 2 to 3 log units and incompatible element contents appropriate to source regions for tholeiites of oceanic island chains such as Hawaii ('hot spot' source regions, abbreviated as 'Hawaiian pyrolite').

The relationships between magmatism at spreading centres, at 'hot spots' or migrating tension fractures (see Figure 6) and the chemically zoned asthenosphere has been fully explored elsewhere (GREEN, 1971, 1972; GREEN and LIEBERMANN, 1976; GREEN *et al.*, 1986) and in this paper we address the possibilities created by interaction of an oxidized subducted lithospheric slab with reduced mantle below the asthenosphere (Figure 6).

It is generally accepted that the peridotite of the lithosphere is variable in composition from lherzolite to harzburgite, probably as a result of prior extraction of basaltic to picritic melts. Local, more extreme chemical variation results from trapped liquids, high-pressure accumulates or metasomatic enrichment from migratory fluid phases. Two examples of chemical variation are illustrated in Figure 8, showing chemical trends in spinel lherzolite inclusions from W. Victoria (NICKEL and GREEN, 1984) and from garnet and spinel lherzolites within the Ronda high-temperature, high-pressure peridotite intrusion (FREY *et al.*, 1985). Even more refractory harzburgite compositions are seen in some ophiolite complexes. These are commonly partially or completely serpentinized and during serpentinization, became highly oxidized with abundant magnetite development.

The evidence from deep focus earthquakes suggests that subducted lithospheric slabs retain their identity to depths of at least 600–700 km. Dehydration reactions in subducted basaltic crust and serpentinized peridotite may lead to migration of H_2O-rich or $H_2O + CO_2$ fluids from the subducted slab into the overlying peridotite wedge, instigating melting on the water-saturated peridotite solidus (solidus 3 of Figure 3, KUSHIRO 1968; GREEN, 1973). Melts formed in this way will have geochemical characteristics reflecting the partially residual character of the remobilized lithosphere together with the imprint of components partitioned into

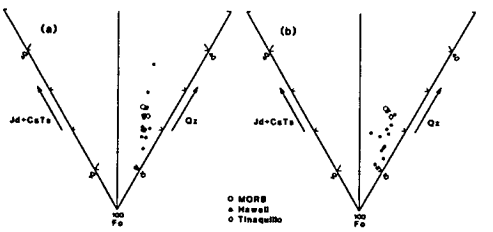

FIG. 8. Two examples of peridotite suites of variable composition from lherzolite to harzburgite, reflecting prior extraction of basaltic to picritic melts, plotted in the normative system Fo–Jd + CaTs–Qz–Di, projected from Di onto the plane Fo–Jd + CaTs–Qz. (a) Ronda, high temperature, high pressure peridotite intrusion FREY *et al.*, 1985; (b) Spinel lherzolite inclusions from Lake Bullenmerri, W. Victoria, NICKEL and GREEN, 1984. Also plotted are 'MORB' pyrolite, 'Hawaiian' pyrolite and Tinaquillo lherzolite compositions, which have been studied experimentally under high pressures and temperatures (JAQUES and GREEN, 1980; FALLOON and GREEN, unpublished data).

nd transported by the fluid phase migrating from ıe subducted slab. A related model suggests that :mperatures on the upper part of the subducted ab (the subducted basaltic/eclogitic crust partic-larly) may be high enough for fluid-saturated or ehydration melting and for melt to migrate from ıe subducted slab to modify and melt the overlying eridotite mantle wedge. The models have been ex-lored and evaluated in many previous publications ee RINGWOOD (1974) and GILL (1981) for review nd references). However the concept of redox-in-raction between deep mantle degassing CH_4 H_2-rich fluids and lithospheric slab with mineral ssemblages reflecting f_{O_2} near FMQ to MW con-itions adds a further dimension to subduction. It possible for dehydrated, very refractory peridotite eclogite of the subducted slab to generate H_2O-ch fluid by reaction of anhydrous oxidized mineral ssemblages (Fe^{3+} in silicates, spinels, carbonates) ith primary $CH_4 + H_2$ fluids. The increased $_{H_2O}$ will cause melting, even of refractory harz-urgite (KUSHIRO, 1972; MYSEN and BOETTCHER, 975; GREEN, 1973). A second, important effect ill be that any redox front bounding a residual ab of subducted lithosphere in contact with normal IORB pyrolite will be a locus for high a_{H_2O}—the echanical effect of this will be to concentrate stress elease (earthquake activity) at such redox fronts. ower temperatures within the subducted slab will enerally inhibit melting of the slab itself but this ay be counteracted by high a_{H_2O} contrasting with igh a_{CH_4} and thus high solidus temperatures in rrounding mantle. A particularly favourable lo-ation for redox interaction coupled with higher mperatures at the edges of a subducted slab will e at trench/transform intersections, *e.g.*, the south nd of the Marianas Trench and the northern end the Tonga Trench, where the subducted slab uts, across a transform fault zone, against normal eanic lithosphere/asthenosphere to deep levels. he movement zone will probably act as a channel-ay for enhanced mantle degassing and by provid-g a temperature contrast across the transform fault ne, will act as a heat input to the subducted slab. In Figure 6, we suggest that the immediate source eridotite for Hawaiian or 'hot spot' volcanism lies the uppermost part of the asthenosphere or al-rnatively within the base of the lithosphere, where is has been enriched by migration, reaction and ystallization of an interstitial melt. The success the 'fixed hot spot' frame of reference in analy-ing relative plate movement over the past 100 illion years shows that the cause or trigger for and chain or 'hot spot trace' volcanism does not within the moving lithospheric plate but lies be-neath this plate and reflects a 'fixed' mantle or a deep mantle in which the convective flow is much slower than and decoupled from the lithospheric plate motions (MORGAN, 1972; DUNCAN, 1981). If large slabs of subducted lithosphere are carried to depths > 600 km and embedded within the return flow or deeper mantle convection pattern (HOFFMAN and WHITE, 1982; RINGWOOD, 1986), then they may act to oxidize $CH_4 + H_2$ fluids passing through them to $CH_4 + H_2O$. This effect could feed $CH_4 + H_2O$ plumes into overlying asthenosphere + lithosphere and trigger 'hot spot volcanism' as depicted in Figure 6. For example we suggest that the great frequency of sea mounts and island chain volcanoes in the West Pacific may be due to the Pacific plate over-riding relict subducted slabs embedded in the 150–650 km depth interval of the upper mantle and reflecting material originally subducted on Palaeozoic-Mesozoic subduction zones along the East Asian margin.

Mantle degassing and magma genesis: Continental lithosphere

In Figure 7 (*cf.* GREEN *et al.*, 1986) we present a summary diagram illustrating mantle degassing of $CH_4 + H_2$ beneath a very old, thick lithosphere characterized by very low geothermal gradient (Shield geotherms C and D of Figure 3). The lithosphere has a zone of amphibole stability in lherzolitic compositions at $P < 28$–29 kbar but at deeper levels subsolidus assemblages contain phlogopite and may contain other hydrous phases such as titanoclinohumite (MCGETCHIN *et al.*, 1970). Carbon will be present as diamond or graphite, or at depths > 150 km, as magnesite if f_{O_2} > FMQ (Figure 5; EGGLER 1975, 1978; GREEN *et al.*, 1986; BREY *et al.*, 1983; WYLLIE, 1978, 1979). Samples of deep continental lithosphere occur as xenoliths in kimberlite pipes and illustrate heterogeneity and variations from possible trapped liquids or relict subducted oceanic crust (eclogite, grosspydite, lherzolite to highly refractory harzburgite, and extremely K- and Ti-rich phlogopite rocks).

If mantle temperatures approach the solidus 3 (Figure 3), then redox melting of lithosphere may occur by interaction of reduced CH_4-rich fluids from deeper levels with oxidized lherzolite, or harzburgite. GREEN *et al.* (1986) have suggested that the distinctive mineral inclusion suite within South African diamonds which is characterized by extremely magnesian olivine, refractory low-Al enstatite and extremely low calcium, Cr-rich pyrope garnet, is a consequence of redox melting (see Figure 7, scenario B).

Although Archaean and Proterozoic cratons preserve a remarkably long history of stability as recorded by cover of undeformed Proterozoic sediments, they are frequently cut by mafic dyke swarms. In the post-Permian breakup of Gondwanaland, stable cratons with thick underlying lithosphere, have rifted and drifted apart so that regions of old, thick lithosphere are now juxtaposed against young lithosphere of oceanic type. An initial situation of rapid temperature change at the base of the lithosphere of a newly rifted craton (*cf.* BOYD 1973; BOYD and NIXON, 1975; NICKEL and GREEN, 1985) will be followed by heating of the sub-craton lithosphere so that the solidus of phlogopite-bearing lherzolite and harzburgite will be exceeded. Small melt fractions of olivine lamproite to leucite lamproite composition (FOLEY, 1986; FOLEY *et al.*, 1986) reflect phlogopite harzburgite source rocks and depths of segregation from 150 km to ~70 km respectively. Source rocks of phlogopite-bearing garnet lherzolite will produce potassic olivine nephelinites to basanites (WEDEPOHL, 1985) with the particular liquid composition being determined by CO_2:H_2O as well as by source rocks and depth of magma segregation (FREY *et al.*, 1978; EGGLER, 1978; GREEN, 1976; BREY and GREEN, 1976; WYLLIE, 1979). If upwelling and diapirism occurs from within the heated former sub-cratonic lithosphere, then magmas produced at lower pressures will retain trace element and isotopic compositions reflecting their source compositions but the magmas will be picritic to tholeiitic or alkali olivine basaltic in character, reflecting higher degrees of melting and shallower depths of magma segregation.

MAGMA SOURCE COMPOSITIONS

Mantle-derived peridotite suites

Compositions of two suites ranging from lherzolite to harzburgite and with high pressure mineral assemblages requiring crystallization at pressures in excess of 10 kbar are projected in Figure 8. The Ronda peridotite suite (FREY *et al.*, 1985) defines a linear trend consistent with extraction of magma lying within the olivine-hypersthene-plagioclase-diopside volume, *i.e.*, an olivine tholeiite or tholeiitic picrite liquid (FREY *et al.*, 1985). The Bullenmerii suite shows more scatter but again a trend implying an olivine tholeiite or tholeiitic picrite extraction (*cf.* NICKEL and GREEN, 1984). Model Hawaiian pyrolite, MORB pyrolite and Tinaquillo lherzolite compositions are also plotted in Figure 8. All three have CaO and Al_2O_3 contents > 3–4 weight percent but the suites differ in Na_2O, TiO_2, K_2O, and incompatible element contents with Tinaquillo being the most refractory composition (JAQUES and GREEN, 1980; GREEN *et al.*, 1979).

The trends in Figure 8 defined by the mantle samples (which could be matched by other xenolith suites or high-temperature, high-pressure intrusive peridotite suites) are considered to result from partial melting and incomplete melt extraction (FREY *et al.*, 1985; NICKEL and GREEN, 1984) and thus we infer that mantle source compositions, prior to melt extraction are at least as 'fertile' as the most plagioclase-rich and diopside-rich limits of the trends shown in Figure 8. If the processes outlined in previous sections, which lead to one or more remelting events, particularly under the fluxing effects of C–H–O fluids, are operative in the earth then the range of potential source peridotite compositions covers at least the range of the samples plotted, *i.e.*, trending from lherzolite towards harzburgite with 80 weight percent Ol, 20 weight per cent En.

Source for mid-ocean ridge basalts

Compositions of (>70) glasses from dredged ocean floor basalts are plotted in Figures 9 and 10—all have 100 Mg/(Mg + Fe^{2+}) > 68, *i.e.*, they are primitive in the sense of suitability as melts in equilibrium with olivine > Mg_{87}. It may be noted tha

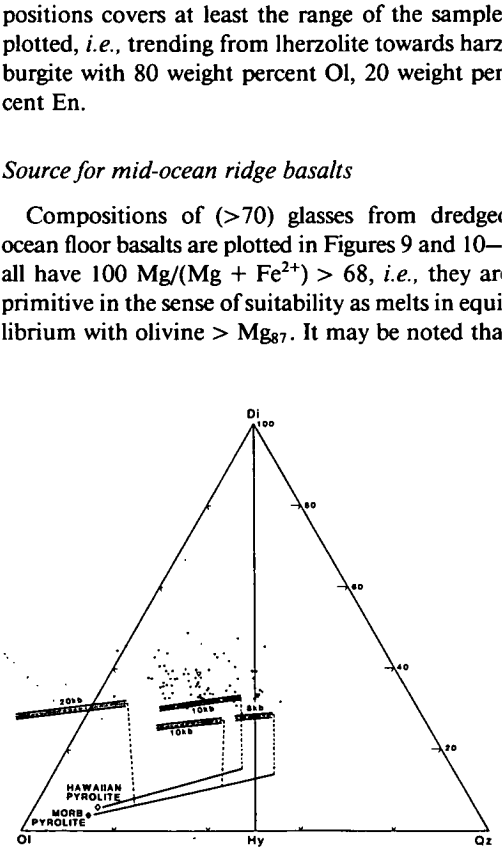

FIG. 9. Equilibrium partial melts of MORB pyrolite a 8, 10 and 20 kbar (FALLOON and GREEN, unpublished data) and 'Hawaiian' pyrolite at 10 kbar (JAQUES and GREEN, 1980) compared with primitive MORB glasses in the normative system Ol-Jd + CaTs-Qz-Di. Compositions are projected from plagioclase (An + Ab) onto the plane Ol-Di-Qz. Cotectics are as follows: (1) stippled line ol + opx + cpx + L cotectic. (2) dashed line, ol + opx + L cotectic. (3) solid line, ol + L cotectic. (▼) is the MORB glass DSDP3-18-7-1, studied by GREEN *et al.*, (1979) and (▽) is the low-olivine parent composition of BRYAN (1979)

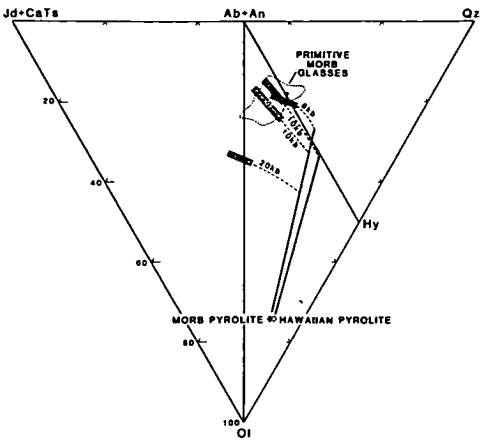

FIG. 10. Equilibrium partial melts of 'MORB' pyrolite at 8, 10 and 20 kbar and 'Hawaiian' pyrolite at 10 kbar compared with the field of primitive MORB glasses in the normative system Ol–Jd + CaTs–Qz–Di. Compositions are projected from Di onto the plane Jd + CaTs–Qz–Ol. Cotectics and symbols as for Figure 9. For purposes of clarity the primitive MORB glasses are not plotted individually as in Figure 9 but outlined by the dotted line.

olivine tholeiite liquids dominate the group but they do spread from quartz-normative compositions (5 points) to nepheline-normative compositions (2 points). The glass DSDP 3–18–7–1, studied experimentally by GREEN *et al.*, (1979) as a primitive MORB lies centrally within the MORB field.

GREEN *et al.* (1979, Table 4, column D) calculated a model source composition for DSDP 3–18–7–1 and we have studied the anhydrous melting relationships of this composition (MORB pyrolite) from 8–20 kbar. A 'sandwich' technique (STOLPER, 1980) was used in which a layer of DSDP 3–18–7–1 glass is placed between two layers of MORB pyrolite. The bulk compositions of these mixtures lie on the join between these two compositions (Figures 9 and 10). This approach avoids the bulk compositional changes inherent in equilibrating diverse liquids within unrelated peridotite layers (FUJII and SCARFE, 1985; TAKAHASHI and KUSHIRO, 1983; STOLPER, 1980) although these studies provide useful comparative data for our purposes.

The results are summarized in Figures 9 and 10, showing 3-phase cotectics (Ol + Opx + Cpx), followed by (Ol + Opx) cotectics until the olivine-control line is reached as the temperature increases. Attention is particularly drawn to the compositional range of liquids along the 3-phase cotectic. For example, at 20 kbar liquids in equilibrium with olivine, orthopyroxene and clinopyroxene range from nepheline-normative picrites to picrites with low normative hypersthene contents, before clinopyroxene disappears. Examination of Figure 10 alone would suggest that MORB glasses may be explained as primary olivine tholeiite melts separating from Ol + Opx + Cpx residues at approximately 8 kbar to 13 kbar pressure. Limited olivine fractionation and variation in percent melting could possibly account for the observed compositional variation of Figure 10. However, it is insufficient to examine only one projection or plot of the many chemical variables involved. From Figure 9, it is clear that almost all MORB glasses are too rich in normative diopside to have formed as primary liquids on Ol + Opx + Cpx cotectics. However, a few exceptions lie close to Ol + Opx + Cpx cotectics at ~8 kbar and these distinctive MORB glasses have low normative olivine contents or are quartz normative. They are similar in composition to the low-olivine parent composition of BRYAN (1979) and are consistent with being close to primary liquids or derived from ~8 kbar primary olivine tholeiite magmas via limited olivine fractionation.

Examination of Figure 9 suggests that liquids formed by small degrees of melting at 10–12 kbar, might fractionate small amounts of olivine to reach MORB glass compositions. In fact, this mechanism does not work as liquids at small degrees of melting have TiO_2 contents, Na/Ca ratio, K_2O contents and P_2O_5 contents that are too high for MORBs.

The data, as illustrated in Figures 9 and 10, but confirmed by other oxide, element ratio and normative plots, show that most MORB glasses are derivative by olivine factionation from primary picritic magmas (*i.e.*, liquids with >20% normative olivine), segregating from residual olivine, orthopyroxene and clinopyroxene at pressures of 15–20 kbar. Melting conditions are essentially anhydrous although small quantities of reduced and oxidised volatiles may be present (BYERS *et al.*, 1983; MATHEZ, 1984). It is inferred from Figure 10 particularly, that we do not see liquids formed by very high degrees of melting along the olivine + orthopyroxene cotectic and we believe that this is unlikely in a single stage melting process as such liquids would require >30–35% melting and melt segregation apparently occurs prior to this (GREEN and RINGWOOD, 1967; MYSEN and KUSHIRO, 1977; JAQUES and GREEN 1980).

Liquids at 10 kbar from the Hawaiian pyrolite melting study (JAQUES and GREEN, 1980) are also plotted in Figure 10. The pattern of liquid variation with progressively higher degrees of melting is similar to that for MORB pyrolite but the Ol + Opx + Cpx cotectic is at much higher normative diopside contents. Although the cotectic overlaps the MORB

field in this projection the liquids have >3 weight percent TiO_2, >0.5 weight percent K_2O and Na/Ca ratios unlike MORB. The Hawaiian pyrolite composition cannot produce MORB liquids in terms of major and minor elements and vice versa—different source compositions are required.

Source for Troodos Upper Pillow Lavas

CAMERON (1985) has subdivided the Troodos Upper Pillow Lavas into three chemical groups with trace element and isotopic abundances requiring chemical differences between the source compositions for each group. DUNCAN and GREEN (1986) studied a parental Group III composition (Arakapas area) experimentally with particular attention to matching of observed phenocryst assemblages with phases crystallized under controlled pressure and temperature conditions. Conditions of magma segregation from residual harzburgite were determined as 1350°C, 8–9 kbar and the magma contained ~0.5–1 percent weight H_2O.

In Figure 11, we plot the Troodos Group III parental lava composition with derivative glasses and aphyric basalts to compare with the area of MORB glasses and the range of liquids derived from MORB pyrolite. The Troodos Group III parental liquid lies marginally outside (*i.e.*, is more refractory than) the olivine–control line from MORB pyrolite. In terms of phase relations a liquid close to Troodos Group III parental magma could be formed by melting of MORB pyrolite at the point of elimination of orthopyroxene from the residual phases, *i.e.*, a dunite residue. However, minor and trace element contents of the MORB–pyrolite derived melt do not match these of Troodos Upper Pillow Lava—a relation readily apparent in the first plagioclase to crystallize (~An_{91} in Troodos UPL and ~An_{78} in DSDP 3 18–7–1).

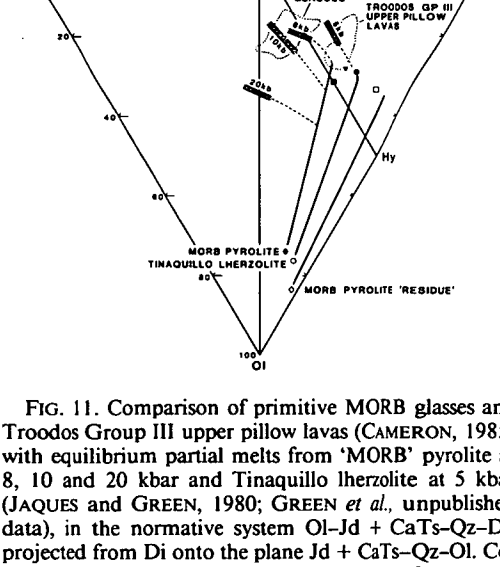

FIG. 11. Comparison of primitive MORB glasses and Troodos Group III upper pillow lavas (CAMERON, 1985) with equilibrium partial melts from 'MORB' pyrolite at 8, 10 and 20 kbar and Tinaquillo lherzolite at 5 kbar (JAQUES and GREEN, 1980; GREEN *et al.*, unpublished data), in the normative system Ol–Jd + CaTs–Qz–Di, projected from Di onto the plane Jd + CaTs–Qz–Ol. Cotectics same as for Figure 9. Symbols are as follows: (■) calculated parental composition for the Troodos Group III upper pillow lavas studied by DUNCAN and GREEN (1986). (▼) refractory primitive magma composition identified from glass inclusions in magnesian (Fo_{94}) olivine phenocrysts from Tonga (FALLOON and GREEN, 1986b). (●) Marianas fore-arc lava (JENNER, 1983). (□) Cape Vogel, boninite parental magma composition calculated by WALKER and CAMERON (1983). (▽) primitive MORB glass DSDP3–18–7–1 studied experimentally by GREEN *et al.* (1979).

If we compare the melting relations of Tinaquillo lherzolite (Figure 11), its more refractory character means that the olivine/orthopyroxene cotectic does not end at but continues through Troodos UPL composition (*cf.* Figure 1). In phase relations, trace element and minor element abundances, the source peridotite for Troodos UPL must be more refractory than MORB pyrolite—we infer that it is a residual lherzolite composition in which melting is enhanced by addition of a very small amount of water (0.5–1 percent weight H_2O in the melt fraction) sufficient to depress the melting temperature by about 30–50°C.

Source for north Tongan arc high magnesium lavas

In 1984, the Japanese research vessel 'Natsushima' dredged an extraordinary variety of high magnesium lavas from water depths in excess of 2000 m at the northern termination of the Tonga arc (FALLOON, 1985; FALLOON and GREEN, 1986a). In detail, the samples show evidence for decoupling of incompatible elements from major plus compatible elements. For example, rocks with similar major element chemistry have REE patterns varying from strongly LREE enriched to strongly LREE depleted. There is also unequivocal evidence for magma mixing involving several magnesian end member liquids, differing principally in their degree of depletion in the more incompatible elements and in ratios such as Na/Ca. One sample contained Fo_9 olivine phenocrysts and within these unusually magnesian olivine crystals occur large glass inclusions with CaO/Na_2O > 20 and magnesian quartz tholeiite compositions (FALLOON and GREEN 1986b). Correction for quench outgrowth on the olivine host enabled calculation of the original liquid (Figure 11). In other samples from the same and

ther dredge sites, extremely calcic plagioclase (up o An_{100}) megacrysts occur and are compatible with rystallization from a liquid matching the compo- ition of the glass inclusions in olivine. The role of vater in depressing the liquidus and fluxing melting f refractory lherzolite composition, is as yet un- ertain. However, the composition of the glass in- lusion is such that the original magma is a possible artial melt of very refractory lherzolite composi- ons, such as Tinaquillo lherzolite, with magma egregation at ~5 kbar (anhydrous) or a slightly igher pressure if OH^- solution expands the olivine hase volume.

Source for boninite or high magnesia andesites

In young West Pacific Arcs, distinctive very high iO_2 (>56 weight percent, high magnesium, low alcium lavas characterized by rare olivine and bundant enstatite or multiply twinned clinoensta- te (inverted from protoenstatite) have been found oth outcropping in emergent islands and dredged rom the sea floor (DALLWITZ *et al.*, 1966; KURODA *t al.*, 1978; CRAWFORD *et al.*, 1981; UMINO, 1985;)IETRICH *et al.*, 1978). Strongly porphyritic char- cter, accumulation of phenocrysts and growth of uench phases makes determination of liquid com- ositions very difficult. Experimental studies (TA- SUMI, 1981; JENNER and GREEN, unpublished) ave established conditions of multiple olivine and rthopyroxene saturation and the latter studies lead s to a preferred petrogenetic model in which liquids ontain ~2 weight percent water and segregate from esidual olivine and orthopyroxene at ~2–5 kbar, ~ 1250–1300°C.

In Figure 11, plots of possible parental magma ompositions lie on the refractory (olivine–enstatite) de of the olivine–control line for peridotite such s MORB pyrolite or Tinaquillo lherzolite. Liquids uch as boninites cannot be derived from lherzolites s calcic as those and require very refractory harz- urgite source rocks (*cf.* Figure 1). Potential source ocks in terms of (Jd + CaTs)–Ol–Qz–Di include ne more refractory compositions of the lherzolite- arzburgite suites of Figure 8. However, examina- on of trace element and minor element contents f boninites reveals great variability (JENNER 1981, ICKEY and FREY 1982, CAMERON *et al.*, 1983) om incompatible elements enriched to V-shaped EE patterns suggesting addition of a minor en- ched component to a previously strongly depleted eridotite. A similar mechanism is required to ex- ain the non-refractory character of the plagioclase vhich appears very late in the crystallization se- uence and lacks a high Ca/Na ratio). The geo- chemistry and petrology of boninites suggests vol- atile-induced (H_2O–rich) melting of very refractory residual harzburgite. There is evidence for signifi- cant addition of incompatible elements either with or prior to the addition of H_2O–rich fluid.

CONCLUSIONS

The genesis of primary magmas in the earth's mantle is controlled by

a) Pressure, temperature variation, *i.e.*, mantle geotherms, which differ in different tectonic settings;
b) The presence and composition of a fluid phase, principally within the system C–H–O; and
c) The bulk compositions of source peridotite.

Experimental studies at high pressure and tem- perature constrain the effects of C–H–O fluid em- phasizing the importance of water–rich and water–methane fluids at oxygen fugacities of IW to IW + 1 to 3 log units. The experimental studies also show that different source peridotite compositions are required for primary magmas from different tectonic settings. These different source composi- tions can be simply related within a framework in which the source compositions for Hawaiian (Hot- spot) and Mid–Ocean Ridge tholeiitic picrites to olivine tholeiites are regarded as 'enriched' and 'de- pleted' variants of the mantle composition within the asthenosphere. The process of enrichment and depletion is attributed to upward migration of a very small (~1%) melt fraction of olivine melilitite or olivine nephelinite character within the astheno- sphere.

Source rocks for back–arc basin tholeiites, island arc tholeiites, high–Mg tholeiites such as Troodos Upper Pillow Lavas or from the Tongan fore–arc, and particularly for boninite parent magmas, are highly refractory lherzolites to harzburgites. The roles of such compositions as source rocks for mag- mas requires second and probably third stage melt- ing, in which residues from extraction of earlier magmatic events are re–melted in different P, T and tectonic settings.

In such multiple melting episodes, a key role is played by C–H–O fluids in fluxing the melting, and in the case of boninite liquids, in introducing in- compatible elements to the source rock prior to or during the melting process. Although the subducted slab has long been regarded as a source for H_2O–rich fluids by dehydration of minerals within the upper parts of the slab, in this paper we suggest that an additional source of water, particularly at deeper levels of the subduction process, comes from redox interaction of reduced $CH_4 + H_2$ fluids from the

deep mantle with the oxidized (FMQ) mineral assemblages of the subducted slab.

Particularly favourable environments for multistage melting, even of extremely refractory harzburgite compositions within the subducted slab, occur at the intersections of subduction zones with transform faults, *e.g.*, northern end of Tongan Trench, southern end of Marianas Trench.

Acknowledgements—We acknowledge the assistance of K. Harris (High Pressure Laboratory), W. Jablonski (microprobe laboratory), P. Robinson (geochemical laboratory) and other technical staff of the Geology Department, University of Tasmania in the research programs summarized in this paper. Mrs. J. Pongratz and Mrs. J. Beattie are thanked for drafting and manuscript preparation. The research is supported by the Australian Research Grants Scheme and research funds from the University of Tasmania.

REFERENCES

ARCULUS R. J., DAWSON J. B., MITCHELL R. H., GUST D. A. and HOLMES R. D. (1984) Oxidation state of the upper mantle recorded by megacryst ilmenite in kimberlite and type A and B spinel lherzolite. *Contrib. Mineral. Petrol.* **85**, 85–94.

BASALTIC VOLCANISM STUDY PROJECT (1981) *Basaltic Volcanism on the Terrestrial Planets.* 1286 pp. Pergamon Press.

BOYD F. R. (1973) A pyroxene geotherm. *Geochim. Cosmochim. Acta* **37**, 2533–254.

BOYD F. R. and NIXON P. H. (1975) Origins of ultramafic rocks from some kimberites of northern Lesotho and the Monastery Mine, South Africa. *Phys. Chem. Earth* **9**, 431–454.

BREY G. P. and GREEN D. H. (1975) The role of CO_2 in the genesis of olivine melilitite. *Contrib. Mineral. Petrol.* **49**, 93–103.

BREY G. P. and GREEN D. H. (1976) Solubility of CO_2 in olivine melilitite at high pressures and role of CO_2 in the Earth's upper mantle. *Contrib. Mineral. Petrol.* **55**, 217–230.

BREY G. P., BRICE W. R., ELLIS D. J., GREEN D. H., HARRIS K. L. and RYABCHIKOV I. D. (1983) Pyroxene–carbonate reactions in the upper mantle. *Earth Planet. Sci. Lett.* **62**, 63–74.

BRYAN W. B. (1979) Regional variation and Petrogenesis of Basalt Glasses from the FAMOUS Area, Mid-Atlantic Ridge. *J. Petrol.* **20**, 293–325.

BYERS C. D., MUENOW D. W. and GARCIA M. D. (1983) Volatiles in basalts and andesites from the Galapagos Spreading Center, 85° to 86°W. *Geochim. Cosmochim. Acta* **47**, 1551–1558.

CAMERON W. E. (1985) Petrology and origin of primitive lavas from the Troodos ophiolite, Cyprus. *Contrib. Mineral. Petrol.* **89**, 239–255.

CAMERON W. E., MCCULLOCH M. R. and WALKER D. A. (1983) Boninite petrogenesis: chemical and Nd–Sr isotopic constraints. *Earth Planet. Sci. Lett.* **65**, 75–89.

CRAWFORD A. J., BECCALUVA A. L. and SERRI G. (1981) Tectonomagmatic evolution of the West Philippine-Mariana region and the origin of boninites. *Earth Planet. Sci. Lett.* **54**, 346–356.

DALLWITZ W. B., GREEN D. H. and THOMPSON J. E. (1966) Clinoenstatite in a volcanic rock from the Cap Vogel area, Papua. *J. Petrol.* **7**, 375–403.

DIETRICH V., EMMERMAN R., OBERHANSLI R. and PUCHELT H. (1978) Geochemistry of basaltic and gabbroic rocks from the West Mariana Basin and the Mariana Trench. *Earth Planet. Sci. Lett.* **39**, 127–144.

DUNCAN R. A. (1981) Hotspots in the Southern Oceans–An absolute frame of reference for motion of the Gondwana Continents. *Tectonophys.* **74**, 29–42.

DUNCAN R. A. and GREEN D. H. (1986) The genesis of refractory melts in the formation of oceanic crust. *Contrib. Mineral. Petrol.*, (Submitted).

EGGLER D. H. (1975) CO_2 as a volatile component of the mantle: The system Mg_2SiO_4–SiO_2–H_2O–CO_2. *Phys. Chem. Earth* **9**, 869–882.

EGGLER D. H. (1978) The effect of CO_2 upon partial melting of peridotite in the system Na_2O–CaO–Al_2O_3–MgO–H_2O–CO_2 to 35 kb, with an analysis of melting in peridotite–H_2O–CO_2 system. *Amer. J. Sci.* **278**, 305–343.

EGGLER D. H. (1983) Upper mantle oxidation state: Evidence from olivine–orthopyroxene–ilmenite assemblages. *Geophys. Res. Lett.* **10**, 365–368.

EGGLER D. H. and BAKER D. R. (1982) Reduced volatiles in the system C–O–H: implications to meltings, fluid formation, and diamond genesis. In *High-Pressure Research in Geophysics,* (eds. S. AKIMOTO and M. MANGHNANI), pp. 237–250 Center for Academic Publications Japan, Tokyo.

FALLOON T. J. (1985) Preliminary petrography and geochemistry of igneous rocks from the Northern Tonga Ridge and adjacent Lau Basin. In *A Marine Geological and Geophysical Survey of the Northern Tonga Ridge and Adjacent Lau Basin,* (eds. E. HONZA, K. B. LEWIS *et al.*), pp. 63–71 Mineral Resources of Tonga Field Report No. 1, Ministry of Lands, Survey and National Resources, Kingdom of Tonga.

FALLOON T. J. and GREEN D. H. (1986a) Dredged igneous rocks from the Northern Termination of the Tofua Magmatic arc, Tonga and adjacent Lau Basin. *Australian Journal of Earth Sciences,* (Submitted).

FALLOON T. J. and GREEN D. H. (1986b) Glass inclusions in magnesian olivine phenocrysts from Tonga: Evidence for highly refractory parental magmas in the Tonga Arc. *Earth Planet. Sci. Lett.*, (In press).

FOLEY, S. F. (1986) The genesis of lamproitic magmas in a reduced fluorine-rich mantle. *Int. Kimb. Conf. Pert. Extended Abstracts 4th,* (In press).

FOLEY S. F., TAYLOR W. R. and GREEN D. H. (1986) The role of fluorine and oxygen fugacity in the genesis of the ultrapotassic rocks. *Contrib. Mineral. Petrol.*, (In press).

FREY F. A. and GREEN D. H. (1974) The mineralogy, geochemistry and origin of lherzolite inclusions in victorian basinites. *Geochim. Cosmochim. Acta* **38**, 1023–1059.

FREY F. A., GREEN D. H. and ROY D. S. (1978) Integrated models of basalt petrogenesis: a study of quartz tholeiites to olivine melilitites from south eastern Australia utilizing geochemical and experimental petrological data. *J. Petrol.* **19**, 463–513.

FREY F. S., SUEN J. C. and STOCKMAN H. W. (1985) The Ronda high temperature peridotite: Geochemistry and petrogenesis. *Geochim. Cosmochim. Acta* **49**, 2469–2491.

FROST B. R. (1979) Mineral equilibria involving mixed

volatiles in a C–O–H fluid phase: the stabilities of graphite and siderite. *Amer. J. Sci.* **279,** 1033–1059.
UJII T. and SCARFE C. M. (1985) Composition of liquids coexisting with spinel lherzolite at 10 kbar and the genesis of MORBS. *Contrib. Mineral. Petrol.* **90,** 18–28.
ILL J. B. (1981) *Orogenic Andesites and Plate Tectonics.* 390 pp. Springer-Verlag.
OLD T. and SOTER S. (1980) The Deep-Earth–Gas hypothesis. *Sci. Amer.* **242,** 130–137.
OLD T. and SOTER S. (1983) Methane and seismicity: a reply. *EOS* **64,** 663.
REEN D. H. (1971) Composition of basaltic magmas as indicators of conditions of origin: application to oceanic volcanism. *Phil. Trans. Roy. Soc. London* **A268,** 707–725.
REEN D. H. (1972) Magmatic activity as the major process in the chemical evolution of the earth's crust and mantle. *Tectonophys.* **13,** 47–71.
REEN D. H. (1973) Experimental melting studies on a model upper mantle composition at high pressure under water-saturated and water-undersaturated conditions. *Earth Planet. Sci. Lett.* **19,** 37–53.
REEN D. H. (1976) Experimental testing of equilibrium partial melting of peridotite under water-saturated, high-pressure conditions. *Can. Mineral.* **14,** 255–268.
REEN D. H. and RINGWOOD A. E. (1967) The genesis of basaltic magmas. *Contrib. Mineral. Petrol.* **15,** 103–190.
REEN D. H. and LIEBERMANN R. C. (1976) Phase equilibria and elastic properties of the pyrolite model for the oceanic upper mantle. *Tectonophys.* **32,** 61–92.
REEN D. H., HIBBERSON W. O. and JAQUES A. L. (1979) Petrogenesis of mid-ocean ridge basalts. In *The Earth: Its Origin, Structure and Evolution,* (ed. M. W. MCELHINNY), pp. 265–299 Academic Press.
REEN D. H., TAYLOR W. R. and FOLEY S. F. (1986) The Earth's upper mantle as a source for volatiles. *Geol. Soc. Aust. Special Pub. 12,* (In press).
UPTA A. K., TAYLOR W. R. and GREEN D. H. (1986) Experimental study of the system forsterite–nepheline–quartz at variable temperatures under 28 kb pressure, (Submitted).
AGGERTY S. E. (1978) The redox state of planetary basalts. *Geophys. Res. Lett.* **5,** 443–446.
ICKEY R. L. and FREY F. A. (1982) Geochemical characteristics of boninite series volcanics: implications for their source. *Geochim. Cosmochim. Acta* **46,** 2099–2115.
OFFMAN A. W. and WHITE W. M. (1982) Mantle plumes from ancient oceanic crust. *Earth Planet. Sci. Lett.* **57,** 421–436.
OLLOWAY J. R. (1973) The system pargasite–H_2O–CO_2: a model for melting of a hydrous mineral with a mixed-volatile fluid—I. Experimental results to 8 kbar. *Geochim. Cosmochim. Acta* **37,** 651–666.
QUES A. L. and GREEN D. H. (1980) Anhydrous melting of peridotite at 0–15 kb pressure and the genesis of tholeiitic basalts. *Contrib. Mineral. Petrol.* **73,** 287–310.
NNER G. A. (1981) Geochemistry of high-Mg andesites from Cape Vogel, Papua New Guinea. *Chem. Geol.* **33,** 307–332.
NNER G. A. (1983) Petrogenesis of high-Mg andesites: An experimental and geochemical study with emphasis on high-Mg andesite from Cape Vogel, P.N.G. Ph.D. Dissertation, Univ. of Tasmania.
URAT G., PALME H., SPETTEL B., BADDENHAUSEN H., HOFMEISTER H., PALME C. and WANKE H. (1980) Geochemistry of ultramafic xenoliths from Kapfenstein, Austria: evidence for a variety of upper mantle processes. *Geochim. Cosmochim. Acta* **44,** 45–60.
KURODA N., SHIRAKI K. and URANO H. (1978) Boninite as a possible calc-alkaline primary magma. *Bull. Volcanol.* **41,** 563–575.
KUSHIRO I. (1968) Melting of a peridotite nodule at high pressures and high water pressures. *J. Geophys. Res.* **73,** 6023–6029.
KUSHIRO I. (1972) Effect of water on the compositions of magmas formed at high pressures. *J. Petrol.* **13,** 311–334.
MATHEZ E. A. (1984) Influence of degassing on oxidation states of basaltic magmas. *Nature* **310,** 371–375.
MATTIOLI G. S. and WOOD B. J. (1986) Upper mantle f_{O_2} recorded by spinel-lherzolites (abstr.) *EOS* **67,** 375.
MCGETCHIN T. R., SILVER L. T. and CHODOS A. A. (1970) Titanoclinohumite: a possible mineralogical site for water in the upper mantle. *J. Geophys. Res.* **75,** 255–259.
MENZIES M. (1983) Mantle ultramafic xenoliths in alkaline magmas: evidence for mantle heterogeneity modified by magmatic activity. In *Continental Basalts and Mantle Xenoliths,* (eds. C. J. HAWKESWORTH and M. J. NORRY), pp. 92–110 Shiva Publ., Cheshire, England.
MORGAN W. J. (1972) Plate motions and deep mantle convection. *Geol. Soc. Amer. Mem.* **132,** 7–22.
MYSEN B. O. and BOETTCHER A. L. (1975) Melting of a hydrous mantle I. Phase relations of natural peridotite at high pressures and temperatures with controlled activities of water, carbon dioxide and hydrogen. *J. Petrol.* **16,** 520–548.
MYSEN B. O. and KUSHIRO I. (1977) Compositional variations of coexisting phases with degree of melting of peridotite in the upper mantle. *Amer. Mineral.* **62,** 843–865.
MYSEN B. O., VIRGO D., HARRISON W. J. and SCARFE C. M. (1980) Solubility mechanisms of H_2O in silicate melts at high pressures and temperatures: A Raman spectroscopic study. *Amer. Mineral.* **65,** 900–914.
NICKEL K. G. and GREEN D. H. (1984) The nature of the upper-most mantle beneath Victoria, Australia as deduced from ultramafic xenoliths. In *Kimberlites II: The Mantle and Crust-Mantle Relationships,* (ed. J. KORNPROBST), pp. 161–178 Elsevier.
NICKEL K. G. and GREEN D. H. (1985) Empirical geothermobarometry for garnet peridotites and implications for the nature of the lithosphere, kimberlites and diamonds. *Earth Planet. Sci. Lett.* **73,** 158–170.
RINGWOOD A. E. (1966) The chemical composition and origin of the earth. In *Advances in Earth Science,* (ed. P. M. HURLEY), pp. 287–356 M.I.T. Press, Cambridge.
RINGWOOD A. E. (1974) The petrological evolution of island arc systems. *J. Geol. Soc. London.* **130,** 183–204.
RINGWOOD A. E. (1986) Dynamics of subducted lithosphere and implications for basalt genesis. *Terra Cognita* **6,** 67–77.
RYABCHIKOV I. D., GREEN D. H., WALL V. J. and BREY G. P. (1981) The oxidation state of carbon in the low-velocity zone. *Geochem. International* **18,** 148–158.
SATO M. (1978) Oxygen fugacity of basaltic magmas and the role of gas-forming elements. *Geophys. Res. Lett.* **5,** 447–449.
SATO M. and VALENZA M. (1980) Oxygen fugacities of the layered series of the Skaergaard Instrusion, East Greenland. *Amer. J. Sci.* **20A,** 134–158.
SCHAIRER J. F. and YODER H. S. JR. (1961) Crystallization

in the system nepheline–forsterite–silica at one atmosphere pressure. *Carnegie Inst. Wash. Yearb.* **60,** 141–144.

STOLPER E. (1980) A Phase Diagram for Mid-ocean ridge basalts: Preliminary results and implications for petrogenesis. *Contrib. Mineral. Petrol.* **74,** 13–27.

TAKAHASHI E. and KUSHIRO I. (1983) Melting of a dry peridotite at high pressures and basalt magma genesis. *Amer. Mineral.* **68,** 859–879.

TATSUMI Y. (1981) Melting experiments on a high-magnesian andesite. *Earth Planet. Sci. Lett.* **54,** 357–365.

TAYLOR W. R. (1985) The role of C–O–H fluids in upper mantle processes: a theoretical, experimental and spectroscopic study. Ph.D. Dissertation, Univ. of Tasmania.

TAYLOR W. R. (1986) A reappraisal of the nature of fluids included by diamond—a window to deep-seated mantle fluids and redox conditions. *Geol. Soc. Aust. Special Publ.* **12,** (In press).

TAYLOR W. R. and GREEN D. H. (1987) The petrogenic role of methane: Effects on liquidus phase relations and the solubility of reduced C–H–O volatiles. In *Magmatic Processes: Physicochemical Principles,* (ed. B. O. MYSEN), pp. 121–138 The Geochemical Society Spec. Publ. No. 1.

UMINO S. (1985) Volcanic geology of Chichijima, the Bonin Islands. *J. Geol. Soc. Japan* **91,** 505–523.

WALKER D. A. and CAMERON W. E. (1983) Boninite primary magmas: evidence from the Cape Vogel Peninsula, P.N.G. *Contrib. Mineral. Petrol.* **83,** 150–158.

WEDEPOHL K. H. (1985) Origin of the Tertiary basaltic volcanism in the northern Hessian Depression. *Contrib. Mineral. Petrol.* **89,** 122–145.

WELHAN J. A. and CRAIG H. (1979) Methane and hydrogen in East Pacific Rise hydrothermal fluids. *Geophys. Res. Lett.* **6,** 829–831.

WELHAN J. A. and CRAIG H. (1983) Methane, hydrogen and helium in hydrothermal fluids at 21°N on the East Pacific Rise. In *Hydrothermal Processes at Seafloor Spreading Centres,* (eds. P. A. RONA, K. BOSTROM, L. LAUBIER and K. L. SMITH), pp. 391–409 Plenum Press, New York.

WENDLANDT R. F. and MYSEN B. O. (1980) Melting phase relations of natural peridotite + CO_2 as a function of degree of melting at 15 and 30 kbar. *Amer. Mineral.* **65,** 37–44.

WINDOM K. E. and BOETTCHER A. L. (1981) Phase relations for the joins jadeite–enstatite and jadeite–forsterite at 28 kb and their bearing on basalt genesis. *Amer. J. Sci.* **281,** 335–351.

WOERMANN E. and ROSENHAUER M. (1985) Fluid phases and the redox state of the Earth's mantle: extrapolations based on experimental, phase-theoretical and petrological data. *Fortschr. Mineral.* **63,** 263–349.

WYLLIE P. J. (1978) Mantle fluid compositions buffered in peridotite–CO_2–H_2O by carbonates, amphibole, phlogopite. *J. Geology* **86,** 687–713.

WYLLIE P. J. (1979) Magmas and volatile components. *Amer. Mineral.* **65,** 469–500.

WYLLIE P. J. (1980) The origin of kimberlites. *J. Geophys. Res.* **85,** 6902–6910.

YODER H. S. JR. and TILLEY C. E. (1962) Origin of basalt magmas: an experimental study of natural and synthetic rock systems. *J. Petrol.* **3,** 342–532.

B38

Magmatic Processes: Physicochemical Principles
© The Geochemical Society, Special Publication No. 1, 1987
Editor B. O. Mysen

The petrogenetic role of methane: Effect on liquidus phase relations and the solubility mechanism of reduced C–H volatiles

W. R. TAYLOR and D. H. GREEN
Geology Department, University of Tasmania, GPO Box 252C, Hobart, Australia 7001

Abstract—Methane and other reduced volatiles may be an important species in the Earth's mantle. The nature of mantle partial melting under reduced conditions in the presence of such volatiles is, however, largely unknown. To evaluate the petrogenetic role of C–H volatiles experimental liquidus studies were undertaken in the system nepheline(Ne)–forsterite(Fo)–silica(Q)–C–O–H at 28 kbar. Methane-dominated fluids are conveniently generated in high pressure experiments from a mixture of Al_4C_3 and $Al(OH)_3$. Compared to the volatile-absent system, the effect of CH_4-rich fluids is to expand the Fo phase field relative to En_{ss} (melt depolymerization) and to bring phases of high octahedral aluminum content onto the liquidus (leading to early appearance of garnet on the liquidus of other compositions). This contrasts with the effect of CO_2 which gives rise to the expansion of the En_{ss} phase field and the effect of H_2O which results in a greater expansion of the Fo field than CH_4. The magnitude of liquidus temperature depressions for C–H fluid–saturated Fo–Ne–Q melts are comparable to that of pure CO_2 (~90°C at 28 kbar).

Infrared (IR) spectroscopic investigations of C–H fluid saturated jadeite and sodamelilite glasses quenched from 30 kbar, establish the presence of both dissolved, oxidized, and reduced components as also required by charge-balance constraints. The former occurs as O–H groups and the latter is consistent with a reduced network component of O:Si stoichiometry <2 ("silicon monoxide" units). There is no spectroscopic evidence for the presence of dissolved molecular CH_4, other C–H groups or carbonate. Pyrolysis/gas chromatographic analyses give dissolved H contents equivalent to ~3 weight percent H_2O and reduced C contents of 1000–2000 ppm (wt) in a form yet to be characterized. Aluminosilicate melts have a strong preference for dissolved H over C under reduced conditions.

INTRODUCTION

[AJOR ADVANCES in understanding the role of vol-ile components in igneous petrogenesis have taken ace over the last ten years. Much of this effort has een directed at determining the petrogenetic role the oxidized volatiles CO_2 and H_2O which are own to have a significant effect on super-solidus ase relations at upper mantle pressures (see review HOLLOWAY, 1981).

Because H_2O and CO_2 are the most abundant ecies in volcanic gases (*e.g.*, ANDERSON, 1975), has been commonly assumed that they will also the most abundant species at depth in the Earth's per mantle. If this basic assumption is incorrect, d this will depend to a large extent on the mantle's idation state, then the role of volatiles other than $_2O$ and CO_2 must be considered (RYABCHIKOV *al.*, 1981).

A variety of evidence exists to support the idea at at least part of the upper mantle is reduced ough to stabilize CH_4 at depth ($f_{O_2} \leq$ IW + 2 log its). This evidence includes intrinsic oxygen fu-city measurements on mantle-derived minerals dicating the prevalence of low f_{O_2} conditions nongst "type A" upper mantle (ARCULUS and ELANO, 1981) and the finding of primordial (^{3}He rrelated) CH_4 as a significant component of fluids tgassing at mid-ocean ridge hydrothermal centers (WELHAN and CRAIG, 1981, 1983). Current views on the redox state of the Earth's mantle have recently been summarized by WOERMANN and ROSENHAUER (1985, in particular see pp. 317–322). Although this area is still one of active debate and inquiry, it seems likely that a range of oxidation states from relatively oxidized ($f_{O_2} \sim$ FMQ) to reduced ($f_{O_2} \sim$ IW) are applicable to the upper mantle. Volatiles in the reduced part of the system C–O–H may therefore be of considerable importance in igneous petrogenesis.

If magma generation involving volatile components takes place in a reduced environment, for example at f_{O_2}'s near the iron-wustite (IW) oxygen buffer, then in the model system "peridotite"–C–O–H, volatiles will be dominantly $CH_4 > H_2O > H_2 > C_2H_6$ mixtures and crystalline carbonates will not be stable relative to diamond or graphite (RYABCHIKOV *et al.*, 1982; EGGLER and BAKER, 1982). To explore the nature of mantle melting under reduced conditions an adequate understanding of the thermodynamic properties of C–O–H fluids at elevated pressures and temperatures is required. Reduced volatile interactions with silicate melts can then be investigated by experimental and spectroscopic means. The first aspect has been considered by TAYLOR (1985, 1987) and the second is the purpose of this paper.

The contrasting effects of oxidized versus reduced volatiles on liquidus phase relations are investigated in the model peridotite system nepheline(Ne)–forsterite(Fo)–silica(Q) under conditions of CH_4, CO_2 and H_2O volatile saturation and in the absence of volatiles. To place constraints on the mechanism of reduced C–H volatile dissolution in aluminosilicate melts, CH_4-saturated, graphite-free glasses of sodamelilite ($NaCaAlSi_2O_7$, Sm) and jadeite ($NaAlSi_2O_6$, Jd) composition have been analysed for carbon and hydrogen and investigated by Fourier Transform infrared (FTIR) spectroscopic methods.

Iron-bearing compositions have not been considered in this study primarily because f_{O_2} conditions in the presence of a C–H fluid will lie well within the Fe-metal stability field. The effect of reduced volatiles on these compositions must instead be investigated in the presence of mixed H_2O–CH_4–H_2 fluids at higher f_{O_2}'s (near the IW buffer for example). In this study we concentrate on identifying the mechanism of reduced C–H volatile dissolution free from interference by other species and thus provide the necessary basis for extension into natural systems.

PREVIOUS WORK ON REDUCED C–H VOLATILE INTERACTIONS WITH SILICATE MELTS

Little is known of how reduced volatiles interact with silicate melts. EGGLER and BAKER (1982) conducted a number of reconnaissance experiments determining the effect of C–H volatiles on the melting and liquidus phase relations of diopside and the composition diopside $(Di)_{35}$ pyrope $(Py)_{65}$ at $P > 20$ kbar. Experimental f_{O_2} conditions were believed to be near the Si–SiO_2 buffer but could not be determined directly. EGGLER and BAKER (1982) found liquidus depressions of ~100°C in diopside at 21 kbar and a large liquidus field of olivine plus garnet extending to at least 40 kbar in $Di_{35}Py_{65}$ coexisting with C–H fluid. In the latter case this differs from the effect of H_2O which does not bring garnet onto the liquidus and the effect of CO_2 which stabilizes orthopyroxene to high pressures. The presence of "depolymerized" phases such as olivine and garnet on the C–H volatile saturated liquidus led to the suggestion that reduced volatiles have a depolymerizing effect on silicate melts. Quench problems did not allow spectroscopic investigation of the glasses produced in their study and a detailed solubility mechanism could not be ascertained. In the only other study involving CH_4-bearing fluids, JAKOBSSON (1984), using a pyrolysis/mass spectrometry technique, determined the dissolved volatile content of quenched albite glasses equilibrated with H_2O–CH_4 fluids at 10–25 kbar (f_{O_2} ~ IW). Gases released at 1200°C consisted mainly of H_2O (>80 mol percent) with smaller amounts of reduced volatiles (CO, CH_4 and H_2). The extent to which dispersed graphite in the samples affected results was not assessed; low total C/H ratios (<0.06), however, suggest reduced carbon solubilities are not large under these conditions. Raman and infrared (IR) spectroscopic measurements confirmed the dominance of dis solved water; carbonate and possibly molecular methan were detected in some samples. Recently, LUTH an BOETTCHER (1986) have demonstrated that H_2, a signi icant component of C–H fluids at high pressures, interact strongly with silicate liquids and may be quite soluble i silicate melts.

In the light of the above studies it is of importance t establish the nature and mechanism of reduced C–H vo atile interaction with silicate systems. Problems of graphit contamination, quench effects and uncertainty in the na ture of the C–H fluids actually generated have limited pre vious studies. Resolution of these problems is essential fo obtaining unambiguous spectroscopic and analytical re sults. The f_{O_2} conditions chosen for the present study ar such that CH_4 is the dominant fluid species. At highe f_{O_2}'s, where H_2O becomes important, the effects of reduce C–H volatiles may not be clearly resolved from thos of H_2O.

EXPERIMENTAL TECHNIQUES

High pressure experiments

All high pressure experiments were performed with 0.5" diameter (1.27 cm) solid-media, high-pressure apparatu using techniques similar to those of GREEN and RINC WOOD (1967). Temperatures were recorded with a P $Pt_{90}Rh_{10}$ thermocouple automatically controlled to withi ±5–7°C of the set value. All experiments were carried ou by using the "piston-in" technique and applying a −10 pressure correction to nominal load pressures; quote pressures are accurate to ±1 kbar.

Silicate compositions in the system nepheline–forsterite silica (Ne–Fo–Q) were prepared from analytical reager grade Al_2O_3, SiO_2, Na_2CO_3 and MgO fired at 900°C afte thorough mixing and repeated grinding under aceton Compositions were checked by microprobe analysis of glas beads prepared from the sintered oxide mixes on an Ir strip heater. Sodamelilite and jadeite starting materials wer powdered glasses prepared from sintered oxides. Sample were melted at 1250°C in Pt-crucibles and quenched i air to colorless glasses; their composition and homogeneit were checked by microprobe analysis.

Methane-saturated experiments

Calculations by TAYLOR (1985, 1987) reveal that unde upper mantle pressure-temperature conditions C–H fluic in equilibrium with graphite contain CH_4 as a major (>8 mol percent) component and H_2 and C_2H_6 as minor (<1 mol percent) components. Such fluids are stable only a f_{O_2}'s below ~IW–4 log f_{O_2} units. Under these condition f_{H_2} is large so that maintenance of fluid excess condition during an experiment requires minimization of diffusiv H_2-loss by employing run durations as short as possibl while still achieving fluid–melt equilibrium. In preliminar studies, we found that the use of complex organic com pounds as a methane-source (such as those used by HOI LOWAY and REESE, 1974; EGGLER and BAKER, 1982) re sults in the formation of disordered graphite which persis in experiments for run durations of less than a few hour To overcome this problem in short duration experimen that do not incorporate a solid f_{O_2} buffer (as those unde taken here), methane should ideally be produced rapidl and by direct reaction.

Methane, together with a small amount of H_2, can be readily generated at 1 bar by the action of H_2O on Al_4C_3 (WADE and BANISTER, 1973). Because this reaction proceeds rapidly to completion and produces a C–H fluid with a CH_4:H_2 ratio of ~9:1 (similar to that calculated for high pressure-temperature equilibrium), it is an ideally suited generation reaction. By including $Al(OH)_3$ as the source of H_2O a convenient solid reactant can be prepared. Overall the methane generation reaction may be written:

$$4Al(OH)_3 + Al_4C_3 \rightarrow 4Al_2O_3 + 3CH_4 (+H_2 + C_2H_6). \quad (1)$$

To give the fluid-generating carbide/hydroxide mixture sufficient bulk, alumina was used as a diluant giving a mixture capable of generating 0.2 mg CH_4/10 mg mix. To eliminate the possibility that adsorbed water or excess air in the capsule might lead to oxidation of methane and production of H_2O, a 1:1 molar ratio of $Al(OH)_3$ to Al_4C_3 (three times carbide excess over reaction stoichiometry) was employed. The presence of excess carbide was confirmed optically and by x-ray diffraction at the end of each experiment. All mixtures containing Al_4C_3 (98 weight percent purity, Goodfellows Metals #AL516010) were stored under vacuum desiccation to prevent reaction with atmospheric moisture.

Experiments with C–H volatiles were carried out in large capacity "buffer" assemblies using Pt outer capsules (3.5 mm O.D.) and inner unsealed Pt capsules containing ~15 mg of silicate sample. Sample-containing capsules were heated briefly to red-heat prior to loading the methane-source to ensure removal of all traces of adsorbed water. The inner capsule was surrounded with sufficient fluid-generating mix to produce ~1 mg of methane. For jadeite and sodamelilite compositions, experiments were of 30 minutes duration at 30 kbar, 1320°C and 1350°C, respectively; run details for system Ne–Fo–Q experiments are listed in the Appendix. Talc was chosen as the pressure transmitting medium to maximize the external f_{H_2} of the system and thus limit H_2 loss from the capsule.

Prior to experiments with silicates a "blank" run was performed at 30 kbar, 1300°C for 15 minutes with the aim of determining whether fluid phase equilibrium is achievable in short run times by this technique. Analysis of the fluid phase following the run was accomplished by mass spectrometry using a capsule piercing technique. The presence of a vapor phase is readily recognized by the distended nature of the capsule. The device used for capsule piercing consists of a modified regulating valve (Whitey #SS-1VS6) with a redesigned stem tip fashioned into a hardened needle point. A removable cradle serves to position and hold the capsule in place during piercing. Gases were released under vacuum (~10^{-6} torr) and directed into the ion-source of a VG-micromass 7070 double focusing mass spectrometer via a modified probe insertion technique. To achieve low background levels, particularly for H_2O caused chiefly by absorbed molecules on metal surfaces, it was found necessary to evacuate the whole system (probe plus piercer) for ~12 hours prior to taking measurements. After piercing, mass spectra were acquired by multiple scans of ~2 sec duration over the mass range 10–70 m/z. The total ion current was monitored during the piercing experiment and both background and sample spectra were recorded at various sensitivities. With the data acquisition system used by the VG instrument, H_2 was below the lower mass-range limit of recorded spectra. The presence of both H^+ and H_2^+ ions was, however, confirmed qualitatively by oscillographic traces down to low mass numbers. Mass spectra are normalized to zero background (mainly residual air and water vapor in the instrument) by reference to the m/z 32 (O_2^+) or 40 (Ar^+) peak. X-ray diffraction (XRD) and optical examination of the solid product showed the presence of Al_2O_3, ordered graphite and excess Al_4C_3. No oxycarbides were identified either optically or by XRD. The presence of abundant ordered graphite indicates that an f_{H_2} buffer reaction of the type: C(graphite) + $2H_2$ = CH_4, has been operative during the experiment. The form of the mass spectra for the blank experiment and for those experiments with silicate present are identical except a finite amount of H_2O (<0.2 mol percent) is found in the latter. Figure 1 shows a typical methane (m/z 12–16) and ethane (m/z 24–30, m/z 28 overlaps with background N_2^+) spectrum for an experiment with silicate present. Trace amounts of C_{3-4} hydrocarbons are also present. Although the C_2H_6/CH_4 ratio of the fluid is slightly higher than predicted by the MRK-equation calculations of TAYLOR (1986): ~25 vs. 18 expected, overall the agreement with theory is good. Derived fluids are thus believed to represent those at graphite-fluid equilibrium. The absence of oxygen-containing volatiles (*i.e.*, H_2O) places an upper limit on the $\log f_{O_2}$ of the system at near IW–5 $\log f_{O_2}$ units under experimental conditions for the "blank" experiments and near IW–4.5 $\log f_{O_2}$ units for those containing silicate. The use of a carbide/hydroxide mixture is thus a rapid and convenient method for preparing fluids dominated by CH_4 at high pressures.

Water, carbon dioxide and volatile-absent experiments

These experiments were performed in talc/pyrex or talc-only (for water-saturated runs) sleeved assemblies using 2.3 mm O.D. Pt or $Ag_{50}Pd_{50}$ capsules. H_2O (~30 weight percent) was added via microsyringe and CO_2 (~15 weight percent) was generated from $Ag_2C_2O_4$. Run times for CO_2 and volatile-absent experiments were kept to <20 min. (see Appendix) to avoid the risk of H_2O formation by hydrogen diffusion into the capsule. All mixes and assembly parts were dried at 120°C, 24 hours prior to use.

Spectroscopic methods

Spectra of C–H fluid—saturated glasses were investigated by Fourier Transform infrared (FTIR) spectroscopy using a Digilab model FTS-20E spectrometer. FTIR spectroscopy offers significant advantages over conventional instrumentation, including increased signal-to-noise ratio, increased sensitivity due to high energy throughput and ready access to computer-based data manipulation procedures such as band fitting and spectrum subtraction. Spectra of both powdered glass and crystalline samples were obtained by the conventional KBr disc method. Aproximately 2 mg (1 mg for crystalline compounds) of sample was ground together with 200 mg of IR-grade KBr in an agate mortar for 10 minutes. After drying the powder at 120°C, pellets were pressed between 1 cm diameter polished stainless steel dies; any cloudy discs were remade. Discs were then dried under P_2O_5 desiccant overnight to remove traces of adsorbed water. Spectra were acquired by signal averaging 200 scans at 4 cm^{-1} resolution referenced against a blank KBr disc.

Difficulties with KBr powder spectroscopy rest largely with its reproducibility. Differences in sample preparation, reflected mainly in particle size distribution and orientation effects may lead to changes in bandwidths and relative

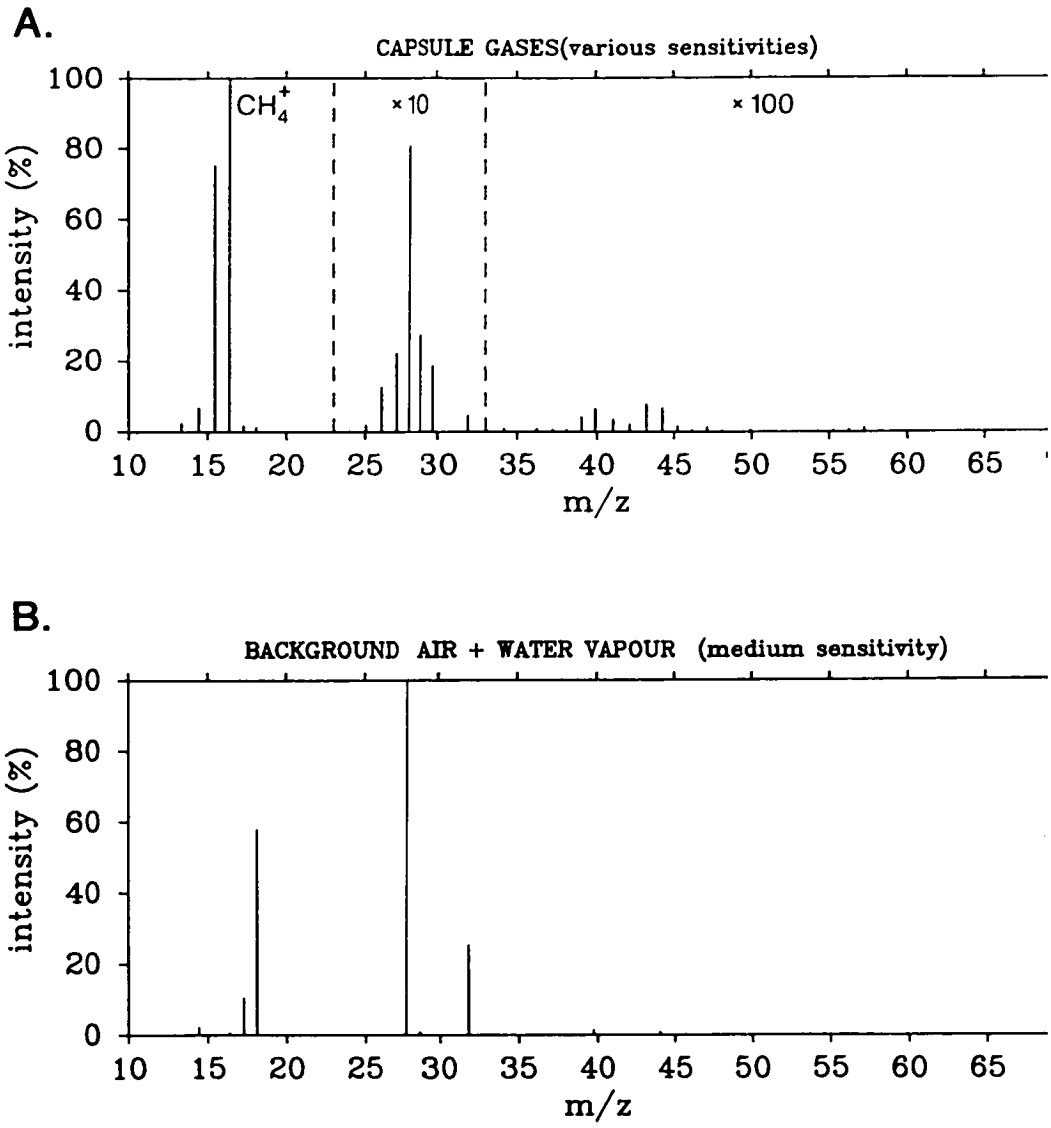

FIG. 1. (A) Mass spectrum of capsule gases released from run T-1341 at low (m/z 10–23), medium (×10, m/z 23–33) and high (×100, m/z >33) sensitivities. Methane: m/z 13–17; ethane: m/z 25–30; C_{3-4} hydrocarbons m/z >36; background water vapour and air: m/z 17–18, 28, 32. (B) Instrumental background at medium sensitivity. Note suppression of background ion intensity due to input of capsule gases (ratios of individual gases, however, remain unchanged).

intensities (MCMILLAN, 1985). Such changes are of critical importance in quantitative studies but are of lesser importance in the interpretative work undertaken here. Nevertheless, reproducibility checks were performed by the preparation of duplicate discs, in all cases using identical preparative methods. Duplicates showed close similarity in spectral features (as illustrated in Figures 7A and 7B). It is believed that the reproducibility of the KBr disc method, provided sample preparation techniques remain consistent, is not a problem in the interpretation of the silicate glass and crystal spectra considered here.

Analytical Methods

Pyrolysis/gas chromatography

Quantitative carbon and hydrogen analyses of t
C-H fluid-saturated glasses were performed with a He
lett-Packard 185B CHN analyser at the Analytical Servi
Section, Research School of Chemistry, Australian N
tional University). The method has been previously appli
by BREY (1976) in the analysis of ~mg quantities of silic
glasses containing dissolved carbonate and water. F

-H fluid-saturated glasses that may contain dissolved educed components, ~0.5 to 1.5 mg of sample was in-mately mixed with 85 mg of $MnO_2/WO_3/Cr_2O_3$ oxidant. amples were then combusted at 1080°C for 90 seconds llowing an initial heating at 70°C to remove atmospheric ases.

In the pyrolysis of reduced C-bearing glasses, the pos-bility exists that crystallites of silicon carbide might form uring the combustion process and remain unreactive to xidation (SiC being known for its chemical inertness and gh thermal stability: ROCHOW, 1973). To determine hether the pyrolysis/gas chromatography technique gives ccurate results for the analysis of substances containing r with the potential to form) Si–C bonds, three standard mpounds consisting of mixtures of finely ground SiC nd silica powder were analysed. Results for unknowns nd standards are listed in Table 1. Standards were com-usted for 90 seconds and 120 seconds (in the latter case ere was a considerable loss in sensitivity).

lectron microprobe

Electron microprobe analyses for carbon were per-rmed at the Electron Optical Centre (E.O.C.), University Adelaide (JEOL 733 microprobe, B. J. Griffin analyst) nd Central Science Laboratory, University of Tasmania EOL JXA50A microprobe). Measurements were ob-ined with a light element (STE crystal) wavelength dis-ersive spectrometer using 15 kV accelerating voltage in e former case and 10 kV in the latter. The beam in both ases was defocussed to a 10–20 μm diameter spot with 0 nA beam current to minimize specimen damage. Pol-hed epoxy mounts containing the samples, blanks and n array of carbon standards (graphite, SiC and various rbonates) were coated with aluminum following the ethod of MATHEZ and DELANEY (1981). Analyses at . O. C., Adelaide, were performed by 60 second counts n the peak and 20 seconds on the backgrounds with the ectrometer positioned 10 mm either side of the peak

able 1. Pyrolysis/gas chromatography analytical results*

ample #	Comp.	C (Weight percent)	H_2O (Weight percent)	Combustion time (sec)
-1296	Jd	0.13 ± 0.03	2.9 ± 0.4	90
-1341	Sm	0.09 ± 0.07	3.0 ± 0.5	90
-1318	Sm	0.12 ± 0.04	1.7 ± 0.1	90
-1250	Sm	not analysed	5.5 ± 0.2	90

tandards iC + SiO_2)	Actual weight percent C	Analysed weight percent C	Combustion time (sec)
A	0.5	0.24 ± 0.04	90
		0.18 ± 0.02	120
B	1.0	0.32 ± 0.03	90
		0.21 ± 0.06	120
C	1.5	0.51 ± 0.07	90

* All samples analysed in duplicate, averages and std viations quoted.
Detection limits: C 0.05 weight percent; H as H_2O 0.18 ight percent.

position. Full ZAF corrections were applied. Surface carbon contamination, derived from cracking of vacuum pump oils under the beam, resulted in a detection limit for carbon of ~0.2 weight percent. Analyses of standards, blanks and unknowns gave results of high consistency mainly due to the good precision obtainable with long counting times at reasonably high count rates. Absolute accuracy is difficult to judge due to the large matrix corrections used and the effects of surface contamination. These uncertainties could amount to errors of as much as ±30%.

CONTRASTING LIQUIDUS PHASE RELATIONS IN THE SYSTEM Ne–Fo–Q–C–O–H

At pressures >25 kbar the system nepheline(Ne)–forsterite(Fo)–silica(Q) contains liquidus phase fields of forsterite (Fo), enstatite$_{ss}$ (En_{ss}) and jadeite$_{ss}$ (Jd_{ss}) analogous to the major minerals of upper mantle peridotite. This system forms the base of the simplified basalt tetrahedron (YODER and TILLEY, 1962) and as such offers a useful model for investigating small degrees of partial melting of mantle peridotite. Liquidus phase relationships in the system Ne–Fo–Q have therefore been widely studied particularly as a function of pressure and activity of volatile species (KUSHIRO, 1968, 1972; EGGLER, 1978; WINDOM and BOETTCHER, 1981). The position of the Fo–En_{ss} two-phase boundary can be used as an indicator of melt-phase silica activity reflecting the relative degree of silicate melt polymerization/depolymerization (as discussed most recently by RYERSON, 1985). The aim of this study is to locate the Fo–En_{ss} two-phase boundary in the system Ne–Fo–Q under conditions dominated by a CH_4-rich vapor phase. Comparisons can then be made with the boundary position under volatile-absent, H_2O-saturated and CO_2-saturated conditions. The resultant phase diagrams can be used to predict the nature of mantle melting under conditions of saturation with different volatile species and hence over a range of f_{O_2}'s.

A pressure of 28 kbar was chosen to allow incorporation of the volatile-absent experimental data of WINDOM and BOETTCHER (1981) along the joins jadeite–enstatite (Jd–En) and jadeite–forsterite (Jd–Fo) as well as duplicating pressure conditions near the top of the oceanic LVZ where ≲2% partial melt is believed to exist (GREEN and LIEBERMANN, 1976). Experiments were conducted along the join $Ne_{55}Q_{45}$–$Ne_{55}Fo_{45}$ to provide approximately 90° intersection with the two-phase boundary at liquidus temperatures that are not prohibitively high (*i.e.*, <1500°C). Vapor saturation was confirmed in each experiment by piercing the sample capsule and noting the weight loss at 25°C and 110°C. All

water-saturated runs produced a fine white precipitate surrounding the fluid exit hole; this arises from solid-phase solubility in high pressure-temperature aqueous fluids as discussed by RYABCHIKOV *et al.* (1982).

Experimental charges were examined optically and by electron microprobe analysis; all showed quench effects of variable extent, mainly as $MgAl_2SiO_6$(MgTs)-rich pyroxene overgrowths sometimes extending to Jd-rich compositions and as individual crystallites on and about En_{ss}. Skeletal olivines are present in some runs. In selected experiments, electron microprobe analyses established liquid and crystal compositions as recorded in the Appendix and Table 2. In practice, only for the volatile-absent runs, showing the least quench effects and only small Na/Al ratio deviations from 1, were we able to analyse liquid compositions directly. This allowed the volatile-absent Fo-En_{ss} boundary to be well constrained with three experiments at $Ne_{55}Fo_{25}Q_{20}$. A liquid composition was estimated for CO_2-saturated run T-1227 from analysis of a large glass-rich area. The composition was projected back into the Na/Al = 1 plane from average quench En. In both H_2O-saturated and C-H fluid-saturated OH-containing glasses the combined effects of quench crystal growth and Na-volatilization under the electron microprobe beam precluded any estimate of liquid composition.

The position (in terms of weight percent Fo) of experimentally determined Fo-En_{ss} two-phase boundaries for the Ne_{55} compositions at P = 28 kbar are listed below:

Volatile species	Fo Weight percent	Estimated liquid temperature (°C
absent	24	1495 ± 5
H_2O-saturated	18 ± 1	1120 ± 15
CH_4-H_2-saturated	21 ± 1	1410 ± 15
CO_2-saturated	34 ± 1	1410 ± 15

These data allow delineation of Fo and En_{ss} liquidu phase fields on the ternary Ne-Fo-Q diagram (Fi ure 2); the volatile-absent fields for Jd_{ss}, S ($MgAl_2O_4$ spinel) and Ne_{ss} (nepheline$_{ss}$) are fro GUPTA *et al.* (1987).

Volatile-absent boundary

The position of the volatile-absent two-pha boundary is consistent with the experimental resul of KUSHIRO (1968) on the composition NFA-($Ne_{62}Fo_{18}Q_{20}$) which has Fo on the liquidus up 30 kbar. The intersection of the boundary with tl Fo-Q binary system is estimated from the data CHEN and PRESNALL (1975) to occur near Fo_2 These constraints place the Fo-En_{ss} boundary at 2 kbar close to the composition $Jd_{32}Fo_{68}$ on the Jc Fo join. WINDOM and BOETTCHER (1981, Figu 2) inferred that this point should lie near $Jd_{50}Fo$ but this position could not be adequately co strained by their experimental data. Recent expe imental work in the dry system by GUPTA *et a* (1987) has refined the position of the three pha Fo-En_{ss}-Jd_{ss} point. Although differing from WI DOM and BOETTCHER's (1981) interpretation, it in agreement with their experimental data alo

Table 2. Sm and Jd composition glasses: experimental results at 30 kbar

Run #	Comp.	Volatile	T°C	Product
T-1158	Sm	absent	1420	Glass
T-1159	Sm	absent	1370	Sm crystals
T-1160	Sm	absent	1395	Glass
T-1178	Sm	CO_2 ~8 weight percent	1300	Clear glass (MH buffer)
T-1250	Sm	H_2O ~6 weight percent	1300	Clear glass (graphite capsul
T-1318	Sm	C-H 9 weight percent	1320	Glass + grossular crystals
T-1341	Sm	C-H 9 weight percent	1350	Clear glass containing smal fluid inclusions <1 μm diam.
T-1442	Sm/SiC	—	1500	Glass + disseminated graphite
T-1296	Jd	C-H 10 weight percent	1320	Clear glass, inclusion-free

Microprobe analyses:	SiO_2	Al_2O_3	CaO	Na_2O	Tota
T-1341 (Av. glass)	44.2 (.4)*	18.6 (.4)	20.9 (.3)	11.8 (.2)	95.5
T-1296 (Av. glass)	56.0 (.6)	23.6 (.5)	—	14.7 (.2)	94.3
T-1318 (grossular)	39.48	22.56	37.56	0.00	99.6

* Figures in brackets are 1σ standard deviations.

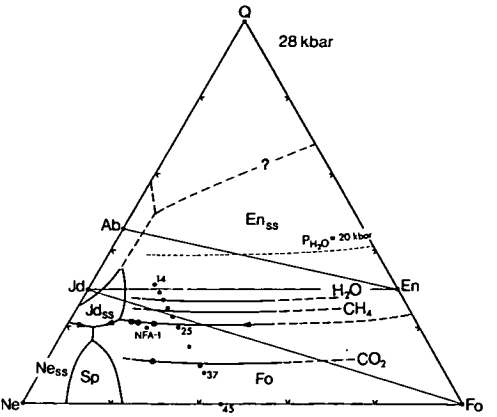

FIG. 2. Ternary liquidus phase diagram (weight percent) or the system Ne–Fo–Q at 28 kbar showing the position f the Fo–En_{ss} two-phase boundary under volatile-absent nd CO_2, H_2O and CH_4–H_2 volatile-saturated conditions. 'olatile-absent phase boundaries are from GUPTA *et al.* 1986) and this work. Dashed phase boundaries are in- erred. Compositions studied are indicated by the filled ircles on the join $Ne_{55}Fo_{45}$–$Ne_{55}Q_{45}$, adjacent numbers ndicate weight percent Fo component. Composition NFA-1 is from KUSHIRO (1968) and the 20 kbar water- aturated Fo–En_{ss} boundary is from KUSHIRO (1972). Double circles are analysed liquid compositions.

ne Jd–Fo and Jd–En joins as well as the earlier ata of KUSHIRO (1968). Figure 3 presents the mended phase diagram for the Jd–Fo pseudobi- ary join. The main change from WINDOM and BOETTCHER (1981) is the expansion of the Fo + L phase field (note also that two points are mislabelled on their original figure).

CO_2-saturated boundary

The shift in position of the Fo–En_{ss} boundary relative to the volatile-absent system is greatest for CO_2-saturation (expansion of En_{ss} field from Fo_{24} to Fo_{34} at Ne_{55}) reflecting CO_2's strong melt polymerizing role. Equilibrium and quench En_{ss} compositions on this boundary are rich in MgTs component (equilibrium crystals contain 15–17 weight percent Al_2O_3) and poor in Na_2O (<3.5 weight percent). This behaviour may arise from a decrease in Na_2O activity in the melt due to sodium–carbonate complex formation and accords with the CO_2 solubility mechanisms discussed by MYSEN and VIRGO (1980b,c).

H_2O-saturated boundary

The depolymerizing role of H_2O dominated fluids is clearly illustrated in Figure 2. Expansion of the Fo phase field at Ne_{55} relative to the volatile-absent system is from $Fo_{24} \rightarrow Fo_{18}$. This shift is not as large as that for CO_2 in the opposite direction; however, there appears to be a substantial pressure effect associated with the H_2O-saturated boundary. At $P_{H_2O} = 20$ kbar this boundary is found near $Ne_{55}Fo_7Q_{38}$ (KUSHIRO, 1972) a difference of Fo_{11}

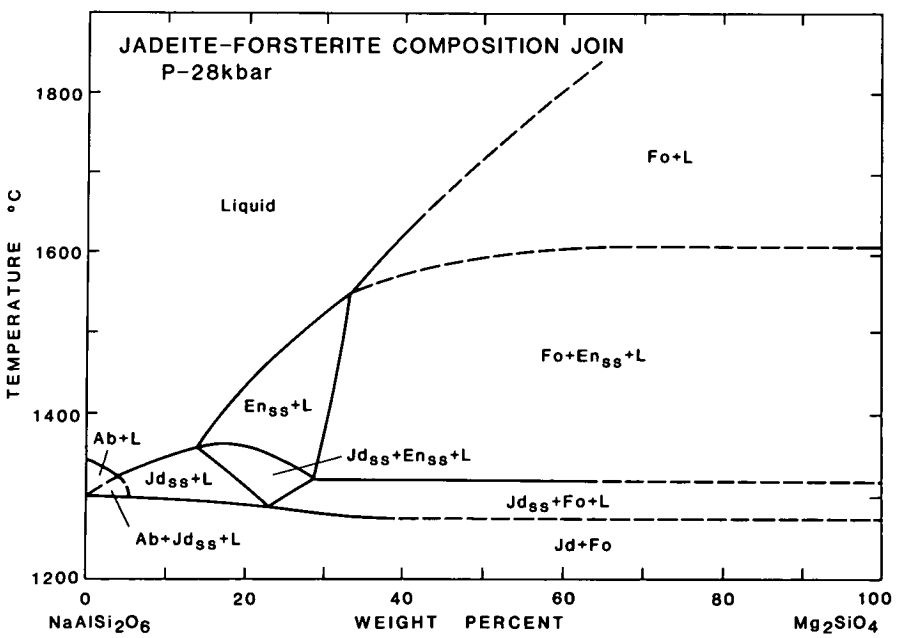

FIG. 3. Amended pseudobinary phase diagram for the join Jd–Fo at 28 kbar.

from the volatile-absent boundary at the same pressure (*cf.* the Fo_6 difference at 28 kbar). This effect may be ascribed to a diminishing ability of H_2O to depolymerize melts at higher pressures and could be due to a number of factors:

(a) changes in the solubility of solid components in co-existing aqueous fluid with pressure;

(b) dissolution of a higher proportion of H_2O in molecular form with increasing P_{H_2O} as shown by STOLPER (1982); because molecular water dissolves without (Si, Al)–O–Si bond cleavage there will be no accompanying network depolymerization;

(c) change in behaviour of H_2O with pressure toward that of a network polymerizer by formation of a greater proportion of alkali cation–hydroxy complexes relative to Si–OH bonds in an analogous fashion to CO_2 dissolution forming carbonate complexes.

If H_2O tends to be more polymerizing with increasing pressure via any of the above mechanisms, then there are important consequences for magma genesis. Thus, CO_2 may not be required in the genesis of highly silica undersaturated magmas (as proposed by EGGLER, 1978, and other workers) if H_2O can perform a melt polymerizing role. Further investigation of the role of H_2O at high pressures is clearly warranted.

C–H fluid—saturated boundary

The Fo–En_{ss} two-phase boundary for saturation with reduced C–H fluids falls between the H_2O and the volatile-absent boundaries implying a depolymerizing role for reduced C–H volatiles. The compositions of equilibrium, quench rim and quench crystal pyroxenes for volatile-absent, C–H fluid, H_2O and CO_2-saturated runs in which Fo and En_{ss} equilibrium crystals coexist are compared in Figures 4A and 4B. The proportion of jadeite component in equilibrium pyroxenes varies with volatile species in the order: CH_4–H_2 > volatile-absent > CO_2 > H_2O (circled in Figure 4B). This order is generally retained for quench rims and quench crystals. In the volatile-absent, CO_2 and C–H fluid—saturated cases, temperature and hence silica activity (buffered by coexisting Fo and En_{ss}), are of similar magnitude. On this basis, we would interpret differences in pyroxene chemistry as due largely to changes in the activity of network modifying oxides in the liquid. The observed enrichment in pyroxene of the jadeite component under conditions of C–H fluid saturation may, therefore, reflect an increase in the activity of network modifying Na_2O and Al_2O_3 relative to the volatile-absent system.

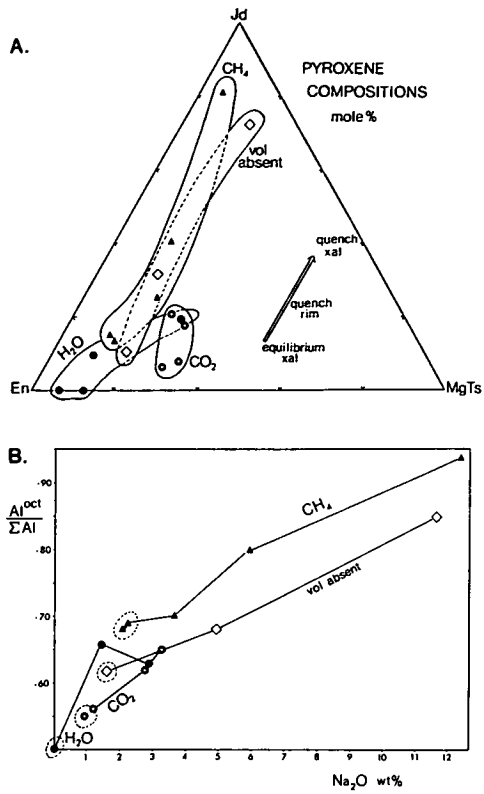

FIG. 4. A. Plot of pyroxene compositions (mol percen coexisting with forsterite for selected runs in the syster Ne–Fo–Q. Quench pyroxenes extend to very Jd-ric compositions in the CH_4 fluid—saturated and volatile absent systems. ▲ C–H fluid—(*i.e.*, CH_4–H_2) saturate (T–1291); ◊ volatile-absent (T–1210); ● CO_2-saturate (T–1227); ● H_2O-saturated (T–1175). Arrow shows th direction of pyroxene quench trends. B. Plot of Al occu pying octahedral sites/ΣAl versus Na_2O (weight percen for pyroxenes of Figure 4A. Dotted areas indicate equilit rium pyroxenes.

The results presented here indicate that C–H volatile dissolution leads to network depolymeriza tion accompanied by changes in the activity of net work modifying oxides. In order to write a mech anism to describe the dissolution process, howeve more detailed information on an atomic or molec ular basis is needed than can be supplied by liquidu studies. This requires spectroscopic and analytica data on samples free from contamination as con sidered below.

SOLUBILITY MECHANISM OF METHANE: ANALYTICAL AND SPECTROSCOPIC CONSTRAINTS

Sodamelilite and jadeite compositions have bee chosen for this investigation because their volatile

ee, H_2O and CO_2–containing glasses have been haracterized structurally by x-ray diffraction and ibrational spectroscopic methods (*e.g.*, TAYLOR nd BROWN, 1979; MYSEN and VIRGO, 1980a; IYSEN *et al.*, 1980; SHARMA and YODER, 1979). n addition, both compositions show good quench-ng behaviour in the presence of volatiles (MYSEN nd VIRGO, 1980a).

olatile-absent melting of sodamelilite and ıdeite at 30 kbar

To determine the magnitude of liquidus depres-ons in the presence of C–H volatiles the volatile-ee melting points of sodamelilite and jadeite are equired at 30 kbar. Crystalline sodamelilite is stable bove 4–5 kbar and at 10 kbar has a melting interval f ~50°C (YODER, 1964). At 20 kbar, the solidus nd liquidus may be regarded as coincident within xperimental precision (KUSHIRO, 1964). Experi-ients at 30 kbar (Table 2) show that crystalline odamelilite melts congruently at 1380 ± 10°C. ıdeite melts congruently to liquid at 1370 ± 10°C, 0 kbar (BELL, 1964).

'–H saturated melting at 30 kbar

Results of the melting experiments at 30 kbar are sted in Table 2. Product glasses are clear and raphite-free. Interaction of C–H fluids and silicate nelts leads to liquidus depressions of ~40°C in odamelilite and at least 50°C in jadeite. This ob-ervation together with the consistently low electron nicroprobe totals reported in Table 2 implies a sig-ificant solubility of a reduced volatile component r components. All experimental charges retain ex-ess carbide and mass spectra of quenched vapor ndicate the presence of only trace quantities of bulk xygen as H_2O. Thus the observed effects cannot e ascribed to absorbed H_2O or other external ources of oxidation.

In some experiments, small blebs of Pt–Si alloy ere occasionally observed at the Pt capsule/silicate nterface. This could be a potential source of oxygen nd hence H_2O) via the reaction:

$$SiO_2(\text{melt}) + y\text{Pt}(\text{capsule}) \rightarrow$$

$$\text{Si}_x\text{Pt}_y(\text{alloy}) + xO_2, \quad \text{where} \quad 0 < x, y < 1. \quad (2)$$

lectron microprobe analyses for silica (see Table), however, show no detectable Si loss to a Pt–Si loy within analytical error: compare 46.5 weight ercent SiO_2 in the sodamelilite starting material ith 46.3 weight percent (std deviation 0.4) found the C–H saturated glass (total normalized to 00%). The amount of oxygen (expressed in the form of dissolved H_2O) that could enter a soda-melilite melt by this process and remain undetected by silica analysis is <0.4 weight percent H_2O.

Under C–H fluid excess conditions the liquidus phase for the sodamelilite composition is grossular and not crystalline sodamelilite as observed under volatile-absent conditions. This observation is consistent with the early appearance of garnet on the liquidus of the C–H volatile—saturated $Di_{35}Py_{65}$ composition (EGGLER and BAKER, 1982). Combined with the results in the system Ne–Fo–Q these observations suggest that, in general, liquidus phases of higher octahedral aluminum content are favored by C–H fluid dissolution.

Spectroscopic results

Fourier Transform infrared (FTIR) spectra of sodamelilite and jadeite glasses are presented over

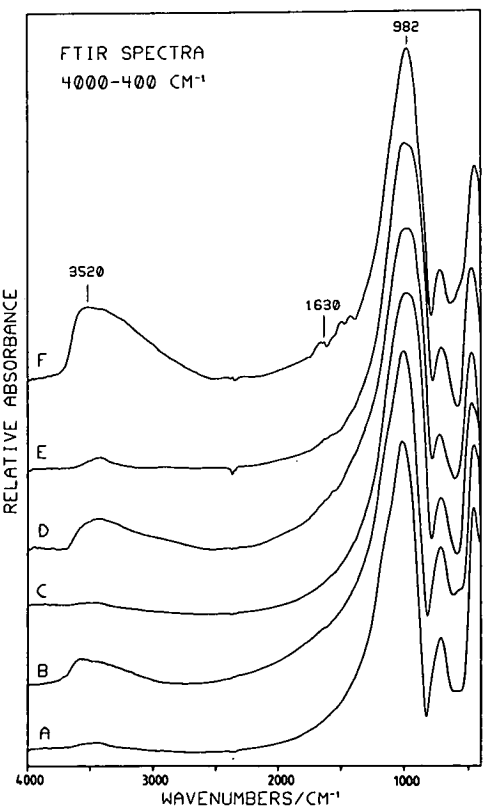

FIG. 5. FTIR spectra (4000–400 cm^{-1}): A. Volatile-free jadeite glass (quenched at 1 bar); B. C–H fluid—saturated jadeite glass (T–1296); C. Volatile-free sodamelilite glass (quenched at 30 kbar); D. C–H fluid—saturated soda-melilite glass (T–1341); E. Sodamelilite glass reduced by interaction with silicon carbide at 1500°C, 30 kbar (see text); F. Hydrous sodamelilite glass (T–1250). Weak positive or negative bands near 2350 cm^{-1} are due to atmospheric CO_2 vapour.

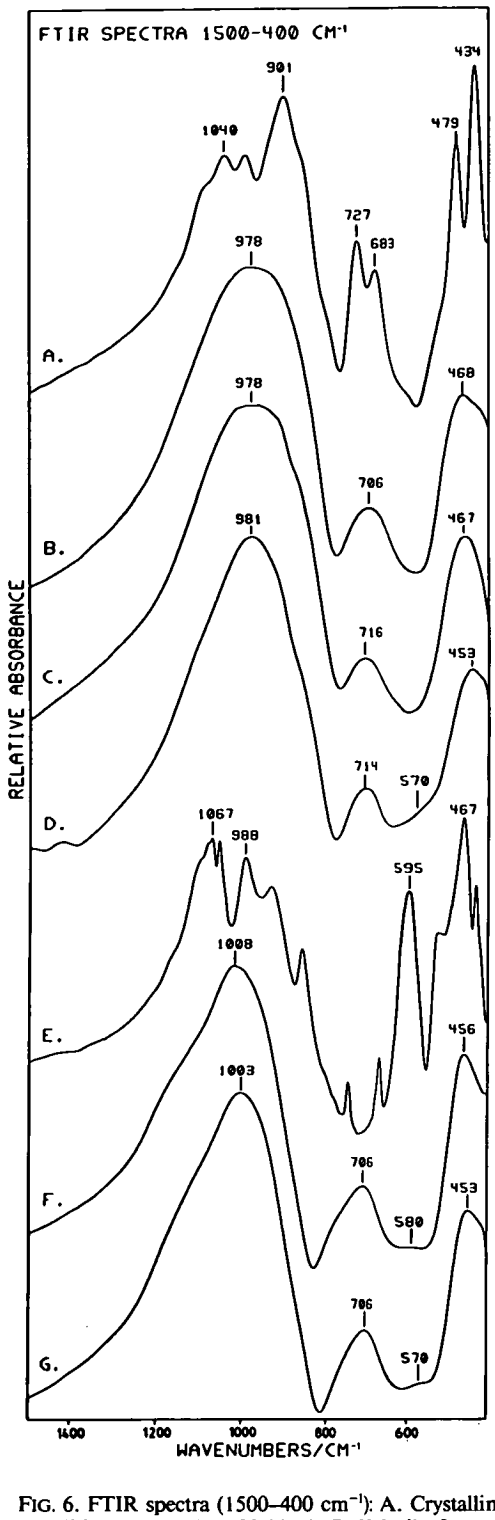

FIG. 6. FTIR spectra (1500–400 cm^{-1}): A. Crystalline sodamelilite (prepared at 30 kbar); B. Volatile-free sodamelilite glass (quenched at 30 kbar); C. C–H fluid—saturated sodamelilite glass (T–1341); D. Sodamelilite glass containing 5.5 ± 0.2 weight percent dissolved H_2O (T–

the ranges 4000–400 cm^{-1} and 1500–400 cm^{-1} Figures 5 and 6. For jadeite, comparisons have bee made between C–H fluid–saturated glass quenche from 30 kbar, 1320°C and the 1 bar volatile-abse jadeite glass. Such comparisons are valid becau the Raman study of MYSEN *et al.* (1980) has show that the spectroscopically resolvable structure quenched jadeite melt remains essentially una fected by pressure up to at least 38 kbar. For s damelilite, the volatile-free glass used for compa ison was quenched from 30 kbar, 1395°C. The fo lowing features distinguish spectra of the C–H flu saturated glasses (Figs 5B, D and 6C, G) from t volatile-free glasses (Figures 5A, C and 6B, F):

High-frequency region 4000–1400 cm^{-1}

A broad, asymmetric O–H stretch band centere at ~3580 cm^{-1} is the most prominent feature the high-frequency region. Comparison of O– peak areas with hydrous sodamelilite glass (Figu 5F) containing 5.5 ± 0.2 weight percent H_2O giv an estimated dissolved hydrogen content equivale to 2.7 ± 0.3 weight percent H_2O (if all H is derive from CH_4 then this would correspond to a metha solubility of ~1 weight percent). The area und the O–H envelope in C–H fluid—saturated jadei suggests a similar dissolved OH content. There a no absorption bands at ~2900 cm^{-1} that could b ascribed to C–H bond stretching in dissolved m lecular methane or other hydrocarbon groups su as $-CH_3$ or $-CH_2-$. No absorptions appear in t frequency range 2600–1700 cm^{-1}. A weak ban appears at ~1630 cm^{-1} (ν_2 H–O–H bending vibr tion) due to the presence of dissolved molecul H_2O (STOLPER, 1982). There is no evidence for di solved carbonate which has a characteristic ν_3 a sorption band or bands at ~1600–1380 cm^{-1}.

Aluminosilicate envelopes 1200–400 cm^{-1}

Changes occur in both the high-frequency ar mid-range envelopes (centered at ~1000 cm^{-1} ar ~700 cm^{-1} respectively) and in the spectral regio near 570 cm^{-1}. These changes reflect structur rearrangements in the aluminosilicate network th result from volatile dissolution. They are mo clearly illustrated in difference spectra (volatil saturated minus volatile-absent glasses) presente in Figure 7. Strong positive features appear

1250). The doublet at 1500–1400 cm^{-1} is due to tra dissolved carbonate; E. Crystalline jadeite (prepared at kbar); F. Volatile-free jadeite glass (quenched at 1 ba G. C–H fluid—saturated jadeite glass (T–1296).

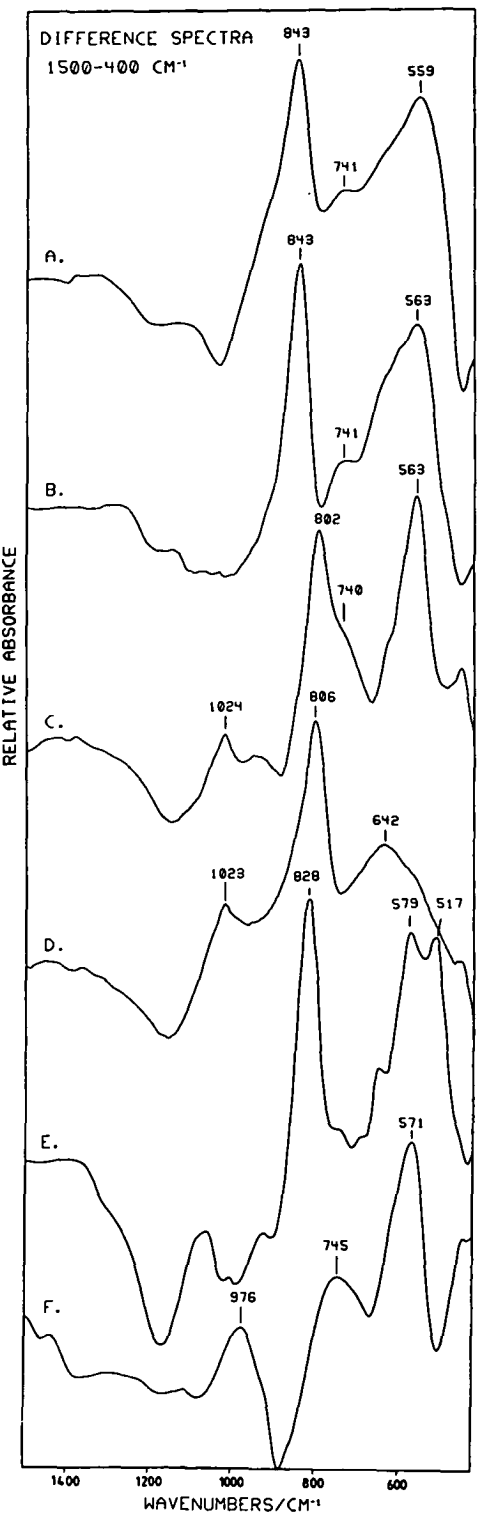

FIG. 7. Difference spectra (1500–400 cm^{-1}) (component-bearing) minus (component-absent): A. (C–H fluid—saturated jadeite glass T-1296) minus (1 bar volatile-free jadeite glass); B. Same as A but duplicate KBr discs were used to record both component-bearing and component-absent spectra (reproducibility check); C. (C–H fluid—saturated sodamelilite glass T-1341) minus (30 kbar volatile-free sodamelilite glass); D. (SiC reduced sodamelilite glass) minus (30 kbar volatile-free sodamelilite glass) [the "reduced component"]; E. (C–H fluid—saturated $Ne_{55}Fo_{25}Q_{20}$ glass containing ~10% enstatite crystals: run T-1289) minus ($Ne_{55}Fo_{25}Q_{20}$ 1 bar glass); F. (Hydrous sodamelilite glass T-1250) minus (30 kbar volatile-free sodamelilite glass) [the "oxidized component"].

~850–800 and ~570 cm^{-1} in C–H fluid—saturated sodamelilite and jadeite glasses. Weaker features are present as shoulders at ~950, ~740 and ~640 cm^{-1} and at ~1020 cm^{-1} in sodamelilite only. Both strong positive difference features appear in the spectrum of Ne–Fo–Q glass (sample from run T-1289) which also has a strong band at 517 cm^{-1} due the presence of crystalline enstatite. Negative difference features are much less pronounced and occur in spectra of both C–H fluid-saturated sodamelilite and jadeite at ~1160 cm^{-1} and in jadeite near 1050 cm^{-1}. These may be due to a decrease of Si–O–(Si, Al) bridging bonds but it is difficult to make specific assignments because of the complex overlapping nature of Si–O symmetric and asymmetric stretching modes of both bridging and non-bridging oxygen in this region of the infrared spectrum. There is little change in the low-frequency envelopes (centred near 450 cm^{-1}) except at <425 cm^{-1} where KBr background effects become noticeable.

Positive difference features related to OH dissolution

The prominent 570 cm^{-1} band is present in the FTIR difference spectrum of hydrous sodamelilite glass (Figure 7F) and therefore may be ascribed to changes in the aluminosilicate network resulting from OH dissolution. Bands in this region in the Raman spectra of aluminosilicate glasses have usually been assigned to in-plane Si–O–Si bridge bending motions or to the presence of 3- or 4-membered ring structures (MCMILLAN, 1984). However, in the 500–600 cm^{-1} region in the infrared TARTE (1965, 1967), FARMER *et al.* (1979) and SERNA *et al.* (1979) have assigned strong absorption bands in aluminosilicate glasses, crystals and gels to vibrations of AlO_6 polyhedra. While such an assignment will require confirmation (perhaps using more definitive techniques such as solid-state NMR), TAYLOR (1985) noted that strong IR bands in the 620–520 cm^{-1} region are found in all crystalline aluminosilicates containing AlO_6 polyhedra

but are absent in structurally related minerals lacking Al or in those containing only AlO_4 polyhedra (exceptions are minerals based on small ring framework structures such as the feldspars or scapolites). This is illustrated (Figures 6A & 6E) in the spectra of crystalline jadeite ($NaAl^{VI}Si_2O_6$, strong band at 595 cm^{-1}) and sodamelilite ($NaCaAl^{IV}Si_2O_7$, no strong absorptions 620–520 cm^{-1}). The weaker 950 and 740 cm^{-1} features identified in the C-H fluid —saturated glasses are also present in the hydrous glass and could be due, respectively, to Si–OH stretching (MYSEN and VIRGO, 1980a) and vibrations of Al–O–Al linkages in aluminate condensates or "clusters" (TARTE, 1967; SERNA *et al.*, 1977).

850–800 cm^{-1} positive difference feature

The ~850–800 cm^{-1} feature is located on the low-frequency limb of the high-frequency envelope in jadeite, sodamelilite and Ne–Fe–Q glasses. This band is not present in hydrous sodamelilite glass and therefore is unlikely to be associated with OH dissolution or network depolymerization. Instead, this band is characteristic of reduced C-H volatile dissolution and may be due to a dissolved reduced component. Spectroscopic identification of such a component in aluminosilicate glasses is verifiable experimentally as discussed later. Possible assignments for the 850–800 cm^{-1} feature are considered below after applying necessary theoretical constraints.

Theoretical constraints

Mechanisms for the dissolution of reduced volatiles in silicate melts have been suggested by very few authors. In a study that investigated the solubility behaviour of CO as a CO_2–CO volatile mixture, EGGLER *et al.* (1979) suggested that CO dissolves by a carbonation reaction of the type:

$$CO + 2O^- = CO_3^{2-} \quad \cdots\cdot A, \quad (3)$$

where "O^-" = non-bridging oxygen. EGGLER and BAKER (1982) proposed two mechanisms for CH_4 dissolution based on analogous reactions for H_2O, *i.e.*

$$4Si\text{–}O\text{–}Si + CH_4 = 4Si\text{–}OH + C \quad \cdots\cdot B \quad (4)$$

$$Si\text{–}O\text{–}Si + CH_4 = Si\text{–}CH_3 + Si\text{–}OH \quad \cdots\cdot C. \quad (5)$$

The validity of mechanisms A and B is, however, questionable because neither reaction can be correctly charge-balanced (at least in a chemically realistic sense in Equation A, "O^-" cannot be equated with NBO for usual oxidation states of oxygen in silicate melts). Because electroneutrality should always be obeyed when balancing any chemical reaction, it is evident that if a reduced volatile dissolves in a silicate melt to give an "oxidized bond' such as O–H or O–C, then this must be balanced at equilibrium by concurrent production of a "reduced bond." Such a bond is one involving an element in a lower oxidation state or one excluding oxygen or both. Candidates in the case of a C–H fluid could include: Si–H, Si–C, C–H, Si–Si and analogous bonds involving Al and other metal cations.

Reference to the FTIR spectra of sodamelilite and jadeite C–H fluid–saturated glasses immediately eliminates metal–hydrogen or C–H bonds as candidates for the "reduced bond." This is because bonds of this type have characteristic IR stretching frequencies in the range ~3000–1700 cm^{-1} where no absorption was noted. C–H bonds are expected at 3050–2850 cm^{-1} and Si–H bonds at 2250–2100 cm^{-1} (POUCHERT, 1981). Thus reaction C, suggested by EGGLER and BAKER (1982), while being properly charge balanced and involving Si–C and C–H as reduced bonds, is not consistent with observed spectroscopic results.

Possible mechanisms of C–H volatile dissolution

The theoretical and spectroscopic constraints discussed above, greatly limit the choice of a reduced component. We suggest that the most likely candidates are either (I) a network unit containing Si–C bonds or (II) a non-stoichiometric network component containing units having an O/Si ratio less than 2, such as found in amorphous silicon monoxide. The former alternative implies that only hydrocarbon species (*i.e.*, dominantly CH_4) are involved in the dissolution process, whereas the latter alternative is a general reduction of the silicate network and could involve H_2 as well as CH_4. Support for candidate (I) is given by the known range of IR active Si–C bond stretching frequencies for molecular compounds (WELTNER and MCLEOD, 1964; POUCHERT, 1981) *e.g.*, organosilicon compounds (Si–CH_3 bonds): 680–740 cm^{-1}; matrix-isolated SiC_2 and SiC molecules: 835 and 1226 cm^{-1} respectively. The range ~700 cm^{-1} to 1226 cm^{-1} encompasses the region that includes the strongest difference spectrum features at ~850–800 cm^{-1}. However, these features would also be consistent with the presence of silicon monoxide or related units. Compared with pure silica glass, the high-frequency envelope in amorphous silicon monoxide is shifted down frequency by some 100 cm^{-1} (PLISKIN and LEHMAN, 1965; KHANNA *et al.*, 1981). A similar shift in band components in aluminosilicate

glasses would be sufficient to extend the high-frequency envelope to lower wavenumbers and hence result in the observed ~850–800 cm^{-1} positive difference features.

Mechanisms (I) and (II) may be described by the following balanced equations (for $[SiO_3]^{2-}$ and sodamelilite melt-units):

Mechanism I: (Silicon–carbon bond formation)

$$2[SiO_3]^{2-} + CH_4 = \{Si\text{–}C\} + 4[OH]^- + [SiO_2]^0 \quad (6)$$

$$2[Al^{IV}Si_2O_7]^{3-} + CH_4 = 2[Al^{NN}O_2]^- + 4[OH]^- + \{Si\text{–}C\} + 3[SiO_2]^0 \quad (7)$$

.... D.

Mechanism II: (Network reduction by CH_4 or H_2, or both)

$$2[SiO_3]^{2-} + CH_4 = 2\{Si\text{–}O\} + 4[OH]^- + \{C^0\} \quad (8)$$

$$2[Al^{IV}Si_2O_7]^{3-} + CH_4 = 2[Al^{NN}O_2]^- + 4[OH]^- + 2\{Si\text{–}O\} + 2[SiO_2]^0 + \{C^0\} \quad (9)$$

.... E

$$[SiO_3]^{2-} + H_2 = \{Si\text{–}O\} + 2[OH]^- \quad (10)$$

$$[Al^{IV}Si_2O_7]^{3-} + H_2 = [Al^{NN}O_2]^- + 2[OH]^- + \{Si\text{–}O\} + [SiO_2]^0 \quad (11)$$

.... F

where

{ } = unidentified location in silicate network
[ ] = melt-unit or complex
$\{C^0\}$ = graphite, diamond or carbon dissolved in the melt in unspecified form
NN = Al in non-network sites (*e.g.*, AlO_6 polyhedra).

For both mechanisms additional equilibria can be written to relate spectroscopically observed species such as dissolved molecular water:

$$[SiO_2] + 2[OH]^- = [H_2O]_{molecular} + [SiO_3]^{2-}. \quad (12)$$

Mechanisms (I) and (II) are similarly constructed; both reactions produce 4 moles of O–H bonds (the "oxidized component") per mole of dissolved methane. For the sodamelilite melt-unit, the solution process is written to accommodate a redistribution of Al between network and non-network sites. The major difference between the mechanisms is in the nature of the reduced bond formed (*i.e.*, the "reduced component"). In mechanism (I), a significant melt-phase solubility of reduced carbon as Si–C bonds is implied. This mechanism is directly analogous to the structural role of nitrogen in Na_2O–CaO–silicon oxynitride glasses recently investigated by BROW and PANTANO (1984). Based on FTIR and x-ray photoelectron spectroscopic results those authors concluded that nitrogen is present in the silicate network of oxynitride glasses in the form of Si–N bonds with N in three-fold and possibly two-fold co-ordination sites. With increasing N content the principle changes in the FTIR spectra are seen in the high-frequency envelope which broadens and shifts to lower wavenumbers (similar to that observed in the C–H fluid—saturated glasses). The maximum amount of nitrogen dissolved in the Na_2O–CaO–silicon oxynitride glasses at 1 bar was ~2.2 weight percent N but the effects of N substitution on the network are clearly seen in the FTIR spectrum at much lower levels.

Mechanism (II) requires the presence of a silicate network unit with an O:Si ratio <2; this is represented in Equations E and F by a {SiO} or "silicon monoxide" group. It is conceivable that such units might resemble those found in amorphous silicon monoxide. The RDF study of YASAITIS and KAPLOW (1972) favors a structure for this compound based on puckered $(SiO)_n$ rings where the average co-ordination number about each Si atom does not deviate significantly from two. Such a structure gives each Si atom a formal valency of II.

Characterization of the "reduced component"

For the sodamelilite composition the "reduced component" was characterized spectroscopically by reducing the silicate network at high pressure under anhydrous conditions. The starting material consisted of sodamelilite glass in which a portion of the SiO_2 was substituted by –SiC [total C = 1.5 weight percent, equivalent to a methane solubility of 2 weight percent via mechanism (I)]. An inner graphite capsule was used to separate the silicate/carbide mix from the outer Pt capsule to prevent Pt–Si alloy formation. Over a run time of 90 min at 30 kbar and 1500°C, SiC was fully decomposed producing a product consisting of clear glass and disseminated graphite. This experiment does not distinguish between mechanisms (I) and (II) because SiC may dissolve to form reduced Si–C bonds or may reduce the silicate network directly via the reaction: $SiC + SiO_2 \rightarrow 2\{SiO\} + C$ [analogous to mechanism (II)]. FTIR spectra are shown in Figures 5E and 7D. Graphite is essentially IR inactive over this spectral range and does not contribute to the observed bands. The difference spectrum Figure 7D has a major positive feature at 806 cm^{-1} and weaker features at 1023 and 642 cm^{-1} corresponding closely

to those present in C–H fluid—saturated sodamelilite. In fact a combination of the hydrous sodamelilite glass difference spectrum (the "oxidized component") and Figure 7D would be almost indistinguishable from the C–H fluid—saturated spectrum. Thus separate "reduced" and "oxidized" components can be characterized spectroscopically; the latter is associated with O–H bond formation and the former is best interpreted as a reduction of the silicate network. Whether or not this reduction involves formation of reduced bonds to carbon must be decided by analytical means.

Analytical constraints

Results of pyrolysis/gas chromatography analyses for C and H for both samples and standards are presented in Table 1. The analysed carbon contents of the standards (SiO_2–SiC mixtures) are between half and one third of the known amounts present. This suggests incomplete oxidation of SiC has occurred with greatest discrepancy occurring at C contents >0.5 weight percent. Carbon values for the glass unknowns must therefore be regarded as minimum quantities only; if α–SiC forms metastably in these samples then analyses may be low by as much as a factor of two for total C contents ≤0.5 weight percent. Hydrogen analyses (converted to weight percent H_2O) are in good agreement with those deduced spectroscopically for sodamelilite. C–H fluid equilibrated glasses therefore contain a minimum of ~1000 ppm C and a maximum of ~2000 ppm C. These results are confirmed by quantitative and semi-quantitative electron microprobe analyses for carbon (Table 3). Carbon contents in the C–H fluid—saturated glasses are near or below the limit of detection (<2000 ppm) consistent with the gas chromatographic analyses.

For mechanism (I) to operate a reduced carbon solubility of 8000–12000 ppm is required. Thus mechanism (II) is supported as the dominant process for reduced volatile interaction with aluminosilicate melts. The small amount of carbon detected could dissolve either by mechanism (I) or perhaps in the form of atomic carbon occupying interstitial sites or cation vacancies as suggested FREUND *et al.* (1980) for oxide and silicate lattices. Carbon dissolved in this manner would be undetectable by IR and Raman spectroscopic methods.

Table 3. Microprobe analyses for carbon*

Sample	Expected weight percent	Weight percent analysed
Graphite (treated as unknown)	100.00	101.22
T–1178 (Sm + CO_2)	2.1 ± 0.2	2.15
T–1296 (Jd + C–H fl.)		
T–1341 (Sm + C–H fl.)	~0.1–0.2	≤0.2†
T–1318 (Sm + C–H fl.)		

* B.J. Griffin, analyst.
† Limit of detection ≃0.2 weight percent.

DISCUSSION

The recognition of mechanism (II) as the dominant process of C–H volatile solubility does not discriminate between the particular reduced volatile species involved. The mechanism is a general reduction of the silicate network that may take place in the presence of any of the reduced volatiles H_2, CH_4 or C_2H_6. In the presence of CH_4-rich fluids the H/C ratio of the melt phase greatly exceeds H/C of the coexisting fluid suggesting that reduced C–H volatile solubility will largely be a function of f_{H_2} and governed by equilibria similar to F above [Equations (10) and (11)]. In the system aluminosilicate–C–O, carbon monoxide is an important reduced volatile at $P < 20$ kbar and is believed to dissolve in melts by a carbonation reaction (EGGLER *et al.*, 1979). Charge balance constraints dictate a solubility mechanism that must involve a reduced component and we can propose reactions analogous to Equations E and F to describe CO dissolution, *e.g.*,

$$CO + [SiO_3]^{2-} = CO_3^{2-} + \{Si\text{–}O\}. \quad (12)$$

If carbonate ions and a reduced melt component such as {SiO} cannot coexist stably in silicate melts, there are real difficulties in proposing CO as a melt-soluble species other than in molecular form. Choice of mechanism (II) also helps rationalize the experimental results of LUTH and BOETTCHER (1986) which show that H_2 gives rise to significant depressions of the albite and diopside solidii implying a strong interaction between H_2 and aluminosilicate liquids as predicted by model F above.

Liquidus phase relations in the system Ne–Fo–Q suggest that dissolution of a C–H fluid, compared to the volatile-absent case, raises melt activities of network modifying Al_2O_3. This is in accord with the observed expansion of the garnet phase volume in other systems. The idea that carbon-rich eclogites could be the products of fractional crystallization of mantle melts under conditions of CH_4–H_2O–H_2 volatile saturation as proposed by EGGLER and BAKER (1982) is supported by the data presented here. KUSHIRO and YODER (1974) stated that ". . . in the presence of water . . . it should be possible for eclogite to form from garnet lherzolite" at depths

greater than the 26 kbar limit in the volatile-absent case, *i.e.*, to within the stability field of diamond. Because both H_2O and CH_4–H_2 fluids have similar melt depolymerizing behaviour, the findings of KUSHIRO and YODER (1974) will apply equally well to CH_4–H_2O–H_2 volatile mixtures as to pure H_2O. The added advantage in the case of carbon-rich eclogites is that the preference of the melt for H compared with C will drive a coexisting CH_4-bearing fluid phase toward carbon saturation leading to precipitation of diamond or graphite via equations similar to E. This is in accord with the origins of graphite-diamond eclogite from the Roberts Victor kimberlite as discussed by HATTON and GURNEY (1979). Those authors propose an origin based on rapid crystallization of melts produced by volatile-induced partial melting of garnet lherzolite where melt volumes are such that gravitational separation of diamond or graphite is ineffective. Whereas the authors propose that carbon is a result of reduction of a CO_2-bearing vapor during cooling, an alternative mechanism in which CH_4–H_2O–H_2 fluids give rise to melting accompanied by carbon precipitation from the fluid phase can equally well explain the origin of these rocks.

The finding that the network portion of silicate melts is quite susceptible to reduction via formation of groups with O/Si < 2, has not been demonstrated previously. For the observed H_2O content of C–H fluid-saturated sodamelilite glass at 30 kbar, 1350°C, we calculate that ~20% of the Si should be present as Si(II) (equivalent to 6–7 weight percent SiO) by mechanism (II). Reduced systems such as the enstatite chondrite group of meteorites have intrinsic oxygen fugacities that lie below IW. Measured values for the equilibrated EL enstatite chondrite group give f_{O_2}'s in the range ~IW–3 to IW–4 $\log f_{O_2}$ units (BRETT and SATO, 1984; WALTER and DOAN, 1969), near the redox conditions of the present C–H fluid experiments. In these rocks Si is distributed amongst three phases: metal (kamacite with ~1–4 weight percent Si), silicate (mainly enstatite), and silicon oxynitride (sinoite, $Si_2N_2O_2$) with graphite and not silicon carbide as an important accessory (SEARS *et al.*, 1982). This solid phase distribution of Si redox environments (at least at relatively low pressures) is consistent with the interpretation of C–H fluid—equilibrated aluminosilicate glasses where a reduced silicate network plus elemental carbon is evidently more stable than the equivalent melt structure containing Si–C bonds. It is possible to express the relationship between solid phases and a corresponding melt at f_{O_2} ~ IW–4 × $\log f_{O_2}$ units via a disproportionation equilibrium of the type:

$$2[Si^{2+}O_x]_{\substack{\text{silicate}\\\text{melt}}} = (2-x)[Si^0]_{\substack{\text{metallic}\\\text{phase}}} + x[Si^{4+}O_2]_{\substack{\text{solid}\\\text{silicate}}} \quad (13)$$

where $1 < x < 2$.

In view of recent hypotheses supporting the early incorporation of large amounts of reduced enstatite chondritic components into the Earth's mantle (SMITH, 1982; JAVOY and PINEAU, 1983; ITO *et al.*, 1984) such equilibria are expected to have an important bearing on the mantle–core segregation of Si.

SUMMARY

In this investigation, a mechanism for C–H volatile solubility in aluminosilicate melts has been proposed from the interpretation of FTIR spectra within theoretical and analytical constraints. The mechanism is supported by phase relations determined in the system Ne–Fo–Q–C–O–H which indicates a melt depolymerizing role for C–H fluids.

On spectroscopic and theoretical grounds reduced C–H volatile dissolution can be resolved into soluble oxidized and reduced components. The former is represented by O–H bonds (as hydroxyl groups and molecular water) and affects melt structure much in the manner of H_2O dissolution. There is no spectroscopic evidence for the presence of dissolved molecular CH_4 or carbonate. The reduced component is somewhat enigmatic. Analytical data establish that the reduced component is consistent with a network silicon-oxygen unit where the formal valency on silicon is reduced from IV to II (O:Si stoichiometry of the system <2). At the f_{O_2} conditions of these experiments, ~IW–4.5 $\log f_{O_2}$ units, a general reduction of the silicate network is evidently favored over formation of Si–C bonds. This is not the case, however, in analogous reduced systems containing nitrogen where Si–N bonding in silicon oxynitride glasses is well characterized. Nevertheless, the reduced carbon solubility in the aluminosilicate melts studied is ~1000 ppm (minimum) in a form yet to be characterized.

These results have been used to (1) propose solubility mechanisms for other reduced volatiles such as CO; (2) help rationalize the observed strong interaction between H_2 and silicate melts; (3) suggest an alternative interpretation for the origin of carbonaceous eclogites as the product of CH_4–H_2O fluid-induced partial melts of garnet lherzolite; (4) suggest a mechanism for mantle–core partitioning of Si and (5) provide a basis for investigating the nature of melting in a reduced mantle as discussed in the accompanying paper by GREEN *et al.* (1987).

Acknowledgements—We are grateful to Dr. B. J. Griffin (University of Adelaide) for much time spent at the microprobe analysing our samples for carbon. We thank J. Bignell, N. Davis, W. Jablonski and K. L. Harris for invaluable technical assistance. This study was supported financially by a Commonwealth Postgraduate Scholarship and Australian National Research Fellowship awarded to WRT and an ARGS grant to DHG.

REFERENCES

ANDERSON A. T. (1975) Some basaltic and andesitic gases. *Rev. Geophys. Space Phys.* **13**, 37–55.

ARCULUS R. J. and DELANO J. W. (1981) Intrinsic oxygen fugacity measurements: techniques and results for spinels from upper mantle peridotites and megacryst assemblages. *Geochim. Cosmochim. Acta* **45**, 899–913.

BELL P. M. (1964) High-pressure melting relations for jadeite composition. *Carnegie Inst. Wash. Yearb.* **63**, 171–174.

BRETT R. and SATO M. (1984) Intrinsic oxygen fugacity measurements on seven chondrites, a pallasite, and a tektite and the redox state of meteorite parent bodies. *Geochim. Cosmochim. Acta* **48**, 111–120.

BREY G. (1976) CO_2 solubility and solubility mechanisms in silicate melts at high pressures. *Contrib. Mineral. Petrol.* **57**, 215–221.

BROW R. K. and PANTANO C. G. (1984) Nitrogen coordination in oxynitride glasses. *J. Amer. Ceram. Soc. Comm.* **67**, C72–C74.

CHEN C-H. and PRESNALL D. C. (1975) The system Mg_2SiO_4–SiO_2 at pressures up to 25 kilobars. *Amer. Mineral.* **60**, 398–406.

EGGLER D. H. (1978) The effect of CO_2 upon partial melting of peridotite in the system Na_2O–CaO–Al_2O_3–MgO–SiO_2–CO_2 to 35 kb, with an analysis of melting in a peridotite–H_2O–CO_2 system. *Amer. J. Sci.* **278**, 305–343.

EGGLER D. H. and BAKER D. R. (1982) Reduced volatiles in the system C–O–H: Implications to mantle melting, fluid formation and diamond genesis. In *High Pressure Research in Geophysics*, (eds. S. AKIMOTO and M. H. MANGHANI), pp. 237–250 Center for Academic Publications.

EGGLER D. H., MYSEN B. O., HOERING T. C. and HOLLOWAY J. R. (1979) The solubility of carbon monoxide in silicate melts at high pressures and its effect on silicate phase relations. *Earth Planet. Sci. Lett.* **43**, 321–330.

FARMER V. C., FRASER A. R. and TAIT J. M. (1979) Characterisation of the chemical structures of natural and synthetic aluminosilicate gels and sols by infrared spectroscopy. *Geochim. Cosmochim. Acta* **43**, 1417–1420.

FREUND F., KATHREIN H., WENGELER H., KNOBEL R. and HEINEN H. J. (1980) Carbon in solid solution in forsterite—a key to the intractable nature of reduced carbon in terrestrial and cosmogenic rocks. *Geochim. Cosmochim. Acta* **44**, 1319–1333.

GREEN D. H. and LIEBERMANN R. C. (1976) Phase equilibria and elastic properties of the pyrolite model for the oceanic upper mantle. *Tectonophys.* **32**, 61–92.

GREEN D. H. and RINGWOOD A. E. (1967) The genesis of basaltic magmas. *Contrib. Mineral. Petrol.* **15**, 103–190.

GREEN D. H., FALLOON T. J. and TAYLOR W. R. (1987) Mantle derived magmas—roles of variable source peridotite and variable C–H–O fluid compositions. In *Magmatic Processes: Physicochemical Principles*, (ed B. O. MYSEN), The Geochemical Society Spec. Publ No. 1, pp. 139–154.

GUPTA A. K., TAYLOR W. R. and GREEN D. H. (1987 Experimental study of the system forsterite–nepheline–jadeite at variable temperatures under 28 kbar pressure *Amer. J. Sci.*, (Submitted).

HATTON C. J. and GURNEY J. J. (1979) A diamond-graphite eclogite from the Roberts Victor Mine. *Proc Int. Kimberlite Conf., 2nd*, Vol. 2, 29–36.

HOLLOWAY J. R. (1981) Volatile interactions in magmas *Adv. Phys. Geochem.* **1** (ed. S. K. SAXENA), pp. 273–293. Springer-Verlag.

HOLLOWAY J. R. and REESE R. L. (1974) The generation of N_2–CO_2–H_2O fluids for use in hydrothermal experimentation. I. Experimental method and equilibrium calculations in the C–O–H–N system. *Amer. Mineral.* **59**, 587–597.

ITO E., TAKAHASHI E. and MATSUI Y. (1984) The mineralogy and chemistry of the lower mantle: an implication of the ultrahigh-pressure phase relations in the system MgO–FeO–SiO_2. *Earth Planet. Sci. Lett.* **67**, 238–248.

JAKOBSSON S. (1984) Melting experiments on basalts in equilibrium with a graphite-iron-wustite buffered C–O–H fluid. Ph.D. Dissertation, Arizona State Univ.

JAVOY M. and PINEAU F. (1983) Stable isotope constraints on a model Earth from a study of mantle nitrogen. *Meteoritics* **18**, 320.

KHANNA R. K., STRANZ D. D. and DONN B. (1981) A spectroscopic study of intermediates in the condensation of refractory smokes: Matrix isolation experiments of SiO. *J. Chem. Phys.* **74**, 2108–2115.

KUSHIRO I. (1964) The join akermanite-soda melilite at 20 kilobars. *Carnegie Inst. Wash. Yearb.* **63**, 90–92.

KUSHIRO I. (1968) Compositions of magmas formed by partial zone melting of the Earth's upper mantle. *J. Geophys. Res.* **73**, 619–634.

KUSHIRO I. (1972) Effect of water on the composition of magmas formed at high pressures. *J. Petrol.* **13**, 311–334.

KUSHIRO I. and YODER H. S. JR. (1974) Formation of eclogite from garnet lherzolite: liquidus relations in a portion of the system $MgSiO_3$–$CaSiO_3$–Al_2O_3 at high pressures. *Carnegie Inst. Wash. Yearb.* **73**, 266–269.

LUTH R. W. and BOETTCHER A. L. (1986) Hydrogen and the melting of silicates. *Amer. Mineral.* **71**, 264–276.

MATHEZ E. A. and DELANEY J. R. (1981) The nature and distribution of carbon in submarine basalts and peridotite nodules. *Earth Planet. Sci. Lett.* **56**, 217–232.

MCMILLAN P. (1984) Structural studies of silicate glasses and melts—applications and limitations of Raman spectroscopy. *Amer. Mineral.* **69**, 622–644.

MCMILLAN P. (1985) Vibrational spectroscopy in the mineral sciences. In *Reviews in Mineralogy, 14* (eds. A. NAVROTSKY and S. KIEFFER), pp. 9–63 Mineralogical Society of America.

MYSEN B. O. and VIRGO D. (1980a) Solubility mechanism of water in basalt melt at high pressures and temperatures: $NaCaAlSi_2O_7$–H_2O as a model. *Amer. Mineral.* **65**, 1176–1184.

MYSEN B. O. and VIRGO D. (1980b) The solubility behaviour of CO_2 in melts on the join $NaAlSi_3O_8$–$CaAl_2Si_2O_8$–CO_2 at high pressures and temperatures: A Raman spectroscopic study. *Amer. Mineral.* **65**, 1166–1175.

MYSEN B. O. and VIRGO D. (1980c) Solubility mecha-

nisms of carbon dioxide in silicate melts: A Raman spectroscopic study. *Amer. Mineral.* **65**, 885–899.

MYSEN B. O., VIRGO D. and SCARFE C. M. (1980) Relations between anionic structure and viscosity of silicate melts—a Raman spectroscopic study. *Amer. Mineral.* **65**, 690–710.

PLISKIN W. A. and LEHMAN H. S. (1965) Structural evaluation of silicon oxide films. *J. Electrochem. Soc.* **112**, 1013–1019.

POUCHERT C. J. (1981) *The Aldrich Library of Infrared Spectra.* 3rd ed., 1203 pp. Aldrich Chemical Co.

ROCHOW E. G. (1973) The chemistry of silicon. In *Comprehensive Inorganic Chemistry,* Vol. 9, pp. 1323–1467 Pergamon Press.

RYABCHIKOV I. D., GREEN D. H., WALL V. J. and BREY G. P. (1981) The oxidation state of carbon in the reduced-velocity zone. *Geochem. Int.* **18**, 148–158.

RYABCHIKOV I. D., SCHREYER W. and ABRAHAM K. (1982) Compositions of aqueous fluids in equilibrium with pyroxenes and olivines at mantle pressures and temperatures. *Contrib. Mineral. Petrol.* **79**, 80–84.

RYERSON F. J. (1985) Oxide solution mechanisms in silicate melts: Systematic variations in the activity coefficient of SiO_2. *Geochim. Cosmochim. Acta* **49**, 637–650.

SEARS D. W., KALLEMEYN G. W. and WASSON J. T. (1982) The compositional classification of chondrites: II. The enstatite chondrite group. *Geochim. Cosmochim. Acta* **46**, 597–608.

SERNA C. J., VELDE B. D. and WHITE J. L. (1977) Infrared evidence of order–disorder in amesites. *Amer. Mineral.* **62**, 296–303.

SERNA C. J., WHITE J. L. and VELDE B. D. (1979) The effect of aluminium on the infra-red spectra of 7 Å trioctahedral minerals. *Mineral. Mag.* **43**, 141–148.

SHARMA S. K. and YODER H. S. JR. (1979) Structural study of glasses of akermanite, diopside and sodium melilite compositions by Raman spectroscopy. *Carnegie Inst. Wash. Yearb.* **78**, 526–532.

SMITH J. V. (1982) Heterogeneous growth of meteorites and planets, especially the Earth and moon. *J. Geol.* **90**, 1–125.

STOLPER E. (1982) Water in silicate glasses: an infrared spectroscopic study. *Contrib. Mineral. Petrol.* **81**, 1–17.

TARTE P. (1965) The determination of cation co-ordination in glasses by infra-red spectroscopy. In *Physics of Non-Crystalline Solids,* (ed. J. A. PRINZ), pp. 549–565. John Wiley.

TARTE P. (1967) Infra-red spectra of inorganic aluminates and characteristic vibrational frequencies of AlO_4 tetrahedra and AlO_6 octahedra. *Spectrochim. Acta* **23A**, 2127–2143.

TAYLOR M. and BROWN G. E. (1979) Structure of mineral glasses—II. The SiO_2–$NaAlSiO_4$ join. *Geochim. Cosmochim. Acta* **43**, 1467–1473.

TAYLOR W. R. (1985) The role of C–O–H fluids in upper mantle processes: a theoretical, experimental and spectroscopic study. Ph.D. Thesis, Univ. of Tasmania.

TAYLOR W. R. (1987) A 5-parameter modified Redlich-Kwong equation of state for C–O–H fluids at upper mantle pressures and temperatures, (In prep.).

WADE K. and BANISTER A. J. (1973) The chemistry of aluminium, gallium, indium and thallium. In *Comprehensive Inorganic Chemistry,* Vol. 12, pp. 993–1064 Pergamon Press.

WALTER L. S. and DOAN A. S. (1969) A determination of oxygen fugacities of chondritic meteorites (abstr.). *Geol. Soc. Amer. Abstr. Prog.* **1**, 232–233.

WELHAN J. A. and CRAIG H. (1979) Methane and hydrogen in East Pacific Rise hydrothermal fluids. *Geophys. Res. Lett.* **6**, 829–831.

WELHAN J. A. and CRAIG H. (1983) Methane, hydrogen and helium in hydrothermal fluids at 21°N on the East Pacific Rise. In *Hydrothermal Processes at Seafloor Spreading Centers,* (eds. P. A. RONA, K. BOSTROM, L. LAUBIER and K. L. SMITH), pp. 391–409 Plenum Press.

WELTNER W. and MCLEOD D. (1964) Spectroscopy of silicon carbide and silicon vapor trapped in neon and argon matrices at 4 K and 20 K. *J. Chem. Phys.* **41**, 235–245.

WINDOM K. E. and BOETTCHER A. L. (1981) Phase relations for the joins jadeite-enstatite and jadeite-forsterite at 28 kb and their bearing on basalt genesis. *Amer. J. Sci.* **281**, 335–351.

WOERMANN E. and ROSENHAUER M. (1985) Fluid phases and the redox state of the Earth's mantle; extrapolations based on experimental, phase-theoretical and petrological data. *Fortschr. Mineral.* **63**, 263–349.

YASAITIS J. A. and KAPLOW R. (1972) Structure of amorphous silicon monoxide. *J. Appl. Phys.* **43**, 995–1000.

YODER H. S. JR. (1964) Soda melilite. *Carnegie Inst. Wash. Yearb.* **63**, 86–89.

YODER H. S. JR. and TILLEY C. E. (1962) Origin of basalt magma: an experimental study of natural and synthetic rock systems. *J. Petrol.* **3**, 342–532.

APPENDIX

Experimental results along the join $Ne_{55}Fo_{45}$–Ne_{55}–O_{45} P = 28 kbar

VOLATILE-ABSENT

Run number	Fo Weight percent	Duration (min.)	T (°C)	Approx. % Cryst.	Products*
T-1210**	25	15	1440	40	Fo, Opx, Liq, Qx
T-1213**	25	10	1500	—	Liq, Qx
T-1215**	25	10	1475	30	Fo, Opx, Liq, Qx
T-1218**	25	12	1490	10	Fo, Liq, Qx
H_2O–SATURATED (~30 Weight percent H_2O added as liquid)					
T-1175	18	60	1100	5–10	Fo, Opx, Liq, Qx
T-1237	14	60	1040	20	Opx, Liq, Qx
T-1304	20	60	1100	5	Fo, Liq, Qx
T-1305	16	60	1060	10	Opx, Liq, Qx
CO_2–SATURATED (~15 Weight percent CO_2 generated from $Ag_2C_2O_4$)					
T-1226	30	12	1390	10	Opx, Liq, Qx
T-1227†	35	12	1390	—	Fo, Opx, Liq, Qx
T-1334	37	12	1400	<2	Fo, Liq, Qx, Qcarb
C-H FLUID—SATURATED (~7 Weight percent CH_4 generated from $Al(OH)_3/Al_4C_3$ mix)					
T-1174	18	25	1280	25	Opx, Liq, Qx, Fo (tr
T-1208	25	20	1350	30	Fo, Opx, Liq, Qx
T-1284	22	20	1380	20	Fo, Opx, Liq, Qx
T-1289††	20	25	1380	10	Opx, Liq, Qx
T-1291	20	25	1360	20	Opx, Fo, Liq, Qx
T-1315	22	30	1395	5	Fo, Liq, Qx

* Fo = forsterite; Opx = enstatite s.s.; Liq = glass; Qx = quench crystals; Qcarb = quench carbonate; tr = trace.
† Liquid composition obtained (see below).
†† FTIR spectrum and difference spectrum obtained (see Figure 7)

Liquid Compositions (Weight percent)

Oxide	T-1213	T-1218	T-1215	T-1210	T-1227*
SiO_2	54.01	54.39	54.55	54.52	48.81
Al_2O_3	19.85	21.51	22.79	23.19	22.93
MgO	14.28	11.03	8.81	8.19	14.32
Na_2O	11.86	13.07	13.85	14.10	13.94
Fe	24.9 (25)†	19.3	15.4	14.3	25.0
Ne	55.3 (55)	59.9	63.5	68.6	63.9
Q	19.8 (20)	20.8	21.1	21.1	11.1

* Liquid projected back into Na/Al = 1 plane from average quench pyroxene: $En_{55}MgTs_{30}Jd_{15}$ (mol percent).
† Expected composition in brackets.

Contrib Mineral Petrol (1987) 96:326–342

Contributions to Mineralogy and Petrology
© Springer-Verlag 1987

B39

The genesis of refractory melts in the formation of oceanic crust

R.A. Duncan* and D.H. Green
Department of Geology, University of Tasmania, Hobart, Tasmania 7001, Australia

Abstract. Refractory, primary liquids arising in various oceanic plate tectonic settings are characterized by high MgO, SiO_2, Ca/Na, low TiO_2 and generally low incompatible element abundances relative to primary liquids parental to MORB. We propose that the former melts segregate from upper mantle peridotite which has earlier been depleted by extraction of picritic melts which were parental to MORB. A compositional range in the 'second-stage' melts is expected, depending on the extent of previous depletion of the peridotite, the temperature and pressure of melt segregation, and the possible influence of volatile phases (C-H-O) present during melting.

An example of a second stage melt is of magnesian quartz tholeiite composition, identified from among the Upper Pillow Lavas, Troodos ophiolite, Cyprus. Experimental studies determine that this composition has appropriate liquidus phases to have segregated from depleted upper mantle peridotite at about 25 km, 1360° C leaving a harzburgite residue. The experimental studies are applied to interpretation of cooling histories and water contents of specific Upper Pillow Lavas. Magma batches are estimated to have contained 0.5–1.0% H_2O. Picritic lavas quenched from olivine + liquid at < 5 kb. Magnesian, pyroxene-phyric lavas exhibit intratelluric crystallization at ~5 kb, 1270° C (Mg_{88} pigeonite and Mg_{89} orthopyroxene).

These and other second-stage melts will crystallize extremely refractory minerals identical to many found in cumulate sequences in ophiolites, in plutonic rocks dredged and drilled from ocean basins, and occurring as xenocrysts in ocean floor basalts. Multistage melting of upper mantle peridotite, with and without presence of water, reconciles some of the present difficulties in relating ophiolite and ocean floor basalt compositions, and is an important process in ocean crust formation in a variety of different oceanic settings (mid-ocean ridges, marginal basins, and island arcs).

Introduction

It is generally accepted that primary basaltic magmas are generated in tensional environments by partial melting following diapiric ascent of upper mantle peridotite. It is also well established from the results of numerous trace element and isotopic studies that a spectrum of source peridotite compositions, differing principally in their incompatible ("LIL" and "HFS") element abundances, is required to account for the variety of observed primary basalts. Experimental petrologists have demonstrated that a given source peridotite composition can produce a continuum of primary nephelinitic, basaltic and picritic magmas by variation of depth of magma segregation and degree of partial melting. The degree of partial melting of a particular peridotite at any pressure and temperature is dependent on the nature and concentration of C-H-O fluids present in the source region. Against this background of complexity in variable upper mantle composition and melting conditions, petrologists are now turning to detailed field, petrological and geochemical studies of specific geological settings, to identify source peridotite compositions and conditions of melting appropriate to particular plate tectonic environments.

The processes of magmatism and oceanic crust formation at mid-ocean ridges have naturally formed a major focus of these investigations. Basalts dredged and drilled from the ocean floor, dredged samples of gabbro and ultramafic cumulates, and of ultramafic tectonite are thought to be complementary components (primary and fractionated liquids, shallow level cumulate minerals, and refractory residues, respectively) in the formation of new oceanic crust at mid-ocean ridges. The most common basalt types found in this spreading environment are olivine tholeiites (Basaltic Volcanism Project, Ch. 1.2.5, 1981). Examination of analyzed glasses and aphyric basalts, using criteria such as Mg# (Mg/(Mg + Fe)) and Ni content, indicates that primary liquids for mid-ocean ridge magmatism range from tholeiitic picrite to olivine-poor tholeiite (Frey et al. 1974; Bryan et al. 1976; Bryan and Moore 1977; Presnall and Hoover 1984; Stolper 1980; Green et al. 1979).

A large number of ocean floor basalts can be related to more olivine-rich parents by pre-eruptional fractional crystallization of olivine, spinel, plagioclase and pyroxene at low pressure (Frey et al. 1974; Bryan et al. 1976; Bryan and Moore 1977) while more complex melting and mixing mechanisms are required to account for some minor and trace element abundance variations (e.g., Langmuir et al. 1977; Shibata et al. 1979; Flower et al. 1977; O'Hara 1977).

Evidence for second-stage melts in the ocean basins

Experimental studies of the phase relationships of primitive ocean floor basalts (Green et al. 1979; Stolper 1980; Elthon and Scarfe 1984) have defined the compositional range of

* *Present address:* College of Oceanography, Oregon State University, Corvallis, Oregon, 97331, USA

Offprint requests to: D.H. Green

Table 1. Contrasted mineral compositions in ocean floor basalt phenocrysts, xenocrysts, and ophiolite layered series

	Low pressure (<5 kb) cumulates from DSDP 3–18[a]	Xenocrysts entrained in MORB's[b]	Ophiolite basal accumulates[c]
OL	$<Mg_{91}$	Mg_{91-89}	$<Mg_{93}$
OPX	$<Mg_{87}$	–	$<Mg_{93}$
CPX	$<Mg_{88}$	$Mg_{90.7}$	$<Mg_{94}$
PL	$<An_{80}$	$An_{91.5-85}$	$<An_{95}$
SP	$\frac{100Cr}{Cr+Al}<60$ (Fig. 1)	–	$\frac{100Cr}{Cr+Al}<90$

[a] Green et al. (1979)
[b] Donaldson and Brown (1977)
[c] England and Davies (1973), Pallister and Hopson (1980), Juteau and Whitechurch (1980), Jaques (1981)

minerals expected to precipitate from picrite and olivine tholeiites during low pressure fractionation (Table 1). Phenocrysts in ocean floor basalts and plutonic cumulate rocks recovered from the ocean basins with these specific mineralogical compositions may be reasonably related to the picritic parental liquids and derivative olivine tholeiites and Fe-, Ti-rich quartz tholeiites from the ocean floor. There is, however, evidence from the mid-ocean ridge environment for more refractory magmas than those described above. Specifically, some ocean floor basalts contain plagioclase xenocrysts (Donaldson and Brown 1977; Dungan et al. 1979) which are much too calcic (An_{85-92}) to have formed from the proposed olivine tholeiitic melts. These calcic plagioclase megacrysts often contain melt inclusions which have high Mg# and very much higher CaO/Na_2O than primitive olivine tholeiite liquids. Highly magnesian (Mg_{89-91}) chrome-diopside megacrysts (Donaldson and Brown 1977) are also refractory relative to their host magmas and may either be xenocrysts of a disaggregated lherzolite (melting residue) or phenocrysts of an admixed refractory liquid. Similarly refractory plagioclase and pyroxenes (ortho-, calcic clino-) are found in cumulate plutonic rocks from the ocean floor (Hodges and Papike 1976; Hamlyn and Bonatti 1980). These extreme mineral compositions cannot have precipitated from the parental tholeiitic picrites or common MORB.

A correlation between ophiolites and the formation of oceanic crust at mid-ocean ridges has been used to apply the results from studies of ophiolite assemblages to model the petrogenesis of MORB and oceanic crustal structure (e.g., Moores and Vine 1971; Christensen and Salisbury 1975). This correspondence, however, is not universally accepted and some authors have argued that many ophiolites form in a convergent margin environment (Miyashiro 1973; Sun and Nesbitt 1979; Cameron et al. 1980). This topic has been recently reviewed in Gass et al. (1984).

Against a background of increasing evidence for a spectrum of primary, mantle-derived tholeiitic liquids (Table 2) and of controversy regarding the plate tectonic environment for genesis of ophiolites, Duncan and Green (1980) and Green et al. (1979) argued for formation of refractory primary magmas of magnesian quartz tholeiite composition. These proposed melts would form by ~10% melting and magma segregation at relatively shallow levels (~25 km) from a peridotite diapir previously depleted by extraction of 20–25% melt of tholeiitic picrite (parental magma for N-MORB DSDP 3–18, Green et al. 1979) at deeper levels (50–70 km). Hence the more refractory liquids were termed 'second-stage' melts. Duncan and Green (1980) specifically applied this multistage melting model to interpret the unusually depleted Upper Pillow Lavas of the Troodos ophiolite, Cyprus, as such a second-stage melt produced in a mid-ocean ridge environment. A parental magma composition for this distinctive sequence of picrites to quartz tholeiites was calculated from geochemical data available at that time (Table 2). Wood (1979) proposed a similar model of incremental melting.

Since proposing this model and specific parental magma composition for the Upper Pillow Lavas at Troodos, we have obtained geochemical, mineralogical and petrological data on samples collected from the Troodos ophiolite. In addition, a large amount of new data on Troodos basaltic rocks has been reported by others. In this paper we report the crystallization behaviour of the model parental magma as a function of pressure and temperature. We find that liquids of this composition are multiply saturated in olivine and orthopyroxene at 7–8 kb (depth of ~25 km) at a temperature of 1360° C and thus may be primary melts, leaving harzburgite residue. The sequence of crystallization in the experiments matches that observed in the natural rocks at Troodos and experimental mineral compositions are appropriately refractory to match phenocrysts in the lavas and in some of the lowermost cumulate sequences of this ophiolite. We discuss the implications of these experimental results for genesis of refractory melts in a variety of oceanic tensional environments.

Refractory lavas from the Troodos ophiolite, Cyprus

One of the most intensively studied ophiolite assemblages is that formed by volcanic and plutonic rocks in the Troodos Mountains, Cyprus. In spite of this attention, however, the petrogenesis and plate tectonic setting of this complex are by no means clear. The Troodos volcanic rocks have been divided into an older sequence of Lower Pillow Lavas (LPL) and a younger sequence of Upper Pillow Lavas (UPL), which are distinguished by a metamorphic discontinuity defined by zeolite mineralogy (Gass and Smewing 1973) or, in places, a stratigraphic unconformity (Smewing et al. 1975). The two extrusive sequences were originally thought to have had separate origins: the LPL derived from mid-ocean ridge or back-arc spreading and the UPL from later off-ridge or possibly initial island arc volcanism (Smewing et al. 1975; Moores and Vine 1971; Pearce 1975; Duncan and Green 1980).

Some confusion about the petrologic affinity of these rocks is due to the chemical alteration present in whole rock samples. However, many recent studies (Robinson et al. 1983; Schmincke et al. 1983; Rautenschlein et al. 1985) using fresh glasses from the entire extrusive section have shown that the lower sequence is predominantly differentiated andesite to dacite, resembling an evolved island-arc tholeiitic series, while the upper sequence is picrite, mafic basalt and basaltic andesite which are similar to rocks drilled and dredged from fore-arc regions (e.g., Marianas Arc, Meijer 1980). The Troodos lavas differ in composition from all mid-ocean ridge tholeiites so far recovered with the possible exception of those at DSDP Sites 236 and 240 in the Somali Basin (Frey et al. 1980).

Of particular interest are the chemically primitive and refractory compositions found within the UPL. These quartz-normative rocks contain phenocrysts of forsteritic olivine or magnesian orthopyroxene, microphenocrysts of olivine, magnesian orthopyroxene, pigeonite and diopside, and a quenched groundmass of clinopyrox-

Table 2. Refractory melts developed in oceanic tensional settings

	Troodos ophiolite		Mid-atlantic Ridge	High-Mg andesite (island arc)	Lau Basin (back-arc)	Stage one melt	DSDP Site 236
	1	2	3	4	5	6	7
SiO_2	52.4	52.9	50.9	57.3	47.0	48.3	53.3
TiO_2	0.3	0.5	0.6	0.1	0.3	0.6	0.6
Al_2O_3	11.7	12.2	14.4	9.8	14.0	13.7	14.4
FeO	8.4	8.1	6.9	9.1	9.4	7.9	9.9
MnO	0.1	0.1	0.1	0.1	0.1	0.1	
MgO	15.8	15.2	12.1	15.2	16.0	16.7	7.8
CaO	10.7	9.1	13.6	5.9	12.1	10.9	12.4
Na_2O	0.7	1.6	1.4	1.6	0.9	1.7	1.7
K_2O	0.1	0.3	0.1	0.9	0.1	0.1	0.1
Total	100.2	100.0	100.1	100.0	99.9	100.0	100.2
Mg/(Mg+Fe)	0.770	0.770	0.757	0.749	0.752	0.790	0.580

1 Inferred Upper Pillow Lava parental liquid (Duncan and Green 1980); *2* Upper Pillow Lava group I parent (Cameron 1985) +8% Fo_{91}; *3* Xenocryst melt inclusions (Donaldson and Brown 1977); *4* Marianas fore-arc lava (Jenner 1983); *5* Primitive basalt (Hawkins 1976) plus 15% Fo_{90}; *6* Olivine tholeiite DSDP 3-18-7-1 (Frey et al. 1974) +17% Fo_{91} (Green et al. 1979); *7* Average basaltic glass from DSDP Site 236, Indian Ocean (Melson et al. 1977)

Table 3. Chemical compositions of Upper Pillow Lavas, Troodos ophiolite, Cyprus

	61367	61369	61370	61351	61371	61373	61375	61377	61358	61359	68799
SiO_2	46.26	46.27	53.53	54.90	53.05	54.21	54.02	53.87	54.08	53.46	54.07
TiO_2	0.29	0.22	0.49	0.32	0.49	0.20	0.29	0.20	0.31	0.32	0.40
Al_2O_3	6.55	6.88	13.27	15.45	13.57	13.20	13.08	12.02	13.45	14.29	14.96
FeO	9.32	9.02	8.35	7.57	8.56	8.05	8.13	9.93	8.06	8.12	7.86
MnO	0.17	0.15	0.16	0.15	0.16	0.16	0.16	0.18	0.15	0.16	0.16
MgO	32.49	31.23	12.15	7.87	12.16	12.68	11.20	12.61	10.81	10.15	9.40
CaO	4.35	5.22	9.98	11.06	10.00	10.63	11.92	10.74	12.11	12.42	11.25
Na_2O	0.53	0.74	1.59	1.86	1.53	0.48	0.94	0.39	0.63	0.69	1.62
K_2O	0.04	0.22	0.41	0.35	0.33	0.33	0.22	0.04	0.26	0.24	0.13
P_2O_5	0.03	0.03	0.06	0.04	0.06	0.03	0.04	0.02	<0.03	<0.03	0.05
Mg#	0.861	0.860	0.722	0.647	0.717	0.737	0.711	0.694	0.705	0.690	0.681
Group	I	I	I	I	I	III	III	III	III	III	II
Ni	1031	1012	195	74	160	208	215	248	205	176	122
Cr	2180	2310	716	345	673	700	723	871	607	586	404
Zr	14	13	31	33	21	<4	8	15	10	9	15
Nb	<2	<2	<2	9	<2	<2	<2	5	2	4	11
Y	5	7	13	16	12	7	9	6	10	10	11
Rb	<2	4	6	8	5	5	2	<2	4	4	3
Sr	26	72	150	100	103	153	199	105	196	204	75
Ba	3	12	18	49	20	49	22	73	33	60	64
Sc	14	18	33	37	32	46	41	44	37	39	36
V	93	102	191	244	189	251	206	237	211	227	245

University of Tasmania sample numbers. Major elements in weight percent oxide, trace elements in ppm: all analyses by XRF. Group classification following criteria of Cameron (1985)

ene, plagioclase and glass, with accessory magnesiochromite and occasionally groundmass hornblende. Three geochemically distinct groups have been recognized (Cameron 1985), based on TiO_2, CaO/Na_2O and Zr contents. Rare earth element abundance patterns and isotopic compositions (Sr, Nd) also distinguish the groups (McCulloch and Cameron 1983). These differences cannot be due to crystal fractionation and are considered to have been generated by incremental melting of a variably depleted source periodotite in the presence of hydrous fluids (Cameron 1985).

Within these very depleted rocks (relative to MORB), group I lavas have the highest TiO_2, Na_2O and Zr concentrations, and ε_{Nd} values slightly less than MORB (McCulloch and Cameron 1983; Rautenschlein et al. 1985). Group III lavas have extremely low TiO_2, Na_2O and Zr, higher CaO and generally much lower ε_{Nd} values than group I. Group II lavas are intermediate in composition between groups I and III. The groups are also geographically separated: group I occurs in the Margi area (Gass 1958; Searle and Vokes 1969), group III occurs principally in the Arakapas Fault Belt (Simonian and Gass 1978) but also in the outlying Akamas and Mamonia outcrop, and group II occurs at various localities around the periphery of the ophiolite and mixed with group III lavas in the Arakapas Fault Belt (Cameron 1985).

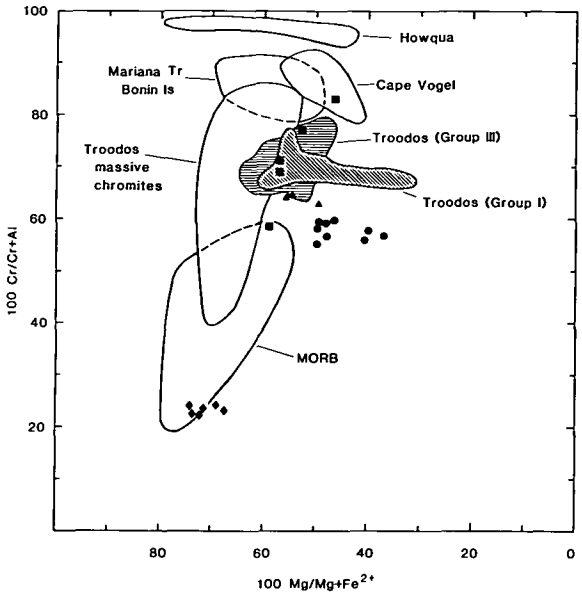

Fig. 1. Cr/(Cr+Al) and Mg/(Mg+Fe) variations in spinels from lavas and plutonic rocks from the Troodos ophiolite compared with those from ocean floor basalts (Frey et al. 1974; Sigurdsson and Schilling 1976), lavas from the Mariana fore-arc and Cape Vogel, PNG (Cameron et al. 1979), and extremely refractory Howqua peridotite (Crawford 1980). Compositions for massive chromites and accessory spinels (*squares*) in Troodos plutonic rocks are from Greenbaum (1977). Spinel compositions in Troodos UPL lavas (groups I and III) and cumulate rocks and tectonite are from this study. ◆ Harzburgite, ● Poikilitic wehrlite, ▲ Dunite

All reported compositional data for Troodos UPL as well as twelve new analyses from this study (Table 3) are plotted in Fig. 2a. Whole rock and glass compositions are shown as molecular normative values in the basalt tetrahedron (Yoder and Tilley 1962), projected from the Di vertex onto the basal plane (Jd+Ts)-Ol-Qz. Most of the compositions plot within the Pl-Opx-Qz field shown. Compositions were grouped using the criteria of Cameron (1985). Group I lavas can be clearly distinguished from group III lavas while group II lavas are intermediate as expected.

From Fig. 2a it is apparent that the group I ultramafic and basaltic lava compositions are principally controlled by removal or addition of olivine with some minor removal of pyroxene. The group II and III lavas also show strong olivine control but pyroxene subtraction or addition has been more significant than in group I lavas. The parental magmas for these groups would plot on olivine-control lines passing through the most primitive lava compositions and near the Pl-Opx join (based on Mg#'s of 0.75 to 0.77, Duncan and Green 1980). Such hypothetical parental magma compositions form a restricted group in Fig. 2a, and vary principally in normative Pl and Opx content. The parental magma composition proposed by Duncan and Green (1980) plots toward the high-Opx content side of this range and appears to be more representative of the group III lava compositions.

Petrography and mineral compositions of Troodos

Our sampling of the UPL sequence was carried out during field excursions associated with the International Ophiolite Symposium in Cyprus in 1979 and our chemical data and grouping of samples match with that of Cameron (1985). However the subtle chemical differences in major element compositions between groups I, II and III must be compared with crystallization histories as revealed in phenocryst phases. For example, we enquired whether magnesian olivine, magnesian calcic clinopyroxene and pigeonite were restricted to chilled lavas of group I (Margi area) or also occurred together with the previously reported magnesian orthopyroxene and clinopyroxene-bearing lavas of group III (Arakapas area). Small compositional differences between parental liquids result in changes in the relative crystallization order among plagioclase, calcic clinopyroxene and pigeonite. Similarly, the effect of load pressure on appearance of olivine or orthopyroxene as liquidus phases is well documented (Green and Ringwood 1967) and the coexistence of three pyroxenes (orthopyroxene, pigeonite and augite) is sensitive to both temperature and pressure of crystallization (Lindsley 1983). By combining experimental studies with observations of natural phenocryst phases it should be possible to deduce the crystallization path, in terms of P and T, for the natural rocks and also to deduce the water content of the primary magma.

The mineralogy of analyzed rocks from the Troodos ophiolite is summarized in Table 4 and selected mineral compositions appear in Table 6.

Group I lavas – near Margi Village (Excursion C, stops 3, 4 and 7a, Pantazis et al. 1979)

Lavas are strongly olivine-phyric and analysed bulk compositions (Table 3) range from picrites (32% MgO) to quartz tholeiites (7.9% MgO). Olivine phenocrysts are up to $Mg_{90.8}$ in picritic lavas but $<Mg_{86.4}$ in quartz tholeiites. Orthopyroxene and magnesian pigeonite are absent and quench pyroxene trends between augite and subcalcic augite are $<Mg_{77}$ (Fig. 4). The second silicate phase to crystallize appears to be augite ($<Mg_{86.8}$) but chromian spinel ($<Mg_{64}$, $<Cr_{78}$; Fig. 1) accompanies the magnesian olivine. Plagioclase phenocrysts were not observed. Samples of a picritic intrusive plug (stop 7a) appear to contain similar olivine to the lavas but also contain magnesian diopside cores ($Mg_{89.2}$) augite rims and separate crystals ($<Mg_{84}$), pigeonite ($<Mg_{80}$) and orthopyroxene ($<Mg_{75.3}$).

Group II, III lavas – Arakapas Fault Belt (Excursion K, stops 2, 3, 4 and 6; Excursion J, stop 5, Pantazis et al. 1979)

Lavas are olivine- and pyroxene-phyric and the pyroxene phenocrysts/microphenocrysts include magnesian orthopyroxene [$Mg_{88.7}-Mg_{85.2}$], magnesian pigeonite [$<Mg_{87.9}$] and diopside [$<Mg_{89.8}$]. Olivine is commonly altered but relict olivines are $<Mg_{90.6}$. Although forming a coherent chemical group, individual samples show apparently distinctive crystallization sequences (Table 4).

Some examples (103A, 68799, 61376, 61355) contain olivine, spinel and pyroxene phenocrysts and microphenocrysts. In these samples the pyroxenes range from cores of calcic diopside (up to $Mg_{89.8}$) through subcalcic (Wo_{20-30}) clinopyroxene ($<Mg_{87.7}$) to rims of subcalcic and more Fe-rich augites. These samples contrast with apparently similarly quenched rocks (61373, 61377) in which minor olivine pseudomorphs are accompanied by *orthopyroxene* microphenocrysts and clinopyroxenes with cores of calcic diopside ($<Mg_{89.4}$). A third variant (61375, 61358) contains olivine phenocrysts and microphenocrysts, and clinopyroxene microphenocrysts, some of which include small, sharply bounded laths of magnesian pigeonite (Fig. 5). Within a single hand specimen and thin section, some 'domains' of the rock consist only of olivine+spinel+glass, others of olivine+spinel+calcic to sub-calcic clinopyroxene (as in 68799, 61376 etc.) and other 'domains' contain the olivine, spinel, pigeonite cores with magnesian diopside and sub-calcic augite overgrowths. Careful microprobe analysis (Fig. 4c) shows closely grouped and consistent magnesian pigeonite (Wo_{9-14}) compositions for the cores illustrated in Fig. 5 and a distinct compositional gap to magnesian diopside (Wo_{30-40}) in the immediately surrounding pyroxene. Outer zones of the pyroxene microphenocrysts show zoning to more Fe-rich augite and subcalcic augite compositions. The SEM contrast (Mean atomic no. contrast) of Fig. 5 and the clustered compositions of Fig. 4c confirm the presence of magnesian pigeonite in some samples of group III lavas and exclude the possibility that the apparent continuity of random 'core' analyses of microphenocrysts (Fig. 4b, c) from high to low calcium contents is an analytical artifact of overlap between orthopyroxene cores and clinopyroxene rims.

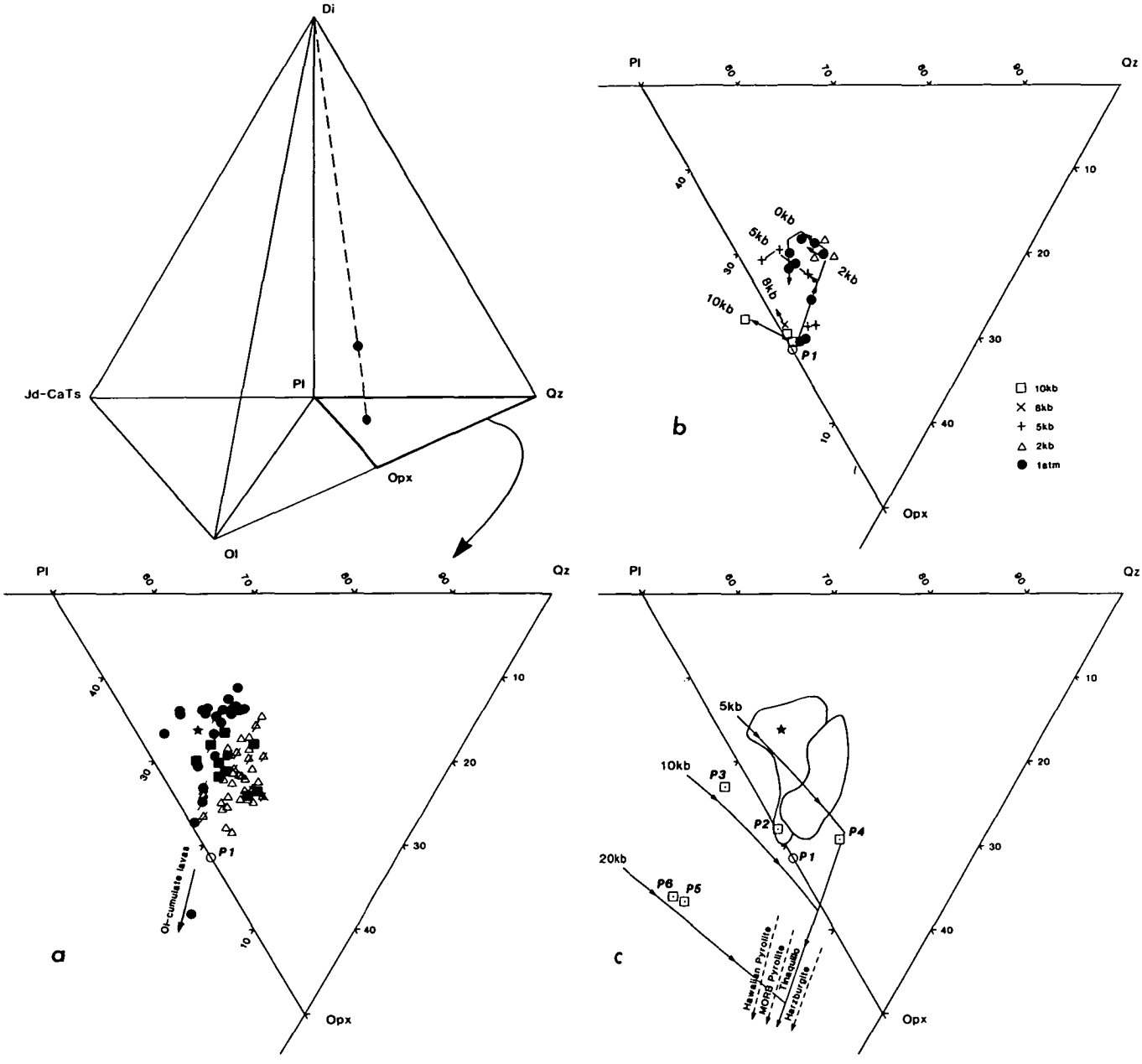

Fig. 2a–c. **a** Molecular normative compositions of natural rocks and glasses from the Upper Pillow Lavas (Troodos ophiolite) plotted in the ternary system (Jd+CaTs)-Ol-Qz, projected from the Di vertex of the basalt tetrahedron. Compositional variation controlled mainly by addition or subtraction of olivine from parental melts represented by the proposed parental composition P1 (*large open circle*). Group I (*circles*), group II (*squares*) and group III (*triangles*), identified by Cameron (1985), form overlapping but distinct clusters and indicate a restricted range of separate parental liquids. Samples examined in this study which exhibit olivine (/) or pyroxene (\) crystallization are indicated. Other analyses are from Gass (1958), Searle and Vokes (1969), Smewing and Potts (1976), Simonian and Gass (1978), Robinson et al. (1983), Schminke et al. (1983), Thy et al. (1985), Cameron (1985) and Rautenschlein et al. (1985). **b** Compositions of glasses from crystallization experiments at 8, 5, 2 kb and 1-atm pressures, same projection as **a**. *Arrows* indicate the path of the liquid composition with progressive crystallization of olivine, pyroxene and plagioclase from the starting composition P1. **c** Refractory melt compositions and peridotite equilibrium melt compositions (after Jaques and Green 1980) same projection as **a**. The fields of groups I and III UPL lavas from **a** are shown with DSDP Site 236 composition (*star*). Parental melts (Table 2) are P1 (Troodos UPL, group I), P2 (Troodos UPL, group III), P3 (MAR melt inclusions), P4 (High-Mg andesite, Mariana fore-arc), P5 (Lau Basin parent) and P6 (N-MORB parent). *Arrows* indicate the path of compositions derived from increasing percent melting at 5, 10 and 20-kb pressure from a somewhat depleted natural peridotite (Tinaquillo, Jaques and Green 1980; Green et al. unpublished). The olivine-only limit of the melting path moves to lower plagioclase content with increasing depletion of the source peridotite composition (Hawaiian pyrolite to harzburgite). The positions of P1, P3, P6 differ from the plotted positions in Falloon and Green (1986) because in this paper all Fe is calculated as FeO whereas in Falloon and Green (1986) $Fe^{2+}:Fe^{3+}$ is assumed to be 9:1

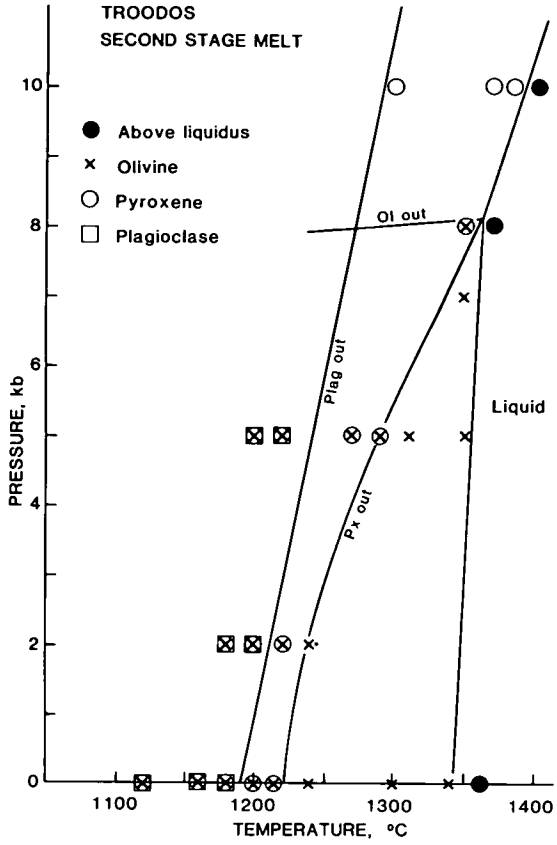

Fig. 3. Phase relations of the proposed parental liquid for the Upper Pillow Lavas (Troodos ophiolite) in pressure-temperature space. Olivine is the liquidus phase alone to 8 kb, while above 8 kb orthopyroxene is the sole liquidus phase. Because this liquid is saturated in olivine and orthopyroxene at 7–8 kb, 1360° C, it can be considered primary, leaving behind a harzburgite residue

Taken together the analyses of individual samples of group III lavas of apparently identical composition show crystallization paths within small, variously quenched domains, which include olivine, spinel, magnesian orthopyroxene ($<Mg_{88.7}$), magnesian pigeonite ($<Mg_{87.9}$), magnesian diopside ($<Mg_{89.8}$). These variously quenched domains may result from turbulent or convective flow in ascending lavas, some domains beginning to crystallize within the conduit system, others remaining above liquidus to surface eruption.

The use of olivine and pyroxene compositions to deduce P, T cooling paths for magmas is explored in later sections. The mineralogical observations on our samples are similar to those of Cameron (1985) and clarify the role of magnesian pigeonite in some group III samples. Spinel compositions are not distinguishable between groups I and III lavas and plagioclase is not a phenocryst phase in any of the samples which were selected for their glassy character.

Plutonic rocks

The mineralogical data on plutonic rock samples are summarized in Table 4. These minerals may be compared with phenocryst phases of the volcanic rocks and with the experimentally determined liquidus phases for Troodos Upper Pillow Lava magma type over the 1 bar to 10 kb interval. It is apparent that the tectonite harzburgite sampled can *not* be related as a residue or cumulate from Troodos Upper Pillow Lava magma segregation. The high Al_2O_3-content of the pyroxenes and low Cr/Cr+Al of spinel (Fig. 1) establish affinities for these harzburgite samples with high temperature spinel lherzolite mineralogies (e.g., Lizard Peridotite, spinel lherzolite xenoliths in basalt) and with residues from basaltic or picritic melt extraction from undepleted lherzolite in the 10–20 kb pressure interval (Jaques and Green 1980; Green et al. 1979).

The cumulate dunite (61361) *may* be a cumulate from a liquid of Troodos UPL type on the basis of similarity of spinel compositions but the clinopyroxene is much more magnesian and calcic than the most magnesian phenocrysts encountered in groups I or III lavas. The effects of sub-solidus re-equilibration in increasing Fe/Mg partitioning between olivine and clinopyroxene may be a further complicating factor. The poikilitic wehrlite is also a possible low pressure cumulate from Troodos UPL group III magma types on the basis of spinel and pyroxene compositions. Again the lower extent of pyroxene mutual solid solution and more magnesian clinopyroxene compositions suggest some degree of sub-solidus re-equilibration in comparison with the volcanic rocks. The layered gabbro samples lack olivine and the less magnesian character of pyroxenes demonstrates derivation from evolved liquids rather than primitive magnesian liquids such as group I or group III lavas. It is notable that the highly calcic cumulate plagioclase of these rocks may be appropriate to group III lavas but not to the lower Ca/Ca+Na ratios of group I lavas.

Results of experimental study of model parental magma

The melt composition (Table 2) proposed by Duncan and Green (1980) as parental to refractory pillow lavas at the Troodos ophiolite was chosen for experimental investigation. This model composition was determined from the reported variation in Troodos lava compositions, using the constraint that its Mg# (0.77) must be appropriate (Roeder and Emslie 1970) for the most magnesian olivines observed ($Mg_{91.7}$). Its characteristics are high SiO_2, MgO and CaO/Na_2O, and low TiO_2, Na_2O relative to inferred parental liquids for mid-ocean ridge and back-arc basin basalts. Trace and rare earth element abundances in the Troodos lavas are consistent with melting from a severely depleted source (Smewing et al. 1975; Smewing and Potts 1976; Kay and Senechal 1976; Simonian and Gass 1978; McCulloch and Cameron 1983; Cameron 1985). In view of the recent geochemical evidence for significant variability among the Troodos lavas (Cameron 1985) no single melt composition can be parental to the entire extrusive suite. However, the model composition is representative of a restricted range of parental liquids, all with the noted depleted characteristics.

We conducted a series of melting and crystallization experiments designed to establish the phase relationships of this model composition in pressure-temperature space (Table 5). We desired first to test whether this composition could be a primary liquid (i.e., whether olivine, orthopyroxene ± clinopyroxene occur together on the liquidus at some pressure and temperature). Secondly, the order of appearance of phases crystallizing at various pressures was determined. Finally, experimental mineral and liquid compositions were analyzed for comparison with Troodos ultramafic and basaltic compositions.

A sintered oxide mix of the model composition was used for the experimental charges. Preparation and experimental methods have been discussed previously (Green et al. 1979). All experiments were carried out under anhydrous conditions in spec-pure Fe capsules. The sample bulk composition was monitored for each run to check for addition of iron from the capsule. Little or no iron addition was recorded in glasses from above-liquidus runs. This established that liquidus temperatures and liquidus phases are correct. In some, but not all, of the longer below-liquidus experiments significant Fe-addition occurred (<10%

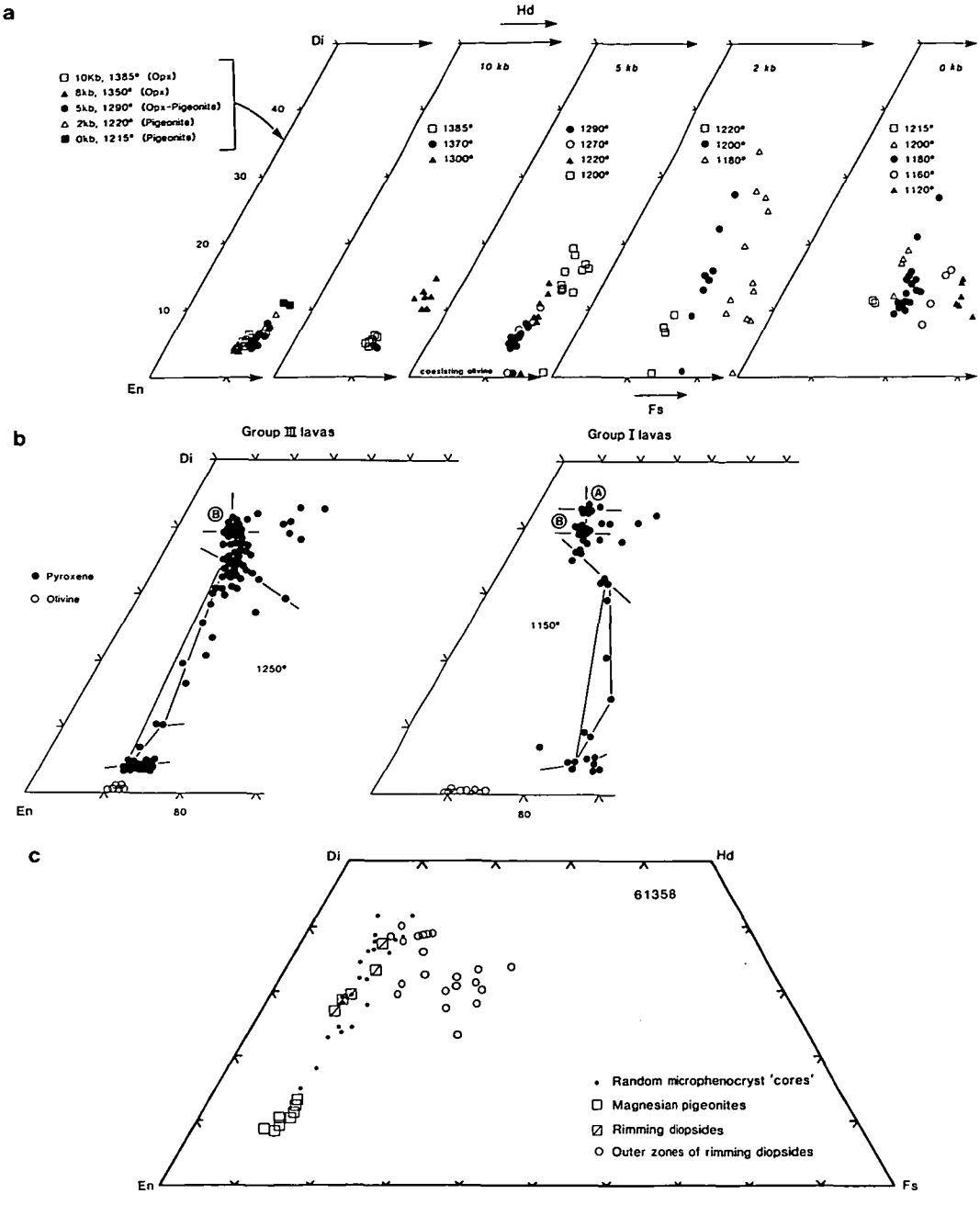

Fig. 4a–c. **a** Pyroxene quadrilateral showing the dependence of first-formed pyroxenes on pressure, and compositions of pyroxenes with falling temperature at various pressures. **b** Also pyroxene quadrilateral for phenocrysts and microphenocrysts of group I (Margi area) and group III lavas. Intersections **a** and **b** mark probable xenocrystal diopside crystals in each lava group. The 3-pyroxene fields for 5 kb, 1250° C and 1 atm, 1150° C are superimposed to illustrate overlap with natural microphenocryst compositions (Lindsley 1983). **c** Analytical data for pyroxenes of 61358 as illustrated in plate 1. Random microphenocryst 'cores' were obtained by point analyses without optimizing back-scattered electron images as in Fig. 5 (cf., Fig. 4b, group III lavas). Magnesian pigeonites are point analyses within the sharply bounded cores of microphenocrysts of Fig. 5. 'Rimming diopside' compositions are analyses immediately outside these cores and 'Outer zones' are near-edge compositions or compositions of small separate quench pyroxenes

of original Fe). This had the effect of reducing the oversaturated character of the glasses through the increased FeO content and is the cause of some scatter of the liquid compositions in normative Qz in Fig. 2b. Because of the low fO_2 of experiments in spec-pure Fe capsules, the crystallization of spinel was probably inhibited, and our experiments cannot be applied to discussion of the stability and composition of spinel (chromite-spinel-magnetite solid solution) in the natural basalts, erupted at fO_2 higher than IW buffer.

Mineral and glass analyses were determined using a JEOL JX-50A electron probe microanalyser fitted with an EDAX energy dispersive analytical system. Operating conditions were accelerating voltage of 15 kV, beam current of 3 nanoamps, beam diameter of < 0.5 μm, and 80-s counting time. Glass analyses with on-line data reduction (Griffin 1979), were made using rapid, reduced area scans to minimize alkali volatilization. All iron abundances are reported as weight percent FeO.

Results of experiments are summarized in Table 5 and illustrated in Fig. 3. Mineral and glass compositions of ex-

Table 4. Mineralogy of volcanic and plutonic rocks from the Troodos ophiolite, Cyprus. Compositions (Mg #) of clinopyroxenes connected by –Q– indicate a population of compositions from sub-calcic augite (~10% CaO) to calcic augite but in addition some samples (61358, 61375) contain small pigeonite cores within more calcic clinopyroxene (Table 6, Fig. 5)

Sample	Olivine Mg #	Ortho-pyroxene (Mg #)	Clinopyroxene			Spinel (Mg #, Cr #)	Plagioclase (An #)
			Lo-Ca	Med-Ca	Hi-Ca		
Volcanic rocks							
Arakapas area							
61373	Altered	88.7–85.2			89.4–81.7	59.6–49.0 77.6–67.5	
61376	Altered	?altered	86.5–83.5 —— Q ——		89.8–83.5	55.7–51.3 74.7–67.9	
61375	88.0–87.6	–	87.1–86.0		–	53.2–51.4 69.5–69.1	
61355	88.0	–	87.0 —— Q ——		88.9–84.6	53.8–49.5 78.2–70.9	
61358	89.4–88.9	–	87.9–86.5 —— Q ——		88.5–85.7	58.2–56.2 74.0–68.0	
61359	88.9–87.9	–		85.3–80.8		55.8–54.8 74.3–67.1	
61377	Altered	88.4–85.2	86.4–86.1 —— Q ——		86.9–82.5	51.3–44.7 80.0–73.0	
103A	90.6–82.7	–	87.7–87.1 —— Q ——		87.5–82.0	63.1–57.9 71.0–66.0	
Kalavasos area							
68799	88.5–85.7	–	85.7–84.8 —— Q ——		83.4–82.0	53.7–48.7 67.1–64.4	
Margi area							
61367	90.8–89.7	–	71.8 ——		89.2	60.4–31.9 72.5–64.0	
61348	90.3–86.9	75.3–70.7	74.1–71.7 ——		89.2–73.9	56.5–37.0 73.0–68.4	
61370	90.0–88.1			Quench		54.3–45.4	
61357				77.6–66.3		78.2–70.1	
61371	88.2	–		74.4		65.1–55.4 74.7–72.7	
Plutonic rocks							
Harzburgite tectonite Excursion A, Stop 6 (61360, 61342)	Altered	91.3–90.7			94.0–92.7	73.2–63.6 26.0–23.6	
Dunite (A,7) (61361)	90.8	–			95.7	54.8–48.9 65.6–63.8	
Poikilitic Wehrlite (A,9) (61345)	87.9–87.5	88.4–87.1			93.6–89.5	56.2–34.7 65.6–55.4	
Olivine Clino-pyroxenite (A,7)	82.9–82.8	–			91.1–89.0	–	
Layered Gabbro (A,8) (61363)	–	80.0–78.2			82.2–81.6	–	91.8–90.3
Layered Gabbro (A,5) (61364)	–	72.2			72.8–71.4	–	94.5–92.8
Massive Gabbro (A,4) (61365)	–	74.3–67.7			73.0	–	89.0–82.8

perimental charges appear in Tables 6 and 7. Liquidus temperatures are high in keeping with the refractory nature of this composition. Olivine is the liquidus phase alone from 1 atm to 7–8 kb where orthopyroxene joins it. At this point, the liquidus slope (dT/dP) becomes steeper, with orthopyroxene alone on the liquidus at 10 kb. A liquid of this composition could then have segregated from an upper mantle peridotite at roughly 25 km and 1360° C, leaving behind a harzburgite residue. Hence it is a possible primary melt.

Of particular interest are the compositions of the mineral assemblage (olivine + orthopyroxene) at the multiple saturation point, 7–8 kb and 1360° C, for these will be the compositions of phases in the harzburgite residue left after segregation of this melt from the upper mantle (and the compositions expected in the most magnesian complementary cumulates at Troodos). In the experiment at 8 kb, 1350° C the olivine is Mg_{90} and the orthopyroxene is Mg_{91} (Table 6). The orthopyroxene contains about 1% Al_2O_3 and 2% CaO. This composition matches the primary orthopyroxene reported from cumulate rocks in some ophiolites (Jaques 1981) although the CaO concentration is somewhat greater than re-equilibrated orthopyroxene (England and Davies 1973; Jaques 1981). The mineralogy is appropriate for the harzburgite tectonite and the lowermost refractory

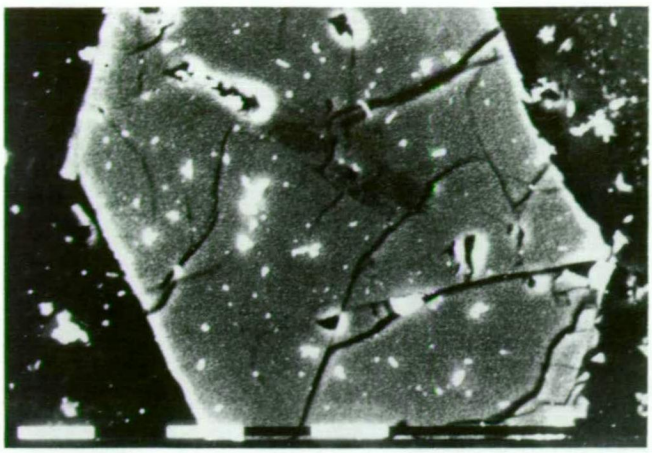

Fig. 5. Back scattered electron image (SEM) of microphenocryst in 61358 showing discrete, sharply bounded core of pigeonite (Table 6, Fig. 4c) within rimming sub-calcic diopside – the latter becoming iron-rich (*brighter*) towards the rim. Scale marks are 10 μm divisions

Table 5. Melting experiments on model liquid composition

Run no.	Pressure (kbar)	Temperature (° C)	Time (h)	Phases present
T-407	10	1400	0.4	Gl
T-409	10	1385	0.4	Gl + Opx
T-404	10	1370	0.7	Gl + Opx
T-509	10	1300	31.0	Gl + Cpx
T-410	8	1370	0.6	Gl
T-411	8	1350	0.7	Gl + Ol + Opx
T-413	7	1350	0.7	Gl + Ol
T-398	5	1350	0.7	Gl + Ol
T-399	5	1310	0.7	Gl + Ol
T-427	5	1290	6.0	Gl + Ol + Opx + Pg
T-400	5	1270	1.5	Gl + Ol + Opx + Pg
T-484	5	1220	6.0	Gl + Ol + Pg + Cpx + Pl
T-490	5	1200	6.0	Gl + Ol + Pg + Cpx + Pl
T-533	2	1240	6.0	Gl + Ol
T-538	2	1220	6.0	Gl + Ol + Pg
T-476	2	1200	8.0	Gl + Ol + Pg + Cpx + Pl
T-475	2	1180	8.0	Gl + Ol + Pg + Cpx + Pl
AT-25	0	1360	0.3	Gl
AT-28	0	1340	0.3	Gl + Ol
AT-24	0	1300	0.5	Gl + Ol
AT-26	0	1240	2.0	Gl + Ol
AT-39	0	1215	6.0	Gl + Ol + Pg
AT-27	0	1200	2.0	Gl + Ol + Pg + Cpx
AT-43	0	1180	120.0	Gl + Ol + Pg + Cpx + Pl
AT-40	0	1160	120.0	Gl + Ol + Pg + Cpx + Pl
AT-42	0	1120	240.0	Gl + Ol + Pg + Cpx + Pl

Gl glass; *Ol* olivine; *Opx* orthopyroxene; *Cpx* clinopyroxene; *Pg* Pigeonite; *Pl* plagioclase. All experiments anhydrous in spec-pure Fe capsules

accumulate sequences seen in *some* ophiolites (e.g., England and Davies 1973; Pallister and Hopson 1980; Juteau and Whitechurch 1980; Jaques 1981) although it is *inappropriate* for the tectonite harzburgite samples described from Troodos in the previous section.

Figure 3 shows that at 5 kb olivine (Mg_{91}) is the first phase to crystallize from 1350° C to 1290° C where it is joined by pigeonite ($Mg_{88.6}$) followed at 1270° C by orthopyroxene ($Mg_{88.7}$) accompanied by pigeonite ($Mg_{87.5}$) and then by plagioclase (An_{85}) with decreasing temperature. At 2 kb pigeonite ($Mg_{87.8}$) follows olivine ($Mg_{91.6}$ inferred on the liquidus), with sub-calcic augite (Mg_{86}) and plagioclase ($An_{88.8}$) at 10–20° C lower temperature. Experiments at 1 bar determined that the first formed olivine is $Mg_{91.6}$ with pigeonite (Mg_{86}) precipitating after a fall in temperature of about 130° C , followed closely by sub-calcic augite (Mg_{84}) and plagioclase ($> An_{91}$).

With falling pressure the field of olivine-alone crystallization broadens so that at low pressures the olivines which co-precipitate with first-formed pyroxene are more iron-rich than those at higher pressures. The composition of first-formed pyroxene is highly pressure dependent as illustrated in Fig. 4. At 10 and 8 kb magnesian orthopyroxene (Mg_{90-91}) crystallizes while at 5 kb less magnesian pigeonite ($Mg_{88.6}$) and orthopyroxene ($Mg_{88.7}$) are followed and then replaced by pigeonite and sub-calcic augite ($< Mg_{87.5}$). Pigeonite is the earliest pyroxene at 2 kb ($Mg_{87.8}$) and at 1 bar (Mg_{86}) pressure. The calcium content of the first-formed pyorxene increases with decreasing pressure.

The low pressure plagioclase compositions reach An_{91} at 1120° C but are no more calcic at 1160° C and 1180° C as would be expected (Drake 1975). The most refractory feldspar compositions reported from ophiolites reach An_{95}. The experimental plagioclase contains significant amounts of FeO and MgO indicating non-equilibrium nucleation which may disrupt the true Ca-Na partitioning. Hence, An_{91} is probably a minimum estimate of the anorthite content of the equilibrium plagioclase crystallizing from this melt at low pressures. The anorthite content of first-formed plagioclase decreases with increasing pressure, $> An_{91}$ (1 bar) to An_{86} (5 kb), as previously reported (Green et al. 1979) – this can be related to increased calcic clinopyroxene crystallization prior to plagioclase appearance.

In Fig. 2b are plotted glass analyses (Table 7) reflecting liquid lines of descent for crystallization from the proposed parental melt, determined from experiments at 8, 5, 2 kb and 1-bar pressures. Initial removal of olivine drives the melt composition away from the olivine vertex. With increasing pressures the field of olivine-alone crystallization shrinks as seen in Fig. 3. Consequently, at the onset of pyroxene crystallization, liquids evolving at lower pressures are more quartz-normative (Fig. 2b). As orthopyroxene, pigeonite and clinopyroxene join olivine crystallization, the melt compositions move toward the plagioclase vertex. Finally, with the addition of plagioclase to the crystallization the liquids move slowly away from the plagioclase vertex.

The compositional field for Troodos natural rocks and glasses matches the experimental melt compositions quite well (Fig. 2a, 2b), although better for the group III lavas than for group I. Olivine removal or accumulation (in group I particularly) or olivine followed by pyroxene removal or addition (group III only), is the major source of chemical variability among the lavas. The variable mineralogy in the lavas noted previously can now be compared with the experimental results to determine the crystallization paths of the natural rocks. Figure 6 illustrates the experimentally determined compositions (Mg#) of mafic minerals crystallizing as a function of pressure and temperature (from Fig. 3). For example, those lavas with olivines from $Mg_{91.5}$ to $Mg_{88.7}$ composition, followed by sub-calcic pyroxene or pigeonite of $< Mg_{87}$, crystallized at relatively shallow

Table 6. Mineral composition from experiments and Troodos UPL

	AT39 1 Atm 1215° C Lo-Ca Cpx	AT43 1 Atm 1180° C			T538 2 kb 1220° C Lo-Ca Cpx	T427 5 kb 1290° C Lo-Ca Cpx	5 kb T400 1270° C		T411 8 kb 1350° C Opx	T409 10 kb 1385° C Opx	T509 10 kb 1300° C Lo-Ca Cpx
		Lo-Ca Cpx	Hi-Ca Cpx	Plag			Opx	Lo-Ca Cpx			
SiO_2	56.4	54.7	53.8	47.6	56.5	56.7	57.4	56.8	57.1	56.8	54.8
Al_2O_3	2.8	0.8	2.8	31.5	1.1	1.5	0.9	1.1	1.1	1.6	2.8
FeO	7.7	12.2	9.2	1.4	7.6	7.1	7.2	7.7	6.6	6.7	9.1
MgO	27.2	27.0	20.8	0.9	30.6	30.8	31.8	30.3	32.8	32.0	27.1
CaO	5.6	5.0	13.0	17.5	3.9	3.6	2.6	4.2	2.4	2.8	6.0
Na_2O	–	–	–	1.2	–	–	–	–	–	–	–
Cr_2O_3	0.3	0.3	0.4	–	0.3	0.3	0.2	–	–	–	0.1
	$Mg_{86.3}$	$Mg_{79.9}$	$Mg_{80.2}$	Ca/Ca+Na = 0.89	$Mg_{87.8}$	$Mg_{88.6}$	$Mg_{88.7}$	$Mg_{87.5}$	$Mg_{90.1}$	$Mg_{89.5}$	$Mg_{84.2}$

	Arakapas area 61373		Arakapas area 61375	Arakapas area 61358			61345 Poikilitic Wehrlite				61361 Dunite		61360 Tectonite Harzburgite		
	Opx	Hi-Ca Cpx	Lo-Ca Cpx	Pig. Cores (mean of 5)	Sub-Calc. diopside	Hi-Ca Cpx	Enstatite	Diopside	Spinel	Spinel	Diopside	Spinel	Enstatite	Diopside	Spinel
SiO_2	56.1	54.1	54.9	55.8	53.4	53.3	55.6	54.0	–	–	54.9		54.2	52.4	–
TiO_2	–			–	0.2	–	–			0.3	–	0.3	–	–	–
Al_2O_3	1.1	1.3	2.0	1.6	3.4	2.1	1.5	0.6	17.7	20.3	–	18.2	4.4	4.1	45.7
FeO	7.4	4.2	8.0	7.6	5.9	4.2	7.9	2.8	18.7	29.1	1.4	20.2	5.8	2.4	13.8
MgO	32.8	19.5	29.3	29.7	21.3	18.7	32.8	17.7	13.4	8.7	18.0	12.3	32.8	17.2	17.3
CaO	2.0	20.2	5.3	4.6	15.4	20.6	1.6	24.5	–	–	25.2		1.6	22.4	–
Na_2O	–	–	–	–	–	–	–	–			–			0.35	–
Cr_2O_3	0.5	0.7	0.5	0.6	0.5	1.1	0.6	0.4	50.2	41.7	0.4	48.7	0.7	1.1	23.3
	$Mg_{88.7}$	$Mg_{89.3}$	$Mg_{86.7}$	$Mg_{87.4}$	$Mg_{86.6}$	$Mg_{88.9}$	$Mg_{88.1}$	Mg_{92}	$Mg_{56.2}$ $Cr_{65.6}$	$Mg_{34.7}$ $Cr_{57.9}$	$Mg_{95.7}$	$Mg_{51.9}$ $Cr_{63.9}$	$Mg_{91.0}$	$Mg_{92.7}$	$Mg_{69.1}$ $Cr_{25.4}$

Table 7. Glass compositions from crystallization experiments on Troodos UPL model composition. Also given are Mg# or An-content of coexisting phases and, for 1-atm runs, the degree of crystallization from mass balance calculations

Run no.	AT-25	AT-28	AT-24	AT-26	AT-39	AT-27	AT-43	AT-40
Pressure	1 Atm	1 Atm	1 Atm	1 Atm	1 Atm	1 Atm	1 Atm	1 Atm
Temperature (° C)	1360	1340	1300	1240	1215	1200	1180	1160
SiO_2	52.6	52.9	53.6	54.3	54.3	53.7	52.5	52.0
TiO_2	0.4	0.4	0.4	0.4	0.4	0.45	0.8	1.1
Al_2O_3	11.5	11.3	12.0	13.0	13.7	13.8	13.7	12.6
FeO	8.4	8.3	8.2	8.4	8.9	8.9	12.0	14.3
MnO	0.1	0.1	0.1	0.1	0.1	0.1	0.1	0.1
MgO	15.5	15.7	13.3	10.5	9.4	9.0	7.6	7.2
CaO	10.9	10.8	11.7	12.5	12.5	13.4	11.8	11.3
Na_2O	0.6	0.6	0.7	0.7	0.9	0.9	1.3	1.3
K_2O	0.1	0.1	0.1	0.1	0.1	0.15	0.3	0.4
Mg#	76.5	77.0	74.3	69.0	65.2	63.7	52.7	47.3
K_D (Ol/liq)	–	0.30	0.32	0.34	0.32	0.32	0.30	0.31
Glass	100%	~100%	92%	86%	82%	75%	~40%	~25%
Olivine	–	<1%, $Mg_{91.7}$	8%, Mg_{90}	14%, $Mg_{86.6}$	16%, $Mg_{85.3}$	15%, $Mg_{84.6}$	5%, $Mg_{78.9}$	~ 5%, $Mg_{74.4}$
Orthopyroxene	–	–	–	–	–	–	–	
Lo-Ca Cpx	–	–	–		2% (Table 6)	* } ~10%	Table 6 } ~40%	* } ~45%
Hi-Ca-Cpx	–	–	–		–	* }	Table 6 }	* }
Plagioclase	–	–	–		–	–	~15%, > An_{89}	~25%, > An_{84}

Run no.	T538	T476	T475	T398	T399	T427	T400	T484
Pressure	2 kb	2 kb	2 kb	5 kb	5 kb	5 kb	5 kb	5 kb
Temperature (° C)	1220	1200	1180	1350	1310	1290	1270	1220
SiO_2	53.9	54.6	53.8	52.6	53.2	53.4	52.6	52.4
TiO_2	0.4	0.8	1.2	0.4	0.4	0.4	0.4	0.5
Al_2O_3	13.6	12.5	12.9	11.4	11.8	13.2	14.0	15.3
FeO	8.4	10.1	13.0	8.9	8.7	9.0	9.1	9.0
MnO	0.1	0.1	0.1	0.1	0.1	0.1	0.1	0.1
MgO	10.4	9.3	6.4	15.3	14.2	11.1	10.4	9.1
CaO	12.4	11.0	11.2	10.6	11.0	12.1	12.7	12.8
Na_2O	0.8	1.0	1.2	0.7	0.75	0.8	0.8	1.0
K_2O	0.1	0.5	0.4	0.1	0.1	0.1	0.1	0.15
Mg#	68.9	62.1	46.7	75.4	74.2	68.2	67.0	64.3
K_D (Ol/liq)	0.34	0.34	0.29	0.33	0.32	0.32	0.30	0.31
Olivine	$Mg_{86.6}$	$Mg_{82.7}$	$Mg_{75.4}$	$Mg_{90.3}$	$Mg_{90.0}$	$Mg_{87.4}$	$Mg_{87.0}$	$Mg_{85.4}$
Orthopyroxene	–	–	–	–	–	?	$Mg_{88.7}$	–
Lo-Ca Cpx	$Mg_{87.8}$	$Mg_{83.3}$	Mg_{75}	–	–	*$Mg_{88.6}$	$Mg_{87.5}$	Mg_{87-86}
Hi-Ca-Cpx	–	$Mg_{83.7}$	Mg_{81}	–	–	–	–	?
Plagioclase	–	An_{89}	$\geqq An_{84}$	–	–			An_{86}

Run no.	T490	T413	T410	T411	T407	T409	T404	T509
Pressure	5 kb	7 kb	8 kb	8 kb	10 kb	10 kb	10 kb	10 kb
Temperature (° C)	1200	1350	1370	1350	1400	1385	1370	1300
SiO_2	51.6	53.0	52.3	52.4	52.6	52.2	52.2	49.8
TiO_2	0.7	0.4	0.4	0.4	0.4	0.4	0.4	0.5
Al_2O_3	14.7	11.8	11.2	12.0	11.3	11.7	12.0	14.5
FeO	11.5	8.8	9.0	9.2	9.1	9.3	9.3	11.4
MnO	0.1	0.1	0.1	0.1	0.1	0.1	0.1	0.1
MgO	8.0	14.0	15.5	14.1	15.3	14.6	14.2	11.0
CaO	12.2	11.2	10.6	11.2	10.7	11.0	11.2	11.7
Na_2O	1.4	0.7	0.7	0.7	0.7	0.7	0.8	1.1
K_2O	0.2	0.1	0.1	0.1	0.1	0.1	0.1	0.1
Mg#	55.3	73.9	75.4	72.7	75.0	73.7	73.0	63.2
K_D (Ol/liq)	0.26	0.33	–	0.32	–	–	–	–
Olivine	$Mg_{82.3}$	$Mg_{89.5}$	–	$Mg_{89.5}$	–	–	–	–
Orthopyroxene	–	–	–	$Mg_{90.1}$	–	$Mg_{89.5}$	$Mg_{89.5}$	–
Lo-Ca Cpx	Mg_{85-83}	–	–	–	–	–	–	Mg_{83}
Hi-Ca-Cpx	–	–	–	–	–	–	–	–
Plagioclase	An_{85}	–	–	–	–	–	–	–

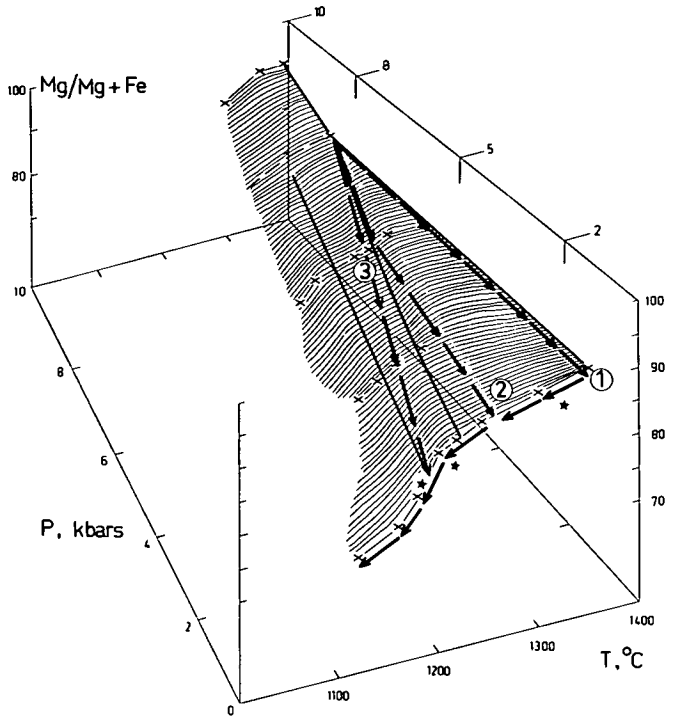

Fig. 6. The ratio Mg/(Mg + Fe) of crystallizing mafic phases is used to construct a surface in P–T space. Primary melts produced at the multiple saturation point (8 kb, 1360° C) may rise and crystallize by a variety of paths as shown by the *solid arrows*. Path (*1*) is picrite sample 61367, (*2*) is olivine-pigeonite basalt 61358, and (*3*) is orthopyroxene-bearing basalt 61373. The eruption (*quench*) temperature of these three samples are indicated by *stars*

depth (< 2 kb) before erupting and quenching. The magnesian and calcic diopside cores ($Mg_{89.2}$) in some of these lavas (Fig. 4), however, must have crystallized at greater depths (5–8 kb) and then been transported to shallow depths to crystallize their less magnesian rims ($< Mg_{86}$). These magnesian diopsides may in fact be xenocrystal to their host magmas, particularly to Group III liquids. The composition of first-formed pyroxenes (Fig. 4) allows distinction of higher and lower pressure crystallization paths. For instance, samples 61373 and 61377 contain altered olivine, magnesian orthopyroxene (Mg_{88-89}) and augite (Mg_{89}) and so began crystallizing pyroxene at $\geqq 5$ kb pressure before erupting and quenching. Samples 61375 and 61358 contain olivine (Mg_{88-89}), pigeonite ($Mg_{86.5-88}$) and augite ($Mg_{88.5}$) and also began crystallizing pyroxene at $\leqq 5$ kb pressure. In general, the group I melts of the Margi locality moved rapidly from source to the surface before significant crystallization, while group III lavas from exhibit Arakapas area show various cooling paths including limited early crystallization in deep crustal (7–15 km) magma conduits.

The variation in Mg # of olivine, pigeonite, orthopyroxene and augite and the sensitivity of the crystallization sequence to pressure and water content (lowering of liquidus temperature) suggest that it should be possible to use these phase relationships to deduce eruption temperature and water contents of the Troodos liquids. Analyses of glasses showing water contents of 2–5% may reflect the known tendency of glasses to hydrate and will also reflect an enrichment by quench olivine and pyroxene crystallization. The presence of quench amphibole (Cameron 1985) in some samples establishes that some water was present during quenching of the Troodos lavas and the combination of the experimental study and geothermometry of the natural pyroxenes further constrains this.

The diagrams of Lindsley (1983) allow us to plot the Mg # of pigeonite in the 3-phase assemblage (orthopyroxene, pigeonite, augite) as a function of pressure and temperature. The diagrams are however not well constrained at high Mg # and high temperatures (Lindsley 1983). Our own experimental data provides additional data e.g. runs at 5 kb, yield orthopyroxene and pigeonite ($Mg_{88.6}$) at 1290° C and orthopyroxene ($Mg_{88.7}$) and pigeonite ($Mg_{87.5}$) at 1270° C. We infer the 3-pyroxene triangle for pigeonite Mg_{88} passes through 5 kb, 1270° C and pigeonite ($Mg_{87.8}$) is also present at 1220° C, 2 kb. The 3-pyroxene triangle for Mg_{90} pigeonite probably lies at $T > 1340$° C at 8 kb. The pyroxene phase relations define a P,T composition grid which can be overlapped with the P,T phase relationships of Fig. 3. Figure 3 shows that it is only at 5 ± 1 kb that the Troodos experimental composition crystallizes low-calcium pyroxene of Mg_{88-89} composition as the first pyroxene after olivine crystallization. The pyroxene data of Lindsley (1983) and from this work show that at $T \sim$ 1270° C, 5 kb the reaction:

Pigeonite (Mg_{88}) → Orthopyroxene ($> Mg_{88}$) + Diopside ($\geqq Mg_{88}$) + Pigeonite ($< Mg_{88}$) occurs. The evidence from the Arakapas lavas for microphenocryst cores of pigeonite $Mg_{88-86.5}$ with sub-calcic diopside rims and of orthopyroxene ($Mg_{88.7-85}$) microphenocrysts argues that these crystals formed at $T \sim 1270$° C, 5 kb – the pressure being fixed by the olivine and pyroxene relations of Fig. 3 and the temperature by the opx-pig-aug relationships discussed above.

If this interpretation of the observed pyroxenes in Arakapas lavas is correct then we may place limits on the water content of Arakapas lavas (cf., Cameron 1985). Addition of water will depress the liquidus temperature and temperature of first appearance of pyroxene, the amount of depression at 5 kb being approximately 25° C, 45° C, 75° C and 150° C by 0.5, 1, 2, and 5 wt% H_2O respectively [estimated from studies by Green (1972), Nicholls and Ringwood (1973), Jenner (1983), Wyllie (1979) and Green (1973)]. Depression of the liquidus and of pyroxene appearance by more than ~50° C would take the first appearance of Mg_{88-89} low-calcium pyroxene down to temperatures well within the orthopyroxene + diopside field.

The data show that no more than a small amount of water was present in the melt producing a depression of the liquidus by up to 50° C. Given the identification of groundmass hornblende (Cameron 1985; Cameron et al. 1980), of significant volatile contents in apparently fresh glasses (Rautenschlein et al. 1985), and of evidence from radiogenic isotopes of addition of hydrous fluids to the source peridotite (McCulloch and Cameron 1983), the experimental results are compatible with 0.5–1 wt% H_2O in the melts.

Second-stage melts in other oceanic settings

The relatively restricted range of major element compositions of basaltic liquids erupted on the ocean floor has led different researchers to develop several distinct petrogenetic models, each of which proposes globally uniform

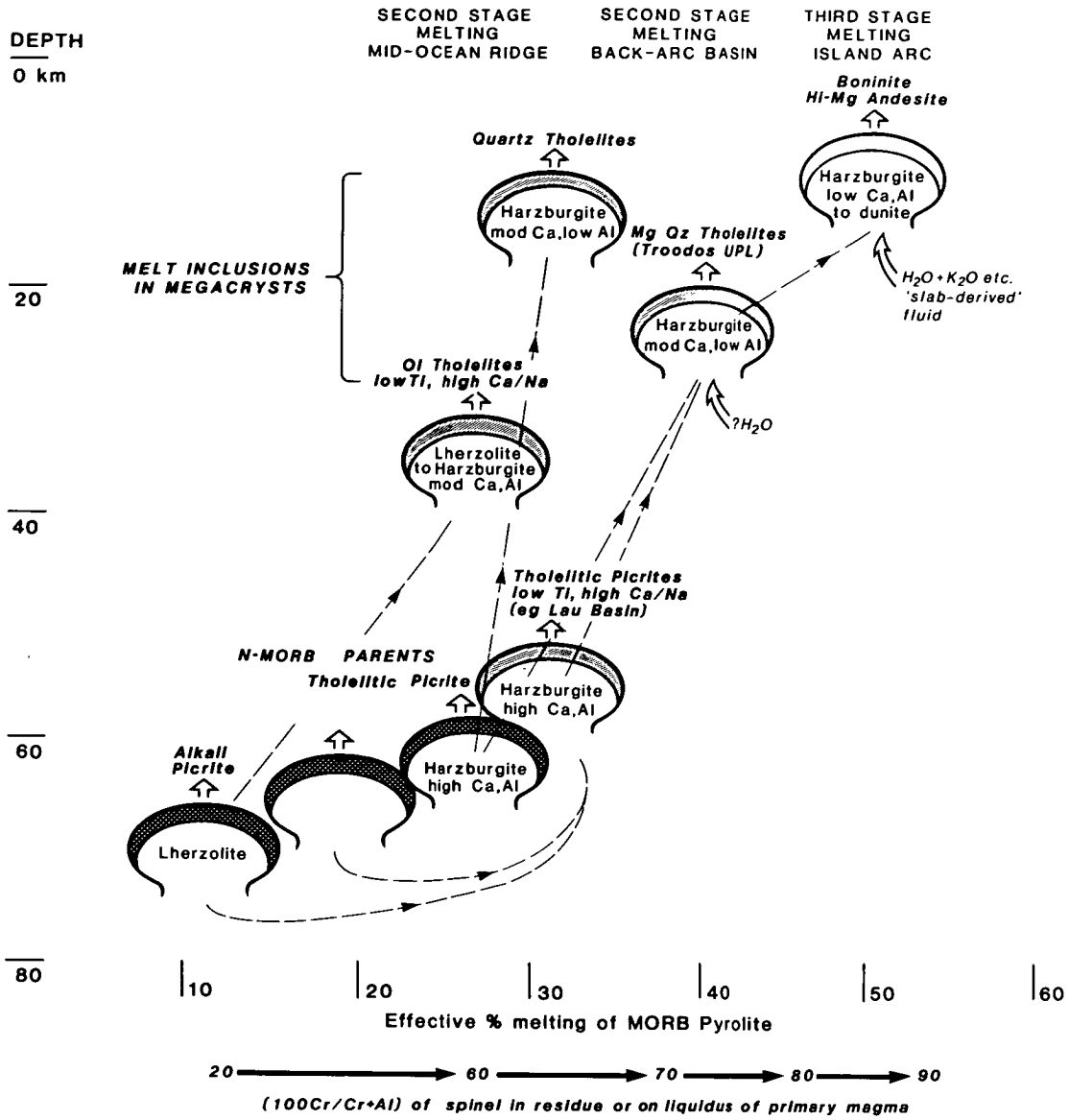

Fig. 7. Diagram illustrating multistage melting of MORB pyrolite, increasingly refractory nature of residual chrome-spinel and control of pressure (*depth*) on character of melts in equilibrium with harzburgite residues: stage I melts shown in *black*, stage II melts shown in *grey*, stage III melts shown in *white*. Mid-Ocean ridge setting is envisaged as essentially anhydrous with 2nd stage melts developed by continued diapiric uprise of residues from variable extraction of MORB parental picritic magmas. Second stage melts may only partially segregate from residual harzburgite leading to low pressure cumulate sequences (c.f., Duncan and Green 1980). In a convergent margin/marginal basin setting residual lherzolite to harzburgite (with high Ca, Al pyroxenes) may undergo 2nd stage melting with fluxing by addition of small water contents (Troodos UPL) or water + K_2O etc. (slab-derived fluids) (Island Arc Tholeiites). If *residual harzburgite* from second stage melting is further fluxed by addition of water + K_2O etc. then boninite or high-Mg andesite magmas may form, characterized by extremely high Cr/Cr + Al in spinel and very low Ca/Al ratios but with "fertile" Ca/Na, K/Na and REE ratios

conditions of primary melt production and segregation beneath mid-ocean spreading ridges (e.g., O'Hara 1968; Presnall et al. 1979; Green et al. 1979). For example, Green et al. (1979) have shown that MORB petrogenesis could be dominated by primary picritic liquids and their derivatives by crystal fractionation. Stolper (1980) has argued that a spectrum of primary melts can be generated at various depths. These primary melts produce derivative olivine tholeiites at the earth's surface by a variety of crystal fractionation paths. We will refer to these MORB liquids as first-stage melts, derived from the initial melting of upper mantle diapirs in the major convective upwelling and mantle differentiation process, i.e., mid-ocean ridges and oceanic crust construction.

There is evidence from mineral compositions and melt inclusions that distinctly more refractory primary melt compositions are also produced in the mid-ocean spreading ridge environment. These primary liquids are termed second-stage (or multistage) melts to reflect melting from a previously depleted source peridotite, probably the residue from first-stage melting. Second-stage melts are found in tensional oceanic settings other than mid-ocean spreading ridges, and their compositions differ considerably in response to varying degrees of melting and melt segregation

conditions as well as variable depletion of the residual source peridotite.

Jaques and Green (unpublished data) have investigated the crystallization behavior of one of the more primitive back-arc basin basalt compositions, Lau Basin 95-1; (Table 2) and an olivine-enriched variant (95-2). This liquid also exhibits high CaO/Na_2O and low TiO_2 contents which indicate melting from a depleted upper mantle source rock. The SiO_2-undersaturated character of this composition relative to Troodos magmas is attributed to small degrees of melting (<10%) and melt segregation at great depth (near 18 kb, 1400° C determined experimentally by Jaques and Green, unpublished data). This is a second-stage melt in its chemical characteristics with respect to MORB and occurred in a back-arc basin setting but the timing and tectonic setting of the inferred first stage melting are a matter of conjecture (Fig. 7).

A tensional regime may also develop in the early stages of oceanic plate convergence, such as at numerous island arcs in the western Pacific Ocean. Rocks with unusually high MgO, SiO_2 and low TiO_2, CaO (Table 2) have been dredged and drilled from the Mariana Trench (Dietrich et al. 1978; Meijer et al. 1982; Bloomer 1983) and reported in volcanic sections at Chichi-Jima in the Bonin Islands (Kuroda and Shiraki 1975), at Cape Vogel, Papua New Guinea (Dallwitz et al. 1966) and at Fiji (J. Gill, personal communication 1982). These have been termed high magnesium andesites or boninites, and are associated with tholeiites and basaltic andesites typical of island arcs. These rocks generally contain abundant magnesian orthopyroxene (some contain clinoenstatite), little or no plagioclase, and may contain olivine (Cameron et al. 1979). Reported rare earth element patterns (Sun and Nesbitt 1978; Hickey and Frey 1982; Cameron et al. 1983) vary from light rare earth element (LREE) depleted (Mariana Trench, DSDP Site 458) to slightly U-shaped (Bonin Islands) to LREE-enriched (Cape Vogel, Papua New Guinea). All exhibit very low abundances of the heavy rare earth elements (<5 times chondrite), however, in keeping with melting from a depleted source which has mixed to varying degrees with an alkali-LREE-rich fluid phase (Sun and Nesbitt 1978; Jenner 1981; Hickey and Frey 1982; Cameron et al. 1979).

Because of their refractory character, boninites have been compared with the Upper Pillow Lavas at the Troodos ophiolite (Cameron et al. 1980). Significant differences between the groups are evident, however. The Troodos lavas are dominated by olivine control whereas compositional variation in boninites is controlled by initial, very minor olivine appearance followed by pyroxene crystallization (clinoenstatite, orthopyroxene, or clinopyroxene). The SiO_2 and alkali contents are much higher in boninites at comparable stages of differentiation, but TiO_2 and CaO are lower. Some of the Troodos UPL exhibit a similar LREE enrichment and isotopic variability to boninites, and McCulloch and Cameron (1983) and Cameron (1985) interpret this as evidence for a LREE-enriched, high $^{87}Sr/^{86}Sr$, low ε_{Nd} fluid phase involved in melting of the source peridotite. Spinel compositions (Fig. 1) are slightly more refractory than for the UPL at Troodos. Cameron (1985) contended that the UPL represent an intermediate step between MORB and boninitic series rocks.

Further evidence for the diversity of primary magma compositions present in convergent margin environments is provided by Falloon and Green (1986) in the identification of extremely refractory olivine (Fo_{94}) containing glass inclusions from the northern end of the Tongan arc. These glasses are more refractory than Troodos Upper Pillow lavas in Mg#, Ca/Na and TiO_2 content and are slightly more silica-rich (quartz normative) (Falloon and Green 1986, Table 2; Figs. 5, 6, 8). These glasses also resemble boninites but differ markedly in high CaO contents and very high Ca/Na ratios. Experimental work by Jenner (1983) and Tatsumi (1981) showed that melts of boninitic composition may derive from quite shallow levels (<5 kb) providing water is present. This is consistent with their generation at the initiation of subduction where sinking hydrated oceanic crust dehydrates to supply hydrous fluids to the surrounding residual upper mantle peridotite. The introduction of water will stimulate melting and segregation of refractory liquids from severely depleted peridotite. The observed enrichment (relative to other second-stage melts) in alkalis, the LREE, high $^{87}Sr/^{86}Sr$, low ε_{Nd} may be inherited from the fluid phase (Sun and Nesbitt 1978; Hickey and Frey 1982; Jenner 1981; McCulloch and Cameron 1983).

The second-stage parental melt compositions discussed are given in Table 2 and plotted in Fig. 2c. All are primary and have similar Mg#. The composition P3 derived from melt inclusions in xenocrysts from Mid-Atlantic Ridge tholeiites (Donaldson and Brown (1977) has the highest TiO_2 and normative diopside and plagioclase contents of the group, and high but not extreme Ca/Na. Melts of this composition could produce calcic plagioclase and magnesian pyroxenes seen as megacrysts in MORB's of olivine tholeiite parentage. Melts of this type could segregate from dry, somewhat depleted upper mantle peridotite at 8 to 10 kb pressure under spreading ridges (Figs. 2c, 7).

The parental magmas for Troodos UPL are lower in TiO_2 and normative diopside and plagioclase content, and have very high Ca/Na. The experimental composition P1 appears to be parental to the group III (Arakapas) lavas and is slightly more refractory than P2, a possible parental composition for the group I (Margi) lavas. These magmas derive from melting of depleted peridotite at 7 to 8 kb pressure with or without small amounts of water (<1 wt%) present (Figs. 2c, 7). The unusual MORB compositions from DSDP Site 236 (Indian Ocean) exhibit the same high SiO_2, MgO, CaO/Na_2O and low TiO_2, Na_2O and K_2O character of many of the Margi area lavas. Olivine and clinopyroxene removal from composition P2 at low pressures could produce the Site 236 compositions.

The high magnesium andesite (boninite) parental composition P4 from Jenner (1983) has extremely low TiO_2 and CaO, high normative hypersthene and low normative diopside and plagioclase. It has moderate Ca/Na. It is clearly different from, and inappropriate as a parent for, any of the Troodos UPL compositions. The higher normative quartz content of this refractory melt composition indicates segregation from a depleted peridotite either at similar depths (7–8 kb) but with higher water contents (2–3% H_2O in melts) or alternatively at somewhat shallower depths (2–3 kb) with water content of <1% in melts.

Experimental studies of the melting behavior of several peridotite compositions (Jaques and Green 1980; Falloon, unpublished data) have determined the compositional paths of melts as a function of pressure and degree of melting. The second-stage melts we have discussed fall between the 10 and 5 kb melt composition paths shown in Fig. 2c (after

Jaques and Green 1980). As expected the melts become more refractory along the trend of increasing melting, or peridotite depletion.

Figure 7 illustrates a range of multistage melting paths by which basaltic liquids could reach mid-ocean ridge spreading centers and other oceanic tensional environments. Upper mantle diapirs of peridotite rise adiabatically, progressively developing greater amounts of melt which maintain chemical equilibrium with the crystal residue until the liquids segregate between 80 and 50 km depth. This is first-stage melting and produces a range of picritic primary liquids which are parental to the majority of ocean floor basalts. At the pressure of melt segregation, the residue from this melting episode is harzburgite, consisting of olivine, aluminous enstatite (2.5% CaO), aluminous spinel, and little or no aluminous clinopyroxene. This residual harzburgite re-equilibrates to spinel or garnet lherzolite at lower pressures and temperatures (due to unmixing of aluminous orthopyroxene).

Residual diapirs may continue to rise adiabatically and generate an additional melt fraction at some shallower depth. This is second-stage melting and produces a high Ca/Na, magnesian olivine tholeiite composition such as that identified from melt inclusions in refractory megacrysts in mid-ocean ridge basalts (Price et al. 1986; Donaldson and Brown 1977; Table 2). From melting studies of depleted peridotite (Jaques and Green 1980), liquids of this composition could be generated at 10–12 kb (35–40 km depth) by ~10% melting. The residue from this is depleted harzburgite or lherzolite with moderately aluminous (2–4% Al_2O_3) pyroxenes. Such crystalline residues may continue diapiric intrusion until emplaced at the base of the oceanic crust, and seen in dredged samples (Hamlyn and Bonatti 1980) and in some ophiolites.

Second-stage melt segregation at ~25 km will produce magnesian quartz tholeiites seen, for example, among the Upper Pillow Lavas at the Troodos ophiolite. These liquids form after about 10% melting of residues from first stage melting and leave an extremely depleted harzburgite residue with low-Al (~1%) pyroxenes, similar to the harzburgite tectonite seen at the base of some ophiolites (England and Davies 1973; Pallister and Hopson 1980; Juteau and Whitechurch 1980; Jaques 1981). These examples illustrate our model of multi-stage melting processes beneath spreading ridges, either of mid-ocean or back arc types, in which the residue left from an earlier melting event is available for further basaltic liquid extraction as it continues its diapiric rise. At convergent plate margins tensional environments and high temperature diapirism of residual refractory peridotite also occur and melting is aided by access of H_2O-rich fluids released from the subduction zone processes (Fig. 7). In these situations we find evidence for melting of the most refractory source peridotites in the extreme values of olivine Mg#, spinel Cr#, plagioclase (Ca/Ca+Na) and high Mg, low Ca enstatite (proto-enstatite).

Conclusions

Experimental study of the phase relations of a melt composition representative of magnesian magmas within the Upper Pillow Lavas (UPL) at the Troodos ophiolite, Cyprus, has demonstrated that:

1) Such a composition may be a primary liquid, segregated as approximately 10% melt fraction at 7–8 kb, 1360° C from a harzburgite residue (olivine, orthopyroxene, chrome-spinel). The presence of a small amount of water (<0.1 wt% in source peridotite) would lower the temperature, and raise the pressure (slightly) of the multiple saturation point.

2) Compositional and mineralogical variation of glasses and phenocrysts within the UPL matches crystallizing phases and complementary liquids determined from the experiments.

3) Mineral compositions found in some but not all of, the lower plutonic sequences at the Troodos ophiolite may be genetically related to the UPL magma type as complementary cumulates.

4) Compositionally distinct groups within the UPL are related to variable parental magma compositions. One group of olivine-phyric and orthopyroxene-free lavas appears to require a slightly more diopside-normative parent magma than the most refractory orthopyroxene-bearing lavas. The first group began crystallization at low pressure (<2 kb), while the second crystallized in deeper (7–15 km) magma conduits, probably from melts containing a small of dissolved water (~0.5 wt%).

Distinct, highly refractory melts can occur in a variety of plate tectonic environments including mid-ocean spreading ridges, back-arc basins and the fore-arc region of island arcs. These refractory melts share the geochemical characteristics of being MgO-rich, TiO_2- and Na_2O-poor, and generally depleted in incompatible elements. Such compositions can arise by multistage melting of the upper mantle, either as a continuous process (as at mid-ocean ridges) or resumed after a significant time period by a change to tensional tectonics with or without access of water (back arc basin or island arc). Pressure, temperature and dissolved volatile species, as well as the specific composition of the depleted source peridotite, will determine the composition of the resulting second-stage melts.

Acknowledgements. K.L. Harris, W.C. Doran, P. Robinson and W. Jablonski provided technical assistance. R.A. Duncan was supported by a Queen's Fellowship in Marine Sciences from the Australian Government. This research was carried out under an ARGS grant to D.H. Green. Reviews by W. Cameron and A.L. Jaques improved the manuscript. T.J. Falloon independently confirmed the presence of magnesian pigeonite microphenocryst cores and obtained the data presented in Fig. 4C and illustrated by Fig. 5. We acknowledge helpful discussions with A.J. Crawford, R. Varne, T. Falloon, M. Rautenschlein, H.U. Schmincke, W. Cameron and A.L. Jaques.

References

Basaltic Volcanism Project (1981) Basaltic volcanism on the terrestrial planets. Pergamon Press Inc., New York, p 1286

Bloomer SH (1983) Distribution and origin of igneous rocks from the landward slopes of the Mariana Trench: implications for its structure and evolution. J Geophys Res 88:7411–7428

Bryan WB, Moore JG (1977) Compositional variations of young basalts in the Mid-Atlantic Ridge rift valley near lat. 36°49′ N. Geol Soc Am Bull 88:556–570

Bryan WB, Thomson G, Frey FA, Dickey JS (1976) Inferred geologic settings and differentiation in basalts from the Deep Sea Drilling Project. J Geophys Res 81:4285–4304

Cameron WE (1985) Petrology and origin of primitive lavas from the Troodos ophiolite, Cyprus. Contrib Mineral Petrol 89:239–255

Cameron WE, Nisbet EG, Dietrich VJ (1979) Boninites, komatiites and ophiolitic basalts. Nature 280:550–553

Cameron WE, Nisbet EG, Dietrich VJ (1980) Petrographic dissimilarities between ophiolitic and ocean floor basalts. In: Panayiotou A (ed) Ophiolites. Geol Surv Dept, Nicosia, pp 182–192

Cameron WE, McCulloch MT, Walker DA (1983) Boninite petrogenesis: chemical and Nd-Sr isotopic constraints. Earth Planet Sci Lett 65:75–89

Christensen FNI, Salisbury MH (1975) Structure and constitution of the lower oceanic crust. Rev Geophys Space Phys 13:57–86

Crawford AJ (1980) A clinoenstatite-bearing cumulate olivine pyroxenite from Howqua, Victoria. Contrib Mineral Petrol 75:353–367

Dallwitz WB, Green DH, Thompson JE (1966) Clinoenstatite in a volcanic rock from the Cape Vogel Area, Papua. J Petrol 7:375–403

Dietrich V, Emmerman R, Oberhansli R, Puchelt H (1978) Geochemistry of basaltic and gabbroic rocks from the West Mariana Basin and the Mariana Trench. Earth Planet Sci Lett 39:127–144

Donaldson CH, Brown RW (1977) Refractory megacrysts and magnesium-rich melt inclusions within spinel in oceanic tholeiite: indicators of magma mixing and parental liquid compositions. Earth Planet Sci Lett 37:81–89

Drake MJ (1975) Plagioclase-melt equilibria. Geochim Cosmochim Acta 40:457–465

Duncan RA, Green DH (1980) The role of multi-stage melting in the formation of oceanic crust. Geology 8:22–26

Dungan MA, Long PE, Rhodes JM (1979) The petrography, mineral chemistry, and one-atmosphere phase relations of basalts from Site 395. In: Initial reports of the Deep Sea Drilling Project, vol 45. US Government Printing Office, Washington, DC, pp 461–477

Elthon D, Scarfe CM (1984) High pressure phase equilibria of a high magnesia basalt and the genesis of primary oceanic basalts. Am Mineral 69:1–15

England RN, Davies HL (1973) Mineralogy of ultramafic cumulates and tectonites from eastern Pacific. Earth Planet Sci Lett 17:416–425

Falloon TJ, Green DH (1986) Glass inclusions in magnesian olivine phenocrysts from Tonga – evidence for highly refractory parent magmas in the Tongan Arc. Earth Planet Sci Lett 81:95–103

Flower MFJ, Robinson PT, Schmincke U, Ohnmacht W (1977) Magma fractionation systems beneath the Mid-Atlantic Ridge at 36–37° N. Contrib Mineral Petrol 64:167–195

Frey FA, Bryan WB, Thompson G (1974) Atlantic ocean floor: geochemistry and petrology of basalts from Legs 2 and 3 of the Deep Sea Drilling Project. J Geophys Res 79:5507–5527

Frey FA, Dickey JS Jr, Thompson G, Bryan WB, Davies HL (1980) Evidence for heterogeneous primary MORB and mantle sources, NW Indian Ocean. Contrib Mineral Petrol 74:387–402

Gass IG (1958) Ultrabasic pillow lavas from Cyprus. Geol Mag 95:241–251

Gass IG, Smewing JD (1973) Intrusion, extrusion and metamorphism at constructive margins: evidence from the Troodos Massif, Cyprus. Nature 242:26–29

Gass IG, Lippard SJ, Shelton AW (eds) (1984) Ophiolites and oceanic lithosphere. Geol Soc Lond Spec Publ 13:1–413

Green TH (1972) Crystallization of calc-alkaline andesite under controlled high pressure hydrous conditions. Contrib Mineral Petrol 34:150–166

Green DH (1973) Conditions of melting of basanite magma from garnet peridotite. Earth Planet Sci Lett 17:456–465

Green DH, Ringwood AE (1967) The genesis of basaltic magmas. Contrib Mineral Petrol 15:103–190

Green DH, Hibberson WO, Jaques AL (1979) Petrogenesis of mid-ocean ridge basalts. In: McElhinny MW (ed) The earth: its origin, structure and evolution. Academic Press, pp 265–290

Greenbaum D (1977) The chromitiferous rocks of the Troodos ophiolite complex, Cyprus. Econ Geol 72:1175–1194

Griffin BJ (1979) Energy-dispersive analysis system calibration and operation with TasSueds, an advanced interactive data-reduction package. Univ Tasmania Dep Geol Publ 343

Hamlyn PR, Bonatti E (1980) Petrology of mantle-derived ultramafics from the Owen F.Z., NW Indian Ocean: implications for the nature of the oceanic upper mantle. Earth Planet Sci Lett 48:65–79

Hawkins JW (1976) Petrology and geochemistry of basaltic rocks of the Lau Basin. Earth Planet Sci Lett 28:283–297

Hickey RL, Frey FA (1982) Geochemical characteristics of boninite series volcanics: implications for their source. Geochim Cosmochim Acta 46:2099–2115

Hodges FN, Papike JJ (1976) DSDP Site 334: magmatic cumulates from oceanic layer 3. J Geophys Res 81:4135–4151

Jaques AL (1981) Petrology and petrogenesis of cumulate peridotites and gabbros from the Marum ophiolite complex, northern Papua New Guinea. J Petrol 22:1–40

Jaques AL, Green DH (1980) Anhydrous melting of peridotite at 0–15 kb pressure and the genesis of tholeiitic basalts. Contrib Mineral Petrol 73:287–310

Jenner GA (1981) Geochemistry of high-Mg andesites from Cape Vogel, Papua New Guinea. Chem Geol 33:307–332

Jenner GA (1983) Petrogenesis of high-Mg andesites: an experimental and geochemical study with emphasis on high-Mg andesites from Cape Vogel, PNG. PhD thesis, University of Tasmania, Hobart

Juteau T, Whitechurch H (1980) The magmatic cumulates of Antalya (Turkey): evidence of multiple intrusions in an ophiolite magma chamber. In: Panayiotou A (ed) Ophiolites. Geol Surv Dep, Nicosia, pp 377–391

Kay RW, Senechal RG (1976) The rare earth geochemistry of the Troodos ophiolite complex. J Geophys Res 81:964–970

Kuroda N, Shiraki K (1975) Boninite and related rocks of Chichijima, Bonin Islands, Japan. Rep Fac Sci Shizuoka Univ 10:145–155

Langmuir CH, Bender JF, Bence AE, Hanson GN, Taylor SR (1977) Petrogenesis of basalts from the Famous area: Mid-Atlantic Ridge. Earth Planet Sci Lett 36:133–156

Lindsley DH (1983) Pyroxene thermometry. Am Mineral 68:477–493

McCulloch MT, Cameron WE (1983) Nd-Sr isotopic study of primitive lavas from the Troodos ophiolite, Cyprus: evidence for a subduction-related setting. Geology 11:727–731

Meijer A (1980) Primitive arc volcanism and a boninite series: examples from western Pacific island arcs. In: Hayes DE (ed) The tectonic and geologic evolution of southeast Asian seas and islands. Am Geophys Union Monogr 23:269–282

Meijer A, Anthony E, Reagan M (1982) Petrology of volcanic rocks from the fore-arc sites. In: Initial reports of the Deep Sea Drilling Project, vol 60, US Government Printing Office, Washington, DC, pp 709–730

Melson WG, Byerly GR, Nelen JA, O'Hearn T, Wright TL, Vallier T (1977) A catalogue of the major element chemistry of abyssal volcanic glasses. Smithsonian Contrib Earth Sci 19:31–60

Miyashiro A (1973) The Troodos ophiolitic complex was probably formed in an island arc. Earth Planet Sci Lett 19:218–224

Moores EM, Vine FJ (1971) The Troodos Massif, Cyprus, and other ophiolites as oceanic crust: evaluation and implications. Philos Trans R Soc London 268:443–466

Nicholls IA, Ringwood AE (1973) Effect of water on olivine stability in tholeiites and the production of silica-saturated magmas in the island arc environment. J Geol 81:289–300

O'Hara MJ (1968) Are ocean-floor basalts primary magmas? Nature 220:683–686

O'Hara MJ (1977) Geochemical evolution during fractional crystallization of a periodically refilled magma chamber. Nature 266:503–507

Pallister JS, Hopson CA (1980) Samail ophiolite plutonic suite: field relations, phase variation, cryptic variation and layering, and a model of a spreading ridge magma chamber. J Geophys Res 86:2593–2644

Pantazis TM, Panayiotou A, Gass I, Adamides N, Simonian K (1979) Field excursion guidebook. International Ophiolite Symposium, Nicosia, Cyprus. Geol Surv Dep Nicosia, p 142

Pearce JA (1975) Basalt geochemistry used to investigate the past tectonic environments on Cyprus. Tectonophys 25:41–67

Presnall DC, Hoover JD (1984) Composition and depth of origin of primary mid-ocean ridge basalts. Contrib Mineral Petrol 87:170–178

Presnall DC, Dixon JR, O'Donnell TH, Dixon SA (1979) Generation of mid-ocean ridge tholeiites. J Petrol 20:3–35

Price RC, Kennedy AK, Riggs-Sneeringer M, Frey FA (1986) Geochemistry of basalts from the Indian Ocean triple junction: implications for the generation and evolution of Indian Ocean ridge basalts. Earth Planet Sci Lett 78:379–386

Rautenschlein M, Jenner GA, Hertogen J, Hofmann AW, Kerrich R, Schminke H-U, White WM (1985) Isotopic and trace element composition of volcanic glasses from the Akaki Canyon, Cyprus: implications for the origin of the Troodos ophiolite. Earth Plant Sci Lett 75:369–383

Robinson PT, Melson WG, O'Hearn T, Schminke H-U (1983) Volcanic glass compositions of the Troodos ophiolite, Cyprus. Geology 11:400–404

Roeder PL, Emslie RF (1970) Olivine-liquid equilibrium. Contrib Mineral Petrol 29:275–289

Schminke H-U, Rautenschlein M, Robinson PT, Mehegan JM (1983) Troodos Extrusive series of Cyprus: a comparison with oceanic crust. Geology 11:405–409

Searle DL, Vokes FM (1969) Layered ultrabasic lavas from Cyprus. Geol Mag 106:515–530

Shibata T, DeLong SE, Walker D (1979) Abyssal tholeiites from the Oceanographer Fracture Zone. I. Petrology and fractionation. Contrib Mineral Petrol 70:89–102

Sigurdsson H, Schilling J-G (1976) Spinels in Mid-Atlantic Ridge basalts: chemistry and occurrence. Earth Planet Sci Lett 29:7–20

Simonian KO, Gass IG (1978) Arakapas fault belt, Cyprus: a fossil transform fault. Geol Soc Am Bull 89:1220–1230

Smewing JD, Potts PJ (1976) Rare-earth abundances in basalts and metabasalts from the Troodos Massif, Cyprus. Contrib Mineral Petrol 57:245–258

Smewing JD, Simonian KO, Gass IG (1975) Metabasalts from the Troodos Massif, Cyprus: genetic implication deduced from petrography and trace element geochemistry. Contrib Mineral Petrol 51:49–64

Stolper EM (1980) A phase diagram for mid-ocean ridge basalts: preliminary results and implications for petrogenesis. Contrib Mineral Petrol 74:13–27

Sun S-S, Nesbitt RW (1979) Geochemical regularities and genetic significance of ophiolitic basalts. Geology 6:689–693

Tatsumi Y (1981) Melting experiments on a high magnesium andesite. Earth Planet Sci Lett 54:357–365

Thy P, Brooks CK, Walsh JN (1985) Tectonic and petrogenetic implications of major and rare earth element chemistry of Troodos glasses, Cyprus. Lithos 18:165–178

Wood DA (1979) Dynamic partial melting: its application to the petrogenesis of basalts erupted in Iceland, the Faeroe Islands, the Isle of Skye (Scotland) and the Troodos Massif (Cyprus). Geochim Cosmochim Acta 43:1031–1046

Wyllie PJ (1979) Magmas and volatile components. Am Mineral 64:469–500

Yoder HS, Tilley CE (1962) Origin of basalt magmas: an experimental study of natural and synthetic rock systems. J Petrol 3:342–532

Received May 20, 1986 / Accepted March 11, 1987

B40

PETROLOGY OF UPPER MANTLE PROCESSES IN THE S.W. PACIFIC

By

D.H. Green, M. Barsdell, A.J. Crawford, S.M. Eggins, T.J. Falloon and M.E. Wallace, Department of Geology, University of Tasmania, Hobart 7001

ABSTRACT

The Earth's Upper Mantle is dominantly
idotitic but in convergent margin
ions, such as the S.W. Pacific,
duction of oceanic crust gives greater
ical and petrological diversity to
er mantle petrology and petrogenesis.
ination of currently active, Quaternary
Tertiary volcanism in the S.W. Pacific,
ticularly seeking information from ocean
or sampling to characterize the basement
island arcs and to investigate active
eading centres, consistently points to
ental magmas of basaltic to picritic
racter. However, these parental magmas
chemically diverse and it is not
sible to designate a characteristic
land arc' or 'convergent margin'
rogenesis in the sense of a
racteristic mantle source composition
a charactistic partial melting regime.
this respect, magma genesis at
vergent margins contrasts with that at
anic spreading centres. Our studies
nasize the importance of source
idotite ranging from 'fertile
rzolite' (i.e. compositions with 3-4%
Al_2O_3, 0.3-0.5% Na_2O) to refractory
zburgite (<1% CaO, Al_2O_3). Secondly,
studies emphasize the importance of C-
fluids in determining the solidus
perature for mantle peridotite.
rdly, the process of magma mixing adds
siderable complexity to magmatic
ution at convergent margins. End
per components for magma mixing range
n picrites to magnesian quartz-
leiites to boninites - all from
idotitic sources - but also include
itic to rhyodacitic melts derived from
ting of subducted basaltic (eclogitic)
st. Since each of these 'primary'
vergent margin magmas may undergo
stal fractionation and magma mixing,
at diversity of magma types in this
tonic setting must be expected.

The S.W. Pacific provides a variety of tectonic settings for which we can attempt to deduce the characteristics of parental magma(s) as a step towards defining the source conditions and source compositions. Our approach is to use the constraints of major element geochemistry and experimental petrology for these purposes with the aim of establishing a petrological framework for interpretation of further complexities revealed by trace-element and isotopic studies. In convergent margin regions, the subduction process carries cool, partially hydrated, carbonated and oxidized crust and lithosphere to mantle depths beneath an over-riding wedge of lithosphere and asthenosphere. At trench-transform fault intersections or where relatively young spreading centres occur on the subducted slab, the effects of heat transfer and of volatile (H_2O-rich) release from the subducted slab act to partially melt refractory lherzolite and harzburgite source rocks. Petrogenetic indicators of these refractory sources are high Ca/Na ratios (and anorthitic plagioclase to An_{100}), high Cr/Cr + Al ratios in liquidus spinels and highly magnesian olivine (to Fo_{94}) and clinopyroxene (to Mg_{94}). The role of H_2O is significant in lowering liquidus temperature by 50-150°C but magmas are apparently water-undersaturated at source. The most water-rich parental magmas in the S.W. Pacific appear to be 'boninites' or 'high magnesian andesites' but even these very high SiO_2, low CaO melts appear to have contained only 2-3% water at source. An additional source of water, applicable to deep levels of subduction zones, may derive from interaction of 'oxidized' crust/lithosphere with (CH_4 + H_2)-rich fluids degassing from the deep interior of the earth.

INTRODUCTION

In the past 30 years the methods of experimental petrology have evolved from studies of simple 2 and 3-component system analogues of igneous rocks, through studies of 'model' or ideal mantle or magma compositions to studies of specific rock suites and samples aiming to precisely quantify their crystallization history and magma petrogenesis in terms of P,T, volatile content and composition. Techniques have evolved rapidly with the application of the electron microprobe and scanning electron microscope to experimental charges, and more recently with the use of mass spectrometry and infrared spectroscopy to analyze fluid compositions from charges and volatile components dissolved in melts.

In recent years the Department of Geology at the University of Tasmania has engaged in investigations in the Tasman Sea, S.W. Pacific and Papua New Guinea with the specific aims of using these methods to understand deep crust and mantle petrogenetic processes in this extremely diverse and tectonically active area which forms parts of the boundary between the Pacific and Australian-Antarctic plates. The experimental approach has included examination of effects of C-H-O, C-H-O-S, and of fluorine-rich fluids on melting and phase relations. These latter studies provide information on sulphur solubility in mantle-derived melts, on thermal regimes in different tectonic settings, on volatile contents, and on roles of fluid degassing from magmas. This information is necessary 'pure science' on which models of ore-metal solution, transport, deposition and concentration must be built. The nature of this paper is thus in the nature of a review of present ideas on mantle petrogenesis and the application of those ideas in the S.W. Pacific, with the specific purpose of providing part of the geological framework on which models of mineralization and methods of mineral exploration are built.

MELTING IN THE UPPER MANTLE

Fig. 1a summarizes the results of experimental studies (Green 1973, Jaques and Green 1980, Green 1987) on a fertile peridotite (designated 'Hawaiian pyrolite' from its suitability as a source composition for Hawaiian olivine tholeiite to olivine melilitite magmas) at pressures to 3.5GPa and under conditions of different water contents. In fig. 1b the results of a similar study (Jaques & Green, 1980; M.E. Wallace, unpublished Ph.D. research) on a more refractory lherzolite composition (Tinaquillo lherzolite) are illustrated. The figures illustrate a fundamental aspect of mantle rheology and petrology, i.e. the control on solidus temperature by volatile (principally H_2O) content and by pargasitic amphibole stability. In fig. 1b we draw attention to the relative positions of the dehydration-solidi or amphibole-peridotite solidi for the two lherzolite compositions. Tinaquillo lherzolite, the more 'refractory' composition has a lower dehydration solidus temperature because the low TiO_2, Na_2O and K_2O contents of this rock determine that the amphibole composition stable at 15-25kb, 1000°C is close to pargasite whereas the amphibole in Hawaiian pyrolite has a higher Ti-pargasite content and is stable to higher temperature, i.e. the more 'fertile' lherzolite has a higher dehydration solidus. We return to this observation in a later section.

In fig. 1a we indicate the conditions of pressure and temperature at which mafic magmas of various types (from olivine lamproites and kimberlites to boninites) segregated from olivine-rich residues (garnet lherzolite to enstatite-bearing dunite). It should be noted that the Tinaquillo lherzolite composition can only produce 'refractory' magma types such as Troodos or Tongan Forearc high-magnesium quartz tholeiites or boninites and is unsuitable as a source composition for Hawaiian or even mid ocean ridge basalts unless 'pre-conditioned' by precursor metasomatic enrichment. However, 'fertile' compositions such as Hawaiian pyrolite may produce magmas with enriched source geochemical signatures ('ocean island' or 'hot spot' geochemical signatures) and then, by a second or third stage melting of residue left after extraction of stage one magmas, these sources may yield magmas with 'depleted' or 'refractory' source geochemical signatures (Duncan & Green, 1987).

In fig. 2, the petrogenetic framework of fig. 1 is applied to the conventional plate tectonic model of divergent plate boundaries (mid-ocean ridges), convergent plate boundaries (subduction zones), secondary spreading centres (back-arc basins) and nemataths (Carey 1958) or 'hot spot' volcanism or island chain volcanism. Fig. 2 does not, of course, illustrate the complexities of 4-dimensional tectonics. For example subduction zones may terminate against transform faults and in this environment will juxtapose cold, refractory, subducted lithosphere against normal 'hot' fertile asthenosphere beneath

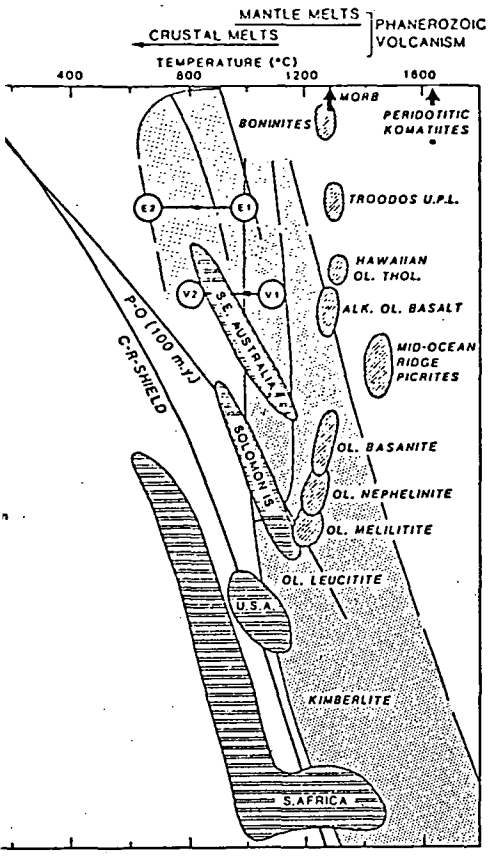

The P,T conditions deduced for melting and magma
on processes in the modern Earth. Lightly
d area is the partial melting region for average
tal crust with solidi shown for anhydrous, water-
d and 'dehydration melting' conditions. The
atterned area illustrates melting conditions for
eridotite ('Hawaiian' pyrolite) with solidi for
$H_2O = P_{Load}$ and for the fluid-absent amphibole +
+ pyroxenes etc. eutectic (dehydration solidus).
al gradients for 100 m.yr old oceanic crust (P-O)
continental shield (C-R) are shown. Evidence for
ure distribution in crust and lithosphere derived
tle xenoliths in different areas is shown by
ally patterned areas. E1-E2 and V1-V2 show
cooling paths deduced for deep continental crust
Land) and for mantle xenolith suites from Victoria
stralia, in each case after disturbance of the
by a major magmatic and thermal event.

itions of magma segregation for a variety of modern
'basaltic' magmas are illustrated (diagonally
reas). These are confined within an envelope
by adiabatic upwelling at divergent plate margins
through 1450°C, 15-20kb - i.e. mid-ocean ridge
segregation) and by the 'shield geotherm' defined
peridotite xenoliths from diamond-bearing
tes from the South African shield.

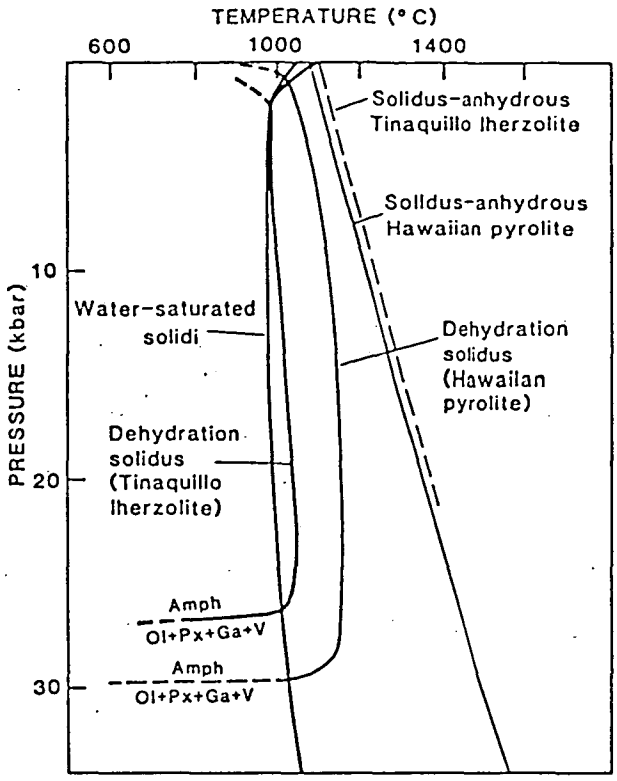

Fig. 1b Phase diagrams for 'fertile' or 'enriched' Hawaiian pyrolite and 'refractory' or 'depleted' Tinaquillo lherzolite compositions. Both have similar major element compositions (Jaques & Green 1980), but the marked differences in the amphibole dehydration solidus are attributable to the higher temperature stability of the Ti-pargasite relative to low Ti-pargasite in the refractory composition. In both cases amphibole is stable to the solidus in the 2-25kb pressure interval.

plates. Similarly the addition of
me dimension' emphasizes that
ion zones may later be cut by
al or rift structures at high angles
trench-arc trends and divergent
may be carried towards and into
ion zones.

fig. 2, in addition to the
ional plate tectonic framework, we
troduced the concept of an Earth
s degassing reduced gases (CH_4 + H_2)
from the deep interior (Gold & Soter 1980, Ryabchikov et. al. 1981, Green et. al. 1987a, b, Taylor & Green 1987, Taylor 1987, Foley 1987, Wyllie 1987). Although the composition of the Earth's early atmosphere remains a topic of debate, there is evidence for hydrogen loss from the upper atmosphere, and for an early reducing atmosphere followed by increasing oxygen content (Cloud 1978). Hydration, carbonation and oxidation of magmatic rocks at the Earth's surface and metamorphism and fluid circulation in the crust, produce a crust/lithosphere section which is oxidized (HM to FMQ) at shallow depths and more reduced (MW to IW + 1 or 2 log units) at deeper levels (Taylor 1987). In fig. 2, subduction is highlighted as a process which introduces oxidized (and at shallow depths, hydrated and carbonated) rocks of the lithosphere into a low fO_2 (IW to IW + 1 log unit) environment in the asthenosphere and upper mantle (Transition Zone).

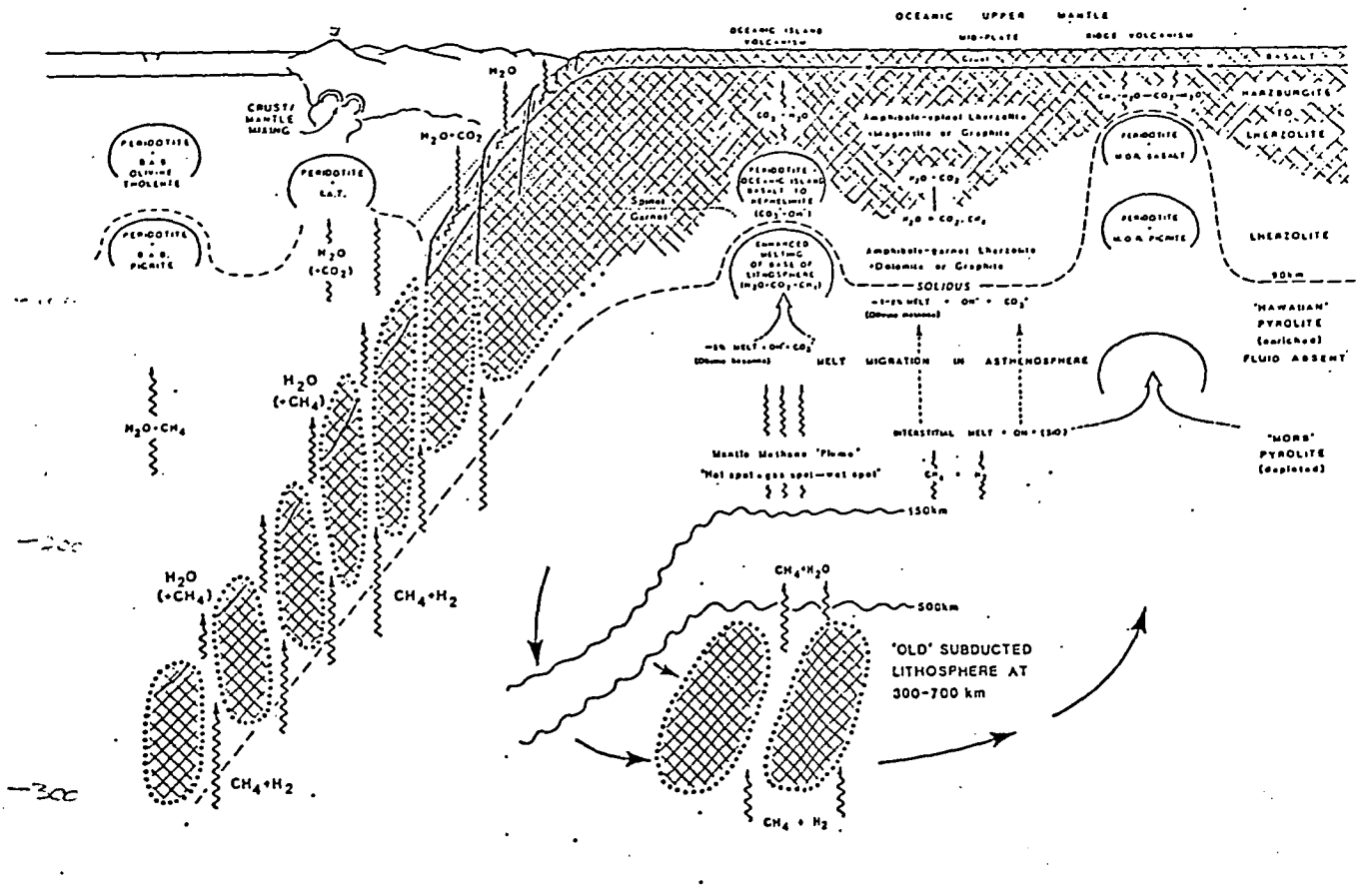

Fig. 2 Schematic model of the oceanic lithosphere and asthenosphere. The lithosphere is variable in composition due to melt extraction and fluid enrichment events and is envisaged as variably oxidized from FMQ (shaded areas) to ~IW + 1, 2 log units (blank areas of lithosphere). The asthenosphere is a fluid absent region in which C-H-O volatiles are dissolved in a small melt fraction (1-2% melt) which migrates towards the top of the asthenosphere or base of the lithosphere. Source regions for Hawaiian-type island chains (hot-spots) are in the upper part of the asthenosphere or base of the lithosphere. Source regions for MORB are in the lower part of the asthenosphere. The mantle is degassing reduced fluids (CH_4 + H_2) and the asthenosphere is a fluid absent region with intrinsic oxygen content and fugacity varying from ~IW to IW + 2, 3 log units - this variation is accommodated in change of melt structure from reduced (Si:O > 1:2)to contain $(OH)^-$ and $(CO_3)^=$ [fO_2 ~IW + 2, 3 log units]. The patterned symbol on the oceanic lithosphere signifies fO_2-FMQ i.e. 'oxidized' lithosphere. In the convergent margin or subduction plate boundary scenario, the oxidized lithosphere is portrayed as penetrated along fracture zones by CH_4 + H_2 fluids from subjacent mantle. The redox inter-action produces H_2O-rich fluids which strongly influence melting relations above or within the subducted lithosphere. Thus, even at depths below those at which hydrated minerals of the oceanic crust and lithosphere have been lost, the 'slab' may be a source of H_2O-rich fluids. Abbreviations for primary magmas developed within the schematic diapirs are: M.O.R. = mid-ocean ridge; I.A.T. = island arc tholeiite; B.A.B. = back-arc basin.

If reduced, CH_4-rich, fluids ascending from the Earth's interior penetrate oxidized lithosphere, for example, along fractures intersecting subducted lithosphere (fig. 2), then the fluids will intersect the carbon saturation surface depositing either graphite or diamond and moving to more water-rich fluid compositions (Taylor & Green 1987, Taylor 1987, Green et. al. 1987a, b). The consequences of generation of water rich-fluids at temperatures $\geq$ 1000^{0}C approx., are to produce melting of peridotitic compositions. This process of 'redox-melting' will occur whenever CH_4-rich fluids intersect interfaces between oxidized and reduced rock volumes in the upper mantle and fig. 2 suggests this mechanism to produce increased mantle (H_2O

CH_4)-fluid generation beneath 'hot-spots' 'wet-spots' without the necessity for a ermal plume or chemically distinctive me from the deep mantle. Redox melting fers a mechanism for generating high fH_2O lues in refractory, anhydrous but dized rocks [e.g. harzburgite containing .5% Fe_2O_3 in enstatite and chromite-gnetite solid solution in spinel] and in g. 2 we suggest that this process may be portant in subduction zones or where jor lithospheric fracture zones ransform faults) intersect subduction nes. Magmas produced by this method uld contain small but significant water ntents and would have low intrinsic fO_2.

An additional characteristic is most lpful in characterizing the source gions for mafic magmas. It is axiomatic at it is not the trace element contents the major element compositions of melts ich determine the nature of their quidus phases, and thus define their ssible residual phases and conditions of lting. In terms of major elements, it not possible for example, to generate a ninite parental liquid from a Hawaiian rolite composition (fig. 11, Green et. 1987a). Similarly, liquids such as e Troodos high magnesia quartz tholeiites quire source compositions at least as fractory (in major and minor elements) as haquillo lherzolite.

The abundances of minor and trace ements commonly referred to as HFS(Ti, Nb, etc.) LIL(K, Rb, Ba, Sr) or (La,Ce....Yb) are <u>not</u> simply related to rtile' or 'refractory' compositions as fined by major and minor elements, and ghly refractory 'boninite source' positions may already possess (or quire by fluid access during melting) ghly enriched LIL or REE trace element ndances. This independence of major ment and trace element signatures has n amply demonstrated for lithosphere ples (lherzolite xenoliths) by many kers (Frey & Green 1974, O'Reilly & ffin, 1987).

To summarize this section and erring to fig. 2, we have emphasized the roles for C-H-O-rich fluids in ermining P,T conditions at which melting urs in the mantle. The stability-field graphite (diamond) divides such fluids o $H_2O + CO_2$ (oxidized) and $H_2O + CH_4$ duced). There is a high probability t the deep-earth (asthenosphere and nsition Zone) is reduced (fO_2 ~ IW + 1 log unit) and degassing CH_4-rich fluids. Subduction of oceanic crust and lithosphere will carry oxidized (fO_2~ FMQ to HM) rocks to depths of $\geq$700 kms and redox interaction, including redox melting, will occur with generation of H_2O-rich fluids. The availability of H_2O-rich fluids to deep levels of the earth and the complex tectonics of subduction-transform-back-arc spreading regions such as in S.W. Pacific create conditions for multistage melting of fertile to highly refractory peridotite bulk compositions. In this environment LIL, HFS and REE trace element abundances in the magma source regions are highly variable and reflect fluid interactions or complex multi-event lithospheric processes. It is nevertheless commonly possible to identify the major element characteristics of the source peridotite as 'fertile', 'moderately refractory' or 'highly refractory' on the basis of major element characteristics of the magmas. In the following sections, the tectonic framework of the S.W. Pacific is briefly reviewed and the magmatic activity evident in different tectonic situations, interpreted using the petrogenetic framework presented in this section.

TECTONIC ELEMENTS OF THE SOUTHWEST PACIFIC

In Figures 3 and 4, we summarize the major known or inferred tectonic processes currently operating in the southwest Pacific, and indicate the areas of our current investigations briefly reported herein. Two areas also being investigated, the Tasmantid seamount chain intraplate volcanism (S.J. Eggins), and the Woodlark Spreading Centre (A.J. Crawford) are outside the region shown in Figures 3 and 4. Referring to Figures 3 and 4, the importance of fracture systems terminating or transecting subduction zones is very apparent. The Vanuatu arc is presently rifting parallel to, and approximately 85km behind the trench, to form the Coriolis and Northern Trough backarc basins. An additional feature of some importance derives from the collision of the D'Entrecasteaux Zone, an elevated northern extension of the New Caledonia-Loyalty Island arc system, with the Vanuatu arc. Major fractures in the over-riding, arc-bearing plate radiate out from the collision site, and conform remarkably well to the fracture pattern suggested by a simple indenter model (Collot et. al. 1983). Where these fractures intersect the active Central Volcanic Chain, volcanoes composed of abundant primitive picritic and olivine basalt magmas (Aoba

and Ambrym) have developed, aligned along the fractures. These fracture zones have apparently provided easy access to the surface for primitive magma, which otherwise would have cooled and differentiated within the arc crust or subvolcanic magma chambers to eventually erupt as basaltic andesites or more evolved lavas. The primitive lavas on Aoba and Ambrym offer a rare glimpse of arc parental magmas.

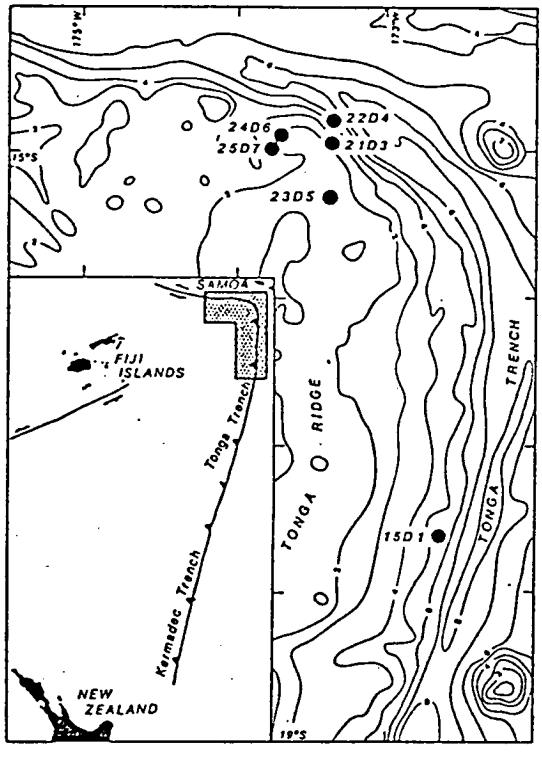

Fig. 3 Bathymetry of the northern termination of the Tonga trench, showing dredge locations of the 1985 'Natsushima' cruise.

The northern termination of the Tongan Trench lies in an area of exceptional tectonic complexity. Here, subduction of the Pacific Plate changes gradually to apparent transform motion, and must involve major tears in the subducting plate. In addition, a short distance further north lies the Samoan Island Chain, a line of 'hot-spot'-related intraplate volcanoes. Dredging in the north Tongan arc and trench (Fig. 3) has sampled a diversity of primitive lavas, including several suites of magnesian arc tholeiites, lavas transitional to boninites, and a plagiogranite chemically suitable as a candidate for a partial melt of subducted slab eclogite (Falloon, Green and Crawford, 1987). This local diversity of magma compositions over a small area is not surprising considering the tectonic setting. Magma generation in the region of the termination of North Tongan Trench could conceivably be affected by 'normal' subduction processes, possible backarc basin-related MORB-source diapirism, processes related to tearing of the down-going Pacific Plate as it swings into transform motion, and perhaps also some thermal or tectonic influence of the nearby Samoan intraplate volcanism.

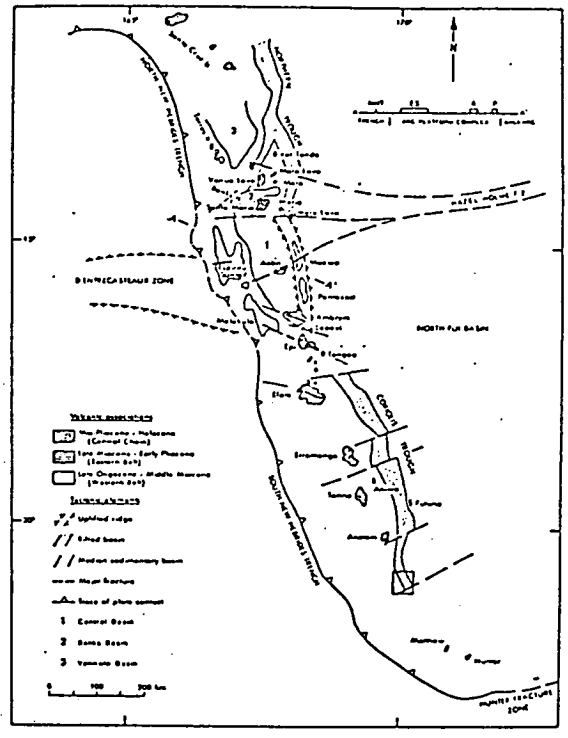

Fig. 4 Localities and major tectonic features of the Vanuatu region, modified from Greene et. al. (1987).

1) TONGAN ARC - VITIAZ FRACTURE ZONE INTERSECTION
(T. J. Falloon)

Dredging of the north Tonga ridge and trench slope in this area has shown that the volcanic basement is dominated by basaltic rocks with the andesitic to dacitic volcanoes of the Tofua magmatic arc (TM-arc) representing a volumetrically minor component to the arc. An important but minor rock type is a fine-grained plagiogranite with extremely depleted heavy rare earth (HREE) element abundances (Falloon et al., 1987a) which has major and trace element abundances indicative of an origin by melting of eclogitic source rock at pressures of ~25kb (i.e. depths of ~80kms) and provides evidence of a component of melting from subducted slab in the island arc setting. However while

etrogenetically important, this magma type lays a minor role compared with the ominance of very magnesian basaltic lavas, any dredged samples of which have ompositions and petrography consistent ith primary magmas derived by partial elting of peridotite (Falloon et al., 987a, b).

Dredged lavas (basaltic andesite) from he mid-trench slope (station 15, Fig. 3) f the Tonga trench have petrographic and eochemical affinities to transitional type T-type) Lau Basin back-arc basalts Hawkins & Melchoir, 1985). The Lau Basin s known to be geochemically zoned with T-ype basalts forming the earlier, western argin and normal- type (N-type) basalts orming the modern central part of the Lau asin (Hawkins & Melchoir, 1985). The astern part of the Lau Basin close to the ctive TM-arc is also considered to be omposed of T-type back-arc basalts, but hese have not been recovered by dredging ue to burial by recent TM-arc volcanism. he recovery of basaltic andesites with T-ype characteristics suggests that early au Basin back-arc crust now forms the rustal basement on which the young TM-arc s built. More primitive basalt ompositions recovered by dredging in the au Basin suggest primary magmas segregate t depths of about 50-60kms during apirism beneath back-arc spreading entres, and are derived from a lherzolite ource peridotite depleted in LIL and LREE lements (i.e. similar to Tinaquillo herzolite compositions).

Dredged rocks from the forearc station 23 Fig. 3) near the termination of he north Tonga ridge, and at the ntersection of the Tonga ridge with the tiaz Fracture Zone (station 21, 24, and , Fig. 3) are characterized by high SiO_2 d MgO contents relative to volcanics of he Tofua magmatic arc. The compositions of hese high-Mg lavas require a mantle eridotite source more depleted in basaltic omponents than either a MORB source mantle represented by MORB pyrolite) or a Lau asin back-arc basalt source mantle represented by Tinaquillo lherzolite) but till of lherzolite character, as indicated the high CaO/Al_2O_3 ratios (0.9-1.1) of he high-Mg lavas and associated glass nclusion compositions in phenocrystal livine. Experimental work (Duncan & Green, 987) on a primitive parental composition the Upper Pillow Lavas of the Troodos hiolite, Cyprus, which is compositionally ry similar to the high-Mg lavas from ations 24 and 25, suggests that such imitive compositions are possible primary gmas at 8kbar pressure at temperatures ~1360°C, in equilibrium with a harzburgite residue under anhydrous conditions. or ~1250-1300°C with water contents of 0.5-1%.

Compositions of glass inclusions trapped in magnesian olivine phenocrysts (Fo_{94}, Falloon & Green, 1986) provide evidence of even more refractory mantle sources. Liquid compositions crystallizing magnesian olivine are characterized by very high CaO/Na_2O ratios (18-29) and provide a ready explanation for the calcic plagioclase phenocryst compositions (>An 90) in Tonga arc lavas. These calcic plagioclase phenocrysts are xenocrystic in magmas with CaO/Na_2O ratios too low for precipitation of such calcic plagioclase. Glasses contain small water contents (~1% approx.) but chromite microphenocrysts are extremely reduced indicating a source containing H_2O-bearing but low fO_2 fluids ($?H_2O + CH_4$ possibly).

The fractional crystallization history of the north Tongan high-Mg lavas is dominated by olivine + orthopyroxene + Cr-spinel as opposed to the plagioclase + clinopyroxene + orthopyroxene ± titanomagnetite control of the young TM-arc volcanics. The more primitive north Tonga high-Mg lavas are not suitable parental magmas to young TM-arc volcanics, as shown by the higher SiO_2 contents of the latter. TM-arc basaltic andesites require parental compositions with <50 wt% SiO_2, suggesting primary magmas segregating from mantle diapirs at pressures > 10kbars. The more evolved TM-arc basaltic andesites are derived from primary magnesian olivine tholeiite and picrite compositions by olivine-dominated fractionation.

The petrography, mineral chemistry and compositions of glass, glass inclusion and wholerock chemistry of the station 23 and 21 high-Mg lavas provide uniquivocal evidence for mixing of relatively evolved and primitive magma batches in a sub-arc magma chamber (Falloon et al., 1987b).

Isotopic (Sr, Nd) and trace element geochemistry of station 24 and 25 high-Mg lavas provide strong evidence for an 'enriched' mantle component similar to that present in ocean island basalts (e.g. Samoa just to the north of the dredged lavas). The geochemistry of the high-Mg lavas from Tonga suggests little involvement of subducted oceanic crust and associated intercalated sediments. However high

LIL/REE element ratios suggest the possible movement of hydrous fluids from the subducted oceanic lithosphere into the overlying mantle peridotite.

2. VANUATU ARC

(M. Barsdell, A.J. Crawford, S.M. Eggins)

Geological Setting: The Vanuatu Arc abuts the western edge of the North Fiji Basin and overlies an easterly dipping subduction zone. The Vanuatu Arc is terminated to the south by the Hunter Fracture Zone, a complex transform fault system which has facilitated the opening of the North Fiji Basin and the clockwise rotation of the basement to the Vanuatu Arc which began about 6-8m.yrs ago (Kroenke 1984). The Vanuatu Arc is composite, with basement rocks, remnants of original Vitiaz Arc, forming the fore-arc (Western Belt) of the modern arc. Vitiaz Arc products also form the basement to the Eastern Belt islands of Pentecost and Maewo. The earliest products of the current ENE subduction are of late Miocene to early Pliocene age and overlie the pre-early Miocene ophiolites and submarine volcanics of the Eastern Belt. The focus of volcanism then apparently shifted westwards during the early Pleistocene age to the currently active Central Chain where submarine volcanism gave way to subaerial effusive volcanism with a dominance of basalts over more evolved products. A data base of 368 published and unpublished analyses of Central Chain volcanic rocks (post-late Pliocene) contains: basalts (<52% SiO_2) = 63%; basaltic andesites (52-56% SiO_2) = 15%; andesites (56-63% SiO_2) = 17.4%; dacites (63-69%) SiO_2) = 4.6%. With one exception, the active volcanoes of the Vanuatu Arc all lie along the axis of the Central Chain. The exception, Merelava volcano, lies at the southern terminus of the northern trough.

Petrology and Geochemistry: The Vitiaz Arc remnants, as exposed on the islands of the Torres Group, Santo and Malekula (Western Belt) and the pre-mid Miocene rocks of Pentecost and Maewo, (Eastern Belt) conform to the classic island arc calc-alkaline and tholeiitic associations. The Western Belt is a calc-alkaline province with a preponderance of submarine basalts intruded by microdiorites and microgabbros, often containing hornblende. Rocks of similar age in the Eastern Belt (and closer to the site of the early Miocene Vitiaz trench) are tholeiitic in character.

The early volcanism associated with the modern Vanuatu Arc is represented by tholeiitic rocks of late Miocene-early Pliocene age on Pentecost and Maewo.

The Central Chain Volcanoes are petrographically diverse, including picrites, ankaramites, olivine and quartz tholeiites, high Al basalts, calc-alkaline andesites and dacites, high K_2O basalts and their differentiates. Little agreement has been reached on the classification of these rocks in terms of volcanic rock series. While most Central Chain basalts show affinities with the tholeiitic series, as demonstrated by pigeonite in the groundmass and marked iron enrichment, andesitic differentiates often show features transitional between tholeiites and calc-alkaline series. Classical calc-alkaline suites such as Merig in the Banks Islands are rare in this arc system.

Lateral Variation in K_2O: Conventionally, island arc volcanism shows increasing K_2O content (at a given SiO_2 content) and K/Na ratio as distance from the trench increases. The reverse pattern is present in the Vanuatu Arc as illustrated by the southern Banks Is. [Gaua (Santa-Maria) to Merelava]. Detailed studies (Barsdell et. al. 1982) show very high K_2O contents and La/Yb ratios particularly in Gaua basalts, and also show that major differences are present between primitive picrites (with 15% MgO and La/Yb ~5.5) from Gaua compared to tholeiitic ankaramite (with 13.5% MgO and La/Yb ~1.2) from Merelava. These systematic variations across the Vanuatu Arc are attributed to variations in K_2O and related incompatible elements in the source region and not primarily to changes in conditions of partial melting (Barsdell et. al. 1982). A second volcanic transect through the arc further south (from Tanna to Futuna) shows little variation in K_2O or La/Yb across the arc and the source region does not appear to have suffered the same extent of precursor incompatible-element enrichment that characterizes the source region for the western (Gaua) part of the Merelava-Gaua section.

Variations along the Central Chain: Volcanoes of the Central Chain show wide variation in K_2O/SiO_2 within single volcanoes but high K_2O basalts occur along the length of the arc, from Gaua to Erromango. On a number of islands, rock series of diverging trends are apparent - a

d to high K_2O differentiates with
easing SiO_2 and decreasing MgO, and a
nd trend maintaining relatively less
as SiO_2 increases through andesite and
te compositions. The latter trend is
ome suites attributable to hornblende
lvement in crystal fractionation, but
ther suites petrographic evidence for
is lacking.

Trace element abundances, including
throughout the Central Chain show
cal 'island arc' characteristics of
ng Nb-depletion and low concentrations
FS elements (Zr,Hf,Ta and Ti) and heavy
High-K_2O basalts are also strongly
ched in LIL elements (Rb,Sr,Ba and
) and have the lowest HREE.

itive Arc Magmas -AOBA
. Eggins)

The large volcanic shield of Aoba
ae) straddles a major fracture, which
sects the Vanuatu Arc in response to
collision of the D'Entrecasteaux zone
the Vanuatu forearc. The voluminous
tions of magnesian basalts on Aoba
ar to have been facilitated by
peded ascent of magma along this
ture from the lithosphere (Ramsay et.
1981).

Two distinct, stratigraphically
rate lava suites are readily identified
he basis of phenocryst mineralogy.
have been derived from lithosphere
profoundly different geochemical
acteristics.

The older suite of lavas is
acterized by the phenocryst assemblage,
esian olivine ($Mg^{\#}$75-89) + magnesian
opyroxene ($Mg^{\#}$80-92) + calcic
ioclase (An 75-94) + titanomagnetite.
e all Aoba lavas belong to the strongly
element enriched, high-K_2O group of arc
ositions, this suite also has
ually high abundances of HFS elements,
sitional to those commonly derived by
ing of more fertile OIB (ocean island
lt) sources.

The younger suite, dominated by
itic and olivine tholeiite
ositions, is composed solely of
esian olivine ($Mg^{\#}$80-93) + magnesian
opyroxene ($Mg^{\#}$80-93) + chrome-spinel
ic lavas. Reconstruction of primitive
id compositions produces a range of
well constrained picritic liquids with up to 18-20wt% MgO ($Mg^{\#}$80). Segregation of these liquids occurred at about 60-70km depth. Whole rock major element compositions, and Cr-spinel with high $Cr^{\#}$ (70-84) encroaching on those of boninites, indicate that this lithosphere has undergone strong depletion through one or more episodes of partial melting. Subsequent lithospheric enrichment event(s) have boosted LREE and LIL element contents to the high levels now manifested in the erupted lavas.

The complex history and diversity of the Aoba source region is further emphasized by the occurrence of a poorly exposed suite of picritic lavas, petrographically indistinguishable from the younger suite, but with twice the LREE and LIL element abundances at equivalent MgO contents.

Petrogenesis: Picritic magmas are present on many islands and provide constraints on primary magma, source composition and residual phases in the upper mantle. Olivine (Fo_{93}), diopside ($Mg^{\#}$=94) and Cr-rich spinel show that the source peridotites were 'refractory' and 'depleted' in terms of major elements (and in HFS and HREE elements). Modelling of the melting processes suggests picritic parental liquids with ~18% MgO (for Gaua) and load pressures at magma separation of 1.5-2.5 GPa. The source rocks for Gaua and Aoba picrites were pre-enriched in K_2O and incompatible elements, including LREE, whereas the source region for Merelava picrites is depleted and refractory in LIL and LREE elements.

We infer that the process of K_2O and LIL enrichment is NOT related to present subduction but rather is a precursor metasomatism, probably by fluids related to earlier, west-dipping subduction beneath the site of the present Central Chain.

3. TASMANTID SEAMOUNTS. (S.M. Eggins)

Basaltic samples have been dredged from five seamounts of the Tasmantid Sea Mount Chain (Vogt et. al. 1971) extending from Gascoyne Seamount in the southern Tasman Sea to Queensland Seamount in the north. The basalts are olivine tholeiitic and transitional to alkali-olivine basalts/hawaiites. Some samples show evidence of moderate pressure (1.5GPa) evolution with the presence of aluminous pyroxene xenocrysts. Although sampling is

very limited, a number of very primitive glassy samples provide excellent evidence for the nature of parental and primitive magmas. Parental magmas are picritic with residual olivine of Mg_{89} composition and liquidus spinels are relativly low in Cr. In sharp contrast to picrites of the Vanuatu Arc or the high-Mg tholeiites of the Tongan Arc, the picrites and olivine basalts of the Tasmantid Sea Mounts, are very rich in TiO_2 and HFS elements - they match extremely closely in chemistry and petrology with the olivine tholeiites, picrites and alkali-olivine basalts etc. of the main cone-building stage of the Hawaiian Volcanoes.

The extremely fractionated REE abundance patterns present in these sea-mount volcanoes are most readily attributable to the role of residual garnet. However, garnet is not a liquidus phase below ~3.5GPa, by which pressure olivine is no longer a liquidus phase for the most primitive liquids of the sea-mounts. The major and trace element studies of the Tasmantid Sea Mount Chain are consistent with rifting of the lithosphere of the northward-moving Australian-Indian plate and diapiric upwelling of enriched lherzolite (Hawaiian pyrolite) composition from the base of the lithosphere or top of the asthenosphere. However these source regions must be enriched prior to this process by migration of a very small melt fraction extracted from underlying garnet lherzolite. The enrichment process is attributed to highly undersaturated C-H-O-bearing melt of olivine-melilitite to olivine nephelinite character. Enrichment in LIL, HFS and LREE in this area differs from the ?fluid-controlled enrichment evident in source regions for the Vanuatu Central Chain in that in the latter case LILE-enrichment exceeds LREE-enrichment and HFS-enrichment does not occur.

CONCLUSIONS

The studies briefly reported herein illustrate the duality of our approach to petrology and geochemistry. Laboratory-based experimental petrology investigations provide important constraints on aspects of magma generation including source, parent and magma fluid compositions, and P/T regimes of melt segregation. In a complementary fashion, land-based and marine geological investigations of the S.W. Pacific provide a natural laboratory in which hypotheses derived from experimental petrology may be tested.

The Southwest Pacific area is remarkable for the diversity of tectonic environments and particularly for the evidence of small scale rifts (back arc basins) forming very close to active arc-volcanism centres. Oceanic trench/volcanic arcs are also cut by fractures of both strike-slip and tensional character. This tectonic complexity is such that it is very much an open question whether source rocks and depths of magma segregation lie above, within or even beneath the subducted slab, i.e. within the mantle/crust wedge above the Benioff Zone, within the subducted crust and lithosphere immediately below the Benioff Zone or even within the asthenosphere below the subducted lithosphere.

The petrological and geochemical studies reported briefly in this paper confirm the dominance of olivine-rich basaltic magmas within the S.W. Pacific convergent margin complex and thus confirm the dominance of peridotitic source rocks. The studies show that these source rocks characteristically have a depleted major element chemical composition in comparison with source rocks for mid-ocean ridge or intra-plate basalts. Superimposed on these source characteristics is evidence for enrichment processes, probably effected by C-H-O (S,Cl) fluid migration and transport and particularly enriching mantle regions in LIL elements and LREE. Melting, diapirism and magma segregation occur at different depths in different tectonic environments and much remains to be learnt in this area. There is clear evidence for multistage melting and for the role of C-H-O fluid in fluxing melting of refractory residual peridotite, but even the most water-rich primary magmas (boninites) requiring the most refractory source rocks wre formed at temperatures of 1200-1250°C with low water contents (2-3%).

Our studies have demonstrated primary magmas ranging from olivine-rich picrites to high-magnesia quartz tholeiites and boninites and have demonstrated that the thermal envelope for magma generation in the S.W. Pacific convergent margin region has a high temperature band passing through ~20kb, 1400°C and ~8kb 1250°C.

REFERENCES

BARSDELL, M., SMITH, I.E.M. and SPORLI, K.B. 1982. The origin of reversed geochemical zoning in the northern New Hebrides Volcanic Arc. Contrib. Mineral. Petrol. 81, 148-155.

, S.W. 1958. A tectonic approach to continental drift. Symp. Continental Drift. Hobart, 177-355.

, P. 1978. Cosmos, Earth and Man. 172 pp. Yale University Press.

T, J.Y., DANIEL, J. and BURNE, R.V. 1985. Recent tectonics associated with the subduction/collision of the d'Entrecasteaux zone in the central New Hebrides. Tectonophysics, v.112, p.325-356.

N, R.A. and GREEN, D.H., 1987. The genesis of refractory melts in the formation of oceanic crust. Contrib. Mineral. Petrol. (in press)

ON, T.J., GREEN, D.H. and CRAWFORD, A.J. 1987a. Dredged igneous rocks from the northern termination of the Tofua magmatic arc, Tonga and adjacent Lau Basin. Australian Journal of Earth Sciences (in press).

ON, T.J., McCULLOCH, M.T., GREEN, D.H. 1987b. The petrogenesis of high-mg lavas and associated island arc tholeiites from north Tonga. In Boninites and related rocks. Crawford, A.J. (ed.) (submitted).

, S.F. 1987. The genesis of lamproitic magmas in a reduced, flourine-rich mantle. Proc. 4th Int. Kimberlite Conf., Geol. Soc. Aust. Special Publ.

F.A. and GREEN, D.H. 1974. The mineralogy, geochemistry and origin of lherzolite inclusions in Victorian basanites. Geochim. Cosmochim. Acta, 38, 1023-1059.

D.H. 1973. Experimental melting studies on a model upper mantle composition at high pressure under water-saturated and water-undersaturated conditions. Earth Planet. Sci. Letters, 19, 37-53.

, D.H., TAYLOR, W.R. and FOLEY, S.F. 1986 The Earth's upper mantle as a source of volatiles. Geol. Soc. Aust. Special Publ., 13, (in press).

, D.H., FALLOON, T.J. and TAYLOR, W.R. 1987. Mantle derived magmas - role of variable source peridotite and variable C-H-O fluid compositions. In: Mysen, B.O. (ed.). Magmatic Processes : Physiochemical Principles. The Geochemical Society Spec. Publ. 1, 139-154.

GREEN, D.H. 1987. The Earth's lithosphere and asthenosphere - concepts and constraints derived from petrology and high pressure experiments. (in prep.).

GREENE, H.G., MACFARLANE, A., FISHER, M.A., JOHNSON, D. and CRAWFORD, A.J. 1987. Structure and tectonics of the New Hebrides arc. In: Greene, H.G. and Wong, F. (Eds.), Geology and Off-shore Resources of Pacific Island Arcs - Vanuatu Region. Circum-Pacific Council for Energy and Mineral Resources, Earth Science Series (in press).

GOLD, T. and SOTER, S. 1982. Abiogenic methane and the origin of petroleum. Energy Explor. Exploit., 1, 89-104.

HAWKINS, J.W. and MELCHOIR, J.T. 1985. Petrology of Mariana Trough and Lau Basin basalts. J. Geophys. Res. 90, 11431-11468.

JAQUES, A.L. and GREEN, D.H. 1980. Anhydrous melting of peridotite at 0-15kbar pressure and the genesis of tholeiitic basalts. Contrib. Mineral. Petrol. 1973, 705-720.

KROENKE, L.W. 1984. Cenozoic tectonic development of the southwest Pacific. U.N. ESCAP, CCOP/SOPAC Tech. Bull. 6.

O'REILLY, S.Y. and GRIFFIN, W.L. 1987. Mantle metasomatism beneath Western Victoria, Australia (submitted to Geochim. Cosmochim. Acta.).

RAMSAY, W.R.H., CRAWFORD, A.J., FODEN, J.D. 1984. Field setting, mineralogy, chemistry and genesis of arc picrites, New Georgia, Solomon Islands. Contrib. Miner. Petrol. 88, 386-402.

RYABCHIKOV, I.D., GREEN, D.H., WALL, V.J. and BREY, G.P. 1981. The oxidation state of carbon in the reduced-velocity zone. Geochem. Int. 18, 148-158.

TAYLOR, W.R. and GREEN, D.H. 1987. The role of reduced C-O-H fluids and mantle melting. Proc. 4th Int. Kimberlite Conf., Geol. Soc. Aust. Spec. Publ.

TAYLOR, W.R. 1987. A reappraisal of the nature of fluids included by diamond - a window to deep-seated mantle fluids and redox conditions. Geol. Soc. Aust. Special Publ., 13, (in press).

VOGT, P.R. and CONNOLLY, J.R. 1971. Tasmantid Guyots, the age of the Tasman Basin, and motion between the Australia plate and the mantle. Bull. Geol. Soc. Am. 82, 2577-2584.

WYLLIE, P.J. 1987. Transfer of subcratonic carbon into kimberlites and rare earth carbonatites. In: Mysen, B.O. (ed.) Magmatic Processes : Physiochemical Principles. The Geochemical Society Spec. Publ. 1, 107-120.

B41

Australian Journal of Earth Sciences (1987) 34, 487–506

Dredged igneous rocks from the northern termination of the Tofua magmatic arc, Tonga and adjacent Lau Basin

T. J. Falloon, D. H. Green and A. J. Crawford

Department of Geology, University of Tasmania, Hobart, Tas. 7001, Australia.

Fresh igneous rocks were dredged from six stations during the 1984 cruise of the *Natsushima* to the North Tonga Ridge and Lau Basin. Samples were recovered from inner trench wall, forearc, arc ridge and backarc basin settings in water depths > 2000 m. The volcanics are unlike those of the subaerial volcanoes of the Tofua magmatic arc, and provide a glimpse of the petrological diversity present in the submarine levels of this intra-oceanic arc-backarc system. Amongst the dredged lavas are unusual olivine- and pyroxene-bearing vitrophyres with high-MgO (13–20 wt%) and SiO_2 (52–56 wt%) contents. These primitive lavas are distinct petrographically and geochemically from boninites in their high CaO/Al_2O_3 ratios (0.7–0.9), high-CaO (> 7 wt%) contents, and the presence of abundant olivine phenocrysts, but are similar to low-Ti ophiolitic basalts such as those of the Upper Pillow Lavas of the Troodos ophiolite, Cyprus. The dredged Tongan high-Mg lavas are therefore an *in situ* occurrence of a low-Ti ophiolitic lava suite, and support an intra-oceanic island arc origin for the Troodos and other ophiolites with these lavas.

Key words: boninite, Fiji, high-Mg lavas, Lau Basin, Lau–Colville Ridge, low-Ti lavas, ophiolites, Tofua magmatic arc, Tonga, Troodos.

INTRODUCTION

During the cruise of the *Natsushima* to the North Tonga Ridge and Lau Basin in 1984, igneous rocks were recovered from seven dredge stations (Falloon 1985). Samples were taken from six different morphotectonic elements of the intra-oceanic arc and from one station in the backarc basin. In this paper, petrographic, wholerock major and trace element data are presented and the geochemical affinities of the dredged rocks are discussed. A more detailed treatment of the petrogenetic implications of this data will be presented elsewhere (T. J. Falloon unpubl. data).

Analysis of the petrogenesis of Tongan arc lavas has been limited to the study of axial chain volcanoes of the Tofua magmatic arc (Ewart & Bryan 1972; Ewart *et al* 1973; Ewart 1976; Ewart *et al* 1977). These volcanoes are constructional features of relatively minor scale in terms of the volume of the Tongan arc. As passage of magmas from the mantle through arc crust to eruption provides ample opportunity for extensive fractionation and mixing of parental and evolved magmas, it is likely that the compositions of lavas erupted from the volcanoes will not be representative of the arc crust as a whole. This possibility emphasizes the importance of the dredged samples. As they were all dredged from water depths generally > 2000 m, they offer an insight into the nature of arc magmatism away from axial chain volcanoes, a topic about which little information exists at present.

The igneous rocks recovered from each dredge station are geochemically distinct from the rocks of the Tonga Is, as well as from each other, indicating considerable geochemical complexity in the Tonga arc. Dredge stations on the North Tonga Ridge and forearc were from a relatively restricted geographical area. Within this area, a range of mantle sources and possibly a range of partial melting conditions are required to explain the geochemistry of the dredged rocks. Amongst the dredged rocks are highly magnesian lavas with affinities to both boninites and low-Ti ophiolitic basalts. The presence of these high-Mg lavas has important implications for the petrogenesis of these distinctive rocks.

GEOLOGICAL AND TECTONIC SETTING

The Tonga Ridge, Trench and Forearc together with the Lau backarc basin and remnant arc (the Lau–Colville Ridge) form an intra-oceanic island

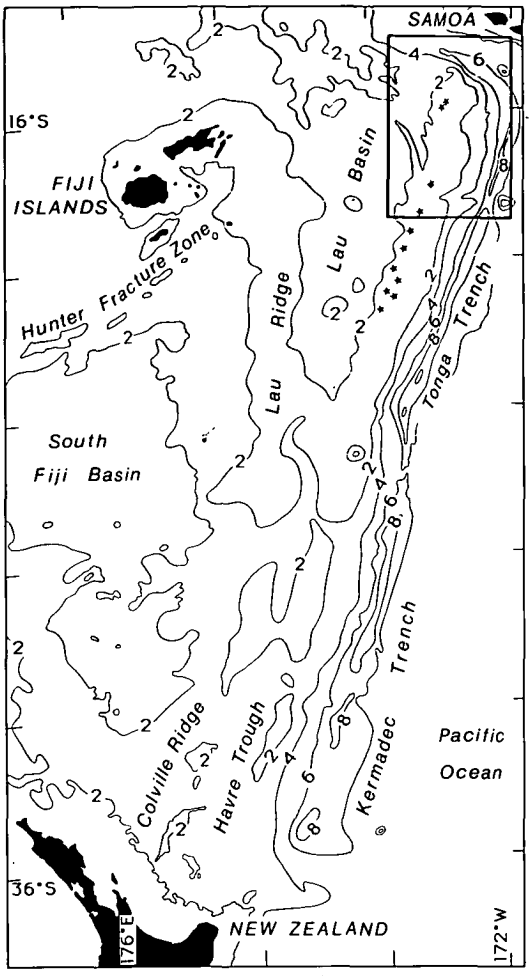

Fig. 1 Locality map of the southwest Pacific, showing the relationship of the Tonga Ridge and Trench to other elements of the southwest Pacific region. Stars represent islands of the young TM-arc. Square outline is the area covered by Fig. 2. Water depth contoured in thousands of metres.

arc system (Fig. 1). The Tonga Ridge itself is morphologically complex, in its southern part consisting of two island chains separated by the 1800 m deep Tofua trough. The eastern chain of islands, the 'Vavua-Eua' block, is covered by limestone and with the exception of Eua lacks exposed volcanic rock. The 'Vavua-Eua' block represents an older Eocene to mid-Miocene forearc, formerly joined to the once active Lau–Colville Ridge (Gill 1976; Gill *et al* 1984; Hawkins *et al* 1984; Duncan *et al* 1985; Hawkins & Falvey 1985); it has since been separated by the opening of the Lau Basin. The western chain o islands is Plio–Pleistocene in age and comprises the presently active island arc, the 'Tofua magmatic arc' (TM-arc). This active chain o volcanic islands extends as far north as the islands of Tafahi and Nuiatoputapu; eruptive products range (in SiO_2 content) from basaltic andesite to dacite, with basaltic andesite being dominant (Ewart *et al* 1973, 1977). The most recent volcanic activity was the 1968 Metis Shoal eruption (Melson *et al* 1970). The TM-arc north of the islands of the Tonga ridge is truncated by a graben subparallel to the bend of the Tonga Trench, where there is a transition from subduction to transform tectonics (Giardini & Woodhouse 1986). The North Tonga Ridge is morphologically distinct from the South Tonga Ridge, as the 'Vavua-Eua' block is no longer present; instead, the North Tonga Ridge has a deeply submerged, gently dipping forearc.

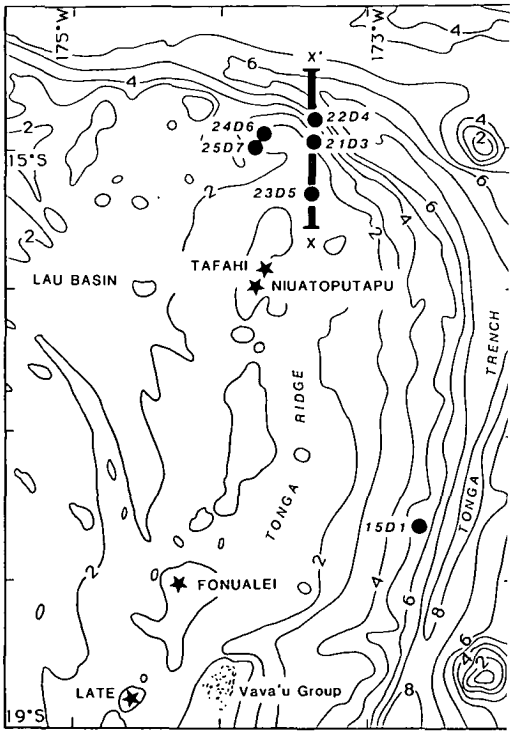

Fig. 2 Locality map of the North Tonga Ridge showing the location of the dredge stations which yielded igneous rock. Station 31, not shown on this map, is located at the southeastern end of the Pegg Ridge in the adjacent Lau Basin. X–X′ is the line of the seismic profile given in Fig. 3.

Table 1 Dredge locations yielding igneous material during the 1984 cruise of the *Natsushima*.

Dredge	Station	Latitude °S	Longitude °W	Water depth (m)	Area	Recovery
1	15	17°37.7′	172°41.5′	4325–4860	Trench wall	Small basalt clasts, volcanogenic conglomerates, volcaniclastics
3	21	14°57.9′	173°23.4′	1500–2000	Transform–Trench wall	Large haul of basaltic rock, volcaniclastics
4	22	14°49.0′	173°23.0′	4400–4500	Transform–Trench wall	Metagabbros, plagiogranite, serpentinite, volcaniclastics
5	23	15°19.6′	173°23.9′	1600–2250	Forearc	Blocks of vesicular basalts, volcaniclastics
6	24	14°53.5′	173°43.8′	3090–3260	North Tonga Ridge	Two large pieces of vesicular pillow basalt, volcaniclastics
7	25	14°59.6′	173°45.6′	2728–2805	North Tonga Ridge	Large haul fresh pillow lavas
11	31	17°21.2′	176°46.7′	2220–2230	Southeast Peggy Ridge, Lau Basin	Volcaniclastics, pumice, one small piece of pillow rind

DREDGE LOCATIONS

Dredge stations which recovered igneous material are shown in Fig. 2 and details are given in Table 1. Station 15, which sampled acoustic basement outcropping on the upper trench slope, yielded several kilograms of small fragments of volcanic and subvolcanic rocks present as clasts in a canyon-fill, debris-flow type deposit of Late Miocene to Early Pliocene age (Honza *et al* 1985). The main clast type is a clinopyroxene + plagioclase-phyric basaltic andesite; dolerite and gabbro clasts with the same mineralogy as the basaltic andesite are also present. The igneous rocks represent an earlier volcanic episode than the young Tofua magmatic arc.

Stations 21 and 22 are on a large isolated block (Fig. 3), separated from the North Tonga Ridge by a major graben. Station 21 provided a large amount of fresh porphyritic and aphyric basaltic

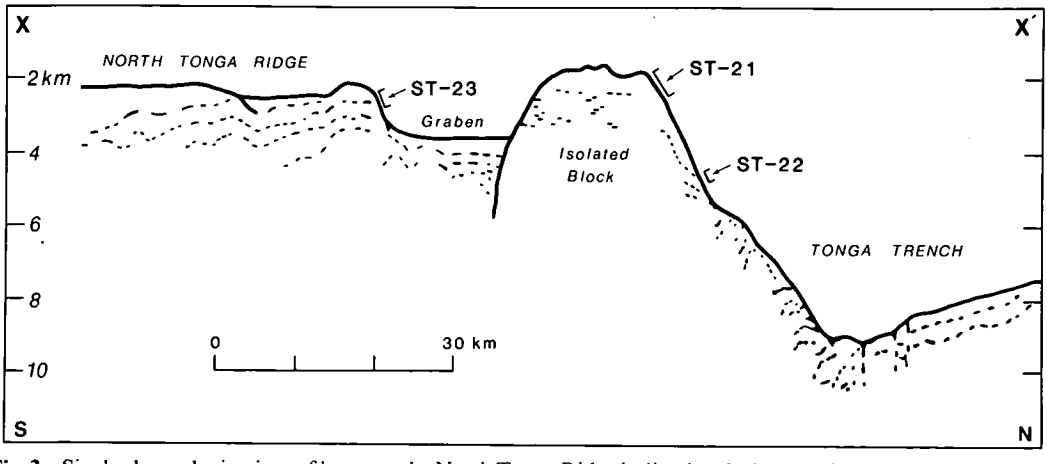

Fig. 3 Single channel seismic profile across the North Tonga Ridge indicating the large graben and isolated block at the termination of the North Tonga Ridge, and positions of dredge stations 21, 22 and 23. Seismic profile from Kitekei'aho *et al* (1985).

andesite and andesite, while large blocks of fresh and altered plutonic rocks (metagabbro and plagiogranite), altered basalt and serpentinite were recovered from station 22.

Station 23, on the southern scarp of the graben (Fig. 3), yielded one large block and several smaller pieces of basaltic andesite and andesite, along with small clasts of highly vesicular olivine + orthopyroxene + clinopyroxene-phyric lava.

Stations 24 and 25 are on knolls aligned subparallel to the curved northern part of the Tonga Trench. Preliminary acoustic profiles show horsts and grabens with normal faults in this area (Honza *et al* 1985). Large amounts of highly vesicular, fresh pillow basalt fragments with fresh glassy rinds were recovered from these stations.

Station 31, located at the southeastern end of the Peggy Ridge in the Lau Basin, in an area sampled extensively by previous dredging (Hawkins 1976), gave rise to one small piece of pillow rind.

Stations 21, 22, 24 and 25 are in an area sampled extensively by the Russian vessel *R/V Kallisto* (Sharaskin *et al* 1983), which dredged mainly in deep water, recovering proportionately larger quantities of altered ultramafic and mafic plutonic material; 'boninite' was reported near stations 24 and 25. Stations 24 and 25 were chosen to confirm the Russian sampling.

ANALYTICAL TECHNIQUES

Major and trace element geochemistry, including REE, of representative samples from each dredge station are presented in Tables 3, 4 and 5. Major element geochemistry was determined by X-ray fluorescence spectrometry (XRF) using the method of Norrish and Hutton (1969). Barium, Rb, Sr, Zr, Nb, Y, Sc, Ni, Cr and V were determined on pressed powdered discs by XRF. REE were also determined by XRF using the method of Robinson *et al* (1986).

Because each dredge station has its own distinctive petrographic and geochemical characteristics, the geochemical affinities of each dredge station will be presented separately. Before the dredge stations are discussed, it is worthwhile outlining briefly the known geochemistry of the TM-arc, because it will serve as a reference point in the discussion of the geochemical affinities of the dredged rocks.

TOFUA MAGMATIC ARC

The TM-arc, defined by the exposed Tongan volcanic islands, and dominated by basaltic andesites, with minor andesites and dacites (Ewart *et al* 1973, 1977), can be subdivided conveniently into two parts on geographic and geochemical criteria. The first part is defined by the volcanic islands of South Tonga which includes the basaltic andesites, andesites and dacites of Fonualei, Late, Hunga Ha'apai and Tofua. The basaltic andesites, which represent the least evolved compositions from the islands, have SiO_2 contents of between 53 and 55 wt% (Ewart *et al* 1973) and form a well defined tholeiitic Fe-enrichment trend on the FeOt/MgO vs SiO_2 diagram (Fig. 4). The basaltic andesites

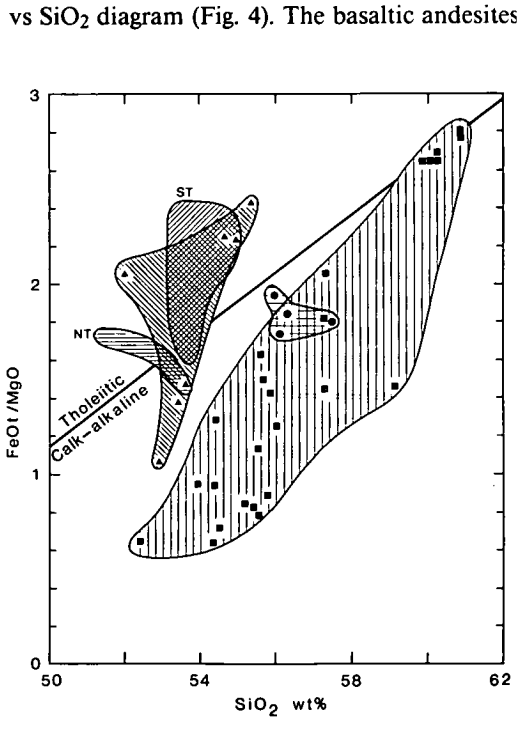

Fig. 4 FeOt/MgO vs SiO_2 relationships of basaltic andesites and andesites from stations 15, 21 and 23 compared with those of the TM-arc. The line is the dividing line between tholeiitic and calc-alkaline suites of Miyashiro (1974). NT and ST are North Tonga and South Tonga, respectively, the two main groups within the TM-arc.
(■) Station 21 basaltic andesites and andesites; data taken from Table 3 and Falloon (unpubl. data).
(●) Station 23 basaltic andesites; data from Table 5.
(▲) Station 15 basaltic andesites; data from Table 3.
Data for North Tonga and South Tonga taken from Ewart *et al* (1973) and Ewart (1976).

Table 2 Petrographic summary of dredged lavas from North Tonga.

Station no.	Group	Phenocrysts and microphenocrysts	Groundmass	Comments
15		plag + cpx	Glass (devitrified), plag + cpx microlites, timg, chlorite and smectite. Hyalopilitic to hyalo-ophitic	Strong resorption in plag mph cores, patchy zoning in cpx mph. Some lavas show more coarse grained subophitic textures
21	I	opx + oliv + (cpx) + (cr-sp)	Fresh glass, plag + cpx microlites minor timg	Six types of glomerocrysts in these lavas: (1) opx, (2) opx + cpx, (3) opx + oliv, (4) opx + cpx + oliv, (5) cpx + opx + plag, (6) plag oliv, opx and plag have euhedral to strongly resorbed grain boundaries.
	II	opx + cpx + oliv	Coarse grained sub-ophitic, minor chlorite and smectite	
		opx + cpx + (oliv) + (plag)	Fresh glass, plag + cpx microlites, minor timg	
	III	opx + plag + cpx + (oliv)	As above	Lavas range from strongly vesicular to non-vesicular
		opx + plag + cpx + oliv + (cr-sp) + (timg)	Fresh glass acicular pyx microlites	
	IV	plag + opx + cpx	Fresh glass plag + cpx microlites, minor timg	
	V	Aphyric	As above	
23	BA	plag + opx + cpx + (oliv)	Fresh glass plag + cpx microlites, minor timg	Similar to station 21 lavas, oliv strongly resorbed
	A	opx + oliv + (cr-sp)	Fresh glass, quench pyroxenes, minor cr-cp euhedra	opx + oliv subhedral, euhedral to strongly resorbed; opx glomerocrysts common
	B	opx + oliv + (cr-sp) + (cpx)	As above	
24		oliv + opx + cr-sp	As above	Many olivine mph have skeletal morphologies
25		oliv + cr-sp	As above	

Phenocrysts and microphenocrysts are listed in order of modal abundance; parentheses indicate trace abundances (<1%). plag = plagioclase, oliv = olivine, opx = orthopyroxene, cpx = clinopyroxene, cr-sp = chromian spinel, timg = titanomagnetite, mph = microphenocryst, ba = basaltic andesite, pyx = pyroxenes.

have high abundances of large ion lithophile (LIL) elements relative to the heavy Rare Earth elements (HREE); REE abundances are low, and chondrite-normalized REE patterns are flat to slightly light Rare Earth element (LREE)-depleted; a representative pattern from Late (sample L1) is shown in Fig. 5d. The second group is defined by the basaltic andesites from the Northern Tongan island of Tafahi and a single andesite from Niuatoputapu (Ewart 1976). The basaltic andesites from Tafahi are distinctly different from those of the South Tonga islands, having slightly lower SiO_2 (51–54 wt%) and TiO_2 (0.36–0.41 wt% compared with 0.49–0.64 wt%) contents, and lower incompatible element abundances. The REE patterns are similar to basaltic andesites from the South Tonga islands, but REE abundances are lower (sample T-116 in Fig. 5d). One distinguishing characteristic of the Tafahi basaltic andesites is their low Zr content (8 parts/10^6; Ewart 1976), reflected in high Ti/Zr ratios compared with those from the South Tonga islands (269–307 cf. 119–144). Such high ratios are characteristic of very depleted (depleted in the abundance of silicate incompatible elements relative to a chondritic mantle model; Gast 1968) sources (Sun & Nesbitt 1978). The low REE and other incompatible abundances, and the lower TiO_2 contents compared with those of the South Tonga islands, are consistent with the basaltic andesites of the North Tonga islands having been derived from a mantle source more depleted in silicate incompatible elements than the basaltic andesites of the South Tonga islands.

In the following sections the petrography, geochemistry and geochemical affinities of the dredged samples are presented. Important petrographic features of the dredged lavas are summarized in Table 2.

STATION 15

Petrography

Lava clasts from station 15 are microphyric basaltic andesites containing plagioclase (~5%) and clinopyroxene (~1–2%) as single euhedral microphenocrysts as well as microglomerocrysts. The clasts display a range of groundmass textures reflecting a range of cooling rates. Some clasts come from the glassy selvages of pillows, where the groundmass consists mainly of brown devitrified glass with sparse plagioclase microlites. Others display more coarse grained subophitic textures. Alteration in coarser grained samples is confined to interstices where chlorite and yellow-green smectite replace original glass.

A single clast of metagabbro, too small for analysis, also from station 15, consists of approximately equal proportions of coarse grained plagioclase and amphibole. The amphibole (actinolite + hornblende) replaces original clinopyroxene. Plagioclase shows signs of saussuritization. Minor anhedral titanomagnetite occurs between plagioclase and amphibole.

Geochemistry and geochemical affinities

Analysed clasts from station 15 (Table 3) are all basaltic andesites of relatively uniform compositions. SiO_2 contents vary from 52 to 55 wt%, while MG# (100 Mg/(Mg + Fet), Fet (total iron as FeO) varies from 59 to 45 wt%. In terms of the FeOt/MgO vs SiO_2 relationships, station 15 basaltic andesites show a tholeiitic trend, overlapping with and extending the TM-arc compositional trend (Fig. 4). However, they differ from the TM-arc basaltic andesites being characterized by relatively high TiO_2 (>1.0 wt%) and Na_2O contents (>2.6 wt%), resulting in lower CaO/TiO_2, Al_2O_3/TiO_2 and CaO/Na_2O ratios, lower Ba (<29 parts/10^6), Sr (130–158 parts/10^6) and REE contents, and higher Zr (57–94 parts/10^6) and Y (22–45 parts/10^6) contents. REE patterns (Fig. 5a) are LREE-depleted with $(La/Yb)_N = 0.47–0.81$; TM-arc basaltic andesites have flat to slightly depleted REE patterns (Ewart *et al* 1973, 1977).

Basaltic andesites from station 15 are of particular significance because they come from the basement sequence underlying the TM-arc, as recognized on single channel seismic profiles (Honza *et al* 1985). Sediment adhering to the clasts gives a preliminary age of mid-Miocene to Early Pliocene (10–3.5 Ma) based on microfossil content (Honza *et al* 1985), providing a minimum age for the lavas. Using this age as a guide, there are four potential sources, of similar or older age, from which the basaltic andesites of station 15 could have been derived; these are discussed separately below.

'Eua–Vavua' block basement sequence

Volcanic rocks of the 'Eua–Vavua' basement sequence are exposed on the island of Eua (Ewart

Table 3 Major, trace and REE geochemistry of basaltic andesites from Station 15.

Sample no.	1-30	1-31	1-33	1-34	1-38	1-39	1-35	123 103-1	ANT 225-1
SiO_2	54.81	55.35	54.59	53.56	53.43	51.49	52.96	53.62	54.10
TiO_2	1.28	1.32	1.25	1.08	0.96	1.46	1.01	1.77	1.06
Al_2O_3	16.03	16.07	16.22	17.11	16.90	15.81	17.37	15.59	14.69
FeOt	10.24	10.10	10.36	8.08	8.47	11.59	8.15	9.60	11.66
MnO	0.19	0.18	0.18	0.16	0.16	0.19	0.15	0.19	0.21
MgO	4.58	4.18	4.64	5.58	6.08	5.65	7.77	4.79	5.32
CaO	9.19	8.79	9.13	10.51	10.84	8.85	9.00	9.49	10.32
Na_2O	2.99	3.02	2.96	3.12	2.58	3.38	3.20	3.39	2.36
K_2O	0.61	0.87	0.58	0.68	0.48	0.49	0.29	0.51	0.11
P_2O_5	0.09	0.11	0.10	0.12	0.10	0.65	0.11	0.51	0.11
LOI	1.54	2.52	1.85	2.08	1.15	2.60	2.59	—	—
MG#	44.37	42.44	44.36	55.17	56.12	46.49	62.94	47.06	44.84
Ba	28	29	24	26	29	16	29		
Rb	9	13	9	10	9	10	4		
Sr	130	131	133	158	132	156	136		
Zr	74	78	76	87	59	94	57		
Nb	<1	<1	1	1	1	<1	<1		
Y	30	31	30	32	29	45	22		
Sc	39	33	39	34	40	32	39		
V	349	357	349	244	259	267	257		
Ni	23	20	25	39	52	18	109		
Cr	46	33	43	131	204	27	234		
La					2.84	4.73	1.98		
Ce					9.23	12.41	7.22		
Pr					1.56	2.19	1.44		
Nd					8.40	12.24	7.34		
Sm					2.84	3.85	2.57		
Eu					1.11	1.53	0.96		
Gd					4.04	5.50	3.37		
Dy					5.03	6.68	3.71		
Er					3.28	4.35	2.25		
Yb					3.20	3.86	2.06		

Samples 123, 103-1 and ANT 225-1 are examples of T-type LBB from Hawkins and Melchoir (1985). Major element geochemistry summed to 100% volatile free, FeOt = total iron as FeO, LOI = Loss on ignition. Major elements are in wt%, trace elements are in parts per million.

& Bryan 1972; Ewart *et al* 1977; Duncan *et al* 1985; Hawkins & Falvey 1985). Radiometric dating has identified three periods of volcanism (Duncan *et al* 1985), namely Late to mid-Eocene (40–41 Ma), Late Oligocene (31–33 Ma) and Early Miocene (17–19 Ma). The mid-Eocene phase of volcanism has been correlated with other Eocene basement sequences in the South-west Pacific, all associated with the ancient 'Vitiaz' arc (Gill 1976, 1984; Gill *et al* 1984). The geochemical data on Eua are limited and lavas have been altered to varying degrees (Ewart & Bryan 1972), making it difficult to characterize lava compositions. Despite these difficulties, there are significant geochemical differences between the Eocene phase of volcanism and basaltic andesites from station 15. Compared with the Eua lavas, those from station 15 have lower Ba, and higher contents of Zr, Y, Ni, Cr and TiO_2. The one published REE analysis from Eocene volcanics, sample E7 (Ewart & Bryan 1972), is LREE-depleted, similar to station 15 REE patterns. The character of Early Oligocene volcanics is poorly constrained but is similar to

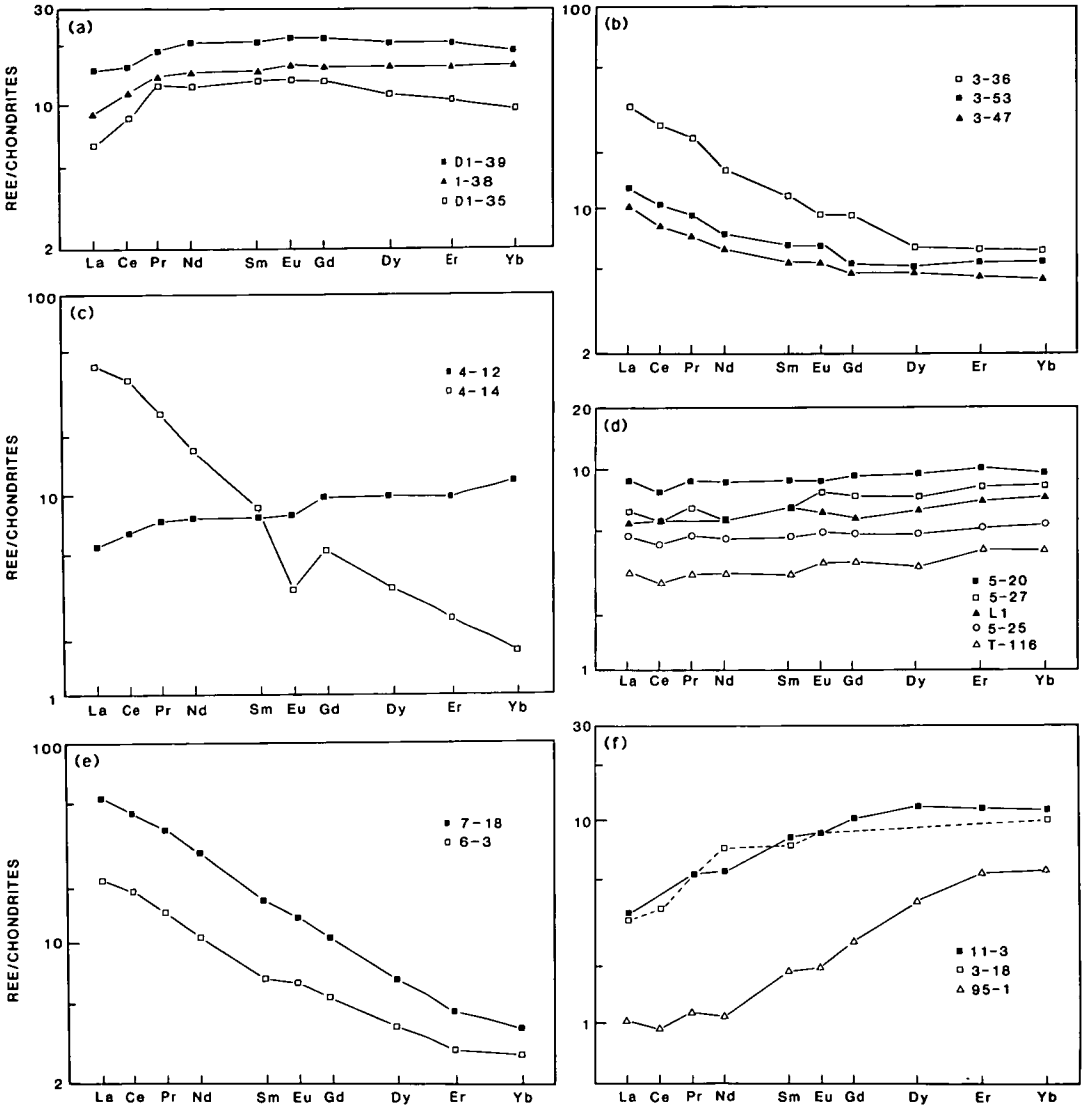

Fig. 5 REE patterns for dredged igneous rocks from the 1984 *Natsushima* cruise. **Fig. 5a** Station 15 basaltic andesites. **Fig. 5b** Station 21 basaltic andesites and one andesite (3-36). **Fig. 5c** Station 22: 4-12 is a metagabbro, 4-14 a plagiogranite. **Fig. 5d** Station 23, and representative patterns from the TM-arc; sample L1 is from South Tonga and sample T-116 from NorthTonga (Ewart *et al* 1977). Samples 5-20 and 5-27 are basaltic andesites; sample 5-25 is a Group B high-Mg lava (Table 2). **Fig. 5e** High-Mg lavas from stations 24 (6-3) and 25 (7-18). **Fig. 5f** REE pattern of glass rind 11-3 from station 31 compared with a primitive MORB glass DSDP3-18-7-1 (Frey *et al* 1974) and a Lau Basin basalt 95-1 (Hawkins 1976; Gill 1976).

the older Eocene volcanics (Hawkins & Fâlvey 1985). The Early Miocene phase of magmatism is represented by dykes, intruding the older volcanic sequence, which range in composition from basaltic andesite to andesite, and are also distinct geochemically from station 15 basaltic andesites.

Remnant arc, the Lau–Colville Ridge

The Lau–Colville Ridge was part of the former volcanic arc before the opening and spreading of the Lau Basin in latest Miocene or Early Pliocene times. The oldest exposed rocks on the Lau–Colville Ridge (Gill 1976), the Lau Volcanics (6.4–9.0 Ma), are calc-alkaline, have a lower FeOt and no Fe-enrichment trend, and higher Ba, Sr, K, Rb and REE than station 15 lavas (Gill 1976); they are also LREE-enriched and have lower Ti/Zr ratios. It is highly unlikely that the station 15 tholeiites were formed during Lau–Colville Ridge volcanism.

Fiji

Basement rocks comprising the Wainimala and Savura Groups on Viti Levu are potential sources for the basaltic andesites of station 15, as Fiji would have been in the vicinity of the present day North Tonga Ridge prior to the opening of the Lau Basin. The basement rocks of Fiji range in age from 33 to 10 Ma and are composed primarily of an island arc tholeiite suite ranging from basalt to rhyolite in composition, which has suffered metamorphism to zeolite or lower greenschist assemblages (Gill 1984).

The Wainimala Group (Gill 1970) displays a wide range in trace and minor element composition compared with the restricted range in composition present in the station 15 rocks. Important differences between the two suites are the higher abundances of Ba (50–124 cf. 16–29 parts/10^6 in station 15 lavas) and the presence of significant LREE enrichment in some of the Wainimala lavas ($[La/Yb]_N = 0.59–2.33$). All station 15 lavas analysed for REE are LREE-depleted. Similarly, the Savura Group differs from station 15 lavas in having higher Ba, Sr and lower Zr contents.

The Namosi Andesites, calc-alkaline lavas 6 Ma old, could be a potential source for station 15 clasts on the basis of age. They are excluded because of their calc-alkaline character, high Ba, Rb, Sr and K_2O contents, and low TiO_2 and LREE-enriched REE patterns (Gill 1970), similar to those of the Lau volcanics.

Early Lau Basin back-arc volcanism

A fourth possibility for the origin of the station 15 basaltic andesites, is that they were erupted during the early stages of development of the Lau back arc basin. The oldest fauna (3.1–3.4 Ma) found in the Lau Basin is in the base of DSDP hole 203. However, the opening of the Lau Basin probably began in the latest Miocene or Early Pliocene (Hawkins *et al.* 1984), meaning that the Lau Basin began to form before the onset of volcanism of the present TM-arc. The TM-arc therefore may have been constructed on early formed Lau Basin backarc crust. Support for this hypothesis is found in the similarity in chondrite-normalized element abundance patterns between the Lau Basin basalt from station 31 and station 15 basaltic andesites (Fig. 6a). The Lau Basin sample 11-3 from station 31 and the station 15 basaltic andesites have similar abundances of incompatible elements and have LREE-depleted REE patterns. In particular, the station 15 basaltic andesites have low Ba/La (1.06–4.62) and Sr/Zr ratios (1.66–2.4), atypical of arc-related volcanics but similar to Lau Basin basalts.

Despite these similarities in trace element signature, station 15 lavas are unlike typical Lau Basin basalts, such as sample 11-3, because they are high in SiO_2 (51–55 wt%), whereas Lau Basin basalts have MORB-like major element chemistry with $SiO_2 < 50$ wt%, and high Al_2O_3 and CaO contents (up to 14 wt%). The recognition of zonation in crustal composition of the Lau Basin by Hawkins and Melchior (1985) is therefore significant. Volcanics from the central part of the basin are N-MORB type basalts; these are flanked by belts of basalt similar to Mariana Trough basalts, designated normal (N)-type Lau Basin Basalt (LBB) and transitional (T)-type LBB, respectively, by Hawkins and Melchior (1985). The zonation is well defined on the western side but is obscure in the eastern side because it is probably buried by the younger TM-arc. In terms of major element chemistry, station 15 basaltic andesites are similar to the T-type LBB from the western margin of the Lau Basin, which have similar SiO_2 (51–54 wt%), TiO_2 (1.06–1.77) and K_2O (0.17–1.02) contents (Table 3). It is suggested that the early stages of development of the Lau Basin involved shallower depths of melt segregation or higher contents of H_2O at higher pressure, producing more silica-saturated parental liquids than magmas parental to lavas currently supplied to the spreading zones. The trace element signature of the mantle source has remained constant despite variations in the

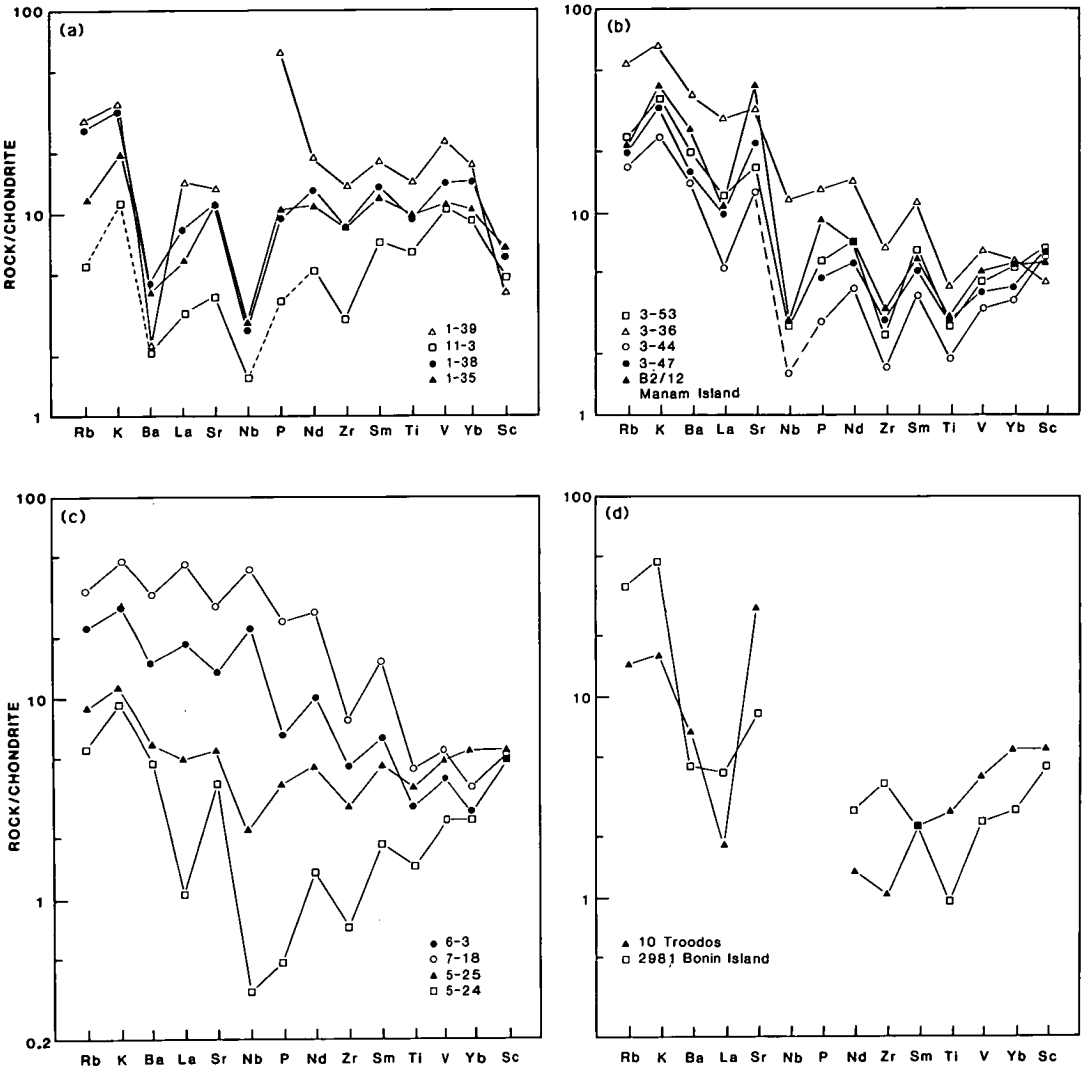

Fig. 6 Representative chondrite normalized element abundance patterns for the dredged igneous rocks and other related rocks. Normalizing values are from Thompson *et al* (1983). **Fig. 6a** Stations 15 and 31. **Fig. 6b** Station 21, and a sample from Manam Is., PNG (B2/12; Johnson *et al* 1985). **Fig. 6c** High-Mg lavas (Stations 23, 24 and 25). **Fig. 6d** Low-Ti ophiolitic basalt (sample 10, from the Troodos Upper Pillow Lavas, Cyprus; Cameron *et al* 1983) and a boninite (sample 2981, Bonin Islands; Hickey & Frey 1982).

conditions of partial melting (P-T-X_{H_2O}) during the evolution of the Lau Basin.

Station 15 basaltic andesites were probably erupted on the eastern side of the Lau Basin, early in its spreading history, and now form the basement to the TM-arc. Compared with conventional models of back-arc basin development (Crawford *et al* 1981), it is unusual to find early Lau Basin crust outcropping on the forearc slope of the north Tonga trench. This implies either

that a significant volume of pre-Lau Basin volcanic arc crust (of which the Lau–Colville Ridge is the remnant arc) has been subducted, despite its location on the over-riding plate, or that initial Lau Basin rifting commenced in the forearc region of the Late Miocene arc. In the latter case, the Lau–Colville Ridge must represent the entire width of the Miocene arc axial ridge supporting the arc volcanoes. In the former case, the presence of *in situ* arc volcanics close to the Mariana Trench axis implies that blocks of Mariana forearc crust have been dragged into the subduction zone and subducted (Beccaluva *et al* 1980). At this stage a forearc rifting model is favoured.

STATION 21

Petrography

Dredged rocks from station 21 are all fresh, porphyritic to aphyric, vesicular to non-vesicular lavas which can be subdivided into five petrographic groups based on the types and abundances of phenocryst phases (Table 2) and major element geochemistry; MgO contents tend to decrease from group I to V. The distinguishing characteristics of these lavas compared with TM-arc lavas are the dominance of orthopyroxene as a phenocryst phase, and the presence of significant amounts of olivine (up to 12 modal %) and Cr-spinel as microphenocrysts and inclusions in phenocryst phases. In contrast, the lavas of the Tonga islands are characterized by a two pyroxene–plagioclase assemblage, with plagioclase being the dominant phenocryst phase (Ewart *et al* 1973). Olivine has only been reported as rare xenocrysts in basaltic andesites from the islands of Tofua and Kao, and in the Metis Shoal dacite (Melson *et al* 1970; Bryan *et al* 1972).

Olivine, orthopyroxene, clinopyroxene and plagioclase are all present as discrete phenocryst and microphenocryst phases and also as glomerophyric clusters, but plagioclase and olivine rarely coexist in the latter. Olivine and orthopyroxene phenocrysts are generally euhedral and vary from >4 mm in size to microphenocrysts. Some larger olivine and orthopyroxene phenocrysts have resorbed margins, the olivines being rimmed by orthopyroxene plus minor clinopyroxene. This evidence for disequilibrium and reaction between olivine and liquid contrasts with the presence of euhedral olivine microphenocrysts. Where olivine is present with orthopyroxene and clinopyroxene in glomerocrysts, it is present in the core of the glomerocryst, suggesting that pyroxene glomerocrysts may be the result of the complete reaction of a large olivine phenocryst with melt.

Plagioclase is most common as large glomeroporphyritic clusters, the glomerocrysts displaying either resorbed or euhedral grain boundaries. The groundmass consists of generally fresh glass, plagioclase and clinopyroxene microlites. Textures range from hyalopilitic to more coarse grained subophitic textures. Titanomagnetite is present as minor anhedral to skeletal granules in the glass. Many samples have abundant feathery quench pyroxene in the groundmass.

Geochemistry and geochemical affinities

Representative analyses of station 21 lavas (Table 4) define a high MgO, low K (Gill 1981), low Ti, tholeiitic suite. Because of their high SiO_2 content, station 21 compositions fall in the calc-alkaline field of Miyashiro (1974) but nevertheless show a distinct Fe-enrichment trend, emphasizing the inadequacy of this classification when dealing with high-Si, high-Mg lava suites. The low initial FeOt/MgO ratios are the result of relatively low FeOt contents (8.7–10.2 wt%), while MgO contents in station 21 lavas range from 15 to 3 wt% (MG# ranges from 41 in evolved aphyric lavas to >70 for the more mafic compositions). At a given MG#, station 21 lavas have lower TiO_2 (0.2–0.45 wt%) and higher SiO_2 contents (52–61 wt%) than TM-arc basaltic andesites (Fig. 7). They have relatively high Ni and Cr contents compared with most island arc basalts and basaltic andesites (Ni up to 265 parts/10^6, Cr up to 1095 parts/10^6), Cr/Ni ratios being high, and >5 in MgO-rich samples, and when compared with TM-arc basaltic andesites, have high abundances of Ba, Rb, Sr and K_2O, but lower abundances of Zr, Y and REE. REE patterns are LREE-enriched (Fig. 5b); $(La/Yb)_N$ varies from 1.36 to 4.97, heavy REE are low, and have relatively flat patterns ($Gd/Yb_N = 0.90$–1.18, 1.52 in sample 3-36). Low Zr, Y and HREE abundances are similar to basaltic andesites from the island of Tafahi, but Tafahi samples differ in having

Table 4 Major, trace and REE geochemistry of representative samples from Stations 21 and 22.

Sample no.	3-44	3-47	3-53	3-36	B2/12	4-11 G	4-12 G	4-15 G	4-14 P
SiO_2	54.35	55.18	57.51	60.17	52.64	58.27	54.59	53.38	73.23
TiO_2	0.20	0.31	0.29	0.42	0.30	0.59	0.44	0.33	0.11
Al_2O_3	10.67	10.94	13.18	15.21	14.93	16.42	15.04	14.65	14.38
FeOt	9.41	10.00	9.22	8.90	8.30	7.60	8.42	10.69	1.79
MnO	0.19	0.19	0.18	0.15	0.17	0.16	0.17	0.19	0.03
MgO	14.99	12.14	8.14	3.35	9.12	5.52	8.65	8.42	0.60
CaO	8.66	9.24	9.53	7.68	11.43	6.50	10.67	10.21	7.45
Na_2O	1.14	1.48	1.35	2.96	2.40	4.63	1.85	1.91	2.30
K_2O	0.35	0.48	0.54	1.01	0.61	0.27	0.13	0.18	0.07
P_2O_5	0.03	0.05	0.06	0.14	0.10	0.04	0.03	0.03	0.04
LOI	0.05	0.98	−0.07	0.86	0.65	6.76	1.25	5.15	0.52
MG#	75.93	70.62	63.61	42.70	66.19	56.41	64.68	58.38	37.38
Ba	106	113	140	271	180	26	29	37	60
Rb	6	7	8	19	8	5	1	3	—
Sr	151	172	202	385	514	82	74	69	550
Zr	12	20	17	44	22	51	45	57	48
Nb	<1	<1	<1	4	<1	1	2	2	16
Y	7	8	9	13	10	19	21	32	7
Sc	50	51	50	34	42	34	51	61	24
V	247	259	275	309	275	203	229	191	41
Ni	275	153	84	21	81	51	93	82	5
Cr	1095	762	365	17	288	108	189	187	9
La		3.25	3.94	9.49	3.33		1.73		13.34
Ce		6.53	7.95	20.85	7.92		5.24		30.60
Pr		0.82	0.94	2.57	—		0.86		2.96
Nd		3.70	4.47	9.29	4.51		4.46		9.65
Sm		1.05	1.31	2.29	1.27		1.53		1.57
Eu		0.39	0.49	0.67	0.47		0.57		<0.24
Gd		1.29	1.34	2.38	—		2.54		1.32
Dy		1.60	1.67	2.06	—		3.20		1.07
Er		1.01	1.19	1.33	—		2.04		0.52
Yb		0.95	1.19	1.26	1.21		2.31		0.37

Letters G and P signify metagabbro and plagiogranite, respectively. Sample B2/12 from Manam Is., PNG (Johnson *et al* 1985). Major element geochemistry summed to 100% volatile free, FeOt = total iron as FeO, LOI = Loss on ignition. Major elements are in wt%, trace elements are in parts per million.

higher REE abundances and LREE-depleted patterns (e.g. sample T116 has a $(La/Yb)_N$ ratio of 0.77; Ewart *et al* 1977). Tafahi basaltic andesites also have lower abundances of Rb, Ba, Sr and K_2O, higher TiO_2 and lower SiO_2 for a given MgO content than lavas from station 21.

Although station 21 lavas are distinctly different from those of the TM-arc suite, they show geochemical affinities with other low-Ti basaltic andesite suites, notably the Manam Is. suite from Papua New Guinea (Johnson *et al* 1985). Both the station 21 and the Manam suites have similar LREE-enriched REE patterns, low abundances of high field strength (HFS) elements (Y, Ti, Zr and P) relative to the REEs on chondrite normalized abundance patterns (Fig. 6b), and have high LIL elements (K, Rb, Ba, Sr) abundances relative to the REE and HFS elements. Overall, rocks from station 21 comprise a more primitive suite than Manam, having higher MgO, Ni and Cr abundances and lower incompatible element abundances.

The Manam and the station 21 suites share many petrogenetic similarities with boninite

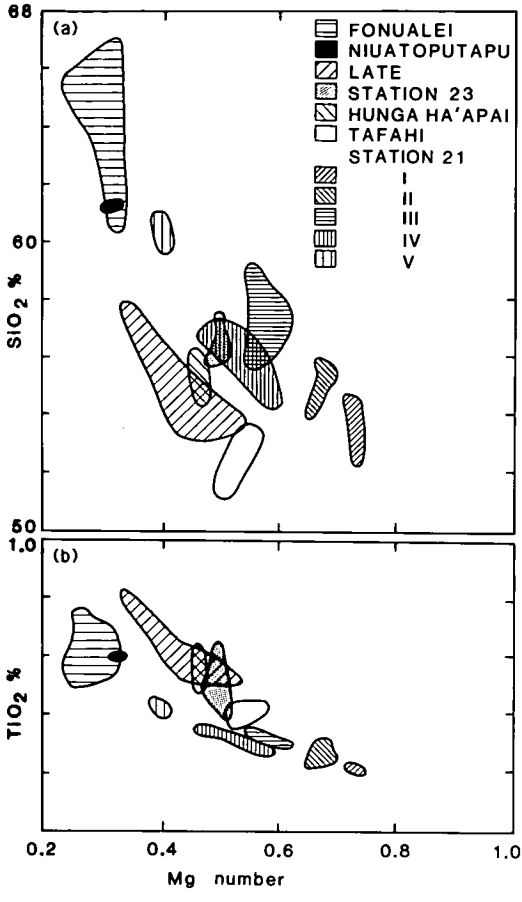

Fig. 7a SiO_2 vs MG# (Mg/(Mg+Fet)) for dredged rocks from station 21 and the basaltic andesites from station 23 compared with rocks from the TM-arc. Roman numerals I–V refer to the petrographic groups from station 21 outlined in Table 2. Field for the station 23 basaltic andesites constructed from data taken from Table 5. Fields for station 21 lavas constructed from data from Table 4 and Falloon (unpubl. data). Fields for the islands of the TM-arc constructed from data from Ewart *et al* (1973) and Ewart (1976). **Fig. 7b** TiO_2 vs MG# for dredged rocks from station 21 and basaltic andesites from station 23 compared with rocks from the TM-arc. Key same as for Fig. 7a.

lavas from Western Pacific arcs (Hickey & Frey 1982; Cameron *et al* 1983; Johnson *et al* 1985), such as evidence for a 'depleted' source peridotite metasomatized by two or more 'enriched' components, but their trace element signatures distinguish them from boninite sources. The most important distinguishing characteristic is the lack of a strong Zr-enrichment. Zircon enrichment in boninite suites is reflected by low Ti/Zr ratios (<70), and a Zr 'peak' relative to Sm on chondrite-normalized element abundance diagrams (Fig. 6b). The station 21 and Manam suites lack both of these features and have geochemical affinities with low-Ti ophiolitic basalts rather than with boninite.

STATION 22

Petrography

Metagabbros from station 22 possess primary pyroxene(s) which have been totally replaced by amphibole (hornblende and actinolite) and chlorite, fresh or slightly saussuritized plagioclase, and accessory titanomagnetite and secondary epidote. The plagiogranite is a fresh medium to fine grained holocrystalline rock with a microgranitic texture, and consists of equal amounts of quartz and plagioclase (An_{60}), plus ~5–10 modal % hornblende with accessory sphene and apatite. Small pieces of serpentinite recovered from station 22 consist of serpentine, except one sample which contains relict cores of olivine and orthopyroxene, suggesting a harzburgititic protolith.

Geochemistry and geochemical affinities

Metagabbros from station 22, characterized by high SiO_2 and low TiO_2 contents, have major element geochemistries similar to station 21 basaltic andesites. However, the metagabbros have significantly lower abundances of Ba and Sr, higher abundances of Zr and Y, and the least altered sample (4-12; Table 4) has a LREE-depleted REE pattern (Fig. 5c). These trace element abundances are not considered to have been significantly affected by alteration because of the consistency of element ratios between samples which have suffered varying degrees of alteration (e.g. LOI which ranges from 1.25 to 6.76 wt%). For similar reasons, metagabbros from station 22 lack genetic relationships with TM-arc rocks. The metagabbros were dredged from depths comparable with those of basaltic andesites from station 15 (4500–4440 m compared with 4325–4860 m). They contain a trace element signature similar to that of the basaltic andesites, having low-Ba and high-Zr contents, and LREE-depleted REE patterns. It is possible that the basement sequence exposed at station

15, characterized by high-Ti basaltic andesites, is continuous along the North Tonga Ridge.

The plagiogranite from station 22 (Table 5) is characterized by high-SiO_2, and low-K_2O contents, consistent with the absence of K-feldspar. Unlike typical MORB-derived or ophiolitic plagiogranites which have flat HREE patterns (Coleman & Donato 1979), this specimen has a strongly HREE-depleted pattern ($[La/Yb]_N = 24$, with a marked Eu anomaly; Fig. 5c). The plagiogranite is high in Sr, and relatively low in Ba and Rb, consistent with the absence of K-feldspar and is unusual in having a significant Nb (16 parts/10^6) content compared with the low Nb contents of other Tongan rocks (mostly below detection limit). The HREE-depleted REE pattern suggests involvement of garnet as a residual or fractionating phase in the petrogenesis of this rock. It is possible that the plagiogranite is derived from a slab-derived (eclogitic residue) as opposed to a mantle-derived (peridotitic residue) parent magma.

STATION 23

Basaltic andesites and high-Mg lavas were recovered from station 23.

Petrography of basaltic andesites

Petrographically, the basaltic andesites are similar to those from station 21, containing 6–14 modal % phenocrysts and microphenocrysts of orthopyroxene, clinopyroxene and plagioclase set in a hyalopilitic groundmass of fresh glass, acicular plagioclase microlites and anhedral clinopyroxene grains. Olivine is present as rare resorbed phenocrysts surrounded by stubby orthopyroxene microphenocrysts, and contains Cr-spinel inclusions. Pyroxene–plagioclase glomerocrysts are common; larger orthopyroxene phenocrysts display blocky and patchy zoning and are frequently rimmed by clinopyroxene.

Geochemistry and geochemical affinities of basaltic andesites

The basaltic andesites are relatively uniform in composition (Table 5) and compared with those of the TM-arc have on average higher SiO_2 contents (55–56 cf. 53–55 wt% for TM-arc compositions), lower FeOt, higher MgO (reflected in lower FeOt/MgO ratios; Fig. 4) and higher Ni and Cr contents. Similarities with TM-arc basaltic andesites include TiO_2 contents (Fig. 8b) and flat to slightly LREE-depleted REE patterns (Fig. 5d); in these respects they contrast with the petrographically similar station 21 lavas. Incompatible element contents are lower than those of TM-arc basaltic andesites, causing significant differences in trace element ratios such as Ba/La and Sr/La. The basaltic andesites from station 23 were derived from a mantle source different from, yet sharing many similar characteristics with, the mantle source of the TM-arc basaltic andesites.

Petrography of high-Mg lavas

Small highly vesicular, highly phyric pieces of high-Mg lavas, also recovered from station 23, can be subdivided into two groups on petrographic and geochemical criteria (Table 2). In both groups olivine occurs as large subhedral to euhedral phenocrysts, sometimes with resorbed margins. Orthopyroxene is present mainly in euhedral glomerophyric clusters, but also as discrete phenocrysts and microphenocrysts, sometimes showing resorption. Orthopyroxene is mostly unzoned, although some phenocrysts show an unusual blocky or patchy zoning and rims of clinopyroxene. Clinopyroxene in Group B lavas (Table 2) is present mainly as small subhedral to euhedral microphenocrysts, and rarely as large resorbed clinopyroxene phenocrysts. The groundmass is hyalopilitic, consists of abundant acicular pyroxene microlites and fresh glass, and contains small euhedral olivine and Cr-spinel microphenocrysts; plagioclase is absent.

Geochemistry of high-Mg lavas

Representative analyses of the high-Mg lavas are presented in Table 5. Samples 5-24 and 5-28 are from Group A and sample 5-25 is from Group B. Both groups are characterized by high MgO (16–21 wt%) at relatively high SiO_2 contents (52–53 wt%). Group A lavas are more 'primitive', containing higher MgO, Ni and Cr, lower TiO_2 and lower abundances of incompatible elements such as Ba, Sr, Zr and Y. Both groups have high MG# (75–69) appropriate

Table 5 Major, trace and REE geochemistry of basaltic andesites from Station 23, high-Mg lavas from Stations 23, 24 and 25, and pillow rind from Station 31.

Sample no.	5-24	5-28	5-25	5-20	5-21	5-23	5-27	St-24 6-3	St-25 7-18	St-31 11-3
SiO_2	52.95	53.72	53.83	56.30	55.92	56.11	57.48	56.04	54.72	50.22
TiO_2	0.15	0.14	0.36	0.62	0.48	0.38	0.44	0.31	0.45	0.65
Al_2O_3	7.92	8.27	9.63	15.20	16.56	16.66	14.80	10.60	10.90	15.33
FeOt	9.70	9.65	9.71	9.77	9.29	8.76	9.66	8.46	8.65	9.57
MnO	0.21	0.20	0.19	0.17	0.17	0.16	0.17	0.17	0.17	—
MgO	20.89	19.65	16.30	5.33	4.75	5.07	5.36	13.61	12.97	8.87
CaO	7.18	7.54	8.50	10.20	10.80	11.03	10.11	9.17	9.65	13.40
Na_2O	0.85	0.69	1.27	2.08	1.80	1.58	1.67	1.14	1.52	1.96
K_2O	0.14	0.12	0.16	0.24	0.19	0.19	0.25	0.43	0.71	—
P_2O_5	0.01	0.02	0.04	0.07	0.04	0.04	0.06	0.07	0.26	—
LOI	0.13	−0.02	0.24	0.71	0.18	0.20	0.57	1.87	1.69	—
MG#	79.33	80.13	76.87	51.93	47.66	50.77	49.71	76.11	74.80	64.73
Ba	34	35	41	55	50	42	57	105	230	14
Rb	2	2	3	4	3	3	4	8	12	2
Sr	46	48	68	126	123	118	108	159	348	48
Zr	5	7	20	39	25	15	25	32	53	21
Nb	<1	<1	<1	−1	<1	<1	<1	8	16	<1
Y	5	6	10	17	14	11	13	8	11	22
Sc	44	43	44	44	46	44	49	43	44	51
V	191	200	225	298	270	231	270	214	223	299
Ni	501	433	341	37	27	29	40	189	199	133
Cr	2027	1767	1294	75	54	94	124	927	760	350
La			1.51	2.82			1.91	6.53	15.98	3.43
Ce			3.34	6.44			4.43	14.74	37.72	—
Pr			0.55	1.01			0.76	1.73	4.48	5.52
Nd			2.72	5.17			3.56	6.36	17.29	5.83
Sm			0.89	1.72			1.24	1.30	3.23	8.17
Eu			0.36	0.62			0.59	0.45	1.02	8.61
Gd			1.27	2.37			1.90	1.35	2.68	10.58
Dy			1.62	3.10			2.46	1.27	1.84	11.57
Er			1.10	2.15			1.78	0.63	0.93	11.74
Yb			1.14	2.07			1.78	0.58	0.79	11.39

For sample St-31 11-3 major element geochemistry determined by electron microprobe; others summed to 100% volatile free. FeOt = total iron as FeO, LOI = Loss on ignition. Major elements are in wt%, trace elements are in parts per million.

for them to be in equilibrium with mantle olivine (> Fo_{88}; Green 1971). Although the high MG# may also reflect the abundance of mafic phenocrysts in these lavas, so that whole rock compositions may not be representative of liquid compositions, the presence of euhedral olivine phenocrysts as magnesian as Fo_{94} strongly supports the claim that the lavas have near-primary compositions.

Group A lavas have low HREE abundances (<3× chondrites) with LREE-depleted patterns. Such low abundances render the Group A samples unsuitable for the XRF-determined REE analytical technique of Robinson *et al* (1986). However, preliminary results suggest that La is <0.35 parts/10^6, with $(La/Yb)_N$ approximately equal to 0.43. Sample 5-25 from Group B has a flat REE abundance pattern (Fig. 5d) with $(La/Yb)_N = 0.87$ and low REE abundances (5×chondrites). The REE pattern of sample 5-25 is similar to those of the basaltic andesites of station 23 and the TM-arc,

suggesting that the high-Mg lavas could be parental to these andesites. This possibility is precluded by the high SiO_2 content > 52 wt%, the parental magma of TM-arc basaltic andesites requiring <50 wt% SiO_2; and a low FeOt of 9.6–9.7 wt% for Group B lavas which produce low initial FeOt/MgO ratios and result in station 23 high-Mg lavas plotting away from the main TM-arc trend (Fig. 4).

The high-Mg lavas from station 23 could be the source of xenocrystal olivine (Fo_{93}), orthopyroxene and Cr-spinel in the Metis Shoal dacite (Melson *et al* 1970), and could therefore be involved in magma mixing processes beneath the young TM-arc. The Group B high-Mg lavas are possibly co-magmatic with basaltic andesites from station 23, which have similar REE patterns. The geochemical affinities of high-Mg lavas from station 23 are discussed separately in conjunction with high-Mg lavas from stations 24 and 25.

STATIONS 24 AND 25

Petrography

The glass rind of pillow lavas from these stations consists of abundant small euhedral olivine microphenocrysts, some with skeletal morphologies, minor small Cr-spinel euhedra and complexly intergrown orthopyroxene laths set in fresh glass. Pillow interiors are characterized by interconnecting elongate orthopyroxene laths, fresh glass and spherulitic pyroxene, with abundant (~10 modal %) euhedral olivine microphenocrysts and phenocrysts. Apart from the absence of large orthopyroxene phenocrysts, the petrography of stations 24 and 25 pillow lavas is similar to that of the high-Mg lavas from station 23 in that the groundmass of both contain abundant olivine microphenocrysts, orthopyroxene and Cr-spinel euhedra. Lavas from stations 24 and 25 may have erupted at temperatures above the orthopyroxene liquidus, whereas those from station 23 quenched below the appearance temperature of orthopyroxene.

Geochemistry

Samples 6-3 and 7-18 (Table 5) are representative of the high-Mg lavas from stations 24 and 25, respectively. Compared with high-Mg lavas from station 23, they are higher in SiO_2 and TiO_2 (0.3–0.45 wt%), lower in MgO and are strongly enriched in incompatible elements Rb, Ba, Sr, Zr, Nb, Y and K. The REE patterns (Fig. 5e) are LREE-enriched ($La/Yb_N = 7.46–13.4$); those from station 25 are more enriched in incompatible elements than lavas from station 24. The geochemical affinities of the pillow lavas are discussed below.

STATION 31

Petrography, geochemistry and geochemical affinities

The pillow rind recovered from station 31 (sample 11-3, Table 5), consisting of minor euhedral plagioclase microlites, euhedral olivine microphenocrysts and fresh glass, has geochemical affinities with primitive MORB glasses (Bryan & Moore 1977; Langmuir *et al* 1977) but differs in its relatively higher FeOt, which produces a MG# lower than primitive MORB.

Sample 11-3 is geochemically and petrographically similar to other Lau Basin basalts (e.g. site 95; Hawkins 1976; Hawkins & Melchoir 1985). Although Hawkins and Melchoir (1985) emphasized their geochemical similarities with N-type MORB, there are significant differences, as illustrated by 11-3, which indicate a distinctive Lau Basin (back-arc basin) magma type. These characteristics include:

(i) Compared with primitive MORB glasses of similar MG# or MgO content, sample 11-3 has significantly lower TiO_2 contents. The more magnesian sample 95-1 has only 0.35 wt% TiO_2 (Gill 1976; Hawkins 1976), whereas primitive MORB glasses have TiO_2 contents >0.63 and mostly between 0.7 and 0.9 wt%.

(ii) High CaO contents and high CaO/Al_2O_3 and CaO/Na_2O ratios. Combined with other Lau Basin samples (e.g. 14.7 wt% CaO in sample 95-12; Hawkins & Melchoir 1985) sample 11-3 has an exceptionally high CaO content even for relatively calcic MORB glasses.

(iii) Lau Basin basalts have low abundances of incompatible elements, especially Sr (48 parts/10^6 in 11-3; 52–155 parts/10^6 in primitive MORB glasses), Zr (21 parts/10^6 in 11-3; 18–51 parts/10^6 in primitive MORB glasses) and Ba (14 parts/10^6 in 11-3; 11–50 parts/10^6 in primitive MORB glasses).

(iv) Sample 11-3 has a strongly LREE-depleted REE pattern (Fig. 5f), with $(La/Yb)_N = 0.3$; sample 95-1 (Gill 1976) has a more depleted pattern $(La/Yb)_N = 0.17$. Few primitive MORB glasses have such depleted patterns.

GEOCHEMICAL AFFINITIES OF THE HIGH-Mg LAVAS

Samples from the flank area of the 'island arc' are remarkable for the consistency and dominance of 'primitive' highly magnesium lavas characterized by highly magnesian olivine and orthopyroxene phenocrysts and glass which has high MG#. In contrast, there is a paucity of such rocks amongst the emergent volcanoes or indeed in the classical rocks comprising the island arc magma series (calc-alkaline, island arc tholeiite and shoshonitic volcanics; Gill 1981). Thus it is significant that these high-Mg lavas, which contain both magnesian olivine and orthopyroxene, imply source compositions of peridotitic rather than eclogitic or pyroxenitic character.

A comparison of the high-Mg lavas from stations 23, 24 and 25 with other primitive lavas indicates strong affinities with low-Ti ophiolitic basalts (Sun & Nesbitt 1978), such as the Upper Pillow Lavas from the Arakapas Fault Belt region, Cyprus (Cameron 1985). In terms of petrography alone, the Tongan high-Mg lavas can be considered exact equivalents of Arakapas-type pillow lavas. Arakapas lavas also contain orthopyroxene-dominated and olivine-dominated lavas, equivalent to rocks from station 23 and stations 24 and 25, respectively. Low-Ti ophiolitic basalts have similar groundmass textures to boninites, leading to confusion in nomenclature (Cameron *et al* 1979, 1983). However, the Tongan high-Mg lavas, together with low-Ti ophiolitic basalts, are distinguished from boninite by the following characteristics:

(i) Whereas Tongan lavas and low-Ti ophiolitic

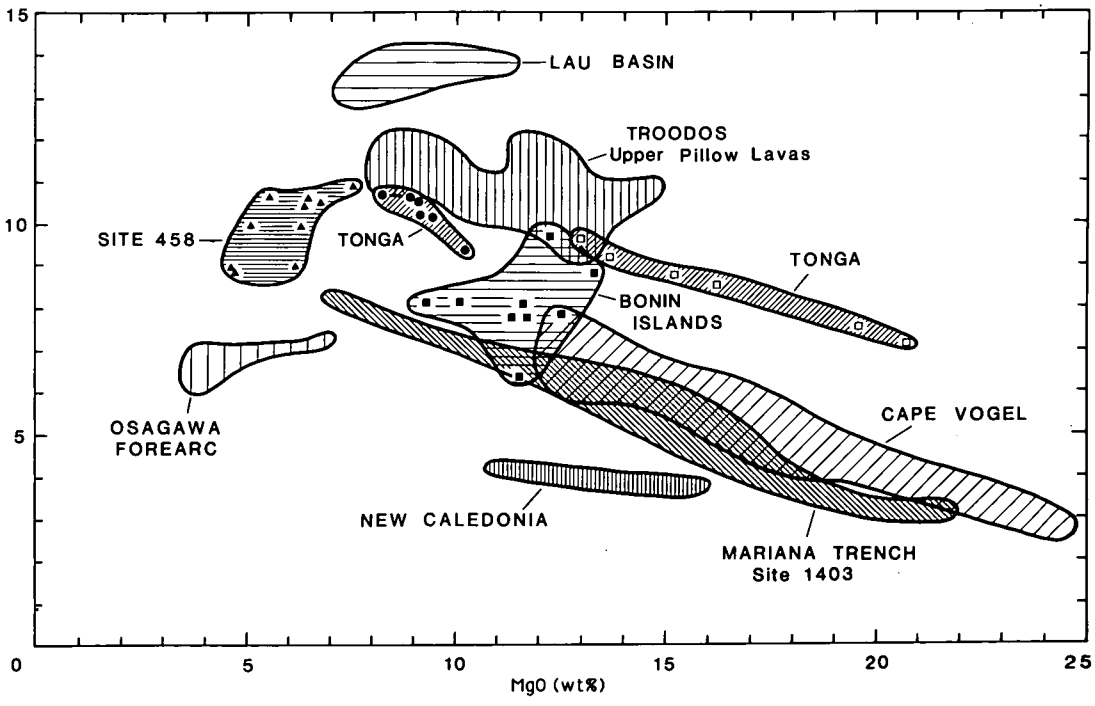

Fig. 8 CaO vs MgO wt% for high-Mg lavas from stations 23, 24 and 25. (□) Whole rock analyses from Table 5. (●) The quenched groundmass compositions of the high-Mg lavas (Falloon unpubl. data). Fields for calcic Lau Basin back-arc basin basalts (Hawkins 1976) and boninites were determined from the following sources. DSDP site 458, Mariana forearc (Meijer 1980; Hickey & Frey 1982); individual data points represented by (▲). Bonin Islands (Komatsu 1980; Hickey & Frey 1982; Cameron *et al* 1983); individual data points represented by (■). Cape Vogel, PNG (Jenner 1981). Mariana Trench, site 1403 (Dietrich *et al* 1978; Sharaskin *et al* 1980). New Caledonia (Cameron *et al* 1983). Ogasawara forearc (Johnson 1985). The Troodos Upper Pillow Lavas from Cameron (1985).

basalts have olivine as an important phenocryst and microphenocryst phase, olivine is rare or absent from boninites (Jenner 1981; Walker & Cameron 1983). The former rocks also lack clinoenstatite as a phenocryst phase.

(ii) SiO_2 contents at a given MgO are lower in the Tongan and low-Ti ophiolitic lavas (Cameron *et al* 1983).

(iii) High CaO contents relative to boninites (Fig. 8) are reflected in high CaO/Al_2O_3 ratios. Pillow lavas from stations 23, 24 and 25 with CaO/Al_2O_3 ratios of between 0.7 and 0.9 are generally higher than primitive MORB glass compositions, and significantly higher than boninites which have characteristically low CaO/Al_2O_3 ratios (Cape Vogel boninites have CaO/Al_2O_3 ratios of 0.66–0.52) because of low CaO contents. In Fig. 8, the CaO content of Tongan high-Mg lavas overlaps with Troodos Upper Pillow Lava compositions and plots well away from clinenstatite-bearing boninite. A clear separation appears to exist between boninite and Tongan lavas but two examples from the Bonin Is plot with the Tongan lavas, while 'boninite' series rocks from site 458 (Meijer 1980) seem to fall between the two fields (Fig. 8). Clinoenstatite is absent from both the two Bonin Is. samples and from site 458. These 'intermediate' lavas could possibly be the result of mixing between a low-CaO boninite-type liquid with a more calcic magma, such as a Troodos-type liquid or even a calcic Lau Basin type liquid.

(iv) Both the Tongan lavas and low-Ti ophiolitic basalts lack the characteristic enrichment of Zr over the middle REE element Sm on normalized abundance patterns present in boninites (see Fig. 6c for the Tongan high-Mg lavas and Fig. 6d where a representative boninite and Troodos pattern are compared). The chondrite-normalized element abundance patterns for the Tongan high-Mg lavas are variable, and different from the boninite and Troodos patterns in Fig. 6d. Sample 5-24 from station 23, with a LREE-depleted pattern, is closest to the Troodos pattern. The differences between the Tongan high-Mg lavas and the Troodos Upper Pillow Lavas can be attributed to a difference in the nature of an 'enriched' metasomatizing component, which invaded a depleted mantle source. The nature of the proposed 'enriched' component and a detailed petrogenetic assessment of these lavas are subjects of another paper (T. J. Falloon unpubl. data).

SUMMARY

Apart from stations 15 and 31, dredging during the cruise of the *Natsushima* in 1984 took place within a small area at the northern termination of the North Tonga Ridge. Each dredge station yielded distinctive suites of rocks which are different both from one another and from the young volcanics of the Tofua magmatic arc, and which are primitive in having high-MG# compatible with derivation from mantle peridotite sources. These characteristics require the existence of a range of mantle sources at the northern end of the Tonga Ridge, as well as a probable range in partial melting conditions ($P\text{-}T\text{-}X_{H_2O}$). Possibly the unique tectonic setting of the dredged rocks, next to the intersection of a volcanic arc and a transform fault-oblique subduction system has allowed contributions from a variety of different sources (slab, mantle wedge, LVZ), through processes such as *en echelon* rifting, and minor spreading.

Basaltic andesites from station 23 display the closest affinities to those from the TM-arc; the higher SiO_2 contents at similar MG# of station 23 lavas could be explained by a shallower depth of melt segregation or alternatively higher P_{H_2O} during partial melting (Green 1976).

The high-Mg lavas have similarities with low-Ti ophiolitic basalts, and support an intra-oceanic island arc setting for ophiolites with these distinctive types of lavas. They are primitive in character (high MG#, Ni and Cr) and are possible mantle-derived primary melts in an island arc setting. Basaltic andesites from station 15, from the basement of the TM-arc, have strong geochemical affinities with early Lau Basin basalts. It is possible that the basement of the young TM-arc along the North Tonga Ridge is old Lau Basin crust, as suggested previously by Hawkins *et al* (1984), Hawkins and Falvey (1985), and Hawkins and Melchoir (1985). The dredged rocks demonstrate that arcs are geochemically complex, and that exposed volcanic islands may not be representative of the volcanism which constructed the arc.

ACKNOWLEDGMENTS

Financial support for this study was provided by a Commonwealth postgraduate award to TJF and a grant from the Department of Science and Technology. Technical assistance was provided by P. Robinson. Thanks are also extended to the captain and crew of the *Natsushima*, to chief scientists E. Honza and K. B. Lewis and to fellow shipboard colleagues.

REFERENCES

BECCALUVA L., MACIOTTA G., SAVELLI C., SERRI G. & ZEDA O. 1980. Geochemistry and K/Ar ages of volcanics dredged in the Philippine Sea (Mariana, Yap, Palau Trenches and Parece Vela Basin). *In* Hayes D. E. ed. The Tectonic and Geologic Evolution of Southeast Asian Seas and Islands. *American Geophysical Union, Geophysical Monogram Series* **23**, 247–260.

BRYAN W. B., STICE G. D. & EWART A. 1972. Geology, petrology and geochemistry of the volcanic islands of Tonga. *Journal of Geophysical Research* **77**, 1566–1585.

BRYAN W. B. & MOORE J. G. 1977. Compositional variations of young basalts in the Mid-Atlantic Ridge ridge valley near lat. 36°39′N. *Geological Society of America Bulletin* **88**, 556–570.

CAMERON W. E. 1985. Petrology and origin of primitive lavas from the Troodos ophiolite, Cyprus. *Contributions to Mineralogy and Petrology* **89**, 239–255.

CAMERON W. E., NISBET E. G. & DIETRICH V. J. 1979. Boninites, komatiites and ophiolitic basalts. *Nature* **280**, 550–553.

CAMERON W. E., MCCULLOCH M. T. & WALKER D. A. 1983. Boninite petrogenesis: chemical and Nd–Sr isotopic constraints. *Earth and Planetary Science Letters* **65**, 75–89.

COLEMAN R. G. & DONATO M. M. 1979. Oceanic plagiogranite revisited. *In* Barker F. ed. *Trondhjemites and Related Rocks*, pp. 78–93. Elsevier, Amsterdam.

CRAWFORD A. J., BECCULUVA L. & SERRI G. 1981. Tectono-magmatic evolution of the West Philippine-Mariana region and the origin of boninites. *Earth and Planetary Science Letters* **54**, 346–356.

DIETRICH V., EMMERMANN R., OBERHANSKI R. & PUCHELT H. 1978. Geochemistry of basaltic and gabbroic rocks from the West Mariana Basin and the Mariana Trench. *Earth and Planetary Science Letters* **39**, 127–144.

DUNCAN R. A., PICKTHORN L. G. & VALLIER T. L. 1985. Volcanic episodes at Eua, Tonga Islands. *In* Vallier T. and Scholl D. ed. Geology and offshore resources of Pacific island-arcs Tonga region. *Circum Pacific Council for Energy and Mineral Resources, Earth Science Series* **2**, 236–245.

EWART A. 1976. A petrological study of the younger Tongan andesites and dacites, and the olivine tholeiites of Niua Fo'ou Island, S.W. Pacific. *Contributions to Mineralogy and Petrology* **58**, 1–21.

EWART A. & BRYAN W. B. 1972. Petrography and geochemistry of the igneous rocks from Eua, Tongan Islands. *Geological Society of America Bulletin* **83**, 3281–3298.

EWART A., BRYAN W. B. & GILL J. B. 1973. Mineralogy and geochemistry of the younger volcanic islands of Tonga, S.W. Pacific. *Journal of Petrology* **14**, 429–465.

EWART A., BROTHERS R. N. & MATEEN A. 1977. An outline of the geology and geochemistry, and the possible petrogenetic evolution of the volcanic rocks of the Tonga–Kermadec–New Zealand island arc. *Journal of Volcanology and Geothermal Research* **2**, 205–250.

FALLOON T. J. 1985. Preliminary petrography and geochemistry of igneous rocks from the northern Tonga ridge and adjacent Lau Basin. *In* Honza E., Lewis K. B. and Shipboard Party. A Marine Geological and Geophysical Survey of the Northern Tonga Ridge and Adjacent Lau Basin. *Natural Resources of Tonga Field Report* **1**, 63–71.

FREY F. A., BRYAN W. B. & THOMPSON G. 1974. Atlantic ocean floor: geochemistry and petrology of basalts from legs 2 and 3 of the DSDP. *Journal of Geophysical Research* **79**, 5507–5527.

GAST P. W. 1968. Trace element fractionation and the origin of tholeiitic and alkaline magma types. *Geochimica et Cosmochimica Acta* **32**, 1057–1086.

GIARDINI D. & WOODHOUSE J. H. 1986. Horizontal shear flow in the mantle beneath the Tonga arc. *Nature* **319**, 551–555.

GILL J. B. 1970. Geochemistry of Viti Levu, Fiji, and its evolution as an island arc. *Contributions to Mineralogy and Petrology* **27**, 179–203.

GILL J. B. 1976. Composition and age of Lau Basin and Ridge volcanic rocks: Implications for evolution of an interarc basin and remnant arc. *Geological Society of America Bulletin* **87**, 1384–1395.

GILL J. B. 1981. *Orogenic Andesites and Plate Tectonics*. Springer-Verlag, New York.

GILL J. B. 1984. Sr–Pb–Nd isotopic evidence that both MORB and OIB sources contribute to oceanic island arc magmas in Fiji. *Earth and Planetary Science Letters* **68**, 443–458.

GILL J. B., STORK A. L. & WHELAN P. M. 1984. Volcanism accompanying back-arc basin development in the southwest Pacific. *Tectonophysics* **102**, 207–224.

GREEN D. H. 1971. Composition of basaltic magmas as indicators of conditions of origin: application to oceanic volcanism. *Philosophical Transactions of the Royal Society of London Academy* **268**, 707–725.

GREEN D. H. 1976. Experimental testing of 'equilibrium' partial melting of peridotite under water-saturated, high-pressure conditions. *Canadian Mineralogist* **14**, 255–268.

HAWKINS J. W. 1976. Petrology and geochemistry of basaltic rocks of the Lau Basin. *Earth and Planetary Science Letters* **28**, 283–297.

HAWKINS J. W., BLOOMER S. H., EVANS C. A. & MELCHIOR J. T. 1984. Evolution of intra-oceanic arc-trench systems. *Tectonophysics* **102**, 175–205.

HAWKINS J. W. & MELCHIOR J. T. 1985. Petrology of Mariana Trough and Lau Basin basalts. *Journal of Geophysical Research* **90**, 11, 431–11, 468.

HAWKINS J. W. & FALVEY D. A. 1985. Petrology of andesitic dikes and flows from Eua, Tonga. *In* Vallier T. L. and Scholl D. W. eds. Geology and offshore resources of Pacific island-arcs Tonga region. *Circum-Pacific Council for Energy and Mineral Resources, Earth Science Series*, **2**, 236–245.

HICKEY R. L. & FREY F. A. 1982. Geochemical characteristics of boninite series volcanics: implications for their source. *Geochimica et Cosmochimica Acta* **46**, 2099–2115.

HONZA E., LEWIS K. B. & SHIPBOARD PARTY 1985. A Marine Geological and Geophysical Survey of the Northern Tonga Ridge and adjacent Lau Basin. *Natural Resources of Tonga, Field Report* **1**.

JENNER G. 1981. Geochemistry of high-Mg andesites from Cape Vogel Papua New Guinea. *Chemical Geology* **33**, 307–332.

JOHNSON K. T. M. 1985. Major, trace and rare earth element abundances in boninitic lavas from the Ogasaware forearc. *Journal of the Faculty of Science Hokkaido University* **21**, 453–463.

JOHNSON R. W., JAQUES A. L., HICKEY R. L., MCKEE C. O. & CHAPPELL B. W. 1985. Manam Island, Papua New Guinea: petrology and geochemistry of a low-TiO_2 basaltic island arc volcano. *Journal of Petrology* **26**, 283–323.

KITEKEI'AHO T., TAPPIN D., HONZA E., OKUDA Y., MIYAZAKI T., YOKOKURA T. & LEWIS K. B. 1985. Seismic profiles from Northern Tonga. *In* Honza E., Lewis K. B. and Shipboard Party. A Marine Geological and Geophysical Survey of the Northern Tonga Ridge and Adjacent Lau Basin. *Natural Resources of Tonga Field Report* **1**, 31–35.

KONATSU M. 1980. Clinoenstatite in volcanic rocks from the Bonin Islands. *Contributions to Mineralogy and Petrology* **74**, 329–338.

LANGMUIR C. H., BENDER J. F., BENCE A. E., HANSON G. N. & TAYLOR S. R. 1977. Petrogenesis of basalts from the FAMOUS area: Mid-Atlantic Ridge. *Earth and Planetary Science Letters* **36**, 133–156.

MEIJER A. 1980. Primitive arc volcanism and a boninite series: examples from Western Pacific island arcs. *In* Hayes D. ed. The Tectonic and Geologic Evolution of Southeast Asian Seas and Islands. *American Geophysical Union Geophysical Monogram* **23**, 269.

MELSON W. G., JAROSEWICH E. & LUNDQUIST C. A. 1970. Volcanic eruption at Metis Shoal, Tonga, 1967–68: description and petrology. *Smithsonian Contributions to the Earth Sciences* **4**, 1–17.

MIYASHIRO A. 1974. Volcanic rock series in island arcs and active continental margins. *American Journal of Science* **274**, 321–355.

NORRISH K. & HUTTON J. T. 1969. An accurate X-ray spectrographic method for the analysis of a wide range of geologic samples. *Geochimica et Cosmochimica Acta* **33**, 431–451.

ROBINSON P., HIGGINS N. C. & JENNER G. A. 1986. Determination of rare-earth elements, Yttrium and Scandium in rocks by an ion exchange x-ray fluorescence technique. *Chemical Geology* **55**, 121–137.

SHARASKIN A. Y., DOBRETSOV N. L. & SOBOLEV N. V. 1980. Marianities: the clinoenstatite bearing pillow-lavas associated with the ophiolite assemblage of Mariana Trench. *In* Panayiotou A. ed. *Ophiolites, Proceedings International Ophiolite Symposium Cyprus 1980.* Ministry of Agricultural and National Resources, Nicosia.

SHARASKIN A. Y., PUTCHIN I. K., ZLOBIN S. K. & KOLESOV G. M. 1983. Two ophiolite sequences from the basement of the Northern Tonga Arc. *Ofioliti* **8**, 411–438.

SUN S. & NESBITT R. W. 1978. Geochemical regularities and genetic significance of ophiolitic basalts. *Geology* **6**, 689–693.

THOMPSON R. N., MORRISON M. A., DICKIN A. P. & HENDRY G. L. 1983. Continental flood basalts . . . arachnids rule ok? *In* Hawkesworth C. J. and Norry M. J. eds. *Continental Basalts and Mantle Xenoliths*, pp. 158–185. Shiva Geology Series, Cheshire.

WALKER D. A. & CAMERON W. E. 1983. Boninite primary magmas: evidence from the Cape Vogel peninsula, PNG. *Contributions to Mineralogy and Petrology* **83**, 150–158.

(*Received* 14 *October* 1986; *accepted* 18 *March* 1987)

B42.

Mineralogy and Petrology (1987) 37: 181–219

Mineralogy and Petrology

© by Springer-Verlag 1987

Anhydrous Partial Melting of MORB Pyrolite and Other Peridotite Compositions at 10 kbar: Implications for the Origin of Primitive MORB Glasses

T. J. Falloon and D. H. Green

Geology Department, University of Tasmania, Hobart, Australia

With 10 Figures

Received April 24, 1987;
accepted August 17, 1987

Summary

Anhydrous partial melting experiments on four peridotite compositions have been conducted at 10 kbar providing a relatively internally consistent set of data on the character of primary melts expected from the oceanic upper mantle in the mid-ocean ridge setting. The four peridotite compositions are: "MORB pyrolite" (considered to be suitable for the production of primitive (Mg#$\geqslant$0.68) MORB glasses at 10 kbar), "Hawaiian pyrolite" (representative of "enriched" upper mantle), Tinaquillo lherzolite (representative of more "depleted" upper mantle), and the spinel lherzolite KLB-1 which is a suitable composition for the production of primitive MORB glasses. The equilibrium liquids were determined by "sandwich" experiments. The primitive MORB glass DSDP 3-18-7-1 was used in experiments using MORB pyrolite and KLB-1, while a calculated 10 kbar liquid composition from *Jaques* and *Green* (1980) was used in experiments with Hawaiian pyrolite and Tinaquillo lherzolite. The results of the experiments are used to test a 10 kbar melt model for the generation of primitive MORB glasses, which are parental magmas to typical MORB compositions. The melt compositions from the four peridotites studied are significantly different from primitive MORB glasses in major element chemistry and plot away from the field of primitive MORB glasses in the CIPW molecular normative "Basalt tetrahedron". The results indicate that primitive MORB glasses are derivative compositions lying on olivine fractionation lines from picritic parents, which themselves are primary magmas at pressures greater than 10 kbar. The results of this study are integrated with previous 10 kbar experimental studies.

Zusammenfassung

Wasserfreie partielle Aufschmelzung von MORB Pyrolit und andere Peridotit-Zusammensetzungen bei 10 kbar: Bedeutung für die Entstehung primitiver MORB Gläser

Vier Peridotit-Zusammensetzungen wurden bei 10 kbar unter wasserfreien Bedingungen partiell aufgeschmolzen, und die Ergebnisse mit möglichen primitiven Schmelzen Mittel-Ozeanischer Rücken verglichen.

Die folgenden perioditischen Zusammensetzungen wurden untersucht: „MORB pyrolite" [mögliche Ausgangszusammensetzung für primitive (Mg# > 0.68) MORB-Glaszusammensetzungen bei 10 kbar]; „Hawaiian pyrolite" (representativ für ‚angereicherten' Oberen Mantel); „Tinaquillo Iherzolite" (representativ für ‚verarmten' Oberen Mantel) und spinel Iherzolite, KLB-1 (im Gleichgewicht mit primitiver MORB-Glaszusammensetzung). Die Schmelzen im Gleichgewicht mit diesen Ausgangszusammensetzungen wurden mittels „Sandwich'-Experimenten ermittelt.
Die primitive MORB-Glaszusammensetzung DSDP 3-18-7-1 wurde mit MORB pyrolite und KLB-1 equilibriert, während eine Modell-Zusammensetzung von *Jaques* and *Green* (1980) in Verbindung mit „Hawaiian pyrolite" und „Tinaquillo Iherzolite" vermischt wurde. Die Resultate der Experimente werden mit einem 10 kbar Aufschmelzungsmodell zur Entstehung primitiver MORB-Gläser verglichen. Die Schmelzen im Gleichgewicht mit den vier Peridotit-Ausgangszusammensetzungen unterscheiden sich wesentlich von primitiven MORB-Gläsern, sowohl hinsichtlich ihrer Hauptelemente als auch ihrer Plot-Parameter im Basalttetraeder. Primitive MORB-Glaszusammensetzungen stellen keine primären Schmelzen dar, sondern sind durch Olivinfraktionierung von primitiven Magmen abzuleiten. Die Resultate dieser Untersuchungen werden mit früheren 10 kbar Experimenten verglichen.

Introduction

The nature, composition and depth of origin of primary magmas parental to Mid Ocean Ridge Basalts (MORB) is at the present time a subject of controversy (*Presnall* and *Hoover*, 1984, 1986; *Fujii* and *Scarfe*, 1985; *Elthon*, 1986). Two differing models of MORB petrogenesis are currently proposed in the literature. The first model termed here the 10 kbar[1] primary melt model states that the most primitive, in the sense of high $Mg/(Mg+Fe^{2+})$ ratio (Mg#), MORB glasses are close to or are in fact primary melts from the melting of upper mantle peridotite composition at relatively shallow depths, 30 km or 10 kbar pressure being the most commonly proposed depth of origin (*Bender* et al., 1978; *Fujii* and *Bougault*, 1983; *Fujii* and *Scarfe*, 1985; *Presnall* et al., 1979; *Presnall* and *Hoover*, 1984; *Green* and *Ringwood*, 1967). The second model, termed here the picrite primary melt model, states that these more primitive MORB glasses are not primary but are fractionated compositions, derived by olivine extraction from more picritic parents. The latter are interpreted as primary melts of mantle peridotite at pressures ranging from 15–20 kbars (*Green* et al., 1979; *Elthon* and *Scarfe* 1980, 1984; *Stolper*, 1980) or higher (30 kbar) pressures (*O'Hara*, 1968).
The two models place differing emphasis on the type of primary magmas which are involved in MORB genesis. In the 10 kbar primary melt model, picritic primary melts are considered to be of minor importance, primary melts being dominated by olivine tholeiite compositions similar to the most primitive of MORB glasses. Similarly in the picrite primary melt model, picritic melts are the dominant primary melts, while the presence of[1] primary olivine and quartz tholeiite melts is considered to be of minor importance.
Experimental petrologists have tested these two models by a combination of two methods, (1) near-liquidus studies of natural MORB glass compositions (*Bender*

[1] In this paper the term "10 kbar primary melt model" is used in a general sense to mean approximately 10 kbar, as some of the experiments discussed in this paper were conducted at pressures of 8, 9 and 10.5 kbar.

et al., 1978; *Green* et al., 1979; *Fujii* and *Bougault*, 1983; *Fujii* et al., 1978; *Kushiro* and *Thompson*, 1972) and (2) by the direct melting studies of peridotite compositions (*Jaques* and *Green*, 1980; *Takahashi* and *Kushiro*, 1983; *Fujii* and *Scarfe*, 1985; *Presnall* et al., 1979; *Sen*, 1982; *Green* et al., 1987). However, despite these efforts disagreement exists, mainly due to differing interpretations of the results from the experimental studies. In this study the second approach has been adopted and melting experiments have been carried out on a MORB pyrolite[2] composition at 10 kbar pressure using a basalt-peridotite sandwich technique. For comparison with MORB pyrolite, 10 kbar experiments on Tinaquillo lherzolite, Hawaiian pyrolite (*Jaques* and *Green*, 1980) and spinel lherzolite KLB-1 (*Takahashi*, 1986) were also performed. The basalt used in the "sandwich" is one of the most primitive MORB glasses recovered from the Mid-Atlantic ridge, DSDP 3-18-7-1 (*Frey* et al., 1974). The liquidus phase relationships of this composition were studied by *Green* et al. (1979). By using the sandwich technique it is possible to obtain information regarding the nature of equilibrium partial melts from a suitable source composition for MORB at 10 kbar. In this way we produce a direct testing of a 10 kbar primary melt model for MORB petrogenesis. The results of the 10 kbar melting experiments on the MORB pyrolite composition demonstrate that the majority of primitive MORB glasses are not primary melts at 10 kbar, thus making the picrite primary melt our preferred model for MORB petrogenesis. Prelimiary results of this study have been presented in *Green* et al. (1987). Before presenting the results of the 10 kbar melting study, it is worthwhile briefly reviewing the results and implications of high pressure near-liquidus experiments on MORB compositions.

Approach 1: High Pressure Near-Liquidus Experiments on MORB

Although the rationale behind this approach is relatively straightforward, the interpretation of the experimental results has been the cause of controversy (*Fujii* and *Bougault*, 1983; *Basaltic Volcanism Study Project*, 1981; *Thompson*, 1987). The rationale is as follows: if primitive MORB glasses are primary magmas then we expect to find at some pressure and temperature multiple saturation at or near the liquidus in the phases olivine, clinopyroxene + orthopyroxene or olivine + orthopyroxene suggesting equilibrium with an lherzolite or harzburgite residue respectively. In evaluating the importance of multiple saturation at or near liquidus temperatures, the glass in equilibrium with olivine, orthopyroxene ± clinopyroxene must be very close to the original bulk composition of the glass.

In this study primitive MORB glasses are defined solely on the basis of the $Mg/(Mg+Fe^{2+})$ ratio (Mg#), where Fe^{2+} is calculated using a $Fe^{2+}/(Fe^{3+}+Fe^{2+})$ ratio which has been set equal to 0.9. This value is appropriate for the reduced oxygen fugacity present in MORB source regions (*Christie* et al., 1986; *Green* et al., 1987). MORB glasses with $Mg\# \geqslant 0.68$ are defined as primitive, as they are consistent with equilibrium with a mantle olivine of $Mg\# \geqslant 0.87$ and are thus potential primary magmas from upper mantle peridotite. Glass compositions have been chosen instead of whole rock data as glass compositions represent liquid compositions, and do not suffer from the effects of crystal accumulation and alteration (*Melson* et al., 1977).

[2] "MORB pyrolite" is the name applied to a model source peridotite composition based on combining liquid (mid ocean ridge basalt) with residual peridotite (*Green* et al., 1979)

Table 1. *Compositions of MORB Glasses for Which the High Pressure Phase Relationships Have Been Experimentally Determined and the Range in Composition of Primitive MORB Glasses*

	1	2	3a	3b	3c	4	5	6
SiO_2	48.20	49.47	49.70	50.80	50.91	50.00	49.68	48.20 - 51.64
TiO_2	0.73	0.82	0.72	0.62	0.56	1.64	1.55	0.50 - 1.30
Al_2O_3	16.30	15.23	16.40	17.28	15.15	15.00	15.49	15.50 - 17.62
FeO^t	8.92	8.15	7.90	7.85	6.52	11.20	9.08	7.30 - 9.40
MgO	10.70	10.66	10.10	10.20	12.61	8.40	9.17	8.10 - 10.70
CaO	12.00	12.21	13.10	12.16	11.68	10.60	10.61	11.23 - 13.57
Na_2O	1.95	1.94	2.00	2.12	1.68	2.70	2.88	1.42 - 2.71
K_2O	0.09	0.16	-	-	-	-	-	0.01 - 0.32
P_2O_5	-	0.10	-	-	-	-	-	0.03 - 0.14
MnO	0.25	0.14	0.12	-	-	0.22	0.18	0.09 - 0.25
Cr_2O_3	0.05	-	0.07	-	-	-	-	0.01 - 0.13
Total	99.19	98.88	100.12	101.03	99.11	99.89	98.75	
Mg#	0.70	0.72	0.72	0.72	0.79	0.60	0.66	0.68 - 0.73
CIPW norm (molecular)								
Qz	-	-	-	-	-	-	-	<8.39
Ne	-	-	-	-	-	-	-	<1.00
Ab	14.51	14.76	15.04	16.03	12.54	20.47	21.77	10.53 - 20.79
An	29.39	27.44	29.95	31.70	28.78	24.02	24.44	24.92 - 34.04
Di	19.95	23.34	24.50	19.11	20.56	20.41	19.90	18.76 - 29.45
Hy	9.32	15.97	11.63	18.33	28.43	15.54	10.78	<24.96
Ol	22.78	13.93	15.34	11.73	6.65	12.27	16.53	<28.33
CaO/Al_2O_3	0.78	0.80	0.79	0.70	0.77	0.71	0.68	0.67 - 0.88
CaO/Na_2O	6.15	6.29	6.55	5.73	6.95	3.92	3.68	4.58 - 9.49
CaO/TiO_2	16.44	14.90	18.19	19.61	20.86	6.50	6.84	9.32 - 25.60
Al_2O_3/TiO_2	22.33	18.57	22.77	27.87	27.05	9.14	9.99	12.00 - 33.80

(1) primitive MORB glass ALV527-1-1 from the FAMOUS area of the Mid-Atlantic Ridge (*Bender* et al., 1978).

(2) primitive MORB glass ARP74-10-16 from the FAMOUS area of the Mid-Atlantic Ridge (*Fujii* and *Bougault*, 1983).

(3a) primitive MORB glass DSDP3-18-7-1 from the South Atlantic (*Frey* et al., 1974; *Green* et al. 1979).

(3b) glass in equilibrium with calcic clinopyroxene, run T-25, 1300°C, 12 kbar (*Green* et al., 1979).

(3c) glass in equilibrium with orthopyroxene, run T-16, 1360°C, 12kbar (*Green* et al., 1979).

(4) aphyric glassy olivine tholeiite, sample Leg45-395A-8-1-9 from the Mid-Atlantic Ridge (*Fujii* and *Kushiro*, 1977).

(5) olivine tholeiite, sample T-87 from the Mid-Atlantic Ridge (*Kushiro* and *Thompson*, 1972; *Kushiro*, 1973).

(6) Minimum and maximum values for over 80 primitive MORB glasses (data sources, see caption to Fig.4).

Listed in Table 1 are the compositions of MORB glasses which have had their high-pressure near liquidus phase relationships determined. Three of the MORBs, DSDP 3-18-7-1, ALV 527-1-1 and ARP 74-10-16 have high Mg# and conform to our definition of primitive MORB glasses. However two of the MORBs, 395 A-8-1-9 and T-87 have significantly lower CaO, Mg# and higher FeO than the three above mentioned primitive MORB glasses and are not considered primitive according to our criteria. In the following sections the results of the high-pressure near liquidus experiments are evaluated to determine whether or not primitive MORB glasses are saturated in orthopyroxene near their liquidi at 10 kbars pressure.

High-Pressure Near-Liquidus Experiments on ALV 527-1-1 and DSDP 3-18-7-1

Both ALV 527-1-1 (*Bender* et al., 1978) and DSDP 3-18-7-1 (*Green* et al., 1979) have very similar phase relationships. Olivine is the liquidus phase until approximately 12 kb when it is replaced by clinopyroxene. Both compositions fail to show multiple saturation at any pressure with the assemblage olivine + orthopyroxene ± clinopyroxene. An orthopyroxene reported in a run at 15 kbar on ALV 527-1-1 (*Bender* et al., 1978) is now considered to be an aberrant result (*Fujii* and *Bougault*, 1983; *Elthon* and *Scarfe*, 1984).

Green et al. (1979) added orthopyxroxene to DSDP3-18-7-1 at 12 kbar to test how close to orthopyroxene saturation DSDP 3-18-7-1 was. They found that between 5 to 9 wt% orthopyroxene had to be added to DSDP 3-18-7-1, significantly changing the bulk composition (see Table 1, 3b and 3c), before orthopyroxene appeared on the liquidus. On the basis of this result *Green* et al. (1979) added olivine to DSDP 3-18-7-1 to evaluate whether at a higher pressure and temperature an olivine-enriched magma could be saturated in olivine + orthopyroxene ± clinopyroxene. A MORB picrite composition (DSDP 3-18-7-1 + 17 wt% olivine) was found to be multiply saturated in olivine + orthopyroxene at 20 kbar, 1430 °C, thus this composition is a possible primary MORB magma in equilibrium with a harzburgite residue.

Fujii and *Bougault* (1983) discussed the validity of the orthopyroxene addition experiments of *Green* et al. (1979); because the topology of the orthopyroxene-olivine phase boundary is unknown or uncertain, permissible topologies could be constructed in which a large amount of added orthopyroxene would be required before orthopyroxene saturation is reached even though the composition of DSDP 3-18-7-1 is close to the olivine-orthopyroxene cotectic (see for example Fig. 3.3.14, *Basaltic Volcanism Study Project*, 1981). Thus the orthopyroxene addition experiments of *Green* et al. (1979) did not fully evaluate the "closeness" to multiple saturation of DSDP 3-18-7-1 nor directly determined the composition of liquids, close to DSDP 3-18-7-1, which were olivine + orthopyroxene ± clinopyroxene saturated at 10 kbar. However the sandwich technique used in this experimental study by its very nature will "force" the composition of DSDP 3-18-7-1 to equilibrate with a peridotite mineralogy. The resulting equilibrium glass composition can then be compared with the bulk composition of DSDP 3-18-7-1. It will be shown that liquids in equilibrium with olivine + orthopyroxene ± clinopyroxene at 10 kbar, as determined by the sandwich technique used in this study, are substantially different from DSDP 3-18-7-1 confirming the conclusions of *Green* et al. (1979) based on the orthopyroxene addition experiments.

High-Pressure Near-Liquidus Experiments on ARP 74-10-16

The experimental results on ARP 74-10-16 (*Fujii* and *Bougault*, 1983) differ from the previous two studies as multiple saturation in olivine + clinopyroxene + orthopyroxene occurred at 10 kbar. The appearance of orthopyroxene could be explained by the fact that ARP 74-10-16 has a higher normative Hy content then DSDP 3-18-7-1 or ALV 527-1-1 (Table 1). On the basis of their experiments *Fujii* and *Bougault* (1983) claim that ARP 74-10-16 is a possible primary magma of spinel or plagioclase lherzolite at 10 kbar, thus giving support to a 10 kbar primary melt model. However the run data presented by *Fujii* and *Bougault* (1983) (their Table 3) shows that the multiple saturation occurred between 25 to 50 °C below the liquidus, at 10 kbar. If ARP 74-10-16 was a primary magma multiple saturation would be expected ~ 5–10 °C below the liquidus. *Fujii* and Bougault (1983) fail to provide electron microprobe (EMP) analyses of the glass composition in equilibrium with olivine + orthopyroxene + clinopyroxene at 10 kbar, making it impossible to evaluate whether or not their conclusions concerning ARP 74-10-16 are valid or not. If the orthopyroxene did in fact crystallize ~ 50 °C below the liquidus at 10 kbar, then it is likely that the charge was highly crystalline making it impossible to obtain unmodified glass compositions, hence explaining the lack of this critical data in *Fujii* and *Bougault* (1983).

High-Pressure Near-Liquidus Experiments on 395 A-8-1, 50 cm and T-87

The experimental results on the two more Fe-rich MORBs 395 A-8-1, 50 cm (*Fujii* et al., 1978) and T-87 (*Kushiro* and *Thompson*, 1972) showed that they were saturated in orthopyroxene approximately 20 °C below the liquidus at approximately 8 kbar for 395 A-8-1, 50 cm and approximately 10 °C below the liquidus at 7.5 kbar for T-87. For these two magmas to be considered primary magmas then we must envisage a mantle source peridotite with olivine $\leqslant Fo_{86}$ (cf. *Wilkinson*, 1982). The liquid in equilibrium with orthopyroxene published by *Kushiro* (1973) has a Mg# of 0.57 and would only be in equilibrium with a mantle olivine of Fo_{82} which differs considerably from previous estimates of mantle peridotite for MORB, which have an olivine of $Fo_{90\pm2}$ (*Green*, 1970, 1971; *Frey* et al., 1985; *Nickel* and *Green*, 1984; *Jaques* and *Green*, 1980). Thus if we accept arguments in favour of a mantle olivine of $Fo_{90\pm2}$ then the two Fe-rich MORBs must be regarded as fractionated compositions, a possibility recognized by *Kushiro* and *Thompson* (1972). The Ni contents of these two compositions are appreciably lower than commonly inferred for primitive magmas (*Allegre* et al., 1977; *Sato*, 1977), supporting the conclusion that T-87 and 395 A-8-1, 50 cm are fractionated compositions, which have reached orthopyroxene saturation at some lower pressure from that of their parental compositions.

In summary the first approach has not been all that successful in demonstrating the primary nature of primtive MORB. However when interpreted correctly the results from the primitive MORBs ALV 527-1-1, DSDP 3-18-7-1 and ARP 74-10-16 suggest that these and MORB of similar composition are not multiply saturated at 10 kbar, near their liquidi. The multiple saturation in ARP 74-10-16 occurs well below its liquidus temperature.

Table 2. *Compositions of Peridotites and Basalt Compositions Used in This Study*

	1	2	3	4	5	6	7	8	9
SiO_2	44.32	44.74	47.15	47.50	47.90	44.48	49.70	49.03	49.76
TiO_2	0.16	0.17	0.28	0.13	1.18	0.16	0.72	0.30	3.20
Al_2O_3	4.33	4.37	7.28	5.35	5.91	3.59	16.40	14.35	14.28
FeO^t	9.82	7.55	7.27	7.51	8.81	8.10	7.90	9.00	8.96
MnO	0.10	0.11	0.12	0.18	0.13	0.12	0.12	0.00	0.00
MgO	36.84	38.57	30.57	32.80	28.80	39.22	10.10	13.63	10.48
CaO	3.34	3.38	5.63	4.97	5.14	3.44	13.10	12.40	9.14
Na_2O	0.39	0.40	0.66	0.30	0.95	0.30	2.00	1.15	3.27
K_2O	0.00	0.00	0.00	0.03	0.22	0.02	0.00	-	0.76
P_2O_5	0.00	0.00	0.00	0.02	0.06	0.03	0.00	-	-
Cr_2O_3	0.44	0.45	0.75	0.75	0.72	0.31	0.07	-	-
NiO	0.25	0.26	0.29	0.43	0.13	0.25	0.03	-	-
Total	99.99	100.00	100.00	99.97	99.95	100.02	100.14	99.86	99.85
Mg#	0.87	0.90	0.88	0.89	0.85	0.90	0.69	0.73	0.67
CIPW norm (molecular)									
Ab	2.14	2.17	3.97	1.79	5.81	1.62	15.09	8.45	23.34
An	6.16	6.12	11.33	8.73	7.64	5.10	30.07	27.82	17.53
Di	3.98	4.01	7.39	7.54	9.47	5.04	24.56	22.53	18.53
Hy	13.20	12.49	22.22	27.97	25.46	12.18	12.10	20.82	3.56
Ol	72.52	73.47	52.56	51.69	45.88	74.37	14.69	18.10	23.22
CaO/Al_2O_3	0.77	0.77	0.77	0.93	0.87	0.96	0.79	0.86	0.64
CaO/Na_2O	8.56	8.45	8.53	16.56	5.41	11.46	6.55	10.78	2.79
CaO/TiO_2	20.87	19.88	20.11	38.23	4.35	21.50	18.19	41.33	2.86
Al_2O_3/TiO_2	27.06	25.70	26.00	41.15	5.01	22.44	22.77	47.83	4.46

(1) MORB pyrolite composition MPY-87.

(2) MORB pyrolite composition MPY-90.

(3) MORB pyrolite MPY-90 minus 40% olivine ($Mg_{91.6}Fe_{8.1}Ni_{0.2}Mn_{0.1}$), MPY-90-40.

(4) Tinaquillo lherzolite minus 40% olivine ($Mg_{91.9}Fe_{8.0}Mn_{0.1}$), TQ-40.

(5) Hawaiian pyrolite minus 40% olivine ($Mg_{91.6}Fe_{8.1}Ni_{0.2}Mn_{0.1}$), HW-40.

(6) Spinel lherzolite KLB-1 (*Takahashi*, 1986).

(7) Primitive MORB glass DSDP3-18-7-1 (*Green* et al., 1979).

(8) *Jaques* and *Green* (1980) calculated melt composition from Tinaquillo at 10kbar, 1300°C. Composition given is the mix composition as determined by broad beam electron microprobe analysis.

(9) *Jaques* and *Green* (1980) calculated melt composition from Hawaiian pyrolite at 10kbar, 1250°C. Composition given is the mix composition as determined by broad beam electron microprobe analysis.

t=total iron as FeO, Mg#=Mg/(Mg + Fe^t), (-) below detection limit.

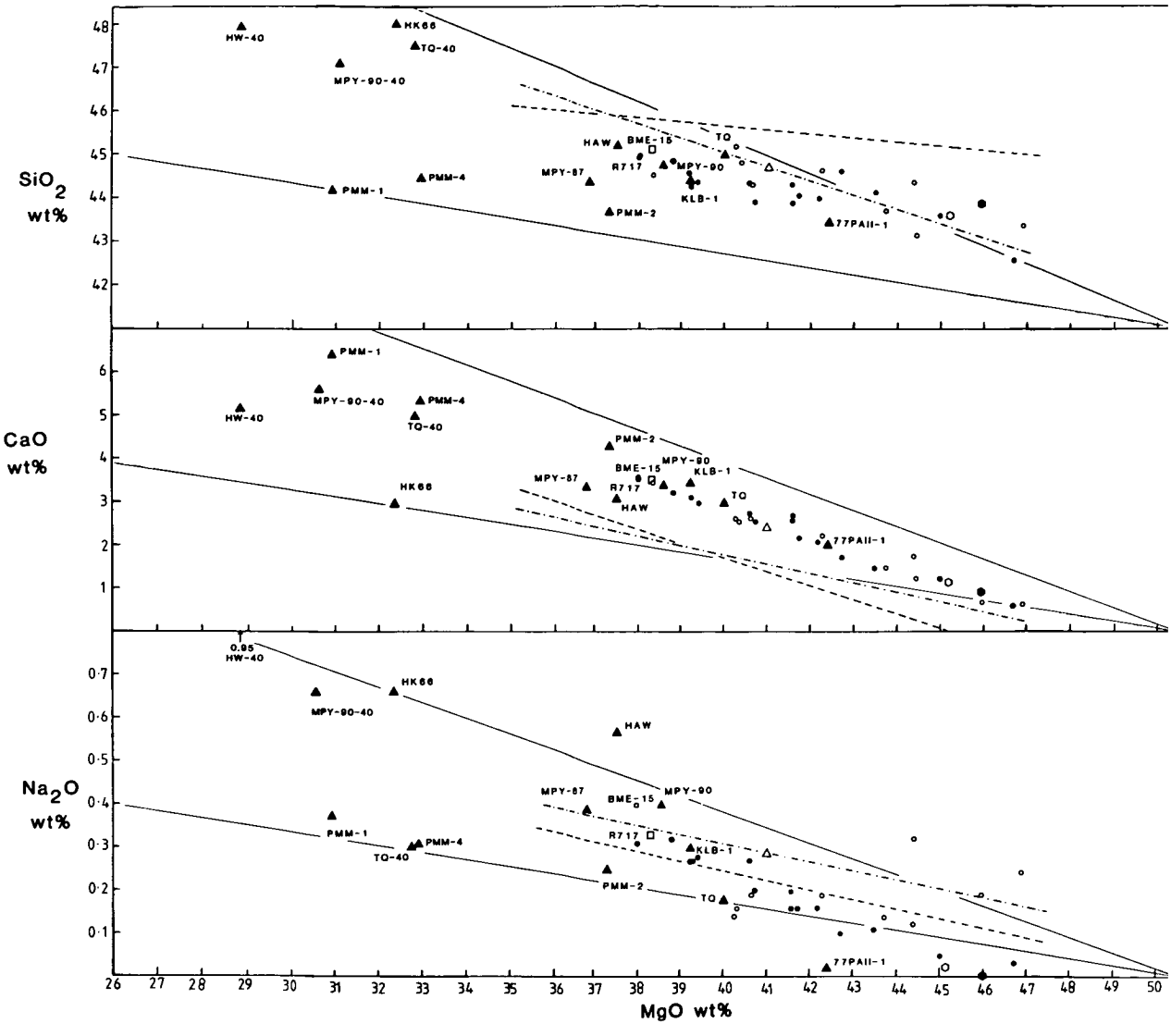

Fig. 1

Fig. 1. Major element oxides SiO_2, CaO, Na_2O, FeOt, Al_2O_3 and TiO_2 versus MgO for peridotite compositions used in 10 kbar melting experiments compared with natural peridotite suites. ● peridotite compositions from the Ronda high temperature peridotite intrusion (*Frey* et al., 1985). R 717 is the most "fertile" composition from the Ronda suite. ○ peridotite xenolith compositions from Lake Bullenmerri, Victoria, (*Nickel* and *Green*, 1984). BME-15 is the most "fertile" peridotite composition from Lake Bullenmerri. △ estimated primitive undepleted mantle composition (*Maaloe* and *Aoki*, 1977). □ estimate of mantle composition (*Jagoutz* et al., 1979). ⬡ average of 50 representative plagioclase-free spinel harzburgites and lherzolites from the ocean ridges and fracture zones (*Dick* and *Fisher*, 1984). ⬢ residue composition based on the extraction of a 24% partial melt of a MORB picrite (DSDP 3-18-7-1 plus 17 wt% olivine) from MORB pyrolite (*Green* et al., 1979). ▲ peridotite compositions used in 10 kbar melting studies, each compositions used

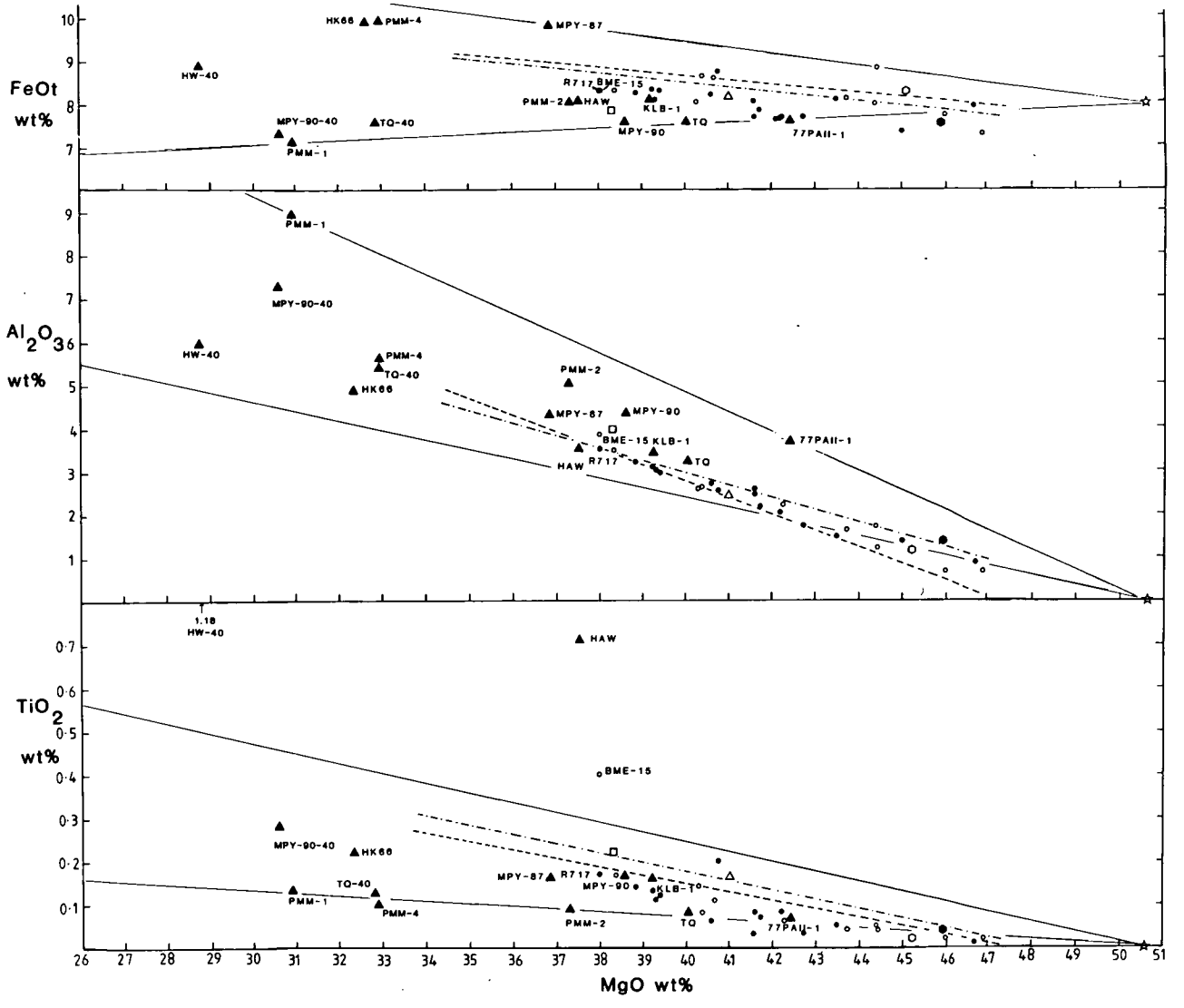

Fig. 1 (continued)

in 10 kbar melting studies, each composition is individually marked as follows: HAW Hawaiian pyrolite (*Jaques* and *Green*, 1980). HW-40 Hawaiian pyrolite minus 40 wt% olivine (*Jaques* and *Green*, 1980). TQ Tinaquillo lherzolite (*Jaques* and *Green*, 1980). TQ-40 Tinaquillo lherzolite minus 40 wt% olivine (*Jaques* and *Green*, 1980). 77 PAII-1 plagioclase and spinel lherzolite from Pali vent no. 2, Oahu (*Sen*, 1982). HK 66 spinel lherzolite from Salt Lake Crater, Hawaii (*Takahashi* and *Kushiro*, 1983). PMM-1, PMM-2, PMM-4 spinel lherzolite compositions studied by *Fujii* and *Scarfe*, 1985. KLB-1 spinel lherzolite inclusion from the Kilbourne Hole Crater, New Mexico (*Takahashi*, 1986). MPY-87, MPY-90, MPY-90-40 MORB pyrolite starting compositions used in this study. $-\cdot-\cdot-\cdot-$ regression line for 83 oceanic spinel lherzolite xenoliths (*Maaloe* and *Aoki*, 1977). $- - - -$ regression line for ocean-floor peridotites (*Shibata* and *Thompson*, 1986). ☆ olivine ($Fo_{91.6}$) composition. ——— olivine control lines from olivine ($Fo_{91.6}$)

Approach 2: Direct Melting Experiments on Peridotite Compositions

The second approach which experimental petrologists have used in the investigation of MORB petrogenesis is the direct melting of upper mantle peridotite. The rationale of this approach is again straightforward: if primitive MORB glasses are primary magmas at 10 kbar then it should be possible to produce similar compositions as equilibrium partial melts from suitable source compositions at 10 kbar. Choosing a suitable starting composition however is of critical importance as numerous studies have shown that liquid compositions are not invariant but are affected by the bulk compositions of the starting material (*Jaques* and *Green*, 1980; *Takahashi* and *Kushiro*, 1983; *Fujii* and *Scarfe*, 1985). The peridotite starting compositions used in this study are listed in Table 2. The main composition used is a MORB pyrolite composition calculated by *Green* et al. (1979) based on combining 24 wt% of the pricrite composition (mix E, *Green* et al., 1979) which was in equilibrium with olivine + orthopyroxene at 20 kb, 1430 °C with a harzburgite residue. The choice of "harzburgite" residue in the calculation of "MORB" pyrolite composition requires some comment as *Fujii* and *Scarfe* (1985) criticize the *Green* et al. (1979) calculation of the model source on the basis that most ultramafic rocks dredged form the ocean floor are not harzburgite but lherzolite. However *Dick* and *Fisher* (1984) calculate an average composition for dredged ultramafic rocks (lherzolites) from the Indian-Antarctic ridge which is remarkably similar to the residual "harzburgite" of *Green* et al. (1979) (see Fig. 1). Reconciliation of the apparently different interpretations lies in recognizing that the orthopyroxene in residual harzburgite at 15–20 kbar, 1400–1450 °C contains >5 wt% Al_2O_3 and >2.5 wt% CaO. Residual harzburgite of this character will recrystallize at lower temperatures to spinel lherzolite.

The other compositions used are Tinaquillo lherzolite minus 40 wt% olivine, Hawaiian pyrolite minus 40 wt% olivine and the spinel lherzolite KLB-1 (powder kindly supplied by *E. Takahashi*). The melting relations of Tinaquillo and Hawaiian pyrolite have been studied previously by *Jaques* and *Green* (1980) and that of KLB-1 has been studied by *Takahashi* (1986). Three different MORB pyrolite compositions were used in the experiments designated MPY-87, MPY-90 and MPY-90-40. MPY-90 is the MORB pyrolite originally calculated by *Green et al.* (1979), MPY-90-40 is MPY-90 minus 40 wt% olivine and MPY-87 is a result of recalculating MPY-90 to a lower Mg# to produce a more Fe-rich pyrolite composition. The more Fe-rich composition is biassed towards yielding MORB olivine tholeiites as primary melts since most primitive olivine tholeiites have Mg# between 0.68–0.70 and if they are primary melts require residual peridotite with olivine $\geq Fo_{87}$ [$(K_D)^{Ol/Liq}_{Fe/Mg} = 0.32$]. Olivine contains only Mg, Fe and Ni in solid solution and the effect of extracting 40 wt% olivine from the model source composition cannot affect phase relations or phase compositions in any way *except* in Mg, Fe, or Ni concentration, as long as olivine is a residual phase. Put another way, the effect of extracting 40 wt% olivine of Fo_{91} composition will only be to lessen the buffering role of olivine in Mg# and Ni content -thus liquids and residues for pyrolite-40 wt% olivine will change a little more rapidly than for pyrolite in Mg# and Ni content with increasing degree of melting. The net result of olivine subtraction is to increase the modal abundance of pyroxene, spinel and melt at the expense of olivine and to slightly underestimate the Mg# of liquids and residues in equilibrium with residual olivine of $<Fo_{91}$ (i.e. low degrees of melting) and to slightly overestimate the Mg#

of liquids and residues in equilibrium with olivine of $> Fo_{91}$. In the following section the suitability of these starting compositions for studies of MORB petrogenesis is discussed with reference to natural peridotite suites.

Natural Peridotite Suites as a Constraint on Suitable Source Compositions for MORB Petrogenesis

An important constraint on the choice of a suitable source composition is the variability in natural peridotite compositions of upper mantle origin. Two peridotite suites which are representative of moderate pressure upper mantle peridotite samples have therefore been chosen to illustrate their chemical coherence and relevance in defining upper mantle source compositions. The peridotite suites are the Ronda high temperature peridotite intrusion (*Frey* et al., 1985) and spinel lherzolite inclusions from Lake Bullenmerri, Victoria (*Nickel* and *Green* 1984). Both suites have suitable major and trace element characteristics for the production of MORB (*Frey* et al., 1985; *Nickel* and *Green*, 1984).

Both the peridotite suites give well-defined linear major element trends when plotted against MgO (Fig. 1). These linear oxide trends are interpreted as being produced by batch partial melting combined with the incomplete extraction of a partial melt of picritic composition (*Frey* et al., 1985; *Nickel* and *Green*, 1984). These picritic melts, which related the more fertile to the more depleted peridotite compositions are suitable parental magmas to MORB (*Frey* et al., 1985; *Nickel* and *Green*, 1984). These linear oxide trends include at their residual or refractory MgO-rich end, the average of 50 representative plagioclase-free spinel harzburgite and lherzolites dredged from oceanic ridges and fracture zones (*Dick* and *Fisher*, 1984) and the very similar residue composition calculated by *Green* et al. (1979) for extraction of 24 wt% partial melt of MORB picrite (DSDP 3-18-7-1 + 17 wt% olivine) from MORB pyrolite composition. The trends also include less refractory primitive mantle composition estimates based on spinel lherzolite suites by *Maaloe* and *Aoki* (1977) and *Jagoutz* et al. (1979).

For comparison the regression line for 83 oceanic lherzolite xenoliths from *Maaloe* and *Aoki* (1977) and the regression line for ocean-floor peridotites from *Shibata* and *Thompson* (1986) are plotted in Fig. 1. Both regression lines plot within the peridotite array defined by Ronda and Bullenmerri for most oxides. However the regression line of *Shibata* and *Thompson* (1986) plots at significantly higher SiO_2 contents and lower CaO contents than the Ronda and Bullenmerri suites. The data set used by *Shibata* and *Thompson* (1986) is of serpentinized peridotite and the process of serpentinization is not always isochemical but may increase the SiO_2/MgO ratios and leach CaO.

Based on the above linear oxide trends displayed by the Ronda and Bullenmerri suites, suitable starting compositions for melting experiments relevant to MORB should lie within or close to the trends defined by the two peridotite suites. In Fig. 1 a number of peridotite compositions used in melting experiments, such as PMM-1 (*Fujii* and *Scarfe*, 1985) and HK 66 (*Takahashi* and *Kushiro*, 1983) plot well away from the peridotite array. However these compositions plot in a similar position to the minus 40 wt% olivine compositions of Tinaquillo lherzolite, Hawaiian and MORB pyrolite (TQ-40, HW-40, MPY-90-40 respectively Fig. 1). Thus the suitability of peridotite starting compositions used in melting experiments must be evaluated on the basis of whether they plot in or near the peridotite array, or

Table 3. *Comparison of Peridotite Starting Compositions with Natural Peridotite Suites on the Basis of Olivine Control Lines from (Fo_{91})*

	SiO_2	CaO	Na_2O	FeO	Al_2O_3	TiO_2
TQ (TQ-40)	OK	OK	LO	OK	OK	OK
HW (HW-40)	OK	LO	HI	OK	OK	HI
MPY-87	LO	OK	OK	HI	OK	OK
MPY-90 (MPY-90-40)	OK	OK	OK	OK	OK	OK
HK66	HI	LO	HI	HI	OK	OK
KLB-1	OK	OK	OK	OK	OK	OK
77PAII-1	OK	OK	LO	OK	OK	OK
PMM-1	LO	HI	OK	OK	HI	OK
PMM-2	LO	HI	OK	OK	HI	OK
PMM-4	LO	OK	OK	HI	OK	OK

The terms OK, LO, HI are used to indicate the relative position of the above peridotite compositions to the natural peridotite array in Fig.1. OK indicates the composition falls near or close to the natural array, HI indicates it falls above and LO indicates it plots below the natural array, see text for a more complete explanation.

whether they would plot in or near the array if olivine was added to them until they plot within the natural peridotite array. For the purposes of this comparison olivine control lines were drawn from an olivine composition of $Fo_{91.6}$. Table 3 summaries the results of this analysis for all the peridotite starting compositions used in 10 kbar melting studies. From Table 3 it can be seen that the compositions KLB-1, Tinaquillo and MORB pyrolite are the most suitable starting materials for MORB petrogenesis. Compositions such as those used by *Fujii* and *Scarfe* (1985) (PMM-1, -2 and -4) are not suitable as they have significantly lower SiO_2 and slightly higher Al_2O_3 and CaO contents than the natural peridotite array. Hawaiian pyrolite is clearly unsuitable as a MORB source in TiO_2 and Na_2O content but not in other major oxides.

Experimental Approach and Techniques

The experimental determination of equilibrium partial melts of peridotite compositions in the past has been fraught with difficulties. The direct EMP analyses of glass in the charge does not give correct glass compositions due to quench modification of the glasses (*Green*, 1973). However if the glass is sufficiently abundant, as is the case in higher degrees of partial melting, then reasonably accurate glass compositions can be obtained.

Jaques and *Green* (1979, 1980) avoided the quench problem by analysis of all the residual crystalline phases, combined with modal analysis of the charge, thus enabling the calculation of the equilibrium partial melt by mass balance. This approach suffers from uncertainties in the modal analysis and in the composition of the residual phases where Fe-loss has occurred in the experiments. Reversal work on the *Jaques* and *Green* (1980) calculated equilibrium liquids has shown many of

them to be too olivine rich, the equilibrium liquids liying at more silica-saturated compositions (*Falloon* et al., 1988). Another successful approach has been the "sandwich" technique where a basalt is placed in between peridotite and allowed to equilibrate with the peridotite and its partial melt at a desired pressure and temperature. This provides a large area of glass to be analysed at the end of the run (*Stolper*, 1980; *Takahashi* and *Kushiro*, 1983; *Fujii* and *Scarfe*, 1985). The character of the resultant partial melts however is very much dependent on the character of the basalt used in the sandwich and the resulting bulk composition of the mixture. In this study we have used the MORB glass DSDP 3-18-7-1 (*Green* et al., 1979; *Frey* et al., 1974) as the basalt in the "sandwich" between layers of MORB pyrolite and because there is a close compositional link between DSDP 3-18-7-1 and the calculated MORB pyrolite compositions of *Green* et al. (1979) the resultant equilibrium melts are an internally consistent and coherent evaluation of the ability of the MORB pyrolite composition to yield MORB basaltic or picritic primary magmas. In the "sandwich" experiments on Hawaiian pyrolite and Tinaquillo lherzolite, the basaltic layers were glasses of the compositions calculated by *Jaques* and *Green* (1980) for the appropriate P and T conditions.

All the starting mixes used (Table 2) except KLB-1 were made up from sintered oxides, crushed in acetone and fired at 1000 °C. Fayalite was then added to the mixes before refiring in a silica evacuated tube at 1000 °C. The mixes were then stored in an oven at 110 °C. The DSDP 3-18-7-1 mix was the same as that used by *Green* et al. (1979). The KLB-1 mix consists of powdered natural peridotite. The mixes were then loaded into graphite capsules and sealed in an outer platinum capsule. Two sizes of graphite capsule were used; in the large bore graphite capsule, a layer of DSDP 3-18-7-1 mix was loaded between layers of MORB pyrolite. In the small bore graphite capsules only two layers were used the basalt layer forming the top layer (DSDSP 3-18-7-1 or *Jaques* and *Green*, 1980 calculated liquids in the case of Tinaquillo lherzolite and Hawaiian pyrolite). The wt% basalt in each bulk composition is given in Table 4.

All experiments were carried out in a high pressure piston cylinder apparatus at the University of Tasmania, a piston-in technique with a pressure correction of minus 10% nominal piston pressure was used. A 0.5 inch diameter, talc-pyrex assembly was used with a graphite heater. A pure alumina thermocouple sheath was used, with sintered alumina components surrounding the capsule. The thermocouple sheath enters the assembly through a mullite sleeve. The bottom spacer is fired pyrophyllite (mullite and silica).

Both $Pt/Pt_{90}Rh_{10}$ and $W_{75}Re_{25}/W_{97}Re_3$ thermocouples were used in the course of the experimental study. Significant thermocouple drift was experienced on long runs when using the $Pt/Pt_{90}Rh_{10}$ thermocouple.

As the composition of olivine above the solidus is sensitive to temperature (*Jaques* and *Green*, 1980; *Roedder* and *Emslie*, 1970), in those runs which had experienced thermocouple drift, the temperature of the run was determined by comparing the equilibrium olivine composition with olivine compositions produced in experiments using $W_{75}Re_{25}/W_{97}Re_3$ thermocouples. The $W_{75}Re_{25}/W_{97}Re_3$ thermocouples were controlled by a Kent P 96 M controller, temperatures being accurate to ± 1 °C. Temperatures listed in Table 4 are in agreement with the experiments of *Takahashi* (1986) on KLB-1 which is similar in composition to the MORB pyrolite composition studied.

Table 4. *10 kbar Peroditite-Basalt Sandwich Experiments*

Run no.	T(°C)	Time(hrs)	Capsule type	Peridotite Composition	Basalt wt%	Phases present
T-1511	1310	24.0	A	MPY-87	5.5	Ol + Opx + Cpx + Sp + m + L
T-1472	1350	3.0	A	MPY-87	9.5	Ol + Opx + Cpx + Sp + L
T-2123	1350	30.0	B	MPY-87	18.0	Ol + Opx + Cpx + Sp + L
T-1493	1350	3.0	A	MPY-87	10.4	Ol + Opx + Cpx + m + L
T-1478	1400	3.5	A	MPY-87	10.3	Ol + Opx + Cpx + m + L
T-2140	1400	32.0	B	MPY-87	23.0	Ol + Opx + Cpx + Sp + L
T-1464	1420	1.5	A	MPY-87	12.0	Ol + Opx + m + L
T-1480	1420	2.0	A	MPY-87	10.2	Ol + Opx + m + L
T-1461	1420	24.0	A	MPY-87	14.0	Ol + Opx + m + L
T-2113	1375	18.0	B	TQ-40	23.5	Ol + Opx + Cpx + Sp + L
T-2117	1325	25.0	B	HW-40	24.0	Ol + Opx + Cpx + L
T-2133	1350	25.0	B	KLB-1	23.0	Ol + Opx + Cpx + Sp + L
T-2121	1230	24.0	B	MPY-90-40	30.0	Ol + Opx + Cpx + Pl + Sp + L
T-2078	1300	25.0	B	MPY-90-40	17.6	Ol + Opx + Cpx + Sp + L
T-2138	1350	24.0	B	MPY-90-40	27.0	Ol + Opx + Cpx + Sp + L
T-2136	1350	24.0	B	MPY-90	24.0	Ol + Opx + Cpx + Sp + L

Ol olivine, Opx orthopyroxene, Cpx clinopyroxene, Sp aluminous spinel, m metallic globule (Fe,Ni), Pl plagioclase, L liquid (Glass), Q quench crystals.

A and B stand for large and small bore graphite capsules respectively

At the end of the run the sample was removed from the graphite capsule and sectioned longitudinally for microprobe analysis. All analyses were done on a JEOL JX 50 A electron microprobe-scanning electron microscope, at the University of Tasmania, fitted with an energy dispersive EDAX analytical system (operating conditions 15 kv, 7×10^{-10} A), calibration was on pure Cu. Back scattered electron photographs were taken of all run products to check on the compositional uniformity of all the phases (Phillips 505 SEM, operating conditions 20 kv, spot size 100 ηm).

Experimental Results

Details of the experimental runs are given in Table 4. The compositions of equilibrium partial melts produced in the experiments are given in Tables 5 and 6. The compositions of the partial melts are compared with primitive MORB glasses in Figs. 4, 5, 6 and 7. Representative residual phase compositions are presented in Table 7.

Attainment of Equilibrium

In most runs the liquid layer was quenched as a coherent glass layer (100–300 μm) between or on top of the peridotite layer(s) which consist of crystals and glass (Fig. 2). In some runs close to the solidus (T-1511 and T-2078) abundant clinopyroxene crystallization occurred within the glass layer and the glass composition was obtained by analysing large pools of glass (50–70 μm) within the charge.

Table 5. *Compositions of Equilibrium Partial Melts at 10 kbar from MORB Pyrolite (MPY-87)*

	1	2	3	4	5	6	7	8	9	10
SiO_2	50.90	50.20	50.36	50.37	50.54	50.78	50.07	50.04	50.38	0.17
TiO_2	0.81	0.65	0.77	0.65	0.60	0.67	0.53	0.57	0.55	0.05
Al_2O_3	19.16	17.21	17.05	17.11	15.94	15.42	14.87	14.61	14.25	0.12
FeO^t	6.82	7.68	7.51	7.54	7.61	7.79	8.15	8.40	8.15	0.13
MgO	8.52	10.50	10.37	10.41	11.34	11.12	13.46	13.57	13.58	0.17
CaO	10.48	11.60	11.53	11.74	11.96	12.10	11.26	11.11	11.74	0.09
Na_2O	3.31	2.18	2.18	2.17	1.89	1.83	1.55	1.53	1.57	0.06
Cr_2O_3	-	-	0.24	-	0.26	0.27	0.24	0.26	0.36	0.04
Total	100.00	100.02	100.01	99.99	100.14	99.98	100.09	100.09	99.86	
Mg#	0.69	0.71	0.71	0.71	0.73	0.72	0.75	0.74	0.75	
CIPW norm (molecular)										
Ab	25.22	16.52	16.63	16.52	14.31	13.98	11.48	11.32	11.67	
An	31.77	31.40	31.22	31.32	29.54	28.83	27.73	27.21	26.37	
Di	12.37	17.20	17.39	18.05	20.52	22.27	18.53	18.24	19.32	
Hy	9.01	17.79	20.14	18.42	22.12	24.74	25.22	26.28	27.60	
Ol	18.10	13.92	10.75	12.56	10.11	6.49	14.04	13.58	11.59	
CaO/Al_2O_3	0.55	0.67	0.67	0.68	0.75	0.78	0.76	0.76	0.78	
CaO/Na_2O	3.16	5.32	5.28	5.41	6.33	6.61	7.26	7.26	7.08	
CaO/TiO_2	12.94	17.85	14.97	18.06	19.93	18.06	21.24	19.49	20.22	
Al_2O_3/TiO_2	23.65	26.47	22.14	26.32	26.56	23.01	28.06	25.63	25.91	

(1) run no. T-1511, (2) run no. T-1472, (3) run no. T-2123, (4) run no. T-1493, (5) run no. T-1478, (6) run no. T-2140, (7) run no. T-1464, (8) run no. T-1480, (9) run no. T-1461, (10) average σ values for the glass analyses.
t= total iron as FeO, Mg#=Mg/(Mg + Fe^t), (-) below detection limit, MnO values all below detection limit, for run details refer to Table 4.

Table 6. *Compositions of Equilibrium Partial Melts at 10 kbar from Various Peridotite Compositions*

	1	2	3	4	5	6	7	8	9
SiO_2	50.47	50.78	50.27	50.55	49.88	50.73	50.69	51.32	50.48
TiO_2	0.42	3.34	0.68	0.96	0.81	0.73	0.70	0.61	0.87
Al_2O_3	15.29	15.45	17.31	17.71	18.99	17.68	16.81	16.11	15.33
FeO^t	7.41	7.78	6.94	7.77	6.92	6.67	6.53	4.89	8.36
MgO	12.05	8.57	10.75	9.31	9.40	10.19	11.14	12.42	10.72
CaO	12.83	9.56	11.95	11.06	11.11	11.71	12.04	12.66	11.84
Na_2O	1.15	3.47	2.03	2.63	2.84	2.19	1.97	1.58	1.88
K_2O	-	0.71	-	-	-	-	-	-	0.17
Cr_2O_3	0.32	0.22	-	-	-	-	-	0.34	nd
MnO	-	-	-	-	-	-	-	-	0.15
P_2O_5	-	-	-	-	-	-	-	-	0.09
Total	99.94	100.08	99.93	99.99	99.95	99.90	99.88	99.93	99.80
Mg#	0.74	0.66	0.73	0.68	0.71	0.73	0.75	0.82	0.69
CIPW norm (molecular)									
Ab	8.84	25.55	15.45	20.11	21.39	16.83	14.99	12.10	14.39
An	31.30	20.09	32.32	31.11	32.79	32.90	31.39	31.45	28.05
Di	23.19	18.82	17.94	15.63	13.47	16.85	21.85	28.04	21.21
Hy	30.87	7.09	19.29	16.53	8.25	21.28	21.85	28.04	23.52
Ol	2.80	13.89	11.86	8.27	20.61	8.57	9.00	3.14	8.01
CaO/Al_2O_3	0.84	0.62	0.69	0.62	0.58	0.66	0.72	0.78	0.77
CaO/Na_2O	11.16	2.75	5.89	4.20	3.91	5.35	6.11	8.01	6.29
CaO/TiO_2	30.55	2.86	17.57	11.52	3.91	16.04	17.20	20.75	13.61
Al_2O_3/TiO_2	36.40	4.62	25.45	18.45	23.44	24.22	24.00	26.41	17.62

(1) TQ-40, run no. T-2113, (2) HW-40, run no. T-2117, (3) KLB-1, run no. T-2133, (4) MPY-90-40, run no. T-2121, (5) MPY-90-40, run no. T-2078, (6) MPY-90-40, run no. T-2138, (7) MPY-90, run no. T-2136, (8) MPY-90-40, run no. T-2098 (this run has suffered Fe loss), (9) P_2, most primitive olivine basalt from FA (*Le Roex* et al., 1981).
t=total iron as FeO, Mg#=Mg/(Mg + Fe^t), for run details please refer to Table 4
(-) below detection limit, nd = not determined.

Due to the nature of the sandwich technique modal homogeneity is not produced during the experiment, and although the melt phase is distributed throughout the charge, being in contact with all grain boundaries, the melt is concentrated in one layer. Due to the presence of this glass layer crystal growth is enhanced resulting in much larger and more abundant clinopyroxene and orthopyroxene crystals near the glass/peridotite (now crystals and glass) contact. All phases near or in the glass layer were found to be compositionally uniform from core to rim even for short run times. Clinopyroxene is commonly attached to orthopyroxene or forms large poikilitic grains enclosing smaller olivine crystals. In run T-2121 plagioclase occurred as large crystals projecting into the glass layer, as well as smaller interstial grains throughout the MORB pyrolite end of the charge. The plagioclase was compositionally uniform from core to rim as well as compositionally uniform throughout the charge (An_{67-69}). However phases away from the glass layer were not compositionally uniform from core to rim. Rim compositions were identical to the cores and rims of phases close to the glass layer, while cores were of a different composition. In general the cores of olivines were less magnesian than the rims, the rim composition being in equilibrium with glass on the basis of a

Table 7. *Representative Residual Phase Compositions from Sandwich Experiments on MORB Pyrolite, Hawaiian Pyrolite, Tinaquillo Llherzolite and Spinel Lherzolite KLB-1*

Run no.	Phase	SiO_2	TiO_2	Al_2O_3	FeO	MgO	CaO	Na_2O	Cr_2O_3	Mg#
T-1511	OL	40.31			12.15	47.54				0.875
	OPX	53.52	0.30	6.31	7.35	29.01	2.66		1.05	0.876
	CPX	51.61	0.35	6.28	4.67	18.79	17.09	0.39	0.82	0.878
	SP			55.76	10.19	20.59			13.46	0.783
T-1472	Ol	40.74		0.22	11.22	47.60	0.24			0.883
	OPX	53.53		5.61	6.80	30.33	2.82		0.91	0.888
	SP		0.50	54.50	9.50	17.00			18.50	0.761
T-2123	OL	40.51			11.51	47.76	0.21			0.881
	OPX	53.56	0.19	5.45	6.93	30.12	2.92		0.82	0.886
	CPX	51.03	0.31	7.04	4.92	19.95	16.69	0.32		0.874
T-1493	OL	40.26			11.47	47.85	0.22		0.20	0.881
	OPX	53.47		5.52	7.00	30.29	2.85		0.88	0.885
	CPX	51.07	0.36	7.52	4.93	19.11	16.69	0.32		0.874
T-1478	OL	40.40			10.81	48.20	0.29		0.30	0.888
	OPX	54.38		3.80	6.84	31.05	2.79		1.14	0.89
	CPX	52.26	0.24	5.86	5.44	21.67	13.28	0.24	1.00	0.876
T-2140	OL	40.79			10.68	48.02	0.28		0.23	0.889
	OPX	54.24		4.89	6.49	30.38	2.64		1.36	0.893
	CPX	52.14	0.21	5.96	4.82	20.67	14.58		1.62	0.884
	SP		0.22	36.12	11.10	18.58			33.99	0.749
T-1461	OL	40.59			10.39	48.57	0.21		0.24	0.893
	OPX	54.64		4.14	6.49	31.18	2.51		1.03	0.895
T-1480	OL	40.52			10.32	48.68	0.21		0.27	0.894
	OPX	55.03		2.98	6.67	31.82	2.35		1.15	0.895

$(K_d)^{Ol/liq}_{Fe/Mg}$ equal to 0.32 (*Takahashi* and *Kushiro*, 1983). Cores of pyroxenes away from the glass layer have lower CaO, Al_2O_3 and slightly lower Mg# than the equilibrium rim compositions. As a result of this zoning in crystals removed from the glass layer, bulk equilibrium was not achieved during the length of even the longest runs (30 h), however local equilibrium was achieved between the glass composition and residual crystals near the glass layer and rims of crystals away from the glass layer. Equilibrium is also confirmed by comparing the glass compositions in short runs (3 h), to compositions in long run times (> 20 h), differences are all within analytical uncertainity. Using the sintered oxide mix as a starting material as opposed to a powdered natural peridotite enables equilibrium to be obtained relatively rapidly. The single experiment performed on KLB-1 (T-2133) resulted in large unreacted cores in the pyroxenes, although compositionally uniform

Table 7 *(continued)*

Run no.	Phase	SiO_2	TiO_2	Al_2O_3	FeO	MgO	CaO	Na_2O	Cr_2O_3	Mg#
T-1464	OL	40.44			10.19	48.97	0.20		0.20	0.895
	OPX	55.51		2.98	6.53	32.13	2.17		0.86	0.90
T-2113	OL	40.73			9.82	48.84	0.40		0.22	0.899
	OPX	54.89		4.02	5.58	31.41	2.73		1.36	0.909
	CPX	51.96	0.19	5.83	4.57	20.84	15.03		1.59	0.891
T-2117	OL	40.22			12.84	46.67	0.27			0.866
	OPX	54.53	0.59	4.12	7.22	29.87	2.53		1.15	0.881
	CPX	51.13	1.40	5.92	5.64	19.46	14.57	0.37	1.57	0.86
T-2133	OL	40.84			10.08	48.65	0.21		0.22	0.896
	OPX	54.06	0.22	7.26	6.33	29.19	2.51		0.43	0.892
	CPX	51.29	0.30	7.00	4.05	19.18	16.81	0.24	1.14	0.885
	SP			48.39	9.46	20.58			21.57	0.795
T-2121	OL	40.21			12.37	47.22	0.21			0.872
	OPX	52.82		7.57	6.11	30.27	2.25		0.98	0.898
	CPX	51.03	0.65	7.08	4.78	18.57	16.44	0.44	1.00	0.874
	SP	0.67	0.34	44.19	11.39	19.49			23.92	0.753
	PLG	52.21		30.61	0.19		13.60	3.39		
T-2078	OL	40.63			10.44	48.66	0.27			0.891
	OPX	54.01	0.23	5.88	6.16	30.14	2.93		0.66	0.897
	CPX	51.68	0.25	6.45	4.22	19.80	16.05	0.35	1.19	0.873
	SP	0.89	0.19	54.00	8.67	21.36	0.15		14.75	0.815
T-2138	OL	41.18			10.03	48.53	0.27			0.896
	OPX	53.99		6.63	5.92	29.97	2.60		0.88	0.90
	CPX	51.76	0.27	6.68	4.59	21.23	13.71		1.51	0.892
	SP	2.00	0.34	43.47	9.75	19.59	0.34		24.51	0.782
T-2136	OL	40.96			9.22	49.59	0.24			0.906
	OPX	53.77		3.74	5.48	33.54	2.22		1.24	0.916
	CPX	51.52	0.26	6.65	3.92	20.06	15.64	0.31	1.63	0.901
	SP		0.18	43.29	9.20	20.39			26.94	0.798

all analyses are normalised to 100%, OL =olivine, OPX= orthopyroxene, CPX =clinopyroxene, SP =spinel, PLG =plagioclase, GA =garnet, NiO contents are all below detection limit.

crystals of pyroxene occurred near the glass layer. Previous workers have shown that longer run times (> 72 h, *Fujii* and *Scarfe*, 1985) still do not eliminate these relict cores. Excessively long run times also run the risk of Fe-loss, as will be discussed later.

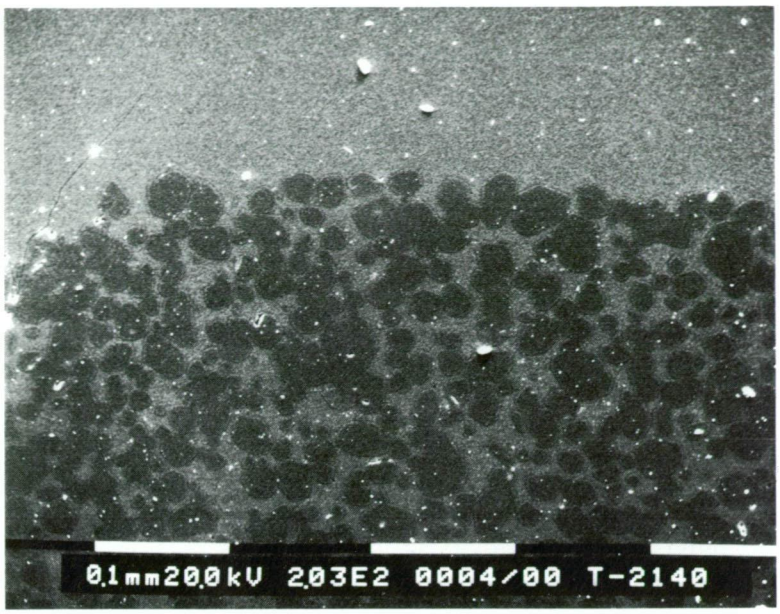

Fig. 2. Back scattered electron image photograph of run no. T-2140. Lightest gray is glass, light gray is clinopyroxene and dark grey is olivine and orthopyroxene. Bright "rims" present on some crystals is due to topography (polishing) not compositional zoning. Scale bar is 100 μm

The results from this study and the studies of *Takahashi* and *Kushiro* (1983) and *Fujii* and *Scarfe* (1985) allow us to evaluate the use of the sandwich technique in obtaining equilibrium partial melts. One of the important unknown factors in using the sandwich technique for determining equilibrium liquid compositions is the effect of changing the bulk composition of the peridotite by adding a basaltic component. The results of this study and those of *Takahashi* and *Kushiro* (1983) and *Fujii* and *Scarfe* (1985) allow us to make the following observations.

(1) Changing the modal proportion of basalt to a peridotite composition does not affect the liquid compositions along a olivine + orthopyroxene + clinopyroxene + liquid cotectic so long as the amount of added basalt mix does not exceed ~40 wt% and provided none of the residual phases are eliminated. For example experiments T-1472 and T-2123 produced similar equilibrium liquid compositions despite having different modal proportions of DSDP 3-18-7-1 (9.5 and 18 wt% respectively). Experiments by *Fujii* and *Scarfe* (1985) showed slight compositional differences in liquid composition with differing proportions of basalt added. These differences (mainly in Mg#, CaO, Na_2O and K_2O content of the glasses) can be readily explained by Fe-loss, as will discussed in another part of this paper.

(2) In general using different basalt compositions with the same peridotite host or vice-versa produces differences in the equilibrium liquid composition. For some of the experiments using HK 66 and PMM-4 differences in the equilibrium liquids were not observed when different basalt compositions were used. This can be explained by the very fertile nature of HK 66 and PMM-4, both being enriched in "melt" components, they were able to "swamp" differences in most basalt com-

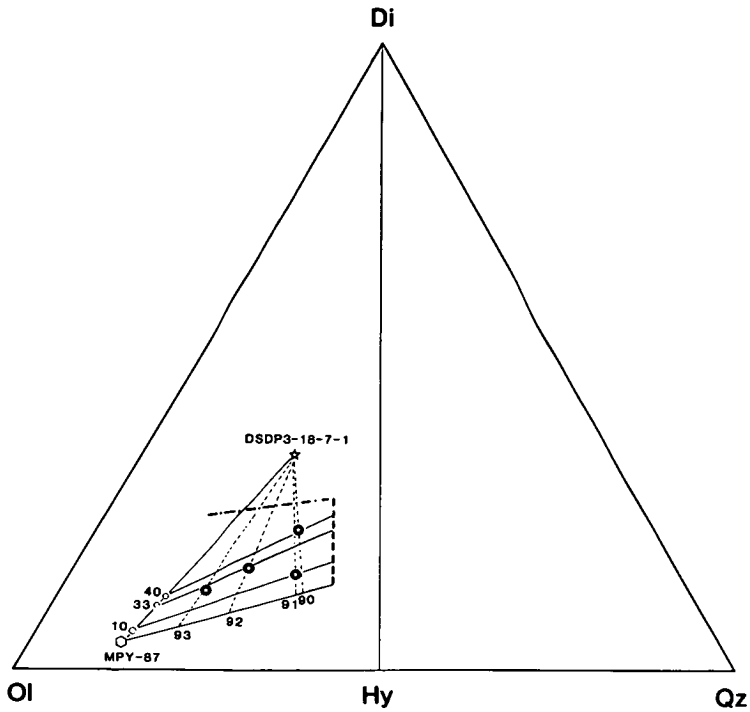

Fig. 3. CIPW molecular normative projection from plagioclase (Ab+An) onto the face olivine(Ol)-diopside(Di)-quartz(Qz) of the "basalt tetrahedron". $-\cdot-\cdot-\cdot-$ represents the locus of liquid compositions in equilibrium with olivine + orthopyroxene + clinopyroxene + spinel from 10 kbar experiments on MORB pyrolite. ------- represents locus of liquid compositions in equilibrium with olivine and orthopyroxene from 10 kbar experiments on MORB pyrolite. ———— represents locus of liquids compositions in equilibrium with olivine only from 10 kbar experiments on MORB pyrolite. $- - - -$ represents a mixing line between DSDP 3-18-7-1 and a liquid composition lying on the olivine + liquid cotectic for MPY-87. Mixing lines pass through the experimentally determined glass compositions. (◘) experimental glass compositions in equilibrium with olivine only from 10 kbar sandwich experiments on MORB pyrolite (DSDP 3-18-7-1 plus MPY-87). *90, 91, 92, 93* represent equilibrium olivine compositions (Fo mole%) along an olivine + liquid cotectic for MPY-87. 10, 33, 40 represent percent DSDP 3-18-7-1 in the bulk composition of the sandwich experiments

positions which were used in the sandwich experiments of *Takahashi* and *Kushiro* (1983) and *Fujii* and *Scarfe* (1985).

Although varying the modal proportions of the added basalt component has little effect on the liquid composition along a olivine + orthopyroxene + clinopyroxene + liquid cotectic, the presence of an added basaltic component does affect the stability of pyroxene, especially orthopyroxene. This illustrated with reference to the glass compositions from runs T-1424, 1447, 1434 and 1437 which were all in equilibrium with olivine only (not reported in Table 4). In Fig. 3 the glass composition from these runs are plotted in the CIPW molecular normative projection from plagioclase (An + Ab). Bulk compositions for the sandwich experiments, which lie on a tie line between DSDP 3-18-7-1 and MPY-87, have been plotted in Fig. 3. Also plotted are the olivine + orthopyroxene + clinopyroxene + spinel + liquid and olivine + orthopyroxene + liquid cotectics determined for MORB pyrolite

in this study. As can be seen from Fig. 3 none of the liquids in equilibrium with olivine fall on an olivine control line through MPY-87, instead they fall on olivine control lines through the respective bulk composition for each sandwich experiment. The liquid compositions represent simple mixtures between DSDP 3-18-7-1 and a melt in equilibrium with olivine lying on a olivine control line through MPY-87. The position on the olivine control line through MPY-87 is determined by drawing a line from DSDP 3-18-7-1 through the respective liquid composition onto the olivine control line through MPY-87 (Fig. 3). At each of these intersections the equilibrium olivine composition (Fo mol%) observed in the experiment is given indicating temperature is increasing from right to left in Fig. 3. The effect of increasing the proportion of DSDP 3-18-7-1 in the sandwich is to rotate the olivine control lines upwards towards DSDP 3-18-7-1. The result of this is to shrink the above-solidus fields of orthopyroxene initially, followed by clinopyroxene, until eventually only olivine is left, which is the liquidus phase of DSDP 3-18-7-1 at 10 kbar (*Green* et al., 1979). Therefore the sandwich technique is limited in that it will not permit access to liquids formed at high degrees of melting of the peridotite composition i.e. compositions in equilibrium with olivine + orthopyroxene near the point at which orthopyroxene is eliminated are not accessible. The liquids near this composition should be determinable by direct melting studies on the peridotite composition alone, provided quenching problems can be evaluated and dismissed. The experimental study of *Sen* (1982) on the spinel lherzolite 77 PAII-1 illustrates a different problem. *Sen* (1982) determined the liquids from 77 PAII-1 by direct EMP analysis of glass pools, and it seems likely that the liquid compositions have been modified by either quench growth or proximity to large residual crystals which have depleted the liquids in Al_2O_3. Other inconsistencies, such as in the erratic behaviour of Na_2O and CaO contents with increasing partial melting, point to quench modification of *Sen* (1982) liquids.

Fe-loss

The problem of Fe-loss to noble metal containers is a major problem to be addressed in experimental petrology (*Merrill* and *Wyllie*, 1973; *Green*, 1976; *Stern* and *Wyllie*, 1975; *O'Hara* and *Humphreys*, 1977; *Jaques* and *Green*, 1979; *Nehru* and *Wyllie*, 1975). The extent of iron loss is dependent on the temperature of the run and run duration. The effect of iron loss is to increase the silica saturation of the equilibrium liquid composition, due to the expansion of the olivine and orthopyroxene phase fields at the expense of clinopyroxene. This expansion also results in more calcic liquid compositions and the stabilization of calcic pyroxene in the residue (*Jaques* and *Green*, 1979). Fe-loss also increases the overall oxygen fugacity in the charge, which is reflected in an increase of the mole ratio $FeO_{1.5}/FeO$ in the melt with time (*Takahashi*, 1980). Some of the possible chemical reactions causing an increase in fO_2 in the charge are listed below;

$$Fe_2SiO_{4\,\text{olivine}} \text{---} > SiO_{2\,\text{melt}} + 2\,(Fe/Pt)_{\text{solid solution}} + O_2 \qquad (1)$$

$$Pt + 3\,FeO_{\text{melt}} \text{---} > (Fe/Pt)_{\text{solid solution}} + Fe_2O_{3\text{melt}} \qquad (2)$$

etc.

The effect of increasing fO_2 during a run in which Fe-loss is occurring is to stabilize chromian spinel (Cr-spinel) to very high degrees of partial melting, as was the case

with the experiments performed by *Jaques* and *Green* (1980) were Cr-spinel was still present even after the elimination of all other phases except olivine. The higher fO_2 occurring in Pt capsules due to iron-loss, compared to experiments performed in graphite is reflected in the trivalent cation ratio $100\,Fe^{3+}/(Fe^{3+}+Al^{3+}+Cr^{3+})$ (Fe#) which is higher in Cr-spinels crystallizing in Pt capsules.

During the course of this experimental study Fe-loss occurred in some experiments (not reported in Table 4) due to leakage of melt through the porous nature of the graphite container. The graphite in this case was of inferior density and quality than that used in the experiments presented in Table 4. This resulted in melt being able to make contact with the outer Pt capsule. The glass composition for one such experiment T-2098 is reported in Table 6. The glass composition compared with equilibrium partial melts from MORB pyrolite, has higher SiO_2, CaO and lower Na_2O contents and has a much higher Mg#. These features are a result of equilibrium being shifted by Fe-loss away from an olivine + orthopyroxene + clinopyroxene + spinel + liquid assemblage to an orthopyroxene + clinopyroxene + liquid assemblage. The important features of Fe-loss in noble metal containers can be summarized below:

(1) Fe-loss stabilizes a more Fe^{3+} and Cr^{3+} rich spinel, due to an increase of fO_2.

(2) Liquid compositions become more silica-saturated, and have higher CaO contents, due to the expansion of the Mg-rich olivine and orthopyroxene fields at the expense of calcic pyroxene.

(3) Mg# of the liquid becomes very high due to loss of Fe to Pt, which is also reflected in magnesian residual phase compositions.

The above features of Fe-loss appear to be present in the experiments of *Fujii* and *Scarfe* (1985). *Fujii* and *Scarfe* (1985) conducted melting experiments on peridotite compositions PMM-1 and PMM-2 between the temperatures of 1250 °C and 1310 °C, within this temperature interval the Mg# of the equilibrium glasses changed from 0.69 for PMM-1 and 0.72 for PMM-2 to 0.78 and 0.80 respectively. Based on the equilibrium $(K_d)^{ol/liq}_{Fe/Mg}$ of 0.32 in graphite determined by *Takahashi* and *Kushiro* (1983) at 10 kbar the change in the Mg# of the glasses represents a change in the olivine composition from Fo_{87} to Fo_{92} in the case PMM-1 and from $Fo_{88.8}$ to Fo_{93} in the case of PMM-2. This change in olivine composition is too large to be explained simply by an increase in temperature of only 60 °C. The large range and high Mg# of the glasses from *Fujii* and *Scarfe* (1985) can be attributed to iron loss occurring over the long run times used, iron loss being more evident in the high temperature runs than the lower temperature runs. The presence of Fe-loss in the higher temperature runs of *Fujii* and *Scarfe* (1985) explains many of the unique features of their experiments. Firstly the very high CaO contents of the higher temperature liquids compared to MORB pyrolite glass compositions can be explained by the contraction of the calcic pyroxene field. Secondly the more chromium rich spinels relative to spinels in graphite experiments reported by *Fujii* and *Scarfe* (1985) can be explained by an increase in fO_2 due to Fe-loss. However complete spinel compositions were not reported by *Fujii* and *Scarfe* (1985) and it is not possible to ascertain if spinel is significantly different from spinels crystallizing in graphite. Thirdly the decrease in iron contents of the glasses from 7.77 to 6.52 wt% for PMM-1 and from 7.25 to 6.03 wt% for PMM-2 is the opposite of that expected with increasing degree of partial melting. FeO contents should gradually increase towards the FeO content of the bulk composition during batch partial melting. The falling FeO contents can be explained by Fe-loss to the Pt container.

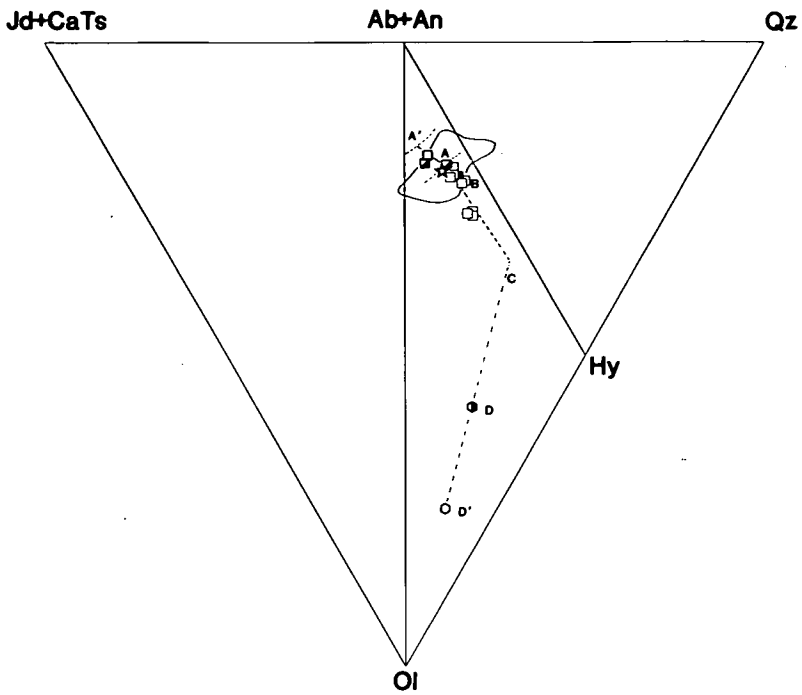

Fig. 4. Equilibrium glass compositions from MORB pyrolite plotted in the CIPW molecular normative projection from diopside (Di) onto the base of the "basalt tetrahedron" jadeite plus calcium Tschermak's molecule (Jd + Cas)-quartz(Qz)-olivine(Ol). ○ MORB pyrolite (MPY-87, MPY-90), ◑ MORB pyrolite minus 40 wt% olivine (MPY-90-40), □ glass compositions from MPY (Table 5), ◪ glass compositions from MPY-90-40 (Table 6), ■ glass compositions from MPY-90 (Table 6), letters *A, A', B, C, D, D'* are referred to in the text. –·–·–·– locus of liquids in equilibrium with olivine, – – – – locus of liquids in equilibrium with olivine + orthopyroxene, ———— locus of liquids in equilibrium with olivine + clinopyroxene + orthopyroxene + spinel, ☆ composition of primitive MORB glass DSDP 3-18-7-1 enclosed by the field of primitive MORB glasses (*Natland* et al., 1984; *Melson* et al., 1977; *Melson* et al., 1976; *Frey* et al., 1973; *Frey* et al., 1974; *Green* et al., 1979; *O'Donnell* and *Presnall*, 1980; *Melson* and *O'Heran*, 1979; *Scarfe* and *Smith*, 1977; *Shipboard S. P.*, 1977; *Hekinian* et al., 1976; *Langmuir* et al., 1977; *Bender* et al., 1978; *Fujii* and *Bougault*, 1983; *Basaltic Volcanism Study Project*, 1981; *Shibata* et al., 1979; *Barker* et al., 1983; *Melson*, 1973; *Stakes* et al., 1984; *Sigurdsson*, 1981; *Bryan*, 1979; *Bryan* and *Moore*, 1977; *Bryan* et al., 1981)

Equilibrium Glass Compositions at 10 kbar

In order to portray the chemical relationships between the composition of the equilibrium partial melts compositions of MORB pyrolite at 10 kbar and primitive MORB glasses a graphical projection based on the molecular CIPW norm is used in Figs. 4 and 5. The normative minerals are assigned to the four end members of a tetrahedron (*Green*, 1970). The tetrahedron is based on the "Basalt tetrahedron" of *Yoder* and *Tilley* (1962). To illustrate the three-dimensional relationships within the tetrahedron, two subprojections onto the faces of the tetrahedron will be used. The first is a projection from diopside (Di) onto the base of the tetrahedron Jadeite plus Ca Tschermak's molecule (Jd + CaTs)-quartz (Qz)-olivine (Ol) as in Fig. 4. The second is a projection from plagioclase (An + Ab) onto the face olivine (Ol)-diopside

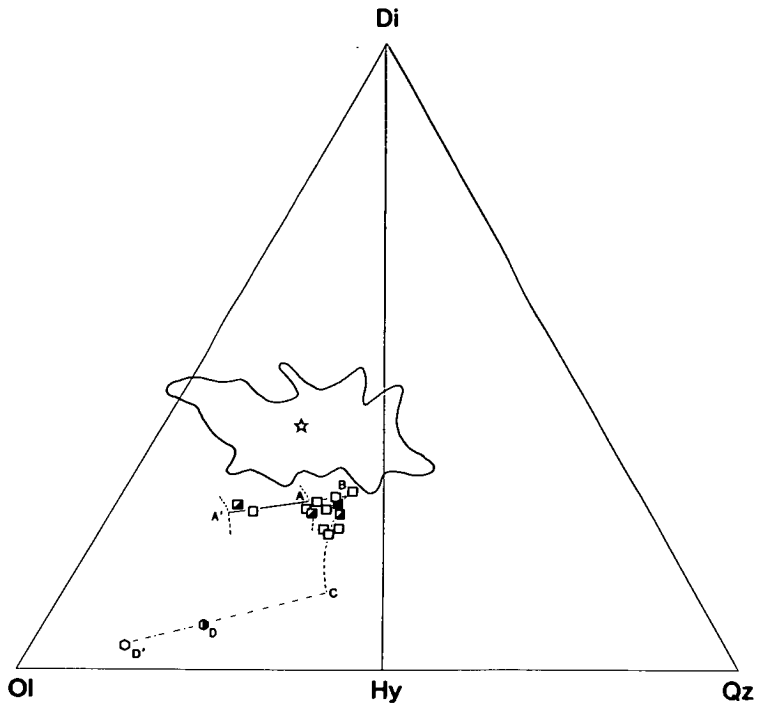

Fig. 5. Equilibrium glass compositions from MORB pyrolite plotted in the CIPW molecular normative projection from plagioclase (Ab+An) onto the face olivine(Ol)-diopside(Di)-quartz(Qz) of the "basalt tetrahedron". Symbols and cotectics as for Fig. 4

(Di)-quartz (Qz) as in Fig. 5. The subprojection from plagioclase is very similar to the projection used by *Walker* et al. (1979) and *Grove* et al. (1982). The projection scheme of *Elthon* (1983) gives a result different from *Walker* et al. (1979) but is very similar to a subprojection from Jd+CaTs onto the face olivine (Ol)-diopside (Di)-quartz (Qz) in our projection scheme.

In the subprojection from diopside (Figs. 4 and 6) equilibrium melt compositions from MPY-87, MPY-90, MPY-90-40, HW-40, TQ-40 and KLB-1 all plot within the primitive MORB glass field, indicating the possibility that primitive MORB glasses are indeed primary melts at 10 kbar. However when viewed from the plagioclase (An+Ab) projection (Figs. 5 and 7), except for the glasses from HW-40, all the 10 kbar equilibrium liquids plot below the spectrum of primitive MORB glasses indicating that primitive MORB glasses are not primary magmas. In a companion study to that reported here (*Falloon* and *Green*, 1988), it is demonstrated that the MORB glasses are derivative compositions lying on olivine control lines from more picritic primary magmas segregating from peridotite at pressures greater than 10 kbar.

Glass Compositions from MORB Pyrolite (MPY-87, MPY-90, MPY-90-40)

The equilibrium liquid compositions from MORB pyrolite are presented in Table 5 and are compared to primitive MORB glasses in Fig. 4 and 5. The liquid compositions define the following equilibrium phase boundaries;

(1) A six phase point (olivine + orthopyroxene + clinopyroxene + spinel + plagioclase + liquid) defined by run no. T-2121.
(2) A olivine + orthopyroxene + clinopyroxene + spinel + liquid cotectic, defined by run nos. T-1511, 1472, 2123, 1493, 1478, 2140, 2078, 2138 and 2136.
(3) A olivine + orthopyroxene + liquid cotectic defined by runs T-1464, 1480 and 1461.

The course of melting of MORB pyrolite is described with reference to letters A, A′, B, C, D and D′ in Figs. 4 and 5. Melting begins at A which represents a six-phase cotectic. The liquid composition represented by T-2121 is high in Al_2O_3, TiO_2 and Na_2O but low in CaO compared to primitive MORB glasses. The plagioclase composition at the six-phase cotectic is An_{68-69}. The six-phase cotectic is not invariant but moves towards A′, where plagioclase is eliminated from the residue. The movement is a consequence of plagioclase melting, which enriches the liquid in Al_2O_3 and Na_2O. Na_2O depolymerizes the melt structure expanding the olivine phase volume (*Kushiro*, 1975). This expansion of the olivine phase volume can be seen best in the projection from Di (Fig. 4). After plagioclase is eliminated continual melting moves liquid compositions from A′ to B, along an olivine + orthopyroxene + clinopyroxene + spinel + liquid cotectic. A large variation in liquid composition is possible along this cotectic due to the solid solution behaviour of olivine, pyroxenes and spinel. At B clinopyroxene is eliminated from the residue. Spinel also is eliminated as a consequence of the low fO_2 within the graphite capsules. Between B and C liquid compositions move along an olivine + orthopyroxene + liquid cotectic. At some point between B and C, depending on bulk composition, orthopyroxene is eliminated from the residue, and the liquids thereafter lie on an olivine control line through the bulk composition. At C orthopyroxene is eliminated from bulk compositions consisting of MORB pyrolite without any added DSDP 3-18-7-1. Important observations from Figs. 4 and 10 are;
(1) The 10 kbar equilibrium liquids from MORB pyrolite plot below primitive MORB glasses and plot well below the composition of DSDP 3-18-7-1.
(2) The 10 kbar equilibrium liquids from MORB pyrolite only span the middle range of the primitive MORB glass spectrum in terms of silica saturation. The range in silica saturation of the 10 kbar liquids is limited due to the plagioclase phase volume which stops liquids from crossing over to the Ne-normative side of the tetrahedron, and the elimination of clinopyroxene stops liquids crossing to the quartz normative side of the diagram. The equilibrium liquids at low degrees of partial melting (<9 wt%, determined from least-squares mass balance calculations) in equilibrium with olivine + clinopyroxene + orthopyroxene + spinel ± plagioclase are distinct from primitive MORB glasses in their high Na_2O_3 and Al_2O_3 contents and low FeO, MgO and CaO contents. Equilibrium liquids at higher degrees of partial melting differ significantly from primitive MORB glasses in having lower TiO_2, Al_2O_3, CaO and Na_2O contents and have higher MgO contents.

In terms of CIPW molecular normative mineralogy, the equilibrium liquids have significantly higher normative Hy than most primitive MORB glasses, which is one of the main causes for the glasses plotting below the primitive MORB in Fig. 4. The high Hy contents of the equilibrium liquids is partly a result of the high SiO_2 contents compared to most primitive MORB glasses. In Fig. 8 the frequency distribution of SiO_2 contents of primitive MORB glasses is presented. Primitive MORB glasses appear to have a bimodal distribution with a maximum between 49.3 to

50.2 and another smaller maximum between 51 and 51.3 wt% SiO_2. Primitive MORB glasses with higher SiO_2 contents than the 10 kbar liquids from MORB pyrolite have low olivine normative contents or are quartz normative and they plot to the right of the 10 kbar cotectic in Fig. 4. These distinctive MORB glasses are therefore possible primary melts at pressures of less than 10 kbar. This possibility will be discussed later. Although primitive MORB glasses plot above the 10 kbar cotectic in Fig. 5, there are some primitive MORB compositions that do fall on the 10 kbar cotectic, an example is given in Table 6 (no. 9) which is the average primitive olivine basalt composition P_2 from the FAMOUS area of the Mid-Atlantic ridge (*Le Roex* et al., 1981). The composition of P_2 is identical to the liquid composition T-1478 (Table 5) except for a slight difference in FeO and MgO contents. Although P_2 is not a glass composition but an average of three sparsely phyric to aphyric olivine basalt compositions it should still be close to a liquid composition. This result suggests that some MORB parental magmas are 10 kbar primary melts in equilibrium with a lherzolite residue. However the overwhelming majority of primitive MORB compositions represented by the glass compositions in Figs. 4 and 5 are not primary melts at 10 kbar. *Le Roex* et al. (1981) demonstrated that the composition of P_2 was not a suitable parental composition to the majority of olivine basalts from FAMOUS. In a companion paper (*Falloon* and *Green*, 1988) primitive olivine basalts from FAMOUS are shown to be near or close (< 10 wt% olivine fractionation) to primary melts segregating from pressures of between 10 to 18 kbars leaving a lherzolitic residue.

Glass Compositions from Tinaquillo Lherzolite (TQ-40) and Hawaiian Pyrolite (HW-40)

The results of the two 10 kbar experiments on TQ-40 and HW-40 are part of a more comprehensive study from 2–30 kb on these two compositions reported in *Falloon* et al. (1988). Due to the uncertainties involved in the modal analyses of experimental charges in order to calculate equilibrium liquids at 10 kbar, the calculated liquids of *Jaques* and *Green* (1980) were reversed by use of the sandwich technique. The results of the sandwich experiments demonstrate a significant shift in the olivine + orthopyroxene + clinopyroxene + liquid cotectics for Tinaquillo lherzolite and Hawaiian pyrolite to more silica saturated compositions (*Falloon* et al., 1988). This shift is seen more clearly in the projection from Di (Fig. 6). Compared with calculated 10 kbar liquids from Tinaquillo, the glass composition of T-2113 (Table 6) has higher SiO_2, Al_2O_3 and CaO. Compared with primitive MORB glasses the composition of run T-2113 plots below the primitive MORB glasses spectrum in Fig. 7 and plots to the right of 10 kbar liquids from MORB pyrolite, which is expected for a more depleted source composition. T-2113 has higher CaO/Al_2O_3 and CaO/Na_2O ratios than most primitive MORB glasses as a result of lower Al_2O_3 and Na_2O contents. T-2113 also has significantly lower TiO_2 and higher MgO contents than primitive MORB glasses.

Compared to calculated liquids from HW-40 the 10 kbar reversal run T-2117 (Table 6) has signficantly higher SiO_2 and Al_2O_3 contents and lower FeO and MgO contents. It is signficant that the composition of run T-2117 plots within the primitive MORB glass spectrum in Fig. 7 indicating it is possible to have peridotite sources which produce melts which define olivine + orthopyroxene + clinopy-

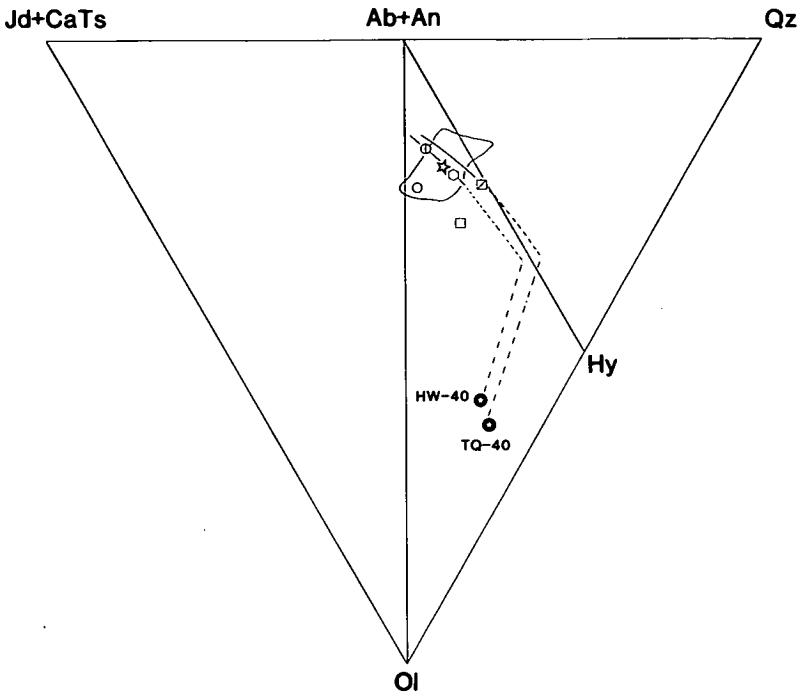

Fig. 6. Equilibrium glass compositions from Hawaiian pyrolite, Tinaquillo lherzolite and spinel lherzolite KLB-1 plotted in the CIPW molecular normative projection from diopside(Di) onto the base of the "basalt tetrahedron" jadeite plus calcium Tschermak's molecule (Jd + CaTs)-quartz(Qz)-olivine(Ol). ○ calculated *Jaques* and *Green* (1980) 10 kbar liquid composition from Hawaiian pyrolite (Table 2), □ calculated *Jaques* and *Green* (1980) 10 kbar liquid composition from Tinaquillo lherzolite (Table 2), ⬡ equilibrium glass composition from KLB-1 (Table 6), ⊠ equilibrium glass composition from Tinaquillo lherzolite (Table 6), ⦶ equilibrium glass composition from Hawaiian pyrolite (Table 6), ☆ primitive MORB glass DSDP 3-18-7-1 enclosed by the field of primitive MORB glasses (references see caption to Fig. 4) cotectics as for Fig. 4

roxene + spinel + liquid cotectics at high normative Di contents in the projection from plagioclase (An + Ab). However such peridotite compositions differ in Na_2O, TiO_2, K_2O contents from typical oceanic upper mantle represented by the Ronda and Bullenmerri peridotite suites (Fig. 1) and the melt compositions are unlike primitive MORB glasses. In the case of HW-40, melt compositions at 10 kbar are lower in Al_2O_3 and CaO than primitive MORB glasses and are enriched in Na_2O, K_2O and TiO_2.

Glass Compositions from KLB-1

The one experiment performed using KLB-1 as the peridotite in the sandwich with DSDP 3-18-7-1 produced a liquid composition very similar to the liquid compositions from MORB pyrolite. The composition of run T-2133 (Table 6) plots in a similar position to liquid compositions from MORB pyrolite, below primitive MORB glasses in Fig. 9. This result is not unexpected due to the very close similarities between MORB pyrolite and KLB-1.

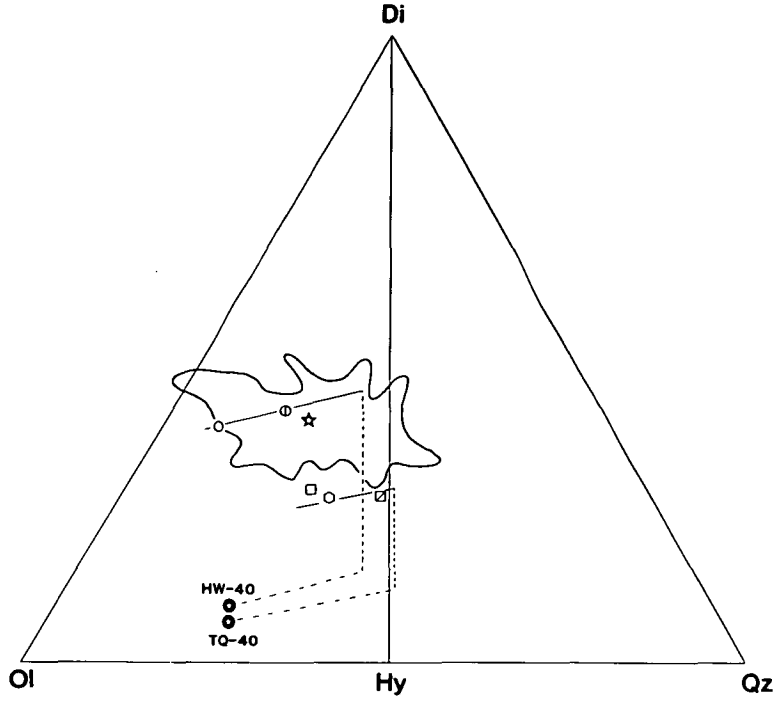

Fig. 7. Equilibrium liquid compositions from Hawaiian pyrolite, Tinaquillo lherzolite and spinel lherzolite KLB-1 plotted in the CIPW molecular normative projection from plagioclase (Ab+An) onto the face olivine (Ol)-diopside(Di)-quartz(Qz) of the "basalt tetrahedron". Symbols as for Fig. 6 and cotectics as for Fig. 4

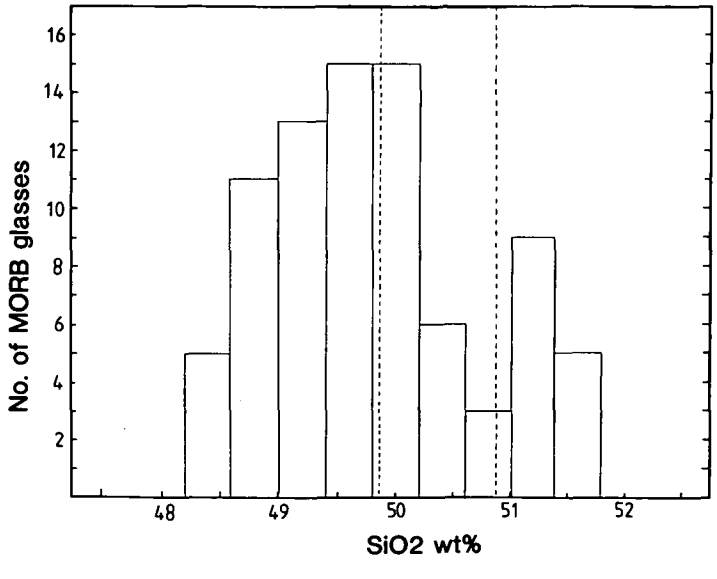

Fig. 8. Frequency histogram of SiO_2 contents of primitive MORB glasses (references see caption to Fig. 4). Dashed lines delineate the range of SiO_2 contents for equilibrium liquid compositions from this study

Summary

The results of the 10 kbar melting study on MORB pyrolite, Hawaiian pyrolite, Tinaquillo lherzolite and the spinel peridotite KLB-1 demonstrate that equilibrium liquids are sufficiently different from primitive MORB glasses to warrant the conclusion that primitive MORB glasses are not primary magmas at 10 kbar. All the 10 kbar liquids except those from Hawaiian pyrolite define olivine + orthopyroxene + clinopyroxene + spinel + liquid cotectics which plot below primitive MORB glasses in Figs. 5 and 7. The following section will attempt to integrate these new results with previous 10 kbar melting studies relevant to MORB petrogenesis.

Comparison with Other 10 kbar Melting Studies

Equilibrium liquid compositions from previous 10 kbar melting studies are plotted in the basalt tetrahedron (Figs. 9 and 10) where they are compared with the spectrum of primitive MORB glasses and equilibrium partial melt compositions from MORB pyrolite at 10 kbar. In the projection from Di (Fig. 9) not all the liquid compositions at 10 kbar define the same olivine + orthopyroxene + clinopyroxene + liquid or olivine + orthopyroxene + liquid cotectics. This could be due to differences in bulk compositions used or to differences in pressure calibration between different laboratories using the piston-cylinder apparatus. With regards to differences in pressure calibration *Falloon* and *Green* (1988) and *Falloon* et al. (1988) demonstrate that for three different peridotite compositions (MORB pyrolite, Hawaiian pyrolite and Tinaquillo lherzolite) equilibrium partial melt compositions overlie each other in the projection from Di, and define the same olivine + clinopyroxene + orthopyroxene + liquid and olivine + orthopyroxene + liquid cotectics at 5, 10, 15, 20 and 30 kbars. Cotectics moving systematically with pressure towards the olivine apex parallel to the Ol-(Jd + CaTs) join. The position of these cotectics is also consistent with 30, 20, 15 and 5 kbar cotectics from HK 66 (*Takahashi* and *Kushiro*, 1983) and 10 and 30 kbar cotectics from KLB-1 (*Takahashi*, 1986; this study). These results provide an internally consistent set of data, upon which other melting studies can be compared and evaluated. The position of cotectics at pressures higher and lower than 10 kbar demonstrate that the position of the 10 kbar cotectics from MORB pyrolite are correctly located. Because different peridotite compositions (Hawaiian pyrolite, MORB pyrolite, Tinaquillo lherzolite, HK 66 spinel lherzolite, KLB-1 spinel lherzolite) define similar cotectics at 30, 20, 15 and 5 kbars, differences in bulk composition are not considered likely in explaining differences in the position of cotectics at 10 kbar in the projection from Di. The most likely explanation is differences in pressure calibration of the piston cylinder apparatus between pressures of 8 to 12 kbars. Previous experimental studies are discussed on an individual basis below.

Stolper (1980)

In the experiments of *Stolper* (1980) a primitive MORB glass ALV 519-4-1 was equilibrated with olivine and orthopyroxene in a sandwich type experiment. The aim of the study was to establish the nature of liquids in equilibrium with orthopyroxene at 10 kbar. The liquids in equilibrium with olivine + orthopyroxene at 10 kbar from *Stolper* (1980) are plotted in Figs. 9 and 10. The liquid compositions

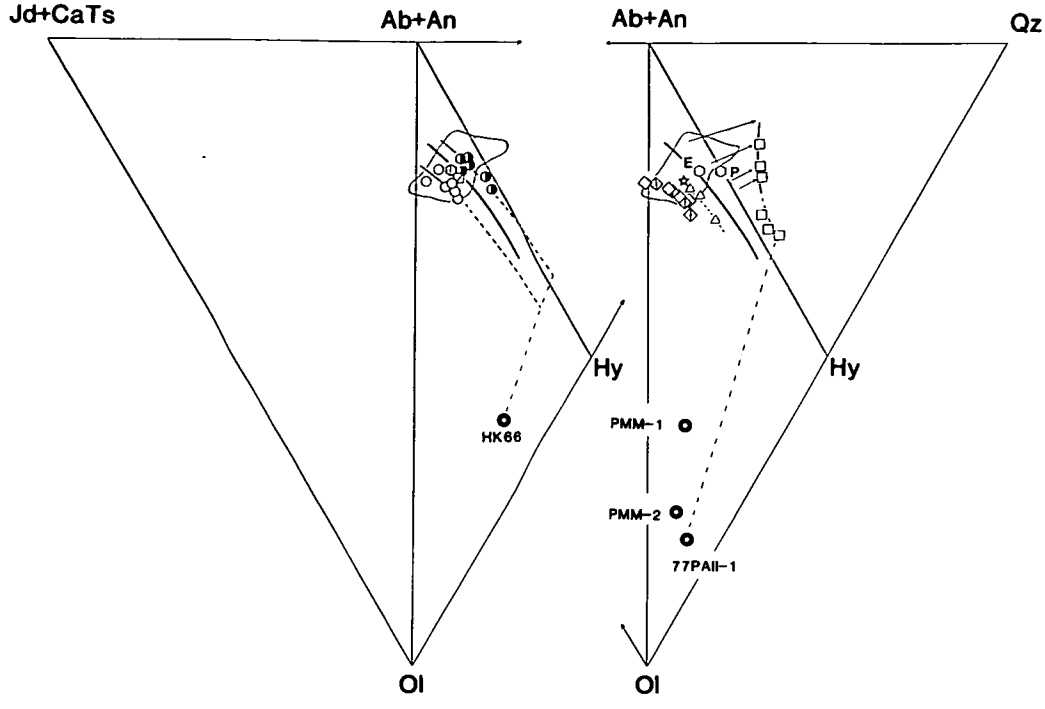

Fig. 9. Glass compositions from various 10 kbar melting studies plotted in the CIPW molecular normative projection from diopside(Di) onto the base of the "basalt tetrahedron" jadeite plus calcium Tschermak's molecule(Jd + CaTs)-quartz(Qz)-olivine(Ol). The field of primitive MORB glasses from Fig. 4 is outlined. ○ glass compositions from HK 66 at 10 kbar (*Takahashi* and *Kushiro*, 1983), ◑ glass compositions from HK 66 at 8 kbar (*Takahashi* and *Kushiro*, 1983), ⌽ MORB composition T-87 (Table 1), ⊠ MORB composition Leg 45-395 A-8-1-9 (Table 1), ☆ MORB composition ARP 74-10-16 (Table 1), ◇, ◈ glass compositions from PMM-1 and PMM-2 respectively (*Fujii* and *Scarfe*, 1985), □ glass compositions from 77 PAII-1 (*Sen*, 1982), △ glass compositions from *Stolper* (1980), ⬡ P six phase invariant point in the system CaO-MgO-Al_2O_3-SiO_2 (*Presnall* et al., 1979), ⬡ E six phase pseudoinvariant point in the complex system from *Elthon* and *Scarfe* (1984), ——— solid line represents the 10 kbar cotectic from MORB pyrolite. ↗..... dotted line represents a possible cotectic for liquids in equilibrium with olivine + orthopyroxene + clinopyroxene at 9 kbar from 77 PAII-1, arrows show the effect of quench modification on equilibrium liquid compositions

define an olivine + orthopyroxene + liquid cotectic almost identical to that from MORB pyrolite, the liquid compositions of *Stolper* (1980) being very similar to the glass compositions of runs T-1464, 1461 and 1480. However the cotectic defined by 10 kbar liquids from *Stolper* (1980) plots slightly away from the MORB pyrolite olivine + orthopyroxene + liquid cotectic towards the olivine apex in Figs. 9 and 10. The liquid compositions from *Stolper* (1980) being more consistent with a 12 kbar olivine + orthopyroxene + liquid cotectic. The results of this experimental study are however still in agreement with the conclusion of *Stolper* (1980), that primitive MORB glasses do not lie close to orthopyroxene saturation at 10 kbar and therefore are not primary melts. The only differences between the study of *Stolper* (1980) and this study are;

(1) *Stolper* (1980) bulk compositions are undefined.

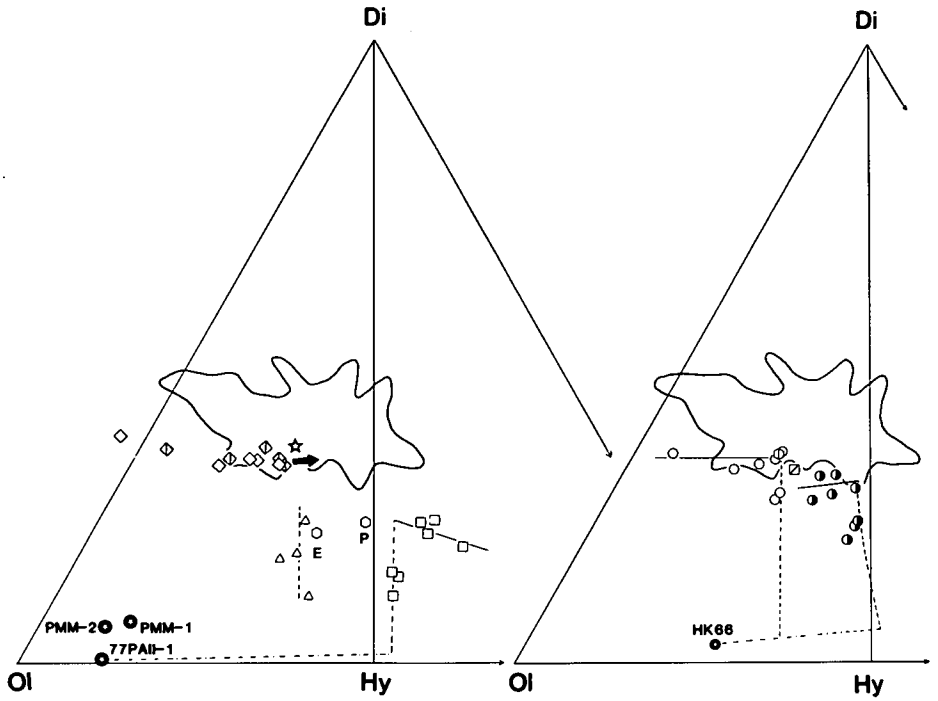

Fig. 10. Glass compositions from various 10 kbar melting studies plotted in the CIPW molecular normative projection from plagioclase (Ab + An) onto the face diopside(Di)-olivine(Ol)-quartz(Qz) of the "basalt tetrahedron". Symbols as for Fig. 9, cotectics as for Fig. 4, ➡ arrow shows expected trend of liquid compositions with progressive Fe-loss at higher temperatures

(2) The olivine + orthopyroxene + clinopyroxene + liquid cotectic is projected as a point in the phase diagram presented by *Stolper* (1980) whereas in reality it projects as a line.
(3) *Stolper* (1980) 10 kbar liquids are more consistent with a 12 kbar olivine + orthopyroxene + liquid cotectic.

Elthon and Scarfe (1984)

Elthon and *Scarfe* (1984) studied the high pressure phase relationships of a high-MgO picrite NT-23 from the Tortuga ophiolite complex, in southern Chile. As a result of this study *Elthon* and *Scarfe* (1984) established the composition of a liquid in equilibrium with olivine + orthopyroxene + clinopyroxene + plagioclase + spinel at 10 kbar (run 333, Table 3, *Elthon* and *Scarfe*, 1984). This liquid composition plots very close to run T-2121 from MORB pyrolite and is similar in major element chemistry, having similar high Al_2O_3 relative to CaO contents. However the composition has a low Mg# of 0.63, in equilibrium with Fo_{83} olivine. The liquid composition therefore can not be regarded as equivalent to a mantle melt from peridotite of $Fo_{90\pm2}$. The liquid composition is substantially different from primitive MORB glasses at 10 kbar. The results of this study are in agreement with the conclusion of *Elthon* and *Scarfe* (1984) that MORB glasses with >9.5 wt% MgO are not primary magmas, but are derived from more picritic parents.

Presnall et al. (1979) and Presnall and Hoover (1984)

Presnall et al. (1979) based on the results of their experimental study in the simple system CaO-MgO-Al_2O_3-SiO_2 (CMAS) presented a model for the generation of Mid-Ocean ridge tholeiites. In the system CMAS the solidus curve for a simplified plagioclase and spinel lherzolite was found to have a cusp at 9 kbar, where the transition from plagioclase to spinel lherzolite intersects the solidus forming an invariant point. In the model of *Presnall* et al. (1979) magma generation is caused by the intersection of a mantle geotherm at the 9 kb cusp, and the composition of the near-solidus liquid produced at the 9 kb cusp models the composition of primitive MORB glasses. The composition of the 9 kb invariant point in the system CMAS is plotted in Figs. 9 and 10. The 9 kbar liquid composition plots close to but outside the field of primitive MORB glasses in Figs. 9 and 10. *Presnall* et al. (1979) predicted that in the complex system, the 9 kbar point would move towards the primitive MORB glass spectrum due to the addition of components such as Na_2O, TiO_2 etc. The results of this experimental study have confirmed the predicted shift except for two important points:

(1) The six-phase point in the complex system represented by T-2121 does indeed fall in the middle of the primitive MORB glass spectrum in the projection from Di in Fig. 4, but in the projection from plagioclase (An + Ab) (Fig. 5) falls below the primitive MORB glasses.

(2) In the model of *Presnall* et al. (1979) the composition of the liquids at the cusp are broadly similar to primitive MORB glasses although Figs. 9 and 10 illustrate important differences. However in the complex system the composition in equilibrium with olivine + orthopyroxene + clinopyroxene + spinel + plagioclase is substantially different from primitive MORB glasses, as are liquids lying along a olivine + orthopyroxene + clinopyroxene + spinel + liquid cotectic. The results of this study do not support the model of *Presnall* et al. (1979).

More recently *Presnall* and *Hoover* (1984) recognizing the fact that there is indeed a range of silica saturation amongst primitive MORB glasses, and as a single pressure of origin in inadequate to explain this feature, proposed that primary MORBs are generated from pressures of between 7 and 11 kbar, based on the results from simple systems (CMAS and SCAMN, N = Na_2O). However in the complex system based on the equilibrium liquids from MORB pyrolite at 8 kbar (*Falloon* and *Green*, 1988), Tinaquillo lherzolite and Hawaiian pyrolite at 5 kbar (*Falloon* et al., 1988; *Jaques* and *Green*, 1980), peridotite partial melts have SiO_2 contents of between 50 to 55 wt%. These compositions are substantially more SiO_2-rich than most primitive MORB glasses.

Takahashi and Kushiro (1983)

In Figs. 9 and 10 the 10 kbar and 8 kbar partial melt compositions from HK 66 are plotted. The partial melts define olivine + orthopyroxene + clinopyroxene + liquid and an olivine + orthopyroxene + liquid cotectics. The 10 kbar and 8 kbar liquids from HK 66 have much higher FeO, Na_2O and TiO_2 contents and lower CaO contents when compared to liquids from MORB pyrolite and are unlike any primitive MORB glass. In the projection from Di (Fig. 9), the 10 kbar cotectic from HK 66 is displaced towards the olivine apex and its position is more consistent with a cotectic lying somewhere between 12 and 15 kbars. The 10 kbar liquids from

HK 66 in Figs. 9 and 10 plot in a similar position to 12–15 kbar partial melts from Hawaiian pyrolite, Tinaquillo lherzolite, and MORB pyrolite. The 10 kbar partial melts from HK 66 also plot very close to 15 kbar partial melts from HK 66 in the projection from Di and overlie 15 kbar partial melts in the projection from plagioclase (Ab + An). The 8 kbar partial melts from HK 66 plot close to the 10 kbar cotectic from MORB pyrolite in the projection from Di and overlie 10 kbar partial melts from MORB pyrolite in the projection from plagioclase (An + Ab) (Fig. 10) and are therefore more likely to represent 10 kbar partial melts than the reported 10 kbar compositions from *Takahashi* and *Kushiro* (1983).

The partial melts from HK 66 at 8 and 10 kbar, although unlike primitive MORB glasses, are very similar in compositions to the more Fe-rich MORB T-87 and 395 A-8-1-9 which were studied by *Kushiro* and *Thompson* (1972) and *Fujii* et al. (1978) respectively. These two MORB compositions are also plotted in Fig. 10. Some of the partial melt compositions from HK 66 are identical to the composition T-87 studied by *Kushiro* and *Thompson* (1972), leading to the possible conclusion that T-87 and similar Fe-rich MORBs are primary magmas from a Fe-rich mantle having an olivine of less than Fo_{86}.

Sen (1982)

Sen (1982) studied the melting relationships of a depleted plagioclase and spinel lherzolite 77 PAII-1. Unfortunately *Sen* (1982) determined liquid compositions by direct EMP analysis of glass pools. The erratic behaviour of Na_2O and CaO, as well as the anomalous CaO/Al_2O_3 ratios of the liquid compositions compared to the CaO/Al_2O_3 ratio of 77 PAII-1 indicate that the liquids presented by *Sen* (1982) have suffered some degree of quench modification. Further evidence for the effects of quench modification of *Sen's* (1982) liquid compositions is seen in the projection from Di (Fig. 9). Partial melt compositions define a olivine + orthopyroxene + clinopyroxene + liquid cotectic which is displaced towards the quartz apex, when compared with the 10 kbar cotectic from MORB pyrolite. The displacement is larger for the lower temperature compositions, where the effects of quench modification will be most evident. Arrows in Fig. 9 indicate the displacement of equilibrium liquids from a predicted 9 kbar cotectic by quench modification to the actual published compositions of *Sen* (1982).

The liquids from 77 PAII-1 have value in establishing the character of melt compositions from depleted compositions at shallow depths. The nature of such melts from depleted peridotite sources has implications for assessing the role of that second-stage melting processes play in MORB petrogenesis (*Duncan* and *Green*, 1987). The glass compositions relative to primitive MORB glasses have high SiO_2 and CaO contents and low TiO_2 and Na_2O contents. The melt compositions are similar in character to those from Tinaquillo lherzolite, which is also a depleted peridotite composition relative to MORB pyrolite.

Fujii and Scarfe (1985)

In Figs. 9 and 10 the glass compositions from equilibrium melting of PMM-1 and PMM-2 are presented (Table 6, *Fujii* and *Scarfe* 1985). The liquid compositions define a olivine + orthopyroxene + clinopyroxene + spinel + liquid cotectic at higher normative Di and higher normative Ol in Fig. 10 and 9 respectively, than

MORB pyrolite. As previously discussed the higher temperature liquid compositions from *Fujii* and *Scarfe* (1985) show evidence of Fe-loss, the arrow in Fig. 9 indicates the direction liquid compositions will lie at even higher temperatures than those run by *Fujii* and *Scarfe* (1985). As Fe-loss progresses, equilibrium moves away from the olivine apex towards more quartz normative, diopside rich liquids, eventually olivine disappears leaving the liquid in equilibrium with Mg-rich calcic pyroxene ± Mg-rich orthopyroxene. The position of lower temperature liquid compositions, which show no evidence of Fe-loss, define a olivine + orthopyroxene + clinopyroxene + spinel + liquid cotectic plotting in a similar position to the 10 kbar cotectic from HK 66. As with the HK 66 cotectic, the cotectic defined by PMM-1 and PMM-2 is more consistent with a 12–15 kbar cotectic. The low temperature liquid compositions from PMM-1 and PMM-2 are unlike primitive MORB glasses, due to their high Al_2O_3, Na_2O and low CaO contents, and low CaO/Na_2O and CaO/Al_2O_3 ratios. Higher temperature liquids have suffered Fe-loss resulting in more CaO-rich liquid compositions, with very high Mg# and low FeO contents. These liquids therefore are not suitable compositions to debate the primary versus evolved character of primitive MORB glasses.

Are Primitive MORB Glasses Primary Magmas at 10 kbar?

Based on the results of the 10 kbar melting study on MORB pyrolite, Tinaquillo lherzolite, Hawaiian pyrolite and KLB-1, primitive MORB glasses with Mg# $\geqslant$ 0.68 are not primary magmas at 10 kbar, nor do most of them lie on olivine control lines from 10 kbar olivine + orthopyroxene + clinopyroxene + spinel + liquid cotectics. However primitive MORB glasses with SiO_2 contents greater than 50 wt% can either be derived from picritic parents or alternatively are primary magmas at depths less than 10 kbar. The SiO_2 rich primitive MORB glasses, which are characterized by low olivine normative contents or are quartz normative, have several compositional characteristics that distinguish them from most other primitive MORB glasses. Compared to most other primitive MORB glasses, these SiO_2 rich glasses have higher CaO contents, lower Na_2O and TiO_2 contents and have higher CaO/Al_2O_3 and CaO/Na_2O ratios. They show geochemical affinities to proposed second-stage melts in the oceanic setting (*Duncan* and *Green*, 1987; *Falloon* and *Green*, 1986).

Second-stage melts result from the remelting of a depleted peridotite diapir at shallow depths (< 30 km) the diapir having lost a first stage melt fraction at some greater depth. Proposed second stage melt compositions include the upper pillow lavas of the Troodos ophiolite, Cyprus (*Cameron*, 1985; *Duncan* and *Green*, 1987), basalt glass compositions from the Lau back arc basin (*Hawkins* and *Melchior*, 1985) and glass inclusions in magnesian olivine (Fo_{94}) phenocrysts from the North Tonga forearc (*Falloon* and *Green*, 1986). Although such compositions have so far not been identified amongst MORB suites, they are necessary to explain the existence of calcic plagioclase megacrysts found within MORB (*Fisk*, 1984; *Donaldson* and *Brown*, 1977; *Autio* and *Rhodes*, 1984; *Stakes* et al., 1984: *Price* et al., 1986). The failure to locate magma batches retaining such refractory compositions may be due to processes such as magma mixing of small volume second-stage melts with dominant and subjacent stage-one picrites (*Duncan* and *Green*, 1980).

The 10 kbar melts from Tinaquillo lherzolite and 77 PAII-1 are similar to those

expected of second-stage melts. However in Fig. 7 and 10 the primitive MORB glasses with low normative olivine or with normative quartz, plot at higher normative Di contents than liquid compositions from Tinaquillo lherzolite and 77 PAII-1. This suggests that these distinctive primitive MORB glass compositions have undergoe some degree of olivine fractionation. These glass compositions do not appear to be primary melts but the characteristics of these distinctive primitive MORB glasses demands a source composition more depleted than MORB pyrolite.

Conclusions

(1) MORB glasses with Mg#$\geq$0.68 encompass a large range of silica saturation in CIPW molecular normative projections (Ne to Qz normative) in the "basalt tetrahedron".
(2) Previous high pressure liquidus studies on some of these primitive MORB glasses have failed to conclusively demonstrate multiple saturation in olivine + orthopyroxene ± clinopyroxene at any pressure.
(3) Equilibrium partial melts at 10 kbar from MORB pyrolite, Hawaiian pyrolite, Tinaquillo lherzolite and the spinel lherzolite KLB-1 form a relatively self consistent data set. The liquid compositions from these four peridotite compositions are all distinctly different from primitive MORB glasses and except for liquid compositions from Hawaiian pyrolite plot below primitive MORB glasses in the projection from plagioclase (An + Ab) in the molecular CIPW normative "basalt tetrahedron". This leads to the preferred interpretation that primitive MORB glasses are not primary melts but are fractionated compositions lying on olivine control lines from more picritic parents.
(4) Many bulk compositions used previously in melting studies relevant to MORB petrogenesis, when compared with natural peridotite suites representative of oceanic upper mantle, such as the Ronda peridotite and Lake Bullenmerri lherzolite nodules, are found to have distinct compositional differences from the natural suites and are inappropriate for use in 10 kbar melting studies.
(5) Silica contents of primitive MORB glasses show a slight bimodal distribution with most primitive MORB glasses having SiO_2 contents <50 wt%, and a small, but significant number, having SiO_2 contents greater than 51 wt%. These more silica rich glasses have characteristics similar to those expected of second-stage melting of depleted mantle peridotite.
(6) Some previous 10 kbar melting studies are shown to have used inappropriate bulk compositions, and have suffered from problems such as quench modification of glasses and Fe-loss.
(7) The experiments of *Takahashi* and *Kushiro* (1983) produced liquid compositions unlike primitive MORB glasses but very similar to more Fe-rich MORB. If Fe-rich mantle is involved in the petrogenesis of MORB then such magmas are possible primary melts at low pressures.
(8) The composition of a liquid in equilibrium with olivine + orthopyroxene + clinopyroxene + spinel + plagioclase is unlike primitive MORB glasses at 10 kbar. The model of *Presnall* et al. (1979) involving melting at a 9 kbar "cusp" can not explain the range in composition of primitive MORB glasses.
(9) At pressures between 7–11 kbars liquid compositions from peridotite in the complex system, as opposed to simple systems (*Presnall* and *Hoover*, 1984, 1986),

will be too silica rich compared to most primitive MORB glasses. Higher pressures and consequently more MgO-rich parents are required.

Acknowledgements

Financial support for this study was provided by a Commonwealth postgraduate award to *T. J. Falloon* and ARGS funds to *D. H. Green*. Technical assistance was provided by *W. Jablonski* and *K. L. Harris*.

References

Allegre CJ, Treuil M, Minster J, Minster B, Albarede F (1977) Systematic use of trace elements in igneous process. Part 1: Fractional crystallization processes in volcanic suites. Contrib Min Petrol 60: 57–65

Autio LK, Rhodes JM (1984) Costa Rica rift zone basalts: geochemical and experimental data from a possible example of multistage melting. In: *Cann JR, Langsetz MG, Honnorez J, von Herzen RP, White SM* (eds) Initial reports of the deep sea drilling project, vol 69, Washington (U.S. Government Printing Office), pp 729–745

Barker SE, Kudo AM, Keil K (1983) Mineral chemistry of basalts from Holes 483 and 483B. In: *Lewis BTR, Robinson P*, et al (eds) Initial reports of the deep sea drilling project, vol 65, Washington (U.S. Government Printing Office), pp 635–642

Basaltic Volcanism Study Project (1981) Basaltic volcanism on the terrestrial planets. Pergamon Press, New York, 1286 pp.

Bender JF, Hodges FN, Bence AE (1978) Petrogenesis of basalts from the project FAMOUS area: experimental study from 0–15 kbars. Earth Planet Sci Lett 41: 277–302

Bryan WB (1979) Regional variation and petrogenesis of basalt glasses from the FAMOUS area, Mid-Atlantic ridge. J Petrol 20: 293–325

— *Moore JG* (1977) Compositional variations of young basalts in the Mid-Atlantic ridge rift valley near lat 36° 49′ N. Geol Soc Am Bull 88: 556–570

— *Thompson G, Ludden JN* (1981) Compositional variation in normal MORB from 22°–25° N: Mid-Atlantic ridge and Kane fracture zone. J Geophys Res 86: 11,815–11,836

Cameron WE (1985) Petrology and origin of primitive lavas from the Troodos ophiolite, Cyprus. Contrib Min Petrol 89: 239–255

Christie DM, Carmichael ISE, Langmuir CH (1986) Oxidation states of mid-ocean ridge basalt glasses. Earth Planet Sci Lett 79: 397–411

Dick HJB, Fisher RL (1984) Mineralogic studies of the residues of mantle melting: abyssal and alpine type-peridotites. In: *Kornprobst J* (ed) Kimberlites II. The mantle and crust-mantle relationships. Elsevier, Amsterdam, pp 295–308

Donaldson CH, Brown RW (1977) Refractory megacrysts and magnesium rich melt inclusions within spinel in oceanic tholeiites: indicators of magma mixing and parental magma composition. Earth Planet Sci Lett 37: 81–89

Duncan RA, Green DH (1980) Role of multistage melting in the formation of oceanic crust. Geology 8: 22–26

— *Green DH* (1987) The genesis of refractory melts in the formation of oceanic crust. Contrib Min Petrol 96: 326–342

Elthon D (1983) Isomolar and isostructural pseudo-liquidus phase diagrams for oceanic basalts. Am Min 68: 506–511

— *Scarfe CM* (1980) High pressure equilibria of a high-mg basalt: implications for the origin of MORB. Carnegie Institute of Washington Yearbook 79: 277–281

— — (1984) High-pressure phase equilibria of a high-magnesia basalt and the genesis of primary oceanic basalts. Am Min 69: 1–15

Falloon TJ, Green DH (1986) Glass inclusions in magnesian olivine phenocrysts from Tonga: evidence for highly refractory parental magmas in the Tongan arc. Earth Planet Sci Lett 81: 95–103

— — *Hatton CJ, Harris KL* (1988) The anhydrous partial melting of a fertile and depleted peridotite from 2–30 kbar and application to basalt petrogenesis. J Petrol (in press)
— — (1987) Anhydrous partial melting of peridotite from 8 to 35 kbars and the petrogenesis of MORB. J Petrol (submitted)
Fisk MK (1984) Depths and temperature of mid-ocean ridge magma chambers and the composition of their source magmas. In: *Gass IG, Lippard SJ, Shelton AW* (eds) Ophiolites and oceanic lithosphere. Blackwell Scientific Publications, Oxford, pp 17–23
Frey FA, Bryan WB, Thompson G (1974) Atlantic Ocean Floor: Geochemistry and Petrology of basalts from Legs 2 and 3 of the DSDP. J Geophys Res 79: 5507–5527
— *Suen CJ, Stockman HW* (1985) The Ronda high temperature peridotite: Geochemistry and petrogenesis. Geochim Cosmochim Acta 49: 2469–2491
— *Bryan WB, Thompson G, Roy S* (1973) Petrological and geochemical results for basalts from DSDP Legs 2 and 3. EOS Trans. AGU, 54: 1004–1006
Fujii T, Kushiro I (1977) Melting relations and viscousity of an abyssal tholeiite. Yb Carnegie Instn Wash 76: 461–465
— *Bougault H* (1983) Melting relations of a magnesian abyssal tholeiite and the origin of MORBs. Earth Planet Sci Lett 62: 283–295
— *Scarfe CM* (1985) Compositions of liquids coexisting with spinel lherzolite at 10 kbar and the genesis of MORBs. Earth Planet Sci Lett 90: 18–28
— *Kushiro I, Hamuro K* (1978) Melting relations and viscosity of an abyssal olivine tholeiite. In: *Melson WG, Rabinowitz PD,* et al. (eds) Initial reports of the deep sea drilling project, vol 45, Washington (U.S. Government Printing Office), pp 513–517
Green DH (1970) The origin of basaltic and nephelinitic magmas. Trans Leicester Lit Phil Society 64: 28–54
— (1971) Composition of basaltic magmas as indicators of conditions of origin: application to oceanic volcanism. Phil Trans Roy Soc Lond 268: 707–725
— (1973) Experimental melting studies on a model upper mantle composition at high pressure under water-saturated and water-undersaturated conditions. Earth Planet Sci Lett 19: 37–53
— (1976) Experimental testing of "equilibrium" partial melting of peridotite under water-saturated, high-pressure conditions. Can Min 14: 255–268
— *Ringwood AE* (1967) The genesis of basaltic magmas. Contrib Min Petrol 15: 103–190
— *Hibberson WO, Jaques AL* (1979) Petrogenesis of mid-ocean ridge basalts. In: *McElhinney MW* (ed) The Earth: its origin structure and evolution. Academic Press London, pp 265–299
— *Falloon TJ, Taylor WR* (1987) Mantle derived magmas role of variable source peridotite and variable C-H-O fluid compositions. In: *Mysen BO* (ed) Magmatic processes: Physicochemical principles. The Geochemical Society Spec Publ 1: 139–154
Grove TL, Gerlach DC, Sando TW (1982) Origin of Calc-Alkaline Series Lavas at Medicine Lake Volcano by fractionation, assimilation and mixing. Contrib Min Petrol 80: 160–182
Hawkins JW, Melchior JT (1985) Petrology of Mariana trough and Lau Basin Basalts. J Geophys Res 90: 11,431–11,468
Hekinian R, Moore JG, Bryan WB (1976) Volcanic rocks and processes of the mid-Atlantic ridge rift valley near 36°49′ N. Contrib Mineral Petrol 58: 83–110
Jagoutz E, Palme H, Baddenhausen H, Blum K, Cendales M, Dreibus G, Spettel B, Lorenz V, Wanke H (1979) The abundance of major, minor and trace elements in the earth's mantle as derived from primitive ultramafic nodules. Proc Lunar planet Sci Conf 10th. Geochim Cosmochim Acta [Suppl] 11: 2031–2050
Jaques AL, Green DH (1979) Determination of liquid compositions in high-pressure melting of peridotite. Am Min 64: 1312–1321
— — (1980) Anhydrous melting of peridotite at 0–15 kbar pressure and the genesis of tholeiitic basalts. Contrib Min Petrol 73: 287–310

Kushiro I (1973) Origin of some magmas in oceanic and circum-oceanic regions. Tectonophysics 17: 211–222

— (1975) On the nature of silicate melt and its significance in magma genesis: regularities in the shift of the liquidus boundaries involving olivine, pyroxene and silica minerals. Am J Sci 275: 411–431

— *Thompson RN* (1972) Origin of some abyssal tholeiites from the mid-Atlantic ridge. Carnegie Inst Washington Yearb 71: 403–406

Langmuir CH, Bender JF, Bence AE, Hanson GN (1977) Petrogenesis of basalts from the FAMOUS area: Mid-Atlantic ridge. Earth Planet Sci Lett 36: 133–156

Le Roex AP, Erlank AJ, Needham HD (1981) Geochemical and mineralogical evidence for the occurrence of at least three distinct magma types in the "FAMOUS" region. Contrib Min Petrol 77: 24–37

Maaloe S, Aoki K (1977) The major element composition of the upper mantle estimated from the composition of lherzolites. Contrib Min Petrol 63: 161–173

Melson WG (1973) Basaltic glasses from the Deep Sea Drilling Project: chemical characteristics, compositions of alteration products, and fission track "ages". EOS 54: 1011

— *O'Hearn T* (1979) Basaltic glass erupted along the mid-Atlantic ridge between 0–37 °N: Relationships between composition and latitude. In: *Talwani M, Hay W, Ryan WBF* (eds) Deep Sea Drilling Results in the Atlantic Ocean: Ocean Crust. Am Geophys Union, Maurice Ewing ser 2: 273–284

— *Vallier T, Wright TL, Bylerly G, Nelen J* (1976) Chemical diversity of abyssal volcanic glass erupted along Pacific, Atlantic, and Indian Ocean sea-floor spreading centers. AGU Geophys Mon 19: 351–368

— *Byerly GR, Nelen JA, O'Hearn T, Wright TL, Vallier T* (1977) A catalog of the major element chemistry of abyssal volcanic glasses. Smithsonian Contrib Earth Sci 19: 31–60

Merrill RB, Wyllie PJ (1973) Absorption of iron by platinum capsules in high pressure rock melting experiments. Am Min 58: 16–20

Natland JH, Adamson AC, Laverne C, Melson WG, O'Hearn T (1984) A compositionally nearly steady-state magma chamber at the Costa Rica Rift: Evidence from basalt glass and mineral data, deep sea drilling project sites 501, 504 and 505. In: *Cann JR, Langseth MG, Honnorez J, von Herzen RP, White SM* et al (eds) Initial reports of the deep sea drilling project, vol 69, Washington (U.S. Government Printing Office), pp 811–858

Nehru CE, Wyllie PJ (1975) Compositions of glasses from St. Pauls peridotite partially melted at 20 kbar. J Geol 83: 455–471

Nickel KG, Green DH (1984) The nature of the upper-most mantle beneath Victoria, Australia as deduced from ultramafic xenoliths. In: *Kornprobst J* (ed) Kimberlites II. The mantle and crust-mantle relationships. Elsevier, Amsterdam, pp 161–178

O'Donnell TH, Presnall DC (1980) Chemical variations of the glass and mineral phases in basalts dredged from 25°–30 °N along the mid-Atlantic ridge. Am J Sci 280: 845–868

O'Hara MJ (1968) Are ocean floor basalts primary magma? Nature 220: 683–686

— *Humphreys DJ* (1977) Problems of iron gain and loss during experimentation on natural rocks: The experimental crystallization of five lunar basalts at low pressure. Phil Trans R Soc Lond 286: 313–330

Presnall DC, Hoover JD (1984) Composition and depth of origin of primary mid-ocean ridge basalts. Contrib Min Petrol 87: 170–178

— — (1986) Composition and depth of origin of primary mid-ocean ridge basalts-reply to D. Elthon. Contrib Min Petrol 94: 257–261

— *Dixon JR, O'Donnell TH, Dixon SA* (1979) Generation of mid-ocean ridge tholeiites. J Petrol 20: 3–35

Price RC, Kennedy AK, Riggs-Sneeringer M, Frey FA (1986) Geochemistry of basalts from the Indian Ocean triple junction: implications for the generation and evolution of Indian Ocean ridge basalts. Earth Planet Sci Lett 78: 379–396

Roeder PL, Emslie RF (1970) Olivine-liquid equilibrium. Contrib Min Petrol 29: 275–289
Sato H (1977) Nickel content of basaltic magmas: identification of primary magmas and a measure of the degree of olivine fractionation. Lithos 10: 113–120
Scarfe CM, Smith DGW, (1977) Secondary minerals in some basaltic rocks from DSDP Leg 37. Can J Earth Sci 14: 903–910
Sen G (1982) Composition of basaltic liquids generated from a partially depleted lherzolite at 9 kbar pressure. Nature 299: 336–338
Shibata T, Thompson G (1986) Peridotites from the mid-Atlantic ridge at 43 °N and their petrogenetic relation to abyssal tholeiites. Contrib Mi Petrol 93: 144–159
— *DeLong SE, Walker D* (1979) Abyssal tholeiites from the oceanographer fracture zone. I. Petrology and fractionation. Contrib Min Petrol 70: 89–102
Shipboard Scientific Party (1977) Initial reports of the deep sea drilling project, vol 37, Washington (U.S. Government Printing Office), pp 15–326
Sigurdsson H (1981) First-order major element variation in basalt glasses from the mid-Atlantic ridge 29 °N to 73 °N. J Geophys Res 86: 9483–9502
Stakes DS, Shervais JW, Hopson CA (1984) The volcanic-tectonic cycle of the FAMOUS and AMAR valleys, Mid-Atlantic ridge (36°47′N): evidence from basalt glass and phenocryst compositional variations for a steady state magma chamber beneath the valley midsections, AMAR 3. J Geophys Res 89: 6995–7028
Stern CR, Wyllie PJ (1975) Effect of iron absorption by noble-metal capsules on phase boundaries in rock melting experiments at 30 kbar. Am Mineral 60: 681–689
Stolper E (1980) A phase diagram for mid-ocean ridge basalts: preliminary results and implications for petrogenesis. Contrib Min Petrol 74: 13–27
Takahashi E (1980) Olivine/liquid nickel partitioning at high pressures: experiments with an olivine capsule. EOS 61: 397
— (1986) Melting of a dry peridotite KLB-1 up to 14 Gpa: Implications on the origin of peridotitic upper mantle. J Geophys Res 91: 9367–9382
— *Kushiro I* (1983) Melting of a dry peridotite at high pressures and basalt magma genesis. Am Min 68: 859–879
Thompson RN (1987) Phase-equilibria constraints on the genesis and magmatic evolution of oceanic basalts. Earth Science Reviews 24: 161–210.
Walker D, Shibata T, DeLong SE (1979) Abyssal tholeiites from the oceanographer fracture zone. II. Phased equilibria and mixing. Contrib Min Petrol 70: 111–125
Wilkinson JFG (1982) The genesis of mid-ocean ridge basalts. Earth Science Reviews 18: 1–57
Yoder HS Jr, Tilley CE (1962) Origin of basalt magmas: an experimental study of natural and synthetic rock systems. J Petrol 3: 342–532

Authors' address: Dr. *T. J. Falloon*, Geology Department, University of Tasmania, Hobart 7001, Australia.

Printed in Austria